

ORGANOMETALLICS

Volume 14, Number 3, March 1995

© Copyright 1995
American Chemical Society

Communications

Asymmetric Induction in the Diels–Alder Reaction Catalyzed by Chiral Metallocene Triflate Complexes: Dramatic Effect of Solvent Polarity

James B. Jaquith, Jinying Guan, Shaotian Wang, and Scott Collins*

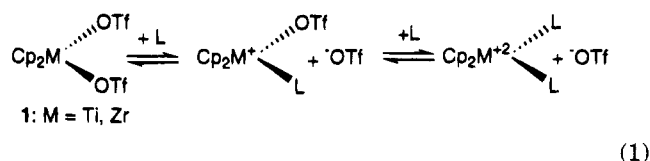
Department of Chemistry, University of Waterloo, Waterloo, Ontario, Canada N2L 3G1

Received October 28, 1994[®]

Summary: The Diels–Alder cycloaddition reaction between oxazolidinone-based dienophiles **4–6** and cyclopentadiene is efficiently catalyzed by the chiral metallocene complex [(*S*)-1,2-ethylenebis(η^5 -tetrahydroindenyl)]Zr(OTf)₂ (**2**) as well as its titanium analog (**3**). The level of asymmetric induction is dramatically affected by solvent polarity; in CH₂Cl₂ solvent the cycloaddition process is essentially nonstereoselective, whereas in CH₃NO₂ or 2-nitropropane, higher enantioselectivity (>70% ee) is observed. This behavior can be partially explained with reference to the results of variable-temperature NMR studies of the complexes derived from *rac*-**2** and dienophile **4**.

The use of electron-deficient metallocene compounds of the group 4 elements in organic synthesis is attracting increasing attention. Achiral and chiral cationic metallocene alkoxide complexes of zirconium have been employed in catalytic amounts in the Diels–Alder reaction and the Mukaiyama cross-aldol condensation.¹ Related applications have also been reported by Bosnich and co-workers, employing achiral metallocene bis(triflate) complexes of titanium and zirconium (**1**)² that were initially prepared and structurally characterized by Thewalt and co-workers.³ They are related to

cationic metallocene complexes in that one (or both) of the triflate ligands is labile, particularly in polar, donor solvents (eq 1).^{2,3}



(1)

It occurred to us that such catalysts might prove advantageous for use with substrates that can coordinate to the metal center in a bidentate fashion; the alkoxide complexes studied previously are unlikely candidates, as the alkoxide ligand functions as, at least a 4 e donor to the metal center.¹ We report here preliminary results concerning the use of chiral metallocene bis(triflate) complexes and bidentate dienophiles in the Diels–Alder reaction.⁴

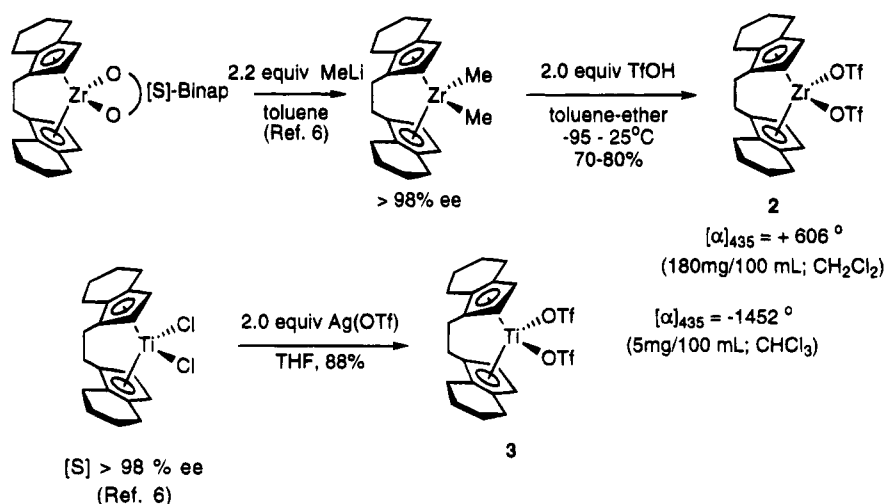
(2) (a) Hollis, T. K.; Robinson, N. P.; Whelan, J.; Bosnich, B. *Tetrahedron Lett.* **1993**, *34*, 4309. (b) Hollis, T. K.; Odenkirk, W.; Robinson, N. P.; Whelan, J.; Bosnich, B. *Tetrahedron* **1993**, *49*, 5415. (c) Hollis, T. K.; Robinson, N. P.; Bosnich, B. *J. Am. Chem. Soc.* **1992**, *114*, 5464. (d) Hollis, T. K.; Robinson, N. P.; Bosnich, B. *Organometallics* **1992**, *12*, 2745. (e) Hollis, T. K.; Robinson, N. P.; Bosnich, B. *Tetrahedron Lett.* **1992**, *33*, 6423.

(3) (a) Thewalt, U.; Klein, H. P. *Z. Kristallogr.* **1980**, *153*, 307. (b) Thewalt, U.; Lasser, W. *Z. Naturforsch., B: Anorg. Chem., Org. Chem.* **1983**, *38B*, 1501.

[®] Abstract published in *Advance ACS Abstracts*, February 15, 1995.

(1) (a) Hong, Y.; Norris, D. J.; Collins, S. *J. Org. Chem.* **1993**, *58*, 3591. (b) Hong, Y.; Kuntz, B. A.; Taylor, N. J.; Collins, S. *Organometallics* **1993**, *12*, 964. (c) Collins, S.; Koene, B. E.; Ramachandran, R.; Taylor, N. *J. Organometallics* **1991**, *10*, 2092.

Scheme 1

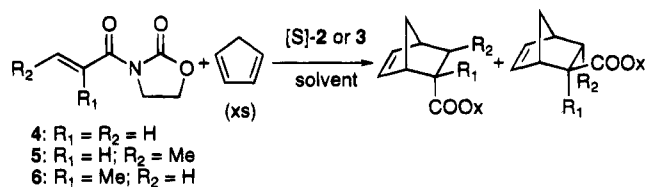


The chiral metallocene bis(triflate) complexes **2** and **3**⁵ were prepared as outlined in Scheme 1⁶ and were used to catalyze the Diels–Alder reaction of cyclopentadiene with oxazolidinone-derived dienophiles **4–6** (Table 1).⁷

As is evident from the experiments summarized in Table 1, the rate and stereoselectivity of the Diels–Alder reaction are significantly influenced by the polarity of the solvent employed. In particular, the rate of the reaction is generally enhanced in the polar solvent CH₃NO₂ and the endo selectivity is somewhat diminished from that seen in CH₂Cl₂ (e.g. entry 1 vs 2).

However, the level of asymmetric induction is dramatically affected; the cycloaddition process involving

Table 1. Diels–Alder Reactions Catalyzed by Complexes **2** and **3**^a



entry no.	catalyst (amt, mol %)	dienophile	solvent	T (°C)	t (h) ^b	Y (%)	endo: exo ^c	% ee ^d
1	3 (10.0)	4	CH ₂ Cl ₂	0	8	91	9:1	~0
2	3 (10.0)	4	CH ₃ NO ₂	0	0.5	94	7:1	88
3	3 (5.0)	4	CH ₃ NO ₂	0	0.5	88	6:1	85
4	3 (5.0)	4	CH ₃ NO ₂	-30	0.5	85	7:1	89
5	2 (1.0)	4	CH ₂ Cl ₂	-78	1	88	30:1	30
6	2 (1.0)	4	CH ₃ NO ₂	-30	1	94	5:1	68
7	2 (5.0)	4	NO ₂ CH(CH ₃) ₂	-78	8	84	6:1	92
8	2 (5.0)	5	CH ₂ Cl ₂	-30	24	40	4:1	70
9	2 (1.0)	5	NO ₂ CH(CH ₃) ₂	-30	24	52	8:1	92
10	2 (5.0)	5	NO ₂ CH(CH ₃) ₂	-30	2	87	7:1	90
11	2 (5.0)	5	NO ₂ CH(CH ₃) ₂	-78	24	84	15:1	95
12	2 (5.0)	6	CH ₂ Cl ₂	-30	24	12	3.1:1	69 ^{e,f}
13	2 (1.0)	6	CH ₃ NO ₂	-30	48	59	1.1:1	78 ^{e,f}
14	2 (5.0)	6	CH ₃ NO ₂	-30	48	88	1.1:1	78 ^{e,f}

^a Reactions were conducted under the following conditions in the indicated solvent: [dienophile] = ~0.5 M; [diene] = ~1.0–2.0 M. ^b The time required for 100% conversion as monitored by TLC. ^c Determined by ¹H NMR and/or HPLC (Chiracel OD column). ^d The % ee is quoted for the endo diastereomer, which was determined by HPLC; the major endo enantiomer possesses the 2R configuration, as revealed by conversion to the known benzyl ester.⁴ ^e The figure quoted is for the exo diastereomer; the endo enantiomers were not resolved by HPLC. ^f The absolute configuration of the major enantiomer was not determined, as the endo and exo diastereomers could not be separated by chromatography.

dienophile **4** is essentially stereorandom in CH₂Cl₂, whereas in CH₃NO₂ much higher enantioselectivity is observed using catalyst **3** (entries 1 and 2). Similar, although less dramatic, effects are observed when using the zirconium catalyst **2** (entries 5–7) or dienophiles **5** and **6** and this catalyst (entries 8 and 10 and 12 and 14, respectively). In both solvents and using either catalyst, the absolute configuration of the major enantiomer is the same.

Insight into the reasons for these dramatic differences was obtained from variable-temperature ¹H and ¹⁹F NMR studies on the complexation of dienophile **4** to racemic zirconium catalyst **2** in CD₂Cl₂ and CD₃NO₂.⁸

(4) For similar approaches employing other chiral catalysts and oxazolidinone-based dienophiles see, inter alia: (a) Evans, D. A.; Miller, S. J.; Lectka, T. *J. Am. Chem. Soc.* **1993**, *115*, 6460 (90 to >98% ee). (b) Corey, E. J.; Imai, N.; Zhang, H.-Y. *J. Am. Chem. Soc.* **1991**, *113*, 728 (80–86% ee). (c) Narasaka, K.; Iwasawa, N.; Inoue, M.; Yamada, T.; Nakashima, M.; Sugimori, J. *J. Am. Chem. Soc.* **1989**, *111*, 5340 (72–84% ee) and references therein. For earlier work employing chiral oxazolidinone-based dienophiles and achiral alkylaluminum catalysts see: Evans, D. A.; Chapman, K. T.; Bisaha, J. *J. Am. Chem. Soc.* **1988**, *110*, 1238.

(5) (a) (S)-**2**: [α]₄₃₅ = +606° (c = 180 mg/100 mL; CH₂Cl₂); ¹H NMR (250 MHz, CDCl₃) δ 6.80 (d, J = 3 Hz, 2H), 5.90 (d, J = 3 Hz, 2H), 3.46 (br s, 4H), 2.63 (m, 8H), 1.83 (m, 4H), 1.61 (m, 4H) ppm; ¹³C NMR (50 MHz, CDCl₃) δ 138.9, 137.4, 128.9, 118.8 (q, J_{CF} = 318 Hz), 118.7, 112.5, 29.0, 24.0, 23.0, 21.6, 21.4 ppm; ¹⁹F NMR (188 MHz, CDCl₃, 25 °C) δ -77.2 (s) ppm; IR (KBr) 3112, 3076, 2950, 2912, 2865, 1677, 1649, 1493, 1469, 1441, 1353, 1314, 1291, 1236, 1197, 1152, 981, 818, 628 cm⁻¹; MS (EI) m/z 652 (M⁺, ⁹⁰Zr). Anal. Calcd for C₂₂H₂₄F₆O₆S₂Zr: C, 40.42; H, 3.70. Found: C, 40.18; H, 3.89. (b) (S)-**3**: [α]₄₃₅ = -1452° (c = 5 mg/100 mL; CHCl₃); ¹H NMR (250 MHz, CDCl₃) δ 6.96 (d, J = 3 Hz, 2H), 5.92 (d, J = 3 Hz, 2H), 3.68 (m, 4H), 2.64 (m, 8H), 1.81 (m, 4H), 1.52 (m, 4H) ppm; ¹³C NMR (62.8 MHz, CDCl₃) δ 146.3, 142.4, 134.7, 124.6, 119.2 (q, J_{CF} = 319 Hz), 117.3, 29.3, 24.7, 23.7, 21.1, 20.9 ppm; ¹⁹F NMR (188 MHz, CD₂Cl₂, 25 °C) δ -77.4 (s) ppm with CFC₃ as an external standard; IR (CHCl₃) 3055, 2942, 2305.67, 1428, 1347, 1265, 1200, 1009, 896, 740, 632 cm⁻¹. Anal. Calcd for C₂₂H₂₄F₆O₆S₂Ti: C, 43.28; H, 3.96; S, 10.50. Found: C, 42.94; H, 3.94; S, 10.88.

(6) (a) Grossman, R. B.; Davis, W. M.; Buchwald, S. L. *J. Am. Chem. Soc.* **1991**, *113*, 2321. (b) Collins, S.; Kuntz, B. A.; Hong, Y. *J. Org. Chem.* **1989**, *54*, 4154 and references therein.

(7) Typical procedure: Oxazolidinone **4** (141 mg, 1.0 mmol) and (S)-**2** (6.5 mg, 0.01 mmol) were combined and dissolved in CH₃NO₂ (2.0 mL). After the solution was cooled to -30 °C, cyclopentadiene (200–500 μL) was added via syringe. After 50 min at this temperature, TLC (silica gel, CH₂Cl₂) revealed the complete consumption of **4**. The mixture was quenched with saturated aqueous NH₄Cl (2 mL) and diluted with CH₂Cl₂ (10 mL) and water (5 mL). The aqueous layer was washed with CH₂Cl₂ (2 × 5 mL) and the combined organic layers dried over anhydrous Na₂SO₄ and filtered and solvent removed in vacuo to provide the crude adduct in ca. 90% yield, substantially pure by ¹H NMR spectroscopy. The adducts could be further purified by flash chromatography on silica gel with CH₂Cl₂ as eluent. The diastereomer and enantiomer ratios summarized in Table 1 were determined using the crude mixture prior to chromatography.

In CD_3NO_2 solvent at -30°C , coordination of **4** to the metal center is favored, even with equimolar amounts of both substrates; signals due to unbound **4** and catalyst **2** were weak in the ^1H and ^{19}F NMR spectra.⁹ In CD_2Cl_2 , more complex behavior is observed. Binding of **4** to **2** is entropically unfavorable; signals due to unbound **4** and **2** are clearly present but diminish in intensity at lower temperatures. The equilibrium constant for exchange of bound and unbound **4** is sensitive to temperature and thus the rate of exchange is also highly temperature dependent.

Two complexes are present in a ratio of $\sim 2:1$ in CD_3NO_2 at -30°C , and this ratio is largely unaffected by the presence of excess dienophile or catalyst.⁹ ^{19}F NMR spectra at this temperature exhibit three signals at $\delta -77.0$, -77.2 , and -78.0 ppm in a ratio of $\sim 1:2.2:2.7$.¹⁰ The signal at highest field is characteristic of free triflate ion in this solvent,² whereas the former two signals are at higher field than that observed for catalyst **2** (-76.8 ppm). ^{13}C NMR spectra in CD_3NO_2 clearly indicate that both $\text{C}=\text{O}$ groups of the dienophile are coordinated to Zr in both complexes.¹¹ From these results, it seems clear that substrate **4** binds to **2** and displaces one triflate ligand from the coordination sphere of the metal.

Similar effects are observed in CD_2Cl_2 at -30°C ; the same two complexes are present (on the basis of the similarity in chemical shifts and coupling constants observed in the ^1H NMR spectra) but in a ratio of $\sim 6:1$. ^{19}F NMR spectra at this temperature exhibit four peaks at $\delta -77.2$, -77.8 , -78.2 , and -78.6 ppm; the first signal is due to catalyst **2**, whereas the last three signals are in a ratio of $\sim 1:5.7:7.3$ with the third signal characteristic of free triflate ion.

The simplest interpretation of the results of the Diels–Alder cycloaddition reactions and the NMR studies is shown in Scheme 2; the two five-coordinate complexes **A** and **B** are present that differ in which $\text{C}=\text{O}$ group of the dienophile occupies the central coordination site.¹² From the observed change in the level of asymmetric induction in the two solvents, coupled with the change in stability between the two complexes, it seems

(8) Similar studies employing catalyst **3** were precluded by the very unfavorable equilibrium constant for binding of **4** to this complex, even in CD_3NO_2 (i.e. less than 5% complexation at -30°C at a 1:1 stoichiometry): Guan, J. Unpublished results.

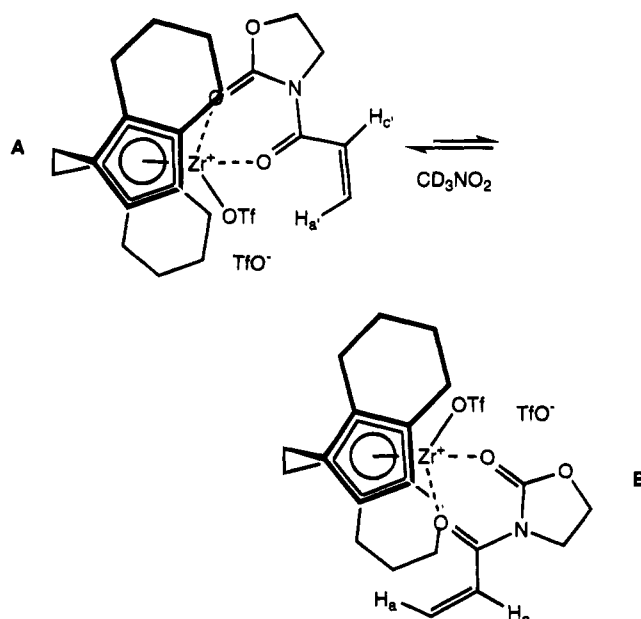
(9) Identical behavior was seen using (*S*)-**2**: Jaquith, J. Unpublished results.

(10) The signal due to free triflate ion is significantly line-broadened, whereas the remaining signals are sharp. Experiments at different catalyst:substrate ratios or using catalyst **2** and $[\text{nBu}_4\text{N}][\text{OTf}]$ demonstrated that free triflate ion is rapidly exchanging with bound triflate in residual catalyst **2** but not with either complex.

(11) See the supplementary material for details. For similar spectroscopic studies employing oxazolidinones such as **4** and other Lewis acids see: Castellano, S.; Dwight, W. J. *J. Am. Chem. Soc.* **1993**, *115*, 2986.

(12) For a discussion of the bonding in five-coordinate bent-metalloene complexes see: Lauher, J. W.; Hoffmann, R. *J. Am. Chem. Soc.* **1976**, *98*, 1729.

Scheme 2



likely that it is the *minor* isomer **B** that reacts most rapidly and selectively with cyclopentadiene. The absolute configuration of the major, *endo* enantiomer formed is also consistent with this hypothesis.¹³

In summary, high enantioselectivity is observed in the Diels–Alder reaction using chiral metallocene complexes and bidentate dienophiles in polar solvents. Future work will be directed toward how metallocene and dienophile structure affect the equilibrium depicted in Scheme 2 and the selectivity of the Diels–Alder reaction.

Acknowledgment. We wish to thank the Natural Sciences and Engineering Research Council for financial support of this work. The assistance of Dr. Sandra Mooibrek and Mrs. Janet Venne with the NMR studies is gratefully acknowledged.

Supplementary Material Available: Text giving experimental procedures and spectroscopic and characterization data for all compounds prepared and figures showing ^1H , ^{13}C , and ^{19}F NMR spectra for the complexes formed from (\pm)-**2** and **4** (26 pages). Ordering information is given on any current masthead page.

OM940825F

(13) Additional support for the hypothesis of complex **B** having the structure shown was obtained by NOE-difference spectra in $\text{CD}_3\text{NO}_2/\text{CD}_2\text{Cl}_2$ solvent mixtures (ca. 5:1) at -55°C . Irradiation of H_a (Scheme 2) led to enhancements (ca. 5%) of two of the CpH protons (on the same ring) in this complex, whereas irradiation of H_a' of the major isomer did not lead to observable NOE for any protons on the tetrahydroindanyl rings. Furthermore, in both complexes, the oxazolidinone adopted the *s-cis* conformation; irradiation of the protons α to N in the oxazolidinone ring led to enhancements of H_c and H_c' , respectively. See the supplementary material for additional details.

Highly Selective Dehydrogenative Silylation of Ethylene Using the Bis(dihydrogen) Complex $\text{RuH}_2(\text{H}_2)_2(\text{PCy}_3)_2$ as Catalyst Precursor

M. Lorraine Christ, Sylviane Sabo-Etienne,* and Bruno Chaudret

Laboratoire de Chimie de Coordination du CNRS, 205, route de Narbonne, 31077 Toulouse Cedex, France

Received December 19, 1994[®]

Summary: The complex $\text{RuH}[(\eta^3\text{-C}_6\text{H}_5)\text{P}(\text{C}_6\text{H}_{11})_2](\text{C}_2\text{H}_4)(\text{PCy}_3)$ (**4**), resulting from the dehydrogenation of a cyclohexyl ring of the bis(dihydrogen) complex $\text{RuH}_2(\text{H}_2)_2(\text{PCy}_3)_2$ (**1**) with C_2H_4 , is a highly efficient catalyst for the selective dehydrogenative silylation of ethylene into the vinylsilane $\text{CH}_2=\text{CHSiEt}_3$ (**2**). Total conversion of 1000 equiv of HSiEt_3 under 20 bar of C_2H_4 is achieved, in less than 15 min at 17 °C, leading to **2** in 93% selectivity.

Although the reactivity of molecular dihydrogen complexes is a very active area, relatively few studies concerning their activity in catalysis have been carried out.¹ Thus, dihydrogen derivatives represent likely catalytic intermediates but more evidence is needed to demonstrate their activity.

As part of our current studies on the properties of the thermally stable bis(dihydrogen) complex $\text{RuH}_2(\text{H}_2)_2(\text{PCy}_3)_2$ (**1**),² we recently reported the stoichiometric reactions of **1** with HER_3 (E = Si, Ge). Dihydrogen substitution leads to the novel compounds $\text{RuH}_2(\text{H}_2)(\text{HER}_3)(\text{PCy}_3)_2$ in which the HER_3 ligand is weakly coordinated.^{2e} We now demonstrate the catalytic activity of **1** toward ethylene and triethylsilane.

The hydrosilylation of olefins catalyzed by transition-metal complexes (eq 1) has been extensively studied,³ but the competitive reaction of dehydrogenative silylation of olefins has been much less documented (eq 2).⁴

[®] Abstract published in *Advance ACS Abstracts*, February 15, 1995.

(1) (a) Kubas, G. *J. Acc. Chem. Res.* **1988**, *21*, 120. (b) Crabtree, R. H. *Acc. Chem. Res.* **1990**, *23*, 95. (c) Crabtree, R. H. *Angew. Chem., Int. Ed. Engl.* **1993**, *32*, 789. (d) Jessop, P. G.; Morris, R. H. *Coord. Chem. Rev.* **1992**, *121*, 155. (e) Heinekey, D. M.; Oldham, W. J., Jr. *Chem. Rev.* **1993**, *93*, 913.

(2) (a) Chaudret, B.; Poilblanc, R. *Organometallics* **1985**, *4*, 1722. (b) Arliguie, T.; Chaudret, B.; Morris, R. H.; Sella, A. *Inorg. Chem.* **1988**, *27*, 598. (c) Chaudret, B.; Chung, G.; Eisenstein, O.; Jackson, S. A.; Lahoz, F. J.; Lopez, J. A. *J. Am. Chem. Soc.* **1991**, *113*, 2314. (d) Arliguie, T.; Chaudret, B.; Chung, G.; Dahan, F. *Organometallics* **1991**, *10*, 2973. (e) Sabo-Etienne, S.; Hernandez, M.; Chung, G.; Chaudret, B.; Castel, A. *New J. Chem.* **1994**, *18*, 175. (f) Christ, M. L.; Sabo-Etienne, S.; Chaudret, B. *Organometallics* **1994**, *13*, 3800. (g) Christ, M. L.; Sabo-Etienne, S.; Chung, G.; Chaudret, B. *Inorg. Chem.* **1994**, *33*, 5316.

(3) Brookhart, M.; Grant, B. E. *J. Am. Chem. Soc.* **1993**, *115*, 2151 and references therein.

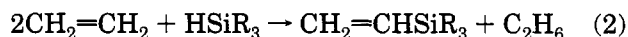
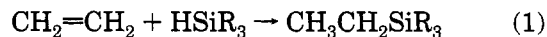
(4) (a) Millan, A.; Fernandez, M.-J.; Bentz, P.; Maitlis, P. M. *J. Mol. Catal.* **1984**, *26*, 89. (b) Tanke, R. S.; Crabtree, R. H. *Organometallics* **1991**, *10*, 415. (c) Corey, J. Y. *Advances in Silicon Chemistry*; Larson, G. L., Ed.; JAI Press: London, 1991; Vol. 1, p 327. (d) Duckett, S. B.; Perutz, R. N. *Organometallics* **1992**, *11*, 90. (e) Kakiuchi, F.; Nogami, K.; Chatani, N.; Seki, Y.; Murai, S. *Organometallics* **1993**, *12*, 4748. (f) Doyle, M. P.; Devora, G. A.; Nefedov, A. O.; High, K. G. *Organometallics* **1992**, *11*, 549. (g) Kesti, M. R.; Waymouth, R. M. *Organometallics* **1992**, *11*, 1095. (h) Seitz, F.; Wrighton, M. S. *Angew. Chem., Int. Ed. Engl.* **1988**, *27*, 289.

Table 1. Reaction of Ethylene with HSiEt_3 Catalyzed by the Ruthenium Complexes **1**, **4**, and **5**

entry no.	catalyst M	$\text{HSiEt}_3:\text{M}$	T (°C)	P (bar)	time (min)	product ratio ^c 2:3
1	1	100	21	1	105	78:22
2	1	100	22	2	30	80:20
3	1	100	60	2	10	79:21
4	1	1000	13	20	30	76:24
5 ^b	1	100	22	1	150	97:3
		+100 ^c	22	1	290	98:2
		+100 ^c	22	1	410	98:2
6	4	100	17	1	80	99:1
7	4	1000	17	20	15	93:7
8	5	100	18	1	90	98:2

^a Determined by GC; in all cases, HSiEt_3 was totally consumed. ^b C_2H_4 was first bubbled into **1** in pentane before addition of HSiEt_3 . ^c 100 additional equiv of HSiEt_3 added.

This alternative reaction has synthetic value because the vinylsilanes are versatile synthetic intermediates.⁵



We describe herein an effective system for the dehydrogenative silylation of ethylene.

The main results are summarized in Table 1. When ethylene is bubbled at room temperature into a mixture of **1** and HSiEt_3 in a 1:100 ratio in pentane solution, total conversion of HSiEt_3 is observed within 2 h, producing the vinylsilane $\text{CH}_2=\text{CHSiEt}_3$ (**2**) in 78% yield together with the hydrosilylated product SiEt_4 (**3**) in 22% yield (entry 1). According to GC analysis, **3** is formed in the early stage of the catalysis (Figure 1). Ethane was detected by GC as well as by ¹H NMR monitoring. The reaction can be run at higher pressure and temperature (entries 2–4) without modification of the selectivity, but this lead to an increase in the reaction rate. High turnover numbers (entry 4) were obtained, and clearly much higher total turnovers can be achieved. Higher selectivity can be simply achieved by bubbling ethylene into a pentane solution of **1** before the addition of HSiEt_3 (entry 5): the vinylsilane **2** is thus obtained in 97% yield. The system is stable since successive additions of HSiEt_3 can be done (entry 5) without any decomposition of the catalyst (even after

(5) (a) Cooke, F.; Moerk, R.; Schwindeman, J.; Magnus, P. *J. Org. Chem.* **1980**, *45*, 1046. (b) Magnus, P. D.; Sarkar, T.; Djuric, S. *Comprehensive Organometallic Chemistry*; Wilkinson, G., Stone, F. G. A., and Abel, E. W., Eds.; Pergamon: New York, 1984; Vol. 7, Chapter 48. (c) Fleming, I.; Dunogues, J.; Smithers, R. H. *Org. React.* **1990**, *37*, 57. (d) Takeuchi, R.; Tanouchi, N. *J. Chem. Soc., Chem. Commun.* **1993**, 1319.

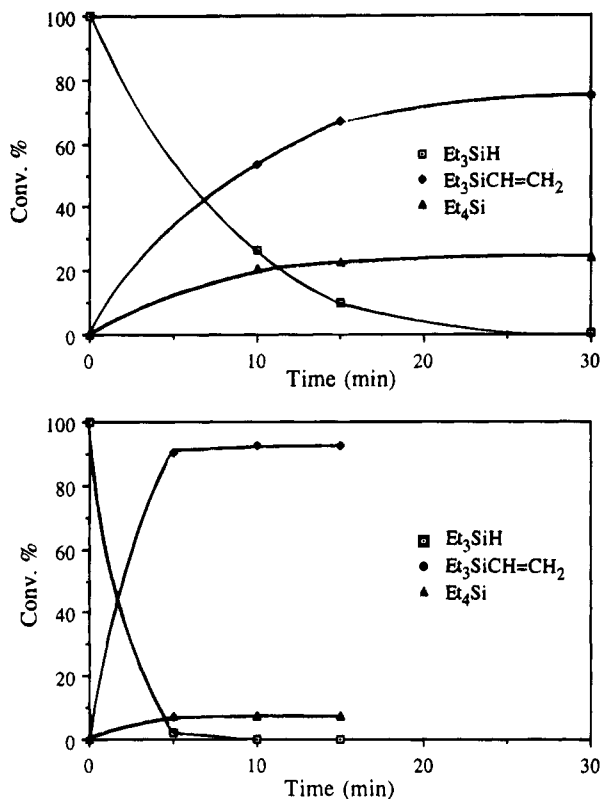


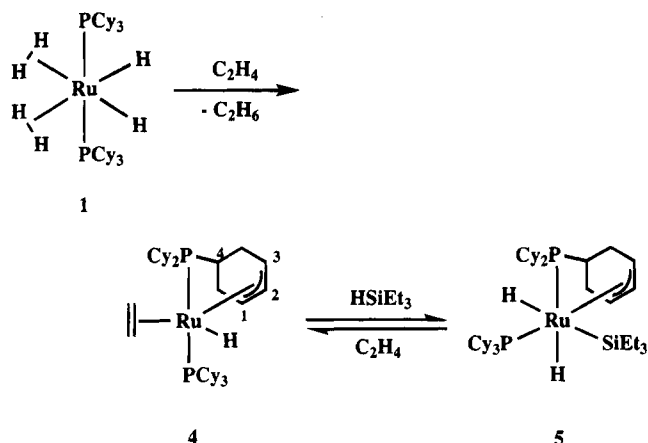
Figure 1. Variation in relative amounts of HSiEt_3 , $\text{CH}_2=\text{CHSiEt}_3$, and SiEt_4 vs time: (top) **1** (0.025 mmol), HSiEt_3 (25 mmol), 20 bar of C_2H_4 , 13 °C; (bottom) **4** (0.025 mmol), HSiEt_3 (25 mmol), 20 bar of C_2H_4 , 17 °C.

the mixture is kept overnight in the absence of ethylene and silane). Finally, when H_2 is bubbled into the reaction mixture at the end of a run (for example such as in entry 2), hydrogenation of the vinylsilane is rapidly achieved and the saturated silane **3** is obtained in 100% yield. We must notice that under the same conditions as entry 1 or 5, less than 5% conversion of HSiEt_3 was obtained using $\text{Ru}_3(\text{CO})_{12}$ or $\text{Ru}(\text{COD})(\text{COT})$ instead of **1** as catalysts.

Having established that **1** is a powerful catalyst, we sought mechanistic information. Bubbling ethylene into a pentane solution of **1** results in the formation of $\text{RuH}[(\eta^3\text{-C}_6\text{H}_8)\text{P}(\text{C}_6\text{H}_{11})_2](\text{C}_2\text{H}_4)(\text{PCy}_3)$ (**4**).⁶ At 223 K, the hydride signal for **4** is observed as a doublet of doublets at $\delta -7.1$, $J_{\text{P-H}} = 18.9$ and 26.2 Hz, and as a singlet upon ^{31}P decoupling. The $^{31}\text{P}\{^1\text{H}\}$ NMR spectrum displays an AB pattern ($\delta 82.2$ and 42.2, $J_{\text{P-P}} = 283$ Hz). Particularly diagnostic for the allyl ligand are the ^{13}C NMR spectra (JMOD and $^{13}\text{C}\{^{31}\text{P}\}$). The doublets at $\delta 77.9$ ($J_{\text{C-H}} = 161$ Hz), $\delta 67.0$ ($J_{\text{C-H}} = 150$ Hz), and

(6) The reaction of **1** with C_2H_4 was previously described as producing a bis(ethylene) complex.^{2a} Additional data, particularly from ^{13}C NMR spectra, lead us to reformulate the complex as $\text{RuH}[(\eta^3\text{-C}_6\text{H}_8)\text{P}(\text{C}_6\text{H}_{11})_2](\text{C}_2\text{H}_4)(\text{PCy}_3)$ (**4**). Complex **4**: A suspension of **1** (500 mg; 0.75 mmol) in pentane (30 mL) was placed in a Fischer-Porter bottle, which was pressurized to 3 bar of ethylene. After immediate dissolution, a white solid precipitated (yield 87%). When ethylene was bubbled, the precipitation was slower. Anal. Calcd for $\text{RuC}_{38}\text{H}_{68}\text{P}_2$: C, 66.3; H, 10.0. Found: C, 66.4; H, 10.4. ^1H NMR (250 MHz, C_6D_6): $\delta -7.1$ (dd, $J_{\text{P-H}} = 18.9$ and 26.2 Hz, Ru-H), 3.24, 3.39, 3.74, 4.26, 5.19, 5.32, 5.54 (all br, 1H each; allylic and ethylenic protons). $^{31}\text{P}\{^1\text{H}\}$ NMR (81.015 MHz, C_6D_6): $\delta 82.2, 42.2$ ($J_{\text{P-P}} = 283$ Hz). ^{13}C NMR (50.32 MHz, C_6D_6): $\delta 77.9$ (d, $J_{\text{C-H}} = 161$ Hz, C_2), 67.0 (d, $J_{\text{C-H}} = 150$ Hz, C_1), 45.8 (d, $J_{\text{C-H}} = 156$ Hz, C_3), 42.3 (dd, $J_{\text{C-H}} = 130$ Hz, $J_{\text{C-P}} = 19$ Hz, C_4); the ethylenic carbons are presumably hidden by the multiplets of the cyclohexyl carbons between $\delta 27$ and 33.

Scheme 1



$\delta 45.8$ ($J_{\text{C-H}} = 156$ Hz) are assigned to the three allylic carbons (see Scheme 1).

Addition of HSiEt_3 to **4** leads to the new complex $\text{Ru}(\text{H})_2(\text{SiEt}_3)[(\eta^3\text{-C}_6\text{H}_8)\text{P}(\text{C}_6\text{H}_{11})_2](\text{PCy}_3)$ (**5**), a formally Ru(IV) complex resulting from oxidative addition (see Scheme 1).⁷ The two hydride ligands for **5** give a broad triplet ($\delta -9.54$, $J_{\text{P-H}} = 17$ Hz) and a doublet of doublets of doublets ($\delta -12.63$, $J_{\text{P-H}} = 57$ Hz, $J_{\text{P-H}} = 25$ Hz, $J_{\text{H-H}} = 5$ Hz), whereas an AB pattern ($\delta 79.9$ and 65.4, $J_{\text{P-P}} = 18$ Hz) is observed in the $^{31}\text{P}\{^1\text{H}\}$ spectrum. The low $J_{\text{P-P}}$ value is in agreement with a formally heptacoordinated structure in which the two phosphines are not in a trans position any more. Finally, upon exposure of **5** to C_2H_4 , we successfully regenerate **4**.

^1H and ^{31}P NMR monitoring of the catalytic reaction at different temperatures revealed that **1** is converted into the complex $\text{RuH}[(\eta^3\text{-C}_6\text{H}_8)\text{P}(\text{C}_6\text{H}_{11})_2](\text{C}_2\text{H}_4)(\text{PCy}_3)$ (**4**).⁸ **4** is observed during all of the catalysis and is the only detected complex after total conversion of HSiEt_3 . Realizing that the catalytic cycle is entered by reaction of **1** with C_2H_4 to produce **4**, we generated a long-lived catalyst system by simply starting with isolated complex **4** (entries 6 and 7); it is noteworthy that there is no reaction between **4** and **2**, which favors the catalytic formation of **2**. When the reaction was carried out under 20 bar of C_2H_4 at 17 °C with the HSiEt_3 :**4** ratio equal to 1000:1, total conversion of HSiEt_3 was observed in less than 15 min and **2** and **3** were obtained in a 93:7 ratio (eq 3).⁹ Finally, **5** was also found to be an effective catalyst precursor (entry 8), therefore suggesting its participation in the catalytic cycle.

(7) Complex **5**: Et_3SiH (89 μL ; 0.56 mmol) was added to a solution of **4** (200 mg; 0.28 mmol) in pentane (200 mL). After the mixture was stirred overnight at room temperature, the yellow solution was concentrated to 20 mL, affording a gray solid on storing at -20 °C for 3 h (yield 91%). Anal. Calcd for $\text{RuC}_{42}\text{H}_{80}\text{P}_2\text{Si}$: C, 65.0; H, 10.41. Found: C, 65.4; H, 10.7. ^1H NMR (250 MHz, C_6D_6): $\delta -12.63$ (ddd, $J_{\text{P-H}} = 57$ and 25 Hz, $J_{\text{H-H}} = 5$ Hz, Ru-H), -9.54 (br t, $J_{\text{P-H}} = 17$ Hz, Ru-H), 1.08 (q, $J_{\text{H-H}} = 8$ Hz, SiCH_2CH_3), 1.48 (t, $J_{\text{H-H}} = 8$ Hz, SiCH_2CH_3), 3.14 (br, 1H), 3.98 (br, 1H), 4.95 (pseudo t, 1H, $J = 6$ Hz). $^{31}\text{P}\{^1\text{H}\}$ NMR (81.015 MHz, C_6D_6): $\delta 79.9, 65.4$ ($J_{\text{P-P}} = 18$ Hz).

(8) We have previously shown that stoichiometric reaction of HSiEt_3 with **1** yields within 5 min the complex $\text{RuH}_2(\text{H}_2)(\text{HSiEt}_3)(\text{PCy}_3)_2$.^{2a} When HSiEt_3 is used, the reaction is much slower and **1** and the new complex $\text{RuH}_2(\text{H}_2)(\text{HSiEt}_3)(\text{PCy}_3)_2$ (**6**) could not be separated. Under ethylene, this mixture regenerates **4** and the organic products **2** and **3**. The competitive formation of **6** and **4** could be responsible for the different selectivity observed when HSiEt_3 is added to **1** prior to bubbling ethylene.

(9) Under conditions of $[\text{4}] = 18$ mg (0.025 mmol) and $[\text{HSiEt}_3] = 4$ mL (25 mmol), the initial turnover rate is ca. 3 s^{-1} (mol of **4**)⁻¹. The reaction is essentially first order in HSiEt_3 .

Oxy Functionalization of Metal-Coordinated Heterocyclic Carbenes^{†,‡}

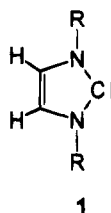
Wolfgang A. Herrmann,* Peter W. Roesky,[§] Martina Elison, Georg Artus, and Karl Öfele

Anorganisch-chemisches Institut der Technischen Universität München,
Lichtenbergstrasse 4, D-85747 Garching bei München, Germany

Received December 6, 1994[®]

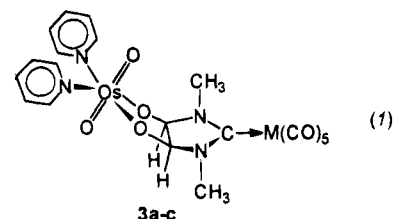
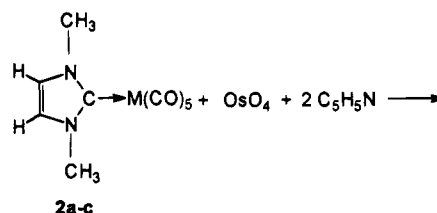
Summary: Metal-coordinated 1,3-dimethylimidazolin-2-ylidene ligands undergo osmylation by means of osmium tetroxide to yield a new type of bimetallic, redox-stable complexes with metals in very different oxidation states (e.g. Cr⁰/Os^{VI}). This oxy functionalization does not influence the metal–carbene bond in a significant way (IR and NMR spectra, single-crystal X-ray diffraction structure).

Carbenes which are derived from imidazolium and pyrazolium salts have long been known as ligands in transition-metal chemistry.² The isolation of the free monomeric ligand **1**³ has spurred renewed interest in



this subject. The attractiveness of these ligands is due both to their easy availability and to their stability. Acting as strongly nucleophilic ligands, heterocyclic carbenes behave in metal coordination chemistry like the widely used phosphines,^{1,4} with π -back-bonding being of little or no importance. In the present paper, we describe the osmylation of metal-attached carbenes.

Treatment of an ether solution of the metal complexes **2a–c** of the CC-unsaturated carbene **1** (R = CH₃) with osmium tetroxide in the presence of pyridine results in the bimetallic complexes **3a–c** as brown precipitates (yields >80%). The products are stable in air and dissolve in polar solvents (eq 1). The crystallographically determined structure of the chromium derivative



2,3	a	b	c
M	Cr	Mo	W

3a (single-crystal X-ray diffraction) and the spectroscopic data reveal a *cis* addition of osmium tetroxide across the C=C bond of the heterocyclic carbene. An osmate ester^{5–7} and a metal carbene,⁸ both of which are known as separate molecules, are connected in **3a–c** by oxy-functionalized 1,3-dimethylimidazolin-2-ylidene ligands (Figure 1). Obviously, the metal carbonyl fragment is kinetically resistant against oxidation; no interaction is observed in the system Os^{VIII}/Cr⁰, with the cyclic voltammetry $E_{1/2}$ data amounting to +1.4 V (irreversible) and –1.1 V (irreversible) vs Ag/AgCl for **3b**.

The individual molecular structures of the components (Cr⁰–carbonyl and Os^{VI}–ester) differ only slightly from the monomolecular examples. The shorter C(carbene)–N bond and the elongated N–C(3,4) bond⁹ may be explained by the disappearance of a certain π -delocalization within the planar carbene moiety of **2a** or by changes in the hybridization at C3 and C4 as a consequence of the CC cross addition of osmium tetroxide. The C–C distance (1.523(6) Å) is in the normal

[†] Heterocyclic Carbenes. 2. Part 1: Reference 1.

[‡] Dedicated to Professor Herbert W. Roesky on the occasion of his 60th birthday.

[§] Kekulé Fellow of the Verband der Chemischen Industrie, Frankfurt am Main, Germany, 1993–1994.

[®] Abstract published in *Advance ACS Abstracts*, February 1, 1995.

(1) Öfele, K.; Herrmann, W. A.; Mihalios, D.; Elison, M.; Herdtweck, E.; Scherer, W.; Mink, J. *J. Organomet. Chem.* **1993**, *459*, 177–184.

(2) (a) Öfele, K. *J. Organomet. Chem.* **1968**, *12*, 42–43. (b) Öfele, K.; Kreiter, C. G. *Chem. Ber.* **1972**, *105*, 529–540. (c) Öfele, K.; Herberhold, M. *Z. Naturforsch.* **1973**, *28B*, 306–309. (d) Öfele, K.; Herberhold, M. *Angew. Chem.* **1970**, *82*, 775–777; *Angew. Chem., Int. Ed. Engl.* **1970**, *9*, 739–740. (e) Wanzlick, H.-W.; Schönherr, H.-J. *Angew. Chem.* **1968**, *80*, 154; *Angew. Chem., Int. Ed. Engl.* **1968**, *7*, 141.

(3) (a) Arduengo, A. J., III; Harlow, R. L.; Kline, M. *J. Am. Chem. Soc.* **1991**, *113*, 361–363. (b) Dixon, D. A.; Arduengo, A. J., III. *J. Phys. Chem.* **1991**, *95*, 4180–4182. (c) Arduengo, A. J., III; Rasika Dias, H. V.; Harlow, R. L.; Kline, M. *J. Am. Chem. Soc.* **1992**, *114*, 5530–5534.

(4) Herrmann, W. A.; Öfele, K.; Elison, M.; Kühn, F. E.; Roesky, P. *J. Organomet. Chem.* **1994**, *480*, C7–C9.

(5) Herrmann, W. A.; Eder, S. J.; Scherer, W. *Chem. Ber.* **1993**, *126*, 39–43.

(6) (a) Criegee, R. *Justus Liebigs Ann. Chem.* **1936**, *522*, 75–96. (b) Criegee, R. *Angew. Chem.* **1937**, *50*, 153–155. (c) Criegee, R.; Marchand, B.; Wannowius, H. *Justus Liebigs Ann. Chem.* **1942**, *550*, 99–133.

(7) (a) Hentges, S. G.; Sharpless, K. B. *J. Am. Chem. Soc.* **1980**, *102*, 4263–4365. (b) Johnson, R. A.; Sharpless, K. B. In *Catalytic Asymmetric Synthesis*; Ojima, I., Ed.; VCH: Weinheim, Germany, 1993; pp 227–272.

(8) Kuhn, N.; Kratz, T.; Boese, R.; Bläser, D. *J. Organomet. Chem.* **1994**, *470*, C8–C11.

(9) Ackermann, K.; Hofmann, P.; Köhler, F. H.; Kratzer, H.; Krist, H.; Öfele, K.; Schmidt, H. R. *Z. Naturforsch.* **1983**, *38B*, 1313–1324.

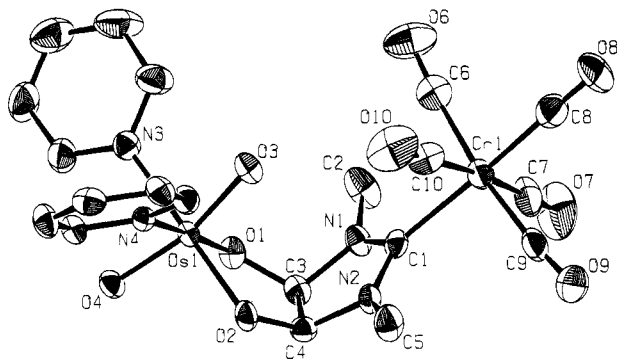


Figure 1. PLATON drawing of the crystal and molecular structure of **3a**. Thermal ellipsoids are drawn at the 50% probability level. Selected distances (Å) and angles (deg): Os1–O1, 1.966(3); Os1–O2, 1.955(3); Cr1–C1, 2.129(4); Cr1–C8, 1.879(5); O1–C3, 1.411(5); O2–C4, 1.405(5); N1–C1, 1.342(5); N1–C3, 1.468(5); N2–C1, 1.349(5); N2–C4, 1.470(5); C3–C4, 1.523(6); O2–Os1–O1, 83.8(1); C8–Cr1–C1, 177.6(2); C3–O1–Os1, 111.5(2); C4–O2–Os1, 112.5(2); C3–N1–C1, 114.2(3); C4–N2–C1, 113.8(3); N1–C1–Cr1, 126.7(3); N2–C1–Cr1, 126.8(3); N2–C1–N1, 106.5(3); N1–C3–O1, 110.9(4); C4–C3–O1, 112.6(4); C4–C3–N1, 102.5(3); N2–C4–O2, 110.1(3); C3–C4–O2, 113.2(4); C3–C4–N2, 102.3(3).

range of single bonds. It is much shorter in **2c** (1.355–(13) Å)⁸ and in the free carbene **1** (1.338(3) Å, R = adamantyl^{3c}). The osmate ester fragment shows the typical *trans* O=Os=O structure.

The osmacycle adopts an *envelope* conformation (Os at a distance of 0.547 Å off the plane of O1,O2,C3,C4). This results in a boat-shaped conformation of the molecule.¹⁰ Cr–Os electron transfer is blocked by the bending of the complex at the C–C bond (N1–C3–O1 angle 110.9(4)°; N2–C4–O2 angle 110.1(3)°).¹⁰

The structure of **3a–c** is retained in solution as shown by IR and NMR spectra. The reduction of the symmetry of the M(CO)₅ fragment which is caused by the OsO₄ addition results in three (instead of two) CO valence vibrations.¹¹ The new oxygenated carbene ligand is

(10) X-ray crystal structure determination: the chromium/osmium complex **3a** of formula C₂₀H₁₈CrN₄O₉Os crystallized from chloroform at 25 °C in the triclinic space group *P*1 with *a* = 8.184(2) Å, *b* = 11.979(3) Å, *c* = 12.227(3) Å, α = 93.91(2)°, β = 95.77(2)°, γ = 93.22(2)°, *V* = 1187.4(5) Å³, *Z* = 2, ρ_{calc} = 1.96 g cm⁻³, *T* = -50 ± 3 °C, *F*₀₀₀ = 676, Mo Kα radiation, CAD4 Enraf-Nonius, ω-scan (maximum 60 s), 4381 measured reflections (1° < Θ < 25.0°), 240 with negative intensity (*I* < 0.01σ(*I*)), 378 reflections merged, 3943 independent reflections, 3943 of which with *I* > 0.0σ(*I*) used for the refinement. The structure solution was obtained by Patterson methods.¹³ All hydrogen atoms were detected from difference Fourier syntheses and were freely refined.¹⁴ No intensity correction was used; the empirical absorption correction is based on ψ-scan data (μ = 58.7 cm⁻¹): *w* = 1/σ²(*F*_o), *R* = Σ(|*F*_o| - |*F*_c|)/Σ|*F*_o| = 0.026; *R*_w = [Σw(|*F*_o| - |*F*_c|)²/Σw|*F*_o|²]^{1/2} = 0.020, residual electron density +1.31 e Å⁻³ (1.01 Å near Os1), minimum -0.87 e Å⁻³. For further details of the crystal structure determination, the Fachinformationszentrum Karlsruhe, Gesellschaft für wissenschaftlich-technische Information mbH, D-76344 Eggenstein-Leopoldshafen, Germany, may be contacted; quote the reference number of this paper, the names of the authors, and the registration number CSD-58805.

(11) Adams, D. M. *Metal-Ligand and Related Vibrations*; Edward Arnold: London, 1960.

seen to be slightly more C-nucleophilic than its precursor **1**: the *trans*-coordinated CO group is less involved in the back-bonding to the zerovalent metal centers (IR data).

The addition of OsO₄ to the C=C bond of the carbene ligands results in a high-field shift of the NMR signals as a consequence of the new CH–O bonds in **3** (¹H NMR: **2a** δ(CH) 7.11, **3a** δ(CH) 5.30; ¹³C NMR: **2a** δ(CH) 124.29, **3a** δ(CH) 103.18). The number of NMR signals shows the symmetrical bonding of the osmate ester to the metal-coordinated carbene ligand. The oxy derivatization has only a small influence on the UV/vis spectra.¹²

Acknowledgment. This work received generous support by the Verband der Chemischen Industrie (Ph.D. Fellowship for P.W.R.) and the Deutsche Forschungsgemeinschaft.

Supplementary Material Available: Text giving a description of the crystal structure determination and tables giving positional and thermal parameters and bond distances and angles for **3a** (8 pages). Ordering information is given on any current masthead page.

OM940929Q

(12) **Pentacarbonyl[O,O'-(bis(pyridine)dioxoosmium)-1,3-dimethyl-4,5-dioxoimidazolidin-2-ylidene]chromium (3a)**: 88 mg (0.35 mmol) of OsO₄ and 0.06 mL (0.70 mmol) of dry pyridine are dissolved in 10 mL of ether. To this solution are added 100 mg of **2a** (0.35 mmol) in 10 mL of ether. The mixture is stirred for 12 h. During the reaction a brown microcrystalline solid precipitate is obtained. After the solvent is decanted, the solid is washed with ether and then dried in vacuo. Yield: 203 mg (83%). IR (KBr; cm⁻¹): 2052 (m, ν(CO)), 1969 (s, ν(CO)), 1912 (vs, ν(CO)), 1431 (m), 1048 (m), 843 (s, ν(O=Os=O)). ¹H-NMR (CDCl₃, 270 MHz, 20 °C): δ 3.32 (s, 6H, NCH₃), 5.30 (s, 2H, NCH), 7.50 (t, 4H, py H-3), 7.92 (t, 2H, py H-4), 8.81 (d, 4H, py H-2). ¹³C{¹H} NMR (CDCl₃, 67.6 MHz, 20 °C): δ = 35.30 (NCH₃), 103.18 (NCH) 125.65 (py C-3), 141.17 (py C-4), 149.31 (py C-2), 188.34 (C carbene), 218.44 (CO), 222.27 (CO). UV/vis (CH₂Cl₂, 20 °C): λ_{max}, nm (ε, L mol⁻¹ cm⁻¹): 246 (20 350), 346 (2400). Mp: >320 °C. Anal. Found (calcd) for C₂₀H₁₈CrN₄O₉Os (700.58): C, 34.29 (33.80); H, 2.59 (2.63); N, 8.00 (7.76). **Pentacarbonyl[O,O'-(bis(pyridine)dioxoosmium)-1,3-dimethyl-4,5-dioxoimidazolidin-2-ylidene]molybdenum (3b)**: Yield: 80%. IR (KBr; cm⁻¹): 2061 (m, ν(CO)), 1974 (s, ν(CO)), 1916 (vs, ν(CO)), 1451 (m), 1048 (m), 842 (s, ν(O=Os=O)), 603 (m). ¹H NMR (CDCl₃, 270 MHz, 20 °C): δ 3.29 (s, 6H, NCH₃), 5.34 (s, 2H, NCH), 7.51 (t, 4H, py H-3), 7.91 (t, 2H, py H-4), 8.82 (d, 4H, py H-2). ¹³C{¹H} NMR (CDCl₃, 67.6 MHz, 20 °C): δ 35.82 (NCH₃), 103.43 (NCH), 125.58 (py C-3), 141.21 (py C-4), 149.32 (py C-2), 186.59 (C carbene), 207.21 (CO), 214.99 (CO). EI-MS (70 eV): *m/z* 192 ([Os]⁺, relative intensity 1%), 128 ([C₅H₅N₂O₂]⁺, 3%), 112 ([C₅H₅N₂O]⁺, 3%), 79 ([C₅H₅N]⁺, 67%). UV/vis (CH₂Cl₂, 20 °C): λ_{max}, nm (ε, L mol⁻¹ cm⁻¹): 248 (16 960), 262 (15 720), 358 (2260). Mp: 310 °C dec. Anal. Found (calcd) for C₂₀H₁₈MoN₄O₉Os (744.52): C, 32.27 (32.25); H, 2.44 (2.47); Mo, 12.89 (12.83); N, 7.53 (7.44); O, 19.34 (19.43). **Pentacarbonyl[O,O'-(bis(pyridine)dioxoosmium)-1,3-dimethyl-4,5-dioxoimidazolidin-2-ylidene]tungsten(3c)**: Yield: 85%. IR (KBr; cm⁻¹): 2060 (s, ν(CO)), 1966 (s, ν(CO)), 1900 (vs, ν(CO)), 1451 (m), 1048 (m), 842 (s, ν(O=Os=O)), 601 (m). ¹H NMR (CDCl₃, 400 MHz, 20 °C): δ 3.30 (s, 6H, NCH₃), 5.35 (s, 2H, NCH), 7.52 (t, 4H, py H-3), 7.92 (t, 2H, py H-4), 8.82 (d, 4H, py H-2). ¹³C{¹H} NMR (CDCl₃, 100.51 MHz, 20 °C): δ 36.69 (NCH₃), 103.22 (NCH), 125.71 (py C-3), 141.21 (py C-4), 149.35 (py C-2), 178.00 (C carbene), 198.77 (CO), 202.04 (CO). UV/vis (CH₂Cl₂, 20 °C): λ_{max}, nm (ε, L mol⁻¹ cm⁻¹): 242 (34 510), 288 (5920), 360 (1550). Mp: >320 °C. Anal. Found (calcd) for C₂₀H₁₈N₄O₉OsW (832.38): C, 28.86 (27.92); H, 2.18 (2.47); N, 6.73 (6.79); O, 17.30 (17.71); W, 22.08 (22.55).

(13) Sheldrick, G. M. SHELXS-86; Universität Göttingen, Göttingen, Germany, 1986.

(14) Watkin, D. J.; Betteridge, P. W.; Carruthers, J. R. CRYSTALS; Oxford University Computing Laboratory, Oxford, U.K., 1986.

Formation of Indenyl Dihydride Complexes from an Iridium Polyhydride Complex: Molecular Structures of $(\eta^5\text{-C}_9\text{H}_7)\text{IrH}_2(\text{PPr}^i_3)_2$ and the η^3 -Indenyl Intermediate $(\eta^3\text{-C}_9\text{H}_7)\text{IrH}_2(\text{PPr}^i_3)_2$

Trang Le Husebo and Craig M. Jensen*

Department of Chemistry, University of Hawaii, Honolulu, Hawaii 96822

Received November 21, 1994[®]

Summary: The reaction of $\text{IrH}_5(\text{PPr}^i_3)_2$ and indene at 60 °C leads to the formation of $(\eta^3\text{-C}_9\text{H}_7)\text{IrH}_2(\text{PPr}^i_3)_2$ and $(\eta^5\text{-C}_9\text{H}_7)\text{IrH}_2(\text{PPr}^i_3)_2$. The molecular structures of these products have been determined by single crystal X-ray diffraction studies. The η^3 -indenyl complex is stable only in the solid state and converts to the η^5 -indenyl complex product upon dissolution.

Recently, Jones reported that the polyhydride complex $\text{ReH}_7(\text{PPh}_3)_2$ reacts with indene to produce hydrido η^5 -indenyl and η^5 -indanyl complexes.¹ We have found that the iridium polyhydride complex $\text{IrH}_5(\text{PPr}^i_3)_2$ (**1**) also reacts with indene to produce a hydrido η^5 -indenyl complex. However, unlike the rhenium system, a hydrido η^3 -indenyl complex is also obtained. We wish to report the synthesis and molecular structures of the iridium indenyl hydride complexes.

The title complexes are obtained in major yield upon heating **1** (0.600 g, 1.2 mmol) with excess indene (2.7 mL, 23 mmol) in benzene (50 mL) at 60 °C for 4 days as seen in Scheme 1. Recrystallization of the crude reaction mixture from pentane gave rise to a mixture of distinctively different, red crystals of $(\eta^3\text{-C}_9\text{H}_7)\text{IrH}_2(\text{PPr}^i_3)_2$ (**2**) and orange crystals of $(\eta^5\text{-C}_9\text{H}_7)\text{IrH}_2(\text{PPr}^i_3)_2$ (**3**). Both types of crystals were suitable for X-ray diffraction. Diagrams of the determined molecular structures² and selected bond distances are presented in Figures 1 and 2, respectively. Although the hydride ligands could not be reliably located, their position can be inferred from the observed molecular geometries. The presence of the hydride ligands was confirmed through solid state infrared spectroscopy of KBr pellets of the complexes. Ir–H stretches were observed at 2213 and 2174 cm^{-1} for **2** and at 2230 and 2159 cm^{-1} for **3**.

The structures determined for **2** and **3** allow the comparison of a pair of highly related η^3 - and η^5 -coordinated indenyl complexes. The η^3 -indenyl ligand of **2** is coordinated in an η^3 -allyl fashion, as the Ir–C(2) bond length is significantly shorter than the Ir–C(1) and Ir–C(3) bond distances. Similar coordination was found

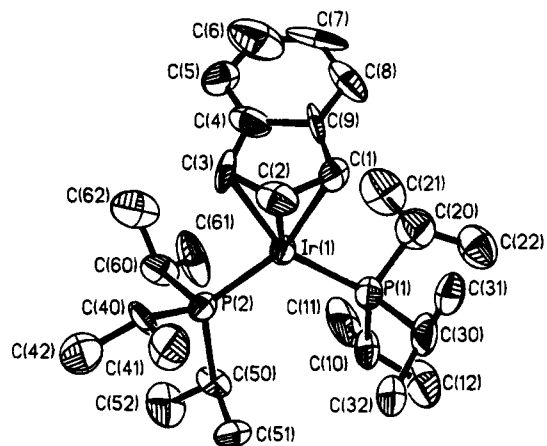
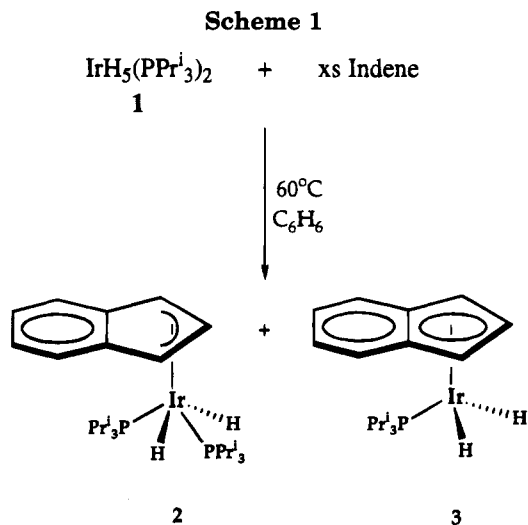


Figure 1. Projection of $(\eta^3\text{-C}_9\text{H}_7)\text{IrH}_2(\text{PPr}^i_3)_2$ (**2**) with the thermal ellipsoids at 50% probability. Selected bond lengths (Å): Ir(1)–C(1) = 2.266(2), Ir(1)–C(2) = 2.121(3), Ir(1)–C(3) = 2.286(2). The hydrogen atoms have been omitted for clarity.



by Merola for the η^3 -indenyl ligand of $(\eta^3\text{-C}_9\text{H}_7)\text{Ir}(\text{PMe}_3)_3$.³ The η^5 -coordination of the five-membered indenyl ring of **3** entails extensive ring slippage, as depicted in Figure 3. The Ir–C bonds involving the carbons also contained in the six-membered ring are pronouncedly lengthened. This is similar to the bonding situation found⁴ for $[(\eta^5\text{-C}_9\text{H}_7)\text{IrH}(\text{PPh}_3)_2]^+$. However, unlike the case for the monohydride complex, the hydride trans influence in **3** also results in a significant lengthening of the Ir(1)–C(3) bond.

The observed orientation of the indenyl and phosphine ligands in **3** is not in accordance with the general trends

(3) Merola, J. S.; Kacmarcik, R. T.; Van Engen, D. *J. Am. Chem. Soc.* **1986**, *108*, 329.

[®] Abstract published in *Advance ACS Abstracts*, February 15, 1995.
 (1) Rosini, G. P.; Jones, W. D. *J. Am. Chem. Soc.* **1993**, *115*, 965.
 (2) (a) Crystallographic data for **2**: monoclinic, $P2_1/n$, $Z = 8$ (2 symmetry-independent molecules of **2** per asymmetric unit), $a = 8.515(8)$ Å, $b = 34.73(2)$ Å, $c = 19.044(11)$ Å, $\beta = 91.45(4)^\circ$, $V = 5630(5)$ Å³, $\rho_{\text{calc}} = 1.479$ g/cm³; Nicolet P3 diffractometer, Mo K α radiation ($\lambda = 0.71073$ Å); 6099 independent reflections with $4^\circ < 2\theta < 40^\circ$ collected, 5310 reflections used in refinement with $I > 3\sigma(I)$; $R = 0.047$, $R_w = 0.057$, GOF = 1.62. Two of the carbons of one of the symmetry-independent molecules of **2** could not be refined anisotropically. (b) Crystallographic data for **3**: triclinic, $P\bar{1}$, $Z = 4$ (2 symmetry-independent molecules of **3** per asymmetric unit), $a = 9.355(2)$ Å, $b = 14.012(3)$ Å, $c = 15.535(3)$ Å, $\alpha = 63.45(3)^\circ$, $\beta = 89.20(3)^\circ$, $\gamma = 88.49(3)^\circ = 1821.0(7)$ Å³, $\rho_{\text{calc}} = 1.705$ g/cm³; Nicolet P3 diffractometer, Mo K α radiation ($\lambda = 0.71073$ Å); 3689 independent reflections with $3^\circ < 2\theta < 40^\circ$ collected, 3408 reflections used in refinement with $I > 3\sigma(I)$; $R = 0.028$, $R_w = 0.037$, GOF = 1.24.

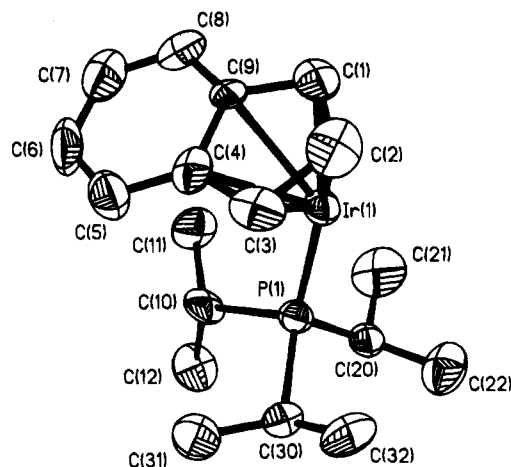


Figure 2. Projection of ($\eta^5\text{-C}_9\text{H}_7$) $\text{IrH}_2(\text{PPr}_3)$ (**3**) with the thermal ellipsoids at 50% probability. Selected bond lengths (\AA): $\text{Ir}(1)\text{-C}(1) = 2.249(1)$, $\text{Ir}(1)\text{-C}(2) = 2.244(1)$, $\text{Ir}(1)\text{-C}(3) = 2.304(1)$, $\text{Ir}(1)\text{-C}(4) = 2.399(1)$, $\text{Ir}(1)\text{-C}(9) = 2.380(1)$. The hydrogen atoms have been omitted for clarity.

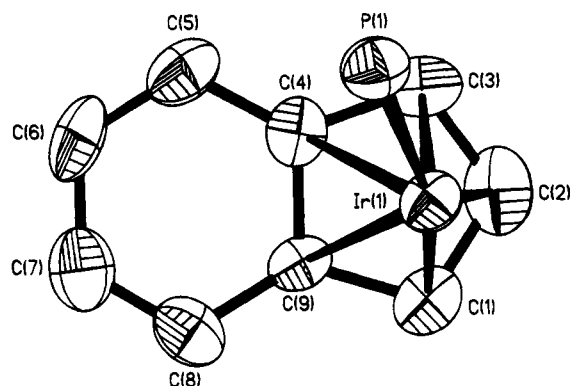


Figure 3. Projection of ($\eta^5\text{-C}_9\text{H}_7$) $\text{IrH}_2(\text{PPr}_3)$ (**3**) along the plane normal to the five-membered ring.

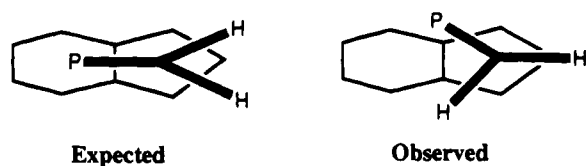
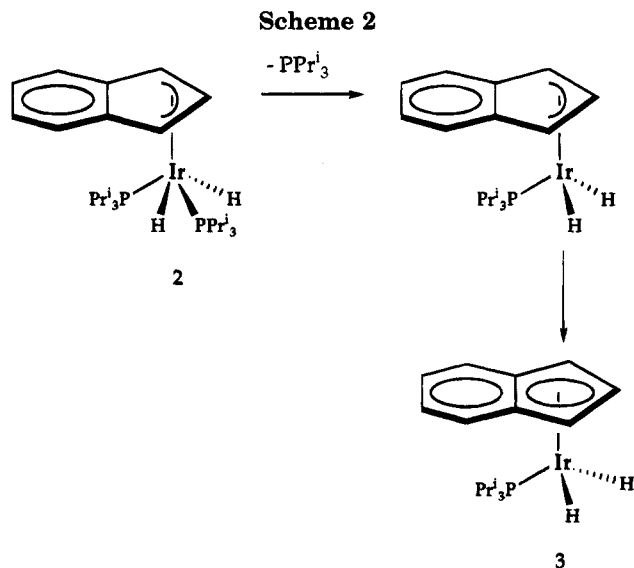


Figure 4. Schematic drawings of the expected and observed conformations of ($\eta^5\text{-C}_9\text{H}_7$) $\text{IrH}_2(\text{PPr}_3)$ (**3**).

in the conformations of indenyl complexes outlined by Faller and Crabtree.⁴ In view of the relative trans influence of hydride and phosphine ligands, the conformation illustrated in Figure 4, in which the phosphine eclipses the indenyl ligand and the hydrides are transoid to the indenyl ligand, would be expected. As seen in Figure 3, the phosphine is found instead to be in a staggered orientation with regard to the indenyl ligand. Apparently, steric factors prevent **3** from assuming the electronically preferred conformation.

In contrast to the case for the solid state, only one complex and free triisopropylphosphine are detected by ^1H , ^{13}C , and ^{31}P NMR spectroscopy of the product mixture dissolved in CD_2Cl_2 .⁵ The observed complex is readily identified as **3**. The doublet resonance observed in the ^1H NMR spectrum for the hydride ligands at -21.9 ppm ($J_{\text{P-H}} = 26.0$ Hz) establishes the monophosphine formulation, and the resonances observed for the



η^5 -indenyl ligand are very similar to those reported by Bergman for ($\eta^5\text{-C}_9\text{H}_7$) $\text{IrH}_2(\text{PMe}_3)$.⁶ We do not observe any of the resonances which Merola has shown to be diagnostic of an iridium η^3 -indenyl complex³ or additional resonances in the hydride region. Infrared spectroscopy of the product mixture dissolved in pentane confirms that a single dihydride complex is present in solution, as only two Ir-H stretches are observed at 2221 and 2142 cm^{-1} . We conclude that **2** undergoes loss of phosphine and conversion to **3** as seen in Scheme 2 upon dissolution. Attempts to reverse this process by addition of excess triisopropylphosphine led instead to a complicated mixture of unidentified products.

The microreverse of the process in Scheme 2, ring slippage followed by capture of a coordination site by an incoming ligand, has often been proposed to occur in the reactions of rhodium and iridium hydrido complexes containing η^5 -aromatic ligands. For example, Jones has proposed that such sequences occur during the displacement of $\text{C}_5\text{Me}_5\text{H}$ from ($\eta^5\text{-C}_5\text{Me}_5$) $\text{RhH}_2(\text{PMe}_3)_2$ (**4**) by PMe_3 .⁷ Previous structural characterizations of η^3 -indenyl complexes^{3,8} have lent support for such mechanisms. Our results provide more direct evidence for η^3 -indenyl intermediates in the reactions of rhodium and iridium hydrido complexes containing η^5 -aromatic ligands. Moreover, these results illustrate that the energetically preferred distribution of complexes containing η^5 - and η^3 -bonded aromatic ligands can be drastically different in solution than in the solid state.

Acknowledgment. The support of this research by the U.S. Department of Energy Hydrogen Program is gratefully acknowledged.

Supplementary Material Available: Tables of crystal data, atomic positions, anisotropic thermal parameters, bond distances, bond angles, and hydrogen atom coordinates for ($\eta^3\text{-C}_9\text{H}_7$) $\text{IrH}_2(\text{PPr}_3)$ (**2**) and ($\eta^5\text{-C}_9\text{H}_7$) $\text{IrH}_2(\text{PPr}_3)$ (**3**) (12 pages). Ordering information is given on any current masthead page.

OM9408876

(5) Spectroscopic data for **3**: ^1H NMR (500.1 MHz, CD_2Cl_2) δ 7.28 (m, 2H), 6.92 (m, 2H), 5.67 (t, 1H, $J_{\text{H-H}} = 2.5$ Hz), 5.57 (m, 2H), 1.54 (m, 3H), 0.71 (dd, 18H, $J_{\text{P-H}} = 14.0$ Hz, $J_{\text{H-H}} = 7.5$ Hz), -21.88 (d, 2H, $J_{\text{H-H}} = 26.0$ Hz); ^{31}P NMR (121.7 MHz, CD_2Cl_2) δ 47.6 (s); ^{13}C NMR (125.7 MHz, CD_2Cl_2) δ 122.9 (s), 122.0 (s), 109.5 (s), 86.3 (s), 64.3 (s), 27.9 (d, $J_{\text{C-P}} = 31.5$ Hz), 20.0 (s).

(6) Foo, T.; Bergman, R. G. *Organometallics* **1992**, *11*, 1801.

(7) Jones, W. D.; Kuydendal, V. L.; Selmezy, A. D. *Organometallics* **1991**, *10*, 1577.

(8) O'Connor, J. M.; Casey, C. P. *Chem. Rev.* **1987**, *87*, 307 and references therein.

(4) Faller, J. W.; Crabtree, R. H.; Habib, A. *Organometallics* **1985**, *4*, 929.

Polymeric Organosilicon Systems. 24. Anionic Polymerization of 4,5,10-Trisilabicyclo[6.3.0]undeca-1(11),8-diene-2,6-diyne

Eiji Toyoda, Atsutaka Kunai, and Mitsuo Ishikawa*

Department of Applied Chemistry, Faculty of Engineering, Hiroshima University, Higashi-Hiroshima 724, Japan

Received November 4, 1994[®]

Summary: Anionic ring-opening polymerization of cyclic silole derivatives has been reported. The reaction of 4,5,10-trisilabicyclo[6.3.0]undeca-1(11),8-diene-2,6-diyne with a catalytic amount of tetrabutylammonium fluoride afforded polymers that have a regular alternating arrangement of a disilanylene unit and 3,4-diethynylene-substituted silole system.

Current interest has focused on the synthesis of silicon-containing polymers that can be used as functionality materials.¹ It is of interest to us to synthesize alternating disilanylene polymers that have an electron-deficient group such as a silole unit in the polymer backbone, because these polymers might produce n-type conducting materials.² Recently, we have found that 1,2,5,6-tetrasilacycloocta-3,7-diyne undergo anionic,^{3a} thermal,^{3b} and radical-induced^{3b} ring-opening polymerization to give poly[(disilanylene)ethynyls] with high molecular weights. As a part of our continuing investigations concerning the design and synthesis of silicon-containing functionality materials, we have prepared a new type of the polymer that has a regular alternating arrangement of a disilanylene unit and 3,4-diethynylene-substituted silole system in the polymer backbone. Our strategy for the synthesis of this type of polymer involves the anionic ring-opening reaction of the cyclic silole derivatives 4,5,10-trisilabicyclo[6.3.0]undeca-1(11),8-diene-2,6-diyne. To our knowledge, only two types of polymers involving silole rings in the main chain have been prepared so far.^{4,5}

The starting siloles 4,4,5,5,10,10-hexamethyl-, 4,4,5,5-tetraethyl-10,10-dimethyl-, and 4,5-dibutyl-4,5,10,10-

tetramethyl-4,5,10-trisilabicyclo[6.3.0]undeca-1(11),8-diene-2,6-diyne (**5a–c**) were prepared by the series of reactions shown in Scheme 1. Treatment of 1,4-bis(trimethylsilyl)butadiyne⁶ with 1,1,2,2-tetramethyldisilane⁷ in the presence of a catalytic amount of dichlorobis(triethylphosphine)nickel(II) in THF at reflux temperature for 26 h gave a mixture of 1,1-dimethyl-2,5-bis(trimethylsilyl)-3,4-bis(trimethylsilyl)ethynylsilole (**1**) and 1,1,4,4-tetramethyl-2,5-bis(trimethylsilyl)-3,6-bis(trimethylsilyl)ethynyl-1,4-disilacyclohexa-2,5-diene (**2**).⁸ The reaction of this mixture with methanol in the presence of a catalytic amount of potassium hydroxide at 50 °C for 1 h afforded the respective desilylated products (**3** and **4**). Diethynylsilole **3**,⁹ thus formed, could be readily separated from **4**¹⁰ by column chromatography. Compounds **3** and **4** were obtained in 27% and 11% isolated yields, respectively, from the starting 1,4-bis(trimethylsilyl)butadiyne. Treatment of **3** with 2 equiv of lithium diisopropylamide at –70 °C for 0.5 h, followed by the reaction of the resulting dilithio compound with 1,2-dichlorotetra-methyldisilane,¹¹ produced the cyclic silole derivative **5a**, with a 4,5,10-trisilabicyclo[6.3.0]undeca-1(11),8-diene-2,6-diyne ring structure,¹² in 8% yield. Similar treatment of the dilithio compound with 1,2-dichlorotetraethyl-^{3a} and 1,2-dibutyl-1,2-dichlorodimethyldisilane^{3a} afforded the respective siloles (**5b**¹³ and **5c**¹⁴) in 54% and 39% yields.

(5) (a) Corriu, R. J. P.; Douglas, W. E.; Yang, Z.-X. *J. Organomet. Chem.* **1993**, *456*, 35. (b) Bréfort, J. L.; Corriu, R. J. P.; Gerbier, P.; Guérin, C.; Henner, B. J. L.; Jean, A.; Kuhlmann, T. *Organometallics* **1992**, *11*, 2500.

(6) Walton, D. R. M.; Waugh, F. J. *Organomet. Chem.* **1972**, *37*, 45. (7) Urenovitch, J. V.; West, R. J. *Organomet. Chem.* **1965**, *3*, 138. For 1,1,2,2-tetramethyldisilane: MS *m/z* 118 (M⁺); ¹H NMR (δ in CDCl₃) 0.14 (d, 12H, MeSi, *J* = 3.3 Hz), 3.69 (m, 2H, HSi).

(8) Okinoshima, H.; Yamamoto, K.; Kumada, M. *J. Am. Chem. Soc.* **1972**, *94*, 9263.

(9) Compound **3**: mp 49–50 °C; MS *m/z* 302 (M⁺); UV λ_{max} (THF solution) 238 nm (ε = 18 600), 333 nm (ε = 2700); IR ν_{C=CH} 3303, ν_{C=C} 2094 cm⁻¹; ¹H NMR (δ in CDCl₃) 0.21 (s, 18H, Me₂Si), 0.24 (s, 6H, Me₂Si), 3.33 (s, 2H, ethynyl protons); ¹³C NMR (δ in CDCl₃) –3.88 (Me₂Si), –0.75 (Me₂Si), 82.57, 82.95 (C=C), 144.44, 156.10 (C=C); ²⁹Si NMR (δ in CDCl₃) –8.07 (Me₂Si), 24.97 (Me₂Si). Anal. Calcd for C₁₆H₂₆Si₃: C, 63.50; H, 8.66. Found: C, 63.34; H, 8.66.

(10) Compound **4**: mp 136–138 °C; MS *m/z* 360 (M⁺); IR ν_{C=CH} 3282 cm⁻¹; ¹H NMR (δ in CDCl₃) 0.25 (s, 18H, Me₂Si), 0.30 (s, 12H, Me₂Si), 3.70 (s, 2H, ethynyl protons); ¹³C NMR (δ in CDCl₃) –0.84 (Me₂Si), 0.70 (Me₂Si), 86.25, 89.94 (C=C), 154.10, 172.36 (C=C); ²⁹Si NMR (δ in CDCl₃) –7.71 (Me₂Si), –24.47 (Me₂Si). Anal. Calcd for C₁₈H₃₂Si₂: C, 59.92; H, 8.94. Found: C, 59.88; H, 8.91.

(11) Kumada, M.; Yamaguchi, M.; Yamamoto, Y.; Nakajima, J.; Shiina, K. *J. Org. Chem.* **1956**, *21*, 1264.

(12) Compound **5a**: mp 198–199 °C dec; MS *m/z* 416 (M⁺); UV λ_{max} (THF solution) 225 nm (ε = 36 900), 250 nm (ε = 24 400), 340 nm (ε = 3400); IR ν_{C=C} 2108 cm⁻¹; ¹H NMR (δ in CDCl₃) 0.206 (s, 18H, Me₂Si), 0.214 (s, 6H, Me₂Si in silole ring), 0.30 (s, 12H, Me₂Si–Si); ¹³C NMR (δ in CDCl₃) –3.65 (Me₂Si in silole ring), –2.78 (Me₂Si–Si), –0.34 (Me₂Si), 105.40, 115.28 (C=C), 147.15, 149.86 (C=C); ²⁹Si NMR (δ in CDCl₃) –31.48 (Me₂Si–Si), –7.63 (Me₂Si), 27.40 (Me₂Si in silole ring). Anal. Calcd for C₂₀H₃₆Si₅: C, 57.62; H, 8.70. Found: C, 57.55; H, 8.58.

[®] Abstract published in *Advance ACS Abstracts*, February 1, 1995.

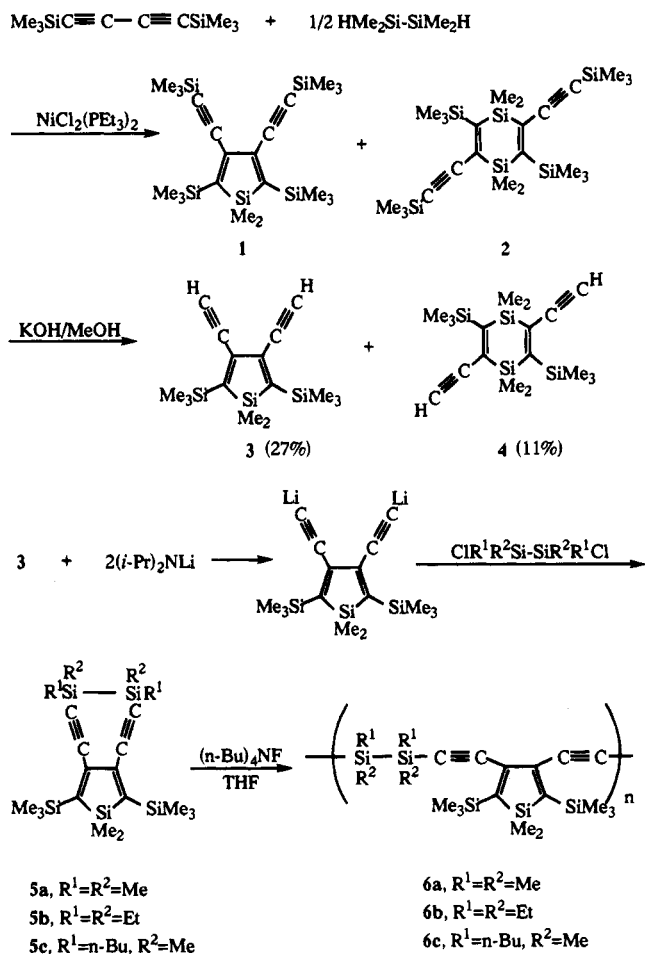
(1) For example: (a) Ishikawa, M.; Nate, K. In *Inorganic and Organometallic Polymers*; Zeldin, M., Wynne, K. J., Allcock, H. R., Eds.; ACS Symposium Series 360; American Chemical Society: Washington, DC, 1988; Chapter 16. (b) Nate, K.; Ishikawa, M.; Ni, H.; Watanabe, H.; Saheki, Y. *Organometallics* **1987**, *6*, 1673. (c) Ohshita, J.; Kanaya, D.; Ishikawa, M.; Yamanaka, T. *J. Organomet. Chem.* **1989**, *369*, C18. (d) Hong, H.; Weber, W. P. *Polym. Bull.* **1989**, *22*, 363. (e) Hu, S.; Weber, W. P. *Polym. Bull.* **1989**, *21*, 133. (f) Ishikawa, M.; Hasegawa, Y.; Kunai, A. *J. Organomet. Chem.* **1990**, *381*, C57. (g) Ohshita, J.; Kanaya, D.; Ishikawa, M.; Koike, T.; Yamanaka, T. *Macromolecules* **1991**, *24*, 2106. (h) Ohshita, J.; Ohsaki, H.; Ishikawa, M. *Bull. Chem. Soc. Jpn.* **1993**, *66*, 1795. (i) Ohshita, J.; Kanaya, D.; Ishikawa, M. *J. Organomet. Chem.* **1994**, *468*, 55.

(2) Although the conducting polymers with semiconducting levels have been obtained by treating the alternating disilanylene polymers having various π-electron systems with SbF₅, FeCl₃, and I₂, all of them are p-type conducting (see ref 3a and also see: Ishikawa, M.; Sakamoto, H.; Ishii, M.; Ohshita, J. *J. Polym. Sci. A: Polym. Chem.* **1993**, *31*, 3281. Fukushima, M. *Industrial Science and Technology Frontier Program: The 2nd Symposium on Silicon-Based Polymers*; Japan High Polymer Center: Tokyo, 1994; extended abstracts pp 183–191).

(3) (a) Ishikawa, M.; Hatano, T.; Hasegawa, Y.; Horio, T.; Kunai, A.; Miyai, A.; Ishida, T.; Tsukihara, T.; Yamanaka, T.; Koike, T.; Shioya, J. *Organometallics* **1992**, *11*, 1604. (b) Ishikawa, M.; Horio, T.; Hatano, T.; Kunai, A. *Organometallics* **1993**, *12*, 2078.

(4) Tamao, K.; Yamaguchi, S.; Shiozaki, M.; Nakagawa, Y.; Ito, Y. *J. Am. Chem. Soc.* **1992**, *114*, 5867.

Scheme 1

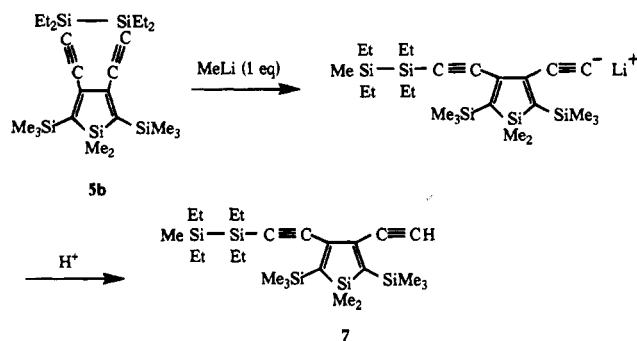


Compounds **5a–c** readily undergo the anionic ring-opening polymerization in the presence of a catalytic amount of tetrabutylammonium fluoride (2 mol %) to give the respective alternating polymers with high molecular weights in high yields. In a typical experiment, a mixture of 195 mg (0.412 mmol) of silole **5b** and 0.008 mmol (2 mol %) of tetrabutylammonium fluoride in 1 mL of THF dried over Na–K alloy was stirred in a sealed tube at room temperature for 20 h. After addition of a few drops of MeI, the mixture was poured into ca. 50 mL of methanol. Then, the resulting solid was filtered off and dried under reduced pressure to give 169 mg (87% yield) of poly[(1,2-diethynyltetraethyldisilanyl)silole(1,1-dimethyl-1-silacyclopenta-2,4-diene-3,4-diyl)] (**6b**)¹⁵ with a molecular weight of $M_w = 30\,300$ ($M_w/M_n = 1.66$). Similar treatment of **5a** and **5c** with

(13) Compound **5b**: mp 104–105 °C; MS m/z 472 (M^+); UV λ_{max} (THF solution) 227 nm ($\epsilon = 39\,300$), 250 nm ($\epsilon = 26\,500$), 340 nm ($\epsilon = 3700$); IR $\nu_{\text{C}\equiv\text{C}}$ 2112 cm^{-1} ; ^1H NMR (δ in CDCl_3) 0.23 (s, 18H, Me_3Si), 0.24 (s, 6H, Me_2Si), 0.72–0.91 (m, 8H, $\text{CH}_3\text{CH}_2\text{Si}$), 1.07 (t, 12H, $\text{CH}_3\text{-CH}_2\text{Si}$, $J = 7.8$ Hz); ^{13}C NMR (δ in CDCl_3) -3.54 (Me_2Si), -0.34 (Me_3Si), 4.55, 8.59 (Et_2Si), 104.37, 116.01 ($\text{C}\equiv\text{C}$), 147.66, 149.08 ($\text{C}=\text{C}$); ^{29}Si NMR (δ in CDCl_3) -20.54 (Et_2Si), -7.35 (Me_3Si), 27.66 (Me_2Si). Anal. Calcd for $\text{C}_{24}\text{H}_{44}\text{Si}_5$: C, 60.94; H, 9.38. Found: C, 60.75; H, 9.47.

(14) Compound **5c** (mixture of cis and trans isomers): MS m/z 500 (M^+); UV λ_{max} (THF solution) 227 nm ($\epsilon = 33\,800$), 251 nm ($\epsilon = 24\,300$), 340 nm ($\epsilon = 3800$); IR $\nu_{\text{C}\equiv\text{C}}$ 2112 cm^{-1} ; ^1H NMR (δ in CDCl_3) 0.20 (s, 18H, Me_3Si), 0.22 (s, 6H, Me_2Si in silole ring), 0.28 (s, 6H, $n\text{-BuMeSi}$), 0.69–0.91, 1.30–1.50 (m, 18H, $n\text{-Bu}$); ^{13}C NMR (δ in CDCl_3) -4.48, -4.40 ($n\text{-BuMeSi}$), -3.63, -3.61, -3.58 (Me_2Si), -0.36 (Me_3Si), 13.76, 26.09, 26.84, 26.94 ($n\text{-Bu}$), 105.21, 115.45 ($\text{C}\equiv\text{C}$), 147.41, 149.40 ($\text{C}=\text{C}$); ^{29}Si NMR (δ in CDCl_3) -28.82, -28.61 ($n\text{-BuMeSi}$), -7.60 (Me_3Si), 27.27 (Me_2Si). Anal. Calcd for $\text{C}_{26}\text{H}_{48}\text{Si}_5$: C, 62.32; H, 9.66. Found: C, 62.10; H, 9.76.

Scheme 2



the fluoride anion in THF afforded polymers **6a** ($M_w = 9400$, $M_w/M_n = 1.38$)¹⁶ and **6c** ($M_w = 46\,300$, $M_w/M_n = 1.76$)¹⁷ in 75% and 80% yields, respectively.

That monomers **5a–c** undergo anionic ring-opening reactions, giving the polymers **6a–c**, was confirmed by the fact that treatment of **5b** with a catalytic amount of methyllithium produced polymer **6b** ($M_w = 47\,900$, $M_w/M_n = 1.26$) in 77% yield.

IR, ^1H NMR, and ^{13}C NMR spectra for this polymer were identical with those for **6b** obtained from the fluoride anion-catalyzed polymerization of **5b**. Furthermore, the reaction of **5b** with 1 equiv of methyllithium at -90 °C for 1 h, followed by treatment of the resulting mixture with dilute hydrochloric acid, produced 3-ethynyl-4-((2-methyltetraethylsilyl)ethynyl)-1,1-dimethyl-2,5-bis(trimethylsilyl)silole (**7**)¹⁸ in 60% yield as the sole volatile product. This result clearly indicates that methyl anion attacks at a silicon atom in the disilanyl unit to give a ring-opened lithioethynylsilole (Scheme 2).

The ^{13}C NMR spectrum for **6b** reveals resonances at δ -3.64, -0.55, 4.93, and 8.67 ppm, attributed to $\text{Me}_2\text{-Si}$, Me_3Si , and Et_2Si carbons, as well as resonances at δ 97.39, 107.32, 145.98, and 155.21 ppm, due to sp and sp^2 carbons, respectively. Its ^{29}Si NMR spectrum shows three resonances at δ -30.11, -8.76, and 24.02 ppm,

(15) Polymer **6b**: mp 79–82 °C; $M_w = 30\,300$ ($M_w/M_n = 1.66$); UV λ_{max} (THF solution) 255 nm ($\epsilon = 25\,000$), 300 nm (sh, $\epsilon = 9400$); IR $\nu_{\text{C}\equiv\text{C}}$ 2130 cm^{-1} ; ^1H NMR (δ in CDCl_3) 0.21 (s, 18H, Me_3Si), 0.23 (s, 6H, Me_2Si), 0.90 (q, 8H, $\text{CH}_3\text{CH}_2\text{Si}$, $J = 7.6$ Hz), 1.12 (t, 12H, $\text{CH}_3\text{-CH}_2\text{Si}$, $J = 7.6$ Hz); ^{13}C NMR (δ in CDCl_3) -3.64 (Me_2Si), -0.55 (Me_3Si), 4.93, 8.67 (Et_2Si), 97.39, 107.32 ($\text{C}\equiv\text{C}$), 145.98, 155.21 ($\text{C}=\text{C}$); ^{29}Si NMR (δ in CDCl_3) -30.11 (Et_2Si), -8.76 (Me_3Si), 24.02 (Me_2Si). Anal. Calcd for $(\text{C}_{24}\text{H}_{44}\text{Si}_5)_n$: C, 60.94; H, 9.38. Found: C, 60.56; H, 9.65.

(16) Polymer **6a**: mp 90–98 °C; $M_w = 9400$ ($M_w/M_n = 1.38$); UV λ_{max} (THF solution) 254 nm ($\epsilon = 16\,100$), 292 nm (sh, $\epsilon = 7800$); IR $\nu_{\text{C}\equiv\text{C}}$ 2136 cm^{-1} ; ^1H NMR (δ in CDCl_3) 0.19 (s, 18H, Me_3Si), 0.21 (s, 6H, Me_2Si in silole ring), 0.36 (s, 12H, $\text{Me}_2\text{Si}-\text{Si}$), ^{13}C NMR (δ in CDCl_3) -3.75 (Me_2Si in silole ring), -2.53 ($\text{Me}_2\text{Si}-\text{Si}$), -0.65 (Me_3Si), 98.60, 106.69 ($\text{C}=\text{C}$), 145.64, 155.36 ($\text{C}=\text{C}$); ^{29}Si NMR (δ in CDCl_3) -37.32 ($\text{Me}_2\text{Si}-\text{Si}$), -8.51 (Me_3Si), 24.57 (Me_2Si in silole ring). Anal. Calcd for $(\text{C}_{20}\text{H}_{36}\text{Si}_5)_n$: C, 57.62; H, 8.70. Found: C, 56.81; H, 8.80.

(17) Polymer **6c**: mp 46–50 °C; $M_w = 46\,300$ ($M_w/M_n = 1.76$); UV λ_{max} (THF solution) 254 nm ($\epsilon = 25\,900$), 301 nm (sh, $\epsilon = 12\,300$); IR $\nu_{\text{C}\equiv\text{C}}$ 2134 cm^{-1} ; ^1H NMR (δ in CDCl_3) 0.19 (s, 18H, Me_3Si), 0.21 (s, 6H, Me_2Si in silole ring), 0.35 (s, 6H, BuMeSi), 0.81–0.89, 1.32–1.47 (m, 18H, $n\text{-Bu}$); ^{13}C NMR (δ in CDCl_3) -4.00 (BuMeSi), -3.73 (Me_2Si), -0.60 (Me_3Si), 13.81, 14.01, 14.12, 26.54, 26.73, 26.78 ($n\text{-Bu}$), 98.24, 106.86 ($\text{C}=\text{C}$), 145.89, 154.82, 154.85, 154.88 ($\text{C}=\text{C}$); ^{29}Si NMR (δ in CDCl_3) -34.93, -34.75 (BuMeSi), -8.17 (Me_3Si), 24.79 (Me_2Si). Anal. Calcd for $(\text{C}_{26}\text{H}_{48}\text{Si}_5)_n$: C, 62.32; H, 9.66. Found: C, 61.66; H, 9.61.

(18) Compound **7**: MS m/z 488 (M^+); IR $\nu_{\text{C}\equiv\text{CH}}$ 3307, $\nu_{\text{C}\equiv\text{C}}$ 2132 cm^{-1} ; ^1H NMR (δ in CDCl_3) 0.11 (s, 3H, MeSi), 0.20, 0.21, 0.23 (3 s, 24H, 2 Me_3Si and Me_2Si), 0.68–1.23 (m, 20H, EtSi), 3.23 (s, 1H, ethynyl proton); ^{13}C NMR (δ in CDCl_3) -6.00 (Et_2MeSi), -3.75 (Me_2Si), -0.68 (Me_3Si), 5.00, 5.38, 8.21, 8.66 (Et), 82.95, 98.99, 106.65 ($\text{C}=\text{C}$), 145.12, 146.02, 153.41, 155.54 ($\text{C}=\text{C}$); ^{29}Si NMR (δ in CDCl_3) -28.47, -11.49 ($\text{Si}-\text{Si}$), -8.42, -8.23 (Me_3Si), 24.79 (Me_2Si). Anal. Calcd for $(\text{C}_{25}\text{H}_{48}\text{Si}_5)_n$: C, 61.40; H, 9.89. Found: C, 61.40; H, 9.87.

due to Et_2Si , Me_3Si , and Me_2Si . No other resonances are detected in its ^{13}C and ^{29}Si NMR spectra. These results indicate that **6b** has a regular alternating arrangement of a disilanylene unit and 3,4-diethynylsilole system in the polymer main chain. The structures of **6a** and **6c** were also verified by spectroscopic and elemental analysis.

Polymers **6a–c** are solids, melt without decomposition, and are soluble in aromatic hydrocarbons, ethers, and chlorocarbons but insoluble in alcohols.

We are continuing to explore the use of the present polymers as functionality materials.

Supplementary Material Available: Text giving experimental details and spectroscopic data for **1** and **2** and figures giving ^1H , ^{13}C , and ^{29}Si NMR spectra for polymers **6a–c** (12 pages). Ordering information is given on any current masthead page.

OM940839L

Lithium and Sodium Complexes of a Tetrasilylethylene Dianion¹

Akira Sekiguchi,* Masaaki Ichinohe, Chizuko Kabuto, and Hideki Sakurai*

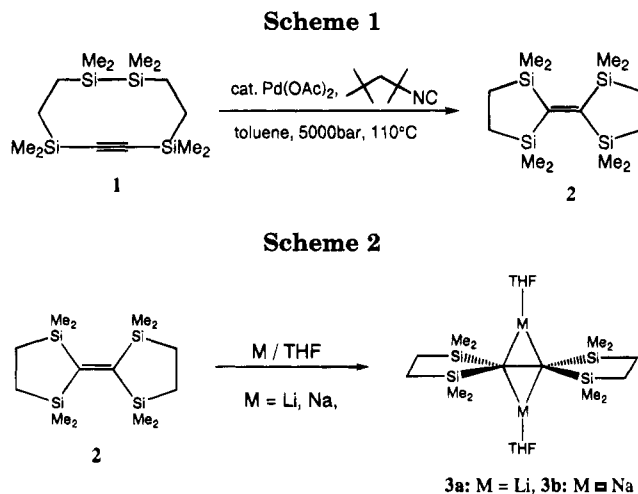
Department of Chemistry and Organosilicon Research Laboratory, Faculty of Science, Tohoku University, Aoba-ku, Sendai 980-77, Japan

Received October 12, 1994[®]

Summary: Reduction of 2,2,2',2',5,5,5',5'-octamethyl-2,2',5,5'-tetrasilabicyclopentylidene (**2**) with lithium and sodium in THF gave the corresponding dianionic dialkali metals. The structures of **2**, (2,2,2',2',5,5,5',5'-octamethyl-2,2',5,5'-tetrasilabicyclopentylidene)bis[(tetrahydrofuran)lithium(I)] (**3a**), and (2,2,2',2',5,5,5',5'-octamethyl-2,2',5,5'-tetrasilabicyclopentylidene)bis[(tetrahydrofuran)sodium(I)] (**3b**) were studied by X-ray crystallography. The central anionic C-C bonds are not twisted for **3a**, whereas they are twisted by 17.1° for **3b**.

Interest in the reactivity, structure, and bonding of organic alkali metal compounds, especially organolithium compounds, has remarkably increased in recent years.² However, the chemistry of sodium derivatives has not been well established.³ We have previously reported the unique structure of (1,1,2,2-tetrakis(trimethylsilyl)ethylene)bis[(tetrahydrofuran)lithium(I)], obtained readily by the reaction of tetrakis(trimethylsilyl)ethylene with lithium metal.⁴ Obviously, four silyl substituents facilitate the reduction of the ethylene.⁵ The highly twisted structure of the anion is an interesting fact to be pointed out, but the parent olefin itself is also twisted (twist angle: 29.5°).⁶ Contrary, however, the reaction of the olefin with sodium or potassium gave only its radical anion, none of the ethylene dianion disodium or dipotassium being produced.

We have designed 2,2,2',2',5,5,5',5'-octamethyl-2,2',5,5'-tetrasilabicyclopentylidene (**2**) as a planar or almost planar tetrasilyl-substituted ethylene appropriately fixed by the rings. Expectedly, the cyclic ethylene **2** underwent facile two electron reduction by Li and Na to give the corresponding dianions. We wish to report herein the crystal structures of **2**, the dilithium derivative **3a**, and the disodium derivative **3b**. The latter



constitutes the first crystal structure of disodioethane without stabilization by phenyl groups.

The tetrasilabicyclopentylidene (**2**) was prepared by the intramolecular double silylation of 3,3,6,6,7,7,10,10-octamethyl-3,6,7,10-tetrasilacyclodecyne (**1**).⁷ Thus, heating the cyclic acetylene **1** at 110 °C with a catalytic amount of Pd(OAc)₂/tert-octyl isocyanide under 5000 bar afforded **2** cleanly in 60% yield (Scheme 1).⁸ Because of the rigid structure fixed by five-membered rings, the olefinic carbons are strictly coplanar with a dihedral angle of 4.8° as determined by the X-ray diffraction method. Neither twisting along the C-C double bond nor pyramidalization of the sp² carbons was observed.

The cyclic ethylene **2** underwent two electron reduction not only with lithium but also with sodium in THF to give dark red solutions of the dianions of **3a** (Li) and **3b** (Na) (Scheme 2).⁹ The 1,2-disodio derivative was isolated as dark red crystals as follows. Reduction of **2** with excess sodium in THF at room temperature gave a dark red solution of the ethylene dianion within 1 h. Evaporation of THF followed by crystallization from toluene afforded (2,2,2',2',5,5,5',5'-octamethyl-2,2',5,5'-tetrasilabicyclopentylidene)bis[(tetrahydrofuran)sodium(I)] (**3b**). All the experiments were carried out by using

(7) The cyclic ethylene **2** was prepared according to the modified procedure reported by Ito; see: (a) Ito, Y.; Suginome, M.; Murakami, M. *J. Org. Chem.* **1991**, *56*, 1948. (b) Murakami, M.; Oike, H.; Sugawara, M.; Suginome, M.; Ito, Y. *Tetrahedron* **1993**, *49*, 3933. (c) Murakami, M.; Suginome, M.; Fujimoto, K.; Ito, Y. *Angew. Chem., Int. Ed. Engl.* **1993**, *32*, 1473.

(8) Spectral data for **2**: pale yellow crystals, mp 118–119 °C; ¹H NMR (CDCl₃, δ) 0.13 (s, 24 H), 0.76 (s, 8 H); ¹³C NMR (CDCl₃, δ) 0.1, 10.5, 189.5; ²⁹Si NMR (CDCl₃, δ) -3.9; UV (hexane) λ_{max}/nm (ε) 235 (15 400), 379 (160); HRMS calcd for C₁₄H₃₂Si₄ m/z 312.1581, found m/z 312.1589.

(9) Reduction of **2** with potassium, rubidium, and cesium in THF also gave dark red solutions of the corresponding dianions. Details and spectral data for these dianions will be reported elsewhere.

[®] Abstract published in *Advance ACS Abstracts*, February 15, 1995.

(1) Chemistry of Organosilicon Compounds. 319.

(2) For reviews, see: (a) Wardell, J. L. In *Comprehensive Organometallic Chemistry*; Wilkinson, G., Stone, F. G. A., Abel, E. W., Eds.; Pergamon Press: New York, 1982. (b) Schleyer, P. v. R. *Pure Appl. Chem.* **1983**, *55*, 355. (c) *Ibid.* **1984**, *56*, 151. (d) Setzer, W. N.; Schleyer, P. v. R. *Adv. Organomet. Chem.* **1985**, *24*, 353. (e) Gunther, H.; Moskau, D.; Bast, P.; Schmalz, D. *Angew. Chem., Int. Ed. Engl.* **1987**, *26*, 1212.

(3) For reviews on sodium derivatives, see: (a) Schade, C.; Schleyer, P. v. R. *Adv. Organomet. Chem.* **1987**, *27*, 169. (b) Bock, H.; Ruppert, K.; Näther, C.; Havlas, Z.; Herrmann, H. F.; Arad, C.; Göbel, I.; John, A.; Meuret, J.; Nick, S.; Rauschenbach, A.; Seitz, W.; Vaupel, T.; Solouki, B. *Angew. Chem., Int. Ed. Engl.* **1992**, *31*, 550.

(4) (a) Sekiguchi, A.; Nakanishi, T.; Kabuto, C.; Sakurai, H. *J. Am. Chem. Soc.* **1989**, *111*, 3748. (b) Sekiguchi, A.; Ichinohe, M.; Nakanishi, T.; Sakurai, H. *Chem. Lett.* **1993**, 267.

(5) See also facile reduction of hexakis(trimethylsilyl)benzene and 1,2,4,5-tetrakis(trimethylsilyl)benzene: (a) Sekiguchi, A.; Ebata, K.; Kabuto, C.; Sakurai, H. *J. Am. Chem. Soc.* **1991**, *113*, 1464. (b) Sekiguchi, A.; Ebata, K.; Kabuto, C.; Sakurai, H. *J. Am. Chem. Soc.* **1991**, *113*, 7081.

(6) Sakurai, H.; Nakadaira, Y.; Tobita, H.; Ito, T.; Toriumi, K.; Ito, H. *J. Am. Chem. Soc.* **1982**, *104*, 300.

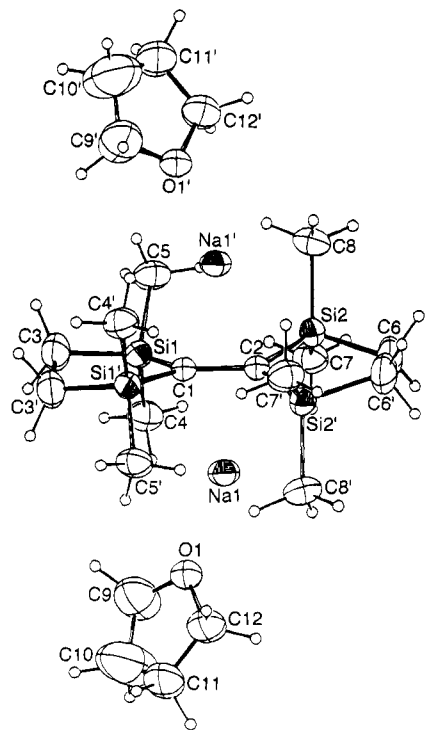


Figure 1. ORTEP drawing of **3b**. Selected bond distances (Å): Si1–C1 1.807(6), Si1–C3 1.879(11), Si2–C2 1.806(7), Si2–C6 1.866(10), C1–C2 1.579(15), O1–Na1 2.293(6), C1–Na1 2.487(4), C2–Na1 2.501(4). Selected bond angles (deg): Si1–C1–Si1' 106.5(5), Si1–C1–C2 126.8(3), Si2–C2–Si2' 106.0(5), Si2–C2–C1 127.0(2), C1–Na1–C2 36.9(3). Dihedral angle (deg): Si1–C1–Si1'/Si2–C2–Si2' 17.1.

the Schlenk tube method. The dilithium derivative **3a** was also isolated by a similar manner.¹⁰

The molecular structures of **3a,b** confirmed by X-ray diffractions are shown in Figures 1 and 2, respectively. The molecule of **3a** has a crystallographic 2-fold axis and mirror symmetry, whereas that of **3b** has only a crystallographic 2-fold axis. Geometries of **2**, **3a**, and **3b** are compared in Table 1.¹¹

Several interesting features for the structures of **3a,b** can be pointed out. The cations in **3a,b** are three-coordinated, being bonded to THF in addition to two anionic carbons. The bond length of the central C–C bond is significantly stretched from 1.369 Å in **2** to 1.575 Å in **3a** and 1.579 Å in **3b**. The bond lengths of Si–C(sp²) bonds (1.825 Å for **3a** and 1.807 Å for **3b**) are remarkably shortened compared to **2** (1.906 Å). In

(10) Spectral data for **3a**: ¹H NMR (toluene-*d*₆, δ) 0.41 (s, 24 H), 1.13 (s, 8 H), 1.30–1.38 (m, 8 H), 3.52–3.59 (m, 8 H); ¹³C NMR (toluene-*d*₆, δ) 5.7 (CH₃), 11.0 (quint, *J*(¹³C–⁶Li) = 3.1 Hz, CLi), 14.5 (CH₂), 25.6 (THF), 69.2 (THF); ²⁹Si NMR (toluene-*d*₆, δ) –6.2; ⁶Li NMR (toluene-*d*₆, δ) 1.72. Spectral data for **3b**: ¹H NMR (toluene-*d*₆, δ) 0.35 (s, 24 H), 1.03 (s, 8 H), 1.26–1.34 (m, 8 H), 3.32–3.40 (m, 8 H); ¹³C NMR (toluene-*d*₆, δ) 6.8 (CH₃), 13.9 (CH₂), 14.7 (CNa), 25.5 (THF), 68.6 (THF); ²⁹Si NMR (toluene-*d*₆, δ) –10.6; ²³Na NMR (toluene-*d*₆, δ) –2.8 (*ν*_{1/2} = 2120 Hz).

(11) Crystal data for **2**: MF = C₁₄H₃₂Si₄, MW = 312.76, monoclinic, *a* = 18.274(3) Å, *b* = 9.200(1) Å, *c* = 13.145(2) Å, β = 116.38(1)°, *V* = 1979.7(6) Å³, space group = *C2/c*, *Z* = 4, *D*_{calc} = 1.049 g/cm³. The final *R* factor was 0.0448 (*R*_w = 0.0456) for 2259 reflections with *F*_o > 3σ(*F*_o). Crystal data for **3a**: MF = C₂₂H₄₈Li₂O₂Si₄, MW = 470.85, monoclinic, *a* = 17.551(18) Å, *b* = 9.438(7) Å, *c* = 9.520(4) Å, β = 108.89(4)°, *V* = 1492.1(20) Å³, space group = *C2/m*, *Z* = 2, *D*_{calc} = 1.048 g/cm³. The final *R* factor was 0.0923 (*R*_w = 0.0913) for 1606 reflections with *F*_o > 3σ(*F*_o). Crystal data of **3b**: MF = C₂₂H₄₈Na₂O₂Si₄, MW = 502.94, monoclinic, *a* = 9.715(1) Å, *b* = 11.383(4) Å, *c* = 13.728(3) Å, β = 99.06(1)°, *V* = 1499.1(6) Å³, space group = *P2/c*, *Z* = 2, *D*_{calc} = 1.114 g/cm³. The final *R* factor was 0.0880 (*R*_w = 0.0921) for 1698 reflections with *F*_o > 3σ(*F*_o).

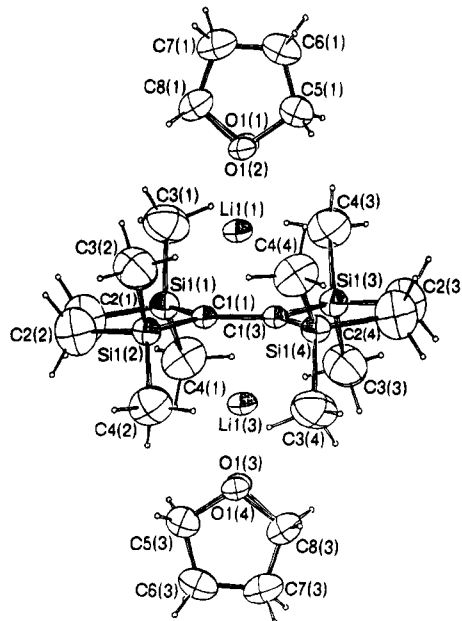


Figure 2. ORTEP drawing of **3a**. Selected bond distances (Å): Si1(1)–C1(1) 1.825(4), Si1(1)–C2(1) 1.868(9), C1(1)–C1(3) 1.575(9), O1(1)–Li1(1) 1.871(11), C1(1)–Li1(1) 2.061(12), C1(1)–Li1(3) 2.065(12). Selected bond angles (deg): Si1(1)–C1(1)–Si1(2) 106.0(4), Si1(1)–C1(1)–C1(3) 127.0(1), C1(1)–Li1(1)–C1(3) 44.9(3). Dihedral angle (deg): Si1(1)–C1(1)–Si1(2)/Si1(3)–C1(3)–Si1(4) 0.0.

Table 1. Selected Bond Lengths (Å), Bond Angles (deg), and Dihedral Angles (deg) of **2**, **3a**, and **3b**^a

	2	3a (Li)	3b (Na)
C–C	1.369(2) ^b	1.575(9) ^c	1.579(15) ^c
C–M		2.063(12)	2.494(4)
C–Si	1.906(2)	1.825(4)	1.807(6)
Si–CH ₃	1.870(2)	1.901(7)	1.919(9)
Si–CH ₂	1.883(2)	1.868(9)	1.873(10)
Si–C–C	127.8(1)	127.0(1)	126.9(2)
Si–C–Si	104.5(1)	106.0(4)	106.3(5)
(Si–C–Si)–(Si–C–Si)	4.8	0.0	17.1

^a Standard deviations are in parentheses. ^b C–C double bond. ^c Anionic C–C bond.

contrast, the bond lengths of Si–CH₃ bonds (1.901 Å for **3a** and 1.919 Å for **3b**) are somewhat elongated with respect to **2** (1.870 Å). The bond angles of Si–C(sp²)–C(sp²) (127.0° for **3a** and 126.9° for **3b**) and C(sp²)–Si–C(sp²) (106.0° for **3a** and 106.3° for **3b**) are almost the same with those of **2** (127.8 and 104.5°, respectively). The dilithium derivative **3a** has a completely planar structure similar to that of the precursor olefin **2** (4.8°), and therefore, the geometry of the cyclopentylidene **2** is essentially retained after the lithiation. On the other hand, disodium derivative **3b** is twisted by 17.1° resulting from the increased electronic repulsion.¹² The twisting angle is evidently influenced by the counter-cation. The dianion halves of **3a,b** are unexpectedly not twisted perpendicularly to each other due to Coulombic attraction between anion and cation centers.¹³

(12) It is a precedent that (tetraphenylethylene)disodium bis(diethyl ether) twists by 56° along the central C–C bond. However, unusual sandwichlike coordination is disclosed in which one of sodium is located between phenyl rings; see: Bock, H.; Ruppert, K.; Fenske, D. *Angew. Chem., Int. Ed. Engl.* **1989**, *28*, 1685.

(13) For theoretical calculations on ethylene dianion dilithium, see: (a) Kos, A. J.; Jemmis, E. D.; Schleyer, P. v. R.; Gleiter, R.; Fischbach, U.; Pople, J. A. *J. Am. Chem. Soc.* **1981**, *103*, 4996. (b) So, S. P. *J. Organomet. Chem.* **1989**, *361*, 283.

The magnitude of such attractive interaction depends on the distance between the anion and cation centers as well as the radii of the cations. The distances of Li^+ and Na^+ from the anionic carbons are 2.063 and 2.494 Å, respectively. These distances are slightly shorter than those of the π -complexed organolithium and sodium derivatives reported so far.^{2d,3a} Therefore, it can be concluded that the group 1 complexes of **2** prefer planar geometry to the perpendicular structure, but larger cations tend to have more twist structures along the central C–C bond. It is interesting to note in this respect that the dianion halves of the charge-transfer salt of decamethylcobaltocene tetracyanoethylene, $\{[\text{Co}(\text{C}_5\text{Me}_5)_2]\}^{2+}[(\text{NC})_2\text{CC}(\text{CN})_2]^{2-}$, are reported to be twisted by 87.1° presumably due to a rather weak interaction between anion and cation centers.¹⁴

Acknowledgment. This work was supported financially by the Ministry of Education, Science, and Culture of Japan (Grant-in-Aid for Specially Promoted Research No. 02102004 and for Scientific Research on Priority Area of Reactive Organometallics No. 05236102). One of the authors (M.I.) thanks the Japan Society for Promotion of Science for the Fellowship for Japan Junior Scientists.

Supplementary Material Available: Tables giving details of the X-ray experiments, atomic parameters, anisotropic temperature factors, and distances and angles and figures showing the structures of **2**, **3a**, and **3b** (19 pages). Ordering information is given on any current masthead page.

OM9407870

(14) Dixon, D. A.; Miller, J. S. *J. Am. Chem. Soc.* **1987**, *109*, 3656.

New Unsaturated Cyclic Carbenes via Direct Activation of Enynols by Ruthenium(II) Complexes

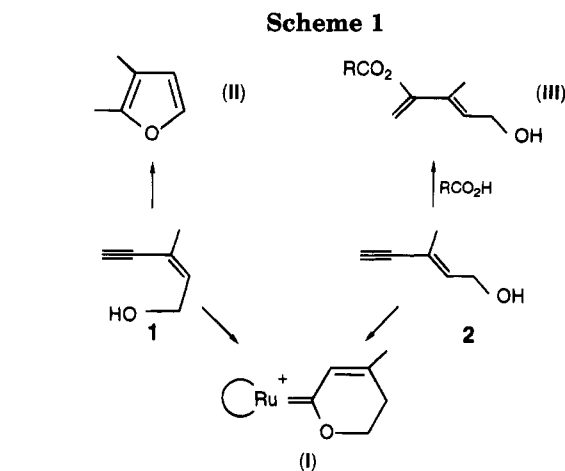
Natividad Ruiz, Daniel Péron, and Pierre H. Dixneuf*

Laboratoire de Coordination Organique, URA-CNRS 415, Campus de Beaulieu, Université de Rennes, 35000 Rennes, France

Received November 22, 1994[⊗]

Summary: $RuCl_2(PMe_3)(C_6Me_6)$ (**3**) reacts with (*Z*)- $HC\equiv CC(Me)=CHCH_2OH$ (**1**) in the presence of $NaPF_6$ to afford a cyclic α,β -unsaturated carbene, the 2-oxacyclohex-5-en-1-ylidene ruthenium complex **4**, and the reaction of $RuCl_2(PMe_3)_2(C_5Me_5)$ (**5**) with both **1** and its *E* isomer **2** leads to the same six-membered unsaturated carbene complex **6**. The activation of (*Z*)- $HC\equiv CC(Me)=CHCH(R)OH$ derivatives ($R = Me$ (**7**), $C\equiv CSiMe_3$ (**9**)) with **5** affords the carbene complexes **8** and **10**, and their formation is explained on the basis of a $Ru=C=C=C(Me)CH_2CH(R)OH$ allenylidene intermediate.

Cyclic metal–carbene complexes, especially α,β -unsaturated derivatives, have been shown to be useful reagents for organic synthesis,^{1–5} and their applications provide impetus to the search for simple, straightforward methods of preparation. Heteroatom-containing cyclic metal–carbene complexes have been conveniently prepared *via* metal ω -haloacyl, carbamoyl, alkoxycarbonyl, or imido intermediates,⁶ opening of epoxides by deprotonated Fischer type carbene complexes,^{3,7} activation of homopropargylic alcohols with low-valent d^6 complexes^{5,8} or ruthenium(II) derivatives,^{9,10} and even direct activation of tetrahydrofuran.¹¹ An important class of unsaturated cyclic carbene complexes, the pyranylidene–metal complexes, requires the previous preparation of functional carbenes—propenylidene–metal derivatives¹² or alkynyl carbene complexes—to react with β -dicarbonyl derivatives,² acrylates,⁴ or enol



ethers.¹³ α,β -Unsaturated cyclic carbenes have been recently obtained from a (4-methoxy-2-oxacyclopentylidene)chromium(0) compound *via* methanol elimination³ and by addition of alkyl radicals generated from epoxides and $(Cp_2TiCl)_2$.¹⁴ We now report the synthesis of novel α,β -unsaturated cyclic carbene metal complexes, the (2-oxacyclohex-5-en-1-ylidene)ruthenium complexes of type **I**, *via* direct activation of (*Z*)- and (*E*)-enynols **1** and **2** (Scheme 1) suggesting the formation of the same allenylidene–ruthenium intermediate.

The activation of (*Z*)-enynol **1** with $RuCl_2(PR_3)(arene)$ catalysts has recently been shown to provide a selective catalytic synthesis of functional furans of type **II** (Scheme 1), whereas such a reaction was inefficient with the *E* isomer **2** as starting material.¹⁵ However, (*E*)-enynol **2** appeared to be an excellent precursor for access to a variety of functional dienes of type **III** *via* addition of carboxylic acids, in the presence of the $Ru_2(O_2CH)_2(CO)_4(PPh_3)_2$ catalyst.¹⁶ Formation of both **II** and **III** proceeded *via* the electrophilic activation with ruthenium(II) complexes of the η^2 -coordinated $HC\equiv C$ bond of **1** or **2** toward regioselective addition to carbon C(2) of the intramolecular hydroxy group in the suitable geometry in **1**¹⁵ or of the carboxylate to give **III**.¹⁶ This led us to investigate the stoichiometric activation of both **1** and **2** in the presence of ruthenium(II) precursors, but under conditions favoring the coordination of the alkyne.¹⁷

The arene–ruthenium(II) complex **3**²² reacts with an excess of (*Z*)- $HC\equiv CC(Me)=CHCH_2OH$ (**1**; 2.5 equiv) and $NaPF_6$ (1.5 equiv) in dichloromethane. After 15 h at room temperature, the orange, cationic carbene complex

[⊗] Abstract published in *Advance ACS Abstracts*, February 1, 1995.

(1) Dötz, K. H.; Fischer, H.; Hofmann, P.; Kreissl, F. R.; Schubert, U.; Weiss, K. *Transition Metal Carbene Complexes*; Verlag Chemie: Weinheim, Germany, 1983.

(2) Wang, S. L. B.; Wulff, W. D. *J. Am. Chem. Soc.* **1990**, *112*, 4550.

(3) (a) Lattuada, L.; Licandro, E.; Maiorana, S.; Molinari, H.; Pagagni, A. *Organometallics* **1991**, *10*, 807. (b) Baldoli, C.; Lattuada, L.; Licandro, E.; Maiorana, S.; Pagagni, A. *Organometallics* **1993**, *12*, 2994.

(4) (a) Camps, F.; Moretó, J. M.; Ricart, S.; Viñas, J. M.; Molins, E.; Miravittles, C. *J. Chem. Soc., Chem. Commun.* **1989**, 1560. (b) Segundo, A.; Moretó, J. M.; Viñas, J. M.; Ricart, S.; Molins, E. *Organometallics* **1994**, *13*, 2467.

(5) Quayle, P.; Rahman, S.; Ward, E. L. M. *Tetrahedron Lett.* **1994**, *35*, 3801.

(6) (a) King, R. B. *J. Am. Chem. Soc.* **1983**, *85*, 1922. (b) Casey, C. P.; Anderson, R. L. *J. Am. Chem. Soc.* **1971**, *93*, 3554. (c) Motschi, H.; Angelici, R. J. *Organometallics* **1982**, *1*, 343. (d) Michelin, R. A.; Zanotto, L.; Braga, D.; Sabatino, P.; Angelici, R. J. *Inorg. Chem.* **1988**, *27*, 93 and references therein.

(7) Casey, C. P.; Brunsvold, W. R.; Scheck, D. M. *Inorg. Chem.* **1977**, *16*, 3059.

(8) (a) Dötz, K. H.; Sturm, W.; Alt, H. G. *Organometallics* **1987**, *6*, 1424. (b) Parlier, A.; Rudler, H. *J. Chem. Soc., Chem. Commun.* **1986**, 514.

(9) Le Bozec, H.; Ouzzine, K.; Dixneuf, P. H. *Organometallics* **1991**, *10*, 2768.

(10) Davies, S. G.; McNally, J. P.; Smallridge, A. J. *Adv. Organomet. Chem.* **1990**, *30*, 1.

(11) Boutry, O.; Gutiérrez, E.; Monge, A.; Nicasio, M. C.; Pérez, P. J.; Carmona, E. *J. Am. Chem. Soc.* **1992**, *114*, 7288.

(12) Juneau, K. N.; Hegedus, L. S.; Roepke, F. W. *J. Am. Chem. Soc.* **1989**, *111*, 4762.

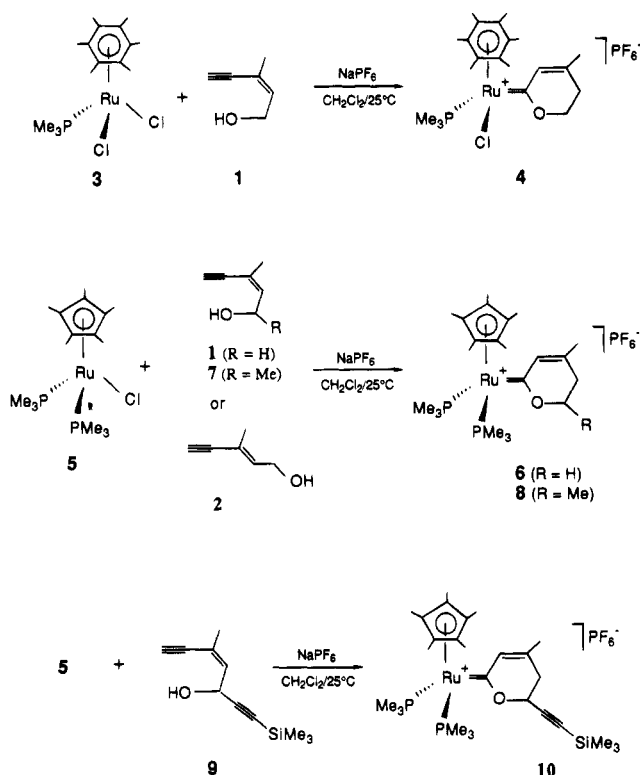
(13) Faron, K. L.; Wulff, W. D. *J. Am. Chem. Soc.* **1990**, *112*, 6419.

(14) Merlic, C. A.; Xu, D. *J. Am. Chem. Soc.* **1991**, *113*, 9855.

(15) Seiller, B.; Bruneau, C.; Dixneuf, P. H. *J. Chem. Soc., Chem. Commun.* **1994**, 493.

(16) Bruneau, C.; Kabouche, Z.; Neveux, M.; Seiller, B.; Dixneuf, P. H. *Inorg. Chim. Acta* **1994**, *222*, 155.

Scheme 2



4 was isolated in 75% yield (Scheme 2). Its analytical and NMR data were consistent with an α,β -unsaturated cyclic carbene derivative (NMR in CDCl_3 (δ , ppm): ^{13}C , 293.73 (Ru=C, d, $^2J_{\text{PC}} = 21.6$ Hz); ^1H , 7.54 (1H, =CH)).²³

This unexpected cyclization reaction suggested the initial formation of the vinylidene intermediate (Z)- $\text{Ru}=\text{C}=\text{CH}-\text{C}(\text{Me})=\text{CHCH}_2\text{OH}$, as for the activation of homopropargylic alcohols,^{9,10} and cyclization allowed by the Z configuration of the double bond, *via* intramolecular addition of the hydroxy group to the electrophilic vinylidene carbon, followed by isomerization to afford the conjugated heterodiene derivative **4**. Such a mechanism suggested that the E isomer **2** would not give a similar type of carbene on reaction with **3**. Actually, complexes **3** and **2** react slowly but the intermediate is not stable.

The stability of **4** is not very high, probably because the unsaturated carbene ligand is electron withdrawing

(17) In the presence of both a polar solvent and a noncoordinating anion salt, these mild conditions were shown to favor the dissociation of the Ru-Cl bond and allow the coordination of terminal alkyne leading to vinylidene^{9,18,19} or allenylidene^{20,21} ruthenium intermediates from $\text{RuCl}_2(\text{PR}_3)(\text{arene})$ ^{9,18,20,21} or $\text{RuCl}(\text{PR}_3)_2(\text{C}_5\text{Me}_5)$ ¹⁹ precursors.

(18) Devanne, D.; Dixneuf, P. H. *J. Organomet. Chem.* **1990**, *390*, 371.

(19) Le Lagadec, R.; Roman, E.; Toupet, L.; Müller, U.; Dixneuf, P. H. *Organometallics* **1994**, *13*, 5030.

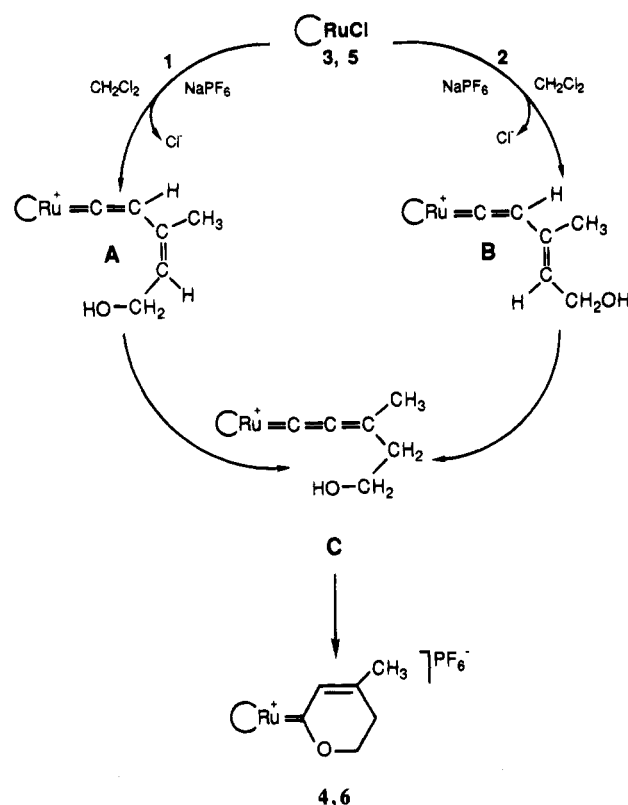
(20) Pilette, D.; Ouzzine, K.; Le Bozec, H.; Dixneuf, P. H.; Rickard, C. E. F.; Roper, W. R. *Organometallics* **1992**, *11*, 809.

(21) Devanne, D.; Dixneuf, P. H. *J. Chem. Soc., Chem. Commun.* **1990**, 641.

(22) (a) Bennett, M. A.; Robertson, G. B.; Smith, A. K. *J. Organomet. Chem.* **1972**, *43*, C41. (b) Bennett, M. A.; Smith, A. K. *J. Chem. Soc., Dalton Trans.* **1974**, 233.

(23) Full details of the synthesis and characterization of **4**, **6**, **8**, and **10** by multinuclear NMR, IR, and elemental analysis are provided in the supplementary material. Selected spectroscopic data for **4**: ^1H NMR (300.134 MHz, CDCl_3) δ 7.54 (broad s, 1H, HC=), 4.81 (m, 1H, OCH₂), 4.65 (m, 1H, OCH₂), 2.46 (m, 2H, CH₂), 2.09 (s, 18H, C₅Me₆), 1.99 (s, =CMe); $^{31}\text{P}\{^1\text{H}\}$ NMR (121.496 MHz, CDCl_3) δ 10.41 (s, PMe₃), -143.96 (sept, $^1J(\text{PF}) = 713$ Hz, PF₆⁻); $^{13}\text{C}\{^1\text{H}\}$ NMR (50.331 MHz, CDCl_3) δ 293.73 (d, $^2J(\text{PC}) = 21.6$ Hz, Ru=C), 151.45 (s, HC=CMe), 134.06 (s, HC=), 72.58 (s, OCH₂), 28.92 (s, CH₂), 23.56 (s, =CMe).

Scheme 3



and is bonded to a cationic electrophilic ruthenium(II) moiety.²⁴ Thus, the activation of both enynols **1** and **2** has been attempted with the more electron releasing²⁴ ruthenium(II) complex $\text{RuCl}(\text{PMe}_3)_2(\text{C}_5\text{Me}_5)$ (**5**).²⁵ Complex **5** reacts with an excess of **1** in the presence of NaPF_6 (CH_2Cl_2) to give 84% of the carbene complex **6** after 15 h at room temperature (Scheme 2). The E isomer **2** under identical conditions reacted with complex **5** and surprisingly led to the same complex **6**, which was isolated in 70% yield. Complex **6** shows in its ^{13}C NMR (CDCl_3) a low-field triplet at δ 280.43 ppm ($^2J_{\text{PC}} = 14.3$ Hz) for the Ru=C carbene carbon nucleus.²⁶

The higher stability of carbene **6** with respect to **4** allowed us to attempt the activation of the C(1)-substituted enynol (Z)- $\text{HC}=\text{CC}(\text{Me})=\text{CHCH}(\text{Me})\text{OH}$ (**7**).²⁷ Complex **5** reacts with **7** to afford the carbene complex **8** (88%). The chirality at the substituted sp^3 carbon in complex **8** caused the nonequivalency of (PMe₃) ^{31}P nuclei.²⁸

The activation of the diynenol **9**²⁷ by complex **5** was also attempted, as both alkyne groups could be activated.²⁹ The reaction led to the formation of a precipi-

(24) The oxidation potentials of **3** and **5**, measured using cyclic voltammetry (CH_3CN , 200 mV/s, Bu₄NPF₆ (0.1 M), Pt/V (SCE)), were $E_{1/2} = +0.77^9$ and $+0.09$ V (SCE), respectively.

(25) Fagan, P. J.; Mahoney, W. S.; Calabrese, J. C.; Williams, I. D. *Organometallics* **1990**, *9*, 1843.

(26) Selected spectroscopic data for **6**: ^1H NMR δ (300.134 MHz, CDCl_3) 6.67 (broad s, 1H, HC=); $^{13}\text{C}\{^1\text{H}\}$ NMR (75.469 MHz, CDCl_3) δ 280.43 (t, $^2J(\text{PC}) = 14.3$ Hz, Ru=C), 139.69 (s, =CMe), 136.26 (s, HC=).

(27) The functional enynols were prepared from the commercially available precursor **1** *via* oxidation into the corresponding aldehyde followed by addition of the suitable lithium reagent.¹⁵

(28) Selected spectroscopic data for **8**: $^{31}\text{P}\{^1\text{H}\}$ NMR (121.496 MHz, CDCl_3) δ 8.83, 7.40 (AB system, $^2J_{\text{PP}} = 40.8$ Hz, PMe₃), -143.76 (sept, $^1J(\text{PF}) = 715$ Hz, PF₆⁻); $^{13}\text{C}\{^1\text{H}\}$ NMR (75.469 MHz, CDCl_3) δ 281.6 (t, $^2J(\text{PC}) = 14.3$ Hz, Ru=C), 139.44 (s, =CMe), 136.08 (s, HC=).

(29) Péron, D.; Romero, A.; Dixneuf, P. H. *Gazz. Chim. Ital.*, in press.

tate which was identified as complex **10**, containing the (trimethylsilyl)ethynyl substituent at the carbon atom linked to oxygen (^{13}C NMR δ 278.1 ppm (Ru=C, t, $^2J_{\text{PC}} = 14.1$ Hz); ^{31}P NMR δ 8.44, 7.51 (AB system, $^2J_{\text{PP}} = 38.9$ Hz); ^1H NMR δ 6.67 (HC=C), 0.16 (SiMe₃) ppm).³⁰ The formation of **10** indicated that in **9** the HC=C bond is more reactive than the MeSiC=C group. Compounds of type **10** offer potential for the access to bimetallic systems linked by an unsaturated bridge *via* further activation of the C=C bond.

The synthesis of **6** from the *E* isomer **2** eliminates the "obvious" mechanism *via* the intramolecular addition of the OH group to the vinylidene carbon of **B**, from which the direct isomerization into **A** is not likely (Scheme 3). It has been shown, on the basis of labeling experiments,²¹ that the first activation step of alkenylacetylenes HC=CC(R)=CH₂ with complexes of type **3** consisted of the formation of an allenylidene intermediate *via* migration of the HC=C proton to the carbon C(4)³¹ and the allenylidene complex L_nRu=C=C=C(R)CH₃

(30) Selected spectroscopic data for **10**: ^1H NMR δ (300.134 MHz, CDCl₃) δ 6.67 (broad s, 1H, HC=), 4.82 (dd, $^3J(\text{HH}) = 5.1$ Hz, $^3J(\text{HH}) = 10.1$ Hz, 1H, OCH), 0.16 (s, 9H, SiMe₃); $^{31}\text{P}\{^1\text{H}\}$ NMR (121.496 MHz, CDCl₃) δ 8.44, 7.51 (AB system, $^2J_{\text{PP}} = 38.9$ Hz, PMe₃), -143.75 (sept, $^1J(\text{PF}) = 714$ Hz, PF₆⁻); $^{13}\text{C}\{^1\text{H}\}$ NMR (75.469 MHz, CDCl₃) δ 278.1 (t, $^2J(\text{PC}) = 14.1$ Hz, Ru=C), 137.31 (s, =CMe), 135.89 (s, HC=), 100.48 (s, CC=), 98.99 (s, C₅Me₅), 93.26 (s, =CSi).

(31) With RuCl₂(PR₃)(arene) complexes the reaction proceeds, in the presence of MeOH, according to the equation²¹ (Ru(η^2 -DC=CC(R)=CH₂) → (Ru=C=C=C(R)CH₂D) → (Ru=C(OMe)CH=C(R)CH₂D.

was isolated from isopropenylacetylene and RuCl₂(Ph₂PCH₂PPh₂)₂.³²

Thus, it can be expected that the activation of both isomers **1** and **2** with complexes **3** and **5** leads to the same allenylidene intermediate **C**, resulting from the migration of the terminal alkyne hydrogen to the carbon C(4), *via* the two different vinylidene derivatives **A** from **1** and **B** from **2**. The carbon C(1) of allenylidene-ruthenium complexes is known to be the electrophilic site for the addition of methanol;³¹ thus, the intramolecular addition of the OH group of **C** to the allenylidene carbon C(1) with proton transfer at carbon C(2) will directly afford the cyclic α,β -unsaturated carbene complex of type **I**.

Acknowledgment. We are grateful to the European Union "Human Capital and Mobility" program for the award of a postdoctoral grant (No. ERBCHBICT 941209) to N.R. (University of Zaragoza).

Supplementary Material Available: A textual presentation of experimental procedures and spectroscopic data for complexes **4**, **6**, **8**, and **10** (3 pages). Ordering information is given on any current masthead page.

OM9408932

(32) Pirio, N.; Touchard, D.; Toupet, L.; Dixneuf, P. H. *J. Chem. Soc., Chem. Commun.* **1991**, 980.

A Stable Bimetallic Copper(I) Titanium Acetylide

Maurits D. Janssen,[†] Mathias Herres,[‡] Laszlo Zsolnai,[‡] David M. Grove,[†]
Anthony L. Spek,[§] Heinrich Lang,^{*,‡} and Gerard van Koten^{*,†}

Debye Institute, Department of Metal-Mediated Synthesis, Utrecht University, Padualaan 8,
3584 CH Utrecht, The Netherlands, Ruprecht-Karls Universität Heidelberg,
Anorganisch-Chemisches Institut, Im Neuenheimer Feld 270, 69120 Heidelberg, Germany, and
Bijvoet Center for Biomolecular Research, Laboratory of Crystal and Structural Chemistry,
Utrecht University, Padualaan 8, 3584 CH Utrecht, The Netherlands

Received November 16, 1994[®]

Summary: The reaction of $[(\eta^5\text{-C}_5\text{H}_4\text{SiMe}_3)_2\text{Ti}(\text{C}\equiv\text{CSiMe}_3)_2]\text{CuCl}$ (**4**) with 1 equiv of $\text{LiC}\equiv\text{CR}$ ($\text{R} = \text{SiMe}_3$ (**5a**), $t\text{-Bu}$ (**5b**), Ph (**5c**)) affords the monomeric complexes $[(\eta^5\text{-C}_5\text{H}_4\text{SiMe}_3)_2\text{Ti}(\text{C}\equiv\text{CSiMe}_3)_2]\text{CuC}\equiv\text{CR}$ ($\text{R} = \text{SiMe}_3$ (**3a**), $t\text{-Bu}$ (**3b**), Ph (**3c**)). Complexes **3** were independently prepared by starting from $(\eta^2\text{-C}_5\text{H}_4\text{SiMe}_3)_2\text{Ti}(\text{C}\equiv\text{CSiMe}_3)_2$ (**1**) and $1/n [\text{CuC}\equiv\text{CR}]_n$ ($\text{R} = \text{SiMe}_3$ (**2a**), $t\text{-Bu}$ (**2b**), Ph (**2c**)) and are the first examples of stable monomeric bis(η^2 -alkyne)(η^1 -alkynyl)copper compounds. Reaction of **1** with $1/4 [\text{CuO-}t\text{-Bu}]_4$ (**6**) results in the formation of the remarkably stable bimetallic acetylide complex $[(\eta^5\text{-C}_5\text{H}_4\text{SiMe}_3)_2\text{Ti}(\text{C}\equiv\text{CSiMe}_3)(\text{C}\equiv\text{CCu})_2]$ (**7**) (mp 157 °C dec) by nucleophilic substitution of one of the alkynyl-SiMe₃ groups in **1**, whereby $t\text{-BuOSiMe}_3$ is eliminated. Other nucleophiles (e.g. F^- and EtO^-) show a similar reactivity, although in this case the substitution is much slower and less selective.

Alkynylcopper(I) compounds are generally encountered as polynuclear species which exist either as discrete aggregates or as oligomers.¹ In these species the alkynyl ligands are σ - and π -bonded to copper(I) centers. Recently we showed that bis(alkynyl)titanocenes are very useful chelating ligands for the stabilization of mononuclear bis(η^2 -alkyne)(η^1 -aryl)copper and -silver compounds, where aryl is for example $\text{C}_6\text{H}_2\text{Me}_3\text{-2,4,6}$.² In order to study intramolecular *vs* intermolecular alkyne to copper coordination, we are interested in the isolation of mononuclear bis(η^2 -alkyne)(η^1 -alkynyl)-copper(I) compounds, using the chelate effect of the alkynyl units in the bis(alkynyl)titanocene $(\eta^5\text{-C}_5\text{H}_4\text{-SiMe}_3)_2\text{Ti}(\text{C}\equiv\text{CSiMe}_3)_2$ (**1**).³

Addition of $(\eta^5\text{-C}_5\text{H}_4\text{SiMe}_3)_2\text{Ti}(\text{C}\equiv\text{CSiMe}_3)_2$ (**1**)^{3f} to solutions or suspensions of alkynylcopper(I) compounds, $[\text{CuC}\equiv\text{CR}]_n$ ($\text{R} = \text{SiMe}_3$ (**2a**), $t\text{-Bu}$ (**2b**), Ph (**2c**)),¹ in a 1:1 molar ratio leads to the quantitative formation of the monomeric complexes $[(\eta^5\text{-C}_5\text{H}_4\text{SiMe}_3)_2\text{Ti}(\text{C}\equiv\text{CSiMe}_3)_2]\text{CuC}\equiv\text{CR}$ ($\text{R} = \text{SiMe}_3$ (**3a**), $t\text{-Bu}$ (**3b**), Ph (**3c**)). An alternative preparative route is the transmetalation of $[(\eta^5\text{-C}_5\text{H}_4\text{SiMe}_3)_2\text{Ti}(\text{C}\equiv\text{CSiMe}_3)_2]\text{CuCl}$ (**4**) with the corresponding alkynyllithium compounds $\text{LiC}\equiv\text{CR}$ ($\text{R} = \text{SiMe}_3$ (**5a**), $t\text{-Bu}$ (**5b**), Ph (**5c**)) (see Scheme 1). Complexes **3** are stable in solution and in the solid state and can be isolated as orange crystalline solids by cooling their diethyl ether solutions to -30 °C. They are soluble in most organic solvents, and solutions of **3** can be handled safely in air for short periods of time. Crystals of **3** are stable to air for a few weeks.

The presence of two different C=C stretching frequencies in the IR spectra of **3** indicates that besides an η^1 -bonded alkynylcopper unit, $\text{CuC}\equiv\text{CR}$, η^2 -bonded disubstituted alkyne ligands are present. Through the η^2 -coordination of these alkyne moieties to the copper atom in **3**, the $\nu(\text{C}\equiv\text{C})$ vibration is shifted from 2012 cm^{-1} in the parent compound **1**^{3f} to 1896 in **3a**, 1902 in **3b**, and 1941 cm^{-1} in **3c**. The η^1 -bonded alkynyl group, $\text{C}\equiv\text{CR}$, is found at $\nu(\text{C}\equiv\text{C})$ 2035 in **3a**, 2095 in **3b**, and 2094 cm^{-1} in **3c**.

The molecular structure of **3a** was determined by a single-crystal X-ray diffraction analysis.⁴

The molecular structure of **3a** (see Figure 1) shows that $[(\eta^5\text{-C}_5\text{H}_4\text{SiMe}_3)_2\text{Ti}(\text{C}\equiv\text{CSiMe}_3)_2]\text{CuC}\equiv\text{CSiMe}_3$ is monomeric. Both alkyne groups from the bis(alkynyl)-titanocene are η^2 -coordinated to the copper atom Cu1,

(3) (a) Lang, H.; Herres, M.; Zsolnai, L.; Imhof, W. *J. Organomet. Chem.* **1991**, *409*, C7-C11. (b) Lang, H.; Herres, M.; Zsolnai, L. *Organometallics* **1993**, *12*, 5008–5011. (c) Lang, H.; Imhof, W. *Chem. Ber.* **1992**, *125*, 1307–1311. (d) Lang, H.; Zsolnai, L. *J. Organomet. Chem.* **1991**, *406*, C5-C8. (e) Lang, H.; Herres, M.; Zsolnai, L. *Bull. Chem. Soc. Jpn.* **1993**, *66*, 429–431. (f) Lang, H.; Seyferth, D. Z. *Naturforsch.* **1990**, *45B*, 212–220.

(4) Single crystals of **3a** were grown by cooling a saturated Et_2O solution to -20 °C. Crystal data for **3a**: $\text{C}_{31}\text{H}_{53}\text{CuSi}_5\text{Ti}$, red crystal ($0.38 \times 0.38 \times 0.63$ mm), monoclinic, space group $P2_1/c$, with $a = 20.9981(9)$ Å, $b = 12.0851(9)$ Å, $c = 15.2434(10)$ Å, $\beta = 100.146(4)^\circ$, $V = 3807.7(4)$ Å³, $Z = 4$, d_{calc} = 1.182 g cm^{-3} , $F(000) = 1440$, $\mu(\text{Mo K}\alpha) = 9.4$ cm^{-1} . A total of 9267 (8447 unique) reflections ($0.99 < \theta < 27.50^\circ$; $\omega/2\theta$ scan; $T = 150$ K) were measured on an Enraf-Nonius CAD-4T rotating anode diffractometer using graphite-monochromated Mo K α radiation ($\lambda = 0.71073$ Å). Data were corrected for Lorentz polarization effects and absorption (DIFABS minimum and maximum correction: 0.826/1.103). The structure was solved by direct methods (SHELXS86) and difference Fourier techniques and refined on F^2 by full-matrix least squares (SHELXL93) to an R_1 value of 0.055 for 5854 reflections with $F_o > 4\sigma(F_o)$ and 343 parameters, $wR_2 = 0.151$, $S = 1.024$, and $w^{-1} = (\sigma^2(F_o^2) + (0.0826P)^2)$, where $P = (\max(F_o^2, 0) + 2F_c^2)/3$. Hydrogen atoms were introduced on calculated positions and refined riding on their carrier atoms. All non-H atoms were refined with anisotropic thermal parameters. A final Fourier map showed no residual density outside -0.43 and 0.58 $\text{e}/\text{Å}^3$ (near Cu1).

* To whom correspondence should be addressed.

[†] Debye Institute, Utrecht University.

[‡] Universität Heidelberg.

[§] Bijvoet Center for Biomolecular Research, Utrecht University.

[®] Abstract published in *Advance ACS Abstracts*, February 1, 1995.

(1) (a) For a review on metal alkynyls: Nast, R. *Coord. Chem. Rev.* **1982**, *47*, 89–124. (b) $[\text{Cu}(\text{C}\equiv\text{CPh})(\text{PMe}_3)_4]$: Corfield, P. W. R.; Shearer, H. M. M. *Acta Crystallogr.* **1966**, *21*, 957–965. (c) $[\text{Ag}(\text{C}\equiv\text{CPh})(\text{PMe}_3)_3]$: Corfield, P. W. R.; Shearer, H. M. M. *Acta Crystallogr.* **1966**, *20*, 502–508. (d) $[\text{Cu}_3(\mu_3\text{-}\eta^1\text{-C}\equiv\text{CPh})_2(\text{dppm})_3]\text{BF}_4$ and $[\text{Cu}_3(\mu_3\text{-}\eta^1\text{-C}\equiv\text{CPh})(\text{dppm})_3](\text{BF}_4)_2$: Díez, J.; Gamasa, M. P.; Gimeno, J.; Lastra, E.; Aguirre, A.; García-Granda, S. *Organometallics* **1993**, *12*, 2213–2220. (e) $[\text{Cu}_3(\mu_3\text{-}\eta^1\text{-C}\equiv\text{C-}t\text{-Bu})(\mu_3\text{-Cl})(\text{dppm})_3]\text{PF}_6$: Yam, V. W.-W.; Lee, W.-K.; Lai, T.-F. *Organometallics* **1993**, *12*, 2383–2387. (f) $[\text{Cu}_3(\text{SAr})_2\text{C}\equiv\text{C-}t\text{-Bu}]_n$: Knotter, D. M.; Spek, A. L.; van Koten, G. *J. Chem. Soc., Chem. Commun.* **1989**, 1738–1739. Knotter, D. M.; Spek, A. L.; Grove, D. M.; van Koten, G. *Organometallics* **1992**, *11*, 4083–4090. (g) $[\text{CuC}\equiv\text{CPh}]_n$: Corfield, P. W. R.; Shearer, H. M. M. In *Organometallic Compounds*; Coates, G. E., Green, M. L. H.; Wade, K., Eds.; Chapman and Hall: London, 1977; Vol. 2. (h) $[\text{CuC}\equiv\text{C-}t\text{-Bu}]_n$: Coates, G. E.; Parkin, C. J. *Inorg. Nucl. Chem.* **1961**, *22*, 59. (i) $[\text{MC}\equiv\text{CCF}_3]_n$ ($\text{M} = \text{Cu}$, Ag): Haszeldine, R. N. *J. Chem. Soc.* **1951**, 588–591.

(2) Janssen, M. D.; Herres, M.; Spek, A. L.; Grove, D. M.; Lang, H.; van Koten, G. To be submitted for publication.

Scheme 1

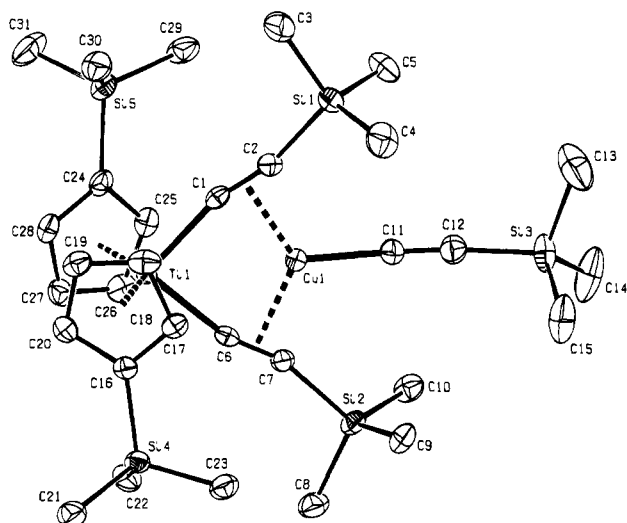
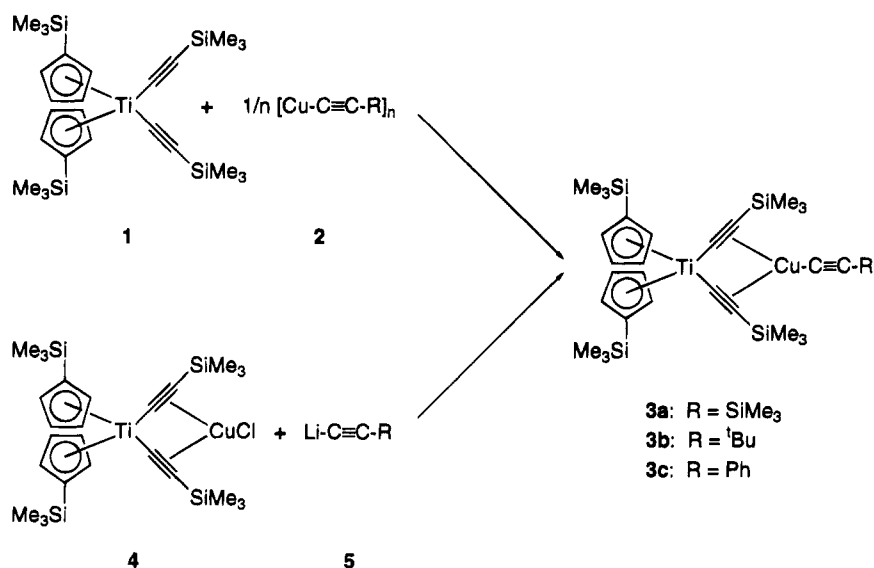


Figure 1. Molecular structure of **3a** (ORTEP, thermal ellipsoids at 50% probability). Selected bond distances (Å) and bond angles (deg): Ti1–Cu1, 2.9665(8); Cu1–C11, 1.898(3); Cu1–C1, 2.074(4); Cu1–C2, 2.112(4); Cu1–C6, 2.069(4); Cu1–C7, 2.111(4); C1–C2, 1.236(5); C6–C7, 1.240(5); C11–C12, 1.215(6); Ti1–C1, 2.081(4); Ti1–C6, 2.095(4); Ti1–C1–C2, 165.0(3); C1–C2–Si1, 162.8(3); Ti1–C6–C7, 165.4(4); C6–C7–Si2, 162.9(4); Cu1–C11–C12, 175.6(3); C11–C12–Si3, 171.4(4).

while the alkynyl ligand from the starting alkynyl-copper(I) compound is exclusively η^1 -coordinated. The C≡C bond lengths of the $Ti(C\equiv CSiMe_3)_2$ unit are lengthened from an average of 1.208 Å in **1^{3b}** to 1.236–(5) Å (C1–C2) and 1.240(5) Å (C6–C7) in **3a**. The copper atom possesses a trigonal-planar geometry and is surrounded by the two η^2 -bonded alkynyl ligands from **1** and by one η^1 -bonded alkynyl ligand and represents the first example in organocopper chemistry for which the monomeric structure is brought about by η^2 -bonded alkyne ligands. The Ti–C≡C–Si units are significantly bent (Ti1–C1–C2 = 165.0(3)°, Ti1–C6–C7 = 165.4(4)°, C1–C2–Si1 = 162.8(3)°, C6–C7–Si2 = 162.9(4)°; see Figure 1) due to the η^2 -coordination of the Ti–C≡C–SiMe₃ ligands to the copper atom. The same behavior is observed in similar bis(η^2 -alkyne)CuX complexes (X = singly bonded organic or inorganic ligand).^{2,3}

The η^1 -bonded (trimethylsilyl)ethynyl unit, $Cu-C\equiv C-SiMe_3$, has a geometry typical for a noncoordinating alkynyl ligand (C11–C12 = 1.215(6) Å, Cu1–C11–C12 = 175.6(3)°, C11–C12–Si3 = 171.4(4)°; see Figure 1).

Surprisingly, complex **1** reacts selectively with 1/4 $[CuO-t-Bu]_4$ (**6**)⁵ in Et₂O at ambient temperature to yield quantitatively the dimeric complex $[(\eta^5-C_5H_4SiMe_3)_2Ti-(C\equiv CSiMe_3)(C\equiv CCu)]_2$ (**7**). The intermediate formation of the bis(η^2 -alkyne) coordination complex $[(\eta^5-C_5H_4SiMe_3)_2Ti(C\equiv CSiMe_3)_2]CuO-t-Bu$ (**8**) is not observed; elimination of *t*-BuOSiMe₃ (as detected with GC–MS) and the formation of **7** is instantaneous and quantitative. Other nucleophiles (e.g. F[–] and EtO[–]) show a similar reactivity toward complexes **3**, although the reaction is much slower and less selective due to competitive cleavage of the Ti–C≡C bond (see Scheme 2).

Complex **7** is a dark red solid which melts with decomposition at 157 °C; it is air-stable and is soluble in most organic solvents. The thermal and kinetic stability of **7** is remarkable, since bimetallic acetylide species of copper(I) ($Cu-C\equiv CM$) are usually very reactive and can be explosive.¹⁵

A cryoscopic molecular weight determination of **7** in benzene indicates that it is dimeric in solution. Variable-temperature ¹H NMR experiments indicate that **7** maintains this aggregation state in solution; in the temperature range 207–353 K the ¹H spectra remain essentially identical.

The molecular structure of **7** (see Figure 2)⁶ comprises

(5) Lemmen, T. H.; Goeden, G. V.; Huffman, J. C.; Geerts, R. L.; Caulton, K. G. *Inorg. Chem.* **1990**, *29*, 3680–3685.

(6) Single crystals of **7** were grown from a saturated diethyl ether solution at –30 °C. **7** contains one molecule of Et₂O in the unit cell: C₄₆H₇₀Cu₂Si₆Ti₂·Et₂O, dark orange crystal (0.30 × 0.20 × 0.40 mm), secured in a glass capillary and sealed under nitrogen, triclinic, space group $P\bar{1}$, with $a = 11.714(3)$ Å, $b = 12.190(4)$ Å, $c = 12.581(3)$ Å, $\alpha = 101.12(2)^\circ$, $\beta = 117.39(2)^\circ$, $\gamma = 90.54(2)^\circ$, $V = 1555.2(8)$ Å³, $Z = 1$, $d_{\text{calc}} = 1.241$ g cm^{–3}, $F(000) = 616$, $\mu(\text{Mo K}\alpha) = 10.7$ cm^{–1}. Diffraction data were collected on a Siemens (Nicolet Syntex) R3m/V diffractometer by using the θ – 2θ technique (2θ limits $2 \leq 2\theta \leq 47^\circ$, scan range 0.75° , scan speed $3 \leq \omega \leq 29.3^\circ$ min^{–1} and Mo K α radiation ($\lambda = 0.71079$ Å). The structure was solved by direct methods (SHELXTL-PLUS) on 4240 unique reflections with $R > 4\sigma(F)$. Non-hydrogen atoms were refined anisotropically, and hydrogen atoms were fixed at calculated positions (number of variables 284). An empirical absorption correction was applied. Final discrepancy indices: $R = 0.030$ and $wR = 0.031$.

Scheme 2

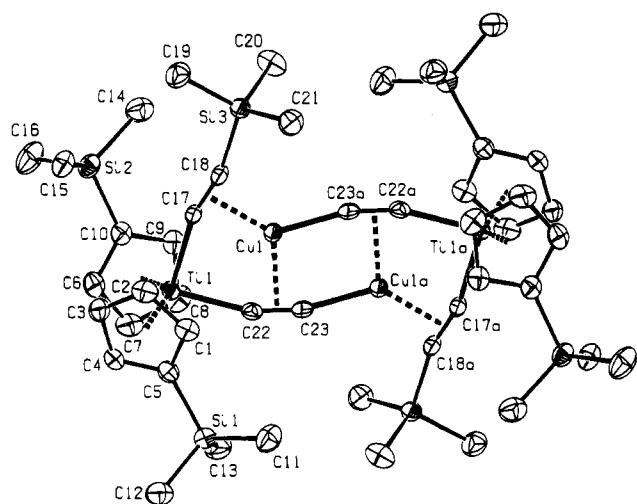
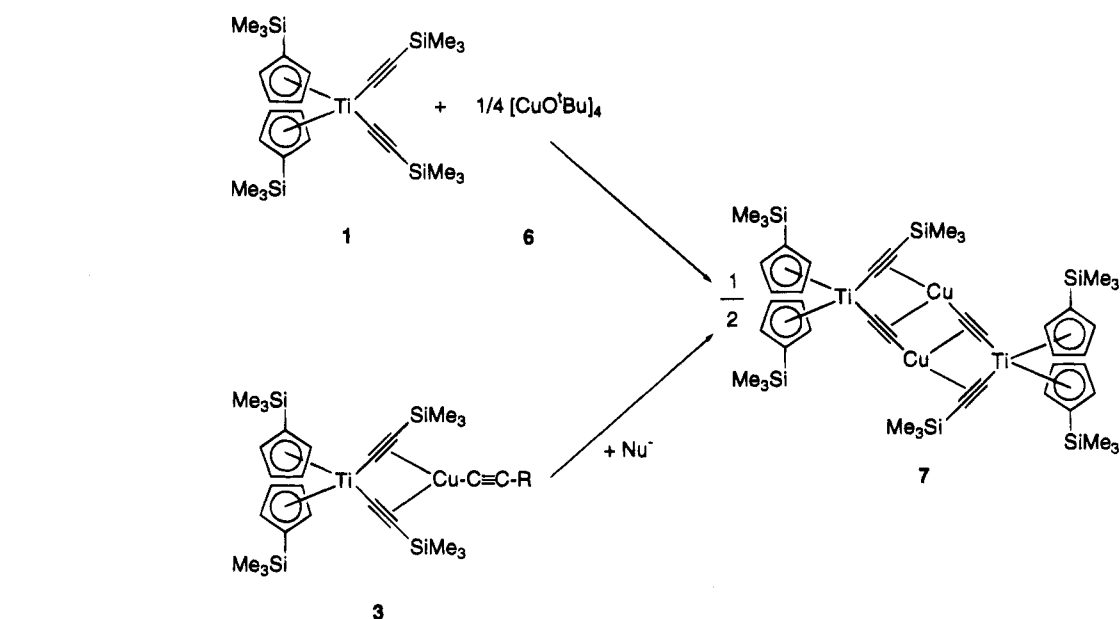


Figure 2. Molecular structure of **7** (ORTEP, thermal ellipsoids at 50% probability). Selected bond distances (Å) and bond angles (deg): Ti1–Cu1, 2.911(1); Cu1–Cu1a, 2.998(1); Cu1–C22, 2.107(2); Cu1–C23, 2.161(3); Cu1–C23a, 1.920(3); Cu1–C17, 2.030(3); Cu1–C18, 2.086(3); C17–C18, 1.234(3); C22–C23, 1.243(4); Ti1–C17, 2.097(3); Ti1–C22, 2.079(3); Ti1–C17–C18, 164.6(2); C17–C18–Si3, 165.0(2); Ti1–C22–C23, 163.4(2); C22–C23–Cu1a, 165.0(2); C17–Ti1–C22, 90.5(1); Cu1–C23–Cu1a, 94.4(1).

a dimer of the bimetallic acetylide ($\eta^5\text{-C}_5\text{H}_4\text{SiMe}_3$)₂Ti-(C≡CSiMe₃)(C≡CCu) in which the alkynyl ligand within the Ti–C≡C–Cu entity is also η^2 -bonded to a second copper atom, thus forming an alkyne-bridged dimer. The C≡C bond lengths of the alkyne ligands within this building block are lengthened from 1.208 Å in **1** to 1.234(3) Å (TiC≡CSi) and 1.243(4) Å (TiC≡CCu) in **7**. Each copper atom exhibits a somewhat distorted trigonal planar geometry with two η^2 - and one η^1 -bonded alkynyl ligands. The Ti–C≡C–Cu moiety deviates from linearity upon its η^2 -coordination to a second copper atom (Cu1) (Ti1–C22–C23 = 163.4(2)°, Cu1a–C23–C22 = 165.0(2)°). The central Cu₂(η^2 -C≡C)₂ core of **7** has a structural arrangement which corresponds to that observed in most polynuclear alkynylcopper(I)

compounds, in which the alkynyl ligands are η^1 - as well as η^2 -bonded to copper atoms, thus forming an infinite zigzag chain.^{1g}

In the IR spectrum of **7** two distinct $\nu(\text{C}\equiv\text{C})$ vibrations at 1896 cm⁻¹ (TiC≡CSi) and 1844 cm⁻¹ (TiC≡CCu) are observed. These IR data are in agreement with the η^2 -coordination of both TiC≡CSi and TiC≡CCu entities to the copper atom. Note that the C≡C vibration frequency for the TiC≡CSi unit in **7** is the same as that found in complex **3a**.

The bis(η^2 -alkyne)(η^1 -alkynyl) complexes **3** and **7** are surprisingly stable. They are selectively formed by self-assembly from alkynylcopper or copper alkoxide aggregates and the bis(alkynyl)titanocene **1**. Moreover, dimeric **7** can be formed from monomeric **3**, when nucleophiles are present in solution (Scheme 2).

The coordination properties of the chelating bis(alkyne) ligand **1** are currently being investigated for the synthesis and isolation of stabilized mononuclear aryl-, alkenyl-, or alkylcopper(I) fragments out of heterocopper and cuprate reagents. As an example, the isolation of [($\eta^5\text{-C}_5\text{H}_4\text{SiMe}_3$)₂Ti(C≡CSiMe₃)₂]Cu{C₆H₄NMe₂-4} from *in situ* prepared Cu{C₆H₄NMe₂-4}⁷ has recently been achieved.²

Acknowledgment. This research was supported in part by the Deutsche Forschungsgemeinschaft, the Volkswagenstiftung, and the Fonds der Chemischen Industrie (Germany) and also in part (A.L.S.) by the Netherlands Foundation for Chemical Research (SON) with financial aid from the Netherlands Organization for Scientific Research (NWO).

Supplementary Material Available: Text giving synthetic procedures and analytical and spectroscopic data for **3** and **7** and tables of all atom parameters for **3a** and **7** (27 pages). Ordering information is given on any current masthead page.

OM940874S

(7) van Koten, G.; Leusink, A. J.; Noltes, J. G. *J. Organomet. Chem.* **1975**, *85*, 105–114.

A Systematic Synthetic Approach to a Novel, Mixed 2,3-C₂B₄– and 2,4-C₂B₄–Erbium(III) Carborane Bent-Sandwich Complex

Narayan S. Hosmane,^{*,†} Ying Wang,[†] Hongming Zhang,[†] Aderemi R. Oki,[†] John A. Maguire,[†] Eberhard Waldhör,[‡] Wolfgang Kaim,[‡] Herbert Binder,[‡] and Reinhard K. Kremer[§]

Department of Chemistry, Southern Methodist University, Dallas, Texas 75275, Institut für Anorganische Chemie, Universität Stuttgart, Pfaffenwaldring 55, D-70550 Stuttgart 80, Germany, and Max-Planck-Institut für Festkörperforschung, Heisenbergstrasse 1, D-70506 Stuttgart, Germany

Received November 14, 1994[®]

Summary: The reaction between *closo-exo*-Li(TMEDA)-1-Li(TMEDA)-2,3-(SiMe₃)₂-2,3-C₂B₄H₄ (**1a**) and anhydrous ErCl₃ in a molar ratio of 2:1, in dry benzene at 0 °C produced, in 93% yield, a novel Er(III) bent-sandwich complex, [Li(TMEDA)₂][1-Cl-1-(μ-Cl)-2,2',3,3'-(SiMe₃)₄-5,6-[(μ-H)₂Li(TMEDA)]-4,4',5'-[(μ-H)₃Li(TMEDA)]-1,1'-*commo*-Er(2,3-C₂B₄H₄)₂] (**2**), as an orange crystalline solid. The reaction of **2** with 1 equiv of *closo-exo*-Li(TMEDA)-1-Li(TMEDA)-2,4-(SiMe₃)₂-2,4-C₂B₄H₄ (**1b**) in dry benzene at 0 °C produces the pink, dimeric Er(III) mixed-carborane bent-sandwich complex {Li(TMEDA)₂}₂{*commo*-1-[2,3-(SiMe₃)₂-2,3-C₂B₄H₄]-1-Er-[2,4-(SiMe₃)₂-2,4-C₂B₄H₄]}₂ (**3**) in 95% yield, thus demonstrating a possible general synthetic route to mixed-carborane metal complexes.

The majority of the metallaborane and metallacarborane sandwich compounds described in the literature are those in which a metal, or metal group, is bonded to *nido*-polyhedral boron cage fragments of the same type.¹ Most of the mixed-ligand complexes that have been prepared are those having either a cyclopentadienide (C₅R₅⁻), or some other cyclic organic π donor, as the companion ligand to a carborane.^{1–3} The scarcity of sandwich complexes containing two different carborane ligands stems mainly from the well-known fact that the simultaneous complexation of a metal moiety with two similar but nonidentical ligands would produce not only mixed-ligand metal complexes but also the species derived from each of the ligands exclusively bonding. The ability to systematically synthesize sandwich complexes containing two similar carborane ligands would allow for the introduction of modifications that might enhance certain desirable properties of the molecules. Recently, Grimes and co-workers have shown that a number of multidecker complexes with different metals and different carborane ligands could be syn-

thesized through a sequential complexation–degradation process.⁴ However, a general systematic approach to the exclusive formation of a complex in which a metal is sandwiched by two different carborane ligands has yet to be demonstrated. We report herein the synthesis of an anionic chloroerbacarborane bent-sandwich complex of a 2,3-C₂B₄ carborane system and its subsequent reaction with the dilithium-complexed [2,4-(SiMe₃)₂-2,4-C₂B₄H₄]²⁻ dianion to produce, in high yield, a dimeric, dianionic, mixed-ligand erbacarborane containing one 2,3-C₂B₄ and one 2,4-C₂B₄ carborane ligand. To our knowledge, these compounds constitute the first reported erbium complexes of any carborane ligand and are some of the few examples of metallacarborane sandwich compounds having two different carborane ligands.^{1,5}

Treatment of *closo-exo*-Li(TMEDA)-1-Li(TMEDA)-2,3-(SiMe₃)₂-2,3-C₂B₄H₄ (**1a**; TMEDA = (Me₂NCH₂)₂)⁶ with anhydrous ErCl₃ in a molar ratio of 2:1 in dry benzene produced an Er(III) bent-sandwich complex, [Li(TMEDA)₂][1-Cl-1-(μ-Cl)-2,2',3,3'-(SiMe₃)₄-5,6-[(μ-H)₂Li(TMEDA)]-4,4',5'-[(μ-H)₃Li(TMEDA)]-1,1'-*commo*-Er(2,3-C₂B₄H₄)₂] (**2**), as an orange crystalline solid, in 93% yield.⁷ This high-yield production of **2** is quite different from the results found for the reaction of the corresponding THF-solvated analogue of **1a** with a number of different LnCl₃ salts, in which the only lanthanide-containing products were the trinuclear clusters {[η⁵-1-Ln-2,3-(SiMe₃)₂-2,3-C₂B₄H₄]₃[(μ-1-Li-2,3-(SiMe₃)₂-2,3-C₂B₄H₄)₃(μ₃-OMe)][μ-Li(C₄H₈O)]₃(μ₃-O)} (Ln = Sm, Gd, Dy, Ho, Tb).^{1e} Further treatment of **2** with 1 equiv of *closo-exo*-Li(TMEDA)-1-Li(TMEDA)-2,4-(SiMe₃)₂-2,4-C₂B₄H₄ (**1b**) in dry benzene at 0 °C resulted in the formation of a pink, dimeric Er(III) mixed-carborane sandwich complex, {Li(TMEDA)₂}₂{*commo*-1-[2,3-(SiMe₃)₂-2,3-C₂B₄H₄]-1-Er-[2,4-(SiMe₃)₂-2,4-C₂B₄H₄]}₂ (**3**), in 95% yields (Scheme 1).⁷ The high-yield substitution of one of the complexed 2,3-C₂B₄ units by a 2,4-C₂B₄ ligand, along with concomitant Cl⁻ elimination and dimerization of the resulting erbacarborane mixed-sandwich complexes, was unexpected. At this point the driving force for this reaction is not known. However, the almost quantitative yield indicates that this present

[†] Southern Methodist University.

[‡] Universität Stuttgart.

[§] Max-Planck-Institut für Festkörperforschung.

[®] Abstract published in *Advance ACS Abstracts*, February 1, 1995.

(1) (a) Grimes, R. N. In *Comprehensive Organometallic Chemistry*; Wilkinson, G., Stone, F. G. A., Abel, E. W., Eds.; Pergamon: Oxford, U.K., 1982; Vol. 1, Chapter 5.5, p 459. (b) *Comprehensive Coordination Chemistry*; Wilkinson, G., Gillard, R. D., McCleverty, J. A., Eds.; Pergamon: New York, 1987. (c) Cotton, F. A.; Wilkinson, G. *Advanced Inorganic Chemistry*, 5th ed.; Wiley: New York, 1988. (d) Stone, F. G. A. *Adv. Organomet. Chem.* **1990**, *31*, 53. (e) Hosmane, N. S.; Maguire, J. A. *J. Cluster Sci.* **1993**, *4*, 297.

(2) Swisher, R. G.; Sinn, E.; Grimes, R. N. *Organometallics* **1984**, *3*, 599.

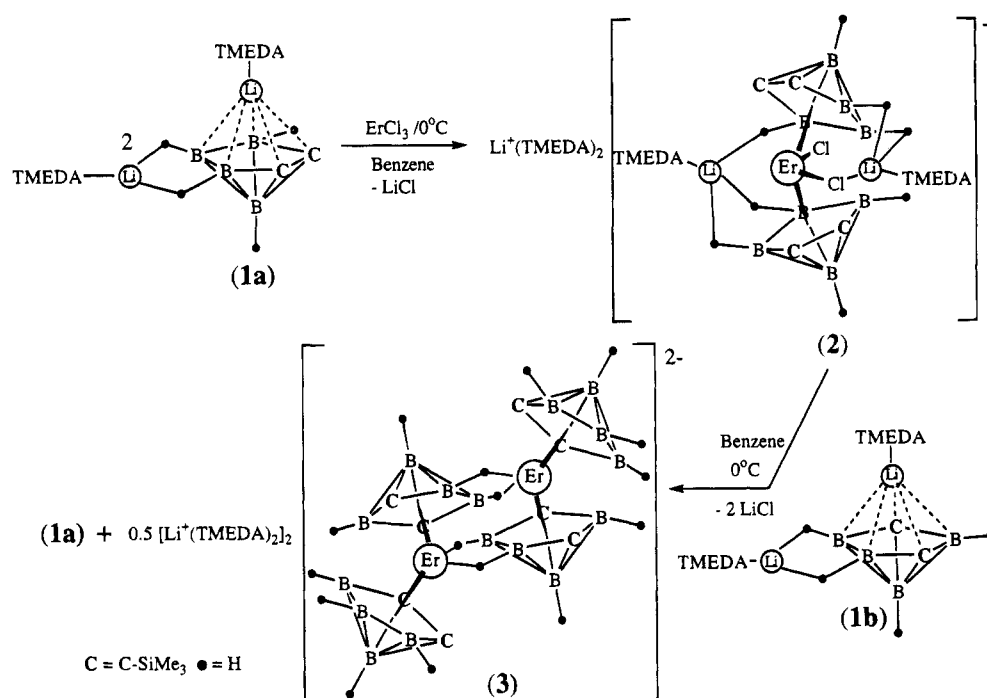
(3) Hosmane, N. S.; Wang, Y.; Zhang, H.; Maguire, J. A.; Waldhör, E.; Kaim, W.; Binder, H.; Kremer, R. K. *Organometallics* **1994**, *13*, 4156.

(4) (a) Grimes, R. N. *Chem. Rev.* **1992**, *92*, 251. (b) Wang, X.; Sabat, M.; Grimes, R. N. *J. Am. Chem. Soc.* **1994**, *116*, 2687.

(5) Wang, Z.-T.; Sinn, E.; Grimes, R. N. *Inorg. Chem.* **1985**, *24*, 834.

(6) Hosmane, N. S.; Saxena, A. K.; Barreto, R. D.; Zhang, H.; Maguire, J. A.; Jia, L.; Wang, Y.; Oki, A. R.; Grover, K. V.; Whitten, S. J.; Dawson, K.; Tolle, M. A.; Siriwardane, U.; Demissie, T.; Fagner, J. S. *Organometallics* **1993**, *12*, 3001.

Scheme 1



methodology may constitute a general, systematic approach to the synthesis of a series of mixed-ligand metallacarborane complexes that would be of both theoretical and practical interest. The generality of this reaction is currently being explored in our laboratories.

Although the paramagnetism of **2** and **3** precluded obtaining useful NMR data, the IR and the microanalytical data for these compounds are consistent with their molecular formulas and solid-state X-ray structures.⁸ The mixed-carborane structure of **3** is the only one that is consistent with the stoichiometry and product yields of its synthetic scheme.⁷ Electron paramagnetic resonance signals could not be detected for either the solid samples of **2** and **3** or their frozen

toluene glasses at 3.1 K, indicating that the complexes have very efficient relaxation or have g factors beyond the range of the X-band spectrometer used for these measurements.⁹ However, both **2** and **3** exhibit Curie law behavior with effective moments per Er atom slightly less than the expected $\mu_{\text{eff}}^{\text{angle}}$ (where $\mu_{\text{eff}}^{\text{angle}}$ is the effective moment of a free Er^{3+} ion). The lower than expected magnetic moments are most likely due to errors in the determination of the sample mass.¹⁰ No indication of magnetic ordering was observed down to 5 K. The X-ray structures of **2** and **3** (see Figures 1 and 2)¹¹ show that the complexes have bent-sandwich geometries that are quite similar to those of the cyclopentadienyl dimer $[\text{Cp}_2\text{ErC}\equiv\text{C}(\text{CH}_3)_3]_2$ ¹² and the metalla-

(7) Synthesis of **2**: A 6.37 mmol (2.96 g) sample of *closo-exo*-Li(TMEDA)-1-Li(TMEDA)-2,3-(SiMe₃)₂-2,3-C₂B₄H₄ (**1a**)⁶ was reacted with 3.19 mmol (0.872 g) of anhydrous ErCl₃ in dry benzene (30 mL) at 0 °C for 12 h, during which time the orange solution turned turbid. The mixture was then filtered in vacuo and the residue washed repeatedly with a solvent mixture of *n*-hexane (10%) and benzene (90%) to obtain a clear orange filtrate. The white solid left on the frit (not measured) was identified as LiCl by qualitative analysis and by ⁷Li NMR spectra. After slow removal of the solvents from the filtrate, an orange, air-sensitive crystalline solid, identified as [Li(TMEDA)₂][1-Cl-1-(μ-Cl)-2,2',3,3'-(SiMe₃)₄-5,6-(μ-H)₂Li(TMEDA)]-4,4',5,5'-[(μ-H)₂Li(TMEDA)]-1,1'-*commo*-Er(2,3-C₂B₄H₄)₂] (**2**), was obtained in 93% yield (3.44 g, 2.97 mmol; soluble in polar and slightly soluble in nonpolar organic solvents; mp 240 °C dec). Synthesis of **3**: A 20 mL benzene solution containing 0.54 g (1.17 mmol) of the dilithiacarborane *closo-exo*-Li(TMEDA)-1-Li(TMEDA)-2,4-(SiMe₃)₂-2,4-C₂B₄H₄ (**1b**) (Zhang, H.; Wang, Y.; Saxena, A. K.; Oki, A. R.; Maguire, J. A.; Hosmane, N. S. *Organometallics* **1993**, *12*, 3983) was poured, in vacuo, into a 10 mL benzene solution containing 1.36 g (1.17 mmol) of **2** at 0 °C, and the resulting solution was stirred for 24 h at this temperature, during which time the pink solution turned turbid. The mixture was then filtered in vacuo and the residue washed repeatedly with dry benzene to obtain a clear, light pink filtrate. The white solid on the frit (not measured) was identified as LiCl by qualitative analysis and by ⁷Li NMR spectra. After slow removal of nearly 60% of the solvent at 0 °C in vacuo, pink, air-sensitive crystals, identified as {Li(TMEDA)₂}₂{*commo*-1-[2,3-(SiMe₃)₂-2,3-C₂B₄H₄]-1-Er-[2,4-(SiMe₃)₂-2,4-C₂B₄H₄]}₂ (**3**), were collected (0.94 g, 0.56 mmol; 95% yield; soluble in polar and slightly soluble in nonpolar organic solvents; mp >250 °C). The remaining solvent was then removed from the filtrate in vacuo, to isolate an off-white solid (0.52 g, 1.12 mmol) which was later identified by ¹H, ¹¹B, and ⁷Li NMR spectra as **1a**.⁶ Compound **1b** was not identified among the products. The X-ray-quality crystals of **2** and **3** were grown from their benzene solutions.

(8) Compound **2**: IR (cm⁻¹) 2514 (s, s), 2465 (s, br), 2413 (br, sh) [ν(B-H)]. Anal. Calcd for C₄₀H₁₀₈N₈B₈Si₄Cl₂Li₃Er: C, 41.46; H, 9.39; N, 9.67; Cl, 6.12. Found: C, 41.48; H, 9.18; N, 9.46; Cl, 5.92. Complex **3**: IR (cm⁻¹) 2580 (sh), 2515 (s, s), 2460 (s, br), 2410 (sh) [ν(B-H)]; Anal. Calcd for C₅₆H₁₅₂N₈B₁₆Si₈Li₂Er₂·1.5 C₆H₆: C, 43.33; H, 9.01; N, 6.22. Found: C, 43.73; H, 10.02; N, 5.75.

(9) EPR spectra of **2** and **3** were recorded on a Bruker ESP 300 spectrometer in the X band (9.6 GHz).

(10) Magnetic susceptibility measurements were made on a MPMS Quantum Design magnetometer at an external field of 0.1 T.

(11) X-ray data for **2** (C₄₀H₁₀₈N₈B₈Si₄Cl₂ErLi₃·0.5 C₆H₆; fw 1198.2; P2₁2₁2) and **3** (C₅₆H₁₅₂N₈B₁₆Si₈Er₂Li₂; fw 1683.9; P2₁/n). Data were collected at 230 K on a Siemens R3m/V diffractometer with $a = 21.051(6)$ and $12.605(3)$ Å, $b = 23.435(6)$ and $23.891(6)$ Å, $c = 14.148(4)$ and $16.400(3)$ Å, $\beta = 90.0$ and $108.73(2)^\circ$, $V = 6980(3)$ and $4647(2)$ Å³, $Z = 4$ and 2 , and $D_{\text{calc'd}} = 1.140$ and 1.196 g/cm³ for **2** and **3**, respectively. Of the 4166 and 5308 reflections collected ($2\theta = 3.5$ – 42°), 2962 and 3209 reflections were considered as observed ($F > 6.0\sigma(F)$) and were corrected for Lorentz, polarization, and absorption effects. Both structures were solved by heavy-atom methods, and block-diagonal least-squares refinements were performed by using SHELXTL-PLUS (Sheldrick, G. M. Structure Determination Software Programs; Siemens Analytical X-ray Instruments, Inc., Madison, WI, 1990). A discrete zwitterionic chloroerborane, a Li(TMEDA) cation, and a half-C₆H₆ molecule of crystallization were located in the asymmetric unit of the structure of **2**. The TMEDA-H in the cationic unit and the lattice C₆H₆ are disordered. All non-H atoms, except for the N and C atoms of the disordered groups in **2** and the disordered Me groups on Si(4) in **3**, were refined anisotropically. Bonds in the disordered groups were restrained during the final cycles of refinements. Methyl and methylene H's in the nondisordered groups were placed in calculated positions, and the cage H's, located in DF maps, were not refined. The final refinements converged at $R = 0.056$ and 0.037 , $R_w = 0.072$ and 0.047 , and GOF = 1.68 and 1.08 for **2** and **3**, respectively.

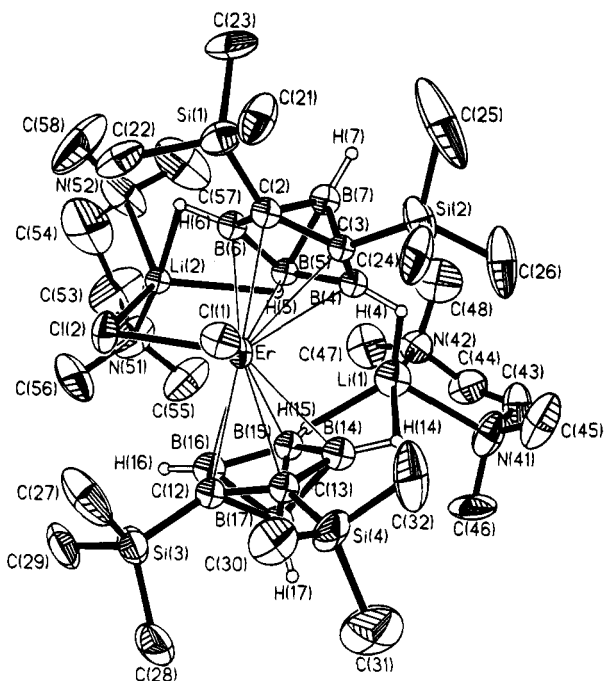


Figure 1. Perspective view of **2** drawn at the 40% probability level. Pertinent distances (Å) and angles (deg): Er–(C₂B₃ centroid 1,2), 2.332, 2.351; Er–Cl(1,2), 2.583(5), 2.666(5); (centroid 1)–Er–(centroid 2), 129.7; Cl(1)–Er–Cl(2), 97.0 (2); (centroid 1,2)–Er–Cl(1, 2), 105.8, 103.0, 110.7, 105.5 (see Supplementary Table S-2 for detailed bond lengths and angles). The cationic Li⁺(TMEDA)₂ unit, the C₆H₆ molecule of crystallization, and the methyl and methylene H's are omitted for clarity.

carborane complexes of the d⁰ metals Y(III),¹³ Ti(IV),³ Zr(IV),¹⁴ and Hf(IV).¹⁵ The Cent(1)–Er–Cent(2) angles 129.7° and 135.5° for **2** and **3**, respectively, are quite close to the Cp–Er–Cp value of 130.2° found for [Cp₂ErC≡C(CH₃)₃]₂¹² and are within the 130–135° range of the analogous angles in the d⁰ metallacarboranes.^{3,13–15} The bent-sandwich geometry allows for the inclusion of two Cl[−] ions in the primary coordination sphere of the Er in **2**, giving a very distorted tetrahedral arrangement about the metal; the Cl(1)–Er–Cl(2) angle is 97.7°, which is substantially smaller than the other ligand–Er–ligand bond angles in **2** (see Figure 1). The average Er–Cl bond distance in **2** is 2.624 Å, which is close to the value of 2.617 Å for the analogous distances in CpErCl₂(THF)₃.¹⁶ However, the two Er–Cl bond distances in **2** differ by about 0.08 Å, which is outside the experimental uncertainties in the measured bond lengths. This unequal bonding may be the result of the rather strong interaction between Cl(2) and one of the bridging Li⁺ ions, Li(2); the Li(2)–Cl(2) distance is 2.435 Å, which is well within the sum of the van der Waals radii of the two substances.¹⁷ The replacement of a 2,3-C₂B₄ carborane with its 2,4-C₂B₄ isomer as one goes from **2** to **3**

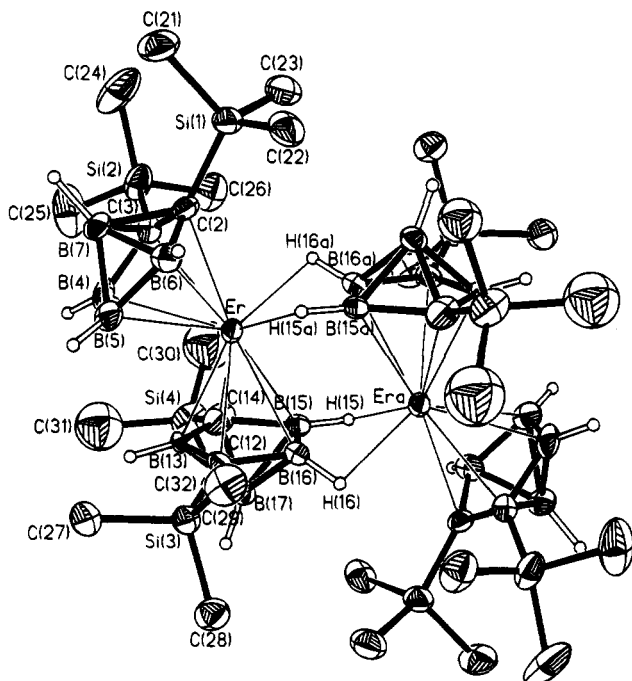


Figure 2. Perspective view of **3** drawn at the 40% probability level. Pertinent distances (Å) and angles (deg): Er–(2,3-C₂B₃ centroid), 2.280; Er–(2,4-C₂B₃ centroid), 2.319; Er–B(15a), 2.634(11); Er–B(16a), 2.653(12); Er(a)–B(15), 2.634(11); Er(a)–B(16), 2.653(12) (see Supplementary Table S-2 for detailed bond lengths and angles). The cationic Li⁺(TMEDA)₂ units and the silylmethyl H's are omitted for clarity.

induces some unexpected changes in geometry. While this replacement does not materially change the Er–carborane interactions (the Er–cent distances in compounds **2** and **3** are similar; see Figures 1 and 2), substantial alterations occur in other parts of the molecule. In addition to the 2,3-C₂B₄ carborane ligand, the two Cl[−] ions, along with their Li⁺ counterions, are displaced and dimerization in **3** is accomplished through two Er–H–B bridging interactions. Such interactions have been observed in the [commo-1-Cp-1-Ti-2,3-(SiMe₃)₂-2,3-C₂B₄H₄]₂ dimer and in a number of main-group metallacarborane complexes.^{1e,18}

The presence of reactive Cl[−] ligands on Er(III) strongly suggests that **2** can also be converted to the corresponding metal alkyl derivatives, which may in turn act as precursors to a number of organic and organometallic transformations. Such an investigation is currently underway in our laboratories.

Acknowledgment. This work was supported in part by grants from the Texas Advanced Technology Program (Grant No. 003613006), the National Science Foundation (Grant No. CHE-9400672), the Robert A. Welch Foundation (Grant No. N-1016), and the donors of the Petroleum Research Fund, administered by the American Chemical Society. We wish to thank Miss E. Bruecher for experimental assistance.

Supplementary Material Available: Tables of positional and thermal parameters and selected bond distances and bond angles for **2** and **3** (12 pages). Ordering information is given on any current masthead page.

OM940861E

(18) Hosmane, N. S.; Maguire, J. A. *Adv. Organomet. Chem.* **1990**, 30, 99 and references therein.

(12) Atwood, J. L.; Hunter, W. E.; Wayda, A. L.; Evans, W. J. *Inorg. Chem.* **1981**, 20, 4115.

(13) Oki, A. R.; Zhang, H.; Hosmane, N. S. *Organometallics* **1991**, 10, 3964.

(14) (a) Siriwardane, U.; Zhang, H.; Hosmane, N. S. *J. Am. Chem. Soc.* **1990**, 112, 9637. (b) Thomas, C. J.; Jia, L.; Zhang, H.; Siriwardane, U.; Maguire, J. A.; Wang, Y.; Brooks, K. A.; Weiss, V. P.; Hosmane, N. S. *Organometallics* **1995**, 14, 1365.

(15) Zhang, H.; Jia, L.; Hosmane, N. S. *Acta Crystallogr., Cryst. Struct. Commun.* **1993**, C49, 453.

(16) Day, C. S.; Day, V. W.; Ernst, R. D.; Vollmer, S. H. *Organometallics* **1982**, 1, 998.

(17) Bondi, A. J. *Phys. Chem.* **1964**, 68, 441.

Selenium Complexes of Permethyltantalocene: Interesting Contrasts with Their Tellurium Analogues

Jun Ho Shin and Gerard Parkin*

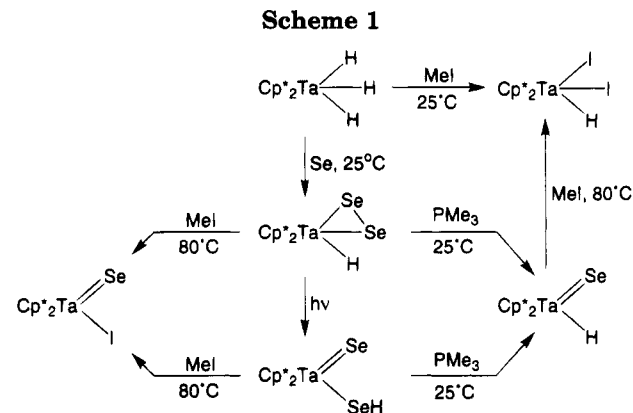
Department of Chemistry, Columbia University, New York, New York 10027

Received November 29, 1994[⊗]

Summary: A series of selenium derivatives of permethyltantalocene, which include $\text{Cp}^*_2\text{Ta}(\eta^2\text{-Se}_2)\text{H}$, $\text{Cp}^*_2\text{Ta}(\text{Se})\text{SeH}$, $\text{Cp}^*_2\text{Ta}(\text{Se})\text{H}$, and $\text{Cp}^*_2\text{Ta}(\text{Se})\text{I}$ have been prepared. The selenido-iodide complex $\text{Cp}^*_2\text{Ta}(\text{Se})\text{I}$ exhibits novel reactivity differences with MeMgI and MeLi , to give the selenido-methyl complex $\text{Cp}^*_2\text{Ta}(\text{Se})\text{-CH}_3$ and selenoformaldehyde-hydride complex $\text{Cp}^*_2\text{Ta}(\eta^2\text{-SeCH}_2)\text{H}$, respectively.

As an extension of our interest in metal-ligand multiple bonding,¹ we have recently described some studies concerned with terminal tellurido and telluroformaldehyde complexes of permethyltantalocene.² Specifically, we reported the syntheses of $\text{Cp}^*_2\text{Ta}(\text{Te})\text{H}$, $\text{Cp}^*_2\text{Ta}(\text{Te})\text{CH}_3$, and $\text{Cp}^*_2\text{Ta}(\eta^2\text{-TeCH}_2)\text{H}$ ($\text{Cp}^* = \eta^5\text{-C}_5\text{Me}_5$), *i.e.* the tellurium analogues of the (i) oxo and formaldehyde and (ii) sulfido and thioformaldehyde derivatives described by Bercaw.^{3–5} In this paper, we report the syntheses of the previously unknown members of this series, namely the selenium derivatives $\text{Cp}^*_2\text{Ta}(\text{Se})\text{H}$, $\text{Cp}^*_2\text{Ta}(\text{Se})\text{CH}_3$, and $\text{Cp}^*_2\text{Ta}(\eta^2\text{-SeCH}_2)\text{H}$. Furthermore, since organotantalum selenium complexes are not common,⁶ comparisons with the analogous tellurium system provide a rare opportunity to demonstrate how the chemistry of these complexes varies as a function of the chalcogen.

A convenient entry to selenium complexes of permethyltantalocene is provided by the synthesis of the diselenido complex $\text{Cp}^*_2\text{Ta}(\eta^2\text{-Se}_2)\text{H}$ upon reaction of $\text{Cp}^*_2\text{TaH}_3$ with elemental selenium at room temperature, in the absence of light (Scheme 1).^{7,8} In the presence of ambient light, however, $\text{Cp}^*_2\text{Ta}(\eta^2\text{-Se}_2)\text{H}$ is smoothly converted to the selenido-hydro-selenido complex $\text{Cp}^*_2\text{Ta}(\text{Se})\text{SeH}$ over a period of days (Scheme 1).^{9,10} The transformation to $\text{Cp}^*_2\text{Ta}(\text{Se})\text{SeH}$ may also be carried out in the dark at 100 °C, although the conversion is accompanied by some decomposition.



The formation of $\text{Cp}^*_2\text{Ta}(\text{Se})\text{SeH}$ provides an interesting contrast to the corresponding tellurium system, for which the ditellurido-hydride derivative $\text{Cp}^*_2\text{Ta}(\eta^2\text{-Te}_2)\text{H}_2$ is stable with respect to $\text{Cp}^*_2\text{Ta}(\text{Te})\text{TeH}$ under comparable conditions. The facile formation of the $\text{Cp}^*_2\text{Ta}(\text{Se})\text{SeH}$ tautomer for the selenium system is most probably a consequence of both (i) stronger Se-H *versus* Te-H bonds¹¹ and (ii) the increased preference for the lighter element to partake in multiple bonding.^{12,13}

The relationship between $\text{Cp}^*_2\text{Ta}(\eta^2\text{-E}_2)\text{H}$ and $\text{Cp}^*_2\text{Ta}(\text{E})\text{EH}$ (eq 1) bears analogies with several other

(8) A mixture of $\text{Cp}^*_2\text{TaH}_3$ (0.27 g, 0.59 mmol) and Se (0.14 g, 1.8 mmol) in benzene (*ca.* 25 mL) was stirred at room temperature for 3 days in the absence of light. After this period the mixture was filtered, the volatile components were removed *in vacuo*, and the residue was washed with cold pentane to give $\text{Cp}^*_2\text{Ta}(\eta^2\text{-Se}_2)\text{H}$ as a purple solid (0.32 g, 88%). The $[\text{Ta}(\eta^2\text{-Se}_2)\text{H}]$ moiety of $\text{Cp}^*_2\text{Ta}(\eta^2\text{-Se}_2)\text{H}$ is characterized by (i) an absorption at 1777 cm^{-1} in the IR spectrum attributable to $\nu(\text{Ta}-\text{H})$, (ii) two ^{77}Se NMR signals at δ -408 and 54 ppm with $^1J_{\text{Se}-\text{Se}} = 295$ Hz, of which the resonance at 54 ppm also exhibits $^2J_{\text{Se}-\text{H}} = 19$ Hz, and (iii) a signal at 1.42 ppm in the ^1H NMR spectrum with ^{77}Se satellites ($^2J_{\text{Se}-\text{H}} = 19$ Hz) assignable to $[\text{Ta}-\text{H}]$.

(9) A mixture of $\text{Cp}^*_2\text{TaH}_3$ (0.32 g, 0.71 mmol) and Se (0.17 g, 2.1 mmol) in toluene (*ca.* 30 mL) was stirred at room temperature for 1 day, without precautions being taken to keep out ambient light. After this period the mixture was filtered and stirred for a further *ca.* 3–8 days, until only $\text{Cp}^*_2\text{Ta}(\text{Se})\text{SeH}$ was observed by ^1H NMR spectroscopy. The volatile components were removed *in vacuo*, and the residue was washed with cold pentane to give $\text{Cp}^*_2\text{Ta}(\text{Se})\text{SeH}$ as a yellow-brown solid (0.33 g, 75%). The $[\text{Ta}(\text{Se})\text{SeH}]$ moiety of $\text{Cp}^*_2\text{Ta}(\text{Se})\text{SeH}$ is characterized by (i) an absorption at 2250 cm^{-1} in the IR spectrum attributable to $\nu(\text{Se}-\text{H})$, (ii) two ^{77}Se NMR signals at δ -209 and 2363 ppm, of which the resonance at -209 ppm exhibits $^1J_{\text{Se}-\text{H}} = 26$ Hz, and (iii) a signal at -3.96 ppm in the ^1H NMR spectrum with ^{77}Se satellites ($^1J_{\text{Se}-\text{H}} = 26$ Hz) assignable to $[\text{TaSe}-\text{H}]$.

(10) Other examples of terminal hydro-selenido complexes include *trans*-Pt(PEt₃)₂(SeH)₂,^{10a} *trans*-Pt(PEt₃)₂(SeH)H,^{10a} $\text{Cp}^*_2\text{Ti}(\text{SeH})_2$ ($^1J_{\text{Se}-\text{H}} = 27$ Hz),^{10b} and (dppe)Ni(SeH)₂.^{10c} (a) Blacklaws, I. M.; Ebsworth, E. A. V.; Rankin, D. W. H.; Robertson, H. E. *J. Chem. Soc., Dalton Trans.* **1978**, 753–758. (b) Bottomley, F.; Chin, T.-T.; Egharevba, G. O.; Kane, L. M.; Pataki, D. A.; White, P. S. *Organometallics* **1988**, 7, 1214–1221. (c) Schmidt, M.; Hoffmann, G. G. *Angew. Chem., Int. Ed. Engl.* **1978**, 17, 598–599.

(11) For reference, the E-H bond energies in H₂Se and H₂Te are 73 and 64 kcal mol⁻¹, respectively. See: Gunn, S. R. *J. Phys. Chem.* **1964**, 68, 949–952.

(12) (a) Norman, N. C. *Polyhedron* **1993**, 12, 2431–2446. (b) Kutzelnigg, W. *Angew. Chem., Int. Ed. Engl.* **1984**, 23, 272–295.

* Abstract published in *Advance ACS Abstracts*, February 15, 1995.

(1) Rabinovich, D.; Parkin, G. *J. Am. Chem. Soc.* **1991**, 113, 5904–5905. (b) Rabinovich, D.; Parkin, G. *J. Am. Chem. Soc.* **1991**, 113, 9421–9422. (c) Rabinovich, D.; Parkin, G. *J. Am. Chem. Soc.* **1993**, 115, 9822–9823. (d) Rabinovich, D.; Parkin, G. *Inorg. Chem.* **1994**, 33, 2313–2314. (e) Howard, W. A.; Waters, M.; Parkin, G. *J. Am. Chem. Soc.* **1993**, 115, 4917–4918. (f) Howard, W. A.; Parkin, G. *J. Am. Chem. Soc.* **1994**, 116, 606–615. (g) Howard, W. A.; Parkin, G. *J. Organomet. Chem.* **1994**, 472, C1–C4. (h) Kuchta, M. C.; Parkin, G. *J. Chem. Soc., Chem. Commun.* **1994**, 1351–1352. (i) Kuchta, M. C.; Parkin, G. *J. Am. Chem. Soc.* **1994**, 116, 8372–8373.

(2) Shin, J. H.; Parkin, G. *Organometallics* **1994**, 13, 2147–2149. (3) van Asselt, A.; Burger, B. J.; Gibson, V. C.; Bercaw, J. E. *J. Am. Chem. Soc.* **1986**, 108, 5347–5349.

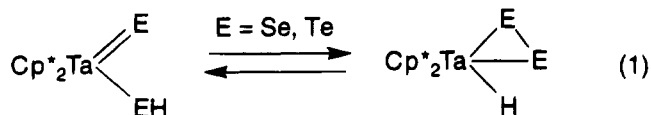
(4) Parkin, G.; Bunel, E.; Burger, B. J.; Trimmer, M. S.; van Asselt, A.; Bercaw, J. E. *J. Mol. Catal.* **1987**, 41, 21–39.

(5) Nelson, J. E.; Parkin, G.; Bercaw, J. E. *Organometallics* **1992**, 11, 2181–2189.

(6) For a recent report of organotantalum selenium complexes, see: Tatsumi, K.; Kawaguchi, H.; Tani, K. *Angew. Chem., Int. Ed. Engl.* **1993**, 32, 591–593.

(7) See the supplementary material for complete synthetic details and characterization data.

systems for which there exist pairs of tautomers of the general types $\text{Cp}^*_2\text{Ta}(\eta^2\text{-XY})\text{H}$ and $\text{Cp}^*_2\text{Ta}(\text{X})\text{YH}$. Some



specific examples include (i) $\text{Cp}^*_2\text{Ta}(\eta^2\text{-ECH}_2)\text{H}$ and $\text{Cp}^*_2\text{Ta}(\text{E})\text{CH}_3$ (E = O, S, Se, Te), (ii) $\text{Cp}^*_2\text{Ta}(\eta^2\text{-CH}_2\text{-NMe})\text{H}$ and $\text{Cp}^*_2\text{Ta}(\text{NMe})\text{CH}_3$, and (iii) $\text{Cp}^*_2\text{Ta}(\eta^2\text{-CH}_2\text{-CH}_2)\text{H}$ and $\text{Cp}^*_2\text{Ta}(\text{CH}_2)\text{CH}_3$.⁴

Both $\text{Cp}^*_2\text{Ta}(\eta^2\text{-Se}_2)\text{H}$ and $\text{Cp}^*_2\text{Ta}(\text{Se})\text{SeH}$ are converted to the selenido-hydride complex $\text{Cp}^*_2\text{Ta}(\text{Se})\text{H}$ upon reaction with PMe_3 (Scheme 1).^{7,14,15} The tellurido-hydride complex $\text{Cp}^*_2\text{Ta}(\text{Te})\text{H}$ was previously synthesized from $\text{Cp}^*_2\text{Ta}(\eta^2\text{-Te}_2)\text{H}$ by a similar method, but, in addition to PMe_3 , mercury was also required in order to provide a more effective driving force.²

The selenido-iodide derivative $\text{Cp}^*_2\text{Ta}(\text{Se})\text{I}$ is readily obtained by reactions of both $\text{Cp}^*_2\text{Ta}(\eta^2\text{-Se}_2)\text{H}$ and $\text{Cp}^*_2\text{Ta}(\text{Se})\text{SeH}$ with MeI (Scheme 1).⁷ Interestingly, however, $\text{Cp}^*_2\text{Ta}(\text{Se})\text{I}$ is not obtained as a product of the reaction of the selenido-hydride $\text{Cp}^*_2\text{Ta}(\text{Se})\text{H}$ with MeI , which gives, preferentially, the diiodido-hydride complex $\text{Cp}^*_2\text{TaHI}_2$.¹⁶

$\text{Cp}^*_2\text{Ta}(\text{Se})\text{I}$ serves as a useful synthetic precursor for other organotantalum selenium derivatives. In this context, $\text{Cp}^*_2\text{Ta}(\text{Se})\text{I}$ exhibits at least two different reaction pathways with alkyllithium and Grignard reagents, which may be regarded to be a result of attack at either the tantalum center or the selenido ligand.¹⁷ The specific pathway followed is a sensitive function of both the alkyl and metal moieties of the $[\text{RM}]$ reagent. For example, the selenido-methyl complex $\text{Cp}^*_2\text{Ta}(\text{Se})\text{-CH}_3$ is produced by the reaction of $\text{Cp}^*_2\text{Ta}(\text{Se})\text{I}$ with MeMgI , whereas the selenoformaldehyde-hydride tautomer $\text{Cp}^*_2\text{Ta}(\eta^2\text{-SeCH}_2)\text{H}$ ¹⁸ is obtained by the reaction of $\text{Cp}^*_2\text{Ta}(\text{Se})\text{I}$ with MeLi . Moreover, Bu^nLi reacts with $\text{Cp}^*_2\text{Ta}(\text{Se})\text{I}$ to give the selenoaldehyde complex $\text{Cp}^*_2\text{Ta}(\eta^2\text{-SeCHPr}^n)\text{H}$, while Bu^nMgCl gives the selenido-alkyl derivative $\text{Cp}^*_2\text{Ta}(\text{Se})\text{Bu}^n$.^{7,19} In contrast, how-

(13) It is interesting to note that the disulfido-hydride complex of niobium ($\eta^2\text{-C}_5\text{Me}_4\text{Et})_2\text{Nb}(\eta^2\text{-S}_2)\text{H}$ has been reported to convert to a mixture of ($\eta^2\text{-C}_5\text{Me}_4\text{Et})_2\text{Nb}(\text{S})\text{SH}$ and ($\eta^2\text{-C}_5\text{Me}_4\text{Et})_2\text{Nb}(\eta^2\text{-S}_2)\text{SH}$ at 110 °C.^{13a} The tantalum disulfido-hydride complex ($\eta^2\text{-C}_5\text{H}_4\text{Bu}^t$)₂Ta($\eta^2\text{-S}_2$)H has also been prepared, but details of possible isomerization were not reported.^{13b} However, the methyl derivative $\text{Cp}_2\text{Ta}(\eta^2\text{-S}_2)\text{CH}_3$ has been shown to be converted photochemically to a mixture that contains $\text{Cp}_2\text{Ta}(\text{S})\text{SMe}$ and $\text{Cp}_2\text{Ta}(\text{S})\text{Me}$.^{13c} (a) Brunner, H.; Gehart, G.; Meier, W.; Wachter, J.; Nuber, B. *J. Organomet. Chem.* **1993**, *454*, 117–122. (b) Bach, H.-J.; Brunner, H.; Wachter, J.; Kubicki, M. M.; Leblanc, J.-C.; Moise, C.; Volpato, F.; Nuber, B.; Ziegler, M. L. *Organometallics* **1992**, *11*, 1403–1407. (c) Proulx, G.; Bergman, R. G. *J. Am. Chem. Soc.* **1994**, *116*, 7953–7954.

(14) The $[\text{Ta}(\text{Se})\text{H}]$ moiety of $\text{Cp}^*_2\text{Ta}(\text{Se})\text{H}$ is characterized by signals at δ 8.91 and 2153 ppm in the ¹H and ⁷⁷Se NMR spectra, respectively, and an absorption assignable to $\nu(\text{Ta}-\text{H})$ at 1844 cm⁻¹ in the IR spectrum.

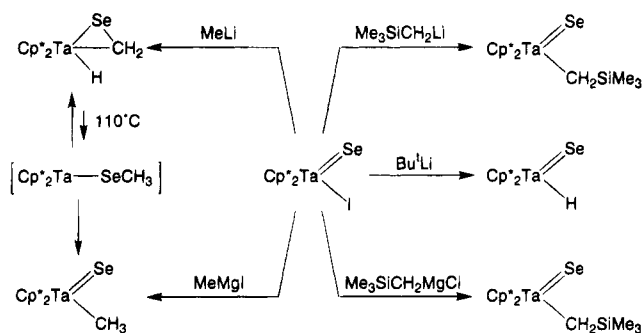
(15) The conversion of $\text{Cp}^*_2\text{Ta}(\eta^2\text{-Se}_2)\text{H}$ to $\text{Cp}^*_2\text{Ta}(\text{Se})\text{H}$ is reversible, in that addition of selenium to $\text{Cp}^*_2\text{Ta}(\text{Se})\text{H}$ slowly regenerates $\text{Cp}^*_2\text{Ta}(\eta^2\text{-Se}_2)\text{H}$ in the dark.

(16) $\text{Cp}^*_2\text{TaHI}_2$ may also be obtained by the direct reaction of $\text{Cp}^*_2\text{TaH}_3$ with MeI .

(17) To a certain degree, the dual reactivity associated with the $[\text{Ta}=\text{Se}]$ moiety has parallels in the reactions of $\text{Cp}^*_2\text{W}=\text{O}$ with electrophiles, in which attack may occur at either the *d*² tungsten center or the oxo ligand. See: Parkin, G.; Bercaw, J. E. *Polyhedron* **1988**, *7*, 2053–2082.

(18) The $[\text{Ta}(\eta^2\text{-SeCH}_2)]$ moiety in $\text{Cp}^*_2\text{Ta}(\eta^2\text{-SeCH}_2)\text{H}$ is characterized by ¹H, ¹³C, and ⁷⁷Se NMR signals at δ 2.45 (d, ³J_{H-H} = 3 Hz), δ 50.5 (t, ¹J_{C-H} = 143 Hz), and δ -595 ppm, respectively.

Scheme 2



ever, both lithium and magnesium (trimethylsilyl)methyl derivatives, $\text{LiCH}_2\text{SiMe}_3$ and $\text{Me}_3\text{SiCH}_2\text{MgCl}$, react with $\text{Cp}^*_2\text{Ta}(\text{Se})\text{I}$ to give the selenido-alkyl derivative $\text{Cp}^*_2\text{Ta}(\text{Se})\text{CH}_2\text{SiMe}_3$.⁷ The isolation of only $\text{Cp}^*_2\text{Ta}(\text{Se})\text{CH}_2\text{-SiMe}_3$ from the latter reactions is presumably a consequence of the greater steric interactions that would exist between the SiMe_3 group and the Cp^* ligands within the selenoaldehyde complex $\text{Cp}^*_2\text{Ta}(\eta^2\text{-SeCHSiMe}_3)\text{H}$. Finally, a further class of reactivity exhibited by $\text{Cp}^*_2\text{Ta}(\text{Se})\text{I}$ is observed with the secondary and tertiary alkyl derivatives Pr^iMgCl , Bu^iMgCl , and Bu^tLi , which yield the selenido-hydride derivative $\text{Cp}^*_2\text{Ta}(\text{Se})\text{H}$ as a consequence of β -H elimination (Scheme 2).

Although mononuclear selenoformaldehyde complexes are known,²⁰ the synthesis of $\text{Cp}^*_2\text{Ta}(\eta^2\text{-SeCH}_2)\text{H}$ by functionalization of the terminal selenido ligand of $\text{Cp}^*_2\text{Ta}(\text{Se})\text{I}$ is of particular significance since $\text{Cp}^*_2\text{Ta}(\eta^2\text{-SeCH}_2)\text{H}$ could not be isolated by adopting an approach analogous to that used for the preparation of $\text{Cp}^*_2\text{Ta}(\eta^2\text{-TeCH}_2)\text{H}$. Thus, whereas $\text{Cp}^*_2\text{Ta}(\eta^2\text{-TeCH}_2)\text{H}$ is obtained by the reaction of the methylidene-hydride complex $\text{Cp}^*_2\text{Ta}(\text{CH}_2)\text{H}$ with elemental Te and PMe_3 ,² the corresponding reaction between $\text{Cp}^*_2\text{Ta}(\text{CH}_2)\text{H}$ and elemental Se produced a mixture, of which both $\text{Cp}^*_2\text{Ta}(\eta^2\text{-SeCH}_2)\text{H}$ and $\text{Cp}^*_2\text{Ta}(\text{Se})\text{Me}$ were only minor components.²¹ Moreover, in contrast to the tellurium analogue, the selenoformaldehyde moiety adopts an orientation in which the CH_2 group is located in the central equatorial position, analogous to the case for $\text{Cp}^*_2\text{Ta}(\eta^2\text{-ECH}_2)\text{H}$ (E = O, S), rather than the lateral position observed for $\text{Cp}^*_2\text{Ta}(\eta^2\text{-TeCH}_2)\text{H}$.^{2,22}

The formation of the $\text{Cp}^*_2\text{Ta}(\eta^2\text{-SeCH}_2)\text{H}$ tautomer in the reaction of $\text{Cp}^*_2\text{Ta}(\text{Se})\text{I}$ with MeLi is a reflection of kinetic control, since $\text{Cp}^*_2\text{Ta}(\eta^2\text{-SeCH}_2)\text{H}$ is unstable

(19) In addition, PhLi and PhMgCl react with $\text{Cp}^*_2\text{Ta}(\text{Se})\text{I}$ to give the spectroscopically characterized derivatives $\text{Cp}^*_2\text{Ta}(\eta^2\text{-SeC}_6\text{H}_4)\text{H}$ and $\text{Cp}^*_2\text{Ta}(\text{Se})\text{Ph}$, respectively.

(20) Mononuclear selenoformaldehyde complexes include $\text{CpRh}(\text{PMe}_3)(\eta^2\text{-CH}_2\text{Se})$,^{20a} $\text{Os}(\eta^2\text{-CH}_2\text{Se})(\text{CO})_2(\text{PPh}_3)_2$,^{20b} $\text{Os}(\eta^2\text{-CH}_2\text{Se})(\text{NO})(\text{Cl})(\text{PPh}_3)_2$,^{20c} and $[\text{CpRe}(\eta^2\text{-CH}_2\text{Se})(\text{NO})(\text{PPh}_3)]^+$.^{20d} (a) Paul, W.; Werner, H. *Angew. Chem., Int. Ed. Engl.* **1983**, *22*, 316–317. (b) Headford, C. E. L.; Roper, W. R. *J. Organomet. Chem.* **1983**, *244*, C53–C56. (c) Hill, A. F.; Roper, W. R.; Waters, J. M.; Wright, A. H. *J. Am. Chem. Soc.* **1983**, *105*, 5939–5940. (d) McCormick, F. B. *Organometallics* **1984**, *3*, 1924–1927.

(21) It is, however, possible that one of the unidentified products of this reaction is the Se-endo isomer of $\text{Cp}^*_2\text{Ta}(\eta^2\text{-SeCH}_2)\text{H}$, analogous to the tellurium system.

(22) The lateral location of selenium is suggested by the observations of (i) magnetization transfer between the hydride and methylene groups and (ii) a coupling of the selenoformaldehyde carbon atom with the Ta-H group (²J_{C-H} = 11 Hz), analogous to the values observed for $\text{Cp}^*_2\text{Ta}(\eta^2\text{-OCH}_2)\text{H}$ (²J_{C-H} = 7 Hz)^{22a} and $\text{Cp}^*_2\text{Ta}(\eta^2\text{-SCH}_2)\text{H}$ (²J_{C-H} = 10 Hz).⁵ In contrast, ²J_{C-H} was not observed for $\text{Cp}^*_2\text{Ta}(\eta^2\text{-TeCH}_2)\text{H}$.² (a) Burger, B. J. Ph.D. Thesis, California Institute of Technology, Pasadena, CA, 1987.

with respect to $\text{Cp}^*_2\text{Ta}(\text{Se})\text{CH}_3$.²³ Furthermore, since $\text{Cp}^*_2\text{Ta}(\eta^2\text{-SeCH}_2)\text{H}$ only isomerizes to $\text{Cp}^*_2\text{Ta}(\text{Se})\text{CH}_3$ at an appreciable rate at ca. 110 °C, the formation of $\text{Cp}^*_2\text{Ta}(\text{Se})\text{CH}_3$ in the reaction with MeMgI also presumably reflects kinetic control.²⁴

The isomerization of $\text{Cp}^*_2\text{Ta}(\eta^2\text{-SeCH}_2)\text{H}$ to $\text{Cp}^*_2\text{Ta}(\text{Se})\text{CH}_3$ is a first-order process ($k = 1.5(2) \times 10^{-3} \text{ s}^{-1}$ at 110 °C), and the conversion of the d_3 derivative $\text{Cp}^*_2\text{Ta}(\eta^2\text{-SeCD}_2)\text{H}$ is characterized by an inverse kinetic isotope effect ($k_{\text{H}}/k_{\text{D}} = 0.6(1)$ at 110 °C). By analogy with the formaldehyde and thioformaldehyde derivatives $\text{Cp}^*_2\text{Ta}(\eta^2\text{-OCH}_2)\text{H}$ and $\text{Cp}^*_2\text{Ta}(\eta^2\text{-SCH}_2)\text{H}$ reported by Bercaw,³⁻⁵ the inverse kinetic isotope effect is indicative of a stepwise sequence involving a preequilibrium with $[\text{Cp}^*_2\text{TaSeCH}_3]$, followed by rate-determining α -methyl elimination (Scheme 2).²⁵

The molecular structures of the terminal selenido complexes $\text{Cp}^*_2\text{Ta}(\text{Se})\text{H}$ ($d(\text{Ta}=\text{Se}) = 2.329(2) \text{ \AA}$) and $\text{Cp}^*_2\text{Ta}(\text{Se})(\text{CH}_2\text{SiMe}_3)$ ($d(\text{Ta}=\text{Se}) = 2.372(1) \text{ \AA}$) have been determined by X-ray diffraction,²⁶ and the Ta=Se bond lengths are similar to the value in $[\eta^4\text{-N}(\text{CH}_2\text{CH}_2\text{NSiMe}_3)_3]\text{TaSe}$ ($2.330(1) \text{ \AA}$).^{27,28} The organotantalum

(23) $\text{Cp}^*_2\text{Ta}(\eta^2\text{-SeCHPr}^n)\text{H}$ is also converted to the selenido complex $\text{Cp}^*_2\text{Ta}(\text{Se})\text{Bu}^n$ at ca. 120 °C.

(24) It should also be noted that the isomerization of $\text{Cp}^*_2\text{Ta}(\eta^2\text{-SeCH}_2)\text{H}$ to $\text{Cp}^*_2\text{Ta}(\text{Se})\text{CH}_3$ is not catalyzed by MeMgI .

(25) Attempts to trap $[\text{Cp}^*_2\text{TaSeCH}_3]$ with, for example, CO or PMe_3 were unsuccessful.

(26) $\text{Cp}^*_2\text{Ta}(\text{Se})\text{H}$ is monoclinic, $P2_1/n$ (No. 14), with $a = 8.388(2) \text{ \AA}$, $b = 14.030(4) \text{ \AA}$, $c = 17.407(5) \text{ \AA}$, $\beta = 103.04(2)^\circ$, $V = 1996(1) \text{ \AA}^3$, and $Z = 4$. $\text{Cp}^*_2\text{Ta}(\text{Se})\text{CH}_2\text{SiMe}_3$ is triclinic, $P\bar{1}$ (No. 2), with $a = 8.972(2) \text{ \AA}$, $b = 9.527(2) \text{ \AA}$, $c = 15.488(3) \text{ \AA}$, $\alpha = 83.55(2)^\circ$, $\beta = 80.30(2)^\circ$, $\gamma = 78.61(2)^\circ$, $V = 1275(1) \text{ \AA}^3$, and $Z = 2$.

(27) Christou, V.; Arnold, J. *Angew. Chem., Int. Ed. Engl.* **1993**, *32*, 1450–1452.

(28) For further comparison, the average Ta=Se bond lengths in $[\text{Cp}^*\text{Ta}(\text{Se})_3\text{Li}_3\text{Cl}(\text{THF})_3]$ and $[\text{Cp}^*\text{Ta}(\text{Se})_3\text{Li}_2(\text{tmeda})_2]$ are 2.40(1) and 2.41(4) Å, respectively.⁶

selenium complexes have also been studied by ⁷⁷Se NMR spectroscopy.⁷ Thus, the terminal selenido complexes are characterized by relatively low field ⁷⁷Se NMR chemical shifts in the range δ 1990–2363 ppm,²⁹ while the singly bonded Se complexes are identified by high-field chemical shifts in the range δ +54 to –595 ppm.

In summary, a series of selenium complexes of permethyltantalocene, $\text{Cp}^*_2\text{Ta}(\eta^2\text{-Se}_2)\text{H}$, $\text{Cp}^*_2\text{Ta}(\text{Se})\text{SeH}$, $\text{Cp}^*_2\text{Ta}(\text{Se})\text{R}$ (R = H, Me, Buⁿ, CH₂SiMe₃, I), and $\text{Cp}^*_2\text{Ta}(\eta^2\text{-SeCHR})\text{H}$ (R = H, Prⁿ), have been prepared. These complexes provide some interesting contrasts to their tellurium analogues. For example, the diselenido-hydride complex $\text{Cp}^*_2\text{Ta}(\eta^2\text{-Se}_2)\text{H}$ is unstable with respect to the selenido-hydroselenide complex $\text{Cp}^*_2\text{Ta}(\text{Se})\text{SeH}$, whereas the ditellurido-hydride complex $\text{Cp}^*_2\text{Ta}(\eta^2\text{-Te}_2)\text{H}$ is stable under comparable conditions.

Acknowledgment. We thank the U.S. Department of Energy, Office of Basic Energy Sciences (No. DE-FG02-93ER14339), and the donors of the Petroleum Research Fund, administered by the American Chemical Society, for partial support of this research. G.P. is the recipient of a Camille and Henry Dreyfus Teacher-Scholar Award (1991–1996) and a Presidential Faculty Fellowship Award (1992–1997).

Supplementary Material Available: Text giving synthetic details and tables of analytical and spectroscopic data for all new complexes and tables of crystallographic data and figures giving structures for $\text{Cp}^*_2\text{Ta}(\text{Se})\text{H}$ and $\text{Cp}^*_2\text{Ta}(\text{Se})(\text{CH}_2\text{SiMe}_3)$ (32 pages). Ordering information is given on any current masthead page.

OM9409128

(29) For comparison, the ⁷⁷Se NMR signal for $[\eta^4\text{-N}(\text{CH}_2\text{CH}_2\text{NSiMe}_3)_3]\text{TaSe}$ is observed at 1518 ppm.²⁷

Inclusion of Al_2Me_6 in the Crystalline Lattice of the Organometallic Complexes $\text{LnAl}_3\text{Me}_{12}$

William J. Evans,* Reiner Anwander, and Joseph W. Ziller

Department of Chemistry, University of California, Irvine, California 92717

Received January 18, 1995[®]

Summary: The homoleptic tetramethylaluminates $\text{Ln}(\text{AlMe}_4)_3$ are formed by reaction of excess AlMe_3 in hexane with $\text{Ln}(\text{NMe}_2)_3(\text{LiCl})_3$ obtained from LnCl_3 and LiNMe_2 . $\text{Nd}[(\mu\text{-Me})_2\text{AlMe}_2]_3$ was characterized by X-ray diffraction, but it was also found that this complex as well as its yttrium analog will cocrystallize with Al_2Me_6 to form the isostructural alkylaluminum inclusion systems $\{\text{Ln}[(\mu\text{-Me})_2\text{AlMe}_2]_3\}_2[\text{Al}_2\text{Me}_6]$.

Alkylaluminum reagents are of tremendous importance to Ziegler/Natta and Kaminsky olefin polymerization catalysis¹ as well as in organic synthesis.² Bimetallic mixed-metal systems are commonly used although much remains to be learned about their mechanism of action and even their precise compositions. For example, it is still not understood why such a large excess of the commonly used catalytic activator methylaluminoxane (MAO) is needed in mixed-metal systems or how many effective equivalents of trimethylaluminum are in MAO.

We describe here a new class of mixed-metal tetramethylaluminates, namely the yttrium and the lanthanide metal complexes $\text{Ln}(\text{AlMe}_4)_3$,³ and report that these organometallic species have the capacity to form 2:1 cocrystallization products with molecular Al_2Me_6 when excess Al_2Me_6 is present. The formation of the trimethylaluminum inclusion products demonstrates that substantial amounts of unreacted trimethylaluminum can be retained in very pure crystalline mixed-metal organometallic compounds.

The tris(tetramethylaluminate) complexes are formed by reaction of excess trimethylaluminum with the insoluble product $\text{Ln}(\text{NMe}_2)_3(\text{LiCl})_3$ ⁴ generated by reaction of LiNMe_2 with the yttrium or lanthanide trihalide, eq 1.⁵ This synthesis is analogous to that used to make

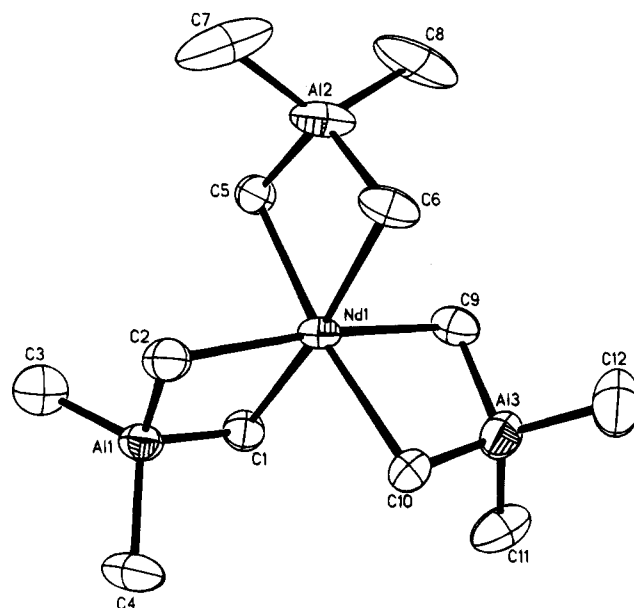
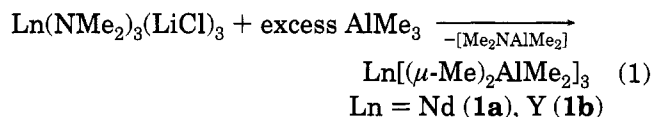


Figure 1. Molecular structure of $\text{Nd}[\text{AlMe}_4]_3$ (**1a**, molecule 1) with numbering identical to that of $\text{Nd}[\text{AlMe}_4]_3(\text{Al}_2\text{Me}_6)_{0.5}$ (**2a**) and $\text{Y}[\text{AlMe}_4]_3(\text{Al}_2\text{Me}_6)_{0.5}$ (**2b**). Thermal ellipsoids are drawn at the 50% probability level. Selected distances (Å) and angles (deg): **1a**: molecule 1, Nd1–C1 = 2.578(13), Nd1–C2 = 2.563(14), Nd1–C5 = 2.605(13), Nd1–C6 = 2.609(14), Nd1–C9 = 2.601(14), Nd1–C10 = 2.595(13); molecule 2, Nd2–C13 = 2.581(14), Nd2–C14 = 2.596(13), Nd2–C17 = 2.566(14), Nd2–C18 = 2.595(14), Nd2–C21 = 2.594(13), Nd2–C22 = 2.588(13). **2a**: Nd–C1 = 2.602(6), Nd–C2 = 2.599(6), Nd–C5 = 2.572(6), Nd–C6 = 2.588(5), Nd–C9 = 2.594(5), Nd–C10 = 2.600(6). **2b**: Y–C1 = 2.505(7), Y–C2 = 2.514(8), Y–C5 = 2.505(7), Y–C6 = 2.505(6), Y–C9 = 2.510(6), Y–C(10) = 2.057(7).

the permethylated mixed-metal neodymium gallium complex $\text{NdGa}_3\text{Me}_{12}$ from GaMe_3 .⁴ It was uncertain if the more reactive AlMe_3 would follow the same reaction pathway. Unlike the hexamethylanthanide “ate” complexes $[\text{Li}(\text{solvent})]_3[\text{LnMe}_6]$ ⁶ and the cyclopentadienyl derivatives $(\text{C}_5\text{H}_5)_2\text{Ln}[(\mu\text{-Me})_2\text{AlMe}_2]$,³ the $\text{Ln}[(\mu\text{-Me})_2\text{AlMe}_2]_3$ complexes are easily available for both early and late lanthanide elements. In addition, these compounds can be stored at room temperature over a long period of time in the absence of any coordinating solvent without decomposition. As such, the $\text{Ln}[\text{AlMe}_4]_3$ complexes represent conveniently obtained, easily handled alternatives to reagents such as $\text{M}[\text{AlMe}_4]$ and $\text{M}[\text{AlMe}_2]$.¹³

The $\text{Ln}[(\mu\text{-Me})_2\text{AlMe}_2]_3$ complexes show only one ¹H NMR signal at room temperature (Nd, 10.56; Sm, –3.11; Y, –0.27 ppm). However, separate resonances for the two types of methyl groups could be resolved at lower temperature for the smaller metals. For Y, the sharp singlet broadens into the baseline at –40 °C and reappears as 1:1 signals at –0.13, and –0.43 ppm below

[®] Abstract published in *Advance ACS Abstracts*, February 15, 1995.

(1) Sinn, H.; Kaminsky, W. *Adv. Organomet. Chem.* **1980**, *18*, 99. Kaminsky, W.; Miri, M.; Sinn, H.; Woldt, R. *Makromol. Chem., Rapid Commun.* **1983**, *4*, 417. Kaminsky, W.; Külper, K.; Brintzinger, H. H.; Wild, F. R. W. P. *Angew. Chem., Int. Ed. Engl.* **1985**, *24*, 507. Ewen, J. A. *J. Am. Chem. Soc.* **1984**, *106*, 6355–6364.

(2) Haushe, J. R. In *Comprehensive Organic Synthesis*; Trost, B. M., Fleming, I., Eds.; Pergamon: Oxford, U.K., 1991; Chapter 1.3.

(3) Note that mixed-ligand lanthanide tetramethylaluminates $(\text{C}_5\text{R}_5)_2\text{Ln}[(\mu\text{-Me}_2\text{AlMe}_2)]_3$ have been reported earlier. (a) Ln = Y, Yb; R = H; Holton, J.; Lappert, M. F.; Ballard, D. G. H.; Pearce, R.; Atwood, J. L.; Hunter, W. E. *J. Chem. Soc., Dalton Trans.* **1979**, 45–53. (b) Ln = Y; R = H; Scollary, G. R. *Aust. J. Chem.* **1978**, 411–414. (c) Ln = Y, Lu; R = Me; Busch, M. A.; Harlow, R.; Watson, P. L. *Inorg. Chim. Acta* **1987**, *140*, 15. (d) Ln = Sm; R = Me; Evans, W. J.; Chamberlain, L. R.; Ulibarri, T. A.; Ziller, J. W. *J. Am. Chem. Soc.* **1988**, *110*, 6423–6432.

(4) Evans, W. J.; Anwander, R.; Doedens, R. J.; Ziller, J. W. *Angew. Chem.* **1994**, *33*, 1641–1644.

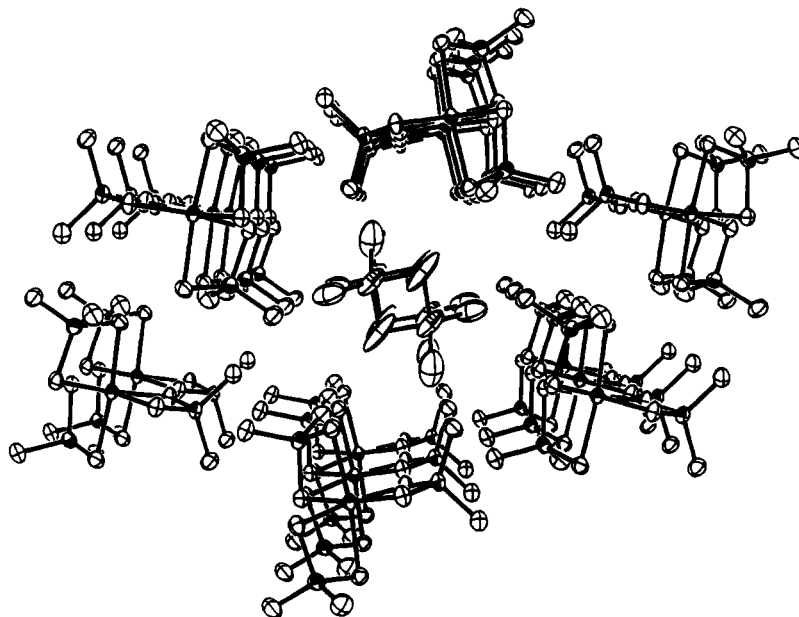


Figure 2. View of $\text{Nd}[\text{AlMe}_4]_3(\text{Al}_2\text{Me}_6)_{0.5}$, **2a**, indicating the location of Al_2Me_6 in channels formed by $\text{Nd}[\text{AlMe}_4]_3$ molecules.

-60°C . At -80°C , ^{89}Y coupling (3.7 Hz) was observed on the -0.13 resonance. For Sm, 1:1 signals at 2.16 and -7.22 ppm are resolved at -80°C , while for Nd only a broadened signal is observed at -80°C . These results are consistent with increased steric unsaturation and more rapid exchange at the larger metal center. $\text{Nd}[(\mu\text{-Me})_2\text{AlMe}_2]_3$, **1a**, was definitively identified by X-ray crystallography (Figure 1) and crystallizes from hexane at room temperature in a dichroic green/purple form with two independent molecules in the unit cell.⁸ The space group is different from that of $\text{Nd}[(\mu\text{-Me})_2\text{-GaMe}_2]_3$.⁴

Crystallization of the $\text{Ln}[(\mu\text{-Me})_2\text{AlMe}_2]_3$ products from the original hexane extract of the reaction mixture in the presence of excess trimethylaluminum at -35°C forms the 2:1 inclusion complexes $\{\text{Nd}[(\mu\text{-Me})_2\text{-}$

$\text{AlMe}_2]_3\}_2[\text{Al}_2\text{Me}_6]$, **2a**, and $\{\text{Y}[(\mu\text{-Me})_2\text{AlMe}_2]_3\}_2[\text{Al}_2\text{Me}_6]$, **2b**, which are isostructural.⁹ As shown in Figure 2, the Al_2Me_6 (mp 15°C) has been trapped in the crystalline lattice and is located in channels which are formed by four $\text{LnAl}_3\text{Me}_{12}$ molecules. Both the Al_2Me_6 and $\text{Ln}[(\mu\text{-Me})_2\text{AlMe}_2]_3$ molecules are arranged in a stacked fashion.

The structures of the $\text{Ln}[(\mu\text{-Me})_2\text{AlMe}_2]_3$ units in **1a**, **2a**, and **2b** are very similar. In each case, three bidentate AlMe_4^- ligands form a pseudooctahedral geometry around the metal. The average $\text{Nd}-\text{C}(\mu\text{-Me})$ distances of 2.589(14) Å in **1a** and 2.590(6) Å in **2a** are very similar to the $\text{Nd}-\text{C}$ distance in $\text{Nd}[(\mu\text{-Me})_2\text{GaMe}_2]_3$ (2.599(11) Å). The 2.508(7) Å average $\text{Y}-\text{C}(\mu\text{-Me})$ distance in **2b** is consistent with these considering the smaller ionic size of yttrium.¹⁰ In comparison, the $\text{Ln}-\text{C}(\mu\text{-Me})$ distances in the eight coordinate complexes $\text{Cp}_2\text{Y}[(\mu\text{-Me})_2\text{AlMe}_2]_3^{\text{b}}$ and $\text{Cp}_2\text{Yb}[(\mu\text{-Me})_2\text{AlMe}_2]_3^{\text{a}}$ are 2.58(3) and 2.58(1) Å, respectively.

The Al_2Me_6 molecules in **2a,b** were not sufficiently ordered to provide metrical parameters of high precision. The terminal $\text{Al}-\text{C}$ distances of 1.936(10) and 1.948(12) Å in **2a** and 1.925(12) and 1.934(10) Å in **2b** are in agreement with those found in pure Al_2Me_6 (1.956(2), 1.949(2) Å).¹¹ The bridging $\text{Al}-\text{C}$ bond lengths of 2.262(11) and 2.236(11) Å for **2a** are elongated compared to **2b** (2.122(11), 2.163(11) Å) and pure Al_2Me_6 (2.125(2), 2.123(2) Å), probably due to disordering.

The inclusion and stabilization of reactive species in

(5) The procedure for the preparations of **1a**, **1b**, **2a**, and **2b** was essentially the same and is illustrated in the case of the neodymium complex **2a**. In the glovebox, addition of excess AlMe_3 (1.75 mL, 18.35 mmol) to a pink hexane suspension of $\text{Nd}(\text{NMe}_2)_3(\text{LiCl})_3^{\text{b}}$ (0.62 g, 1.53 mmol) causes soluble products to be extracted into the hexane phase and a white precipitate to form. After being stirred for 24 h, the mixture was centrifuged to remove the precipitate, and the solution was stirred for an additional 24 h. Analytical and spectroscopic data were collected on crystals grown from concentrated hexane solutions at -35°C . Data for **2a** (0.64 g, 88%) are as follows. Anal. Calcd for $\text{C}_{15}\text{H}_{45}\text{Al}_4\text{Nd}$ (477.7): C, 37.72; H, 9.49. Found: C, 37.92; H, 9.44. ^1H NMR (500 MHz, C_7D_8): 30°C , δ -0.31 (s, Al_2Me_6), 10.56 (s, $\Delta\nu_{1/2} = 40$ Hz). IR (Nujol): 1249 m, 721 vs, 683 vs, 571 vs, 552 vs, 466 s, 367 m, 316 s, 223 cm^{-1} . Data for **2b** (0.60 g, 83%) are as follows. Anal. Calcd for $\text{C}_{15}\text{H}_{45}\text{Al}_4\text{Y}$ (422.3): C, 42.66; H, 10.74. Found: C, 42.84; H, 10.04. ^1H NMR (300 MHz, C_6D_6 , 20°C): δ -0.26 (s), -0.37 (s, $\text{Al}_2\text{-Me}_6$). IR (Nujol): 1248 m, 1216 s, 1195 s, 722 vs, 696 vs, 571 vs, 553 vs, 466 m, 453 m, 367 w, 313 s, 245 cm^{-1} . The Sm analog of **2a** was also obtained (Anal. Calcd for $\text{C}_{15}\text{H}_{45}\text{Al}_4\text{Sm}$ (483.8): C, 37.24; H, 9.37. Found: C, 37.20; H, 9.06. ^1H NMR (500 MHz, C_7D_8): 30°C , δ -0.34 (s, Al_2Me_6), -3.11 (s, $\Delta\nu_{1/2} = 30$ Hz). IR (Nujol): 1250 m, 1197 vs, 727 vs, 698 vs, 569 vs, 556 vs, 465 s, 368 w, 313 s, 223 cm^{-1}).

(6) (a) Schumann, H.; Pickardt, J.; Bruncks, N. *Angew. Chem.* **1981**, *93*, 127–128; *Angew. Chem., Int. Ed. Engl.* **1981**, *20*, 120–121. (b) Schumann, H.; Müller, J.; Bruncks, N.; Lauke, H.; Pickardt, J. *Organometallics* **1984**, *3*, 69–74. (c) Schumann, H.; Lauke, H.; Hahn, E.; Pickardt, J. *J. Organomet. Chem.* **1984**, *263*, 29–35.

(7) Mole, T.; Jeffery, E. A. *Organoaluminum Compounds*; Elsevier: Amsterdam, 1972.

(8) Crystal data, Siemens R3m/V diffractometer, are as follows. **1a** (-110°C): monoclinic, $P2_1/c$, $a = 7.437(2)$ Å, $b = 17.855(3)$ Å, $c = 32.423(5)$ Å, $\beta = 92.109(14)^\circ$, $V = 4302.5(14)$ Å³, and $D_{\text{calcd}} = 1.252$ g cm^{-3} for $Z = 8$; 4839 reflections ($|F_o| > 3.0\sigma(F_o)$); $R = 0.064$, $R_w = 0.084$.

(9) Crystal data, Siemens R3m/V diffractometer, are as follows. **2a** (-110°C): monoclinic, $P2_1/n$, $a = 7.516(1)$ Å, $b = 19.953(4)$ Å, $c = 17.965(3)$ Å, $\beta = 97.22(1)^\circ$, $V = 2672.9(9)$ Å³, and $D_{\text{calcd}} = 1.187$ g cm^{-3} for $Z = 4$; 3983 reflections ($F \geq 3\sigma(F)$), $R = 0.039$, $R_w = 0.046$. **2b** (-110°C): monoclinic, $P2_1/n$, $a = 7.452(2)$ Å, $b = 19.896(4)$ Å, $c = 17.770(3)$ Å, $\beta = 96.61(2)^\circ$, $V = 2617.1(10)$ Å³, and $D_{\text{calcd}} = 1.072$ g cm^{-3} for $Z = 4$; 2675 reflections ($F \geq 3.0\sigma(F)$), $R = 0.062$, $R_w = 0.067$.

(10) Shannon, R. D. *Acta Crystallogr.* **1976**, *A32*, 751.

(11) (a) Lewis, P. H.; Rundle, R. E. *J. Chem. Phys.* **1953**, *21*, 986. (b) Vranka, R. G.; Amma, E. L. *J. Am. Chem. Soc.* **1967**, *89*, 3121–3126. (c) Byram, S. K.; Fawcett, J. K.; Nyburg, S. C.; O'Brien, R. J. *Chem. Commun.* **1970**, 16–17. (d) Huffman, J. C.; Streib, W. E. *Chem. Commun.* **1971**, 911–912.

host molecules has been broadly studied.¹² Many examples of organic host guest combinations are known, and recently the use of inorganic metalloporphyrin "sponges" as crystalline hosts for small organic guests has been detailed.¹³ The cocrystallization of two different reactive neutral *organometallic* compounds as in crystalline **2a,b** is not common, however.¹⁴ The facile stoichiometric incorporation of trimethylaluminum into these mixed-metal organometallic aluminum complexes may explain why reactivity consistent with the presence of trimethylaluminum is unexpectedly found in orga-

nometallic systems thought to be free of trimethylaluminum. Moreover, since the $\text{Ln}[\text{AlMe}_4]_3$ complexes form high-quality single crystals both with and without Al_2Me_6 , single crystal formation is not a sufficient criterion to exclude the presence of Al_2Me_6 .

Acknowledgment. We thank the Division of Chemical Sciences of the Office of Basic Energy Sciences of the Department of Energy for support for this research and the Deutsche Forschungsgemeinschaft for a postdoctoral fellowship (to R.A.).

Supplementary Material Available: Molecular structure diagrams of **1** and **2** and tables of crystal data, positional parameters, bond distances and angles, and thermal parameters (38 pages). Ordering information is given on any current masthead page.

OM950036D

(12) For leading references, see: Helgeson, R. C.; Selle, B. J.; Goldberg, I.; Knobler, C. B.; Cram, D. J. *J. Am. Chem. Soc.* **1993**, *115*, 11506–11511. Yang, X.; Knobler, C. B.; Zheng, Z.; Hawthorne, M. F. *J. Am. Chem. Soc.* **1994**, *116*, 7142–7159.

(13) Byrn, M. P.; Curtis, C. J.; Hsiou, Y.; Khan, S. I.; Sawin, P. A.; Tendick, S. K.; Terzis, A.; Strouse, C. E. *J. Am. Chem. Soc.* **1993**, *115*, 9480–9497 and references therein.

(14) The X-ray crystal structure of the inorganic system $[\text{W}_2(\text{NMe}_2)_6]_2[\text{W}(\text{NMe}_2)_6]$ has been reported: Chisholm, M. H.; Cotton, F. A.; Extine, M.; Stults, B. R. *J. Am. Chem. Soc.* **1976**, *98*, 4477–4485.

Articles

Preparation and X-ray Crystal and Molecular Structure of *cis*-[(dppp)Pd(H₂O)(OSO₂CF₃)]⁺(OSO₂CF₃)⁻ and *cis*-[(dppp)Pd(H₂O)₂]²⁺(OSO₂CF₃)⁻₂. Coordinated Water-Triflate Hydrogen Bonds[†]

Peter J. Stang,* Danh H. Cao, Gregory T. Poulter, and Atta M. Arif*

Department of Chemistry, The University of Utah, Salt Lake City, Utah 84112

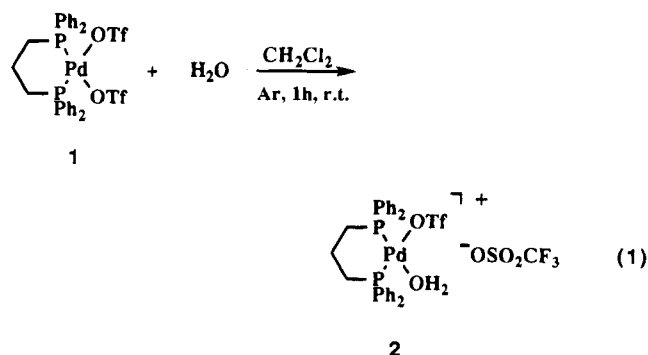
Received October 28, 1994[®]

Reaction of 1 and 2 equiv of water, respectively, with *cis*-(1,3-bis(diphenylphosphino)propane)palladium(II) triflate yields the corresponding monoquo and diaquo cationic Pd complexes 2 and 3 in 86% and 99% yield respectively, as yellow, air-stable, microcrystalline solids. The molecular structures of [(dppp)Pd(OH₂)(OSO₂CF₃)₂], (2) and [(dppp)Pd(OH₂)₂(OSO₂CF₃)₂], (3) have been determined by single-crystal X-ray crystallography. Complex 2 crystallizes in the monoclinic space group *P*2₁/*n* with *Z* = 4, *a* = 13.857(5) Å, *b* = 13.335(5) Å, *c* = 19.054(8) Å, β = 102.98(2)°, *R* = 0.0461, and *R*_w = 0.0614 at 298 K. Complex 3 crystallizes in the triclinic space group *P*1̄ with *Z* = 2, *a* = 11.440(1) Å, *b* = 11.800(1) Å, *c* = 14.269(1) Å, α = 95.66(1)°, β = 94.49(1)°, γ = 109.15(1)°, *R* = 0.0301, and *R*_w = 0.0467 at 298 K.

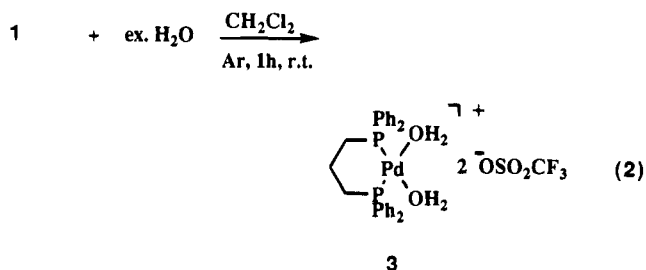
There is considerable current interest in transition-metal solvent complexes in general and water complexes in particular.^{1,2} Although several monoquo cationic transition-metal complexes are known,² there is much less information on diaquo complexes and the molecular structure of aquo complexes in general. Moreover, whereas a number of platinum aquo complexes are known, there have been very few palladium aquo complexes reported. Therefore, in this paper we wish to report the ready, high-yield preparation and the X-ray crystal molecular structures of both the monoquo and diaquo palladium(II) cationic complexes 2 and 3.

Results and Discussion

Reaction of exactly 1 equiv of water with anhydrous [(dppp)Pd(OSO₂CF₃)₂] (1)³ in CH₂Cl₂ at room temperature under an argon atmosphere results in an 86% yield of the monoquo complex 2 (eq 1). Likewise,



interaction of 1 with 2 equiv or more of water yields the diaquo complex 3 in 99% isolated yield (eq 2). Complexes 2 and 3 are respectively light yellow and yellow, air-stable, microcrystalline solids.



Single-Crystal Molecular Structure Determination. Suitable single crystals for X-ray structure determination of 2 and 3, were obtained by careful layering of diethyl ether over a CH₂Cl₂ solution of 2 and 3, respectively, at room temperature. Both compounds crystallize as hexagonal platelets. Crystallographic data are summarized in Table 1, and the final atomic coordinates of the heavy atoms are given in Tables 2 and 3. Relevant bond distances and bond angles are reported in Table 4. ORTEP diagrams are displayed in Figures 1 and 2, respectively.

(1) Beck, W.; Sünkel, K. *Chem. Rev.* **1988**, *88*, 1405 and references therein.

(2) For key recent references see: (a) Kubas, G. J.; Burns, C. J.; Khalsa, G. R. K.; Van Der Sluys, L. S.; Kiss, G.; Hoff, C. D. *Organometallics* **1992**, *11*, 3390. (b) Leoni, P.; Sommovigo, M.; Pasquali, M.; Midollini, S.; Braga, D.; Sabatino, P. *Organometallics* **1991**, *10*, 1038. (c) Rauscher, D. J.; Thaler, E. G.; Huffman, J. C.; Caulton, K. G. *Organometallics* **1991**, *10*, 2209. (d) Branan, D. M.; Huffman, N. W.; McElroy, E. A.; Prokopuk, N.; Salazar, A. B.; Robbins, M. J.; Hill, W. E.; Webb, T. R. *Inorg. Chem.* **1991**, *30*, 1200. (e) Bergmeister, J. J., III; Hanson, B. E.; Merola, J. S. *Inorg. Chem.* **1990**, *29*, 4831. (f) Steed, J. W.; Tocher, D. A. *J. Chem. Soc., Chem. Commun.* **1991**, 1609.

[†] Dedicated to Professor William M. Jones on the occasion of his 65th birthday.

[®] Abstract published in *Advance ACS Abstracts*, February 15, 1995.

Table 1. Crystal and Data Collection Parameters for Compounds **2** and **3**

	2	3
molecular formula	PdS ₂ P ₂ F ₆ O ₇ C ₂₉ H ₂₈	PdS ₂ P ₂ F ₆ O ₈ C ₂₉ H ₃₀
fw	835.009	853.024
space group	P2 ₁ /n	P1̄
space group no.	14	2
cryst syst	monoclinic	triclinic
cell constants		
<i>a</i> (Å)	13.857(5)	11.440(1)
<i>b</i> (Å)	13.335(5)	11.800(1)
<i>c</i> (Å)	19.054(8)	14.269(1)
α (deg)		95.66(1)
β (deg)	102.98(2)	94.49(1)
γ (deg)		109.15(1)
<i>V</i> (Å ³)	3431.08	1798.15
<i>Z</i>	4	2
<i>D</i> _{calc} (g cm ⁻³)	1.618	1.575
cryst dimens (mm)	0.33 × 0.30 × 0.27	0.29 × 0.32 × 0.37
abs coeff (cm ⁻¹)	8.158	7.809
radiation	Mo (0.710 73 Å)	Mo (0.710 73 Å)
no. of unique rflns	5337	6310
2θ range (deg)	2.00–50.00	2.00–50.00
scan technique	θ/2θ	θ/2θ
scan speed (deg min ⁻¹)	variable	4.5
scan width (deg)	0.8000 + 0.3400 (tan θ)	K -1.2 to K +1.2
no of rflns between stds	1 X-ray h	
abs cor	empirical	empirical
min transmissn (%)	84.8748	90.03
max transmissn (%)	99.9052	99.99
highest peak, final diff Fourier (e Å ⁻³)	1.151 (about 1.050 Å from Pd)	0.698
weighting scheme	non-Poisson contribn	non-Poisson contribn
ignorance factor, <i>P</i>	0.04	0.05
data rejected if <i>I</i>	<3.00σ(<i>I</i>)	<3.00σ(<i>I</i>)
data rejected if (sin θ)/λ	<0.0500	<0.0500
no. of observs	4198	5566
no. of variables	509	554
data to param ratio	8.248	10.047
shift to error ratio	0.018	0.016
error in an observn of unit wt (GOF)	2.2949	1.3400
<i>R</i> (<i>R</i> _w)	0.0461 (0.0614)	0.0301 (0.0467)

Perusal of the data in Table 4 reveals a number of unusual and interesting aspects about the molecular structures of complexes **2** and **3**. In both complexes the Pd(II) atom has a distorted-square-planar coordination: the two cis sites are occupied by the dppp ligand, while the remaining two sites are taken up by the coordinated water and a covalently bound triflate in **2** and two coordinated water molecules in **3**.

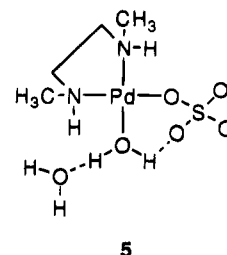
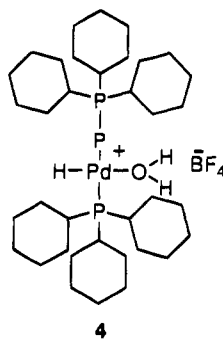
The bond angles around the palladium atom are close to the expected values of 90°, ranging in values from 86.1 to 93.2° for **2** and 87.66 to 93.38° for **3**. The P–Pd–P chelation angle is just over 90° in both **2** and **3**, whereas the O₁–Pd–O₂ angles are 86.1 and 87.66° for **2** and **3**, respectively. The palladium–phosphorus bond distances of 2.226–2.237 Å are in the normal range for cis-chelated phosphorus. The Pd–OH₂ distance in **2** is 2.159 Å, whereas in **3** these distances are 2.127 and 2.135 Å. These values compare favorably with the corresponding bond angles and bond distances in the related Pd–OH₂ complex *trans*-[(Cy₃P)₂Pd(H)(OH₂)]⁺BF₄⁻ (**4**), recently reported by Leoni and co-workers.^{2b}

Particularly noteworthy are the hydrogen-bonding patterns in complexes **2** and **3**. In the monoquo complex **2**, the hydrogens of the complexed water molecule are hydrogen-bonded intramolecularly to the coordinated triflate and intermolecularly to the anionic triflate counterion with an O–H...O distance of approximately 2.0 Å. A comparable hydrogen-bonding

Table 2. Positional Parameters and Estimated Standard Deviations for Compound **2**

atom	<i>x</i>	<i>y</i>	<i>z</i>
Pd	0.21098(2)	0.16094(3)	0.47998(2)
S1	0.3985(1)	0.1034(1)	0.61921(7)
S2	0.1414(1)	-0.2548(1)	0.48825(7)
P1	0.19812(8)	0.32802(9)	0.48256(6)
P2	0.12216(8)	0.15671(9)	0.36697(6)
F1	0.4719(3)	0.1155(3)	0.5051(2)
F2	0.5124(3)	0.2364(3)	0.5796(3)
F3	0.5802(3)	0.0934(3)	0.6037(3)
F4	0.3092(3)	-0.3188(5)	0.5632(4)
F5	0.2537(5)	-0.1942(4)	0.6078(3)
F6	0.1927(4)	-0.3369(4)	0.6139(3)
O1	0.2331(3)	0.0046(3)	0.4843(2)
O2	0.3142(3)	0.1655(3)	0.5833(2)
O3	0.4377(4)	0.1298(4)	0.6917(2)
O4	0.3855(3)	-0.0010(3)	0.6041(2)
O5	0.1231(3)	-0.3515(3)	0.4565(3)
O6	0.0573(3)	-0.2150(4)	0.5111(2)
O7	0.1862(3)	-0.1844(4)	0.4490(2)
C1	0.0853(3)	0.3862(4)	0.4326(3)
C2	0.0624(4)	0.3601(4)	0.3525(3)
C3	0.0280(3)	0.2521(3)	0.3375(2)
C4	0.2981(3)	0.3837(3)	0.4496(2)
C5	0.3060(4)	0.4861(5)	0.4440(4)
C6	0.3838(5)	0.5252(5)	0.4170(4)
C7	0.4516(4)	0.4687(5)	0.3981(3)
C8	0.4457(4)	0.3667(5)	0.4034(3)
C9	0.3689(4)	0.3237(4)	0.4278(3)
C10	0.2095(3)	0.3691(4)	0.5741(2)
C11	0.3029(4)	0.3895(4)	0.6185(3)
C12	0.3101(4)	0.4196(5)	0.6877(3)
C13	0.2298(5)	0.4302(5)	0.7166(3)
C14	0.1391(4)	0.4076(5)	0.6752(3)
C15	0.1277(4)	0.3776(4)	0.6040(3)
C16	0.0536(3)	0.0401(3)	0.3513(2)
C17	0.0661(4)	-0.0268(4)	0.2991(3)
C18	0.0065(5)	-0.1112(4)	0.2860(3)
C19	-0.0652(5)	-0.1273(4)	0.3236(3)
C20	-0.0775(4)	-0.0619(4)	0.3757(3)
C21	-0.0178(4)	0.0215(4)	0.3906(3)
C22	0.2077(3)	0.1591(4)	0.3075(2)
C23	0.1919(4)	0.2193(4)	0.2462(3)
C24	0.2589(4)	0.2175(5)	0.2031(3)
C25	0.3399(4)	0.1576(5)	0.2187(3)
C26	0.3564(4)	0.0982(5)	0.2779(3)
C27	0.2911(4)	0.0989(5)	0.3228(3)
C28	0.4960(4)	0.1390(5)	0.5743(4)
C29	0.2277(5)	-0.2760(5)	0.5703(5)

pattern was observed in the chelated Pt–OH₂ complex [Pt(NH(CH₃)C₂H₄NH(CH₃))(H₂O)(SO₄)]·H₂O (**5**), reported by Rochon and Melanson.⁵ In complex **3**, how-



ever, both coordinated water molecules are doubly hydrogen-bonded to the two triflate counterions. Interestingly, the two water molecules are each hydrogen-bonded to different triflates rather than the same one, as seen in the ORTEP representation. Similarly, both hydrogens in the aquo complex **4** are hydrogen-bonded to the fluorines of the BF₄⁻ anion.^{2b} The role of

Table 3. Positional Parameters and Estimated Standard Deviations for Compound 3

atom	x	y	z
Pd	0.17963(1)	0.12857(1)	0.29772(1)
S1	-0.04504(6)	-0.22004(7)	0.41900(5)
S2	0.29620(6)	-0.12651(7)	0.13519(5)
P1	0.07386(5)	0.23363(5)	0.23057(4)
P2	0.34196(5)	0.29797(5)	0.34223(4)
F1	-0.0166(3)	-0.4258(2)	0.4330(3)
F2	-0.1936(3)	-0.4389(3)	0.3622(3)
F3	-0.0309(3)	-0.3856(3)	0.2918(2)
F4	0.2059(3)	-0.3318(2)	0.0261(2)
F5	0.3438(2)	-0.3277(2)	0.1361(2)
F6	0.1648(3)	-0.3390(2)	0.1707(2)
O1	0.0388(2)	-0.0347(2)	0.2339(1)
O2	0.2649(2)	0.0199(2)	0.3691(1)
O3	-0.1023(2)	-0.2306(2)	0.5033(2)
O4	-0.1055(2)	-0.1800(2)	0.3439(2)
O5	0.0880(2)	-0.1652(3)	0.4332(2)
O6	0.1820(2)	-0.1067(2)	0.1130(2)
O7	0.3448(2)	-0.0991(2)	0.2347(2)
O8	0.3866(2)	-0.0920(3)	0.0708(2)
C1	0.0917(2)	0.3787(2)	0.2969(2)
C2	0.2224(2)	0.4681(2)	0.3200(2)
C3	0.3058(2)	0.4287(2)	0.3888(2)
C4	-0.0898(2)	0.1501(2)	0.2288(2)
C5	-0.1306(2)	0.1123(3)	0.3123(2)
C6	-0.2557(3)	0.0527(4)	0.3155(3)
C7	-0.3381(3)	0.0284(3)	0.2356(3)
C8	-0.2980(3)	0.0648(4)	0.1538(3)
C9	-0.1739(3)	0.1249(3)	0.1472(2)
C10	0.1057(2)	0.2546(2)	0.1105(2)
C11	0.1023(3)	0.3554(3)	0.0707(2)
C12	0.1264(4)	0.3661(3)	-0.0213(2)
C13	0.1534(3)	0.2773(3)	-0.0746(2)
C14	0.1563(3)	0.1769(3)	-0.0363(2)
C15	0.1328(3)	0.1642(3)	0.0557(2)
C16	0.4478(2)	0.2746(2)	0.4338(2)
C17	0.5652(3)	0.2760(3)	0.4162(2)
C18	0.6421(3)	0.2528(3)	0.4872(3)
C19	0.6047(3)	0.2310(3)	0.5722(3)
C20	0.4887(4)	0.2301(3)	0.5904(2)
C21	0.4086(3)	0.2519(3)	0.5212(2)
C22	0.4281(2)	0.3391(2)	0.2433(2)
C23	0.4306(3)	0.2497(3)	0.1738(2)
C24	0.4973(4)	0.2791(5)	0.0984(3)
C25	0.5562(4)	0.3974(5)	0.0899(3)
C26	0.5562(4)	0.4874(4)	0.1566(3)
C27	0.4908(3)	0.4580(3)	0.2344(3)
C28	-0.0735(4)	-0.3772(4)	0.3725(3)
C29	0.2512(4)	-0.2893(3)	0.1166(3)

hydrogen bonding in the formation of aquo transition-metal complexes has long been recognized⁵⁻⁷ and is important in stabilizing the solid-state structure of these molecules.⁸⁻¹⁰ In both of our complexes **2** and **3** and complex **5** the S-O bond distance of the coordinated oxygen is significantly longer than the remaining non-coordinated S-O bonds. Finally, reaction of the mono-aquo complex **2** with additional water readily forms the diaquo complex **3**.

Experimental Section

General Methods. All reactions were conducted under a dry nitrogen atmosphere using Schlenk techniques, unless

- (3) Stang, P. J.; Cao, D. H. *J. Am. Chem. Soc.* **1994**, *116*, 4981.
- (4) The H atoms were located by X-ray, and since they are based on X-ray-derived H-atom positions with considerable uncertainties, all H-atom structural parameters need to be interpreted with caution.
- (5) Rochon, F. D.; Melanson, R. *Inorg. Chem.* **1987**, *26*, 989.
- (6) Britten, J. F.; Lippert, B.; Lock, C. J.; Pilon, P. *Inorg. Chem.* **1982**, *21*, 1936.
- (7) Hollis, L. S.; Lippard, S. J. *Inorg. Chem.* **1983**, *22*, 2605.
- (8) Brown, I. D. *Structure and Bonding in Crystals*; Academic Press: New York, 1981, Vol. II.
- (9) Braga, D.; Grepioni, F. *Acc. Chem. Res.* **1994**, *27*, 51.
- (10) Braga, D.; Grepioni, F.; Sabatino, P.; Desiraju, G. R. *Organometallics* **1994**, *13*, 3532.

Table 4. Relevant Bond Distances (Å) and Angles (deg) for Compounds 2 and 3^a

Compound 2			
Pd-O1	2.106(4)	P2-C3	1.819(5)
Pd-O2	2.159(3)	P2-C16	1.812(5)
Pd-P1	2.237(1)	P2-C22	1.815(5)
Pd-P2	2.228(1)	S1-O2	1.469(4)
P1-C1	1.812(5)	S1-O3	1.411(5)
P1-C4	1.805(5)	S1-O4	1.425(5)
P1-C10	1.801(5)	S2-O5	1.424(4)
O1-H1	0.71(6)	S2-O6	1.435(5)
O1-H2	0.74(6)	S2-O7	1.426(5)
O4--H2	2.04(6)	S1-C28	1.817(8)
O7--H1	2.00(7)	S2-C29	1.76(1)
P1-Pd-P2	90.98(4)	P2-Pd-O2	172.3(1)
O1-Pd-O2	86.1(2)	P1-Pd-O1	175.5(1)
P1-Pd-O2	89.5(1)	H1-O1-H2	107(7)
P2-Pd-O1	93.2(1)	O1-H1-O7	153(7)
		O1-H2-O4	157(7)
Compound 3			
Pd-O1	2.127(2)	P2-C3	1.804(3)
Pd-O2	2.135(2)	P2-C16	1.815(3)
Pd-P1	2.2264(7)	P2-C22	1.799(3)
Pd-P2	2.2309(7)	S1-O3	1.411(2)
P1-C1	1.814(3)	S1-O4	1.431(3)
P1-C4	1.804(3)	S1-O5	1.434(3)
P1-C10	1.803(3)	S2-O6	1.419(2)
O1-H1	0.72(4)	S2-O7	1.448(3)
O1-H2	0.76(4)	S2-O8	1.423(3)
O2-H3	0.74(3)	S1-C28	1.820(6)
O2-H4	0.83(4)	S2-C29	1.804(5)
O4--H2	1.93(5)		
O5--H3	2.00(3)		
O6--H1	2.03(4)		
O7--H4	1.83(4)		
P1-Pd-P2	90.33(2)	P2-Pd-O1	170.37(9)
P1-Pd-O1	89.42(6)	P1-Pd-O2	174.23(8)
P2-Pd-O2	93.38(6)	H1-O1-H2	114(5)
O1-Pd-O2	87.66(8)	H3-O2-H4	109(4)
O1-H1-O6	163(4)		
O1-H2-O4	172(4)		
O2-H3-O5	172(4)		
O2-H4-O7	173(4)		

^aNumbers in parentheses are estimated standard deviations in the least significant digits.

otherwise noted. IR spectra were recorded on a Mattson Polaris FT-IR spectrophotometer. NMR spectra were recorded on a Varian XL-300 spectrometer. ¹H NMR spectra were recorded at 300 MHz, and all chemical shifts (δ) are reported in ppm relative to the proton resonance resulting from incomplete deuteration of the NMR solvent CD₂Cl₂ (5.32 ppm). ¹³C NMR spectra were recorded at 75 MHz, and all chemical shifts (δ) are reported in ppm relative to the carbon resonance of the deuterated NMR solvent CD₂Cl₂ (53.8 ppm). ³¹P NMR spectra were recorded at 121 MHz, and all chemical shifts (δ) are reported in ppm relative to external 85% H₃PO₄ at 0.00 ppm. ¹⁹F NMR spectra were recorded at 282 MHz, and all chemical shifts are reported upfield relative to external CFC1₃ at 0.00 ppm. Microanalyses were performed by Atlantic Microlab Inc., Norcross, GA. Melting points were obtained with a Mel-Temp capillary melting point apparatus and were not corrected.

Preparation of [(dppp)Pd(OH₂)(OSO₂CF₃)]⁺(OSO₂CF₃)⁻ (2**).** A 25 mL Schlenk flask flame-dried under argon and equipped with a stirbar and rubber septum was charged with (dppp)Pd(OTf)₂ (0.100 g, 0.122 mmol) and 15 mL of CH₂Cl₂. To the homogeneous yellow mixture was added via syringe deionized water (2.0 mL, 0.11 mmol). The reaction mixture was stirred for 1 h at ambient temperature, followed by reduction of the solvent to 4 mL under vacuum. Via syringe 20 mL of dry *n*-pentane was added immediately, yielding a yellow precipitate. The solvent was decanted via syringe, and the residue was dried under vacuum to afford **2**, as a light

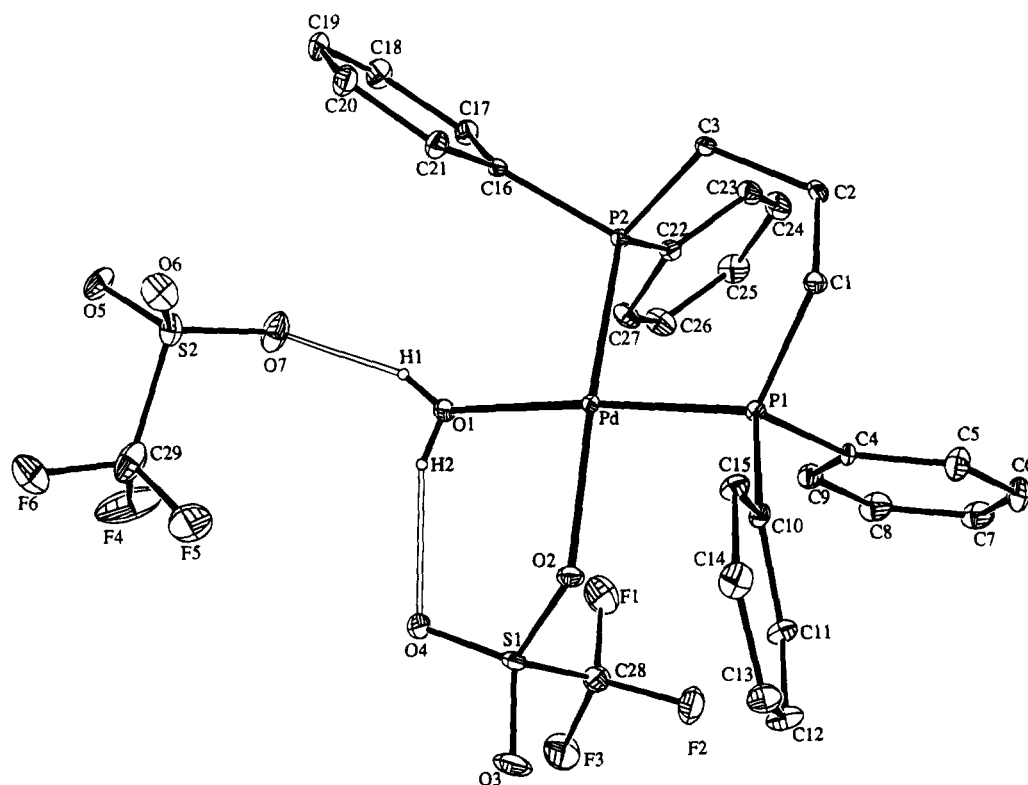


Figure 1. ORTEP plot of $[(\text{dppp})\text{Pd}(\text{OH})_2(\text{OSO}_2\text{CF}_3)_2]$ (**2**).

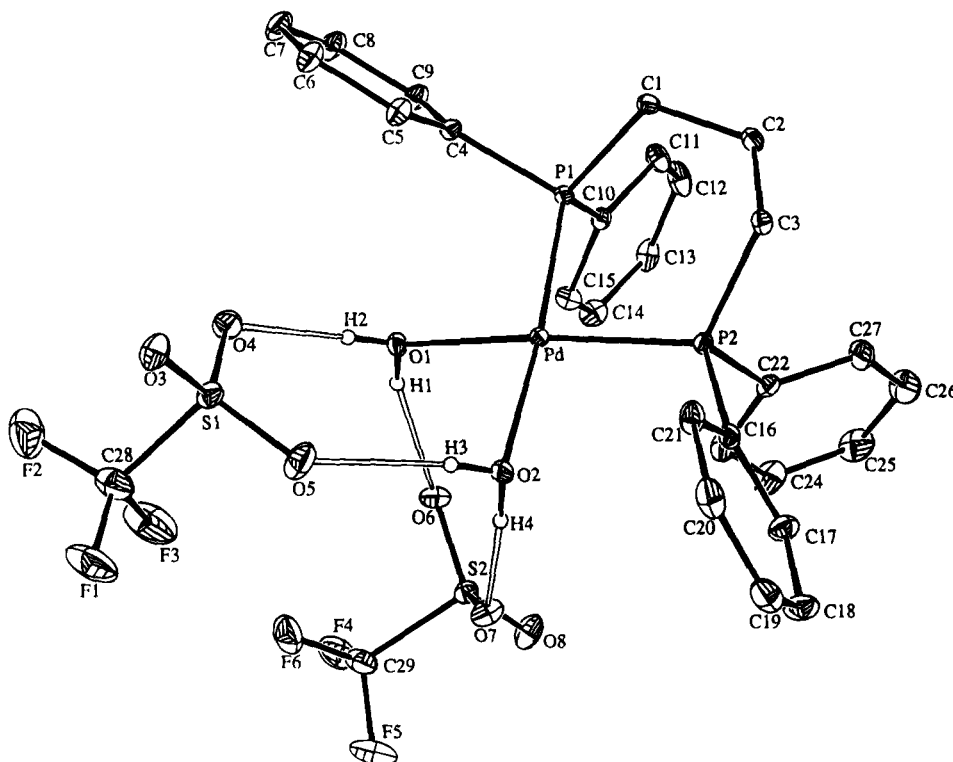


Figure 2. ORTEP plot of $[(\text{dppp})\text{Pd}(\text{OH})_2(\text{OSO}_2\text{CF}_3)_2]$ (**3**).

yellow microcrystalline solid; yield 87.4 mg (86%); mp 206–209 °C dec; IR (KBr, cm^{-1}) 3222 (m, OH), 2919 (w), 1229 (m), 1168 (m), 1098 (w), 1020 (m); ^1H NMR (CD_2Cl_2) 7.3–7.7 (m, 20H, C_6H_5), 5.1 (s, 2H, H_2O), 2.7–2.9 (m, 4H, CH_2), 2.1–2.4 (m, 2H, CH_2); ^{31}P NMR (CD_2Cl_2) 20.4 (s); ^{19}F NMR (CD_2Cl_2) –76. Anal. Calcd for $\text{C}_{29}\text{H}_{26}\text{PdP}_2\text{S}_2\text{O}_6\text{F}_6\text{H}_2\text{O}$: C, 41.71; H, 3.38; S 7.68. Found: C, 41.61; H, 3.49; S, 7.48.

X-ray-quality crystals were grown by careful layering with a CH_2Cl_2 /diethyl ether mixture at ambient temperature.

Preparation of $[(\text{dppp})\text{Pd}(\text{OH})_2]^{+}(\text{OSO}_2\text{CF}_3)^{-}_2$ (3**).** A 25 mL Schlenk flask flame-dried under argon and equipped with a stirbar and rubber septum was charged with $(\text{dppp})\text{Pd}(\text{OTf})_2$ (137 mg, 0.168 mmol) and 20 mL of CH_2Cl_2 . To the homogeneous yellow mixture was added via syringe an excess of deionized water (10 mL, 0.55 mmol). The reaction mixture was stirred for 1 h at ambient temperature, followed by reduction of the solvent to 4 mL under vacuum. Via syringe 20 mL of dry *n*-pentane was added immediately, yielding a

yellow precipitate. The solvent was decanted via syringe, and the residue was dried under vacuum to afford **3**, as a light yellow microcrystalline solid: yield 137 mg (99%); mp 232–238 °C dec; IR (KBr, cm^{-1}) 3285 (s, OH), 2917 (m), 1252 (m), 1167 (s), 1099 (m), 1031 (m); ^1H NMR (CD_2Cl_2) 7.3–7.7 (m, 20H, C_6H_5), 4.1 (s, 4H, H_2O), 2.7–2.9 (m, 4H, CH_2), 2.2–2.5 (m, 2H, CH_2); ^{31}P NMR (CD_2Cl_2) 20.4 (s); ^{19}F NMR (CD_2Cl_2) –76. Anal. Calcd for $\text{C}_{29}\text{H}_{26}\text{PdP}_2\text{S}_2\text{O}_6\text{F}_6 \cdot 2\text{H}_2\text{O}$: C, 40.83; H, 3.54; S, 7.52. Found: C, 40.57; H, 3.56; S, 7.55.

X-ray-quality crystals were grown by careful layering with a CH_2Cl_2 /diethyl ether mixture at ambient temperature.

X-ray Crystallographic Analysis of 2. A light yellow crystal, 0.33 mm \times 0.30 mm \times 0.27 mm, was glued onto a glass fiber and mounted for data collection on a CAD4 diffractometer. The unit cell parameters were obtained by a least-squares refinement of 25 centered reflections in the range $20 < 2\theta < 30^\circ$. The space group was determined from systematic absences ($h0l$, $h + l = 2n + 1$, $0k0$, $k = 2n + 1$) and subsequent least-squares refinement. The data were collected by the θ – 2θ scan technique, with variable scanning rate, using monochromatic Mo radiation. A total of 5337 unique reflections were measured in the range of $2.0 < 2\theta < 50^\circ$, of which 4198 were considered observed; i.e., $I > 3\sigma(I)$. Standard reflections showed no decay during data collection. Lorentz and polarization corrections, and an empirical absorption correction based upon a series of ψ scans, were applied to the data. Intensities of equivalent reflections were averaged.

The structure was solved by the standard heavy-atom techniques with the Molen/VAX package. Non-hydrogen atoms were refined with anisotropic thermal parameters. All hydrogen atoms were located and refined with fixed isotropic thermal parameter. Scattering factors, and $\Delta f'$ and $\Delta f''$ values, were taken from the literature.

X-ray Crystallographic Analysis of 3. A yellow crystal, 0.29 mm \times 0.32 mm \times 0.37 mm, was glued onto a glass fiber and mounted for data collection on a Syntex P1 diffractometer. The unit cell parameters were obtained by a least-squares refinement of 30 centered reflections in the range $10 < 2\theta < 20^\circ$. The space group was determined from subsequent least-squares refinement. The data were collected by the θ – 2θ scan technique, with fixed rate, using monochromatic Mo radiation. A total of 6310 unique reflections were measured in the range of $2.0 < 2\theta < 50^\circ$, of which 5566 were considered observed; i.e., $I > 3\sigma(I)$. Standard reflections showed no decay during data collection. Lorentz and polarization corrections, and an empirical absorption correction based upon a series of ψ scans, were applied to the data. Intensities of equivalent reflections were averaged.

The structure was solved by the standard heavy-atom techniques with the Molen/VAX package. Non-hydrogen atoms were refined with anisotropic thermal parameters. All hydrogen atoms were located and refined isotropically. Scattering factors, and $\Delta f'$ and $\Delta f''$ values, were taken from the literature.

Acknowledgment. We thank the NSF (Grant No. CHE 9101767) for financial support and Johnson-Matthey for the generous loan of $\text{PdCl}_2 \cdot x\text{H}_2\text{O}$.

Supplementary Material Available: Crystal structure data for compounds **2** and **3**, including tables of calculated positional parameters for the hydrogen atoms and anisotropic displacement parameters and extended lists of bond lengths, bond angles, and torsion angles (22 pages). Ordering information is given on any current masthead page.

OM940823V

Spectroelectrochemical (IR, UV/Vis) Determination of the Reduction Pathways for a Series of $[\text{Re}(\text{CO})_3(\alpha\text{-diimine})\text{L}']^{0/+}$ ($\text{L}' = \text{Halide}, \text{Otf}^-, \text{THF}, \text{MeCN}, n\text{-PrCN}, \text{PPh}_3, \text{P}(\text{OMe})_3$) Complexes

G. J. Stor, F. Hartl,* J. W. M. van Outersterp, and D. J. Stufkens

Anorganisch Chemisch Laboratorium, Universiteit van Amsterdam, Nieuwe Achtergracht 166, 1018 WV Amsterdam, The Netherlands

Received April 14, 1994[®]

The reduction pathways were investigated for a series of $[\text{Re}(\text{CO})_3(\alpha\text{-diimine})\text{L}']^{0/+}$ ($\text{L}' = \text{Cl}^-, \text{Br}^-, \text{I}^-, \text{Otf}^-, \text{THF}, \text{MeCN}, n\text{-PrCN}, \text{PPh}_3, \text{P}(\text{OMe})_3$; $\alpha\text{-diimine} = \text{bpy}, i\text{-Pr-PyCa}, \text{dapa}, \text{dpp}, \text{abpy}$) complexes. The individual one-electron reduction steps were studied mainly in THF, by a combination of cyclic voltammetry and *in situ* FTIR and UV/vis spectroscopy. The stability of the reduced $[\text{Re}(\text{CO})_3(\alpha\text{-diimine})\text{L}']^{-/}$ complexes depends on the ability of the $\alpha\text{-diimine}$ radical ligand to accommodate the unpaired electron in its lowest empty π^* orbital, which increases in the order $\text{bpy} < i\text{-Pr-PyCa} < \text{dapa} < \text{dpp} < \text{abpy}$. The higher the energy of this π^* orbital, the more pronounced is the donor character of the $\alpha\text{-diimine}$ radical. Concomitant polarization of the radical complex and increased electron density within the $\text{Re}-(\alpha\text{-diimine})$ chelate ring labilize the $\text{Re}-\text{L}'$ bond and may cause dissociation of L' and dimerization of the Re radicals, or substitution of L' by a better π acceptor. The kinetic stability of the $\text{Re}-\text{L}'$ bond increases in the order $\text{halide} \ll \text{THF} < \text{PPh}_3, n\text{-PrCN} < \text{P}(\text{OMe})_3$. The labilizing effect of the strong donating power of the reduced $\alpha\text{-diimine}$ ligand on the $\text{Re}-\text{L}'$ bond becomes much more apparent upon the second one-electron reduction step. For $\alpha\text{-diimine} = \text{bpy}, i\text{-Pr-PyCa}, \text{dpp}$, the products of the first one-electron reduction were converted in this step into the five-coordinated anionic $[\text{Re}(\text{CO})_3(\alpha\text{-diimine})]^-$ complexes, in which the π -electron density is largely delocalized over the $\text{Re}-(\alpha\text{-diimine})$ chelate bond, as indicated by their low $\nu(\text{CO})$ frequencies and average $\text{C}=\text{O}$ force constants. For $\alpha\text{-diimine} = \text{dapa}$, the anionic $[\text{Re}(\text{CO})_3(N,N,N)\text{-dapa}]^-$ species was produced, in which the third imine nitrogen atom interacts only weakly with the Re center. Importantly, for $\text{L}' = \text{P}(\text{OMe})_3$, the strongest π acceptor employed, the stable six-coordinated $[\text{Re}(\text{CO})_3(N,N\text{-dapa})(\text{P}(\text{OMe})_3)]^-$ anion was formed. The only stable six-coordinated $[\text{Re}(\text{CO})_3(\alpha\text{-diimine})\text{L}']^-$ anions with $\text{L}' = \text{THF}$ or PPh_3 in the axial position were obtained for $\alpha\text{-diimine} = \text{abpy}$. The abpy ligand is a strong π acceptor due to its very low-lying π^* LUMO of the azo bond character. In this case, even a third one-electron reduction step was observed, which is probably more localized on the aromatic rings of abpy and converted the abpy ligand into a strong donor. As a result, the interaction of the ligand $\text{L}' = \text{THF}, \text{PPh}_3$ with the Re center in the dianionic product $\{[\text{Re}(\text{CO})_3(\text{abpy})]^{2-} \cdots \text{L}'\}$ is very weak.

Introduction

Complexes of the type $[\text{Re}(\text{CO})_3(\alpha\text{-diimine})\text{L}']^{0/+}$, in which L' is a halide, bridging ligand, organic donor/acceptor, nitrogen donor or some other monodentate ligand, have been the subject of a large number of studies. In large part, this permanently growing interest stems from the ability of these complexes and their reduced forms to act as efficient sensitizers for energy and electron transfer processes,¹ and as catalysts in the selective reduction of CO_2 .² Thus, the complexes were successfully applied in the photochemical^{2a,c,e,h,j,m} and electrochemical^{2b,d,h,i,k,l,m,n} conversion of CO_2 into CO. In order to elucidate the role of these complexes as electrocatalysts in C_1 chemistry, most fundamental studies have mainly been confined to cyclic voltammetry^{2d,f,k} ^{3b-d}

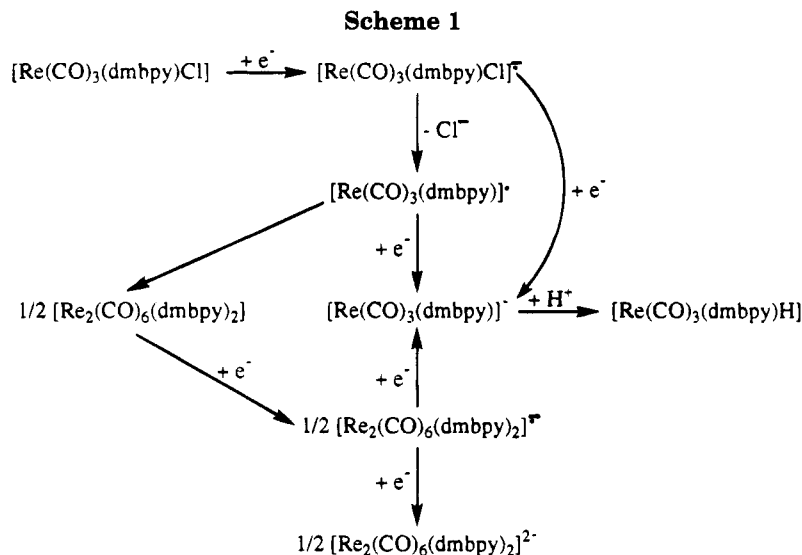
and ESR spectroscopy.^{3a,c,d} It has been established that the one-electron reduction of $[\text{Re}(\text{CO})_3(\alpha\text{-diimine})\text{L}']$ (L'

(2) (a) Hawecker, J.; Lehn, J. M.; Ziessel, R. *J. Chem. Soc., Chem. Commun.* **1983**, 536. (b) Hawecker, J.; Lehn, J. M.; Ziessel, R. *J. Chem. Soc., Chem. Commun.* **1984**, 328. (c) Sullivan, B. P.; Meyer, T. J. *J. Chem. Soc., Chem. Commun.* **1984**, 1244. (d) Sullivan, B. P.; Bolinger, C. M.; Conrad, D.; Vining, W. J.; Meyer, T. J. *J. Chem. Soc., Chem. Commun.* **1985**, 1414. (e) Kutal, C.; Weber, M. A.; Ferraudi, G.; Geiger, D. *Organometallics* **1985**, *4*, 2161. (f) Breikss, A. J.; Abruña, H. D. *J. Electroanal. Chem.* **1986**, *201*, 347. (g) Sullivan, B. P.; Meyer, T. J. *Organometallics* **1986**, *5*, 1500. (h) Hawecker, J.; Lehn, J. M.; Ziessel, R. *Helv. Chim. Acta* **1986**, *69*, 1990. (i) Cabrera, C. R.; Abruña, H. D. *J. Electroanal. Chem.* **1986**, *209*, 101. (j) Kutal, C.; Corbin, J.; Ferraudi, G. *Organometallics* **1987**, *6*, 553. (k) O'Toole, T. R.; Sullivan, B. P.; Bruce, M. R. M.; Margerum, L. D.; Murray, R. W.; Meyer, T. J. *J. Electroanal. Chem.* **1989**, *259*, 217. (l) Sullivan, B. P.; Bruce, M. R. M.; O'Toole, T. R.; Bolinger, C. M.; Megehee, E.; Thorp, H.; Meyer, T. J. In *Catalytic Activation of Carbon Dioxide*; Ayers, W. M., Ed.; A. C. S. Symp. Ser. 363; The American Chemical Society: Washington, DC, 1988. (m) Calzaferri, G.; Hadener, K.; Li, J. *J. Photochem. Photobiol. A: Chem.* **1992**, *64*, 259. (n) Shu, C.-F.; Wrighton, M. S. Unpublished work.

(3) (a) Kaim, W.; Kohlmann, S. *Chem. Phys. Lett.* **1987**, *139*, 365. (b) Kaim, W.; Kramer, H. E. A.; Vogler, C.; Rieker, J. *J. Organomet. Chem.* **1989**, *367*, 107. (c) Kaim, W.; Kohlmann, S. *Inorg. Chem.* **1990**, *29*, 2909. (d) Vogler, C. Thesis, Universität Stuttgart, 1990.

[®] Abstract published in *Advance ACS Abstracts*, February 1, 1995.

(1) See for example: (a) Luong, J. C.; Nadjo, L.; Wrighton, M. S. *J. Am. Chem. Soc.* **1978**, *100*, 5790. (b) Stufkens, D. *J. Comments Inorg. Chem.* **1992**, *13*, 359 and references therein. (c) Yoon, D. I.; Berg-Brennan, C. A.; Lu, H.; Hupp, J. T. *Inorg. Chem.* **1992**, *31*, 3192.



= halide) is exclusively localized on the α -diimine ligand, while in the subsequent one-electron reduction the Re center might also be involved. For $[\text{Re}(\text{CO})_3(\text{bpy})\text{Cl}]$, a full description of the reduction pathways has been proposed,^{2f,k} which is mainly based on the data obtained by cyclic voltammetry. Quite recently, an analogous reaction sequence for $[\text{Re}(\text{CO})_3(\text{dmbpy})\text{Cl}]$ (dmbpy = 4,4'-dimethyl-2,2'-bipyridine) has been reported by Christensen et al.⁴ They followed for the first time the redox behavior of $[\text{Re}(\text{CO})_3(\text{dmbpy})\text{Cl}]$ by means of in situ FTIR reflection spectroscopy. In this way they were able to identify all reduction intermediates and products involved, as summarized in Scheme 1. The results obtained from these studies have clearly shown that the one-electron reduction of the bpy or dmbpy ligand in $[\text{Re}(\text{CO})_3(\alpha\text{-diimine})\text{L}']$ results in the fast dissociation of the halide ligand L' .

Vogler et al.^{3d} have demonstrated for another series of $[\text{Re}(\text{CO})_3(\alpha\text{-diimine})\text{L}']$ ($\text{L}' = \text{Cl}^-, \text{Br}^-$) complexes that the labilization of the halide ligand upon the one-electron reduction, as studied by cyclic voltammetry and in situ ESR spectroscopy, depends strongly on the π -acceptor properties of the α -diimine ligand and the character of the halide ligand itself. Thus, in the $[\text{Re}(\text{CO})_3(\alpha\text{-diimine})\text{L}']^{\bullet+}$ radical complexes, Br^- was more readily replaced by donor-solvent molecules (THF, MeCN) or by PPh_3 than Cl^- . In addition, the rate of this substitution reaction appeared to decrease significantly with increasing π -acceptor ability of the α -diimine ligand.

In this paper, we report electrochemical data for a representative series of complexes $[\text{Re}(\text{CO})_3(\alpha\text{-diimine})\text{L}']^{0/+}$ ($\text{L}' = \text{Cl}^-, \text{Br}^-, \text{I}^-, \text{Otf}^-$, donor solvent molecule, PR_3 ; α -diimine = 2,2'-bipyridine (bpy), pyridine-2-carbaldehyde *N*-isopropylimine (*i*-Pr-PyCa), 2,6-diacetylpyridine bis(anil) (dapa), 2,3-di(2-pyridyl)pyrazine (dpp), azo-2,2'-bipyridine (abpy)). These complexes were carefully chosen with the aim to vary systematically the influence of both the α -diimine and L' ligands on the reduction routes, and to investigate trends in the stability and the spectroscopic properties of the reduction products. The individual one-electron reduction steps and the following homogeneous reactions were

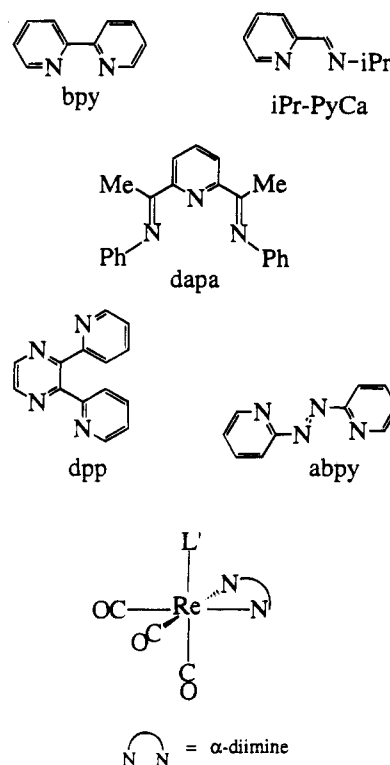


Figure 1. Structures of the α -diimine ligands and the general molecular geometry of the $[\text{Re}(\text{CO})_3(\alpha\text{-diimine})\text{L}']^{0/+}$ complexes.

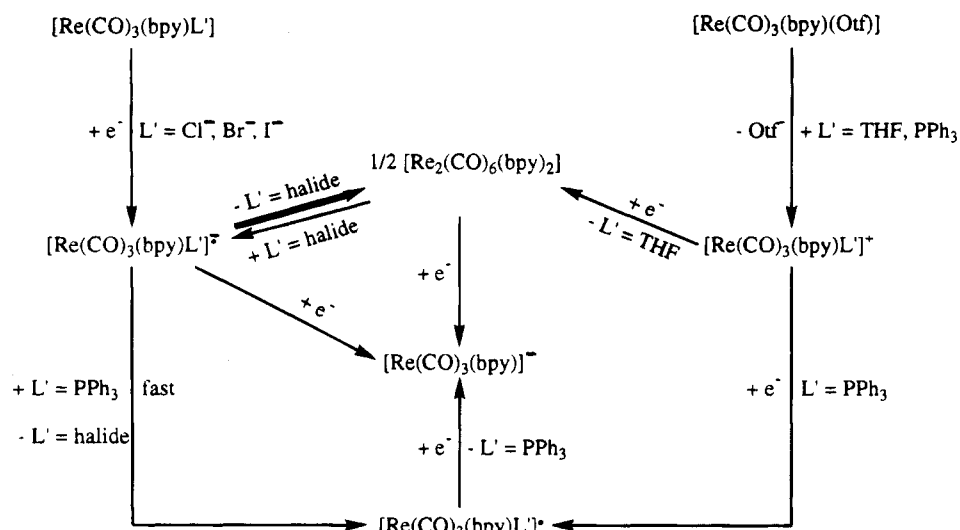
studied by conventional cyclic voltammetry and, for the spectroscopic characterization, by FTIR and UV/vis spectroelectrochemistry, performed in air-tight optically transparent thin-layer electrochemical (OTTLE) cells. The complexes studied are $[\text{Re}(\text{CO})_3(\text{bpy})\text{L}']^{0/+}$ ($\text{L}' = \text{Cl}^-, \text{Br}^-, \text{I}^-, \text{Otf}^-$, THF, PPh_3), $[\text{Re}(\text{CO})_3(\text{i-Pr-PyCa})\text{L}']^{0/+}$ ($\text{L}' = \text{Br}^-, \text{Otf}^-$, THF, *n*-PrCN, PPh_3), $[\text{Re}(\text{CO})_3(\text{dpp})\text{Br}]$, $[\text{Re}(\text{CO})_3(\text{abpy})\text{L}']^{0/+}$ ($\text{L}' = \text{Br}^-, \text{Otf}^-$, THF, PPh_3), and $[\text{Re}(\text{CO})_3(\text{N,N-dapa})\text{L}']^{0/+}$ ($\text{L}' = \text{Br}^-, \text{Otf}^-$, THF, MeCN, *n*-PrCN, PPh_3 , $\text{P}(\text{OMe})_3$). The structures of the α -diimine ligands and the complexes $[\text{Re}(\text{CO})_3(\alpha\text{-diimine})\text{L}']^{0/+}$ are schematically depicted in Figure 1.

Experimental Section

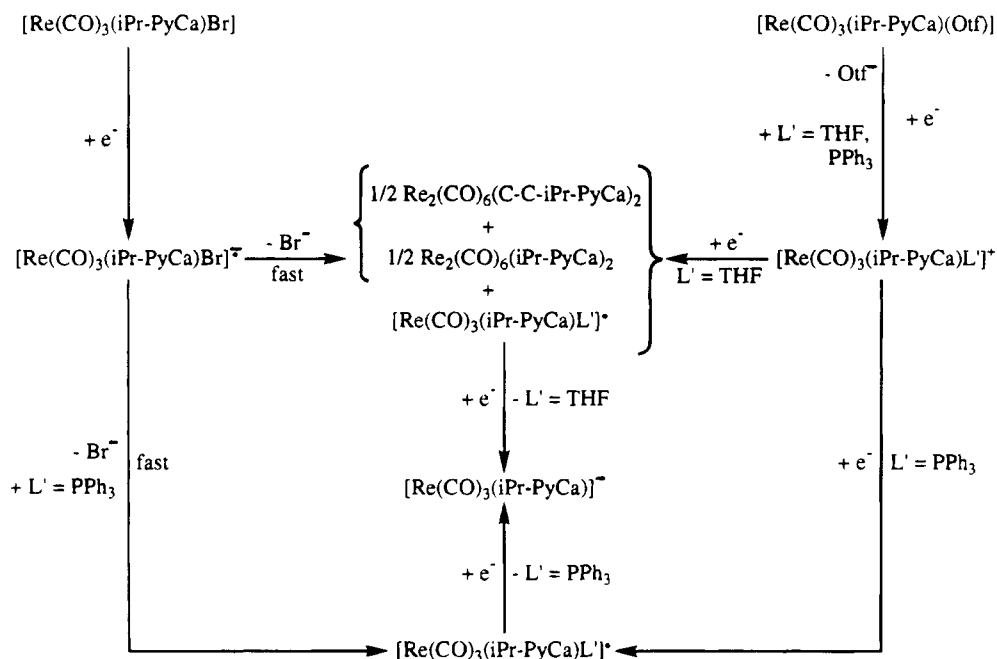
Materials and Preparations. Tetrahydrofuran (THF, Janssen) and acetonitrile (MeCN, Janssen) were distilled from

(4) Christensen, P.; Hamnett, A.; Muir, A. V. G.; Timney, J. A. *J. Chem. Soc., Dalton Trans.* **1992**, 1455.

Scheme 2



Scheme 3



a Na/benzophenone mixture and from P_2O_5 , respectively, under a nitrogen atmosphere. Butyronitrile (*n*-PrCN, Aldrich) was distilled from CaH_2 prior to use. The supporting electrolyte Bu_4NPF_6 (Fluka) was dried overnight under vacuum at 80°C . $\text{P}(\text{OMe})_3$ was distilled under vacuum from CaH_2 . Ferrocene (Fc) (BDH), bpy (Merck), dpp, PPh_3 , and Ag^+Otf^- ($\text{Otf}^- = \text{CF}_3\text{SO}_3^-$) (all Aldrich) were used as received.

The ligands *i*-Pr-PyCa,⁵ dapa,⁶ and abpy⁷ were synthesized according to literature procedures. The $[\text{Re}(\text{CO})_3(\alpha\text{-diimine})\text{(halide)}]$ complexes ($\alpha\text{-diimine} = \text{bpy},^8 \text{ } i\text{-Pr-PyCa},^8 \text{ dapa}^9$) were prepared as previously described, with the modification that the reactions were performed by refluxing the components in toluene for 3 h. The synthesis of the $[\text{Re}(\text{CO})_3(\text{dpp})\text{Br}]$ complex

was performed following reported methods.¹⁰ For the synthesis of $[\text{Re}(\text{CO})_3(\text{abpy})\text{Br}]$ the same procedure was followed as for the dinuclear $\{[\text{Re}(\text{CO})_3\text{Br}]_2(\mu\text{-abpy})\}$ species, except that a molar ratio $[\text{Re}(\text{CO})_5\text{Br}]/\text{abpy}$ of 1:3 was used in order to favor the formation of the mononuclear species. All the $[\text{Re}(\text{CO})_3(\alpha\text{-diimine})\text{(halide)}]$ complexes were purified by column chromatography on Silica 60, activated by heating overnight under vacuum at 150°C , with gradient elution of *n*-hexane/THF. The $[\text{Re}(\text{CO})_3(\alpha\text{-diimine})\text{(Otf)}]$ complexes were synthesized according to literature procedures,^{2c} except that Ag^+Otf^- instead of H^+Otf^- was used as a reactant. All electrochemical and spectroelectrochemical samples were degassed by several freeze-pump-thaw cycles and handled carefully under a nitrogen atmosphere.

Spectroscopic Measurements and Instrumentation.

IR spectra were measured on a Bio-Rad FTS-7 FTIR spectrometer (five scans, resolution 2 cm^{-1}). Electronic absorption spectra were recorded on a Perkin-Elmer Lambda 5 UV/vis spectrophotometer, equipped with a 3600 data station. For IR and UV/vis spectroelectrochemical experiments at room

(5) Bock, H.; tom Dieck, H. D. *Chem. Ber.* **1967**, *100*, 228.
 (6) (a) Alyea, E. C.; Merrel, P. H. *Syn. React. Inorg. Metalorg. Chem.* **1974**, *4*, 535. (b) Lavery, A.; Nelson, S. M. *J. Chem. Soc., Dalton Trans.* **1984**, 615.

(7) Kirpal, A.; Reiter, L. *Ber. Dtsch. Chem. Ges.* **1927**, *60*, 664.
 (8) Staal, L. H.; Oskam, A.; Vrieze, K. *J. Organomet. Chem.* **1979**, *170*, 235.

(9) Albon, J. M.; Edwards, D. A.; Moore, P. J. *Inorg. Chim. Acta* **1989**, *159*, 19.

(10) Ruminski, R.; Cambron, R. T. *Inorg. Chem.* **1990**, *29*, 1575.

Table 1. CO-Stretching Frequencies of [Re(CO)₃(α-diimine)L'] (L' = Cl⁻, Br⁻, I⁻, Otf⁻; α-Diimine = bpy, *i*-Pr-PyCa) and Their Reduction Products in THF, unless Stated Otherwise

complex	$\nu(\text{CO})$ (cm ⁻¹)	k_{av} (Nm ⁻¹)
[Re(CO) ₃ (bpy)Cl]	2019 s, 1917 s, 1895 s	1527
[Re(CO) ₃ (bpy)Br]	2019 s, 1919 s, 1895 s	1528
[Re(CO) ₃ (bpy)I]	2020 s, 1921 s, 1900 s	1532
[Re(CO) ₃ (bpy)(Otf)]	2034 s, 1930 s, 1914 s	1551
[Re(CO) ₃ (bpy)(THF)] ⁺	2019 s, 1917 s, 1894 s	1526
[Re(CO) ₃ (bpy)(PPh ₃)] ⁺	2037 s, 1950 s, 1922 s	1568
[Re(CO) ₃ (bpy)Cl] ⁻	1996 s, 1883 s, 1868 s	1483
[Re(CO) ₃ (bpy)Br] ⁻	1997 s, 1888 s, 1867 s	1486
[Re(CO) ₃ (bpy)I] ⁻	1995 s, 1889 s, 1866 s	1485
[Re(CO) ₃ (bpy)(PPh ₃)] ⁻	2015 s, 1919 s, 1892 s	1524
[Re ₂ (CO) ₆ (bpy) ₂]	1988 s, 1951 s, 1887 s	
	1859 s	
[Re(CO) ₃ (bpy)] ⁻	1947 m, 1843 s, br	1425
[Re(CO) ₃ (<i>i</i> -Pr-PyCa)Br]	2020 s, 1919 s, 1897 s	1529
[Re(CO) ₃ (<i>i</i> -Pr-PyCa)(Otf)]	2034 s, 1934 s, 1912 s	1552
[Re(CO) ₃ (<i>i</i> -Pr-PyCa)(THF)] ⁺	2020 s, 1919 s, 1896 s	1529
[Re(CO) ₃ (<i>i</i> -Pr-PyCa)(<i>n</i> -PrCN)] ⁺ ^b	2036 s, 1930 s, br	1561
[Re(CO) ₃ (<i>i</i> -Pr-PyCa)(PPh ₃)] ⁺	2037 s, 1951 s, 1923 s	1569
[Re(CO) ₃ (<i>i</i> -Pr-PyCa)Br] ⁻	1994 s, 1875 s, 1849 s	1469
[Re(CO) ₃ (<i>i</i> -Pr-PyCa)(THF)] ⁻	1995 s, 1875 s, 1851 s	1470
[Re(CO) ₃ (<i>i</i> -Pr-PyCa)(<i>n</i> -PrCN)] ^{-b}	2005 s, 1886 s, br	1499
[Re(CO) ₃ (<i>i</i> -Pr-PyCa)(PPh ₃)] ⁻	2011 s, 1914 s, 1887 s	1517
[Re ₂ (CO) ₆ (<i>i</i> -Pr-PyCa) ₂] ^c	1984 s	
[Re ₂ (CO) ₆ (C-C- <i>i</i> -Pr-PyCa) ₂] ^a	2014 s, 1993 s, 1907 m, 1890 vs, 1871 s	
[Re ₂ (CO) ₆ (C-C- <i>i</i> -Pr-PyCa) ₂] ^{a,b}	2017 s, 1994 s, 1913 m, 1893 vs, 1874 sh	
[Re(CO) ₃ (<i>i</i> -Pr-PyCa)] ⁻	1948 m, 1840 s, br	1422
[Re(CO) ₃ (<i>i</i> -Pr-PyCa)] ^{-b}	1946 m, 1845 s, br	1426
[Re(CO) ₃ (<i>i</i> -Pr-PyCa)(<i>n</i> -PrCN)] ^{-b,c}	1980 m	

^a The imine-carbon atoms of the *i*-Pr-PyCa ligands are coupled. ^b In *n*-PrCN at room temperature. ^c Other $\nu(\text{CO})$ bands could not be observed.

temperature an OTTLE cell¹¹ was used, equipped with a Pt-minigrid working electrode (32 wires/cm). Spectroelectrochemistry at low temperature was performed in a homemade cryostated OTTLE cell, which has been described in detail elsewhere.¹² Either NaCl or CaF₂ windows were utilized for IR OTTLE measurements and CaF₂ or quartz windows were employed for UV/vis OTTLE measurements. The working electrode surroundings were carefully masked to avoid the spectral beam passing through the nonelectrolyzed solution. Cyclic voltammetry and controlled-potential electrolyses within the OTTLE cell were carried out by using a PAR Model 174 potentiostat. For all spectroelectrochemical samples, the concentrations of [Re(CO)₃(α-diimine)L']^{0/+} and Bu₄NPF₆ were 10⁻² M and 3 × 10⁻¹ M, respectively. Cyclic voltammograms were recorded under the following conditions: 10⁻³ M [Re(CO)₃(α-diimine)L']^{0/+} in THF in the presence of 10⁻¹ M Bu₄NPF₆, Pt disk electrode of 0.8 mm² area. All potentials are reported with respect to the standard¹³ ferrocene/ferrocenium (Fc/Fc⁺) couple.

Results

IR Spectroelectrochemistry. All [Re(CO)₃(α-diimine)L']^{0/+} complexes studied undergo two subsequent reduction steps which may be followed by secondary chemical reactions (see Schemes 2–6). Infrared spectra of the reduction products were investigated in the CO-stretching region, and the frequencies are summarized in Tables 1–3. Reduction of the carbonyl complexes will be accompanied by a lowering of the stretching frequen-

Table 2. CO-Stretching Frequencies of [Re(CO)₃(α-diimine)L'] (L' = , Br⁻, Otf⁻; α-Diimine = dpp, abpy) and Their Reduction Products in THF

complex	$\nu(\text{CO})$ (cm ⁻¹)	k_{av} (Nm ⁻¹)
[Re(CO) ₃ (dpp)Br]	2023 s, 1924 s, 1903 s	1537
[Re(CO) ₃ (dpp)Br] ⁻	2000 s, 1891 s, 1875 s	1493
[Re(CO) ₃ (dpp)(THF)] ⁻	2008 s, 1898 s, 1881 s	1504
[Re(CO) ₃ (dpp)(PPh ₃)] ⁻	2014 s, 1922 s, 1896 s	1527
[Re(CO) ₃ (dpp)] ⁻	1960 m, 1855 s, br	1444
[Re(CO) ₃ (abpy)Br]	2028 s, 1943 s, 1917 s	1556
[Re(CO) ₃ (abpy)(Otf)] ⁻	2039 s, 1953 s, 1928 s	1573
[Re(CO) ₃ (abpy)(THF)] ⁺	2026 s, 1941 s, 1915 s	1553
[Re(CO) ₃ (abpy)(PPh ₃)] ⁺	2044 s, 1972 s, 1946 s	1596
[Re(CO) ₃ (abpy)Br] ⁻	2004 s, 1900 s, 1871 s	1498
[Re(CO) ₃ (abpy)(THF)] ⁻	2017 s, 1915 s, 1893 s	1524
[Re(CO) ₃ (abpy)(PPh ₃)] ⁻	2019 s, 1934 s, 1896 s	1536
[Re(CO) ₃ (abpy)(THF)] ⁻	1984 s, 1880 s, 1854 s	1468
[Re(CO) ₃ (abpy)(PPh ₃)] ⁻	1991 s, 1891 s, 1860 s	1481
{[Re(CO) ₃ (abpy)] ^{2-••} ·THF}	1966 s, 1845 s, 1807 s	1418
{[Re(CO) ₃ (abpy)] ^{2-••} ·PPh ₃ }	1970 s, 1840 s, 1813 s	1421

cies and force constants of the CO ligands in the products. In particular, the changes in force constants along the redox series are good indicators of the changing donor/acceptor character of the α-diimine ligand. The CO-stretching vibrations of the mononuclear tricarbonyl complexes, having C_s symmetry, are described by four C≡O force constants, viz. k_{ax} , k_{eq} , $k_{\text{ax,eq}}$, and $k_{\text{eq,eq}}$. These force field parameters can only be calculated, using the Cotton-Kraihanzel Energy Factored Force Fields method,^{14a,b} when the frequencies of the ¹³CO-enriched positional isotopomers are also known.^{14c} This allows then the correct assignment of the two low-frequency $\nu(\text{CO})$ bands to the A'' and (A')₂ normal vibrational modes for all members of a redox series. The empirical method by Timney^{14d} requires knowledge of the geometry of the complexes which may vary appreciably, see e.g. the formation of pentacoordinated species [Re(CO)₃(α-diimine)]⁻ (vide infra). Therefore, only the average C≡O force constants k_{av} ^{14e} were calculated according to eq 1 (see Tables 1–3) and employed in a qualitative discussion of the electronic effects:

$$k_{\text{av}} = 4.0383 \times 10^{-4} \frac{\sum_i g_i \nu_i^2}{\sum_i g_i} \quad (1)$$

where g_i is the degeneracy of the *i*th CO-stretching mode, of frequency ν_i (cm⁻¹).

A lowering of k_{av} as a result of the reduction means that the Re→CO π-back-bonding increased. This clearly indicates that the added electrons are at least partly delocalized within the Re-(α-diimine) chelate ring, which in turn increases the electron density on the Re center. The delocalization plays an important role for the stability and composition of the reduction products and depends considerably on the varying π-acceptor/σ,π-donor properties of the α-diimine ligands under study (vide infra).

One-Electron Reduction of [Re(CO)₃(α-diimine)-L'] (α-Diimine = bpy, L' = Cl⁻, Br⁻, I⁻; α-Diimine = *i*-Pr-PyCa, dpp, abpy, L' = Br⁻) in THF. One-electron reduction of [Re(CO)₃(bpy)Br] in THF/Bu₄NPF₆

(11) Krejčík, M.; Daněk, M.; Hartl, F. *J. Electroanal. Chem.* **1991**, *317*, 179.

(12) Hartl, F.; Luyten, H.; Schoemaker, G. C. *Appl. Spectrosc.* **1995**, in press.

(13) Gritzner, G.; Kuta J. *Pure Appl. Chem.* **1984**, *56*, 461.

(14) (a) Cotton, F. A.; Kraihanzel, C. S. *J. Am. Chem. Soc.* **1962**, *84*, 4432. (b) Kraihanzel, C. S.; Cotton, F. A. *Inorg. Chem.* **1963**, *2*, 533. (c) Turner, J. J.; Grevels, F. W.; Howdle, S. M.; Jacke, J.; Haward, M. T.; Klotzbücher, W. E. *J. Am. Chem. Soc.* **1991**, *113*, 8347. (d) Timney, J. A. *Inorg. Chem.* **1979**, *18*, 2502. (e) Braterman, P. S. *Metal Carbonyl Spectra*; Academic Press: London, 1975; p 36.

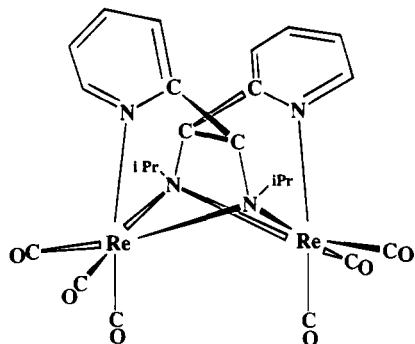


Figure 2. Structure of the C–C-coupled dimer $[\text{Re}_2(\text{CO})_6(\text{C-C-}i\text{-Pr-PyCa})_2]$.¹⁶

at 293 K afforded the radical anion $[\text{Re}(\text{CO})_3(\text{bpy})\text{Br}]^-$ ($\nu(\text{CO})$ at 1997, 1888, and 1867 cm^{-1})⁴ only in very low yield. The formation of the closely related radical $[\text{Re}(\text{CO})_3(\text{bpy})(\text{THF})]$ can be excluded here since this radical appeared to be very unstable when formed by one-electron reduction of $[\text{Re}(\text{CO})_3(\text{bpy})(\text{THF})]^+$ (vide infra). The second, major product formed upon reduction of $[\text{Re}(\text{CO})_3(\text{bpy})\text{Br}]$ was identified as the metal–metal-bonded dimer $[\text{Re}_2(\text{CO})_6(\text{bpy})_2]$ ($\nu(\text{CO})$ at 1988, 1951, 1887, and 1859 cm^{-1} ; UV/vis $\lambda_{\text{max}} = 805, 600, 470 \text{ nm}$), in accordance with literature data.^{1f,h,i,15} The concentration of $[\text{Re}(\text{CO})_3(\text{bpy})\text{Br}]^-$ gradually decreased in the course of the electrolysis. Most probably, the radical anion lost Br^- and transformed into $[\text{Re}_2(\text{CO})_6(\text{bpy})_2]$.

One-electron reduction of the complexes $[\text{Re}(\text{CO})_3(\text{bpy})\text{Cl}]$ and $[\text{Re}(\text{CO})_3(\text{bpy})\text{I}]$ also gave $[\text{Re}_2(\text{CO})_6(\text{bpy})_2]$ as the main product, together with a small amount of $[\text{Re}(\text{CO})_3(\text{bpy})\text{Cl}]^-$ ($\nu(\text{CO})$ at 1996, 1883, and 1868 cm^{-1}) and $[\text{Re}(\text{CO})_3(\text{bpy})\text{I}]^-$ ($\nu(\text{CO})$ at 1995, 1889, and 1866 cm^{-1}), respectively. From the radical anions $[\text{Re}(\text{CO})_3(\text{bpy})\text{L}]^-$, the Cl derivative appeared to be most stable and could be generated at much higher concentration than the corresponding Br and I complexes under identical conditions. A similar trend has been observed for the closely related $[\text{Re}(\text{CO})_3(\text{dab})\text{L}]^-$ ($\text{L}' = \text{Cl}^-, \text{Br}^-$) species.^{3d}

One-electron reduction of $[\text{Re}(\text{CO})_3(i\text{-Pr-PyCa})\text{Br}]$ in THF yielded both $[\text{Re}(\text{CO})_3(i\text{-Pr-PyCa})\text{Br}]^-$ ($\nu(\text{CO})$ at 1994, 1875, and 1849 cm^{-1}) and the metal–metal-bonded dimer $[\text{Re}_2(\text{CO})_6(i\text{-Pr-PyCa})_2]$ ($\nu(\text{CO})$ at 1984 cm^{-1} , other bands obscured; UV/vis $\lambda_{\text{max}} = 785 \text{ nm}$) only as minor products. Instead, a novel complex was obtained with $\nu(\text{CO})$ bands at 2014, 1993, 1907, 1890, and 1871 cm^{-1} . Quite recently, this product has been isolated and structurally characterized by X-ray diffraction.¹⁶ It appeared to be a C–C-coupled dimer containing two $\text{Re}(\text{CO})_3(i\text{-Pr-PyCa})$ fragments and no Re–Re bond. The imine nitrogen atoms of the two $i\text{-Pr-PyCa}$ ligands have adopted a bridging coordination to the two Re centers and the imine carbon atoms of these two ligands are coupled (see Figure 2). The formation of this complex, which will be denoted as $[\text{Re}_2(\text{CO})_6(\text{C-C-}i\text{-Pr-PyCa})_2]$, most likely occurs by a radical coupling reaction. A detailed description of its structure will be given in a forthcoming article.¹⁶

One-electron reduction of $[\text{Re}(\text{CO})_3(\text{dpp})\text{Br}]$ in THF (Scheme 4) also led to the formation of the radical

anionic complex $[\text{Re}(\text{CO})_3(\text{dpp})\text{Br}]^-$, as evidenced by its CO-stretching frequencies at 2000, 1891, and 1875 cm^{-1} which closely resemble those of $[\text{Re}(\text{CO})_3(\text{bpy})\text{Br}]^-$ (Table 1). However, contrary to the related bpy and $i\text{-Pr-PyCa}$ complexes, the radical anion did not easily lose Br^- and did not transform into the dimer $[\text{Re}_2(\text{CO})_6(\text{dpp})_2]$. Instead, $[\text{Re}(\text{CO})_3(\text{dpp})\text{Br}]^-$ slowly converted into a new, stable product with $\nu(\text{CO})$ frequencies at 2008, 1898, and 1881 cm^{-1} . These frequencies closely resemble those of the solvated radicals $[\text{Re}(\text{CO})_3(\alpha\text{-diimine})(\text{THF})]$ ($\alpha\text{-diimine} = i\text{-Pr-PyCa}, \text{abpy}$) (see Tables 1 and 2) and are therefore attributed to $[\text{Re}(\text{CO})_3(\text{dpp})(\text{THF})]$.

In sharp contrast to the above-mentioned complexes, no dissociation of Br^- occurred upon one-electron reduction of $[\text{Re}(\text{CO})_3(\text{abpy})\text{Br}]$ in THF (see Figure 3). The radical anionic product $[\text{Re}(\text{CO})_3(\text{abpy})\text{Br}]^-$ ($\nu(\text{CO})$ at 2004, 1900, and 1871 cm^{-1}) did not decompose at the applied reduction potential of the parent complex even 30 min after the reduction had been completed. It is thus the most stable member of the series of $[\text{Re}(\text{CO})_3(\alpha\text{-diimine})\text{Br}]^-$ complexes under study.

All complexes $[\text{Re}(\text{CO})_3(\alpha\text{-diimine})\text{Br}]$ appeared to be thermally stable in the presence of a 100-fold excess of PPh_3 . However, substitution of Br^- by the better π acceptor PPh_3 was observed upon the one-electron reduction of the parent complexes. The substitution was very fast for $[\text{Re}(\text{CO})_3(\text{bpy})\text{Br}]^-$ since this radical anion was formed in the course of the electrolysis only as a minor product with a very weak $\nu(\text{CO})$ band at 1997 cm^{-1} (Table 1). The main product was identified as the radical $[\text{Re}(\text{CO})_3(\text{bpy})(\text{PPh}_3)]$ ($\nu(\text{CO})$ at 2017, 1918, and 1894 cm^{-1}) by the close similarity of its $\nu(\text{CO})$ frequencies with those of $[\text{Mn}(\text{CO})_3(\text{bpy})(\text{P}(\text{nBu})_3)]$ at 2012, 1923, and 1891 cm^{-1} .¹⁷ No dimer $[\text{Re}_2(\text{CO})_6(\text{bpy})_2]$ was detected in this case. This observation again illustrates that the Re–Br bond in the reduced complex $[\text{Re}(\text{CO})_3(\text{bpy})\text{Br}]^-$ is strongly labilized. $[\text{Re}(\text{CO})_3(\text{bpy})(\text{PPh}_3)]$ was reoxidized to give initially a product with $\nu(\text{CO})$ bands at 2037, 1950, and 1922 cm^{-1} , which are assigned to the cation $[\text{Re}(\text{CO})_3(\text{bpy})(\text{PPh}_3)]^+$.¹⁸ $[\text{Re}(\text{CO})_3(\text{bpy})(\text{PPh}_3)]^+$ reacted back thermally with Br^- , still present in the solution, to give the parent complex $[\text{Re}(\text{CO})_3(\text{bpy})\text{Br}]$.

In contrast to this, the conversion of the initially generated radical anions $[\text{Re}(\text{CO})_3(\text{dpp})\text{Br}]^-$ and, in particular, $[\text{Re}(\text{CO})_3(\text{abpy})\text{Br}]^-$ into the radicals $[\text{Re}(\text{CO})_3(\text{dpp})(\text{PPh}_3)]$ ($\nu(\text{CO})$ at 2014, 1922, and 1896 cm^{-1}) and $[\text{Re}(\text{CO})_3(\text{abpy})(\text{PPh}_3)]$ ($\nu(\text{CO})$ at 2019, 1934, and 1896 cm^{-1}) was a very slow process which required typically more than 10 min for its completion.

One-Electron Reduction of $[\text{Re}(\text{CO})_3(\alpha\text{-diimine})\text{L}]$ ($\alpha\text{-Diimine} = \text{bpy}, i\text{-Pr-PyCa}, \text{abpy}, \text{L}' = \text{Otf}^-$). One-electron reduction of the complexes $[\text{Re}(\text{CO})_3(\alpha\text{-diimine})(\text{Otf})]$ with the weakly coordinated Otf^- (CF_3SO_3^-) ligand was studied by IR spectroelectrochemistry with the aim to provide more evidence for correct assignment of the various reduction products obtained from the secondary chemical reactions of the radical anions $[\text{Re}(\text{CO})_3(\alpha\text{-diimine})\text{Br}]^-$ (vide supra). This strategy was particularly helpful in those cases where the

(15) Servaas, P. C.; Stor, G. J.; Stufkens, D. J.; Oskam, A. *Inorg. Chim. Acta* **1991**, *178*, 185.

(16) Rossenaar, B. D.; Kleverlaan, C.; Stufkens, D. J.; Oskam, A. To be published.

(17) Stor, G. J.; Morrison, S. L.; Stufkens, D. J.; Oskam, A. *Organometallics* **1994**, *13*, 2641.

(18) van Dijk, H. K.; van der Haar, J.; Stufkens, D. J.; Oskam, A. *Inorg. Chem.* **1989**, *28*, 75.

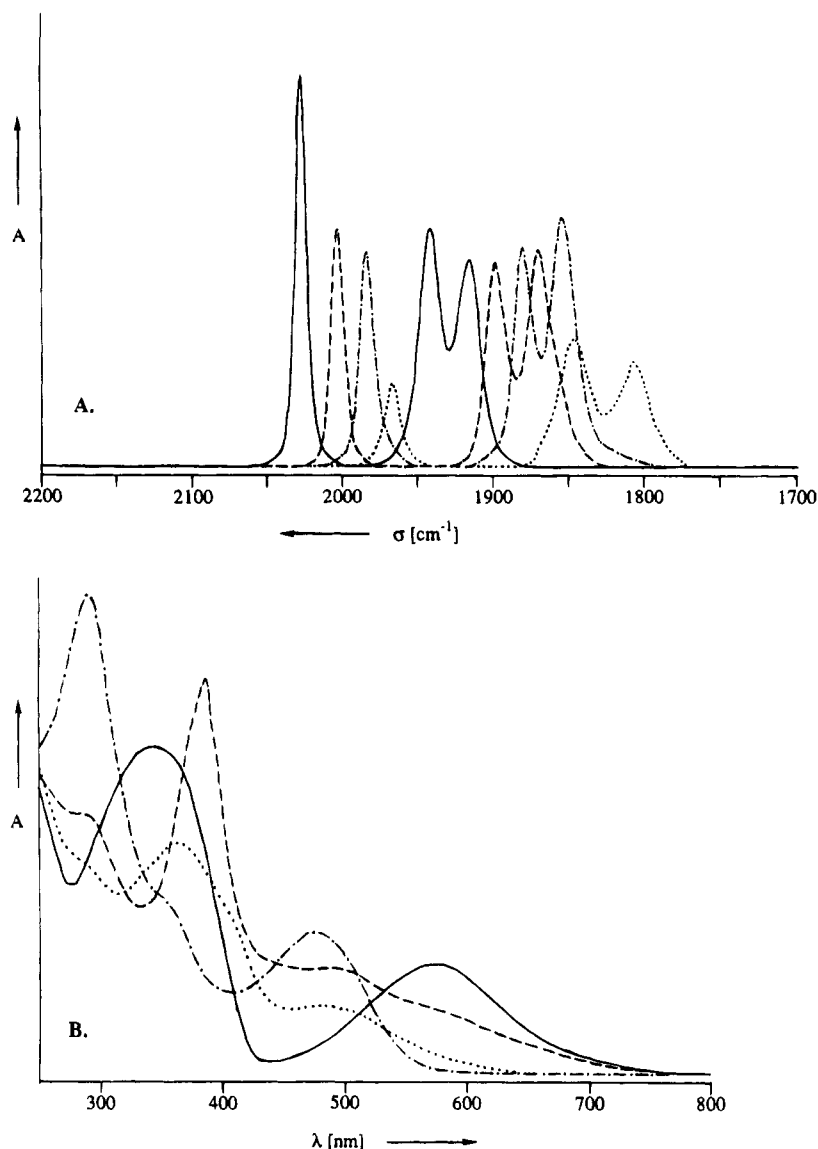
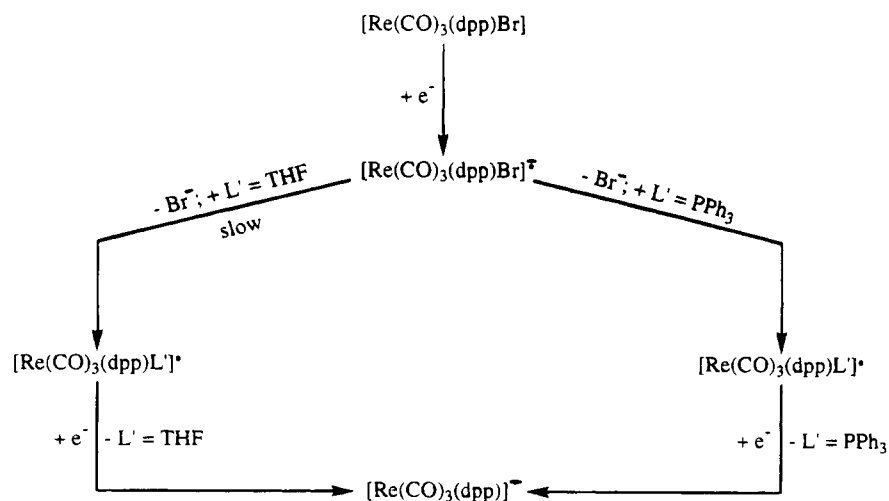


Figure 3. IR (CO-stretching region) (A) and UV/vis (B) spectra of the products formed during the three-step one-electron reduction of $[\text{Re}(\text{CO})_3(\text{abpy})\text{Br}]$ in THF: (—) $[\text{Re}(\text{CO})_3(\text{abpy})\text{Br}]$; (---) $[\text{Re}(\text{CO})_3(\text{abpy})\text{Br}]^{\cdot -}$; (-·-) $[\text{Re}(\text{CO})_3(\text{abpy})(\text{THF})]^{\cdot -}$; (···) $\{[\text{Re}(\text{CO})_3(\text{abpy})]_2^{\cdot -} \cdot \text{THF}\}$.

Scheme 4



dissociation of the Br^- ligand was a slow process, or when the assignment of the $\nu(\text{CO})$ bands was not straightforward due to near coincidence of the $\nu(\text{CO})$

frequencies for different compounds, such as $[\text{Re}(\text{CO})_3(\text{bpy})\text{Br}]/[\text{Re}(\text{CO})_3(\text{bpy})(\text{THF})]^{\cdot -}$ or $[\text{Re}(\text{CO})_3(i\text{-PrPyCa})\text{Br}]/[\text{Re}(\text{CO})_3(i\text{-Pr-PyCa})(\text{THF})]^{\cdot -}$ (Table 1).

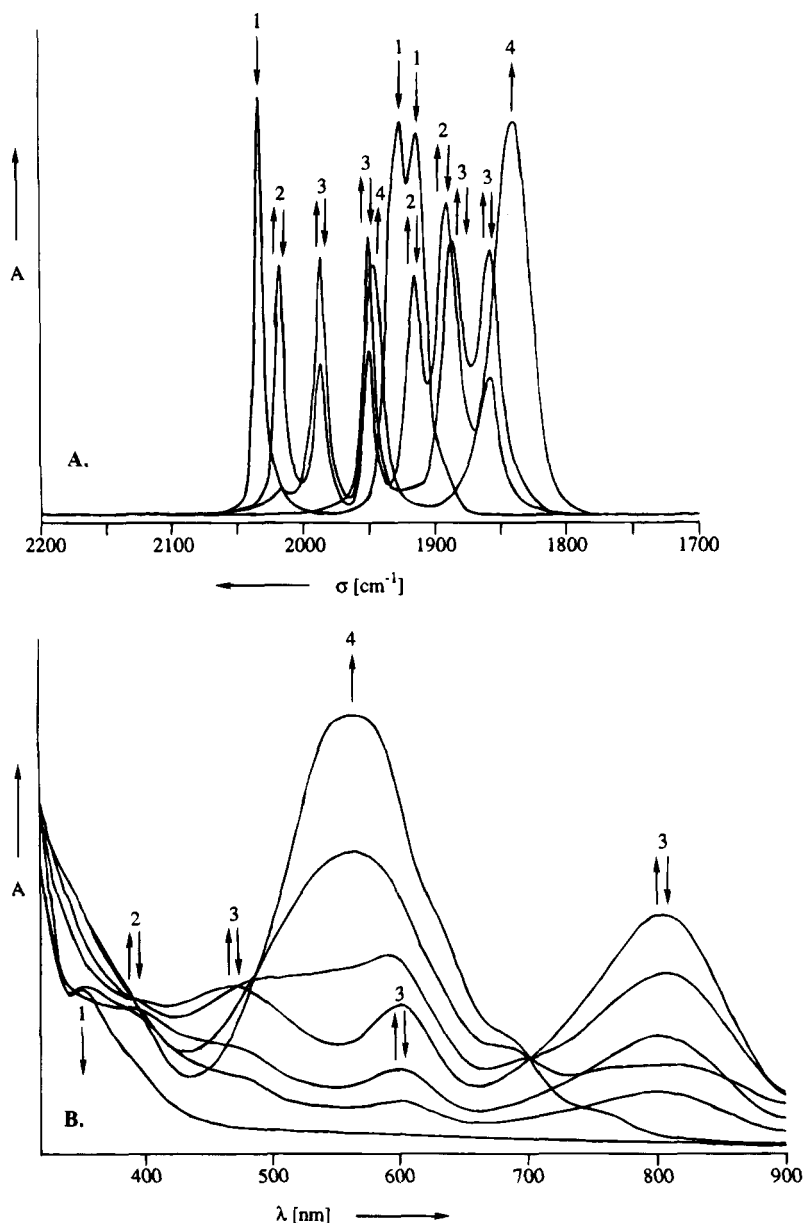


Figure 4. IR (CO-stretching region) (A) and UV/vis (B) spectral changes during two successive one-electron reductions of $[\text{Re}(\text{CO})_3(\text{bpy})(\text{Otf})]$ in THF: (1) $[\text{Re}(\text{CO})_3(\text{bpy})(\text{Otf})]$; (2) $[\text{Re}(\text{CO})_3(\text{bpy})(\text{THF})]^+$; (3) $[\text{Re}_2(\text{CO})_6(\text{bpy})_2]$; (4) $[\text{Re}(\text{CO})_3(\text{bpy})]^-$.

All complexes $[\text{Re}(\text{CO})_3(\alpha\text{-diimine})(\text{Otf})]$ ($\alpha\text{-diimine} = \text{bpy}, i\text{-Pr-PyCa}, \text{abpy}$) (Tables 1 and 2) were transformed already at the onset of the one-electron reduction in THF into the cationic complexes $[\text{Re}(\text{CO})_3(\alpha\text{-diimine})(\text{THF})]^+$ (see Figure 4A). Similarly, the cations $[\text{Re}(\text{CO})_3(\alpha\text{-diimine})(\text{PPh}_3)]^+$ were obtained in the presence of a 100-fold excess of PPh_3 in THF. For example, the corresponding thermal substitution of Otf^- by THF or PPh_3 in the complex $[\text{Re}(\text{CO})_3(\text{bpy})(\text{Otf})]$ took several hours at ambient temperature. This electrocatalytic ligand substitution reaction was not further investigated and most likely occurs via the same mechanism as proposed by Kochi et al.¹⁹ for the related electrocatalytic substitution of MeCN in $[(\text{MeCp})\text{Mn}(\text{CO})_2(\text{MeCN})]$ by PR_3 or $\text{P}(\text{OR})_3$. In our case, the radical chain process is initiated by substitution of the labile Otf^- ligand in the reduced complex $[\text{Re}(\text{CO})_3(\alpha\text{-diimine})(\text{Otf})]^-$ by either THF or PPh_3 to give the radicals $[\text{Re}(\text{CO})_3(\alpha\text{-diimine})\text{L}']^{\cdot}$

($\text{L}' = \text{THF}$ or PPh_3). As follows from Table 7, both radicals can transfer the unpaired electron to parent $[\text{Re}(\text{CO})_3(\alpha\text{-diimine})(\text{Otf})]$, by which process they are oxidized to the corresponding cations (the propagation step). The electrocatalytic reaction is terminated by one-electron oxidation of the radicals $[\text{Re}(\text{CO})_3(\alpha\text{-diimine})\text{L}']^{\cdot}$ at the electrode potential applied. The latter, heterogeneous electron transfer at the electrode surface may significantly compete with the homogeneous electron transfer provided that both processes are outer-sphere electron transfers. Since this is likely the case, both, radical chain and electrode mediated,¹⁹ electrocatalytic mechanisms may operate.

One-electron reduction of the cations $[\text{Re}(\text{CO})_3(\alpha\text{-diimine})\text{L}']^+$ ($\alpha\text{-diimine} = \text{bpy}$ (see Figure 4), $i\text{-Pr-PyCa}, \text{abpy}$; $\text{L}' = \text{THF}, \text{PPh}_3$) at a lower electrode potential gave primarily the corresponding radicals $[\text{Re}(\text{CO})_3(\alpha\text{-diimine})\text{L}']^{\cdot}$ (see Schemes 2, 3, and 5 and Tables 1 and 2). The radicals $[\text{Re}(\text{CO})_3(\alpha\text{-diimine})(\text{PPh}_3)]^{\cdot}$ were formed as single, stable species. Contrary to this, stable

(19) Hershberger, J. W.; Klingler, R. J.; Kochi, J. K. *J. Am. Chem. Soc.* **1983**, *105*, 61.

radicals $[\text{Re}(\text{CO})_3(\alpha\text{-diimine})(\text{THF})]^\cdot$ were obtained only for the abpy and dpp (see above, and Scheme 4) complexes. $[\text{Re}(\text{CO})_3(\text{bpy})(\text{THF})]^\cdot$ converted to the dimer $[\text{Re}_2(\text{CO})_6(\text{bpy})_2]^\cdot$ as the only detectable product. $[\text{Re}(\text{CO})_3(i\text{-Pr-PyCa})(\text{THF})]^\cdot$ was formed only in low yield, together with a very small amount of the metal-metal-bonded dimer $[\text{Re}_2(\text{CO})_6(i\text{-Pr-PyCa})_2]^\cdot$. The C-C-coupled dimer $[\text{Re}_2(\text{CO})_6(\text{C-C-}i\text{-Pr-PyCa})_2]^\cdot$ (Figure 2) was the main product in this case.

A different reaction sequence was observed for $[\text{Re}(\text{CO})_3(i\text{-Pr-PyCa})(\text{Otf})]^\cdot$ in *n*-PrCN. The complex transformed thermally into a product with $\nu(\text{CO})$ bands at 2036 and 1930 (broad) cm^{-1} . The two lowest frequency $\nu(\text{CO})$ bands coincide. This effect has also been observed for several $[\text{Re}(\text{CO})_3(\alpha\text{-diimine})(\text{MeCN})]^\cdot$ complexes.^{3d} This $\nu(\text{CO})$ pattern is a typical property of $[\text{Re}(\text{CO})_3(\text{N})_3]^\cdot$ complexes, having three N-donor atoms trans to the carbonyls (a local C_{3v} symmetry). Therefore, we identify the product as $[\text{Re}(\text{CO})_3(i\text{-Pr-PyCa})(n\text{-PrCN})]^\cdot$. One-electron reduction of this cation afforded two products in comparable concentrations: the C-C-coupled dimer $[\text{Re}_2(\text{CO})_6(\text{C-C-}i\text{-Pr-PyCa})_2]^\cdot$ and a second complex with $\nu(\text{CO})$ bands at 2005 and 1886 (broad) cm^{-1} . Again on the basis of the broadness of the 1886 cm^{-1} band,^{3d} the latter frequencies are assigned to the $[\text{Re}(\text{CO})_3(i\text{-Pr-PyCa})(n\text{-PrCN})]^\cdot$ radical. Both processes, the thermal conversion of $[\text{Re}(\text{CO})_3(i\text{-Pr-PyCa})(\text{Otf})]^\cdot$ into $[\text{Re}(\text{CO})_3(i\text{-Pr-PyCa})(n\text{-PrCN})]^\cdot$ and the formation of the solvent-stabilized radical $[\text{Re}(\text{CO})_3(i\text{-Pr-PyCa})(n\text{-PrCN})]^\cdot$, show that *n*-PrCN coordinates more strongly to the Re center than THF.

In Situ Electrochemical Generation of Doubly Reduced Anions $[\text{Re}(\text{CO})_3(\alpha\text{-Diimine})]^{2-}$ ($\alpha\text{-Diimine} = \text{bpy}, i\text{-Pr-Pyca}, \text{dpp}$) and $[\text{Re}(\text{CO})_3(\alpha\text{-diimine-}L')^{2-}$ ($\alpha\text{-Diimine} = i\text{-Pr-PyCa}, L' = n\text{-PrCN}; \alpha\text{-Diimine} = \text{abpy}, L' = \text{THF}, \text{PPh}_3$). All singly reduced $\text{Re}(\alpha\text{-diimine})$ complexes, described in the preceding text, could be reduced in a subsequent one-electron, $\alpha\text{-diimine-localized}$ step. The composition of the doubly reduced species was mainly dependent on the particular $\alpha\text{-diimine}$ ligand used (see schemes 2–5 and Figures 3 and 4).

Reduction of $[\text{Re}(\text{CO})_3(\text{bpy})L']^\cdot$ ($L' = \text{Cl}^-, \text{Br}^-, \text{I}^-$), stabilized by an excess of L' in the solution, of the metal-metal-bonded dimer $[\text{Re}_2(\text{CO})_6(\text{bpy})_2]^\cdot$, and of the radical $[\text{Re}(\text{CO})_3(\text{bpy})(\text{PPh}_3)]^\cdot$ produced the same compound possessing $\nu(\text{CO})$ bands at 1947 and 1843 (broad) cm^{-1} (see Figure 4A). These frequencies are assigned to the five-coordinated anionic complex $[\text{Re}(\text{CO})_3(\text{bpy})]^{2-}$, in accordance with previous results obtained by cyclic voltammetry,^{2f,k} with the results of Christensen et al.,⁴ and with its invariable $\nu(\text{CO})$ frequencies, regardless the composition of the parent complexes. Similarly, $[\text{Re}(\text{CO})_3(\text{dpp})]^\cdot$ ($\nu(\text{CO})$ at 1960 and 1855 (broad) cm^{-1}) was obtained by one-electron reduction of both $[\text{Re}(\text{CO})_3(\text{dpp})(\text{THF})]^\cdot$ and $[\text{Re}(\text{CO})_3(\text{dpp})(\text{PPh}_3)]^\cdot$. It should be noted that all reductions were fully chemically reversible. Reoxidation of $[\text{Re}(\text{CO})_3(\text{bpy})]^{2-}$ in THF in the presence of 1 equiv of Br^- led both to $[\text{Re}_2(\text{CO})_6(\text{bpy})_2]^\cdot$ and a small amount of $[\text{Re}(\text{CO})_3(\text{bpy})\text{Br}]^\cdot$. This observation indicates existence of an equilibrium between the two products (see Scheme 2).

The closely related anion $[\text{Re}(\text{CO})_3(i\text{-Pr-PyCa})]^\cdot$ ($\nu(\text{CO})$ at 1948 and 1840 (broad) cm^{-1}) was formed in THF by reduction of $[\text{Re}(\text{CO})_3(i\text{-Pr-PyCa})\text{Br}]^\cdot$, $[\text{Re}(\text{CO})_3(i\text{-Pr-}$

$\text{PyCa})(\text{THF})]^\cdot$ (both generated in low concentration in THF, see above) and the stable radical $[\text{Re}(\text{CO})_3(i\text{-Pr-PyCa})(\text{PPh}_3)]^\cdot$, and of the dimers $[\text{Re}_2(\text{CO})_6(i\text{-Pr-PyCa})_2]^\cdot$ and $[\text{Re}_2(\text{CO})_6(\text{C-C-}i\text{-Pr-PyCa})]^\cdot$. Only in *n*-PrCN, the reduction of $[\text{Re}(\text{CO})_3(i\text{-Pr-PyCa})(n\text{-PrCN})]^\cdot$, present in equilibrium with $[\text{Re}_2(\text{CO})_6(\text{C-C-}i\text{-Pr-PyCa})]^\cdot$ (see above), afforded a small amount of the six-coordinated anion $[\text{Re}(\text{CO})_3(i\text{-Pr-PyCa})(n\text{-PrCN})]^{2-}$ having a weak $\nu(\text{CO})$ band at 1981 cm^{-1} . The lower $\nu(\text{CO})$ frequencies of this anion were obscured by those of dominant $[\text{Re}(\text{CO})_3(i\text{-Pr-PyCa})]^\cdot$ ($\nu(\text{CO})$ at 1946 and 1845 (broad) cm^{-1}). Nevertheless, the assignment of the 1981 cm^{-1} band to $[\text{Re}(\text{CO})_3(i\text{-Pr-PyCa})(n\text{-PrCN})]^{2-}$ is strongly supported by the IR spectra of $[\text{Re}(\text{CO})_3(N,N\text{-dapa})(n\text{-PrCN})]^{2-}$ (see below, Table 3) and $[\text{Re}(\text{CO})_3(\text{bpy})(n\text{-PrCN})]^\cdot$ ($\nu(\text{CO})$ at 1980, 1861, and 1851 cm^{-1}). The latter six-coordinated anion was recently generated²⁰ in high yield in *n*-PrCN at 213 K.

A remarkable difference in behavior upon reduction was observed for the radical complexes containing the abpy ligand. In THF, both stable radicals $[\text{Re}(\text{CO})_3(\text{abpy})\text{Br}]^\cdot$ and $[\text{Re}(\text{CO})_3(\text{abpy})(\text{THF})]^\cdot$ were converted in separate experiments into the same product with three distinct $\nu(\text{CO})$ bands at 1984, 1880, and 1854 cm^{-1} (see Scheme 5 and Figure 3A). In contrast, $[\text{Re}(\text{CO})_3(\text{abpy})(\text{PPh}_3)]^\cdot$ was reduced to give a different species which exhibited $\nu(\text{CO})$ vibrations at 1991, 1891, and 1860 cm^{-1} . The appearance of three new $\nu(\text{CO})$ bands indicates that the doubly reduced complexes have retained a six-coordinated geometry since the related six-coordinated complexes $[\text{Re}(\text{CO})_3(\text{DBCat})L']^{2-}$ ($L' = \text{PPh}_3$)²¹ and adducts $[\text{Mn}(\text{CO})_3(\text{DBCat})]^{2-}L'$ (DBCat = 3,5-di-*tert*-butylcatecholate, $L' = \text{pyridine}, \text{PPh}_3, \text{P}(\text{cHex})_3$)²² also exhibit three well-separated $\nu(\text{CO})$ bands. Up to now, only five-coordinated anions such as $[\text{Mn}(\text{CO})_3(\text{DBCat})]^{2-}$,²² $[\text{W}(\text{CO})_3(\text{DBCat})]^{2-}$,²³ $[\text{Mn}(\text{CO})_3(\text{bpy})]^{2-}$,¹⁷ and $[\text{Re}(\text{CO})_3(\alpha\text{-diimine})]^\cdot$ ($\alpha\text{-diimine} = \text{bpy}, i\text{-Pr-PyCa}, \text{dpp}$) (see Tables 1 and 2) appeared to be characterized by only two $\nu(\text{CO})$ bands. The doubly reduced products are therefore assigned as $[\text{Re}(\text{CO})_3(\text{abpy})(\text{THF})]^{2-}$ and $[\text{Re}(\text{CO})_3(\text{abpy})(\text{PPh}_3)]^{2-}$, respectively.

Contrary to the other complexes, both $[\text{Re}(\text{CO})_3(\text{abpy})(\text{THF})]^\cdot$ and $[\text{Re}(\text{CO})_3(\text{abpy})(\text{PPh}_3)]^\cdot$ could even be reduced in a third one-electron step. The resulting products showed three well-separated CO-stretching vibrations of equal intensities at 1966, 1845, and 1807 cm^{-1} , and at 1970, 1840, and 1813 cm^{-1} , respectively. The small difference between the corresponding average CO force constants k_{av} (see Table 2) implies that the sixth ligand $L' = \text{THF}, \text{PPh}_3$ only weakly interacts with the Re center. Hence, both dianionic complexes are formulated as $\{[\text{Re}(\text{CO})_3(\text{abpy})]^{2-} \cdot L'\}$.

Reduction of $[\text{Re}(\text{CO})_3(N,N\text{-dapa})L']^\cdot$ ($L' = \text{Br}^-, \text{Otf}^-$). In both starting complexes, the dapa ligand is bidentately coordinated to the Re center via the pyridine nitrogen atom and one of the imine nitrogen atoms, as

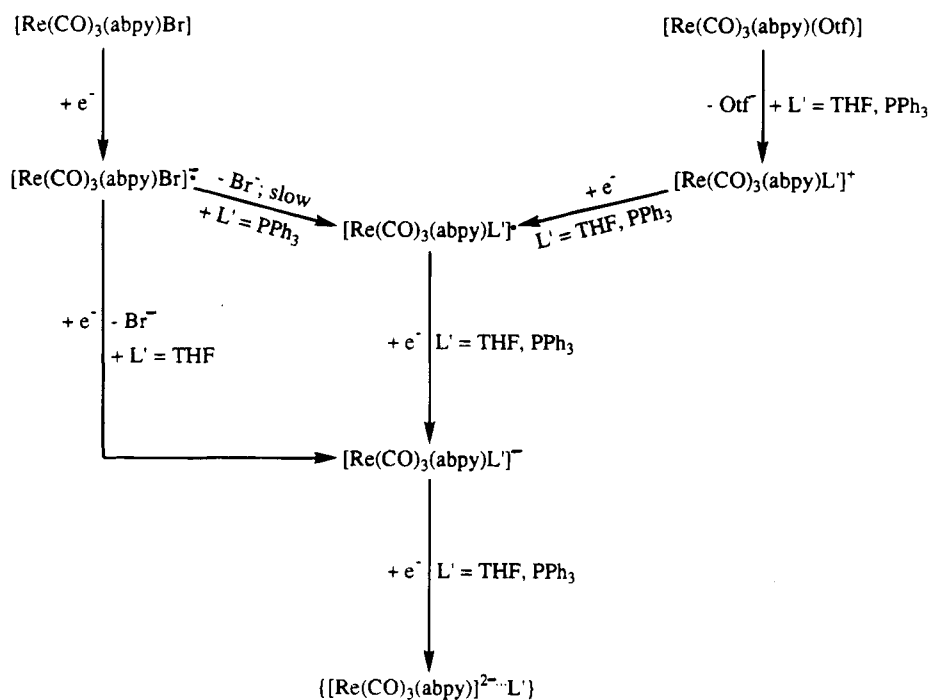
(20) van Outersterp, J. W. M.; Hartl, F.; Stufkens, D. J. *Organometallics* **1995**, in press.

(21) Hartl, F.; Vlček, A., Jr. *Inorg. Chem.* **1992**, *31*, 2869.

(22) Hartl, F.; Stufkens, D. J.; Vlček, A., Jr. *Inorg. Chem.* **1992**, *31*, 1687.

(23) Darensbourg, D. J.; Klausmeyer, K. K.; Mueller, B. L.; Reibenspies, J. H. *Angew. Chem., Int. Ed. Engl.* **1992**, *31*, 1503.

Scheme 5



evidenced by the ^1H NMR spectra.^{9,24e} Contrary to the other complexes discussed so far, this ligand may, however, use its nitrogen-donor sidearm to adopt a tridentate coordination. In order to find out if this property plays an important role in the redox chemistry we studied the reduction pathways of $[\text{Re}(\text{CO})_3(\text{N,N-dapa})\text{L}']$ in detail.

When $[\text{Re}(\text{CO})_3(\text{N,N-dapa})(\text{Otf})]$ was dissolved in THF, a slow thermal reaction occurred to give a product with CO-stretching vibrations at 2022, 1925, and 1900 cm^{-1} . As such a reaction was not observed for $[\text{Re}(\text{CO})_3(i\text{-Pr-PyCa})(\text{Otf})]$ (see above), these frequencies are attributed to the six-coordinated $[\text{Re}(\text{CO})_3(\text{N,N,N-dapa})]^+$ complex, in which the Otf^- anion has been substituted by the third nitrogen atom of the dapa ligand. This indicates that this donor atom coordinates more strongly than THF. All $[\text{Re}(\text{CO})_3(\text{N,N-dapa})(\text{Otf})]$, not yet thermally transformed into $[\text{Re}(\text{CO})_3(\text{N,N,N-dapa})]^+$, reacted to give the latter product in 100% yield prior to the onset of the first one-electron reduction step. The thermal lability of $[\text{Re}(\text{CO})_3(\text{N,N-dapa})(\text{Otf})]$ became evident when the complex was dissolved in THF/100-fold excess of PPh_3 , or in MeCN or *n*-PrCN. In the former case, a mixture of $[\text{Re}(\text{CO})_3(\text{N,N,N-dapa})]^+$ and $[\text{Re}(\text{CO})_3(\text{N,N-dapa})(\text{PPh}_3)]^+$ was obtained, whereas in the latter case, $[\text{Re}(\text{CO})_3(\text{N,N-dapa})\text{L}']^+$ ($\text{L}' = \text{MeCN}$ or *n*-PrCN) was exclusively formed (see Table 3 for the corresponding $\nu(\text{CO})$ frequencies). These thermal reactions clearly illustrate that there is a competition between PPh_3 and the third nitrogen atom of the dapa ligand regarding their coordination to Re, and that MeCN and *n*-PrCN coordinate more firmly than PPh_3 in the cationic

Table 3. CO-Stretching Frequencies of $[\text{Re}(\text{CO})_3(\text{N,N-dapa})\text{L}']$ ($\text{L}' = \text{Br}^-, \text{Otf}^-$) and Their Reduction Products in THF, unless Stated Otherwise

complex	$\nu(\text{CO})$ (cm^{-1})	k_{av} (Nm^{-1})
$[\text{Re}(\text{CO})_3(\text{N,N-dapa})\text{Br}]$	2022 s, 1924 s, 1901 s	1535
$[\text{Re}(\text{CO})_3(\text{N,N-dapa})(\text{Otf})]$	2033 s, 1935 s, 1916 s	1555
$[\text{Re}(\text{CO})_3(\text{N,N-dapa})(\text{MeCN})]^+{}^a$	2037 s, 1934 s, br	1566
$[\text{Re}(\text{CO})_3(\text{N,N-dapa})(n\text{-PrCN})]^+{}^b$	2038 s, 1936 s, br	1568
$[\text{Re}(\text{CO})_3(\text{N,N,N-dapa})]^+$	2022 s, 1925 s, 1900 s	1535
$[\text{Re}(\text{CO})_3(\text{N,N-dapa})(\text{PPh}_3)]^+$	2036 s, 1949 s, 1927 s	1569
$[\text{Re}(\text{CO})_3(\text{N,N-dapa})(\text{P}(\text{OMe})_3)]^+$	2044 s, 1963 s, 1929 s	1582
$[\text{Re}(\text{CO})_3(\text{N,N-dapa})(\text{MeCN})]^+{}^a$	2009 s, 1899 s, br	1514
$[\text{Re}(\text{CO})_3(\text{N,N-dapa})(n\text{-PrCN})]^+$	2012 s, 1901 s, br	1518
$[\text{Re}(\text{CO})_3(\text{N,N,N-dapa})]^+$	2000 s, 1887 s, 1860 s	1483
$[\text{Re}(\text{CO})_3(\text{N,N,N-dapa})]^+{}^a$	1998 s, 1886 s, 1852 s	1478
$[\text{Re}(\text{CO})_3(\text{N,N,N-dapa})]^+{}^b$	2000 s, 1891 s, 1853 s	1481
$[\text{Re}(\text{CO})_3(\text{N,N-dapa})(\text{PPh}_3)]^+$	2013 s, 1916 s, 1898 s	1525
$[\text{Re}(\text{CO})_3(\text{N,N-dapa})(\text{PPh}_3)]^+{}^a$	2011 s, 1914 s, 1891 s	1519
$[\text{Re}(\text{CO})_3(\text{N,N-dapa})(\text{P}(\text{OMe})_3)]^+$	2020 s, 1929 s, 1898 s	1535
$[\text{Re}(\text{CO})_2(\text{N,N-dapa})(\text{P}(\text{OMe})_3)_2]^+$	1940 s, 1862 s	1460
$[\text{Re}(\text{CO})_3(\text{N,N,N-dapa})]^+$	1964 s, 1856 s, 1840 s	1439
$[\text{Re}(\text{CO})_3(\text{N,N-dapa})(\text{MeCN})]^+{}^a$	1983 s, 1865 s, 1842 s	1454
$[\text{Re}(\text{CO})_3(\text{N,N-dapa})(n\text{-PrCN})]^+{}^b$	1980 s, 1856 s, 1842 s	1448
$[\text{Re}(\text{CO})_3(\text{N,N-dapa})(n\text{-PrCN})]^+{}^c$	1980 s, 1865 s, 1843 s	1453
$[\text{Re}(\text{CO})_3(\text{N,N-dapa})(\text{P}(\text{OMe})_3)]^+$	1997 s, 1892 s, 1872 s	1490

^a In MeCN at 243 K. ^b In *n*-PrCN at 233 K. ^c In *n*-PrCN at room temperature.

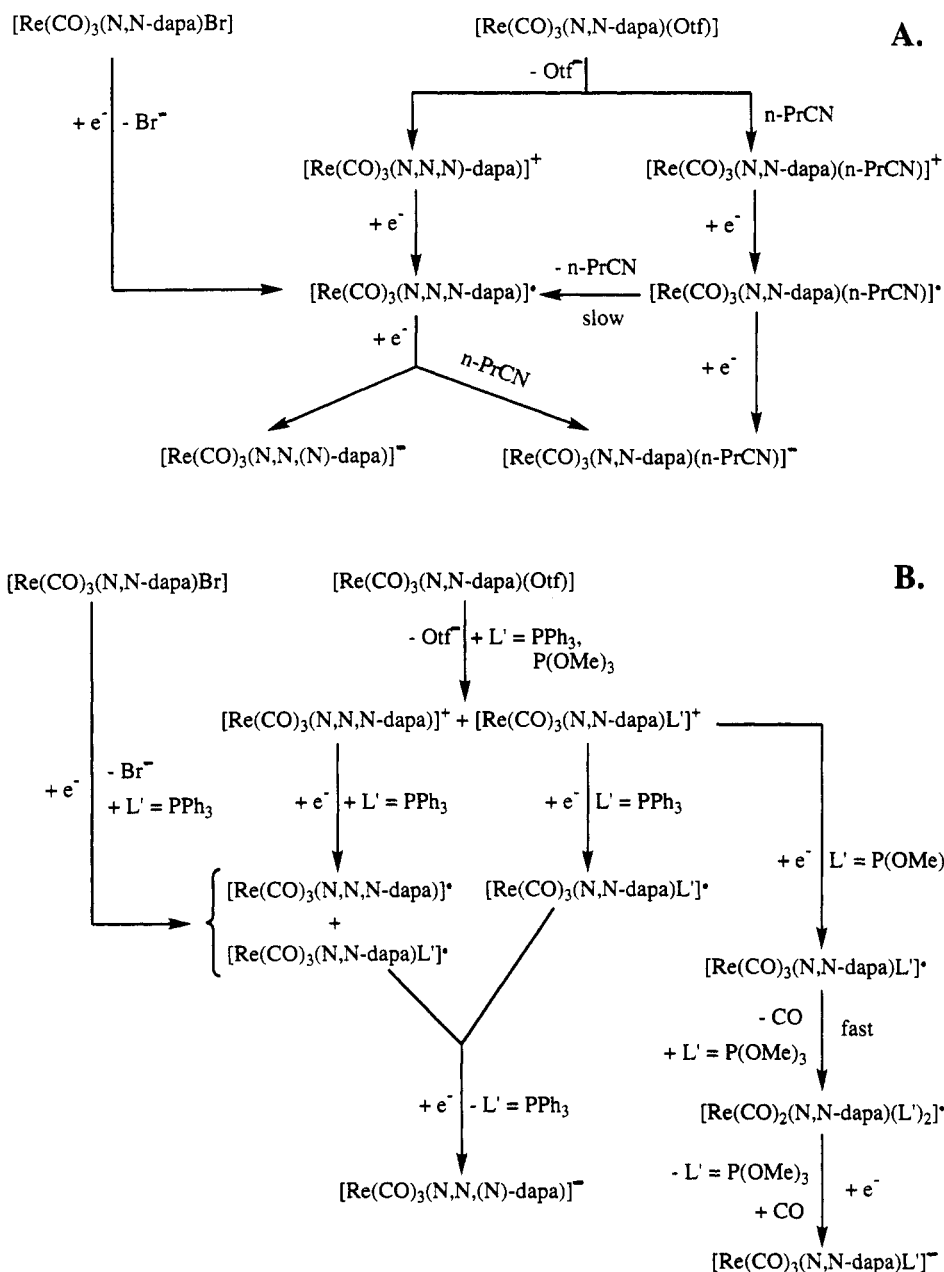
complexes when used as solvents. In accordance, no $[\text{Re}(\text{CO})_3(\text{N,N-dapa})(\text{PPh}_3)]^+$ appeared in MeCN or *n*-PrCN.

Similar competitive substitution reactions took place even during the one-electron reduction of the aforementioned dapa complexes (see Scheme 6). Upon passing the one-electron reduction step in THF, $[\text{Re}(\text{CO})_3(\text{N,N,N-dapa})]^+$ was smoothly converted into a product

(24) (a) Alyea, E. C.; Ferguson, G.; Restivo, R. J. *Inorg. Chem.* **1975**, *14*, 2491. (b) Restivo, R. J.; Ferguson, G. *J. Chem. Soc., Dalton Trans.* **1976**, 518. (c) Blake, A. J.; Lavery, A. J.; Hyde, T. I.; Schröder, M. *J. Chem. Soc., Dalton Trans.* **1989**, 965. (d) Edwards, D. A.; Mahon, M. F.; Martin, W. R.; Molloy, K. C.; Fanwick, P. E.; Walton, R. A. *J. Chem. Soc., Dalton Trans.* **1990**, 3161. (e) Stor, G. J.; van der Vis, M.; Stufkens, D. J.; Oskam, A. To be published.

(25) (a) Angelici, R. J.; Basolo, F.; Poè, A. *J. Am. Chem. Soc.* **1963**, *85*, 2215. (b) Reimann, R. H.; Singleton, E. *J. Chem. Soc., Dalton Trans.* **1973**, 841. (c) Wuyts, L. F.; van der Kelen, G. P. *Inorg. Chim. Acta* **1977**, *23*, 19. (d) Bond, A. M.; Colton, R.; McDonald, M. E. *Inorg. Chem.* **1978**, *17*, 2842. (e) Bombin, F.; Carriedo, G. A.; Miguel, J. A.; Riera, V. *J. Chem. Soc., Dalton Trans.* **1981**, 2049. (f) Carriedo, G. A.; Riera, V. *J. Organomet. Chem.* **1981**, *205*, 371. (g) Bond, A. M.; Colton, R.; McCormick, M. J. *Inorg. Chem.* **1977**, *16*, 155.

Scheme 6



with CO-stretching vibrations at 2000, 1887, and 1860 cm^{-1} . These frequencies can reasonably be assigned to the radical $[\text{Re}(\text{CO})_3(\text{N},\text{N},\text{N}-\text{dapa})]^\bullet$, as coordination of THF has been found to be too weak (see above) to compete significantly. It should be noted that the intensity pattern of the $\nu(\text{CO})$ bands of both $[\text{Re}(\text{CO})_3(\text{N},\text{N},\text{N}-\text{dapa})]^\bullet$ and $[\text{Re}(\text{CO})_3(\text{N},\text{N},\text{N}-\text{dapa})]^\bullet$ (see Table 3) rules out their meridional geometry with in-plane coordinated dapa.^{16,24,25}

One-electron reduction of $[\text{Re}(\text{CO})_3(\text{N},\text{N}-\text{dapa})\text{L}']^\bullet$ ($\text{L}' = \text{MeCN}$ or $n\text{-PrCN}$) initially afforded the corresponding radicals $[\text{Re}(\text{CO})_3(\text{N},\text{N}-\text{dapa})\text{L}']^\bullet$ with typically coincident lower $\nu(\text{CO})$ frequencies (see Table 3). However, in contrast to the cations $[\text{Re}(\text{CO})_3(\text{N},\text{N}-\text{dapa})\text{L}']^+$ ($\text{L}' = \text{MeCN}$ or $n\text{-PrCN}$), the radicals appeared to be thermally more labile, as they slowly transformed to $[\text{Re}(\text{CO})_3(\text{N},\text{N},\text{N}-\text{dapa})]^\bullet$, even when the temperature was decreased to 243 K (in MeCN) or to 223 K (in $n\text{-PrCN}$). In the presence of PPh_3 , the radical $[\text{Re}(\text{CO})_3(\text{N},\text{N}-\text{dapa})\text{L}']^\bullet$ was obtained as the major product besides a

small amount of $[\text{Re}(\text{CO})_3(\text{N},\text{N},\text{N}-\text{dapa})]^\bullet$. These results clearly indicate that, in particular, coordination of a better π -acceptor is more important for the stability of the radicals, than for that of the parent cationic complexes.

Exactly the same conclusion can be drawn for the complexes $[\text{Re}(\text{CO})_3(\text{N},\text{N}-\text{dapa})\text{Br}]^{0/+}$ and $[\text{Re}(\text{CO})_3(\text{N},\text{N}-\text{dapa})(\text{P}(\text{OMe})_3)]^{+/+}$ (see Scheme 6). The only exception to the reactivity pattern of the tricarbonyl complexes, as outlined above, was an occurrence of a CO-substitution reaction for the radical $[\text{Re}(\text{CO})_3(\text{N},\text{N}-\text{dapa})(\text{P}(\text{OMe})_3)]^\bullet$ in the presence of excess $\text{P}(\text{OMe})_3$ which afforded a bis(carbonyl) product with two intense $\nu(\text{CO})$ bands at 1940 and 1862 cm^{-1} . As such a CO substitution was not observed in the presence of excess PPh_3 , it is concluded that $[\text{Re}(\text{CO})_2(\text{N},\text{N}-\text{dapa})(\text{P}(\text{OMe})_3)_2]^\bullet$ had been formed.

In a subsequent one-electron reduction step, $[\text{Re}(\text{CO})_2(\text{N},\text{N}-\text{dapa})(\text{P}(\text{OMe})_3)_2]^\bullet$ was converted into a tricarbonyl complex with $\nu(\text{CO})$ bands at 1997, 1892, and 1872 cm^{-1} .

Table 4. Absorption Maxima in the Visible Region of $[\text{Re}(\text{CO})_3(\alpha\text{-diimine})\text{L}]$ ($\text{L}' = \text{Cl}^-, \text{Br}^-, \text{I}^-, \text{Otf}^-$; $\alpha\text{-Diimine} = \text{bpy}, i\text{-Pr-PyCa}$) and Their Reduction Products in THF

complex	λ_{max} (nm)
$[\text{Re}(\text{CO})_3(\text{bpy})\text{Br}]$	385
$[\text{Re}(\text{CO})_3(\text{bpy})(\text{Otf})]$	355
$[\text{Re}(\text{CO})_3(\text{bpy})(\text{THF})]^+$	385
$[\text{Re}(\text{CO})_3(\text{bpy})(\text{PPh}_3)]^+$	365, 330
$[\text{Re}(\text{CO})_3(\text{bpy})(\text{PPh}_3)]^-$	500, 390
$[\text{Re}_2(\text{CO})_6(\text{bpy})_2]$	805, 600, 470
$[\text{Re}(\text{CO})_3(\text{bpy})]^-$	750 sh, 680 sh, 630 sh, 560
$[\text{Re}(\text{CO})_3(i\text{-Pr-PyCa})\text{Br}]$	410
$[\text{Re}(\text{CO})_3(i\text{-Pr-PyCa})(\text{Otf})]$	365, 270
$[\text{Re}(\text{CO})_3(i\text{-Pr-PyCa})(\text{THF})]^+$	380
$[\text{Re}(\text{CO})_3(i\text{-Pr-PyCa})(\text{PPh}_3)]^+$	375
$[\text{Re}(\text{CO})_3(i\text{-Pr-PyCa})(\text{THF})]^-$	395, 330
$[\text{Re}(\text{CO})_3(i\text{-Pr-PyCa})(\text{PPh}_3)]^-$	450 sh, 395
$[\text{Re}_2(\text{CO})_6(\text{C-C-}i\text{-Pr-PyCa})_2]$	390
$[\text{Re}_2(\text{CO})_6(i\text{-Pr-PyCa})_2]$	785
$[\text{Re}(\text{CO})_3(i\text{-Pr-PyCa})]^-$	510, 285

The shift of these frequencies with respect to those of $[\text{Re}(\text{CO})_3(\text{N,N-dapa})(\text{P}(\text{OMe})_3)]^-$ (see Table 3) is almost equal to the frequency shifts observed upon the reduction of $[\text{Re}(\text{CO})_3(\text{abpy})(\text{PPh}_3)]^-$ to give $[\text{Re}(\text{CO})_3(\text{abpy})(\text{PPh}_3)]^-$ (see Table 2). The above frequencies are therefore assigned to the doubly reduced six-coordinated $[\text{Re}(\text{CO})_3(\text{N,N-dapa})(\text{P}(\text{OMe})_3)]^-$ complex. This means that one of the coordinated $\text{P}(\text{OMe})_3$ ligands is substituted by CO, still present in the thin solution layer of the OTTLE cell.

Two different anionic complexes were obtained by one-electron reduction of $[\text{Re}(\text{CO})_3(\text{N,N,N-dapa})]$. In *n*-PrCN at 233–293 K, the six-coordinated anion $[\text{Re}(\text{CO})_3(\text{N,N-dapa})(n\text{-PrCN})]^-$ ($\nu(\text{CO})$ at 1980, 1856, and 1842 cm^{-1} , 233 K) was most likely formed as the only, stable product which did not even react with a 100-fold excess of PPh_3 . In THF at 293 K, another species was generated which exhibited $\nu(\text{CO})$ bands at 1964, 1856, and 1840 cm^{-1} , i.e. at much lower wavenumbers than those of six-coordinated $[\text{Re}(\text{CO})_3(\text{N,N-dapa})(n\text{-PrCN})]^-$, but at apparently higher wavenumbers than those of the five-coordinated, closely related anion $[\text{Re}(\text{CO})_3(i\text{-Pr-PyCa})]^-$ (see Table 1). We therefore attribute the $\nu(\text{CO})$ frequencies in THF to a six-coordinated anion $[\text{Re}(\text{CO})_3(\text{N,N,N-dapa})]^-$, in which, however, coordination of the third N-atom of dapa to the Re center is very weak.

Scheme 6 summarizes the reduction pathways of $[\text{Re}(\text{CO})_3(\text{N,N-dapa})\text{L}']$ ($\text{L}' = \text{Br}^-, \text{Otf}^-$) in THF or *n*-PrCN in the absence (A) and presence (B) of PPh_3 or $\text{P}(\text{OMe})_3$.

UV/Vis Spectroelectrochemistry. Several redox reactions described in the preceding section were also followed by UV/vis spectroscopy under the same conditions (concentration, temperature). The UV/vis data of the starting complexes and the products are summarized in Tables 4–6.

The $[\text{Re}(\text{CO})_3(\alpha\text{-diimine})\text{Br}]$ complexes under study show one ($\alpha\text{-diimine} = \text{bpy}, i\text{-Pr-PyCa}, \text{dapa}$) or two ($\alpha\text{-diimine} = \text{dpp}, \text{abpy}$) absorption bands in the visible region. The lowest energy bands of all parent complexes belong to CT transitions from π -interacting $\text{Re } d_{\pi}$ -halide p_{π} orbitals to the lowest π^* orbital of $\alpha\text{-diimine}$ (L) (i.e. to transitions of a mixed MLCT/LCT character).²⁶ For $[\text{Re}(\text{CO})_3(\text{dpp})\text{Cl}]$, the band at higher energy

Table 5. Absorption Maxima in the Visible Region of $[\text{Re}(\text{CO})_3(\alpha\text{-diimine})\text{L}']$ ($\text{L}' = \text{Br}^-, \text{Otf}^-$; $\alpha\text{-Diimine} = \text{dpp}, \text{abpy}$) and Their Reduction Products in THF

complex	λ_{max} (nm)
$[\text{Re}(\text{CO})_3(\text{dpp})\text{Br}]$	415, 320 sh
$[\text{Re}(\text{CO})_3(\text{dpp})\text{Br}]^-$	425, 310
$[\text{Re}(\text{CO})_3(\text{dpp})(\text{THF})]^-$	425, 310
$[\text{Re}(\text{CO})_3(\text{dpp})(\text{PPh}_3)]^-$	450
$[\text{Re}(\text{CO})_3(\text{dpp})]^-$	530, 410 sh, 320
$[\text{Re}(\text{CO})_3(\text{abpy})\text{Br}]$	570, 345
$[\text{Re}(\text{CO})_3(\text{abpy})\text{Br}]^-$	500, 380
$[\text{Re}(\text{CO})_3(\text{abpy})(\text{THF})]^-$	470, 350 sh, 290
$[\text{Re}(\text{CO})_3(\text{abpy}) \cdot \text{THF}]^{2-}$	480, 360

Table 6. Absorption Maxima in the Visible Region of $[\text{Re}(\text{CO})_3(\text{N,N-dapa})\text{L}']$ ($\text{L}' = \text{Br}^-, \text{Otf}^-$) and Their Reduction Products in THF

complex	λ_{max} (nm)
$[\text{Re}(\text{CO})_3(\text{N,N-dapa})\text{Br}]$	415
$[\text{Re}(\text{CO})_3(\text{N,N-dapa})(\text{Otf})]$	375
$[\text{Re}(\text{CO})_3(\text{N,N,N-dapa})]^+$	390
$[\text{Re}(\text{CO})_3(\text{N,N-dapa})(\text{PPh}_3)]^+$	375
$[\text{Re}(\text{CO})_3(\text{N,N,N-dapa})]^-$	405
$[\text{Re}(\text{CO})_3(\text{N,N-dapa})(\text{PPh}_3)]^-$	430
$[\text{Re}(\text{CO})_3(\text{N,N,N-dapa})]^-$	540

has been assigned to an intraligand $\pi \rightarrow \pi^*$ transition of the dpp ligand.¹⁰

Upon the one-electron reduction of $[\text{Re}(\text{CO})_3(\text{bpy})\text{L}']$ ($\text{L}' = \text{Cl}^-, \text{Br}^-, \text{I}^-, \text{Otf}^-$) the metal–metal-bonded dimer $[\text{Re}_2(\text{CO})_6(\text{bpy})_2]$ was formed, which shows an intense band at 805 nm, and two weaker bands at 600 and 470 nm, respectively (Figure 4B). The 805 nm band most probably belongs to $\text{Re } d_{\pi} \rightarrow \pi^*$ (bpy) MLCT transitions,¹⁵ analogous to the related $[\text{Mn}_2(\text{CO})_6(\text{bpy})_2]$ dimer.²⁷ One-electron reduction of $[\text{Re}(\text{CO})_3(i\text{-Pr-PyCa})\text{L}']$ ($\text{L}' = \text{Br}^-, \text{Otf}^-$) only produced a very small amount of $[\text{Re}_2(\text{CO})_6(i\text{-Pr-PyCa})_2]$ which showed again a low-energy band at 785 nm. For the C–C-coupled dimer $[\text{Re}_2(\text{CO})_6(\text{C-C-}i\text{-Pr-PyCa})_2]$, formed as the main product, the lowest-energy MLCT transition had shifted to 390 nm due to loss of conjugation between the pyridine and imine groups.

The final reduction product, the five-coordinated anion $[\text{Re}(\text{CO})_3(\text{bpy})]^-$, exhibits a broad and intense absorption band at 560 nm with shoulders at 630, 680, and 750 nm (Figure 4B). Similarly, $[\text{Re}(\text{CO})_3(i\text{-Pr-PyCa})\text{L}']$ ($\text{L}' = \text{Br}^-, \text{Otf}^-$) and $[\text{Re}(\text{CO})_3(\text{dpp})\text{Br}]$ afforded the five-coordinated anions $[\text{Re}(\text{CO})_3(i\text{-Pr-PyCa})]^-$ (λ_{max} 510 nm) and $[\text{Re}(\text{CO})_3(\text{dpp})]^-$ (λ_{max} 530, 410 (sh), 320 nm), respectively. The absorption band between 500 and 600 nm might be assigned either to an intraligand transition in the $\alpha\text{-diimine}$ ligand or, more probably, to an electronic transition with a partial $\text{bpy}^{2-} \rightarrow \text{Re}^{\text{I}} \text{CT}$ character.²²

The UV/vis spectra of the reduction products formed in the course of the successive reduction of $[\text{Re}(\text{CO})_3(\text{abpy})\text{Br}]$ in THF, i.e. those of the radical anion $[\text{Re}(\text{CO})_3(\text{abpy})\text{Br}]^-$, the anion $[\text{Re}(\text{CO})_3(\text{abpy})(\text{THF})]^-$, and the dianion $\{[\text{Re}(\text{CO})_3(\text{abpy})] \cdot \text{THF}\}^{2-}$, are depicted in Figure 3B.

Cyclic Voltammetry. Cyclic voltammograms of the complexes $[\text{Re}(\text{CO})_3(\alpha\text{-diimine})\text{L}']^{0/+}$ ($\text{L}' = \text{Cl}^-, \text{Br}^-, \text{I}^-, \text{Otf}^-, \text{PPh}_3$) were recorded in THF. The electrode

(26) Stor, G. J.; Stufkens, D. J.; Vernooijs, P.; Baerends, E. J.; Fraanje, J.; Goubitz, K. *Inorg. Chem.* **1994**, *33*, in press.

(27) (a) Kokkes, M. W.; de Lange, W. G. J.; Stufkens, D. J.; Oskam, A. J. *Organomet. Chem.* **1985**, *294*, 59. (b) Stufkens, D. J. *Coord. Chem. Rev.* **1990**, *104*, 39. (c) van der Graaf, T.; Stufkens, D. J.; Oskam, A.; Goubitz, K. *Inorg. Chem.* **1991**, *30*, 599.

Table 7. Reduction Potentials (V vs Fc/Fc⁺) of the Complexes [Re(CO)₃(α-diimine)L]^{0/+j}

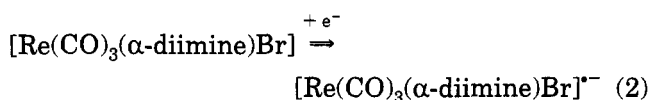
complex	$E_{p,c}^{I a}$	(ΔE_p)	$E_{p,c}^{II a}$
[Re(CO) ₃ (bpy)Cl]	-1.91	(110)	-2.38
[Re(CO) ₃ (bpy)Br]	-1.91	(110)	-2.33
[Re(CO) ₃ (bpy)I]	-1.91	(105)	-2.27
[Re ₂ (CO) ₆ (bpy) ₂] ^b	-2.08	(100)	
[Re(CO) ₃ (bpy)(Otf)] ^c	-1.54	(95)	
[Re(CO) ₃ (bpy)(THF)] ^{+ d}	-1.73	(75)	-2.23
[Re(CO) ₃ (bpy)(PPh ₃)] ^{+ e}	-1.62	(75)	-2.10
[Re(CO) ₃ (<i>i</i> -Pr-PyCa)Br]	-1.75	(90)	-2.37
[Re ₂ (CO) ₆ (C-C- <i>i</i> -Pr-PyCa) ₂]	-1.96		
[Re(CO) ₃ (<i>i</i> -Pr-PyCa)(Otf)] ^c	-1.36	(90)	
[Re(CO) ₃ (<i>i</i> -Pr-PyCa)(THF)] ^{+ d}	-1.64	(120)	-2.21
[Re(CO) ₃ (<i>i</i> -Pr-PyCa)(PPh ₃)] ^{+ e}	-1.45	(85)	-2.08
[Re(CO) ₃ (<i>N,N</i> -dapa)Br]	-1.64	(90)	-2.16
[Re(CO) ₃ (<i>N,N,N</i> -dapa)(Otf)] ^c	-1.29	(100)	
[Re(CO) ₃ (<i>N,N,N</i> -dapa)] ^{+ f}	-1.59	(105)	-2.16
[Re(CO) ₃ (<i>N,N,N</i> -dapa)(P(OMe) ₃)] ^{+ f}	-1.40	(70)	-1.95
[Re(CO) ₃ (<i>N,N,N</i> -dapa)(PPh ₃)] ^{+ e}	-1.35	(80)	-1.82
[Re(CO) ₃ (dpp)Br] ^g	-1.56	(80)	-2.05
[Re(CO) ₃ (abpy)Br] ^h	-0.80	(90)	-1.49
[Re(CO) ₃ (abpy)(Otf)] ^c	-0.46	(115)	
[Re(CO) ₃ (abpy)(THF)] ^{+ d,h}	-0.62	(70)	-1.36 ⁱ
[Re(CO) ₃ (abpy)(PPh ₃)] ^{+ e,h}	-0.51	(80)	-1.46 ⁱ

^a Peak potentials of the first and second reductions. ^b Oxidation of [Re₂(CO)₆(bpy)₂] at -0.29 and -0.60 V vs Fc/Fc⁺. ^c No second reduction observed. ^d Measured in situ in a [Re(CO)₃(α-diimine)(Otf)]/THF solution. ^e Measured in situ in a [Re(CO)₃(α-diimine)(Otf)]/excess PPh₃/THF solution. ^f Measured in situ in a [Re(CO)₃(abpy)(Otf)]/excess P(OMe)₃/THF solution. ^g Both in the absence and presence of excess PPh₃. ^h A third, electrochemically quasireversible, chemically reversible reduction at $E_{p,c} = -2.86$ V vs Fc/Fc⁺. ⁱ $\Delta E_p = 90$ mV. ^j CV of 10⁻³ M solutions in THF/10⁻¹ M Bu₄NPF₆ at $v = 100$ mV/s, 0.8 mm² Pt disk electrode, 293 K.

potentials, presented in Table 7, were measured against the standard Fc/Fc⁺ redox couple.^{13,28}

The cyclic voltammograms (CV) of the complexes [Re(CO)₃(α-diimine)Br] (α-diimine = bpy, *i*-Pr-PyCa, dapa, dpp), measured without excess Br⁻ in the THF solution, exhibited two one-electron cathodic peaks separated by approximately 400–600 mV (see Table 7). The only exception was the CV of the complex [Re(CO)₃(abpy)Br] in which the two cathodic peaks were found at significantly more positive potentials (Table 7) and were separated by 690 mV (see Figure 5A). In this case, even a third cathodic peak appeared at $E_{p,c} = -2.86$ V.

On the basis of previous results,^{2d,f,k,3b,d} the first reduction is assigned to



For all [Re(CO)₃(α-diimine)Br] studied, this process was electrochemically reversible and diffusion controlled, as evidenced by identical or slightly different ΔE_p values for the [Re(CO)₃(α-diimine)Br]/[Re(CO)₃(α-diimine)Br]^{·-} and Fc/Fc⁺ redox couples²⁸ and by a constant value of the current function $i_p v^{-1/2}$, respectively. The reduction was chemically reversible on the CV time scale, corresponding to the scan rate range of $v = 50$ – 500 mV/s, only for the complexes [Re(CO)₃(α-diimine)Br], α-diimine = dpp and abpy (the current ratio $i_p^a/i_p^c = 1$). The one-electron reduction of these two [Re(CO)₃(α-diimine)Br] complexes was chemically reversible even in the presence of a 100-fold excess of PPh₃ in the THF

(28) Electrochemical reversibility of all electrode processes was compared with that of the Fc/Fc⁺ couple in the same solution to account for effects such as uncompensated iR drop, electrode passivation, etc.

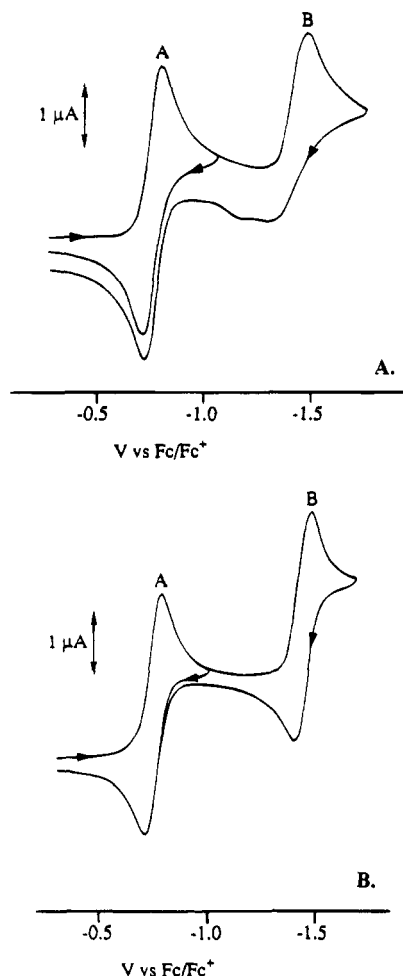
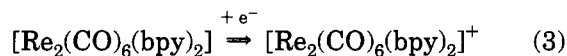


Figure 5. Cyclic voltammogram of [Re(CO)₃(abpy)Br] in the absence (A) and presence (B) of PPh₃. Conditions: 10⁻³ M solution in THF/10⁻¹ M Bu₄NPF₆ (A), and 10⁻¹ M PPh₃ (B); Pt disk electrode, 293 K, $v = 100$ mV/s.

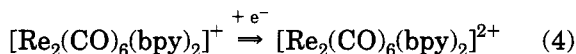
solution. This observation is in full agreement with the IR spectroelectrochemical results (see above) which indicated only slow substitution of Br⁻ by THF (α-diimine = dpp) or by PPh₃ (α-diimine = dpp, abpy).

The radical anions [Re(CO)₃(α-diimine)Br]^{·-} (α-diimine = bpy, *i*-Pr-PyCa, dapa) were not stable on the CV time scale (i_p^a/i_p^c was less than 1 within $v = 50$ – 500 mV/s and did not change significantly with the increasing scan rate). On the reverse scan, a small anodic peak appeared in all cyclic voltammograms at a more positive potential than that of the anodic counterpeak of the [Re(CO)₃(α-diimine)Br]/[Re(CO)₃(α-diimine)Br]^{·-} redox couple. On the basis of the IR OTTLE results (see above) and on comparison with cyclic voltammograms of the related complexes [Re(CO)₃(α-diimine)(Otf)] (see below, Table 7), the small anodic peaks are assigned to reoxidation of the radicals [Re(CO)₃(α-diimine)(THF)]^{·-} (α-diimine = bpy, *i*-Pr-PyCa) and [Re(CO)₃(*N,N,N*-dapa)]^{·-}, formed from the labile radical anions [Re(CO)₃(α-diimine)Br]^{·-} by dissociation of Br⁻ and rapid coordination of the solvent or the third nitrogen atom of the dapa ligand, respectively. It is noteworthy that the radical [Re(CO)₃(bpy)(THF)]^{·-} was not detected on the OTTLE time scale due to its fast conversion to [Re₂(CO)₆(bpy)₂] (see above). The formation of the dimer on the CV time scale was revealed by the presence of two additional anodic peaks in the CV of [Re(CO)₃(bpy)Br] at $E_{p,a} = -0.60$ and -0.29 V,

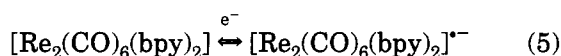
observed on the reverse scan after passing the first cathodic process, and a new, electrochemically reversible, redox couple at $E_{1/2} = -2.03$ V, observed during repeated potential sweeps between the two cathodic processes of parent $[\text{Re}(\text{CO})_3(\alpha\text{-diimine})\text{Br}]$ (Table 7). In accordance with literature data, the chemically irreversible anodic processes^{2f} are assigned to



and



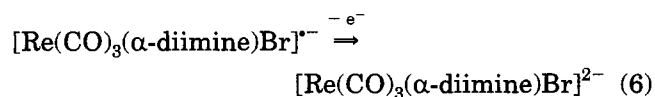
respectively. Both positively charged dimers readily decompose to give parent $[\text{Re}(\text{CO})_3(\text{bpy})\text{Br}]$, the only product detected on the IR OTTLE time scale. The redox couple at -2.03 V is attributed^{2d,f,k} to



No peaks due to redox reactions of $[\text{Re}(\text{CO})_3(\text{bpy})\text{-(THF)}]^-$ and $[\text{Re}_2(\text{CO})_6(\text{bpy})_2]$ were found in the CV of $[\text{Re}(\text{CO})_3(\text{bpy})\text{Cl}]$. The one-electron reduction of this complex (Table 7) was chemically reversible on the CV time scale ($i_p^a/i_p^c = 1$) having thus manifested, in accordance with the IR OTTLE experiments, higher stability of $[\text{Re}(\text{CO})_3(\text{bpy})\text{Cl}]^-$ in comparison with the Br derivative.

In the presence of PPh_3 , one-electron reduction of $[\text{Re}(\text{CO})_3(\alpha\text{-diimine})\text{Br}]$ ($\alpha\text{-diimine} = \text{bpy}, i\text{-Pr-PyCa}, \text{dapa}$) led to the stable radicals $[\text{Re}(\text{CO})_3(\alpha\text{-diimine})(\text{PPh}_3)]$ (see the IR OTTLE results). In the corresponding cyclic voltammograms, the fast follow-up conversion of the primary reduction product $[\text{Re}(\text{CO})_3(\alpha\text{-diimine})\text{Br}]^-$ to $[\text{Re}(\text{CO})_3(\alpha\text{-diimine})(\text{PPh}_3)]$ was again evidenced by the appearance of small anodic peaks after switching the scan direction behind the cathodic peak of the chemically irreversible reduction of parent $[\text{Re}(\text{CO})_3(\alpha\text{-diimine})\text{Br}]$. These small peaks could reasonably be assigned to reoxidation of $[\text{Re}(\text{CO})_3(\alpha\text{-diimine})(\text{PPh}_3)]$ as their $E_{p,a}$ values agreed well with those obtained from cyclic voltammograms of corresponding $[\text{Re}(\text{CO})_3(\alpha\text{-diimine})(\text{PPh}_3)]^+$ (see below, Table 7). For $\alpha\text{-diimine} = \text{bpy}$, all CV peaks of $[\text{Re}_2(\text{CO})_6(\text{bpy})_2]$ (Table 7) disappeared upon addition of PPh_3 , in line with the spectroelectrochemical results described in preceding sections.

The second, more negative, redox couple in the CV of $[\text{Re}(\text{CO})_3(\alpha\text{-diimine})\text{Br}]$ ($\alpha\text{-diimine} = \text{bpy}, i\text{-Pr-PyCa}, \text{dapa}, \text{dpp}, \text{abpy}$) (Table 7) was chemically irreversible ($i_p^a/i_p^c < 1$), independent of $\alpha\text{-diimine}$ or addition of excess PPh_3 into the THF solution (see Figure 5A). The irreversibility may best be explained by attributing^{2d,f,k} the second reduction step to



As evidenced by the spectroelectrochemical results, the doubly reduced complexes $[\text{Re}(\text{CO})_3(\alpha\text{-diimine})\text{Br}]^{2-}$ are extremely labile and readily lose Br^- to give either five-coordinated anions $[\text{Re}(\text{CO})_3(\alpha\text{-diimine})]^-$ ($\alpha\text{-diimine} = \text{bpy}, i\text{-Pr-PyCa}, \text{dpp}$) or six-coordinated anions

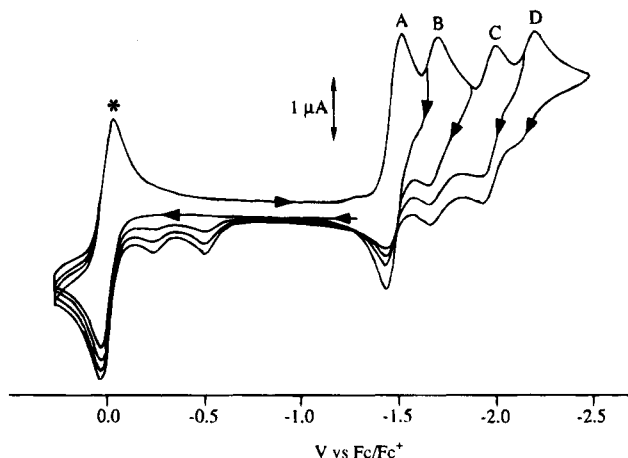


Figure 6. Cyclic voltammogram of $[\text{Re}(\text{CO})_3(\text{bpy})(\text{Otf})]$. Conditions: 10^{-3} M solution in THF/ 10^{-1} M Bu_4NPF_6 , Pt disk electrode, 293 K, $v = 100$ mV/s; * = Fc/Fc^+ .

$[\text{Re}(\text{CO})_3(\text{abpy})\text{L}']$ ($\text{L}' = \text{THF}, \text{PPh}_3$). The remaining anion in the series, $[\text{Re}(\text{CO})_3(\text{N,N,N})\text{-dapa}]^-$, can be considered as a transient case (see above). All anions should undergo one-electron reoxidation which, however, was not clearly detectable in the cyclic voltammograms of most $[\text{Re}(\text{CO})_3(\alpha\text{-diimine})\text{Br}]$ studied. An exception is the cyclic voltammogram of $[\text{Re}(\text{CO})_3(\text{abpy})\text{Br}]$ (Figure 5A) which exhibits a small, positively shifted, anodic peak at -1.22 V which can reasonably be assigned to the reoxidation of stable $[\text{Re}(\text{CO})_3(\text{abpy})\text{-(THF)}]^-$. For, the chemically reversible redox couple $[\text{Re}(\text{CO})_3(\text{abpy})(\text{THF})]/[\text{Re}(\text{CO})_3(\text{abpy})(\text{THF})]^-$ was found at $E_{1/2} = -1.31$ V ($\Delta E_p = 90$ mV) in the cyclic voltammogram of $[\text{Re}(\text{CO})_3(\text{abpy})(\text{Otf})]$ in THF (see below). The small difference in $E_{p,a}$ can be ascribed to an influence of kinetics of the irreversible reduction of $[\text{Re}(\text{CO})_3(\text{abpy})\text{Br}]^-$, involving dissociation of Br^- from $[\text{Re}(\text{CO})_3(\text{abpy})\text{Br}]^{2-}$ and concomitant coordination of THF.

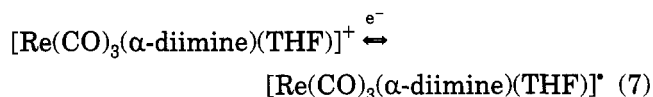
The one-electron reduction of $[\text{Re}(\text{CO})_3(\text{abpy})\text{Br}]^-$ in the presence of excess PPh_3 appeared to be chemically reversible ($i_p^a/i_p^c = 1$ within $v = 20\text{--}500$ mV/s) (see B in Figure 5B), which seemed to be in contradiction with the above interpretation. However, the reversible redox couple B in Figure 5B is in fact composed of two different redox couples, $[\text{Re}(\text{CO})_3(\text{abpy})\text{Br}]^-/[\text{Re}(\text{CO})_3(\text{abpy})\text{Br}]^{2-}$ and $[\text{Re}(\text{CO})_3(\text{abpy})(\text{PPh}_3)]/[\text{Re}(\text{CO})_3(\text{abpy})(\text{PPh}_3)]^-$, that accidentally coincide (see Table 7).

Both six-coordinated anions $[\text{Re}(\text{CO})_3(\text{abpy})\text{L}']^-$ ($\text{L}' = \text{THF}, \text{PPh}_3$) could subsequently be reduced at -2.86 V in an electrochemically quasireversible ($\Delta E_p = 130$ mV vs 90 mV for Fc/Fc^+ and chemically reversible ($i_p^a/i_p^c = 1$ at $v = 100$ mV/s) one-electron step to give, according to the IR OTTLE results (see above), the stable dianions $\{[\text{Re}(\text{CO})_3(\text{abpy})]^{2-} \cdot \text{L}'\}$. Very weak coordination of L' to the Re center in the dianions, as evidenced by their very similar average CO force constants (see Table 2), is probably responsible for the observed electrochemically quasireversible character of this reduction step.

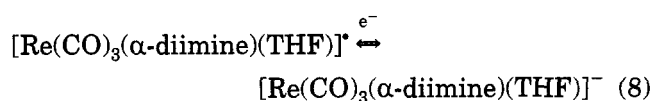
Cyclic voltammograms of the complexes $[\text{Re}(\text{CO})_3(\alpha\text{-diimine})(\text{Otf})]$ ($\alpha\text{-diimine} = \text{bpy}, i\text{-Pr-PyCa}, \text{dapa}$ and abpy) in THF are, in general, more complex than those of corresponding $[\text{Re}(\text{CO})_3(\alpha\text{-diimine})\text{Br}]$. They exhibit three characteristic cathodic peaks (denoted as A, B, and D, see Figure 6) which were accompanied, in the case of $\alpha\text{-diimine} = \text{bpy}$ and $i\text{-Pr-PyCa}$, by a fourth cathodic peak at -2.08 (C in Figure 6) and -1.96 V, respectively.

The cathodic peak current, $i_{p,c}$, of the redox couples B and D was typically observed to be significantly lower in comparison with $i_{p,c}$ of the most positive redox couple A (see Figure 6). This means that the cathodic peak of the redox couple A can be assigned to one-electron reduction of parent $[\text{Re}(\text{CO})_3(\alpha\text{-diimine})(\text{Otf})]$ (see Table 7). The reduction is followed by a secondary reaction producing a species which can successively be reduced at more negative potentials.

The IR OTTLE experiments have demonstrated that $[\text{Re}(\text{CO})_3(\alpha\text{-diimine})(\text{Otf})]$ ($\alpha\text{-diimine} = \text{bpy}, i\text{-Pr-PyCa}, \text{abpy}$) are converted in an electrochemically initiated electron-transfer chain (ETC) step to the corresponding cations $[\text{Re}(\text{CO})_3(\alpha\text{-diimine})(\text{THF})]^+$. In these cases, we therefore attribute the redox couples B and D to



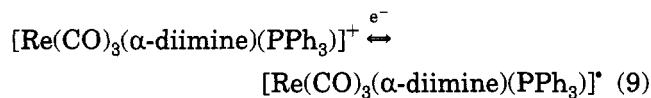
and



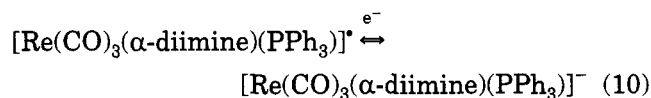
respectively (see Table 7). A similar reaction sequence can be applied for $[\text{Re}(\text{CO})_3(N,N\text{-dapa})(\text{Otf})]$ which is reduced at -1.29 V. On the basis of the IR OTTLE experiments (see above), the reduction initiated transformation of $[\text{Re}(\text{CO})_3(N,N\text{-dapa})(\text{Otf})]$ to $[\text{Re}(\text{CO})_3(N,N,N\text{-dapa})]^+$ which was subsequently reduced in two steps to give $[\text{Re}(\text{CO})_3(N,N,N\text{-dapa})]^+$ and $[\text{Re}(\text{CO})_3(N,N,N\text{-dapa})]^-$. These reductions were observed in the CV of $[\text{Re}(\text{CO})_3(N,N\text{-dapa})(\text{Otf})]$ as two cathodic peaks at -1.59 V (B) and -2.16 V (D), respectively.

Comparison of the cyclic voltammograms of $[\text{Re}(\text{CO})_3(\text{bpy})\text{L}']$ ($\text{L}' = \text{Br}^-$ and Otf^-) revealed, in accordance with literature data,^{2d,f,k} that the redox couple C in the CV of $[\text{Re}(\text{CO})_3(\text{bpy})(\text{Otf})]$ (see Figure 6) can be assigned according to eq 5. In agreement with this assignment, the two successive oxidations of $[\text{Re}_2(\text{CO})_6(\text{bpy})_2]$, as described by eqs 3 and 4, were also found in the CV of $[\text{Re}(\text{CO})_3(\text{bpy})(\text{Otf})]$ at -0.51 and -0.23 V, respectively (Figure 6). Similarly, the cathodic peak of the redox couple C in the CV of related $[\text{Re}(\text{CO})_3(i\text{-Pr-PyCa})(\text{Otf})]$ was assigned to one-electron reduction of the C-C-coupled dimer $[\text{Re}_2(\text{CO})_6(\text{C-C-}i\text{-Pr-PyCa})_2]$ (Table 7), the major product formed upon the reduction of the parent complex (see above). It is important to note that the cathodic peak C of $[\text{Re}_2(\text{CO})_6(\text{C-C-}i\text{-Pr-PyCa})_2]$ was much less developed than that of $[\text{Re}_2(\text{CO})_6(\text{bpy})_2]$ under identical conditions, i.e. concentration of parent $[\text{Re}(\text{CO})_3(\alpha\text{-diimine})(\text{Otf})]$, temperature, scan rate. This observation is not surprising, as it is likely to assume that the formation of $[\text{Re}_2(\text{CO})_6(\text{C-C-}i\text{-Pr-PyCa})_2]$ is a slower process than the formation of the metal-metal-bonded dimer $[\text{Re}_2(\text{CO})_6(\text{bpy})_2]$.

In the presence of excess PPh_3 , all complexes $[\text{Re}(\text{CO})_3(\alpha\text{-diimine})(\text{Otf})]$ ($\alpha = \text{bpy}, i\text{-Pr-PyCa}, \text{dapa}, \text{abpy}$) were thermally converted to $[\text{Re}(\text{CO})_3(\alpha\text{-diimine})(\text{PPh}_3)]^+$ prior to the CV experiments. Consequently, only two redox couples were observed during negative CV scans (see Table 7) which are assigned to



and



The second reduction (10) was chemically and electrochemically reversible only for $\alpha\text{-diimine} = \text{abpy}$. This result once more confirms the inherent stability of $[\text{Re}(\text{CO})_3(\alpha\text{-diimine})(\text{PPh}_3)]^-$, as was revealed by the above described IR OTTLE experiments.

Discussion

The experimental results clearly show that the nature of the products, formed by reduction of the complexes $[\text{Re}(\text{CO})_3(\alpha\text{-diimine})\text{L}']^{0/+}$, is mainly determined by the $\alpha\text{-diimine}$ ligand. A schematic MO diagram of the parent complexes is presented in Figure 7.

The relative positions of the orbitals are derived from MO calculations performed on $[\text{Mn}(\text{CO})_3(\text{bpy})\text{L}']$ complexes ($\text{L}' = \text{Cl}^-, \text{Br}^-, \text{I}^-$).²⁶ The HOMO consists of two close-lying orbitals which are an antibonding $\text{Re } d_{\pi}\text{-L}' p_{\pi}$ combination with a variable halide p_{π} contribution. Apart from this weak π interaction, there is a much stronger $\text{Re-L}' \sigma$ interaction, giving rise to a filled bonding orbital and an empty antibonding orbital, which are mainly $\text{L}' p\sigma$ and $\text{Re } d\sigma^*$ in character, respectively. The LUMO is mainly $\alpha\text{-diimine } \pi^*$ in character. The energy of the π^* LUMO decreases in the order $\text{bpy} > i\text{-Pr-PyCa} > \text{dapa} > \text{dpp} > \text{abpy}$, as evidenced by both the shift of the CT band of $[\text{Re}(\text{CO})_3(\alpha\text{-diimine})\text{L}']^{0/+}$ to higher energy (Tables 4–6) and the negative shift of the one-electron reduction potential of these complexes (Table 7) in the same order. The lower the energy of the π^* orbital, the better the $\alpha\text{-diimine}$ ligand is able to accommodate the added electron(s). The stability of the products of the first, second, and (for abpy) third one-electron reduction steps is strongly influenced by this property and will be discussed in this section.

The First One-Electron Reduction Step. One-electron reduction of the complexes $[\text{Re}(\text{CO})_3(\alpha\text{-diimine})\text{L}']^{0/+}$ destabilizes the π^* LUMO of the $\alpha\text{-diimine}$ ligand, which is expected to accommodate the unpaired electron. However, the resulting decrease of the $\nu(\text{CO})$ frequencies by $20\text{--}30 \text{ cm}^{-1}$ clearly points to an increase of the electron density also on Re and the CO ligands. In full line with the Koopmans theorem, the relative energies of the frontier orbitals are not considerably changed upon reduction and the electronic effects are delocalized over the whole complex. Only the π^* SOMO of the $\alpha\text{-diimine}$ ligand is slightly shifted to higher energy, for example in comparison with the empty $d\sigma^*$ orbital. Hence, the observed labilization of the $\text{Re-L}'$ bond is ascribed to profound changes in the $\alpha\text{-diimine}$ nature, from a π acceptor in $[\text{Re}(\text{CO})_3(\alpha\text{-diimine})\text{L}']^{0/+}$ to a rather strong σ donor in the $[\text{Re}(\text{CO})_3(\alpha\text{-diimine})\text{L}']^{-/}$ products. Its extent appears to increase with a negative shift in the one-electron reduction potential of the parent complexes which reflects a lower tendency of $\alpha\text{-diimine}$ to accommodate the unpaired electron. The most labile $\text{Re-L}'$ bonds can therefore be expected for

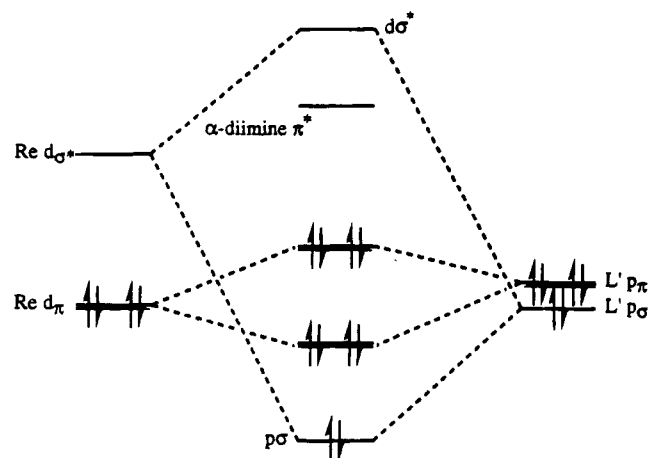


Figure 7. Schematic MO diagram of $[\text{Re}(\text{CO})_3(\alpha\text{-diimine})\text{L}']^{0/+}$, derived from MO calculations performed²⁶ on $[\text{Mn}(\text{CO})_3(\text{bpy})\text{L}']$ ($\text{L}' = \text{Cl}^-, \text{Br}^-, \text{I}^-$).

the reduction products with the bpy and *i*-Pr-PyCa ligands, especially if L' is a negatively charged halide or a hard Lewis base like THF.

Indeed, one-electron reduction of $[\text{Re}(\text{CO})_3(\alpha\text{-diimine})\text{L}']^{0/+}$ ($\text{L}' = \text{halide, THF}$; $\alpha\text{-diimine} = \text{bpy, } i\text{-Pr-PyCa}$) resulted in the fast dissociation of L' from $[\text{Re}(\text{CO})_3(\alpha\text{-diimine})\text{L}']^{-/}$. For $\alpha\text{-diimine} = \text{bpy}$, the $[\text{Re}(\text{CO})_3(\text{bpy})]^\cdot$ radicals readily dimerized to give the metal-metal-bonded complex $[\text{Re}_2(\text{CO})_6(\text{bpy})_2]$, whereas the $[\text{Re}(\text{CO})_3(i\text{-Pr-PyCa})]^\cdot$ radicals reacted to give the C-C-coupled dimer $[\text{Re}_2(\text{CO})_6(\text{C-C-}i\text{-Pr-PyCa})_2]$ as the main product, together with a very small amount of the metal-metal-bonded dimer $[\text{Re}_2(\text{CO})_6(i\text{-Pr-PyCa})_2]$. Obviously, the *i*-Pr-PyCa ligand in $[\text{Re}(\text{CO})_3(i\text{-Pr-PyCa})]^\cdot$ tends to accommodate the unpaired electron in the π^* orbital localized mainly on the nonaromatic imine group which exerts higher reactivity toward a C-C-coupling reaction than an aromatic imine group.

The observed slow substitution of Br^- by THF in the $[\text{Re}(\text{CO})_3(\text{dpp})\text{Br}]^-$ radical anion indicates that the Re-Br bond is still considerably labilized. The reduction potential of $[\text{Re}(\text{CO})_3(\text{dpp})(\text{THF})]^+$ is expected to be more positive than that of $[\text{Re}(\text{CO})_3(\text{dpp})\text{Br}]$, as observed for the analogous bpy and *i*-Pr-PyCa complexes (Table 7). Apparently, the dpp radical ligand is still a sufficiently strong donor in the $[\text{Re}(\text{CO})_3(\text{dpp})\text{Br}]^-$ radical anion to cause dissociation of the negatively charged Br^- ligand. This reasonably explains the observed lability of $[\text{Re}(\text{CO})_3(\text{dpp})\text{Br}]^-$ toward the attack of THF. The donor power of the dpp radical anion in the product $[\text{Re}(\text{CO})_3(\text{dpp})\text{THF}]$ decreases to such an extent that the Re-THF bond is relatively stable.

One-electron reduction of $[\text{Re}(\text{CO})_3(\text{abpy})\text{L}']^{0/+}$ ($\text{L}' = \text{Br}^-, \text{THF}$) gave rise to the formation of the stable $[\text{Re}(\text{CO})_3(\text{abpy})\text{L}']^{-/}$ complexes. In this case, the rather positive reduction potentials of the parent species indicate that the added electron is completely localized on the azo bond of the abpy ligand. The polarization effect of the abpy radical on the Re-Br bond in $[\text{Re}(\text{CO})_3(\text{abpy})\text{Br}]^-$ is therefore very limited and the complex is able to withstand the attack of THF.

The same arguments can be used to explain the experimentally observed stability of the radicals $[\text{Re}(\text{CO})_3(\alpha\text{-diimine})(\text{PPh}_3)]^\cdot$ ($\alpha\text{-diimine} = \text{bpy, } i\text{-Pr-PyCa, dpp, and abpy}$). The π^* LUMO of the $\alpha\text{-diimine}$ is relatively low in energy in the parent complexes $[\text{Re}(\text{CO})_3(\alpha\text{-diimine})\text{PPh}_3]^+$ (see Table 7), thereby making it more able to accommodate the unpaired electron. Also, the Re-PPh₃ bond is more resistant toward a cleavage in comparison with the THF and Br^- ligands due to the stronger π acceptor and weaker σ donor character of PPh₃. Consequently, it is not surprising that, although $[\text{Re}(\text{CO})_3(\text{abpy})\text{Br}]^-$ is stable enough to withstand the substitution of Br^- by THF (vide supra), the Re-Br bond is labilized sufficiently for the substitution of Br^- by PPh₃. This experimental result is fully in accord with the above interpretation. In this respect, an even higher stability can be predicted for the axial Re-CO bond in the $[\text{Re}(\text{CO})_4(\alpha\text{-diimine})]^\cdot$ radicals. Recent electrochemical results on $[\text{Re}(\text{CO})_4(\text{bpy})]^+$ seem to support this trend.²⁹

The increased localization of the unpaired electron on the $\alpha\text{-diimine}$ should also be reflected in an increase of the CO-stretching frequencies and k_{av} for the $[\text{Re}(\text{CO})_3(\alpha\text{-diimine})\text{Br}]^-$ and $[\text{Re}(\text{CO})_3(\alpha\text{-diimine})(\text{PPh}_3)]^\cdot$ radicals in the order $\alpha\text{-diimine} = \text{bpy} < i\text{-Pr-PyCa} < \text{dpp} < \text{abpy}$. With the exception of the complexes with the bpy ligand, all reduced complexes indeed comply with this expected trend (Tables 1-3).

The Second One-Electron Reduction Step. One-electron reduction of the metal-metal-bonded dimer $[\text{Re}_2(\text{CO})_6(\alpha\text{-diimine})_2]$ ($\alpha\text{-diimine} = \text{bpy, } i\text{-Pr-PyCa}$) resulted in the formation of the five-coordinated anionic $[\text{Re}(\text{CO})_3(\alpha\text{-diimine})]^-$ complex. This reduction step is localized with all probability on the $\alpha\text{-diimine } \pi^*$ LUMO of the dimers. As a consequence of the strong polarization effect caused by a considerable σ -donor character of coordinated bpy^- and *i*-Pr-PyCa⁻ (see above), the Re-Re bond in $[\text{Re}_2(\text{CO})_6(\alpha\text{-diimine})_2]^-$ is rapidly split upon generation of both the five-coordinated anionic $[\text{Re}(\text{CO})_3(\alpha\text{-diimine})]^-$ and radical $[\text{Re}(\text{CO})_3(\alpha\text{-diimine})]^\cdot$ complexes. The latter radical complex is readily reduced at the applied potential to give $[\text{Re}(\text{CO})_3(\alpha\text{-diimine})]^-$. Alternatively, the radical dimeric species $[\text{Re}_2(\text{CO})_6(\alpha\text{-diimine})_2]^\cdot$ might be stable, so that a second one-electron reduction is needed to induce the splitting of the Re-Re bond. However, the experimental results are not in favor of the latter explanation, since reduced $[\text{Re}_2(\text{CO})_6(\alpha\text{-diimine})_2]^-$ were not detected in the course of the spectroelectrochemical experiments, but only on the CV time scale. Similarly, it has recently been shown that the related metal-metal-bonded complexes $[(\text{CO})_5\text{MnMn}(\text{CO})_3(\alpha\text{-diimine})]$ were readily split into $[\text{Mn}(\text{CO})_5]^-$ and $[\text{Mn}(\text{CO})_3(\alpha\text{-diimine})]^\cdot$ upon one-electron reduction.³⁰

One-electron reduction of the C-C-coupled $[\text{Re}_2(\text{CO})_6(\text{C-C-}i\text{-Pr-PyCa})_2]$ dimer was also shown to produce the five-coordinated $[\text{Re}(\text{CO})_3(i\text{-Pr-PyCa})]^-$ complex. The mechanism of this reaction remains to be established.

One-electron reduction of $[\text{Re}(\text{CO})_3(\alpha\text{-diimine})\text{L}']^\cdot$ ($\text{L}' = \text{PPh}_3, \alpha\text{-diimine} = \text{bpy, } i\text{-Pr-PyCa, dpp}$; $\text{L}' = \text{THF, } \alpha\text{-diimine} = \text{dpp}$) also led to the formation of the five-coordinated anionic $[\text{Re}(\text{CO})_3(\alpha\text{-diimine})]^-$ complex. Apparently, the donor ability of the $\alpha\text{-diimine}$ dianionic ligand in $[\text{Re}(\text{CO})_3(\alpha\text{-diimine})]^-$ is extremely enhanced. It prevents even the coordination of PPh₃ as a weak π -acceptor molecule, which occurs during the first one-electron reduction step. Instead, a strong π -interaction

(29) Shaver, R. J.; Rillema, D. P. *Inorg. Chem.* **1992**, *31*, 4101.

(30) van der Graaf, T.; Hofstra, R. M. J.; Schilder, P. G. M.; Rijkhoff, M.; Stufkens, D. J.; Oskam, A. *Organometallics* **1991**, *10*, 3668.

may take place between the π^* HOMO of the α -diimine dianion and the asymmetric member of the set of LUMO orbitals of the $\text{Re}(\text{CO})_3^+$ fragment, like in the isoelectronic $[\text{Mn}(\text{CO})_3(\text{DBCat})]^-$ ²² and $[\text{W}(\text{CO})_3(\text{DBCat})]^{2-}$ ²³ (DBCat = 3,5-di-*tert*-butylcatecholate) complexes. This interaction in the five-coordinated $[\text{Re}(\text{CO})_3(\alpha\text{-diimine})]^-$ anion allows the α -diimine dianion to exert very strong π -donor character and to increase considerably the electron density on Re. Experimentally, this π -delocalization is evidenced by much lower $\nu(\text{CO})$ frequencies and average CO force constants of the $[\text{Re}(\text{CO})_3(\alpha\text{-diimine})]^-$ anions in comparison with the stable six-coordinated anions $[\text{Re}(\text{CO})_3(\alpha\text{-diimine})\text{L}]^-$ (α -diimine = dapa, $\text{L}' = \text{P}(\text{OMe})_3$, *n*-PrCN; α -diimine = abpy, $\text{L}' = \text{THF}$, PPh_3) (Tables 1–3).

One-electron reduction of $[\text{Re}(\text{CO})_3(\text{abpy})\text{Br}]^-$ or $[\text{Re}(\text{CO})_3(\text{abpy})(\text{THF})]^-$ produced the doubly reduced six-coordinated $[\text{Re}(\text{CO})_3(\text{abpy})(\text{THF})]^{2-}$ complex. The six-coordinated geometry of the latter anionic complex indicates a relatively low donor ability of the abpy dianion. This implies that both added electrons are accommodated completely in the lowest π^* orbital of the abpy ligand localized³¹ on its azo bond. Such a distribution of the electron density over the abpy ligand induces only the dissociation of the negatively charged halide, but the Re–THF bond remains thermally stable. The one-electron reduction of $[\text{Re}(\text{CO})_3(\text{abpy})(\text{PPh}_3)]^-$ to give $[\text{Re}(\text{CO})_3(\text{abpy})(\text{PPh}_3)]^{2-}$ may obviously be explained in the same way.

The Third One-Electron Reduction Step. The third reduction step at rather negative potentials was observed only for the abpy complexes. One-electron reduction of $[\text{Re}(\text{CO})_3(\text{abpy})(\text{THF})]^-$ or $[\text{Re}(\text{CO})_3(\text{abpy})(\text{PPh}_3)]^-$ resulted in the formation of complexes with slightly different CO-stretching frequencies. Therefore, it was decided that $\{[\text{Re}(\text{CO})_3(\text{abpy})]^{2-} \cdot \text{THF}\}$ and $\{[\text{Re}(\text{CO})_3(\text{abpy})]^{2-} \cdot \text{PPh}_3\}$ were formed, respectively. The weak interaction of the donor solvent and/or phosphine molecule with five-coordinated $[\text{Re}(\text{CO})_3(\text{abpy})]^{2-}$ suggests that the abpy ligand can partly accommodate even the third added electron, probably on the pyridyl rings. Thus, only the third reduction step led in this case to the splitting of the Re– L' bond ($\text{L}' = \text{THF}$, PPh_3). This behavior reflects the considerably increased π -donor character of formally abpy^{3-} , which corresponds to the population of another π^* orbital of much higher energy. Noteworthy, two one-electron and one two-electron reduction steps, localized on abpy, have recently been reported³¹ for the $[(\text{Ru}(\text{bpy})_2)_2(\mu\text{-abpy})]^{4+}$ complex. The exceptional π -acceptor ability of the bridging, easily reducible abpy ligand has been explained by a considerably low energy of its frontier π^* orbitals.

The $[\text{Re}(\text{CO})_3(\text{N,N-dapa})\text{L}']$ ($\text{L}' = \text{Br}^-$, Otf^-) Complexes. The energy of the π^* SOMO of the dapa ligand in the complexes $[\text{Re}(\text{CO})_3(\text{N,N-dapa})\text{L}']^{0/+}$ is comparable with the energy of the π^* SOMO of *i*-Pr-PyCa (Table 7). Nevertheless, no dimeric products, characteristic for the *i*-Pr-PyCa complexes, were formed upon one-electron reduction of $[\text{Re}(\text{CO})_3(\text{N,N-dapa})\text{Br}]$. Apart from possible, but less important steric reasons, this is presumably due to the ability of the third nitrogen atom of the dapa ligand to coordinate at the open site on the Re center, created by dissociation of Br^- from $[\text{Re}(\text{CO})_3$

$(\text{N,N-dapa})\text{Br}]^-$. This was manifested by the one-electron reduction of $[\text{Re}(\text{CO})_3(\text{N,N-dapa})\text{L}']^{0/+}$ ($\text{L}' = \text{Br}^-$, Otf^-) in the presence of excess PPh_3 . Although in both reactions the $[\text{Re}(\text{CO})_3(\text{N,N-dapa})(\text{PPh}_3)]^-$ complex was formed as the main product, the $[\text{Re}(\text{CO})_3(\text{N,N,N-dapa})]$ complex was observed as the second, minor product. It is obvious from these results that the third nitrogen atom of the reduced dapa ligand can compete even with PPh_3 for coordination at the open site on Re, due to energetically convenient closure of the second chelate bond.

In view of the above-mentioned, it is not surprising that the one-electron reduction of the radical complexes $[\text{Re}(\text{CO})_3(\text{N,N,N-dapa})]$ and $[\text{Re}(\text{CO})_3(\text{N,N-dapa})(\text{PPh}_3)]^-$ gave rise to the formation of the anionic $[\text{Re}(\text{CO})_3(\text{N,N,N-dapa})]^-$ complex. Due to the same reasons as already discussed for the analogous $[\text{Re}(\text{CO})_3(\alpha\text{-diimine})(\text{PPh}_3)]^-$ (α -diimine = bpy, *i*-Pr-PyCa, dpp) complexes, $[\text{Re}(\text{CO})_3(\text{N,N-dapa})(\text{PPh}_3)]^-$ loses the PPh_3 ligand after one-electron reduction. Like the *i*-Pr-PyCa dianion, coordinated dapa^{2-} also possesses strong donor character, which in turn makes the interaction of its third nitrogen with the Re center in $[\text{Re}(\text{CO})_3(\text{N,N,N-dapa})]^-$ rather weak.

One-electron reduction of $[\text{Re}(\text{CO})_3(\text{N,N-dapa})(\text{P}(\text{OMe})_3)]^+$ in the presence of excess $\text{P}(\text{OMe})_3$ produced $[\text{Re}(\text{CO})_3(\text{N,N-dapa})(\text{P}(\text{OMe})_3)]^-$. Subsequently, this complex readily transformed into $[\text{Re}(\text{CO})_2(\text{N,N-dapa})(\text{P}(\text{OMe})_3)_2]^-$. Recently, a similar reduction-induced CO-substitution reaction has been observed³² for $[\text{Ru}(\text{CO})_2(\text{i-Pr-DAB})(\text{Me})(\text{P}(\text{OMe})_3)]^+$, which was reduced in the presence of excess $\text{P}(\text{OMe})_3$ to give $[\text{Ru}(\text{CO})(\text{i-Pr-DAB})(\text{Me})(\text{P}(\text{OMe})_3)_2]^-$. For both the Re and Ru complex, no CO substitution was observed in the presence of excess PPh_3 . This may be due to the stronger π -acceptor character and smaller cone angle of $\text{P}(\text{OMe})_3$ compared with PPh_3 . Nevertheless, the electron density on the Re center strongly increases upon substitution of CO by $\text{P}(\text{OMe})_3$, as displayed by the much lower k_{av} value of $[\text{Re}(\text{CO})_2(\text{N,N-dapa})(\text{P}(\text{OMe})_3)_2]^-$ ($k_{\text{av}} = 1460 \text{ Nm}^{-1}$) compared with $[\text{Re}(\text{CO})_3(\text{N,N-dapa})(\text{P}(\text{OMe})_3)]^-$ ($k_{\text{av}} = 1535 \text{ Nm}^{-1}$). Therefore, it is understandable that one-electron reduction of $[\text{Re}(\text{CO})_2(\text{N,N-dapa})(\text{P}(\text{OMe})_3)_2]^-$ leads to a dissociation of one of the $\text{P}(\text{OMe})_3$ ligands. Noteworthy, one $\text{P}(\text{OMe})_3$ ligand still remains coordinated in the anionic $[\text{Re}(\text{CO})_3(\text{N,N-dapa})(\text{P}(\text{OMe})_3)]^-$ product due to its significant π -acceptor character, which can compensate for the strongly increased donor power of dapa upon its reduction to formal dianion. The open site on the Re center is reoccupied by CO still present in the solution. A similar reaction has been observed for the $[\text{Re}(\text{CO})_2(\text{DBSQ})(\text{PPh}_3)_2]$ complex, which reacted to give $[\text{Re}(\text{CO})_3(\text{DBCat})(\text{PPh}_3)]^-$ upon one-electron reduction in the presence of CO.²¹ The reverse substitution of $\text{P}(\text{OMe})_3$ by CO strongly decreases the electron density in the Re d_{π} orbitals. This is evidenced by the increase of k_{av} when $[\text{Re}(\text{CO})_2(\text{N,N-dapa})(\text{P}(\text{OMe})_3)_2]^-$ ($k_{\text{av}} = 1460 \text{ Nm}^{-1}$) transforms into $[\text{Re}(\text{CO})_3(\text{N,N-dapa})(\text{P}(\text{OMe})_3)]^-$ ($k_{\text{av}} = 1490 \text{ Nm}^{-1}$), despite a second electron is added to the complex.

Summary and Conclusions

(1) The combination of cyclic voltammetry and in situ spectroelectrochemical FTIR and UV/vis measurements

(31) Krejčík, M.; Zális, S.; Klíma, J.; Sýkora, D.; Matheis, D.; Klein, A.; Kaim, W. *Inorg.Chem.* **1993**, *32*, 3362.

(32) Nieuwenhuis, H. A.; Hartl, F.; Stufkens, D. J. To be published.

provided an excellent tool for the elucidation of the reduction pathways for a series of complexes $[\text{Re}(\text{CO})_3(\alpha\text{-diimine})\text{L}]^{0/+}$ ($\alpha\text{-diimine} = \text{bpy}, i\text{-Pr-PyCa}, \text{dapa}, \text{dpp}, \text{abpy}$; $\text{L}' = \text{Br}^-$, donor solvent, PR_3 , $\text{P}(\text{OR})_3$).

(2) The stability of the $\text{Re-L}'$ bond in the radical products of the first one-electron reduction, $[\text{Re}(\text{CO})_3(\alpha\text{-diimine})\text{L}]^{-/}$, appeared to increase in the order $\text{bpy} < i\text{-Pr-PyCa} < \text{dapa} < \text{dpp} < \text{abpy}$, i.e. with the ability of the $\alpha\text{-diimine}$ ligand to accommodate the unpaired electron in its π^* LUMO, as was manifested by the less negative reduction potentials of the parent complexes and by the increasing CO force constants of the radical products in the same order.

(3) The second one-electron reduction step drastically destabilizes the coordination of the ligand L' and leads to the delocalized $\text{Re}^{-(\alpha\text{-diimine}^{2-})} \pi$ bonding in the five-coordinated anions $[\text{Re}(\text{CO})_3(\alpha\text{-diimine})]^-$ ($\alpha\text{-diimine} = \text{bpy}, i\text{-Pr-PyCa}, \text{dpp}$).

(4) The six-coordinated anionic complexes $[\text{Re}(\text{CO})_3(\alpha\text{-diimine})\text{L}]^-$ may be formed under the following circumstances: (a) $\alpha\text{-diimine}$ accommodates completely both added electrons (abpy with the easily reducible azo bond); (b) L' is an efficient π -acceptor ligand like $\text{P}(\text{OR})_3$ or $\text{CO}^{2\ominus}$; (c) L' is present in a very large excess (the $n\text{-PrCN}$ solvent); (d) $\alpha\text{-diimine}$ coordinates as a tripodate ligand (dapa: L' is then the third nitrogen atom).

Acknowledgment. Dr. A. Vlček, Jr. is thanked for his critical reading of the manuscript. Thanks are due to the Netherlands Foundation for Chemical Research (SON) and the Netherlands Organization for the Advancement of Pure Research (NWO) for their financial support.

OM9402832

Formation of Antiferromagnetic Heteronuclear Thiolate- and Sulfide-Bridged Complexes. 4. Synthesis of Triangular Clusters with CrRe₂ and Cr₂Re Cores

Igor L. Eremenko, Sergei Nefedov, and Heinz Berke*

Institute of Inorganic Chemistry, University of Zurich, Winterthurerstrasse 190, CH-8057 Zurich, Switzerland

Boris I. Kolobkov and Vladimir M. Novotortsev

Institute of General and Inorganic Chemistry of the Russian Academy of Sciences, Leninsky prosp. 31, 117907 Moscow, Russia

Received June 13, 1994[®]

The thermolysis of Cp₂Cr₂(μ-SCMe₃)₂(μ₃-S)Re(CO)₂(NO)Cl₂ (**4**) either in benzene under an atmosphere of CO (70–80 °C) or in the presence of Co₂(CO)₈ (70 °C) was studied. In both cases the formation of the tetranuclear cluster [CpCr(μ-SCMe₃)₂(μ₃-S)Re(CO)(NO)]₂ (**5**) was observed. Under a CO atmosphere **5** transformed into two main products: the known antiferromagnetic Cp₂Cr₂(μ-SCMe₃)₂(μ₃-S)₂Re(CO)(NO) cluster (**2a**) and the paramagnetic CpCr(μ-SCMe₃)Re(CO)(NO)(μ₃-S)₂(μ-SCMe₃)Re(CO)₂(NO) compound (**6**; Cr–Re(1) = 3.068(2) Å, Cr–Re(2) = 3.391(2) Å, Re(1)–Re(2) = 3.317(1) Å, μ_{eff} = 3.80 μ_B (289–282 K)). Carbonylation of **5** was achieved in the presence of Co₂(CO)₈. One NO group was lost, producing a CpCr(μ-SCMe₃)Re(CO)(NO)(μ₃-S)(μ₃-SCMe₃)(μ-SCMe₃)Re(CO)₃ cluster (**7**; Cr–Re(2) = 3.150(2) Å, Cr–Re(1) = 3.668(2) Å, Re(1)–Re(2) = 3.454(1) Å, μ_{eff} = 3.68 μ_B (289–282 K)) and **2a**. The oxidation of **2a** by I₂ (CH₂Cl₂, 22 °C) led to the antiferromagnetic Cp₂Cr₂(μ-SCMe₃)₂(μ₃-S)₂Re(NO)I complex (**9**; Cr(1)–Re = 2.744(5) Å, Cr(2)–Re = 3.034(5) Å, Cr(1)–Cr(2) = 3.139(6) Å) containing three magnetically coupled metal centers (–2J(Cr–Cr) = 70 cm^{–1}, –2J(Cr–Re)_{av} = 302 cm^{–1}). **9** can be reconverted into **2a** through reaction with an excess of Co₂(CO)₈. Compounds **6**, **7**, and **9** were characterized by X-ray analyses. Crystal data: **6**, space group P2₁/c, a = 17.133(7) Å, b = 12.294(4) Å, c = 11.672(5) Å, β = 92.61(3)°, Z = 4, V = 2456(2) Å³; **7**, space group P2₁/c, a = 15.979(7) Å, b = 12.065(4) Å, c = 16.424(7) Å, β = 104.95(2)°, Z = 4, V = 3059(2) Å³; **9**, space group P2₁, a = 9.669(4) Å, b = 11.758(6) Å, c = 11.913(5) Å, β = 107.56(2)°, Z = 2, V = 1291(1) Å³.

Introduction

Recently we have shown that remetallation processes can be utilized for the synthesis of triangular antiferromagnetic clusters with Cr₂Re¹ and Cr₂W^{2,3} cores. The reaction of the binuclear Cp₂Cr₂(μ-SCMe₃)₂(μ-S) complex (**1**) with sources of halogen and nitrosyl-containing Re or W fragments afforded Cp₂Cr₂(μ-SCMe₃)₂(μ₃-S)₂M(NO)X clusters (**2a**, M(NO)X = Re(NO)(CO); **2b**, M(NO)X = W(NO)₂; **2c**, M(NO)X = W(NO)(SCMe₃); **2d**, M(NO)X = W(NO)Cl). These reactions proceeded via the intermediacy of short-lived heterobinuclear CpCr(μ-SCMe₃)₂(μ-S)M(NO)L_n species (**3**; M = Re, W), which at elevated temperatures incorporated a CpCrS fragment (from **1**) to yield the clusters **2**.^{1–3} The binuclear complexes **3** may be applied as basic blocks in subsequent cluster-building processes. Following this idea, we now report about the preparation of two new paramagnetic clusters with CrRe₂ cores and about another Cr₂Re cluster containing three magnetically coupled metal centers.

Results and Discussion

Thermolysis of the Cp₂Cr₂(μ-SCMe₃)₂(μ₃-S)Re(NO)(CO)₂Cl₂ Adduct under a CO Atmosphere or in the Presence of Co₂(CO)₈. It was found earlier that the thermolysis of the Cp₂Cr₂(μ-SCMe₃)₂(μ₃-S)Re(NO)(CO)₂Cl₂ (**4**) adduct leads to formation of the tetranuclear [CpCr(μ-SCMe₃)₂(μ₃-S)Re(CO)(NO)]₂ complex (**5**) as a decarbonylated dimeric form of **3**.¹ For the reincorporation of CO in **3** we tried two sources of CO: CO gas and the Co₂(CO)₈ complex. The reaction of **4** with CO takes place in benzene solution at 70–80 °C with a concomitant color change. After some minutes the intermediate formation of **5** was observed. Further heating leads to the complete disappearance of **4** and **5**. Two major products, the clusters Cp₂Cr₂(μ-SCMe₃)₂(μ₃-S)₂Re(CO)(NO) (**2a**) and CpCr(μ-SCMe₃)Re(CO)(NO)(μ₃-S)₂(μ-SCMe₃)Re(CO)₂(NO) (**6**), were finally formed in approximately equal amounts (Scheme 1).

In the IR spectrum **6** shows characteristic ν(CO) (2073, 2062, 1990, and 1973 cm^{–1}) and ν(NO) (1741 and 1707 cm^{–1}) bands. The structure of **6** was determined by an X-ray diffraction study (Figure 1, Table 1). It contains the CpCr(μ-SCMe₃)Re(CO)(NO) unit (Cr(1)–Re(1) = 3.068(2) Å, Cr(1)–SR = 2.359(3) Å, Re(1)–SR = 2.435(2) Å, Cp(cen)–Cr–Re = 176.8(2)°, which is also part of **5**. The Cr(1) and Re(1) centers are additionally

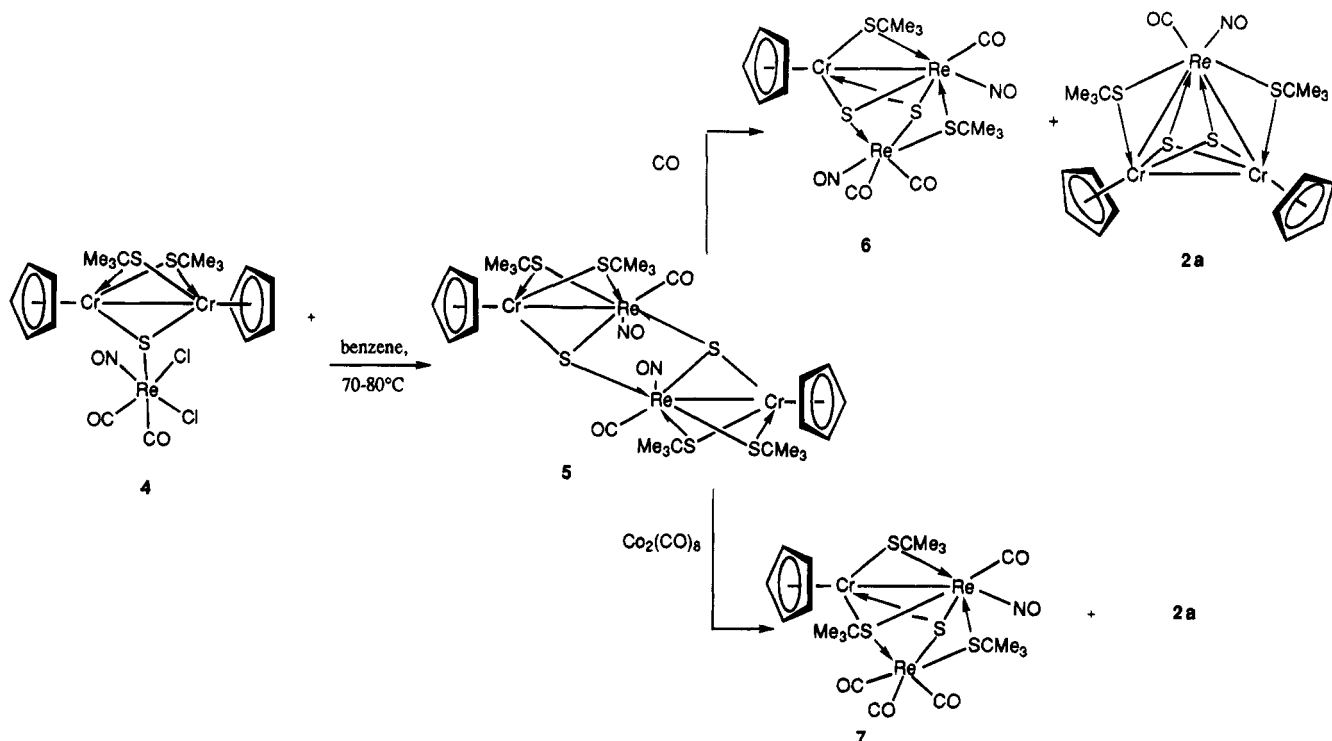
[®] Abstract published in *Advance ACS Abstracts*, February 1, 1995.

(1) Eremenko, I. L.; Berke, H.; Kolobkov, B. I.; Novotortsev, V. M. *Organometallics* 1994, 13, 244.

(2) Eremenko, I. L.; Berke, H.; Van der Zeijden, A. A. H.; Kolobkov, B. I.; Novotortsev, V. M. *J. Organomet. Chem.* 1994, 471, 123.

(3) Eremenko, I. L.; Rosenberger, S.; Nefedov, S. E.; Berke, H.; Novotortsev, V. M. *Inorg. Chem.*, in press.

Scheme 1



bridged by two sulfide ligands ($\text{Cr}-\text{S} = 2 \times 2.374(3) \text{ \AA}$, $\text{Re}(1)-\text{S} = 2.515(2)$ and $2.519(2) \text{ \AA}$). These two sulfur atoms are also involved in binding to the $\text{Re}(\text{CO})_2(\text{NO})$ moiety ($\text{Re}(2)-\text{S} = 2.484(2)$ and $2.499(2) \text{ \AA}$). The second thiolate group in **6** bridges the $\text{Re}(1)$ and $\text{Re}(2)$ atoms ($\text{Re}(1)-\text{S}(3) = 2.443(2) \text{ \AA}$, $\text{Re}(2)-\text{S}(3) = 2.491(2) \text{ \AA}$). Judging from the bond distances there are no bonding contacts between $\text{Re}(2)$ and the $\text{Cr}(1)$ and $\text{Re}(2)$ centers ($\text{Re}(2)-\text{Cr}(1) = 3.391(2) \text{ \AA}$, $\text{Re}(2)-\text{Re}(1) = 3.317(1) \text{ \AA}$).

In the presence of $\text{Co}_2(\text{CO})_8$ the thermolysis of **4** takes a course similar to the reaction under a CO atmosphere. At $70-80 \text{ }^\circ\text{C}$ in benzene evolution of CO and formation of **5** are observed. After 10–15 min the starting materials and **5** have disappeared and **2a** and a $\text{CpCr}(\mu\text{-SCMe}_3)\text{Re}(\text{CO})(\text{NO})(\mu_3\text{-S})(\mu_3\text{-SCMe}_3)(\mu\text{-SCMe}_3)\text{Re}(\text{CO})_3$ compound (**7**) are formed as the main components of the reaction mixture (Scheme 1). The IR spectrum of **7** exhibits $\nu(\text{CO})$ ($2010, 1964, 1952, 1908$ and 1882 cm^{-1}) and $\nu(\text{NO})$ (1716 cm^{-1}) bands. The structure of this molecule was also established by single-crystal X-ray diffraction (Figure 2, Table 2). **7** contains, like **5** and **6**, the heterobinuclear $\text{CpCr}(\mu\text{-SCMe}_3)\text{Re}(\text{CO})(\text{NO})$ unit ($\text{Cr}(1)-\text{Re}(2) = 3.150(2) \text{ \AA}$, $\text{Cr}(1)-\text{S}(3) = 2.369(4) \text{ \AA}$, $\text{Re}(2)-\text{S}(3) = 2.442(3) \text{ \AA}$) bearing a practically linear $\text{Cp}(\text{cen})\text{-Cr-Re}$ arrangement ($178.3(2)^\circ$). **7** has two other bridges: one thiolate ($\text{Cr}-\text{S} = 2.399(3) \text{ \AA}$, $\text{Re}(2)-\text{S} = 2.501(3) \text{ \AA}$) and one sulfide ($\text{Cr}-\text{S} = 2.360(3) \text{ \AA}$, $\text{Re}(2)-\text{S} = 2.504(3) \text{ \AA}$), which connect to the $\text{Re}(\text{CO})_3$ fragment ($\text{Re}(1)-\text{SR} = 2.556(3) \text{ \AA}$, $\text{Re}(2)-\text{S} = 2.517(3) \text{ \AA}$, $\text{Re}(1)-\text{Cr}(1) = 3.668(2) \text{ \AA}$). In addition a third SCMe_3 bridge holds the rhenium atoms in **7** together ($\text{Re}(1)-\text{S} = 2.516(3) \text{ \AA}$, $\text{Re}(2)-\text{S} = 2.432(3) \text{ \AA}$, $\text{Re}(1)-\text{Re}(2) = 3.454(1) \text{ \AA}$).

($\text{CO})_3$ compound (**7**) are formed as the main components of the reaction mixture (Scheme 1). The IR spectrum of **7** exhibits $\nu(\text{CO})$ ($2010, 1964, 1952, 1908$ and 1882 cm^{-1}) and $\nu(\text{NO})$ (1716 cm^{-1}) bands. The structure of this molecule was also established by single-crystal X-ray diffraction (Figure 2, Table 2). **7** contains, like **5** and **6**, the heterobinuclear $\text{CpCr}(\mu\text{-SCMe}_3)\text{Re}(\text{CO})(\text{NO})$ unit ($\text{Cr}(1)-\text{Re}(2) = 3.150(2) \text{ \AA}$, $\text{Cr}(1)-\text{S}(3) = 2.369(4) \text{ \AA}$, $\text{Re}(2)-\text{S}(3) = 2.442(3) \text{ \AA}$) bearing a practically linear $\text{Cp}(\text{cen})\text{-Cr-Re}$ arrangement ($178.3(2)^\circ$). **7** has two other bridges: one thiolate ($\text{Cr}-\text{S} = 2.399(3) \text{ \AA}$, $\text{Re}(2)-\text{S} = 2.501(3) \text{ \AA}$) and one sulfide ($\text{Cr}-\text{S} = 2.360(3) \text{ \AA}$, $\text{Re}(2)-\text{S} = 2.504(3) \text{ \AA}$), which connect to the $\text{Re}(\text{CO})_3$ fragment ($\text{Re}(1)-\text{SR} = 2.556(3) \text{ \AA}$, $\text{Re}(2)-\text{S} = 2.517(3) \text{ \AA}$, $\text{Re}(1)-\text{Cr}(1) = 3.668(2) \text{ \AA}$). In addition a third SCMe_3 bridge holds the rhenium atoms in **7** together ($\text{Re}(1)-\text{S} = 2.516(3) \text{ \AA}$, $\text{Re}(2)-\text{S} = 2.432(3) \text{ \AA}$, $\text{Re}(1)-\text{Re}(2) = 3.454(1) \text{ \AA}$).

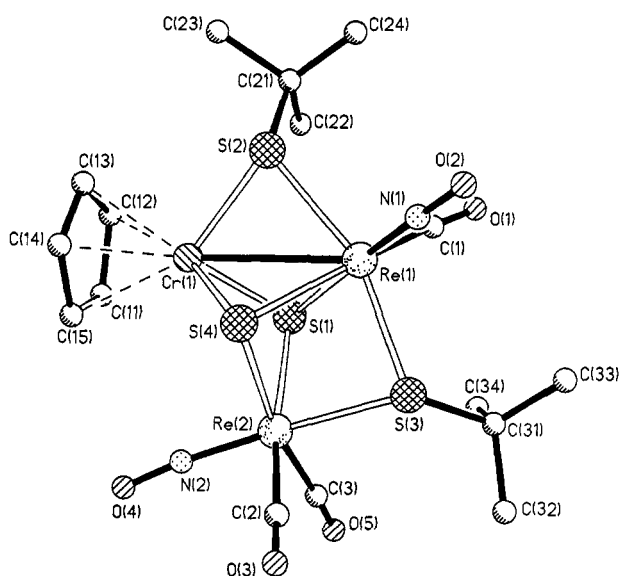


Figure 1. Molecular structure of $\text{CpCr}(\mu\text{-SCMe}_3)\text{Re}(\text{CO})(\text{NO})(\mu_3\text{-S})_2(\mu\text{-SCMe}_3)\text{Re}(\text{CO})_2(\text{NO})$ (**6**).

Table 1. Selected Bond Lengths (\AA) and Bond Angles (deg) for **6**

$\text{Re}(1)-\text{Cr}(1)$	3.068(2)	$\text{Re}(1)-\text{S}(1)$	2.515(2)
$\text{Re}(1)-\text{S}(2)$	2.435(2)	$\text{Re}(1)-\text{S}(3)$	2.443(2)
$\text{Re}(1)-\text{S}(4)$	2.519(3)	$\text{Re}(1)-\text{N}(1)$	1.767(8)
$\text{Re}(1)-\text{C}(1)$	1.918(9)	$\text{Re}(2)-\text{S}(1)$	2.484(2)
$\text{Re}(2)-\text{S}(3)$	2.491(2)	$\text{Re}(2)-\text{S}(4)$	2.499(2)
$\text{Re}(2)-\text{N}(2)$	1.839(9)	$\text{Re}(2)-\text{C}(2)$	1.974(10)
$\text{Re}(2)-\text{C}(3)$	1.945(10)	$\text{Cr}(1)-\text{S}(1)$	2.374(3)
$\text{Cr}(1)-\text{S}(2)$	2.359(3)	$\text{Cr}(1)-\text{S}(4)$	2.374(3)
$\text{N}(1)-\text{O}(1)$	1.199(11)	$\text{N}(2)-\text{O}(2)$	1.162(13)
$\text{C}(1)-\text{O}(1)$	1.163(12)	$\text{C}(2)-\text{O}(2)$	1.127(14)
$\text{C}(3)-\text{O}(3)$	1.150(13)		
$\text{S}(1)-\text{Re}(1)-\text{S}(2)$	86.9(1)	$\text{Re}(1)-\text{S}(4)-\text{Cr}(1)$	77.6(1)
$\text{S}(2)-\text{Re}(1)-\text{S}(3)$	158.4(1)	$\text{S}(1)-\text{Re}(1)-\text{S}(4)$	77.6(1)
$\text{S}(1)-\text{Re}(1)-\text{S}(4)$	80.2(1)	$\text{S}(3)-\text{Re}(1)-\text{S}(4)$	78.5(1)
$\text{S}(1)-\text{Re}(2)-\text{S}(3)$	84.6(1)	$\text{S}(2)-\text{Cr}(1)-\text{S}(4)$	84.8(1)
$\text{S}(3)-\text{Re}(2)-\text{S}(4)$	78.0(1)	$\text{Re}(1)-\text{S}(1)-\text{Re}(2)$	83.1(1)
$\text{S}(1)-\text{Cr}(1)-\text{S}(4)$	83.3(1)	$\text{Re}(1)-\text{S}(2)-\text{Cr}(1)$	79.6(1)
$\text{Re}(1)-\text{S}(1)-\text{Cr}(1)$	77.7(1)	$\text{Re}(1)-\text{S}(4)-\text{Re}(2)$	82.8(1)
$\text{Re}(2)-\text{S}(1)-\text{Cr}(1)$	88.5(1)	$\text{Re}(2)-\text{S}(4)-\text{Cr}(1)$	88.2(1)
$\text{Re}(1)-\text{S}(3)-\text{Re}(2)$	84.5(1)		

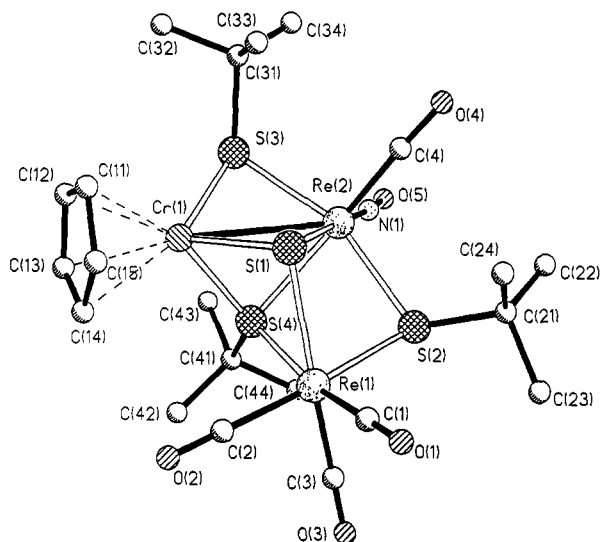
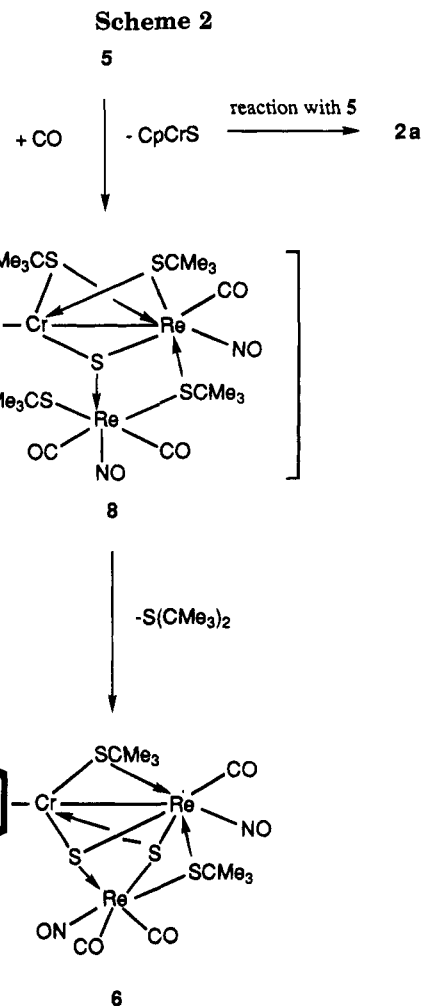


Figure 2. Perspective view of the molecular structure of $\text{CpCr}(\mu\text{-SCMe}_3)\text{Re}(\text{CO})(\text{NO})(\mu_3\text{-S})(\mu_3\text{-SCMe}_3)(\mu\text{-SCMe}_3)\text{Re}(\text{CO})_3$ (**7**).

Table 2. Selected Bond Lengths (Å) and Bond Angles (deg) for **7**

Re(1)–S(1)	2.556(3)	Re(1)–S(2)	2.516(3)
Re(1)–S(4)	2.517(3)	Re(1)–C(1)	1.943(15)
Re(1)–C(2)	1.960(11)	Re(1)–C(3)	1.896(15)
Re(2)–Cr(1)	3.150(2)	Re(2)–S(1)	2.504(3)
Re(2)–S(2)	2.432(3)	Re(2)–S(3)	2.442(3)
Re(2)–S(4)	2.501(3)	Re(2)–N(1)	1.775(10)
Re(2)–C(4)	1.908(15)	Cr(1)–S(1)	2.360(3)
Cr(1)–S(3)	2.369(4)	Cr(1)–S(4)	2.399(3)
N(1)–O(5)	1.195(16)	C(1)–O(1)	1.111(19)
C(2)–O(2)	1.150(16)	C(3)–O(3)	1.145(21)
C(4)–O(4)	1.176(18)		
S(1)–Re(1)–S(2)	81.6(1)	S(1)–Re(1)–S(4)	70.8(1)
S(2)–Re(1)–S(4)	76.8(1)	S(1)–Re(2)–S(2)	84.3(1)
S(1)–Re(2)–S(3)	86.1(1)	S(1)–Re(2)–S(4)	71.9(1)
S(2)–Re(1)–S(3)	159.9(1)	S(2)–Re(2)–S(4)	78.7(1)
S(3)–Re(2)–S(4)	81.6(1)	S(1)–Cr(1)–S(3)	91.1(1)
S(1)–Cr(1)–S(4)	76.2(1)	S(3)–Cr(1)–S(4)	85.3(1)
Re(1)–S(1)–Re(2)	86.1(1)	Re(1)–S(1)–Cr(1)	96.4(1)
Re(2)–S(1)–Cr(1)	80.7(1)	Re(1)–S(2)–Re(2)	88.5(1)
Re(2)–S(3)–Cr(1)	81.8(1)	Re(1)–S(4)–Re(2)	87.0(1)
Re(2)–S(4)–Cr(1)	96.5(1)	Re(2)–S(4)–Cr(1)	80.0(1)

It has been mentioned earlier that the primary intermediate of reactions of **4** under CO or in the presence of $\text{Co}_2(\text{CO})_8$ is the cluster **5**. Further carbonylation of it then takes place, causing rupture of one of the binuclear Cr,Re fragments. The intermediate **8** and a CpCrS unit are generated (Scheme 2). **8** stabilizes itself with elimination of a SR_2 moiety to yield the cluster **6**. The released CpCrS unit attacks another molecule of **5**, forming **2a** with a Cr_2Re core. The same step sequence was observed when **2a** was formed from the reaction of **5** with **1**.¹ It has been reported earlier that $\text{Co}_2(\text{CO})_8$ can act as a carbonylating agent at elevated temperatures.⁴ Thus, **8** might also appear as a reactive intermediate in this case. However, the presence of coordinatively unsaturated Co-containing fragments might then induce ligand exchange between one NO group and one terminal SR ligand from the peripheral Re center in **8**. Uptake of a CO group at this atom completes the $\text{Re}(\text{CO})_3$ moiety, which is additionally coordinated by one of the SR bridges of the



heterobinuclear Cr,Re unit. The formal replacement of one three-electron NO donor at the Re center in **6** with the two-electron-donor CO ligand in **7** makes it necessary to count the tridentate SR bridge in **7** as a five-electron ligand. Instead, the sulfide atom in **6** has to act as a four-electron donor.

The paramagnetism of both compounds is caused by the presence of a Cr(III) atom containing three unpaired electrons. The effective magnetic moments of **6** ($3.80 \mu_{\text{B}}$) and of **7** ($3.68 \mu_{\text{B}}$) are close to the pure spin-only value and are not dependent on temperature (289–282 K). From the presence of half-occupied orbitals at the Cr and from the 18-electron configuration at the Re centers in the linear CpCrRe units of **5–7** follows a 3-electron and therefore half-order bond between the Cr and the Re atom. An analogous electron count is given for one of the isomers of **2a**.³ For the formation of a single Re–Cr bond it would be necessary to remove one electron from the Cr_2Re core, which could principally be achieved by oxidation of the Re(I) center in **2a**.

Formation of the $\text{Cp}_2\text{Cr}_2(\mu\text{-SCMe}_3)_2(\mu_3\text{-S})_2\text{Re}(\text{NO})\text{I}$ Cluster. The oxidation was attempted by the reaction of the $\text{Cp}_2\text{Cr}_2(\mu\text{-SCMe}_3)_2(\mu_3\text{-S})_2\text{Re}(\text{NO})(\text{CO})$ cluster (**2a**) with various sources of atomic selenium such as Se_8 (powder) in THF or in CH_2Cl_2 (20–65 °C) or KNCS in THF/EtOH solution (20–70 °C); these attempts, however, were not successful. The oxidation of **2a** was then accomplished at room temperature in CH_2Cl_2 with I_2 . A single soluble product, the antiferromagnetic $\text{Cp}_2\text{Cr}_2(\mu\text{-SCMe}_3)_2(\mu_3\text{-S})_2\text{Re}(\text{NO})\text{I}$ cluster (**9**) was formed ($\mu_{\text{eff}}/\text{Cr}$ at = 1.40 (284 K)–1.043 (111 K) μ_{B})

(4) See for example: Pasynskii, A. A.; Eremenko, I. L.; Nefedov, S. E.; Yanovsky, A. A.; Struchkov, Yu. T.; Shaposhnikova, A. D.; Stadnichenko, R. A. *Russ. J. Inorg. Chem. (Engl. Transl.)* **1993**, *38*, 423.

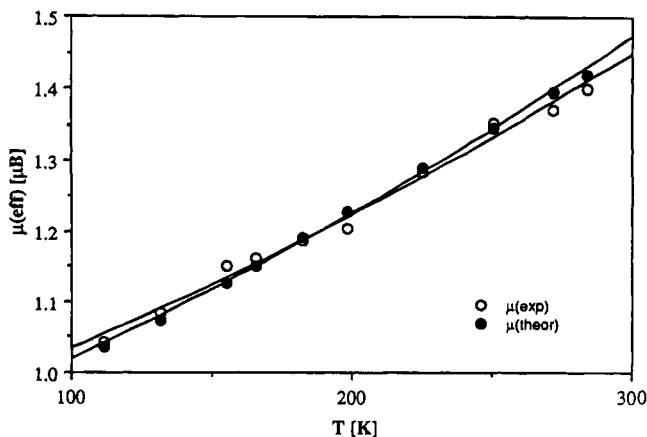
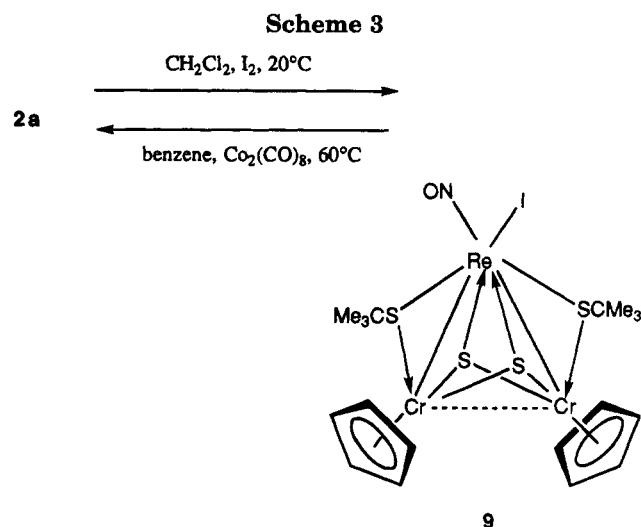


Figure 3. Plot of the theoretical and experimental temperature dependence of the magnetic moment μ_{eff} for **9**.



(Figure 3) (Scheme 3). **9** cannot be further oxidized to a corresponding cation with excess I_2 or with TCNQ. The reduction of **9** by $\text{Co}_2(\text{CO})_8$ leads to a practically quantitative yield of **2a**. This reaction is accompanied by the formation of $\text{Co}_4(\text{CO})_{12}$.

The IR spectrum ($2100\text{--}1500\text{ cm}^{-1}$) of **9** showed only one $\nu(\text{NO})$ (1687 cm^{-1}) band. The single-crystal X-ray investigation of **9** confirmed that it had the same Cr₂Re core as **2a** (Figure 4, Table 3). However there is one electron less at the 17-electron Re center in **9**, since a CO group is replaced by an I atom ($\text{Re}\text{--}\text{I} = 2.764(3)\text{ \AA}$, $\text{Re}\text{--}\text{N} = 1.901(21)\text{ \AA}$). This leads to a dramatic structural distortion of the metal triangle. In **9** one Re–Cr bond ($3.034(5)\text{ \AA}$) is long and close to the value of **2a** ($2 \times 3.080(2)\text{ \AA}$ in the isomer with half-order Re–Cr bonds;³ $2 \times 2.940(5)\text{ \AA}$ in the other isomer of **2a**¹). The second Re–Cr distance in **9** is short ($2.744(5)\text{ \AA}$) and represents a single bond. There is a significant elongation of the Cr–Cr separation ($3.139(6)\text{ \AA}$) in **9** compared with the related distances in **2a** ($3.002(4)$ ³ and $3.010(6)\text{ \AA}$ ¹ in both isomers). The spin–spin exchange energies between the Cr(III) centers of the magnetic $\text{Cp}_2\text{Cr}_2\text{S}_2$ system in **2a** ($-2J(\text{Cr}\text{--}\text{Cr}) = 231\text{ cm}^{-1}$) and in **9** ($-2J(\text{Cr}\text{--}\text{Cr}) = 70\text{ cm}^{-1}$) therefore strongly differ. The latter value (below 100 cm^{-1}) is typical for binuclear $\text{Cp}_2\text{X}_2\text{Cr}^{\text{III}}_2$ species with two bridges and a bent geometry without Cr–Cr interaction. For example, the $\text{Cp}_2\text{Cr}_2(\text{OCMe}_3)_2(\mu\text{--OCMe}_3)_2$ complex has a $-2J$ value of 70

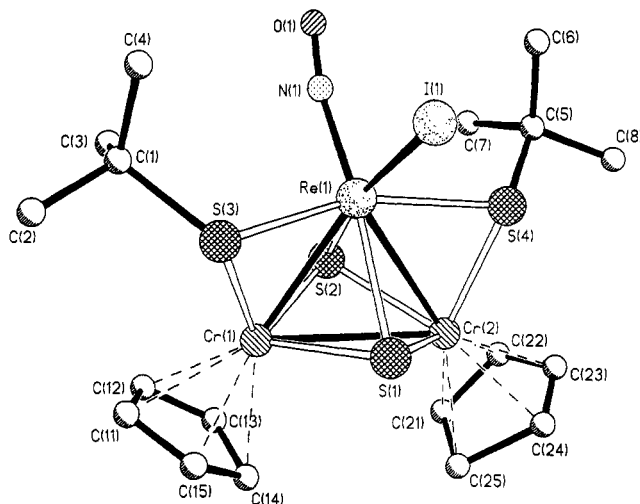


Figure 4. Perspective view of the molecular structure of $\text{Cp}_2\text{Cr}_2(\mu\text{--SCMe}_3)_2(\mu_3\text{--S})_2\text{Re}(\text{NO})\text{I}$ (**9**).

Table 3. Selected Bond Lengths (\AA) and Bond Angles (deg) for **9**

Re(1)–I(1)	2.764(3)	Re(1)–Cr(1)	2.744(5)
Re(1)–Cr(2)	3.034(5)	Re(1)–S(1)	2.474(9)
Re(1)–S(2)	2.433(9)	Re(1)–S(3)	2.380(8)
Re(1)–S(4)	2.462(7)	Re(1)–N(1)	1.901(21)
Cr(1)–S(1)	2.314(12)	Cr(1)–S(2)	2.301(11)
Cr(1)–S(3)	2.364(9)	Cr(2)–S(1)	2.351(11)
Cr(2)–S(2)	2.293(10)	Cr(2)–S(4)	2.399(10)
N(1)–O(2)	1.011(34)		
I(1)–Re(1)–S(1)	95.1(2)	I(1)–Re(1)–S(2)	168.3(2)
I(1)–Re(1)–S(3)	90.2(2)	I(1)–Re(1)–S(4)	85.2(2)
I(1)–Re(1)–N(1)	93.5(7)	S(1)–Re(1)–S(2)	81.5(3)
S(1)–Re(1)–S(3)	78.3(3)	S(1)–Re(1)–S(4)	81.2(3)
S(2)–Re(1)–S(3)	100.0(3)	S(2)–Re(1)–S(4)	83.2(3)
S(3)–Re(1)–S(4)	158.6(3)	S(1)–Re(1)–N(1)	170.9(8)
Re(1)–S(1)–Cr(1)	69.8(3)	Re(1)–S(1)–Cr(2)	77.9(3)
Cr(1)–S(1)–Cr(2)	84.6(4)	Re(1)–S(2)–Cr(1)	70.8(3)
Re(1)–S(2)–Cr(2)	79.8(3)	Cr(1)–S(2)–Cr(2)	86.2(3)
Re(1)–S(3)–Cr(1)	70.7(2)	Re(1)–S(4)–Cr(2)	77.2(3)
Re(1)–N(1)–O(1)	157.5(26)		

cm^{-1} .⁵ It was shown in a theoretical study and from investigations of the structure and magnetic properties of chromium alkoxide compounds⁵ that there is no overlap between the semiooccupied orbitals of the chromium atoms. The Cp_2Cr_2 moiety in **9** adopts a bent structure ($\text{Cp}(\text{cen})\text{--}\text{Cr}(1)\text{--}\text{Cr}(2) = 120.2(5)^\circ$, $\text{Cp}(\text{cen})\text{--}\text{Cr}(2)\text{--}\text{Cr}(1) = 130.3(5)^\circ$); however, the $\text{Cp}(\text{cen})\text{--}\text{Cr}\text{--}\text{Re}$ arrangements are almost linear ($\text{Cp}(\text{cen})\text{--}\text{Cr}(1)\text{--}\text{Re} = 177.3(3)^\circ$, $\text{Cp}(\text{cen})\text{--}\text{Cr}(2)\text{--}\text{Re} = 175.9(3)^\circ$). The Re(II) center carries one unpaired electron. An average $-2J(\text{Re}\text{--}\text{Cr})$ value (302 cm^{-1}) was calculated by the Heisenberg–Dirac–Van Vleck (HDVV) model⁶ for a side-equal triangle.⁷ This value, however, does not realistically describe the magnetic behavior of a strongly distorted structure with quite different Re–Cr bonds (spin–spin exchange by a direct mechanism). In cases of a strong asymmetry, as in **9**, there are as yet no models for the proper theoretical treatment. It is hoped that this simulation problem can be solved in the future

(5) Nefedov, S. E.; Pasynskii, A. A.; Eremenko, I. L.; Orazsakhmatov, B.; Novotortsev, V. M.; Ellert, O. G.; Shestakov, A. F.; Yanovsky, A. I.; Struchkov, Yu. T. *J. Organomet. Chem.* **1990**, *384*, 279.

(6) Van Vleck, J. H. *The Theory of Electronic and Magnetic Susceptibilities*; Oxford University Press: London, 1932.

(7) In this case the spin Hamiltonian takes the form $H = -2J_1S_1S_2 - 2J_2(S_1S_3 + S_2S_3) + g\beta H(S_{1z} + S_{2z})$, where J_1 and J_2 are the isotropic exchange parameters, g is the isotropic g factor, and S values are the spins of the exchange-coupled metal atoms ($S_1 = S_2 = 3/2$, $S_3 = 1/2$).

Table 4. Data Collection and Processing Parameters of 6, 7, and 9

	6	7	9
compd	6	7	9
formula	C ₁₆ H ₂₃ CrN ₂ O ₅ Re ₂ S ₄	C ₂₁ H ₃₂ CrNO ₅ Re ₂ S ₄	C ₁₈ H ₂₈ Cr ₂ INOReS ₄
mol wt	876.0	931.1	819.8
color and habit	brown prism	green-brown prism	brown prism
space group	P2 ₁ /c	P2 ₁ /c	P2 ₁
a, Å	17.133(7)	15.979(7)	9.669(4)
b, Å	12.294(4)	12.065(4)	11.758(5)
c, Å	11.672(5)	16.424(7)	11.913(5)
β, deg	92.61(3)	104.95(2)	107.56(2)
V, Å ³	2456(2)	3059(2)	1291(1)
Z	4	4	2
Q _{calcd} , g cm ⁻³	2.369	2.022	2.108
abs coeff, cm ⁻¹	107.51	85.45	70.31
cryst size, mm	0.32 × 0.25 × 0.25	0.30 × 0.35 × 0.20	0.35 × 0.25 × 0.05
scan type	ω-2θ	ω-2θ	ω-2θ
scan speed, deg min ⁻¹	variable; 2.00-14.65	variable; 2.02-14.65	variable; 1.50-14.65
scan width	1.60	1.60	1.80
colcn range	+h,+k,+l	+h,+k,+l	+h,+k,+l
2θ range, deg	3-52	4-52	3-52
no. of unique data	4669	6039	2677
no. of rfl vs obsd (F ≥ 4σ(F))	3880	3567	1683
no. of variables	271	307	252
weighting scheme	w ⁻¹ = σ ² (F) + 0.0050F ²	w ⁻¹ = σ ² (F) + 0.0100F ²	w ⁻¹ = σ ² (F) + 0.0100F ²
R	0.032	0.041	0.058
R _w	0.057	0.059	0.077
residual extrema in final diff map, e Å ⁻³	+0.95 to -1.15	+1.79 to -1.67	+1.72 to -1.59

Table 5. Atomic Coordinates (×10⁴) and Equivalent Isotropic Displacement Coefficients (Å² × 10³) for 6

atom	x	y	z	U(eq) ^a
Re(1)	1921(1)	452(1)	971(1)	21(1)
Re(2)	3706(1)	-148(1)	1997(1)	29(1)
Cr(1)	3056(1)	2373(1)	1261(1)	22(1)
S(1)	2708(1)	1123(2)	2701(2)	23(1)
S(2)	1784(1)	2351(2)	402(2)	23(1)
S(3)	2563(1)	-1289(2)	1374(2)	29(1)
S(4)	3245(1)	768(2)	178(2)	28(1)
O(1)	523(5)	233(6)	2524(7)	44(3)
O(2)	953(6)	-422(6)	-986(7)	55(3)
O(3)	4643(5)	-1790(8)	586(8)	65(3)
O(4)	5194(5)	1024(7)	2651(9)	68(3)
O(5)	3981(5)	-1264(7)	4357(7)	55(3)
N(1)	1372(5)	-70(6)	-223(7)	30(2)
N(2)	4600(6)	626(7)	2373(9)	45(3)
C(1)	1049(5)	331(7)	1936(8)	28(3)
C(2)	4303(6)	-1220(8)	1132(9)	38(3)
C(3)	3862(5)	-868(8)	3474(8)	33(3)
C(11)	3895(6)	3358(8)	2362(8)	33(3)
C(12)	3243(6)	4034(8)	2037(9)	39(3)
C(13)	3259(6)	4126(7)	806(8)	29(3)
C(14)	3894(6)	3503(8)	408(9)	38(3)
C(15)	4277(6)	3033(7)	1395(8)	34(3)
C(21)	1012(6)	3181(7)	1102(8)	32(3)
C(22)	1086(6)	3079(8)	2407(8)	36(3)
C(23)	1156(7)	4355(8)	768(9)	39(3)
C(24)	240(6)	2803(9)	594(9)	40(3)
C(31)	2117(7)	-2221(7)	2456(8)	38(3)
C(32)	2710(8)	-3158(9)	2632(12)	62(5)
C(33)	1341(8)	-2580(9)	1883(9)	50(4)
C(34)	1991(6)	-1657(7)	3618(8)	34(3)

^a Equivalent isotropic *U*, defined as one-third of the trace of the orthogonalized *U*_{ij} tensor.

by an appropriate adjustment of the available standard program package.⁸

Conclusion

Heating of 4 in the presence of CO gas or Co₂(CO)₈ led to the cluster 5 with a Cr₂Re₂ core. The same product was observed when 4 was heated under N₂.¹ The subsequent uptake of the soft CO ligand at one of

Table 6. Atomic Coordinates (×10⁴) and equivalent isotropic displacement coefficients (Å² × 10³) for 7

atom	x	y	z	U(eq) ^a
Re(1)	2514(1)	1467(1)	769(1)	42(1)
Re(2)	2695(1)	-1377(1)	641(1)	36(1)
Cr(1)	1380(1)	-654(2)	1677(1)	40(1)
S(4)	2848(2)	-62(2)	1847(2)	34(1)
S(2)	3445(2)	165(2)	185(2)	43(1)
S(3)	1901(2)	-2440(2)	1462(2)	41(1)
S(1)	1417(2)	-99(2)	309(2)	35(1)
O(1)	1826(8)	3002(10)	-733(8)	97(5)
O(2)	1411(7)	2929(8)	1655(7)	80(5)
O(3)	4015(10)	3060(12)	1403(11)	147(8)
O(4)	2024(8)	-2512(10)	-1087(7)	95(5)
O(5)	4212(8)	-2885(10)	1107(10)	108(6)
N(1)	3618(7)	-2253(9)	905(8)	56(4)
C(1)	2088(10)	2426(12)	-200(10)	68(6)
C(2)	1839(6)	2381(8)	1354(6)	31(3)
C(3)	3438(11)	2477(12)	1167(11)	78(7)
C(4)	2266(9)	-2080(13)	-426(9)	66(6)
C(11)	10(8)	-706(14)	1751(8)	62(5)
C(12)	534(10)	-1141(14)	2507(9)	70(6)
C(13)	1089(9)	-306(14)	2928(8)	59(5)
C(14)	921(9)	625(12)	2432(8)	59(5)
C(15)	246(9)	400(13)	1739(8)	60(5)
C(21)	3381(9)	273(12)	-961(9)	61(5)
C(22)	3832(11)	-735(14)	-1183(10)	83(7)
C(23)	3858(12)	1317(12)	-1067(11)	85(8)
C(24)	2442(10)	280(15)	-1503(10)	83(7)
C(31)	1101(9)	-3469(10)	843(9)	56(5)
C(32)	594(10)	-3921(14)	1463(10)	78(7)
C(33)	440(10)	-2932(14)	76(9)	73(6)
C(34)	1630(11)	-4386(11)	592(10)	77(7)
C(41)	3764(7)	-125(10)	2816(7)	45(4)
C(42)	3641(12)	758(14)	3380(10)	92(8)
C(43)	3780(10)	-1260(13)	3191(10)	81(7)
C(44)	4606(9)	75(12)	2533(10)	71(6)

^a Equivalent isotropic *U*, defined as one-third of the trace of the orthogonalized *U*_{ij} tensor.

the Re(I) centers of 5 initiated a breakdown of the Cr₂-Re₂ core into two clusters, 2a and 6 (CO atmosphere) or 7 (Co₂(CO)₈), with Cr₂Re and CrRe₂ cores, respectively. The presence of an unsaturated Co-containing fragment also induced NO/CO exchange between a Co and a Re center with formation of a Re(CO)₃ unit in 7, instead of a Re(CO)₂(NO) moiety in 6. The difference of one electron between these units is compensated for by the presence of a tridentate SR group (five electrons)

(8) Rikitin, Yu. V.; Novotortsev, V. M.; Kalinnikov, V. T.; Pasynskii, A. A.; Larin, G. M.; Philatov, A. V.; Idrisov, T. C. *Koord. Khim.* 1977, 3, 807.

Table 7. Atomic Coordinates ($\times 10^4$) and Equivalent Isotropic Displacement Coefficients ($\text{\AA}^2 \times 10^3$) for **9**

atom	x	y	z	$U(\text{eq})^a$
Re(1)	3531(1)	9521	6713(1)	31(1)
I(1)	1772(2)	7840(2)	7166(2)	51(1)
Cr(1)	5539(4)	9545(6)	5506(3)	38(1)
Cr(2)	6637(5)	9848(5)	8251(5)	50(2)
S(1)	5686(10)	8286(8)	7031(9)	50(2)
S(2)	5318(9)	10987(7)	6746(8)	43(2)
S(3)	3180(9)	8768(7)	4793(7)	43(2)
S(4)	4503(8)	9686(9)	8870(6)	45(2)
O(1)	1323(23)	11201(19)	6492(26)	131(2)
N(1)	2025(22)	10626(18)	6342(21)	46(2)
C(1)	1815(26)	9553(29)	3552(22)	64(2)
C(2)	1983(30)	9058(29)	2447(22)	89(3)
C(3)	2062(28)	10807(25)	3508(26)	76(3)
C(4)	320(25)	9223(27)	3748(24)	77(2)
C(5)	3909(28)	10988(25)	9532(25)	73(2)
C(6)	2374(29)	10777(29)	9349(28)	94(3)
C(7)	4145(30)	12086(26)	8973(30)	95(3)
C(8)	4915(35)	10886(33)	10886(26)	172(3)
C(11)	6003(30)	9228(32)	3844(24)	130(2)
C(12)	6270(30)	10383(28)	4010(29)	113(2)
C(13)	7431(32)	10406(27)	5237(24)	111(2)
C(14)	7778(32)	9350(27)	5371(27)	107(3)
C(15)	6832(31)	8619(26)	4595(24)	73(2)
C(21)	8717(28)	10718(32)	8575(29)	134(3)
C(22)	8167(33)	10922(34)	9490(29)	191(3)
C(23)	8107(28)	10204(32)	10178(23)	117(2)
C(24)	8476(31)	9170(30)	9564(26)	109(3)
C(25)	9040(24)	9394(27)	8631(25)	75(2)

^a Equivalent isotropic U , defined as one-third of the trace of the orthogonalized U_{ij} tensor.

in **7**, in comparison with the μ_3 -sulfide bridge (four electrons) in **6**. **6** and **7** are the first cluster derivatives with the heterobinuclear $\text{CpCr}(\mu\text{-SCMe}_3)_n(\mu\text{-S})_m\text{Re}(\text{CO})(\text{NO})$ "block" displaying a Cr–Re bond order of half. For the triangular antiferromagnetic cluster **9** the presence of a single Cr–Re bond is suggested. In this molecule there are three coupled metal centers: two Cr(III) atoms and one Re(II) atom; the latter results from the removal of one electron from the Re(I) center in **2a** by oxidation.

Experimental Section

General Comments. All operations, including the syntheses of the starting compounds, were carried out under dry oxygen-free nitrogen by standard Schlenk techniques. Benzene and THF were purified by distillation from sodium/benzophenone ketyl. Hexane and heptane were dried by boiling over sodium. Dichloromethane (CH_2Cl_2) was purified by double distillation from P_2O_5 . Thin-layer chromatography (TLC) (Merck, 5×7.5 cm, Kieselgel 60 F₂₅₄) was used to monitor the progress of the reaction. Column chromatography was applied to separate the reaction mixtures (Kieselgel 60, Merck, 70–230 mesh ASTM). The starting compounds **2a**, **4**, and **5** were prepared as described earlier.¹ Infrared spectra were recorded on a Bio-Rad FTS-45 spectrometer in KBr pellets. Mass spectra (EI or FAB) were measured on a Finnigan MAT 8320 (70 eV). The temperature dependence of the magnetic susceptibilities (χ_m) of the compounds **6**, **7**, and **9** were determined by the Faraday technique in the range 296–277 K, using an instrument devised in the Institute of General and Inorganic Chemistry of the Russian Academy of Sciences.⁹

Thermolysis of $\text{Cp}_2\text{Cr}_2(\mu\text{-SCMe}_3)_2(\mu_3\text{-S})\text{Re}(\text{CO})_2(\text{NO})\text{Cl}_2$ (4**) under a CO Atmosphere.** A black solution of **4** (500 mg, 0.63 mmol) was stirred in benzene (50 mL) at 70–80 °C, and a permanent stream of CO was bubbled through the solution.

(9) Novotortsev, V. M. Ph.D. Thesis, Institute of General and Inorganic Chemistry Moscow, 1974.

After 10–15 min the formation of the $[\text{CpCr}(\mu\text{-SCMe}_3)_2(\mu_3\text{-S})\text{Re}(\text{CO})(\text{NO})_2]$ cluster (**5**) was observed (IR and TLC monitoring), and after 4 h the reaction was finished. The color of the solution had changed from black to brown-green. TLC indicated the absence of **4** and **5** and the presence of a new brown-green band together with **2a** as major products. These compounds were separated by column chromatography into two fractions (5×30 cm, silica gel).

(I) A brown-green solution in benzene (70 mL), after concentration to 10 mL and cooling to 10 °C, afforded brown prismatic crystals of $\text{CpCr}(\mu\text{-SCMe}_3)\text{Re}(\text{CO})(\text{NO})(\mu_3\text{-S})_2(\mu\text{-SCMe}_3)\text{Re}(\text{CO})_2(\text{NO})$ (**6**; 80 mg, 0.091 mmol, 43.5%). Anal. Calcd for $\text{CpCr}(\text{SCMe}_3)_2(\text{S})_2\text{Re}_2(\text{CO})_3(\text{NO})_2$: C, 21.92; H, 2.63; N, 3.20. Found: C, 22.02; H, 2.68; N, 3.07. MS(FAB; m/z): 876, $\text{CpCr}(\text{SCMe}_3)_2(\text{S})_2\text{Re}_2(\text{CO})_3(\text{NO})_2$. IR (ν , cm^{-1}): 3113 (w), 2966 (m), 2924 (m), 2895 (m), 2859 (w), 2073 (s), 2062 (vs), 1990 (vs), 1973 (vs), 1741 (s), 1707 (vs), 1465 (w), 1453 (m), 1431 (m), 1384 (w), 1363 (m), 1156 (m), 1057 (w), 1018 (m), 1005 (w), 844 (w), 812 (m), 667 (w), 602 (w), 593 (m), 548 (m), 539 (m), 481 (m). μ_{eff} (289–282 K) = 3.80 μ_B .

(II) A green solution in CH_2Cl_2 (50 mL), after addition of heptane (15 mL), concentration to 20 mL, and cooling (–30 °C), gave green plates of **2a** (55 mg, 0.076 mmol, 36.3%).

Thermolysis of **4 in the Presence of $\text{Co}_2(\text{CO})_8$.** A black-brown solution of **4** (500 mg, 0.63 mmol) and $\text{Co}_2(\text{CO})_8$ (200 mg, 0.58 mmol) in benzene (50 mL) was stirred at 70 °C. After 10 min formation of **5** was observed (TLC monitoring). Further heating of the reaction mixture for 2.5 h led to a brown-green solution. TLC (benzene/ CH_2Cl_2) assured the absence of **4** and **5**. The newly formed products were separated by column chromatography (5×30 cm, silica gel) with evolution of two main bands.

(I) A brown-green solution in benzene (50 mL), after addition of heptane (10 mL) and concentration to 10 mL, afforded green-brown prisms of $\text{CpCr}(\mu\text{-SCMe}_3)\text{Re}(\text{CO})(\text{NO})(\mu_3\text{-S})(\mu_3\text{-SCMe}_3)(\mu\text{-SCMe}_3)\text{Re}(\text{CO})_3$ (**7**; 92 mg, 0.099 mmol, 47.1%). Anal. Calcd for $\text{CpCr}(\text{SCMe}_3)_3(\text{S})\text{Re}_2(\text{CO})_4(\text{NO})$: C, 27.07; H, 3.44; N, 1.50. Found: C, 26.88; H, 3.57; N, 1.65. MS (EI; m/z): 931, $\text{CpCr}(\text{SCMe}_3)_3(\text{S})\text{Re}_2(\text{CO})_4(\text{NO})$; 903, $\text{CpCr}(\text{SCMe}_3)_3(\text{S})\text{Re}_2(\text{CO})_3(\text{NO})$; 846, $\text{CpCr}(\text{SCMe}_3)_2(\text{S})_2\text{Re}_2(\text{CO})_3(\text{NO})$; 789, $\text{CpCr}(\text{SCMe}_3)(\text{S})_3\text{Re}_2(\text{CO})_3(\text{NO})$; 761, $\text{CpCr}(\text{SCMe}_3)(\text{S})_3\text{Re}_2(\text{CO})_2(\text{NO})$; 733, $\text{CpCr}(\text{SCMe}_3)(\text{S})_3\text{Re}_2(\text{CO})(\text{NO})$; 705, $\text{CpCr}(\text{SCMe}_3)(\text{S})_3\text{Re}_2(\text{NO})$; 703, $\text{CpCr}(\text{SCMe}_3)(\text{S})_3\text{Re}_2(\text{CO})$; 675, $\text{CpCr}(\text{SCMe}_3)(\text{S})_3\text{Re}_2$; 646, $\text{CpCr}(\text{S})_4\text{Re}_2(\text{NO})$; 616, $\text{CpCr}(\text{S})_4\text{Re}_2$; 551, CrRe_2S_4 . IR (ν , cm^{-1}): 3101 (w), 2975 (m), 2959 (m), 2917 (m), 2889 (m), 2855 (w), 2010 (vs), 1964 (s), 1952 (vs), 1908 (s), 1882 (vs), 1716 (vs), 1455 (m), 1387 (w), 1364 (m), 1156 (m), 1062 (w), 1015 (m), 1008 (w), 819 (m), 636 (m), 617 (m), 580 (w), 545 (w), 524 (m), 516 (w), 493 (w), 483 (w). μ_{eff} (289–282 K) = 3.68 μ_B .

(II) A green solution in CH_2Cl_2 (45 mL), after concentration to 8–10 mL and cooling (–30 °C), yielded deep green plates of **2a** (50 mg, 0.069 mmol, 33%).

Reaction of $\text{Cp}_2\text{Cr}_2(\mu\text{-SCMe}_3)_2(\mu_3\text{-S})_2\text{Re}(\text{CO})(\text{NO})$ (2a**) with I_2 .** A green-brown solution of **2a** (350 mg, 0.485 mmol) and I_2 (65 mg, 0.256 mmol) in CH_2Cl_2 (30 mL) was stirred at room temperature for 30 min until the formation of a dark brown solution was observed. TLC indicated the presence of a single brown band. It was separated by column chromatography (5×30 cm, silica gel, CH_2Cl_2). The solution (35 mL) was concentrated to 8–10 mL and after cooling to –30 °C gave brown needle-shaped crystals of $\text{Cp}_2\text{Cr}_2(\mu\text{-SCMe}_3)_2(\mu_3\text{-S})_2\text{Re}(\text{NO})$ (**9**) (260 mg, 0.317 mmol, 65.4%). Anal. Calcd for $\text{Cp}_2\text{Cr}_2(\text{SCMe}_3)_2(\text{S})_2\text{Re}(\text{NO})$: C, 26.34; H, 3.41; N, 1.71. Found: C, 26.52; H, 3.44; N, 1.72. MS (EI or FAB; m/z): 820, $\text{Cp}_2\text{Cr}_2(\text{SCMe}_3)_2(\text{S})_2\text{Re}(\text{NO})$; 636, $\text{Cp}_2\text{Cr}_2(\text{SCMe}_3)(\text{S})_3\text{Re}(\text{NO})$; 579, $\text{Cp}_2\text{Cr}_2(\text{S})_4\text{Re}(\text{NO})$; 549, $\text{Cp}_2\text{Cr}_2(\text{S})_4\text{Re}$; 484, $\text{CpCr}_2(\text{S})_4\text{Re}$; 419, Cr_2ReS_4 . IR (ν , cm^{-1}): 3102 (w), 3063 (w), 2967 (m), 2954 (m), 2911 (m), 2884 (m), 2846 (m), 1687 (vs), 1466 (w), 1443 (m), 1432 (m), 1389 (w), 1362 (m), 1153 (m), 1069 (w), 1012 (m), 833 (w), 817 (m), 806 (m), 667 (w), 592 (w), 474 (w). μ_{eff} Cr atom = 1.40 (284 K)–1.043 (111 K) μ_B .

Reaction of 9 with $\text{Co}_2(\text{CO})_8$. A brown solution of **9** (100 mg, 0.122 mmol) and $\text{Co}_2(\text{CO})_8$ (60 mg, 0.175 mmol) was stirred at 50–60 °C for 2 h. TLC indicated the presence of $\text{Co}_4(\text{CO})_{12}$ and **2a** and the absence of **9**. The black precipitate, which displayed no $\nu(\text{CO})$ and $\nu(\text{NO})$ bands in the IR spectrum, was filtered off from the green-brown solution. The filtrate was chromatographed on silica gel (5 × 30 cm, benzene). Yield of $\text{Co}_4(\text{CO})_{12}$: 15 mg, 0.028 mmol, 31.5%. Yield of **2a**: 85 mg, 0.118 mmol, 96%.

Crystal Structure Determination. The crystals of **6**, **7**, and **9** were mounted in air on glass fibers using 5 min epoxy resin. The unit cell parameters were determined and refined from 24 equivalent reflections with $2\theta \geq 22\text{--}24^\circ$ obtained by a Nicolet R3 ($T = 22^\circ\text{C}$, for **7** and **9**) or a Siemens R3/m ($T = -80^\circ\text{C}$, for **6**) four-circle diffractometer. Intensity data (Mo $K\alpha$, $\lambda = 0.71073 \text{ \AA}$) were corrected for Lorentz and polarization effects. Backgrounds were scanned for 25% (for **7** and **9**) and 12.5% (for **6**) of the peak widths on each end of the scans. Three reflections were monitored for crystal decomposition or movement. No significant variations in these standards were observed, and therefore no correction was applied. Details of the crystal parameters, the data collection, and structure refinement are given in Table 4.

All structures were solved by direct methods to locate the transition metals and sulfur atoms. The other non-hydrogen atoms were found in difference Fourier maps. The DIFABS method¹⁰ was used for the absorption correction of all clusters at the stage of the isotropic approximation. An anisotropic

refinement was applied to all non-hydrogen atoms. The H atoms in all structures were generated geometrically (C–H bonds fixed at 0.96 Å), and all H atoms were assigned the same isotropic temperature factor of $U = 0.08 \text{ \AA}^2$. Computations were performed using the SHELXTL PLUS program package¹¹ on a VAXstation 3100 (for **6**) or on a 486 IBM PC (for **7** and **9**) computer. Selected bond lengths and bond angles are given in Tables 1–3, and positional and equivalent isotropic thermal parameters are listed in Tables 5–7. Additional information is available as supplementary material.

Acknowledgment. We thank Mrs. B. Spichtig for the recording of the mass spectra and the Swiss National Science Foundation and the Russian Fundamental Science Foundation (Grant No. 93-03-5394) for financial support.

Supplementary Material Available: Tables of the crystal data, anisotropic thermal parameters, hydrogen atom coordinates, and bond distances and angles for **6**, **7**, and **9** (23 pages). Ordering information is given on any current masthead page.

OM940450Y

(10) Walker, N.; Stuart, D. *Acta Crystallogr.* **1983**, *A39*, 158.

(11) Sheldrick, G. M. In *Crystallographic Computing 3: Data Collection, Structure Determination, Proteins, and DataBases*; Clarendon Press: New York, 1985; p 175.

Chromium and Molybdenum Carbonyl Complexes of C₇Ph₇H and C₇Ph₅Me₂H and of C₇Ph₇H(CO), the Diels–Alder Adduct of Tetracyclone and Triphenylcyclopropene: Variable-Temperature NMR and X-ray Crystallographic Study[†]

Lisa C. F. Chao, Hari K. Gupta, Donald W. Hughes, James F. Britten, Suzie S. Rigby, Alex D. Bain, and Michael J. McGlinchey*

Department of Chemistry, McMaster University, Hamilton, Ontario L8S 4M1, Canada

Received July 28, 1994[⊗]

The Diels–Alder reaction of tetraphenylcyclopentadienone (tetracyclone) with triphenylcyclopropene yields the adduct **2** with an *endo* hydrogen at C(7); thermal elimination of CO produces heptaphenylcycloheptatriene (**1a**). This initially formed isomer with a pseudo-equatorial phenyl substituent at the sp³ position is sterically hindered and undergoes a conformational flip, forming **1b**, which allows the phenyl group to occupy the favored pseudo-axial site. However, the remaining phenyls are sterically encumbered and slowed rotation of these rings can be monitored by ¹H and ¹³C NMR spectroscopy. The intermediacy of conformer **1a** is shown by the formation of isomers of C₇(*p*-tolyl)₂Ph₅H, arising via a series of [1,5] hydrogen shifts that are possible only for **1a** and not for **1b**. Similarly, use of 2,5-dimethyl-3,4-diphenylcyclopentadienone yields C₇Me₂Ph₅H, **3**, in which [1,5]-hydrogen shifts occur. **1** crystallizes in the triclinic space group *P* $\bar{1}$ with *a* = 9.8320(10) Å, *b* = 10.0260(10) Å, *c* = 19.166(2) Å, α = 92.194(1)°, β = 90.57(1)°, γ = 108.94(1)°, and *V* = 1785.2(3) Å³ for *Z* = 2. **2** crystallizes in the monoclinic space group *P*2₁/*n* with *a* = 12.829(4) Å, *b* = 16.456(2) Å, *c* = 18.226(3) Å, β = 110.06(1)°, and *V* = 3614.3(13) Å³ for *Z* = 4. The reaction of Cr(CO)₆ with C₇Ph₇H leads to incorporation of a Cr(CO)₃ group on a peripheral phenyl ring rather than on the seven-membered ring. However, the tricyclic ketone **2**, which is the precursor to **1**, reacts with Mo(CO)₆ to give the π -allyl complex (η^5 -C₃Ph₄OH)Mo(CO)₂(η^3 -C₃Ph₃H₂) (**10**), in which the triphenylcyclopropene ring has been opened. **10** crystallizes in the triclinic space group *P* $\bar{1}$ with *a* = 13.265(3) Å, *b* = 13.561(3) Å, *c* = 13.635(4) Å, α = 71.84(2)°, β = 65.04(2)°, γ = 61.20(1)°, and *V* = 1930.3(12) Å³ for *Z* = 2.

Introduction

Recent work on the fluxional behavior of organometallic fragments bonded to sterically demanding ligands has included such molecules as (C₆Et₆)Cr(CO)L/L'', where L' and L'' can be CO, CS, NO⁺ or PR₃,¹ (C₆Et₅C(=O)Me)Cr(CO)₃,^{2a} [C₆Et₄(CH₂CH₂C(=O)R)₂]Cr(CO)₃,^{2b} [(C₆H₅)Cr(CO)₃](C₆H₅)₂COH,³ (C₅Ph₅)Fe(CO)(CHO)(PMe₃),⁴ and (C₆Ph₆)Cr(CO)₃.⁵ In each case, the barrier associated with tripodal rotation was measurably different from that observed for the rotation of the peripheral ethyl or phenyl substituents.

It is well-established that, for molecules of the type C_nAr_n,^{6–8} peripheral ring rotation can be slowed on the NMR time-scale when bulky *ortho*-substituents are present. In the solid state these molecules adopt propeller-type conformations in which the external phenyls make a dihedral angle, θ , of \approx 50–60° with the plane of the central ring.⁹ Such a geometry provides a compromise between the coplanar arrangement $\theta = 0^\circ$, which maximizes π overlap but leads to severe steric strain, and the orthogonal structure $\theta = 90^\circ$, in which interactions between bulky groups are minimized. One can view these species in terms of the angle ω , subtended by adjacent phenyls at the center of the internal ring: in C₅Ph₅, $\omega = 72^\circ$, in C₆Ph₆, $\omega = 60^\circ$, and in C₇Ph₇, $\omega = 51.4^\circ$. While it is true that increasing the ring size lengthens the radial distance of the external phenyls from the center of the molecule, this is more than compensated for by the diminishing value of ω .

We thus chose to study potential routes to organometallic complexes of the type (C₇Ph₇)ML_n in which the

[†] Dedicated to Professor C. W. Jefford (University of Geneva, Geneva, Switzerland) on the occasion of his 65th birthday.

* Abstract published in *Advance ACS Abstracts*, February 1, 1995.

(1) (a) Mailvaganam, B.; Frampton, C. S.; Sayer, B. G.; Top, S.; McGlinchey, M. J. *J. Am. Chem. Soc.* **1991**, *113*, 1177. (b) Iverson, D. J.; Hunter, G.; Blount, J. F.; Damewood, J. R., Jr.; Mislow, K. *J. Am. Chem. Soc.* **1981**, *103*, 6073. (c) Hunter, G.; Blount, J. F.; Damewood, J. R., Jr.; Iverson, D. J.; Mislow, K. *Organometallics* **1981**, *1*, 448. (d) McGlinchey, M. J. *Adv. Organomet. Chem.* **1992**, *34*, 285 and references therein.

(2) (a) Downton, P. A.; Mailvaganam, B.; Frampton, C. S.; Sayer, B. G.; McGlinchey, M. J. *J. Am. Chem. Soc.* **1990**, *111*, 27. (b) Kilway, K. V.; Siegel, J. S. *J. Am. Chem. Soc.* **1991**, *113*, 2332. (c) Kilway, K. V.; Siegel, J. S. *J. Am. Chem. Soc.* **1992**, *114*, 255.

(3) Malisza, K. L.; Chao, L. F. C.; Britten, J. F.; Sayer, B. G.; Jaouen, G.; Top, S.; Decken, A.; McGlinchey, M. J. *Organometallics* **1993**, *12*, 2462.

(4) Li, L.; Decken, A.; Sayer, B. G.; McGlinchey, M. J.; Brégaint, P.; Thépot, J.-Y.; Toupet, L.; Hamon, J.-R.; Lapinte, C. *Organometallics* **1994**, *13*, 682.

(5) Mailvaganam, B.; Sayer, B. G.; McGlinchey, M. J. *J. Organomet. Chem.* **1990**, *395*, 177.

(6) Gust, D.; Patton, A. *J. Am. Chem. Soc.* **1978**, *100*, 8175.

(7) (a) Mislow, K.; Gust, D.; Finocchiaro, P.; Boettcher, R. *J. Top. Curr. Chem.* **1973**, *47*, 1. (b) Willem, R.; Gielen, M.; Hoogzand, C.; Pepermans, H. in *Advances in Dynamic Stereochemistry*; Gielen, M., Ed.; Freund: London, 1985; p 207.

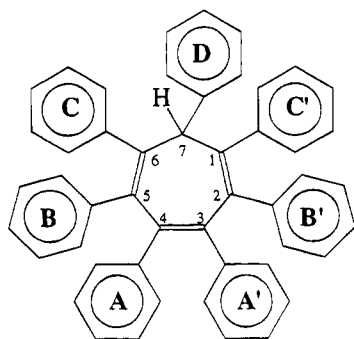
(8) Janiak, C.; Schumann, H. *Adv. Organomet. Chem.* **1991**, *33*, 291.

(9) (a) Bart, J. C. *J. Acta Crystallogr., Sect. B* **1968**, *24*, 1277. (b) Almenningsen, A.; Bastiansen, O.; Skancke, P. N. *Acta Chem. Scand.* **1958**, *12*, 1215.

Table 1. ^1H and ^{13}C NMR Data for $\text{C}_7\text{Ph}_7\text{H}$ (1) and $\text{C}_7\text{Ph}_5\text{Me}_2\text{H}$ (3)

	phenyl A/A'		phenyl B/B'		phenyl C/C'		phenyl D		other	
	^1H , δ	^{13}C , δ	^1H , δ	^{13}C , δ	^1H , δ	^{13}C , δ	^1H , δ	^{13}C , δ	^1H , δ	^{13}C , δ
$\text{C}_7\text{Ph}_7\text{H}$ (1) ^a										
ortho	6.29 (4H) d of d, 8.2, 1.5 Hz	130.71	7.09 (4H, m) ^b	131.04	7.18 (4H) d of d, 8.1, 1.4 Hz	129.22	8.00 (2H) d of t, 8.3, 1.2 Hz	126.26		
meta	6.63 (4H, m)	125.39	7.08 (4H, m) ^c	126.55	7.03 (4H, m)	126.95	7.51 (2H) d of d, 8.3, 7.5 Hz	127.84		
para	6.67 (2H, m)	124.44	7.03 (2H, m)	125.39	7.03 (2H, m)	125.71	7.40 (1H) t of q, 7.5, 1.2 Hz	126.26		
ipso carbon		140.00		140.24		143.10		142.53		
ring carbon		142.75		136.35		138.72		57.17		
sp ³ H									5.35 (1H, s)	57.17
$\text{C}_7\text{Ph}_5\text{Me}_2\text{H}$ (3) ^d										
ortho	6.51 (2H, b)	130.27	B 7.07 (2H, m); B' 7.23 (2H, m)	B 130.71; B' 131.62	7.17 (2H, m)	130.44	7.61 (2H) d of t, 8.3, 1.2 Hz	126.43		
meta	6.94 (2H, m)	127.35	B 7.17 (2H, m); B' 7.23 (2H, m)	B 127.74; ^e B' 128.21 ^e	7.16 (2H, m)	128.21 ^e	7.34 (2H) d of d, 7.5, 8.3 Hz	128.03		
para	6.91 (1H, m)	125.94	B 7.61 (1H, m); B' 7.08 (1H, m)	B 126.64; ^f B' 126.19 ^f	7.14 (1H, m)	126.77 ^f	7.20 (1H, m)	126.43		
sp ³ H									4.84 (1H, s)	56.90
1-Me									1.87 (3H, s)	25.03
4-Me									1.20 (3H, s)	20.43

^a Spectra obtained in CD_2Cl_2 on 500 MHz NMR spectrometer. Legend: d = doublet, q = quartet, s = singlet, t = triplet, m = multiplet, b = broad. ^b At -90°C , splits into two peaks at 7.5 and 6.7 ppm. ^c At -90°C , splits into two peaks at 7.3 and 6.9 ppm. ^d ^{13}C spectra obtained in CD_2Cl_2 at 125.721 MHz. ^e Peak assignments of meta carbons may be interchanged. ^f Peak assignments of para carbons may be interchanged.

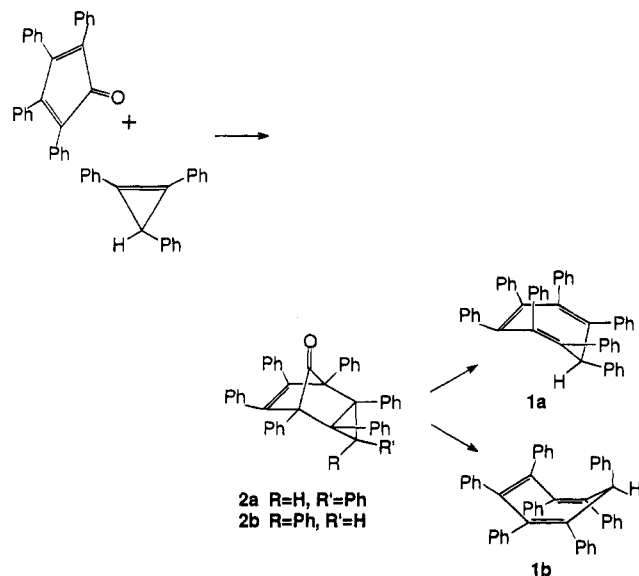
Figure 1. Labelling scheme for $\text{C}_7\text{Ph}_7\text{H}$ (1).

spinning of the organometallic moiety about the C_7 axis and the rotation of the peripheral phenyls might be correlated, as in the molecular bevel gears discussed by Iwamura and Mislow.^{10,11} Heptaphenylcycloheptatriene, $\text{C}_7\text{Ph}_7\text{H}$ (1), was originally synthesized by Battiste in 1961,¹² and the C_7Ph_7^+ and C_7Ph_7^- ions and also the C_7Ph_7 radical have since been reported.^{13,14} We are unaware of any structural or molecular dynamics studies on these systems; moreover, despite the elegant work of a number of groups on $(\text{C}_7\text{H}_7)\text{ML}_n$ derivatives,¹⁵ there are, to our knowledge, no reports of organometallic complexes containing the C_7Ph_7 unit. We here describe the dynamic behavior and structures of heptaphenyl- and of dimethylpentaphenylcycloheptatriene and also their reactions with chromium and molybdenum carbonyls.

Results and Discussion

Structure of $\text{C}_7\text{Ph}_7\text{H}$. Heptaphenylcycloheptatriene (1), is conveniently synthesized by the Diels–Alder addition of tetraphenylcyclopentadienone (commonly known as tetracyclone) and 1,2,3-triphenylcyclopropene

to give the tricyclic ketone 2. The reaction is normally



carried out at elevated temperatures, and loss of CO yields $\text{C}_7\text{Ph}_7\text{H}$ directly;¹² however, if the Diels–Alder addition is performed at room temperature, the intermediate ketone 2, can be isolated.

The 500 MHz ^1H and 125 MHz ^{13}C NMR spectra of $\text{C}_7\text{Ph}_7\text{H}$ can be completely assigned by means of ^1H – ^1H COSY and ^1H – ^{13}C shift-correlated experiments, together with selected NOE measurements, and the NMR data for 1 are collected in Table 1. The protons of the unique phenyl (ring D in Figure 1) are markedly deshielded relative to those of the A rings; moreover, the NOE data reveal a clear interaction between the *ortho* protons of the D and A rings, suggesting the structure 1b, whereby the D ring is pseudo-axial and the single hydrogen substituent is sited equatorially. At

(10) Iwamura, H.; Mislow, K. *Acc. Chem. Res.* **1988**, *21*, 175.
 (11) For a very recent example of a molecular brake, see: Kelly, T. R.; Bowyer, M. C.; Bhaskar, K. V.; Bebbington, D.; Garcia, A.; Lang, F.; Kim, M. H.; Jette, M. P. *J. Am. Chem. Soc.* **1994**, *116*, 3657.
 (12) Battiste, M. A. *Chem. Ind.* **1961**, 550.
 (13) Battiste, M. A. *J. Am. Chem. Soc.* **1961**, *83*, 4101.
 (14) (a) Breslow, R.; Chang, H. W. *J. Am. Chem. Soc.* **1965**, *87*, 2200.
 (b) Battiste, M. A. *J. Am. Chem. Soc.* **1962**, *84*, 3780.

(15) (a) Elschenbroich, Ch.; Salzer, A. *Organometallics—A Concise Introduction*, 2nd ed.; VCH: Weinheim, Germany, 1992; pp 358–361.
 (b) Bennett, M. J.; Pratt, J. L.; Simpson, K. A.; LiShingMan, L. K. K.; Takats, J. *J. Am. Chem. Soc.* **1976**, *98*, 4810. (c) Heinekey, D. M.; Graham, W. A. *J. Am. Chem. Soc.* **1979**, *101*, 6115. (d) Airoldi, M.; Deganello, G.; Gennaro, G.; Moret, M.; Sironi, A. *Organometallics* **1993**, *12*, 3694 and references therein.

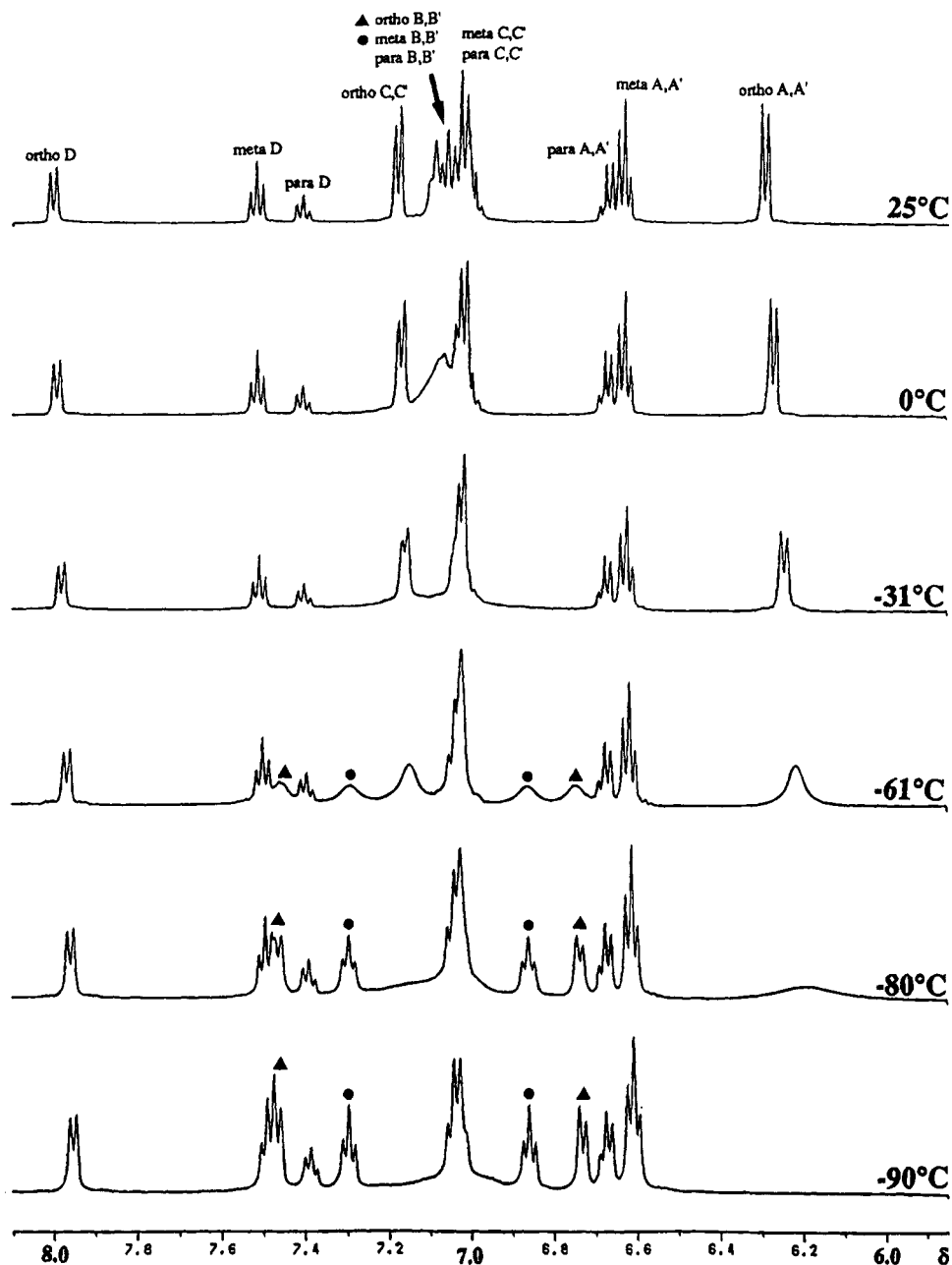


Figure 2. Variable-temperature 500 MHz ^1H NMR spectra of $\text{C}_7\text{Ph}_7\text{H}$ (1).

room temperature, the **B** and **C** phenyl protons are heavily overlapped. However, when the sample is cooled, the doublet attributable to the *ortho* protons of the **B** rings broadens and splits to give a pair of doublets separated by no less than 0.73 ppm; likewise, as shown in Figure 2, the *meta* protons of the **B** rings also decoalesce to give a pair of triplets 0.44 ppm apart. At -90°C , the *ortho* protons of the **A** rings, and of the **C** rings, have also broadened and disappeared into the base line. Comparable splittings are seen in the variable-temperature ^{13}C spectra of $\text{C}_7\text{Ph}_7\text{H}$ (see Figure 3), and the barrier to rotation of the **B** rings may be evaluated as $11.0 \pm 0.5 \text{ kcal mol}^{-1}$. This relatively high barrier tells us that these phenyls are in a very crowded environment; moreover, the large chemical shift differences observed for the protons of the **B** ring when its rotation is slow on the NMR time scale suggest that the *ortho* protons in particular experience ring current effects very different from their neighboring phenyls.

To clarify these points, $\text{C}_7\text{Ph}_7\text{H}$ (1), was structurally

characterized by X-ray crystallography and views of the molecule are shown in Figure 4. In the solid state, 1 possesses close to C_s symmetry such that the pseudo mirror plane contains the sp^3 carbon and bisects the double bond bearing the phenyl **A** rings. It is also evident that the unique phenyl group (the **D** ring in our notation), in accord with the NMR evidence, is axial and also straddles the pseudo mirror plane. As expected, the C_7 ring adopts a boat conformation such that the dihedral angles between the planes containing $\text{C}(6)-\text{C}(7)-\text{C}(1)$ [plane 1], $\text{C}(1)-\text{C}(2)-\text{C}(5)-\text{C}(6)$ [plane 2], and $\text{C}(2)-\text{C}(3)-\text{C}(4)-\text{C}(5)$ [plane 3] are 125° for [plane 1]/[plane 2] and 145° for [plane 2]/[plane 3]. These may be compared with the corresponding interplanar angles in C_7H_8 , which are 144° for [plane 1]/[plane 2] and 140° for [plane 2]/[plane 3].¹⁶ Thus, the conformation of the seven-membered boat in $\text{C}_7\text{Ph}_7\text{H}$ is markedly different from that found in cycloheptatriene itself, especially

(16) Traetteberg, M. *J. Am. Chem. Soc.* 1964, 86, 4265.

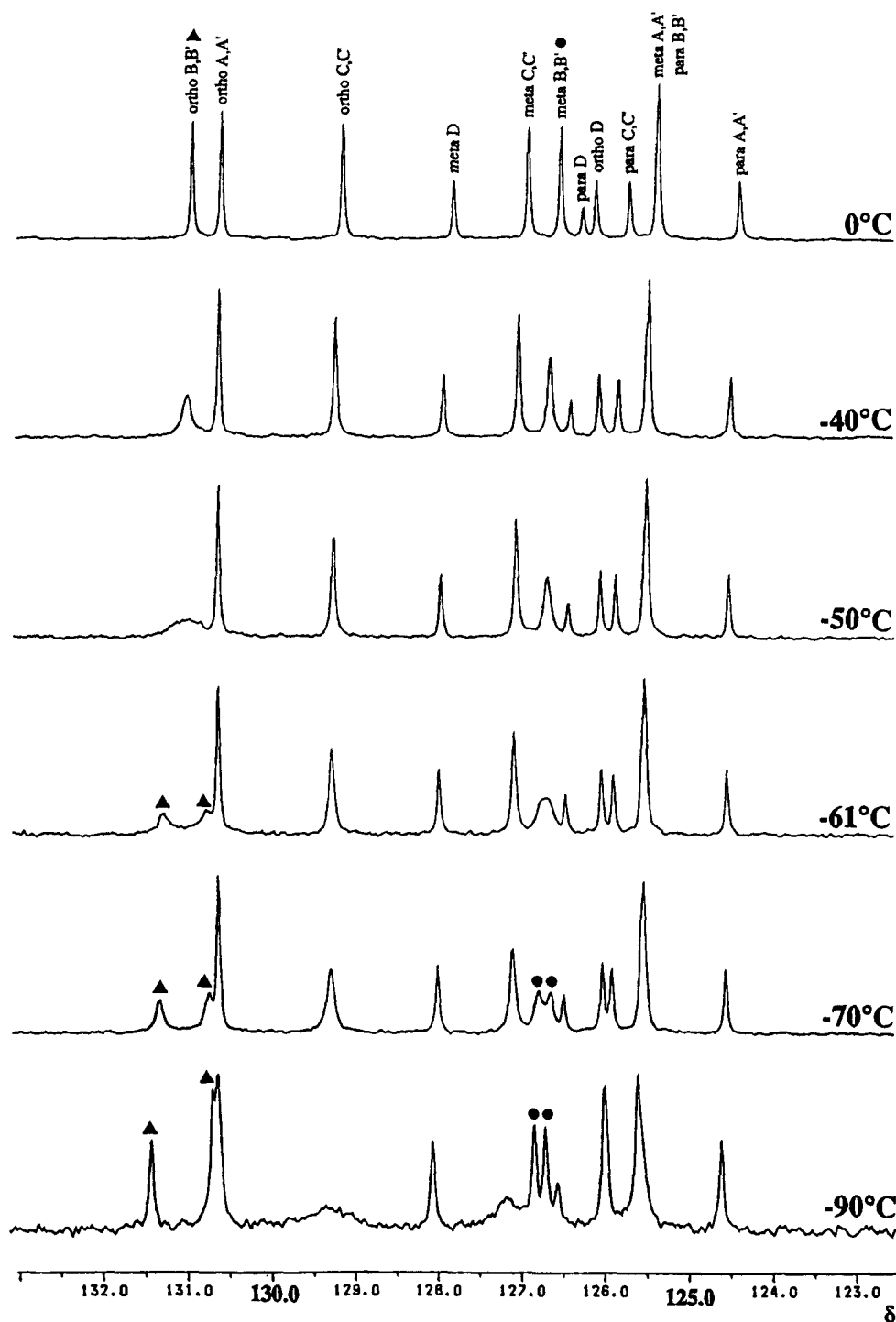


Figure 3. Variable temperature 125 MHz ^{13}C NMR spectra of $\text{C}_7\text{Ph}_7\text{H}$ (**1**).

with respect to the bending of the sp^3 carbon out of the $\text{C}(1)\text{--C}(2)\text{--C}(5)\text{--C}(6)$ plane. In C_7H_8 , this deviation from planarity is 36° , but in $\text{C}_7\text{Ph}_7\text{H}$ it has become 55° , presumably to minimize steric interactions between the phenyl substituents.

Our major interest lies with the orientations of the peripheral phenyl rings relative to the central C_7 ring. The phenyl **A** rings are almost perpendicular to their portion of the central ring; typically, the dihedral angles $\text{C}(2)\text{--C}(3)\text{--C}(31)\text{--C}(32)$ and $\text{C}(2)\text{--C}(3)\text{--C}(31)\text{--C}(36)$ are 92° and 87° , respectively. The **B** rings take up an orientation of $63 \pm 4^\circ$, while the **C** phenyls are twisted through 50° relative to the plane defined by $\text{C}(7)\text{--C}(1)\text{--C}(2)$ of the central ring. The net result is to place the **B** phenyls in a very restricted locale, and this is

illustrated in the space-filling model which appears as Figure 5. Furthermore, we can see from Figure 5 that the *ortho* hydrogens of the **B** rings are in very different magnetic environments. One proton, H(22), is sandwiched between the adjacent **A** and **C** phenyls and so is unusually highly shielded; its *ortho* partner in the same **B** ring, H(26), is situated on the molecular periphery, far from any aromatic fragments whose ring currents could affect its chemical shift. Since it is clear that the X-ray structure of **1** provides a rationale for the large chemical shift separation between protons on opposite edges of the **B** phenyl rings, one can conclude that the solid-state data provide an excellent model for the most favored conformation in solution.

The marked shielding of the *ortho* protons of the **A**

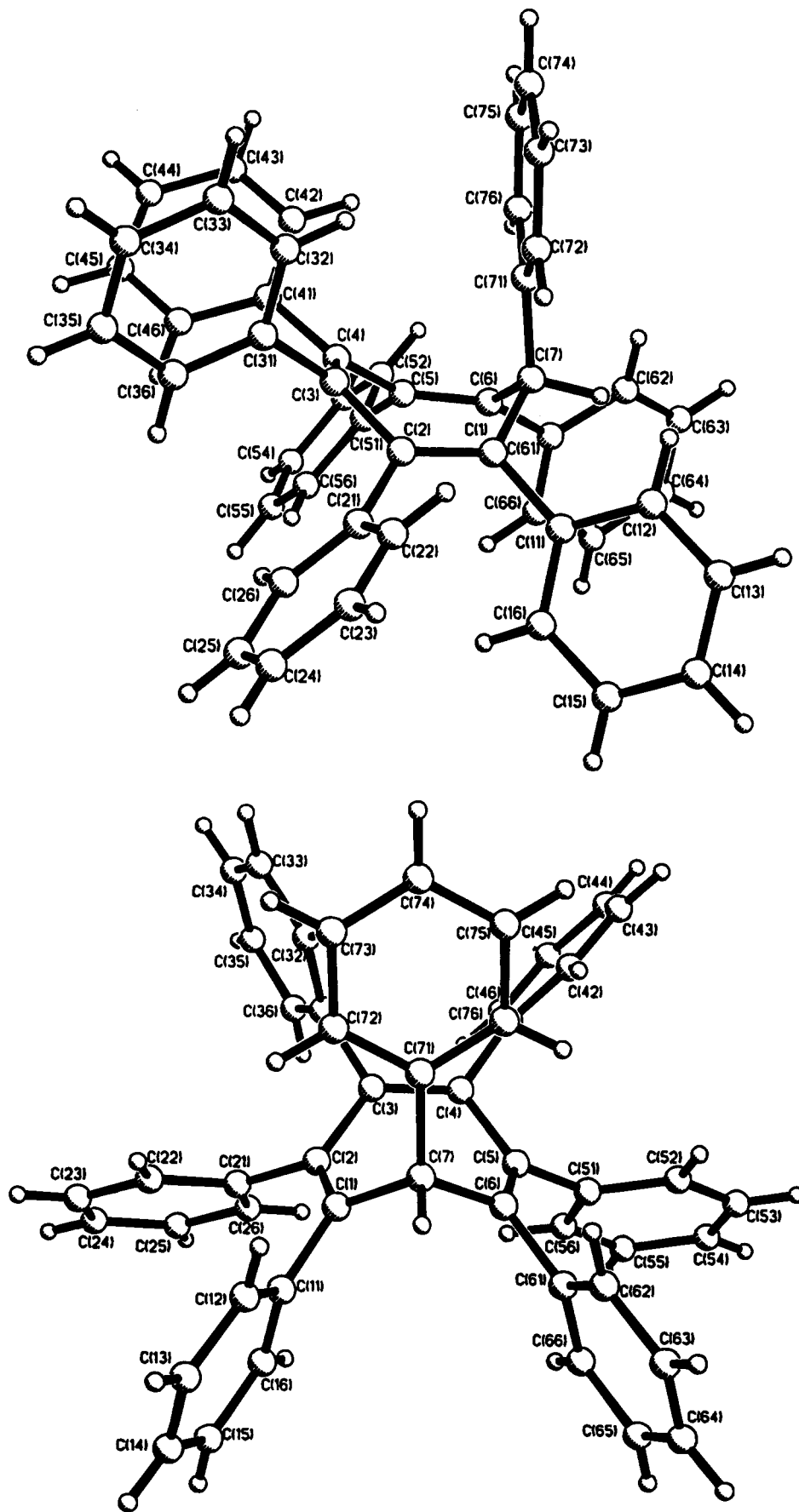


Figure 4. Molecular structures of C₇Ph₇H (1), showing the atom-numbering scheme: (a, top) side view; (b, bottom) view depicting the pseudo mirror plane.

rings may be accounted for by their proximity to the unique phenyl (ring D). Indeed, in the room-tempera-

ture ¹H spectrum, these protons exhibit a doublet at δ 6.2, which is, of course, the time-averaged chemical shift

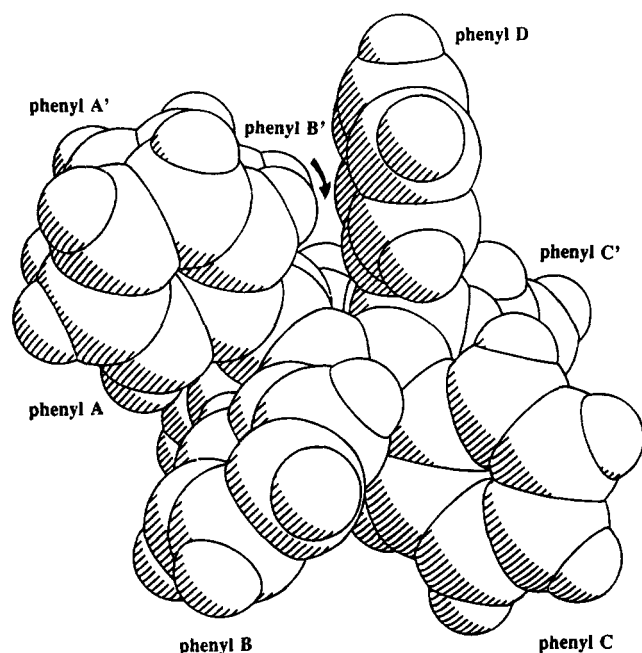


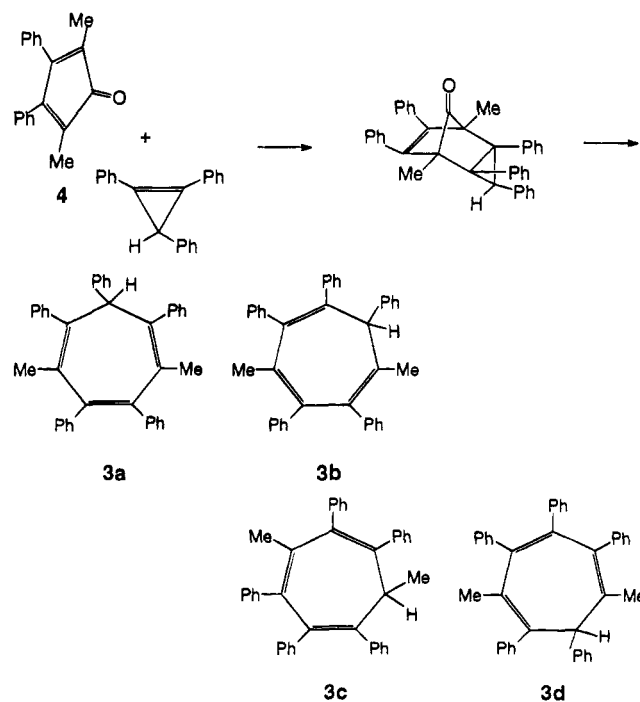
Figure 5. Space-filling model of C_7Ph_7H (**1**).

for the two environments H(32)/H(42) and H(36)/H(46). At $-70\text{ }^\circ\text{C}$, this resonance has broadened considerably, and by $-90\text{ }^\circ\text{C}$ it has completely disappeared into the base line. Since solubility limitations do not allow the observation of a limiting spectrum for slowed **A** ring rotation, it is not possible to extract a barrier for this process. Nevertheless, knowing the coalescence temperature ($\sim -70\text{ }^\circ\text{C}$), one could estimate this barrier if the approximate chemical shift difference between H(32) and H(36) could be evaluated. Making the (admittedly naive) assumption that the major contributor to this chemical shift separation is the sum of the ring current effects of the neighboring phenyls, then a simple calculation leads to an estimate of $\Delta\nu$. To test the validity of such an approach, the ring current induced chemical shift difference between the *ortho* protons H(22) and H(26) was evaluated; the X-ray structure of **1** places H(22) 3.51 \AA from the centroid of the phenyl **C** ring bonded to C(1) such that the vector connecting these two points makes an angle of 124° with the ring plane. The Johnson–Bovey ring current tables¹⁷ (based on the original model of Waugh and Fessenden¹⁸) predict that the **C** ring induces an incremental shielding of 0.69 ppm for a proton sited in such a position. In a similar manner, one can evaluate the shielding of H(22) caused by the anisotropic character of the phenyl **A** ring at C(3); the Johnson–Bovey approach yields a shielding of 0.34 ppm . By using this method, the incremental shifts predicted for H(26), and for the *meta* protons H(23) and H(25), were evaluated. Overall, this calculatory approach suggests chemical shift differences of $0.73 \pm 0.1\text{ ppm}$ for the *ortho* H's of the **B** rings, and $0.31 \pm 0.1\text{ ppm}$ for the *meta* H's; the experimental shift differences are 0.73 and 0.44 ppm , respectively.

The corresponding calculations for the *ortho* proton chemical shifts in the **A** and **C** phenyl rings yield a $\Delta\delta$ value of 0.65 ppm in each case. We note that the **A** ring protons which face the unique **D** ring are particularly

strongly shielded. These estimates of $\Delta\nu$, in conjunction with a coalescence temperature of $\sim 203\text{ K}$, yield a ΔG^\ddagger value of approximately 9.1 kcal mol^{-1} for the barrier to **A** ring rotation. Likewise, the barrier to **C** ring rotation was also estimated to be $\approx 9\text{ kcal mol}^{-1}$. After making due allowances for the errors associated with such an approach, the energy requirements for rotation of the **A** and **C** phenyls appear to be considerably less than the 11 kcal mol^{-1} barrier found experimentally for the **B** phenyls. Although the chemical shift differences between *ortho* protons in the **A** and **C** rings have been estimated from ring current calculations rather than measured directly, the experimental coalescence temperatures are available. It is easy to show that, for the **A** and **C** rings to have rotational barriers of $\sim 11\text{ kcal mol}^{-1}$, the $\delta\Delta$ values for their *ortho* protons would have to be $\sim 3\text{ Hz}$ rather than the estimated separation of approximately 325 Hz . Therefore, we can conclude that the phenyl rotations are not correlated in C_7Ph_7H .

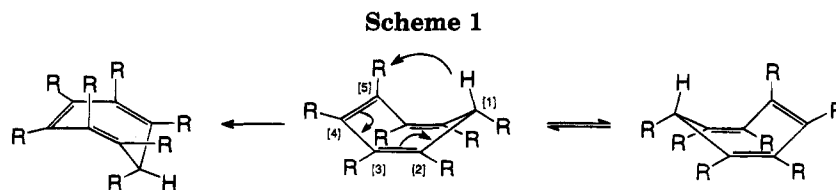
Hydrogen Migrations in $C_7Ph_5Me_2H$. The analogous synthesis of $C_7Ph_5Me_2H$ (**3**), can be readily envisaged from the Diels–Alder reaction of 1,2,3-triphenylcyclopropene with 2,5-dimethyl-3,4-diphenylcyclopentadienone (**4**). This latter molecule, unlike C_4Ph_4CO , which is monomeric, occurs as its Diels–Alder dimer and so must be cracked before use.¹⁹ When **4** and C_3Ph_3H are either melted together or heated in refluxing xylenes for 4 days, CO is evolved and $C_7Ph_5Me_2H$ is produced. However, the complexity of the NMR spectra, in particular the nonequivalence of the methyl groups in both the 1H and ^{13}C regimes, reveals that **3** cannot be the anticipated symmetrical isomer **3a**. Indeed, the singlet character of both methyl signals in the 1H spectrum eliminates **3c** and leaves **3b** and **3d** as the only two viable candidates.



The choice between these two isomers can be made by using a combination of 2D and NOE experiments.

(17) Johnson, C. E., Jr.; Bovey, F. A. *J. Chem. Phys.* **1958**, *29*, 1012.
 (18) Waugh, J. S.; Fessenden, R. W. *J. Am. Chem. Soc.* **1957**, *79*, 846; **1958**, *80*, 6697.

(19) Allen, C. F. H. *Chem. Rev.* **1962**, *62*, 653.



These spectra allowed the ready identification of the phenyl **D** ring (whose *ortho* protons were coupled to the methine hydrogen) and of the methyl and phenyl in the **C** environment (both of which showed NOE's to this same methine proton). Irradiation of the *ortho* H's of the **D** ring enhanced the other methyl as well as the single phenyl in the **A** environment. These data were confirmed by irradiation of each methyl in turn; all the data were consistent with structure **3b**, in which the methine hydrogen again occupied the pseudo-equatorial site at C(7). Although this structure possesses two phenyl **B** rings, they each have a phenyl and a methyl neighbor, thus avoiding the severe steric crowding which is observed in C_7Ph_7H .

Such molecules must arise via hydrogen migrations, but the symmetry-allowed [1,5]-suprafacial sigmatropic shift can only occur when the migrating hydrogen is positioned axially so as to facilitate the rearrangement shown in Scheme 1. Since the methine hydrogen at C(7) is positioned pseudo-equatorially, any attempt to equilibrate the methyl environments must first surmount the barrier to cycloheptatriene ring flipping. The 1H spectrum of **3** was recorded at various temperatures up to 137 °C (410 K), but no broadening or coalescence of the methyl signals was evident. This result yields a minimum barrier of 19.4 kcal mol⁻¹ for C_7 ring inversion. Consequently, we carried out a series of selective inversion experiments, since this technique is capable of detecting slow exchange without the need to take the sample to inconveniently high temperatures.²⁰ However, even at 410 K, no magnetization transfer between methyl sites could be detected, and so we must revise our estimate of the minimum barrier for ring inversion to 25 kcal mol⁻¹. We note that this minimum estimate for ΔG^\ddagger exceeds the quoted value of 23.8 kcal mol⁻¹ for 1,2:3,4:5,6-tribenzocycloheptatriene.²¹

Structure of the Tricyclic Ketone 2. A crucial factor in such rearrangements is the ring conformation; it may well be the case that [1,5]-hydrogen shifts also occur during the formation of C_7Ph_7H but, since such a process would be degenerate, the same final product would result.²² The crystallographically characterized molecule **1b** could not undergo [1,5]-hydrogen shifts without flipping to the other boat conformer, as in Scheme 1. The activation energies for such conformational flips vary from 6.3 kcal mol⁻¹ for C_7H_8 to more than 20 kcal mol⁻¹ for cycloheptatrienes bearing bulky

groups.²³ Clearly, the conformation of the initially formed C_7Ph_7H is dependent on the structure of the precursor tricyclic ketone, **2a** or **2b**. The geometry of **2** could not be assigned unequivocally since, even at 500 MHz, overlap of the phenyl peaks is too severe. Consequently, the problem was again resolved by X-ray crystallography and the resulting structure, **2a**, appears as in Figure 6. It is evident that all three phenyls derived from the cyclopropane ring are mutually *cis* in the Diels–Alder adduct.

The tricyclic ketone **2a** possesses several interesting structural features. We note that the C(1)–C(6) distance is rather long at 1.569(6) Å, reflecting its somewhat strained environment as a member of three different-sized rings (a cyclopropane, a cyclopentanone, and a cyclohexene). It is this bond that is broken when CO is lost and C_7Ph_7H is formed. However, it is also interesting that the C(1)–C(2) and C(5)–C(6) bonds are also long, 1.607(6) and 1.600(6) Å, respectively;²⁴ these are the bonds that are made during the Diels–Alder reaction to form **2a**, and their weakness may account for the ready reversibility of this process. Indeed, as we shall see presently, this factor presumably comes into play during the reaction of **2a** with $Mo(CO)_6$. It is apparent that cheletropic loss of CO from **2a** will yield **1a**,²⁵ in which [1,5]-hydrogen shifts are viable. However, the structure determined for C_7Ph_7H is **1b**, in which a boat-to-boat conformational flip has occurred. An examination of molecular models confirms that the initially formed conformer, **1a**, engenders severe steric problems between the pseudo-equatorial phenyl (ring **D**) and its neighbors in the **C** positions.

To demonstrate the intermediacy of conformer **1a**, we used 2,5-diphenyl-3,4-di-*p*-tolylcyclopentadienone to prepare **1'** and **2'**, analogous to **1** and **2**. Thermolysis of **2'** resulted in elimination of CO and formation of the isomers depicted in Figure 7. The peripheral tolyl rings in the isomers of **1'** give rise to seven equally intense 1H methyl resonances; moreover, the aromatic protons in the **D**-ring environment clearly reveal the presence of both phenyl and tolyl groups in a 5:2 ratio. We can therefore conclude that conformation **1a** is sufficiently long-lived to allow rapid [1,5]-suprafacial sigmatropic hydrogen shifts before ring flipping to **1b** prevents any further rearrangement.

(23) (a) Anet, F. A. L. *J. Am. Chem. Soc.* **1964**, *86*, 458. (b) Anet, F. A. L.; Anet, R. In *Dynamic NMR Spectroscopy*; Jackman, L. M., Cotton, F. A., Eds., Academic Press: New York, 1975; pp 592–597. (c) Aonuma, S.; Komatsu, K.; Takeuchi, K. *Chem. Lett.* **1989**, 2107.

(24) We are aware of only one closely related structure, *viz.* the Diels–Alder adduct of tetracyclone with cyclopentadiene, where both the *endo* and *exo* isomers are known. In the *endo* adduct, the bonds formed in the Diels–Alder addition (corresponding to C(1)–C(2) and C(5)–C(6) in **2**) average 1.569 Å, reflecting the less crowded nature of this product: Coxon, J. M.; O'Connell, M. J.; Steel, P. J. *Aust. J. Chem.* **1965**, *38*, 1223.

(25) Battiste has noted that *endo*-tricyclo[3.2.1.0^{2,4}]octen-8-ones undergo facile decarbonylation to yield cycloheptatrienes directly, while their *exo* isomers apparently decompose via norcaradiene intermediates: Halton, B.; Battiste, M. A.; Rehberg, R.; Deyrup, C. L.; Brennan, M. E. *J. Am. Chem. Soc.* **1967**, *89*, 5964.

(20) (a) Sanders, J. K. M.; Hunter, B. K. *Modern NMR Spectroscopy*; Oxford University Press: Oxford, U.K., 1987; pp 224–229. (b) Forsén, S.; Hoffman, R. A. *J. Chem. Phys.* **1963**, *39*, 2892. (c) Forsén, S.; Hoffman, R. A. *J. Chem. Phys.* **1964**, *40*, 1189. (d) Forsén, S.; Hoffman, R. A. *J. Chem. Phys.* **1966**, *45*, 2049. (e) Bain, A. D.; Cramer, J. A. *J. Magn. Reson.* **1993**, *A103*, 217. (f) Bain, A. D.; Cramer, J. A. *J. Chem. Phys.* **1993**, *97*, 2884.

(21) Nográdi, M.; Ollis, W. D.; Sutherland, I. O. *J. Chem. Soc. D* **1970**, 158.

(22) It has been reported that, after 45 min at 300 °C, C_7Ph_7H shows evidence of [1,5]-phenyl shifts. Harvey, J. A.; Ogliaruso, M. A. *J. Org. Chem.* **1976**, *41*, 3374.

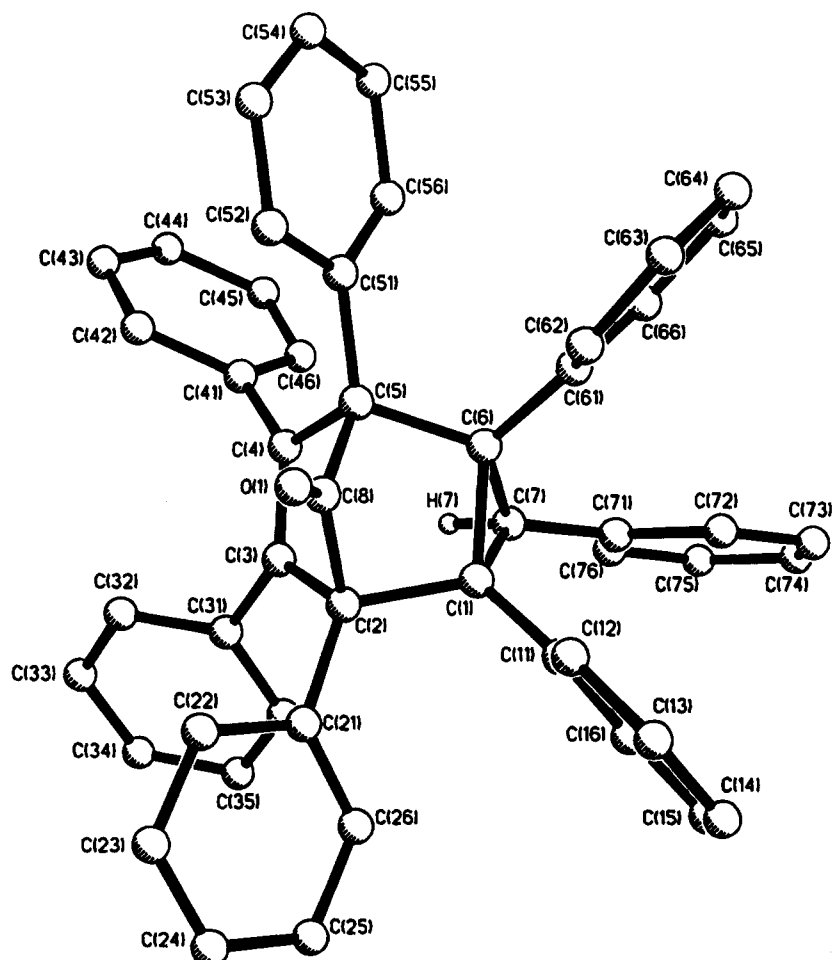


Figure 6. Molecular structure of C_7Ph_7HCO (**2**), showing the atom-numbering scheme.

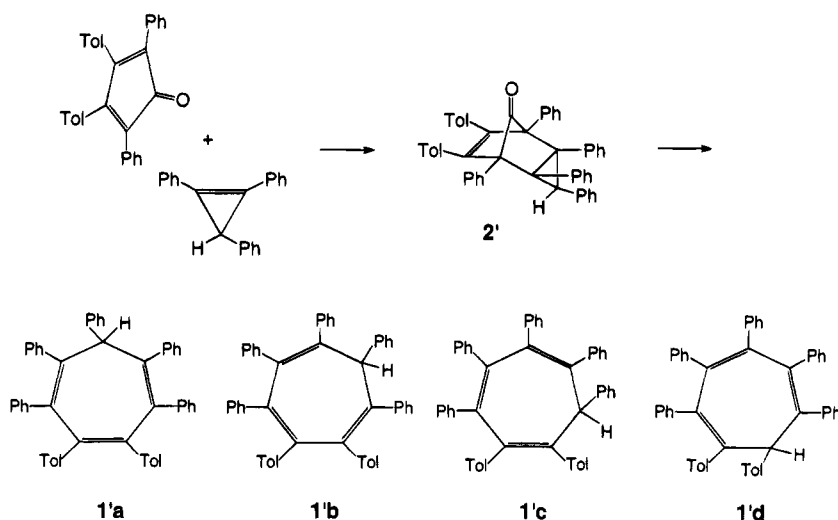


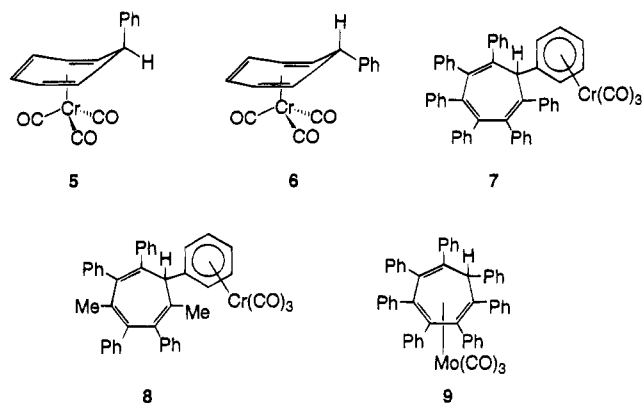
Figure 7. Isomers of $C_7(p\text{-tolyl})_2Ph_5H$ (**1'**).

Reactions of C_7Ph_7H with Metal Carbonyls. It is known that 7-phenylcycloheptatriene reacts with $Cr(CO)_6$ or $(pyridine)_3Cr(CO)_3$ to give the *exo*- and *endo*-phenyl isomers, **5** and **6**, respectively, in which the metal is η^6 -coordinated to the 7-membered ring.²⁶

Treatment of C_7Ph_7H with $Cr(CO)_6$ yields a yellow complex, **7**, in which the $Cr(CO)_3$ moiety is attached to an external phenyl ring. The marked shielding of the

1H and ^{13}C resonances in the chromium-complexed ring, together with the symmetrical character of the remaining phenyl ^{13}C signals, indicates that the metal is coordinated to the unique **D** ring. Whether the metal merely attacked the most sterically accessible ring, or rather the product resulted from hydrogen migration after complexation, remains an open question at present. Analogously, $(C_7Ph_5Me_2H)Cr(CO)_3$ (**8**), was prepared, and the observation of five distinct protons in the complexed phenyl ring suggests that, like **3**, the molecule lacks a mirror plane. We should, however, recall

(26) Pauson, P. L.; Smith, G. H.; Valentine, J. H. *J. Chem. Soc. C* **1967**, 1061.



that hydrogen migrations proceed 10^3 times more rapidly in $(\eta^6\text{-C}_7\text{H}_8)\text{Mo}(\text{CO})_3$ than they do in free cycloheptatriene; deuterium labeling studies suggest that, in the complex, it is the *endo* hydrogen which migrates, presumably through a metal hydride intermediate.²⁷

The reactions of $\text{Mo}(\text{CO})_6$ or $(\text{CH}_3\text{CN})_3\text{W}(\text{CO})_3$ with $\text{C}_7\text{Ph}_7\text{H}$ gave relatively unstable products that are still the subject of investigation, but a more interesting result was obtained when the tricyclic ketone **2a** was heated under reflux with $\text{Mo}(\text{CO})_6$. The intent was to try to coordinate a molybdenum carbonyl fragment onto the open face of **2a** in the expectation that subsequent metal-assisted cyclopropane ring opening and loss of CO would yield a complex in which the molybdenum was bonded to the central ring, as in **9**. However, when the reactants were heated, a blue coloration appeared, indicating the formation of tetracyclone, presumably as the result of a retro-Diels–Alder reaction. The product, **10**, that was finally isolated was shown by mass spectrometry to possess a molecular weight corresponding to $\text{C}_7\text{Ph}_7\text{H}_3\text{Mo}(\text{CO})_3$, and its identity was not immediately evident from the NMR data. The structure of **10**, determined by X-ray crystallography, is shown in Figure 8 and reveals that it contains an η^5 -1-hydroxy-2,3,4,5-tetraphenylcyclopentadienyl ligand and also an η^3 -1,2,3-triphenylallyl moiety coordinated to a dicarbonylmolybdenum center. Although the $\text{Ph}_4\text{C}_5\text{OH}$ moiety is not a common ligand, ruthenium and molybdenum complexes are known.^{28,29} The molybdenum– C_5 (centroid) distance of 2.052 Å in **10** compares well with the value of 2.034 Å found in $[\text{Mo}_2(\text{CO})_3(\mu\text{-}\sigma\text{-}\eta^5\text{-C}_4\text{Ph}_4\text{CO})(\eta^5\text{-C}_5\text{Ph}_4\text{OH})]$.²⁹

The four peripheral rings of the η^5 - $\text{Ph}_4\text{C}_5\text{OH}$ ligand adopt a propeller-type geometry in which the phenyls are twisted relative to the central five-membered ring by θ values of 41, 52, 66, and 44°. This is in contrast with their orientations in $[\text{Mo}_2(\text{CO})_3(\mu\text{-}\sigma\text{-}\eta^5\text{-C}_4\text{Ph}_4\text{CO})(\eta^5\text{-C}_5\text{Ph}_4\text{OH})]$, where they were described as taking up a cup-shaped arrangement.²⁹

Subsequently, it was shown that the molybdenum complex **10** (and also its dimethyl analogue **11**) can be prepared by heating $\text{Mo}(\text{CO})_6$, $\text{C}_3\text{Ph}_3\text{H}$, and tetracyclone (or $\text{C}_4\text{Ph}_2\text{Me}_2\text{CO}$ (**4**)) in refluxing toluene; it is not necessary to use the tricyclic ketone **2** as the precursor. The reaction of $\text{Mo}(\text{CO})_6$ with tetracyclone has been investigated previously.²⁹ In the presence of acetonitrile,

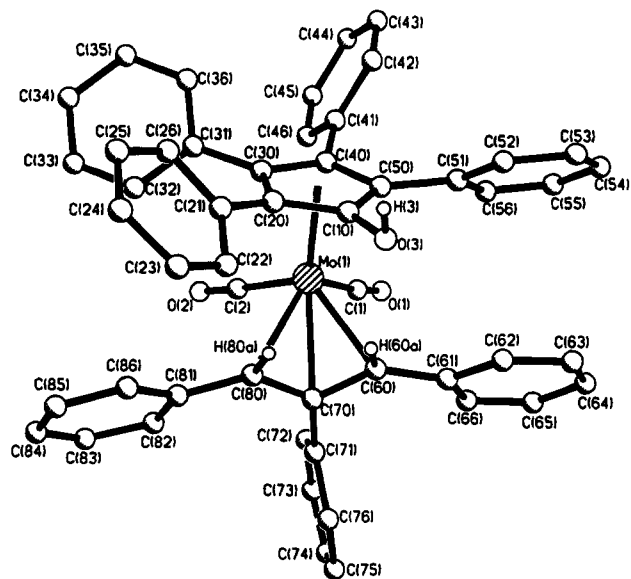
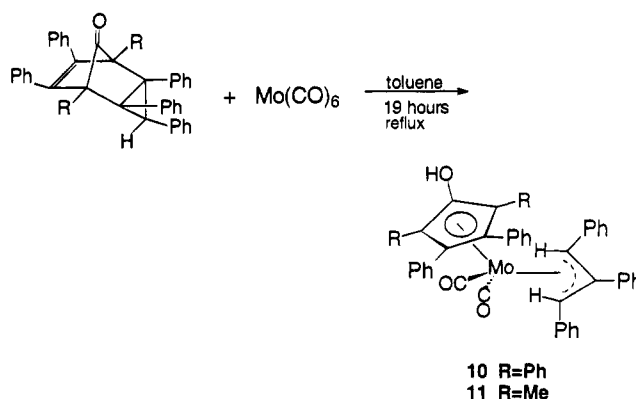
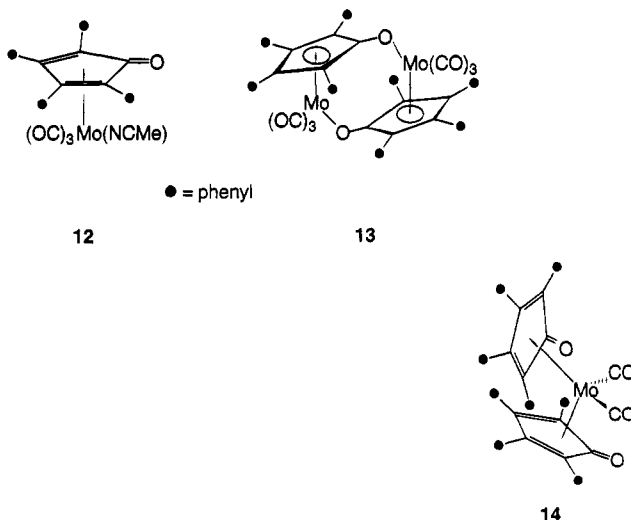


Figure 8. Molecular structure of $(\text{C}_5\text{Ph}_4\text{OH})(\text{C}_3\text{Ph}_3\text{H}_2)\text{Mo}(\text{CO})_2$ (**10**) showing the atom-numbering scheme.



trile, the $(\text{dienone})\text{Mo}(\text{CO})_3(\text{NCCH}_3)$ complex **12** is formed, but in the absence of a coordinating solvent, one can obtain either the oxygen-bridged dimer **13**, or the bis(dienone) $\text{Mo}(\text{CO})_2$ species **14**, depending on the ratio of reactants.



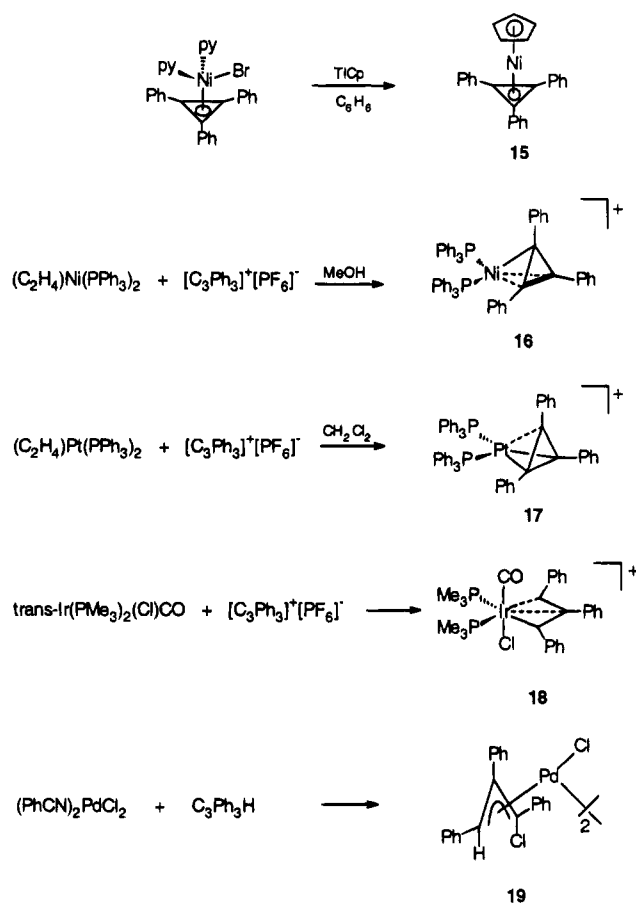
(27) Roth, W. R.; Grimme, W. *Tetrahedron Lett.* **1966**, 2347.

(28) Mays, M. J.; Morris, M. J.; Raithby, P. R.; Shvo, Y.; Czarkie, D. *Organometallics* **1989**, *8*, 1162.

(29) Adams, H.; Bailey, N. A.; Hempstead, P. D.; Morris, M. J.; Riley, S.; Beddoes, R. L.; Cook, E. S. *J. Chem. Soc., Dalton Trans.* **1993**, 91.

A number of reactions of $\text{C}_3\text{Ph}_3\text{H}$ or of the C_3Ph_3^+ cation with organometallics have been reported.³⁰ Schrock³¹ and Hughes³² have investigated the experimental barrier to rotation of the $\eta^3\text{-C}_3\text{R}_3$ ligand, where

Scheme 2



R is a bulky substituent such as *tert*-butyl or phenyl, in a series of tungsten, molybdenum and ruthenium complexes. It was shown that in $\text{CpMX}_2(\text{C}_3\text{R}_3)$ systems the frontier orbitals of the CpMX_2 fragment play a crucial role in determining the rotational barrier.^{30h,32}

Of particular relevance to this work are a series of products, **15**–**19**, resulting from the treatment of $[\text{Ph}_3\text{C}_3]^+[\text{PF}_6]^-$ or $\text{C}_3\text{Ph}_3\text{H}$ with several coordinatively unsaturated organometallics. In the first four cases shown in Scheme 2, the opening of the cyclopropenyl ring has proceeded to a different extent, culminating in the iridacycle **18**.^{30c} In **10**, the cyclopropene ring opening is now complete, and the addition of hydrogen has generated the η^3 -1,2,3-triphenylallyl ligand. We note that $\text{C}_3\text{Ph}_3\text{H}$ is reported to react with $(\text{PhCN})_2\text{PdCl}_2$ to give $[(\eta^3\text{-1-chloro-1,2,3-triphenylallyl})\text{PdCl}]_2$ (**19**),^{30g} however, we are unaware of any X-ray crystallographic data on this molecule. One might envisage a route to **10** that involves an intermediate of the type (tetracyclone) $\text{Mo}(\text{CO})_3(\text{C}_3\text{Ph}_3\text{H})$ that subsequently undergoes cyclopropene ring opening, perhaps via a

metallacyclobutene.³⁰ⁱ However, such mechanistic proposals must remain speculative until deuterium-labeling studies can establish the source of the additional two hydrogens.

To conclude, the Diels–Alder reaction of tetracyclone (or of $\text{C}_4\text{Ph}_2\text{Me}_2\text{CO}$) with triphenylcyclopropene yields the adduct with an *endo* hydrogen at C(7); thermolysis to bring about elimination of CO produces the appropriately substituted cycloheptatriene in which [1,5]-hydrogen shifts can occur. However, this initially formed isomer with a pseudo-equatorial phenyl substituent at the sp^3 position is sterically hindered and undergoes a conformational flip which allows the phenyl group to occupy the favored pseudo-axial site. Nevertheless, the remaining phenyls are sterically encumbered and slowed rotation of these rings can be monitored by ^1H and ^{13}C NMR spectroscopy.

The reaction of $\text{Cr}(\text{CO})_6$ with $\text{C}_7\text{Ph}_7\text{H}$ leads to incorporation of a $\text{Cr}(\text{CO})_3$ group on a peripheral phenyl ring; attempts to coordinate $\text{Mo}(\text{CO})_3$ or $\text{W}(\text{CO})_3$ to the seven-membered ring have so far been unsuccessful. It is well-known that the corresponding $(\eta^6\text{-C}_7\text{H}_8)\text{M}(\text{CO})_3$ complexes, where $\text{M} = \text{Cr}, \text{Mo}, \text{W}$, adopt geometries whereby the six coordinated sp^2 carbons are almost coplanar, and only the methylene group is bent substantially out of this plane.³³ Such a conformation may be energetically disfavored for the $\text{C}_7\text{Ph}_7\text{H}$ ligand, and it has not yet been possible to characterize any molecules in which a metal is coordinated to the central ring of the heptaphenylcycloheptatriene ligand. However, the tricyclic ketone **2**, which is the precursor to **1**, reacts with $\text{Mo}(\text{CO})_6$ to give the complex $(\eta^5\text{-C}_5\text{Ph}_4\text{OH})\text{Mo}(\text{CO})_2(\eta^3\text{-C}_3\text{Ph}_3\text{H}_2)$. Experiments designed to generate centrally bonded metal complexes of the $\text{C}_7\text{Ph}_7\text{H}$ ligand are continuing.

Experimental Section

All syntheses were carried out under a dry nitrogen atmosphere utilizing conventional benchtop and glovebag techniques. Solvents were dried and distilled according to standard procedures.³⁴ Silica gel (200–400 mesh) was employed for flash column chromatography. The 1D and 2D ^1H and ^{13}C NMR were recorded on a Bruker AM-500, AC-300, or AC-200 spectrometer. IR spectra were recorded on a Bio-Rad FTS-40 instrument using NaCl plates. Mass spectra were collected on a VG analytical ZAB-E spectrometer by direct electron impact and direct chemical ionization (NH_3) methods. Melting points were determined on a Thomas Hoover melting point apparatus and are uncorrected.

Preparation of $\text{C}_7\text{Ph}_7\text{H}$ (1). **1** was prepared from 2,3,4,5-tetraphenylcyclopentadienone and 1,2,3-triphenylcyclopropene according to the literature procedure.¹² Recrystallization from $\text{CHCl}_3/\text{ether}$ gave a 72% yield of colorless crystals, mp 284–286 °C (lit.¹² 285–287.5 °C). ^1H and ^{13}C NMR data are listed in Table 1. Mass spectrum (DEI): m/z (%) 624 (100) $[\text{M}]^+$, 546 (32) $[\text{M} - \text{Ph} - \text{H}]^+$, 469 (35) $[\text{M} - 2\text{Ph} - \text{H}]^+$, 391 (17) $[\text{M} - 3\text{Ph} - 2\text{H}]^+$.

Preparation of $\text{C}_7\text{Ph}_7\text{HCO}$ (2). 2,3,4,5-Tetraphenylcyclopentadienone (2.341 g, 6 mmol) and 1,2,3-triphenylcyclopropene (0.806 g, 3 mmol) in benzene were stirred at room temperature for 6 days. **2** was purified by flash chromatography using 3:2 $\text{CH}_2\text{Cl}_2/\text{hexanes}$ as the eluent. The first band gave **2** (1.568 g, 2.4 mmol, 80%), which recrystallized from $\text{CH}_2\text{Cl}_2/\text{hexane}$ as colorless plates. ^1H NMR (200 MHz, CD_2Cl_2):

(30) (a) Mealli, C.; Midolloni, S.; Moneti, S.; Sacconi, L. *Angew. Chem., Int. Ed. Engl.* **1980**, *19*, 931. (b) McClure, M. D.; Weaver, D. L. *J. Organomet. Chem.* **1973**, *54*, C59. (c) Tuggle, R. M.; Weaver, D. L. *Inorg. Chem.* **1972**, *11*, 2237. (d) Keasey, A.; Maitlis, P. M. *J. Chem. Soc., Dalton Trans.* **1978**, 1830. (e) Frisch, P. D.; Khare, G. P. *Inorg. Chem.* **1979**, *18*, 781. (f) Kettle, S. F. A. *Inorg. Chem.* **1964**, *3*, 604. (g) Muskak, P.; Battiste, M. A. *J. Organomet. Chem.* **1969**, *17*, 46. (h) Mealli, C.; Midolloni, S.; Moneti, S.; Sacconi, L.; Silvestre, J.; Albright, T. A. *J. Am. Chem. Soc.* **1982**, *104*, 95. (i) Li, R. T.; Nguyen, S. T.; Grubbs, R. H.; Ziller, J. W. *J. Am. Chem. Soc.* **1994**, *116*, 10032.

(31) Churchill, M. R.; Fettingner, J. C.; McCullough, L.; Schrock, R. R. *J. Am. Chem. Soc.* **1984**, *106*, 3356.

(32) Ditchfield, R.; Hughes, R. P.; Tucker, D. S.; Bierwagen, E. P.; Robbins, J.; Robinson, D. J.; Zakutansky, J. A. *Organometallics* **1993**, *12*, 2258.

(33) Dunitz, J.; Pauling, P. *Helv. Chim. Acta* **1960**, *43*, 2188.

(34) Perrin, D. D.; Armarego, W. L. F.; Perrin, D. R. *Purification of Laboratory Chemicals*; Pergamon Press: New York, 1980.

Table 2. Structure Determination Summary

	1	2	10
empirical formula	C ₄₉ H ₃₆	C ₅₀ H ₃₆ O	C ₅₂ H ₃₈ MoO ₃
fw	624.78	652.79	806.76
cryst size (mm)	0.25 × 0.25 × 0.25	0.1 × 0.1 × 0.05	0.2 × 0.2 × 0.1
color, habit	colorless, parallelepiped	colorless, plate	red-brown, plate
temp (K)	298(2)	300(2)	298(2)
wavelength	0.710 73	0.710 73	0.710 73
cryst syst	triclinic	monoclinic	triclinic
space group	P $\bar{1}$	P2 ₁ /n	P $\bar{1}$
unit dimens			
<i>a</i> (Å)	9.8320(10)	12.829(4)	13.265(3)
<i>b</i> (Å)	10.0260(10)	16.456(2)	13.561(3)
<i>c</i> (Å)	19.166(2)	18.226(3)	13.635(4)
α (deg)	92.194(1)	90.0	71.84(2)
β (deg)	90.57(1)	110.06(1)	65.04(2)
γ (deg)	108.94(1)	90.0	61.20(1)
<i>V</i> (Å ³)	1785.2(3)	3614.3(13)	1930.3(12)
<i>Z</i>	2	4	2
calcd density (Mg/m ³)	1.162	1.200	1.388
abs coeff (mm ⁻¹)	0.066	0.070	0.385
<i>F</i> (000)	660	1376	832
θ range (deg)	2.13–25.00	2.09–22.50	2.23–24.98
index ranges	−1 ≤ <i>h</i> ≤ 11, −11 ≤ <i>k</i> ≤ 11, −22 ≤ <i>l</i> ≤ 22	−1 ≤ <i>h</i> ≤ 15, −1 ≤ <i>k</i> ≤ 19, −21 ≤ <i>l</i> ≤ 20	−1 ≤ <i>h</i> ≤ 12, −14 ≤ <i>k</i> ≤ 13, −15 ≤ <i>l</i> ≤ 14
no. of rflns collected	7480	6396	5717
no. of indep rflns	6282	4666	4929
no. of params	446	461	513
goodness of fit on <i>F</i> ²	1.028	0.981	1.042
final <i>R</i> indices (<i>I</i> > 2σ(<i>I</i>))	<i>R</i> 1 = 0.0527, <i>wR</i> 2 = 0.1176	<i>R</i> 1 = 0.0702, <i>wR</i> 2 = 0.1238	<i>R</i> 1 = 0.0658, <i>wR</i> 2 = 0.1008
<i>R</i> indices (all data)	<i>R</i> 1 = 0.0884, <i>wR</i> 2 = 0.1398	<i>R</i> 1 = 0.1602, <i>wR</i> 2 = 0.1628	<i>R</i> 1 = 0.1325, <i>wR</i> 2 = 0.1231
extinction coeff	0.0063(10)	N/A	0.0005(4)
largest diff peak (Å ⁻³)	0.221	0.170	0.342
largest diff hole (Å ⁻³)	−0.210	−0.180	−0.445

δ 7.30–6.77 (m, 35H, phenyl protons), 3.60 (s, 1H, H7). ¹³C NMR (50.288 MHz, CD₂Cl₂): δ 194.16 (C8), 142.97 (C3/C4), 137.04, 135.38, 135.10, 133.55, 133.41, 131.72, 130.01, 127.81, 127.37, 127.10, 126.98, 126.75, 126.39, 126.13 (phenyl carbons), 68.77 (C2/C5), 38.56 (C1/C6), 31.95 (C7). IR (CH₂Cl₂): ν_{CO} 1768 cm⁻¹. Mass spectrum (DEI): *m/z* (%) 652 (5) [M]⁺, 624 (100) [M - CO]⁺, 547 (5) [M - CO - Ph]⁺.

Preparation of C₇(*p*-tolyl)₂Ph₃H (1'). 1' was prepared analogously to 1 from 2,5-diphenyl-3,4-ditolylcyclopentadienone (0.118 g, 0.29 mmol) and 1,2,3-triphenylcyclopropene (0.077 g, 0.29 mmol). The product was chromatographed over silica gel with ether/pentane (2:98) as eluent. The major band was separated and gave 1' as an oily yellow solid (0.123 g, 0.18 mmol, 65%), a mixture of isomers 1'a–1'd. ¹H NMR (500 MHz, CD₂Cl₂): δ 7.97 (d, 10H, *ortho* of phenyl D), 7.85 (d, 4H, *ortho* of tolyl D), 7.49 (m, 10H, *meta* of phenyl D), 7.39 (d, 5H, *para* of phenyl D), 7.32 (d, 4H, *meta* of tolyl D), 7.16–6.14 (m, 198H, tolyl/phenyl protons), 5.31 (s, 5H, sp³ H), 5.28 (s, 2H, sp³ H), 2.44 (s, 1 CH₃), 2.22 (s, 2 CH₃'s), 2.17 (s, 1 CH₃), 2.16 (s, 1 CH₃), 1.98 (s, 1 CH₃), 1.97 (s, 1 CH₃). ¹³C NMR (125.76 MHz, CD₂Cl₂): δ 144.19, 143.72, 143.54, 141.36, 141.20, 140.42, 139.72, 139.60, 138.04, 137.28, 136.86, 136.41, 136.03 (ipso and ring carbons), 132.05, 131.84, 131.76, 131.55, 130.22, 130.08, 129.38, 128.79, 128.66, 128.28, 127.91, 127.51, 127.21, 127.17, 126.61, 126.35, 126.32, 125.34 (phenyl carbons), 58.27, 57.98 (sp³ ring carbons), 21.24, and 20.92 (CH₃'s). Mass spectrum (DEI): *m/z* (%) 652 (100) [M]⁺, 561 (17) [M - Tol]⁺, 483 (14) [M - Tol - Ph - H]⁺.

Preparation of C₇Ph₅Me₂H (3). 2,5-Dimethyl-3,4-diphenylcyclopentadienone dimer (1.30 g, 2.5 mmol) was heated in refluxing xylenes (25 mL) for 1 h. Formation of the monomer was indicated by a red coloration of the solution. 1,2,3-Triphenylcyclopropene (1.315 g, 4.9 mmol) was then added and the mixture heated under reflux for 4 days, after which time the xylenes were removed by distillation. The product was recrystallized from pentane to give colorless crystals of 3 (0.80 g, 30%), mp 181–185 °C. ¹H and ¹³C NMR data are listed in Table 1. Mass spectrum (DEI): *m/z* (%) 500 (100) [M]⁺, 485 (10) [M - CH₃]⁺, 407 (39) [M - Ph - H]⁺.

Trace amounts of the ketone intermediate C₇Ph₅Me₂HCO,

a yellow solid, also recrystallized and were isolated. ¹H NMR (200 MHz, CD₂Cl₂): δ 7.28–6.23 (m, 25H, phenyl protons), 2.96 (s, 1H, H7), 1.15 (s, 6H, 2CH₃). ¹³C NMR (50.288 MHz, CD₂Cl₂): δ 197.13 (C8), 147.78 (C3/C4), 135.22, 133.53, 132.93, 131.17, 130.28, 128.24, 128.0, 127.73, 127.54, 126.71, 125.55 (phenyl carbons), 65.21 (C2/C5), 55.23 (C1/C6), 38.65 (C7), 9.82 (CH₃). IR (CH₂Cl₂): ν_{CO} 1752 cm⁻¹. Mass spectrum (DEI): *m/z* (%) 528 (32) [M]⁺, 500 (100) [M - CO]⁺, 485 (17) [M - CO - CH₃]⁺, 407 (68) [M - CO - CH₃ - Ph - H]⁺.

Preparation of (C₇Ph₇H)Cr(CO)₃ (7). A mixture of C₇-Ph₇H (1; 0.413 g, 0.661 mmol) and Cr(CO)₆ (0.189 g, 0.859 mmol) in dry *n*-butyl ether (15 mL) and dry THF (15 mL) was heated under reflux for 48 h. The yellow solution was then cooled and the solvent removed under reduced pressure. The residue was recrystallized from toluene and hexane to give 7, a yellow solid (0.201 g, 0.263 mmol, 40%). ¹H NMR (300 MHz, CDCl₃): δ 7.07–6.19 (m, 30H, noncoordinated phenyls), 5.60–5.32 (m, 5H, coordinated phenyl). ¹³C NMR (75.432 MHz, CDCl₃): δ 143.58, 142.02, 140.03, 139.91, 138.27, 137.25 (ipso and ring carbons), 131.51, 131.30, 129.83, 127.75, 127.39, 127.14, 126.77, 126.41, 126.01, 125.58 (noncoordinated phenyl carbons), 93.18, 92.77, 92.03 (coordinated phenyl carbons), 55.82 (C7). IR (CH₂Cl₂): ν_{CO} 1968, 1894 cm⁻¹. Mass spectrum (DEI): *m/z* (%) 760 (5) [M]⁺, 676 (100) [M - 3CO]⁺, 623 (70) [M - Cr(CO)₃ - H]⁺, 546 (30) [M - Cr(CO)₃ - Ph - H]⁺, 469 (25) [M - Cr(CO)₃ - 2Ph - H]⁺. Anal. Calcd for C₅₂H₃₆O₃Cr: C, 82.10; H, 4.74. Found: C, 82.37; H, 4.52.

Preparation of (C₇Ph₅Me₂H)Cr(CO)₃ (8). To a mixture of C₇Ph₅Me₂H (0.5 g, 1 mmol) and Cr(CO)₆ (0.22 g, 1 mmol) were added 5 mL of dry *n*-butyl ether and 3 mL of dry THF, and the reaction mixture was heated under reflux for 2 days. After the mixture was cooled to room temperature, most of the solvent was removed and the remaining greenish yellow residue was chromatographed over silica gel with hexane/CH₂-Cl₂ (1:1) as eluent. The yellow band was separated and concentrated under reduced pressure and kept for crystallization at -20 °C. The yellow amorphous solid (0.064 g, 0.1 mmol, 10%) of 8 precipitated and was filtered. ¹H NMR (200 MHz, CD₂Cl₂): δ 7.60–6.50 (m, 20H, noncoordinated phenyls), 5.83–5.28 (m, 5H, coordinated phenyl), 4.82 (s, 1H, H7), 1.89

Table 3. Atomic Coordinates ($\times 10^4$) and Equivalent Isotropic Displacement Parameters ($\text{\AA}^2 \times 10^3$) for $\text{C}_7\text{Ph}_7\text{H}$ (1)

	<i>x</i>	<i>y</i>	<i>z</i>	<i>U</i> (eq) ^a
C(1)	1177(2)	-142(2)	8347(1)	43(1)
C(11)	2156(2)	727(2)	8908(1)	43(1)
C(12)	1749(3)	1711(2)	9310(1)	59(1)
C(13)	2613(3)	2489(3)	9854(1)	70(1)
C(14)	3919(3)	2341(3)	9991(1)	69(1)
C(15)	4362(3)	1407(3)	9590(1)	66(1)
C(16)	3489(2)	601(2)	9057(1)	54(1)
C(2)	827(2)	-1561(2)	8281(1)	43(1)
C(21)	1308(2)	-2376(2)	8813(1)	46(1)
C(22)	945(3)	-2316(2)	9507(1)	57(1)
C(23)	1365(3)	-3076(3)	9996(1)	75(1)
C(24)	2143(3)	-3916(3)	9807(2)	80(1)
C(25)	2530(3)	-4009(3)	9127(2)	78(1)
C(26)	2111(3)	-3228(3)	8625(1)	64(1)
C(3)	-64(2)	-2417(2)	7696(1)	45(1)
C(31)	-1210(3)	-3760(2)	7884(1)	53(1)
C(32)	-2544(3)	-3717(3)	8015(2)	101(1)
C(33)	-3642(4)	-4925(5)	8211(2)	139(2)
C(34)	-3367(5)	-6164(5)	8257(2)	118(2)
C(35)	-2065(5)	-6234(4)	8111(2)	117(1)
C(36)	-982(4)	-5033(3)	7941(2)	92(1)
C(4)	101(2)	-2032(2)	7021(1)	46(1)
C(41)	-742(2)	-2984(2)	6435(1)	51(1)
C(42)	-1667(3)	-2573(3)	6028(2)	83(1)
C(43)	-2395(4)	-3387(4)	5458(2)	103(1)
C(44)	-2213(4)	-4629(4)	5291(2)	101(1)
C(45)	-1306(4)	-5079(4)	5688(2)	101(1)
C(46)	-569(3)	-4264(3)	6259(2)	79(1)
C(5)	1142(2)	-698(2)	6798(1)	44(1)
C(51)	1933(2)	-846(2)	6151(1)	49(1)
C(52)	1754(3)	-269(3)	5528(1)	68(1)
C(53)	2483(4)	-481(3)	4945(1)	88(1)
C(54)	3398(4)	-1252(3)	4973(2)	89(1)
C(55)	3598(3)	-1821(3)	5584(2)	78(1)
C(56)	2858(3)	-1631(2)	6168(1)	62(1)
C(6)	1377(2)	561(2)	7143(1)	44(1)
C(61)	2430(2)	1910(2)	6923(1)	48(1)
C(62)	2009(3)	3094(3)	6872(1)	71(1)
C(63)	2956(4)	4358(3)	6669(2)	95(1)
C(64)	4342(4)	4469(3)	6522(2)	96(1)
C(65)	4792(3)	3321(3)	6582(2)	85(1)
C(66)	3843(3)	2046(3)	6779(1)	64(1)
C(7)	599(2)	657(2)	7820(1)	45(1)
C(71)	-1030(2)	273(2)	7768(1)	48(1)
C(72)	-1865(3)	-94(2)	8355(1)	56(1)
C(73)	-3326(3)	-336(3)	8328(1)	68(1)
C(74)	-3997(3)	-236(3)	7709(1)	78(1)
C(75)	-3190(3)	147(3)	7124(1)	79(1)
C(76)	-1725(3)	403(3)	7154(1)	62(1)

^a *U*(eq) is defined as one third of the trace of the orthogonalized U_{ij} tensor.

(s, 3H, 1-Me), 1.17 (s, 3H, 4-Me). ¹³C NMR (50.288 MHz, CD_2Cl_2): δ 144.05, 143.11, 141.84, 136.99 (ring carbons), 131.61, 130.70, 130.45, 130.28, 128.44, 128.20, 128.02, 127.90, 127.73, 127.34, 127.08, 126.77, 126.64, 126.42, 126.19, 125.94 (non-coordinated phenyl carbons), 92.78, 93.35, 93.53 (coordinated phenyl carbons), 56.87 (C7), 25.04 (1-Me), 20.44 (4-Me). IR (CH_2Cl_2): ν_{CO} 1966, 1889 cm^{-1} . Mass spectrum (DEI): *m/z* (%) 636 (12) [M^+], 552 (55) [$\text{M} - 3\text{CO}^+$], 500 (100) [$\text{M} - \text{Cr}(\text{CO})_3^+$], 407 (85) [$\text{M} - \text{Cr}(\text{CO})_3 - \text{Ph} - \text{Me} - \text{H}^+$]. Mass spectrum (DCI, NH_3^+): *m/z* (%) 654 (15) [$\text{M} + \text{NH}_4^+$].

Preparation of $(\text{C}_5\text{Ph}_4\text{OH})(\text{C}_3\text{Ph}_3\text{H}_2)\text{Mo}(\text{CO})_2$ (10). To a mixture of $\text{C}_7\text{Ph}_7\text{HCO}$ (0.148 g, 0.23 mmol) and $\text{Mo}(\text{CO})_6$ (0.068 g, 0.26 mmol) was added 20 mL of dry toluene. The reaction mixture was heated under reflux in the dark for 20 h. After cooling, filtration under vacuum, and removal of solvent, the brown residue was flash-chromatographed on silica gel using 1:4 CH_2Cl_2 /hexanes as the eluent. After removal of $\text{C}_7\text{Ph}_7\text{H}$ and tetracyclone, a brown-red band gave **10** (0.057 g, 0.07 mmol, 31%). Recrystallization from CH_2Cl_2 /hexanes yielded red-brown plates, mp 220–222 °C. ¹H NMR (500 MHz, CD_2Cl_2): 7.21–6.79 (m, 35H, phenyl protons), 5.04

Table 4. Atomic Coordinates ($\times 10^4$) and Equivalent Isotropic Displacement Parameters ($\text{\AA}^2 \times 10^3$) for $\text{C}_7\text{Ph}_7\text{HCO}$ (2)

	<i>x</i>	<i>y</i>	<i>z</i>	<i>U</i> (eq) ^a
O(1)	1740(3)	540(2)	9509(2)	61(1)
C(1)	895(4)	1555(3)	7883(2)	40(1)
C(11)	1839(4)	1450(3)	7595(3)	46(1)
C(12)	2866(4)	1167(3)	8074(3)	57(2)
C(13)	3716(5)	1032(3)	7788(4)	73(2)
C(14)	3570(6)	1170(3)	7016(4)	84(2)
C(15)	2552(6)	1450(3)	6524(3)	73(2)
C(16)	1701(5)	1581(3)	6805(3)	57(2)
C(2)	422(4)	743(3)	8147(2)	41(1)
C(21)	655(4)	-65(3)	7845(3)	46(1)
C(22)	786(5)	-741(3)	8314(3)	60(2)
C(23)	938(5)	-1504(3)	8057(4)	81(2)
C(24)	938(5)	-1602(4)	7314(4)	87(2)
C(25)	773(6)	-956(4)	6819(4)	82(2)
C(26)	635(5)	-189(3)	7093(3)	68(2)
C(3)	-765(4)	863(3)	8129(3)	42(1)
C(31)	-1753(4)	457(3)	7562(2)	45(1)
C(32)	-2533(5)	72(3)	7792(3)	62(2)
C(33)	-3463(5)	-272(3)	7251(3)	75(2)
C(34)	-3609(5)	-229(3)	6469(3)	76(2)
C(35)	-2842(5)	152(4)	6232(3)	80(2)
C(36)	-1917(5)	500(3)	6767(3)	65(2)
C(4)	-771(4)	1410(3)	8687(2)	41(1)
C(41)	-1742(4)	1715(3)	8863(3)	46(1)
C(42)	-2072(5)	1367(4)	9435(3)	79(2)
C(43)	-2958(6)	1689(5)	9619(4)	101(2)
C(44)	-3502(6)	2355(5)	9223(4)	107(3)
C(45)	-3173(6)	2713(5)	8665(4)	99(2)
C(46)	-2304(5)	2402(4)	8484(3)	73(2)
C(5)	407(4)	1709(3)	9099(2)	42(1)
C(51)	593(4)	2092(3)	9887(2)	48(1)
C(52)	1072(4)	1667(3)	10576(3)	57(2)
C(53)	1190(5)	2044(4)	11288(3)	73(2)
C(54)	826(5)	2814(4)	11310(3)	79(2)
C(55)	321(5)	3235(4)	10626(3)	73(2)
C(56)	200(5)	2867(3)	9922(3)	61(2)
C(6)	852(4)	2198(3)	8506(2)	37(1)
C(61)	1737(4)	2807(3)	8908(2)	46(1)
C(62)	2768(4)	2554(3)	9433(3)	57(2)
C(63)	3535(5)	3109(4)	9873(3)	71(2)
C(64)	3302(6)	3926(4)	9802(3)	74(2)
C(65)	2306(6)	4185(3)	9276(3)	70(2)
C(66)	1523(5)	3637(3)	8835(2)	54(2)
C(7)	109(4)	2275(3)	7656(2)	42(1)
C(71)	166(4)	2941(3)	7117(2)	41(1)
C(72)	1118(5)	3320(3)	7104(3)	53(1)
C(73)	1107(5)	3934(3)	6576(3)	64(2)
C(74)	92(6)	4166(4)	6041(3)	70(2)
C(75)	-866(5)	3819(3)	6030(3)	65(2)
C(76)	-832(5)	3197(3)	6565(2)	53(1)
C(8)	1007(4)	908(3)	9034(3)	45(1)

^a *U*(eq) is defined as one third of the trace of the orthogonalized U_{ij} tensor.

(s, 1H, H3), 2.70 (s, 2H, H60a/H80a). ¹³C NMR (125.721 MHz, CD_2Cl_2): δ 243.97, 240.54 (CO's), 140.94, 137.97, 133.83, 133.38, 133.21, 132.77, 131.02, 130.06, 129.52, 128.87, 128.70, 128.03, 127.99, 127.89, 127.69, 126.15 (phenyl carbons and ring CO), 114.61, 104.04, 97.26 (C20/C50, C30/C40, C70), 73.36 (C60/C80). IR (CH_2Cl_2): ν_{CO} 1945, 1874 cm^{-1} . Mass spectrum (DEI): *m/z* (%) 808 (39) [M^+], 752 (98) [$\text{M} - 2\text{CO}^+$], 482 (84) [$\text{M} - 2\text{CO} - \text{C}_3\text{Ph}_3\text{H}_2 - \text{H}^+$], 384 (100) [$\text{C}_5\text{Ph}_4\text{O}^+$]. Anal. Calcd for $\text{C}_{52}\text{H}_{38}\text{O}_3\text{Mo}$: C, 77.42; H, 4.71. Found: C, 77.31; H, 4.92.

Preparation of $(\text{C}_5\text{Ph}_2\text{Me}_2\text{OH})(\text{C}_3\text{Ph}_3\text{H}_2)\text{Mo}(\text{CO})_2$ (11). A mixture of 1,2,3-triphenylcyclopropene (0.268 g, 1 mmol) and 2,5-dimethyl-3,4-diphenylcyclopentadienone dimer (0.260 g, 0.5 mmol) and $\text{Mo}(\text{CO})_6$ (0.264 g, 1 mmol) in dry *n*-butyl ether (12 mL) was refluxed under nitrogen for 18 h. After cooling to room temperature and filtration through Celite, the solvent was removed by vacuum. The residue was chromatographed over silica gel using CH_2Cl_2 /hexanes as eluent in a 1:4 ratio. The major band gave **11** (0.16 g, 0.234 mmol, 23%), a yellow powder. ¹H NMR (200 MHz, CD_2Cl_2): δ 7.51–6.92 (m, 25H,

Table 5. Atomic Coordinates ($\times 10^4$) and Equivalent Isotropic Displacement Parameters ($\text{\AA}^2 \times 10^3$) for $(\text{C}_5\text{Ph}_4\text{OH})(\text{C}_3\text{Ph}_3\text{H}_2)\text{Mo}(\text{CO})_2$ (10)

	x	y	z	$U(\text{eq})^a$
Mo(1)	1458(1)	1506(1)	2170(1)	29(1)
C(1)	740(8)	463(7)	2343(6)	34(2)
C(2)	721(7)	1231(6)	3769(7)	34(2)
C(10)	1788(7)	2929(6)	594(6)	30(2)
C(20)	1494(7)	3406(6)	1521(6)	30(2)
C(21)	2205(7)	3957(6)	1583(6)	27(2)
C(22)	3467(8)	3521(7)	1181(6)	38(2)
C(23)	4075(9)	4112(7)	1159(7)	49(3)
C(24)	3468(9)	5125(8)	1537(7)	48(3)
C(25)	2214(8)	5588(7)	1920(7)	43(2)
C(26)	1580(7)	5017(6)	1941(6)	34(2)
C(30)	300(7)	3458(6)	2208(6)	26(2)
C(31)	-434(7)	3987(6)	3240(6)	30(2)
C(32)	37(8)	3702(7)	4076(7)	39(2)
C(33)	-659(9)	4208(8)	5012(7)	49(3)
C(34)	-1827(10)	5043(8)	5137(8)	60(3)
C(35)	-2301(8)	5344(7)	4309(7)	49(3)
C(36)	-1606(8)	4815(6)	3375(6)	35(2)
C(40)	-134(7)	3038(6)	1689(6)	25(2)
C(41)	-1412(7)	3205(6)	1999(6)	28(2)
C(42)	-2055(8)	3905(7)	1294(7)	42(2)
C(43)	-3263(9)	4131(8)	1582(8)	53(3)
C(44)	-3868(9)	3691(8)	2578(8)	55(3)
C(45)	-3226(8)	2976(7)	3289(7)	44(2)
C(46)	-2007(7)	2734(7)	2989(6)	37(2)
C(50)	809(7)	2708(6)	665(6)	29(2)
C(51)	744(7)	2362(6)	-245(6)	30(2)
C(52)	1242(8)	2786(7)	-1307(6)	45(2)
C(53)	1181(8)	2495(8)	-2157(7)	52(3)
C(54)	655(9)	1762(7)	-1963(7)	54(3)
C(55)	163(8)	1348(7)	-909(7)	50(3)
C(56)	221(8)	1635(7)	-75(7)	45(2)
C(60)	3251(7)	238(7)	1141(7)	33(2)
C(61)	3295(7)	-415(7)	432(6)	36(2)
C(62)	3612(8)	-55(7)	-676(7)	41(2)
C(63)	3589(9)	-531(8)	-1413(7)	57(3)
C(64)	3253(8)	-1422(8)	-1044(8)	54(3)
C(65)	2958(9)	-1829(8)	36(8)	57(3)
C(66)	2969(8)	-1336(8)	769(8)	57(3)
C(70)	3258(7)	-78(7)	2262(7)	33(2)
C(71)	3467(8)	-1256(6)	2844(7)	36(2)
C(72)	2577(8)	-1616(7)	3592(7)	44(2)
C(73)	2891(10)	-2755(8)	4047(7)	55(3)
C(74)	4076(10)	-3521(8)	3760(8)	64(3)
C(75)	4963(9)	-3173(8)	3040(8)	73(3)
C(76)	4669(9)	-2037(8)	2583(8)	62(3)
C(80)	3210(8)	818(7)	2636(7)	37(2)
C(81)	3255(7)	832(7)	3710(7)	38(2)
C(82)	2983(8)	134(8)	4671(7)	52(3)
C(83)	3062(9)	232(9)	5609(8)	66(3)
C(84)	3473(9)	985(9)	5592(8)	68(3)
C(85)	3774(9)	1678(8)	4645(9)	63(3)
C(86)	3660(8)	1604(7)	3729(8)	49(3)
O(1)	232(6)	-64(5)	2477(5)	59(2)
O(2)	235(6)	1098(5)	4680(5)	55(2)
O(3)	2829(5)	2785(4)	-290(4)	41(2)

^a $U(\text{eq})$ is defined as one third of the trace of the orthogonalized U_{ij} tensor.

phenyl protons), 4.78 (s, 1H, OH), 2.66 (s, 2H, allyl 2CH), 1.85 (s, 6H, 2CH₃). ¹³C NMR (50.288 MHz, CD₂Cl₂): δ 141.98, 138.63, 135.48, 133.58, 133.23, 131.95, 128.72, 128.53, 128.02, 127.97, 127.34, 125.86 (phenyl carbons and ring CO), 112.85, 102.70, 91.35 (ring and allyl C-Ph), 70.35 (allyl CH-Ph), 9.19 (2CH₃). IR (CH₂Cl₂): ν_{CO} 1947, 1876 cm⁻¹. Mass spectrum (DEI): m/z (%) 684 (3) [M]⁺, 626 (5) [M - 2CO - 2H]⁺, 366 (12) [M - C₅Ph₂Me₂OH - 2CO - 1H]⁺, 260 (100) [M - C₃Ph₃H₂ - H - Mo(CO)₂]⁺.

Ring Current Induced Chemical Shift Calculation. These calculations were performed using the program LARC,³⁵ and a list of induced chemical shifts can be found in Table S19 (supplementary material).

Table 6. Selected Bond Lengths (\AA) and Bond Angles (deg) for 1, 2, and 10

$\text{C}_7\text{Ph}_7\text{H}$ (1)			
C(1)-C(2)	1.352(3)	C(4)-C(5)	1.477(3)
C(2)-C(3)	1.476(3)	C(5)-C(6)	1.351(3)
C(3)-C(4)	1.360(3)	C(6)-C(7)	1.529(3)
C(6)-C(5)-C(4)	123.6(2)	C(2)-C(1)-C(7)	120.4(2)
C(1)-C(2)-C(3)	123.2(2)	C(5)-C(6)-C(7)	120.4(2)
$\text{C}_7\text{Ph}_7\text{HCO}$ (2)			
C(1)-C(2)	1.607(6)	C(5)-C(8)	1.548(6)
C(2)-C(3)	1.526(6)	C(2)-C(8)	1.559(6)
C(3)-C(4)	1.353(6)	C(8)-O(1)	1.194(5)
C(4)-C(5)	1.519(6)	C(1)-C(7)	1.518(6)
C(5)-C(6)	1.600(6)	C(6)-C(7)	1.525(6)
C(1)-C(6)	1.569(6)		
C(3)-C(2)-C(1)	111.1(4)	C(5)-C(8)-C(2)	98.1(4)
C(4)-C(5)-C(6)	111.0(3)	C(7)-C(6)-C(1)	58.7(3)
C(7)-C(6)-C(5)	118.9(4)	C(7)-C(1)-C(6)	59.2(3)
C(7)-C(1)-C(2)	117.0(4)	C(1)-C(7)-C(6)	62.0(3)
$(\text{C}_5\text{Ph}_4\text{OH})\text{C}_3\text{Ph}_3\text{H}_2\text{Mo}(\text{CO})_2$ (10)			
C(10)-C(20)	1.421(10)	C(1)-O(1)	1.131(8)
C(20)-C(30)	1.440(10)	C(2)-O(2)	1.135(8)
C(30)-C(40)	1.437(10)	Mo(1)-centroid	2.052
C(40)-C(50)	1.446(10)	Mo(1)-C(60)	2.309(8)
C(10)-C(50)	1.427(11)	Mo(1)-C(80)	2.337(8)
C(10)-O(3)	1.371(8)	Mo(1)-C(70)	2.339(8)
C(60)-C(70)	1.456(11)	Mo(1)-C(1)	1.964(9)
C(70)-C(80)	1.424(11)	Mo(1)-C(2)	1.972(8)
C(10)-C(20)-C(30)	105.9(7)	C(20)-C(10)-C(50)	110.8(7)
C(40)-C(30)-C(20)	109.4(6)	C(2)-Mo(1)-C(1)	77.4(3)
C(30)-C(40)-C(50)	107.3(7)	C(80)-C(70)-C(60)	111.2(7)
C(10)-C(50)-C(40)	106.7(7)		

X-ray Crystallography. X-ray crystallographic data were collected on a Siemens P4 diffractometer with a rotating anode and graphite-monochromated Mo K α radiation ($\lambda = 0.71073$ \AA). The background measurements were obtained by using a stationary crystal and stationary counter at the beginning and end of the scan, each for 25% of the total scan time. The scan type used was $\theta-2\theta$. In each case a variable scan speed was used, 5.00-60.00°/min in ω for **1** and **2**, 4.00-60.00°/min in ω for **10**. Three standard reflections which were measured after every 97 reflections showed no instrument instability and only minor crystal decay. The molecules **1** and **2** were solved by using the direct method, while for **10** the Patterson method was used; both are contained in the SHELXTL-PLUS program library.³⁶ All hydrogen atoms were refined isotropically. The method of refinement was full-matrix least squares in each case. Crystal data collection parameters are listed in Table 2. Atom coordinates and selected bond lengths and angles for **1**, **2**, and **10** are collected in Tables 3-6.

Acknowledgment. Financial support from the Natural Sciences and Engineering Research Council of Canada is gratefully acknowledged. Mass spectra were obtained courtesy of Dr. Richard Smith of the McMaster Regional Centre for Mass Spectrometry.

Supplementary Material Available: Tables of thermal parameters, bond lengths and angles, and positional parameters for hydrogen atoms for **1**, **2**, and **10**, plots of molecules **1**, **2**, and **10** showing thermal ellipsoids, and a list of calculated ring current shifts (21 pages). Ordering information is given on any current masthead page.

OM940603H

(35) Agarwal, A.; Barnes, J. A.; Fletcher, J. L.; McGlinchey, M. J.; Sayer, B. G. *Can. J. Chem.* **1977**, *55*, 2575.

(36) SHELXTL-Plus was written by G. M. Sheldrick, Nicolet XRD, Madison, WI.

Chiral Recognition in Platinum Complexes of 1,2-Diphenyl-*N,N'*-bis[(2,4,6-trimethylphenyl)methyl]-1,2-diaminoethane. Stereoselective Coordination of Olefins and Molecular Structure of a Trigonal Bipyramidal Adduct

Maria Elena Cucciolito, Mohamud A. Jama, Federico Giordano, and Aldo Vitagliano*

Dipartimento di Chimica, Università di Napoli "Federico II", via Mezzocannone 4, 80134 Napoli, Italy

Vincenzo De Felice

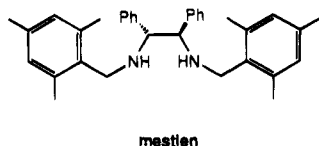
Facoltà di Agraria, Università del Molise, via Tiberio 21/A, 86100 Campobasso, Italy

Received July 5, 1994[®]

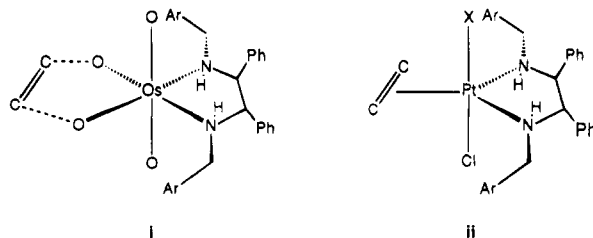
Trigonal bipyramidal olefin–platinum complexes of the title chiral diamine (mestien) have been synthesized and their stereochemistry has been investigated by ¹H and ¹³C NMR spectroscopy. The molecular structure of the complex PtClMe ((*E*)-ClCH=CHCl) (mestien) has been determined by X-ray diffraction analysis. The coordinated nitrogen atoms display a single configuration, and a high enantioface selectivity is observed in the coordination of prochiral olefins having a moderate lateral bulk. The selectivity can be correlated to the conformation adopted by the diamine ligand, which shows a remarkable similarity to those calculated for a proposed intermediate in the enantioselective dihydroxylation of olefins by osmium tetroxide.

Introduction

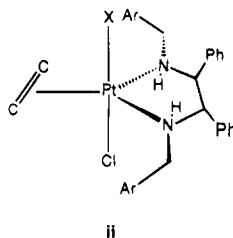
The title diamine (henceforth referred as mestien) has been recently used as a very effective controller ligand for the enantioselective¹ and diastereoselective² dihydroxylation of olefins by osmium tetroxide. Although molecular mechanics models have been developed^{1,3} to explain the observed selectivities, no metal complexes of mestien have been described so far. One of the proposed intermediates has a *C*₂ symmetric structure (i), with the double bond lying in the same plane



droxylation of olefins by osmium tetroxide. Although molecular mechanics models have been developed^{1,3} to explain the observed selectivities, no metal complexes of mestien have been described so far. One of the proposed intermediates has a *C*₂ symmetric structure (i), with the double bond lying in the same plane



containing the two nitrogen atoms and the metal. From a geometrical point of view, species i closely resembles a bipyramidal complex (ii), whose structure can be



thought as derivable from i by removing the two oxygen atoms and approaching the olefin to the metal by 1–1.5 Å. Species ii could be anticipated to reveal strong chiral induction effects in the coordination of olefins. In addition, if species i correctly represents the active dihydroxylation intermediate (which is still under debate⁴), species ii could offer a useful stereochemical model for such an intermediate. Following the above considerations and our general interest in five-coordinate olefin complexes of Pt(II),⁵ we were prompted to synthesize complexes of the type ii and to investigate their stereochemical properties, also in view of possible uses in other stereoselective processes.

Results and Discussion

Synthesis of the Complexes. Bipyramidal Pt(II) complexes of mestien were prepared by described procedures,⁵ according to Scheme 1. Path A was used with olefins bearing electron-releasing substituents, while path B was used with olefins bearing electron-withdrawing substituents. The reason for this choice resides in the effect of the substituents on the stability of platinum–olefin complexes, which follows opposite trends in four- and five-coordinate complexes.^{5b,6} Accordingly, ethene is easily displaced from the starting dimer 1 by electron-rich olefins, while electron-withdrawing sub-

(4) Jorgensen, K. A.; Schiott, B. *Chem. Rev.* **1990**, *90*, 1483.

(5) (a) Albano, V. G.; Braga, D.; De Felice, V.; Panunzi, A.; Vitagliano, A. *Organometallics* **1987**, *6*, 517. (b) Cucciolito, M. E.; De Felice, V.; Panunzi, A.; Vitagliano, A. *Organometallics* **1989**, *8*, 1180. (c) Albano, V. G.; Demartin, F.; De Renzi, A.; Morelli, G.; Saporito, A. *Inorg. Chem.* **1985**, *24*, 2032.

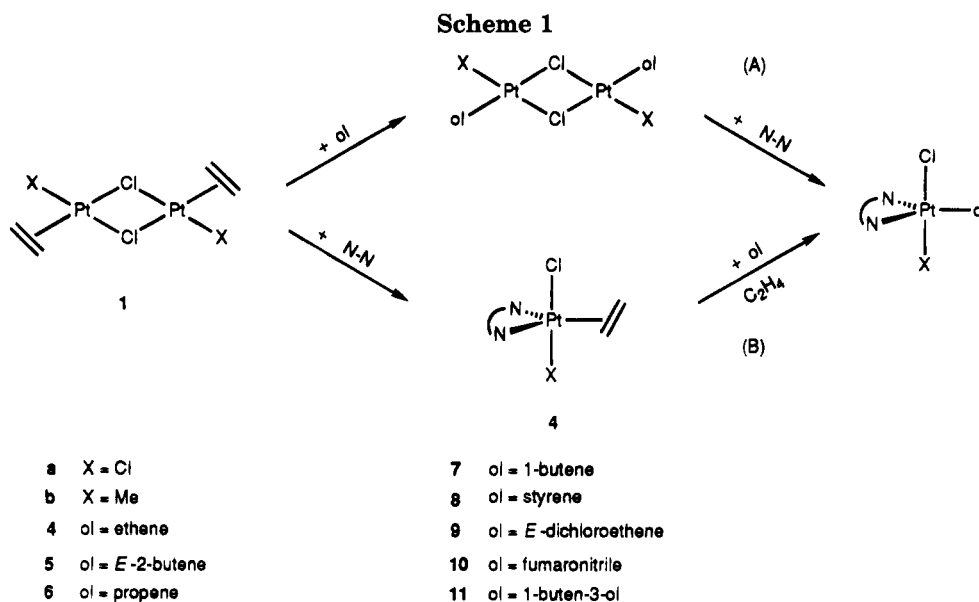
(6) Albano, V. G.; Natile, G.; Panunzi, A. *Coord. Chem. Rev.* **1994**, *133*, 67.

[®] Abstract published in *Advance ACS Abstracts*, January 15, 1995.

(1) Corey, E. J.; DaSilva Jardine, P.; Virgil, S.; Yuen, P. W.; Connell, R. D. *J. Am. Chem. Soc.* **1989**, *111*, 9243.

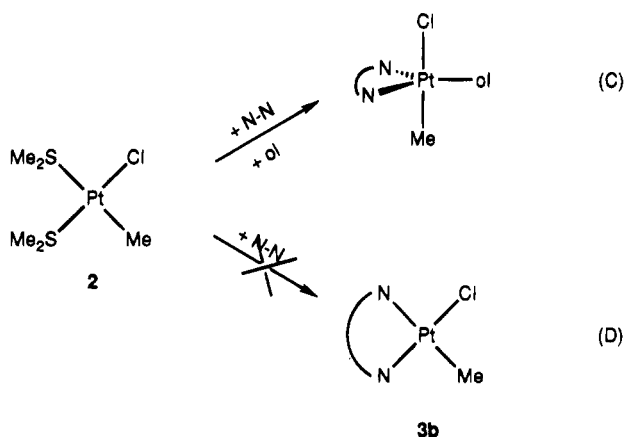
(2) Wang, Y.; Babirad, S. A.; Kishi, Y. *J. Org. Chem.* **1992**, *57*, 468.

(3) Wu, Y. D.; Wang, Y.; Houk, K. N. *J. Org. Chem.* **1992**, *57*, 1362.



stituents are generally required to displace ethene from the bipyramidal complexes **4**.

The complexes containing a σ -bonded methyl group (type **b**) could be prepared by an alternative procedure starting from the dimethyl sulfide complex **2** (path C).^{5b}



However, the latter method worked nicely only in the case of ethene and olefins bearing electron-withdrawing substituents. The reaction was sluggish with propene and did not take place at all with (*E*)-2-butene, most likely as a consequence of the above cited trend controlling the stability of five-coordinate complexes. Some attempts to prepare the four-coordinate complex **3b** by directly displacing dimethyl sulfide from complex **2** (path D) failed. Either no reaction was observed or decomposition took place when drastic conditions (e.g., refluxing toluene) were used.

A number of (mestien)(olefin)PtCl₂ complexes (**4a**–**8a**) and (mestien)(olefin)PtClMe complexes (**4b**, **5b**, **8b**–**11b**) were synthesized and characterized by ¹H and ¹³C NMR spectroscopy. Elemental analyses were performed only when crystalline products were obtained. Racemic mestien was used in all cases, except that of **11b**, which was made with pure (*S,S*)-(+)-mestien. The bipyramidal structure was confirmed in all cases by the multiplicity of the NMR signals and by the high field at which the olefinic ¹H and ¹³C resonances were observed.^{5,6}

The original purpose for preparing the methyl-substituted complexes **b** was to enable the observation

of olefin association–dissociation equilibria, which were previously shown to be facilitated by the presence of σ -bonded carbon ligands.^{5a,b} Actually, olefin loss was observed upon warming (at 60 °C) a chloroform solution of the (*E*)-2-butene complexes **5a** and **5b**. The dichloro complex **5a** gave the expected four-coordinate complex **3a**, while **5b** gave a mixture of products which we did not further characterize. In both cases, the olefin loss was not reversible. We have no evidence allowing us to state whether the lack of reversibility was due to kinetic or thermodynamic reasons. However, since in the present work we are mainly concerned with the stereochemical features of the complexes, we did not try to investigate further the thermodynamical aspects of the olefin coordinations in these species.

Stereochemistry of the Complexes. General Considerations. The diamine mestien contains, besides the two chiral carbon centers, two chiral nitrogen atoms, which of course very quickly epimerize in the free ligand as a consequence of fast nitrogen inversion. The nitrogen chirality is “frozen” upon coordination, so that in principle different diastereomers can be formed, depending on the configuration adopted by the coordinated nitrogen centers. The number of possible diastereomers can further increase, according to the overall symmetry of the PtClX(olefin) fragment. In the simplest case of a metal–olefin fragment having *C*_{2v} symmetry, as for complex **4a**, three diastereomers could be formed. When a chiral (racemic) olefin is used and the diamine–metal fragment lacks the *C*₂ axis (complex **11b**), up to 32 different diastereomers are possible! At first glance, the diastereomeric population of a given complex could be straightforwardly determined by inspection of the NMR spectra. However, the number of isomers that would actually be observed by NMR depends not only on their relative abundances (matching their relative stabilities, in the case an equilibrium is attained) but also on their interconversion rates. Three different dynamic processes can take place in solution, each one interconverting a subset of all the possible isomers: (a) nitrogen inversion; (b) olefin rotation; (c) olefin exchange. A general discussion of the actual occurrence of these three processes for complexes **4**–**11** seems worthwhile.

Table 1. Diastereomeric Distribution of [PtClX(olefin)(mestien)] Complexes

complex	possible isomers ^a	obsd isomers (within 95% of total)	% of major Isomer ^b	suggested configuration of the olefinic carbon(s) ^c
4a	3	1	100	
5a	6	2	92	<i>S, S</i>
6a	6	2	84	<i>S</i>
7a	6	2	91	<i>S</i>
8a	6	2	55	
4b	4	1	100	
5b	8	2	85	<i>S, S</i>
8b	16	4	41	
9b	8	2	88	<i>R, R</i> ^d
10b	8	2	57	
11b	32	2	86 ^e	

^a Only isomers retaining the usual *tbp* structure, with equatorial N–N and olefinic ligands, are considered. ^b Approximate equilibrium population. ^c Referred to the major diastereomer in the complex containing (*R,R*)-mestien. ^d Unequivocally assigned *via* X-ray structure. ^e Isomeric population in the actually isolated complex.

(a) Nitrogen Inversion. This was shown to be fast at room temperature for some (diamine)(C₂H₄)PtCl₂ complexes,⁷ with the nitrogen atoms displaying the same configuration (*trans* arrangement of the substituents) in the largely predominating isomer.^{7,8} In our case, this process could be directly revealed by variable-temperature NMR only if appreciable amounts of different diastereomers were present at equilibrium. As a matter of fact, only one isomer was detected in a wide temperature range for complexes **4a** and **4b**. In the case of other complexes, minor species were detected (see Table 1), which could be ascribed to the coordination of different olefinic enantiofaces (see later). Therefore, we can reasonably infer that the nitrogen atoms selectively adopt one configuration, (*trans* configuration according to the retention of the C₂ axis in complexes **4a** and **5a**), but we lack direct evidence about the *rate* of nitrogen inversion. However, we can consider that this could occur either via proton dissociation or via nitrogen dissociation, and in both cases proton exchange should occur at a comparable rate. With the possible exception of the (*E*)-2-butene complex **5a**, at room temperature proton exchange is slow on the NMR ν time scale, since coupling to the vicinal CH protons was invariably observed. In most cases it is also slow on the laboratory time scale, since deuterium exchange (CDCl₃ saturated with D₂O) occurred with half-lives ranging between 1 min (**4a**) and 1 day (**9b**). The above observations give indirect evidence that nitrogen inversion in most if not all complexes is slow at room temperature on the NMR ν time scale.

(b) Olefin Rotation. When both the olefin and the metal fragment lack a C₂ axis, this process interconverts two different rotamers. We found that at room temperature olefin rotation is slow on the NMR ν time scale and sometimes also slow on the T₁ time scale. Thus, in the case of the propene complex **6a**, at 300 K two separate couples of sharp singlets are observed for the mesityl methyl groups belonging to opposite sides of the diamine ("slow" rotation), which at 330 K are coalesced into a single couple of sharp singlets ("fast" rotation). In the case of the dichloroethene complex **9b**, rotation

is much slower, as evidenced by the nonequivalence of the two olefinic protons ($\delta = 4.68$ ppm and $\delta = 3.62$ ppm, respectively) at 330 K, and by the absence of saturation transfer between the two protons even at this temperature.

(c) Olefin Exchange (Dissociation–Association).

This process can interconvert all the isomers that differ by the spatial orientation of the olefin (rotamers and *re-si* isomers) or by the enantiomeric olefin being coordinated (in the case of racemic chiral alkenes). We found that at room temperature and in the presence of free olefin in all cases the exchange occurs with half-lives larger than 1 min, since no saturation transfer was ever observed between the signals of free and coordinated olefin. The exchange was actually monitored in a few cases, and half-lives of the order of 10–30 min were observed for olefins bearing electron-releasing substituents. The exchange is accelerated by traces of acid (CF₃COOH), in agreement with a mechanism involving the dissociation of one nitrogen atom, as suggested by van Koten et al.⁹ The exchange is much slower for electron-withdrawing olefins (several days in the case of the fumaronitrile complex **10b**), but ultimately an equilibrium is reached between the possible diastereomers.

The above observations point to the conclusion that at room temperature for all the complexes investigated the NMR signals of the possible isomers are not averaged by exchange phenomena. Therefore the actual populations of the various isomers can be directly inferred by the multiplicity and intensity of the signals observed in the NMR spectra. The number of isomers that were observed and the abundance of the major one are listed in Table 1, in comparison with the total number of the possible diastereomers. Inspection of Table 1 shows that in most cases a remarkable stereoselectivity controls the formation of the five-coordinate adducts. Before discussing in detail some stereochemical features of the complexes, as inferred by the NMR data, we shall present the results of the X-ray structural analysis of complex **9b**.

Molecular Structure of PtClMe(*E*)-(1-*R*,2-*R*)-CHCl=CHCl[(*R*-C,*R*-C',4*S*-N,*S*-N')mestien] (9b**).** The crude complex **9b** consisted of a mixture of diastereomers containing a major component in nearly 90% abundance. Crystallization from methylene chloride–ethanol gave single crystals of the major isomer which were suitable for X-ray diffraction. Crystals (space group *P*2₁/*c*) contained enantiomorphous molecules, (racemic mestien was used in the preparation) displaying the trigonal bipyramidal (*tbp*) structure that is usual for five-coordinated olefin complexes of platinum(II).⁶ An ORTEP drawing of the molecule, showing the atom numbering scheme, is shown in Figure 1. Relevant geometric parameters are given in Tables 2 and 3. The Pt–C(2) and Pt–C(3) distances (2.04(1) and 1.98(1) Å, respectively) are the shortest observed for similar complexes.⁶ The short Pt–C distances are accompanied by a considerable lengthening of the C(2)–C(3) double bond (1.50(2) Å) and by a large bending-back of the two chlorine atoms (torsion angle Cl(2)–C(2)–C(3)–Cl(3) = –123(1)°). All together, the above data indicate a strong metal–olefin bond, with a contribution of π -back-dona-

(7) Fanizzi, F. P.; Maresca, L.; Natile, G.; Lanfranchi, M.; Manotti-Lanfredi, A. M.; Tiripicchio, A. *Inorg. Chem.* **1988**, *27*, 2422.

(8) De Renzi, A.; Di Blasio, B.; Saporito, A.; Scalone, M.; Vitagliano, A. *Inorg. Chem.* **1980**, *19*, 960.

(9) van der Poel, H.; van Koten, G.; van Stein, G. C. *J. Chem. Soc., Dalton Trans.* **1981**, 2164.

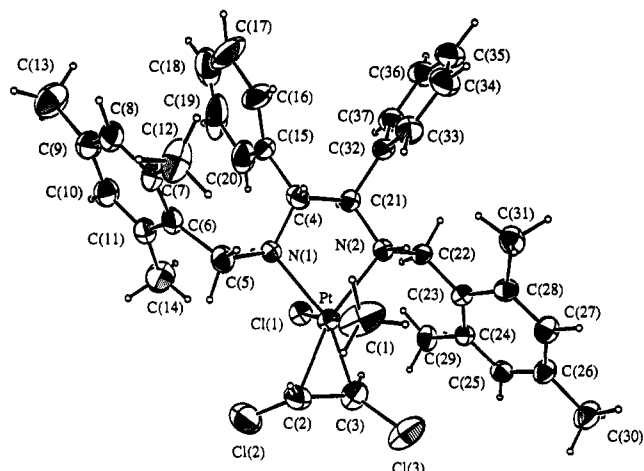


Figure 1. ORTEP view of PtClMe[(*E*)-ClCH=CHCl]-mestien (**9b**) showing the atom labeling scheme. Thermal ellipsoids are drawn at the 25% probability level.

Table 2. Fractional Atomic Coordinates and Equivalent Thermal Parameters (\AA^2) of the Non-Hydrogen Atoms^a

	<i>x</i>	<i>y</i>	<i>z</i>	B_{eq}^b
Pt	0.45657(4)	0.24069(3)	0.60620(4)	4.65(1)
Cl(1)	0.3611(3)	0.2453(2)	0.4292(2)	6.0(1)
Cl(2)	0.5049(5)	0.0948(3)	0.5145(4)	11.5(2)
Cl(3)	0.7311(3)	0.2410(3)	0.6832(4)	11.3(2)
N(1)	0.2876(7)	0.2210(5)	0.5973(7)	5.1(3)
N(2)	0.4018(7)	0.3475(5)	0.6220(6)	4.3(2)
C(1)	0.531(1)	0.2460(9)	0.760(1)	11.1(5)
C(2)	0.548(1)	0.1551(8)	0.607(1)	7.8(4)
C(3)	0.601(1)	0.2221(8)	0.598(1)	7.0(4)
C(4)	0.238(1)	0.2825(6)	0.626(1)	5.8(3)
C(5)	0.275(1)	0.1544(7)	0.647(1)	6.2(4)
C(6)	0.156(1)	0.1294(6)	0.613(1)	5.5(3)
C(7)	0.100(1)	0.1292(7)	0.671(1)	5.8(3)
C(8)	-0.010(1)	0.1156(8)	0.635(1)	7.4(4)
C(9)	-0.069(1)	0.0980(8)	0.542(1)	7.3(4)
C(10)	-0.010(1)	0.0922(8)	0.483(1)	7.6(4)
C(11)	0.102(1)	0.1056(7)	0.515(1)	6.9(4)
C(12)	0.154(1)	0.1457(9)	0.780(1)	9.5(5)
C(13)	-0.195(1)	0.0905(9)	0.499(1)	10.4(6)
C(14)	0.163(1)	0.0995(9)	0.449(1)	10.2(5)
C(15)	0.110(1)	0.2858(7)	0.580(1)	7.1(4)
C(16)	0.049(1)	0.2977(9)	0.636(1)	12.8(5)
C(17)	-0.066(1)	0.3013(9)	0.597(2)	21(1)
C(18)	-0.117(2)	0.2903(9)	0.499(2)	16(1)
C(19)	-0.058(2)	0.2786(9)	0.442(3)	24(2)
C(20)	0.055(1)	0.2757(9)	0.481(2)	11.4(8)
C(21)	0.279(1)	0.3487(6)	0.594(1)	4.8(3)
C(22)	0.432(1)	0.4066(6)	0.569(1)	4.7(3)
C(23)	0.552(1)	0.4186(6)	0.602(1)	4.5(3)
C(24)	0.609(1)	0.4111(6)	0.541(1)	5.0(3)
C(25)	0.718(1)	0.4247(7)	0.571(1)	5.4(3)
C(26)	0.780(1)	0.4502(8)	0.664(1)	5.8(3)
C(27)	0.723(1)	0.4606(8)	0.724(1)	6.1(4)
C(28)	0.612(1)	0.4466(7)	0.698(1)	5.4(3)
C(29)	0.548(1)	0.3890(8)	0.435(1)	6.3(4)
C(30)	0.902(1)	0.4627(9)	0.698(1)	8.2(5)
C(31)	0.556(1)	0.4628(8)	0.766(1)	7.1(4)
C(32)	0.245(1)	0.4126(6)	0.636(1)	5.5(3)
C(33)	0.281(1)	0.4246(8)	0.734(1)	6.7(4)
C(34)	0.253(1)	0.4840(9)	0.769(1)	8.5(5)
C(35)	0.185(1)	0.5323(9)	0.702(1)	8.9(5)
C(36)	0.146(1)	0.5210(8)	0.608(1)	8.4(5)
C(37)	0.176(1)	0.4609(8)	0.573(1)	7.0(4)

^a ESDs in parentheses. ^b $B_{eq} = 4/3 \sum_i \sum_j \beta_{ij} a_i a_j$.

tion which seems to be relevant even within the class of five-coordinate complexes.⁶ The Pt–N(1) and Pt–N(2) bond distances (2.210(9) and 2.223(9) Å, respectively) are also slightly shorter than those observed for

Table 3. Selected Bond Lengths (Å) and Relevant Valence Angles (deg)^a

Bond Lengths					
Pt–Cl(1)	2.450(2)	N(2)–C(21)	1.50(1)	Cl(3)–C(3)	1.73(1)
Pt–N(1)	2.210(9)	C(2)–C(3)	1.50(2)	N(1)–C(5)	1.52(1)
Pt–C(2)	2.04(1)	Pt–C(1)	2.12(1)	N(2)–C(22)	1.52(1)
Cl(2)–C(2)	1.72(1)	Pt–N(2)	2.223(9)	C(4)–C(21)	1.53(2)
N(1)–C(4)	1.49(1)	Pt–C(3)	1.98(1)		
Bond Angles					
N(1)–Pt–N(2)	78.8(5)	C(2)–Pt–C(3)	43.7(9)		
N(1)–Pt–C(2)	116.1(8)	N(2)–Pt–C(3)	122.1(8)		
Cl(1)–Pt–N(1)	81.6(4)	Cl(1)–Pt–N(2)	91.6(4)		
Cl(1)–Pt–C(2)	95.2(7)	Cl(1)–Pt–C(3)	92.7(7)		
C(1)–Pt–C(2)	90.4(9)	C(1)–Pt–C(3)	91.0(9)		
N(1)–Pt–C(1)	96.4(8)	N(2)–Pt–C(1)	82.9(8)		
Pt–C(2)–C(3)	66(1)	Pt–C(3)–C(2)	70(1)		
Pt–C(2)–Cl(2)	122(1)	Pt–C(3)–Cl(3)	128(1)		
Cl(2)–C(2)–C(3)	122(2)	Cl(3)–C(3)–C(2)	119(2)		
Pt–N(1)–C(4)	113(1)	Pt–N(1)–C(5)	114(1)		
Pt–N(2)–C(21)	110(1)	Pt–N(2)–C(22)	119(1)		
C(4)–N(1)–C(5)	113(1)	C(21)–N(2)–C(22)	108(1)		
N(1)–C(5)–C(6)	113(2)	N(2)–C(22)–C(23)	114(1)		
N(1)–C(4)–C(15)	115(2)	N(1)–C(4)–C(21)	109(1)		
C(15)–C(4)–C(21)	107(2)	N(2)–C(21)–C(4)	112(1)		
N(2)–C(21)–C(32)	111(1)	C(4)–C(21)–C(32)	110(1)		
Cl(1)–Pt–C(1)	174.4(7)				

^a ESDs in parentheses.

other five-coordinate olefin complexes with diamine ligands.⁶ This could be a secondary consequence of the larger π -back-donation, which in turn should promote a better σ -donation by the nitrogen ligand on the opposite side.

Concerning the stereochemistry of the diamine ligand, the two nitrogen atoms display the same configuration, which is the opposite of that of the two chiral carbon centers. The torsion angles Pt–N(1)–C(5)–C(6) and Pt–N(2)–C(22)–C(23) ($-161(1)^\circ$ and $-63(1)^\circ$, respectively) are such that one of the two mesityl groups is extended toward the olefin ligand, while the other one is withdrawn and stacked in front of one of the phenyl rings in the back of the molecule. In a recent MM2 modeling of a postulated dihydroxylation intermediate,³ the same configuration was found for the two chiral nitrogen atoms, and two conformations very similar to the above were calculated to be the only acceptable. The two conformations were close in energy, differing by ~ 2 kJ/mol for each mesityl group. The conformational similarity found between two chemically different species (**i** and **ii**) suggests that the steric constraints arising in the diamine frame after chelation are strong enough to overwhelm the effects of the packing forces and those resulting from the difference in the remaining molecular fragment. The chiral environment created around the platinum center by the outstretched diamine "arm" is most likely responsible for the high selectivity observed in the olefin coordination. As pointed out in the previously cited MM2 work,³ no selectivity would be expected in the case where both "arms" of the diamine were withdrawn toward the back of the molecule.

Stereochemistry of the Complexes. Specific Aspects. Having in mind the molecular structure of **9b**, we shall now discuss the stereochemical features of a number of selected complexes, as inferred by the NMR data.

4a. The presence of only one species can be detected from the ^1H NMR spectrum of this compound in the range 190–300 K. As mentioned before, the chemical equivalence of the two halves of the diamine indicates that the C_2 axis is retained in the complex molecule,

which means that the two nitrogen atoms adopt the same configuration (most likely the opposite to that of the chiral carbon atoms, according to the structure of **9b**). A remarkable molecular rigidity is revealed by variable-temperature ^1H NMR spectroscopy. In the room-temperature spectrum (270 MHz), the protons of the phenyl groups give rise to a single broad band centered at $\delta = 7.2$ ppm. At 253 K, this is split into five different broad signals which at 233 K become two sharp doublets and three sharp triplets (2 H each). This indicates restricted rotation around the C–phenyl bonds, causing nonequivalence of the two ortho (and meta) protons within each phenyl group, but retaining the chemical equivalence between the two halves of the coordinated diamine. On lowering the temperature to 203 K, the ortho methyls of the mesityl groups, which at room temperature give rise to a singlet (12 H) at $\delta = 2.31$, also split into two broad singlets (6 H each) at $\delta = 2.13$ ppm and 2.48 ppm, respectively. This indicates restricted rotation around the C–mesityl bond. It is worth noting that the observed rigidity is a consequence of the coordination, since no splitting whatsoever is observed for the resonances of the free ligand, down to 180 K. The rigidity of the coordinated diamine indicates that a limited conformational space is available to the complex. This is consistent with the previously cited MM2 analysis and with the high selectivity observed upon coordination of prochiral olefins (see later).

5a. The ^1H and ^{13}C NMR spectra (298 K) show the presence of one dominant isomer ($92 \pm 2\%$ abundance). Similarly to the ethene complex **4a**, a C_2 axis is present in the molecule, indicating that the two nitrogen atoms adopt the same configuration, which is most likely the opposite of that of the chiral carbon atoms, as shown by the crystal structure of complex **9b**. A minor species ($\sim 8\%$ abundance) is also detectable through the signal of the olefinic methyl groups (doublet at $\delta = 1.12$ ppm, $^3J_{\text{H-Pt}} = 40$ Hz). Other signals from the minor species are not positively assignable in the proton spectrum due to overlapping by the resonances of the major isomer. Further evidence of the minor isomer is provided by the carbon spectrum (see Experimental Section). Since the C_2 symmetry is retained by the minor species, the latter is most likely due to the coordination of the other olefinic enantioface. This assignment was confirmed by preparing the complex *in situ*, mixing equivalent amounts of the starting dimer **1** and mestien directly in the NMR tube. The first spectrum, recorded ~ 2 min after mixing, showed comparable amounts (ratio 55:45) of the two isomers. The mixture then evolved to the final equilibrium composition with a half-life of ~ 8 min, a figure that gives the estimate of the (E)-2-butene exchange rate.

The ^1H NMR spectrum (270 MHz) of **5a** shows a temperature dependence which resembles that of the ethene complex **4a**, with the addition of some more complicated features. The behavior of the phenyl proton signals and that of the mesityl CH_3 and aromatic protons is similar to that of the ethene complex **4a**. Most interesting is the temperature behavior of the olefin methyl resonances. In the temperature range explored (190–320 K), the methyl groups give rise to a single resonance signal, which at 320 K appears as a doublet, with the expected ^{195}Pt satellite peaks ($J_{\text{Pt}} \approx 40$ Hz). At 293 K the signal is broad, such that the Me–CH coupling is not longer detectable and the ^{195}Pt satellites

appear as shoulders of the main peak. At 250 K the signal is sharp again, the Me–CH coupling and satellite peaks are easily measurable. Further cooling results in broadening, such that at 210 K no coupling is detectable. The chemical shift of the butene methyl protons (and, to a lesser extent, that of the olefinic protons) is strongly affected by the temperature, moving from $\delta = +0.25$ ppm at 320 K to $\delta = -0.42$ ppm at 190 K. (The =CH protons move from $\delta = 3.5$ ppm to $\delta = 3.0$ ppm in the same temperature range.) The successive sharpening–broadening–sharpening of the butene methyl signal that occurs upon warming from 190 to 320 K is consistent with the occurrence of two or more exchange processes in two different temperature ranges. In the temperature range where either dynamic process is frozen, splitting of the butene resonances should occur. Since no splitting is actually observed, most likely both exchange processes involve minor species, whose signals are not easily detected. We tentatively suggest that the high-temperature process (range 290–320 K) involves inversion of configuration at nitrogen. Indeed, complex **5a** is the only one for which fast NH proton exchange can be observed at 320 K (loss of coupling to CH and CH_2 protons), consistent with the possibility of fast nitrogen inversion as discussed above. The low-temperature process might result from a progressive freezing of the conformational mobility of the diamine “arms”, allowing the existence at low temperature of different atropoisomers of the complex. The temperature dependence of the chemical shifts of the butene methyl protons deserves some further discussion. At 320 K, the methyl groups display their resonance at an unusually high field ($\delta = 0.25$ ppm), while in a more usual range is the corresponding chemical shift of the minor diastereomer ($\delta = 1.15$ ppm). This strongly points to a dynamically averaged conformation similar to that observed in the solid state for the sterically analogous complex **9b**, where one of the chlorine atoms is just facing the middle of a mesityl benzene ring, thus experiencing its paramagnetic shielding. The shielding increases upon cooling, and at 190 K the methyl signal moves to $\delta = -0.4$ ppm. This suggests the dominance at low temperature of the more stable conformation³ in which both the diamine mesityl groups are extended toward the olefin and facing its methyl substituents. In such conformation, a higher enantioface selectivity should be expected. Accordingly, the observed population of the minor diastereomer was lower at 240 K ($6 \pm 2\%$) than at 320 K ($11 \pm 2\%$). The above data, in connection to the molecular structure of **9b**, suggest that the butene methyl groups in **5a** experience the same sterical environment as the chlorine atoms in **9b**. It seems very likely, therefore, that in the molecules containing (R,R)-mestien, the (E)-2-butene adopts the S,S configuration¹⁰ in the major diastereomer. A NOE experiment was performed at 298 K to get independent configurational evidence. The result was a partial success, in that the only nontrivial NOE was detected between the butene methyl protons and the mesityl CH protons. Although this observation is consistent with all the above considerations, it does not give any conclusive evidence about the butene configuration.

(10) The formal inversion with respect to complex **9b** is due to a change in the priority sequence of the substituents when methyl is substituted for chlorine.

6a. The ^1H and ^{13}C NMR spectra show the presence of one dominant isomer in $84 \pm 2\%$ abundance at 298 K. Also, in this case the population of the major isomer increases upon cooling ($89 \pm 2\%$ at 253 K). In the range 213–300 K, the diamine signals show a temperature dependence similar to that of the ethene and (E)-2-butene complexes **4a** and **5a**, indicating comparable skeletal rigidity. In the low-temperature range, the signal of the propene methyl group behaves similarly to the (E)-2-butene complex **5a**, although a lesser variation of the chemical shift is observed ($\delta = +0.18$ ppm at 313 K, $\delta = -0.11$ ppm at 213 K). As in the case of **5a**, this can be explained by conformational changes of the diamine side chains, and the high field at which the methyl signal is observed is consistent with it facing the mesityl benzene ring and experiencing its paramagnetic shielding. As for **5a**, the only nontrivial NOE was observed between the propene methyl protons and the mesityl CH protons. In analogy to **5a**, we suggest the S configuration for the coordinated propene carbon (when (R,R)-mestien is bound). At room temperature and below, the two halves of the diamine ligand are not equivalent, due to restricted rotation around the Pt–double bond axis. Rotation of the olefin becomes apparent after warming at 320 K. At this temperature, the mesityl CH and Me signals, which at 298 K (400 MHz) appear as three couples of singlets (δ 6.76, 6.79, 2 + 2 H; δ 2.29, 2.34, 6 + 6 H; δ 2.20, 2.22, 3 + 3 H), coalesce into three sharp singlets. The NH protons, which have a larger difference of chemical shift ($\Delta\delta \approx 1$ ppm) still give separate resonances.

11b. This compound was obtained by displacing ethene from complex **4b** (pure (S,S)-(+)-mestien was used in this case) with an excess of the racemic allylic alcohol 1-buten-3-ol. Several attempts to crystallize the product failed, and the complex was only obtained as a crude vitreous solid after evaporation of the solvent. The ^1H and ^{13}C NMR spectra indicated the presence of two isomers **11b'** and **11b''** in $\sim 6:1$ ratio. A third species, in $\sim 4\%$ abundance, was detected through its Pt–Me proton signal at $\delta = 0.10$ ppm. Even excluding configurational isomerism of the coordinated nitrogen atoms, the two major species **11b'** and **11b''** could in principle differ according to three kinds of isomerism: coordination of different enantiomers of the olefin, coordination of different faces of the same enantiomeric olefin, and rotational isomerism around the Pt–double bond axis. In order to clarify the stereochemical relation between the two major species, we added to a sample of the complex **4** equiv of racemic free olefin. The ^1H NMR spectrum of the mixture showed the increase of the population of the minor isomer **11b''** to $\sim 19\%$. Moreover, we also prepared the complex by olefin exchange on the starting dimer **1** and successive addition of the optically pure diamine (S,S)-(+)-mestien (path A in Scheme 1). The ^1H NMR spectrum of the product showed the presence of the two isomers **11b'** and **11b''** in about equimolar amounts. Thus, **11b'** and **11b''** differ by the coordination of enantiomeric olefins, and the equilibrium constant for the exchange between the two enantiomeric olefins can be estimated to be ~ 4 .

When we observed the fair chiral discrimination reported above, we argued that the same would probably be observed in the case of complexes having a different metal but similar symmetry. While this work was in

progress, we exploited the idea by investigating Cu(I) olefin complexes of mestien. Apart from the absence of axial ligands, these are expected to display the same trigonal arrangement of ligands around the metal center¹¹ as the five-coordinate platinum species **ii**. By using (S,S)-(+)-mestien, crystalline Cu(I) complexes were obtained with many olefins.¹² In the case of racemic secondary allylic alcohols, selective coordination of one enantiomer (better than 90% ee) was indeed observed, disclosing a very effective method for the resolution of allylic alcohols.¹² It is worth noting that the coordination of the same enantiomer ((R)-(-)-1-buten-3-ol) is preferred both in Cu(I) and in Pt(II) complexes of (S,S)-(+)-mestien. This was shown by comparing the allylic alcohol, isolated after treatment of **11b'** with NaCN, with an authentic sample obtained through the resolution procedure using the Cu(I) complex. From the above comparison, **11b'** turned out to be the complex with (R)-(-)-1-buten-3-ol. The enantiomeric alcohol (S)-(+)-1-buten-3-ol is therefore contained in **11b''**.

Conclusions

The results we have reported, including the remarkable steric similarity between **9b** and the MM2 model of the postulated osmium intermediate **i**, indicate that a limited number of conformations are available to the diamine skeleton after coordination. The whole structure is scarcely flexible, and the mesityl groups either point toward the olefin on the opposite side (resulting in good chiral induction) or are withdrawn toward the phenyl groups in the back of the molecule (resulting in poor chiral induction). Inspection of Table 1 shows that in most cases a very high selectivity was observed in the coordination of prochiral olefins. The two olefins that gave poor selectivity were fumaronitrile and styrene. Both have in common a rigid substituent on the double bond, a "stick" in the former case and a ring in the latter. A reasonable explanation for the poor selectivity comes from the inspection of the molecular structure of **9b** (Figure 1). The Cl(3) substituent is close to a fair van der Waals contact with one mesityl benzene ring (distance from the mean plane of the ring, 3.81 Å). A methyl group (complexes **5a** and **6a**) or a flexible alkyl chain (complex **7a**) should be easily accommodated in about the same position. By contrast, a rigid substituent in the same position would hit the mesityl ring, thus forcing the diamine "arm" to turn back in the alternative conformation, with consequent loss of selectivity. In conclusion, mestien appears to be very efficient in creating a "chiral pocket" around the metal. The size and shape of the pocket are suitable for the enantioselective "in-plane" coordination of olefins in a trigonal environment. The scope of the chiral induction is limited to moderately sized olefins. Rigid substituents creating a large lateral bulk result in the opening of the "pocket" with consequent loss of selectivity.

Experimental Section

^1H NMR and ^{13}C spectra were recorded on a Bruker WH-400 or a Bruker AC-270 spectrometer, respectively. ^1H NMR

(11) Masuda, H.; Machida, K.; Munakata, M.; Kitagawa, S.; Shimono, H. *J. Chem. Soc., Dalton Trans.* **1988**, 1907.

(12) Cucciolito, M. E.; Ruffo, F.; Vitagliano, A.; Funicello, M. *Tetrahedron Lett.* **1994**, 35, 169.

chemical shifts are reported in δ (ppm) relative to the solvent (CHCl_3 , 7.26; CDCl_2 , 5.33). ^{13}C NMR chemical shifts are given in δ values relative to the solvent (CDCl_3 , 77.0 ppm). Unless otherwise stated, the reported data refer to spectra recorded at 25 °C. The following abbreviations are used in descriptions of NMR multiplicities: s, singlet; d, doublet; t, triplet; q, quartet; m, multiplet; app, apparent, br, broadened; J_{Pt} = coupling constant to ^{195}Pt (when satellite peaks are unambiguously detected). Protons are identified as shown in footnote.¹³ When necessary, the NMR assignments were done using decoupling techniques. Solvents and reagents were of AnalaR grade and were used without further purification. Unless otherwise stated, platinum complexes were prepared and stored in air.

Materials. The diamine mestien was prepared¹ and resolved as previously described.¹⁴ $[\text{PtClMe}(\eta^2\text{-ethene})_2]^{15}$ and $[\text{PtClMe}(\text{SMe}_2)_2]^{16}$ were prepared as previously described.

Synthesis of $[\text{PtCl}_2(\text{mestien})(\eta^2\text{-olefin})]$. General Procedure.^{5c} A 0.285 g (0.5 mmol) sample of $[\text{PtCl}_2(\eta^2\text{-ethene})_2]$ was dissolved in 4 mL of methylene chloride at 0 °C, and a large excess of the appropriate olefin was added. The solution was evaporated in vacuo, the residue was dissolved again in methylene chloride, and the above sequence was repeated once. The residue was dissolved in 10 mL of methanol at 0 °C, and 1.1 mmol of mestien was added under stirring at 0 °C. A yellow precipitate formed, which after 30 min of stirring was collected on a filter and dried, giving the required $[\text{PtCl}_2(\text{mestien})(\eta^2\text{-olefin})]$ in 85–90% yield.

Synthesis of $[\text{PtClMe}(\text{mestien})(\eta^2\text{-olefin})]$. General Procedure A.^{5b} The procedure was the same as above except that the starting compound was $[\text{PtClMe}(\eta^2\text{-ethene})_2]^{15}$ and diethyl ether was used as solvent in place of methanol in the second step.

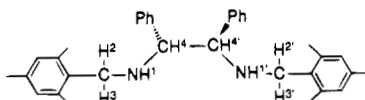
General Procedure B. A 0.5 mmol sample of the ethene or (E)-2-butene complexes (obtained through procedure A) was dissolved in 10 mL of methylene chloride, and a large excess of appropriate olefin was added. The solution was evaporated in vacuo, the residue was dissolved again in methylene chloride, and the above sequence was repeated once giving the required complex, which was recrystallized from methylene chloride–diethyl ether.

General Procedure C. Some complexes could be prepared from $[\text{PtClMe}(\text{SMe}_2)_2]^{16}$ according to a previously reported procedure.^{5b}

$[\text{PtCl}_2(\text{mestien})(\eta^2\text{-ethene})]$ (4a): ^1H NMR (270 MHz, CDCl_3) δ 2.20 (s, 6 H, Ar-Me), 2.31 (s, 12 H, Ar-Me), 2.30 (2 H, =CHH),¹⁷ 2.42 (m, 2 H, $J_{\text{Pt}} \approx 70$ Hz, =CHH),¹⁸ 3.56 (dd, 2 H, $J_{\text{Pt}} \approx 35$ Hz, H^2 , $H^{2'}$), 4.15 (m, 4 H, H^3 , $H^{3'}$, H^4 , $H^{4'}$), 4.30 (m, 2 H, H^1 , $H^{1'}$), 6.73 (s, 4 H, Ar-H), 7.17 (br, 10 H, Ph). Anal. Calcd for $\text{PtC}_{36}\text{H}_{44}\text{Cl}_2\text{N}_2$: C, 56.10; H, 5.75; N, 3.63. Found: C, 55.83; H, 5.72; N, 3.45.

$[\text{PtCl}_2(\text{mestien})(\eta^2\text{-E-2-butene})]$ (5a): ^1H NMR (400 MHz, CDCl_3) δ 0.11 (br s, 6 H, MeCH=), 2.18 (s, 6 H, Ar-Me), 2.34 (s, 12 H, Ar-Me), 3.39 (br s, 2 H, CH=), 3.59 (br d, 2 H, H^2 , $H^{2'}$), 4.17 (br s, 2 H, H^4 , $H^{4'}$), 4.3 (m, 4 H, H^1 , $H^{1'}$, H^3 , $H^{3'}$), 6.76 (s, 4 H, Ar-H), 7.12 (m, 10 H, Ph); ^{13}C NMR (67.9 MHz, CDCl_3) δ 17.3 ($J_{\text{Pt}} = 35$ Hz, MeCH=), 20.6 (Ar-Me), 20.7 (Ar-Me), 47.8 (NCH_2 , $\text{N}'\text{C}'\text{H}_2$), 54.2 (br, $J_{\text{Pt}} = 290$ Hz, CH=), 69.2 (CHPh, CHPh), 127.9, 128.3, 129.3, 131.1, 136.9, 137.4, 138.1. Signals from the minor isomer (~8%) are detectable. ^{13}C NMR δ 17.9 (MeCH=), 49.5 (NCH_2 , $\text{N}'\text{C}'\text{H}_2$), 70.0 (CHPh, CHPh),

(13)



(14) Saigo, K.; Kubota, N.; Takebayashi, S.; Hasegawa, M. *Bull. Chem. Soc. Jpn.* **1986**, *59*, 931.

(15) Scott, J. D.; Puddephatt, R. J. *J. Chem. Soc., Chem. Commun.* **1984**, 193.

(16) Scott, J. D.; Puddephatt, R. J. *Organometallics* **1983**, *2*, 1643.

(17) Overlapped by Ar-Me signals.

(18) A part of AA'BB' multiplet.

Anal. Calcd for $\text{PtC}_{38}\text{H}_{48}\text{Cl}_2\text{N}_2$: C, 57.14; H, 6.06; N, 3.51. Found: C, 56.68; H, 5.81; N, 3.32.

$[\text{PtCl}_2(\text{mestien})(\eta^2\text{-propene})]$ (6a): ^1H NMR (400 MHz, CD_2Cl_2) δ 0.05 (d, 3 H, $J_{\text{Pt}} \approx 40$ Hz, =CHMe), 2.20 (1 H, =CHH),¹⁷ 2.20 (s, 3 H, Ar-Me), 2.22 (s, 3 H, Ar-Me), 2.29 (s, 6 H, Ar-Me), 2.34 (s, 6 H, Ar-Me), 2.41 (d, 1 H, =CHH), 3.24 (d app quartet, 1 H, $J_{\text{Pt}} \approx 75$ Hz, =CHMe), 3.50 (app d, 2 H, H^2 , $H^{2'}$), 4.00 (br app t, 1 H, $H^{1'}$), 4.2 (m, 4 H, H^3 , $H^{3'}$, H^4 , $H^{4'}$), 4.40 (br app t, 1 H, H^1), 6.76 (s, 2 H, Ar-H), 6.79 (s, 2 H, Ar-H), 7.0–7.4 (br, 10 H, Ph). Minor isomer (~15%) ^1H NMR δ 0.62 (d, 3 H, =CHMe). ^{13}C NMR (100 MHz, CDCl_3) δ 17.9 (MeCH=), 20.7 (Ar-Me), 37.1 ($J_{\text{Pt}} = 290$ Hz, CH₂=), 47.2 (NCH_2), 48.1 ($\text{N}'\text{C}'\text{H}_2$), 51.4 ($J_{\text{Pt}} = 310$ Hz, CH=), 68.6 (PhCH), 70.2 (PhCH), 128.1, 128.3, 128.6, 129.0, 129.1, 129.4, 131.0, 131.9, 136.7, 136.8, 137.0, 137.1, 137.4, 137.6, 138.0. Signals from the minor isomer are detectable. ^{13}C NMR δ 17.6 (MeCH=), 37.8 (CH₂=) 47.5 (NCH_2), 49.7 ($\text{N}'\text{C}'\text{H}_2$ or CH=), 69.8 (PhCH), 70.6 (PhCH). Anal. Calcd for $\text{PtC}_{37}\text{H}_{46}\text{Cl}_2\text{N}_2$: C, 56.63; H, 5.91; N, 3.57. Found: C, 56.40; H, 5.80; N, 3.36.

$[\text{PtCl}_2(\text{mestien})(\eta^2\text{-1-butene})]$ (7a): ^1H NMR (270 MHz, CDCl_3) δ 0.01 (m, 1 H, =CHCHH), 0.68 (t, 3 H, CH₂Me), 0.95 (m, 1 H, =CHCHH), 2.18 (s, 3 H, Ar-Me), 2.21 (s, 3 H, Ar-Me), 2.3 (1 H, =CHH),¹⁷ 2.30 (s, 6 H, Ar-Me), 2.32 (s, 6 H, Ar-Me), 2.47 (d, 1 H, =CHH), 3.17 (d app q, 1 H, $J_{\text{Pt}} = 75$ Hz, =CH), 3.1–3.3 (m, 4 H, H^3 , $H^{3'}$, H^4 , $H^{4'}$), 3.53 (app d, 1 H, H^2), 3.60 (app d, 1 H, $H^{2'}$), 4.05 (app t, 1 H, $H^{1'}$), 4.40 (app t, 1 H, H^1), 6.75 (s, 4 H, Ar-H), 7.1–7.2 (br, 10 H, Ph). Minor isomer (~8%) ^1H NMR δ 0.87 (t, 3 H, CH₂Me). Anal. Calcd for $\text{PtC}_{38}\text{H}_{48}\text{Cl}_2\text{N}_2$: C, 57.14; H, 6.06; N, 3.51. Found: C, 56.81; H, 5.90; N, 3.26.

$[\text{PtCl}_2(\text{mestien})(\eta^2\text{-styrene})]$ (8a). Complex 5a (80 mg, 0.1 mmol) was dissolved in 2 mL of methylene chloride, and 0.1 mL of styrene was added. The solution was evaporated to dryness, and the procedure was repeated once. The crude residue was washed with pentane and dried, giving a yellow powder (70 mg, 82% yield). The complex decomposes in solution in a few hours, giving 3a and free styrene. ^1H NMR (270 MHz, CDCl_3), only the methyl singlets are assignable (approximate relative intensities in parentheses) at δ 1.98 (3), 1.99 (6), 2.02 (6), 2.06 (2.5), 2.12 (5), 2.28 (2.5), 2.42 (3), 2.45 (5). Complex overlapping multiplets appear in the δ range 3.4–5.3 and 6.4–7.5. The observed pattern of methyl singlets is consistent with the presence of two isomers in ~6:5 ratio, both displaying hindered rotation of the olefin around the Pt–double bond axis.

$[\text{PtCl}_2(\text{mestien})]$ (3a). The complex was obtained as crystalline precipitate by decomposition of 8a in methanol solution, recrystallized from methylene chloride–diethyl ether: ^1H NMR (270 MHz, CDCl_3) δ 1.99 (s, 6 H, Ar-Me), 2.10 (s, 12 H, Ar-Me), 3.97 (dd, 2 H, H^4 , $H^{4'}$), 4.64 (dd, 2 H, H^2 , $H^{2'}$), 5.30 (dd, 2 H, H^3 , $H^{3'}$), 5.48 (m, 2 H, H^1 , $H^{1'}$), 6.39 (s, 4 H, Ar-H), 6.9 (m, 10 H, Ph); ^{13}C NMR (100 MHz, CDCl_3) δ 20.5 (Ar-Me), 20.7 (Ar-Me), 54.4 (NCH_2 , $\text{N}'\text{C}'\text{H}_2$), 77.4 (CHPh, CHPh), 126.3, 128.0, 129.0, 129.4, 129.9, 136.4, 137.0, 137.5. Anal. Calcd for $\text{PtC}_{34}\text{H}_{40}\text{Cl}_2\text{N}_2$: C, 54.99; H, 5.43; N, 3.77. Found: C, 54.65; H, 5.30; N, 3.57.

$[\text{PtClMe}(\text{mestien})(\eta^2\text{-ethene})]$ (4b). Procedures A and C: ^1H NMR (400 MHz, $\text{CDCl}_3\text{-CD}_3\text{OD}$ 10:1)¹⁹ δ -0.16 (s, 3 H, $J_{\text{Pt}} = 70$ Hz, Pt-Me), 0.81 (app t, 1 H, $J_{\text{Pt}} = 65$ Hz, =CH), 0.89 (app t, 1 H, $J_{\text{Pt}} = 65$ Hz, =CH), 1.81 (app t, 1 H, $J_{\text{Pt}} = 85$ Hz, =CH), 2.00 (app t, 1 H, $J_{\text{Pt}} = 85$ Hz, =CH), 2.10 (s, 3 H, Ar-Me), 2.13 (s, 3 H, Ar-Me), 2.16 (s, 6 H, Ar-Me), 2.25 (s, 6 H, Ar-Me), 3.48 (d, 1 H, H^3), 3.55 (d, 1 H, $H^{3'}$), 3.72 (d, 1 H, H^4), 3.78 (d, 1 H, $H^{4'}$), 4.18 (d, 1 H, H^2), 4.54 (d, 1 H, H^4), 6.62 (s, 2 H, Ar-H), 6.67 (s, 2 H, Ar-H), 6.9–7.3 (m, 10 H, Ph); ^{13}C NMR (100 MHz, $\text{CDCl}_3\text{-CD}_3\text{OD}$ 10:1) δ -12.6 ($J_{\text{Pt}} = 730$ Hz, Pt-Me), 20.1 (Ar-Me), 20.3 (Ar-Me), 20.5 (Ar-Me), 20.6 (Ar-Me), 28.1 ($J_{\text{Pt}} = 355$ Hz, =CH₂), 29.5 ($J_{\text{Pt}} = 375$ Hz, =CH₂), 47.6 (NCH_2 , $\text{N}'\text{C}'\text{H}_2$), 69.5 (PhCH), 70.5 (PhCH), 127.8, 128.2,

(19) In pure CDCl_3 the NH protons signals appear as double triplets at δ 3.09 ($J_{\text{Pt}} = 30$ Hz) and 4.35 ($J_{\text{Pt}} = 45$ Hz).

128.4, 128.5, 128.8, 128.9, 131.5, 131.7, 136.2, 136.6, 136.7, 137.6, 137.9. Anal. Calcd for PtC₃₇H₄₇ClN₂: C, 59.23; H, 6.31; N, 3.73. Found: C, 58.85; H, 6.38; N, 3.58.

[PtClMe(mestien)(η^2 -(E)-2-butene)] (5b). Procedure A: ¹H NMR (270 MHz, CDCl₃) δ -0.03 (d, 3 H, J_{Pt} = 65 Hz, =CHMe), 0.10 (s, 3 H, J_{Pt} = 75 Hz, Pt-Me), 0.45 (d, 3 H, J_{Pt} = 60 Hz, MeHC=), 1.8 (m, 1 H, =CHMe), 2.22 (s, 12 H, Ar-Me), 2.35 (s, 6 H, Ar-Me), 2.86 (m, 1 H, MeHC=), 3.04 (m, 1 H, H¹), 3.62 (m, 1 H, H³), 3.78 (app t, 1 H, H⁴), 3.98 (app t, 1 H, H²), 4.50 (app t, 1 H, H²), 4.62 (app t, 1 H, H⁴), 4.75 (m, 1 H, H¹), 6.70 (s, 2 H, Ar-H), 6.76 (s, 2 H, Ar-H), 7.0-7.3 (m, 10 H, Ph). Minor isomer (~15%) ¹H NMR δ 0.48 (s, 3 H, J_{Pt} = 75 Hz, Pt-Me).

[PtClMe(mestien)(η^2 -styrene)] (8b). Procedure A: ¹H NMR (270 MHz, CDCl₃). The only clearly assignable signals are four Pt-Me singlets at δ -0.10 (J_{Pt} = 70 Hz), -0.04 (J_{Pt} = 75 Hz), 0.47 (J_{Pt} = 75 Hz), 0.68 (J_{Pt} = 66 Hz) (relative abundances 7:4:3:3). The Ar-Me groups give several signals (at least nine) in the range 2.0-2.5 ppm, and the rest of the spectrum is made of complex overlapping multiplets as in the case of 8a. The composition of 8b was indirectly confirmed by bubbling ethylene through a solution of the compound in methylene chloride, which quantitatively yielded 4b and free styrene.

[PtClMe(mestien)(η^2 -(E)-dichloroethene)] (9b). Procedures B and C: ¹H NMR (400 MHz, CDCl₃) δ 0.51 (s, 3 H, J_{Pt} = 70 Hz, Pt-Me), 2.01 (s, 3 H, Ar-Me), 2.05 (s, 3 H, Ar-Me), 2.16 (s, 6 H, Ar-Me), 2.24 (s, 6 H, Ar-Me), 3.27 (d app t, 1 H, H¹), 3.43 (d, 1 H, J_{Pt} = 42 Hz, =CH), 3.75 (m, 3 H, H², H^{2'}, H⁴), 4.13 (dd, 1 H, H³), 4.48 (d, 1 H, J_{Pt} = 83 Hz, =CH), 4.49 (app t, 1 H, H⁴), 4.54 (app t, 1 H, H³), 4.92 (m, 1 H, H¹), 6.53 (s, 2 H, Ar-H), 6.62 (s, 2 H, Ar-H), 6.6-7.6 (br, 8 H),²⁰ 6.96 (app t, 1 H, Ph), 7.03 (app t, 1 H, Ph); ¹³C NMR (100 MHz, CDCl₃) δ 0.6 (J_{Pt} = 725 Hz, Pt-Me), 20.2 (Ar-Me), 20.4 (Ar-Me), 42.6 (J_{Pt} = 475 Hz, =CH), 42.9 (J_{Pt} = 425 Hz, =CH), 49.2, 49.4 (NCH₂, N'C'H₂), 70.9, 71.3 (PhCH, PhC'H), 128.5, 128.7, 128.8, 129.3, 129.6, 129.7, 130.0, 136.0, 136.3, 136.5, 136.6, 137.1, 137.2. Anal. Calcd for PtC₃₇H₄₅Cl₂N₂: C, 54.25; H, 5.54; N, 3.42. Found: C, 53.67; H, 5.40; N, 3.24.

[PtClMe(mestien)(η^2 -fumaronitrile)] (10b). Procedures B and C: ¹H NMR (270 MHz, CDCl₃) isomer A (43% abundance) δ 0.51 (s, 3 H, J_{Pt} = 67 Hz, Pt-Me), 1.64 (d, 1 H, J_{Pt} = 61 Hz, =CH), 2.21 (s, 3 H, Ar-Me), 2.22 (s, 3 H, Ar-Me), 2.27 (s, 6 H, Ar-Me), 2.34 (s, 6 H, Ar-Me), 2.95 (d, 1 H, J_{Pt} = 86 Hz, =CH), 3.6-4.6 (6 H),²¹ 4.82 (app t, 1 H, H²), 5.52 (m, 1 H, H¹), 6.81 (s, 2 H, Ar-H), 6.84 (s, 2 H, Ar-H), 6.6-7.6 (br, 10 H, Ph); isomer B (57% abundance) ¹H NMR δ 0.93 (s, 3 H, J_{Pt} = 65 Hz, Pt-Me), 2.09 (s, 3 H, Ar-Me), 2.14 (s, 3 H, Ar-Me), 2.27 (s, 6 H, Ar-Me), 2.29 (d, 1 H, J_{Pt} = 61 Hz, =CH), 2.34 (s, 6 H, Ar-Me), 3.35 (d, 1 H, J_{Pt} = 81 Hz, =CH), 3.6-4.6 (7 H),²¹ 5.60 (m, 1 H, H¹), 6.56 (s, 2 H, Ar-H), 6.64 (s, 2 H, Ar-H), 6.6-7.6 (br, 10 H, Ph). Anal. Calcd for PtC₃₉H₄₅ClN₄: C, 58.53; H, 5.67; N, 7.00. Found: C, 57.98; H, 5.51; N, 6.88.

[PtClMe(S,S)-(+)-mestien](η^2 -1-buten-3-ol)] (11b). Procedure B: ¹H NMR (400 MHz, CDCl₃) δ 0.01 (s, 3 H, J_{Pt} = 70 Hz, Pt-Me), 0.74 (dd, 1 H, J_{Pt} = 81 Hz, =CHH), 0.84 (d, 3 H, CHMe), 1.86 (dd, 1 H, =CH), 2.18 (app s, 12 H, Ar-Me), 2.31 (app s, 6 H, Ar-Me), 2.38 (dd, 1 H, =CHH), 2.51 (app q, 1 H, CHOH), 2.91 (d app t, 1 H, H¹), 3.52 (dd, 1 H, H³), 3.59 (dd, 1 H, H³), 3.76 (app t, 1 H, H⁴), 3.85 (app t, 1 H, H²), 4.28 (app t, 1 H, H²), 4.64 (app t, 1 H, H⁴), 4.77 (d app t, 1 H, H¹), 6.72 (s, 4 H, Ar-H), 6.8-7.4 (br, 10 H, Ph); ¹³C NMR (67.9 MHz, CDCl₃) δ -10.0 (J_{Pt} = 730 Hz, Pt-Me), 20.2 (Ar-Me), 20.5 (Ar-Me), 20.6 (Ar-Me), 23.5 (CHMe), 24.6 (J_{Pt} = 350 Hz, =CH₂), 47.2 (NCH₂), 47.3 (N'C'H₂), 53.5 (J_{Pt} = 380 Hz, =CH), 66.6 (J_{Pt} = 35 Hz, CHOH), 68.1 (PhCH), 70.3 (PhC'H), 127-138 (Ar, Ph).²²

(20) At 25 °C the signals are coalesced in a single flat band.

(21) Overlapped multiplets from both A and B isomers.

(22) The aromatic carbon resonances overlap in that range.

Table 4. Summary of Crystallographic Data

crystal size/mm	0.10 × 0.12 × 0.30
formula	PtCl ₃ N ₂ C ₃₇ H ₄₅
fw	819.2
crystal system	monoclinic
space group	P2 ₁ /c
a/Å	13.163(2)
b/Å	19.274(4)
c/Å	14.906(2)
β	112.56(2)
V/Å ³	3492(2)
Z	4
F(000)	1640
D _c /g cm ⁻³	1.56
D _m /g cm ⁻³	1.53
λ (Cu K α)/Å	1.5418
θ_{max} /deg	72
μ /cm ⁻¹	99.6
no. of indep. refls.	6859
no. of refls. above 3 σ (I)	3918
no. of refined parameters	388
goodness of fit	1.075
R	0.059
R _w	0.069

11b". This diastereomer, which contains the opposite enantiomer of the butenol, was obtained in equimolar mixture with 11b' by using procedure A for the preparation: ¹H NMR (270 MHz, CDCl₃) δ 0.13 (s, 3 H, J_{Pt} = 70 Hz, Pt-Me), 1.30 (d, 3 H, CHMe), 2.10 (app s, 6 H, Ar-Me), 2.25 (app s, 12 H, Ar-Me), 3.12 (app t, 1 H, H¹), 4.52 (app t, 1 H, H² or H⁴). Other signals are not assignable due to overlapping with the signals of the other diastereomer. ¹³C NMR (67.9 MHz, CDCl₃) δ -9.3 (Pt-Me), 19.0 (Ar-Me), 20.5 (Ar-Me), 22.8 (CHMe), 31.1 (=CH₂), 45.6 (NCH₂), 47.6 (N'C'H₂), 53.6 (=CH), 63.0 (CHOH), 69.7 (PhCH), 71.1 (PhC'H), 127-138 (Ar, Ph).²⁰

Structure Determination and Refinement of [PtClMe(mestien)((E)-dichloroethene)] (9b). Crystals suitable for X-ray analysis were obtained as follows. The complex (0.06 mmol) was dissolved in 30 mL of CH₂Cl₂-ethanol (25:75 v/v) at T = 40 °C. The resulting solution was kept at room temperature, producing colorless crystals, which were isolated. Many of the details of the structure analysis are listed in Table 4. X-ray data were collected at room temperature on an Enraf-Nonius CAD4-F automatic diffractometer using Cu K α graphite-monochromated radiation operated in the ω/θ scan mode. The unit cell parameters were obtained by a least-squares fitting of the setting values of 25 strong reflections in the θ range 23 ≤ θ ≤ 29°. Three monitoring reflections, measured every 500, showed intensity fluctuations within 5%. The structure was solved by routine application of the Patterson and Fourier techniques. The full-matrix least-squares refinement minimized the quantity $\sum w(\Delta F)^2$ with $w^{-1} = [\sigma^2(F_o) + (0.02F_o)^2 + 1]$ where σ is derived from counting statistics. All non-hydrogen atoms were refined anisotropically. The H atoms were added at calculated positions with isotropic thermal parameters 1.2 times larger than the B of the carrier atoms and held fixed during the refinement. A correction for absorption effects was applied according to Walker and Stuart,²³ by using the computer program DIFABS (maximum and minimum values of the absorption correction were 1.4 and 0.7). The final Fourier difference map was within 1.3 e Å⁻³. Neutral atomic scattering factors were taken from the literature.²⁴ All calculations, carried out on a Vax 750 at the Centro Interdipartimentale di Metodologie Chimico-fisiche of the Università di Napoli, were performed with the Enraf-Nonius (SDP) set of programs.²⁵ Complete lists of bond distances and angles, hydrogen atom parameters, and anisotropic thermal param-

(23) Walker, N.; Stuart, D. *Acta Crystallogr.* **1983**, A39, 158.

(24) North, A. C. T.; Phillips, D. C.; Mathews, F. S. *Acta Crystallogr.* **1968**, A24, 351.

(25) B. A. Frenz & Associates Inc. Structure Determination Package (SDP), College Station, TX, and Enraf-Nonius, Delft, The Netherlands, 1982.

eters of the non-hydrogen atoms have been deposited as supplementary material.

Acknowledgment. We thank the Consiglio Nazionale delle Ricerche (CNR) and the Ministero della Università e della Ricerca Scientifica e Tecnologica (MURST) for financial support, the Ministero degli Affari Esteri for a grant to M.A.J. (1991–1992), and the Centro Interdipartimentale di Metodologie Chimico-

fisiche, Università di Napoli for the use of NMR spectrometers and X-ray and computer facilities.

Supplementary Material Available: Tables of positional and thermal parameters of the H atoms (Table 5s), anisotropic thermal parameters of the non-hydrogen atoms (Table 6s), and complete bond distances and angles (Table 7s) (4 pages). Ordering information is given on any current masthead page.

OM940523D

Platinum-Catalyzed Oxidations with Hydrogen Peroxide: The (Enantioselective) Epoxidation of α,β -Unsaturated Ketones

Carla Baccin, Andrea Gusso, Francesco Pinna, and Giorgio Strukul*

Department of Chemistry, University of Venice, Dorsoduro 2137, 30123 Venezia, Italy

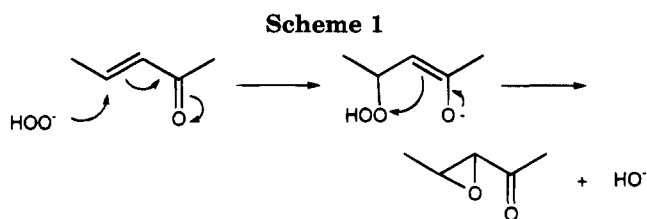
Received July 8, 1994[⊗]

The catalytic epoxidation of α,β -unsaturated ketones with hydrogen peroxide catalyzed by a variety of (P-P)Pt(CF₃)(solv)⁺ and (P-P)Pt(2-van) complexes (P-P = a variety of diphosphines, including chiral diphosphines; 2-van = the bis anion of 2-vanillin) is reported. The reaction can be carried out at room temperature under mild conditions and is moderately selective. Loss of chemical selectivity is related to the acidity of the medium with both classes of catalysts. The enantioselective transformation can be easily accomplished with chiral diphosphine modified catalysts, but a significant loss of enantioselectivity is observed during the course of the reaction. If the reaction is carried out stoichiometrically with the use of (P-P)Pt(CF₃)(OOH) oxidants, the ee can be as high as 63% and stable with time.

Introduction

The epoxidation of α,β -unsaturated ketones with hydrogen peroxide under basic conditions was first discovered by Weitz and Scheffer in 1921 and is one of the oldest applications of hydrogen peroxide as oxidant in synthetic organic chemistry.¹ As was later demonstrated,² the reaction involves (Scheme 1), as the rate-determining step, the nucleophilic attack of the hydroperoxide anion generated in the alkaline medium at the carbon-carbon double bond made electrophilic by the electron-withdrawing carbonyl substituent. The requirement of a nucleophilic peroxy oxygen appears to be the main reason why metal catalysis with the traditional d⁰ transition metal complexes was never applied to this interesting synthetic reaction. On the other hand, the efficiency and versatility of the purely organic system³ provided no incentive to search for other possible transition-metal catalysts.

The enantioselective version of the Weitz-Scheffer oxidation was first reported by Wynberg,⁴ utilizing a chiral organic base (a quininium salt) and hydrogen peroxide under phase-transfer conditions. In the oxidation of chalcones, ee values in the range 25–55% were observed. Alternatively, but still limited to the oxidation of chalcones, Julià and co-workers⁵ employed the traditional alkaline system, but carried out the reaction within the α -helix of a poly(α -amino acid).⁶ With this methodology ee values up to 93% were reported. The need for a more versatile synthetic approach (not limited



to chalcones) to the asymmetric transformation suggests that transition-metal catalysis should be investigated. Indeed, the diastereoselective epoxidation of (already) chiral β -hydroxy enones has been reported recently by Markò et al.⁷ using the Sharpless system and is an elegant application of the well-known epoxidation of allylic alcohols. In the general case of α,β -unsaturated ketones, given the nature of the substrates, only catalysts able to increase the nucleophilicity of hydrogen peroxide seem to be suited to this purpose.

Over the years we have investigated the catalytic properties of a class of platinum(II) complexes of the type (P-P)Pt(CF₃)X (P-P = various diphosphines; X = solvent, -OH) that are still the only transition-metal catalysts capable of increasing the nucleophilicity of hydrogen peroxide,⁸ similarly to alkali metals. In this work we report our attempts to accomplish with these catalysts the Weitz-Scheffer oxidation along with the enantioselective version of the same reaction.

Results and Discussion

Catalysts. The catalysts employed in the present study are shown in Chart 1. The first type (1) of

* To whom correspondence should be addressed. FAX: (39) 41 529 8517. e-mail: strukul@vega.cicsd.unive.it.

[⊗] Abstract published in *Advance ACS Abstracts*, January 15, 1995.

(1) Weitz, E.; Scheffer, A. *Ber. Dtsch. Chem. Ges.* **1921**, *54*, 2327.

(2) Bunton, C. A.; Minkoff, G. J. *J. Chem. Soc.* **1949**, 665.

(3) (a) Plesnicar, B. In *Oxidation in Organic Chemistry*; Trahanovsky, W. S., Ed.; Academic Press: New York, 1978; Part C, p 243.

(b) Plesnicar, B. In *The Chemistry of Peroxides*; Patai, S., Ed.; Wiley-Interscience: New York, 1983; Chapter 17, p 566. (c) Hudlicky, M.

Oxidations in Organic Chemistry; American Chemical Society: Washington, DC, 1990; p 60.

(4) (a) Helder, R.; Hummelen, J. C.; Laane, R. W. P. M.; Wynberg, H. *Tetrahedron Lett.* **1976**, 1831. (b) Hummelen, J. C.; Wynberg, H. *Tetrahedron Lett.* **1978**, 1089. (c) Wynberg, H.; Greijdanus, B. *J. Chem. Soc., Chem. Commun.* **1978**, 427. (d) Wynberg, H.; Marsman, B. *J. Org. Chem.* **1980**, *45*, 158. (e) Meijer, E. W.; Wynberg, H. *Angew. Chem., Int. Ed. Engl.* **1988**, *27*, 975.

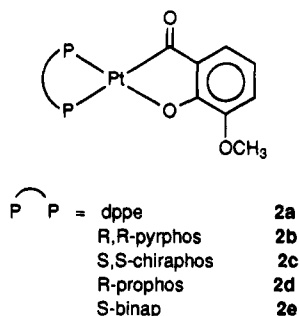
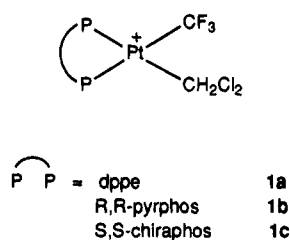
(5) (a) Julià, S.; Guixer, J.; Masana, J.; Vega, J. *Angew. Chem., Int. Ed. Engl.* **1980**, *19*, 929. (b) Julià, S.; Guixer, J.; Masana, J.; Rochas, J.; Colonna, S.; Annunziata, R.; Molinari, H. *J. Chem. Soc., Perkin Trans. 1* **1982**, 1317. (c) Colonna, S.; Molinari, H.; Banfi, S.; Julià, S.; Masana, J.; Alvarez, A. *Tetrahedron* **1983**, *39*, 1635.

(6) Aglietto, M.; Chiellini, E.; D'Antone, S.; Ruggeri, G.; Solaro, R. *Pure Appl. Chem.* **1988**, *60*, 415 and references therein.

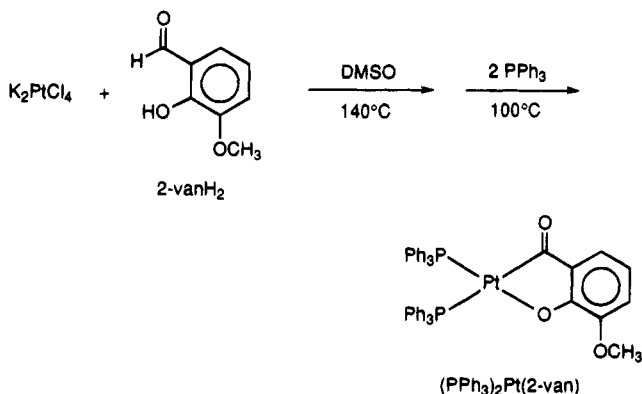
(7) (a) Bailey, M.; Markò, I. E.; Ollis, W. D. *Tetrahedron Lett.* **1990**, *31*, 4509. (b) Bailey, M.; Markò, I. E.; Ollis, W. D. *Tetrahedron Lett.* **1991**, *32*, 2687.

(8) Strukul, G. In *Catalytic Oxidations with Hydrogen Peroxide as Oxidant*; Strukul, G., Ed.; Kluwer: Dordrecht, The Netherlands, 1992; p 177, and references therein.

Chart 1



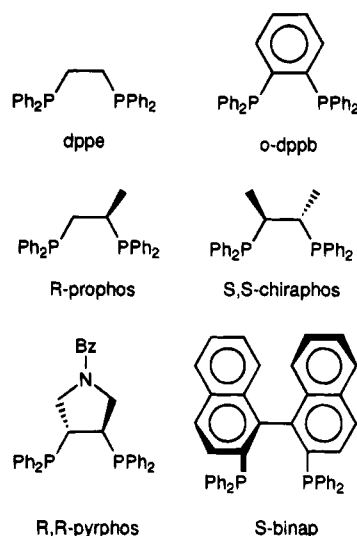
Scheme 2



compounds belongs to the general class of Pt(II) complexes reported above, that were found active in a variety of other catalytic oxidations.^{8,9} The synthetic procedure for these and other complexes of the same type is reported elsewhere.¹⁰ The second class of complexes (**2**) was recently reported to catalyze the Baeyer–Villiger oxidation of cyclic ketones¹¹ (including the enantioselective transformation) and were synthesized according to the procedure (Scheme 2) reported by Pregosin et al. some years ago¹² for $(\text{PPh}_3)_2\text{Pt}(\text{2-van})$ (2-van = the bis anion of 2-vanillin). Details on the synthesis and characterization of these complexes is reported in ref 11. For the meaning of the diphosphine acronyms, see Chart 2.

General Reactivity. For the screening procedure toward a class of different α,β -unsaturated ketones (Chart 3), the two prototype complexes $[(\text{dppe})\text{Pt}(\text{CF}_3)(\text{CH}_2\text{Cl}_2)]\text{BF}_4$ (**1a**) and $(\text{dppe})\text{Pt}(\text{2-van})$ (**2a**) were chosen, while in the search for the best operating

Chart 2



conditions catalyst **1a** and 2-cyclohexen-1-one (**3**) were tested.

The epoxidation of **3** was carried out at room temperature under N_2 atmosphere using 35% H_2O_2 as the oxidant. Since the catalyst is moderately soluble in the substrate, reactions were tested in the absence of solvent. Under these conditions a two-phase (ketone/ H_2O) reaction medium forms. A summary of the data observed when the operating conditions are changed is shown in Table 1. All reactions start immediately upon addition of the oxidant and display a relatively constant initial rate that is maintained for about 1 h. A progressive slowdown follows, reaching asymptotically the maximum conversion. Although even at low catalyst concentration (Table 1, entry 6) the maximum epoxide productivity is still acceptable, an increase of the catalyst amount is obviously beneficial. As can be seen from Table 1, the maximum amount of epoxide is in all cases much lower than the amount of oxidant used. Similarly to previous oxidations with H_2O_2 when the carbonyl functional group is present in the substrate,^{11,13} even in this case no more than 30–35% of the H_2O_2 introduced is converted into products. As was already suggested, this is probably due to catalytic decomposition of the oxidant via formation of dioxirane species.¹³ The use of a solvent (DCE) is detrimental, resulting in a lowering of both the initial rate and the maximum productivity (entry 2), and similar effects are observed when the catalyst is changed from the solvato cationic complex **1a** to the complex $(\text{dppe})\text{Pt}(\text{CF}_3)(\text{OH})$ (entry 3).

Comparison with previous results obtained with cyclohexene (no epoxidation was observed)¹⁴ indicates that the presence of an electron-withdrawing substituent in the substrate molecule strongly increases the reactivity of the system, in agreement with the mechanistic suggestion¹⁴ that the effect of Pt is to increase the electrophilicity of the olefin through coordination while, at the same time, increasing the nucleophilicity of H_2O_2 .

The operating conditions of Table 1, entry 1 were applied to the epoxidation of the α,β -unsaturated ke-

(9) Strukul, G. In *Advances in Catalyst Design*; Graziani, M., Rao, C. N. R., Eds.; World Scientific: Singapore, 1993; Vol. 2, p 53, and references therein.

(10) (a) Sinigaglia, R.; Michelin, R. A.; Pinna, F.; Strukul, G. *Organometallics* **1987**, *6*, 728. (b) Zanardo, A.; Michelin, R. A.; Pinna, F.; Strukul, G. *Inorg. Chem.* **1989**, *28*, 1648.

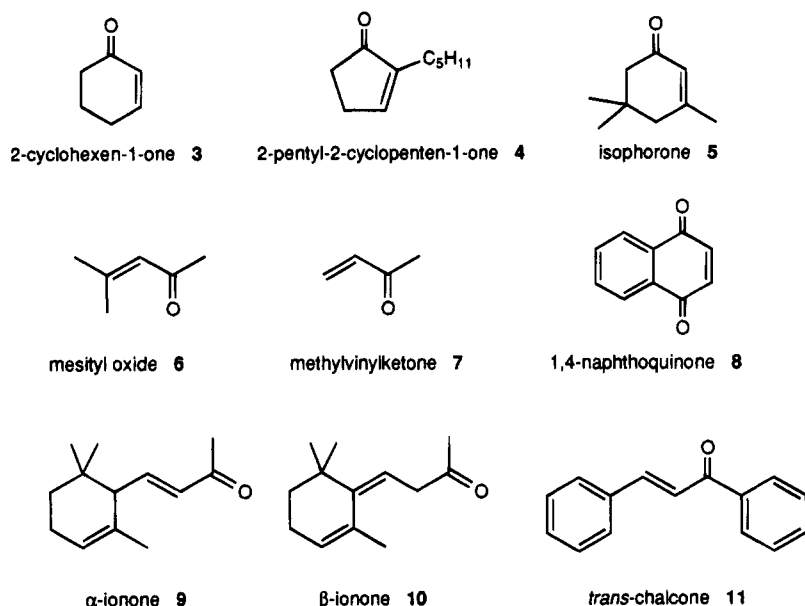
(11) Gusso, A.; Baccin, C.; Pinna, F.; Strukul, G. *Organometallics* **1994**, *13*, 3442.

(12) Pregosin, P. S.; Anklin, C.; Bachechi, F.; Mura, P.; Zambonelli, L. *J. Organomet. Chem.* **1981**, *222*, 175.

(13) (a) Del Todesco Frisone, M.; Giovanetti, R.; Pinna, F.; Strukul, G. *Stud. Surf. Sci. Catal.* **1991**, *66*, 405. (b) Del Todesco Frisone, M.; Pinna, F.; Strukul, G. *Organometallics* **1993**, *12*, 148.

(14) Strukul, G.; Michelin, R. A. *J. Chem. Soc., Chem. Commun.* **1984**, 1538.

Chart 3

**Table 1. Epoxidation of 2-Cyclohexen-1-one (3): Effect of Catalyst Amount on the Productivity of the Reaction^a**

entry no.	amt of catalyst (mmol)	max amt of epoxide (mmol)	time (min)	10 ⁴ (init rate) (M s ⁻¹)
1	0.05	1.67	384	2.1
2 ^b	0.05	0.11	1669	0.03
3 ^c	0.05	0.89	7065	0.22
4	0.02	1.14	160	1.1
5	0.01	1.26	357	0.65
6	0.005	1.07	255	0.41

^a Experimental conditions: catalyst [(dpe)Pt(CF₃)(CH₂Cl₂)]BF₄; 2-cyclohexen-1-one, 10 mmol; 35% H₂O₂, 5 mmol; T, 25 °C; N₂, 1 atm. ^b DCE (2 mL) added as solvent. ^c Catalyst used (dpe)Pt(CF₃)(OH).

Table 2. Epoxidation of α,β -Unsaturated Ketones with Hydrogen Peroxide Catalyzed by Complexes 1a and 2a^a

entry no.	catalyst	substrate	max amt of epoxide ^b (mmol)	time (h)	T (°C)
1	1a	3	1.67	7	25
2	2a		1.77	4	25
3	1a	4	1.37	164	25
4	2a		1.56	30	25
5	<i>c</i>	5	0.66 (39)	4	50
6	1a		0.56 (40)	26	50
7	2a		0.61 (40)	27	25
8	1a	6	0.48 (12)	82	25
9	2a		0.49 (11)	92	25
10 ^d			0.35 (9)	84	25
11	1a	7	0.26 (10)	124	25
12	2a		0.98 (12)	146	25
13 ^d			0.60 (10)	180	25

^a Experimental conditions: catalyst, 0.05 mmol; substrate, 10 mmol; 35% H₂O₂, 5 mmol; N₂, 1 atm. With catalyst **2a**, HClO₄ (0.05 mmol) added prior to reaction (see Experimental Section). ^b When other products are formed, numbers in parentheses refer to the percent selectivity with respect to the epoxide. ^c [(*o*-dppb)Pt(CF₃)(CH₂Cl₂)]ClO₄ as catalyst. ^d DCE (2 mL) added as solvent.

tones shown in Chart 3. No reaction was observed with substrates **8–11** even for long reaction times (up to 120 h) or an increase in the reaction temperature up to 80 °C. Similarly, no reaction was observed when two α,β -unsaturated esters were tested, namely ethyl acrylate and ethyl crotonate. The results obtained in the epoxidation of substrates **3–7** are reported in Table 2. The following general comments can be made.

(1) The reactivity of catalyst **2a** is generally higher than that of catalyst **1a** (entries 2, 4, 7, and 12). The

use of **2a** as catalyst requires activation with a stoichiometric amount of perchloric acid. The evolution of **2a** to produce the catalytically active species has already been reported.¹¹

(2) As was already observed in the epoxidation of 1-octene,^{10b} the substitution of dppe in **1a** with a flat, less sterically demanding diphosphine such as *o*-dppb results in a higher catalytic activity (entry 5).

(3) With the exception of substrates **3** and **4**, where epoxides are the only oxidation products, in the other cases (entries 5–13) the yield of epoxide is rather poor and relatively independent of the catalyst used. This point will be further discussed below.

Byproduct Formation. The problem of the formation of byproducts has been fully addressed in the case of mesityl oxide (**6**). Typically, after an initial time (about 1 h) where only epoxide is observed, a series of byproducts start forming that eventually become the main products. These have been identified as acetone (38%), the terminal epoxide (10%), and the two glycols (internal 36%, terminal 5%) arising from the epoxides, with the use of GC-MS analysis in comparison with authentic samples. The selectivities given refer to the final reaction mixture for **1a** as catalyst and are typical. As to the pathways with which these compounds form, these have been identified with the following experiments.

A mixture of **6** and the corresponding epoxide in CH₂-Cl₂ was independently synthesized with the traditional (NaOH/H₂O₂) Weitz-Scheffer procedure.² When this mixture was placed in contact with an aqueous solution containing an amount of H₂SO₄ or HClO₄ identical with the amount of catalyst used in the catalytic experiments, formation in solution of acetone and the glycol arising from the epoxide were observed.

When the same mixture of **6** and the corresponding epoxide were contacted with **1a** in the absence of water, no reaction was observed.

A possible reaction pathway summarizing these observations is shown in Scheme 3. It is known¹⁴ that the catalytic activity of [(P-P)Pt(CF₃)(solvent)]⁺ complexes is related to the Pt⁺/PtOOH hydrolysis equilibrium

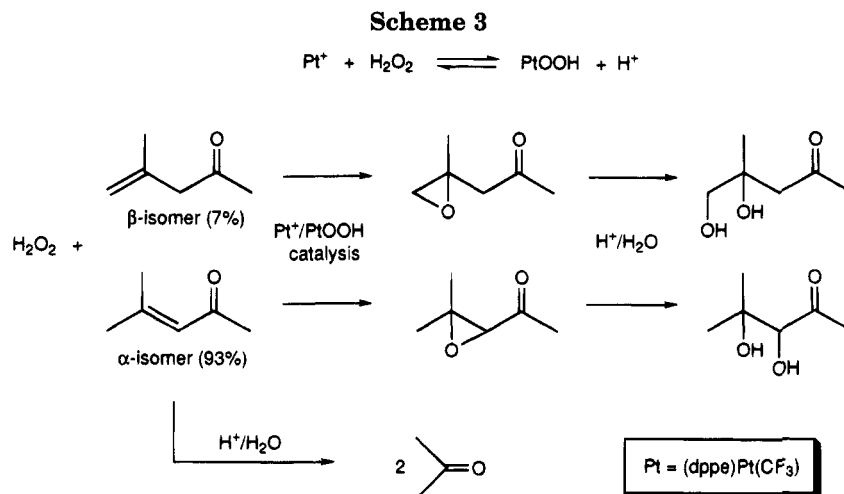


Table 3. Enantioselective Epoxidation of 2-Cyclohexen-1-one (3) with Hydrogen Peroxide Catalyzed by [(pyrphos)Pt(CF₃)(CH₂Cl₂)]BF₄ (1b)^a

entry no.	amt of catalyst (mmol)	T (°C)	time (h)	init amt of epoxide (mmol) (% ee)	final time (h)	final amt of epoxide (mmol) (% ee)
1	0.05	-10	1.4	0.02 (72)	25	0.30 (39)
2	0.05	0	1.1	0.08 (60)	45	0.45 (49)
3	0.05	25	0.7	0.10 (34)	32	0.58 (7)
4	0.05	50	0.5	0.10 (22)	28	1.52 (4)
5	0.025	25	0.8	0.09 (44)	45	0.53 (5)
6	0.02	25	0.8	0.10 (49)	28	0.53 (10)
7	0.01	25	0.8	0.20 (56)	166	1.32 (1)
8	0.005	25	2.6	0.08 (72)	127	1.25 (1)

^a Experimental conditions: 2-cyclohexen-1-one, 10 mmol; 35% H₂O₂, 5 mmol; N₂, 1 atm.

shown in Scheme 3, where protons are produced, making the system acidic. Due to their moderate solubility in the (acidic) water phase of the catalysis medium, the epoxides, once formed, can be hydrolyzed to produce the corresponding glycols. Furthermore, it has to be pointed out that the commercial (Janssen) mesityl oxide used as substrate is a mixture of α - and β -isomers. Since the latter is a terminal olefin and the present system is very reactive toward terminal olefins, significant amounts of terminal epoxide (and the corresponding glycol) are produced. As to the formation of acetone, it should be pointed out that mesityl oxide is the dimer of acetone made by aldol condensation, the most likely explanation for its presence being the inverse reaction,¹⁵ again due to the acidic aqueous medium.

In summary, our experiments seem to demonstrate that transition-metal catalysis is involved only in the epoxide formation, thereby confirming the good intrinsic selectivity of the catalysts, which are only *indirectly* responsible for the (probably unavoidable) formation of the byproducts.

In the epoxidation of **5**, acetone (18%) (isophorone is the trimer of acetone), the unsaturated lactone (29%), arising from Pt-catalyzed Baeyer–Villiger oxidation, and two unidentified products (14% in total) are formed as byproducts. Finally, in the epoxidation of **7**, in addition to the epoxide, also the formation of acetone (58%), glycol (10%), and an unidentified product (20%) (formaldehyde could not be detected) were observed in the reaction mixture.

Enantioselective Epoxidation. Catalysts **1b,c** and **2b–e** were employed in the enantioselective epoxidations. These were carried out in pure substrate using 35% H₂O₂ as oxidant. Evaluation of the ee in the course of the reaction was performed by GC using a commercial (Chrompack) β -cyclodextrin capillary column.

Prior to the complete screening of the substrates reported in Chart 3, a search for the best operating conditions was carried out with catalyst **1b** on substrate **3**. Results are reported in Table 3. The reaction was checked at different temperatures and changing catalyst amounts. As can be seen, independent of the conditions used, there is always a strong decrease of the ee during the course of the reaction. In fact, at the beginning of the reaction, when low amounts of epoxide are produced, a relatively high asymmetric induction is observed, while at the end of the reaction, almost complete loss of ee may occur. This fact, coupled with the small size of the catalytic runs, prevented the possible determination of the absolute configuration of the preferred enantiomer. A dramatic case (Table 3, entry 8) showing the decrease of the ee during the course of the reaction is shown in Figure 1. In general, if the final ee is compared with the values observed during the reaction, a simple mass balance seems to show that the dropping down of the ee is indeed due to a (partial) racemization of the epoxide rather than a loss of the enantioselective properties of the catalyst. Major factors affecting the initial ee are the reaction temperature (Table 3, entries 1–4) and the catalyst amount (entries 3 and 5–8). The lower the catalyst amount, the higher the initial ee. Therefore, it seems that the catalyst is actively involved in the loss of ee. On the other hand, the final ee seems to be related mainly to the duration of the experiment.

(15) See for example: Reeves, R. L. In *The Chemistry of the Carbonyl Group*; Patai, S., Ed.; Wiley-Interscience: New York, 1971; Chapter 12, p 580.

Table 4. Catalytic Enantioselective Epoxidation of α,β -Unsaturated Ketones 4–6 with Hydrogen Peroxide^a

entry no.	catalyst	substrate	T (°C)	time (h)	init amt of epoxide (mmol) (% ee)	final time (h)	final amt of epoxide (mmol) (% ee)
1	1b	4	25	0.4	0.04 (13)	96	0.5 (1)
2			50	0.5	0.06 (28)	28	0.6 (1)
3	1c		25	0.4	0.06 (38)	53	0.3 (2)
4	2b		0	0.6	0.04 (42)	98	0.08 (0)
5			50	0.1	0.04 (5)	3	1.3 (0)
6	2c		0	1	0.06 (39)	98	1.5 (4)
7			25	0.5	0.05 (1)	53	1.4 (0)
8	2d		0	0.2	0.06 (57)	98	0.1 (0)
9			50	0.1	0.04 (2)	3	1.0 (0)
10	2e		0	1.5	0.09 (41)	98	1.0 (18)
11			25	0.6	0.08 (22)	31	0.9 (11)
12			50	0.1	0.09 (5)	3	0.9 (4)
13	2b	5	0	1.7	0.04 (11)	45	0.3 (2)
14			25	1.4	0.05 (47)	73	0.5 (4)
15			50	0.8	0.04 (5)	23	0.3 (1)
16	2c		25	2.9	0.07 (14)	49	0.6 (3)
17	2d		0	1.8	0.06 (4)	48	0.2 (1)
18	2d	6	0	0.1	0.08 (12)	26	0.5 (4)
19			25	0.02	0.09 (9)	4	0.6 (0)
20	2e		0	0.1	0.06 (10)	27	0.6 (7)
21			25	0.05	0.08 (5)	5	0.6 (0)

^a Experimental conditions: catalyst, 0.05 mmol; substrate, 10 mmol; 35% H₂O₂, 5 mmol; N₂, 1 atm. With catalysts 2b–e, HClO₄ (0.05 mmol) added prior to reaction (see Experimental Section).

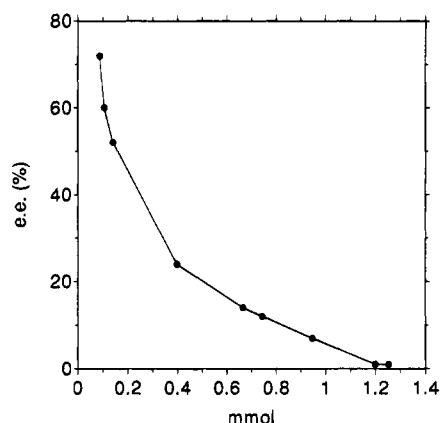
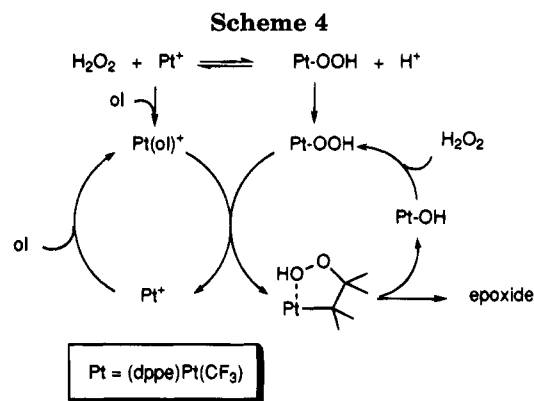


Figure 1. Decrease of the ee of 2,3-epoxycyclohexanone with the amount produced in the epoxidation of 2-cyclohexen-1-one with H₂O₂ catalyzed by [(pyrphos)Pt(CF₃)(CH₂-Cl₂)]BF₄ (1b). See Table 3, entry 8.

Since, from a practical point of view, what is important is the final asymmetric induction, in order to shorten the reaction time, the other catalysts and substrates were checked at high catalyst concentration, i.e. under the conditions of entries 1–4 (Table 3).

The results obtained in the epoxidation of substrates 4–6 with catalysts 1b,c and 2b–e are reported in Table 4. As can be seen, although in several cases the initial ee may be interesting, with the exception of entries 9 and 10 the extent of the asymmetric induction at the end of the catalytic reaction is almost negligible. Again, this made the determination of the absolute configuration impossible.

Loss of Enantiomeric Excess. The role of the catalyst in the apparent racemization process was investigated in the case of substrate 4 with catalyst 1b. It is known from previous kinetic studies on the epoxidation of 1-octene¹⁶ that the catalytic reaction proceeds through the mechanism shown in Scheme 4. On this basis the enantiotopic discrimination will occur at the time of metal–olefin complex formation.^{10a} Since ep-

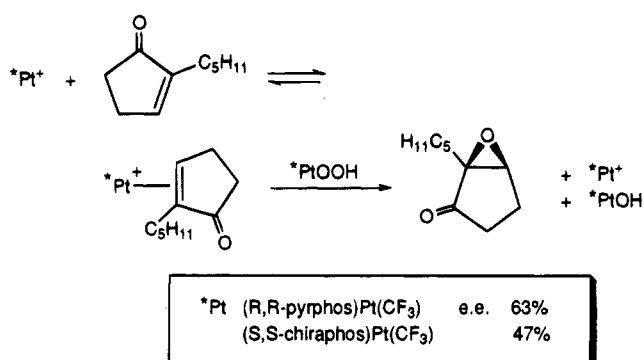


oxide forms from the interaction between the metal–olefin complex and the actual oxidant PtOOH, a stoichiometric reaction leading to the formation of 1 equiv of chiral epoxide can be set up. This will mimic the early stage of the catalytic reaction and, in the absence of aqueous H₂O₂, give the *intrinsic enantiodifferentiating properties* of the catalyst.

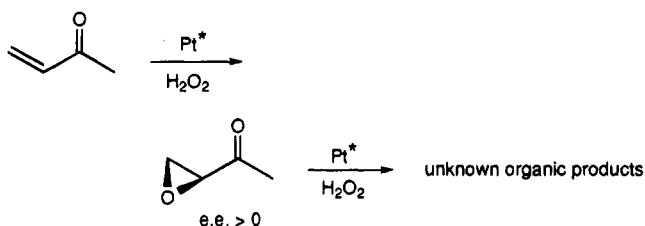
Complex 1b (0.05 mmol) was dissolved in pure 4 (1 mL) at 25 °C, and to this solution was added (*R,R*-pyrphos)Pt(CF₃)(OOH) (0.05 mmol). GC analysis revealed the immediate formation of the epoxy ketone with an optical purity of 63%, significantly higher than the initial ee of the catalytic reaction (13%, Table 4, entry 1); this value remained constant for many hours. The same experiment was repeated with complex 1c and (*S,S*-chiraphos)Pt(CF₃)(OOH), yielding 1 equiv of epoxy ketone with ee 47%, again constant with time (see Scheme 5 for a summary).

These experiments demonstrate that the intrinsic enantiodifferentiating properties of the catalysts (at least for 1b,c) are good and seem to support the idea that the reaction intermediates involved in Scheme 5 have no direct role in the apparent racemization process. However, the catalytic reaction differs from the stoichiometric one in the presence of excess water and hydrogen peroxide. Other pathways, involving the acidity of the medium (formed from the hydrolysis equilibrium in Scheme 3) and leading to reversible enol

Scheme 5



Scheme 6



formation via protonation of the carbonyl functional group, might be plausible but would apply only to substrate **6**, where only one chiral center is produced. Indeed, the loss of ee in the catalytic reaction would be accounted for in the presence of a consecutive reaction, probably a further oxidation, leading to products undetectable by GLC analysis. This possibility is illustrated in Scheme 6: if the further reaction of the epoxide is mediated by the catalyst, the transformation will be stereoselective and, if mismatched with respect to the first step, will lead to a decrease of the observed ee in the remaining epoxide.

This possibility was tested by checking the feasibility of the second step of Scheme 6, using racemic 2-pentyl-2,3-epoxycyclopentanone and complex **1b** in the presence of 35% H₂O₂. GLC analysis in the presence of an internal reference (cyclooctane) revealed no reaction. Therefore, a tentative explanation can be offered only for catalysts **2b–e**, which constitute the majority of the catalysts tested and where the nature of the active species involved in the oxygen-transfer step is still undefined. The complexity of the catalyst activation process evidenced in a previous paper¹¹ leads to the formation of a variety of potential catalytically active intermediates. These may produce opposing effects on the asymmetric induction, and this fact may be a possible explanation for the observed loss of optical purity.

Conclusions

The results reported in this work represent the *first successful example of transition-metal catalysis* applied to the Weitz–Scheffer oxidation reaction. Given the nature of the carbon–carbon double bond in α,β -unsaturated ketones, this is undoubtedly due to the unique ability of the Pt(II) catalysts here reported to increase the nucleophilicity of hydrogen peroxide. Although the potential applications seem limited by the low selectivity displayed in some cases and attributed to the acidity generated by the catalysts, the system

seems promising and deserves further investigation. This is particularly important with respect to the enantioselective epoxidation, since it represents the first example of asymmetric catalysis applied to this class of substrates and the intrinsic enantioselective properties of the catalysts, as demonstrated by the stoichiometric reactions, appear to be interesting.

Experimental Section

Apparatus. IR spectra were taken on a Perkin-Elmer 683 spectrophotometer and on a Digilab FTS 40 interferometer either in Nujol mulls using CsI plates or in CH₂Cl₂ solution using CaF₂ windows. GLC measurements were taken on a Hewlett-Packard 5790A gas chromatograph equipped with a 3390 automatic integrator. GLC–MS measurements were performed on a Hewlett-Packard 5971 mass selective detector connected to a Hewlett-Packard 5890 II gas chromatograph. Identification of products was made with GLC or GLC–MS by comparison with authentic samples. Optical rotation measurements were performed on a Perkin-Elmer 241 polarimeter operating at 589 nm.

Materials. Solvents were dried and purified according to standard methods. α,β -Unsaturated ketone substrates were purified by passing through neutral alumina, prior to use. 1,4-Naphthoquinone was purified by recrystallization from EtOH; methyl vinyl ketone was distilled in vacuo and stored at 0 °C. Hydrogen peroxide (35% from Fluka), 90% *m*-chloroperbenzoic acid (MCPBA, Janssen), 85% *t*-BuOOH (Aldrich), dppe, *o*-dppb, *R*-prophos, and *S,S*-chiraphos (Strem), *R,R*-pyrphos (Degussa), and *S*-binap (Janssen) were commercial products and were used without purification.

The following compounds were prepared according to literature procedures: [(dppe)Pt(CF₃)(CH₂Cl₂)]BF₄,¹⁷ [(*o*-dppb)Pt(CF₃)(CH₂Cl₂)]BF₄,^{10b} [(*S,S*-chiraphos)Pt(CF₃)(CH₂Cl₂)]BF₄,^{10a} [(*R,R*-pyrphos)Pt(CF₃)(CH₂Cl₂)]BF₄,^{10b} (dppe)Pt(2-van),¹² (*R,R*-pyrphos)Pt(2-van),¹¹ (*S,S*-chiraphos)Pt(2-van),¹¹ (*R*-prophos)-Pt(2-van),¹¹ and (*S*-binap)Pt(2-van).¹¹

Synthesis of Epoxy Ketones. Epoxy ketones used as standards for gas chromatographic determinations in the individual catalytic reactions were synthesized¹⁸ from the starting α,β -unsaturated ketone (10 mmol) in 10 mL of MeOH (or THF), to which 30 mmol of 35% H₂O₂ was added under N₂ with stirring at 0 °C. After a few minutes 30 μ L of a 10% aqueous solution of NaOH was added, and after ~30 min the solution was extracted from CH₂Cl₂/H₂O. The dry organic phase containing 45–60% epoxy ketone was used for qualitative identification and for the determination of the separation conditions of the lactone enantiomers on the chiral β -cyclodextrin GC column.

In the cases of the epoxidation of α -ionone, β -ionone, *trans*-chalcone, and isophorone, *t*-BuOOH was used instead of H₂O₂.

Catalytic Reactions. These were carried out in a 25 mL round-bottomed flask equipped with a stopcock for vacuum/N₂ operations and a side arm fitted with a screw-capped silicone septum to allow sampling. Constant temperature (± 0.1 °C) was maintained by water circulation through an external jacket connected with a thermostat. For reactions carried out at temperatures >25 °C the reaction vessel was equipped with a reflux condenser. Stirring was performed by a Teflon-coated bar driven externally by a magnetic stirrer. Absence of diffusional problems below the 3×10^{-4} M s⁻¹ initial rate was determined by the conversion vs time plot independence of the stirring rate in randomly selected catalytic experiments. The concentration of the commercial H₂O₂ solution was checked iodometrically prior to use.

The following general procedure was followed. The required amount of catalyst was placed as the solid in the reactor, which

(17) Michelin, R. A.; Napoli, M.; Ros, R. *J. Organomet. Chem.* **1979**, *175*, 239.

(18) MacAlpine, G. A.; Warkentin, J. *Can. J. Chem.* **1978**, *56*, 308.

was evacuated and filled with N₂. Purified, N₂-saturated substrate was added under N₂ flow, followed, if necessary, by the required amounts of solvent. After it was thermostated at the required temperature with stirring for a few minutes, the H₂O₂ solution in the appropriate amount was injected through the septum and the time was started. When (P-P)-Pt(2-van) catalysts were used, an amount of 70% HClO₄ equivalent to the amount of catalyst was added prior to H₂O₂ addition. The solution was stirred for 1 h, and then H₂O₂ was injected.

All reactions were monitored with GLC by direct injection of samples taken periodically from the reaction mixtures with a microsyringe. Where appropriate, initial rate data were determined from conversion vs time plots. Prior quenching of the catalyst with LiCl did not show any differences in randomly selected analyses. Separation of the products was performed on 25 m HP-5 capillary columns using a flame ionization detector.

The amount of residual H₂O₂ at different times was determined by sampling 10 μL aliquots from the aqueous phase. These were diluted in water and titrated iodometrically.

Determination of ee. The ee values during the catalytic reaction were determined by GLC using a 25 m Chrompack

CP-β-cyclodextrin-2,3,6-M-19 capillary column. Since even for racemic mixtures there is an apparent ee which depends on the peak area, a calibration curve (apparent ee/peak area) was first determined using the racemic lactones synthesized according to the above procedure. This calibration curve was used to correct the experimental values obtained in the enantioselective reactions. ee data reported in Tables 3 and 4 for short times refer to the first detectable amount of product formed after addition of H₂O₂.

Acknowledgment. This work was supported jointly by MURST (40% programs) and the CNR (Progetto Finalizzato Chimica Fine II). Thanks are expressed to Professor O. De Lucchi of this department and Professor F. Di Furia (University of Padova) for many helpful discussions and to Dr. M. Selva for help in the interpretation of the mass spectra. We thank also Miss T. Fantinel for skillful technical assistance.

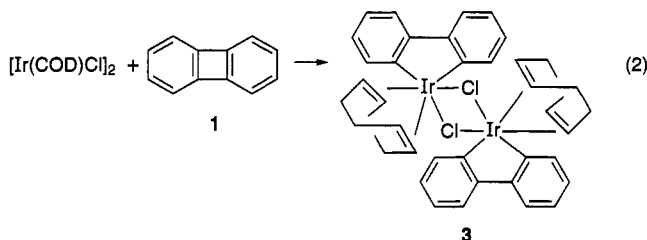
OM940537J

showed that some of the Ir(III) complexes can be oxidized quasi-reversibly to Ir(IV) species, one of which can also be isolated. The EPR spectroscopic data confirmed that the oxidation is metal-centered. We also interpreted the easy oxidation of {Ir(biph)} complexes using extended Hückel (EHT) studies. Part of this work has appeared as a communication.^{8c}

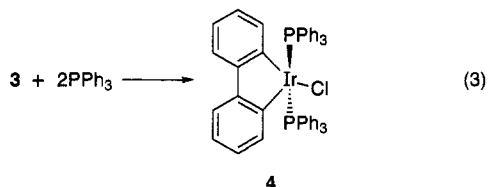
Results and Discussion

Heats of combustion¹² and quantum-chemical calculations¹³ show that biphenylene has a relatively low resonance energy of about 15 kcal/mol. X-ray diffraction studies¹⁴ suggest that the central ring of biphenylene has little delocalization. The distances of the C–C bonds joining the two phenylene groups are 1.52 Å, close to a C–C single bond, while the other two bond-lengths in the central four-membered ring are 1.46 Å. The strain energy of the four-membered ring is high, about 63 kcal/mol.¹⁵ This facilitates making a metallacycle from biphenylene by breaking one of the two C–C bonds linking the two phenyl groups.

Preparation and Structure of [Ir^{III}(PPh₃)₂(biph)Cl] (4). Biphenylene (1) reacts with [Ir(COD)Cl]₂ at 90 °C over 2 h in CH₂Cl₂ (sealed tube) to give [Ir(COD)(biph)Cl]₂ (3; 89%, eq 2) as a yellow powder by a known



type⁵ of C–C cleavage reaction. The reaction is probably driven by the large ring strain. No reaction was observed under milder thermal conditions, however: for example, reflux in CH₂Cl₂ for 2 days. 3 does not dissolve in any organic solvent, and we are therefore unable to recrystallize it or to obtain any spectroscopic data to confirm the ring-opened structure. Replacement of COD by PPh₃ can be achieved by reaction at room temperature for 5 h in CH₂Cl₂ to give [Ir(PPh₃)₂(biph)Cl] (4; eq 3). This complex was isolated in high yield



(90%) as air-stable red crystals. ¹H and ³¹P NMR data show that 4 has only two bound PPh₃ groups, suggesting that 4 has a five-coordinate (16-electron) geometry. The sixth site in 4 cannot be saturated by addition of PPh₃,

(12) Cass, R. C.; Springall, H. D.; Quincey, P. G. *J. Chem. Soc.* **1955**, 1188.

(13) Dewar, M. J. S. *The Molecular Orbital Theory of Organic Chemistry*; McGraw-Hill: New York, 1969.

(14) Mark, T. C. W.; Trotter, J. *Proc. Chem. Soc. London* **1961**, 163.

(15) Cava, M. P.; Mitchell, M. J. *Cyclobutadienes and Related Compounds*; Academic Press: New York, 1967.

(16) Esteruelas, M. A.; Werner, H. *J. Organomet. Chem.* **1986**, 303, 221. Milstein, D. *J. Am. Chem. Soc.* **1982**, 104, 5227. Wright, S. C.; Baird, M. C. *J. Am. Chem. Soc.* **1985**, 107, 6899.

Table 1. X-ray Crystallographic Data for [Ir(PPh₃)₂(biph)Cl] (4)

formula	C ₄₈ H ₃₈ ClP ₂ Ir
space group	P2 ₁ /c (No. 14)
a, Å	23.259(2)
b, Å	18.955(2)
c, Å	19.096(2)
β, deg	114.143(9)
V, Å ³	7682(3)
mol wt	904.45
ρ _{calcd} , g/cm ³	1.564
Z	8
T, °C	23
scan type	ω-2θ
max 2θ, deg	50.0
no. of data used	8026
no. of params refined	937
esd of unit wt	1.39
radiation	Mo Kα (λ = 0.710 69 Å)
convergence, largest shift/error	0.20
R	0.035 ^a
R _w	0.039

^a Function minimized: $R = \sum ||F_o| - |F_c|| / \sum |F_o|$ and $R_w = [\sum w(|F_o| - |F_c|)^2 / \sum w F_o^2]^{1/2}$, where $w = 4F_o^2 / \sigma^2(F_o^2)$.

Table 2. Selected Bond Distances (Å) and Angles (deg) for 4

Bond Distances			
Ir–Cl	2.380(3)	Ir–C(12)	2.00(1)
Ir–P(1)	2.345(3)	C(1)–C(6)	1.43(1)
Ir–P(2)	2.342(3)	C(6)–C(7)	1.44(1)
Ir–C(1)	2.00(1)	C(7)–C(12)	1.40(1)
Bond Angles			
Cl–Ir–P(1)	92.92(9)	P(1)–Ir–C(1)	89.6(3)
Cl–Ir–P(2)	90.40(9)	P(1)–Ir–C(12)	87.7(3)
Cl–Ir–C(1)	131.1(3)	P(2)–Ir–C(1)	92.4(3)
Cl–Ir–C(12)	151.4(3)	P(2)–Ir–C(12)	86.8(3)
P(1)–Ir–P(2)	173.5(1)	C(1)–Ir–C(12)	77.4(4)

regardless of the amount added (1–20 equiv/Ir). This may reflect the steric bulk of the PPh₃ ligand. The ring-opened structure of 4 was further characterized by X-ray crystallographic studies (Figure 1).

X-ray Crystallographic and Geometric Studies on 4. X-ray-quality single crystals of 4 were obtained by slowly evaporating a CH₂Cl₂ solution. The resulting crystallographic data (Table 1) were solved, and an ORTEP diagram of the structure is shown in Figure 1. Selected bond distances and angles are listed in Table 2. As shown in Figure 1, 4 has an electron- and ligand-deficient five-coordinate geometry.

The bond angles Cl–Ir–C(1) (131.1°), Cl–Ir–C(12) (151.4°), and C(1)–Ir–C(12) (77.4°) differ from each other and from the value of 120° characteristic of a five-coordinate TBP structure.

Several d⁶ Ir^{III}(PR₃)₂ZZ'X systems similar to ours have been studied by EHT and ab initio calculations.¹⁷ It has been shown that the TBP structure is unfavorable for a diamagnetic d⁶ configuration because the e' set is only partially filled. A geometrical distortion of the three equatorial ligands (ZZ'X) leading to the stabilization of one of the two e' orbitals and thus to an opening of the HOMO–LUMO gap has been found to be favorable. The equatorial ligand arrangements for each case are as follows:

(17) (a) Rachidi, I. E.-I.; Eisenstein, O.; Jean, Y. *New J. Chem.* **1990**, 14, 671. (b) Riehl, J.-F.; Jean, Y.; Eisenstein, O.; Pélissier, M. *Organometallics* **1992**, 11, 729. (c) Albinati, A.; Bakmutov, V. I.; Caulton, K. G.; Clot, E.; Eckert, J.; Eisenstein, O.; Gusev, D. G.; Grushin, V. V.; Hauger, B. E.; Klooster, W.; Koetzle, T. F.; McMullan, R. K.; O'Loughlin, T. J.; Pélissier, M.; Ricci, J. S.; Sigalas, M. P.; Vymenits, A. B. *J. Am. Chem. Soc.* **1993**, 115, 7300.

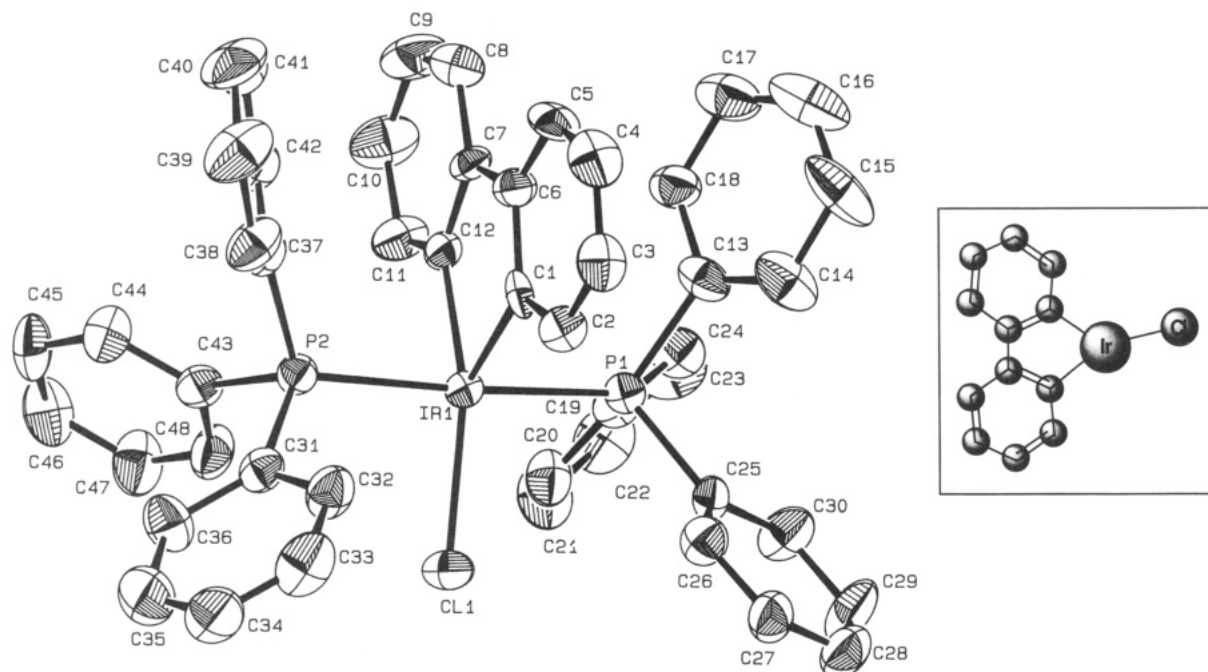
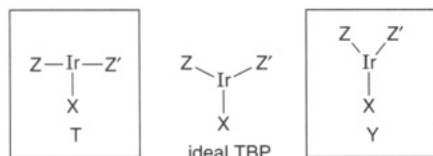


Figure 1. ORTEP drawing of $[\text{Ir}(\text{PPh}_3)_2(\text{biph})\text{Cl}]$ (**4**) with the (biph)IrCl fragment in the insert. Hydrogen atoms are omitted for clarity.



The two axial ligands, not shown, lie above and below the plane of the page. The Z, Z', and X ligands take up a Y or T shape. For equatorial ligands that are pure σ donors the T shape is preferred and the ligand (Z for instance) with the highest σ -donating ability occupies the site which is at the foot of the T (a structure called T_Z). In contrast, if X is a π donor and if the Z and Z' ligands do not themselves carry any π orbitals, a Y structure with the X ligand at the foot of the Y (Y_X) becomes more stable. In this structure, a π bond between one of the lone pair of the π -donor ligand X and the metal empty orbital can be established and leads to electron transfer from X to the electron-deficient complex. This metal-X π bond is the factor responsible for the stability of the Y_X structure. The stabilization is however small in magnitude, especially for weak π -donor ligands such as Cl, and it has been shown that the Y structure lies in a shallow valley.¹⁷ This valley connects the Y_X minimum to a structure of $T_{Z(Z')}$ type with Z (or Z') at the foot of the T. In T_Z the π bond between X and the metal cannot be established since all symmetry-adapted d (xy , xz , yz) orbitals are filled. The small energy difference between Y_X and T_Z comes from the competition between the π effect, which leads to a preference for Y_X , and the σ -donating effect of Z, which leads to a preference for T_Z . This last T structure has not been found as a minimum on the potential energy surface (PES), but the presence of constraints such as steric factors in the system have been shown to displace the absolute minimum from a pure Y_X structure (with a C_{2v} symmetry when $Z = Z'$) to a situation intermediate between Y_X and T_Z .^{17c} Any other constraint, such as a rigid bite angle within the equatorial ligands, would necessarily produce a similar displace-

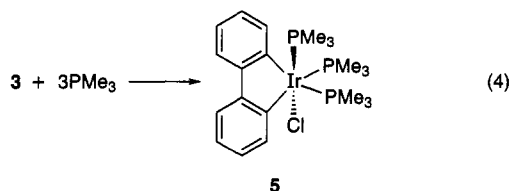
ment of the minimum away from the C_{2v} structure if the angle between the two constrained ligands does not correspond to the angle calculated for the optimal structure.

In the previous ab initio calculations on the model complex $[\text{Ir}(\text{PH}_3)_2\text{ClMe}_2]$ it was found that the Y_{Cl} type structure was the most stable.¹⁷ The calculated C-Ir-C angle is 81.9° , close to that in complex **4**. EHT calculations were performed on the model complex $\text{Ir}(\text{biph})\text{Cl}(\text{PH}_3)_2$.¹⁸ Because the C-Ir-C angle (77.4°) in $\text{Ir}(\text{biph})$ does not correspond to the optimal C-Ir-C angle for two monodentate Ir-C bonds, the C_{2v} Y_{Cl} structure is not calculated to be the minimum. A slightly distorted form in which the Cl group lies off the C_2 axis is preferred. The structure is thus an intermediate between the Y_{Cl} and T_{C} forms, where T_{C} describes a geometry in which one of the carbons of the biph ring is at the foot of the T structure. The angle between the C_2 axis and the Ir-Cl bond was calculated to be 23° , which is in fair agreement with the experimental value (10.3°). If the Cl is replaced by a pure σ donor, such as H, the resulting calculated structure lies much closer to a T. A similar distortion has been discussed for a Rh(III) metallacyclic complex.¹⁹ As a result of the existence of the Ir-Cl π bond in a structure of Y type (or very close to it), the Ir-Cl bond length (2.38 Å) is shorter than the sum of the covalent radii of the Ir and Cl atoms (2.45 Å).

Preparation of $[\text{Ir}^{\text{III}}(\text{PMe}_3)_3(\text{biph})\text{Cl}]$ (5**).** Treatment of **3** with PMe_3 in CH_2Cl_2 at room temperature under nitrogen affords $[\text{Ir}(\text{PMe}_3)_3(\text{biph})\text{Cl}]$ (**5**) as an air-stable white powder (eq 4). The biph group is therefore stable to reductive elimination under these conditions. The coordination site of the Cl group in **5**, determined by ^{31}P NMR (δ -42.29, d, 2P; -54.70, t, 1P), is axial, not equatorial, as in the case of $[\text{Ir}(\text{PPh}_3)_2(\text{biph})\text{Cl}]$ (**4**).

(18) Ammeter, J. H.; Bürgi, H.-B.; Thibault, J. C.; Hoffmann, R. *J. Am. Chem. Soc.* **1978**, *100*, 3686. Atomic parameters for Ir are taken from ref 17.

(19) Thorn, D. L.; Hoffmann, R. *Nouv. J. Chem.* **1979**, *3*, 39.

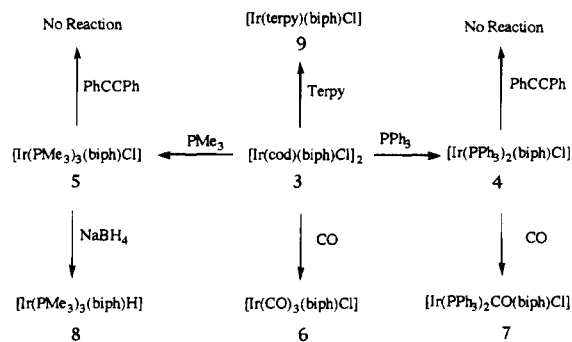


This may be a result of the lower steric bulk of PMe_3 versus PPh_3 and perhaps the larger trans effect of PR_3 versus Cl .²⁰

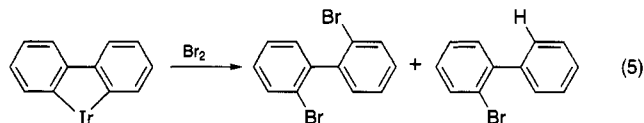
Reactivity of {Ir(biph)} Complexes. If biph is to be a useful ligand, it should be stable under a variety of conditions. We find that the {Ir(biph)} group of **3** can persist unchanged on treatment with CO , PhCCPh , PR_3 , or NaBH_4 . The reaction of **3** with CO gives the unstable compound $[\text{Ir}(\text{CO})_3(\text{biph})\text{Cl}]$ (**6**), but the CO insertion product fluorenone is not formed, even on heating (CH_2Cl_2 , 90°C). The IR spectroscopic data ($\nu(\text{CO})$ 2155, 2116, and 2092 cm^{-1}) suggest that **6** has a meridional structure. The instability of this complex is consistent with the unusually high-energy CO absorptions in the IR which occur at a frequency close to that of free CO (2143 cm^{-1}), indicating that metal to CO back-bonding is weak. **4** does not react with H_2 or PPh_3 but reacts rapidly with CO at room temperature to form $[\text{Ir}(\text{PPh}_3)_2(\text{biph})(\text{CO})\text{Cl}]$ (**7**; $\nu(\text{CO})$ 2001 cm^{-1}). Other small donor molecules such as NH_3 can also react with **4** in a similar way.

As shown in Scheme 1, **6** and NaBH_4 (CH_2Cl_2 -EtOH,

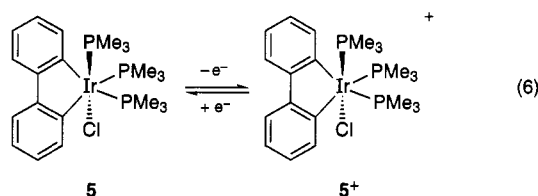
Scheme 1. Reactivities of {Ir(biph)} Complexes



90°C , 5 h) give $[\text{Ir}(\text{PMe}_3)_3(\text{biph})\text{H}]$ (**8**; 68%). The hydride in **8** is cis to both biph Ir-C bonds, as shown by ^1H NMR (Ir-H, -11.05 ppm , $J(\text{H,P trans}) = 133\text{ Hz}$, $J(\text{H,P cis}) = 22.7\text{ Hz}$). Reductive elimination with the cis hydride is not observed under our conditions. The reaction of **3** with 2,2',2''-terpyridine (terpy) did not cleave the Ir-C bond of the metallacycle but gave the new complex $[\text{Ir}(\text{terpy})(\text{biph})\text{Cl}]$ (**9**). **9** has an unusually well-resolved ^1H NMR, showing the aromatic protons at chemical shifts ranging from 5.6 to 8.8 ppm. Treatment of **9** with AgBF_4 in CH_2Cl_2 under a CO atmosphere gives $[\text{Ir}(\text{terpy})(\text{biph})\text{CO}]$ (**9a**) with $\nu(\text{CO})$ 2059 cm^{-1} . Of all the reagents we have used, only Br_2 cleaves the Ir-C bond of the {Ir(biph)} group. In the best-studied case, $[\text{Ir}(\text{COD})(\text{biph})(\text{O}_2\text{CCF}_3)]$, formed from **3** and AgO_2CCF_3 , reacts with Br_2 to give 2,2'-dibromobiphenyl (50%) and 2-bromobiphenyl (49%) (eq 5).



Electrochemical Studies. The quasi-reversible electrochemical reduction of $[\text{Pt}(\text{biph})(\text{bpy})]$ has been briefly reported,⁵ but in this case it is unclear which of the two ligands, bpy or biph, promotes the observed redox activity. In many of our {Ir(biph)} complexes we find that biph alone can promote electrochemical oxidation to give stable odd-electron Ir(IV) complexes. For example, the CV of **5** in CH_2Cl_2 showed a quasi-reversible ($\Delta E = 108\text{ mV}$) diffusion-controlled oxidation wave at $E = 836\text{ mV}$ vs SCE (Figure 2a). Multiple-cycle experiments show that no new species are formed having CV waves in the region of 0.0–1.0 V. The number of electrons transferred, determined by exhaustive electrolysis, was $1.0 \pm 0.1\text{ e}$. The resulting Ir(IV) species, which can also be generated by bulk electrolysis (eq 6), has been detected by its EPR ($g_x = 2.37$, $g_y =$



2.28, $g_z = 1.84$; Figure 3). The reversibility of the CV suggests that this Ir(IV) cation is best formulated as $[\text{Ir}^{\text{IV}}(\text{PMe}_3)_3(\text{biph})\text{Cl}]^+$ (**5⁺**). Isolation and crystallization of **5⁺** was unsuccessful, probably as a result of decomposition.

The 16 e complex $[\text{Ir}(\text{PPh}_3)_2(\text{biph})\text{Cl}]$ (**4**) also showed quasi-reversible one-electron oxidation in CH_2Cl_2 at room temperature, but the oxidation wave shifts to 950 mV vs SCE, a potential more positive than in **5** (Figure 2b). This shift indicates that the 16 e Ir(III) system is more electron-deficient than **5**. The resulting Ir(IV) product was not stable enough for detection by EPR in this case. The CV of $[\text{Ir}(\text{PPh}_3)_2(\text{biph})(\text{CO})\text{Cl}]$ (**7**) in CH_2Cl_2 showed an even more positive oxidation wave at 1120 mV vs SCE, reflecting the strong back-donation from Ir to CO which makes the Ir even more electron-deficient. The complex $[\text{Ir}(\text{terpy})(\text{biph})\text{Cl}]$ (**9**), formed in the reaction of **3** with terpy in methanol, shows only an irreversible oxidation wave at 930 mV but a nearly reversible reduction wave at -1.47 V vs SCE ($\Delta E = 77.2\text{ mV}$).

The EHT calculations suggest²¹ that the easy oxidation of the biph system is due to the presence of a high-energy HOMO. The highest filled π level of biph combines in an antibonding way with the filled Ir yz orbital, which results in a high-lying HOMO with large metal character (Figure 4). Good overlap and a good energy match between the metal d and π ligand orbitals are responsible for the strong destabilization of the HOMO.

In the case of complex **5**, the axial Cl group can also interact with the Ir yz orbital. One of the lone pairs of Cl further destabilizes the yz orbital by mixing into this

(20) (a) Hel'man, A. D.; Karandashova, E. F.; Essen, L. N. *Dokl. Akad. Nauk. SSSR*, **1948**, *63*, 37. (b) Basolo, F.; Pearson, R. G. *Prog. Inorg. Chem.* **1962**, *4*, 381. (c) Pidcock, A. *J. Chem. Soc. A* **1966**, 1707.

(21) Lu, Z.; Jun, C.-H.; de Gala, S. R.; Sigalas, M.; Eisenstein, O.; Crabtree, R. H. *J. Chem. Soc., Chem. Commun.* **1993**, 1877 (supplementary material).

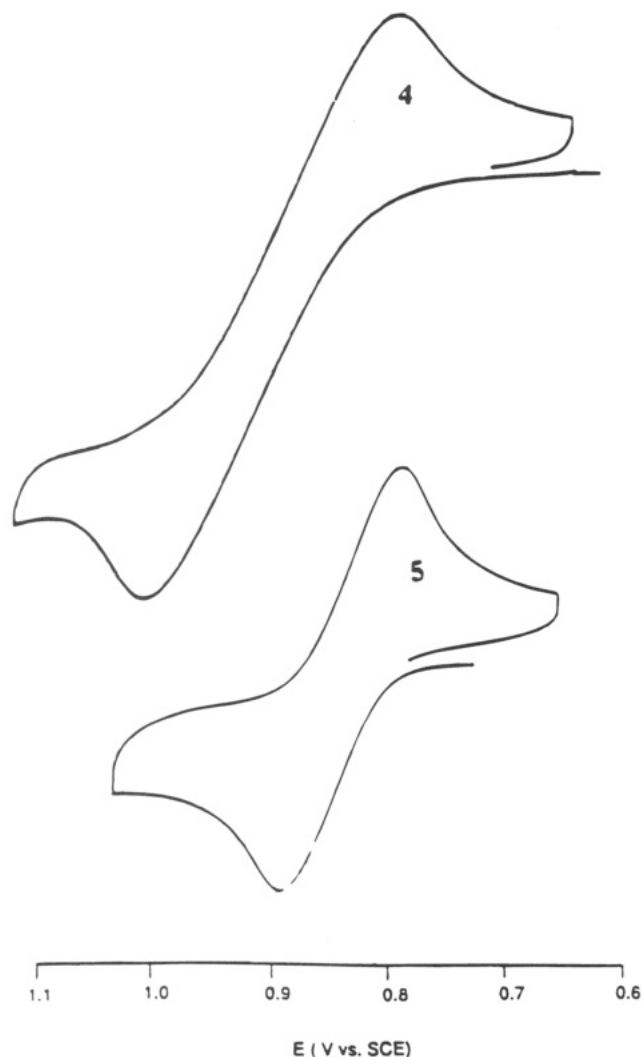


Figure 2. Comparative cyclic voltammetry of 1.0×10^{-3} mol/L $[\text{Ir}(\text{PPh}_3)_2(\text{biph})\text{Cl}]$ (**4**) and 3.0×10^{-4} mol/L $[\text{Ir}(\text{PMe}_3)_3(\text{biph})\text{Cl}]$ (**5**).

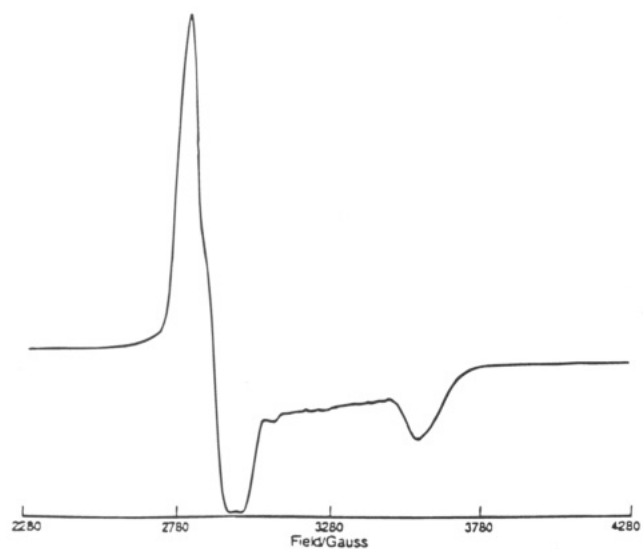


Figure 3. X-Band EPR spectrum of $[\text{Ir}(\text{PMe}_3)_3(\text{biph})\text{Cl}]^+$ (**6**⁺) at 7 K.

molecular orbital in an antibonding fashion. This suggests why **5** can be oxidized more easily than compound **4** and permits the occurrence of an Ir(IV) structure.

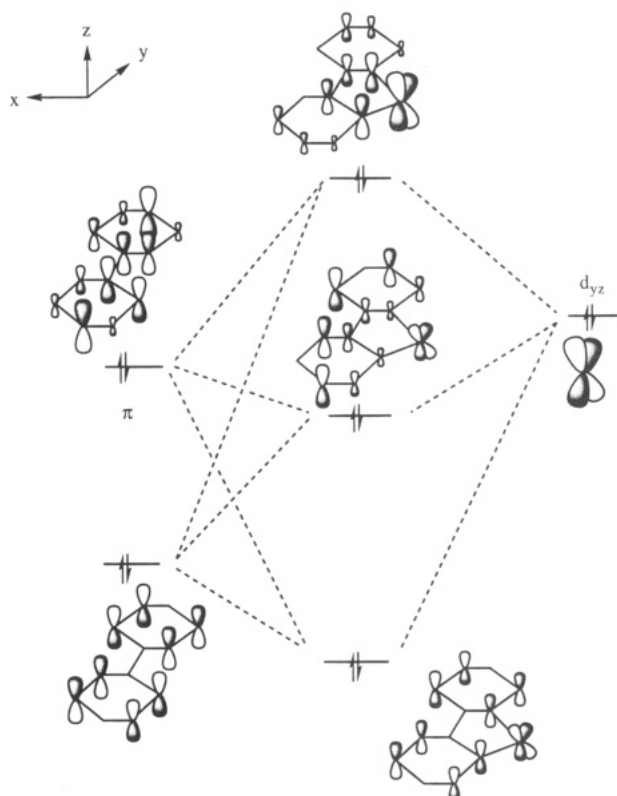
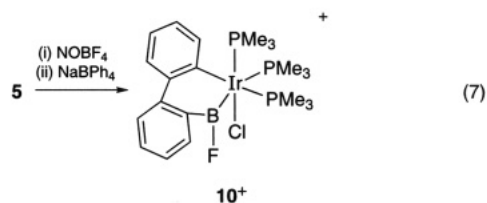


Figure 4. Orbital interaction in $[\text{Ir}(\text{PMe}_3)_3(\text{biph})\text{Cl}]$ (**6**) derived from EHT studies.

Synthesis, Characterization, and Crystal Structure of $[\text{Ir}^{\text{IV}}(\text{PMe}_3)_3(\text{biphBF})\text{Cl}]$ (10**⁺).** In aiming for oxidation catalysts involving air, we wondered whether it would be possible to make a stable $\{\text{Ir}^{\text{IV}}(\text{biph})\}$ system. Complex **5**⁺ formed by bulk electrolysis of **5** could not be obtained in crystalline form. A rapid reaction occurred, however, when **5** was treated with NOBF_4 in CH_2Cl_2 to give a dark greenish solution, which gave a dark brown solid on isolation. This new complex gives EPR signals ($g_{xy} = 2.15$ and $g_z = 1.96$; Figure 5) different from those for **5**⁺. Stable crystals of the product $[\text{Ir}(\text{PMe}_3)_3\text{Cl}(\text{biphBF})][\text{BPh}_4]$ (**10** $[\text{BPh}_4]$) are formed in 46% yield after isolation with NaBPh_4 (eq 7). NaBPh_4



provides the essential large counterion needed to obtain crystals. The X-ray crystal structure (Figure 6) shows it to be an Ir(IV) organometallic boryl compound with a BF unit inserted into one of the Ir–C bonds. Organometallic Ir(IV) complexes are not common,²² and no Ir(IV) boryl compounds have been reported.²³ This insertion may take place via electrophilic attack of BF_3 , which could come from either NOBF_4 or BF_4^- , on the Ir–Ar bond. High-resolution mass spectroscopy confirms the formulation, both from the mass of the molecular ion peak of **10**⁺ (638.1344 amu, observed; 638.1347 amu, calculated) and from its characteristic seven-line isotope pattern (computer simulation), which cannot be accommodated by any other group than BF.

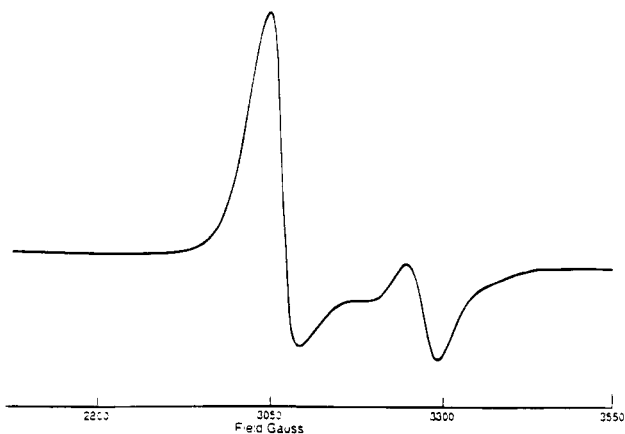


Figure 5. X-Band EPR spectrum of $[\text{Ir}(\text{PMe}_3)_3(\text{biphBF})\text{Cl}]^+$ (10^+) at 5 K.

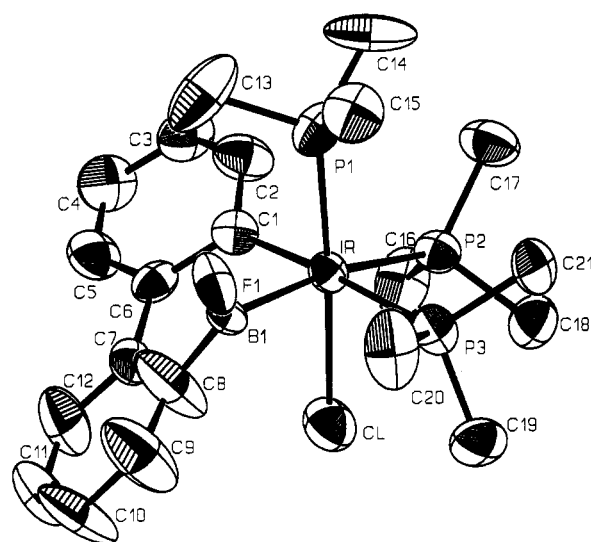


Figure 6. ORTEP drawing of $[\text{Ir}(\text{PMe}_3)_3\text{Cl}(\text{biphBF})]^+$ (10^+). Hydrogen atoms are omitted for clarity.

A single crystal of $10[\text{BPh}_4]$ was obtained from slow diffusion of diethyl ether into a solution of $10[\text{BPh}_4]$ in CH_2Cl_2 . The resulting data (Table 3) were solved by using Patterson methods to give the ORTEP diagram shown in Figure 6. The BPh_4^- counterion is not shown for clarity. Selected bond distances and angles are listed in Table 4.

The electron density map showed a very unusual structure with a BF group in the six-membered metallacyclic ring. As expected, the structure shows a coplanar arrangement of the boryl group (F, B, Ir, and C atoms). The $\text{C}_6\text{H}_4\text{B}-\text{F}$ fragment shows unusually

(22) (a) Hay-Motherwell, R. S.; Wilkinson, G.; Hussain-Bates, B.; Hursthouse, M. B. *Polyhedron* **1991**, 1457. (b) Hay-Motherwell, R. S.; Wilkinson, G.; Hussain-Bates, B.; Hursthouse, M. B. *J. Chem. Soc., Dalton Trans.* **1992**, 3477. (c) Serpone, N.; Jamieson, M. A. In *Comprehensive Coordination Chemistry*; Wilkinson, G., Ed.; Pergamon Press: Oxford, U.K., 1987; Vol. 4. (d) Gulliver, D. J.; Levason, W. *Coord. Chem. Rev.* **1982**, 46, 1. (e) Leigh, G. J.; Richards, R. L. In *Comprehensive Organometallic Chemistry*; Wilkinson, G., Ed.; Pergamon Press: Oxford, U.K., 1982; Vol. 5. (f) Zemva, B.; Lutar, K.; Jesih, A.; Casteel, W. J.; Bartlett, N. *J. Chem. Soc., Chem. Commun.* **1989**, 346.

(23) (a) Schmid, G.; Nöth, H. *Angew. Chem., Int. Ed. Engl.* **1963**, 2, 623. (b) Baker, R. T.; Ovenall, D. W.; Calabrese, J. C.; Westcott, S. A.; Taylor, N. J.; Williams, I. D.; Marder, T. B. *J. Am. Chem. Soc.* **1990**, 112, 9399. (c) Knorr, J. R.; Merola, J. S. *Organometallics* **1990**, 9, 3008. (d) Westcott, S. A.; Taylor, N. J.; Marder, T. B.; Baker, R. T.; Jones, N. J.; Calabrese, J. C. *J. Chem. Soc., Chem. Commun.* **1991**, 304. (e) Hartwig, J. F.; Huber, S. *J. Am. Chem. Soc.* **1993**, 115, 4908.

Table 3. X-ray Crystallographic Data for $[\text{Ir}(\text{PMe}_3)_3(\text{biphBF})\text{Cl}]^+$ (10^+)

formula	$\text{C}_{45}\text{H}_{55}\text{B}_2\text{FP}_3\text{ClIr}$
fw	957.14
cryst habit	dark brown cut plate
space group	$P2_1/n$ (No. 14)
a , Å	9.689(2)
b , Å	35.555(6)
c , Å	12.576(2)
β , deg	94.44(1)
V , Å ³	4320(2)
Z	4
ρ_{calcd} , g/cm ³	1.472
$F(000)$	1932
$\mu(\text{Mo K}\alpha)$, cm ⁻¹	32.85
radiation	Mo K α ($\lambda = 0.71069$ Å)
T , °C	23
scan type	$2\theta/\omega$
max 2θ , deg	49.9
no. of unique rflns	7841
cor	Lorentz-polarization (transmission factor 0.71-1.29; -28% decline)
no. of observns	4459
R	0.051 ^a
R_w	0.061

^a Function minimized $\sum w(|F_o| - |F_c|)^2$, where least-squares weights $w = 4F_o^2/\sigma^2(F_o)^2$.

Table 4. Selected Bond Distances (Å) and Angles (deg) for 10^+

Bond Distances			
Ir-Cl	2.504(4)	F(1)-B(1)	1.09(1)
Ir-P(1)	2.333(4)	C(8)-B(1)	1.47(2)
Ir-P(2)	2.348(3)	C(1)-C(6)	1.42(2)
Ir-P(3)	2.432(3)	C(6)-C(7)	1.48(2)
Ir-C(1)	2.07(1)	C(7)-C(8)	1.39(2)
Ir-B(1)	2.00(1)		
Bond Angles			
Cl-Ir-P(1)	176.5(1)	P(2)-Ir-P(3)	92.3(1)
Cl-Ir-P(2)	78.9(1)	P(2)-Ir-B(1)	165.5(4)
Cl-Ir-P(3)	87.6(1)	P(2)-Ir-C(1)	88.5(3)
Cl-Ir-C(1)	88.7(4)	P(3)-Ir-C(1)	176.0(4)
Cl-Ir-B(1)	87.3(4)	P(3)-Ir-B(1)	91.5(4)
P(1)-Ir-P(2)	102.6(1)	C(1)-Ir-B(1)	86.7(5)
P(1)-Ir-P(3)	95.5(1)	Ir-B(1)-F(1)	118(1)
P(1)-Ir-C(1)	88.2(4)	Ir-B(1)-C(8)	114(1)
P(1)-Ir-B(1)	90.9(5)	F(1)-B(1)-C(8)	127(2)

large anisotropic thermal ellipsoids, probably due to conformational flexibility of the metallacycle. This leads to an artificially short B-F distance of 1.09 Å (the sum of covalent radii of B and F is 1.26 Å), which should not be regarded as well determined. No disorder model we tried was satisfactory.

The structure of 10^+ is essentially octahedral, with the Cl and one of the PMe_3 groups axial. The Ir-Cl bond, which is now cis to the biphBF group, shows a lengthened distance (2.504 Å) as a result of the trans effect of the PMe_3 group. The observed Ir-P(3) bond distance (2.43 Å) is unusual, being longer than that of the other Ir-P bonds (2.33-2.35 Å), suggesting that an aryl group may have a stronger trans effect than a boryl group.

Catalytic Activity. Unlike complexes of most other unsaturated metallacycles,^{22,23} our biph complexes can survive reaction conditions commonly used in catalytic chemistry, showing the stability of the $\{\text{Ir}(\text{biph})\}$ group. As we have published elsewhere,²⁴ 4 and 5 are active

(24) Jun, C.-H.; Lu, Z.; Crabtree, R. H. *Tetrahedron Lett.* **1992**, 33, 7119.

catalysts for the unusual head-to-head dimerization of terminal alkynes.

Conclusion. We have synthesized and characterized a series of new iridium complexes which are obtained from a C–C bond cleavage of biphenylene. Rather than having a pure T or Y structure, the d^6 five-coordinate species $[\text{Ir}(\text{PPh}_3)_2(\text{biph})\text{Cl}]$ has an intermediate structure. EHT calculations suggest that this is caused by the angular constraint within the rigid biph group. The complex $[\text{Ir}(\text{PMe}_3)_3(\text{biph})\text{Cl}]$ has a quasi-reversible CV with an oxidation wave at 836 mV vs SCE and can be oxidized to an Ir(IV) species by bulk electrolysis. The unusual Ir(IV) boryl complex $[\text{Ir}(\text{PMe}_3)_3(\text{biphBF})\text{Cl}]$ was produced when $[\text{Ir}(\text{PMe}_3)_3(\text{biph})\text{Cl}]$ was treated with NOBF_4 . The insertion of the BF group probably occurs via an electrophilic attack of BF_3 on an Ir–C bond of the metallacycle. Calculations suggest that the easy oxidation of a Ir(biph) system is a result of the metal-centered HOMO of the molecule being high-lying as a consequence of the repulsive interaction between an occupied π orbital of biph and an occupied Ir yz orbital. This permits the existence of an Ir(IV) form. The biph system seems suitable for use as a stabilizing ligand in organometallic chemistry, where it can promote redox and catalytic activities in its metal complexes.

Experimental Section

General Considerations. All manipulations were carried out under a nitrogen atmosphere. Solvents such as dichloromethane, diethyl ether, and toluene were distilled from calcium hydride or sodium benzophenone ketyl. All the reagents were used as received without further purification.

Spectroscopy. Samples for EPR studies were prepared by taking a CH_2Cl_2 solution of the complex (**10**) or from the bulk electrolysis experiment (**5**⁺) under an Ar atmosphere and freezing to -77°C . In order to form a good glass, an equal volume of toluene was added. Continuous-wave X-band ($\nu = 9.0519$ GHz) EPR investigations were carried out at 7 K (**5**⁺) and 5 K (**10**) on a home-built X-band instrument with an Oxford ESR-900 cryostat.²⁵

Infrared spectra were recorded as CH_2Cl_2 solutions in a KBr liquid cell on a Nicolet 5-SX FTIR spectrometer. ^1H and ^{31}P NMR measurements were obtained on a Bruker WM-250 or WM-500 spectrometer.

Electrochemistry. Cyclic voltammetry on **4** and **5** was carried out in CH_2Cl_2 solution under N_2 using a PAR273 electrochemical setup with 0.1 M TBAP as supporting electrolyte. Three electrodes were used: a saturated calomel reference electrode (SCE), a 3.0 mm polished glassy-carbon working electrode, and a Pt-wire counter electrode. The solution volume was 5 mL, and the scan rate was 100 mV/s.

Chloro(biphenyl-2,2'-diyl)(1,5-cyclooctadiene)iridium(III) (3). A red solution of $[\text{Ir}(\text{COD})\text{Cl}]_2$ (0.441 g, 1.31 mmol) in 1.5 mL of anhydrous CH_2Cl_2 was treated with 0.200 g (1.31 mmol) of biphenylene under nitrogen and heated for 2 h at 90°C in a screw-cap vial. The red solution gave a bright yellow precipitate, which was filtered and washed with cooled CH_2Cl_2 . Yield: 0.571 g, 89%. Anal. Calcd (found) for $\text{IrC}_{20}\text{H}_{20}\text{Cl}$: C, 49.23 (49.41); H, 4.13 (4.22).

Chloro(biphenyl-2,2'-diyl)bis(triphenylphosphine)iridium(III) (4). This red-orange complex was prepared by reacting 0.500 g (1.02 mmol) of **3** and 0.54 g (2.05 mmol) of triphenylphosphine in 15 mL of CH_2Cl_2 at room temperature for 5 h under N_2 . The majority of the CH_2Cl_2 was removed under reduced pressure, diethyl ether was added, and **4** crystallized at 0°C . Yield: 0.834 g, 90%. Anal. Calcd (found)

for $\text{IrC}_{48}\text{H}_{38}\text{ClP}_2$: C, 63.74 (63.55); H, 4.24 (4.18). ^1H NMR (CH_2Cl_2 , 500 Hz): 7.33 (dd, Ph), 7.25 (br s, Ph and biph), 7.17 (t, Ph), 6.47 (t, 2 H, biph), 6.28 (dt, 1.5 and 7.5 Hz, 2 H, biph), 6.25 ppm (dd, 1.5 and 7.5 Hz, 2 H, biph). ^{31}P NMR (CH_2Cl_2 , 500 Hz): 21.77 ppm (s, 2 P, PPh_3).

Chloro(biphenyl-2,2'-diyl)tris(trimethylphosphine)iridium(III) (5). A yellow suspension of 0.500 g (1.02 mmol) of **3** in 10 mL of CH_2Cl_2 turned buff upon adding 0.234 g (3.06 mmol) of trimethylphosphine. After it was stirred for 2 h at room temperature under N_2 , the solution became colorless. The solvent was removed under reduced pressure, and the residue was washed with hexane and filtered on a glass frit. Yield: 0.492 g, 78%. Anal. Calcd (found): C, 41.48 (41.53); H, 5.80 (5.56). ^{31}P NMR (CD_2Cl_2 , 500 Hz): -42.29 (d, 22.2 Hz, 2 P, eq PMe_3), -54.70 ppm (t, 1 P, ax PMe_3). ^1H NMR (CD_2Cl_2 , 500 Hz): 8.19 (t, 6.0 Hz, 1 H, biph), 7.41 (d, 6.1 Hz, 2 H, biph), 7.26 (d, 7.5 Hz, 1 H, biph), 6.99 (t, 7.2 Hz, 1 H, biph), 6.92 (d, 7.4 Hz, 1 H, biph), 6.88 (d, 7.4 Hz, 1 H, biph), 6.71 (t, 7.4 Hz, 1 H, biph), 1.74 (d, 7.3 Hz, 9 H, ax PMe_3), 0.94 ppm (dd, 3.7 Hz, 18 H, eq PMe_3).

Observation of Chloro(biphenyl-2,2'-diyl)tricarbonyliridium(III) (6). CO (20 mL/min) was bubbled through a yellow suspension of **3** (0.500 g, 1.02 mmol) in CH_2Cl_2 at room temperature. The yellow solid, **3**, slowly disappeared over 15 min to give a yellow solution. The solvent then was removed under reduced pressure to produce a yellow residue of the product. This material was unstable and gave a brown species rapidly. IR: 2155.4, 2116.2, 2092.9 cm^{-1} .

Chloro(biphenyl-2,2'-diyl)(terpyridine)iridium(III) (9). A mixture of 0.500 g (1.02 mmol) of **3** and 0.239 g (1.02 mmol) of terpy in 20 mL of methanol was stirred at room temperature for 3 days. The resulting greenish precipitate was filtered, washed with hexane, and purified by recrystallization from DMF. Yield: 0.505 g, 80.4%. Anal. Calcd (found): C, 52.89 (52.44); H, 3.12 (3.42); N, 6.86 (6.65). ^1H NMR (CD_2Cl_2 , 250 Hz): 8.79 (d, 2 H, terpy), 8.57 (d, 2 H, terpy), 8.45 (dd, 1 H, biph), 8.33 (t, 1 H, terpy), 7.96 (t, 2 H, terpy), 7.84 (d, 2 H, terpy), 7.51 (dd, 1 H, biph), 7.37 (t, 2 H, terpy), 7.28 (d, 1 H, biph), 7.02 (d, 1 H, biph), 7.00 (d, 1 H, biph), 6.52 (t, 1 H, biph), 6.20 (t, 1 H, biph), 5.58 ppm (d, 1 H, biph).

Chloro(2-(fluoroboryl)biphenyl- $C^{2,2}$)tris(trimethylphosphine)iridium(IV) (10⁺). To a red-orange solution of **5** (0.200 g, 0.33 mmol) in CH_2Cl_2 was added NOBF_4 (0.0384 g, 0.33 mmol). An immediate color change to greenish black was observed. The mixture was stirred for an additional 20 min at room temperature. The solvent was then removed under reduced pressure and NaBPh_4 (0.15 g) was added. The complex was purified by recrystallization from CH_2Cl_2 /hexane. Yield: 0.097 g, 46%. Exact mass: calcd (found) for **10**⁺ 638.1344 (638.1347) amu. X-Band EPR (5 K): $g_{xy} = 2.15$, $g_z = 1.96$.

X-ray Crystallographic Analysis of 4. Crystals of **4** grew as irregularly shaped, flat plates of orange crystals from CH_2Cl_2 /hexane. A crystal of approximate dimensions $0.85 \times 0.50 \times 0.18$ mm was mounted in a random orientation on a glass fiber. Diffraction measurements were made on a four-circle Enraf-Nonius CAD4 fully automated diffractometer, equipped with a graphite monochromator (Mo $K\alpha$ radiation, $\lambda = 0.71069$ Å). The cell constants and an orientation matrix for data collection were obtained from least-squares refinement using setting angles of 25 carefully centered reflections. A total of 13 948 unique reflections were collected with $2\theta \leq 50^\circ$; of those, 8026 with $I \geq 3\sigma(I)$ were adjudged observed. The data were corrected for Lorentz and polarization effects. The linear absorption coefficient for Mo $K\alpha$ is 36.48 cm^{-1} . Owing to the irregular shape of the crystal, the DIFABS program was used to correct for absorption. The structure was solved using SHELXS86. There are two independent but essentially identical $\text{C}_{48}\text{H}_{38}\text{ClP}_2\text{Ir}$ molecules in the unit cell. All hydrogen positions were calculated and assigned isotropic thermal parameters which were 20% greater than the equivalent value of the atom to which they were bound. The standard deviation

(25) Beck, W. F.; Innes, J. B.; Lynch, J. B.; Brudvig, G. W. *J. Magn. Reson.* **1991**, *91*, 12.

of an observation of unit weight was 1.39. The weighting scheme was based on counting statistics and included a factor ($p = 0.03$) to downweight the intense reflections. The maximum and minimum peaks on the final difference Fourier map corresponded to 1.16 and $-1.20 \text{ e}/\text{\AA}^3$.

X-ray Crystallographic Analysis of 10. Single crystals of **10** were obtained by slow diffusion of diethyl ether into a solution of **10** in CH_2Cl_2 . A dark brown cut plate crystal of **10** having the approximate dimensions $0.10 \times 0.35 \times 0.35 \text{ mm}$ was mounted on a glass fiber. X-ray crystallographic measurements were made on an Enraf-Nonius CAD4 diffractometer with graphite-monochromated $\text{Mo K}\alpha$ radiation. Cell constants and an orientation matrix for data collection were obtained from a least-squares refinement using the setting angle of 25 carefully centered reflections in the range $19.00 < 2\theta < 32.00^\circ$. Moving-crystal–moving-counter background measurements were made by scanning an additional 25% above and below the scan range. Of the 8198 reflections collected, 7841 were unique ($R_{\text{int}} = 0.021$). The intensities of two representative reflections measured every 60 min decreased by 28%. A linear correction factor was applied to the data to account for this. The linear absorption coefficient for $\text{Mo K}\alpha$ is 32.9 cm^{-1} . The data were corrected for Lorentz and

polarization effects. The structure was solved by the Paterson method. The standard deviation of an observation of unit weight was 2.26. The weighting scheme was based on counting statistics and included a factor ($p = 0.03$) to downweight the intense reflections. The maximum and minimum peaks on the final difference Fourier map corresponded to 1.04 (located 1.2 \AA from the Cl atom) and $-0.91 \text{ e}/\text{\AA}^3$.

Acknowledgment. We thank the National Science Foundation for financial support of this research. The Laboratoire de Chimie Théorique is associated with the CNRS and is a member of ICMO and IPCM.

Supplementary Material Available: Full tables of data collection parameters, atom coordinates, bond distances and angles, and anisotropic thermal parameters for $[\text{Ir}(\text{PPh}_3)_2(\text{biph})\text{Cl}]$ (**4**) and $[\text{Ir}(\text{PMe}_3)_3(\text{biphBF})\text{Cl}][\text{BPh}_4]$ (**10**), figures giving additional views of **4** and **10**, and text giving full experimental details for determination of the structures of **4** and **10** (35 pages). Ordering information is given on any current masthead page.

OM940515X

Axial Shielding of 5d⁸ and 5d⁷ Metal Centers in Dimesitylplatinum Complexes with Unsaturated Chelate Ligands: Spectroscopic and Spectroelectrochemical Studies of Four Different Oxidation States

Axel Klein and Wolfgang Kaim*

Institut für Anorganische Chemie der Universität Stuttgart,
Pfaffenwaldring 55, D-70550 Stuttgart, Germany

Received August 1, 1994[®]

Platinum(II) complexes (N[∧]N)PtMes₂, Mes = mesityl, were synthesized with the α-dimine chelate ligands N[∧]N = 2,2'-bipyridine, 2,2'-bipyrazine, 2,2'- and 4,4'-bipyrimidine, 1,4,7,10-tetraazaphenanthrene, and dipyrldo[3,2-*a*:2',3'-*c*]phenazine. The compounds can be reversibly reduced to EPR and UV/Vis/near-IR spectroelectrochemically detectable radical complexes [(N[∧]N⁻¹)Pt^{II}Mes₂]⁻ and to dianions [(N[∧]N^{-II})Pt^{II}Mes₂]²⁻. Reversible one-electron oxidation is also possible, leading to cations [(N[∧]N)Pt^{III}Mes₂]⁺, which are EPR-silent even at 4 K but exhibit the typical ligand-field transitions for planar low-spin d⁷ ions. The unusual persistence of the Pt(III) state results from an effective protection of the axial positions by two mesityl groups which also block oxidative addition reactions. In contrast, the complexes (bpy)PtClMes and (bpy)Pt(*o*-CF₃Ph)₂, *o*-CF₃Ph = *o*-(trifluoromethyl)phenyl, have better accessible axial positions and are no longer oxidized reversibly. In agreement with the spectroelectrochemical results for the singly oxidized and reduced states, the neutral precursor molecules are distinguished by low-lying MLCT excited states which give rise to solvatochromic absorption and emission features. Comparison of the data from optical spectroscopy and from reversible one-electron redox processes allowed us to determine the solvent-dependent contributions from intra- and intermolecular reorganization following MLCT excitation.

Complexes of platinum(II) are generally distinguished by high substitutional stability and by a square planar coordination geometry at the metal center. These compounds have received much attention because of their prototypical oxidative addition reactivity,^{1,2} their aggregation tendencies,³ their therapeutical potential,⁴ and their photophysical properties, in particular their often intense luminescence.⁵ Light-emitting Pt(II) complexes frequently contain π-acceptor ligands, and the resulting metal-to-ligand charge transfer (MLCT) excited states are thus available for emission.^{2e,5} However, the presence of the 5d element platinum in such complexes causes a complicated electronic situation because of the high spin-orbit coupling constant of the element and because of the possible interaction of 5d and 6s metal orbitals with ligand MOs.^{5f,g} Furthermore,

the coordinatively unsaturated square planar situation invites aggregation, e.g., via Pt-Pt contacts or other stacking interactions.^{3,5a,i,k,q} It is not surprising, therefore, that intermolecular interactions have to be considered in the photo-^{5a,i,k,q} and electrochemistry of Pt(II) systems; for instance, the removal of one electron from Pt(II) usually proceeds irreversibly^{2e} due to the attack by nucleophiles in the axial position of the thus primarily obtained Pt(III) species. In contrast to low-spin d⁸ states, the low-spin d⁷ configuration generally favors

(5) (a) Miskowski, V. M.; Houlding, V. H. *Inorg. Chem.* **1989**, *28*, 1529. (b) Ballardini, R.; Gandolfi, M. T.; Prodi, L.; Ciano, M.; Balzani, V.; Kohnke, F. H.; Zavareh, H. S.; Spencer, N.; Stoddart, J. F. *J. Am. Chem. Soc.* **1989**, *111*, 7072. (c) Zuleta, J. A.; Chesta, C. A.; Eisenberg, R. *J. Am. Chem. Soc.* **1989**, *111*, 8916. (d) Che, C.-M.; Wan, K.-T.; He, L.-Y.; Poon, C.-K.; Yam, V. W.-W. *J. Chem. Soc., Chem. Commun.* **1989**, 943. (e) Che, C.-M.; He, L.-Y.; Poon, C.-K.; Mak, C. W. *Inorg. Chem.* **1989**, *28*, 3081. (f) Biedermann, J.; Gliemann, G.; Klement, U.; Range, K.-J.; Zabel, M. *Inorg. Chem.* **1990**, *29*, 1884. (g) Biedermann, J.; Gliemann, G.; Klement, U.; Range, K.-J.; Zabel, M. *Inorg. Chim. Acta* **1990**, *169*, 63. (h) Kunkely, H.; Vogler, A. *J. Am. Chem. Soc.* **1990**, *112*, 5625. (i) Wan, K.-T.; Che, C.-M.; Cho, K.-C. *J. Chem. Soc., Dalton Trans.* **1991**, 1077. (k) Miskowski, V. M.; Houlding, V. H. *Inorg. Chem.* **1991**, *30*, 4446. (l) Vogler, A.; Kunkely, H. *Angew. Chem.* **1982**, *94*, 217; *Angew. Chem., Int. Ed. Engl.* **1982**, *21*, 209. (m) Chassot, L.; von Zelewsky, A. *Helv. Chim. Acta* **1986**, *69*, 1855. (n) Miskowski, V. M.; Houlding, V. H.; Che, C. M.; Wang, Y. *Inorg. Chem.* **1993**, *32*, 2518. (o) Zuleta, J. A.; Bevilacqua, J. M.; Eisenberg, R. *Coord. Chem. Rev.* **1991**, *111*, 237. (p) Zuleta, J. A.; Bevilacqua, J. M.; Proserpio, D. M.; Harvey, P. D.; Eisenberg, R. *Inorg. Chem.* **1992**, *31*, 2396. (q) Houlding, V. H.; Miskowski, V. M. *Coord. Chem. Rev.* **1991**, *111*, 145. (r) Cornioley-Deuschel, C.; von Zelewsky, A. *Inorg. Chem.* **1987**, *26*, 3354. (s) Maestri, M.; Sandrini, D.; Balzani, V.; von Zelewsky, A.; Deuschel-Cornioley, C.; Jolliet, P. *Helv. Chim. Acta* **1988**, *71*, 1053. (t) von Zelewsky, A.; Belser, P.; Hayoz, P.; Dux, R.; Husa, X.; Suckling, A.; Stoekli-Evans, H. *Coord. Chem. Rev.* **1994**, *132*, 75. (u) Chan, C.-W.; Cheng, L.-K.; Che, C.-M. *Coord. Chem. Rev.* **1994**, *132*, 87. (v) Bevilacqua, J. M.; Eisenberg, R. *Inorg. Chem.* **1994**, *33*, 1886.

[®] Abstract published in *Advance ACS Abstracts*, January 15, 1995.

(1) Collman, J. P.; Hegedus, L. S.; Norton, J. R.; Finke, R. G. *Principles and Applications of Organotransition Metal Chemistry*; University Science Books: Mill Valley, CA, 1987; Chapter 5.

(2) (a) Chaudhury, N.; Puddephatt, R. J. *J. Organomet. Chem.* **1975**, *84*, 105. (b) Scott, J. D.; Puddephatt, R. J. *Organometallics* **1986**, *5*, 1538. (c) Aye, R. J.; Ferguson, G.; Lough, A. J.; Puddephatt, R. J. *Angew. Chem.* **1989**, *101*, 765; *Angew. Chem., Int. Ed. Engl.* **1989**, *28*, 767. (d) Achar, S.; Puddephatt, R. J. *Angew. Chem.* **1994**, *106*, 895; *Angew. Chem., Int. Ed. Engl.* **1994**, *33*, 847. (e) Vogler, C.; Schwederski, B.; Klein, A.; Kaim, W. *J. Organomet. Chem.* **1992**, *436*, 367.

(3) (a) Krogmann, K.; Hausen, H.-D. *Z. Anorg. Allg. Chem.* **1968**, *358*, 67. (b) Thomas, T. W.; Underhill, A. E. *Chem. Soc. Rev.* **1972**, *1*, 99. (c) Gencheva, G.; Mitewa, M.; Bontchev, P. R.; Gochev, G.; Macicek, J.; Zhecheva, E.; Yordanov, N. D. *Polyhedron* **1992**, *11*, 365. (d) Coyer, M. J.; Herber, R. H.; Chen, J.; Croft, M.; Szu, S. P. *Inorg. Chem.* **1994**, *33*, 716. (e) Harvey, P. D.; Truong, K. D.; Aye, K. T.; Drouin, M.; Bandrauk, A. D. *Inorg. Chem.* **1994**, *33*, 2347. (f) Herber, R. H.; Croft, M.; Coyer, M. J.; Bilash, B.; Sahiner, A. *Inorg. Chem.* **1994**, *33*, 2422.

(4) (a) Sundquist, W. I.; Lippard, S. J. *Coord. Chem. Rev.* **1990**, *100*, 293. (b) Lippert, B. *Prog. Inorg. Chem.* **1989**, *37*, 1.

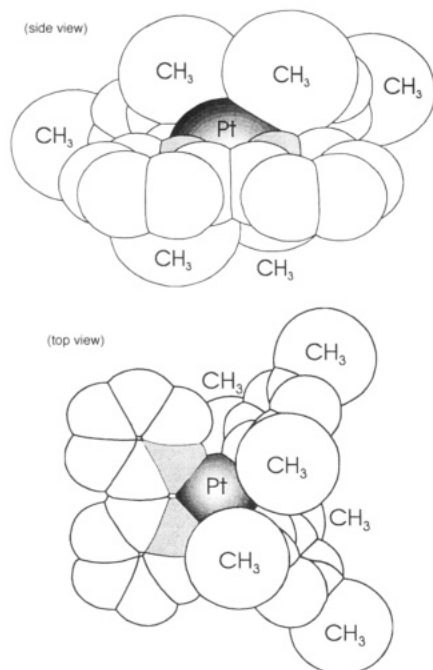
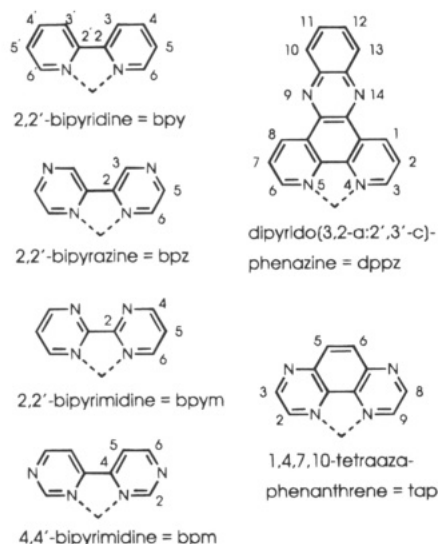


Figure 1. Space-filling model representations of the molecular structure of (bpy)PtMes₂.

higher coordination numbers than four, approaching the low-spin d⁶ situation with its extreme preference for hexacoordination.

In this paper we describe the consequences of axial shielding of essentially square planar coordinated platinum in mononuclear complexes (N[∞]N)Pt(Mes)₂ where Mes is mesityl (2,4,6-trimethylphenyl) and N[∞]N are α-diimine ligands of the 2,2'-bipyridine type.



In a recent structural study⁶ of (bpy)PtMes₂, the first mesitylplatinum compound to be characterized,⁷ we pointed out that two such axially protecting aryl ligands can block the access of molecules to these open coordination sites, thereby preventing one of the most typical reactions of Pt(II) compounds, viz., oxidative addition by alkyl halides.² Figure 1 illustrates the structural

situation of (bpy)PtMes₂ using a space-filling model.

Results from cyclic voltammetry and EPR as well as UV/Vis/near-IR spectroelectrochemistry (one-electron oxidation, two one-electron reductions) are being presented now for various complexes (N[∞]N)PtMes₂ and for the related species (bpy)PtClMes and (bpy)Pt(o-CF₃-Ph)₂. There have been some recent studies of singly reduced Pt(II) complexes with heterocyclic anion radical ligands;^{2e,6,8} on the other hand, the number of persistent mononuclear Pt(III) species is still rather small^{9,10} although such states have been discussed as intermediates.¹¹ There are of course several stable oligonuclear species formally involving Pt(III).¹² Room-temperature absorption and emission spectra of the neutral Pt(II) complexes will also be reported here, including the effects of different solvents (solvatochromism).^{2e,5o}

Experimental Section

Materials. The ligands bpm¹³ and dppz,¹⁴ which are not commercially available, and the platinum precursor complexes (DMSO)₂PtMes₂ and (DMSO)₂Pt(o-CF₃Ph)₂¹⁵ were obtained following literature procedures. Although the solid Pt(II) complexes are air-stable, their preparation and investigation was carried out under argon in dried solvents.

General Synthetic Procedure for Complexes (N[∞]N)-PtMes₂. In a typical reaction, 150 mg (0.225 mmol) of bis(dimethylsulfoxido)dimesitylplatinum(II) was suspended together with 0.26 mmol of the corresponding α-diimine ligand in 40 mL of toluene and heated under reflux for ~3 days; less basic ligands N[∞]N required longer reaction times. The course of the reaction could be monitored via the disappearance of the sulfoxide vibration ν(S=O) at 1130 cm⁻¹.¹⁶ The products that precipitated on cooling to 4 °C were collected, washed with *n*-hexane, and treated with 1,2-dichloroethane. After filtration through a microporous frit to remove colloidal platinum, the

(8) (a) Braterman, P. S.; Song, J.-I.; Vogler, C.; Kaim, W. *Inorg. Chem.* **1992**, *31*, 222. (b) Braterman, P. S.; Song, J. I.; Wimmer, F. M.; Wimmer, S.; Kaim, W.; Klein, A.; Peacock, R. D. *Inorg. Chem.* **1992**, *31*, 5084. (c) MacGregor, S. A.; McInnes, E.; Sorbie, R. J.; Yellowlees, L. J. In *Molecular Electrochemistry of Inorganic, Bioinorganic and Organometallic Compounds*; Pombeiro, A. J. L., McCleverty, J. A., Eds.; Kluwer Academic Publishers: Dordrecht, The Netherlands, 1993; p 503.

(9) (a) Uson, R.; Fornies, J.; Tomas, M.; Menjon, B.; Bau, R.; Sünkel, K.; Kuwabara, E. *Organometallics* **1986**, *5*, 1576. (b) Uson, R.; Fornies, J.; Tomas, M.; Ara, I.; Menjon, B. *J. Organomet. Chem.* **1987**, *226*, 129. (c) Blake, A. J.; Gould, R. O.; Holder, A. J.; Hyde, T. I.; Lavery, A. J.; Odulate, M. O.; Schröder, M. *J. Chem. Soc., Chem. Commun.* **1987**, 118. (d) Blake, A. J.; Holder, A. J.; Hyde, T. I.; Schröder, M. *J. Chem. Soc., Chem. Commun.* **1987**, 987. (e) Pandey, K. K. *Coord. Chem. Rev.* **1992**, *121*, 1.

(10) Matrix-stabilized Pt(III) transients: (a) Geoffroy, M.; Bernardinelli, G.; Castan, P.; Chermette, H.; Deguenon, D.; Nour, S.; Weber, J.; Wermeille, M. *Inorg. Chem.* **1992**, *31*, 5056. (b) Wermeille, M.; Geoffroy, M.; Arrizabalaga, P.; Bernardinelli, G. *Inorg. Chim. Acta* **1993**, *211*, 81. (c) Waltz, W. L.; Lillie, J.; Walters, R. T.; Woods, R. J. *Inorg. Chem.* **1980**, *19*, 3284. (d) Boucher, H. A.; Lawrance, G. A.; Lay, P. A.; Sargeson, A. M.; Bond, A. M.; Sangster, D. F.; Sullivan, J. C. *J. Am. Chem. Soc.* **1983**, *105*, 4652.

(11) (a) Halpern, J.; Pribanic, M. *J. Am. Chem. Soc.* **1968**, *90*, 5942. (b) Glennon, C. S.; Hand, T. D.; Sykes, A. G. *J. Chem. Soc., Dalton Trans.* **1980**, 19.

(12) (a) Hollis, L. S.; Lippard, S. J. *J. Am. Chem. Soc.* **1981**, *103*, 6761. (b) Renn, O.; Albinati, A.; Lippert, B. *Angew. Chem.* **1990**, *102*, 71. *Angew. Chem., Int. Ed. Engl.* **1990**, *29*, 84. (c) Matsumoto, K.; Sakai, K.; Nishio, K.; Tokisue, Y.; Ito, R.; Nishide, T.; Shichi, Y. *J. Am. Chem. Soc.* **1992**, *114*, 8110. (d) Baxter, L. A. M.; Heath, G. A.; Raptis, R. G.; Willis, A. C. *J. Am. Chem. Soc.* **1992**, *114*, 6944. (e) Uson, R.; Fornies, J.; Tomas, M.; Casas, J. M.; Cotton, F. A.; Falvello, L. R.; Feng, X. *J. Am. Chem. Soc.* **1993**, *115*, 4145.

(13) Effenberger, F. *Chem. Ber.* **1965**, *98*, 2260.

(14) Amoyal, E.; Homsí, A.; Chambron, J. C.; Sauvage, J. P. *J. Chem. Soc., Dalton Trans.* **1990**, 1841.

(15) Eaborn, C.; Kundu, K.; Pidcock, A. *J. Chem. Soc., Dalton Trans.* **1981**, 933.

(16) Cotton, F. A.; Francis, R.; Horrocks, W. D. Jr., *J. Phys. Chem.* **1960**, *64*, 1534.

(6) Klein, A.; Hausen, H.-D.; Kaim, W. *J. Organomet. Chem.* **1992**, *440*, 207.

(7) For a later report of a structurally characterized mesitylplatinum(II) compound, see: Fallis, K. A.; Anderson, G. K.; Rath, N. P. *Organometallics* **1993**, *12*, 2435.

dissolved complex was precipitated by dropwise addition of *n*-hexane and dried *in vacuo*. Typical yields were 85%; the yellow to dark-red compounds gave satisfactory analyses (C, H, N; available as supplementary material).

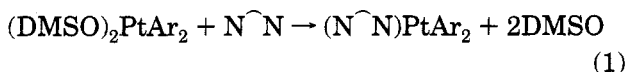
(bpy)PtClMes. In analogy to a published procedure,¹⁷ a solution of 9.5 mg (0.12 mmol) of acetyl chloride in 10 mL of toluene was slowly added to a suspension of 60 mg (0.1 mmol) of (bpy)PtMes₂⁶ in 30 mL of toluene/ethanol (5/1). After ~1 h the color change from red to yellow indicated the completion of the reaction. Removal of the solvent, washing with pentane, and drying under vacuum yielded 43 mg (85%) of the yellow compound. Analysis (C, H, N). ¹H NMR ((CD₃)₂SO): δ 9.33 (d, 1H, H₆), 8.62 (d, 1H, H₃), 8.56 (d, 1H, H_{3'}), 8.38 (t, 1H, H₄), 8.32 (t, 1H, H_{4'}), 8.08 (d, 1H, H_{6'}), 7.93 (t, 1H, H₅), 7.52 (t, 1H, H_{5'}), 6.59 (s, 2H, H_{Mes}), 2.29 (s, 3H, *p*-CH₃), 2.20 (s, 6H, *o*-CH₃). UV/Vis (λ_{max}): 465, 436, 407, 388, 362 nm (toluene); 450 sh, 422, 379, 353 nm (THF). The compound could also be obtained by using hydrochloric acid and stopping the reaction after ~30 min; longer reaction times produced (bpy)PtCl₂.¹⁸

(bpy)Pt(*o*-CF₃Ph)₂. A suspension of 164 mg (0.255 mmol) of (DMSO)₂Pt(*o*-CF₃Ph)₂ and 41 mg (0.26 mmol) of 2,2'-bipyridine in 40 mL of toluene was heated under reflux for 2 days. After cooling to 4 °C for 24 h, the yellow precipitate was collected by filtration, washed with hexane, and recrystallized several times from 1,2-dichloroethane/heptane (1/3) to yield 133 mg (81%) of yellow microcrystals. Analysis (C, H, N). ¹H NMR (Table 1). UV/Vis (λ_{max}): 441 sh, 436, 420, 365 nm (toluene).

Instrumentation. EPR spectra were recorded in the X band on a Bruker System ESP 300 equipped with a Bruker ER035M gaussmeter and a HP 5350B microwave counter. ¹H-NMR spectra were taken on a Bruker AC 250 spectrometer, infrared spectra were obtained using Perkin-Elmer 684 and 283 instruments. UV/Vis/near-absorption spectra were recorded on Shimadzu UV160 and Bruins Instruments Omega 10 spectrophotometers. A Perkin-Elmer fluorescence spectrometer LS-3B served to record emission spectra. Cyclic voltammetry and differential pulse voltammetry were carried out in THF, 1,2-dichloroethane, or acetonitrile/0.1 M Bu₄NPF₆, using a three-electrode configuration (glassy carbon electrode, Pt counter electrode, Ag/AgCl reference) and a PAR 273 potentiostat and function generator. The ferrocene/ferrocenium couple served as internal reference. Spectroelectrochemical measurements were performed using an optically transparent thin-layer electrode (Ottle) cell¹⁹ for UV/Vis spectra and a two-electrode capillary for EPR studies.²⁰

Results

Due to the steric requirements of two mesityl groups and the general sluggishness of substitution reactions at Pt(II) the formation (eq 1) of the complexes (N̂N)-



PtMes₂ required long reaction times at elevated temperatures with the eventual formation of some decomposition products such as elemental platinum. The use of (DMSO)PtMes₂ gave the best results in terms of purity and yield. Nevertheless, reactions with the weakly basic ligand bpm²¹ required longer times, and N=N function-containing ligands such as 3,3'-bipy-

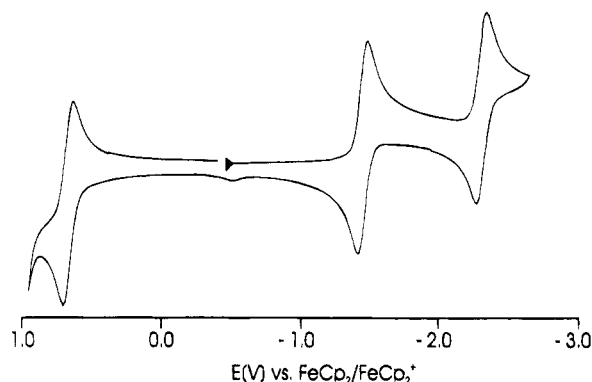


Figure 2. Cyclic voltammogram of (tap)PtMes₂ in THF/0.1 M Bu₄NPF₆ at 100 mV/s scan rate.

ridazine²¹ or 2,2'-azobispyridine²² failed to show any significant conversion to the corresponding compounds (N̂N)PtMes₂ although the analogous dichloroplatinum(II) complexes could be obtained.^{23a} The use of 3,6-bis(2-pyridyl)-1,2,4,5-tetrazine²² and longer reaction times in the case of N̂N = 2,2'-bipyrimidine produced little soluble dinuclear complexes, which will be described separately.^{23b} Brief (<30 min) action of hydrochloric acid on (bpy)PtMes₂ gave the mixed product (bpy)PtClMes, which could also be synthesized in a more controlled fashion by the action of acetyl chloride in a protic solvent mixture; (bpy)PtCl₂ is the reaction product after longer reaction times. The DMSO substitution method (eq 1) was also employed to prepare (bpy)Pt(*o*-CF₃Ph)₂, which was desired in order to evaluate the steric shielding of the *o*-(trifluoromethyl)phenyl substituent and to test the suitability of carbon-bonded fluoride atoms for protection of cationic Pt(III).

The complexes were identified primarily by ¹H-NMR spectroscopy, which revealed solvent-dependent chemical shifts of the protons of the heterocyclic ligands and variable spin-spin coupling involving the ¹⁹⁵Pt nuclei (*I* = 1/2, 33.8%); Table 1 summarizes the relevant data.

The ability of complexes (N̂N)PtMes₂ to add or lose electrons was studied by cyclic voltammetry with very similar results in THF, acetonitrile, or 1,2-dichloroethane, Figure 2 shows a typical cyclovoltammogram, and Table 2 contains the electrochemical data.

All complexes (N̂N)PtMes₂ show a reversible one-electron reduction wave, a mostly reversible second one-electron reduction step, and one reversible oxidation wave with the same current, as determined by cyclic voltammetry, differential pulse voltammetry and coulometry. Whereas the first reduction and oxidation processes meet all reversibility criteria even at scan rates of 20 mV/s, the second reduction becomes fully reversible only at 1000 mV/s for some complexes, as indicated by the large peak potential differences in Table 2. The second oxidation is always irreversible as is the first oxidation of complexes (bpy)PtClMes, (bpy)Pt(*o*-CF₃Ph)₂, (bpy)PtCl₂, and (DMSO)PtMes₂.

The generally reversible first reduction processes allowed us to generate persistent anionic species for EPR and UV/Vis/near-IR spectroelectrochemistry. EPR spectra were recorded in fluid solution at room temperature and in the frozen state; Figure 3 shows typical

(17) Clark, H. C.; Manzer, L. E. *J. Organomet. Chem.* **1973**, *59*, 411.

(18) Morgan, G. T.; Burstall, F. H. *J. Chem. Soc.* **1954**, 965.

(19) Krejci, M.; Danek, M.; Hartl, F. *J. Electroanal. Chem.* **1991**, *317*, 179.

(20) Kaim, W.; Ernst, S.; Kasack, V. *J. Am. Chem. Soc.* **1990**, *112*, 173.

(21) Ernst, S.; Kaim, W. *J. Am. Chem. Soc.* **1987**, *108*, 3578.

(22) Kaim, W.; Kohlmann, S. *Inorg. Chem.* **1987**, *26*, 68.

(23) (a) Klein, A. Ph.D. Thesis, Universität Stuttgart, 1994. (b) Klein, A.; Kaim, W. Manuscript in preparation.

Table 1. $^1\text{H-NMR}$ Data^a of Complexes ($\text{N}^{\wedge}\text{N}$)PtAr₂

complex	$\text{N}^{\wedge}\text{N}$ ligand		PtAr ₂ fragment	
	δ^a	J^b	δ^a	J^b
(bpy)PtMes ₂		In (CD ₃) ₂ SO		
	8.58 dd (3,3')	7.80 (H3, H4)	6.51 s ^c (HMes)	14.80 (Pt, HMes)
	8.31 dd (4,4')	7.30 (H4, H5)	2.34 s (oCH ₃)	
	8.14 dd (6,6')	5.57 (H5, H6)	2.10 s (pCH ₃)	
(bpm)PtMes ₂	7.61 dd (5,5')			
	9.48 d (5,5')	5.30 (H5, H6)	6.51 s ^c (HMes)	15.72 (Pt, HMes)
	8.79 dd ^c (6,6')	7.43 (Pt, H6)	2.36 s (oCH ₃)	
	8.71 d ^c (2,2')	13.60 (Pt, H2)	2.13 s (pCH ₃)	
(bpz)PtMes ₂	9.96 s (3,3')	<1.0 (H3, H5)	6.56 s ^c (HMes)	15.67 (Pt, HMes)
	8.96 d (6,6')	3.01 (H5, H6)	2.31 s (oCH ₃)	
	8.20 dd (5,5')		2.14 s (pCH ₃)	
(bpym)PtMes ₂	9.38 dd (6,6')	2.17 (H4, H6)	6.52 s ^c (HMes)	14.69 (Pt, HMes)
	8.33 dd (4,4')	5.56 (H4, H5)	2.35 s (oCH ₃)	
	7.86 dd (5,5')	4.74 (H5, H6)	2.11 s (pCH ₃)	
	9.96 d (5,6)	1.10 (H2, H5)	6.57 s ^c (HMes)	14.47 (Pt, HMes)
(tap)PtMes ₂	8.95 d (3,8)	3.04 (H2, H3)	2.31 s (oCH ₃)	22.00 (Pt, H2, H9)
	8.20 dd (2,9)		2.14 s (pCH ₃)	
	9.83 dd (1,8)	8.19 (H7, H8)	6.58 s (HMes)	
	8.57 dd (3,6)	5.22 (H6, H7)	2.43 s (oCH ₃)	
(dppz)PtMes ₂	8.47 dd (10,13)	6.58 (H10, H11)	2.16 s (pCH ₃)	
	8.14 dd (11,12)	3.41 (H10, H12)	8.12 dd (2,7)	1.42 (H6, H8)
	8.65 d (3,3')	8.09 (H3, H4)	7.94 dd (6,6') ^d	
	8.34 dd (4,4')	7.65 (H4, H5)	7.80 t (3,3') ^d	
(bpy)Pt(o-CF ₃ Ph) ₂	7.62 dd (5,5')	5.55 (H5, H6)	7.13 t (5,5') ^d	
	7.45 dd (6,6')	1.94 (H4, H6)	7.01 m (4,4') ^d	
		In CD ₂ Cl ₂		
	9.32 d (5,5')	5.23 (H5, H6)	6.67 s ^c (HMes)	15.74 (Pt, HMes)
(bpm)PtMes ₂	9.07 d ^c (2,2')	12.87 (Pt, H2,2')	2.42 s ^c (oCH ₃)	6.66 (Pt, oCH ₃)
	8.04 dd (6,6')	1.27 (H2, H6)	2.21 s (pCH ₃)	
	9.47 dd (5,5')	1.30 (H2, H5)	6.69 s ^c (HMes)	15.33 (Pt, HMes)
	8.76 d ^c (3,8)	3.00 (H2, H3)	2.37 s ^c (oCH ₃)	5.99 (Pt, oCH ₃)
(tap)PtMes ₂	8.48 dd (2,9)	20.62 (Pt, H2,9)	2.23 s (pCH ₃)	7.72 (Pt, H3,8)

^a Chemical shifts δ in ppm (positions in parentheses). ^b Coupling constants J in hertz (coupling nuclei in parentheses); HMes, meta protons; oCH₃, ortho methyl groups; pCH₃, para methyl groups of mesityl ligand. ^c ¹⁹⁵Pt isotope coupling ($I = 1/2$; 33.8% natural abundance). ^d CF₃ substituent in position 2 (ortho position); J values not available due to insufficient resolution.

Table 2. Electrochemical Data^a of Complexes ($\text{N}^{\wedge}\text{N}$)PtAr₂ and Related Species

complex	$E_{\text{pa}}^{\text{oxII}}$	$E_{1/2}^{\text{oxI}}$	$E_{1/2}^{\text{redI}}$	$E_{1/2}^{\text{redII}}$
(bpy)PtMes ₂ ^b	1.01	0.45 (60)	-2.05 (60)	-2.73 (80)
(bpm)PtMes ₂ ^b	1.02	0.53 (60)	-1.37 (62)	-2.12 (78)
(bpz)PtMes ₂ ^b	1.06	0.59 (62)	-1.47 (63)	-2.34 (135)
(bpym)PtMes ₂ ^b	0.98	0.54 (63)	-1.67 (61)	-2.38 (102)
(tap)PtMes ₂ ^b	1.05	0.60 (68)	-1.49 (65)	-2.35 (68)
(dppz)PtMes ₂ ^b	1.00	0.49 (67)	-1.50 (62)	-2.24 (95)
(bpy)PtClMes ^c	1.19	0.83 (irr) ^d	-1.80 (69)	-2.47 (114)
(bpy)Pt(o-CF ₃ Ph) ₂ ^c	0.91 (irr) ^d	0.52 (irr) ^d	-1.86 (66)	-2.56 (91)
(bpy)PtPh ₂ ^c	0.52 (irr) ^d	0.52 (irr) ^d	-2.08 (60)	-2.75 (83)
(bpy)PtCl ₂ ^b	1.19	0.67 (irr) ^d	-1.64 (83)	-2.30 (84)
(DMSO) ₂ PtMes ₂ ^b	1.18	0.89 (irr) ^d		

^a From cyclic voltammetry in 0.1 M Bu₄NPF₆ solutions at 100 mV/s scan rate. Potentials $E_{1/2}$ (in V) vs FeCp₂^{2+/+}, peak potential differences (in mV) in parentheses. Anodic peak potentials E_{pa} for the second oxidation step (oxII). ^b In THF. ^c In acetonitrile. ^d Anodic peak potential E_{pa} .

spectra and Table 3 contains a summary of pertinent data. The rather high line width and the significant deviations of isotropic g factors, g_{iso} , from the free electron value of 2.0023 are not unexpected for radial complexes of a 5d element; furthermore, the frequently observed isotropic ¹⁹⁵Pt satellite splitting, α_{iso} (¹⁹⁵Pt), allowed us to obtain a corresponding correlation between g_{iso} and α_{iso} (Figure 4).

All attempts to observe EPR spectra of electrogenerated cations failed. These attempts included *intra muros* electrolysis at 293 K as well as brief (1 min) *extra muros* electrolyses at room temperature or slightly longer low-temperature electrolyses (at 240 K) and then rapid freezing to a glassy solution at 77 K. EPR

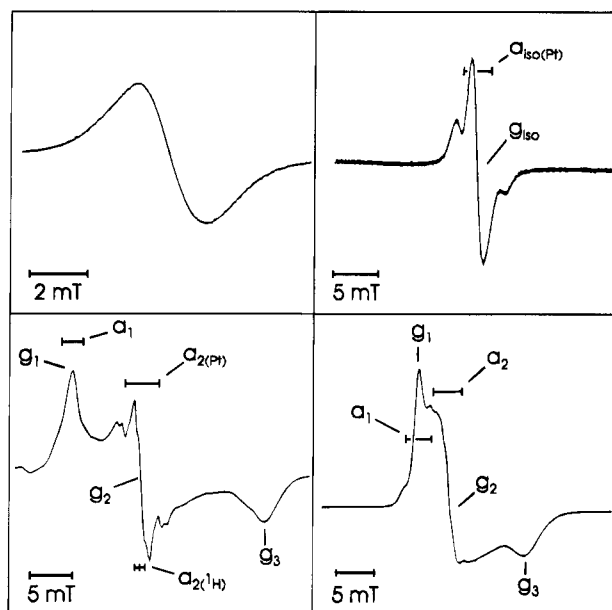


Figure 3. EPR spectra of [(tap)PtMes₂]⁻ (left) and [(bpym)PtMes₂]⁻ (right), electrogenerated in THF/0.1 M Bu₄NPF₆, in fluid solution at 293 K (top) and in glassy frozen solution at 150 K (bottom).

measurements of all thus generated complexes [($\text{N}^{\wedge}\text{N}$)PtMes₂]⁺ between 4 and 300 K failed to exhibit any signals for Pt(III) centers.

Absorption and emission spectra of the complexes were recorded at room temperature in solution. Figure

Table 3. EPR Data^a of Anion Radical Complexes^b $[(N\ N)PtAr_2]^{-}$

radical complex	$g_{iso}(293K)$	g components			Δg^c	$a(Pt)_{iso}$	$a(Pt)$ components			further hyperfine splitting
		g_1	g_2	g_3			a_1	a_2	a_3	
$[(bpy)PtMes_2]^{-}$	1.9898	2.0312	2.0071	1.9340 ^d	972	4.0	5.2	3.8	<3.4 ^d	
$[(bpm)PtMes_2]^{-e}$	1.9972	2.0302	2.0054	1.954 ^f	762	<1.7	<1.6	2.2	<2.5 ^f	
$[(bpz)PtMes_2]^{-}$	1.9964	2.0573	2.0056	1.9200 ^d	1373	2.8	3.5	nd ⁱ	<2.1 ^d	0.53 ⁱ
$[(bpym)PtMes_2]^{-}$	1.9927	2.0291	2.0051	1.9453 ^d	838	3.0	3.6	~3.0	<2.5 ^d	
$[(tap)PtMes_2]^{-}$	1.9964	2.0579	2.0058	1.9213 ^d	1366	<2.4	2.5	4.1	<2.5 ^d	0.62 ^j
$[(dppz)PtMes_2]^{-}$	2.0035	2.0069	2.0039	2.0039 ^g	30	<0.2		nd	g	0.52 ^k
$[(bpy)Pt(o-CF_3Ph)_2]^{-}$	1.9937	2.0236	2.0065	1.9502 ^g	734	2.1	2.6	2.8	<2.5 ^g	
$[(bpy)PtClMes]^{-e}$	1.9914	2.031	2.004	1.931 ^f	1000	4.7	3.0	4.5	<3.8 ^f	
$[(bpy)PtCl_2]^{-h}$	1.9988	2.038	2.009	1.935 ^h	1030	5.8	5.9	10.1	2.5 ^h	

^a Coupling constants for nuclei ¹H, ¹⁴N, or ¹⁹⁵Pt ($I = 1/2$, 33.8% natural abundance) (in mT). Data from graphical spectra analysis (see Figure 3); errors estimated for a_1 , a_2 , and a_3 are ± 0.3 mT. ^b Generated from neutral precursors by cathodic reduction in 1,2-dichloroethane/0.1 M Bu₄NPF₆ or Bu₄NClO₄. ^c $\Delta g = (g_1 - g_3) \times 10^4$. ^d At 150 K. ^e In THF/0.1 M Bu₄NPF₆. ^f At 110 K. ^g At 120 K. ^h At 77 K in DMF/0.1 M Bu₄NBF₄, from ref 8c. ⁱ Triplet coupling (H5,5') at 150 K. ^j Triplet coupling (Figure 3) $a_2(H3, 8)$, at 150 K. ^k Quintet coupling (N9,14), at 293 K. ^l nd, not detected.

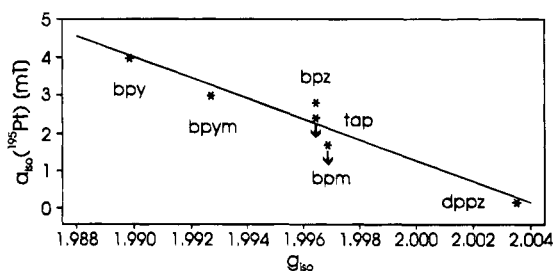


Figure 4. Correlation of isotropic g factors g_{iso} with isotropic hyperfine coupling constants $a_{iso}(^{195}Pt)$ of radical complexes $[(N\ N)PtMes_2]^{-}$ (\downarrow , upper limit). Least-squares fit: $a_{iso} = 543.096 \text{ mT} - (g_{iso} - 270.915 \text{ mT})$; $r = 0.969$ (correlation coefficient).

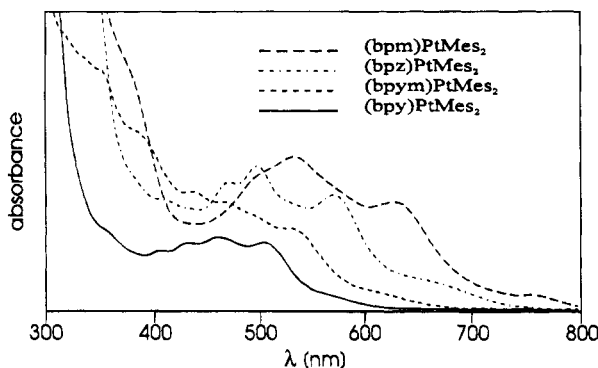


Figure 5. Absorption spectra of complexes $(N\ N)PtMes_2$ in toluene. Intensities different for each spectrum.

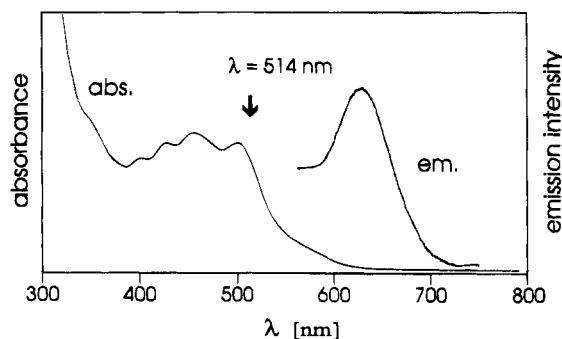


Figure 6. Emission spectrum of $(bpy)PtMes_2$ at 293 K in toluene solution; excitation wavelength 514 nm.

5 contains representative absorption spectra; Figure 6 illustrates the absorption and emission spectrum of the bpy complex. Absorption and emission maxima are summarized in Tables 4 and 5.

The absorption maxima of the complexes exhibit the typical^{2e,5o,24-26} negative solvatochromism, i.e., a high-

Table 4. Absorption Maxima^a of Complexes $(N\ N)PtMes_2$ in Toluene

$N\ N$	λ_{max}		
	³ MLCT ^b	¹ MLCT	
bpy	570 (sh);	504, 459, 432, 406;	352 (sh)
bpm	760;	631, 535, 503 (sh);	372 (sh)
bpz	650 (sh);	573, 499, 483;	406
bpym	610 (sh);	529, 494sh, 472, 430;	382 (sh), 352 (sh)
tap	660 (sh);	567, 498, 470, 408 (sh)	
dppz	570 (sh);	500 sh, 436 (sh);	378, 362, 345

^a Wavelengths λ in nanometers. Most intense band within a group italic. ^b Weak bands.

Table 5. Long-Wavelength Emission and Absorption Data^a for Complexes $(N\ N)PtAr_2$

complex	emission (excitation)		absorption	Stokes shift
	λ_{max}^{em}	$\tilde{\nu}_{max}^{em}$		
$(bpy)PtMes_2$	610	16 390 (506)	19 840	3450
$(bpz)PtMes_2$	590 sh	16 959 (470)	17 640	690
$(bpym)PtMes_2$	591	16 920 (500)	18 900	1980
$(tap)PtMes_2$	580	17 240 (488)	17 640	400
$(dppz)PtMes_2$	592	16 890 (514)	19 490	2600
$(bpy)Pt(o-CF_3Ph)_2$	508	19 680 (430)	22 670	3000
$(bpy)PtClMes$	558	17 920 (470)	21 500	3580

^a From measurements in toluene at 293 K. Wavelengths in nanometers; wavenumbers and Stokes shifts $\Delta = \tilde{\nu}_{max}^{abs} - \tilde{\nu}_{max}^{em}$ in reciprocal centimeters. No emission was observed for $(bpm)PtMes_2$.

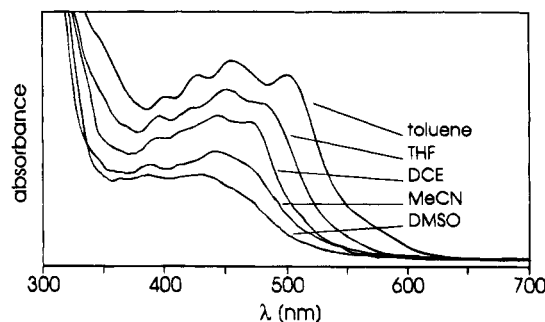


Figure 7. Solvatochromism of $(bpy)PtMes_2$ in different solvents at room temperature (DCE = 1,2-dichloroethane). Intensities different for each spectrum.

energy shift in more "polar" solvents (Figure 7, Table 6). Table 6 summarizes the solvent dependence for the long-wavelength absorption features; higher energy MLCT absorption components, e.g., of $(bpy)PtMes_2$, show a similar extent of the negative solvatochromic

(24) Kaim, W.; Kohlmann, S.; Ernst, S.; Olbrich-Deussner, B.; Bessenbacher, C.; Schulz, A. *J. Organomet. Chem.* **1987**, 321, 215.
 (25) Manuta, D. M.; Lees, A. J. *Inorg. Chem.* **1983**, 22, 3825.
 (26) Reichardt, C. *Solvents and Solvent Effects in Organic Chemistry*, 2nd ed.; VCH: Weinheim, Germany, 1988.

Table 6. Solvent Dependence of Long-Wavelength Absorption Maxima $\tilde{\nu}_{\max}$ of Complexes $(\widehat{N}\widehat{N})\text{PtMes}_2$

$(\widehat{N}\widehat{N})$	$\tilde{\nu}_{\max}$ [cm ⁻¹]				correlation parameters ^a		
	toluene	THF	MeCN	DMSO	A (cm ⁻¹)	B (cm ⁻¹)	r
bpy	19 840	20 830	21 505 (sh) ^a	21 840 (sh) ^a	19 180	2670	0.966
bpm	15 850	17 330	17 920	18 250 (sh)	14 880	3440	0.997
bpz	17 450	18 620	19 120	19 420	16 790	2680	0.979
bpym	18 900	20 370	20 700 (sh)	20 920 (sh)	17 700	3125	0.984
tap	17 640	18 620 (sh)	19 420	19 380 (sh)	16 870	2730	0.986
dppz	19 490	20 280 (sh)	21 510	21 640 (sh)	18 480	3230	0.995

^a Linear regression $\tilde{\nu}_{\max} = A + BE^*_{\text{MLCT}}$; correlation coefficient r. $E^*_{\text{MLCT}} = 0.30$ (toluene), 0.59 (THF), 0.90 (MeCN), and 1.00 (DMSO).

Table 7. Absorption Data^a of Complexes $[(\widehat{N}\widehat{N})\text{PtMes}_2]^{n-}$ in THF/0.1 M Bu₄NPF₆

$\widehat{N}\widehat{N}$	λ_{\max} ($\epsilon \times 10^{-3}$) for n = 0; MLCT	λ_{\max} ($\epsilon \times 10^{-3}$) for n = 1				λ_{\max} for n = 2; IL
		IL1	IL2	IL3	IL4	
bpy	480 (2.46), 441 (2.69), 418 (sh), 393	1356 (0.2), 1120 (sh), 942 (1.2);	832 (1.3), 744 (1.0);	530 (5.2), 494 (4.9), 473 (sh);	371 (10.8)	529 (br), 397
bpm	577 (1.70), 487 (2.38)	737 (1.9), 666 (2.7);	603 (2.7), 551 (3.5);	492 (10.0), 461 (8.0), 440 (sh);	337 (12.0)	358 (br)
bpz	537 (2.58), 517 (sh), 480 (2.82), 458	1199 (2.9), 1077 (sh), 1027 (3.2);	526 (sh);	502 (6.0), 466 (5.0);	327 (sh)	500 (sh), 368
bpym	491 (1.50), 423 (sh)	1150 (sh), 950 (0.5), 828 (0.4);		506 (6.1), 477 (5.9), 453 (sh);	356 (sh)	377
tap	537 (sh), 532, 483, 457	1202, 1085 (sh), 1027;	523 (sh);	502, 466;	333 (sh)	
dppz	493 (sh), 423 (sh)	1345, 1208;		588, 558 (sh), 452;	342	825, 726, 453

^a Wavelengths λ (in nm); molar extinction coefficients (in M⁻¹ cm⁻¹). MLCT, Metal-to-ligand charge transfer bands; IL, intraligand bands.

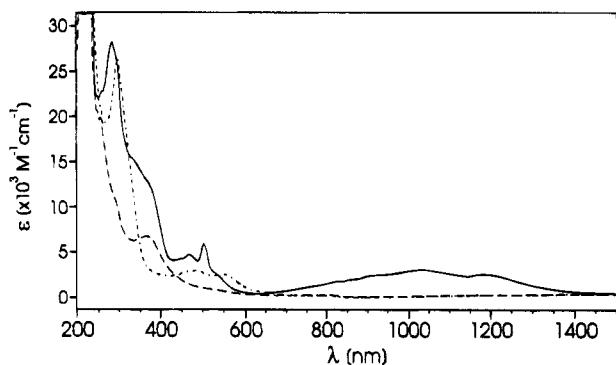


Figure 8. UV/Vis/near-IR absorption spectra from reductive spectroelectrochemistry of $(\text{bpz})\text{PtMes}_2$ in THF/0.1 M Bu₄NPF₆: neutral complex (---); monoanion (—); dianion (---).

effect. Table 6 also contains parameters of the linear correlation with the best suitable solvent parameter, E^*_{MLCT} , which had been empirically derived from MLCT transitions of complexes $(\text{bpy})\text{M}(\text{CO})_4$, M = Mo, W, by Manuta and Lees.²⁵ Attempts to obtain correlations with E_T , ϵ_r ,²⁶ or $E_{\text{CT}}(\pi)$ ²⁷ were less successful.

While the MLCT absorption maxima of the complexes $(\widehat{N}\widehat{N})\text{PtMes}_2$ exhibit negative solvatochromism (Table 6), the emission maxima show the opposite behavior, as noted here for $(\text{bpy})\text{PtMes}_2$: ν_{\max}^{em} 16 390 (powder or toluene solution), 15 080 (1,2-dichloroethane), 14 140 cm⁻¹ (MeCN solution). Both effects are characteristic of a low-lying MLCT excited and emissive state.²⁸

UV/Vis/near-IR spectroelectrochemical data were obtained for both the monoanions and the monocations. Figures 8 and 9 show typical such spectra; Tables 7 and 8 contain the pertinent data.

While the monoanions show the expected^{8,29,30}

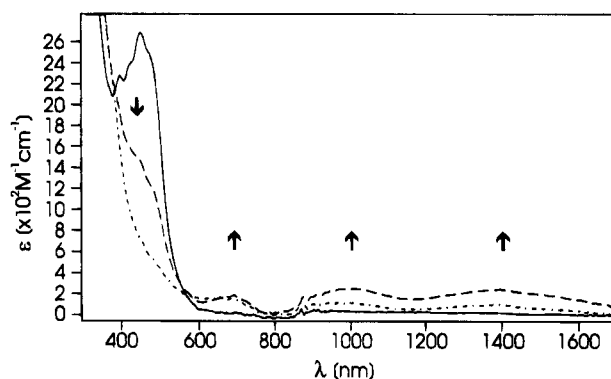


Figure 9. UV/Vis/near-IR absorption spectra from oxidative spectroelectrochemistry of $(\text{bpy})\text{PtMes}_2$ in THF/0.1 M Bu₄NPF₆: neutral complex (—); monocation after 2 min (---); partially decomposed monocation after 4 min (---).

Table 8. Ligand-Field Absorption Maxima^a of Spectroelectrochemically Generated Complexes $[(\widehat{N}\widehat{N})\text{PtMes}_2]^+$

$\widehat{N}\widehat{N}$	λ_1	$\tilde{\nu}_1$	(ϵ)	λ_2	$\tilde{\nu}_2$	(ϵ)	λ_3	$\tilde{\nu}_3$	(ϵ)
bpy	687	14540	(257)	1001	9980	(316)	1394	7170	(320)
bpm	647	15450	(430)	956	10460	(474)	1387	7210	(618)
bpz	638	15660		948	10540		1376	7260	
bpz ^b	640	15610	(190)	944	10590	(275)	1408	7100	(480)
bpym	670 (sh)	14920 (sh)	(180)	970	10310	(135)	1440	6940	(208)
bpym ^b	671	14900		965	10360		1402	7130	
tap	721 (sh)	13860 (sh)		972	10290		1380	7240	
dppz	703	14220		969	10330		1404	7120	

^a In THF/0.1 M Bu₄NPF₆, except where noted. Wavelengths λ (in nm); wavenumbers $\tilde{\nu}$ (in cm⁻¹); molar extinction coefficients ϵ (in M⁻¹ cm⁻¹).

^b In 1,2-dichloroethane/0.1 M Bu₄NPF₆.

features of the individual ligand radical anions, $(\widehat{N}\widehat{N})^{\cdot-}$, all monocations are distinguished by three weak bands at long wavelengths (600–1500 nm, Table 8). The typically slow electrolysis time in an Otte cell showed that the monoanions are generally stable under those conditions whereas the cations undergo a degradation reaction within minutes (Figure 9), despite the fully reversible redox process in the more rapid cyclic voltammetry experiment.

(27) Kaim, W.; Olbrich-Deussner, B.; Roth, T. *Organometallics* **1991**, *10*, 410.

(28) Zulu, M. M.; Lees, A. *J. Inorg. Chem.* **1988**, *27*, 3325.

(29) Krejčík, M.; Zalis, S.; Ladwig, M.; Matheis, W.; Kaim, W. *J. Chem. Soc., Perkin Trans. 2* **1992**, 2007.

(30) Fees, J.; Kaim, W.; Moscherosch, M.; Matheis, W.; Klima, J.; Krejčík, M.; Zalis, S. *Inorg. Chem.* **1993**, *32*, 166.

Discussion

Reactivity and Stability of Oxidation States.

The consequences of an apparently efficient axial protection of the platinum(II) center in complexes $(\widehat{N}N)PtMes_2$ (Figure 1) can be summarized as follows. First, the mere synthesis of these species requires fairly long reaction times due to the sterically hindered substitution reaction of $(DMSO)_2PtMes_2$ (eq 1). As shown quantitatively in a previous report on oxidative addition behavior,^{2e} the ligand basicity can be correlated with the reaction rate; similarly, the comparatively electron-rich bpy ligand substitutes for DMSO within 3 days whereas the weakly basic²¹ bpm requires at least 4 days under the same conditions.

Second, thermal^{1,2} and photoinduced^{5r,s} oxidative addition reactions are blocked. This is evident from the addition of the standard reagent iodomethane to the prototypical complex $(bpy)PtMes_2$, which does not show any sign of conversion after more than 6 months at room temperature, with or without light.^{6,23a} A similar result had been reported for $(dppm)PtMes_2$, $dppm = bis(diphenylphosphino)methane$.³² While hydrochloric acid reacts to hydrolyze the Pt–C bonds, it does so rather slowly with the formation of $(bpy)PtClMes$ as isolable intermediate. Acetyl chloride does not react with, e.g., $(bpy)PtMes_2$ in dry THF, CH_2Cl_2 , or MeCN; however, the HCl produced after addition of ethanol leads to $(bpy)PtClMes$. In contrast to the species $(\widehat{N}N)PtMes_2$, the complex $(bpy)Pt(o-CF_3Ph)_2$ readily adds iodomethane, which already suggests a lesser degree of axial shielding in this compound. In summary, the dimesitylplatinum complexes appear sterically shielded against external attack in the axial position, except for attacks by the smallest of electrophiles, H^+ .

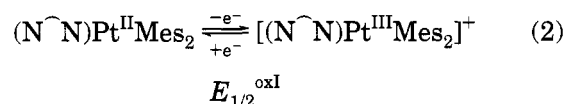
The most intriguing consequence of this axial shielding of the coordinatively unsaturated metal center by intramolecularly attached and seemingly inert mesityl substituents is the stabilization of the one-electron oxidized state, involving the rare^{9,10} mononuclear Pt(III) center. This oxidation occurs at rather low potentials for all complexes $(\widehat{N}N)PtMes_2$ because of the electron-donating substituent effect from two mesityl groups; a smaller contribution from the varying donor capacity of the different heterocyclic ligands $\widehat{N}N$ is also evident from Table 2. Axial protection by particularly bulky ligands should not only preclude any dimerization or other aggregation, more importantly, it should also prevent nucleophilic solvent molecules or electrolyte ions from attacking at the very reactive electrophilic metal center in the paramagnetic cations $[(\widehat{N}N)PtMes_2]^+$. Previous studies on the irreversible oxidation of complexes $(\widehat{N}N)PtPh_2$ have shown a very pronounced solvent dependence of the anodic peak potential.^{2e}

In fact, all dimesitylplatinum(II) complexes are oxidized in a clean, cyclovoltammetrically reversible one-electron step, as evident also from comparison (differential pulse voltammetry, coulometry) with the fully reversible one-electron reduction waves (Figure 2). However, the exchange of only one mesityl group by chloride as in $(bpy)PtClMes$ makes the metal center

susceptible again to irreversible oxidation at a slightly higher potential (Table 2). It is thus evident that *both* mesityl substituents are necessary to provide the necessary axial protection (Figure 1) for stabilization of the Pt(III) state. Even so, the stability of that extremely reactive form is not high enough to obtain it as an isolable material. As the UV/Vis/near-IR spectroelectrochemical experiments show (Figure 9), the decay of electrogenerated Pt(III) cations proceeds within a few minutes at room temperature, thus permitting spectroscopic studies but not crystallization. Protection by one *o*-trifluoromethyl substituent instead of two *o*-methyl groups on each of the two aryl rings also proved detrimental to the stability of the Pt(III) form; irreversible anodic oxidation occurs for $(bpy)Pt(o-CF_3Ph)_2$ at a relatively high potential (Table 2). In addition to a still insufficient axial protection against external attack, the possible intramolecular activation of the CH(methyl) bonds in mesityl substituents and the abstraction of fluoride in the case of $(bpy)Pt(o-CF_3Ph)_2$ are conceivable causes for the decomposition of the Pt(III) species with their assumed reactive $(5d_z^2)^1$ configuration. (The shortest nonbonded Pt–C(*o*-CH₃) distance in $(bpy)PtMes_2$ is ~320 pm). Whereas the affinity of high oxidation state platinum for fluoride ligation is well established,³³ the oxidative addition of the C–H bond via an agostic intermediate to activated metal sites has recently been demonstrated in a number of cases.^{34,35}

It should be noted here that the hitherto reported stable complexes of monomeric Pt(III) do not contain C–H bonds close to the metal center: The anion $[Pt(C_6Cl_5)_4]^-$ contains no H at all,^{9a,b} and the metal in $[Pt(ttn)_2]^{3+}$ ^{9c,d} is coordinated exclusively to the sulfur donor atoms of 1,4,7-trithiacyclononane (ttn).

After the fully reversible first oxidation to a Pt(III) cation (eq 2) which is persistent on the time scale (<1 min) of the cyclovoltammetry experiment, the second



oxidation wave is completely irreversible. It thus remains speculative whether this process is a straight Pt(III) → Pt(IV) transition or an oxidation involving the carbanionic aryl ligands.³⁶ As a d^6 center, Pt(IV) requires hexacoordination, which can be provided in sterically unhindered cases by solvent donor molecules such as MeCN or by halide ions.³⁷

The stepwise reduction (eqs 3 and 4) of the complexes concerns primarily the heterocyclic acceptor ligands $\widehat{N}N$, the corresponding potentials thus show a variation and separation $E_{1/2}^{redI} - E_{1/2}^{redII}$ that is typical for

(33) (a) Anderson, C. M.; Crespo, M.; Ferguson, G.; Lough, A. J.; Puddephatt, R. J. *Organometallics* **1992**, *11*, 1177. (b) Crespo, M.; Martinez, M.; Sales, J. *J. Chem. Soc., Chem. Commun.* **1992**, 822.

(34) Crabtree, R. H.; Hamilton, D. G. *Adv. Organomet. Chem.* **1988**, *28*, 299.

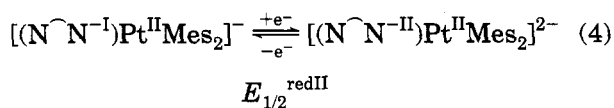
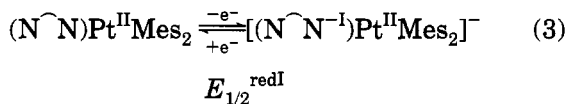
(35) Ankaniec, B. C.; Hardy, D. T.; Thomson, S. K.; Watkins, W. N.; Young, G. B. *Organometallics* **1992**, *11*, 2591.

(36) (a) Kaim, W. *Top. Curr. Chem.* **1994**, *169*, 231. (b) Hasenzahl, S.; Kaim, W.; Stahl, T. *Inorg. Chim. Acta* **1994**, *225*, 23.

(37) (a) Davies, J. A.; Chen, L.; Eagle, C. T.; Staples, R. J. In *Molecular Electrochemistry of Inorganic, Bioinorganic and Organometallic Compounds*; Pombeiro, A. J. L., McCleverty, J. A., Eds.; Kluwer Academic Publishers: Dordrecht, The Netherlands, 1993; p 351. (b) Watzky, M. A.; Wankine, D.; Heeg, M. J.; Endicott, J. F.; Ochrymowycz, L. A. *Inorg. Chem.* **1993**, *32*, 4882.

(31) Shida, T. *Electronic Absorption Spectra of Radical Ions*; Elsevier Science Publishers: Amsterdam, 1988.

(32) Hassan, F. S. M.; McEwan, D. M.; Pringle, P. G.; Shaw, B. L. *J. Chem. Soc., Dalton Trans* **1985**, 1501.



the free ligands and their organometallic or other complexes.^{21,22,30,38} The susceptibility for the reduction of $(\widehat{N}\widehat{N})\text{PtMes}_2$ thus increases along the following sequence for $\widehat{N}\widehat{N}$: bpy < bpym < dppz \approx tap \approx bpz < bpm. In essence, this is also the sequence of increasing reducibility for the free ligands.²¹

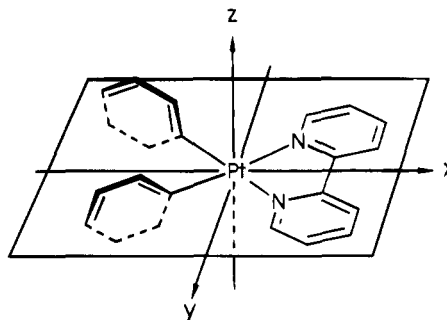
In comparison to PtPh_2 , the PtMes_2 complex fragment is a little less electrophilic and thus induces slightly more negative reduction potentials; the opposite is true for $\text{Pt}(o\text{-CF}_3\text{Ph})_2$ and, of course, for PtCl_2 (Table 2). A particular stabilization of the monoanions or dianions due to steric shielding could not be established; usually it is the small H^+ electrophile that attacks such reduced compounds.³⁰

EPR and UV/Vis/Near-IR Spectroelectrochemistry. Both EPR and optical absorption spectroscopy are well suited to determine the nature of neighboring paramagnetic states of a complex with low-lying MLCT excited states. With respect to EPR, the unexpected result of these studies was the absence of any detectable signals for the one-electron oxidized form, even at 4 K. EPR spectra with rather small g anisotropy and ^{195}Pt hyperfine coupling of ~ 5 mT were observed for persistent hexacoordinate Pt(III) species with exclusively S or N heteroatom donors,^{9c-e,10d} on the other hand, no EPR signals were reported for the square planar organometallic ion $[(\text{Pt}(\text{C}_6\text{Cl}_5)_4)]^-$.^{9a,b} With $2.57 \mu_B$ at room temperature, the magnetic moment for the latter complex ion^{9a} already suggests that spin-orbit coupling effects contribute significantly to the ground and magnetically excited states of that $5d^7$ species. Higher metal isotope coupling constants and much more pronounced g anisotropies were observed for Pt(III) centers, which can be generated via irradiation of single crystals containing "normal" Pt(II) salts; however, the exact structural situation of these centers with respect to the ligation at the unprotected axial sites is not known.¹⁰

In contrast to approximately octahedral low-spin d^7 species, the corresponding square planar centers have several close-lying d orbitals to accommodate the electrons.^{39,40} In addition to the large spin-orbit coupling constant of $\sim 5000 \text{ cm}^{-1}$ for platinum,⁴¹ this particular d orbital situation can cause very rapid EPR relaxation for species such as $[(\text{Pt}(\text{C}_6\text{Cl}_5)_4)]^-$ or $[(\widehat{N}\widehat{N})\text{PtMes}_2]^+$. Additional evidence for this argument comes from a comparison with the low-spin d^7 complex $(\text{PEt}_2\text{Ph})_2\text{CoMes}_2$, which has g_1 3.72, g_2 1.96 and g_3 1.74,^{40a} i.e., a large g anisotropy despite a much smaller spin-orbit coupling constant of $\sim 500 \text{ cm}^{-1}$ for Co(II).⁴¹ If there is a good analogy between $[(\widehat{N}\widehat{N})\text{PtMes}_2]^+$ and

$(\text{PEt}_2\text{Ph})_2\text{CoMes}_2$, the EPR silence of the former species would thus be not unexpected.

The analogy between square planar low-spin Co(II) and Pt(III) centers does indeed exist, as is obvious from UV/Vis/near-IR spectroelectrochemistry (Figure 9, Table 8). Three long-wavelength absorptions λ_{1-3} or ν_{1-3} due to ligand-field (LF) transitions from doubly occupied d orbitals to the singly occupied d orbital are expected,^{39,40b,42} e.g., for square planar low-spin Co(II) complexes such as $(\text{PEt}_2\text{Ph})_2\text{CoMes}_2$,^{40b} and are observed here for the electrogenerated Pt(III) complexes. The higher intensity of the LF transitions in case of the platinum complexes is due to the higher extent of orbital mixing in the $5d^7$ relative to the $3d^7$ situation; unfortunately, most reported optical spectra of transient Pt(III) species were restricted to the UV and visible regions.^{10,43} Exact spectral assignments for square planar low-spin d^7 systems are difficult to make,^{39,40b,42} the strongest dependence of the second-lowest transition on the heterocyclic ligand suggests a tentative d orbital sequence $(d_{xz})^2, (d_{x^2-y^2})^2, (d_{yz})^2, (d_z)^1$ for complexes $[(\widehat{N}\widehat{N})\text{PtMes}_2]^+$ see Scheme 1).



All one-electron reduced complexes $[(\widehat{N}\widehat{N})\text{PtAr}_2]^-$ exhibit EPR signals at room temperature which, however, are rarely sufficiently resolved to show ligand hyperfine structure (Figure 3, Table 3). The exception is the complex with $\widehat{N}\widehat{N} = \text{dppz}$, where the unpaired electron resides in the 1,4-diazine part of the molecule with little participation of the α -diimine/metal site.³⁰ Despite being predominantly anionic complexes of Pt(II),^{2e,6,8} most anionic complexes exhibit a well-detectable rhombic g anisotropy in frozen solution (which explains the poor resolution of room-temperature spectra). This effect is favored both by the very large spin-orbit coupling factor of the $5d$ metal and by the not totally negligible participation of platinum at the singly occupied MO (SOMO).^{8c} This metal participation is also evident from the sizeable ^{195}Pt isotope coupling, observed both in fluid solution and for the g_1 and g_2 components in the frozen state (Figure 1). The smallest metal splitting for the g_3 component has similarly been observed for $[(\text{bpy})\text{PtCl}_2]^-$ (Table 3).^{8c} Small g anisotropies Δg were found for the complexes with the ligands bpm and dppz. The latter shows virtually no metal participation at the SOMO as evident from the virtually unchanged isotropic g factor relative to the value of 2.003 21 for $\text{dppz}^{\cdot-}$.³⁰ As mentioned before, the reason

(38) Ernst, S. D.; Kaim, W. *Inorg. Chem.* **1989**, *28*, 1520.

(39) Lever, A. B. P. *Inorganic Electronic Spectroscopy*, 2nd eds.; Elsevier Science Publishers: Amsterdam, 1984; p 503.

(40) (a) McKenzie, E. D.; Moore, R. D.; Worthington, J. M. *Inorg. Chim. Acta* **1975**, *14*, 37. (b) Falvello, L.; Gerloch, M. *Inorg. Chem.* **1980**, *19*, 472.

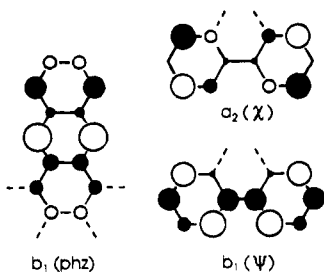
(41) Goodman, B. A.; Raynor, J. B. *Adv. Inorg. Chem. Radiochem.* **1970**, *13*, 136.

(42) For a discussion, see: Ceulemans, A.; Dendooven, M.; Vanquickenborne, L. G. *Inorg. Chem.* **1985**, *24*, 1159.

(43) (a) Goursot, A.; Chermette, H.; Waltz, W. L.; Lilie, J. *Inorg. Chem.* **1989**, *28*, 2241. (b) Goursot, A.; Chermette, H.; Waltz, W. L.; Lilie, J. *Inorg. Chem.* **1989**, *28*, 2247.

(44) Kaim, W. *J. Am. Chem. Soc.* **1982**, *104*, 3833.

for this effect lies in the occupation of an orbital $b_1(\text{phz})$, which is almost exclusively confined to the phenazine part of the molecule.³⁰



The total amount Δg of g anisotropy (Table 3) thus shows a variation which is closely related to the extent of orbital interaction between the singly occupied π^* orbital of N^-N and the appropriate orbital ($5d_{xz}$) at the metal. This interaction depends on the π^* orbital coefficients at the coordination centers, which are highest for bpz (and the related tap) ligand and lower for the bpm and bpm isomers.²¹

Except for the dppz complex where the metal participates very little at the SOMO, the g factors show a deviation to lower values relative to the free electron value g_e of 2.0023. According to an established concept,⁴⁵ this sign for the deviation of the isotropic g value suggests a frontier orbital situation with strong contributions from close-lying excited states with nonzero angular momentum involving low-lying unoccupied MOs, such as $5d_{xy}$ or $6p_z$. In comparison, the contribution from those excited states involving occupied MOs such as the other $5d$ orbitals should be small.

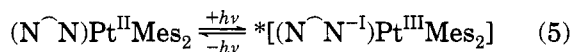
The relation $g_1 > g_2 > g_e > g_3$ is very different from the one expected for a square planar $\text{Pt}(\text{I}) = 5d^9$ system, viz., $g_{\parallel} > g_{\perp} > g_e$.⁴⁶ Nevertheless, the series of complexes $[(\text{N}^-\text{N})\text{PtMes}_2]^-$ has allowed us to correlate the isotropic g factors with the metal isotope hyperfine splitting (Figure 4) as is often done successfully for metal-centered paramagnetic species.^{46,47} A rather satisfactory linear correlation was obtained, the bpy complex showing the strongest effect due to a specific combination of σ -donor and π -acceptor capability. The anion $[(\text{bpy})\text{PtMes}_2]^-$ also exhibits a lower g_{iso} than the $\text{bpy}^{\cdot-}$ complexes of PtPh_2 , $\text{Pt}(o\text{-CF}_3\text{Ph})_2$ and PtCl_2 , indicating a closer situation of π^* (N^-N) and low-lying unoccupied metal orbitals in the radical complexes with PtMes_2 .

UV/Vis/near-IR spectroelectrochemistry of the anionic complexes confirms the notion of a predominant N^-N ligand-based electron uptake (eqs 3 and 4). The observed spectra (Figure 8, Table 7) show close similarity to those of the free ligand ions²⁹⁻³¹ and their complexes,^{30,48} the spectra in the Vis/near-IR region of the radical complexes are dominated by intraligand ($\pi \rightarrow \pi$) transitions which involve the SOMO. Many of these transitions show characteristic vibrational structuring; forbidden transitions that are very weak in the free ligands^{29,31} gain in intensity after metal coordination.^{30,48} While the absorption bands of the dimesitylplatinum complexes of the anion radical ligands show

slight hypsochromic shifts of $\sim 1000 \text{ cm}^{-1}$ relative to those of free $(\text{N}^-\text{N})^{\cdot-}$, their similarity encourages us to transfer the previous assignments^{29,30,48} to the complexes reported here. As has been noted previously for complexes of anion radicals,⁴⁸ the MLCT absorption bands which dominate the spectra of the precursor complexes are diminished in intensity and shifted into the UV region where they are often obscured by intense intraligand absorption bands. In most instances, the radical anions and their complexes exhibit transitions at longer wavelengths than the doubly reduced species (Figure 8, Table 7).

Absorption and Emission Spectroscopy, Solvatochromism, and Reorganization Energies. On the basis of the collected information on neighboring oxidation states we can interpret the optical absorption and emission spectra of the neutral complexes $(\text{N}^-\text{N})\text{-PtMes}_2$ as follows.

In contrast to complexes $(\text{N}^-\text{N})\text{M}(\text{CO})_4$, $\text{M} = \text{Cr}, \text{Mo}, \text{W}$,²¹ $[(\text{N}^-\text{N})\text{Ru}(\text{bpy})_2]^{2+,38}$ or $[(\text{N}^-\text{N})\text{Cu}(\text{PPh}_3)_2]^{+,49}$ the absorption spectra show generally structured bands (Figure 5) of medium intensity (ϵ 1500–4000 $\text{M}^{-1} \text{ cm}^{-1}$; Table 4) in the visible region. While part of this effect may be due to vibrational structuring in rather rigid complexes with low-coordinate metal centers, there appear to be several close-lying electronic transitions with comparable intensity. From the EPR and UV/Vis/near-IR spectroelectrochemical results (eqs 2–4), we can deduce that the lowest lying transitions should have MLCT character (eq 5).



The observed negative solvatochromism of the long-wavelength absorptions, i.e., their hypsochromic shift in more polar solvents (coupled with diminished structuring, Figure 7) is also indicative of "normal" MLCT transitions where the direction of the transition moment (metal to ligand) is opposite to the dipole moment in the ground state: $(\text{N}^-\text{N})^{\delta+}\text{-Pt}^{\delta-}$.²⁴⁻²⁸

Successful correlations with the E^*_{MLCT} parameters²⁵ (Table 6) also confirm the MLCT character underlying the long-wavelength band system; not only the direction but also the extent of the solvatochromism are typical for complexes between electron-rich metal centers and π -acceptor ligands²⁴ which are not engaging significantly in π/π interaction with solvent donor molecules.²⁷ The latter is due to the moderate acceptor character of complexes $(\text{N}^-\text{N})\text{PtMes}_2$ and to the steric bulk of the mesityl groups, which precludes a π/π solvation interaction.²⁷ There is a small variation in the solvent sensitivity of the longest wavelength absorption feature which, however, is not without precedent;^{2e,50} the bpm complex exhibits the most pronounced such sensitivity whereas $(\text{bpy})\text{PtMes}_2$ shows a relatively small solvatochromism. In comparison, the solvent sensitivity of PtMes_2 complexes is smaller than that of PtPh_2 analogues,^{2e} indicating a higher dipole moment in the ground state for the latter complexes with the less electron-rich diarylplatinum fragment. The band positions for individual solvents and the calculated inter-

(45) Kaim, W. *Coord. Chem. Rev.* **1987**, *76*, 187.

(46) Symons, M. *Chemical and Biochemical Aspects of Electron-Spin Resonance*; Van Nostrand Reinhold Co.: New York, 1978.

(47) Moscherosch, M.; Kaim, W. *J. Chem. Soc., Perkin Trans. 2* **1992**, 1493.

(48) Braterman, P. S.; Song, J.-I.; Kohlmann, S.; Vogler, C.; Kaim, W. *J. Organomet. Chem.* **1991**, *411*, 207.

(49) Vogler, C.; Kaim, W. *Z. Naturforsch.* **1992**, *47B*, 1057.

(50) Ernst, S.; Kurth, Y.; Kaim, W. *J. Organomet. Chem.* **1986**, *302*, 211.

cepts A at $E_{\text{MLCT}}^* = 0.0$ (Table 6) show the expected and established^{21,38,49,50} dependence on the π -acceptor ligands $\widehat{N\widehat{N}}$, which can also be deduced from the electrochemical potential differences $E_{1/2}^{\text{oxI}} - E_{1/2}^{\text{redI}}$ (see below, Table 9).

In addition to the intense absorption bands with their irregular structuring, there are weak long-wavelength shoulders observable for each of the complexes $(\widehat{N\widehat{N}})\text{PtMes}_2$ (Figure 5). These features may be attributed to ³MLCT transitions which have sufficient intensity here because of the involvement of a heavy element.

Platinum(II) complexes show frequently emission from intraligand, MLCT, LF, or metal/metal excited states.⁵ The complexes $(\widehat{N\widehat{N}})\text{PtMes}_2$ offer the opportunity to study systems that exhibit systematically variable electronic structures and are shielded against aggregation or "direct" solvation in the first coordination sphere. On the other hand, the structural situation as indicated in Figure 1 is characterized by a certain rigidity which should not only improve the resolution of absorption features but also enhance the emission intensity due to the restriction of quenching processes.⁵

While a more detailed low-temperature emission study of some selected complexes $(\widehat{N\widehat{N}})\text{PtMes}_2$ will be reported elsewhere,⁵¹ the preliminary results of room-temperature luminescence in toluene solution summarized here (Figure 6, Table 5) already suggest that the typical emission bands with maxima between 580 and 620 nm result from MLCT excited states. In agreement with a hypsochromically shifted absorption, the compound $(\text{bpy})\text{Pt}(\text{o-CF}_3\text{Ph})_2$ exhibits an emission band at 508 nm, i.e., at a much shorter wavelength than the dimesitylplatinum analogue. On the other hand, $(\text{bpm})\text{PtMes}_2$ exhibits no detectable emission below 750 nm, as was also observed for $(\text{bpm})\text{PtPh}_2$.^{2e} The reason for this latter result lies in the very low-lying MLCT excited state and in the facile quenching of this state by interaction with the peripheral nucleophilic $\text{N}^{1,1'}$ centers.⁵² Both the solvatochromism of the emission maximum of $(\text{bpy})\text{PtMes}_2$ and the decreasing Stokes shift for the complexes with better π -acceptor ligands suggest an emission from a ³MLCT excited state, as was discussed previously for related systems.^{5a,9,4}

The availability of both oxidation and reduction potentials for complexes with low-lying MLCT absorption and emission has allowed us to correlate (eq 6) the

$$\Delta E = E_{1/2}^{\text{oxI}} - E_{1/2}^{\text{redI}} \text{ (in V)} = E_{\text{op}} \text{ (in eV)} - \chi \quad (6)$$

electrochemical differences ΔE with the optical data. Such correlations have been obtained before for ruthenium(II) "polypyridine" complexes⁵³ and some other complexes of d^6 metals.⁵⁴ Here we report a first such correlation with calculated contributions χ from inter- and intramolecular reorganization⁵⁵ for a series of d^8 -configured systems in two different solvents (Table 9).

Table 9. Correlation^a between Optical and Electrochemical Data for Complexes $(\widehat{N\widehat{N}})\text{PtMes}_2$ in Two Different Solvents

$\widehat{N\widehat{N}}$	$\Delta E = E_{1/2}^{\text{oxI}} - E_{1/2}^{\text{redI}}$ (V)		E_{op} (eV) ^b		χ ((eV) ^b	
	THF	MeCN	THF	MeCN	THF	MeCN
bpy	2.37	2.27	2.58	2.67	0.21	0.43
bpm	1.90	1.78	2.09	2.22	0.20	0.44
bpz	2.06	1.99	2.31	2.37	0.25	0.38
bpym	2.21	2.11	2.45	2.57	0.24	0.46
tap	2.09	1.98	2.31	2.41	0.22	0.43
dppz	1.99	1.91	2.51	2.67	0.52	0.76

^a $\chi = E_{\text{op}} - \Delta E$. ^b 1 eV = 8065.5 cm^{-1} .

Scheme 1

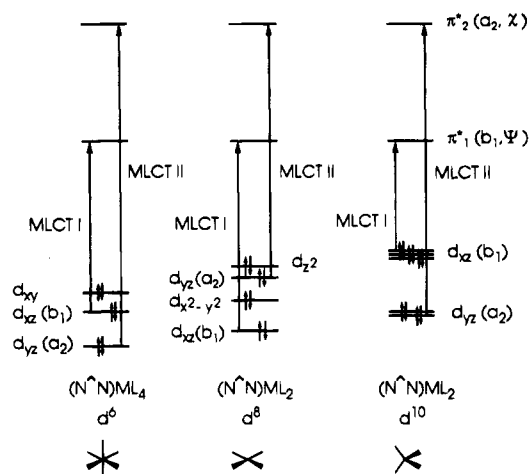


Table 9 shows that the reorganization energies are generally larger by ~ 0.2 eV in the more polar acetonitrile (intermolecular contribution) than in THF, where most values χ are similar to the $\chi \sim 0.2$ V obtained for complexes of $(\widehat{N\widehat{N}})_2\text{Ru}^{2+}$.⁵³ This result indicates both a fairly high degree of conformational rigidity due to steric crowding (Figure 1) and little geometrical restructuring in going from $(\widehat{N\widehat{N}})^0$ to $(\widehat{N\widehat{N}})^-$ and from Pt(II) to Pt(III) (intramolecular contributions to χ). Large deviations of $\chi > 0.5$ (eV) are observed and expected^{15,30} for the dppz complex because the "redox orbital" $b_1(\text{phz})$ is different from the "optical orbital" $b_1(\psi)$ in this case.

An excellent correspondence between optical and electrochemical data is obtained when information from absorption and emission in the same solvent are combined. For $(\text{bpy})\text{PtMes}_2$ in MeCN, the average between the absorption maximum at 2.67 eV (21 505 cm^{-1} , 465 nm) and the emission maximum at 1.75 eV (14 140 cm^{-1} , 707 nm) lies at 2.21 eV and thus very close to the ΔE value of 2.27 V in that solvent (Table 9).

In view of all available information from electrochemistry and EPR and UV/Vis/near-IR spectroscopy of complexes $(\widehat{N\widehat{N}})\text{PtMes}_2$,^{2e} we can assign the absorption spectra of the neutral forms as follows: The weak long-wavelength shoulders of the main intense band system are due to ³MLCT transitions, which owe their visibility to the presence of a $5d^8$ metal center. The highly solvatochromic and always structured group of absorptions in the visible and near-UV region involves apparently two ¹MLCT absorption band systems which exhibit vibrational splitting. Whereas the resolution of vibrational splitting in nonpolar solvents is favored by the low coordination number of the d^8 system⁵⁶ and by

(51) Stückl, A. C.; Klein, A., in preparation.
 (52) Kaim, W.; Matheis, W. *Chem. Ber.* **1990**, *123*, 1323.
 (53) Dodsworth, E. S.; Lever, A. B. P. *Chem. Phys. Lett.* **1985**, *119*, 61; **1986**, *124*, 152.
 (54) (a) Bruns, W.; Kaim, W.; Waldhör, E.; Krejčík, M. *Inorg. Chem.*, in press. (b) Kaim, W.; Bruns, W.; Kohlmann, S.; Krejčík, M. *Inorg. Chim. Acta* **1995**, *229*, 143.
 (55) Kober, E. M.; Goldsby, K. A.; Narayana, D. N. S.; Meyer, T. J. *J. Am. Chem. Soc.* **1983**, *105*, 4303.

(56) Ladwig, M.; Kaim, W. *J. Organomet. Chem.* **1992**, *439*, 79.

the geometrical rigidity, the closeness of both overlap-favored MLCT transitions MLCT1 ($d_{yz} \rightarrow \pi^*_{1}(\psi)$) and MLCT2 ($d_{xz} \rightarrow \pi^*_{2}(\chi)$) is due to an orbital situation (Scheme 1) where the d_{xz} orbital lies *lower* than d_{yz} .

This situation is thus different from that of essentially octahedral complexes $(\widehat{N})ML_4$ of d^6 metal centers^{21,57} and from that of approximately tetrahedral complexes $(\widehat{N})ML_2$ of d^{10} metals,⁴⁹ where the differences between MLCT1 and MLCT2 are much larger.

(57) Balk, R.; Stufkens, D. J.; Oskam, A. *Inorg. Chim. Acta* **1978**, *28*, 133.

Acknowledgment. This work was supported by Deutsche Forschungsgemeinschaft (SFB 270), Volkswagen-Stiftung, and Fonds der Chemischen Industrie. We thank J. Fees for the dppz ligand.

Supplementary Material Available: Table of reaction times, yields, and elemental analyses for complexes $(\widehat{N})Pt(\text{Mes})_2$ (1 page). Ordering information is given on any current masthead page.

OM9406097

Electrochemistry of Octamethyl[3]ruthenocenophane: Synthesis and Structure of the First Dicationic Derivative of Ruthenocene, $[\{\eta^5:\eta^5\text{-C}_5\text{Me}_4(\text{CH}_2)_3\text{C}_5\text{Me}_4\}\text{Ru}(\text{NCMe})](\text{PF}_6)_2$

Kiyonari Hashidzume, Hiromi Tobita,* and Hiroshi Ogino*

Department of Chemistry, Faculty of Science, Tohoku University, Sendai 980-77, Japan

Received August 25, 1994[⊗]

The octamethyl[3]ruthenocenophane $\{\eta^5:\eta^5\text{-C}_5\text{Me}_4(\text{CH}_2)_3\text{C}_5\text{Me}_4\}\text{Ru}$ (**1**) was synthesized by the reaction of $\text{RuCl}_3 \cdot 3\text{H}_2\text{O}$ with $\text{HC}_5\text{Me}_4(\text{CH}_2)_3\text{C}_5\text{Me}_4\text{H}$ in triethylene glycol at 200 °C. Other sterically congested ruthenocene derivatives, $(\eta^5\text{-C}_5\text{Me}_5)_2\text{Ru}$ (**2**) and $(\eta^5\text{-C}_5\text{Me}_4\text{H})_2\text{Ru}$ (**3**), were also prepared in high yields by this simple method. The cyclic voltammogram of **1** in CH_2Cl_2 shows a reversible 1e oxidation wave at $E_{1/2} = +0.36$ V vs SCE, while that in CH_3CN exhibits a 2e oxidation wave at +0.30 V vs SCE and a smaller 2e reduction wave at -0.04 V vs SCE. The bulk electrolysis of **1** at +0.30 V vs SCE in 0.1 M $\text{NH}_4\text{PF}_6/\text{CH}_3\text{CN}$ gave the dication salt containing CH_3CN as an additional ligand, $[\{\eta^5:\eta^5\text{-C}_5\text{Me}_4(\text{CH}_2)_3\text{C}_5\text{Me}_4\}\text{Ru}(\text{NCMe})](\text{PF}_6)_2$ (**4**), almost quantitatively. The ECE mechanism including the CH_3CN coordination/dissociation process was suggested for the redox reaction between **1** and its dication $[\mathbf{1} \cdot \text{NCCH}_3]^{2+}$ based on the cyclic voltammograms of **1**–**4** as well as the crystal structure analysis of **1** and **4**. Crystal data for **1**: $\text{C}_{21}\text{H}_{30}\text{Ru}$, space group $P2_1/a$, $a = 15.272(2)$ Å, $b = 11.090(1)$ Å, $c = 10.991(2)$ Å, $\beta = 101.07(2)^\circ$, $V = 1826.8(4)$ Å³, $Z = 4$, $R = 0.052$, and $R_w = 0.084$ based on 4435 reflections with $[|F_o| > 3\sigma(F_o)]$. Crystal data for **4**: $\text{C}_{23}\text{H}_{33}\text{F}_{12}\text{NP}_2\text{Ru}$, space group $Pmnm$, $a = 11.031(1)$ Å, $b = 14.883(1)$ Å, $c = 8.973(1)$ Å, $V = 1473.1(2)$ Å³, $Z = 2$, $R = 0.059$, and $R_w = 0.085$ based on 2528 reflections with $[|F_o| > 3\sigma(F_o)]$.

Introduction

The redox behavior of group 8 metallocenes has been extensively studied since the discovery of ferrocene in 1951.¹ Nevertheless, the redox chemistry of ruthenocene and osmocene has made only slow advances relative to that of ferrocene. Ruthenocene has been known to exhibit an irreversible 2e oxidation wave by cyclic voltammetry (CV) since 1960.² But, in spite of some efforts,² the isolation of the electrochemical 2e oxidation product has not yet succeeded. Only chemical oxidation of Cp_2Ru ($\text{Cp} = \eta^5\text{-C}_5\text{H}_5$) with halogens gave isolable Ru(IV) species, $[\text{Cp}_2\text{Ru-X}]^+$ ($\text{X} = \text{Cl, Br, I}$),³ and the reactivity⁴ and electron-transfer reactions^{5,6} of these monocations have been thoroughly investigated. In the case of osmocene, which shows two successive irreversible oxidation waves, the Os(IV) species $[\text{Cp}_2\text{Os-X}]^+$ ($\text{X} = \text{Cl, Br, I, NO}_3$) have been prepared chemically and the reactivity investigated.⁵ Moreover, the osmocene

dications ligated by a Lewis base $[\text{Cp}_2\text{Os-L}]^{2+}$ ($\text{L} = \text{NCCH}_3, \text{SC}(\text{NH}_2)_2$) have been synthesized as the first group 8 metallocene(IV) dications by the disproportionation of dimeric osmocenium ion $[(\text{Cp}_2\text{Os})_2]^{2+}$.⁷ Despite these advances of the synthesis of oxidized group 8 metallocenes, the redox behavior of ruthenocene and osmocene has not been well interpreted yet because of the irreversibility of their CV's.

Recently, Hill et al. reported that all parent group 8 metallocenes Cp_2M ($\text{M} = \text{Fe, Ru, Os}$) exhibit a single, quasi-reversible 1e oxidation in CH_2Cl_2 solutions of the noncoordinating electrolyte tetrabutylammonium tetrakis[3,5-bis(trifluoromethyl)phenyl]borate.⁸ On the basis of these results, they suggested that the above-mentioned irreversible 2e oxidation of ruthenocene is the result of the coordination of even weakly coordinating species in the solution. This phenomenon could be avoided by steric blocking of the electrophilic metal center. In fact, sterically congested decamethylruthenocene and -osmocene exhibit a reversible 1e oxidation in CH_2Cl_2 even in the presence of usual supporting electrolytes such as $\text{Bu}_4\text{N}^+\text{PF}_6^-$.⁹ Furthermore, Kölle et al. succeeded in the isolation of the decamethylruthenocene monocation, although it is thermally unstable.⁹ Interestingly, Kölle et al. also reported that in CH_3CN the CV of decamethylruthenocene at low sweep rate shows a small reduction wave at 0.05 V vs SCE on

[⊗] Abstract published in *Advance ACS Abstracts*, February 1, 1995.

(1) (a) Mann, C. K.; Barnes, K. K. *Electrochemical Reactions in Nonaqueous Systems*; Marcel Dekker: New York, 1970; p 418. (b) Janz, G. J.; Tomkins, R. P. T. *Nonaqueous Electrolytes Handbook*; Academic Press: New York, 1978; Vol. 2, p 611.

(2) (a) Kuwana, T.; Publitz, D. E.; Hoh, G. *J. Am. Chem. Soc.* **1960**, *82*, 5811. (b) Gubin, S. P.; Smirnova, S. A.; Denisovich, L. I.; Lubovich, A. A. *J. Organomet. Chem.* **1971**, *30*, 243. (c) Denisovich, L. I.; Zakurin, N. V.; Bezrukova, A. A.; Gubin, S. P. *J. Organomet. Chem.* **1974**, *81*, 207. (d) Gale, R. J.; Job, R. *Inorg. Chem.* **1981**, *20*, 42.

(3) Sohn, Y. S.; Schlucter, A. W.; Hendrickson, D. N.; Gray, H. B. *Inorg. Chem.* **1974**, *13*, 301.

(4) (a) Smith, T. P.; Kwan, K. S.; Taube, H.; Bino, A.; Cohen, S. *Inorg. Chem.* **1984**, *23*, 1943. (b) Kirchner, K.; Taube, H. *J. Am. Chem. Soc.* **1991**, *113*, 7039. (c) Kirchner, K.; Taube, H.; Scot, B.; Willet, R. D. *Inorg. Chem.* **1993**, *32*, 1430.

(5) Smith, T. P.; Iverson, D. J.; Droegge, M. W.; Kwan, K. S.; Taube, H. *Inorg. Chem.* **1987**, *26*, 2882.

(6) Kirchner, K.; Dodgen, H. W.; Wherland, S.; Hunt, J. P. *Inorg. Chem.* **1990**, *29*, 2381.

(7) Droegge, M. W.; Harman, W. D.; Taube, H. *Inorg. Chem.* **1987**, *26*, 1309.

(8) Hill, M. G.; Lamanna, W. M.; Mann, K. R. *Inorg. Chem.* **1991**, *30*, 4687.

(9) (a) Kölle, U.; Salzer, A. *J. Organomet. Chem.* **1983**, *243*, C27. (b) O'Hare, D.; Green, J. C.; Chadwick, T. P.; Miller, J. S. *Organometallics* **1988**, *7*, 1335.

the backward scan besides a large reversible 1e oxidation wave. From these facts, it is obvious that the redox behavior of the ruthenocene derivatives changes depending on the solvent, substituents on the cyclopentadienyl rings, and supporting electrolyte, but there has been very little information about the mechanism of this phenomenon.

We have recently succeeded in the synthesis and structure determination of the first dicationic derivative of ferrocene, $[\{\eta^5\text{-}\eta^5\text{-C}_5\text{Me}_4(\text{CH}_2)_3\text{C}_5\text{Me}_4\}\text{Fe}(\text{NCMe})](\text{PF}_6)_2$.¹⁰ This prompted us to complete the iron triad with respect to the metallocene dication. We report here the synthesis and electrochemistry of octamethyl[3]-ruthenocenophane, $\{\eta^5\text{-}\eta^5\text{-C}_5\text{Me}_4(\text{CH}_2)_3\text{C}_5\text{Me}_4\}\text{Ru}$, and the synthesis and structure of the first dicationic derivative of ruthenocene, $[\{\eta^5\text{-}\eta^5\text{-C}_5\text{Me}_4(\text{CH}_2)_3\text{C}_5\text{Me}_4\}\text{Ru}(\text{NCMe})](\text{PF}_6)_2$. We also show the first clear evidence for the 2e redox behavior of ruthenocene derivatives.

Experimental Section

All manipulations were performed under an inert atmosphere using standard Schlenk techniques. All solvents were dried and deoxygenated by standard methods. $\text{HC}_5\text{Me}_4(\text{CH}_2)_3\text{C}_5\text{Me}_4\text{H}$,¹¹ $\text{C}_5\text{Me}_5\text{H}$,¹² $\text{C}_5\text{Me}_4\text{H}_2$,¹³ and $[\text{Cp}_2\text{Fe}]\text{PF}_6$ ¹⁴ were prepared by the published procedures. Bu_4NPF_6 was recrystallized from EtOH. Other reagents were purchased and used without further purification. ^1H and ^{13}C NMR spectra were recorded on Bruker AM-600 and Varian XL-200 spectrometers, IR spectra on JASCO IR-810 and Bruker IFS66v spectrophotometers, mass spectra on JEOL-HX100 and Hitachi M-2500 spectrometers, and UV-vis spectra on a Shimadzu UV-265 spectrophotometer. Cyclic voltammograms were recorded by use of an electrochemical analysis system consisting of a FUSO potential scanning unit (Model 321) and a potentiostat (Model 311). Measurements were made with a three-electrode system containing a Pt-rod working electrode, a Pt-coil auxiliary electrode, and a saturated calomel reference electrode (SCE). A measured solution was coupled through a salt bridge filled with a 0.1 M supporting electrolyte solution to the reference electrode. Bu_4NPF_6 was used as supporting electrolyte and was dissolved in acetonitrile or dichloromethane to make 0.1 M solutions. Bulk electrolysis was carried out using a HOKUTO DENKO HA 501 potentiostat/galvanostat, and the current was monitored on a FUSO coulometer (Model 343). A Pt net was used as a working electrode, a carbon rod as a counter electrode which was separated from the electrolysis solution by a sintered glass filter, and a saturated calomel electrode as a reference electrode.

$\{\eta^5\text{-}\eta^5\text{-C}_5\text{Me}_4(\text{CH}_2)_3\text{C}_5\text{Me}_4\}\text{Ru}$ (1). A mixture of $\text{RuCl}_3\cdot 3\text{H}_2\text{O}$ (1.05 g, 4.06 mmol), $\text{HC}_5\text{Me}_4(\text{CH}_2)_3\text{C}_5\text{Me}_4\text{H}$ (3.19 g, 11.2 mmol), and triethylene glycol (100 mL) was heated at 200 °C for 3.5 h with vigorous stirring because of the poor solubility of the ligand precursor in the solvent. The reaction mixture was extracted with hexane (80 mL \times 6), and the solvent was removed from the combined extract. The residue was chromatographed on alumina (eluent hexane) to afford **1** as colorless crystals. Yield after recrystallization from ethanol: 404 mg (1.04 mmol, 26%). Mp: 254–258 °C dec. ^1H NMR (600 MHz, C_6D_6): δ 1.50 (12H, s, CH_3), 1.59 (4H, broad dd, CH_2), 1.72 (2H, broad quin, CH_2), 1.76 (12H, s, CH_3). ^{13}C NMR (50 MHz, C_6D_6): δ 10.0 ($^1J_{\text{CH}} = 125$ Hz, CH_3), 11.1 ($^1J_{\text{CH}} =$

125 Hz, CH_3), 21.4 ($^1J_{\text{CH}} = 124$ Hz, $^2J_{\text{CH}} = 4.5$ Hz, CH_2), 38.6 ($^1J_{\text{CH}} = 125$ Hz, $^2J_{\text{CH}} = 4.5$ Hz, CH_2), 81.4 (ring C), 83.6 (ring C), 84.8 (ring C). IR (KBr, cm^{-1}): 2960 (m), 2900 (m), 1635 (m), 1470 (w), 1380 (m), 1120 (w), 1070 (w), 1025 (m). MS (EI): m/z 384 (100, M^+), 369 (21.7, $\text{M}^+ - \text{CH}_3$), 148 (95.2, $\text{C}_5\text{-Me}_4(\text{CH}_2)_2^+$), 135 (21.6, C_5Me_5^+). UV (λ_{max} , nm (ϵ)): 311 (808). Anal. Calcd for $\text{C}_{21}\text{H}_{30}\text{Ru}$: C, 65.76; H, 7.88. Found: C, 65.99; H, 7.86.

$(\eta^5\text{-C}_5\text{Me}_5)_2\text{Ru}$ (2).⁹ A mixture of $\text{RuCl}_3\cdot 3\text{H}_2\text{O}$ (203 mg, 0.780 mmol), $\text{C}_5\text{Me}_5\text{H}$ (230 mg, 1.35 mmol), and ethylene glycol (15 mL) was heated at 140 °C for 14.5 h. During this reaction, $(\eta^5\text{-C}_5\text{Me}_5)_2\text{Ru}$ sublimed onto the surface of the flask as white crystals. The reaction mixture was extracted with hexane (30 mL \times 3), and the solvent was removed from the extract to afford crude $(\eta^5\text{-C}_5\text{Me}_5)_2\text{Ru}$. Sublimation of the crude sample at 85 °C/0.3 Torr gave pure **2** as colorless crystals. Yield: 174 mg (0.47 mmol, 70%). ^1H NMR (90 MHz, CDCl_3): δ 1.63 (30 H, s, CH_3) (lit.⁹ 1.63 ppm); MS (EI): m/z 372 (100, M^+), 357 (42.5, $\text{M}^+ - \text{CH}_3$), 135 (25.0, C_5Me_5).

$(\eta^5\text{-C}_5\text{Me}_4\text{H})_2\text{Ru}$ (3).¹⁵ In a similar manner, heating of $\text{RuCl}_3\cdot 3\text{H}_2\text{O}$ (205 mg, 0.793 mmol) and $\text{C}_5\text{Me}_4\text{H}_2$ (285 mg, 70% in purity, 1.5 mmol) in ethylene glycol (40 mL) gave **3** as colorless crystals. Yield: 189 mg (0.551 mmol, 75%). ^1H NMR (300 MHz, CDCl_3): δ 1.67 (12H, s, CH_3), 1.69 (12H, s, CH_3), 4.04 (2H, s, $\text{C}_5\text{Me}_4\text{H}$); MS (EI): m/z 344 (100, M^+), 329 (55.0, $\text{M}^+ - \text{CH}_3$).

$[\{\eta^5\text{-}\eta^5\text{-C}_5\text{Me}_4(\text{CH}_2)_3\text{C}_5\text{Me}_4\}\text{Ru}(\text{NCMe})](\text{PF}_6)_2$ (4). (1) **Electrochemical Oxidation.** A solution of **1** (101 mg, 0.264 mmol) in CH_3CN (120 mL) containing 0.1 M NH_4PF_6 as supporting electrolyte was electrolyzed at +0.30 V vs SCE. Before the current decreased to almost zero, 41.0 C (corresponding to 1.6 electron per molecule) had passed through the cell. After filtration, the orange filtrate was evaporated and the residue was washed with water to remove white crystals of NH_4PF_6 to afford a red powder of $[\{\eta^5\text{-}\eta^5\text{-C}_5\text{Me}_4(\text{CH}_2)_3\text{C}_5\text{Me}_4\}\text{Ru}(\text{NCMe})](\text{PF}_6)_2$ (**4**; 175 mg, 0.245 mmol, 93%). Recrystallization of **4** from MeCN/ether gave red needles of pure **4**.

(2) **Chemical Oxidation.** Acetonitrile (20 mL) was added to **1** (303 mg, 0.789 mmol) and $[\text{Cp}_2\text{Fe}]\text{PF}_6$ (553 mg, 1.67 mmol), and the mixture was stirred at room temperature, which changed from blue to red within several minutes. After further stirring for 1.5 h, the solution was concentrated to ca. 10 mL and Et_2O was added to afford crude **4** as a red powder. This powder was collected by filtration and dissolved again in MeCN (50 mL). The solution was filtered and the filtrate was evaporated to give pure **4** (483 mg, 0.676 mmol, 86%) as a red solid. ^1H NMR (200 MHz, CD_3CN): δ 1.65 (12H, s, CH_3), 1.92 (12 H, s, CH_3), 1.7–2.4 (6H, m, CH_2), 2.85 (3H, s, CH_3CN). ^{13}C NMR (50 MHz, CD_3CN): δ 6.3 (CH_3CN), 9.1 (CH_3), 11.6 (CH_3), 18.1 (CH_2), 36.1 (CH_2), 108.1 (ring C), 108.5 (ring C), 115.9 (ring C), 136.4 (CH_3CN). IR (KBr, cm^{-1}): 2970 (w), 2940 (m), 2860 (w), 1735 (w), 1640 (m), 1520 (m), 1460 (m), 1445 (m), 1403 (m), 1390 (m), 1330 (w), 1265 (w), 1095 (w), 1090 (w), 1020 (m), 844 (vs, ν_{PF_6}), 560 (s, δ_{PF_6}). MS (EI): m/z 383 (75.0, $\text{M}^+ - 2\text{PF}_6 - \text{CH}_3\text{CN} - \text{H}^+$). UV (λ_{max} , nm (ϵ)): 367 (1710), 490 sh (240). Anal. Calcd for $\text{C}_{23}\text{H}_{33}\text{F}_{12}\text{N}_2\text{Ru}$: C, 38.66; H, 4.66; N, 1.96. Found: C, 38.68; H, 4.44; N, 1.92.

X-ray Crystal Structure Determination of 1. Crystals of **1** suitable for X-ray analysis were grown by gradually cooling the hot ethanol solution to room temperature over 2 days. Reflection data were collected on a Rigaku AFC-6A four-circle diffractometer with graphite-monochromated Mo K α radiation at 20 °C. Crystallographic data are listed in Table 1. From the crystal system and the lattice constants, the crystal of **1** was thought to be isomorphous with that of the iron analogue. Therefore, the analysis was started by assuming that all of the atomic positions of **1** except for those of the central methylene carbon of the trimethylene chain and

(10) Ogino, H.; Tobita, H.; Habazaki, H.; Shimoi, M. *J. Chem. Soc., Chem. Commun.* **1989**, 828.

(11) Tobita, H.; Habazaki, H.; Shimoi, M.; Ogino, H. *Chem. Lett.* **1988**, 1041.

(12) Threlkel, R. S.; Bercaw, J. E. *J. Organomet. Chem.* **1977**, 136, 1.

(13) Kohl, F. X.; Jutzi, P. *J. Organomet. Chem.* **1983**, 243, 119.

(14) Hendrickson, D. N.; Sohn, Y. S.; Gray, H. B. *Inorg. Chem.* **1971**, 10, 1559.

(15) Li, L.; Jiang, S.; Yang, G.; Liu, J.; Liang, Y. *Youji Huaxue* **1989**, 9, 217. *Chem. Abstr.* **1990**, 112, 119078c.

Table 1. Crystal Data for $\{\eta^5\text{-}\eta^5\text{-C}_5\text{Me}_4(\text{CH}_2)_3\text{C}_5\text{Me}_4\}\text{Ru}$ (1) and $[\{\eta^5\text{-}\eta^5\text{-C}_5\text{Me}_4(\text{CH}_2)_3\text{C}_5\text{Me}_4\}\text{Ru}(\text{NCMe})](\text{PF}_6)_2$ (4)

sample	1	4
formula	C ₂₁ H ₃₀ Ru	C ₂₃ H ₃₃ F ₁₂ NP ₂ Ru
fw	383.54	714.52
cryst syst	monoclinic	orthorhombic
space group	<i>P</i> 2 ₁ / <i>a</i>	<i>P</i> <i>mnm</i>
syst absence	(<i>h</i> 0 <i>l</i>), <i>h</i> = 2 <i>n</i> + 1 (0 <i>k</i> 0), <i>k</i> = 2 <i>n</i> + 1	(<i>h</i> 0 <i>l</i>), <i>h</i> + <i>l</i> = 2 <i>n</i> + 1
<i>a</i> /Å	15.272(2)	11.031(1)
<i>b</i> /Å	11.090(1)	14.883(1)
<i>c</i> /Å	10.991(2)	8.973(1)
β /deg	101.07(2)	
<i>V</i> /Å ³	1826.8(4)	1473.1(2)
<i>Z</i>	4	2
<i>d</i> _{calc} /g cm ⁻³	1.39	1.61
<i>d</i> _{meas} /g cm ⁻³	1.38	
μ (Mo K α)/cm ⁻¹	8.37	6.51
cryst size/mm	0.38 × 0.33 × 0.18	0.43 × 0.33 × 0.28
radiation	Mo K α (λ = 0.710 73 Å)	Mo K α (λ = 0.710 73 Å)
monochromator	graphite	graphite
temp/°C	20	20
rfIns measd	$\pm h, k, l$	<i>hkl</i>
2 θ range/deg	3–70	3–70
scan mode	ω –2 θ	ω –2 θ
ω -scan width/deg	1.0 + 0.35 tan θ	1.1 + 0.35 tan θ
bkgd(count time)/s	10.0	10.0
ω -scan rate/deg min ⁻¹	2.0	2.0
no. of unique data	6917	3554
no. of data used with $ F_o > 3\sigma(F_o)$	4435	2528
no. of params refined	176	171
<i>R</i> ^a	0.052	0.059
<i>R</i> _w ^b	0.084	0.085
quality-of-fit indicator ^c	0.915	1.59
largest shift/esd, final cycle	0.68	0.01
max resid electron dens/e Å ⁻³	1.1	1.48

^a $R = \sum ||F_o| - |F_c|| / \sum |F_o|$. ^b $R_w = [\sum w(|F_o| - |F_c|)^2 / \sum w|F_o|^2]^{1/2}$; $w = [\sigma^2(|F_o|) + aF_o^2]^{-1}$, where $a = 0.005$ for 1 and 0.002 for 4. ^c $[\sum w(|F_o| - |F_c|)^2 / (N_{\text{observns}} - N_{\text{params}})]^{1/2}$.

hydrogen atoms are the same as those of the iron analogue.¹⁶ Those were refined by the block-diagonal least-squares method with individual anisotropic thermal parameters. The central methylene carbon C(20) was found out in Fourier synthesis and was refined with an isotropic thermal parameter. There is a disorder for this carbon occupying the positions between C(10) and C(15) and between C(11) and C(16) with the occupancy factors 0.43 and 0.57, respectively. Positions of hydrogen atoms could not be determined. The final atomic parameters and temperature factors of non-hydrogen atoms are listed in Table 2.

X-ray Crystal Structure Determination of 4. Red needles of 4 were grown by diffusion of Et₂O vapor into the MeCN solution of 4 in a desiccator at 5 °C. Crystallographic data are listed in Table 1. The structure was solved by the heavy-atom method and refined by the block-diagonal least-squares method with individual anisotropic thermal parameters for non-hydrogen atoms. Positions of all hydrogen atoms of the methyl groups on the Cp rings were derived by difference-Fourier synthesis and refined by applying isotropic thermal parameters. Positions of other hydrogen atoms could not be determined. The final atomic parameters and temperature factors of non-hydrogen atoms are listed in Table 3.

All calculations were performed on a Nippon Electric Co. ACOS-2000 computer system at the Computer Center of Tohoku University with the Universal Crystallographic Computation Program System UNICS III.¹⁷

Results and Discussion

Synthesis of $\{\eta^5\text{-}\eta^5\text{-C}_5\text{Me}_4(\text{CH}_2)_3\text{C}_5\text{Me}_4\}\text{Ru}$ (1). The reaction of RuCl₃·3H₂O with cyclopentadiene in

Table 2. Final Atomic Coordinates ($\times 10^4$) and Equivalent Isotropic Temperature Factors for $\{\eta^5\text{-}\eta^5\text{-C}_5\text{Me}_4(\text{CH}_2)_3\text{C}_5\text{Me}_4\}\text{Ru}$ (1)

atom	<i>x</i>	<i>y</i>	<i>z</i>	<i>B</i> _{eqv} , Å ²
Ru	2753.5(2)	551.1(3)	559.8(3)	2.8
C(0)	2053(3)	–25(5)	782(4)	3.7
C(1)	3514(3)	–673(4)	1573(4)	3.3
C(2)	1982(3)	1166(4)	3883(4)	3.6
C(3)	2937(3)	2448(4)	3077(4)	3.5
C(4)	2887(3)	947(4)	4541(4)	3.4
C(5)	1274(4)	647(6)	15(8)	6.6
C(6)	4501(4)	–823(6)	1726(6)	5.1
C(7)	1182(5)	521(6)	4154(9)	6.6
C(8)	3289(4)	3434(5)	2354(6)	5.1
C(9)	3154(4)	118(6)	5598(5)	5.1
C(10)	1201(4)	–1443(8)	2101(7)	6.9
C(11)	1274(4)	647(6)	15(8)	6.6
C(12)	3320(5)	973(7)	–171(5)	5.5
C(13)	4501(4)	–823(6)	1726(6)	5.1
C(14)	3209(5)	–2347(5)	3095(6)	5.3
C(15)	1182(5)	521(6)	4154(9)	6.6
C(16)	1248(4)	2628(7)	2081(6)	5.8
C(17)	3289(4)	3434(5)	2354(6)	5.1
C(18)	4456(4)	1842(6)	4504(6)	5.3
C(19)	3154(4)	118(6)	5598(5)	5.1
C(20A) ^b	714(10)	–325(13)	2780(13)	4.6(0.3)
C(20B) ^b	814(9)	1547(12)	1109(12)	6.0(0.3)

^a The equivalent isotropic temperature factors for non-hydrogen atoms were computed using the following expression: $B_{\text{eqv}} = \frac{1}{3}(B_{11}a^2 + B_{22}b^2 + B_{33}c^2 + B_{13}ac \cos \beta)$. The B_{ij} 's are defined by $\exp[-(h^2B_{11} + k^2B_{22} + l^2B_{33} + 2hkB_{12} + 2hlB_{13} + 2klB_{23})]$. ^b These atoms were refined isotropically.

Table 3. Final Atomic Coordinates ($\times 10^4$) and Equivalent Isotropic Temperature Factors for Non-Hydrogen Atoms of $[\{\eta^5\text{-}\eta^5\text{-C}_5\text{Me}_4(\text{CH}_2)_3\text{C}_5\text{Me}_4\}\text{Ru}(\text{NCMe})](\text{PF}_6)_2$ (4)

atom	<i>x</i>	<i>y</i>	<i>z</i>	<i>B</i> _{eqv} , Å ²
Ru	2500	2468.7(3)	2500	2.8
P(1)	2500	4540(2)	7500	4.5
P(2)	2500	8955(2)	7500	4.6
F(1)	2500	3564(5)	7500	22.4
F(2)	2500	4595(9)	5832(6)	17.7
F(3)	1048(4)	4547(3)	7500	6.3
F(4)	2500	5584(6)	7500	15.4
F(5)	2500	9980(5)	7500	15.4
F(6)	1528(4)	9008(4)	6252(5)	13.4
F(7)	2500	7973(7)	7500	29.7
N	2500	3861(4)	2500	3.3
C(1)	1184(4)	1337(3)	2500	4.0
C(2)	947(3)	1864(3)	3793(4)	3.7
C(3)	595(3)	2719(3)	3311(4)	3.5
C(4)	1361(6)	316(4)	2500	6.2
C(5)	910(4)	1576(4)	5385(5)	5.7
C(6)	100(4)	3461(3)	4273(5)	5.1
C(7) ^b	2500	–56(7)	2977(14)	5.5
C(8)	2500	4591(6)	2500	5.0
C(9)	2500	5593(7)	2500	9.1

^a The equivalent isotropic temperature factors for non-hydrogen atoms were computed using the following expression: $B_{\text{eqv}} = \frac{1}{3}(B_{11}a^2 + B_{22}b^2 + B_{33}c^2)$. The B_{ij} 's are defined by $\exp[-(h^2B_{11} + k^2B_{22} + l^2B_{33} + 2hkB_{12} + 2hlB_{13} + 2klB_{23})]$. ^b Atomic occupancy factor: 50%.

ethanol in the presence of zinc dust is known to give Cp₂Ru in high yield.^{18,19} On the other hand, it is reported that similar methods in the presence or absence of zinc dust provide the decamethyl derivative ($\eta^5\text{-C}_5\text{Me}_5)_2\text{Ru}$ in only low to moderate yields, sometimes together with a large amount of $[(\eta^5\text{-C}_5\text{Me}_5)\text{RuCl}_2]_2$.^{9,20} Although a high-yield preparative method of ($\eta^5\text{-C}_5\text{Me}_5)_2\text{Ru}$ has been reported by Singleton et al., it utilizes

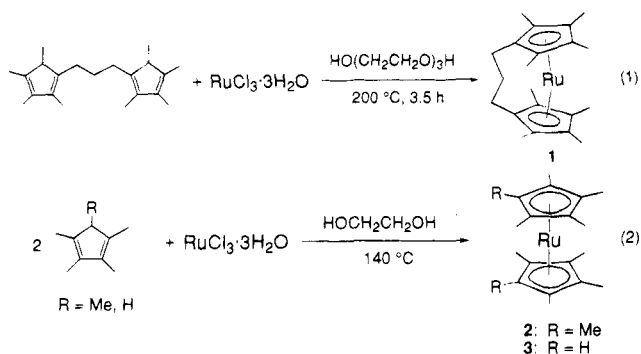
(18) (a) Rubezhov, A. Z.; Ivanov, A. S.; Bezrukova, A. A. *Izv. Akad. Nauk SSSR, Ser. Khim.* **1979**, 1608. (b) Pertici, P.; Vitulli, G.; Paci, M.; Porri, L. *J. Chem. Soc., Dalton Trans.* **1980**, 1961. (c) Vol'kenau, N. A.; Bolesova, I. N.; Shul'pina, L. S.; Kitaigorodskii, A. N.; Kravtsov, D. N. *J. Organomet. Chem.* **1985**, 288, 341.

(16) Tobita, H., unpublished results.

(17) Sakurai, T.; Kobayashi, M. *Rikagaku Kenkyusho Houkoku* **1979**, 55, 69.

relatively special precursors, $[\text{RuCl}_2(\text{COD})]_n$ and $n\text{-Bu}_3\text{SnC}_5\text{Me}_5$.^{19e,f}

For the synthesis of ruthenocenophane **1**, we first tried to apply the former method, i.e. the reaction of $\text{RuCl}_3 \cdot 3\text{H}_2\text{O}$ with $\text{HC}_5\text{Me}_4(\text{CH}_2)_3\text{C}_5\text{Me}_4\text{H}$ in ethanol. However, this resulted in only the formation of black solid, perhaps the chloride $[\{\text{C}_5\text{Me}_4(\text{CH}_2)_3\text{C}_5\text{Me}_4\}\text{Ru}_2\text{Cl}_4]_n$, and the desired product was not obtained. However, by changing the solvent from ethanol to high-boiling triethylene glycol, we succeeded in synthesizing **1** in a fair yield. Thus, the reaction of $\text{RuCl}_3 \cdot 3\text{H}_2\text{O}$ with $\text{HC}_5\text{Me}_4(\text{CH}_2)_3\text{C}_5\text{Me}_4\text{H}$ in triethylene glycol at 200 °C gave **1** as colorless crystals in 26% yield (eq 1). It was also found that other sterically congested ruthenocenes, $(\eta^5\text{-C}_5\text{Me}_5)_2\text{Ru}$ (**2**)^{9,20} and $(\eta^5\text{-C}_5\text{Me}_4\text{H})_2\text{Ru}$ (**3**),¹⁵ can also be prepared in high yields by a similar procedure (eq 2).



The ¹H NMR spectrum of **1** shows two sharp singlets for α - and β -methyl groups of tetramethylcyclopentadienyl moieties at δ 1.50 and 1.76 ppm, respectively, and a broad quintet for a central methylene and a broad double doublet for two methylenes next to the Cp rings at δ 1.72 and 1.59 ppm, respectively. The assignment of the methyl groups is based on the ¹H NMR spectrum of the β -monoethyl derivative of **1**, $\{\eta^5\text{-}\eta^5\text{-C}_5\text{Me}_4(\text{CH}_2)_3\text{C}_5\text{Me}_3\text{Et}\}\text{Ru}$, which shows the signals of α -methyl groups at higher field than that of a β -methyl group.²¹ The ¹³C NMR spectrum, mass spectrum, and elemental analysis are also consistent with the structure of ruthenocenophane **1**.

Electrochemistry. The cyclic voltammograms (CV's) of **1** and its dication $[\{\eta^5\text{-}\eta^5\text{-C}_5\text{Me}_4(\text{CH}_2)_3\text{C}_5\text{Me}_4\}\text{Ru}(\text{NCMe})](\text{PF}_6)_2$ (**4**; vide infra) are depicted in Figure 1 and the CV's of **2** and **3** in Figure 2. The redox potentials of **1**–**4** and Cp_2Ru are listed in Table 4. It is known that Cp_2Ru shows an irreversible one-step 2e oxidation wave under the usual conditions in CH_2Cl_2 or CH_3CN .² A similar redox behavior has also been

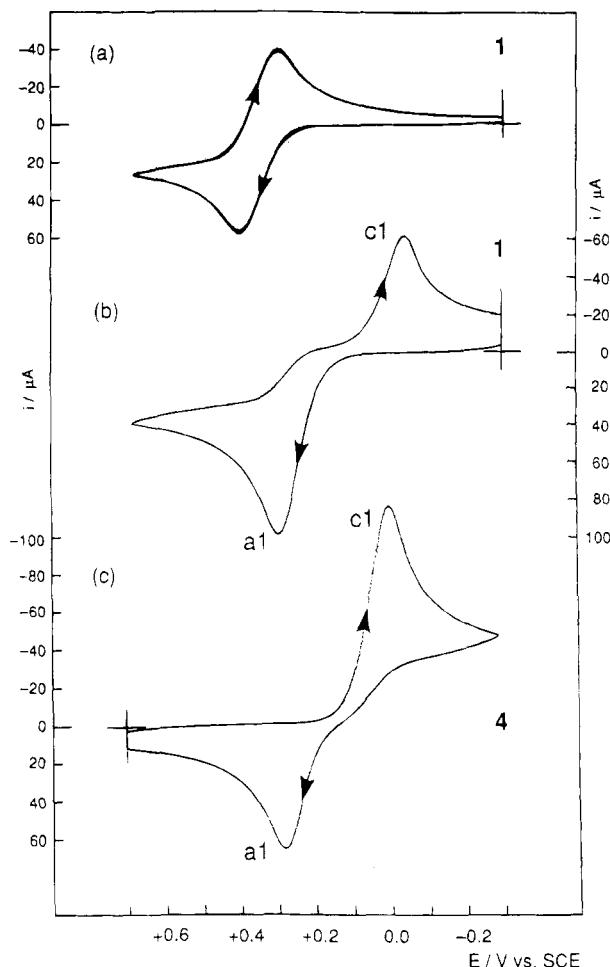


Figure 1. Cyclic voltammograms of (a) $\{\eta^5\text{-}\eta^5\text{-C}_5\text{Me}_4(\text{CH}_2)_3\text{C}_5\text{Me}_4\}\text{Ru}$ (**1**) in CH_2Cl_2 , (b) **1** in CH_3CN , and (c) $[\{\eta^5\text{-}\eta^5\text{-C}_5\text{Me}_4(\text{CH}_2)_3\text{C}_5\text{Me}_4\}\text{Ru}(\text{NCMe})](\text{PF}_6)_2$ (**4**) in CH_3CN at room temperature and a sweep rate of 50 mV s^{-1} . [**1**] = 1.02 mM (CH_2Cl_2) and 0.96 mM (CH_3CN); [**4**] = 1.00 mM .

observed for [3]- and [4]ruthenocenophanes in CH_3CN .²² The only exceptional redox behavior of Cp_2Ru has been observed when noncoordinating $[\text{Bu}_4\text{N}][\text{B}\{3,5\text{-C}_6\text{H}_3(\text{CF}_3)_2\}_4]$ is used as supporting electrolyte in CH_2Cl_2 : a reversible 1e oxidation wave has been observed in the CV.⁸

In contrast with these relatively noncongested ruthenocene derivatives, the oxidation of extremely congested $(\eta^5\text{-C}_5\text{Me}_5)_2\text{Ru}$ (**2**) is reported to proceed by a reversible 1e process in CH_2Cl_2 even in the presence of the usual supporting electrolyte (Figure 2a).⁹ A similar reversible oxidation wave is also observed for **2** in CH_3CN , but it is accompanied by a small irreversible reduction wave at a more negative region ($E_{\text{pc}} = +0.05 \text{ V}$ vs SCE) on the backward scan at a normal scan rate (Figure 2b).⁹ The irreversible redox behaviors of ruthenocene derivatives have been attributed to the susceptibility of ruthenocene monocations toward nucleophilic attack⁸ or dimerization,^{7,23} which might be suppressed by steric hindrance in the case of **2**. However, no direct evidence has been given for the binding of nucleophiles on the ruthenium center of oxidized ruthenocenes.

(19) For other preparative methods of Cp_2Ru , see: (a) Wilkinson, G. J. *Am. Chem. Soc.* **1952**, *74*, 6146. (b) Bublitz, D. E.; McEwen, W. E.; Kreinberg, J. *Org. Synth.* **1961**, *41*, 96. (c) Ritchie, G. L. D.; Cooper, M. K.; Calvert, R. L.; Dennis, G. R.; Phillips, L.; Vrbancich, J. J. *Am. Chem. Soc.* **1983**, *105*, 5215. (d) Gauthier, G. J. *J. Chem. Soc. D* **1969**, 690. (e) Liles, D. C.; Shavor, A.; Singleton, E.; Weige, M. B. *J. Organomet. Chem.* **1985**, *288*, C37. (f) Albers, M. O.; Liles, D. C.; Robinson, D. J.; Shavor, A.; Singleton, E.; Weige, M. B.; Boeyens, J. C. A.; Leventis, D. C. *Organometallics* **1986**, *5*, 2321. (g) Winter, C. H.; Pirzad, S.; Cao, D. H. *J. Chem. Soc., Chem. Commun.* **1991**, 1026. (h) Winter, C. H.; Pirzad, S.; Graf, D. D.; Cao, D. H.; Heeg, M. J. *Inorg. Chem.* **1993**, *32*, 3654.

(20) (a) Tilley, T. D.; Grubbs, R. H.; Bercaw, J. E. *Organometallics* **1984**, *3*, 274. (b) Oshima, N.; Suzuki, H.; Moro-oka, Y. *Chem. Lett.* **1984**, 1161. (c) Kudinov, A. R.; Rybinskaya, M. I.; Struchkov, Y. T.; Yanovskii, A. I.; Petrovskii, P. V. *J. Organomet. Chem.* **1987**, *336*, 187.

(21) Hashidzume, K., unpublished results.

(22) Kamiyama, S.; Ikeshoji, T.; Kasahara, A.; Matsue, T.; Osa, T. *Denkikagaku Oyobi Kougyoubuturikagaku* **1986**, 608.

(23) Mueller-Westerhoff, U. T.; Rheingold, A. L.; Swiegers, G. F. *Angew. Chem., Int. Ed. Engl.* **1992**, *31*, 1352.

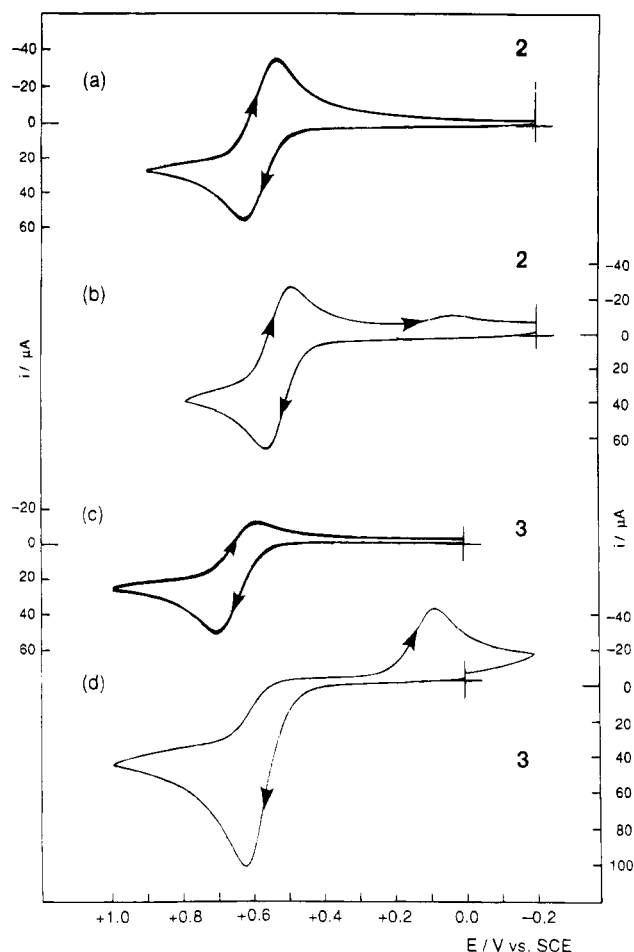


Figure 2. Cyclic voltammograms of (a) $(\eta^5\text{-C}_5\text{Me}_5)_2\text{Ru}$ (**2**) in CH_2Cl_2 , (b) **2** in CH_3CN , (c) $(\eta^5\text{-C}_5\text{Me}_4\text{H})_2\text{Ru}$ (**3**) in CH_2Cl_2 , and (d) **3** in CH_3CN at room temperature and a sweep rate of 50 mV s^{-1} . $[\mathbf{2}] = 1.02 \text{ mM}$ (CH_2Cl_2) and 1.01 mM (CH_3CN); $[\mathbf{3}] = 0.92 \text{ mM}$ (CH_2Cl_2) and 0.95 mM (CH_3CN).

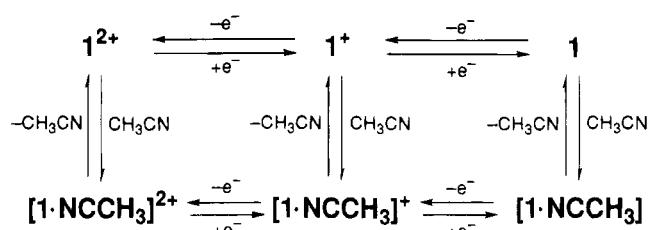
Table 4. Redox Potentials of **1–3** and Cp_2Ru (vs SCE) in CH_3CN at Room Temperature^a

compd	solvent	E_{pa}/V	E_{pc}/V	$E_{1/2}/\text{V}$	$\Delta E_p/\text{mV}$	n^b
1	CH_2Cl_2	+0.41	+0.30	+0.36	110	1
	CH_3CN	+0.30	-0.04		340	2
2	CH_2Cl_2	+0.62	+0.53	+0.58	90	1
	CH_3CN	+0.57	+0.49	+0.53	80	~1
3	CH_2Cl_2	+0.70	+0.59	+0.65	110	1
	CH_3CN	+0.62	+0.08		540	2
4	CH_3CN	+0.29	-0.01		300	2
	Cp_2Ru					
	CH_2Cl_2	+1.07	+0.58		490	2
Cp_2Ru	CH_2Cl_2^c	+1.08	+0.98	+1.03	95	1
	CH_3CN	+0.96	+0.47		490	2

^a Conditions and legend: supporting electrolyte, Bu_4NPF_6 ; E_{pa} , anodic peak potential; E_{pc} , cathodic peak potential; $E_{1/2}$, half-wave potential; ΔE_p , $E_{\text{pa}} - E_{\text{pc}}$. ^b Number of electrons involved in the electrode reactions. ^c Reference 8; supporting electrolyte $[\text{Bu}_4\text{N}][\text{B}\{3,5\text{-C}_6\text{H}_3(\text{CF}_3)_2\}_4]$.

The CV of **1** shows a reversible 1e oxidation wave in CH_2Cl_2 (Figure 1a) exactly like that of $(\eta^5\text{-C}_5\text{Me}_5)_2\text{Ru}$. In CH_3CN , on the other hand, the CV of **1** is completely different from that of **2**: **1** shows an oxidation wave a1 at +0.30 V vs SCE and a smaller reduction wave c1 at -0.04 V vs SCE on the backward scan after oxidation (Figure 1b). The fundamental shape of the CV is kept even at much higher scan rate (350 mV/s). The oxidation potential of **1** is the lowest among all known ruthenocene derivatives to date.

Scheme 1. Fence Scheme for the Redox Reactions between **1** and $[\mathbf{1}\cdot\text{NCCH}_3]^{2+}$ in CH_3CN

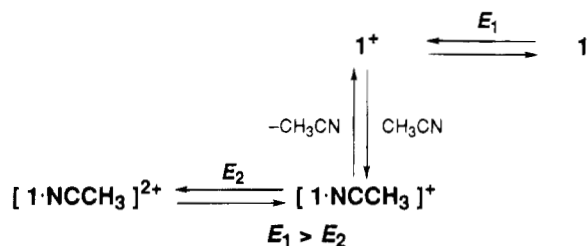


As will be discussed below, the oxidation product of **1** in CH_3CN at +0.30 V vs SCE has been isolated and characterized as the dication in which a CH_3CN molecule is coordinated to the Ru center, $[\{\eta^5\text{-C}_5\text{Me}_4(\text{CH}_2)_3\text{C}_5\text{Me}_4\}\text{Ru}(\text{NCMe})](\text{PF}_6)_2$ (**4**; see eq 4). This result clearly shows that the oxidation wave a1 corresponds to a 2e oxidation process and is accompanied by a chemical process: the ligation of CH_3CN . The reduction wave c1 on the backward scan can be assigned to a 2e reduction of the dication to regenerate **1** and is also accompanied by a chemical process: the dissociation of CH_3CN . The latter assignment is confirmed by the CV of the dication salt **4**, which shows the reduction wave c1 and oxidation wave a1 on the backward scan at positions identical with those of **1** (Figure 1c, Table 4). The only, but important, difference of the CV of **4** from that of **1** is that the wave height of c1 is larger than that of a1. In other words, in the CV's of both **1** and **4**, the wave on the backward scan is smaller than that of the forward scan. This is apparently due to the loss of the generated species by diffusion from the surface of the electrode. This loss occurs when the potential is scanned through the range between the waves a1 and c1, because in this range neither **1** nor **4** is electrolyzed substantially on the surface of the working electrode.

Scheme 1 shows the fence scheme for the redox reaction between **1** and $[\mathbf{1}\cdot\text{NCCH}_3]^{2+}$ including electron-transfer processes at the electrode surface coupled with homogeneous chemical reactions: the coordination and dissociation of a CH_3CN molecule. Three routes are possible from **1** to $[\mathbf{1}\cdot\text{NCCH}_3]^{2+}$, i.e. CEE, ECE, and EEC mechanisms, where E and C designate electrochemical and chemical steps, respectively.²⁴ Among them, the possibility of the CEE mechanism seems to be low because the 18e complex **1** is unlikely to be coordinated with CH_3CN to give a 20e complex or a ring-slippage product with a η^3 -cyclopentadienyl ring. Although several examples of these types of complexes are known, there seems to be no factors which stabilize the CH_3CN -coordinated derivative of **1**. Only a small difference in the oxidation potentials of **1** in CH_2Cl_2 ($E_{\text{pa}} = +0.41 \text{ V}$ vs SCE) and in CH_3CN ($E_{\text{pa}} = +0.30 \text{ V}$ vs SCE) supports the very weak interaction between **1** and CH_3CN . The EEC mechanism can be ruled out because, in CH_2Cl_2 , **1** shows only a reversible 1e oxidation wave. This means that the second oxidation from the monocation to the dication is only achieved by the vast lowering of the oxidation potential of the monocation as a result of the coordination of CH_3CN . Thus, the ECE mechanism is the most probable for this system.

(24) (a) Evans, D. H. *Chem. Rev.* **1990**, *90*, 739. (b) Bard, A. J.; Faulkner, L. R. *Electrochemical Methods: Fundamentals and Applications*; Wiley: New York, 1980; Chapter 11.

Scheme 2. ECE Scheme for the Redox Reaction between 1 and [1·NCCH₃]²⁺ in CH₃CN



To explain the CV's of **1** and **4** by the ECE mechanism, the following two prerequisites must be fulfilled: (1) the redox potential for [1·NCCH₃]⁺/[1·NCCH₃]²⁺ (E_2) must be more negative than that for 1/1⁺ (E_1) and (2) a fast equilibrium must exist between 1⁺ and [1·NCCH₃]⁺ in CH₃CN. Thus, in the oxidation of **1** to [1·NCCH₃]²⁺, 1⁺ generated on the electrode surface at the potential E_1 quickly equilibrates with [1·NCCH₃]⁺. Since E_2 is more negative than E_1 , [1·NCCH₃]⁺ is instantly oxidized on the electrode or by 1⁺ to give [1·NCCH₃]²⁺. The inverse process, the reduction of [1·NCCH₃]²⁺ to **1**, can be also explained in a similar ECE mechanism. These situations are illustrated in Scheme 2.

The CV of the iron analogue of **1**, { η^5 : η^5 -C₅Me₄(CH₂)₃C₅Me₄}Fe (**5**), shows two successive reversible and quasi-reversible 1e oxidation waves at $E_{1/2} = -0.049$ and 1.054 V vs SCE, respectively, in CH₃CN/0.1 M Bu₄NBF₄.¹⁰ This can be attributed to a very weak interaction between the monocation **5**⁺ and CH₃CN which only slightly shifts the oxidation potential to the negative side. In this case, the oxidation of **5** apparently proceeds in an EEC mechanism to give [5·NCCH₃]²⁺. Comparison of the CV's of **1** and **5** clearly shows that the interaction of CH₃CN with the ruthenium center of 1⁺ is much stronger than that with the iron center of 5⁺. In general, the large difference of the electrochemical behavior of ruthenocene in comparison with ferrocene is attributable to the much stronger interaction of ruthenocenium ion with nucleophilic solvents or supporting electrolytes compared with that of ferrocenium ion. Our demonstration of the ECE mechanism for the redox reaction between **1** and [1·NCCH₃]²⁺ strongly support this interpretation.

The strong interaction probably also exists between [(η^5 -C₅Me₅)₂Ru]⁺ (**2**⁺) and CH₃CN. As mentioned above, the CV of **2** in CH₃CN shows a small reduction wave on the backward scan (Figure 2b), and it has been assigned to the reduction of some decomposition product formed by the attack of CH₃CN on highly electrophilic 2⁺.⁹ However, from the close similarity of the structure and redox potentials between **1** and **2**, we think the small reduction wave might be better assigned to the reduction of dicationic [(η^5 -C₅Me₅)₂Ru·NCCH₃]²⁺ ([2·NCCH₃]²⁺). In this case, due to the difficulty of taking the bent-metalocene structure, the equilibrium shown in eq 3 (R = Me) would lie far to the left. Thus,



1⁺: R₂ = -(CH₂)₃-

2⁺: R = Me

3⁺: R = H

[1·NCCH₃]⁺: R₂ = -(CH₂)₃-

[2·NCCH₃]⁺: R = Me

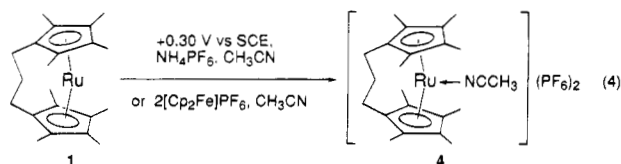
[3·NCCH₃]⁺: R = H

the second oxidation of [2·NCCH₃]⁺ to [2·NCCH₃]²⁺ at

the surface of the electrode or with 2⁺ must be slow owing to the low concentration of [2·NCCH₃]⁺ and gives only a small amount of [2·NCCH₃]²⁺ within a certain sweep time, while most of 2⁺ is left unchanged. This situation gives the large reduction wave of 2⁺ at $E_{pc} = 0.49$ V vs SCE and the small reduction wave of [2·NCCH₃]²⁺ at $E_{pc} = 0.05$ V vs SCE.

This hypothesis is further supported by the CV of [(η^5 -C₅Me₄H)₂Ru] (**3**) in CH₃CN (Figure 2d). The CV of **3** obviously resembles that of **1** (Figure 1b) better than that of **2** (Figure 2b) and shows a large 2e reduction wave at 0.08 V vs SCE. This denotes that the equilibrium in eq 3 (R = H) would not lie as far to the left as that of **2**. A plausible explanation for this is as follows: The bulkiness of the cyclopentadienyl ligand in **3** is apparently less than that of **2**. Therefore, **3** can take the bent-back structure more easily than **2**. The results described above suggest that the steric factor is critical to determine the equilibrium constant of eq 3, and the ruthenocene, which can take a more bent structure, can accommodate an CH₃CN molecule on the ruthenium center more easily and gives a more stable, CH₃CN-ligated ruthenocene monocation.

Synthesis of 4. Bulk electrolysis of **1** at +0.30 V vs SCE in 0.1 M NH₄PF₆/CH₃CN gave the dicationic salt [{ η^5 : η^5 -C₅Me₄(CH₂)₃C₅Me₄}Ru(NCMe)](PF₆)₂ (**4**) as red crystals in 93% yield. This compound was also obtained in 86% yield by the chemical oxidation of **1** with 2 equiv of [Cp₂Fe]PF₆ in CH₃CN (eq 4).



The ¹H NMR spectrum of **4** in CD₃CN shows three sharp signals at δ 1.65, 1.92, and 2.85 ppm, which clearly indicate that **4** is diamagnetic. The first two signals are assigned to the methyl groups on the bridged cyclopentadienyl rings and the last one to the coordinated CH₃CN. The coordinated CH₃CN of **4** does not exchange with solvent CD₃CN at room temperature. This is in sharp contrast with the iron analogue **5**, on which the exchange occurs rapidly under the same conditions.¹⁶ This fact as well as the significant downfield shift of ¹H and ¹³C NMR signals of the coordinated CH₃CN in comparison with those of free CH₃CN is consistent with the strong bonding interaction between Ru and CH₃CN in **4**.

Structures of 1 and 4. The ORTEP drawings for **1** and **4** are shown in Figures 3 and 4. Selected bond distances and angles in **1** and **4** are listed in Tables 5 and 6, respectively. In both complexes, two cyclopentadienyl rings have the eclipsed form as in all other structurally determined ruthenocene derivatives. Also in both complexes, the central methylene of the trimethylene chain is disordered in two sites. Namely, the central methylene in **1** is located at C(20A) (between C(10) and C(15)) and C(20B) (between C(11) and C(16)), as shown in Figure 3 with the occupancy factors 0.43 (C(20A)) and 0.57 (C(20B)), respectively. The central methylene in **4** (C(7)) is disordered between the two sites shown in Figure 4 from the requirement of the mirror plane. These disorders may cause unusualness of some

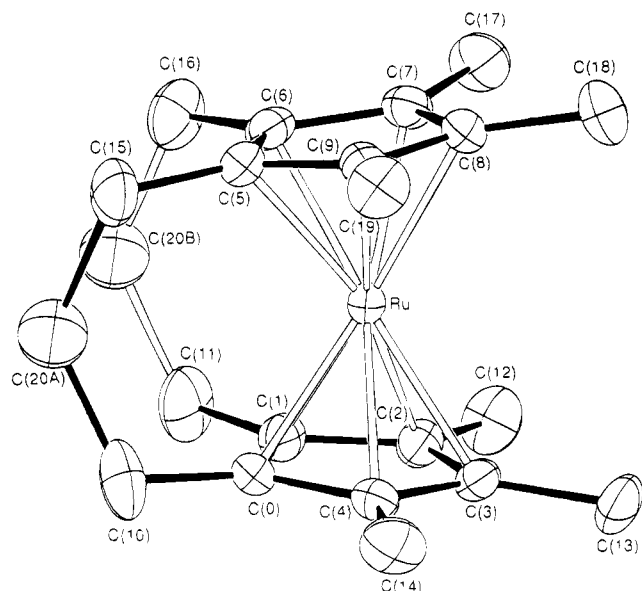


Figure 3. ORTEP drawing of $\{\eta^5:\eta^5\text{-C}_5\text{Me}_4(\text{CH}_2)_3\text{C}_5\text{Me}_4\}\text{Ru}$ (**1**) showing 30% probability thermal ellipsoids.

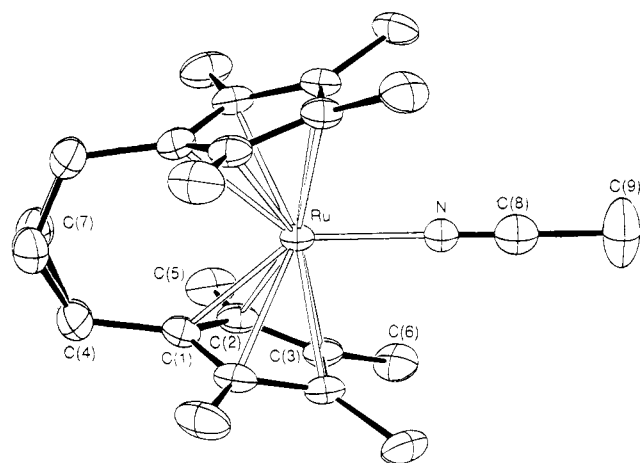


Figure 4. ORTEP drawing of $[\{\eta^5:\eta^5\text{-C}_5\text{Me}_4(\text{CH}_2)_3\text{C}_5\text{Me}_4\}\text{Ru}(\text{NCMe})](\text{PF}_6)_2$ (**4**) showing 30% probability thermal ellipsoids.

bond lengths determined around the trimethylene chains of **1** and **4**, i.e. very long C–C distances between C(20A) or C(20B) and other carbons (1.66(2)–1.81(2) Å) in **1** and a fairly short C(4)–C(7) distance (1.438(9) Å) in **4** for the C–C single bond.

Two cyclopentadienyl rings of **1** are slightly bent back by the trimethylene chain, and the dihedral angle between the least-squares planes is 11.2°. On the other hand, the corresponding dihedral angle for **4** is much larger, 34.8°, apparently due to the coordination of an CH_3CN molecule. The latter value is comparable with those of the iron analogue of **4** (34.5°)¹⁰ and the iodo-coordinated ruthenocenene cation $[\text{Cp}_2\text{Ru}-\text{I}]^+\text{I}_3^-$ (32.2°).³ The CH_3CN molecule is coordinated to the ruthenium center in **4** in end-on form with the nitrogen atom bound to the ruthenium atom. The Ru–N≡C–C unit is linear and lies on the intersection of two crystallographic mirror planes. This coordination mode is in sharp contrast with the isoelectronic molybdenocene–acetonitrile complex $\text{Cp}_2\text{Mo}(\text{NCCH}_3)$, in which the CH_3CN molecule is coordinated to the metal in side-on form.²⁵ The Ru–N bond length (2.072(6) Å) is comparable with those of other Ru–NCCH₃ complexes such as $[\text{CpRu}$

Table 5. Selected Bond Distances (Å) and Angles (deg) in $\{\eta^5:\eta^5\text{-C}_5\text{Me}_4(\text{CH}_2)_3\text{C}_5\text{Me}_4\}\text{Ru}$ (**1**)

Distances			
Ru–C(0)	2.147(5)	Ru–C(1)	2.137(6)
Ru–C(2)	2.176(7)	Ru–C(3)	2.203(5)
Ru–C(4)	2.183(5)	Ru–C(5)	2.151(6)
Ru–C(6)	2.151(5)	Ru–C(7)	2.183(5)
Ru–C(8)	2.201(5)	Ru–C(9)	2.193(6)
C(0)–C(1)	1.465(9)	C(1)–C(2)	1.434(7)
C(2)–C(3)	1.443(7)	C(3)–C(4)	1.433(8)
C(4)–C(0)	1.441(6)	C(5)–C(6)	1.452(8)
C(6)–C(7)	1.441(7)	C(7)–C(8)	1.433(7)
C(8)–C(9)	1.441(7)	C(9)–C(5)	1.452(6)
C(0)–C(10)	1.494(10)	C(1)–C(11)	1.515(9)
C(2)–C(12)	1.510(11)	C(3)–C(13)	1.493(7)
C(4)–C(14)	1.506(9)	C(5)–C(15)	1.495(10)
C(6)–C(16)	1.493(9)	C(7)–C(17)	1.510(9)
C(8)–C(18)	1.498(7)	C(9)–C(19)	1.476(10)
C(10)–C(20A)	1.69(2)	C(11)–C(20B)	1.81(2)
C(15)–C(20A)	1.81(2)	C(16)–C(20B)	1.66(2)
Angles			
C(0)–C(1)–C(2)	107.0(4)	C(1)–C(2)–C(3)	109.3(5)
C(2)–C(3)–C(4)	107.2(4)	C(3)–C(4)–C(0)	109.1(4)
C(4)–C(0)–C(1)	107.3(5)	C(5)–C(6)–C(7)	107.3(4)
C(6)–C(7)–C(8)	108.9(5)	C(7)–C(8)–C(9)	108.1(4)
C(8)–C(9)–C(5)	107.8(5)	C(9)–C(5)–C(6)	107.9(4)
C(0)–C(10)–C(20A)	109.7(8)	C(1)–C(11)–C(20B)	105.4(8)
C(5)–C(15)–C(20A)	106.9(9)	C(6)–C(16)–C(20B)	107.8(7)
C(10)–C(20A)–C(15)	127.8(10)	C(11)–C(20B)–C(16)	132.1(10)

dihedral angle between two cyclopentadienyl rings 11.18

Table 6. Selected Bond Distances (Å) and Angles (deg) in $[\{\eta^5:\eta^5\text{-C}_5\text{Me}_4(\text{CH}_2)_3\text{C}_5\text{Me}_4\}\text{Ru}(\text{NCMe})](\text{PF}_6)_2$ (**4**)^a

Distances			
Ru–N	2.072(6)	Ru–C(2)	2.257(4)
Ru–C(1)	2.224(5)	Ru–C(3)	2.255(3)
C(1)–C(2)	1.425(6)	C(1)–C(4)	1.531(8)
C(2)–C(3)	1.399(5)	C(2)–C(5)	1.492(7)
C(3)–C(3')	1.456(8)	C(3)–C(6)	1.504(6)
C(4)–C(7)	1.438(9)		
N–C(8)	1.086(11)	C(8)–C(9)	1.491(14)
C(5)–H(51)	0.88(5)	C(6)–H(61)	0.90(5)
C(5)–H(52)	0.96(5)	C(6)–H(62)	0.86(4)
C(5)–H(53)	0.99(4)	C(6)–H(63)	0.89(4)
Angles			
C(1)–C(2)–C(3)	107.5(4)	C(3)–C(2)–C(5)	123.4(4)
C(2)–C(1)–C(2')	109.1(4)	C(2)–C(3)–C(6)	126.3(4)
C(2)–C(3)–C(3')	108.0(3)	C(3')–C(3)–C(6)	125.0(4)
C(2)–C(1)–C(4)	124.7(4)	C(1)–C(4)–C(7)	119.6(5)
C(1)–C(2)–C(5)	128.8(4)	C(4)–C(7)–C(4'')	121.7(9)
Ru–N–C(8)	180.0(7)	N–C(8)–C(9)	180.0(10)

dihedral angle between two cyclopentadienyl rings 34.8

^a Key to the symmetry operation: single prime, $x, y, 1/2 - z$; double prime, $1/2 - x, y, z$.

$(\text{NCCH}_3)_3]^+$ (2.090(1) Å) and $[(\eta^6\text{-C}_6\text{H}_6)\text{Ru}(\text{NCCH}_3)_3]^{2+}$ (2.059(4) Å)²⁶ with a formal Ru(II), and $[\text{Ru}(\text{SC}_6\text{Me}_4\text{H})_4(\text{NCCH}_3)]$ (2.096(5) Å)²⁷ and $[\text{Ru}(\text{SC}_6\text{Me}_4\text{H})_3(\text{NCCH}_3)]^+$ (2.03(2) Å)²⁸ with a formal Ru(IV). The N≡C bond length (1.086(11) Å) is significantly shorter than the corresponding distances in the iron analogue (1.150(11) Å)¹⁰ and free CH_3CN (1.1571 Å).²⁹ It is known that a stronger donor–acceptor interaction between an end-on CH_3CN and a Lewis acid gives a shorter N≡C bond.^{30,31} Thus, the shorter N≡C distance in **4** also

(25) Wright, T. C.; Wilkinson, G.; Moteralli, M.; Hursthouse, M. B. *J. Chem. Soc., Dalton Trans.* **1986**, 2017.

(26) Luginbühl, W.; Zbinden, P.; Pittet, P. A.; Armbruster, T.; Bürgi, H.-B.; Merbach, A. E.; Ludi, A. *Inorg. Chem.* **1991**, *30*, 2350.

(27) Koch, S. A.; Millar, M. *J. Am. Chem. Soc.* **1983**, *105*, 3362.

(28) Satsangee, S. P.; Hain, J. H., Jr.; Cooper, P. T.; Koch, S. A. *Inorg. Chem.* **1992**, *31*, 5160.

(29) Costain, C. C. *J. Chem. Phys.* **1958**, *29*, 864.

supports the stronger metal–NCCH₃ bonding interaction in **4** compared with that in the iron analogue **5**.

The Ru–C bond lengths of **1** (average 2.17 Å) are almost the same as those of Cp₂Ru (2.186(3) Å)³² and (η⁵-C₅Me₅)₂Ru (2.17(1) Å).^{19e,f} In contrast, the Ru–C bonds of **4** (average 2.25 Å) are the longest among structurally determined ruthenocene derivatives, including [Cp₂RuI]⁺I₃⁻ (2.20 Å).³ The same tendency has been also seen in the iron derivatives: **5**, 2.04 Å,¹⁶ [5-NCCH₃](PF₆)₂, 2.169 Å.¹⁰ Considering that on oxidation the electrons of **1** are removed from the HOMO (a_{1g} orbital) with essentially nonbonding character, and this orbital becomes the 2a₁ orbital of **4** which is mainly used to make a bond with CH₃CN, this bond lengthening can be attributed to the steric repulsion between the permethylcyclopentadienyl rings and a coordinated CH₃CN in **4**. This is supported by the fact that the deviation of methyl groups (bent away from Ru) from the cyclopentadienyl ring planes is much larger in **4** (average 0.187 Å) than in **1** (average 0.076 Å).

Conclusions

Sterically congested ruthenocenes, {η⁵:η⁵-C₅Me₄(CH₂)₃-C₅Me₄}Ru (**1**), (η⁵-C₅Me₅)₂Ru (**2**), and (η⁵-C₅Me₄H)₂Ru (**3**), can be prepared conveniently in moderate to high yields by heating the corresponding cyclopentadienes and RuCl₃·3H₂O in high-boiling glycols. Electrochemical or chemical oxidation of **1** afforded the first dicationic derivative of ruthenocene, [{η⁵:η⁵-C₅Me₄(CH₂)₃C₅Me₄}Ru(NCMe)](PF₆)₂ (**4**), almost quantitatively. Crystal structure determinations of **1** and **4** demonstrated that the CH₃CN in **4** is coordinated to Ru at the nitrogen atom in end-on form and wedges itself into the two Cp rings of **4** to make them bent back. On the basis of the cyclic voltammograms of **1–4** as well as the structures of **1** and **4**, we suggested the ECE mechanism, including the CH₃CN coordination/dissociation process for the redox behavior of ruthenocene derivatives **1–4**.

Supplementary Material Available: Tables of positional and thermal parameters for hydrogen atoms in **4** and of anisotropic thermal parameters for non-hydrogen atoms, additional bond distances and angles, and least-squares planes and atomic deviations for **1** and **4** and packing diagrams for **1** and **4** (11 pages). Ordering information is given on any current masthead page.

OM940684H

(30) Storhoff, B. N.; Lewis, H. C., Jr. *Coord. Chem. Rev.* **1977**, *23*, 1.

(31) (a) Purcell, K. F.; Drago, R. S. *J. Am. Chem. Soc.* **1966**, *88*, 919. (b) Swanson, B.; Shriver, D. F.; Ibers, J. A. *Inorg. Chem.* **1969**, *10*, 2182.

(32) Seiler, D.; Dunitz, J. D. *Acta Crystallogr.* **1980**, *B36*, 46.

Restricted Rotation about the Metal–Aryl Bond in Platinum–Aryl Complexes of Chiral Diphosphines

John M. Brown* and Jesús J. Pérez-Torrente

Dyson Perrins Laboratory, South Parks Road, Oxford OX1 3QY, U.K.

Nathaniel W. Alcock

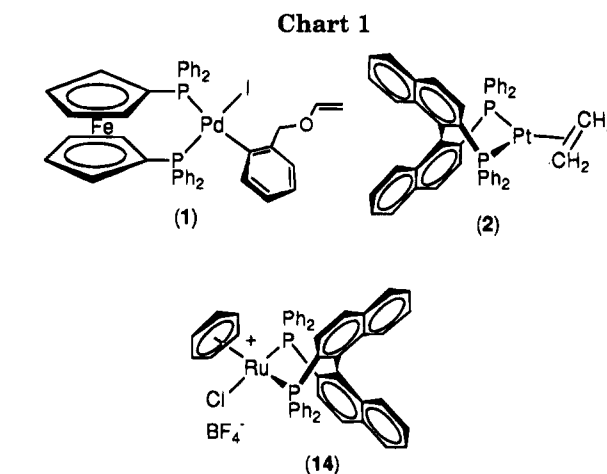
Department of Chemistry, University of Warwick, Coventry CV4 7AL, U.K.

Received August 1, 1994[⊗]

Square-planar bromo aryl, iodo aryl, and diaryl platinum(II) diphosphine complexes were prepared from the corresponding Pt(0) ethene complex by direct reaction with the haloarene, or from the Pt(II) dichloride complex by reaction with 2 equiv of aryllithium. These complexes exhibit restricted rotation about the metal–aryl bond in different ways. The diastereotopic pair of *ortho* hydrogens of the arylplatinum moiety in (DIOP)Pt(3,5-dibromophenyl)(I) (**3**) were sharp and distinct in the ¹H NMR spectrum below ambient temperature. (DIOP)Pt-(2-methoxyphenyl)(I) (**6**) exists as two distinct diastereomers discernable in the ambient-temperature ¹H NMR spectrum. The bis(2-methoxyphenyl) complexes behaved similarly, since three distinct diastereomers were observed in solution for both the DIOP and BINAP complexes **11** and **13** (but not for the CHIRAPHOS complex **12**). Only the BINAP complex **13** is dynamic on the NMR time scale at ambient temperature. The X-ray structure of complex **13** in one stereoisomeric *anti* form is reported: Monoclinic, space group *C*2, unit cell dimensions *a* = 36.08(5) Å, *b* = 12.12(1) Å, *c* = 12.45(2) Å, β = 104.5(1)°, *Z* = 4. The structure was refined to an *R* value of 0.063 (*R*_w = 0.087) for 3011 observed reflections. Examination of the corresponding DPPF complex **15** indicates separate *syn* and *anti* diastereomers. In the course of the synthetic work, significant differences between the reactivity of the ligands was encountered, and trends in rotation barriers with changing complex structure are discussed.

Introduction

In the course of mechanistic studies on the intramolecular Heck reaction, restricted rotation was observed about the Pd–aryl bond in complex **1** and close relatives, manifested by diastereotopic side-chain methylene groups in the ¹H NMR spectrum.¹ There was no evidence for interconversion at ambient temperature, and although related observations had been made for *cis*-² or *trans*-bis(triethylphosphine)nickel aryls³ and a palladium analog,⁴ their generality had not been established. For this reason, a series of thermally stable⁵ (diphosphine)-platinum aryls was synthesized and restricted rotation evaluated by NMR. The objectives were to discover (a) the effects, if any, of the ligand bite angle on the extent of rotational freedom and (b) the necessity or otherwise of *ortho*-aryl substituents, and (c) the extent of stereoselection between isomers in chiral diphosphine complexes. X-ray structural studies of square-planar palladium⁶ and platinum aryls have established that the aryl group prefers to lie orthogonal to the coordination plane, as is the case with related metal vinyls,⁷ or acyls.⁸ Aside from any electronic preference for orthogonal



geometry, an in-plane aryl will experience greater steric hindrance between the *ortho*-H or *ortho* substituents and the *cis*-adjacent ligands.⁹

(6) For recent examples of Pd aryls see: Kramer, R.; Polborn, K.; Beck, W. *J. Organomet. Chem.* **1992**, *441*, 333. Markies, B. A.; Canty, A. J.; Janssen, M. D.; Spek, A. L.; Boersma, J.; van Koten, G. *Recl. Trav. Chim. Pays-Bas* **1991**, *110*, 477–479; de Graaf, W.; van Wegen, J.; Boersma, J.; Spek, A. L.; van Koten, G. *Recl. Trav. Chim. Pays-Bas* **1989**, *108*, 275–277. Huser, M.; Youinou, M.-T.; Osborn, J. A. *Angew. Chem., Int. Ed. Engl.* **1989**, *28*, 1386–1387.

(7) Calhorda, M. J.; Brown, J. M.; Cooley, N. A. *Organometallics* **1991**, *10*, 1431–1439.

(8) For recent examples of the X-ray structure of Pd acyls see: Grushin, V. V.; Alper, H. *Organometallics* **1993**, *12*, 1890–1895; Huang, L.; Ozawa, F.; Osakada, K.; Yamamoto, A. *J. Organomet. Chem.* **1990**, *383*, 587. Bardi, R.; Piazzesi, A. M.; Del Pra, A.; Cavinato, G.; Toniolo, L. *Inorg. Chim. Acta.* **1985**, *99*, 102.

[⊗] Abstract published in *Advance ACS Abstracts*, January 15, 1995.

(1) Brown, J. M.; Pérez-Torrente, J. J.; Alcock, N. W.; Clase, H. J. *Organometallics* **1995**, *14*, 207–213.

(2) Miki, K.; Tanaka, M.; Kasai, N.; Wada, M. *J. Organomet. Chem.* **1988**, *352*, 385–396.

(3) Griffiths, D. B.; Young, G. B. *Organometallics* **1986**, *5*, 1744–1746.

(4) Alster, P. L.; Boersma, J.; Smeets, W. J. J.; Spek, A. L.; van Koten, G. *Organometallics* **1993**, *12*, 1639–1647.

(5) Brown, J. M.; Cooley, N. A. *Chem. Rev.* **1988**, *88*, 1031–1048 and references therein.

Results and Discussion

Synthesis of Complexes. In catalytic asymmetric synthesis employing diphosphine complexes, three of the most commonly used ligands are CHIRAPHOS,¹⁰ BINAP,¹¹ and DIOP.¹² The three are distinguished by chelate ring size (respectively 5, 7, and 7) and variation in the degree of flexibility of the chelate backbone (with BINAP significantly more rigid than DIOP)¹³ and in the bite angles of the ligand, which are typically 85, 90, and 99°, respectively. For comparison, complexes of the achiral ligand DPPF¹⁴ were prepared. Two aryl groups were chosen. Coordinated 3,5-dibromophenyl residues exhibit magnetic inequivalence of the *ortho* hydrogens in the slow rotation limit provided that the complex possesses chirality: i.e. if the diphosphine is chiral, but not otherwise. For a single coordinated *o*-methoxyphenyl group, the same applies, but restricted rotation in a bis(*o*-methoxyphenyl) complex allows for the possibility of diastereoisomerism; with a symmetrical achiral chelating ligand, there are simply *syn* and *anti* isomers, but with a C₂ symmetrical chiral chelating ligand an additional species is possible because there are two possible *anti* isomers which are diastereomeric. These possibilities are outlined in Figure 1.

Two strategies were applied to synthesize the desired complexes. The halides in both series were prepared from the corresponding Pt(0) ethene complex and the required aryl iodide or bromide. The new BINAP derivative **2** was synthesized by the previously described method¹⁵ from (BINAP)PtCl₂, which involves reduction of the Pt dihalide with NaBH₄ under an atmosphere of ethylene. Because it had proved impossible to prepare (CHIRAPHOS)Pt(C₂H₄) by this route, no attempt was made to prepare its η¹-aryl, η¹-halide complexes. The reactions which were successful are indicated in Scheme 1. For DIOP and DPPF, the preparations of complexes **3**, **5**, and **6** proved straightforward, giving stable products which were fully characterized. Difficulties were encountered in attempted preparation of the BINAP complexes **4** and **7** in both aryl halide series. Reaction of complex **2** with 3,5-dibromiodobenzene¹⁶ did not occur at a significant rate below 100 °C in toluene, and under those conditions competitive formation of a second species, possibly the corresponding PtI₂ complex, was observed; the components could not be separated. The reaction with 1,3,5-tribromobenzene occurred under similar conditions with comparable results. Complex **2** was unreactive toward *o*-iodoanisole. In that case the bis(aryl) complex **13** (q.v.) was reacted with HBr/MeOH at low temperatures to give predominantly bromide **7**, but **7** was mixed with some of the corresponding dibromide and again not easily separated.

The η¹,η¹-diaryl complexes were prepared from the corresponding (diphosphine)platinum dihalides by nu-

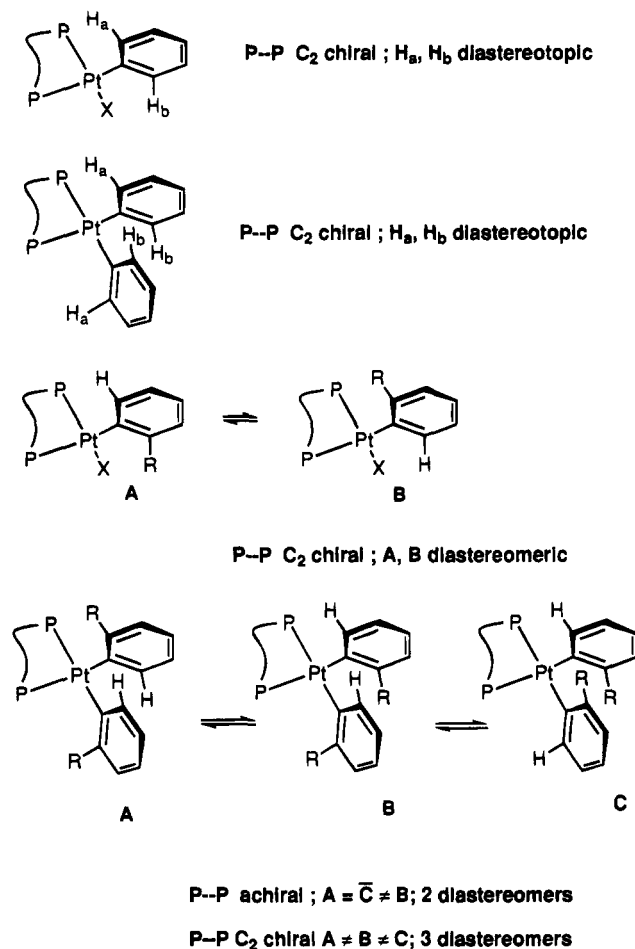


Figure 1. Stereochemical consequences of restricted rotation in chiral Pt diphosphine aryl complexes.

cleophilic displacement with the relevant organolithium species, as indicated in Scheme 2. In the 3,5-dibromophenyl series, the DIOP-derived species could not be obtained cleanly despite several attempts, but others were synthesized and characterized without incident.

NMR Observations on (3,5-Dibromophenyl)platinum Halides. The DIOP complex **3** shows interesting behavior. Its ³¹P NMR spectrum is a temperature-invariant AB quartet, while broadening is seen in the ¹H NMR spectrum below ambient temperature. At -10 °C in CD₂Cl₂, the two *o*-H's of the Pt-aryl residue, identified by their strong Pt and P coupling (*J*_{Pt-H} = 40 Hz, *J*_{P-H} = 6.5 Hz) are separate and distinct (Figure 2), while on warming to ambient probe temperature the same signals have become two broad humps centered at 6.95 and 7.05 ppm, close to coalescence. Similar behavior is observed in C₇D₈, where the relevant protons are partially obscured by other aryl protons in the 7.4 ppm region. This set of observations is consistent with restricted rotation about the aryl-Pt bond with an approximate rate constant of 10² s⁻¹ at ambient temperature. This explanation was strengthened by comparison with the related DPPF complex **5**, where the corresponding *ortho* protons are equivalent and sharp, while still possessing the distinctive coupling pattern (c.f. Figure 2).

NMR Observations on (2-Methoxyphenyl)platinum Halides. Only the DIOP complex **6** was obtained pure in this series. It exists as two distinct rotamers in 57:43 ratio, demonstrated by the doubling of resonances in the ¹H NMR (e.g. OCH₃ 3.199, 3.131 ppm; Ar

(9) For preliminary communication of part of this work see: Alcock, N. W.; Brown, J. M.; Pérez-Torrente, J. J. *Tetrahedron Lett.* **1992**, *33*, 389-393.

(10) Fryzuk, M. J.; Bosnich, B. *J. Am. Chem. Soc.* **1977**, *99*, 6262-6269.

(11) Miyashita, A.; Yasuda, A.; Takaya, H.; Toriumi, K.; Ito, T.; Souchi, T.; Noyori, R. *J. Am. Chem. Soc.* **1980**, *102*, 7932-7934.

(12) Kagan, H. B.; Dang, T.-P., *J. Am. Chem. Soc.* **1972**, *94*, 6429-6433.

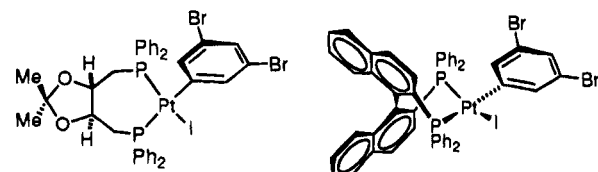
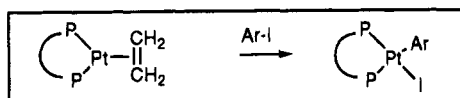
(13) Brown, J. M.; Evans, P. L. *Tetrahedron* **1988**, *44*, 4905-4918.

(14) Hayashi, T.; Konishi, M.; Kobori, Y.; Kumada, M.; Higuchi, T.; Hirotsu, K. *J. Am. Chem. Soc.* **1984**, *106*, 158, and references therein.

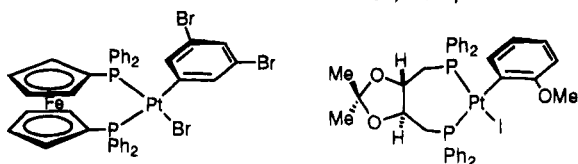
(15) Brown, J. M.; Cooley, N. A. *Organometallics* **1990**, *9*, 353-359.

(16) Benkeser, R. A.; Hickner, R. A.; Hoke, D. L.; Thomas, U. H. *J. Am. Chem. Soc.* **1958**, *80*, 5289.

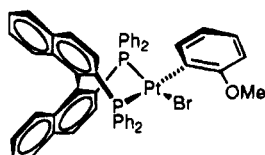
Scheme 1



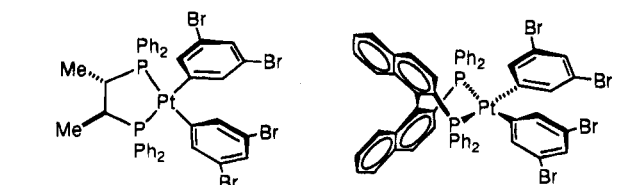
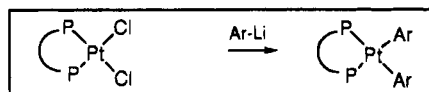
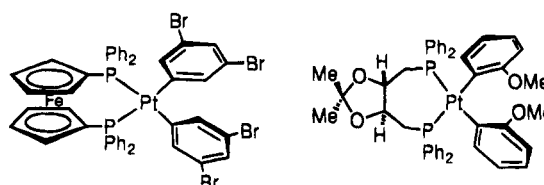
(3) THF, reflux 2.5 h; 75%

(4) ArI, toluene, 100°C
8h, main product(5) ArBr, THF, reflux
5.5 h.; 80%

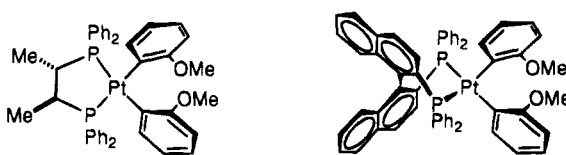
(6) THF, reflux, 3h., 86%

(7) Ex PtAr₂, HBr, -40°C
main product

Scheme 2

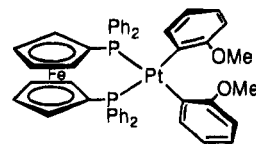
(8) Et₂O, -78°C - RT, 3h., 93%(9) Et₂O, -78°C - RT, 3h., 86%(10) Et₂O, -78°C - RT, 3h., 87%

(11) THF, -78°C - RT, 3h., 80%



(12) THF, -78°C - RT, 3h., 91%

(13) THF, -78°C - RT, 3h., 91%



(15) THF, -78°C - RT, 3h., 92%

H6 7.62, 7.58 ppm [C₇D₈] with P and Pt couplings). The ³¹P NMR demonstrates this more clearly, exhibiting two well-defined AB quartets with the expected P and ¹⁹⁵Pt couplings. The relevant signals were sharp, in contrast to complex **2**, indicating a rotational barrier of at least 80 kJ mol⁻¹ for the Pt-aryl bond at ambient temperature. As indicated above, attempts to make the BINAP analog **7** directly were unsuccessful, and an indirect procedure led to impure material.

NMR Observations on Bis(3,5-dibromophenyl)platinum Complexes. The ¹H NMR spectra of CHIRAPHOS and BINAP complexes **8** and **9** exhibited a single sharp multiplet at ambient temperature for the *o*-aryl-Pt protons consistent with fast rotation; the spectra were similar in that respect to the DPPF complex **10**. When the BINAP-derived species **9** was cooled to 233 K, the ¹H NMR spectrum showed no more broadening than was observed for other protons in the aryl region. The conclusion is that rapid aryl rotation occurs in the diaryl complexes, in contrast to the DIOP-derived aryl iodide **3**. In the absence of *ortho* substituents it is feasible that the aryl-Pt bond rotations are geared¹⁷ in such a way as to maintain C₂ symmetry.

NMR and X-ray Structural Observations on Bis-(2-methoxyphenyl)platinum Complexes. It proved possible to prepare and characterize all four complexes in this series. The DIOP complex **11** possessed a complex ¹H NMR spectrum, signals in the OMe region being consistent with the presence of two symmetrical and one unsymmetrical isomer. This was affirmed by the ³¹P NMR spectrum (Figure 3) taken at 201 MHz;

all three possible stereoisomeric forms were present in approximately 3:1:1 ratio, with the *syn*-diaryl-Pt isomer exhibiting inequivalent phosphorus nuclei (*J*_{PP} = 12 Hz). This indicated both a small difference in free energy between the different rotamers and a high barrier to their interconversion. In contrast, both ³¹P and ¹H NMR spectra of the CHIRAPHOS complex **12** showed a single set of resonances; for example OCH₃ resonates at 3.162 ppm and the aromatic region shows distinct resonances for H3, H5, and H6 of Pt-aryl rings. Given the smaller bite angle of the ligand, fast rotation about the P-aryl bond at ambient temperature is a more probable explanation than stereospecific formation of one *anti* rotamer.

For the BINAP complex **13**, the overall spectral features were quite similar to those of the DIOP complex **11**, with two distinct differences. All three rotamers were seen in the ¹H and ³¹P NMR spectra (Figure 3), but the selectivity in favor of one form was more marked and interconversion was apparent on variable-temperature analysis over the temperature range 0–60 °C in C₇D₈. Analysis of the OCH₃ region of the ¹H NMR using DNMR3¹⁸ to simulate the line broadening indicated a barrier of around 70 kJ mol⁻¹ at 25 °C. The main *anti*

(17) Cozzi, F.; Guenzi, A.; Johnson, C. A.; Mislow, K.; Hounshell, W. D.; Blount, J. F. *J. Am. Chem. Soc.* **1981**, *103*, 957–958.

(18) We thank the late Dr. A. E. Derome for help with this determination.

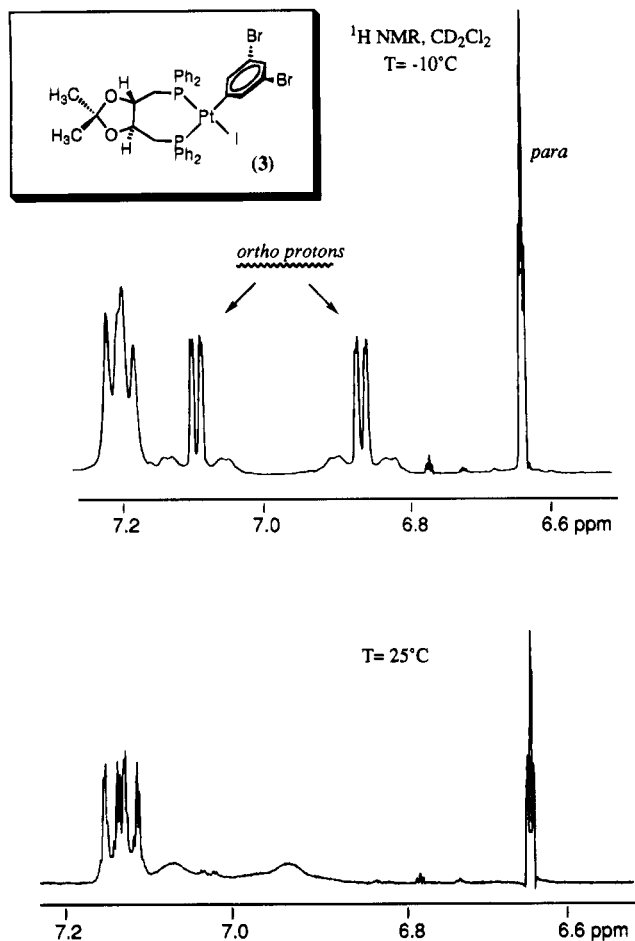


Figure 2. Restricted aryl–Pt rotation in complex **3** manifested by the temperature dependence of the *o*-aryl protons of the σ -aryl group.

rotamer was present to the extent of 80% in C_7D_8 and 85% in CD_2Cl_2 , and most of the remainder was the *syn* rotamer.

Slow crystallization of complex **13** from acetone/ethanol at $-40^\circ C$ gave X-ray-quality crystals, and the structure obtained is shown in Figure 4. This provides support for the observed restricted rotation through enforced stacking of the *o*-anisyl and adjacent face-oriented P–aryl rings. This nonbonded interaction could be responsible for the large binaphthyl twist angle of 81° and the large P–Pt–P angle of 93° , in comparison to published structures for BINAP complexes.^{19,20} The increased biaryl inter-ring angle swings the two ligating phosphines further apart, and this is compensated by torsional strain, unevenly distributed between the two (P–C)–(C–C[biaryl]) linkages, which possess torsion angles of 8.7° and 24.0° . The ruthenium complex **14** has a similar biaryl twist angle and a related unsymmetrical distortion of the C–P bonds with respect to the biaryl linkage.²⁰ All other BINAP ruthenium complexes reported exhibit values between 0 and 15.6° for the

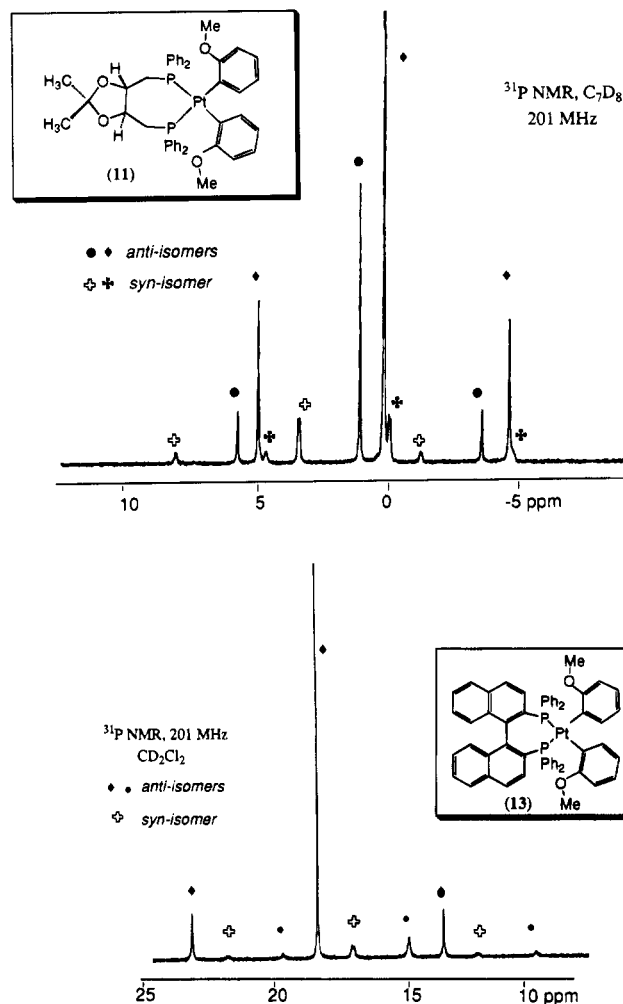


Figure 3. Ambient-temperature ^{31}P spectra of complexes **11** and **13**, illustrating the presence of three distinct rotamers.

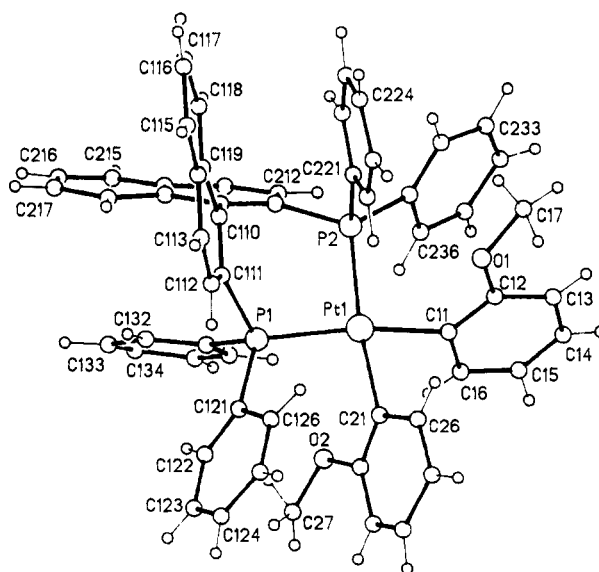


Figure 4. X-ray crystal structure of the *R,S,S* form of complex **13**.

relevant torsion angle and between 64 and 74° for the biaryl twist angle. The potential for torsional strain involving out-of-plane aryl–C–P distortion within a chelate diphosphine has not previously been recognized, although it is seen together with distortion of the Pd–N bond away from the direction of the lone-pair vector in

(19) Kawano, H.; Ikariya, T.; Ishii, Y.; Kodama, T.; Saburi, M.; Yoshikawa, S.; Uchida, Y.; Akutagawa, S. *Bull. Chem. Soc. Jpn.* **1992**, *65*, 1595. Mashima, K.; Hino, T.; Takaya, H. *J. Chem. Soc., Dalton Trans* **1992**, 2099. Mashima, K.; Hino, T.; Takaya, H. *Tetrahedron Lett.* **1991**, *32*, 3101. Ashby, M. T.; Khan, M. A.; Halpern, J. *Organometallics* **1991**, *10*, 2011. Kawano, H.; Ishii, Y.; Kodama, T.; Saburi, M.; Ichida, Y. *Chem. Lett.* **1987**, 1311. Ohta, T.; Takaya, H.; Noyori, R. *Inorg. Chem.* **1988**, *27*, 566.

(20) Kawano, H.; Ikariya, T.; Ishii, Y.; Kodama, T.; Saburi, M.; Yoshikawa, S.; Uchida, Y.; Akutagawa, S. *J. Org. Chem.* **1994**, *59*, 3064 and references therein.

related P–N chelate complexes.²¹ Other features of the X-ray structure are of interest. The square plane is distorted toward tetrahedral with P–Pt–C angles of 168.3 and 169.6°, respectively. The Pt–aryl rings are twisted away from orthogonality with the mean coordination plane, average torsion angles (C_{ortho}–C_{ipso})–(Pt–C_{ipso}) being 71 and 72°. For a range of square-planar *cis*-diarylplatinum complexes retrieved from the CSSR database,⁷ the corresponding or equivalent angles range between 70 and 90°. It is assumed, but not proved, that the crystals correspond to the main rotamer observed by NMR, so that the proportion in C₇D₈ solution is 85% *R,S,S* (*anti*), 1.5% *R,R,R* (*anti'*), and 18.5% *R,R,S* (*syn*).²²

The source of stereoselectivity leading to predominant formation of the *R,R,R* diastereomer must be quite subtle, since rotation of one of the Pt–aryl rings of complex **13** through 180° in a molecular model based on the X-ray structure (Chem 3D), which causes the *anti*–*syn* conversion, fails to introduce any increase in nonbonded interactions between the OMe group and the adjacent face-on P–aryl group of the diphosphine ligand. An explanation for the selective formation of one rotamer must then have an electronic origin. Face to face arene–arene stacking as seen here is not the optimum orientation but arises from enforced proximity, the preferred alignment of aryl rings being edge-to-face unless there is strong charge transfer.²³ Here the spatial disposition of P–aryl and Pt–aryl groups is sustained by the rigidity of the binaphthyl backbone, and in the preferred diastereomer the C–OMe bond dipole is forced away from the centroid of the neighboring P–aryl ring (Figure 5a). This interaction is more favorable than the alternative shown in Figure 5b, where that bond dipole is in proximity to the P–aryl centroid. Note that the structure in Figure 5a corresponds to the *R,S,S* (*anti*) rotamer and the structure in Figure 5b to the disfavored *R,R,R* (*anti'*) rotamer.

The final compound in this series is the DPPF complex **15**. The ³¹P spectrum of analytically pure material showed two signals at 11.6 and 13.3 ppm in a 97:3 ratio. In the ¹H NMR a second OMe peak at 3.08 ppm was seen to high field of the main peak at 3.20 ppm, again in the ratio 97:3. The minor peak diminished in intensity on irradiation of the main OCH₃ and decreased in proportion on cooling the sample. It is then possible to attribute the observations to the existence of *anti* and *syn* rotamers about the Pt–aryl linkage, with a high energy barrier. The preferred rotamer is not known, but we note that the X-ray structure of *cis*-(PPh₃)₂Pt(*o*-anisyl)₂ reveals *anti*-related Pt–aryl groups.²⁴ All other symmetrical bis(aryl) complexes with a single *ortho* substituent adopt the *anti* form in the solid state.²⁵

Mechanism of Atropisomerism. Although a σ -aryl group possesses an intrinsic electronic preference for orthogonality to the square plane in Pt(II) complexes,

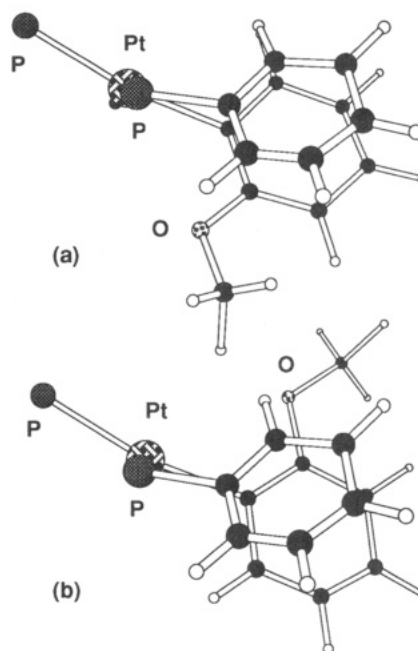


Figure 5. (a) Model of a fragment of complex **13** derived from the X-ray coordinates indicating the geometry of P–aryl/Pt–aryl stacking. (b) The same view of an alternative structure corresponding to the disfavored *anti* isomer, created by a rotation of 180° about the Pt–aryl bond in the model shown in (a).

as discussed, that preference is strongly augmented by steric pressures in the present case. Within the range of accuracy amenable to analysis of the dynamic NMR results, it appears that the interconversion of *anti* and *anti'* atropisomers is not favored over the interconversion of *anti* and *syn* atropisomers of **13**. This means that there is no special role for gearing the motions of the two Pt–aryl groups in a conrotation process, which would bring about the former but not the latter isomerization. If the *anti*–*syn* interconversion is carried out with the Chem 3D model, rotating the left-hand Pt–aryl in **13** so that the OMe group moves inwards toward its Pt–aryl neighbor, there is a severe nonbonded interaction between the *ortho* H of the Pt aryl and the adjacent P–phenyl group, involving both the *ipso* and *ortho* carbons of the latter. Without allowing for bond angle distortions, the approach between C_{ipso} and H_{ortho} as specified comes as close as 0.820 Å. There is limited scope for averting this interaction by movement of the P–phenyl group, itself constrained by proximity to the binaphthyl framework. In order to avoid this close approach, which would lead to an activation free energy far in excess of the observed 80 kJ mol⁻¹, other distortions need to occur concurrent with Pt–aryl rotation. For example, the C–Pt bonds can follow a twisting motion which maintains the C₂ symmetry of the complex while moving toward an overall tetrahedral geometry. This has the overall effect of making the space around the rotating aryl group more open. In addition some opening of the C_{aryl}–P–Pt angle from the aryl group and moderate narrowing of the C–Pt–C angle will diminish the residual nonbonded repulsions. In consequence, the steric energy associated with the interconversion of atropisomers will be distributed over several angle bending and torsional modes.

Conclusions. The objective of the work was to delineate the scope of restricted rotation about P–aryl linkages in *cis*-(diphosphine)platinum complexes. A

(21) Alcock, N. W.; Brown, J. M.; Pearson, M.; Woodward, S. *Tetrahedron: Asymmetry* **1992**, *3*, 17–20. Alcock, N. W.; Brown, J. M.; Hulmes, D. I. *Tetrahedron: Asymmetry* **1993**, *4*, 743–756.

(22) Using the standard Cahn–Ingold–Prelog conventions for the assignment of atropisomeric chirality and treating the trans P–Pt–C' as one pair of substituents about the Pt–C axis; Prelog, V.; Helmchen, G. *Angew. Chem., Int. Ed. Engl.* **1982**, *21*, 567–583.

(23) Hunter, C. A. *Chem. Soc. Rev.* **1994**, *23*, 101–109.

(24) Debaerdemaker, T.; Klein, H.-P.; Wiege, M.; Brune, H. A. *Z. Naturforsch., B* **1981**, *36*, 958.

(25) Brune, H. A.; Wiege, M.; Debaerdemaker, T. *Z. Naturforsch., B* **1984**, *39*, 359. Cf. Debaerdemaker, T.; Weisemann, C.; Brune, H. A. *Acta Crystallogr., Sect. C* **1987**, *43*, 1253.

complete survey was thwarted by difficulty in obtaining pure samples of two of the key compounds, but sufficiently diverse results were obtained that several general conclusions can be drawn.

First, an *ortho* substituent is not a necessary condition for slow rotation on the NMR time scale under ambient conditions. The dynamic behavior of complex **3**, which exhibits distinct resonances for the 2- and 6-hydrogens at $-10\text{ }^{\circ}\text{C}$ that coalesce above room temperature, shows this clearly. The bis(aryl) complexes **8** and **9** did not show evidence of restricted rotation, however. Second, the presence of an *ortho* substituent (OMe) enhances the probability of observing restricted rotation and slows the rate of interconversion of atropisomers. This is shown by comparison of the two DIOP complexes **3** and **6**. The NMR spectrum of the former has rapidly interconverting diastereotopic *o*-H atoms at ambient temperature, but the latter exists as two diastereomers whose interconversion is slow on the NMR time scale. Third, there is qualitative evidence for a correlation between the diphosphine bite angle and the Pt-aryl rotation barrier. In the 3,5-dibromophenyl series, the DIOP complex alone exhibits slow rotation. In the bis(*o*-methoxyphenyl) series, where all four complexes were characterized, the CHIRAPHOS complex, with the smallest bite angle, is the only one which does not exhibit diastereoisomerism.

These observations of large rotational barriers about the metal-aryl bond in square-planar complexes, associated with a high level of stereoselectivity in the case of the BINAP complex, suggest that it may be fruitful to look for further examples of asymmetric cross-coupling of *ortho*-substituted aryl halides.²⁶

Experimental Section

General Information. All reactions were carried out under dry argon by using Schlenk glassware and vacuum line techniques. All solvents were freshly distilled from standard drying agents and degassed by three freeze/thaw cycles before use. ^1H NMR spectra were recorded on a Bruker WH-300 (300 MHz) or a Bruker AM-500 (500 MHz) spectrometer and are referenced to residual protic solvents with chemical shifts being reported as δ (ppm) from TMS. ^{31}P NMR spectra were recorded on a Bruker AM-250 spectrometer operating at 101.26 MHz using 85% H_3PO_4 as external reference. Elemental analyses were performed by the Dyson Perrins Laboratory Analytical Service using a Carlo Erba 1106 elemental analyzer.

The starting materials [(dppf)PtCl₂]²⁷ (dppf = 1,1'-bis(diphenylphosphino)ferrocene), [(*R*-BINAP)PtCl₂] (*R*-BINAP = (*R*)-(+)-2,2'-bis(diphenylphosphino)-1,1'-binaphthyl), [(*R,R*-CHIRAPHOS)PtCl₂] (*R,R*-CHIRAPHOS = (2*R*,3*R*)-(+)-2,3-bis(diphenylphosphino)butane), [(*S,S*-DIOP)PtCl₂]^{28,29} and [(*S,S*-DIOP)Pt(η^2 -ethene)]³⁰ (*S,S*-DIOP = (+)-(2*S*,3*S*)-2,3-isopropylidene-2,3-dihydroxy-1,4-bis(diphenylphosphino)butane), and [(dppf)Pt(η^2 -ethene)]¹ were prepared according to literature methods. 1,3,5-Tribromobenzene was purchased from Aldrich; 3,5-dibromoiodobenzene was prepared by following the described procedure.¹⁶

Synthesis of [(*R*-BINAP)Pt(η^2 -ethene)] (2**).** Ethylene was bubbled through a solution of [(*R*-BINAP)PtCl₂] (0.120 g,

0.135 mmol) in a dichloromethane-ethanol (1:1) mixture (5 mL). The solution was cooled to $-78\text{ }^{\circ}\text{C}$, and then solid NaBH_4 (0.017 g, 0.405 mmol) was added. The resulting solution was slowly warmed to room temperature (1 h), maintaining a steady flow of ethylene through the solution. Addition of ethanol (10 mL) and concentration under vacuum rendered the complex as an orange-yellow solid which was isolated by filtration, washed with water (15 mL) and EtOH, and dried under vacuum (0.108 g, 94%). Anal. Calcd for $\text{C}_{46}\text{H}_{36}\text{P}_2\text{Pt}$: C, 65.32; H, 4.28. Found: C, 65.60; H, 4.36. ^1H NMR (300 MHz, CDCl_3): 8.01 (m, 4H), 7.47-7.24 (m, 16H), 7.12 (m, 2H), 7.06 (m, 2H), 6.90 (m, 2H), 6.56 (m, 2H), 6.43 (m, 4H) (BINAP), 2.41 (m, 2H, =CH₂, $J_{\text{Pt-H}} = 62\text{ Hz}$), 2.03 (d, 2H, =CH₂, $J_{\text{Pt-H}} = 62\text{ Hz}$, $J_{\text{H-H}} = 5\text{ Hz}$). ^{31}P NMR (250 MHz, toluene/ D_2O): 34.56 (s, $J_{\text{Pt-P}} = 3473\text{ Hz}$).

Synthesis of [(*S,S*-DIOP)Pt(I)(3,5-Br₂C₆H₃)] (3**).** To a solution of [(*S,S*-DIOP)Pt(η^2 -ethene)] (0.060 g, 0.083 mmol) in THF (10 mL) was added solid 3,5-dibromoiodobenzene (0.033 g, 0.091 mmol) and the mixture refluxed for 2.5 h. The solvent was removed under vacuum to give a light brown residue, which was washed with a diethyl ether-MeOH (1:2) mixture (5 mL). The white solid was collected by filtration and washed with cold MeOH. Recrystallization from dichloromethane/MeOH gave the complex as colorless microcrystals (0.066 g, 75%). Anal. Calcd for $\text{C}_{37}\text{H}_{35}\text{Br}_2\text{IO}_2\text{P}_2\text{Pt}$: C, 42.10; H, 3.34. Found: C, 42.24; H, 3.33. ^1H NMR (500 MHz, CD_2Cl_2 , 263 K): 7.81 (m, 2H, Ph), 7.75 (m, 2H, Ph), 7.56 (m, 3H, Ph), 7.50 (m, 6H, Ph), 7.37 (m, 3H, Ph), 7.30 (m, 2H, Ph), 7.19 (m, 2H, Ph), 7.09 (dd, 1H, *o*-H, $\text{C}_6\text{H}_3\text{Br}_2$, $J_{\text{H-Pt}} = 48\text{ Hz}$, $J_{\text{H-P}} = 6.7\text{ Hz}$, $J_{\text{H-H}} = 1.5\text{ Hz}$), 6.86 (dd, 1H, *o*-H, $\text{C}_6\text{H}_3\text{Br}_2$, $J_{\text{H-Pt}} = 40\text{ Hz}$, $J_{\text{H-P}} = 6.7\text{ Hz}$, $J_{\text{H-H}} = 1.3\text{ Hz}$), 6.62 (t, 1H, *p*-H, $\text{C}_6\text{H}_3\text{Br}_2$, $J_{\text{H-H}} = 1.8\text{ Hz}$), 3.97 (m, 1H, -CH₂P), 3.72 (m, 1H, -CH₂P), 3.31 (t, 1H, CH), 2.91 (m, 1H, -CH₂P), 2.73 (t, 1H, -CH), 2.39 (m, 1H, -CH₂P), 1.18 (s, 3H, CH₃), 1.04 (s, 3H, CH₃). ^{31}P NMR (250 MHz, toluene/ D_2O) 8.33 (d, $J_{\text{Pt-P}} = 3864\text{ Hz}$, $J_{\text{P-P}} = 17\text{ Hz}$), -4.73 (d, $J_{\text{Pt-P}} = 1768\text{ Hz}$, $J_{\text{P-P}} = 17\text{ Hz}$).

Reaction of [(*R*-BINAP)Pt(η^2 -ethene)] (2**) with Haloarenes.** [(*R*-BINAP)Pt(η^2 -ethene)] (**2**) (0.080 g, 0.094 mmol) was dissolved in THF or toluene (10 mL); then 3,5-dibromoiodobenzene (0.100 mmol) was added and the reaction monitored by ^{31}P NMR. No reaction was observed in THF at reflux (2 h) or in toluene at $80\text{ }^{\circ}\text{C}$. The reaction started at $100\text{ }^{\circ}\text{C}$ in toluene and was completed in 8 h to give mainly a mixture whose ^{31}P NMR spectrum was consistent with the presence of the desired compound as the major component [(*R*-BINAP)Pt(I)(3,5-Br₂C₆H₃)] (**3**), contaminated by a second product. Attempts to isolate **4** pure were unsuccessful. ^{31}P NMR (250 MHz, toluene/ D_2O): **4**, 5.02 (d, $J_{\text{Pt-P}} = 1775\text{ Hz}$, $J_{\text{P-P}} = 20\text{ Hz}$), 4.86 (d, $J_{\text{Pt-P}} = 3871\text{ Hz}$, $J_{\text{P-P}} = 20\text{ Hz}$); impurity, 3.09 (s, $J_{\text{Pt-P}} = 1708\text{ Hz}$).

Synthesis of [(dppf)Pt(Br)(3,5-Br₂C₆H₃)] (5**).** To a solution of [(dppf)Pt(η^2 -ethene)] (0.105 g, 0.135 mmol) in THF (10 mL) was added solid 1,3,5-tribromobenzene (0.057 g, 0.174 mmol). The mixture was refluxed for 5.5 h to give an orange solution. The solvent was removed under vacuum to give an orange residue which was dissolved in acetone (1 mL); slow addition of pentane gave the complex as an orange microcrystalline solid which was filtered, washed with pentane, and dried under vacuum (0.115 g, 80%). Anal. Calcd for $\text{C}_{40}\text{H}_{31}\text{Br}_3\text{FeP}_2\text{Pt}$: C, 45.14; H, 2.93. Found: C, 44.97; H, 2.91. ^1H NMR (300 MHz, CD_2Cl_2): 8.02 (m, 4H), 7.53 (m, 6H), 7.43 (m, 6H), 7.19 (m, 4H), 7.02 (dd, 2H, *o*-H, $\text{C}_6\text{H}_3\text{Br}_2$, $J_{\text{H-Pt}} = 39.7\text{ Hz}$, $J_{\text{H-P}} = 7.1\text{ Hz}$, $J_{\text{H-H}} = 1.8\text{ Hz}$), 6.75 (s, 1H, *p*-H, $\text{C}_6\text{H}_3\text{Br}_2$), 4.78 (s, 2H), 4.54 (s, 2H), 4.16 (s, 2H), 3.61 (s, 2H) (Cp). ^{31}P NMR (250 MHz, THF/ D_2O): 16.13 (d, $J_{\text{Pt-P}} = 4211\text{ Hz}$, $J_{\text{P-P}} = 16\text{ Hz}$), 12.39 (d, $J_{\text{Pt-P}} = 1784\text{ Hz}$, $J_{\text{P-P}} = 16\text{ Hz}$).

Synthesis of [(*S,S*-DIOP)Pt(I)(*o*-C₆H₄-OMe)] (6**).** To a solution of [(*S,S*-DIOP)Pt(η^2 -ethene)] (0.095 g, 0.131 mmol) in THF (10 mL) was added 2-iodoanisole (0.12 mL, 0.854 mmol, $\rho = 1.795\text{ g cm}^{-3}$). The mixture was refluxed for 3 h to give a pale yellow solution. The solvent was evaporated to dryness and the residue redissolved in diethyl ether (2 mL); addition of MeOH and cooling to $-15\text{ }^{\circ}\text{C}$ afforded a white solid which

(26) Hayashi, T.; Hayashizaki, K.; Kiyoh, T.; Ito, Y. *J. Am. Chem. Soc.* **1988**, *110*, 8153-8156.

(27) Whitesides, G. M.; Gaasch, J. F.; Stedronsky, E. R. *J. Am. Chem. Soc.* **1972**, *94*, 5258.

(28) Doyle, M. M.; Jackson, W. R.; Perlmutter, P. *Tetrahedron Lett.* **1989**, *30*, 5357.

(29) McDermott, J. X.; White, J. F.; Whitesides, G. M. *J. Am. Chem. Soc.* **1976**, *98*, 6521.

(30) Brown, J. M.; Cook, S. J.; Kimber, S. J. *J. Organomet. Chem.* **1984**, *269*, C58.

was filtered, washed with cold MeOH, and vacuum-dried. Recrystallization from dichloromethane/MeOH gave colorless microcrystals (0.106 g, 86%). Anal. Calcd for $C_{38}H_{39}IO_3Pt$: C, 49.20; H, 4.23. Found: C, 49.20; H, 4.22. 1H NMR (500 MHz, CD_2Cl_2): major isomer, 7.99 (m, 2H), 7.70 (m, 2H), 7.65 (m, 2H), 7.55–7.40 (m, 6H), 7.36 (m, 2H), 7.30–7.18 (m, 4H), 7.13 (m, 2H), 6.49 (m, 2H), 5.88 (m, 2H) (Ph and *o*-anisyl), 4.29 (m, 1H, $-CH_2P$), 3.79 (m, 1H, $-CH_2P$), 3.340 (s, 3H, OMe), 3.11 (td, 1H, $-CH$), 2.82 (m, 1H, $-CH$), 2.51 (m, 1H, $-CH_2P$), 2.45 (m, 1H, $-CH_2P$), 1.18 (s, 3H, CH_3), 0.80 (s, 3H, CH_3); minor isomer, 7.93 (m, 2H), 7.78 (m, 2H), 7.65 (m, 2H), 7.55–7.40 (m, 8H), 7.26–7.23 (m, 4H), 7.07 (m, 2H), 7.02 (m, 2H), 6.45 (m, 2H) (Ph and *o*-anisyl), 4.12 (m, 1H, $-CH_2P$), 3.95 (m, 1H, $-CH_2P$), 3.343 (s, 3H, OMe), 3.25 (td, 1H, $-CH$), 2.90 (m, 1H, $-CH$), 2.78 (m, 1H, $-CH_2P$), 2.20 (m, 1H, $-CH_2P$), 1.19 (s, 3H, CH_3), 1.09 (s, 3H, CH_3). ^{31}P NMR (250 MHz, CH_2Cl_2/D_2O): major isomer, -1.73 (d, $J_{Pt-P} = 4054$ Hz, $J_{P-P} = 17.5$ Hz), -5.93 (d, $J_{Pt-P} = 1914$ Hz, $J_{P-P} = 17.5$ Hz); minor isomer, -2.53 (d, $J_{Pt-P} = 4063$ Hz, $J_{P-P} = 17$ Hz), -2.96 (d, $J_{Pt-P} = 1755$ Hz, $J_{P-P} = 17$ Hz).

Reaction of [(*R*-BINAP)Pt(*o*- C_6H_4 -OMe) $_2$] with HBr. To a solution of complex **13** (*vide infra*) (0.040 mmol) in THF was slowly added 1 equiv of HBr (0.047 M in MeOH) at 0 °C. Monitoring of the reaction by ^{31}P NMR shows unreacted starting material and the complex [(*R*-BINAP)PtBr $_2$] ($\delta = 5.99$, $J_{Pt-P} = 3585$ Hz) as the major species, the desired complex [(*R*-BINAP)Pt(Br)(*o*- C_6H_4 -OMe)] (**7**) only being observed as a minor component. When the reaction was carried out in toluene at -40 °C using HBr (3.7×10^{-3} M), the same mixture was obtained with complex **7** being the dominant species (two isomers, $\delta = 15.99$ (d, $J_{Pt-P} = 1765$ Hz, $J_{P-P} = 19$ Hz), 15.33 (d, $J_{Pt-P} = 1760$ Hz, $J_{P-P} = 19$ Hz), 12.06 (d, $J_{Pt-P} = 4200$ Hz, $J_{P-P} = 20$ Hz), 11.85 (d, $J_{Pt-P} = 4224$ Hz, $J_{P-P} = 20$ Hz)]. Attempts to isolate pure complex **7** were unsuccessful.

Synthesis of [(*R,R*-CHIRAPHOS)Pt(3,5- $Br_2C_6H_3$) $_2$] (8**) and [(*R*-BINAP)Pt(3,5- $Br_2C_6H_3$) $_2$] (**9**).** A solution of 3,5-dibromophenyllithium³¹ was prepared by addition of a solution of *n*-BuLi (1.67 mL, 2.0 M in hexane) in diethyl ether (10 mL) to a solution of 1,3,5-tribromobenzene (0.378 g, 1.200 mmol) in diethyl ether (10 mL) at -78 °C. The appropriate [(diphosphine)PtCl $_2$] (0.1 mmol) was added, and the solutions were warmed to room temperature (3 h) to give an orange-brown solution. Addition of MeOH (2 mL) gave a pale yellow solution. The solvent was removed under vacuum and the residue extracted with toluene and filtered through Celite. Concentration of the solution to ca. 1 mL and slow addition of *n*-hexane gave the complexes as white cream-colored solids which were filtered, washed with *n*-hexane, and dried under vacuum.

[(*R,R*-CHIRAPHOS)Pt(3,5- $Br_2C_6H_3$) $_2$] (8**).** Yield: 93%. Anal. Calcd for $C_{40}H_{34}Br_4P_2Pt$: C, 44.02; H, 3.13. Found: C, 43.58; H, 2.54. 1H NMR (300 MHz, d_8 -toluene): 7.65 (m, 4H), 7.43 (t, 2H, *p*-H, $C_6H_3Br_2$), 7.29 (m, 4H, *o*-H, $C_6H_3Br_2$, $J_{Pt-H} = 62$ Hz, $J_{P-H} = 5.3$ Hz, $J_{H-H} = 1.8$ Hz), 7.20–6.90 (m, 12H), 6.86 (m, 4H), 2.21 (m, 2H, $-CH$), 1.04 (m, 6H, $-CH_3$). ^{31}P NMR (250 MHz, CH_2Cl_2/D_2O): 45.12 (s, $J_{Pt-P} = 1828$ Hz).

[(*R*-BINAP)Pt(3,5- $Br_2C_6H_3$) $_2$] (9**).** Yield: 86%. Anal. Calcd for $C_{56}H_{38}Br_4P_2Pt$: C, 52.23; H, 2.97. Found: C, 52.42; H, 2.80. 1H NMR (500 MHz, d_8 -toluene): 7.76 (t, 2H), 7.49 (m, 4H) (BINAP), 7.38 (m, 2H, *o*-H, $C_6H_3Br_2$), 7.35 (m, 4H), 7.21 (t, 4H), 7.07 (m, 2H), 7.02 (t, 4H), 6.92 (t, 4H) (BINAP), 6.80 (t, 2H, *p*-H, $C_6H_3Br_2$), 6.50 (td, 2H), 6.40 (m, 2H), 6.36 (m, 4H), 6.22 (d, 2H) (BINAP). ^{31}P NMR (250 MHz, CH_2Cl_2/D_2O): 17.1 (s, $J_{Pt-P} = 1903$ Hz).

Synthesis of [(dppf)Pt(3,5- $Br_2C_6H_3$) $_2$] (10**).** The complex was prepared from [(dppf)PtCl $_2$] (0.150 g, 0.182 mol) and 3,5-dibromophenyllithium (2.194 mmol) following the procedure described above for complexes **7** and **8**. Complex **9** is isolated as a yellow solid (0.195 g, 87%). Anal. Calcd for $C_{46}H_{34}Br_4FeP_2Pt$: C, 45.31; H, 2.81. Found: C, 45.31; H, 2.67. 1H NMR (300 MHz, CD_2Cl_2): 7.54–7.36 (m, 20H), 6.88 (m, 4H, *o*-H,

$C_6H_3Br_2$, $J_{Pt-H} = 69$ Hz), 6.74 (s, 2H, *p*-H, $C_6H_3Br_2$), 4.33 (s, 4H), 4.28 (s, 4H) (Cp). ^{31}P NMR (250 MHz, CH_2Cl_2/D_2O): 15.02 (s, $J_{Pt-P} = 1947$ Hz).

Synthesis of [(DIPHOS)Pt(*o*- C_6H_4 -OMe) $_2$] Complexes (DIPHOS = *S,S*-DIOP (11**), *R,R*-CHIRAPHOS (**12**), *R*-BINAP (**13**)).** To a solution of *o*- C_6H_4 (OMe)Li (1.80 mmol), prepared *in situ* by reaction of 2-iodoanisole (0.24 mL, 1.80 mmol, $\rho = 1.795$ g cm^{-3}) with *n*-BuLi (0.9 mL, 2.0 M, 1.80 mmol) in THF (10 mL) at -78 °C, the appropriate [(diphosphine)PtCl $_2$] complex (0.150 mmol) was added. The solution was slowly warmed to room temperature (3 h), and then MeOH (2 mL) was added. The solvent was removed under vacuum to give a white residue which was washed with cold hexane (2 \times 5 mL) and then dissolved in toluene (5 mL) and filtered through Celite. Concentration of the pale yellow solutions under vacuum to ca. 1 mL and slow addition of cold pentane gave the complexes **11** and **12** as white solids which were collected by filtration, washed with cold pentane, and vacuum-dried. Complex **13** is obtained as a white solid after washing the obtained residue with cold MeOH.

[(*S,S*-DIOP)Pt(*o*- C_6H_4 -OMe) $_2$] (11**).** Yield: 80%. Anal. Calcd for $C_{46}H_{46}O_4P_2Pt$: C, 59.53; H, 5.10. Found: C, 59.67; H, 5.14. 1H NMR (500 MHz, d_8 -toluene): isomer A, 8.30 (m, 4H, Ph), 7.50 (m, 4H, Ph), 7.20 (m, 4H, Ph), 7.18 (m, 2H, *o*-anisyl), 6.80 (m, 8H, Ph), 6.58 (t, 2H, *o*-anisyl), 6.42 (t, 2H, *o*-anisyl), 5.88 (d, 2H, *o*-anisyl), 3.80 (m, 2H, $-CH_2P$), 3.12 (m, 2H, $-CH_2P$), 2.68 (td, 2H, $-CH$), 3.32 (s, 6H, OMe), 1.16 (s, 6H, CH_3); isomer B, 4.18 (s, 3H, OMe), 4.00 (s, 3H, OMe), 1.23 (s, 3H, $-CH_3$), 1.04 (s, 3H, $-CH_3$); isomer C, 3.38 (m, 2H, $-CH_2P$), 3.26 (s, 6H, OMe), 3.02 (m, 2H, $-CH_2P$), 2.51 (m, 2H, CH), 1.31 (s, 6H, CH_3). ^{31}P NMR (500 MHz, d_8 -toluene): isomer A, 0.33 (s, $J_{Pt-P} = 1952$ Hz); isomer B, 3.63 (d, $J_{Pt-P} = 1891$ Hz, $J_{P-P} = 12$ Hz), 0.13 (d, $J_{Pt-P} = 1903$ Hz, $J_{P-P} = 12$ Hz); isomer C, 1.25 (s, $J_{Pt-P} = 1901$ Hz).

[(*R,R*-CHIRAPHOS)Pt(*o*- C_6H_4 -OMe) $_2$] (12**).** Yield: 91%. Anal. Calcd for $C_{42}H_{42}O_2P_2Pt$: C, 60.35; H, 5.06. Found: C, 60.51; H, 5.21. 1H NMR (300 MHz, CD_2Cl_2): 8.07 (t, 4H, Ph), 7.47 (m, 6H, Ph), 7.30 (t, 2H, *o*-anisyl), 7.18 (m, 6H, Ph), 6.85 (t, 4H, Ph), 6.64 (t, 2H, *o*-anisyl), 6.38 (t, 2H, *o*-anisyl), 6.20 (d, 2H, *o*-anisyl), 3.13 (s, 6H, $-OMe$), 2.13 (m, 2H, $-CH$), 1.02 (m, 6H, $-CH_3$). ^{31}P NMR (250 MHz, acetone/ D_2O): 43.2 (s, $J_{Pt-P} = 1903$ Hz).

[(*R*-BINAP)Pt(*o*- C_6H_4 -OMe) $_2$] (13**).** Yield: 91%. Anal. Calcd for $C_{56}H_{46}O_2P_2Pt$: C, 67.50; H, 4.49. Found: C, 67.50; H, 4.54. 1H NMR (300 MHz, CD_2Cl_2): isomer A, 7.79 (m, 4H), 7.52 (m, 4H), 7.45 (m, 4H), 7.27–6.88 (m, 10H), 6.65 (m, 8H), 6.38 (m, 8H), 5.70 (m, 2H) (BINAP and *o*-anisyl), 2.73 (s, 6H, OMe); isomer B, 3.75 (s, 3H, OMe), 3.40 (s, 3H, OMe); isomer C, 3.97 (s, 6H, OMe). ^{31}P NMR (500 MHz, CD_2Cl_2): isomer A, 18.57 (s, $J_{Pt-P} = 1954$ Hz); isomer B, 17.27 (d, $J_{Pt-P} = 1941$ Hz), 16.19 (d, $J_{Pt-P} = 1941$ Hz); isomer C, 15.08 (s, $J_{Pt-P} = 1967$ Hz).

Synthesis of [(dppf)Pt(*o*- C_6H_4 -OMe) $_2$] (15**).** The complex was prepared from [(dppf)PtCl $_2$] (0.100 g, 0.122 mol) and *o*- C_6H_4 (OMe)Li (1.464 mmol) by following the procedure described above for complex **11**. Complex **15** is obtained as a yellow microcrystalline solid (0.108 g, 92%). Anal. Calcd for $C_{48}H_{42}FeO_2P_2Pt$: C, 59.82; H, 4.39. Found: C, 59.38; H, 4.48. 1H NMR (300 MHz, CD_2Cl_2): major isomer, 8.62 (m, 4H, Ph), 7.61 (m, 6H, Ph), 7.06 (d, 2H, *o*-anisyl), 7.02 (m, 2H, Ph), 6.83 (m, 4H, Ph), 6.57 (m, 4H, Ph), 6.49 (t, 2H, *o*-anisyl), 6.24 (t, 2H, *o*-anisyl), 5.85 (d, 2H, *o*-anisyl), 4.75 (s, 2H, Cp), 4.25 (s, 2H, Cp), 4.19 (s, 2H, Cp), 3.93 (s, 2H, Cp), 3.31 (s, 6H, OMe); minor isomer, 3.20 (s, 6H, OMe). ^{31}P NMR (250 MHz, CH_2Cl_2/D_2O): 11.61 (s, $J_{Pt-P} = 2059$ Hz).

Crystal Structure Determination for Complex 13. Crystals were obtained as colorless plates from acetone/ethanol at 233 K and readily lost solvent. Attempts to mount them in Lindemann tubes were not successful, but it was found to be possible to cool a mounted crystal and retain reasonable diffraction (though with very broad peaks, which led to poor precision in the cell constants). Crystal data collection parameters are summarized in Table 3.

(31) Chen, L. S.; Chen, G. J.; Tamborski, C. J. *Organomet. Chem.* **1981**, *215*, 281.

Table 1. Atom Coordinates ($\times 10^4$) and Isotropic Thermal Parameters ($\text{\AA}^2 \times 10^3$)

atom	x	y	z	U^a	atom	x	y	z	U^a
Pt(1)	8893.8(2)	5000.0	7941.9(6)	26(1)*	C(131)	8484(8)	4218(21)	10108(25)	38(10)*
P(1)	8378(2)	4768(4)	8695(5)	24(2)*	C(132)	8188(7)	3833(19)	10511(21)	24(5)
P(2)	8923(2)	3153(6)	7543(7)	31(3)*	C(133)	8285(9)	3431(26)	11593(26)	52(11)*
O(1)	9193(5)	4712(17)	5768(15)	54(8)*	C(134)	8678(11)	3321(25)	12187(23)	59(11)*
O(2)	9006(5)	6682(15)	9924(14)	38(6)*	C(135)	8934(7)	3741(19)	11747(19)	25(5)
O(001)	6007(17)	2676(49)	5988(49)	203(20)	C(136)	8850(7)	4170(19)	10747(22)	29(9)*
O(002)	10347(11)	-725(29)	7483(29)	113(10)	C(21)	8833(10)	6707(33)	7993(29)	55(11)
C(001)	6345(21)	2630(62)	6436(57)	140(19)	C(22)	8924(9)	7321(23)	8963(21)	42(10)*
C(002)	6471(22)	1415(65)	6663(65)	166(22)	C(23)	8881(9)	8461(24)	8956(25)	38(7)
C(003)	6533(18)	3404(55)	6537(49)	126(17)	C(24)	8753(9)	9026(27)	8014(25)	48(7)
C(004)	10053(15)	-1013(43)	7558(43)	98(13)	C(25)	8713(9)	8443(27)	6942(24)	50(11)*
C(005)	9941(20)	-837(57)	8538(58)	144(20)	C(26)	8761(9)	7260(23)	6973(28)	42(10)*
C(11)	9418(8)	5333(20)	7579(19)	39(10)*	C(27)	8990(8)	7258(28)	10936(24)	52(10)*
C(12)	9492(7)	5152(33)	6582(18)	41(9)*	C(211)	8769(7)	2210(21)	8531(19)	21(5)
C(13)	9859(7)	5271(26)	6445(20)	49(11)*	C(212)	9080(7)	1700(19)	9304(20)	22(8)*
C(14)	10161(9)	5608(27)	7340(27)	56(8)	C(213)	9023(7)	1090(20)	10207(19)	31(8)*
C(15)	10063(9)	5836(44)	8267(27)	104(14)*	C(214)	8619(7)	959(19)	10299(21)	31(8)*
C(16)	9711(8)	5740(28)	8485(20)	50(10)*	C(215)	8566(9)	366(22)	11182(20)	47(10)*
C(17)	9277(10)	4248(35)	4753(23)	69(12)*	C(216)	8204(7)	252(25)	11302(22)	44(10)*
C(111)	8011(12)	3790(29)	7935(28)	47(12)*	C(217)	7900(7)	778(19)	10549(22)	35(9)*
C(112)	7665(7)	4264(18)	7204(22)	29(9)*	C(218)	7962(6)	1393(22)	9672(22)	33(8)*
C(113)	7440(7)	3666(20)	6456(19)	28(8)*	C(219)	8338(6)	1481(19)	9531(18)	22(5)
C(114)	7505(7)	2520(19)	6323(23)	30(8)*	C(210)	8420(9)	2110(21)	8667(21)	40(9)*
C(115)	7256(9)	1898(25)	5495(22)	45(10)*	C(221)	8609(6)	2744(20)	6228(19)	20(7)*
C(117)	7623(7)	291(26)	6114(18)	40(10)*	C(222)	8412(8)	3523(21)	5504(19)	33(9)*
C(118)	7882(7)	898(24)	6909(22)	38(9)*	C(223)	8201(8)	3220(25)	4516(21)	40(10)*
C(119)	7817(7)	2051(19)	7068(20)	25(8)*	C(224)	8127(8)	2148(25)	4189(21)	41(9)*
C(110)	8087(8)	2713(22)	7827(21)	26(9)*	C(225)	8322(7)	1349(24)	4865(23)	43(9)*
C(121)	8127(7)	6044(19)	8822(21)	28(8)*	C(226)	8574(9)	1645(26)	5919(25)	49(10)*
C(122)	8093(8)	6497(21)	9787(24)	36(9)*	C(231)	9413(11)	2658(25)	7459(21)	58(11)*
C(123)	7943(8)	7506(24)	9920(31)	49(10)*	C(232)	9471(9)	2039(26)	6622(26)	50(11)*
C(124)	7808(8)	8130(34)	8993(30)	64(12)*	C(233)	9816(9)	1753(23)	6612(25)	44(10)*
C(124)	7808(8)	8130(34)	8993(30)	64(12)*	C(234)	10130(9)	2062(29)	7384(35)	67(13)*
C(125)	7834(9)	7725(24)	7933(30)	51(11)*	C(235)	10080(8)	2654(35)	8357(33)	74(13)*
C(126)	8007(9)	6684(31)	7897(37)	52(13)*	C(236)	9695(8)	3010(25)	8320(25)	44(10)

^a Asterisks denote equivalent isotropic U values, defined as one-third of the trace of the orthogonalized U_{ij} tensor.

Table 2. Selected Bond Distances (\AA) and Angles (deg)

Pt(1)–P(1)	2.302(8)	P(2)–C(211)	1.861(27)
Pt(1)–P(2)	2.301(8)	P(2)–C(221)	1.812(22)
Pt(1)–C(11)	2.090(31)	P(2)–C(231)	1.897(41)
Pt(1)–C(21)	2.084(40)	O(1)–C(12)	1.390(29)
P(1)–C(111)	1.852(36)	O(1)–C(17)	1.483(39)
P(1)–C(121)	1.819(24)	O(2)–C(22)	1.393(31)
P(1)–C(131)	1.830(30)	O(2)–C(27)	1.455(37)
P(1)–Pt(1)–P(2)	93.1(3)	C(22)–O(2)–C(27)	115.5(21)
P(1)–Pt(1)–C(11)	168.3(6)	O(1)–C(12)–C(11)	115.9(24)
P(2)–Pt(1)–C(11)	92.8(7)	O(1)–C(12)–C(13)	122.9(23)
P(1)–Pt(1)–C(21)	90.4(11)	O(2)–C(22)–C(21)	113.8(26)
P(2)–Pt(1)–C(21)	169.6(10)	O(2)–C(22)–C(23)	123.9(24)
C(11)–Pt(1)–C(21)	85.6(12)	P(1)–C(111)–C(110)	122.2(27)
C(12)–O(1)–C(17)	118.6(22)	P(2)–C(221)–C(210)	126.3(19)

Data were collected with a Siemens R3m four-circle diffractometer in ω - 2θ mode. The crystal was held at 220 K with an Oxford Cryosystems Cryostream cooler. Maximum 2θ was 45° with scan range $+0.7^\circ(\omega)$ around the $K\alpha_1$ – $K\alpha_2$ angles, scan speed 3 – $15^\circ \text{ min}^{-1}(\omega)$, depending on the intensity of a 2 s prescan; backgrounds were measured at each end of the scan for 0.25 of the scan time. hkl ranges were: 0 – 38 , 0 – 12 , and -12 to 13 . Three standard reflections were monitored every 200 reflections and showed no decrease during data collection. Unit cell dimensions and standard deviations were obtained by least-squares fit to 17 reflections ($20 < 2\theta < 22^\circ$). Reflections were processed using profile analysis and were corrected for Lorentz, polarization, and absorption effects (by the Gaussian method); minimum and maximum transmission factors were 0.55 and 0.88. Systematic reflection conditions hkl , $k + l = 2n$ indicate one of the space groups $C2$, Cm , and $C2/m$. The intensity statistics and the chemical structure suggested that $C2/m$ was unlikely; $C2$ was selected for initial testing and shown to be correct by the successful refinement. Heavy atoms were located by the Patterson interpretation section of SHELXL-TL and the light atoms then found by E-map expansion and successive Fourier syntheses. One molecule of ethanol and

Table 3. Crystallographic Data for 13

molecular formula	$C_{58}H_{44}O_2Pt_2C_2H_6O \cdot C_3H_6O$
M_r	1134.2
cryst syst	monoclinic
cryst size (mm)	$0.067 \times 0.40 \times 0.26$
space group	$C2$
a (\AA)	36.08(5)
b (\AA)	12.12(1)
c (\AA)	12.45(2)
β (deg)	104.5(1)
V (\AA^3)	5272(2)
Z	4
D_c (g cm^{-3})	1.43
T (K)	220
diffractometer	Siemens R3m
radiation; λ (\AA)	Mo $K\alpha$; 0.710 69
μ , mm^{-1}	2.76
scan method	ω - 2θ
$2\theta(\text{max})$, deg	45
no. of unique rflns	3658
no. of obsd rflns	3011
criterion for observn	$I > 2\sigma(I)$
no. of params refined	561
S (goodness of fit)	0.91
$\Delta/\sigma_{\text{max}}$	0.3
R	0.063
R_w	0.087
residual electron density	+0.6 / -1.0

one of acetone of solvation are present in the asymmetric unit; both had high thermal parameters but were treated with full occupancy.

Anisotropic temperature factors were used for all non-H atoms. Hydrogen atoms were given fixed isotropic temperature factors; $U = 0.08 \text{\AA}^2$. Those defined by the molecular geometry were inserted at calculated positions and not refined. The absolute structure of the individual crystal chosen was checked by refinement of a $\Delta f''$ multiplier. The y coordinate of the Pt atom was fixed to define the origin.

A weighting scheme of the form $w = 1/(\sigma^2(F) + gF^2)$ with $g = 0.008$ was used and shown to be satisfactory by a weight analysis. All computing was performed on a DEC Microvax-II using SHELXTL PLUS (Sheldrick, 1986).³² Scattering factors in the analytical form and anomalous dispersion factors were taken from ref 33. Final atomic coordinates are given in Table 1 and selected bond lengths and angles in Table 2.

Acknowledgment. We thank Johnson-Matthey for the loan of Pt salts and the Spanish Ministry of Education for a Fellowship (to J.J.P.-T.).

(32) Sheldrick, G. M. *SHELXTL User's Manual*; Nicolet Instrument Co.: Madison, WI, 1983, 1986.

(33) *International Tables for X-Ray Crystallography*; Kynoch Press: Birmingham, U.K., 1974; Vol. IV (present distributor Kluwer Academic Publishers, Dordrecht, The Netherlands).

Supplementary Material Available: Tables of crystal data, anisotropic thermal parameters, additional bond distances and angles, and H atom positional parameters for **13** (8 pages). Ordering information is given on any current masthead page. Lists of anisotropic thermal parameters, H atom coordinates, full bond lengths and angles and structure factors have been deposited with the British Library Lending Division as Supplementary Publication. Copies may be obtained through The Executive Secretary, International Union of Crystallography, 5 Abbey Square, Chester CH1 2HU, England. Additional data available from the Cambridge Crystallographic Centre comprises H atom coordinates, thermal parameters, and full bond lengths and angles.

OM9406106

Silicon-Carbon Unsaturated Compounds. 52. Thermal Reaction of 1-Mesityl-, 1-*o*-Tolyl-, and 1-*p*-Tolyl-3-phenyl-1,2-bis(trimethylsilyl)silacycloprop-2-enes

Atsutaka Kunai,* Yoichi Matsuo, Joji Ohshita, Mitsuo Ishikawa,* Yoshio Aso, Tetsuo Otsubo, and Fumio Ogura

Department of Applied Chemistry, Faculty of Engineering, Hiroshima University, Kagamiyama, Higashi-Hiroshima 724, Japan

Received August 8, 1994[⊙]

Thermal reaction of 1-mesityl-, 1-*o*-tolyl-, and 1-*p*-tolyl-3-phenyl-1,2-bis(trimethylsilyl)silacycloprop-2-enes (**1a–1c**) has been studied. The thermolysis of **1b** afforded 3,3-dimethyl-4-phenyl-1-*o*-tolyl-5-(trimethylsilyl)-1,3-disilacyclopent-4-ene (**2b**), 1-*o*-tolyl-1,3-bis(trimethylsilyl)-1-silaindene (**3b**), and 1-*o*-tolyl-2,3-bis(trimethylsilyl)-1-silaindene (**4b**), while the thermolysis of **1c** produced 3,3-dimethyl-4-phenyl-1-*p*-tolyl-5-(trimethylsilyl)-1,3-disilacyclopent-4-ene (**2c**), 1-*p*-tolyl-1,3-bis(trimethylsilyl)-1-silaindene (**3c**), and 1-*p*-tolyl-2,3-bis(trimethylsilyl)-1-silaindene (**4c**). The thermolysis of **1b** in the presence of phenyl(trimethylsilyl)acetylene afforded (*Z*)-3-phenyl-1-[2-phenyl-1,2-bis(trimethylsilyl)ethenyl]-1-*o*-tolyl-2-(trimethylsilyl)silacycloprop-2-ene (**7b**), together with **2b**, **3b**, and **4b**, while the similar reaction of **1c** produced (*Z*)- and (*E*)-1-[2-phenyl-1,2-bis(trimethylsilyl)ethenyl]-1-*o*-tolyl-2-(trimethylsilyl)-1-silaindene, in addition to **2c**, **3c**, and **4c**. The reactions of **1b** and **1c** in the presence of methyl-diphenylsilane produced *Z* and *E* isomers of 1-(2-methyl-2,2-diphenyl-1-*o*-tolyl-disilanyl)- and 1-(2-methyl-2,2-diphenyl-1-*p*-tolyl-disilanyl)-2-phenyl-1,2-bis(trimethylsilyl)ethene, respectively. The structure of 1-mesityl-5-phenyl-4,6,7-tris(trimethylsilyl)-1-silabenzob[n]bornadiene (**6a**), which is produced from the reaction of **1a** with phenyl(trimethylsilyl)acetylene, was reinvestigated. **6a** crystallizes in the space group $P2_1/a$ with cell dimensions of $a = 23.955(7)$ Å, $b = 12.664(1)$ Å, $c = 11.514(1)$ Å, $\alpha = \gamma = 90^\circ$, $\beta = 98.76(2)^\circ$, $V = 3452(1)$ Å³, $Z = 4$, and $D_{\text{calcd}} = 1.095$ g/cm³. **7b** crystallizes in the space group $P2_1/c$ with cell dimensions of $a = 18.880(1)$ Å, $b = 9.4251(7)$ Å, $c = 20.938(3)$ Å, $\alpha = \gamma = 90.0^\circ$, $\beta = 115.069(6)^\circ$, $V = 3374.9(3)$ Å³, $Z = 4$, and $D_{\text{calcd}} = 1.065$ g/cm³.

Introduction

Silacyclopropenes, which can readily be prepared by the photolysis of phenylethynepolysilanes,¹ undergo a wide variety of reactions, depending on the substituents on the silicon atom and the reaction conditions.^{2–9} For example, the reaction of 1-mesityl-3-phenyl-1,2-bis(trimethylsilyl)silacycloprop-2-ene (**1a**) with a Ni(PPh₃)₄ catalyst produces a nickelasilacyclobutene which isomerizes to a silapropadiene–nickel complex. The silapropadiene–nickel complex undergoes further rearrangement to give two isomers of a benzodisilacyclohexene derivative as the final products, via C–H bond activation of a methyl group on the mesityl ring (Scheme 1).^{6,7}

[⊙] Abstract published in *Advance ACS Abstracts*, February 1, 1995.

(1) (a) Ishikawa, M.; Fuchikami, T.; Kumada, M. *J. Am. Chem. Soc.* **1977**, *99*, 245. (b) Sakurai, H.; Kamiyama, Y.; Nakadaira, Y. *J. Am. Chem. Soc.* **1977**, *99*, 3879.

(2) Ishikawa, M.; Kovar, D.; Fuchikami, T.; Nishimura, K.; Kumada, M.; Higuchi, T.; Miyamoto, S. *J. Am. Chem. Soc.* **1981**, *103*, 2324.

(3) Ishikawa, M.; Nishimura, K.; Ochiai, H.; Kumada, M. *J. Organomet. Chem.* **1982**, *236*, 7.

(4) Ishikawa, M.; Sugisawa, H.; Fuchikami, T.; Kumada, M.; Yamabe, T.; Kawakami, H.; Ueki, Y.; Shizuka, H. *J. Am. Chem. Soc.* **1982**, *104*, 2872.

(5) Ishikawa, M.; Matsuzawa, S.; Sugisawa, H.; Yano, F.; Kamitori, S.; Higuchi, T. *J. Am. Chem. Soc.* **1985**, *107*, 7706.

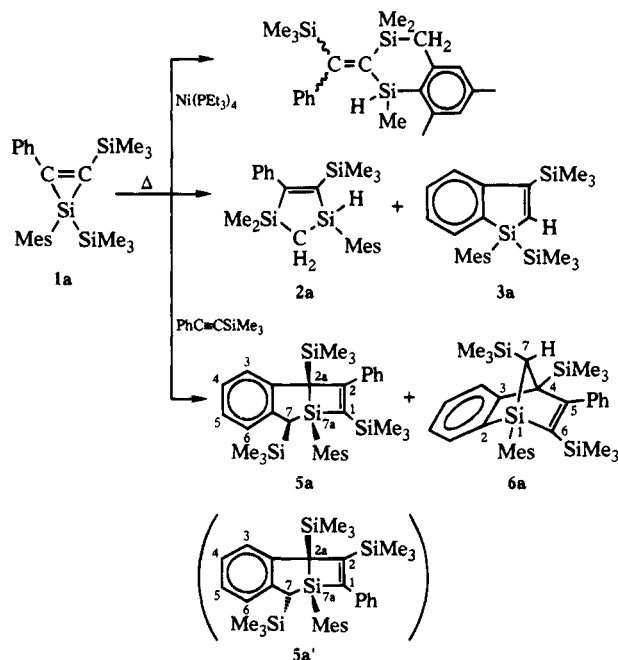
(6) Ishikawa, M.; Ohshita, J.; Ito, Y.; Iyoda, J. *J. Am. Chem. Soc.* **1986**, *108*, 7417.

(7) Ohshita, J.; Isomura, Y.; Ishikawa, M. *Organometallics* **1989**, *8*, 2050.

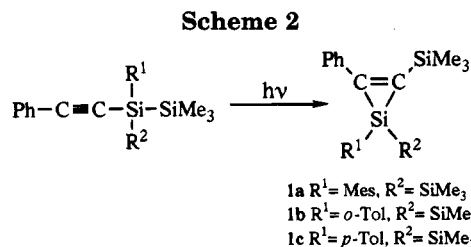
(8) Ishikawa, M.; Yuzuriha, Y.; Horio, T.; Kunai, A. *J. Organomet. Chem.* **1991**, *402*, C20.

(9) Ishikawa, M.; Horio, T.; Yuzuriha, Y.; Kunai, A.; Tsukihara, T.; Naitou, H. *Organometallics* **1992**, *11*, 597.

Scheme 1



More recently, we have reported that the thermolysis of **1a** in the absence of a trapping agent produces 1-mesityl-3,3-dimethyl-4-phenyl-5-(trimethylsilyl)-1,3-disilacyclopent-4-ene (**2a**) and 1-mesityl-1,3-bis(trimethylsilyl)-1-silaindene (**3a**),⁸ while in the presence of



phenyl(trimethylsilyl)acetylene, **1a** affords two adducts, along with **2a** and **3a** (Scheme 1).⁹ The structure of one of two adducts was confirmed to be *c*-7a-mesityl-2-phenyl-1,*r*-2a,*c*-7-tris(trimethylsilyl)cyclobutenosilaindan (**5a**) by an X-ray crystallographic study.¹⁰ Since all spectral data for the other product were quite similar to those of **5a**, we concluded this compound as a regio isomer of **5a**, *c*-7a-mesityl-1-phenyl-2,*r*-2a,*t*-7-tris(trimethylsilyl)cyclobutenosilaindan (**5a'**). NOE-FID difference experiments at 270 MHz also suggested the structure proposed for **5a'**. However, during the course of further study on the reaction of silacyclopropenes, we suspected that erroneous structural assignment had been made for **5a'** and found that this compound must be 1-mesityl-5-phenyl-4,6,7-tris(trimethylsilyl)-1-silabenzob[*b*]norborene (**6a**). We also found that the thermal behavior of related compounds, 1-*o*-tolyl- and 1-*p*-tolyl-3-phenyl-1,2-bis(trimethylsilyl)silacycloprop-2-enes (**1b** and **1c**) in the presence of phenyl(trimethylsilyl)acetylene is quite different from that of **1a**. In this paper, we report the thermal reaction of **1a**–**1c** in the presence or absence of trapping agents and the results of an X-ray diffraction study for **6a**.

Results and Discussion

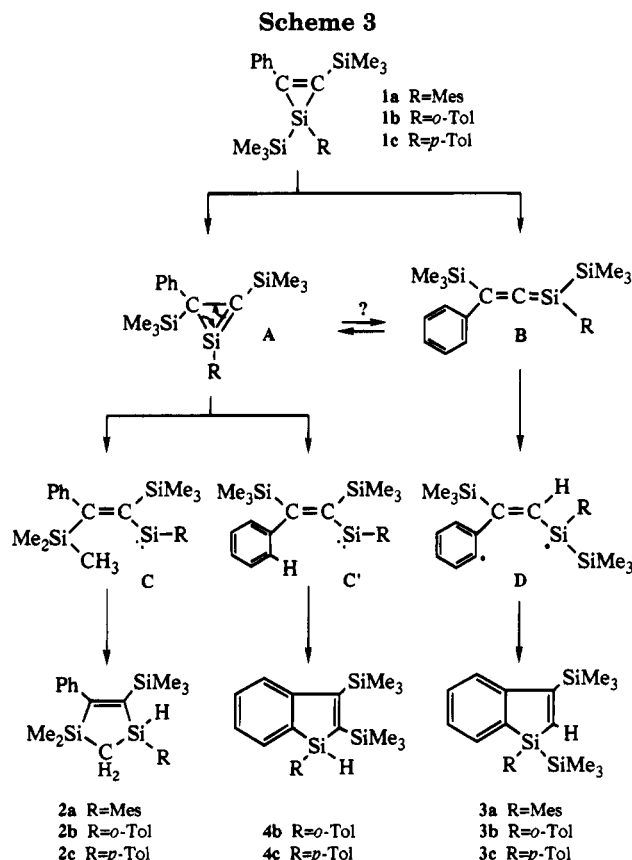
Silacyclopropene **1a** used as the starting compound was prepared by irradiating 2-mesityl-2-(phenylethynyl)hexamethyltrisilane with a low-pressure mercury lamp in hexane, followed by distillation as reported previously (Scheme 2).⁷ Similarly, **1b** and **1c** were prepared by the photolysis of 2-*o*-tolyl- and 2-*p*-tolyl-2-(phenylethynyl)hexamethyltrisilanes in 41–46% and 25–36% yields, respectively.¹¹

As reported previously,^{8,9} the thermolysis of **1a** at 280 °C for 6 h produces isomerization products **2a** and **3a** in 49% and 28% yields, respectively. The thermolysis of **1b** and **1c** also produced isomerization products analogous to **2a** and **3a** (Table 1).¹² Thus, when **1b** was heated in a degassed sealed tube at 130 °C for 6 h, 3,3-dimethyl-4-phenyl-1-*o*-tolyl-5-(trimethylsilyl)-1,3-disilacyclopent-4-ene (**2b**) and 1-*o*-tolyl-1,3-bis(trimethylsilyl)-1-silaindene (**3b**) were obtained in 7% and 58% yields, together with a 5% yield of 1-*o*-tolyl-2,3-bis(trimethylsilyl)-1-silaindene (**4b**) (Scheme 3). Similar thermolysis of **1c** under the same conditions produced 3,3-dimethyl-4-phenyl-1-*p*-tolyl-5-(trimethylsilyl)-1,3-disilacyclopent-4-ene (**2c**), 1-*p*-tolyl-1,3-bis(trimethylsilyl)-1-silaindene (**3c**), and 1-*p*-tolyl-2,3-bis(trimethylsilyl)-1-silaindene (**4c**) in 11%, 36%, and 9% yields, respectively. The

Table 1. Thermal Reaction of Silacycloprop-2-enes 1a–1c in the Presence or Absence of Trapping Agent

compd	additive ^a	temp, °C	time, h	product (yield, %)				
1a ^b	none	280	6	2a (49)	3a (28)			
1b	none	280	6	2b (6)	3b (3)	4b (4)		
1b	none	250	6	2b (5)	3b (5)	4b (8)		
1b	none	150	6	2b (7)	3b (8)	4b (4)		
1b	none	130	6	2b (7)	3b (58)	4b (5)		
1b ^c	none	100	6	2b (7)	3b (21)	4b (10)		
1c	none	280	6	2c (5)	3c (10)	4c (10)		
1c	none	250	6	2c (6)	3c (9)	4c (6)		
1c	none	200	6	2c (3)	3c (4)	4c (4)		
1c	none	150	6	2c (5)	3c (20)	4c (14)		
1c	none	130	6	2c (11)	3c (36)	4c (9)		
1c ^c	none	100	6	2c (0)	3c (0)	4c (0)		
1a ^b	PTA	280	6	2a (13)	3a (23)	5a (26)	6a (26)	
1b	PTA	280	6	2b (6)	3b (12)	4b (20)	7b (17)	
1b	PTA	230	6	2b (11)	3b (4)	4b (17)	7b (44)	
1b	PTA	200	6	2b (4)	3b (4)	4b (1)	7b (44)	
1c	PTA	280	6	2c (5)	3c (8)	4c (8)	8c (13)	9c (10)
1c	PTA	250	6	2c (5)	3c (2)	4c (11)	8c (75)	9c (11)
1b	MDS	280	6	2b (6)	3b (7)	4b (11)	10b (4)	11b (1)
1b	MDS	250	6	2b (9)	3b (6)	4b (13)	10b (14)	11b (10)
1b	MDS	230	6	2b (3)	3b (7)	4b (13)	10b (1)	11b (1)
1c	MDS	280	6	2c (2)	3c (8)	4c (4)	10c (4)	11c (2)
1c	MDS	250	6	2c (2)	3c (3)	4c (4)	10c (60)	11c (18)
1c	MDS	200	6	2c (2)	3c (3)	4c (2)	10c (0)	11c (0)

^a PTA and MDS stand for phenyl(trimethylsilyl)acetylene and methyl-diphenylsilane, respectively. ^b Results of previous work.⁹ ^c Conversion of starting material was very low.



thermolysis of **1b** and **1c** at temperatures higher than 150 °C resulted in the decrease of yields of main products **3b** and **3c**. At 100 °C, however, the rate of isomerization of **1b** and **1c** was extremely slow, and most of the starting compound was recovered after 6-h reaction.

The structures of these products were verified by spectrometric analysis, as well as by elemental analysis. Like **2a**,⁸ the ¹H NMR spectrum of disilacyclopentene

(10) The positions of the trimethylsilyl and phenyl groups in **5a** were inversely shown in Scheme II of the previous paper (ref 9). The correct form for **5a** is exhibited in the stereoview (Figure 1) of the same paper. See also erratum shown in *Organometallics* **1992**, *11*, No. 10, p 3486.

(11) **1b** and **1c** are thermally stable at room temperature but sensitive to oxygen and moisture in air.

(12) In contrast to silacyclopropanes, silacyclopropenes do not eliminate silylenes thermally, but undergo thermal isomerization.

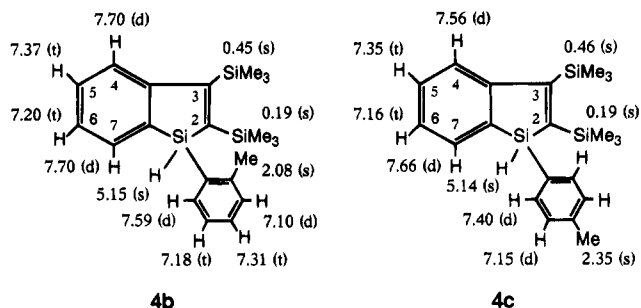


Figure 1. ^1H NMR chemical shifts of silaindenes **4b** and **4c**.

2b reveals two singlet resonances due to nonequivalent dimethylsilyl protons at δ -0.08 and 0.22 ppm and resonances due to an ABX spin system of the ring $\text{CH}_2\text{-SiH}$ unit at δ -0.05 (dd), 0.23 (dd), and 5.19 (dd) ppm. The ^1H NMR spectrum of **2c** also shows similar signals at δ 0.13 , 0.20 (MeSi), -0.11 (dd), 0.19 (dd), and 5.11 (dd) ppm (CH_2SiH). As observed for **3a**,⁸ the ^1H NMR spectrum of silaindene **3c** reveals resonances characteristic to the silaindene ring at δ 6.93 (s, C2-H), 7.20 (t, C6-H), 7.34 (t, C5-H), 7.52 (d, C4-H), and 7.65 (d, C7-H) ppm, together with resonances due to *p*-tolyl ring protons at δ 7.13 (d, 2H, *m*-H) and 7.42 (d, 2H, *o*-H) ppm. A similar pattern is also observed in the ^1H NMR spectrum of **3b**. In contrast to **3b** and **3c**, a proton signal due to SiH appears at δ 5.15 ppm for **4b** and δ 5.14 ppm for **4c**, but the signal characteristic to C2-H is not observed for these compounds. The ^1H NMR chemical shifts for silaindenes **4b** and **4c** are shown in Figure 1. The location of protons on the silaindenyl ring as well as protons in the tolyl ring for **3b,c** and **4b,c** was confirmed by ^1H - ^1H COSY experiments at 270 MHz. These results are wholly consistent with the structures proposed for these products.

The formation of products **2a-c**, **3b,c**, and **4a-c** can best be understood by a series of reactions shown in Scheme 3.^{8,9} A 1,2-trimethylsilyl shift from the silicon atom to the sp^2 carbon at the C3 position in the silacyclopropenyl ring would produce silacycloprop-1-ene intermediate (**A**), which isomerizes to give silylene species (**C** and **C'**) as the reactive intermediates. The silylenes thus formed insert intramolecularly into a C-H bond of either the trimethylsilyl group or phenyl group, which is located on the same side as the silylene center with respect to a carbon-carbon double bond to give **2a-c** or **4a-c**, respectively. The products **3a-c** may be explained by isomerization of the silacyclopropenes **1a-c** to a silapropadiene (**B**), followed by a hydrogen shift from the ortho position of the phenyl ring to the internal carbon of the silapropadiene and then coupling of the resulting diradical (**D**) to form a silaindene ring.

Previously, we reported that the thermolysis of **1a** in the presence of a large excess of phenyl(trimethylsilyl)acetylene at 280°C for 6 h gives two adducts **5a** and **5a'** in 20% and 26% yields, along with **2a** (13%) and **3a** (23%).⁹ The structure of **5a'** was reexamined by an X-ray diffraction study and verified to be 1-mesityl-5-phenyl-4,6,7-tris(trimethylsilyl)-1-silabenzob[n]bornadiene (**6a**) (see below).

In the thermolysis of **1a** in the presence of phenyl(trimethylsilyl)acetylene, the yield of **2a** decreases markedly, compared with that of the reaction in the

absence of the acetylene, but no change is observed in the yield of **3a**. These results indicate that silacycloprop-1-ene **A** was trapped by the acetylene (Scheme 4).^{13,14} Therefore, the formation of **5a** may be explained by [2 + 2] cycloaddition of **A** with phenyl(trimethylsilyl)acetylene giving intermediate (**E**) (path a), followed by isomerization of **E** to another intermediate (**F**). A 1,3-hydrogen shift in intermediate **F** to restore the aromatic sextet would produce **5a** as proposed previously.^{10,15} An alternative pathway involving scission of a C-C bond in the silacycloprop-1-enyl ring of **A** (path b), leading to intermediate (**G**) and silene (**H**), and then [2 + 2] cycloaddition of silene **H** with the acetylene would produce **5a**. However, examination of stereo models indicates that [2 + 2] cycloaddition of silene **H** with the acetylene seems to be unfavorable because of a large steric hindrance.

In contrast to the formation of **5a**, adduct **6a** can be understood in terms of a series of the reaction involving scission of an Si-C bond of the silacycloprop-1-enyl ring of **A** (path c).¹⁶ As shown in Scheme 4, a 1,3-hydrogen shift in intermediate (**J**) derived from ring enlargement of **A** would produce another silene intermediate (**K**). The [4 + 2] cycloaddition of this intermediate with the acetylene would produce **6a**. In this reaction, intermediate (**L**) might be formed from intermediate **J** via a 1,3-hydrogen shift.¹⁷ However, no products arising from silene **L** were detected in the reaction mixture. Presumably, [2 + 2] cycloaddition of this silene with the acetylene is sterically unfavorable, as in the case of the reaction of silene **H**.

We also carried out the thermolysis of **1b** and **1c** in the presence of phenyl(trimethylsilyl)acetylene. Interestingly, the thermolysis of **1b** in the presence of the acetylene afforded a product quite different from those of **1a**. Thus, heating **1b** in the presence of phenyl(trimethylsilyl)acetylene at 230°C for 6 h produced (*Z*)-3-phenyl-1-[2-phenyl-1,2-bis(trimethylsilyl)ethenyl]-1-*o*-tolyl-2-(trimethylsilyl)silacycloprop-2-enes (**7b**) in 44% yield, together with **2b** (11%), **3b** (4%), and **4b** (17%), while at 280°C for 6 h, the similar reaction of **1b** gave **7b** only in low yield. Product **7b** is thermally and oxidatively stable. For example, when **7b** was heated in a degassed sealed tube at 200°C for several hours, **7b** was recovered quantitatively. **7b** can be recrystallized from ethanol without decomposition even under aerobic conditions.

(13) Barton and his co-workers^{14a,b} have reported that, in the thermal rearrangement of methylvinylsilylene to ethynylmethylsilane, the intermediacy of 1-methylsilacycloprop-1-ene seems to be thermodynamically unfavorable on the basis of ab initio calculations for structural isomers with the formula C_2SiH_4 reported by Gordon et al.,^{14c} and the reaction may proceed via 1-methylsilacycloprop-2-ene, which is in equilibrium with the starting vinylsilylene. However, in the case of silacyclopropenes having bulky substituents on the ring, especially in the case of **1a**, the formation of **5a** and **6a** can best be rationalized in terms of intermediate **A**.

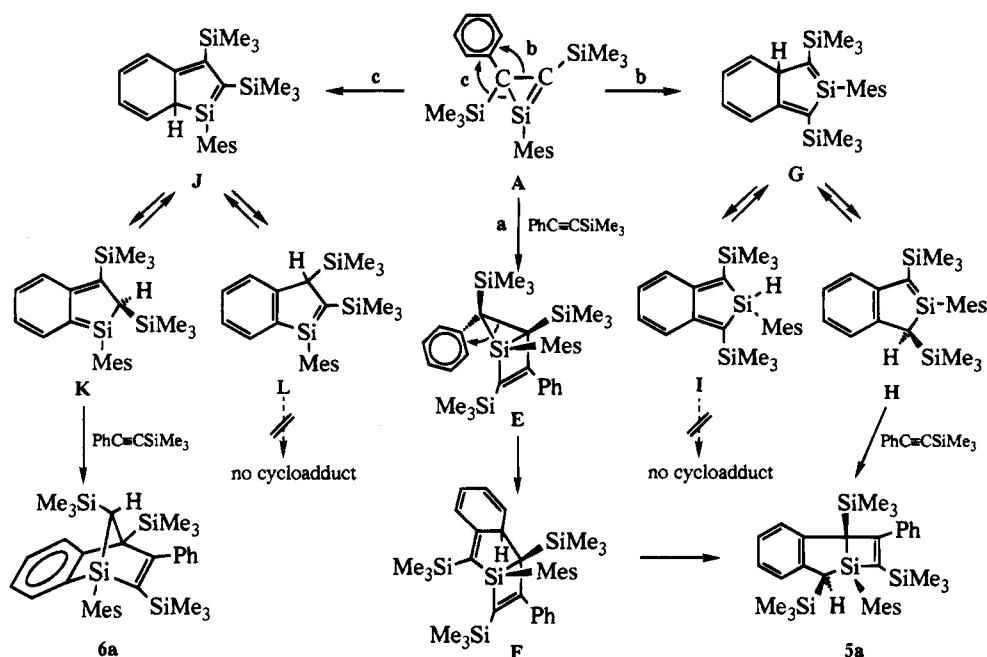
(14) (a) Barton, T. J.; Burns, G. T.; Coure, W. F.; Wulff, W. D. *J. Am. Chem. Soc.* **1982**, *104*, 1149. (b) Barton, T. J.; Burns, S. A.; Burns, G. T. *Organometallics* **1983**, *2*, 199. (c) Gordon, M. S.; Koob, R. D. *J. Am. Chem. Soc.* **1981**, *103*, 2939.

(15) The addition of phenyl(trimethylsilyl)acetylene to intermediate **A** may occur from the side of the phenyl group, although alternative geometry for intermediate **E** has been shown in ref 9.

(16) It seems likely that **5a** and **6a** may be formed by different pathways, because no interconversion between **5a** and **6a** is observed under the conditions used.

(17) Thermal and photochemical 1,3-hydrogen shifts in a silacyclopropadienyl ring system has been reported: Khabashesku, V. N.; Balaji, V.; Boganov, S. E.; Nefedov, O. M.; Michl, J. *J. Am. Chem. Soc.* **1994**, *116*, 320.

Scheme 4



On the other hand, when the reaction of **1c** with phenyl(trimethylsilyl)acetylene was carried out at 250 °C for 6 h, no silacyclopene analogous to **7b** was detected in the reaction mixture. Instead, (*Z*)- and (*E*)-1-[2-phenyl-1,2-bis(trimethylsilyl)ethenyl]-1-*o*-tolyl-2-(trimethylsilyl)-1-silaindenes (**8c** and **9c**) were obtained in 75% and 11% yields, as main products.

The structures of **8c** and **9c** were verified by spectroscopic analysis, and the location of substituents was confirmed by NOE-FID difference experiments at 270 MHz. For **9c**, saturation of trimethylsilyl protons ($\delta -0.05$) at the C2 position caused a positive NOE of a proton (s, $\delta 7.80$) at the C3 position, as well as *o*-protons (d, 2H, $\delta 7.43$) in the *p*-tolyl ring, while saturation of trimethylsilyl protons ($\delta -0.08$) at the β position of the olefinic unit resulted in enhancement of trimethylsilyl protons ($\delta 0.28$) at the α position, *o*-protons in the *p*-tolyl ring, and *o*-protons (d, $\delta 6.71$) in the phenyl ring. Irradiation of trimethylsilyl protons at the α position caused enhancement of a proton (d, $\delta 7.62$) at the C7 position and the trimethylsilyl protons at the β position. In the similar NOE-FID difference experiments for geometric isomer **8c**, saturation of trimethylsilyl protons at the α position ($\delta 0.44$) with respect to the olefinic unit caused enhancement of a proton ($\delta 7.61$) at the C7 position and trimethylsilyl protons ($\delta 0.38$) at the C2 position, but no enhancement was observed for trimethylsilyl protons at the β position ($\delta -0.29$), indicating that these trimethylsilyl groups are located in a *trans* fashion. Irradiation of trimethylsilyl protons at the C2 position resulted in enhancement of a proton at the C3 position (s, $\delta 8.05$), as well as *o*-protons (d, 2H, $\delta 7.55$) in the *p*-tolyl ring and trimethylsilyl protons at the α and β positions. These results unambiguously support the structures proposed for **8c** and **9c**.

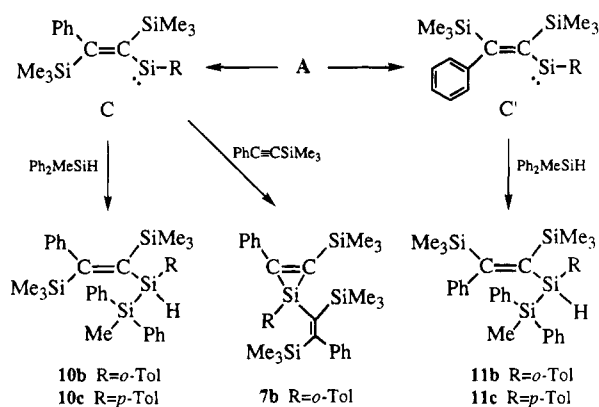
In order to obtain more information for the reactive species leading to these products, we carried out the reaction of **1b** and **1c** in the presence of a hydrosilane. Thus, heating **1b** at 250 °C for 6 h in the presence of methyl-diphenylsilane afforded (*Z*)-1-(2-methyl-2,2-diphenyl-1-*o*-tolyl-disilanyl)-2-phenyl-1,2-bis(trimethyl-

silyl)ethene (**10b**) and (*E*)-1-(2-methyl-2,2-diphenyl-1-*o*-tolyl-disilanyl)-2-phenyl-1,2-bis(trimethylsilyl)ethene (**11b**) in 14% and 10% yields, along with **3b** (9%), **4b** (6%), and **5b** (13%), while the similar reaction of **1c** produced (*Z*)-1-(2-methyl-2,2-diphenyl-1-*p*-tolyl-disilanyl)-2-phenyl-1,2-bis(trimethylsilyl)ethene (**10c**) and (*E*)-1-(2-methyl-2,2-diphenyl-1-*p*-tolyl-disilanyl)-2-phenyl-1,2-bis(trimethylsilyl)ethene (**11c**) in 60% and 18% yields, respectively, together with **3c** (2%), **4c** (3%), and **5c** (4%). The production of these compounds clearly indicates that silylene species C and C' play an important role in the thermal reactions for **1b** and **1c** (see Scheme 3).

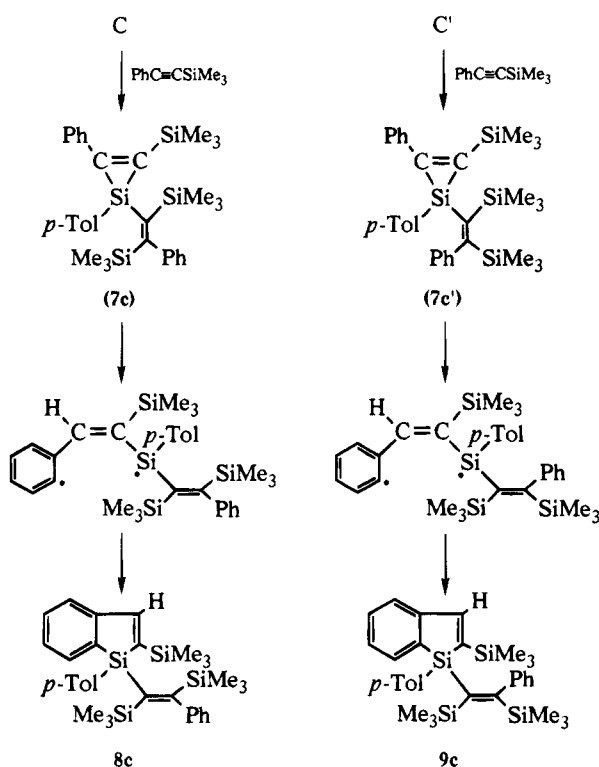
The structures of **10b**, **10c**, **11b**, and **11c** were verified by spectroscopic analysis, and their *Z* and *E* geometries were established by NOE-FID difference experiments at 270 MHz. For **11c**, irradiation of trimethylsilyl protons at the position β ($\delta -0.24$) to the disilanyl group caused a strong enhancement of trimethylsilyl protons at the α position ($\delta 0.30$), while saturation of the trimethylsilyl protons at $\delta 0.30$ ppm resulted in enhancement of the trimethylsilyl protons at $\delta -0.24$ ppm as well as a proton at $\delta 5.33$ ppm (SiH), indicating that **11c** must have the *E* configuration. For **10c**, however, irradiation of trimethylsilyl protons at the α ($\delta -0.05$) and β ($\delta -0.45$) positions, respectively, caused no effect for the trimethylsilyl protons, as expected for the *Z* configuration. For **10b** and **11b**, all attempts to separate these two isomers using recycling HPLC were unsuccessful. The isolated samples were always contaminated with a small amount of the other isomer. Nevertheless, their *E* and *Z* configurations could be readily confirmed by NOE-FID difference experiments in a manner similar to the above.

Scheme 5 illustrates a possible mechanistic interpretation for the formation of **7b**, **10b**, **10c**, **11b**, and **11c** in the reaction of **1b** and **1c**. The silylene species C and C' derived from A insert into an Si-H bond of the hydrosilane to afford **10b,c** and **11b,c**, respectively. The formation of **7b** can be understood by cycloaddition of

Scheme 5



Scheme 6



silylene **C** generated from **1b** to the triple bond of phenyl(trimethylsilyl)acetylene.

As shown in Scheme 6, products **8c** and **9c** may be explained by isomerization of silacyclopropenes (**7c** and **7c'**) which would be produced by the cycloaddition of **C** and **C'** derived from **1c** to the acetylene. Homolytic scission of a silicon-carbon bond in the silacyclopropene ring of **7c** and **7c'**, followed by a 1,3-hydrogen shift from the ortho position of the phenyl ring to the α position of the carbon-carbon double bond would produce diradical intermediates. The coupling reaction of the resulting diradicals produces **8c** and **9c**, respectively.

X-ray Analysis of 6a and 7b. The colorless crystals of **6a** and **7b** were obtained by recrystallization from ethanol, and their structures were solved by an X-ray crystallographic analysis. The experimental conditions and summary of structural refinement for **6a** and **7b** are listed in Table 2.

For **6a**, the final atomic coordinates and equivalent isotropic temperature factors are given in Table 3. The ORTEP view of the molecular structure with the atomic

Table 2. Crystal Data, Experimental Conditions, and Summary of Structural Refinement for **6a** and **7b**

compound	6a	7b
mol formula	C ₃₄ H ₄₈ Si ₄	C ₃₂ H ₄₄ Si ₄
mol wt	569.10	541.04
space group	<i>P</i> 2 ₁ / <i>a</i>	<i>P</i> 2 ₁ / <i>c</i>
cell dimens		
<i>a</i> , Å	23.955(7)	18.880(1)
<i>b</i> , Å	12.664(1)	9.4251(7)
<i>c</i> , Å	11.514(1)	20.938(3)
α , deg	90.0	90.0
β , deg	98.76(2)	115.069(6)
γ , deg	90.0	90.0
<i>V</i> , Å ³	3452(1)	3374.9(3)
<i>Z</i>	4	4
<i>D</i> _{calcd} , Mg/m ³	1.095	1.065
cryst size, mm	0.9 × 0.8 × 0.8	0.5 × 0.3 × 0.3
cryst color	colorless	colorless
μ , mm ⁻¹	1.62	1.63
diffractometer	Rigaku AFC-6C	Rigaku AFC-6C
temp, K	298	298
wavelength, Å	1.5418 (Cu K α)	1.5418 (Cu K α)
monochromator	graphite crystal	graphite crystal
scan type	$\omega - 2\theta$	$\omega - 2\theta$
scan speed, deg/min	6	4
scan width, deg	0 ≤ 2θ ≤ 126	0 ≤ 2θ ≤ 126
diffraction geometry	symmetrical A	symmetrical A
range of <i>h, k, l</i>		
<i>h</i>	-28 ≤ <i>h</i> ≤ 28	-24 ≤ <i>h</i> ≤ 24
<i>k</i>	0 ≤ <i>k</i> ≤ 15	0 ≤ <i>k</i> ≤ 10
<i>l</i>	0 ≤ <i>l</i> ≤ 13	0 ≤ <i>l</i> ≤ 21
no. of unique reflns	5258	5177
no. of obsd reflns ($ F_o \geq 3\sigma(F_o)$)	4953	3788
<i>R</i> _{sym}	0.013	0.043
<i>F</i> (000)	1232	992
<i>R</i>	0.096	0.085
<i>R</i> _w ^a	0.142	0.079

^a Weighting scheme is $(\sigma(F_o)^2 + 0.0004|F_o|^2)^{-1}$.

numbering scheme is shown in Figure 2, and selected bond distances and angles are listed in Table 4. The thermal parameters of the methyl carbon atoms attached to Si4 are large, suggesting an orientational disorder by rotation about the C5-Si4 bond. For **7b**, the final atomic coordinates and equivalent isotropic temperature factors are given in Table 5. The ORTEP view and the atomic numbering scheme of the molecule are shown in Figure 3, and selected bond distances and angles are listed in Table 6. The data reveal some lengthening of the bond between Si3 and C7 (1.981(6) Å), indicating the existence of a large steric repulsion caused by trimethylsilyl, phenyl, and silacyclopropenyl substituents. For **6a** and **7b**, there are no close intermolecular contacts.

Experimental Section

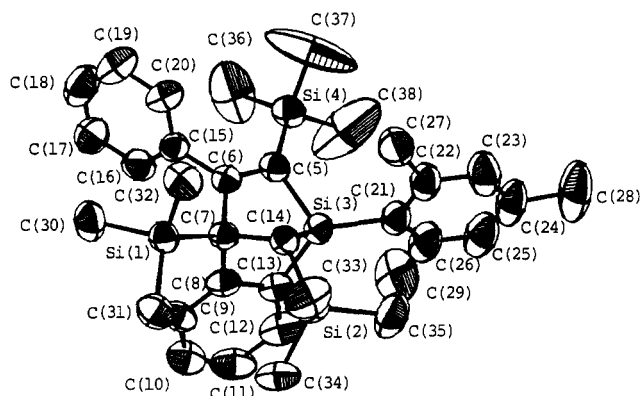
General Procedures. All thermal reactions were carried out in a 10 cm × 0.8 cm degassed sealed glass tube by heating with an electric furnace. The yields of the products were determined by gas-liquid chromatography (GLC) on OV-17 using pentadecane as an internal standard on the basis of the starting silacyclopropenes. Analytical samples were isolated by recycling high-pressure liquid chromatography (HPLC). ¹H, ¹³C, and ²⁹Si NMR spectra were measured with JEOL JNM-EX-270 and Bruker AM-X-400 spectrometers. Infrared spectra were recorded on a Perkin-Elmer 1600-FT-IR spectrophotometer. Mass spectra were recorded on Shimadzu Model GCMS QP-1000 and Hitachi M-80B spectrometers.

X-ray Analysis of 6a and 7b. Colorless crystals of **6a** and **7b** were obtained by recrystallization from ethanol. The experimental conditions and summary of structural refinement for **6a** and **7b** are listed in Table 2. The X-ray diffraction data were collected with a Rigaku AFC-6C automated four-circle

Table 3. Atomic Coordinates and Equivalent Isotropic Thermal Parameters (\AA^2) for 6a with ESDs in Parentheses

atom	x	y	z	B_{eq}^a
Si(1)	0.30402(5)	0.4257(1)	0.9799(1)	4.31(6)
Si(2)	0.44635(5)	0.3492(1)	1.1585(1)	4.96(6)
Si(3)	0.36267(5)	0.3487(1)	1.3475(1)	4.15(6)
Si(4)	0.23458(6)	0.2921(1)	1.4220(1)	5.14(6)
C(5)	0.28360(19)	0.3345(4)	1.3193(4)	4.15(13)
C(6)	0.27058(18)	0.3766(4)	1.2102(4)	3.86(12)
C(7)	0.32162(18)	0.4156(4)	1.1480(4)	3.77(12)
C(8)	0.34299(19)	0.5176(4)	1.2154(4)	4.33(14)
C(9)	0.33676(22)	0.6194(4)	1.1699(5)	5.03(15)
C(10)	0.36113(26)	0.7037(5)	1.2370(6)	6.23(20)
C(11)	0.38881(29)	0.6891(5)	1.3459(7)	6.96(22)
C(12)	0.39457(25)	0.5828(6)	1.3985(5)	6.23(19)
C(13)	0.37096(19)	0.4966(4)	1.332(4)	4.41(14)
C(14)	0.37091(18)	0.3334(4)	1.1870(4)	3.78(12)
C(15)	0.21139(19)	0.3993(4)	1.1544(4)	4.20(13)
C(16)	0.18811(22)	0.4980(5)	1.1664(6)	5.50(17)
C(17)	0.13220(25)	0.5199(6)	1.1176(7)	6.93(21)
C(18)	0.09978(25)	0.4374(7)	1.0586(7)	7.74(26)
C(19)	0.12236(25)	0.3388(7)	1.0475(6)	7.15(23)
C(20)	0.17845(20)	0.3178(5)	1.0952(5)	5.45(17)
C(21)	0.40087(20)	0.2610(5)	1.4661(4)	4.98(16)
C(22)	0.40268(23)	0.1516(6)	1.4437(5)	5.96(18)
C(23)	0.43232(28)	0.0818(7)	1.5291(7)	7.77(24)
C(24)	0.45975(28)	0.1246(8)	1.6363(6)	7.90(26)
C(25)	0.45548(29)	0.2295(8)	1.6583(6)	7.93(27)
C(26)	0.42570(25)	0.2984(7)	1.5776(5)	6.71(21)
C(27)	0.37262(29)	0.0993(5)	1.3302(6)	6.65(20)
C(28)	0.49158(40)	0.0399(11)	1.7219(8)	11.84(40)
C(29)	0.42170(47)	0.4142(8)	1.6128(7)	10.58(36)
C(30)	0.23929(25)	0.5045(6)	0.9182(5)	6.22(19)
C(31)	0.36248(25)	0.4898(5)	0.9120(5)	6.17(18)
C(32)	0.29322(26)	0.2878(5)	0.9248(5)	5.91(18)
C(33)	0.45820(25)	0.2697(6)	1.0292(6)	7.13(22)
C(34)	0.46944(23)	0.4920(5)	1.1454(6)	6.26(19)
C(35)	0.49662(25)	0.2929(8)	1.2839(7)	8.24(26)
C(36)	0.16911(50)	0.3667(11)	1.4113(12)	14.58(53)
C(37)	0.21491(81)	0.1585(10)	1.3957(13)	19.94(84)
C(38)	0.27255(53)	0.2872(20)	1.5685(9)	21.50(104)

$$^a B_{eq} = (1/3)(B_{11}a^2 + B_{22}b^2 + B_{33}c^2 + B_{13}ac \cos \beta).$$

**Figure 2.** ORTEP view of 6a, showing the atom-numbering scheme.

diffractometer using graphite-monochromatized Cu K α radiation ($\lambda = 1.5418 \text{ \AA}$). The structures were solved by the Monte-Carlo direct method,¹⁸ using the MULTAN78 program system¹⁹ for the selection of the initial set of phase, and refined by the full-matrix least-squares program with analytical absorption correction.²⁰ Atomic scattering factors were taken from *International Tables for X-ray Crystallography*.²¹ Aniso-

Table 4. Selected Bond Lengths (\AA) and Bond Angles (deg) for 6a with Their ESDs in Parentheses

Bond Lengths					
Si(1)-C(7)	1.921(5)	C(18)-C(19)	1.375(12)	C(7)-C(14)	1.588(6)
Si(3)-C(5)	1.881(5)	C(21)-C(22)	1.412(10)	C(8)-C(13)	1.443(6)
Si(3)-C(14)	1.898(5)	C(22)-C(23)	1.428(10)	C(10)-C(11)	1.339(10)
Si(4)-C(5)	1.868(5)	C(23)-C(24)	1.414(10)	C(12)-C(13)	1.395(8)
C(6)-C(7)	1.587(7)	C(24)-C(28)	1.573(14)	C(15)-C(20)	1.410(7)
C(7)-C(8)	1.552(7)	C(26)-C(29)	1.529(13)	C(17)-C(18)	1.412(11)
C(8)-C(9)	1.392(7)	Si(2)-C(14)	1.896(5)	C(19)-C(20)	1.398(8)
C(9)-C(10)	1.392(8)	Si(3)-C(13)	1.894(6)	C(21)-C(26)	1.412(8)
C(11)-C(12)	1.475(10)	Si(3)-C(21)	1.886(6)	C(22)-C(27)	1.543(9)
C(15)-C(16)	1.385(8)	C(5)-C(6)	1.356(7)	C(24)-C(25)	1.360(15)
C(16)-C(17)	1.399(8)	C(6)-C(15)	1.493(6)	C(25)-C(26)	1.390(11)
Bond Angles					
C(5)-Si(3)-C(13)	101.2(2)	C(5)-Si(3)-C(14)	94.2(2)		
C(5)-Si(3)-C(21)	115.8(2)	C(13)-Si(3)-C(14)	89.4(2)		
C(13)-Si(3)-C(21)	126.9(2)	C(14)-Si(3)-C(21)	122.3(2)		
Si(3)-C(5)-Si(4)	129.2(3)	Si(3)-C(5)-C(6)	101.9(4)		
Si(4)-C(5)-C(6)	128.4(4)	C(5)-C(6)-C(7)	117.1(4)		
C(5)-C(6)-C(15)	123.0(4)	C(7)-C(6)-C(15)	119.5(4)		
Si(1)-C(7)-C(6)	114.2(3)	Si(1)-C(7)-C(8)	117.0(3)		
Si(1)-C(7)-C(14)	111.6(3)	C(6)-C(7)-C(8)	104.5(4)		
C(6)-C(7)-C(14)	105.0(4)	C(8)-C(7)-C(14)	103.3(3)		
C(7)-C(8)-C(9)	125.0(4)	C(7)-C(8)-C(13)	112.8(4)		
C(9)-C(8)-C(13)	122.2(5)	C(8)-C(9)-C(10)	119.3(5)		
C(9)-C(10)-C(11)	121.3(6)	C(10)-C(11)-C(12)	120.8(6)		
C(11)-C(12)-C(13)	119.2(5)	Si(3)-C(13)-C(8)	103.0(4)		
Si(3)-C(13)-C(12)	140.0(4)	C(8)-C(13)-C(12)	117.0(5)		
Si(2)-C(14)-Si(3)	113.6(2)	Si(2)-C(14)-C(7)	124.7(3)		
Si(3)-C(14)-C(7)	91.4(3)	C(6)-C(15)-C(16)	120.2(4)		
C(6)-C(15)-C(20)	119.4(5)	C(16)-C(15)-C(20)	120.3(4)		
C(15)-C(16)-C(17)	121.0(5)	C(16)-C(17)-C(18)	117.9(7)		
C(17)-C(18)-C(19)	121.4(6)	C(18)-C(19)-C(20)	120.4(7)		
C(15)-C(20)-C(19)	119.0(6)	Si(3)-C(21)-C(22)	118.1(4)		
Si(3)-C(21)-C(26)	123.5(5)	C(22)-C(21)-C(26)	118.3(6)		
C(21)-C(22)-C(23)	120.5(6)	C(21)-C(22)-C(27)	123.6(5)		
C(23)-C(22)-C(27)	115.9(6)	C(22)-C(23)-C(24)	118.7(8)		
C(23)-C(24)-C(25)	119.9(7)	C(23)-C(24)-C(28)	113.8(9)		
C(25)-C(24)-C(28)	126.3(7)	C(24)-C(25)-C(26)	122.3(7)		
C(21)-C(26)-C(25)	120.0(7)	C(21)-C(26)-C(29)	121.9(6)		
C(25)-C(26)-C(29)	118.2(6)				

tropic temperature factors were used for refinement. Hydrogen atoms were not included in the refinement for 6a but included in that for 7b. The final atomic coordinates and equivalent isotropic temperature factors are given in Tables 3 and 5. ORTEP views of the molecular structure were shown in Figures 2 and 3,²² and selected bond distances and angles are listed in Tables 4 and 6.^{23,24}

Materials. Solvent hexane was dried over lithium aluminum hydride and distilled before use. Silacyclopropene 1a was prepared by the photolysis of 2-mesityl-2-(phenylethynyl)-hexamethyltrisilane in hexane, as described in the previous paper.⁷ Silacyclopropenes 1b and 1c were prepared by the similar photolysis of 2-(phenylethynyl)-2-o-tolylhexamethyltrisilane and 2-(phenylethynyl)-2-p-tolylhexamethyltrisilane in 41–46% and 25–36% yields, respectively. After evaporation of the solvent, the silacyclopropene thus obtained was transferred directly into the reaction tube by vacuum distillation.¹¹ For 1b: ¹H NMR (δ in C₆D₆) 0.24 (s, 9H, SiMe₃), 0.38 (s, 9H, SiMe₃), 2.53 (s, 3H, Me), 7.01–7.83 (m, 9H, aromatic ring H); ¹³C NMR (δ in C₆D₆) -0.14, 0.28 (SiMe₃), 24.1 (Me), 125.5, 128.6, 128.9, 129.6, 129.7, 130.1, 136.4 (aromatic ring CH), 136.1, 136.6, 143.6, 151.7, 169.2 (ipso and olefinic C); ²⁹Si NMR (δ in C₆D₆) -115.3 (ring Si), -14.2, -4.8 (SiMe₃); MS *m/z* 366 (M⁺), 351 (M⁺ - CH₃); HRMS *m/z* calcd for C₂₁H₃₀Si₃

(21) *International Tables for X-Ray Crystallography*; Kynoch Press: Birmingham, U.K., 1974; Vol. 4.

(22) Johnson, C. K. ORTEP; Report ORNL-3794; Oak Ridge National Laboratory, Oak Ridge, TN, 1965.

(23) All computations were performed on the HITAC M-680/180E system at the Information Processing Center of Hiroshima University using the CRYSTAN program system.²⁴

(24) Katayama, C.; Honda, M. CRYSTAN, The Computer Center of Nagoya University Library Program, 1985.

(18) Furusaki, A. *Acta Crystallogr., Sect. A* **1979**, *35*, 220.

(19) Main, P.; Hull, S. E.; Lessinger, L.; Germain, G.; Declercq, J.-P.; Woolfson, M. *MULTAN78, A System of Computer Programs for the Automatic Solution of Crystal Structures from X-Ray Diffraction Data*; University of York, England and Louvain, Belgium, 1978.

(20) Katayama, C.; Sakabe, N.; Sakabe, K. *Acta Crystallogr., Sect. A* **1972**, *28*, S207.

Table 5. Atomic Coordinates and Equivalent Isotropic Thermal Parameters (Å²) for 7b with ESDs in Parentheses

atom	x	y	z	B _{eq} ^a
Si(1)	0.76214(6)	0.3585(1)	0.52050(6)	5.03(3)
Si(2)	0.8959(1)	0.5882(2)	0.65511(9)	7.95(6)
Si(3)	0.6432(1)	0.6164(2)	0.45853(9)	8.17(6)
Si(4)	0.73349(7)	0.2645(2)	0.35028(7)	6.15(4)
C(5)	0.8451(3)	0.4614(5)	0.5828(2)	5.4(2)
C(6)	0.8669(2)	0.3543(5)	0.5520(2)	5.1(2)
C(7)	0.6948(3)	0.4521(6)	0.4369(3)	6.7(2)
C(8)	0.6889(3)	0.4181(6)	0.3754(4)	7.4(2)
C(9)	0.7105(4)	0.2258(6)	0.5502(3)	7.5(2)
C(10)	0.7409(7)	0.1469(8)	0.6089(5)	11.7(4)
C(11)	0.6893(8)	0.037(1)	0.6250(6)	13.4(6)
C(12)	0.6187(9)	0.031(1)	0.5766(6)	15.0(6)
C(13)	0.5817(6)	0.112(2)	0.5120(8)	18.2(7)
C(14)	0.6275(7)	0.2017(9)	0.5020(8)	14.8(6)
C(15)	0.8139(7)	0.153(1)	0.6591(5)	13.2(5)
C(16)	0.9421(3)	0.2932(5)	0.5610(3)	5.6(2)
C(17)	1.0035(4)	0.3784(7)	0.5666(4)	9.0(3)
C(18)	1.0736(4)	0.321(1)	0.5747(5)	11.8(4)
C(19)	1.0859(4)	0.180(1)	0.5813(4)	10.4(3)
C(20)	1.0262(4)	0.0929(8)	0.5768(4)	8.7(3)
C(21)	0.9538(3)	0.1482(6)	0.5646(3)	6.9(2)
C(22)	0.6429(3)	0.5226(7)	0.3130(3)	7.4(2)
C(23)	0.6807(4)	0.6422(7)	0.3042(3)	7.6(2)
C(24)	0.6424(6)	0.7310(8)	0.2470(4)	9.9(3)
C(25)	0.5680(7)	0.701(1)	0.1999(4)	10.5(4)
C(26)	0.5304(5)	0.586(1)	0.2067(4)	9.7(3)
C(27)	0.5682(4)	0.4903(9)	0.2635(4)	9.5(3)
C(28)	0.929(1)	0.745(1)	0.6183(8)	18.3(8)
C(29)	0.9852(7)	0.505(2)	0.7210(6)	15.4(6)
C(30)	0.8311(6)	0.644(2)	0.6905(6)	14.3(6)
C(31)	0.6329(4)	0.578(1)	0.5409(4)	9.8(3)
C(32)	0.7146(9)	0.7701(9)	0.4790(7)	15.2(6)
C(33)	0.541(1)	0.648(4)	0.3900(6)	20.6(9)
C(34)	0.7415(5)	0.1009(7)	0.4014(4)	8.8(3)
C(35)	0.8315(4)	0.3150(9)	0.3585(4)	9.0(3)
C(36)	0.6712(5)	0.212(1)	0.2565(4)	9.7(3)

$$^a B_{eq} = (4/3)(B_{11}a^2 + B_{22}b^2 + B_{33}c^2 + B_{13}ac \cos \beta).$$

366.1653, found 366.1574. For **1c**: ¹H NMR (δ in C₆D₆) 0.32 (s, 9H, SiMe₃), 0.39 (s, 9H, SiMe₃), 2.10 (s, 3H, Me), 7.00–7.80 (m, 9H, aromatic ring H); ¹³C NMR (δ in C₆D₆) 0.19, 0.42 (SiMe₃), 21.4 (Me), 128.6, 128.8, 129.1, 130.1, 134.8 (aromatic ring CH), 132.2, 135.9, 139.2, 149.7, 166.1 (ipso and olefinic C); ²⁹Si NMR (δ in C₆D₆) –120.1 (ring Si), –11.4, –9.9 (SiMe₃); MS *m/z* 366 (M⁺), 351 (M⁺ – CH₃); HRMS *m/z* calcd for C₂₁H₃₀Si₃ – CH₃ 351.1419, found 351.1337.

Thermolysis of 1b. A mixture of 0.34 mmol of **1b** and 0.71 mmol of pentadecane as an internal standard was heated in a sealed tube at 130 °C for 6 h. The mixture was analyzed by GLC as being **2b** (7%), **3b** (58%), and **4b** (5%). **2b**, **3b**, and **4b** were isolated by recycling HPLC. For **2b**: IR 2112 (ν_{Si-H}) cm⁻¹; ¹H NMR (δ in CDCl₃) –0.29 (s, 9H, SiMe₃), –0.08 (s, 3H, SiMe), –0.05 (dd, 1H, HCH, *J* = 14.5 Hz, *J* = 2.5 Hz), 0.22 (s, 3H, SiMe), 0.23 (dd, 1H, HCH, *J* = 14.5 Hz, *J* = 4.3 Hz), 2.48 (s, 3H, Me), 5.19 (dd, 1H, SiH, *J* = 4.3 Hz, *J* = 2.5 Hz), 6.97–7.55 (m, 9H, phenyl and tolyl H); ¹³C NMR (δ in CDCl₃) –6.6 (SiCH₂Si), –0.8 (SiMe), –0.5 (SiMe), 0.8 (SiMe₃), 22.5 (Me), 125.0, 125.6, 125.9, 127.1, 127.8, 129.5, 136.1, 136.6, 143.5, 146.6 (aromatic ring carbons), 161.3, 185.3 (olefinic carbons); MS *m/z* 366 (M⁺). Anal. Calcd for C₂₁H₃₀Si₃: C, 68.78; H, 8.25. Found: C, 68.51; H, 8.46. For **3b**: IR 1438 (ν_{C-C}), 1247 (ν_{Si-C}) cm⁻¹; ¹H NMR (δ in CDCl₃) 0.07 (s, 9H, SiSiMe₃), 0.32 (s, 9H, C(3)-SiMe₃), 2.42 (s, 3H, Me), 7.03 (s, 1H, C(2)-H), 7.15 (t, 1H, tolyl *m*-H, *J* = 7.5 Hz), 7.16 (d, 1H, tolyl *m'*-H, *J* = 7.5 Hz), 7.24 (t, 1H, C(6)-H, *J* = 7.5 Hz), 7.27 (td, 1H, tolyl *p*-H, *J* = 7.5 Hz, *J* = 1.5 Hz), 7.36 (td, 1H, C(5)-H, *J* = 7.5 Hz, *J* = 1.5 Hz), 7.55 (d, 1H, tolyl *o*-H, *J* = 7.5 Hz), 7.67 (d, 1H, C(4)-H, *J* = 7.5 Hz), 7.76 (d, 1H, C(7)-H, *J* = 7.5 Hz); ¹³C NMR (δ in CDCl₃) –1.33 (SiSiMe₃), –0.54 (C(3)-SiMe₃), 23.4 (Me), 125.1, 125.5, 125.8, 128.8, 129.4 (two), 133.3, 135.9, 143.6 (aromatic ring CH), 132.9, 139.1, 144.1, 152.5, 165.6 (ipso and fused C); MS *m/z* 366 (M⁺). Anal. Calcd for C₂₁H₃₀Si₃: C,

68.78; H, 8.25. Found: C, 68.79; H, 8.27. For **4b**: IR 2125 (ν_{Si-H}), 1248 (ν_{Si-C}) cm⁻¹; ¹H NMR (δ in CDCl₃) 0.19 (s, 9H, C(2)-SiMe₃), 0.45 (s, 9H, C(3)-SiMe₃), 2.08 (s, 3H, Me), 5.15 (s, 1H, SiH), 7.10 (d, 1H, tolyl *m'*-H, *J* = 7.5 Hz), 7.18 (t, 1H, tolyl *m*-H, *J* = 7.5 Hz), 7.20 (t, 1H, C(6)-H, *J* = 7.5 Hz), 7.31 (td, 1H, tolyl *p*-H, *J* = 7.5 Hz, *J* = 1.5 Hz), 7.37 (td, 1H, C(5)-H, *J* = 7.5 Hz, *J* = 1.5 Hz), 7.59 (d, 1H, tolyl *o*-H, *J* = 7.5 Hz), 7.70 (2d, 2H, C(4)-H and C(7)-H, *J* = 7.5 Hz); ¹³C NMR (δ in CDCl₃) 2.50 (C(3)-SiMe₃), 2.75 (C(2)-SiMe₃), 21.3 (Me), 125.2, 126.1, 126.5, 129.5, 129.6, 130.2, 132.5, 137.8 (aromatic ring CH), 132.0, 136.3, 144.9, 155.4, 158.2, 176.9 (ipso and fused C); MS *m/z* 366 (M⁺). Anal. Calcd for C₂₁H₃₀Si₃: C, 68.78; H, 8.25. Found: C, 68.51; H, 8.30.

Thermolysis of 1c. A mixture of 0.24 mmol of **1c** and 0.94 mmol of pentadecane as an internal standard was heated in a sealed tube at 130 °C for 6 h. The mixture was analyzed by GLC as being **2c** (11%), **3c** (36%), and **4c** (9%). Compounds **2c**, **3c**, and **4c** were isolated by recycling HPLC. For **2c**: IR 2113 (ν_{Si-H}), 1245 (ν_{Si-C}) cm⁻¹; ¹H NMR (δ in CDCl₃) –0.31 (s, 9H, SiMe₃), –0.11 (dd, 1H, HCH, *J* = 14.9 Hz, *J* = 1.7 Hz), 0.13 (s, 3H, SiMe), 0.19 (dd, 1H, HCH, *J* = 14.9 Hz, *J* = 4.3 Hz), 0.20 (s, 3H, SiMe), 2.38 (s, 3H, Me), 5.11 (dd, 1H, SiH, *J* = 4.3 Hz, *J* = 1.7 Hz), 6.96–7.48 (m, 9H, aromatic ring H); ¹³C NMR (δ in CDCl₃) –5.68 (SiCH₂Si), –0.63 (two SiMe), 0.85 (SiMe₃), 21.5 (Me), 125.6, 126.0, 127.7, 128.7, 134.7 (aromatic ring CH), 134.4, 139.1, 146.6, 160.9, 185.3 (olefinic and ipso C); MS *m/z* 366 (M⁺). Anal. Calcd for C₂₁H₃₀Si₃: C, 68.78; H, 8.25. Found: C, 68.55; H, 8.15. For **3c**: IR 1438 (ν_{C-C}), 1247 (ν_{Si-C}) cm⁻¹; ¹H NMR (δ in CDCl₃) 0.10 (s, 9H, SiSiMe₃), 0.30 (s, 9H, C(3)-SiMe₃), 2.31 (s, 3H, Me), 6.93 (s, 1H, C(2)-H), 7.13 (d, 2H, tolyl *m*-H, *J* = 7.5 Hz), 7.20 (t, 1H, C(6)-H, *J* = 6.5 Hz), 7.34 (t, 1H, C(5)-H, *J* = 7.5 Hz), 7.42 (d, 2H, tolyl *o*-H, *J* = 7.5 Hz), 7.52 (d, 1H, C(4)-H, *J* = 7.5 Hz), 7.65 (d, 1H, C(7)-H, *J* = 6.5 Hz); ¹³C NMR (δ in CDCl₃) –1.53 (SiSiMe₃), –0.54 (C(3)-SiMe₃), 21.5 (Me), 125.3, 125.9, 128.93, 132.8, 135.0, 139.2, 143.7 (aromatic ring CH), 123.7, 128.84, 128.88, 156.7, 165.9 (ipso and fused C); MS *m/z* 366 (M⁺). Anal. Calcd for C₂₁H₃₀Si₃: C, 68.78; H, 8.25. Found: C, 68.78; H, 8.24. For **4c**: IR 2126 (ν_{Si-H}), 1248 (ν_{Si-C}) cm⁻¹; ¹H NMR (δ in CDCl₃) 0.19 (s, 9H, C(2)-SiMe₃), 0.46 (s, 9H, C(3)-SiMe₃), 2.35 (s, 3H, Me), 5.14 (s, 1H, SiH), 7.15 (d, 2H, tolyl *m*-H, *J* = 7.5 Hz), 7.16 (t, 1H, C(6)-H, *J* = 7.5 Hz), 7.35 (t, 1H, C(5)-H, *J* = 7.5 Hz), 7.40 (d, 2H, tolyl *o*-H, *J* = 7.5 Hz), 7.56 (d, 1H, C(4)-H, *J* = 7.5 Hz), 7.66 (d, 1H, C(7)-H, *J* = 7.5 Hz); ¹³C NMR (δ in CDCl₃) 2.63 (C(2)-SiMe₃), 2.86 (C(3)-SiMe₃), 21.6 (Me), 125.8, 126.5, 128.9, 129.5, 132.5, 135.3 (aromatic ring CH), 128.8, 136.6, 139.8, 155.6, 158.1, 176.9 (ipso and fused C); MS *m/z* 366 (M⁺). Anal. Calcd for C₂₁H₃₀Si₃: C, 68.78; H, 8.25. Found: C, 68.61; H, 8.08.

Thermolysis of 1b in the Presence of Phenyl(trimethylsilyl)acetylene. A mixture of 0.43 mmol of **1b**, 3.0 mmol of phenyl(trimethylsilyl)acetylene, and 0.94 mmol of pentadecane as an internal standard was heated in a sealed tube at 230 °C for 6 h. The mixture was analyzed by GLC as being **2b** (11%), **3b** (4%), **4b** (17%), and **7b** (44%). **7b** was isolated by recycling HPLC. For **7b**: IR 1480 (ν_{C-C}), 1247 (ν_{Si-C}) cm⁻¹; ¹H NMR (δ in CDCl₃) –0.58 (s, 9H, =CPhSiMe₃), –0.41 (s, 9H, ring SiMe₃), –0.04 (s, 9H, =C(Si)SiMe₃), 2.67 (s, 3H, Me), 6.35–8.21 (m, 14H, aromatic ring H); ¹³C NMR (δ in CDCl₃) 0.11 (=CPhSiMe₃), 1.49 (ring SiMe₃), 1.64 (=C(Si)SiMe₃), 24.0 (Me), 124.3, 125.2, 125.4, 126.6, 126.7, 127.5, 127.6, 127.7, 128.1, 129.8, 130.6, 132.8, 134.2, 135.0, 144.6, 145.2, 145.7, 157.4, 185.7 (aromatic and olefinic carbons); ²⁹Si NMR (δ in C₆D₆) –104.7 (ring Si), –11.3, –7.3, –5.6 (SiMe₃); MS *m/z* 540 (M⁺). Anal. Calcd for C₃₂H₄₄Si₄: C, 71.04; H, 8.20. Found: C, 70.88; H, 8.11.

Thermolysis of 1c in the Presence of Phenyl(trimethylsilyl)acetylene. A mixture of 0.45 mmol of **1c**, 2.6 mmol of phenyl(trimethylsilyl)acetylene, and 1.2 mmol of pentadecane as an internal standard was heated in a sealed tube at 250 °C for 6 h. The mixture was analyzed by GLC as being **2c** (5%), **3c** (2%), **4c** (11%), **8c** (75%), and **9c** (11%). **8c** and

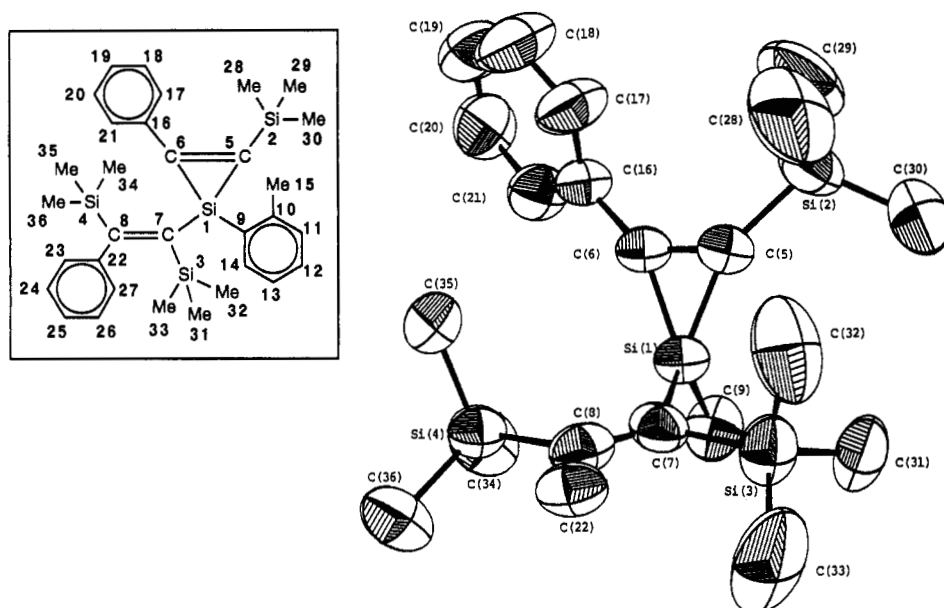


Figure 3. ORTEP view (right) and the atom-numbering scheme (left) of **7b**. In the view, an *o*-tolyl group on Si1 and a phenyl group on C8 are represented by single carbons, C9 and C22, respectively.

Table 6. Selected Bond Lengths (Å) and Angles (deg) for **7b** with Their Esd's in Parentheses

Bond Lengths			
Si(1)–C(5)	1.834(4)	C(17)–C(18)	1.37(1)
Si(1)–C(7)	1.891(5)	C(19)–C(20)	1.37(1)
Si(2)–C(5)	1.848(5)	C(22)–C(23)	1.39(1)
Si(4)–C(8)	1.859(7)	C(23)–C(24)	1.39(1)
C(6)–C(16)	1.470(7)	C(25)–C(26)	1.33(2)
C(8)–C(22)	1.573(8)	Si(1)–C(6)	1.801(4)
C(9)–C(14)	1.488(1)	Si(1)–C(9)	1.848(7)
C(10)–C(15)	1.34(1)	Si(3)–C(7)	1.981(6)
C(12)–C(13)	1.45(2)	C(5)–C(6)	1.352(7)
C(16)–C(17)	1.373(9)	C(7)–C(8)	1.29(1)
C(9)–C(10)	1.34(1)	C(18)–C(19)	1.35(1)
C(10)–C(11)	1.56(2)	C(20)–C(21)	1.38(1)
C(11)–C(12)	1.29(2)	C(22)–C(27)	1.385(8)
C(13)–C(14)	1.29(2)	C(24)–C(25)	1.36(1)
C(16)–C(21)	1.381(8)	C(26)–C(27)	1.42(1)
Bond Angles			
C(5)–Si(1)–C(6)	43.7(2)	C(5)–Si(1)–C(7)	116.7(2)
C(5)–Si(1)–C(9)	122.2(3)	C(6)–Si(1)–C(7)	123.6(3)
C(6)–Si(1)–C(9)	121.1(2)	C(7)–Si(1)–C(9)	112.5(3)
Si(1)–C(5)–Si(2)	156.3(4)	Si(1)–C(5)–C(6)	66.9(3)
Si(2)–C(5)–C(6)	135.8(3)	Si(1)–C(6)–C(5)	69.5(3)
Si(1)–C(6)–C(16)	155.2(4)	C(5)–C(6)–C(16)	134.8(4)
Si(1)–C(7)–Si(3)	110.9(3)	Si(1)–C(7)–C(8)	123.4(5)
Si(3)–C(7)–C(8)	125.6(4)	Si(4)–C(8)–C(7)	128.3(5)
Si(4)–C(8)–C(22)	114.2(5)	C(7)–C(8)–C(22)	117.3(5)
Si(1)–C(9)–C(10)	127.0(6)	Si(1)–C(9)–C(14)	115.6(6)
C(10)–C(9)–C(14)	117.4(9)	C(9)–C(10)–C(11)	120.3(9)
C(9)–C(10)–C(15)	127(1)	C(11)–C(10)–C(15)	113.0(9)
C(10)–C(11)–C(12)	113(1)	C(11)–C(12)–C(13)	130(1)
C(12)–C(13)–C(14)	114(1)	C(9)–C(14)–C(13)	125(1)
C(6)–C(16)–C(17)	121.1(5)	C(6)–C(16)–C(21)	121.2(5)
C(17)–C(16)–C(21)	117.8(5)	C(16)–C(17)–C(18)	121.1(6)
C(17)–C(18)–C(19)	121.0(8)	C(18)–C(19)–C(20)	119.1(8)
C(19)–C(20)–C(21)	120.6(7)	C(16)–C(21)–C(20)	120.3(6)
C(8)–C(22)–C(23)	119.0(4)	C(8)–C(22)–C(27)	120.9(6)
C(23)–C(22)–C(27)	119.9(6)	C(22)–C(23)–C(24)	119.7(6)
C(23)–C(24)–C(25)	120.0(8)	C(24)–C(25)–C(26)	121.6(8)
C(22)–C(27)–C(26)	118.6(8)		

9c were isolated by recycling HPLC. For **8c**: IR 1249 ($\nu_{\text{Si-C}}$) cm^{-1} ; $^1\text{H NMR}$ (δ in CDCl_3) -0.29 (s, 9H, $=\text{CPhSiMe}_3$), 0.38 (s, 9H, C(2)- SiMe_3), 0.44 (s, 9H, $=\text{C}(\text{Si})\text{SiMe}_3$), 2.31 (s, 3H, Me), 7.12 (d, 2H, tolyl *m*-H, $J = 7.5$ Hz), 7.15 – 7.35 (m, 7H, C(5)-H, C(6)-H, phenyl *o*-, *m*-, *p*-H), 7.55 (d, 2H, tolyl *o*-H, $J = 7.5$ Hz), 7.61 (d, 1H, C(7)-H, $J = 7.5$ Hz), 7.64 (d, 1H, C(4)-H, $J = 7.5$ Hz), 8.05 (s, 1H, C(3)-H); $^{13}\text{C NMR}$ (δ in CDCl_3) 1.48 , 2.81 , 3.90 (SiMe_3), 21.5 (Me), 126.0 , 126.3 , 127.3 , 127.5 , 127.8 , 128.6 , 129.0 , 132.3 , 135.6 (aromatic ring CH), 131.2 , 139.1 , 140.1 , 140.2 , 142.6 (ipso and fused C), 154.6 (C(2)), 162.2 (C(3)), 160.3 , 176.4 (olefinic C); $^{29}\text{Si NMR}$ (δ in C_6D_6) -10.0 , -7.7 , -6.2 (SiMe_3), 4.5 (ring Si); MS m/z 540 (M^+). Anal. Calcd for

$\text{C}_{32}\text{H}_{44}\text{Si}_4$: C, 71.04; H, 8.20. Found: C, 71.00; H, 8.20. For **9c**: IR 1544 ($\nu_{\text{C=C}}$), 1246 ($\nu_{\text{Si-C}}$) cm^{-1} ; $^1\text{H NMR}$ (δ in CDCl_3) -0.08 (s, 9H, $=\text{CPhSiMe}_3$), -0.05 (s, 9H, C(2)- SiMe_3), 0.28 (s, 9H, $=\text{C}(\text{Si})\text{SiMe}_3$), 2.28 (s, 3H, Me), 6.71 (d, 2H, phenyl *o*-H, $J = 7.5$ Hz), 6.94 (t, 2H, phenyl *m*-H, $J = 7.5$ Hz), 7.01 (d, 2H, tolyl *m*-H, $J = 7.5$ Hz), 7.03 (t, 1H, phenyl *p*-H, $J = 7.5$ Hz), 7.27 (t, 1H, C(6)-H, $J = 7.5$ Hz), 7.38 (t, 1H, C(5)-H, $J = 7.5$ Hz), 7.43 (d, 2H, tolyl *o*-H, $J = 7.5$ Hz), 7.62 (d, 1H, C(7)-H, $J = 7.5$ Hz), 7.75 (d, 1H, C(4)-H, $J = 7.5$ Hz), 7.80 (s, 1H, C(3)-H); $^{13}\text{C NMR}$ (δ in CDCl_3) 1.15 , 2.77 , 3.22 (SiMe_3), 21.5 (Me), 126.2 , 126.3 , 127.3 (two), 128.1 , 128.3 , 128.8 , 132.5 , 135.9 (aromatic ring CH), 131.6 , 138.8 , 139.7 , 140.6 , 141.1 (ipso and fused C), 155.2 (C(3)), 158.5 (C(2)), 163.6 , 171.1 (olefinic C); MS m/z 540 (M^+); HRMS m/z calcd for $\text{C}_{32}\text{H}_{44}\text{Si}_4$ 540.2517, found 540.2485.

Thermolysis of 1b in the Presence of Methylphenylsilane. A mixture of 0.34 mmol of **1b**, 2.7 mmol of methylphenylsilane, and 0.94 mmol of pentadecane as an internal standard was heated in a sealed tube at 250 °C for 6 h. The mixture was analyzed by GLC as being **2b** (9%), **3b** (6%), **4b** (13%), **10b** (14%), and **11b** (10%). **10b** and **11b** were isolated by recycling HPLC. Since all attempts to separate **10b** from **11b** using recycling HPLC were unsuccessful, samples containing a small amount of the other isomer were subjected to spectrometric and elemental analysis. For a mixture of **10b** and **11b**: IR 2137 ($\nu_{\text{Si-H}}$), 1246 ($\nu_{\text{Si-C}}$) cm^{-1} ; $^1\text{H NMR}$ (δ in CDCl_3) -0.41 , -0.23 , -0.08 , 0.24 (s, 9H, SiMe_3), 0.46 , 0.90 (s, 3H, SiMe), 2.13 , 2.40 (s, 3H, Me), 5.43 , 5.51 (s, 1H, SiH), 6.84 – 7.69 (m, 19H, aromatic ring H); $^{13}\text{C NMR}$ (δ in CDCl_3) -3.56 , -1.38 (SiPh_2Me), 2.05 , 2.90 , 2.99 , 3.76 (SiMe_3), 23.2 , 23.9 (Me), 124.7 , 124.8 , 125.5 , 126.8 , 127.1 , 127.2 , 127.3 , 127.7 , 127.82 , 127.85 , 127.89 , 128.75 , 128.79 , 128.9 , 129.0 , 129.1 , 129.3 , 129.5 , 129.7 , 135.0 , 135.2 , 135.5 , 135.6 , 137.5 (aromatic ring CH), 132.9 , 134.5 , 137.0 , 137.2 , 137.3 , 137.7 , 144.3 , 144.5 , 149.0 , 149.7 (ipso C), 154.3 , 169.1 , 171.5 , 182.4 (olefinic C). Anal. Calcd for $\text{C}_{34}\text{H}_{44}\text{Si}_4$: C, 72.27; H, 7.85. Found: C, 72.24; H, 7.85. For **10b**: $^1\text{H NMR}$ (δ in CDCl_3) -0.41 (s, 9H, $=\text{CPhSiMe}_3$), -0.08 (s, 9H, $=\text{C}(\text{Si})\text{SiMe}_3$), 0.90 (s, 3H, SiMe), 2.40 (s, 3H, Me), 5.51 (s, 1H, SiH); $^{13}\text{C NMR}$ (δ in CDCl_3) -1.38 (SiPh_2Me), 2.05 , 2.90 (SiMe_3), 23.9 (Me); MS m/z 564 (M^+). For **11b**: $^1\text{H NMR}$ (δ in CDCl_3) -0.23 (s, 9H, $=\text{CPhSiMe}_3$), 0.24 (s, 9H, $=\text{C}(\text{Si})\text{SiMe}_3$), 0.46 (s, 3H, SiMe), 2.13 (s, 3H, Me), 5.43 (s, 1H, SiH); $^{13}\text{C NMR}$ (δ in CDCl_3) -3.56 (SiPh_2Me), 2.99 , 3.76 (SiMe_3), 23.2 (Me); MS m/z 564 (M^+).

Thermolysis of 1c in the Presence of Methylphenylsilane. A mixture of 0.44 mmol of **1b**, 3.9 mmol of methyl-

diphenylsilane, and 1.2 mmol of pentadecane as an internal standard was heated in a sealed tube at 250 °C for 6 h. The mixture was analyzed by GLC as being **2c** (2%), **3c** (3%), **4c** (4%), **10c** (60%), and **11c** (18%). **10c** and **11c** were isolated by recycling HPLC, followed by recrystallization from ethanol. For **10c**: IR 2148 ($\nu_{\text{Si-H}}$), 1244 ($\nu_{\text{Si-C}}$) cm^{-1} ; ^1H NMR (δ in CDCl_3) -0.45 (s, 9H, =CPhSiMe₃), -0.05 (s, 9H, =C(Si)SiMe₃), 0.89 (s, 3H, SiMe), 2.34 (s, 3H, Me), 5.44 (s, 1H, SiH), 6.78–7.71 (m, 19H, aromatic ring H); ^{13}C NMR (δ in CDCl_3) -1.90 (SiPh₂Me), 2.18, 2.63 (SiMe₃), 21.5 (Me), 125.5, 126.7, 127.3, 127.4, 127.8, 127.9, 128.8, 129.0, 129.1, 135.4, 135.7, 135.8 (aromatic ring CH), 131.1, 137.1, 137.7, 138.8, 149.2 (ipso C), 153.5, 183.7 (olefinic C); MS m/z 564 (M^+). Anal. Calcd for C₃₄H₄₄Si₄: C, 72.27; H, 7.85. Found: C, 72.08; H, 7.78. For **11c**: IR 2148 ($\nu_{\text{Si-H}}$), 1244 ($\nu_{\text{Si-C}}$) cm^{-1} ; ^1H NMR (δ in CDCl_3) -0.24 (s, 9H, =CPhSiMe₃), 0.30 (s, 9H, =C(Si)SiMe₃), 0.45 (s, 3H, SiMe), 2.30 (s, 3H, Me), 5.33 (s, 1H, SiH), 7.00–7.50 (m, 19H, aromatic ring H); ^{13}C NMR (δ in CDCl_3) -3.86 (SiPh₂Me), 2.75, 4.06 (SiMe₃), 21.4 (Me), 126.6, 127.71, 127.76, 127.80, 128.4, 128.6, 128.8, 129.0, 135.1, 135.3, 136.2 (aromatic ring CH), 129.4, 136.9, 137.1, 138.7, 149.2 (ipso C), 168.1, 171.1

(olefinic C); MS m/z 564 (M^+). Anal. Calcd for C₃₄H₄₄Si₄: C, 72.27; H, 7.85. Found: C, 72.08; H, 7.78.

Acknowledgment. This research was supported in part by a Grant-in-Aid on Priority Area of Reactive Organometallics (05236102) from the Ministry of Education, Science and Culture, to which our thanks are due. We also express our appreciation to Shin-Etsu Chemical Co. Ltd., Nitto Electric Industrial Co. Ltd., Dow Corning Asia Ltd., Toshiba Silicone Co. Ltd., Sumitomo Electric Co. Ltd., Kaneka Corp., and Japan High Polymer center for financial support.

Supplementary Material Available: Tables of bond distances and angles and anisotropic thermal parameters for **6a** and **7b** and an ORTEP view of **7b** with full carbons (10 pages). Ordering information is given on any current masthead page.

OM9406310

Preparation of Ethereal Lithium Dimethylcuprates $(\text{Me}_2\text{CuLi})_2$ and $\text{Me}_2\text{CuLi}\cdot\text{LiI}$ Displaying Narrow Line Width ^{13}C NMR Resonances^{1a}

Steven H. Bertz^{*,1b}

AT & T Bell Laboratories, Murray Hill, New Jersey 07974

A. Samuel Vellekoop and Robin A. J. Smith^{1c}

Department of Chemistry, University of Otago, P.O. Box 56, Dunedin, New Zealand

James P. Snyder^{1d}

Istituto di Ricerche di Biologia Molecolare P. Angeletti, 00040 Pomezia, Italy

Received August 10, 1994[®]

Halide-free lithium dimethylcuprate $(\text{Me}_2\text{CuLi})_2$ (**1**) and the Gilman reagent $\text{Me}_2\text{CuLi}\cdot\text{LiI}$ (**2**) have been generated from an ether-soluble form of solid MeLi obtained by transmetalation between BuLi and MeI. The ^{13}C NMR spectra of these cuprates show single narrow resonances at -9.25 and -9.28 ppm ($W_{1/2} < 4$ Hz), respectively. The preparative procedure can be adapted to allow for ^{13}C enrichment and is thus suitable for mechanistic studies using ^{13}C NMR. Ab initio geometry optimization and subsequent calculation of the cuprate ^{13}C chemical shifts indicates that the structural environment around the methyl carbons in the two compounds is remarkably similar. Modeling of the LiI-mediated equilibrium between $\text{Me}_2\text{CuLi}\cdot\text{LiI}$ and $(\text{Me}_2\text{CuLi})_2$ suggests strongly that the Gilman reagent consists primarily of dimer $(\text{Me}_2\text{CuLi})_2$ and free LiI. The virtually identical ^{13}C NMR shifts observed for **1** and **2** are thereby explained, along with the effect of lithium halide on line width.

Introduction

Organocuprates have found wide application in many areas of organic synthesis.^{2a} Despite the great variety of carbon–carbon bond forming reactions which can be achieved with these reagents, in many cases the mechanistic details remain undetermined.^{2b} Two reasons for this apparent paucity of mechanistic information are the complex nature of the reagents themselves^{2c} and the difficulty in monitoring the reagents during reactions. A promising approach to solving these problems is the use of NMR spectroscopy to investigate the nature of the reagents in solution, preferably under conditions similar to those employed for maximum synthetic efficiency, and also to directly observe some of the reaction intermediates.^{2d}

The preferential use of ^{13}C rather than ^1H NMR for studies of these species in solution³ is based upon its relatively large natural chemical shift range and the fact

that carbon nuclei, being directly attached to the metal site, are more sensitive to electronic perturbations than hydrogen nuclei two or more bonds removed. The problem with this potentially useful approach is related to the low NMR sensitivity of the ^{13}C nucleus, particularly if used at natural abundance. Early work involving the direct NMR investigation of conjugate addition reactions with methyl cuprates demonstrated the formation of cuprate–enoate complexes and also reported a significant broadening of the ^{13}C resonance of the methyl carbon attached to the metal.⁴ A ^{13}C -enriched substrate was necessary in order to obtain publication-quality spectra.^{4b} In order to effectively investigate fundamental cuprate structures and also to accurately monitor the organocopper species during reactions, a methyl cuprate with a narrow line width ^{13}C NMR methyl resonance produced by a route readily amenable to ^{13}C enrichment is highly desirable.

Methylcuprates are normally prepared by reaction of 2 equiv of MeLi with a suitable copper(I) salt, typically CuI or CuBr, which affords $\text{Me}_2\text{CuLi}\cdot\text{LiI}$ or $\text{Me}_2\text{CuLi}\cdot\text{LiBr}$, respectively. Low-halide lithium dimethylcuprate $(\text{Me}_2\text{CuLi})_2$ (**1**) is used less often in normal synthetic procedures and has usually been prepared by the reaction of MeLi with methylcopper, $(\text{MeCu})_n$, which is an insoluble yellow solid in the usual hydrocarbon and ethereal solvents.⁵ We represent pure lithium

[®] Abstract published in *Advance ACS Abstracts*, January 15, 1995.

(1) (a) New Copper Chemistry, 23. For part 22, see: He, X.; Ruhlandt-Senge, K.; Power, P. P.; Bertz, S. H. *J. Am. Chem. Soc.* **1994**, *116*, 6963. (b) Present address: Lonza Inc., 79 Route 22 East, Annandale, NJ 08801. (c) Inquiries concerning MeLi preparation should be addressed to this author. (d) Inquiries concerning computational aspects should be addressed to this author. Present address: Department of Chemistry, Emerson Center for Scientific Computation, Emory University, Atlanta, GA 30322.

(2) (a) Reviews: Bertz, S. H.; Fairchild, E. H. *Encyclopedia of Reagents for Organic Synthesis*; Wiley: New York, in press. Lipshutz, B. H.; Sengupta, S. *Org. React.* **1992**, *41*, 135. Posner, G. H. *An Introduction to Synthesis Using Organocopper Reagents*; John Wiley & Sons: New York, 1980. Rossiter, B. E.; Swingle, N. M. *Chem. Rev.* **1992**, *92*, 771. (b) Review: Smith, R. A. J.; Vellekoop, A. S. *Advances in Detailed Reaction Mechanisms Vol. 3*, Coxon, J. M., Ed.; JAI Press: Greenwich, CT, 1994; p 79. (c) For a recent review of organocuprate structures, see: Power, P. P. *Prog. Inorg. Chem.* **1991**, *39*, 75. (d) For an outstanding recent example, see: Krause, N.; Wagner, R.; Gerold, A. *J. Am. Chem. Soc.* **1994**, *116*, 381.

(3) (a) Bertz, S. H.; Dabbagh, G.; He, X.; Power, P. P. *J. Am. Chem. Soc.* **1993**, *115*, 11640. (b) Bertz, S. H. *J. Am. Chem. Soc.* **1991**, *113*, 5470. (c) Bertz, S. H. *J. Am. Chem. Soc.* **1990**, *112*, 4031.

(4) (a) Hallnemo, G.; Olsson, T.; Ullenius, C. *J. Organomet. Chem.* **1985**, *282*, 133. (b) Christenson, B.; Olsson, T.; Ullenius, C. *Tetrahedron* **1989**, *45*, 523. (c) Ullenius, C.; Christenson, B. *Pure Appl. Chem.* **1988**, *60*, 57.

(5) Gilman, H.; Jones, R. G.; Woods, L. A. *J. Org. Chem.* **1952**, *17*, 1630.

dimethylcuprate in ether as a dimer (Me_2CuLi)₂, based on the studies of Pearson⁶ and Ashby.⁷ X-ray structures of **1** and $\text{Me}_2\text{CuLi}\cdot\text{LiI}$ (**2**) have not yet been determined. Solvent molecules are undoubtedly coordinated by the Li atoms, based upon analogy with known organocopper structures^{2c} and the observations of Ullenius and Christenson.^{4c}

Initial NMR investigations of methylcuprates in diethyl ether at low temperature reported a single ¹H NMR resonance at -1.16 ppm^{8a} and a single ¹³C NMR peak ranging from -8.8 to -9.6 ppm.^{8b} During the course of our studies on cuprate–enone complexes, we found that the ¹³C NMR spectra of various preparations of ethereal lithium dimethylcuprate generally showed a single methyl resonance at ca. -9.2 ppm in diethyl ether,⁹ but that the line widths varied dramatically. We now report details of the preparation and characterization of especially pure solutions of (Me_2CuLi)₂ and $\text{Me}_2\text{CuLi}\cdot\text{LiI}$ with extremely sharp ¹³C NMR spectra. We also describe an improved preparation of ether-soluble MeLi, which is easily adapted to the preparation of (¹³CH₃)₂CuLi·LiI. In addition, we present theoretical calculations which shed considerable light on the experimental data.

Results and Discussion

The ¹³C NMR resonance of $\text{Me}_2\text{CuLi}\cdot\text{LiI}$ prepared from commercial “low-halide” MeLi in diethyl ether-*d*₁₀ is a single broad peak (-9.2 ppm, $W_{1/2} = 15\text{--}20$ Hz). $\text{Me}_2\text{CuLi}\cdot\text{LiI}$ prepared initially from commercial MeLi in diethyl ether followed by evaporative solvent removal and replacement with diethyl ether-*d*₁₀ gave a similar broad resonance ($W_{1/2} = 22$ Hz). In addition, the ¹H NMR spectrum of the latter solution displayed several new high-field resonances, which indicated chemical change had taken place during the solvent manipulation.⁹

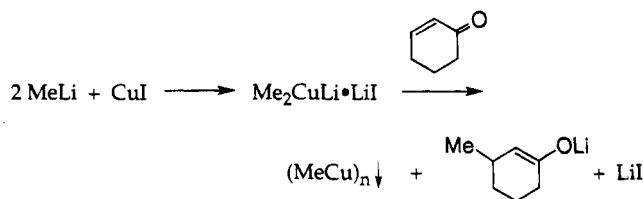
Methods for the preparation of low-halide (Me_2CuLi)₂ are beset by several difficulties related to the preparation of pure methylcopper. Methylcopper was originally obtained by the reaction of a suspension of CuI with an equimolar amount of MeLi in diethyl ether followed by filtration or decantation of the ethereal LiI solution.⁵ Fresh diethyl ether was added, and after stirring or shaking, the ether was again removed along with the dissolved salts.

The first problem is the thermal instability of methylcopper, which makes the production of byproducts during the precipitation and washing process a significant consideration. Consequently, one cannot wash the organometallic an arbitrary number of times with fresh solvent. Another difficulty arises directly from the methylcopper washing procedure, as there is no convenient method for rapidly determining the amount of LiI removed or the amount of methylcopper lost during manipulation. Subsequent reaction of the methylcopper prepared in this manner with 1 equiv of ethereal low-halide MeLi gives a solution characterized by a ¹³C NMR

methyl carbon resonance at -9.2 ppm with line width $W_{1/2} = 10$ Hz, only marginally better than the material made without removal of LiI (*vide supra*).

Even with extensive washing at low temperature, significant amounts of iodide (5–10%) are still present, as determined by atomic absorption spectroscopy. We speculate that CuI units are trapped in the 3-dimensional MeCu lattice, since both the starting material (CuI)_n and the product (MeCu)_n are very insoluble in ether. These problems with the purification of MeCu ultimately raise questions concerning the exact composition of the low-halide lithium dimethylcuprate subsequently prepared from it.

MeCu from a Homogeneous Solution. We therefore desired a preparation of MeCu from homogeneous solution in order to avoid contamination by entrainment. The key to developing such a procedure was House's observation that $\text{Me}_2\text{CuLi}\cdot\text{LiI}$ reacts with α -enones to afford MeCu and the corresponding Li enolate.¹⁰ We have found that the MeCu prepared in this way is pure enough that only two or three washes are required to obtain (Me_2CuLi)₂ with a very low halide content (<3%) and with a minimal loss of Cu. This halide level cannot be achieved with the previous procedure even with six washings, and the loss of Cu is unacceptably high. The initial formation of a homogeneous cuprate solution before precipitation of methylcopper appears to promote more effective halide removal.



We believe that the formation of a mixed lithium enolate–lithium halide cluster may be involved in our procedure, thereby facilitating efficient removal of the lithium halide. Such complexes are a subject of growing synthetic and mechanistic interest.^{11,12} Lithium enolate–lithium alkoxide clusters are well-characterized.¹³

Soluble Methylithium Etherate. Since solvent exchange is not satisfactory for high-quality cuprates (*vide supra*), we needed a source of ether-soluble, solid MeLi. Methylithium is usually prepared in diethyl ether by the direct reaction of elemental lithium with a halomethane.¹⁴ An alternative preparation of a solution of methylithium by transmetalation between BuLi and MeI in diethyl ether or tetrahydrofuran (THF) at low temperature has been described.¹⁵

The preparation of solid MeLi by transmetalation has also been achieved with hexane as the reaction medium.¹⁶ This material was soluble in THF or triethyl-

(10) House, H. O.; Wilkins, J. M. *J. Org. Chem.* **1976**, *41*, 4031.

(11) Miller, S. A.; Griffiths, S. L.; Seebach, D. *Helv. Chim. Acta* **1993**, *76*, 563.

(12) Seebach, D. *Angew. Chem., Int. Ed. Engl.* **1988**, *27*, 1624.

(13) DeLong, G. T.; Pannell, D. K.; Clarke, M. T.; Thomas, R. D. *J. Am. Chem. Soc.* **1993**, *115*, 7013.

(14) Lusch, M. J.; Phillips, W. V.; Sieloff, R. F.; Nomura, G. S.; House, H. O. *Org. Synth.* **1984**, *62*, 101.

(15) Reiffers, S.; Vaalburg, W.; Wiegman, T.; Beerling-Van der Molen, H. D.; Paans, A. M. J.; Woldring, M. G.; Wynberg, H. *J. Labelled Compd. Radiopharm.* **1979**, *16*, 56.

(16) (a) McKeever, L. D.; Waack, R.; Doran, M. A.; Baker, E. B. *J. Am. Chem. Soc.* **1969**, *91*, 1057. (b) Hatch, H. B. Lithium Corporation of America, personal communication, April 1989.

(6) Pearson, R. G.; Gregory, C. D. *J. Am. Chem. Soc.* **1976**, *98*, 4098.

(7) Ashby, E. C.; Watkins, J. J. *J. Am. Chem. Soc.* **1977**, *99*, 5312.

(8) (a) House, H. O.; Respass, W. L.; Whitesides, G. M. *J. Org. Chem.* **1966**, *31*, 3128. (b) House, H. O.; Chu, C.-Y. *J. Org. Chem.* **1976**, *41*, 3083.

(9) (a) Bertz, S. H.; Smith, R. A. *J. Am. Chem. Soc.* **1989**, *111*, 8276. (b) Vellekoop, A. S.; Smith, R. A. *J. Am. Chem. Soc.* **1994**, *116*, 2902.

amine,^{16a} and it likewise dissolved in toluene provided 2 equiv of THF was present.^{16b} This transmetalation procedure gave a white solid, which was found to be insoluble in diethyl ether at 0 °C despite vigorous attempts to promote solution, as has been noted previously.¹⁷

The insolubility of solid methyllithium in weakly coordinating solvents such as diethyl ether can be rationalized on the basis of the published crystal structure of a sample prepared in the absence of electron donor ligands.¹⁸ This shows that the material consists of a polymeric array of tetrameric units. Methyllithium in diethyl ether is known to be tetrameric,^{19a} although the degree of ether coordination in solution is unknown. Solid methyllithium prepared in the presence of diethyl ether has been found to have the empirical formula MeLi·OEt₂,^{19b} but its solid state structure has not been reported. By analogy with the X-ray structure of MeLi·THF,²⁰ it seems reasonable that solid methyllithium etherate is tetrameric and that diethyl ether occupies the fourth coordination site on each metal atom.

It was therefore envisioned that the solubility of solid MeLi precipitated from hexane could be improved, if at least 1 molar equiv of diethyl ether per lithium were included in the reaction mixture. Examination of the effect of a stoichiometric amount of diethyl ether on the preparation of MeLi by transmetalation in hexane at -78 °C resulted in the production of low yields of methyllithium (40–50%) and high levels of residual base (20–30%). These difficulties were effectively resolved by repetition of the reaction at -40 °C, where satisfactory yields (80–90%) of an ether-soluble form of solid MeLi with an encouragingly low level of residual base (<10%) were realized. Most of the residual base in the product was traced to residual base in the commercial BuLi used. In addition, the halide content of the product was found to be very low (<2%), but not as low as that of commercial low-halide MeLi (<0.5%).

NMR-Clean (Me₂CuLi)₂ and Me₂CuLi·LiI. The ¹³C NMR of "halide-free" (Me₂CuLi)₂ prepared from the solid MeLi showed a sharp (*W*_{1/2} = 3.1 Hz) peak at -9.25 ppm at -80 °C (peak broadening takes place above -60 °C). When commercial low-halide MeLi was used in our improved preparation of (Me₂CuLi)₂, the width at half-height was a remarkably low 2.5 Hz. The narrow low-temperature line widths allow accurate determination of the resonance positions. Hence quotation of chemical shifts to ±0.01 ppm can now be made in a meaningful way (see Experimental Section). From the analytical results and consideration of the NMR spectra (Table 1), it appears that the organocuprate ¹³C NMR line width of low-halide (Me₂CuLi)₂ is related to the amount of residual halide present. This can be attributed to an equilibrium between **2** and **1** plus free LiI (*vide infra*).

Elemental analysis of low-halide (Me₂CuLi)₂, prepared by combining traditional MeCu methodology^{5,6} and our methyllithium preparation, showed a Cu:Li:I ratio of 1.00:0.97:0.06. The result was comparable with

Table 1. NMR Spectral Data for Lithium Dimethylcuprates in Diethyl Ether at -80 °C

cuprate	MeLi source	MeCu source	chem shift ^a (ppm)		¹³ C NMR line width ^b (Hz)
			¹ H	¹³ C	
(Me ₂ CuLi) ₂	commercial	MeLi + CuI	-1.09	-9.2	10 ^c
(Me ₂ CuLi) ₂	commercial	Me ₂ CuLi·LiI + C ₆ H ₈ O ^d	-1.15	-9.2	2.5 ^c
(Me ₂ CuLi) ₂	MeLi(s)	Me ₂ CuLi·LiI + C ₆ H ₈ O ^d	-1.09	-9.25	3.1
Me ₂ CuLi·LiI	commercial		-1.10	-9.2	15 ^c
Me ₂ CuLi·LiI	MeLi(s)		-1.05	-9.28	<4

^a All resonances appear upfield from TMS. ^b Half-height line width. ^c Previous work.^{9a} ^d Cyclohex-2-enone.

that obtained by utilizing commercial low-halide MeLi in which the halide to copper ratio was found to be 5–10%. In contrast, halide-free (Me₂CuLi)₂ prepared via MeCu from Me₂CuLi·LiI and 2-cyclohexenone showed a Cu:Li:I ratio of 1.00:0.97:0.03 using our MeLi. With commercial low-halide MeLi, 2% halide was found.

As the presence of extraneous species in the low-halide (Me₂CuLi)₂ preparation seemed to influence the line width of the ¹³C NMR resonance, the effect of using ether-soluble solid methyllithium on the line width of the methyl resonance of the stoichiometric material Me₂CuLi·LiI was investigated. When Me₂CuLi·LiI was synthesized by use of the MeLi solution prepared in this work, it consistently had a single ¹³C NMR resonance at -9.28 ppm with a line width *W*_{1/2} < 4 Hz at -80 °C. Appreciable broadening of the ¹³C resonance was observed at temperatures above -50 °C. This experimental result was reproducible over several runs and is significantly better than previous results (Table 1). Therefore, narrow-line spectra can be obtained for Me₂CuLi·LiI, provided appropriate reagents and methods are employed.

A bonus from these studies is the availability of ¹³C-enriched **1** and **2** derived from ¹³C-labeled MeI. Repetition of the MeLi preparation with MeI (¹³C, 50%) gave ¹³CH₃Li and (¹³CH₃)₂CuLi·LiI with the same level of enrichment. This mixture displayed a sharp resonance which was readily discernible at normal reaction concentrations and has allowed effective monitoring of the methyl carbon resonance during subsequent mechanistic investigations in ether.^{9b}

Molecular Geometries and Charge Distributions for 1–3. The near identity of the ¹³C chemical shifts of (Me₂CuLi)₂ and MeCuLi·LiI reagents (-9.25 and -9.28 ppm, respectively) can arise from three sources. The compounds possess similar structures with virtually identical carbon shifts. The structures are different, but the NMR shifts are coincidentally the same. Both reagents lead to a common species by equilibrium partition. To examine these possibilities, we have performed calculations on the most likely structures for **1a** and **2a** and compared them for bonding and chemical shift patterns at carbon.

The halide-free species is presumed to exist in solution with the nonplanar dimeric structure **1** (R = H), surmised by NMR^{6,7} and determined crystallographically for a tetrakis(trimethylsilyl) derivative (**1d**, R = Si(CH₃)₃) in which each lithium cation is solvated by a molecule of dimethyl sulfide solvent of crystallization²¹

(17) Reynolds, K. A.; O'Hagan, D.; Gani, D.; Robinson, J. A. *J. Chem. Soc., Perkin Trans. 1* **1988**, 3195.

(18) Weiss, E.; Hencken, G. *J. Organomet. Chem.* **1970**, *21*, 265.

(19) (a) West, P.; Waack, R. *J. Am. Chem. Soc.* **1967**, *89*, 4395. (b) Tavaleeva, T. V.; Rodionov, A. N.; Kocheshkov, K. A. *Dokl. Akad. Nauk SSSR* **1961**, *140*, 847.

(20) Ogle, C. A.; Huckabee, B. H.; Johnson, H. C., IV; Sims, P. F.; Winslow, S. D.; Pinkerton, A. A. *Organometallics* **1993**, *12*, 1960.

(21) Olmstead, M. M.; Power, P. P. *Organometallics* **1990**, *9*, 1720.

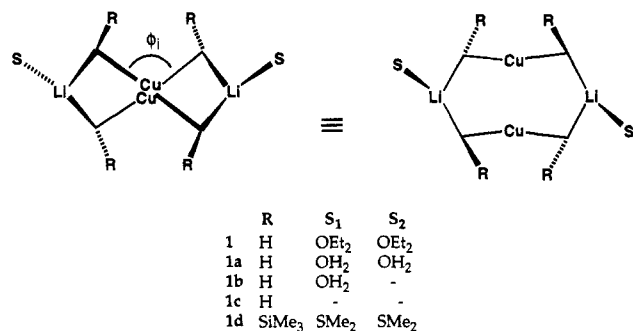
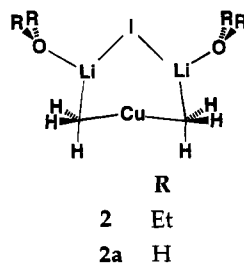


Figure 1. Two spatial representations of the $((\text{RCH}_2)_2\text{CuLi})_2$ Gilman dimer. The interplane angle ϕ_i is defined on the left.

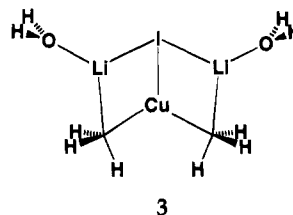
(Figure 1). Diarylcuprates in the solid state^{22–24} and in solution²⁵ uniformly display the same molecular topology. To generate a model for **1**, the silyl groups and sulfide molecules of **1d** were replaced by protons and H₂O, respectively, to give $(\text{Me}_2\text{CuLi})_2(\text{H}_2\text{O})_2$ (**1a**, Figure 1). Thus, the water molecules serve as generalized first solvation shell ether surrogates. First, structure **1a** was optimized (LANL2DZ/MP2) by constraining the interplane angle to its experimental value ($\phi_i = 96.8^\circ$). In a second geometry optimization, lifting the constraint leads to a moderate molecular flattening ($\phi_i = 117.0^\circ$) for the fully relaxed structure, accompanied by the relatively small energy gain of 3.6 kcal/mol (Table 2). The diminutive stabilization suggests the possibility that crystal packing forces may be responsible for the near-orthogonal $\phi_i = 96.8^\circ$ twist observed in the solid state. This notion is compatible with the interpretation that cuprate molecular fragments are assembled largely by ionic forces.²⁶ In support of this conclusion, diarylcuprates sustain a range of angles ϕ_i (94.4,²² 112.0,²³ 124.3,²⁴ and 130.9°²³). Empirical values in solution are unknown.

We have not explored the structure of $\text{Me}_2\text{CuLi}\cdot\text{LiI}$ extensively. However, the theoretical lowest energy isomer for solvated $\text{Me}_2\text{CuLi}\cdot\text{LiCN}(\text{H}_2\text{O})_2$ ²⁷ has been applied to $\text{Me}_2\text{CuLi}\cdot\text{Li}(\text{H}_2\text{O})_2$. The resulting structure **2a** is best described by a lower-order dimethylcuprate anion bridged by the Li₂I cation.



Given the existence of discrete copper(I) triiodide anions in the solid state,²⁸ we have likewise considered

the tricoordinate copper species **3**. As for the cyano²⁷ and methyl²⁹ series, $\text{Me}_2\text{CuLi}\cdot\text{LiX}$ (X = CN, CH₃), full optimization of **3** leads downhill to **2a**. Consequently, the Cu–I bond was constrained to 2.546 Å, the LANL2DZ/MP2 value derived for CuI alone. Subjecting the remaining variables to optimization provides bicycle **3**, 25.4 kcal/mol above isomer **2a**. The energy gap is comparable to that obtained previously for the cyano and methyl congeners.^{26,27,29}



While LANL2DZ/MP2 methodology tends to lengthen Cu–C bonds by 0.05 Å against experimental values,²⁶ a comparison of relative internal variables for optimized **1a** and **2a** is instructive for discerning significant structural variations, particularly around the methyl groups. As can be seen from Figure 2, the C–Cu and C–Li bond lengths and the C–Cu–C and Li–C–Cu bond angles are virtually identical. Within the cyclic structures the methyl groups would appear to be essentially uninfluenced by distal metal or halogen atoms. In **1a** the long C---Cu distances are 3.90 and 4.30 Å; in **2**, $r(\text{C---I}) = 4.84$ Å. In addition, natural population analysis (NPA) of the two structures **1a/2a** places very similar atomic charges of $-1.31/-1.29$, $+0.56/+0.55$ and $+0.87/+0.80$ at C, Cu and Li respectively. Both structures display NPA Cu–C bond orders of 0.36 (Figure 2). On the whole, the methyl carbons of **1a** and **2a** appear to be topologically, geometrically and electronically congruent.

¹³C NMR Predictions for 1a and 2a. To examine the influence of the latter factors on the ¹³C NMR spectrum, carbon shieldings for the optimized cuprates have been predicted with the LORG/RPAC methodology.^{30,31} In general, reasonable chemical shift results are obtained with the LORG approach for first- and second-row elements when a basis set of double- ζ quality is utilized.³¹ In the present work we focus on the relative chemical shifts of carbon ligands bonded to copper in Gilman cuprates.

As a result of the very large temporary memory requirements for integral storage during the post-SCF shielding calculations, the most extensive LORG treatment for $(\text{Me}_2\text{CuLi})_2$ involved monohydrate **1b** (Figure 1). As will be discussed below, this expediency has no significant effect on the quality of the ¹³C shift estimates. Relaxed and unsymmetrical forms of **1b** with two different methyl carbons elicit absolute shielding tensor values ranging from 209 to 217 ppm (Table 3).

(22) Koten, G. v.; Jastrzebski, J. T. B. H. *J. Am. Chem. Soc.* **1985**, *107*, 697.

(23) Lorenzen, N. P.; Weiss, E. *Angew. Chem., Int. Ed. Engl.* **1990**, *29*, 300.

(24) Olmstead, M. M.; Power, P. P. *J. Am. Chem. Soc.* **1990**, *112*, 8008.

(25) Koten, G. v.; Noltes, J. G. *J. Am. Chem. Soc.* **1979**, *101*, 6593.

(26) Snyder, J. P. submitted for publication in *J. Am. Chem. Soc.*

(27) Snyder, J. P.; Spangler, D. P.; Behling, J. R.; Rossiter, B. E. *J. Org. Chem.* **1994**, *59*, 2665.

(28) Bowmaker, G. A.; Clark, G. R.; Rogers, D. A.; Camus, A.; Marsich, N. *J. Chem. Soc., Dalton Trans.* **1984**, 37.

(29) Snyder, J. P.; Tipword, G. E.; Spangler, D. P. *J. Am. Chem. Soc.* **1992**, *114*, 1507.

(30) Bouman, T. D.; Hansen, A. E. *RPAC Molecular Properties Package, Version 9.0*; Southern Illinois University at Edwardsville, 1991.

(31) (a) Hansen, A. E.; Bouman, T. D. *J. Chem. Phys.* **1985**, *82*, 5035. (b) Bouman, T. D.; Hansen, A. E. *Chem. Phys. Lett.* **1988**, *149*, 510. (c) Hansen, A. E.; Bouman, T. D. *J. Chem. Phys.* **1989**, *91*, 3552. (d) Bouman, T. D.; Hansen, A. E. *Int. J. Quantum Chem., Quantum Chem. Symp.* **1989**, *23*, 381. (e) Bouman, T. D.; Hansen, A. E. *Chem. Phys. Lett.* **1990**, *175*, 292. (f) Facelli, J. C.; Grant, D. M.; Bouman, T. D.; Hansen, A. E. *J. Comput. Chem.* **1990**, *11*, 32.

Table 2. Absolute Energies, Zero Point Energies (ZPE), and Selected Variables of the LANL2DZ/MP2 Optimized Geometries^a

	E_{tot} , hartrees	ZPE, kcal	$r(\text{Cu}-\text{C})$	$r(\text{Li}-\text{C})$	$r(\text{I}-\text{X})^a$	$\theta(\text{C}-\text{Cu}-\text{C})$	$\phi(\text{C}-\text{Cu}-\text{C}-\text{Li})$	$\phi(\text{C}-\text{Cu}\cdots\text{Cu}-\text{C})^b$
1a (exp ϕ_1)	-716.494 02 (-715.409 41)	(127.6)	2.004 (2.066)	2.262 (2.259)		176.6 (178.7)	-136.6 (167.0)	94.5 (94.5)
			2.009 (2.067)	2.309 (2.263)		176.6 (178.7)	-150.0 (-89.5)	"96.8" ("96.8")
1a (relaxed)	-716.499 83 (-715.411 30)	(128.0)	2.001 (2.068)	2.216 (2.095)		169.8 (172.4)	-146.3 (-139.3)	115.7 (113.5)
			2.009 (2.071)	2.297 (2.098)		170.0 (172.7)	-159.2 (-156.4)	117.0 (113.9)
1d (exp) ^c			1.950	2.198		171.5		94.5
			1.959	2.219		173.7		96.8
2a	-453.156 73 (-452.474 53)	76.6 (80.9)	2.007 (2.079)	2.188 (2.152)	4.102 (3.978) ^d	169.4 (169.2)	180.0 (180.0)	
					2.756 (2.789) ^e			
3	-453.116 30	33.5 (34.9)	2.162	2.088	"2.546" ^d	118.4	179.7	
					2.794 ^e			
4	-189.833 84 (-189.539 11)			$r(\text{Li}\cdots\text{Li})$ 3.193 (3.282)	2.731 (2.759) ^d	$\theta(\text{Li}-\text{Li}-\text{I})$ 54.2 (53.5)	$\phi(\text{O}-\text{Li}-\text{I}-\text{Li})$ 180.0 (180.0)	

^a LANL2DZ/SCF values in parentheses; Å, deg. Values in quotation marks were constrained during geometry optimization. ^b Dihedral angle (ϕ_1) between planes defined by $[\text{CH}_3-\text{Cu}(1)-\text{CH}_3]\text{Cu}(2)$ and $[\text{CH}_3-\text{Cu}(2)-\text{CH}_3]\text{Cu}(1)$. ^c The two values reported represent the extremes for the bond lengths. ^d $r(\text{I}-\text{Cu})$. ^e $r(\text{I}-\text{Li})$.

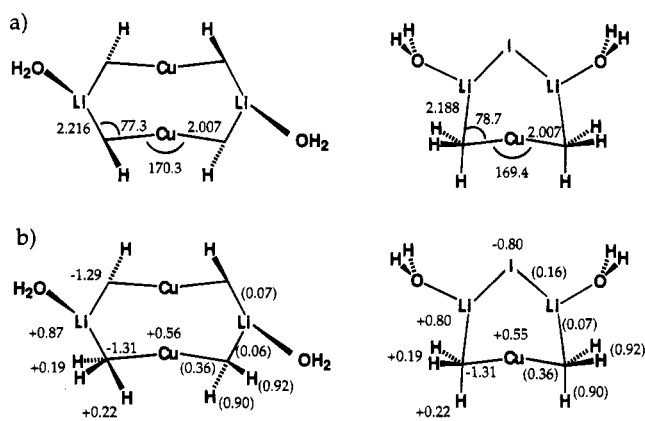


Figure 2. Comparison of LANL2DZ/MP2 optimized Gilman dimer **1a** (fully relaxed) and the iodide-bridged cuprate **2a**: (a) optimized variables (Å, deg). The unequal, long Cu···C distances for **1a** are 3.90 and 4.30 Å. In **2a** $r(\text{C}\cdots\text{I}) = 4.84$ Å. (b) NPA charges and bond orders (in parentheses).

Table 3. LORG/RPAC ¹³C NMR Chemical Shifts Relative to TMS for Structural Variations of **1** and **2** (ppm)^a

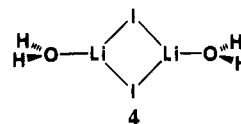
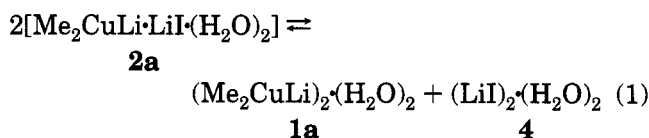
structure	exp geometry	LANL2DZ ^c	LANL2DZ/MP2 ^c
TMS		(201.4)	(198.4)
1b ($\phi_1 = 96.8^\circ$)	-11.6 ^d (213.0)	-13.6 (215.0)	-11.6 (210.0)
	-14.6 ^e (213.0)	-13.9 (215.3)	-12.9 (211.3)
1c ($\phi_1 = 96.8^\circ$)		-13.8 (215.2)	-11.5 (209.9)
		-14.2 (215.6)	-13.3 (211.7)
1b (relaxed)		-13.1 (214.5)	-10.9 (209.3)
		-15.2 (216.6)	-13.7 (212.1)
1c (relaxed)		-13.0 (214.4)	-10.8 (209.2)
		-15.0 (216.4)	-13.6 (212.0)
2a		-13.8 (215.2)	-12.0 (210.4)
2b		-14.3 (215.7)	-13.0 (211.4)

^a LANL2DZ/LORG absolute values for the ¹³C shifts in parentheses. ^b dihydrate **2a**; monohydrate **1b**; unhydrated **1c** and **2b**; cf. Figure 1. ^c Geometries optimized at these levels. ^d Relative to TMS (LANL2DZ opt). ^e Relative to TMS (LANL2DZ/MP2 opt).

These values were scaled by ¹³C shifts of 201.4 and 198.4 ppm derived by optimizing the geometry of the TMS molecule with LANL2DZ and LANL2DZ/MP2, respectively. Fully relaxed **1b** is predicted to show ¹³C chemical shifts for C₁/C₂ of -13.1/-15.2 and -10.9/-13.7 ppm (LANL2DZ and LANL2DZ/MP2 respectively) in excellent agreement with the observed value of -9.25 ppm for (Me₂CuLi)₂ at -80 °C in THF. The corresponding shifts for **2a** with equivalent carbons are -13.8 and -12.0 ppm (Table 3). In accord with the similar structural surroundings of the methyl groups in **1a** and **2a** (Figure 2), the relative ¹³C shifts are

predicted to vary by less than 2 ppm between the two structures. Separate ether solutions of the lithium organocuprates can therefore be expected to exhibit very similar ¹³C NMR spectra.

Equilibrium Partition between 1a and 2a. While Me₂CuLi·LiI is capable of independent existence as evidenced by the appearance of **2** as a local, if not global, minimum, it may nonetheless serve as a partner in a perturbable equilibrium with dimer **1**. Equation 1



applies under the assumption that a solvated dimer³² modeled by **4** is the predominant aggregate for lithium iodide under the present conditions. Lithium halide dimers are favored in the gas phase^{32a} and in solution.^{33,34} The pseudo-halogen salt LiNCS is observed as a dimer in diethyl ether.³⁵ Formation of (LiNCS)₄ is strongly endothermic and promoted only in sterically hindered ether solvents.³⁶ Furthermore, a study of LiI and LiSCN mixed aggregates in the same solvents illustrates lithium iodide's reluctance to form tetramers.³⁷ Thus, it is reasonable to assume that LiI is a dimer in the Et₂O solvent utilized herein.

The LANL2DZ/MP2 energy for eq 1 favors a shift to the right by 6.3 kcal/mol. When corrected for zero point energies (cf. Experimental and Computational Section), the gap falls to 4.4 kcal/mol (0.01% of **2a** at -80 °C).

(32) (a) Chabanel, M. *Pure Appl. Chem.* **1990**, *62*, 35. (b) Durant, F.; Govillon, Y.; Piret, P.; Van Meerssche, M. *Bull. Soc. Chim. Belg.* **1966**, *75*, 1777. (c) Amstutz, R.; Dunitz, J. D.; Laube, T.; Schweizer, W. B.; Seebach, D. *Chem. Ber.* **1986**, *119*, 434.

(33) Solomonik, V. G.; Krasnov, K. S. *Russ. J. Phys. Chem. (Engl. Transl.)* **1979**, *53*, 161, and references cited.

(34) (a) Turner, W. E. S.; Bissett, C. C. *J. Chem. Soc.* **1915**, 105, 1777. (b) Menard, D.; Chabanel, M. *J. Phys. Chem.* **1975**, *79*, 1081.

(35) (a) Paoli, D.; Luçon, M.; Chabanel, M. *Spectrochim. Acta* **1979**, *35A*, 593. (b) Vaes, J.; Chabanel, M.; Martin, M. L. *J. Phys. Chem.* **1978**, *82*, 2420.

(36) (a) Chabanel, M.; Luçon, D.; Paoli, D. *J. Phys. Chem.* **1981**, *85*, 1058. (b) Kim, Y. H.; Paoli, D.; Chabanel, M. *C. R. Acad. Sci., Ser. 2* **1985**, *301*, 1113.

(37) Goralski, P.; Chabanel, M. *Inorg. Chem.* **1987**, *26*, 2169.

Were LiI, like LiCH_3 ,^{18–20,38} to prefer a tetramer rather than a dimer in a given solvent system, the equilibrium would be displaced even further in the direction of **1a** and **4**. The conclusion to be drawn from this study is that solutions of pure $\text{Me}_2\text{CuLi}\cdot\text{LiI}$ may dissociate to give solutions composed largely of halide-free $(\text{Me}_2\text{CuLi})_2$ and LiI aggregates. The identical ^{13}C NMR spectra measured for the two reagents as well as their parallel chemical behavior (*vide infra*) is thereby reconciled. At the same time, the ^{13}C line width broadening in the presence of nonstoichiometric quantities of LiI is readily understood as the result of an equilibrium shift of eq 1 back in the direction of the bridged iodide **2a**. Thus, for situations in which the concentration of **2a** is $\geq 10\%$ of the total cuprate concentration, slow exchange between **1a** and **2a** with similar but nonidentical ^{13}C chemical shifts may obtain even at low temperatures. Peak broadening is the result. This interpretation accommodates the experimentally observed line widths described in this report and highlights the importance of eliminating residual lithium halides from cuprate reagents intended for mechanistic studies by NMR.

^{13}C chemical shifts have frequently been used to detect the presence of cuprates in solution^{9b} and to probe alternate bonding schemes at copper.³ The calculations described above pose an interpretive challenge in the use of ^{13}C NMR for assigning structures to closely related cuprates. Single- and variable-temperature NMR would appear to be insufficient for distinguishing individual bridged species such as **1** and **2** from an equilibrium partition between them. In these and related alkyl cases,^{27,29} bonding at copper and carbon is essentially unaltered. Thus while ^{13}C NMR might help to account for the invariability of cuprate chemical shifts in different media,^{3a} it will fail to provide specific structural insight unless perturbing centers (e.g., aryl groups or chiral auxiliaries) are present in the organometallic complex. By contrast, it can be anticipated that different bonding patterns at the metal center will occasion a range of chemical shifts at the ligand carbons. Some π complexes,^{2d,4,9} as well as compounds with tetracoordinated copper,³⁹ fall in this category relative to Cu–bivalent Gilman reagents.

Chemical Similarity of 1 and 2. Conjugate addition of each of the $(\text{Me}_2\text{CuLi})_2$ and $\text{Me}_2\text{CuLi}\cdot\text{LiI}$ preparations with a common substrate, 10-methyl-(19)-octal-2-one, in diethyl ether gave similar results,⁹ which tends to confirm the chemical similarity of the two reagents. Nevertheless, the halide-free cuprate gave a small but significant amount of 1,2-addition product.⁹ All things considered, the more easily prepared $\text{Me}_2\text{CuLi}\cdot\text{LiI}$ is superior for most synthetic applications.^{2a}

Conclusions

In summary, a soluble form of solid methylolithium can be prepared by transmetalation in hexane provided 1 equiv of diethyl ether is present at -40°C . This material is particularly useful for spectroscopic studies, as the derived $\text{Me}_2\text{CuLi}\cdot\text{LiI}$ displays narrow line width spectra. Comparable spectral line widths can be obtained from halide-free $(\text{Me}_2\text{CuLi})_2$, provided it is prepared by our improved procedure using MeCu precipi-

tated from homogeneous solution. With reproducible syntheses of well-defined methylcuprates now in hand, it may be hoped that our understanding of the alkylcuprates will catch up to the more complete understanding we have of arylcuprates from ^{13}C NMR spectroscopy.³ Utilization of this preparation of MeLi for structural and mechanistic investigations with metals other than copper is receiving attention in ongoing experiments. Finally, theoretical calculations permit spectroscopic and mechanistic insights into factors underlying the experimental observables for organocopper compounds. Extensions of the computational work to examine issues such as additives, solvent effects, and aggregation are underway.

Experimental and Computational Section

Caution. Dry methylcopper is explosive. In the present work, we never tried to pump off all the solvent or to blow it all off with an inert gas.

General Procedures. CuI was purified by continuous extraction using THF according to Posner and Whitten.⁴⁰ The purified CuI was then dried *in vacuo* (2 Torr) and the solid obtained was powdered and stored *in vacuo*. MeI (^{13}C , 99%) was obtained from Aldrich and used without further purification. Diethyl ether-*d*₁₀ was obtained from Cambridge Isotope Laboratories and dried over 4A molecular sieves ($1/16$ in. beads) before use. BuLi was obtained from Aldrich as a 1.6 M solution in hexanes. Standardization of alkyllithiums was carried out using the Gilman double titration technique⁴¹ with 1,2-dibromoethane or 3-bromopropene.

^1H NMR (16K data points) and ^{13}C NMR (32K) spectra were recorded at 300 and 75 MHz, respectively, and taken with spectral windows of 4000 and 9000 Hz on a Varian VXR 300 NMR spectrometer. This corresponds to 0.25 and 0.28 Hz/point, respectively. Atomic absorption analyses were carried out on a Philips Pye Unicam PU9000 atomic absorption spectrometer. All reactions were run under a positive argon atmosphere. Diethyl ether and *n*-hexane were distilled from LiAlH_4 and stored over sodium wire.

Halide Analysis. Halide analyses of MeLi solutions were carried out by the Volhard method.⁴² Halide analyses of cuprate solutions were carried out as follows: H_2O (5 mL) was added to an ethereal organocuprate solution (~ 8 mL), followed by 10% NH_3 solution (10 mL). The mixture was aspirated with air for ~ 15 min, by which time all the inorganic material had dissolved and the ether had evaporated. Zinc dust was then added slowly at room temperature to the blue aqueous solution with vigorous stirring until the solution decolorized. The solution was then filtered under gravity and the precipitate washed thoroughly with water (50 mL). The combined filtrate was analyzed for halide by the Volhard method.⁴²

Metal Analysis. Copper and lithium analyses of cuprate solutions (~ 8 mL) were undertaken as follows: an ethereal cuprate solution was added to H_2O (5 mL) and the ether was distilled off at atmospheric pressure. The residue was then cooled, and concentrated HNO_3 (5 mL) was added cautiously. The mixture was boiled in a fume hood until the evolution of brown vapor ceased and a clear blue solution remained, whereupon the solution was cooled to room temperature. The heating and cooling steps were repeated until a consistent blue solution color was obtained at room temperature. The residual solution was then diluted with H_2O to give a concentration in the range 5.5–7.0 $\mu\text{g}/\text{mL}$ for copper and 1.0–1.7 $\mu\text{g}/\text{mL}$ for lithium and analyzed by atomic absorption spectroscopy. Concentrations of Li^+ and Cu^{2+} were determined by comparison of the atomic absorption of the sample with atomic

(38) Kaufmann, E.; Raghavachari, K.; Reed, A. E.; Schleyer, P. v.

R. Organometallics **1988**, *7*, 1597, and references cited.

(39) Pesek, J. J.; Mason, W. R. *Inorg. Chem.* **1979**, *18*, 924.

(40) Posner, G. H.; Whitten, C. E. *Org. Synth.* **1976**, *55*, 122.

(41) Gilman, H.; Cartledge, F. K. *J. Organomet. Chem.* **1964**, *2*, 447.

(42) Vogel, A. I. *Quantitative Inorganic Analysis*, 2nd ed.; Longmans: London, 1960; p 259.

absorptions of standard solutions containing known amounts of both Li^+ and Cu^{2+} .

Preparation of Solid and Ethereal MeLi. (a) A hexane solution of BuLi (50 mL, 1.56 M, 78 mmol, 0.11 M residual base) was placed in a dry 100 mL Schlenk tube and cooled to -78°C under argon. Dry, degassed diethyl ether (8.65 mL, 78 mmol) was added, and the solution was agitated with a stream of argon gas. The cold solution was then added dropwise *via* a cannula over 15 min to a solution of MeI (4.87 mL, 78 mmol) in dry, degassed *n*-hexane (30 mL) held under argon at -40°C in a 200 mL Schlenk tube. A white precipitate formed ~ 5 min after the start of the addition. The suspension was stirred for 2 h at -40°C and then transferred under argon into two dry, septum-capped 50 mL centrifuge tubes, each containing a magnetic spin bar and precooled to -78°C . The suspensions were centrifuged at -78°C for 10 min and the supernatants removed by decantation at -78°C using a cannula. Dry, degassed *n*-hexane (15 mL) precooled to -78°C was added to the residue in each centrifuge tube held at -78°C . After 15 s agitation, the solid was separated by centrifugation and decantation, maintaining the temperature at -78°C as much as possible. The cold wash process was repeated two further times. Dry, degassed diethyl ether (25 mL, precooled to -78°C) was then added to the residue in each tube held at -78°C ; the suspensions were allowed to warm to 0°C with stirring and then held at 0°C for 16 h. The resulting mixtures were centrifuged at 0°C , and analysis of the combined supernatant showed MeLi (65 mL, 1.03 M, 86%) with residual base (0.11 M) and halide (0.02 M).

(b) Repetition of (a) without diethyl ether for 3 h at -78°C followed by centrifugation and decantation gave a white residue. Dry, degassed diethyl ether (50 mL, precooled to -78°C) was then added to the residue, and the suspension was allowed to warm to 0°C with vigorous stirring. After standing at 0°C for 16 h, the resulting suspension was centrifuged, and analysis of the supernatant showed MeLi (60 mL, 0.05 M, 5% yield) with a residual base titer of 0.35 M. Repetition of this reaction at -40°C and at -20°C gave total base analyses of 0.11 and 0.10 M, respectively.

Preparation of Ethereal MeLi (50% ^{13}C). A hexane solution of BuLi (6.80 mL, 1.55 M, 0.09 M residual base, 10.53 mmol) was cooled to -78°C under argon. Dry, degassed diethyl ether (1.09 mL, 10.54 mmol) was added, and the mixture was agitated with a stream of argon gas. The cold (-78°C) solution was added over 3 min to a solution of MeI (0.35 mL, 5.64 mmol) and MeI (^{13}C , 99%) (0.31 mL, 4.90 mmol) in dry, degassed *n*-hexane (8 mL) under argon in a dry, septum-capped 50 mL centrifuge tube, containing a magnetic spin bar and held at -40°C . A white precipitate formed ~ 5 min after the start of the addition. The suspension was stirred for 2 h at -40°C and then centrifuged, the supernatant decanted, and the solid washed at -78°C with *n*-hexane as described in (a) for MeLi. Dry, degassed diethyl ether (11 mL, precooled to -78°C) was added to the residue at 78°C , and the suspension was allowed to warm to 0°C with stirring. The solution was allowed to stand at 0°C for 16 h and then centrifuged. Analysis of the isolated supernatant showed MeLi (11 mL, 0.47 M, 50% ^{13}C) with residual base (0.14 M).

Preparation of Halide-Free (Me_2CuLi)₂. (a) **By Metathesis.** An ethereal solution of MeLi (1.00 mL, 1.02 M, 0.15 M residual base; 1.02 mmol) was added to a stirred suspension of CuI (0.19 g, 1.01 mmol) in dry, degassed diethyl ether (5 mL) at 0°C under argon in a 100 mL Schlenk tube. The resultant yellow suspension was stirred for 1 min at 0°C , cooled to -78°C , and transferred using a 1.5 mm cannula under argon into a dry 25 mL centrifuge tube, containing a magnetic spin bar and precooled to -78°C . The mixture was centrifuged at -78°C for 10 min. The supernatant was decanted using a cannula and then dry, degassed diethyl ether (10 mL, precooled to -78°C) was added to the solid. The resultant slurry was stirred until a consistent suspension was obtained (~ 0.5 h). The suspension was then centrifuged at

-78°C for 10 min and the supernatant removed by decantation at -78°C using a cannula. This washing procedure was repeated two more times. Dry, degassed diethyl ether (10 mL, precooled to -78°C) was then added to the residual yellow solid, followed by ethereal MeLi (0.75 mL, 1.02 M, 0.76 mmol, 0.15 M residual base). The resultant mixture was warmed to 0°C and stirred for 5 min. The cloudy reaction mixture was centrifuged at 0°C for 10 min and the supernatant was decanted and analyzed. Found: Cu, 0.64 mmol; Li, 0.70 mmol; I, 0.04 mmol. Allowing for the lithium content of residual base originally present in the MeLi, a Cu:Li:I ratio of 1.00:0.97:0.06 was determined.

(b) **By the 2-Cyclohexenone Method.** An ethereal solution of MeLi (2.00 mL, 1.02 M, 0.15 M residual base; 2.04 mmol) was added to a stirred suspension of CuI (0.19 g, 1.03 mmol) in dry, degassed diethyl ether (5 mL) at 0°C under argon. The resultant clear solution was stirred for 5 min and then 2-cyclohexenone (0.11 g, 1.14 mmol) in dry diethyl ether (1 mL) was added. The resultant yellow suspension was stirred for 1 min at 0°C and then cooled to -78°C . The mixture was transferred using a 1.5 mm cannula under argon to a dry, septum-capped 25 mL centrifuge tube, containing a magnetic spin bar and precooled to -78°C . Centrifugation, decantation, and washing was carried out as described in (a). Dry, degassed diethyl ether (10 mL, precooled to -78°C) was added to the residual yellow solid, followed by ethereal MeLi (0.90 mL, 1.02 M, 0.15 M residual base; 0.92 mmol). The reaction mixture was allowed to warm to 0°C and stirred for 5 min. The slightly cloudy mixture was then centrifuged at 0°C for 10 min, and the supernatant was decanted and analyzed. Found: Cu, 0.76 mmol; Li, 0.83 mmol; I, 0.02 mmol. Allowing for the lithium content of residual base originally present in the MeLi, a Cu:Li:I ratio of 1.00:0.97:0.03 was calculated. Analysis of the combined washes showed 10% of the Cu was left.

Preparation of $\text{Me}_2\text{CuLi}\cdot\text{LiI}$. An ethereal solution of MeLi (2.00 mL, 1.03 M, 0.11 M residual base, 2.06 mmol) was added to a stirred suspension of CuI (0.19 g, 1.03 mmol) in dry, degassed diethyl ether (5 mL) in a 30 mL Schlenk tube at 0°C under argon and stirred for 5 min at 0°C . The slightly cloudy solution was allowed to stand at 0°C for 5 min and the supernatant (~ 7 mL) was analyzed and used for spectroscopic measurements. Halide analysis was carried out on a preparation separate from that used for metal determination. Found: Cu, 1.04 mmol; Li, 2.21 mmol; I, 1.02 mmol. Calculated Cu, 1.03 mmol; Li, 2.22 mmol; I, 1.03 mmol. Allowing for the lithium content of the residual base originally present in the MeLi, a Cu:Li:I ratio of 1.00:1.92:0.98 was calculated for the material.

Low-Temperature NMR Analysis of Cuprate Solutions. From independent experiments with a diethyl ether-TMS mixture, it was found that the relative position of the ^{13}C methyl resonance of diethyl ether with respect to TMS varied with temperature and that at -80°C it was 15.72 ppm. Subsequent spectra were referenced to the methyl resonance of diethyl ether. Cuprate solutions, prepared in diethyl ether at 0°C as described above, were transferred by using a cannula into septum-capped 5 or 10 mm NMR tubes containing diethyl ether- d_{10} (0.10 or 1.0 mL, respectively) and benzene (15 μL , internal standard) and precooled to 0°C . The cuprate solutions were cooled to -80°C in the probe of the NMR spectrometer before spectra were obtained. The methyl resonance of diethyl ether in these cuprate solutions typically showed a width at half-height $W_{1/2} = 2.5$ Hz. All methylcuprate resonances appeared upfield of TMS.

(Me_2CuLi)₂, prepared as in (b), showed single ^1H and ^{13}C resonances at -1.09 and -9.25 ppm, respectively, over a temperature range of -80 to -40°C . The ^{13}C resonance had $W_{1/2} = 3.1$ Hz at -80°C .

$\text{Me}_2\text{CuLi}\cdot\text{LiI}$, prepared as described above, showed single ^1H and ^{13}C resonances at -1.05 and -9.28 ppm, respectively, over a temperature range of -80 to -30°C . The ^{13}C resonance

observed in several experiments consistently had $W_{1/2} < 4$ Hz at -80 °C.

[^{13}C]Me₂CuLiLiI, prepared from MeLi (^{13}C , 50%) showed a single ^{13}C resonance at -9.28 ppm that was ~ 50 times more intense than the corresponding resonance observed for natural abundance Me₂CuLiLiI.

Computational Methods. The structures described in Table 2 were optimized with Gaussian-92⁴³ at both Hartree-Fock (HF) and MP2 levels with the ECP-2 or LANL2DZ basis set incorporating Hay-Wadt relativistic effective core potentials (ECP) at Cu(I) and I.⁴⁴ For Cu(I), 10 1s-2p core electrons were replaced by the pseudopotential leaving 18 electrons in the AO space ((8s5p5d)/[3s3p2d], split (341/311/41)). For iodide the inner electrons are accommodated by a 36 electron krypton core potential; the 8 valence electrons treated explicitly ((3s3p)/[2s2p], split (21/21)). The remaining atoms are described by the all-electron D95V double- ζ basis ((9s5p)/[3s2p], split (721/41)). Electron correlation effects were included with Møller-Plesset perturbation to the second order (MP2) within the frozen core approximation.⁴⁵

For geometry optimization of **1a**, the backbone of the tetrakis(trimethylsilyl) derivative X-ray crystal structure²¹ (**1d**) was utilized as a starting point. The silyl groups were replaced with a proton, and the dimethyl sulfide solvent molecules coordinated to lithium were mutated to water molecules (Figure 1). The molecule was optimized in two stages. First, geometry relaxation proceeded with no assumptions concerning symmetry, all atoms treated as independent. However, the X-ray-determined angle between the two planes defined by [CH₃-Cu(1)-CH₃]Cu(2) and [CH₃-Cu(2)-CH₃]Cu(1), $\phi_1 = 96.8^\circ$ (cf. Figure 1) was retained as a constant. Second, this constraint was lifted to give an optimized interplane angle of 117.0° . Optimizations for **2a** and **3** were performed by assuming a plane of symmetry containing the Cu and I atoms (*C_s* symmetry). Both yielded planar structures. Dimer **4** was treated within the *C_{2h}* point group, but settled into *C_{2v}* symmetry. The latter is a common motif for LiX³² and CuX⁴⁶ (X = halide) dimers in the solid state.

Zero point energy corrections were calculated at both

LANL2DZ/SCF and LANL2DZ/MP2 for **2a** and **3**, but only at the SCF level for **1a** (Table 2). The SCF/MP2 ZPE ratio for cuprates obtained here and elsewhere²⁶ ranges from 0.95 to 0.98. Thus we take $0.965 \times 128.0 = 123.5$ kcal/mol as an estimate for the ZPE of the LANL2DZ/MP2 optimized structure **1a** (relaxed, Table 2). The ΔZPE for eq 1 is then $((123.5 + 33.5)/2) - 76.6 = 1.9$ kcal/mol.

Population and bonding analyses are based on the natural population (NPA) and natural bond orbital (NBO) formalisms.⁴⁷ Chemical shift calculations were carried out at the Hartree-Fock level (LANL2DZ) with the RPAC Molecular Properties Package, version 9.0.³⁰ The resulting magnetic shieldings were obtained by employing the first-order, localized orbital/local origin variant (LORG) of coupled Hartree-Fock theory over Foster-Boys localized orbitals.^{30,31} In order to compare with experimental values referred to tetramethylsilane, TMS was optimized (both LANL2DZ and LANL2DZ/MP2) and its absolute ^{13}C chemical shift calculated at the LANL2DZ level to be 201.4 and 198.4 ppm, respectively. All estimates of empirical cuprate carbon shifts reported in Table 3 were derived by subtracting their absolute values from these numbers. To ascertain the influence of geometric factors on predicted ^{13}C shifts, both constrained-optimized **1b** ($\phi_1 = 96.8^\circ$) and unoptimized (Me₂CuLi)₂ (i.e., with backbone and proton positions of the X-ray structure **1d**²¹) were subjected to the LORG/RPAC treatment. As is evident from Table 3, the calculated shieldings differ by no more than 3 ppm. Furthermore, elimination of the solvent surrogate H₂O's altogether for either **1a** or **2a** (i.e., **1c** and **2b**, respectively) changes the ^{13}C NMR shifts by no more than 1.0 ppm. Other workers have successfully employed the RPAC methodology for evaluating both the optical properties⁴⁸ and the NMR spectra⁴⁹ of organometallic compounds.

Acknowledgment. This research has been assisted by grants from the Research Committee of the University of Otago and the New Zealand Universities Grants Committee.

OM9406409

(43) Frisch, M. J.; Trucks, G. W.; Head-Gordon, M.; Gill, P. M. W.; Wong, M. W.; Foresman, J. B.; Johnson, B. G.; Schlegel, H. B.; Robb, M. A.; Replogle, E. S.; Gomperts, R.; Andres, J. L.; Raghavachari, K.; Binkley, J. S.; Gonzalez, C.; Martin, R. L.; Fox, D. J.; Defrees, D. J.; Baker, J.; Stewart, J. J. P.; Pople, J. A. *Gaussian 92*, Revision A; Gaussian, Inc., Pittsburgh, PA, 1992.

(44) Hay, P. J.; Wadt, W. R. *J. Chem. Phys.* **1985**, *82*, 299.

(45) (a) Møller, C.; Plesset, M. S. *Phys. Rev.* **1934**, *46*, 618. (b) Binkley, J. S.; Pople, J. A. *Int. J. Quantum Chem.* **1975**, *9*, 229, and references therein.

(46) Bowmaker, G. A.; Camp, D.; Hart, R. D.; Healy, P. C.; Skelton, B. W.; White, A. H. *Aust. J. Chem.* **1992**, *45*, 1155.

(47) (a) Reed, A. E.; Weinstock, R. B.; Weinhold, F. *J. Chem. Phys.* **1985**, *83*, 735. (b) Reed, A. E.; Weinhold, F. *J. Chem. Phys.* **1985**, *83*, 1736. (c) Reed, A. E.; Curtis, L. A.; Weinhold, F. *Chem. Rev.* **1988**, *88*, 899.

(48) Ernst, M. C.; Royer, D. *J. Inorg. Chem.* **1993**, *32*, 1226.

(49) (a) Combarizia, J. E.; Enemark, J. H.; Barfield, M.; Facelli, J. *C. J. Am. Chem. Soc.* **1989**, *111*, 7619. (b) Combarizia, J. E.; Barfield, M.; Enemark, J. H. *J. Phys. Chem.* **1991**, *95*, 5463. (c) Ellis, P. D.; Odum, J. D.; Lipton, A. S.; Gulick, J. M. *J. Am. Chem. Soc.* **1993**, *115*, 755.

Syntheses and Reactivities of Indole and Indolyl Complexes of (Cymene)ruthenium(II)

Sylvia Chen, V. Carperos, B. Noll, R. Jeffrey Swope, and M. Rakowski DuBois*
 Department of Chemistry and Biochemistry, University of Colorado, Boulder, Colorado 80309

Received August 8, 1994[®]

The reaction of [(*p*-cymene)Ru(OTf)₂]_x with a series of indoles has led to the synthesis of new Ru(II) indole complexes of the formula [(cymene)Ru(ind)](OTf)₂, where ind = indole (**3a**), 1-methylindole (**3b**), 2,3-dimethylindole (**3c**), and 2-methylindole (**3d**). Complex **3b** has been characterized by an X-ray diffraction study. The complex crystallized in space group *P2₁/n* with *a* = 16.180(3) Å, *b* = 9.028(2) Å, *c* = 18.827(4) Å, *β* = 109.54(2)°, *V* = 2591.7(9) Å³, and *Z* = 4. The structural study confirmed that the dication has a sandwich structure with parallel η⁶-cymene and η⁶-1-methylindole ligands. Complexes **3a**, **c**, and **d** can be deprotonated at the indole nitrogen to form monocations [(cymene)Ru(indolyl)]OTf, **4a** for indolyl, **4c** for 2,3-dimethylindolyl, and **4d** for 2-methylindolyl. The aqueous p*K*_a values for the indole ligands in **3a**, **c**, and **d** have been determined from titration data to be 7.71, 8.15, and 8.02, respectively. A tetraphenylborate salt of an indolyl derivative, [(cymene)Ru(2,3-dimethylindolyl)]BPh₄, was obtained as a single crystal. The complex crystallized in space group *C2/c* with *a* = 40.050(14) Å, *b* = 11.049(4) Å, *c* = 16.778(6) Å, *β* = 109.70(3)°, and *Z* = 8. A preliminary X-ray diffraction study confirmed a sandwich structure with the indolyl ligand coordinated through the carbocyclic ring in an η⁶-bonding mode. Complex **4c** reacted with PdCl₂PPh₃(CH₃CN) to form a heteronuclear complex, [(cymene)Ru(2,3-dimethylindolyl)PdCl₂PPh₃]OTf (**5**), in which the indolyl ligand undergoes η⁶-coordination to ruthenium and η¹-N-coordination to Pd. The reaction of **4c** with [CuOTf]₂·C₆H₆ led to the formation of a trinuclear product {[(cymene)Ru(2,3-dimethylindolyl)]₂Cu}(OTf)₃ (**6**), in which the copper ion is proposed to coordinate to two indolyl nitrogens. Reactions of **3**, **4**, and **6** with nucleophiles have been compared. Although the reactions of **3** and **4** gave complex mixtures of products, the reaction of **6** with LiAl(*O*-*t*-Bu)₃H at -78 °C resulted in the clean formation of a single isomer, formulated as {[(cymene)Ru(2,3-dimethylindolyl-H)]₂Cu}(OTf) (**7a**). The latter is proposed to result from hydride addition to C4 in each indolyl ligand of **6**.

Introduction

We have recently synthesized and characterized the reaction chemistry of the sandwich complexes containing the tetramethylpyrrolyl ligand [(cymene)Ru(NC₄-Me₄)]OTf (**1**) and the neutral pentamethylpyrrole ligand [(cymene)Ru(MeNC₄Me₄)](OTf)₂ (**2**).¹ We found that both complexes reacted with nucleophiles such as hydride or methoxide ion. Nucleophilic addition to **1** occurred at the cymene ligand to give η⁵-cyclohexadienyl derivatives, while nucleophilic addition to **2** occurred at the α-carbon atom of the pentamethylpyrrole ligand. Further protonation at the nitrogen heterocycle in the latter product led to dissociation of a reduced cyclic iminium ion.

In this paper, we report the synthesis and characterization of related sandwich complexes of (cymene)Ru(II) containing the indole and indolyl ligands. We wished to compare the effect of metal π-coordination on the reactivities of the pyrrole and indole rings. Previous reports of π-bound indole complexes²⁻⁶ include (indole)Cr(CO)₃,² Cp^{*}Ru(X-indole),^{3,4} and [(CO)₃Mn(indole)]⁺⁵ derivatives. These complexes were proposed to involve η⁶-coordination of the heterocycle and were found to promote regioselective nucleophilic substitution or ad-

dition reactions or metalation reactions at the indole six-membered ring. These reactions are of considerable interest because of their potential application in the synthesis of natural products based on the indole structure.

Relatively few syntheses of metal complexes involving π-coordination of the anionic indolyl ligand have been reported.^{6c,7} Deprotonation of an η⁶-indole derivative of Ir(III) was proposed to result in a ring shift isomerization to an η⁵-indolyl complex, eq 1,^{6c} but reactivity

(2) (a) Semmelhack, M. F.; Wulff, W.; Garcia, J. L. *J. Organomet. Chem.* **1982**, 240, C5. (b) Kozikowski, A. P.; Isobe, K. *J. Chem. Soc., Chem. Commun.* **1978**, 1076. (c) Beswick, P. J.; Greenwood, C. S.; Mowlem, T. J.; Nechvatal, G.; Widdowson, D. A. *Tetrahedron* **1988**, 44, 7325. (d) Masters, N. F.; Mathews, N.; Nechvatal, G.; Widdowson, D. A. *Tetrahedron* **1989**, 45, 5955.

(3) (a) Moriarty, R. M.; Ku, Y. Y.; Gill, U. S. *Organometallics* **1988**, 7, 660. (b) Moriarty, R. M.; Gill, U. S.; Ku, Y. Y. *J. Organomet. Chem.* **1988**, 350, 157. (c) Gill, U. S.; Moriarty, R. M.; Ku, Y. Y.; Butler, I. R. *J. Organomet. Chem.* **1991**, 417, 313.

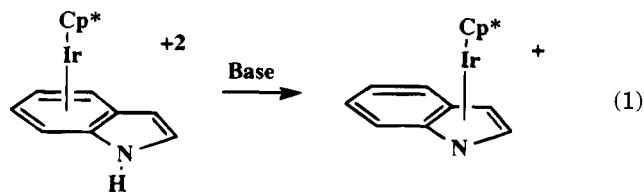
(4) Lomenzo, S. A.; Nolan, S. P.; Trudell, M. L. *Organometallics* **1994**, 13, 676.

(5) Ryan, W. J.; Peterson, P. E.; Cao, Y.; Williard, P. G.; Sweigart, D. A.; Baer, C. D.; Thompson, C. F.; Chung, Y. K.; Chung, T. M. *Inorg. Chim. Acta* **1993**, 211, 1.

(6) (a) Fish, R. H.; Barolt, E.; Kim, H. S. *Organometallics* **1991**, 10, 1965. (b) Fairhurst, G.; White, C. *J. Chem. Soc., Dalton Trans.* **1979**, 1531. (c) White, C.; Thompson, S. J.; Maitlis, P. M. *J. Chem. Soc., Dalton Trans.* **1977**, 1654.

(7) (a) Pauson, P. L.; Qazi, A. R.; Rockett, B. W. *J. Organomet. Chem.* **1967**, 7, 325. (b) Ji, L. N.; Kerschner, D. L.; Derek, M. E.; Basolo, F. *J. Organomet. Chem.* **1985**, 296, 83. (c) Jeffrey, J. A. D.; Metters, C. *J. Chem. Soc., Dalton Trans.* **1977**, 1624.

[®] Abstract published in *Advance ACS Abstracts*, February 15, 1995.
 (1) Kvietok, F.; Allured, V.; Carperos, V.; Rakowski DuBois, M. *Organometallics* **1994**, 13, 60.

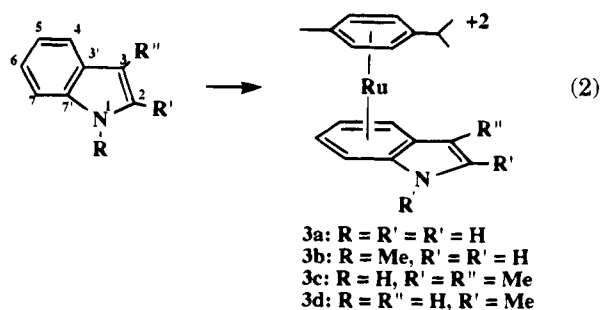


studies of such derivatives have not been carried out. η^5 -Coordination of indolyl to a cationic metal ion has the potential for activating the pyrrolic ring to reduction or ring-opening reactions. Such processes would provide important potential models for proposed steps in the commercial hydrodenitrogenation reactions catalyzed by heterogeneous metal catalysts.⁸ The Ru complexes reported here permit us to further explore the coordination modes and reactivities of the neutral and anionic ligand forms of this ring system.

Results and Discussion

Syntheses and Characterization of Indole Derivatives. The reaction of [(cymene)Ru(OTf)₂]_x with a neutral indole ligand in diethyl ether at room temperature resulted in the formation of the dicationic [(cymene)Ru(ind)](OTf)₂, where ind = indole (**3a**), 1-methylindole (**3b**), 2,3-dimethylindole (**3c**), and 2-methylindole (**3d**), eq 2. Deprotonation of **3c** followed by alkylation with

[(Cymene)Ru(OTf)₂]_x +



methyl triflate gave the dication with the 1,2,3-trimethylindole ligand, **3e**. The products were characterized by ¹H and ¹³C NMR and FAB mass spectroscopic data. Single crystals of [(cymene)Ru(1-methylindole)](OTf)₂ (**3b**) were isolated from a THF/ether solution, and an X-ray diffraction study of this product is discussed below.

The ¹H NMR data for the new complexes are listed in Table 1. Two-dimensional COSY (¹H–¹H) NMR data were used to assign the resonances of the aromatic protons. Chemical shifts for the protons of the cymene ligand lie generally between 6 and 7 ppm; shifts for *H*3, *H*5, and *H*6 of the indole ligand are also in this range, while two lower field resonances (7.3–7.9 ppm) are assigned to *H*4 and *H*7. The resonance assigned to *H*2 in the indole ligands in **3a,b** (~8.2 ppm) is shifted downfield by 1.0–1.6 ppm relative to that of the free ligands.⁹

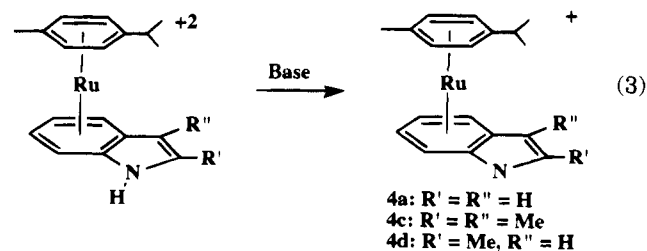
(8) Ho, T. C. *Catal. Rev.-Sci. Eng.* **1988**, *30*, 117.

(9) (a) Chadwick, D. J. In *Comprehensive Heterocyclic Chemistry*; Bird, C. W., Cheeseman, G. W. H., Eds.; Pergamon Press: Oxford, U.K., 1984; Vol. 4, p 155, and references within. (b) The structure of free indole is subject to disorder problems, but comparisons of structural data of **3b** with those of 3-substituted indoles were made.^{9a} (c) Rosenberg, E.; Williamson, K. L.; Roberts, J. D. *Org. Magn. Res.* **1976**, *8*, 117.

In the ¹³C spectra of the dication, the expected number of resonances were observed for the aromatic carbons. For some of the derivatives, ¹H–¹³C HETCOR data were used to distinguish the quaternary and methine carbons and to assign the resonances of the latter. These data are summarized in Table 2. For example, in the spectra of **3a**, **c**, and **e**, resonances for the methine carbons of the cymene and carbocyclic indole rings were found in the region between 78 and 93 ppm. These are shifted significantly upfield from those of the free cymene and indole ligands. Shifts of the indole carbocyclic ring in this range are similar to those observed for the CpRu indole systems^{3a} and are consistent with an η^6 -coordination of indole. The resonances of the pyrrole carbons in the coordinated ligand of **3a** (C2, 145 ppm; C3, 104 ppm) are shifted downfield relative to those of the free ligand (C2, 123 ppm; C3, 102 ppm).^{9c}

X-ray Diffraction Study of [(Cymene)Ru(1-methylindole)](OTf)₂ (3b**).** Single crystals of **3b** were grown by diffusion of diethyl ether into a THF solution of the compound. The complex crystallized in space group *P*2₁/*n* with four molecules per unit cell. A perspective drawing is shown in Figure 1, and selected bond distances are given in Table 3. The data confirm a sandwich structure with two parallel η^6 -arene ligands. The angle between the ruthenium ion and the center of each ring is 178.9°. The distance between Ru and the center of the cymene ring (1.706 Å) is somewhat longer than the average distance in other cymene complexes (1.678 Å),¹⁰ but it is significantly shorter than the Ru–indole distance of 1.761 Å. A similar trend was observed in [(*p*-cymene)Ru(NC₄Me₄)]⁺, where Ru–cym(centroid) = 1.698 Å and Ru–TMP(centroid) = 1.812 Å.¹ Within the accuracy of the data, the bond lengths of the indole ligand are not significantly different from those reported for a η^6 -indole–manganese complex⁵ or for a free indole molecule.^{9a,b}

Syntheses and Characterization of [(Cymene)Ru(indolyl)]⁺ Derivatives. When the dicationic complexes containing an NH group, **3a,c,d**, were eluted through a neutral alumina column with EtOH, an immediate color change from yellow to red or orange was observed. The resulting products were isolated as oily noncrystalline materials and identified as the N-deprotonated derivatives [(cymene)Ru(indolyl)]OTf, **4a,c,d**, eq 3. The deprotonations could also be achieved



with other bases in solution. For example, **4c** could be isolated from the reaction of **3c** with NaOH in aqueous solution, and the addition of triflic acid to the monocation regenerated its conjugate acid, **3c**. Only one previous example has been reported in which both the indole and indolyl derivatives of a complex have been

(10) McCormick, G. B.; Cox, D. D.; Gleason, W. B. *Organometallics* **1993**, *12*, 610, and references within.

Table 1. ¹H NMR Data for Indole and Indolyl Complexes (Triflate Salts)^a

complex	cymene	indole		
		carbocyclic ring	pyrrole ring	upfield region
[(cym)Ru(indole)] ²⁺ (3a)	6.40 ^b	7.47 (d, <i>J</i> = 5, H4) ^c	8.26 (d, <i>J</i> = 3, H2)	2.58 (spt, cym-CHMe ₂)
	6.36	6.39 (t, <i>J</i> = 5 H5)	6.72 (d, <i>J</i> = 3, H3)	1.93 (s, cym-Me)
	6.27	6.43 (t, <i>J</i> = 6, H6)	10.84 (br s, NH)	1.20 (d, cym- <i>i</i> -Pr)
	6.25	7.62 (d, <i>J</i> = 6, H7) ^c		1.19 (d, cym- <i>i</i> -Pr)
[(cym)Ru(1-methylindole)] ²⁺ (3b)	6.60	7.52 (d, <i>J</i> = 6, H4)	8.19 (d, <i>J</i> = 3, H2)	3.85 (s, NMe)
	6.45	6.45 (m, H5,6)	6.71 (d, <i>J</i> = 3, H3)	2.60 (spt, cym-CHMe ₂)
	6.29	7.63 (d, <i>J</i> = 6, H7)		1.92 (s, cym-Me)
				1.19 (d, cym- <i>i</i> -Pr)
[(cym)Ru(2,3-dimethylindole)] ²⁺ (3c)	6.82 ^d	7.76 (d, <i>J</i> = 6, H4)	11.8 (br s, NH)	1.16 (d, cym- <i>i</i> -Pr)
	6.79	6.21 (t, <i>J</i> = 6, H5)		2.70 (spt, <i>i</i> -Pr-CH)
	6.78	6.64 (t, <i>J</i> = 6, H6)		2.51 (s, NCCH ₃)
	6.65	7.88 (d, <i>J</i> = 6, H7)		2.30 (s, NC=CCH ₃)
				1.88 (s, cym-Me)
[(cym)Ru(2-methylindole)] ²⁺ (3d)	6.43	7.34 (m, H4)	11.0 (br s, NH)	1.19 (d, <i>i</i> -Pr)
	6.39	6.31 (2t, <i>J</i> = 6, H5, 6)	6.42 (s, H3)	2.58 (spt, <i>i</i> -Pr-CH)
	6.30	7.49 (m, H7)		2.54 (s, NCCH ₃)
	6.25			1.96 (s, cym-Me)
				1.20 (d, <i>i</i> -Pr)
[(cym)Ru(1,2,3-trimethylindole)] ²⁺ (3e)	6.54	7.34 (m, H4)		3.72 (s, NMe)
	6.49	6.34 (m, H5, 6)		2.63 (spt <i>i</i> -Pr-CH)
	6.43	7.48 (m, H7)		2.43 (s, NCCH ₃)
	6.34			2.25 (s, NC=CCH ₃)
				1.87 (s, cym-Me)
[(cym)Ru(indolyl)] ⁺ (4a)	6.23 ^d	7.30 (d, <i>J</i> = 5, H4)	8.60 (d, <i>J</i> = 1, H2)	1.20, 1.17 (2d, cym- <i>i</i> -Pr)
	6.13	6.05 (m, H ₅ , H ₆)	6.33 (d, <i>J</i> = 1, H3)	2.41 (sept, CHMe ₂)
	6.01	7.40 (d, <i>J</i> = 5, H7)		1.80 (s, cym-Me)
	5.96			1.16, 1.15 (2d, cym- <i>i</i> -Pr)
[(cym)Ru(2,3-dimethylindolyl)] ⁺ (4c)	6.31 ^d	7.01 (d, <i>J</i> = 6, H4)		2.52 (sept, CHMe ₂)
	6.17	5.84 (t, <i>J</i> = 6, H5)		2.45 (s, NCM _e)
	6.10	6.09 (t, <i>J</i> = 6, H6)		2.22 (s, NC=CMe)
	5.86	7.23 (d, <i>J</i> = 6, H7)		1.77 (s, cym-Me)
				1.21 (d, cym- <i>i</i> -Pr)
[(cym)Ru(2-methylindolyl)] ⁺ (4d)	6.29 ^d	7.15 (d, <i>J</i> = 6, H4)	6.12 (s, H3)	1.18 (d, cym- <i>i</i> -Pr)
	6.18	6.04 (t, <i>J</i> = 6, H5)		2.54 (s, NCM _e)
	6.05	5.98 (t, <i>J</i> = 6, H6)		2.47 (sept, CHMe ₂)
		7.32 (d, <i>J</i> = 6, H7)		1.86 (s, cym-Me)
		6.84 (d, <i>J</i> = 6, H4)		1.21, 1.20 (2d, cym- <i>i</i> -Pr)
[(cym)Ru(2,3-dimethylindolyl)PdCl ₂ PPh ₃] ⁺ (5)	6.58 ^e	6.84 (d, <i>J</i> = 6, H4)		2.56 (sept, CHMe ₂)
	6.52	5.96 (t, <i>J</i> = 6, H5)		2.48 (s, NCM _e)
	6.30	5.83 (t, <i>J</i> = 6, H6)		1.99 (s, NC=CMe)
		7.40 (d, <i>J</i> = 6, H7)		1.58 (s, cym-Me)
				1.14, 1.08 (2d, cym- <i>i</i> -Pr)
{[(cym)Ru(2,3-dimethylindolyl)] ₂ Cu} ³⁺ (6)	6.45	7.27 (d, <i>J</i> = 6, H4)		2.59 (sept, CHMe ₂)
	6.40	6.27 (m, H4, 5)		2.45 (s, NCM _e)
	6.27	7.44 (d, <i>J</i> = 6, H7)		2.22 (s, NC=CMe)
				1.86 (s, cym-Me)
{[(cym)Ru(2,3-dimethylindolyl-H)] ₂ Cu} ⁺ (7a)	6.01	3.54 (dd, <i>J</i> = 14, <i>J</i> = 5, H4 endo)		1.19, 1.17 (2d, cym- <i>i</i> -Pr)
	5.81			2.27 (spt, CHMe ₂)
	5.41	3.01 (d, <i>J</i> = 14, H4 exo)		2.04 (s, NCM _e)
	4.93	3.75 (t, <i>J</i> = 6, H5)		1.89 (s, NCCMe)
		4.62 (t, <i>J</i> = 6, H6)		1.79 (s, cym-Me)
		6.54 (d, <i>J</i> = 5, H7)		1.14, 1.11 (2d, cym- <i>i</i> -Pr)
{[(cym)Ru(2,3-dimethylindolyl-H)] ₂ Cu} ⁺ (7b)	6.00	6.35 (d, H4)		2.3 (spt, CHMe ₂)
	5.83	4.55 (t, H5)		2.12 (s, NCM _e)
	5.08	3.66 (t, H6)		1.86 (s, NCCMe)
	4.62	3.42 (dm, <i>J</i> = 15, H7 endo)		1.75 (s, cym-Me)
		3.23 (d, <i>J</i> = 15, H7 exo)		1.1 (d, cym- <i>i</i> -Pr)

^a Chemical shifts are reported in ppm. Assignments were made on the basis of COSY spectra recorded in CD₃CN, unless otherwise specified. *J* values are reported in hertz. The numbering scheme for the indole positions is shown in eq 2. ^b The cymene resonances are doublets with *J* ≈ 6 Hz. Mutually coupled doublets are indicated. ^c Resonances of H4 and H7 are not distinguished by COSY data. We have tentatively assigned the lower field resonance to H7 by analogy to assignments made for other indole complexes.^{3a,5,6c} We should note, however, that the lower field resonance in free indole is assigned to H4.^{9a,c} ^d Spectrum recorded in CDCl₃. ^e Spectrum recorded in DMSO-*d*₆. Phenyl resonances of the triphenylphosphine ligand were also observed as a multiplet at 7.26–7.53 ppm.

isolated. While [Cp*Ir(indole)]²⁺ and [Cp*Ir(indolyl)]⁺ have been characterized,^{6c} similar attempts to deprotonate the analogous Co and Rh indole derivatives led to decomposition.^{6b,c}

We have considered the possibility that the deprotonation of **3** promotes a ring shift isomerization of the indolyl ligand to produce η⁵-coordination of the hetero-

cycle in **4**. π-Bonding through the five-membered heterocycle might be favored because of the high electron density in this anionic ring. A similar shift has been proposed, but not verified by structural data, for the indole and indolyl complexes of iridium; see eq 1.^{6c} However, spectroscopic data do not support the suggested ring shift isomerization for the ruthenium com-

Table 2. ^{13}C NMR Data for Indole and Indolyl Complexes (Triflate Salts)^{a,b}

complex	quaternary C	aromatic methine C	upfield region
[(cym)Ru(indole)] ²⁺ (3a)	172.7 (OTf)	145.3 (C2)	31.6 (CHMe ₂)
	124.0	104.2 (C3)	22.3, 22.1 (CHMe ₂)
	119.8	93.4 (cym)	17.2 (PhMe)
	113.7	92.8 (cym)	
	109.0	90.7 (cym)	
		90.5 (cym)	
		89.1 (C5 or 6)	
		88.7 (C5 or 6)	
		88.1 (C4)	
		81.3 (C7)	
		92.1	31.2 (CHMe ₂)
[(cym)Ru(2,3-dimethylindole)] ²⁺ (3c)	154.1 (OTf)	92.1	21.9, 21.8 (CHMe ₂)
	117.7	91.9	16.8 (PhMe)
	117.3	89.4	12.5 (NCMe)
	112.2	87.3	7.5 (NC = CMe)
	108.8	87.0 (cym)	
	108.7	86.9 (cym)	
	104.6	84.9 (C4)	
		79.8 (C7)	
[(cym)Ru(1,2,3-trimethylindole)] ²⁺ (3e)	156.4 (OTf)	92.6	32.2 NMe
	124.1	92.4	32.0 CHMe ₂
	119.8	90.1	22.5 CHMe ₂
	114.6	89.8	17.8 Me
	109.8	87.6 (2)	12.2 Me
	109.7	85.7	8.7 Me
	103.5	78.9	
[(cym)Ru(indolyl)] ⁺ (4a)	173.1 (OTf) ^c	164.0 (C2)	30.9 CHMe ₂
	123.1	101.0 (C3)	22.8 CHMe ₂
	114.1	90.8 (cym)	18.7 PhMe
	109.6	90.1 (cym)	
	104.1	87.6 (2, cym)	
		86.3 (C7)	
		84.7 (C5 or C6)	
		84.4 (C4)	
		83.8 (C5 or C6)	
		89.8 (cym)	31.1 (CHMe ₂)
[(cym)Ru(2,3-dimethylindolyl)] ⁺ (4c)	171.5 (OTf) ^c	89.3 (cym)	22.9, 22.7 (CHMe ₂)
	122.4	86.6 (cym)	17.3 (NCMe)
	113.6	86.5 (cym)	16.8 (PhMe)
	111.3	83.4 (C4 or C7)	8.8 (NC = CMe)
	106.5	83.3 (C4 or C7)	
	104.2 (2)	82.7 (C5)	
		82.5 (C6)	
		98.4 (C3)	30.5 (CHMe ₂)
		90.2 (cym)	22.4, 22.3 (CHMe ₂)
		89.2 (cym)	19.0 (NCMe)
[(cym)Ru(2-methylindolyl)] ⁺ (4d)	176.8 (OTf) ^c	86.8 (cym)	16.2 (PhMe)
	123.2	86.5 (cym)	
	113.3	84.0 (C7)	
	112.4	83.1 (C6)	
	103.9 (2)	82.9 (C5)	
		82.8 (C4)	
		134.5 (d, J = 10, PPh ₃)	30.4 (CHMe ₂)
		133.9 (d, J = 10, PPh ₃)	22.1
		131.2 (s, p-C of PPh ₃)	22.0
		128.3 (d, J = 11, PPh ₃)	17.2
[(cym)Ru(2,3-dimethylindolyl)PdCl ₂ PPh ₃] ⁺ (5)	162.2 (OTf) ^d	91.7	15.6
	127.7	89.2	8.4
	119.0	87.8	
	113.6	87.2	
	107.9	84.9	
	106.2	83.0	
	105.6	82.6	
		80.6	
		91.0 (2)	31.6 (CHMe ₂)
		85.2	22.5, 22.3 (CHMe ₂)
{[(cym)Ru(2,3-dimethylindolyl) ₂ Cu] ³⁺ (6)	168.5 (OTf)	84.8	17.1 (NCMe)
	124.2 ^e	88.1 (2)	16.8 (PhMe)
	122.2	84.1 (C4)	8.5 (NC = CMe)
	119.9	83.3 (C7)	
	115.3		
	108.1		
	107.8		
106.6			

^a Assignments are based on two-dimensional heteronuclear correlation (HETCOR) spectra. ^b In CD₃CN unless otherwise specified. ^c In CDCl₃. ^d In DMSO-*d*₆. ^e Only six quaternary ring carbons are expected for this compound. The impurity peak has not been identified.

plexes, but rather suggest that derivatives of **4** retain η^6 -coordination of the indole ligand. In the ^1H NMR

spectra of **4a**, **c**, and **d**, the resonances of the indole ligand are shifted upfield (0.2–0.7 ppm) relative to those

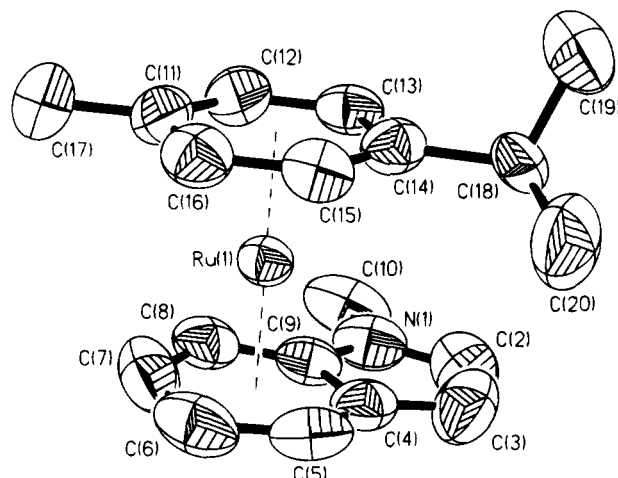


Figure 1. Perspective drawing for [(cymene)Ru(1-methylindole)](OTf)₂ (**3b**). Thermal ellipsoids are shown at the 50% probability level.

of the dications **3a**, **c**, and **d**. These shifts are consistent with the increased shielding expected for the monocation and are similar to those reported for [CpRu(η^6 -indole-Cl)]⁺.^{3a}

Perhaps more diagnostic data are provided by the ¹³C NMR spectra of **4a**, **c**, and **d**. In each case, resonances for the methine carbons of the indolyl six-membered ring (82–90 ppm) occur significantly upfield from those of the free ligand and are characteristic of η^6 -coordination in these Ru complexes. The spectral data can be compared to that reported for [(cymene)Ru(naphthalene)]²⁺. The ¹³C resonances for the coordinated ring of naphthalene are shifted upfield to 94 ppm while the resonances for the uncoordinated ring of the ligand occur from 100 to 140 ppm.¹¹ A comparison of the reported ¹³C data for the proposed [Cp*Ir(η^6 -indolyl)]⁺ shows that the resonances for the carbocyclic indole ring are also found in the region from 80 to 90 ppm, upfield from those of the free ligand, and a η^6 -indole formulation may be more appropriate for this system as well. ¹³C NMR data for other proposed η^5 -indolyl complexes have not been reported,^{7a,b} but a structural study has confirmed the η^5 coordination of the ligand in (2-methylindolyl)Mn(CO)₃.^{7c}

In order to confirm the structural assignment suggested by the spectroscopic data, we attempted to obtain single crystals of a derivative of **4**. The triflate salts of **4** were not successfully crystallized, but the metathesis reaction of **4c** with NaBPh₄ resulted in the formation of an orange microcrystalline product, identified as [(cymene)Ru(2,3-dimethylindolyl)]BPh₄. Single crystals of this product were obtained by diffusion of EtOH into a CH₂Cl₂ solution of the compound. However, the crystalline sample diffracted poorly and complete refinement of the structure has been hampered by a disorder problem.¹² Nevertheless, the preliminary structural data confirm that the cation is a sandwich structure with both η^6 -cymene and η^6 -indolyl ligands. A perspective drawing of the major orientation of the molecule is shown in Figure 2, and tables of the preliminary data are given in the supplementary material. The η^6 -indolyl ligand is slightly tilted with respect to the cymene ring, and the angle between the center of each ring and the ruthenium ion is 173.4°, somewhat

more acute than in the structure of the dication **3b**. The distances between Ru and the center of each ring were determined to be Ru–cymene(centroid) = 1.705 Å and Ru–indolyl(centroid) = 1.760 Å. These are similar to the values observed for the structure of **3b**.

The acidity of pyrrole rings has been found to increase dramatically upon π -coordination to a metal ion.^{1,13} A similar qualitative effect can be predicted for indole coordination, but no pK_a data for π -coordinated indole ligands have been reported. pH titrations of **3c** and **d** were carried out with NaOH in aqueous solutions, and **4a** was titrated with HCl. Each titration gave a curve with a single inflection point. The pK_a values of the coordinated indole ligands, determined at the half-equivalence point of each curve, were found to be 7.71 ± 0.06 for **3a**, 8.02 ± 0.04 for **3d**, and 8.15 ± 0.05 for **3c**. The pK_a values increase, as expected, as the methyl substitution on the indole ring increases. The results demonstrate that the η^6 -coordination of indole significantly increases the acidity of the ligand, as the aqueous pK_a value for free indole was reported to be 16.97.¹⁴

Reactions of Indole and Indolyl Complexes With Nucleophiles. As noted above, previous metal indole complexes have been used to carry out nucleophilic substitution and addition reactions on the activated indole ligand. Addition reactions at the C4 and C7 carbon atoms of the unsubstituted ligand were favored.^{2–5} A survey of the reactivity of [(cymene)Ru(1-methylindole)](OTf)₂ (**3b**) with nucleophiles was carried out in order to compare the electrophilic activation by the cymene–Ru(II) fragment. The reaction of **3b** with LiCH(CO₂Et)₂ in THF at –78 °C led to the formation of two major product isomers in a ~2:1 ratio. The NMR spectrum of this mixture was too complex to make structural assignments for the products. However, some assignments for cymene and indole protons have been made on the basis of COSY data (see Experimental Section). In particular, the triplet patterns of H5 and/or H6 of the indole ring could be distinguished in the region 4.8–4.4 ppm, and these upfield shifts relative to those of **3b** suggest that nucleophilic addition to the carbocyclic ring may have occurred. Reactions of **3b** with other nucleophiles, including LiAl(O-*t*-Bu)₃H, LiBEt₃H, MeLi, or NaOMe, led to a mixture of products or to decomposition. Attempts at purification by column chromatography were unsuccessful, and no identification of products was possible on the basis of the very complicated NMR spectra.

The reactions of the monocationic complex [(cymene)Ru(2,3-dimethylindolyl)]OTf (**4c**) with nucleophiles were also surveyed in order to compare the reactivity to that characterized previously for [(cymene)Ru(NC₄Me₂)]OTf. In the latter system, hydride and alkoxide nucleophiles

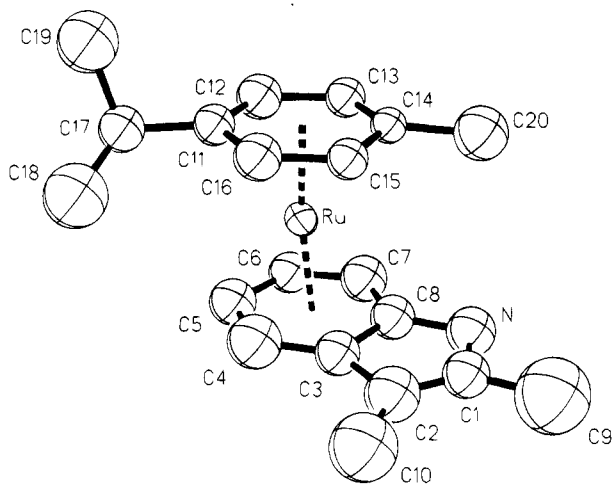
(12) A crystal was selected and mounted on a Siemens P4RA diffractometer. Crystal data: $a = 40.050(14)$ Å, $b = 11.049(4)$ Å, $c = 16.778(6)$ Å, $\beta = 109.70(3)^\circ$. Space group C2/c (No. 15), $Z = 8$. Final $R = 0.114$ for 146 parameters and 1854 data, $F \geq 4\sigma(F)$. The structure was solved via direct methods. Solution and refinement used the SHELXTL PLUS suite of programs. The largest residual electron density peaks, 2.19 and 2.12 e/Å³, could not be satisfactorily resolved but are consistent with a disorder that exchanges the cymene ligand with the indolyl. Examination of thermal parameters also supports such a conclusion. Analysis of the crystal structure indicates these ligands are similarly sized and sufficient space appears to exist to accommodate such disorder. The ratio between the two forms is ~65:35. Full details are provided in the supplementary material. Further studies are under way to better resolve this structure.

(13) Kuhn, N.; Schulten, M.; Zauder, E.; Augart, N.; Boese, R. *Chem. Ber.* **1989**, *122*, 1891.

(14) Yagil, G. *Tetrahedron* **1967**, *23*, 2855.

Table 3. Selected Bond Distances (Å) for [(Cymene)Ru(1-methylindole)](OTf)₂ (3b)

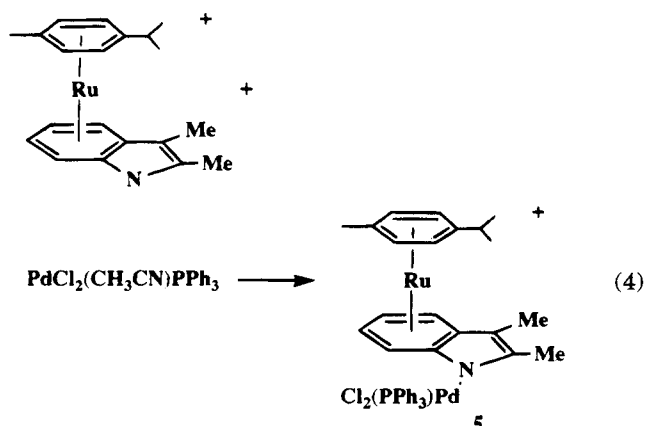
Ru (1)–C (4)	2.327 (11)	C (3)–C (4)	1.400 (17)	Ru (1)–C (14)	2.242 (11)
Ru (1)–C (6)	2.207 (16)	C (4)–C (9)	1.443 (15)	Ru (1)–C (16)	2.189 (13)
Ru (1)–C (8)	2.246 (13)	C (6)–C (7)	1.420 (20)	N (1)–C (9)	1.328 (18)
Ru (1)–C (11)	2.220 (11)	C (8)–C (9)	1.415 (13)	C (2)–C (3)	1.394 (24)
Ru (1)–C (13)	2.240 (11)	Ru (1)–C (5)	2.218 (11)	C (4)–C (5)	1.381 (19)
Ru (1)–C (15)	2.213 (11)	Ru (1)–C (7)	2.172 (15)	C (5)–C (6)	1.396 (17)
N (1)–C (2)	1.406 (16)	Ru (1)–C (9)	2.350 (13)	C (7)–C (8)	1.389 (22)
N (1)–C (10)	1.438 (23)	Ru (1)–C (12)	2.200 (10)		

**Figure 2.** Perspective drawing for [(cymene)Ru(2,3-dimethylindolyl)]BPh₄. Thermal ellipsoids are shown at the 50% probability level.

reacted cleanly with the cymene ligand at room temperature to form cyclohexadienyl derivatives.¹ In contrast, the reactions of the indolyl complex with hydride or alkoxide reagents under similar conditions led to a complicated mixture of products which were not identified.

Syntheses of Heteronuclear Indolyl Complexes.

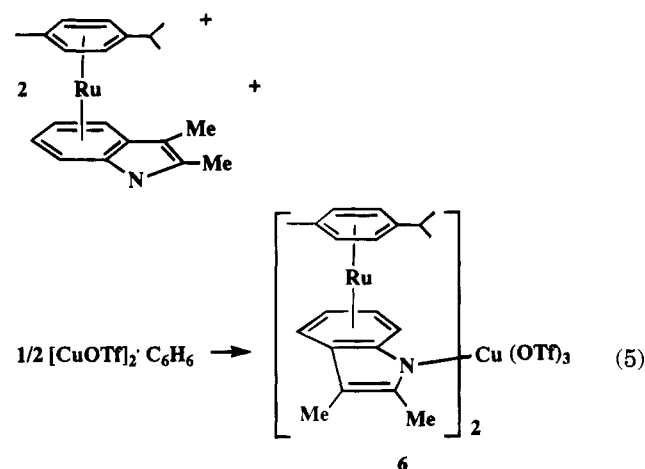
As discussed above, the indolyl ligand in the (cymene)-Ru(II) derivatives can be protonated or alkylated at the anionic nitrogen site. We attempted to extend this reactivity in reactions with electrophilic transition metal derivatives. Related examples of bi- and trinuclear pyrrolyl complexes that make use of η^1 -N, η^5 -bonding modes of the pyrrolyl ligand have been synthesized.¹⁵ The reaction of **4c** with PdCl₂(PPh₃)(CH₃CN) proceeded in dichloromethane to give a single product, which was identified as [(cymene)Ru(η^6 -indolyl)- η^1 -PdCl₂(PPh₃)]-OTf (**5**), eq 4. The FAB mass spectrum of the product



showed an envelope that corresponded to the parent ion of the proposed cation at m/e 818. ¹H and ¹³C NMR

data (Tables 1 and 2) were consistent with the formation of a single product in which the Ru π -coordination of the carbocyclic ring of the indolyl ligand is maintained, and the nitrogen atom of the ligand serves as a donor to the palladium ion. The ³¹P NMR spectrum of **5**, which showed a singlet at 27.6 ppm, supported the formation of only one isomer, but the stereochemistry at palladium in **5** (or in the starting Pd reagent) has not been determined. Previous examples of the interaction of palladium(II) with the nitrogen atom in rearranged indole ligands and in indolyls have been reported.¹⁶

The reaction of **4c** with [CuOTf]₂·C₆H₆ also proceeded to form a new yellow heteronuclear complex which was formulated as {[(cymene)Ru(η^6 -indolyl)]₂- η^1 -Cu}(OTf)₃ (**6**), eq 5. Evidence for the trinuclear formulation was



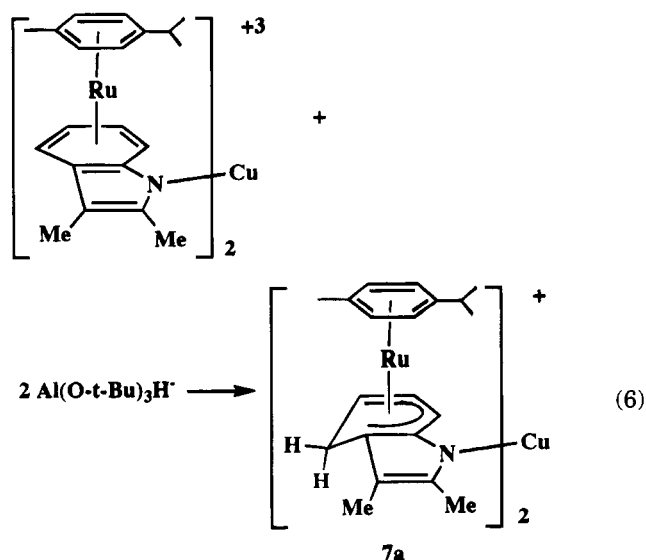
observed in the FAB mass spectrum. An envelope at m/e 1270, which corresponded to the parent ion of **6**, showed good agreement with calculated intensity ratios for two rutheniums and one copper ion in the proposed formulation. Fragments that corresponded to loss of OTf and to loss of one (cymene)Ru(indolyl) unit were also observed. No evidence was observed for the formation of a 1:1 Ru–Cu complex. For example, complete conversion to **6** was achieved regardless of whether $1/2$ or 1 equiv of copper ion was used in the synthesis. The ¹H NMR spectrum of **6** at room temperature gave no indication of ligand dissociation at the copper ion. A sharp spectrum was observed that was similar to that of the starting ruthenium complex **4c**. The chemical shifts for the ring hydrogens in the dimethylindolyl ligand of **6** were shifted downfield by ~ 0.2 ppm relative

(15) (a) Pyshnograeva, N. I.; Batsanov, A. S.; Struchkov, Y. T.; Ginsberg, A. G.; Setkina, V. N. *J. Organomet. Chem.* **1985**, *297*, 69. (b) Pyshnograeva, N. I.; Setkina, V. N.; Andrianov, V. G.; Struchkov, Y. T.; Kursanov, D. N. *J. Organomet. Chem.* **1978**, *157*, 431. (c) Losilkina, V. I.; Pyshnograeva, N. I.; Baranetskaya, N. K.; Setkina, V. N. *Izv. Akad. Nauk SSSR, Ser. Khim.* **1985**, 2780. (d) Kuhn, N. *Bull. Soc. Chem. Belg.* **1990**, *99*, 707.

(16) (a) Yamauchi, O.; Takani, M.; Toyoda, K.; Masuda, H. *Inorg. Chem.* **1990**, *29*, 1856. (b) Robson, R. *Inorg. Chim. Acta* **1982**, *57*, 71.

to those in **4c**. ^1H and ^{13}C NMR data for **6** are included in Tables 1 and 2.

Reaction of the Heteronuclear Complex **6 with Nucleophiles.** We were interested in determining whether simultaneous η^6, η^1 -coordination of the indolyl ligand in the heteronuclear complexes would lead to altered or enhanced selectivity in the reactions of the coordinated ligand with nucleophiles. In reactions of **6** with a hydride reagent, we found no evidence that coordination to the Cu^+ ion activated the nitrogen ring toward nucleophilic addition. However, we did find that the selectivity of the attack on the carbocyclic ring was significantly improved. The reaction of **6** with excess (5–6 equiv) $\text{LiAl}(\text{O}-t\text{-Bu})_3\text{H}$ in THF at -78°C resulted in much cleaner product formation than was observed for the mononuclear Ru–indole or indolyl complexes. A single isomer of a new complex was isolated by solvent evaporation and extraction with CH_2Cl_2 at 0°C . The product was formulated on the basis of ^1H NMR, COSY, and mass spectral data as $\{[(\text{cymene})\text{Ru}(2,3\text{-dimethylindolyl-H})_2\text{Cu}]\text{OTf}(\mathbf{7a})\}$, a symmetrical isomer which resulted from hydride addition to an equivalent atom in each indolyl ligand of **6**, eq 6.



The mass spectrum of the product gave an envelope consistent with the parent cation of the proposed formulation. The COSY spectrum of **7a** gave coupling patterns which indicated that this product was the result of hydride addition to either $C4$ or $C7$ in each indolyl ligand. Although the NMR data do not distinguish the two possibilities, we propose that $C4$ is the preferred site of addition in **7a**. The presence of the $\text{Cu}(\text{I})$ moiety on the nitrogen atom is expected to cause steric hindrance to nucleophilic addition to $C7$ with the bulky hydride reagent. The reactions of $(\text{CO})_3\text{Cr}(\text{indole})$ and $[(\text{CO})_3\text{Mn}(\text{indole})]^+$ complexes with nucleophiles were reported to show a similar selectivity for addition to $C4$ over $C7$ in most cases, especially when a bulky group (e.g., $\text{SiPh}_2(t\text{-Bu})$, CH_2Ph) was present on the indole nitrogen.^{2a,5} The hydride additions are also presumed to be exo to the Ru ions on the basis of the established stereochemistries of other nucleophilic additions to arene ruthenium complexes.^{1,3c}

The ^1H NMR spectrum of **7a** is shown in Figure 3, and the COSY spectrum of the expanded region from 3 to 7 ppm is shown in Figure 4. The most diagnostic

signal in the spectrum was the doublet for the external hydride substituents (H_{exo}) on the indolyl ligands at 3.00 ppm ($J = 14$ Hz). The large J value arose from geminal coupling with the endo hydrogen substituent. The upfield chemical shift and large geminal coupling constant for the exo hydrogens are similar to those seen in the ^1H NMR spectra of other hydride addition products.^{1,2,5} A doublet of doublets at 3.54 ppm was assigned to the endo hydrogen at the 4 position of the indolyl ring. The multiplicity was the result of both geminal coupling to the exo hydride substituent ($J = 14$ Hz) and vicinal coupling to the adjacent hydrogen, $\text{H}5$ ($J = 5.4$ Hz). The dihedral angle between the $\text{C}-\text{H}$ bonds of H_{exo} and $\text{H}5$ was estimated to be close to 90° , and the vicinal coupling between these two hydrogens was therefore not observed.¹⁷

Regioselectivity in the formation of **7** was found to be dependent upon temperature. When the product work-up was carried out at 20°C instead of 0°C , the ^1H NMR spectrum of the product displayed resonances for an approximate 1.5:1 mixture of isomers. In addition to the resonances identified for **7a**, a second set for the minor isomer were observed and assigned to the product of hydride addition to $C7$ in each indolyl ligand, **7b**. A resonance at 3.13 ppm with $J = 15$ Hz was assigned to the exo hydrogen of **7b**. Distinct resonances for the other indolyl hydrogens were also observed and have been tentatively assigned on the basis of the COSY NMR data, Table 1. Statistically, the isomer resulting from hydride addition to $C4$ of one indolyl ligand and $C7$ of the other is also expected to form. However, the ^1H NMR spectrum does not show separate resonances for the "mixed" isomer.

Summary and Conclusions

Both indole and indolyl derivatives of (cymene)Ru(II) have been synthesized and characterized. The η^6 -coordination of the carbocyclic ring of the bicyclic ligand has been confirmed by X-ray diffraction studies for both the indole and indolyl complexes. The aqueous $\text{p}K_{\text{a}}$ values of the coordinated indole, 2-methyl- and 2,3-dimethylindole ligands were determined to be 7.71, 8.02, and 8.15, respectively. Coordination of a second metal ion to $[(\text{cymene})\text{Ru}(2,3\text{-dimethylindolyl})]\text{OTf}$ occurred at the anionic nitrogen of the pyrrolyl ring and the heteronuclear $\eta^6-\eta^1$ complexes $[(\text{cymene})\text{Ru}(2,3\text{-dimethylindolyl})\text{PdCl}_2\text{PPh}_3]\text{OTf}$ (**5**) and $\{[(\text{cymene})\text{Ru}(2,3\text{-dimethylindolyl})_2\text{Cu}](\text{OTf})_3(\mathbf{6})\}$ have been isolated. The coordination of the $\text{Cu}(\text{I})$ ion in the indolyl complex led to a pattern of nucleophilic addition for **6** similar to that observed for $[(\text{cymene})\text{Ru}(1\text{-methylindole})]^{2+}$ (**3b**). However, the selectivity of the reaction with **6** was significantly enhanced, and only a single regioisomer of the hydride addition product was formed at -78°C . In these studies of the (cymene)Ru(II) derivatives, no evidence for η^5 -coordination of the indolyl ligand or for activation of the heterocyclic ring toward nucleophilic attack has been observed. Further studies of how metal ion coordination might affect the reactivity of the indole and indolyl ligands are in progress.

(17) The coupling constant is proportional to $\cos^2 \phi$, where ϕ is the dihedral angle between $\text{C}-\text{H}$ bonds: Silverstein, R. M.; Bassler, G. C.; Morrill, T. C. *Spectrometric Identification of Organic Compounds*, 5th ed.; Wiley: New York, 1991; p 196.

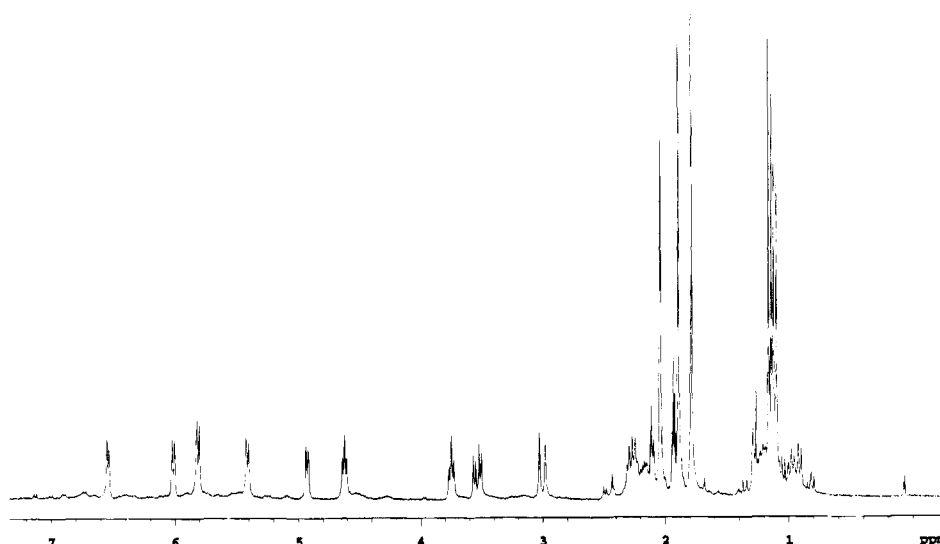


Figure 3. 300 MHz ^1H NMR spectrum of **7a** in CD_3CN . See Table 1 for assignments.

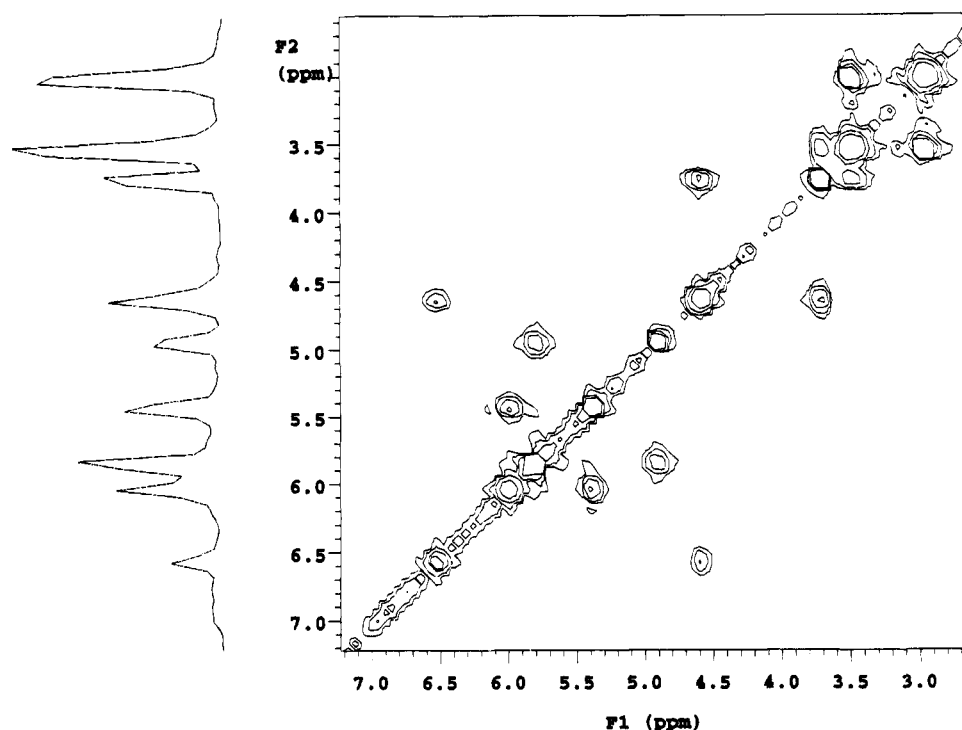


Figure 4. COSY spectrum for **7a** in the region from 3.0 to 7.0 ppm.

Experimental Section

Materials. $[(p\text{-Cymene})\text{RuCl}_2]_2$ and $[(p\text{-cymene})\text{Ru}(\text{OTf})_2]_2$ were synthesized by literature procedures.^{18,19} $\text{PdCl}_2(\text{CH}_3\text{CN})_2$ was obtained from Strem, and $[\text{Cu}(\text{OTf})_2(\text{C}_6\text{H}_6)]$ was obtained from Johnson Matthey. Indoles and other reagents were obtained from Aldrich and used as received. Dichloromethane and acetonitrile were distilled from CaH_2 . Tetrahydrofuran and diethyl ether were distilled from sodium/benzophenone. Reactions were carried out under nitrogen using standard Schlenk techniques. Column chromatography was carried out with Fischer Scientific neutral alumina absorption (80–200 mesh). Elemental analyses were performed by Desert Analytical Laboratory, Tucson, AZ, and National Chemical Consulting, Inc., Tenafly, NJ.

Instrumentation. ^1H NMR spectra were recorded at 300 MHz and ^{13}C NMR spectra at 75.4 MHz on a Varian VXR-300 NMR spectrometer. Chemical shifts, given in ppm, were referenced to TMS by using the solvent signal as a secondary reference. ^{31}P NMR spectra were recorded at 75.4 MHz on this instrument using phosphoric acid as an external standard. Mass spectra were obtained on a VG Analytical 7070 EQ-HF mass spectrometer. 3-Nitrobenzyl alcohol was used as a matrix for the FAB spectra.

The COSY spectra were collected by use of 1024 points in t_2 that were collected over the bandwidth necessary to include the desired resonances with 512 t_1 blocks and 1024 scans per block. These were zero filled to 1024 $t_2 \times 1024 t_1$.

Solution pH measurements were taken with an Orion Research Model 701A digital ionalyzer. Electrochemical mea-

(18) Bennett, M. A.; Huang, T. N.; Matheson, T. W.; Smith, A. K. *Inorg. Synth.* **1982**, *21*, 74.

(19) Ganja, E. A.; Rauchfuss, T. B.; Stern, C. L. *Organometallics* **1991**, *10*, 270.

surements were obtained on a Cypress Systems CYSY-1 analytical system. The cell consisted of a platinum working electrode, platinum auxiliary electrode, and copper reference electrode. Cyclic voltammograms were run in acetonitrile solutions of ~0.1 M tetrabutylammonium hexafluorophosphate or tetrabutylammonium perchlorate at scan rates of 100 mV/s. Ferrocene was used as an internal reference for all potentials.

[(η^6 -*p*-Cymene)Ru(η^6 -indole)][OTf]₂ (3a). [(*p*-Cymene)-RuCl₂]₂ (0.315 g, 0.515 mmol) was suspended in 30 mL of Et₂O. To the red suspension was added AgOTf (0.60 g, 2.3 mmol), and the orange solution was stirred under N₂ for 3 h. The resulting solution of [(*p*-cymene)Ru(OTf)₂]₂ was filtered away from the white solids into a flask containing indole (0.135 g, 0.115 mmol). A yellow precipitate formed immediately. After 20 min, the clear supernatant was decanted and the yellow solid was washed with Et₂O. The crude product, which contained free indole, was recrystallized from THF (10 mL)/Et₂O (30 mL) to give a tan solid, which was dried under vacuum. Yield: 0.266 g, 40%. MS (FAB⁺): *m/e* 852 (853 calcd for the [Ru(cymene)(indolyl)₂(OTf)⁺], 352 (M - H - 2OTf). MS (FAB⁻): *m/e* 799 (M + OTf - H), 650 (M - H). Anal. Calcd for C₂₀H₂₁NO₆S₂F₆Ru: C, 36.92; H, 3.25; N, 2.15. Found: C, 36.61; H, 3.09; N, 2.15.

The procedures for the syntheses of the indole derivatives **3b-d** were similar to that described for **3a**.

[(η^6 -*p*-Cymene)Ru(η^6 -1-methylindole)][OTf]₂ (3b) yield: 0.198 g, 48%. ¹³C NMR (CD₃CN): δ 148.6 (q, OTf); δ 129.6, 117.6, 114.1, 108.6, 103.2, 102.2, 92.7, 91.7, 89.9, 89.8, 88.2, 87.6, 79.0, 67.6 (aromatic quat C and CH); δ 34.2 (NCH₃); δ 31.1 (CHCH₃); δ 21.9, 21.4, 17.0 (CH₃). Cyclic voltammetry: *E*_{pc} = -1.49 V (irrev). Anal. Calcd for C₂₁H₂₃NF₆O₆S₂Ru: C, 37.95; H, 3.49; N, 2.11. Found: C, 37.70; H, 3.46; N, 2.32.

X-ray Diffraction Study of [(Cymene)Ru(1-methylindole)(OTf)₂ (3b). Single crystals of **3b** were grown by slow diffusion of Et₂O into a THF solution of the compound. The structure was solved by Patterson techniques on a Siemens P3/F diffractometer using the SHELXTL PLUS program package. The non-hydrogen atoms were included in ideal positions. One of the CF₃SO₃ anions was disordered and was refined with bond distance constraints.²⁰ Information on the crystal data, experimental conditions, and solution and refinement procedures are given in Table 4, and full details are given in the supplementary material.

[(η^6 -*p*-Cymene)Ru(η^6 -2,3-dimethylindole)][OTf]₂ (3c). Yield: 0.284 g, 87%. The cyclic voltammogram of **3c** showed an irreversible reduction (*E*_{pc}) at -1.22 V and a quasi-reversible couple with *E*_{p/2} = -1.60 V (ΔE_p = 260 mV). A plot of the peak current of the cathodic wave at -1.73 V vs the square root of the scan rate between 50 and 500 mV/s was linear. MS (FAB⁺): *m/e* 380 (M - 2OTf); 909 ([Cymene)-Ru(2,3-dimethylindolyl)₂(OTf)⁺). Anal. Calcd for C₂₂H₂₅NO₆S₂F₆Ru: C, 38.94; H, 3.71; N, 2.06. Found: C, 38.69; H, 3.53; N, 1.93.

[(η^6 -*p*-Cymene)Ru(η^6 -2-methylindole)][OTf]₂ (3d). Yield: 0.154 g, 44%. MS (FAB⁺): *m/e* 366 (M - H - 2OTf). MS (FAB⁻): *m/e* 814 (M + OTf), 664 (M - H).

[(η^6 -*p*-Cymene)Ru(η^6 -1,2,3-trimethylindole)][OTf]₂ (3e). To a red solution of **4c** (see below) (0.137 g, 0.259 mmol) in 20 mL of CH₂Cl₂ was added MeOTf (0.050 mL, 0.44 mmol). The solution immediately turned yellow. After 1 h, solvent was evaporated to give a yellow sticky solid, which was washed with Et₂O and dried under vacuum.

[(η^6 -*p*-Cymene)Ru(η^6 -indolyl)][OTf] (4a). Complex **3a** was prepared in CH₂Cl₂ solution, and the crude product was chromatographed on a neutral alumina column. Elution with CH₃CN defined a slow moving yellow band which was then

Table 4. Selected Crystallographic and Data Collection Parameters for [(Cymene)Ru(1-methylindole)](OTf)₂ (3b)

formula	C ₂₁ H ₂₃ NO ₆ F ₆ S ₂ Ru
FW, amu	664.6
color, habit	yellow, parallelepiped
crystal system	monoclinic
crystal dimens, mm	0.1 × 0.2 × 0.4
space group	<i>P</i> 2 ₁ / <i>n</i>
<i>a</i> , Å	16.180(3)
<i>b</i> , Å	9.028(2)
<i>c</i> , Å	18.827(4)
β , deg	109.54(2)
<i>V</i> , Å ³	2591.7(9)
<i>Z</i>	4
<i>D</i> _{calcd} , g/cm ³	1.703
μ , mm ⁻¹	0.825
<i>F</i> (000)	1336
radiation	Mo K α (λ = 0.710 73 Å)
temp, °C	22–24
2 θ range, deg	3.0–50.0
scan type	θ – θ
scan speed	variable; 4.00–60.00°/min
scan range	from 1.00° below 2 θ for <i>K</i> _{α1} to 1.00° above 2 θ for <i>K</i> _{α2}
total no. of reflectns	5535
no. of obsd reflectns	2166 (<i>F</i> > 4.0 σ (<i>F</i>))
<i>R</i> , <i>R</i> _w	0.0528, 0.0589
goodness of fit	1.27
largest difference peak, e ⁻ /Å ³	0.55
largest difference hole, e ⁻ /Å ³	-0.35

moved quickly down the column with EtOH. Solvent was evaporated to give an orange-yellow oily solid, which was dried under vacuum. Yield: 0.049 g, 52%. MS (FAB⁺): *m/e* 852 (853 calcd for the [Ru(cymene)(indolyl)₂(OTf)⁺]; 352 (M - H - 2OTf). MS (FAB⁻): *m/e* 799 (M + OTf - H), 650 (M - H).

[(η^6 -*p*-Cymene)Ru(2,3-dimethylindolyl)][OTf] (4c). Complex **3c** was prepared in CH₂Cl₂ solution. The crude product was washed with Et₂O and then loaded onto a neutral alumina column with CH₂Cl₂. Upon contact with the alumina, it underwent a color change from yellow to red. About 500 mL of CH₂Cl₂ was passed through the column to remove any remaining 2,3-dimethylindole. The red band was then eluted with EtOH, and solvent was evaporated to give a red oily solid, which was dried under vacuum. Yield: 0.534 g, 88%. Attempts to recrystallize the triflate salt from CH₂Cl₂/Et₂O, CH₂Cl₂/hexane, CH₃CN/Et₂O, and THF/Et₂O were unsuccessful. The product was stored at -18 °C, at which it remained stable for up to 3 days. MS (FAB⁺): *m/e* 380 (M - OTf). A fragment at *m/e* 909 (M + 2,3-dimethylindolyl) was also observed. Cyclic voltammetry: *E*_{pc} = -1.72 V (irrev). High-resolution MS (FAB⁺): calcd *m/e* 380.0952, found *m/e* 380.0988.

The tetraphenylborate salt [(*p*-cymene)Ru(2,3-dimethylindolyl)][BPh₄] was prepared by adding 1 equiv NaBPh₄ to an ethanol solution of **4c**. The product precipitated out of solution as a red solid. After stirring for 1 h, the air-stable solid was collected by filtration, washed with ethanol, and dried under vacuum. Anal. Calcd for C₄₄H₄₄NBRu: C, 75.64; H, 6.35; N, 2.00. Found: C, 75.26; H, 6.50; N, 2.02.

[(η^6 -*p*-Cymene)Ru(2-methylindolyl)][OTf] (4d). Complex **3d** was synthesized in CH₂Cl₂ solution, washed with Et₂O, and loaded onto a neutral alumina column with CH₂Cl₂ as the elutant. About 400 mL of CH₂Cl₂ was eluted through the column to remove any free 2-methylindole. The solvent was then changed to ethanol, which eluted an orange-yellow band down the column. Solvent was evaporated to give an orange-yellow oil, which was dried under vacuum. The product could be stored in the drybox at -18 °C for up to 4 days.

Reaction of 3c with Sodium Hydroxide. Complex **3c** (0.15 g, 0.22 mmol) was added to a 0.015 M solution of NaOH (30 mL, 0.45 mmol) to form an orange-red solution, which was stirred under N₂ for 1 h. The solvent was evaporated to give a mixture of red and black solids, which were dried under vacuum for 40 min. The red solid was redissolved in CH₃CN

(20) The bond distance constraints, given as distances in angstroms (ESDs), are as follows: CF₃SO₃⁻, S–O = 1.43(20), S–C = 1.80(12), C–F = 1.33(19), and F–F = 2.17.

and filtered away from the black solid. Solvent was evaporated from the red filtrate. ^1H NMR spectroscopy showed that the red product was the monocationic complex **4c**.

Reaction of 4c with Triflic Acid. Complex **4c** (0.035 g, 0.066 mmol) was dissolved in 8 mL of CH_2Cl_2 to form a red solution. Triflic acid (0.006 mL, 0.07 mmol) was added via syringe, causing an immediate color change from red to yellow. The solution was stirred for 20 min before the solvent was evaporated. The yellow solid was washed with Et_2O and dried under vacuum. The ^1H NMR spectrum of the yellow product showed that it was the dicationic complex **3c**.

Determination of pK_a Values for 3a, c, and d. An aqueous solution of **3c** (25.0 mL of 0.00150 M) was titrated with 0.00170 M NaOH. The solution slowly changed color from yellow to orange-red. The pH of the solution was measured after every 2 mL of NaOH was added. Complex **3d** (25.0 mL of 0.00497 M) was titrated with 0.00595 M NaOH in a similar fashion, and the pH was measured every 1–2 mL of NaOH added. The pK_a of **3a** was determined by titrating an aqueous solution of the deprotonated derivative **4a** (10.0 mL of 0.0300 M) with 0.0107 M HCl. The pK_a of each complex was determined at the half-equivalence point of each titration curve. The pK_a of **3a** was found to be 7.71 (± 0.06), that of **3c** was 8.15 (± 0.05), and that of **3d** was 8.02 (± 0.04). The errors in the pK_a values are based on calculations of pK_a at individual points on the titration curves.

$\text{PdCl}_2(\text{CH}_3\text{CN})(\text{PPh}_3)$. To a yellow solution of $\text{PdCl}_2(\text{NCCH}_3)_2$ (0.302 g, 0.116 mmol) in 30 mL of CH_2Cl_2 was added PPh_3 (0.306 g, 0.116 mmol). The solution turned orange-yellow in color. After stirring under N_2 for 30 min, solvent was evaporated to give an orange-yellow solid, which was washed with Et_2O and dried under vacuum. Yield: 0.477 g, 85%. ^1H NMR (CDCl_3): δ 7.66–7.74 (m, 6H, *m*-H of PPh_3), 7.53–7.54 (m, 3H, *p*-H of PPh_3), 7.40–7.47 (m, *o*-H of PPh_3), 1.23 (s, 3H, CH_3CN). ^{31}P NMR ($\text{DMSO}-d_6$): δ 32.0.

$[(p\text{-Cymene})\text{Ru}(2,3\text{-dimethylindolyl})\text{Pd}(\text{PPh}_3)\text{Cl}_2]\text{[OTf]}$ (5**).** To a mixture of complex **4** (0.232 g, 0.438 mmol) and $\text{Cl}_2\text{Pd}(\text{PPh}_3)(\text{NCCH}_3)$ (0.212 g, 0.441 mmol) was added 30 mL of CH_2Cl_2 . The solution gradually turned from red to orange. After stirring for 2 h, solvent was evaporated to give an orange solid, which was dried under vacuum. Yield: 0.338 g, 80%. The air-stable product was recrystallized from $\text{CH}_2\text{Cl}_2/\text{Et}_2\text{O}$. ^{31}P NMR ($\text{DMSO}-d_6$): δ 27.6 (s). MS (FAB^+): *m/e* 818 (M – OTf), Anal. Calcd for $\text{C}_{39}\text{H}_{39}\text{NPSO}_3\text{F}_3\text{Cl}_2\text{RuPd}$: C, 48.38; H, 4.06; N, 1.45. Found: C, 48.17; H, 4.46; N, 1.48.

$[(\eta^6\text{-}p\text{-Cymene})\text{Ru}(2,3\text{-dimethylindolyl})_2\text{Cu}]\text{[OTf]}_3$ (6**).** To a mixture of **4c** (0.223 g, 0.422 mmol) and $[\text{Cu}(\text{OTf})_2(\text{C}_6\text{H}_6)]$ (0.126 g, 0.250 mmol) was added 25 mL of CH_2Cl_2 . The color of the solution changed from red to yellow-orange within 10 min. After stirring for 1 h, the solution was filtered, and solvent was evaporated from the filtrate to give a yellow solid. The product was dried under vacuum. Yield: 0.192 g, 72%. MS (FAB^+): *m/e* 1270 (M – e), 1208 (M + H – Cu), 1122 (M + H – OTf), 1058 (M – OTf – Cu), 908 (909 calcd for M – Cu – 2OTf), 530 (**4c** + H), 380 (**4c** – OTf). Anal. Calcd for $\text{C}_{43}\text{H}_{48}\text{N}_2\text{S}_3\text{O}_9\text{F}_9\text{Ru}_2\text{Cu}$: C, 40.68; H, 3.81; N, 2.21. Found: C, 40.90; H, 3.77; N, 2.33.

$[(\eta^6\text{-}p\text{-Cymene})\text{Ru}(2,3\text{-dimethylindolyl-H})_2\text{Cu}]\text{[OTf]}$ (7**).** Complex **6** (0.0493 g, 0.0388 mmol) and $\text{LiAl}(\text{O}-t\text{-Bu})_3\text{H}$ (0.0497 g, 0.195 mmol) were combined in a Schlenk flask, which was cooled to -78°C . To the solid mixture was added 25 mL of THF, and the resulting orange solution was stirred at -78°C for 8 h. The flask was warmed to 20°C and solvent was evaporated, leaving a mixture of yellow and white solids. Addition of 30 mL of CH_2Cl_2 to the solid mixture resulted in a yellow solution, which was filtered away from the white solids. Solvent was evaporated from the filtrate, and the resulting yellow solid was dried under vacuum. The ^1H NMR of the product (in CD_3CN) showed resonances for two isomers in a $\sim 1.5:1$ molar ratio. Both isomers have incorporated two hydride equivalents. On the basis of coupling patterns given by the COSY spectrum, one isomer is the result of hydride

addition to C4 in both indolyl ligands, and the other is the result of addition to C7 of both indolyl ligands of **6**. (See Table 1 for ^1H NMR assignments.) MS (FAB^+): 824 (M – OTf); 380 (**4c** – OTf).

The above reaction was repeated with 6 equiv of $\text{LiAl}(\text{O}-t\text{-Bu})_3\text{H}$ at -78°C . After 6 h the yellow solution was placed in an ice bath at 0°C , and solvent was evaporated to give a brownish-yellow solid. Extraction with CH_2Cl_2 followed by solvent evaporation gave a yellow solid which was dried under vacuum. The ^1H NMR (in CD_3CN) showed clean formation of the major isomer observed above, **7a**, which was assigned to the C4 addition product.

Reaction of $[(\text{Cymene})\text{Ru}(1\text{-methylindole)](\text{OTf})_2$ with $\text{LiCH}(\text{CO}_2\text{Et})_2$. To a yellow solution of **3b** (0.0227 g, 0.0341 mmol) in 30 mL of THF was added lithium diethyl malonate (0.0057 g, 0.034 mmol) at -78°C . The solution was stirred at this temperature for 2.5 h. The flask was then warmed to 20°C , and solvent was evaporated. The crude product was extracted with CH_2Cl_2 , and the resulting yellow solution was filtered away from green solids. Solvent was evaporated to give a yellow solid. The ^1H NMR indicated that two major products were present in a 3:2 ratio. The following tentative assignments are based on ^1H NMR integrations and coupling patterns given by the COSY spectrum. Chemical shifts for the major isomer: δ 7.17 (d, H_4 or H_7 of ind, $J = 4.5$ Hz), 7.15 (d, H_2 of ind, $J = 2.7$ Hz), 6.30 (m, 2H of cym), 5.77 (d, H_3 of ind, $J = 3.0$ Hz), 5.47 (d, 1H of cym, $J = 6.0$ Hz), 5.29 (d, 1H of cym, $J = 6.4$ Hz), 4.71 (t, H_5 or H_6 of ind, $J = 5.7$ Hz), 3.62 (s, 3H, NCH_3), 1.81 (s, 3H, PhCH_3). Chemical shifts for the minor isomer: δ 7.10 (d, H_2 of ind, $J = 3.3$ Hz), 6.75 (d, H_4 or H_7 of ind, $J = 5.1$ Hz), 6.14 (d, H_3 of ind, $J = 3.6$ Hz), 6.04 (d, 1H of cym, $J = 5.7$ Hz), 5.79 (d, 1H of cym, $J = 6.6$ Hz), 5.47 (d, 1H of cym, $J = 6.0$ Hz), 5.38 (d, 1H of cym, $J = 6.0$ Hz), 4.84 (t, H_5 or H_6 of ind, $J = 5.4$ Hz), 4.43 (t, H_5 or H_6 of ind, $J = 6.6$ Hz), 3.48 (s, 3H, NCH_3), 1.88 (s, 3H, PhCH_3). The remaining resonances were not assigned because of the complexity of the spectrum in the regions 3.6–4.2, 2.2–2.4, and 1.0–1.3 ppm.

Reactions of 3 with Other Nucleophiles. Complex **3b** (0.198 g, 0.298 mmol) was combined with $\text{LiAl}(\text{O}-t\text{-Bu})_3\text{H}$ (0.48 g, 1.8 mmol) in THF at -78°C . After stirring for 7.5 h, the yellow solution was warmed to 0°C , and solvent was evaporated. The resulting green-yellow oil was redissolved in 20 mL of CH_2Cl_2 and filtered under N_2 , and the product was then eluted as a broad yellow band on a neutral alumina column. This fraction was collected and solvent was removed to give a yellow oil. The ^1H NMR spectrum suggested two major products in approximately a 1:1 ratio: δ 3.48, 3.44 (2 s, NMe); 1.95, 1.93 (2 s, PhMe); 1.1 to 1.3 (2 dd, CHMe_2). These two compounds may be the expected products of hydride addition to C4 and C7 of the 1-methylindole ligand. However, the ^1H NMR spectrum was not clean enough to allow for definite assignments.

Reactions of **3b** with MeLi at -78°C and at room temperature, and with NaBH_4 at room temperature, were also carried out, but complex mixtures of products were formed in each case, and these were not successfully separated or identified. Reactions of **3a** with $\text{LiAl}(\text{O}-t\text{-Bu})_3\text{H}$ at room temperature and LiEt_3BH at -78°C also failed to give characterizable products.

Reactions of $[(\text{Cymene})\text{Ru}(2,3\text{-dimethylindolyl})]\text{[OTf]}$ (4c**) with Nucleophiles.** A solid mixture of **4c** (0.292 g, 0.553 mmol) and $\text{LiAl}(\text{O}-t\text{-Bu})_3\text{H}$ (0.4463 g, 1.82 mmol) was cooled to -78°C , and 30 mL of EtOH was added to form a light orange solution. After 3 h, CH_3CN (10 mL) was added to increase the solubility of **4c**. After another 4 h at -78°C , the solution was darker orange, and there appeared to be no undissolved solids present. The solution was stirred at 0°C for 4 h and then warmed to 30°C and solvent was evaporated, leaving a mixture of brown-orange and white solids. The crude product was redissolved in 30 mL of CH_2Cl_2 and filtered. The solvent was evaporated from the filtrate, and the brown-orange solid was eluted on a neutral alumina column with CH_3CN . A

yellow band was collected and solvent evaporated to give a yellow oil. The ^1H NMR spectrum of the oil displayed resonances for free indole and three major new products which have not yet been identified. However, resonances characteristic of nucleophilic addition to indole were not observed. ^1H NMR (CD_3CN): δ 5.4–7.2 (multiple resonances); 4.0–4.6 (3 d, $J = 5$ Hz); 2.32–2.06 (7s, Me); 1.28, 1.27 (2 s, Me); 0.5–1.0 (3 d, CHMe_2).

Reaction of 4c with Sodium Methoxide. Complex **4c** (0.100 g, 0.189 mmol) was dissolved in 30 mL of MeOH to form a red solution. A solution of NaOMe was prepared by dissolving sodium metal (0.035 g, 1.4 mmol) in 15 mL of MeOH, and this was added to the solution of **4c**. After stirring under N_2 for 15 h, the solution was still red. The solvent was evaporated, and 30 mL of CH_2Cl_2 was added to form an orange solution, which was filtered. Solvent was evaporated from the filtrate to give an orange oil, which was dried under vacuum.

The ^1H NMR (in CDCl_3) displayed a complicated series of broad peaks throughout the spectrum suggesting decomposition, and there was no evidence for starting material (**4c**) remaining.

Acknowledgment. Support for this work by the Division of Chemical Sciences, Office of Basic Energy Sciences, Office of Energy Research, U.S. Department of Energy, is gratefully acknowledged.

Supplementary Material Available: Details of data collection and refinement and tables of bond distances and angles and positional and thermal parameters for **3b** and for [(cymene)Ru(2,3-dimethylindolyl)]BPh₄ (19 pages). Ordering information is given on any current masthead page.

OM940632S

Synthesis, Characterization, and Molecular Structure of Bis(tetraphenylcyclopentadienyl)rhodium(II)[†]

James E. Collins,[‡] Michael P. Castellani,^{*,‡} Arnold L. Rheingold,^{*,§}
Edward J. Miller,^{⊥||} William E. Geiger,^{*,⊥} Anne L. Rieger,^{#,} and
Philip H. Rieger^{*,#}

Departments of Chemistry, Marshall University, Huntington, West Virginia 25755,
University of Delaware, Newark, Delaware, 19716, University of Vermont,
Burlington, Vermont, 05405, and Brown University, Providence, Rhode Island, 02912

Received August 24, 1994[®]

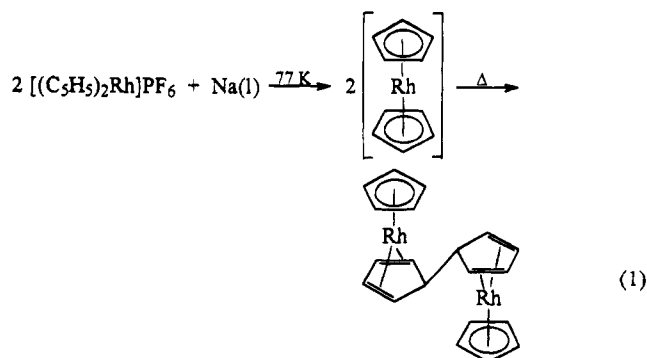
A 5 day diglyme reflux of Rh(acac)₃ and K(C₅HPh₄), followed by treatment with aqueous HPF₆, produces orange-yellow [(C₅HPh₄)₂Rh]PF₆ in 40–50% yield. Reduction of [(C₅HPh₄)₂Rh]PF₆ with sodium amalgam in THF yields olive green (C₅HPh₄)₂Rh in 70% yield. (C₅HPh₄)₂Rh crystallizes in the triclinic space group P1̄ with unit-cell parameters of *a* = 8.622(3) Å, *b* = 10.778(4) Å, *c* = 12.894(5) Å, α = 65.58(3)°, β = 72.66(3)°, γ = 83.52(3)°, and *Z* = 1. The least-squares data refined to *R*_F = 7.63% and *R*_{wF} = 10.12% for the 2479 independent observed reflections with *F*_o > 5σ(*F*_o). The metal–centroid distance is 1.904 Å and all other bond lengths and angles are similar to known octaphenylmetallocenes. ESR spectra of (C₅HPh₄)₂Rh in low-temperature glasses display a rhombic *g* tensor with resolution of Rh hyperfine splitting on one *g* component. Analysis of the spectral parameters is consistent with a d⁷ configuration derived from a nearly degenerate d_{xz}, d_{yz} ground state. Voltammetry and coulometry establish the electron-transfer series (C₅HPh₄)₂Rh^{1+/0/1-} with *E*^o values of –1.44 V and –2.13 V *vs* ferrocene. The heterogeneous charge transfer rate of the second reduction is about 3 orders of magnitude lower than that of the first.

Introduction

Neutral metallocenes of most of the first-row transition metals exist as thermally stable, crystalline solids. Although many of these compounds are paramagnetic, far fewer examples of open-shell metallocenes are known for the lower rows. Low-temperature studies have provided some such examples.^{1,2} In 1985 Cloke and co-workers prepared decamethylrhocenene, (η⁵-C₅-Me₅)₂Re,³ which represents the only isolable, open-shell, lower row neutral metallocene proven to exist.⁴ Decaphenylmolybdocene⁵ and (η⁵-C₅Me(CO₂Me)₄)₂Rh⁶ have been reported; however, definitive proof of their identi-

ties was not provided. In this paper we report the synthesis and characterization of octaphenylrhodocene and its oxidation product.

In 1953, Wilkinson and co-workers⁷ reported the synthesis of the rhodocenium cation, Cp₂Rh⁺, from the reaction of Rh(acac)₃ and CpMgBr (acac = 2,4-pentanedionate, Cp = η⁵-C₅H₅). Keller and Wawersik trapped Cp₂Rh on a liquid nitrogen-cooled ESR probe after a reductive sublimation of Cp₂Rh⁺ by molten sodium.⁸ Warming above 77 K resulted in the complex dimerizing through one ligand on each of two rhodocene molecules to yield a closed-shell product (eq 1).⁹ Thus,



spectroscopic characterization of rhodocene is largely limited to its ESR spectrum. The transient existence

(6) Bruce, M. I.; Humphrey, P. A.; Williams, M. L.; Skelton, B. W.; White, A. H. *Aust. J. Chem.* **1989**, *42*, 1847.

(7) Cotton, F. A.; Whipple, R. O.; Wilkinson, G. *J. Am. Chem. Soc.* **1953**, *75*, 3586.

(8) Keller, H. J.; Wawersik, H. *J. Organomet. Chem.* **1967**, *8*, 185.

(9) Fischer, E. O.; Wawersik, H. *J. Organomet. Chem.* **1966**, *5*, 559.

[†] Dedicated to Professor Harry E. Persinger on the occasion of his 75th birthday.

[‡] Marshall University.

[§] University of Delaware.

[⊥] University of Vermont.

^{||} Brown University.

[#] Permanent address: State University of New York, College at Plattsburgh, Plattsburgh, NY 12901.

[®] Abstract published in *Advance ACS Abstracts*, February 1, 1995.

(1) (a) Mo, W. Re: Graham, R. G.; Grinter, R.; Perutz, R. N. *J. Am. Chem. Soc.* **1988**, *110*, 7036. (b) Mo, W.; Chetwynd-Talbot, J.; Grebenik, P.; Perutz, R. N. *Inorg. Chem.* **1982**, *21*, 3647. (c) Re: Chetwynd-Talbot, J.; Grebenik, P.; Perutz, R. N.; Powell, M. H. A. *Inorg. Chem.* **1983**, *22*, 1675.

(2) Nb: (a) Elson, I. H.; Kochi, J. K. *J. Am. Chem. Soc.* **1975**, *97*, 1262. (b) Lemonovskii, D. A.; Fedin, V. P. *J. Organomet. Chem.* **1977**, *132*, C11. (c) Nesmeyanov, A. N.; Lemonovskii, D. A.; Fedin, V. P.; Perevalova, E. G. *Dokl. Akad. Nauk SSSR* **1979**, *245*, 609; *Dokl. Akad. Nauk SSSR, Engl. Transl.* **1979**, *245*, 142.

(3) (a) Cloke, F. G. N.; Day, J. P. *J. Chem. Soc., Chem. Commun.* **1985**, 967. (b) Bandy, J. A.; Cloke, F. G. N.; Cooper, G.; Day, J. P.; Girling, R. B.; Graham, R. G.; Green, J. C.; Grinter, R.; Perutz, R. N. *J. Am. Chem. Soc.* **1988**, *110*, 5039.

(4) Two lower row metallocene cations have been prepared: (η⁵-C₅-Me₅)₂Os⁺, which can be isolated (O'Hare, D.; Green, J. C.; Chadwick, T. P.; Miller, J. S. *Organometallics* **1988**, *7*, 1335) and (η⁵-C₅Me₅)₂-Ru⁺, which was not isolated (Koelle, U.; Salzer, A. *J. Organomet. Chem.* **1983**, *243*, C27. Kölle, U.; Grub, J. *J. Organomet. Chem.* **1985**, *289*, 133).

(5) Hübel, W.; Merényi, R. *J. Organomet. Chem.* **1964**, *2*, 213.

of rhodocene at ambient temperature has also been observed in electrochemical¹⁰ and mass spectral¹¹ studies of Cp₂Rh⁺.

Polyphenylated cyclopentadienyl ligands frequently reduce the reactivity of complexes in which they are incorporated.¹² The very large size of the tetraphenylcyclopentadienyl ligand (η^5 -C₅HPh₄) suggested that the dimerization reaction that occurred for Cp₂Rh would not happen for (C₅HPh₄)₂Rh. The phenyl substituents should also prevent close approach of substrates that might displace a cyclopentadienyl ligand. Finally, an internal reaction (e.g. orthometalation) would probably generate a complex with an unstable metal oxidation state, electron count, or ligand geometry.

Experimental Section

General Data. All reactions of air- and moisture-sensitive materials were performed under an argon atmosphere employing standard Schlenk techniques, unless otherwise noted. Solids were manipulated under argon in a Vacuum Atmospheres glovebox equipped with an HE-493 dri-train. Hydrated rhodium(III) chloride, hydrated iridium(III) chloride (Johnson-Mathey), 2,4-pentanedione (Aldrich), and 60% aqueous HPF₆ (Strem) were used as received. K(C₅HPh₄)_{0.5}THF¹³ and Tl(C₅HPh₄)¹⁴ were prepared according to literature procedures. Solvents were distilled from an appropriate drying agent under argon: diglyme, triglyme (Aldrich), toluene, and hexane (Fisher) (sodium/benzophenone ketyl), benzene and tetrahydrofuran (THF) (Fisher) (potassium/benzophenone ketyl), and dichloromethane (Fisher) (CaH₂). All other solvents were used as received. Elemental analyses were performed by Schwarzkopf Microanalytical Laboratory, Woodside, NY.

¹H NMR spectra (200.06 MHz) were obtained on a Varian XL-200 NMR spectrometer equipped with a Motorola data system upgrade. Melting points are uncorrected.

Electrochemistry. Voltametric and coulometric experiments were conducted as previously described.¹⁵ Potentials are referred to the ferrocene (Fc)/ferrocenium couple. The supporting electrolyte was [Bu₄N][PF₆] in all cases. Voltammetry simulations employed the method of Grosser.¹⁶

ESR Spectroscopy. X-band ESR spectra were obtained using a Bruker ESP300E spectrometer at the University of Bristol. The spectrometer was equipped with a liquid nitrogen Dewar flask and a variable-temperature unit; field-frequency calibration relied on a Hewlett-Packard microwave frequency counter and the Bruker Hall probe, the offset of which was checked from time to time with DPPH. Toluene solutions of (C₅HPh₄)₂Rh were prepared for ESR spectral studies in several ways, including the use of a nitrogen-filled glovebox, modified Schlenk techniques, and a vacuum line.

Tris(acetylacetonato)rhodium(III) (1). Tris(acetylacetonato)rhodium(III) was prepared by modifying a literature procedure.¹⁷ All steps were carried out in the air. Hydrated rhodium(III) chloride (2.50 g, 9.50 mmol) was dissolved in distilled H₂O (20 mL). The pH of the solution was adjusted

to the range 4.00–5.00 by dropwise addition of aqueous 10% NaHCO₃. When necessary, 0.1 M HCl was used as a back-titrating reagent. The deep purple solution was then treated with 2,4-pentanedione (9.0 mL, 87 mmol) and refluxed for 30 min. After allowing the solution to cool to room temperature, the pH of the system was readjusted to the range 4.00–5.00. Precipitation of Rh(acac)₃ occurred during this process. This mixture (without filtering) was refluxed for 24 h during which time the color of the reaction solution lightened considerably. The orange-yellow solid was collected by vacuum filtration and recrystallized from boiling methanol. The hot methanol solution was slowly cooled, followed by further cooling in an ice-water bath to produce orange-yellow, crystalline **1** (2.78 g, 73%): mp 260–263 °C (lit.¹⁷ mp 260 °C).

Tris(acetylacetonato)iridium(III). This synthesis was the same as for **1** except that IrCl₃·nH₂O was used in place of RhCl₃·nH₂O in the same molar amount: yield 45%.

Bis(tetraphenylcyclopentadienyl)rhodium(III) Hexafluorophosphate (2). Diglyme (15 mL) was added to a solid mixture of Rh(acac)₃ (0.25 g, 0.62 mmol) and K(C₅HPh₄)_{0.5}THF (0.55 g, 1.2 mmol). The reaction mixture was refluxed for 5 days. The dark green/brown solution was transferred to a plastic cup in the air while cooling to room temperature and the green color immediately disappeared. Aqueous HPF₆ (1 mL) was added to solution with stirring. After 1 h the solution was filtered, and the resulting yellow powder was washed with diethyl ether followed by water. The yellow solid was oven dried at 100 °C for 24 h and then extracted with CH₂Cl₂. The resulting solution was gravity filtered into a test tube and layered with an equal volume of hexane. Slow diffusion of the layers yielded large, straw-like yellow crystals of **2** (0.28 g, 46%): mp 409 °C dec; ¹H NMR (CD₂Cl₂) δ 6.8–7.5 (m). Anal. Calcd for C₅₅H₄₂F₆PRh: C, 70.59; H, 4.29. Found: C, 70.95; H, 4.52.

Bis(tetraphenylcyclopentadienyl)rhodium(II) (3). A THF slurry (25 mL) of **2** (0.20 g, 0.20 mmol) was degassed by the freeze-pump-thaw method. This mixture was transferred via cannula onto a 0.1% sodium amalgam (9.3 mg, 0.41 mmol Na). The reaction mixture was stirred vigorously until there was no evidence of the yellow rhodocenium salt suspension (ca. 45 min). The olive green solution was transferred to another flask via cannula to prevent further reduction,¹⁸ and the THF was removed *in vacuo*. The solid was extracted into boiling toluene and frit filtered, and the resulting solution was concentrated to near saturation. Hexane (10 mL) was added, and the resulting solution was cooled to –20 °C overnight to yield deep olive green microcrystals of **3** (0.12 g, 70%). Recrystallization of **3** was performed by slow diffusion of hexane into a saturated benzene solution of **3**: mp 311–313 °C; visible λ_{max} (THF) 715 nm ($5.79 \times 10^3 \text{ M}^{-1}\text{cm}^{-1}$). Anal. Calcd for C₅₅H₄₂Rh: C, 82.75; H, 5.03. Found: C, 82.74; H, 4.84.

X-ray Diffraction Study of Bis(tetraphenylcyclopentadienyl)rhodium(II). A crystal of (C₅HPh₄)₂Rh was grown by layer diffusion of hexane into a saturated THF solution of **3**. Crystal data and parameters used during the collection of intensity data are given in Table 1. A dark green crystal was mounted on a fine glass fiber with epoxy cement. It crystallized in the triclinic space group P $\bar{1}$ and is isomorphous with the other, previously reported octaphenylmetallocenes.^{13,19,20} Unit-cell dimensions were derived from a least-squares fit of the angular settings of 25 reflections with 20° < 2 θ < 25°. A profile fitting procedure was applied to all intensity data to

(10) (a) El Murr, N.; Sheats, J. E.; Geiger, W. E.; Holloway, J. D. L. *Inorg. Chem.* **1979**, *18*, 1443. (b) Gusev, O. V.; Denisovich, L. I.; Peterleitner, M. G.; Rubezhov, A. Z.; Ustynuk, N. A.; Maitlis, P. M. *J. Organomet. Chem.* **1993**, *452*, 219.

(11) Zagorevskii, D. V.; Holmes, J. L. *Organometallics* **1992**, *11*, 3224.

(12) Janiak, C.; Schumann, H. *Adv. Organomet. Chem.* **1991**, *33*, 291.

(13) Castellani, M. P.; Geib, S. J.; Rheingold, A. L.; Trogler, W. C. *Organometallics* **1987**, *6*, 1703.

(14) Schumann, H.; Janiak, C.; Khani, H. *J. Organomet. Chem.* **1987**, *330*, 347.

(15) Hoobler, R. J.; Hutton, M. A.; Dillard, M. M.; Castellani, M. P.; Rheingold, A. L.; Rieger, A. L.; Rieger, P. H.; Richards, T. C.; Geiger, W. E. *Organometallics* **1993**, *12*, 116.

(16) Grosser, D. K. *Cyclic Voltammetry*; VCH Publishers: New York, 1993.

(17) (a) Dwyer, F. P.; Sargeson, A. M. *J. Am. Chem. Soc.* **1953**, *75*, 984. (b) Belyaev, A. V.; Venediktov, A. B.; Fedotov, M. A.; Khramenko, S. P. *Koord. Khim.* **1985**, *11*, 794.

(18) Prolonged exposure of (C₅HPh₄)₂Rh to the sodium amalgam produces a brown solid that is insoluble in THF.

(19) Castellani, M. P.; Wright, J. M.; Geib, S. J.; Rheingold, A. L.; Trogler, W. C. *Organometallics* **1986**, *5*, 1116.

(20) Hoobler, R. J.; Adams, J. V.; Hutton, M. A.; Francisco, T. W.; Haggerty, B. S.; Rheingold, A. L.; Castellani, M. P. *J. Organomet. Chem.* **1991**, *412*, 157.

Table 1. Crystal and Refinement Data for Octaphenylrhodocene

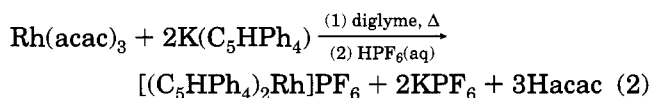
a. Crystal Data	
formula	C ₅₈ H ₄₂ Rh
FW	841.8
cryst system	triclinic
space group	P $\bar{1}$
a, Å	8.622(3)
b, Å	10.778(4)
c, Å	12.894(5)
α , deg	65.58(3)
β , deg	72.66(3)
γ , deg	83.52(3)
V, Å ³	1041.4(7)
Z	1
color	dark green
crystal Size, mm	0.22 × 0.31 × 0.40
D (calcd), g/cm ³	1.342
abs coeff, cm ⁻¹	4.50
b. Data Collection	
diffractometer	Siemens P4
radiation	graphite-monochromated Mo K α ($\lambda = 0.71073$ Å)
temp, K	298
2 θ scan range, deg	4.0 to 48.0
scan type	ω
reflns colld	3137
obsd rflns	2479 ($F > 5.0\sigma(F)$)
c. Solution and Refinement	
solution	direct methods
refinement method	full-matrix least-squares
quantity minimized	$\sum w(F_o - F_c)^2$
weighting scheme	$w^{-1} = \sigma^2(F) + 0.0010F^2$
number of parameters refined	281
final R indices (obs. data), %	R = 7.63, wR = 10.12
R indices (all data), %	R = 15.77, wR = 13.62
GOF	1.88
data-to-parameter ratio	8.8:1
largest difference peak, eÅ ⁻³	2.08
largest difference hole, eÅ ⁻³	-1.04

improve the precision of the measurement of weak reflections. Reflections were corrected for absorption effects using the program XABS (H. Hope), which is based on deviations in F_o and F_c values.

The structure was solved by taking the coordinates of the previously determined octaphenylferrocene, replacing Rh for Fe, and allowing the structure to refine. All hydrogen atoms were treated as idealized, isotropic contributions ($d(C-H) = 0.96$ Å, $U = 1.2 U_{iso}$ of attached C). Atomic positions and bond distances, and bond angles are collected in Tables 2 and 3, respectively. All computer programs used in the data collections and refinements are contained in the Siemens programs P3 and SHELXTL PLUS (VMS).

Results and Discussion

Synthesis and Reactivity. A 5 day reflux of Rh(acac)₃ and K(C₅HPh₄) in diglyme, after treatment with aqueous HPF₆, produces [(C₅HPh₄)₂Rh]PF₆ (**2**) in 40–50% yield as an orange-yellow, crystalline solid (eq 2).



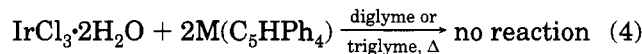
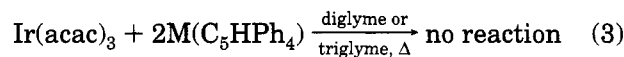
The Rh(acac)₃ was prepared by a modified literature procedure (*vide supra*).¹⁷ Substantial yield reductions occur with shorter reaction times and reactions employing lower boiling THF as solvent produce none of the desired product. [(C₅HPh₄)₂Rh]PF₆ is soluble in CH₂-Cl₂, slightly soluble in THF and acetone, and poorly soluble or insoluble in most other solvents. It is air-stable.

Table 2. Atomic Coordinates (x10⁴) and Equivalent Isotropic Displacement Coefficients (Å² × 10³) for Octaphenylrhodocene

	x	y	z	U ^a
Rh	0	0	0	32(1)
C(1)	2187(9)	1193(8)	-377(7)	43(4)
C(2)	2364(9)	924(9)	-1415(7)	44(4)
C(3)	2376(9)	-551(8)	-1021(7)	41(4)
C(4)	2312(8)	-1138(8)	230(7)	39(3)
C(5)	2304(9)	-48(8)	576(7)	40(4)
C(21)	1670(10)	1777(9)	-3357(7)	47(4)
C(22)	1663(13)	2804(11)	-4430(9)	67(5)
C(23)	2375(16)	4042(12)	-4788(9)	86(6)
C(24)	3111(14)	4252(11)	-4087(9)	78(6)
C(25)	3152(11)	3213(10)	-2986(8)	57(4)
C(26)	2411(9)	1973(9)	-2611(7)	46(4)
C(31)	1814(11)	-2484(10)	-1469(9)	58(5)
C(32)	2187(16)	-3208(12)	-2182(13)	85(7)
C(33)	3437(21)	-2807(17)	-3201(14)	103(10)
C(34)	4298(16)	-1646(15)	-3525(9)	87(7)
C(35)	3936(11)	-914(11)	-2828(8)	64(5)
C(36)	2672(9)	-1312(9)	-1795(7)	45(4)
C(41)	4147(10)	-3096(10)	586(8)	55(4)
C(42)	4479(14)	-4453(13)	1116(11)	79(6)
C(43)	3251(15)	-5336(12)	1940(12)	84(7)
C(44)	1701(14)	-4878(11)	2199(11)	74(6)
C(45)	1364(11)	-3510(9)	1652(9)	57(4)
C(46)	2588(9)	-2601(8)	836(7)	42(4)
C(51)	2752(12)	-1324(11)	2610(9)	64(5)
C(52)	2615(13)	-1421(12)	3731(9)	73(5)
C(53)	2004(12)	-366(12)	4053(9)	68(5)
C(54)	1585(12)	793(12)	3237(9)	70(6)
C(55)	1716(10)	920(10)	2105(8)	52(4)
C(56)	2259(9)	-158(9)	1775(7)	45(4)

^a Equivalent isotropic U defined as one-third of the trace of the orthogonalized U_{ij} tensor.

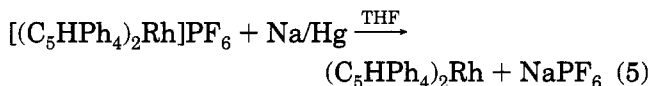
Attempts to prepare the analogous octaphenyliridium complex, (C₅HPh₄)₂Ir⁺, using a variety of reagents and conditions were unsuccessful (eq 3 and 4, M = K or Tl). Refluxes were carried out for up to 7 days



with periodic checks made for the generation of (C₅HPh₄)₂Ir⁺. The behavior observed in this system is reminiscent of that which occurs for the metals of the iron group.²¹

Reduction of [(C₅HPh₄)₂Rh]PF₆ by 0.1% sodium amalgam in THF produces olive green (C₅HPh₄)₂Rh (**3**), in 70% yield (eq 5). Octaphenylrhodocene is the most air-

(21) For all of the iron and cobalt group elements, the unsubstituted metallocene or metallocenium ion is formed under relatively mild conditions (generally a reflux below 80 °C for up to 24 h results in >70% yield). For the syntheses of (C₅HPh₄)₂Fe and (C₅HPh₄)₂Co comparable conditions to Cp₂M are employed with only small yield reductions.^{13,19} For both second-row compounds (C₅HPh₄)₂Ru (160 °C, 48 h, 30% yield) and (C₅HPh₄)₂Rh⁺ (160 °C, 5 d, 50% yield), the conditions are much harsher than for their respective C₅H₅ compound (Cp₂Ru 80 °C, 2 h, 70% yield; Cp₂Rh⁺ 65 °C, 1 d, 70% yield). In each case, the third-row complexes, (C₅HPh₄)₂Os and (C₅HPh₄)₂Ir⁺, did not form even at 215 °C over several days. The third-row C₅H₅ analogues are prepared under similar conditions to their second-row counterparts, albeit with somewhat reduced yields. Since the second- and third-row metals are larger than those of the first row, the differences in reactivity cannot arise from steric considerations. Rather the difference may arise from the fact that lower row metals frequently bind substrates more strongly than first-row metals. In the case of the lower row metals, the C₅HPh₄⁻ anion may have to displace a strongly bound ligand. This would be difficult for a ligand as large and bulky as C₅HPh₄⁻.



sensitive of the octaphenylmetallocenes reported to date, decomposing instantly in solution and in minutes as a solid upon exposure to the air. Thus **3** is dramatically more oxygen-sensitive than its congener $(C_5HPh_4)_2Co$, but is similar to $(C_5HPh_4)_2V$.¹³ This is probably because of the greater accessibility of the metal in **3** and the lower stability of Rh(II) as compared to Co(II). Compound **3** reacts slowly with CH_2Cl_2 , although it does so more rapidly than $(C_5HPh_4)_2Co$. This behavior is also consistent with the phenyl rings preventing close approach of even small substrates to the rhodium center. Complex **3** is quite thermally stable; however, and melts sharply at 311 °C. It is soluble in benzene, toluene, and THF.

Molecular Structure. The crystal structure of $(C_5HPh_4)_2Rh$ is isomorphous to the other known octaphenylmetallocenes.^{13,19,20} It crystallizes as discrete, well-separated molecules with a staggered C_5 configuration and a Rh atom on a crystallographic center of symmetry (Figure 1). Bond distances and angles are collected in Table 3. The M–CNT distance increases from 1.771 Å in $(C_5HPh_4)_2Co$ to 1.904 Å in $(C_5HPh_4)_2Rh$ which is close to the corresponding increase in metal covalent radius (0.09 Å).²² The average Rh–C distances in **3** (2.26 Å) also increase in comparison to $(C_5HPh_4)_2Ru$ (2.20 Å)²⁰ and $(C_5H_3(CO_2Me)_3)_2Rh^+$ (2.17 Å).²³ This is consistent with the 19th electron residing in an antibonding orbital. The phenyl torsion angles (Table 4) are similar to those of $(C_5HPh_4)_2Ru$.

Electrochemistry. Solutions of substituted rhodocenium cation **2** gave two well-defined voltammetric waves (Figure 2) in nonaqueous solvents such as CH_3CN , DMF, and THF. As shown below, they are consistent with the stepwise formation of the neutral complex **3** and the nominally 20e anion $(C_5HPh_4)_2Rh^-$ (**4**). Although the anion is much longer lived than its unsubstituted analogue (the lifetime of Cp_2Rh^- is *ca.* 0.02 s at room temperature^{10a}), it splits off $C_5HPh_4^-$ on the bulk electrolysis time scale. It will also be shown that the heterogeneous electron transfer rate for reduction of **3** to **4** is much slower than that of the oxidation of **3** to **2**.

Reduction of 2 to 3. The first reduction of **2** is essentially Nernstian at both Pt and Hg electrodes, with $E_{2/3}^\circ = -1.44$ V vs Fc. Over the scan rate range of $v = 0.05$ to 0.50 V/s, values of $\Delta E_p (= E_{pa} - E_{pc})$ and $\delta E_p (= E_{pc/2} - E_{pc})$ of 63 ± 5 and 64 mV were measured, respectively, close to the values expected for electrochemically reversible couples.²⁴ The k_s value for the couple appears to be > 1 cm/s.

Bulk coulometry confirmed the one-electron nature of this reduction. Electrolysis ($E_{appl} = -1.7$ V) in THF at ambient temperatures of *ca.* 0.5 mM solutions of **2** in DMF or THF consumed 1.0 F per mole and resulted in green solutions of **3** that were stable for weeks if kept under N_2 . Voltammetry of the electrolysis solution at

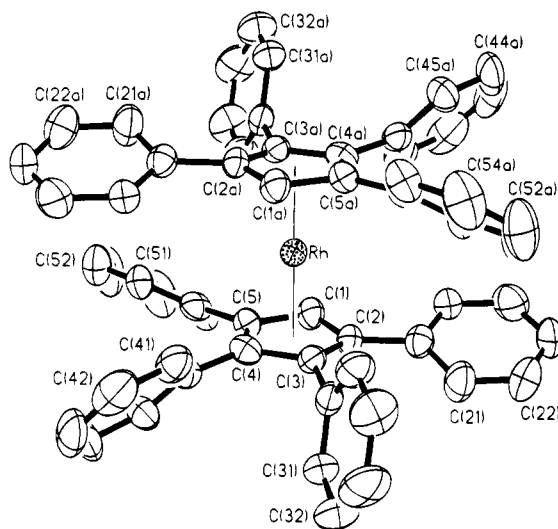


Figure 1. Molecular structure and labeling scheme for $(\eta^5-C_5HPh_4)_2Rh$.

Table 3. Selected Bond Distances (Å) and Angles (deg) for Octaphenylrhodocene

Rh–CNT ^a	1.904	C(1)–Rh–C(2)	37.4(4)
C(1)–C(2)	1.444(14)	C(2)–Rh–C(3)	37.5(3)
C(2)–C(3)	1.455(12)	C(3)–Rh–C(4)	37.7(3)
C(3)–C(4)	1.455(12)	C(1)–Rh–C(5)	36.3(3)
C(4)–C(5)	1.418(14)	C(4)–Rh–C(5)	36.2(4)
C(1)–C(5)	1.411(10)	C(1)–C(2)–C(3)	106.4(7)
Rh–C(1)	2.220(9)	C(2)–C(3)–C(4)	107.5(9)
Rh–C(2)	2.283(7)	C(3)–C(4)–C(5)	107.6(7)
Rh–C(3)	2.247(7)	C(1)–C(5)–C(4)	108.9(8)
Rh–C(4)	2.251(7)	C(2)–C(1)–C(5)	108.9(8)
Rh–C(5)	2.307(9)	C(1)–C(2)–C(26)	125.3(8)
		C(2)–C(3)–C(36)	126.0(7)
		C(3)–C(4)–C(46)	120.5(9)
		C(4)–C(5)–C(56)	126.8(7)
		C(1)–C(5)–C(56)	124.0(9)
		C(5)–C(4)–C(46)	130.5(8)
		C(4)–C(3)–C(36)	125.8(7)
		C(3)–C(2)–C(26)	128.2(9)

^a CNT = centroid of the cyclopentadienyl ring.

Table 4. Phenyl Ring Torsion Angles (deg)

Cp Carbon	angle
2	33.6
3	50.0
4	77.2
5	19.5

the rotating Pt electrode (RPE) showed that conversion from **2** to **3** was quantitative (Figure 3).

The second reduction of **2** involves irreversibility, in both the electrochemical and chemical senses. The stoichiometry of the second reduction is best established by high overpotential methods such as RPE voltammetry and chronoamperometry. Figure 2 (top) shows that the reduction with $E_{1/2}$ *ca.* -2.2 V is a one-electron process, with a relative plateau current equal to that of the **2/3** couple. The same 1e stoichiometry is implied by chronoamperometry results on solutions of **2**, which show that stepping beyond the second wave gives an $it^{1/2}$ constant ($42.0 \mu A s^{-1/2}$) about double that of the first wave ($19.6 \mu A s^{-1/2}$) for a 5 s pulse.

The one-electron product **4** implied by these results is not stable over the time scale of a bulk electrolysis (*ca.* 20 min). Electrolysis potentials past the second wave ($E_{appl} = -2.6$ V) required 2–3e beyond that required to form **3** and resulted in a partially reversible product wave with $E_{pa} = -0.74$ V, exactly the potential

(22) Pauling, L. *The Nature of the Chemical Bond*, 3rd ed.; Cornell University Press: Ithaca, NY, p 256.

(23) Bruce, M. I.; Rodgers, J. R.; Walton, J. K. *J. Chem. Soc., Chem. Commun.* **1981**, 1253.

(24) Bard, A. J.; Faulkner, L. F. *Electrochemical Methods*; John Wiley and Sons: New York, 1980; pp 218–220.

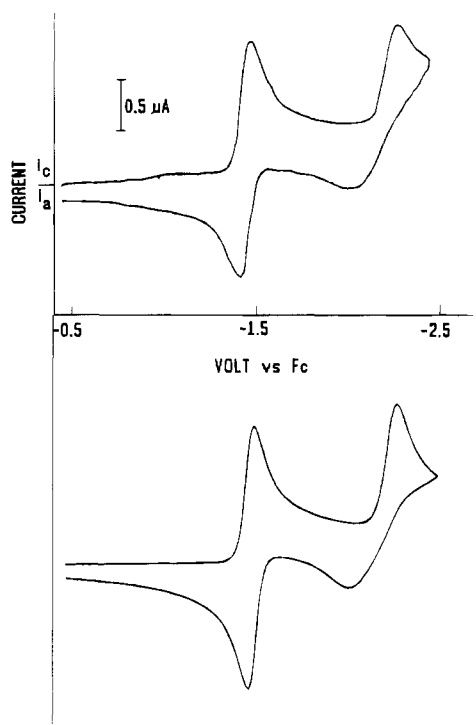


Figure 2. CV traces ($\nu = 0.2$ V/s) of reduction of $(\eta^5\text{-C}_5\text{HPh}_4)_2\text{Rh}^+$: (top, experimental) 0.4 mM solution of $[\text{PF}_6]$ salt in DMF at Pt electrode, $T = \text{ambient}$; (bottom, theoretical) $E_1^\circ = -1.44$ V, $k_{s1} = 3$ cm/s, $\alpha_1 = 0.50$, $E_2^\circ = -2.13$ V, $k_{s2} = 1.0 \times 10^{-3}$ cm/s, $\alpha_2 = 0.68$.

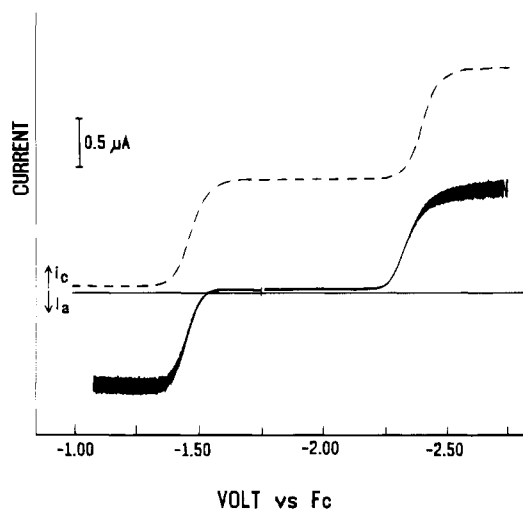
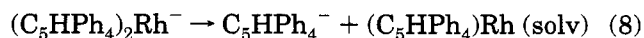
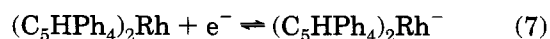
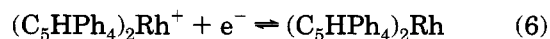


Figure 3. Voltammetry at rotating Pt electrode before (dotted line) and after (solid line) cathodic electrolysis of 0.5 mM solution of $[(\eta^5\text{-C}_5\text{HPh}_4)_2\text{Rh}][\text{PF}_6]$ in THF at $E_{\text{appl}} = -1.7$ V, $T = \text{ambient}$.

measured for a sample of $\text{K}(\text{C}_5\text{HPh}_4)$. Thus it appears that **4** eventually releases at least one of its ligands. The overall electron transfer series involving this rhodocenium analogue can therefore be written as



It is likely that a solvated complex (eq 8) is formed when C_5HPh_4^- splits off, although the counterion might

also coordinate to the metal fragment, especially in $\text{CH}_2\text{-Cl}_2$. The half-sandwich fragment is also electroactive at the E_{appl} of the electrolysis and undergoes reduction by at least one more electron, resulting in higher coulometric counts and most likely the release of the second tetraphenylcyclopentadienyl ligand from the metal.

The anion **4** appears to be stable, however, at room temperature, on the cyclic voltammetry (CV) and chronoamperometry (5 s) time scales. As the following discussion will show, the couple $\mathbf{3} + e^- \rightleftharpoons \mathbf{4}$ is complicated by slow charge transfer kinetics, so that its CV waves may be analyzed as an (electrochemically) irreversible system.

CV scans of **2** yield the following qualitative observations concerning the behavior of the second wave: (1) it has a lower cathodic peak height than the first (ca. 0.8 for i_{p2}/i_{p1}), (2) its (anodic) reverse response is broader than that of the cathodic wave, and (3) the ΔE_p value is greatly increased over the Nernstian value. Further experiments show that the positions of both the cathodic wave and coupled anodic wave are highly dependent on sweep rate, moving to more negative and positive values, respectively, with higher ν . Each of these observations is consistent with a couple that is *chemically reversible* (stable **3** and **4** on the experimental time scale) but *electrochemically irreversible* (slow heterogeneous electron transfer kinetics for $\mathbf{3} + e^- \rightleftharpoons \mathbf{4}$). It should also be noted that the peak separations for this couple, while qualitatively similar, were somewhat electrode (Hg, Au, Pt) and solvent dependent. A typical set of data taken in DMF at Pt and Hg electrodes is discussed below.

Slow charge-transfer (quasi-reversible or irreversible) systems are characterized by the parameters E° , α (transfer coefficient), and k_s (heterogeneous electron-transfer rate at E°).²⁵ Three methods employed for measurement of α gave consistent results with $\alpha = \text{ca. } 0.6$. The breadth of the wave, given by $\delta E_p = E_{p/2} - E_p$ gives α from the relationship $\delta E_p = 48 \text{ mV}/\alpha n$.²⁶ Over the scan rate range of 0.05 to 0.50 V/s, the experimental average of 80 mV for δE_p suggests an α value of 0.60. This value of α predicts a negative shift for E_p of 50 mV ($= 48 \text{ mV}/\alpha n$)²⁶ per 10-fold increase in ν , approximately what is observed for the couple at a Hg electrode.²⁷ Lastly, the cathodic peak height for an irreversible system with $\alpha = 0.6$ should be about 85% of that of a reversible system with the same diffusion coefficient,²⁸ consistent with our observation that the ratio of the second cathodic peak current (extrapolated from the continuation of the first wave) is about 0.80 times the value of the first cathodic peak current.

Some attempts were made at digital simulation of the two waves assuming the stepwise EE mechanism for the reduction of **2**, with the second reduction being much slower than the first. Moderate success was observed matching experiments at slower scan rates, but the data at higher sweep rates (above ca. 2 V/s) could not be fit with the same theoretical parameters, perhaps because of the very unusual shape of the anodic portion of the reverse wave. Figure 2 (bottom) shows a typical low

(25) Reference 24; pp 222–232.

(26) Reference 24; pp 223.

(27) Somewhat larger shifts with ν were observed at Pt electrodes.

(28) Reference 24; pp 225–227.

Table 5. Formal Potentials of Some Rhodocenium Derivatives

compound	couple	solvent	E° vs Fc	reference
[(C ₅ HPh ₄) ₂ Rh] ⁿ	$n = +1/0$	DMF	-1.44 V	this work
	$n = 0/1-$	DMF	-2.19 V ^a	this work
[(C ₅ H ₅) ₂ Rh] ⁿ	$n = +1/0$	CH ₃ CN	-1.81 V	10a
	$n = 0/1-$	CH ₃ CN	-2.58 V	10a
[(C ₅ Me ₅) ₂ Rh] ⁿ	$n = +1/0$	THF	-2.38 V ^c	10b
	$n = 0/1-b$	THF	-3.34 V ^c (irrev)	10b
[(C ₅ H ₅)Rh(C ₅ Me ₅)] ⁿ	$n = +1/0$	THF	-2.07 V ^c	10b
	$n = 0/1-b$	THF	-3.06 V (irrev)	10b
[(C ₅ Me ₅)Rh(C ₉ H ₇)] ⁿ	$n = +1/0$	THF	-1.74 V	10b
	$n = 0/1-b$	THF	-2.44 V	10b

^a Value from CV simulation at Pt electrode. ^b Potential vs Fc obtained by subtracting 0.56 V from quoted potential vs SCE. ^c $n = +1/0$ is only partially chemically reversible, so assignment of second wave to 0/1- is in doubt.

scan rate fit. The best fits at a Pt electrode were obtained with $E^\circ = -2.13$ V vs Fc, $k_s = ca. 10^{-3}$ cm/s, $\alpha = 0.63$ to 0.68.

We cannot rule out the possibility that the second reduction should be treated as an EC mechanism, in which a slow charge transfer is followed by a very fast structural rearrangement. The voltammetry seems to be suggesting that the anion 4 undergoes a significant structural rearrangement compared to 3, as might be expected for a nominally 20e species. Certainly, ring slippage from η^5 to η^4 or η^3 is a possibility.²⁹ If such a distortion occurs, the present data do not allow us to say how much of the structure change occurs during, as opposed to subsequent to, the electron-transfer transition state.

It is of interest to compare the potentials measured for the system 2/3/4 with those reported for the reduction of other rhodocenium-type complexes. These are collected in Table 5. It is perhaps most relevant to compare the separation of the two E° values for reduction of the 18/19e and 19/20e couples. The value of -690 mV measured for $E^\circ_{3/4} - E^\circ_{2/3}$ for the present system is very close to that (-770 mV) measured by Holloway and co-workers, for the parent system, Cp₂Rh^{+0/-} at severely reduced temperatures.^{10a} A similar separation (-700 mV) has been recently reported for reduction of the indenyl derivative (η^5 -C₅Me₅)Rh(η^5 -C₉H₇)⁺ by Gusev and co-workers.^{10b} On the other hand, the much larger separations reported for the reduction of (C₅Me₅)Rh-(C₅R₅) cations (R = H, Me)¹⁶ suggest that the second reduction waves of the latter systems involve a structure other than the 19e radical intermediate, perhaps one with a dimeric structure.

Finally, it is worth noting that the substitution of two tetraphenylcyclopentadienyl units for cyclopentadienyl units shifts the E° values of the Rh sandwich complexes 370 mV more positive, reflecting an appreciable thermodynamic stabilization of the lower oxidation state by the C₅HPh₄ ligand compared to C₅H₅. This value is larger than those (50-200 mV) reported for a number other octaphenylmetallocenes reported earlier.¹³

ESR Spectra. Spectra of (C₅HPh₄)₂Rh in a toluene glass at 77 or 90 K show three features, characteristic of a rhombic g tensor and quite different from the broad, apparently axial, spectrum reported for Cp₂Rh.⁸ Al-

(29) The dangers inherent to invoking structural changes to account for slow heterogeneous charge transfer reactions have been noted by a number of researchers, including one of the authors; see: Geiger, W. E. In *Progress in Inorganic Chemistry*; Lippard, S. J., Ed.; John Wiley and Sons: New York, 1985; Vol 33.

Table 6. ESR Parameters for (C₅HPh₄)₂M

M	T, K	g_x	g_y	g_z	tan α	kV
Rh	77	1.952	2.030	1.771	3.79(4)	0.452(5)
Rh	90	1.958	2.020	1.784	4.08(5)	0.458(5)
Rh	90	1.959	2.021	1.784	4.12(5)	0.462(6)
Rh	90	1.959	2.024	1.771	4.11(5)	0.488(6)
Rh	90	1.955	2.028	1.779	3.90(4)	0.445(5)
Co	77	1.999	2.095	1.884	5.84(14)	0.350(8)
Ni ⁺	77	2.018	2.072	1.884		

though the spectrum was generally reproducible, thawing and refreezing of a sample resulted in slightly different positions of the features. The measured g tensor components for five spectra are given in Table 6. The low-field feature is a singlet at 90 K, but is resolved into a doublet at 77 K ($a^{\text{Rh}} = 26$ G, component widths $ca. 20$ G), but the central and high-field features remain unresolved with widths of $ca. 40$ and 70 G, respectively.

In a d⁷ metallocene with D_{5h} symmetry, d_{xz} and d_{yz} belong to the e_1'' representation and the ground state is degenerate, leading to dynamic Jahn-Teller distortions. In (C₅HPh₄)₂Rh, with at most C_i symmetry, the d_{xz}/d_{yz} degeneracy is lifted, at least in principle, and one of these orbitals is expected to be singly occupied with the other low lying and empty. If the splitting of the d_{xz} - and d_{yz} -based MO's is big enough, we would expect $g_z \ll g_e$ and $g_x, g_y > g_e$.³⁰ Such reasoning gives a good account of the g tensor components in other Rh(II) complexes,³¹ but for (C₅HPh₄)₂Rh, one of the "perpendicular" components is found to be less than g_e . Thus d_{xz} and d_{yz} are apparently nearly degenerate such that vibronic mixing of these orbitals must be taken into account.

Ammeter has described a model to account for the ESR spectra of metallocenes with degenerate or near-degenerate ground states.³² In the model for d⁷ metallocenes, it is assumed that the SOMO is a vibronic admixture of the static MO's with d_{xz} and d_{yz} character

$$|\text{SOMO}\rangle = c'(c_\pi |d_{xy}\rangle - c_\pi' |\phi_{xz}^L\rangle) \chi_{xz} + is'(c_\pi |d_{yz}\rangle - c_\pi' |\phi_{yz}^L\rangle) \chi_{yz} \quad (9)$$

where $|\phi_{xz}^L\rangle$ and $|\phi_{yz}^L\rangle$ are appropriate combinations of ligand orbitals and χ_{xz} and χ_{yz} are relevant vibrational functions. According to this model, the g tensor components are given by³²

$$g_z = g_e - 2kV \cos \alpha \quad (10a)$$

$$g_\perp = 1/2(g_x + g_y) = (g_e + 5x) \sin \alpha \quad (10b)$$

$$g_y - g_x = 6x (1 + V \cos \alpha) \quad (10c)$$

where tan α described the degree of d_{xz}/d_{yz} mixing

$$\tan \alpha = \frac{c'^2 - s'^2}{2c's'} \quad (11)$$

(30) Rieger, P. H. *Organometallic Radical Processes*; Troglor, W. C., Ed.; Elsevier: Amsterdam, 1990; pp 270-305.

(31) (a) Dunbar, K. R.; Haefner, S. C. *Organometallics* **1992**, *11*, 1431. (b) Haefner, K. R.; Dunbar, K. R.; Bender, C. *J. Am. Chem. Soc.* **1991**, *113*, 9540.

(32) (a) Ammeter, J. H. *J. Magn. Reson.* **1978**, *299*. (b) Rajasekharan, M. V.; Giezynski, S.; Ammeter, J. H.; Oswald, N.; Michaud, P.; Hamon, J. R.; Astruc, D. *J. Am. Chem. Soc.* **1982**, *104*, 2400. (c) Zoller, L.; Moser, E.; Ammeter, J. H. *J. Phys. Chem.* **1986**, *90*, 6632.

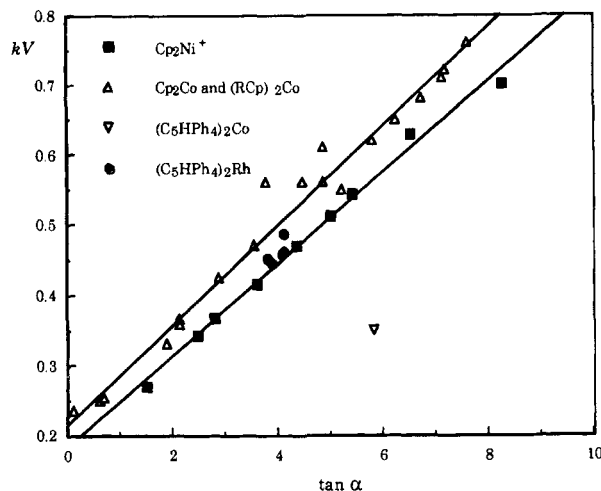


Figure 4. Correlation of total reduction factor kV with increasing "orthorhombicity" $\tan \alpha$ for d^7 metallocenes, after Ammeter.³²

V is the vibrational overlap integral

$$V = \langle \chi_{xz} | \chi_{yz} \rangle \quad (12)$$

x is proportional to $\zeta/\Delta E$ where ζ is the spin-orbital coupling parameter and ΔE is an average one-electron excitation energy, and k is the orbital angular momentum reduction factor resulting from delocalization of spin into ligand orbitals

$$k = 1 - c'^2_{\pi} (1 - \langle \phi_{xz}^L | \mathbf{l}_z | \phi_{yz}^L \rangle) \quad (13)$$

Ammeter finds $k = 0.85$ for the first-row metallocenes. If we assume $k = 0.85 \pm 0.10$ for octaphenylrhodocene and that the g tensor components are accurate to ± 0.001 , we obtain the values of $\tan \alpha$ and kV listed in Table 6.

A plot of kV vs $\tan \alpha$, after Ammeter,^{32a} is shown in Figure 4. The plot includes data for Cp_2Co and $(\text{RCp})_2\text{Co}$, $\text{R} = \text{Me}, \text{Et}, \text{Bu}^t$, in a variety of host lattices, and Cp_2Ni^+ in nine cobalticinium salt lattices; good linear correlations of kV with $\tan \alpha$ are obtained. The variation in these parameters with host lattice was ascribed to lattice-dependent vibronic mixing. The points for $(\text{C}_5\text{HPh}_4)_2\text{Rh}$, plotted on the same graph, lie very close to the cobaltocene correlation line, suggesting (i) that the electronic structure and degree of vibronic mixing are similar for octaphenylrhodocene and cobaltocene and (ii) that toluene glasses contain a variety of solvation sites, the distribution of which depends on the thermal history of the sample, in which various vibrational modes are differentially enhanced or suppressed.

The g tensor components for $(\text{C}_5\text{HPh}_4)_2\text{Co}$ and $[(\text{C}_5\text{HPh}_4)_2\text{Ni}]^+$ from Trogler and co-workers¹³ are also given in Table 6, and values of $\tan \alpha$ and kV are listed for octaphenylcobaltocene. The point corresponding to these values, plotted in Figure 4, is seen to lie far from the correlation line, suggesting that the Ammeter model is a poor approximation for $(\text{C}_5\text{HPh}_4)_2\text{Co}$. The param-

eters for the Ni(III) derivative cannot be fitted to eqs 10; it appears that $\alpha \approx 90^\circ$, implying a large static splitting and negligible vibronic mixing of the d_{xz} - and d_{yz} -based MO's. Indeed, the g components for $[(\text{C}_5\text{HPh}_4)_2\text{Ni}]^+$ are consistent with the static model discussed above.

For $(\text{C}_5\text{HPh}_4)_2\text{M}$, $\text{M} = \text{Rh}, \text{Co}$, and Ni , the X-ray structures show that the $\text{M}-\text{C}(1)$ distance is significantly shorter than the average of the other $\text{M}-\text{C}$ distances (by 2.3, 3.6, and 4.4% for Rh, Co , and Ni , respectively). This distortion from 5-fold symmetry lifts the d_{xz}/d_{yz} degeneracy. Since the $\text{Ni}-\text{C}$ distances are expected to be shorter in the cation, the relative difference between $\text{Ni}-\text{C}(1)$ and the other $\text{Ni}-\text{C}$ distances is probably even greater. Apparently the d_{xz}/d_{yz} splitting in $[(\text{C}_5\text{HPh}_4)_2\text{Ni}]^+$ is big enough to essentially eliminate vibronic mixing. In the Co(II) complex, the static splitting is apparently significant, but not large enough to completely eliminate vibronic mixing, and in octaphenylrhodocene, the splitting is sufficiently small that the molecule behaves as if it had a degenerate ground state.

Summary. This work describes the synthesis and characterization of $[(\text{C}_5\text{HPh}_4)_2\text{Rh}]\text{PF}_6$ and $(\text{C}_5\text{HPh}_4)_2\text{Rh}$. The compound represents the first isolated rhodocene and only the second isolated lower row, open-shell neutral metallocene. Aside from a high sensitivity to oxidation, it appears to be relatively nonreactive. ESR spectra of $(\text{C}_5\text{HPh}_4)_2\text{Rh}$ in low-temperature glasses display a rhombic g tensor with resolution of Rh hyperfine splitting on one g component. Analysis of the spectral parameters is consistent with a d^7 configuration derived from a nearly degenerate d_{xz}, d_{yz} ground state. Voltammetry and coulometry establish the electron-transfer series $(\text{C}_5\text{HPh}_4)_2\text{Rh}^{1+/0/1-}$ with E° values of -1.44 and -2.19 V vs Fc. The heterogeneous charge-transfer rate of the second reduction is much lower than that of the first.

Acknowledgment. The research at Marshall University was supported by a Cottrell College Science Award of the Research Corporation, the National Science Foundation (Grant NSF CHE-9123178), and the Marshall University Foundation and that at the University of Vermont was supported by the National Science Foundation (Grant NSF CHE-9116332). The NSF provided funds toward the University of Delaware diffractometer. We thank the School of Chemistry, University of Bristol, for their hospitality during a sabbatical leave (A.L.R. and P.H.R.) and Dr. P. L. Timms for assistance with ESR sample preparation. J.E.C. thanks Ashland Oil Corp. for a fellowship. We thank Mr. A. Harvath for translating ref 17b. Aesar/Johnson-Matthey made generous loans of $\text{RhCl}_3 \cdot n\text{H}_2\text{O}$ and $\text{IrCl}_3 \cdot n\text{H}_2\text{O}$.

Supplementary Material Available: Tables of anisotropic displacement coefficients and hydrogen-atom coordinates for $(\text{C}_5\text{HPh}_4)_2\text{Rh}$ (3 pages). Ordering information is given on any current masthead page.

OM940679D

New Ruthenium(IV) Complexes via Oxidative Cp*–Ru Bond Rupture and Methyl Activation in Decamethylruthenocene

Samitha P. Deraniyagala[†] and T. David Westmoreland*

Department of Chemistry, Wesleyan University, Middletown, Connecticut 06459

Received August 8, 1994

The two-phase reaction of decamethylruthenocene (Cp*₂Ru) in toluene with Br₂ in weak aqueous acids (HF or CH₃COOH) led to a mixture of [Cp*₂RuBr]Br₃ ([1]Br₃) and [Cp*(C₅(CH₃)₄(CH₂OH))RuBr]Br₃ ([2]Br₃), as confirmed by ¹H NMR and elemental analysis. Recrystallization of this mixture from acetonitrile/ether at –4 °C gave a mixture of [1]Br and [2]Br. A second crop of crystals also contained salts of the Ru(IV) anions [Cp*₂RuBr₄][–] ([3][–]) and [(C₅(CH₃)₄(CH₂OH))RuBr₄][–] ([4][–]). X-ray crystallographic analysis of a selected crystal confirmed the presence of the salt [1][4]. C₃₀H₄₅Br₅ORu₂ crystallizes in the triclinic space group P1̄ (No. 2), with *a* = 9.598(1) Å, *b* = 12.0786(8) Å, *c* = 14.750(1) Å, α = 88.380°, β = 79.977(8)°, γ = 88.321(7)°, and *Z* = 2. This system exhibits both facile activation of a methyl C–H bond and a novel oxidative cleavage of the Cp*–Ru bond.

Introduction

The pentamethylcyclopentadienyl anion ([C₅(CH₃)₅][–], Cp*[–]) is a common ligand in organometallic chemistry and generally binds to d- and f-block metals strongly.¹ Although cleavage of Cp–M bonds has been documented,² examples of the facile displacement of Cp*[–] are relatively uncommon and such reactions generally involve reductive elimination of HCp* from a metal hydride complex.³ Partial decomplexation of Cp*[–] to form a stable η²-tetramethylfulvene complex of palladium has also been reported.⁴

The Cp*[–] ligand exhibits considerable internal stability and the low reactivities of the ring positions as well as the methyl groups^{5,6} account for its frequent use as a “spectator” ligand. We report herein some novel reactivity of Cp*₂Ru incorporating both facile ring functionalization at one of the methyl groups and Cp*–Ru bond rupture under oxidative conditions. These reactions have resulted in the formation of three new ions, [2]⁺, [3][–], and [4][–], shown in Chart 1.

Experimental Section

General Considerations. All reagents were obtained commercially and used as received. Elemental analyses were

[†] Permanent address: Department of Chemistry, University of Sri Jayawardenepura, Nugegoda, Sri Lanka.

* Abstract published in *Advance ACS Abstracts*, February, 1, 1995.
 (1) (a) King, R. B.; Bisnette, M. B. *J. Organomet. Chem.* **1967**, *8*, 287–297. (b) King, R. B. *Coord. Chem. Rev.* **1976**, *20*, 155–169. (c) Maitlis, P. M. *Acc. Chem. Res.* **1978**, *11*, 301–307. (d) Schumann, H. *Angew. Chem., Int. Ed. Engl.* **1984**, *23*, 474–493. (e) Collman, J. P.; Hegedus, L. S.; Norton, J. R.; Finke, R. G. *Principles and Applications of Organotransition Metal Chemistry*; University Science Books: Mill Valley, CA, 1987; p 167. (f) Poli, R. *Chem. Rev.* **1991**, *91*, 509–551.

(2) O'Connor, J. M.; Casey, C. P. *Chem. Rev.* **1987**, *87*, 307–318 and references therein.

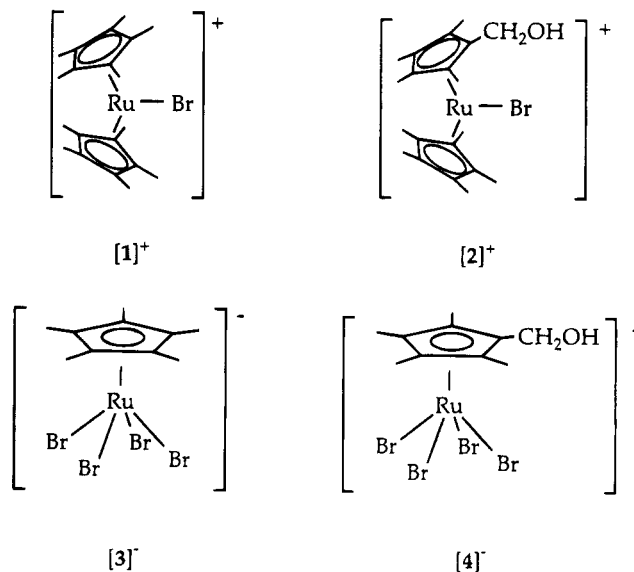
(3) (a) Paneque, M.; Maitlis, P. M. *J. Chem. Soc., Chem. Commun.* **1989**, 105–106. (b) Kubas, G. J.; Kiss, G.; Hoff, C. D. *Organometallics* **1991**, *10*, 2870–2876.

(4) Werner, H.; Crisp, G. T.; Jolly, P. W.; Kraus, H.-J.; Krüger, C. *Organometallics* **1983**, *2*, 1369–1377.

(5) Wei, C.; Aigbirhio, F.; Adams, H.; Bailey, N. A.; Hempstead, P. D.; Maitlis, P. M. *J. Chem. Soc., Chem. Commun.* **1991**, 883–884.

(6) Fan, L.; Turner, M. L.; Hursthouse, M. B.; Malik, K. M. A.; Gusev, O. V.; Maitlis, P. M. *J. Am. Chem. Soc.* **1994**, *116*, 385–386 and references therein.

Chart 1



performed by Atlantic Microlab, Inc. ¹H and ¹³C NMR spectra were obtained in dry CD₃CN on a Varian XL400 spectrometer. Proton chemical shifts were referenced to CHD₂CN (=1.930 ppm), and carbon shifts were referenced to TMS. IR data were obtained using a Perkin-Elmer 1600 FTIR spectrophotometer.

Synthesis. [Cp*₂RuBr]Br₃ ([1]Br₃). A solution of 0.100 g (0.269 mmol) of Cp*₂Ru in 10 mL of toluene was vigorously stirred with a solution of 12 drops of Br₂ (~0.13 g = 0.84 mmol) in 10 mL of 4 M HBr(aq) for 45 min. The aqueous layer was filtered and washed with small portions of water, ethanol, and ethyl ether to give 0.167 g (0.242 mmol) of the green solid [Cp*₂RuBr]Br₃ (90% yield). ¹H NMR spectroscopy (δ 1.82 ppm) agreed with an authentic sample of [1]PF₆.⁷

Oxidation of Cp*₂Ru with Br₂ in HF(aq). A solution of 0.10 g (0.27 mmol) of Cp*₂Ru in 10 mL of toluene was vigorously stirred with a solution of 14 drops of Br₂ (~0.16 g = 0.98 mmol) in 10 mL of 4 M HF(aq) for 45 min. The precipitated green solid (0.14 g) was collected and washed with small portions of water, ethanol, and ether. Spectroscopic

(7) Smith, T. P.; Iverson, D. J.; Droegge, M. W.; Kwan, K. S.; Taube, H. *Inorg. Chem.* **1987**, *26*, 2882–2884.

Table 1. Crystallographic Data for [1][4]

Crystal Parameters			
formula	C ₃₀ H ₄₄ Ru ₂ Br ₅ O	fw	1022.34
space group	P $\bar{1}$ (No. 2)	cryst dimens (mm)	0.27 × 0.20 × 0.15
a, Å	9.598(1)	α , deg	88.380(6)
b, Å	12.0786(8)	β , deg	79.977(8)
c, Å	14.750(1)	γ , deg	88.321(7)
V, Å ³	1682.6(5)	ρ_{calc} , g cm ⁻³	2.018
Z	2	T, °C	23
Intensity Measurements			
radiation	Mo K α	rlins measd	+h, ±k, ±l
max 2 θ , deg	50.0	no. of unique data	5899
Solution and Refinement			
no. of data,	4456	no. of params	343
$F^2 \geq 3\sigma(F^2)$			
R	0.040	R _w	0.049

evidence indicated that the product was a mixture of two complexes, [1]Br₃ and [2]Br₃, as described below. Anal. Found: C, 34.39; H, 4.30; Br, 46.02.

Recrystallization of the crude product was performed by slow diffusion of ethyl ether into an acetonitrile solution at low temperature (−4 °C). Two crops were collected, one at 24 h (~50% mass yield) and another after an additional 48 h (~20% mass yield). The first crop was found by spectroscopic characterization and elemental analysis to consist of a mixture of [1]Br and [2]Br. The characterization of the second crop is described below. A crystal from the second crop, later determined to be [1][4], was selected for crystallographic analysis.

Oxidation of Cp*₂Ru with Br₂ in HA(aq) (A[−] = Cl[−], OAc[−]). In each case the reaction was carried out as described above, using 4 M HOAc or 0.01 M HCl. The precipitated products were collected by filtration and spectroscopically characterized.

X-ray Crystallography. The crystallographic analysis was performed by the Yale University Instrumentation Center. All calculations were performed using the TEXSAN (version 5.0) crystallographic software package developed by Molecular Structure Corporation. The compound C₃₀H₄₄Ru₂Br₅O grew as dark-colored parallelepipeds. A crystal of approximate dimensions 0.27 mm × 0.20 mm × 0.15 mm was mounted in a glass capillary. Diffraction measurements were made on a four-circle Enraf-Nonius CAD4 diffractometer using graphite-monochromated Mo K α radiation ($\lambda = 0.71069$ Å). The cell constants and orientation matrix for data collection, which were obtained from a least-squares refinement using the setting angles of 25 carefully centered reflections, corresponded to a triclinic cell with dimensions given in Table 1. On the basis of packing considerations, a statistical analysis of intensity distribution, and the successful solution and refinement of the structure, the space group was determined to be P $\bar{1}$, (No. 2), Z = 2, with the complex [1][4] forming the asymmetric unit.

There were 5899 unique reflections collected with $2\theta \leq 50^\circ$, 4456 of which had $I \geq 3\sigma(I)$. The data were corrected for Lorentz and polarization effects. An empirical absorption correction was applied, which resulted in transmission factors ranging from 0.82 to 1.10.

The structure was solved using direct methods by locating all non-hydrogen atoms from the difference Fourier. The hydrogens were calculated and assigned isotropic thermal parameters which were 20% greater than the equivalent value of the atom to which they were bonded. The final cycle of full-matrix least-squares anisotropic refinement was based on the 4456 observed reflections with $I \geq 3\sigma(I)$ and 343 variable parameters. There was one large peak left in the final difference Fourier map about 1 Å away from Br(4). The maximum and minimum peaks on the final difference Fourier map corresponded to +1.17 and −0.93 e, respectively. Complete tables of fractional coordinates, bond distances, bond and torsional angles, and anisotropic temperature factors are given in the supplementary material.

Results and Discussion

When Cp*₂Ru in toluene is stirred vigorously with a solution of Br₂ in 4 M aqueous HBr, the green ruthenium(IV) complex [Cp*₂RuBr]Br₃ is formed in high yield. It was suspected that a similar route might be used to obtain [Cp*₂RuF]⁺ salts. When Cp*₂Ru in toluene was treated with Br₂ in 4 M HF(aq), a green solid was isolated. The green solid contained the two components 1[Br₃] and 2[Br₃] in an approximately 2:3 ratio, on the basis of spectroscopic evidence, elemental analysis, and the further reactivity described below.

A solution of the green solid in CD₃CN gave a ¹H NMR resonance at 1.82 ppm for the cation [1]⁺. Cation [2]⁺ gave peaks at 1.84 (C₅(CH₃)₅), 2.00 and 1.79 (C₅(CH₃)₄CH₂OH), 4.01 (C₅(CH₃)₄CH₂OH), and 2.26 ppm⁸ (C₅(CH₃)₄CH₂OH), with the expected relative intensities. These values are shifted from, but comparable to, those reported for the neutral complex Cp*(C₅(CH₃)₄(CH₂OH))Ru.⁹ The proton-decoupled ¹³C NMR spectrum was also consistent with these assignments. ¹³C chemical shifts (ppm relative to TMS) were as follows: 11.13, (C₅(CH₃)₅)₂RuBr⁺; 10.98, (C₅(CH₃)₅)-(C₅(CH₃)₄(CH₂OH))RuBr⁺; 11.65 and 10.13, Cp*(C₅(CH₃)₄(CH₂OH))RuBr⁺; 24.93, Cp*(C₅(CH₃)₄(CH₂OH))-RuBr⁺; 111.11, 107.72, 106.48, and 105.39, quaternary carbons. The assignment of the methylene carbon was confirmed from the ¹H-coupled spectrum, which gave J_{CH} = 159 Hz. Elemental analysis gave good agreement for a mixture of [1]Br₃ and [2]Br₃ in proportions determined by the NMR integrations.¹⁰ The solid mixture is moderately stable in the solid state or in CH₃CN or CH₂Cl₂ solutions.

Separation of [1]⁺ and [2]⁺ was attempted by fractional recrystallization employing slow diffusion of ether into an acetonitrile solution of the green solid at −4 °C. The first (major) crop of crystals obtained after 24 h was found to consist of an intimate mixture of [1]Br and [2]Br. An additional crop of crystals was obtained from the filtrate after 2 days more at −4 °C. X-ray diffraction studies of a selected crystal from the second crop confirmed the presence of an unusual new complex salt, [Cp*₂RuBr][(C₅(CH₃)₄CH₂OH)RuBr₄]. Structural data are given in Figure 1. The overall structural features of the cation, [1]⁺, are similar to those of the related [Cp₂Ru]⁺ cation.¹¹ In each case the C₅R₅ rings are bent back from the coordinated halogen and are eclipsed. The anion, [(C₅(CH₃)₄CH₂OH)RuBr₄][−] ([4][−]), is unusual since relatively few complexes of Ru(IV) containing only one cyclopentadienyl ring or a derivative have been reported.^{5,12} Although most of the structural parameters of the anion are unremarkable, the crystallographic confirmation of the hydroxymethyl group proved problematic. The crystallographically determined C–O bond distance is 1.66 Å, much longer than expected for a carbon–oxygen single bond. On the other hand, the C(32)–C(37)–O angle is 119°, implying an

(8) The chemical shift of the hydroxyl proton varied somewhat, depending on the water content of the solvent. The reported value is for the driest conditions obtained.

(9) (a) Kölle, U.; Grub, J. *J. Organomet. Chem.* **1985**, *289*, 133–139. (b) Kreindlin, A. Z.; Petrovskii, P. V.; Rybinskaya, M. I.; Yanovshii, A. I.; Struchkov, Y. T. *J. Organomet. Chem.* **1987**, *319*, 229–237.

(10) Anal. Found: C, 34.39; H, 4.30; Br, 46.02. Calcd on the basis of a 2:3 ratio of [1]Br₃ (C₂₀H₃₀Br₄Ru) to [2]Br₃ (C₂₀H₃₀Br₄ORu): C, 34.29; H, 4.32; Br, 45.62.

(11) Sohn, Y. S.; Schlueter, A. W.; Hendrickson, D. N.; Gray, H. B. *Inorg. Chem.* **1974**, *13*, 301–304.

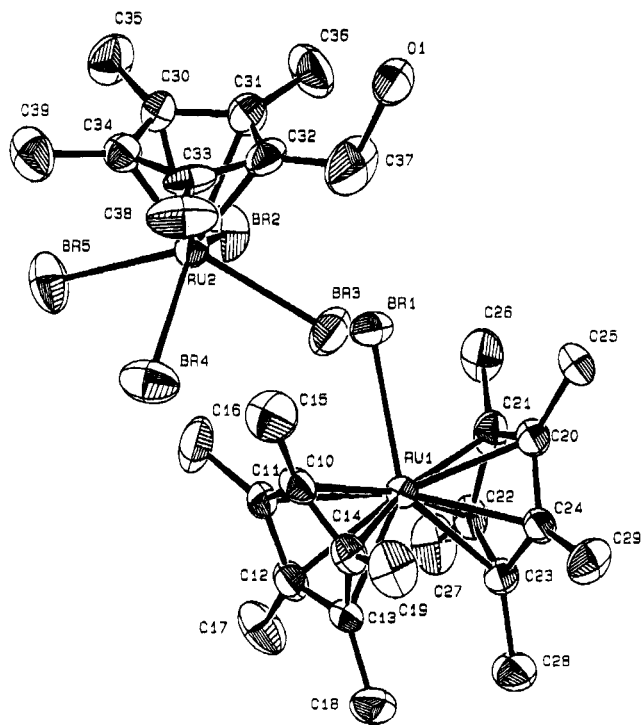


Figure 1. ORTEP plot of the complex salt [1][4]. Hydrogens have been omitted. Selected bond lengths (Å) for [1]⁺: Ru(1)–Br(1) = 2.5479(9); average Ru(1)–C(ring) = 2.26(2); average adjacent C(ring)–C(ring) = 1.42(2); average C(ring)–C(methyl) = 1.50(1). Selected bond lengths (Å) and angles (deg) for [4][−]: Ru(2)–Br(2) = 2.5493(9); Ru(2)–Br(3) = 2.5480(9); Ru(2)–Br(4) = 2.550(1); Ru(2)–Br(5) = 2.5454(9); average Ru(2)–C(ring) = 2.26(7); average adjacent C(ring)–C(ring) = 1.42(1); average C(ring)–C(methyl) = 1.50(1); C(32)–C(37) = 1.50(1); C(37)–O(1) = 1.66(1); C(32)–C(37)–O(1) = 119(7); average Br–Ru(2)–Br = 80.0(7).

sp²-hybridized aldehydic C(37) with a carbonyl oxygen. No carbonyl stretch was present in the IR spectrum of the complex, however. These structural features also cannot be reconciled with the NMR data, which support the formulation given above.

The ¹H NMR of the second crop of crystals revealed the presence of new resonances in addition to those of [1]⁺, including evidence for small amounts of [2]⁺ and for [3][−] (1.47 ppm) in the precipitated solid. Other new resonances could be assigned to the methylene (4.67, 2H), hydroxyl (2.11, 1H), and methyl (1.41, 6H; 1.70, 6H) protons of [4][−]. The assignment of the hydroxyl proton was further confirmed by shaking a solution of the compound with D₂O. The OH resonance was

considerably reduced in magnitude and shifted under the DOH resonance. Integration of the NMR spectra gave mole ratios (relative to [1]⁺) of 0.25 for [3][−] and 0.05 for [4][−].

The strength of the spectroscopic evidence and the highly unusual structural parameters suggest that there are artifacts in the crystallographic data and the identity of the complex is, in fact, as indicated. The most probable origin of the unusual structural parameters would seem to be crystallographic disorder due to cocrystallization of a small amount of an analogous anion with bromine substituted for the hydroxyl group. The use of such a model, however, does not improve the structure solution, nor is there independent spectroscopic evidence for a significant amount of such an anion.

The oxidation of the Cp* methyl group to give [2]⁺ and [4][−] is remarkably facile under these conditions. It is interesting to note that cation [2]⁺ only forms in the presence of relatively weak acids, e.g., aqueous HF or HOOCCH₃. When the oxidation was carried out in HBr, [1]⁺ was formed exclusively. In 0.01 M HCl only small quantities (10–15%) of [2]⁺ were formed. The most reasonable mechanistic possibility for activation of the methyl group is through an intermediate tetramethylfulvene complex⁵ generated by deprotonation of the oxidized complex. The incorporated oxygen atom would then originate from water. No such intermediate has been identified, however, under the conditions used to generate [2]⁺.

The most unusual feature of the chemical transformations described above is the rupture of the Cp*–Ru bond to form the [3][−] and [4][−] anions. Few previous examples of oxidative cleavage of Cp–M bonds are known.¹³ Cp ring loss has also been observed for ruthenocene under similar conditions, but the products have not yet been identified.¹⁴ The ultimate fate of the displaced Cp*[−] is not clear at this point. NMR and mass spectra of the mother liquor from the recrystallization are complex but are consistent with the presence of a variety of brominated Cp* derivatives. The oxidative cleavage of the Cp*–Ru bond by Br₂ represents a new reactivity pathway for Cp*M complexes.

Acknowledgment. The donors of The Petroleum Research Fund, administered by the American Chemical Society, are gratefully acknowledged for partial support of this research.

Supplementary Material Available: Text giving details of the crystallographic analysis of [1][4] and tables of fractional atomic coordinates, complete intramolecular bond distances, bond angles, torsional angles, and anisotropic thermal parameters (22 pages). Ordering information is given on any current masthead page.

OM9406308

(13) (a) Gorsich, R. D. *J. Am. Chem. Soc.* **1960**, *82*, 4211–4214. (b) Ryan, O. B.; Tilst, M.; Parker, V. D. *Organometallics* **1991**, *10*, 298–304.

(14) Deraniyagala, S. P.; Westmoreland, T. D., unpublished results.

(12) (a) Nowell, I. W.; Tabatabaian, K.; White, C. *J. Chem. Soc., Chem. Commun.* **1979**, 547–548. (b) Oshima, N.; Suzuki, H.; Morooka, Y.; Nagashima, H.; Itoh, K. *J. Organomet. Chem.* **1986**, *314*, C46–C48. (c) Bruce, M. I.; Tomkins, I. B.; Wong, F. S.; Skelton, B. W.; White, A. H. *J. Chem. Soc., Dalton Trans.* **1982**, 687–692. (d) Manzano, B. R.; Jalon, F. A.; Lahoz, F. J.; Chaudret, B.; de Montauzon, D. *J. Chem. Soc., Dalton Trans.* **1992**, 977–979. (e) Rao, K. M.; Day, C. L.; Jacobson, R. A.; Angelici, R. J. *Organometallics* **1992**, *11*, 2303–2304. (f) Ditchfield, R.; Hughes, R. P.; Tucker, D. S.; Bierwagen, E. P.; Robbins, J.; Robinson, D. J.; Zakutansky, J. A. *Organometallics* **1993**, *12*, 2258–2267.

Characterization and Thermolysis Reactions of CO₂-Bridged Iron–Tin and Rhenium–Tin Complexes. Structure–Reactivity Correlations

Dorothy H. Gibson,* Ming Ye, Bradley A. Sleadd, Jayesh M. Mehta, Okey P. Mbadike, John F. Richardson, and Mark S. Mashuta

Department of Chemistry, University of Louisville, Louisville, Kentucky 40292

Received September 20, 1994[⊗]

The synthesis, characterization, and thermolysis reactions of the CO₂-bridged iron–tin complexes CpFe(CO)(PPh₃)(CO₂)SnR₃ (**1a–c**; R = Ph, Me, *n*-Bu), Cp*Fe(CO)₂(CO₂)SnR₃ (**2a–c**; R = Ph, Me, *n*-Bu), Cp*Fe(CO)(PPh₃)(CO₂)SnPh₃ (**4a**), and CpFe(CO)₂(CO₂)SnPh₃ (**5a**) and the rhenium–tin complexes Cp*Re(CO)(NO)(CO₂)SnR₃ (**3a,b**; R = Ph, Me) are described. Four of the compounds have been structurally characterized. Crystal data for **1b**: *a* = 10.574(3) Å, *b* = 13.329(8) Å, *c* = 23.346(9) Å, β = 94.71(4)°, with *Z* = 4 in space group *P*2₁/*c*. Crystal data for **1c**: *a* = 13.695(10) Å, *b* = 14.251(9) Å, *c* = 10.475(5) Å, α = 90.99(5)°, β = 90.04(5)°, γ = 83.05(5); with *Z* = 2 in space group *P*1̄. Crystal data for **2a**: *a* = 12.318(3) Å, *b* = 11.907(4) Å, *c* = 19.399(4) Å, β = 100.81(2)°, with *Z* = 4 in space group *P*2₁/*c*. Crystal data for **3b**: *a* = 11.072(2) Å, *b* = 15.403(7) Å, *c* = 7.108(2) Å, α = 92.91(3)°, β = 106.91(2)°, γ = 89.58(3)°, with *Z* = 2 in space group *P*1. All compounds have been characterized by solid-state IR spectral methods which allow a determination of the μ₂-η² or μ₂-η³ bonding mode in each compound when compared with structural data on representative compounds of each type. Factors which control the ease of thermolysis and the mode of decomposition are the bonding type, the presence of electron-donating or electron-withdrawing groups on the tin atom as well as those on iron or rhenium, metal–carbon bond strength, the orientation of the bridging CO₂ ligand between the two metal centers, and, most importantly, the stability of the corresponding metal (iron or rhenium) anion. Simple decarboxylation takes place with **2a–c**, **3b**, and **5a**; disproportionation takes place with **1a–c** and **4a**. Extensive degradation occurs with **3a**. Reaction mechanisms are proposed which are consistent with structural and electronic differences that lead to separate thermolysis paths.

Introduction

Bimetallic complexes with bridging CO₂ ligands are of interest as models for intermediates in catalytic conversions of carbon dioxide.¹ Such compounds exhibit three types of bonding of the CO₂ ligand: μ₂-η², in which the carboxyl carbon and one oxygen are bound to different metal centers,² and two types of μ₂-η³ bonding, in which the carboxyl carbon is bound to one metal and both oxygens are bound to the second metal center. In the μ₂-η³ complexes, symmetrical bonding (C–O and O–M) is found for compounds having two late transition metals,³ whereas unsymmetrical bonding, particularly with the O–M bonds, has been found for complexes having the oxygens bonded to a main-group metal^{3b,4} (Sn) or to an early transition metal (Ti).⁵ The few tin complexes which have been structurally characterized

previously have five-coordinate tin atoms with distorted trigonal-bipyramidal geometry. Many related structures, bearing chelated organic carboxylates, have been characterized by X-ray crystallography. Some of the latter have six-coordinate, octahedral tin atoms, but both five-coordinate and six-coordinate compounds show unsymmetrical bonding of the carboxylate oxygens to the tin atoms.⁶

Gladysz et al.^{4a} were the first to report the structural characterization of a μ₂-η³ CO₂-bridged complex having tin bound to the two carboxyl oxygen atoms. The complex, CpRe(NO)(PPh₃)(CO₂)SnPh₃ (Cp = η⁵-C₅H₅), extruded CO₂ cleanly upon thermolysis at high temperature. This group also found that the analogous PbPh₃ complex, thought to have μ₂-η³ coordination of the carboxyl ligand on the basis of IR spectral comparisons with the previous compound, lost CO₂ at room temperature. We later prepared CpFe(CO)(PPh₃)(CO₂)SnPh₃,⁷ characterized it by X-ray crystallography,^{4b} and found that it degraded upon prolonged heating at

[⊗] Abstract published in *Advance ACS Abstracts*, January 15, 1995.

(1) (a) Fachinetti, G.; Floriani, C.; Zanazzi, P. F. *J. Am. Chem. Soc.* **1978**, *100*, 7405. (b) Gambarotta, S.; Arena, F.; Floriani, C.; Zanazzi, P. F. *J. Am. Chem. Soc.* **1982**, *104*, 5082.

(2) (a) Audett, J. D.; Collins, T. J.; Santarsiero, B. D.; Spies, G. H. *J. Am. Chem. Soc.* **1982**, *104*, 7352. (b) Gibson, D. H.; Ye, M.; Richardson, J. F. *J. Am. Chem. Soc.* **1992**, *114*, 9716. (c) Field, J. S.; Haines, R. J.; Sundermeyer, J.; Woolam, S. F. *J. Chem. Soc., Dalton Trans.* **1993**, 784. (d) Szalda, D.; Chou, M. H.; Fujita, E.; Creutz, C. *Inorg. Chem.* **1992**, *31*, 4712. (e) Yang, Y.-L.; Chen, J.-D.; Lin, Y.-C.; Cheng, M.-C.; Wang, Y. *J. Organomet. Chem.* **1994**, *467*, C6.

(3) (a) Pilato, R. S.; Housmekerides, C. E.; Jernakoff, P.; Rubin, D.; Geoffroy, G. L.; Rheingold, A. L. *Organometallics* **1990**, *9*, 2333. (b) Gibson, D. H.; Mehta, J. M.; Ye, M.; Richardson, J. F.; Mashuta, M. S. *Organometallics* **1994**, *13*, 1070. (c) Gibson, D. H.; Ye, M.; Richardson, J. F.; Mashuta, M. S. *Organometallics* **1994**, *13*, 4559.

(4) (a) Senn, D. R.; Gladysz, J. A.; Emerson, K.; Larsen, R. D. *Inorg. Chem.* **1987**, *26*, 2737. (b) Gibson, D. H.; Richardson, J. F.; Ong, T.-S. *Acta Crystallogr.* **1991**, *C47*, 259. (c) Gibson, D. H.; Richardson, J. F.; Mbadike, O. P. *Acta Crystallogr.* **1993**, *B49*, 784.

(5) Housmekerides, C. E.; Ramage, D. L.; Kretz, C. M.; Shontz, J.; Pilato, R. S.; Geoffroy, G. L.; Rheingold, A. L.; Haggerty, B. S. *Inorg. Chem.* **1992**, *31*, 4453.

(6) For a recent review of the structural chemistry of organotin carboxylates, see: Tiekink, E. R. T. *Appl. Organomet. Chem.* **1991**, *5*, 1.

(7) Gibson, D. H.; Ong, T.-S.; Ye, M. *Organometallics* **1991**, *10*, 1811.

Table 1. ¹³C NMR Chemical Shifts for Carbonyl and Carboxylate Ligands in the Tin Complexes (Multiplicity, *J_{PC}* in Hz)

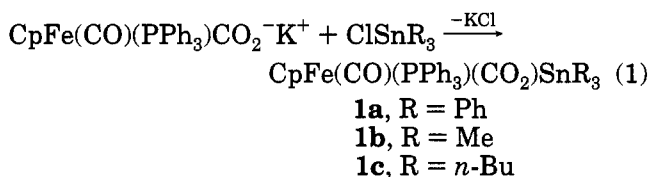
compd	data in CDCl ₃		data in THF- <i>d</i> ₈	
	CO ₂	CO	CO ₂	CO
CpFe(CO)(PPh ₃)(CO ₂)SnPh ₃ (1a)	226.78 (d, 28.4)	219.08 (d, 30.0)	228.16 (d, 31.5)	220.11 (d, 29.4)
CpFe(CO)(PPh ₃)(CO ₂)SnMe ₃ (1b)	219.63 (d, 30.2)	222.05 (d, 32.0)	220.42 (d, 32.5)	220.67 (d, 30.2)
CpFe(CO)(PPh ₃)(CO ₂)Sn(<i>n</i> -Bu) ₃ (1c)	219.56 (d, 30.9)	219.96 (d, 30.6)	220.29 (d, 31.4)	220.63 (d, 30.2)
Cp*Fe(CO) ₂ (CO ₂)SnPh ₃ (2a)	217.74 (s)	215.10 (s)	218.35 (s)	216.27 (s)
Cp*Fe(CO) ₂ (CO ₂)SnMe ₃ (2b)	214.55 (s)	215.72 (s)	209.57 (s)	217.40 (s)
Cp*Fe(CO) ₂ (CO ₂)Sn(<i>n</i> -Bu) ₃ (2c)	213.09 (s)	215.62 (s)	209.80 (s)	217.29 (s)
Cp*Re(CO)(NO)(CO ₂)SnPh ₃ (3a)	200.37 (s)	206.43 (s)	201.01 (s)	207.91 (s)
Cp*Re(CO)(NO)(CO ₂)SnMe ₃ (3b)	197.58 (s)	207.85 (s)	196.10 (s)	210.08 (s)
Cp*Fe(CO)(PPh ₃)(CO ₂)SnPh ₃ (4a)	232.01 (d, 28.2)	221.52 (d, 27.0)	233.36 (d, 28.4)	222.40 (d, 27.0)
CpFe(CO) ₂ (CO ₂)SnPh ₃ (5a)	209.85 (s)	213.32 (s)	210.69 (s)	214.89 (s)

moderate temperatures. While the present work was in progress, Cutler and Pinkes⁸ reported that a different iron–tin complex, Cp*Fe(CO)₂(CO₂)SnMe₃ (Cp* = η⁵-C₅Me₅), which was thought to have a μ₂-η²-coordinated carboxyl group on the basis of IR data, would lose CO₂ at room temperature. The SnPh₃ analog, which appeared to have μ₂-η³ coordination of the bridging CO₂ ligand, was stable at room temperature. Differences in the two bonding types were proposed to account for differences in stability.

Recently we have reported results which indicate a correlation between the orientation of the bridging CO₂ ligand in μ₂-η³ iron–rhenium complexes and their behavior upon thermolysis.^{3c} We report here our studies of the thermolysis behavior of iron–tin complexes and related rhenium–tin complexes and new structural data which allow further correlations to be made between thermolysis activity and bonding parameters involving the CO₂ ligand.

Results and Discussion

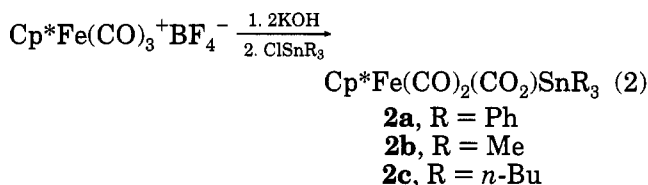
Synthesis and ¹³C NMR Spectral Characterization of the CO₂-Bridged Complexes. The first series of compounds CpFe(CO)(PPh₃)(CO₂)SnR₃ (**1a**, R = Ph; **1b**, R = Me; **1c**, R = *n*-Bu) were synthesized by reactions between the corresponding metalcarboxylate anion and R₃SnCl as shown in eq 1; the preparation of **1a** has been described previously.⁷ All were obtained as crys-



talline solids and have been characterized by elemental analyses and spectral data. The ¹³C NMR spectral characteristics of the products are tabulated in Table 1 and are helpful in characterizing the compounds. Both the terminal carbonyl carbon and the carboxyl carbon appear as low-field doublets. In the case of **1a**, the carboxyl carbon resonance (in THF) has been assigned to the lower field doublet, at 228.16 ppm, because the chemical shift of the terminal carbonyl ligand in related model iron complexes typically appears at 219.6 ± 0.5 ppm. On the basis of comparisons with these model compounds, and for other reasons discussed below in the IR section, the higher field doublet is tentatively assigned to the carboxyl carbon in compounds **1b,c**,

although the closeness of the doublets makes this assignment less certain.

The second series of complexes, Cp*Fe(CO)₂(CO₂)SnR₃ (**2a**, R = Ph; **2b**, R = Me; **2c**, R = *n*-Bu), were prepared by generating the metalcarboxylate anion *in situ* and allowing it to react with the tin halide as we have done previously for another unstable metalcarboxylate anion;^{4c} the sequence is shown in eq 2.

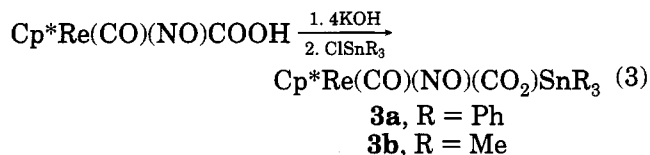


Product yields were high (85–90%). Compounds **2a,b** have been generated previously by a different method.⁸ Although acceptable elemental analysis data was obtained for **2a**, it was not obtained in crystalline form; compound **2b** was obtained only as the major component (60%) of a mixture. By our method, both have been obtained as solids and satisfactory elemental analysis data have been obtained for **2b**. The new compound **2c** is an oil and has been characterized by elemental analysis and spectral data and through its decarboxylation to Cp*Fe(CO)₂Sn(*n*-Bu)₃, which has been synthesized independently and fully characterized. The decarboxylated analogs of **2a,b** were characterized previously; samples of the compounds were prepared for comparison purposes. It is much easier to assign the carboxyl carbon and terminal carbonyl chemical shifts in **2a–c** than in the previous series because the presence of two terminal carbonyls enhances the intensity of these relative to the one carboxyl carbon. Data for the metalcarboxylates are summarized in Table 1. The terminal carbonyls appear at 216.3 ± 1.2 ppm in all of the compounds, but the position of the carboxyl carbon varies with the solvent used as well as with the substituents on the tin atom. Both resonances move upfield in THF, but the carboxyl carbon is affected more in each case. Furthermore, the alkyl tin complexes, **2b,c**, show the largest shifts of the carboxyl carbons in THF. As with **1a**, the carboxyl carbon in the triphenyltin derivative **2a** appears at lower field than the terminal carbonyls. The stability of **2b,c** in solution is also solvent dependent; **2b** is particularly unstable in THF (see discussion below).

The CO₂-bridged rhenium–tin complexes Cp*Re(CO)(NO)(CO₂)SnR₃ (**3a**, R = Ph; **3b**, R = Me) were prepared by reaction between the rhenium metalcarboxylic acid and R₃SnCl in the presence of KOH. Compound **3a** formed in this way was identical with the product we

(8) Pinkes, J. R.; Cutler, A. R. *Inorg. Chem.* **1994**, *33*, 759.

reported previously from a similar method.^{3b} The procedures for **3a,b** are illustrated in eq 3. Both com-



pounds were formed in very good yield (88% in both cases) and could be obtained as crystalline solids which were characterized by elemental analysis and spectral data. The ¹³C NMR resonances were assigned on the basis of comparisons with model compounds of the type Cp*Re(CO)(NO)X (X = halogen); terminal carbonyls in the series appear, typically, at 206.5 ± 1.5 ppm. Also, the carboxyl carbon in Cp*Re(CO)(NO)(CO₂)Re(CO)₃(PPh₃) appears as a doublet, while the terminal carbonyl on the Cp*Re side appears as a singlet at 206.37 ppm.^{3b} Thus, in CDCl₃, the carboxyl carbon in **3a** is assigned to the resonance at 200.37 ppm while in **3b** this carbon is assigned to the resonance at 197.58 ppm.

A sample of compound **4a**, Cp*Fe(CO)(PPh₃)(CO₂)SnPh₃, which is structurally related to the two series of iron complexes described above, was available from our previous work.⁷ Its ¹³C NMR spectrum in CDCl₃ showed the terminal carbonyl and carboxyl carbonyl resonances as doublets at δ 221.52 and 232.01, respectively. The lower field doublet was assigned to the carboxyl carbon after comparisons with ¹³C NMR spectra obtained on other compounds with the Cp*Fe(CO)(PPh₃) fragment.

Compound **5a**, CpFe(CO)₂(CO₂)SnPh₃, was obtained from the corresponding metal carbonyl cation by the method described for **2a** above, except that an excess of the cation was needed to ensure conversion of all ClSnPh₃. The compound is thermally labile and could not be obtained except as the predominant component (91%) of a mixture containing CpFe(CO)₂SnPh₃ (5%) and a small amount of the dimer [CpFe(CO)₂]₂ (4%). The ¹³C NMR spectrum of this mixture allows easy assignment of the resonances due to **5a**; in CDCl₃ the carboxyl carbon appears as a singlet at 209.85 ppm and the terminal carbonyls appear as a singlet at 213.32 ppm.

Clearly, the choice of synthetic method is very important for success in isolating and characterizing the CO₂-bridged tin complexes. Although it is certainly desirable to demonstrate that model compounds such as these can be synthesized directly from CO₂, the necessity of using solvents such as THF to stabilize the requisite metal carbonyl anions can be detrimental to the stability of their metallocarboxylate analogs or to CO₂-bridged compounds derived from them. While this is clearly evident with some of the alkyltin complexes, certainly the most dramatic case is that of **5a**, which could not be observed at all by the previous synthetic method.⁸

Structural Characterizations. The solid-state structures of **1a–c** have been established by X-ray crystallography; we have reported the data for **1a** previously.^{4b} The ORTEP diagram for **1b** is shown in Figure 1; the diagram for **1c** is shown in Figure 2. The crystal data for both compounds are in Table 2. Atomic positional parameters for **1b** are given in Table 3, and those for **1c** are in Table 4. Selected bond distances and angles are shown in Tables 5 and 6 for **1b,c**, respec-

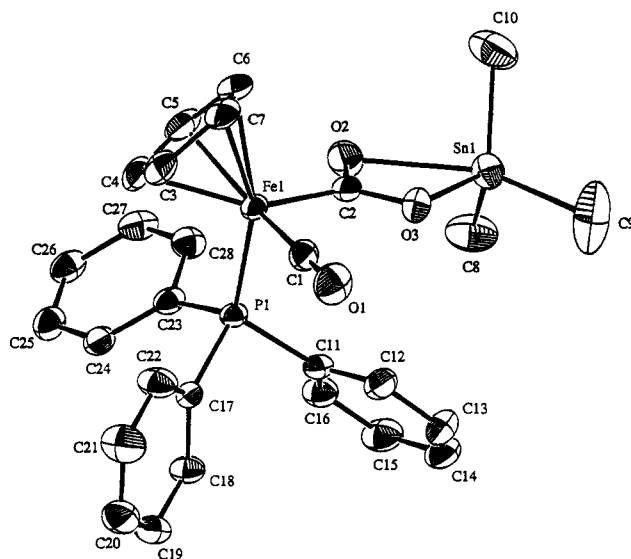


Figure 1. ORTEP drawing of **1b** with thermal ellipsoids shown at the 50% probability level.

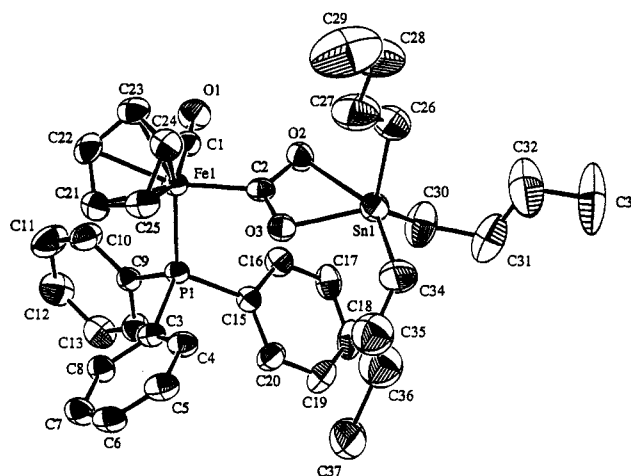


Figure 2. ORTEP drawing of **1c** with thermal ellipsoids shown at the 50% probability level.

tively. All three compounds show $\mu_2\text{-}\eta^3$ bonding of the bridging carboxyl ligand, and all three show unsymmetrical bonding of this group, particularly with regard to the O–Sn bond lengths. Figure 3 shows diagrams for **1a–c** from a different perspective which indicates that the orientation of the carboxyl plane, in all three cases, is approximately coplanar with the Fe–C–O plane. The same orientation of the CO₂ ligand is maintained in the corresponding indenyl iron-tin complex; this complex is the most unsymmetrical of the $\mu_2\text{-}\eta^3$ type iron– or rhenium–tin complexes studied to date.^{4c} In all of these complexes, one O–Sn bond is always axial and this bond is longer than the equatorial one. In **1b** this axial O–Sn bond is up near the Cp ring; in **1a,c** it is away from the Cp ring. Furthermore, methyl derivative **1b** shows the longest axial O–Sn bond in this series; also, this complex exhibits the largest difference between the two O–Sn bond lengths. The most symmetrical complex of this set is **1a**. The carboxyl O–C–O internal angles of **1b,c** are slightly more than 114°, while that of **1a** is smaller by 1°. The iron–carboxyl carbon bond lengths in the compounds are closely similar with an average of 1.934(6) Å.

The structure of **2a** has also been determined by

Table 2. Summary of Crystallographic Data for **1b**, **2a**, and **3b**

	1b	1c	2a	3b
formula	C ₂₈ H ₂₉ O ₃ PFeSn·C ₇ H ₈	C ₃₇ H ₄₇ O ₃ PFeSn·C ₇ H ₈	C ₃₁ H ₃₀ O ₄ FeSn	C ₁₅ H ₂₄ O ₄ NReSn·CHCl ₃
cryst syst	monoclinic	triclinic	monoclinic	triclinic
space group	<i>P</i> 2 ₁ / <i>c</i>	<i>P</i> 1	<i>P</i> 2 ₁ / <i>c</i>	<i>P</i> 1
<i>a</i> , Å	10.574(3)	13.695(10)	12.318(3)	11.072(2)
<i>b</i> , Å	13.329(8)	14.251(9)	11.907(4)	15.403(7)
<i>c</i> , Å	23.346(9)	10.475(5)	19.399(4)	7.108(2)
α , deg		90.99(5)		92.91(3)
β , deg	94.71(4)	90.04(5)	100.81(2)	106.91(2)
γ , deg		83.05(5)		89.58(3)
<i>V</i> , Å ³	3279(2)	2029(2)	2795(1)	1158(6)
<i>Z</i>	4	2	4	2
<i>D_c</i> , g/cm ³	1.44	1.37	1.52	2.03
cryst dimens, mm	0.10 × 0.40 × 0.40	0.10 × 0.35 × 0.37	0.43 × 0.36 × 0.30	0.54 × 0.45 × 0.36
cryst descriptn	orange plate	orange plate	yellow block	orange block
μ (Mo K α), cm ⁻¹	12.84	10.49	14.46	66.66
abs cor	DIFABS	DIFABS	PSI	DIFABS
transmissn factors: min/max	0.883/1.117	0.805/1.245	0.898/1.000	0.792/1.438
radiation (λ , Å)	Mo K α (0.710 93)			
diffractometer	Enraf Nonius CAD4			
monochromator	graphite cryst			
temp, °C	-96(5)	-96(5)	22(1)	-80(5)
scan range	0.75 + 0.35 tan θ	0.85 + 0.35 tan θ	0.75 + 0.35 tan θ	0.80 + 0.35 tan θ
scan speed, deg/min	1–5	1–5	1–5	1–5
max 2 θ , deg	50.0	50.0	50.0	54.0
no. of unique rflns collected	4402	7125	5197	5019
no. of rflns included (<i>I</i> _o > 3 σ (<i>I</i> _o))	3494	6023	4119	4674
no. of params	341	414	425	236
computer hardware	Silicon Graphics IRIS INDIGO			
computer software	teXsan			
ext coeff	could not be refined	could not be refined	2.11 × 10 ⁻⁷	2.01 × 10 ⁻⁷
agreement factors ^a				
<i>R</i>	0.033	0.053	0.022	0.031
<i>R_w</i>	0.034	0.067	0.022	0.031
function minimized	$\sum w(F_o - F_c)^2$			
GOF	1.87	3.65	1.70	2.70
weighting scheme	[$\sigma^2(F_o)$] ⁻¹			
high peak in final diff map, e	0.46	1.01	0.26	1.63

$$^a R = \sum |F_o| - |F_c| / \sum |F_o|; R_w = [\sum w(|F_o| - |F_c|)^2 / \sum w F_o^2]^{1/2}.$$

crystallography; the ORTEP diagram is shown in Figure 4. Crystal data for this compound are also shown in Table 2. Atomic positional parameters for **2a** are given in Table 7, and selected bond distances and bond angles are given in Table 8. Figure 5 shows a view of this compound which is similar to that presented for **1a–c** in Figure 3 and clearly indicates an orientation for the bridging carboxyl group different from that found for **1a–c**; the plane of the carboxyl group in **2a** approximately bisects the C–Fe–C angle between the two terminal carbonyl groups on iron. Also, the axial bond length, O(2)–Sn, in **2a** is nearly 0.3 Å longer than the equatorial one, a greater difference than that seen in **1a**. Furthermore, this axial O–Sn bond is up and next to the Cp* ligand.

Structural data for **3a** have been reported by us previously and clearly indicated $\mu_2\text{-}\eta^3$ coordination of the bridging carboxyl group.^{3b} A view of **3a** comparable to that of **2a** is shown in Figure 5 for comparison. Compound **3a** also shows the “upright” conformation for the carboxyl group. As with **2a**, the axial O–Sn bond length is approximately 0.3 Å longer than the equatorial one, and the longer O–Sn bond is up and near to the Cp* ligand. The structure of **3b** has also been established by X-ray crystallography; the ORTEP diagram is shown in Figure 6. Crystal data for **3b** are shown in Table 2, and atomic positional parameters are given in Table 9. Selected bond distances and bond angles for **3b** are given in Table 10. The carboxyl C–O bonds differ in length by 0.074 Å in this compound as compared to 0.082 Å in **3a**, and the shorter C–O bond in **3b** is only

slightly shorter (0.003 Å) than the one in **3a**. However, compound **3b** has the largest difference in the carboxyl oxygen to tin distances (0.752 Å) of any of the CO₂-bridged compounds which have been structurally characterized and shows distorted-tetrahedral geometry about the tin atom, further indicating no bonding between the tin atom and one of the carboxyl oxygens. Compound **3a** shows carboxyl oxygen to tin distances which differ by approximately 0.3 Å, and both are within normal bonding distances. Furthermore, it exhibits distorted-trigonal-bipyramidal geometry about the tin atom. Also, the carboxyl O–C–O bond angle is larger (117.0(5)° versus 114.6(7)°) in **3b** than that for **3a**. On the basis of these properties, compound **3b** clearly shows $\mu_2\text{-}\eta^2$ coordination of the bridging CO₂ ligand. The diagram of **3b** shown in Figure 5 also indicates that the nonbonded carboxyl oxygen is oriented away from the Cp* ring. Interestingly, there is very little difference in the Re–carboxyl carbon bond lengths in the two compounds (2.100(9) Å in **3a** and 2.103(5) Å in **3b**); in both, this bond is short enough to exhibit substantial carbene character as discussed previously for **3a**.^{3b} The major differences between these two types of CO₂-bridged complexes are in the carboxyl oxygen to tin distances and in the larger internal O–C–O angle for **3b**. These two compounds are distinct from the symmetrical type of $\mu_2\text{-}\eta^3$ CO₂-bridged complex, exemplified by Cp*Re(CO)(NO)(CO₂)Re(CO)₃(PPh₃), which shows nearly equal carboxyl oxygen to rhenium bond distances (0.010 Å difference), nearly equal carboxyl carbon–oxygen bond distances (0.007 Å difference), a shorter

Table 3. Atomic Positional Parameters for 1b

atom	x	y	z	$B_{eq},^a \text{ \AA}^2$
Sn(1)	0.01016(2)	0.18374(2)	-0.17620(1)	2.730(7)
Fe(1)	0.19199(4)	0.14561(3)	0.00983(2)	1.88(1)
P(1)	0.28829(7)	0.29110(6)	0.00394(4)	1.74(2)
O(1)	-0.0312(3)	0.2288(3)	0.0554(2)	3.68(7)
O(2)	0.1977(3)	0.1358(3)	-0.1115(1)	3.27(6)
O(3)	0.0160(2)	0.1885(2)	0.0866(1)	2.46(5)
C(1)	0.0568(3)	0.1986(3)	0.0353(2)	2.37(7)
C(2)	0.1322(3)	0.1576(3)	-0.0705(2)	2.13(7)
C(3)	0.2438(4)	0.0594(3)	0.0850(2)	3.19(8)
C(4)	0.3514(4)	0.0801(3)	0.0554(2)	3.37(9)
C(5)	0.3353(4)	0.0395(3)	-0.0004(2)	3.24(9)
C(6)	0.2153(4)	-0.0078(3)	-0.0061(2)	3.02(8)
C(7)	0.1584(4)	0.0046(3)	0.0460(2)	3.12(8)
C(8)	0.1386(6)	0.2818(4)	-0.2139(2)	4.3(1)
C(9)	-0.1742(6)	0.2520(9)	-0.1890(3)	7.2(2)
C(10)	0.0039(7)	0.0343(5)	-0.2056(2)	5.0(1)
C(11)	0.2224(3)	0.3835(3)	-0.0490(2)	2.12(6)
C(12)	0.0946(4)	0.4085(3)	-0.0491(2)	2.75(8)
C(13)	0.0430(4)	0.4836(3)	-0.0853(2)	3.38(9)
C(14)	0.1187(5)	0.5333(3)	-0.1220(2)	3.72(9)
C(15)	0.2446(5)	0.5085(3)	-0.1226(2)	3.43(9)
C(16)	0.2964(4)	0.4336(3)	-0.0865(2)	2.66(7)
C(17)	0.2969(3)	0.3684(3)	0.0691(2)	1.93(6)
C(18)	0.3337(3)	0.4690(3)	0.0671(2)	2.51(7)
C(19)	0.3417(4)	0.5269(3)	0.1165(2)	2.95(8)
C(20)	0.3114(4)	0.4871(4)	0.1678(2)	3.39(9)
C(21)	0.2733(5)	0.3884(4)	0.1705(2)	3.90(10)
C(22)	0.2670(4)	0.3287(3)	0.1211(2)	3.09(8)
C(23)	0.4540(3)	0.2785(3)	-0.0127(2)	2.14(6)
C(24)	0.5546(3)	0.3151(3)	0.0232(2)	2.42(7)
C(25)	0.6791(3)	0.2964(3)	0.0104(2)	2.85(8)
C(26)	0.7037(3)	0.2417(3)	-0.0372(2)	2.72(7)
C(27)	0.6025(4)	0.2044(3)	-0.0733(2)	2.86(8)
C(28)	0.4787(3)	0.2230(3)	-0.0616(2)	2.63(7)
C(29a)	0.588(1)	0.1095(10)	0.1815(5)	5.6(2)
C(29b)	0.6340	0.1241	0.1777	5.3(4)
C(30a)	0.492(1)	0.1523(9)	0.2101(5)	5.7(2)
C(30b)	0.5464	0.1742	0.2002	6.2(4)
C(31b)	0.4483	0.1291	0.2227	4.3(3)
C(31a)	0.416(1)	0.083(1)	0.2361(6)	6.8(2)
C(32a)	0.421(1)	-0.0206(10)	0.2275(6)	6.0(2)
C(32b)	0.4042	0.0372	0.2355	4.9(3)
C(33a)	0.527(1)	-0.049(1)	0.1934(7)	6.9(2)
C(33b)	0.4758	-0.0269	0.2079	7.2(5)
C(34ab)	0.5992(6)	0.0114(6)	0.1747(3)	5.5(1)
C(35a)	0.662(1)	0.185(1)	0.1562(6)	7.0(2)
C(35b)	0.7252	0.1691	0.1503	7.1(5)

$$^a B_{eq} = \frac{8}{3}\pi^2(U_{11}(aa^*)^2 + U_{22}(bb^*)^2 + U_{33}(cc^*)^2 + 2U_{12}aa^*bb^* \cos\gamma + 2U_{13}aa^*cc^* \cos\beta + 2U_{23}bb^*cc^* \cos\alpha).$$

rhenium-carboxyl carbon bond (2.089(6) Å), and a smaller O-C-O internal angle (113.2(5)°).^{3b} Similar distinctions can be made among **1a** and the two types of CO₂-bridged iron-rhenium complexes which we have characterized structurally.^{2b,3c}

IR Spectral Data. In our previous work we have employed the DRIFTS technique (see Experimental Section) in order to obtain IR spectra of the solid bimetallic CO₂-bridged compounds which would allow us to make direct correlations between these data and X-ray crystallographic data.^{2b,3b,c,7} We have not previously given data obtained from "thin films" as reported recently.⁸ It appeared to us, after examining the DRIFTS data from the three types of CO₂-bridged bimetallic complexes, that each type could be identified by this type of spectra. Band assignments were made only after examining the DRIFTS spectra of related model complexes in each series in order to identify the characteristics of each group in the spectral regions in question. The μ_2 - η^2 complexes of the noncyclic type showed the ν_{asym} and ν_{sym} bands for the CO₂ ligand near 1500 and 1140 cm⁻¹, respectively. The two types of μ_2 -

Table 4. Atomic Positional Parameters for 1c

atom	x	y	z	$B_{eq},^a \text{ \AA}^2$
Sn(1)	0.71227(3)	0.19190(3)	0.41726(4)	3.434(10)
Fe(1)	0.64164(5)	0.50308(5)	0.29869(6)	2.35(2)
P(1)	0.78607(9)	0.49718(9)	0.2059(1)	2.19(3)
O(1)	0.7017(3)	0.5904(3)	0.5323(3)	3.92(10)
O(2)	0.6892(3)	0.3584(3)	0.4800(3)	3.29(9)
O(3)	0.6811(3)	0.3029(3)	0.2872(3)	3.15(8)
C(1)	0.6805(4)	0.5543(4)	0.4386(5)	2.6(1)
C(2)	0.6755(3)	0.3776(4)	0.3637(4)	2.6(1)
C(3)	0.7840(3)	0.4660(4)	0.0347(4)	2.6(1)
C(4)	0.7498(4)	0.3804(4)	0.0002(5)	3.0(1)
C(5)	0.7369(4)	0.3581(4)	-0.1281(5)	3.5(1)
C(6)	0.7567(4)	0.4210(5)	-0.2217(5)	3.8(1)
C(7)	0.7921(4)	0.5040(5)	-0.1883(5)	3.7(1)
C(8)	0.8056(4)	0.5265(4)	-0.0595(5)	3.0(1)
C(9)	0.8422(3)	0.6075(4)	0.2101(4)	2.4(1)
C(10)	0.7877(4)	0.6913(4)	0.2437(6)	4.0(1)
C(11)	0.8304(5)	0.7759(5)	0.2481(7)	5.2(2)
C(12)	0.9284(5)	0.7752(5)	0.2176(6)	4.4(2)
C(13)	0.9838(4)	0.6920(5)	0.1838(6)	3.8(1)
C(14)	0.9414(4)	0.6089(4)	0.1797(5)	3.1(1)
C(15)	0.8893(3)	0.4176(4)	0.2689(4)	2.4(1)
C(16)	0.9114(4)	0.4247(4)	0.3986(5)	3.1(1)
C(17)	0.9939(4)	0.3748(4)	0.4481(5)	3.6(1)
C(18)	1.0554(4)	0.3144(4)	0.3704(6)	4.2(1)
C(19)	1.0329(4)	0.3051(4)	0.2447(6)	4.3(2)
C(20)	0.9510(4)	0.3564(4)	0.1930(5)	3.4(1)
C(21)	0.5700(4)	0.5630(5)	0.1372(5)	3.5(1)
C(22)	0.5355(4)	0.6164(4)	0.2453(6)	3.7(1)
C(23)	0.4926(4)	0.5541(5)	0.3277(5)	3.7(1)
C(24)	0.4993(4)	0.4656(5)	0.2680(5)	3.7(1)
C(25)	0.5481(4)	0.4711(5)	0.1512(5)	3.7(1)
C(26)	0.5841(5)	0.1720(5)	0.5240(6)	5.0(2)
C(27)	0.4918(6)	0.1808(7)	0.4509(8)	7.2(2)
C(28)	0.4034(6)	0.1494(8)	0.5219(9)	8.3(3)
C(29)	0.3193(9)	0.149(1)	0.445(1)	13.3(5)
C(30)	0.8485(5)	0.1882(5)	0.5171(8)	5.5(2)
C(31)	0.8917(6)	0.0903(5)	0.5579(9)	6.5(2)
C(32)	0.8342(8)	0.0476(8)	0.655(1)	9.9(4)
C(33)	0.878(1)	-0.046(1)	0.703(2)	11.2(5)
C(34)	0.7245(6)	0.0818(5)	0.2686(7)	6.1(2)
C(35A)	0.815(2)	0.133(2)	0.153(2)	8.0(5)
C(36A)	0.874(2)	0.110(2)	0.167(2)	7.7(5)
C(37)	0.9245(7)	0.1159(7)	0.012(1)	9.3(3)
C(38A)	0.354(1)	0.184(1)	1.025(1)	8.3(3)
C(39A)	0.416(1)	0.233(1)	1.097(1)	8.4(3)
C(40A)	0.511(1)	0.211(1)	1.054(1)	10.0(4)
C(41A)	0.561(1)	0.149(1)	0.944(2)	11.4(5)
C(42A)	0.496(1)	0.091(1)	0.867(1)	9.9(4)
C(43A)	0.3983(9)	0.1201(9)	0.920(1)	7.4(3)
C(44A)	0.312(2)	0.221(2)	1.110(3)	5.3(6)
C(35B)	0.775(1)	0.092(1)	0.155(2)	7.1(4)
C(36B)	0.847(1)	0.059(1)	0.067(2)	7.3(4)
C(38B)	0.4698	0.1395	0.9583	4.3
C(39B)	0.4862	0.2293	1.0888	4.3
C(40B)	0.5570	0.1933	1.0070	4.3
C(41B)	0.5717	0.1070	0.8854	4.3
C(43B)	0.3598	0.1338	0.9511	4.3
C(44B)	0.2607	0.1925	1.0657	4.3

^a See footnote a in Table 3.

Table 5. Selected Bond Distances (Å) and Bond Angles (deg) for 1b

Bond Distances			
C(2)-O(2)	1.260(6)	Sn-O(2)	2.476(3)
C(2)-O(3)	1.321(5)	Sn-O(3)	2.089(3)
Fe-C(2)	1.936(4)		
Bond Angles			
O(2)-C(2)-O(3)	114.3(3)	O(3)-Sn-C(9)	94.5(2)
O(2)-Sn-O(3)	55.94(9)	O(3)-Sn-C(10)	110.6(2)
Fe-C(2)-O(2)	124.1(3)	O(2)-Sn-C(8)	84.5(2)
Fe-C(2)-O(3)	121.6(3)	O(2)-Sn-C(9)	149.9(2)
O(3)-Sn-C(8)	115.4(2)	O(2)-Sn-C(10)	87.6(2)

η^3 complexes (having either a late transition metal or tin bound to the two oxygens) differed from this and also

Table 6. Selected Bond Distances (Å) and Bond Angles (deg) for **1c**

Bond Distances			
C(2)–O(2)	1.266(7)	Sn–O(2)	2.432(4)
C(2)–O(3)	1.316(7)	Sn–O(3)	2.105(4)
Fe–C(2)	1.934(6)		
Bond Angles			
O(2)–C(2)–O(3)	114.2(5)	O(2)–Sn–C(30)	84.8(2)
O(2)–Sn–O(3)	56.5(1)	O(2)–Sn–C(34)	149.8(3)
Fe–C(2)–O(2)	124.7(4)	O(3)–Sn–C(26)	110.9(3)
Fe–C(2)–O(3)	121.1(4)	O(3)–Sn–C(30)	115.7(2)
O(2)–Sn–C(26)	89.3(2)	O(3)–Sn–C(34)	93.5(3)

from one another. The tin complexes showed the higher frequency band near 1430 cm⁻¹ and the lower frequency band appeared in about the same place as the corresponding one in the $\mu_2\text{-}\eta^2$ compounds, while the compounds with two transition metals show the higher frequency band at about 1435 cm⁻¹ and the lower frequency band at approximately 1260 cm⁻¹. Thus the frequency difference, $\Delta\nu$, as well as the band positions appeared to be diagnostic of the class of compounds to which a particular one belonged.

In order to make direct comparisons, all DRIFTS data in the present work, including those for compounds reported previously, have been obtained from KCl dispersions in the same way, on the same FT-IR instrument and at 1 cm⁻¹ resolution. Thus, small differences in band positions are seen here in comparison to previously reported data; these differences do not change the conclusions summarized above about the spectral characteristics of the three classes of compounds or any structural assignments.

FT-IR spectra of **1a–c** have been obtained by the DRIFTS method (see Table 11), as Nujol mulls and in solution in CHCl₃ and THF. Spectra of model compounds containing the CpFe(CO)(PPh₃) moiety and the spectra of the tin halides were recorded for comparison to the CO₂-bridged compounds. The data for **1a** clearly show that only the $\mu_2\text{-}\eta^3$ form is present under all conditions. The data for **1b,c**, however, revealed that both forms are present in DRIFTS and Nujol mull spectra obtained from solid samples, whereas solution spectra indicate that the $\mu_2\text{-}\eta^2$ form is predominant (if not exclusive). Figure 7 shows the region from 1600 to 1300 cm⁻¹ in the spectra of **1b** obtained by these four methods. Spectrum a (DRIFTS method) indicates the presence of the $\mu_2\text{-}\eta^2$ form (1491 and 1134 cm⁻¹) and the $\mu_2\text{-}\eta^3$ form (1438 or 1433 and 1134 cm⁻¹), as does spectrum b, obtained as a Nujol mull. However, the solution spectra (c and d) indicate the presence of only the $\mu_2\text{-}\eta^2$ form. The spectra clearly show that the carboxyl ν_{asym} band of the $\mu_2\text{-}\eta^2$ form changes position depending upon the method and moves to much higher frequency in THF solution. Also, the band broadens in solution spectra as compared to the spectra obtained from solid samples. The spectra of **1c** show similar changes. It is possible to reconcile these observations with the results of the X-ray structural determinations, which showed only the $\mu_2\text{-}\eta^3$ form, by noting that the solid samples used in the IR analysis were obtained from normal recrystallizations but the single crystals obtained for X-ray analysis were obtained by the slow diffusion method at low temperature and the X-ray data were obtained at very low temperatures. Solution NMR spectra showed evidence for only one form for **1b** or **1c** which, on the basis of IR data obtained in solution, must

be the $\mu_2\text{-}\eta^2$ form. NMR spectra for **1b** were obtained over the temperature range of -50 to +50 °C and showed no evidence for small amounts of a second form or significant changes in chemical shift positions which would indicate averaging.

Full characterization of the second series of compounds by diffuse reflectance is made more difficult by the lability of **2b,c** toward CO₂ loss (see thermolysis section below); some sample degradation occurred because of the necessity of obtaining approximately 100 scans for the DRIFTS spectrum. In all three cases, however, spectra of the corresponding iron–tin complexes were available for comparison. Spectral data for **2b** clearly indicate $\mu_2\text{-}\eta^2$ coordination of the CO₂ ligand. Data for **2c** were obtained by dispersing the oil in KCl and, again, indicate $\mu_2\text{-}\eta^2$ coordination of the CO₂ ligand. DRIFTS spectra of **2a** (Table 11) indicate $\mu_2\text{-}\eta^3$ coordination of the CO₂ ligand as shown by the crystallographic data for the solid-state structure. Note, also, that the carboxyl carbon chemical shift in the ¹³C NMR spectrum of **2a** is substantially lower than those of **2b,c**, as seen for **1a** as compared to **1b,c**. IR band positions obtained from solution spectra of **2a,b** are comparable to those reported by Cutler (see Experimental Section).⁸

DRIFTS spectra of the very stable **3a,b** are also reported in Table 11. The data for **3a** are consistent with $\mu_2\text{-}\eta^3$ coordination of the bridging CO₂, as demonstrated in the solid-state structure;^{3b} spectra obtained by the other methods (see Experimental Section) support the same conclusion. Furthermore, it is clear that **3b** has the $\mu_2\text{-}\eta^2$ type of coordination, since this compound shows a broad, weak band in the 1500 cm⁻¹ region which is absent in the DRIFTS spectrum of its decarboxylation product, Cp*Re(CO)(NO)SnMe₃ (see Experimental Section). Band positions of the ν_{asym} band in **3b** shift slightly, depending upon the spectral method, as discussed above for other compounds of the $\mu_2\text{-}\eta^2$ type.

The DRIFTS spectrum of **4a** shows bands at 1418 and 1140 cm⁻¹, consistent with the assignment of $\mu_2\text{-}\eta^3$ bonding; Nujol mull and solution spectra of **4a** indicate the same form. By comparison of the DRIFTS spectrum of impure **5a** with those obtained from the two impurities, the carboxyl bands can be identified as 1499 and 1159 cm⁻¹. These band positions are indicative of $\mu_2\text{-}\eta^2$ coordination of the bridging CO₂; compound **5a** is thus the only triphenyltin derivative to exhibit this type of bonding of the carboxyl group.

Clearly, the IR spectral data of the CO₂-bridged compounds are not directly comparable unless these data have been obtained by the same method. There are qualitative differences in the IR spectral data obtained by the DRIFTS method and those obtained in solution. The ν_{asym} and ν_{sym} bands for coordinated CO₂ are weak in intensity, and both are broadened in solution spectra as compared to those obtained by the DRIFTS method or in Nujol (see Figure 7 for comparisons in this region of spectral data obtained on **1b**). The position of the higher frequency (ν_{asym}) band, particularly in the complexes having $\mu_2\text{-}\eta^2$ coordination of the CO₂ ligand, varies with the method used for obtaining spectral data. Also, as the data for **1b,c** show, the forms present in solution and in solid samples may differ.

Although comparisons are best made within the same series of compounds, $\Delta\nu$ (the frequency difference between these two characteristic bands) does indicate

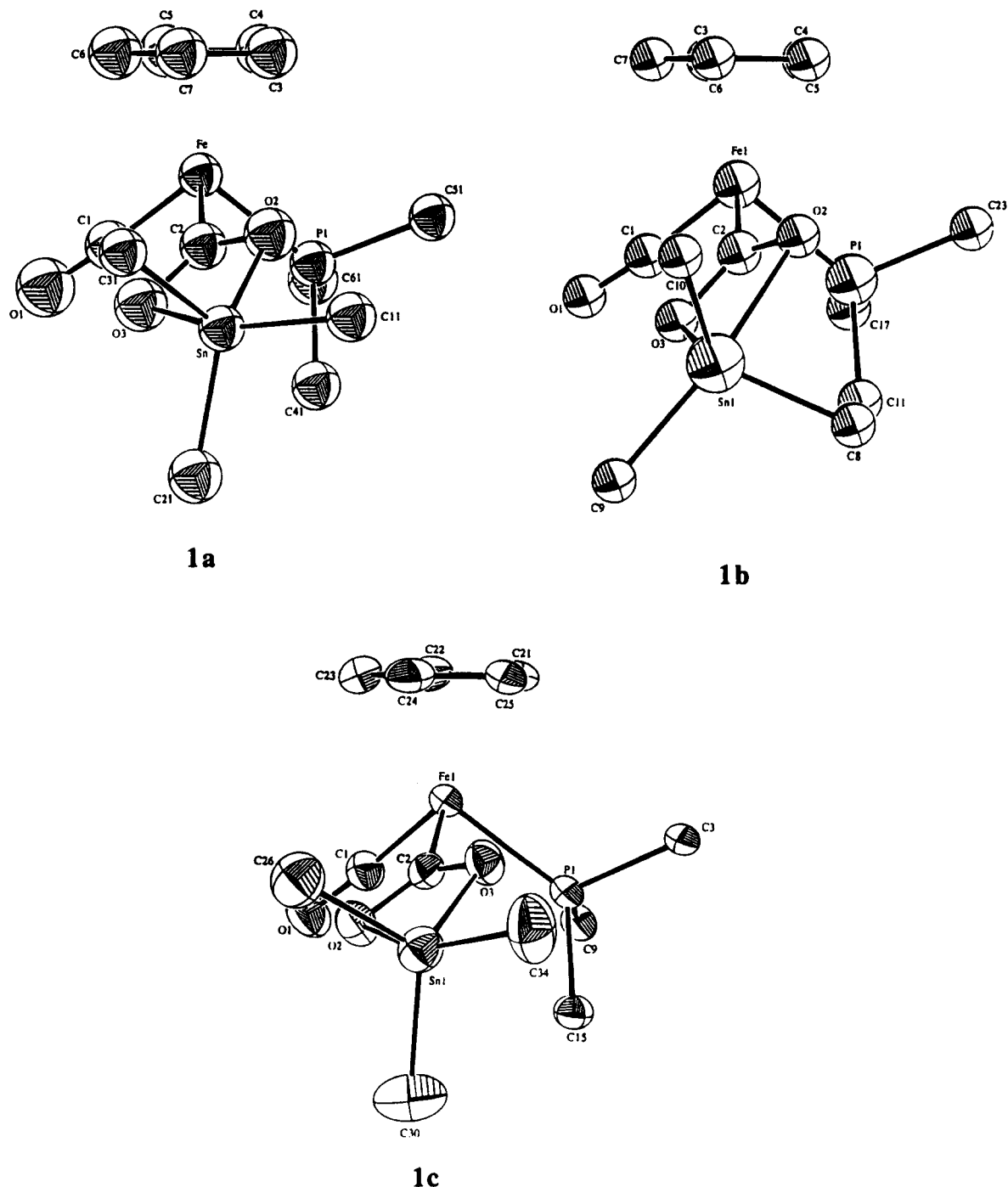


Figure 3. ORTEP diagrams of **1a–c** shown with the tin atoms projecting forward and the plane of the cyclopentadienyl group perpendicular to the plane of the page. The tin and phosphorus atoms are shown with α -bonded atoms only for clarity.

whether a compound exhibits $\mu_2\text{-}\eta^2$ or $\mu_2\text{-}\eta^3$ bonding in the solid state. The first type typically show the ν_{asym} near 1500 cm^{-1} , while those of the second type show this band at lower frequency, in the $1418\text{--}1450\text{ cm}^{-1}$ region. The ν_{sym} band, in both types, appears in the region $1110\text{--}1160\text{ cm}^{-1}$ and sometimes cannot be resolved in the two forms. In some cases, as shown in Table 11, the presence of two bands in the same area (due to different groups) prevents specific assignments. However, in no case would this problem change the assignment of bonding type. Isotopic labeling studies, where the experiments yield pure compounds, are, of course, best for unambiguous assignments of these bands. In the absence of labeling studies, comparisons with the corresponding decarboxylated compounds work

well. Less satisfactory are comparisons with other kinds of model compounds, but a combination of this with IR spectral data obtained by several methods can usually resolve ambiguities.

Thermolysis Reactions and the Relationships between Structure and Decarboxylation Activity.

Efforts to conduct the thermolysis reactions of some of the tin complexes in solution resulted in extensive degradation of the compounds. In order to minimize this problem and to be able to compare the results on all compounds, the thermolysis reactions were done in the solid state.

We reported previously that prolonged heating of **1a** at low temperatures led to extensive degradation.⁷ Higher temperature thermolyses give somewhat better

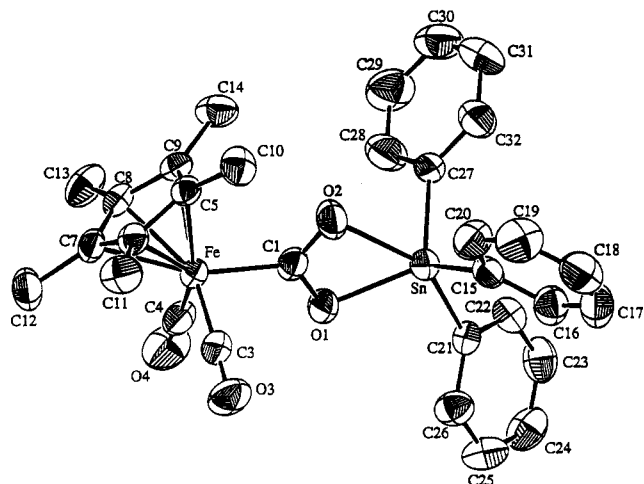


Figure 4. ORTEP drawing of **2a** with thermal ellipsoids shown at the 50% probability level.

Table 7. Atomic Positional Parameters for **2a**

atom	x	y	z	$B_{eq},^a \text{Å}^2$
Sn	0.22244(1)	0.02579(2)	0.119464(9)	3.196(8)
Fe	0.50297(3)	0.04329(3)	0.31348(2)	2.661(8)
O(1)	0.3873(1)	0.0135(2)	0.17251(9)	4.03(4)
O(2)	0.2792(2)	0.0675(2)	0.24163(9)	4.42(5)
O(3)	0.5786(2)	0.2386(2)	0.2477(1)	5.58(6)
O(4)	0.6288(2)	-0.1105(2)	0.2427(1)	6.33(7)
C(1)	0.3756(2)	0.0410(2)	0.2362(1)	3.32(6)
C(3)	0.5472(2)	0.1621(2)	0.2733(1)	3.57(6)
C(4)	0.5767(2)	-0.0505(2)	0.2690(1)	3.85(7)
C(5)	0.4186(2)	0.0955(2)	0.3932(1)	2.91(5)
C(6)	0.5323(2)	0.1257(2)	0.4121(1)	3.08(6)
C(7)	0.5964(2)	0.0266(2)	0.4159(1)	3.26(6)
C(8)	0.5226(2)	-0.0661(2)	0.4011(1)	3.21(6)
C(9)	0.4128(2)	-0.0236(2)	0.3870(1)	3.08(6)
C(10)	0.3226(3)	0.1742(3)	0.3876(2)	4.31(8)
C(11)	0.5748(3)	0.2425(3)	0.4282(2)	4.74(8)
C(12)	0.7204(3)	0.0172(3)	0.4367(2)	5.19(9)
C(13)	0.5557(3)	-0.1877(3)	0.4066(2)	4.95(9)
C(14)	0.3094(3)	-0.0930(3)	0.3733(2)	4.62(8)
C(15)	0.1423(2)	0.1860(2)	0.1032(1)	3.45(6)
C(16)	0.1013(3)	0.2207(3)	0.0354(2)	4.41(8)
C(17)	0.0389(3)	0.3169(3)	0.0219(2)	5.33(9)
C(18)	0.0167(3)	0.3795(3)	0.0759(2)	5.81(10)
C(19)	0.0574(3)	0.3492(3)	0.1435(2)	6.0(1)
C(20)	0.1202(3)	0.2527(3)	0.1572(2)	4.88(8)
C(21)	0.2562(2)	-0.0226(2)	0.0186(1)	3.08(5)
C(22)	0.1865(2)	-0.0981(2)	-0.0219(2)	3.81(7)
C(23)	0.2012(3)	-0.1297(3)	-0.0880(2)	4.61(8)
C(24)	0.2874(3)	-0.0852(3)	-0.1143(2)	4.97(8)
C(25)	0.3581(3)	-0.0109(3)	-0.0761(2)	5.03(9)
C(26)	0.3433(3)	0.0201(2)	-0.0095(2)	4.21(7)
C(27)	0.1211(2)	-0.1050(2)	0.1489(1)	3.32(6)
C(28)	0.1634(3)	-0.2090(3)	0.1684(2)	5.46(9)
C(29)	0.0979(4)	-0.2955(3)	0.1861(2)	6.4(1)
C(30)	-0.0117(3)	-0.2773(3)	0.1836(2)	6.0(1)
C(31)	-0.0555(3)	-0.1757(4)	0.1647(2)	6.4(1)
C(32)	0.0103(3)	-0.0903(3)	0.1473(2)	4.97(8)

^a See footnote *a* in Table 3.

results, but degradation is still a major problem. Compound **1a** requires 10 h at 130 °C, compound **1b** requires 8 h at 100 °C, and compound **1c** requires 10 h at 100 °C for complete thermolysis. All liberate PPh₃ and give small yields (22–44%) of the iron–tin complex CpFe(CO)₂SnR₃ (R = Ph, Me, *n*-Bu). Compound **4a** liberates PPh₃ and gives the dimer [Cp*Fe(CO)₂]₂ in 53% yield. Triphenylphosphine oxide is not a product of any of these thermolyses.

In contrast, the CO₂-bridged iron–tin complexes **2a–c** undergo simple decarboxylation to the corresponding iron–tin complexes Cp*Fe(CO)₂SnR₃ (R = Ph, Me,

Table 8. Selected Bond Distances (Å) and Bond Angles (deg) for **2a**

Bond Distances			
C(1)–O(1)	1.312(3)	Sn–O(1)	2.102(2)
C(1)–O(2)	1.252(3)	Sn–O(2)	2.394(2)
Fe–C(1)	1.956(3)		
Bond Angles			
O(1)–C(1)–O(2)	114.5(2)	O(2)–Sn–C(21)	152.20(8)
O(1)–Sn–O(2)	56.90(6)	O(2)–Sn–C(27)	87.90(8)
Fe–C(1)–O(2)	124.7(2)	O(1)–Sn–C(15)	120.65(9)
Fe–C(1)–O(1)	120.7(2)	O(1)–Sn–C(21)	95.32(8)
O(2)–Sn–C(15)	90.13(9)	O(1)–Sn–C(27)	112.15(9)

n-Bu) and are thermolyzed at lower temperatures during shorter reaction periods than **1a–c**. Compound **2a** requires 3 h at 120 °C, **2b** requires 1 h at 70 °C, and **2c** requires 1.5 h at 90 °C for complete thermolysis; all give the corresponding iron–tin complexes in greater than 70% yield. Compound **5a** also decarboxylates to the corresponding iron–tin complex and is one of the most labile of this group, requiring 2 h at 70 °C for complete thermolysis. We have observed significant differences in stability of these compounds in solution. All three are stable in chloroform at temperatures up to 45 °C. Compound **2a** is also stable in THF (up to 45 °C at least), while **2b** showed significant decarboxylation at 0 °C and **2c** decomposed in this solvent at 25 °C.

Rhenium complexes **3a,b** require higher temperatures and much longer times than iron complexes **2a,b** for complete thermolysis. Compound **3b** decarboxylates to the rhenium–tin complex in 73% yield after 20.5 h at 90 °C. Compound **3a** requires 2 h at 185 °C (or longer times at lower temperatures) for complete thermolysis but degrades, extensively, under all conditions. Only a small amount of product whose spectral properties are consistent with those observed for the rhenium–tin complex is obtained.

It was suggested previously that the $\mu_2\text{-}\eta^2$ type of bridged complex may be more susceptible to simple decarboxylation than ones with $\mu_2\text{-}\eta^3$ coordination.⁸ In a given series of compounds, such as **2a–c**, which decarboxylate readily, this is certainly true. However, the samples of **1b,c** which were used in the thermolysis studies contained major amounts of the $\mu_2\text{-}\eta^2$ form: these compounds did not exhibit simple decarboxylation at all and required prolonged heating at elevated temperatures to complete the thermolysis reactions. Compound **3b** has the $\mu_2\text{-}\eta^2$ form but also requires long heating at high temperature for complete decarboxylation.

The results from our thermolysis reactions, when taken together with the results from structural and spectral characterizations of the compounds, suggest that there are several factors which determine the ease of thermolysis and whether simple decarboxylation will occur or not. Some of the factors that determine which type of bridged complex will result in a particular case also appear to influence the ease of decarboxylation. Note that the ancillary ligands on the two metal centers have strong influences on the type of bridging carboxyl group present. The strongly electron-donating Cp* ligand can be expected to enhance the nucleophilic character of the carboxyl oxygens and promote formation of a fully chelated carboxyl group. The presence of an electron-withdrawing ligand such as phenyl would decrease the electron density on the tin atom and enhance the stability of the $\mu_2\text{-}\eta^3$ form further. Electron-

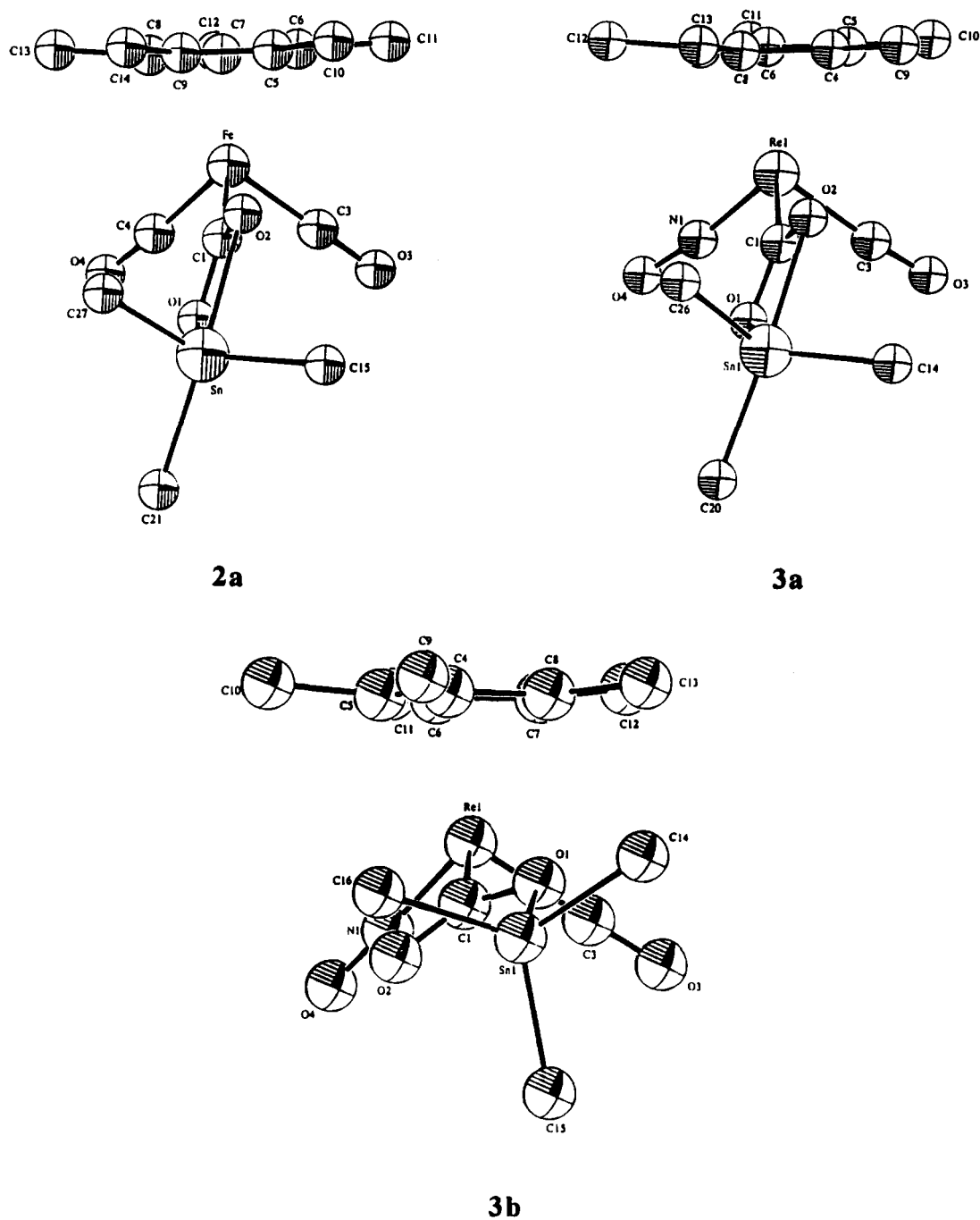


Figure 5. ORTEP diagrams of **2a** and **3a,b** shown with the tin atoms projecting forward and the plane of the pentamethylcyclopentadienyl group perpendicular to the plane of the page. The tin and phosphorus atoms are shown with α -bonded atoms only for clarity.

donating alkyl groups would exert an opposite effect. Compound **5a** has the weakest electron-donor ligands on the carboxyl carbon side, and this species, alone among all the triphenyltin complexes which have been studied to date, exists in the μ_2 - η^2 form in the solid state. Compound **5a** is also one of the most thermally labile systems studied. Differences in the ease of thermolysis of **2a** and **3a** or differences between **2b** and **3b** indicated that metal-carbon bond strengths play a major role in determining the ease of decarboxylation and can take precedence over the type of CO_2 coordination. Less information is available about the effects of the metal center bonded to one or both carboxyl oxygens. The PbPh_3 complex studied by Gladysz^{4a} decarboxylates much more easily than its SnPh_3 analog. Although both compounds exhibit μ_2 - η^3 bonding of the CO_2 ligand, as

indicated by IR spectral data, there are no structural data available on the lead complex.

An additional major factor in determining the ease of decarboxylation appears to be the conformation of the bridging carboxyl group between the two metal centers and whether the longer, axial, O-Sn bond is, as expected, broken more easily. In compounds **1a-c** the plane of the carboxyl group is approximately coplanar with the Fe-C-O plane (see Figure 3). Compounds **2a** and **3a** have an "upright" conformation of the CO_2 in which the plane of the bridging ligand bisects the angle which includes the two terminal carbonyls (in **2a**) or terminal carbonyl and nitrosyl (in **3a**) and the metal atom (see Figure 5). Dechelation (breaking of one O-Sn bond) may occur most easily in the "upright" conformation to give a μ_2 - η^2 form. Decarboxylation should occur

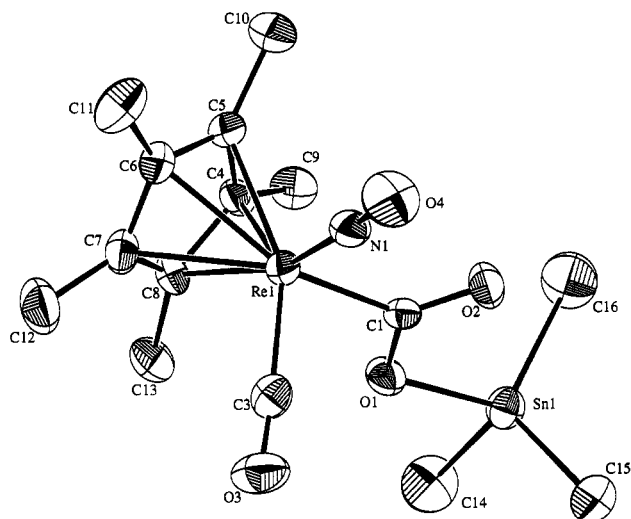


Figure 6. ORTEP drawing of **3b** with thermal ellipsoids shown at the 50% probability level.

Table 9. Atomic Positional Parameters for **3b**

atom	x	y	z	<i>B</i> _{eq} , ^a Å ²
Re(1)	0.17283(2)	-0.17905(1)	0.08356(3)	2.007(5)
Sn(1)	0.25082(4)	-0.48519(2)	0.19991(5)	2.581(8)
Cl(1)	0.3409(2)	0.2669(1)	0.2743(3)	5.76(5)
Cl(2)	0.3359(2)	0.2659(1)	0.6756(3)	5.69(5)
Cl(3)	0.4043(2)	0.1113(1)	0.4870(3)	4.93(4)
O(1)	0.1753(3)	-0.3693(2)	0.0916(5)	2.68(8)
O(2)	0.3213(4)	-0.3143(2)	0.3438(5)	2.96(9)
O(3)	-0.0821(4)	-0.2154(3)	0.1502(7)	4.4(1)
O(4)	0.2756(5)	-0.0749(3)	0.4584(6)	4.6(1)
N(1)	0.2346(4)	-0.1192(3)	0.3121(6)	2.8(1)
C(1)	0.2338(5)	-0.3009(3)	0.1943(7)	2.0(1)
C(3)	0.0157(6)	-0.2031(3)	0.1291(8)	2.8(1)
C(4)	0.2559(5)	-0.2253(3)	-0.1702(7)	2.3(1)
C(5)	0.3000(5)	-0.1402(3)	-0.1053(7)	2.4(1)
C(6)	0.1952(5)	-0.0833(3)	-0.1420(7)	2.5(1)
C(7)	0.0832(5)	-0.1322(4)	-0.2292(8)	2.9(1)
C(8)	0.1198(5)	-0.2205(4)	-0.2455(7)	2.5(1)
C(9)	0.3334(6)	-0.3039(4)	-0.1804(9)	3.0(1)
C(10)	0.4353(6)	-0.1126(5)	-0.035(1)	3.8(2)
C(11)	0.2047(9)	0.0150(4)	-0.107(1)	4.3(2)
C(12)	-0.0461(7)	-0.0958(6)	-0.310(1)	4.4(2)
C(13)	0.0337(7)	-0.2952(5)	-0.3470(10)	3.8(2)
C(14)	0.1468(8)	-0.5645(5)	-0.049(1)	4.5(2)
C(15)	0.1936(7)	-0.5043(4)	0.4539(9)	3.4(1)
C(16)	0.4475(8)	-0.4875(6)	0.231(1)	4.9(2)
C(17)	0.4129(6)	0.2245(4)	0.5037(10)	3.9(2)

^a See footnote *a* in Table 3.

Table 10. Selected Bond Distances (Å) and Bond Angles (deg) for **3b**

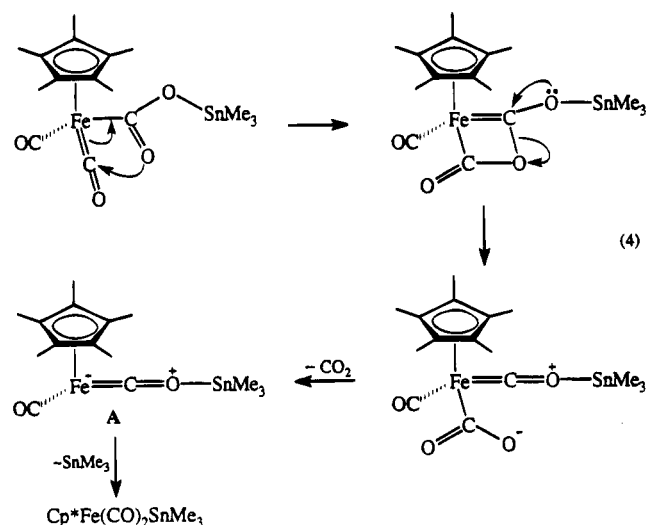
Bond Distances			
C(1)–O(1)	1.311(6)	Sn–O(1)	2.054(4)
C(1)–O(2)	1.237(6)	Sn–O(2)	2.806(4)
Re–C(1)	2.103(5)		
Bond Angles			
O(1)–C(1)–O(2)	117.0(5)	O(1)–Sn–C(16)	110.2(3)
Re–C(1)–O(1)	116.6(4)	C(14)–Sn–C(15)	112.5(3)
Re–C(1)–O(2)	126.3(4)	C(15)–Sn–C(16)	117.4(3)
O(1)–Sn–C(14)	95.7(2)	C(14)–Sn–C(16)	111.6(3)
O(1)–Sn–C(15)	107.0(2)		

most easily when the dechelated oxygen atom is on the face of the molecule away from the Cp or Cp* ligand, as in **3b**. Finally, it must be noted that simple decarboxylation occurs *only* in those compounds for which the corresponding metal anion is known to be stable. Where that species is not known (e.g., CpFe(CO)(PPh₃)⁻ and Cp*Fe(CO)(PPh₃)⁻), the thermolysis reactions do not occur with simple decarboxylation.

Table 11. DRIFTS Spectra (ν_{OCO} in cm⁻¹) for the Tin Metallo-carboxylates

compd	μ_2 - η^2 form	μ_2 - η^3 form
1a		1431, 1161
1b	1491, 1134	1438 or 1433, 1134
1c	1491, 1113	1433, 1113
2a		1450, 1152
2b	1516, 1150 or 1122	
2c	1534, 1118	
3a		1429, 1188 or 1175
3b	1510, 1179	
4a		1418, 1140
5a	1499, 1159	

With all these considerations in mind, the following reaction pathway is suggested as a profile of the decarboxylation reactions which occur in **2a–c**, **3b**, and **5a**; it is illustrated with compound **2b** in eq 4. Note that



the orientation of the nucleophilic carboxyl oxygen must be on the face of the molecule opposite the Cp* ligand to initiate the sequence. Where both oxygens are bound to tin, dechelation must be the first step. This pathway involves oxygen atom transfer, as suggested previously to account for ¹³C scrambling in thermolyses of **2b**,⁸ but also includes the intermediate dipolar species **A**, which is closely related to the corresponding metal carbonyl anion. We suggest that it is the stability of this species, in particular, which determines whether simple decarboxylation occurs or not. The more vigorous conditions needed for thermolysis of triphenyltin complexes, as compared to the analogous compounds with alkyl groups on the tin atom, are probably a reflection of the need to dechelate one carboxyl oxygen to start the decarboxylation sequence as well as the reduced nucleophilicity of the freed carboxyl oxygen caused by the presence of the electron-withdrawing aryl ligands. With **3a**, dechelation of the longer O–Sn bond would leave the freed carboxyl oxygen on the wrong face of the molecule. These factors, together with the strong metal–carboxyl carbon bond and the lowered opportunity (due to a single terminal carbonyl on rhenium) to form the metalloanhydride intermediate as compared to **2a**, are believed to be responsible for the extensive degradation which occurs with **3a**.

Other mechanisms must be considered for the systems studied by Gladysz,^{4a} CpRe(NO)(PPh₃)(CO)₂MR₃, which are known to decarboxylate but cannot achieve an intermediate such as **A** in eq 4 even though the

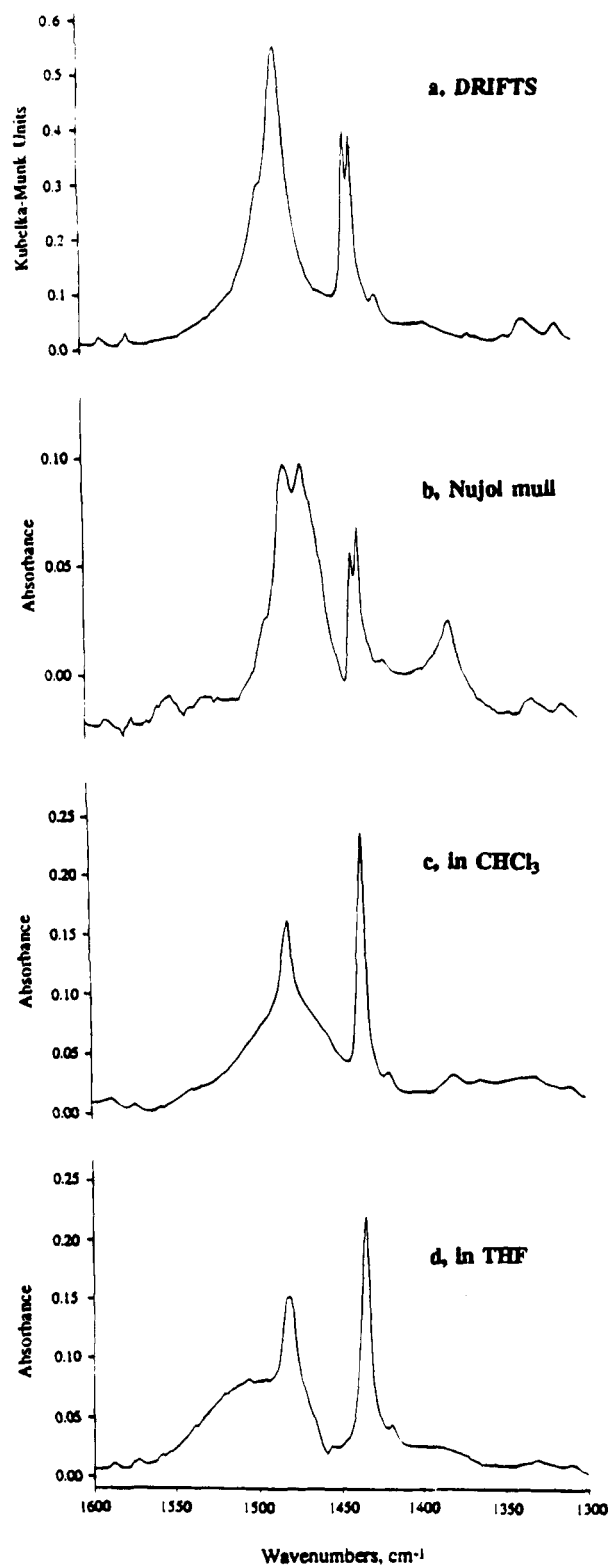
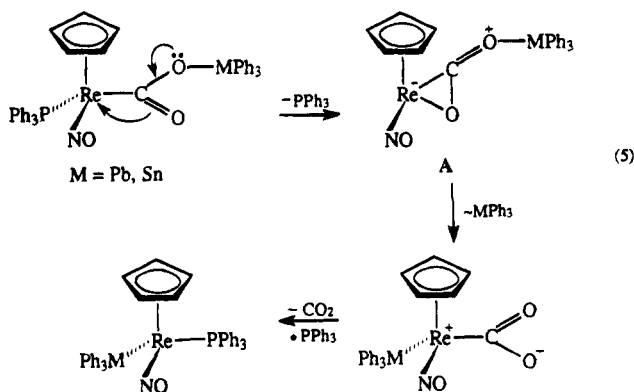


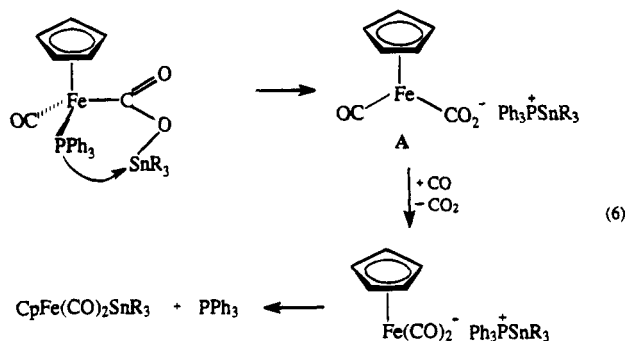
Figure 7. Infrared spectra (1600–1300 cm^{-1} region only) of $\text{CpFe(CO)(PPh}_3\text{)(CO}_2\text{)SnMe}_3$ (**1b**) recorded by different methods.

corresponding metal anion is known here also. When $M = \text{Pb}$, the compound is thought to have $\mu_2\text{-}\eta^3$ bonding of the CO_2 . The triphenyltin complex has a $\mu_2\text{-}\eta^3$ -coordinated CO_2 , and the longer O-Sn bond is known to be on the face opposite the cyclopentadienyl ring. Again, dechelation to the $\mu_2\text{-}\eta^2$ type must precede further reaction. The pathway shown in eq 5 is suggested to account for the decarboxylations exhibited by



compounds in this series. Intermediate **A** in this equation initiates the decarboxylation sequence; its structure bears a close similarity to an $\eta^2\text{-CO}_2$ complex which has added an electrophilic metal center; precedent is available for such a species.⁹

As discussed above, compounds **1a–c** and **4a** do not undergo simple decarboxylation. With **1a–c**, however, significant quantities of the related $\text{CpFe(CO)}_2\text{SnR}_3$ product are formed instead; but degradation also occurs, particularly with **1a,b**. We believe that the behavior of these systems is directly related to the observed ligand rearrangements which we have recently observed with iron–rhenium complexes involving the same metallocarboxylate fragment, $\text{CpFe(CO)(PPh}_3\text{)CO}_2$.^{3b} In those systems, formation of a coordination vacancy on the rhenium center is followed by migration of the PPh_3 ligand from iron to rhenium. An analogous pathway allows us to explain the unusual behavior of the tin complexes with this metal fragment as shown in eq 6.



Intermediate **A** in this sequence would be very unstable and decarboxylation could precede or follow CO scavenging; degradation of **A** can also be expected. With **4a**, similar behavior may be involved, but no iron–tin product is observed from the thermolysis reaction.

Experimental Section

General Data. Reactions and manipulations were carried out under an atmosphere of prepurified nitrogen in Schlenkware or in a Vacuum Atmospheres glovebox (with Dri-train). All glassware was dried in the oven before use. Reagent grade solvents dichloromethane and chloroform were used as received. Benzene, toluene, and hexane were dried over concentrated sulfuric acid and fractionally distilled before use. Solvents used in the glovebox were distilled under nitrogen from the following drying agents: sodium benzophenone ketyl for tetrahydrofuran (THF) and P_2O_5 for dichloromethane,

(9) Fu, P.-F.; Khan, M. A.; Nicholas, K. M. *Organometallics* **1992**, *11*, 2607.

pentane, hexane, benzene, and toluene. Triphenylphosphine, trimethyltin chloride, tri-*n*-butyltin chloride, triphenyltin chloride, *n*-butyllithium, tetramethylethylenediamine (TMEDA), benzene-*d*₆, and chloroform-*d* were obtained from Aldrich; dichloromethane-*d*₂, THF-*d*₈, and toluene-*d*₈ were obtained from Cambridge Isotope Laboratories or Aldrich. Anhydrous CpFe(CO)(PPh₃)CO₂-K⁺,⁷ Cp*Re(CO)(NO)COOH,^{5b} Cp*Fe(CO)₃⁺BF₄⁻,¹⁰ CpFe(CO)₃⁺BF₄⁻,¹¹ CpFe(CO)(PPh₃)(CO₂)-SnPh₃ (**1a**),⁷ and Cp*Fe(CO)(PPh₃)(CO₂)SnPh₃ (**4a**)⁷ were prepared as described previously. Spectral data were obtained on the following instruments: FT-NMR, Bruker AMX-500; FT-IR, Mattson Galaxy series 5000. Diffuse reflectance FT-IR data were obtained on the Mattson instrument with a DRIFTS accessory (Spectra Tech, Inc., Barnes Analytical Division) as KCl dispersions and at 1 cm⁻¹ resolution.¹² ¹H and ¹³C NMR chemical shifts were referenced to residual protons in the deuterated solvents; ³¹P NMR chemical shifts were referenced to external 85% H₃PO₄. Melting points were obtained on a Thomas-Hoover capillary melting point apparatus and are uncorrected. Elemental analyses were performed by Midwest Microlab, Indianapolis, IN.

CpFe(CO)(PPh₃)(CO₂)SnMe₃ (1b). In the glovebox, CpFe(CO)(PPh₃)CO₂-K⁺ (0.50 g, 0.91 mmol) was slurried in 50 mL of THF and chilled to -50 °C. Me₃SnCl (0.22 g, 1.10 mmol) was added, and the mixture was warmed to -10 °C and stirred for 1 h. The resulting yellow mixture was cooled to -30 °C and filtered. The filtrate was evaporated to dryness at -4 °C under vacuum. The crude product was purified by recrystallization from toluene/pentane at -20 °C to give 0.44 g of yellow crystals (86%), mp 89–90 °C.

Anal. Calcd for C₂₈H₂₉FeO₃PSn: C, 54.32; H, 4.72. Found: C, 54.41; H, 4.83. IR ν_{CO} (CH₂Cl₂): 1935 cm⁻¹. IR ν_{OCO}: in Nujol, 1467, 1437 or 1433, 1132 cm⁻¹; in CHCl₃, 1480, 1121 cm⁻¹; in THF, 1507, 1131 cm⁻¹. ¹H NMR (THF-*d*₈): δ 7.54 (m), 7.35 (m), 4.43 (s), -0.01 (t, J_{SnH} = 55.0 Hz). ¹³C NMR (CDCl₃): δ 222.05 (CO, d, J_{PC} = 32.0 Hz), 219.63 (CO₂, d, J_{PC} = 30.2 Hz), 136.67 (d, J_{PC} = 44.0 Hz), 129.91 (d, J_{PC} = 8.8 Hz), 129.65 (s), 127.94 (d, J_{PC} = 8.9 Hz), 84.88 (s), -2.49 (s, br). ¹³C NMR (THF-*d*₈): δ 220.67 (CO, d, J_{PC} = 30.2 Hz), 220.42 (CO₂, d, J_{PC} = 32.5 Hz), 137.99 (d, J_{PC} = 44.0 Hz), 134.39 (d, J_{PC} = 8.8 Hz), 130.37 (s), 128.64 (d, J_{PC} = 9.1 Hz), 85.54 (s), -2.24 (s, br). ³¹P NMR (C₆D₆): δ 79.00 (s).

CpFe(CO)(PPh₃)(CO₂)Sn(*n*-Bu)₃ (1c). In the glovebox CpFe(CO)(PPh₃)CO₂-K⁺ (0.50 g, 1.01 mmol) was slurried in 50 mL of dried THF and chilled to -50 °C. (*n*-Bu)₃SnCl (0.36 g, 1.10 mmol) was added, and the mixture was warmed to -10 °C and stirred for 1 h. The resulting yellow mixture was cooled to -30 °C and filtered. The filtrate was evaporated to dryness at -5 °C under vacuum. The crude yellow product was recrystallized from toluene/pentane at -20 °C. Yellow crystals were collected by filtration (0.67 g, 89%); mp 94–95 °C.

Anal. Calcd for C₃₇H₄₇FeO₃PSn: C, 59.63; H, 6.36. Found: C, 59.44; H, 6.34. IR ν_{CO} (CH₂Cl₂): 1935 cm⁻¹. IR ν_{OCO}: in Nujol, 1489, 1433, 1113 cm⁻¹; in CHCl₃, 1480, 1132 cm⁻¹; in THF, 1507, 1119 cm⁻¹. ¹H NMR (toluene-*d*₈): δ 7.55 (m), 7.35 (m), 4.45 (s), 1.46 (m), 1.27 (m), 0.88 (t, J = 7.6 Hz), 0.72 (m). ¹³C NMR (CDCl₃): δ 219.96 (CO, d, J_{PC} = 30.6 Hz), 219.56 (CO₂, d, J_{PC} = 30.9 Hz), 137.63 (d, J_{PC} = 43.0 Hz), 134.29 (d, J_{PC} = 10.1 Hz), 129.56 (s), 127.85 (d, J_{PC} = 10.1 Hz), 84.64 (s), 28.19 (s), 27.10 (s), 15.92 (s), 13.70 (s). ¹³C NMR (THF-*d*₈): δ 220.63 (CO, d, J_{PC} = 30.2 Hz), 220.29 (CO₂, d, J_{PC} = 31.4 Hz), 138.04 (d, J_{PC} = 43.0 Hz), 134.41 (d, J_{PC} = 10.0 Hz), 130.39 (s), 128.65 (d, J_{PC} = 10.0 Hz), 85.52 (s), 29.36 (s), 28.04 (s), 16.84 (t, J_{SnC} = 366.9 Hz), 14.17 (s). ³¹P NMR (C₆D₆): δ 78.92 (s).

Cp*Fe(CO)₂(CO₂)SnPh₃ (2a). In a Schlenk flask under

N₂, Cp*Fe(CO)₃⁺BF₄⁻ (0.22 g, 0.61 mmol) and Ph₃SnCl (95%, 0.24 g, 0.62 mmol) were dissolved in ca. 20 mL of CH₂Cl₂ and the solution was cooled to 0 °C. KOH (85%, 0.11 g, 1.67 mmol) was dissolved in ca. 0.5 mL of water; the solution was cooled to 0 °C and added dropwise to the CH₂Cl₂ solution. After the mixture was stirred for 15 min, the solvent was removed under vacuum. The residue was extracted with hexane (2 × 20 mL), and the extract was dried over MgSO₄ and filtered through a glass pad. The solvent was stripped from the filtrate, leaving an orange-yellow solid (0.35 g, 90% yield); mp 110 °C. IR and ¹H and ¹³C NMR spectral data were in good agreement with those reported previously.⁸

IR ν_{CO} (hexane): 2015 and 1960 cm⁻¹. IR ν_{OCO}: in CHCl₃, 1470, 1146 cm⁻¹; in THF, 1471, 1160 cm⁻¹. ¹H NMR (CDCl₃): δ 7.73 (m), 7.39 (m), 1.75 (s). ¹³C NMR (CDCl₃): δ 217.74 (CO₂), 215.10 (CO), 141.53, 137.02 (t, J_{SnC} = 47.8 Hz), 129.14, 128.37 (t, J_{SnC} = 61.6 Hz), 96.92, 9.75; singlets except as noted (J_{SnC} could not be determined for other carbons). ¹H NMR (THF-*d*₈): δ 7.70 (m), 7.34 (m), 1.77 (s). ¹³C NMR (THF-*d*₈): δ 218.35 (CO₂), 216.27 (CO), 142.86, 137.79 (t, J_{SnC} = 47.8 Hz), 129.77, 129.02 (t, J_{SnC} = 61.6 Hz), 98.01, 9.78; singlets except as noted (J_{SnC} could not be determined for other carbons).

Cp*Fe(CO)₂(CO₂)SnMe₃ (2b). In a Schlenk flask under N₂, Cp*Fe(CO)₃⁺BF₄⁻ (0.20 g, 0.55 mmol) and Me₃SnCl (0.11 g, 0.55 mmol) were added to 10 mL of CH₂Cl₂, and the solution was cooled to 0 °C. A solution of 85% KOH (0.08 g, 1.2 mmol) in ca. 0.2 mL of water was added dropwise to the reaction mixture, causing a color change from yellow to orange-red. The mixture was stirred for 5 min and the solvent was removed under vacuum. The resulting residue was extracted with hexane/CHCl₃ (70/30, 20 mL). The extract was filtered and the solvent removed under vacuum, leaving 0.22 g (88% yield) of a yellow solid, mp 42 °C.

Anal. Calcd for C₁₆H₂₄FeO₄Sn: C, 42.24; H, 5.32. Found: C, 42.28; H, 5.45. IR ν_{CO} (CHCl₃): 2011 and 1954 cm⁻¹. IR ν_{OCO}: in CHCl₃, 1517, 1132 cm⁻¹; in THF, 1532, 1125 cm⁻¹ (lit.⁸ 1540 and 1123 cm⁻¹). ¹H NMR (CDCl₃, -30 °C): δ 0.35 (t, J_{SnH} = 52.4 Hz), 1.77 (s). ¹³C NMR (CDCl₃, -30 °C): δ -2.16, 9.84, 96.54, 214.55 (CO₂), 215.72 (CO); all singlets (J_{SnC} could not be resolved). ¹H NMR (THF-*d*₈, -30 °C): δ 0.31 (t, J_{SnH} = 52.4 Hz), 1.81 (s). ¹³C NMR (THF-*d*₈, -30 °C): δ -1.82, 9.94, 97.38, 209.57 (CO₂), 217.40 (CO); all singlets (J_{SnC} could not be resolved).

Cp*Fe(CO)₂(CO₂)Sn(*n*-Bu)₃ (2c). In a Schlenk flask under N₂, Cp*Fe(CO)₃⁺BF₄⁻ (0.20 g, 0.55 mmol) and (*n*-Bu)₃SnCl (0.19 g, 0.56 mmol) were added to 10 mL of CH₂Cl₂ and the solution was cooled to 0 °C. A solution of 85% KOH (0.08 g, 1.2 mmol) in ca. 0.2 mL of water was added dropwise to the reaction mixture, causing a color change from yellow to amber. The mixture was stirred for 15 min, cooled to -30 °C for 1 h, and filtered cold, and the solvent was stripped from the filtrate under vacuum, leaving an amber viscous liquid (0.29 g, 91% yield).

Anal. Calcd for C₂₅H₄₂FeO₄Sn: C, 51.67; H, 7.29. Found: C, 51.28; H, 7.62. IR ν_{CO} (CHCl₃): 2012 and 1955 cm⁻¹. IR ν_{OCO}: in CHCl₃, 1524, 1128 cm⁻¹; in THF, 1534, 1120 cm⁻¹. ¹H NMR (CDCl₃, -30 °C): δ 0.85 (t, J = 7.3 Hz), 1.07 (m), 1.27 (m), 1.52 (m), 1.77 (s). ¹³C NMR (CDCl₃, -30 °C): δ 10.01, 13.89, 16.48 (q, J_{SnC} = 358.1 and 342.3 Hz), 27.21 (t, J_{SnC} = 61.6 Hz), 28.34 (t, J_{SnC} = 20.5 Hz), 96.48, 213.09 (CO₂), 215.62 (CO); singlets except as noted. ¹H NMR (THF-*d*₈, -30 °C): δ 0.90 (t, J = 7.3 Hz), 1.05 (m), 1.34 (m), 1.64 (m), 1.83 (s). ¹³C NMR (THF-*d*₈, -30 °C): δ 9.94, 14.40, 17.13 (t, J_{SnC} = 358.1 Hz), 28.17, 29.18, 97.34, 209.80 (CO₂), 217.29 (CO); singlets except as noted.

Cp*Re(CO)(NO)(CO₂)SnPh₃ (3a). To Cp*Re(CO)(NO)-COOH (0.10 g, 0.23 mmol) and Ph₃SnCl (95%, 0.09 g, 0.23 mmol) dissolved in 10 mL of THF and cooled to 0 °C was added an excess of KOH (0.05 g, 0.94 mmol). The mixture was stirred for 30 min at 0 °C and then warmed to room temperature. After this time, 2 mL of water was added and the mixture was stirred for an additional 10 min. The resulting orange solution

(10) Stasunik, A.; Malisch, W. *J. Organomet. Chem.* **1983**, *247*, C47.

(11) Kochhar, R. K.; Pettit, R. *J. Organomet. Chem.* **1966**, *6*, 272.

(12) Griffiths, P. W.; deHaseth, J. A. *Fourier Transform Infrared Spectroscopy*; Wiley: New York, 1986; Chapter 5.

(13) Chinn, M. S.; Heinekey, D. M.; Payne, N. G.; Sofield, C. D. *Organometallics* **1989**, *8*, 1824.

was extracted with CH_2Cl_2 (3×10 mL). The extracts were combined, dried over MgSO_4 , and filtered through a glass pad. Removal of the solvent, in vacuo, gave a bright orange solid. The crude product was recrystallized from CH_2Cl_2 /pentane (1:1, v/v), which afforded an orange solid (0.16 g, 88% yield). The physical and spectral properties were identical with those previously reported for $\text{Cp}^*\text{Re}(\text{CO})(\text{NO})(\text{CO})_2\text{SnPh}_3$.^{3b}

¹H NMR (CDCl_3): δ 7.43–7.82 (m), 2.11 (s). ¹³C NMR (CDCl_3): δ 206.43 (CO), 200.37 (CO₂), 142.02, 137.10, 129.05, 128.71, 104.68, 10.33 (all singlets, J_{SnC} could not be resolved). ¹H NMR ($\text{THF}-d_6$): δ 7.30–7.70 (m), 2.07 (s). ¹³C NMR ($\text{THF}-d_6$): δ 207.91 (CO), 201.01 (CO₂), 143.25, 137.76, 129.69, 128.98, 105.71, 10.18 (all singlets, J_{SnC} could not be resolved).

Cp*Re(CO)(NO)(CO)₂SnMe₃ (3b). A suspension of $\text{Cp}^*\text{Re}(\text{CO})(\text{NO})\text{COOH}$ (0.20 g, 0.47 mmol) and Me_3SnCl (0.09 g, 0.47 mmol) in 10 mL of CH_2Cl_2 was cooled to 0 °C. Excess KOH (0.10 g, 1.88 mmol) was then added and the mixture stirred for 30 min at 0 °C before being warmed to room temperature. After this time, 2 mL of water was added and the mixture was stirred for an additional 10 min and then extracted with CH_2Cl_2 . The extracts were collected, dried over MgSO_4 , and filtered through a glass pad. Removal of the solvent in vacuo gave a dark orange solid. The crude product was recrystallized from CH_2Cl_2 /hexane (1:1, v/v), which afforded an orange crystalline solid (0.25 g, 90% yield); mp 106–108 °C dec.

Anal. Calcd for $\text{C}_{15}\text{H}_{24}\text{NO}_4\text{ReSn}$: C, 30.68; H, 4.12. Found: C, 30.79; H, 4.14. IR ν_{CO} (DRIFTS): 1954 cm^{-1} . IR ν_{NO} (DRIFTS): 1684 cm^{-1} . IR ν_{OCO} : in CHCl_3 , 1512, 1162 cm^{-1} ; in THF, 1524, 1161 cm^{-1} . ¹H NMR (CDCl_3): δ 0.36 (t, $J_{\text{SnH}} = 56.7$ Hz), 2.06 (s). ¹³C NMR (CDCl_3): δ 207.85 (s, CO), 197.58 (s, CO₂), 104.32 (s), 10.20 (s), –2.00 (s). ¹H NMR ($\text{THF}-d_6$): δ 0.61 (t, $J_{\text{SnH}} = 59.2$ Hz), 2.39 (s). ¹³C NMR ($\text{THF}-d_6$): δ 210.08, 196.10, 105.31, 10.25, –2.02 (all singlets, J_{SnC} could not be resolved).

CpFe(CO)₂(CO)₂SnPh₃ (5a). $\text{CpFe}(\text{CO})_3^+\text{BF}_4^-$ (0.22 g, 0.76 mmol) was slurried in 2 mL of CH_2Cl_2 and chilled to 0 °C under N_2 . A solution of KOH (85%, 0.10 g, 1.51 mmol) in 0.5 mL of water was chilled and then added dropwise, with stirring, to the solution of the cation. A red suspension formed quickly. Ph_3SnCl (0.16 g, 0.43 mmol) in 1 mL of CH_2Cl_2 was immediately added, and the mixture was stirred for 2 min. The mixture was then filtered through a glass fiber pad and the filtrate evaporated to dryness, leaving an orange-red, tacky solid which was shown by ¹H NMR analysis to be **5a**, $\text{CpFe}(\text{CO})_2\text{SnPh}_3$, and $[\text{CpFe}(\text{CO})_2]_2$ in a ratio of 91:5:4, respectively; the yield of **5a** was 84% (based on Ph_3SnCl). Compound **5a** could not be purified further. Authentic samples of the two impurities were available for comparison, and the spectral properties of **5a** could be easily identified.

IR ν_{CO} (CHCl_3): 2038, 1988 cm^{-1} . IR ν_{OCO} : in CHCl_3 , 1510, 1157 cm^{-1} . ¹H NMR (CDCl_3): δ 7.70–7.41 (m), 4.93 (s). ¹³C NMR (CDCl_3): δ 213.32 (s, CO), 209.85 (s, CO₂), 140.79 (s), 136.17 (t, $J_{\text{SnC}} = 46.8$ Hz), 129.20 (s), 128.61 (t, $J_{\text{SnC}} = 61.1$ Hz), 85.93 (s). ¹H NMR ($\text{THF}-d_6$): δ 7.78–7.41 (m), 5.07 (s). ¹³C NMR ($\text{THF}-d_6$): δ 214.89 (s, CO), 210.69 (s, CO₂), 141.02 (s), 137.05 (t, $J_{\text{SnC}} = 46.5$ Hz), 130.45 (s), 129.44 (t, $J_{\text{SnC}} = 60.1$ Hz), 87.26 (s).

Cp*Fe(CO)₂Sn(*n*-Bu)₃. $\text{Cp}^*\text{Fe}(\text{CO})_3^+\text{BF}_4^-$ (0.20 g, 0.55 mmol) and (*n*-Bu)₃SnCl (0.18 g, 0.55 mmol) were dissolved in 5 mL of acetone. KOH (0.07 g, 1.11 mmol), in 2 mL of water, was added dropwise to the solution. The color then changed from yellow to brownish yellow. The solvent was evaporated to dryness. The residue was extracted with 20 mL of pentane. After filtration and removal of the solvent, an oil was obtained (0.22 g, 74% yield). The product was purified by column chromatography on Florisil with pentane as the eluent.

Anal. Calcd for $\text{C}_{24}\text{H}_{42}\text{FeO}_2\text{Sn}$: C, 53.66; H, 7.88. Found: C, 53.73; H, 7.86. IR ν_{CO} (CH_2Cl_2): 1964, 1913 cm^{-1} . ¹H NMR (CDCl_3): δ 1.80 (s), 1.59 (m), 1.12 (t, $J = 7.1$ Hz), 0.98 (t, $J = 7.1$ Hz), 0.85 (m). ¹³C NMR (CDCl_3): δ 217.54, 93.46, 30.73, 27.70, 13.77, 12.17, 10.40; all singlets.

Cp*Re(CO)(NO)SnMe₃. A sample of **3b** (0.20 g, 34 mmol) was placed in a small glass tube which was then evacuated and sealed. After heating at 90 °C for 20.5 h, the sample had darkened. The tube was opened, and the residue was extracted with pentane. After filtration and concentration of the pentane extracts, orange crystals were obtained (0.13 g, 73% yield); mp 97 °C.

Anal. Calcd for $\text{C}_{14}\text{H}_{24}\text{NO}_2\text{ReSn}$: C, 30.95; H, 4.45. Found: C, 31.20; H, 4.51. IR ν_{CO} (DRIFTS): 1938 (s) cm^{-1} . IR ν_{NO} (DRIFTS): 1678 (s) cm^{-1} . ¹H NMR (CDCl_3): δ 0.21 (s), 2.13 (s). ¹³C NMR (CDCl_3): 215.41, 100.71, 10.71, –7.91; all singlets.

Cp*Re(CO)(NO)SnPh₃. In the glovebox, a mixture of *n*-butyllithium (0.47 mL, 1.18 mmol) and TMEDA (0.18 mL, 1.18 mmol) in 10 mL of THF was cooled to –20 °C. To this was added dropwise a cold solution of $\text{Cp}^*\text{Re}(\text{CO})(\text{NO})\text{H}$ (0.30 g, 0.79 mmol) in 10 mL of THF. After addition was complete, the mixture was stirred for an additional 10 min at –20 °C. Then, Ph_3SnCl (0.30 g, 0.79 mmol) in 10 mL of THF was added dropwise; stirring was continued for 30 min at –20 °C and, finally, the mixture was warmed to room temperature with continued stirring for 1 h. Removal of solvent, in vacuo, afforded a dark orange solid which was chromatographed on Florisil with 80:20 (v/v) pentane/ether as eluent. After solvent removal, the product was recrystallized from CH_2Cl_2 /hexane and gave 0.32 g (56% yield) of the product; mp 156 °C.

Anal. Calcd for $\text{C}_{25}\text{H}_{30}\text{NO}_2\text{ReSn}$: C, 47.75; H, 4.15. Found: C, 47.56; H, 4.04. IR ν_{CO} (DRIFTS): 1943 cm^{-1} . IR ν_{NO} (DRIFTS): 1687 cm^{-1} . ¹H NMR (CDCl_3): δ 7.44 (m), 2.03. ¹³C NMR (CDCl_3): δ 213.27 (s), 144.64 (s), 137.20 (t, $J_{\text{SnC}} = 37.7$ Hz), 127.81 (t, $J_{\text{SnC}} = 41.5$ Hz), 127.45 (t, $J_{\text{SnC}} = 8.5$ Hz), 100.79 (s), 10.62 (s).

Thermolysis of the Tin Complexes. General Procedures. Small samples, typically 0.10 g of each compound, were placed in glass tubes which were then evacuated and sealed. The reaction conditions (time, temperature) needed for complete thermolysis and the results are detailed for each compound below. The same analysis procedures were followed for each compound. After thermolysis was complete (established by trial and error), the tube was cooled to room temperature and opened and a small amount of CDCl_3 added. The mixture was then filtered and the filtrate analyzed by ¹H and ¹³C NMR spectroscopy using ferrocene as an internal standard.

1a: Thermolysis was complete after 10 h at 130 °C. Extensive degradation was evident, since some of the residue was not soluble in CDCl_3 (or in dichloromethane). Analysis of the soluble components, by NMR, revealed a 22% yield of $\text{CpFe}(\text{CO})_2\text{SnPh}_3$ (identified by comparison with an authentic sample¹⁴). Also, PPh_3 was liberated in 79% yield.

1b: Thermolysis was complete after 8 h at 100 °C, and degradation was again evident. NMR analysis indicated a 26% yield of $\text{CpFe}(\text{CO})_2\text{Sn}(\text{CH}_3)_3$ (identified by comparison with an authentic sample¹⁵), a 15% yield of $[\text{CpFe}(\text{CO})_2]_2$, and a 44% yield of PPh_3 .

1c: Complete thermolysis resulted after 10 h at 100 °C. Again, there was considerable degradation. However, NMR analysis indicated a 44% yield of $\text{CpFe}(\text{CO})_2\text{Sn}(\textit{n}\text{-Bu})_3$ (identified by comparison with an authentic sample¹⁵) and a 75% yield of PPh_3 .

2a: Completion of the thermolysis required 3 h at 120 °C. NMR spectral analysis indicated a 71% yield of $\text{Cp}^*\text{Fe}(\text{CO})_2\text{SnPh}_3$ (identical with an authentic sample⁸) and a 23% yield of $[\text{Cp}^*\text{Fe}(\text{CO})_2]_2$ (also identical with an authentic sample). Additionally, a small amount of a third, unidentified, component was observed.

2b: After 1 h at 70 °C, thermolysis was complete. NMR spectral analysis indicated a 73% yield of $\text{Cp}^*\text{Fe}(\text{CO})_2\text{SnMe}_3$

(14) Ellis, J. E.; Flour, E. *J. Organomet. Chem.* **1975**, *99*, 263.

(15) Dalton, J.; Paul, T.; Stone, F. G. A. *J. Chem. Soc. A* **1969**, 2744.

(16) Goodman, B. A.; Greatrex, R.; Greenwood, N. N. *J. Chem. Soc. A* **1971**, 1868.

(compared with an authentic sample⁸) and showed the dimer [Cp*Fe(CO)₂]₂ as a significant product also.

2c: Thermolysis was complete after 1.5 h at 90 °C. NMR analysis of the product mixture indicated a 78% yield of Cp*Fe(CO)₂Sn(*n*-Bu)₃ (compared with an authentic sample, see above), a 5% yield of the dimer, [Cp*Fe(CO)₂], and small amounts of several products which could not be identified.

3a: Thermolysis was complete after 2 h at 185 °C; degradation was extensive. NMR analysis of the product mixture indicated a very small yield of a compound, whose spectral properties were in agreement with those of an authentic sample of Cp*Re(CO)(NO)SnPh₃.

3b: Complete thermolysis required 20.5 h at 90 °C. The product, isolated in 73% yield, was Cp*Re(CO)(NO)SnMe₃ (see characterization data above for this compound). At 185 °C, thermolysis was complete after 2 min, but degradation was extensive.

4a: Thermolysis required 8 h at 120 °C. Some degradation of the sample was evident; NMR analysis indicated a 53% yield of [Cp*Fe(CO)₂]₂ and a 77% yield of PPh₃.

5a: Thermolysis was complete after 2 h at 70 °C. NMR analysis of the product mixture indicated CpFe(CO)₂SnPh₃ (89%), [CpFe(CO)₂]₂ (10%), and small amounts of unidentified products (note that the sample used for thermolysis consisted of a 91:5:4 mixture of **5a** to iron–tin complex to iron dimer).

X-ray Crystal Structure of 1b. A suitable crystal was grown by layering a saturated toluene solution of **1b** with pentane and then cooling the sample to –30 °C. Data were collected on an Enraf-Nonius CAD4 diffractometer at –96 °C (to prevent solvent loss and degradation of the crystal); the data are outlined in Table 2. Selected bond distances and bond angles are shown in Table 5. Of 4402 unique reflections, 3494 were considered observed ($I > 3\sigma(I)$). The structure was solved using Patterson methods and refined with anisotropic thermal parameters for all non-hydrogen atoms, while the calculated positions and thermal parameters for the hydrogen atoms were kept constant. The temperature factors of the hydrogen atoms were set to 1.2 times the temperature factors of the carbon atoms to which they were bonded. The toluene solvate was found to be orientationally disordered about a common atom (C34ab). The disorder model is comprised of two groups having occupancies of $\frac{2}{3}$ (the “a” group) and $\frac{1}{3}$ (the “b” group). A final *R* index of 0.033 with *R*_w = 0.034 was obtained for 341 variables. All computations were performed using the teXsan¹⁷ package (Molecular Structure Corp.).

X-ray Crystal Structure of 1c. A suitable crystal was grown by layering a saturated toluene solution of **1c** with hexane and then cooling the sample to –30 °C. Data were collected on an Enraf-Nonius CAD4 diffractometer at –96 °C (to prevent solvent loss and degradation of the crystal); the data are outlined in Table 2. Selected bond distances and bond angles are shown in Table 6. Of 7125 unique reflections, 6023 were considered observed ($I > 3\sigma(I)$). The structure was solved using Patterson methods and refined with anisotropic thermal parameters for all non-hydrogen atoms, while the calculated positions and thermal parameters for the hydrogen atoms were kept constant. The temperature factors of the hydrogen atoms were set to 1.2 times the temperature factors of the carbon atoms to which they were bonded. Two sites of disorder were observed. The first, an *n*-butyl group, has two distinct

orientations of the two central atoms (C35, C36), each modeled at 50% occupancy. The second site of disorder is found with the toluene solvate. The model consists of two groups ($\frac{2}{3}$ and $\frac{1}{3}$ occupancy) as described for **1b**. A final *R* index of 0.053 with *R*_w = 0.067 was obtained for 414 variables. All computations were performed using the teXsan¹⁷ package (Molecular Structure Corp.).

X-ray Crystal Structure of 2a. A suitable crystal was grown by layering a saturated ether solution of **2a** with pentane and then cooling the sample to –30 °C. Data were collected on an Enraf-Nonius CAD4 diffractometer and are outlined in Table 2. Selected bond distances and bond angles are shown in Table 8. Of 5197 unique reflections, 4119 were considered observed ($I > 3\sigma(I)$). The structure was solved using Patterson methods and refined with anisotropic thermal parameters for all non-hydrogen atoms, while the calculated positions and thermal parameters for the hydrogen atoms were kept constant. The temperature factors of the hydrogen atoms were set to 1.2 times the temperature factors of the carbon atoms to which they were bonded. A final *R* index of 0.022 with *R*_w = 0.022 was obtained for 425 variables. All computations were performed using the teXsan¹⁷ package (Molecular Structure Corp.).

X-ray Crystal Structure of 3b. A suitable crystal was grown by layering a saturated chloroform solution of **3b** with hexane and then allowing the sample to stand. Data were collected on an Enraf-Nonius CAD4 diffractometer at –80 °C (to prevent solvent loss and degradation of the crystal); the data are outlined in Table 2. Selected bond distances and bond angles are shown in Table 10. Of 5019 unique reflections, 4674 were considered observed ($I > 3\sigma(I)$). The structure was solved using Patterson methods and refined with anisotropic thermal parameters for all non-hydrogen atoms, while the calculated positions and thermal parameters for the hydrogen atoms were kept constant. The temperature factors of the hydrogen atoms were set to 1.2 times the temperature factors of the carbon atoms to which they were bonded. A final *R* index of 0.031 with *R*_w = 0.031 was obtained for 311 variables. All computations were performed using the teXsan¹⁷ package (Molecular Structure Corp.).

Acknowledgment. Support of this work by the United States Department of Energy, Division of Chemical Sciences (Office of Basic Energy Sciences), Office of Energy Research, is gratefully acknowledged. The X-ray equipment was purchased with assistance from the National Science Foundation (Grant No. CHE-9016978). Support of the Molecular Structure Laboratory through the NSF/KY EPSCoR program (Grant No. EHR-9108764) is also gratefully acknowledged. B.A.S. gratefully acknowledges support from a GAANN Fellowship from the United States Department of Education (Grant No. P200A10139).

Supplementary Material Available: Tables of anisotropic thermal parameters, H atom positional parameters, bond distances, bond angles, and torsional angles for **1b,c**, **2a**, and **3b** (56 pages). This material is contained in many libraries on microfiche, immediately follows this article in the microfilm version of the journal, and can be ordered from the ACS; ordering information is given on any current masthead page.

(17) teXsan: Single Crystal Structure Analysis Software, Version 1.6; Molecular Structure Corp., The Woodlands, TX 77381, 1993.

Crystal Structures and Solution Conformations of the Meso and Racemic Isomers of (Ethylenebis(1-indenyl))zirconium Dichloride

Fabrizio Piemontesi,* Isabella Camurati, Luigi Resconi, and Davide Balboni

Himont Italia (Montedison Group), G. Natta Research Center, P.le Donegani 12,
44100 Ferrara, Italy

Angelo Sironi* and Massimo Moret

Istituto di Chimica Strutturistica Inorganica, Università di Milano, Via Venezian 21,
20133 Milano, Italy

Robert Zeigler

Himont U.S.A. (Montedison Group), Inc., Research & Development Center, 912 Appleton Road,
Elkton, Maryland 21921

Nicoletta Piccolrovazzi†

Institut für Polymere, Swiss Federal Institute of Technology, ETH-Zentrum,
8092 Zürich, Switzerland

Received September 14, 1994[®]

The crystal and molecular structures of the C_2 symmetric *rac*-(EBI)ZrCl₂ (**1r**) [monoclinic, space group $I2/c$, No. 15, $a = 11.957(1)$ Å, $b = 10.627(1)$ Å, $c = 13.775(2)$ Å, $\beta = 106.06(1)^\circ$] and of its *meso* isomer (**1m**) [monoclinic, space group $P2_1/n$, No. 14, $a = 11.119(3)$ Å, $b = 10.467(1)$ Å, $c = 14.949(2)$ Å, $\beta = 100.94(2)^\circ$] have been solved. **1r** is in the indenyl-forward (Π) conformation, as is the case for most of the chiral *ansa* ethylene-bridged bisindenyl-type metallocenes. In solution however, already at room temperature there is a rapid (NMR time scale) interconversion between the two Π and Y (indenyl-backward) conformations, as shown by conformational analysis on the proton spectra of the bridge methylenes. This equilibrium is shifted toward the lower energy conformation δ at lower temperatures and is influenced by both the solvent and the σ -ligands. The solid state structure of **1m** shows that this *meso* form is actually in a chiral conformation (C_1 symmetry) because of the staggered placement of the two indenyl ligands ($\text{Ind}^{\wedge}\text{Ind} = 10.0^\circ$). In solution this specific zirconocene gives a perfectly symmetric ¹H NMR spectrum, indicating that, as in the case of the *rac*-isomer, there is a rapid interconversion between the two equienergetic, mirror-image limit conformations.

Introduction

The reports by Ewen¹ and Kaminsky² that the homogeneous catalyst systems composed of *racemic* (ethylenebis(1-indenyl))MCl₂ or *racemic* (ethylenebis(4,5,6,7-tetrahydro-1-indenyl))MCl₂ (group 4 bent metallocenes of the class of chiral *ansa*-metallocenes developed by Brintzinger;³ M = Ti, Zr, Hf) and methylalumoxane (MAO) produce isotactic polypropylene (iPP) have started a frantic research activity on the isospecific polymeri-

zation of olefins with metallocene catalysts in both academic and industrial laboratories. Although less suitable than MgCl₂-supported Ti-based catalysts^{4,5} for the industrial production of polypropylene, the now classic *rac*-(ethylenebis(1-indenyl))zirconium dichloride (*rac*-(EBI)ZrCl₂, **1r**) and *rac*-(ethylenebis(4,5,6,7-tetrahydro-1-indenyl))zirconium dichloride (*rac*-(EBTHI)-

(3) (a) Schnutenhaus, H.; Brintzinger, H. H. *Angew. Chem., Int. Ed. Engl.* **1979**, *18*, 777. (b) Wild, F.; Zsolnai, L.; Huttner, G.; Brintzinger, H. H. *J. Organomet. Chem.* **1982**, *232*, 233. (c) Collins, S.; Kuntz, B.; Taylor, N.; Ward, D. *J. Organomet. Chem.* **1988**, *342*, 21. (d) Wild, F.; Wasjucionek, M.; Huttner, G.; Brintzinger, H. H. *J. Organomet. Chem.* **1985**, *288*, 63. (e) Schäfer, A.; Karl, E.; Zsolnai, L.; Huttner, G.; Brintzinger, H. H. *J. Organomet. Chem.* **1987**, *328*, 87. (f) Wiesenfeldt, H.; Reinmuth, A.; Barsties, E.; Evertz, K.; Brintzinger, H. H. *J. Organomet. Chem.* **1989**, *369*, 359. (g) Burger, P.; Hortmann, K.; Diebold, J.; Brintzinger, H. H. *J. Organomet. Chem.* **1991**, *417*, 9. (h) Brintzinger, H. H. In *Transition Metals and Organometallics as Catalysts for Olefin Polymerization*; Kaminsky, W., Sinn, H., Eds.; Springer-Verlag: Berlin, 1988; p 249.

(4) These are found to produce iPP which is not suitable for current commercial applications: at practical polymerization temperatures, in fact, molecular weight, isotacticity, and regioregularity are relatively low, and these molecular properties are reflected in very high solvent soluble fractions, low melting temperatures, and poor mechanical properties.⁵

† Current Address: Dow Europe SA, Bachtobelstr. 3, 8810 Horgen, Switzerland.

[®] Abstract published in *Advance ACS Abstracts*, January 1, 1995. (1) (a) Ewen, J. *J. Am. Chem. Soc.* **1984**, *106*, 6355. (b) Ewen, J. U.S. Patent 4,522,982 to Exxon, 1985. (c) Ewen, J. In *Catalytic Polymerization of Olefins*; Studies in Surface Science Catalysis Vol. 25; Keii, T., Soga, K., Eds.; Elsevier: Amsterdam, 1986; p 271. (d) Ewen, J.; Haspeslagh, L.; Atwood, J.; Zhang, H. *J. Am. Chem. Soc.* **1987**, *109*, 6544.

(2) (a) Kaminsky, W.; Külper, K.; Brintzinger, H.; Wild, F. *Angew. Chem., Int. Ed. Engl.* **1985**, *24*, 507. (b) Kaminsky, W.; Külper, K.; Buschermöhle, M.; Lüker, H. U.S. Patent 4,769,510 to Hoechst, 1988. (c) Kaminsky, W. *Angew. Makromol. Chem.* **1986**, *145/146*, 149. (d) Drögemüller, H.; Niedoba, S.; Kaminsky, W. *Polym. React. Eng.* **1986**, *299*. (e) Kaminsky, W. In *Catalytic Polymerization of Olefins*; Keii, T., Soga, K., Eds.; Elsevier: Amsterdam, 1986; p 293.

ZrCl₂) are often used as the comparison catalysts when new metallocenes are introduced. They are also excellent model compounds for theoretical⁶ and mechanistic⁷ studies and have found interesting applications as enantioselective catalysts.⁸ For chiral *ansa*-metallocenes, the metal-*ansa*-ligand framework dictates substrate enantioface selectivity, and ligand-substrate nonbonded interactions can be affected by conformational changes of the catalyst. Brintzinger⁹ has shown that there is a rapid (NMR time scale) interconversion between two conformations in the achiral C_{2v}-symmetric *ansa*-titanocene (ethylenebis(cyclopentadienyl)titanium dichloride. Chien^{9g,h} and Rieger¹⁰ have proposed that the two conformers of the active species in **1r** might have different stereoregulating abilities in propylene polymerization.

Hence, a better knowledge of the basic properties of these chiral zirconocenes, especially in solution, should be of general interest. We have already reported on the effect of monomer concentration on the molecular weight and stereo- and regioregularity of polypropylene produced with **1r**.¹¹ In this paper we present the molecular structures of **1r** and its stereoisomer *meso*-(EBI)ZrCl₂ (**1m**), and aiming at establishing the differences between solid state and solution conformations of these *ansa*-zirconocene precatalysts, we present their dynamics in solution through a detailed ¹H and ¹³C NMR analysis.¹²

Results and Discussion

1. Synthesis of the Zirconocenes. After the first report by Brintzinger and Wild,^{3d} who prepared pure *rac*-(EBI)ZrCl₂ (**1r**) in 30% yield from ZrCl₄ and (ethylene(bisindenyl))Li₂ ((EBI)Li₂), this synthesis has been largely improved. By using higher dilution and slow, simultaneous addition of the two reactants, ZrCl₄(THF)₂ and (EBI)Li₂ in THF, Collins¹³ reported a 52% yield of the pure racemic product. By the use of KH as the deprotonating agent, Buchwald¹⁴ increased the yields up to 75% but at the expense of specificity, as a mixture of isomers (*rac*:*meso* 2:1) is obtained. Although this does not represent a major problem in the synthesis of *rac*-(EBTHI)ZrCl₂, for the two isomers are easily separated given their very different solubilities in toluene, this is a major drawback if one wishes to obtain pure *rac*-(EBI)ZrCl₂, as the two isomers are not easily separated by solvent extraction. However, repeated crystallization from THF of the **1r/1m** mixture prepared according to Buchwald finally yielded pure **1m** as orange crystals suitable for X-ray diffraction. Collins' procedure results in isomerically pure **1r** directly and ultimately in the highest yield.

However, Collins' protocol requires a washing step with HCl/H₂O which can lead, if not carried out very rapidly and on the perfectly dried reaction mixture (given the instability of (EBI)ZrCl₂ in solution toward hydrolysis), to some decomposition products which are not completely removed (e.g. zirconium oxy chlorides) by the subsequent washings with EtOH and Et₂O, leading to highly varying chemical purities (and catalytic activity!) of the final product. A simple way of purifying this product consists of a CH₂Cl₂ Soxhlet extraction of the crude reaction mixture after filtration of the THF/Et₂O slurry and drying. Provided the usual precautions in the handling of moisture-sensitive compounds are observed, *rac*-(EBI)ZrCl₂ is stable in refluxing CH₂Cl₂ for at least 2 days. Furthermore, if little enough solvent is used, the product crystallizes during extraction and is recovered quantitatively upon solvent removal. We recommend this simpler, highly reproducible purification procedure if **1r** is to be used for catalytic purposes.

2. Crystal and Molecular Structure of *rac*- and *meso*-(EBI)ZrCl₂. *rac*-(EBI)ZrCl₂ (**1r**) has a crystallographically imposed C₂ symmetry and is isomorphous and isostructural to *rac*-(EBI)HfCl₂^{1d} and to the related *rac*-(EBTHI)TiCl₂,^{3b} *rac*-(EBTHI)ZrCl₂,^{3c,d} and *rac*-(EBTHI)HfCl₂^{1d} tetrahydro derivatives. Conversely, *meso*-(EBI)ZrCl₂ (**1m**), *meso*-(EBTHI)ZrCl₂¹⁵ and *meso*-(EBTHI)TiCl₂^{3b} are not isomorphous, possibly because the lack of any internal symmetry element (to be aligned with a crystallographic one) leaves a larger packing conformational freedom to the *meso* derivatives which, as a consequence, have systematically larger *U/Z* (volume per molecule; see Table 1) values than their *rac* counterparts (*i.e.* less-bound systems have a larger conformational freedom). Figures 1 and 2 report two different ORTEP views of *rac*- and *meso*-(EBI)ZrCl₂

(5) (a) Grassi, A.; Zambelli, A.; Resconi, L.; Albizzati, E.; Mazzocchi, R. *Macromolecules* **1988**, *21*, 617. (b) Cheng, H.; Ewen, J. *Makromol. Chem.* **1989**, *190*, 1931. (c) Tsutsui, T.; Ishimaru, N.; Mizuno, A.; Toyota, A.; Kashiwa, N. *Polymer* **1989**, *30*, 1350. (d) Tsutsui, T.; Mizuno, A.; Kashiwa, N. *Makromol. Chem.* **1989**, *190*, 1177. (e) Tsutsui, T.; Kioka, M.; Toyota, A.; Kashiwa, N. In *Catalytic Olefin Polymerization*; Studies on Surface Science and Catalysis Vol. 56; Keii, T., Soga, K., Eds.; Elsevier: Amsterdam, 1990; p 493. (f) Rieger, B.; Chien, J. *Polym. Bull.* **1989**, *21*, 159. (g) Rieger, B.; Mu, X.; Mallin, D.; Rausch, M.; Chien, J. *Macromolecules* **1990**, *23*, 3559. (h) Chien, J.; Sugimoto, R. *J. Polym. Sci. A: Polym. Chem.* **1991**, *29*, 459.

(6) (a) Corradini, P.; Guerra, G.; Vacatello, M.; Villani, V. *Gazz. Chim. Ital.* **1988**, *118*, 173. (b) Cavallo, L.; Guerra, G.; Oliva, L.; Vacatello, M.; Corradini, P. *Polym. Commun.* **1989**, *30*, 16. (c) Cavallo, L.; Corradini, P.; Guerra, G.; Vacatello, M. *Polymer* **1991**, *32*, 1329. (d) Cavallo, L.; Guerra, G.; Vacatello, M.; Corradini, P. *Chirality* **1991**, *3*, 299. (e) Castonguay, L.; Rappé, A. *J. Am. Chem. Soc.* **1992**, *114*, 5832.

(7) (a) Pino, P.; Cioni, P.; Wei, J. *J. Am. Chem. Soc.* **1987**, *109*, 6189. (b) Pino, P.; Cioni, P.; Galimberti, M.; Wei, J.; Piccolrovazzi, N. In *Transition Metals and Organometallics as Catalysts for Olefin Polymerization*; Kaminsky, W., Sinn, H., Eds.; Springer-Verlag: Berlin, 1988; pp 269. (c) Pino, P.; Galimberti, M. *J. Organomet. Chem.* **1989**, *370*, 1. (d) Pino, P.; Galimberti, M.; Prada, P.; Consiglio, G. *Makromol. Chem.* **1990**, *191*, 1677. (e) Kaminsky, W.; Ahlers, A.; Möller-Lindenhof, N. *Angew. Chem., Int. Ed. Engl.* **1989**, *28*, 1216. (f) Krauledat, H.; Brintzinger, H. H. *Angew. Chem., Int. Ed. Engl.* **1990**, *29*, 1412. (g) Ewen, J.; Elder, M.; Jones, R.; Haspelslagh, L.; Atwood, J.; Bott, S.; Robinson, K. *Makromol. Chem., Macromol. Symp.* **1991**, *48/49*, 253. (h) Horton, A.; Frijns, J. *Angew. Chem., Int. Ed. Engl.* **1991**, *30*, 1152. (i) Chien, J.; Tsai, W.; Rausch, M. *J. Am. Chem. Soc.* **1991**, *113*, 8570. (j) Coates, G.; Waymouth, R. *J. Am. Chem. Soc.* **1993**, *115*, 91. (k) Busico, V.; Cipullo, R.; Corradini, P. *Makromol. Chem., Rapid Commun.* **1993**, *14*, 97.

(8) (a) Waymouth, R.; Pino, P. *J. Am. Chem. Soc.* **1990**, *112*, 4911. (b) Grossman, R.; Davis, W.; Buchwald, S. *J. Am. Chem. Soc.* **1991**, *113*, 2321. (c) Hong, Y.; Kuntz, B.; Collins, S. *Organometallics* **1993**, *12*, 964. (d) Hoveyda, A.; Morken, J. *J. Org. Chem.* **1993**, *58*, 4237.

(9) Smith, J.; von Seyerl, J.; Huttner, G.; Brintzinger, H. H. *J. Organomet. Chem.* **1979**, *173*, 175.

(10) Rieger, B. *J. Organomet. Chem.* **1992**, *428*, C33.

(11) Balbontin, G.; Fait, A.; Piemontesi, M.; Resconi, L.; Rychlicki, H. Presented in part at the International Symposium on Synthetic, Structural and Industrial Aspects of Stereospecific Polymerization (STEPOL '94), Milano, Italy, June 6-10, 1994; book of Abstracts pp 205-206.

(12) Camurati, I.; Piemontesi, F.; Resconi, L.; Zeigler, R. Presented in part at the International Symposium on Synthetic, Structural and Industrial Aspects of Stereospecific Polymerization (STEPOL '94), Milano, Italy, June 6-10, 1994; book of Abstracts pp 245-246.

(13) Lee, I.; Gauthier, W.; Ball, J.; Iyengar, B.; Collins, S. *Organometallics* **1992**, *11*, 2115.

(14) Grossman, R.; Doyle, R.; Buchwald, S. *Organometallics* **1991**, *10*, 1501.

(15) Collins, S.; Gauthier, W.; Holden, D.; Kuntz, B.; Taylor, N.; Ward, D. *Organometallics* **1991**, *10*, 2061.

Table 1. Reduced Cell Parameters for Known Racemic and Meso *ansa*-Bisindenyl or Tetrahydroindenyl Derivatives

	<i>a</i> (Å)	<i>b</i> (Å)	<i>c</i> (Å)	β (deg)	<i>Z</i>	<i>V</i>	SG ^b	ref
<i>rac</i> -(EBTH)Ti	12.340	10.088	14.144	104.97	4	1701	<i>I2/c</i>	3b
<i>rac</i> -(EBTH)Zr	12.598	10.092	14.302	105.38	4	1753	<i>I2/c</i>	3c,d
<i>rac</i> -(EBTH)Hf ^a	12.574	10.115	14.296	105.47	4	1752	<i>I2/c</i>	1d
<i>rac</i> -(EBI)Zr	11.957	10.627	13.775	106.06	4	1682	<i>I2/c</i>	this work
<i>rac</i> -(EBI)Hf ^a	11.945	10.612	13.718	106.09	4	1671	<i>I2/c</i>	1d
<i>meso</i> -(EBTH)Ti	14.952	13.633	17.352		8	3537	<i>Pbca</i>	3b
<i>meso</i> -(EBTH)Zr	12.051	15.184	9.939	92.94	4	1816	<i>P2₁/c</i>	15
<i>meso</i> -(EBI)Zr	11.119	10.467	14.949	100.94	4	1708	<i>P2₁/n</i>	this work

^a Originally described in the (equivalent) standard *C2/c* space group.

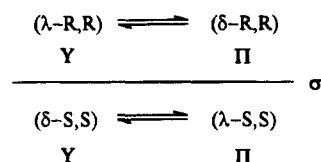
^b SG = space group.

while Tables 2 (lengths), 3 (angles), and 4 (least-squares planes and slip-fold indicators) contain most of their relevant bonding parameters.

The *rac*-C₂H₄(indenyl)₂M fragment has been previously structurally characterized in *rac*-(EBI)HfCl₂,^{1d} [*rac*-(EBI)ZrC(SiMe₃)=CMe₂]⁺,¹⁶ and [*rac*-(EBI)Zr{CH(SiMe₂Cl)(SiMe₃)}]⁺,¹⁷ while this is the first structural characterization of the *meso* one, which unfortunately is affected by some conformational disorder problem (see Experimental Section), and the bonding parameters are not sufficiently accurate to allow a detailed comparison of C–C and Zr–C interactions in the *rac* and *meso* fragments. Nevertheless it is clear that in both the derivatives the Zr–C bond interactions involving the bridgehead carbon atoms are longer than the other carbon–metal bonds within the η^5 -moiety. Incipient $\eta^5 \rightarrow \eta^3$ distortions are normally observed for η^5 -indenyl complexes and are commonly measured by the so called slip-fold parameters Ψ , Ω , and Δ defined in ref 18. Moreover on moving from *rac* to *meso*, the indenyl ligands take more room around the Zr atom at the expense of the chlorine atoms as shown by the widening of the Cp–Zr–Cp' angle, the shrinking of the Cl–Zr–Cl angle, and the lengthening of the average Zr–Cl bond distance. Besides, because the two Zr–Cl bonds in the *meso* derivative are not related by symmetry and, more importantly, their local environments are dissimilar, they are markedly different. The *rac* stereoisomer, reported in Figure 1, according to an adaptation by Schlogl of the Cahn–Ingold–Prelog rules has clearly an *R,R* configuration of the bridgehead carbon atoms and a δ conformation of the Zr–C1,C8,C8',C1' "metallacycle". Conversely the *meso* stereoisomer reported in Figure 2 has λ,R,S stereochemistry. However, both in solution and in the solid state, as they crystallize in a centrosymmetric space groups, their enantiomers (λ,S,S and δ,R,S , respectively) are also present. In Table 5 we report the distances and torsional angles between the bridge protons H8 and the indenyl back protons H2 and H7 in **1r** and **1m**.

3. NMR Analysis and Solution Conformations. Spectral Assignments. One of the key questions in evaluating the catalytic performance of organometallic complexes is whether their solid state structure is maintained in solution. In the case of the *rac*-(EBI)-ZrCl₂ precatalyst, the first point to be established is whether the only conformation observed in its crystal structure (indenyl-forward, here called Π from the Greek $\pi\omega\omega$, in front) is maintained in solution, or if also

the higher energy indenyl-backward conformation (Υ , from the Greek $\nu\sigma\tau\epsilon\omega\omega$, behind) can be present (Figure 3).^{3h} We use here a nomenclature for the two different conformations (Π and Υ) different from that commonly used for this class of compounds (λ and δ). The λ and δ nomenclature changes also by changing enantiomer, by simple reflection, and can thus generate confusion in racemic compounds as **1r** (see Scheme 1; σ represents a mirror plane).

Scheme 1

Our interest in determining the solution conformations for **1r** and **1m** stems from the fact that it is the metal–*ansa* ligand framework, which remains intact during catalysis, that dictates enantioface selectivity in a number of enantioselective and diastereoselective transformations, and ligand–substrate nonbonded interactions are expected to be slightly different in the two conformations.

In order to elucidate this point we carried out a detailed NMR analysis of **1r** and **1m**. Complete spectral assignments of the ¹H and ¹³C NMR spectra of *rac*- and *meso*-(EBI)ZrCl₂ were first made through bidimensional NMR techniques and are reported in Table 6a; their proton spectra are overlapped in Figure 4.

The following discussion is based on the numbering system reported in Chart 1 according to the atom numbering of the molecular structures (Figures 1 and 2). The ¹H NMR spectrum of **1r** exhibits three recognizable groups of signals, the multiplet of the bridge protons (H8), the doublets of the C5 ring protons (H2, H3), and the C6 ring protons (H4, H5, H6 and H7).

COSY¹⁹ and NOESY²⁰ 2-D sequences, showing correlations of resonances from *J*-coupled (COSY) and dipolar-coupled (NOESY) protons, were used to establish a biunivocal correspondence between each proton in the molecule and each resonance in the 1-D spectrum. Figure 5 shows an expanded region of the COSY spectrum of *rac*-(EBI)ZrCl₂ together with the more significant coupling patterns between H2–H3, H3–H7, H4–H5, H5–H6, and H6–H7. In addition to some of the cross-peaks found in the COSY spectrum, the NOESY spectrum (Figure 6) shows the correlations between H8–H2, H8–H7, H2–H7', and H3–H4 (a prime indicates a proton on the opposite indenyl), thus confirming the assignments made through COSY.

The DEPT 135 sequence was used to separate the resonances of CH₂, CH, and quaternary carbons in the ¹³C spectrum. Assignments of the protonated carbons were then obtained using a heteronuclear COSY (XH-CORR)²¹ which correlates each carbon to its directly bound protons. Unambiguous attribution of the quaternary carbons from the heteronuclear long-range COSY (COLOC)²² spectrum was not possible. We present here a tentative assignment based on nuclear

(19) (a) Aue, W. P.; Bartholdi, E.; Ernst, R. R. *J. Chem. Phys.* **1976**, *64*, 2229. (b) Nagayama, K.; et al. *J. Magn. Reson.* **1980**, *40*, 321.

(20) States, D. J.; Haberkorn, R. A.; Ruben, D. J. *J. Magn. Reson.* **1982**, *48*, 286.

(21) Bax, A.; Morris, G. J. *J. Magn. Reson.* **1981**, *42*, 501.

(16) Horton, A.; Orpen, G. *Organometallics* **1991**, *10*, 3910.

(17) Horton, A.; Orpen, G. *Organometallics* **1992**, *11*, 1193.

(18) Faller, J. W.; Crabtree, R. H.; Habib, A. *Organometallics* **1985**, *4*, 929.

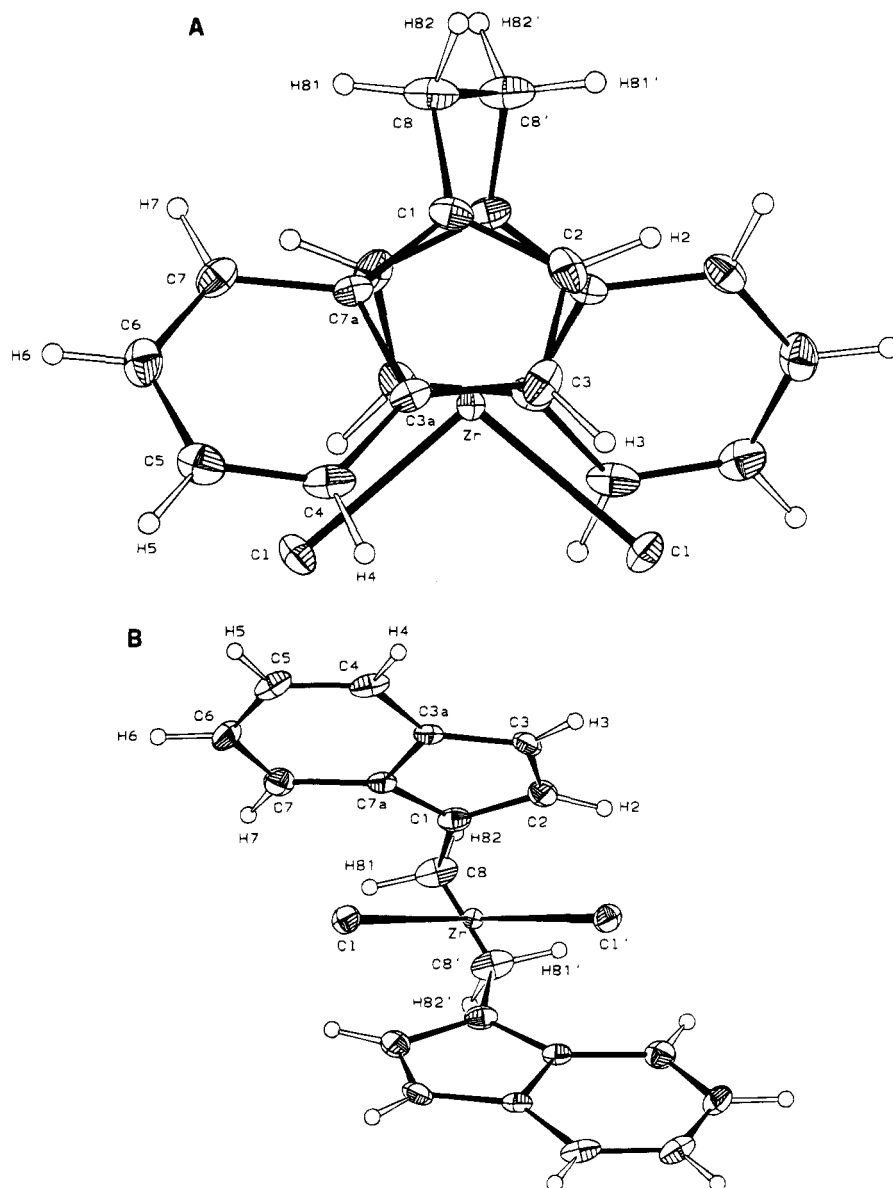


Figure 1. Top (A) and front (B) ORTEP views of **1r**. Thermal ellipsoids are drawn at the 30% probability level. Hydrogen atoms were given arbitrary radii.

Overhauser enhancement (NOE) experiments. We can assign the ^{13}C peak at 121.81 ppm to the carbon 1 due to its coupling to only two protons, the large NOE seen upon irradiation of the ethylene bridge protons, and the sharpening of the peak when the aromatic protons on the five-membered ring are irradiated. The two resonances at 123.12 and 129.62 ppm cannot be unambiguously assigned. Through the combination of NOE data and the comparison with the spectrum²³ of a similar chiral zirconocene (*rac*-(ethylenebis(4,7-dimethyl-1-indenyl))zirconium dichloride¹³), we can tentatively assign the peak at 123.12 ppm to carbon 7a and the peak at 129.62 ppm to carbon 3a.

The same analysis was performed on **1m**. Chemical shifts for both hydrogens and carbons are reported in Table 6b. Assignments of the ^1H spectrum were obtained from the COSY of Figure 7. The spectrum exhibits correlations between H3 and H7 (due to the 5J coupling constant), H2–H3, H6–H7, H5–H6, and H4–

H5. In the *meso* form the two bridge protons give well-separated multiplets at 3.5 and 3.8 ppm which were assigned from the NOESY spectrum of Figure 8 exhibiting cross-peaks between H81 and H2 and H82 and H7.

Assignments of the protonated carbons were obtained from the XH-CORR spectrum; again no univocal assignments were possible for the quaternary carbons. However, as we observed little dependence of the chemical shifts on the zirconocene symmetry, we give assignments for these carbons based on those obtained for the *rac* isomer **6r**.

Conformational Analysis. The $\text{CH}_2\text{--CH}_2$ bridge protons of **1r** form an AA'BB' spin system which gives rise to a 24 line spectrum (centrosymmetric about $1/2(\nu_A + \nu_B)$). Its form depends on the values of chemical shift difference ($\Delta\delta$) and coupling constants (J)²⁴ which are influenced by the molecular conformation. Particularly, while the geminal coupling constants (2J) do not

(22) Kessler, H.; Griesinger, C.; Zarbock, J.; Loosli, H. R. *J. Magn. Reson.* **1984**, *57*, 331.

(23) Unpublished results from our laboratories.

(24) In an AA'BB' spin system coupling constants and chemical shifts cannot be directly obtained from the peak distances in the spectrum but must be calculated by computer analysis of the spectral region of interest: the Bruker program PANIC, a version of the LAOCOON type programs (see ref 25, p 186), was used.

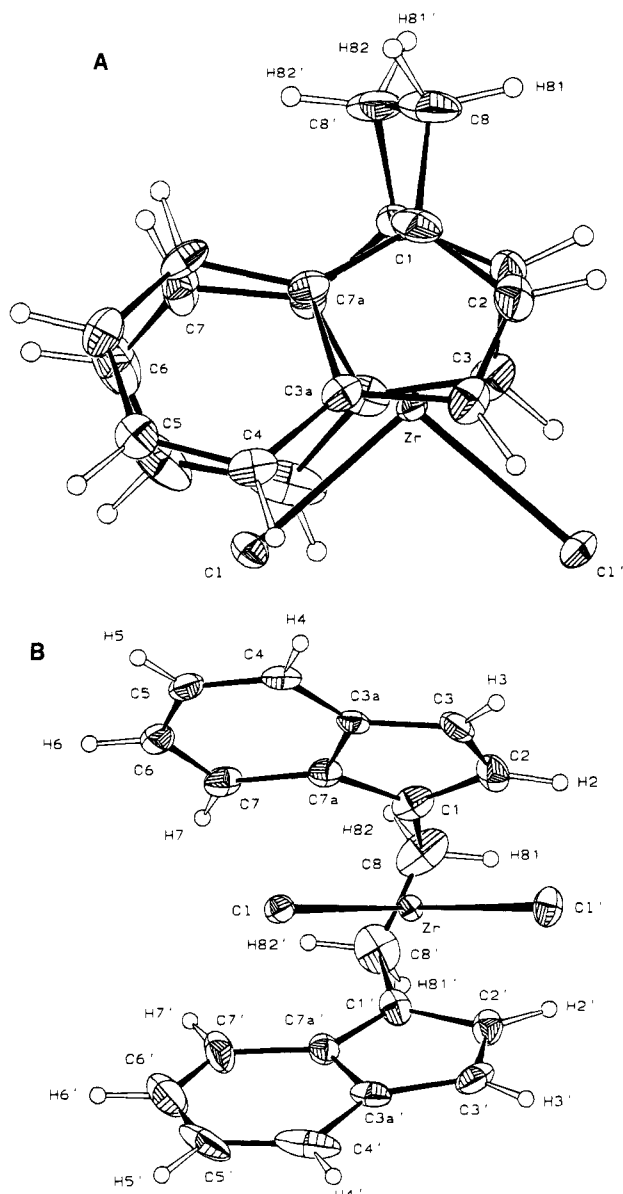


Figure 2. Top (A) and front (B) ORTEP views of **1m**. Thermal ellipsoids are drawn at the 30% probability level. Hydrogen atoms were given arbitrary radii.

change, the vicinal coupling constants (3J) strongly depend on the dihedral angle ϑ between the CH bonds according to the Karplus relation:²⁵

$$^3J = A + B \cos \vartheta + C \cos 2\vartheta \quad (1)$$

where A , B , and C are constants. For our system, the best results were obtained with $A = 7.23$, $B = -0.51$, and $C = 5.16$.

Both Π and Y structures are expected to approach a staggered ethylene bridge conformation,^{3e,26} and ϑ is likely to be between 30 and 60°. Two sets of coupling constants, one for each limit conformation, were then calculated according to eq 1 for ϑ values in the ranging from 0 to 60° (Table 7).

None of these calculated sets of J values fit the experimental coupling constants at 298 K (reported in Table 8), and our data can be interpreted only if a fast (NMR time scale) exchange occurs (Pachler-type equi-

Table 2. Bond Lengths (Å)^a

	<i>rac</i> -(EBI)ZrCl ₂	<i>meso</i> -(EBI)ZrCl ₂	
		I	II
Zr—Cl	2.3884(5)	2.3968(8)	2.4551(8)
Zr—C1	2.438(2)	2.476(3)	2.481(3)
Zr—C2	2.443(2)	2.457(3)	2.470(3)
Zr—C3	2.531(2)	2.526(3)	2.514(4)
Zr—C3a	2.624(2)	2.646(3)	2.596(3)
Zr—C7a	2.553(2)	2.557(3)	2.563(3)
C1—C2	1.401(4)	1.401(5)	1.393(5)
C1—C7a	1.404(3)	1.429(4)	1.417(4)
C1—C8	1.470(3)	1.489(6)	1.544(7)
C2—C3	1.388(4)	1.396(5)	1.393(5)
C3—C3a	1.398(4)	1.420(5)	1.428(5)
C3a—C4	1.413(3)	1.425(4)	1.438(5)
C3a—C7a	1.415(3)	1.423(5)	1.405(5)
C4—C5	1.352(4)	1.344(4)	1.350(6)
C5—C6	1.402(5)	1.409(5)	1.401(8)
C6—C7	1.334(4)	1.344(4)	1.326(5)
C7—C7a	1.433(3)	1.429(4)	1.430(4)
C8—C8'	1.518(5)	1.452(7)	

^a I, II indicate atoms (I) and primed atoms (II) of **1m** as shown in Figure 2B.

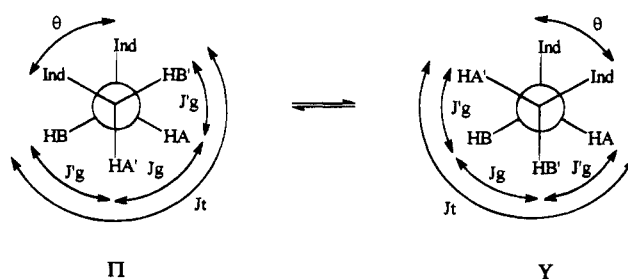
Table 3. Selected Bond and Torsional Angles (deg)^a

	<i>rac</i> -(EBI)ZrCl ₂	<i>meso</i> -(EBI)ZrCl ₂	
		I	II
<i>cp</i> —Zr— <i>cp</i> '	125.3(1)	126.2(1)	
C1—Zr—Cl'	99.09(3)	97.62(3)	
<i>cp</i> —Zr—Cl	106.5(1)	106.0(1)	107.8(1)
<i>cp</i> —Zr—Cl'	108.9(1)	107.0(1)	108.6(1)
C7a—C1—C2	107.5(2)	106.8(4)	108.0(4)
C7a—C1—C8	124.6(2)	128.3(4)	126.5(4)
C2—C1—C8	127.9(2)	124.7(4)	125.9(4)
C1—C2—C3	109.0(2)	109.5(4)	108.8(4)
C2—C3—C3a	108.0(2)	108.1(4)	108.3(4)
C3—C3a—C4	134.3(2)	132.5(3)	136.6(5)
C3—C3a—C7a	107.9(2)	107.5(3)	106.2(3)
C4—C3a—C7a	117.7(2)	120.0(3)	117.2(4)
C3a—C4—C5	120.2(2)	118.9(3)	120.2(6)
C4—C5—C6	122.4(2)	121.3(3)	120.5(6)
C5—C6—C7	119.5(3)	121.9(3)	123.3(6)
C7a—C7—C6	120.5(2)	119.5(3)	116.5(5)
C1—C7a—C3a	107.7(2)	107.9(3)	108.7(3)
C1—C7a—C7	132.6(2)	133.7(4)	129.1(4)
C3a—C7a—C7	119.7(2)	118.3(3)	122.2(4)
C1—C8—C8'—C1'	45.6(3)	-40.9(6)	
<i>bz</i> — <i>cp</i> — <i>cp</i> '— <i>bz</i> '	48.6(1)	-10.0(3)	

^a *cp* and *bz* refer to the center of mass of the five- and six-membered rings of the indenyl ligands. I, II indicate atoms (I) and primed atoms (II) of **1m** as shown in Figure 2B.

librium,²⁷ Scheme 2; Π and Y conformations are arbitrarily assigned and will be used without any reference to the real ones. Due to the AA'BB' spin system symmetry the bridge protons cannot be individually assigned, i.e., HA = H81 or H82, HB = H82 or H81, HA' = H81' or H82', and HB' = H82' or H81').

Scheme 2



(25) Günther, H. *NMR Spectroscopy*; Wiley: New York, 1980; p 106.
 (26) Jordan, R. F.; LaPointe, R. E.; Baenzinger, N.; Hinch, G. D. *Organometallics* **1990**, *9*, 1539.

(27) (a) Pachler, K. G. R. *Spectrochim. Acta* **1963**, *19*, 2085–2092.
 (b) *Spectrochim. Acta* **1964**, *20*, 581.

Table 4. Angles between Relevant Least-Squares Planes and Slip-Fold Parameters^a

	<i>rac</i> -(EBI)ZrCl ₂	<i>meso</i> -(EBI)ZrCl ₂	
		I	II
<i>Al/Bz</i> (deg)	5.3(1)	4.7(3)	2.8(3)
<i>ZrCl₂/In</i> (deg)	31.89(4)	31.01(5)	31.26(8)
<i>In/In'</i> (deg)	63.47(4)	62.3(1)	
Ψ (deg)	5.36	4.84	3.48
Ω (deg)	2.28	2.07	1.74
Δ (Å)	0.206	0.188	0.135

^a *Al*, *Bz*, *In*, and *ZrCl₂* refer to the least-squares planes defined by the allylic moieties (C7a, C1, C2), the six-membered rings, the indenyl ligands, and the ZrCl₂ atoms, respectively. I, II indicate atoms (I) and primed atoms (II) of **1m** as shown in Figure 2B.

The vicinal coupling constants are then given by the following equations:

$$J_{AA'} = aJ_g^\Pi + bJ_t^Y \quad (2)$$

$$J_{BB'} = aJ_t^\Pi + bJ_g^Y \quad (3)$$

$$J_{A'B} = J_{AB'} = aJ_g^\Pi + bJ_g^Y \quad (4)$$

where *a* and *b* are the relative residence times for the Π and *Y* conformations respectively (*a* + *b* = 1), and *J_t*, *J_g*, and *J_g'* are the vicinal coupling constants of the limit conformation, given by

$$J_t^\Pi = 7.23 - 0.51 \cos(120 + \vartheta_\Pi) + 5.16 \cos[2(120 + \vartheta_\Pi)] \quad (5a)$$

$$J_g^\Pi = 7.23 - 0.51 \cos(120 - \vartheta_\Pi) + 5.16 \cos[2(120 - \vartheta_\Pi)] \quad (5b)$$

$$J_g^\Pi = 7.23 - 0.51 \cos(\vartheta_\Pi) + 5.16 \cos(2\vartheta_\Pi) \quad (5c)$$

$$J_t^Y = 7.23 - 0.51 \cos(120 + \vartheta_Y) + 5.16 \cos[2(120 + \vartheta_Y)] \quad (6a)$$

$$J_g^Y = 7.23 - 0.51 \cos(120 + \vartheta_Y) + 5.16 \cos[2(120 - \vartheta_Y)] \quad (6b)$$

$$J_g^Y = 7.23 - 0.51 \cos(\vartheta_Y) + 5.16 \cos(2\vartheta_Y) \quad (6c)$$

Introducing the experimental *J*s in eqs 2–4 and using eqs 5a–6c, we can obtain ϑ_Π (48.8°), ϑ_Y (35.3°), *a*, and *b* (see Table 8). These results show that at room temperature one of the two conformations is slightly preferred and that the dihedral angles ϑ_Π and ϑ_Y have different values.

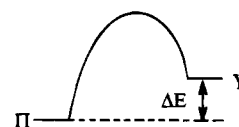
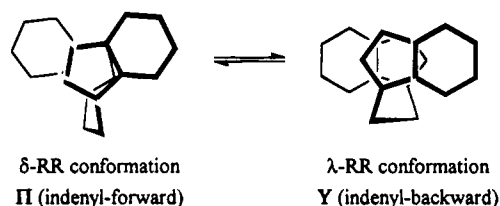
The conformational equilibrium was more deeply investigated in the same way by analyzing NMR spectra in a temperature range between 298 and 193 K.

As the temperature goes down, the spectrum changes due to the increase of the chemical shift difference and the change of the coupling constants (see Figure 9 and Table 8). The behavior of ³*J*s with 1/*T* is showed in Figure 10. As the angles ϑ_Π and ϑ_Y should not depend on the temperature, while *J_{AB'}* changes with *T*, we can deduce from eq 4 that *J_g^Π* ≠ *J_g^Y*. This is possible only if *J_Π* ≠ *J_Y*, confirming our results at room temperature.

Table 5. Selected H··H Lengths (Å) and Torsional Angles (deg)^a

	<i>rac</i> -(EBI)ZrCl ₂	<i>meso</i> -(EBI)ZrCl ₂	
		I	II
H81–H2	3.78	2.55	4.50
H81–H2'	2.66	2.77	3.76
H82–H2	3.08	3.45	4.38
H82–H2'	3.99	4.05	3.02
H81–H7	2.41	4.13	2.46
H81–H7'	4.95	4.86	2.36
H82–H7	3.56	3.03	3.94
H82–H7'	4.56	4.38	3.55
H81–C8–C8'–H81'	165.9	–160.7	
H81–C8–C8'–H82'	49.3	41.9	
H82–C8–C8'–H81'	47.3	–41.6	
H82–C8–C8'–H82'	–71.3	77.1	

^a I, II indicate bridge atoms (I) and primed bridge atoms (II) of **1m** as shown in Figure 2B.

**Figure 3.** Π and *Y* conformations in **1r**. (The ZrCl₂ fragment is omitted for clarity.)**Table 6. Carbon and Proton Assignments for *rac*-(EBI)ZrCl₂ and *meso*-(EBI)ZrCl₂**

atom	¹ H-NMR	multipl (<i>J</i> , Hz)	¹³ C-NMR
(a) <i>rac</i> -(EBI)ZrCl ₂			
1			121.81
2	6.20	d (3.35)	113.98
3	6.58	dd (3.35, 0.85)	110.83
4	7.50	d t	125.73
5	7.35	m	126.69
6	7.20	m	126.63
7	7.65	d q	121.42
8	3.6–3.9	m (AA'BB')	29.06
3a			129.62
7a			123.12
(b) <i>meso</i> -(EBI)ZrCl ₂			
1			121.21
2	6.55	d	115.28
3	6.70	dd	112.61
4	7.46	dt	125.64
5	7.15	m	126.30
6	7.07	m	126.74
7	7.50	dq	122.24
81 ^a	3.50–3.75	m (AA')	29.33
82 ^a	3.85–4.10	m (BB')	29.33
3a			129.39
7a			123.98

^a Hydrogens 81 = 81' and 82 = 82'.

The values of *a* and *b*, calculated using the room temperature ϑ_Π and ϑ_Y values (Table 8), show that, upon cooling, the conformational equilibrium is slowed down and one of the two limit conformations becomes predominant. As we said before, from our NMR data it is not possible to decide whether this conformation is really Π or *Y*, but as nonbonding interactions between

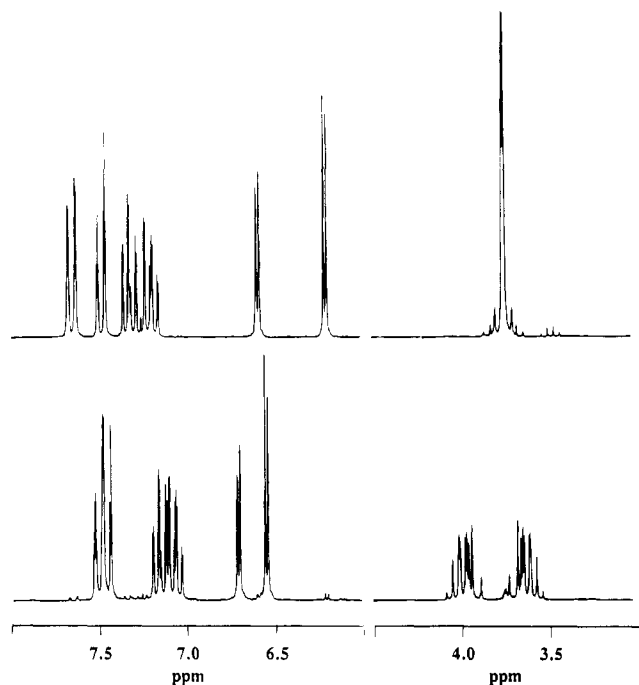
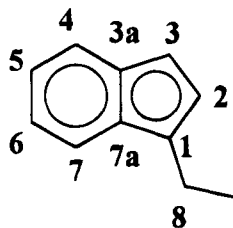


Figure 4. ^1H NMR spectrum of **1r** (top) and **1m** (bottom) in CDCl_3 at room temperature.

Chart 1



the bridge and indenyl fragments are higher in the latter,²⁸ we suggest the more stable conformation to be the II one.

Plotting of $\ln(a/b)$ versus $1/T$ (Figure 11) gave a linear correlation ($r = 0.993$) according to the following expression:

$$\ln(a/b) = \Delta G_{\text{IIY}}/RT$$

As the entropy difference for conformational isomers is usually assumed to be negligible, that is $\Delta G \approx \Delta H$, from the slope we obtain a value of $\Delta H_{\text{IIY}} = 0.945$ kcal/mol.

The experimental spectra for **1r** in different solvents are reported in Figure 12 together with the calculated set of coupling constants (Table 9). It can be seen that the conformational equilibrium is slightly influenced by the solvent.

In the case of **1m** a highly symmetric spectrum is observed at room temperature (only one signal for each type of proton on the two indenyl rings is present).

Two cases are then possible: (a) The molecule is in a completely eclipsed (e) conformation leading to a calculated J set of 11, 11, 5, 5 Hz for the bridge signal (see Table 10). (b) The molecule is rapidly exchanging between two staggered (s' and s'') conformations through a completely eclipsed (e) conformation (Figure 13). The

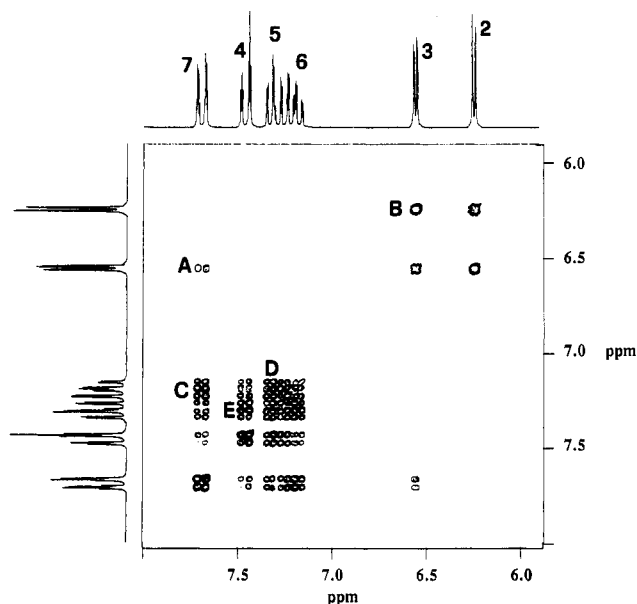


Figure 5. Expanded region of the COSY spectrum of **1r**. The cross-peak **A** at (6.6–7.65 ppm) due to a long-range coupling (5J) typical of indenyl systems allows the identification of H3 and H7. All other assignments were obtained from the cross-peaks **B** at 6.6–6.2 ppm (H3 and H2), **C** at 7.65–7.2 ppm (H7 and H6), **D** at 7.2–7.35 ppm (H6 and H5), and **E** at 7.35–7.5 ppm (H5 and H4).

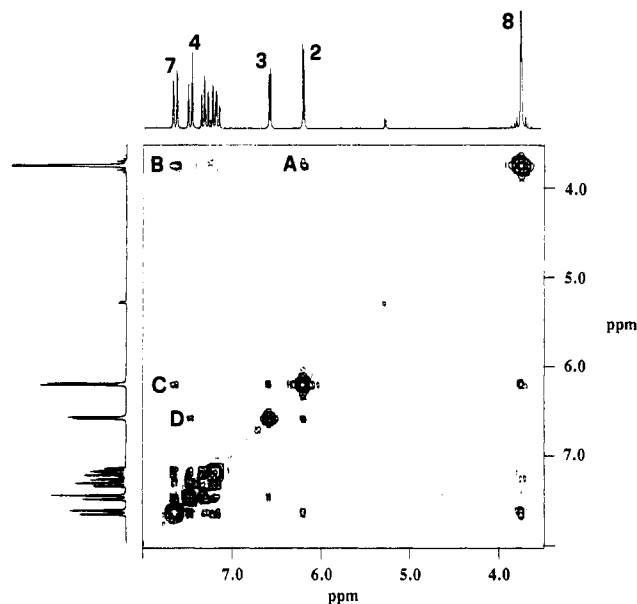


Figure 6. Expanded region of the NOESY spectrum of **1r** showing correlations between the bridge protons H8 with H2 (cross peak **A**) and H7 (**B**), between H2 and H7' (**C**), and between H3 and H4 (**D**).

two staggered conformations are mirror images, hence equienergetic, and have two symmetric sets of calculated coupling constants; the observed coupling constants are the average between those of the two limit conformations (Table 10).

Our results (see Table 11) are in favor of the equilibrium hypothesis and were confirmed by the VT-NMR spectra in the temperature range between 298 and 193 K (Figure 14; Table 11).

Conclusions

We have solved the solid state structure of Brintzinger's C_2 symmetric $\text{rac}-(\text{EBI})\text{ZrCl}_2$ and found it to be

(28) Collins, S.; Hong, Y.; Ramachandran, R.; Taylor, N. J. *Organometallics* **1991**, *10*, 2349.

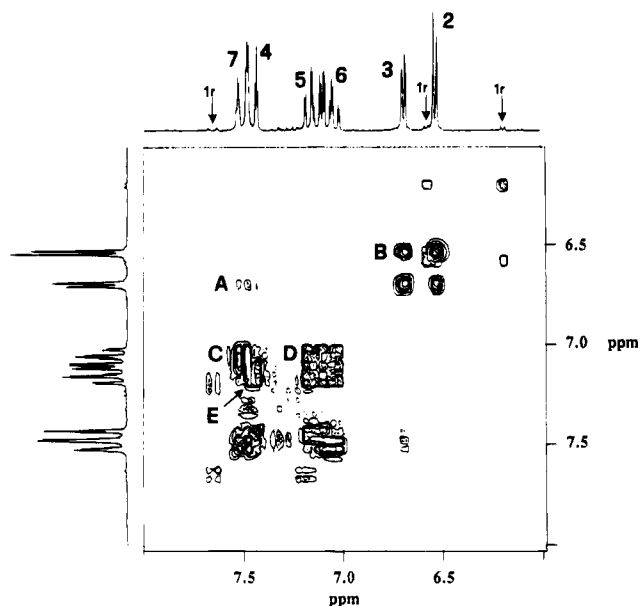


Figure 7. COSY spectrum of **1m**. The cross-peak **A** at 6.7–7.5 ppm due to the typical indenyl long-range coupling (5J) identifies H3 and H7. Cross-peak **B** at 6.55–6.7 with H3 identifies H2; cross-peak **C** at 7.5–7.07 ppm with H7 identifies H6; cross-peaks **D** at 7.07–7.15 and **E** at 7.15–7.46 identify H5 and H4, respectively.

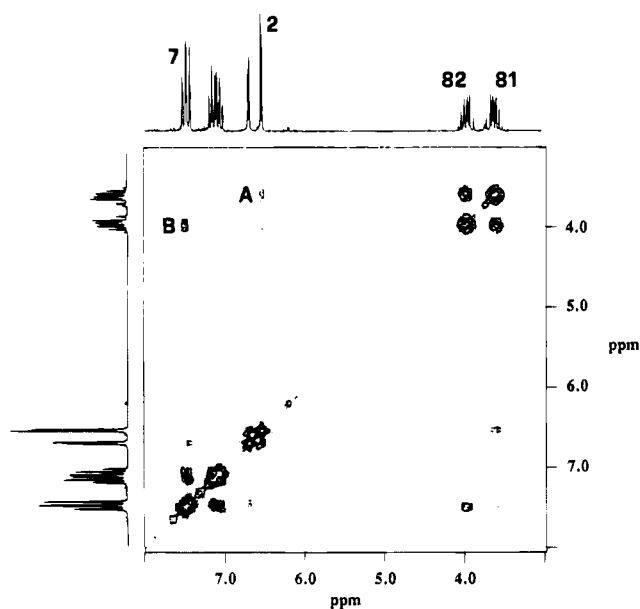


Figure 8. NOESY spectrum of **1m** showing correlations between the two bridge protons and H2 (cross peak **A**) and H7 (**B**) allowing the assignment of H81 (=H81') and H82 (=H82') as the multiplets at 3.5 and 3.8 ppm, respectively.

in the Π (indenyl-forward) conformation, as is the case for most of the chiral ethylene bridged bisindenyl-type metallocenes. In solution, however, already at room temperature there is a rapid (NMR time scale) interconversion between the two Π and Y (indenyl-backward) conformations, as shown by conformational analysis of the bridge methylenes done on their proton spectra and as found by Brintzinger⁹ for the *ansa* C_{2v} -symmetric (ethylenebis(cyclopentadienyl))titanium dichloride.

This equilibrium is shifted toward the lower energy conformation Π at lower temperatures. Solvent effects are also present. Also the solid state structure of the *meso* isomer has been compared to its solution conformation equilibrium. In the solid state *meso*-(EBI)ZrCl₂

Table 7. Coupling Constants (Hz) Calculated with the Karplus Relation for the Different Conformations of *rac*-(EBI)ZrCl₂ and for Different ϑ Values

ϑ	Π conformation			Y conformation		
	$J_{AA'}$	$J_{BB'}$	$J_{AB'} = J_{A'B}$	$J_{AA'}$	$J_{BB'}$	$J_{AB'} = J_{A'B}$
0	4.91	4.91	11.88	4.91	4.91	11.88
10	6.66	3.45	11.58	3.45	6.66	11.58
20	8.52	2.47	10.70	2.47	8.52	10.70
25	9.41	2.19	10.08	2.19	9.41	10.08
30	10.25	2.07	9.37	2.07	10.25	9.37
35	11.01	2.10	8.58	2.10	11.01	8.58
40	11.66	2.29	7.74	2.29	11.66	7.74
45	12.19	2.63	6.87	2.63	12.19	6.87
50	12.58	3.10	6.01	3.10	12.58	6.01
55	12.82	3.70	5.17	3.70	12.82	5.17
60	12.90	4.40	4.40	4.40	12.90	4.40

Table 8. *rac*-(EBI)ZrCl₂ VT-NMR Data: Experimental and Calculated Coupling Constants (in Parentheses) and Residence Times

T (K)	$J_{AB} = J_{A'B}$ (Hz)	$J_{AA'}$ (Hz)	$J_{BB'}$ (Hz)	$J_{AB'} = J_{A'B}$ (Hz)	a	b	L.S. ^a
298	-14.626	6.310	8.138	7.137	0.583	0.417	0.0037
		(6.345)	(8.173)	(7.172)			
273	-14.609	6.125	8.457	7.083	0.611	0.389	0.0006
		(6.122)	(8.460)	(7.108)			
253	-14.628	5.795	8.738	7.052	0.643	0.357	0.0080
		(5.866)	(8.789)	(7.035)			
233	-14.726	5.853	9.155	7.005	0.665	0.335	0.0463
		(5.686)	(9.021)	(6.983)			
223	-14.797	5.471	9.319	6.826	0.694	0.306	0.0084
		(5.451)	(9.323)	(6.915)			
213	-14.619	5.268	9.559	6.807	0.717	0.283	0.0030
		(5.262)	(9.567)	(6.861)			
193	-14.946	4.744	9.993	6.404	0.772	0.228	0.1352
		(4.825)	(10.130)	(6.736)			

$${}^a \text{L.S.} = \sum (J_{\text{exp}} - J_{\text{calc}})^2.$$

is actually in a chiral conformation (C_1 symmetry) because of the staggered placement of the two indenyl ligands ($\text{Ind}^{\wedge}\text{Ind} = 10.0^\circ$). In solution this asymmetric zirconocene gives a highly symmetric NMR spectrum indicating that, as in the case of the *rac* isomer, there is a rapid interconversion between the two equienergetic, mirror-image limit conformations. These results show that ethylene-bridged zirconocenes are less rigid than previously realized, and in the case where multiple spatial arrangements of the π -ligands are possible, the X-ray structure should not be used as a rigid model for the active site.

It is reasonable to assume that the energy of $\Pi \leftrightarrow Y$ conformation interconversion in the catalytically active species *rac*-(EBI)ZrP⁺ is higher due to the bulkiness of the growing polymer chain. As proposed by Rieger¹⁰ and Chien,^{5g,h} different conformations are likely to have different effects on catalyst stereospecificity. This might explain the high T_p dependence of the stereospecificity of **1r**/MAO observed in propylene polymerization.

Experimental Section

General Procedures. All operations were performed under nitrogen by using conventional Schlenk-line techniques. Solvents were distilled from blue benzophenone ketyl (THF), LiAlH₄ (Et₂O), P₄O₁₀ (CH₂Cl₂, CHCl₃), or AlⁱBu₃ (hydrocarbons) and stored under nitrogen. Indene (Aldrich) was distilled from CaH₂. 1,2-Dibromoethane (Aldrich) was stored over molecular sieves. MeLi (Aldrich) and BuLi (Aldrich) were used as received. All compounds were analyzed by ¹H NMR (200 MHz, CDCl₃, referenced against the peak of residual CHCl₃ at 7.25 ppm) or ¹³C NMR (50.3 MHz, CDCl₃, referenced against the central line of CDCl₃ at 77.00 ppm). All NMR solvents were dried over LiAlH₄ and distilled before use. Preparation of the

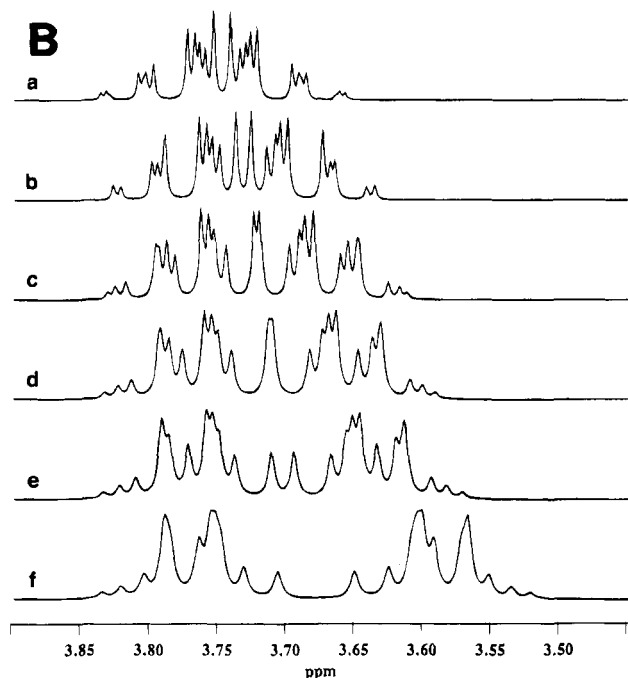
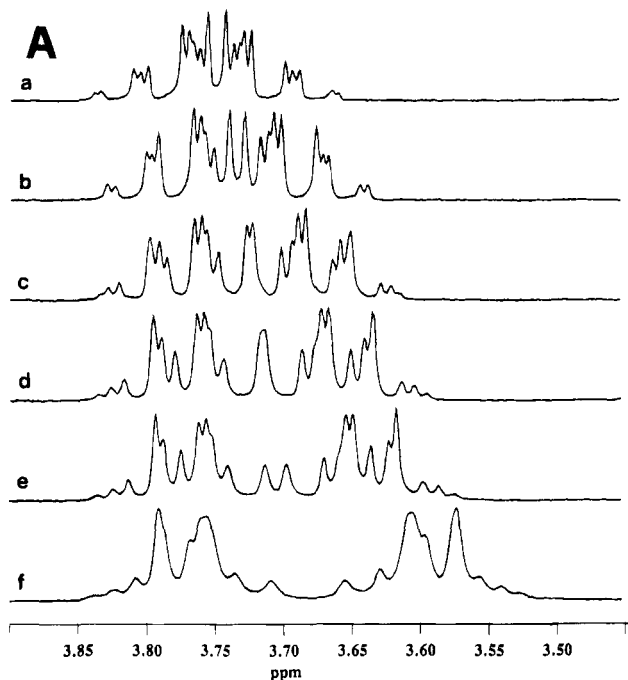


Figure 9. Experimental (A) and calculated (B) spectra of ethylene bridge region of **1r** in CD_2Cl_2 , at 25 (a), 0 (b), -20 (c), -40 (d), -50 (e), and -80 °C (f).

samples was carried out under dry, oxygen-free nitrogen using standard inert atmosphere techniques. Due to the low solubility of these compounds, the samples were dissolved in 0.5 mL of solvent to obtain a saturated solution in a 5-mm NMR tube.

Room-temperature spectra were recorded on an AC 200 Bruker spectrometer operating at 200.13 MHz for ^1H and 50.323 MHz for ^{13}C , in the Fourier transform mode. A 90° pulse of 6.5 s for ^1H , of 28 s for the decoupler ($\text{DP} = 1\text{H}$), and of 6.0 s for ^{13}C was used. Variable-temperature experiments were run on a Varian 300 spectrometer. All the ^{13}C spectra were acquired in the broad band decoupling mode. A $0.5/J(\text{CH}) = 0.0033$ s value, corresponding to $J = 150$ Hz, was used for DEPT135.

COSY and NOESY were obtained with a 1200-Hz spectral window, 0.426 s acquisition time, and 1 s relaxation delay. A total of 64 transients were collected for each of 256 t_1

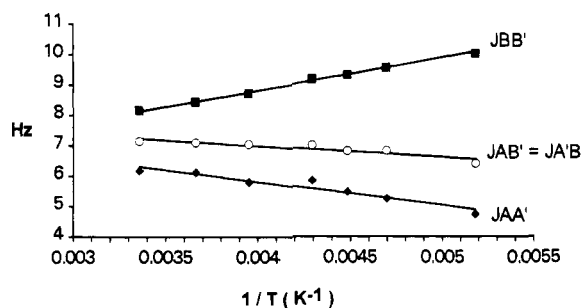


Figure 10. Temperature dependence of the bridge protons vicinal coupling constants.

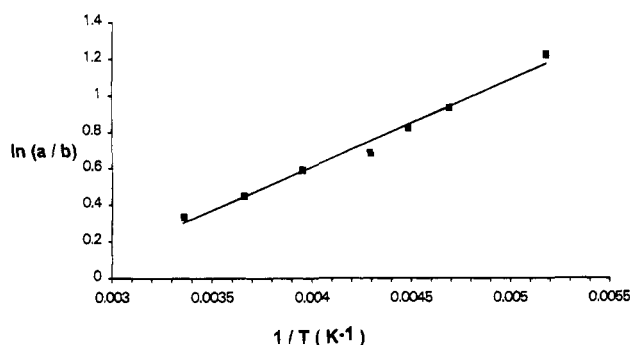


Figure 11. Linear relationship of $\ln(a/b)$ vs $1/T$ (Arrhenius plot).

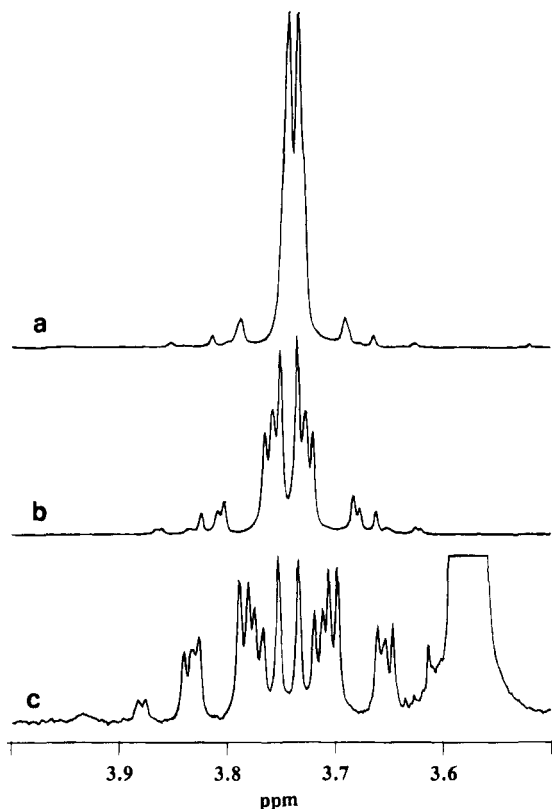


Figure 12. Ethylene bridge region of **1r** in CDCl_3 (a), CD_2Cl_2 (b), and $\text{THF-}d_8$ (c).

increments. Data were zero filled in the first dimension to 512W points before Fourier transformation. A 2 s mixing time (generally used for small molecules) was used in the NOESY experiment.

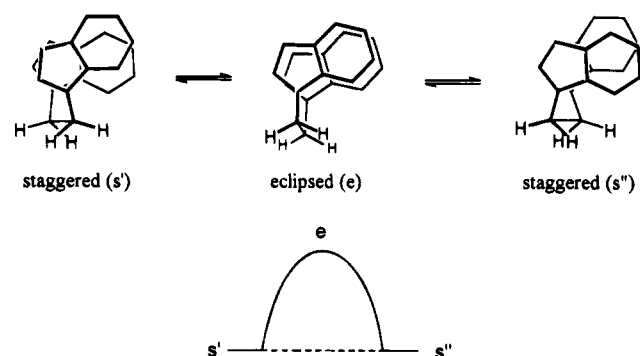
For XH-CORR and COLOC the recycling time was 2 s with 256 transients being collected for each t_1 increment. A total of 512 spectra, each consisting of 4K data points, were accumulated, and the data matrix was zero filled in the first dimension to $4\text{K} \times 512\text{W}$ before Fourier transformation with

Table 9. Coupling Constants (Hz) for *rac*-(EBI)ZrCl₂ in Different Solvents

	CDCl ₃	THF-d ₈	CD ₂ Cl ₂
$J_{A'B'} = J_{AB}$	-14.69	-14.50	-14.36
$J_{AA'}$	7.54	8.38	7.96
$J_{AB'} = J_{A'B}$	7.08	7.36	7.36
$J_{BB'}$	7.54	6.06	5.80

Table 10. Coupling Constants (Hz) Calculated with Karplus Relation for the Staggered (s) and Eclipsed (e) Conformations of *meso*-(EBI)ZrCl₂

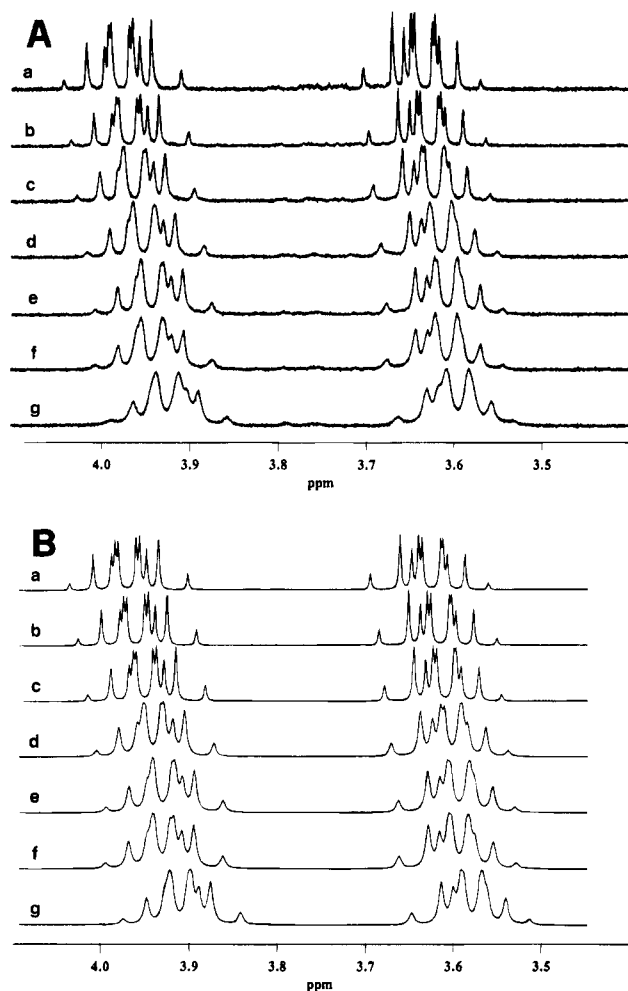
	<i>meso</i> s'		<i>meso</i> e		<i>meso</i> s''		$s' \rightleftharpoons s''$ J_{av}
	θ (deg)	J_{calc}	θ (deg)	J_{calc}	θ (deg)	J_{calc}	
H81-H82'	160.7	10.8	120	5.2	77	3.3	7.0
H81-H81'	41.9	7.5	0	11.3	41.6	7.5	7.5
H82-H82'	41.6	7.5	0	11.3	41.9	7.5	7.5
H82-H81'	77	3.3	120	5.2	160.7	10.8	7.0

**Figure 13.** Staggered (*s'* and *s''*) and eclipsed (*e*) conformations in **1m** (ZrCl₂ fragment omitted for clarity).**Table 11. *meso*-(EBI)ZrCl₂ VT-NMR Data: Experimental Coupling Constants**

<i>T</i> (K)	$J_{AB} = J_{A'B'}$ (Hz)	$J_{AA'}$ (Hz)	$J_{BB'}$ (Hz)	$J_{AB'} = J_{A'B}$ (Hz)
298	-14.678	7.064	7.147	7.384
273	-14.544	7.046	7.138	7.420
253	-14.473	7.019	7.130	7.510
233	-14.216	6.975	7.121	7.867
223	-14.451	6.991	7.064	7.522
213	-14.164	6.973	7.192	7.851
193	-14.187	7.135	7.149	7.535

a frequency range of 8000 Hz in ¹³C and of 1200 Hz in ¹H. $\Delta_1 = 3.45$ ms and $\Delta_2 = 1.72$ ms (corresponding to J (CH) of 150 Hz) and $\Delta_1 = 50$ ms and $\Delta_2 = 33$ ms (J (CH) = 10 Hz) were used for XH-CORR and COLOC respectively.

1,2-Bis(3-indenyl)ethane (Slightly Modified from Buchwald).¹⁴ Distilled indene (20 mL, 172 mmol) and THF (200 mL) were placed in a 500 mL flask equipped with a nitrogen inlet connected to an oil bubbler for pressure release, a stirring bar, and a 250 mL dropping funnel. After the apparatus was cooled to -78 °C by means of a dry ice/acetone bath, 110 mL of a 1.6 M solution of MeLi in Et₂O (176 mmol) was added dropwise with stirring. At the end of the addition, the flask was allowed to warm slowly to room temperature and stirred for 3 h (darkening of the red-orange solution was observed). The so obtained red solution was cooled to -78 °C, and 7.5 mL of 1,2-dibromoethane (87 mmol) in 50 mL THF was added dropwise to it (some gas evolution was observed throughout the addition). The flask was removed from the dry ice/acetone bath, stirred overnight at room temperature, and then quenched with 1 mL of H₂O (color changed from red to brown); the solvents were removed in vacuo until a light brown mass was obtained, to which (under normal atmosphere) 95% EtOH (200 mL) was added. The mixture was refluxed for 30 min and then allowed to cool slowly to room temperature. A microcrystalline ochre solid precipitated upon cooling, which was filtered off, redissolved in CHCl₃ on the filter to remove the small amount of insoluble tars present, dried in vacuo, washed

**Figure 14.** Experimental (A) and calculated (B) spectra of ethylene bridge region of **1m** in CD₂Cl₂, at 25 (a), 0 (b), -20 (c), -40 (d), -50 (e), -60 (f), and -80 °C (g).

with hexane (2 × 20 mL), and finally dried in vacuo to yield 11.35 g (51.3%) of a light yellow microcrystalline solid. The final washing steps afford a product of high (99.4% by GC) and reproducible purity. All the mother liquors collected and brought to dryness yielded, after extraction with CHCl₃ and washing with hexane, an additional 2.48 g of darker and less pure (82% by GC) product (discarded). ¹H NMR (δ , ppm, CDCl₃, 200 MHz): 2.95 (s, 4H), 3.35 (s, 4H), 6.30 (s, 2H), 7.1–7.6 (m, 8H).

***rac*- and *meso*-(Ethylenebis(1-indenyl))ZrCl₂ ((EBI)-ZrCl₂, **1r** and **1m**).** Pure **1r** was prepared according to Collins,¹³ modifying the final purification procedure. After precipitation of the reaction crude with Et₂O, the mixture was filtered under nitrogen in a filtration apparatus equipped with a side arm (to allow solvent refluxing) connecting the system above and below the frit, a receiving flask on the bottom, and bubble condenser on the top. The yellow solid was washed with Et₂O (washings discarded), dried, and then extracted with 50 mL of refluxing CH₂Cl₂ until the filtrate was colorless. The extraction process required several hours when done on a 10-g scale using a 100 mL extraction apparatus with a 30 mm diameter G3 frit (a gray solid is left on the frit). Most of the product precipitates during extraction. After removal of the solvent, pure **1r** was obtained as a yellow microcrystalline solid in 40% yield. Crystallization from CH₂Cl₂ afforded yellow crystals suitable for X-ray analysis. **1m** of 95% purity was obtained by cooling a 1/1 **1m/1r** THF solution, which was in turn obtained by extracting with CH₂Cl₂ the mixture of isomers obtained according to Buchwald.¹⁴ Cooling of a 95% **1m** THF solution afforded orange crystals of pure **1m**.

Table 12. Summary of Crystal Data and Data-Collection/Analysis Parameters

	<i>rac</i> -(EBI)ZrCl ₂	<i>meso</i> -(EBI)ZrCl ₂
formula	C ₂₀ H ₁₆ Cl ₂ Zr	C ₂₀ H ₁₆ Cl ₂ Zr
<i>M_r</i>	418.5	418.5
cryst system	monoclinic	monoclinic
space group	<i>I</i> 2/ <i>c</i> (No. 15)	<i>P</i> 2 ₁ / <i>n</i> (No. 14)
<i>a</i> , Å	11.957(1)	11.119(3)
<i>b</i> , Å	10.627(1)	10.467(1)
<i>c</i> , Å	13.775(2)	14.949(2)
β , deg	106.06(1)	100.94(2)
<i>V</i> , Å ³	1682(1)	1708(1)
<i>Z</i>	4	4
<i>d</i> , g/cm ³	1.652	1.627
<i>F</i> (000)	840	840
cryst dimens, mm	0.15 × 0.10 × 0.07	0.20 × 0.12 × 0.10
μ (Mo K α), cm ⁻¹	9.6	9.4
min rel transm factor	0.95	0.95
no. of reflns for Ψ scan	3	3
θ range, deg	3–27.5	3–25
scan mode	ω	ω
scan range, deg	1.0 + 0.35 tan θ	1.0 + 0.35 tan θ
required $\sigma(I)/I$	0.01	0.01
max scan time, s	70	70
octants of recipr space colld	$\pm h, k, l$	$\pm h, k, l$
cryst decay	no	9%
no. of colld reflns (at RT)	1912	3288
no. of unique obsd reflns	1808	2718
[<i>I</i> > 3 σ (<i>I</i>)]		
no. of refined params	106	216
weights (<i>a</i> , <i>b</i>) ^a	1.0, 0.004 668	1.0, 0.001 402
max shift/error	<0.01	<0.01
<i>R</i> ^b	0.026	0.032
<i>R'</i> ^c	0.034	0.045
max peak diff Fourier map, e Å ⁻³	0.40	0.57

^a $\omega = a/(\sigma^2(F_o) + bF_o^2)$. ^b $R = \sum(|F_o - k|F_c|)/\sum F_o$. ^c $R' = [\sum w(F_o - k|F_c|)^2/\sum wF_o^2]^{1/2}$.

Table 13. Atomic Coordinates and Equivalent Isotropic Displacements Parameters^a for *rac*-(EBI)ZrCl₂

	<i>x</i>	<i>y</i>	<i>z</i>	<i>U</i> (Å ²)
Zr	0.00000	0.47772(2)	0.25000	2.210(8)
Cl1	0.07003(4)	0.32677(5)	0.38511(4)	3.87(1)
C1	0.1143(2)	0.6733(2)	0.2463(2)	3.65(4)
C2	0.0951(2)	0.6145(3)	0.1513(2)	4.28(5)
C3	0.1587(2)	0.4998(3)	0.1618(2)	4.12(6)
C3a	0.2229(2)	0.4884(2)	0.2630(2)	3.10(5)
C4	0.3087(2)	0.4007(2)	0.3173(2)	4.38(6)
C5	0.3599(2)	0.4199(3)	0.4168(2)	4.88(6)
C6	0.3297(2)	0.5239(3)	0.4705(3)	4.73(7)
C7	0.2501(2)	0.6099(2)	0.4220(2)	4.07(5)
C7a	0.1943(2)	0.5955(2)	0.3162(2)	2.91(4)
C8	0.0658(2)	0.7965(2)	0.2709(3)	5.13(7)

^a Equivalent isotropic *U* defined as one-third of the trace of the orthogonalized *U_{ij}* tensor.

X-ray Structure Determination and Refinements. Crystal data and experimental conditions for compounds **1r** and **1m** are reported in Table 12. Unit cell parameters were determined by least-squares fit of the setting angles of 25 intense reflections having a θ value in the range 10.0–14.0°. The intensity data were recorded on an Enraf-Nonius CAD-4 automated diffractometer at room temperature using the scan conditions and sampling the reciprocal lattice as reported in Table 12.

The crystal stability was checked by monitoring three standard reflections every 60 min. Final drift corrections, when applied, are reported in Table 12. The diffracted intensities were corrected for Lorentz, polarization, and background effects. An empirical absorption correction was applied according to the method developed by North *et al.*, based on Ψ scans ($\Psi = 0$ –360°, every 10°) of three reflections having χ values near 90°. Scattering factors for neutral atoms and

(29) North, A. C. T.; Phillips, D. C.; Mathews, F. S. *Acta Crystallogr.* **1968**, *A24*, 351.

Table 14. Atomic Coordinates and Equivalent Isotropic Displacements Parameters^a for *meso*-(EBI)ZrCl₂

	<i>x</i>	<i>y</i>	<i>z</i>	<i>U</i> (Å ²)
Zr	0.21032(2)	0.18919(2)	-0.01677(2)	2.83(1)
Cl1	0.41532(7)	0.26800(8)	0.02789(5)	3.91(2)
Cl'	0.20862(9)	0.04984(9)	0.11509(6)	5.21(2)
C1	0.1216(3)	0.1191(4)	-0.1736(2)	5.6(1)
C2	0.1248(4)	0.0122(4)	-0.1169(3)	5.9(1)
C3	0.2461(4)	-0.0247(3)	-0.0856(3)	5.3(1)
C3a	0.3225(3)	0.0559(3)	-0.1270(2)	3.91(7)
C4	0.4510(3)	0.0564(3)	-0.1256(2)	4.73(8)
C5	0.4984(4)	0.1483(4)	-0.1713(3)	5.03(9)
C6	0.4234(4)	0.2425(4)	-0.2210(3)	5.5(1)
C7	0.3016(4)	0.2449(4)	-0.2251(2)	5.2(1)
C7a	0.2456(3)	0.1490(3)	-0.1786(2)	4.03(7)
C8	0.0076(5)	0.1832(6)	-0.2210(3)	8.4(2)
C1'	0.0451(3)	0.3356(3)	-0.0898(3)	4.88(9)
C2'	0.0013(3)	0.2718(4)	-0.0208(3)	4.99(9)
C3'	0.0675(4)	0.3121(4)	0.0630(3)	5.9(1)
C3a'	0.1533(3)	0.4070(3)	0.0470(3)	5.25(9)
C4'	0.2435(5)	0.4875(6)	0.1015(5)	10.2(2)
C5'	0.3076(6)	0.5718(6)	0.0608(6)	12.5(3)
C6'	0.2901(5)	0.5792(5)	-0.0344(6)	11.6(3)
C7'	0.2087(4)	0.5089(4)	-0.0897(4)	7.4(2)
C7a'	0.1385(3)	0.4203(3)	-0.0479(3)	4.49(8)
C8'	0.0010(5)	0.3155(5)	-0.1931(4)	7.9(2)

^a Equivalent isotropic *U* defined as one-third of the trace of the orthogonalized *U_{ij}* tensor.

anomalous dispersion corrections for scattering factors were taken from refs 30 and 31, respectively.

The structures were solved by standard Patterson and Fourier methods and refined by full-matrix least-squares minimizing the function $\sum w(F_o - k|F_c|)^2$. Weights were assigned to individual observations according to the formula and the parameters reported in Table 12. Anisotropic thermal parameters were assigned to all non-hydrogen atoms. Hydrogen atoms were placed in idealized positions (C–H = 0.95 Å) and refined riding on their parent atom with a common (refined) isotropic thermal parameter (*U* = 0.085(4) and 0.116(5) Å² for **1r** and **1m**, respectively).

The structure of **1m** is affected by a slight disorder of the ethylenebis(1-indenyl) ligand, which seems to be due to some conformational freedom around the ethylene hinge. We were not able to refine a consistent disordered model, possibly because of the closeness of the separated individual conformers. Hence, in order to favor the convergence toward a stereochemically significant result, the chemically equivalent C–C interactions within the indenyl ligands were restrained (with σ of 0.005 Å) to have similar bond distances. The disorder is nevertheless still manifested by the moderately large thermal ellipsoids of the carbon atoms and by the unreasonably short C8–C8' bond distances. In keeping with the observed disorder, even if does not explain it, the "ordered" stereoisomer is packed more efficiently than the "disordered" ones (i.e. **1r** has a smaller *U*/*Z* values than **1m**).

The final values of the agreement indices, *R* and *R_w*, and of maximum residuals in the final difference Fourier synthesis are reported in Table 12. The final positional parameters are reported in Tables 13 and Table 14 for **1r** and **1m**, respectively. All the calculations were performed on a Personal IRIS 35 using SHELX.³²

OM9407215

(30) Cromer, D. T.; Waber, J. T. *International Tables for X-Ray Crystallography*; The Kynoch Press: Birmingham, U.K., 1974; Vol. 4, Table 2.2.b (present distributor: Kluwer Academic Publishers, Dordrecht, The Netherlands).

(31) Cromer, D. T. *International Tables for X-Ray Crystallography*; The Kynoch Press: Birmingham, U.K., 1974; Vol. 4, Table 2.3.1 (present distributor: Kluwer Academic Publishers, Dordrecht, The Netherlands).

(32) Sheldrick, G. M. SHELX76, Program for crystal structure determination. Univ. of Cambridge, England, 1976.

Insertion Reactions of Benzyne-Nickel(0) Complexes with Acetylenes

Martin A. Bennett* and Eric Wenger

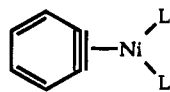
Research School of Chemistry, Australian National University, Canberra, ACT 0200, Australia

Received September 29, 1994[®]

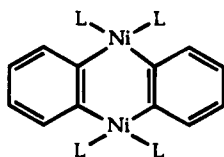
Complexes of nickel(0) containing η^2 -4,5-difluorobenzynes, $\text{Ni}((1,2-\eta)\text{-}4,5\text{-F}_2\text{C}_6\text{H}_2)(\text{PET}_3)_2$ (**10**) and $\text{Ni}((1,2-\eta)\text{-}4,5\text{-F}_2\text{C}_6\text{H}_2)(\text{dcpe})$ (**11**; dcpe = 1,2-bis(dicyclohexylphosphino)ethane, $\text{Cy}_2\text{PCH}_2\text{-CH}_2\text{PCy}_2$) have been synthesized by alkali-metal reduction of the appropriate (2-halo-phenyl)nickel(II) halides. Spectroscopic measurements (^{13}C NMR, FAB-MS) indicate that **10**, **11**, and the parent benzyne complex $\text{Ni}((1,2-\eta)\text{-C}_6\text{H}_4)(\text{PET}_3)_2$ (**2**) are monomeric, analogous to the structurally characterized species $\text{Ni}((1,2-\eta)\text{-C}_6\text{H}_4)(\text{Cy}_2\text{PCH}_2\text{CH}_2\text{PCy}_2)$. Complexes **2** and **10** undergo rapid intermolecular exchange with PEt_3 at room temperature and react with disubstituted acetylenes by double insertion into the metal-benzyne bond to form 1,2,3,4-tetrasubstituted naphthalenes. With electrophilic acetylenes ($\text{MeO}_2\text{CC}_2\text{CO}_2\text{Me}$, $\text{MeC}_2\text{-CO}_2\text{Me}$, $\text{HC}_2\text{CO}_2\text{Me}$, and $\text{CF}_3\text{C}_2\text{CF}_3$) an aromatic cyclootrimer is also formed; exceptionally, hexafluorobut-2-yne also gives with **10** a phenanthrene derived from two benzyne units and the acetylene. The unsymmetrical acetylenes *tert*-butylacetylene and methyl 2-butyne give rise to good regioselectivity in the resulting naphthalenes, the favored isomers being very dependent on the steric and electronic influence of the substituents. The dcpe complexes react similarly but more slowly with acetylenes, and with $\text{MeO}_2\text{CC}_2\text{CO}_2\text{Me}$ the monoinsertion complexes $\text{Ni}\{\text{C}(\text{CO}_2\text{Me})=\text{C}(\text{CO}_2\text{Me})\text{C}_6\text{H}_2\text{R}_2\text{-o}\}(\text{dcpe})$ ($\text{R} = \text{H}, \text{F}$) can be observed.

Introduction

Bis(tertiary phosphine) complexes, ML_2 , of zerovalent nickel and platinum form stable complexes with many unsaturated compounds and have been used to stabilize highly reactive, nonisolable species such as small cycloalkynes and benzyne.¹ The monomeric benzyne complexes $\text{Ni}(\eta^2\text{-C}_6\text{H}_4)\text{L}_2$ ($\text{L}_2 = \text{dcpe}$ (**1**),² 2 *P*-*i*-Pr₃) have



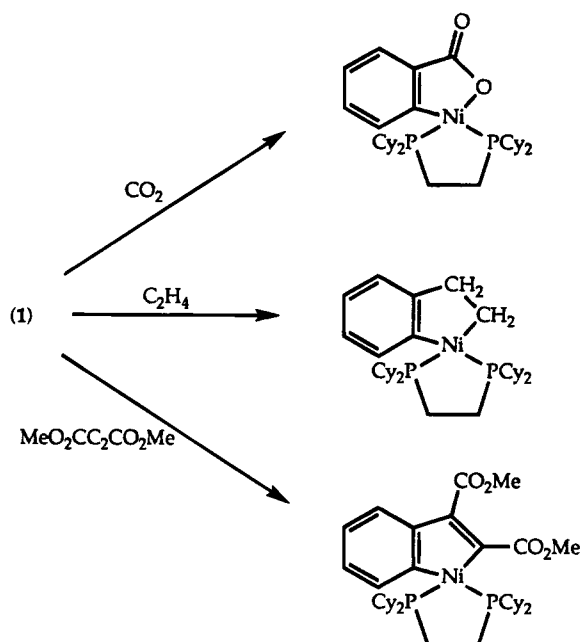
2L = dcpe (**1**), 2*P*-*i*-Pr₃, 2PEt₃ (**2**)



L = PEt₃ (**3**)

been made by reduction of the corresponding (2-bromophenyl)nickel(II) chloro complexes $\text{NiCl}(2\text{-BrC}_6\text{H}_4)\text{-L}_2$ with 0.5–1% sodium amalgam,^{3,4} and the dcpe complex has been structurally characterized.³ In contrast, reduction with lithium of $\text{NiCl}(2\text{-BrC}_6\text{H}_4)(\text{PEt}_3)_2$ has been reported by Dobson *et al.*⁵ to give a thermally sensitive solid of empirical formula $\text{Ni}(\text{C}_6\text{H}_4)(\text{PEt}_3)_2$

Scheme 1



which, on the basis of ^1H NMR and solution molecular weight data, was formulated as a dimeric bis(μ -*o*-phenylene)dinickel(II) complex (**3**) rather than a monomeric η^2 -benzyne complex (**2**). Although **1** has been shown to undergo stoichiometric insertions with carbon dioxide, ethylene, and dimethyl acetylenedicarboxylate (Scheme 1), little else is known about the reactivity of (η^2 -benzyne)nickel(0) complexes. In this paper we report the preparation and characterization of several new complexes of this class and examine their reaction with various acetylenes.

[®] Abstract published in *Advance ACS Abstracts*, February 1, 1995.

(1) (a) Bennett, M. A.; Schwemlein, H. P. *Angew. Chem., Int. Ed. Engl.* **1989**, *28*, 1296. (b) Bennett, M. A. *Pure Appl. Chem.* **1989**, *61*, 1695.

(2) Abbreviations: dcpe = 1,2-bis(dicyclohexylphosphino)ethane, $(\text{C}_6\text{H}_{11})_2\text{PCH}_2\text{CH}_2\text{P}(\text{C}_6\text{H}_{11})_2$; COD = 1,5-cyclooctadiene, C_8H_{12} ; AIBN = azobis(isobutyronitrile).

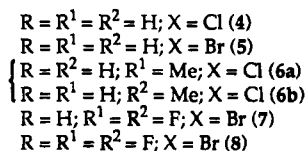
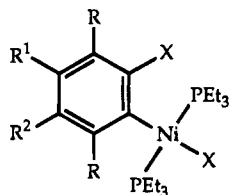
(3) Bennett, M. A.; Hambley, T. W.; Roberts, N. K.; Robertson, G. B. *Organometallics* **1985**, *4*, 1992.

(4) Bennett, M. A.; Griffiths, K. D.; Okano, T.; Parthasarathi, V.; Robertson, G. B. *J. Am. Chem. Soc.* **1990**, *112*, 7047.

(5) Dobson, J. E.; Miller, R. G.; Wigen, J. P. *J. Am. Chem. Soc.* **1971**, *93*, 554.

Results and Discussion

Nickel(II) Precursors. The (2-halogenophenyl)-nickel(II) halide precursors $\text{NiX}(\text{Ar})(\text{PET}_3)_2$ (**4–8**) were made in good yields by oxidative addition of the appropriate dihaloarene to $\text{Ni}(\text{COD})_2$ in the presence of triethylphosphine (2 equiv).^{6,7} The dibromoarenes re-



acted faster than the dichloroarenes, in agreement with literature reports on this type of reaction.^{7,8} 3,4-Dichlorotoluene gave an inseparable mixture of the 2-chloro-4-methyl and 2-chloro-5-methyl nickel(II) complexes **6a** and **6b** in a 1:4 ratio, as shown by NMR (¹H, ¹³C, and ³¹P NMR) spectroscopy (see Experimental Section). Although 1,2-dibromo-4,5-difluorobenzene gave the organonickel(II) complex **7** in good yield, 1,2-dibromo-3,4,5,6-tetrafluorobenzene gave an inseparable mixture of organonickel(II) complex **8** and $\text{NiBr}_2(\text{PET}_3)_2$. More electron-rich arenes such as 1,2-dibromo-4,5-dimethoxybenzene, 1,2-dibromo-3,4,5,6-tetramethylbenzene, 1,2-dibromo-4,5-dimethylbenzene, and 1,2,4,5-tetrabromobenzene gave only small amounts of the required organonickel(II) complexes; the main products were $\text{NiBr}_2(\text{PET}_3)_2$ and organic compounds formed by dehalogenation of the dihaloarene and coupling of the aryl residues. The lower stability of chelate (σ -aryl)-nickel(II) complexes $\text{NiBr}\{\text{C}_6\text{H}_2(\text{CH}_2\text{NMe}_2)_2\text{-2,6-R-4}\}$ when the *para* substituent R is electron-donating has been noted recently.⁸

These qualitative results are consistent with current views about the mechanism of oxidative addition of unactivated aromatic halides (ArX) to nickel(0) complexes.^{7,9,10} In the first step, an electron is transferred from nickel(0) to the C–X bond, generating the nickel(I) radical anion intermediate $\text{L}_2\text{Ni}(\text{XAr})^{\cdot-}$. This can either rearrange rapidly to the oxidative-addition product $\text{NiX}(\text{Ar})\text{L}_2$ or can decompose to the nickel(I) species NiXL_2 , which can react with more ArX to give NiX_2L_2 and the aryl radical Ar^{\cdot} . The radical anion is likely to be less stable for an electron-rich aromatic system; therefore, the second pathway will be favored in this case. In 3,4-dichlorotoluene, the 4-position *para* to CH_3 is probably more electron-rich than the 3-position; hence, the initial electron transfer from nickel(0) should occur preferentially to the latter site. In agreement, 4-bromotoluene reacts about 4 times less rapidly with $\text{Ni}(\text{PET}_3)_4$ than does bromobenzene and about 3 times less rapidly than does 2-bromotoluene.⁹

The complex $\text{NiCl}(2\text{-BrC}_6\text{H}_4)(\text{dcpe})$ was prepared previously in two steps from $\text{NiCl}_2(\text{dcpe})$.³ Reduction with lithium under ethylene gave $\text{Ni}(\eta^2\text{-C}_2\text{H}_4)(\text{dcpe})$, which was treated with *o*-dibromobenzene to give $\text{NiBr}(2\text{-BrC}_6\text{H}_4)(\text{dcpe})$; reaction in situ with LiCl gave $\text{NiCl}(2\text{-BrC}_6\text{H}_4)(\text{dcpe})$. A simpler route to this type of compound has been developed from the observation that reduction of $\text{NiX}_2(\text{PPh}_3)_2$ with zinc dust in the presence of an aromatic halide and a catalytic amount of AIBN gives the σ -aryl complex $\text{NiX}(\text{Ar})(\text{PPh}_3)_2$ in good yield.¹¹ In this way, we have made from 1,2-dibromo-4,5-difluorobenzene the complex $\text{NiBr}(2\text{-Br-4,5-F}_2\text{C}_6\text{H}_2)(\text{PPh}_3)_2$ and displaced the PPh_3 ligands with *dcpe* on heating in toluene to give the required complex $\text{NiBr}(2\text{-Br-4,5-F}_2\text{C}_6\text{H}_2)(\text{dcpe})$ (see Experimental Section).

η^2 -Benzyne Complexes. Reduction of $\text{NiBr}(2\text{-BrC}_6\text{H}_4)(\text{PET}_3)_2$ (**5**) by lithium in ether at -40°C gives $\text{Ni}(\text{C}_6\text{H}_4)(\text{PET}_3)_2$, which can be isolated as a sticky, thermally unstable solid from hexane at -60°C but becomes a viscous oil at room temperature. The compound is difficult to obtain in crystalline form, possibly because it tenaciously retains traces of PET_3 . The ¹H NMR spectrum agrees with that reported by Dobson *et al.*⁵ for the compound they isolated from lithium reduction of $\text{NiCl}(2\text{-BrC}_6\text{H}_4)(\text{PET}_3)_2$ and formulated as **3**. However, the fast-atom bombardment mass spectrum (FAB-MS) of our compound dissolved in a degassed aprotic matrix (tetraglyme) gave the highest mass peak at m/z 370, as expected for monomeric $\text{Ni}(\text{C}_6\text{H}_4)(\text{PET}_3)_2$, with an isotopic pattern characteristic of a compound containing only one nickel atom. The IR spectrum in hexane shows a strong band at 1590 cm^{-1} , similar to that at 1583 cm^{-1} in the spectrum of monomeric $\text{Ni}(\eta^2\text{-C}_6\text{H}_4)(\text{dcpe})$ (**1**), which was assigned tentatively to a C≡C stretch modified by coordination.³ These bands are notably more intense than the $\nu(\text{CC})$ band at $1560\text{--}1570\text{ cm}^{-1}$ observed in *o*- $\text{C}_6\text{H}_4\text{X}_2$ ($\text{X} = \text{Cl}, \text{Br}$) and at 1554 cm^{-1} in the μ -*o*-phenylene complex $\text{Ir}_2(\eta^5\text{-C}_5\text{Me}_5)_2(\text{CO})_2(\mu\text{-C}_6\text{H}_4)$.¹² The ³¹P{¹H} NMR spectrum at room temperature consists of a broad singlet at δ 28.5. A sharper signal is obtained if the solution is cooled to -30°C (no further sharpening is observed at -60°C) or if the original sample is repeatedly recrystallized from hexane and held in vacuo for extended periods to remove as much residual PET_3 as possible. These features point to intermolecular associative exchange of the monomer **2** with PET_3 rather than dissociative exchange from a dimer **3**; a similar conclusion has been drawn from

similar observations on the metallacycle $\text{Ni}(\text{C}_6\text{H}_4\text{CMe}_2\text{-CH}_2)(\text{PMe}_3)_2$.¹³ Finally, the ¹³C NMR spectrum of **2** at 25°C shows a singlet at δ 143.3 which can be assigned to the coordinated carbon atoms of η^2 -benzyne, by analogy with the spectrum of **1**.³ In contrast to **1**, ³¹P coupling is not observed at room temperature owing to the rapid intermolecular exchange with PET_3 , but at -60°C there is a doublet of doublets at δ 144.09 attributable to the X part of an AA'X spectrum ($\text{A} = ^{31}\text{P}$, $\text{X} = ^{13}\text{C}$). The separation between the outer lines 1 and 4 ($J(\text{PC}) + J(\text{P}'\text{C})$) is 73.7 Hz, and that between lines 1 and 2 (or 3 and 4) is 16.5 Hz. The evidence indicates that the reduction product of **4** and **5** is a monomer, $\text{Ni}(\eta^2\text{-C}_6\text{H}_4)$ -

(6) Fahey, D. R. *J. Am. Chem. Soc.* **1970**, *92*, 402.

(7) Fahey, D. R.; Mahan, J. E. *J. Am. Chem. Soc.* **1977**, *99*, 2501.

(8) van de Kuil, L. A.; Luitjes, H.; Grove, D. M.; Zwikker, J. W.; van der Linden, J. G. M.; Roelofs, A. M.; Jennekens, L. W.; Drenth, W.; van Koten, G. *Organometallics* **1994**, *13*, 468.

(9) Tsou, T. T.; Kochi, J. K. *J. Am. Chem. Soc.* **1979**, *101*, 6319.

(10) Kochi, J. K. *Pure Appl. Chem.* **1980**, *55*, 571.

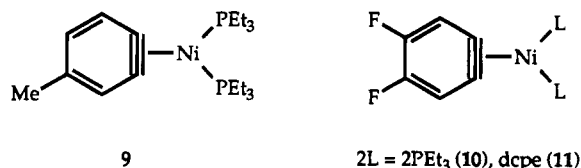
(11) Bennett, M. A.; Roberts, N. K., unpublished work.

(12) Graham, W. A. G., personal communication.

(13) Carmona, E.; Gutiérrez-Puebla, E.; Marín, J. M.; Monge, A.; Paneque, M.; Poveda, M. L.; Ruiz, C. *J. Am. Chem. Soc.* **1989**, *111*, 2883.

(PEt₃)₂ (**2**), rather than a dimer (**3**), although the reported molecular weight data⁵ are not easily explained.

In contrast to NiCl(2-BrC₆H₄)(PEt₃)₂ or NiBr(2-BrC₆H₄)(PEt₃)₂, the 2-chlorophenyl complex NiCl(2-ClC₆H₄)(PEt₃)₂ (**4**) is inert toward lithium, but it is reduced to **2** by 1% Na/Hg. Similarly, reduction of the isomeric mixture **6a/6b** with 1% Na/Hg gives the 4-methylbenzyne complex **9** in *ca.* 80% yield, as estimated



by ³¹P NMR spectroscopy, but this also was too unstable to be purified. The difference in reactivity between **4** and **5** toward lithium indicates that the first step in the reduction of the 2-halophenyl complexes by alkali metals is abstraction of halide ion from the *σ*-aryl group, not from nickel(II).

Reduction of **7** with lithium in ether gives the 4,5-difluorobenzyne complex Ni((1,2- η)-4,5-F₂C₆H₂)(PEt₃)₂ (**10**), which can be isolated in 78% yield as a yellow-brown solid melting at *ca.* 20 °C. Although very air-sensitive, it is thermally more stable than **2**. The FAB mass spectrum shows the highest mass peak at *m/z* 406 due to the parent ion. The ¹H NMR spectrum consists of a two-proton triplet at δ 7.40 (³J_{HF} = 5 Hz) due to equivalent aromatic protons, in addition to multiplets arising from the PEt₃ protons, and there is just a singlet at δ -142.1 in the ¹⁹F NMR spectrum (*cf.* the precursor **7**, whose ¹⁹F NMR spectrum exhibits a pair of multiplets in a 1:1 ratio). The ³¹P{¹H} NMR spectrum shows a broad singlet at δ 28.0, which shifts to low frequency on addition of a small amount of PEt₃. In the presence of PEt₃ (1 equiv) there is a very broad signal at δ 6, approximately midway between that of **10** and free PEt₃ (δ -19.2). Clearly, **10**, like **2**, undergoes rapid intermolecular exchange with PEt₃ on the NMR time scale at room temperature.

Reduction of NiBr(2-Br-4,5-F₂C₆H₂)(dcpe) with lithium, either in ether or toluene at room temperature, gave the 4,5-difluorobenzyne complex Ni((1,2- η)-4,5-F₂C₆H₂)(dcpe) (**11**) as a yellow solid in 85% yield, which is much easier to handle than **10**. It can also be made by treatment of **10** with dcpe, which provides further evidence of the lability of the PEt₃ ligands in **10**. The complex is only slightly soluble in benzene and hexane and decomposes immediately in dichloromethane. The FAB mass spectrum shows a parent ion peak at *m/z* 592, and the ³¹P{¹H} and ¹⁹F NMR spectra each show a sharp singlet. The ¹³C NMR spectrum shows a symmetrical five-line multiplet at δ 137.60, the central line being less intense than the other four lines. This pattern is typical of a AA'X system, and the parameters are similar to these observed for **1**: the separation between the outer lines 1 and 5 (*J*(PC) + *J*(P'C)) is 85.7 Hz, and that between lines 1 and 2 (or 4 and 5) is 14.3 Hz.

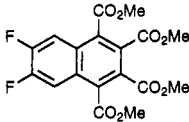
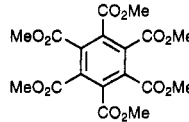
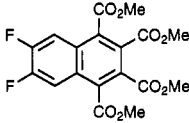
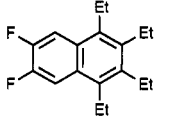
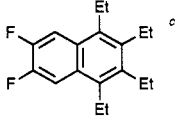
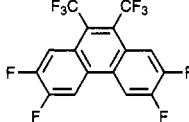
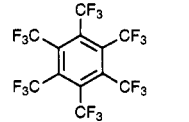
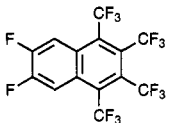
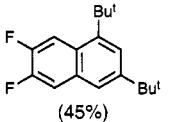
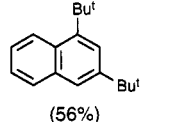
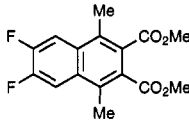
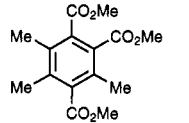
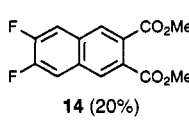
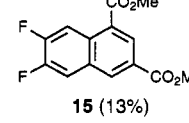
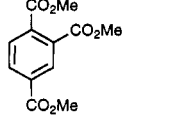
Reactions with Acetylenes. We have concentrated on the reactions of the 4,5-difluorobenzyne complex **10** with acetylenes because of its relative stability and because the combination of ¹⁹F and ¹H NMR spectroscopy aided product identification. These reactions did

not give isolable nickel(II) complexes arising from monoinsertion into the Ni-benzyne bond. In most cases, the main products that could be isolated were the aromatic compound formed by cyclotrimerization of the acetylene and a naphthalene arising from double insertion of the acetylene into the Ni-benzyne bond and subsequent reductive elimination; formation of the aromatic cyclotrimer was generally favored with more electrophilic acetylenes. The results are summarized in Table 1. Thus, a solution of **10** in hexane reacted rapidly with dimethyl acetylenedicarboxylate (*ca.* 2 mol/mol of **10**) at -30 °C to give, after chromatography on silica gel, hexamethyl benzenehexacarboxylate (48% yield) and tetramethyl 6,7-difluoronaphthalene-1,2,3,4-tetracarboxylate (*ca.* 5% yield based on **10**), which were identified by NMR (¹H, ¹⁹F) spectroscopy and mass spectrometry. The crude reaction product showed a ³¹P NMR singlet at δ 26.6, which may be due to Ni-(PEt₃)₂(η^2 -MeO₂CC₂CO₂Me). Evidently, this species acts as a catalyst precursor for the cyclotrimerization of dimethyl acetylenedicarboxylate. The reaction of **10** with 3-hexyne occurred only at room temperature to give, as the main product, 6,7-difluoro-1,2,3,4-tetraethylnaphthalene, which was isolated in 89% yield; there was no evidence in this case for the aromatic cyclotrimer C₆Et₆.

The more electrophilic acetylene hexafluoro-2-butyne reacted vigorously with **10** to give a large amount of unidentified polymeric material, but extraction with ether afforded a mixture containing C₆(CF₃)₆, 6,7-difluoro-1,2,3,4-tetrakis(trifluoromethyl)naphthalene (**12**), and, unexpectedly, 9,10-bis(trifluoromethyl)-2,3,6,7-tetrafluorophenanthrene (**13**) in a ratio of 1.4:1:2.4, as estimated by integration of the peaks in the ¹⁹F NMR spectrum; the last compound was isolated by crystallization from CH₂Cl₂ in 25% yield. Each component showed a parent ion peak in the EI mass spectrum. The ¹H NMR spectrum of the mixture showed a triplet at δ 8.23 (*J*_{HF} = 9.4 Hz) due to the equivalent aromatic protons of **12** and a pair of doublets of doublets at δ 8.10 and 8.23 due to the two pairs of aromatic protons of **13**. In the region δ -50 of the ¹⁹F NMR spectrum there was observed a singlet due to C₆(CF₃)₆, a pair of doublets due to the two pairs of CF₃ groups of **12**, and a singlet due to the equivalent CF₃ groups of **13**. Correspondingly, in the region δ -130, there was a triplet due to the equivalent aromatic fluorine atoms of **12** and a pair of triplets due to the two pairs of fluorine atoms of **13**.

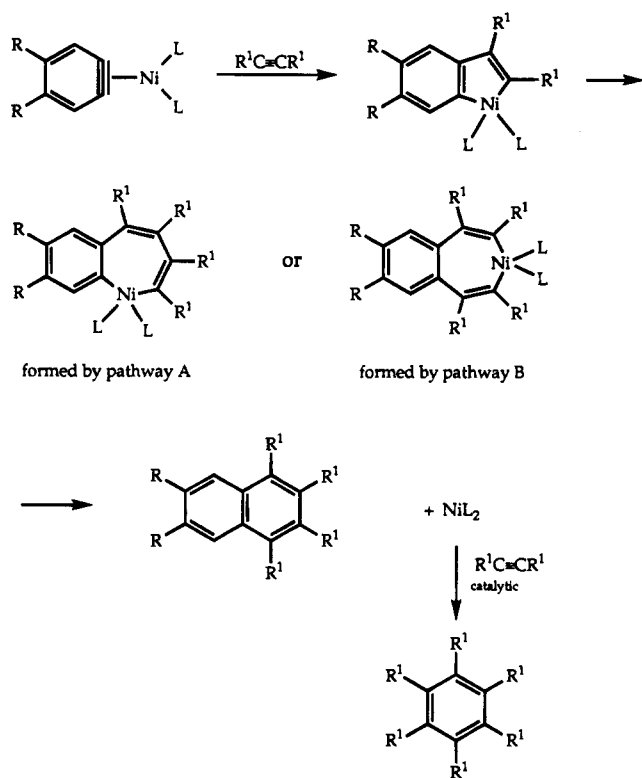
Products arising from double insertion are also obtained from the reaction of **2** and **10** with unsymmetrically substituted alkynes; the position of the substituents in the resulting naphthalene depends on the nature of the substituents. Thus, the reaction of *tert*-butylacetylene with **2** and **10** gave respectively 1,3-di-*tert*-butylnaphthalene and 1,3-di-*tert*-butyl-6,7-difluoronaphthalene. In contrast, the reaction of methyl 2-butyrate with **10** gave an approximately 1:1 mixture of the aromatic cyclotrimer trimethyl 3,5,6-trimethyl-1,2,4-benzenetricarboxylate and the symmetrically substituted derivative dimethyl 6,7-difluoro-1,4-dimethyl-2,3-naphthalenedicarboxylate, whose structure was assigned unambiguously by a nuclear Overhauser (NOE) experiment. The corresponding reaction of **10** with methyl propiolate was not regioselective, giving a 1.3:1 mixture of the symmetrically disubstituted dimethyl 6,7-difluoro-2,3-naphthalenedicarboxylate (**14**) and the unsymmetri-

Table 1. Reactions of Acetylenes with (η^2 -Benzyne)nickel(0) Complexes

η^2 -benzyne complex ^a	acetylene	organic products (yields) ^b	
10	MeO ₂ CC≡CCO ₂ Me	 (5%)	 (48%)
11	MeO ₂ CC≡CCO ₂ Me	 (43%)	
10	EtC≡CEt	 (89%)	
11	EtC≡CEt	 c	
10	CF ₃ C≡CCF ₃	 13 (25%)	 (16%)
		 12 (10%)	polymer
10	Bu ^t C≡CH	 (45%)	
2	Bu ^t C≡CH	 (56%)	
10	MeC≡CCO ₂ Me	 (57%)	 (11%)
10	HC≡CCO ₂ Me	 14 (20%)	 15 (13%)
		 (12%)	

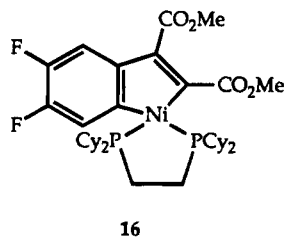
^a Ni((1,2- η)-C₆H₄)(PEt₃)₂ (2), Ni((1,2- η)-4,5-F₂C₆H₂)(PEt₃)₂ (10), Ni((1,2- η)-4,5-F₂C₆H₂)(dcpe) (11). ^b Yields of naphthalene are based on the benzyne complex, yields of aromatic cyclotrimer are based on acetylene. ^c Yield not determined but probably almost quantitative.

Scheme 2



cally disubstituted dimethyl 6,7-difluoro-1,3-naphthalenedicarboxylate (**15**), together with trimethyl benzene-1,2,4-tricarboxylate.

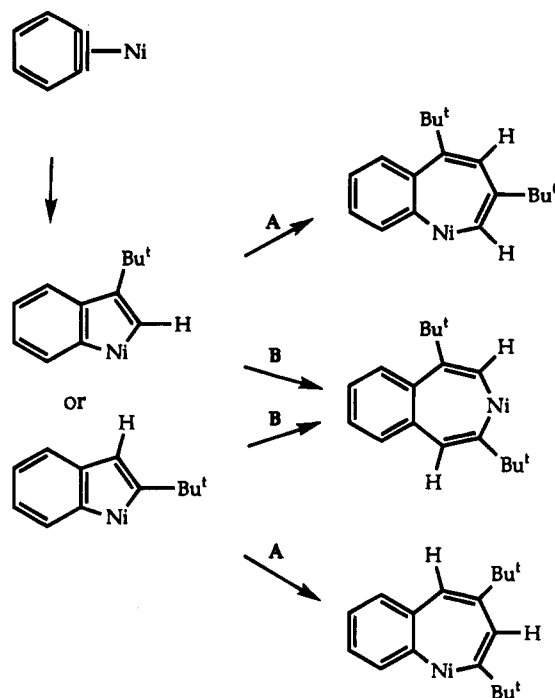
The apparent difference in behavior of the Ni(η^2 -benzyne)(PEt₃)₂ (**2** and **10**) and Ni(η^2 -C₆H₄)(dcpe) (**1**) complexes toward dimethyl acetylenedicarboxylate led us to investigate the latter in more detail. The 4,5-difluorobenzyne complex Ni((1,2- η)-4,5-F₂C₆H₂)(dcpe) (**11**) reacted with MeO₂CC₂CO₂Me and with EtC₂Et to give the same naphthalene compounds obtained from Ni((1,2- η)-4,5-F₂C₆H₂)(PEt₃)₂ (**10**). In the case of MeO₂CC₂CO₂Me, however, it was possible to identify the intermediate monoinsertion product (**16**) by NMR spec-



copy, although it decomposed on attempted isolation.

Similarly, we found that the monoinsertion product Ni{C₆H₄C(CO₂Me)=C(CO₂Me)}(dcpe)³ was formed only if a very dilute solution of MeO₂CC₂CO₂Me was added slowly to **1** at -10 °C. Rapid addition, or use of an excess of the acetylene, led to the formation of the double-insertion product tetramethyl naphthalene-1,2,3,4-tetracarboxylate.

As mentioned above, the formation of the organic compounds can be rationalized by assuming that the acetylene undergoes sequential double insertion into the Ni–benzyne bond, as illustrated for a symmetrical acetylene in Scheme 2. The initially formed nickelain-

Scheme 3^a

^a Phosphine ligands are omitted for clarity.

dene complex could undergo insertion of the second molecule of acetylene either into the nickel–vinyl bond, giving a 1,3-nickelabenzocycloheptatriene (pathway A), or into the nickel–aryl bond, giving a 1,4-isomer (pathway B). Pathway A is directly analogous to one of the mechanisms invoked for alkyne cyclooligomerization at transition-metal centers.^{14,15} Irrespective of the route followed, reductive elimination of the nickel–carbon σ -bonds then forms the naphthalene and generates the highly reactive 14e species NiL₂, which is capable of catalyzing the cyclotrimerization of acetylenes.¹⁶

The pathway adopted in the insertion of an unsymmetrical acetylene in the two successive steps clearly determines the substitution pattern in the resulting naphthalene. The exclusive formation of 1,3-di-*tert*-butylnaphthalenes from **2** or **10** and *tert*-butylacetylene can be accounted for if the insertions take place by pathway A, probably under steric control, independently of the orientation of the coordinated acetylene; i.e., the *tert*-butyl group could be placed on the carbon atom not directly attached to nickel or on that directly bonded to the nickel. If pathway B were operative, the direction of the first and the second insertions would have to differ, which seems less likely (Scheme 3). In the insertion of phenylpropyne and other unsymmetrical acetylenes into the nickel–methyl bonds of NiMe(acac)-(PPh₃)¹⁷ and *trans*-NiClMe(PMe₃)₂,¹⁸ the carbon atom bearing the sterically bulkier substituent is attached to the metal in the resulting η^1 -vinyl product (eqs 1 and 2). In the first case, however, it has been established

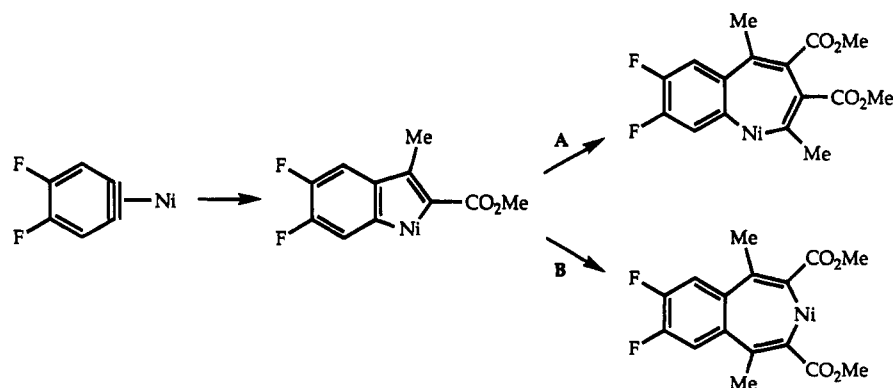
(14) Winter, M. J. In *The Chemistry of the Metal-Carbon Bond*; Hartley, F. R., Patai, S., Eds.; Wiley: New York, 1985; Vol. 3, Chapter 5, p 259.

(15) Collman, J. P.; Hegedus, L. S.; Norton, J. R.; Finke, R. G. *Principles and Applications of Organotransition Metal Chemistry*; University Science Books: Mill Valley, CA, 1987; pp 613, 870.

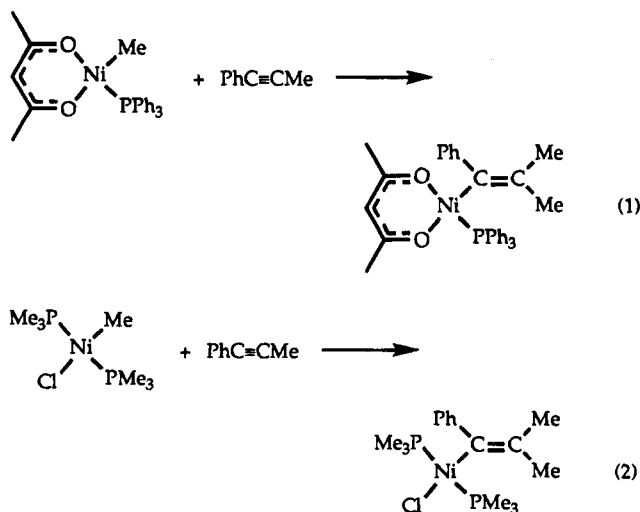
(16) Jolly, P. W. In *Comprehensive Organometallic Chemistry*; Wilkinson, G., Stone, F. G. A., Abel, E. W., Eds.; Pergamon: Oxford, U.K., 1982; Vol. 8, p 649.

(17) Huggins, J. M.; Bergman, R. G. *J. Am. Chem. Soc.* **1981**, *103*, 3002.

(18) Klein, H.-F.; Reitzel, L. *Chem. Ber.* **1988**, *121*, 1115.

Scheme 4^a

^a Phosphine ligands are omitted for clarity.



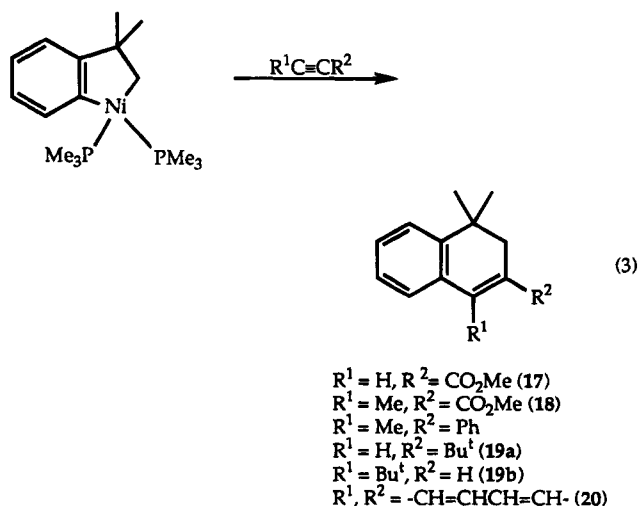
that the insertion proceeds by initial dissociation of PPh₃, probably via the intermediate NiMe(acac)(η²-alkyne). In this intermediate, repulsion between the bulkier substituent of the unsymmetrical acetylene and the methyl group on nickel causes the latter to migrate to the sterically less hindered carbon atom. It is not known whether the acetylene insertions into **1**, **2**, **10**, and **11** are preceded by dissociation of PPh₃ (**2** and **10**) or by one-ended dissociation of dppe (**1** and **11**); therefore, it is not clear whether the same steric argument can be invoked or whether repulsion between the bulky substituent and one of the phosphine groups is predominant.

The reaction of **10** with methyl 2-butynoate is probably under electronic control and could proceed by either pathway A or B, as shown in Scheme 4. In both cases, the observed regiochemistry can be accounted for by invoking dipolar intermediates or transition states.¹⁹ As shown in Scheme 5, the coordinated benzyne can be imagined to attack the electron-deficient carbon atom (C³) of coordinated methyl 2-butynoate to give the first insertion product (I). Coordination of a second molecule of methyl 2-butynoate and a similar nucleophilic attack of C² of the alkyne on the electron-deficient, bound carbon atom of the metallacycle leads, after cyclization, to complex II and, after reductive elimination, to the observed naphthalene (pathway A). Pathway B in this case involves a nucleophilic attack of the nickel-aryl bond of I on the positively charged carbon atom of the incoming acetylene to give, after ring closure, isomer

III. A mechanism similar to that suggested for pathway A has been postulated for the formation of the unsymmetrical cyclotrimer trimethyl 1,2,4-benzenetricarboxylate from the reaction of methyl 2-butynoate with various nickel(0) precursors;^{16,20} this is also the only cyclotrimerization product we observe.

The reaction of **10** with methyl propiolate is much less selective than those with methyl 2-butynoate or *tert*-butylacetylene, which may indicate that both steric and electronic controls are operative. An interesting feature of this reaction is its incompleteness: even when a large excess of methyl propiolate was used, only about half the starting complex reacted to form the double-insertion products. Presumably, as soon as enough Ni(PMe₃)₂ had been generated from reductive elimination to catalyze cyclotrimerization, this reaction took precedence over the double insertion.

The regioselectivity of the acetylene insertions of **2** and **10** can be compared with those into the nickel-phenyl bond of Ni(C₆H₄CMMe₂CH₂)(PMe₃)₂, which give, after reductive elimination, dihydronaphthalenes (eq 3).^{13,21} In this case, it is suggested that the PMe₃ ligand

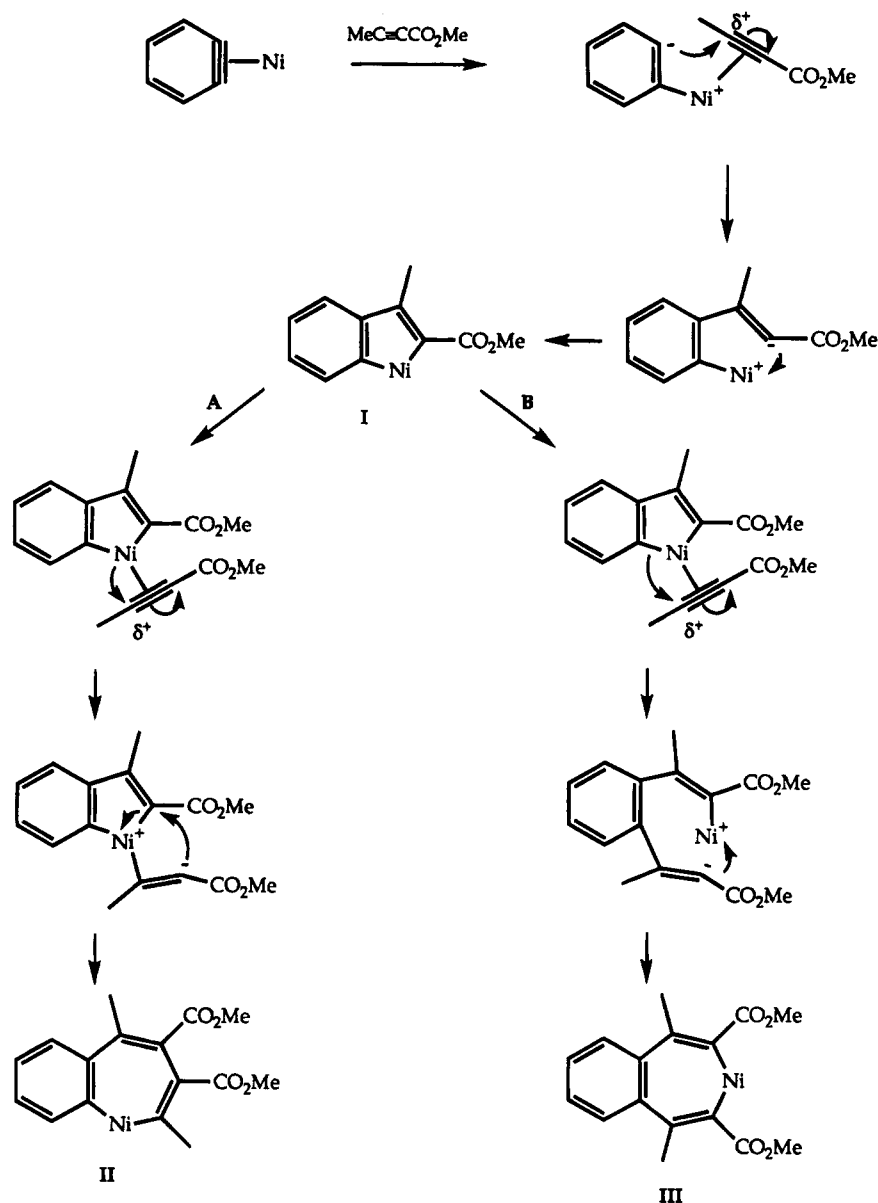


trans to the Ni-C(sp³) bond is more labile than that trans to the Ni-C(sp²) bond; hence, the alkyne coordinates cis to the nickel-phenyl bond and insertion occurs at this site. The reactions with methyl propiolate and methyl 2-butynoate to give **17** and **18** occur with the

(20) Dierks, R.; tom Dieck, H. *Z. Naturforsch., B: Anorg. Chem., Org. Chem.* **1984**, *39*, 180.

(21) Cámpora, J.; Llebaria, A.; Moretó, J. M.; Poveda, M. L.; Carmona, E. *Organometallics* **1993**, *12*, 4032.

(19) Maitlis, P. M. *Pure Appl. Chem.* **1972**, *30*, 427.

Scheme 5^a

^a Phosphine ligands are omitted for clarity.

same regioselectivity as we observe for the latter acetylene and are undoubtedly under electronic control. However, *tert*-butylacetylene gives a 2.2:1 mixture of isomers **19a** and **19b**, so that in this case the sterically more crowded intermediate having the *tert*-butyl group close to the PMe_3 ligand seems to be slightly favored.

The phenanthrene **13** obtained from **10** and hexafluoro-2-butyne formally arises by coupling of two benzyne units and the acetylene. A closely related reaction is

the addition of benzyne to $\text{Ni}(\text{C}_6\text{H}_4\text{CMe}_2\text{CH}_2)(\text{PMe}_3)_2$ to give the dihydrophenanthrene **20** (eq 3). Similarly, **13** could be formed by insertion of one molecule of $\text{CF}_3\text{C}\equiv\text{CCF}_3$ into the nickel–benzyne bond of **10** and insertion of benzyne (either coordinated or liberated by decomposition of **10**) into the resulting nickelacyclopentadiene complex.

Finally, the reactions reported here can be compared with the insertions of acetylenes with other η^2 -benzyne complexes, either isolated as such or generated in situ. The fragments $\text{M}(\eta^2\text{-C}_6\text{H}_4)(\eta^5\text{-C}_5\text{H}_5)_2$ ($\text{M} = \text{Ti},^{22} \text{Zr}^{23}$) and the complex $\text{Ru}(\eta^2\text{-C}_6\text{H}_4)(\text{PMe}_3)_4$ ²⁴ undergo monoinsertion of disubstituted alkynes to give isolable metallain-

denes, but these are apparently resistant to further insertion, presumably because there is no readily available coordination site for an additional acetylene molecule (see below). It is worth noting that steric effects appear to determine the formation of the predominant regioisomer arising from the insertion of toluene into the *o*-fluorobenzyne–metal bond of $\text{Ti}((1,2\text{-}\eta)\text{-3-FC}_6\text{H}_3)(\eta^5\text{-C}_5\text{H}_5)_2$.²⁵ One example of sequential double insertion is provided by the reactions of triphenylchromium(III) with 2-butyne or toluene, which give 1,2,3,4-tetramethylnaphthalene or 1,2,3,4-tetraphenylnaphthalene, respectively, in addition to the cyclotrimer of the acetylene.^{26,27} The naphthalenes could arise from the reaction

(22) (a) Masai, H.; Sonogashira, K.; Hagihara, N. *Bull. Chem. Soc. Jpn.* **1968**, *41*, 750. (b) Mattia, J.; Humphrey, M. B.; Rogers, R. D.; Atwood, J. L.; Rausch, M. D. *Inorg. Chem.* **1978**, *17*, 3257. (c) Rausch, M. D.; Mintz, E. A. *J. Organomet. Chem.* **1980**, *190*, 65.

(23) (a) Buchwald, S. L.; Watson, B. T.; Huffman, J. C. *J. Am. Chem. Soc.* **1986**, *108*, 7411. (b) Buchwald, S. L.; Nielsen, R. B. *Chem. Rev.* **1988**, *88*, 1047.

(24) Hartwig, J. F.; Bergman, R. G.; Andersen, R. A. *J. Am. Chem. Soc.* **1991**, *113*, 3404.

(25) Butler, I. R.; Cullen, W. R.; Einstein, F. W. B.; Jones, R. H. *J. Organomet. Chem.* **1993**, *463*, C6.

of the acetylene with an intermediate (benzyne)chromium species formed by elimination of benzene from triphenylchromium(III).²⁸ In agreement, bis(benzyne) complexes have been isolated from reactions of homoleptic σ -aryl metalates of the heavier elements Nb, Ta, Mo, W, and Re.²⁹

Conclusions

(a) Success in the preparation of (2-halogenoaryl)-nickel(II) halide complexes by oxidative addition of *o*-dihaloarenes to Ni(COD)₂ in the presence of PEt₃ depends very much on the nature of the arene substituents and fails when these are strongly electron-donating, such as OMe.

(b) The benzyne complexes Ni(η^2 -C₆H₄)(PEt₃)₂ (**2**), Ni((1,2- η)-4,5-F₂C₆H₂)(PEt₃)₂ (**10**), and Ni((1,2- η)-4,5-F₂C₆H₂)(dcp) (**11**) have been prepared by alkali-metal reduction of the (2-halogenoaryl)nickel(II) halides and have been shown to be monomeric. Our data suggest that the previously reported *mu*-*o*-phenylene complex Ni₂(μ -C₆H₄)₂(PEt₃)₄ (**3**) is probably monomeric Ni(η^2 -C₆H₄)(PEt₃)₂.

(c) These benzyne complexes undergo double-insertion reactions with alkynes to give substituted naphthalenes, the reactivity being dependent on the nature of the auxiliary phosphine ligands. The insertion reactions of complexes **1** and **11**, containing dcp, with dimethyl acetylenedicarboxylate are slower than the reactions of their PEt₃ analogues **2** and **10**, and monoinsertion intermediates are observed.

(d) The unsymmetrically substituted acetylenes *tert*-butylacetylene and methyl 2-butyrate give double-insertion products with good but different regioselectivities, which can be accounted for by invoking steric or electronic arguments, respectively, in each case.

Experimental Section

General Procedures. All experiments were performed under an inert atmosphere with use of standard Schlenk techniques, and all solvents were dried and degassed prior to use. All reactions involving benzyne complexes were carried out under argon. NMR spectra were recorded on a Varian XL-200E (¹H at 200 MHz, ¹³C at 50.3 MHz, ¹⁹F at 188.1 MHz, and ³¹P at 80.96 MHz), a Varian Gemini-300 BB (¹H at 300 MHz and ¹³C at 75.4 MHz), or a Varian VXR-300 instrument (¹H at 300 MHz and ¹³C at 75.4 MHz). The chemical shifts (δ) for ¹H and ¹³C are given in ppm relative to residual signals of the solvent, to external 85% H₃PO₄ for ³¹P, and to internal CFCl₃ for ¹⁹F. The spectra of all nuclei (except ¹H and ¹⁹F) were ¹H-decoupled. The coupling constants (*J*) are given in Hz. Infrared spectra were measured in solution (NaCl cells) on a Perkin-Elmer 683 instrument. Mass spectra of the complexes were obtained on a VG ZAB2-SEQ spectrometer by the fast-atom bombardment (FAB) technique. Solutions of the samples were prepared in dry THF (for benzyne complexes) or CH₂Cl₂ and added to a matrix of glycerol or 3-nitrobenzyl alcohol or, for benzyne complexes, degassed tetraglyme. Mass spectra of organic compounds were obtained by the electron

impact method (EI) on a VG Micromass 7070F spectrometer. Microanalyses were done in-house.

Starting Materials. 1,2-Dichlorobenzene, 1,2-dibromobenzene, 1,2-dichloro-4-methylbenzene, 1,2,4,5-tetrabromobenzene, 1,2-dibromo-4,5-difluorobenzene and 1,2-dibromo-3,4,5,6-tetrafluorobenzene were obtained commercially and used as received. 1,2-Dibromo-4,5-dimethylbenzene and 1,2-dibromo-3,4,5,6-tetramethylbenzene were prepared by bromination of *o*-xylene and 1,2,3,4-tetramethylbenzene in CH₃CO₂H.³⁰ 1,2-Dibromo-4,5-dimethoxybenzene was prepared by bromination of 1,2-dimethoxybenzene in EtOH.³¹ The complexes NiBr₂(PPh₃)₂³² and Ni(COD)₂³³ were prepared according to the literature.

Preparations of Nickel(II) Precursors. (a) NiCl(2-CIC₆H₄)(PEt₃)₂ (**4**). To a vigorously stirred suspension of Ni(COD)₂ (3.155 g, 11.5 mmol) and hexane (80 mL) under nitrogen was added dropwise PEt₃ (3.7 mL, 28.7 mmol) at room temperature. After 5 min, 1,2-dichlorobenzene (1.8 mL, 16 mmol) was added to the red solution and the mixture was stirred at room temperature for 40 min, refluxed for 2 h, and then stirred again at room temperature for 16 h. The solution was filtered through Celite, and the residue was washed with toluene. The orange solution was evaporated *in vacuo* to 20 mL, methanol (40 mL) was added, and the solution was cooled to -78 °C. Solvent was decanted, and the resulting orange crystals were washed with methanol (2 × 10 mL) and dried *in vacuo* to yield 4.25 g of **4** (84%). IR (CH₂Cl₂): 3045 (w), 2975 (s), 2945 (m), 2920 (m), 2890 (m), 1565 (m), 1550 (w), 1460 (m), 1440 (m), 1415 (m), 1380 (w), 1235 (w), 1040 (s), 1015 (m) cm⁻¹. ¹H NMR (200 MHz, C₆D₆): δ 1.03 (quint, 18H, ³J = 7.5, CH₃), 1.27–1.44 (m, 12H, CH₂), 6.65 (tq, 1H, ³J = 7.7, ⁴J = 1.65, H⁴), 6.79 (dt, 1H, ³J = 7.4, ⁴J = 1.4, H⁵), 7.07 (dd, 1H, ³J = 7.7, ⁴J = 1.4, H³), 7.37 (dq, 1H, ³J = 7.4, ⁴J = 1.65, H⁶). ¹³C{¹H} NMR (75.4 MHz, C₆D₆): δ 8.09 (CH₃), 13.96 (t, *J*_{CP} = 12.8, CH₂), 123.22 (CH), 124.13 (CH), 127.07 (CH), 138.75 (t, *J*_{CP} = 3.2, C⁶-H), 141.43 (t, *J*_{CP} = 3.2, C²), 154.36 (t, *J*_{CP} = 34.1, C¹). ³¹P{¹H} NMR (80.96 MHz, C₆D₆): δ 11.7 (s). FAB-MS (glycerol, C₁₈H₃₄Cl₂NiP₂): *m/z* 295 (6), 293 (16), Ni(PEt₃)₂, 231 (41), 229 (100, 2-Cl-1-PEt₃C₆H₄); the molecular ion at *m/z* 440 was not observed.

(b) NiBr(2-BrC₆H₄)(PEt₃)₂ (**5**). By the same procedure, PEt₃ (6.9 mL, 46.4 mmol) was added to Ni(COD)₂ (5.1 g, 18.6 mmol) in hexane (120 mL). 1,2-Dibromobenzene (3.14 mL, 26 mmol) was added, and the red solution was stirred for 1.25 h at room temperature, 2 h under reflux, and 16 h at room temperature. After filtration through Celite and crystallization, 8.87 g of brown solid (**5**) was isolated (90%). IR (CH₂Cl₂): 3045 (w), 2975 (s), 2945 (m), 2920 (m), 2890 (m), 1560 (w), 1545 (w), 1460 (m), 1434 (m), 1418 (m), 1383 (w), 1233 (m), 1079 (m), 1040 (s), 1003 (m) cm⁻¹. ¹H NMR (200 MHz, C₆D₆): δ 1.00 (quint, 18H, ³J = 7.5, CH₃), 1.30–1.60 (m, 12H, CH₂), 6.55 (tt, 1H, ³J = 8, ⁴J = 1.5, H⁴), 7.78 (tt, 1H, ³J = 7, ⁴J = 1.5, H⁵), 7.18–7.26 (m, 2H, H^{3,6}). ¹³C{¹H} NMR (75.4 MHz, C₆D₆): δ 8.41 (CH₃), 14.88 (t, *J*_{CP} = 12.7, CH₂), 123.85 (CH), 124.56 (CH), 130.46 (CH), 133.35 (t, *J*_{CP} = 4.4, C²), 139.68 (t, *J*_{CP} = 3.3, C⁶-H), 159.55 (t, *J*_{CP} = 34, C¹). ³¹P{¹H} NMR (80.96 MHz, C₆D₆): δ 10.65 (s). FAB-MS (glycerol, C₁₈H₃₄Br₂NiP₂): *m/z* 295 (7), 293 (16, Ni(PEt₃)₂), 275 (100), 273 (97, 2-Br-1-PEt₃C₆H₄); the molecular ion at *m/z* 528 was not observed. Anal. Calcd for C₁₈H₃₄Br₂NiP₂: C, 40.72; H, 6.45; P, 11.67. Found: C, 40.09; H, 6.57; P, 11.64.

(c) NiCl(2-Cl-4-MeC₆H₃)(PEt₃)₂ (**6a**) and NiCl(2-Cl-5-MeC₆H₃)(PEt₃)₂ (**6b**). A mixture of PEt₃ (6 mL, 40.3 mmol) and Ni(COD)₂ (4.43 g, 16.1 mmol) in hexane (100 mL) was treated with 3,4-dichlorotoluene (2.9 mL, 22.6 mmol) and worked up as above to give 6.95 g (95%) of yellow powder which was a 4:1 mixture of **6b** and **6a** (as determined by ¹H NMR spectroscopy). The structures were assigned on the basis of

(26) (a) Zeiss, H. H.; Herwig, W. *J. Am. Chem. Soc.* **1958**, *80*, 2913. (b) Herwig, W.; Metlesics, W.; Zeiss, H. H. *J. Am. Chem. Soc.* **1959**, *81*, 6203. (c) Sneed, R. P. A.; Zeiss, H. H. *J. Organomet. Chem.* **1969**, *20*, 153; **1972**, *40*, 163.

(27) Sneed, R. P. A. *Organochromium Compounds*; Academic Press: New York, 1975; p 255.

(28) A (benzyne)chromium species may also be implicated in the classic Hein reaction, i.e. the conversion of triphenylchromium(III) to bis(η^6 -benzene)chromium(I) and bis(η^6 -benzene)(η^6 -biphenyl)chromium(I): Reference 27, p 275.

(29) Reference 1a, p 1309, and references cited therein.

(30) Smith, L. I.; Moyle, C. L. *J. Am. Chem. Soc.* **1933**, *55*, 1676.

(31) Underwood, H. W., Jr.; Baril, O. L.; Toone, G. C. *J. Am. Chem. Soc.* **1930**, *52*, 4087.

(32) Venanzi, L. M. *J. Chem. Soc.* **1958**, 719.

(33) Schunn, R. A. *Inorg. Synth.* **1974**, *15*, 5.

the different NMR coupling constants in a ^{13}C APT NMR experiment and by comparison with similar complexes.³⁴ **6a**: ^1H NMR (200 MHz, C_6D_6) δ 1.04 (quint, 18H, $^3J = 7.5$, CH_3), 1.30–1.50 (m, 12H, CH_2), 2.03 (s, 3H, $\text{C}^4\text{-Me}$), 6.68 (br d, 1H, $J = 7.5$, H^5), 6.95 (d, 1H, $^3J = 7.5$, H^6), 7.25 (br s, 1H, H^3); $^{13}\text{C}\{^1\text{H}\}$ NMR (50.3 MHz, C_6D_6) δ 8.54 (CH_3), 14.35 (t, $J_{\text{CP}} = 12.5$, CH_2), 20.58 ($\text{C}^4\text{-Me}$) (more shielded than in **6b**, which indicates the methyl group to be *para* to nickel), 125.77 (t, $J_{\text{CP}} = 2.6$, $\text{C}^5\text{-H}$), 128.29 (m, $\text{C}^3\text{-H}$), 132.83 (t, $J_{\text{CP}} = 2.1$, C^4), 138.51 (t, $J_{\text{CP}} = 3.6$, $\text{C}^6\text{-H}$), resonances due to C^1 and C^2 were not located. $^{31}\text{P}\{^1\text{H}\}$ NMR (80.96 MHz, C_6D_6) δ 11.70 (s). **6b**: IR (CH_2Cl_2) 3045 (w), 2975 (s), 2945 (m), 2920 (m), 2890 (m), 2835 (w), 1575 (w), 1555 (w), 1460 (m), 1448 (m), 1419 (m), 1383 (w), 1243 (w), 1137 (w), 1093 (m), 1040 (s), 1009 (m), 819 (m), 807 (m) cm^{-1} ; ^1H NMR (200 MHz, C_6D_6) δ 1.04 (quint, 18H, $^3J = 7.5$, CH_3), 1.30–1.50 (m, 12H, CH_2), 2.09 (s, 3H, $\text{C}^5\text{-Me}$), 6.46 (br d, 1H, $^3J = 8$, H^4), 7.00 (d, 1H, $^3J = 8$, H^3), 7.30 (br s, 1H, H^6); $^{13}\text{C}\{^1\text{H}\}$ NMR (50.3 MHz, C_6D_6) δ 8.54 (CH_3), 14.43 (t, $J_{\text{CP}} = 12.5$, CH_2), 21.14 ($\text{C}^5\text{-Me}$), 124.43 (t, $J_{\text{CP}} = 2.3$, $\text{C}^4\text{-H}$) (smallest coupling; on *para* position), 126.86 (t, $J_{\text{CP}} = 2.9$, $\text{C}^3\text{-H}$), 133.28 (t, $J_{\text{CP}} = 2.6$, C^5), 138.70 (t, $J_{\text{CP}} = 4$, C^2), 139.45 (t, $J_{\text{CP}} = 3.7$, $\text{C}^6\text{-H}$), 154.97 (t, $J_{\text{CP}} = 34$, C^1); $^{31}\text{P}\{^1\text{H}\}$ NMR (80.96 MHz, C_6D_6) δ 11.56 (s). FAB-MS (glycerol, $\text{C}_{18}\text{H}_{36}\text{Cl}_2\text{NiP}_2$): m/z 295 (6), 293 (15, $\text{Ni}(\text{PEt}_3)_2$), 245 (46), 243 (100, 2-Cl-5-Me-1- $\text{PEt}_3\text{C}_6\text{H}_3$); the molecular ion at m/z 454 was not observed.

(d) **NiBr(2-Br-4,5- $\text{F}_2\text{C}_6\text{H}_2$)(PEt_3)₂ (**7**)**. To a suspension of $\text{Ni}(\text{COD})_2$ (1.9 g, 6.9 mmol) in hexane (60 mL) at 0 °C was added successively PEt_3 (2.6 mL, 17.3 mmol) and 1,2-dibromo-4,5-difluorobenzene (2.64 g, 9.7 mmol) in solution in hexane (10 mL). The brown solution was stirred for 10 min at 0 °C and 4 h at room temperature. The solvent was removed under reduced pressure, and the brown residue was extracted with hexane (4 × 10 mL, 3 × 5 mL). The solution was filtered through Celite and evaporated to half-volume *in vacuo*. The complex was crystallized at -78 °C to yield **7** (2.9 g, 74%) as a brown solid. IR (CH_2Cl_2): 2975 (s), 2945 (m), 2920 (m), 2890 (m), 1597 (w), 1578 (w), 1458 (vs), 1215 (m), 1165 (m), 1041 (s), 876 (m) cm^{-1} . ^1H NMR (200 MHz, C_6D_6): δ 0.93 (quint, 18H, $^3J = 7.5$, CH_3), 1.20–1.50 (m, 12H, CH_2), 6.91 (dd, 1H, $J_{\text{HF}} = 10.5$, $J_{\text{HF}} = 7.5$, H^3), 7.04 (ddt, 1H, $J_{\text{HF}} = 11$, $J_{\text{HF}} = 9$, $J_{\text{HF}} = 1.8$, H^6). $^{13}\text{C}\{^1\text{H}\}$ NMR (50.3 MHz, C_6D_6): δ 8.59 (CH_3), 15.02 (t, $J_{\text{CP}} = 12.9$, CH_2), 119.02 (d, $J_{\text{CF}} = 17.9$, $\text{C}^3\text{-H}$), 124.62 (C^2), 125.56 (d, $J_{\text{CF}} = 13.1$, $\text{C}^6\text{-H}$), 147.14 (dd, $J_{\text{CF}} = 245.1$, $J_{\text{CF}} = 13.8$, C-F), 148.54 (dd, $J_{\text{CF}} = 250.5$, $J_{\text{CF}} = 11.3$, C-F), 155.18 (dt, $J_{\text{CP}} = 34.1$, $J_{\text{CF}} = 3.9$, C^1). ^{19}F NMR (188.1 MHz, C_6D_6): δ -144.8 (m), -142.3 (m). $^{31}\text{P}\{^1\text{H}\}$ NMR (80.96 MHz, C_6D_6): δ 10.89 (s). FAB-MS (glycerol, $\text{C}_{18}\text{H}_{32}\text{Br}_2\text{F}_2\text{NiP}_2$): m/z 565 (0.7, $\text{M} + 1$), 539 (2), 537 (5), 312 (13), 311 (95), 310 (14), 309 (100, 2-Br-4,5- F_2 -1- $\text{PEt}_3\text{C}_6\text{H}_2$), 295 (6), 293 (15, $\text{Ni}(\text{PEt}_3)_2$). Anal. Calcd for $\text{C}_{18}\text{H}_{32}\text{Br}_2\text{F}_2\text{NiP}_2$: C, 38.14; H, 5.69; P, 10.93; Br, 28.19. Found: C, 38.52; H, 5.95; P, 10.66; Br, 28.97.

(e) **NiBr(2-Br- C_6F_4)(PEt_3)₂ (**8**)**. As described for **7**, a suspension of $\text{Ni}(\text{COD})_2$ (1.36 g, 4.9 mmol) in hexane (40 mL) was treated with PEt_3 (1.82 mL, 12.4 mmol). After 5 min, the solution was cooled to 0 °C and 1,2-dibromo-3,4,5,6-tetrafluorobenzene (0.95 mL, 6.9 mmol) was added slowly. The solution instantly became dark brown. After 4 h at 0 °C, the solvent was evaporated off and the brown oil was extracted with hexane. Filtration and crystallization at -78 °C gave 2.33 g of a 2:1 mixture of **8** (57%) and $\text{NiBr}_2(\text{PEt}_3)_2$. **8**: ^1H NMR (200 MHz, C_6D_6) δ 0.92 (quint, 18H, $^3J = 7.5$, CH_3), 1.20–1.40 (m, 12H, CH_2); $^{13}\text{C}\{^1\text{H}\}$ NMR (75.4 MHz, C_6D_6) δ 8.18 (CH_3), 15.34 (t, $^1J_{\text{CP}} = 13.2$, CH_2), 109.19 (dt, $J = 18$, $J_{\text{CP}} = 3.2$, C^2), 136.60 (dt, $^1J_{\text{CF}} = 246.0$, $J = 15.4$, C-F), 138.47 (ddd, $^1J_{\text{CF}} = 258.1$, $J = 24.1$, $J = 12.1$, C-F), 138.87 (dt, $J = 53.8$, $J_{\text{CP}} = 30.8$, C^1), 143.86 (ddd, $^1J_{\text{CF}} = 250.4$, $J = 12.1$, $J = 3.3$, C-F), 146.01 (d, $^1J_{\text{CF}} = 224.1$, C-F) (this complicated system was not well enough resolved to assign all the coupling constants and the C-F carbon atoms); ^{19}F NMR (188.1 MHz, C_6D_6) δ -159.5 (t, $^3J_{\text{FF}} = 20.7$, F^4), -158.2 (dd, $^3J_{\text{FF}} = 19.9$ and 31.7, F^5), -128.5

(dd, $^3J_{\text{FF}} = 20.8$, $^5J_{\text{FF}} = 11.2$, F^3), -113.5 (dd, $^3J_{\text{FF}} = 31.9$, $^5J_{\text{FF}} = 11.2$, F^6); $^{31}\text{P}\{^1\text{H}\}$ NMR (80.96 MHz, C_6D_6) δ 11.60 (s). $\text{NiBr}_2(\text{PEt}_3)_2$: ^1H NMR (200 MHz, C_6D_6) δ 1.11 (t, 18H, $^3J = 7.5$, CH_3), 1.72 (q, 12H, $^3J = 7.5$, CH_2); $^{13}\text{C}\{^1\text{H}\}$ NMR (75.4 MHz, C_6D_6) δ 8.69 (CH_3), 15.93 (CH_2). This ^1H NMR spectrum of $\text{NiBr}_2(\text{PEt}_3)_2$ agreed with that of an independently prepared sample and that reported in the literature.³⁵ Attempts to record a $^{31}\text{P}\{^1\text{H}\}$ NMR spectrum of $\text{NiBr}_2(\text{PEt}_3)_2$ were unsuccessful, perhaps because of the presence of a small amount of tetrahedral paramagnetic isomer.^{36,37} Crude reaction mixtures often showed a singlet at δ 11.60 that subsequently disappeared, which may be due to $\text{NiBr}_2(\text{PEt}_3)_2$.

(f) **NiBr(2-Br-4,5- $\text{F}_2\text{C}_6\text{H}_2$)(PPh_3)₂**. A suspension of zinc dust (1.9 g, 29 mmol) in THF (20 mL) was activated by ultrasound for 30 min at room temperature and treated successively with solutions of 1,2-dibromo-4,5-difluorobenzene (6.7 g, 24.9 mmol) in THF (10 mL) and of $\text{NiBr}_2(\text{PPh}_3)_2$ (15.8 g, 21 mmol) in THF (60 mL) containing AIBN (0.25 g). The green mixture was stirred for 1.5 h at room temperature to give a brown solution. The solvent was removed by evaporation, and the complex was extracted with CH_2Cl_2 . The solution was then filtered through Celite and evaporated to dryness. The yellow-brown solid was washed with hot ethanol to yield $\text{NiBr}(2\text{-Br-4,5-}\text{F}_2\text{C}_6\text{H}_2)(\text{PPh}_3)_2$ (11.5 g, 64%). ^1H NMR (200 MHz, C_6D_6): δ 6.26 (dd, 1H, $J_{\text{HF}} = 10.5$, $J_{\text{HF}} = 7.2$, H^3), 6.36–6.53 (app. t, 1H, $J_{\text{HF}} = 9$, H^6), 6.99 (br s, 18H, PPh_3), 7.82–7.95 (m, 12H, PPh_3). ^{19}F NMR (188.1 MHz, C_6D_6): δ -147.38 (m), -142.72 (m). $^{31}\text{P}\{^1\text{H}\}$ NMR (80.96 MHz, C_6D_6): δ 21.53 (s).

(g) **NiBr(2-Br-4,5- $\text{F}_2\text{C}_6\text{H}_2$)(*dcpe*)**. A suspension of $\text{NiBr}(2\text{-Br-4,5-}\text{F}_2\text{C}_6\text{H}_2)(\text{PPh}_3)_2$ (6.27 g, 7.3 mmol) and *dcpe* (3.41 g, 8 mmol) in toluene (140 mL) was heated for 4 h at 50 °C. The brown solution was filtered through Celite, the residue was extracted with CH_2Cl_2 , and the solvent was removed by evaporation. The complex was purified by column chromatography (silica gel, diethyl ether) and crystallized from CH_2Cl_2 /hexane (1:1) to yield $\text{NiBr}(2\text{-Br-4,5-}\text{F}_2\text{C}_6\text{H}_2)(\text{dcpe})$ (3.31 g, 60%). IR (CH_2Cl_2): 2930 (s), 2850 (m), 1590 (w), 1445 (s), 1155 (w), 1000 (w) cm^{-1} . ^1H NMR (200 MHz, CD_2Cl_2): δ 1.10–2.15 (m, 40H, CH_2 of C_6H_{11}), 2.18–2.52 (m, 4H, CH_2), 2.80–3.00 (m, 4H, CH of C_6H_{11}), 6.89 (tdd, 1H, $J = 10$, 6, 2, H^{arom}), 7.05 (ddd, 1H, $J = 10$, 7, 2, H^{arom}). ^{13}C NMR (75.4 MHz, CD_2Cl_2): δ 19.00–38.00 (m, CH_2 and C_6H_{11}), 119.10 (app d, $^2J_{\text{CF}} = 17.6$, CH), 125.06 (dd, $^2J_{\text{CF}} = 13.2$, $^3J_{\text{CF}} = 2.2$, CH), 126.18 (br s, C^2), 147.30 (dd, $^1J_{\text{CF}} = 244.8$, $^2J_{\text{CF}} = 14.3$, C-F), 148.76 (dt, $^1J_{\text{CF}} = 249.3$, $^2J_{\text{CF}} = 8.8$, C-F), 156.92 (ddd, $J_{\text{CP}} = 85.6$, $J_{\text{CP}} = 34.0$, $^3J_{\text{CF}} = 4.4$, C^1). ^{19}F NMR (188.1 MHz, CD_2Cl_2): δ -145.71 (m), -143.68 (m). $^{31}\text{P}\{^1\text{H}\}$ NMR (80.96 MHz, CD_2Cl_2): δ 66.77 (dd, $J_{\text{PP}} = 30.5$, $J_{\text{FP}} = 3.4$), 69.01 (d, $J_{\text{PP}} = 30.5$). Anal. Calcd for $\text{C}_{32}\text{H}_{50}\text{Br}_2\text{F}_2\text{NiP}_2$: C, 51.03; H, 6.69. Found: C, 50.49; H, 6.79.

Preparation of η^2 -Benzyne Complexes. (a) **Ni((1,2- η)- C_6H_4)(PEt_3)₂ (**2**)**. (i) To a 1% sodium amalgam prepared from sodium (0.43 g, 18.7 mmol) in mercury (3.15 mL) was added successively THF (20 mL) and **4** (0.52 g, 1.18 mmol). The mixture was stirred vigorously at room temperature for 23 h. The solution was then cooled to -40 °C, and hexane (20 mL) was added. The solution was filtered through Celite into a flask at 0 °C, and the solvent was evaporated *in vacuo*. The dark red residue was extracted with hexane at -40 °C, the extract was filtered, and the orange filtrate was cooled to -78 °C. The yellow powder obtained was decanted, washed with hexane at -78 °C, and dried *in vacuo* at -78 °C. The yield of **2** was 261 mg (45%).

(ii) Glass beads (10 mL volume) and lithium dispersion (30%, 100 mg) were placed in a flask under argon. The lithium was washed with hexane and dried *in vacuo*, and diethyl ether was added (30 mL). The mixture was cooled to -45 °C, and **5** (1.07 g, 2.03 mmol) was added. The mixture was stirred at -40 °C

(35) Fergusson, J. E.; Heveltdt, P. F. *Inorg. Chim. Acta* **1978**, *31*, 145.

(36) Que, L.; Pignolet, L. H. *Inorg. Chem.* **1973**, *12*, 156.

(37) Grimes, C. G.; Pearson, R. G. *Inorg. Chem.* **1974**, *13*, 970.

(34) Granell, J.; Muller, G.; Rocamora, M.; Vilarrasa, J. *Magn. Reson. Chem.* **1986**, *24*, 243.

for 4 h, and the solvent was removed *in vacuo* at this temperature. The brown residue was extracted with hexane (6 × 5 mL) at 0 °C, and the brown extract was filtered through Celite into a flask at -78 °C and maintained at this temperature overnight. The supernatant liquid was decanted, and after it was dried *in vacuo* at -40 °C, **5** was isolated as a yellow-brown solid containing traces of starting complex (745 mg, 80% yield by ³¹P NMR). IR (hexane): 3040 (w), 3000 (w), 2980 (w), 1598 (s), 1435 (m), 1125 (vs), 1030 (s), 760 (s), 730 (s) cm⁻¹. ¹H NMR (200 MHz, C₆D₆): δ 0.85–1.10 ([A₃B₂X] m, 18H, *J* = 7.5, CH₃), 1.45–1.63 ([A₃B₂X] m, 12H, *J* = 7.5, CH₂), 7.28–7.36 ([AA'BB'] m, 2H, H^{4,5}), 7.75–7.85 ([AA'BB'] m, 2H, H^{3,6}). ¹³C{¹H} NMR (50.3 MHz, C₆D₆): δ 9.28 (CH₃), 19.33 (m, CH₂), 122.91, 127.20 (CH), 143.34 (C^{1,2}). ¹³C{¹H} NMR (75.4 MHz, THF-*d*₈, -60 °C): δ 9.14 (CH₃), 19.88 (m, CH₂), 122.72 (t, CH, *J*_{CP} = 4.9), 126.71 (CH), 144.09 [dd, C^{1,2}, separations 73.6, 16.5 (see text)]. ³¹P{¹H} NMR (80.96 MHz, C₆D₆): δ 28.5 (br s). FAB-MS (tetraglyme, C₁₈H₃₄NiP₂): *m/z* 370 (100, M); no peaks due to dimer detected.

(b) Ni((1,2-η)-4-MeC₆H₃)(PEt₃)₂ (**9**). Following the procedure described above, the isomeric mixture **6a/6b** (777 mg, 1.7 mmol) was stirred for 18.5 h at room temperature over a 1% Na/Hg amalgam (615 mg/4 mL) in THF. The solution was decanted from the amalgam and evaporated to dryness, the residue was extracted with hexane at -40 °C (8 × 5 mL), and this solution was filtered through Celite into a flask at -78 °C. After evaporation of the solvent, the black residue was recrystallized from hexane at -78 °C to yield a brown solid which contained **9** as well as some unchanged **6a/6b**. Attempts to purify the solid further caused its decomposition. The estimated yield (³¹P NMR) of **9** was >70%. ³¹P{¹H} NMR (80.96 MHz, C₆D₆): δ 27.64 (br s).

(c) Ni((1,2-η)-4,5-F₂C₆H₂)(PEt₃)₂ (**10**). A flask containing glass beads was charged with lithium (242 mg) and diethyl ether (100 mL) and cooled to -50 °C. Complex **7** (3.1 g, 5.49 mmol) in ether (2 × 20 mL) was added, and the mixture was stirred for 5 h at -40 °C. The solvent was evaporated, and the brown solid was extracted with hexane (5 × 20 mL) at -30 °C. The extract was filtered through Celite into a flask at -78 °C and cooled to -78 °C to yield 1.73 g (78%) of **10** as a brown solid. IR (hexane): 3030 (w), 1535 (w), 1440 (s), 1410 (m), 1325 (m), 1255 (m), 1240 (vs), 1140 (m), 1025 (m), 840 (m), 815 (s), 760 (s), 660 (s) cm⁻¹. ¹H NMR (200 MHz, C₆D₆): δ 0.78–1.05 ([A₃B₂X] m, 18H, *J* = 7.5, CH₃), 1.38–1.50 ([A₃B₂X] m, 12H, *J* = 7.5, CH₂), 7.40 (t, 2H, ³*J*_{HF} = 5, H^{3,6}). ¹³C{¹H} NMR (50.3 MHz, C₆D₆): δ 8.77 (CH₃), 19.82 (d, *J*_{CP} = 21.4, CH₂), 108.38–108.96 ([ABX] m, CH) (assigned by APT experiment), 135.16 (C^{1,2}), 150.44 (dd, ¹*J*_{CF} = 249.1, ²*J*_{CF} = 16.7, C-F). ¹⁹F NMR (188.1 MHz, C₆D₆): δ -142.08 (s). ³¹P{¹H} NMR (80.96 MHz, C₆D₆): δ 28.0 (br s). FAB-MS (tetraglyme, C₁₈H₃₂F₂NiP₂): *m/z* 406 (41, M), 377 (9, M - Et), 296 (37), 294 (100, Ni(PEt₃)₂), 282 (6), 280 (18), 265 (8), 263 (11).

(d) Attempted Preparation of Ni((1,2-η)-C₆F₄)(PEt₃)₂. A suspension of **8** (456 mg, 0.76 mmol) in ether (20 mL) was treated with lithium (37 mg) for 4 h at -40 °C. The solvent was removed by evaporation, and the resulting solid was extracted with hexane at -40 °C. The extract was filtered through Celite into a flask at -78 °C. The extract was taken to dryness, and the impure residue was extracted again with hexane. Crystallization at -78 °C gave 117 mg of solid containing the benzyne complex, traces of OPet₃ (³¹P NMR: δ 46.40), and some other unidentified impurities. ³¹P{¹H} NMR (80.96 MHz, C₆D₆): δ 26.44 (br s).

(e) Ni((1,2-η)-4,5-F₂C₆H₂)(dcpe) (**11**). (i) A 30% Li dispersion (200 mg) was washed with hexane, and toluene (40 mL) was added. The suspension was cooled to -78 °C, and NiBr-(2-Br-4,5-F₂C₆H₂)(dcpe) (0.624 g, 0.88 mmol) was added. The mixture was stirred for 45 h at room temperature, and the solution was filtered through Celite. The solvent was evaporated to a volume of 20 mL, hexane (40 mL) was added, and the complex was precipitated at -78 °C. Crystallization of the solid from THF/hexane yielded 404 mg (85%) of **11**. IR (THF): 1535 (w), 1440 (vs), 1320 (m), 1235 (s), 1135 (m), 1005

(m), 815 (m), 747 (s), 665 (s) cm⁻¹. ¹H NMR (200 MHz, THF-*d*₈): δ 1.10–2.20 (m, 48H, CH₂ and C₆H₁₁), 7.17 (dt, 2H, *J* = 5.3, *J* = 1.7, H^{3,6}). ¹³C NMR (75.4 MHz, THF-*d*₈): δ 22.53 (t, *J*_{CP} = 19.8, CH₂), 25.32 (quint, *J*_{CP} = 19.7, CH₂), 27.09, 27.96, 28.02, 30.10, 30.46 (CH₂ of C₆H₁₁), 35.56 (t, *J*_{CP} = 11.0, CH of C₆H₁₁), 111.15 (m, C^{3,6}-H), 137.60 [5-line m, C^{1,2}, separations 85.7, 14.3 (see text)], 151.41 (dd, ¹*J*_{CF} = 245.9, ²*J*_{CF} = 16.5, C^{4,5}). ¹⁹F NMR (188.1 MHz, THF-*d*₈): δ -142.13 (s). ³¹P{¹H} NMR (80.96 MHz, THF-*d*₈): δ 79.21 (s). FAB-MS (tetraglyme, C₃₂H₅₀F₂NiP₂): *m/z* 592 (22, M).

(ii) A solution of **10** (21 mg, 0.052 mmol) in THF-*d*₈ (0.45 mL) and dcpe (24 mg, 0.057 mmol) was prepared in a NMR tube at -78 °C. After 10 min at room temperature, ³¹P NMR spectroscopy confirmed total conversion of **10** into **11**.

Reaction with Acetylenes. (a) **Dimethyl Acetylenedicarboxylate.** (i) A solution of **10** (360 mg, 0.9 mmol) in hexane (10 mL) was cooled to -30 °C, and dimethyl acetylenedicarboxylate (0.27 mL, 2.2 mmol) was added; there was an immediate reaction. The mixture was stirred for 1.5 h at -30 °C, and a red solid was formed. The solvent was removed by evaporation, and the residue was extracted with ether. The solution was filtered through Celite, and the solvent was evaporated to dryness to yield 599 mg of red oil which showed a ³¹P NMR singlet at δ 26.64. Purification by column chromatography (silica gel, hexane/ether 5:1) yielded 150 mg of hexamethyl benzenehexacarboxylate, C₆(CO₂Me)₆, and 18 mg of tetramethyl 6,7-difluoro-1,2,3,4-naphthalenetetracarboxylate, 1,2,3,4-(CO₂Me)₄-6,7-F₂C₁₀H₂, which eluted first: IR (CHCl₃) 2960 (w), 1740 (s), 1528 (m), 1465 (m), 1445 (m), 1360 (w), 1270 (m), 1237 (m), 1165 (m) cm⁻¹; ¹H NMR (200 MHz, CDCl₃) δ 3.90 (s, 6H, OCH₃), 3.99 (s, 6H, OCH₃), 7.92 (t, 2H, *J*_{HF} = 9.6, H^{5,8}); ¹³C{¹H} NMR (75.4 MHz, CDCl₃) δ 53.24 (OCH₃), 53.33 (OCH₃), 113.15 (dd, ²*J*_{CF} = 13.2, ³*J*_{CF} = 7.7, C⁵-H and C⁸-H), 127.69 (t, ³*J*_{CF} = 4.4, C^{4a,8a}), 128.70 (C^{2,3}), 132.83 (C^{1,4}), 152.09 (dd, ¹*J*_{CF} = 259.2, ²*J*_{CF} = 17.6, C^{6,7}), 166.33 (C=O), 166.51 (C=O); ¹⁹F NMR (188.1 MHz, CDCl₃) δ -129.45 (t, *J*_{HF} = 9.3); EI-MS (C₁₈H₁₄F₂O₈) *m/z* 396 (40, M), 365 (100), 162 (16), 86 (16), 84 (24). C₆(CO₂Me)₆: IR (CHCl₃) 2960 (w), 1745 (s), 1447 (m), 1365 (w), 1335 (w), 1237 (m), 1210 (m) cm⁻¹; ¹H NMR (200 MHz, CDCl₃) δ 3.86 (s, 18H); ¹³C{¹H} NMR (75.4 MHz, CDCl₃) δ 53.42 (OCH₃), 133.88 (C), 165.14 (C=O); EI-MS (glycerol, C₁₈H₁₈O₁₂) *m/z* 426 (1, M), 395 (100, C₆(CO₂Me)₆(CO)), 182 (12), 104 (11).

(ii) A solution of **11** (0.23 g, 0.39 mmol) in THF (10 mL) cooled to -78 °C was treated dropwise with a solution of dimethyl acetylenedicarboxylate (0.048 mL, 0.39 mmol) in THF (5 mL), and the mixture was stirred for 30 min at -40 °C. The ¹⁹F NMR spectrum showed no evidence for the presence of the monoinertion complex **14** (see below) but did show signals due to 1,2,3,4-(CO₂Me)₄-6,7-F₂C₁₀H₂ (see above). Purification by column chromatography (silica gel, hexane/ether (5:1)) yielded 33 mg of tetramethyl 6,7-difluoro-1,2,3,4-naphthalenetetracarboxylate (43% based on dimethyl acetylenedicarboxylate).

(iii) When the dimethyl acetylenedicarboxylate solution was added over a 20 min period to a solution of **11** at -10 °C, the monoinertion complex **16** was formed. After the mixture was stirred for 20 min at -10 °C, the solvent was removed by evaporation and the residue was washed with hexane. Attempted crystallization from CH₂Cl₂/hexane (1:5) caused decomposition; therefore, the product **16** was identified spectroscopically. ¹H NMR (200 MHz, CD₂Cl₂): δ 1.10–2.50 (m, 48H, CH₂ and C₆H₁₁), 3.68 (s, 3H, OCH₃), 3.70 (s, 3H, OCH₃), 6.72–6.92 (m, 1H, H³ or H⁶), 6.97–7.15 (m, 1H, H³ or H⁶). ³¹P{¹H} NMR (80.96 MHz, CD₂Cl₂): δ 63.77 (dd, *J*_{PP} = 24.5, *J*_{FP} = 3.7), 69.34 (d, *J*_{PP} = 24.5).

(b) **3-Hexyne.** (i) As described above, a solution of **10** (360 mg, 0.9 mmol) in hexane (10 mL) was cooled to -30 °C and 3-hexyne (0.25 mL, 2.2 mmol) was added dropwise. The mixture was stirred for 15 h at 65 °C. The workup yielded 472 mg of a brown oily solid which showed ³¹P NMR resonances at δ 26.72 and 27.06. Purification by column chromatography (silica gel, hexane/ether (5:1)) yielded 6,7-difluoro-

1,2,3,4-tetraethylnaphthalene (221 mg, 89%). IR (CHCl₃): 2975 (m), 2940 (w), 2910 (w), 2880 (w), 1528 (m), 1450 (m), 1267 (s), 1100 (m), 1015 (m), 817 (m) cm⁻¹. ¹H NMR (200 MHz, CDCl₃): δ 1.21 (t, 6H, ³J = 7.6, 2 × CH₃), 1.25 (t, 6H, ³J = 7.6, 2 × CH₃), 2.80 (q, 4H, ³J = 7.5, 2 × CH₂), 2.98 (q, 4H, ³J = 7.6, 2 × CH₂), 7.71 (t, 2H, J_{HF} = 10.9, H^{5,8}). ¹³C{¹H} NMR (75.4 MHz, CDCl₃): δ 15.14 (CH₃), 15.58 (CH₃), 22.00 (CH₂), 22.68 (CH₂), 110.62 (dd, ²J_{CF} = 10.5, ³J_{CF} = 6.6, C⁵-H and C⁸-H), 128.21 (C^{4a,8a}), 134.93 (C^{2,3}), 138.38 (C^{1,4}), 148.97 (dd, ¹J_{CF} = 248.2, ²J_{CF} = 17.6, C^{6,7}). ¹⁹F NMR (188.1 MHz, CDCl₃): δ -139.96 (t, J_{HF} = 10.4). EI-MS (C₁₈H₂₂F₂): *m/z* 276 (61, M), 261 (44), 118 (21), 106 (67), 105 (66), 90 (49), 78 (57), 77 (72), 62 (100), 55 (59).

(ii) To a solution of **11** (50 mg, 0.08 mmol) in THF-*d*₈ (0.5 mL) in a NMR tube was added 3-hexyne (0.03 mL). The sample was heated for 16 h at room temperature. The ¹⁹F NMR spectrum showed quantitative transformation of the benzyne complex into 6,7-difluoro-1,2,3,4-tetraethylnaphthalene.

(c) **Hexafluoro-2-butyne**. Complex **10** was prepared *in situ* from **7** (505 mg, 0.89 mmol) by reduction with 30% Li dispersion (118 mg) in ether (20 mL) for 3 h at -30 °C, the reaction progress being monitored by ³¹P NMR spectroscopy. The solvent was evaporated, the residue was washed with hexane at -30 °C, and the extract was filtered through Celite and its volume reduced *in vacuo* to 20 mL. Exposure of the solution at -30 °C to an atmosphere of hexafluoro-2-butyne caused an instantaneous reaction. After the mixture was stirred for 30 min at -20 °C and 1 h at room temperature, the solvent was evaporated to yield 1.8 g of a brown insoluble polymer. The solid was extracted with ether and purified by column chromatography (silica gel, hexane/ether (5:1)) to yield 194 mg of a 2.4:1.4:1 mixture (ratio calculated from the ¹⁹F NMR spectrum) of 9,10-bis(trifluoromethyl)-2,3,6,7-tetrafluorophenanthrene (**13**), hexakis(trifluoromethyl)benzene, and 6,7-difluoro-1,2,3,4-tetrakis(trifluoromethyl)naphthalene (**12**); 44 mg (25%) isolated by crystallization from CH₂Cl₂. C₆(CF₃)₆: ¹⁹F NMR (188.1 MHz, CDCl₃) δ -52.24 (s, CF₃); EI-MS (C₁₂F₁₈) *m/z* 486 (13, M), 467 (40), 417 (34), 69 (100, CF₃). 6,7-F₂-1,2,3,4-(CF₃)₄-C₁₀H₂ (**12**): ¹H NMR (200 MHz, CDCl₃) δ 8.23 (t, J_{HF} = 9.4, H^{5,8}); ¹⁹F NMR (188.1 MHz, CDCl₃) δ -50.74 (d, J = 12.2, CF₃), -53.55 (d, J = 12.2, CF₃), -125.46 (t, J = 9.8, F^{6,7}); EI-MS (C₁₄H₂F₁₄) *m/z* 436 (51, M), 417 (25, M - F), 386 (22), 367 (56, M - CF₃), 348 (4), 317 (20), 298 (7), 229 (7), 149 (14), 77 (11), 69 (100, CF₃). 2,3,6,7-F₄-9,10-(CF₃)₂-C₁₄H₄ (**13**): ¹H NMR (200 MHz, CDCl₃) δ 8.10 (br dd, 2H, J = 11.8, J = 8.3, H^{arom}), 8.23 (dd, 2H, J = 11.4, J = 7.6, H^{arom}); ¹⁹F NMR (188.1 MHz, CDCl₃) δ -52.49 (s, CF₃), -130.54 (t, J = 10.5, F^{arom}), -133.33 (t, J = 10.5, F^{arom}); EI-MS (C₁₆H₄F₁₀) *m/z* 386 (57, M), 367 (9), 336 (6), 317 (34), 85 (31), 71 (50), 69 (68, CF₃), 57 (100).

(d) **tert-Butylacetylene**. (i) A solution of **2** (0.38 g, 1 mmol) in hexane (20 mL) was cooled to -30 °C, and *tert*-butylacetylene (0.45 mL, 4 mmol) in ether (2 mL) was added. The mixture was stirred for 1 h at -30 °C and 4.5 h at room temperature, the progress of the reaction being monitored by ³¹P NMR spectroscopy. The solvent was removed by evaporation, and the residue, taken up in ether, was filtered through a silica gel column. The compound was purified by preparative TLC (silica gel, hexane/ether (1:1)), and 135 mg (56%) of 1,3-di-*tert*-butylnaphthalene was isolated: ¹H NMR (200 MHz, CDCl₃): δ 1.53 (s, 9H, C(CH₃)₃), 1.75 (s, 9H, C(CH₃)₃), 7.48-7.56 (m, 2H, H^{6,7}), 7.70-7.76 (m, 2H, H^{2,4}) (no coupling observed with the other protons), 7.92-7.98 (m, 1H, H⁵), 8.46-8.54 (m, 1H, H⁸) (H^{5,8} became approximate doublets by irradiation at δ 7.47). ¹³C NMR (75.4 MHz, CDCl₃): δ 31.22 (CH₃), 31.84 (CH₃), 34.92 (C), 36.26 (C), 122.18 (CH), 122.34 (CH), 123.94 (CH), 124.56 (CH), 126.55 (CH), 129.66 (CH), 135.13 (C^{4a,8a}), 145.40 (C^{1 or 3}), 147.19 (C^{1 or 3}). EI-MS (C₁₈H₂₄): *m/z* 240 (30, M), 225 (100), 141 (11), 77 (10), 57 (73).

(ii) A solution of **10** (0.331 g, 0.8 mmol) in THF (20 mL) was prepared at -50 °C, and *tert*-butylacetylene (0.5 mL, 4.5 mmol) in solution in THF (5 mL) was added. The mixture was stirred

for 1 h at -30 °C and 20 h at room temperature. Workup as described above and crystallization from CH₂Cl₂/hexane gave 99 mg (45%) of 1,3-di-*tert*-butyl-6,7-difluoronaphthalene. ¹H NMR (300 MHz, CD₂Cl₂): δ 1.40 (s, 9H, C(CH₃)₃), 1.60 (s, 9H, C(CH₃)₃), 7.57 (dd, 1H, J = 8.7, 8.1, H⁴), 7.57 (dt, 1H, J_{HF} = 21, J = 0.5, H⁸), 7.62 (br s, 1H, H²), 8.15 (dd, 1H, J_{HF} = 14.7, J = 8.7, H⁵). ¹³C NMR (75.4 MHz, CD₂Cl₂): δ 31.36 (CH₃), 31.87 (CH₃), 35.36 (C), 36.57 (C), 113.63 (d, ²J_{CF} = 15.6, C^{5 or 8}-H), 115.07 (d, ²J_{CF} = 15.4, C^{5 or 8}-H), 122.05 (d, J = 3.2, C^{2 or 4}-H), 123.20 (d, J = 2.3, C^{2 or 4}-H), 126.78 (d, ³J_{CF} = 5.9, C^{4a or 8a}), 132.91 (d, ³J_{CF} = 7.7, C^{4a or 8a}), 145.77 (d, J = 4.4, C^{1 or 3}), 148.49 (dd, ¹J_{CF} = 244.8, ²J_{CF} = 15.4, C-F), 148.61 (d, J = 2.2, C^{1 or 3}), 149.20 (dd, ¹J_{CF} = 248.1, ²J_{CF} = 15.4, C^{1 or 3}). ¹⁹F NMR (188.1 MHz, CD₂Cl₂): δ -140.57 (m), -138.86 (m).

(e) **Methyl 2-Butynoate**. A solution of **10** (0.345 mg, 0.85 mmol) in THF (20 mL) was cooled to -78 °C, and a solution of methyl 2-butyrate (0.34 mL, 3.4 mmol) in THF (5 mL) was added. The solution was stirred for 5.5 h while being warmed to room temperature. The solvent was removed by evaporation. Filtration of an ether solution through a silica gel column yielded 257 mg of a clean 1.3:1 mixture of dimethyl 6,7-difluoro-1,4-dimethyl-2,3-naphthalenedicarboxylate (57%) and trimethyl 1,2,4-benzenetricarboxylate.¹⁹ The compounds were separated by column chromatography (silica gel, hexane/ether (1:1)), and the structure of the naphthalene compound was assigned unambiguously by ¹H NMR spectroscopy. A nuclear Overhauser effect (NOE) experiment yielded a 18% response from the naphthalenic protons in C^{5,8} on irradiation of the signal attributed to the methyl protons (δ 2.62). IR (CH₂Cl₂): 3010 (w), 2955 (m), 1730 (vs, C=O), 1525 (s), 1435 (s), 1230 (vs), 1170 (s), 1080 (m), 1030 (m), 873 (m), 860 (m), 805 (w) cm⁻¹. ¹H NMR (200 MHz, CDCl₃): δ 2.62 (s, 6H, 2 × CH₃), 3.90 (s, 6H, 2 × CO₂CH₃), 7.82 (t, 2H, J_{HF} = 10.1, H^{5,8}). ¹³C NMR (75.4 MHz, CDCl₃): δ 16.34 (CH₃), 52.75 (OCH₃), 112.40 (m, CH), 129.38 (C), 130.46 (C), 131.65 (C), 150.79 (dd, ¹J_{CF} = 252.5, ²J_{CF} = 16.4, CF), 169.13 (C=O). ¹⁹F NMR (188.1 MHz, CD₂Cl₂): δ -134.38 (t, J_{HF} = 10.2). EI-MS (C₁₆H₁₄F₂O₄): *m/z* 308 (26, M), 277 (77), 276 (100), 261 (33), 218 (87), 190 (73), 151 (31), 57 (53).

(f) **Methyl Propiolate**. A solution of **10** (331 mg, 0.82 mmol) in THF (20 mL) was cooled to -50 °C, and a solution of methyl propiolate (0.36 mL, 4 mmol) in THF (5 mL) was added. The solution was stirred for 1 h at -30 °C and 20 h at room temperature, but the reaction was not complete as shown by ³¹P NMR spectroscopy. An excess of methyl propiolate was added, but no decrease in the residual amount of **10** was observed. The solvent was removed by evaporation, and the crude red oil, as an ether extract, was filtered through a silica gel column. The ¹⁹F NMR spectrum of the crude compound showed a 1.3:1 mixture of the symmetrically substituted dimethyl 6,7-difluoro-2,3-naphthalenedicarboxylate (**14**) and the unsymmetrical dimethyl 6,7-difluoro-1,3-naphthalenedicarboxylate (**15**). Separation on preparative TLC (silica gel, hexane/ether (1:1)) yielded 30 mg (13%) of **15** and 171 mg of a 3:1 mixture of trimethyl 1,2,4-benzenetricarboxylate and **14** (20%). The structure of **14** was assigned by a NOE experiment. Irradiation of the signal due to H^{5,8} (δ 7.71) gave a 16% response from the remaining aromatic protons. 2,3-(CO₂Me)₂-6,7-F₂-C₁₀H₄ (**14**): ¹H NMR (200 MHz, CD₂Cl₂) δ 3.91 (s, 6H, 2 × OCH₃), 7.71 (t, 2H, J_{HF} = 9.2, H^{5,8}), 8.18 (s, 2H, H^{1,4}); ¹⁹F NMR (188.1 MHz, CD₂Cl₂) δ -133.32 (t, J_{HF} = 9.2). 1,3-(CO₂Me)₂-6,7-F₂-C₁₀H₄ (**15**): IR (CH₂Cl₂) 2950 (w), 1715 (s), 1515 (s), 1465 (m), 1435 (w), 1375 (w), 1285 (w), 1235 (s), 1220 (m), 1130 (m), 855 (m) cm⁻¹; ¹H NMR (200 MHz, CD₂Cl₂) δ 3.98 (s, 3H, OCH₃), 4.00 (s, 3H, OCH₃), 7.77 (dd, 1H, J_{HF} = 10.4, J_{HF} = 8.3, H^{5 or 8}), 8.68 (br s, 1H, H^{2 or 4}), 8.77 (br s, 1H, H^{2 or 4}), 8.91 (dd, 1H, J_{HF} = 13.4, J_{HF} = 8.3, H^{5 or 8}); ¹⁹F NMR (188.1 MHz, CD₂Cl₂) δ -135.88 (m), -130.56 (m).

Acknowledgment. We thank the Swiss National Science Foundation for the award of a Fellowship (E.W.) (Grant No 8220-033162).

OM940753S

Titanium Alkylidenes via Dineopentyl Complexes

Johannes A. van Doorn and Harry van der Heijden*

Koninklijke/Shell-Laboratorium, Amsterdam (Shell Research BV), P.O. Box 3003,
1003 AA Amsterdam, The Netherlands

A. Guy Orpen

Department of Inorganic Chemistry, The University, Bristol BS8 1TS, United Kingdom

Received September 29, 1994[®]

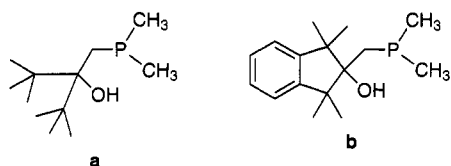
Mono(cyclopentadienyl)titanium neopentylidene complexes with bulky phosphinoalkoxide ancillary ligands were prepared via the corresponding dineopentyl complexes. The structure of **3b** was determined by an X-ray analysis. Crystal data: Ti(η^5 -C₅H₅)(CHMe₃)(PMe₂-CH₂C(O)-CMe₂-o-C₆H₄CMe₂), monoclinic, space group *P*2₁/*c* (No. 14), *a* = 10.728(3) Å, *b* = 12.881(4) Å, *c* = 18.553(6) Å, β = 104.36(3)°, *Z* = 4, *N*_o = 3419, *R* = 0.045. The titanium alkylidene readily reacts with ethene, initially forming a metallacycle, while subsequent reactions produce a stable ethene complex. Reaction of the alkylidene with CO to form ketene derivatives was briefly studied.

Introduction

Recently we reported a route to novel mononuclear titanium alkylidene complexes containing a bulky (phenylphosphino)alkoxide¹ and a cyclopentadienyl ligand. The alkylidene complex was not isolated in a pure state due to a subsequent addition of a CH bond of one of the phenyl groups of the ligand across the double-bond system of the metal alkylidene,¹ forming the cyclometalated complex **4**. The insertion reaction is reversible, but it complicates a study of reactions of the alkylidene with olefins. In order to avoid the ortho-metalation reaction, we have replaced the phenyl groups at the phosphorus atom with methyl groups. This allowed the isolation of well-defined neopentylidene species suitable for structural characterization and reactivity studies.

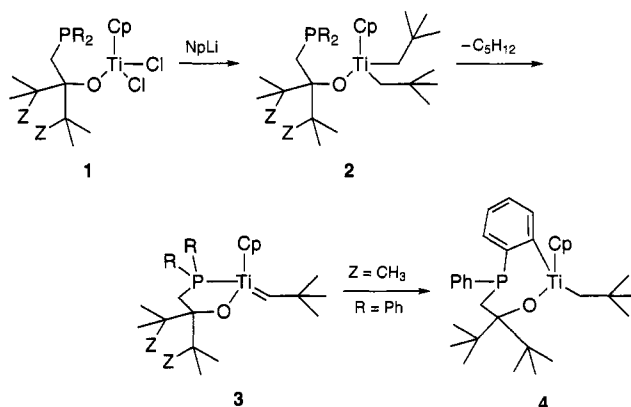
Results and Discussion

The precursors of the (methylphosphino)alkoxide ligands, the alcohols **a** and **b**, were prepared according to Lappert² by addition of (CH₃)₂PCH₂Li³ to the appropriate ketone followed by hydrolysis. The dichloro-



rotitanium alkoxide complexes **1** were prepared by reaction between cyclopentadienyltitanium trichloride and (**a**)Li or (**b**)Li. The ³¹P NMR spectra of these products **1a** or **1b** suggest that the phosphorus atom is

Scheme 1^a



^a Legend: **a**, R = Z = CH₃; **b**, R = CH₃, Z + Z = 1,2-phenylene.

only weakly bonded to the titanium atom. The signal is usually broad, and the chemical shift is strongly dependent on the solvent (see Experimental Section). This may indicate that a rapid exchange occurs between a bonded and a nonbonded situation. Reaction of the dichlorides **1** with neopentyl lithium readily leads to the corresponding dineopentyl complexes, which are not stable at room temperature. The spectroscopic data for **2b** are given in the Experimental Section together with the synthetic procedure for **3b**. Both **2a** and **2b** form stable alkylidene complexes by expulsion of neopentane. They show characteristic resonances in the NMR spectra. The alkylidene hydrogen resonance is found around 12 ppm and is a doublet due to coupling to phosphorus. The alkylidene carbon atom resonance is found at ca. 280 ppm; the signal is a doublet due to coupling to phosphorus. The relatively low value of the ¹J(¹H¹³C) coupling constant (approximately 95 Hz) may indicate an agostic interaction of the alkylidene hydrogen with the titanium atom.

Compound **3a** was obtained as a green oil which crystallized very slowly with difficulty from a concentrated pentane solution. In contrast, the alkylidene **3b** readily forms dark green crystals which were suitable for an X-ray structure determination.

[®] Abstract published in *Advance ACS Abstracts*, February 1, 1995.
(1) van Doorn, J. A.; van der Heijden, H.; Orpen, A. G. *Organometallics* **1994**, *13*, 4271.

(2) Engelhardt, L. M.; Harrowfield, J. M.; Lappert, M. F.; MacKinnon, I. A.; Newton, B. H.; Raston, C. L.; Skeleton, B. W.; White, A. H. *J. Chem. Soc., Chem. Commun.* **1986**, 846.

(3) (a) Karsch, H. H.; Appelt, A. *Z. Naturforsch.* **1983**, *38B*, 1399.
(b) Engelhardt, L. M.; Jacobsen, G. E.; Raston, C. L.; White, A. H. *J. Chem. Soc., Chem. Commun.* **1984**, 220.

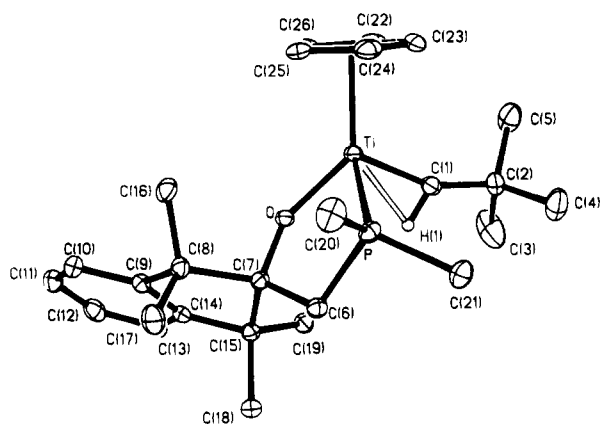


Figure 1. Molecular structure of **3b** showing the full labeling scheme. Non-hydrogen atoms are represented as ellipsoids enclosing 30% probability density. Cyclopentadienyl, methylene, aryl, and methyl hydrogens have been omitted for clarity.

Table 1. Selected Bond Lengths (Å) and Bond Angles (deg) for **3b**

Ti-P	2.534(1)	Ti-O	1.869(2)	Ti-C(1)	1.911(3)
Ti-C(22)	2.377(3)	Ti-C(23)	2.419(3)	Ti-C(24)	2.409(4)
Ti-C	2.373(3)	Ti-C(26)	2.341(3)	P-C(6)	1.839(3)
P-C(20)	1.821(4)	P-C(21)	1.814(3)	O-C(7)	1.415(3)
C(1)-C(2)	1.516(4)	C(2)-C(3)	1.533(7)	C(2)-C(4)	1.515(5)
C(2)-C(5)	1.515(5)	C(6)-C(7)	1.551(4)	C(7)-C(8)	1.599(4)
C(7)-C(15)	1.577(4)	C(8)-C(9)	1.523(4)	C(8)-C(16)	1.534(4)
C(8)-C(17)	1.546(4)	C(9)-C(10)	1.399(4)	C(9)-C(14)	1.390(4)
C(10)-C(11)	1.384(5)	C(11)-C(12)	1.373(5)	C(12)-C(13)	1.385(5)
C(13)-C(14)	1.391(5)	C(14)-C(15)	1.513(4)	C(15)-C(18)	1.542(4)
C(15)-C(19)	1.538(4)	C(22)-C(23)	1.415(5)	C(22)-C(26)	1.404(5)
C(23)-C(24)	1.403(5)	C(24)-C(25)	1.400(5)	C(25)-C(26)	1.403(5)

P-Ti-O	77.1(1)	P-Ti-C(1)	96.5(1)
O-Ti-C(1)	107.2(1)	P-Ti-C(22)	141.2(1)
O-Ti-C(22)	135.9(1)	C(1)-Ti-C(22)	91.6(1)
P-Ti-C(23)	107.6(1)	O-Ti-C(23)	161.8(1)
C(1)-Ti-C(23)	89.8(1)	C(22)-Ti-C(23)	34.3(1)
P-Ti-C(24)	86.5(1)	O-Ti-C(24)	132.5(1)
C(1)-Ti-C(24)	118.8(1)	C(22)-Ti-C(24)	56.8(1)
C(23)-Ti-C(24)	33.8(1)	P-Ti-C(25)	100.2(1)
O-Ti-C(25)	105.6(1)	C(1)-Ti-C(25)	145.7(1)
C(22)-Ti-C(25)	57.2(1)	C(23)-Ti-C(25)	56.6(1)
C(24)-Ti-C(25)	34.0(1)	P-Ti-C(26)	134.8(1)
O-Ti-C(26)	106.8(1)	C(1)-Ti-C(26)	123.1(1)
C(22)-Ti-C(26)	34.6(1)	C(23)-Ti-C(26)	57.1(1)
C(24)-Ti-C(26)	57.0(1)	C(25)-Ti-C(26)	34.6(1)
Ti-P-C(6)	96.5(1)	Ti-P-C(20)	125.5(1)
C(6)-P-C(20)	105.5(2)	Ti-P-C(21)	122.6(1)
C(6)-P-C(21)	103.4(1)	C(20)-P-C(21)	100.1(2)
Ti-O-C(7)	138.3(2)	Ti-C(1)-C(2)	158.7(2)
C(1)-C(2)-C(3)	110.6(3)	C(1)-C(2)-C(4)	109.8(3)
C(3)-C(2)-C(4)	107.9(3)	C(1)-C(2)-C(5)	112.2(3)
C(3)-C(2)-C(5)	108.0(3)	C(4)-C(2)-C(5)	108.2(3)
P-C(6)-C(7)	112.2(2)	O-C(7)-C(6)	107.3(2)
O-C(7)-C(8)	108.2(2)	C(6)-C(7)-C(8)	116.7(2)
O-C(7)-C(15)	108.7(2)	C(6)-C(7)-C(15)	111.2(2)
C(8)-C(7)-C(15)	104.5(2)	C(7)-C(8)-C(9)	101.1(2)
C(7)-C(8)-C(16)	112.3(2)	C(9)-C(8)-C(16)	109.7(2)
C(7)-C(8)-C(17)	115.0(2)	C(9)-C(8)-C(17)	110.9(2)
C(16)-C(8)-C(17)	107.7(3)	C(8)-C(9)-C(14)	112.4(2)
C(9)-C(14)-C(15)	110.8(3)	C(7)-C(15)-C(14)	102.0(2)

X-ray Structure of 3b. The molecular structure of **3b** is given in Figure 1. Pertinent bond distances and bond angles are given in Table 1. The molecule is monomeric, with a distorted three-legged piano-stool geometry around the metal center. The phosphinoalkoxide ligand is bidentate with a Ti-P distance of 2.534(1) Å and a Ti-O distance of 1.869(2) Å (cf. average Ti-O for terminal alkoxides of 1.847 Å quoted in ref 4 and 1.787(2) Å for the alkoxide in the metalated compound

Table 2. Atomic Coordinates ($\times 10^4$) and Equivalent Isotropic Displacement Parameters ($\text{Å}^2 \times 10^3$) for **3b**

atom	x	y	z	U_{eq}^a
Ti	764(1)	547(1)	1340(1)	22(1)
P	2092(1)	643(1)	2674(1)	27(1)
O	2112(2)	-376(2)	1347(1)	22(1)
C(1)	1264(3)	1869(2)	1036(2)	28(1)
C(2)	1127(3)	2974(2)	746(2)	34(1)
C(3)	2090(5)	3189(4)	275(3)	86(2)
C(4)	1404(4)	3729(3)	1392(2)	61(1)
C(5)	-211(4)	3196(3)	269(2)	55(1)
C(6)	3564(3)	70(2)	2505(2)	26(1)
C(7)	3270(3)	-703(2)	1844(2)	23(1)
C(8)	3120(3)	-1898(2)	2041(2)	27(1)
C(9)	3584(3)	-2432(2)	1423(2)	27(1)
C(10)	3409(3)	-3470(2)	1198(2)	34(1)
C(11)	3849(3)	-3806(3)	597(2)	40(1)
C(12)	4462(3)	-3130(3)	227(2)	38(1)
C(13)	4665(3)	-2106(3)	452(2)	32(1)
C(14)	4217(3)	-1754(2)	1051(2)	26(1)
C(15)	4374(3)	-697(2)	1419(2)	26(1)
C(16)	1716(3)	-2197(2)	1988(2)	34(1)
C(17)	3930(3)	-2241(3)	2814(2)	39(1)
C(18)	5736(3)	-620(2)	1939(2)	33(1)
C(19)	4245(3)	204(2)	862(2)	29(1)
C(20)	1776(4)	-79(3)	3453(2)	47(1)
C(21)	2646(3)	1863(3)	3130(2)	40(1)
C(22)	-1378(3)	769(3)	611(2)	36(1)
C(23)	-1349(3)	1232(3)	1307(2)	35(1)
C(24)	-1092(3)	447(3)	1848(2)	37(1)
C(25)	-974(3)	-495(3)	1495(2)	36(1)
C(26)	-1140(3)	-296(3)	733(2)	36(1)

^a Equivalent isotropic U , defined as one-third of the trace of the orthogonalized U_{ij} tensor.

4.1 The Ti-O-C angle in **3b** is significantly smaller than that in the metalated complex **4**, reflecting the larger ring size¹ and probably an increased O-Ti π -donation contribution in **4**. The Ti=C double-bond distance is 1.911(3) Å (cf. 2.120(4) Å for the neopentyl ligand of **4**). The Ti-C(1)-C(2) angle of 158.7(2)° together with the Ti-C(1)-H(1) angle of 85(3)° (Ti-H(1) = 2.05(5) Å) suggests an α -agostic type distortion of the alkylidene, as is commonly found in d^0 metal alkylidenes.⁵ The d^0 complex **3b** makes an interesting comparison with the related d^2 -metal three-legged piano-stool alkylidene complex CpV(CHCMe₃)dmpe.⁶ In the latter the alkylidene unit is rotated 90° with respect to the orientation relative to the Cp ligand and is much more distorted (angle V-C-C = 173.3(3)°, angle V-C-H = 65(3)°).

Reactions of the Alkylidene. At room temperature alkylidene **3b** reacts smoothly with ethylene to form the metallacyclobutane complex **5**. This compound can be crystallized from pentane. The ¹H NMR spectrum shows characteristic downfield shifts (δ 3.8–2.9) for the α -protons, and one of the β -protons is strongly shifted upfield (δ -0.40). These characteristics are comparable with those of bis(cyclopentadienyl)titanacyclobutanes.^{7,8}

(4) Orpen, A. G.; Brammer, L.; Allen, F. H.; Kennard, O.; Watson, D. G.; Taylor, R. *J. Chem. Soc., Dalton Trans.* **1989**, S1.

(5) (a) Demolliens, A.; Jean, Y.; Eisenstein, O. *Organometallics* **1986**, *5*, 1457. (b) Nugent, W. A.; Mayer, J. M. *Metal-Ligand Multiple Bonds*; Wiley: New York, 1988; Chapter 5, and references cited therein. (c) Goddard, R. J.; Hoffman, R.; Jemmis, E. D. *J. Am. Chem. Soc.* **1980**, *102*, 7667.

(6) (a) Hessen, B.; Meetsma, A.; Teuben, J. H. *J. Am. Chem. Soc.* **1989**, *111*, 5977. (b) Hessen, B.; Buijink, J. K. F.; Meetsma, A.; Teuben, J. H.; Helgesson, G.; Håkansson, M.; Jagner, S.; Spek, A. L. *Organometallics* **1993**, *12*, 2268.

(7) (a) Howard, T. R.; Lee, J. B.; Grubbs, R. H. *J. Am. Chem. Soc.* **1980**, *102*, 6876. (b) Gilliom, L. R.; Grubbs, R. H. *J. Am. Chem. Soc.* **1986**, *108*, 733.

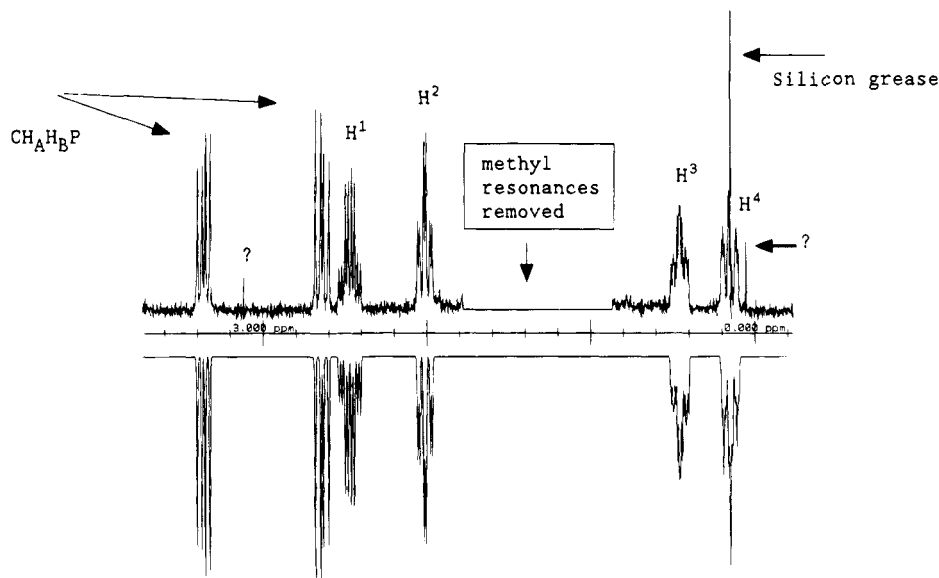
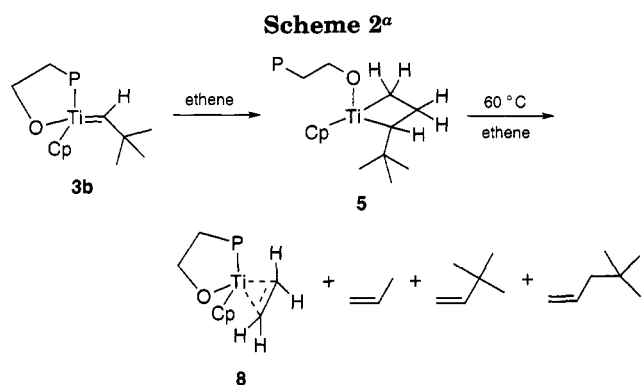


Figure 2. Selected resonances of the titanium ethene complex **8** together with the simulated spectrum. The data are given in the Experimental Section.



^a The phosphinoalkoxide ligand is drawn schematically.

The ³¹P resonance appears at -63.6 ppm, and this indicates that the phosphorus atom in this complex is not coordinated. These data are consistent with structure **5**.

When the reaction is performed at a higher temperature (60 °C) with an excess of ethene, the purple ethene complex **8** is obtained in addition to three olefins: propene (0.5 equiv), 3,3-dimethyl-1-butene (0.6 equiv), and 4,4-dimethyl-1-pentene (0.4 equiv) (GLC).

The formation of these olefins suggests that the metallacyclobutane complex **5** reacts in two different ways. A β-H elimination leads to a hydrido alkyl complex which rearranges to a 4,4-dimethylpentene complex by reductive elimination. Subsequently, the olefin is displaced by ethene, leading to the ethene complex **8**. The other olefins, 3,3-dimethylbutene and propene, are the result of metathesis reactions. Metathesis of the metallacyclobutane **5** leads to 3,3-dimethylbutene and a methylene complex. Reaction of this methylene compound with ethene leads to a metallacycle which gives propene and the ethene complex **8** by a route similar to that for the formation of 4,4-dimethylpentene.

The purple titanium ethylene adduct **8** was characterized by NMR spectroscopy. Figure 2 shows the

hydrogen resonances of the ethene fragment. The structure of **8** was confirmed by an independent synthesis from **1b** and diethylmagnesium. The ³¹P NMR spectrum of **8** shows a sharp resonance at +17.7 ppm, suggesting that the phosphinoalkoxide is bidentate in this complex. The ¹³C chemical shifts of the coordinated ethene and the C-H coupling constants ($\delta(\text{CH}^1\text{H}^2)$ 58.8, $^1J(\text{CH}) = 144$ Hz, $\delta(\text{CH}^3\text{H}^4)$ 55.0, $^1J(\text{CH}) = 147$ Hz) compare well with those in Cp*₂Ti(η²-ethene).⁹ The resonances of the two ethene protons with the largest PH coupling constants appear at relatively high field.

Both the ¹H and ¹³C chemical shifts and the ¹H-¹H and ¹H-¹³C coupling constants are consistent with a carbon hybridization between an sp² and an sp³ situation.

A similar complex of 1-butene could be obtained as well. Reaction of titanium chloride **1b** with BuLi in hexane leads to a mixture of two isomeric 1-butene complexes (ratio 3:2). Exactly the same mixture of compounds was obtained from a reaction of **1b** with *s*-butyllithium; no 2-butene complex was formed. The 1-butene ligand can be readily replaced with ethene by adding ethene to a solution of the butene complexes.

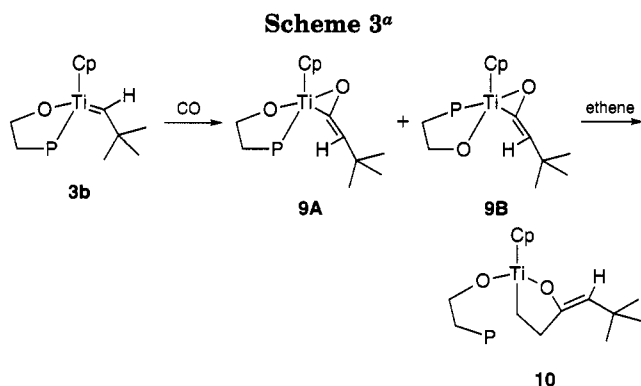
Attempts to use the alkylidene complexes for catalytic olefin conversion were not very successful. Reaction of the alkylidene **3a** with propene and 2-pentene at 60 °C gives the expected metathesis products. The turnover number, however, is very low (<5), and the rate rapidly falls off.

The alkylidene **3b** reacts with CO to give a ketene complex.¹⁰ We have obtained a mixture of two red compounds, the ketene complexes **9A** and **9B**, in the ratio 2:1. Spectroscopic data suggest a structure for **9A** with the ketene carbonyl carbon quasi-cis to the phosphorus atom ($^2J(^{13}\text{C}^{31}\text{P}) = 4.8$ Hz, $\delta(^{31}\text{P})$ 2.4 ppm) and for **9B** with the ketene carbonyl carbon quasi-trans to

(9) (a) Cohen, S. A.; Auburn, P. R.; Bercaw, J. E. *J. Am. Chem. Soc.* **1983**, *105*, 1136. (b) Hill, J. E.; Fanwick, P. E.; Rothwell, I. P. *Organometallics* **1992**, *11*, 171. (c) Luinstra, G. A.; ten Cate, L. C.; Heeres, H. J.; Pattiasina, J. W.; Meetsma, A.; Teuben, J. H. *Organometallics* **1991**, *10*, 3227.

(10) Schrock, R. R. *Acc. Chem. Res.* **1979**, *12*, 98.

(8) Anslyn, E. V.; Grubbs, R. H. *J. Am. Chem. Soc.* **1987**, *109*, 4880.



^a Configurations around the double bonds are not known. Phosphinoalkoxide ligands are drawn schematically.

the phosphorus atom ($^2J(^{13}\text{C}^{31}\text{P}) = 28.3 \text{ Hz}$, $\delta(^{31}\text{P}) - 7.5 \text{ ppm}$). The results of the elemental analysis are in accord with an 1:1 adduct of the alkylidene and CO. The mixture of these isomers reacts with ethene, forming one new compound, the orange titanium bis(alkoxide) **10** with a 1-oxa-2-titanacyclopentane fragment.¹¹ In compound **10** the phosphorus atom is not coordinated to the metal center.

Concluding Remarks

Stable titanium alkylidene complexes have been readily prepared via the corresponding dineopentyl compound. These complexes bear a bulky chelating phosphinoalkoxide and one cyclopentadienyl ligand. The ready synthesis of these alkylidene complexes does not agree with the current opinion that titanium alkylidenes are not accessible through the corresponding dineopentyl complexes. Our successful synthesis may be allowed by particular properties of phosphinoalkoxide ligands. Alternatively, these results may suggest that the synthesis of bis(cyclopentadienyl) alkylidenes via the dineopentyl compounds has to be revisited. The alkylidenes react readily with α -olefins at room temperature, forming metallacycles. The reaction products of the alkylidene with ethene show that a metathesis reaction has occurred, but in low yield. Eventually, a stable titanium ethene complex is obtained.

Experimental Section

General Information. All operations with air-sensitive materials were either performed in an argon atmosphere using Schlenk techniques or under nitrogen in a glovebox. THF, hexane, and ether were freshly distilled from sodium/benzophenone. Ligand **a** was prepared according to Lappert.² Trimethylphosphine was obtained from Strem, and CpTiCl_3 from Aldrich. 1,1,3,3-Tetramethylindane,¹⁴ neopentyl lithium,¹⁶ $\text{Me}_2\text{PCH}_2\text{Li}\cdot\text{TMEDA}$,¹⁷ and diethylmagnesium^{18,19} were prepared by published methods.

(11) Meinhart, J. D.; Santarsiero, B. D.; Grubbs, R. H. *J. Am. Chem. Soc.* **1986**, *108*, 3318.

(12) Sheldrick, G. M. *SHELXTL-PLUS* Rev. 4.2; University of Göttingen: Göttingen, FRG, 1990.

(13) *International Tables for X-ray Crystallography*; Kynoch Press: Birmingham, U.K., 1974; Vol. IV.

(14) Langhals, E.; Langhals, H. *Tetrahedron Lett.* **1990**, 859.

(15) *genMR Package*; Ivorysoft Scientific Software, Amerbos 330, Amsterdam.

(16) Schrock, R. R.; Fellmann, J. D. *J. Am. Chem. Soc.* **1978**, *100*, 3359.

(17) Engelhardt, L. M.; Jacobsen, G. E.; Raston, C. L.; White, A. H. *J. Chem. Soc., Chem. Commun.* **1984**, 220.

Table 3. Crystallographic Data for 3b

chem formula	$\text{C}_{26}\text{H}_{39}\text{OPTi}$
M_r	446.5
space group	$P2_1/c$ (No. 14)
a , Å	10.728(3)
b , Å	12.881(4)
c , Å	18.553(6)
β , deg	104.36(3)
V , Å ³	2483.8(12)
D_{exptl} , g cm ⁻³	1.19
Z	4
λ , Å	0.710 69
$\mu(\text{Mo K}\alpha)$, cm ⁻¹	4.2
spec size, mm	0.45 × 0.45 × 0.8
$2\theta_{\text{max}}$, deg	50
N_v	265
N_o	3419
R^a	0.045
R_w^a	0.063
S^a	2.06

$$^a R = \sum |\Delta| / \sum |F_o|; R_w = [\sum w\Delta^2 / \sum wF_o^2]^{1/2}; S = [\sum w\Delta^2 / (N_o - N_v)]^{1/2}; \Delta = F_o - F_c.$$

The NMR data were obtained with Varian 200 and 300 MHz apparatus. The data are given with the experimental procedures. Coupling constants (in Hz) with phosphorus are given in parentheses; $^1\text{H}^{13}\text{C}$ couplings are given in brackets.

X-ray Structure Analysis. A single crystal of **3b** was mounted in a thin-walled glass capillary under N_2 and held in place with silicone grease. All diffraction measurements were made at low temperature (200 K) on a Nicolet P3m diffractometer fitted with an LT-1 crystal cooling device, using graphite-monochromated $\text{Mo K}\alpha$ X-radiation. Unit cell dimensions were determined from 42 centered reflections in the range $15.0 < 2\theta < 30.0^\circ$. A total of 6103 diffracted intensities, including check reflections, were measured in a unique quadrant of reciprocal space by Wyckoff ω scans. Three check reflections (4,2-11, 720, and 093) remeasured after every 100 ordinary data showed ca. 5% decay and variation of $\pm 2\%$ over the period of data collection; an appropriate correction was therefore applied. Of the 5899 intensity data (other than checks) collected, 4393 unique observations remained after averaging of duplicate and equivalent measurements and deletion of systematic absences; of these, 3419 with $I > 3\sigma(I)$ were retained for use in structure solution and refinement. An absorption correction was applied in the basis of 348 azimuthal scan data; maximum and minimum transmission coefficients were 0.788 and 0.692, respectively. Lorentz and polarization corrections were applied.

The structure was solved by Patterson and Fourier methods. All non-hydrogen atoms were assigned anisotropic displacement parameters and all hydrogen atoms fixed isotropic displacement parameters. All non-hydrogen atoms and the hydrogen atom H(1) (which was located in a difference Fourier synthesis) were refined without positional constraints. All other hydrogen atoms were constrained to idealized geometries ($\text{C}-\text{H} = 0.96 \text{ \AA}$, $\text{H}-\text{C}-\text{H} = 109.5^\circ$). Full-matrix least-squares refinement of this model (265 parameters) converged to final residual indices given in Table 3. Weights, w , were set equal to $[\sigma_c^2(F_o) + gF_o^2]^{-1}$, where $\sigma_c^2(F_o)$ is the variance in F_o due to counting statistics and $g = 0.0005$ was chosen to minimize the variation in S as a function of $|F_o|$. Final difference electron density maps showed no features outside the range $+0.43$ to -0.26 e \AA^{-3} , the largest of these being close to the center of a P-C bond. All calculations were carried out on a Nicolet R3m/V structure determination system using programs of the SHELXTL-PLUS package.¹² Complex neutral-atom scattering factors were taken from ref 13.

Ligand b. A solution of butyllithium in hexane (1.6 M, 70 mmol) was added to a stirred solution of trimethylphosphine

(18) Strohmeier, W.; Seifert, F. *Chem. Ber.* **1961**, *94*, 2356.

(19) Dryden, N. H.; Legzdins, P.; Trotter, J.; Yee, V. C. *Organometallics* **1991**, *10*, 2857.

(5.10 g, 67 mmol) and TMEDA (8.08 g, 69.5 mmol) in 50 mL of hexane. This solution was stirred overnight. The resulting mixture was cooled to $-78\text{ }^{\circ}\text{C}$, and solid 1,1,3,3-tetramethyl-2-indanone (13.18 g, 70 mmol) was added. The mixture was allowed to reach room temperature. After 2 h the mixture was concentrated and 50 mL of water and 100 mL of diethyl ether was added. The organic layer was separated, washed twice with water, and dried on MgSO_4 . After filtration the solvent was removed in vacuo. The resulting material was dried in vacuo at $80\text{ }^{\circ}\text{C}$. It was difficult to purify the product: yield ca. 90%; purity ca. 90%. It was used as such, and the resulting titanium complex was readily purified.

The pure ligand can be obtained when the lithiated trimethylphosphine is isolated prior to reaction with the indanone. A mixture of 5.77 g (29.1 mmol) of $(\text{CH}_3)_2\text{PCH}_2\text{Li}\cdot\text{TMEDA}$ in 20 mL of pentane was slowly added to a solution of 1,1,3,3-tetramethyl-2-indanone in 30 mL of pentane at $0\text{ }^{\circ}\text{C}$. The resulting mixture was stirred for 1 h at room temperature, and subsequently the product was extracted with 30 mL of water. A foam was formed. The water layer was separated and the organic materials were extracted two more times with water. The combined water layers were neutralized with HCl until pH 7. The resulting alcohol was extracted with dichloromethane. After separation the dichloromethane layer was filtered over 1 cm of silica. The solvent was removed in vacuo, leaving 6.41 g (83.1%) of the pure alcohol as a white solid. NMR (CDCl_3): ^1H , CH_3P δ 1.16 (2.5), CH_2P 1.79 (3.2), CH_3 1.31 and 1.46, Ar 7.05–7.27, OH 1.59 (1.5); ^{13}C , CH_3P δ 16.4 (11.6), CH_2P 36.7 (16.2), CH_3 29.8 (1.6) and 23.8 (7.7), COH 87.5 (4.9), $\text{C}(\text{CH}_3)_2$ 50.8, Ar 149.0 (1.1), 127.2, 122.9; ^{31}P , δ -61.1 .

Titanium Dichloride Complex 1a. To a stirred mixture of 1.76 g (8 mmol) of (cyclopentadienyl)titanium trichloride and 60 mL of dichloromethane was added 1.8 g (8 mmol) of the lithium alkoxide derived from the alcohol **a** at $0\text{ }^{\circ}\text{C}$. The mixture was stirred for 16 h. The precipitate was removed by centrifugation, washed with dichloromethane, and centrifuged again. The combined dichloromethane layers were concentrated to ca. 3 mL. Then pentane was slowly added to induce crystallization of the product. The yellow material was filtered and dried in vacuo. Yield 2.7 g (67%). Anal. Calcd: C, 50.90; H, 7.79; Cl, 17.67; P, 7.72; Ti, 11.93. Found: C, 50.77; H, 7.67; Cl, 17.80; P, 7.95; Ti, 11.85. NMR (C_6D_6): ^1H , CH_3P δ 0.95 (6.7), CH_2P 1.96 (10.0), *t*-Bu 1.10, Cp 6.33 (2.0); ^{31}P , δ -1.8 . NMR (CD_2Cl_2): ^1H , CH_3P δ 1.62 (8.8), CH_2P 1.74 (10.8), *t*-Bu 1.24, Cp 6.64 (2.2); ^{31}P , δ $+9.7$.

Titanium Dichloride Complex 1b. A solution of butyllithium in hexane (19.7 mmol, 1.6 M) was added to a stirred solution of 5.2 g (ca. 19.7 mmol) of the alcohol **b** in 25 mL of hexane at $0\text{ }^{\circ}\text{C}$. The resulting mixture was concentrated to ca. 15 mL, and then 4.32 g (19.7 mmol) of (cyclopentadienyl)titanium trichloride was added at $0\text{ }^{\circ}\text{C}$. The mixture was stirred for another 16 h at room temperature. The precipitate was removed and washed four times with dichloromethane. The dichloromethane layers were combined and concentrated to ca. 5 mL. Subsequently, pentane was added slowly to induce crystallization. The yellow material was filtered and dried in vacuo; yield 4.6 g (52%). Anal. Calcd: C, 56.40; H, 6.54; Cl, 15.85; P, 6.93; Ti, 10.71. Found: C, 56.26; H, 6.48; Cl, 16.11; P, 7.14; Ti, 10.45. NMR (CD_2Cl_2): ^1H , CH_3P δ 1.58 (4.3), CH_2P 2.46 (8.5), CH_3 1.34 and 1.60, Ar 7.2–7.4, Cp 6.44 (1.6); ^{31}P , δ -17.2 (broadened).

Alkylidene Complex 3a. This compound was prepared as described for **3b**. The product was isolated as a green oil in ca. 90% yield. Crystals were obtained from a concentrated pentane solution at $-40\text{ }^{\circ}\text{C}$. Anal. Calcd: C, 65.99; H, 10.32; Ti, 11.96. Found: C, 66.71; H, 10.15; Ti, 12.00. NMR (C_6D_6): ^1H , *CH-t*-Bu δ 12.27 (3.8), $\text{C}(\text{CH}_3)_3$ 1.22, Cp 6.11 (1.7), PMe_2 1.31 (6.4) and 0.71 (5.8), $\text{CH}_A\text{H}_B\text{P}$ 3.19 (10.4) and 2.40 (10.0), $J(\text{H}_A\text{H}_B)$ = 16, *t*-Bu 0.97 and 1.44; ^{13}C , neopentylidene, TiC δ 283.5 (11.4) [96], $\text{C}(\text{CH}_3)_3$ 42.6, $\text{C}(\text{CH}_3)_2$ 34.0 (3.6) [124], Cp 106.7 [171], alkoxide, PMe_2 23.2 (21.5) [128] and 15.0 (9.1)

[127], CH_2P 51.7 (22.0) [125], CO 93.5 (4.5), $\text{C}(\text{CH}_3)_3$ 47.2 (1.4) and 45.8 (2.3), CH_3 30.8 [126] and 30.1 [125]; ^{31}P , δ 0.53.

Alkylidene Complex 3b. Solid neopentyllithium (585 mg, 7.5 mmol) was added to a stirred suspension of **1b** in pentane at $0\text{ }^{\circ}\text{C}$. After the mixture was stirred for 2 h at room temperature, the precipitate was removed by centrifugation. The liquid fraction was kept at room temperature for 24 h; then the solvent was removed, leaving a green solid, yield 90%. Crystals for the X-ray structure determination were prepared by recrystallization from a concentrated pentane solution at $-40\text{ }^{\circ}\text{C}$.

NMR of the intermediate dialkyl complex **2b**: ^1H (C_6D_6 , $20\text{ }^{\circ}\text{C}$), Cp δ 5.92, neopentyl, CH_3 1.07, CH_AH_B , 2.35 H_B was not observed due to overlap, $J(\text{H}_A\text{H}_B)$ = 11 Hz, phosphinoalkoxide, Me_2P 1.20, CH_2P 2.01 (5), CH_3 1.46 and 1.19, ArH, 5.9–7.2; ^{13}C ($[\text{D}_8]\text{toluene}$, $-30\text{ }^{\circ}\text{C}$), neopentyl, TiC δ 94.7 (3.2) [111], $\text{C}(\text{CH}_3)_3$ 36.7, CH_3 32.6 [125], Cp 110.8 [172], alkoxide, PMe_2 16.2 (14) [125], CH_2P 37.7 (17.9) [125], CO 102.0 (8.6), $\text{C}(\text{CH}_3)_2$ 51.1 (2.7), $\text{C}(\text{CH}_3)_2$ 22.1 (7.8) [125] and 29.8 [126], Ar 126.2, 121.4, and 148.8; $^{31}\text{P}(\text{C}_6\text{D}_6)$, δ -63.8 .

NMR of **3b**: ^1H (C_6D_6), δ *CH-t*-Bu 11.92 (3.8), $\text{C}(\text{CH}_3)_3$ 1.22, Cp 5.90 (1.7), PMe_2 1.23 (7.3) and 0.88 (6.2), $\text{CH}_A\text{H}_B\text{P}$ 3.41 (9.0) and 2.26 (8.7), $J(\text{H}_A\text{H}_B)$ = 14.9, CH_3 2.08, 1.28, 1.19, and 1.14; ^{13}C ($[\text{D}_8]\text{toluene}$), neopentylidene, TiC 278.1 (12.2) [95], $\text{C}(\text{CH}_3)_3$ 45.8 (1.4), $\text{C}(\text{CH}_3)_2$ 32.5 (3.2) [124], Cp 105.1 [169], alkoxide, PMe_2 19.9 (220) [127] and 13.7 (8.5) [127], CH_2P 44.7 (22.0) [125], CO 96.1 (5.8), $\text{C}(\text{CH}_3)_2$ 52.8 (4.8) and 49.8, $\text{C}(\text{CH}_3)_2$ 30.2 [125], 29.4 [125], 25.7 [125], and 22.6 [125], Ar, CH 125.9 [155], 126.0 [155], 121.6 [155], and 121.5 [155], C, 148.9 and 148.8; ^{31}P ($[\text{D}_8]\text{toluene}$), δ 1.03.

Metallacycle 5. At room temperature 0.5 mL (ca. 0.04 mmol) of ethene gas was added to a solution of 80 mg (0.018 mmol) of alkylidene **3b** in 3 mL of pentane. The resulting solution was cooled to $-40\text{ }^{\circ}\text{C}$. Orange crystals of the metallacycle were obtained (55 mg, 65% of theory). Anal. Calcd: C, 70.88; H, 9.13. Found: 70.66; H, 8.91. NMR: ^1H , Ar δ 7.0–7.2, Cp 5.46, CH_3 1.50, 1.42, 1.15, and 1.12, CH_3P 0.93 (3.5) and 0.91 (3.8), PCH_2 1.64 (4.6), *t*-Bu 1.04. The metallacyclobutane resonances could be simulated¹⁵ with the following data: H^1 δ 3.09, H^2 2.917, H^3 1.738, H^4 -0.400 , H^5 3.845, $J(\text{H}^1\text{H}^2)$ = 9.05, $J(\text{H}^1\text{H}^3)$ = 9.60, $J(\text{H}^1\text{H}^4)$ = 12.5, $J(\text{H}^2\text{H}^3)$ = 3.20, $J(\text{H}^2\text{H}^4)$ = 10.50, $J(\text{H}^3\text{H}^4)$ = 10.0, $J(\text{H}^3\text{H}^5)$ = 12.0, $J(\text{H}^4\text{H}^5)$ = 10.0, $J(\text{H}^5\text{P})$ = 2.5; ^{31}P δ -63.6 .

Ethene Complex 8. To a mixture of the dichloride **1b** and C_6D_6 was added 1.3 equivalents of Et_2Mg -dioxane. The reaction was monitored by NMR. The resulting precipitate was removed by filtration, and the solvent was removed. The resulting purple solid ethene complex was identical with that derived from the reaction of the alkylidene **3b** with ethene. NMR (C_6D_6): the ^1H spectrum could be simulated¹⁵ with the data H^1 δ 2.47, H^2 2.01, H^3 0.46, H^4 0.15, CH_AP 3.36, CH_BP 2.64, $J(\text{H}^1\text{H}^2)$ = 10.9, $J(\text{H}^2\text{H}^4)$ = 11.9, $J(\text{H}^1\text{H}^3)$ = 5.2, $J(\text{H}^2\text{P})$ = 3.1, $J(\text{H}^1\text{H}^4)$ = 12.0, $J(\text{H}^4\text{P})$ = 3.6, $J(\text{H}^1\text{P})$ = 11.5, $J(\text{H}_A\text{H}_B)$ = 14.7, $J(\text{H}^2\text{H}^3)$ = 11.9, $J(\text{H}_A\text{P})$ = 8.4, $J(\text{H}^2\text{H}^4)$ = 3.6, $J(\text{H}_B\text{P})$ = 10.0; ^{13}C , ethene, δ 58.8 (5) [144 t], 55.0 [147, t], Cp 107.6 [170, d], alkoxide, Ar 122.7 [155], one signal masked by benzene resonance, and 149.8, PMe_2 , 15.1 (4) [128, q] and 12.2 (20) [129, q], CH_2P 42.8 (19) [126, t], CO 99.0 (8), $\text{C}(\text{CH}_3)_2$ 53.5 (4) and 50.2, CH_3 31.0 [126, q], 30.6 [126, q], 26.1 [126, q], and 22.8 [126, q]; ^{31}P , δ 17.7.

Ketene Complexes 9A and 9B. Carbon monoxide was bubbled through a green solution of the alkylidene **3b** (ca. 80 mg, 0.02 mmol) in pentane. The red precipitate was filtered and dried in vacuo; yield ca. 80%. The product consists of two isomers, **9A** and **9B**. Anal. Calcd: C, 68.35; H, 8.29; P, 6.53; Ti, 10.09. Found: C, 68.20; H, 8.20; P, 6.68; Ti, 10.25.

NMR (C_6D_6) **9A**: ^1H , CH δ 4.19 (2.7), *t*-Bu 1.60, $\text{CH}_A\text{H}_B\text{P}$, H_A 2.58, H_B 2.12, $J(\text{H}_A\text{H}_B)$ = 15, $J(\text{H}_A\text{P})$ = 10, $J(\text{H}_B\text{P})$ = 10.5, Cp 5.88 (2); ^{13}C , CO δ 189.5 (4.8), *C-t*-Bu 89.4 (3.7), *t*-Bu, C 33.7 (2.8), CH_3 32.0, Cp 110.2; ^{31}P δ 2.4.

NMR (C_6D_6) **9B**: ^1H , CH δ 3.95 (1.8), *t*-Bu 1.59, $\text{CH}_A\text{H}_B\text{P}$, H_A 2.47, H_B 1.95, $J(\text{H}_A\text{H}_B)$ = 15, $J(\text{H}_A\text{P})$ = 10.2, $J(\text{H}_B\text{P})$ = 10.2,

Cp 5.82 (2); ^{13}C , δ CO 196.9 (28.3), C-*t*-Bu 95.8 (2.4), *t*-Bu, C 33.2 (2.6), CH_3 31.8, Cp 110.3; ^{31}P δ -7.5.

Bis(alkoxide) Complex 10. The mixture of ketene complexes **9A** and **9B** was dissolved in C_6D_6 , and ethene was bubbled through the solution. The color changed from red to orange. NMR (C_6D_6): ^1H , δ CH 4.19 (1.3), CH_2CH_2 3.41 (m) and 3.14 (m), *t*-Bu 1.33, Cp 5.97 (1.5), PCH_3 1.03 (4.4) and 0.81 (3.9), PCH_2 1.83 (8.9), CH_3 1.50 and 1.46; ^{13}C , CO δ 164.6 (8.1), C-*t*-Bu 102.4, $\text{CH}_2\text{C}=\text{C}$ 48.0 (4.4), TiCH_2 64.8 (10.6), *t*-Bu, C 31.5, CH_3 31.6; ^{31}P , δ -21.8.

Acknowledgment. We are indebted to Dr. B. Hessen for helpful discussions.

Supplementary Material Available: Full tables of atomic coordinates, thermal parameters, and bond lengths and angles for **3b** (3 pages). Ordering information is given on any current masthead page.

OM940754K

Relativistic Effects in Cationic Gold(I) Complexes: A Comparative Study of ab Initio Pseudopotential and Density Functional Methods

Jan Hrušák,* Roland H. Hertwig, Detlef Schröder, Peter Schwerdtfeger,[†]
Wolfram Koch,* and Helmut Schwarz*

Institut für Organische Chemie der Technischen Universität Berlin,
Strasse des 17. Juni 135, D-10623 Berlin, Germany

Received September 9, 1994[®]

The cationic gold(I) complexes Au⁺(H₂O), Au⁺(CO), Au⁺(NH₃), and Au⁺(C₂H₄) have been examined by different ab initio and density functional methods using nonrelativistic and relativistic ECPs and a quasi-relativistic approach, where relativistic effects are explicitly taken into account. On the one hand, Au⁺(H₂O) and Au⁺(CO) exhibit binding energies (35.9 and 44.1 kcal/mol, respectively, at the CCSD(T) level of theory) which are comparable with those of the complexes of the group 11 congeners Cu⁺ and Ag⁺. While for Au⁺(NH₃) and Au⁺(C₂H₄) a large relativistic stabilization is observed, such that the binding energies (65.3 and 68.8 kcal/mol, respectively, at the CCSD(T) level of theory) are almost twice as high as for M⁺(NH₃) and M⁺(C₂H₄) for M = Cu and Ag. With respect to the computational methods applied, structural features and energetics obtained with different ab initio (MP2, CCSD(T)) and DFT (ADF/BP, B3LYP) methods are in reasonable agreement with each other. In general, the relativistic effects on structures and energetics of these gold(I) compounds are quite large, and the interplay of electron correlation and relativistic effects is discussed.

Introduction

Complexes of transition-metal cations with small ligands L, e.g., water, ammonia, and small hydrocarbons, deserved considerable interest within the last decade, especially with respect to bond activations and other catalytic processes. Numerous experimental studies^{1,2} have established accurate bond dissociation energies (BDEs) of M⁺(L) complexes, thus providing a detailed insight into the nature of the metal–ligand bonding.³ Due to the large amount of data available for first-row transition-metal cations, these compounds represent valuable test systems for theoretical investigations.^{4–8} Nowadays, the results of quantum-mechanical calculations are in good agreement with the

experimental findings, provided the basis set is sufficiently flexible and the effects of electron correlation are adequately described, which usually requires sophisticated methods such as multireference configuration interaction (MRCI) or coupled-cluster (CC) techniques.^{9–11}

Much less is known experimentally about metal–ligand interactions for singly charged second- and third-row transition metals, as for example for gold(I) compounds. Wilkins et al.¹² reported lower bounds of bond energies for a number of Au⁺(L) complexes as derived from gas-phase reactions of Au⁺ with a series of organic compounds and made comparisons with the behavior

[†] Permanent address: Computational Material Science and Engineering Research Centre, Department of Chemistry and the School of Engineering, University of Auckland, Private Bag 92019, Auckland, New Zealand.

[®] Abstract published in *Advance ACS Abstracts*, January 15, 1995.

(1) (a) Armentrout, P. B. *Annu. Rev. Phys. Chem.* **1990**, *41*, 313. (b) Eller, K.; Schwarz, H. *Chem. Rev.* **1991**, *91*, 1121. (c) Weishaar, J. C. *Acc. Chem. Res.* **1993**, *26*, 213.

(2) (a) Irikura, K. K.; Beauchamp, J. L. *J. Am. Chem. Soc.* **1989**, *111*, 75. (b) Buckner, S. W.; MacMahon, T. J.; Byrd, G. L.; Freiser, B. S. *Inorg. Chem.* **1989**, *28*, 3511. (c) Ashcroft, T.; Cheetham, A. K.; Foord, J. S.; Green, M. L. H.; Grey, C. P.; Murrell, A. J.; Vernon, P. D. F. *Nature* **1990**, *334*, 319. (d) Stojka, Z.; Herman, R. G.; Klier, K. *J. Chem. Soc., Chem. Commun.* **1991**, 185. (e) Irikura, K. K.; Beauchamp, J. L. *J. Am. Chem. Soc.* **1991**, *113*, 2769. (f) Irikura, K. K.; Beauchamp, J. L. *J. Phys. Chem.* **1991**, *95*, 8344. (g) Clemmer, D. E.; Armentrout, P. B. *J. Phys. Chem.* **1991**, *95*, 3084. (h) Capitán, M. J.; Malet, P.; Centeno, M. A.; Munoz-Páez, A.; Carrizos, I.; Ódrizola, J. A. *J. Phys. Chem.* **1993**, *97*, 9233.

(3) (a) Schilling, J. B.; Goddard, W. A., III; Beauchamp, J. L. *J. Am. Chem. Soc.* **1987**, *109*, 5573. (b) Rösch, N.; Göring, A.; Ellis, D. E.; Schmidbaur, H. *Angew. Chem.* **1989**, *101*, 1410; *Angew. Chem., Int. Ed. Engl.* **1989**, *28*, 1357. (c) Hill, Y. D.; Freiser, B. S.; Bauschlicher, C. W., Jr. *J. Am. Chem. Soc.* **1991**, *113*, 1507.

(4) (a) Li, J.; Pyykkö, P. *Inorg. Chem.* **1993**, *32*, 2630. (b) Häberlen, O. D.; Rösch, N. *J. Phys. Chem.* **1993**, *97*, 4970.

(5) (a) Fiedler, A.; Hrušák, J.; Schwarz, H. Z. *J. Phys. Chem.* **1992**, *175*, 15. (b) Magnusson, E.; Moriaty, N. W. *J. Comput. Chem.* **1993**, *8*, 961.

(6) (a) Mavridis, A.; Herrera, F. L.; Harrison, J. F. *J. Phys. Chem.* **1991**, *95*, 2854. (b) Sodupe, M.; Bauschlicher, C. W., Jr. *Chem. Phys. Lett.* **1993**, *212*, 624.

(7) (a) Merchan, M.; Nebot-Gill, I.; González-Luque, R.; Orti, E. *J. Chem. Phys.* **1987**, *87*, 1690. (b) Barnes, L. A.; Rosi, M.; Bauschlicher, C. W., Jr. *J. Chem. Phys.* **1990**, *93*, 609. (c) Smith, G. W.; Carter, E. A. *J. Phys. Chem.* **1991**, *95*, 2327.

(8) (a) Nicolas, G.; Barthelat, J. C. *J. Phys. Chem.* **1986**, *90*, 2870. (b) Miralles-Sabater, J.; Merchan, M.; Nebot-Gil, I.; Viruela-Martin, P. M. *J. Phys. Chem.* **1988**, *92*, 4853. (c) Nicolas, G.; Spiegelman, F. *J. Am. Chem. Soc.* **1990**, *112*, 5410. (d) Sodupe, M.; Bauschlicher, C. W., Jr. *J. Phys. Chem.* **1991**, *95*, 8640. (e) Guo, B. C.; Castleman, A. W., Jr. *Chem. Phys. Lett.* **1991**, *181*, 16. (f) Basch, H.; Hoz, T. (private communication) In *The chemistry of triple bonded functional groups*; Patai, S., Ed.; Wiley: New York, Vol. 2, Suppl. C, in press.

(9) (a) Alvarado-Swaisgood, A. E.; Harrison, J. F. *J. Phys. Chem.* **1985**, *89*, 2517. (b) Alvarado-Swaisgood, A. E.; Harrison, J. F. *J. Phys. Chem.* **1988**, *92*, 2757.

(10) (a) Bauschlicher, C. W., Jr.; Partridge, H.; Sheehy, J. A.; Langhoff, S. R.; Rosi, M. *J. Phys. Chem.* **1992**, *96*, 6969. (b) Bauschlicher, C. W., Jr.; Partridge, H.; Scuseria, G. E. *J. Chem. Phys.* **1992**, *97*, 7471.

(11) (a) Musaev, G. D.; Morokuma, K.; Koga, N.; Nguyen, K. A.; Gordon, M. S.; Cundari, T. R. *J. Phys. Chem.* **1993**, *97*, 11435. (b) Musaev, D. G.; Koga, N.; Morokuma, K. *J. Phys. Chem.* **1993**, *97*, 4064. (c) Musaev, D. G.; Morokuma, K. *Isr. J. Chem.* **1993**, *33*, 307. (d) Blomberg, M. R. A.; Siegbahn, P. E. M.; Svensson, M. *J. Phys. Chem.* **1994**, *98*, 2062.

(12) (a) Weil, D. A.; Wilkins, C. L. *J. Am. Chem. Soc.* **1985**, *107*, 7316. (b) Chowdhury, A. K.; Wilkins, C. L. *J. Am. Chem. Soc.* **1987**, *109*, 5336.

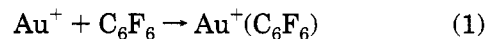
of the analogous Cu⁺ and Ag⁺ ions. Similar techniques have been applied for the determination and characterization of the bond energy of the elusive gold(I) fluoride¹³ by Schröder et al.¹⁴ Here, the predicted bond energy is in excellent agreement with results of ab initio calculations by Schwerdtfeger et al.¹⁵

In addition to the problem caused by correlation energy, systems containing heavy elements ($Z > 50$) exhibit relativistic effects,¹⁶ which have significant influence on physicochemical properties such as bond lengths, energetics, and ionization energies in particular. In fact, for third-row transition metals, the relativistic contributions to the bonding are of the same order as the effects of correlation energy. As pointed out by Pyykkö and Desclaux,¹⁷ relativistic effects reach a local maximum for group 11 compounds within a period of the periodic table. A convenient possibility to introduce relativistic effects into theoretical approaches is the use of spin-orbit averaged relativistic effective core potentials (RECPs).¹⁸ In this paper, the corresponding nonrelativistic potential is denoted as ECP. The relativistic effect (Δ_R) on an atomic or molecular property P is defined as $\Delta_R P = P_{NR} - P_R$; where P_{NR} is the property as derived from the nonrelativistic (NR) calculation and P_R is derived from the scalar relativistic (R) calculation at a certain level of theory.

Whereas a number of theoretical calculations on neutral gold compounds have been performed using a variety of methods (for a review, see ref 16c), so far only a few ab initio studies addressed structures and energetics of cationic gold compounds. The smallest positively charged, diatomic system, i.e., the AuH⁺ cation, has been studied in great detail,^{19–21} establishing a theoretical prediction for BDE (Au⁺–H) in the order of 44 kcal/mol. Furthermore, the Au⁺(PH₃) system has been examined at the HF level by Schwerdtfeger et al.,^{20a} leading to a relativistic BDE of 47 kcal/mol, whereas the nonrelativistic bond energy was calculated to 25 kcal/mol only. Recently, Veldkamp and Frenking²² performed MP2 and QCISD(T) calculations on Au⁺(CO)_{*n*} systems and found the first CO molecule ($n = 1$) to be

bound by 45 kcal/mol. Further, Hrušák et al.²³ reported CCSD(T) calculations on the Au⁺(H₂O) complex, possessing a nonplanar geometry with a BDE of 36 kcal/mol. Most recently, Basch and Hoz^{8f} computed the BDE of Au⁺(C₂H₄) as 71.2 and 62.5 kcal/mol at the MP2 and QCISD(T)//MP2 levels, respectively.

In a previous study,²⁴ we used the radiative association reaction of bare Au⁺ cations with hexafluorobenzene (eq 1) for the formation of the Au⁺(C₆F₆) complex



in the low-pressure regime of a Fourier–transform ion cyclotron resonance mass spectrometer. Due to the relatively small bond dissociation energy of Au⁺(C₆F₆), this complex can be used as a versatile precursor for the generation of other Au⁺(L) complexes by subsequent ligand-exchange reactions. Ion–molecule reactions employing the bracketing technique provided a relative gold(I) cation affinity scheme for the various ligands L, which follows the order C₆F₆ < H₂O < CO < C₂H₄ ≈ C₆H₆ ≈ NH₃ ≈ C₃H₆ < C₄H₆.²⁴

Here, we report a computational study of the cationic complexes of Au⁺ with the small ligands CO, H₂O, NH₃, and C₂H₄. The principal aims of this study are to evaluate the BDEs at a uniform level of theory and to discuss the relativistic effects on the energetics and structures of these cationic species. In addition to the standard ECP and RECP ab initio calculations performed at the SCF as well as correlated levels, approximate density functional theory (DFT)²⁵ has been applied, where relativistic effects were either accounted for through the use of a RECP or through an explicit quasirelativistic approach. Recently, it has been shown that gradient-corrected DFT methods can give accurate binding energies for both main-group and transition-metal systems.²⁶ The inclusion of DFT methods is of particular interest in order to obtain further information on the performance of these methods in the theoretical description of bare metal–cation complexes with respect to the relativistic effects.

Theoretical Methods

Ab initio calculations have been performed by employing the GAUSSIAN92 program.²⁷ For the gold atom we used the multi-electron adjusted relativistic (RECP) and nonrelativistic (ECP) effective core potentials derived by Schwerdtfeger et al.²⁰ covering 60 electrons ([Kr]4d¹⁰4f¹⁴). The original basis set was augmented by additional diffuse and polarization functions,^{23,24} resulting in a [10s/8p/7d/1f]/(9s/5p/6d/1f) basis set for both the relativistic and nonrelativistic calculations. For the other atoms we used Dunning TZ2P basis sets²⁸ with an additional *f*-polarization function ($\alpha_f = 1.85$) for the oxygen, nitrogen, and carbon atoms, i.e., the [10s/6p/2d/1f]/(5s/3p/2d/1f) contraction

- (13) Saenger, K. L.; Sun, C. P. *Phys. Rev.* **1992**, *46*, 670.
 (14) Schröder, D.; Hrušák, J.; Tornieporth-Oetting, I. C.; Klapötke, T. M.; Schwarz, H. *Angew. Chem.* **1994**, *106*, 223; *Angew. Chem., Int. Ed. Engl.* **1994**, *33*, 212.
 (15) Schwerdtfeger, P.; McFeaters, J. S.; Stephens, R. L.; Liddell, M. J.; Dolg, M.; Hess, B. A. *Chem. Phys. Lett.* **1994**, *218*, 362.
 (16) (a) Barthelat, J. C.; Durand, P.; Pelissier, M. *Phys. Rev. A* **1980**, *21*, 1773. (b) Balasubramanian, K.; Pitzer, K. S. *Adv. Chem. Phys.* **1987**, *67*, 287. (c) Pyykkö, P. *Chem. Rev.* **1988**, *88*, 563. (d) Pisani, L.; André, J.-M.; André, M.-C.; Clementi, E. *J. Chem. Educ.* **1993**, *70*, 894.
 (17) Pyykkö, P.; Desclaux, J. P. *Acc. Chem. Res.* **1979**, *12*, 276.
 (18) (a) Durand, P.; Barthelat, J. C. *Theor. Chim. Acta* **1975**, *38*, 283. (b) Ermler, W. C.; Ross, R. B.; Christiansen, P. A. *Int. J. Quantum Chem.* **1991**, *40*, 829. (c) Küchle, W.; Dolg, M.; Stoll, H.; Preuss, H. *Mol. Phys.* **1991**, *74*, 1245. (d) Dolg, M.; Küchle, W.; Stoll, H.; Preuss, H.; Schwerdtfeger, P. *Mol. Phys.* **1991**, *74*, 1245. (e) Stevens, W. J.; Krauss, M.; Basch, H.; Jasien, P. G. *Can. J. Chem.* **1992**, *70*, 612. (f) Cundari, T. R.; Stevens, W. J. *J. Chem. Phys.* **1993**, *98*, 5555.
 (19) (a) Ohanessian, G.; Brusich, M. J.; Goddard, W. A., III *J. Am. Chem. Soc.* **1990**, *112*, 7179. (b) Ohanessian, G.; Goddard, W. A., III *Acc. Chem. Res.* **1990**, *23*, 386. (c) Ishikawa, Y.; Malli, G. L.; Pyper, N. C. *Chem. Phys. Lett.* **1992**, *194*, 481.
 (20) (a) Schwerdtfeger, P.; Dolg, M.; Schwarz, W. H. E.; Bowmaker, G. A.; Boyd, P. D. W. *J. Chem. Phys.* **1989**, *91*, 1762. (b) Schwerdtfeger, P. *J. Am. Chem. Soc.* **1989**, *111*, 7261. (c) Schwerdtfeger, P.; Boyd, P. D. W.; Burrell, A. K.; Robinson, W. T.; Taylor, M. J. *Inorg. Chem.* **1990**, *29*, 3593. (d) Ishikawa, Y.; Malli, G. L.; Pyper, N. C. *Chem. Phys. Lett.* **1992**, *194*, 481.
 (21) A recent relativistic MR-CCSD approach leads to BDE(Au⁺–H) = 45.2 kcal/mol: Kaldor, U.; Hess, B. A., private communication.
 (22) Veldkamp, A.; Frenking, G. *Organometallics* **1993**, *12*, 4613.

- (23) Hrušák, J.; Schröder, D.; Schwarz, H. *Chem. Phys. Lett.* **1994**, *225*, 416.
 (24) Schröder, D.; Hrušák, J.; Hertwig, R. H.; Koch, W.; Schwerdtfeger, P.; Schwarz, H. *Organometallics*, in press.
 (25) Ziegler, T. *Chem. Rev.* **1991**, *91*, 651.
 (26) (a) Tschinke, V.; Ziegler, T. *Theor. Chim. Acta* **1991**, *81*, 65. (b) Becke, A. D. *J. Chem. Phys.* **1992**, *96*, 2155.
 (27) GAUSSIAN92-DFT Rev. F.2 Frisch, M. J.; Trucks, G. W.; Schlegel, H. W.; Gill, P. M. W.; Johnson, B. G.; Wong, M. W.; Foresman, J. B.; Robb, M. A.; Head-Gordon, M.; Replogle, E. S.; Gomperts, R.; Andres, J. L.; Raghavachari, K.; Binkley, J. S.; Gonzales, C.; Martin, R. L.; Fox, D. J.; Defrees, D. J.; Baker, J.; Stewart, J. J. P.; Pople, J. A. GAUSSIAN Inc.: Pittsburgh, PA, 1992.
 (28) Feller, D.; Davidson, E. P. In *Reviews in Computational Chemistry*; VCH Publishers: New York, 1990; Vol. 1.

scheme. For hydrogen atoms, a $[5s/2p/1d]/(3s/2p/1d)$ contracted basis set was used. The RECP corrects due to the parametrization procedure only for the relativistic Darwin and mass velocity terms. The spin-orbit interaction (SO) is not included. However, since all the systems under study are closed shell singlets, resulting from the gold (1S) interaction with singlet ligands, the SO contribution to the bond energy is zero.

Full geometry optimizations have been performed by using standard procedures at the SCF and MP2 levels of theory for both the relativistic and nonrelativistic approaches. Further improvement of the geometries was obtained by optimization at the CCSD(T) level of theory; here, the 1s electrons of oxygen, carbon, nitrogen, and also the 5s and 5p electrons of gold were kept frozen in the CC calculations. Due to the technical limitations, no CCSD(T) geometry optimization for $Au^+(C_2H_4)$ and $Au^+(NH_3)$ was possible, and we restricted ourselves to the MP2-optimized geometry in the CCSD(T) energy calculation. However, as can be seen from the comparison of optimized geometries for the other ligands (vide infra), the MP2 and CCSD(T) computed structures do not differ substantially. Furthermore, since all systems under study correspond to closed-shell singlets, it can be assumed that a limited perturbational treatment such as MP2 should be a sufficient approach to account for the correlation effects on the geometries.²² For the same reasons, the harmonic frequencies have been calculated at the MP2 level of theory only.

The DFT calculations were carried out using the Amsterdam density functional (ADF) suite of programs²⁹ with the inner-shell electrons ([He] for C, O, N, and [Xe]4f¹⁴ for Au) treated in the frozen core approximation.³⁰ The valence orbitals were expanded as linear combinations of Slater-type basis functions. Triple- ζ basis sets with additional polarization functions on carbon, oxygen, nitrogen, and hydrogen were used throughout, while for the gold atom a triple- ζ basis set was employed. All molecular and atomic energies were calculated using the local spin density approximation (LDA) with Slater's exchange functional and the Vosko-Wilk-Nusair parametrization (VWN)³¹ on the homogeneous electron gas for correlation,³² augmented by Becke's³³ and Perdew's³⁴ (BP) gradient corrections for the exchange and correlation potential, respectively,³⁵ this method will be referred to as ADF/BP.

In the ADF/BP scheme, relativistic effects on the electronic structures were evaluated by using the quasi-relativistic approach of Ziegler et al.³⁶ This leads to a quasi-relativistic SCF procedure, resulting in quasi-relativistic densities and corresponding energies, which involves the sum of the relativistic Darwin and mass velocity operators. Applications of this quasi-relativistic methodology³⁷ have demonstrated that it can be successfully employed to investigate relativistic effects on bonding; this holds true in particular for third-row transition metals and heavier elements for which relativistic influences on the valence density become essential.¹⁶ Since our ADF program implementation does not allow a gradient-oriented geometry optimization within the relativistic treatment, only the gold ligand distance was optimized by a series

of single-point calculations, while the ligand substructure was kept frozen at the nonrelativistic geometry.

For the analysis of the different contributions to the bonding, the decomposition scheme developed by Morokuma, Ziegler, and co-workers³⁸ was employed: The total binding energy BDE is expressed as the sum of the steric interaction ΔE_{steric} and the orbital interaction ΔE_{Or} . The orbital interaction term ΔE_{Or} contains all contributions arising from donor-acceptor interactions as well as the relaxation of the individual fragments due to the presence of the bonding partner.

In order to check the suitability of standard ab initio ECP parametrizations in density functional approaches, relativistic and nonrelativistic DFT calculations have been performed with the GAUSSIAN92-DFT²⁷ program by using both the RECP and ECP augmented with basis sets as described above. In these calculations we employed the ECP and RECP, respectively, and a hybrid HF-DFT method, in which the exchange functional consists of a mixture between HF and LDA exchange corresponding to a three-parameter fit according to Becke. The correlation functional uses a combination of the nonlocal functional derived by Lee, Yang, and Parr⁴⁰ and the local correlation functional from the homogeneous electron gas. In analogy to the GAUSSIAN keyword, this semiempirical hybrid method will be referred to as B3LYP. Most recently, Pople and co-workers⁴¹ have shown that for main-group elements B3LYP reproduces physical properties of polyatomic molecules with accuracy (i.e., ± 2 kcal/mol) similar to the G2 contraction scheme.⁴² In addition, we performed test calculations with the GAUSSIAN92-DFT program using the following: (i) the BP method mentioned above; however, instead of the quasi-relativistic approach of ADF, the RECP was applied; (ii) Becke's three-parameter fit and the VWN functional for correlation (to be referred as B3P); and (iii) for $Au^+(H_2O)$, we also performed geometry optimization on the CISD level of theory.

Results and Discussion

Atomic gold assumes a $^2S_{1/2}$ ($d^{10}s^1$), while the cation has a 1S_0 ($d^{10}s^0$) ground state. The experimental ionization energy (IE) of gold amounts to 9.225 eV,⁴³ whereas the calculations result in 8.54 (CCSD(T)/RECP), 8.61 (MP2/RECP), and 9.34 eV (B3LYP/RECP). As far as these discrepancies are concerned, we refer to previous studies,⁴⁴ which have shown that polarization functions of higher l -quantum number (i.e., g -type functions in the case of Au) are needed in order to describe the IEs with an accuracy better than 0.2 eV.

With respect to the species of interest, i.e., $Au^+(H_2O)$, $Au^+(CO)$, $Au^+(C_2H_4)$, and $Au^+(NH_3)$, our previous experimental study revealed the following:²⁴ Whereas the BDEs of $Au^+(H_2O)$ and $Au^+(CO)$ are moderate and within the range of the BDE values for first- and second-row transition-metal cations, the BDEs of $Au^+(NH_3)$ and

(29) ADF (version 1.0.2): (a) Baerends, E. J.; Ellis, D. E. *Chem. Phys.* **1973**, *2*, 71. (b) teVelde, G.; Baerends, E. J. *J. Comput. Phys.* **1992**, *99*, 84, and references cited therein.

(30) Snijders, J. G.; Baerends, E. J. *Mol. Phys.* **1977**, *33*, 1651.

(31) Vosko, S. H.; Wilk, L.; Nusair, M. *Can. J. Phys.* **1980**, *58*, 1200.

(32) Parr, R. G.; Yang, W. *Density Functional Theory of Atoms and Molecules*, Oxford University Press: New York, 1989.

(33) Becke, A. D. *J. Chem. Phys.* **1986**, *84*, 4524.

(34) Perdew, J. P. *Phys. Rev. B* **1986**, *33*, 8822.

(35) Levy, M.; Perdew, J. P. *Int. J. Quantum Chem.* **1994**, *49*, 539.

(36) (a) Ziegler, T.; Tschinke, V.; Baerends, E. J.; Snijders, J. G.; Ravenek, W. *J. Phys. Chem.* **1989**, *93*, 3050. For earlier relativistic calculations by these authors, see: (b) Snijders, J. G.; Baerends, E. J. *Mol. Phys.* **1978**, *36*, 1789. (c) Snijders, J. G.; Baerends, E. J.; Roos, P. *J. Mol. Phys.* **1979**, *38*, 1909. (d) Ziegler, T.; Snijders, J. G.; Baerends, E. J. *J. Chem. Phys.* **1981**, *74*, 1271.

(37) van Wezenbeek, E. M.; Baerends, E. J.; Snijders, J. G. *Theor. Chim. Acta* **1991**, *81*, 139.

(38) (a) Kitaura, K.; Morokuma, K. *Int. J. Quantum Chem.* **1976**, *10*, 325. (b) Ziegler, T.; Rauk, A. *Theor. Chim. Acta* **1977**, *46*, 1.

(39) Becke, A. D. *Phys. Rev. A* **1988**, *38*, 3098.

(40) Lee, C.; Yang, W.; Parr, R. G. *Phys. Rev. B* **1988**, *37*, 785.

(41) Gill, P. M. W.; Johnson, B. G.; Pople, J. A. *Chem. Phys. Lett.* **1992**, *197*, 499.

(42) (a) Pople, J. A.; Head-Gordon, M.; Fox, D. J.; Raghavachari, K.; Curtis, L. A. *J. Chem. Phys.* **1989**, *90*, 5622. (b) Curtis, L. A.; Raghavachari, K.; Jones, C.; Trucks, G. W.; Pople, J. A. *J. Chem. Phys.* **1990**, *93*, 2537.

(43) Additional thermochemical data were taken from: (a) Lias, S. G.; Bartmess, J. E.; Liebman, J. F.; Holmes, J. L.; Levin, R. D.; Mallard, W. G. *J. Phys. Chem. Ref. Data* **1988**, *17*, Suppl. 1. (b) Moore, C. E. *Atomic Energy Levels*; National Standard Reference Data Series; National Bureau of Standards: Washington DC, 1971; NSRDS-NBS 35. (c) Herzberg, G. *Electronic Spectra and Electronic Structure of Polyatomic Molecules*; Van Nostrand: New York, 1966.

(44) (a) Bauschlicher, C. W. Jr.; *J. Chem. Phys.* **1987**, *86*, 5591. (b) Schwerdtfeger, P. *Chem. Phys. Lett.* **1991**, *183*, 457.

Table 1. Geometries (r in Å, angles in degrees) and Bond Dissociation Energies (kcal/mol) for Au⁺(OH₂)

		SCF	MP2	CISD	CCSD(T) ^a	ADF/BP	B3LYP
$r(\text{Au}-\text{O})$	R	2.306	2.132	2.133	2.158	2.175	2.198
	NR	2.505	2.377			1.992	2.397
$r(\text{O}-\text{H})$	R	0.944	0.964	0.964	0.964	0.997	0.968
	NR	0.944	0.963			0.997	0.964
$\alpha(\text{Au}-\text{O}-\text{H})$	R	126.0	118.8	119.9	119.9	113.5	117.4
	NR	126.7	127.1			113.5	119.9
θ^b	R	180.0	133.3	133.3	133.3	125.9	131.0
	NR	180	180			180	180
BDE	R	25.9	38.8	38.5	35.9	41.2	37.0
	NR	21.4	25.5			4.7	23.6

^a Only the $r(\text{Au}-\text{O})$ distance optimized at the CCSD(T) level; the geometry of the water ligand is frozen at the CISD geometry.²³ ^b The planar structure is a TS at the quasi-relativistic MP2 and B3LYP levels (b_1 i270 cm^{-1}).

particularly Au⁺(C₂H₄) are much higher as compared to their group 11 congeners Cu⁺ and Ag⁺. Unfortunately, the ion-molecule reaction bracketing technique did not allow a precise evaluation of experimental bond energies, since these were either too large or accurate thermochemical reference data were not known. However, it was observed experimentally that ethene is capable of replacing not only the benzene ligand in Au⁺(C₆H₆), but also the covalently bound iodine in AuI⁺ to yield Au⁺(C₂H₄). The latter observation implies that BDE (Au⁺-C₂H₄) exceeds 59 kcal/mol.¹² In contrast, the BDEs of Cu⁺(C₂H₄) and Ag⁺(C₂H₄) are 36 and 34 kcal/mol, respectively.⁸

These results further emphasize that relativistic effects are essential in gold(I) chemistry. In the following sections, we first address the computational results for each species separately and then discuss the interplay of relativistic and correlation effects on structures and energetics. In addition, we compare our theoretical results to some experimental findings to shed more light on the accuracy of our computational approach.

Au⁺(H₂O). Table 1 summarizes the results for the cationic gold-water complex. As stated in our previous study, the relativistic MP2/RECP calculations²³ predict the complex to deviate from planarity by 49°. The planar structure was found to be a transition structure with an imaginary frequency of i270 cm^{-1} , being less stable by 3.1 kcal/mol than the corresponding minimum. The nonplanarity of this system can be attributed to the relativistic stabilization of the gold 6s orbital leading to a relatively high ionization energy (9.225 eV) as compared to Cu (7.726 eV) and Ag (7.576 eV), resulting in a larger covalent contribution to the bonding in Au⁺(H₂O). In terms of the Lewis acidity, this high ionization energy forces a significant electron transfer from H₂O toward Au and thus, in analogy to H₃O⁺, a rehybridization of the water ligand leads to the nonplanar structure. The fact that the distortion (C_{2v} to C_s) of Au⁺(H₂O) is caused by relativistic effects is verified by the results of an MP2 geometry optimization using the nonrelativistic ECP, which predicts a planar C_{2v} -symmetrical structure as the minimum (Table 1). Furthermore, the relatively long Au-O distance of 2.377 Å obtained in the nonrelativistic scheme is in line with the mainly electrostatic nature of the interaction and is reflected by the low stabilization energy of only 25.5 kcal/mol.

When the RECP is applied, the geometrical changes of Au⁺(H₂O) are quite small when either the MP2,

CISD, or CCSD(T) methods is used for the geometry optimization, whereas on the SCF level, the Au-O distance is lengthened significantly. Furthermore, it is not surprising that the largest differences are observed for the Au-O distance ($\Delta r = 0.025$ Å), while the ligand geometry is only slightly changed. However, the magnitude of these geometry differences indicates that all theoretical approaches beyond SCF suffice for the geometry optimization of the gold(I) water complex. A similar conclusion applies for the DFT methods: The RECP-based B3LYP density functional predicts a nonplanar Au⁺(H₂O) structure which is very close to the CCSD(T) results. The Au-O distance is slightly elongated from 2.158 to 2.198 Å, and the ligand substructure is almost unperturbed. The deviation in the Au-O bond length ($\Delta r = 0.040$ Å) by using the B3LYP method (as compared to CCSD(T)) is probably caused in the evaluation of the correlation by the LYP functional,⁴⁰ since a test calculation using the B3P/RECP procedure, where the correlation effects are described by a different functional, predicted the Au-O bond length to be shorter (2.167 Å) as compared to B3LYP.

The results of the nonrelativistic ADF/BP calculation lead to erroneous data: Similar to the other nonrelativistic approaches, the optimized Au⁺(H₂O) structure is planar; however, the optimized Au-O distance is much too short as compared to other methods (Table 1). Further, according to the NR calculation, the stabilization energy is only 4.7 kcal/mol. This failure of the ADF program for the nonrelativistic Au⁺(H₂O) structure can most likely be traced back to the implemented optimizer which is not capable to deal with potential energy surfaces that are very flat, such as here. As a consequence, numerical problems hamper the geometry optimization procedure. However, as compared to the other relativistic approaches, the salient geometrical features of the Au⁺(H₂O) complex are well reproduced by the quasi-relativistic ADF/BP method. With respect to the nonrelativistic computation, the Au-O bond is significantly elongated (2.175 Å) and differs by only 0.017 Å as compared to the CCSD(T)/RECP calculation.

In addition to the geometries, a uniform picture can be deduced for the BDEs from the data in Table 1. Independent of the method used for the electron correlation treatment, the bond energies scatter around the CCSD(T) value of ca. 36 kcal/mol, with a slight tendency for overbinding as compared to CCSD(T). The difference between MP2- and CCSD(T)-calculated BDEs is small (2.9 kcal/mol), and the values compare well also to the B3LYP/RECP results. A slightly larger deviation as compared to the CCSD(T) result (35.9 kcal/mol) is calculated with the quasi-relativistic ADF/BP density functional method (41.2 kcal/mol). In fact, it is well-known from previous studies that this method tends to overestimate stabilization energies.^{25,26} Note, however, that the NR values are severely too low, further emphasizing that the inclusion of relativistic effects is essential in the evaluation of the energetics of gold compounds.¹⁷

Au⁺(CO). Ligand-exchange experiments²⁴ have demonstrated that the CO molecule exhibits a larger gold(I) affinity than H₂O. This finding is in agreement with the QCISD(T)//MP2-calculated relativistic bond energy for Au⁺(CO) of 45.1 kcal/mol as reported by Veldkamp

Table 2. Geometries (r in Å, angles in degrees) and Bond Dissociation Energies (kcal/mol) for $\text{Au}^+(\text{CO})$

		SCF	MP2	MP2 ^a	CCSD(T)	ADF/BP	B3LYP
$r(\text{Au}-\text{C})$	R	2.175	1.907	1.975	1.954	1.890	1.972
	NR	2.679	2.347			2.249	2.396
$r(\text{C}-\text{O})$	R	1.088	1.125	1.143	1.119	1.125	1.113
	NR	1.092	1.125			1.125	1.113
$\alpha(\text{Au}-\text{CO})$	R	180	180	180	180	180	180
	NR	180	180			180	180
BDE	R	18.5	50.1	45.1	44.1	59.5	43.6
	NR	8.4	18.9			18.4	18.0

^a Data taken from ref 22. A single-point calculation with an additional f-polarization function leads to BDE (Au^+-CO) = 51.1 kcal/mol.

and Frenking.²² These authors used the relativistic effective core potential parametrization of Hay and Wadt,⁴⁵ a slightly smaller basis set on gold, and the 6-31G(d) basis set on C and O atoms, such that the differences (especially in the CO bond length) can be attributed to basis set effects and the different RECP parameters used. For comparative purposes, the results of their calculations are also included in Table 2, which contains our theoretical predictions.

Both, the relativistic and nonrelativistic calculations result in linear $C_{\infty v}$ -symmetrical structures⁴⁶ for $\text{Au}^+(\text{CO})$; however, the relativistic changes in the Au-C bond lengths are significant. For example, at MP2 the relativistic contraction of the Au-C bond ($\Delta R_r = 0.440$ Å) is much larger as compared to the $\text{Au}^+(\text{H}_2\text{O})$ complex ($\Delta R_r = 0.245$ Å) and is also accompanied by a sizable stabilization ($\Delta_R E = 31.2$ kcal/mol). Similar to the $\text{Au}^+(\text{H}_2\text{O})$ case, the relativistic B3LYP density functional method predicts a slightly longer Au-L distance (1.972 Å) as compared to the CCSD(T) result (1.954 Å). By using the complementary density functional (ADF/BP), the relativistic Au-C bond distance is calculated shorter (1.890 Å) as compared to the RECP-based CCSD(T) and B3LYP methods; however, these geometry changes are within the computational error of the methods as indicated by the comparison of the Au-C bond lengths obtained with the MP2 approach described in ref 22 and our MP2 results. The C-O bond length as calculated using different correlated methods compare well within 0.01 Å; the slight increase of the C-O bond distance in the previous study²² is probably due to basis set effects (vide supra). Because our ADF/BP calculation is an entirely different approach (Slater orbitals, a direct evaluation of the mass velocity and Darwin terms), the agreement in structure is a further verification for the reliability of the present results.

When RECPs are used, the binding energy of $\text{Au}^+(\text{CO})$ converges at CCSD(T) and B3LYP to 44 kcal/mol; this is also in agreement with the QCISD(T)/RECP//MP2/RECP value of 45.1 kcal/mol given in ref 22. In contrast, the BDE (Au^+-CO) is calculated as 59.5 kcal/mol by using the quasi-relativistic ADF/BP method; i.e., the ligand seems to be strongly overbound. As mentioned above, the same tendency holds true in the comparison of the calculated BDEs for the $\text{Au}^+(\text{H}_2\text{O})$ complex. Finally, in the comparison of the results for $\text{Au}^+(\text{H}_2\text{O})$ and $\text{Au}^+(\text{CO})$, it becomes apparent that the interplay between correlation and relativistic effects is very different for both gold(I) complexes. These differ-

Table 3. Geometries (r in Å, angles in degrees) and Bond Dissociation Energies (kcal/mol) for $\text{Au}^+(\text{C}_2\text{H}_4)$

		SCF	MP2	CCSD(T) ^a	ADF/BP	B3LYP
$r(\text{Au}-\text{C})$	R	2.381	2.098	2.098	2.070	2.231
	NR	2.690	2.451		2.395	2.582
$r(\text{C}-\text{C})$	R	1.356	1.402	1.402	1.365	1.390
	NR	1.331	1.358		1.365	1.351
$r(\text{C}-\text{H})$	R	1.074	1.077	1.077	1.097	1.083
	NR	1.075	1.080		1.097	1.083
$\alpha(\text{C}-\text{C}-\text{H})$	R	120.9	119.9	119.9	121.1	120.7
	NR	121.4	120.8		121.1	121.3
$\theta(\text{H}-\text{CC}-\text{H})$	R	169.5	162.7	162.7	169.9	165.8
	NR	173.6	171.2		169.9	171.6
BDE	R	34.5	73.1	68.8	70.0	68.6
	NR	12.3	30.2		26.0	27.2

^a Calculated at the MP2-optimized geometry.

ent contributions of relativistic and correlation effects on the structure and energetics of $\text{Au}^+(\text{CO})$ as compared to $\text{Au}^+(\text{H}_2\text{O})$ and other complexes are probably due to the different nature of the bonding in $\text{Au}^+(\text{CO})$, as will be discussed below.

$\text{Au}^+(\text{C}_2\text{H}_4)$. Neutral $\text{Au}(\text{C}_2\text{H}_4)$ has been recently studied by Nicolas and Spiegelman^{8c} in the context of a comparison with the analogous copper and silver $\text{M}(\text{C}_2\text{H}_4)$ complexes ($\text{M} = \text{Cu}, \text{Ag}, \text{Au}$). It has been found that all three systems possess C_{2v} symmetrical minima with weakly bound (ca. 12 kcal/mol) 2A_1 ground states. Miralles-Sabater et al.^{8b} performed CI calculations on $\text{Cu}^+(\text{C}_2\text{H}_4)$ and $\text{Ag}^+(\text{C}_2\text{H}_4)$ complexes and found that the bonding can be described mainly in terms of electrostatic forces. In contrast, Guo and Castleman^{8e} determined by a combination of mass spectrometric experiments and theoretical calculations the BDE of $\text{Ag}^+(\text{C}_2\text{H}_4)$ as 33.7 kcal/mol and argued that the interaction should have a large covalent contribution. As mentioned above, our previous experimental study demonstrated that the BDE ($\text{Au}^+-\text{C}_2\text{H}_4$) is surprisingly high and is almost twice that of the analogous copper and silver complexes.²⁴ Most recently, Basch and Hoz^{8f} reported a BDE of 62.5 kcal/mol for the $\text{Au}^+(\text{C}_2\text{H}_4)$ complex by using a QCISD(T)/RECP//MP2/RECP method, which could also reproduce the experimental binding energies of $\text{Cu}^+(\text{C}_2\text{H}_4)$ and $\text{Ag}^+(\text{C}_2\text{H}_4)$.

The results of our calculations (Table 3) support these previously reported findings. For example, at the highest level of theory applied, i.e., CCSD(T), the bond dissociation energy of $\text{Au}^+(\text{C}_2\text{H}_4)$ is calculated as 68.8 kcal/mol, indicating a much larger gold(I) affinity of C_2H_4 , as compared to H_2O and CO. Furthermore, the computed BDE ($\text{Au}^+-\text{C}_2\text{H}_4$) agrees well with the lower bound of 59 kcal/mol as derived from the displacement of the iodine ligand in AuI^+ by ethene²⁴ and is slightly higher than the QCISD(T) value.^{8f}

As far as structural features of $\text{Au}^+(\text{C}_2\text{H}_4)$ are concerned, most of the conclusions drawn for $\text{Au}^+(\text{H}_2\text{O})$ also hold true. For example, the relativistic MP2 and ADF/BP geometries agree quite well with each other, whereas the B3LYP functional leads to a somewhat longer bond distance to the ligand, e.g., $r_{\text{Au}-\text{C}}(\text{MP2}) = 2.098$ Å and $r_{\text{Au}-\text{C}}(\text{ADF/BP}) = 2.070$ Å versus $r_{\text{Au}-\text{C}}(\text{B3LYP}) = 2.231$ Å. Albeit the geometry was optimized with restriction to C_{2v} symmetry, at all levels of theory applied, frequency analyses reveal that these structures are indeed true minima (Table 4). Whereas the ligand substructures in $\text{Au}^+(\text{H}_2\text{O})$ and $\text{Au}^+(\text{CO})$ were found to be hardly perturbed by the presence of the Au^+ cation, in the Au^+ -

(45) Hay, P. J.; Wadt, W. R. *J. Chem. Phys.* **1985**, *82*, 299.

(46) Schwerdtfeger, P.; Bowmaker, G. A. *J. Chem. Phys.* **1994**, *100*, 4487.

Table 4. Calculated Harmonic Frequencies (cm⁻¹) for Au⁺(C₂H₄)

mode	MP2 ^a	BP ^b	ADF/BP ^c	B3LYP
b ₂	371	346	445	317
a ₁	350	356	451	322
b ₁	667	605	590	620
b ₁	832	842	679	812
a ₂	1053	1013	763	932
b ₂	1073	1068	924	1037
a ₁	1099	1083	1146	1051
a ₂	1232	1232	1268	1183
a ₁	1260	1280	1307	1223
b ₂	1488	1482	1676	1428
a ₁	1575	1571	1907	1503
b ₂	3187	3136	2908	3053
a ₁	3174	3140	2918	3054
a ₂	3272	3227	3123	3145
b ₁	3289	3245	3132	3162

^a Calculated by Basch and Hoz using a relativistic potential (ref 8f; private communication). ^b Calculated with the GAUSSIAN program using the RECP. ^c Calculated with the ADF program in the quasi-relativistic scheme.

(C₂H₄) complex the C–C bond distance is elongated significantly as compared to free ethene (MP2, 1.336 Å; experimental, 1.339 Å^{43c}) and the ethene substructure is pyramidalized significantly (θ_{HCCH} (MP2) 17.3), indicating covalent contributions to the bonding in terms of the formation of a metallacyclopropane.⁴⁸ A plausible explanation for the large distortion of the ligand is the relativistically increased donation–back–donation interaction as proposed in the Dewar–Chatt–Duncanson model.⁴⁹ Both components of this electron transfer (i.e., the donation of the π electrons of ethene into an sp or sd hybrid of Au and the back-donation of the 5d electrons into the π^* orbital) lead to a weakening of the C–C double bond. Moreover, the small energy gap ($\Delta\text{IE} = 1.28$ eV) between the gold 6s orbital (IE = 9.225 eV) and the ethene π orbital (IE = 10.51 eV) result in significant charge transfer from the ethene to the gold; this is also reflected in the Mulliken population analysis in which the partial positive charge of the gold atom is only 0.58.²⁴ This charge transfer also accounts for the significant stabilization of Au⁺(C₂H₄) as compared to Cu⁺(C₂H₄) ($\Delta\text{IE} = 2.78$ eV) and Ag⁺(C₂H₄) ($\Delta\text{IE} = 2.93$ eV), which cannot be explained by geometrical arguments only. The large relativistic distortion of the C₂H₂ moiety ($\Delta_{\text{R}}r_{\text{C-C}}$ (MP2) = 0.044 Å, $\Delta_{\text{R}}\theta_{\text{HCCH}}$ (MP2) = 7.5°) can be viewed as a further verification of this proposed interaction scheme.

Except for the SCF result, the BDE (Au⁺–C₂H₄) is ca. 70 kcal/mol at all levels of theory, when relativistic contributions are included. In contrast, the nonrelativistic BDEs are only of the magnitude of an electrostatic interaction. The relativistic effects are also quite large as far as geometry is concerned; for example, the relativistic bond contraction $\Delta_{\text{R}}r_{\text{Au-C}}$ is 0.353 Å at the MP2 level of theory concomitant with an increase of the BDE from 30.2 (ECP) to 73.1 kcal/mol (RECP), i.e., a relativistic stabilization of $\Delta_{\text{R}}E = 42.9$ kcal/mol. In fact, it becomes apparent that the relativistic bond amplification even exceeds the effect of electron correlation. As mentioned above, the differences between the optimized

Table 5. Geometries (f in Å, angles in degrees; optimized in C_{3v}) and Bond Dissociation Energies (kcal/mol) for Au⁺(NH₃)

		SCF	MP2	CCSD(T) ^a	ADF/BP	B3LYP
$r(\text{Au-N})$	R	2.194	2.028	2.028	2.062	2.103
	NR	2.486	2.322		2.325	2.392
$r(\text{N-H})$	R	1.002	1.014	1.014	1.026	1.018
	NR	1.002	1.013		1.026	1.016
$\alpha(\text{Au-N-H})$	R	111.4	110.6	110.6	111.0	110.3
	NR	112.3	112.3		111.0	111.9
BDE	R	42.2	68.6	65.3	72.5	63.5
	NR	27.5	37.7		36.0	38.1

^a Calculated at the MP2-optimized geometry.

geometries of Au⁺(H₂O) and Au⁺(CO) at the various levels of theory applied (except SCF) are small. Thus, we refrained from a complete geometry optimization of Au⁺(C₂H₄) in the CCSD(T) calculations. Furthermore, it was not possible to perform a complete geometry optimization at the quasi-relativistic ADF level, and therefore, we varied only the Au–C distance and kept the geometry of the ethene moiety frozen at the non-relativistic optimized geometry. In order to estimate the error made, we performed a single-point ADF/BP calculation at the MP2/RECP-optimized geometry. The bond energy calculated in such a way is 70.3 kcal/mol as compared to 70.0 kcal/mol listed in Table 3. Within this context, it is worth mentioning that the apparent overbinding obtained for Au⁺(H₂O) and Au⁺(CO) with the ADF/BP approach is not present for the Au⁺(C₂H₄) complex.

Finally, we note that the harmonic frequencies of Au⁺–(C₂H₄), as obtained via three different DFT approaches, are in reasonable agreement with each other (Table 4) and compare quite well with the MP2/RECP values as well as the data reported in ref 8f. Thus, the nonclassical π -bridged structure is a real minimum on the potential energy surface of Au⁺(C₂H₄). Due to the high polarizability of ethene, which gives rise to the ion-induced-dipole interaction, other coordinations (i.e., in-plane bridging structure or the classical σ -bound system) could also be possible; however, the large quadrupole moment⁴⁷ of C₂H₄ should lead to a large ion–quadrupole interaction and thus favor the π bridging.^{8f} However, the low frequencies associated with the Au⁺–(C₂H₄) motion indicate a flat PES for the movement of Au along the C–C axis, and the search for other minima would need further investigations.

Au⁺(NH₃). The results for the Au⁺(NH₃) complex are listed in Table 5; as mentioned above, the CCSD(T) energy was obtained in a single-point calculation at the MP2 geometry. Furthermore, the geometry has been optimized under the restriction of C_{3v} symmetry; however, a subsequent frequency analysis proved the C_{3v} structure to be a minimum.

As found for the other gold(I) complexes, the structural parameters of Au⁺(NH₃) optimized by using different methods are in good agreement with each other. Once again, B3LYP slightly overestimates the Au–N bond length as compared to the other computational approaches; i.e., $r_{\text{Au-N}}$ (B3LYP) = 2.103 Å versus $r_{\text{Au-N}}$ (MP2) = 2.028 Å and $r_{\text{Au-N}}$ (ADF/BP) = 2.062 Å. The relativistic bond contraction $\Delta_{\text{R}}r$ is still substantial, and ranges from 0.26 and 0.29 Å, depending on the level of theory used.

As far as the binding energies are concerned, the BDEs of Au⁺(NH₃) scatter around the CCSD(T) result

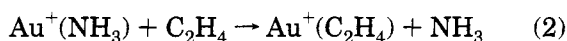
(47) Spackman, M. A. *J. Phys. Chem.* **1989**, *93*, 7594.

(48) (a) For the formation of metallacycles in gas-phase ion–molecule reactions, see: Jacobson, D. B.; Freiser, B. S. *Organometallics* **1983**, *3*, 513. (b) For theoretical aspects, see: Swanström, P.; Jørgensen, K. A. *J. Chem. Soc., Dalton Trans.* **1990**, 115.

(49) (a) Dewar, M. J. S. *Bull. Soc. Chim. Fr.* **1951**, C79, 18. (b) Chatt, J.; Duncanson, L. A. *J. Chem. Soc.* **1953**, 2939.

of 65 kcal/mol; similar to $\text{Au}^+(\text{C}_2\text{H}_4)$, no overestimation of the BDE by the ADF/BP method takes place. Although the computed BDEs of $\text{Au}^+(\text{C}_2\text{H}_4)$ and $\text{Au}^+(\text{NH}_3)$ are quite close to another, the different nature of the bonding already becomes apparent in the comparison of nonrelativistic and relativistic calculations: Due to the dipolar character of ammonia, the ion-dipole interaction between Au^+ and NH_3 is quite large, such that even BDE (SCF/NR) is 27.5 kcal/mol and this effect further increases upon inclusion of correlation. However, the relativistic stabilization of the Au^+-NH_3 bond is still substantial, e.g., $\Delta_{\text{R}}E(\text{MP2}) = 30.9$ kcal/mol. As outlined above, part of this relativistic stabilization is due to electron transfer from ammonia (IE = 10.16 eV) to the gold atom (IE = 9.225 eV); this is also evidenced by the partial positive charge of the gold atom, i.e., 0.63 according to Mulliken population analysis.²⁴

Albeit the computed BDE for $\text{Au}^+(\text{NH}_3)$ is quite large, it is somewhat smaller than $\text{Au}^+(\text{C}_2\text{H}_4)$ for all but the ADF/BP method. For example, at the MP2 level of theory, the computed $\Delta\Delta E$ (0 K) for the ligand exchange reaction of $\text{Au}^+(\text{NH}_3)$ with ethene (eq 2) is +4.5 kcal/mol,



and converting this value to $\Delta\Delta G$ (298 K) does not affect the relative computed gold(I) affinity scheme at all; i.e., $\Delta\Delta G$ (298 K) = +4.5 kcal/mol, since the $\Delta\Delta H$ and $\Delta\Delta S$ terms cancel each other. The CCSD(T) and B3LYP calculations predict similar $\Delta\Delta E$ values for the ligand-exchange reaction 2 (+3.5 and +5.1 kcal/mol, respectively), whereas the ADF/BP procedure results in a reverse value of $\Delta\Delta E = -2.5$ kcal/mol.

Experimentally, it was found that ammonia exhibits a larger gold(I) affinity than ethene, i.e., $\text{BDE}(\text{Au}^+-\text{NH}_3) > \text{BDE}(\text{Au}^+-\text{C}_2\text{H}_4)$, and measurement of the thermal equilibrium constant resulted in $\Delta\Delta G = -2.3$ kcal/mol for the ligand-exchange reaction 2. As far as the relative gold(I) affinities of the ligands are concerned, only the ADF/BP approach predicts the same order as found experimentally, i.e., $\text{H}_2\text{O} < \text{CO} < \text{C}_2\text{H}_4 < \text{NH}_3$, whereas the other methods lead to the reverse order for ethene and ammonia.

Relativistic Effects. A problem often addressed in the literature is the question of the interplay of relativistic and/or correlation energy contributions to the bonding in heavy element containing systems.^{44a} It is an accepted fact that both effects are important and lead to significant bond stabilization. In order to evaluate both effects, often the additivity assumption (eq 3) is made.

$$E_{\text{corr}}^{\text{R}} \equiv E_{\text{SCF}}^{\text{R}} + \Delta E_{\text{corr}}^{\text{R}} \quad (3)$$

According to this approach, the total relativistic energy $E_{\text{corr}}^{\text{R}}$ can be obtained from the uncorrelated relativistic energy $E_{\text{SCF}}^{\text{R}}$ by adding the correlation energy contribution $\Delta E_{\text{corr}}^{\text{R}}$. To a first approximation, one can assume that $\Delta E_{\text{corr}}^{\text{R}} = \Delta E_{\text{corr}}^{\text{NR}}$ and the latter term is easily derived from a nonrelativistic ab initio calculation by using any correlated method. Using this additivity assumption, it seems to be trivial to compute that total energies as E_{Add} (eq 4).

$$E_{\text{Add}} \equiv E_{\text{SCF}}^{\text{R}} + \Delta E_{\text{corr}}^{\text{NR}} \quad (4)$$

However, the errors made by neglecting the relativistic effects on the correlated wave function can be large. Moreover, recently it has been demonstrated for group 11 dipole polarizabilities that relativistic and electron correlation contributions are not additive.⁴⁶ In order to analyze this in more detail for the $\text{Au}^+(\text{L})$ systems, we have calculated the different contributions to the bond energy by using the advantages of the ECP/RECP approach. For the purpose of this study we modified eq 3 to obtain eq 5.⁴⁶

$$E_{\text{Corr}}^{\text{R}} = E_{\text{SCF}}^{\text{NR}} + \Delta_{\text{R}}E + \Delta_{\text{corr}}E + \Delta_{\text{mix}}E \quad (5)$$

For all closed-shell ions under study, it can be assumed that the uncorrelated relativistic effect on the energy ($\Delta_{\text{R}}E$; eq 6) can be calculated from the difference of the SCF energies by use of the relativistic and nonrelativistic effective core potentials.

$$\Delta_{\text{R}}E = E_{\text{SCF}}^{\text{R}} - E_{\text{SCF}}^{\text{NR}} \quad (6)$$

On the other hand, the pure nonrelativistic correlation energy contribution ($\Delta_{\text{corr}}E$) can be evaluated by use of the nonrelativistic wave function (eq 7).

$$\Delta_{\text{corr}}E^{\text{NR}} = E_{\text{corr}}^{\text{NR}} - E_{\text{SCF}}^{\text{NR}} \quad (7)$$

As can be seen from a comparison of MP2-, CCSD(T)-, and B3LYP-calculated BDEs values, the correlation energy is sufficiently described even at the MP2 level; thus, we use the ECP/MP2 data for the evaluation of $\Delta_{\text{corr}}E^{\text{NR}}$. The last term in eq 5 ($\Delta_{\text{mix}}E$) contains the relativistic effect on the correlation energy contribution. Assuming that correlation and relativistic effects are independent of each other and additive, the total energy can be obtained in a first approximation by setting $\Delta_{\text{mix}}E = 0$, thus eq 5 becomes equal to eq 4 leading to $E_{\text{Add}} = E_{\text{corr}}^{\text{R}}$.

The contributions of the various effects to the BDEs of the $\text{Au}^+(\text{L})$ complexes are displayed in Figure 1. As can be seen for $\text{Au}^+(\text{H}_2\text{O})$, even the nonrelativistic SCF computation describes the predominantly electrostatic nature of the bonding qualitatively correct and accounts for 60% of the BDE as compared to the CCSD(T) value. As a consequence, the relativistic and correlation effects on the BDE are quite small, whereas the bond length contraction remains substantial (vide supra). In contrast, for $\text{Au}^+(\text{CO})$, $\text{Au}^+(\text{NH}_3)$, and $\text{Au}^+(\text{C}_2\text{H}_4)$ electron correlation and relativistic effects are much more important. For example, the contributions of $\Delta_{\text{R}}E$ and $\Delta_{\text{corr}}E^{\text{NR}}$ to the total binding energy of $\text{Au}^+(\text{C}_2\text{H}_4)$ are 22 and 18 kcal/mol, respectively. However, as can be easily seen in Figure 1, the evaluation of the BDE in terms of E_{Add} underestimates the bonding substantially. In fact, for $\text{Au}^+(\text{C}_2\text{H}_4)$, the relativistic contribution to correlation energy $\Delta_{\text{mix}}E$ represents 28% of the total binding energy. Similar conclusions can be drawn for $\text{Au}^+(\text{NH}_3)$, and for $\text{Au}^+(\text{CO})$ the weight of $\Delta_{\text{mix}}E$ is even more pronounced (42% of the BDE). As a consequence, the determination of BDE by combining a relativistic SCF calculation with a nonrelativistic treatment of correlation is obviously inadequate. Finally, it is evident from Figure 1 that the relativistic MP2 method tends to overestimate the bond energies as compared to CCSD(T) and B3LYP; however, an ultimate evaluation of the performance of the methods is not feasible

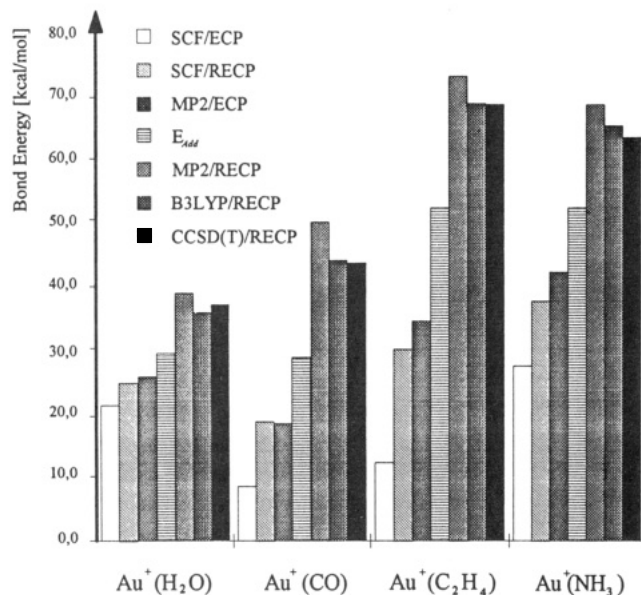


Figure 1. Comparison of the computed BDE (Au^+-L) as obtained by various computational methods using either the nonrelativistic or relativistic potentials, i.e., SCF/ECP, SCF/RECP, MP2/ECP, MP2/RECP, B3LYP/RECP, and CCSD(T)/RECP. The term E_{add} denotes the BDE obtained when correlation and relativistic effects are assumed to behave additively (see text).

since precise and accurate experimental and theoretical data for $Au^+(L)$ complexes are not available.

By comparing the individual energy contributions to the total BDEs, one may be surprised by the fact that the weight of the mixed term ($\Delta_{mix}E$) in $Au^+(CO)$ covers almost half (42%) of the bond energy, whereas for the other ligands, i.e., H_2O , NH_3 , and C_2H_4 , the effect of $\Delta_{mix}E$ is of the order of 25%. By applying the Morokuma bond analysis³⁸ to the results of the ADF/BP method, one may compare $Au^+(CO)$, for example, with the $Au^+(NH_3)$ system. In $Au^+(CO)$, the Au–C bond is shorter than the Au–N bond in $Au^+(NH_3)$, and further, the relativistic bond contraction (Δ_{R^r}) in $Au^+(CO)$ is very large (0.504 Å) as compared to 0.292 Å for $Au^+(NH_3)$. Consequently, the changes in the repulsive steric interaction energy ($\Delta_{R^r}E_{steric}$) are twice as large for $Au^+(CO)$ with respect to $Au^+(NH_3)$; i.e., 94.5 and 46.3 kcal/mol, respectively. On the other hand the relativistic change in the attractive σ overlap $\Delta_{R^r}E_{OI}(\sigma)$, associated with the σ orbital in $Au^+(CO)$ and the a_1 orbital in $Au^+(NH_3)$, is much stronger for $Au^+(CO)$ than for $Au^+(NH_3)$, i.e., 197.1 and 96.4 kcal/mol, respectively. In addition, concomitant to the bond contraction in $Au^+(CO)$ is an

increase of the π - and δ -bonding partition ($\Delta_{R^r}E_{OI}(\pi) = 13.3$ kcal/mol, $\Delta_{R^r}E_{OI}(\delta) = 6.8$ kcal/mol), whereas the contributions of the a_2 and e_1 orbitals to the bonding in $Au^+(NH_3)$ are even destabilizing. Thus, for $Au^+(CO)$, the role of the relativistic correlation energy (ΔE_{mix}) is essential. Furthermore, this explanation accounts for the relatively large deviation (6 kcal/mol) of BDE (Au^+-CO) between the MP2 and CCSD(T) approaches. From a chemical point of view, in $Au^+(CO)$ the 5d orbitals of gold are actively involved in the bonding, whereas for $Au^+(NH_3)$, the bonding is dominated by the electron transfer from the ligand to gold.²⁴

Conclusions

In general, the results of the present study demonstrate that for gold(I) compounds density functional methods are in reasonable good agreement with ab initio MP2 and CCSD(T) approaches. This applies not only for geometries and energetics, but also for relativistic effects if an appropriate RECP scheme is used or the relativistic effects are included directly as in the quasi-relativistic ADF/BP treatment. More precisely, the MP2 and ADF/BP approaches exhibit a slight tendency to overestimate the binding energies as compared to CCSD(T) and B3LYP. In addition, the B3LYP hybrid method leads to an elongation of the corresponding Au^+-L bonds as compared to the other approaches.

For the $Au^+(L)$ complexes under study, correlation and relativistic effects are of the same order of magnitude and both affect the binding severely. As far as the interplay between both effects is concerned, our study emphasizes the necessity for the evaluation of correlation energy using a relativistic approach. However, the agreement of the calculated values with the scarce experimental findings in gold(I) chemistry is not excellent, and there is still room for further improvement in the future.

Acknowledgment. Financial support by the Deutsche Forschungsgemeinschaft, the Fonds der Chemischen Industrie, and the Gesellschaft von Freunden der Technischen Universität Berlin as well as a gift of transition metals from Degussa AG, Hanau, are gratefully acknowledged. P.S. is grateful to the Auckland University Research Committee and to NY/FRG for financial support. Furthermore, we express our thanks to Dipl.-Chem. C. Heinemann for helpful discussions. H. Basch is acknowledged for providing us with a copy of his work prior publication.

OM940709C

Theoretical Study of the Pyramidal Geometry around the Sulfur in the S-Bound Mode of Coordination of Thiophene to the $[\text{Cp}(\text{CO})_2\text{Fe}]^+$ Fragment

Luis Rincón,^{*,†} Joice Terra,[‡] Diana Guenzburger,[‡] and Roberto A. Sánchez-Delgado[†]

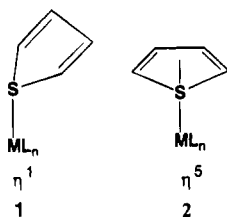
Centro de Química, Instituto Venezolano de Investigaciones Científicas (IVIC), Apartado 21827, Caracas 1020-A, Venezuela, and Centro Brasileiro de Pesquisas Físicas (CBPF), Rua Dr. Xavier Sigaud 150, 22290 Rio de Janeiro, Rio de Janeiro, Brazil

Received September 6, 1994[®]

Density functional calculations have been carried out to study the pyramidal coordination of the sulfur in the thiophene complex $[\text{Cp}(\text{CO})_2\text{Fe}(\eta^1\text{-T})]^+$ (Cp = cyclopentadienyl; T = thiophene). Total energy calculations showed the optimal value of the angle between the Fe–S bond and the thiophene plane to be 120° . An analysis of the changes in the orbitals brought about by the angular variation reveals that the mechanism by which this process takes place is the reduction of the antibonding interaction between the occupied Fe d_{π} orbitals and the S π canonical lone pair in free thiophene. The mechanism found is consistent with the idea of $sp^2 \rightarrow sp^3$ rehybridization of the S atom in thiophene. Calculations performed with and without inclusion of the S 3d basis orbitals show a similar mechanism for the pyramidal distortion.

Introduction

In the last few years the coordination chemistry of thiophenes has developed rapidly;¹ several modes of coordination to discrete metal centers or metal clusters have been identified or proposed. Recent advances in this field are centered in the study of models at the molecular level for the hydrosulfurization (HDS) reaction, which is one of the most important industrial applications of transition metal catalysis.² Of the known thiophene coordination modes, the S or η^1 (1) and the η^5 (2) forms are most frequently suggested for initial



thiophene adsorption to catalyst surfaces.³ Therefore, the understanding of the nature of the thiophene–metal bonding in modes 1 and 2 is crucial for the future development of this field. The nature of the bonding

and geometrical preferences in the η^1 -coordination mode of thiophene is the central topic of this paper.

In examples of the S-bonding mode which have been well-characterized by X-ray diffraction, a pyramidal geometry around the sulfur has been found.¹ The same geometry around the sulfur was found for the adsorption of thiophene on the surface of Pt[111]⁴ and on Cu[100],⁵ in thiaporphyrin complexes⁶ and S-alkylthiophenes.⁷ This result has been interpreted as a tendency of sulfur in the S-bound thiophene complexes to move toward a pyramidal sp^3 hybridization. In terms of molecular orbital theory, there is no clear understanding of the driving force that causes the $sp^2 \rightarrow sp^3$ rehybridization of sulfur in thiophene nor of the contribution of the 3d valence orbitals of S to this process.

The aim of this paper was to elucidate the mechanisms leading to a pyramidal geometry in the S-bound coordination mode of thiophene to a metal center. To this purpose, we studied the well-known complex $[\text{CpFe}(\text{CO})_2(\eta^1\text{-T})]^+$ (Cp = cyclopentadienyl, T = thiophene).⁸ The S-bound mode has been examined theoretically for the $\text{Mo}(\text{CO})_5$ fragment using the CNDO/2 method,⁹ for the RuS_5^{6-} complex using the scattered-wave method,¹⁰ and for $[\text{CpFe}(\text{CO})_2(\eta^1\text{-Th})]^+$ (Th = T, DBT) with the

(4) (a) Stohr, J.; Gland, J.; Kollin, E. B.; Koestner, R. J.; Johnson, A. L.; Muettterties, E. L.; Sette, F. *Phys. Rev. Lett.* **1984**, *53*, 2161. (b) Lang, J. F.; Masel, R. I. *Surf. Sci.* **1985**, *183*, 44.

(5) Sexton, B. A. *Surf. Sci.* **1985**, *163*, 99.

(6) (a) Latos-Grazynski, L.; Lisowski, L.; Olmstead, M. M.; Balch, A. L. *J. Am. Chem. Soc.* **1987**, *109*, 4428. (b) Latos-Grazynski, L.; Lisowski, L.; Olmstead, M. M.; Balch, A. L. *Inorg. Chem.* **1989**, *28*, 1183. (c) Latos-Grazynski, L.; Lisowski, L.; Olmstead, M. M.; Balch, A. L. *Inorg. Chem.* **1989**, *28*, 4065. (d) Latos-Grazynski, L.; Lisowski, L.; Olmstead, M. M.; Balch, A. L. *Inorg. Chem.* **1989**, *28*, 3328.

(7) Gillespie, R. J.; Murray-Rust, P.; Porter, A. E. A. *J. Chem. Soc., Chem. Commun.* **1978**, 83.

(8) (a) Kuhn, N.; Schumman, H. *J. Organomet. Chem.* **1984**, *276*, 55. (b) Goodrich, J. D.; Nickias, P. N.; Selegue, J. P. *Inorg. Chem.* **1987**, *26*, 3424.

(9) Ruette, F.; Valencia, N.; Sanchez-Delgado, R. A. *J. Am. Chem. Soc.* **1989**, *111*, 40.

(10) Smit, T. S.; Johnson, K. H. *Chem. Phys. Lett.* **1993**, *212*, 525.

[†] IVIC.

[‡] CBPF.

[®] Abstract published in *Advance ACS Abstracts*, February 1, 1995.

(1) (a) Angelici, R. J. *Acc. Chem. Res.* **1988**, *21*, 387. (b) Angelici, R. J. *Coord. Chem. Rev.* **1990**, *105*, 61. (c) Rauchfuss, T. B. *Prog. Inorg. Chem.* **1991**, *39*, 259. (d) Sánchez-Delgado, R. A. *J. Mol. Catal.* **1994**, *86*, 287.

(2) (a) Prins, R.; de Beer, V. H.; Somorjai, G. A. *Catal. Rev.—Sci. Eng.* **1989**, *31*, 1. (b) Grange, P. *Catal. Rev.—Sci. Eng.* **1980**, *21*, 135. (c) Gates, B. C.; Katzer, J. R.; Scuit, G. C. A. *Chemistry of Catalytic Processes*; McGraw-Hill: New York, 1979. (d) Mitchell, P. C. H. *Catalysis*; Kemball, C., Ed.; The Chemical Society: London, 1977; Vol. 1. (e) Schuman, S. C.; Shalit, H. *Catal. Rev.* **1970**, *4*, 245.

(3) (a) Wiegand, B. C.; Friend, C. M. *Chem. Rev.* **1992**, *92*, 491. (b) Sauer, N. N.; Markel, E. J.; Schrader, G. L.; Angelici, R. J. *J. Catal.* **1989**, *117*, 295. (c) Markel, E. J.; Schrader, G. L.; Sauer, N. N.; Angelici, R. J. *Catal.* **1989**, *116*, 11.

Fenske–Hall method,¹¹ but a detailed study of the pyramidal coordination mechanism has not been presented previously.

Computational Details

Density functional calculations in the local density approximation¹² were carried out by employing the discrete variational method (DVM) developed by Ellis and Painter.¹³ The local exchange-correlation potential of Hedin and Lundqvist was used.¹⁴

Symmetrized molecular orbitals were formed from numerical atomic orbitals, and the atomic configurations for atoms in the molecule (self-consistent within the framework of a Mülliken type population analysis¹⁵) were determined numerically.¹⁶ Valence basis functions employed here include those for Fe (3s, 3p, 3d, 4s, and 4p), C and O (2s and 2p), H (1s), and S (3s and 3p). Calculations were also performed including the 3d function of S, as shall be discussed later. Core orbitals were kept frozen.

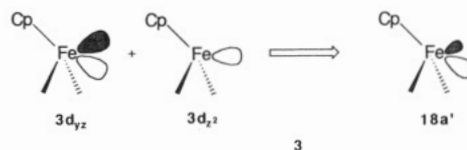
Standard numerical integration methods were used.^{17,18} The molecular charge density was fitted to a multipolar expansion.¹⁹ The method for calculating the total energy is described in detail in ref 20.

The application of density functional theory to organometallic complexes has been reviewed recently.²¹ The geometrical parameters for $[CpFe(CO)_2(\eta^1-T)]^+$ were those given by Goodrich et al.⁸ for the dibenzothiophene analogue. These parameters are as follows: bond distances, Fe–S = 2.289 Å, Fe–C(O) = 1.780 Å, Fe–Cp(centroid) = 1.725 Å, C–O = 1.15 Å; bond angles, S–Fe–C(O) = 94.3° (mean), S–Fe–Cp(centroid) = 121.3°, C(O)–Fe–C(O) = 94.8°, Fe–C–O = 180°. Standard geometries were adopted for thiophene²² and cyclopentadiene (bond distance C–C = 1.44 Å, C–H = 1.09 Å).

Results and Discussion

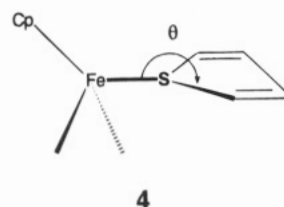
The electronic structure of the coordinatively unsaturated complex d^6 -CpM(CO)₂ has been studied by Schilling et al. using the extended Hückel method;²³ therefore, only a brief description is given here. The more appropriate axis choice for CpM(CO)₂ is one in which the *z* axis is along the future Fe–thiophene bond. The mirror plane of this complex lies in the *yz* plane. The $[CpFe(CO)_2]^+$ fragment of *C_s* point group symmetry has at low energy three occupied metal-based orbitals (see left side of Figure 1): 17a' (*z*², 3%; *yz*, 18%; *x*² – *y*², 52%), 18a' (*z*², 18%; *yz*, 58%; *x*² – *y*², 6%) and 12a'' (*xz*, 65%; *xy*, 5%).²⁴ In the 3d_{*yz*} based orbital 18a', the small contribution of the 3d_{*z*²} orbital causes a dissymmetry in the nodal π character as is shown in 3. At higher energy

is the LUMO low-lying acceptor metal-based orbital 19a' (4s, 5%; 4y, 8%; 4z, 2%; *z*², 54%; *yz*, 3%; *x*² – *y*², 2%).



The well-known frontier orbitals of thiophene²⁵ are shown in the right side of Figure 1. For the η^1 coordination the crucial orbitals of thiophene are the high-energy occupied sulfur "lone pairs": the π lone pair 2b₁ (S(*p_x*), 45%) and the σ lone pair 6a₁ (S(3s), 25%; S(3p_{*z*}), 58%) separated by 0.801 eV. In free thiophene, these canonical "lone pairs" of S come from different symmetries due to the sp² hybridization.

There are many possible conformations for the complex $[CpFe(CO)_2(\eta^1-T)]^+$ corresponding to different values of the angle θ in 4.



We have carried out calculations changing the angle θ of 4 from 100 to 260°. The energy profile for this process is shown in Figure 2. The calculation of Figure 2a does not include the 3d orbitals in S. Figure 2a shows two minima, one deeper well of –3.399 eV (–76.89 kcal mol^{–1}) at 120° and one small well of –0.289 eV (–6.66 kcal mol^{–1}) at 240°. The reference energy was taken as the coplanar geometry. The first well corresponds to the case where thiophene is oriented toward the cyclopentadiene and the second one where it is oriented toward the carbonyls. Our equilibrium theoretical angle θ agrees reasonably well with the Cp(CO)₂Fe(η^1 -DBT) (DBT = dibenzothiophene) complex⁸ which presents an angle of 119.5° and with the rhenium complex Cp*(CO)₂Re(η^1 -T)²⁶ which presents an angle of 140° toward the Cp*. A dynamic nuclear magnetic resonance study on the benzothiophene (BT) complex, $[Cp(CO)_2Fe(\eta^1-BT)]^+$, shows a clear double well potential as in Figure 2, and the ΔG^* was calculated to be 0.404 eV (9.30 kcal mol^{–1}); the barrier for the phenylmethyl sulfide complex $[CpFe(CO)_2(SMePh)]^+$ was 0.539 eV (12.41 kcal mol^{–1}).^{1c} Probably our theoretical higher values of the energy barrier for the isomerization processes are due to not relaxing other geometrical parameters besides the angle θ and to the use of a local exchange-correlation potential. These results cannot be compared with other theoretical studies, because to the best of our knowledge ours is the first theoretical investigation of the pyramidal coordination of S in the η^1 -thiophene complexes. In the following paragraphs

(11) Harris, S. *Organometallics* **1994**, *13*, 2628.

(12) Parr, R. G.; Yang, W. *Density Functional Theory of Atoms and Molecules*, Oxford University Press: New York, 1989.

(13) Ellis, D. E.; Painter, G. S. *Phys. Rev.* **1970**, *B2*, 2887.

(14) Hedin, L.; Lundqvist, B. I. *J. Phys.* **1971**, *C4*, 1971.

(15) Umrigar, C.; Ellis, D. E. *Phys. Rev.* **1980**, *B21*, 852.

(16) Terra, J.; Guenzburger, D. *Phys. Rev.* **1991**, *B44*, 8584.

(17) Stroud, A. H. *Approximate Calculation of Multiple Integrals*; Prentice-Hall: Englewood Cliffs, NJ, 1971.

(18) Ellis, D. E. *Int. J. Quantum Chem.* **1968**, *S2*, 35.

(19) Delley, B.; Ellis, D. E. *J. Chem. Phys.* **1982**, *76*, 1949.

(20) (a) Delley, B.; Ellis, D. E.; Freeman, A. J.; Baerends, E. J.; Post, D. *Phys. Rev.* **1983**, *B27*, 2132. (b) Guenzburger, D.; Ellis, D. E. *Phys. Rev.* **1992**, *B45*, 285.

(21) (a) Ziegler, T. *Chem. Rev.* **1991**, *91*, 651. (b) Ziegler, T. *Pure Appl. Chem.* **1991**, *63*, 873.

(22) Harshbarger, W. R.; Bauer, S. H. *Acta Crystallogr.* **1970**, *B26*, 1010.

(23) Schilling, B. E. R.; Hoffmann, R.; Lichtenberger, D. L. *J. Am. Chem. Soc.* **1979**, *101*, 585.

(24) In order to describe the molecular orbitals eigenvectors, *s*, *x*, *y*, *z*, *xz*, *yz*, *x*² – *y*², and *z*² are used to denote the corresponding *ns*, *np*, and (*n* – 1)*d* atomic orbitals of sulfur or transition metal.

(25) Zonneville, M. C.; Hoffmann, R.; Harris, S. *Surf. Sci.* **1988**, *199*, 320.

(26) Chi, M.-G.; Angelici, R. J. *Organometallics* **1991**, *10*, 2436.

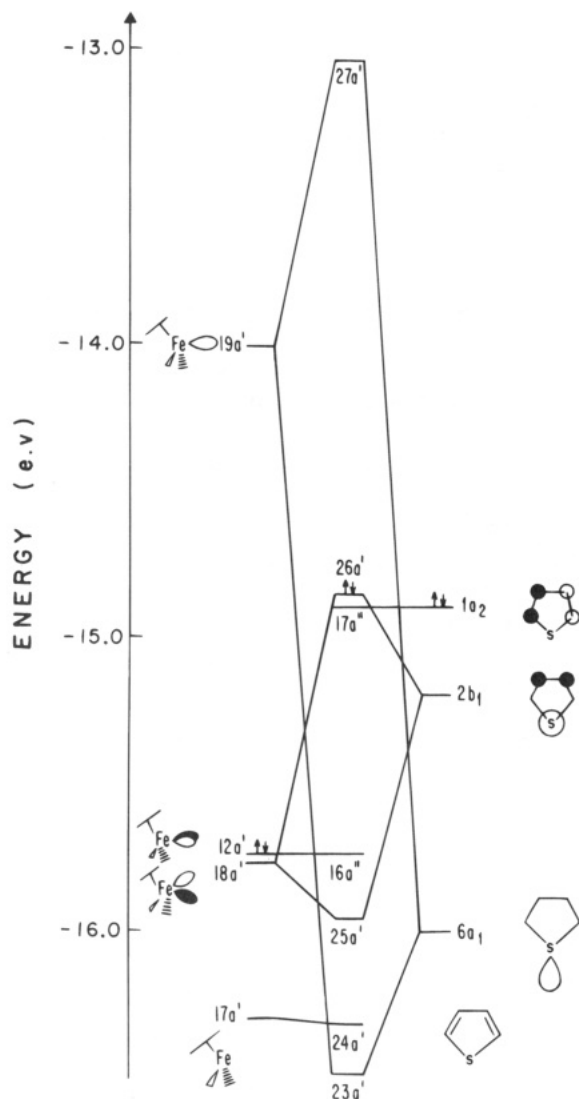


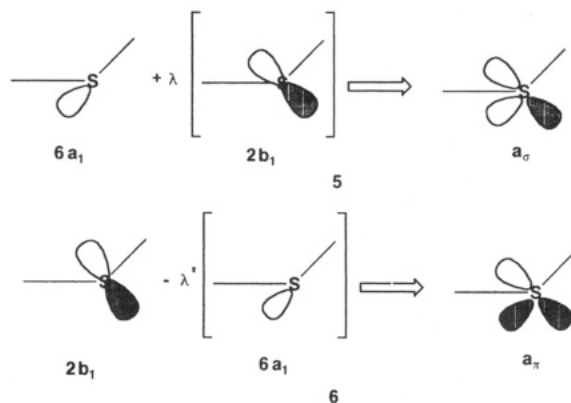
Figure 1. Orbital interaction diagram for $[\text{CpFe}(\text{CO})_2]^+$ and thiophene in the coplanar orientation.

Figure 2a is rationalized by analyzing the fragment molecular orbitals.²⁷

Our discussion will begin with a brief examination of the orbitals at the coplanar geometry. As shown in Figure 1 the coplanar geometry of the complex $[\text{CpFe}(\text{CO})_2(\eta^1\text{-T})]^+$ has at low energy six occupied orbitals: the HOMO $26a'$ (Fe(yz), 11%; S(y), 40%), $17a''$, $16a''$ (Fe($4x$), 2%; Fe(xz), 60%; Fe(xy), 7%), $25a'$ (Fe(z^2), 16%; Fe(yz), 30%; Fe($x^2 - y^2$), 14%), $24a'$ (Fe(yz), 31%; Fe($x^2 - y^2$), 38%) and $23a'$ (Fe(z^2), 10%; Fe($x^2 - y^2$), 3%; S(s), 15%; S(z), 57%). At somewhat higher energy is the unoccupied metal-based d_{z^2} orbital $27a'$ (Fe($4s$), 1%; Fe($4y$), 2%; Fe(z^2), 60%; Fe(yz), 4%; Fe($x^2 - y^2$), 2%; S(s), 14%; S(z), 8%). Due to a small overlap integral the orbitals $12a''$ in $[\text{CpFe}(\text{CO})_2]^+$ and $1a_2$ in thiophene are mainly nonbonding. The $23a'$ and $27a'$ orbitals come from the bonding and antibonding interaction of the unoccupied $19a'$ metal orbital with the $6a_1$ σ lone pair in thiophene. The $23a'$ orbital represents the σ donation from the thiophene to the LUMO orbital in the metal fragment. The occupied $25a'$ and $26a'$ levels are the

bonding and antibonding combinations of $18a'$ in the metal fragment and the $2b_1$ π lone pair in thiophene. The occurrence of this destabilizing interaction in the coplanar conformation provides an important clue for understanding why the S coordination in the η^1 geometry is pyramidal. The different interactions of a' symmetry are a consequence of the S lone pair orientation in the coplanar structure. We shall refer to the metal-based orbital $19a'$ as d_σ and the $18a'$ as d_π .

Now, as the angle θ in **4** changes from 180° , the overlap integral of the d_σ metal orbital and the σ lone pair of thiophene decreases, but in compensation the overlap integral with the π lone pair increases. Similar arguments are applicable to the d_π metal orbital. Then it is expected that the four orbitals d_σ and d_π in the metal fragment and the two lone pairs of thiophene will mix together along the distortion. This mixing complicates the analysis. A simplification may be made by considering linear combinations of thiophene lone pairs, one of σ symmetry (a_σ , **5**) and the other one of π symmetry (a_π , **6**). These combinations are appropriate for a larger overlap with d_σ and d_π .



On the basis of only the values of λ and λ' for **5** and **6**, we can distinguish the following cases:

(a) $\lambda > \lambda'$. In this case, the changes in the overlap integral of a_σ and d_σ orbitals is large compared with the overlap of a_π and d_π for angles different from 180° . This situation rehybridizes the a_π orbital away from d_π and therefore reduces its antibonding character. In this case an energy decrease is expected at angles far from 180° as a consequence of a decrease in the antibonding $26a'$ interaction.

(b) $\lambda = \lambda'$. In this case the situation is similar to the case of coplanar geometry. A smooth energy profile is expected. This is the case in which the hybridization of the S along the whole process is sp^2 .

(c) $\lambda < \lambda'$. This is the antithesis of case a. The overlap integrals of a_π and d_π are large compared with a_σ and d_σ . In this case the bonding interaction between the metal LUMO d_σ and the thiophene σ lone pair is reduced for $\theta \neq 180^\circ$, and the energy profile displays a minimum at $\theta = 180^\circ$, in order to preserve the σ bond and reduce the π antibonding interaction.

As expected from the preceding discussion, the larger variation of the energy is for the orbital $26a'$ of antibonding character. With the angle change from 180° this orbital drops in energy and presents two minima of similar depth, 0.576 and 0.589 eV at 120° and 240° respectively. Bond order calculations for the Fe–S bond shows that the pyramidal distortion increases the Fe–S bond order from 0.344 at 180° to 0.356 at 140° and 0.354

(27) (a) Fujimoto, H.; Hoffmann, R. *J. Phys. Chem.* **1974**, *78*, 1167. (b) Fujimoto, H.; Inagaki, S. *J. Am. Chem. Soc.* **1977**, *99*, 7424. (c) Fujimoto, H.; Osamura, Y.; Minato, T. *J. Am. Chem. Soc.* **1978**, *100*, 2954. (d) Kato, S.; Fujimoto, H.; Yamabe, S.; Fukui, K. *J. Am. Chem. Soc.* **1974**, *96*, 2024. (e) Fujimoto, H.; Kato, S.; Yamabe, S.; Fukui, K. *J. Chem. Phys.* **1974**, *60*, 572.

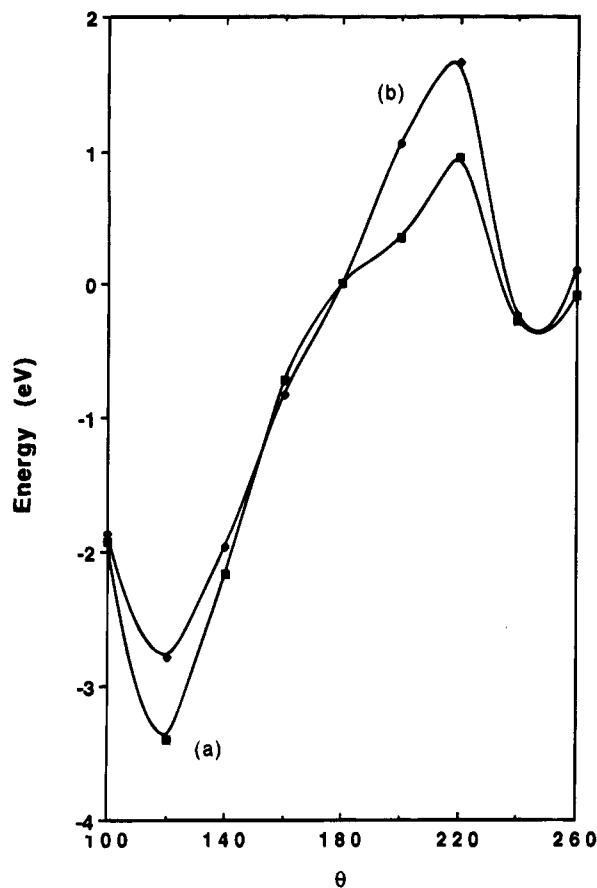


Figure 2. Variation of the calculated total energy as a function of θ , defined in **5**: (a) without 3d orbitals on the S; (b) with 3d orbitals on the S. The reference energy was taken as the coplanar geometry ($\theta = 180^\circ$).

at 220° . In other words, the Fe–S bond is equally strong in both extremes of θ in Figure 2. On the basis of changes of the orbital $26a'$ or in the Fe–S bond order the difference in energy of the two minima in Figure 2a cannot be explained.

The asymmetry of Figure 2a may be caused by the dissymmetry of d_π shown in **3**. Figure 3 shows that the overlap integral of d_π ($18a'$) with the $2b_1$ thiophene orbital is larger for angles near 180° and larger for the right part of the curve than for the left part. In the case of $\langle 18a'|6a_1 \rangle$ the integral increases more rapidly in the right part than in the left part for angles near 180° . The latter effect does not compensate the antibonding interaction between $18a'$ and $2b_1$ which causes a large overlap repulsion at angles larger than 180° as well as the dissymmetry of Figure 2.

Let us now explore the validity of our conclusion that $\lambda > \lambda'$ in **5** and **6** implies a pyramidal coordination in thiophene. This is carried out by focusing on the contribution of the thiophene lone pair orbitals ($2b_1$ and $6a_1$) in the molecular orbitals $26a'$ and $27a'$. By inspection of the contribution of the thiophene $2b_1$ orbital in $27a'$ we obtain an estimate of λ ; in a similar form the contribution of $6a_1$ in $26a'$ represents an estimate of λ' . Figure 4 shows that the contribution of $2b_1$ in $27a'$ is larger than the contribution of $6a_1$ in $26a'$ at $\theta \neq 180^\circ$ in accordance with the hypothesis of $\lambda > \lambda'$.

The rehybridization of S was analyzed by inspection of the S(3s)/S(3p) Mülliken-type population ratio shown in Figure 5. In this Figure we observe that the S(3s)/S(3p) ratio increases from 0.40 at 180° to 0.45 at 120° and 0.45 at 260° . Formally if the Fe–S bond is perfectly

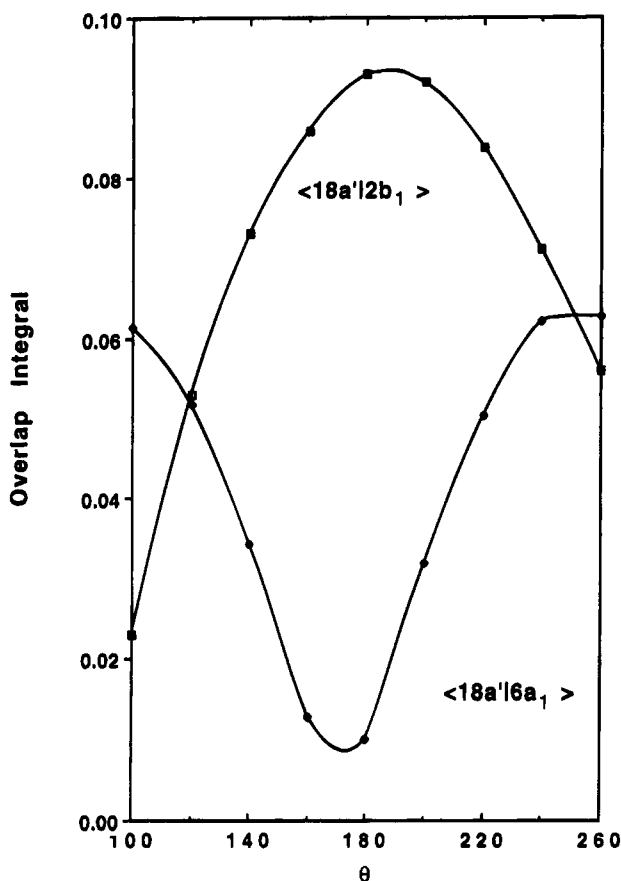


Figure 3. Variation of the overlap integral between the $18a'$ orbital of the $[\text{CpFe}(\text{CO})_2]^+$ fragment and the two lone pair orbitals in thiophene as a function of θ , defined in **5**.

covalent, a rehybridization on S from sp^2 to sp^3 represents a theoretical change from 0.29 to 0.33 in the S(3s)/S(3p) ratio. Our calculations show a strong variation from this hypothetical case but essentially the same tendency. This result is in accord with the hypothesis of a rehybridization in the thiophene molecule in the direction $sp^2 \rightarrow sp^3$.

This description can be easily extended to other compounds because in a good number of known metal- η^1 -S-thiophene complexes the metal fragment presents an unoccupied d_σ orbital of low energy and an occupied d_π orbital; in such cases all the orbital interactions occurring during the pyramidal distortion are similar to the one herein described, and thus we expect as a general rule the pyramidal geometry around the S. Our analysis indicates that coordinatively unsaturated 16-electron fragments in which, by an appropriate ligand field, both d_σ and d_π metal orbitals are unoccupied can coordinate thiophene in a coplanar geometry. In the latter case, a formal four-electron double metal–thiophene bond is to be expected.

While this work was in progress, Fenske–Hall calculations by Harris on $\text{CpFe}(\text{CO})_2(\text{Th})$ (Th = T, DBT) were published.¹¹ A number of features of those calculations are qualitatively similar to our findings, notably the importance of the antibonding interaction of the metal d_π orbital with the π S lone pair of the ligand as a driving force for the pyramidal distortion. However, in contrast with our results, Harris concluded that tipping of the DBT ligand did not indicate rehybridization of the sulfur orbitals. No mention of the energy differences for the coplanar and pyramidal geometries

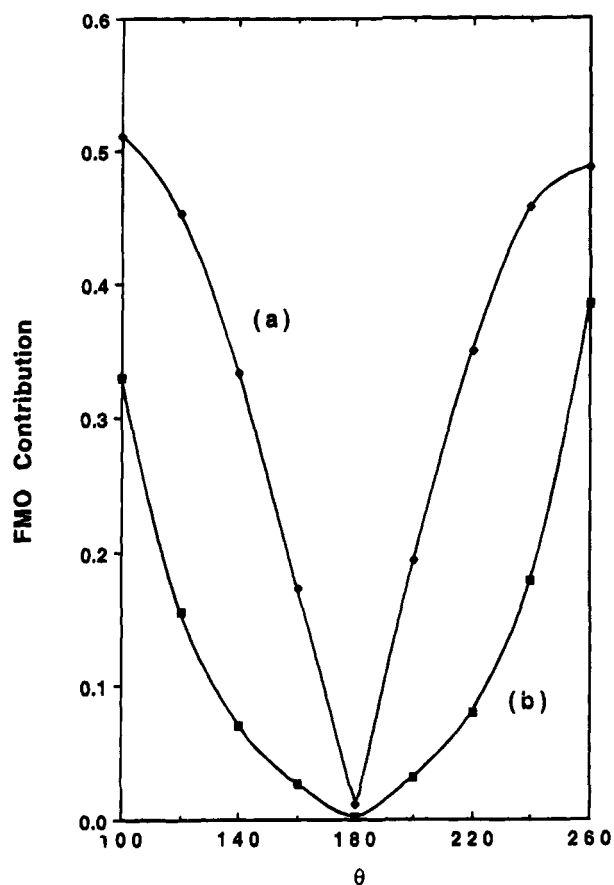


Figure 4. (a) Variation of the contribution of the $6a_1$ orbital of thiophene in the $26a'$ orbital of the η^1 complex as a function of θ . (b) Variation of the contribution of the $2b_1$ orbital of thiophene in the $27a'$ molecular orbital of the η^1 complex as a function of θ .

was provided in that paper, and therefore no comparisons can be made with our data.

Smit and Johnson,¹⁰ using a standard scattered-wave calculation with fractional occupation numbers and populating the orbitals by Fermi-Dirac distributions at 673 K, found that for the C_{2v} thiophene-RuS₅⁶⁻ complex the orbital interaction between the Fermi level orbital $2b_1$ (thiophene π lone pair) and the metal fragment $7e$ orbitals is the dominant one at long distances. In this case, the d_{π} metal orbital can interact in a bonding form with the thiophene π lone pair in a coplanar geometry ($\theta = 180^\circ$), in contrast with our organometallic Fe complex. Strongly pyramidal coordination was found by Calhorda et al.²⁸ in a study of the coordination and reaction of ethylene sulfide and trimethylene sulfides with the fragments Mo(CO)₅ and MoH₄⁴⁻ using the Extended Hückel method. They found that the pyramidal geometry is related to the lowering of the weak four-electron destabilizing interaction between the π -lone pair of sulfides and the $d_{\pi}(yz)$ orbital of the metal fragment.

We have also investigated the role of the 3d basis orbitals on S in this process. The energy profile including 3d orbitals is presented in Figure 2b. This figure shows, with some numerical value variations, the same qualitative features of Figure 2a. A deeper minimum of -2.291 eV (-52.75 kcal mol⁻¹) is obtained. With a detailed study of the Walsh diagram and population and

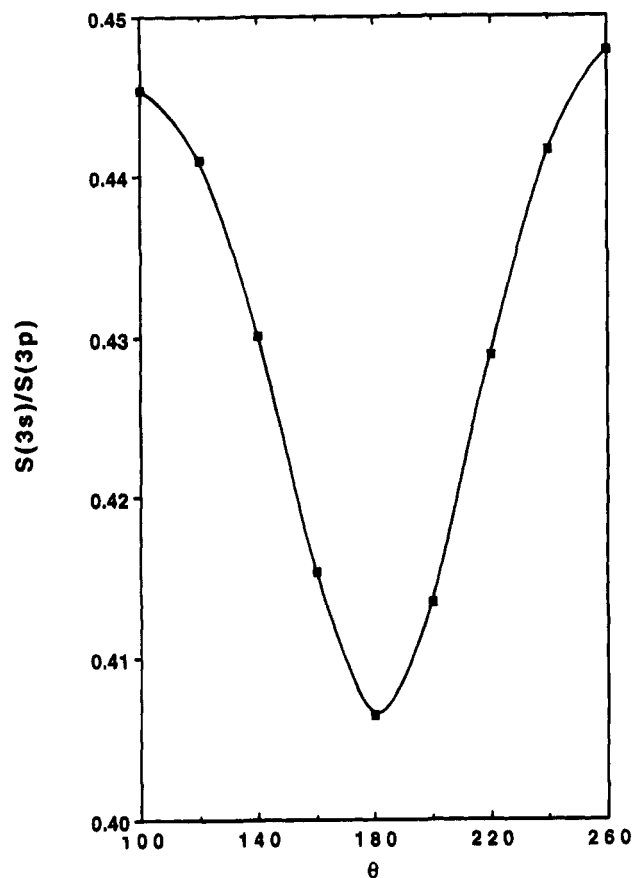


Figure 5. Variation of the S(3s)/S(3p) population ratio as a function of θ , defined in 5.

fragment orbital variations, we arrived at the same conclusions as in the case in which S(3d) orbitals are excluded. Thus the inclusion of S 3d orbitals does not have any significant influence on the previous orbital analysis.

Conclusions

Density functional calculations performed for the complex $[\text{Cp}(\text{CO})_2\text{Fe}(\eta^1\text{-T})]^+$ have provided insight into the pyramidal coordination of thiophene in the S-bound mode. Total energy calculations indicate a value of 120° for the dihedral angle between the Fe-S bond and the plane of thiophene; larger energies of stabilization are found as compared to the experimental values for the similar complexes $[\text{Cp}(\text{CO})_2\text{Fe}(\eta^1\text{-BT})]^+$ and $[\text{Cp}(\text{CO})_2\text{Fe}(\text{SMePh})]^+$. We have rationalized this process in terms of the reduction of the antibonding interaction between the occupied Fe d_{π} orbital and the S π lone pair of thiophene. The nonsymmetrical form of the distortion process causes a preference of coordination with bending toward the cyclopentadienyl ligand. This preference is due in part to the dissymmetry in the nodal π character of d_{π} . Finally, the inclusion of S(3d) orbitals reveals the same features as the calculations without S(3d) orbitals.

Acknowledgment. We thank to the Brazilian National Supercomputer Center—CESUP UFRGS—for access to the Cray Y-MP2E. L.R. thanks the FUNDAY-ACUCHO (Venezuela) for making his travel to CBPF possible. The authors also thank Dr. D. E. Ellis (Northwestern University) and M. Boves (IVIC) for their interest and discussions.

(28) Calhorda, M. J.; Hoffmann, R.; Friend, C. M. *J. Am. Chem. Soc.* **1990**, *112*, 50.

Synthesis of Coinage Metal Cation Adducts of $\text{Nb}(\text{C}_5\text{H}_4\text{SiMe}_3)_2\text{H}(\text{CO})$. X-ray Crystal Structure of $[\{\text{Nb}(\text{C}_5\text{H}_4\text{SiMe}_3)_2(\text{CO})\}_2(\mu\text{-H})_2\text{Cu}]\text{PF}_6$

Antonio Antiñolo,[†] Fernando Carrillo,[†] Bruno Chaudret,^{*,‡} Mariano Fajardo,[§] Santiago García-Yuste,[†] Fernando J. Lahoz,^{||} Maurizio Lanfranchi,[⊥] José A. López,^{||} Antonio Otero,^{*,†} and Maria Angela Pellinghelli[⊥]

Departamento de Química Inorgánica, Orgánica y Bioquímica, Facultad de Químicas, Campus Universitario, Universidad de Castilla-La Mancha, 13071-Ciudad Real, Spain, Laboratoire de Chimie de Coordination du CNRS, 205, route de Narbonne, 31077 Toulouse Cedex, France, Departamento de Química Inorgánica, Campus Universitario, Universidad de Alcalá, 28871-Alcalá de Henares, Spain, Departamento de Química Inorgánica, Instituto de Ciencia de Materiales de Aragón, Universidad de Zaragoza-CSIC, E-50009 Zaragoza, Spain, and Dipartimento di Chimica Generale ed Inorganica, Chimica Analitica, Chimica Fisica, Università degli Studi di Parma, Centro di Studio per la Strutturistica Diffraattometrica del CNR, Viale delle Scienze 78, I-43100 Parma, Italy

Received September 27, 1994[⊗]

The reactions of $\text{Nb}(\text{C}_5\text{H}_4\text{SiMe}_3)_2\text{H}(\text{CO})$ (**2**) with $[\text{Cu}(\text{MeCN})_4]\text{BF}_4$, $\text{CuPPh}_3\text{Cl}/\text{TIPF}_6$, AgBF_4 , $\text{AgPPh}_3\text{Cl}/\text{TIPF}_6$, and $\text{Au}(\text{THT})\text{Cl}/\text{TIPF}_6$ lead to the new adducts $[\{\text{Nb}(\text{C}_5\text{H}_4\text{SiMe}_3)_2(\text{CO})\}_2(\mu\text{-H})_2\text{M}]^+$ ($\text{M} = \text{Cu}$ (**3**), Ag (**4**, **5**), Au (**6**)), in which the coinage metal cation is only linked to the hydride of each niobium center, whereas the reaction with $[\text{Au}(\text{PPh}_3)]^+$ leads to $[\{\text{Nb}(\text{C}_5\text{H}_4\text{SiMe}_3)_2(\text{CO})\}(\mu\text{-H})\text{Au}(\text{PPh}_3)]\text{PF}_6$ (**7**). The crystal structure of **3** has been determined by X-ray diffraction methods. The crystals are monoclinic, space group $P2_1/c$, with $Z = 4$ in a unit cell of dimensions $a = 13.048(5)$ Å, $b = 12.490(4)$ Å, $c = 30.131(9)$ Å, $\beta = 94.52(2)^\circ$. The structure has been solved from diffractometer data by Patterson and Fourier methods and refined by blocked full-matrix least squares on the basis of 3001 observed reflections to R and R_w values of 0.0460 and 0.0608, respectively.

Introduction

Bis(cyclopentadienyl)niobium hydride derivatives have long been of interest for both their high reactivity and their spectroscopic properties.¹ Thus, the NMR properties of Cp_2NbH_3 were known to be anomalous for a long time² until they were recognized as due to exchange couplings.³ By varying the electronic density on the metal using trimethylsilyl substituents on the cyclopentadienyl ring, we were able to produce new compounds displaying large, temperature-dependent exchange couplings.⁴ In the course of our studies on the origin of these couplings, we reacted a series of bis(cyclopentadienyl)niobium trihydride derivatives with coinage element cations, namely "Cu⁺", "Ag⁺",⁵ and "Au⁺",⁶ with the purpose of inhibiting the in-plane deformation mode of the central Nb–H bonds. This vibration was first assumed to be at the origin of the

tunneling phenomenon responsible for the appearance of the exchange couplings.^{7,8} However, instead of the expected inhibition, a strong increase of the couplings was observed in the case of the reaction with "Au⁺".⁶

An alternative model to explain these couplings was to involve rotational tunneling of dihydrogen in a thermally accessible dihydrogen state.⁹ In the case of the coinage element adducts of niobium trihydrides, such a proposal would imply that only one hydride would remain firmly bound to the coinage cation while the two other would form a dihydrogen molecule. In order to test this hypothesis, we describe in this paper the substitution of two hydrides by a molecule of carbon monoxide and the synthesis of new coinage element adducts as well as the crystal structure of the new copper adduct $[\{\text{Nb}(\text{C}_5\text{H}_4\text{SiMe}_3)_2(\text{CO})\}_2(\mu\text{-H})_2\text{Cu}]\text{PF}_6$. Adducts involving copper, silver, and gold with transition metal polyhydrides are known,¹⁰ and several examples where only one hydride links a coinage element to a transition metal have been reported, for example in the adducts $[(\text{PPh}_3)_3\text{H}_2\text{Ir}(\mu\text{-H})\text{MPR}_3]^+$ ($\text{M} = \text{Ag}, \text{Au}$;

[†] Universidad de Castilla-La Mancha.

[‡] Laboratoire de Chimie de Coordination du CNRS.

[§] Universidad de Alcalá.

^{||} Universidad de Zaragoza.

[⊥] Università degli Studi di Parma.

[⊗] Abstract published in *Advance ACS Abstracts*, February 1, 1995.

(1) (a) Tebbe, F. N.; Parshall, G. W. *J. Am. Chem. Soc.* **1971**, *93*, 3793. (b) Klabunde, U.; Parshall, G. W. *J. Am. Chem. Soc.* **1972**, *94*, 9081. (c) Tebbe, F. N. *J. Am. Chem. Soc.* **1973**, *95*, 5412.

(2) (a) Labinger, J. A. In *Comprehensive Organometallic Chemistry*; Wilkinson, G.; Stone, F. G. A.; Abel, E. X., Eds.; Pergamon Press: Oxford, U.K., 1983; Vol. 3, p 707. (b) Curtis, M. D.; Bell, L. G.; Butler, W. *Organometallics* **1985**, *4*, 701.

(3) Heinekey, D. M. *J. Am. Chem. Soc.* **1991**, *113*, 6074.

(4) Antiñolo, A.; Chaudret, B.; Commenges, G.; Fajardo, M.; Jalon, F.; Morris, R. H.; Otero, A.; Schweitzer, C. T. *J. Chem. Soc., Chem. Commun.* **1988**, 211.

(5) Antiñolo, A.; Carrillo, F.; Fernandez-Baeza, J.; Otero, A.; Fajardo, M.; Chaudret, B. *Inorg. Chem.* **1992**, *31*, 5156.

(6) Antiñolo, A.; Carrillo, F.; Chaudret, B.; Fajardo, M.; Fernandez-Baeza, J.; Lanfranchi, M.; Limbach, H.-H.; Maurer, M.; Otero, A.; Pellinghelli, M. A. *Inorg. Chem.* **1994**, *33*, 5163.

(7) (a) Zilm, K. W.; Heinekey, D. M.; Millar, J. M.; Payne, N. G.; Demou, P. *J. Am. Chem. Soc.* **1989**, *111*, 3088. (b) Zilm, K. W.; Heinekey, D. M.; Millar, J. M.; Payne, N. G.; Neshyba, S. P.; Duchamp, J. C.; Szczyrba, J. *J. Am. Chem. Soc.* **1990**, *112*, 92.

(8) Jones, D.; Labinger, J. A.; Weitekamp, D. P. *J. Am. Chem. Soc.* **1989**, *111*, 3087.

(9) Limbach, H.-H.; Maurer, M.; Scherer, G.; Chaudret, B. *Angew. Chem., Int. Ed. Engl.* **1992**, *31*, 1369.

(10) See for example: (a) Venanzi, L. M. *Coord. Chem. Rev.* **1982**, *43*, 251. (b) Rhodes, F. L.; Huffman, J. C.; Caulton, K. G. *Inorg. Chim. Acta* **1992**, *198*, C39.

R = Et, Ph).¹¹ Bimetallic complexes involving a carbonylniobium complex such as $\text{Cp}_2(\text{CO})\text{Nb}(\mu\text{-H})\text{M}(\text{CO})_x$ (M = Fe, $x = 4$;¹² M = Ni, $x = 3$)¹³ have also been reported.

Results and Discussion

Preparation of the Adducts. The reaction of Nb($\text{C}_5\text{H}_4\text{SiMe}_3$)₂H₃ (**1**) with 1 atm of CO in THF at 65 °C for 3 h yields the carbonyl complex Nb($\text{C}_5\text{H}_4\text{SiMe}_3$)₂H(CO) (**2**).¹⁴ **2** was isolated and was reacted in situ with a variety of salts of coinage elements, namely [Cu(MeCN)₄BF₄]¹⁵ "Cu(PPh₃)PF₆" prepared in situ by reacting Cu(PPh₃)Cl¹⁶ with TlPF₆ in THF, AgBF₄, "Ag(PPh₃)PF₆" prepared in situ by reacting Ag(PPh₃)Cl¹⁷ with TlPF₆, and "Au(L)PF₆" prepared in situ by reacting Au(L)Cl (L = PPh₃,¹⁸ THT¹⁹) with TlPF₆.

The reactions with the copper salts are rapid in THF at 0 °C and yield orange solutions from which, after workup and recrystallization from THF/Et₂O, red crystals of [$\{\text{Nb}(\text{C}_5\text{H}_4\text{SiMe}_3)_2(\text{CO})\}_2(\mu\text{-H})_2\text{Cu}\}]\text{PF}_6$ (**3**) were obtained in ca. 90% yield. Interestingly, **3** is air stable for several days in the solid state but decomposes slowly in solution even in the absence of air. Similarly, both silver complexes react rapidly with **2** in THF at 0 °C to give after a similar procedure red microcrystalline compounds identified as [$\{\text{Nb}(\text{C}_5\text{H}_4\text{SiMe}_3)_2(\text{CO})\}_2(\mu\text{-H})_2\text{Ag}\}]\text{X}$ (X = BF₄, **4**; X = PF₆, **5**). The behavior of **4** and **5** with air and in solution is similar to that of **3**. The two gold reagents react differently with **2**. Hence, the reaction with "Au(THT)PF₆" produces at 0 °C in THF the trinuclear species [$\{\text{Nb}(\text{C}_5\text{H}_4\text{SiMe}_3)_2(\text{CO})\}_2(\mu\text{-H})_2\text{Au}\}]\text{PF}_6$ (**6**), whereas that with "Au(PPh₃)PF₆" under the same conditions yields [$\{\text{Nb}(\text{C}_5\text{H}_4\text{SiMe}_3)_2(\text{CO})\}(\mu\text{-H})(\text{AuPPh}_3)\text{PF}_6$] (**7**). **6** and **7** are again air stable in the solid state.

Spectroscopic Characterization of Complexes 3–7. Complexes **3–7** show a ν_{CO} absorption near 1900 cm⁻¹. Using PF₆⁻ as counteranion, the exact values are 1900 cm⁻¹ for **3**, 1917 cm⁻¹ for **5**, 1932 cm⁻¹ for **6**, and 1936 cm⁻¹ for **7**, whereas this band is found at 1910 cm⁻¹ for **2**. This variation is at first sight surprising, since the electrophilicity is expected to decrease from Cu⁺ to Au⁺, but using the CO stretching frequency as a probe, the electron density on **3** seems similar to that on **2** and higher than that on **6**. However, this could result both from the bonding interaction found in the X-ray structure (vide infra) between the copper center and the two carbonyl ligands which behave as semibridging and, on the other side, from the better overlap between the niobium and the gold orbitals which could form a direct metal–metal bond. The effect of this bonding would be a decrease of the electron density on niobium. It is interesting to note that this last effect would be in agreement with the observation that exchange couplings are much larger in the gold adducts of niobocene trihydrides than in the copper adducts.

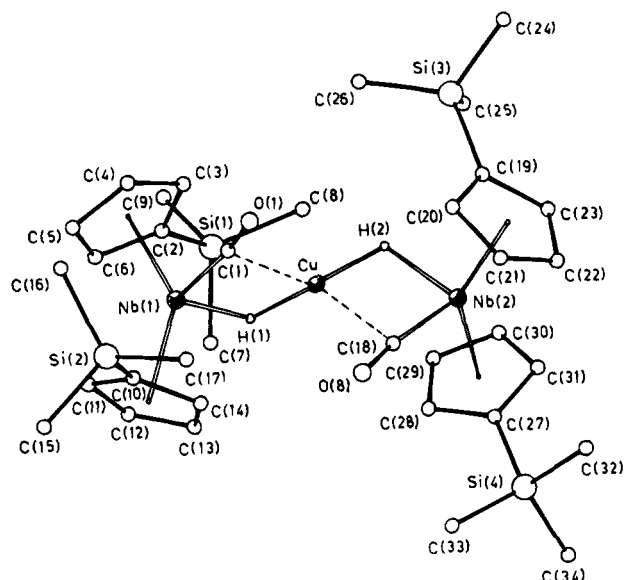


Figure 1. View of the structure of the cationic complex **3** with the atomic labeling scheme.

The ¹H NMR spectra of **3–7** all show a singlet near 0.24 ppm for the SiMe₃ group and several signals between 5 and 6 ppm for the cyclopentadienyl protons. In particular, complexes **3** and **4,5** show four signals, respectively, at 5.91, 5.68, 5.47, and 5.38 ppm and at 5.88, 5.59, 5.42, and 5.35 ppm. The two downfield signals are attributed to the protons in positions 3 and 4 on the Cp ring, whereas the two upfield ones are attributed to protons 2 and 5. The observation of four signals for each Cp ring indicates a lack of symmetry for the structure. In the gold complexes, protons 2 and 5 resonate at the same frequency, respectively 5.36 (**6**) and 5.46 (**7**) ppm. The bridging hydride is observed at δ -7.67 in **3**, -7.10 in **4** and **5**, -3.75 in **6**, and -5.62 in **7**. In addition **4** and **5** show a coupling to silver ($J_{\text{H-Ag}} = 101$ Hz: the signals are broad; therefore, the two different couplings to ¹⁰⁷Ag and ¹⁰⁹Ag are not resolved) and **7** shows a coupling to phosphorus ($J_{\text{H-P}} = 77.1$ Hz). It is difficult to deduce any structural information from these chemical shift variations except perhaps that in **3–5** the hydride lies close to niobium, whereas in **6** it is slightly further away in agreement with a stronger coordination to gold.

These data all agree with a structure involving a coinage metal cation linked to the hydride of two different niobium moieties in the case of **3–6**, whereas **7** would only contain one niobium moiety linked to a "(AuPPh₃)⁺" fragment. The nature of this bonding and the geometry around the coinage cation are, however, not known, which led us to carry out an X-ray crystal structure determination for **3**.

Description of the X-ray Structure of [C₃₄H₅₄CuO₂Nb₂Si₄]⁺PF₆⁻C₄H₉O (3**).** In the crystals of **3**, heterotrinary cationic complexes—formed by two "Nb^{III}(C₅H₄SiMe₃)₂(CO)" moieties linked to a Cu(I) atom through two bridging hydride ligands—PF₆⁻ anions, and THF molecules of solvation are present. The structure of the cation is depicted in Figure 1 together with the atomic numbering scheme; the most important bond distances and angles are given in Table 1 and the atomic coordinates for all non-hydrogen atoms appear in Table 2. To the best of our knowledge, complex **3** represents the first structurally characterized compound containing niobium and copper simultaneously in a molecule.

(11) Albinati, A.; Eckert, J.; Hoffmann, P.; Ruegger, H.; Venanzi, L. M. *Inorg. Chem.* **1993**, *32*, 2377.

(12) Wong, K. S.; Scheidt, W. R.; Labinger, J. A. *Inorg. Chem.* **1979**, *18*, 136.

(13) Skripkin, Y. V.; Paoyuskii, A. A.; Kaliunikov, V. T.; Porai-Koshits, M. A.; Minachova, L. K.; Autsyshkina, A. S.; Ostrikova, V. N. *J. Organomet. Chem.* **1982**, *231*, 205.

(14) Antiñolo, A.; Fajardo, M.; Jalon, F.; Lopez-Mardomingo, C.; Otero, A.; Sanz-Bernabe, C. *J. Organomet. Chem.* **1989**, *369*, 187.

(15) Kubas, G. J. *Inorg. Synth.* **1989**, *19*, 90.

(16) Hall, K. P.; Mingos, D. M. P. *Inorg. Chem.* **1984**, *32*, 237.

(17) Hoffman, R. *Angew. Chem., Int. Ed. Engl.* **1982**, *21*, 711.

(18) Know, S. A. R.; Stone, F. G. A. *J. Chem. Soc. A* **1969**, 2559.

(19) Uson, R.; Laguna, A.; Laguna, M. *Inorg. Synth.* **1989**, *26*, 86.

Table 1. Selected Bond Distances (Å) and Angles (deg) with Esd's in Parentheses for Compound 3^a

Nb(1)–CE(1)	2.064(12)	Cu–C(1)	2.351(13)
Nb(1)–CE(2)	2.061(11)	Cu–C(18)	2.510(13)
Nb(1)–Cu	2.700(2)	C(1)–O(1)	1.146(17)
Nb(1)–C(1)	2.072(15)	C(18)–O(2)	1.146(17)
Nb(2)–CE(3)	2.058(13)	Nb(1)–H(1)	1.83(12)
Nb(2)–CE(4)	2.070(14)	Nb(2)–H(2)	1.95(12)
Nb(2)–Cu	2.732(2)	Cu–H(1)	1.86(11)
Nb(2)–C(18)	2.048(14)	Cu–H(2)	1.54(12)
CE(1)–Nb(1)–CE(2)	137.3(4)	C(1)–Cu–C(18)	96.0(5)
CE(1)–Nb(1)–C(1)	103.5(5)	C(1)–Cu–H(1)	90(4)
CE(2)–Nb(1)–C(1)	107.7(5)	C(1)–Cu–H(2)	134(5)
CE(1)–Nb(1)–H(1)	101(3)	C(18)–Cu–H(1)	133(3)
CE(2)–Nb(1)–H(1)	101(4)	C(18)–Cu–H(2)	89(4)
C(1)–Nb(1)–H(1)	101(4)	H(1)–Cu–H(2)	119(6)
CE(3)–Nb(2)–CE(4)	140.9(5)	CE(5)–Cu–H(1)	122(3)
CE(3)–Nb(2)–C(18)	102.2(6)	CE(5)–Cu–H(2)	119(4)
CE(4)–Nb(2)–C(18)	105.7(6)	Nb(1)–C(1)–O(1)	173.4(12)
CE(3)–Nb(2)–H(2)	104(3)	Nb(2)–C(18)–O(2)	172.2(12)
CE(4)–Nb(2)–H(2)	101(3)	Nb(1)–H(1)–Cu	94(5)
C(18)–Nb(2)–H(2)	94(4)	Nb(2)–H(2)–Cu	102(6)
Nb(1)–Cu–Nb(2)	167.1(1)		

^a CE(1), CE(2), CE(3), and CE(4) are the centroids of the C(2), ..., C(6), C(10), ..., C(14), C(19), ..., C(23), and C(27), ..., C(31) rings, respectively, and CE(5) is the midpoint of C(1)–C(18).

The metal coordination description obviously requires positioning of the light hydride atoms. These two ligands were clearly in evidence in the final ΔF map and were refined as free isotropic atoms (an indirect location by means of a "potential energy" technique validated this assignment²⁰). The resultant coordination sphere around the two independent niobium atoms may be described as distorted tetrahedral with very similar bond distances and angles about both metals. In each niobium center the two Cp' rings are almost eclipsed with the bulky SiMe₃ groups *pseudo-trans* to each other. The intermetallic separations Nb–Cu, 2.700(2) and 2.732(2) Å, are slightly longer than the sum of the atomic radii (~2.67 Å) and are analogous to those reported in related Mo–Cu complexes also containing linear semibridging carbonyls (Mo–Cu ≈ 2.721 Å), where the existence of a direct metal–metal bond has been proposed.²¹ However, only the Nb–Cu distance should not be considered conclusive to assign the presence of the metal–metal bond (see below). The arrangement of the three metals is essentially linear (Nb(1)–Cu–Nb(2) = 167.1(1)°). The two μ -hydride atoms form around the Cu^I atom an angle of 119(6)°.

The most intriguing geometrical features of the structure are the two short intramolecular distances observed between the copper atom and the two supposedly terminal carbonyls (Cu–C(1) = 2.351(13) Å and Cu–C(18) = 2.510(13) Å).²² These Cu–C distances clearly suggest the presence of a bonding interaction between the copper atom and the carbonyls, conferring to these ligands a semibridging character. Interestingly, however, this interaction does not modify the linearity of the carbonyl groups (Nb–C–O angles 173.4(12) and 172.2(12)°), which places this complex among the rare group of compounds containing linear semibridging carbonyls.²³ According to the geometrical parameters and electronic characteristics of the metals, 3

Table 2. Atomic Coordinates ($\times 10^4$) and Isotropic Thermal Parameters ($\text{\AA}^2 \times 10^4$) with Esd's in Parentheses for the Non-Hydrogen Atoms of Compound 3

atom	<i>x/a</i>	<i>y/b</i>	<i>z/c</i>	<i>U</i>
Nb(1)	2594(1)	1297(1)	430(1)	381(4) ^a
Nb(2)	2327(1)	3955(1)	1828(1)	401(4) ^a
Cu	2693(1)	2595(1)	1149(1)	519(6) ^a
Si(1)	4023(3)	-541(3)	1273(1)	608(14) ^a
Si(2)	1170(3)	2738(3)	-562(2)	663(16) ^a
Si(3)	5270(3)	4321(3)	1833(2)	670(16) ^a
Si(4)	-491(3)	4328(3)	2088(2)	669(16) ^a
O(1)	3149(7)	3790(8)	335(3)	768(42) ^a
O(2)	915(7)	4285(8)	927(4)	851(45) ^a
C(1)	2931(9)	2915(12)	395(4)	529(50) ^a
C(2)	3957(8)	153(9)	711(4)	443(43) ^a
C(3)	4393(8)	1166(10)	616(5)	535(49) ^a
C(4)	4249(9)	1338(13)	150(5)	670(58) ^a
C(5)	3752(9)	447(12)	-43(5)	617(54) ^a
C(6)	3573(8)	-275(11)	309(5)	528(48) ^a
C(7)	2767(11)	-1152(12)	1359(6)	935(73) ^a
C(8)	4458(12)	473(12)	1716(5)	912(71) ^a
C(9)	5005(12)	-1612(12)	1257(6)	1062(84) ^a
C(10)	1196(8)	1756(10)	-92(5)	485(48) ^a
C(11)	1359(8)	632(10)	-114(5)	506(48) ^a
C(12)	1128(9)	182(12)	296(5)	635(58) ^a
C(13)	821(8)	962(13)	559(5)	652(56) ^a
C(14)	885(8)	1939(11)	342(4)	516(50) ^a
C(15)	110(11)	2340(15)	-977(5)	1054(81) ^a
C(16)	2404(11)	2755(13)	-833(6)	936(74) ^a
C(17)	864(13)	4060(12)	-341(6)	1080(85) ^a
C(18)	1465(9)	4114(10)	1234(5)	556(50) ^a
C(19)	3946(9)	4894(10)	1844(4)	497(47) ^a
C(20)	3283(10)	5261(10)	1484(5)	651(59) ^a
C(21)	2449(10)	5800(10)	1659(6)	681(63) ^a
C(22)	2539(11)	5722(11)	2113(7)	807(73) ^a
C(23)	3468(10)	5174(10)	2241(5)	677(58) ^a
C(24)	6150(10)	5470(12)	1971(6)	944(76) ^a
C(25)	5487(12)	3230(11)	2236(6)	980(79) ^a
C(26)	5415(11)	3843(13)	1269(5)	1003(77) ^a
C(27)	745(8)	3544(9)	2137(4)	476(46) ^a
C(28)	1021(10)	2609(10)	1897(5)	579(52) ^a
C(29)	1916(12)	2183(11)	2096(6)	756(70) ^a
C(30)	2247(11)	2791(13)	2455(5)	729(64) ^a
C(31)	1537(10)	3644(11)	2478(4)	587(50) ^a
C(32)	-237(12)	5769(12)	2169(7)	1137(90) ^a
C(33)	-1157(11)	4131(15)	1549(5)	1024(79) ^a
C(34)	-1267(12)	3794(16)	2519(6)	1357(98) ^a
P	7893(3)	770(4)	1424(1)	810(16) ^a
F(1)	7188(9)	74(10)	1712(4)	1589(41)
F(2)	8539(11)	1095(12)	1876(5)	2029(55)
F(3)	8670(10)	1410(11)	1159(4)	1761(47)
F(4)	7305(14)	433(15)	1002(6)	2581(75)
F(5)	7209(11)	1708(12)	1435(5)	1994(55)
F(6)	8621(13)	-199(15)	1417(6)	2484(72)
O(3)	7975(12)	2351(13)	4761(6)	1726(56)
C(35)	8152(16)	2251(18)	5228(7)	1633(83)
C(36)	7192(17)	1816(19)	5382(7)	1722(89)
C(37)	6533(15)	1538(17)	4956(7)	1394(70)
C(38)	7226(14)	1615(16)	4630(7)	1302(65)

^a Equivalent isotropic *U*, defined as one-third of the trace of the orthogonalized U_{ij} tensor.

should be included in type III of Crabtree's recent classification of semibridging linear carbonyls,²³ which are characterized by the presence of a metal not known to form stable carbonyls (Cu in 3). Considering these Cu–CO bonding interactions, the geometry around the Cu atom could be described as flattened distorted tetrahedral ($\tau[H(1)CuH(2)|cpC(1)CuC(18)] = 123(4)^\circ$). The Cu, H(1), Nb(1), and C(1) atoms are coplanar (maximum deviation 0.10(11) Å for H(1)), as are the Cu, H(2), Nb(2), and C(18) atoms (maximum deviation 0.32(11) Å for H(2)). The dihedral angle between the two planes is 119.2(4)°.

In summary, the most astonishing aspect of this structural determination is that copper is only bound to two hydrides, while the short intramolecular Cu–C

(20) Orpen, A. G. *J. Chem. Soc., Dalton Trans.* **1980**, 2509.

(21) Sargent, A. L.; Hall, M. B. *J. Am. Chem. Soc.* **1989**, *111*, 1563.

(22) Typical values of direct Cu–CO bonds lie between 1.75 and 1.78 Å: Itajima, N. K.; Fujisawa, K.; Fujimoto, C.; Moro-Oka, Y.; Hashimoto, S.; Kitagawa, T.; Toriumi, K.; Tatsumi, K.; Nakamura, A. *J. Am. Chem. Soc.* **1992**, *114*, 1277.

(23) Crabtree, R. H.; Lavin, M. *Inorg. Chem.* **1986**, *25*, 805.

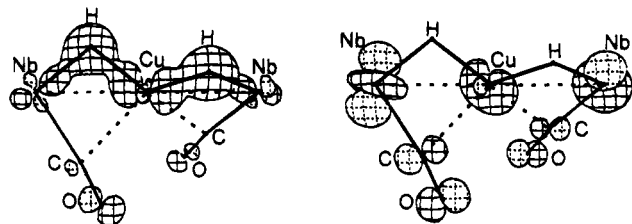


Figure 2. Representation of two MO bonding orbitals (see text). Cyclopentadienyl ligands have been omitted for clarity.

distances, together with the *pseudo*-tetrahedral geometry around copper, suggest a weak interaction between copper and the carbon of the carbonyl groups linked to niobium. Unfortunately, although we have attempted to visualize the presence of such interactions by ^{13}C NMR, with the exception of **7**, all complexes decomposed at least partially in solution during the experiments.

In an attempt to obtain a deeper understanding of the peculiar bridging bonding system in this complex, a theoretical analysis based on extended Hückel MO calculations has been carried out with the CACAO program.²⁴ For this purpose we have used a model based on the crystallographic coordinates of the molecule but changed the $\text{C}_5\text{H}_4\text{Si}(\text{CH}_3)_3$ ligands into ideal C_5H_5 rings for the sake of simplicity. Using the fragment molecular orbital analysis (FMO), we have built up the $[\{\text{Cp}_2\text{Nb}(\text{CO})\text{H}\}_2\text{Cu}]^+$ molecule with two "Cp₂-Nb(CO)H" fragments plus a Cu(I) atom. Each of the Nb fragments present two filled orbitals revealed to be important in our study: the HOMO, formed by a Nb d-type orbital plus a π^* carbonyl orbital in a bonding arrangement ($\pi_{\text{Nb-CO}}$), and the bonding interaction between the niobium and the hydride ligand ($\sigma_{\text{Nb-H}}$). These two orbitals also have weak contributions from the Cp rings, but these we found to be insignificant in our analysis.

In the whole molecule, we can observe the in-phase and out-of-phase combinations of these two orbitals ($\pi_{\text{Nb-CO}}$ and $\sigma_{\text{Nb-H}}$) interacting with those of the copper atom. The stronger interactions are formed by the in-phase and out-of-phase combinations of the $\sigma_{\text{Nb-H}}$ orbitals of the $\text{Cp}_2\text{Nb}(\text{CO})\text{H}$ fragments with the Cu atom, developing two clear intermetallic bridging hydrides. The in-phase bonding orbital is represented in Figure 2 (left side). These hydrides are linked to the metals in a slightly asymmetric manner, as indicated by the Mulliken population calculated for these four bonds: Nb-H = 0.514 and 0.483; Cu-H = 0.171 and 0.207, showing a stronger interaction with the Nb center.

The two noticeable remaining interactions correspond to the combinations of the two filled $\pi_{\text{Nb-CO}}$ orbitals (in-phase and out-of-phase) with the valence shell orbitals of the central Cu atom, forming two three-center-two-electron interactions between the niobium, the carbonyl carbon, and the copper atom. Similar models have been proposed to explain the bonding situation in related linear semibridging carbonyls.²⁵ Interestingly, the two HOMO's of the whole molecule are the corresponding bonding orbitals of this interaction ($\pi_{\text{Nb-CO-Cu}}$ orbitals), one of which is also depicted in Figure 2 (right side). The Mulliken populations calculated between the atoms involved in these interactions are Nb-C = 0.809 and

0.832, Nb-Cu = 0.172 and 0.182, and Cu-C = 0.130 and 0.079. Due to these facts, only a weak direct niobium-copper interaction could be suggested, in spite of the intermetallic separation observed, and consequently the stabilization of the trinuclear complex is fundamentally due to the bridging ligands: hydrides and the linear semibridging carbonyls.

Referring to the controversy on the donor/acceptor nature of the linear semibridging carbonyl groups,²⁶ we can state that in **3** the niobium-carbonyl fragment—as a whole—is donating electron density to the highly acidic metal, as the charge on the Cu atom was observed to increase when the fragment is moved away from the proximity of the Cu atom by opening the angle Cu-H-Nb while the Cu-H distance is kept constant.

Besides the d-type copper orbitals, the s and p orbitals also make significant contributions to the aforementioned interactions, but only for the s and, to a lesser extent one p orbital is this clear-cut. The electron populations in these four atomic orbitals, from the Mulliken analysis, are 0.637, 0.148, 0.055, and 0.040 for the s and p orbitals, respectively, with a total calculated charge for the Cu(I) atom of 0.267. Therefore, we can conclude that the copper atom is receiving electron density through four molecular orbitals, in a *pseudo*-tetrahedral environment, using up to, but not all, four initially empty atomic orbitals. This means that the copper is linked by four bonding interactions through the bridging ligands (hydrides and carbonyls) but clearly not by four bonds of bond order 1, which is also in good agreement with the geometrical data. Unfortunately, the lack of symmetry in this compound makes a more detailed explanation difficult.

In conclusion, we describe in this paper the preparation of a new series of adducts of $\text{Nb}(\text{C}_5\text{H}_4\text{SiMe}_3)_2\text{H}(\text{CO})$ with coinage element cations. The most important result of this study is that the formation of the adducts essentially involves binding of the hydride of a niobium moiety to the Lewis acidic cation. In addition, a weak interaction between the Lewis acid and CO is present, at least in the copper case. A similar type of bonding was recently proposed to explain the NMR properties of adducts of Cp_2NbH_3 (Cp = C_5H_5 , $\text{C}_5\text{H}_4\text{SiMe}_3$, $\text{C}_5\text{H}_3(\text{SiMe}_3)_2$) with M^+ (M = Cu,⁵ Ag,⁵ Au⁶). This study shows that such a bonding can indeed exist, at least in the case of hydrido carbonyl derivatives.

Experimental Section

General Procedures. All manipulations were performed under an inert atmosphere of dry nitrogen or argon using standard Schlenk-tube techniques. Solvents were purified by distillation from appropriate drying agents and degassed before use.

The complexes $\text{Nb}(\text{C}_5\text{H}_4\text{SiMe}_3)_2\text{H}_3$ and $\text{Nb}(\text{C}_5\text{H}_4\text{SiMe}_3)_2\text{H}(\text{CO})$ were prepared as described earlier.^{1,2} $[\text{Cu}(\text{MeCN})_4]\text{BF}_4$, $[\text{CuPPh}_3\text{Cl}]_4$, $[\text{AgPPh}_3\text{Cl}]_4$, AuPPh_3Cl , and $\text{Au}(\text{THT})\text{Cl}$ were prepared according to known procedures.¹⁵⁻¹⁹ Other reagents were used as purchased. NMR spectra were obtained on a Varian Unity FT-300 instrument. IR spectra were recorded as Nujol mulls between CsI plates (in the region between 4000 and 200 cm^{-1}) on a Perkin-Elmer PE883 IR spectrophotometer. Elemental analyses were performed on a Perkin-Elmer 2400 microanalyzer.

$[\{\text{Nb}(\text{C}_5\text{H}_4\text{SiMe}_3)_2(\text{CO})(\mu\text{-H})\}_2\text{M}]\text{X}$ (M = Cu, X = PF_6 (**3**); M = Ag, X = BF_4 (**4**), PF_6 (**5**); M = Au, X = PF_6 (**6**)). A THF

(24) Mealli, C.; Proserpio, D. M. *J. Chem. Educ.* **1990**, *67*, 399.

(25) Morris-Sherwood, B. J.; Powell, C. B.; Hall, M. B. *J. Am. Chem. Soc.* **1984**, *106*, 5079.

(26) Simpson, C. Q., II; Hall, M. B. *J. Am. Chem. Soc.* **1992**, *114*, 1641 and references therein.

solution of $CuPPh_3PF_6$ (0.40 mmol), prepared "in situ" by reaction of $[CuPPh_3Cl_4]$ (300 mg, 0.10 mmol) with $TlPF_6$ (150 mg, 0.40 mmol) (the precipitate of $TlCl$ was eliminated by filtration) was added to a THF solution (30 mL) of $Nb(C_5H_4SiMe_3)_2H(CO)$ (0.81 mmol) at 0 °C. After the mixture was stirred for 15 min, an orange solution with a precipitate was obtained, which was filtered, and the solvent was removed in vacuo. The solid was washed with diethyl ether and then extracted with a mixture of THF and Et_2O (1:1). Complex **3** was isolated on cooling as red crystalline needles (92% yield). **3** was similarly prepared using $[Cu(MeCN)_4]BF_4$ as precursor. Complexes **4–6** were prepared using $AgBF_4$, $AgPPh_3PF_6$, and $Au(THT)PF_6$, respectively, as red crystalline needles (61% yield) for **4** and **5** and brown crystals (94% yield) for **6**, by a procedure similar to that described for **3**. In the reaction with $AuPPh_3PF_6$, the complex $[[Nb(C_5H_4SiMe_3)_2(CO)(\mu-H)](AuPPh_3)]PF_6$ (**7**) was obtained as deep orange crystalline needles (91% yield).

3: IR (Nujol) ν_{CO} 1900 cm^{-1} , ν_{PF_6} 840 cm^{-1} ; 1H NMR (CD_3COCD_3 , in ppm, referenced to TMS) δ -7.67 (s, 2H, H), 0.26 (s, 36H, SiMe₃), 5.38 (4H), 5.47 (4H), 5.68 (4H), 5.91 (4H) (16H, $C_5H_4SiMe_3$). Anal. Calcd for $C_{34}H_{54}O_2Si_4PNb_2CuF_6$: C, 40.8; H, 5.4. Found: C, 40.5; H, 5.3.

4: IR (Nujol) ν_{CO} 1920 cm^{-1} , ν_{BF_4} 1030 cm^{-1} ; 1H NMR (CD_3COCD_3 , in ppm, referenced to TMS): δ -7.10 (d, $J_{HA_g} = 101$ Hz, 2H, $\mu-H$), 0.27 (s, 36H, SiMe₃), 5.35 (4H), 5.41 (4H), 5.59 (4H), 5.88 (4H) (16H, $C_5H_4SiMe_3$). Anal. Calcd for $C_{34}H_{54}O_2Si_4BNb_2AgF_4$: C, 41.3; H, 5.5. Found: C, 41.4; H, 5.5.

5: IR (Nujol) ν_{CO} 1917 cm^{-1} , ν_{PF_6} 840 cm^{-1} ; 1H NMR (CD_3COCD_3 , in ppm, referenced to TMS): δ -7.10 (d, $J_{HA_g} = 101$ Hz, 2H, $\mu-H$), 0.26 (s, 36H, SiMe₃), 5.35 (4H), 5.41 (4H), 5.59 (4H), 5.88 (4H) (16H, $C_5H_4SiMe_3$). Anal. Calcd for $C_{34}H_{54}O_2Si_4PNb_2AgF_6$: C, 41.3; H, 5.5. Found: C, 41.2; H, 5.3.

6: IR (Nujol) ν_{CO} 1932 cm^{-1} , ν_{PF_6} 840 cm^{-1} ; 1H NMR (CD_3COCD_3 , in ppm, referenced to TMS) δ -3.75 (s, 2H, $\mu-H$), 0.26 (s, 36H, SiMe₃), 5.36 (8H), 5.74 (4H), 5.84 (4H) (16H, $C_5H_4SiMe_3$). Anal. Calcd for $C_{34}H_{54}O_2Si_4PNb_2AuPF_6$: C, 35.5; H, 4.6. Found: C, 35.4; H, 4.6.

7: IR (Nujol) ν_{CO} 1936 cm^{-1} , ν_{PF_6} 840 cm^{-1} ; 1H NMR (CD_3COCD_3 , in ppm, referenced to TMS) δ -5.62 (d, $J_{HP} = 77.1$ Hz, 1H, $\mu-H$), 0.25 (s, 18H, SiMe₃), 5.64 (4H), 5.99 (2H), 6.00 (2H) (8H, $C_5H_4SiMe_3$). Anal. Calcd for $C_{25}H_{42}Si_2NbOAU_2P_2F_6$: C, 41.9; H, 4.6. Found: C, 41.4; H, 4.6.

X-ray Data Collection, Structure Determination, and Refinement for $[[Nb(C_5H_4SiMe_3)_2(CO)]_2(\mu-H)_2Cu]PF_6 \cdot C_4H_8O$ (3**).** A single crystal of **3** was sealed in a Lindemann capillary under dry nitrogen and used for data collection. The crystallographic data are summarized in Table 3. Unit cell parameters were determined from the θ values of 25 carefully centered reflections, having $10 < \theta < 16^\circ$. Data ($3 < \theta < 27^\circ$) were collected at 22 °C on Enraf-Nonius CAD4 four-circle single-crystal diffractometer, using the graphite-monochromated Mo K α radiation and the $\omega/2\theta$ scan type. The reflections were collected with a maximum scan speed of 3.3° min⁻¹ and a scan range of 0.80 + 0.35 tan θ (the ω scan area was extended at each side of 25% for background determination). Two standard reflections were monitored every 200 measurements; no significant decay was noticed over the time of data collection. Intensities were corrected for Lorentz and polarization effects. Of 10 604 independent reflections, 3001 having $I \geq 2\sigma(I)$ were considered observed and used in the analysis.

The structure was solved by Patterson and Fourier methods. A THF molecule of solvation was found in the ΔF map. The refinement was carried out first by full-matrix least squares with isotropic thermal parameters and then by blocked full-matrix least squares with anisotropic thermal parameters for all the non-hydrogen atoms of the cation and the P atom of the anion. The two hydrides were well located on a final ΔF map and refined isotropically; all the other hydrogen atoms

Table 3. Crystallographic Data for Compound **3**

mol formula	$[C_{34}H_{54}CuO_2Nb_2Si_4]PF_6 \cdot C_4H_8O$
mol wt	1073.573
cryst syst	monoclinic
space group	$P2_1/c$
radiation	graphite-monochromated Mo K α ($\lambda = 0.710 73 \text{ \AA}$)
<i>a</i> , \AA	13.048(5)
<i>b</i> , \AA	12.490(4)
<i>c</i> , \AA	30.131(9)
β , deg	94.52(2)
<i>V</i> , \AA^3	4895(3)
<i>Z</i>	4
<i>D</i> _{calcd} , g cm ⁻³	1.457
<i>F</i> (000)	2200
cryst dimens, mm	0.16 × 0.18 × 0.20
linear abs (μ), cm ⁻¹	10.76
diffractometer	Enraf-Nonius CAD4
<i>T</i> , °C	22
unique total no. of data	10 604
no. of unique obsd data ($I \geq 2\sigma(I)$)	3001
<i>R</i> ^a	0.0460
<i>R</i> _w ^b	0.0608

$$^a R = \sum ||F_o| - |F_c|| / \sum |F_o|, \quad ^b R_w = [\sum w(|F_o| - |F_c|)^2 / \sum w(F_o)^2]^{1/2}.$$

were placed at their geometrically calculated positions (C–H = 0.96 Å) and refined "riding" on the corresponding carbon atoms. The positions of the hydride ligands were calculated also by minimization of the potential energy of the intramolecular nonbonded interactions involving the two hydrides by using the HYDEX program,²⁰ and they were in good agreement with those found in the final ΔF map. The final cycles of refinement were carried out on the basis of 451 variables; after the last cycles no parameters shifted by more than 0.62 esd. The biggest remaining peak in the final difference map was equivalent to about 0.91 e/Å³. In the final cycles of refinement a weighting scheme, $w = k[\sigma(F_o) + gF_o^2]^{-1}$, was used; at convergence the *k* and *g* values were 0.5929 and 0.0095, respectively. The analytical scattering factors, corrected for the real and imaginary parts of anomalous dispersions, were taken from ref 27. All calculations were carried out on the Gould Povernode 6040 and Encore 91 computers of the "Centro di Studio per la Strutturistica Diffraattometrica" del CNR, Parma, Italy, using the SHELX-86 and SHELX-76 systems of crystallographic computer programs.²⁸ The final atomic coordinates for the non-hydrogen atoms are given in the supplementary material.

Acknowledgment. A.A., F.C., S.G.-Y., M.F., and A.O. gratefully acknowledge financial support from the DGICYT (Grant No. PB 89-0206) of Spain. M.L. and M.A.P. gratefully acknowledge financial support from the Ministero dell'Università e della Ricerca Scientifica e Tecnologica (MURST) and the Consiglio Nazionale delle Ricerche (CNR) (Rome, Italy).

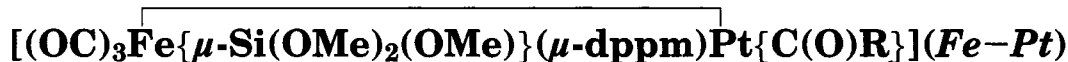
Supplementary Material Available: Hydrogen atom coordinates (Table SI), anisotropic and isotropic thermal parameters for the non-hydrogen atoms (Table SII), complete bond distances and angles (Table SIII), least-squares planes (Table SIV), and complete crystallographic data (Table SV) (14 pages). Ordering information is given on any current masthead page.

OM940750F

(27) *International Tables for X-Ray Crystallography*; Kynoch Press: Birmingham, England, 1974; Vol. IV.

(28) Sheldrick, G. M. SHELXS-86 Program for the Solution of Crystal Structures; University of Göttingen, Göttingen, Germany, 1986. Sheldrick, G. M. SHELX-76 Program for Crystal Structure Determination; University of Cambridge, Cambridge, England, 1976.

Phosphine-Induced Silyl Migration in Heterodinuclear Acyl Complexes



Leading to μ -Siloxycarbene Complexes. Crystal Structure of



Michael Knorr*[†] and Pierre Braunstein*

Laboratoire de Chimie de Coordination, Associé au CNRS (URA 0416), Université Louis Pasteur, 4 rue Blaise Pascal, F-67070 Strasbourg Cedex, France

André DeCian and Jean Fischer

Laboratoire de Cristallochimie et de Chimie Structurale, Associé au CNRS (URA 424), Université Louis Pasteur, 4 rue Blaise Pascal, F-67070 Strasbourg Cédex, France

Received September 28, 1994[®]

Carbon monoxide reacts with the heterodinuclear complexes $[(OC)_3Fe\{\mu-Si(OMe)_2(OMe)\}(\mu-dppm)Pt(R)]$ ($R = Me, Et$) by opening the alkoxysilyl bridge, followed by insertion into the *cis* Pt–alkyl bond to yield the bimetallic acyl complexes $[(OC)_3Fe\{\mu-Si(OMe)_2(OMe)\}(\mu-dppm)Pt\{C(O)R\}]$ (**1a,b**) in which the acyl ligand is *trans* with respect to the metal–metal bond. The driving force for the isomerization of the acyl ligand comes from the tendency to restore the μ -Si–O bridge. Surprisingly, these acyl complexes were not obtained in the reaction of the metalate $K[Fe\{Si(OMe)_3\}(CO)_3(\eta^1-dppm)]$ with *trans*-[PtCl{C(O)R}(PPh₃)₂]; instead the stable μ -siloxycarbene complexes $[(OC)_3Fe\{\mu-C(R)OSi(OMe)_3\}(\mu-dppm)Pt(PPh_3)]$ (**2a**, $R = Me$; **2b**, $R = Et$) were isolated in ca. 75% yield. Similar complexes were obtained in almost quantitative yields from the reaction of **1a** with phosphine or phosphite ligands. The migration of the silyl ligand from iron to the oxygen atom of an acyl ligand bound to the neighboring platinum atom involves silicon–oxygen (acyl) and iron–carbon (acyl) bond formation. The C–O unit found in the carbene ligand stems from the acyl group (¹³C labeling experiment). The phosphorus donor is believed to make the acyl oxygen more electron rich, thus favoring Si migration, and stabilizes the acyl ligand *cis* with respect to the metal–metal bond long enough to allow Si migration to occur. This silyl migration could not be induced by isonitrile ligands although the μ -siloxycarbene complexes $[(OC)_3Fe\{\mu-C(R)OSi(OMe)_3\}(\mu-dppm)Pt(C\equiv NR')]$ (**4a**, $R = Me$, $R' = t-Bu$; **4b**, $R = Et$, $R' = 2,5$ -xylyl) were isolated from the reactions of **2a,b** with the corresponding isonitrile. Cleavage of the C–O bond of **2b** afforded the cationic μ -carbyne complex $[(OC)_3Fe(\mu-CEt)(\mu-dppm)Pt(PPh_3)][CF_3SO_3]$ (**5**). The crystal structure of **2b**·2C₇H₈ has been determined by X-ray diffraction and appears to be the first one for a polymetallic siloxycarbene complex: monoclinic space group $P2_1/c$ with $Z = 4$ in a unit cell of dimensions $a = 11.014(1)$, $b = 21.148(1)$, $c = 26.063(1)$ Å, $\beta = 94.57(2)^\circ$. The structure has been solved from diffractometer data by Patterson and Fourier methods and refined by full-matrix least squares on the basis of 8375 observed reflections ($I > 3\sigma(I)$) to $R(F)$ and $R_w(F)$ values of 0.039 and 0.055.

Introduction

The intramolecular migration of transition metal bound SiR₃ ligands to organic groups has been increas-

ingly studied over the last few years.^{1–23} Such a reactivity of the metal–silicon bond, which may sometimes also be regarded as an insertion of the organic ligand into the metal–silicon bond, plays a key role in some hydrosilation catalytic cycles.^{24–29} We communi-

[†] Present address: Universität des Saarlandes, Anorganische Chemie, D-66041 Saarbrücken, Germany.

[®] Abstract published in *Advance ACS Abstracts*, February 1, 1995.

(1) Aylett, B. J. *Adv. Inorg. Chem. Radiochem.* **1982**, *25*, 1.

(2) Gladysz, J. A. *Acc. Chem. Res.* **1984**, *17*, 326.

(3) Tilley, T. D. In *Transition-metal silyl derivatives*; Patai, S., Rappoport, Z., Eds.; John Wiley, New York, 1991; pp 245.

cated recently the first example of a CO-induced silyl group transfer from one metal center to the adjacent metal in phosphido-bridged Fe–Pt complexes of the type

$[(OC)_3(R_3Si)Fe(\mu-PPh_2)Pt(PPh_3)_2]$. Since this migration is concomitant with CO migration from Pt to Fe, it leads

to the isomeric heterobimetallics $[(OC)_4Fe(\mu-PPh_2)Pt(SiR_3)(PPh_3)]$.³⁰ In related dpmm-bridged Fe–Pt complexes (dpmm = Ph₂PCH₂PPh₂) containing a Pt–alkyl bond trans with respect to the metal–metal bond, facile CO insertion has been found to yield bimetallic acyl

complexes of the type $[(OC)_3Fe\{\mu-Si(OMe)_2(OMe)\}(\mu-dppm)Pt\{C(O)R\}]$ in which the acyl ligand is also situated in the trans position with respect to the metal–metal bond.^{31,32} In the course of these studies, we have observed that migration of a silyl ligand from iron to the neighboring platinum atom could take place and afford in high yields complexes with a bridging siloxycarbene ligand. Very few crystal structures have been reported for siloxycarbene complexes,³³ and that reported below

for $[(OC)_3Fe\{\mu-C(Et)OSi(OMe)_3\}(\mu-dppm)Pt(PPh_3)]$ (**2b**) appears to be the first one in polymetallic chemistry.

Experimental Section

All reactions were performed in Schlenk flasks under purified nitrogen. Solvents were dried and distilled under nitrogen before use (tetrahydrofuran over sodium benzophenone ketyl; toluene, benzene, and hexane over sodium; dichloromethane from P₂O₅). Nitrogen (Air liquide, R-grade) was passed through BASF R3-11 catalyst and molecular sieve columns to remove residual oxygen or water. Elemental C, H, and N analyses were performed by the Service Central de Microanalyses du CNRS. Infrared spectra were recorded in the 4000–400 cm⁻¹ region on Perkin-Elmer 398 and on Bruker IFS 66 spectrophotometers. The ¹H, ³¹P-¹H, and ¹³C-¹H NMR spectra were recorded at 300, 121.5, and 75.5 MHz respectively, on a Bruker AC 300 instrument. Phosphorus chemical shifts were externally referenced to 85% H₃PO₄ in H₂O with downfield chemical shifts reported as positive. ¹⁹⁵Pt chemical shifts were measured on a Bruker AM 400 instrument (85.9 MHz) and externally referenced to K₂PtCl₄ in water with downfield chemical shifts reported as positive. *J* values are reported in hertz. Mass spectra were measured on a

Fisons ZAB-HF spectrometer. The reactions were generally monitored by IR in the ν(CO) region.

$[(OC)_3Fe\{\mu-C(R)OSi(OMe)_3\}(\mu-dppm)Pt(PPh_3)]$ (**2a**, **R** = **Me**; **2b**, **R** = **Et**). **Method A.** A solution of K[Fe(CO)₃{Si(OMe)₃}(dpmm-P)] (0.380 g, 0.55 mmol) in THF (20 mL) was added to a suspension of *trans*-[PtCl{C(O)R}(PPh₃)₂] (0.50 mmol) in THF (5 mL). The reaction mixture was stirred for ca. 24 h during which the sparingly soluble *trans*-[PtCl{C(O)R}(PPh₃)₂] gradually dissolved. The resulting clear orange solution was filtered through Celite and the solvent was removed under reduced pressure. Extraction of the residue with two portions of Et₂O (2 × 20 mL) and addition of hexane to the combined fractions led to the precipitation of **2a,b** on reducing the volume under reduced pressure. The orange yellow products, which are air-stable for short periods of time in the solid state, were isolated in ca. 50% yield. The filtrate was left standing for 12 h at –30 °C and yielded a second crop of the product (total yield ca. 75%).

2a: IR (THF) ν(CO) 1986 m, 1925 vs, 1907 sh; (CH₂Cl₂) 1985 m, 1918 vs, 1905 sh; NMR ¹H (CDCl₃), δ 2.54 (dd, br 3H, CH₃, ⁴*J*(P–H) = 10.2, 2.9), 3.52 (s, 9H, OCH₃), 3.35–3.75 (m, partially obscured by the Si(OMe)₃ resonance, 2H, PCH₂P), 7.04–7.95 (m, 35H, C₆H₅); ³¹P-¹H (CDCl₃), δ 63.9 (d, P³(Fe), ²⁺³*J*(P²–P³) = 117, ²*J*(P–Pt) = 69), 33.0 (d, P¹(Pt), ²*J*(P¹–P²) = 13, ¹*J*(P–Pt) = 4226), 24.1 (dd, P²(Pt), ¹*J*(P–Pt) = 2092; ¹³C-¹H (CDCl₃), δ 220.2 (s, br, FeCO, ²*J*(P–C) not resolved), 219.1 (d, FeCO, ²*J*(P–C) = 18), 216.8 (d, FeCO, ²*J*(P–C) = 20), 184.5 (dd, μ-C, ²*J*(P–C) = 15, 86), 51.2 (s, OCH₃), 45.5 (m, PCP), 43.7 (s, C-CH₃, ²*J*(Pt–C) = 62). Anal. Found: C, 53.88; H, 4.69. Calcd for C₅₁H₄₉FeO₇P₃PtSi (*M* = 1145.88): C, 53.46; H, 4.31.

2b: IR (THF) ν(CO): 1986 m, 1924 vs, 1907 sh; (CH₂Cl₂) 1986 m, 1918 vs, 1906 sh; NMR ¹H (CDCl₃), δ 1.27 (t, 3H, CH₃, ³*J*(H–H) = 6.5), 2.05 (m, 1H, CH₂), 2.62 (m, 1H, CH₂), 3.54 (s, 9H, OCH₃), 3.45 (m, partially obscured by the Si(OMe)₃ resonance, 1H, PCH₂P), 3.75 (m, 1H, PCH₂P), 7.08–7.88 (m, 35H, C₆H₅); ³¹P-¹H (CDCl₃), δ 62.4 (d, P³(Fe), ²⁺³*J*(P²–P³) = 116, ²*J*(P–Pt) = 69), 34.5 (d, P¹(Pt), ²*J*(P¹–P²) = 14, ¹*J*(P–Pt) = 4238), 22.3 (dd, P²(Pt), ¹*J*(P–Pt) = 2039); ¹³C-¹H (CDCl₃), δ 219.6 (d, FeCO, ²*J*(P–C) = 6), 218.9 (d, FeCO, ²*J*(P–C) = 19), 216.3 (d, FeCO, ²*J*(P–C) = 23), 192.0 (dd, μ-C, ²*J*(P–C) = 14, 84), 51.3 (s, OCH₃), 49.0 (s, C-CH₂, ²*J*(Pt–C) = 66), 44.6 (dt, PCP, *J*(P–C) = 12, 17), 18.3 (dd, CH₂CH₃, ⁴*J*(P–C) = 5, 12); ¹⁹⁵Pt-¹H (CH₂Cl₂/CDCl₃), δ –2592.6 (ddd, ¹*J*(Pt–P) =

- (4) Schubert, U. *Transition Met. Chem.* **1991**, *16*, 136.
- (5) Seebald, S.; Mayer, B.; Schubert, U. *J. Organomet. Chem.* **1993**, *462*, 225.
- (6) Arnold, J.; Tilley, T. D. *J. Am. Chem. Soc.* **1985**, *22*, 6409.
- (7) Arnold, J.; Tilley, T. D. *J. Am. Chem. Soc.* **1987**, *109*, 3318.
- (8) Berryhill, S. R.; Clevenger, G. L.; Burdulu, F. Y. *Organometallics* **1985**, *4*, 1509.
- (9) Berryhill, S. R.; Corriu, R. J. P. *J. Organomet. Chem.* **1989**, *370*, C1.
- (10) Crocco, G. L.; Young, C. S.; Lee, K. E.; Gladysz, J. A. *Organometallics* **1988**, *7*, 2158.
- (11) Handwerker, H.; Beruda, H.; Kleine, M.; Zybilla, C. *Organometallics* **1992**, *11*, 3542.
- (12) Harris, P. J.; Howard, J. A. K.; Knox, S. A. R.; McKinney, R. J.; Phillips, R. P.; Stone, F. G. A.; Woodward, P. *J. Chem. Soc. Dalton Trans.* **1978**, 403.
- (13) Ingle, W. M.; Preti, G.; McDiarmid, A. G. *J. Chem. Soc., Chem. Commun.* **1973**, 497.
- (14) Ojima, I.; Ingallina, P.; Donovan, R. J.; Clos, N. *Organometallics* **1991**, *10*, 38.
- (15) Ojima, I.; Donovan, R. J.; Clos, N. *Organometallics* **1991**, *10*, 2606.
- (16) Rickard, C. E. F.; Roper, W. R.; Salter, D. M.; Wright, L. J. *Organometallics* **1992**, *11*, 3931.

- (17) Schubert, U.; Schenkel, A. *Chem. Ber.* **1988**, *121*, 939.
- (18) Sharma, S.; Kapoor, R. N.; Lee, F. C.; Pannell, K. H. *Polyhedron* **1991**, *10*, 1177.
- (19) Thum, G.; Ries, W.; Greisinger, D.; Malisch, W. *J. Organomet. Chem.* **1983**, *252*, C67.
- (20) Vargas, R. M.; Hossain, M. M. *Inorg. Chim. Acta* **1993**, *204*, 139.
- (21) Akita, M.; Oku, T.; Tanaka, M.; Moro-oka, Y. *Organometallics* **1991**, *10*, 3080.
- (22) Chatani, N.; Fukumoto, Y.; Ida, T.; Murai, S. *J. Am. Chem. Soc.* **1993**, *115*, 11614.
- (23) Lin, W.; Wilson, S. R.; Girolami, G. S. *J. Am. Chem. Soc.* **1993**, *115*, 3022.
- (24) Randolph, C. L.; Wrighton, M. S. *J. Am. Chem. Soc.* **1986**, *108*, 3366.
- (25) Seitz, F.; Wrighton, M. S. *Angew. Chem., Int. Ed. Engl.* **1988**, *27*, 289.
- (26) Brookhart, M.; Grant, B. E. *J. Am. Chem. Soc.* **1993**, *115*, 2151.
- (27) Duckett, S. B.; Perutz, R. N. *Organometallics* **1992**, *11*, 90.
- (28) Ojima, I.; Ingallina, P.; Donovan, R. J.; Clos, N.; Shay, W. R.; Eguhi, M.; Zeng, Q.; Korda, A. *J. Cluster Sci.* **1992**, *3*, 423.
- (29) Tanke, R. S.; Crabtree, R. H. *J. Chem. Soc., Chem. Commun.* **1990**, 1056.
- (30) Braunstein, P.; Knorr, M.; Hirle, B.; Reinhard, G.; Schubert, U. *Angew. Chem., Int. Ed. Engl.* **1992**, *31*, 1583.
- (31) Braunstein, P.; Faure, T.; Knorr, M.; Stährfeldt, T.; DeCian, A.; Fischer, J. *Gazz. Chim. Ital.*, in press.
- (32) Braunstein, P.; Knorr, M.; Stährfeldt, T. *J. Chem. Soc., Chem. Commun.* **1994**, 1913.
- (33) Schubert, U. Solid-State Structures of Carbene Complexes. In *Transition Metal Carbene Complexes*; Verlag Chemie: Weinheim, 1983; pp 74–111.

4246, 2040, $^2J(\text{Pt}-\text{P}) = 69$). Anal. Found: C, 53.96; H, 4.50. Calcd for $\text{C}_{52}\text{H}_{51}\text{FeO}_7\text{P}_3\text{PtSi}$ ($M = 1159.91$): C, 53.85; H, 4.43.

Method B. $[(\text{OC})_3\text{Fe}\{\mu\text{-C}(\text{Me})\text{OSi}(\text{OMe})_3\}(\mu\text{-dppm})\text{Pt}(\text{PR}_3)]$ (**2c**, $\text{L} = \text{PEt}_3$; **2d**, $\text{L} = \text{P}(\text{p-tolyl})_3$; **2e**, $\text{L} = \text{P}(\text{OMe})_3$). To a solution of **1a** (0.088 g, 0.1 mmol) in CH_2Cl_2 (6 mL) was added 1 equiv of the corresponding phosphine or 1.1 equiv of $\text{P}(\text{OMe})_3$. After the solution was stirred at ambient temperature (30 min for **2c**, 1 h for **2d** and **2e**), all volatiles were removed under vacuum. The yellow residue was triturated with hexane (ca. 5 mL) and dried again to give the products in ca. 95% yield.

2c: IR (CH_2Cl_2) 1978 m, 1907 vs, br; NMR ^1H (CDCl_3), δ 0.85 (m, 9H, CH_2CH_3), 1.18 (m, 3H, $\text{PCH}^{\text{A}}\text{H}^{\text{B}}$), 1.52 (m, 3H, $\text{PCH}^{\text{A}}\text{H}^{\text{B}}$), 3.08 (ddd, 3H, CH_3 , $^4J(\text{P}-\text{H}) = 9.1, 4.8, 1.1$), 3.66 (s, 9H, OCH_3), 3.40–3.75 (m, partially obscured by the $\text{Si}(\text{OMe})_3$ resonance, 2H, PCH_2P), 7.04–7.85 (m, 20H, C_6H_5); $^{31}\text{P}\{-^1\text{H}\}$ (CDCl_3), δ 67.4 (d, $\text{P}^1(\text{Fe})$, $^{2+3}J(\text{P}^1-\text{P}^2) = 119$, $^2J(\text{P}-\text{Pt}) = 64$), 24.0 (d, $\text{P}^1(\text{Pt})$, $^2J(\text{P}^1-\text{P}^2) = 10$, $^1J(\text{P}-\text{Pt}) = 4161$), 22.7 (dd, $\text{P}^2(\text{Pt})$, $^1J(\text{P}-\text{Pt}) = 2047$); $^{13}\text{C}\{-^1\text{H}\}$ (CDCl_3), δ 220.2 (d, FeCO , $^2J(\text{P}-\text{C}) = 5$), 218.9 (d, FeCO , $^2J(\text{P}-\text{C}) = 20$), 213.8 (d, FeCO , $^2J(\text{P}-\text{C}) = 19$), 182.5 (dd, $\mu\text{-C}$, $^2J(\text{P}-\text{C}) = 13, 87$), 51.8 (s, OCH_3), 44.9 (m, PCP), 43.8 (s, CCH_3), 17.8 (dd, PCH_2CH_3 , $^1J(\text{P}-\text{C}) = 28$, $^3J(\text{P}-\text{C}) = 4$), 8.4 (s, PCH_2CH_3 , $^3J(\text{Pt}-\text{C}) = 25$). Anal. Found: C, 46.48; H, 4.75. Calcd for $\text{C}_{39}\text{H}_{49}\text{FeO}_7\text{P}_3\text{PtSi}$ ($M = 1001.75$): C, 46.76; H, 4.93.

2d: IR (CH_2Cl_2) 1984 m, 1916 vs, 1904 sh; NMR ^1H (CDCl_3), δ 2.28 (s, 9H, PhCH_3), 2.54 (m, br 3H, CH_3), 3.51 (s, 9H, OCH_3), 3.35–3.75 (m, partially obscured by the $\text{Si}(\text{OMe})_3$ resonance, 2H, PCH_2P), 6.81–7.73 (m, 32H, C_6H_5); $^{31}\text{P}\{-^1\text{H}\}$ (CDCl_3), δ 64.1 (d, $\text{P}^3(\text{Fe})$, $^{2+3}J(\text{P}^2-\text{P}^3) = 117$, $^2J(\text{P}-\text{Pt}) = 68$), 31.0 (d, $\text{P}^1(\text{Pt})$, $^2J(\text{P}^1-\text{P}^2) = 13$, $^1J(\text{P}-\text{Pt}) = 4244$), 24.0 (dd, $\text{P}^2(\text{Pt})$, $^1J(\text{P}-\text{Pt}) = 2087$). Anal. Found: C, 54.86; H, 4.32. Calcd for $\text{C}_{54}\text{H}_{55}\text{FeO}_7\text{P}_3\text{PtSi}$ ($M = 1187.98$): C, 54.60; H, 4.67.

2e: IR (KBr) $\nu(\text{OSiC}-\text{H})$ 2840w; $\nu(\text{CO})$ 1986 m, 1909 vs; NMR ^1H (CDCl_3), δ 3.11 (dt, 3H, CH_3 , $^4J(\text{P}-\text{H}) = 10.1, 4.1$), 3.37 (d, 9H, POCH_3 , $^3J(\text{P}-\text{H}) = 12.9$), 3.65 (s, 9H, SiOCH_3), 3.48–3.88 (m, partially obscured by the $\text{Si}(\text{OMe})_3$ resonance, 2H, PCH_2P), 7.04–7.77 (m, 20H, C_6H_5); $^{31}\text{P}\{-^1\text{H}\}$ (CDCl_3), δ 150.3 (d, $\text{P}^1(\text{Pt})$, $^2J(\text{P}^1-\text{P}^2) = 9$, $^1J(\text{P}-\text{Pt}) = 6832$), 67.0 (d, $\text{P}^3(\text{Fe})$, $^{2+3}J(\text{P}^2-\text{P}^3) = 122$, $^2J(\text{P}-\text{Pt}) = 64$), 26.2 (dd, $\text{P}^2(\text{Pt})$, $^1J(\text{P}-\text{Pt}) = 1938$). Anal. Found: C, 42.66; H, 4.43. Calcd for $\text{C}_{36}\text{H}_{43}\text{FeO}_{10}\text{P}_3\text{PtSi}$ ($M = 1007.67$): C, 42.91; H, 4.30.

$[(\text{OC})_3\text{Fe}\{\mu\text{-C}(\text{Et})\text{OSi}(\text{OMe})_3\}(\mu\text{-dppm})\text{Pt}(\text{2,6-xylyl-NC})]$ (**4b**). Solid 2,6-xylyl isonitrile (0.020 g, 0.15 mmol) was added to a solution of **2b** (0.116 g, 0.1 mmol) in CH_2Cl_2 (6 mL). After the solution was stirred for 0.5 h, the solvent was removed *in vacuo*. The residue was then triturated with hexane (ca. 5 mL) and dried again to give the bright yellow product. Due to remaining traces of free PPh_3 and isonitrile no satisfactory elemental analysis could be obtained: IR (KBr) $\nu(\text{OSiC}-\text{H})$ 2840w; $\nu(\text{CN})$ 2174 m; $\nu(\text{CO})$ 1984 m, 1913 vs; NMR ^1H (CDCl_3), δ 1.54 (t, 3H, CH_3 , $^3J(\text{H}-\text{H}) = 6.9$), 2.22 (s, 6H, PhCH_3), 3.10 (m, 1H, $\text{CCH}^{\text{A}}\text{H}^{\text{B}}$), 3.27 (m, 1H, $\text{CCH}^{\text{A}}\text{H}^{\text{B}}$), 3.59 (s, 9H, OCH_3), 3.79 (t, 2H, PCH_2P , $^2J(\text{P}-\text{H}) = 10.4$), 7.02–7.90 (m, 23H, aromatic); $^{31}\text{P}\{-^1\text{H}\}$ (CDCl_3), δ 66.2 (d, $\text{P}^3(\text{Fe})$, $^{2+3}J(\text{P}^2-\text{P}^3) = 124$, $^2J(\text{P}-\text{Pt}) = 66$), 22.1 (d, $\text{P}^2(\text{Pt})$, $^1J(\text{P}-\text{Pt}) = 2046$).

$[(\text{OC})_3\text{Fe}(\mu\text{-Cet})(\mu\text{-dppm})\text{Pt}(\text{PPh}_3)][\text{CF}_3\text{SO}_3]$ (**5**). Pure $\text{CF}_3\text{SO}_3\text{H}$ was added in excess at -30°C to a solution of **2b** (0.116 g, 0.1 mmol) in CH_2Cl_2 (6 mL). After the solution was stirred for 5 min all volatiles were removed *in vacuo* and the residue was triturated with Et_2O (ca. 5 mL) and dried again. Extraction of the solid with CH_2Cl_2 (10 mL) afforded spectroscopically pure yellow **5** as an Et_2O solvate. Mass spectrum for the cationic fragment (FAB^+ , tetraglyme matrix). 1022 ($\text{M}^+ - 30$), 970 ($\text{M}^+ - 2\text{CO}$, 6), 938 ($\text{M}^+ - 3\text{CO}$, 28), 897 ($\text{M}^+ - 3\text{CO} - \text{C}_3\text{H}_5$, 15); IR (CH_2Cl_2) 2039 s, 1994 s, 1951 m, br; NMR ^1H (CDCl_3), δ 1.68 (m, br 3H, CH_3), 4.1–5.2 (br, not resolved, $\text{CH}_2\text{-CH}_3$ and PCH_2P), 6.9–8.42 (m, 35H, C_6H_5); $^{31}\text{P}\{-^1\text{H}\}$ (CDCl_3), δ 54.7 (dd, $\text{P}^3(\text{Fe})$, $^{2+3}J(\text{P}^2-\text{P}^3) = 41$, $^{3+4}J(\text{P}^1-\text{P}^3) = 24$, $^{2+3}J(\text{P}^3-$

Table 1. Crystal Data and Data Collection Parameters for $2\text{b}\cdot 2\text{C}_7\text{H}_8$

formula	$\text{C}_{52}\text{H}_{46}\text{O}_7\text{SiP}_3\text{FePt}\cdot 2\text{C}_7\text{H}_8$
molecular weight	1339.2
color	yellow
crystal system	monoclinic
a (Å)	11.014(1)
b (Å)	21.148(1)
c (Å)	26.063(1)
β (deg)	94.57(2)
V (Å ³)	6051.4
Z	4
D_{calc} (gcm ⁻³)	1.470
wavelength (Å)	0.7107
μ (cm ⁻¹)	27.204
space group	$P2_1/c$
crystal dimm (mm)	0.24 × 0.20 × 0.20
temperature (°C)	-100
radiation	Mo K α graphite monochromated
mode	$\theta/2\theta$
scan speed	variable
scan width (deg)	0.90 + 0.34 tg(θ)
octants	$\pm h+k+l$
θ min/max (deg)	2/26
data collected	13822
data with $I > 3\sigma(I)$	8375
number of variables	650
abs min/max	0.87/1.00
$R(F)^a$	0.039
$R_w(F)^a$	0.055
P	0.06
largest peak in final diff (eÅ ⁻³)	0.13
GOFF	1.270

$$^a R = \sum |F_o| - |F_c| / \sum |F_o|; R_w = [\sum w(|F_o| - |F_c|)^2 / \sum w|F_o|^2]^{1/2}.$$

Pt) = 50), 33.7 (dd, $\text{P}^1(\text{Pt})$, $^2J(\text{P}^1-\text{P}^2) = 16$, $^1J(\text{P}^1-\text{Pt}) = 3724$), 7.9 (dd, $\text{P}^2(\text{Pt})$, $^1J(\text{P}^2-\text{Pt}) = 2444$).

X-ray Crystal Structure Determination of $2\text{b}\cdot 2\text{C}_7\text{H}_8$

Crystallographic details are given in Table 1. Suitable single crystals were obtained by slow diffusion of hexane into a chlorobenzene/toluene solution at -20°C . A single crystal was mounted on a rotation-free goniometer head. Systematic searches in reciprocal spaces using an Enraf-Nonius CAD4-F automatic diffractometer showed that the crystals belong to the monoclinic system. Lattice parameters and intensity data were obtained at -100°C . The resulting data sets were transferred to a VAX computer, and for all subsequent calculations the Enraf-Nonius SDP/VAX package was used.³⁴

Three standard reflections measured every hour during the entire data collection periods showed no significant trend. The raw data were converted to intensities and corrected for Lorentz and polarization factors.³⁵ Absorption corrections derived from ψ scans of four reflections were applied. The structure was solved using the heavy atom method. The atoms of one solvent molecule were introduced as fixed contributors. After refinement of the heavy atoms, difference Fourier maps revealed maxima of residual electronic density close to the positions expected for hydrogen atoms; they were introduced in structure factor calculations by their computed coordinates ($\text{C}-\text{H} = 0.95 \text{ \AA}$) and isotropic temperature factors such as $B(\text{H}) = 1.3B_{\text{eq}}(\text{C}) \text{ \AA}^2$ but not refined. The hydrogen atoms of one solvent molecule were omitted. Full least-squares refinements: $w = 1/\sigma^2(F^2)$; $\sigma^2(F^2) = \sigma^2_{\text{counts}} + (pI)^2$. Final difference maps revealed no significant maxima. The scattering factor coefficients and anomalous dispersion coefficients come from refs 36a and 36b, respectively. Final atomic coordinates are given in Table 2.

(34) Frenz, B. A. The Enraf-Nonius CAD4-SDP. In *Computing in Crystallography*; Schenk, H., Olthoff-Hazekamp, R., van Koningveld, H., Bassi, G. C., Eds.; Delft University Press: Delft, The Netherlands, 1978; p 64.

(35) Walker, N.; Stuart, D. *Acta Crystallogr., Sect. A* **1983**, *39*, 158.
(36) Cromer, D. T.; Waber, J. T. *International Tables for X-ray Crystallography*; The Kynoch Press: Birmingham, 1974; Vol. IV, (a) Table 2.2b; (b) Table 2.3.1.

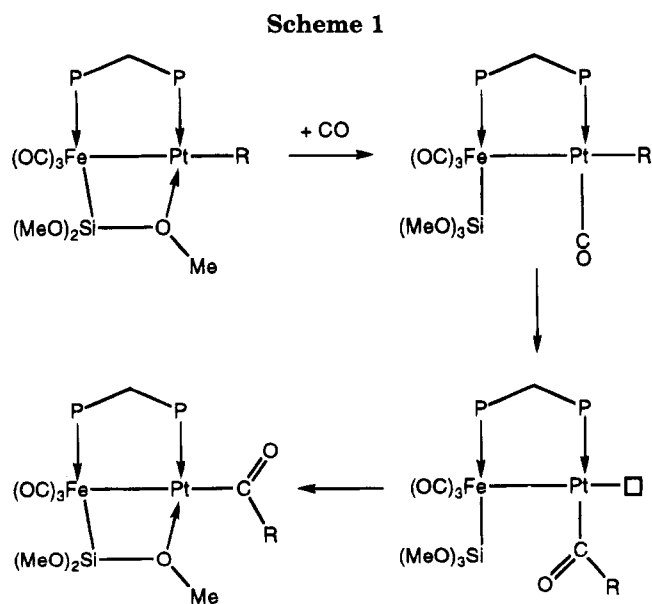
Table 2. Positional Parameters with ESD's for the Non-Hydrogen Atoms of 2b·2C₇H₈

atom	x	y	z	B (Å ²) ^a	atom	x	y	z	B (Å ²) ^a
Pt	0.14512(2)	0.11286(1)	0.16751(1)	1.355(4)	C31	-0.0619(6)	-0.0174(3)	0.1651(3)	1.8(1)
Fe	0.08762(8)	0.16433(4)	0.24874(3)	1.52(2)	C32	-0.1277(6)	0.0192(3)	0.1279(3)	2.1(1)
C1	0.1674(6)	0.2070(3)	0.1885(3)	1.6(1)	C33	-0.2442(7)	0.0010(4)	0.1101(3)	2.7(2)
C2	0.2957(7)	0.2345(4)	0.1951(3)	2.7(2)	C34	-0.2968(7)	-0.0528(4)	0.1291(3)	3.1(2)
C3	0.3079(8)	0.2918(4)	0.2319(3)	3.3(2)	C35	-0.2315(7)	-0.0887(4)	0.1658(3)	2.6(1)
O1	0.0928(4)	0.2509(2)	0.1581(2)	2.2(1)	C36	-0.1152(7)	-0.0713(3)	0.1839(3)	2.3(1)
Si	0.0068(2)	0.3111(1)	0.15641(8)	2.42(4)	C37	0.0812(6)	0.0078(3)	0.2606(2)	1.7(1)
O2	-0.0952(5)	0.2951(3)	0.1101(2)	3.1(1)	P3	0.0175(2)	0.08009(8)	0.28849(6)	1.59(3)
C4	-0.1795(8)	0.3410(5)	0.0884(4)	4.2(2)	C38	0.0607(6)	0.0700(3)	0.3574(3)	1.9(1)
O3	0.0824(5)	0.3741(3)	0.1450(2)	3.8(1)	C39	0.0478(8)	0.0124(4)	0.3825(3)	3.1(2)
C5	0.1673(9)	0.3769(5)	0.1066(4)	5.2(2)	C40	0.0770(9)	0.0073(4)	0.4347(3)	3.8(2)
O4	-0.0544(5)	0.3299(3)	0.2084(2)	3.6(1)	C41	0.1202(9)	0.0578(4)	0.4630(3)	3.6(2)
C6	-0.1708(8)	0.3118(4)	0.2228(3)	3.8(2)	C42	0.1318(9)	0.1151(4)	0.4395(3)	4.2(2)
P1	0.2295(2)	0.10474(8)	0.09156(6)	1.60(3)	C43	0.1043(8)	0.1210(4)	0.3866(3)	3.2(2)
C7	0.2476(6)	0.0268(3)	0.0630(2)	1.7(1)	C44	-0.1469(6)	0.0671(4)	0.2866(3)	2.1(1)
C8	0.1433(7)	-0.0071(4)	0.0470(3)	2.6(2)	C45	-0.2250(6)	0.1191(4)	0.2857(3)	2.6(1)
C9	0.1490(7)	-0.0652(4)	0.0229(3)	2.7(2)	C46	-0.3503(7)	0.1106(4)	0.2850(3)	3.7(2)
C10	0.2601(8)	-0.0906(4)	0.0145(3)	3.1(2)	C47	-0.3987(7)	0.0509(4)	0.2852(4)	3.8(2)
C11	0.3652(8)	-0.0583(4)	0.0293(3)	3.7(2)	C48	-0.3234(7)	-0.0009(4)	0.2872(4)	3.9(2)
C12	0.3590(7)	0.0004(4)	0.0539(3)	2.8(2)	C49	-0.1985(7)	0.0059(4)	0.2875(3)	2.8(2)
C13	0.3833(6)	0.1364(3)	0.0947(3)	1.8(1)	C50	0.2350(6)	0.1378(4)	0.2717(3)	2.4(1)
C14	0.4259(7)	0.1793(4)	0.0607(3)	2.6(1)	O5	0.3285(5)	0.1182(3)	0.2875(2)	3.6(1)
C15	0.5447(7)	0.2017(4)	0.0663(3)	3.6(2)	C51	0.0664(6)	0.2301(3)	0.2897(3)	2.0(1)
C16	0.6223(6)	0.1827(4)	0.1066(3)	2.9(2)	O6	0.0539(6)	0.2718(3)	0.3169(2)	3.5(1)
C17	0.5830(7)	0.1391(4)	0.1419(3)	3.0(2)	C52	-0.0467(6)	0.1631(3)	0.2056(3)	2.2(1)
C18	0.4641(6)	0.1169(4)	0.1365(3)	2.6(1)	O7	-0.1351(4)	0.1643(3)	0.1791(2)	2.9(1)
C19	0.1496(6)	0.1458(3)	0.0368(3)	2.0(1)	C53	0.4941(9)	0.1038(6)	0.5723(4)	5.6(3)
C20	0.0603(7)	0.1890(4)	0.0467(3)	2.6(2)	C54	0.4973(9)	0.1330(6)	0.6208(5)	6.2(3)
C21	0.0009(8)	0.2232(4)	0.0058(3)	3.6(2)	C55	0.559(1)	0.1060(9)	0.6616(5)	9.1(5)
C22	0.0314(8)	0.2120(4)	-0.0444(3)	3.2(2)	C56	0.617(1)	0.0523(8)	0.6570(5)	8.3(4)
C23	0.1164(7)	0.1685(4)	-0.0540(3)	2.6(2)	C57	0.619(1)	0.0218(7)	0.6116(7)	9.2(4)
C24	0.1764(7)	0.1347(4)	-0.0137(3)	2.6(1)	C58	0.554(1)	0.0482(6)	0.5655(6)	8.6(4)
P2	0.0878(2)	0.01198(8)	0.18963(6)	1.58(3)	C59	0.423(2)	0.132(1)	0.5293(6)	13.3(6)
C25	0.1951(6)	-0.0521(3)	0.1809(3)	1.9(1)	C64	0.458	0.183	0.397	13.4(3)*
C26	0.3166(7)	-0.0408(4)	0.2004(3)	2.7(2)	C60	0.658	0.157	0.433	15.0*
C27	0.4053(7)	-0.0865(4)	0.1947(3)	3.4(2)	C61	0.670	0.217	0.454	15.0*
C28	0.3754(8)	-0.1420(4)	0.1698(3)	4.1(2)	C62	0.577	0.260	0.446	15.0*
C29	0.2581(8)	-0.1527(4)	0.1496(3)	3.3(2)	C63	0.471	0.244	0.417	15.0*
C30	0.1689(7)	-0.1083(3)	0.1562(3)	2.4(1)	C65	0.551	0.140	0.405	15.0*
					C66	0.760	0.108	0.441	18.0*

^a Anisotropically refined atoms are given in the form of the isotropic equivalent displacement parameter defined as $\langle u^2 \rangle = \frac{1}{3} [a^2\beta(1,1) + b^2\beta(2,2) + c^2\beta(3,3) + ab(\cos \delta)\beta(1,2) + ac(\cos \beta)\beta(1,3) + bc(\cos \alpha)\beta(2,3)]$.

Results and Discussion

We reported recently on the facile insertion reaction of CO into the Pt–R bond (R = Me, Et, norbornyl) of dppm-bridged bimetallic complexes $[(OC)_3Fe\{\mu-Si(OMe)_2(OMe)\}(\mu-dppm)Pt(R)]$ which led to the stable complexes $[(OC)_3Fe\{\mu-Si(OMe)_2(OMe)\}(\mu-dppm)Pt\{C(O)R\}]$ (1) in which the acyl ligand occupies a position trans to the metal–metal bond.^{31,32} This was rationalized by assuming that opening of the $\mu-Si-O$ bridge liberates a vacant coordination site which is occupied by CO to give the spectroscopically characterized CO adducts $[(OC)_3\{(MeO)_3Si\}Fe(\mu-dppm)Pt(CO)(R)]$ (Scheme 1). Subsequent cis migration of the R group should result in a complex with the acyl ligand trans to phosphorus and we believe that the very fast isomerization leading to 1 must be driven, at least in part, by the tendency to restore the $\mu-Si-O$ bridge.



This isomerization must be very rapid as it could not be observed spectroscopically. In view of the stability

(37) Braunstein, P.; Knorr, M.; Schubert, U.; Lanfranchi, M.; Tiripicchio, A. *J. Chem. Soc., Dalton Trans.* **1991**, 1507.

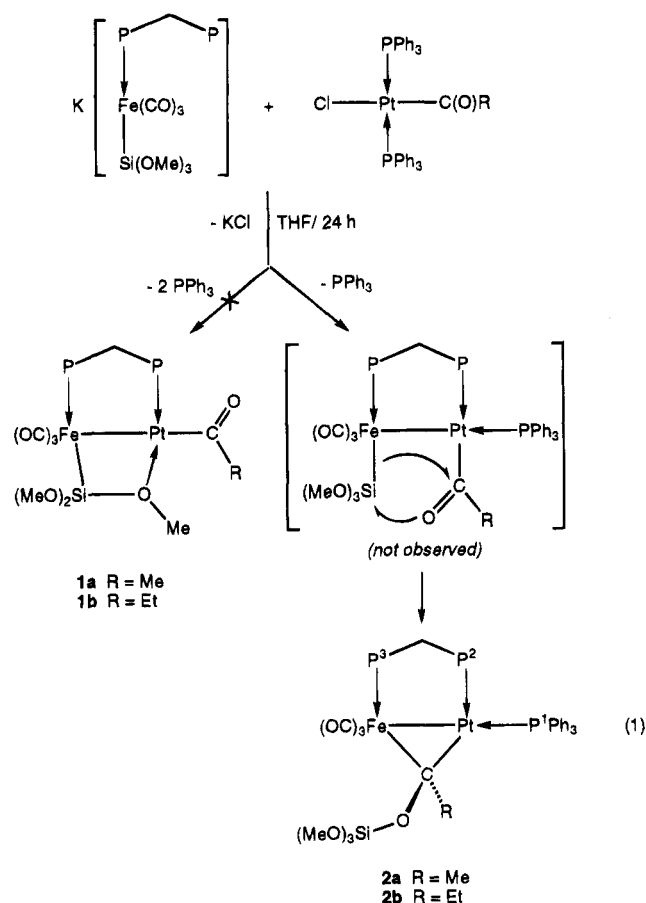
(38) Cook, C. D.; Jauhal, G. S. *Can. J. Chem.* **1967**, *45*, 301.

(39) Knorr, M.; Faure, T.; Braunstein, P. *J. Organomet. Chem.* **1993**, *447*, C4.

(40) Mead, K. A.; Moore, I.; Stone, F. G. A.; Woodward, P. *J. Chem. Soc., Dalton Trans.* **1983**, *9*, 2083.

(41) Awang, M. R.; Jeffery, J. C.; Stone, F. G. A. *J. Chem. Soc., Dalton Trans.* **1983**, *9*, 2091.

of **1**, we attempted its synthesis by another approach: the reaction of the metalate $\text{K}[\text{Fe}\{\text{Si}(\text{OMe})_3\}(\text{CO})_3(\eta^1\text{-dppm})]^{37}$ with $\text{trans-}[\text{PtCl}\{\text{C}(\text{O})\text{R}\}(\text{PPh}_3)_2]^{38}$ (eq 1). This



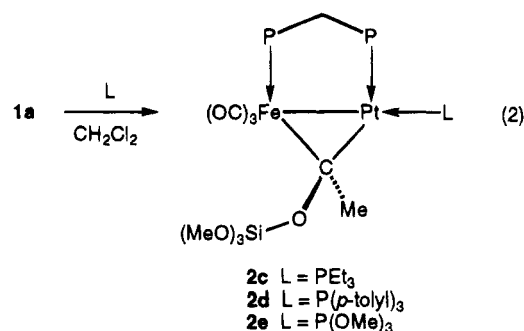
reaction was performed at 293 K in THF for 24 h.

Unexpectedly, the stable μ -carbene complexes $[(\text{OC})_3\text{Fe}\{\mu\text{-C}(\text{R})\text{OSi}(\text{OMe})_3\}(\mu\text{-dppm})\text{Pt}(\text{PPh}_3)]$ (**2a**, R = Me; **2b**, R = Et) were isolated in ca. 75% yield instead of the heterobimetallic acyls **1a,b**.

The existence of a metal-metal bond in complexes **2** confers to the Pt and Fe centers their usual 16 and 18 e count. The structures suggested for **2** were deduced by IR and multinuclear NMR spectroscopic methods, as exemplified for **2b**; the $^{31}\text{P}\{^1\text{H}\}$ NMR spectrum shows a doublet at δ 62.4 for the iron-bound phosphorus atom, which is strongly coupled ($^{2+3}J(\text{P-P}) = 116$ Hz) with the platinum-bound dppm phosphorus, which resonates at δ 22.3. This signal is further split owing to the presence of the PPh_3 ligand which appears at δ 34.5 as a doublet with a typical cis coupling of 14 Hz. The ^{195}Pt NMR spectrum contains a ddd resonance at -2592.6 ppm with a $^1J(\text{Pt-P})$ coupling of 2040 Hz with the dppm phosphorus, a further $^1J(\text{Pt-P})$ coupling of 4246 Hz with the PPh_3 ligand, and a $^{2+3}J(\text{Pt-P})$ coupling of 69 Hz. In the $^{13}\text{C}\{^1\text{H}\}$ NMR spectrum three doublets are observed for the inequivalent Fe carbonyls. The μ -carbenic carbon appears as a doublet of doublets centered at δ 192.0 with $^2J(\text{P-C})$ couplings of 14 and 84 Hz which suggests an unsymmetrically bridged carbene ligand. This stereogenic carbon atom induces inequivalence of the PCH_2P protons (AB spin system with phosphorus and platinum couplings) and of the C-CH_2 protons of the ethyl group which appear as two multiplets (ABX₃

spin system with additional phosphorus couplings) at δ 2.05 and δ 2.62 in the ^1H NMR spectrum. The overall geometry of complexes **2** is therefore similar to that of the μ -aminocarbyne complexes $[(\text{OC})_3\text{Fe}(\mu\text{-CNRR}')(\mu\text{-dppm})\text{Pt}(\text{PPh}_3)][\text{BF}_4]$.³⁹ Related heterobimetallic W-Pt μ -carbene complexes have been prepared by reaction of a mononuclear tungsten carbene complex with $\text{Pt}(\text{COD})_2$ and dppm, affording e.g. $[(\text{OC})\text{Pt}(\mu\text{-dppm})\{\mu\text{-C}(\text{OMe})\text{-Me}\}\text{W}(\text{CO})_4]$ which possesses a ligand arrangement very similar to that in **2** and an asymmetrically bridged carbene ligand, which is closer to platinum than to tungsten.^{40,41}

We felt that a reason for the formation of complexes **2** instead of **1** in reaction 1 could be the presence of PPh_3 . Indeed, the direct reaction of **1a** with 1 equiv of PR_3 in CH_2Cl_2 at ambient temperature also yielded complexes of type **2** (eq 2). The derivatives **2c-e** were



obtained in nearly quantitative yields. The basicity of the PR_3 ligand seems to play a more important role than its cone angle on the rate of this transformation. IR monitoring of the reaction revealed completion with PEt_3 within ca. 30 min (disappearance of the acyl stretch at 1635 cm^{-1}), whereas in the case of $\text{P}(\text{OMe})_3$, even in slight excess, more than 1 h was needed. With AsPh_3 (in slight excess) no reaction was observed even after 3 h. In an attempt to build up a heterotrinary μ -carbene complex, we reacted **1a** with the metallophosphine $[(\text{OC})_5\text{Mo}(\eta^1\text{-Ph}_2\text{PNHPPH}_2)]^{42}$ under similar conditions. Unfortunately, IR and ^{31}P NMR monitoring of the reaction showed only slow intramolecular CO substitution by the pendant phosphorus on Mo and formation of the chelate complex $\text{cis-}[(\text{OC})_4\text{Mo}(\eta^2\text{-Ph}_2\text{PNHPPH}_2)]$ ($^{31}\text{P}\{^1\text{H}\}$ NMR δ 70.3⁴³), the CO adduct $[(\text{OC})_3\{\text{Fe}(\text{MeO})_3\text{-Si}\}\text{Fe}(\mu\text{-dppm})\text{Pt}(\text{CO})\{\text{C}(\text{O})\text{Me}\}]$ ³¹ (formed by reaction with the liberated CO), and **1a**.

These findings suggest that a bimetallic acyl complex is initially formed during the synthesis of complexes **2** according to eq 1 and that this is followed by silyl migration from Fe to O (acyl). However, we have no direct spectroscopic evidence for this acyl intermediate. Evidence that the C-O unit found in the carbene ligand stems from the acyl group was provided by a ^{13}C labeling experiment. Complex **1a** was ^{13}C labeled on the acyl group (by purging a solution of $[(\text{OC})_3\text{Fe}\{\mu\text{-Si}(\text{OMe})_2(\text{OMe})\}(\mu\text{-dppm})\text{Pt}(\text{Me})]$ for 4 min with 99% enriched ^{13}CO) and reacted with tri-*p*-tolylphosphine. The ^{13}C NMR resonance for the labeled carbon appears

(42) Knorr, M. Unpublished results.

(43) Payne, D. S.; Walker, A. P. *J. Chem. Soc. (C)* **1966**, 498.

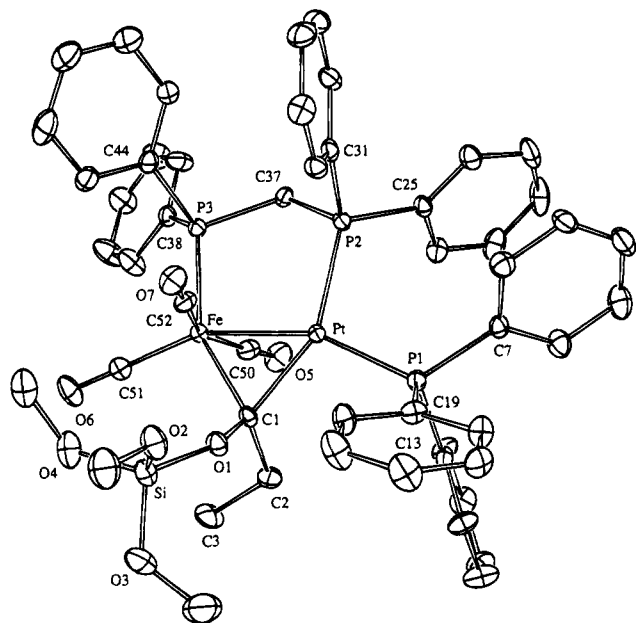


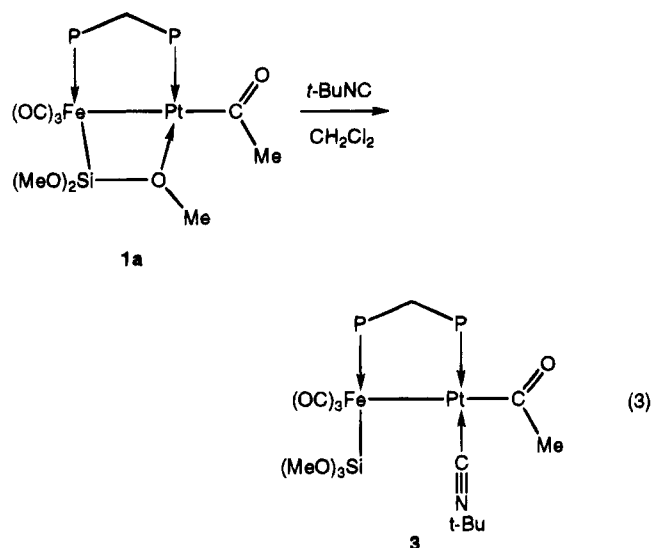
Figure 1. View of the structure of $[(OC)_3Fe\{\mu-C(Et)OSi(OMe)_3\}(\mu-dppm)Pt(PPh_3)]$ (**2b**) in the crystal. Thermal ellipsoids enclose 50% of the electron density.

at δ 184.2 as a doublet of doublets with $^2J(P-C) = 13$ and 85 Hz and shows a strong coupling of 860 Hz with the ^{195}Pt nucleus. The $^{31}P\{-^1H\}$ NMR spectrum of the labeled complex **2c** also enabled us to assign the larger $^2J(P-C)$ value of 85 Hz to the coupling with the dppm phosphorus coordinated on Pt and the 13 Hz coupling to the P nucleus coordinated on Fe. On the basis of these very different $^2J[P-(\mu-C)]$ coupling constants, one would anticipate that the carbene ligand bridges the Fe–Pt bond in an unsymmetrical manner, with the larger value being associated with a shorter Pt–($\mu-C$) distance. However, the crystal structure determination of **2b** revealed an almost symmetrical bridging position for the carbene ligand (see below).

Two possible functions may be envisaged for the phosphine ligand in the reactions of eqs 1 and 2: (i) it will render the acyl oxygen more electron rich, thus favoring Si migration; (ii) it may stabilize the acyl ligand in a cis arrangement with respect to the metal–metal bond long enough to allow Si migration to occur. Conversely, the lack of Si migration during the synthesis of **1** (Scheme 1) is due to the preferred μ -Si–O bridge formation. A rather comparable silicon–oxygen coupling has been reported by Gladysz *et al.* in the case of the mononuclear acyl–silyl complex *cis*- $[(OC)_4Fe\{C(O)Me\}SiMe_3]$.⁴⁴ This labile compound rearranged rapidly via a 1,3 silatropic shift to afford the siloxy carbene complex $[(OC)_4Fe=C(Me)(OSiMe_3)]$. Formation of a strong silicon–oxygen bond is obviously assumed to be the driving force in these reactions. A more recent example of phosphine-induced silyl migration may be found with the conversion of the silyl–alkylidene complex $[Cp_2Ta(=CH_2)\{SiH(t-Bu)_2\}]$ to $[Cp_2Ta(PMe_3)\{CH_2SiH(t-Bu)_2\}]$.⁴⁵

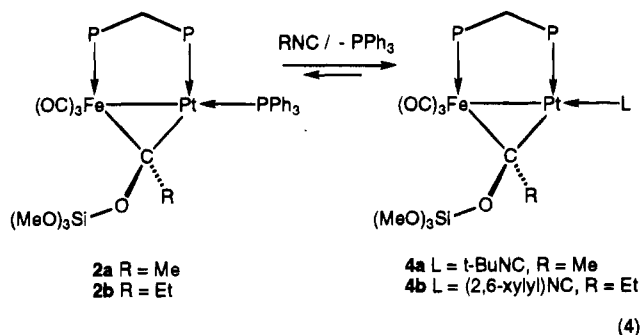
No silyl shift could be induced in complexes **1a** in the presence of *t*-BuNC. Ring opening of the μ -Si–O bridge

occurred instead, and the stable isonitrile adduct **3** was formed in quantitative yield (eq 3).³¹ The isonitrile



ligand is strongly bound in a position cis to the metal–metal bond, thus preventing the acyl ligand to occupy this position and therefore a subsequent silyl migration. We therefore suggest that the phosphine-induced silyl migration is *not* initiated by ring opening of the μ -Si–O bridge of **1** leading to an intermediate with a square planar Pt center. The initial formation of a five-coordinate Pt center should however facilitate the required position change of the acyl group to come in closer contact with the silicon atom.

The isonitrile-substituted carbene complexes **4**, which represent an isomeric form of **3**, can however be obtained from **2** by simple PPh_3 exchange in the presence of an excess of isonitrile, according to eq 4.



After addition of only 1 equiv of *t*-BuNC to a solution of **2a**, ^{31}P NMR monitoring revealed the coexistence of

2a and $[(OC)_3Fe\{\mu-C(Me)OSi(OMe)_3\}\{\mu-dppm\}Pt(t-BuNC)]$ **4a** in a ca. 50:50 ratio, together with a broad resonance of free PPh_3 at δ -4.6, indicating a dynamic equilibrium at ambient temperature. After addition of 3 equiv of *t*-BuNC the equilibrium is completely shifted in favor of **4a**. This complex exhibits a simple AX pattern in the ^{31}P NMR spectrum consisting of a doublet at δ 65.7 for the phosphorus on Fe ($^{2+3}J(P-P) = 122$, $^{2+3}J(Pt-P) = 66$ Hz) and another doublet at δ 22.9 for the P nucleus on platinum ($^1J(Pt-P) = 2068$ Hz). However we failed to isolate pure **4a**, since after removal of volatile *t*-BuNC or attempts of crystallization in the presence of *t*-BuNC only mixtures of **2a** and **4a** were isolated. Addition of 1.1 equiv of 2,6-xylyl isonitrile to

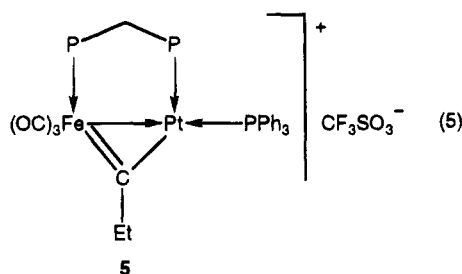
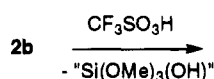
(44) Brinkmann, K. C.; Blakeny, A. J.; Krone-Schmidt, W.; Gladysz, J. A. *Organometallics* **1984**, *3*, 1325.

(45) Berry, D. H.; Koloski, T. S.; Carroll, P. J. *Organometallics* **1990**, *9*, 2952.

a solution of **2b** afforded a 30:70 mixture of **2b** and **4b** and in the presence of 1.5 equiv less than 10% of **2b** were detected by spectral integration.

The cleavage of the C–O bond of μ -alkoxy-carbene complexes by electrophiles under elimination of ROH or ROR' offers a convenient method to prepare cationic μ -alkylidyne complexes.^{46–49} However no reaction took place after stirring a CH₂Cl₂ solution of **2b** with 2 equiv of ethyl triflate, whereas upon addition of excess triflic acid to a cold CH₂Cl₂ solution of **2b** instantaneous silanol elimination occurred and the stable μ -carbyne

complex $[(OC)_3Fe(\mu-CEt)(\mu-dppm)Pt(PPh_3)][CF_3SO_3]$ (**5**) was isolated after extraction from insoluble material(s), probably resulting from condensation of the initially formed (MeO)₃SiOH (eq 5).



The ³¹P-^{[1}H] NMR spectrum of **5** consists of three doublets of doublets for three mutually coupled phosphorus nuclei. A ²J(Pt–P) coupling of 50 Hz is observed for the resonance of the Fe-bound P atom which indicates that the overall geometry found for **2b** has been maintained. The formulation of **5** is further confirmed by the FAB⁺ mass spectrum, which displays an intense peak for the cation, whose simulated isotopic distribution was in excellent agreement with the experimental pattern. Successive loss of the carbonyl and of the \equiv CEt ligands was observed.

In conclusion, we have found in dppm-stabilized bimetallic complexes that migration of the silyl group from iron to an acyl oxygen of a neighboring Pt center results in stable complexes with a bridging siloxycarbene ligand. This reaction may be viewed as the trapping by a silyl group of an intermediate in the cis migration of the R group on the Pt–CO ligand where the acyl ligand is situated in cis position with respect to the metal–metal bond. It is interesting to note that with phosphido-bridged complexes of the same metal couple, silyl migration from iron to platinum has been observed.³⁰ The formation of complexes containing a bridging carbene also extends our previous studies on Si(OMe)₃-substituted Fe–Pt complexes bearing terminal carbene ligands on platinum.⁵⁰ Further studies with Fe–Pd complexes will illustrate the specific role of the metals in this chemistry.

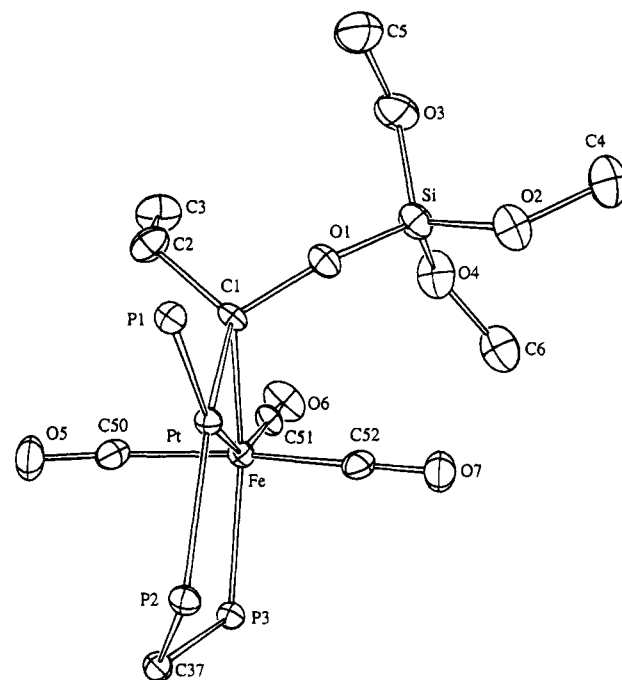


Figure 2. View of the core structure of $[(OC)_3Fe\{\mu-C(Et)OSi(OMe)_3\}(\mu-dppm)Pt(PPh_3)]$ (**2b**) showing the orientation of the bridging siloxycarbene ligand. Thermal ellipsoids enclose 50% of the electron density.

Table 3. Selected Bond Distances (Å) and Angles (deg) in **2b**·2C₇H₈^a

Pt–Fe	2.5062(9)	P1–C7	1.826(7)
Pt–C1	2.074(7)	P1–C13	1.817(7)
Pt–P1	2.260(2)	P1–C19	1.834(7)
Pt–P2	2.311(2)	P2–C25	1.824(7)
Fe–C1	2.066(7)	P2–C31	1.829(7)
Fe–P3	2.230(2)	P2–C37	1.860(7)
Fe–C50	1.776(8)	C50–O5	1.155(9)
Fe–C51	1.781(7)	C51–O6	1.147(8)
Fe–C52	1.786(7)	C52–O7	1.148(8)
C1–C2	1.525(9)	C37–P3	1.854(7)
C1–O1	1.436(8)	P3–C38	1.834(7)
C2–C3	1.55(1)	P3–C44	1.828(7)
O1–Si	1.585(5)		
Si–O2	1.618(6)		
Si–O3	1.611(6)		
Si–O4	1.610(6)		
Fe–Pt–C1	52.6(2)	C1–Fe–C52	84.8(3)
Fe–Pt–P1	157.27(5)	P3–Fe–C50	86.1(2)
Fe–Pt–P2	95.62(5)	P3–Fe–C51	106.2(2)
C1–Pt–P1	104.8(2)	P3–Fe–C52	88.9(2)
C1–Pt–P2	148.1(2)	C50–Fe–C51	101.8(3)
P1–Pt–P2	106.74(6)	C50–Fe–C52	153.8(3)
Pt–Fe–C1	52.9(2)	C51–Fe–C52	104.3(3)
Pt–Fe–P3	99.54(6)	C2–C1–O1	107.5(6)
Pt–Fe–C50	82.1(2)	C1–C2–C3	113.7(6)
Pt–Fe–C51	154.2(2)	C1–O1–Si	148.1(4)
Pt–Fe–C52	73.4(2)	O1–Si–O2	103.4(3)
C1–Fe–P3	152.4(2)	O1–Si–O3	110.6(3)
C1–Fe–C50	87.8(3)	O1–Si–O4	117.7(3)
C1–Fe–C51	101.5(3)	P2–C37–P3	113.4(4)

^a Numbers in parentheses are estimated standard deviations in the least significant digits.

Crystal Structure of $[(OC)_3Fe\{\mu-C(Et)OSi(OMe)_3\}(\mu-dppm)Pt(PPh_3)]\cdot 2C_7H_8$ (2b**·2C₇H₈).** Views of the structure of **2b** are shown in Figures 1 and 2, and selected bond distances and angles are given in Table 3. The Fe–Pt distance of 2.5062(9) Å indicates the

(46) Kao, S. C.; Lu, P. P. Y.; Pettit, R. *Organometallics* **1982**, *1*, 911.
 (47) Gracey, B. P.; Knox, S. A. R.; Macpherson, K. A.; Orpen, A. G.; Stobart, S. R. *J. Chem. Soc., Dalton Trans.* **1985**, *9*, 1935.
 (48) Stone, F. G. A. *Angew. Chem., Int. Ed. Engl.* **1984**, *23*, 89.
 (49) Adams, R. D. *Chem. Rev.* **1989**, *89*, 1703.
 (50) Braunstein, P.; Faure, T.; Knorr, M.; Balegroune, F.; Grandjean, D. *J. Organomet. Chem.* **1993**, *462*, 271.

presence of a metal–metal bond and is close to those found in other complexes of these metals.^{51–54} The iron and platinum atoms are linked by a dppm bridge forming a five-membered ring which has an envelope conformation, with the P(2),C(37),P(3) plane forming an angle of 142.7(2)° with the Fe,P(3),P(2),Pt mean plane. The bridging carbene ligand is symmetrically situated between the metals, with Fe–C(1) and Pt–C(1) distances of 2.066(7) and 2.074(7) Å, respectively. This was not expected on the basis of the spectroscopic data (see above) and differs from the situation found in [(OC)Pt(μ-dppm){μ-C(OMe)(4-MeC₆H₄)}W(CO)₄] where a significant asymmetry was noted.⁴⁰ The angle between the Pt,P(2),P(3),Fe and Fe,C(1),Pt planes amounts to 177.6°. Interestingly, the crystal structure of the related heterometallic complex [(OC)₃Fe(μ-dppm)(μ-CO)Pt(PPh₃)] shows the presence of a symmetrically bridging CO

ligand.⁵⁴ The O(1),C(1),C(2) and Fe,C(1),Pt planes make an angle of 90.6(3)°. The Si–O(1)–C(1) angle is less bent (148.1(4)°) than the other Si–O–C angles, which range from 122.9(6) to 127.2(5)°. The O(1)–Si–O angles are found between 103.4(3) and 117.7(3)°. The coordination about the Fe atom is completed by three terminal CO ligands and may be viewed as distorted octahedral, with C(1)–Fe–P(3), C(50)–Fe–C(52), and Pt–Fe–C(51) angles of 152.4(2), 153.8(3), and 154.2(2)°, respectively. The coordination geometry about the Pt atom is almost planar (max deviation from the mean plane passing through Pt, Fe, P(1), P(2), and C(1) for Pt, 0.0537(2) Å) and the terminal PPh₃ ligand makes an angle of 157.27(5)° with the Fe–Pt bond. The torsion angle P(1)–Pt–Fe–C(51) is 15.3(5)°.

Acknowledgment. We thank the Centre National de la Recherche Scientifique for financial support, the Deutsche Forschungsgemeinschaft for a grant to M.K. and Johnson Matthey PLC for a generous loan of PtCl₂.

Supplementary Material Available: Tables of atomic coordinates including H-atom coordinates, thermal parameters and complete listings of bond distances and angles (16 pages). Ordering information is given on any current masthead page.

OM9407520

(51) Braunstein, P.; Richert, J.-L.; Dusauroy, Y. *J. Chem. Soc., Dalton Trans.* **1990**, 3801.

(52) Braunstein, P.; Colomer, E.; Knorr, M.; Tiripicchio, A.; Tiripicchio-Camellini, M. *J. Chem. Soc., Dalton Trans.* **1992**, 903.

(53) Fontaine, X. L. R.; Jacobsen, G. B.; Shaw, B. L.; Thornton-Pett, M. *J. Chem. Soc., Dalton Trans.* **1988**, 1185.

(54) Fontaine, X. L. R.; Jacobsen, G. B.; Shaw, B. L.; Thornton-Pett, M. *J. Chem. Soc., Dalton Trans.* **1988**, 741.

Heterobridged Dinuclear Gold(I) and Gold(II) Complexes with Xanthate Ligands. X-ray Structures of $[\text{Au}_2\{\mu\text{-(CH}_2)_2\text{PPh}_2\}\{\mu\text{-S}_2\text{CO}^i\text{Pr}\}]$ and $[\text{Au}_2\{\mu\text{-(CH}_2)_2\text{PPh}_2\}\{\mu\text{-S}_2\text{COMe}\}]\text{Br}_2$

Manuel Bardají,[†] Peter G. Jones,[‡] Antonio Laguna,^{*,†} and Mariano Laguna[†]

Departamento de Química Inorgánica, Instituto de Ciencia de Materiales de Aragón, Universidad de Zaragoza-CSIC, E-50009 Zaragoza, Spain, and Institut für Anorganische und Analytische Chemie, Technische Universität Braunschweig, Postfach 3329, D-38023 Braunschweig, Germany

Received September 20, 1994[®]

The reaction of $[\text{Au}_n(\text{S}_2\text{COR})_n]$ ($\text{R} = \text{Me, Et, } ^i\text{Pr}$) with $[\text{Au}_2(\mu\text{-L-L})_2]^{z+}$ ($z = 0, \text{L-L} = \text{CH}_2\text{-PPh}_2\text{CH}_2$; $z = 2, \text{L-L} = \text{PPh}_2\text{CH}_2\text{PPh}_2, \text{PPh}_2\text{CH}_2\text{CH}_2\text{PPh}_2$) leads through a bidentate ligand transfer to heterobridged dinuclear complexes $[\text{Au}_2(\mu\text{-S}_2\text{COR})(\mu\text{-L-L})]^{z+}$ ($z = 0, 1$). The crystal structure of $[\text{Au}_2\{\mu\text{-(CH}_2)_2\text{PPh}_2\}\{\mu\text{-S}_2\text{CO}^i\text{Pr}\}]$ shows a short intramolecular gold–gold distance of 2.8809(9) Å. It crystallizes in the monoclinic space group $P2_1/c$ with $a = 8.571(3)$ Å, $b = 10.219(4)$ Å, $c = 23.210(6)$ Å, $\beta = 97.37(3)^\circ$, and $Z = 4$ (at -100°C). The oxidative addition of halogen affords the corresponding neutral gold(II) complexes containing xanthate ligands $[\text{Au}_2\{\mu\text{-(CH}_2)_2\text{PPh}_2\}\{\mu\text{-S}_2\text{COR}\}\text{X}_2]$ ($\text{R} = \text{Me, Et, } ^i\text{Pr}$; $\text{X} = \text{Cl, Br, I}$). $[\text{Au}_2\{\mu\text{-(CH}_2)_2\text{PPh}_2\}\{\mu\text{-S}_2\text{COMe}\}]\text{Br}_2$ crystallizes in the triclinic space group $P\bar{1}$ with $a = 12.917(4)$ Å, $b = 13.864(3)$ Å, $c = 15.975(5)$ Å, $\alpha = 106.05(2)^\circ$, $\beta = 96.27(2)^\circ$, $\gamma = 113.78(2)^\circ$, and $Z = 4$ (at -100°C). The molecule possesses the general features of dinuclear gold(II) complexes, including a short gold–gold bond of 2.566(1) Å.

Introduction

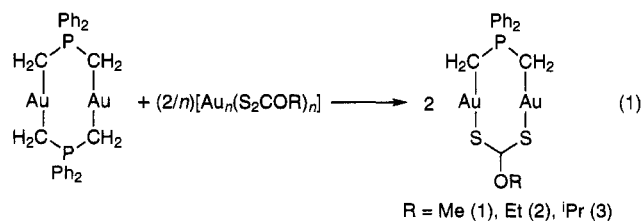
Dithiocarbamate gold(I),¹ gold(III),^{1a,2} and even gold(II)³ complexes have been extensively studied. Gold(I) derivatives have attracted much interest because of the presence of very short intra- and intermolecular gold–gold distances. In contrast, although the first gold(I) xanthate complexes $[\text{Au}_n(\text{S}_2\text{COR})_n]$ were obtained in 1945,⁴ only a few gold(I) or gold(III) compounds of stoichiometry $[\text{Au}(\text{S}_2\text{COR})(\text{PR}_3)_n]$ ($n = 1, 2$)⁵ or $[\text{AuMe}_2(\text{S}_2\text{COR})]$,⁶ have been described, and no gold(II) xanthate complexes have been reported.

In this paper we describe the syntheses not only of several new gold(I) complexes (via bidentate ligand transfer) but also of gold(II) complexes containing xanthate ligands. All the products are heterobridged dinuclear complexes with a xanthate and a (bis)ylide or diphosphine ligand bridging the two gold centers. The molecular structures of $[\text{Au}_2\{\mu\text{-(CH}_2)_2\text{PPh}_2\}\{\mu\text{-S}_2\text{CO}^i\text{Pr}\}]$

and $[\text{Au}_2\{\mu\text{-(CH}_2)_2\text{PPh}_2\}\{\mu\text{-S}_2\text{COMe}\}]\text{Br}_2$ have been established by single-crystal X-ray analysis and are the first crystal structures of dinuclear gold xanthate derivatives.

Results and Discussion

We have recently described^{7,8} ylides transfer reactions of the bis(ylide) derivative $[\text{Au}_2\{\mu\text{-(CH}_2)_2\text{PPh}_2\}_2]$ that allowed us to synthesize di- and trinuclear gold(I) complexes. Now we have synthesized a series of neutral heterobridged gold(I) complexes using a bidentate ligand transfer reaction. Thus, the reaction in dichloromethane of the homobridged complex $[\text{Au}_2\{\mu\text{-(CH}_2)_2\text{PPh}_2\}_2]$ with the insoluble complex $[\text{Au}_n(\text{S}_2\text{COR})_n]$ ($\text{R} = \text{Me, Et, } ^i\text{Pr}$) leads to green solutions from which heterobridged complexes **1–3** can be isolated (eq 1).



These complexes were obtained as green (**1**, **3**) or yellow (**2**) solids, air- and moisture-stable at room temperature. Their acetone solutions are nonconducting, and their IR spectra show medium-intensity bands at ca. 570 cm^{-1} (Table 1) due to $\nu(\text{Au-C}_{\text{ylide}})$.⁹ The $^{31}\text{P}\text{-}\{^1\text{H}\}$ NMR spectra show a singlet at ca. δ 35 ppm for

(7) Cerrada, E.; Gimeno, M. C.; Jiménez, J.; Laguna, A.; Laguna, M.; Jones, P. G. *Organometallics* 1994, 13, 1470.

(8) Bardají, M.; Connelly, N. G.; Gimeno, M. C.; Jiménez, J.; Jones, P. G.; Laguna, A.; Laguna, M. *J. Chem. Soc., Dalton Trans.* 1994, 1163.

[†]Universidad de Zaragoza-CSIC.

[‡]Technische Universität Braunschweig.

[®] Abstract published in *Advance ACS Abstracts*, January 15, 1995.

(1) (a) Coucouvanis, D. *Prog. Inorg. Chem.* 1979, 26, 301 and references therein. (b) Nazrul, M.; Khan, I.; King, C.; Heinrich, D. D.; Fackler, J. P., Jr.; Porter, L. C.; *Inorg. Chem.* 1989, 28, 2150. (c) Heinrich, D. D.; Wang, J.; Fackler, J. P., Jr. *Acta Crystallogr., Sect. C* 1990, 46, 1444 and references therein.

(2) (a) Beckett, M. A.; Crook, J. E.; Greenwood, N. N.; Kennedy, J. D. *J. Chem. Soc., Dalton Trans.* 1984, 1427. (b) Usón, R.; Laguna, A.; Laguna, M.; Castilla, M. L. *J. Organomet. Chem.* 1987, 336, 453. (c) Murray, H. H.; Garzón, G.; Raptis, R. G.; Mazany, A. M.; Porter, L. C.; Fackler, J. P., Jr. *Inorg. Chem.* 1988, 27, 836. (d) Criado, J. L.; López, J. A.; Macías, B.; Fernández-Lago, L. R.; Sala, J. M. *Inorg. Chim. Acta* 1992, 193, 229.

(3) Calabro, C.; Harrison, B. A.; Palmer, G. T.; Moguel, M. K.; Rebbert, L.; Burmeister, J. L. *Inorg. Chem.* 1981, 20, 4311.

(4) Denko, C. W.; Anderson, A. K. *J. Am. Chem. Soc.* 1945, 67, 2241.

(5) (a) Siasios, G.; Tiekink, E. R. T. *Z. Kristallogr.* 1993, 203, 117 and references therein. (b) Assefa, Z.; Staples, R. J.; Fackler, J. P., Jr. *Inorg. Chem.* 1994, 33, 2790.

(6) Pappas, C.; Fackler, J. P., Jr. *Inorg. Chem.* 1980, 19, 2886.

Table 1. Analytical and Spectroscopic Data for Complexes 1–17

complex	anal. (%) ^a		³¹ P{ ¹ H} NMR ^b		¹ H NMR ^c δ(CH ₂ -Au)	IR ^d ν(Au-C _{ylide})
	C	H	δ _{ylide}	δ _{phos}		
[Au ₂ {μ-(CH ₂) ₂ PPh ₂ }(μ-S ₂ COMe)] (1)	27.1 (26.9)	2.35 (2.4)	34.7 (s)		1.96 (d) (12.7)	568
[Au ₂ {μ-(CH ₂) ₂ PPh ₂ }(μ-S ₂ COEt)] (2)	28.05 (28.05)	2.55 (2.65)	34.8 (s)		1.95 (d) (12.7)	572
[Au ₂ {μ-(CH ₂) ₂ PPh ₂ }(μ-S ₂ CO ⁱ Pr)] (3)	29.5 (29.1)	2.85 (2.85)	34.5 (s)		1.93 (d) (12.6)	572
[Au ₂ {μ-S ₂ COMe}(μ-(PPh ₂) ₂ CH ₂)ClO ₄] (4)	33.0 (32.9)	2.65 (2.55)		37.5 (s)		
[Au ₂ {μ-S ₂ COEt}(μ-(PPh ₂) ₂ CH ₂)ClO ₄] (5)	34.0 (33.65)	2.9 (2.7)		37.3 (s)		
[Au ₂ {μ-S ₂ COMe}(μ-(PPh ₂) ₂ CH ₂ CH ₂)ClO ₄] (6)	33.5 (33.65)	2.55 (2.7)		33.7 (s)		
[Au ₂ {μ-S ₂ COEt}(μ-(PPh ₂) ₂ CH ₂ CH ₂)ClO ₄] (7)	34.5 (34.4)	2.95 (2.9)		33.7 (s)		
[Au ₂ {μ-S ₂ CO ⁱ Pr}(μ-(PPh ₂) ₂ CH ₂ CH ₂)ClO ₄] (8)	34.9 (35.1)	2.9 (3.05)		33.7 (s)		
[Au ₂ {μ-(CH ₂) ₂ PPh ₂ }(μ-S ₂ COMe)Cl ₂] (9)	24.3 (24.45)	2.05 (2.2)	42.2 (s)		2.83 (d) (8.8)	574
[Au ₂ {μ-(CH ₂) ₂ PPh ₂ }(μ-S ₂ COMe)Br ₂] (10)	21.9 (22.0)	2.15 (1.95)	45.6 (s)		2.91 (d) (8.8)	572
[Au ₂ {μ-(CH ₂) ₂ PPh ₂ }(μ-S ₂ COMe)I ₂] (11)	19.65 (19.85)	1.95 (1.75)	52.9 (s)		2.97 (d) (9.0)	570
[Au ₂ {μ-(CH ₂) ₂ PPh ₂ }(μ-S ₂ COEt)Cl ₂] (12)	25.05 (25.55)	2.35 (2.4)	42.4 (s)		2.78 (d) (8.8)	576
[Au ₂ {μ-(CH ₂) ₂ PPh ₂ }(μ-S ₂ COEt)Br ₂] (13)	22.85 (23.0)	2.0 (2.15)	45.7 (s)		2.85 (d) (8.8)	574
[Au ₂ {μ-(CH ₂) ₂ PPh ₂ }(μ-S ₂ COEt)I ₂] (14)	20.8 (20.8)	1.65 (1.95)	52.9 (s)		2.93 (d) (9.1)	570
[Au ₂ {μ-(CH ₂) ₂ PPh ₂ }(μ-S ₂ CO ⁱ Pr)Cl ₂] (15)	27.0 (26.6)	2.8 (2.6)	42.2 (s)		2.81 (d) (8.8)	572
[Au ₂ {μ-(CH ₂) ₂ PPh ₂ }(μ-S ₂ CO ⁱ Pr)Br ₂] (16)	23.95 (23.95)	2.45 (2.35)	45.6 (s)		2.89 (d) (8.8)	567
[Au ₂ {μ-(CH ₂) ₂ PPh ₂ }(μ-S ₂ CO ⁱ Pr)I ₂] (17)	21.65 (21.7)	2.35 (2.1)	52.7 (s)		2.91 (d) (9.1)	570

^a Calculated values are given in parentheses. ^b Recorded in CDCl₃, referenced to external H₃PO₄; values in ppm. ^c In CDCl₃ at 300 MHz, referenced to external SiMe₄; values in ppm. Coupling constants in Hz are given in parentheses: s = singlet, d = doublet. ^d Values in cm⁻¹.

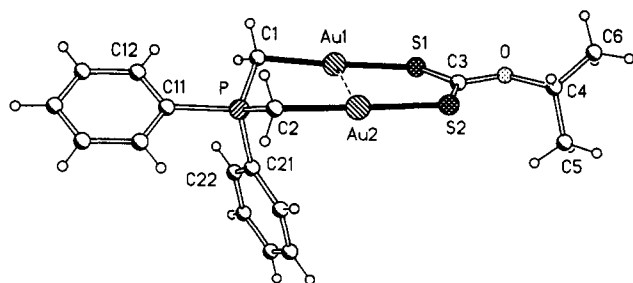


Figure 1. Molecular structure of complex 3, with the atom-numbering scheme. Radii are arbitrary.

the phosphorus atom (Table 1), displaced slightly to low field from the bis(ylide) starting material (δ 34.2 ppm).¹⁰ The ¹H NMR spectra show the ylide methylene proton resonances as doublets at ca. δ 1.95 ppm (Table 1), again low-field displaced (δ 1.30 ppm),¹⁰ showing a stronger influence of the *trans* ligand than do the phosphorus resonances. The positive-ion fast atom bombardment (FAB) mass spectra show in all cases the molecular cation peak (M) at *m/z* (%), complex) 716 (48, 1), 729 (65, 2) and 743 (15, 3).

The cyclic voltammograms of complexes 1 and 2 in CH₂Cl₂ show reversible oxidation waves at 0.47 and 0.48 V, respectively (scan rates 50–200 mV s⁻¹), although they are complicated by the presence of a second irreversible oxidation at 0.62 (1) and 0.59 V (2). These potential values are close to those found by us⁸ in similar dithiocarbamate complexes and show that our complexes are more difficult to oxidize than the starting material [Au₂{μ-(CH₂)₂PPh₂CH₂}] (0.11 V vs Ag–AgCl).¹¹

The structure of complex 3 has been confirmed by X-ray diffraction analysis (Figure 1). The structure consists of a dinuclear gold compound with a central eight-membered ring and a short transannular gold-gold contact of 2.8809(9) Å, similar to that found in [Au₂{μ-(CH₂)₂PPh₂}(μ-S₂CNEt₂)] (2.868(1) and 2.867(1) Å)⁸ or in metallic gold (2.884 Å)^{1c} and shorter than in

(9) (a) Schmidbaur, H.; Franke, R. *Inorg. Chim. Acta.* **1975**, *13*, 85.

(b) Schmidbaur, H.; Franke, R. *Chem. Ber.* **1975**, *108*, 1321.

(10) Usón, R.; Laguna, A.; Laguna, M.; Tartón, M. T.; Jones, P. G. *J. Chem. Soc., Chem. Commun.* **1988**, 740.

(11) Basil, J.; Murray, H. H.; Fackler, J. P., Jr.; Tocher, J.; Mazany, A. M.; Trzcinska-Bancroft, B.; Knachel, H.; Dudis, D.; Delord, T. J.; Marler, D. O. *J. Am. Chem. Soc.* **1985**, *107*, 6908.

Table 2. Atomic Coordinates ($\times 10^4$) and Equivalent Isotropic Displacement Parameters ($\text{Å}^2 \times 10^3$) for 3^a

	x	y	z	U(eq)
Au(1)	2453.0 (4)	6030.7 (4)	5508.3 (1)	32.1 (1)
Au(2)	4846.2 (4)	7522.2 (4)	5037.5 (2)	35.1 (1)
S(1)	2973 (3)	6996 (3)	6405.8 (11)	44.7 (6)
S(2)	5708 (3)	8433 (4)	5932.6 (11)	50.6 (7)
P	2242 (3)	6150 (3)	4157.1 (10)	30.2 (5)
O	5022 (8)	8296 (8)	7000 (3)	43 (2)
C(1)	1935 (11)	5063 (10)	4722 (4)	34 (2)
C(2)	4221 (10)	6695 (12)	4223 (4)	38 (2)
C(3)	4626 (12)	7943 (10)	6444 (4)	38 (2)
C(4)	6373 (12)	9166 (11)	7192 (5)	46 (2)
C(5)	5824 (16)	10546 (12)	7099 (5)	64 (3)
C(6)	6859 (13)	8831 (13)	7816 (4)	51 (3)
C(11)	1691 (10)	5342 (10)	3456 (4)	35 (2)
C(12)	967 (12)	4147 (11)	3429 (4)	47 (2)
C(13)	539 (13)	3552 (12)	2890 (4)	53 (3)
C(14)	800 (12)	4154 (11)	2389 (4)	47 (2)
C(15)	1548 (13)	5332 (12)	2415 (4)	51 (3)
C(16)	1997 (13)	5943 (11)	2949 (4)	49 (2)
C(21)	929 (10)	7529 (9)	4172 (4)	29 (2)
C(22)	-670 (10)	7320 (10)	4192 (4)	42 (2)
C(23)	-1691 (10)	8354 (11)	4212 (4)	43 (2)
C(24)	-1120 (11)	9609 (11)	4220 (4)	46 (2)
C(25)	434 (11)	9856 (10)	4203 (4)	42 (2)
C(26)	1471 (10)	8831 (10)	4176 (4)	38 (2)

^a U(eq) is defined as one-third of the trace of the orthogonalized U_{ij}.

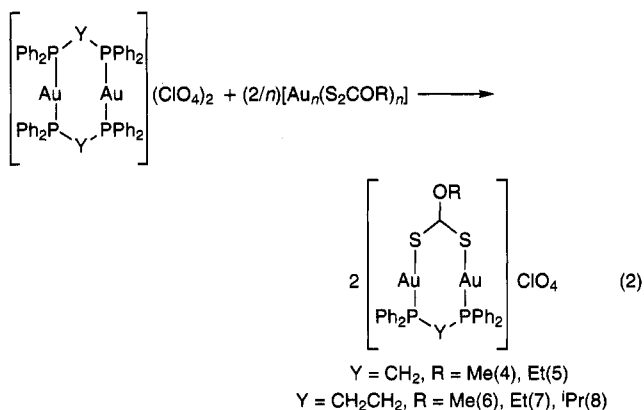
Table 3. Selected Bond Lengths (Å) and Angles (deg) for 3

Au(1)–C(1)	2.073 (10)	Au(1)–S(1)	2.296 (3)
Au(1)–Au(2)	2.8809 (9)	Au(2)–C(2)	2.077 (9)
Au(2)–S(2)	2.309 (3)	S(1)–C(3)	1.708 (10)
S(2)–C(3)	1.674 (10)	P–C(1)	1.764 (9)
P–C(2)	1.773 (9)	P–C(21)	1.806 (10)
P–C(11)	1.831 (10)	O–C(3)	1.341 (12)
O–C(4)	1.483 (12)		
C(1)–Au(1)–S(1)	176.6 (3)	C(1)–Au(1)–Au(2)	90.1 (2)
S(1)–Au(1)–Au(2)	92.98 (7)	C(2)–Au(2)–S(2)	176.3 (3)
C(2)–Au(2)–Au(1)	91.0 (3)	S(2)–Au(2)–Au(1)	91.91 (7)
C(3)–S(1)–Au(1)	110.7 (3)	C(3)–S(2)–Au(2)	112.0 (4)
C(1)–P–C(2)	111.4 (5)	C(1)–P–C(21)	108.9 (4)
C(2)–P–C(21)	110.2 (5)	C(1)–P–C(11)	109.3 (5)
C(2)–P–C(11)	110.7 (4)	C(21)–P–C(11)	106.2 (4)
C(3)–O–C(4)	122.8 (8)	P–C(1)–Au(1)	108.6 (5)
P–C(2)–Au(2)	109.8 (4)	O–C(3)–S(2)	120.5 (8)
O–C(3)–S(1)	107.9 (7)	S(2)–C(3)–S(1)	131.6 (6)
O–C(4)–C(5)	107.6 (9)	O–C(4)–C(6)	105.3 (9)

the bis(ylide)digold(I) complex [Au₂{μ-(CH₂)₂PPh₂}] (2.977(1) Å)¹¹ or in [Au₂{μ-(CH₂)₂S(O)NMe₂}]{μ-(PPh₂)₂-

$\text{CH}_2\text{]} \text{BF}_4$ (2.984(1) Å).¹² The main difference from these two heterobridged dinuclear gold(I) complexes is the absence of intermolecular gold-gold contacts; although the molecules pack in loose pairs antiparallel to each other, the shortest such gold-gold distance is 4.571 Å. The conformation of the eight-membered ring is an "envelope" form, with the ylide P atom lying 0.75 Å out of the plane of the other seven atoms. The coordination around the gold atoms is almost linear, with C-Au-S angles of 176.3(3) and 176.6(3)°. The Au-C bond lengths, 2.073(10) and 2.077(9) Å, are similar to those found in $[\text{Au}_2\{\mu\text{-(CH}_2\text{)}_2\text{PPh}_2\}_2]$ (2.091(7) and 2.085(7) Å), and the Au-S bond distances, 2.296(3) and 2.309(3) Å, are close to those found in the gold(I) xanthate complexes $[\text{Au}(\text{S}_2\text{COR})(\text{PR}_3)]$.⁵

The bidentate ligand transfer processes shown in eq 1 can involve donor-acceptor intermediates, as described for ylide transfer reactions. Thus, we can carry out reactions involving the homoleptic gold(I) xanthate $[\text{Au}_n(\text{S}_2\text{COR})_n]$ (R = Me, Et, ⁱPr) with cationic gold(I) diphosphine complexes $[\text{Au}_2\{\mu\text{-(PPh}_2\text{)}_2\text{Y}\}_2](\text{ClO}_4)_2$ (Y = CH₂, CH₂CH₂) (the former acting as donor and the latter as acceptor), from which we have succeeded in obtaining heterobridged dinuclear gold(I) complexes (eq 2). These reactions proceed even faster than reaction 1.



Complexes 4–8 are air- and moisture-stable yellow solids. They behave as 1:1 electrolytes in acetone solutions, and their IR spectra show bands at 1100 (s, br) and 623 (m) cm⁻¹ which are characteristic of the ClO₄⁻ anion.¹³ The ³¹P{¹H} NMR spectra show a singlet at ca. δ 37 ppm (4, 5) or 34 ppm (6–8) for the phosphorus atoms (Table 1), which imply a dinuclear structure as in complexes 1–3, rather than a tetranuclear structure, in which we should expect complicated spectra as found in $[\text{Au}_4(\mu\text{-dmit})_2\{\mu\text{-(PPh}_2\text{)}_2\text{-CH}_2\}_2]$ ¹⁴ (dmit = 4,5-dimercapto-1,3-dithiole-2-thionate) or in $[\text{Au}_4(\text{MNT})(\text{dppee})_2\text{Cl}_2]$ ¹⁵ (MNT = 1,2-dicyanoethene-1,2-dithiolate; dppee = *cis*-bis(diphenylphosphino)ethylene). The ¹H NMR spectra show the resonances of both ligands in the correct ratio (Experimental Section). Complexes 4–8 were characterized by positive-ion FAB mass spectrometry. In all cases the parent

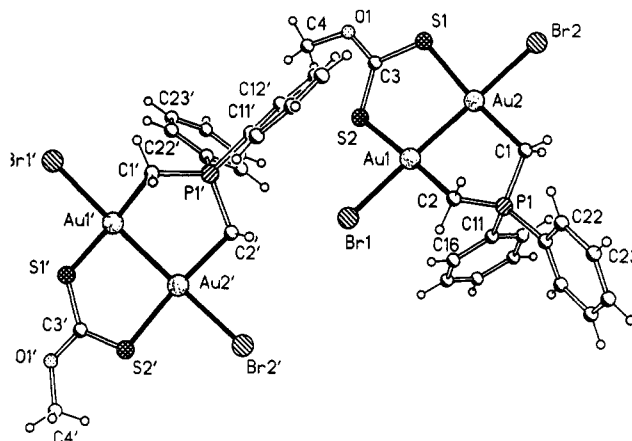
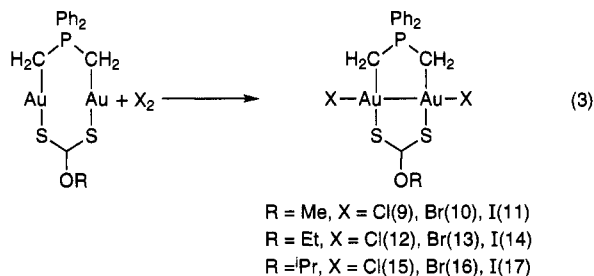


Figure 2. The two molecules of complex 10 in the crystal, with the atom-numbering scheme. Radii are arbitrary.

ion $[\text{M} - \text{ClO}_4]^+$ is the base peak of the spectrum at m/z 885, 899, 899, 913, and 927, respectively.

The neutral dinuclear complexes 1–3 are potential precursors to gold(II) compounds by oxidative addition of halogen, and such reactions are indeed observed, according to eq 3. To the best of our knowledge, they represent the first examples of gold(II) complexes containing xanthate as ligand.



Complexes 9–17 are orange (9, 10, 13, 16), garnet (11, 14, 17), or yellow (12, 15) solids, air- and moisture-stable at room temperature, and are nonconducting in acetone solution. The IR spectra show medium-intensity bands at ca. 570 cm⁻¹ (Table 1) assignable to $\nu(\text{Au}-\text{C}_{\text{ylide}})$ and at 263 (9), 260 (12), or 266 (15) cm⁻¹ due to $\nu(\text{Au}^{\text{II}}-\text{Cl})$.¹⁶ The ³¹P{¹H} NMR spectra show a singlet at ca. δ 42 (9, 12, 15), 46 (10, 13, 16), or 53 (11, 14, 17) ppm for the phosphorus atom of the ylide group (Table 1). These resonances are markedly low-field-shifted compared with 1–3 and follow the trend $\delta_{\text{I}} > \delta_{\text{Br}} > \delta_{\text{Cl}}$, as already observed in $[\text{Au}_2\{\mu\text{-(CH}_2\text{)}_2\text{PPh}_2\}\{\mu\text{-S}_2\text{CNR}_2\}\text{-X}_2]$ ¹⁷ and the symmetrical complexes $[\text{Au}_2\{\mu\text{-(CH}_2\text{)}_2\text{-PPh}_2\}_2\text{X}_2]$.¹¹ In the ¹H NMR spectra the ylide methylene proton resonances appear as doublets, which fall in the range δ 2.78–2.97 ppm (Table 1); again they are low-field-shifted and display the same order $\delta_{\text{I}} > \delta_{\text{Br}} > \delta_{\text{Cl}}$.¹⁷ The FAB⁺ mass spectra do not show the molecular cation peak, although in every spectrum the $[\text{M} - \text{X}]^+$ peak appears at m/z (%) 749 (54), 795 (38), 841 (70), 763 (72), 808 (100), 855 (100), 777 (10), 823 (4), and 869 (12), respectively.

The crystal structure of complex 10 has been determined by X-ray crystallography (Figure 2). The asymmetric unit consists of two molecules of 10 and two

(12) Lin, I. J. B.; Liu, C. W.; Liu, L. K.; Wen, Y. S. *Organometallics* **1992**, *11*, 1447.

(13) Gowda, M. N.; Naikar, S. B.; Reddy, G. K. N. *Adv. Inorg. Chem. Radiochem.* **1984**, *28*, 255.

(14) Cerrada, E.; Jones, P. G.; Laguna, A.; Laguna, M. *J. Chem. Soc., Dalton Trans.* **1994**, 1325.

(15) Dávila, R. M.; Staples, R. J.; Fackler, J. P., Jr. *Organometallics* **1994**, *13*, 418.

(16) Usón, R.; Laguna, A.; Laguna, M.; Fraile, M. N.; Jones, P. G.; Sheldrick, G. M. *J. Chem. Soc., Dalton Trans.* **1986**, 291.

(17) Bardají, M.; Gimeno, M. C.; Jones, P. G.; Laguna, A.; Laguna, M. *Organometallics* **1994**, *13*, 3415.

Table 4. Atomic Coordinates ($\times 10^4$) and Equivalent Isotropic Displacement Parameters ($\text{\AA}^2 \times 10^3$) for 10^a

	x	y	z	U(eq)
Au(1)	2430.3 (4)	6396.1 (4)	3783.6 (3)	26.5 (1)
Au(2)	419.5 (4)	5866.8 (4)	4127.7 (3)	25.6 (1)
Br(1)	4430.6 (11)	6969.4 (10)	3503.1 (9)	38.2 (3)
Br(2)	-1513.9 (10)	5273.3 (10)	4537.3 (8)	31.0 (3)
S(1)	-388 (3)	4075 (2)	3007 (2)	32.6 (7)
S(2)	1677 (3)	5166 (3)	2277 (2)	33.7 (7)
P(1)	2484 (3)	8330 (2)	5373 (2)	29.2 (6)
O(1)	-122 (8)	3164 (7)	1516 (5)	43 (2)
C(1)	978 (9)	7420 (10)	5162 (8)	31 (3)
C(2)	3168 (10)	7458 (9)	5117 (7)	28 (2)
C(3)	388 (11)	4102 (10)	2218 (8)	31 (2)
C(4)	417 (15)	3084 (13)	747 (9)	54 (4)
C(11)	2725 (10)	9196 (9)	4692 (8)	34 (2)
C(12)	2024 (11)	9732 (10)	4638 (8)	41 (2)
C(13)	2204 (11)	10426 (10)	4116 (9)	43 (3)
C(14)	3058 (11)	10569 (11)	3653 (9)	43 (3)
C(15)	3747 (11)	10035 (10)	3699 (8)	37 (2)
C(16)	3593 (10)	9360 (9)	4226 (8)	36 (2)
C(21)	3088 (10)	9241 (9)	6537 (8)	32 (2)
C(22)	3009 (11)	8719 (10)	7179 (8)	42 (3)
C(23)	3565 (13)	9400 (12)	8094 (8)	53 (4)
C(24)	4160 (13)	10546 (11)	8339 (9)	51 (3)
C(25)	4226 (12)	11059 (11)	7701 (8)	49 (3)
C(26)	3673 (12)	10405 (10)	6794 (8)	42 (3)
Au(1')	7582.1 (4)	4393.6 (4)	1587.6 (3)	25.8 (1)
Au(2')	8148.7 (4)	6333.0 (4)	2762.5 (3)	26.5 (1)
Br(1')	6935.2 (12)	2508.5 (10)	385.7 (8)	39.6 (3)
Br(2')	8695.4 (12)	8211.8 (11)	3937.3 (9)	43.4 (3)
S(1')	8970 (3)	5129 (3)	809 (2)	33.5 (7)
S(2')	10060 (3)	7121 (3)	2573 (2)	33.9 (7)
P(1')	5514 (3)	4375 (3)	2419 (2)	29.7 (7)
O(1')	10956 (7)	6780 (7)	1199 (5)	40 (2)
C(1')	6392 (9)	3662 (10)	2265 (7)	26 (2)
C(2')	6481 (11)	5804 (9)	3029 (8)	34 (3)
C(3')	10042 (9)	6386 (9)	1537 (7)	26 (2)
C(4')	12003 (12)	7813 (12)	1742 (10)	54 (4)
C(11')	4486 (10)	3873 (10)	3066 (8)	35 (2)
C(12')	3339 (11)	3662 (12)	2837 (9)	51 (3)
C(13')	2627 (12)	3369 (13)	3414 (10)	55 (3)
C(14')	3044 (11)	3278 (11)	4198 (8)	45 (3)
C(15')	4183 (12)	3495 (12)	4426 (9)	48 (3)
C(16')	4918 (11)	3819 (11)	3884 (9)	43 (3)
C(21')	4701 (10)	4198 (9)	1351 (7)	32 (2)
C(22')	4445 (12)	3291 (11)	583 (8)	46 (3)
C(23')	3783 (12)	3143 (12)	-222 (9)	51 (3)
C(24')	3344 (13)	3900 (11)	-256 (8)	48 (3)
C(25')	3596 (12)	4812 (11)	494 (8)	44 (3)
C(26')	4278 (11)	4963 (11)	1304 (8)	39 (3)
C(5)	2331 (25)	136 (25)	136 (19)	129 (9)
Cl(1)	3782 (7)	560 (6)	1083 (8)	196 (5)
Cl(2)	1582 (12)	428 (15)	768 (11)	270 (7)
C(6)	9520 (33)	9753 (30)	2326 (24)	175 (13)
Cl(3)	9121 (11)	8793 (8)	1367 (6)	188 (4)
Cl(4)	9665 (10)	10963 (8)	2643 (10)	224 (6)

^a See footnote a in Table 2.

molecules of dichloromethane. As in **3**, the structure consists of an eight-membered dimetallacycle in which the two gold atoms are doubly bridged by a xanthate and a bis(ylide) ligand. The C–Au–S angles lie in the range 173.7–176.9(3)°, slightly smaller than that in **3**. In addition, the “envelope” has become a twisted conformation, probably because of the Au–Au bond formation upon oxidation. The Au–Au distances are 2.566(1) and 2.5710(11) Å, shorter than in the symmetrical $[\text{Au}_2\{\mu\text{-(CH}_2)_2\text{PPh}_2\}_2\text{Br}_2]^{18}$ (2.614(1) Å) and close to that found in the analogous complex $[\text{Au}_2\{\mu\text{-(CH}_2)_2\text{PPh}_2\}\{\mu\text{-S}_2\text{CN(CH}_2\text{Ph)}_2\}\text{Br}_2]^{17}$ (2.5653(10) Å). There are inter-

(18) Usón, R.; Laguna, A.; Laguna, M.; Jiménez, J.; Jones, P. G. *J. Chem. Soc., Dalton Trans.* **1991**, 1361.

Table 5. Selected Bond Lengths (Å) and Angles (deg) for **10**

Au(1)–C(2)	2.075 (11)	Au(1)–S(2)	2.351 (3)
Au(1)–Br(1)	2.510 (2)	Au(1)–Au(2)	2.5660 (10)
Au(2)–C(1)	2.100 (12)	Au(2)–S(1)	2.346 (3)
Au(2)–Br(2)	2.5178 (14)	S(1)–C(3)	1.693 (12)
S(2)–C(3)	1.693 (12)	P(1)–C(2)	1.753 (12)
P(1)–C(1)	1.770 (11)	P(1)–C(11)	1.793 (12)
P(1)–C(21)	1.804 (13)	O(1)–C(3)	1.314 (14)
O(1)–C(4)	1.48 (2)	Au(1')–C(1')	2.067 (11)
Au(1')–S(1')	2.348 (3)	Au(1')–Br(1')	2.516 (2)
Au(1')–Au(2')	2.5710 (11)	Au(2')–C(2')	2.111 (13)
Au(2')–S(2')	2.357 (3)	Au(2')–Br(2')	2.516 (2)
S(1')–C(3')	1.700 (12)	S(2')–C(3')	1.678 (11)
P(1')–C(2')	1.763 (11)	P(1')–C(1')	1.776 (10)
P(1')–C(21')	1.801 (11)	P(1')–C(11')	1.808 (12)
O(1')–C(3')	1.329 (13)	O(1')–C(4')	1.46 (2)
C(2)–Au(1)–S(2)	176.9 (3)	C(2)–Au(1)–Br(1)	90.0 (3)
S(2)–Au(1)–Br(1)	87.60 (9)	C(2)–Au(1)–Au(2)	87.9 (3)
S(2)–Au(1)–Au(2)	94.49 (8)	Br(1)–Au(1)–Au(2)	177.89 (4)
C(1)–Au(2)–S(1)	174.2 (3)	C(1)–Au(2)–Br(2)	86.7 (3)
S(1)–Au(2)–Br(2)	87.48 (9)	C(1)–Au(2)–Au(1)	93.8 (3)
S(1)–Au(2)–Au(1)	91.98 (8)	Br(2)–Au(2)–Au(1)	175.69 (3)
C(3)–S(1)–Au(2)	109.8 (4)	C(3)–S(2)–Au(1)	107.0 (4)
C(2)–P(1)–C(1)	106.2 (6)	C(2)–P(1)–C(11)	110.8 (5)
C(1)–P(1)–C(11)	111.1 (6)	C(2)–P(1)–C(21)	109.3 (5)
C(1)–P(1)–C(21)	111.3 (5)	C(11)–P(1)–C(21)	108.1 (5)
C(3)–O(1)–C(4)	118.3 (10)	P(1)–C(1)–Au(2)	113.2 (6)
P(1)–C(2)–Au(1)	108.5 (5)	O(1)–C(3)–S(1)	112.0 (9)
O(1)–C(3)–S(2)	121.2 (9)	S(1)–C(3)–S(2)	126.8 (7)
C(1')–Au(1')–S(1')	176.2 (3)	C(1')–Au(1')–Br(1')	90.9 (3)
S(1')–Au(1')–Br(1')	86.49 (9)	C(1')–Au(1')–Au(2')	89.0 (3)
S(1')–Au(1')–Au(2')	93.76 (8)	Br(1')–Au(1')–Au(2')	176.63 (4)
C(2')–Au(2')–S(2')	173.7 (3)	C(2')–Au(2')–Br(2')	86.5 (3)
S(2')–Au(2')–Br(2')	87.24 (9)	C(2')–Au(2')–Au(1')	92.9 (3)
S(2')–Au(2')–Au(1')	93.35 (8)	Br(2')–Au(2')–Au(1')	178.78 (4)
C(3')–S(1')–Au(1')	107.8 (4)	C(3')–S(2')–Au(2')	107.9 (4)
C(2')–P(1')–C(1')	106.2 (6)	C(2')–P(1')–C(21')	111.3 (5)
C(1')–P(1')–C(21')	110.7 (5)	C(2')–P(1')–C(11')	108.3 (6)
C(1')–P(1')–C(11')	112.2 (5)	C(21')–P(1')–C(11')	108.1 (5)
C(3')–O(1')–C(4')	120.4 (9)	P(1')–C(1')–Au(1')	107.6 (5)
P(1')–C(2')–Au(2')	113.8 (6)	O(1')–C(3')–S(2')	119.8 (9)
O(1')–C(3')–S(1')	111.8 (8)	S(2')–C(3')–S(1')	128.3 (7)

molecular contacts between gold atoms (Au(2)Au(2') $;-1+x,y,z$), 3.833 Å; Au(2)Au(2') $;-x,1-y,1-z$), 4.121 Å) and between gold and bromine (Au(2)Br(2') $;-x,1-y,1-z$), 3.472 Å; Au(2') $;-1+x,y,z$)Br(2), 3.597 Å).

The Au–Br bond lengths range from 2.510(2) to 2.518(1) Å, similar to those in $[\text{Au}_2\{\mu\text{-(CH}_2)_2\text{PPh}_2\}_2\text{Br}_2]$ (2.516(1) Å) or in $(\text{NBu}_4)[\text{Au}_2\{\mu\text{-MNT}\}_2\text{Br}_2]^{19}$ (2.510(8) Å). The values do not display the unexpected difference observed in $[\text{Au}_2\{\mu\text{-(CH}_2)_2\text{PPh}_2\}\{\mu\text{-S}_2\text{CN(CH}_2\text{Ph)}_2\}\text{Br}_2]$ (2.5022(14) and 2.5253(14) Å). The Au–S bond lengths (2.346(3)–2.357(3) Å) are longer than in **3** and marginally longer than in $[\text{Au}_2\{\mu\text{-(CH}_2)_2\text{PPh}_2\}\{\mu\text{-S}_2\text{CN(CH}_2\text{Ph)}_2\}\text{Br}_2]$ (2.337(3) and 2.338(3) Å), in which an elongation of the Au–S distances as one goes from dithiocarbamate–gold(I) to –gold(II) derivatives had already been remarked upon. The Au–C distances 2.067(11)–2.111(13) Å are similar to those found in other gold(II) ylide complexes. The coordination around the gold atoms is essentially square planar. The chains Br–Au–Au–Br are almost linear; Br–Au–Au angles are 175.69(3)–178.78(4)°.

The reaction of the cationic complexes **4**–**8** with halogen proceeds in a different way; the gold(II) derivatives are not obtained and the $^{31}\text{P}\{^1\text{H}\}$ NMR spectra show a mixture of products, including the starting material. In the case of **4** and **5** with chlorine,

(19) Khan, N. I.; Wang, S.; Fackler, J. P., Jr. *Inorg. Chem.* **1989**, *28*, 3579.

the previously described complexes $[\text{Au}_3\text{Cl}_2\{\mu\text{-(PPh}_2)_2\text{-CH}_2\}_2]\text{ClO}_4$ and $[(\text{AuCl})_2\{\mu\text{-(PPh}_2)_2\text{CH}_2\}]^{20,21}$ were detected by $^{31}\text{P}\{^1\text{H}\}$ NMR.

These results can be rationalized by considering that strongly σ -donating ligands, such as bis(ylide), should support oxidative addition much better than weaker σ -donating and stronger π -accepting ligands.²² This could be the reason the combination of bis(ylide) and xanthate, but not diphosphine and xanthate, yields gold(II) derivatives. Moreover, the positive charge of the diphosphine complex, in contrast to the neutral character of the xanthate-bis(ylide) pair, could be an additional reason; very few cationic gold(II) complexes are known.^{18,23}

Experimental Section

General Data. IR spectra were recorded on a Perkin-Elmer 559 or 883 spectrophotometer, over the range 4000–200 cm^{-1} , by using Nujol mulls between polyethylene sheets. ^1H and ^{31}P NMR spectra were measured on a Varian UNITY 300 in CDCl_3 solutions; chemical shifts are quoted relative to SiMe_4 (^1H) and H_3PO_4 (external, ^{31}P). C, H, and N analyses were performed with a Perkin-Elmer 2400 microanalyzer. Conductivities were measured in acetone solution with a Philips PW 9509 apparatus. Melting points were measured on a Büchi apparatus and are uncorrected. Mass spectra were recorded on a VG Autospec using FAB^+ techniques.

Electrochemical studies were carried out using an EG and G Model 273 potentiostat, in conjunction with a three-electrode cell. The auxiliary electrode was a platinum wire, and the working electrode was a platinum bead. The reference was an aqueous saturated calomel electrode (SCE) separated from the test solution by a fine-porosity frit and an agar bridge saturated with KCl. CH_2Cl_2 solutions were 5×10^{-4} M in complex and 0.1 M in $[\text{NBu}_4][\text{PF}_6]$ as the supporting electrolyte.

C, H, and N analyses and $^{31}\text{P}\{^1\text{H}\}$ and some ^1H NMR data are listed in Table 1. All reactions were carried out at room temperature.

Syntheses. $[\text{Au}_2\{\mu\text{-(CH}_2)_2\text{PPh}_2\}(\mu\text{-S}_2\text{COR})]$ (**R = Me (1), Et (2), ^iPr (3)**). To a solution of $[\text{Au}_2\{\mu\text{-(CH}_2)_2\text{PPh}_2\}_2]^{11}$ (0.123 g, 0.15 mmol) in dichloromethane (40 mL) was added the stoichiometric amount of $[\text{Au}_n(\mu\text{-S}_2\text{COR})_n]$ (obtained by addition of $[\text{AuCl}(\text{tht})]^{24}$ to an alcoholic KS_2COR solution⁴) (**R = Me**, 0.092 g (**1**); **R = Et**, 0.096 g (**2**); **R = ^iPr** , 0.099 g (**3**)). After the suspension was stirred for about 6 h, the solution was filtered off to remove the unreacted starting material. Then the clear solution was evaporated to ca. 5 mL. Addition of diethyl ether led to precipitation of **1–3**. Solids were washed with diethyl ether (2×5 mL). **1**: yield 80%; mp 194 °C dec; ^1H NMR (not included in Table 1) δ 7.83–7.39 (m, 10H, Ph), 4.13 (s, 3H, Me); $\Lambda_M = 1 \Omega^{-1} \text{cm}^2 \text{mol}^{-1}$. **2**: yield 85%; mp 175 °C; ^1H NMR δ 7.83–7.44 (m, 10H, Ph), 4.49 (q, 2H, $J(\text{HH}) = 7.1$ Hz, $\text{CH}_2\text{-O}$), 1.42 (t, 3H, CH_3); $\Lambda_M = 1 \Omega^{-1} \text{cm}^2 \text{mol}^{-1}$. **3**: yield 78%; mp 160 °C; ^1H NMR δ 7.81–7.43 (m, 10H, Ph), 5.40 (sept, 1H, $J(\text{HH}) = 6.2$ Hz, CH-O), 1.38 (d, 6H, Me); $\Lambda_M = 1 \Omega^{-1} \text{cm}^2 \text{mol}^{-1}$. Other mass spectra peaks at m/z (%) 517 (50, **1**) and 545 (12, **3**) are due to $[\text{M} - \text{Au}]^+$.

$[\text{Au}_2(\mu\text{-S}_2\text{COR})\{\mu\text{-(PPh}_2)_2\text{Y}\}]\text{ClO}_4$ (**Y = CH}_2**, **R = Me (4), Et (5)**; **Y = CH}_2\text{CH}_2**, **R = Me (6), Et (7), ^iPr (8)**). To a solution of $[\text{Au}_2\{\mu\text{-(PPh}_2)_2\text{Y}\}_2](\text{ClO}_4)_2^{16,25}$ (0.05 mmol; **X = CH}_2** (0.068 g), **CH}_2\text{CH}_2** (0.069 g)) in dichloromethane (40 mL) was added the stoichiometric amount of $[\text{Au}_n(\mu\text{-S}_2\text{COR})_n]$ (**R = Me** (0.030 g), **Et** (0.032 g), **^iPr** (0.033 g)). After the mixture was stirred for 5 h (**4**) or 2 h (**5–8**), the solution was filtered. Concentration of the filtered solution to ca. 5 mL and addition of diethyl ether led to precipitation of **4–8**. Solids were washed with diethyl ether (2×5 mL). **4**: yield 82%; mp 240 °C dec; ^1H NMR δ 7.79–7.33 (m, 20H, Ph), 4.33 (s, 3H, Me), 4.19 (t, 2H, $J(\text{PH}) = 12.4$ Hz, PCH_2P); $\Lambda_M = 110 \Omega^{-1} \text{cm}^2 \text{mol}^{-1}$. **5**: yield 72%; mp 160 °C; ^1H NMR δ 7.80–7.33 (m, 20H, Ph), 4.69 (q, 2H, $J(\text{HH}) = 7.1$ Hz, $\text{CH}_2\text{-O}$), 4.19 (t, 2H, $J(\text{PH}) = 12.5$ Hz, PCH_2P), 1.42 (t, 3H, CH_3); $\Lambda_M = 111 \Omega^{-1} \text{cm}^2 \text{mol}^{-1}$. **6**: yield 94%; mp 202 °C; ^1H NMR δ 7.81–7.50 (m, 20H, Ph), 4.36 (s, 3H, Me), 3.10 ("d", 4H, $J(\text{PH}) = 12.4$ Hz, $\text{PCH}_2\text{CH}_2\text{P}$); $\Lambda_M = 130 \Omega^{-1} \text{cm}^2 \text{mol}^{-1}$. **7**: yield 78%; mp 218 °C; ^1H NMR δ 7.83–7.51 (m, 20H, Ph), 4.72 (q, 2H, $J(\text{HH}) = 7.1$ Hz, $\text{CH}_2\text{-O}$), 3.10 ("d", 4H, $J(\text{PH}) = 12.2$ Hz, $\text{PCH}_2\text{CH}_2\text{P}$), 1.58 (t, 3H, CH_3); $\Lambda_M = 127 \Omega^{-1} \text{cm}^2 \text{mol}^{-1}$. **8**: yield 72%; mp 190 °C; ^1H NMR δ 7.81–7.50 (m, 20H, Ph), 5.53 (sept, 1H, $J(\text{HH}) = 6.0$ Hz, CH-O), 3.09 (br, 4H, $\text{PCH}_2\text{CH}_2\text{P}$), 1.56 (d, 6H, Me); $\Lambda_M = 103 \Omega^{-1} \text{cm}^2 \text{mol}^{-1}$.

$[\text{Au}_2\{\mu\text{-(CH}_2)_2\text{PPh}_2\}(\mu\text{-S}_2\text{COR})\text{X}_2]$ (**R = Me, X = Cl (9), Br (10), I (11)**; **R = Et, X = Cl (12), Br (13), I (14)**; **R = ^iPr , X = Cl (15), Br (16), I (17)**). To a solution of $[\text{Au}_2\{\mu\text{-(CH}_2)_2\text{PPh}_2\}(\mu\text{-S}_2\text{COR})]$ (0.1 mmol; **1** (0.071 g), **2** (0.073 g), **3** (0.074 g)) in dichloromethane (20 mL) was added the stoichiometric amount of halogen X_2 (0.1 mmol; $\text{X}_2 = \text{Cl}_2, \text{Br}_2$, in CCl_4 solution; I_2 , 0.025 g). After the mixture was stirred for about 20 min at room temperature, the solution was concentrated to ca. 5 mL. Addition of diethyl ether (20 mL) afforded complexes **9–17**. Solids were washed with diethyl ether (2×5 mL). **9**: yield 77%; mp 148 °C dec; ^1H NMR (not included in Table 1) δ 7.74–7.54 (m, 10H, Ph), 4.22 (s, 3H, Me); $\Lambda_M = 3 \Omega^{-1} \text{cm}^2 \text{mol}^{-1}$. **10**: yield 80%; mp 124 °C dec; ^1H NMR δ 7.74–7.53 (m, 10H, Ph), 4.22 (s, 3H, Me); $\Lambda_M = 4 \Omega^{-1} \text{cm}^2 \text{mol}^{-1}$. **11**: yield 90%; mp 130 °C dec; ^1H NMR δ 7.71–7.63 (m, 10H, Ph), 4.19 (s, 3H, Me); $\Lambda_M = 3 \Omega^{-1} \text{cm}^2 \text{mol}^{-1}$. **12**: yield 89%; mp 146 °C; ^1H NMR δ 7.75–7.56 (m, 10H, Ph), 4.59 (q, 2H, $J(\text{HH}) = 7.1$ Hz, $\text{CH}_2\text{-O}$), 1.46 (t, 3H, CH_3); $\Lambda_M = 5 \Omega^{-1} \text{cm}^2 \text{mol}^{-1}$. **13**: yield 90%; mp 120 °C dec; ^1H NMR δ 7.73–7.53 (m, 10H, Ph), 4.57 (q, 2H, $J(\text{HH}) = 7.1$ Hz, $\text{CH}_2\text{-O}$), 1.44 (t, 3H, CH_3); $\Lambda_M = 3 \Omega^{-1} \text{cm}^2 \text{mol}^{-1}$. **14**: yield 83%; mp 98 °C dec; ^1H NMR δ 7.71–7.52 (m, 10H, Ph), 4.55 (q, 2H, $J(\text{HH}) = 7.1$ Hz, $\text{CH}_2\text{-O}$), 1.44 (t, 3H, CH_3); $\Lambda_M = 2 \Omega^{-1} \text{cm}^2 \text{mol}^{-1}$. **15**: yield 70%; mp 163 °C dec; ^1H NMR δ 7.76–7.37 (m, 10H, Ph), 5.45 (sept, 1H, $J(\text{HH}) = 6.1$ Hz, CH-O), 1.43 (d, 6H, Me); $\Lambda_M = 2 \Omega^{-1} \text{cm}^2 \text{mol}^{-1}$. **16**: yield 73%; mp 162 °C dec; ^1H NMR δ 7.80–7.37 (m, 10H, Ph), 5.44 (sept, 1H, $J(\text{HH}) = 6.1$ Hz, CH-O), 1.43 (d, 6H, Me); $\Lambda_M = 4 \Omega^{-1} \text{cm}^2 \text{mol}^{-1}$. **17**: yield 78%; mp 110 °C; ^1H NMR δ 7.71–7.47 (m, 10H, Ph), 5.41 (sept, 1H, $J(\text{HH}) = 6.1$ Hz, CH-O), 1.41 (d, 6H, Me); $\Lambda_M = 23 \Omega^{-1} \text{cm}^2 \text{mol}^{-1}$.

X-ray Structure Determination of Compounds 3 and 10. Crystals were mounted on glass fibers in inert oil and transferred to the cold gas stream of the diffractometer (Siemens R3 with LT-2 low temperature attachment). Data were collected at -100 °C in the ω -scan mode using monochromated $\text{Mo K}\alpha$ radiation ($\lambda = 0.71073$ Å) to $2\theta_{\text{max}} = 50^\circ$. Cell constants were refined from setting angles of ca. 50 reflections in the 2θ range $20\text{--}23^\circ$. Absorption corrections were based on ψ scans. Structures were solved with the heavy-atom method and refined anisotropically on F^2 .²⁶ Hydrogen atoms were included as rigid methyl groups or using a riding model.

(25) Schmidbaur, H.; Wohlleben, A.; Schubert, U.; Frank, A.; Huttner, G. *Chem. Ber.* **1977**, *110*, 2751.

(26) Sheldrick, G. M. SHELXL-93: A Program for Crystal Structure Refinement (prerelease version 1992); University of Göttingen, Göttingen, Germany.

(20) Usón, R.; Laguna, A.; Laguna, M.; Fernández, E.; Villacampa, M. D.; Jones, P. G.; Sheldrick, G. M. *J. Chem. Soc., Dalton Trans.* **1983**, 1679.

(21) Schmidbaur, H.; Wohlleben, A.; Wagner, F.; Orama, O.; Huttner, G. *Chem. Ber.* **1977**, *110*, 1748.

(22) Schmidbaur, H. *Acc. Chem. Res.* **1975**, *8*, 62.

(23) (a) Vicente, J.; Chicote, M. T.; Saura-Llamas, I. *J. Chem. Soc., Dalton Trans.* **1990**, 1941. (b) Laguna, A.; Laguna, M.; Jiménez, J.; Lahoz, F. J.; Olmos, E. *J. Organomet. Chem.* **1992**, *435*, 235. (c) Bardají, M.; Blasco, A.; Jiménez, J.; Jones, P. G.; Laguna, A.; Laguna, M.; Merchán, F. *Inorg. Chim. Acta* **1994**, *223*, 55.

(24) Usón, R.; Laguna, A.; Laguna, M. *Inorg. Synth.* **1989**, *26*, 85.

Compound 3: monoclinic, space group $P2_1/c$, $a = 8.571(3)$ Å, $b = 10.219(4)$ Å, $c = 23.210(6)$ Å, $\beta = 97.37(3)^\circ$, $V = 2016.1$ Å³, $Z = 4$, $\mu = 14.8$ mm⁻¹, $D_{\text{exptl}} = 2.446$ Mg m⁻³; pale brown tablet cut to $0.8 \times 0.25 \times 0.1$ mm, 6108 reflections, 3566 independent ($R_{\text{int}} = 0.061$); 219 parameters, 150 restraints, $R_w(F^2) = 0.097$, $R(F, >4\sigma(F)) = 0.033$, $S = 1.05$, maximum $\Delta\rho = 2.3$ e Å⁻³.

Compound 10-CH₂Cl₂: triclinic, space group $P\bar{1}$, $a = 12.917(4)$ Å, $b = 13.864(3)$ Å, $c = 15.975(5)$ Å, $\alpha = 106.05(2)^\circ$, $\beta = 96.27(2)^\circ$, $\gamma = 113.78(2)^\circ$, $V = 2435.5$ Å³, $Z = 4$, $\mu = 15.8$ mm⁻¹, $D_{\text{exptl}} = 2.616$ Mg m⁻³; orange prism $0.5 \times 0.3 \times 0.15$ mm, 10 360 reflections, 8618 independent ($R_{\text{int}} = 0.024$); 479 parameters, 296 restraints, $R_w(F^2) = 0.112$, $R(F, >4\sigma(F)) = 0.040$, $S = 1.01$, maximum $\Delta\rho = 1.8$ e Å⁻³.

Acknowledgment. We thank the Dirección General de Investigación Científica y Técnica (No. PB91-0122) and the Fonds der Chemischen Industrie for financial support and Ministerio de Educación y Ciencia for a grant (to M.B.).

Supplementary Material Available: Descriptions of the crystal structure determinations, including tables of crystal data, data collection, and solution and refinement parameters, atomic coordinates of H atoms, bond distances and angles, and thermal parameters (10 pages). Ordering information is given on any current masthead page.

OM940733Q

Organometallic Mixed-Valent Ions with d^7d^8 and d^8d^9 Electronic Configurations Derived from (fulvalenediyl) $\text{Co}_2(\text{COD})_2$

Teen T. Chin and William E. Geiger*

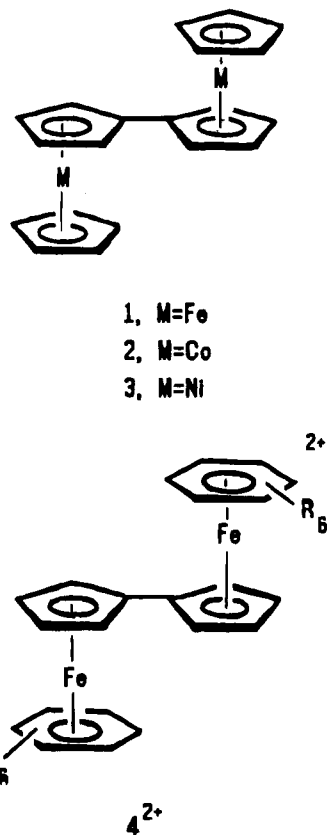
Department of Chemistry, University of Vermont, Burlington, Vermont 05405

Received September 30, 1994[⊗]

The dinuclear complex (fulvalenediyl) $\text{Co}_2(1,5\text{-C}_8\text{H}_{12})_2$ ($\text{FvCo}_2(\text{COD})_2$), **5**, has four one-electron redox reactions in the potential range +1.0 to -3.1 V vs ferrocene, three of which are chemically reversible. Two oxidations are observed with formal potentials of -0.300 and -0.072 V, the E° separation of 228 mV being diagnostic of a moderate M-M interaction. ESR spectra of the d^7d^8 mixed-valent monocation **5**⁺ show that it is valence trapped. The reduction **5**/**5**⁻ has a formal potential of -2.86 V. The d^8d^9 monoanion **5**⁻ produced by Na/K reduction of **5** in THF is also valence trapped according to ESR spectroscopy. The series **5**⁺/**5**⁻ is the first one in which two different mixed-valent states are characterized for a single fulvalenediyl-bridged complex.

Introduction

Mixed-valent (MV) ions derived from fulvalenediyl-bridged complexes have been intensely investigated. The preponderance of these studies has involved formally d^5d^6 ions, most frequently with ferrocenyl groups as the electron-transfer (ET) centers.¹ A rather sophisticated knowledge of the factors affecting their electronic delocalization has emerged, especially for ions in solid-state matrices.² Although fulvalenediyl-bridged MV complexes with electronic configurations other than d^5d^6 are also of interest, few investigations of such systems have been reported. The d^6d^7 monocation of bicobaltocene, **2**⁺, has a greater metal-metal interaction than that found in the biferrocene cation, **1**⁺,³ and is reported to be delocalized on the ESR time scale.⁴ The information published to date on the binickelocene system **3** is insufficient to warrant a conclusion about delocalization in the d^7d^8 monocation, **3**⁺.⁵ An analogous electron-rich fulvalenediyl system is that derived from the reduction of the d^6d^6 dications, **4**²⁺.⁶ The question of delocalization in the d^6d^7 monocation **4**⁺ is most clear in the arene = hexamethylbenzene case, for which both Mössbauer and



[⊗] Abstract published in *Advance ACS Abstracts*, February 1, 1995.

(1) Cowan, D. O.; LeVanda, C.; Park, J.; Kaufman, F. *Acc. Chem. Res.* **1973**, *6*, 1. For leading references to the electrochemical behavior of biferrocene and its derivatives, see: Kotz, J. C. In *Topics in Organic Electrochemistry*; Fry, A. J., Britton, W. E., Eds.; Plenum Press: New York, 1986; pp 100–113.

(2) Dong, T.-Y.; Hendrickson, D. N.; Iwai, K.; Cohn, M. J.; Geib, S. J.; Rheingold, A. L.; Sano, H.; Motoyama, I.; Nakashima, S. *J. Am. Chem. Soc.* **1985**, *107*, 7996.

(3) McManis, G. E.; Nielson, R. M.; Weaver, M. J. *Inorg. Chem.* **1987**, *27*, 1827.

(4) Morrison, W. H., Jr.; Hendrickson, D. N. *Inorg. Chem.* **1980**, *19*, 3330.

(5) Binickelocene is reported to undergo a two-electron oxidation in a single process, implying noninteracting metal centers (Schottenberger, H.; Ingram, G.; Obendorf, D. *J. Organomet. Chem.* **1992**, *426*, 109), whereas $\text{FvNi}_2(\eta^5\text{-C}_6\text{Me}_6)_2$ is reported to be oxidized in sequential one-electron steps with a large (385 mV) potential separation (Hudeczek, P.; Köhler, F. H. *Organometallics* **1992**, *11*, 1773).

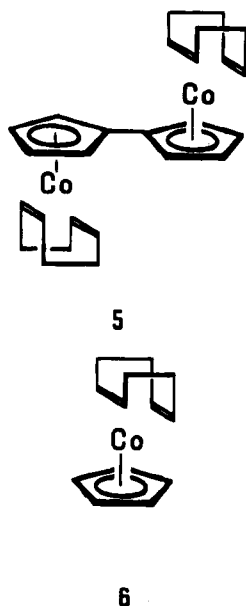
(6) (a) Desbois, M.-H.; Astruc, D.; Guillin, J.; Mariot, J.-P.; Varret, F. *J. Am. Chem. Soc.* **1985**, *107*, 5280. (b) Desbois, M.-H.; Astruc, D.; Guillin, J.; Varret, F.; Trautwein, A. X.; Villeneuve, G. *J. Am. Chem. Soc.* **1989**, *111*, 5800. (c) Desbois, M.-H.; Astruc, D. *Organometallics* **1989**, *8*, 1841. (d) Delville, M.-H.; Rittinger, S.; Astruc, D. *J. Chem. Soc., Chem. Commun.* **1992**, 519.

IR spectroscopy suggest an inherently delocalized SOMO.^{6d}

These literature precedents demonstrate that metal-metal interactions across a fulvalene spacer may be drastically different for different metal electronic configurations. We are pursuing studies to expand our knowledge about the role played by electronic configuration in intramolecular ET across polyolefin bridging ligands, and offer in this paper some observations on d^7d^8 and d^8d^9 systems.

The starting material for generation of the MV species is (fulvalenediyl) $\text{Co}_2(\eta^4\text{-1,5-cyclooctadiene})$, $\text{FvCo}_2(\text{COD})_2$,

5. This complex containing two Co(I), d⁸, metals,



reported earlier by Rausch et al.,⁷ was chosen with the expectations that (a) the monocation and monoanion would each be sufficiently stable to allow for characterization of the desired MV ions and (b) cobalt hyperfine splittings would allow probing of delocalization in those ions by ESR spectroscopy. The mononuclear analogue CpCo(η^4 -1,5-COD), **6**, is known to undergo one-electron oxidation⁸⁻¹⁰ and one-electron reduction¹¹ to the corresponding d⁷, Co(II), and d⁹, Co(0), species, respectively. Both *mononuclear* ions are subject to moderately rapid decomposition reactions and lack the long-term chemical reversibility of, e.g., the Cp₂Fe⁺/Cp₂Fe couple. Nevertheless, both **6**⁺ and **6**⁻ have been studied by ESR spectroscopy.^{10,12} We were able to obtain spectra under similar conditions for the MV ions derived from **5** which show that both the d⁷d⁸ ion (**5**⁺) and the d⁸d⁹ ion (**5**⁻) are *valence trapped* in frozen solutions. We believe that this is the first instance in which a single fulvalenediyl-bridged complex has been characterized in two *different* mixed-valent states.

Although the observation of a single Co hyperfine interaction in both MV ions clearly implies valence trapping, the quantitative significance of the ESR spectra was unclear for **5**⁺ until a successful analysis of the unusual spectrum of **6**⁺ by Rieger et al.¹⁰ Our knowledge of the ESR spectra of these systems is now such that we can say that the degrees of metal character in the SOMOs of **5**⁺ and **5**⁻ are roughly the same, in spite of the much lower Co hyperfine splittings in the cation compared to the anion.

Full details of the electrochemical behavior of **5** are also included. They are consistent with a moderate degree of metal-metal interaction across the fulvalenediyl ligand.

(7) Rausch, M. D.; Spink, W. C.; Conway, B. G.; Rogers, R. D.; Atwood, J. L. *J. Organomet. Chem.* **1990**, *383*, 227.

(8) Moraczewski, J. M.; Geiger, W. E. *Organometallics* **1982**, *1*, 1385.

(9) Kölle, U. *Inorg. Chim. Acta* **1981**, *47*, 13.

(10) Rieger, P. H.; Chin, T. T.; Sharp, L. I.; Geiger, W. E. *Organometallics* **1995**, *14*, 1322.

(11) Moraczewski, J. M.; Geiger, W. E. *J. Am. Chem. Soc.* **1981**, *103*, 4779.

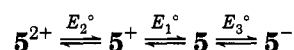
(12) Rieger, P. H. In *Organometallic Radical Processes*; Troglor, W. C., Ed.; Elsevier: Amsterdam, 1990; pp 290-294.

Experimental Section

All operations were conducted with dried and distilled solvents under an atmosphere of dinitrogen, unless otherwise noted. Literature methods were followed for the preparation of [NBu₄][PF₆]¹³ and FvCo₂(COD)₂.⁷ The identity and purity of the latter were checked by NMR and EIMS and by elemental analysis (Robertson Labs) (Calc for C₂₆H₃₂Co₂: C, 67.50; H, 6.93. Found: C, 67.17; H, 7.00). This compound was found to be sparingly soluble in CH₂Cl₂, THF, 1,2-dimethoxyethane, and DMF at temperatures below 270 K. The oxidant [N(p-BrC₆H₄)₃][BF₄] was prepared by a variation of the method of Bell et al.¹⁴ Electrochemical procedures were as previously described.^{15a} The supporting electrolyte was in all cases 0.1 M [NBu₄][PF₆]. Reference electrodes of Ag/AgCl or SCE were employed, but all potentials are referred to the standard ferrocene/ferrocenium couple, added as an internal standard at appropriate points in the experiments, as recommended by IUPAC.¹⁶ The working electrode was generally a Pt bead or disk, the former being pretreated with an HNO₃/Fe(II) cycle, the latter by polishing with diamond paste. Some scans of the reduction waves were obtained at a hanging Hg drop electrode, and rotating electrode voltammograms were obtained with a Pt bead at 1800 rpm. The area of the Pt disk employed for chronoamperometry experiments (0.400 cm²) was calibrated with ferricyanide.^{15b} A luggin probe was employed to minimize ohmic loss in CV experiments. ESR spectra were recorded on a modified Varian E-4 spectrometer using DPPH as a reference standard.

Results

Electrochemistry of FvCo₂(COD)₂. I. Oxidations. Complex **5** displays two diffusion-controlled, one-electron, chemically- and electrochemically-reversible¹⁷ oxidations at mild potentials, $E_1^\circ = -0.300$ V and $E_2^\circ = -0.072$ V vs Fc, in CH₂Cl₂ (Figure 1). When considered with the reduction of **5** (other solvents, vide infra), the dinuclear complex exhibits the reversible ET series (potentials collected in Table 1):



The one-electron stoichiometry of the oxidation processes was confirmed by chronoamperometry and bulk coulometry experiments. For the former, 5 s pulses were employed in stepping from -0.5 V to either -0.2 V (first oxidation) or +0.1 V (second oxidation). The *it*^{1/2} constant for the more positive step was approximately double that of the less positive (38.5 vs 19.6 $\mu\text{A s}^{1/2}$). A diffusion coefficient of 1.12×10^{-5} cm²/s was calculated for **5** from these data. The first oxidation wave was irreversible in more polar solvents such as DMF ($E_{\text{pa}} = -0.41$ V, irrev to $v = 20$ V/s) and THF, consistent with findings for the mononuclear analogue **6**.^{8,9} A third

(13) Tulyathan, B.; Geiger, W. E. *J. Am. Chem. Soc.* **1985**, *107*, 5960.

(14) Bell, F. A.; Ledwith, A.; Sherrington, D. C. *J. Chem. Soc. C* **1969**, 2719.

(15) (a) Pierce, D. T.; Geiger, W. E. *J. Am. Chem. Soc.* **1992**, *114*, 6063. (b) Adams, R. *Electrochemistry at Solid Electrodes*; Marcel Dekker: New York, 1969; p 124.

(16) Gritzner, G.; Kuta, J. *Pure Appl. Chem.* **1984**, *56*, 461.

(17) Voltammetry was studied quantitatively over the scan rate range 0.02 to 1.0 V/s. The anodic current functions were constant to within 10%, ratios of i_p/i_a were approximately unity, and ΔE_p values were essentially the same as those of ferrocene. At a scan rate of 0.1 V/s, ΔE_p was ca. 60 mV for both waves. The slopes of rotating Pt electrode voltammograms were also consistent with Nernstian charge transfer reactions {slopes of plots of $-E_{\text{app}} \text{ vs } \log[i/(i_a - i)]$ were 50 and 54 mV for the first and second oxidation waves at 253 K, respectively, compared to 50 mV for theory at this temperature}.

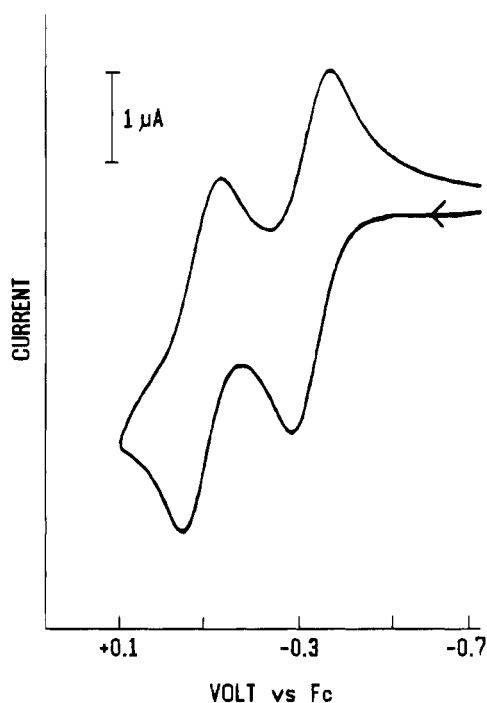


Figure 1. CV scan of 0.27 mM $\text{FvCo}_2(\text{COD})_2$ in $\text{CH}_2\text{Cl}_2/0.1 \text{ M } [\text{NBu}_4][\text{PF}_6]$ at a Pt electrode, $\nu = 0.2 \text{ V/s}$, $T = \text{ambient}$, showing waves for the $5/5^+/5^{2+}$ sequence.

Table 1. Formal Potentials (V vs Fc) of Cobalt–COD Complexes in Nonaqueous Solvents Containing 0.1 M $[\text{NBu}_4][\text{PF}_6]$

complex	solvent	temp, K	couple	E°	ref
$\text{FvCo}_2(\text{COD})_2$, 5	CH_2Cl_2	298	2+/1+	-0.072	this work
5	CH_2Cl_2	298	1+/0	-0.300	this work
5	DME ^a	273	0/1-	-2.86	this work
$\text{CpCo}(\text{COD})$, 6	CH_2Cl_2	298	1+/0	-0.22	ref 8
6	THF	298	0/1-	-3.01	ref 11

^a DME = 1,2-dimethoxyethane.

oxidation of **5** was irreversible even in CH_2Cl_2 at 243 K ($E_{\text{pa}} = +0.84 \text{ V}$).

Exhaustive electrolysis at a Pt basket was conducted on **5** in CH_2Cl_2 at 243 K. With $E_{\text{appl}} = -0.1 \text{ V}$ (first oxidation), after passage of ca. 0.5 F/equiv, the solution had turned from yellow to dark green and a sample aliquot (rapidly frozen at 77 K) was removed for ESR analysis. The rotating Pt electrode (RPE) scans before and after this partial electrolysis (Figure 2) showed that about half the starting material had been converted to the monocation 5^+ . Note in Figure 2 that the overall current height of the two waves after partial electrolysis (Figure 2, middle) is slightly greater than that before electrolysis (Figure 2, top). This almost certainly arises from the fact that neutral **5** is sparingly soluble in CH_2Cl_2 at this temperature, whereas the solubility of 5^+ is sufficient to dissolve all monocation formed in the electrolysis. This solubility problem does not affect the coulometry, which is based on moles electrolyzed rather than on concentrations.

Allowing the electrolysis to continue at the potential of the second wave ($E_{\text{appl}} = +0.3 \text{ V}$) gave the total release of 2.0 F/equiv when the reaction was complete. The resulting deep blue solution was ESR silent. According to CV and RPE scans (e.g., Figure 2, bottom), it contained 5^{2+} at a concentration of about 40% of the

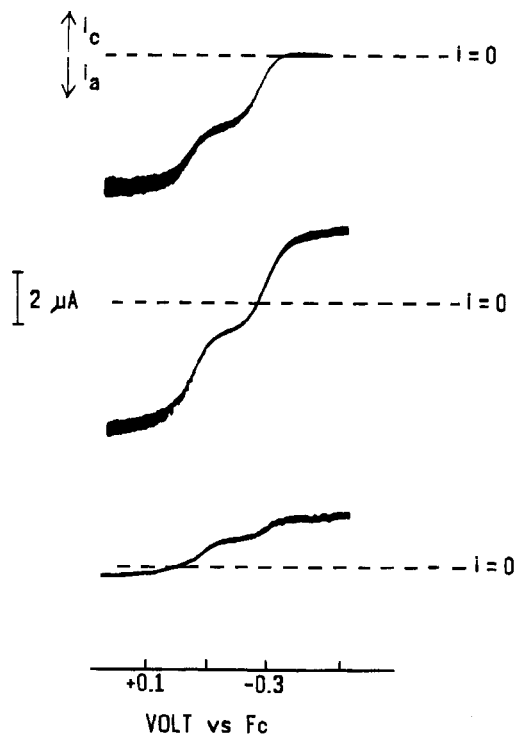


Figure 2. RPE voltammograms during anodic electrolysis of 0.56 mM $\text{FvCo}_2(\text{COD})_2$ in $\text{CH}_2\text{Cl}_2/0.1 \text{ M } [\text{NBu}_4][\text{PF}_6]$ at $T = 243 \text{ K}$. (top) prior to electrolysis; (middle) after oxidation by 0.5 F/equiv at $E_{\text{appl}} = -0.1 \text{ V}$ (first oxidation plateau); (bottom) after oxidation by a total of 1.8 F/equiv ($E_{\text{appl}} = +0.2 \text{ V}$, second oxidation plateau). The zero current line shows the dominant forms in the bulk of solution are (top) **5**, (middle) ca. 1:1 $5:5^+$, and (bottom) 5^{2+} .

starting material and new cathodic waves at $E_{\text{pc}} = -1.45$ and -1.56 V due to unidentified¹⁸ decomposition products.

The CV, chronoamperometry, and coulometry results tell us that the monocation of **5** is somewhat longer lived than that of the mononuclear analogue **6**, which does not exhibit complete chemical reversibility in slow CV scans at room temperature.⁸

Two aspects of the potentials, E_1° and E_2° , of **5** are important. One is that E_1° is shifted 80 mV negative from the comparable Co(II)/Co(I) couple of **6**: -0.30 vs -0.22 V^8 vs Fc. This is typical of homodinuclear systems exhibiting a moderate metal–metal interaction: the first redox process of the dinuclear system occurs at a more facile potential than that of the mononuclear analogue. For example, the first oxidation of **1** is about 90 mV negative of Fc,²⁰ as is that of the dichromium diaryl complex (diaryl)[Cr(CO)₂PR₃]₂ ($x = 2$) compared to $x = 1$.²¹ Both cations in these literature examples exhibited class II MV behavior in solution, in the Robin–Day classification.²²

(18) By analogy with the detailed studies of the fate of 6^+ in ref 8, decomplexation of COD from the metal center is expected over long reaction times for the dication 5^{2+} . The cathodic waves did not match up with those reported in the literature for dicobaltocene,^{3,19} a possible product.

(19) Davison, A.; Smart, J. C. *J. Organomet. Chem.* **1973**, *49*, C43. For electrochemical data on the Cp* analogue $\text{FvCo}_2(\eta^5\text{-C}_5\text{Me}_5)_2$, see Hudeczek and Köhler in ref 5.

(20) Morrison, W. H., Jr.; Hendrickson, D. N. *J. Chem. Phys.* **1973**, *59*, 380.

(21) Pierce, D. T.; Geiger, W. E. *Inorg. Chem.* **1994**, *33*, 373.

(22) Robin, M. B.; Day, P. *Adv. Inorg. Chem. Radiochem.* **1967**, *10*, 247.

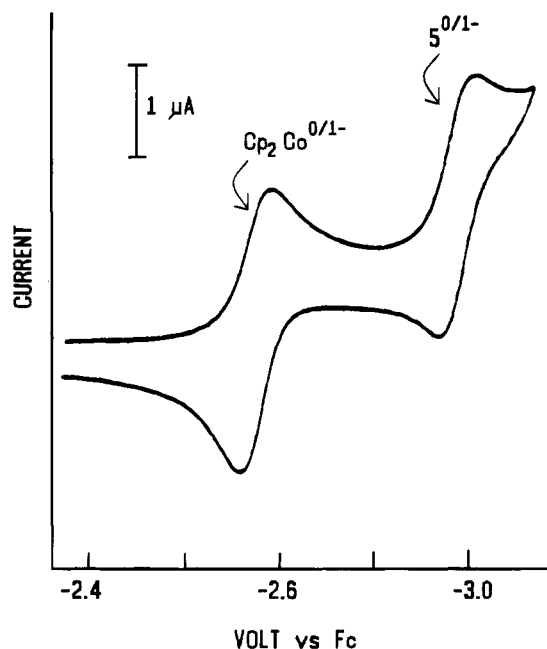


Figure 3. CV scan of 0.29 mM FvCo₂(COD)₂ and 0.27 mM Cp₂Co⁺ in dimethoxyethane/0.1 M [NBu₄][PF₆] at Pt electrode, $T = 273$ K, $v = 0.2$ V/s. The wave at -2.6 V is the second reduction of the cobaltocenium ion (Cp₂Co^{0/-}).

The second point relevant to MV studies is that there is a moderate (228 mV) difference between E_2° and E_1° in **5**, separations of this magnitude being commonly associated with class II valence-trapped systems.^{21,23}

II. Reduction. A single reduction of one-electron height (compared with the internal standard cobaltocenium,²⁴ Figure 3) is observed for **5**, $E_3^\circ = -2.86$ V in dimethoxyethane at 268 K. Peak separations were quasi-Nernstian (e.g., $\Delta E_p = 90$ mV at $v = 0.1$ V/s, compared to 80 mV for Cp₂Co^{0/-}). Coulometry of the reduction processes at -3.0 V was unsuccessful, in the sense that regeneration of neutral **5** gave abnormally high coulomb counts, most likely owing to the reaction of **5**⁻ with adventitious weak oxidants.

Efforts were made to search for the second reduction of **5**, which comes beyond the solvent cathodic breakdown (-3.1 V in our work). The low-temperature conditions known to give more negative potential windows in DMF²⁵ and other solvents²⁶ were not useful in the present case owing to the low solubility of **5** at reduced temperatures. Given the fact that the monoanion, **5**⁻, is not inherently delocalized (vide infra), the second reduction of **5** is likely to occur within about 350 mV²⁷ of the first, but our experiments can only put a lower limit of -240 mV on the value of $E_4^\circ - E_3^\circ$, where E_4° would describe the hypothetical reaction $5^- + e^- \rightleftharpoons 5^{2-}$.

The fact that E_3° (-2.86 V) is less negative than the value reported for reduction of the analogous mononuclear complex, **6**, -3.01 V in THF,¹¹ is again consistent with a moderate metal–metal interaction in **5**.

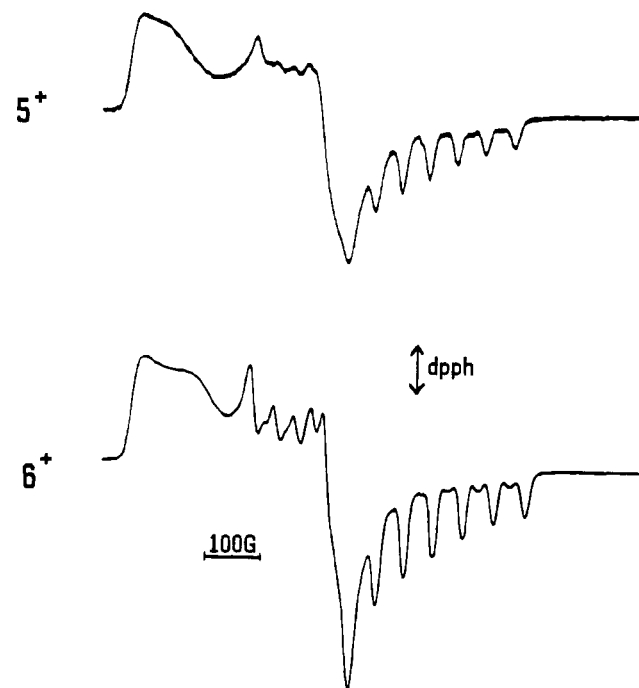


Figure 4. ESR spectra of (top) [FvCo₂(COD)₂]⁺ (**6**⁺) and (bottom) [CpCo(COD)]⁺ (**5**⁺) at 77 K in 1:1 CH₂Cl₂:1,2-C₂H₄Cl₂ generated by oxidation of the precursor with 1 equiv of [(*p*-BrC₆H₄)₃N][BF₄] at low temperatures under vacuum.

ESR Spectroscopy of 5⁺ and 5⁻. ESR-active samples of the monocation **5**⁺ were produced when **5** was oxidized either (a) by bulk electrolysis at the potential of the first anodic process or (b) by 1 equiv of the oxidizing agent “magic blue”, [N(*p*-BrC₆H₄)₃]⁺, in either CH₂Cl₂ or a 1:1 mixture of CH₂Cl₂:1,2-C₂H₄Cl₂. Identical spectra were obtained by the two methods. The deep green solutions were ESR-silent in fluid media at 205 K, but solutions frozen at 77 K produced intense spectra. The chemical oxidation with the imminium radical was conducted at 218 K under high-vacuum conditions, followed by rapid freezing of the sample, so there is a high degree of certainty that the spectra do not arise from decomposition products.

Immediately apparent from the glassy spectrum (Figure 4) are the hyperfine interactions with a *single* Co nucleus, as demonstrated in the high-field *g* component ($g = 2.00$). Seven of the eight expected Co lines ($I = 7/2$) are resolved ($A_{Co} = 55$ G). The splittings along the other two *g* components are smaller and incompletely resolved. Except for minor differences in resolution, the spectrum of **5**⁺ is a virtual overlay of the spectrum of **6**⁺, a fact which establishes that the SOMO of the MV system [FvCo₂(COD)₂]⁺ has essentially the same composition as that of the 17e, d⁷, radical cation [CpCo(COD)]⁺. This establishes that the formal d⁷d⁸ system of **5**⁺ is *valence trapped* under these conditions.

Rieger's analysis of the ESR spectrum of **6**⁺ showed that although there are considerable ligand contributions, the SOMO has about two-thirds metal character, mostly d_{xz} with some mixing in of the d_{x²-y²} orbital. It is noteworthy that, in spite of the much lower metal hyperfine splittings in **5**⁺ (and **6**⁺) as compared to **5**⁻ (and **6**⁻), vide infra, the SOMOs of the MV cation and MV anion of **5** can both be said to be metal-based, with about the same degree of metal–ligand covalency.

(23) Richardson, D. E.; Taube, H. *Coord. Chem. Rev.* **1984**, *60*, 107.

(24) Current functions for equimolar **5** and Cp₂Co were within 5%. For cobaltocenium reduction, see: Geiger, W. E. *J. Am. Chem. Soc.* **1974**, *96*, 2632.

(25) Van Duyne, R. P.; Reilly, C. N. *Anal. Chem.* **1972**, *44*, 158.

(26) Meerholz, K.; Heinze, J. *J. Am. Chem. Soc.* **1989**, *111*, 2325 and references therein.

(27) Lee, M.-T.; Foxman, B. M.; Rosenblum, M. *Organometallics* **1985**, *4*, 539.

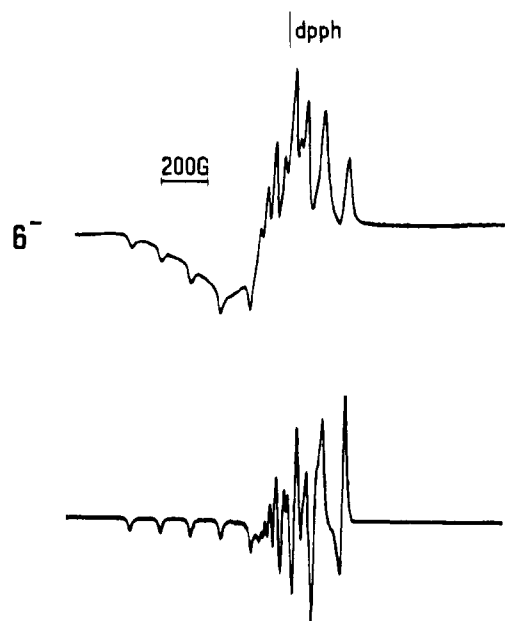
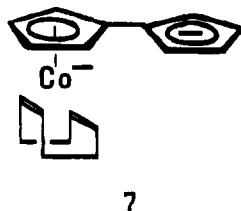


Figure 5. Experimental (top) and simulated (bottom) ESR spectra $[\text{FvCo}_2(\text{COD})_2]^-$ (6^-) (spectrum at 77 K). The anion was generated by reduction of a dimethoxyethane solution of **6** by NaK under vacuum. Simulation parameters are in Table 2.

The anion 5^- was readily produced upon reduction of the neutral complex with NaK in dimethoxyethane under high vacuum. The yellow solution of **5** immediately changed to dark yellow upon contact with NaK, whereupon the solution was frozen, giving the ESR spectrum of Figure 5 (top) which was simulated (Figure 5, bottom) with the parameters in Table 2. Interaction with a *single* Co nucleus is indicated, demonstrating that the MV ion 5^- is *valence trapped*. It is also worth noting that the ESR parameters of 5^- are virtually the same as those of the mononuclear analogue 6^- under the same conditions (see ref 12; results duplicated in present work). Having the benefit of the previous quantitative analysis of ref 12, we can state that the SOMO of the formal d^8d^9 MV ion, 5^- , is composed of $2/3$ d_{yz} with significant ligand covalency.

Because the reduction of **5** required alkali metal conditions as opposed to controlled potential electrolysis, we were concerned about the possibility that the ESR-active ion might be a decomposition product such as **7**,



rather than 5^- . There is precedence for such a partial decomplexation from the work of Bard et al. on the reduction of $\text{FvFe}_2(\eta^5\text{-C}_5\text{H}_4\text{COOMe})_2$.²⁸ We therefore allowed a solution of **5** to react for an extended time period with NaK at 218 K, the familiar color changes being observed, then oxidized the solution with 1 equiv of Cp_2Co^+ , and investigated the final solution by CV

Table 2. ESR Parameters for Fulvalenyl- and Cyclopentadienylcobalt Cyclooctadiene Radicals at 77 K (Coefficients in Units of 10^4 cm^{-1})

radical	electronic configuration	g_1	g_2	g_3	A_1	A_2	A_3
5^- ^a	d^8d^9	2.150	2.009	1.970	140	25	28
6^- ^b	d^9	2.171	2.027	1.985	159	37	46
5^+ ^c	d^7d^8	2.329	2.120	2.003	20	<i>e</i>	56
6^+ ^d	d^7						

^a In dimethoxyethane after NaK reduction of **5**, present work. ^b In DMF/0.1 M $[\text{NBu}_4][\text{PF}_6]$ after electrolysis of **6**.¹² ^c In $\text{CH}_2\text{Cl}_2:\text{C}_2\text{H}_4\text{Cl}_2/0.1 \text{ M } [\text{NBu}_4][\text{PF}_6]$ after electrolysis, present work. ^d In $\text{CH}_2\text{Cl}_2:\text{C}_2\text{H}_4\text{Cl}_2/0.1 \text{ M } [\text{NBu}_4][\text{PF}_6]$ after electrolysis, see ref 10. ^e Too small to be resolved.

scans in dimethoxyethane. Only the waves of Cp_2Co and **5** were observed. This experiment gives strong evidence that the ESR-active radical is 5^- when $\text{FvCo}_2(\text{COD})_2$ reacts with NaK.

Discussion

The conclusions concerning mixed valency in the monocation and monoanion of **5** are relatively straightforward from the ESR results: both ions exhibit trapped-valent behavior on the ESR time scale (ca. 10^{-8} s) in frozen glasses. No spectroscopic data were obtained, however, on the MV ions in fluid solutions. The lack of ESR spectra for solutions of 5^+ or 5^- most likely arises from severe line broadening consequent to rapid electronic relaxation of the radicals. No attempts were made to obtain optical absorption spectra, owing to the relatively short lifetimes of the radicals.

Voltammetry results give indirect support to a model of trapped valency in solution as well. The separation of the formal potentials of the two oxidation waves of **5** (228 mV) is about the same as with other trapped-valent analogues.^{21,23} The E° separation is affected by various phenomena²³ and must be used with caution in drawing conclusions about delocalization. The present value is well below that, however, noted empirically to be associated with delocalized systems.²⁷ All indications are, therefore, that the d^7d^8 ion (5^+) is valence trapped in both the liquid and solid state. Our inability to observe the second reduction of **5** by CV means that we cannot make conclusions about the MV ion 5^- in liquid media, but this ion is clearly trapped-valent at 77 K. Although there may possibly be conditions, therefore, under which 5^- becomes detrapped, the d^8d^9 system does *not* appear to be inherently delocalized.

One reason why the results on **5** are noteworthy is that the mixed-valency of the single complex is investigated in two different MV electronic configurations. It has heretofore not been possible, to our knowledge, to produce two different sets of MV ions for the *same* fulvalenediyl-bridged homodinuclear system. For example, the reduction of biferrocene has not been reported, nor has the oxidation of the diarene complexes 4^{2+} . The three reductions reported for the dicobaltoceum dication should produce both the d^6d^7 and d^7d^8 ions, but no spectroscopic data on the latter have yet appeared.^{5,19} Study of different mixed-valence forms of the same molecule, as opposed to those that are merely isoelectronic, has the obvious benefit of testing the dependence on electronic structure without complications wrought by changes in ligand substituent effects (e.g., substitution of H by CO_2Me in a cyclopentadienyl

ligand) or overall charge in the complex (e.g., the Fe^{II}-Fe^{II} system in **1** is neutral, whereas that in **4** is dicationic). Given the great variety of cyclopentadienyl-bonded metal radicals,²⁹ there appear to be opportunities to "tune" into various MV metal oxidation states

by judicious choices of metals (with ancillary ligands) bonded to the fulvalenediyl spacer.

Acknowledgment. We are grateful to the National Science Foundation for support of this work under NSF CHE91-16332.

OM9407619

(29) Connelly, N. G.; Geiger, W. E. *Adv. Organomet. Chem.* **1984**, *23*, 41-63 (examples through 1983).

Characterization of the 17-Electron Radical Cation [CpCo(1,5-COD)]⁺ by ESR Spectroscopy

Teen T. Chin, Laura Inman Sharp, and William E. Geiger*

Department of Chemistry, University of Vermont, Burlington, Vermont 05405

Philip H. Rieger*

Department of Chemistry, Brown University, Providence, Rhode Island 02912

Received September 30, 1994[⊗]

The 17e cation, [CpCo(1,5-COD)]⁺, generated by chemical or electrochemical oxidation of the neutral 18e complex in CH₂Cl₂/C₂H₄Cl₂, exhibits an intense, reasonably well resolved ESR spectrum at 77 K. The spectrum can be interpreted to yield the spin Hamiltonian matrices, $g = (2.120, 2.329, 2.003)$, $A^{\text{Co}} = (55.7, 20, 0.5) \times 10^{-4} \text{ cm}^{-1}$ where the x - and z -principal axes of the hyperfine matrix are rotated, relative to the g -matrix axes, by $\beta = 65^\circ$. With the inclusion of spin-orbit coupling corrections, the ESR parameters lead to a singly occupied molecular orbital with 57% $3d_{xz}$, 6% $3d_{x^2-y^2}$, and 3% 4s cobalt character.

Introduction

A number of half-sandwich d⁷ complexes of cobalt containing 17 valence electrons have been generated,¹⁻⁶ usually, but not always,⁶ through oxidation of their 18e precursors. The latter are known to promote alkyne trimerizations and other synthetically useful transformations.⁷ In certain cases, complexes are known in which CpCo is bound to two olefin bonds of biologically active ligands, and in at least one case, the 17e cation [CpCo(η^4 -ligand)]⁺ has been postulated as the key intermediate in the oxidatively induced cyclization of a precursor to strychnine.⁸ The spin density distribution, specifically the relative makeup of metal and tetrahapto-bound hydrocarbon in the SOMO, is therefore of more than nominal interest for this class of 17e radicals, especially in light of the possibility of generating 17e CpCo "spin tags" on pharmacologically and catalytically useful complexes.

Very few data are available, however, on the ESR behavior of these radicals. The cation [CpCo(CO)(PR₃)]⁺ has a single broad line,³ whereas the neutral alkyne complex, (η^6 -C₆Ph₆)Co(η -C₂Ph₂) has a resolved ⁵⁹Co hyperfine structure in fluid media.⁶ The pentamethylcyclopentadienyl complex [Cp*Co(1,5-COD)]⁺ displays ⁵⁹Co hyperfine structure in frozen solution.⁵ In the last case, the largest hyperfine component, ca. 55 G, was only about one-third of the largest component for d⁹ Co(0) analogues such as [CpCo(diolefin)]⁻.^{9,10} We felt that

it was important to learn whether the smaller coupling is due to greater delocalization into the ligand framework, a possibility that might have important implications for magnetic resonance studies on [CpCo(diolefin)]⁺ systems. At the same time, we were investigating dinuclear systems containing the (C₅H₄R)Co(diolefin) fragment (see accompanying paper)¹¹ and desired an analysis of the ESR spectra which would allow conclusions to be drawn concerning the electronic structure of mixed-valent ions spin trapped on one of these fragments.

Some years ago, one of us reported that the oxidation of CpCo(1,5-COD) (1) is chemically reversible in CH₂-Cl₂ on the cyclic voltammetry (CV) time scale, but that bulk electrolysis at ambient temperatures yielded only Cp₂Co⁺ and 1,5-COD as recognized products.⁵ Although the pentamethylcyclopentadienyl analogue, [Cp*Co(1,5-COD)]⁺, was more stable, its frozen solution ESR spectrum was poorly resolved.^{5,12}

In the present investigation, we found that the parent radical, [CpCo(1,5-COD)]⁺ (1⁺), was sufficiently long-lived at subambient temperatures to give an intense ESR spectrum with sufficient resolution to allow a detailed interpretation of the spectrum. In the following, we describe the generation of the radical cation, the analysis of its ESR spectrum, and a detailed spin-orbit coupling treatment needed to interpret the highly anisotropic g -matrix and noncoincident g - and ⁵⁹Co hyperfine matrix principal axes which arose in the spectral analysis. The noncoincident principal axes imply a small but significant distortion of the complex from pseudo-C_{2v} symmetry.

Experimental Section

CpCo(1,5-COD) was prepared by the literature method.¹³ The oxidant, [N(*p*-BrC₆H₄)₃][BF₄] ("magic blue"), was prepared

(9) Connelly, N. G.; Geiger, W. E.; Lane, G. A.; Raven, S. J.; Rieger, P. H. *J. Am. Chem. Soc.* **1986**, *108*, 6219 and references therein.

(10) Rieger, P. H. In *Organometallic Radical Processes*, Troglor, W. C., Ed.; Elsevier: Amsterdam, 1990; pp 290-294.

(11) Chin, T. T.; Geiger, W. E., *Organometallics* **1995**, *14*, 1316.

(12) Moraczewski, J. Ph.D. Dissertation, University of Vermont, 1980.

(13) King, R. B.; Treichel, P. M.; Stone, F. G. A. *J. Am. Chem. Soc.* **1961**, *83*, 3593.

[⊗] Abstract published in *Advance ACS Abstracts*, February 1, 1995.

(1) Co(II) π -radicals with formal d⁹ electronic configurations are not considered here. For references to such systems (e.g., cobaltocene), see: (a) Kölle, U.; Fuss, B.; Rajasekharan, M. W.; Ramakrishna, B. L.; Ammeter, J. H.; Böhm, M. C. *J. Am. Chem. Soc.* **1984**, *106*, 4152. (b) Ammeter, J. H. *J. Magn. Reson.* **1978**, *10*, 299. (c) Castellani, M. P.; Geib, S. J.; Rheingold, A. L.; Troglor, W. C. *Organometallics* **1987**, *6*, 1703 and references therein.

(2) McKinney, R. J. *Inorg. Chem.* **1982**, *21*, 2051.

(3) Broadley, K.; Connelly, N. G.; Geiger, W. E. *J. Chem. Soc., Dalton Trans.* **1983**, 121.

(4) Kölle, U. *Inorg. Chim. Acta* **1981**, *47*, 13.

(5) Moraczewski, J.; Geiger, W. E. *Organometallics* **1982**, *1*, 1385.

(6) Bagini, P.; Funaioli, T.; Fachinetti, G.; Laschi, F.; Zanazzi, P. F. *J. Chem. Soc. Chem. Commun.* **1989**, 405.

(7) Jonas, K. *Angew. Chem., Intl. Ed. Engl.* **1985**, *24*, 295.

(8) Grotjahn, D. B.; Vollhardt, K. P. C. *J. Am. Chem. Soc.* **1990**, *112*, 5653.

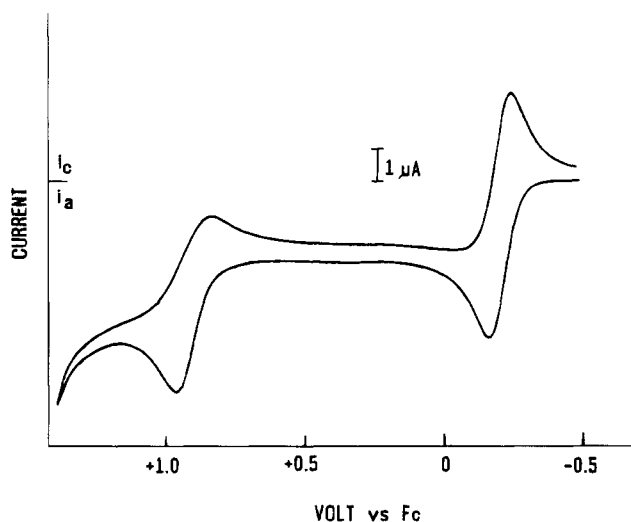


Figure 1. Cyclic voltammogram of 5×10^{-4} M $\text{CpCO}(1,5\text{-COD})$ in $\text{CH}_2\text{Cl}_2/0.1$ M $[\text{NBu}_4][\text{PF}_6]$, $\nu = 0.1$ V s^{-1} , $T = 233$ K.

by a modification of the method of Bell.¹⁴ Potentials in this paper are referred to the ferrocene/ferrocenium couple,¹⁵ although Ag/AgCl was usually used as the experimental reference electrode. All operations were conducted under an atmosphere of nitrogen inside a Vacuum Atmospheres drybox. The temperature of the electrochemical cell was controlled to a precision of $\pm 0.1^\circ$ by immersion in a heptane bath for which an FTS electrical cooling system provided the thermal control. The supporting electrolyte was 0.1 M $[\text{NBu}_4][\text{PF}_6]$, and the working electrode was Pt. All other electrochemical techniques are as described in the accompanying paper. ESR spectra were recorded on a modified Varian E-4 spectrometer equipped with a frequency counter, using DPPH as an external standard. Analysis and simulation of ESR spectra employed computer programs described elsewhere.¹⁶

Results

Electrochemical Generation of 1^+ . Before discussing the ESR results, we first present evidence that the spectrally active radical is indeed 1^+ . Figure 1 shows a CV scan for **1** at 233 K, $\nu = 0.1$ V s^{-1} . Two one-electron oxidations are observed, the first ($E^\circ = -0.22$ V vs Fc) corresponding to the couple $1/1^+$. The second wave ($E^\circ = +0.90$ V) corresponds to $1^+/1^{2+}$ and is of limited chemical reversibility. Bulk electrolysis of this solution was conducted at 230 K, $E_{\text{appl}} = +0.2$ V, until the current was less than 5% of its original value (ca. 20 min, $n_{\text{app}} = 1.1$ e). After the electrolysis, voltammetry at the rotating Pt electrode (Figure 2) gave a cathodic response ($E_{1/2} = -0.25$ V) with limiting current about 40% of that of the original solution. Thus a reasonable concentration of the cation 1^+ was present. This solution gave an ESR spectrum nearly identical to that obtained from solutions of **1** which had been oxidized by chemical one-electron oxidants.

Chemical Oxidation of **1.** In order to obtain a higher radical concentration, **1** was oxidized by $[\text{N}(p\text{-BrC}_6\text{H}_4)_3]^+$ ("magic blue"). The potential of magic blue is $+0.72$ V vs Fc, sufficient to form the monocation of **1** but not so positive as to form the dication. To a mixture of solids containing approximately equimolar equiva-

lents of **1** and magic blue was distilled under vacuum a 1:1 mixture of CH_2Cl_2 and 1,2- $\text{C}_2\text{H}_4\text{Cl}_2$. The mixture was allowed to melt, brought briefly to 218 K, and then frozen in liquid nitrogen. The resulting frozen glass gave an intense ESR spectrum shown in Figure 3a. Fluid solutions of 1^+ were ESR-silent.

Interpretation of the ESR Spectrum. The ESR spectrum consists of three groups of features: an unresolved group of positive-going features at low field, four or five divergences in the middle, and seven negative-going features at high field. The high-field end of the central group and the low-field end of the high-field group overlap. The g - and A -matrix components corresponding to the low-field group (labeled y) were estimated on the basis of the center and width of the unresolved envelope. The spacing of the central features is markedly uneven, even after second-order corrections; the high-field features are also unevenly spaced, though not so obviously. This behavior is characteristic of noncoincident g and hyperfine matrix principal axes. With this hypothesis, the positions of the resolved features can be analyzed¹⁶ to obtain the other two g - and A -matrix components (the larger g component is labeled x) and the angle β between the corresponding g - and A -matrix principal axes.¹⁷ For large noncoincidences such as that observed here, there is an ambiguity in labeling; for $\beta = 25^\circ$, the larger hyperfine component corresponds to z , but the x - and z -axes are reversed if we take $\beta = 65^\circ$. Both sets of parameters are given in Table 1, and a computer-simulated spectrum (independent of the choice of axes) is shown in Figure 3b. The coordinate system assumed here is shown in Figure 4.

Careful inspection of Figure 3a shows small features of regular spacing between the hyperfine components of the lowest g value. These were present in all spectra of the radical, no matter what its method of preparation. They are also present in the spectra of the valence-trapped dinuclear cation $[\text{FvCo}_2(\text{COD})_2]^+$ and are not accounted for by the spectral simulation. It is possible that these features arise from a minor isomer or rotamer of the cation radical.

Interpretation of ESR Parameters. MO calculations by Albright, et al.¹⁸ and by Wakatsuki et al.¹⁹ predict that the singly-occupied molecular orbital (SOMO) in 1^+ is primarily metal d_{xz} in character.^{18,19} A filled MO with d_{z^2} character lies just below the SOMO and nearly degenerate MOs with $d_{x^2-y^2}$ and d_{xy} character are found at somewhat lower energies. Other MOs with d_{xz} or d_{yz} character are well separated from the SOMO. We have performed extended Hückel MO calculations which lead to similar qualitative predictions. Spin-orbit coupling (*vide infra*) then is expected to lead to g -matrix components, $g_y > g_x > g_z$, and the g -matrix components of Table 1 are labeled accordingly. The observed noncoincidence of the g - and A -matrix principal axes suggests significant d -orbital hybridization, most likely through admixture of d_{xz} with the nearby d_{z^2} , $d_{x^2-y^2}$, or d_{xy} orbitals. All three of these possibilities (as well as

(17) There is no experimental reason to suppose that the principal axes corresponding to the low-field group are coincident, but if the SOMO is a $d_{xz}/d_{x^2-y^2}/d_{z^2}$ hybrid, the y -axes are expected to be coincident; similarly, for a d_{xz}/d_{yz} hybrid, the z -axes should be coincident and, for a d_{xz}/d_{xy} hybrid, the x -axes should be coincident.

(18) Albright, T. A.; Geiger, W. E.; Moraczewski, J.; Tulyathan, B. *J. Am. Chem. Soc.* **1981**, *103*, 4787.

(19) Wakatsuki, Y.; Yamazaki, H.; Kobayashi, T.; Sugawara, Y. *Organometallics* **1987**, *6*, 1191.

(14) Bell, F. A.; Ledwith, A.; Sherrington, D. C. *J. Chem. Soc. C* **1969**, 2719.

(15) Gritzner, G.; Kuta, J. *Pure Appl. Chem.* **1984**, *56*, 461.

(16) (a) DeGray, J. A.; Rieger, P. H. *Bull. Magn. Reson.* **1987**, *8*, 95.

(b) Rieger, P. H. *Electron Spin Reson.* **1993**, *13B*, 178.

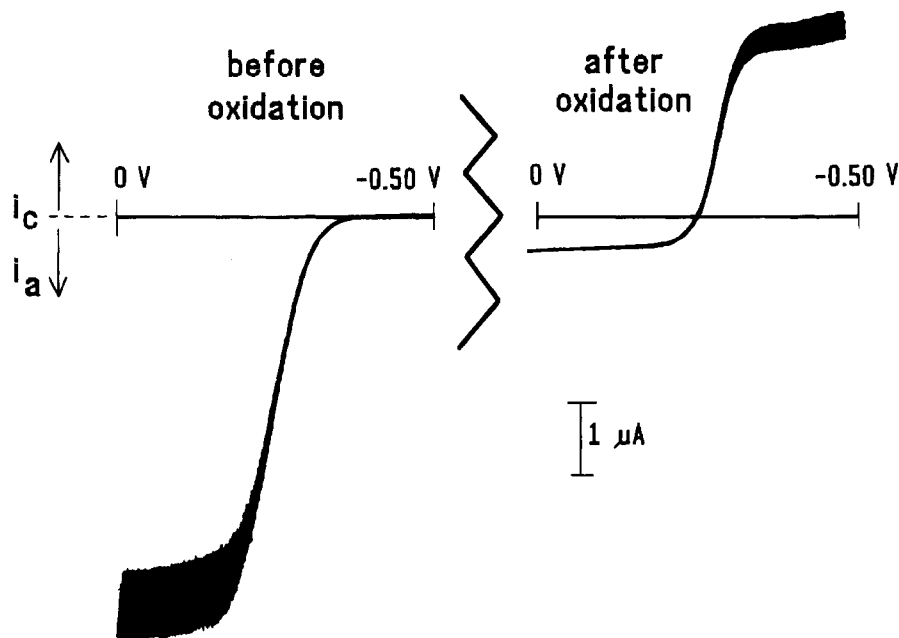


Figure 2. Rotating Pt electrode scans before (left) and after (right) anodic electrolysis of 5×10^{-4} M CpCo(1,5-COD) in $\text{CH}_2\text{Cl}_2/0.1$ M $[\text{NBu}_4][\text{PF}_6]$ at 230 K. Note that $E_{1/2}$ is unchanged but that the wave after electrolysis consists mainly of cathodic current arising from reduction of 1^+ .

Table 1. ESR Parameters

g_x	g_y	g_z	A_x^a	A_y^a	A_z^a	β , deg
2.120 ± 0.001	2.329 ± 0.005	2.003 ± 0.001	$(+)55.7 \pm 0.3$	$(-)20 \pm 3$	$(-)0.5 \pm 0.3$	65.0 ± 0.5
			or $(-)0.5 \pm 0.3$		or $(+)55.7 \pm 0.3$	or 25.0 ± 0.5

^a In units of 10^{-4} cm^{-1} .

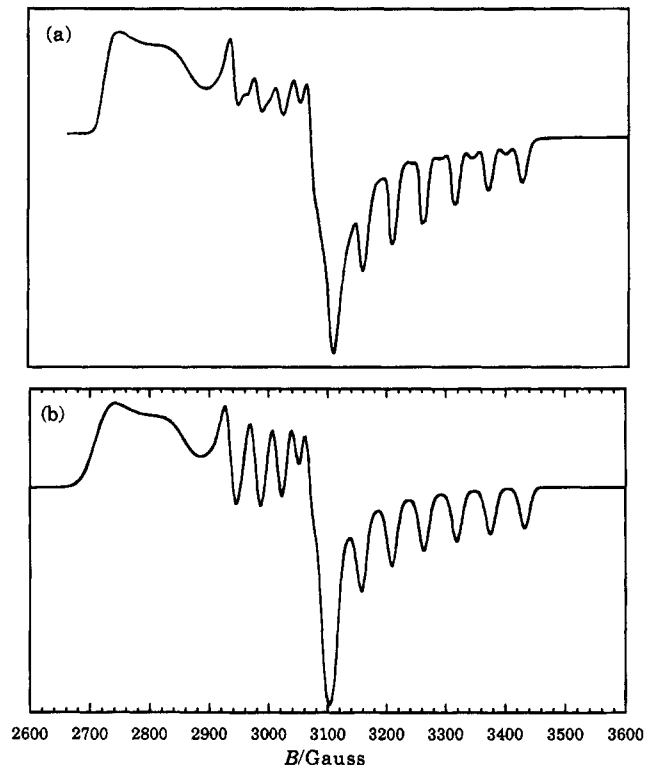


Figure 3. (a) ESR spectrum of $[\text{CpCo}(\text{COD})]^+$ in $\text{CH}_2\text{Cl}_2/\text{C}_2\text{H}_2\text{Cl}_2$ at 77 K. (b) Computer simulated spectrum using the parameters of Table 1.

d_{xz}/d_{yz} hybrids) were examined in some detail. The large g anisotropy suggests that spin-orbit coupling corrections to the dipolar coupling matrix are significant, and accordingly, spin-orbit coupling corrections were ap-

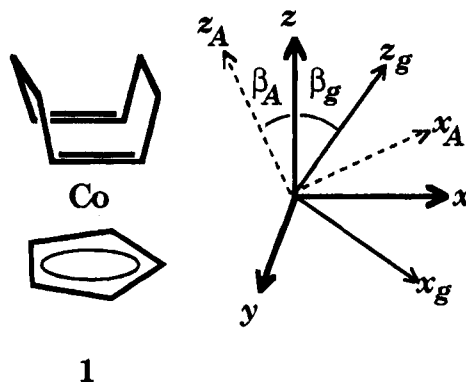


Figure 4. Structure of **1** showing the molecular coordinate system and the principal axes of the g and ^{59}Co hyperfine interaction matrices.

plied to all four hybridization schemes. In the end, however, only $d_{xz}/d_{x^2-y^2}$ hybridization can account for the magnitudes of the hyperfine matrix components and the noncoincidence of the principal axes.

For a SOMO of the form

$$|\text{SOMO}\rangle = a_1|xz\rangle + a_2|x^2 - y^2\rangle + \dots \quad (1)$$

the g -matrix components are

$$g_{xx} = g_e + 2\zeta \left(\frac{a_1^2}{\Delta_{xy}} + \frac{a_2^2}{\Delta_{yz}} \right) \quad (2a)$$

$$g_{yy} = g_e + 2\zeta \left(\frac{\alpha_1^2}{\Delta_{x^2-y^2}} + \frac{3a_1^2}{\Delta_{xz}} + \frac{a_2^2}{\Delta_{yz}} \right) \quad (2b)$$

$$g_{zz} = g_e + 2\zeta \left(\frac{a_1^2}{\Delta_{yz}} + \frac{4a_2^2}{\Delta_{xy}} \right) \quad (2c)$$

$$g_{xz} = 2\zeta \left(\frac{\alpha_1 \alpha_2}{\Delta_{yz}} - \frac{2\alpha_1 \alpha_2}{\Delta_{xy}} \right) \quad (2d)$$

where, for example,

$$\frac{1}{\Delta_{x^2-y^2}} = \sum_{i \neq 0} \frac{c_i^2}{E_i - E_0} \quad (3)$$

In eq 3, the sum extends over all MOs (except the SOMO) with energies E_i and $d_{x^2-y^2}$ LCAO coefficient c_i . We assume that only MOs with $d_{x^2-y^2}$, d_{z^2} , and d_{xy} character are sufficiently close in energy to the SOMO that spin-orbit coupling is significant and thus that terms in Δ_{xz} and Δ_{yz} can be ignored. The matrix is diagonalized by rotation about the y -axis by the angle β_g :

$$\tan 2\beta_g = \frac{4\alpha_1 \alpha_2}{\alpha_1^2 - 4\alpha_2^2} \quad (4)$$

The g -components then are

$$g_X = g_e + 2\zeta \left(\frac{a_1^2 + 4a_2^2}{\Delta_{xy}} \right) \quad (5a)$$

$$g_Y = g_e + 2\zeta \left(\frac{a_1^2}{\Delta_{x^2-y^2}} + \frac{3a_1^2}{\Delta_{z^2}} \right) \quad (5b)$$

$$g_Z = g_e \quad (5c)$$

Ignoring spin-orbit coupling to MOs with d_{xz} or d_{yz} character yields the dipolar hyperfine interaction matrix elements

$$(A_{xx})_{\text{dipolar}} = P \left[\frac{2}{7}(a_1^2 + a_2^2) + \frac{2\zeta a_1^2}{\Delta_{xy}} + \frac{3\zeta a_1^2}{7\Delta_{x^2y^2}} - \frac{3\zeta a_1^2}{7\Delta_{z^2}} \right] \quad (6a)$$

$$(A_{yy})_{\text{dipolar}} = P \left[\frac{2}{7}(-2a_1^2 + a_2^2) + \frac{2\zeta a_1^2}{\Delta_{x^2-y^2}} + \frac{3\zeta a_1^2}{7\Delta_{xy}} + \frac{6\zeta a_1^2}{\Delta_{z^2}} \right] \quad (6b)$$

$$(A_{zz})_{\text{dipolar}} = P \left[\frac{2}{7}(a_1^2 - 2a_2^2) + \frac{8\zeta a_2^2}{\Delta_{xy}} - \frac{3\zeta a_1^2}{7\Delta_{xy}} - \frac{3\zeta a_1^2}{7\Delta_{x^2-y^2}} + \frac{3\zeta a_1^2}{7\Delta_{z^2}} \right] \quad (6c)$$

$$(A_{xz})_{\text{dipolar}} = P \left[\frac{6}{7}a_1 a_2 - \frac{34\zeta a_1 a_2}{7\Delta_{xy}} - \frac{4\zeta a_1 a_2}{7\Delta_{x^2-y^2}} \right] \quad (6d)$$

$$(A_{zy})_{\text{dipolar}} = P \left[\frac{6}{7}a_1 a_2 - \frac{4\zeta a_1 a_2}{\Delta_{xy}} - \frac{2\zeta a_1 a_2}{7\Delta_{x^2-y^2}} - \frac{6\zeta a_1 a_2}{7\Delta_{z^2}} \right] \quad (6e)$$

where P is the dipolar parameter ($282 \times 10^{-4} \text{ cm}^{-1}$).²⁰

Assuming that $\Delta_{x^2-y^2} \approx \Delta_{xy}$, these expressions simplify to

$$(A_{xx})_{\text{dipolar}} = P \left[\frac{2}{7}(a_1^2 + a_2^2) + \frac{9}{7}\Delta g_{xx} - \frac{1}{14}\Delta g_{yy} \right] \quad (7a)$$

$$(A_{yy})_{\text{dipolar}} = P \left[\frac{2}{7}(-2a_1^2 + a_2^2) + \Delta g_{yy} + \frac{3}{14}\Delta g_{xx} \right] \quad (7b)$$

$$(A_{zz})_{\text{dipolar}} = P \left[\frac{2}{7}(a_1^2 - 2a_2^2) + \Delta g_{zz} - \frac{1}{2}\Delta g_{xx} + \frac{1}{14}\Delta g_{yy} \right] \quad (7c)$$

$$(A_{xz})_{\text{dipolar}} = P \left[\frac{6}{7}a_1 a_2 + \frac{19}{14}g_{xz} \right] \quad (7d)$$

$$(A_{zx})_{\text{dipolar}} = P \left[\frac{6}{7}a_1 a_2 + g_{xz} - \frac{1}{7}a_2 \Delta g_{yy} \right] \quad (7e)$$

The matrix is approximately diagonalized by rotation about the y -axis by the angle β_A :

$$\tan 2\beta_A = - \frac{2a_1 a_2 + \frac{11}{4}g_{xz} - \frac{a_2}{6a_1}\Delta g_{yy}}{a_2^2 - \frac{7}{6}\Delta g_{zz} - \frac{1}{6}\Delta g_{yy} + \frac{25}{12}\Delta g_{xx}} \quad (8)$$

to give the components

$$A_Y = A_s + P \left[\frac{2}{7}(-2a_1^2 + a_2^2) + \Delta g_{yy} + \frac{3}{14}\Delta g_{xx} \right] \quad (9a)$$

$$A_X A_Z = A_s + P \left[\frac{1}{7}(2a_1^2 - a_2^2) + \frac{1}{2}\Delta g_{zz} + \frac{11}{28}\Delta g_{xx} \right] \pm \frac{3}{7}P(a_2^4 + 4a_1^2 a_1^2 a_2^2 + 11a_1 a_2 g_{xz} + Q)^{1/2} \quad (9b)$$

where

$$Q = -a_2^2 \left(\Delta g_{yy} - \frac{25}{6}\Delta g_{xx} + \frac{7}{3}\Delta g_{zz} \right) + \left(\frac{1}{6}\Delta g_{yy} - \frac{25}{12}\Delta g_{xx} + \frac{7}{6}\Delta g_{zz} \right)^2 + \frac{19}{18}g_{xz} \left(7g_{xz} - \frac{a_2}{a_1}\Delta g_{yy} \right)$$

Analysis of the ESR parameters proceeded as follows.

(1) Assuming a value of the hybridization ratio, $R = (a_2/a_1)^2$, we used eq 4 to compute β_g and eq 5 to compute Δg_{xx} , Δg_{zz} , and g_{xz} from the experimental parameters, Δg_x and Δg_z .

(2) The isotropic hyperfine coupling is given by

$$\langle A \rangle = \frac{1}{3}(A_X + A_Y + A_Z) = A_s + P \Delta \langle g \rangle \quad (10)$$

where

$$\Delta \langle g \rangle = \langle g \rangle - g_e = \frac{1}{3}(g_X + g_Y + g_Z) - g_e \quad (11)$$

Depending on the signs of A_Y and A_Z , $\langle A \rangle = \pm(12 \pm 1) \times 10^{-4}$ or $\pm(25 \pm 1) \times 10^{-4} \text{ cm}^{-1}$. However, since

$$A_Y - \langle A \rangle = P \left[-\frac{4}{7}a_1^2 + \frac{2}{7}a_2^2 + \Delta g_{yy} + \frac{3}{14}\Delta g_{xx} - \Delta \langle g \rangle \right] \quad (12)$$

is expected to be negative, only $\langle A \rangle = +12 \times 10^{-4} \text{ cm}^{-1}$ ($A_s = -30 \times 10^{-4} \text{ cm}^{-1}$) makes physical sense. Thus

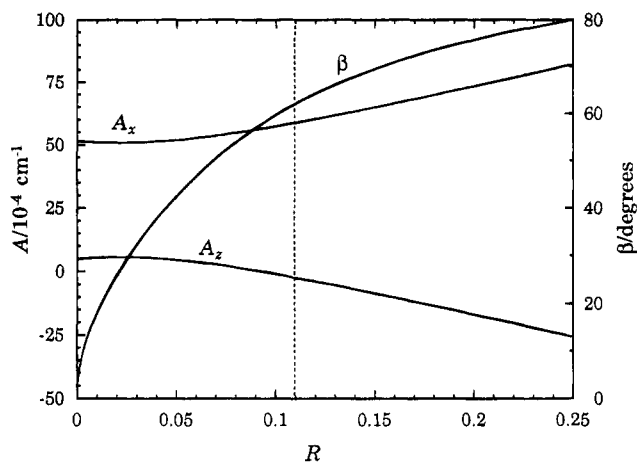


Figure 5. Computed values of A_Y and A_Z and the noncoincidence angle β as functions of the hybridization ratio, $R = (a_2/a_1)^2$. The dashed vertical line shows the position of best fit to the experimental parameters.

given A_Y and Δg_Y , the assumed value of R , and the computed Δg_{xx} , we compute a_1^2 and a_2^2 using eq 12.

(3) Values of β_A , A_Y , and A_Z are then computed using eqs 8 and 9 and compared with the experimental values. Although the signs of β_A and β_g depend on the sign of a_2/a_1 , the magnitude of the difference, $\beta = |\beta_A - \beta_g|$, is independent of sign; β , A_X , and A_Z are plotted vs R in Figure 5.

(4) Minimum error in β , A_X , and A_Z is obtained for $R = 0.11$ with $\beta = 62^\circ$, $A_X = 58.7 \times 10^{-4} \text{ cm}^{-1}$, $A_Z = -2.4 \times 10^{-3} \text{ cm}^{-1}$, $a_1^2 = 0.574$, $a_2^2 = 0.063$, and $q^d = 0.637$. The fit is quite acceptable given the experimental uncertainties, particularly in A_Y .

The parameter A_s has contributions from spin polarization and the direct contribution of Co 4s character,

$$A_s = Q_d q^d + Q_s q^s \quad (13)$$

where $Q_s = +1984 \times 10^{-4} \text{ cm}^{-1}$ ²⁰ and $Q_d \approx -131 \times 10^{-4} \text{ cm}^{-1}$.²¹ Thus $A_s = -30 \times 10^{-4} \text{ cm}^{-1}$ leads to $q^s \approx 0.026$.

Discussion

The total cobalt spin density estimated for 1^+ , $q = 0.66$, is comparable to that found for the corresponding $19e$ anion, 1^- , where the SOMO is 68% cobalt $3d_{yz}$.¹⁰ Thus both the HOMO and LUMO of the neutral parent complex are primarily metal based and are only weakly delocalized onto the ligands. This picture is entirely consistent with the MO calculations of Albright et al.¹⁸ and Wakatsuki et al.¹⁹ who found that for a CpCo(diolefin) complex, the LUMO is metal-olefin antibonding with predominant Co $3d_{yz}$ character while the HOMO is weakly metal-olefin bonding with predominant Co $3d_{xz}$ character. The closely spaced MO with d_{z^2} character implied by the large value of g_Y is consis-

tent with the MO calculations of Wakatsuki et al.¹⁹ and with the assignment of the photoelectron spectrum of **1**.²²

As shown by the $R = 0$ intercept of Figure 5, most of the difference, $A_x - A_z$, is due to spin-orbit coupling effects which are unusually large in this system. The angle between the g and A hyperfine matrix principal axes has unusually large contributions from both β_g and β_A (33.6 and -28.4° , respectively, assuming like signs for a_1 and a_2). Spin-orbit coupling also has an effect on β_A ; neglecting the correction terms, eq 8 gives $\beta_A = -40.3^\circ$ for $R = 0.11$. This result provides a hint to the significance of the angle. For a pure d_{xz} orbital, the dipolar matrix principal axes are conventionally taken as the molecular x , y , and z axes, but the orientations of x and z are, in fact, arbitrary since the matrix is axial. When even a trace of $d_{x^2-y^2}$ is mixed in, however, the lobes become unequal and the principal axes are then oriented along the lobes; eq 8 gives $\beta_A = -45^\circ$, neglecting spin-orbit coupling terms. Thus the large value of β is rather misleading; in fact, the lobes of an $R = 0.11$ hybrid are rotated only about 5° from those of a pure d_{xz} orbital. Although the extent of hybridization is small, it is unclear why it should have occurred at all.

We have considered the possibility of ligand isomerization to 1,3- or 1,4-COD. The lower symmetry of such a complex and the nonequivalence of the olefin carbon atoms would be expected to lead to metal d-orbital hybridization of the type observed. However, the electrochemical experiments described above show no change in the potential of the $1/1^+$ couple over the course of an electrolysis experiment. Thus isomerization would have to be very fast on the CV time scale, essentially concerted with electron transfer in both directions, and this appears to be very unlikely.

It is possible that tilting of the 1,5-COD ligand about an axis perpendicular to the double bonds could give rise to the observed d-orbital hybridization. It is conceivable that binding of a solvent dipole on one side of the metal might lead to such a distortion, but it seems unlikely that the present solvent- $\text{CH}_2\text{Cl}_2/\text{C}_2\text{H}_4\text{-Cl}_2$ -would give a sufficiently sharply defined solvate to produce the well-resolved ESR spectrum observed.

Extended Hückel MO calculations were performed to test the hypothesis of ring tilting. In these calculations, the Co-C(Cp) and Co-C(COD) distances were 2.10 and 1.995 Å, respectively, and the Cp and COD rings were of idealized geometry with 105, 120, and 109.5° bond angles. The Cp ring was oriented so as to preserve a plane of symmetry passing between the COD double bonds, and default CAChe²³ EHMO parameters were employed. These calculations show that there is a small but significant admixture of $d_{x^2-y^2}$ into d_{xz} in the undistorted structure which increases when the COD ring is tilted away from the in-plane Cp carbon atom and decreases for the opposite rotation. Thus it is probably safest to say that the observed d-orbital hybridization reflects the lower-than- C_{2v} symmetry when the Cp ring is not freely rotating.

Acknowledgment. This work was supported in part by the National Science Foundation (CHE 91-16332). We are grateful to Pfizer, Inc., for a summer fellowship to L. I. S.

OM940760G

(21) Peake, B. M.; Rieger, P. H.; Robinson, B. H.; Simpson, J. J. *Am. Chem. Soc.* **1980**, *102*, 156.

(22) Green, J. C.; Powell, P.; Tiborg, E. *Organometallics* **1984**, *3*, 211.

(23) CAChe Scientific, Inc., Box 500, Beaverton, OR 97077.

Organoiron Thermochemistry. Solution Thermochemical Investigation of Tertiary Phosphine Ligand Electronic Effects in *trans*-(P(*p*-XC₆H₄)₃)₂Fe(CO)₃ Complexes

Chunbang Li and Steven P. Nolan*

Department of Chemistry, University of New Orleans, New Orleans, Louisiana 70148

Received October 11, 1994[®]

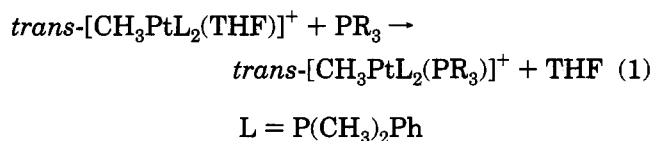
The enthalpies of reaction of (BDA)Fe(CO)₃ (BDA = (C₆H₅)CH=CHC(O)(CH₃), benzylideneacetone) with a series of para-substituted triphenylphosphine ligands, leading to the formation of *trans*-(P(*p*-XC₆H₄)₃)₂Fe(CO)₃ complexes (X = H, CH₃O, CH₃, Cl, F, CF₃), have been measured by solution calorimetry in THF at 50 °C. The range of reaction enthalpies spans some 7.7 kcal/mol and helps establish a relative order of complex stability for 14 compounds in the iron tricarbonyl system. The relative enthalpy scale for tertiary phosphine complexes, *trans*-(P(*p*-XC₆H₄)₃)₂Fe(CO)₃, is as follows (X, Δ*H*_{reacn} in kcal/mol): CF₃, 22.4(0.3); Cl, 25.0(0.1); F, 25.8(0.2); H, 26.9(0.2); CH₃, 28.2(0.3); CH₃O, 30.1(0.2). The thermodynamic investigation of these isosteric tertiary phosphine ligands helps to independently determine the importance of phosphine electronic contribution to the enthalpy of reaction in this system. Correlations of various factors gauging the electron-donating properties of the phosphine ligands clearly show the electronic factor to be the overwhelming contributor to the enthalpy of reaction in the *trans*-(PR₃)₂Fe(CO)₃ system.

Introduction

The field of organometallic thermochemistry has gained recognition as one of great relevance to catalysis.¹ Such valuable investigations have led to a better understanding of bonding and reactivity patterns in a small number of organometallic systems.^{2,3} These studies have also proven to be powerful tools in predicting the thermodynamic feasibility of given reactions or individual steps comprising catalytic cycles.^{3,4} In spite of the general view that such studies are fundamental to a better understanding of organometallic systems,

this area remains one where few complete investigations have been performed.

Tertiary phosphines and chelating tertiary diphosphines have been widely used as ligands in organometallic chemistry.⁵ Kinetic, catalytic, and structural studies have been conducted on such complexes.⁶ In spite of the vast amount of information focusing on transition-metal phosphine complexes, few thermodynamic data regarding heats of binding of these ligands to metal centers exist. Manzer and Tolman⁷ have reported on the solution calorimetry of square-planar platinum(II) complexes, shown in eq 1, for a series of



phosphine ligands. A similar series was then investigated for Ni(0) complexes,⁸ shown in eq 2.



More recently, detailed thermochemical investigations of two related Mo(0) systems have been reported by Hoff and co-workers.⁹

* Abstract published in *Advance ACS Abstracts*, February 1, 1995.

(1) For leading references in this area see: (a) Nolan, S. P. *Bonding Energetics of Organometallic Compounds*; In *Encyclopedia of Inorganic Chemistry*; Wiley: New York, 1994. (b) Hoff, C. D. *Prog. Inorg. Chem.* **1992**, *40*, 503–561. (c) Martinho Simões, J. A.; Beauchamp, J. L. *Chem. Rev.* **1990**, *90*, 629–688. (d) Marks, T. J., Ed. *Bonding Energetics in Organometallic Compounds*; ACS Symposium Series 428; American Chemical Society: Washington, DC, 1990. (e) Marks, T. J., Ed. *Metal-Ligand Bonding Energetics in Organotransition Metal Compounds*; Polyhedron Symposium-in-Print 7; Pergamon Press: Oxford, U.K., 1988. (f) Skinner, H. A.; Connor, J. A. In *Molecular Structure and Energetics*; Liebman, J. F., Greenberg, A., Eds.; VCH: New York, 1987; Vol. 2, Chapter 6. (g) Skinner, H. A.; Connor, J. A. *Pure Appl. Chem.* **1985**, *57*, 79–88. (h) Pearson, R. G. *Chem. Rev.* **1985**, *85*, 41–59. (i) Mondal, J. U.; Blake, D. M. *Coord. Chem. Rev.* **1982**, *47*, 205–238. (j) Mansson, M. *Pure Appl. Chem.* **1983**, *55*, 417–426. (k) Pilcher, G.; Skinner, H. A. In *The Chemistry of the Metal-Carbon Bond*; Harley, F. R., Patai, S., Eds.; Wiley: New York, 1982; pp 43–90. (l) Connor, J. A. *Top. Curr. Chem.* **1977**, *71*, 71–110.

(2) (a) Nolan, S. P.; Hoff, C. D.; Stoutland, P. O.; Newman, L. J.; Buchanan, J. M.; Bergamn, R. G.; Yang, G. K.; Peters, K. G. *J. Am. Chem. Soc.* **1987**, *109*, 3143–3145, and references therein. (b) Nolan, S. P.; Lopez de la Vega, R.; Hoff, C. D. *Organometallics* **1986**, *5*, 2529–2537.

(3) (a) Nolan, S. P.; Porchia, M. Marks, T. J. *Organometallics* **1991**, *10*, 1450–1457. (b) Nolan, S. P.; Stern, D.; Marks, T. J. *J. Am. Chem. Soc.* **1989**, *111*, 7844–7854.

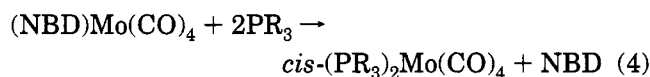
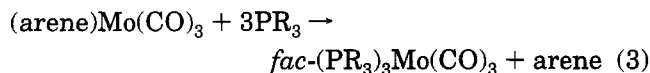
(4) (a) Nolan, S. P.; Stern, D.; Hedden, D.; Marks, T. J. In ref 1d, pp 159–174. (b) Nolan, S. P.; Lopez de la Vega, R.; Mukerjee, S. L.; Gonzalez, A. A.; Hoff, C. D. In ref 1e, pp 1491–1498. (c) Marks, T. J.; Gagné, M. R.; Nolan, S. P.; Schock, L. E.; Seyam, A. M.; Stern, D. L. *Pure Appl. Chem.* **1989**, *61*, 1665–1672. (d) Schock, L. E.; Marks, T. J. *J. Am. Chem. Soc.* **1988**, *110*, 7701.

(5) Tolman, C. A. *Chem. Rev.* **1977**, *77*, 313–348. (6) Pignolet, L. H., Ed. *Homogeneous Catalysis with Metal Phosphine Complexes*; Plenum: New York, 1983.

(7) Manzer, L. E.; Tolman, C. A. *J. Am. Chem. Soc.* **1975**, *97*, 1955–1986.

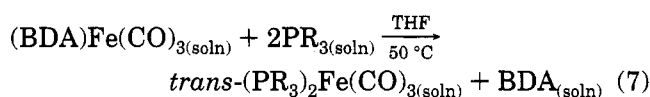
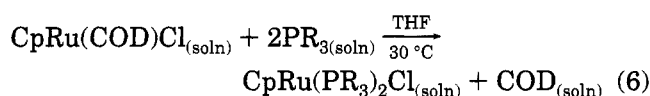
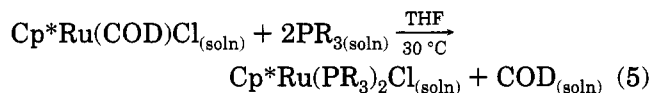
(8) Tolman, C. A.; Reutter, D. W.; Seidel, W. C. *J. Organomet. Chem.* **1976**, *117*, C30–C33.

(9) (a) Nolan, S. P.; Hoff, C. D. *J. Organomet. Chem.* **1985**, *290*, 365–373. (b) Mukerjee, S. L.; Nolan, S. P.; Hoff, C. D.; de la Vega, R. *Inorg. Chem.* **1988**, *27*, 81–85.



NBD = norbornadiene

In an effort to remedy this dearth of thermodynamic information on metal–phosphine complexes, we have recently reported on three organogroup 8 systems:^{10,11}



Cp = C₅H₅; Cp* = C₅Me₅; BDA = PhCH=CHCOMe; PR₃ = tertiary phosphine

Noteworthy is that in every one of the phosphine-based organometallic thermochemical investigations mentioned above, interpretations of results are provided in terms of phosphine steric and electronic contributions to the overall enthalpy of reaction. A number of relationships have been used to determine or gauge these relative steric and electronic contributions in kinetic and thermodynamic studies.^{12,13} In the present contribution, we extend our solution calorimetric work on organoiron-based systems¹¹ and report on the relative importance of the tertiary phosphine ligand electronic parameter as it affects metal–ligand bond enthalpies and complex stability. The present thermochemical investigation focuses on a series of isosteric

phosphine ligands binding the iron tricarbonyl system (–Fe(CO)₃).

Experimental Section

General Considerations. All manipulations involving organoiron complexes were performed under inert atmospheres of argon or nitrogen using standard high-vacuum or Schlenk tube techniques or in a Vacuum Atmospheres glovebox containing less than 1 ppm of oxygen and water. Tetrahydrofuran was stored over sodium wire, distilled from sodium benzophenone ketyl, stored over Na/K alloy, and vacuum-transferred into flame-dried glassware prior to use. Infrared spectra were recorded using a Perkin-Elmer FTIR Model 2000 spectrometer in 0.1 mm NaCl cells. NMR spectra were recorded using a Varian Gemini 300 MHz spectrometer. Calorimetric measurements were performed using a Calvet calorimeter (Setaram C-80), which was periodically calibrated using the TRIS reaction¹⁴ or the enthalpy of solution of KCl in water.¹⁵ The experimental enthalpies for these two standard reactions compared very closely to literature values. This calorimeter has been previously described,¹⁶ and typical procedures are described below. The organoiron complex (BDA)Fe(CO)₃ (1) was synthesized according to literature procedures.¹⁷ Only materials of high purity as indicated by IR and NMR spectroscopy were used in the calorimetric experiments. All organoiron complexes have been previously reported,¹⁸ with the exception of the *trans*-(*p*-CF₃C₆H₄)₃P)₂Fe(CO)₃ complex, which was synthesized as described below. All ligands were purchased from Strem Chemicals (Newburyport, MA) or Organometallics, Inc. (East Hampstead, NH), and used as received.

Synthesis and Characterization of *trans*-(*p*-CF₃-C₆H₄)₃P)₂Fe(CO)₃. A 100 mL flask was charged with 510 mg of P(*p*-CF₃C₆H₄)₃ (1.09 mmol), 140 mg (0.49 mmol) of (BDA)Fe(CO)₃ (BDA = benzylideneacetone), and 15 mL of THF. The clear orange solution was stirred at room temperature for 88 h, after which time the solvent was removed under vacuum. The residue was dissolved in 20 mL of CH₂Cl₂ and slowly cooled to –50 °C using a dry ice–acetone bath. Following filtration, washing with 2 mL of pentane and drying under vacuum afforded 288 mg of a golden yellow product (yield 57%). ¹H NMR (*d*₈-THF): 7.87 ppm (24 H, m, Ph). IR (THF): ν_{CO} 1899 cm^{–1}. Anal. Calcd for C₄₆H₂₄FeP₂O₃F₁₈: C, 50.40; H, 2.26. Found: C, 50.71; H, 2.43.

Calorimetric Measurement for Reaction Involving (BDA)Fe(CO)₃ and P(*p*-CF₃C₆H₄)₃. The mixing vessels of the Setaram C-80 were cleaned, dried in an oven maintained at 120 °C, and then taken into the glovebox. A 20–30 mg sample of recrystallized (BDA)Fe(CO)₃ was accurately weighed into the lower vessel; it was closed and sealed with 1.5 mL of mercury. Four milliliters of a stock solution of the phosphine ligand (2 g of the phosphine ligand in 25 mL of THF) was added and the remainder of the cell was assembled, removed from the glovebox, and inserted in the calorimeter. The reference vessel was loaded in an identical fashion with the exception that no organoiron complex was added to the lower vessel. After the calorimeter had reached thermal equilibrium at 50.0 °C (about 2 h) the reaction was initiated by inverting the calorimeter. At the end of the reaction (1–2 h) the vessels were removed from the calorimeter, taken into the glovebox, and opened, and the infrared cell was filled under an inert atmosphere. An infrared spectrum of each product was

(10) For organoruthenium systems see: (a) Nolan, S. P.; Martin, K. L.; Stevens, E. D.; Fagan, P. J. *Organometallics* **1992**, *11*, 3947–3953. (b) Luo, L.; Fagan, P. J.; Nolan, S. P. *Organometallics* **1993**, *12*, 3405–3411. (c) Luo, L.; Zhu, N.; Zhu, N.-J.; Stevens, E. D.; Nolan, S. P.; Fagan, P. J. *Organometallics* **1994**, *13*, 669–675. (d) Li, C.; Cucullu, M. E.; McIntyre, R. A.; Stevens, E. D.; Nolan, S. P. *Organometallics* **1994**, *13*, 3621–3627. (e) Luo, L.; Nolan, S. P. *Organometallics* **1994**, *13*, 4781–4786. (f) Luo, L.; Li, C.; Cucullu, M. E.; Nolan, S. P. *Organometallics* **1995**, *14*, 1333–1338.

(11) For organoiron systems see: (a) Luo, L.; Nolan, S. P. *Organometallics* **1992**, *11*, 3483–3486. (b) Luo, L.; Nolan, S. P. *Inorg. Chem.* **1993**, *32*, 2410–2415.

(12) (a) Rahman, M. M.; Liu, H.-Y.; Eriks, K.; Prock, A.; Giering, W. P. *Organometallics* **1989**, *8*, 1–7. (b) Liu, H.-Y.; Eriks, K.; Prock, A.; Giering, W. P. *Inorg. Chem.* **1989**, *28*, 1759–1763. (c) Poe, A. J. *Pure Appl. Chem.* **1988**, *60*, 1209–1216 and references cited therein. (d) Gao, Y.-C.; Shi, Q.-Z.; Kersher, D. L.; Basolo, F. *Inorg. Chem.* **1988**, *27*, 188–191. (e) Baker, R. T.; Calabrese, J. C.; Krusic, P. J.; Therien, M. J.; Trogler, W. C. *J. Am. Chem. Soc.* **1988**, *110*, 8392–8412. (f) Rahman, M. M.; Liu, H.-Y.; Prock, A.; Giering, W. P. *Organometallics* **1987**, *6*, 650–658.

(13) (a) Huynh, M. H. V.; Bessel, C. A.; Takeuchi, K. J. *Abstracts of Papers*, 208th National Meeting of the American Chemical Society, Washington, DC, Fall 1994; American Chemical Society: Washington, DC, 1994; Abstract INOR 165. (b) Perez, W. J.; Bessel, C. A.; See, R. F.; Lake, C. H.; Churchill, M. R.; Takeuchi, K. J. *Abstracts of Papers*, 208th National Meeting of the American Chemical Society, Washington, DC, Fall 1994; American Chemical Society: Washington, DC, 1994; INOR 166. (c) Ching, S.; Shriver, D. F. *J. Am. Chem. Soc.* **1989**, *111*, 3238–3243. (d) Lee, K.-W.; Brown, T. L. *Inorg. Chem.* **1987**, *26*, 1852–1856.

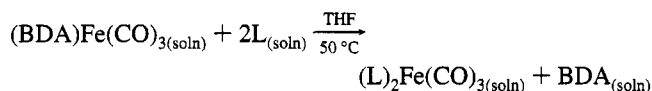
(14) Ojelund, G.; Wadso, I. *Acta Chem. Scand.* **1968**, *22*, 1691–1699.

(15) Kilday, M. V. *J. Res. Natl. Bur. Stand. (U.S.)* **1980**, *85*, 467–481.

(16) Nolan, S. P.; Hoff, C. D. *J. Organomet. Chem.* **1985**, *282*, 357–362.

(17) Howell, J. A. S.; Johnson, B. F. G.; Josty, P. L.; Lewis, J. J. *Organomet. Chem.* **1972**, *39*, 329–333.

(18) (a) Inoue, H.; Takei, T.; Heckmann, G.; Fluck, E. Z. *Naturforsch.* **1991**, *46B*, 682–686. (b) Sowa, J. R.; Zanolli, V.; Facchin, G.; Angelici, R. J. *J. Am. Chem. Soc.* **1991**, *113*, 9185–9192.

Table 1. Enthalpies of Substitution (kcal/mol) in the Reaction

L	complex	δ_{CO} (cm ⁻¹) ^a	$-\Delta H_{\text{reacn}}$ ^b
AsPh ₃	(Ph ₃ As) ₂ Fe(CO) ₃	1886	10.2(0.2) ^c
P(<i>p</i> -CF ₃ C ₆ H ₄) ₃	[(<i>p</i> -CF ₃ C ₆ H ₄) ₃ P] ₂ Fe(CO) ₃	1899	22.4(0.3) ^d
AsEt ₃	(Et ₃ As) ₂ Fe(CO) ₃	1865	24.5(0.3) ^c
P(<i>p</i> -ClC ₆ H ₄) ₃	[(<i>p</i> -ClC ₆ H ₄) ₃ P] ₂ Fe(CO) ₃	1893	25.0(0.1) ^d
P(<i>p</i> -FC ₆ H ₄) ₃	[(<i>p</i> -FC ₆ H ₄) ₃ P] ₂ Fe(CO) ₃	1891	25.8(0.2) ^d
P(C ₆ H ₅) ₃	[(C ₆ H ₅) ₃ P] ₂ Fe(CO) ₃	1887	26.9(0.2) ^c
P(<i>p</i> -CH ₃ C ₆ H ₄) ₃	[(<i>p</i> -CH ₃ C ₆ H ₄) ₃ P] ₂ Fe(CO) ₃	1884	28.2(0.3) ^d
P(<i>p</i> -CH ₃ OC ₆ H ₄) ₃	[(<i>p</i> -CH ₃ OC ₆ H ₄) ₃ P] ₂ Fe(CO) ₃	1882	30.1(0.2) ^d
PPh ₂ Me	(Ph ₂ MeP) ₂ Fe(CO) ₃	1878	34.1(0.3) ^c
PPhMe ₂	(PhMe ₂ P) ₂ Fe(CO) ₃	1875	37.3(0.3) ^c
PMe ₃	(Me ₃ P) ₂ Fe(CO) ₃	1871	38.9(0.2) ^c
P ⁿ Bu ₃	(ⁿ Bu ₃ P) ₂ Fe(CO) ₃	1865	41.7(0.3) ^c
PEt ₃	(Et ₃ P) ₂ Fe(CO) ₃	1867	42.4(0.2) ^c

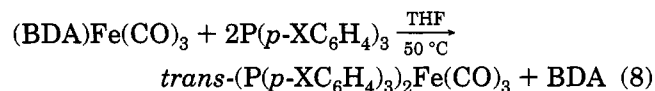
^a Infrared spectra were recorded in THF. ^b Enthalpy values are reported with 95% confidence limits. ^c Taken from ref 11. ^d This work.

recorded using this procedure. Conversion to *trans*-(P(*p*-CF₃C₆H₄)₃)₂Fe(CO)₃ was found to be quantitative under these reaction conditions. The enthalpy of reaction, -15.9 ± 0.1 kcal/mol, represents the average of five individual calorimetric determinations.

Calorimetric Determination of the Enthalpy of Solution of (BDA)Fe(CO)₃ in THF. In order to consider all species in solution, the enthalpy of solution of **1** had to be directly measured. The calorimeter cells were loaded in the exact fashion as in the example described above, with the exception that no ligands were introduced in the reaction cell. The measured enthalpy is 6.5 ± 0.1 kcal/mol and represents seven separate determinations. To ensure that no decomposition had occurred during the thermal equilibration at 50 °C, a THF solution of (BDA)Fe(CO)₃ was maintained at 50 °C for 3 h; the solvent was then removed and the residue examined by NMR and IR spectroscopy. Both analytical techniques clearly showed the complex to have remained intact during this thermal treatment.

Results

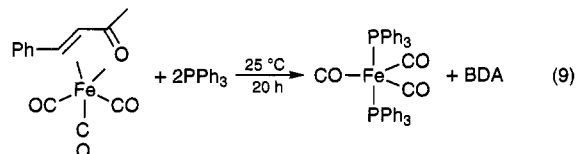
The (BDA)Fe(CO)₃ complex (BDA = PhCH=CHCOMe, benzylideneacetone) was selected as the entryway into the thermochemistry of the iron tricarbonyl system in view of the labile nature of the BDA ligand. In the present study, a series of isosteric tertiary phosphine ligands were investigated by batch solution calorimetry:



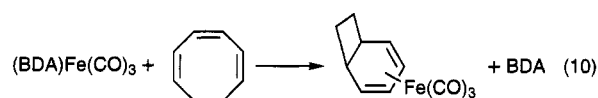
All reactions investigated led to a unique product under the calorimetric conditions as determined by infrared and NMR spectroscopy. A list of all enthalpies of reaction involving para-substituted triphenylphosphine ligands is provided in Table 1. All reported enthalpies of reaction are solution-phase values and take into account the enthalpy of solution of (BDA)Fe(CO)₃ (6.5 ± 0.1 kcal/mol).

Discussion

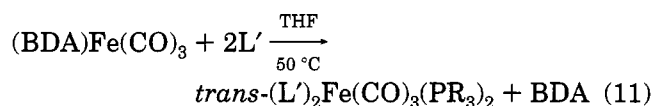
With the exception of the few thermodynamic investigations reported by Muetterties¹⁹ and Connor,²⁰ thermodynamic information focusing on organoiron systems remains scarce. The (BDA)Fe(CO)₃ complex (BDA = PhCH=CHCOMe, benzylideneacetone) provides easy access to iron tricarbonyl complexes and thermochemical data, in view of the labile nature of the BDA ligand as illustrated by Angelici and co-workers,¹⁸ who have reported its usefulness as a synthon leading to high yields of (phosphine)tricarbonyliron complexes:



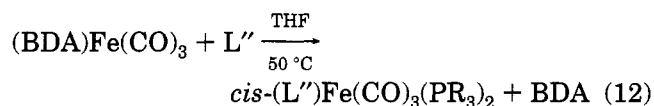
The labile nature of the BDA complex has also previously been noted by Brookhart and co-workers in their use of this complex as a diene trapping agent:²¹



We have recently reported the enthalpies of reaction of (BDA)Fe(CO)₃ with a series of mono- and bidentate ligands using solution calorimetry in THF at 50 °C according to eqs 11 and 12.¹¹



L' = monodentate ligand



L'' = bidentate ligand

In the monodentate phosphine study, we have interpreted contributions of steric and electronic phosphine effects by using a relationship first proposed by Tolman and co-workers:⁵

$$-\Delta H^\circ = A_0 + A_1\theta + A_2\nu \quad (13)$$

where enthalpies of reaction are correlated to steric (θ , cone angle) and electronic (ν , A_2 carbonyl stretching frequency in Ni(CO)₃L (L = tertiary phosphine) factors. The A_1/A_2 ratio can be taken as a measure of the relative importance of steric versus electronic factors. It would be expected that steric factors play only a minor role in this iron system in view of the final *trans* arrangement

(19) Putnik, C. F.; Welter, J. J.; Stucky, G. D.; D'Aniello, M. J.; Sosinsky, B. A.; Kirner, J. F.; Muetterties, E. L. *J. Am. Chem. Soc.* **1978**, *100*, 4107–4109.

(20) (a) Brown, D. L. S.; Connor, J. A.; Leung, M. L.; Paz Andrade, M. I.; Skinner, H. A.; Zafarani-Moattar, M. T. *J. Organomet. Chem.* **1976**, *110*, 79–89. (b) Connor, J. A.; Demain, C. P.; Skinner, H. A.; Zafarani-Moattar, M. T. *J. Organomet. Chem.* **1979**, *170*, 117–130.

(21) (a) Graham, C. R.; Scholes, G.; Brookhart, M. *J. Am. Chem. Soc.* **1977**, *99*, 1180–1188. (b) Brookhart, M.; Nelson, G. O. *J. Organomet. Chem.* **1979**, *164*, 193–202.

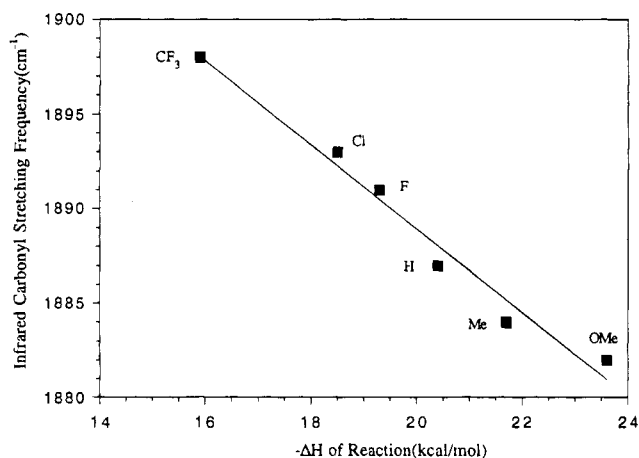


Figure 1. Carbonyl stretching frequency vs enthalpy of phosphine substitution reaction for *trans*-(P(*p*-XC₆H₄)₃)₂Fe(CO)₃ complexes (slope -2.21 , $R = 0.99$).

of ligands. A value of 0.008 was calculated for the A_1/A_2 ratio and quantitatively denoted the overwhelming influence of electronic factors. Excellent relationships were established when the electronic factor was solely considered. However, this analysis dealt with phosphine ligands with varied steric demands and an examination of enthalpies of reaction as a function of electronic variations is warranted in order to shed light on the unique importance of this parameter in the present iron system.

A number of measurable properties reflect the electron donation of the phosphine ligands, and these can be examined in terms of possible relationships with the measured enthalpies of reaction listed in Table 1. Two different but equally useful approaches can be used. One can examine the overall electron donation from the phosphine to the metal by examining the carbonyl stretch associated with the bis(phosphine)iron tricarbonyl product. The CO stretch is notable for gauging such quantities.²² The amount of back-donation into CO as reflected by the position of the CO stretch is then a gauge of phosphine electron donation. In our preceding report on organoiron thermochemistry,^{11a} a relationship between carbonyl stretching frequencies and enthalpies of reaction was established and showed remarkable linearity. This is not entirely surprising, since the carbonyl stretching modes are directly influenced by the electronic donation provided by ancillary ligands allowing for modulation in the metal electron density available for back-donation to the CO groups. The overall effect seen in the present system is due to the electronic nature of phosphine ligand providing electron density that will account for the amount of back-donation to CO as reflected by the CO stretching frequency. A relationship exists (with an excellent fit, $R = 0.99$) between the enthalpy of reaction of phosphine ligands investigated in the present study and the carbonyl stretching frequency observed in the corresponding bis(phosphine)iron tricarbonyl product (Figure 1). All thermochemical data measured up to now can be included in order to test the general validity of such a relationship. The fit of the relationship is clearly indicative of the principal role played by the ligand electronic parameter in all complexes investigated (Figure 2).

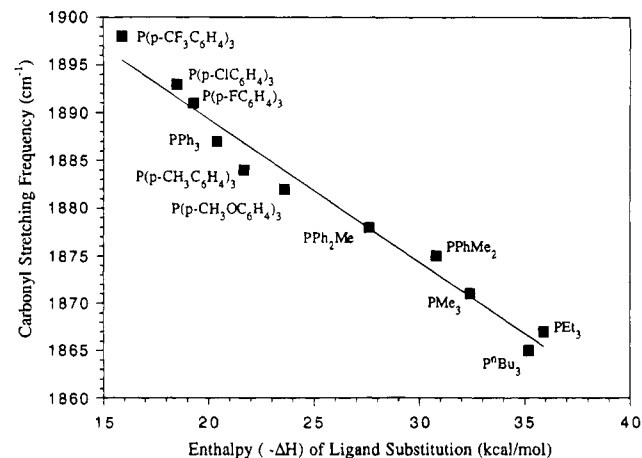


Figure 2. Carbonyl stretching frequency vs enthalpy of phosphine substitution reaction in a series of *trans*-(L)₂Fe(CO)₃ complexes (slope -1.50 , $R = 0.99$).

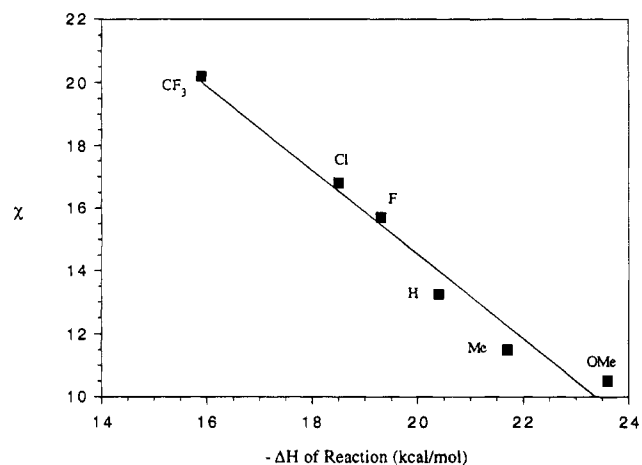


Figure 3. Phosphine electronic parameter (χ) vs enthalpy of phosphine substitution reaction for a series of *trans*-(P(*p*-XC₆H₄)₃)₂Fe(CO)₃ complexes (slope -1.34 , $R = 0.99$).

The second approach deals with the donating ligands themselves, in this case, the tertiary phosphine ligands. Recently, attempts have been made to extract information about the stereoelectronic factors influencing the thermodynamics and kinetics of reactions by quantitative analysis of ligand effects (QALE).²³ Steric and electronic ligand characteristics represent the foundation of a QALE treatment. Correlations obtained using this method oftentimes are linear and offer insights into structure and reactivity patterns. Such a treatment was performed for the present thermochemical data, only utilizing the electronic parameter, and results are graphically represented in Figure 3.

As can be clearly seen, since the series of tertiary phosphine ligands is isosteric, only the electronic parameter will be the origin of any variations in measured enthalpies of reaction. Enthalpies of reaction correlate in a linear fashion with the ligand electronic parameter (χ).²³ Here it can be seen that a difference of some 8 kcal/mol results from modifying the electronics of the para-substituted group on the triphenylphosphine phenyl group. This effect is substantial when considering the stereoelectronic range of phosphine ligands previ-

(22) Collman, J. P.; Hegedus, L. S.; Norton, J. R.; Finke, R. G. *Principles and Applications of Organotransition Metal Chemistry*, 2nd ed.; University Science: Mill Valley, CA, 1987.

(23) (a) Fernandez, A. L.; Prock, A.; Giering, W. P. *Organometallics* **1994**, *13*, 2767–2772 and references cited therein. (b) Liu, H.-Y.; Eriks, K.; Prock, A.; Giering, W. P. *Organometallics* **1990**, *9*, 1758–1766.

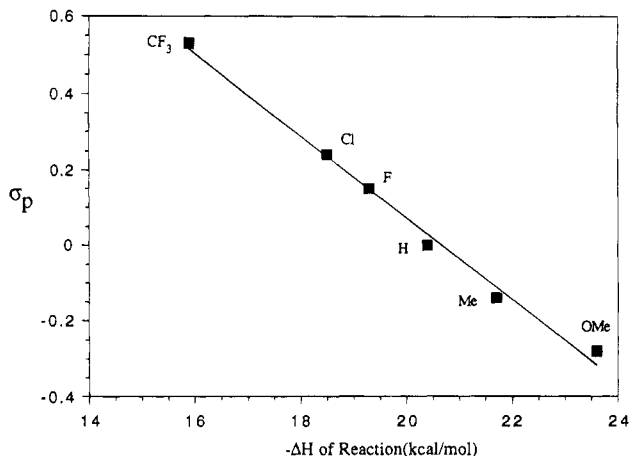
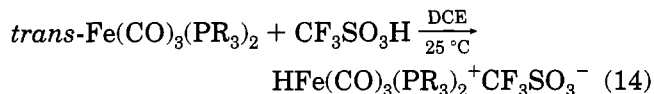


Figure 4. Hammett σ_p parameter vs enthalpy of phosphine substitution reaction for a series of *trans*-(P(*p*-XC₆H₄)₃)₂Fe(CO)₃ complexes (slope -0.11 , $R = 1.00$).

ously studied in this system, which lead to a total enthalpy scale spanning some 20 kcal/mol.¹¹ This 8 kcal/mol range clearly illustrates the importance of electronic ligand parameters in the present system. Table 1 lists all enthalpies of reactions measured with corresponding carbonyl stretching frequencies for all *trans*-(PR₃)₂Fe(CO)₃ complexes so far investigated by solution calorimetry.

An alternative to the QALE treatment is possible in this study of isosteric phosphines if the overall donor properties of the phosphine can be regarded as depending solely on the electronic nature of the para substituent on the aryl fragment. This brings to mind an LFER (linear free energy relationship) treatment.²⁴ Such a simple correlation can be established with remarkable fit ($R = 1.00$). It is then concluded that the para substituent on the phosphine aryl group is entirely responsible for the modulation in enthalpy of ligand substitution reaction within the present series.

Angelici and co-workers have recently reported on the enthalpies of protonation of *trans*-(PR₃)₂Fe(CO)₃ complexes¹⁸ (eq 14). In their study, the investigators were



principally interested in gauging the metal basicity as a function of ancillary ligation. Having established that electronic parameters were of utmost importance in the present *trans*-(P(*p*-X-C₆H₄)₃)₂Fe(CO)₃ system, comparison with the measured enthalpies of protonation should shed light on whether ligand electronic characteristics in the form of enthalpies of ligand substitution also correlate with heats of protonation. The relationship shows a good fit, and it may therefore be concluded that phosphine electronic contributions also affect the magnitude of enthalpies of protonation and therefore metal basicity.

The magnitude of the reported enthalpy values provide insight into reactivity patterns. The (PPh₃)₂Fe(CO)₃ complex has previously been found to possess one

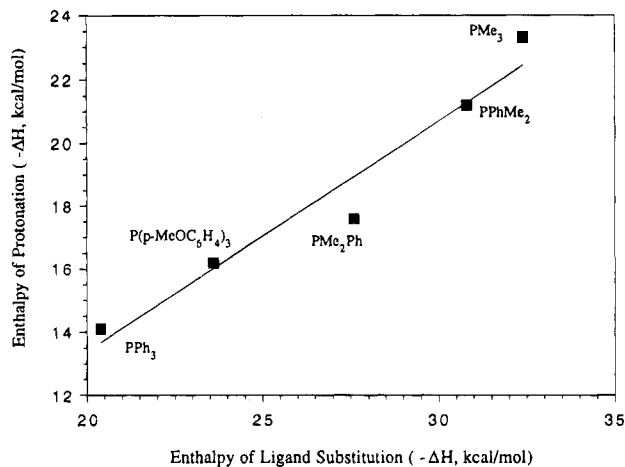
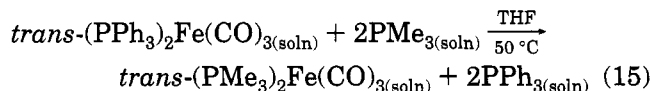
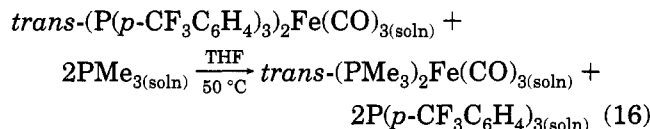


Figure 5. Enthalpy of protonation vs enthalpy of phosphine substitution reaction in a series of *trans*-(P(*p*-XC₆H₄)₃)₂Fe(CO)₃ complexes (slope 0.73 , $R = 0.98$).

of the weakest Fe-PR₃ bonds. With the present data, we see that the Fe-P bond can be further destabilized by appending an electron-withdrawing para substituent on the phenyl ring of the triphenylphosphine ligands. This has a net effect of weakening the Fe-P bond by some 2 kcal/mol compared to the Fe-PPh₃ bond. This also means that any substitution reaction that can be carried out from the *trans*-(PPh₃)₂Fe(CO)₃ complex will prove more exothermic by some 4.5 kcal/mol if it is carried out instead from the *trans*-(*p*-CF₃C₆H₄)₃P₂Fe(CO)₃ complex (eqs 15 and 16) and conversely, of course,

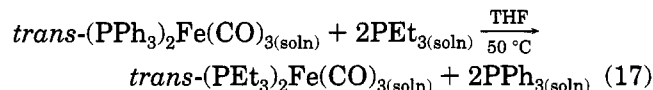


$$\Delta H_{\text{calcd}} = -12.0 \pm 0.3 \text{ kcal/mol}$$

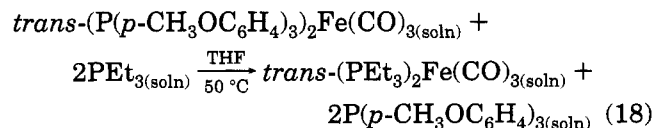


$$\Delta H_{\text{calcd}} = -16.5 \pm 0.4 \text{ kcal/mol}$$

any substitution reaction carried out from the *trans*-(PPh₃)₂Fe(CO)₃ complex will prove more exothermic by some 3.2 kcal/mol than if it were carried out from the *trans*-(*p*-CH₃OC₆H₄)₃P₂Fe(CO)₃ complex (eqs 17 and 18).



$$\Delta H_{\text{calcd}} = -15.5 \pm 0.3 \text{ kcal/mol}$$



$$\Delta H_{\text{calcd}} = -12.3 \pm 0.3 \text{ kcal/mol}$$

Conclusion

The reported solution calorimetric investigation represents the first detailed thermochemical study of ligand

(24) (a) Wells, P. R. *Linear Free Energy Relationships*; Academic Press: New York, 1968. (b) Charton, M. *Prog. Org. Chem.* **1973**, *10*, 81-204. (c) March, J. *Advanced Organic Chemistry*; Wiley-Interscience: New York, 1992; pp 278-286.

substitution reactions involving isosteric tertiary phosphine ligands for an organometallic system. The results allow for a quantitative evaluation of electronic effects in the present iron system. The present iron tricarbonyl system allows for simple relationships to be established between enthalpies of reaction and a variety of quantitative factors reflecting the overall electronic effect of phosphine binding. Excellent correlations are established with the carbonyl stretching frequency of the product, the phosphine electronic parameter χ , and the Hammett σ parameters associated with the phenyl para substituent of triphenylphosphine ligands. An excellent correlation is established with all enthalpy data vs carbonyl stretching frequency. This fact clearly illustrates the major role of the electronic contribution in the present system. The degree of variation observed

in enthalpies of reaction as a function of simple modification in para-substituted triphenylphosphine ligands shows important insights into reactivity fine tuning. Studies focusing on the enthalpic contributions of other ligands in this and related systems are presently underway.

Acknowledgment. The National Science Foundation (Grant No. CHE-9305492) and the Louisiana Education Quality Support Fund are gratefully acknowledged for support of this research. The Louisiana Board of Regents is also acknowledged for allocating funds allowing the purchase of the FT-IR spectrophotometer (Grant No. ENH-TR-41, 1993-1994).

OM9407823

Organoruthenium Thermochemistry. Absolute Metal–Ligand Bond Disruption Enthalpies in the $(\eta^5\text{-C}_5\text{Me}_5)(\text{CO})_2\text{Ru-X}$ System (X = H, Cl, Br, I) and Thermodynamic Influences of Ancillary Ligand Variation on the Ru–X Bond Disruption Enthalpy

Lubin Luo, Chunbang Li, Michèle E. Cucullu, and Steven P. Nolan*

Department of Chemistry, University of New Orleans, New Orleans, Louisiana 70148

Received October 31, 1994[®]

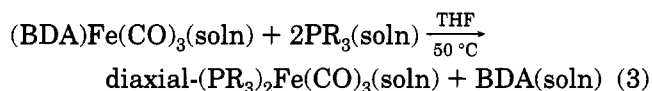
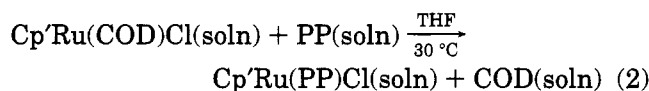
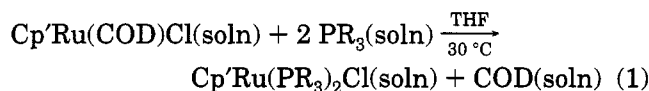
The enthalpies of reaction of $(\eta^5\text{-C}_5\text{Me}_5)(\text{CO})_2\text{Ru-H}$ (1) with CCl_4 , CBr_4 , and CH_3I leading to the formation of $(\eta^5\text{-C}_5\text{Me}_5)(\text{CO})_2\text{Ru-X}$ complexes (X = Cl, Br, I) have been measured by solution calorimetry in THF at 30 °C. On the basis of enthalpies of reaction and the recently reported Ru–H in $(\text{C}_5\text{H}_5)\text{Ru}(\text{CO})_2\text{H}$ (65 ± 1.0 kcal/mol), an absolute Ru–X bond disruption enthalpy (BDE) scale can be established for ruthenium halide complexes. The absolute BDE scale for ruthenium halide complexes, $(\eta^5\text{-C}_5\text{Me}_5)(\text{CO})_2\text{Ru-X}$, is as follows (X, kcal/mol): Cl, 80.7; Br, 61.1; and I, 55.6, respectively. These ruthenium BDE values can be directly compared with other metal-based systems and lead to a clearer understanding of general BDE trends in M–X systems. In addition, a number of enthalpies of reaction were measured involving organoruthenium hydride complexes with varied ancillary ligands in order to examine the ancillary ligand effects on the relative Ru–X bond enthalpies.

Introduction

The field of organometallic thermochemistry has gained recognition as one of great relevance to chemistry and catalysis.¹ Such valuable investigations have led to a better understanding of bonding and reactivity patterns in a small number organometallic systems.^{2–4} In spite of the general view that such studies are fundamental to a better understanding of organometallic systems, this area remains one where few absolute metal–ligand bond disruption enthalpy investigations have been performed in solution.

We have recently reported on ligand substitution

reactions focusing on group 8 metal-centered organometallic systems.^{5,6}



$\text{Cp}' = \text{C}_5\text{H}_5$ or C_5Me_5 ; BDA = $\text{PhCH}=\text{CHCOMe}$;

$\text{PR}_3 =$ tertiary phosphine;

PP = chelating diphosphine

These data are of utility in calculating enthalpies of ligand exchange and in estimating equilibrium constants for a number of reactions. There are however much less thermochemical data available for homolytic cleavage of the M–X bond to produce radical fragments. A series of papers on the $\text{X}_2\text{Mo}(\text{C}_5\text{H}_5)_2$ complexes has led to generation of Mo–X bond estimates.^{7–10} Hoff and co-workers have investigated the related X–Mo(CO)₃–

[®] Abstract published in *Advance ACS Abstracts*, February 1, 1995.

(1) For leading references in this area, see: (a) Nolan, S. P. *Bonding Energetics of Organometallic Compounds*. In *Encyclopedia of Inorganic Chemistry*; J. Wiley and Sons: New York, 1994. (b) Hoff, C. D. *Prog. Inorg. Chem.* **1992**, *40*, 503–561. (c) Martinho Simões, J. A.; Beauchamp, J. L. *Chem. Rev.* **1990**, *90*, 629–688. (d) Marks, T. J., Ed. *Bonding Energetics in Organometallic Compounds*; ACS Symposium Series; American Chemical Society: Washington, DC, 1990; p 428. (e) Marks, T. J., Ed. *Metal-Ligand Bonding Energetics in Organotransition Metal Compounds*; Polyhedron Symposium-in-Print; Pergamon: London, 1988; p 7. (f) Skinner, H. A.; Connor J. A. In *Molecular Structure and Energetics*; Liebman, J. F., Greenberg, A., Eds.; VCH: New York, 1987; Vol. 2, Chapter 6. (g) Skinner, H. A.; Connor, J. A. *Pure Appl. Chem.* **1985**, *57*, 79–88. (h) Pearson, R. G. *Chem. Rev.* **1985**, *85*, 41–59. (i) Mondal, J. U.; Blake, D. M. *Coord. Chem. Rev.* **1983**, *47*, 204–238. (j) Mansson, M. *Pure Appl. Chem.* **1983**, *55*, 417–426. (k) Pilcher, G.; Skinner, H. A. In *The Chemistry of the Metal-Carbon Bond*; Harley, F. R., Patai, S., Eds.; Wiley: New York, 1982; pp 43–90. (l) Connor, J. A. *Top. Curr. Chem.* **1977**, *71*, 71–110.

(2) (a) Nolan, S. P.; Hoff, C. D.; Stoutland, P. O.; Newman, L. J.; Buchanan, J. M.; Bergman, R. G.; Yang, G. K.; Peters, K. G. *J. Am. Chem. Soc.* **1987**, *109*, 3143–3145 and references therein. (b) Nolan, S. P.; Lopez de la Vega, R.; Hoff, C. D. *Organometallics* **1986**, *5*, 2529–2537.

(3) (a) Nolan, S. P.; Porchia, M.; Marks, T. J. *Organometallics* **1991**, *10*, 1450–1457. (b) Nolan, S. P.; Stern, D.; Marks, T. J. *J. Am. Chem. Soc.* **1989**, *111*, 7844–7854.

(4) (a) Nolan, S. P.; Stern, D.; Hedden, D.; Marks, T. J. In ref 1d, pp 159–174. (b) Nolan, S. P.; Lopez de la Vega, R.; Mukerjee, S. L.; Gongalez, A. A.; Hoff, C. D. In ref 1e, pp 1491–1498. (c) Marks, T. J.; Gagné, M. R.; Nolan, S. P.; Schock, L. E.; Seyam, A. M.; Stern, D. L. *Pure Appl. Chem.* **1989**, *61*, 1665–1672. (d) Schock, L. E.; Marks, T. J. *J. Am. Chem. Soc.* **1988**, *110*, 7701.

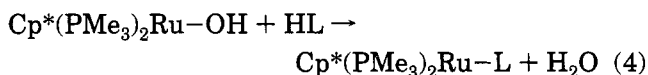
(5) For organoruthenium systems, see: (a) Nolan, S. P.; Martin, K. L.; Stevens, E. D.; Fagan, P. J. *Organometallics* **1992**, *11*, 3947–3953. (b) Luo, L.; Fagan, P. J.; Nolan, S. P. *Organometallics* **1993**, *12*, 4305–4311. (c) Luo, L.; Zhu, N.; Zhu, N.-J.; Stevens, E. D.; Nolan, S. P.; Fagan, P. J. *Organometallics* **1994**, *13*, 669–675. (d) Li, C.; Cucullu, M. E.; McIntyre, R. A.; Stevens, E. D.; Nolan, S. P. *Organometallics* **1994**, *13*, 3621–3627.

(6) For organoiron systems, see: (a) Luo, L.; Nolan, S. P. *Organometallics* **1992**, *11*, 3483–3486. (b) Luo, L.; Nolan, S. P. *Inorg. Chem.* **1993**, *32*, 2410–2415. (c) Li, C.; Nolan, S. P. *Organometallics* **1995**, *14*, 1327–1332.

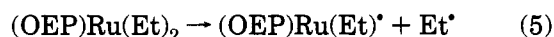
(7) Calado, J. C. G.; Dias, A. R.; Marthinho-Simões, J. A.; Ribeiro da Silva, M. A. V. *Rev. Port. Quim.* **1979**, *21*, 129–131.

(8) Calado, J. C. G.; Dias, A. R.; Marthinho-Simões, J. A. *J. Organomet. Chem.* **1980**, *195*, 203–206.

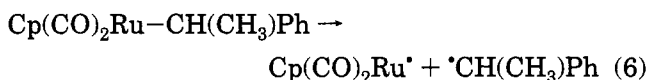
(C₅H₅) system and derived Mo–X BDE values.¹¹ Hoff and Bergman have performed such a study for the X₂Ir-(PMe₃)(C₅Me₅) system.^{2a} The few thermodynamic studies focusing on organoruthenium complexes have included the kinetic determination of relative bond enthalpy data for the Cp*(PMe₃)₂Ru–X system reported by Bercaw and co-workers.¹²



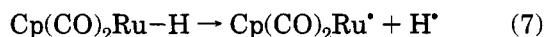
Collman has examined the kinetics of cleavage of one of the Ru–ethyl bonds (21.7 ± 1.5 kcal/mol) in the (OEP)Ru(Et)₂ system.¹³



Halpern and Mancuso have reported a kinetic determination of *D*(Ru–R) (33 kcal/mol) in Cp(CO)₂RuCH(CH₃)C₆H₅.¹⁴



and Parker and Tilset have most recently estimated absolute bond disruption enthalpies for a number of transition metal hydrides including H–Ru(CO)₂Cp.¹⁵



We now report new thermochemical data which allow for estimation of Ru–X bond disruption enthalpy values for the X–Ru(CO)₂(C₅Me₅) system and also report on reaction enthalpy variations as a function of ancillary ligand modifications.

Experimental Section

General Considerations. All manipulations involving organoruthenium complexes were performed under inert atmospheres of argon or nitrogen using standard high vacuum or Schlenk tube techniques or in a Vacuum/Atmospheres glovebox containing less than 1 ppm oxygen and water. Tetrahydrofuran was stored over sodium wire, distilled from sodium benzophenone ketyl, stored over Na/K alloy, and vacuum transferred into flame-dried glassware prior to use. Infrared spectra were recorded using a Perkin-Elmer FTIR Model 2000 spectrometer in 0.1 mm NaCl cells. NMR spectra were recorded using a Varian Gemini 300 MHz spectrometer. Calorimetric measurements were performed using a Calvet calorimeter (Setaram C-80) which was periodically calibrated using the TRIS reaction¹⁶ or the enthalpy of solution of KCl

(9) (a) Calado, J. C. G.; Dias, A. R.; Marthinho-Simões, J. A.; Ribeiro da Silva, M. A. V. *J. Organomet. Chem.* **1979**, *174*, 77–80. (b) Calado, J. C. G.; Dias, A. R.; Minas de Piedades, M. E.; Marthinho-Simões, J. A. *Rev. Port. Quim.* **1980**, *22*, 53–58.

(10) Calado, J. C. G.; Dias, A. R.; Salem, M. S.; Marthinho-Simões, J. A. *J. Chem., Soc., Dalton Trans.* **1981**, 1174–1177.

(11) Nolan, S. P.; Lopez de la Vega, R.; Hoff, C. D. *J. Organomet. Chem.* **1986**, *315*, 187–199.

(12) Bryndza, H. E.; Fong, L. K.; Paciello, R. A.; Tam, W.; Bercaw, J. E. *J. Am. Chem. Soc.* **1987**, *109*, 1444–1456.

(13) Collman, J. P.; McElwee-White, L.; Brothers, P. J.; Rose, E. J. *Am. Chem. Soc.* **1986**, *108*, 1332–1333.

(14) Mancuso, C.; Halpern, J. *J. Organomet. Chem.* **1992**, *428*, C8–C11.

(15) Tilset, M.; Parker, V. D. *J. Am. Chem. Soc.* **1989**, *111*, 6711–6717; **1990**, *112*, 2843.

(16) Ojelund, G.; Wadsö, I. *Acta Chem. Scand.* **1968**, *22*, 1691–1699.

in water.¹⁷ The experimental enthalpies for these two standard reactions compared very closely to literature values. This calorimeter has been previously described,¹⁸ and typical procedures are described below. The organoruthenium complexes Cp*Ru(CO)₂H,¹⁹ CpRu(PPh₃)₂H,²⁰ CpRu(dppe)H,²⁰ and CpRu(PMe₃)₂H²¹ were synthesized according to literature procedures. Only materials of high purity as indicated by IR and NMR spectroscopies were used in the calorimetric experiments. All ligands were purchased from Strem Chemicals (Newburyport, MA) and used as received.

¹H NMR Titrations. Prior to every set of calorimetric experiments involving a new reaction, an accurately weighed amount (±0.1 mg) of the organoruthenium complex was placed in a Wilmad screw-capped NMR tube fitted with a septum, and THF-*d*₈ was subsequently added. The solution was titrated with a solution of the reactant of interest by injecting the latter in aliquots through the septum with a microsyringe, followed by vigorous shaking. The reactions were monitored by ¹H NMR spectroscopy, and the reactions were found to be rapid and quantitative, conditions necessary for accurate and meaningful calorimetric results. These criteria were satisfied for all organoruthenium reactions investigated.

Calorimetric Measurement for Reaction Involving Cp*(CO)₂Ru–H (1) and CCl₄. The mixing vessels of the Setaram C-80 were cleaned, dried in an oven maintained at 120 °C, and then taken into the glovebox. A 20–30 mg sample of recrystallized Cp*(CO)₂RuH (1) was accurately weighed into the lower vessel, and it was closed and sealed with 1.5 mL of mercury. A 4 mL amount of a stock solution of CCl₄ (5 mL of the phosphine ligand in 25 mL of THF) was added, and the remainder of the cell was assembled, removed from the glovebox, and inserted in the calorimeter. The reference vessel was loaded in an identical fashion with the exception that no organoruthenium complex was added to the lower vessel. After the calorimeter had reached thermal equilibrium at 30.0 °C (about 2 h), the reaction was initiated by inverting the calorimeter. At the end of the reaction (1–2 h), the vessels were removed from the calorimeter, taken into the glovebox, and opened, and the infrared cell was filled under inert atmosphere. An infrared spectrum of each product was recorded using this procedure. Conversion to Cp*(CO)₂RuCl was found to be quantitative under these reaction conditions. The enthalpy of reaction, –36.7 ± 0.6 kcal/mol represents the average of five individual calorimetric determinations. This methodology represents a typical procedure involving all organometallic compounds and all reactions investigated in the present study.

Calorimetric Determination of the Enthalpy of Solution of Cp*(CO)₂RuH (1) in THF. In order to consider all species in solution, the enthalpy of solution of 1 had to be directly measured. The calorimeter cells were loaded in the exact fashion as in the example described above with the exception that no ligands were introduced in the reaction cell. The measured enthalpy is 4.4 ± 0.3 kcal/mol and represents seven separate determinations. To ensure that no decomposition had occurred during the thermal equilibration at 30 °C, a THF solution of Cp*(CO)₂RuH was maintained at 30 °C for 3 h, the solvent was then removed, and the residue was examined by NMR and IR spectroscopies. Both analytical techniques clearly showed the complex to have remained intact during this time.

(17) Kilday, M. V. *J. Res. Natl. Bur. Stand. (U.S.)* **1980**, *85*, 467–481.

(18) (a) Nolan, S. P.; Hoff, C. D. *J. Organomet. Chem.* **1985**, *290*, 365–373. (b) Mukerjee, S. L.; Nolan, S. P.; Hoff, C. D.; de la Vega, R. *Inorg. Chem.* **1988**, *27*, 81–85.

(19) Fagan, P. J.; Mahoney, W. S.; Calabrese, J. C.; Williams, I. D. *Organometallics* **1990**, *9*, 1843–1852.

(20) Bruce, M. I.; Humphrey, M. G.; Swincer, A. G.; Wallis, R. C. *Aust. J. Chem.* **1984**, *37*, 1747–1755.

(21) Mayer, J. M.; Calabrese, J. C. *Organometallics* **1984**, *3*, 1292–1298.

Table 1. Ru–X Bond Disruption Enthalpy Estimates for Cp*Ru(CO)₂X Complexes (kcal/mol)

$$\text{Cp}^*\text{Ru}(\text{CO})_2\text{H}(\text{soln}) + \text{XR}(\text{soln}) \xrightarrow[30^\circ\text{C}]{\text{THF}} \text{Cp}^*\text{Ru}(\text{CO})_2\text{X}(\text{soln}) + \text{HR}(\text{soln})$$

X–R	–ΔH ^{rxn}	D(Ru–H) ^a	D(X–R) ^b	D(R–H) ^b	D(Ru–X)
Cl–Cl ₃	41.1(0.6)	65	70.4	95.8	80.7
Br–CBr ₃	44.4(0.4)	65	56.2	96.0	61.1
I–CH ₃	39.3(0.5)	65	56.3	105	55.6

^a D(Ru–H) Taken from ref 15. ^b Ancillary thermodynamic data taken from ref 22.

Table 2. Enthalpies of Reactions of Cp'Ru(L)₂H with RX (kcal/mol)

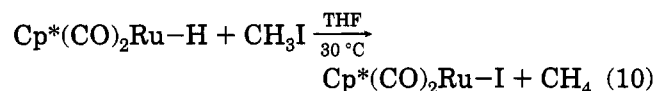
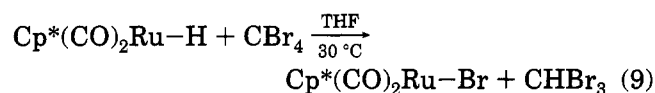
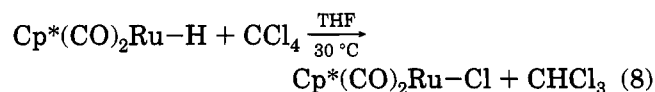
$$\text{Cp}'\text{Ru}(\text{L})\text{H}(\text{soln}) + \text{XR}(\text{soln}) \xrightarrow[30^\circ\text{C}]{\text{THF}} \text{Cp}'\text{Ru}(\text{L})_2\text{X}(\text{soln}) + \text{HR}(\text{soln})$$

entry	Cp'	L	X–R ^a	–ΔH ^{rxn}
1	Cp*	CO	Cl–CCl ₃	41.1(0.6)
2	Cp*	CO	Br–CBr ₃	44.4(0.4)
3	Cp*	CO	I–CH ₃	39.3(0.5)
4	Cp*	PMe ₃	I–CH ₃	45.0(0.7)
5	Cp	PMe ₃	I–CH ₃	44.1(0.4)
6	Cp	dppe	I–CH ₃	35.2(0.3)
7	Cp	dppe	Cl–CCl ₃	40.4(0.2)

^a Ancillary thermodynamic data taken from ref 22.

Results

A number of reactions involving halogenating agents have been used in organometallic thermochemistry to extract metal–halide BDE values and trends.^{1c,3} In the present study, we have found reactions 8–10 to provide direct solution calorimetric access to enthalpies of reaction that allow for a determination of absolute ruthenium–halide BDE values.



Enthalpies of reaction with appropriate halogenating agents are reported in Table 1. All reactions where enthalpies of reaction values are reported were subjected to NMR titrations prior to performing the calorimetric experiments and were determined to be rapid and quantitative under calorimetric conditions. All reactions investigated lead to a unique product under the calorimetric conditions as determined by NMR spectroscopy.

All reported enthalpies of reaction are solution phase values and take into account the enthalpy of solution of the appropriate ruthenium hydride complex. These enthalpies of solution have been included in halogenation enthalpies of reaction reported in Table 2.

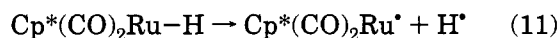
Table 3. Bond Disruption Enthalpy Estimates (kcal/mol) for Cp*Ru(CO)₂X and Related Systems

	Cp*Ru- X (CO) ₂ X ^a	Cp ₂ Mo(X) ₂ ^b	CpMo(CO) ₃ X ^c	Cp*Ir- (PMe ₃) ₂ (X) ₂ ^d	Cl(CO)Ir- (PR ₃) ₂ (X) ₂ ^e
H	65.0	60.0	66.0	74.2	60
Cl	80.7	72.9	72.4	90.3	71
Br	61.1	57.8	60.5	76.0	53
I	55.6	49.4	58.1	63.8	35

^a This work, average uncertainties in absolute bond disruption enthalpy values are on the order of ±5 kcal/mol. For experimental errors on specific measurements, see text. ^b Taken from refs 7–10. ^c Taken from ref 11. ^d Taken from ref 2a. ^e Taken from ref 23.

Discussion

The Cp*(CO)₂RuH (1) complex (Cp* = η⁵-C₅Me₅) was selected as the entryway into the thermochemistry of the Cp*(CO)₂RuX system in view of the recent thermochemical determination of the Ru–H bond disruption enthalpy (BDE) in CpRu(CO)₂H. Parker and Tilset have recently determined the BDE of a number of metal–hydride species one of which is Cp(CO)₂RuH where the Ru–H BDE is estimated to be worth some 65 ± 1.0 kcal/mol in acetonitrile.¹⁵ In this study, two other second row metal–hydride BDE's were also determined: Cp(CO)₃Mo–H (62 kcal/mol) and Cp*(CO)₃Mo–H (61 kcal/mol). These values are the same within experimental error. Substitution of Cp for Cp*, as ancillary ligation, does not appear to greatly affect the strength of the Ru–H bond. Furthermore, Hoff and co-workers have determined the Mo–H BDE in the Cp(CO)₃Mo–H system as 66 ± 5 kcal/mol in THF solution.^{18a} It is based on these BDE trends that we assign a value of 65 kcal/mol to the Cp*(CO)₂RuH bond.

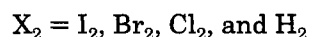
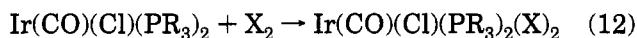


$$D(\text{Ru–H}) \approx 65 \pm 2.0 \text{ kcal/mol}$$

Having measured enthalpies of reaction 8–10 and established a thermodynamic anchor point for this system, we could derive absolute ruthenium–halide BDE values utilizing known thermochemical data for organic compounds involved in the halogenation reactions.²² This absolute BDE scale for Cp*(CO)₂Ru–X complexes (Table 1) allows for comparisons with other known M–X BDE values and for the examination or existence of any bonding trends in L_nM–X (L_n = ancillary ligands) systems.

The solution thermochemistry of two iridium(III) systems has been investigated. The binding of halides has been investigated by Blake and co-workers²³ for Vaska's complex (Table 3).

These reactions result in the oxidative addition of halogens producing Ir(CO)(Cl)(PR₃)₂(X)₂ complexes.



The other Ir system investigated is Cp*Ir(PMe₃)(X)₂, whose solution thermochemistry was investigated by

(22) (a) Weast, R. C., Ed. *Handbook of Chemistry and Physics*, 62th ed.; CRC Press: Cleveland, OH, 1981; p F-180. (b) Cox, J. D.; Pilcher, G. *Thermochemistry of Organic and Organometallic Compounds*; Academic Press: New York, 1970.

(23) Yoneda, G.; Blake, D. M. *Inorg. Chem.* **1981**, *20*, 67–71 and references therein.

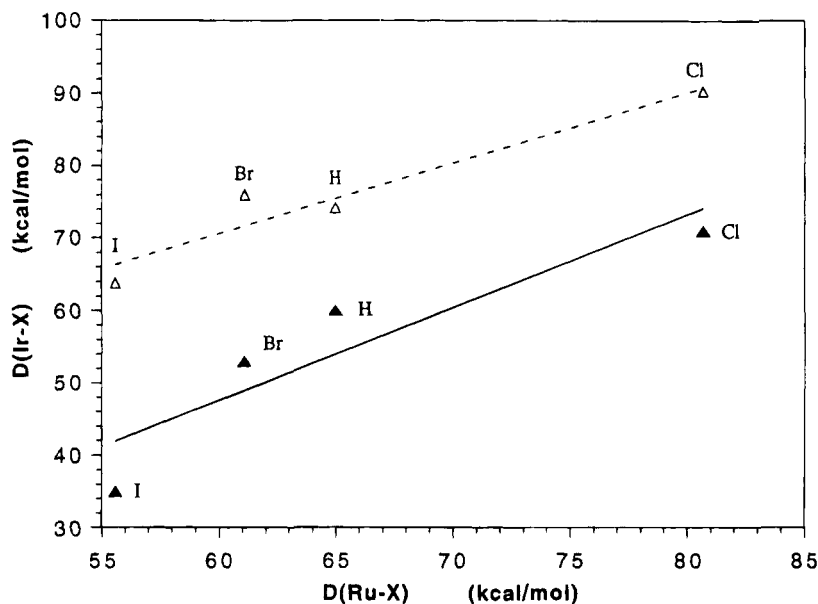


Figure 1. Metal-X (X = H, Cl, Br, I) bond disruption enthalpy data in $\text{Cp}^*(\text{CO})_2\text{Ru-X}$ vs $\text{Ir}(\text{CO})(\text{Cl})(\text{PR}_3)_2$ (\blacktriangle) ($R = 0.92$; slope = 1.28) and $\text{Cp}^*\text{Ir}(\text{PMe}_3)(\text{X})_2$ (\triangle) ($R = 0.96$; slope = 0.97) systems.

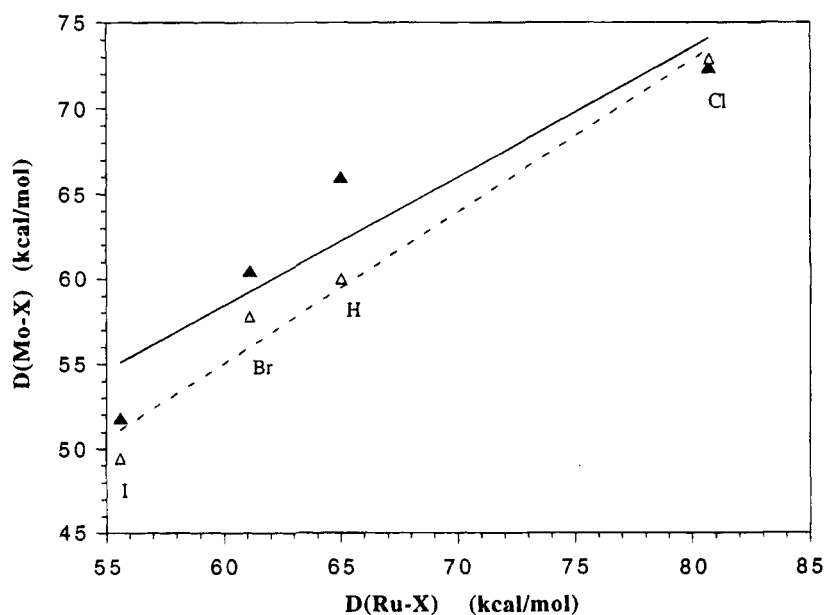
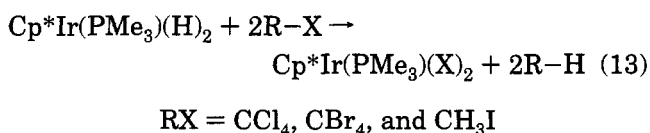


Figure 2. Metal-X (X = H, Cl, Br, I) bond disruption enthalpy data in $\text{Cp}^*(\text{CO})_2\text{Ru-X}$ vs $\text{CpMo}(\text{CO})_3\text{X}$ (\blacktriangle) ($R = 0.93$; slope = 0.76) and $\text{Cp}_2\text{Mo}(\text{X})_2$ (\triangle) ($R = 0.99$; slope = 0.89) systems.

Hoff and Bergman.^{2a}



Both these iridium systems have the metal center in a formal M^{3+} (d^6) oxidation state rendering them iso-electronic with the present Ru^{2+} (d^6) system. The BDE correlation between the two systems is depicted in Figure 1.

The point could be made, that in view of similar ancillary ligation, a better correlation should be expected for the $\text{Cp}^*\text{Ir}(\text{PMe}_3)(\text{X})_2$ system, and in fact a better correlation coefficient is found for this relationship ($R = 0.96$) versus the Vaska system ($R = 0.92$). In both these iridium systems, however, the average of two

BDE's is considered and a direct correlation with the ruthenium system, where a single halide bond is formed, is presented. Regardless of this fact, the relative Ru-X bond disruption enthalpy trend found follows that of previously investigated systems: $\text{M-Cl} > \text{M-H} > \text{M-Br} > \text{M-I}$.^{1c}

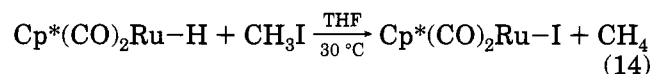
A more appropriate comparison may exist with organometallic complexes of second row transition metals since ruthenium falls in this category. The only systems investigated are the $\text{CpMo}(\text{CO})_3\text{X}$ (Mo^{2+})¹¹ and Cp_2MoX_2 (Mo^{4+})⁷⁻¹⁰ systems. A graphic representation of possible correlations with the present ruthenium data can be found in Figure 2.

With the similar Cp ligation, it might be expected that the two second row molybdenum systems correlate more closely to their ruthenium neighbor. In fact, correlation coefficients of 0.93 and 0.99 are calculated for the $\text{CpMo}(\text{CO})_3\text{X}$ and Cp_2MoX_2 systems, respectively. Both sec-

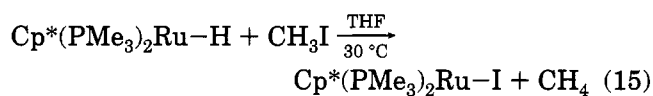
and row systems show good correlations with the present ruthenium data (slopes of 0.76 and 0.89, respectively).

In an effort to compare enthalpies or reaction involving the cleavage of the Ru–H bond in different ligand environments, the reactivity of a number of phosphine-substituted ruthenium hydride complexes were tested under calorimetric conditions. Only a few of the complexes tested reacted rapidly and cleanly enough to be investigated by solution calorimetry. Results are presented in Table 2. The enthalpies of reaction associated with variation in the ancillary ligation provide insights into the factors influencing the strength of the Ru–H/Ru–X bonds and can be explained in terms of ligand donor/acceptor properties.²⁴

The difference in enthalpy of reaction between reactions 14 and 15, some 5.7 kcal/mol, can be attributed to



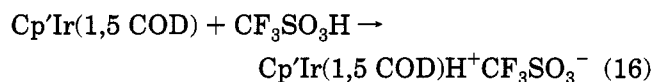
$$\Delta H = -39.3(0.5) \text{ kcal/mol}$$



$$\Delta H = -45.0(0.7) \text{ kcal/mol}$$

the change in electronic properties of the ancillary ligands. The substitution of trimethyl phosphine for CO in the Cp*Ru(L)₂H system makes these species less acidic. This effect is consistent with the greater σ donor, poorer π acceptor character of PMe₃, relative to CO. This substitution results in a strengthening of the Ru–H bond. The strength of the Ru–H bond in reaction 15 is increased, relative to the reaction involving CO, as a result of the change in metal–hydride acidity. These trends in metal basicities on going to increased σ donation have previously been observed.²⁵

The relative metal basicity has been shown to decrease on going from Cp to Cp* as ancillary ligations. This has been observed by Angelici and Sowa²⁶ in their studies of enthalpies of protonation reaction:



$$\text{Cp}' = \text{C}_5\text{Me}_x\text{H}_{x-5}; x = 0, 1, 3-5$$

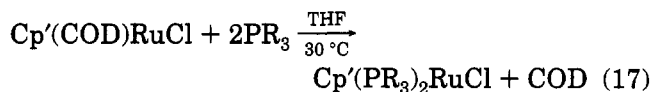
A difference in enthalpies of protonation of some 5 kcal/mol was found to exist between the Cp and Cp* complexes. This enthalpy difference of 5 kcal/mol was also apparent in our calorimetric investigations of ligand substitution reactions.^{5b,27}

(24) (a) Tolman, C. A. *Chem. Rev.* **1977**, *77*, 313–348. (b) Manzer, L. E.; Tolman, C. A. *J. Am. Chem. Soc.* **1975**, *97*, 1955–1986. (c) Pignolet, L. H., Ed. *Homogeneous Catalysis with Metal Phosphine Complexes*; Plenum: New York, 1983.

(25) (a) Tolman, C. A. *J. Am. Chem. Soc.* **1970**, *92*, 2953–2956. (b) Walker, H. W.; Pearson, R. G.; Ford, P. C. *J. Am. Chem. Soc.* **1983**, *105*, 1179–1186. (c) Collman, J. P.; Hegedus, L. S.; Norton, J. R.; Finke, R. G. *Principles and Applications of Organotransition Metal Chemistry*, 2nd ed.; University Science: Mill Valley, CA, 1987.

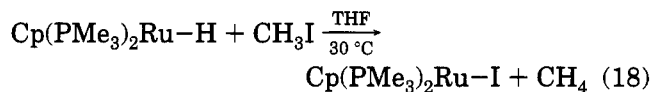
(26) Sowa, J. R.; Angelici, R. J. *J. Am. Chem. Soc.* **1991**, *113*, 2537–2544.

(27) Cucullu, M. E.; Luo, L.; Nolan, S. P.; Fagan, P. J.; Jones, N. L.; Calabrese, J. C. *Organometallics* **1995**, *14*, 289–296.



$$\text{Cp}' = \text{C}_5\text{H}_5 \text{ and } \text{C}_5\text{Me}_5$$

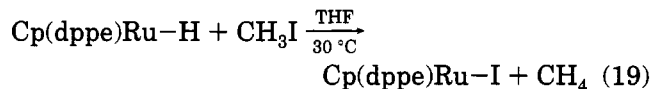
However, as in complexes studied by Tilset and Parker, the thermochemical results illustrated by reactions 15 and 18 display no measurable M–L BDE difference on going from Cp* to Cp as ancillary ligation.¹⁵



$$\Delta H = -44.1(0.4) \text{ kcal/mol}$$

It would therefore appear that Ru–X bonds are not significantly affected by a change in ancillary ligation. Alternatively, it could be argued that there is, on going from Cp* to Cp, a constant factor affecting both the strength of the Ru–H and Ru–I bonds which would result in no apparent difference in enthalpy of reaction between the two pairs of complexes. At this point, in view of a lack of absolute Ru–H BDE data as a function of ancillary ligand variation, the exact reason for the almost constant enthalpy data seen in reactions 15 and 18 cannot be unequivocally explained.

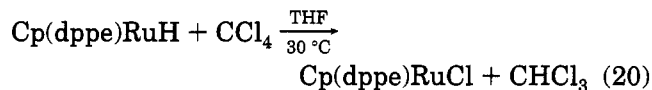
There is however a significant difference in enthalpy values between reactions 18 and 19.



$$\Delta H = -35.2(0.3) \text{ kcal/mol}$$

dppe = bis(diphenylphosphino)ethane

In this case, it appears that the poorer σ donation of dppe, compared to 2 equiv of PMe₃, is the source of the enthalpy difference. This σ donation term may be the overall factor dictating the magnitude of the Ru–H bond enthalpy in these complexes. A relative σ donation scale can therefore be constructed for the present system and proceeds in increasing donating ability in the following order: 2PMe₃ > 2CO > dppe. This relative scale has also been tested for reaction 20, which has a measured



$$\Delta H = -40.4(0.2) \text{ kcal/mol}$$

enthalpy of reaction less exothermic than its Cp*(CO)₂Ru–X analog. On the basis of the σ donation scale and arguments presented above, a less exothermic enthalpy value would have been predicted.

Conclusion

The reported solution calorimetric investigation represents the first detailed thermochemical study of metal–halogen bond enthalpies in organoruthenium systems. The present study allows for the determina-

tion of the first absolute Ru–halide BDE values in the Cp*Ru(CO)₂X system. The absolute BDE scale parallels those of other systems investigated by solution calorimetry. Enthalpies of reactions were also measured for complexes bearing phosphine ancillary ligands. The stability scale and the magnitude in enthalpies of reaction point toward the degree of σ donation from the ancillary ligand to be an important factor in dictating the strength of the Ru–H interaction. Further studies are underway in order to clarify factors influencing metal–ligand bond disruption enthalpies.

Acknowledgment. The National Science Foundation (Grant CHE-9305492) and the Louisiana Education Quality Support Fund are gratefully acknowledged for support of this research. The Louisiana Board of Regents is also acknowledged for allocating funds allowing the purchase of the FT-IR spectrophotometer (Grant ENH-TR-41, 1993–1994). We are also indebted to Johnson Matthey/Aesar for a generous loan of ruthenium salts.

OM940829K

1,4-Bis(trimethylsilyl)but-2-ene-1,4-diyl Complexes of Lithium, Magnesium, Aluminum, and Gallium

Michael G. Gardiner and Colin L. Raston*

Faculty of Science and Technology, Griffith University,
Nathan, Brisbane, Queensland 4111, Australia

F. Geoffrey N. Cloke and Peter B. Hitchcock

School of Chemistry and Molecular Sciences, University of Sussex,
Brighton BN1 9QJ, United Kingdom

Received October 12, 1994[®]

(*Z*)-1,4-Dilithio-1,4-bis(trimethylsilyl)but-2-ene has been prepared as a THF (\equiv tetrahydrofuran) adduct, $[(\text{CH}(\text{Me}_3\text{Si})\text{CH})_2\text{Li}_2(\text{THF})_2]_2$ (**4**), via demetalation of the (*E*)-but-2-ene precursor using *n*-BuLi in THF and by reduction of (*E,E*)-1,4-bis(trimethylsilyl)buta-1,3-diene by lithium in THF. The complex is dimeric in the solid state with two lithium atoms bridging the (*Z*)-but-2-ene-1,4-diyl units; the other two lithium atoms are external to the dianion moieties and are solvated by two THF molecules, forming a Li(dianion)Li₂(dianion)-Li inverted double-decker sandwich structure. Treatment of the (*Z*)-1,4-dilithio-1,4-bis(trimethylsilyl)but-2-ene adduct of TMEDA ($\equiv N,N,N',N'$ -tetramethylethylenediamine), $[(\text{CH}(\text{Me}_3\text{Si})\text{CH})_2\{\text{Li}(\text{TMEDA})\}_2]$ (**3**), with (a) MgCl₂ or *i*-PrMgCl in diethyl ether results in formation of the TMEDA adduct of the magnesacyclopent-3-ene, isolated as [*meso*-(CH-(Me₃Si)CH)₂Mg}(TMEDA)] (**5**) or (b) MeAlCl₂, Et₂AlCl, or GaCl₃ in diethyl ether results in stereospecific formation of the corresponding metallacyclopent-3-enes, isolated as [*meso*-HC(Me₃Si)HC)₂MR]₂(TMEDA) (M = Al, R = Me (**6a**), Et (**6b**); M = Ga, R = Cl (**7**)). Assignment of the *meso* isomers for **5**–**7** is based on NMR data and X-ray crystal structure determination for **5**, **6b**, and **7**. Crystals of **4** are monoclinic, space group *P2₁/n* (No. 14), with *a* = 9.874(5) Å, *b* = 19.691(5) Å, *c* = 12.563(7) Å, β = 94.46(3)°, *V* = 2435(2) Å³, and *Z* = 2. Crystals of **5** are monoclinic, space group *P2₁/c* (No. 14), with *a* = 13.535(5) Å, *b* = 12.464(5) Å, *c* = 16.128(7) Å, β = 101.69(3)°, *V* = 2660(10) Å³, and *Z* = 4. Crystals of **6b** are orthorhombic, space group *Pbca* (No. 61), with *a* = 17.689(2) Å, *b* = 16.743(2) Å, *c* = 14.091(5) Å, *V* = 4173(1) Å³, and *Z* = 4. Crystals of **7** are monoclinic, space group *P2₁/n* (No. 14), with *a* = 14.118(5) Å, *b* = 17.309(2) Å, *c* = 16.000(6) Å, β = 91.96(2)°, *V* = 3908(2) Å³, and *Z* = 4.

Introduction

There has been recent renewed interest in the synthesis, structure, and reactivity of main-group-metal-butadiene complexes. 1,1,4,4-Tetraphenylbutadiene-sodium and -potassium complexes as DME (\equiv 1,2-dimethoxyethane) adducts¹ and 2,3-dimethyl-1,4-diphenylbutadiene-magnesium, -calcium, and -strontium complexes as THF (\equiv tetrahydrofuran) adducts² are accessible by reduction of the corresponding butadiene. The unsubstituted magnesium derivative $[(\text{C}_4\text{H}_6)\text{-Mg}(\text{THF})_2]_n$ is the reagent of choice in the preparation of many transition-metal complexes, but despite this the only structurally characterized examples for butadiene-magnesium complexes are [(1,4-diphenylbutadiene)Mg-(THF)₃]³ and [(2,3-dimethyl-1,4-diphenylbutadiene)Mg-(DME)₂]₂,² and the mode of bonding remains uncertain for other analogues. 2,3-Dimethylbut-2-ene-1,4-diyl complexes of aluminum and gallium are formed *via* the

low-temperature condensation of aluminum(I) chloride⁴ with butadienes and metathetical exchange reactions of gallium(III) chlorides⁵ and butadiene complexes of highly electropositive metals and have oligomeric metal bridging structures and monomeric metallacyclopent-3-ene structures. Paramagnetic⁶ and anionic alumina-cyclopent-3-ene complexes⁷ have been prepared by low-temperature condensation of butadiene with aluminum vapor and the Na reduction of AlMe₃ in the presence of butadiene. Structural information on lithium-butadiene complexes was limited to theoretical molecular orbital calculations⁸ and the X-ray structure determination of the bis(TMEDA) ($\equiv N,N,N',N'$ -tetramethylethylenediamine) adduct of the 1,4-dilithio-1,4-diphenylbut-2-ene derivative.⁹ The complexes studied so far have revealed binding modes of the butadienes as varied as

(4) Dohmeier, C.; Mattes, R.; Schnöckel, H. *J. Chem. Soc., Chem. Commun.* **1990**, 358.

(5) (a) Herberich, G. E.; Englert, U.; Posselt, D. *J. Organomet. Chem.* **1993**, 461, 21. (b) Schumann, H.; Just, O.; Seuss, T. D.; Görlitz, F. H.; Weimann, R. *J. Organomet. Chem.* **1994**, 466, 5.

(6) Chenier, J. H. B.; Howard, J. A.; Tse, J. S.; Mile, B. *J. Am. Chem. Soc.* **1985**, 107, 7290.

(7) Lehmkuhl, H.; Culjkovic, J.; Nehl, H. *Justus Liebig's Ann. Chem.* **1973**, 666.

(8) Kos, A. J.; Stein, P.; Schleyer, P. v. R. *J. Organomet. Chem.* **1985**, 280, C1.

[®] Abstract published in *Advance ACS Abstracts*, January 15, 1995.

(1) Bock, H.; Näther, C.; Ruppert, K. *J. Chem. Soc., Chem. Commun.* **1992**, 765.
(2) Mashima, K.; Sugiyama, H.; Kanehisa, N.; Kai, Y.; Yasuda, H.; Nakamura, A. *J. Am. Chem. Soc.* **1994**, 116, 6977.
(3) Kai, Y.; Kanehisa, N.; Miki, K.; Kasai, N.; Mashima, K.; Yasuda, H.; Nakamura, A. *Chem. Lett.* **1982**, 1277.

those established in the well-studied field of transition-metal–diene chemistry.

Herein we report the synthesis and crystal structures of some lithium, magnesium, aluminum, and gallium butadiene complexes as an extension to our previously published reports on the synthesis of TMEDA adducts of 1,4-bis(trimethylsilyl)but-2-ene-1,4-diyl complexes of lithium and aluminum chloride.¹⁰ Included are (a) the dimeric THF adduct of the dilithio derivative, $[(\text{CH}(\text{Me}_3\text{Si})\text{CH})_2\text{Li}_2(\text{THF})_2]_2$ (**4**), prepared by metalation and reduction reactions, and its fluxional behavior in benzene solution, (b) the preparation of the magnesium complex $[\textit{meso}-(\text{CH}(\text{Me}_3\text{Si})\text{CH})_2\text{Mg}](\text{TMEDA})$ (**5**) as a mild anionic transfer reagent for the 1,4-bis(trimethylsilyl)but-2-ene-1,4-diyl dianion, with note being made of the potent reducing ability of the TMEDA adduct of the lithium derivative, *viz.* reduction of CaCl_2 to calcium metal, and (c) alkylaluminum, $[\textit{meso}-(\text{HC}(\text{Me}_3\text{Si})\text{HC})_2\text{AlR}]_2(\text{TMEDA})$ ($\text{R} = \text{Me}$ (**6a**), Et (**6b**)), and chlorogallium analogues as TMEDA adducts, $[\textit{meso}-(\text{HC}(\text{Me}_3\text{Si})\text{HC})_2\text{GaCl}]_2(\text{TMEDA})$ (**7**), by metathetical exchange reactions. The complexes show a progression in structure from exhibiting η^4 -(*Z*)-but-2-ene-1,4-diyl geometries in the case of the lithium complex to highly puckered metallacyclopent-3-ene structures for the magnesium complex and finally to metallacyclopent-3-ene structures for the group 13 complexes without any interaction of the metal with the π -electrons of the dianion. NMR data for the four complexes are correlated with the observed solid-state binding modes, providing useful indicators of the extent of π -complexation in main-group-metal–butadiene compounds.

Experimental Section

Syntheses. All manipulations were carried out using standard Schlenk and glovebox techniques under an atmosphere of high-purity argon or nitrogen. Solvents were dried and then freeze/thaw-degassed prior to use. Compounds **1–3** were prepared according to our literature procedures.^{10a} (*E*)-1,1,4,4-Tetrakis(trimethylsilyl)but-2-ene was prepared by literature procedures.¹¹ Finely milled MgCl_2 was obtained from ICI; all other reagents were obtained from Aldrich. ^1H NMR spectra were recorded on Bruker WM-360 and Varian Gemini-200 and Unity-400 spectrometers in deuterated benzene or toluene and referenced to the residual ^1H resonances of the solvent (δ 7.15 and 6.98, respectively). ^7Li NMR spectra were recorded on a Varian Unity-400 spectrometer in deuterated benzene or toluene and referenced to external LiNO_3 (1 M in D_2O , δ 0.00). ^{13}C NMR spectra were recorded in deuterated benzene on Bruker WM-360 and Varian Gemini-200 spectrometers operating at 90 and 50 MHz, respectively, using broadband proton decoupling and were referenced to the ^{13}C resonances of the deuterated solvent (δ 128.00). EI mass spectra were recorded on a Kratos MS80 spectrometer. Elemental analyses were performed by the Canadian Microanalytical Services Ltd., Vancouver, BC, Canada, and the Chemical and Micro Analytical Services Pty. Ltd., Melbourne, Australia. Melting points were determined in sealed glass capillaries under argon and are uncorrected.

(9) Wilhelm, D.; Clark, T.; Schleyer, P. v. R.; Dietrich, H.; Mahdi, W. J. *Organomet. Chem.* **1985**, *280*, C6.

(10) (a) Field, L. D.; Gardiner, M. G.; Kennard, C. H. L.; Messerle, B. A.; Raston, C. L. *Organometallics* **1991**, *10*, 3167. (b) Field, L. D.; Gardiner, M. G.; Messerle, B. A.; Raston, C. L. *Organometallics* **1992**, *11*, 3566. (c) Gardiner, M. G.; Raston, C. L. *Organometallics* **1993**, *12*, 81.

(11) Laguerre, M.; Dunogues, J.; Calas, N. D. e. R. *J. Organomet. Chem.* **1980**, *193*, C17.

Synthesis of $[(\text{CH}(\text{Me}_3\text{Si})\text{CH})_2\text{Li}_2(\text{THF})_2]_2$ (4**).** **Method a.** To a stirred solution of *n*-BuLi (31.3 mL, 1.60 M, 50.0 mmol) in THF (10 mL) was added (*E*)-1,4-bis(trimethylsilyl)but-2-ene (**1**; 5.00 g, 25.0 mmol) dropwise over 10 min at 0 °C. The solution was warmed to room temperature and became deep red after 15 min. After a further 12 h the volatiles were removed *in vacuo* to yield an orange solid. Hexane (100 mL) was then added and the resulting orange solution filtered, concentrated, and cooled to -30 °C, yielding pale orange crystals of the *title compound* in three crops (6.32 g, 72% yield): mp 126–130 °C; ^1H NMR (360 MHz, C_6D_6) δ 0.33 (36 H, s, SiMe_3), 0.37 (4 H, AA'XX', CHSi), 1.26 (16 H, m, CH_2), 3.41 (24 H, m, OCH_2), 5.47 (4 H, AA'XX', =CH); ^{13}C NMR (90 MHz, C_6D_6) δ 3.6 (SiMe_3), 25.3 (CHSi), 25.6 (CH_2), 68.8 (OCH_2), 105.3 (=CH); ^7Li NMR (155.5 MHz, C_6D_6) δ -1.87 . Anal. Found: C, 60.21; H, 10.82. Calcd: C, 60.64; H, 10.74.

Method b. To a solution of (*E,E*)-1,4-bis(trimethylsilyl)buta-1,3-diene (**2**; 1.13 g, 5.71 mmol) in THF (5 mL) was added freshly cut lithium (0.21 g, 30.3 mmol) at room temperature. The solution became orange-red after 15 min and was allowed to stand for 12 h, resulting in a red solution. The mixture was filtered to remove excess lithium metal, and then the volatiles were removed *in vacuo* to yield an orange solid. Hexane (20 mL) was added and the orange solution filtered, concentrated (*ca.* 5 mL), and cooled to -30 °C, yielding pale orange crystals of the *title compound* in two crops (1.45 g, 76% yield). (This product was spectroscopically identical with the above synthesis).

Synthesis of $[\textit{meso}-(\text{CH}(\text{Me}_3\text{Si})\text{CH})_2\text{Mg}](\text{TMEDA})$ (5**).**

Method a. To a solution of *i*-PrMgCl (2.25 mL, 2 M, 4.50 mmol) in Et_2O (20 mL) at *ca.* -80 °C was added a solution of **3** (1.00 g, 2.25 mmol) in Et_2O (20 mL) dropwise over 10 min with stirring. When the mixture was warmed to room temperature, a yellow solution with a white precipitate formed, which was stirred for a further 30 min. The solution was filtered, and volatiles were removed *in vacuo* to yield a yellow oil. Hexane (10 mL) was added and the resulting solid broken up, yielding a colorless solution which was filtered and concentrated *in vacuo* to yield crystals of *i*-Pr₂Mg(TMEDA). Et_2O (20 mL) was added to the hexane-insoluble yellow residue and the solution filtered; concentrating to *ca.* 5 mL and cooling to *ca.* -30 °C yielded pale yellow rods of the *title compound* in three crops (0.59 g, 78% yield): mp 185 °C dec; ^1H NMR (360 MHz, C_6D_6) δ 0.42, 0.44 (18 H, s, SiMe_3), 0.67, 0.73 (2 H, AA'XX', CHSi), 1.38 (4 H, s, NCH_2), 1.72, 1.78 (12H, s, NMe), 6.00, 6.28 (2 H, AA'XX', =CH); ^{13}C NMR (90 MHz, C_6D_6) δ 3.3, 3.4 (SiMe_3), 17.7, 20.7 (CHSi), 45.1, 45.6 (NMe), 55.2 (NCH_2), 119.1, 124.6 (=CH); MS *m/e* 338 (M^+ , 22%). Anal. Found: C, 56.59; H, 11.90; N, 8.66. Calcd: C, 56.70; H, 11.30; N, 8.26.

Method b. To a solution of MgCl_2 (0.17 g, 1.79 mmol) in Et_2O (10 mL) at *ca.* -80 °C was added a solution of **3** (0.72 g, 1.62 mmol) in Et_2O (10 mL) dropwise over 5 min with stirring. When the mixture was warmed to room temperature, a yellow solution with a white precipitate formed, which was stirred for a further 2 h. The solution was filtered; concentrating to *ca.* 5 mL and cooling to *ca.* -30 °C yielded pale yellow rods of the *title compound* in four crops (0.44 g, 81% yield) (this product was spectroscopically identical with that from method a).

Synthesis of $[\textit{meso}-(\text{HC}(\text{Me}_3\text{Si})\text{HC})_2\text{AlMe}]_2(\text{TMEDA})$ (6a**).**

To a solution of MeAlCl_2 (2 mL, 1 M, 2.00 mmol) in Et_2O (10 mL) at *ca.* -80 °C was added a solution of **3** (0.89 g, 2.00 mmol) in Et_2O (20 mL) dropwise over 5 min with stirring. When this mixture was warmed to room temperature, a colorless solution with a white precipitate formed, which was stirred for a further 1 h. The solution was filtered, and volatiles were removed *in vacuo*. The resulting oil was heated *in vacuo* at *ca.* 100 °C for 2 h to give a white solid, whereupon hexane (50 mL) was added, the solution filtered, and the filtrate concentrated to *ca.* 20 mL. Slow cooling to *ca.* -30 °C yielded colorless crystals of the *title compound* in two crops

Table 1. Summary of X-ray Diffraction Data and Overall Refinement Parameters for $[(\text{CH}(\text{Me}_3\text{Si})\text{CH})_2\text{Li}_2(\text{THF})_2]_2$ (**4**), $[\{\text{meso}-(\text{CH}(\text{Me}_3\text{Si})\text{CH})_2\text{Mg}\}(\text{TMEDA})]\cdot\text{THF}$ (**5**), $[\{\text{meso}-(\text{HC}(\text{Me}_3\text{Si})\text{HC})_2\text{AlEt}\}_2(\text{TMEDA})]$ (**6b**), and $[\{\text{meso}-(\text{HC}(\text{Me}_3\text{Si})\text{HC})_2\text{GaCl}\}_2(\text{TMEDA})]$ (**7**)

	4	5	6b	7
formula	$\text{C}_{36}\text{H}_{76}\text{Li}_4\text{O}_4\text{Si}_4$	$\text{C}_{16}\text{H}_{38}\text{N}_2\text{MgSi}_2$	$\text{C}_{30}\text{H}_{70}\text{N}_2\text{Al}_2\text{Si}_4$	$\text{C}_{26}\text{H}_{60}\text{N}_2\text{Ga}_2\text{Cl}_2\text{Si}_4$
mol wt	713.10	338.97	625.20	723.46
space group	$P2_1/n$ (No. 14)	$P2_1/c$ (No. 14)	$Pbca$ (No. 61)	$P2_1/n$ (No. 14)
<i>a</i> , Å	9.874(5)	13.535(5)	17.689(2)	14.118(5)
<i>b</i> , Å	19.691(5)	12.464(5)	16.743(2)	17.309(2)
<i>c</i> , Å	12.563(7)	16.128(7)	14.091(5)	16.000(6)
α , deg	90	90	90	90
β , deg	94.46(3)	101.69(3)	90	91.96(2)
γ , deg	90	90	90	90
<i>V</i> , Å ³	2435(2)	2660(10)	4173(1)	3908(2)
<i>Z</i>	2	4	4	4
<i>D</i> (calcd), g cm ⁻³	0.972	1.025	0.995	1.230
<i>F</i> (000), e	784	912	1384	1528
temp, K	297	173	297	297
radiation		Mo K α (0.710 69 Å, graphite monochromator)		
μ , cm ⁻¹	1.48	1.70	2.03	16.58
2 θ limit, deg	50	46	50	50
no. of unique rflns	2695	3911	3664	7120
no. of obsd rflns (<i>I</i> > 2.5 σ (<i>I</i>))	1215	1971	1759	3723
<i>R</i> ^a	0.056	0.080	0.050	0.048
<i>R</i> _w ^b	0.056	0.080	0.050	0.048
final residue, e Å ⁻³	-0.3/+0.3	-0.7/+0.7	-0.4/+0.5	-1.0/+0.7
<i>s</i>	1.52	3.05	2.19	2.65

$$^a R = \sum ||F_o| - |F_c|| / \sum |F_o|, \quad ^b R_w = (\sum w||F_o| - |F_c||^2 / \sum w|F_o|^2)^{1/2}.$$

with difficulty (0.23 g, 38% yield): mp 177–180 °C (>200 °C dec); ¹H NMR (200 MHz, C₆D₆) δ -0.49 (6 H, s, AlMe), -0.07 (4 H, s, CHSi), 0.28 (36 H, s, SiMe₃), 1.75 (12 H, s, NMe), 2.46 (4 H, s, NCH₂), 6.28 (4 H, s, =CH); ¹³C NMR (50 MHz, C₆D₆) δ -8.9 (AlMe), 1.2 (SiMe₃), 17.9 (CHSi), 44.5 (NMe), 53.2 (NCH₂), 134.5 (=CH). Anal. Found: C, 55.95; H, 11.93; N, 5.81. Calcd: C, 56.32; H, 11.14; N, 4.69.

Synthesis of $[\{\text{meso}-(\text{HC}(\text{Me}_3\text{Si})\text{HC})_2\text{AlEt}\}_2(\text{TMEDA})]$ (6b**).** To a solution of Et₂AlCl (4.5 mL, 1 M, 4.50 mmol) in Et₂O (10 mL) at ca. -80 °C was added a solution of **3** (1.00 g, 2.25 mmol) in Et₂O (10 mL) dropwise over 5 min with stirring. When this mixture was warmed to room temperature, a colorless solution with a white precipitate formed, which was stirred for a further 2 h. The solution was filtered and volatiles were removed *in vacuo* to yield an oil which crystallized after 7 days. The crystals of the *title compound* were washed with cold hexane (2 × 10 mL) and collected (0.47 g, 72% yield): mp 164–166 °C dec; ¹H NMR (360 MHz, C₆D₆) δ -0.11 (4 H, s, CHSi), 0.19 (4 H, q, ³J_{H-H} = 8.14 Hz, AlCH₂), 0.29 (36 H, s, SiMe₃), 1.30 (6 H, t, ³J_{H-H} = 8.14 Hz, Me), 1.75 (12 H, s, NMe), 2.50 (4 H, s, NCH₂), 6.26 (4 H, s, =CH); ¹³C NMR (90 MHz, C₆D₆) δ 0.9 (SiMe₃), 1.8 (AlCH₂), 11.5 (Me), 17.8 (CHSi), 43.9 (NMe), 51.9 (NCH₂), 134.2 (=CH); MS *m/e* 254 ((HC(Me₃Si)HC)₂AlEt⁺, 28%), 225 ((HC(Me₃Si)HC)₂Al⁺, 21%). Anal. Found: C, 56.34; H, 11.15; N, 4.27. Calcd: C, 57.64; H, 11.28; N, 4.48.

Synthesis of $[\{\text{meso}-(\text{HC}(\text{Me}_3\text{Si})\text{HC})_2\text{GaCl}\}_2(\text{TMEDA})]$ (7**).** To a solution of GaCl₃ (0.50 g, 2.84 mmol) in Et₂O (20 mL) at ca. -80 °C was added a solution of **3** (1.26 g, 2.83 mmol) in Et₂O (20 mL) dropwise over 5 min with stirring. When this mixture was warmed to room temperature, the red color of the solution dissipated after 30 min to yield a yellow solution with a white precipitate, which was stirred for a further 30 min. The solution was filtered, and volatiles were removed *in vacuo* to yield an oil which was heated *in vacuo* at ca. 80 °C for 1 h to give an off-white solid. Hexane (50 mL) was added, the solution filtered, and the filtrate concentrated to ca. 10 mL. Slow cooling to ca. -30 °C yielded colorless crystals of the *title compound* in two crops with difficulty (0.47 g, 46% yield): mp 114 °C dec; ¹H NMR (200 MHz, C₆D₆) δ 0.31 (4 H, s, CHSi), 0.33 (36 H, s, SiMe₃), 1.89 (12 H, s, NMe), 2.71 (4 H, s, NCH₂), 6.24 (4 H, s, =CH); ¹³C NMR (50 MHz, C₆D₆) δ 0.5 (SiMe₃), 19.1 (CHSi), 45.4 (NMe), 54.0 (NCH₂), 132.7 (=CH). Anal. Found: C, 43.47; H, 8.77; N, 5.00. Calcd: C, 43.17; H, 8.36; N, 3.87.

Structure Determination. Crystals of **4**, **6b**, and **7** suitable for X-ray structure determination were grown from hexane solutions at -30 °C and were mounted in sealed capillaries under an argon atmosphere. Crystals of **5** suitable for X-ray structure determination could be grown from either Et₂O or THF solutions at -30 °C; crystals obtained from THF solution were sensitive to loss of solvent and were handled under a THF-saturated argon atmosphere. Unique diffractometer data sets were measured using Enraf-Nonius CAD4 diffractometers. Reflections with *I* > 2.5 σ (*I*) were considered "observed" and used in the full-matrix least-squares refinements, minimizing $\sum w\delta^2$ after solution of the structures by direct methods. Conventional residuals on *F* at convergence are quoted. No extensive, significant extinction effects were found. Neutral-atom complex scattering factors were employed.¹² Computation used the XTAL 3.0¹³ and SHELXS-86¹⁴ program systems. Molecular core geometries, atom coordinates, and crystal data are given in Tables 1–9, and molecular projections showing numbering schemes are given in Figures 1–4. Averaged structural parameters will be used in the structural comparisons of the complexes where appropriate and are distinguished by the absence of the least-squares error term from the determined quantity. Anisotropic thermal parameters were refined for all non-hydrogen atoms in all four structure determinations. Methine hydrogen atoms were located and refined in (*x*, *y*, *z*), and all other hydrogen atoms were calculated and constrained at estimated values (C–H = 1.0 Å). Temperature factors for methyl hydrogen atoms were estimated at 1.5 U_{ii} (average) of the attached carbon atom and 1.25 U_{ii} (average) for other hydrogen atoms. Disorder in the ethyl group of **6b** was apparent in Fourier difference maps and was modeled anisotropically as a population refined complementary site occupancy disorder; no hydrogens were included on these atoms. A second data set was obtained for compound **5** on a rod-shaped crystal crystallized from Et₂O, which yielded an inaccurate and highly disordered structure.¹⁵ Structural commentary will be restricted to the former structure determination; suffice it to say that the molecular

(12) *International Tables for X-ray Crystallography*; Ibers, J. A., Hamilton, W. C., Eds.; Kynoch Press: Birmingham, England, 1974; Vol. 4.

(13) *XTAL User's Manual-Version 3.0*; Hall, S. R., Stewart, J. M., Eds., the Universities of Western Australia and Maryland, 1990.

(14) Sheldrick, G. M. SHELXS-86, Program for Crystal Structure Solution; Universität Göttingen: Göttingen, Germany, 1986.

Table 2. Non-Hydrogen Atom (and Methine Hydrogen Atom) Coordinates and Isotropic Thermal Parameters for $[\{(\text{CH}(\text{Me}_3\text{Si})\text{CH})_2\text{Li}_2(\text{THF})_2\}_2] \text{ (4)}$

atom	<i>x/a</i>	<i>y/b</i>	<i>z/c</i>	$U, \text{\AA}^2$
Li1	0.768(2)	0.3364(7)	0.024(1)	0.10(1)*
Li2	0.972(2)	0.4874(7)	0.098(1)	0.087(8)*
C1	0.8896(9)	0.4263(4)	-0.0723(6)	0.057(4)*
Si1	0.8756(3)	0.4013(1)	-0.2109(2)	0.072(1)*
C11	0.780(1)	0.4692(5)	-0.2893(7)	0.110(5)*
C12	0.787(1)	0.3184(5)	-0.2442(7)	0.123(5)*
C13	1.048(1)	0.3885(5)	-0.2639(7)	0.106(5)*
C2	0.971(1)	0.3879(4)	0.0092(7)	0.072(5)*
C3	0.941(1)	0.3833(4)	0.1180(7)	0.072(5)*
C4	0.830(1)	0.4144(4)	0.1646(6)	0.058(4)*
Si4	0.7849(3)	0.4018(1)	0.2978(2)	0.078(1)*
C41	0.636(1)	0.4580(5)	0.3191(8)	0.124(6)*
C42	0.736(1)	0.3126(5)	0.3301(8)	0.160(7)*
C43	0.921(1)	0.4240(6)	0.4020(7)	0.144(6)*
O1	0.8059(8)	0.2386(3)	0.0316(6)	0.109(3)*
C1o	0.735(1)	0.1871(6)	-0.023(1)	0.139(7)*
C2o	0.827(2)	0.1293(7)	-0.021(1)	0.187(9)*
C3o	0.929(2)	0.1415(7)	0.063(1)	0.173(9)*
C4o	0.920(1)	0.2092(6)	0.086(1)	0.186(9)*
O2	0.5680(8)	0.3364(4)	-0.0112(7)	0.098(4)*
C5o	0.480(2)	0.3063(8)	0.056(1)	0.152(9)*
C6o	0.361(2)	0.348(1)	0.060(2)	0.20(1)*
C7o	0.376(2)	0.4003(9)	-0.021(2)	0.23(1)*
C8o	0.493(2)	0.3871(8)	-0.068(1)	0.164(9)*
H1	0.814(8)	0.450(3)	-0.037(5)	0.076
H2	1.058(9)	0.367(4)	-0.020(6)	0.095
H3	1.031(7)	0.357(3)	0.167(5)	0.090
H4	0.766(7)	0.444(3)	0.103(5)	0.073

* Asterisks denote isotropic equivalent thermal parameters.

Table 3. Non-Hydrogen Atom (and Methine Hydrogen Atom) Coordinates and Isotropic Thermal Parameters for $[\{meso\text{-}(\text{CH}(\text{Me}_3\text{Si})\text{CH})_2\text{Mg}\}(\text{TMEDA})]\cdot\text{THF} \text{ (5)}$

atom	<i>x/a</i>	<i>y/b</i>	<i>z/c</i>	$U, \text{\AA}^2$
Mg	0.2236(2)	0.7686(2)	0.4209(2)	0.0220(9)*
C1	0.2331(7)	0.6381(7)	0.3310(5)	0.021(3)*
Si1	0.2410(2)	0.4925(2)	0.3360(2)	0.0306(9)*
C11	0.3762(8)	0.4515(8)	0.3746(6)	0.045(4)*
C12	0.1629(9)	0.4313(8)	0.4054(7)	0.055(4)*
C13	0.1976(9)	0.4265(8)	0.2298(6)	0.054(4)*
C2	0.1421(7)	0.6931(7)	0.2890(5)	0.027(3)*
C3	0.1338(7)	0.8032(7)	0.2793(5)	0.025(3)*
C4	0.2197(7)	0.8747(7)	0.3120(5)	0.026(3)*
Si4	0.2083(2)	1.0206(2)	0.2973(2)	0.0288(8)*
C41	0.3373(8)	1.0849(8)	0.3291(6)	0.044(4)*
C42	0.1236(8)	1.0844(8)	0.3600(6)	0.046(4)*
C43	0.1550(8)	1.0582(8)	0.1838(6)	0.051(4)*
C5	0.0690(9)	0.669(1)	0.5069(8)	0.064(5)*
C6	0.0130(8)	0.838(1)	0.4477(6)	0.052(4)*
N1	0.1020(6)	0.7768(6)	0.4897(5)	0.034(3)*
C7	0.1483(8)	0.8313(9)	0.5700(6)	0.049(4)*
C8	0.2490(8)	0.7860(9)	0.6083(5)	0.044(4)*
N2	0.3200(6)	0.7869(7)	0.5484(4)	0.037(3)*
C9	0.396(1)	0.703(1)	0.5708(7)	0.083(6)*
C10	0.369(1)	0.892(1)	0.5507(7)	0.082(6)*
O	0.590(1)	0.8562(8)	0.4337(7)	0.133(6)*
C14	0.660(1)	0.774(1)	0.4481(8)	0.086(6)*
C15	0.610(1)	0.682(1)	0.3967(9)	0.090(7)*
C16	0.533(1)	0.730(1)	0.333(1)	0.112(8)*
C17	0.528(1)	0.841(1)	0.355(1)	0.095(7)*
H1	0.291(6)	0.670(7)	0.311(5)	0.029
H2	0.076(7)	0.658(7)	0.272(5)	0.033
H3	0.066(6)	0.829(7)	0.256(5)	0.029
H4	0.293(7)	0.842(6)	0.304(5)	0.030

* Asterisks denote isotropic equivalent thermal parameters.

geometry in the latter determination approximates that of the former.

Results and Discussion

Syntheses. Lithium Chemistry. The synthesis of **4** by metalation and reduction routes is summarized in

Table 4. Non-Hydrogen Atom (and Methine Hydrogen Atom) Coordinates, Isotropic Thermal Parameters, and Population Parameters for $[\{meso\text{-}(\text{HC}(\text{Me}_3\text{Si})\text{HC})_2\text{AlEt}_2(\text{TMEDA})\}_2] \text{ (6b)}$

atom	<i>x/a</i>	<i>y/b</i>	<i>z/c</i>	$U, \text{\AA}^2$	PP
Al	0.616(1)	0.5960(1)	0.3771(1)	0.0506(6)*	
C1	0.7259(4)	0.6234(4)	0.3790(4)	0.057(2)*	
Si1	0.7627(1)	0.7227(1)	0.3425(1)	0.0674(7)*	
C11	0.7283(7)	0.8003(5)	0.4236(8)	0.172(6)*	
C12	0.7378(7)	0.7469(5)	0.2200(6)	0.156(5)*	
C13	0.8691(5)	0.7271(6)	0.3491(9)	0.159(6)*	
C2	0.7572(4)	0.5548(4)	0.3236(5)	0.068(3)*	
C3	0.7130(4)	0.5005(4)	0.2824(5)	0.068(3)*	
C4	0.6281(3)	0.5039(4)	0.2885(4)	0.053(2)*	
Si4	0.5822(1)	0.5039(1)	0.1696(1)	0.0628(7)*	
C41	0.4791(4)	0.4846(6)	0.1819(5)	0.100(4)*	
C42	0.6212(5)	0.4229(6)	0.0920(5)	0.113(4)*	
C43	0.5953(6)	0.6002(6)	0.1061(5)	0.134(5)*	
C5	0.5306(4)	0.6721(5)	0.3588(6)	0.092(3)*	
C6a	0.5098(9)	0.7327(9)	0.422(1)	0.157(9)*	0.72(2)
C6b	0.538(1)	0.741(2)	0.298(3)	0.13(2)*	0.28(2)
N	0.5976(3)	0.5494(3)	0.5134(3)	0.063(2)*	
C1n	0.5164(4)	0.5292(4)	0.5346(4)	0.071(3)*	
C2n	0.6470(4)	0.4787(5)	0.5295(5)	0.084(3)*	
C3n	0.6201(4)	0.6131(5)	0.5819(5)	0.097(3)*	
H1	0.744(4)	0.626(4)	0.432(4)	0.070	
H2	0.809(4)	0.552(4)	0.314(4)	0.085	
H3	0.736(4)	0.459(3)	0.247(4)	0.085	
H4	0.607(3)	0.456(3)	0.313(4)	0.068	

* Asterisks denote isotropic equivalent thermal parameters.

Scheme 1. Lithiation of the (*E*)-but-2-ene precursor **1** with 2 equiv of *n*-BuLi in THF leads to proton abstraction from the 1- and 4-positions of the butene, giving the dimeric THF adduct of (*Z*)-1,4-dithio-1,4-bis(trimethylsilyl)but-2-ene, $[\{(\text{CH}(\text{Me}_3\text{Si})\text{CH})_2\text{Li}_2(\text{THF})_2\}_2] \text{ (4)}$. Compound **4** has also been prepared by reduction of (*E,E*)-1,4-bis(trimethylsilyl)buta-1,3-diene (**2**) by lithium in THF. Complex **4** can be isolated in high yield as a very air- and moisture-sensitive orange crystalline solid from each synthetic route.

Attempted lithiation of **1** in noncoordinating solvent systems and the relatively weak donor solvent Et₂O by alkylolithium reagents were unsuccessful. Here the increased reactivity of the alkylolithium reagents in strong oxygen and nitrogen donors is apparently required to effect the dilithiation of **1**. This has been well noted for acidic hydrocarbons devoid of Lewis base functionalities and has been attributed to the lowered association of the alkylolithium reagents in strong donor solvents and/or the increased nucleophilicity of the anion in the Lewis base adducts of the lithiating reagents. Attempted selective monolithiation of **1** by *n*-BuLi(PMDETA) (PMDETA ≡ *N,N,N',N',N''*-penta-

(15) Complex **5** crystallizes from Et₂O as prismatic crystals in the orthorhombic space group *Pmmm* (No. 59), with two molecules in the unit cell. Molecules of **5** reside on sites of *mm* symmetry, ($1/4, 1/4, z$), the asymmetric unit containing one-fourth of a molecule. The structure is disordered over the mirror plane (*x, 1/4, z*), with the trimethylsilyl moiety, the allylic carbon, and one methylene carbon of the TMEDA molecule being common to both orientations; all other atoms were refined with fixed site occupancies of 0.5. All non-hydrogen atoms were refined anisotropically, with the exception of the magnesium atom, which was refined isotropically owing to its proximity to the mirror plane. Further details of this structure determination are available as supplementary material. Crystal data: C₁₆H₃₈N₂MgSi₂, *M_r* = 338.97, orthorhombic, space group *Pmmm* (No. 59), *a* = 12.287(1) Å, *b* = 12.215(2) Å, *c* = 7.9912(6) Å, *V* = 1199.3(3) Å³, *Z* = 2, *D*(calcd) = 0.941 g cm⁻³, *F*(000) = 378 electrons, temperature 297 K, radiation Mo Kα, λ = 0.710 69 Å (graphite monochromated), μ = 1.71 cm⁻¹, no absorption correction applied, 2θ_{max} = 50°, 1169 independent reflections measured, 538 of these considered as "observed" (*I* > 2.5σ(*I*)) and used in the refinement, min/max final residual density -0.8/0.3 e Å⁻³, *R* = 0.088, *R_w* = 0.088, *s* = 1.22.

Table 5. Non-Hydrogen Atom (and Methine Hydrogen Atom) Coordinates and Isotropic Thermal Parameters for $[\{meso-(HC(Me_3Si)HC)_2GaCl\}_2(TMEDA)]$ (7)

atom	<i>x/a</i>	<i>y/b</i>	<i>z/c</i>	<i>U</i> , Å ²
Ga1	-0.11884(6)	0.34986(4)	0.62350(5)	0.0486(3)*
Ga2	0.12218(6)	0.60135(5)	0.81995(6)	0.0539(3)*
Cl1	-0.1365(2)	0.4252(1)	0.5121(1)	0.0749(9)*
Cl2	0.1343(2)	0.4960(1)	0.8963(2)	0.087(1)*
C1	-0.1144(6)	0.2357(4)	0.6169(5)	0.057(3)*
Si1	-0.1481(2)	0.1828(1)	0.5192(2)	0.0665(9)*
C11	-0.0627(8)	0.2076(7)	0.4384(7)	0.114(5)*
C12	-0.1461(9)	0.0768(5)	0.5398(7)	0.111(5)*
C13	-0.2693(7)	0.2088(6)	0.4818(6)	0.083(4)*
C2	-0.1737(7)	0.2175(5)	0.6911(5)	0.067(3)*
C3	-0.2163(6)	0.2720(4)	0.7337(5)	0.060(3)*
C4	-0.2122(5)	0.3569(4)	0.7137(5)	0.054(3)*
Si4	-0.3271(2)	0.4046(1)	0.6924(2)	0.0633(8)*
C41	-0.3880(7)	0.3671(7)	0.5967(7)	0.110(5)*
C42	-0.3095(7)	0.5096(5)	0.6803(7)	0.100(5)*
C43	-0.4073(7)	0.3887(7)	0.7807(8)	0.121(6)*
C5	0.1202(6)	0.7054(4)	0.8712(5)	0.061(3)*
Si5	0.1528(2)	0.7168(2)	0.9843(2)	0.073(1)*
C51	0.2707(8)	0.6754(7)	1.0101(6)	0.109(5)*
C52	0.1579(9)	0.8218(6)	1.0124(7)	0.112(5)*
C53	0.0627(9)	0.6701(8)	1.0485(7)	0.133(6)*
C6	0.1826(6)	0.7468(4)	0.8117(5)	0.062(3)*
C7	0.2234(6)	0.7105(5)	0.7497(5)	0.061(3)*
C8	0.2140(5)	0.6251(4)	0.7323(5)	0.054(3)*
Si8	0.3299(2)	0.5743(1)	0.7322(2)	0.0713(9)*
C81	0.3116(8)	0.4728(6)	0.700(1)	0.148(7)*
C82	0.3924(7)	0.5785(7)	0.8357(7)	0.104(5)*
C83	0.4093(8)	0.6214(8)	0.6570(7)	0.122(6)*
C1n	0.0814(6)	0.3682(5)	0.5896(6)	0.076(3)*
C2n	0.0502(6)	0.3419(4)	0.7346(5)	0.067(3)*
N1	0.0180(4)	0.3870(3)	0.6600(4)	0.051(2)*
C3n	0.0296(5)	0.4717(4)	0.6756(5)	0.054(3)*
C4n	-0.0358(5)	0.5000(4)	0.7424(5)	0.059(3)*
N2	-0.0151(4)	0.5809(3)	0.7698(4)	0.056(2)*
C5n	-0.0344(6)	0.6350(5)	0.7006(6)	0.078(4)*
C6n	-0.0829(6)	0.5967(5)	0.8385(6)	0.087(4)*
H1	-0.054(5)	0.219(4)	0.626(5)	0.071
H2	-0.180(5)	0.164(5)	0.709(5)	0.084
H3	-0.258(5)	0.256(4)	0.771(5)	0.074
H4	-0.180(5)	0.383(4)	0.767(4)	0.068
H5	0.062(5)	0.725(5)	0.868(5)	0.076
H6	0.190(5)	0.802(5)	0.817(5)	0.078
H7	0.261(5)	0.739(4)	0.716(5)	0.076
H8	0.184(5)	0.619(4)	0.677(4)	0.068

* Asterisks denote isotropic equivalent thermal parameters.

Table 6. Selected Structural Parameters for $[\{(CH(Me_3Si)CH)_2Li_2(THF)_2\}_2]$ (4)^a

Bond Distances (Å)					
Li1-C1	2.50(2)	Li2-C1	2.53(2)	C1-C2	1.46(1)
Li1-C2	2.27(2)	Li2-C2	2.25(2)	C2-C3	1.42(1)
Li1-C3	2.20(2)	Li2-C3	2.09(2)	C3-C4	1.42(1)
Li1-C4	2.38(2)	Li2-C4'	2.22(2)	C1-Si1	1.805(7)
Li1-O1	1.96(2)	Li2-Li2'	2.61(2)	C4-Si4	1.781(8)
Li1-O2	1.99(2)	Li2-C1'	2.22(2)		
Bond Angles (deg)					
C1-Li1-C4	78.3(5)	Si1-C1-C2		122.0(6)	
C1-Li1-O1	128(1)	C1-C2-C3		124.0(8)	
C1-Li1-O2	113.4(7)	C2-C3-C4		126.4(8)	
O1-Li1-O2	101.1(8)	Si4-C4-C3		125.7(6)	
C1-Li2-C4	80.7(5)				

^a A prime denotes the symmetry operator $-x, -y, -z$.

methyl-diethylenetriamine) in hexane afforded a mixture of unreacted **1** and mono- and dilithiated products (GC/MS analysis of ClSiMe₃-quenched product). This result is in contrast to the lithiation of *o*-(Me₃SiCH₂)₂C₆H₄ with the aforementioned reagent, in which case selective monolithiation resulted, the product being isolable as a crystalline solid, [*o*-C₆H₄(CH₂SiMe₃)(CH{Li(PMDETA)}-SiMe₃)]¹⁶

Table 7. Selected Structural Parameters for $[\{meso-(CH(Me_3Si)CH)_2Mg\}(TMEDA)]\cdot THF$ (5)

Bond Distances (Å)					
Mg-C1	2.200(9)	Mg-N1	2.17(1)	C3-C4	1.48(1)
Mg-C2	2.381(8)	Mg-N2	2.213(7)	C1-Si1	1.819(9)
Mg-C3	2.399(8)	C1-C2	1.45(1)	C4-Si4	1.836(9)
Mg-C4	2.191(9)	C2-C3	1.38(1)		
Bond Angles (deg)					
C1-Mg-C4	85.0(3)	N1-Mg-N2		83.4(4)	
C1-Mg-N1	121.6(3)	Si1-C1-C2		121.9(6)	
C1-Mg-N2	125.9(3)	C1-C2-C3		124.3(8)	
C4-Mg-N1	119.0(3)	C2-C3-C4		121.2(8)	
C4-Mg-N2	126.6(3)	Si4-C4-C3		120.8(6)	

Table 8. Selected Structural Parameters for $[\{meso-(HC(Me_3Si)HC)_2AlEt\}_2(TMEDA)]$ (6b)

Bond Distances (Å)					
Al-C1	1.995(6)	C1-C2	1.49(1)	C4-Si4	1.836(6)
Al-C4	1.995(6)	C2-C3	1.33(1)	C5-C6a	1.40(2)
Al-N	2.099(5)	C3-C4	1.505(9)	C5-C6b	1.45(4)
Al-C5	1.996(8)	C1-Si1	1.859(7)		
Bond Angles (deg)					
C1-Al-C4	94.7(3)	C5-Al-N		103.7(3)	
C1-Al-C5	126.3(3)	Si1-C1-C2		114.4(5)	
C4-Al-C5	119.6(3)	C1-C2-C3		122.3(6)	
C1-Al-N	103.0(2)	C2-C3-C4		122.3(6)	
C4-Al-N	107.6(2)	Si4-C4-C3		112.6(4)	

Table 9. Selected Structural Parameters for $[\{meso-(HC(Me_3Si)HC)_2GaCl\}_2(TMEDA)]$ (7)

Bond Distances (Å)					
Ga1-C1	2.215(2)	Ga1-N1	2.100(6)	C4-Si4	1.842(8)
Ga2-C12	2.199(3)	Ga2-N2	2.102(6)	C5-C6	1.50(1)
Ga1-C1	1.981(7)	C1-C2	1.51(1)	C6-C7	1.32(1)
Ga1-C4	1.991(8)	C2-C3	1.32(1)	C7-C8	1.51(1)
Ga2-C5	1.978(8)	C3-C4	1.51(1)	C5-Si5	1.864(9)
Ga2-C8	1.985(8)	C1-Si1	1.859(8)	C8-Si8	1.858(8)
Bond Angles (deg)					
C11-Ga1-C1	123.2(2)	C5-Ga2-N2		106.6(3)	
C11-Ga1-C4	119.2(2)	C8-Ga2-N2		112.4(3)	
C12-Ga2-C5	121.8(3)	Si1-C1-C2		115.2(6)	
C12-Ga2-C8	121.6(2)	C1-C2-C3		122.1(7)	
C1-Ga1-C4	97.1(3)	C2-C3-C4		124.5(8)	
C5-Ga2-C8	97.0(3)	Si4-C4-C3		115.9(6)	
C11-Ga1-N1	97.0(2)	Si5-C5-C6		115.7(6)	
C12-Ga2-N2	97.2(2)	C5-C6-C7		121.9(7)	
C1-Ga1-N1	106.8(3)	C6-C7-C8		124.4(8)	
C4-Ga1-N1	113.9(3)	Si8-C8-C7		113.1(6)	

Attempted lithiations of the butenes (*E*)- and (*Z*)-1,1,4,4-tetrakis(trimethylsilyl)but-2-ene, under a variety of conditions were unsuccessful, including the specific conditions necessary for the lithiation of the sterically demanding tris(trimethylsilyl)methane¹⁷ (MeLi under reflux in a 10/3 THF/Et₂O solvent mixture). Here the added steric hindrance to metalation afforded by the extra trimethylsilyl substituents does not allow lithiation to occur, despite the likely increased thermodynamic acidity of the allylic protons relative to the bis(trimethylsilyl)-substituted analogues (based on polarization considerations by silicon). In addition, any metalation of the tetrakis(trimethylsilyl)-substituted butenes would result in nonplanarity of an sp²-metalated center and the vinylic moiety.

Exposure of benzene solutions of isolated **4** to atmospheric oxygen leads to oxidation of the but-2-ene-1,4-diyl group, quantitatively yielding the free butadiene

(16) Lappert, M. F.; Raston, C. L.; Skelton, B. W.; White, A. H. *J. Chem. Soc., Chem. Commun.* **1982**, 14.

(17) Cook, M. A.; Eaborn, C.; Jukes, A. E.; Walton, D. R. M. *J. Organomet. Chem.* **1970**, *24*, 529.

Scheme 1

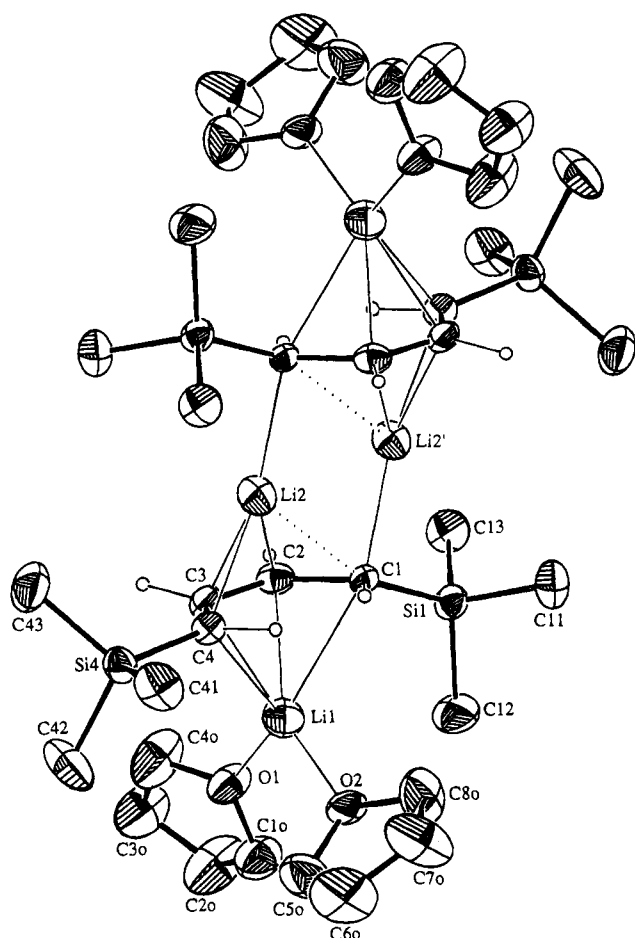
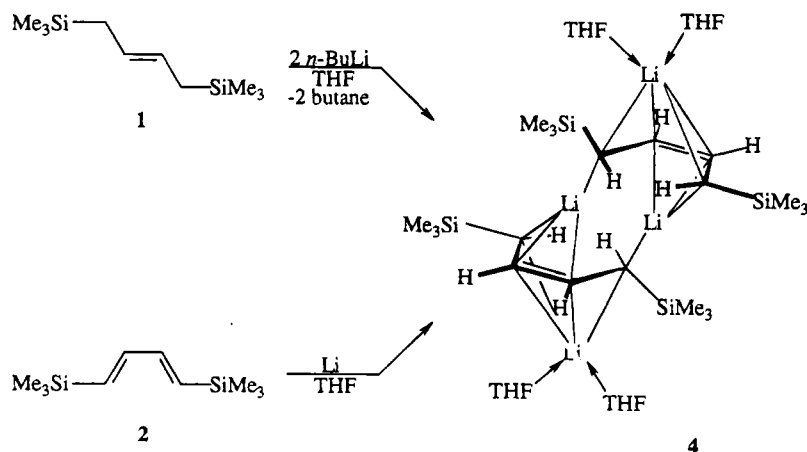


Figure 1. Molecular projection of $[(\text{CH}(\text{Me}_3\text{Si})\text{CH})_2\text{Li}_2(\text{THF})_2]_2$ (4), showing the labeling scheme. Thermal ellipsoids are drawn at the 20% probability level. For clarity, only methine hydrogens are shown as spheres of arbitrary radii.

(*E,E*)-1,4-bis(trimethylsilyl)buta-1,3-diene (2) (by NMR). Similar reaction of the crude lithiation product is not so clean, and we still recommend our published procedure for the synthesis of 2.^{10a}

The differing levels of association of 4 and the analogous monomeric TMEDA adduct $[(\text{CH}(\text{Me}_3\text{Si})\text{Si})\text{CH}_2\{\text{Li}(\text{TMEDA})\}_2]$ (3) are consistent with the well-accepted ability of bidentate Lewis bases to reduce the association of organolithium complexes more effectively than their monofunctional counterparts. While the coordination

sphere of the lithium atoms can be saturated by monodentate Lewis bases, very often oligomers result from partial solvation of the metal centers unless the added stability of chelation by the Lewis base is offered. Examples illustrating this point include the polymeric structure of $[(\eta^3\text{-exo,exo-1,3-diphenylallyl})\{\mu\text{-Li}(\text{OEt}_2)\}]_n$ ¹⁸ and monomeric $[(\eta^3\text{-exo,exo-1,3-bis(trimethylsilyl)allyl})\text{-Li}(\text{TMEDA})]$,¹⁹ where adduct formation is at the expense of π -complexation only when the Lewis base is at least bidentate. This generality has far from blanket applicability though, and the TMEDA adduct of the MeLi tetramer²⁰ $[(\text{MeLi})_4(\text{TMEDA})_2]_n$ is a much-cited example in which the integrity of the unsolvated $(\text{MeLi})_4$ unit retains its integrity and is capped on the lithium atom vertices by a single nitrogen donor of a TMEDA molecule to form a three-dimensional polymer.

There is very little structural information in the literature pertaining to unsolvated and partially solvated structures of organolithium compounds containing π metal-ligand interactions, owing to their preparation generally involving lithiation in the presence of Lewis bases or electron exchange reactions in donor solvents. The polymeric structure of $[(\eta^3\text{-exo,exo-1,3-diphenylallyl})\{\mu\text{-Li}(\text{OEt}_2)\}]_n$ and the lithium-bridged substituted-fulvalene dimer²¹ $[\{\text{C}_{24}\text{H}_{14}(\text{SiMe}_3)_2(\mu\text{-Li})\{\text{Li}(\text{THF})_2\}\}_2]$ represent typical structures in which the bonding observed in the completely solvated monomeric analogues is reflected on the other side of the anion plane and an oligomeric stack containing alternating Li cations and anionic groups results. The dimeric structure of 4 relates to this generality and indicates that the likely structure of the unsolvated compound, if accessible, would be a linear polymer, consisting of alternating dianions bridged by pairs of lithium atoms.

Magnesium Chemistry. The TMEDA adduct of (*Z*)-1,4-magnesia-1,4-bis(trimethylsilyl)but-2-ene, $[\text{meso}(\text{CH}(\text{Me}_3\text{Si})\text{CH})_2\text{Mg}\{\text{TMEDA}\}]$ (5) has been prepared by metathetical exchange reactions between MgCl_2 and *i*-PrMgCl and 4 in Et_2O at low temperature (*ca.* -80°C) (Scheme 2). The complex can be isolated in high

(18) Boche, G.; Etzrodt, H.; Marsch, M.; Massa, W.; Baum, G.; Dietrich, H.; Mahdi, W. *Angew. Chem.* **1986**, *98*, 84; *Angew. Chem., Int. Ed. Engl.* **1986**, *25*, 104.

(19) Boche, G.; Fraenkel, G.; Cabral, J.; Harms, K.; Hommes, N. J. R. v. E.; Lhorencz, J.; Marsch, M.; Schleyer, P. v. R. *J. Am. Chem. Soc.* **1992**, *114*, 1562.

(20) Köster, H.; Thoennes, D.; Weiss, E. *J. Organomet. Chem.* **1978**, *160*, 1.

(21) Malaba, D.; Chen, L.; Tessier, C. A.; Youngs, W. J. *Organometallics* **1992**, *11*, 1007.

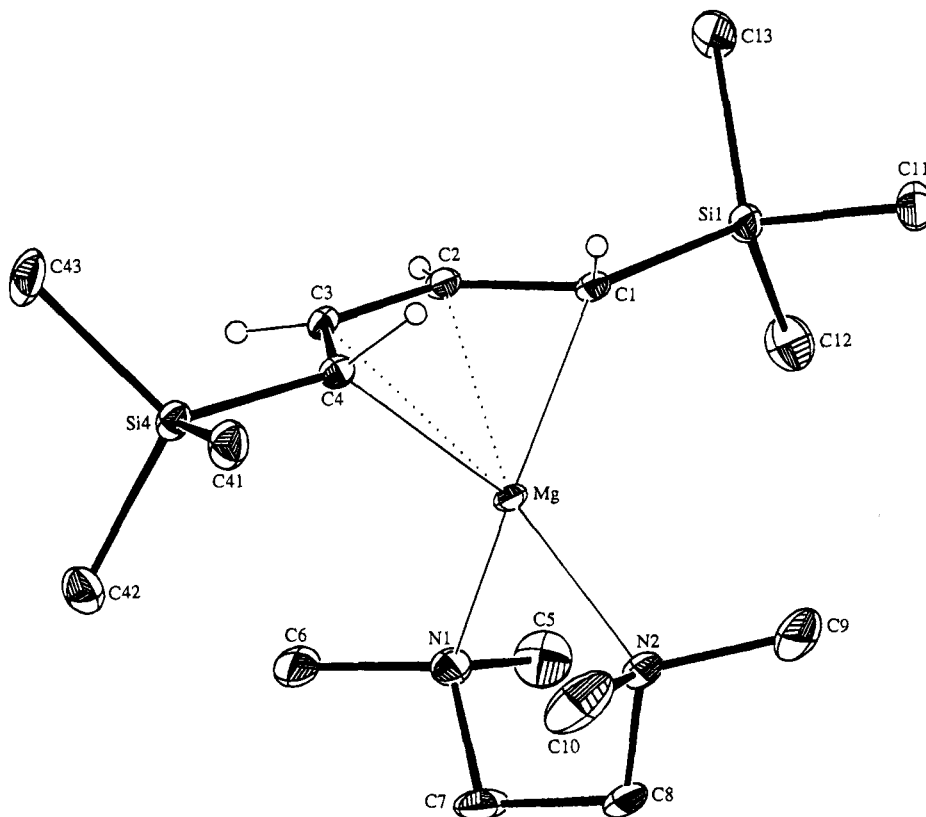
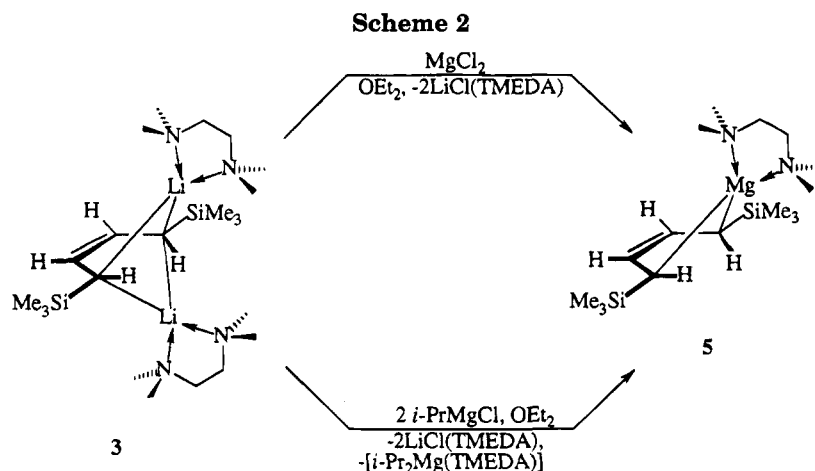


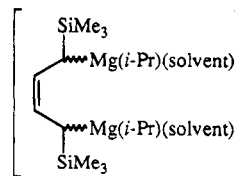
Figure 2. Molecular projection of $[\{meso\text{-}(\text{CH}(\text{Me}_3\text{Si})\text{CH})_2\text{Mg}\}(\text{TMEDA})]\cdot\text{THF}$ (**5**), showing the labeling scheme. Thermal ellipsoids are drawn at the 20% probability level. For clarity, only methine hydrogens are shown as spheres of arbitrary radii.



yield as a very air- and moisture-sensitive yellow crystalline solid from both synthetic routes.

The two organomagnesium products obtained from the metathetical exchange involving *i*-PrMgCl are readily isolable owing to their differing solubilities in alkane solvents, the insolubility of **5** precluding the obtainment of even the ^1H NMR spectrum of the complex in cyclohexane- d_{12} . The products from this reaction can be seen to result from a shift in the Schlenk equilibrium of the Grignard reagent prior to reaction with the lithium complex, which is plausible, given the presence of TMEDA. Alternatively, the products could result from elimination of the diisopropylmagnesium complex from an initially formed dimagnesium complex (**I**). This relates to the shift in the Schlenk equilibrium by the addition of 1,4-dioxane to ethereal solutions of Grignard reagents. No attempt was made at low-temperature

isolation or spectroscopic identification of such an intermediate. Given the similarities which exist be-



I

tween but-2-ene-1,4-diyl and metallabenzocyclopentene complexes, the concentration and temperature dependence observed in the magnesium halide elimination from the di-Grignard reagent of *ortho*-bis(chloromethyl)-benzene to give $[\{o\text{-CH}_2\text{C}_6\text{H}_4\text{CH}_2\}\text{Mg}(\text{THF})_2]_3$ is noteworthy.²²

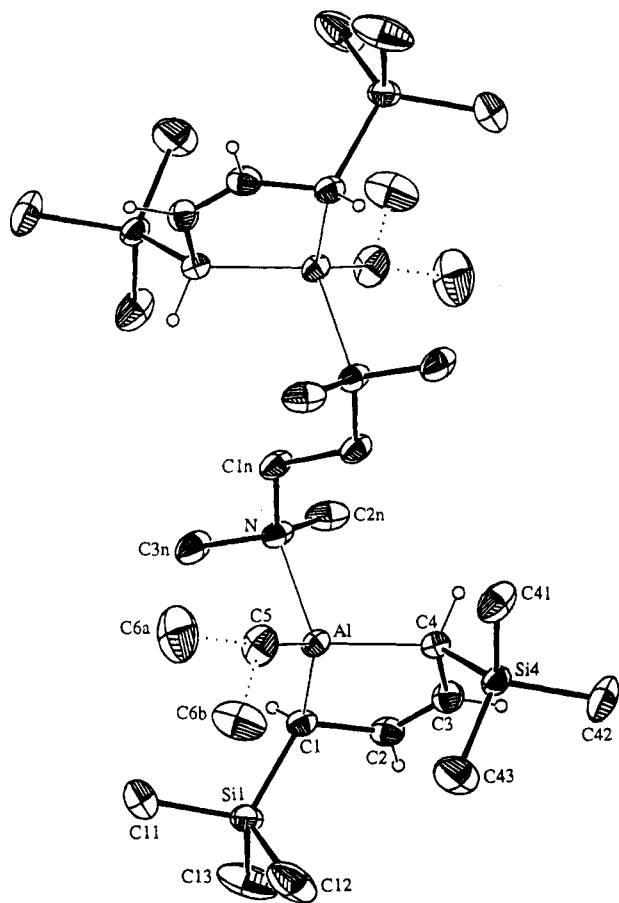


Figure 3. Molecular projection of [*meso*-(HC(Me₃Si)-HC)₂AlEt]₂(TMEDA)] (**6b**), showing the labeling scheme. Thermal ellipsoids are drawn at the 20% probability level. For clarity, only methine hydrogens are shown as spheres of arbitrary radii. Bonds to the disordered ethyl group are dashed.

Attempts to prepare **5** by the metalation of **1** using *n*-Bu-*s*-BuMg and the direct reaction of activated magnesium metal and **2** were unsuccessful. The latter synthetic approach is the most common method for the preparation of the THF adduct of the unsubstituted analogue, [(C₄H₆)Mg(THF)₂]_n. The reaction of magnesium metal with dienes is prone to prolonged initiation periods, and this is the most likely reason for the failure of the magnesium metal to react in this case. The lack of metalation of **1** using *n*-Bu-*s*-BuMg with TMEDA reflects the decreased nucleophilicity of organomagnesium compounds relative to the more polar Li-C bonds found in lithium alkyls, which readily metalate the allylic positions of the same substrate. In this context it has been noted that metalation by Grignard and dialkylmagnesium complexes often only occurs to a significant extent in heteroatom Lewis base functionalized organic compounds, even despite the favorable thermodynamic acidity of the hydrocarbon.

The reactivity of compound **5** has been investigated in order to further investigate the nature of the bonding in the complex. When treated with ClSiMe₃ and H₂O, the complex behaves as a but-2-ene-1,4-diyl, yielding the (*Z*)-butenes (*Z*)-1,1,4,4-tetrakis(trimethylsilyl)but-2-ene and (*Z*)-1,4-bis(trimethylsilyl)but-2-ene, respectively. Reaction with oxygen gives (*E,E*)-1,4-bis(trimethylsilyl)-

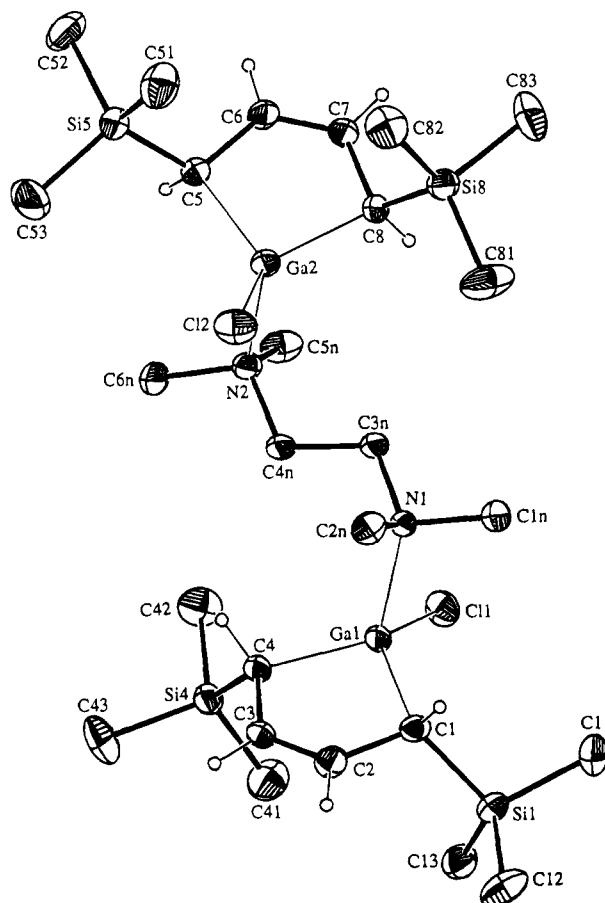


Figure 4. Molecular projection of [*meso*-(HC(Me₃Si)-HC)₂GaCl]₂(TMEDA)] (**7**), showing the labeling scheme. Thermal ellipsoids are drawn at the 20% probability level. For clarity, only methine hydrogens are shown as spheres of arbitrary radii.

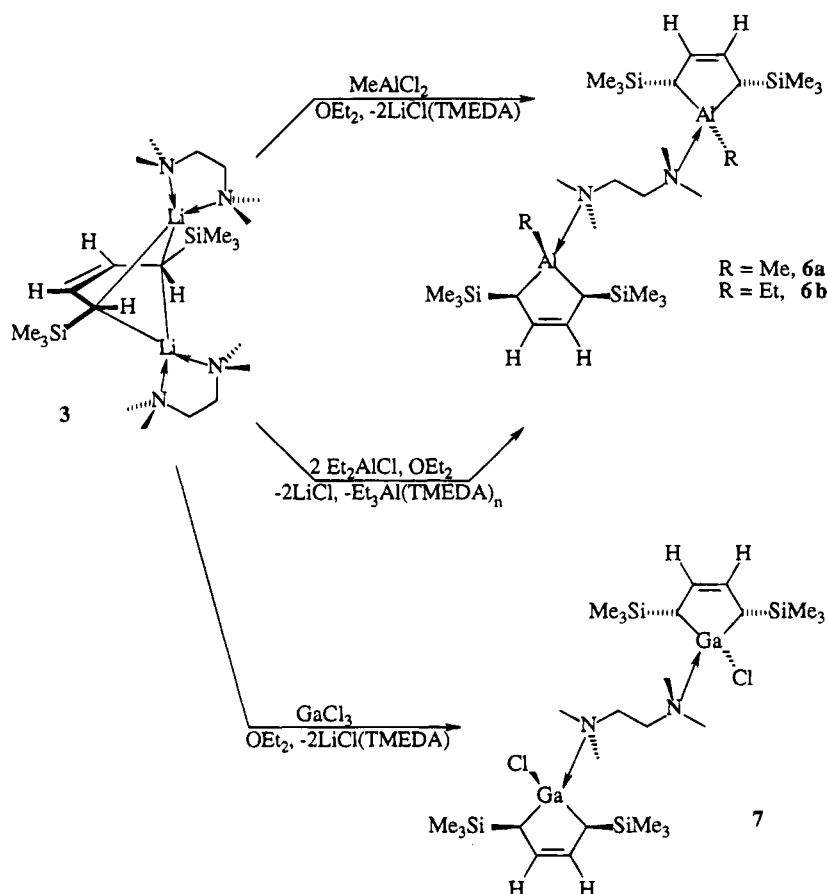
buta-1,3-diene (**2**), the complex here behaving as an η^4 -coordinated diene. Similarly, the complex decomposes at temperatures greater than 185 °C to give (*E,E*)-1,4-bis(trimethylsilyl)buta-1,3-diene (**2**), magnesium metal, and TMEDA.

Aluminum and Gallium Chemistry. The synthesis of **6a,b** and **7** in moderate yield as air- and moisture-sensitive colorless crystalline solids is summarized in Scheme 3. The TMEDA adducts of the 2,5-bis(trimethylsilyl)-substituted *meso*-methylaluminumcyclopent-3-ene [*meso*-(HC(Me₃Si)HC)₂AlMe]₂(TMEDA)] (**6a**) and *meso*-ethylaluminumcyclopent-3-ene complexes [*meso*-(HC(Me₃Si)HC)₂AlEt]₂(TMEDA)] (**6b**) have been prepared by metathetical exchange reactions between MeAlCl₂ and Et₂AlCl and **3** in Et₂O at low temperature (*ca.* -80 °C). Similarly, the TMEDA adduct of the 2,5-bis(trimethylsilyl)-substituted *meso*-chlorogallacyclopent-3-ene complex [*meso*-(HC(Me₃Si)HC)₂GaCl]₂(TMEDA)] (**7**) has been prepared by a metathetical exchange reaction between GaCl₃ and **3** under the same temperature and solvent conditions.

Treatment of InCl₃ with **3** in Et₂O at low temperature (*ca.* -80 °C) results in reduction, affording indium metal and free (*E,E*)-1,4-bis(trimethylsilyl)butadiene (**2**). Indeed, attempted synthesis of the gallium complex **7** by the reverse addition of GaCl₃ to **3** also yields deposited gallium metal.^{10c} Decomposition of [*meso*-(HC(Me₃Si)-HC)₂AlCl]₂(TMEDA)] and **7**, yielding free (*E,E*)-1,4-bis(trimethylsilyl)butadiene (**2**) and metal, occurs at tem-

(22) Lappert, M. F.; Martin, T. R.; Raston, C. L.; Skelton, B. W.; White, A. H. *J. Chem. Soc., Dalton Trans.* **1982**, 1959.

Scheme 3



temperatures exceeding 290 and 114 °C, respectively. In this context, the chlorometallacyclopent-3-ene complexes can be viewed as trapped metal(I) chloride species, MCl ($\text{M} = \text{Al}, \text{Ga}$), thermally decomposing to **2** and presumably the metal(I) chloride, which under these conditions disproportionates to metal and the metal(III) chloride.²³ While the β -hydrogen elimination pathway is inhibited because of geometry constraints in the metallacyclopent-3-enes studied here, a reductive elimination/ $\text{M}-\text{C}$ bond homolysis decomposition pathway is favored by the stability of the byproduct, **2**. The decrease in the thermal stability of the metal(III) oxidation state in this series of complexes mirrors the periodic trend of the instability of metals in their higher oxidation state for the lower members of the group 13 elements.

The alkylaluminacyclopent-3-ene complexes prepared according to Scheme 3 also thermally decompose to give aluminum metal and (*E,E*)-1,4-bis(trimethylsilyl)butadiene **2**, at temperatures exceeding 200 and 164 °C, for the methyl (**6a**) and ethyl (**6b**) analogues, respectively. The decreased thermal stability of the ethylaluminum species relative to that of the methyl analogue possibly is attributable to the β -hydrogen elimination decomposition pathway available in this case; however $\text{Al}-\text{C}$ bond homolysis cannot be ruled out given the relative stability of the ethyl radical over that of the methyl radical.²⁴ Less bulky alkylaluminum complexes decompose via β -hydrogen elimination at far milder temperatures; for

instance, trialkylaluminum complexes decompose initially to dialkylaluminum hydride species at 100 °C and then to aluminum metal.²⁵ For the β -hydrogen elimination decomposition pathway to be facile, a vacant coordination site is necessary on the metal center for the hydride transfer in the transition state and the $(\beta\text{-H})-\text{C}-\text{C}-\text{M}$ dihedral angle must be allowed to approach 0° to allow the hydride transfer to occur. In this context we note that the EI mass spectrum of complex **6b** exhibits no molecular ion peak; the largest fragment observed is that of the Lewis base free species $[\{\text{HC}(\text{Me}_3\text{Si})\text{HC}\}_2\text{AlEt}]^+$ (*m/e* 254, 28%), which is presumably three-coordinate and coordinatively unsaturated, making β -hydrogen elimination a feasible process for this species. However, no fragment corresponding to $[\{\text{HC}(\text{Me}_3\text{Si})\text{HC}\}_2\text{AlH}]^+$ is apparent. A molecular ion with a mass to charge ratio of 225 (21%), corresponding to the ion $[\{\text{HC}(\text{Me}_3\text{Si})\text{HC}\}_2\text{Al}]^+$, is also observed. We have not performed an analysis on the gaseous products from this thermal decomposition and a suggestion of the mechanism is only tentative at this stage; indeed, loss of (*E,E*)-1,4-bis(trimethylsilyl)butadiene (**2**) may be the primary process here.

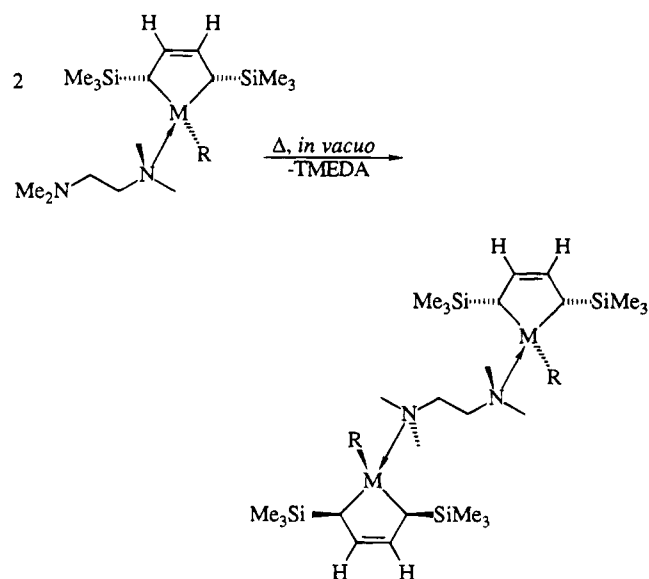
In all cases the reactions outlined in Schemes 2 and 3 are stereospecific, giving the *meso* isomers as the only isolable products, this assignment being made on the basis of ^1H and ^{13}C NMR data and crystal structure determinations (**5**, **6b**, and **7** only). The remaining assignment of stereochemistry about the metal centers concerning the site of coordination of the nitrogen center

(23) Paetzold, P. *Angew. Chem.* **1991**, *103*, 559; *Angew. Chem., Int. Ed. Engl.* **1991**, *30*, 544.

(24) Cowley, A. H.; Corbelin, S.; Jones, R. A.; Lagow, R. J.; Nail, J. W. *J. Organomet. Chem.* **1994**, *464*, C1.

(25) Ziegler, K.; Gellert, H.-G.; Lehmkuhl, H.; Pfohl, W.; Zosel, K. *Justus Liebig's Ann. Chem.* **1960**, *629*, 1.

Scheme 4

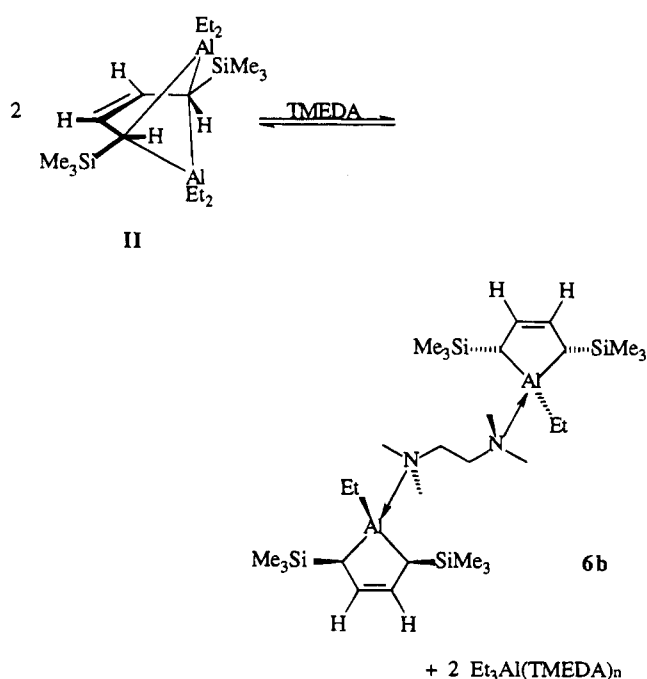


of the bridging TMEDA molecule is made solely on the basis of the crystal structure determinations and is consistent with steric considerations. Coordination to the face of the metallacycle bearing the trimethylsilyl substituents would result in unreasonably close contacts between the TMEDA methyl groups and the trimethylsilyl substituents. The steric hindrance of the trimethylsilyl substituents may block chelation of the TMEDA molecule, forming five-coordinate species. Any chelation would likely lead to the formation of four-coordinate ionic species;^{26,27} cf., $[t\text{-Bu}_2\text{Al}(\text{TMEDA})]^+\text{Cl}^-$, $[t\text{-Bu}_2\text{Al}(\text{TMEDA})]^+[t\text{-Bu}_2\text{AlCl}_2]^-$ and $[\{2\text{-(Me}_3\text{Si)}_2\text{CC}_5\text{-H}_4\text{N}\}_2\text{Al}]^+[\text{AlCl}_4]^-$.

The isolation of the crystalline metallacyclopent-3-ene complexes outlined in Scheme 3 was dependent on the use of isolated crystalline organolithium reagents; the use of crude reaction mixtures derived from treating **1** with $n\text{-BuLi}(\text{TMEDA})$ in hexane gave intractable oils. The Et_2O -insoluble residues from these reactions contained no trimethylsilyl-substituted compounds, negating the possibility of other ionic byproducts being formed in these reactions. The extended heating *in vacuo* during the reaction workup (ca. 5 h at 100 °C) necessary to isolate the complexes possibly is required due to an initial 1:1 metallacycle-TMEDA adduct, $[\{\text{meso}-(\text{HC}(\text{Me}_3\text{Si})\text{HC})_2\text{MR}\}(\text{TMEDA})]$, which then loses $1/2$ equiv of TMEDA to yield $[\{\text{meso}-(\text{HC}(\text{Me}_3\text{Si})\text{HC})_2\text{MR}\}_2(\text{TMEDA})]$ (Scheme 4). The nature of such an intermediate was not investigated.

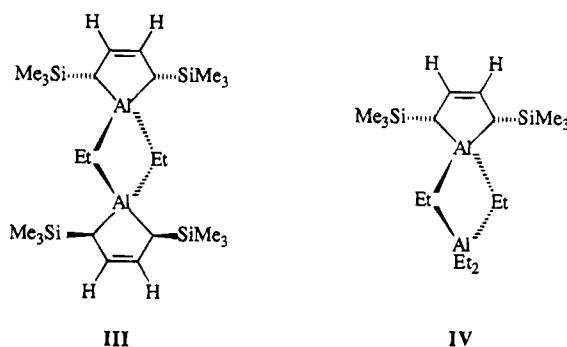
The two organoaluminum products obtained from the reaction of **3** with 2 equiv of Et_2AlCl can be rationalized similarly to the synthesis of **5** from the same lithium transfer reagent and 2 equiv of $i\text{-PrMgCl}$. In this case, however, the byproduct triethylaluminum complex was not isolated. Literature reviews have stressed the point that dimers of the type $(\text{R}_2\text{AlR}')_2$ are stabilized only when R' is a good bridging group, such as Me, Et, and

Scheme 5



Ph.²⁸ In this case it is not surprising that the equilibrium in Scheme 5 lies to the right; the orbitals of the bridging (*Z*)-but-2-ene-1,4-diyl unit in **II** which are available to bond to the aluminum centers are not compatible with those of the favored bonding descriptions of electron-deficient alkyl bridge bonding in aluminum chemistry.²⁹

In the absence of TMEDA in the reaction mixture, alternative redistribution reactions giving products of the type $[\{\text{meso}-(\text{HC}(\text{Me}_3\text{Si})\text{HC})_2\text{Al}(\mu\text{-Et})_2\{\text{meso}-(\text{HC}(\text{Me}_3\text{Si})\text{HC})_2\}\}_2]$ (**III**) and $[\{\text{meso}-(\text{HC}(\text{Me}_3\text{Si})\text{HC})_2\text{Al}(\mu\text{-Et})_2\text{AlEt}_2\}]$ (**IV**) would be favorable here. There is ample



precedence for such redistribution behavior in both laboratory and industrial synthesis in aluminum chemistry, the organolithium sesquihalides $\text{Me}_3\text{Al}_2\text{Cl}_3$, for example, redistribute *via* chloro- and alkyl-bridged dimer equilibrations, and a number of species are present in solution.

X-ray Structure Commentary. Structure of 4. Complex **4** crystallizes as prismatic crystals in the monoclinic space group $P2_1/n$, with two molecules in the unit cell, the asymmetric unit comprising half of the dimer of composition $[\{(\text{CH}(\text{Me}_3\text{Si})\text{CH})_2\text{Li}_2(\text{THF})_2\}_2]$, the

(26) Uhl, W.; Wagner, J.; Fenske, D.; Baum, G. *Z. Anorg. Allg. Chem.* **1992**, 612, 25.

(27) Engelhardt, L. M.; Kynast, U.; Raston, C. L.; White, A. H. *Angew. Chem.* **1987**, 99, 702; *Angew. Chem., Int. Ed. Engl.* **1987**, 26, 681.

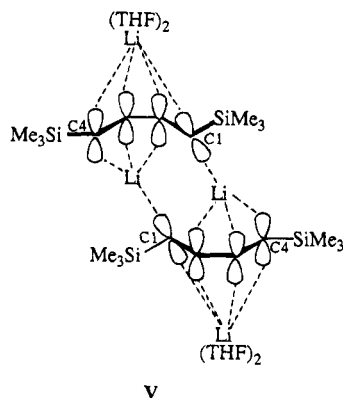
(28) Eisch, J. J. In *Comprehensive Organometallic Chemistry*; Wilkinson, G., Stone, F. G. A., Abel, E. W., Eds.; Pergamon: Oxford, England, 1982; Vol. 1, Chapter 6.

(29) Wade, K. *Electron Deficient Compounds*; Nelson: London, 1971.

other half being generated by an inversion center at $(1, \frac{1}{2}, 0)$ (Figure 1).

The dimeric structure of **4** can be seen to arise from the association of two η^4 -bound (*Z*)-1,4-dilithiobut-2-ene units, being held together by two lithium atoms bridging the dianions. The structure contains two "external" six-coordinate lithium atoms in distorted pseudotetrahedral environments, considering the lithium atoms to be principally bound to the two allylic carbons, the other two sites being occupied by oxygen atoms of the coordinating THF molecules. The two "internal" lithium atoms are devoid of neutral donor ligands and are formally four-coordinate, being bound in η^3 and η^1 fashion to each of the (*Z*)-but-2-ene-1,4-diyl units which they bridge. The overall molecular symmetry is crystallographically imposed to be C_i .

Selected geometrical parameters are given in Table 6. The exterior lithium atoms are bound asymmetrically to the outside faces of the dianions, having been slipped away from the allylic carbon, C1, which is bound principally η^1 to an interior lithium atom and toward the allylic carbon, C4, which is also bound to an interior lithium atom as part of an η^3 -allyl type interaction. The exterior Li–C distances measure 2.50(2), 2.27(2), 2.20(2), and 2.38(2) Å for C1–C4, respectively. This asymmetry is a consequence of the trimethylsilyl group attached to C1 having been shifted out of the dianion plane defined by C1–C4 by some 0.78(1) Å to accommodate the two interior lithium atoms binding to the internal face of the dianion. This has the effect of directing the p orbital of C1 in the direction of the exterior lithium atoms, allowing them to bind more closely to C4 (V).



The exterior lithium atoms lie 1.88(2) Å from the dianion plane in **4**, which compares with the same parameter in the monomeric structure of **3**, 1.81(2) Å.^{10b} The distance of the interior lithium atom to the dianion to which it is η^3 bound is similar at 1.79(2) Å, but significantly shorter than its distance from the ligand with which it is bound in η^1 fashion, 2.06(2) Å. The interior Li–C bond lengths measure 2.22(2) Å for the η^1 bond to C1 and 2.25(2), 2.09(2), and 2.22(2) Å for the η^3 linkages to C2, C3, and C4, respectively. The Li–C distances to the interior lithium atoms are on average shorter than those to the exterior lithium atoms, in agreement with the additional solvation of the exterior lithium atoms by the THF molecules. The η^3 -allyl type Li–C distances in **4** compare with the those found in the structure of $[(\eta^3\text{-}exo,exo\text{-}1,3\text{-bis(trimethylsilyl)allyl})\text{-lithium(TMEDA)}]_2$,¹⁹ 2.229(9)–2.27(1) Å for the terminal

Li–C distances and 2.170(9) Å for the Li–C distance to the central carbon of the anion.

The Li–O distances of 1.96(2) and 1.99(2) Å are typical for THF solvates of organolithium complexes. The O–Li–O plane is approximately orthogonal to the C1–Li–C4 plane, the interplanar angle measuring 90.1(3)°.

The Li–Li contact distance between the two interior lithium atoms in **4** is 2.61(2) Å and compares with 2.56(1) Å observed in the two-coordinate lithium centrosymmetric dimer $[(\text{Li}\{2\text{-(Me}_3\text{Si)}_2\text{CC}_5\text{H}_4\text{N}\})_2]^{30}$ and 2.57 Å in $[(\text{MeLi})_4(\text{TMEDA})_2]_n$.²⁰ The bonding importance of these close lithium–lithium contacts is uncertain, with evidence from NMR and *ab initio* molecular orbital studies suggesting that the Li–Li bond order is near zero in organolithium compounds.

The η^3 -allyl type bonding to C2, C3, and C4 by the interior lithium atoms in **4** has a marked effect on the electronic configuration of the dianion. The C1–C2 distance is 1.46(1) Å, significantly longer than the C2–C3 and C3–C4 distances of 1.42(1) Å, and can be contrasted with the analogous distances in **3**, which were consistent with the electronic configuration being but-2-ene-1,4-diyl; i.e., C1–C2, C2–C3, and C3–C1' measured 1.49(3), 1.34(3), and 1.45(3) Å, respectively.^{10b}

Charge stabilization onto the polarizing silicon substituents of **4** is suggested by the contraction of the Si–C bond distance to the metalated carbons C1 and C4, 1.805(7) and 1.781(8) Å, respectively, relative to the average Si–C(methyl) bond distance of 1.88 Å, the silicon atom lying close to the plane defined by the carbon atoms C1–C4 exhibiting the shortest of the two Si–C distances. The extent of silicon–carbon bond distance contraction observed here is similar to that observed in **3**, 1.76(1) Å.^{10b} Other bond distances and angles within the molecule are unexceptional.

Structure of 5. Complex **5** crystallizes as rod-shaped crystals in the monoclinic space group $P2_1/c$, with four molecules in the unit cell, with the asymmetric unit containing one molecule of **5** and one molecule of uncoordinated THF (Figure 2).

The structure of **5** is best described as a magnesacyclopent-3-ene containing a four-coordinate magnesium center in a distorted-tetrahedral environment, with two of the coordination sites being occupied by carbon atoms from a single but-2-ene-1,4-diyl moiety and the other two sites being occupied by nitrogen atoms of a chelating TMEDA molecule. The molecule is devoid of crystallographic symmetry, but the molecular symmetry approximates to C_s , with torsion in the ethylene linkage of the TMEDA chelate ring being the largest deviation from mirror symmetry.

Selected geometrical parameters are given in Table 7. Given the length of the Mg–C bonds to the allylic carbons, 2.200(9) and 2.191(9) Å, there is a large puckering of the magnesium atom out of the ligand plane, resulting in a secondary interaction between the magnesium atom and the vinylic carbons, 2.381(8) and 2.399(8) Å to C2 and C3, respectively, represented by dashed bonds in the molecular structure figure. This is reflected in the large fold angle ($\phi = 73.9(5)^\circ$) of the magnesium atom out of the ligand plane, which is defined by the angle between the ligand plane, C1–C2–

(30) Colgan, D.; Papasergio, R. I.; Raston, C. L.; White, A. H. *J. Chem. Soc., Chem. Commun.* **1984**, 1708.

C3–C4, and the C1–Mg–C4 plane. The deviation of the magnesium atom from the ligand plane is 1.555(9) Å.

A comparison with the crystal structure of the closest acyclic analogue to **5**, [Me₂Mg(TMEDA)],³¹ whose Mg–C distance measured 2.166(6) Å, negates any possibility that the large puckering of the metallacyclic ring is attributable to the interaction of the magnesium atom with the vinylic carbons with concomitant π -complex formation. The average Mg–N distance of 2.19 Å in **5** is significantly shorter than in [Me₂Mg(TMEDA)], 2.242 Å, giving further evidence that the carbanion is acting only as a four-electron σ -donor and does not offer additional electron density to the magnesium atom through π -bonding. These bond distance variations are in common with all other four-coordinate, mononuclear bis(sp³-nitrogen) donor adducts of magnesium alkyl and aryl compounds covered in recent literature reviews.³²

The most striking angular deviation observed in the structure of **5** in comparison to that of [Me₂Mg(TMEDA)] is the acute C–Mg–C bond angle in **5**, 85.0(3)°, compared to 130.0(4)° in the acyclic dialkylmagnesium, and is clearly a consequence of the small ligand bite angle of the dianion. The ligand bite angle in the puckered magnesacyclopent-3-ene **5** is opened up relative to that observed in the lithium analogue **3**, in which case the fold angle (ϕ) is 90° and the ligand bite angle measures 81.3(6)°. The ligand bite angle of the chelating TMEDA molecule, 83.4(4)°, further contributes to the angular distortion from tetrahedral geometry of the magnesium atom. The N–Mg–N plane is approximately orthogonal to the C–Mg–C plane, the interplanar angle measuring 88.4(3)°.

Bond distances within the dianion moiety are in agreement with the electronic configuration of the dianion being best described as a but-2-ene-1,4-diyl, with some evidence for charge delocalization through the carbon–carbon double bond. The C2–C3 bond distance of 1.38(1) Å is longer than that of an isolated carbon–carbon double bond, and the C1–C2 and C3–C4 bond distances of 1.45(1) and 1.48(1) Å are diminished relative to a standard carbon (sp³)–carbon (sp²) single bond. The displacements of the positionally refined hydrogen atoms bound to C1 and C4 from the least-squares plane defined by the carbons C1–C4, 0.66(9) and 0.63(9) Å, respectively, lend further support to the metalated carbons having significant sp³ character.

Some degree of charge stabilization onto the polarizing silicon substituents is again suggested by the contraction of the average Si–C bond distance to the metalated carbons, 1.82 Å, relative to the average Si–C(methyl) bond distance of 1.87 Å; the silicon atoms lie within 0.1 Å of the plane defined by the carbon atoms C1–C4, presumably to maximize such charge stabilization. The extent of silicon–carbon distance contraction observed in **5** is less than in the lithium analogue **3**, which reflects the smaller charge density on the allylic carbons in the magnesium complex relative to the lithium complex. Other bond distances and angles within the molecule are unexceptional.

Structures of 6b and 7. Complex **6b** crystallizes as prismatic crystals in the orthorhombic space group *Pbca*, with four molecules in the unit cell, the asymmetric unit containing half of a centrosymmetric molecule of [{*meso*-(HC(Me₃Si)HC)₂AlEt₂}(TMEDA)] centered on (1/2, 1/2, 1/2) (Figure 3). Complex **7** crystallizes as prismatic crystals in the monoclinic space group *P2₁/n*, with four molecules in the unit cell, the asymmetric unit consisting of one molecule of [{*meso*-(HC(Me₃Si)HC)₂GaCl₂}(TMEDA)] (Figure 4).

Though the crystal packing in **6b** and **7** is different, the overall molecular geometry of the complexes varies little and the structures are best described as TMEDA adducts of substituted metallacyclopent-3-enes. The metallacyclopent-3-enes contain four-coordinate metal centers in distorted-tetrahedral environments, with two of the coordination sites being occupied by carbon atoms from a single but-2-ene-1,4-diyl moiety, the two remaining sites being occupied by a nitrogen atom of the metal bridging TMEDA molecules and a carbon atom of the metal-bound ethyl group (**6b**) or the chloride substituent (**7**). The molecular symmetry in both structures is centrosymmetric, being crystallographically imposed in the case of **6b**, with the symmetry of the metallacyclic rings approximating to C_s.

Selected geometrical parameters are given in Tables 8 and 9. The length of the metal–C bonds in both complexes, 1.995 (**6b**) and 1.984 Å (**7**), necessitate only a small puckering of the metallacyclic rings, the fold angles measuring 7.7 and 7.0°, respectively, and there is no interaction between the metal atoms and the vinylic carbons as a result of this. The deviation of the metal atoms from the ligand planes measure only 0.18 and 0.16 Å for **6b** and **7**, respectively. The Al–C bond length to the ethyl group in **6b** is similar to the Al–C bond distances within the metallacycle, measuring 1.996(5) Å, and compares with the Al–C distances in [{*meso*-(MeC(Me₃Si)HC)₂AlCl₂}(TMEDA)]^{10c} (1.961 Å) and [(3,4-Me₂C₄H₄)Al(μ -Cl)]₆⁴ (1.952(7) Å) and the computed structure of [(C₄H₆)AlCl(NMe₃)],^{10c} 1.985 Å. The Ga–C distances in **7** are close to those in the only other structurally characterized gallium metallacycles,

[(CH₂)₅GaCH₂CH(R)CH₂NMe₂] (R = H, Me;^{5b} 1.967–1.993 Å) [(3,4-Me₂C₄H₄)Ga(μ -NEt₂)₂]^{5a} (1.972–1.983 Å), [(CH₂)₄Ga(μ -As(tBu)₂)₂]²⁵ (1.997 Å), and its acyclic analogue, [(Me₂Ga(μ -As(tBu)₂)₂)]₂ (2.016–2.028 Å).³³

The Ga–Cl distance of **7** (2.207 Å) is comparable to the terminal Ga–Cl distances seen in the four-coordinate dialkylgallium chloride arsine complex [(*neo*-Pent)₂GaCl{As(SiMe₃)₃}]³⁴ (2.241(1) Å) and the aluminum analogue of **7**, [{*meso*-(MeC(Me₃Si)HC)₂AlCl₂}(TMEDA)]^{10c} (2.165 Å). The Ga–Cl distance seen for the five-coordinate dialkylgallium chloride complex [Me₂GaCl(1,10-phenanthroline)]³⁵ is much longer at 2.440(3) Å.

The metal–N distances in both complexes, 2.099(5) (**6b**) and 2.101 Å (**7**), compare well with other four-coordinate amine adducts of trialkylaluminum species,

(33) Arif, A. M.; Benac, B. L.; Cowley, A. H.; Geerts, R.; Jones, R. A.; Kidd, K. B.; Power, J. M.; Schwab, S. T. *J. Chem. Soc., Chem. Commun.* **1986**, 1543.

(34) Wells, R. L.; McPhail, A. T.; Pasterczyk, J. W.; Alvanipour, A. *Organometallics* **1992**, *11*, 226.

(35) McPhail, A. T.; Miller, R. W.; Pitt, C. G.; Gupta, G.; Srivastava, S. C. *J. Chem. Soc., Dalton Trans.* **1976**, 1657.

(31) Greiser, T.; Kopf, J.; Thoennes, D.; Weiss, E. *J. Organomet. Chem.* **1980**, *191*, 1.

(32) (a) Weiss, E. *Angew. Chem.* **1993**, *105*, 1565; *Angew. Chem., Int. Ed. Engl.* **1993**, *32*, 1501. (b) Holloway, C. E.; Melnik, M. *J. Organomet. Chem.* **1994**, *465*, 1.

e.g., $[\text{Me}_3\text{Al}\{\text{N}(\text{CH}_2\text{CH}_2)_3\text{CH}\}]^{36}$ (2.06(1) Å), but are longer than seen in $[\text{Cl}_3\text{Al}(\text{NMe}_3)]^{37}$ (1.96(1) Å), in line with the greater Lewis acidity of the AlCl_3 unit relative to R_2AlCl , which also accounts for the different Al–N distances between **6b** and $[\{\text{meso}-(\text{MeC}(\text{Me}_3\text{Si})\text{HC})_2-\text{AlCl}\}_2(\text{TMEDA})]$ (2.047 Å), R_3Al units having decreased Lewis acidity relative to R_2AlCl units. Overall, the bond distances to the metal centers observed in the structures of $[\{\text{meso}-(\text{MeC}(\text{Me}_3\text{Si})\text{HC})_2\text{AlCl}\}_2(\text{TMEDA})]$ and **7** reflect the near-equal covalent radii of the two metals. Further, the variation in metal–N distances of 2.047 and 2.101 Å, respectively, compared to those of the metal–C distances, 1.961 and 1.984 Å, respectively, and metal–Cl distances, 2.165 and 2.207 Å, respectively, reflect the weaker Lewis acidic nature of gallium compared to aluminum in their organometallic compounds.

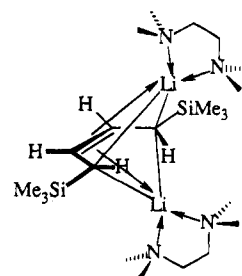
The metal cores of **6b** and **7** are considerably distorted from tetrahedral coordination. The largest deviation is attributable to the small ligand bite angles for the complexes, which measure 94.7(3) (**6b**) and 97.1° (**7**). These ligand bite angles can be compared to those observed in the analogous lithium (**3**) and magnesium (**5**) complexes, 81.3(6) and 85.0(3)°, respectively, in which cases the fold angles of the metallacyclic rings are far greater, 90 and 73.9(5)°, respectively, and the more polarized metal–C(allylic) bonds are longer at 2.39 and 2.20 Å, respectively. In comparison the cyclic hexamer⁴ $[\{(3,4-\text{Me}_2\text{C}_4\text{H}_4)\text{Al}(\mu\text{-Cl})\}_6]$ exhibits a much wider C–Al–C bond angle of 128.1(3)°; in this case there is no condition of placing the metal into a five-membered ring, and the geometry about the metal can adopt a more preferable arrangement. Similarly the C–Ga–C angle in the gallacycle $[\{(\text{CH}_2)_4\text{Ga}(\mu\text{-As}(\text{tBu})_2)_2\}]$,²⁴ 93.6(2)°, is more acute compared to that in the acyclic analogue $[\{\text{Me}_2\text{Ga}(\mu\text{-As}(\text{tBu})_2)_2\}]$,³³ 109.3(3)°. The N–M–Cl(Et) plane in **6b** and **7** is approximately orthogonal to the C–M–C plane in both complexes, the interplanar angles measuring 93.7 and 94.0(2)°, respectively.

Consistent with the largely covalent nature of Al– and Ga–C bonds, there is no significant contraction of the average Si–C bond distances to the metalated carbons of **6b** and **7**, 1.861 and 1.856 Å, respectively, relative to the average Si–C(Me) bond distances of 1.856 and 1.853 Å, respectively, reflecting the smaller charge density on the carbons in these complexes compared to the analogous lithium and magnesium complexes, which exhibit significant bond distance contractions.

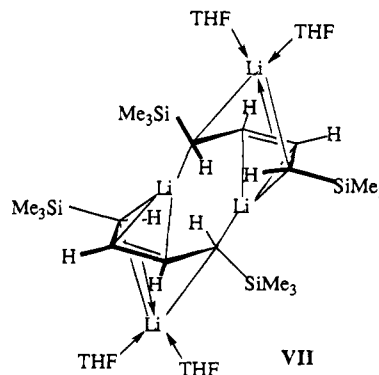
Bond distances and angles within the but-2-ene-1,4-diyl moieties are unexceptional for a (*Z*)-but-2-ene structure, with C–C bond distances ranging over 1.49–1.51 Å and the C=C distances occurring within 1.32–1.33 Å. The endocyclic C–C–C bond angles in both complexes approximate to 122(1)° and are seemingly not affected by being in the metallacycle. Other bond angles within the molecule are unexceptional.

NMR Spectroscopy: Solution-State Structures. The assignment of the electronic structure of the dianion in **4–7** as (*Z*)- η^4 -but-2-ene-1,4-diyl is supported by both the carbon–carbon bond lengths of the dianion in the

solid state and the one-bond ^{13}C – ^1H coupling constants for the vinylic and allylic carbons of the complexes observed in the proton-coupled ^{13}C NMR spectra. The $^1J_{\text{C-H}}$ values measure 152 and 123 Hz for the vinylic and allylic carbons, respectively, in complex **4**. These compare with the analogous coupling constants of 157 and 131 Hz in (*E,E*)-1,4-bis(trimethylsilyl)buta-1,3-diene (**2**), 153 and 115 Hz in (*Z*)-1,4-bis(trimethylsilyl)but-2-ene, and 152 and 127 Hz in the related complex^{10a} $[(\text{CH}(\text{Me}_3\text{Si})\text{CH})_2\{\text{Li}(\text{TMEDA})\}_2]$ (**3**) and are in agreement with the assignment of substantial sp^3 character to the allylic carbons in the lithium complexes. The high-field resonance of the allylic carbons at 23.6–27.8 ppm for **3** and **4** is consistent with the assignment of sp^3 character for the same carbons and suggests substantial negative charge density on the allylic carbons. The ^{13}C NMR resonances for the vinylic carbons of **3** and **4** are shifted to higher field by some 20 ppm relative to the but-2-ene precursors, suggesting some amount of charge delocalization through the double bond. Overall the structures of **3** and **4** are best represented as in **VI** and **VII**. This relates to the interpretation of



VI



VII

butadiene complexes of the early transition metals as being highly puckered metallacyclopent-3-ene or (*Z*)- η^4 -but-2-ene-1,4-diyl complexes which contain carbon–carbon bond lengths alternating in the order long–short–long. In comparison to complex **4**, the same $^1J_{\text{C-H}}$ coupling constants of 155 and 110 Hz measured for the nearly planar aluminacyclopent-3-ene **6a** indicate essentially pure sp^3 character for the allylic carbons of the group 13 complexes. The $^1J_{\text{C-H}}$ values of 150 and 114 Hz for the same carbon nuclei in the highly puckered magnesacyclopent-3-ene **5** indicate that the hybridization at the allylic carbons also has very little sp^2 character. The chemical shifts of the vinylic and allylic carbons in compounds **4–7** show a progression which is in line with the aforementioned proposed electronic structure of the dianions.

In solution complex **4** is fluxional; the room-temperature ^7Li NMR spectrum (Figure 5) shows the presence

(36) Whitt, C. D.; Parker, L. M.; Atwood, J. L. *J. Organomet. Chem.* **1971**, *32*, 291.

(37) Grant, D. F.; Killean, R. G. C.; Lawrence, J. L. *Acta Crystallogr., Sect. B* **1969**, *25*, 377.

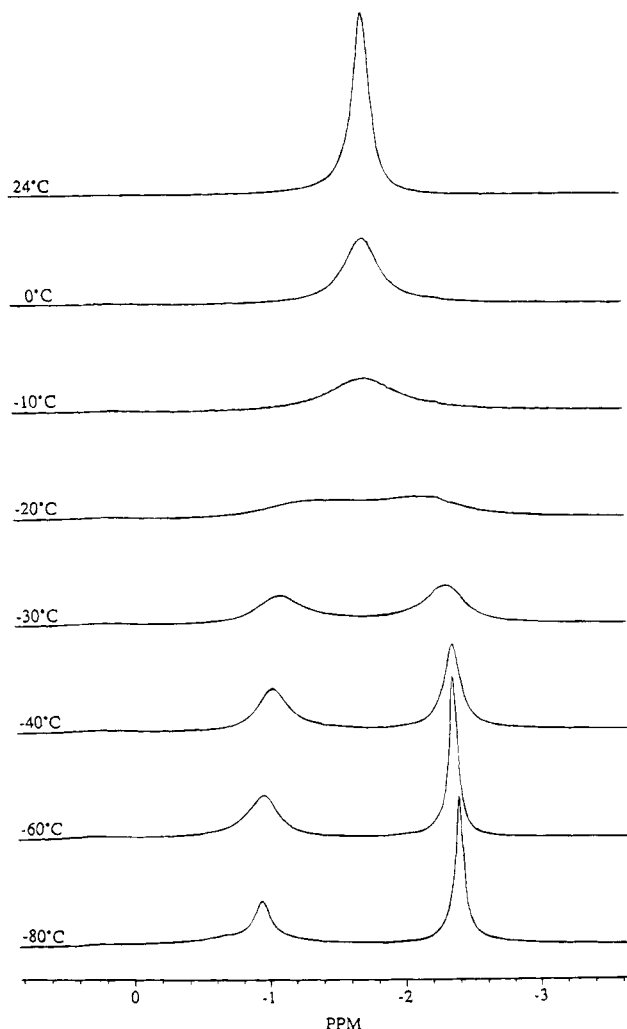


Figure 5. Variable-temperature ^7Li NMR spectra of $[(\text{CH}(\text{Me}_3\text{Si})\text{CH})_2\text{Li}_2(\text{THF})_2]_2$ (**4**) in $\text{C}_6\text{D}_5\text{CD}_3$ (155.5 MHz).

of a single broad resonance at -1.87 ppm. Cooling the sample results in the resonance broadening further still and coalescing at *ca.* -20 °C. Further cooling gives two resonances at -1.08 and -2.40 ppm of near-equal intensity, consistent with the crystal structure of the dimeric complex. The process which exchanges the solvated and unsolvated lithium atoms is most likely a monomer–dimer equilibration, which is frozen out at low temperature. Solution molecular weight measurements support this, giving an association of 1.0 in benzene at room temperature (Signer method).³⁸

Variable-temperature ^1H NMR spectra of complex **4** show no marked temperature dependence in the range $+24$ to -100 °C, indicating that a second, more facile equilibration between the η^1 and η^3 bonding modes observed for the ligand-bridging lithium atoms cannot be frozen out and the dianions are swaying in solution to give time-averaged equivalence of both ends of the but-2-ene-1,4-diyl group. The broadened resonance at -1.08 ppm in the low-temperature ^7Li NMR spectrum of the complex is possibly for the unsolvated lithium atom associated with this process; however, line widths in ^7Li NMR spectra are, in addition to exchange process broadening, often dominated by the quadrupolar relax-

ation contribution to the relaxation of the nucleus and are dependent on the electric field gradient across the nucleus, governed by the coordination environment of the nucleus, and are not readily predicted or calculable.³⁹

In solution complex **5** is present as a mixture of two species in near-equal proportions. The ^1H NMR spectrum, acquired immediately after dissolution in the deuterated solvent, shows the presence of two chemically inequivalent but-2-ene-1,4-diyl moieties and three resonances for the protons of the TMEDA molecules in deuterated THF, benzene, toluene, and cyclohexane solutions. The presence of the AA'XX' spin systems for the vinylic and allylic protons of the dianions discounts the alternative interpretation of the spectrum as resulting from one species in solution in which the symmetry of the dianion is lowered, having each end of the but-2-ene-1,4-diyl moiety distinguishable. In that particular case, a first-order ABXY spin system would be observed for the same protons. ^1H – ^1H COSY and ^1H – ^{13}C HMQC experiments were also consistent with the presence of two symmetric but-2-ene-1,4-diyl units being present. The third alternative interpretation of the spectrum arising from a single oligomer in solution which contains two inequivalent but-2-ene-1,4-diyl units can be ruled out, owing to the observation of a kinetically unreproducible redistribution of the two species in solution. ^1H NMR spectra of **5** on occasion contain single resonances for each of the methyl, allylic, and vinylic protons of the but-2-ene-1,4-diyl moiety and single resonances for the methyl and methylene protons of the TMEDA molecule when acquired immediately after dissolution, consistent with a single species being present in solution. Over a period of several minutes, a spectrum identical with that described above is obtained. The appearance of the second species in solution is at the expense of the initial species, and at equilibrium the solution contains a *ca.* 1:1 mixture of the two species in benzene, toluene, THF, and cyclohexane. The spectrum exhibits no marked concentration or temperature dependence over the range -100 to 30 °C. In this context, we note that 1,7-dimagnesacyclododecane has been reported to be in equilibrium with the monomer magnesacyclohexane and 1,6-dimagnesacyclododecane exists exclusively as a dimer in THF,⁴⁰ but we reserve comment on the oligomeric nature of **5** in solution at this stage. The ^{13}C NMR spectrum of complex **5** gives little more information on the behavior of the complex in solution over and above that determined from the ^1H NMR spectrum. Resonances are observed for two different but-2-ene-1,4-diyl units, and the resonances assigned to the TMEDA molecule consist of two methyl and one methylene signals, perhaps due to fortuitous signal overlap.

The appearance of the spin system for the protons attached to the backbone of the metallacycle **5** suggests that both of the species present in solution maintain the highly puckered metallacyclic structure observed in the crystal structure or adopt structures containing π -complexation. In such structures the allylic protons deviate only slightly from the plane defined by the four carbons of the but-2-ene-1,4-diyl unit. Similar coupling systems are observed in (*E,E*)-1,4-bis(trimethylsilyl)-

(38) Burger, B. J.; Bercaw, J. E. In *Experimental Organometallic Chemistry*; Wayda, A. L., Darensbourg, M. Y., Eds.; American Chemical Society: Washington, DC, 1987; Chapter 4.

(39) Hartwell, G. E.; Allerhand, A. *J. Am. Chem. Soc.* **1971**, *93*, 4415.
(40) Spek, A. L.; Schat, G.; Holtkamp, H. C.; Blomberg, C.; Bickelhaupt, F. *J. Organomet. Chem.* **1977**, *131*, 331.

buta-1,3-diene (**2**), complexes **3** and **4**, and (*Z*)-1,1,4,4-tetrakis(trimethylsilyl)but-2-ene,^{10a} in which cases the dihedral angle between the allylic and vinylic protons is close to 180°; in the last case, the crystal structure shows that the allylic protons are locked into this geometry by the restricted rotation about the C–C single bond of the (*Z*)-but-2-ene unit.

In solution complexes **6** and **7** retain the slightly puckered metallacyclic structures found for the crystal structures of **6b** and **7**. The ¹H NMR spectra of the complexes show the expected resonances for the but-2-ene-1,4-diyl moiety and the signals from the aluminum-bound ethyl group in addition to two resonances for the TMEDA molecule, which moved somewhat relative to their uncoordinated chemical shifts. The vinylic and allylic protons of the but-2-ene-1,4-diyl unit appears as singlets, being consistent with the dihedral angles between the allylic and vinylic protons near to 90° in

the crystal structures of the complexes, giving coupling constants that are expected to be small by the vicinal Karplus relationship.

Acknowledgment. We gratefully acknowledge support of this work by the Australian Research Council and the Department of Industry, Science and Technology (Australia) for travel support (M.G.G. and C.L.R.). We thank Colin Kennard and Karl Byriel for collecting some of the X-ray diffraction data.

Supplementary Material Available: Lists of U_{ij} values, hydrogen atom parameters, and bond distances and angles for compounds **4**, **5**, **6b**, and **7** and a figure giving an additional view of **5** (16 pages). Ordering information is given on any current masthead page.

OM9407868

Configurational Assignment of Acyclic (π -Allyl)palladium Complexes: Analytical Application of Chelating Nitrogen Ligands

Adolf Gogoll,* João Gomes, Magnus Bergkvist, and Helena Grennberg

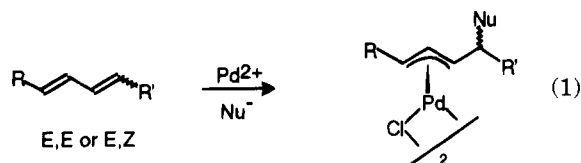
Department of Organic Chemistry, University of Uppsala, Box 531, 751 21 Uppsala, Sweden

Received October 20, 1994[®]

A method for assignment of the relative stereochemistry in acyclic (π -allyl)palladium complexes by ¹H NMR H–H coupling constants has been developed. It is based on the introduction of nitrogen chelating ligands of the bipyridyl type into the complexes. The analytical suitability of several other types of nitrogen chelating ligands has also been investigated. A model for rationalization of the observed relation between stereochemistry and spectral parameters is proposed. Introduction of the chelating ligand also affects the syn,anti equilibrium of the complexes. Isomer ratios depend upon the relative stereochemistry of the side chain as well as on the chelating ligand.

Introduction

In the formation of (π -allyl)palladium complexes by nucleophilic addition to 1,3-dienes, the relative stereochemistry between the metal and the stereogenic center formed by attack of the first nucleophile is of interest (eq 1). This stereochemistry is dependent upon both the



nature of the nucleophile and the reaction conditions.¹ Since the attack of the second nucleophile may be directed toward the (π -allyl)palladium complex either syn or anti to the metal,² it is highly desirable to directly determine the stereochemistry of the first reaction step.

The position of the metal relative to the π -allyl ligand in (π -allyl)palladium complexes has previously been investigated using chelating nitrogen ligands, so-called reporter ligands.^{3a,b} So far, only cyclic, sterically rigid, or very simple acyclic (π -allyl)palladium complexes have been studied.³ The main obstacle for a direct investigation of the steric relationship between the metal and the substituent Nu in acyclic systems (eq 1) is the rotation about the C–C bond between the stereogenic center and the neighboring π -allyl carbon, which makes this relationship less clear. In the present paper we demonstrate a method for direct structural characterization of these complexes by ¹H NMR using nitrogen chelating ligands. The purpose of our investigations is twofold: (i) the unequivocal assignment of the relative stereochemistry between the metal and the nucleophile

and (ii) the characterization of the interactions between the π -allyl group and other ligands on palladium in such nonrigid complexes. This is important because these are the same types of interactions which eventually determine the stereoselectivity of further transformations, e.g. if chiral ligands are attached to the metal.⁴

Results

As a model system, the pair of diastereomeric complexes **2** (R = Me) was prepared from (*E,E*)- and (*E,Z*)-2,4-hexadiene (**1**) with palladium chloride in methanol in the presence of an excess of chloride ions (Scheme 1). The relative stereochemistry between the metal and the methoxy substituent has been determined previously by chemical transformations.⁵ The chloro dimers were transformed into complexes with chelating nitrogen ligands (N[∧]N; Chart 1) by known procedures (Scheme 2).^{3a}

Assignments. Unequivocal assignment of the ¹H NMR signals was a precondition in the development of this method. In particular, no recourse to trends for chemical shifts or coupling constants which might be known from other similar complexes was allowed.⁶ This was especially important because all complexes form equilibrium mixtures between three isomers due to syn–anti isomerization⁷ of the substituents on the π -allyl system (Chart 2 and Figure 1). Sequential assignment of the alkyl chain protons, i.e. Me1 to Me6, was straightforward from coupling information. How-

[®] Abstract published in *Advance ACS Abstracts*, February 1, 1995.

(1) Åkermark, B.; Zetterberg, K. In *Inorganic Reactions and Methods*; Zuckerman, J. E., Ed.; VCH: Weinheim, Germany, 1991; Vol. 12A, p 148.

(2) Bäckvall, J. E.; Nyström, J. E.; Nordberg, R. E. *J. Am. Chem. Soc.* **1985**, *107*, 3676.

(3) (a) Albinati, A.; Ammann, C. J.; Pregosin, P. S.; Rügger, H. *Organometallics* **1990**, *9*, 1826. (b) Albinati, A.; Kunz, R. W.; Ammann, C. W.; Pregosin, P. S. *Organometallics* **1991**, *10*, 1800. (c) Bäckvall, J. E.; Granberg, K. L.; Andersson, P. G.; Gatti, R.; Gogoll, A. *J. Org. Chem.* **1993**, *58*, 5445.

(4) (a) Ohkita, K.; Kurosawa, H.; Hasegawa, T.; Hirao, T.; Ikeda, I. *Organometallics* **1993**, *12*, 3211. (b) Leutenegger, U.; Umbricht, G.; Fahrni, C.; von Matt, P.; Pfaltz, A. *Tetrahedron* **1992**, *48*, 2143. (c) Frost, C. G.; Williams, J. M. J. *Tetrahedron Lett.* **1993**, *34*, 2015. (d) Dawson, G. J.; Frost, C. G.; Williams, J. M. J. *Tetrahedron Lett.* **1993**, *34*, 3149. (e) Sprinz, J.; Helmchen, G. *Tetrahedron Lett.* **1993**, *34*, 1769.

(5) (a) Bäckvall, J. E.; Nordberg, R. E.; Wilhelm, D. *J. Am. Chem. Soc.* **1985**, *107*, 6892. (b) An earlier report did not resolve the stereochemistry: Lukas, J.; van Leeuwen, P. W. N. M.; Volger, H. C.; Kouwenhoven, A. P. *J. Organomet. Chem.* **1973**, *47*, 153.

(6) This is important in view of possible anisotropic shifts induced by the heteroaromatic ligands.^{3a}

(7) Faller, J. W.; Thomsen, M. E.; Mattina, M. J. *J. Am. Chem. Soc.* **1971**, *93*, 2642. The free energy of formation of the anti isomer was found to be ca. 12.7 kJ/mol higher than for the syn isomer for a methyl group. The free energy of activation for the conversion was found to be around 87.5 kJ/mol.

Scheme 1

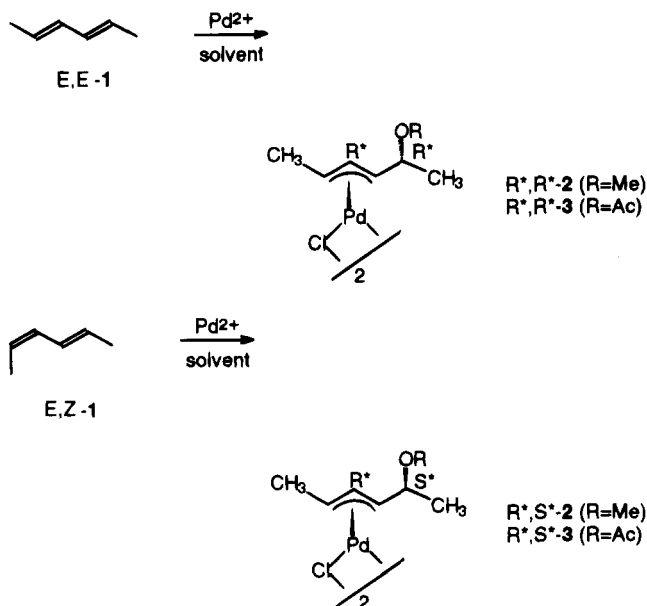
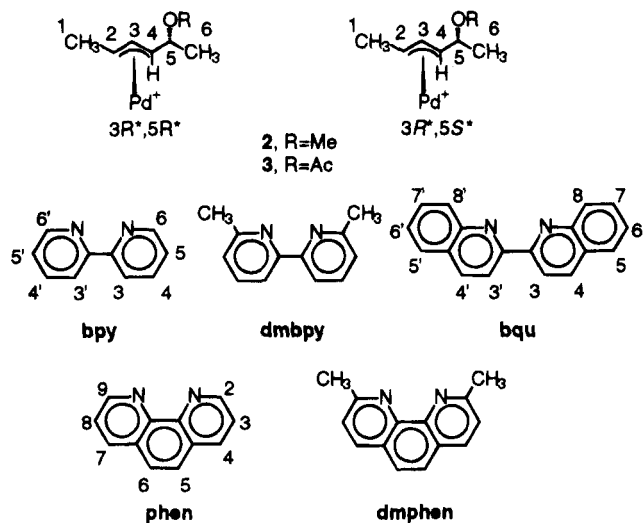
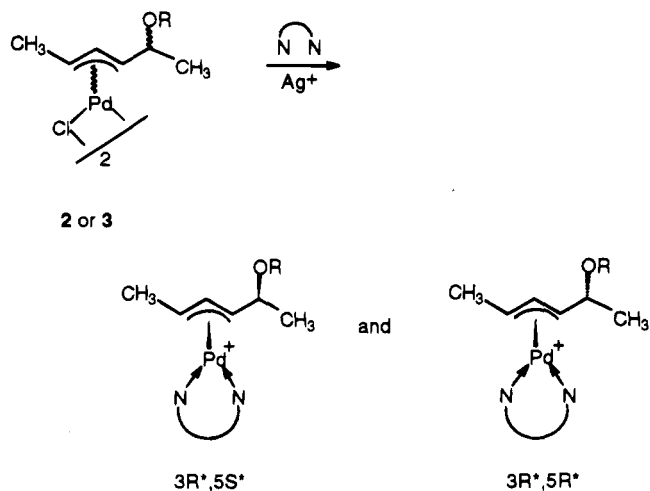


Chart 1

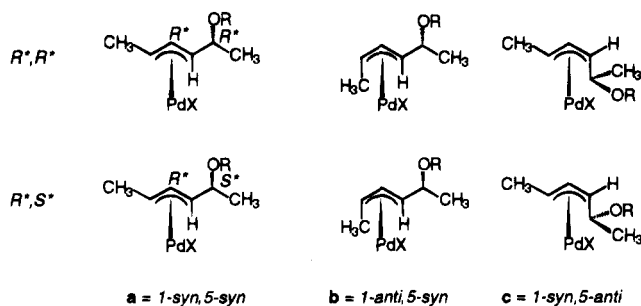


Scheme 2



ever, the crucial distinctions between H2 and H5 (both dq) and between H3 and H4 (both dd) could not be made by chemical shift arguments. Unambiguous entry points for the assignment were as follows: (i) the NOE

Chart 2



with the methoxy group identified H5 and Me6, (ii) the two lines of the Me1 doublets were always broader than those of the Me6 doublet due to a small allylic coupling with H3 ($J = 0.7$ Hz, $\nu_{1/2} = 2-2.2$ Hz for Me1 and $\nu_{1/2} = 1-1.5$ Hz for Me6), and (iii) NOEs between protons on the chelating ligand and the methyl groups are larger for Me1 than for Me6. *Post festum*, it was also found that (iv) H3 always has a higher chemical shift than H4. The three syn-anti isomers a-c (Chart 2) were identified by the following NOEs: between H2 and H4 in the 1-syn,5-syn isomer (a), between Me1 and H4 in the 1-anti,5-syn isomer (b), and between H2 and H5 in the 1-syn,5-anti isomer (c). No 1-anti,5-anti isomer was observed for any complex. Again, with this evidence in hand, several other parameters turned out to be reliable indicators for the isomer structure: (v) J_{H2-H3} is always larger in c than in b, (vi) J_{H3-H4} is always larger in b than in c, and (vii) J_{H4-H5} is always larger in c than in b.

Assignment of Relative Stereochemistry. If the chelating nitrogen ligands operated as reporter ligands in the present complexes, two related complexes (e.g. $(R^*,R^*)-2$ and $(R^*,S^*)-2$ with the same chelating ligand) might be distinguished by different NOEs between chelating ligand protons and one of the substituents on C-5. For example, if the π -allyl ligand carbon chain in the syn,syn isomer a was stretched out in a zigzag manner, then H5 would point toward the chelating ligand in the R^*,R^* isomer but away from the chelating ligand in the R^*,S^* isomer. However, no such difference was observed, not even in NOESY spectra recorded at low temperature. This indicates a rather high mobility of the side chain, i.e. a low barrier of rotation about the C4-C5 bond, also indicated by an NOE between H3 and Me6 in isomers a. Nor could a difference between the R^*,R^* and R^*,S^* series be observed in the sterically more congested 1-syn,5-anti isomers (c), although one here might expect a larger barrier because of steric interactions with H2.

Chelating ligands with larger steric interactions with the π -allyl ligands might increase the rotational barrier about the C4-C5 bond and result in larger differences of NOEs. However, the ligands bqu, which has been reported to have larger steric interactions with π -allyl ligands than bpy,^{3a} and phen showed effects similar to those observed for bpy. Nor did the methyl-substituted ligands dmbpy and dmphen, which should have a still larger interaction, improve the situation. One reason for the inability of these ligands to lock the free rotation of the side chain might be the dynamic behavior of the ligands themselves. As has recently been shown, rotation about the ligand-metal axis by this type of ligands

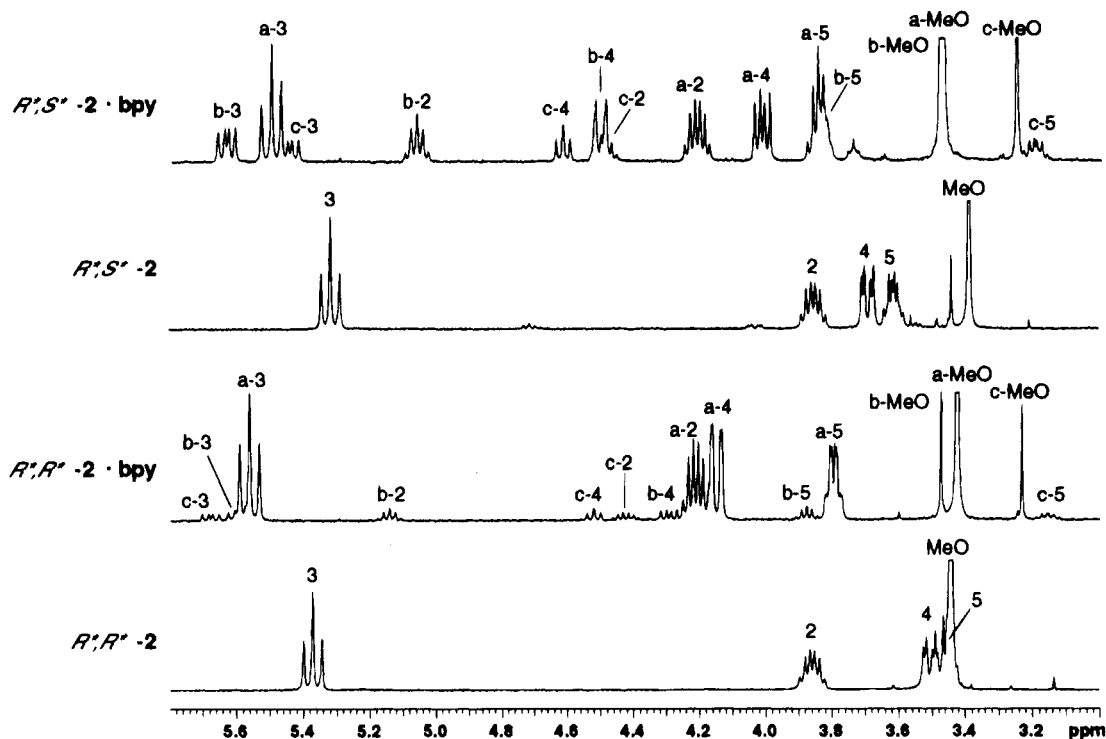


Figure 1. π -Allyl proton region of the ^1H NMR spectra (400 MHz, CDCl_3 , 25 $^\circ\text{C}$) of (R^*,R^*) -2 and (R^*,S^*) -2 and their bpy complexes. Signals have been assigned to the three isomers a–c (Chart 2).

Table 1. ^1H NMR Chemical Shifts for the π -Allyl Ligand Protons of the Complexes 2 and 3 with bpy and bqu Ligands

ligand	(R^*,R^*) -2			(R^*,S^*) -2			(R^*,R^*) -3			(R^*,S^*) -3			
	a	b	c	a	b	c	a	b	c	a	b	c	
bpy	Me1	1.62	1.34	1.69	1.63	1.36	1.69	1.64	1.37	1.7	1.67	1.36	1.69
	H2	4.21	5.14	4.42	4.21	5.06	4.45	4.31	5.30	4.49	4.42	5.20	4.50
	H3	5.56	5.60	5.68	5.50	5.64	5.45	5.61	5.77	5.59	5.67	5.72	5.62
	H4	4.15	4.30	4.52	4.02	4.51	4.62	4.07	4.29	4.82	4.01	4.36	4.82
	H5	3.80	3.88	3.16	3.85	3.82	3.20	5.31	5.40	4.73	5.34	5.42	4.60
	Me6	1.48	1.45	1.45	1.49	1.46	1.29	1.57	1.52	1.50	1.53	1.58	1.42
	R	3.43	3.47	3.23	3.47	3.48	3.25	2.00	2.01	2.12	2.11	2.05	1.64
bqu	Me1	1.02	1.62	1.36	1.07	1.51	1.11	1.07	1.69	1.42	1.11	1.65	1.19
	H2	4.74	5.23	4.66	4.81	5.16	4.87	4.90	5.35	4.60	4.90	5.21	4.88
	H3	5.35	5.49	5.65	5.39	5.56	5.30	5.33	5.57	5.72	5.48	5.49	5.54
	H4	4.62	4.87	4.84	4.70	4.78	5.05	4.64	4.78	4.98	4.53	4.86	5.04
	H5	3.21	3.43	3.11	3.49	3.26	3.55	4.64	5.01	4.52	5.09	4.72	4.75
	Me6	1.23	0.88	0.86	0.61	1.28	1.37	1.31	0.91	0.69	0.64	1.34	1.47
	R	2.12	3.18	3.17	3.26	2.55	3.62	1.22	1.91	1.90	2.00	1.42	1.79

is accompanied by release of one nitrogen–metal bond.^{8,9} Therefore, the effective distance for nuclear Overhauser effects between chelating ligand protons and π -allyl protons would be considerably larger than indicated by molecular models or X-ray crystallography, and the steric strain upon the π -allyl ligand would be released.

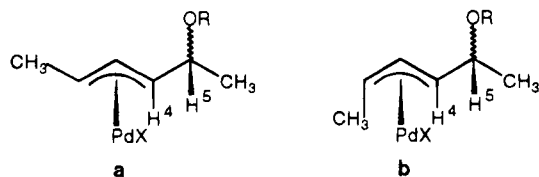
Since the relative stereochemistry of the complexes could not be assigned from NOE data, the question arose whether there might be any reliable relationship between chemical shifts or coupling constants and complex

structure. Such a relationship can indeed be noticed. Both ^1H NMR and ^{13}C NMR chemical shifts show regular patterns depending upon the nature of the chelating ligand and its proposed relative orientation toward the π -allyl unit (Table 1 and Experimental Section). However, their variation does not allow unambiguous assignment of the stereochemistry.

Such information is provided by the coupling constant between H4 and H5: the value of $J_{\text{H4-H5}}$ is between 2.0 and 2.6 Hz for the R^*,R^* isomers, whereas $J_{\text{H4-H5}}$ is always larger, between 4.0 and 6.6 Hz, for the R^*,S^* isomers (Table 2). This is independent of the choice of chelating ligand. The chloro dimers do not follow this pattern. A comparison of the important regions of the ^1H NMR spectra is shown in Figure 1. It is reasonable to assume that upon the introduction of the chelating ligands a change in the equilibrium of rotamers about the C4–C5 bond occurs. The source of this change can be of an electronic nature, i.e. change of electron density on the metal, or of steric nature, i.e. through-space

(8) (a) Gogoll, A.; Örnebro, J.; Grennberg, H.; Bäckvall, J. E. *J. Am. Chem. Soc.* **1994**, *116*, 3631. A similar effect might result from different binding modes of the ligands. Single-bonded dmphen: (b) Taira, Z.; Yamazaki, S. *Bull. Chem. Soc. Jpn.* **1986**, *59*, 649. (c) Yamazaki, S. *Polyhedron* **1985**, *4*, 1915. dmphen destabilizes square-planar coordination environments with respect to trigonal ones: (d) Sjögren, M. P. T.; Hansson, S.; Åkermark, B.; Vitagliano, A. *Organometallics* **1994**, *13*, 1963.

(9) (a) Activation energies for the observed apparent ligand rotation^{3a,b,8,9b} were in the usually observed range; e.g., $\Delta G^\ddagger = 63$ kJ/mol for (R^*,R^*) -2-bpy and (R^*,S^*) -2-bpy (from signal coalescence, CDCl_3 solution, 25 $^\circ\text{C}$). (b) Gogoll, A.; Grennberg, H. *Magn. Reson. Chem.* **1993**, *31*, 954.

Table 2. J_{H4-H5} (Hz) in the Syn,Syn Isomers (a) and Anti,Syn Isomers (b) of 2 (Chart 2)

X	R	J_{H4-H5} , isomer a		J_{H4-H5} , isomer b	
		R^*,R^*	R^*,S^*	R^*,R^*	R^*,S^*
Cl	Me	4.1	3.5		
bpy	Me	2.0	6.4	7.0	1.9
bqu	Me	2.7	4.0	4.7	2.3
phen	Me	2.4	6.6	7.2	2.3
dmphen	Me	2.6	5.7	5.3	2.3
dmbpy	Me	2.3	4.2	6.1	2.0

Table 3. J_{H4-H5} (Hz) in the Syn,Syn Isomers (a) and Anti,Syn Isomers (b) of 3 (Chart 2)

X	R	J_{H4-H5} , isomer a		J_{H4-H5} , isomer b	
		R^*,R^*	R^*,S^*	R^*,R^*	R^*,S^*
Cl	Ac	6.5	4.8		
bpy	Ac	2.0	4.4	5.3	2.2
bqu	Ac	nd ^a	4.3	4.2	2.5
phen	Ac	2.2		4.4	
dmphen	Ac	2.8		4.5	
dmbpy	Ac	3.1		4.6	

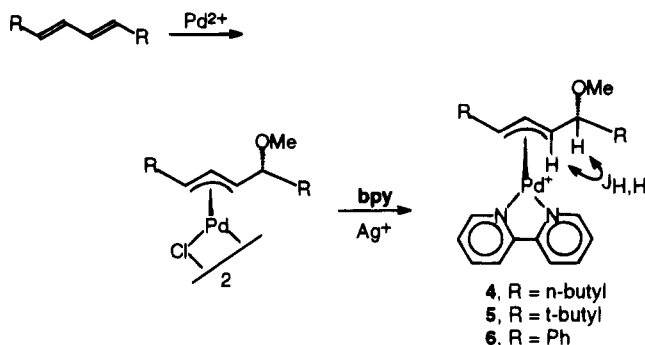
^a H4 and H5 have the same chemical shift.

interactions between the chelating ligand and the stereogenic center on the π -allyl group, or both.¹⁰

It was important to investigate whether the observed regularity extends to other substituents, e.g. the synthetically more versatile acetoxy group. Thus, the complexes (R^*,R^*)-**3** and (R^*,S^*)-**3** and the corresponding reporter ligand complexes were prepared (Scheme 2, R = Ac). As can be seen from the data (Table 3), the regularity of the coupling constant J_{H4-H5} for the chelating nitrogen ligand complexes is unaltered.

Further Examples. Having established our analytical method with the model compounds derived from 2,4-hexadiene, it was of interest to test it on complexes with other substituents on the π -allyl system. Thus, the chloro dimer complexes **4** (from (E,E)-5,7-dodecadiene), **5** (from (E,E)-2,2,7,7-tetramethyl-3,5-octadiene) and the corresponding nitrate complex **6** (from (E,E)-1,4-diphenyl-1,3-butadiene) were prepared and converted into the corresponding bpy complexes (Scheme 3). Their analytically significant spectral parameters are presented in Table 4 and follow very closely the reference data determined on the model complexes **2** and **3**. Also the spectral regions containing the π -allyl and CH-OR protons have very similar appearances (Figure 2). The reactivity of (E,E)-1,4-diphenyl-1,3-butadiene was too low to give detectable amounts of the corresponding (π -allyl)palladium complex under the usual reaction conditions. Therefore, the reaction was carried out in the presence of silver nitrate, which obviously results in the formation of a more reactive palladium-diene complex. A further difference observed with this ligand is that no isomer **b** is formed for **6**-bpy. A likely explanation is that in this isomer the steric interaction with the anti- π -allyl proton would

(10) Such an interaction has previously been proposed to explain the stereoselectivity of nucleophilic substitutions in complexes **2**.^{5b}

Scheme 3**Table 4.** Analytically Relevant Parameters for the Complexes 4–6 (CDCl₃ Solution, 25 °C)

complex	isomer ratio a:b:c	$J_{H-H(a)}$ (Hz) ^a	$J_{H-H(b)}$ (Hz) ^a
4	84:9:7	2.1	7.1
5	83:10:7	0.9	9.1
6	86:0:14 ^b	2.9	nd ^b

^a Coupling constant corresponding to J_{H4-H5} in the model complexes derived from **2** and **3** (Scheme 3). ^b Only isomers **a** and **c** were observed.

force the phenyl ring to rotate out of the plane of the π -allyl system, resulting in an increase of energy because conjugation is no longer possible.

Isomer Equilibria. Ligands on the metal may alter the syn,anti equilibrium in (π -allyl)palladium complexes.^{7,8d,11} The chloro dimers **2** and **3** occur exclusively as syn,syn isomers, whereas introduction of the chelating nitrogen ligands leads to equilibria of the three isomers **a–c** (Chart 2 and Figure 1). Quite unexpectedly, the relative amounts of isomers provided a further indication of the relative stereochemistry of the complexes (Table 5). Namely, the equilibrium distribution of isomers shows a direct dependence upon the relative stereochemistry of the stereogenic center and, interestingly, methoxy and acetoxy derivatives, i.e. **2** and **3**, show similar distributions. In the R^*,R^* series, isomer **a** dominates if the chelating ligand is bpy, phen, or bqu, whereas the R^*,S^* series is characterized by a larger amount of isomers **b** and **c** with these ligands. Changing the chelating nitrogen ligand to the sterically more demanding dmbpy and dmphen almost reverses the pattern of isomer distribution for the two series: the syn,syn isomer **a** is suppressed in the R^*,R^* series, and one isomer dominates in the R^*,S^* series, although this is now isomer **b**.

Discussion

Having empirically established J_{H4-H5} as an unambiguous analytical indicator for the stereochemistry of the complexes, it was desirable to find a rationalization for this finding. This is also of importance for an extension of the method to other substituents, e.g. those obtained from nitrogen, sulfur, or carbon nucleophiles.

Primarily, the coupling constant J_{H4-H5} is indicative of the dihedral angle between H4 and H5. Since the NOE measurements indicate relatively free rotation about the C4–C5 bond, the observed value must be the weighted average of the possible rotamers.¹² The approximate coupling constants for the individual rotam-

(11) Equilibration times between 2 min and several days have been reported for comparable complexes: Sjögren, M.; Hansson, S.; Norrby, P.-O.; Åkermark, B. *Organometallics* **1992**, *11*, 3954.

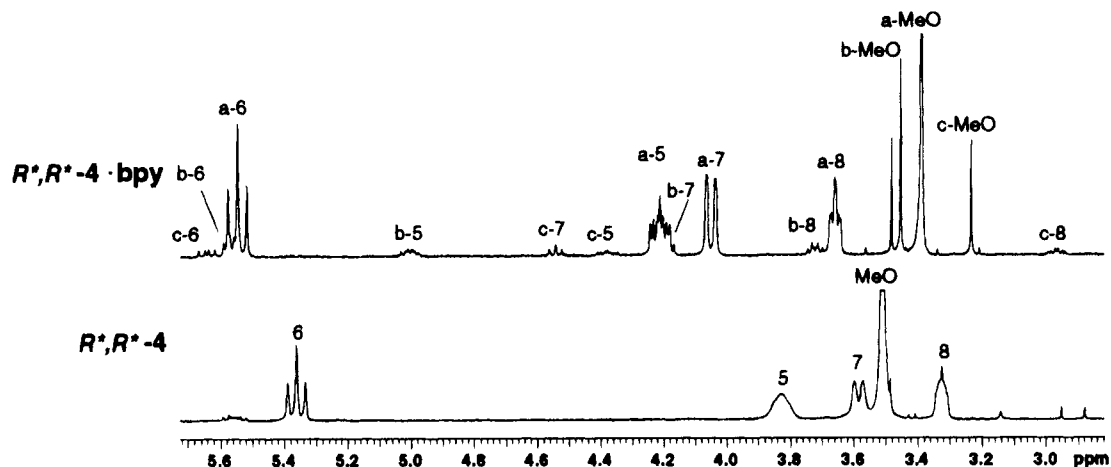


Figure 2. π -Allyl proton region of the ^1H NMR spectra (400 MHz, CDCl_3 , 25 $^\circ\text{C}$) of (R^*,R^*) -4 and its bpy complex.

Table 5. Isomer Ratios a:b:c of the Equilibrium Mixtures of $[(\pi\text{-Allyl})\text{palladium-chelating ligand}]$ Complexes^a

ligand	R	R^*,R^* complex	R^*,S^* complex
bpy	Me	82:9:8	47:33:20
bpy	Ac	83:7:10	37:29:34
phen	Me	85:8:7	60:28:12
phen	Ac	86:7:7	
bqu	Me	87:7:6	42:32:26
bqu	Ac	88:8:4	46:22:32
dmbpy	Me	59:22:19	11:70:19
dmbpy	Ac	57:29:14	
dmphen	Me	48:26:26	16:64:20 ^b
dmphen	Ac	46:41:13	

^a Determined by integration of ^1H NMR spectra (CDCl_3 solution, 25 $^\circ\text{C}$). ^b CD_3OD solution.

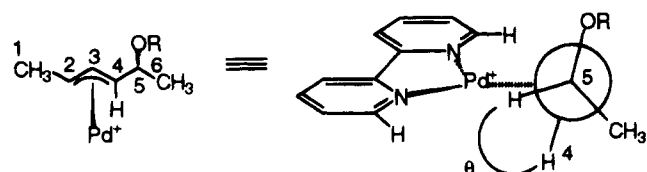


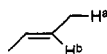
Figure 3.

ers could be calculated from a Karplus equation for alkenes¹³ if their geometry, i.e. in particular the dihedral angle θ (Figure 3), was known. Likely rotamer geometries are shown in Chart 3.¹⁴ In both series, the calculated coupling constants for these rotamers are 3.6 Hz for I, 3.6 Hz for II, and 11.6 Hz for III, without accounting for additional effects from substituent electronegativities, which are likely to reduce these values somewhat.

The observed coupling constants (R^*,R^* series, 2.0–3.1 Hz; R^*,S^* series, 4.0–6.6 Hz) can be accommodated

(12) Rotational barriers in comparable alkene derivatives are low (a few kJ/mol) and give rise to rapidly exchanging rotamers also at low temperature (ca. -60 $^\circ\text{C}$): (a) Bothner-By, A. A.; Castellano, S.; Ebersole, S. J.; Günther, H. *J. Am. Chem. Soc.* **1966**, *88*, 2466. (b) Gung, B. W.; Wolf, M. A.; Zhu, Z. *J. Org. Chem.* **1993**, *58*, 3350.

(13) Garbisch, E. W. *J. Am. Chem. Soc.* **1964**, *86*, 5561.

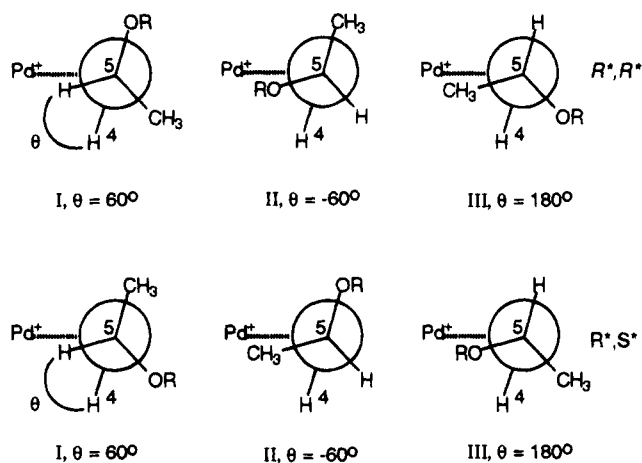


$$J_{a,b} = 6.6(\cos^2 \theta) + 2.6(\sin^2 \theta) \text{ for } 0^\circ < \theta < 90^\circ;$$

$$J_{a,b} = 11.6(\cos^2 \theta) + 2.6(\sin^2 \theta) \text{ for } 90^\circ < \theta < 180^\circ.$$

(14) For geometries in comparable olefins, see ref 12. The angles between the N–Pd–N plane and the plane of the π -allyl system have been determined as 104 and 109.5 $^\circ$ in comparable complexes by X-ray crystallography.^{3a,b}

Chart 3



by assuming that rotamer I or II is dominating for R^*,R^* complexes, whereas rotamer III is dominating for R^*,S^* complexes. A reason could be electrostatic or dipole–dipole interactions between the metal and the electronegative group OR,¹⁵ which would favor rotamers II (R^*,R^* series) and III (R^*,S^* series), respectively. The same coupling constant $J_{\text{H4-H5}}$ is indicative of the stereochemistry also in the isomers **b**, where the relative order is reversed; i.e., $J_{\text{H4-H5}}$ is larger in R^*,R^* complexes (4.2–7.2 Hz) than in R^*,S^* complexes (1.9–2.5 Hz). This can be explained as follows (Figure 4): in isomers **a**, the π -allyl ligand may be tilted about the ligand–metal axis in order to avoid steric interaction between the syn substituents on the π -allyl system (CH_3 or $\text{CH}(\text{OR})\text{CH}_3$) and the chelating ligand,¹⁶ and conformation II can easily be accommodated. In the formation of **b**, Me1 has avoided some of the strain imposed on it by the chelating ligand by going into the anti position. This results in a less tilted π -allyl ligand which, however, puts the OR group into an unfavorable position with respect to the chelating ligand. Rotation about the

(15) (a) This interaction is likely to be less pronounced in the chloro dimers, where the positive charge on the metal is compensated to a larger extent by the closely attached chloride anions. It is known that the anions in $(\pi\text{-allyl})\text{palladium}$ complexes with chelating nitrogen ligands are dislocated from the metal.^{3a} (b) A similar interaction has been proposed before.^{5b}

(16) Such ligand tilt in $(\pi\text{-allyl})\text{Pd}$ complexes with chelating nitrogen ligands has been described before: (a) Fanizzi, F. P.; Intini, F. P.; Maresca, L.; Natile, G.; Lanfranchi, M.; Tiripicchio, A. *J. Chem. Soc., Dalton Trans.* **1991**, 1007. (b) Reference 11.

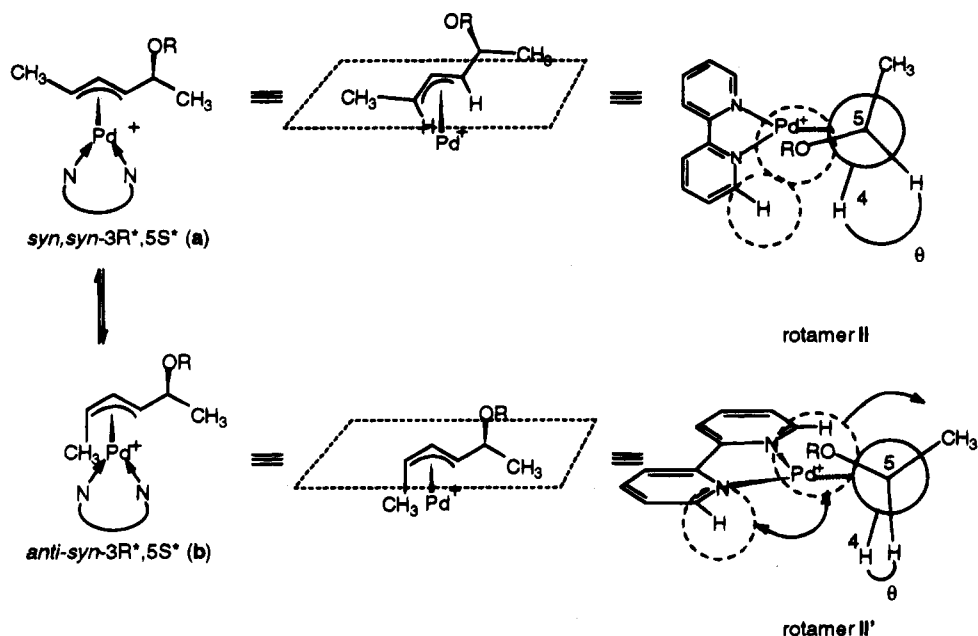


Figure 4.

C4–C5 bond (Figure 4) decreases this interaction and results in a smaller H4–H5 dihedral angle and thus a larger coupling constant (rotamer II'). The situation is reversed in the proposed main rotamer III of the R^*,S^* complexes, where the **b** isomers show a smaller coupling constant J_{H4-H5} than the **a** isomers (Tables 2 and 3).

In the **c** isomers, the side chain with the stereogenic center is moved away from the chelating ligand by occupying the anti position. Therefore, steric interactions as in **a** and **b** are absent and similar coupling constants are obtained for both the R^*,R^* and the R^*,S^* series.

The similar behavior of methoxy- and acetoxy-substituted π -allyl ligands can also be explained by the interaction between the substituent and the metal as described above. In addition, steric effects should be similar since both groups have the same conformational energy of 2.5 kJ/mol.¹⁷

The influence of the chelating ligands on the syn-anti isomer equilibrium can be rationalized using the same model. It is known that the nitrogen chelating ligands show a stronger steric interaction with the substituent in the syn position than in the anti position.^{3a,10} In the series of R^*,R^* complexes rotamer II would dominate (Chart 3). Here, the bulky methyl substituent is rotated away from the chelating ligand and isomer **a** predominates. In the R^*,S^* complexes, the methyl group is oriented toward the chelating ligand. The resulting steric strain is relieved by formation of isomers **b** and **c**. The larger steric strain imposed by the methyl derivatives dmbpy and dmphen results in the formation of a larger amount of isomers **b** and **c** in both series. The ligand bqu behaves like the small ligands bpy and phen. Obviously, not the rigidity of the

ligand (i.e. bpy in comparison to phen) but the presence of the bulky methyl substituents is decisive. The present results imply that the anti selectivity of a ligand is not just a function of its own structure but is also very much dependent on the relative stereochemistry of the (π -allyl)palladium complexes. There is no advantage as far as an anti-directing effect is concerned in using phen instead of bpy. Usage of ligands with larger steric interactions, i.e. dmphen or dmbpy, results in an anti selectivity which is lower in the R^*,R^* series than in the R^*,S^* series.^{18,19} The ligand dmphen has also been described in Pt complexes, where it induces distortion of the complex away from the usually observed square-planar geometry.²⁰

Conclusions

The relative stereochemistry between the metal and a methoxy or acetoxy substituent on the carbon adjacent to the π -allyl system in acyclic (π -allyl) palladium complexes can reliably be determined by introducing nitrogen chelating ligands into the complexes. These ligands, previously used as so-called "reporter" ligands, interfere with the rotamer equilibrium about the C–C bond adjacent to the π -allyl system. The coupling constant between the protons on these carbons was found to be an unambiguous indicator for the structure of the complexes. In addition, the introduction of the chelating ligand alters the equilibrium of syn,anti isomers of the π -allyl system. This equilibrium depends

(18) However, a nicely matching example is (R^*,S^*)-dmphen, where the ratio $a:(b+c) = 16:84$ is equal to the one reported by Åkermark and co-workers for the symmetric π -allyl ligand in (2,9-dimethyl-1,10-phenanthroline)[(2-4- η)-3-pentenyl]palladium tetrafluoroborate.¹¹

(19) The higher amount of anti isomers (**b** and **c**) in the R^*,S^* series resembles better the results reported for unsubstituted π -allyl groups.¹¹ A possible explanation might be that the rotamer III, in contrast to II, has the alkyl chain in an orientation which is likely to be found in the absence of the Pd–OR interaction.

(20) (a) Cf. ref 16a. Steric interactions with the methyl groups induced a narrowed Cl–Pt–Cl angle. In addition, the chlorides were displaced from the N–Pt–N plane (by 0.286 and 0.372 Å). The phenanthroline was bent (17°), and there was a rotated overall ligand plane with respect to the Pt coordination plane (28°). (b) Monodentate dmphen has also been observed.^{5b,c}

(17) (a) This comparison is not strictly correct, because the conformational energy describes the energy difference between substituted cyclohexanes with these groups in either axial or equatorial position.^{17b} On the other hand, the molecular volumes of MeO and AcO are 63 and 88 Å³, respectively, which are rather similar because those parts of the substituent (CH₃ and (C=O)CH₃) which differ are oriented away from the chelating ligand (calculated with PC-MODEL, Serena Software, Bloomington, IN). (b) Potapov, V. M. *Stereochemistry*; MIR Publishers: Moscow, 1979.

on the chelating ligand as well as on the relative stereochemistry of the complex. The present results can be rationalized by a model involving electrostatic or dipole-dipole interaction between the metal and the methoxy or acetoxy substituent and steric interaction between the π -allyl ligand and the reporter ligand. A further development of this method will involve new types of ligands, which by increased steric interaction with the flexible side chains to the π -allyl system might produce unambiguous NOEs and thus act as true reporter ligands in the original sense of the term.^{3a,b}

Experimental Section

NMR spectra were obtained, for solutions containing 5–10 mg of the compound in 0.6 mL of CDCl₃ at 25 °C unless stated otherwise, on a Varian Unity 400 instrument at 400 MHz for ¹H and 100.6 MHz for ¹³C. Chemical shifts for ¹H and ¹³C are referenced to TMS via the solvent signals (¹H, CHCl₃ at 7.26 ppm, CHD₂OD at 3.30 ppm; ¹³C, CDCl₃ at 77.0 ppm, CD₃OD at 49.0 ppm). Chemical shift correlation was performed using TOCSY²¹ and HSQC²² experiments. Chemical exchange and NOEs were measured by NOESY²³ spectra, using mixing times between 1 and 1.5 s.

(*Z,E*)-2,4-Hexadiene and a commercially available mixture of (*E,E*)- and (*Z,E*)-2,4-hexadiene were obtained from Aldrich and used as supplied. The (π -allyl)palladium chlorodimers **2**^{5a} and **3**²⁴ were prepared using literature procedures. The use of the diene mixture resulted in the formation of the expected two palladium complexes, i.e. both (*R**,*R**)- and (*R**,*S**)-**2** or (*R**,*R**)- and (*R**,*S**)-**3**, which could be separated by flash chromatography. (*E,E*)-Dodeca-5,7-diene was prepared from 1-hexyne. ²⁵ (*E,E*)-2,2,7,7-Tetramethyl-3,5-octadiene was prepared from 3,3-dimethyl-1-butyne.²⁵ (*E,E*)-1,4-Diphenyl-1,3-butadiene was prepared from cinnamic aldehyde and sodium 1-phenylacetate.²⁶ 6,6'-Dimethyl-2,2'-bipyridyl²⁷ (dmbpy) was prepared from 2-chloro-6-methylpyridine.²⁸ The other nitrogen chelating ligands were commercially available and used as supplied (abbreviations are given in Chart 1). Because of the straightforward method of preparation, elemental analyses were performed only for a selection of complexes.

Nitrogen chelating ligands were introduced into chloro dimers **2** and **3** in analogy to previous descriptions.^{3a} General procedure: The chloro dimer (30 mg) was dissolved or suspended in methanol (2 mL). Addition of AgCF₃SO₃ (2 equiv) afforded immediate precipitation of AgCl. Stirring was continued for 10 min and, after filtration, bpy (2 equiv) was added to the filtrate. Addition of diethyl ether and storage at -20 °C afforded yellowish crystals, which were recrystallized from CHCl₃/Et₂O. Bq complexes were recrystallized from MeOH/Et₂O. The *R**,*R** and *R**,*S** isomers of **2** and **3** were separated from a solution in diethyl ether by flash chromatography on silica using diethyl ether/pentane (30/70) as eluent. Ratios of syn-anti isomers (Chart 2; syn:syn:anti:syn:syn:anti = a:b:c) were determined by integration of corresponding proton signals for each of the three isomers. In general, a stable equilibrium was achieved after not longer than a few hours.¹¹

In some cases, the chelating nitrogen ligand protons were broadened by dynamic processes,⁹ and only the π -allyl ligand proton shifts are reported.

6,6'-Dimethyl-2,2'-bipyridyl (dmbpy). To a solution of NiCl₂ (2.124 g, 5 mmol) and P(Ph)₃ (9.36 g, 36 mmol) in tetrahydrofuran (50 mL) at 50 °C under a nitrogen atmosphere was added zinc powder (0.58 g, 9 mmol). After the mixture was stirred for 1 h, 2-chloro-6-methylpyridine (1 mL, 9 mmol) was added and stirring continued for another 3 h. The solution was poured into dilute NH₃ (6 mL concentrated NH₃ in 94 mL of H₂O), and the mixture was extracted with chloroform (3 × 50 mL). The combined organic phases were washed with H₂O (3 × 50 mL). After drying (MgSO₄) and evaporation, the crude product was purified by flash chromatography (CH₂Cl₂/MeOH, 98:2): colorless crystals, 310 mg (1.68 mmol, 37%), mp 89–90 °C (lit.²⁷ mp 88–90 °C). ¹H NMR (CDCl₃): δ 8.17 (d, *J* = 7.7 Hz, 2H), 7.68 (dd, *J* = 7.7 Hz, 7.5 Hz, 2H), 7.15 (d, *J* = 7.5 Hz, 2H), 2.63 (s, 3H).

(*R,*S**)-Bis[(5-methoxy-(2-4- η^3)-hexenyl)palladium chloride] ((*R**,*S**)-**2**).^{5a} ¹H NMR (CDCl₃): δ 5.37 (H3), 3.87 (H2), 3.52 (H4), 3.45 (MeO), 3.44 (H5), 1.34 (Me6), 1.31 (Me1). ¹³C NMR (CDCl₃): δ 108.3 (C3), 80.9 (C4), 78.8 (C2), 75.8 (C5), 57.6 (MeO), 20.6 (Me6), 18.0 (Me1).**

(*R,*S**)-Bis[(5-methoxy-(2-4- η^3)-hexenyl)palladium chloride] ((*R**,*S**)-**2**).^{5a} ¹H NMR (CDCl₃): δ 5.32 (H3), 3.87 (H2), 3.70 (H4), 3.62 (H5), 3.39 (MeO), 1.37 (Me6), 1.31 (Me1). ¹³C NMR (CDCl₃): 107.6 (C3), 79.2 (C4), 79.1 (C2), 74.7 (C5), 56.4 (MeO), 17.8 (Me1), 17.1 (Me6).**

(*R,*S**)-Bis[(5-acetoxy-(2-4- η^3)-hexenyl)palladium chloride] ((*R**,*S**)-**3**).²⁴ ¹H NMR (CDCl₃): δ 5.39 (H3), 5.01 (H5), 3.86 (H2), 3.43 (H4), 2.07 (AcO), 1.45 (Me6), 1.30 (Me1). ¹³C NMR (CDCl₃): δ 170.2 (C=O), 110.4 (C3), 80.7 (C2), 78.2 (C4), 70.4 (C5), 21.6 (AcO), 20.6 (Me6), 18.3 (Me1).**

(*R,*S**)-Bis[(5-acetoxy-(2-4- η^3)-hexenyl)palladium chloride] ((*R**,*S**)-**3**).²⁴ ¹H NMR (CDCl₃): δ 5.25 (H3), 5.06 (H5), 3.88 (H2), 3.59 (H4), 2.07 (AcO), 1.44 (Me6), 1.31 (Me1). ¹³C NMR (CDCl₃): δ 170.3 (C=O), 107.8 (C3), 80.0 (C2), 77.0 (C4), 69.2 (C5), 21.2 (AcO), 18.9 (Me6), 17.9 (Me1).**

(2,2'-Bipyridyl)[(*R,*S**)-[(5-methoxy-(2-4- η^3)-hexenyl)palladium]] Trifluorosulfonate ((*R**,*R**)-**2-bpy**): light yellow crystals; mp 129 °C. ¹H NMR: isomer a, δ 8.98 (1H, H6_{bpy}), 8.50 (1H, H6'_{bpy}), 8.6 (2H, H4,4'_{bpy}), 8.2 (2H, H3,3'_{bpy}), 7.69 (2H, H5,5'_{bpy}), 5.56 (dd, *J* = 11.7 Hz, 11.7 Hz, 1H, H3), 4.21 (dq, *J* = 11.7 Hz, 6.1 Hz, 1H, H2), 4.15 (dd, *J* = 11.7 Hz, 2.0 Hz, 1H, H4), 3.80 (dq, *J* = 2.0 Hz, 6.2 Hz, 1H, H5), 3.43 (s, 3H, MeO), 1.62 (d, *J* = 6.1 Hz, 3H, Me1), 1.48 (d, *J* = 6.2 Hz, 3H, Me6); isomer b, δ 9.31 (1H, H6_{bpy}), 8.89 (1H, H6'_{bpy}), 8.6 (2H, H4,4'_{bpy}), 8.2 (2H, H3,3'_{bpy}), 7.60 (2H, H5,5'_{bpy}), 5.60 (dd, *J* = 12.4 Hz, 7.9 Hz, 1H, H3), 5.14 (dq, *J* = 7.9 Hz, 6.7 Hz, 1H, H2), 4.30 (dd, *J* = 12.4 Hz, 7.0 Hz, 1H, H4), 3.88 (dq, *J* = 7.0 Hz, 6.3 Hz, 1H, H5), 3.47 (s, 3H, MeO), 1.45 (d, *J* = 6.3 Hz, 3H, Me6), 1.34 (d, *J* = 6.7 Hz, 3H, Me1); isomer c, δ 8.81 (1H, H6_{bpy}), 8.62 (1H, H6'_{bpy}), 8.6 (2H, H4,4'_{bpy}), 8.2 (2H, H3,3'_{bpy}), 7.76 (2H, H5,5'_{bpy}), 5.68 (dd, *J* = 12.4 Hz, 8.1 Hz, 1H, H3), 4.52 (dd, *J* = 8.1 Hz, 8.1 Hz, 1H, H4), 4.42 (dq, *J* = 12.4 Hz, 6.1 Hz, 1H, H2), 3.23 (s, 3H, MeO), 3.16 (dq, *J* = 8.1 Hz, 6.2 Hz, 1H, H5), 1.69 (d, *J* = 6.1 Hz, 3H, Me1), 1.45 (d, *J* = 6.2 Hz, 3H, Me6). ¹³C NMR (π -allyl ligand): isomer a, δ 112.7 (C3), 81.4 (C4), 77.3 (C2), 74.6 (C5), 56.7 (MeO), 19.6 (C1), 17.0 (C6). Ratio a:b:c = 82:9:8. Anal. Calcd for C₁₈H₂₁N₂O₄F₃PdS: C, 41.19; H, 4.03; N, 5.34. Found: C, 41.19; H, 3.90; N, 5.34.**

(2,2'-Biquinolyl)[(*R,*S**)-[(5-methoxy-(2-4- η^3)-hexenyl)palladium]] Trifluorosulfonate ((*R**,*R**)-**2-bqu**). ¹H NMR: isomer a, δ 8.60 (4H, H3,3'_{bqu} and H4,4'_{bqu}), 8.37 (2H, H8,8'_{bqu}), 7.96 (2H, H7,7'_{bqu}), 7.89 (2H, H5,5'_{bqu}), 7.64 (2H, H6,6'_{bqu}), 5.35 (dd, *J* = 11.5 Hz, 11.5 Hz, H3), 4.74 (dq, *J* = 11.5 Hz, 6.0 Hz, H2), 4.62 (dd, *J* = 11.5 Hz, 2.7 Hz, H4), 3.21 (dq, *J* = 2.7 Hz, 6.3 Hz, H5), 2.12 (s, 3H, MeO), 1.23 (d, *J* = 6.3 Hz, 3H, Me6), 1.02 (d, *J* = 6.0 Hz, 3H, Me1); isomer b, δ 8.78 (2H, H3,3'_{bqu}), 8.72 (2H, H4,4'_{bqu}), 8.30 (2H, H8,8'_{bqu}),**

(21) Braunschweiler, L.; Ernst, R. R. *J. Magn. Reson.* **1983**, *53*, 521.
(22) (a) Bodenhausen, G.; Ruben, D. J. *Chem. Phys. Lett.* **1980**, *69*, 185. (b) Torres, A. M.; Nakashima, T. T.; McClung, R. E. D. *J. Magn. Reson.* **1993**, *A102*, 219.

(23) (a) States, D. J.; Haberkorn, R. A.; Ruben, D. J. *J. Magn. Reson.* **1983**, *48*, 286. (b) Wider, G.; Macura, S.; Kumar, A.; Ernst, R. R.; Wüthrich, K. *J. Magn. Reson.* **1984**, *56*, 207.

(24) Bökmann, F.; Gogoll, A.; Bohman, O.; Pettersson, L. G. M.; Siegbahn, H. O. G. *Organometallics* **1992**, *11*, 1784.

(25) Zweifel, G.; Miller, R. L. *J. Am. Chem. Soc.* **1970**, *92*, 6678.

(26) Corson, B. B. In *Organic Syntheses*; Blatt, A. H., Ed.; Wiley: New York, 1943; Collect. Vol. II, p 229.

(27) Fabian, R. H.; Klassen, D. M.; Sonntag, R. W. *Inorg. Chem.* **1980**, *19*, 1977.

(28) Nasielski, J.; Standaert, A.; Nasielski-Hinkens, R. *Synth. Commun.* **1991**, *21*, 901.

8.00 (2H, H7,7'_{bqu}), 7.92 (2H, H5,5'_{bqu}), 7.69 (2H, H6,6'_{bqu}), 5.49 (dd, $J = 12.4$ Hz, 7.9 Hz, 1H, H3), 5.23 (dq, $J = 7.9$ Hz, 6.6 Hz, 1H, H2), 4.87 (dd, $J = 12.4$ Hz, 4.7 Hz, 1H, H4), 3.43 (dq, $J = 4.7$ Hz, 6.7 Hz, 1H, H5), 3.18 (s, 3H, MeO), 1.62 (d, $J = 6.6$ Hz, 3H, Me1), 0.88 (d, $J = 6.7$ Hz, 3H, Me6); isomer **c**, δ 8.80 (2H, H3,3'_{bqu}), 8.69 (2H, H4,4'_{bqu}), 8.22 (2H, H8,8'_{bqu}), 7.95 (2H, H7,7'_{bqu}), 7.91 (2H, H5,5'_{bqu}), 7.71 (2H, H6,6'_{bqu}), 5.65 (dd, $J = 12.4$ Hz, 7.6 Hz, 1H, H3), 4.84 (dd, $J = 8.5$ Hz, 7.6 Hz, 1H, H4), 4.66 (dq, $J = 12.4$ Hz, 6.1 Hz, 1H, H2), 3.17 (s, 3H, MeO), 3.11 (dq, $J = 8.5$ Hz, 6.4 Hz, 1H, H5), 1.36 (d, $J = 6.1$ Hz, 3H, Me1), 0.86 (d, $J = 6.4$ Hz, 3H, Me6). ¹³C NMR (π -allyl ligand): isomer **a**, δ 113.3 (C3), 83.2 (C4), 79.2 (C2), 73.7 (C5), 55.4 (MeO), 19.8 (C6), 18.3 (C1). Ratio **a:b:c** = 87:7:6. Anal. Calcd for C₂₆H₂₅N₂O₄F₃PdS: C, 49.82; H, 4.03; N, 4.48. Found: C, 49.56; H, 3.94; N, 4.33.

(1,10-Phenanthroline)-[(3R*,5R*)-(5-methoxy-(2-4- η^3)-hexenyl)palladium] Trifluorosulfonate ((R*,R*)-2-phen). ¹H NMR: isomer **a**, δ 9.39 (1H, H2_{phen}/H9_{phen}), 8.93 (1H, H2_{phen}/H9_{phen}), 8.68 (2H, H4,7_{phen}), 8.07 (2H, H3,8_{phen}), 8.03 (2H, H5,6_{phen}), 5.65 (t, $J = 11.7$ Hz, 1H, H3), 4.36 (ddq, $J = 11.7$ Hz, 0.8 Hz, 6.2 Hz, 1H, H2), 4.32 (ddd, $J = 11.7$ Hz, 2.4 Hz, 0.8 Hz, 1H, H4), 3.94 (dq, $J = 2.4$ Hz, 6.2 Hz, 1H, H5), 3.48 (s, 3H, MeO), 1.74 (d, $J = 6.2$ Hz, 3H, Me1), 1.54 (d, $J = 6.2$ Hz, 3H, Me6); isomer **b**, δ 9.62 (1H, H2,9_{phen}), 8.72 (3H, H2,9_{phen}, H4,7_{phen}), 8.07 (2H, H3,8_{phen}), 8.05 (2H, H5,6_{phen}), 5.72 (dd, $J = 12.7$ Hz, 8.1 Hz, 1H, H3), 5.46 (dq, $J = 8.1$ Hz, 6.8 Hz, 1H, H2), 4.44 (dd, $J = 12.7$ Hz, 7.2 Hz, 1H, H4), 4.01 (dq, $J = 7.2$ Hz, 6.3 Hz, 1H, H5), 3.56 (s, 3H, MeO), 1.54 (d, $J = 6.3$ Hz, 3H, Me6), 1.40 (d, $J = 6.8$ Hz, 3H, Me1); isomer **c**, δ 9.22 (1H, H2,9_{phen}), 9.06 (1H, H2,9_{phen}), 8.68 (2H, H4,7_{phen}), 8.08 (2H, H5,6_{phen}), 8.07 (2H, H3,8_{phen}), 5.77 (dd, $J = 12.6$ Hz, 7.9 Hz, 1H, H3), 4.79 (dd, $J = 8.7$ Hz, 7.9 Hz, 1H, H4), 4.63 (dq, $J = 12.6$ Hz, 6.2 Hz, 1H, H2), 3.24 (m, 1H, H5), 3.26 (s, 3H, MeO), 1.81 (d, $J = 6.2$ Hz, 3H, Me1), 1.50 (d, $J = 6.3$ Hz, 3H, Me6). Ratio **a:b:c** = 85:8:7.

(6,6'-Dimethyl-2,2'-bipyridyl)[(3R*,5R*)-(5-methoxy-(2-4- η^3)-hexenyl)palladium] Trifluorosulfonate ((R*,R*)-2-dmbpy). ¹H NMR: isomer **a**, δ 8.22 (2H, H3,3'_{dmbpy}), 8.03 (2H, H4,4'_{dmbpy}), 7.49 (2H, H5,5'_{dmbpy}), 5.47 (dd, $J = 11.5$ Hz, 11.1 Hz, 1H, H3), 4.43 (dq, $J = 11.5$ Hz, 6.0 Hz, 1H, H2), 4.19 (dd, $J = 11.1$ Hz, 2.3 Hz, 1H, H4), 3.46 (dq, $J = 2.3$ Hz, 6.3 Hz, 1H, H5), 2.91 (s, 3H, Me_{dmbpy}), 2.90 (s, 3H, MeO), 1.33 (d, $J = 6.3$ Hz, 3H, Me6), 1.30 (d, $J = 6.0$ Hz, 3H, Me1); isomer **b**, δ 8.29 (2H, H3,3'_{dmbpy}), 8.05 (2H, H4,4'_{dmbpy}), 7.51 (2H, H5,5'_{dmbpy}), 5.51 (dd, $J = 7.6$ Hz, 6.4 Hz, 1H, H2), 5.44 (m, 1H, H3), 4.41 (m, 1H, H4), 3.54 (dq, $J = 6.1$ Hz, 6.4 Hz, 1H, H5), 3.17 (s, 3H, MeO), 2.89 (s, 3H, Me_{dmbpy}), 1.42 (d, $J = 6.4$ Hz, 3H, Me1), 1.17 (d, $J = 6.4$ Hz, 3H, Me6); isomer **c**, δ 8.32 (2H, H3,3'_{dmbpy}), 8.07 (2H, H4,4'_{dmbpy}), 7.53 (2H, H5,5'_{dmbpy}), 5.44 (m, 1H, H3), 4.98 (dd, $J = 7.5$ Hz, 7.5 Hz, 1H, H4), 4.62 (dq, $J = 12.0$ Hz, 6.2 Hz, 1H, H2), 3.30 (m, 1H, H5), 3.30 (s, 3H, MeO), 2.85 (s, 3H, Me_{dmbpy}), 1.40 (d, $J = 6.2$ Hz, 3H, Me1), 1.23 (Me6). Ratio **a:b:c** = 59:22:19.

(2,9-Dimethyl-1,10-phenanthroline)[(3R*,5R*)-(5-methoxy-(2-4- η^3)-hexenyl)palladium] Trifluorosulfonate ((R*,R*)-2-dmphen). ¹H NMR: isomer **a**, δ 8.46 (2H, H4,4'_{dmphen}), 7.91 (2H, H5,5'_{dmphen}), 7.81 (2H, H3,3'_{dmphen}), 5.49 (dd, $J = 11.3$ Hz, 11.3 Hz, 1H, H3), 4.65 (dq, $J = 11.3$ Hz, 5.9 Hz, 1H, H2), 4.42 (dd, $J = 11.3$ Hz, 2.6 Hz, 1H, H4), 3.45 (dq, $J = 2.6$ Hz, 6.3 Hz, 1H, H5), 3.11 (s, 3H, Me_{dmphen}), 2.91 (s, 3H, MeO), 1.36 (d, $J = 6.3$ Hz, 3H, Me6), 1.35 (d, $J = 5.9$ Hz, 3H, Me1); isomer **b**, δ 8.53 (2H, H4,4'_{dmphen}), 7.96 (2H, H5,5'_{dmphen}), 7.86 (2H, H3,3'_{dmphen}), 5.78 (dq, $J = 7.8$ Hz, 6.7 Hz, 1H, H2), 5.53 (dd, $J = 11.7$ Hz, 7.8 Hz, 1H, H3), 4.59 (dd, $J = 11.7$ Hz, 5.3 Hz, 1H, H4), 3.68 (dq, $J = 5.3$ Hz, 6.3 Hz, 1H, H5), 3.21 (s, 3H, MeO), 3.11 (s, 3H, Me_{dmphen}), 1.49 (d, $J = 6.7$ Hz, 3H, Me1), 1.15 (d, $J = 6.3$ Hz, 3H, Me6); isomer **c**, δ 8.52 (2H, H4,4'_{dmphen}), 7.94 (2H, H5,5'_{dmphen}), 7.87 (2H, H3,3'_{dmphen}), 5.56 (dd, $J = 11.6$ Hz, 7.6 Hz, 1H, H3), 5.27 (dd, $J = 7.6$ Hz, 7.6 Hz, 1H, H4), 4.70 (dq, $J = 11.6$ Hz, 6.0 Hz, 1H, H2), 3.36 (dq, $J = 7.6$ Hz, 6.3 Hz, 1H, H5), 3.32 (s, 3H,

MeO), 3.10 (s, 3H, Me_{dmphen}), 1.44 (d, $J = 6.0$ Hz, 3H, Me1), 1.29 (d, $J = 6.3$ Hz, 3H, Me6). Ratio **a:b:c** = 48:26:26.

(2,2'-Bipyridyl)[(3R*,5S*)-(5-methoxy-(2-4- η^3)-hexenyl)palladium] Trifluorosulfonate ((R*,S*)-2-bpy): yellow crystals; mp 142 °C. ¹H NMR: isomer **a**, δ 9.20 (1H, H6_{bpy}), 8.62 (2H, H4,4'_{bpy}), 8.57 (1H, H6'_{bpy}), 8.22 (2H, H3,3'_{bpy}), 7.71 (1H, H5_{bpy}), 7.65 (1H, H5_{bpy}), 5.50 (dd, $J = 11.5$ Hz, 11.5 Hz, 1H, H3), 4.21 (dq, $J = 11.5$ Hz, 6.1 Hz, 1H, H2), 4.02 (dd, $J = 11.5$ Hz, 6.4 Hz, 1H, H4), 3.85 (dq, $J = 6.4$ Hz, 6.3 Hz, 1H, H5), 3.47 (s, 3H, MeO), 1.63 (d, $J = 6.1$ Hz, 3H, Me1), 1.49 (d, $J = 6.3$ Hz, 3H, Me6); isomer **b**, δ 9.16 (1H, H6_{bpy}), 8.86 (1H, H6'_{bpy}), 8.6 (2H, H4,4'_{bpy}), 8.3 (2H, H3,3'_{bpy}), 7.72 (1H, H5_{bpy}), 7.66 (1H, H5_{bpy}), 5.64 (dd, $J = 12.5$ Hz, 7.9 Hz, 1H, H3), 5.06 (dq, $J = 7.9$ Hz, 6.7 Hz, 1H, H2), 4.51 (dd, $J = 12.5$ Hz, 1.9 Hz, 1H, H4), 3.82 (dq, $J = 1.9$ Hz, 6.3 Hz, 1H, H5), 3.48 (s, 3H, MeO), 1.46 (d, $J = 6.3$ Hz, 3H, Me6), 1.36 (d, $J = 6.7$ Hz, 3H, Me1); isomer **c**, δ 9.06 (1H, H6_{bpy}), 8.6 (2H, H4,4'_{bpy}), 8.59 (1H, H6'_{bpy}), 8.3 (2H, H3,3'_{bpy}), 7.73 (1H, H5_{bpy}), 7.58 (1H, H5_{bpy}), 5.45 (dd, $J = 12.5$ Hz, 8.5 Hz, 1H, H3), 4.62 (dd, $J = 8.5$ Hz, 8.5 Hz, 1H, H4), 4.45 (dq, $J = 12.5$ Hz, 6.2 Hz, 1H, H2), 3.25 (s, 3H, MeO), 3.20 (dq, $J = 8.5$ Hz, 6.7 Hz, 1H, H5), 1.69 (d, $J = 6.2$ Hz, 3H, Me1), 1.29 (d, $J = 6.7$ Hz, 3H, Me6). ¹³C NMR (π -allyl ligand): isomer **a**, δ 114.0 (C3), 79.8 (C4), 77.9 (C2), 76.5 (C5), 55.6 (MeO), 20.2 (C6), 17.0 (C1); isomer **b**, δ 109.0 (C3), 80.0 (C2), 78.5 (C4), 75.4 (C5), 56.9 (MeO), 19.6 (C6), 16.4 (C1); isomer **c**, δ 111.8 (C3), 82.6 (C4), 76.0 (C5), 75.9 (C2), 56.7 (MeO), 21.8 (C6), 17.2 (C1). Ratio **a:b:c** = 47:33:20. Anal. Calcd for C₁₈H₂₁N₂O₄F₃PdS: C, 41.19; H, 4.03; N, 5.34. Found: C, 41.03; H, 3.95; N, 5.37.

(2,2'-Biquinoly)[(3R*,5S*)-(5-methoxy-(2-4- η^3)-hexenyl)palladium] Trifluorosulfonate ((R*,S*)-2-bqu): yellow crystals; mp 180 °C dec. ¹H NMR: isomer **a**, δ 8.7–8.8 (4H, H3,3' and H4,4'_{bqu}), 8.40 (2H, H-8,8'_{bqu}), 7.96 (2H, H7,7'_{bqu}), 7.91 (2H, H5,5'_{bqu}), 7.68 (2H, H6,6'_{bqu}), 5.39 (dd, $J = 11.6$ Hz, 11.6 Hz, 1H, H3), 4.81 (dq, $J = 11.6$ Hz, 6.0 Hz, 1H, H2), 4.70 (dd, $J = 11.6$ Hz, 4.0 Hz, 1H, H4), 3.49 (dq, $J = 4.0$ Hz, 6.5 Hz, 1H, H5), 3.26 (s, 3H, MeO), 1.07 (d, $J = 6.0$ Hz, 3H, Me1), 0.61 (d, $J = 6.5$ Hz, 3H, Me6); isomer **b**, δ 8.7–8.8 (4H, H3,3' and H4,4'_{bqu}), 8.32 (2H, H8,8'_{bqu}), 8.02 (2H, H7,7'_{bqu}), 7.92 (2H, H5,5'_{bqu}), 7.70 (2H, H6,6'_{bqu}), 5.56 (dd, $J = 11.9$ Hz, 7.8 Hz, 1H, H3), 5.16 (dq, $J = 7.8$ Hz, 6.6 Hz, 1H, H2), 4.78 (dd, $J = 11.9$ Hz, 2.3 Hz, 1H, H4), 3.26 (dq, $J = 2.3$ Hz, 6.3 Hz, 1H, H5), 2.55 (s, 3H, MeO), 1.51 (d, $J = 6.6$ Hz, 3H, Me1), 1.28 (d, $J = 6.3$ Hz, 3H, Me6); isomer **c**, δ 8.75 (2H, H8,8'_{bqu}), 8.7–8.8 (4H, H3,3' and H4,4'_{bqu}), 7.98 (2H, H7,7'_{bqu}), 7.90 (2H, H5,5'_{bqu}), 7.67 (2H, H6,6'_{bqu}), 5.30 (dd, $J = 11.9$ Hz, 7.9 Hz, 1H, H3), 5.05 (dd, $J = 8.9$ Hz, 7.9 Hz, 1H, H4), 4.87 (dq, $J = 11.9$ Hz, 6.1 Hz, 1H, H2), 3.62 (s, 3H, MeO), 3.55 (dq, $J = 8.9$ Hz, 6.1 Hz, 1H, H5), 1.37 (d, $J = 6.1$ Hz, 3H, Me6), 1.11 (d, $J = 6.1$ Hz, 3H, Me1). ¹³C NMR (π -allyl ligand): isomer **a**, δ 114.9 (C3), 80.6 (C2), 79.4 (C4), 74.0 (C5), 56.4 (MeO), 18.4 (C1), 17.0 (C6); isomer **b**, δ 106.5 (C3), 81.0 (C2), 80.8 (C4), 74.5 (C5), 56.0 (MeO), 20.0 (C6), 17.0 (C1); isomer **c**, δ 110.8 (C3), 86.7 (C4), 76.4 (C5), 75.5 (C2), 57.3 (MeO), 21.9 (C6), 18.5 (C1). Ratio **a:b:c** = 42:32:26. Anal. Calcd for C₂₆H₂₅N₂O₄F₃PdS: C, 49.82; H, 4.03; N, 4.48. Found: C, 49.76; H, 4.03; N, 4.57.

(1,10-Phenanthroline)[(3R*,5S*)-(5-methoxy-(2-4- η^3)-hexenyl)palladium] Trifluorosulfonate ((R*,S*)-2-phen). ¹H NMR: isomer **a**, δ 9.55 (1H, H2,9_{phen}), 9.32 (1H, H2,9_{phen}), 8.68 (2H, H4,7_{phen}), 8.09 (2H, H3,8_{phen}), 8.05 (2H, H5,6_{phen}), 8.02 (2H, H3,8_{phen}), 5.61 (dd, $J = 11.8$ Hz, 11.6 Hz, 1H, H3), 4.36 (dq, $J = 11.8$ Hz, 6.2 Hz, 1H, H2), 4.14 (dd, $J = 11.6$ Hz, 6.6 Hz, 1H, H4), 3.98 (dq, $J = 6.6$ Hz, 6.3 Hz, 1H, H5), 3.53 (s, 3H, MeO), 1.74 (d, $J = 6.2$ Hz, 3H, Me1), 1.52 (d, $J = 6.3$ Hz, 3H, Me6); isomer **b**, δ 9.51 (1H, H2,9_{phen}), 8.95 (1H, H2,9_{phen}), 8.65 (2H, H4,7_{phen}), 8.03 (2H, H5,6_{phen}), 7.49 (2H, H3,8_{phen}), 5.71 (dd, $J = 12.6$ Hz, 7.8 Hz, 1H, H3), 5.38 (dq, $J = 7.8$ Hz, 6.8 Hz, 1H, H2), 4.66 (dd, $J = 12.6$ Hz, 2.3 Hz, 1H, H4), 3.94 (dq, $J = 2.3$ Hz, 6.2 Hz, 1H, H5), 3.54 (s, 3H, MeO), 1.50 (d, $J = 6.2$ Hz, 3H, Me6), 1.42 (d, $J = 6.8$ Hz, 3H, Me1); isomer **c**, δ 9.39 (1H, H2,9_{phen}), 9.01 (1H, H2,9_{phen}), 8.65 (2H, H4,7_{phen}), 8.13

(2H, H3,8_{phen}), 8.03 (2H, H5,6_{phen}), 7.95 (2H, H3,8_{phen}), 5.53 (dd, $J = 12.8$ Hz, 7.9 Hz, 1H, H3), 4.83 (dd, $J = 9.1$ Hz, 7.9 Hz, 1H, H4), 4.70 (dq, $J = 12.8$ Hz, 6.1 Hz, 1H, H2), 3.26 (dq, $J = 9.1$ Hz, 6.1 Hz, 1H, H5), 3.23 (s, 3H, MeO), 1.81 (d, $J = 6.1$ Hz, 3H, Me1), 1.33 (d, $J = 6.1$ Hz, 3H, Me6). Ratio a:b:c = 60:28:12.

(6,6'-Dimethyl-2,2'-bipyridyl)[(3R*,5S*)-(5-methoxy-(2-4- η^3)-hexenyl)palladium] Trifluorosulfonate ((R*,S*)-2-dmbpy). ¹H NMR: isomer a, δ 8.23 (2H, H3,3'_{dmbpy}), 8.05 (2H, H4,4'_{dmbpy}), 7.50 (2H, H5,5'_{dmbpy}), 5.41 (dd, $J = 11.2$ Hz, 1H, H3), 4.32 (dq, $J = 6.1$ Hz, 1H, H2), 4.12 (dd, $J = 11.2$ Hz, 4.2 Hz, 1H, H4), 3.63 (dq, $J = 4.2$ Hz, 6.4 Hz, 1H, H5), 3.25 (s, 3H, MeO), 2.90 (s, 3H, Me_{dmbpy}), 1.27 (d, $J = 6.1$ Hz, 3H, Me1), 1.02 (d, $J = 6.4$ Hz, 3H, Me6); isomer b, δ 8.31 (2H, H3,3'_{dmbpy}), 8.10 (2H, H4,4'_{dmbpy}), 7.80 (2H, H5,5'_{dmbpy}), 5.51 (dd, $J = 11.5$ Hz, 8.0 Hz, 1H, H3), 5.38 (dq, $J = 8.0$ Hz, 6.6 Hz, 1H, H2), 4.40 (dd, $J = 11.5$ Hz, 2.0 Hz, 1H, H4), 3.45 (dq, $J = 2.0$ Hz, 6.2 Hz, 1H, H5), 2.93 (s, 3H, MeO), 2.88 (s, 3H, Me_{dmbpy}), 1.38 (d, $J = 6.6$ Hz, 3H, Me1), 1.31 (d, $J = 6.2$ Hz, 3H, Me6); isomer c, δ 8.29 (2H, H3,3'_{dmbpy}), 8.03 (2H, H4,4'_{dmbpy}), 7.53 (2H, H5,5'_{dmbpy}), 5.36 (dd, $J = 12.0$ Hz, 7.8 Hz, H3), 5.13 (dd, $J = 8.6$ Hz, 7.8 Hz, H4), 4.47 (dq, $J = 12.0$ Hz, 6.3 Hz, H2), 3.07 (dq, $J = 8.6$ Hz, 6.1 Hz, H5), 3.27 (s, 3H, MeO), 2.88 (s, 3H, Me_{dmbpy}), 1.38 (d, $J = 6.3$ Hz, 3H, Me1), 1.22 (d, $J = 6.1$ Hz, 3H, Me6). Ratio a:b:c = 11:70:19.

(2,9-Dimethyl-1,10-phenanthroline)[(3R*,5R*)-(5-methoxy-(2-4- η^3)-hexenyl)palladium] Trifluorosulfonate ((R*,S*)-2-dmphen). ¹H NMR (CD₃OD, 25 °C): isomer a, δ 8.54 (2H, H4,4'_{dmphen}), 8.01 (2H, H5,5'_{dmphen}), 7.89 (2H, H3,3'_{dmphen}), 5.57 (dd, $J = 10.1$ Hz, 6.2 Hz, 1H, H3), 3.80 (dq, $J = 10.1$ Hz, 6.2 Hz, 1H, H2), 3.42 (dd, $J = 10.1$ Hz, 5.7 Hz, 1H, H4), 3.30 (dq, $J = 5.7$ Hz, 6.4 Hz, 1H, H5), 3.22 (s, 3H, Me_{dmphen}), 2.91 (s, 3H, MeO), 1.11 (d, $J = 6.2$ Hz, 3H, Me1), 0.98 (d, $J = 6.4$ Hz, 3H, Me6); isomer b, δ 8.63 (2H, H4,4'_{dmphen}), 8.05 (2H, H5,5'_{dmphen}), 7.95 (2H, H3,3'_{dmphen}), 5.77 (dq, $J = 7.8$ Hz, 6.6 Hz, 1H, H2), 5.62 (dd, $J = 11.5$ Hz, 7.8 Hz, 1H, H3), 4.78 (dd, $J = 11.5$ Hz, 2.3 Hz, 1H, H4), 3.69 (dq, $J = 2.3$ Hz, 6.3 Hz, 1H, H5), 3.14 (s, 3H, Me_{dmphen}), 2.87 (d, 3H, MeO), 1.47 (d, $J = 6.6$ Hz, 3H, Me1), 1.36 (d, $J = 6.3$ Hz, 3H, Me6); isomer c, δ 8.62 (2H, H4,4'_{dmphen}), 8.05 (2H, H5,5'_{dmphen}), 7.94 (2H, H3,3'_{dmphen}), 5.51 (m, 1H, H3), 5.50 (m, 1H, H4), 4.76 (dq, $J = 10.9$ Hz, 6.1 Hz, 1H, H2), 3.32 (dq, $J = 5.7$ Hz, 6.1 Hz, 1H, H5), 3.33 (s, 3H, MeO), 3.17 (s, 3H, Me_{dmphen}), 1.41 (d, $J = 6.1$ Hz, 3H, Me1), 1.25 (d, $J = 6.1$ Hz, 3H, Me6). Ratio a:b:c = 16:64:20.

(2,2'-Bipyridyl)[(3R*,5R*)-(5-acetoxy-(2-4- η^3)-hexenyl)-palladium] Trifluorosulfonate ((R*,R*)-3-bpy): almost colorless crystals; mp 139 °C. ¹H NMR: isomer a, δ 8.72 (1H, H6_{bpy}), 8.56 (3H, H6' and H3,3'_{bpy}), 8.20 (2H, H4,4'_{bpy}), 7.71 (1H, H5_{bpy}), 7.62 (1H, H5'_{bpy}), 5.61 (dd, $J = 11.6$ Hz, 11.6 Hz, 1H, H3), 5.31 (dq, $J = 2.0$ Hz, 6.4 Hz, 1H, H5), 4.31 (dq, $J = 11.6$ Hz, 6.1 Hz, 1H, H2), 4.07 (dd, $J = 11.6$ Hz, 2.0 Hz, 1H, H4), 2.00 (s, 3H, AcO), 1.64 (d, $J = 6.1$ Hz, 3H, Me1), 1.57 (d, $J = 6.4$ Hz, 3H, Me6); isomer b, δ 8.90 (1H, H6_{bpy}), 8.81 (1H, H6'_{bpy}), 8.57 (2H, H3,3'_{bpy}), 8.18 (2H, H4,4'_{bpy}), 7.72 (1H, H5_{bpy}), 7.66 (1H, H5'_{bpy}), 5.77 (dd, $J = 12.5$ Hz, 8.1 Hz, H3), 5.40 (dq, $J = 5.3$ Hz, 6.1 Hz, 1H, H5), 5.30 (dq, $J = 8.1$ Hz, 6.8 Hz, 1H, H2), 4.29 (dd, $J = 12.5$ Hz, 5.3 Hz, 1H, H4), 2.01 (s, 3H, AcO), 1.52 (d, $J = 6.1$ Hz, 3H, Me6), 1.37 (d, $J = 6.8$ Hz, 3H, Me1); isomer c, δ 8.90 (1H, H6_{bpy}), 8.60 (2H, H3,3'_{bpy}), 8.56 (1H, H6'_{bpy}), 8.24 (2H, H4,4'_{bpy}), 7.21 (2H, H5,5'_{bpy}), 5.59 (dd, $J = 12.5$ Hz, 7.6 Hz, 1H, H3), 4.82 (dd, $J = 7.6$ Hz, 8.2 Hz, 1H, H4), 4.73 (dq, $J = 8.2$ Hz, 6.6 Hz, 1H, H5), 4.49 (dq, $J = 12.5$ Hz, 6.2 Hz, 1H, H2), 2.12 (s, 3H, AcO), 1.70 (d, $J = 6.2$ Hz, 3H, Me1), 1.50 (d, $J = 6.6$ Hz, 3H, Me6). ¹³C NMR (π -allyl ligand): isomer a, δ 169.8 (C=O), 112.3 (C3), 78.8 (C2), 77.9 (C4), 67.9 (C5), 21.3 (C1), 21.1 (Ac), 17.0 (C6). Ratio a:b:c = 83:7:10. Anal. Calcd for C₁₉H₂₁N₂O₅F₃PdS: C, 41.28; H, 3.83; N, 5.07. Found: C, 41.06; H, 3.75; N, 5.05.

(2,2'-Biquinoly)[(3R*,5R*)-(5-acetoxy-(2-4- η^3)-hexenyl)-palladium] Trifluorosulfonate ((R*,R*)-3-bqu): yellow crystals; mp 141 °C. ¹H NMR: isomer a, δ 8.57 (4H, H3,3'

and H4,4'_{bqu}), 8.37 (2H, H8,8'_{bqu}), 7.93 (2H, H7,7'_{bqu}), 7.85 (2H, H5,5'_{bqu}), 7.62 (2H, H6,6'_{bqu}), 5.33 (dd, $J = 11.4$ Hz, 11.4 Hz, H3), 4.90 (dq, $J = 11.4$ Hz, 6.0 Hz, H2), 4.64 (m, 2H, H4 and H5), 1.31 (d, $J = 6.2$ Hz, Me6), 1.22 (s, 3H, AcO), 1.07 (d, $J = 6.0$ Hz, Me1); isomer b, δ 8.77 (2H, H3,3'_{bqu}), 8.71 (2H, H4,4'_{bqu}), 8.29 (2H, H8,8'_{bqu}), 8.04 (2H, H7,7'_{bqu}), 7.95 (2H, H6,6'_{bqu}), 7.71 (2H, H6,6'_{bqu}), 5.57 (dd, $J = 11.9$ Hz, 7.8 Hz, H3), 5.35 (dq, $J = 7.8$ Hz, 6.6 Hz, H2), 5.01 (dq, $J = 4.2$ Hz, 6.7 Hz, H5), 4.78 (dd, $J = 11.9$ Hz, 4.2 Hz, H4), 1.91 (s, 3H, AcO), 1.69 (d, $J = 6.6$ Hz, Me1), 0.91 (d, $J = 6.7$ Hz, Me6); isomer c, δ 8.73 (2H, H3,3'_{bqu}), 8.67 (2H, H4,4'_{bqu}), 8.20 (2H, H8,8'_{bqu}), 7.95 (2H, H7,7'_{bqu}), 7.92 (2H, H5,5'_{bqu}), 7.69 (2H, H6,6'_{bqu}), 5.72 (dd, $J = 12.4$ Hz, 7.5 Hz, H3), 4.98 (dd, $J = 8.4$ Hz, 7.5 Hz, H4), 4.60 (dq, $J = 12.4$ Hz, 6.2 Hz, H2), 4.52 (dq, $J = 8.4$ Hz, 6.4 Hz, H5), 1.90 (s, 3H, AcO), 1.42 (d, $J = 6.2$ Hz, Me1), 0.69 (d, $J = 6.4$ Hz, 3H, Me6). ¹³C NMR (π -allyl ligand): isomer a, δ 113.2 (C3), 80.7 (C2), 79.0 (C4), 68.0 (C5), 21.2 (C6), 20.1 (Ac), 18.3 (C1). Ratio a:b:c = 88:8:4. Anal. Calcd for C₂₇H₂₅N₂O₅F₃PdS: C, 49.67; H, 3.86; N, 4.29. Found: C, 49.42; H, 3.80; N, 4.22.

(1,10-Phenanthroline)[(3R*,5R*)-(5-acetoxy-(2-4- η^3)-hexenyl)palladium] Trifluorosulfonate ((R*,R*)-3-phen). ¹H NMR: isomer a, δ 9.15 (1H, H2,9_{phen}), 9.02 (1H, H2,9_{phen}), 8.69 (2H, H4,7_{phen}), 8.07 (2H, H5,6_{phen}), 8.05 (2H, H3,8_{phen}), 5.71 (dd, $J = 12.0$ Hz, 11.2 Hz, 1H, H3), 5.46 (dq, $J = 2.2$ Hz, 6.3 Hz, 1H, H5), 4.51 (ddq, $J = 12.0$ Hz, 0.8 Hz, 6.3 Hz, 1H, H2), 4.27 (ddd, $J = 11.2$ Hz, 2.2 Hz, 0.8 Hz, 1H, H4), 2.02 (s, 3H, Ac), 1.78 (d, $J = 6.3$ Hz, 3H, Me1), 0.64 (d, $J = 6.3$ Hz, 3H, Me6); isomer b, δ 5.89 (dd, $J = 12.0$ Hz, 7.7 Hz, H3), 5.70 (m, 1H, H2), 5.54 (m, 1H, H5), 4.46 (dd, $J = 12.0$ Hz, 4.4 Hz, 1H, H4), 2.17 or 2.04 (s, 3H, Ac), 1.59 (d, $J = 6.6$ Hz, 3H, Me6), 1.43 (d, $J = 6.2$ Hz, 3H, Me1); isomer c, δ 5.70 (m, 1H, H3), 5.14 (dd, $J = 9.0$ Hz, 7.7 Hz, 1H, H4), 4.81 (m, 1H, H5), 4.66 (m, 1H, H2), 2.17 or 2.04 (s, 3H, Ac), 1.77 (d, $J = 6.2$ Hz, 3H, Me1), 1.57 (d, $J = 6.4$ Hz, 3H, Me6). Ratio a:b:c = 86:7:7.

(6,6'-Dimethyl-2,2'-bipyridyl)[(3R*,5R*)-(5-acetoxy-(2-4- η^3)-hexenyl)palladium] Trifluorosulfonate ((R*,R*)-3-dmbpy). ¹H NMR: isomer a, δ 8.22 (2H, H3,3'_{dmbpy}), 8.01 (2H, H4,4'_{dmbpy}), 7.45 (2H, H5,5'_{dmbpy}), 5.46 (dd, $J = 11.2$ Hz, 11.2 Hz, 1H, H3), 5.15 (dq, $J = 3.1$ Hz, 6.4 Hz, 1H, H5), 4.54 (dq, $J = 11.2$ Hz, 6.0 Hz, 1H, H2), 4.21 (dd, $J = 11.2$ Hz, 3.1 Hz, 1H, H4), 2.91 (s, 3H, Me_{dmbpy}), 1.61 (s, 3H, Ac), 1.42 (d, $J = 6.4$ Hz, 3H, Me6), 1.34 (d, $J = 6.0$ Hz, 3H, Me1); isomer b, δ 8.30 (2H, H3,3'_{dmbpy}), 8.08 (2H, H4,4'_{dmbpy}), 7.53 (2H, H5,5'_{dmbpy}), 5.66 (m, 1H, H2), 5.62 (m, 1H, H3), 5.19 (dq, $J = 4.6$ Hz, 6.7 Hz, 1H, H5), 4.38 (dd, $J = 10.8$ Hz, 4.6 Hz, 1H, H4), 2.91 (s, 3H, Me_{dmbpy}), 1.97 (s, 3H, Ac), 1.46 (d, $J = 5.9$ Hz, 3H, Me1), 1.16 (d, $J = 6.7$ Hz, 3H, Me6); isomer c, δ 5.46 (m, 1H, H3), 5.10 (dd, $J = 7.6$ Hz, 7.6 Hz, 1H, H4), 4.82 (m, 1H, H5), 4.61 (m, 1H, H2), 2.87 (s, 3H, Me_{dmbpy}), 2.03 (s, 3H, Ac), 1.42 (3H, Me6), 1.28 (d, $J = 6.5$ Hz, 3H, Me1). Ratio a:b:c = 57:29:14.

(2,9-Dimethyl-1,10-phenanthroline)[(3R*,5R*)-(5-acetoxy-(2-4- η^3)-hexenyl)palladium] Trifluorosulfonate ((R*,R*)-3-dmphen). ¹H NMR: isomer a, δ 8.43 (2H, H4,4'_{dmphen}), 7.91 (2H, H5,5'_{dmphen}), 7.75 (2H, H3,3'_{dmphen}), 5.48 (dd, $J = 10.8$ Hz, 10.8 Hz, 1H, H3), 5.25 (dq, $J = 2.8$ Hz, 6.4 Hz, 1H, H5), 4.79 (dq, $J = 10.8$ Hz, 6.0 Hz, 1H, H2), 4.41 (dd, $J = 10.8$ Hz, 2.8 Hz, 1H, H4), 3.11 (s, Me_{dmphen}), 1.47 (s, 3H, Ac), 1.44 (d, $J = 6.4$ Hz, 3H, Me6), 1.38 (d, $J = 6.0$ Hz, 3H, Me1); isomer b, δ 8.52 (2H, H4,4'_{dmphen}), 7.95 (2H, H5,5'_{dmphen}), 7.86 (2H, H3,3'_{dmphen}), 5.95 (dq, $J = 7.9$ Hz, 6.4 Hz, 1H, H2), 5.72 (dd, $J = 11.5$ Hz, 7.9 Hz, 1H, H3), 5.30 (dq, $J = 4.5$ Hz, 6.9 Hz, 1H, H5), 4.51 (dd, $J = 11.5$ Hz, 4.5 Hz, 1H, H4), 3.13 (s, 3H, Me_{dmphen}), 1.96 (s, 3H, Ac), 1.52 (d, $J = 6.4$ Hz, 3H, Me1), 1.15 (d, $J = 6.9$ Hz, 3H, Me6); isomer c, δ 8.52 (2H, H4,4'_{dmphen}), 7.96 (2H, H5,5'_{dmphen}), 7.87 (2H, H3,3'_{dmphen}), 5.57 (dd, $J = 11.7$ Hz, 7.8 Hz, 1H, H3), 5.41 (dd, $J = 7.8$ Hz, 7.8 Hz, 1H, H4), 4.91 (dq, $J = 7.8$ Hz, 6.7 Hz, 1H, H5), 4.68 (dq, $J = 11.7$ Hz, 7.0 Hz, H2), 3.11 (s, 3H, Me_{dmphen}), 2.03 (s, 3H, Ac), 1.38 (d, $J = 7.0$ Hz, 3H, Me1), 1.32 (d, $J = 6.7$ Hz, 3H, Me6). Ratio a:b:c = 46:41:13.

(2,2'-Bipyridyl)[(3*R,5*S**)-(5-acetoxy-(2-4- η^3)-hexenyl)-palladium] trifluorosulfonate ((*R**,*S**)-3-bpy):** yellowish crystals; mp 114 °C. ¹H NMR: isomer **a**, δ 8.64 (4H, H6,6' and H3,3'_{bpy}), 8.24 (2H, H4,4'_{bpy}), 7.70 (2H, H5,5'_{bpy}), 5.67 (dd, $J = 11.6$ Hz, 1H, H3), 5.34 (dq, $J = 4.4$ Hz, 6.7 Hz, 1H, H5), 4.42 (dq, $J = 11.6$ Hz, 6.2 Hz, 1H, H2), 4.01 (dd, $J = 11.6$ Hz, 4.4 Hz, 1H, H4), 2.11 (s, 3H, AcO), 1.67 (d, $J = 6.2$ Hz, 3H, Me1), 1.53 (d, $J = 6.7$ Hz, 3H, Me6); isomer **b**, δ 8.91 (1H, H6_{bpy}), 8.86 (1H, H6'_{bpy}), 8.54 (2H, H3,3'_{bpy}), 8.24 (2H, H4,4'_{bpy}), 7.62 (2H, H5,5'_{bpy}), 5.72 (dd, $J = 12.4$ Hz, 8.0 Hz, 1H, H3), 5.42 (dq, $J = 2.2$ Hz, 6.4 Hz, 1H, H5), 5.20 (dq, $J = 8.0$ Hz, 6.8 Hz, 1H, H2), 4.36 (dd, $J = 12.4$ Hz, 2.2 Hz, 1H, H4), 2.05 (s, 3H, AcO), 1.58 (d, $J = 6.4$ Hz, 3H, Me6), 1.36 (d, $J = 6.8$ Hz, 3H, Me1); isomer **c**, δ 8.96 (1H, H6_{bpy}), 8.64 (2H, H3,3'_{bpy}), 8.55 (1H, H6'_{bpy}), 8.24 (2H, H4,4'_{bpy}), 7.70 (2H, H5,5'_{bpy}), 5.62 (dd, $J = 12.5$ Hz, 7.6 Hz, 1H, H3), 4.82 (dd, $J = 9.9$ Hz, 7.6 Hz, 1H, H4), 4.60 (dq, $J = 9.9$ Hz, 6.3 Hz, 1H, H5), 4.50 (dq, $J = 12.5$ Hz, 6.3 Hz, 1H, H2), 1.69 (d, $J = 6.3$ Hz, 3H, Me1), 1.64 (s, 3H, AcO), 1.42 (d, $J = 6.3$ Hz, 3H, Me6). ¹³C NMR (π -allyl ligand): isomer **a**, δ 114.2 (C3), 81.0 (C2), 73.6 (C4), 69.1 (C5), 21.1 (Ac), 18.7 (C6), 17.0 (C1); isomer **b**, δ 108.5 (C3), 81.4 (C2), 75.3 (C4), 68.3 (C5), 21.2 (C6), 21.1 (Ac), 16.5 (C1); isomer **c**, δ 112.5 (C3), 79.9 (C4), 75.2 (C2), 69.6 (C5), 22.9 (C6), 21.0 (Ac), 17.0 (C1). Ratio **a:b:c** = 37:29:34. Anal. Calcd for C₁₉H₂₁N₂O₅F₃PdS: C, 41.28; H, 3.83; N, 5.07. Found: C, 41.19; H, 3.71; N, 5.03.

(2,2'-Biquinolyl)[(3*R,5*S**)-(5-acetoxy-(2-4- η^3)-hexenyl)-palladium] trifluorosulfonate ((*R**,*S**)-3-bqu):** yellow crystals; mp 160 °C dec. ¹H NMR: isomer **a**, δ 8.8–8.6 (4H, H3,3' and H4,4'_{bqu}), 8.38 (2H, H8,8'_{bqu}), 8.01 (2H, H5,5'_{bqu}), 8.00 (2H, H7,7'_{bqu}), 7.71 (2H, H6,6'_{bqu}), 5.48 (dd, $J = 11.5$ Hz, 11.5 Hz, 1H, H3), 5.09 (dq, $J = 4.3$ Hz, 6.7 Hz, 1H, H5), 4.90 (dq, $J = 11.5$ Hz, 6.0 Hz, 1H, H2), 4.53 (dd, $J = 11.5$ Hz, 4.3 Hz, 1H, H4), 2.00 (s, 3H, AcO), 1.11 (d, $J = 6.0$ Hz, 3H, Me1), 0.64 (d, $J = 6.7$ Hz, 3H, Me6); isomer **b**, δ 8.8–8.6 (4H, H3,3' and H4,4'_{bqu}), 8.30 (2H, H8,8'_{bqu}), 8.04 (2H, H7,7'_{bqu}), 7.91 (2H, H5,5'_{bqu}), 7.71 (2H, H6,6'_{bqu}), 5.49 (dd, $J = 11.9$ Hz, 7.7 Hz, 1H, H3), 5.21 (dq, $J = 7.7$ Hz, 6.6 Hz, 1H, H2), 4.86 (dd, $J = 11.9$ Hz, 2.5 Hz, 1H, H4), 4.72 (dq, $J = 2.5$ Hz, 6.4 Hz, 1H, H5), 1.65 (d, $J = 6.6$ Hz, 3H, Me1), 1.42 (s, 3H, AcO), 1.34 (d, $J = 6.4$ Hz, 3H, Me6); isomer **c**, δ 8.8–8.6 (4H, H3,3' and H4,4'_{bqu}), 8.48 (2H, H8,8'_{bqu}), 8.00 (2H, H7,7'_{bqu}), 7.94 (2H, H5,5'_{bqu}), 7.75 (2H, H6,6'_{bqu}), 5.54 (dd, $J = 12.0$ Hz, 7.6 Hz, 1H, H3), 5.04 (dd, $J = 9.2$ Hz, 7.6 Hz, 1H, H4), 4.88 (dq, $J = 12.0$ Hz, 6.1 Hz, 1H, H2), 4.75 (dq, $J = 9.2$ Hz, 6.2 Hz, 1H, H5), 1.79 (s, 3H, AcO), 1.47 (d, $J = 6.2$ Hz, 3H, Me6), 1.19 (d, $J = 6.1$ Hz, 3H, Me1). ¹³C NMR (π -allyl ligand): isomer **a**, δ 114.9 (C3), 81.7 (C2), 74.9 (C4), 68.1 (C5), 21.0 (Ac), 18.4 (C1), 16.6 (C6); isomer **b**, δ 106.6 (C3), 82.4 (C2), 77.2 (C4), 68.3 (C5), 21.3 (C6), 20.4 (Ac), 17.1 (C1); isomer **c**, δ 110.5 (C3), 80.8 (C4), 76.7 (C2), 69.7 (C5), 22.8 (C6), 21.1 (Ac), 18.7 (C1). Ratio **a:b:c** = 46:22:32. Anal. Calcd for C₂₇H₂₅N₂O₅F₃PdS: C, 49.67; H, 3.86; N, 4.29. Found: C, 49.66; H, 3.88; N, 4.24.

(6*R,8*R**)-Bis[(8-methoxy-(5-7- η^3)-dodecenyloxy)palladium chloride] ((*R**,*R**)-4)** was prepared from (*E,E*)-dodeca-5,7-diene by following the procedure for the preparation of (*R**,*R**)-2: yellow solid; mp 65 °C. ¹H NMR: δ 5.36 (t, $J = 11.1$ Hz, 1H, H6), 3.83 (br s, 1H, H5), 3.58 (br d, $J = 11.1$ Hz, 1H, H7), 3.51 (br s, 3H, MeO), 3.32 (br, 1H, H8), 1.8–1.2 (m, 12H), 0.90 (t, $J = 7.3$ Hz, 3H, Me), 0.89 (t, $J = 7.0$ Hz, 3H, Me). ¹³C NMR: δ 132.9, 130.3, 106.2, 83.4, 80.4, 79.3, 58.9, 35.1, 32.0, 31.0, 27.3, 22.7, 22.3, 14.0, 13.9.

(2,2'-Bipyridyl)[(6*R,8*R**)-(8-methoxy-(5-7- η^3)-dodecenyloxy)palladium] tetrafluoroborate ((*R**,*R**)-4-bpy):** colorless crystals; mp 144–146 °C. ¹H NMR: isomer **a**, δ 8.84 (1H, H6_{bpy}), 8.57 (2H, H3,3'_{bpy}), 8.45 (1H, H6'_{bpy}), 8.22 (1H, H4'_{bpy}), 8.21 (1H, H4_{bpy}), 7.71 (1H, H5_{bpy}), 7.68 (1H, H5'_{bpy}), 5.55 (dd, $J = 11.7$ Hz, 11.7 Hz, 1H, H6), 4.21 (dddd, $J = 11.7$ Hz, 8.9 Hz, 4.0 Hz, 0.8 Hz, 1H, H5), 4.05 (ddd, $J = 11.7$ Hz, 2.1 Hz, 0.9 Hz, 1H, H7), 3.66 (ddd, $J = 5.9$ Hz, 5.9 Hz, 2.1 Hz, 1H, H8), 3.40 (s, 3H, MeO), 2.04 (m, 1H, H4), 1.88–1.73 (m,

4H, 2H9, H4, H3), 1.56–1.45 (m, 5H, 2H10, H3, 2H2), 1.40 (m, 2H, 2H11), 0.98 (t, $J = 7.2$ Hz, 3H, Me1), 0.96 (t, $J = 7.2$ Hz, 3H, Me12); isomer **b**, δ 5.59 (dd, $J = 12.6$ Hz, 7.9 Hz, 1H, H6), 4.76 (ddd, $J = 8.9$ Hz, 7.9 Hz, 5.6 Hz, 1H, H5), 4.19 (dd, $J = 12.6$ Hz, 7.1 Hz, 1H, H7), 3.72 (ddd, $J = 7.1$ Hz, 5.4 Hz, 5.4 Hz, 1H, H8), 3.45 (s, 3H, MeO), 0.88 (t, $J = 7.2$ Hz, 3H, Me1); isomer **c**, δ 5.66 (dd, $J = 12.6$ Hz, 7.8 Hz, 1H, H6), 4.57 (dd, $J = 8.1$ Hz, 7.8 Hz, 1H, H7), 4.40 (ddd, $J = 12.6$ Hz, 9.2 Hz, 3.9 Hz, 1H, H5), 3.23 (s, 3H, MeO), 2.98 (ddd, $J = 8.6$ Hz, 8.1 Hz, 3.5 Hz, 1H, H8), 0.8 (t, $J = 7.2$ Hz, 3H, Me12). ¹³C NMR (CDCl₃): isomer **a**, δ 154.6, 154.2, 152.1, 150.4, 141.05, 140.98, 127.6, 127.5, 123.9, 123.7, 111.0 (C7), 82.5 (C8), 79.5 (C6), 78.1 (C5), 57.4 (MeO), 34.1 (C4), 31.9 (C10), 30.9 (C9), 26.7 (C3), 22.7 (C2), 22.2 (C11), 14.0 (C1), 13.9 (C12). Ratio **a:b:c** = 84:9:7. Anal. Calcd for C₂₉H₃₃N₂OBF₄Pd: C, 50.53; H, 6.08; N, 5.12. Found: C, 50.97; H, 6.06; N, 5.26.

(4*R,6*R**)-Bis[(6-methoxy-2,2,7,7-tetramethyl-(3-5- η^3)-octenyl)palladium chloride] ((*R**,*R**)-5)** was obtained from (*E,E*)-2,2,7,7-tetramethyl-3,5-octadiene as a poorly soluble solid and directly converted into the bpy complex ((*R**,*R**)-5-bpy). A solution of the diene (300 mg, 0.55 mmol) in 3 mL of MeOH/CH₂Cl₂ (2:1) was added to a solution containing palladium chloride (150 mg, 0.85 mmol) and NaCl (75 mg, 1.3 mmol) in MeOH (1 mL), and this mixture was stirred at room temperature for 11 h. The precipitated, yellowish solid was collected and dried, yielding 121 mg of (*R**,*R**)-5 (0.18 mmol, 65% from diene). A portion of the solid (46 mg, 0.07 mmol) was suspended in acetone (2 mL), and a solution of bpy (21 mg, 0.135 mmol) in acetone (1 mL) was added. AgBF₄ (27.7 mg, 0.14 mmol) was added, which resulted in the precipitation of AgCl. The mixture was stirred for 2 h at room temperature, the precipitate removed, and the remaining solution evaporated, leaving a light yellow solid (51 mg, 0.1 mmol, 70%). The complex was recrystallized from MeOH. ((*R**,*R**)-5-bpy): yellow crystals; mp >220 °C dec. ¹H NMR: isomer **a**, δ 5.64 (dd, $J = 13.1$ Hz, 10.8 Hz, 1H, H4), 4.65 (d, $J = 13.1$ Hz, 1H, H3), 3.81 (ddd, $J = 10.8$ Hz, 0.9 Hz, 0.9 Hz, 1H, H5), 3.32 (s, MeO), 3.08 (br s, 1H, H6), 1.37 (s, 9H, Me1, 2Me2), 1.05 (s, 9H, 2Me7, Me8); isomer **b**, δ 5.26 (dd, $J = 12.9$ Hz, 8.7 Hz, 1H, H4), 5.14 (d, $J = 8.7$ Hz, 1H, H3), 4.37 (dd, $J = 12.9$ Hz, 9.1 Hz, 1H, H5), 3.27 (s, 3H, MeO), 2.99 (d, $J = 9.1$ Hz, 1H, H6), 1.18 (s, 9H, 2Me7, Me8), 1.05 (s, 9H, Me1, 2Me2); isomer **c**, δ 5.59 (dd, $J = 13.3$ Hz, 8.8 Hz, 1H, H4), 4.93 (d, $J = 13.3$ Hz, 1H, H3), 4.60 (dd, $J = 8.8$ Hz, 3.3 Hz, 1H, H5), 3.43 (s, 3H, MeO), 3.18 (d, $J = 3.3$ Hz, 1H, H6), 1.32 (s, 9H, Me1, 2Me2), 1.01 (s, 9H, 2Me7, Me8). The bpy signals were broad due to dynamic processes. Ratio **a:b:c** = 83:10:7.

(2,2'-Bipyridyl)[(2*R,4*R**)-(4-methoxy-1,4-diphenyl-(1-3- η^3)-butenyl)palladium] nitrate ((*R**,*R**)-6-bpy)** was prepared from (*E,E*)-1,4-diphenyl-1,3-butadiene by a modified procedure. PdCl₂ (118 mg, 0.67 mmol) and NaCl (182 mg, 3.12 mmol) were dissolved in MeOH (2.5 mL) under gentle warming. (*E,E*)-1,4-Diphenyl-1,3-butadiene (147 mg, 0.71 mmol) dissolved in chloroform (2 mL) was added to the cooled solution, and this mixture was stirred for 1 h at room temperature. AgNO₃ (770 mg, 4.53 mmol) was added to the clear red solution, giving after 10 min a clear yellow solution and a gray precipitate. The precipitate was filtered off and washed repeatedly with chloroform, and to the combined organic solutions (ca. 20 mL) was added a solution of bpy (120 mg, 0.76 mmol) in chloroform (0.5 mL). After addition of 4 mL of diethyl ether, the solution was put into the refrigerator, resulting in the formation of light yellow crystals (338 mg (0.60 mmol, 90% from PdCl₂), mp 160–162 °C) of (*R**,*R**)-6-bpy. In solution, the complex decomposes slowly into a mixture of the diene, methanol, and a yellow solid; therefore the bpy signals were not assigned. It is only sparingly soluble in CDCl₃, better in hot CD₃OD. ¹H NMR (CDCl₃, 25 °C): isomer **a**, δ 6.33 (dd, $J = 11.9$ Hz, 11.3 Hz, 1H, H2), 4.83 (d, $J = 2.9$ Hz, 1H, H4), 4.80 (d, $J = 11.9$ Hz, 1H, H1), 4.48 (dd, $J = 11.3$ Hz, 2.9 Hz, 1H, H3), 3.36 (s, 3H, MeO); isomer **c**, δ 6.27 (dd,

$J = 12.6$ Hz, 7.5 Hz, 1H, H2), 5.49 (d, $J = 12.6$ Hz, 1H, H1), 4.82 (dd, $J = 9.5$ Hz, 7.5 Hz, 1H, H3), 4.31 (d, $J = 9.5$ Hz, 1H, H4), 3.29 (s, 3H, MeO). Ratio (CDCl₃) a:b:c = 86:0:14; ¹H NMR (CD₃OD, 45 °C): isomer a, δ 7.68 (2H, *o*-Ph₁), 7.60 (2H, *o*-Ph₄), 7.54 (1H, *p*-Ph₁), 7.47 (2H, *m*-Ph₁), 7.44 (2H, *m*-Ph₄), 7.38 (1H, *p*-Ph₄), 6.45 (dd, $J = 11.3$ Hz, 1H, 11.9 Hz, H2), 4.99 (d, $J = 11.9$ Hz, 1H, H1), 4.86 (d, $J = 3.1$ Hz, 1H, H4), 4.50 (dd, $J = 11.3$ Hz, 3.1 Hz, 1H, H3), 3.37 (s, 3H, MeO); isomer c, δ 7.83 (2H, *o*-Ph₁), 7.55 (4H, *o*-Ph₄ and *m*-Ph₁), 7.49 (1H, *p*-Ph₁), 7.14 (2H, *m*-Ph₄), 7.08 (1H, *p*-Ph₄), 6.48 (dd, $J = 12.6$ Hz, 7.5 Hz, 1H, H2), 5.63 (d, $J = 12.6$ Hz, 1H, H1), 5.00 (dd, $J = 9.6$ Hz, 7.5 Hz, 1H, H3), 4.34 (d, $J = 9.6$ Hz, 1H, H4), 3.30 (s, 3H, MeO). Ratio (CD₃OD, 45 °C) a:b:c = 70:0:30. Anal.

Calcd for C₂₇H₂₅N₃O₄Pd: C, 57.71; H, 4.48; N, 7.48. Found: C, 53.26; H, 4.38; N, 8.27.

Acknowledgment. Financial support from the Swedish Natural Science Research Council and the Erasmus project (J.G.; Grant No. ICP-93-UK-1346/13) is gratefully acknowledged.

Supplementary Material Available: Tables giving ¹H NMR shifts and coupling constants for the π -allyl and nitrogen ligands of the Pd complexes (3 pages). Ordering information is given on any current masthead page.

OM940807Y

Chemistry of C-Trimethylsilyl-Substituted Heterocarboranes. 17. Syntheses, Structures, and Reactivities of Bent-Sandwich, d^0 Zirconacarboranes of the "Carbons Adjacent" C_2B_4 Carborane Systems

Colacot J. Thomas, Lei Jia, Hongming Zhang, Upali Siriwardane,[†] John A. Maguire, Ying Wang, Karen A. Brooks, Vikram P. Weiss, and Narayan S. Hosmane*

Department of Chemistry, Southern Methodist University, Dallas, Texas 75275

Received October 7, 1994[⊗]

The reaction of $ZrCl_4$ with *closo-exo*-Li(THF)-1-Na(THF)-2-(SiMe₃)-3-(R)-2,3- $C_2B_4H_4$ (R = SiMe₃, Me, H) in a benzene/THF solvent mixture produced 1-Cl-1-(THF)-2,2'-(SiMe₃)₂-3,3'-(R)₂-4,4',5,5'-Li(THF)-1,1'-*commo*-Zr(2,3- $C_2B_4H_4$)₂ (R = SiMe₃ (I), Me (II), H (III)), in 68%, 61%, and 59% yields, respectively. Compound I was found to be resistant to chloride substitution with common alkylating agents. Instead, the reaction of I with Me₃SiCH₂-MgCl in a 1:1 molar ratio in a THF/Et₂O solvent mixture produced, in 40% yield, the salt [Mg(THF)₆][1-Cl-1-(THF)-2,2',3,3'-(SiMe₃)₄-1,1'-*commo*-Zr(2,3- $C_2B_4H_4$)₂]₂·4THF (IV), while a 1:2 molar reaction gave 1-Cl-1-(CH₂SiMe₃)-2,2',3,3'-(SiMe₃)₄-4,4',5,5'-[(μ -H)₄Li](μ_3 -Cl)[Mg-(μ_2 -Cl)(THF)₃]₂-1,1'-*commo*-Zr(2,3- $C_2B_4H_4$)₂ (V), in 65% yield. All compounds were characterized by chemical analyses, infrared spectroscopy, and ¹H, ¹¹B, and ¹³C NMR spectroscopy. Compounds I, II, and V were further characterized by ⁷Li NMR spectroscopy and I, II, IV, and V by single crystal X-ray diffraction. Compound I crystallizes as I·THF, in the triclinic space group $P\bar{1}$, while II, IV, and V crystallized in the monoclinic space groups $P2_1/c$, $P2_1/c$, and $C2/c$, respectively. The unit cell parameters of I·THF are $a = 11.428(3)$ Å, $b = 12.140(3)$ Å, $c = 17.685(4)$ Å, $\alpha = 93.27(2)^\circ$, $\beta = 90.35(2)^\circ$, $\gamma = 114.91(2)^\circ$, $V = 2220.4(8)$ Å³, and $Z = 2$, while those of II, IV, and V are $a = 16.928(8)$, $13.129(2)$, and 25.602 Å, $b = 16.373(6)$, $22.429(5)$, and $22.541(4)$ Å, $c = 12.048(5)$, $19.217(3)$, and $24.740(5)$ Å, $\beta = 90.37(3)$, $90.16(2)$, and $90.17(2)^\circ$, $V = 3339(2)$, $5660(2)$, and $14277(5)$ Å³, and $Z = 4$, 2 , and 8 , respectively. Full-matrix least-squares refinements of I·THF, II, IV, and V converged at $R = 0.044$, 0.059 , 0.051 , and 0.078 and $R_w = 0.057$, 0.073 , 0.065 , and 0.086 , respectively.

Introduction

Because of their role in olefin polymerization systems, the d^0 complexes of the type $[(\eta^5-C_5R_5)_2M(L)]^+$ have received a great deal of attention.¹ Much of the research involved studies of the structural and electronic changes induced by different substituents on the cyclopentadienide ligands and the effect of those changes on the catalytic efficacy of the complex.² Another way to introduce structural and electronic changes is to replace the cyclopentadienide ligands with other cyclic six-electron π -donors. The carborane dianions of the type *nido*-[7,8- $R_2C_2B_9H_9$]²⁻ and *nido*-[2,3- $R_2C_2B_4H_4$]²⁻ (R = H or a cage carbon substituent) are formal six-electron donors and have ligating properties that are quite similar to those of the cyclopentadienides. Their simi-

larities to the Cp system have been demonstrated through the syntheses and structural characterizations of a number of sandwich and half-sandwich metalla-carborane complexes.³ However, within this group, examples of d^0 transition-metal complexes are underrepresented. Jordan and co-workers⁴ have reported the syntheses of several mixed-ligand complexes of the form $Cp^*(C_2B_9H_{11})M(R)$ (M = Zr, Hf; R = anionic hydrocarbon unit; $Cp^* = C_5Me_5$), with structures being reported for the complex where M = Zr and R = C(Me)=C(Me)₂ as well as for the dimer $[Cp^*(C_2B_9H_{11})Zr]_2(\mu-CH_2)$. The complexes were found to be similar to the parent zirconocenes in that they were bent-sandwich complexes in which both the Cp^* and the carborane ligands were η^5 -bonded to the metal. More recently, Bercaw has reported the structures of two dimeric scandium complexes, $\{[Cp^*(C_2B_9H_{11})ScCH(SiMe_3)_2]_2Li\}Li(THF)_3$ and $[Cp^*(C_2B_9H_{11})ScH]_2[Li(THF)_2]_2$, which also showed bent-sandwich geometries.⁵ The scandium hydride complex was found to be surprisingly unreactive, presumably

* To whom correspondence should be addressed.

[†] Present address: Department of Chemistry, Louisiana Tech University, Ruston, LA 71272.

[⊗] Abstract published in *Advance ACS Abstracts*, February 1, 1995.

(1) (a) Jordan, R. F. *Adv. Organomet. Chem.* **1991**, *32*, 325 and references therein. (b) Cardin, D. J.; Lappert, M. F.; Raston, C. L. *Chemistry of Organo-Zirconium and -Hafnium Compounds*; Ellis Horwood: West Sussex, England, 1986. (c) Kaminsky, W.; Sinn, H. *Transition Metals and Organometallics as Catalysts for Olefin Polymerization*; Springer-Verlag: Berlin, 1987 (see references therein).

(2) (a) Spaleck, W. A.; Antberg, M.; Rohrmann, J.; Winter, A.; Bachmann, B.; Kiprof, P.; Behm, J.; Herrmann, W. *Angew. Chem., Int. Ed. Engl.* **1992**, *31*, 1347. (b) Kaminsky, W.; Kulper, K.; Brintzinger, H. H.; Wild, F. R. W. *P. Angew. Chem., Int. Ed. Engl.* **1985**, *24*, 507. (c) Woo, T. K.; Fan, L.; Ziegler, T. *Organometallics* **1994**, *13*, 2252.

(3) (a) Hawthorne, M. F.; Young, D. C.; Wegner, P. A. *J. Am. Chem. Soc.* **1965**, *87*, 1818. (b) Hanusa, T. P. *Polyhedron* **1982**, *1*, 663. (c) Grimes, R. N. In *Comprehensive Organometallic Chemistry*; Wilkinson, G., Stone, F. G. A., Abel, E. W., Eds.; Pergamon: Oxford, U.K., **1982**; Vol. 1, Chapter 5.5, p 459. (d) Hosmane, N. S.; Maguire, J. A. *Adv. Organomet. Chem.* **1990**, *30*, 99.

(4) Crowther, D. J.; Baenziger, N. C.; Jordan, R. F. *J. Am. Chem. Soc.* **1991**, *113*, 1455.

(5) Bazan, G. C.; Schaefer, W. P.; Bercaw, J. E. *Organometallics* **1993**, *12*, 2126.

due to strong B-H-Sc bridges present in the dimer. There is even less information available on the smaller, C_2B_4 -cage complexes. Grimes reported the structure of the air-stable complex $(\eta^8-C_8H_8)Ti[(C_2H_5)_2C_2B_4H_4]$ in which a titanium, in a formal +4 state, was sandwiched between the planar 10-electron donor, $[C_8H_8]^{2-}$ and a *nido*- $[(C_2H_5)_2C_2B_4H_4]^{2-}$ unit, with the cyclooctatetraenyl and the C_2B_3 bonding faces being essentially parallel to one another.⁶ This is in contrast to the structure of the mixed-ligand Ti(IV) sandwich $1-(\eta^5-C_5H_5)-1-Cl-1-(THF)-2,3-(SiMe_3)_2-1,2,3-TiC_2B_4H_4$, which has a bent-sandwich structure typical of the titanocenes.⁷ There have also been some very recent preliminary reports on several d^0 mixed Cp-($R_2C_2B_4H_4$) complexes of Nb and Ta, which show bent structures.⁸ To our knowledge, the only structural description of a full-sandwich, *commo*-metallacarborane of a d^0 transition metal was that given in our preliminary report on the zirconacarborane $1-Cl-1-(THF)-2,2',3,3'-(SiMe_3)_4-4,5,5'-Li(THF)_2-1,1'-commo-Zr(2,3-C_2B_4H_4)_2$.⁹ We report herein the details of the synthesis and structure of this compound as well as the C_{cage} -substituted derivatives along with the results of an investigation of their reaction chemistry, which turns out to be quite different from that of the mixed-ligand zirconium sandwich complexes or the zirconocenes.

Experimental Section

Materials. 2,3-Bis(trimethylsilyl)-2,3-dicarba-*nido*-hexaborane(8), 2-(trimethylsilyl)-3-methyl-2,3-dicarba-*nido*-hexaborane(8) and 2-(trimethylsilyl)-2,3-dicarba-*nido*-hexaborane(8), were prepared by the methods of Hosmane et al.¹⁰ $ZrCl_4$ (Aldrich Chemical Co.) was dried at $120^\circ C/10^{-4}$ mmHg for 12 h before use. Benzene, tetrahydrofuran (THF), diethyl ether (Et_2O), and *n*-hexane were dried over $LiAlH_4$ and doubly distilled before use. All other solvents were dried over 4–8 mesh molecular sieves (Aldrich) and either saturated with dry argon or degassed. Sodium hydride (NaH), *tert*-butyllithium (*t*-BuLi, 1.7 M solution in pentane), and Me_3SiCH_2MgCl (1 M solution in Et_2O) were obtained from Aldrich Chemical Co. and used as received. Solutions of the Na/Li complexes of the *nido*-carborane *closo-exo*-Li(THF)-1-Na(THF)-2-($SiMe_3$)-3-(R)-2,3- $C_2B_4H_4$ (R = $SiMe_3$, Me, H) in THF/benzene mixture were prepared by the methods described elsewhere.¹¹

Spectroscopic and Analytical Procedures. Proton, lithium-7, boron-11, and carbon-13 pulse Fourier transform NMR spectra, at 200, 77.7, 64.2, and 50.3 MHz, respectively, were recorded on an IBM-WP200 SY multinuclear NMR spectrometer. Infrared spectra were obtained on a Perkin-Elmer Model 283 infrared spectrophotometer and a Nicolet Magna-550 FT-IR spectrophotometer. Elemental analyses were obtained from Oneida Research Services (ORS) Inc.,

Whitesboro, NY, and E&R Microanalytical Laboratory, Inc., Corona, NY.

Synthetic Procedures. All experiments were carried out in Pyrex glass round-bottom flasks of 250 mL capacity, containing magnetic stirring bars and fitted with high-vacuum Teflon valves. Nonvolatile substances were manipulated in either a Vacuum Atmospheres drybox or evacuable glovebags under an atmosphere of dry nitrogen. All known compounds among the products were identified by comparing their mp/bp and IR and NMR spectra with those of the authentic samples.

Synthesis of 1-Cl-1-(C_4H_8O)-2,2'-($SiMe_3$)₂-3,3'-(R)₂-4,4',5,5'-Li(C_4H_8O)-1,1'-*commo*-Zr(2,3- $C_2B_4H_4$)₂ (R = $SiMe_3$ (I), Me (II), H (III)). A benzene/THF solution (20 mL/1 mL) of *closo-exo*-Li(C_4H_8O)-1-Na(C_4H_8O)-2-($SiMe_3$)-3-(R)-2,3- $C_2B_4H_4$ (1.76 g, 4.5 mmol, R = $SiMe_3$; 1.13 g, 3.4 mmol, R = Me; 1.31 g, 4.13 mmol, R = H) was poured onto anhydrous $ZrCl_4$ (0.52 g, 2.25 mmol; 0.39 g, 1.70 mmol; 0.42 g, 2.06 mmol) *in vacuo* at $-78^\circ C$, and the resulting heterogeneous mixture was stirred for 12 h, during which time the solution turned yellow. The solvents were then removed, the residue was dissolved in diethyl ether, and the mixture was stirred further for 30 min to precipitate NaCl out of the reaction mixture as an off-white solid. This mixture was filtered through a frit *in vacuo* to collect an orange filtrate. The solvent was removed from the filtrate under reduced pressure to obtain an orange-yellow solid which was identified as 1-Cl-1-(C_4H_8O)-2,2'-($SiMe_3$)₂-3,3'-(R)₂-4,4',5,5'-Li(C_4H_8O)-1,1'-*commo*-Zr(2,3- $C_2B_4H_4$)₂ (1.20 g, 1.53 mmol, 68% yield, I; 0.70 g, 1.04 mmol, 61% yield, II; 0.78 g, 1.21 mmol, 59% yield, III). Compounds I–III are soluble in polar solvents and have melting points of 160, 141, and $134^\circ C$, respectively. Anal. Calcd for $C_{24}H_{60}B_8O_2ClSi_2LiZr$ (I): C, 40.44; H, 8.43; B, 12.13. Found: C, 40.20; H, 8.24; B, 12.39. Calcd for $C_{20}H_{48}B_8O_2ClSi_2LiZr$ (II): C, 40.27; H, 8.05; Li, 1.10; Si, 9.41. Found: C, 40.65; H, 8.33; Li, 0.96; Si, 9.49. Calcd for $C_{18}H_{44}B_8O_2ClSi_2LiZr$ (III): C, 38.00; H, 7.80; Li, 1.20. Found: C, 37.27; H, 7.32; Li, 0.95. While compound I was recrystallized from dry THF to form a THF-solvated species, I·THF, II was recrystallized from anhydrous benzene solution and was subsequently used for X-ray analyses.

Reaction of I with Me_3SiCH_2MgCl (in 1:1 Mole Ratio). A THF (20 mL) solution of 1-Cl-1-(C_4H_8O)-2,2',3,3'-($SiMe_3$)₄-4,4',5,5'-Li(C_4H_8O)-1,1'-*commo*-Zr(2,3- $C_2B_4H_4$)₂ (I; 3.30 g, 4.23 mmol) was added to an ether solution of Me_3SiCH_2MgCl (1M, 4.23 mL) *in vacuo* at $-78^\circ C$, over a period of 30 min. The reaction mixture was slowly warmed to room temperature with constant stirring, which continued for another 48 h. The mixture was then filtered *in vacuo* to remove some insoluble white solid (uncharacterized). Removal of solvents from the filtrate resulted in the formation of a fine, yellow fluffy (crystallite) material. Upon addition of 20 mL of C_6H_6 , the crystallite dissolved readily, with immediate formation of an almost colorless crystalline solid. When this product was recrystallized from THF, pale yellow crystals formed slowly. Subsequent analysis showed the final product to be the salt $[Mg(THF)_6][1-Cl-1-(C_4H_8O)-2,2',3,3'-(SiMe_3)_4-1,1'-commo-Zr(2,3-C_2B_4H_4)_2]_2 \cdot 4THF$ (IV; 3.4 g, 1.69 mmol, 40% yield; mp $96^\circ C$ dec). Anal. Calcd for $C_{80}H_{184}B_{16}O_{12}Cl_2Si_8MgZr_2$ (IV): C, 47.73; H, 9.23; Mg, 1.21. Found: C, 47.50; H, 9.40; Mg, 1.23. The X-ray-quality crystals of IV were grown from THF solution.

Reaction of I with Me_3SiCH_2MgCl (in 1:2 Mole Ratio). An Et_2O /THF (25 mL/5 mL) solution of I (3.30 g, 4.23 mmol) was added over a period of 30 min, with constant stirring, to an Et_2O solution of Me_3SiCH_2MgCl (1 M, 8.5 mL) *in vacuo* at $-78^\circ C$. The reaction mixture was slowly warmed to room temperature and was stirred for about 3 days, during which time no observable color change occurred. After 3 days, the solvent was removed under reduced pressure to obtain a gray-white crystallite material, which was redissolved in a mixture of C_6D_6 and $CDCl_3$ (5 mL/5 mL). Removal of solvents from the solution produced a gelatinous solid, which on treatment

(6) Swisher, R. G.; Sinn, E.; Grimes, R. N. *Organometallics* **1984**, *3*, 599.

(7) Hosmane, N. S.; Wang, Y.; Zhang, H.; Maguire, J. A.; Waldhör, E.; Kaim, W.; Binder, H.; Kremer, R. K. *Organometallics* **1994**, *13*, 4156.

(8) (a) Stockman, K. E.; Finn, M. G.; Sabat, M.; Grimes, R. N. Abstract No. 9, BUSA IV, Syracuse, NY, July 1994. (b) Houseknecht, K.; Finn, M. G.; Sabat, M.; Grimes, R. N. Abstract No. 68, BUSA IV, Syracuse, NY, July 1994.

(9) Siriwardane, U.; Zhang, H.; Hosmane, N. S. *J. Am. Chem. Soc.* **1990**, *112*, 9637.

(10) (a) Hosmane, N. S.; Sirmokadam, N. N.; Mollenhauer, M. N. *J. Organomet. Chem.* **1985**, *279*, 359. (b) Hosmane, N. S.; Mollenhauer, M. N.; Cowley, A. H.; Norman, N. C. *Organometallics* **1985**, *4*, 1194. (c) Hosmane, N. S.; Maldar, N. N.; Potts, S. B.; Rankin, D. W. H.; Robertson, H. E. *Inorg. Chem.* **1986**, *25*, 1561. (d) Hosmane, N. S.; Islam, M. S.; Burns, E. G. *Inorg. Chem.* **1987**, *26*, 3236.

(11) (a) Hosmane, N. S.; Saxena, A. K.; Barreto, R. D.; Maguire, J. A.; Jia, L.; Wang, Y.; Oki, A. R.; Grover, K. V.; Whitten, S. J.; Dawson, K.; Tolle, M. A.; Siriwardane, U.; Demissie, T.; Fagner, J. S. *Organometallics* **1993**, *12*, 3001. (b) Barreto, R. D.; Hosmane, N. S. *Inorg. Synth.* **1992**, *29*, 89.

Table 1. Crystal Data^a for I·THF, II, IV and V

	I·THF	II	IV	V
formula	C ₂₈ H ₆₈ O ₃ B ₈ Si ₄ ClLiZr	C ₂₀ H ₄₈ O ₂ B ₈ Si ₂ ClLiZr	[C ₂₀ H ₅₂ O ₂ B ₈ Si ₄ ClZr] ₂ · [MgC ₂₄ H ₄₈ O ₆] ₄ ·4THF	[C ₄₄ H ₁₀₃ O ₆ B ₈ Si ₅ Cl ₄ · LiMg ₂ Zr] _{1/2} ·Et ₂ O
fw	785.3	596.9	2013.6	1280.8
cryst system	triclinic	monoclinic	monoclinic	monoclinic
space group	<i>P</i> $\bar{1}$	<i>P</i> 2 ₁ / <i>c</i>	<i>P</i> 2 ₁ / <i>c</i>	<i>C</i> 2/ <i>c</i>
<i>a</i> , Å	11.428(3)	16.928(8)	13.129(2)	25.602(6)
<i>b</i> , Å	12.140(3)	16.373(6)	22.429(5)	22.541(4)
<i>c</i> , Å	17.685(4)	12.048(5)	19.217(3)	24.740(5)
β , deg ^d	90.35(2)	90.37(3)	90.16(2)	90.17(2)
<i>V</i> , Å ³	2220.4(8)	3339(2)	5660(2)	14277(5)
<i>Z</i>	2	4	2	8
<i>D</i> _{calcd} , Mg/m ³	1.174	1.187	1.182	1.191
abs coeff, mm ⁻¹	0.435	0.489	0.370	0.442
crystal dimens, mm	0.25 × 0.20 × 0.15	0.20 × 0.30 × 0.05	0.20 × 0.30 × 0.10	0.05 × 0.30 × 0.15
scan type	$\theta/2\theta$	$\theta/2\theta$	$w/2\theta$	$w/2\theta$
scan speed in ω : min, max	5.0, 25.0	6.0, 30.0	6.0, 30.0	6.0, 30.0
2 θ range, deg	3.0–46.0	3.0–40.0	3.5–42.0	3.5–38.0
<i>T</i> , K	298	230	230	230
decay, %	0	0	0	0
no. of data collected	6556	3509	6413	5947
obsd reflns, <i>I</i> > 3.0 σ (<i>I</i>)	4842	2363	3813	3195
no. of params refined	415	292	523	652
GOF	2.01	2.93	1.44	1.66
χ^2	0.0003	0.0003	0.001	0.001
$\Delta\rho_{\max, \min}$, e/Å ³	+0.64, -0.70	+0.63, -0.41	+0.65, -0.53	+0.56, -0.41
<i>R</i> ^b	0.044	0.059	0.051	0.078
<i>R</i> _w	0.057	0.073	0.065	0.086

^a Graphite-monochromatized Mo K α radiation, $\lambda = 0.71073$ Å. ^b $R = \sum |F_o| - |F_c| / \sum F_o$; $wR = [\sum w(F_o - F_c)^2 / \sum w(F_o)^2]^{1/2}$. ^c $w = 1/[\sigma^2(F_o) + g(F_o)^2]$. ^d For **I**, $\alpha = 93.27(2)^\circ$ and $\gamma = 114.91(8)^\circ$.

with diethyl ether (50 mL) resulted in a clear solution and an off-white solid residue (300 mg); the mixture was then filtered *in vacuo* to collect a pale yellow filtrate. The solid residue, collected on the frit, failed to burn with a green flame during the flame test, indicating the absence of boron in the residue; therefore, it was discarded. The filtrate was concentrated and allowed to stand in a vacuum flask at room temperature. On standing for 2 days, pale yellow crystals slowly formed from the filtrate and were identified as 1-Cl-1-(C₄H₉O)-2,2',3,3'-(SiMe₃)₄-4,4',5,5'-[(μ -H)₄Li](μ_3 -Cl)[Mg(μ_2 -Cl)(THF)₃]₂-1,1'-*commo*-Zr(2,3-C₂B₄H₄)₂ (**V**); (3.16 g, 2.54 mmol, 65% yield; mp 145 °C). Anal. Calcd for C₄₄H₁₀₃B₈O₆Cl₄Si₅LiMg₂Zr (**V**): C, 42.49; H, 8.34; B, 6.96. Found: C, 42.33; H, 8.24; B, 7.14. The X-ray-quality crystals of **V** were grown from Et₂O solution.

X-ray Analyses of 1-Cl-1-(C₄H₉O)-2,2',3,3'-(SiMe₃)₄-4,4',5,5'-Li(C₄H₉O)-2,2'-1,1'-*commo*-Zr(2,3-C₂B₄H₄)₂ (I**·THF), 1-Cl-1-(C₄H₉O)-2,2'-(SiMe₃)₂-3,3'-(Me)₂-4,4',5,5'-Li(C₄H₉O)-1,1'-*commo*-Zr(2,3-C₂B₄H₄)₂ (**II**), [Mg(THF)₆][1-Cl-1-(C₄H₉O)-2,2',3,3'-(SiMe₃)₄-1,1'-*commo*-Zr(2,3-C₂B₄H₄)₂]₂·4THF (**IV**), and 1-Cl-1-CH₂SiMe₃-2,2',3,3'-(SiMe₃)₄-4,4',5,5'-[(μ -H)₄Li](μ_3 -Cl)[Mg(μ_2 -Cl)(THF)₃]₂-1,1'-*commo*-Zr(2,3-C₂B₄H₄)₂ (**V**). The crystals were coated with epoxy resin and mounted sequentially on a Siemens R3m/V diffractometer under a low-temperature nitrogen stream. The pertinent crystallographic data and conditions for data collection are summarized in Table 1. Final unit cell parameters were obtained by a least-squares fit of the angles of 24 accurately centered reflections (15° < 2 θ < 29° for **I**·THF, 18° < 2 θ < 30° for **II**, 19° < 2 θ < 26° for **IV**, 16° < 2 θ < 26° for **V**). Three standard reflections, monitored after every 150 reflections, did not show any significant change in intensity during the data collection. The data were corrected for Lorentz and polarization effects. Semi-empirical absorption studies (ψ scan) were also applied, with the minimum and maximum transmission factors of 0.840 and 0.980 for **I**·THF, 0.659 and 0.820 for **II**, 0.723 and 0.756 for **IV**, and 0.725 and 0.764 for **V**, respectively. All structures were solved by heavy-atom methods and subsequent difference Fourier syntheses using the SHELXTL-Plus package.¹² Scattering factors, as well as anomalous-dispersion corrections for Zr, Mg, Cl, and**

Si atoms, were taken from literature values.¹³ Full-matrix least-squares refinement was performed for each structure. Compounds **II**, **IV**, and **V** all showed disordered THF molecules that limited the extent to which these structures could be refined, at least compared to **I**·THF. In **II** the disoriented THF was one attached to the Li (labeled O(26)–C(30) in Table 2); in **IV** one of the four THF's of crystallization was disordered, while in **V** all six of the magnesium-coordinating THF's plus the ethyl groups of the Et₂O of crystallization were disordered. All of the disordered segments were elastically constrained in the final cycles of refinements. All carborane cage H atoms were located in DF maps, while the methyl and methylene H atoms, except the disordered ones, were placed at calculated positions. The final refinements converged at *R* = 0.044 and *R*_w = 0.057 for structure **I**·THF, 0.059 and 0.073 for **II**, 0.051 and 0.065 for **IV**, and 0.078 and 0.086 for **V**, respectively. The final atomic coordinates are given in Table 2; selected bond distances and bond angles are listed in Table 3. Additional geometric information is given in the supplementary material.

Results and Discussion

Synthesis. The reaction of ZrCl₄ with 2 equiv of the sodium/lithium compounds *closo-exo*-Li(THF)-1-Na(THF)-2-(SiMe₃)-3-(R)-2,3-C₂B₄H₄ (R = SiMe₃, Me, H) in C₆H₆/THF mixtures produced the *commo*-zirconocarboranes 1-Cl-1-(THF)-2,2'-(SiMe₃)₂-3,3'-(R)-2,4,4',5,5'-Li(THF)-1,1'-*commo*-Zr(2,3-C₂B₄H₄)₂ (R = SiMe₃ (**I**), Me (**II**), H (**III**)), in 60–70% yields (see Scheme 1). One of the characteristics of these compounds is their ability, and tendency, to incorporate varying numbers of THF molecules of solvation, depending on the complex and conditions. The crystal structure of **I**·THF shows three THF molecules, two solvating the lithium and one coordinated to the zirconium (see Figure 1). However, the powdery sample of **I** sent for analysis clearly shows the presence of only two THF molecules, presumably

(12) Sheldrick, G. M. *Structure Determination Software Programs*; Siemens X-Ray Analytical Instruments Inc.: Madison, WI, 1991.

(13) *International Tables for X-ray Crystallography*; Kynoch Press: Birmingham, U.K., 1974; Vol. IV.

Table 2. Atomic Coordinates ($\times 10^4$) and Equivalent Isotropic Displacement Coefficients ($\text{\AA}^2 \times 10^3$)

	<i>x</i>	<i>y</i>	<i>z</i>	<i>U</i> (eq)		<i>x</i>	<i>y</i>	<i>z</i>	<i>U</i> (eq)
Compound I-THF									
Zr	2208(1)	3249(1)	2759(1)	38(1)	C(25)	6070(6)	1773(6)	1966(4)	85(3)
Li	-840(8)	742(8)	1763(5)	61(4)	C(26)	6140(6)	4156(6)	1608(4)	90(3)
Cl	4229(1)	5050(1)	3099(1)	58(1)	C(27)	3713(6)	7633(5)	2196(4)	86(3)
Si(1)	3911(2)	1595(1)	4100(1)	64(1)	C(28)	2472(8)	6967(6)	3659(4)	110(4)
Si(2)	5706(1)	3046(1)	2348(1)	56(1)	C(29)	885(7)	7083(6)	2362(6)	131(5)
Si(3)	2177(2)	6624(1)	2624(1)	73(1)	C(30)	4287(5)	5705(5)	873(3)	79(3)
Si(4)	2501(1)	4940(1)	767(1)	59(1)	C(31)	2109(7)	3711(6)	3(3)	90(3)
C(2)	3191(4)	1814(4)	3197(3)	46(2)	C(32)	1868(7)	6015(6)	433(4)	91(3)
C(3)	3919(4)	2411(4)	2519(3)	41(2)	O(40)	1635(3)	3138(3)	4004(2)	58(1)
B(4)	3006(5)	2108(5)	1804(3)	47(2)	C(41)	408(6)	2249(5)	4267(3)	79(3)
B(5)	1548(5)	1166(5)	2079(3)	53(2)	C(42)	241(10)	2738(9)	4983(5)	191(7)
B(6)	1724(6)	1039(5)	2983(4)	55(2)	C(43)	1262(10)	3857(8)	5171(5)	156(6)
B(7)	2868(6)	894(5)	2370(3)	52(2)	C(44)	2129(7)	4171(6)	4566(3)	89(3)
C(12)	1570(4)	4939(4)	2384(3)	50(2)	O(45)	-1777(5)	176(4)	800(3)	109(2)
C(13)	1697(4)	4277(4)	1664(3)	47(2)	C(46)	-2976(9)	-625(10)	659(6)	165(7)
B(14)	691(5)	2903(5)	1623(3)	50(2)	C(47)	-3588(13)	-442(16)	79(7)	274(17)
B(15)	-142(5)	2738(5)	2399(3)	51(2)	C(48)	-2587(21)	587(10)	-246(8)	330(21)
B(16)	475(5)	4064(5)	2869(4)	56(3)	C(49)	-1549(14)	662(14)	148(7)	486(18)
B(17)	162(5)	4037(5)	1889(4)	59(3)	O(50)	-1803(4)	-629(3)	2336(2)	75(2)
C(21)	4676(7)	3029(5)	4707(3)	91(3)	C(51)	-2486(8)	-699(6)	3004(5)	111(4)
C(22)	2621(7)	473(6)	4651(4)	99(4)	C(52)	-2772(11)	-1862(8)	3298(5)	149(6)
C(23)	5055(6)	900(6)	3937(4)	90(4)	C(53)	-2271(11)	-2470(8)	2791(7)	171(8)
C(24)	6808(5)	3873(5)	3175(3)	77(3)	C(54)	-1637(9)	-1712(6)	2227(6)	131(5)
Compound II									
Zr	2225(1)	503(1)	1326(1)	67(1)	B(15)	2350(8)	1109(8)	3279(10)	104(6)
Li	3719(13)	1010(14)	3028(21)	144(10)	B(16)	2659(6)	121(7)	3293(9)	84(5)
Cl	1516(1)	-595(1)	362(2)	83(1)	B(17)	1758(8)	359(9)	3979(11)	118(6)
Si(1)	2682(2)	375(2)	-1960(3)	109(1)	C(17)	414(6)	-235(6)	2782(9)	110(5)
Si(2)	1966(2)	-1544(2)	3197(2)	92(1)	C(18)	2921(5)	-1909(6)	2616(9)	108(5)
C(2)	2986(5)	493(5)	-498(8)	77(4)	C(19)	1923(7)	-1768(7)	4695(8)	133(6)
C(3)	3377(5)	-82(6)	286(9)	89(4)	C(20)	1171(6)	-2138(6)	2487(8)	116(5)
B(4)	3730(7)	309(7)	1312(12)	99(6)	O(21)	1388(3)	1438(3)	644(5)	80(2)
B(5)	3523(7)	1293(7)	1146(12)	100(5)	C(22)	561(5)	1283(6)	385(8)	89(4)
B(6)	3059(6)	1380(6)	8(11)	87(5)	C(23)	250(6)	2093(7)	6(9)	115(5)
B(7)	3924(7)	781(7)	18(13)	103(6)	C(24)	731(6)	2686(6)	631(10)	105(5)
C(7)	3594(6)	-936(6)	-101(9)	110(5)	C(25)	1492(6)	2316(5)	730(10)	105(5)
C(8)	3430(9)	814(10)	-2834(11)	205(9)	O(26)	4574(5)	1312(5)	3946(8)	134(4)
C(9)	2500(9)	-669(7)	-2373(10)	175(8)	C(27)	5307(7)	1391(21)	3629(15)	343(21)
C(10)	1760(7)	916(8)	-2191(10)	156(7)	C(28)	5746(11)	1751(18)	4457(18)	308(17)
C(12)	1932(5)	-396(5)	2999(6)	74(3)	C(29)	5258(9)	1917(17)	5333(14)	248(14)
C(13)	1234(6)	141(6)	2826(8)	86(4)	C(30)	4547(9)	1801(17)	4803(17)	333(19)
B(14)	1415(8)	1079(9)	2936(10)	102(6)					
Compound IV									
Zr	4517(1)	1583(1)	7655(1)	32(1)	O(41)	4776(4)	2337(2)	8433(3)	46(2)
Mg	10000	0	10000	37(1)	C(42)	5249(8)	2898(4)	8281(5)	71(4)
Cl	4943(2)	2221(1)	6640(1)	47(1)	C(43)	5639(12)	3122(5)	8954(7)	140(8)
Si(1)	2125(2)	2785(1)	7671(1)	49(1)	C(44)	5408(12)	2727(6)	9477(7)	122(7)
Si(2)	2330(2)	1749(1)	6084(1)	53(1)	C(45)	4753(8)	2260(4)	9195(4)	62(4)
Si(3)	5932(2)	341(1)	6382(1)	55(1)	O(51)	9886(4)	156(2)	11079(3)	47(2)
Si(4)	7521(2)	1660(1)	7066(1)	49(1)	C(52)	8937(6)	109(5)	11469(4)	69(4)
C(2)	2688(5)	2017(3)	7630(4)	38(3)	C(53)	9144(9)	374(8)	12144(5)	143(8)
C(3)	2781(5)	1628(4)	7003(4)	41(3)	C(54)	10194(8)	391(6)	12254(5)	93(5)
B(4)	3033(7)	965(4)	7224(5)	45(4)	C(55)	10690(7)	313(4)	11556(4)	63(4)
B(5)	3045(7)	952(4)	8094(5)	45(4)	O(56)	9659(4)	917(2)	9832(3)	49(2)
B(6)	2849(7)	1656(4)	8327(5)	42(3)	C(57)	9602(9)	1211(4)	9159(5)	78(4)
B(7)	2042(8)	1357(4)	7671(5)	50(4)	C(58)	9468(14)	1821(5)	9278(7)	153(9)
C(12)	5725(6)	789(3)	7202(4)	40(3)	C(59)	9374(11)	1950(5)	9994(7)	105(6)
C(13)	6382(5)	1292(5)	7471(4)	36(3)	C(60)	9441(7)	1369(3)	10348(5)	59(4)
B(14)	6211(7)	1374(4)	8263(5)	45(4)	O(61)	11548(4)	218(2)	10076(3)	45(2)
B(15)	5361(8)	879(5)	8502(5)	49(4)	C(62)	12394(6)	-186(4)	10206(5)	52(3)
B(16)	5052(7)	513(4)	7796(5)	45(4)	C(63)	13332(7)	143(4)	10064(6)	82(5)
B(17)	6364(8)	647(4)	7961(5)	47(4)	C(64)	13052(6)	775(4)	10183(6)	72(4)
C(21)	2047(8)	3041(4)	8588(5)	80(4)	C(65)	11977(7)	818(4)	9972(5)	60(4)
C(22)	2875(7)	3366(4)	7214(5)	72(4)	O(71)	7148(4)	1199(3)	11124(3)	66(2)
C(23)	792(7)	2782(4)	7339(5)	78(4)	C(72)	6536(7)	1556(4)	10697(5)	64(4)
C(24)	975(7)	1531(5)	6009(5)	88(5)	C(73)	5482(7)	1330(4)	10748(5)	63(4)
C(25)	3038(8)	1267(5)	5479(5)	93(5)	C(74)	5455(7)	1044(5)	11440(6)	91(5)
C(26)	2451(8)	2513(5)	5725(5)	83(5)	C(75)	6518(7)	972(4)	11658(5)	69(4)
C(27)	5075(9)	-314(4)	6388(5)	97(5)	O(76)	8070(10)	4268(9)	8968(9)	381(12)
C(28)	5667(8)	751(4)	5563(4)	81(4)	C(77)	8715(13)	4496(6)	9444(8)	278(12)
C(29)	7273(8)	34(4)	6359(5)	81(4)	C(78)	9727(11)	4352(7)	9214(9)	236(10)
C(30)	8673(6)	1228(5)	7347(5)	71(4)	C(79)	9547(11)	3779(6)	8903(8)	204(8)
C(31)	7557(7)	1714(4)	6094(4)	66(4)	C(80)	8472(11)	3719(7)	9023(8)	259(11)
C(32)	7656(7)	2437(4)	7398(5)	77(4)					

Table 2. (Continued)

	x	y	z	U(eq)		x	y	z	U(eq)
Compound V									
Zr	2628(1)	4873(1)	973(1)	67(1)	C(29)	3041(9)	3070(9)	2070(8)	200(16)
Li	3427(14)	6063(16)	863(11)	110(16)	C(30)	2893(10)	4371(10)	2803(8)	243(20)
Mg(1)	3997(2)	7893(3)	1352(2)	78(2)	C(31)	4051(12)	4098(14)	2564(10)	358(30)
Mg(2)	4782(2)	7230(2)	548(2)	70(2)	C(32)	3704(11)	5360(11)	2662(8)	282(23)
Cl(1)	2120(2)	4302(2)	1643(2)	107(2)	O(51)	4095(6)	8752(6)	1627(6)	116(7)
Cl(2)	4295(2)	8167(2)	434(2)	96(2)	C(52)	4567(8)	8917(8)	1876(13)	264(23)
Cl(3)	4923(2)	7587(2)	1494(2)	88(2)	C(53)	4598(7)	9577(9)	1859(9)	178(17)
Cl(4)	3926(2)	6863(2)	932(2)	84(2)	C(54)	4228(11)	9750(7)	1421(9)	225(21)
Si(5)	2578(2)	4326(2)	-466(2)	77(2)	C(55)	3844(7)	9253(10)	1410(9)	163(15)
C(41)	2389(6)	4307(6)	254(5)	65(7)	O(56)	3216(4)	8048(5)	1172(5)	98(6)
C(42)	1995(7)	4386(8)	-912(6)	106(9)	C(57)	3034(6)	8056(13)	635(4)	221(19)
C(43)	2907(7)	3639(7)	-666(7)	116(10)	C(58)	2470(7)	7897(10)	646(8)	150(13)
C(44)	3024(6)	4946(7)	-658(6)	101(9)	C(59)	2306(4)	8070(13)	1201(10)	153(19)
C(2)	1768(6)	5450(7)	832(7)	63(7)	C(60)	2792(6)	8022(20)	1530(5)	342(31)
C(3)	2033(7)	5710(8)	1301(7)	90(9)	O(61)	3804(4)	7623(8)	2126(4)	111(7)
B(4)	2549(10)	5992(9)	1145(8)	87(11)	C(62)	3851(10)	7040(6)	2323(8)	179(16)
B(5)	2627(8)	5883(9)	509(7)	68(9)	C(63)	3673(13)	7045(10)	2896(7)	189(17)
B(6)	2107(8)	5521(9)	315(8)	71(9)	C(64)	3536(12)	7671(14)	3025(5)	222(21)
B(7)	2019(9)	6131(10)	728(9)	85(11)	C(65)	3731(10)	8021(7)	2556(8)	250(22)
C(12)	3337(7)	4141(9)	1289(9)	98(10)	O(66)	5487(4)	7588(5)	267(5)	94(6)
C(13)	3382(8)	4643(10)	1656(8)	102(10)	C(67)	5513(6)	8150(7)	22(8)	166(14)
B(14)	3535(10)	5202(11)	1361(9)	96(11)	C(68)	6076(8)	8296(7)	-50(8)	150(13)
B(15)	3604(7)	5019(10)	724(8)	70(9)	C(69)	6338(5)	7936(9)	377(10)	167(15)
B(16)	3451(8)	4344(10)	676(8)	74(10)	C(70)	5979(7)	7427(9)	470(12)	238(20)
B(17)	3884(10)	4563(12)	1201(11)	112(13)	O(71)	5125(4)	6406(4)	708(6)	99(6)
Si(1)	1068(2)	5240(3)	758(3)	108(3)	C(72)	5414(7)	6056(9)	346(6)	225(19)
Si(2)	1766(4)	5936(3)	1978(3)	162(4)	C(73)	5379(10)	5431(7)	536(10)	196(18)
Si(3)	3308(3)	3318(3)	1407(3)	134(4)	C(74)	5253(10)	5488(8)	1121(10)	160(15)
Si(4)	3481(4)	4596(4)	2414(3)	201(6)	C(75)	5061(9)	6105(9)	1200(5)	153(14)
C(21)	913(6)	5114(8)	42(8)	133(12)	O(76)	4573(4)	6950(6)	-231(4)	92(6)
C(22)	907(6)	4548(7)	1096(8)	136(11)	C(77)	4245(8)	6455(8)	-296(7)	269(23)
C(23)	625(7)	5848(8)	964(9)	160(13)	C(78)	4174(9)	6360(9)	-888(9)	184(16)
C(24)	1509(10)	6727(9)	1933(10)	263(20)	C(79)	4306(15)	6945(12)	-1133(7)	258(22)
C(25)	1284(9)	5412(9)	2264(8)	217(16)	C(80)	4570(12)	7297(7)	-703(7)	213(18)
C(26)	2299(12)	5933(13)	2452(8)	313(28)	O(81)	5000	1645(17)	2500	346(20)
C(27)	2894(8)	2947(8)	909(8)	152(12)	C(82)	4745(14)	1940(9)	2082(12)	311(20)
C(28)	3976(9)	3026(10)	1346(10)	240(20)	C(83)	4510(12)	1485(15)	1729(12)	244(14)

^a Equivalent isotropic U , defined as one-third of the trace of the orthogonalized U_{ij} tensor.

one solvating a Li and the other bound to the Zr. The ^{13}C NMR spectrum of the crystalline sample of **I** (**I**·THF) agrees more with the X-ray structure in that it shows two different sets of THF resonances, with 1:2 peak area ratios, one set at 76.43 and 33.24 ppm, due to the Zr-bound THF, and the other set, ascribed to the Li-bound molecules, having resonances at 68.63 and 25.49 ppm.⁹ On the other hand, the results found for **II**, in which a Me replaces a SiMe_3 on each of the carboranes, shows somewhat different results. Both the X-ray study and ^{13}C and ^1H NMR spectra show two THF molecules, one each on the Li and Zr (see Figure 2 and Table 4). Although no X-ray data could be obtained for **III**, the analytical and NMR spectral data suggest that the structure of **III** is similar to that of **II** in that both have single THF molecules coordinating the Li and Zr atoms. The alterations in the appearances and characteristics of the solids found in the preparation and purification steps of **IV** and **V**, as described in the Experimental Section, are also what one would expect for species exhibiting variable solvation patterns.

The most surprising and, from a practical standpoint, disappointing results were the products obtained from the reactions of **I** with $\text{Me}_3\text{SiCH}_2\text{MgCl}$ (see Scheme 1). A 1:1 molar ratio of **I** and the Grignard reagent resulted in the replacement of two Li^+ 's by a Mg^{2+} , giving the ionic compound **IV** (Figures 3 and 4). The only major alteration is that a cation no longer occupies a bridging position on the zirconacarborane anions (see Figures 1

and 2). Reaction of **I** with excess $\text{Me}_3\text{SiCH}_2\text{MgCl}$ resulted in the formation of a complex double salt, **V**, which is shown in Figure 5 and Scheme 1. The 65% yield of this compound indicates that **V** is the major solid product formed in this reaction. Compound **V** was also the only identified product of the reaction of the chlorozirconacarborane with the Grignard reagent, in that $[\text{Me}_3\text{SiCH}_2]^-$ replaced the THF in the primary coordination sphere of the zirconium. The actual mass balances of the reactions of **I** with the Grignard reagent are not known. With the exception of the replacement of the one zirconium-bound THF by a Me_3SiCH_2 in **V**, the Grignard alkyl groups were not found among the products. Presumably, they react with some proton source in the reaction mixture and leave as Me_4Si . Also, the stoichiometry of compound **V** is such that it would require the reaction of 3 mol of Grignard reagent for every 1 mol of **V** formed, not the 2:1 molar ratio of the reaction; the 65% yield would allow for such a 3:1 stoichiometry. Compound **I** also failed to react with other standard alkylating agents such as AlMe_3 , MeLi , $t\text{-BuLi}$, and $\text{Me}_3\text{SiCH}_2\text{Li}$. At this point it is not known whether compounds **IV** and **V** are the results of bonding preferences or solubility differences. Irrespective of the driving force, the results do demonstrate the inertness of the Cl that is coordinated to the zirconium; this is quite different from the behavior of corresponding chlorozirconocenes.¹

Table 3. Selected Bond Lengths (Å) and Bond Angles (deg)^a

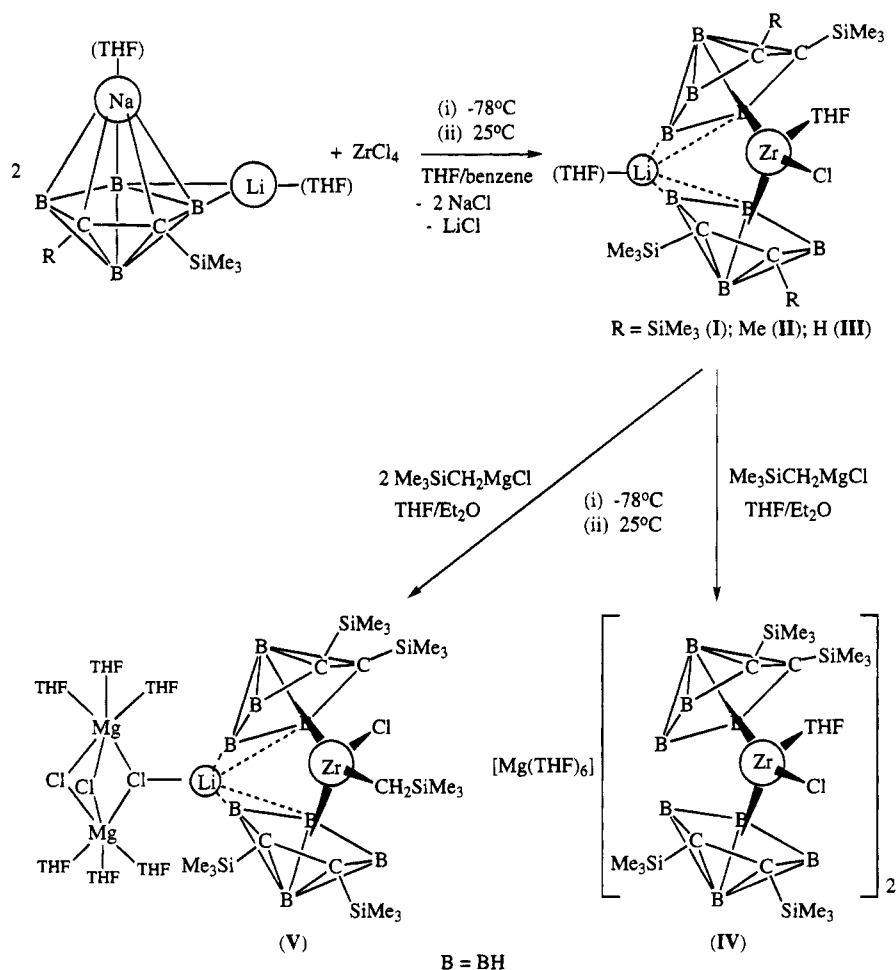
Bond Lengths							
Compound I·THF							
Zr-Cnt(1)	2.176	Zr-Cnt(2)	2.172	C(2)-B(6)	1.570(7)	C(2)-B(7)	1.727(7)
Zr-Cl	2.461(1)	Zr-C(2)	2.587(6)	C(3)-B(4)	1.559(7)	C(3)-B(7)	1.727(6)
Zr-C(3)	2.583(5)	Zr-B(4)	2.534(6)	B(4)-B(5)	1.670(7)	B(4)-B(7)	1.781(9)
Zr-B(5)	2.538(6)	Zr-B(6)	2.557(6)	B(5)-B(6)	1.633(9)	B(5)-B(7)	1.755(10)
Zr-C(12)	2.567(6)	Zr-C(13)	2.553(5)	B(6)-B(7)	1.762(9)	C(12)-C(13)	1.506(7)
Zr-B(14)	2.542(6)	Zr-B(15)	2.556(6)	C(12)-B(16)	1.558(7)	C(12)-B(17)	1.716(7)
Zr-B(16)	2.563(7)	Zr-O(40)	2.296(3)	C(13)-B(14)	1.574(6)	C(13)-B(17)	1.706(8)
Li-B(5)	2.606(11)	Li-B(14)	2.494(6)	B(14)-B(15)	1.648(8)	B(14)-B(17)	1.764(10)
Li-B(15)	2.413(10)	Li-O(45)	1.935(10)	B(15)-B(16)	1.632(8)	B(15)-B(17)	1.768(9)
Li-O(50)	1.916(9)	C(2)-C(3)	1.502(6)	B(16)-B(17)	1.764(9)		
Compound II							
Zr-Cnt(3)	2.179	Zr-Cnt(4)	2.169	C(3)-B(4)	1.512(17)	C(3)-B(7)	1.722(15)
Zr-Cl	2.450(2)	Zr-C(2)	2.554(9)	C(3)-C(7)	1.520(14)	B(4)-B(5)	1.662(17)
Zr-C(3)	2.513(10)	Zr-B(4)	2.566(11)	B(4)-B(7)	1.773(20)	B(5)-B(6)	1.582(18)
Zr-B(5)	2.559(11)	Zr-B(6)	2.570(11)	B(5)-B(7)	1.739(19)	B(6)-B(7)	1.763(15)
Zr-C(12)	2.548(8)	Zr-C(13)	2.544(9)	C(12)-C(13)	1.485(13)	C(12)-B(16)	1.534(14)
Zr-B(14)	2.563(12)	Zr-B(15)	2.561(12)	C(12)-B(17)	1.735(16)	C(13)-B(14)	1.572(17)
Zr-B(16)	2.554(11)	Zr-O(21)	2.240(5)	C(13)-B(17)	1.682(16)	C(13)-C(17)	1.518(14)
Li-B(4)	2.364(28)	Li-B(5)	2.335(28)	B(14)-B(15)	1.634(19)	B(14)-B(17)	1.816(19)
Li-B(15)	2.344(26)	Li-B(16)	2.333(25)	B(15)-B(16)	1.700(18)	B(15)-B(17)	1.799(19)
Li-O(26)	1.883(25)	C(2)-C(3)	1.487(13)	B(16)-B(17)	1.783(18)		
C(2)-B(6)	1.579(14)	C(2)-B(7)	1.766(14)				
Compound IV							
Zr-Cnt(5)	2.173	Zr-Cnt(6)	2.152	C(3)-B(4)	1.582(13)	C(3)-B(7)	1.721(13)
Zr-Cl	2.485(2)	Zr-C(2)	2.592(7)	B(4)-B(5)	1.672(14)	B(4)-B(7)	1.791(14)
Zr-C(3)	2.600(7)	Zr-B(4)	2.530(10)	B(5)-B(6)	1.660(14)	B(5)-B(7)	1.792(14)
Zr-B(5)	2.541(10)	Zr-B(6)	2.551(9)	B(6)-B(7)	1.776(14)	C(12)-C(13)	1.510(11)
Zr-C(12)	2.541(8)	Zr-C(13)	2.560(7)	C(12)-B(16)	1.573(12)	C(12)-B(17)	1.710(12)
Zr-B(14)	2.552(9)	Zr-B(15)	2.523(10)	C(13)-B(14)	1.549(12)	C(13)-B(17)	1.726(12)
Zr-B(16)	2.515(9)	Zr-O(41)	2.283(5)	B(14)-B(15)	1.642(14)	B(14)-B(17)	1.744(14)
Mg-O(51)	2.109(5)	Mg-O(56)	2.129(5)	B(15)-B(16)	1.636(13)	B(15)-B(17)	1.759(14)
Mg-O(61)	2.095(5)	C(2)-C(3)	1.493(11)	B(16)-B(17)	1.776(14)		
C(2)-B(6)	1.580(12)	C(2)-B(7)	1.709(13)				
Compound V							
Zr-Cnt(7)	2.196	Zr-Cnt(8)	2.222	Li-Cl(4)	2.216(36)	C(41)-Si(5)	1.847(14)
Zr-Cl(1)	2.471(5)	Zr-C(41)	2.271(13)	C(42)-Si(5)	1.860(17)	C(43)-Si(5)	1.831(17)
Zr-C(2)	2.580(15)	Zr-C(3)	2.558(18)	C(44)-Si(5)	1.867(17)	C(2)-C(3)	1.465(24)
Zr-B(4)	2.567(20)	Zr-B(5)	2.551(19)	C(2)-B(6)	1.556(26)	C(2)-B(7)	1.685(27)
Zr-B(6)	2.561(20)	Zr-C(12)	2.574(19)	C(3)-B(4)	1.518(30)	C(3)-B(7)	1.706(28)
Zr-C(13)	2.614(20)	Zr-B(14)	2.617(24)	B(4)-B(5)	1.606(27)	B(4)-B(7)	1.732(32)
Zr-B(15)	2.597(18)	Zr-B(16)	2.533(20)	B(5)-B(6)	1.633(28)	B(5)-B(7)	1.743(30)
Mg(1)-Cl(2)	2.476(7)	Mg(1)-Cl(3)	2.492(7)	B(6)-B(7)	1.729(30)	C(12)-C(13)	1.456(30)
Mg(1)-Cl(4)	2.547(7)	Mg(1)-O(51)	2.068(14)	C(12)-B(16)	1.612(30)	C(12)-B(17)	1.708(31)
Mg(1)-O(56)	2.077(11)	Mg(1)-O(61)	2.070(12)	C(12)-Si(3)	1.878(22)	C(13)-B(14)	1.508(32)
Mg(2)-Cl(2)	2.468(7)	Mg(2)-Cl(3)	2.499(7)	C(13)-B(17)	1.722(33)	C(13)-Si(4)	1.894(20)
Mg(2)-Cl(4)	2.532(7)	Mg(2)-O(66)	2.096(12)	B(14)-B(15)	1.639(30)	B(14)-B(17)	1.742(36)
Mg(2)-O(71)	2.092(11)	Mg(2)-O(76)	2.097(12)	B(15)-B(16)	1.576(31)	B(15)-B(17)	1.722(34)
Li-B(4)	2.361(42)	Li-B(5)	2.263(39)	B(16)-B(17)	1.774(33)		
Li-B(14)	2.316(41)	Li-B(15)	2.421(41)				
Bond Angles							
Compound I·THF							
Cnt(1)-Zr-Cl	108.0	Cnt(2)-Zr-Cl	110.1	C(3)-B(7)-B(5)	95.3(4)	B(4)-B(7)-B(5)	56.4(3)
Cnt(1)-Zr-O(40)	105.1	Cnt(2)-Zr-O(40)	104.9	C(2)-B(7)-B(6)	53.5(3)	C(3)-B(7)-B(6)	93.0(4)
Cnt(1)-Zr-Cnt(2)	130.4	Cl-Zr-O(40)	90.5(1)	B(4)-B(7)-B(6)	95.9(5)	B(5)-B(7)-B(6)	55.3(4)
B(5)-Li-B(14)	67.2(3)	B(5)-Li-B(15)	81.2(3)	C(13)-C(12)-B(16)	110.6(4)	C(13)-C(12)-B(17)	63.6(3)
B(5)-Li-O(45)	128.0(5)	B(14)-Li-O(45)	105.7(4)	B(16)-C(12)-B(17)	65.0(3)	C(12)-C(13)-B(14)	110.9(4)
B(15)-Li-O(45)	127.1(5)	B(5)-Li-O(50)	103.1(5)	C(12)-C(13)-B(17)	64.2(3)	B(14)-C(13)-B(17)	64.9(4)
B(14)-Li-O(50)	153.8(5)	B(15)-Li-O(50)	117.3(5)	C(13)-B(14)-B(15)	105.7(4)	C(13)-B(14)-B(17)	61.2(3)
O(45)-Li-O(50)	99.3(4)	C(3)-C(2)-B(6)	110.9(4)	B(15)-B(14)-B(17)	62.3(4)	B(14)-B(15)-B(16)	105.9(4)
C(3)-C(2)-B(7)	64.2(3)	B(6)-C(2)-B(7)	64.4(3)	B(14)-B(15)-B(17)	62.1(4)	B(16)-B(15)-B(17)	62.4(4)
C(2)-C(3)-B(4)	111.4(4)	C(2)-C(3)-B(7)	64.2(3)	C(12)-B(16)-B(15)	106.9(5)	C(12)-B(16)-B(17)	61.8(3)
B(4)-C(3)-B(7)	65.4(3)	C(3)-B(4)-B(5)	105.6(4)	B(15)-B(16)-B(17)	62.6(4)	C(12)-B(17)-C(13)	52.2(3)
C(3)-B(4)-B(7)	61.8(3)	B(5)-B(4)-B(7)	61.0(4)	C(12)-B(17)-B(14)	93.6(4)	C(13)-B(17)-B(14)	53.9(3)
B(4)-B(5)-B(6)	105.6(4)	B(4)-B(5)-B(7)	62.6(4)	C(12)-B(17)-B(15)	94.8(4)	C(13)-B(17)-B(15)	95.3(4)
B(6)-B(5)-B(7)	62.6(4)	C(2)-B(6)-B(5)	106.5(4)	B(14)-B(17)-B(15)	55.6(4)	C(12)-B(17)-B(16)	53.2(3)
C(2)-B(6)-B(7)	62.1(3)	B(5)-B(6)-B(7)	62.1(4)	C(13)-B(17)-B(16)	93.1(4)	B(14)-B(17)-B(16)	95.8(5)
C(2)-B(7)-C(3)	51.6(2)	C(2)-B(7)-B(4)	92.3(4)	B(15)-B(17)-B(16)	55.0(3)	Zr-O(40)-C(41)	123.9(3)
C(3)-B(7)-B(4)	52.8(3)	C(2)-B(7)-B(5)	95.0(4)	Zr-O(40)-C(44)	124.0(3)		

Table 3 (Continued)

Bond Angles							
Compound II							
Cnt(1)-Zr-Cl	106.8	Cnt(2)-Zr-Cl	106.7	C(3)-B(7)-B(5)	92.1(8)	B(4)-B(7)-B(5)	56.5(7)
Cnt(1)-Zr-O(21)	106.1	Cnt(2)-Zr-O(21)	104.3	C(2)-B(7)-B(6)	53.2(6)	C(3)-B(7)-B(6)	90.6(7)
Cnt(1)-Zr-Cnt(2)	133.6	Cl-Zr-O(21)	91.2(2)	B(4)-B(7)-B(6)	95.2(8)	B(5)-B(7)-B(6)	53.7(7)
B(4)-Li-B(15)	99.2(9)	B(5)-Li-B(15)	88.7(9)	C(13)-C(12)-B(16)	110.0(8)	C(13)-C(12)-B(17)	62.4(7)
B(4)-Li-B(16)	80.0(8)	B(5)-Li-B(16)	98.8(9)	B(16)-C(12)-B(17)	65.8(7)	C(12)-C(13)-B(14)	114.3(8)
B(4)-Li-O(26)	129.1(12)	B(5)-Li-O(26)	128.5(12)	C(12)-C(13)-B(17)	66.1(7)	B(14)-C(13)-B(17)	67.7(8)
B(15)-Li-O(26)	131.5(13)	B(16)-Li-O(26)	132.2(13)	C(12)-C(13)-C(17)	119.4(9)	B(14)-C(13)-C(17)	125.2(9)
C(3)-C(2)-B(6)	107.7(8)	C(3)-C(2)-B(7)	63.3(6)	B(17)-C(13)-C(17)	126.3(9)	C(13)-B(14)-B(15)	103.8(9)
B(6)-C(2)-B(7)	63.3(6)	C(2)-C(3)-B(4)	115.0(8)	C(13)-B(14)-B(17)	59.0(7)	B(15)-B(14)-B(17)	62.6(8)
C(2)-C(3)-B(7)	66.3(7)	B(4)-C(3)-B(7)	66.1(8)	B(14)-B(15)-B(16)	105.8(9)	B(14)-B(15)-B(17)	63.7(8)
C(2)-C(3)-C(7)	119.7(9)	B(4)-C(3)-C(7)	123.1(9)	B(16)-B(15)-B(17)	61.2(7)	C(12)-B(16)-B(15)	106.0(8)
B(7)-C(3)-C(7)	124.5(8)	C(3)-B(4)-B(5)	103.3(10)	C(12)-B(16)-B(17)	62.6(7)	B(15)-B(16)-B(17)	62.1(8)
C(3)-B(4)-B(7)	62.6(8)	B(5)-B(4)-B(7)	60.7(8)	C(12)-B(17)-C(13)	51.5(6)	C(12)-B(17)-B(14)	92.7(8)
B(4)-B(5)-B(6)	107.1(9)	B(4)-B(5)-B(7)	62.8(8)	C(13)-B(17)-B(14)	53.2(7)	C(12)-B(17)-B(15)	94.0(8)
B(6)-B(5)-B(7)	63.9(8)	C(2)-B(6)-B(5)	106.8(8)	C(13)-B(17)-B(15)	92.8(8)	B(14)-B(17)-B(15)	53.7(7)
C(2)-B(6)-B(7)	63.5(6)	B(5)-B(6)-B(7)	62.4(8)	C(12)-B(17)-B(16)	51.7(9)	C(13)-B(17)-B(16)	91.1(8)
C(2)-B(7)-C(3)	50.4(5)	C(2)-B(7)-B(4)	91.2(7)	B(14)-B(17)-B(16)	95.3(8)	B(15)-B(17)-B(16)	56.7(7)
C(3)-B(7)-B(4)	51.2(7)	C(2)-B(7)-B(5)	92.8(7)	Zr-O(21)-C(22)	124.4(5)	Zr-O(21)-C(25)	125.1(5)
Compound IV							
Cnt(5)-Zr-Cl	107.9	Cnt(6)-Zr-Cl	109.4	B(14)-C(13)-B(17)	64.1(6)	C(13)-B(14)-B(15)	107.2(7)
Cnt(5)-Zr-O(41)	104.6	Cnt(6)-Zr-O(41)	104.6	C(13)-B(14)-B(17)	62.9(5)	B(15)-B(14)-B(17)	62.5(6)
Cnt(5)-Zr-Cnt(6)	130.5	Cl-Zr-O(41)	93.1(1)	B(14)-B(15)-B(16)	105.9(7)	B(14)-B(15)-B(17)	61.6(6)
C(3)-C(2)-B(6)	111.9(7)	C(3)-C(2)-B(7)	64.6(5)	B(16)-B(15)-B(17)	63.0(6)	C(12)-B(16)-B(15)	105.5(7)
B(6)-C(2)-B(7)	65.2(6)	C(2)-C(3)-B(4)	110.6(7)	C(12)-B(16)-B(17)	61.1(5)	B(15)-B(16)-B(17)	61.9(6)
C(2)-C(3)-B(7)	63.8(5)	B(4)-C(3)-B(7)	65.5(6)	C(12)-B(17)-C(13)	52.2(4)	C(12)-B(17)-B(14)	93.0(6)
C(3)-B(4)-B(5)	106.6(7)	C(3)-B(4)-B(7)	61.0(5)	C(13)-B(17)-B(14)	53.0(5)	C(12)-B(17)-B(15)	94.8(6)
B(5)-B(4)-B(7)	62.2(6)	B(4)-B(5)-B(6)	104.7(7)	C(13)-B(17)-B(15)	94.9(6)	B(14)-B(17)-B(15)	55.9(5)
B(4)-B(5)-B(7)	62.2(6)	B(6)-B(5)-B(7)	61.8(6)	C(12)-B(17)-B(16)	53.6(5)	C(13)-B(17)-B(16)	93.4(6)
C(2)-B(6)-B(5)	106.2(7)	C(2)-B(6)-B(7)	60.9(5)	B(14)-B(17)-B(16)	96.0(6)	B(15)-B(17)-B(16)	55.1(5)
B(5)-B(6)-B(7)	62.8(6)	C(2)-B(7)-C(3)	51.6(5)	Zr-O(41)-C(42)	125.5(5)	Zr-O(41)-C(45)	124.0(5)
C(2)-B(7)-B(4)	92.4(6)	C(3)-B(7)-B(4)	53.5(5)	O(51)-Mg-O(56)	88.5(2)	O(51)-Mg-O(61)	87.9(2)
C(2)-B(7)-B(5)	95.5(6)	C(3)-B(7)-B(5)	95.9(6)	O(56)-Mg-O(61)	89.4(2)	O(51)-Mg-O(51A)	180.0(1)
B(4)-B(7)-B(5)	55.6(5)	C(2)-B(7)-B(6)	53.9(5)	O(56)-Mg-O(51A)	91.5(2)	O(61)-Mg-O(51A)	92.1(2)
C(3)-B(7)-B(6)	93.4(6)	B(4)-B(7)-B(6)	95.4(6)	O(56)-Mg-O(56A)	180.0(1)	O(61)-Mg-O(56A)	90.6(2)
B(5)-B(7)-B(6)	55.5(5)	C(13)-C(12)-B(16)	111.5(6)	Mg-O(51)-C(52)	123.8(5)	Mg-O(51)-C(55)	127.8(5)
C(13)-C(12)-B(17)	64.4(5)	B(16)-C(12)-B(17)	65.3(6)	Mg-O(56)-C(57)	125.7(5)	Mg-O(56)-C(60)	127.9(5)
C(12)-C(13)-B(14)	110.0(6)	C(12)-C(13)-B(17)	63.4(5)	Mg-O(61)-C(62)	127.4(4)	Mg-O(61)-C(65)	125.1(4)
Compound V							
Cnt(7)-Zr-Cl(1)	108.1	Cnt(8)-Zr-Cl(1)	106.0	B(17)-C(13)-Si(4)	122.9(15)	C(13)-B(14)-B(15)	106.6(18)
Cnt(7)-Zr-C(41)	102.7	Cnt(8)-Zr-C(41)	106.7	C(13)-B(14)-B(17)	63.5(15)	B(15)-B(14)-B(17)	61.1(14)
Cnt(7)-Zr-Cnt(8)	132.0	Cl(1)-Zr-C(41)	95.3(4)	B(14)-B(15)-B(16)	106.6(16)	B(14)-B(15)-B(17)	62.4(14)
B(4)-Li-B(14)	84.1(13)	B(5)-Li-B(14)	99.3(15)	B(16)-B(15)-B(17)	64.9(14)	C(12)-B(16)-B(15)	104.5(16)
B(4)-Li-B(15)	98.9(14)	B(5)-Li-B(15)	86.6(13)	C(12)-B(16)-B(17)	60.4(13)	B(15)-B(16)-B(17)	61.5(14)
B(5)-Li-Cl(4)	134.2(17)	B(14)-Li-Cl(4)	125.0(15)	C(12)-B(17)-C(13)	50.2(12)	C(12)-B(17)-B(14)	90.5(16)
B(15)-Li-Cl(4)	134.0(16)	Zr-C(41)-Si(5)	132.2(7)	C(13)-B(17)-B(14)	51.6(13)	C(12)-B(17)-B(15)	94.6(15)
C(3)-C(2)-B(6)	110.6(14)	C(3)-C(2)-B(7)	65.2(12)	C(13)-B(17)-B(15)	94.3(15)	B(14)-B(17)-B(15)	56.5(13)
B(6)-C(2)-B(7)	64.3(12)	C(3)-C(2)-Si(1)	128.5(13)	C(12)-B(17)-B(16)	55.1(13)	C(13)-B(17)-B(16)	92.4(15)
B(6)-C(2)-Si(1)	119.0(12)	B(7)-C(2)-Si(1)	125.7(12)	B(14)-B(17)-B(16)	94.3(16)	B(15)-B(17)-B(16)	53.6(13)
C(2)-C(3)-B(4)	111.6(15)	C(2)-C(3)-B(7)	63.7(12)	Cl(2)-Mg(1)-Cl(3)	84.4(2)	Cl(2)-Mg(1)-Cl(4)	82.9(2)
B(4)-C(3)-B(7)	64.7(13)	C(2)-C(3)-Si(2)	130.2(14)	Cl(3)-Mg(1)-Cl(4)	82.7(2)	Cl(2)-Mg(1)-O(51)	91.7(5)
B(4)-C(3)-Si(2)	115.6(13)	B(7)-C(3)-Si(2)	125.6(13)	Cl(3)-Mg(1)-O(51)	95.6(5)	Cl(4)-Mg(1)-O(51)	174.4(5)
C(3)-B(4)-B(5)	107.2(16)	C(3)-B(4)-B(7)	62.9(13)	Cl(2)-Mg(1)-O(56)	93.4(4)	Cl(3)-Mg(1)-O(56)	172.5(5)
B(5)-B(4)-B(7)	62.8(13)	B(4)-B(5)-B(6)	105.2(15)	Cl(4)-Mg(1)-O(56)	89.9(4)	O(51)-Mg(1)-O(56)	91.6(6)
B(4)-B(5)-B(7)	62.1(13)	B(6)-B(5)-B(7)	61.5(12)	Cl(2)-Mg(1)-O(61)	175.3(5)	Cl(3)-Mg(1)-O(61)	91.0(4)
C(2)-B(6)-B(5)	105.4(14)	C(2)-B(6)-B(7)	61.4(12)	Cl(4)-Mg(1)-O(61)	95.3(5)	O(51)-Mg(1)-O(61)	90.0(6)
B(5)-B(6)-B(7)	62.4(12)	C(2)-B(7)-C(3)	51.2(11)	O(56)-Mg(1)-O(61)	90.9(5)	Cl(2)-Mg(2)-Cl(3)	84.4(2)
C(2)-B(7)-B(4)	92.5(14)	C(3)-B(7)-B(4)	52.4(12)	Cl(2)-Mg(2)-Cl(4)	83.3(2)	Cl(3)-Mg(2)-Cl(4)	82.9(2)
C(2)-B(7)-B(5)	95.5(14)	C(3)-B(7)-B(5)	93.6(14)	Cl(2)-Mg(2)-O(66)	93.9(4)	Cl(3)-Mg(2)-O(66)	93.8(4)
B(4)-B(7)-B(5)	55.0(12)	C(2)-B(7)-B(6)	54.2(11)	Cl(4)-Mg(2)-O(66)	175.8(4)	Cl(2)-Mg(2)-O(71)	173.2(5)
C(3)-B(7)-B(6)	92.6(14)	B(4)-B(7)-B(6)	96.0(15)	Cl(3)-Mg(2)-O(71)	92.9(5)	Cl(4)-Mg(2)-O(71)	90.2(4)
B(5)-B(7)-B(6)	56.1(12)	C(13)-C(12)-B(16)	110.6(17)	O(66)-Mg(2)-O(71)	92.5(5)	Cl(2)-Mg(2)-O(76)	91.4(4)
C(13)-C(12)-B(17)	65.4(15)	B(16)-C(12)-B(17)	64.5(14)	Cl(3)-Mg(2)-O(76)	173.4(4)	Cl(4)-Mg(2)-O(76)	91.6(4)
C(13)-C(12)-Si(3)	132.4(16)	B(16)-C(12)-Si(3)	115.8(15)	O(66)-Mg(2)-O(76)	91.6(5)	O(71)-Mg(2)-O(76)	90.7(6)
B(17)-C(12)-Si(3)	127.1(14)	C(12)-C(13)-B(14)	111.5(17)	Mg(1)-Cl(2)-Mg(2)	80.7(2)	Mg(1)-Cl(3)-Mg(2)	79.8(2)
C(12)-C(13)-B(17)	64.4(14)	B(14)-C(13)-B(17)	64.9(15)	Li-Cl(4)-Mg(1)	144.4(9)	Li-Cl(4)-Mg(2)	137.4(8)
C(12)-C(13)-Si(4)	125.7(16)	B(14)-C(13)-Si(4)	119.5(15)	Mg(1)-Cl(4)-Mg(2)	78.1(2)		

^a Legend: Cnt(1) and Cnt(2) are the centroids of the C₂B₃ rings of I and Cnt(3) and Cnt(4) for II, Cnt(5) and Cnt(6) for IV, and Cnt(7) and Cnt(8) for V, respectively.

Scheme 1



Crystal Structures of I·THF, II, IV, and V. The solid-state structures of I·THF, II, IV, and V are shown in Figures 1–5, respectively. The unit cell of IV (Figure 4) shows that the two zirconacarborane anions are well separated and symmetrically placed on either side of a

solvated magnesium cation, giving a total population of four metallacarborane anions, two $[\text{Mg}(\text{THF})_6]^{2+}$ cations, and eight additional solvated THF's. In Figure 3, the $[\text{Mg}(\text{THF})_6]^{2+}$ cation is deleted, and only one of the two equivalent chlorozirconacarboranes of IV is shown. Table 2 gives the atomic coordinates of the complexes, while some selected bond distances and bond

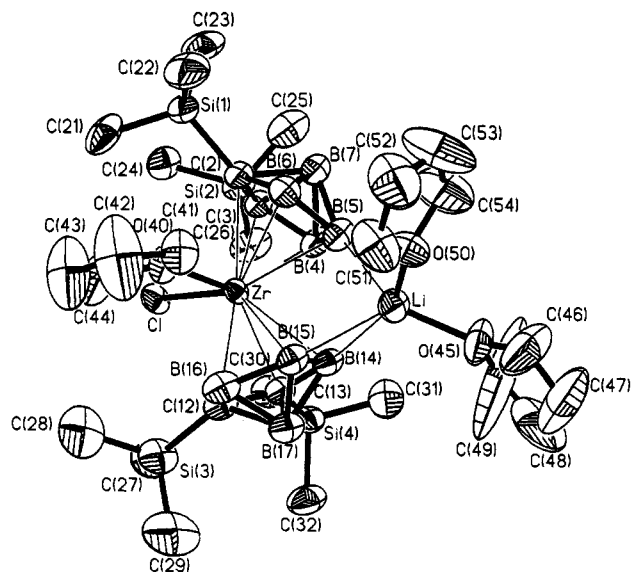


Figure 1. Perspective view of 1-Cl-1-(THF)-2,2',3,3'-(SiMe₃)₄-4,5,5'-Li(THF)₂-1,1'-commo-Zr(2,3-C₂B₄H₄)₂ (I·THF) showing the atom-numbering scheme. The thermal ellipsoids are drawn at the 40% probability level. The SiMe₃, THF, and the cage H's are omitted for clarity.

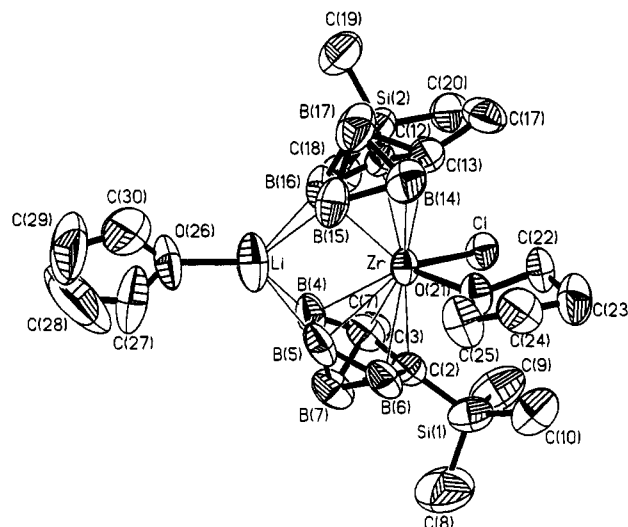


Figure 2. Perspective view of 1-Cl-1-(THF)-2,2'-(SiMe₃)₂-3,3'-(Me)₂-4,4',5,5'-Li(THF)-1,1'-commo-Zr(2,3-C₂B₄H₄)₂ (II) showing the atom-numbering scheme. The thermal ellipsoids are drawn at the 40% probability level. The SiMe₃, THF, and cage H's are omitted for clarity.

Table 4. FT NMR Spectral Data^a

compd	δ splitting, assign [$^1J(^{11}\text{B}-^1\text{H})$ or $^1J(^{13}\text{C}-^1\text{H})$, Hz]	rel area
200.13-MHz ^1H NMR Data		
I	3.82, s, THF; 3.6, br, ill-defined peak, basal H [$^1J(^{11}\text{B}-^1\text{H})$ unresolved]; 3.35, s, THF; 2.6, br, ill-defined peak, apical H [$^1J(^{11}\text{B}-^1\text{H})$ unresolved]; 1.15, s, THF; 1.09, s, THF; 0.30, s, Me ₃ Si; 0.21, s, Me ₃ Si	2:3:2:1:2:2:9:9
II	4.15, s, THF; 3.90, br, ill-defined peak, basal H [$^1J(^{11}\text{B}-^1\text{H})$ unresolved]; 3.62, s, THF; 2.83, br, ill-defined peak, apical H [$^1J(^{11}\text{B}-^1\text{H})$ unresolved]; 2.68, s, Me; 2.60, s, Me; 1.33, s, THF; 1.24, s, THF; 0.52, s, Me ₃ Si; 0.47, s, Me ₃ Si	4:6:4:2:3:3:4:4:9:9
III	6.44, s, cage CH; 4.04, br, ill defined peak, basal H [$^1J(^{11}\text{B}-^1\text{H})$ unresolved]; 3.67, s, THF; 1.8, br, ill-defined peak, apical H [$^1J(^{11}\text{B}-^1\text{H})$ unresolved]; 1.42, s, THF; 0.46, s, Me ₃ Si	1:3:4:1:4:9
IV^b	3.57, br, THF; 1.60, br, THF; 0.42, s, Me ₃ Si	2:2:3
V^b	3.73, s, THF; 3.60, br, ill-defined peak, basal H [$^1J(^{11}\text{B}-^1\text{H})$ unresolved]; 1.78, s, THF; 1.6, br, ill-defined peak, apical H [$^1J(^{11}\text{B}-^1\text{H})$ unresolved]; 0.61, s, Me ₃ Si-C _{cage} ; 0.57, s Me ₃ Si-C _{cage} ; 0.45, s, Me ₃ Si; 0.11, s, CH ₂	12:3:12::1:9:9:4.5:1
64.21-MHz ^{11}B NMR Data ^c		
I	33.16, br, ill-defined peak, basal BH [$^1J(\text{B}-\text{H})$ unresolved]; 25.48, br, ill-defined peak, basal BH [$^1J(\text{B}-\text{H})$ unresolved]; -16.32, br, ill-defined peak, apical BH [$^1J(\text{B}-\text{H})$ unresolved]	1:2:1
II	30.08, br, basal BH [$^1J(\text{B}-\text{H})$ unresolved]; 22.65, br, basal BH [$^1J(\text{B}-\text{H})$ unresolved]; -14.04, d (br), apical BH (120)	1:2:1
III	28.80, vbr, ill-defined peak, basal BH [$^1J(\text{B}-\text{H})$ unresolved]; 22.69, br, basal BH [$^1J(\text{B}-\text{H})$ unresolved]; -17.27, br, apical BH [$^1J(\text{B}-\text{H})$ unresolved]	1:2:1
IV	30.0, vbr, basal BH [$^1J(\text{B}-\text{H})$ unresolved]; 24.0, br, basal BH [$^1J(\text{B}-\text{H})$ unresolved]; -16.6, br, apical BH [$^1J(\text{B}-\text{H})$ unresolved]	1:2:1
V	29.47, br, ill-defined peak, basal BH [$^1J(\text{B}-\text{H})$ unresolved]; 19.86, br, ill-defined peak, basal BH [$^1J(\text{B}-\text{H})$ unresolved]; -19.83, br, ill-defined peak, apical BH [$^1J(\text{B}-\text{H})$ unresolved]	1:2:1
50.32-MHz ^{13}C NMR data ^{a,d}		
I	123.92, s (br), cage C(SiCB); 123.42, s (br), cage C(SiCB); 76.43, t, Zr-THF(150); 68.63, t, Li-THF(148); 33.24, t, Zr-THF(127); 25.49, t, Li-THF(134); 3.65, q, Me ₃ Si (119.8); 3.25, q, Me ₃ Si (118.8)	1:1:1:1:1:1:3:3
II	123.03, s(br), cage C(SiCB); 119.91, s(br), cage C(MeCB); 119.03, s(br), cage C(MeCB); 76.06, t, Zr-THF(154.5); 69.03, t, Li-THF (149.3); 25.40, t, Zr-THF(135); 25.28, t, Li-THF(134); 24.29, q, Me (127); 22.93, q, Me (126.2); 2.15, q, Me ₃ Si (118)	2:1:1:2:2:2:2:1:1:6
III	117.96, s (br), cage C(SiCB); 113.85, d (br), cage C(HCB)(181.28); 76.46, t, Zr-THF(155.1); 69.07, t, Li-THF(147.5); 25.44, t, THF(133.3); 0.10, q, Me ₃ Si (119.51)	2:2:2:2:4:6
IV	116.36, s, cage C(SiCB); 66.57, m, THF; 24.35, m, THF; 3.19, q, Me ₃ Si (122.5)	1:3:3:3
V	116.78, s, cage C(SiCB); 113.2, s, cage C(SiCB); 112.5, s, cage C(SiBC); 68.12, m, THF; 25.68, m, THF; 4.43, q, C-SiMe ₃ (118.16); 4.30, q, C-SiMe ₃ (118.16); 3.91, q, C-SiMe ₃ (120.32); 1.99, q, Me ₃ Si (119.8); 0.16, t, CH ₂ (104.7)	2:1:1:1:12:3:3:6:3:1
77.7-MHz ^7Li NMR Data ^e		
I	-0.96	
II	-0.34	
V	-1.70	

^a C₆D₆ was used as solvent and as an internal standard with δ 7.15 ppm (in the ^1H NMR spectra) and δ 128.0 ppm (in the ^{13}C NMR spectra) for compounds, with a positive sign indicating a downfield shift. ^b C₄D₈O was used as solvent. Legend: s = singlet, d = doublet, t = triplet, q = quartet, v = very, br = broad. ^c Shifts relative to external BF₃·OEt₂. ^d Since relaxations of the cage carbons are slower than that of a protonated C, the relative areas of these carbons could not be measured accurately. ^e Shifts relative to external aqueous LiNO₃.

angles are listed in Table 3. An inspection of Table 3 shows that the structures of all the chlorozirconacarboranes are quite similar; therefore, unless otherwise noted, average bond distances and bond angles will be quoted. Each structure shows that the zirconium, in a formal +4 oxidation state, is sandwiched between two *nido*-C₂B₄ cages. The pentagonal C₂B₃ bonding faces are essentially planar, and the Zr is η^5 -bonded to the ring atoms; the average Zr-ring atom distance is 2.559 \pm 0.018 Å.¹⁴ The Zr-Cent distance is 2.170 \pm 0.018 Å (Cent = the C₂B₃ ring centroid), which is greater than the Zr-Cent distances of 2.045 and 2.091 Å found for the mixed-sandwich complexes (Cp*)(C₂B₉H₁₁)Zr[C-(Me)=CMe₂] and [(Cp*)(C₂B₉H₁₁)Zr]₂(μ -CH₂), respectively.⁴ The zirconacarboranes in this study are similar to the zirconocenes in that they are bent-sandwich complexes with Cent-Zr-Cent angles ranging from 130.4° for **I-THF** to 133.6° for **II** (see Table 3). Analogous angles for the early-transition-metal Cp sandwich complexes range generally around 120°.¹⁵⁻¹⁷ The reason for the larger bending angles found in **I-THF**, **II**, **IV**, and **V** is not apparent and may not be significant,

since a large variation exists in the bending angles of the zirconocenes. For example, a bending angle of 140.7° was found for the zwitterionic complex Cp*₂Zr⁺(*m*-C₆H₄)B⁻(C₆H₄Et)₃.¹⁸ The bending allows for the additional coordination of the Zr so that the zirconacarboranes in **I-THF**, **II**, **IV**, and **V** and, presumably, in **III**, also contain Zr-Cl and Zr-THF (**I-THF**, **II**, and **IV**) or Zr-CH₂SiMe₃ (**V**) bonds. This results in a very distorted tetrahedral geometry about the zirconium atom; the Cl-Zr-R angles (R = THF, CH₂SiMe₃) range from 90.5° for **I-THF** to 95.3° for **V**, which are considerably smaller than the Cent-Zr-Cent angles (see Table 3). The average Zr-Cl bond distance in **I-THF**, **II**, **IV**, and **V** is 2.467 \pm 0.011 Å, which is quite similar to the Zr-Cl distances of 2.452 Å and 2.447 Å for (η^5 -C₅H₄-XMe₃)Zr[CH(SiMe₃)₂]Cl, (X = C, Si, respectively) and the value of 2.441 Å in [(η^5 -C₅H₄)₂(CH₂)₃]ZrCl₂.¹⁹ The

(16) (a) Bush, M. A.; Sim, G. A. *J. Chem. Soc. A* **1971**, 2225. (b) Jeffery, J.; Lappert, M. F.; Luong-Thi, N. T.; Webb, M.; Atwood, J. L.; Hunter, W. E. *J. Chem. Soc. Dalton Trans.* **1981**, 1593. (c) Lappert, M. F.; Riley, P. I.; Yarrow, P. I. W.; Atwood, J. L.; Hunter, W. E.; Zaworotko, M. J. *J. Chem. Soc., Dalton Trans.* **1981**, 814.

(17) Crowther, D. J.; Borkowsky, S. L.; Swenson, D.; Meyer, T. Y.; Jordan, R. F. *Organometallics* **1993**, *12*, 2897.

(18) Hlatky, G. G.; Turner, H. W.; Eckman, R. R. *J. Am. Chem. Soc.* **1989**, *111*, 2728.

(19) Saldarriaga-Molina, C. H.; Clearfield, A.; Bernal, I. *J. Organomet. Chem.* **1974**, *80*, 79.

(14) The uncertainties given with the averages are the average deviations.

(15) Prout, K.; Cameron, T. S.; Forder, R. A.; Critchley, S. R.; Denton, B.; Rees, G. V. *Acta Crystallogr.* **1974**, *B30*, 2290.

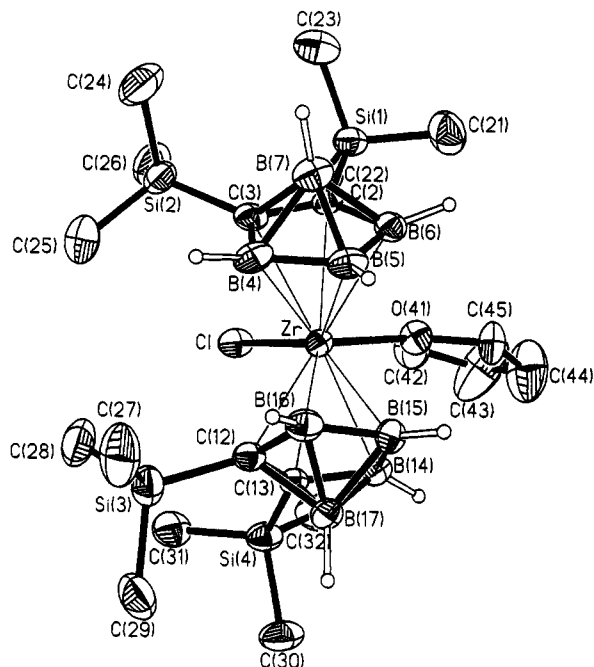


Figure 3. Perspective view of $[\text{Mg}(\text{THF})_6][1\text{-Cl-1-(THF)-2,2',3,3'-(\text{SiMe}_3)_4\text{-1,1'-}i\text{commo-Zr}(2,3\text{-C}_2\text{B}_4\text{H}_4)_2]_2\cdot 4\text{THF}$ (**IV**) showing the atom-numbering scheme. The thermal ellipsoids are drawn at the 40% probability level. The $[\text{Mg}(\text{THF})_6]^{2+}$ cation and the THF's of crystallization are deleted, and only one of the two equivalent chlorozirconacarboranes of **IV** is shown. The SiMe_3 and THF H's are omitted for clarity.

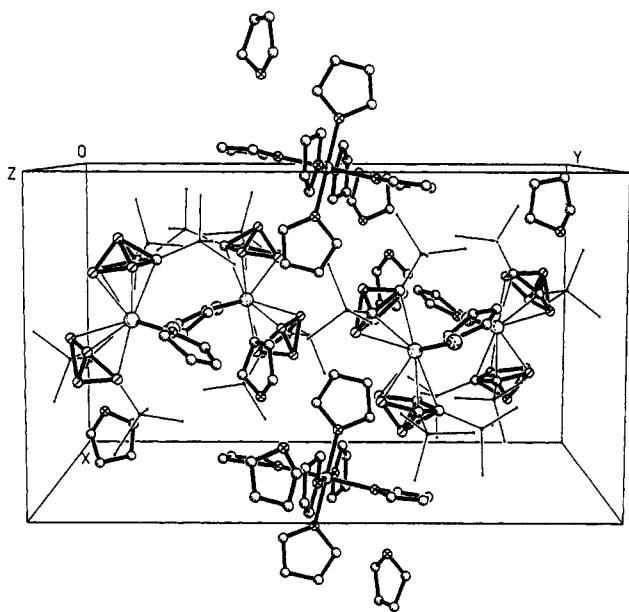


Figure 4. Crystal packing diagram of **IV**.

$\text{Zr}-\text{CH}_2\text{SiMe}_3$ distance of 2.271 Å in **V** is essentially the same as the values of 2.278 and 2.281 Å found for the analogous distances in $(\text{Cp})_2\text{Zr}(\text{CH}_2\text{SiMe}_3)_2$.^{16b} Coordination of the Cl^- ion in **I-THF-IV** imparts an overall negative charge to the zirconacarboranes, while the additional coordination of the $[\text{CH}_2\text{SiMe}_3]^-$ in **V** results in a dianionic zirconacarborane. In compounds **I-THF**, **II**, and **V**, charge compensation is accomplished by a Li^+ ion that bridges the two carborane cages of the zirconacarboranes. The complexes differ in the connectivity of the Li to the cages and in the other groups bonded to the Li. Through a series of $\text{Li}-\text{H}-\text{B}$ bonds

in **II** and **V**, the Li is equally bridged between the basal and a unique boron on each carborane (the equivalent of B(4), B(5), B(15) and B(16) in Figure 2) and is also bonded to one other group, THF in **II** and $[\text{Mg}_2\text{Cl}_3(\text{THF})_6]^+$ in **V**. On the other hand, Figure 1 shows that the Li in **I-THF** is coordinated to two THF molecules and is equally bound to $\text{H}-\text{B}(14)$ and $\text{H}-\text{B}(15)$ ($\text{Li}-\text{B}$ distances 2.45 ± 0.04 Å) and more weakly bound to $\text{H}-\text{B}(5)$ of the other cage (the $\text{Li}-\text{B}(5)$ distance is 2.61 Å). In all cases the Li groups bridge on the side of the carboranes located away from the large THF or $\text{CH}_2\text{-SiMe}_3$ ligands. The bridged Li's do not seem to exert any systematic effect on the extent of bending of the complexes; Table 3 and Figures 3 and 4 show that the $\text{Cent}-\text{Zr}-\text{Cent}$ bond angle of **IV**, which does not have bridging Li's, is essentially the same as that of **I-THF**, in which Li bridging exists.

Some insight into the substitutional inertness of **I** can be obtained by inspection of Figure 6, which shows the usual ball-and-stick model of **V** as well as a space-filling drawing of the complex at the same orientation. For clarity, the bridging Li group is not shown. It is apparent from Figure 6 that, even though the complex is bent, the SiMe_3 groups attached to the cage carbons of the carboranes effectively shield the Cl ligand so that any substitution process which has a large, or moderate, associative component to it would be greatly inhibited. The orientation of the cage carbons, and their attached derivative groups, above and below the Zr-bound Cl ligand is dictated by steric requirements. In these positions, the SiMe_3 groups are on the open side of the bent structure and away from the bulky THF (or $\text{CH}_2\text{-SiMe}_3$) group; any change in the relative orientations of the carborane ligands should result in increased ligand-ligand repulsion.

Spectroscopy. All compounds were characterized by ^1H , ^{11}B , and ^{13}C pulse Fourier transform NMR spectra and IR spectra. Compounds **I**, **II**, and **V** were also characterized by ^7Li NMR spectroscopy. The results of these spectroscopic studies are given in Tables 4 and 5.

The ^1H NMR spectra of **I-V** show appropriate resonances for the carborane protons, those associated with SiMe_3 , Me, or H cage carbon substituents, and THF. In addition, **V** showed two sharp singlets at 0.45 and 0.11 ppm ascribed to the SiMe_3 and CH_2 protons of the $\text{Zr}-\text{CH}_2\text{SiMe}_3$ moiety, respectively (see Table 4). The 0.11 ppm peak is in the range reported for a number of Zr-bound methyl and methylene hydrogen resonances.^{20,21}

The ^{11}B NMR spectra of compounds **I-V** are all similar to one another and exhibit the characteristic three-peak pattern (1:2:1 peak area ratio) of the 1,2,3- MC_2B_4 cage metallacarboranes.³ Table 4 shows that all compounds have an apical boron (the equivalent of B(7) in Figure 1) resonance in the -14 to -20 ppm region and a unique boron (the equivalent of B(5) in Figure 1) resonance in the 20 to 25 ppm region, with the basal borons (the equivalent of B(4) and B(6) in Figure 1) having resonances around 29–33 ppm. Complexation of the *nido*-carborane dianionic ligands by zirconium draws electron density away from the cage, thereby deshielding the cage borons, which results in downfield

(20) Bochmann, M.; Lancaster, S. J.; Hursthouse, M. B.; Abdul Malik, K. M. *Organometallics* **1994**, *13*, 2235.

(21) Siedle, A. R.; Newmark, R. A.; Lamanna, W. M.; Schroeffer, J. N. *Polyhedron* **1990**, *9*, 301.

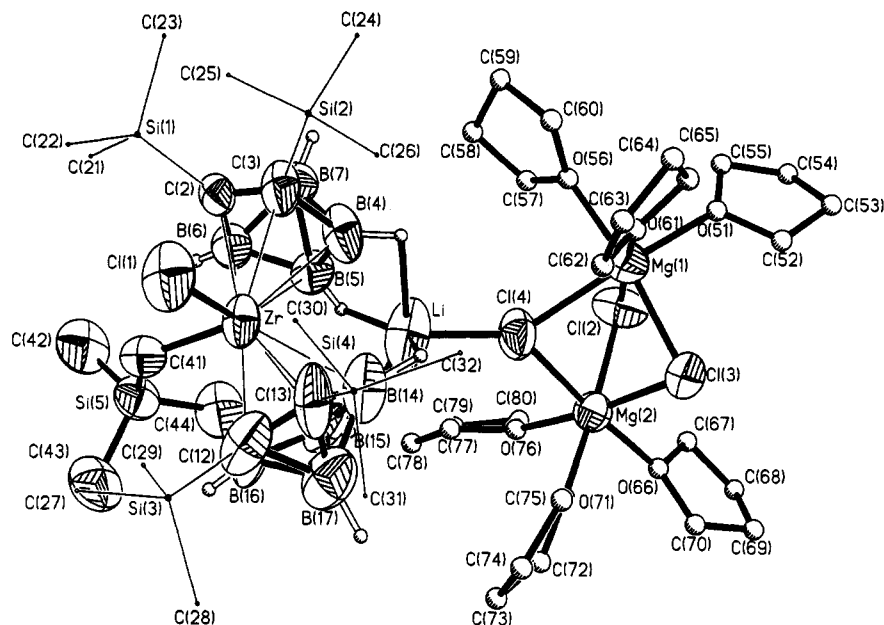


Figure 5. Perspective view of 1-Cl-1-(CH₂SiMe₃)-2,2',3,3'-(SiMe₃)₄-4,4',5,5'-[(μ-H)₄Li](μ₃-Cl)[Mg(μ₂-Cl)(THF)₃]₂-1,1'-*commo*-Zr(2,3-C₂B₄H₄)₂ (V) showing the atom-numbering scheme. The thermal ellipsoids are drawn at the 40% probability level. The atoms of the C_{cage}-SiMe₃ and the THF groups are drawn with the circles of arbitrary radii. Except for the cage BH's, the H atoms are omitted for clarity.

Table 5. Infrared Absorptions (cm⁻¹)^a

I	2954 (vs), 2896 (sh) [ν(C-H)], 2543 (vs), 2496 (sh), 2449 (sh) [ν(B-H)], 1443 (w, br), 1402 (w, br) [δ(CH) _{asym}], 1355 (w, br), 1337 (w), 1249 (vs) [δ(CH) _{sym}], 1179 (ms), 1126 (w, br), 1067 (w, sh), 1044 (m), 1002 (m, br), 914 (w, sh), 844 (vvs, br) [ρ(CH)], 761 (s, s), 703 (w, br), 632 (m, s), 602 (w, sh), 532 (w, br), 479 (w, br)
II	2941 (vs), 2880 (vs) [ν(C-H)], 2530 (vs), 2480 (vs), 2420 (vs, sh) [ν(B-H)], 2370 (w), 2260 (vs), 1610 (s), 1540 (vw), 1445 (s) [δ(CH) _{asym}], 1385 (w, br), 1360 (vw), 1325 (s), 1240 (vs), 1210 (m) [δ(CH) _{sym}], 1155 (w), 1060 (w, sh), 1030 (m), 995 (m), 935 (vw), 910 (w, sh), 845 (vvs, br) [ρ(C-H)], 750 (s), 679 (m), 621 (m), 560 (w), 490 (vvs,br), 415 (w)
III	2940 (vs), 2880 (vs, sh) [ν(C-H)], 2520 (vs), 2440 (s, sh), 2340 (m, sh) [ν(B-H)], 2100 (w, br), 1465 (w), 1400 (w) [δ(CH) _{asym}], 1350 (w, br), 1240 (vs) [δ(CH) _{sym}], 1175 (m), 1130 (w, sh), 1075 (s, sh), 1035 (s), 990 (m, sh), 880 (vs), 840 (s, sh) [ρCCH)], 770 (m, sh), 750 (s), 670 (m), 615 (m), 390 (m), 350 (w)
IV	2580 (m, sh), 2510 (vs) [ν(B-H)], 1400 (w, br), 1340 (w), 1310 (w), 1233 (s), 1160 (vw, sh), 1115 (vw), 1010 (w), 978 (w), 824 (vs), 752 (s), 678 (m), 625 (m), 600 (w), 520 (w) 428 (m), 405 (m)
V	3037-2813 (vs, br) [ν(C-H)], 2705 (s) [ν(C-H)], 2522 (m) [ν(B-H)], 2298 (w), 1973 (w), 1478 (vs) [δ(C-H)], 1369 (vs) [δ(C-H)], 1335 (s) [δ(C-H)], 1288 (vs), 1240 (vs), 1200 (vs), 1071 (vs, br), 894 (vs, br), 758 (s), 665 (s), 640 (s, sh), 507 (vs)

^a For I-IV C₆D₆ was used as solvent; THF was used for V; reference standard. Legend: v = very, s = strong or sharp, m = medium, w = weak, sh = shoulder, br = broad.

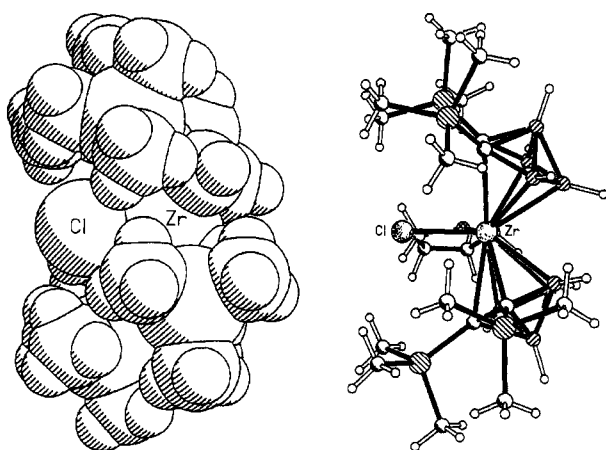


Figure 6. Space-filling and ball-and-stick models of V drawn at the same orientation showing a blockage of the Cl ligand by bulky SiMe₃ substituents on the cage carbons. The bridging groups are not shown for clarity.

shifts of the boron resonances by 20–30 ppm, from their positions in the ¹¹B NMR spectra of the starting Na/Li carboranes.^{10,11} These ¹¹B NMR shifts are similar to those found when other metals bond to the C₂B₄ carboranes and have been explained in terms of a

transfer of electron density out of the cages on metal coordination.²² In general, the peaks are much broader than those found in the Na/Li carborane precursors, hence accurate determinations of B-H coupling constants for compounds I-V could not be obtained.

The ¹³C NMR spectra of I-III show resonances for both Li-coordinated and Zr-coordinated THF molecules. For example, compound I has resonances at 76.43 and 33.24 ppm due to the carbons of the Zr-THF molecule, while the analogous resonances for the Li-THF molecule are at 68.63 and 25.49 ppm, respectively (see Table 4). These results are consistent with the solid-state structures of compounds I and II, which show that both the Zr and Li metals have coordinated THF molecules. Compound IV, which also has THF molecules attached to different metal centers (six bonded to a Mg and one bonded to Zr), exhibits only a single set of ¹³C resonances at 66.57 and 24.35 ppm. In all probability the Zr-THF resonances of this compound are masked by the more intense resonances due to the Mg-bound molecules. The ¹H NMR spectra of I and II parallel their ¹³C NMR results in that two sets of methylene hydrogens are found. For example, the ¹H NMR spectrum of I exhibits

(22) Hosmane, N. S.; Lu, K.-J.; Zhang, H.; Maguire, J. A.; Jia, L.; Barreto, R. D. *Organometallics* 1992, 11, 2458 and references therein.

one set at 3.82 and 1.15 ppm, associated with the Li-THF molecules and another at 3.6 and 1.09 ppm, attributable to the Zr-bound molecules. When the ^1H NMR spectrum of **I** was run as a function of time in a $\text{C}_4\text{D}_8\text{O}/\text{C}_6\text{D}_6$ mixture, the 3.82/1.15 ppm signals slowly disappeared, while the upfield set did not change, even after 5 days had elapsed. These observations indicate that exchange of the Li-bound THF molecules, while slow, is much faster than that of the Zr-bound molecules.

With the exception of compound **IV**, the ^{13}C NMR spectra of all the zirconacarborane cage carbons, and those of their substituent groups, showed multiple resonances indicating nonequivalent cage carbons (see Table 4). Since the cage carbons of **II** and **III** have different substituent groups attached (SiMe_3 , Me, or H), nonequivalence is expected. However, the splitting pattern in **II**, that is, three cage carbon resonances in a 2:1:1 peak area ratio, is more complex than would arise from just the different groups bonded to these atoms, and **I**, which has the same cage carbon substituents, also shows nonequivalent cage carbons. An inspection of various cage carbon-THF, -Cl, and -Li distances in the structures shown in Figures 1, 2, and 5 reveals that the cage carbons of a particular carborane are not equidistant from either the Zr-bound THF (or $\text{CH}_2\text{-SiMe}_3$) ligand or the bridging Li group. At this point it is not possible to assess the relative importance of the two inequalities in determining the multiplicity of the ^{13}C NMR resonances found in the zirconacarboranes. The fact that the ^{13}C NMR spectrum of compound **IV**, which does not have lithium bridges, shows equivalent cage carbons argues for the importance of lithium placement. However, it should be noted that, with the exception of compound **IV**, none of the solid-state structures correctly predicts the solution ^{13}C NMR spectra of the compounds investigated in this study. In addition, the observation that the resonances in both the ^{11}B and ^{13}C NMR spectra of **IV** are much sharper than those of the other zirconacarboranes suggests that some fluxionality involving the bridged lithium groups exists in solution. The ^7Li NMR spectra of **I**, **II**, and **V**

show single resonances at -0.96 , -0.34 , and -1.70 ppm, respectively, which are typical of *exo*-polyhedrally bound lithiums found in the group 1 C_2B_4 cage carboranes.^{11a,23}

The infrared spectra of the compounds show absorptions expected from the structures and formulas of the compounds. These absorptions are listed in Table 5 for the purposes of qualitative analysis.

Conclusion. Although the full-sandwich carboranes 1-Cl-1-(THF)-2,2'-(SiMe_3)₂-3,3'-(R)₂-4,4',5,5'-Li(THF)-1,1'-*commo*-Zr(2,3- $\text{C}_2\text{B}_4\text{H}_4$)₂ (R = SiMe_3 (**I**), Me (**II**), H (**III**)) form readily and are structurally similar to the bent-sandwich chlorozirconocenes, they differ markedly in their reactivities. The coordinated chloride ligands in **I-III** were found to be substitutionally inert in the presence of the Grignard reagent $\text{Me}_3\text{SiCH}_2\text{MgCl}$ or other alkylating agents, such as AlMe_3 and LiR (R = Me, *t*-Bu, Me_3SiCH_2). The solid-state structures of **I**, **II**, and several of the reaction products of **I** and the Grignard reagent showed that the Cl ligand was well protected by the large SiMe_3 groups on the carborane cage carbons. The effects of different substituents on the cage carbons of the carborane ligands of the chlorozirconacarborane and chlorohafnacborane sandwich complexes are currently under investigation in our laboratories.

Acknowledgment. This work was supported in part by grants from the Texas Advanced Technology Program (Grant No. 003613006), the National Science Foundation (Grant No. CHE-9400672), the Robert A. Welch Foundation (Grant No. N-1016), the Southern Methodist University Research Council, and the donors of the Petroleum Research Fund, administered by the American Chemical Society.

Supplementary Material Available: Tables of anisotropic thermal parameters and H atom positional parameters for **I**, **THF**, **II**, **IV**, and **V** (9 pages). Ordering information is given on any current masthead page.

OM9407767

(23) Wang, Y.; Zhang, H.; Maguire, J. A.; Hosmane, N. S. *Organometallics* 1993, 12, 3781.

Cyclobutyne Ligands. 6. Reactions of Alkynes with the (Cyclobutyne)triosmium Complex

$\text{Os}_3(\text{CO})_9(\mu_3\text{-C}_2\text{CH}_2\text{C}(\text{Me})^t\text{Bu})(\mu_3\text{-S})$ in the Presence of UV Irradiation

Richard D. Adams,* Xiaosu Qu, and Wengan Wu

Department of Chemistry and Biochemistry, University of South Carolina,
Columbia, South Carolina 29208

Received October 28, 1994[⊗]

The reactions of the substituted-cyclobutyne triosmium cluster complex $\text{Os}_3(\text{CO})_9[\mu_3\text{-C}_2\text{-CH}_2\text{C}(\text{Me})^t\text{Bu}](\mu_3\text{-S})$ (**1**) with diphenylacetylene and diethylacetylene in the presence of UV irradiation have been investigated. From these reactions the new compounds $\text{Os}_3(\text{CO})_8[\mu_3\text{-SCC}(\text{Me})^t\text{BuCH}_2\text{CCPhCPh}]$ (**2**) and $\text{Os}_3(\text{CO})_8[\mu_3\text{-SCC}(\text{Me})^t\text{BuCH}_2\text{CCEtC}^t\text{Et}]$ (**5**) were obtained when the **1** to alkyne ratios were kept low. Small amounts of the two dimeric isomers *trans*- $[\text{Os}_3(\text{CO})_8\{\mu_3\text{-C}_2\text{CH}_2\text{C}(\text{Me})^t\text{Bu}\}(\mu_4\text{-S})]_2$ (**3**) and *cis*- $[\text{Os}_3(\text{CO})_8\{\mu_3\text{-C}_2\text{CH}_2\text{C}(\text{Me})^t\text{Bu}\}(\mu_4\text{-S})]_2$ (**4**) were formed in both reactions. Compounds **2–4** were characterized by single-crystal X-ray diffraction analyses. Compound **2** contains an open triosmium cluster with a bridging $\text{SCC}(\text{Me})^t\text{BuCH}_2\text{CCPhCPh}$ ligand formed by the cleavage of the formal C–C “triple” bond of the cyclobutyne and coupling of its carbon atoms to the sulfido ligand and the added diphenylacetylene molecule. Compounds **3** and **4** are dimers of the unit $\text{Os}_3(\text{CO})_8[\mu_3\text{-C}_2\text{-CH}_2\text{C}(\text{Me})^t\text{Bu}](\mu_3\text{-S})$ formed simply by the decarbonylation of **1** and formation of Os–S bonds between the two triosmium units. Compounds **3** and **4** were obtained in better yields by the irradiation of **1** in the absence of the alkynes. UV irradiation of solutions of diethylacetylene and **1** in a 30/1 ratio yielded the new compound $\text{Os}_3(\text{CO})_8[\mu\text{-EtCCEtC}_2\text{-CH}_2\text{C}(\text{Me})^t\text{Bu}][\mu\text{-S}(\text{Et})\text{C}=\text{C}(\text{Et})\text{C}=\text{O}]$ (**6**). Compound **6** was also characterized by a single-crystal X-ray diffraction analysis. This compound contains a closed triosmium cluster with

a bridging $\text{EtCCEtC}_2\text{CH}_2\text{C}(\text{Me})^t\text{Bu}$ ligand formed by the coupling of one molecule of $\text{EtC}\equiv\text{CEt}$ to the cyclobutyne ligand and a bridging $\text{S}(\text{Et})\text{C}=\text{C}(\text{Et})\text{C}=\text{O}$ ligand formed by the coupling of a molecule of $\text{EtC}\equiv\text{CEt}$ and a CO ligand to the sulfido ligand. Crystal data: for **2**, space group $P2_1/n$, $a = 11.557(2)$ Å, $b = 11.964(2)$ Å, $c = 22.954(3)$ Å, $\beta = 92.83(1)^\circ$, $Z = 4$, 2748 reflections, $R = 0.026$; for **3**, space group $P2_1/c$, $a = 18.746(4)$ Å, $b = 15.090(2)$ Å, $c = 19.104(4)$ Å, $\beta = 114.88(2)^\circ$, $Z = 4$, 2659 reflections, $R = 0.040$; for **4**, space group $C2/c$, $a = 15.521(4)$ Å, $b = 18.375(3)$ Å, $c = 16.419(3)$ Å, $\beta = 104.65(2)^\circ$, $Z = 4$, 1466 reflections, $R = 0.041$. For **6**, space group $P2_12_12_1$, $a = 17.805(2)$ Å, $b = 18.277(3)$ Å, $c = 9.927(1)$ Å, $Z = 4$, 2307 reflections, $R = 0.023$.

Introduction

We have recently reported the preparation and characterization of several metal cluster complexes that contain the first examples of cyclobutyne and substituted-cyclobutyne ligands.^{1–3} Although theoretical calculations have indicated that the free cyclobutyne molecule $\text{C}\equiv\text{CCH}_2\text{CH}_2$ exists on a potential minimum, uncomplexed cyclobutyne has not yet been isolated.⁴ This is attributed to the presence of substantial ring strain. In our complexes the cyclobutyne ligands are stabilized through bridging coordinations that apparently relieve

some of the ring strain. Indeed, the stabilization is so great that we have found only limited evidence for ring-opening transformations of our coordinated cyclobutyne. It appears to be easier to open the rings of coordinated cyclobutenyl ligands than those of our cyclobutyne ligands.⁵ Our studies have shown that the cyclobutyne ligand has spectroscopic and reactivity properties similar to those of unstrained alkyne complexes.^{1–3,5} In a previous study we reported that the reaction of the cyclobutyne complex $\text{Os}_3(\text{CO})_9(\mu_3\text{-}\eta^2\text{-C}_2\text{-CH}_2\text{CH}_2)(\mu\text{-SPh})$ (**A**) with diphenylacetylene yielded the

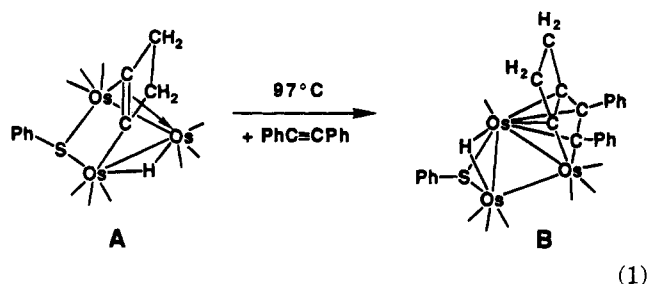
complex $\text{Os}_3(\text{CO})_7[\mu\text{-C}(\text{Ph})\text{C}(\text{Ph})\text{CCCH}_2\text{CH}_2](\mu\text{-SPh})(\mu\text{-H})$ (**B**), in which the cyclobutyne ligand had become coupled to a molecule of diphenylacetylene (eq 1).⁶

We have recently reported the preparation of sulfide cluster complex $\text{Os}_3(\text{CO})_9(\mu_3\text{-C}_2\text{CH}_2\text{C}(\text{Me})^t\text{Bu})(\mu_3\text{-S})$ (**1**),

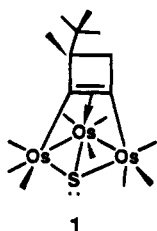
(5) Adams, R. D.; Chen, L.; Qu, X. *Organometallics* 1994, 13, 1992.

(6) Adams, R. D.; Chen, G.; Qu, X.; Wu, W.; Yamamoto, J. H. *Organometallics* 1993, 12, 3426.

[⊗] Abstract published in *Advance ACS Abstracts*, February 1, 1995.
(1) (a) Adams, R. D.; Chen, G.; Qu, X.; Wu, W.; Yamamoto, J. H. *Organometallics* 1993, 12, 3029. (b) Adams, R. D.; Chen, G.; Qu, X.; Wu, W.; Yamamoto, J. H. *J. Am. Chem. Soc.* 1992, 114, 10977.
(2) Adams, R. D.; Qu, X.; Wu, W. *Organometallics* 1993, 12, 4117.
(3) Adams, R. D.; Qu, X.; Wu, W. *Organometallics* 1994, 13, 1272.
(4) (a) Carlson, H. A.; Quelch, G. E.; Schaefer, H. F., III. *J. Am. Chem. Soc.* 1992, 114, 5344. (b) Fitzgerald, G.; Saxe, P.; Schaefer, H. F., III. *J. Am. Chem. Soc.* 1983, 105, 690.



which contains the triply bridging substituted cyclobutene ligand $\overline{C_2CH_2C(Me)^tBu}$.²



We have now investigated the reaction of **1** with diphenylacetylene and diethylacetylene in the presence of UV irradiation. In both cases, products containing ligands formed by the addition of an alkyne to the cyclobutene ligand and a rupture of the C–C multiple bond of the cyclobutene ligand were observed. In the presence of a large excess of diethylacetylene a product formed by the addition of two alkynes without an opening of the cyclobutene ring was observed. The results of this study are reported here.

Experimental Section

General Procedures. Reactions were performed under a dry nitrogen atmosphere. Reagent grade solvents were purified by distillation under nitrogen from the appropriate drying agents (sodium/benzophenone for benzene, CaH_2 for CH_2Cl_2 and hexane). They were stored over molecular sieves and deoxygenated by purging with nitrogen prior to use. $Os_3(CO)_9[\mu_3-C_2CH_2C(Me)^tBu](\mu_3-S)$ (**1**) was prepared according to the published procedure.² IR spectra were recorded on a Nicolet 5DXB FT-IR spectrophotometer. ¹H NMR spectra were recorded on either a Bruker AM-300 or a Bruker AM-500 FT-NMR spectrometer. Mass spectra were recorded on a VG Model 70SQ mass spectrometer by the direct inlet method. Elemental microanalyses were performed by Desert Analytics Organic Microanalysis, Tucson, AZ. UV irradiations were performed by using an externally positioned 360-W medium-pressure mercury arc lamp purchased from Gates Engineering, Long Island, NY, or a 500-W medium-pressure mercury arc lamp purchased from American Ultraviolet Company, Murray Hill, NJ, on solutions in Pyrex glassware. TLC separations were performed in the open air using silica gel (60 Å, F_{254}) on plates (Analtech, 0.25 mm).

Reaction of $Os_3(CO)_9[\mu_3-C_2CH_2C(Me)^tBu](\mu_3-S)$ (1**) with Diphenylacetylene.** A 28.0-mg amount of **1** (0.029 mmol) and a 10.2-mg amount of diphenylacetylene (0.057 mmol) were dissolved in 30 mL of hexane. The solution was irradiated for 2 h. The solvent was removed via rotary evaporation, and the residue was then separated by TLC using hexane solvent to yield (in the order of elution) 18.0 mg of yellow unreacted **1**, 4.0 mg of yellow $Os_3(CO)_8[\mu_3-SCC(Me)^tBuCH_2CPhCPh]$; (**2**; 35% yield), 2.3 mg of yellow *trans*- $[Os_3(CO)_8[\mu_3-C_2CH_2C(Me)^tBu](\mu_4-S)]_2$ (**3**; 24% yield), and 1.0 mg of orange *cis*-

$[Os_3(CO)_8[\mu_3-C_2CH_2C(Me)^tBu](\mu_4-S)]_2$ (**4**; 10% yield). All yields were calculated on the basis of the amount of **1** consumed. Longer irradiation periods did not produce higher yields. Spectroscopic data for the products are as follows. IR (ν_{CO} in hexane, cm^{-1}) for **2**: 2079 (m), 2061 (vs), 2029 (m), 2006 (vs), 1999 (w), 1994 (w), 1986 (s), 1981 (m), 1975 (w). ¹H NMR (δ in $CDCl_3$) for **2**: 7.30–7.08 (m, 10H), 3.96 (d, 1H, ² J_{HH} = 13.8 Hz), 3.87 (d, 1H, ² J_{HH} = 13.8 Hz), 1.31 (s, 3H), 1.01 (s, 9H). Anal. Calcd (found) for **2**: C, 33.00 (33.05); H, 2.13 (2.05). IR (ν_{CO} in hexane, cm^{-1}) for **3**: 2085 (s), 2057 (vs), 2027 (vs), 2008 (m), 2000 (m), 1995 (m), 1955 (m). ¹H NMR (δ in $CDCl_3$) for **3**: 3.51 (d, 1H, ² J_{HH} = 14.4 Hz), 3.44 (d, 1H, ² J_{HH} = 14.4 Hz), 2.38 (d, 1H, ² J_{HH} = 14.4 Hz), 2.34 (d, 1H, ² J_{HH} = 14.4 Hz), 1.16 (s, 3H), 1.06 (s, 3H), 1.00 (s, 9H), 0.94 (s, 9H). The mass spectrum of **3** showed the parent ion at m/e 1898 for ¹⁹²Os₆ and ions corresponding to the loss of each of the 2 *tert*-butyl groups and 16 carbonyl ligands. IR (ν_{CO} in hexane, cm^{-1}) for **4**: 2083 (vs), 2062 (s), 2031 (vs), 2006 (s), 1998 (m), 1990 (w), 1964 (w). ¹H NMR (δ in $CDCl_3$) for **4**: 3.60 (d, 2H, ² J_{HH} = 14.7 Hz), 2.53 (d, 2H, ² J_{HH} = 14.7 Hz), 1.20 (s, 6H), 1.10 (s, 18H). The mass spectrum of **4** showed the parent ion at m/e 1898 for ¹⁹²Os₆ and ions corresponding to the loss of each of the 2 *tert*-butyl groups and 16 carbonyl ligands.

Reaction of **1 with 5 Equiv of Diethylacetylene.** A 29.5-mg amount of **1** (0.0302 mmol) and a 17- μ L amount of diethylacetylene (0.15 mmol, 5 equiv) were dissolved in 180 mL of hexane. The solution was irradiated with a 360 W medium-pressure mercury arc lamp for 3 h with a slow purge of nitrogen through the solution. The solvent was then removed via rotary evaporation, and the residue was separated on TLC using hexane solvent to yield in the order of elution: 10.3 mg of yellow unreacted **1** (35%), 5.5 mg of yellow $Os_3(CO)_8[\mu_3-SCC(Me)^tBuCH_2CCEtCEt]$ (**5**; 27%, calculated yield is based on the amount of **1** consumed), 1.0 mg of **3** (5%), and a trace amount of **4** as detected by IR spectroscopy. Spectroscopic data for compound **5** are as follows. IR (ν_{CO} in hexane, cm^{-1}) for **5**: 2077 (m), 2058 (vs), 2025 (m), 2001 (vs), 1994 (m), 1983 (s), 1976 (m), 1969 (w). ¹H NMR (δ in $CDCl_3$) for **5**: 3.66 (d, 1H, ² J_{HH} = 13 Hz), 3.52 (d, 1H, ² J_{HH} = 13 Hz), 2.99 (dq, 2H, ² J_{HH} = 15 Hz, ³ J_{HH} = 7 Hz), 2.19 (dq, 1H, ² J_{HH} = 14 Hz, ³ J_{HH} = 8 Hz), 1.90 (dq, 1H, ² J_{HH} = 14 Hz, ³ J_{HH} = 8 Hz), 1.24 (t, 3H, ³ J_{HH} = 8 Hz), 1.19 (s, 3H), 1.16 (t, 3H, ³ J_{HH} = 7 Hz), 0.98 (s, 9H). The mass spectrum of **5** showed the parent ion at m/e 1032 and ions corresponding to the loss of each of eight carbonyl ligands.

Reaction of **1 with 30 Equiv of Diethylacetylene.** A 18.0-mg amount of **1** (0.018 mmol) and a 63- μ L amount of diethylacetylene (0.55 mmol, 30 equiv) were dissolved in 150 mL of hexane. The solution was irradiated for 2 h. The solvent was then removed via rotary evaporation, and the residue was separated by TLC using hexane solvent to yield (in the order of elution) 12.3 mg of yellow unreacted **1** and 2.5 mg of orange $Os_3(CO)_8[\mu_3-EtCCEtC_2CH_2C(Me)^tBu](\mu_4-S)(Et)C=C(Et)C=O]$ (**6**; 39% yield based on the amount of **1** consumed). Longer irradiation periods did not produce higher yields. This would be possible if the product **6** were also sensitive to UV irradiation. Spectroscopic data for the product are as follows. IR (ν_{CO} in hexane, cm^{-1}) for **6**: 2085 (w), 2066 (s), 2028 (s), 2012 (vs), 1995 (vs), 1988 (m), 1975 (m), 1956 (w). ¹H NMR (δ in $CDCl_3$) for **6**: 3.79 (d, 1H, ² J_{HH} = 13.8 Hz), 3.34 (d, 1H, ² J_{HH} = 13.8 Hz), 2.93 (dq, 1H, ² J_{HH} = 12.7 Hz, ³ J_{HH} = 7.5 Hz), 2.80 (dq, 1H, ² J_{HH} = 14.4 Hz, ³ J_{HH} = 7.5 Hz), 2.73 (dq, 1H, ² J_{HH} = 12.7 Hz, ³ J_{HH} = 7.5 Hz), 2.55–2.45 (m, 2H), 2.25 (dq, 1H, ² J_{HH} = 13.0 Hz, ³ J_{HH} = 7.5 Hz), 2.18 (dq, 1H, ² J_{HH} = 14.4 Hz, ³ J_{HH} = 7.5 Hz), 1.96 (dq, 1H, ² J_{HH} = 13.0 Hz, ³ J_{HH} = 7.5 Hz), 1.69 (s, 3H), 1.25 (t, 3H, ³ J_{HH} = 7.5 Hz), 1.24 (t, 3H, ³ J_{HH} = 7.5 Hz), 1.10 (t, 3H, ³ J_{HH} = 7.5 Hz), 1.04 (s, 9H), 0.78 (t, 3H, ³ J_{HH} = 7.5 Hz). Anal. Calcd (found) for **6**: C, 31.26 (31.57); H, 3.05 (3.01).

Photolysis of $Os_3(CO)_8[\mu_3-C_2CH_2C(Me)^tBu](\mu_3-S)$ (1**) in**

Table 1. Crystal Data for Compounds 2–6

	2	3	4	6
formula	Os ₃ S ₈ O ₈ C ₃₁ H ₂₄	Os ₆ S ₂ O ₁₆ C ₃₄ H ₂₈ ·C ₆ H ₆	Os ₆ S ₂ O ₁₆ C ₃₄ H ₂₈	Os ₃ S ₈ O ₈ C ₂₉ H ₃₄
formula wt	1127.19	1976.02	1897.91	1113.24
cryst syst	monoclinic	monoclinic	monoclinic	orthorhombic
lattice params				
<i>a</i> (Å)	11.557(2)	18.746(4)	15.521(4)	17.805(2)
<i>b</i> (Å)	11.964(2)	15.090(2)	18.375(3)	18.277(3)
<i>c</i> (Å)	22.954(3)	19.104(4)	16.419(3)	9.927(1)
α (deg)	90	90	90	90
β (deg)	92.83(1)	114.88(2)	104.65(2)	90
γ (deg)	90	90	90	90
<i>V</i> (Å ³)	3170(1)	4902(2)	4530(3)	3230.4(7)
space group	<i>P</i> 2 ₁ / <i>n</i> (No. 14)	<i>P</i> 2 ₁ / <i>c</i> (No. 14)	<i>C</i> 2/ <i>c</i> (No. 15)	<i>P</i> 2 ₁ 2 ₁ 2 ₁ (No. 19)
<i>Z</i> value	4	4	4	4
ρ_{calc} (g/cm ³)	2.36	2.68	2.78	2.29
μ (Mo K α) (cm ⁻¹)	121.17	156.51	169.31	118.89
temp (°C)	20	20	20	20
2 θ_{max} (deg)	43.0	40	43.0	46
no. of obs rflns (<i>I</i> > 3 σ (<i>I</i>))	2748	2659	1466	2307
goodness of fit (GOF)	1.20	1.40	1.18	1.34
residuals: ^a <i>R</i> ; <i>R</i> _w	0.026; 0.025	0.040; 0.033	0.041; 0.037	0.023; 0.025
largest peak in final diff map	0.58	1.80	1.28	0.57
abs cor, max/min	empirical, 1.0/0.54	empirical, 1.0/0.83	empirical, 1.0/0.44	DIFABS, 1.09/0.87

$$^a R = \sum_{hkl} (||F_o| - |F_c|| / \sum_{hkl} |F_o|); R_w = [\sum_{hkl} w(|F_o| - |F_c|)^2 / \sum_{hkl} w |F_o|^2]^{1/2}, w = 1/\sigma^2(F_o); \text{GOF} = [\sum_{hkl} (|F_o| - |F_c|/\sigma(F_o))] / (n_{\text{data}} - n_{\text{vari}}).$$

Hexane. A 20.0-mg amount of **1** (0.0205 mmol) was dissolved in 10 mL of hexane. The solution was irradiated with a medium-pressure 500-W mercury lamp for 3 h with a slow purge of nitrogen through the solution. The solvent was then removed via rotary evaporation, and the residue was separated on TLC using hexane solvent. An 11.5-mg amount of yellow **1** was recovered (58%), and 4.2 mg of yellow **2** (51% yield, based on the amount of **1** consumed) and 1.0 mg of orange **3** (12%, based on the amount of **1** consumed) were isolated. Longer irradiation periods did not lead to increased yields.

Reaction of 3 with CO. A 5.0-mg amount of **3** (0.0026 mmol) was dissolved in 10 mL of CH₂Cl₂ and placed in a 45-mL Parr high-pressure reaction vessel. The vessel was pressurized with CO to 15 atm and then heated at 50 °C for 12 h. After the mixture was cooled, the solvent was removed in vacuo. The residue was dissolved in the minimum amount of CH₂Cl₂ and was separated by TLC using hexane solvent. This yielded 4.8 mg of **1** as the only product (93% yield).

Reaction of 4 with CO. A 5.0-mg amount of **4** (0.0026 mmol) was dissolved in 10 mL of CH₂Cl₂ and placed in a 45-mL Parr high-pressure reaction vessel. The vessel was pressurized with CO to 15 atm and then heated at 50 °C for 12 h. After the mixture was cooled, the solvent was removed in vacuo. The residue was dissolved in the minimum amount of CH₂Cl₂ and was separated by TLC using hexane solvent. This yielded 4.6 mg of **1** as the only product (90% yield).

Crystallographic Analyses. Crystals of **2** and **5** suitable for X-ray diffraction analysis were grown from a solution in a dichloromethane and hexane solvent mixture by slow evaporation of the solvent at -14 °C. Crystals of **3** suitable for X-ray diffraction analysis were grown from a solution in a benzene and hexane solvent mixture by slow evaporation of the solvent at 25 °C. Crystals of **4** suitable for X-ray diffraction analysis were grown from a solution in a dichloromethane and methanol solvent mixture by slow evaporation of the solvent at 25 °C. All crystals used in intensity measurements were mounted in thin-walled glass capillaries. Diffraction measurements were made on a Rigaku AFC6S automatic diffractometer by using graphite-monochromated Mo K α radiation. Unit cells were determined from 25 randomly selected reflections obtained by using the AFC6 automatic search, center, index, and least-squares routines. Crystal data, data collection parameters, and results of the analyses are listed in Table 1. All data processing was performed on a Digital Equipment Corp. VAXstation 3520 computer by using the TEXSAN structure solving program library obtained from Molecular Structure Corp., The Woodlands, TX. Lorentz-polarization (*L*_p) and

absorption corrections were applied to the data in each analysis. Neutral atom scattering factors were calculated by the standard procedures.^{7a} Anomalous dispersion corrections were applied to all non-hydrogen atoms.^{7b} All structures were solved by a combination of direct methods (MITHRIL) and difference Fourier syntheses. Full-matrix least-squares refinements minimized the function $\sum_{hkl} w(|F_o| - |F_c|)^2$, where $w = 1/\sigma(F)^2$, $\sigma(F) = \sigma(F_o^2)/2F_o$, and $\sigma(F_o^2) = [\sigma(I_{\text{raw}})^2 + (0.02I_{\text{net}})^2]^{1/2}/Lp$. For all four analyses, the positions of the hydrogen atoms on the ligands were calculated by assuming idealized geometry (C-H = 0.95 Å). The scattering contributions of all hydrogen atoms were added to the structure factor calculations, but their positions were not refined.

Compound **2** crystallized in the monoclinic crystal system. The space group *P*2₁/*n* was established on the basis of the patterns of systematic absences observed in the data. All non-hydrogen atoms were refined with anisotropic thermal parameters.

Compound **3** crystallized in the monoclinic crystal system. The space group *P*2₁/*c* was established on the basis of the patterns of systematic absences observed in the data. All atoms heavier than carbon were refined with anisotropic thermal parameters. The carbon atoms were refined with isotropic thermal parameters. In the final stages of the refinement a molecule of benzene for the crystallization solvent was located in the lattice. It was added to the analysis and was satisfactorily refined with isotropic thermal parameters for the carbon atoms.

Compound **4** crystallized in the monoclinic crystal system. The patterns of systematic absences observed in the data were consistent with both of the space groups *Cc* and *C2/c*. The centric space group was selected and confirmed by the successful solution and refinement of the structure. All atoms heavier than carbon were refined with anisotropic thermal parameters. The carbon atoms were refined with isotropic thermal parameters.

Compound **6** crystallized in the orthorhombic crystal system. The space group *P*2₁2₁2₁ was assumed and confirmed by the successful solution and refinement of the structure. All non-hydrogen atoms were refined with anisotropic thermal parameters. At the completion of refinement the values of all positional parameters were inverted and the structure was refined again to test for the correctness of the enantiomorph.

(7) (a) *International Tables for X-ray Crystallography*; Kynoch Press: Birmingham, England, 1975; Vol. IV, Table 2.2B, pp 99–101. (b) *Ibid.*, Table 2.3.1, pp 149–150.

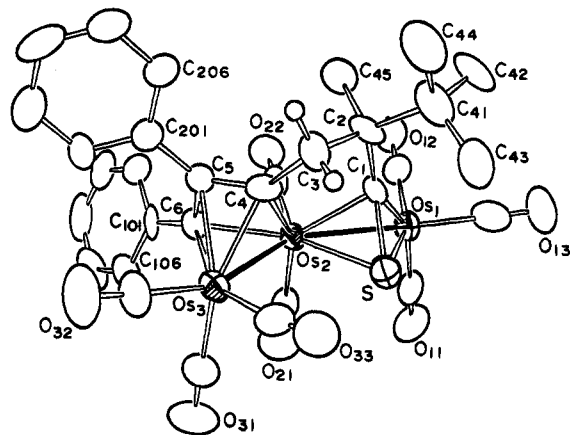


Figure 1. ORTEP diagram of $\text{Os}_3(\text{CO})_8[\mu_3\text{-SCC}(\text{Me})\text{-}^t\text{BuCH}_2\text{CCPhCPh}]$ (**2**) showing 50% probability thermal ellipsoids.

The residuals from this refinement were significantly poorer, and thus, the original set of positional parameters was used in the final calculations.

Results

From the reaction of complex **1** with $\text{PhC}\equiv\text{CPh}$ in the presence of UV irradiation, we have isolated three new compounds: $\text{Os}_3(\text{CO})_8[\mu_3\text{-SCC}(\text{Me})\text{-}^t\text{BuCH}_2\text{CCPhCPh}]$ (**2**; 35% yield), *trans*- $\{\text{Os}_3(\text{CO})_8[\mu_3\text{-C}_2\text{CH}_2\text{C}(\text{Me})\text{-}^t\text{Bu}](\mu_4\text{-S})\}_2$ (**3**; 24% yield), and *cis*- $\{\text{Os}_3(\text{CO})_8[\mu_3\text{-C}_2\text{CH}_2\text{C}(\text{Me})\text{-}^t\text{Bu}](\mu_4\text{-S})\}_2$ (**4**; 10% yield). The obtained yields are actually quite low. The given yields are based on the amount of **1** consumed, and most of the reagent **1** was recovered after the reaction. Unfortunately, longer irradiation periods did not produce higher yields.

UV irradiation of solutions of diethylacetylene and **1** in a 5/1 ratio yielded the new compound $\text{Os}_3(\text{CO})_8[\mu_3\text{-}(\text{EtC}(\text{Et})\text{CCH}_2\text{C}(\text{Me})\text{-}^t\text{Bu})\text{CS}]$ (**5**) in 27% yield. A small amount of **3** (5%) and a trace of **4** were obtained in this reaction also. The IR spectrum of **5** is virtually identical with that of **2**, indicating that the two compounds are structurally similar. Compounds **2**–**4** were further characterized by single-crystal X-ray diffraction analyses.

An ORTEP diagram of the molecular structure of **2** is shown in Figure 1. Final atomic positional parameters are listed in Table 2, and selected interatomic distances and angles are listed in Tables 3 and 4. The molecule consists of an open triangular cluster of three osmium atoms. It has the very unusual bridging organosulfur ligand $\text{SCC}(\text{Me})\text{-}^t\text{BuCH}_2\text{CCPhCPh}$, which is terminated at one end with the sulfur atom. The sulfur atom and the adjacent carbon atom can be viewed as a thioacyl grouping. It is coordinated perpendicular to the $\text{Os}(1)\text{-Os}(2)$ bond. There are only a few previous reports of such groupings.⁸ The $\text{C}(1)\text{-S}$ distance of 1.76(1) Å is similar to those observed for the $\mu\text{-SCR}$ ligands in the complexes $\text{CpMoFe}(\text{CO})_5(\mu\text{-SC-}p\text{-tolyl})$ (1.735(2) Å^{8b}) and $(\text{MeC}_5\text{H}_4)_2\text{Mo}_2(\text{CO})_2(\mu\text{-SEt})(\mu\text{-SCMe})$ (1.751(2) Å^{8c}). The six-carbon chain was formed by a

Table 2. Positional Parameters and $B(\text{eq})$ Values (Å²) for **2**

atom	x	y	z	$B(\text{eq})$
Os(1)	0.65632(04)	0.45437(04)	0.87409(02)	3.04(2)
Os(2)	0.44402(04)	0.33952(04)	0.86983(02)	2.50(2)
Os(3)	0.28155(04)	0.23177(04)	0.79968(02)	3.04(2)
S	0.5677(03)	0.3637(03)	0.78996(13)	3.3(1)
O(11)	0.5875(09)	0.7043(08)	0.8672(04)	6.0(6)
O(12)	0.7296(08)	0.4497(08)	1.0026(04)	5.0(5)
O(13)	0.9015(08)	0.4931(09)	0.8360(05)	6.8(6)
O(21)	0.3228(08)	0.5710(07)	0.8626(04)	5.6(6)
O(22)	0.4729(07)	0.3452(08)	1.0017(04)	4.7(5)
O(31)	0.1315(09)	0.4288(09)	0.7606(04)	6.7(6)
O(32)	0.0940(09)	0.0628(09)	0.7672(04)	6.9(6)
O(33)	0.4096(08)	0.2016(09)	0.6867(04)	5.9(6)
C(1)	0.6200(08)	0.2938(09)	0.8535(05)	2.6(5)
C(2)	0.6485(09)	0.1672(09)	0.8599(05)	3.2(6)
C(3)	0.5427(10)	0.1072(10)	0.8295(05)	3.7(6)
C(4)	0.4369(09)	0.1670(09)	0.8502(05)	2.8(5)
C(5)	0.3414(09)	0.1372(09)	0.8814(05)	2.7(5)
C(6)	0.2874(09)	0.2436(09)	0.8916(05)	2.6(5)
C(11)	0.6152(11)	0.6132(12)	0.8707(06)	4.1(7)
C(12)	0.7006(11)	0.4545(10)	0.9530(06)	3.9(7)
C(13)	0.8102(12)	0.4785(10)	0.8498(06)	4.3(7)
C(21)	0.3682(11)	0.4870(11)	0.8653(05)	3.5(6)
C(22)	0.4623(10)	0.3402(11)	0.9518(06)	3.7(6)
C(31)	0.1867(11)	0.3546(11)	0.7748(06)	4.3(7)
C(32)	0.1643(11)	0.1281(10)	0.7781(06)	4.0(7)
C(33)	0.3562(12)	0.2163(11)	0.7267(06)	4.5(7)
C(41)	0.7663(11)	0.1333(12)	0.8325(06)	4.9(8)
C(42)	0.8694(11)	0.1755(11)	0.8720(07)	5.5(8)
C(43)	0.7760(11)	0.1843(13)	0.7720(06)	5.4(8)
C(44)	0.7771(13)	0.0082(10)	0.8282(07)	7(1)
C(45)	0.6537(10)	0.1372(10)	0.9260(05)	4.0(6)
C(101)	0.2072(09)	0.2731(09)	0.9381(05)	2.8(6)
C(102)	0.2227(10)	0.2289(10)	0.9945(06)	3.9(7)
C(103)	0.1501(12)	0.2584(12)	1.0370(06)	4.8(8)
C(104)	0.0597(12)	0.3262(13)	1.0262(07)	5.3(8)
C(105)	0.0402(10)	0.3714(12)	0.9710(07)	5.0(8)
C(106)	0.1131(10)	0.3430(10)	0.9272(06)	4.0(6)
C(201)	0.2940(10)	0.0262(09)	0.8974(05)	3.2(6)
C(202)	0.1777(10)	0.0084(10)	0.9054(06)	4.2(7)
C(203)	0.1367(12)	-0.0941(12)	0.9211(07)	5.4(8)
C(204)	0.2118(15)	-0.1837(11)	0.9296(06)	5.7(9)
C(205)	0.3264(13)	-0.1683(11)	0.9220(07)	5.2(8)
C(206)	0.3689(10)	-0.0647(10)	0.9075(05)	4.0(7)

Table 3. Intramolecular Distances for **2**^a

Os(1)–Os(2)	2.8097(7)	Os(3)–C(6)	2.11(1)
Os(1)–S	2.400(3)	S–C(1)	1.76(1)
Os(1)–C(1)	2.02(1)	C(1)–C(2)	1.56(1)
Os(2)–Os(3)	2.7353(8)	C(2)–C(3)	1.55(2)
Os(2)–S	2.397(3)	C(2)–C(41)	1.58(2)
Os(2)–C(1)	2.16(1)	C(3)–C(4)	1.51(1)
Os(2)–C(4)	2.11(1)	C(4)–C(5)	1.39(1)
Os(2)–C(6)	2.22(1)	C(5)–C(6)	1.44(1)
Os(3)–C(4)	2.23(1)	Os–C (av)	1.91(2)
Os(3)–C(5)	2.27(1)	C–O (av)	1.14(1)

^a Distances are in angstroms. Estimated standard deviations in the least significant figure are given in parentheses.

Table 4. Intramolecular Bond Angles for **2**

Os(1)–Os(2)–Os(3)	145.47(2)	Os(2)–C(4)–C(5)	99.5(7)
C(1)–Os(2)–C(4)	75.1(4)	Os(3)–C(4)–C(3)	130.1(7)
C(4)–Os(2)–C(6)	61.3(4)	C(3)–C(4)–C(5)	136(1)
Os(2)–C(1)–C(2)	115.3(7)	C(4)–C(5)–C(6)	102.5(9)
S–C(1)–C(2)	127.0(8)	C(6)–C(5)–C(201)	125(1)
C(1)–C(2)–C(3)	104.4(9)	Os(2)–C(6)–C(5)	93.2(6)
C(2)–C(3)–C(4)	106(1)	C(5)–C(6)–C(101)	128(1)
Os(2)–C(4)–C(3)	120.3(8)	Os–C–O (av)	177(2)

^a Angles are in degrees. Estimated standard deviations in the least significant figure are given in parentheses.

combination of 1 equiv of diphenylacetylene with the cyclobutene ligand; the latter, however, has undergone a rupture of one of the C–C bonds in the ring. On the basis of the location of the substituents on the carbon atoms in the product, it is clear that the bond that was

(8) Linford, L.; Raubenheimer, H. G. *Adv. Organomet. Chem.* **1991**, *32*, 1. (b) Alper, H.; Einstein, F. W. P.; Hartstock, F. W.; Willis, A. C. *J. Am. Chem. Soc.* **1985**, *107*, 173. (c) Byrne, P. G.; Garcia, M. E.; Jeffrey, J. C.; Sherwood, P.; Stone, F. G. A. *J. Chem. Soc., Dalton Trans.* **1987**, 1215.

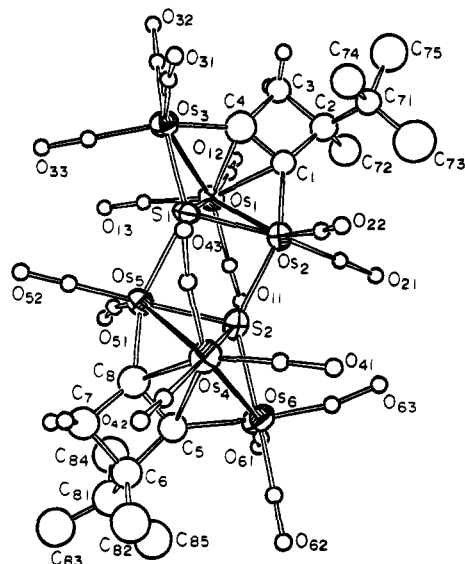


Figure 2. ORTEP diagram of *trans*-[Os₃(CO)₈{μ₃-C₂-CH₂C(Me)^tBu}(μ₄-S)]₂ (**3**) showing 50% probability thermal ellipsoids.

cleaved was the coordinated C–C multiple bond. The bonds C(1)–C(2), C(2)–C(3), and C(3)–C(4) are single (1.56(1), 1.55(1), and 1.58(2) Å, respectively), but the bonds C(4)–C(5) and C(5)–C(6) have multiple-bond character (1.39(1) and 1.44(1) Å). The three-carbon unit C(4), C(5), and C(6) can be described as a dimetallaallyl grouping that is π-bonded to Os(3) and σ-bonded to Os(2). Dimetallaallyl ligands bridging dimetal centers have been observed previously.⁹ The molecule has no overall symmetry. Accordingly, the hydrogen atoms of the methylene group C(3) are inequivalent and they appear as an AB quartet in the ¹H NMR spectrum (δ 3.96 (d, ²J_{HH} = 13.8 Hz) and 3.87 (d, ²J_{HH} = 13.8 Hz) ppm), as expected. Compound **5** exhibits an analogous AB quartet for the corresponding methylene group in it (δ 3.66 (d, 1H, ²J_{HH} = 13 Hz) and 3.52 (d, 1H, ²J_{HH} = 13 Hz) ppm).

The products **3** and **4** contain neither diphenylacetylene nor diethylacetylene ligands or groupings derived from these molecules. This explains why they were formed in both reactions. They are byproducts of the photolysis of **1** formed by simple decarbonylation of the complex and the combination of two Os₃(CO)₈{μ₃-C₂-CH₂C(Me)^tBu}(μ₃-S) fragments. Indeed, they can be formed in better yields when the irradiation reactions are performed in the absence of the alkynes.

ORTEP diagrams of **3** and **4** are shown in Figures 2 and 3, respectively. Positional parameters and selected bond distances and angles are listed in Tables 5–10. Both molecules are dimers of the unit Os₃(CO)₈{μ₃-C₂-CH₂C(Me)^tBu}(μ₃-S). The Os₃(CO)₈{μ₃-C₂-CH₂C(Me)-

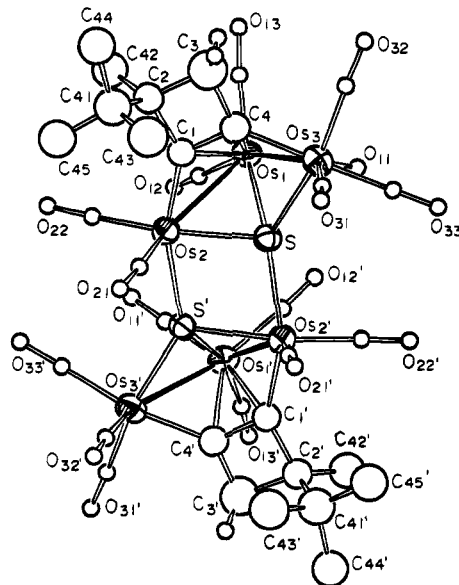


Figure 3. ORTEP diagram of *cis*-[Os₃(CO)₈{μ₃-C₂CH₂C(Me)^tBu}(μ₄-S)]₂ (**4**) showing 50% probability thermal ellipsoids.

^tBu}(μ₃-S) groupings in both molecules are structurally very similar to that of **1** and consist of an open triosmium cluster with the sulfido ligand coordinated to all three osmium atoms and the C–C triple bond of the substituted cyclobutyne coordinated to all three metal atoms on the other side of the cluster. The osmium–osmium bond distances in the dimers are similar to those in **1**, but the difference in lengths between the two metal–metal bonds within a given Os₃ grouping is significantly larger in the dimers (0.039(2) and 0.045(2) Å in **3** and 0.077(2) Å in **4**) than in the parent monomer (0.0213(9) Å). In both molecules the cluster units are linked by two mutually reinforcing sulfur to osmium donor–acceptor bonds (S(1) to Os(5) and S(2) to Os(2) in **3**) and two symmetry-equivalent donor–acceptor bonds (S to Os(2') and S' to Os(2) in **4**). These donor–acceptor bonds are significantly longer in **3** (S(1)–Os(5) = 2.515(7) Å, S(2)–Os(2) = 2.495(8) Å, and S–Os(2') = 2.488(7) Å) than those within the triosmium units, which range from 2.378(7) to 2.452(7) Å in both molecules. The coordinated C–C multiple bonds of the cyclobutyne ligands are also similar to that found in **1** (C(1)–C(4) = C(5)–C(8) = 1.43(3) Å in **3** and C(1)–C(4) = 1.41(3) Å in **4** vs C(1)–C(4) = 1.40(2) Å in **1**). Compound **4** contains a crystallographic 2-fold rotation axis and was formed by the coupling of two

structurally similar Os₃(CO)₈{μ₃-C₂CH₂C(Me)^tBu}(μ₃-S) fragments. The molecule is chiral, but the crystal consists of a racemic mixture of both enantiomers. Compound **3**, on the other hand, was formed by the

coupling of two diastereomeric Os₃(CO)₈{μ₃-C₂CH₂C(Me)^tBu}(μ₃-S) fragments: one formed by the loss of CO from the osmium atom in **1** proximate to the ^tBu-substituted carbon of the cyclobutyne ligand, Os(2), and the other formed by the loss of CO from the osmium atom proximate to the methylene carbon atom of the cyclobutyne ligand; see Scheme 1, which shows the combinations of the monomer units with the identities of the different metal atoms labeled. The formation of **3** thus indicates that decarbonylation of **1** can occur at both of

(9) (a) Adams, R. D.; Babin, J. E.; Tasi, M.; Wang, J.-G. *Organometallics* **1988**, *7*, 755. (b) Jeffrey, J. C.; Went, M. J. *Polyhedron* **1988**, *7*, 775 and references therein. (c) Hein, J.; Jeffrey, J. C.; Sherwood, P.; Stone, F. G. A. *J. Chem. Soc., Dalton Trans.* **1987**, 2211. (d) Delgado, E.; Garcia, M. E.; Jeffrey, J. C.; Sherwood, P.; Stone, F. G. A. *J. Chem. Soc., Dalton Trans.* **1988**, 207. (e) Chisholm, M. H.; Heppert, J. A.; Huffman, J. C. *J. Am. Chem. Soc.* **1984**, *106*, 1151. (f) Churchill, M. R.; Ziller, J. W.; Shapley, J. R.; Yeh, W. Y. *J. Organomet. Chem.* **1988**, *353*, 103.

Table 5. Positional Parameters and $B(\text{eq})$ Values (\AA^2) for 3

atom	x	y	z	$B(\text{eq})$
Os(1)	0.33257(07)	0.42885(08)	0.58470(07)	3.10(6)
Os(2)	0.27950(07)	0.47015(08)	0.42510(07)	3.07(6)
Os(3)	0.20246(07)	0.31781(08)	0.55463(07)	3.41(6)
Os(4)	0.09340(07)	0.66222(09)	0.33464(07)	3.70(6)
Os(5)	0.15167(07)	0.61359(08)	0.49297(07)	2.99(6)
Os(6)	0.22725(08)	0.76493(09)	0.36302(08)	4.22(7)
S(1)	0.1980(04)	0.4572(05)	0.4932(04)	2.9(3)
S(2)	0.2292(04)	0.6239(05)	0.4214(04)	3.2(3)
O(11)	0.4119(12)	0.6069(14)	0.5784(11)	5(1)
O(12)	0.4885(14)	0.3484(15)	0.6979(13)	8(1)
O(13)	0.2993(12)	0.4818(13)	0.7230(12)	5(1)
O(21)	0.4188(12)	0.5111(15)	0.3901(12)	6(1)
O(22)	0.1727(13)	0.4315(16)	0.2586(12)	8(1)
O(31)	0.0655(12)	0.2259(15)	0.4230(11)	6(1)
O(32)	0.2553(14)	0.1524(14)	0.6519(13)	7(1)
O(33)	0.1117(13)	0.3926(17)	0.6435(13)	7(1)
O(41)	0.1041(13)	0.6328(17)	0.1818(12)	8(1)
O(42)	-0.0721(14)	0.7379(19)	0.2449(15)	11(2)
O(43)	0.0256(13)	0.4764(16)	0.3312(11)	6(1)
O(51)	0.2621(13)	0.6741(14)	0.6527(12)	7(1)
O(52)	0.0188(12)	0.5919(13)	0.5393(11)	5(1)
O(61)	0.3760(12)	0.8495(16)	0.4791(14)	8(1)
O(62)	0.1762(16)	0.9254(18)	0.2582(17)	11(2)
O(63)	0.3048(12)	0.6756(16)	0.2725(13)	7(1)
C(1)	0.3154(14)	0.3463(17)	0.4699(14)	2.8(6)
C(2)	0.3725(16)	0.2727(19)	0.4690(16)	3.6(7)
C(3)	0.3512(15)	0.2228(17)	0.5286(14)	2.9(6)
C(4)	0.2872(17)	0.300(02)	0.5183(17)	4.7(7)
C(5)	0.1471(15)	0.7954(18)	0.4096(15)	3.5(6)
C(6)	0.1012(16)	0.8732(19)	0.4195(16)	3.7(7)
C(7)	0.0599(16)	0.8057(20)	0.4531(16)	4.1(7)
C(8)	0.1204(16)	0.7352(19)	0.4514(16)	4.2(7)
C(11)	0.3777(16)	0.5427(19)	0.5766(15)	2.8(6)
C(12)	0.4317(19)	0.376(02)	0.6528(18)	4.4(7)
C(13)	0.3142(19)	0.458(02)	0.6746(19)	4.6(8)
C(21)	0.365(02)	0.495(02)	0.4026(19)	5.3(8)
C(22)	0.2167(20)	0.447(02)	0.318(02)	5.1(8)
C(31)	0.1140(18)	0.2554(19)	0.4731(18)	3.8(7)
C(32)	0.2360(19)	0.216(02)	0.6156(19)	5.0(8)
C(33)	0.1413(18)	0.365(02)	0.6047(18)	4.2(7)
C(41)	0.1040(18)	0.644(02)	0.2476(19)	5.0(8)
C(42)	-0.009(02)	0.715(02)	0.285(02)	6.2(9)
C(43)	0.050(02)	0.552(03)	0.337(02)	7(1)
C(51)	0.2165(17)	0.6429(20)	0.5948(18)	4.0(7)
C(52)	0.0713(17)	0.5998(19)	0.5215(16)	3.7(7)
C(61)	0.3211(19)	0.818(02)	0.4319(18)	4.8(7)
C(62)	0.195(02)	0.865(02)	0.296(02)	6.0(9)
C(63)	0.273(02)	0.720(03)	0.305(02)	7(1)
C(71)	0.3472(15)	0.2232(17)	0.3930(15)	2.8(6)
C(72)	0.4592(17)	0.301(02)	0.5014(17)	5.1(8)
C(73)	0.368(02)	0.275(03)	0.336(02)	8(1)
C(74)	0.2606(17)	0.2053(20)	0.3567(16)	4.7(7)
C(75)	0.3868(19)	0.134(02)	0.4082(19)	6.2(8)
C(81)	0.1543(19)	0.941(02)	0.4867(18)	5.6(8)
C(82)	0.0460(19)	0.925(02)	0.3500(18)	5.8(8)
C(83)	0.1041(19)	0.998(02)	0.5110(18)	6.2(8)
C(84)	0.2147(19)	0.892(02)	0.5571(19)	6.1(8)
C(85)	0.2030(19)	1.003(02)	0.4597(19)	6.4(8)
C(101)	0.425(02)	0.015(03)	0.678(02)	8(1)
C(102)	0.462(02)	0.081(03)	0.731(02)	8(1)
C(103)	0.520(02)	0.131(02)	0.729(02)	7(1)
C(104)	0.544(02)	0.116(03)	0.670(02)	9(1)
C(105)	0.511(02)	0.052(03)	0.621(02)	7(1)
C(106)	0.454(02)	0.004(03)	0.624(02)	8(1)

the external metal atoms of the cluster. Compound **3** has no overall symmetry, but the crystal does contain an equimolar mixture of its two enantiomers. Compound **3** is isostructural and isomorphous with the

ruthenium homologue $\{\text{Ru}_3(\text{CO})_8[\mu_3\text{-C}_2\text{CH}_2\text{C}(\text{Me})^t\text{Bu}](\mu_4\text{-S})_2\}$, which we recently obtained in a very low yield from the reaction of $\text{Ru}_3(\text{CO})_{12}$ with 4-*tert*-butyl-4-methyl-1-(phenylthio)cyclobutene.³ Similar dimers were obtained by the decarbonylation of the related phenylacetylene complexes $\text{Ru}_3(\text{CO})_9(\mu_3\text{-}\eta^2\text{-PhC}_2\text{H})(\mu_3\text{-S})$ and

Table 6. Intramolecular Distances for 3^a

Os(1)—Os(2)	2.850(2)	Os(5)—S(1)	2.515(7)
Os(1)—Os(3)	2.811(2)	Os(5)—S(2)	2.382(7)
Os(1)—S(1)	2.427(7)	Os(5)—C(8)	1.99(3)
Os(1)—C(1)	2.42(2)	Os(6)—S(2)	2.396(8)
Os(1)—C(4)	2.28(3)	Os(6)—C(5)	2.09(3)
Os(2)—S(1)	2.395(8)	C(1)—C(2)	1.55(3)
Os(2)—S(2)	2.495(8)	C(1)—C(4)	1.43(3)
Os(2)—C(1)	2.05(3)	C(2)—C(3)	1.55(3)
Os(3)—S(1)	2.392(7)	C(3)—C(4)	1.62(4)
Os(3)—C(4)	2.00(3)	C(5)—C(6)	1.51(4)
Os(4)—Os(5)	2.846(2)	C(5)—C(8)	1.43(3)
Os(4)—Os(6)	2.801(2)	C(6)—C(7)	1.57(4)
Os(4)—S(2)	2.452(7)	C(7)—C(8)	1.57(4)
Os(4)—C(5)	2.43(3)	Os—C (av)	1.89(4)
Os(4)—C(8)	2.34(3)	O—C (av)	1.16(4)

^a Distances are in angstroms. Estimated standard deviations in the least significant figure are given in parentheses.

Table 7. Intramolecular Bond Angles for 3^a

Os(2)—Os(1)—Os(3)	91.66(5)	Os(4)—S(2)—Os(6)	70.6(2)
Os(5)—Os(4)—Os(6)	91.41(6)	Os(5)—S(2)—Os(6)	115.5(8)
Os(1)—S(1)—Os(2)	72.4(2)	C(2)—C(1)—C(4)	96(2)
Os(1)—S(1)—Os(3)	71.4(2)	C(1)—C(2)—C(3)	87(2)
Os(1)—S(1)—Os(5)	114.9(3)	C(2)—C(3)—C(4)	88(2)
Os(2)—S(1)—Os(3)	116.0(3)	C(1)—C(4)—C(3)	89(2)
Os(2)—S(1)—Os(5)	102.8(3)	C(6)—C(5)—C(8)	94(2)
Os(3)—S(1)—Os(5)	140.1(3)	C(5)—C(6)—C(7)	87(2)
Os(2)—S(2)—Os(4)	120.8(3)	C(6)—C(7)—C(8)	87(2)
Os(2)—S(2)—Os(5)	103.8(3)	C(5)—C(8)—C(7)	90(2)
Os(2)—S(2)—Os(6)	140.4(3)	Os—C—O (av)	174(4)
Os(4)—S(2)—Os(5)	72.1(2)		

^a Angles are in degrees. Estimated standard deviations in the least significant figure are given in parentheses.

Table 8. Positional Parameters and $B(\text{eq})$ Values (\AA^2) for 4

atom	x	y	z	$B(\text{eq})$
Os(1)	0.65462(07)	0.23673(05)	0.21223(07)	3.14(5)
Os(1)	0.61468(07)	0.12910(06)	0.32480(06)	2.94(5)
Os(3)	0.64352(08)	0.13052(07)	0.08757(07)	3.67(5)
S	0.5460(04)	0.1387(04)	0.1780(04)	2.9(3)
O(11)	0.5430(14)	0.3288(10)	0.0684(12)	6(1)
O(12)	0.6083(15)	0.3301(13)	0.3463(14)	7(1)
O(13)	0.8219(16)	0.3277(12)	0.2162(18)	10(2)
O(21)	0.6044(14)	-0.0275(10)	0.3697(13)	6(1)
O(22)	0.6980(13)	0.1738(10)	0.5044(10)	5(1)
O(31)	0.638(02)	-0.0320(11)	0.0589(18)	11(2)
O(32)	0.7910(18)	0.1614(13)	0.0009(17)	9(2)
O(33)	0.4967(18)	0.1685(14)	-0.0728(14)	9(2)
C(1)	0.7279(16)	0.1313(14)	0.2865(15)	3.2(5)
C(2)	0.8304(17)	0.1262(15)	0.3230(15)	3.6(5)
C(3)	0.839(02)	0.1351(19)	0.2310(20)	6.3(7)
C(4)	0.7370(17)	0.1334(15)	0.2030(15)	3.6(5)
C(11)	0.5853(20)	0.2965(15)	0.1191(18)	4.2(6)
C(12)	0.6265(19)	0.2920(15)	0.2992(18)	4.0(6)
C(13)	0.760(02)	0.2947(16)	0.2182(17)	4.6(6)
C(21)	0.6066(17)	0.0329(14)	0.3504(15)	3.1(5)
C(22)	0.6648(19)	0.1560(14)	0.4370(18)	3.7(6)
C(31)	0.638(02)	0.0291(17)	0.0664(19)	4.8(6)
C(32)	0.738(02)	0.1492(18)	0.035(02)	5.9(8)
C(33)	0.551(02)	0.1540(17)	-0.013(02)	5.9(7)
C(41)	0.861(02)	0.0480(17)	0.3606(19)	5.5(7)
C(42)	0.873(02)	0.1856(15)	0.3856(18)	5.1(7)
C(43)	0.819(02)	-0.0124(18)	0.302(02)	6.5(8)
C(44)	0.9633(20)	0.0420(15)	0.3693(19)	5.3(7)
C(45)	0.845(02)	0.0347(16)	0.4456(19)	5.6(7)

$\text{Ru}_3(\text{CO})_8(\text{PMe}_2\text{Ph})(\mu_3\text{-}\eta^2\text{-PhC}_2\text{H})(\mu_3\text{-S})$.¹⁰ When treated with CO at elevated pressures (15 atm) and 50 °C, **3** and **4** were both converted back to **1** in good yields.

Irradiation of solutions of diethylacetylene and **1** in a 30/1 ratio produced no **5** but gave instead the new compound $\text{Os}_3(\text{CO})_8[\mu_3\text{-EtCCeT}_2\text{C}_2\text{CH}_2\text{C}(\text{Me})^t\text{Bu}][\mu\text{-S}(\text{Et})\text{-}$

(10) Adams, R. D.; Babin, J. E.; Wolfe, T. A. *Polyhedron* **1989**, *8*, 1123.

Table 9. Intramolecular Distances for 4^a

Os(1)–Os(2)	2.879(2)	Os(3)–S	2.378(7)
Os(1)–Os(3)	2.802(2)	Os(3)–C(4)	2.08(2)
Os(2)–Os(3)	4.031(2)	C(1)–C(2)	1.55(3)
Os(1)–S	2.434(7)	C(1)–C(4)	1.41(3)
Os(1)–C(1)	2.42(3)	C(2)–C(3)	1.56(4)
Os(1)–C(4)	2.32(3)	C(3)–C(4)	1.54(4)
Os(2)–S	2.383(6)	Os–C (av)	1.90(4)
Os(2)–S'	2.488(7)	O–C (av)	1.14(3)
Os(2)–C(1)	2.01(3)		

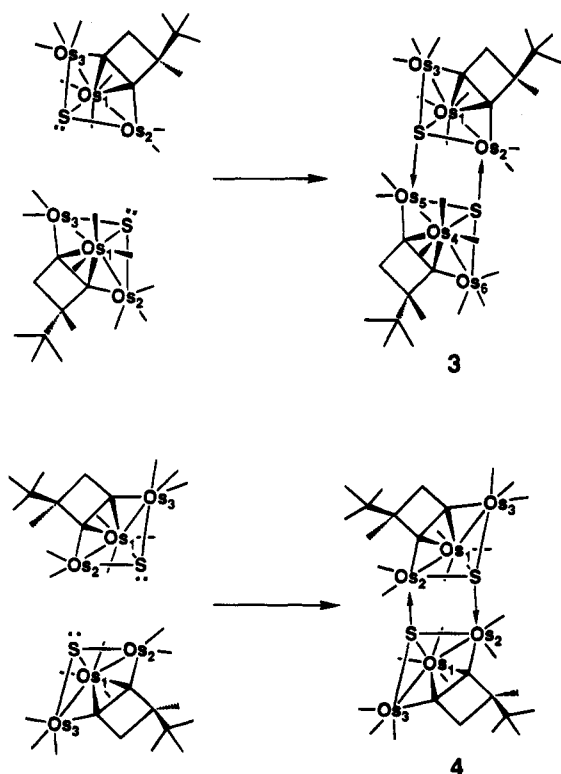
^a Distances are in angstroms. Estimated standard deviations in the least significant figure are given in parentheses.

Table 10. Intramolecular Bond Angles for 4^a

Os(2)–Os(1)–Os(3)	90.40(4)	C(1)–C(2)–C(3)	87(2)
S–Os(2)–S	77.6(2)	C(2)–C(3)–C(4)	87(2)
Os(2)–S–Os(2)	101.7(2)	C(1)–C(4)–C(3)	93(2)
C(2)–C(1)–C(4)	92(2)	Os–C–O (av)	177(3)

^a Angles are in degrees. Estimated standard deviations in the least significant figure are given in parentheses.

Scheme 1



$\text{C}=\text{C}(\text{Et})\text{C}=\text{O}]$ (**6**) in 39% yield based on the amount of **1** consumed. Again the actual yield is quite low since the conversion is poor. Most of the starting material was recovered, but longer irradiation periods and increased amounts of alkyne did not produce better yields. Compound **6** was characterized crystallographically, and an ORTEP diagram of its molecular structure is shown in Figure 4. Final atomic positional parameters are listed in Table 11, and selected interatomic distances and angles are listed in Tables 12 and 13. This molecule consists of a closed triangular triosmium cluster with seven linear terminal carbonyl ligands. The cyclobutyne ligand was coupled to one molecule of $\text{EtC}\equiv\text{C}(\text{Et})$ to form a metallacyclopentadienyl grouping Os(3), C(1), C(4), C(5), and C(6)). The four carbon atoms of this group are π -bonded to Os(2). Interestingly, the four-membered ring of the cyclobutyne grouping was not opened in the course of the formation of the metallacycle. The coupling of two alkynes to form metallacyclopentadienyl

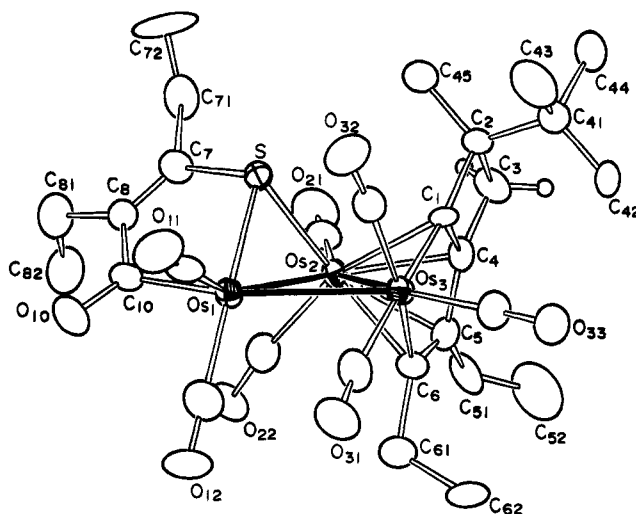


Figure 4. ORTEP diagram of $\text{Os}_3(\text{CO})_8[\mu\text{-EtCCEtC}_2\text{-CH}_2\text{C}(\text{Me})^2\text{Bu}][\mu\text{-S}(\text{Et})\text{C}=\text{C}(\text{Et})\text{C}=\text{O}]$ (**6**) showing 50% probability thermal ellipsoids.

Table 11. Positional Parameters and $B(\text{eq})$ Values (\AA^2) for **6**

atom	x	y	z	$B(\text{eq})$
Os(1)	-0.87665(3)	-0.22302(3)	-0.97462(5)	3.19(2)
Os(2)	-0.88990(3)	-0.09883(3)	-0.81643(6)	3.02(2)
Os(3)	-1.00365(3)	-0.11166(3)	-1.00186(6)	3.16(2)
S	-0.9198(2)	-0.2225(2)	-0.7515(3)	3.3(1)
O(10)	-0.7407(5)	-0.3141(6)	-0.962(1)	5.9(6)
O(11)	-0.9365(7)	-0.3599(6)	-1.098(1)	6.5(7)
O(12)	-0.7805(6)	-0.1956(7)	-1.224(1)	6.2(7)
O(21)	-0.8177(7)	-0.0639(7)	-0.546(7)	7.0(7)
O(22)	-0.7322(5)	-0.1044(6)	-0.932(1)	5.9(6)
O(31)	-0.9578(7)	-0.1573(8)	-1.290(1)	7.4(8)
O(32)	-1.0927(7)	-0.2525(6)	-0.943(1)	6.7(7)
O(33)	-1.1297(6)	-0.0271(7)	-1.138(1)	7.0(7)
C(1)	-1.0185(6)	-0.0700(6)	-0.811(1)	2.8(6)
C(2)	-1.0598(8)	-0.0606(7)	-0.670(1)	3.6(7)
C(3)	-1.0089(7)	0.0061(8)	-0.638(2)	4.3(7)
C(4)	-0.9751(7)	-0.0087(7)	-0.775(1)	3.2(6)
C(5)	-0.9188(8)	0.0161(8)	-0.868(2)	4.3(8)
C(6)	-0.9219(6)	-0.0259(7)	-0.992(2)	3.4(6)
C(7)	-0.8381(7)	-0.2571(7)	-0.668(1)	3.2(6)
C(8)	-0.7817(7)	-0.2810(8)	-0.744(1)	3.7(7)
C(10)	-0.7877(8)	-0.2824(8)	-0.896(1)	3.7(7)
C(11)	-0.9122(8)	-0.3071(8)	-1.049(1)	4.3(8)
C(12)	-0.818(1)	-0.206(1)	-1.131(2)	4.9(9)
C(21)	-0.8441(8)	-0.0768(8)	-0.649(2)	4.1(7)
C(22)	-0.7953(8)	-0.1079(8)	-0.892(1)	3.9(7)
C(31)	-0.9722(8)	-0.1424(9)	-1.181(2)	4.8(8)
C(32)	-1.0605(8)	-0.2005(8)	-0.968(2)	4.4(8)
C(33)	-1.0840(8)	-0.0587(8)	-1.085(1)	4.1(7)
C(41)	-1.1452(7)	-0.0381(9)	-0.688(2)	4.4(7)
C(42)	-1.155(1)	0.027(1)	-0.784(2)	6(1)
C(43)	-1.1908(8)	-0.102(1)	-0.742(2)	7(1)
C(44)	-1.1762(8)	-0.0136(9)	-0.549(2)	4.8(8)
C(45)	-1.0535(8)	-0.1266(9)	-0.576(2)	4.9(8)
C(51)	-0.8685(9)	0.0842(8)	-0.839(2)	6(1)
C(52)	-0.907(1)	0.151(1)	-0.851(3)	9(1)
C(61)	-0.8748(8)	-0.0034(9)	-1.111(2)	4.7(8)
C(62)	-0.919(1)	0.039(1)	-1.212(2)	6(1)
C(71)	-0.841(1)	-0.256(1)	-0.518(2)	5.4(8)
C(72)	-0.886(1)	-0.316(1)	-0.458(2)	9(1)
C(81)	-0.7074(8)	-0.3066(8)	-0.687(2)	5.0(8)
C(82)	-0.6508(8)	-0.247(1)	-0.687(2)	6(1)

groupings is a well-known reaction,¹¹ and we have previously observed a similar cyclobutyne–alkyne coupling in the formation of compound **B** (eq 1). The formation of **6** also involved the addition of a second equivalent of $\text{EtC}\equiv\text{C}(\text{Et})$. The second $\text{EtC}\equiv\text{C}(\text{Et})$ molecule was added to the sulfido ligand, but it was also coupled to a CO group to form a thia enone ligand. The carbonyl

Table 12. Intramolecular Distances for 6^a

Os(1)–Os(2)	2.7702(8)	S–C(7)	1.79(1)
Os(1)–Os(3)	3.0543(8)	O(10)–C(10)	1.21(2)
Os(1)–S	2.344(3)	C(1)–C(2)	1.59(2)
Os(1)–C(10)	2.07(1)	C(1)–C(4)	1.41(2)
Os(2)–Os(3)	2.7468(8)	C(2)–C(3)	1.55(2)
Os(2)–S	2.410(4)	C(3)–C(4)	1.52(2)
Os(2)–C(1)	2.35(1)	C(4)–C(5)	1.44(2)
Os(2)–C(4)	2.28(1)	C(5)–C(6)	1.45(2)
Os(2)–C(5)	2.22(1)	C(7)–C(8)	1.33(2)
Os(2)–C(6)	2.27(1)	C(8)–C(10)	1.51(2)
Os(3)–C(1)	2.06(1)	Os–C (av)	1.89(2)
Os(3)–C(6)	2.14(1)	C–O (av)	1.15(2)

^a Distances are in angstroms. Estimated standard deviations in the least significant figure are given in parentheses.

Table 13. Intramolecular Bond Angles for 6^a

Os(2)–Os(1)–Os(3)	56.02(2)	C(3)–C(4)–C(5)	143(1)
Os(1)–Os(2)–Os(3)	67.23(2)	C(4)–C(5)–C(6)	111(1)
Os(1)–Os(3)–Os(2)	56.75(2)	C(4)–C(5)–C(51)	122(1)
C(1)–Os(3)–C(6)	76.9(5)	C(6)–C(5)–C(51)	127(1)
Os(1)–S–C(7)	99.8(5)	Os(3)–C(6)–C(5)	117(1)
Os(1)–C(1)–C(2)	119.7(8)	S–C(7)–C(8)	118(1)
Os(3)–C(1)–C(4)	117(1)	C(7)–C(8)–C(10)	121(1)
C(2)–C(1)–C(4)	87(1)	Os(1)–C(10)–O(10)	125(1)
C(1)–C(2)–C(3)	90(1)	Os(1)–C(10)–C(8)	115(1)
C(2)–C(3)–C(4)	84(1)	O(10)–C(10)–C(8)	120(1)
C(1)–C(4)–C(3)	99(1)	Os–C–O (av)	177(1)
C(1)–C(4)–C(5)	118(1)		

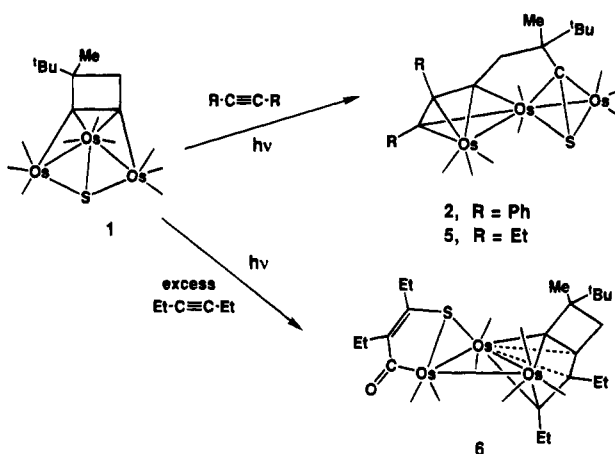
^a Angles are in degrees. Estimated standard deviations in the least significant figure are given in parentheses.

carbon atom C(10) is σ -bonded to Os(1) (Os(1)–C(10) = 2.07(1) Å). Interestingly, the Os(1)–Os(3) bond distance (3.0543(8) Å) is much longer than those of the other two metal–metal bonds (Os(1)–Os(2) = 2.7702(8) Å and Os(2)–Os(3) = 2.7468(8) Å). This may be the result of a high structural trans influence of the σ -bonded acyl carbon C(10). An increase in the length of the metal–metal bond trans to a carbonyl function was also observed in the complex Os₃(CO)₁₀[μ -SCH₂CM₂CH₂-C=O], which contains a thiaosmacyclohexanone ring, but the increase in that complex was not as large as that observed in **6**.¹² The bond between atoms C(7) and C(8) is short (1.33(2) Å), as expected since it is formally a C–C double bond. The formation of the thia enone ligand is clearly a result of the coupling of the alkyne to the sulfido ligand with an additional coupling of a CO ligand to the other end of the alkyne. The addition of alkynes to sulfido ligands in a variety of sulfide-containing metal cluster complexes has been observed previously.¹³ Overall, the cluster is electron-precise with a total of 48 valence electrons about the three metal atoms.

(11) (a) Adams, R. D.; Daran, J.-C.; Jeannin, Y. *J. Cluster Sci.* **1992**, *3*, 1. (b) Fehlhhammer, W. B.; Stolzenberg, H. In *Comprehensive Organometallic Chemistry*; Wilkinson, G., Stone, F. G. A., Abel, E., Eds.; Pergamon: Oxford, U.K., 1982; Chapter 31.4. (c) Slater, S.; Muetterties, E. L. *Inorg. Chem.* **1981**, *20*, 946. (d) Beck, J.; Knox, S. A. K.; Stansfield, R. F. D.; Stone, F. G. A.; Woodward, P. J. *J. Chem. Soc., Dalton Trans.* **1982**, 195. (e) Knox, S. A. K.; Stansfield, R. F. D.; Stone, F. G. A.; Winter, M. J.; Woodward, P. J. *J. Chem. Soc., Dalton Trans.* **1982**, 173.

(12) Adams, R. D.; Belinski, J. A.; Pompeo, M. P. *Organometallics* **1992**, *11*, 2016.

(13) (a) Adams, R. D.; Wang, S. *Organometallics* **1985**, *4*, 1902. (b) Adams, R. D.; Chen, G.; Tanner, J. T.; Yin, J. *Organometallics* **1990**, *9*, 595. (c) Shibahara, T.; Sankane, G.; Mochida, S. *J. Am. Chem. Soc.* **1993**, *115*, 10408. (d) Rakowski DuBois, M.; VanDerveer, M. C.; DuBois, D. L.; Haltiwanger, R. C.; Miller, W. K. *J. Am. Chem. Soc.* **1980**, *102*, 7456. (e) Bolinger, C. M.; Rauchfuss, T. B.; Rheingold, A. L. *J. Am. Chem. Soc.* **1983**, *105*, 6321.

Scheme 2

Discussion

The results of our studies of the reaction of **1** with PhC≡CPh and EtC≡CEt are shown in Scheme 2. When the alkynes were combined with **1** in relatively low concentrations in the presence of UV irradiation, the compounds **2** and **5** were formed by coupling of the alkyne to the cyclobutene ligand and cleavage of the C–C multiple bond of the cyclobutene. We have not been able to pinpoint the circumstances that lead to the cleavage of the C–C multiple bond of the cyclobutene. Clearly, the UV irradiation plays a role in this, since these products are not obtained in the absence of UV irradiation. We believe that the addition of 1 equiv of alkyne is also essential, since at the low alkyne concentrations the two dimeric side products **3** and **4** were formed by the decarbonylation of **1** and combination of the two fragments, and there were no ruptures of bonds in the cyclobutene ligands in the formation of these products. However, the addition of 2 equiv of alkyne appears to have prevented the occurrence of carbon–carbon bond ruptures in the cyclobutene group as demonstrated by the formation of **6**. It is tempting to speculate that the formation of **6** in the presence of excess EtC≡CEt was the result of the capture of some intermediate that existed prior to the occurrence of C–C bond ruptures in the cyclobutene grouping that led to **2** and **5**. It is also possible that the coupling of the cyclobutene grouping to the sulfur atom may have played some part in the the cyclobutene bond rupture process, since the cyclobutene fragment is coupled to the sulfur atoms in **2** and **5** and there was no such coupling in **3**, **4**, and **6**, but this is only speculative since the C–C bond rupture in the cyclobutene could have occurred prior to its coupling to sulfur.

Acknowledgment. This research was supported by the Office of Basic Energy Science of the U.S. Department of Energy.

Supplementary Material Available: Tables of positional parameters for the hydrogen atoms and anisotropic thermal parameters for all of the structural analyses (13 pages). Ordering information is given on any current masthead page.

OM940824N

Reductive Coupling of Group 5 Dicarboxyls to Disiloxyacetylene Complexes: Ring Formation and Effects of Increasing Steric Demands

Brian S. Bronk, John D. Protasiewicz, and Stephen J. Lippard*

Department of Chemistry, Massachusetts Institute of Technology,
Cambridge, Massachusetts 02139

Received October 7, 1994[®]

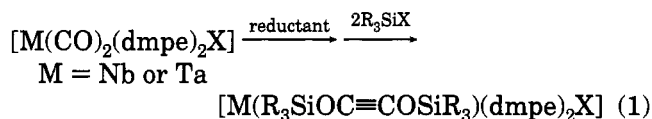
Convenient syntheses of dicarbonyl complexes of the type $[M(\text{CO})_2(\text{depe})_2\text{Cl}]$ (depe = 1,2-bis(diethylphosphino)ethane, $M = \text{Ta}$ (1), Nb (3)) and $[M(\text{CO})_2(\text{dbpe})_2\text{Cl}]$ (dbpe = 1,2-bis(dibutylphosphino)ethane, $M = \text{Ta}$ (2), Nb (4)) having increased steric demands at the high coordinate metal centers are described. Reductive coupling of the CO ligands of 1–4 occurs to provide products of the type $[M(\text{R}'_3\text{SiOC}\equiv\text{COSiR}'_3)(\text{R}_2\text{PCH}_2\text{CH}_2\text{PR}_2)_2\text{X}]$. Single crystal X-ray structural studies were carried out for two reductively coupled products prepared with 1,2-bis(chlorodimethylsilyl)ethane as the electrophile, $[\text{V}(\text{Me}_2\text{SiOC}\equiv\text{COSiMe}_2)(\text{dmpe})_2\text{Cl}]$ (monoclinic, space group $C2/c$, $a = 9.349(2) \text{ \AA}$, $b = 20.548(3) \text{ \AA}$, $c = 16.146(4) \text{ \AA}$, $\beta = 104.79(1)^\circ$, and $V = 2999(1) \text{ \AA}^3$) and $[\text{Ta}(\text{Me}_2\text{SiOC}\equiv\text{COSiMe}_2)(\text{depe})_2\text{Cl}]$ (monoclinic, space group Cc , $a = 11.512(1) \text{ \AA}$, $b = 18.311(3) \text{ \AA}$, $c = 18.493(3) \text{ \AA}$, $\beta = 97.322(7)^\circ$, and $V = 3875(1) \text{ \AA}^3$). In these complexes, the acetylene is contained within a newly formed eight-membered ring, and the ligands are arranged in a pentagonal bipyramid geometry comprising two axial phosphorus atoms and five equatorial ligands, the coupled carbons, a trans chloride, and the remaining two phosphorus atoms.

Introduction

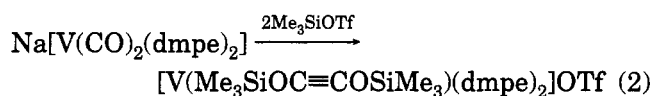
The chemistry of low-valent niobium and tantalum complexes continues to receive considerable attention.¹ Such complexes effect a variety of carbon–carbon bond-forming reactions, including alkyne activation,^{2,3} Reformatsky-type reactions,⁴ and the reductive coupling of isocyanide^{5–7} and carbon monoxide ligands.^{8–14}

The work described here is part of an ongoing investigation of the reductive coupling of two carbon monoxide molecules promoted by transition metal ions. Previous synthetic work demonstrated that two CO ligands in $[M(\text{CO})_2(\text{dmpe})_2\text{Cl}]$ ($M = \text{Nb}$, Ta)^{15,16} com-

plexes can be converted to a coordinated disiloxyacetylene ligand (eq 1). Later studies of the corresponding



vanadium system revealed that similar compounds could be obtained, but lacking a coordinated anion (eq 2).¹⁷ This difference was ascribed in part to the smaller



atomic radius of vanadium, which affords a sterically more congested metal center. Similar steric arguments were invoked to account for the formation of $[\text{V}(\eta^2\text{-C}(\text{O})\text{-Et})(\text{CO})(\text{dmpe})_2]$ upon addition of EtOTf to $\text{Na}[\text{V}(\text{CO})_2(\text{dmpe})_2]$, a reaction that gave only $[\text{Ta}(\text{CO})_2(\text{dmpe})_2\text{Et}]$ for $\text{Na}[\text{Ta}(\text{CO})_2(\text{dmpe})_2]$.¹⁸

In order to determine whether steric congestion would affect the reductive coupling chemistry of niobium and tantalum dicarbonyl complexes, an expanded series of $[M(\text{CO})_2(\text{depe})_2\text{Cl}]$ (depe = 1,2-bis(diethylphosphino)ethane, $M = \text{Ta}$ (1), Nb (3), and $[M(\text{CO})_2(\text{dbpe})_2\text{Cl}]$ (dbpe = 1,2-bis(dibutylphosphino)ethane, $M = \text{Ta}$ (2), Nb (4), compounds was prepared. The ability of these compounds to undergo the coupling reaction with silyl-based electrophiles was investigated. As described in the present article, the most significant consequence of

(16) Datta, S.; Wreford, S. S. *Inorg. Chem.* **1977**, *16*, 1134.

(17) Protasiewicz, J. D.; Lippard, S. J. *J. Am. Chem. Soc.* **1991**, *113*, 6564.

(18) Bronk, B. S.; Protasiewicz, J. D.; Pence, L. E.; Lippard, S. J. *Organometallics*, submitted for publication.

[®] Abstract published in *Advance ACS Abstracts*, January 15, 1995.

(1) See for example: Ellis, J. E. *Adv. Organomet. Chem.* **1990**, *31*, 1.

(2) Kataoka, Y.; Takai, K.; Oshima, K.; Utimoto, K. *J. Org. Chem.* **1992**, *57*, 1615, and references cited therein.

(3) Hurtung, J. B.; Pedersen, S. F. *J. Am. Chem. Soc.* **1989**, *111*, 5468.

(4) Aoyagi, Y.; Tanaka, W.; Ohta, A. *J. Chem. Soc., Chem. Commun.* **1994**, 1225.

(5) Carnahan, E. M.; Lippard, S. J. *J. Am. Chem. Soc.* **1990**, *112*, 3230.

(6) Carnahan, E. M.; Rardin, R. L.; Bott, S. G.; Lippard, S. J. *Inorg. Chem.* **1992**, *31*, 5193.

(7) Carnahan, E. M.; Lippard, S. J. *J. Am. Chem. Soc.* **1992**, *114*, 4166.

(8) Vrtis, R. N.; Liu, S.; Rao, C. P.; Bott, S. G.; Lippard, S. J. *Organometallics* **1991**, *10*, 275.

(9) Vrtis, R. N.; Bott, S. G.; Rardin, R. L.; Lippard, S. J. *Organometallics* **1991**, *10*, 1364.

(10) Protasiewicz, J. D.; Masschelein, A.; Lippard, S. J. *J. Am. Chem. Soc.* **1993**, *115*, 808.

(11) Bianconi, P. A.; Williams, I. D.; Engeler, M. P.; Lippard, S. J. *J. Am. Chem. Soc.* **1986**, *108*, 311–313.

(12) Bianconi, P. A.; Vrtis, R. N.; Rao, C. P.; Williams, I. D.; Engeler, M. P.; Lippard, S. J. *Organometallics* **1987**, *6*, 1968.

(13) Vrtis, R. N.; Lippard, S. J. *Isr. J. Chem.* **1990**, *30*, 331.

(14) Protasiewicz, J. D.; Bronk, B. S.; Masschelein, A.; Lippard, S. J. *Organometallics* **1994**, *13*, 1300.

(15) Burt, R. J.; Leigh, G. J.; Hughes, D. L. *J. Chem. Soc., Dalton Trans.* **1981**, 793.

the steric congestion at these metal centers is their greater ability to form cyclic disiloxyacetylenes, a reaction previously observed only for $\text{Na}[\text{V}(\text{CO})_2(\text{dmpe})_2]$, details of which are reported here for the first time.¹⁹ The syntheses and structure determinations of this complex and the Ta-depe analogue are described.

Experimental Section

General Considerations. All reactions and manipulations were carried out either in a Vacuum Atmospheres drybox under a dinitrogen atmosphere or by standard Schlenk techniques under argon. Solutions were stirred magnetically with a Teflon-covered stir bar unless otherwise noted. $\text{Na}[\text{V}(\text{CO})_2(\text{dmpe})_2]$ was prepared by a published procedure.¹⁷ Solvents (THF, DME, pentane) were distilled under dinitrogen from sodium benzophenone ketyl. Benzene-*d*₆ was dried by passage through a column of alumina and stored under dinitrogen. Tetramethylsilane was distilled from calcium hydride and stored under dinitrogen. All other reagents were used as received after degassing. Proton chemical shifts were referenced to residual solvent peaks and are reported relative to tetramethylsilane. ¹H and ³¹P NMR spectra were recorded on a Varian XL300 instrument at 300 and 121 MHz, respectively. ³¹P NMR spectra were referenced to external phosphoric acid. Infrared (IR) spectra were recorded on a Biorad FTS-7 spectrophotometer.

[Ta(CO)₂(depe)₂Cl] (1). This material was prepared from TaCl_5 (0.860 g, 2.4 mmol) according to a literature procedure,²⁰ except that the reduction of $[\text{Ta}(\text{depe})_2\text{Cl}_4]$ with magnesium/catalytic anthracene under an atmosphere of carbon monoxide was allowed to proceed for 7 d. The desired product, 0.956 g (58%), was obtained as a yellow solid, the spectral properties of which were consistent with those reported previously.²⁰

[Ta(CO)₂(dbpe)₂Cl] (2). A 100-mL, one-necked, pear-shaped flask fitted with a rubber septum was charged with TaCl_5 (1.125 g, 3.14 mmol) and 50 mL of toluene. A solution of 1,2-bis(dibutylphosphino)ethane (2.0 g, 6.3 mmol) in 10 mL of THF was added in one portion with rapid stirring, followed by sodium amalgam, prepared from sodium (0.162 g, 7.05 mmol) and mercury (21.5 g, 107 mmol). The reaction mixture was stirred vigorously for 12 h, after which time stirring was halted in order to allow the solids to settle.

The solution was decanted into a 50-mL, one-necked, pear-shaped flask, and the solvents were removed under vacuum, providing a gummy green solid. The residue was dissolved in 15 mL of THF, and a slurry containing magnesium (0.115 g, 4.7 mmol), mercuric chloride (0.128 g, 0.47 mmol), and a catalytic amount of anthracene (3–5 mg) in 5 mL of THF was added in one portion. The flask was purged with a CO atmosphere for 15 min and then allowed to stir under a CO atmosphere for 72 h. Column chromatography on alumina (elution with THF) followed by recrystallization from pentane at -30°C afforded 1.37 g (48% based on TaCl_5) of the desired product as an orange solid. IR (Nujol): 1811, 1747, 1418, 1342, 1210, 1092, 1050, 979, 899, 721 cm^{-1} . ¹H NMR (C_6D_6): δ 2.33–2.44 (m, 4 H), 2.11–2.18 (m, 4 H), 1.84–2.00 (m, 8 H), 1.32–1.71 (m, 36 H), 1.04–1.21 (m, 4 H), 0.93–1.13 (m, 24 H). ³¹P NMR (C_6D_6): δ 38.5. Anal. Calcd for $\text{C}_{38}\text{H}_{50}\text{ClO}_2\text{P}_4\text{Ta}$: C, 50.19; H, 8.87; N, 0.00. Found: C, 50.04; H, 8.62; N, 0.00.

[Nb(CO)₂(depe)₂Cl] (3). A 50-mL, one-necked pear-shaped flask fitted with a rubber septum was charged with NbCl_5 (0.648 g, 2.4 mmol) and 30 mL of toluene. A solution of 1,2-bis(diethylphosphino)ethane (1.0 g, 4.8 mmol) in 5 mL of THF was added in one portion with rapid stirring, followed by sodium amalgam, prepared from sodium (0.124 g, 5.4 mmol) and mercury (16.5 g, 82 mmol). The reaction mixture was

stirred vigorously for 13 h, after which time stirring was halted in order to allow the solids to settle.

The solution was decanted into a 25-mL, one-necked, pear-shaped flask, and the solvents were removed under vacuum, providing a gummy gray-green solid. The residue was dissolved in 10 mL of THF, and a slurry containing magnesium (0.088 g, 3.6 mmol), mercuric chloride (0.098 g, 0.36 mmol), and catalytic anthracene in 5 mL of THF was added in one portion. The flask was purged with a CO atmosphere for 15 min and then allowed to stir under a CO atmosphere for 72 h. Column chromatography on alumina (elution with THF) followed by recrystallization from THF at -30°C afforded 0.643 g (45% based on NbCl_5) of the desired product as an orange solid. IR (Nujol): 1828, 1753, 1419, 1237, 1040, 1026, 979, 871, 757, 706 cm^{-1} . ¹H NMR (C_6D_6): δ 2.21–2.34 (m, 4 H), 1.85–1.95 (m, 4 H), 1.46–1.83 (m, 12 H), 0.93–1.13 (m, 28 H). Anal. Calcd for $\text{C}_{22}\text{H}_{48}\text{ClO}_2\text{P}_4\text{Nb}$: C, 44.27; H, 8.11; N, 0.00. Found: C, 44.54; H, 8.49; N, 0.00.

[Nb(CO)₂(dbpe)₂Cl] (4). A 100-mL, one-necked, round-bottomed flask fitted with a rubber septum was charged with NbCl_5 (2.12 g, 7.85 mmol) and 50 mL of toluene. A solution of 1,2-bis(dibutylphosphino)ethane (5.0 g, 15.7 mmol) in 10 mL of THF and 10 mL of toluene was added in one portion with rapid stirring, followed by sodium amalgam, prepared from sodium (0.406 gm, 17.7 mmol) and mercury (53.5 g, 267 mmol). The reaction mixture was stirred vigorously for 15 h, after which time stirring was halted in order to allow the solids to settle.

The solution was decanted into a 100-mL, one-necked, round-bottomed flask, and the solvents were removed under vacuum, providing a gummy gray-green solid. The residue was dissolved in 50 mL of THF, and a slurry of magnesium (0.268 g, 11.0 mmol), mercuric chloride (0.320 g, 1.18 mmol), and a catalytic amount of anthracene in 10 mL of THF was added in one portion. The flask was purged with a CO atmosphere for 15 min and then allowed to stir under a CO atmosphere for 7 d. Column chromatography on alumina (elution with THF) followed by recrystallization from THF at -30°C afforded 3.39 g (53% based on NbCl_5) of the desired product as an orange solid. IR (Nujol): 1818, 1755, 1420, 1301, 1210, 1089, 1051, 1020, 915, 893, 816, 722 cm^{-1} . ¹H NMR (C_6D_6): δ 2.31–2.44 (m, 4 H), 1.98–2.11 (m, 4 H), 1.34–1.94 (m, 44 H), 1.08–1.22 (m, 4 H), 0.90–1.12 (m, 24 H). Anal. Calcd for $\text{C}_{38}\text{H}_{50}\text{ClO}_2\text{P}_4\text{Nb}$: C, 55.57; H, 9.82; N, 0.00. Found: C, 55.42; H, 9.59; N, 0.00.

[Ta(Me₃SiOC=COSiMe₃)(depe)₂Cl] (5a). A solution of $[\text{Ta}(\text{CO})_2(\text{depe})_2\text{Cl}]$ (0.230 g, 0.336 mmol) in 10 mL of THF was rapidly stirred with excess 40% Na/Hg for 4 h to generate $\text{Na}[\text{Ta}(\text{CO})_2(\text{depe})_2]$. This solution was decanted into another flask, and Me_3SiCl (0.043 mL, 0.037 g, 0.336 mmol) was added by syringe. The solution quickly turned deep red and was allowed to stir for 5 min. The solvent was removed under vacuum, and the red product was triturated with pentane and then extracted with 10 mL of pentane. The red oil obtained after removal of the pentane displayed ν_{CO} bands in its IR (Nujol) spectrum at 1787 and 1308 cm^{-1} , consistent with the presence of $[\text{Ta}(\text{COSiMe}_3)(\text{CO})(\text{depe})_2]$.⁸ The red oil was taken up into 10 mL of THF, Me_3SiCl (0.050 mL, 0.043 g, 0.394 mmol) was added, and the solution was allowed to stir overnight. The solvent was removed under vacuum and the solid recrystallized from pentane (-30°C) to obtain 0.177 g (63%) of the product as dark brown-green crystals. IR (Nujol): 1558, 1413, 1303, 1250, 1143, 1028, 901, 840, 809, 755, 724, 685, 655, 608 cm^{-1} . ¹H NMR (C_6D_6): δ 1.74–2.12 (m, 16 H), 1.54–1.75 (m, 4 H), 1.36–1.53 (m, 4 H), 0.90–1.28 (m, 24 H), 0.21 (s, 18 H). ³¹P NMR (C_6D_6): δ 45.1 (s). Anal. Calcd for $\text{C}_{28}\text{H}_{66}\text{O}_2\text{P}_4\text{Si}_2\text{ClTa}$: C, 40.46; H, 8.00; N, 0.00. Found: C, 40.71; H, 7.98; N, 0.00.

[Ta(Me₃SiOC=COSiMe₃)(depe)₂OTf] (5b). A 25-mL, one-necked, pear-shaped flask fitted with a rubber septum was charged with $[\text{Ta}(\text{CO})_2(\text{depe})_2\text{Cl}]$ (0.068 g, 0.1 mmol) and 10 mL of DME. Upon dissolution, excess 40% sodium amalgam was added in one portion and the reaction mixture was stirred

(19) Carnahan, E. M.; Protasiewicz, J. D.; Lippard, S. J. *Acc. Chem. Res.* **1993**, *26*, 90.

(20) Protasiewicz, J. D.; Bianconi, P. A.; Williams, I. D.; Liu, S.; Rao, C. P.; Lippard, S. J. *Inorg. Chem.* **1992**, *31*, 4134.

vigorously for 4 h. The orange solution was decanted from the solids into a second 25-mL, one-necked, pear-shaped flask fitted with a rubber septum, and TMSOTf (0.039 mL, 0.044 g, 0.2 mmol) was added in one portion via syringe. The reaction mixture was stirred for 1 h, providing a green solution. Upon removal of the solvents under vacuum, the green product was extracted with pentane and the pentane solution was filtered and concentrated under vacuum to provide 0.088 g of a green solid. Recrystallization from pentane at $-30\text{ }^{\circ}\text{C}$ yielded 0.062 g (66%) of the desired product as green crystals. IR (Nujol): 1581, 1419, 1377, 1313, 1259, 1232, 1203, 1168, 1152, 1030, 1015, 902, 855, 844, 722 cm^{-1} . ^1H NMR (C_6D_6): δ 1.94–2.12 (m, 8 H), 1.74–1.84 (m, 12 H), 1.46–1.54 (m, 4 H), 0.95–1.24 (m, 24 H), 0.13 (s, 18 H). ^{31}P NMR (C_6D_6): δ 50.3. Anal. Calcd for $\text{C}_{29}\text{H}_{66}\text{F}_3\text{O}_5\text{P}_4\text{SSi}_2\text{Ta}$: C, 36.86; H, 7.04; N, 0.00. Found: C, 36.68; H, 6.83; N, 0.00.

[Nb(Me₃SiOC=CO₂SiMe₃)(depe)₂Cl] (6a). A 25-mL, one-necked, pear-shaped flask fitted with a rubber septum was charged with $[\text{Nb}(\text{CO})_2(\text{depe})_2\text{Cl}]$ (0.119 g, 0.2 mmol) and 10 mL of THF. Upon dissolution, excess 40% sodium amalgam was added in one portion and the reaction mixture was stirred vigorously for 3 h. The orange solution was decanted from the solids into a second 25-mL, one-necked, pear-shaped flask fitted with a rubber septum, and TMSCl (0.102 mL, 0.087 g, 0.8 mmol) was added in one portion via syringe. The reaction mixture was stirred for 13 h, providing a green solution. Upon removal of the solvents under vacuum, the green product was extracted with pentane and the pentane solution was filtered and concentrated under vacuum to provide 0.133 g of a green solid. Recrystallization from pentane at $-30\text{ }^{\circ}\text{C}$ afforded 0.108 g (72%) of the desired product as green crystals. IR (Nujol) 1569, 1417, 1259, 1247, 1144, 1036, 1017, 894, 843, 808, 759, 721, 690 cm^{-1} . ^1H NMR (C_6D_6): δ 1.98–2.12 (m, 4 H), 1.66–1.89 (m, 16 H), 1.53–1.65 (m, 4 H), 1.03–1.11 (m, 24 H), 0.22 (s, 18 H). Anal. Calcd for $\text{C}_{28}\text{H}_{66}\text{ClO}_2\text{P}_4\text{Si}_2\text{Nb}$: C, 45.25; H, 8.95; N, 0.00. Found: C, 45.66; H, 9.11; N, 0.00.

[Nb(Me₃SiOC=CO₂SiMe₃)(depe)₂OTf] (6b). A 25-mL, one-necked, pear-shaped flask fitted with a rubber septum was charged with $[\text{Nb}(\text{CO})_2(\text{depe})_2\text{Cl}]$ (0.119 g, 0.2 mmol) and 10 mL of DME. Upon dissolution, excess 40% sodium amalgam was added in one portion and the reaction mixture was stirred vigorously for 4 h. The orange solution was decanted from the solids into a second 25-mL, one-necked, pear-shaped flask fitted with a rubber septum and TMSOTf (0.077 mL, 0.089 g, 0.4 mmol) was added in one portion via syringe. The reaction mixture was stirred for 1 h, providing a green solution. Upon removal of the solvents under vacuum, the green product was extracted with pentane and the pentane solution was filtered and concentrated under vacuum to provide 0.163 g of a green solid. Recrystallization from pentane at $-30\text{ }^{\circ}\text{C}$ yielded 0.146 g (85%) of the desired product as green crystals. IR (Nujol): 1593, 1308, 1259, 1232, 1208, 1165, 1152, 1017, 893, 854, 844 cm^{-1} . ^1H NMR (C_6D_6): δ 1.87–2.09 (m, 10 H), 1.61–1.72 (m, 10 H), 1.05–1.14 (m, 14 H), 0.94–1.03 (m, 14 H), 0.12 (s, 18 H). Anal. Calcd for $\text{C}_{29}\text{H}_{66}\text{F}_3\text{O}_5\text{P}_4\text{SSi}_2\text{Nb}$: C, 40.65; H, 7.76; N, 0.00. Found: C, 40.65; H, 7.79; N, 0.00.

[Ta(Me₃SiOC=CO₂SiMe₃)(dbpe)₂Cl] (7a). A 25-mL one-necked, pear-shaped flask fitted with a rubber septum was charged with $[\text{Ta}(\text{CO})_2(\text{dbpe})_2\text{Cl}]$ (0.046 g, 0.05 mmol) and 10 mL of THF. Upon dissolution, excess 40% sodium amalgam was added in one portion and the reaction mixture was stirred vigorously for 2.5 h. The orange solution was decanted from the solids into a second 25-mL, one-necked, pear-shaped flask fitted with a rubber septum, and TMSCl (0.025 mL, 0.022 g, 0.2 mmol) was added in one portion via syringe. The reaction mixture was stirred for 14 h, providing a green solution. Upon removal of the solvents under vacuum, the green product was extracted with pentane and the pentane solution was filtered and concentrated under vacuum to provide 0.050 g of a green oil. Recrystallization from pentane at $-30\text{ }^{\circ}\text{C}$ yielded 0.029 g (55%) of the desired product as green crystals. IR (Nujol): 1560, 1411, 1341, 1246, 1123, 1090, 1016, 898, 847, 743, 713 cm^{-1} . ^1H NMR (C_6D_6): δ 1.40–2.07 (m, 56 H), 1.04 (t, $J = 7.2$

Hz, 12 H), 0.96 (t, $J = 7.2$ Hz, 12 H), 0.27 (s, 18 H). ^{31}P NMR (C_6D_6): δ 41.0. Anal. Calcd for $\text{C}_{44}\text{H}_{98}\text{ClO}_2\text{P}_4\text{Si}_2\text{Ta}$: C, 50.06; H, 9.36; N, 0.00. Found: C, 50.34; H, 9.38; N, 0.00.

[Ta(Me₃SiOC=CO₂SiMe₃)(dbpe)₂OTf] (7b). A 25-mL, one-necked, pear-shaped flask fitted with a rubber septum was charged with $[\text{Ta}(\text{CO})_2(\text{dbpe})_2\text{Cl}]$ (0.046 g, 0.05 mmol) and 10 mL of DME. Upon dissolution, excess 40% sodium amalgam was added in one portion and the reaction mixture was stirred vigorously for 3 h. The orange solution was decanted from the solids into a second 25-mL, one-necked, pear-shaped flask fitted with a rubber septum, and TMSOTf (0.019 mL, 0.022 g, 0.1 mmol) was added in one portion via syringe. The reaction mixture was stirred for 30 min, providing a green solution. Upon removal of the solvents under vacuum, the green product was extracted with pentane and the pentane solution was filtered and concentrated under vacuum to provide 0.053 g of a green oil. Recrystallization from TMS at $-30\text{ }^{\circ}\text{C}$ yielded 0.028 g (48%) of the desired product as a green solid. IR (Nujol): 1576, 1419, 1323, 1260, 1233, 1203, 1167, 1142, 1092, 1014, 900, 854, 750, 711, 632 cm^{-1} . ^1H NMR (C_6D_6): δ 1.89–2.11 (m, 20 H), 1.38–1.68 (m, 36 H), 0.93–1.02 (m, 24 H), 0.20 (s, 18 H). ^{31}P NMR (C_6D_6): δ 45.8. Anal. Calcd for $\text{C}_{45}\text{H}_{98}\text{F}_3\text{O}_5\text{P}_4\text{SSi}_2\text{Ta}$: C, 46.22; H, 8.45; N, 0.00. Found: C, 46.50; H, 7.82; N, 0.00.

[Nb(Me₃SiOC=CO₂SiMe₃)(dbpe)₂Cl] (8a). A 50-mL, one-necked, pear-shaped flask fitted with a rubber septum was charged with $[\text{Nb}(\text{CO})_2(\text{dbpe})_2\text{Cl}]$ (0.411 g, 0.5 mmol) and 30 mL of THF. Upon dissolution, excess 40% sodium amalgam was added in one portion and the reaction mixture was stirred vigorously for 3.5 h. The orange solution was decanted from the solids into a second 50-mL, one-necked, pear-shaped flask fitted with a rubber septum, and TMSCl (0.254 mL, 0.217 g, 2.0 mmol) was added in one portion via syringe, followed by Bu_4NBPh_4 (0.281 g, 0.5 mmol). The reaction mixture was stirred for 14 h, providing a green solution. Upon removal of the solvents under vacuum, the green product was extracted with pentane and the pentane solution was filtered and concentrated under vacuum to provide 0.462 g of a green solid. Recrystallization from pentane at $-30\text{ }^{\circ}\text{C}$ yielded 0.353 g (73%) of the desired product as a green solid. IR (Nujol): 1585, 1417, 1308, 1259, 1247, 1121, 1009, 972, 890, 846 cm^{-1} . ^1H NMR (C_6D_6): δ 1.37–2.20 (m, 56 H), 1.03 (t, $J = 7.1$ Hz, 12 H), 0.97 (t, $J = 7.1$ Hz, 12 H), 0.27 (s, 18 H). Anal. Calcd for $\text{C}_{44}\text{H}_{98}\text{ClO}_2\text{P}_4\text{Si}_2\text{Nb}$: C, 54.61; H, 10.21; N, 0.00. Found: C, 54.92; H, 10.49; N, 0.00.

[Nb(Me₃SiOC=CO₂SiMe₃)(dbpe)₂OTf] (8b). A 25-mL, one-necked, pear-shaped flask fitted with a rubber septum was charged with $[\text{Nb}(\text{CO})_2(\text{dbpe})_2\text{Cl}]$ (0.082 g, 0.1 mmol) and 10 mL of DME. Upon dissolution, excess 40% sodium amalgam was added in one portion and the reaction mixture was stirred vigorously for 4 h. The orange solution was decanted from the solids into a second 25-mL, one-necked, pear-shaped flask fitted with a rubber septum, and TMSOTf (0.039 mL, 0.044 g, 0.2 mmol) was added in one portion via syringe. The reaction mixture was stirred for 4 h, providing a green solution. Upon removal of the solvent under vacuum, the green product was extracted with pentane and the pentane solution was filtered and concentrated under vacuum to provide a green-brown solid. Recrystallization from TMS at $-30\text{ }^{\circ}\text{C}$ yielded 0.057 g (53%) of the desired product as a green solid. IR (Nujol): 1586, 1319, 1250, 1234, 1205, 1162, 1141, 1015, 892, 846 cm^{-1} . ^1H NMR (C_6D_6): δ 1.36–2.19 (m, 56 H), 0.95–1.05 (m, 24 H), 0.20 (s, 18 H).

[V(Me₂SiOC=CO₂SiMe₂)(dmpe)₂Cl] (9). A 25-mL, one-necked, pear-shaped flask fitted with a rubber septum was charged with a solution of $[\text{V}(\text{CO})_2(\text{dmpe})_2]$ (0.200 g, 0.496 mmol) in 10 mL of THF; $\text{ClMe}_2\text{SiCH}_2\text{CH}_2\text{SiMe}_2\text{Cl}$ (0.107 g, 0.496 mmol) in a few milliliters of THF was added. The solution immediately turned deep red. After stirring for 2 h, a small amount of a brown microcrystalline product appeared. This material was filtered and the filtrate was placed in the $-30\text{ }^{\circ}\text{C}$ freezer, yielding 0.099 g (34%) of the desired product as golden brown crystals. IR (Nujol): 1624, 1254, 1178, 1112,

Table 1. Crystallographic Information for
[V(Me₂SiOC≡COSiMe₂)(dmpe)₂Cl] (9) and
[Ta(Me₂SiOC≡COSiMe₂)(depe)₂Cl] (10)^a

empirical formula	C ₂₀ H ₄₈ O ₂ P ₄ Si ₂ VCl	C ₂₈ H ₆₄ O ₂ P ₄ Si ₂ TaCl
fw	587.06	829.28
<i>a</i> (Å)	9.349(2)	11.512(1)
<i>b</i> (Å)	20.548(3)	18.311(3)
<i>c</i> (Å)	16.146(4)	18.493(3)
β(deg)	104.79(1)	96.322(7)
<i>V</i> (Å ³)	2999(1)	3875(1)
<i>T</i> (°C)	-80	-83
<i>Z</i>	4	4
<i>Q</i> _{calc} (g cm ⁻³)	1.30	1.42
space group	C2/c	Cc
2θ limits (deg)	3-48	3-50
data limits	± <i>h+k+l</i>	+ <i>h+k±l</i>
scan type	<i>ω</i> -2θ	<i>ω</i> -2θ
μ (cm ⁻¹)	7.28	31.5
total no. of data collected	3540	7516
no. of unique data ^b	1756	3054
no. of param refined	209	341
<i>p</i> factor	0.03	0.04
abs correction	none	empirical
trans factor range	0.91-1.00	0.67-1.00
<i>R</i> _{merge}	0.028	0.036
GOF	1.152	1.170
<i>R</i> ^c	0.036	0.032
<i>R</i> _w	0.039	0.039

^a Data were collected on an Enraf Nonius CAD-4F kappa geometry diffractometer with Mo Kα radiation. ^b Observation criterion *I* > 3σ(*I*). ^c *R* = Σ||*F*_o| - |*F*_c||/Σ|*F*_o|, *R*_w = [Σw(|*F*_o| - |*F*_c||)²/Σw|*F*_o|²]^{1/2}, where *w* = 1/σ(*F*), as defined in ref 6.

986, 932, 834, 784, 719, 692, 632 cm⁻¹. ¹H NMR (THF-*d*₈): δ 1.71-1.94 (m, 8 H), 1.22 (br s, 24 H), 0.72 (s, 4 H), 0.09 (s, 12 H). ³¹P NMR (THF-*d*₈): δ 60.9 (partially collapsed octet, 64-57). Anal. Calcd for C₂₀H₄₈O₂P₄Si₂V: C, 40.92; H, 8.24; N, 0.00. Found: C, 40.69; H, 7.98; N, 0.00.

[Ta(Me₂SiOC≡COSiMe₂)(depe)₂Cl] (10). A 25-mL, one-necked, pear-shaped flask fitted with a rubber septum was charged with [Ta(CO)₂(depe)₂Cl] (0.136 g, 0.2 mmol) and 20 mL of THF. Upon dissolution, excess 40% sodium amalgam was added in one portion and the reaction mixture was allowed to stir vigorously for 3.5 h. The solids were allowed to settle, the solution was decanted into a second 25-mL pear-shaped flask, and a solution of (ClMe₂SiCH₂)₂ (0.044 g, 0.2 mmol) in 3 mL of THF was added in one portion via pipet. The reaction mixture was allowed to stir for 2 h, providing a green solution. The solvents were removed under vacuum, and the residue was triturated with two 5-mL portions of pentane. The product was extracted with pentane and filtered, and the solvents were removed under vacuum. Recrystallization from pentane at -30 °C afforded 0.124 g (75%) of the desired product as a brown solid. IR (Nujol): 1570, 1249, 1137, 1036, 1001, 832, 785, 730, 721, 695 cm⁻¹. ¹H NMR (C₆D₆): δ 2.02-2.11 (m, 4H), 1.82-1.97 (m, 16H), 1.60-1.71 (m, 4H), 1.05-1.17 (m, 24H), 0.63 (s, 4H), 0.12 (s, 12H). ³¹P NMR (C₆D₆): δ 44.7. Anal. Calcd for C₂₈H₆₄O₂P₄Si₂ClTa: C, 40.55; H, 7.78; N, 0.00. Found: C, 40.18; H, 8.17; N, 0.00.

X-Ray Crystallography. [V(Me₂SiOC≡COSiMe₂)(dmpe)₂Cl]. Golden brown crystals of **9** were grown by slow cooling of a concentrated THF solution to -30 °C. A plate (dimensions 0.12 × 0.25 × 0.25 mm) was cut from a larger specimen and mounted on the end of a quartz fiber with silicon grease on a cold stage. Unit cell parameters and intensity data were obtained by methods standard in our laboratory,⁶ details of which are provided in Table 1. The crystal was judged to be acceptable on the basis of open counter ω-scans of several low-angle reflections (Δ*ω*_{1/2} = 0.22°) and by axial photographs. The vanadium atom was located by the SHELXS-86²¹ direct

methods option in the TEXSAN software package.²² Remaining non-hydrogen atoms were revealed by subsequent least-squares refinements and difference Fourier maps. All non-hydrogen atoms were refined anisotropically. Hydrogen atoms were included at calculated positions in the final refinement cycles. The largest residual peak in the final difference Fourier map was 0.30 e⁻/Å³ near P1.

[Ta(Me₂SiOC≡COSiMe₂)(depe)₂Cl]. Brown crystals were grown by cooling a saturated solution of **10** in pentane at -30 °C. An irregularly shaped crystal (dimensions 0.3 × 0.3 × 0.2 mm) was mounted from a cold stage onto the end of a quartz fiber with silicon grease. Unit cell parameters and intensity data were obtained by standard methods,⁶ details of which are provided in Table 1. The crystal was judged to be acceptable on the basis of open counter ω-scans of several low-angle reflections (Δ*ω*_{1/2} = 0.27°) and by axial photographs. The tantalum atom was located by the SHELXS-86²¹ direct methods option in the teXsan software package.²³ Remaining non-hydrogen atoms were revealed by alternating DIRDIF²⁴ cycles and difference Fourier maps followed by subsequent least-squares refinements and difference Fourier maps. All non-hydrogen atoms were refined anisotropically. Hydrogen atoms were included at calculated positions in the final refinement cycles. The largest residual peak in the final difference Fourier map was 1.33 e⁻/Å³ near Ta. Although the Durbin-Watson statistics indicated a centric space group, the choice of acentric space group *Cc* was confirmed by the deviations from Friedel's law for (*hkl*) and (-*h*-*k*-*l*).

Results and Discussion

Synthesis and Properties of Dicarboxyl Complexes. The synthesis of [Ta(CO)₂(dmpe)₂Cl] was first reported in 1977.¹⁶ Later work revealed that the dicarbonyl complex could be prepared in good yields with slight modifications of the original procedure and without isolation of the two intermediates, [Ta(dmpe)₂Cl₄] and [Ta(dmpe)₂Cl₂]. Similar procedures resulted in good yields of the corresponding niobium complex. This reaction sequence was also used to prepare [Ta(CO)₂(depe)₂Cl], although the yields were not optimized.²⁰

The synthesis of compounds of the type [M(CO)₂(R₂PCH₂CH₂PR₂)₂Cl] has now been broadened and improved to include both the depe and dbpe derivatives for niobium and tantalum. Reduction of either TaCl₅ or NbCl₅ with sodium amalgam in the presence of the appropriate chelating phosphine ligand readily afforded a blue-green product, presumed to be [M(R₂PCH₂CH₂PR₂)₂Cl₄]. Further reduction with magnesium and a catalytic amount of anthracene under an atmosphere of CO provided the desired products after column chromatography on alumina and/or recrystallization. Important to the success of these reactions were the extended reaction times employed for the reduction under a CO atmosphere (Scheme 1). Shorter reaction times resulted in lower overall yields and made purification of the dicarbonyl complex tedious for the butyl derivatives. Under the described conditions, however, the reactions afforded good yields of the desired product with minimal effort required for purification. Similar conditions employing dppe (1,2-bis(diphenylphosphino)ethane) as the chelating diphosphine did not lead to isolation of [Ta(CO)₂(dppe)₂Cl], however. Possibly, the larger steric demands of the dppe ligand or its different

(22) TEXSAN: Single Crystal Structure Analysis Software, Version 5.0, Molecular Structure Corp.: The Woodlands, TX, 1989.

(23) teXsan: Single Crystal Structure Analysis Software, Version 1.6c, Molecular Structure Corp.: The Woodlands, TX, 1994.

(24) Pathasarathi, V.; Beurskens, P. T.; Slot, H. J. B. Acta Crystallogr. 1983, A24, 860.

(21) Sheldrick, G. M. In *Crystallographic Computing*; Krüger, C., Goddard, R., Eds.; Oxford University Press: Oxford, U.K., 1985; p 175.

Scheme 1

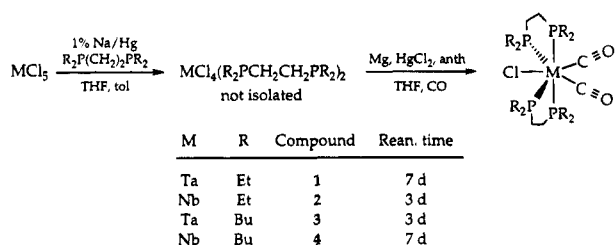


Table 2. Spectroscopic Information for Selected Seven-Coordinate Group V Dicarbonyl Phosphine Halide Complexes

compound	IR ν_{CO} (Nujol) (cm^{-1})	^{31}P NMR (C_6D_6) (ppm)
[Ta(CO) $_2$ (dmpe) $_2$ Cl] a	1740, 1810	24.0
[Ta(CO) $_2$ (depe) $_2$ Cl] (1)	1746, 1819	42.0
[Ta(CO) $_2$ (dbpe) $_2$ Cl] (2)	1747, 1811	38.5
[Nb(CO) $_2$ (dmpe) $_2$ Cl] a	1747, 1810	
[Nb(CO) $_2$ (depe) $_2$ Cl] (3)	1753, 1828	
[Nb(CO) $_2$ (dbpe) $_2$ Cl] (4)	1755, 1818	

a Data from ref 20.

electronic properties preclude formation of either intermediate, [Ta(dppe) $_2$ Cl $_4$] or [Ta(dppe) $_2$ Cl $_2$]. Alternate syntheses of [Nb(CO) $_2$ (dppe) $_2$ Cl] and [Ta(CO) $_2$ (dppe) $_2$ Cl] have been reported, although in multistep, less convenient routes. 25,26

Spectroscopic properties of 1–4 mimic those of the parent dmpe dicarbonyl compounds, as summarized in Table 2. All of the compounds exhibit two low-frequency CO stretches in their infrared spectra around 1820 and 1750 cm^{-1} , confirming the cis orientation of the two carbonyl ligands. The ^{31}P NMR spectra of the tantalum complexes all display a singlet at room temperature.

The solubilities of 1–4 differ from those of their dmpe analogues. The latter are virtually insoluble in nonpolar solvents such as pentane and hexane. In contrast, the corresponding depe derivatives are slightly soluble in aliphatic hydrocarbon solvents, and the dbpe derivatives are highly soluble in these same solvents. Although this difference does not significantly influence the yields of the dicarbonyl complexes, the ramifications are quite important in the subsequent workup of products from the reductive coupling reactions (vide infra).

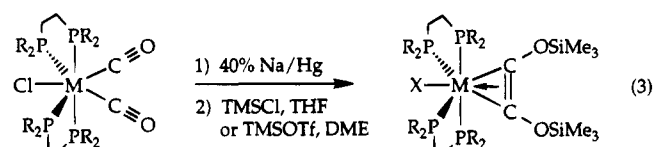
Reductive Coupling Reactions of 1–4 Using Silyl Reagents. Previous investigations of the reductive coupling reaction revealed the sequence of events portrayed in Scheme 2. Reduction of the dicarbonyl complex with excess sodium amalgam yields a highly reduced, six-coordinate M(-1) complex. Upon addition of 1 equiv of an appropriate silylating reagent, a siloxycarbyne can be isolated. Treatment of this species with an additional equivalent of a silylating reagent eventually affords the coupled product. Kinetics studies on the conversion of the carbyne to the coupled product indicated electrophilic attack of the silyl reagent on the CO ligand in the rate-determining step. These experiments, however, left open the question of the timing of the C–C bond-forming event. Scheme 2 depicts two possible intermediates (A and B), either one or even both of which could be important for the coupling reaction. 10,14

(25) Fornalczyk, M.; Süßmilch, F.; Priebisch, W.; Rehder, D. J. *Organomet. Chem.* **1992**, *426*, 159.

(26) Felten, C.; Richter, J.; Priebisch, W.; Rehder, D. *Chem. Ber.* **1989**, *122*, 1617.

Significant differences were observed for reactions of the Na[M(CO) $_2$ (depe or dbpe) $_2$] salts with silyl reagents. Addition of 1 equiv of Me $_3$ SiCl appeared to generate [M(COSiMe $_3$)(CO)(depe or dbpe) $_2$], whereas the corresponding anion obtained from [Ta(CO) $_2$ (dmpe) $_2$ Cl] produced the dinuclear species [(dmpe) $_2$ (CO)Ta≡COTa-(Me $_3$ SiOC≡COSiMe $_3$)(dmpe) $_2$]. 27 The increased steric demands of the depe and dbpe have thus prevented formation of the corresponding dinuclear complex. It is also noteworthy that a similar dinuclear species did not form in reactions of the analogous vanadium dmpe complex. 17

Addition of 2 equiv or more of silyl reagent led to carbon–carbon bond formation, affording the acetylene complexes in good yield (eq 3). Reactions of the niobium



dbpe coupled complexes were sluggish, so the “high-salt effect”, discovered during the kinetics studies of the carbyne–CO coupling step, 10 was used. Addition of 1 equiv of $^n\text{Bu}_4\text{NBPh}_4$ shortened the reaction times significantly.

As illustrated in Table 3, the spectroscopic properties of the new chloride-capped coupled products are in good agreement with previously reported values. 8 Infrared spectroscopy revealed a characteristic stretch between 1550 and 1590 cm^{-1} , attributed to the newly formed C–C bond. The ^1H NMR spectra displayed a singlet arising from the trimethylsilyl moieties at ca. 0.2 ppm, as well as resonances from the phosphine ligands. The ^{31}P NMR spectra of the tantalum species all displayed a sharp singlet, characteristic of complexes containing a freely rotating, four-electron-donating acetylene ligand. 28

Despite the increased crowding imposed by the phosphine ligands, no tantalum or niobium species of the form [M(Me $_3$ SiOC≡COSiMe $_3$)(depe or dbpe) $_2$]OTf was obtained in the present work. Reactions employing TMSOTf proceeded more rapidly than the corresponding reactions with TMSCl, however, obviating the need for high-salt conditions. The yields of the dbpe derivatives were somewhat lower than the corresponding depe compounds, especially for the triflates. As mentioned previously, the butyl derivatives of the dicarbonyl complexes are soluble in pentane. With the dmpe and depe derivatives, purification of the reductive coupling products was readily effected by extraction of the crude product with pentane followed by recrystallization from the same solvent. For the butyl derivatives, however, separation of the crude product was hindered by the solubility of the starting dicarbonyl compound, which was often present in small amounts. In most cases, the reactions proceeded smoothly, affording crude product of fairly high purity. Recrystallization of [M(Me $_3$ SiOC≡COSiMe $_3$)(dbpe) $_2$]OTf (M = Nb, Ta) proved to be quite tedious, however, and was virtually impossible when performed on a small scale, hindering attempts to obtain analytically pure material.

(27) Vrtis, R. N.; Bott, S. G.; Lippard, S. J. *Organometallics* **1992**, *11*, 270.

(28) Templeton, J. L. *Adv. Organomet. Chem.* **1989**, *29*, 1.

Scheme 2

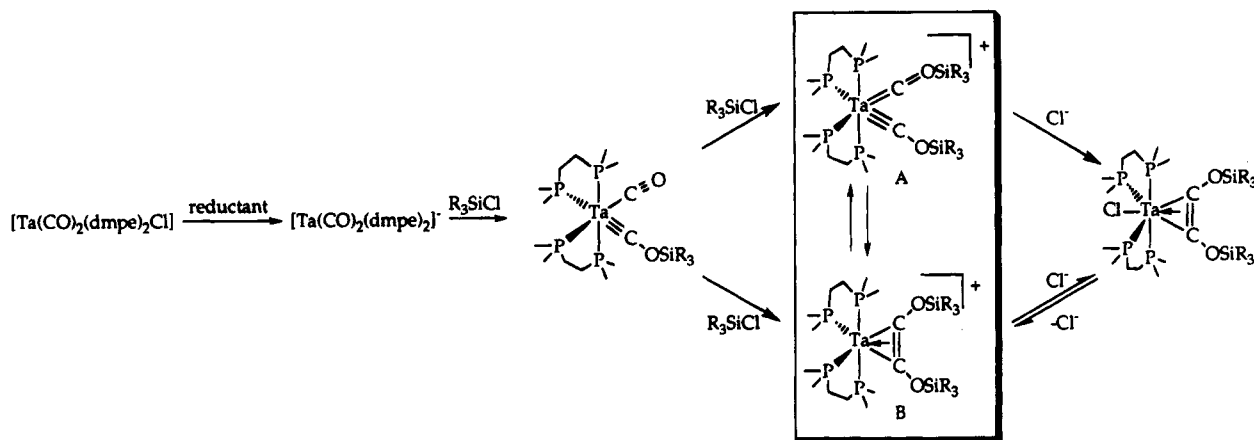


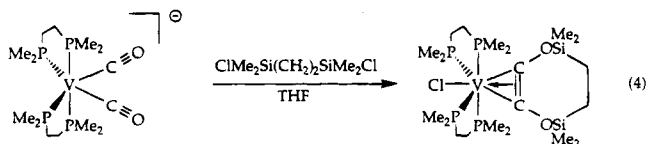
Table 3. Spectroscopic Data and Yields for $[M(\text{Me}_3\text{SiOC}\equiv\text{COSiMe}_3)(\text{R}_2\text{PCH}_2\text{CH}_2\text{PR}_2)_2\text{X}]^a$

compd	(M, R, X)	$\nu_{\text{C}\equiv\text{C}}$ (cm^{-1})	$^1\text{H NMR}$ (Me_3Si) (ppm)	$^{31}\text{P NMR}$ (ppm)	yield (%)
	(Ta, Me, Cl) ^b	1547 ^c	0.26	25 ^d	67
5a	(Ta, Et, Cl)	1558	0.21	45.1	63
6a	(Nb, Et, Cl)	1569	0.22		72
7a	(Ta, Bu, Cl)	1560	0.27	41.0	55
8a	(Nb, Bu, Cl)	1585	0.27		73 ^e
	(Ta, Me, OTf) ^b	1575		28.8 ^d	39
5b	(Ta, Et, OTf)	1581	0.13	50.3	66
6b	(Nb, Et, OTf)	1593	0.12		85
7b	(Ta, Bu, OTf)	1576	0.20	45.8	48
8b	(Nb, Bu, OTf)	1586	0.20		53

^a IR spectra were recorded in Nujol mulls, and NMR spectra were obtained in benzene-*d*₆, unless otherwise specified. ^b From ref 8. ^c KBr pellet. ^d Pentane solution. ^e Run with 1 equiv of Bu₄NBPh₄.

Formation of Cyclic Acetylene Ligands via Reductive Coupling. In order to elaborate the reductive coupling chemistry, we explored the reaction of the highly reduced anions with 1,2-bis(chlorodimethylsilyl)ethane. Our goal was to synthesize a coupled ligand that was part of an eight-membered heterocycle. In addition to affording such a novel acetylene ligand, this reaction would represent the first example of an annulation strategy in dicarbonyl reductive coupling.

Treatment of Na[V(CO)₂(dmpe)₂] with 1,2-bis(chlorodimethylsilyl)ethane in THF resulted in an immediate color change from red to brown. Recrystallization from THF afforded golden brown crystals, the spectroscopic properties of which were consistent with the formation of the desired coupled product (eq 4), especially the



infrared band at 1624 cm^{-1} . The $^1\text{H NMR}$ spectrum showed two singlets at 0.72 and 0.09 ppm integrating for 4 and 12 hydrogens, respectively.

Confirmation of the structure was obtained through a single crystal X-ray study. An ORTEP representation of the molecule is presented in Figure 1, and Tables 4 and 5 list atomic coordinates and some important bond distances and angles, respectively. As anticipated, the newly formed acetylene is incorporated within an eight-membered ring. The C1–C1* bond length of 1.308(6) Å is slightly shorter than the value of 1.348(9) Å found in $[\text{V}(\text{Me}_3\text{SiOC}\equiv\text{COSiMe}_3)(\text{dmpe})_2\text{Br}]$,¹⁷ perhaps a con-

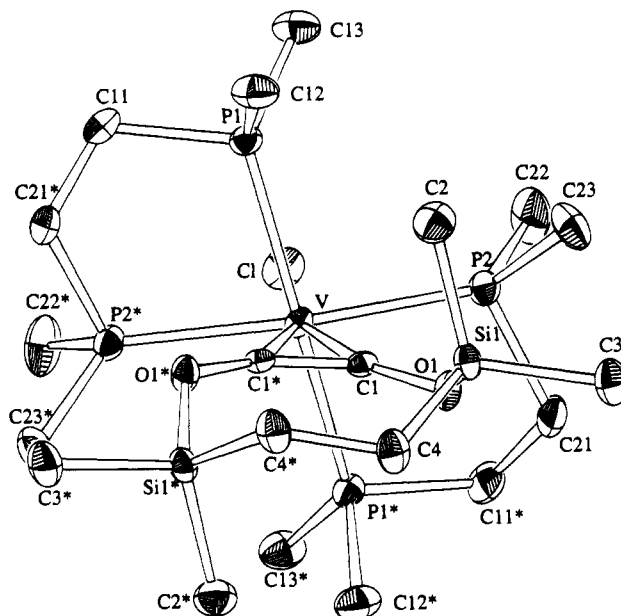


Figure 1. Structure of $[\text{V}(\text{Me}_2\text{SiOC}\equiv\text{COSiMe}_2)(\text{dmpe})_2\text{Cl}]$ showing 40% thermal ellipsoids for all non-hydrogen atoms.

Table 4. Positional Parameters and $B(\text{eq})$ for $[\text{V}(\text{Me}_2\text{SiOC}\equiv\text{COSiMe}_2)(\text{dmpe})_2\text{Cl}]$ (9)^a

atom	x	y	z	$B(\text{eq})^b$ (Å ²)
V	0	0.38391(4)	0.75	1.36(3)
Cl	0	0.26146(6)	0.75	2.51(5)
P(1)	0.0738(1)	0.36900(5)	0.61780(6)	1.79(4)
P(2)	0.2419(1)	0.36764(5)	0.84775(6)	1.92(4)
Si(1)	0.2074(1)	0.59129(5)	0.80617(6)	1.74(4)
O(1)	0.1483(3)	0.5199(1)	0.8344(1)	1.9(1)
C(1)	0.0593(4)	0.4751(2)	0.7820(2)	1.4(1)
C(2)	0.2733(5)	0.5837(2)	0.7080(3)	2.9(2)
C(3)	0.3644(5)	0.6133(2)	0.8973(3)	2.7(2)
C(4)	0.0627(5)	0.6550(2)	0.7919(3)	2.4(2)
C(11)	-0.0897(5)	0.3442(2)	0.5311(3)	3.2(2)
C(12)	0.1357(6)	0.4412(2)	0.5718(3)	2.9(2)
C(13)	0.2086(5)	0.3086(2)	0.6037(3)	2.9(2)
C(21)	0.2249(5)	0.3803(2)	0.9583(3)	3.1(2)
C(22)	0.3364(6)	0.2891(2)	0.8597(3)	3.8(2)
C(23)	0.4002(5)	0.4193(2)	0.8470(3)	3.2(2)

^a Atoms are labeled as indicated in Figure 1. Estimated standard deviations in the least significant figure are given in parentheses. ^b $B(\text{eq}) = \frac{1}{3}[a^2\beta_{11} + b^2\beta_{22} + c^2\beta_{33} + 2ab \cos(\gamma)\beta_{12} + 2ac \cos(\beta)\beta_{13} + 2bc \cos(\alpha)\beta_{23}]$.

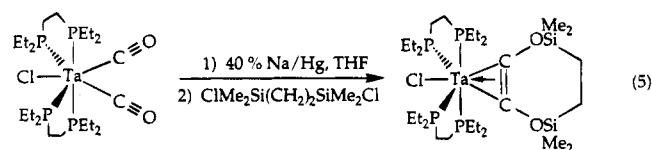
sequence of the ring system. The C1–V–C1* angle of 38.5(2)° is correspondingly smaller than the 40.4(3)° value in the acyclic analogue.

Table 5. Selected Intramolecular Bond Distances (Å) and Angles (deg) Involving the Non-Hydrogen Atoms for**[V(Me₂SiOC≡COSiMe₂)(dmpe)₂Cl] (9)^a**

Bond Distances			
V-P(1)	2.425(1)	O(1)-C(1)	1.377(4)
V-P(2)	2.428(1)	Si(1)-O(1)	1.671(2)
V-C(1)	1.985(3)	C(4)-C(4*)	1.548(7)
C(1)-C(1*)	1.308(6)	V-Cl	2.516(2)
Bond Angles			
V-C(1)-O(1)	151.1(2)	P(1)-V-P(2*)	80.66(4)
C(1)-V-C(1*)	38.5(2)	P(1)-V-C(1)	103.0(1)
Si(1)-O(1)-C(1)	127.6(2)	P(1)-V-C(1*)	90.78(9)
Cl-V-P(1)	82.74(3)	P(1)-V-P(2)	80.66(4)
Cl-V-P(2)	82.09(3)	P(1*)-V-P(2*)	97.33(4)
Cl-V-C(1)	160.76(9)	P(2)-V-P(2*)	164.17(6)
P(1)-V-P(1*)	165.48(6)	P(2)-V-C(1)	79.0(1)
P(1)-V-P(2)	97.33(4)	P(2)-V-C(1*)	116.8(1)

^a Atoms are labeled as indicated in Figure 1. Estimated standard deviations in the least significant figure are given in parentheses.

Attempts to perform the analogous reaction with [Ta(CO)₂(dmpe)₂Cl] resulted in very low yields of the desired heterocyclic product. Although the reasons for this result were not fully explored, one possibility is that dinuclear species form.²⁷ Reaction of Na[Ta(CO)₂(depe)₂] with 1 equiv of 1,2-bis(chlorodimethylsilyl)ethane, however, produced an immediate orange to red color change, indicating formation of a siloxycarbyne species. When the reaction was allowed to continue for an additional 2 h, a green solution formed, suggestive of reductive coupling. Upon workup of the reaction mixture and recrystallization from pentane at -30 °C, green crystals were obtained, the spectroscopic properties of which indicated formation of the desired cyclic acetylene ligand (eq 5). The infrared spectrum exhibited

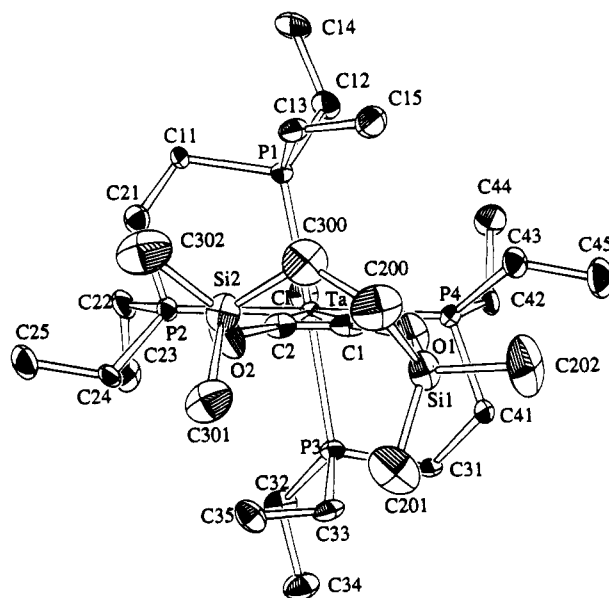


a characteristic $\nu_{C\equiv C}$ band at 1570 cm^{-1} , and there were two singlets in the ¹H NMR spectrum at 0.63 and 0.12 ppm, values similar to those in the spectrum of the corresponding vanadium complex. The ³¹P NMR spectrum consisted of a single, sharp resonance at 44.7 ppm, also consistent with formation of a coupled product.

Confirmation of the structure was provided by an X-ray analysis of a single crystal grown from pentane at -30 °C, an ORTEP representation of which is provided in Figure 2. A list of atomic coordinates may be found in Table 6, and a summary of important bond distances and angles may be found in Table 7. As had been deduced from the spectral data, the product contained the desired cyclic acetylene ligand as part of the eight-membered heterocycle, analogous to the results obtained from the reaction with Na[V(CO)₂(dmpe)₂].

Attempts to synthesize coupled products containing a seven-membered ring, from reactions of Na[M(CO)₂(dmpe)₂] and Na[M(CO)₂(depe)₂] (M = Nb, Ta) with dichlorosilanes (Me₂SiCl₂, ^tBuPhSiCl₂, Ph₂SiCl₂), were unsuccessful.

Summary. Optimized syntheses of three new M(I) dicarbonyl halide complexes have been achieved, where M = Nb or Ta. In addition, an improved synthesis of [Ta(CO)₂(depe)₂Cl] was obtained. The new compounds

**Figure 2. Structure of [Ta(Me₂SiOC≡COSiMe₂)(depe)₂Cl] showing 40% thermal ellipsoids for all non-hydrogen atoms.****Table 6. Positional Parameters and B(eq) for****[Ta(Me₂SiOC≡COSiMe₂)(depe)₂Cl] (10)^a**

atom	x	y	z	B(eq) ^b (Å ²)
Ta	0	0.19466(2)	0.25	1.36(1)
Cl	-0.1964(3)	0.1939(2)	0.2970(2)	2.7(1)
P(1)	-0.0925(3)	0.1102(2)	0.1496(2)	1.8(1)
P(2)	-0.0995(3)	0.2860(2)	0.1579(2)	1.7(1)
P(3)	0.0685(3)	0.2824(2)	0.3527(2)	1.7(1)
P(4)	0.0530(3)	0.1076(2)	0.3565(2)	1.7(1)
Si(1)	0.4202(3)	0.1485(2)	0.2535(2)	3.5(2)
Si(2)	0.2862(3)	0.2366(2)	0.0801(2)	3.5(2)
O(1)	0.2819(7)	0.1348(5)	0.2620(5)	3.8(4)
O(2)	0.1882(9)	0.2560(5)	0.1338(5)	4.3(4)
C(1)	0.174(1)	0.1726(7)	0.2358(7)	2.2(5)
C(2)	0.139(1)	0.2174(7)	0.1882(6)	2.0(5)
C(11)	-0.179(1)	0.1669(7)	0.0786(8)	2.3(5)
C(12)	-0.191(1)	0.0360(7)	0.1682(7)	2.9(5)
C(13)	0.008(1)	0.0662(7)	0.0928(7)	2.6(5)
C(14)	-0.261(2)	0.0000(8)	0.103(1)	4.9(7)
C(15)	0.083(1)	0.0079(8)	0.1284(8)	4.0(7)
C(21)	-0.121(1)	0.2377(9)	0.0696(8)	2.5(6)
C(22)	-0.247(1)	0.3162(7)	0.166(1)	2.8(6)
C(23)	-0.025(1)	0.3692(6)	0.1344(7)	2.3(5)
C(24)	-0.262(1)	0.3682(8)	0.2280(8)	3.1(6)
C(25)	-0.080(1)	0.4138(8)	0.069(1)	4.0(7)
C(31)	0.098(1)	0.2332(8)	0.4407(7)	2.4(5)
C(32)	-0.020(1)	0.3598(8)	0.3789(7)	2.8(6)
C(33)	0.214(1)	0.3242(8)	0.3470(8)	2.7(6)
C(34)	0.032(1)	0.4068(9)	0.4422(8)	3.5(6)
C(35)	0.216(1)	0.3770(7)	0.2833(8)	3.1(6)
C(41)	0.153(1)	0.1542(8)	0.4257(8)	2.5(6)
C(42)	-0.057(1)	0.0764(6)	0.4151(6)	2.2(5)
C(43)	0.134(1)	0.0230(7)	0.3440(7)	2.7(5)
C(44)	-0.140(1)	0.0186(8)	0.3820(8)	3.5(6)
C(45)	0.183(2)	-0.0205(8)	0.4131(8)	4.5(7)
C(200)	0.448(1)	0.130(1)	0.155(1)	7(1)
C(201)	0.475(1)	0.241(1)	0.285(1)	7(1)
C(202)	0.497(1)	0.078(1)	0.311(1)	8(1)
C(300)	0.342(1)	0.145(1)	0.094(1)	5.7(9)
C(301)	0.406(2)	0.307(1)	0.096(1)	6(1)
C(302)	0.211(2)	0.243(1)	-0.009(1)	8(1)

^a Atoms are labeled as indicated in Figure 2. Estimated standard deviations in the least significant figure are given in parentheses. ^b B(eq) = $\frac{1}{3}[a^2\beta_{11} + b^2\beta_{22} + c^2\beta_{33} + 2ab \cos(\gamma)\beta_{12} + 2ac \cos(\beta)\beta_{13} + 2bc \cos(\alpha)\beta_{23}]$.

are useful precursors for reductive coupling reactions of the CO ligands, providing an expanded family of disiloxycarbyne complexes. Increasing the steric de-

Table 7. Selected Intramolecular Bond Distances (Å) and Angles (deg) Involving the Non-Hydrogen Atoms for**[Ta(Me₂SiOC≡COSiMe₂)(depe)₂Cl] (10)^a**

Bond Distances			
Ta-P(1)	2.558(4)	Ta-P(2)	2.565(4)
Ta-P(3)	2.546(4)	Ta-P(4)	2.555(4)
Ta-C(1)	2.09(1)	Ta-C(2)	2.11(1)
Ta-Cl	2.511(3)	C(1)-C(2)	1.24(2)
C(1)-O(1)	1.46(1)	C(2)-O(2)	1.40(1)
Si(1)-O(1)	1.637(8)	Si(2)-O(2)	1.623(8)
Bond Angles			
Ta-C(1)-O(1)	148(1)	Ta-C(2)-O(2)	152(1)
C(1)-Ta-C(2)	34.2(5)	Si(1)-O(1)-C(1)	134.2(8)
Si(2)-O(2)-C(2)	133.8(8)		
Cl-Ta-P(1)	86.0(1)	Cl-Ta-P(2)	83.1(1)
Cl-Ta-P(3)	87.8(1)	Cl-Ta-P(4)	82.9(1)
Cl-Ta-C(1)	162.9(4)	Cl-Ta-C(2)	162.9(4)
P(1)-Ta-P(2)	78.0(1)	P(1)-Ta-P(3)	173.5(1)
P(1)-Ta-P(4)	103.11(9)	P(1)-Ta-C(1)	96.9(3)
P(1)-Ta-C(2)	90.4(3)	P(2)-Ta-P(3)	99.40(9)
P(2)-Ta-P(4)	165.9(1)	P(2)-Ta-C(1)	114.0(4)
P(2)-Ta-C(2)	79.8(4)	P(3)-Ta-P(4)	77.9(1)
P(3)-Ta-C(1)	89.6(3)	P(3)-Ta-C(2)	95.0(3)
P(4)-Ta-C(1)	79.9(4)	P(4)-Ta-C(2)	114.1(4)

^a Atoms are labeled as indicated in Figure 2. Estimated standard deviations in the least significant figure are given in parentheses.

mands of the phosphine ligands had a minimal effect on the formation of the seven-coordinate coupled products. When 1,2-bis(chlorodimethylsilyl)ethane was em-

ployed as the electrophile, the reductively coupled acetylene complexes contained an eight-membered heterocycle. The structures of a vanadium and a tantalum product of this kind confirmed the formation of the ring, and the vanadium complex revealed a newly formed carbon-carbon bond that was slightly shorter than that in the acyclic analogue. The tantalum depe complex illustrates the value of employing more bulky phosphine ligands, affording a much higher yield of the reductively coupled products than the corresponding dmpe complex. Preliminary experiments indicate that the cyclic ligand can be readily removed as the corresponding olefin upon hydrogenation,²⁹ a reaction previously described for the acyclic derivatives.^{9,17}

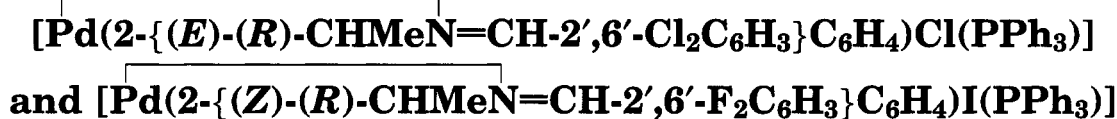
Acknowledgment. This work was supported by a grant from the National Science Foundation. We also thank Dr. L. E. Pence for helpful discussion.

Supplementary Material Available: Tables of bond distances and angles and anisotropic temperature factors for **9** and **10** (8 pages). Ordering information is given on any current masthead page.

OM940780I

(29) Bronk, B. S.; Protasiewicz, J. D.; Lippard, S. J. Unpublished results.

Optically Active Exocyclic Cyclopalladated Derivatives of Benzylidene-(*R*)-(1-phenylethyl)amines: Syntheses and X-ray Molecular Structures of



Joan Albert,* Jaume Granell, and Joaquim Sales

Departament de Química Inorgànica, Universitat de Barcelona, Diagonal 647,
08028-Barcelona, Spain

Mercè Font-Bardía and Xavier Solans

Departament de Cristal·lografia, Minerologia i Dipòsits Minerals, Universitat de Barcelona,
Martí i Franqués, s/n, 08028-Barcelona, Spain

Received October 17, 1994*

The action of Pd(AcO)₂ on benzylidene-(*R*)-(1-phenylethyl)amines, RCH=NCHMePh (R = 2,6-Cl₂C₆H₃ (**1a**), 2,6-F₂C₆H₃ (**1b**), 2,4,6-(MeO)₃C₆H₂ (**1c**)), and subsequent treatment with LiCl, LiBr, or KI gives the corresponding halogen-bridged exocyclic cyclopalladated dimers

[Pd(C–N)X]₂ (X = Cl, Br, I) in which the C=N bond is not included in the metallacycle (compounds **2–4**, respectively). In relation to the *Z* or *E* form adopted by the imines in these cyclopalladated dimers, **2a,b–4a,b** consist of a mixture of (*Z,Z*), (*Z,E*), and (*E,E*) isomers, whereas **2c–4c** consist of only the (*E,E*) isomer. The equilibrium (*Z,Z*) + (*E,E*) ⇌ 2(*Z,E*) is observed in chloroform solutions of **2a,b–4a,b**. According to this equilibrium, when **2a,b** and **3a,b** are eluted through a column of SiO₂ with CHCl₃, the initial band which contains a mixture of (*Z,Z*), (*Z,E*), and (*E,E*) isomers splits into two bands: the first contains the (*Z,Z*) isomer and the second the (*E,E*) isomer. The action of PPh₃ on **2a,b–4a,b** yields

the corresponding cyclopalladated monomers [Pd(C–N)X(PPh₃)]. When this reaction is carried out with dimers **2c–4c**, demethylation of one of the *ortho* methoxy groups is also observed, giving the tridentate species [Pd(C–N–O)(PPh₃)]. The X-ray crystal structure of

two monomers with PPh₃ has been determined. [Pd(2- $\{ (E)\text{-}(R)\text{-CHMeN}=\text{CH-2',6'-Cl}_2\text{C}_6\text{H}_3 \}$ -C₆H₄)Cl(PPh₃)] crystallizes in the monoclinic space group *P*2₁ with *a* = 16.996(4) Å, *b* = 9.006(2) Å, *c* = 9.655(2) Å, β = 91.63(3)°, and *Z* = 2. [Pd(2- $\{ (Z)\text{-}(R)\text{-CHMeN}=\text{CH-2',6'-F}_2\text{C}_6\text{H}_3 \}$ -C₆H₄)I(PPh₃)] crystallizes in the orthorhombic space group *P*2₁2₁2₁ with *a* = 18.017(3) Å, *b* = 14.204(2) Å, *c* = 11.978(2) Å, and *Z* = 4.

Introduction

Since the first examples of cyclometalation reactions were described,¹ there has been a continuous interest in this process, because it permits the selective activation of C–H bonds in heterosubstituted organic molecules.² Although a large number of cyclometalated compounds have been described, few of them are optically active.³ The preparation of such compounds is a field of great interest as a consequence of their useful

applications. It has been shown that (+)-bis(*μ*-chloro)-bis[(*S*)-dimethyl(1-phenylethyl)amine-2*C,N*]dipalladium-(II) and (+)-bis(*μ*-chloro)bis[(*R*)-dimethyl(1-(2-naphthyl)-

* Abstract published in *Advance ACS Abstracts*, February 1, 1995.
(1) (a) Kleiman, J. P.; Dubeck, M. *J. Am. Chem. Soc.* **1963**, *85*, 1544. (b) Cope, A. C.; Siekman, R. W. *J. Am. Chem. Soc.* **1965**, *87*, 3272. (c) Cope, A. C.; Friedrich, E. C. *J. Am. Chem. Soc.* **1968**, *90*, 909.
(2) (a) Bruce, M. I. *Angew. Chem., Int. Ed. Engl.* **1977**, *16*, 73. (b) Newkome, G. R.; Puckett, W. E.; Gupta, V. K.; Kiefer, G. E. *Chem. Rev.* **1986**, *86*, 451. (c) Omae, I. *Coord. Chem. Rev.* **1988**, *83*, 137. (d) Dunina, V. V.; Zalevskaia, O. A.; Potatov, V. M. *Russ. Chem. Rev. (Engl. Transl.)* **1988**, *57*, 250. (e) Ryabov, A. D. *Chem. Rev.* **1990**, *90*, 403.

(3) (a) Otsuka, S.; Nakamura, A.; Kano, T.; Tani, K. *J. Am. Chem. Soc.* **1971**, *93*, 4301. (b) Sokolov, V. I.; Troitskaya, L. L.; Reutov, O. A. *J. Organomet. Chem.* **1977**, *133*, C28. (c) Sokolov, V. I.; Troitskaya, L. L.; Reutov, O. A. *J. Organomet. Chem.* **1979**, *182*, 537. (d) Sokolov, V. I.; Bashilov, V. V.; Musaev, A. A.; Reutov, O. A. *J. Organomet. Chem.* **1982**, *225*, 57. (e) Allen, D. G.; McLaughlin, G. M.; Robertson, G. B.; Steffen, W. L.; Salem, G.; Wild, S. B. *Inorg. Chem.* **1982**, *21*, 1007. (f) Sokolov, V. I.; Troitskaya, L. L.; Rozhkova, T. I. *Gazz. Chim. Ital.* **1987**, *117*, 525. (g) Maassarani, F.; Pfeffer, M.; Le Borgne, G.; Jastrzebski, J. T. B. H.; van Koten, G. *Organometallics* **1987**, *6*, 1111. (h) Wehman-Ooyevaar, I. C. M.; Grove, D. M.; Kooijman, H.; van der Sluis, P.; Spek, A. L.; van Koten, G. *J. Am. Chem. Soc.* **1992**, *114*, 9916. (i) Yang, H.; Khan, M. A.; Nicholas, K. M. *J. Chem. Soc., Chem. Commun.* **1992**, 210. (j) Vicente, J.; Saura-Llamas, I.; Jones, P. G. *J. Chem. Soc., Dalton Trans.* **1993**, 3619. (k) Baena, M. J.; Buey, J.; Espinet, P.; Kitzerow, H. S.; Heppke, G. *Angew. Chem., Int. Ed. Engl.* **1993**, *32*, 1201. (l) Baena, M. J.; Espinet, P.; Ros, M. B.; Serrano, J. L.; Ezcurra, A. *Angew. Chem., Int. Ed. Engl.* **1993**, *32*, 1203. (m) Baena, M. J.; Barberá, J.; Espinet, P.; Ezcurra, A.; Ros, M. B.; Serrano, J. L. *J. Am. Chem. Soc.* **1994**, *116*, 1899. (n) Gorla, F.; Togni, A.; Venanzi, L. M.; Albinati, A.; Lianza, F. *Organometallics* **1994**, *13*, 1607.

ethyl)amine-3*C,N*]dipalladium(II) may be applied to optical resolution of racemic phosphines, arsines, and amines^{3a,e,4} and to the determination by NMR spectroscopy of (a) the optical purity of chiral phosphines and amines⁵ and (b) the absolute configuration of chiral phosphines.⁶ Recently, metallomesogens displaying cholesteric behavior or improved ferroelectric properties have been obtained from cyclopalladated imine derivatives, containing a chiral center in the carboxylate ligand^{3k} or in an alkyl chain.^{3l,m}

Although the utility of cyclometalated complexes in organic synthesis is well-known,⁷ few applications to asymmetric synthesis have been described with optically active cyclometalated compounds.^{3c,n,8} Prostaglandin precursors,^{8b,c} 1,2-disubstituted ferrocenes,^{3c} alcohols,^{8c-e} phosphines,^{8a,f} and oxazolines³ⁿ have been prepared in moderate to high enantiomeric or distereomeric excess, using such compounds as starting materials^{3c,8} or as catalyst precursors.³ⁿ One of the reasons for the scarce application of compounds of this kind to asymmetric synthesis is that few of them contain prochiral organic functions susceptible to asymmetric elaboration.^{3i-m,8f}

Over the last few years we have been working on cyclopalladation of benzylidenebenzylamines (Chart 1). We and others have shown that cyclopalladation of these ligands gives, regioselectively, endocyclic compounds (in which the C=N bond is included in the metallacycle).⁹ We have also shown that the exocyclic compounds can be obtained if the *ortho* positions of the benzal ring (which leads to the formation of endocyclic compounds) are blocked by substituents such as chlorine atoms¹⁰ or methyl groups.¹¹ It is noteworthy that the formation of the exocyclic cyclopalladated compounds is accompanied by the *E* → *Z* isomerization of the benzylidenebenzylamines.

Following and expanding this strategy to prepare exocyclic cyclopalladated compounds of benzylidenebenzylamines, here we describe the preparation of a new

Chart 1

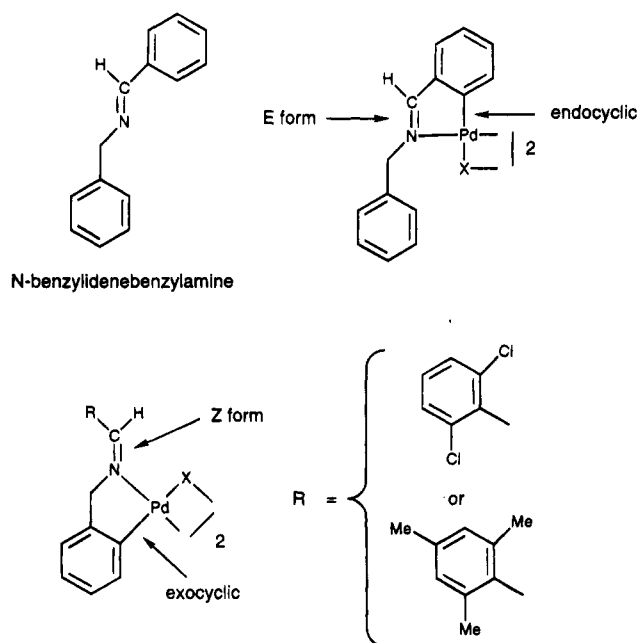
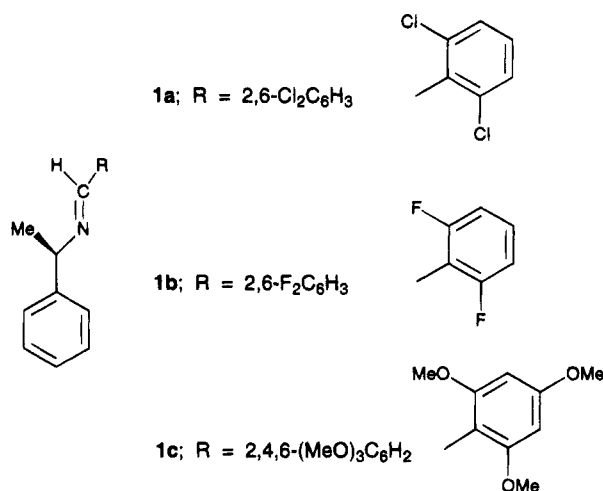


Chart 2



series of optically active exocyclic cyclopalladated compounds derived from benzylidene-(*R*)-(1-phenylethyl)-amines **1a–c** (Chart 2), which have the *ortho* positions of the benzal ring occupied by chlorine atoms, fluorine atoms, and methoxy groups, respectively.

Cyclopalladation of imines **1a–c** proceeds in reasonable yields (up to 50%), furnishing a new series of optically active cyclopalladated compounds containing a homochiral palladacycle with an exocyclic N=CHR group, susceptible to asymmetric elaboration.

Results and Discussion

Cyclopalladation of Imines 1a,b. Synthesis of the Cyclopalladated Compounds. Imines **1a,b** were treated with Pd(AcO)₂ in acetic acid, for 2 h at 80 °C (**1a**) or 45 min at reflux (**1b**). Subsequent treatment of the reaction residues with LiCl, LiBr, or KI in ethanol resulted in the formation of voluminous precipitates which contained the corresponding halogen-bridged exocyclic cyclopalladated dimers **2–4** as major compounds (Scheme 1). Compounds **2** and **3** were obtained in pure form after purification by SiO₂ column chroma-

(4) For recent references on this subject see: (a) Chooi, S. Y. M.; Siah, S. Y.; Leung, P. H.; Mok, K. F. *Inorg. Chem.* **1993**, *32*, 4812. (b) Gabbitas, N.; Salem, G.; Sterns, M.; Willis, A. C. *J. Chem. Soc., Dalton Trans.* **1993**, 3271. (c) Alcock, N. W.; Brown, J. M.; Hulmes, D. I. *Tetrahedron: Asymmetry* **1993**, *4*, 743. (d) Gladiali, S.; Dore, A.; Fabbri, D.; De Lucchi, O.; Manassero, M. *Tetrahedron: Asymmetry* **1994**, *5*, 511. (e) Tani, K.; Tashiro, H.; Yoshida, M.; Yamagata, T. *J. Organomet. Chem.* **1994**, *469*, 229. (f) Chooi, S. Y. M.; Ranford, J. D.; Leung, P. H.; Mok, K. F. *Tetrahedron: Asymmetry* **1994**, *5*, 1805.

(5) (a) Kyba, E. P.; Rines, S. P. *J. Org. Chem.* **1982**, *47*, 4800. (b) Chooi, S. Y. M.; Leung, P. H.; Lim, C. C.; Mok, K. F.; Quek, G. H.; Sim, K. Y.; Tan, M. K. *Tetrahedron: Asymmetry* **1992**, *3*, 529.

(6) Bookham, J. L.; McFarlane, W. *J. Chem. Soc., Chem. Commun.* **1993**, 1352.

(7) (a) Ryabov, A. D. *Synthesis* **1985**, 233. (b) Pfeffer, M. *Recl. Trav. Chim. Pays-Bas* **1990**, *109*, 567.

(8) (a) Sokolov, V. I.; Troitskaya, L. L.; Reutov, O. A. *J. Organomet. Chem.* **1980**, *202*, C58. (b) Sokolov, V. I.; Troitskaya, L. L.; Khrushchova, N. S. *J. Organomet. Chem.* **1983**, *250*, 439. (c) Sokolov, V. I. *Pure Appl. Chem.* **1983**, *55*, 1837. (d) Troitskaya, L. L.; Sokolov, V. I. *J. Organomet. Chem.* **1985**, *285*, 389. (e) Gruselle, M.; Malezieux, B.; Troitskaya, L. L.; Sokolov, V. I.; Epstein, L. M.; Shubina, Y. S.; Vaissermann, J. *Organometallics* **1994**, *13*, 200. (f) Aw, B. H.; Leung, P. H. *Tetrahedron: Asymmetry* **1994**, *5*, 1167.

(9) (a) Albert, J.; Granell, J.; Sales, J. *J. Organomet. Chem.* **1984**, *273*, 393. (b) Albert, J.; Granell, J.; Sales, J.; Solans, X.; Font-Altaba, M. *Organometallics* **1986**, *5*, 2567. (c) Clark, P. W.; Dyke, S. F.; Smith, G.; Kennard, C. H. L. *J. Organomet. Chem.* **1987**, *330*, 447. (d) Chakladar, S.; Paul, P.; Venkatsubramanian, K.; Nag, K. *J. Chem. Soc., Dalton Trans.* **1991**, 2669. (e) Navarro-Ranninger, C.; López-Solera, I.; Alvarez-Valdés, A.; Rodríguez-Ramos, J. H.; Masaguer, J. R.; García-Ruano, J. L.; Solans, X. *Organometallics* **1993**, *12*, 4104.

(10) Albert, J.; Gómez, M.; Granell, J.; Sales, J.; Solans, X. *Organometallics* **1990**, *9*, 1405.

(11) Albert, J.; Ceder, R. M.; Gómez, M.; Granell, J.; Sales, J. *Organometallics* **1992**, *11*, 1536.

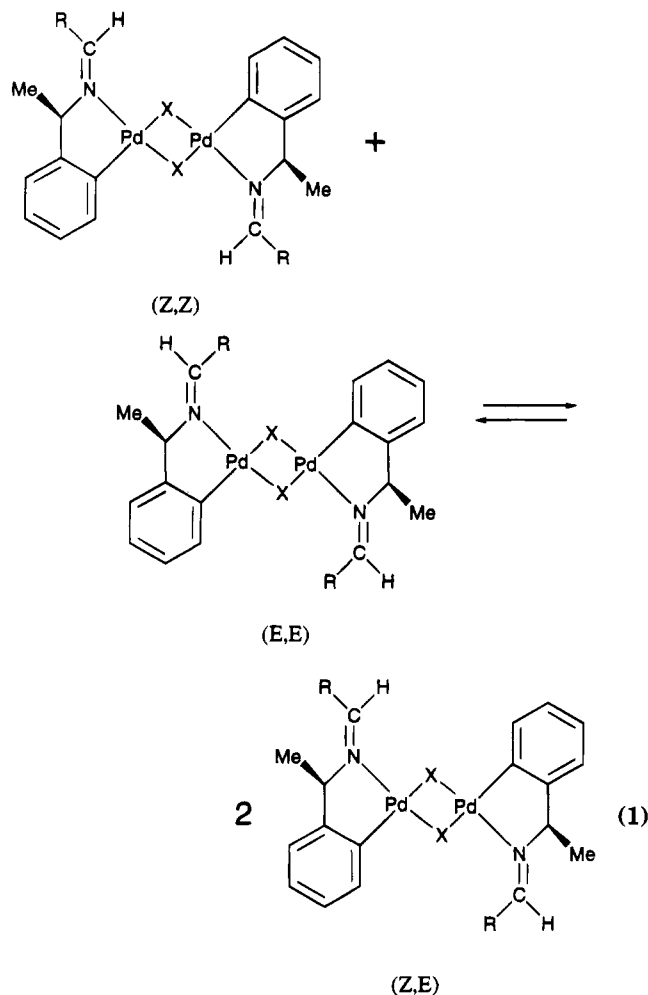
tography, using $\text{CHCl}_3/\text{MeOH}$ (100/2) as eluant, whereas compounds **4** were eluted with CHCl_3 .

^1H and $^{13}\text{C}\{^1\text{H}\}$ NMR in CDCl_3 of compounds **2–4** are quite informative about their structure and behavior in solution. Due to the presence of different isomers, which lead to quite complex NMR spectra, we center the NMR discussion mainly on the chemical shift of the methinic proton ($\text{CH}=\text{N}$). Nevertheless, overall NMR data, chemical reactivity, elemental analyses,¹² and X-ray structures of compounds **5a–(E)** and **7b–(Z)** are consistent with their exocyclic cyclopalladated nature.

In general, it is assumed that halogen-bridged cyclometalated dimers dissolved in benzene, chloroform, or acetone maintain their dimeric structure. Nevertheless, Vicente *et al.*^{3j} have recently proposed that, in acetone solution, the bromo-bridged cyclopalladated dimer of racemic (1-phenylethyl)amine forms a solvated monomeric species, on the basis of its ^1H NMR at 300 MHz, in CD_3COCD_3 solution, which shows only one set of signals. In our case, due to the poor coordinating properties of CDCl_3 and to the presence of more than one set of signals in the NMR spectra, we propose that for compounds **2–4** the species present in CDCl_3 solution are dimers.

^1H NMR at 200 MHz of compounds **2–4** presents, in all the cases, three sets of signals (see Experimental Section), which suggests that these cyclopalladated dimers consist of three isomers that are referred to hereafter as *(Z,Z)*, *(Z,E)*, and *(E,E)* according to the *Z* or *E* form adopted by the imines. This assumption is reinforced by the fact that, in most cases, $^{13}\text{C}\{^1\text{H}\}$ NMR at 75.43 MHz, also shows four singlets for the methinic carbon atoms. Furthermore, the NMR signals of the methinic protons are broad at room temperature, suggesting the equilibrium depicted in eq 1 in CDCl_3 solution.

Recently, van Koten *et al.*¹³ have found that the ^1H NMR at 300 MHz of the chloro-bridged cyclopalladated dimers of 2-[(dimethylamino)methyl]naphthalene and 4,4-dimethyl-2-(2-naphthyl)oxazoline show two sets of signals, which indicates (the presence of solvated species and conformational isomers is excluded) that these dimers consist of a mixture of *cis* and *trans* isomers (this nomenclature refers to the relative arrangements of the cyclometalated ligands around the central $\text{M}(\mu\text{-X})_2\text{M}$ unit). Nevertheless, in the solid state, the halogen-bridged cyclometalated dimers studied so far by X-ray diffraction¹⁴ consist of only the *trans* isomer. Furthermore, the fact that there is usually only one set of signals in the NMR of halogen-bridged cyclometalated dimers is interpreted as indicating that the *trans* isomer is also present in solution.^{3m} In our case, we propose that the *(Z,Z)*, *(Z,E)*, and *(E,E)* cyclopalladated dimers



which form compounds **2–4** consist of only the *trans* isomer, since mixtures of *trans* and *cis* isomers for each dimer would result in more complex ^1H NMR spectra at 200 MHz, with a maximum of six sets of signals.

The exocyclic cyclopalladated character of compounds **2–4** and their proposed structure are consistent with the results obtained when an excess of deuterated pyridine is added to CDCl_3 solutions of these compounds. Thus, the ^1H NMR spectra at 200 MHz of the reaction solutions show the formation of a mixture of

cyclopalladated monomers $[\text{Pd}(\text{C}-\text{N})\text{X}(\text{py}-d_5)]^{15}$ with the imine in the *Z* and *E* forms, since two sets of signals are observed for nearly all the protons.¹⁶ The methinic proton signal appears at δ 9.3–9.4 for the *Z* derivatives and at δ 8.4–8.5 for the *E* derivatives, in good agreement with published results.^{10,11} The deuterated pyridine is located in a *cis* position relative to the palladated carbon,¹⁷ which is inferred by the high-field shift of ca. 1 ppm of the aromatic proton in a *ortho* position to the palladated carbon, this effect being caused by the pyridine ring.¹⁸

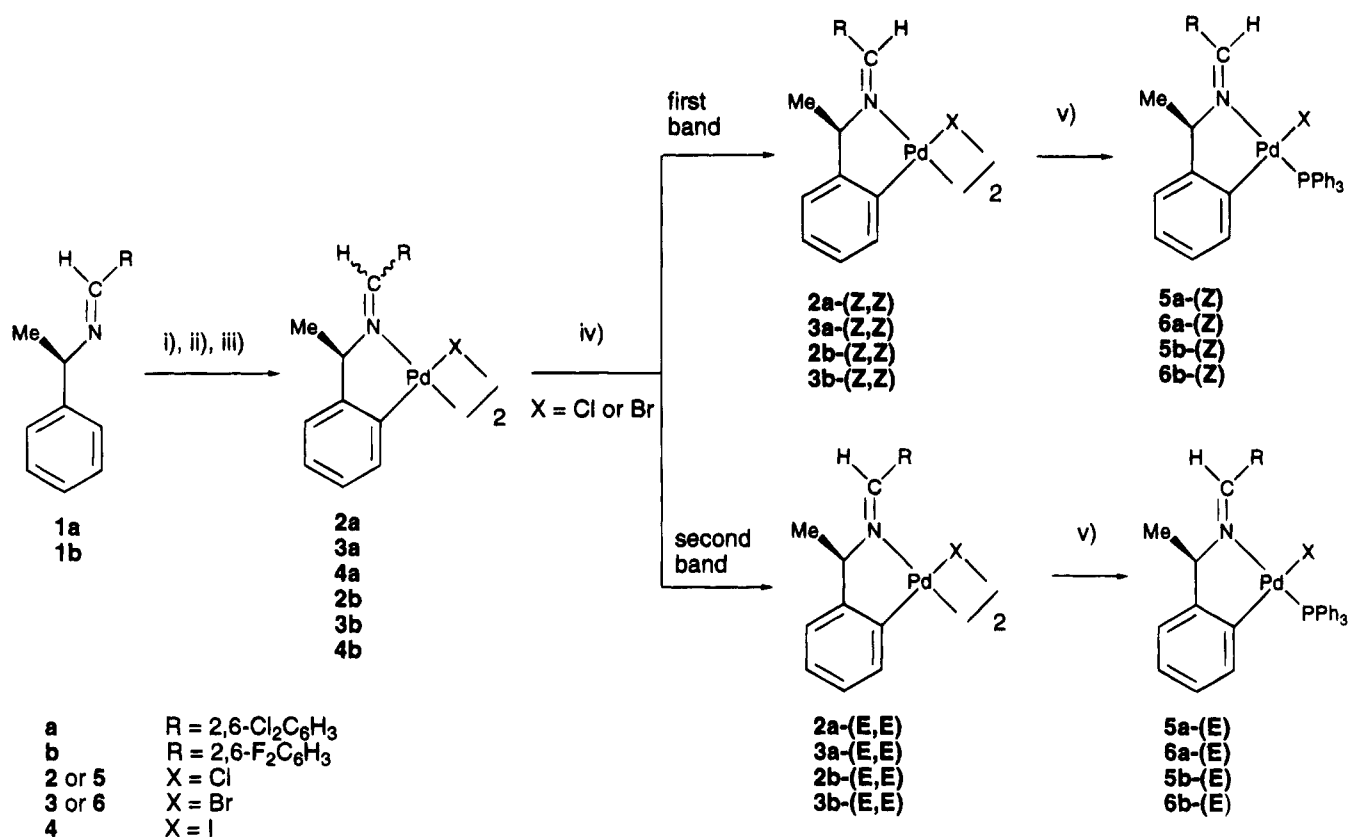
(15) Cleavage of the Pd–N bond and formation of a monomer of formula $[\text{Pd}(\text{C}-\text{N})\text{X}(\text{py})_2]$ has been observed only for a very labile eight-membered metallacycle: Dupont, J.; Pfeffer, M.; Theurel, L.; Rotteveel, M. A.; de Cian, A.; Fischer, J. *New J. Chem.* **1990**, *15*, 551.

(16) The monomers with the imine in the *E* form show broad signals or, in their turn, two groups of signals for the methinic, the benzylic, and the methyl protons. We interpret these results as showing that the rotation around their $\text{C}_{\text{aromatic}}-\text{C}_{\text{methinic}}$ bond is slow or stopped at room temperature.

(12) Compounds **4a,b** in solution slowly liberate palladium(0), precluding any attempt to obtain solid samples of analytical purity of these compounds.

(13) Valk, J. M.; Maasarani, F.; van der Sluis, P.; Spek, A. L.; Boersma, J.; van Koten, G. *Organometallics* **1994**, *13*, 2320.

(14) For recent studies on crystal structures of halogen-bridged cyclometalated dimers see: (a) Vila, J. M.; Gayoso, M.; Pereira, M. T.; Romar, A.; Fernández, J. J.; Thornton-Pett, M. *J. Organomet. Chem.* **1991**, *401*, 385. (b) Crispini, A.; De Munno, G.; Ghedini, M.; Neve, F. *J. Organomet. Chem.* **1992**, *427*, 409. (c) Vila, J. M.; Gayoso, M.; Pereira, M. T.; Ortigueira, J. M.; Fernández, A. *Polyhedron* **1993**, *12*, 171. (d) Barro, J.; Granell, J.; Sainz, D.; Sales, J.; Font-Bardía, M.; Solans, X. *J. Organomet. Chem.* **1993**, *456*, 147. (e) Navarro-Raninger, C.; López-Solera, I.; Alvarez-Valdés, A.; Rodríguez, J. H.; Masaguer, J. R.; García-Ruano, J. L.; Solans, X. *J. Organomet. Chem.* **1994**, *476*, 19.

Scheme 1^a

^a Legend: (i) Pd(AcO)₂ HAcO, 80 °C, 2 h for **1a** or reflux, 45 min for **1b**; (ii) LiCl, LiBr, or KI, EtOH; (iii) SiO₂, CHCl₃/MeOH (100/2); (iv) SiO₂, CHCl₃; (v) PPh₃, acetone.

To confirm the equilibrium depicted in eq 1 in CDCl₃ solutions of compounds **2–4**, we recorded the ¹H NMR at 300 MHz of compound **3a** at different temperatures. Thus, we found that at 50 °C the width of the signals increases in relation to the spectrum at room temperature. This fact is consistent with a faster exchange of cyclopalladated units between the (Z,Z), (Z,E), and (E,E) cyclopalladated dimers at 50 °C, although this dynamic process is still below the coalescence temperature. At -50 °C, however, the NMR becomes extremely complex and 13 signals of the methinic protons appear.

It is known that halogen-bridged cyclometalated dimers can exist as two conformational isomers due to the fact that the M(μ-X)₂M central unit in these dimers is not always planar and, due to steric factors, it frequently adopts a folded conformation.¹⁹ Furthermore, the five-membered metallacycle in compounds **2–4** is not planar, since it has an envelope structure (see X-ray crystallographic studies); therefore, different conformational isomers could appear. Thus, when the temperature decreases, some of the dynamic processes which interconvert extreme conformations of the (Z,Z), (Z,E) and (E,E) cyclopalladated dimers become slow, leading to a very complex spectrum.

¹H NMR spectra at 200 MHz of compounds **2–4**, at room temperature, do not show the presence of conformational isomers.²⁰ According to the literature,²¹ the most likely explanation is that, at room temperature, all the extreme conformations of each of the (Z,Z), (Z,E), and (E,E) cyclopalladated dimers are interconverting at a fast rate, which results in only one set of signals for each of the (Z,Z), (Z,E), and (E,E) cyclopalladated dimers.

Synthesis of the (Z,Z) and (E,E) Cyclopalladated Dimers. Surprisingly, when compounds **2** and **3** are eluted with a less polar eluant (CHCl₃) through a column of SiO₂, the initial yellow band, which contains the mixture of (Z,Z), (Z,E) and (E,E) cyclopalladated dimers, splits into two yellow bands; the first contains the (Z,Z) cyclopalladated dimers and the second the (E,E) cyclopalladated dimers (Scheme 1). The (Z,Z) and (E,E) cyclopalladated dimers are isolated as yellow solids after concentration of the solvent of the corresponding eluted band and subsequent addition of ethanol to the residues. Their elemental analyses were consistent with the proposed formulas, and the ¹H NMR confirmed the Z or E form adopted by the imines. Thus, in the (Z,Z) compounds, the methinic proton is downfield-shifted ca. 0.20–0.30 ppm relative to free imines. This effect is caused by the palladium atom and shows

(17) In reactions of cyclopalladated dimers of N-donor ligands with Lewis bases, which give monomers of formula [Pd(C-N)XL], the Lewis base (L) is found in a *cis* position relative to the palladated carbon which is the thermodynamic control isomer. In analogous cycloplatinated compounds, mixtures of kinetic (L *trans* to the metalated carbon) and thermodynamic isomers can be found: Pregosin, P. S.; Wombacher, F.; Albinati, A.; Lianza, F. *J. Organomet. Chem.* **1991**, *418*, 249.

(18) Fuchita, Y.; Tsuchiya, H. *Polyhedron* **1993**, *12*, 2079.

(19) Crispini, A.; Ghedini, M.; Neve, F. *J. Organomet. Chem.* **1993**, *448*, 241 and references therein.

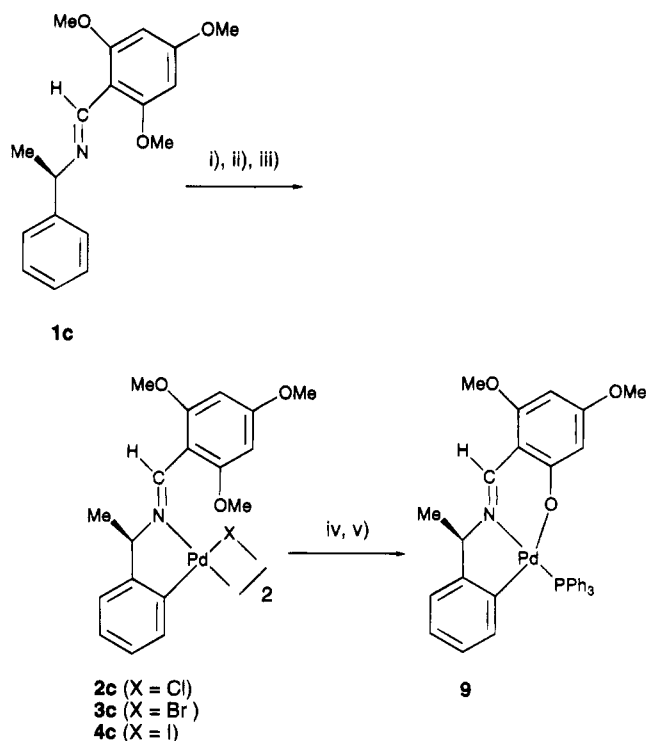
(20) Compound **2a-(Z,Z)** shows two close singlets for the methinic protons at 8.77 and 8.74 ppm, which indicates that this compound consists of two isomers. This has been confirmed by a ¹H NMR at 500 MHz of this compound, which shows two sets of signals for nearly all the protons. At this point, it is difficult to establish whether they are geometrical or conformational isomers.

(21) Ciriano, M. A.; Espinet, P.; Lalinde, E.; Ros, M. B.; Serrano, J. L. *J. Mol. Struct.* **1989**, *196*, 327.

the proximity in space between the methinic proton and the palladium atom.^{10,11} However, in the (*E,E*) dimers, the methinic proton appears slightly upfield- or slightly downfield-shifted (up to *ca.* 0.10 ppm) relative to free imines. It is interesting to note that in endocyclic cyclopalladated benzylideneamines which contain the imine in the *E* form, in general, the largest high-field shifts of the methinic proton up to *ca.* 1 ppm are observed.^{9,11} Consequently, in cyclopalladation reactions of benzylideneamines, the shift of the methinic proton relative to the free imine allows us to determine the endocyclic or exocyclic character of the reaction product and, in the case of the formation of an exocyclic cyclopalladated compound, the *Z* or *E* form adopted by the imine.

The (*Z,Z*) and (*E,E*) exocyclic cyclopalladated dimers **2** and **3** do not undergo change in the *Z* or the *E* form adopted by the imines either in the solid state or in solution. Moreover, when a mixture of (*E,E*) and (*Z,Z*) dimers was prepared in CDCl₃ solution, the NMR spectrum showed the formation of the (*Z,E*) isomer, in good agreement with the equilibrium depicted in eq 1. These results indicate that the process found during chromatography, which transforms (*Z,E*) dimers into (*Z,Z*) and (*E,E*) dimers, is related to this equilibrium, which only involves cleavage and formation of palladium-halogen bonds. Thus, as (*Z,Z*) dimers have higher *R_f* values than (*E,E*) dimers, at the beginning of the column the central part of the band becomes poor in (*Z,Z*) and (*E,E*) isomers; the (*Z,E*) dimers therefore reestablish the equilibrium and reorganize into (*Z,Z*) and (*E,E*) dimers. This process continues during column chromatography, until the original band splits into two bands: the less polar band contains the (*Z,Z*) isomer and the more polar band the (*E,E*) isomer. We have described a similar process for palladated monomers of formula [Pd(C-N)Br(PPh₃)₂], which in solution are in equilibrium with the cyclometalated complexes [Pd(C-N)Br(PPh₃)₃] and PPh₃. In this case, starting the column with the palladated compounds [Pd(C-N)Br(PPh₃)₂], we obtained a first band containing PPh₃ and a second more polar band containing the cyclopalladated monomers [Pd(C-N)Br(PPh₃)].^{11,22}

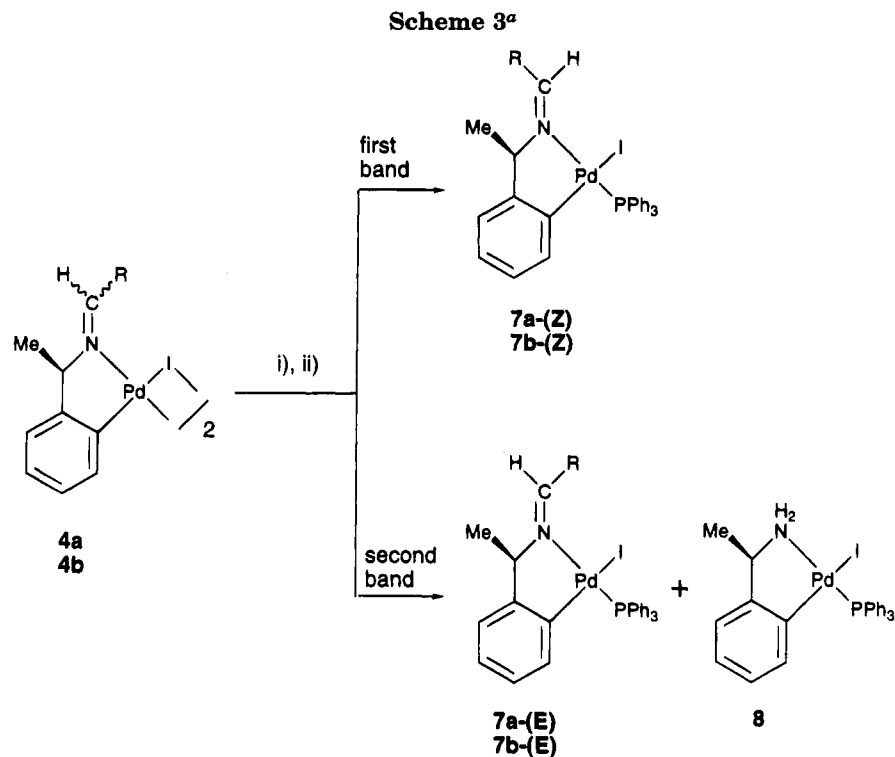
***E* → *Z* Isomerization.** The presence of cyclopalladated units with the imine in the *E* form in dimers **2**–**4** is consistent with our previous proposal that the *E* → *Z* isomerization is controlled by steric effects. Thus, in the bromo-bridged exocyclic cyclopalladated dimers of (2,6-dichlorobenzylidene)benzylamine¹⁰ and (2,4,6-trimethylbenzylidene)benzylamine¹¹ (Chart 1), the imines adopt the *Z* form in order to avoid the steric repulsion between their aromatic group bonded to the methinic carbon and the halogen *trans* to their palladated carbon. For imines **1a,b**, the presence of the methyl bonded to the benzylic carbon results in a less favorable steric situation for the cyclopalladated units with the imine in the *Z* form, and the formation of mixtures of both isomers is observed. The cyclopalladated units with the imine in the *Z* form are the major components, the ratio of cyclopalladated units with the imine in the *Z* form and in the *E* form varying in the interval from 2:1 to 1:1.

Scheme 2^a

^a Legend: (i) Pd(AcO)₂, HAcO, reflux, 45 min; (ii) LiCl, LiBr, or KI, EtOH; (iii) SiO₂, CHCl₃/MeOH (100/2) for runs with LiCl and LiBr or CHCl₃ for run with KI; (iv) PPh₃, acetone, reflux, 24 h; (v) SiO₂, CHCl₃.

Cyclopalladation of Imine 1c. The action of Pd(AcO)₂ on the imine **1c** in acetic acid at reflux for 45 min and subsequent treatment of the reaction residue with LiCl, LiBr, or KI in ethanol results in the formation of a voluminous precipitate which contains the corresponding halogen-bridged exocyclic cyclopalladated dimer as the major compound, which is purified by SiO₂ column chromatography (Scheme 2).

The halogen-bridged exocyclic cyclopalladated dimers **2c**–**4c** show only one set of signals in the ¹H NMR at 200 MHz, in contrast with dimers **2a,b**–**4a,b**. The signal of the methinic proton appears nearly at the same chemical shift as that of the free imine, indicating that the imine adopts the *E* form. The exocyclic cyclopalladated nature of compounds **2c**–**4c** is consistent with the presence of all the signals corresponding to the 2,4,6-trimethoxyphenyl group and with the loss of one of the aromatic protons of the benzylic ring. Moreover, compound **4c** gives well-separated signals for all the protons of the benzylic ring, showing the characteristic pattern of two doublets and two triplets (see Experimental Section) of a 1,2-disubstituted aromatic ring. Another interesting feature of the ¹H NMR at 200 MHz of compounds **2c**–**4c** is that the signal corresponding to the *ortho* methoxy groups is a broad singlet, which indicates that the rotation around the C_{aromatic}–C_{methinic} bond is slow at room temperature. This slow rotation suggests some sort of interaction between the oxygen atom of the *ortho* methoxy groups and the palladium atom, which would explain the *E* form adopted by the imine in compounds **2c**–**4c**, and also the later demethylation of one of the *ortho* methoxy groups which takes place when these compounds react with PPh₃ (see below).



^a Legend: (i) PPh₃, acetone; (ii) SiO₂, CHCl₃.

Reactions with PPh₃. To obtain more soluble and crystalline mononuclear compounds, the reactivity toward triphenylphosphine of the new cyclopalladated dimers was studied.

The action of PPh₃ on cyclopalladated dimers **2a,b-(Z,Z)** and **-(E,E)** and **3a,b-(Z,Z)** and **-(E,E)** in a 2:1 molar ratio gives the corresponding cyclopalladated monomers **5a,b-(Z)** and **-(E)** and **6a,b-(Z)** and **-(E)** (Scheme 1). The chemical shift of the phosphorus in the interval 41–42 ppm and the high-field shift of the aromatic protons of the palladated ring, due to the aromatic rings of PPh₃, confirm the *cis* arrangement of the PPh₃ relative to the metalated carbon.^{10,11} Transformation of the cyclopalladated dimers in the corresponding monomeric complexes proceeds without changes in the *Z* or *E* form adopted by the imines. Thus, in the monomers **5a,b-(Z)** and **6a,b-(Z)**, the downfield shift of the methinic proton relative to free imines (*ca.* 0.80 ppm) and its coupling constant with phosphorus of *ca.* 5 Hz confirm the *Z* form adopted by the imine.^{10,11} However, in compounds **5a,b-(E)** and **6a,b-(E)**, the slightly upfield or slightly downfield shift (up to *ca.* 0.10 ppm) of the methinic proton relative to free imines and its coupling constant with phosphorus of 10–12 Hz confirm the *E* form adopted by the imine.

The stability of the Pd–N bond in cyclometalated derivatives is highly dependent on the basicity of the nitrogen atom. Thus, the action of an excess of PPh₃ on cyclopalladated *N*-benzylideneanilines gives monomers without Pd–N bonds of formula [Pd(C–N)X(PPh₃)₂],²³ whereas cyclopalladated benzylidenebenzylamines give metallacycles of formula [Pd(C–N)X(PPh₃)₂],^{9a} according to the electronic effects of benzyl and phenyl groups bonded to the iminic nitrogen.

The reaction of PPh₃ with dimers **3a-(Z,Z)** and **3b-(Z,Z)**, in a molar ratio of 4:1, did not produce the cleavage of the Pd–N bond, giving only the monomers **5a-(Z)** and **5b-(Z)**. In contrast, an excess of PPh₃ added to the bromo-bridged exocyclic cyclopalladated dimer of (2,6-dichlorobenzylidene)benzylamine produced a monomer of formula [Pd(C–N)X(PPh₃)₂],¹⁰ without a Pd–N bond. These results can be explained by the electron-donating effect of the methyl group, which reinforces the Pd–N bond in compounds **3**.

To obtain compounds analogous to **5a,b-(Z)** and **-(E)** and **6a,b-(Z)** and **-(E)**, the action of PPh₃ on compounds **4a,b**, which consist of a mixture of (*Z,Z*), (*Z,E*), and (*E,E*) isomers, was studied (Scheme 3). Thus, by treatment of compounds **4a,b** with PPh₃ and elution of the residues of reaction through a column of SiO₂ with CHCl₃, two yellow bands were obtained. The first contains compounds **7a,b-(Z)**. However, the second contains a mixture of compounds **7a,b-(E)** and the cyclopalladated monomer of (*R*)-(1-phenylethyl)amine with triphenylphosphine (compound **8**). We propose that compound **8** is formed in the column by hydrolysis of the iminic function of compounds **7a,b-(E)**, which would be induced by the steric repulsion between the aromatic group bonded to the methinic carbon atom and the iodine atom.

Elemental analyses and ¹H and ³¹P{¹H} NMR data of compounds **7a,b-(Z)** are consistent with their proposed structure. ¹H NMR of the mixtures of compounds **7a-(E)** and **8** or **7b-(E)** and **8** confirms the presence of the cyclopalladated monomer of the imine in the *E* form, together with monomer **8**. Thus, evidence for the presence of the cyclopalladated monomer of the imine in the *E* form comes from the doublet at *ca.* 8.6–8.5 ppm having a coupling constant with phosphorus of *ca.* 12 Hz, which is assigned to the methinic proton. Evidence for the presence of the cyclopalladated monomer **8** comes

(23) (a) Onoue, H.; Moritani, I. *J. Organomet. Chem.* **1972**, *43*, 431.
 (b) Granell, J.; Sainz, D.; Sales, J.; Solans, X.; Font-Altaba, M. *J. Chem. Soc., Dalton Trans.* **1986**, 1785.

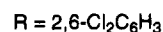
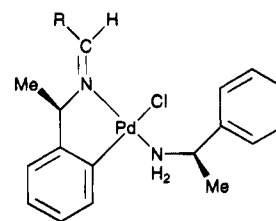
from the broad signals at 4.10 and 3.58 ppm, corresponding to the protons of the amino group.

Interestingly, the action of PPh_3 , at room temperature, on acetone solutions of dimers **2c–4c** gives, as a minor compound, the tridentate species **9** (Scheme 2) together with the corresponding cyclopalladated monomers of formula $[\text{Pd}(\text{C}=\text{N})\text{X}(\text{PPh}_3)]$, which are the major compounds. Yields of compound **9** increase notably when the reaction is carried out in refluxing acetone for 24 h. Compound **9** is easily separated by column chromatography ($\text{SiO}_2/\text{CHCl}_3$), and its elemental analyses and NMR data are consistent with the formula proposed. Thus, the chemical shift of the phosphorus atom of 41.2 ppm, the downfield shift of the methinic proton of 0.11 ppm relative to the free imine, and its coupling constant with phosphorus of 12 Hz confirm the *cis* arrangement of the phosphine in relation to the palladated carbon and the *E* form of the imine. Its exocyclic cyclopalladated nature is consistent with the presence of four well-separated signals with the appropriate multiplicity for the aromatic protons of the benzylic ring (see Experimental Section). Demethylation of one of the *ortho* methoxy groups is inferred from the presence of two well-separated singlets for the remaining methoxy groups, each of them integrated as three protons.

Therefore, the splitting reaction of dimers **2c–4c** with PPh_3 under more drastic conditions (refluxing acetone) induces an intramolecular O–C(sp³) bond activation. This is a rare process, which is limited to some phosphino esters, alkoxyphosphines, or alkoxyphenanthrolines, but has a clear application to the synthesis of new acetato or phenoxo mono- or polynuclear organometallic or coordination compounds.²⁴ The first study on this kind of process carried out by Shaw *et al.*²⁵ with dihalobis(alkoxyphosphine)platinum(II) compounds suggests that the demethylation reaction occurs *via* a four-center transition state which involves the formation of the metal–oxygen and carbon–halogen bonds and the cleavage of the metal–halogen and carbon–oxygen bonds, simultaneously. It is remarkable that the overall process described with imine **1c** involves sequential regioselective activation of two different bonds in the same organic molecule.

Reactions with Chiral Amines. Cyclopalladation of imines **1a–c** proceeded without racemization of the chiral center. This has been demonstrated by reactions of compound **2a-(Z,Z)** with an excess of (*R*)-(+)-(1-phenylethyl)amine and racemic (1-phenylethyl)amine. These reactions, which were performed in an NMR tube, proceeded instantaneously with quantitative yield, giving the corresponding monomers of formula $[\text{Pd}(\text{C}=\text{N})\text{Cl}(\text{amine})]$. ¹H NMR at 200 MHz of the reaction of **2a-(Z,Z)** with (*R*)-(+)-(1-phenylethyl)amine shows only one set of signals for the monomer $[\text{Pd}(\text{C}=\text{N})\text{Cl}(\text{amine})]$, while ¹H NMR at 200 MHz of the reaction of **2a-(Z,Z)** with racemic (1-phenylethyl)amine gives two sets of

Chart 3



signals in a nearly 1:1 ratio, according to the formation of two diastereomeric monomers. These results show that **2a-(Z,Z)** was homochiral.

The quantitative yield of these reactions is inferred from the absence of the signals corresponding to **2a-(Z,Z)**. Moreover, integrals of the signals of the monomers $[\text{Pd}(\text{C}=\text{N})\text{Cl}(\text{amine})]$ show that there is only one coordinated amine per palladium atom. Thus, an excess of amine did not cleave the Pd–N bond. Furthermore, the presence of only one set of signals in the reaction with (*R*)-(+)-(1-phenylethyl)amine indicates that the monomer $[\text{Pd}(\text{C}=\text{N})\text{Cl}(\text{amine})]$ consists of only a geometrical isomer which, in accordance with the literature,¹⁷ we propose to be that with the amine located in a position *cis* to the palladated carbon (Chart 3).

It is interesting to note that, at 200 MHz, the methinic protons of the two diastereoisomeric monomers obtained in the reaction of **2a-(Z,Z)** with racemic (1-phenylethyl)amine appear separated by 10 Hz, which is a promising result for the application of homochiral cyclopalladated compounds of this kind to the determination of the optical purity of chiral amines.

X-ray Crystallographic Studies. Figures 1 and 2 show the molecular structures of **5a-(E)** and **7b-(Z)**, together with the numbering scheme, and Tables 1–3 give selected bond distances and angles as well as final atomic coordinates.

X-ray crystallographic studies of **5a-(E)** and **7b-(Z)** confirm the structures proposed by NMR data. Thus, the molecular structures (Figures 1 and 2) confirm the *R* absolute configuration of the chiral center, the *E* or *Z* form adopted by the imine, the *cis* arrangement of the PPh_3 in relation to the palladated carbon, and the exocyclic cyclopalladated nature of the compounds.

Molecular structures of **5a-(E)** and **7b-(Z)** do not show significant differences from molecular structures of the closely structurally related cyclopalladated compounds of (1-phenylethyl)amine, dimethyl(1-phenylethyl)amine, and dimethyl(1-(2-naphthyl)ethyl)amine.^{3a,e,j,4} Thus, bond distances and angles around the palladium atom are in the normal intervals. The palladium atom is in a roughly distorted-square-planar geometry, this distortion being larger in **5a-(E)** than in **7b-(Z)**. Thus, in **5a-(E)** deviations from the coordination plane of palladium (the plane formed by palladium and atoms directly bonded to it (P, Cl(1), N(1), C(10))) are as follows: Pd, 0.061 Å; P, 0.171 Å; Cl(1), –0.192 Å; N, 0.212 Å; C(10), –0.253 Å. For **7b-(Z)**, however, these deviations are as follows: Pd, 0.009 Å; P, 0.080 Å; Cl(1), –0.094 Å; N, –0.116 Å; C(1), 0.122 Å. The greater distortion of the sphere of coordination of the palladium in **5a-(E)** than in **7b-(Z)** is consistent with a more demanding steric situation around the palladium in compound **5a-(E)**

(24) For recent references on this subject see: (a) Dunbar, K. R. *Comments Inorg. Chem.* **1992**, *13*, 313. (b) Berthon, R. A.; Colbran, S. B.; Craig, D. C. *Polyhedron* **1992**, *11*, 243. (c) Dunbar, K. R.; Matonic, J. H.; Saharan, V. P. *Inorg. Chem.* **1994**, *33*, 25. (d) Dunbar, K. R.; Sun, J. S.; Quillevéré, A. *Inorg. Chem.* **1994**, *33*, 3598. (e) Steinert, P.; Werner, H. *Organometallics* **1994**, *13*, 2677.

(25) Jones, C. E.; Shaw, B. L.; Turtle, B. L. *J. Chem. Soc., Dalton Trans.* **1974**, 992.

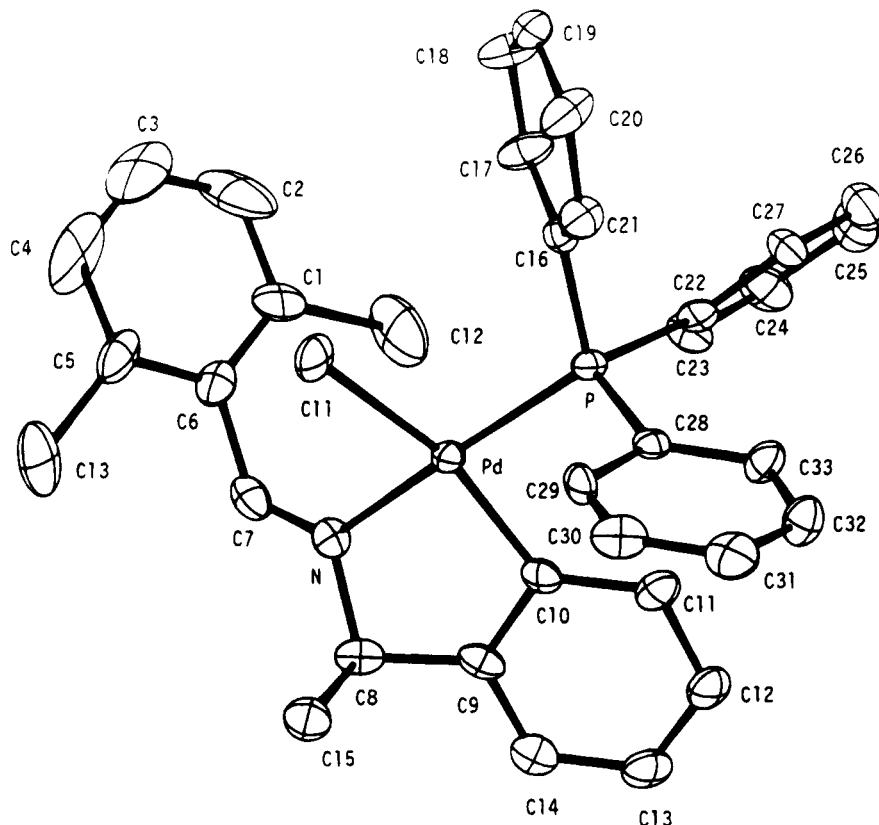


Figure 1. Molecular structure of **5a-(E)**.

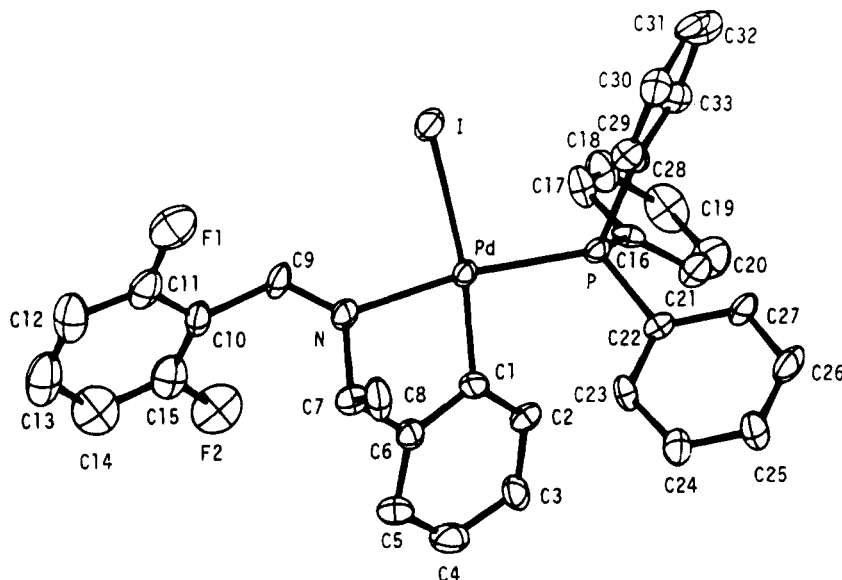


Figure 2. Molecular structure of **7b-(Z)**.

which has the imine in the *E* form. The five-membered metallacycle is not planar but has an envelope structure with the nitrogen atom out of the plane defined by the remaining four atoms of the metallacycle: 0.509 Å for **5a-(E)** and 0.772 Å for **7b-(Z)**. Selected angles between normals to planes of atoms for **5a-(E)** and **7b-(Z)** are listed in Table 4.

Experimental Section

^1H NMR at 200 MHz, $^{13}\text{C}\{^1\text{H}\}$ NMR at 75.43 MHz, and $^{31}\text{P}\{^1\text{H}\}$ NMR at 32.8 MHz were recorded respectively on Varian Gemini 200, Varian XL-300, and Bruker WP 80 SY instruments. Chemical shifts (in ppm) were measured relative to

SiMe_4 for ^1H and ^{13}C NMR and relative to 85% H_3PO_4 for ^{31}P NMR. The solvents used were CDCl_3 in ^1H and ^{13}C NMR and CHCl_3 in ^{31}P NMR. Microanalyses were performed at the Institut de Química Bio-Orgànica de Barcelona (CSIC) and the Serveis Científico-Tècnics de la Universitat de Barcelona.

Materials and Syntheses. All chemicals and solvents were of commercial grade and used as received, except for ethanol, chloroform, dichloromethane, and acetone, which were dried over CaCl_2 and distilled before use.

(E)-(R)-2,6- $\text{Y}_2\text{C}_6\text{H}_3\text{CH}=\text{NCHMeC}_6\text{H}_5$ ($\text{Y} = \text{Cl}$, **1a**; $\text{Y} = \text{F}$, **1b**) and **(E)-(R)-2,4,6-(MeO) $_3\text{C}_6\text{H}_2\text{CH}=\text{NCHMeC}_6\text{H}_5$** (**1c**). Imines **1a-c** were prepared by an adaptation of one of the general methods:²⁶ 20 mmol of the appropriate aldehyde was treated with 20 mmol (2.424 g) of (*R*)-(+)-(1-phenylethyl)amine

Table 1. Selected Bond Distances (Å) and Angles (deg) for 5a-(E) and 7b-(Z)

5a-(E)		7b-(Z)	
P-Pd	2.248(2)	P-Pd	2.244(3)
Cl(1)-Pd	2.382(3)	I-Pd	2.668(1)
N-Pd	2.102(8)	N-Pd	2.112(9)
C(10)-Pd	2.000(10)	C(1)-Pd	2.004(11)
C(7)-N	1.309(13)	C(9)-N	1.254(15)
C(8)-N	1.501(14)	C(7)-N	1.506(16)
C(9)-C(8)	1.485(16)	C(7)-C(6)	1.494(21)
C(10)-C(9)	1.401(15)	C(6)-C(1)	1.400(17)
Cl(1)-Pd-P	92.2(1)	I-Pd-P	96.1(1)
N-Pd-P	170.8(3)	N-Pd-P	170.6(3)
N-Pd-Cl(1)	94.6(2)	N-Pd-I	91.3(3)
C(10)-Pd-P	95.3(3)	C(1)-Pd-P	92.5(4)
C(10)-Pd-Cl(1)	163.3(3)	C(1)-Pd-I	170.4(4)
C(10)-Pd-N	79.8(4)	C(1)-Pd-N	80.7(5)
C(8)-N-Pd	112.9(6)	C(7)-N-Pd	103.9(7)
C(9)-C(8)-N	103.8(8)	C(6)-C(7)-N	104.7(11)
C(10)-C(9)-C(8)	121.7(9)	C(7)-C(6)-C(1)	116.8(12)
C(9)-C(10)-Pd	113.1(7)	C(6)-C(1)-Pd	111.9(9)

Table 2. Final Atomic Coordinates ($\times 10^4$) for 5a-(E)

	x/a	y/b	z/c	B_{eq} (Å ²) ^a
Pd	19328(3)	60133	8955(6)	2.35(2)
P	2968(1)	4912(3)	1972(2)	2.34(8)
Cl(1)	1018(2)	4649(4)	2218(3)	4.19(12)
Cl(2)	1629(3)	9571(7)	2531(6)	8.71(29)
Cl(3)	-1000(2)	6579(5)	1110(6)	7.26(22)
N	1071(5)	7358(10)	-79(9)	3.01(33)
C(1)	793(8)	8706(17)	2965(12)	4.84(59)
C(2)	519(14)	8746(26)	4356(18)	9.45(121)
C(3)	-202(16)	8139(42)	4708(36)	12.15(224)
C(4)	-676(14)	7362(38)	3663(40)	11.52(182)
C(5)	-390(8)	7415(20)	2330(16)	5.73(70)
C(6)	314(6)	8015(13)	1957(12)	3.65(44)
C(7)	491(6)	8049(14)	511(12)	3.68(44)
C(8)	1204(7)	7570(12)	-1597(11)	3.52(43)
C(9)	2073(7)	7489(12)	-1705(10)	3.43(41)
C(10)	2548(6)	6832(11)	-666(10)	3.02(38)
C(11)	3364(8)	6655(15)	-936(12)	3.97(46)
C(12)	3686(7)	7267(15)	-2173(11)	3.74(45)
C(13)	3192(8)	7904(15)	-3160(12)	4.23(52)
C(14)	2402(7)	8040(11)	-2913(12)	3.48(43)
C(15)	817(7)	6224(23)	-2328(13)	4.89(61)
C(16)	2810(5)	3983(11)	3625(9)	2.61(33)
C(17)	2589(8)	4872(14)	4711(11)	4.04(47)
C(18)	2524(9)	4284(15)	6007(12)	4.82(60)
C(19)	2702(7)	2743(19)	6265(13)	4.54(56)
C(20)	2903(9)	1844(21)	5139(15)	6.53(78)
C(21)	2974(7)	2500(14)	3848(12)	3.81(47)
C(22)	3746(5)	6124(17)	2534(9)	3.13(35)
C(23)	3689(7)	7718(15)	2316(12)	3.96(48)
C(24)	4230(8)	8682(17)	2819(14)	4.85(60)
C(25)	4901(9)	8034(22)	3565(15)	5.74(74)
C(26)	4951(7)	6594(19)	3808(16)	5.22(65)
C(27)	4412(6)	5626(18)	3298(12)	4.87(64)
C(28)	3382(5)	3439(11)	932(8)	2.50(33)
C(29)	2868(6)	2358(15)	476(12)	3.71(46)
C(30)	3116(8)	1222(10)	-209(12)	4.03(51)
C(31)	3909(7)	1094(21)	-527(13)	4.86(52)
C(32)	4431(7)	2090(17)	-125(15)	4.53(54)
C(33)	4186(6)	3333(14)	615(11)	3.57(44)

$$^a B_{eq} = (8\pi^2/3) \sum_{ij} U_{ij} A_i^* A_j^* A_i A_j$$

in ethanol (50 mL) at reflux for 4 h and the resulting solution concentrated *in vacuo*. The oils obtained contain the imines (>95%) and were used without further purification. Characterization data are as follows. **1a**: ¹H NMR 8.52 s [CH=N],

(26) See for example: (a) Tennant, G. In *Comprehensive Organic Chemistry*; Barton, D., Ollis, W. D., Eds.; Pergamon: Oxford, U. K., 1979; Vol. 2, Part 8. (b) Dayagi, S.; Yair, D. In *The Chemistry of the Carbon-Nitrogen Double Bond*; Patai, S., Ed.; Wiley: Chichester, U. K., 1970; Chapter 2. (c) Bigelow, L. A.; Eatough, H. In *Organic Syntheses*; Blatt, A. H., Ed.; Wiley: New York, 1994; Vol. 1, p 80.

Table 3. Final Atomic Coordinates ($\times 10^4$) for 7b-(Z)

	x/a	y/b	z/c	B_{eq} (Å ²) ^a
Pd	8281(4)	11054(5)	10482(6)	2.63(3)
I	-5515(4)	12298(5)	2510(7)	4.31(4)
P	637(2)	-200(2)	2063(3)	2.65(13)
N	1179(6)	2237(7)	34(9)	3.61(48)
F(1)	333(6)	3370(8)	-2427(9)	7.26(58)
F(2)	2021(6)	4148(7)	383(9)	7.65(59)
C(1)	1869(6)	1247(9)	1613(11)	3.40(53)
C(2)	2180(7)	1064(10)	2658(11)	3.46(55)
C(3)	2879(8)	1355(9)	2949(14)	4.24(68)
C(4)	3291(9)	1879(12)	2161(20)	6.01(97)
C(5)	3025(8)	2095(12)	1109(16)	5.03(78)
C(6)	2313(7)	1759(9)	870(13)	3.71(61)
C(7)	1976(8)	2006(10)	-231(15)	4.43(71)
C(8)	1975(9)	1244(11)	-1064(13)	5.54(78)
C(9)	851(9)	2956(9)	-319(12)	3.88(60)
C(10)	1179(7)	3713(9)	-1029(12)	3.76(58)
C(11)	894(9)	3936(12)	-2039(13)	5.19(77)
C(12)	1138(12)	4626(13)	-2715(16)	6.39(101)
C(13)	1698(13)	5181(13)	-2338(19)	7.74(120)
C(14)	2002(12)	4997(13)	-1284(17)	7.59(115)
C(15)	1713(10)	4296(11)	-645(14)	5.56(87)
C(16)	510(6)	89(8)	3518(10)	2.97(48)
C(17)	50(9)	844(10)	3738(12)	4.54(71)
C(18)	-91(9)	1115(11)	4857(14)	5.12(74)
C(19)	263(12)	653(14)	5722(14)	6.07(101)
C(20)	724(10)	-76(13)	5480(14)	5.83(92)
C(21)	839(8)	-387(10)	4419(12)	4.45(67)
C(22)	1350(6)	-1117(9)	1926(10)	3.03(47)
C(23)	1969(7)	-981(8)	1265(10)	3.39(56)
C(24)	2479(8)	-1731(11)	1123(14)	4.29(71)
C(25)	2333(9)	-2573(10)	1579(14)	4.83(78)
C(26)	1719(9)	-2718(10)	2232(15)	5.02(77)
C(27)	1203(8)	-2017(9)	2425(13)	4.10(65)
C(28)	-195(7)	-872(8)	1704(12)	2.97(53)
C(29)	-236(7)	-1268(10)	658(11)	4.05(59)
C(30)	-855(9)	-1789(9)	360(13)	4.41(67)
C(31)	-1421(7)	-1918(10)	1070(16)	4.41(74)
C(32)	-1401(8)	-1548(11)	2122(14)	4.72(78)
C(33)	-762(8)	-1036(9)	2447(12)	3.81(58)

$$^a B_{eq} = (8\pi^2/3) \sum_{ij} U_{ij} A_i^* A_j^* A_i A_j$$

Table 4. Selected Angles (deg) between Normals to Planes for 5a-(E) and 7b-(Z)

planes	angle	
	5a-(E)	7b-(Z)
1 and 2	13.5	26.5
1 and 3	12.5	26.2
1 and 4	40.4	33.8
1 and 5	33.4	12.9
2 and 3	4.1	3.8
2 and 4	39.6	50.4
2 and 5	22.1	30.3
3 and 4	43.2	47.6
3 and 5	25.8	28.4
4 and 5	31.2	22.1

plane	definition	
	5a-(E)	7b-(Z)
1 (coordination)	Pd, P, Cl(1), N, C(10)	Pd, I, P, N, C(1)
2 (palladated phenyl)	Pd, C(10), C(11), C(12), C(13), C(14), C(9)	Pd, C(1), C(2), C(3), C(4), C(5), C(6)
3 (metallacycle) ^a	Pd, C(8), C(9), C(10)	Pd, C(1), C(6), C(7)
4 (iminic function)	N, C(6), C(7), C(8)	N, C(7), C(9), C(10)
5 (methinic phenyl)	C(1), C(2), C(3), C(4), C(5), C(6)	C(10), C(11), C(12), C(13), C(14), C(15)

^a The nitrogen atom is out of the plane defined by the remaining atoms of the metallacycle.

7.49–7.13 m [3H, Cl₂C₆H₃ and 5H, C₆H₅], 4.65 q ³J_{HH} = 6.0 Hz [CHMe], 1.64 d ³J_{HH} = 6.0 Hz [CHMe]. **1b**: ¹H NMR 8.57 s [CH=N], 7.42–7.25 m [1H, F₂C₆H₃ and 5H, C₆H₅], 6.92 t ³J_{HH} = ³J_{HH} = 8.4 Hz [2H, F₂C₆H₃], 4.55 q ³J_{HH} = 6.6 Hz [CHMe], 1.62 d ³J_{HH} = 6.6 Hz [CHMe]. **1c**: ¹H NMR 8.54 s [CH=N],

7.48 d $^3J_{\text{HH}} = 7.2$ Hz [2H, C₆H₅], 7.36–7.10 m [3H, C₆H₅], 6.11 s [2H, (MeO)₃C₆H₂], 4.51 q $^3J_{\text{HH}} = 6.6$ Hz [CHMe], 3.83 s [9H, (MeO)₃C₆H₂], 1.61 d $^3J_{\text{HH}} = 6.6$ Hz [CHMe].

[Pd(2-{(R)-CHMeN=CH-2',6'-Cl₂C₆H₃}C₆H₄)X)₂ (X = Cl, 2a; X = Br, 3a; X = I, 4a; Mixture of (Z,Z), (Z,E), and (E,E) Isomers). A stirred suspension of Pd(AcO)₂ (2.2 mmol, 0.5 g) in acetic acid (25 mL) was treated with 2.2 mmol (0.612 g) of 1a at 80 °C for 2 h, and the resulting solution was concentrated *in vacuo*. The reaction residue was treated with 4.4 mmol of LiCl, LiBr, or KI in ethanol (25 mL), and the suspension was stirred at room temperature for 15 min. The precipitate was filtered, dried *in vacuo*, and purified by SiO₂ column chromatography. Compounds 2a and 3a were eluted with CHCl₃/MeOH (100/2) and isolated as yellow powders in yields ranging from 20 to 50%, after concentration of the solvents and addition of ethanol (10 mL). Compound 4a was eluted with CHCl₃ and isolated as a brown powder in yields of 40–50%, after concentration of the solvent and addition of ethanol (10 mL). Characterization data are as follows. 2a: ¹H NMR (selected data) 8.75 br asymmetric s [CH=N, 2a-(Z,Z)], 8.59 and 8.46 br signals and 8.51 s [CH=N, 2a-(Z,E) and 2a-(E,E)], 5.10–4.70 overlapped quartets [CHMe], 1.98 d and 1.38 d $^3J_{\text{HH}} = 6.5$ Hz [CHMe, 2a-(Z,E)], 1.85 d $^3J_{\text{HH}} = 6.5$ Hz [CHMe, 2a-(E,E)], 1.49 d $^3J_{\text{HH}} = 6.5$ Hz [CHMe, 2a-(Z,Z)]; ¹³C NMR (selected data) 163.2, 162.7, 162.2 [CH=N], 81.0, 80.5, 72.8 [CHMe], 27.5, 25.9 [CHMe]. Anal. Calcd (found) for C₃₀H₂₄Cl₂N₂Pd₂: C, 42.99 (42.8); H, 2.88 (2.8); N, 3.34 (3.3). 3a: ¹H NMR (selected data) 8.84 s [CH=N, 3a-(Z,Z)], 8.64 and 8.45 br signals and 8.52 s [CH=N, 3a-(Z,E) and 3a-(E,E)], 5.10–4.70 overlapped quartets [CHMe], 2.10–1.90 and 1.57–1.44 overlapped doublets [CHMe]; ¹³C NMR (selected data) 163.4, 162.9, 162.5, 162.1 [CH=N], 81.2, 81.0, 73.1, 72.9 [CHMe], 27.5, 26.1 [CHMe]. Anal. Calcd (found) for C₃₀H₂₄Br₂Cl₄N₂-Pd₂: C, 38.36 (38.1); H, 2.61 (2.5); N, 3.02 (2.9). 4a: ¹H NMR (selected data) 8.94 s, 8.73 s, 8.43 s, and 8.35 br s [CH=N], 5.10–4.70 overlapped quartets [CHMe], 2.08 d, 2.00 d, 1.63 d, and 1.57 d $^3J_{\text{HH}} = 6.5$ Hz [CHMe]; ¹³C NMR (selected data) 163.9, 163.6, 161.5, 161.2 [CH=N], 81.8, 81.7, 73.2, 73.1 [CHMe], 27.8, 27.7, 26.6, 26.5 [CHMe].

[Pd(2-{(R)-CHMeN=CH-2',6'-F₂C₆H₃}C₆H₄)X)₂ (X = Cl, 2b; X = Br, 3b; X = I, 4b; Mixture of (Z,Z), (Z,E), and (E,E) Isomers). A stirred suspension of Pd(AcO)₂ (4.4 mmol, 1.0 g) in acetic acid (25 mL) was treated with 4.4 mmol of 1b (1.08 g) at reflux for 45 min, and the resulting solution was concentrated *in vacuo*. The reaction residue was treated with 8.8 mmol of LiCl, LiBr, or KI in ethanol (25 mL), and the suspension was stirred at room temperature for 15 min. The precipitate was filtered, dried *in vacuo*, and purified by SiO₂ column chromatography. Compounds 2b and 3b were eluted with CHCl₃/MeOH (100/2) and isolated as yellow powders in yields of 20–50%, after concentration of the solvents and addition of ethanol (10 mL). Compound 4b was eluted with CHCl₃ and isolated as a brown powder in yields of 40–50%, after concentration of the solvent and addition of ethanol (10 mL). Characterization data are as follows. 2b: ¹H NMR (selected data) 8.78 br s [CH=N, 2b-(Z,Z)], 8.74 br s, 8.42 br s, and 8.51 br s [CH=N, 2b-(Z,E) and 2b-(E,E)], 5.00–4.80 four overlapped quartets [CHMe], 1.99 d, 1.91 d, and 1.56–1.45 overlapped doublets $^3J_{\text{HH}} = 6.5$ Hz [CHMe]; ¹³C NMR (selected data) 158.2, 158.1, 158.0, 157.6, [CH=N], 81.1, 73.6 [CHMe], 27.7, 26.5 [CHMe]. Anal. Calcd (found) for C₃₀H₂₄Cl₂F₂N₂Pd₂: C, 46.66 (47.1); H, 3.13 (3.0); N, 3.63 (3.5). 3b: ¹H NMR (selected data) 8.86 br s [CH=N, 3b-(Z,Z)], 8.75 br s and 8.49 br asymmetric s [CH=N, 3b-(Z,E) and 3b-(E,E)], 5.10–4.80 overlapped quartets [CHMe], 2.10–1.95 and 1.65–1.55 overlapped doublets [CHMe]; ¹³C NMR (selected data) 158.2 [CH=N], 81.4, 73.7 [CHMe], 27.7, 26.9 [CHMe]. Anal. Calcd (found) for C₃₀H₂₄Br₂F₂N₂Pd₂: C, 41.84 (41.7); H, 2.81 (2.7); N, 3.25 (3.2). 4b: ¹H NMR (selected data) 8.91 s, 8.75, and 8.36 broad signals and 8.42 s [CH=N], 5.10–4.80 overlapped quartets [CHMe], 2.11–2.04 overlapped doublets, 1.73

d, 1.65 d $^3J_{\text{HH}} = 6.5$ Hz [CHMe]; ¹³C NMR (selected data) 158.4 [CH=N], 81.8, 81.5, 73.9 [CHMe], 27.9, 27.8, 27.3 [CHMe].

Reactions with py-d₅. A 20 mg amount of compound 2a, 3a, 4a, 2b, 3b, or 4b (mixture of (Z,Z), (Z,E), and (E,E) isomers) was placed in an NMR tube and dissolved in 0.7 mL of CDCl₃, and the solution obtained was treated with an excess of py-d₅ (0.060 mL). An instantaneous change of color indicated the quantitative transformation of compounds 2–4

in the corresponding monomers [Pd(2-{(R)-CHMeN=CH-2',6'-Y₂C₆H₃}C₆H₄)X(py-d₅)]. Characterization data are as follows. 2a + py-d₅: ¹H NMR (selected data) 9.33 s [CH=N, monomer Z], 8.54 and 8.53 [CH=N, two rotational isomers of monomer E], 5.11 two overlapped quartets [CHMe, two rotational isomers of monomer E], 4.90 q $^3J_{\text{HH}} = 6.5$ Hz [CHMe, monomer Z], 2.09 d and 2.02 d $^3J_{\text{HH}} = 6.5$ Hz [CHMe, two rotational isomers of monomer E], 1.53 d $^3J_{\text{HH}} = 6.5$ Hz [CHMe, monomer Z]. 3a + py-d₅: ¹H NMR (selected data) 9.43 s [CH=N, monomer Z], 8.53 and 8.50 [CH=N, two rotational isomers of monomer E], 5.12 two overlapped quartets, [CHMe, two rotational isomers of monomer E], 4.90 q $^3J_{\text{HH}} = 6.5$ Hz [CHMe, monomer Z], 2.12 d, 2.04 d, $^3J_{\text{HH}} = 6.5$ Hz [CHMe, two rotational isomers of monomer E], 1.56 d $^3J_{\text{HH}} = 6.5$ Hz [CHMe, monomer Z]. 4a + py-d₅: ¹H NMR (selected data) 9.44 br s [CH=N, monomer Z], 8.37 br asymmetric s [CH=N, monomer E], 5.12 br asymmetric q [CHMe, monomer E], 4.74 q $^3J_{\text{HH}} = 6.5$ Hz [CHMe, monomer Z], 2.06 br asymmetric d [CHMe, monomer E], 1.56 d $^3J_{\text{HH}} = 6.5$ Hz [CHMe, monomer Z]. 2b + py-d₅: ¹H NMR (selected data) 9.40 s [CH=N, monomer Z], 8.53 br asymmetric s [CH=N, monomer E], 4.99 q $^3J_{\text{HH}} = 6.5$ Hz [CHMe, monomers E and Z], 2.03 br asymmetric d [CHMe, monomer E], 1.59 d $^3J_{\text{HH}} = 6.5$ Hz [CHMe, monomer Z]. 3b + py-d₅: ¹H NMR (selected data) 9.46 s [CH=N, monomer Z], 8.51 s [CH=N, monomer E], 4.96 q $^3J_{\text{HH}} = 6.5$ Hz [CHMe, monomers E and Z], 2.08 br signal [CHMe, monomer E], 1.63 d $^3J_{\text{HH}} = 6.5$ Hz [CHMe, monomer Z]. 4b + py-d₅: ¹H NMR (selected data) 9.50 br s [CH=N, monomer Z], 8.50 s [CH=N, monomer E], 5.02 q $^3J_{\text{HH}} = 6.5$ Hz [CHMe, monomers E and Z], 2.12 br signal [CHMe, monomer E], 1.69 d $^3J_{\text{HH}} = 6.5$ Hz [CHMe, monomer Z].

[Pd(2-{(Z)-(R)-CHMeN=CH-2',6'-Y₂C₆H₃}C₆H₄)X)₂ (Y = Cl, X = Cl, 2a-(Z,Z); Y = Cl, X = Br, 3a-(Z,Z); Y = F, X = Cl, 2b-(Z,Z); Y = F, X = Br, 3b-(Z,Z)) and [Pd(2-{(E)-(R)-CHMeN=CH-2',6'-Y₂C₆H₃}C₆H₄)X)₂ (Y = Cl, X = Cl, 2a-(E,E); Y = Cl, X = Br, 3a-(E,E); Y = F, X = Cl, 2b-(E,E); Y = F, X = Br, 3b-(E,E)). A 300 mg amount of compound 2a, 3a, 2b, or 3b (mixture of (Z,Z), (Z,E), and (E,E) isomers) was dissolved in 10 mL of CHCl₃, and the solution was eluted through a column of SiO₂ with CHCl₃. Concentration of the solvent of the first yellow band eluted and addition of ethanol (10 mL) produced the precipitation of the corresponding (Z,Z) compound as a yellow powder in yields of 30–70%. Concentration of the solvent of the second yellow band eluted and addition of ethanol (10 mL) produced the precipitation of the corresponding (E,E) compound as a yellow powder in yields of 10–20%. Characterization data are as follows. 2a-(Z,Z): ¹H NMR 8.77 s and 8.74 s [CH=N, two isomers], 7.42–7.26 m [3H, Cl₂C₆H₃ and 1H, C₆H₄], 6.97 m [2H, C₆H₄] and 6.78 d $^3J_{\text{HH}} = 7.2$ Hz [1H, C₆H₄], 4.84 q $^3J_{\text{HH}} = 6.5$ Hz [CHMe], 1.49 d $^3J_{\text{HH}} = 6.5$ Hz [CHMe]. Anal. Calcd (found) for C₃₀H₂₄Cl₆N₂-Pd₂: C, 42.99 (42.4); H, 2.88 (2.8); N, 3.34 (3.3). 2a-(E,E): ¹H NMR 8.48 br s [CH=N], 7.39 br signal [3H, Cl₂C₆H₃], 7.02–6.62 m [4H, C₆H₄], 4.96 q $^3J_{\text{HH}} = 6.5$ Hz [CHMe], 1.87 d $^3J_{\text{HH}} = 6.5$ Hz [CHMe]. Anal. Calcd (found) for C₃₀H₂₄Cl₆N₂Pd₂: C, 42.99 (42.9); H, 2.88 (2.8); N, 3.34 (3.3). 3a-(Z,Z): ¹H NMR 8.84 s [CH=N], 7.50 d $^3J_{\text{HH}} = 6.7$ Hz [1H, C₆H₄], 7.42 br signal [3H, Cl₂C₆H₃], 7.00–6.89 m [2H, C₆H₄], 6.81 d $^3J_{\text{HH}} = 6.7$ Hz [1H, C₆H₄], 4.85 q $^3J_{\text{HH}} = 6.5$ Hz [CHMe], 1.55 d $^3J_{\text{HH}} = 6.5$ Hz [CHMe]. Anal. Calcd (found) for C₃₀H₂₄Br₂Cl₄N₂Pd₂: C, 38.36 (38.4); H, 2.61 (2.6); N, 3.02 (3.0). 3a-(E,E): ¹H NMR 8.44 s [CH=N], 7.35 br signal [3H, Cl₂C₆H₃], 7.02–6.81 m [4H,

C_6H_4], 4.98 q $^3J_{HH} = 6.5$ Hz [CHMe], 1.94 d $^3J_{HH} = 6.5$ Hz [CHMe]. Anal. Calcd (found) for $C_{30}H_{24}Br_2Cl_4N_2Pd_2$: C, 38.36 (38.4); H, 2.61 (2.6); N, 3.02 (3.0). **2b-(Z,Z)**: 1H NMR 8.78 s [CH=N], 7.60–7.30 m [1H, $F_2C_6H_3$ and 1H, C_6H_4], 7.09–6.92 m [2H, $F_2C_6H_3$ and 2H, C_6H_4], 6.79 d $^3J_{HH} = 6.5$ Hz [1H, C_6H_4], 4.94 q $^3J_{HH} = 6.5$ Hz [CHMe], 1.56 d $^3J_{HH} = 6.5$ Hz [CHMe]. Anal. Calcd (found) for $C_{30}H_{24}Cl_2F_4N_2Pd_2$: C, 46.66 (46.6); H, 3.13 (3.1); N, 3.63 (3.6). **2b-(E,E)**: 1H NMR 8.48 s [CH=N], 7.60–7.30 m [1H, $F_2C_6H_3$], 7.10–6.70 m [2H, $F_2C_6H_3$ and 3H, C_6H_4], 6.62 d $^3J_{HH} = 7.7$ Hz [1H, C_6H_4], 4.95 br q $^3J_{HH} = 6.5$ Hz [CHMe], 1.93 d $^3J_{HH} = 6.5$ Hz [CHMe]. Anal. Calcd (found) for $C_{30}H_{24}Cl_2F_4N_2Pd_2$: C, 46.66 (46.2); H, 3.13 (3.1); N, 3.63 (3.5). **3b-(Z,Z)**: 1H NMR 8.85 br s [CH=N], 7.60–7.45 m [1H, $F_2C_6H_3$ and 1H, C_6H_4], 7.08–6.86 m [2H, $F_2C_6H_3$ and 2H, C_6H_4], 6.81 d $^3J_{HH} = 6.7$ Hz [1H, C_6H_4], 4.93 q $^3J_{HH} = 6.5$ Hz [CHMe], 1.63 d $^3J_{HH} = 6.5$ Hz [CHMe]. Anal. Calcd (found) for $C_{30}H_{24}Br_2F_4N_2Pd_2$: C, 41.84 (41.6); H, 2.81 (2.7); N, 3.25 (3.2). **3b-(E,E)**: 1H NMR 8.45 s [CH=N], 7.60–7.30 m [1H, $F_2C_6H_3$], 7.02–6.89 m [2H, $F_2C_6H_3$ and 4H, C_6H_4], 4.95 q $^3J_{HH} = 6.5$ Hz [CHMe], 1.97 d $^3J_{HH} = 6.5$ Hz [CHMe]. Anal. Calcd (found) for $C_{30}H_{24}Br_2F_4N_2Pd_2$: C, 41.84 (41.1); H, 2.81 (2.8); N, 3.25 (3.0).

[Pd(2-{(E)-(R)-CHMeN=CH-2',4',6'-(MeO)₃C₆H₂}C₆H₄-X)₂ (X = Cl, **2c**; X = Br, **3c**; X = I, **4c**). A stirred suspension of Pd(AcO)₂ (2.2 mmol, 0.5 g) in acetic acid (25 mL) was treated with 2.2 mmol (0.658 g) of imine **1c** at reflux for 45 min, and the resulting solution was concentrated *in vacuo*. The reaction residue was treated with 4.4 mmol of LiCl, LiBr, or KI in ethanol (25 mL), and the suspension was stirred at room temperature for 15 min. The precipitate was filtered, dried *in vacuo*, and purified by SiO₂ column chromatography. Compounds **2c** and **3c** were eluted with CHCl₃/MeOH (100/2) and isolated as yellow powders in yields of 30–40%, after concentration of the solvents and addition of ethanol (10 mL). Compound **4c** was eluted with CHCl₃ and isolated as a brown powder in yields of 40–50%, after concentration of the solvent and addition of ethanol (10 mL). Characterization data are as follows. **2c**: 1H NMR 8.58 s [CH=N], 7.60 d $^3J_{HH} = 7.9$ Hz [1H, C_6H_4], 7.00–6.80 m [3H, C_6H_4], 6.24 s [2H, (MeO)₃C₆H₂], 4.92 q $^3J_{HH} = 6.8$ Hz [CHMe], 4.09 br s [6H, (MeO)₃C₆H₂], 3.88 s [3H, (MeO)₃C₆H₂], 1.64 d $^3J_{HH} = 6.8$ Hz [CHMe]. Anal. Calcd (found) for $C_{36}H_{40}Cl_2N_2O_6Pd_2$: C, 49.11 (48.2); H, 4.58 (4.6); N, 3.18 (3.1). **3c**: 1H NMR 8.53 s [CH=N], 7.80 d $^3J_{HH} = 7.9$ Hz [1H, C_6H_4], 6.89 t $^3J_{HH} = 8.0$ Hz [1H, C_6H_4], 6.85 m [2H, C_6H_4], 6.24 s [2H, (MeO)₃C₆H₂], 4.95 q $^3J_{HH} = 6.6$ Hz [CHMe], 4.09 br s [6H, (MeO)₃C₆H₂], 3.88 s [3H, (MeO)₃C₆H₂], 1.64 d $^3J_{HH} = 6.8$ Hz [CHMe]. Anal. Calcd (found) for $C_{36}H_{40}Br_2N_2O_6Pd_2$: C, 44.60 (44.5); H, 4.16 (4.1); N, 2.89 (2.9). **4c**: 1H NMR 8.42 s [CH=N], 8.10 d $^3J_{HH} = 8.0$ Hz [1H, C_6H_4], 6.96 t $^3J_{HH} = 8.0$ Hz [1H, C_6H_4], 6.83 d $^3J_{HH} = 8.0$ Hz [1H, C_6H_4], 6.72 t $^3J_{HH} = 8.0$ Hz [1H, C_6H_4], 6.23 s [2H, (MeO)₃C₆H₂], 4.98 q $^3J_{HH} = 6.8$ Hz [CHMe], 4.08 br s [6H, (MeO)₃C₆H₂], 3.87 s [3H, (MeO)₃C₆H₂], 1.71 d $^3J_{HH} = 6.8$ Hz [CHMe]. Anal. Calcd (found) for $C_{36}H_{40}I_2N_2O_6Pd_2$: C, 40.66 (40.6); H, 3.79 (3.7); N, 2.63 (2.7).

[Pd(2-{(Z)-(R)-CHMeN=CH-2',6'-Y₂C₆H₃}C₆H₄-X)(PPh₃)₂] (Y = Cl, X = Cl, **5a-(Z)**; Y = Cl, X = Br, **6a-(Z)**; Y = F, X = Cl, **5b-(Z)**; Y = F, X = Br, **6b-(Z)**) and [Pd(2-{(E)-(R)-CHMeN=CH-2',6'-Y₂C₆H₃}C₆H₄-X)(PPh₃)₂] (Y = Cl, X = Cl, **5a-(E)**; Y = Cl, X = Br, **6a-(E)**; Y = F, X = Cl, **5b-(E)**; Y = F, X = Br, **6b-(E)**). A suspension formed by 0.12 mmol of **2a**, **3a**, **2b**, or **3b** ((Z,Z) or (E,E)), 0.24 mmol of PPh₃ (0.062 g), and 20 mL of acetone was stirred at room temperature for 15 min, and the resulting suspension or solution was concentrated *in vacuo*. Addition of ether (10 mL) to the reaction residue produced the precipitation of compounds **5a**, **6a**, **5b**, or **6b** ((Z) or (E)) as white or pale yellow powders in yields of 60–90%. Characterization data are as follows. **5a-(Z)**: 1H NMR 9.32 d $^4J_{PH} = 5.0$ Hz [CH=N], 7.81–7.75 m [6H, PPh₃], 7.43–7.31 m [9H, PPh₃ and 3H, Cl₂C₆H₃], 6.94 d $^3J_{HH} = 7.8$ Hz [1H, C_6H_4],

6.85 m [1H, C_6H_4], 6.40 m [2H, C_6H_4], 4.92 m [CHMe], 1.67 d $^3J_{HH} = 6.5$ Hz [CHMe]; ^{31}P NMR 41.5 s. Anal. Calcd (found) for $C_{33}H_{27}Cl_3NPPd$: C, 58.17 (57.6); H, 3.99 (4.1); N, 2.05 (2.0). **6a-(Z)**: 1H NMR 9.46 d $^4J_{PH} = 5.0$ Hz [CH=N], 7.85–7.74 m [6H, PPh₃], 7.40–7.35 m [9H, PPh₃ and 3H, Cl₂C₆H₃], 6.92 d $^3J_{HH} = 7.7$ Hz [1H, C_6H_4], 6.84 m [1H, C_6H_4], 6.40 m [2H, C_6H_4], 4.90 m [CHMe], 1.72 d $^3J_{HH} = 7.7$ Hz [CHMe]; ^{31}P NMR 41.2 s. Anal. Calcd (found) for $C_{33}H_{27}BrCl_2NPPd$: C, 54.60 (54.5); H, 3.75 (3.9); N, 1.93 (1.8). **5b-(Z)**: 1H NMR 9.30 d $^4J_{PH} = 5.5$ Hz [CH=N], 7.86–7.75 m [6H, PPh₃], 7.48–7.35 m [9H, PPh₃ and 1H, $F_2C_6H_3$], 7.03 t $^3J_{FH} = ^3J_{HH} = 7.7$ Hz [2H, $F_2C_6H_3$], 6.90 m [2H, C_6H_4], 6.41 m [2H, C_6H_4], 4.97 m [CHMe], 1.81 d $^3J_{HH} = 6.3$ Hz [CHMe]; ^{31}P NMR 40.3 s. Anal. Calcd (found) for $C_{33}H_{27}ClF_2NPPd$: C, 61.62 (60.9); H, 4.20 (4.4); N, 2.16 (2.1). **6b-(Z)**: 1H NMR 9.35 d $^4J_{PH} = 5.5$ Hz [CH=N], 7.84–7.74 m [6H, PPh₃], 7.47–7.33 m [9H, PPh₃ and 1H, $F_2C_6H_3$], 7.01 t $^3J_{FH} = ^3J_{HH} = 7.6$ Hz [2H, $F_2C_6H_3$], 6.89 m [2H, C_6H_4], 6.39 m [2H, C_6H_4], 4.95 m [CHMe], 1.87 d $^3J_{HH} = 6.0$ Hz [CHMe]; ^{31}P NMR 41.1 s. Anal. Calcd (found) for $C_{33}H_{27}BrF_2NPPd$: C, 57.20 (57.3); H, 3.93 (4.1); N, 2.02 (2.0). **5a-(E)**: 1H NMR 8.62 d $^4J_{PH} = 10$ Hz [CH=N], 7.72–7.63 m [6H, PPh₃], 7.34–7.25 m [9H, PPh₃ and 3H, Cl₂C₆H₃], 7.01 d $^3J_{HH} = 7.7$ Hz [1H, C_6H_4], 6.85 t $^3J_{HH} = 7.7$ Hz [1H, C_6H_4], 6.32 m [2H, C_6H_4], 5.05 m [CHMe], 2.15 d $^3J_{HH} = 6.5$ Hz [CHMe]; ^{31}P NMR 40.6 s. Anal. Calcd (found) for $C_{33}H_{27}Cl_3NPPd$: C, 58.17 (58.1); H, 3.99 (4.0); N, 2.05 (2.1). **6a-(E)**: 1H NMR 8.60 d $^4J_{PH} = 12$ Hz [CH=N], 7.73–7.64 m [6H, PPh₃], 7.34–7.25 m [9H, PPh₃ and 3H, Cl₂C₆H₃], 7.02 d $^3J_{HH} = 7.6$ Hz [1H, C_6H_4], 6.84 t $^3J_{HH} = 7.6$ Hz [1H, C_6H_4], 6.40–6.20 m [2H, C_6H_4], 5.06 m [CHMe], 2.17 d $^3J_{HH} = 6.5$ Hz [CHMe]; ^{31}P NMR 41.3 s. Anal. Calcd (found) for $C_{33}H_{27}BrCl_2NPPd$: C, 54.60 (55.2); H, 3.75 (3.9); N, 1.93 (1.8). **5b-(E)**: 1H NMR 8.55 d $^4J_{PH} = 12$ Hz [CH=N], 7.76–7.66 m [6H, PPh₃], 7.35–7.28 m [9H, PPh₃ and 1H, $F_2C_6H_3$], 7.00 d $^3J_{HH} = 7.7$ Hz [1H, C_6H_4], 6.86 m [2H, $F_2C_6H_3$ and 1H, C_6H_4], 6.40 t $^3J_{HH} = 7.3$ Hz [1H, C_6H_4], 6.25 t $^3J_{HH} = ^4J_{PH} = 7.3$ Hz [1H, C_6H_4], 4.95 m [CHMe], 2.17 d $^3J_{HH} = 6.6$ Hz [CHMe]; ^{31}P NMR 39.6 s. Anal. Calcd (found) for $C_{33}H_{27}ClF_2NPPd$: C, 61.62 (62.0); H, 4.20 (4.3); N, 2.16 (2.1). **6b-(E)**: 1H NMR 8.55 d $^4J_{PH} = 11$ Hz [CH=N], 7.81–7.67 m [6H, PPh₃], 7.40–7.31 m [9H, PPh₃ and 1H, $F_2C_6H_3$], 7.00–6.80 m [2H, $F_2C_6H_3$ and 2H, C_6H_4], 6.39 t $^3J_{HH} = 7.7$ Hz [1H, C_6H_4], 6.26 t $^3J_{HH} = ^4J_{PH} = 7.7$ Hz [1H, C_6H_4], 4.95 m [CHMe], 2.17 d $^3J_{HH} = 6.5$ Hz [CHMe]; ^{31}P NMR 42.1 s. Anal. Calcd (found) for $C_{33}H_{27}BrF_2NPPd$: C, 57.20 (57.2); H, 3.93 (4.0); N, 2.02 (2.0).

[Pd(2-{(Z)-(R)-CHMeN=CH-2',6'-Y₂C₆H₃}C₆H₄)I(PPh₃)₂] (Y = Cl, **7a-(Z)**; Y = F, **7b-(Z)**), [Pd(2-{(E)-(R)-CHMeN=CH-2',6'-Y₂C₆H₃}C₆H₄)I(PPh₃)₂] (Y = Cl, **7a-(E)**; Y = F, **7b-(E)**), and [Pd(2-{(R)-CHMeNH₂}C₆H₄)I(PPh₃)₂] (**8**). A suspension formed by 0.12 mmol of **4a** or **4b** (mixture of (Z,Z), (Z,E), and (E,E) isomers), 0.24 mmol of PPh₃ (0.062 g), and 20 mL of acetone was stirred at room temperature for 15 min and the resulting suspension concentrated *in vacuo*. The reaction residue was dissolved in CHCl₃ (10 mL) and the solution was eluted through a column of SiO₂ with CHCl₃. Concentration of the solvent of the first yellow band eluted and addition of ether (10 mL) produced the precipitation of **7a-(Z)** or **7b-(Z)** as a pale orange powder in a yield of 44 or 52%, respectively. Concentration of the solvent of the second yellow band eluted and addition of ether (10 mL) produced the precipitation of 40 or 12 mg of a ca. 4:1 or 1:1 mixture of compounds **7a-(E)** and **8** or **7b-(E)** and **8**, respectively. Characterization data are as follows. **7a-(Z)**: 1H NMR 9.64 d $^4J_{PH} = 5.0$ Hz [CH=N], 7.84–7.74 m [6H, PPh₃], 7.40–7.35 m [9H, PPh₃ and 3H, Cl₂C₆H₃], 6.94 d $^3J_{HH} = 7.6$ Hz [1H, C_6H_4], 6.82 t $^3J_{HH} = 7.6$ Hz [1H, C_6H_4], 6.38 m [2H, C_6H_4], 4.90 m [CHMe], 1.82 d $^3J_{HH} = 6.3$ Hz [CHMe]; ^{31}P NMR 41.5 s. Anal. Calcd (found) for $C_{33}H_{27}Cl_3INPPd$: C, 51.29 (51.2); H, 3.52 (3.6); N, 1.81 (1.8). **7b-(Z)**: 1H NMR 9.55 d $^4J_{PH} = 5.5$ Hz [CH=N], 7.86–7.74 m [6H, PPh₃], 7.43–7.33 m [9H, PPh₃ and

1H, F₂C₆H₃], 7.00 t ³J_{FH} = ³J_{HH} = 7.6 Hz [2H, F₂C₆H₃], 6.92 d ³J_{HH} = 7.7 Hz [1H, C₆H₄], 6.62 t ³J_{HH} = 7.7 Hz [1H, C₆H₄], 6.36 m [2H, C₆H₄], 4.98 br q [CHMe], 1.94 d ³J_{HH} = 6.0 Hz [CHMe]; ³¹P NMR 41.1 s. Anal. Calcd (found) for C₃₃H₂₇F₂INPPd: C, 53.57 (53.3); H, 3.68 (3.7); N, 1.89 (1.8). **7a-(E)** + **8**: ¹H NMR (selected data) 8.62 d ⁴J_{PH} = 12 Hz [CH=N, **7a-(E)**], 5.11 m [CHMe, **7a-(E)**], 4.60 m [CHMe, **8**], 4.10 m and 3.58 m [NH₂, **8**], 2.19 d ³J_{HH} = 6.5 Hz [CHMe, **7a-(E)**], 1.75 d ³J_{HH} = 6.5 Hz [CHMe, **8**]. **7b-(E)** + **8**: ¹H NMR (selected data) 8.55 d ⁴J_{PH} = 12 Hz [CH=N, **7b-(E)**], 5.05 m [CHMe, **7b-(E)**], 4.60 m [CHMe, **8**], 4.10 m and 3.58 m [NH₂, **8**], 2.20 d ³J_{HH} = 6.5 Hz [CHMe, **7b-(E)**], 1.75 d ³J_{HH} = 6.5 Hz [CHMe, **8**].



(PPh₃)] (**9**). A suspension formed by 0.12 mmol of **2c**, **3c**, or **4c**, 0.24 mmol of PPh₃ (0.062 g), and 20 mL of acetone was refluxed for 24 h and the resulting solution concentrated *in vacuo*. The reaction residue was purified by SiO₂ column chromatography with CHCl₃ as eluant. Concentration of the solvent of the first pale yellow eluted band and addition of ether (10 mL) produced the precipitation of compound **9** as a pale yellow powder in a yield of 28, 60, or 77%, respectively. Characterization data are as follows. **9**: ¹H NMR 8.65 d ⁴J_{PH} = 12 Hz [CH=N], 7.80–7.60 m [6H, PPh₃], 7.45–7.28 m [9H, PPh₃], 7.06 d ³J_{HH} = 7.7 Hz [1H, C₆H₄], 6.91 t ³J_{HH} = 7.7 Hz [1H, C₆H₄], 6.55 t ³J_{HH} = 7.7 Hz [1H, C₆H₄], 6.45 t ³J_{HH} = ³J_{PH} = 7.7 Hz [1H, C₆H₄], 5.56 d ⁴J_{HH} = 2.5 [1H, (MeO)₂C₆H₂], 5.27 d ⁴J_{HH} = 2.5 [1H, (MeO)₂C₆H₂], 5.10 m [CHMe], 3.77 s [3H, (MeO)₂C₆H₂], 3.61 s [3H, (MeO)₂C₆H₂], 1.63 d ³J_{HH} = 6.8 Hz [CHMe]; ³¹P NMR 41.2 s. Anal. Calcd (found) for C₃₆H₃₂NO₃PPd: C, 64.47 (63.3); H, 4.95 (4.9); N, 2.15 (2.1).

Reaction of 2a-(Z,Z) with (R)-(+)-(1-Phenylethyl)amine and Racemic (1-Phenylethyl)amine. A 20 mg amount of compound **2a-(Z,Z)** was placed in an NMR tube and dissolved in 0.7 mL of CDCl₃, and the solution was treated with an excess (0.020 mL) of (R)-(+)-(1-phenylethyl)amine or racemic (1-phenylethyl)amine. An instantaneous change of color from pale yellow to colorless indicated the quantitative

formation of the corresponding monomers [Pd(2-{(Z)-(R)-CHMe-N=CH-2',6'-Cl₂C₆H₃}C₆H₄)Cl(NH₂CHMeC₆H₅)]. Characterization data are as follows. **2a-(Z,Z)** + (R)-(+)-(1-phenylethyl)amine: ¹H (selected data) NMR 9.10 [CH=N], 4.83 q ³J_{HH} = 6.5 Hz [CH=NCHMe], 4.44 m [NH₂CHMe], 3.76 br m and 3.26 br d [NH₂], 1.95 d ³J_{HH} = 6.7 Hz [NH₂CHMe], 1.49 d ³J_{HH} = 6.5 Hz [CH=NCHMe]. **2a-(Z,Z)** + racemic (1-phenylethyl)amine: ¹H NMR (selected data) 9.15 [CH=N, monomer (R,S)], 9.10 [CH=N, monomer (R,R)], 4.83 q ³J_{HH} = 6.5 Hz [CH=NCHMe, monomers (R,S) and (R,R)], 4.63 m [NH₂CHMe, monomer (R,S)], 4.44 m [NH₂CHMe, monomer (R,R)], 3.76 br m and 3.26 br signal [NH₂, monomers (R,S) and (R,R)], 1.95 d ³J_{HH} = 6.7 Hz [NH₂CHMe, monomer (R,R)], 1.85 d ³J_{HH} = 6.7 Hz [NH₂CHMe, monomer (R,S)], 1.49 d ³J_{HH} = 6.5 Hz [CH=NCHMe, monomer (R,R)], 1.44 d ³J_{HH} = 6.5 Hz [CH=NCHMe, monomer (R,S)].

Crystallographic Studies. A summary of crystallographic data is given in Table 5. Crystals of **5a-(E)** and **7b-(Z)** suitable for X-ray diffraction were grown from CH₂Cl₂/MeOH (1/1). In both cases, a prismatic crystal (0.1 × 0.1 × 0.2) was selected and mounted on a Philips PW-1100 diffractometer. Unit cell parameters were determined from automatic centering of 25 reflections (8° ≤ θ ≤ 12°) and refined by the least-squares method. Intensities were collected with graphite-monochromated Mo Kα radiation, using the ω/2θ scan technique. Three reflections were measured every 2 h as orientation and intensity control, and no significant variation was observed

Table 5. Summary of Crystallographic Data

	5a-(E)	7b-(Z)
formula	C ₃₃ H ₂₇ Cl ₃ NPPd	C ₃₃ H ₂₇ F ₂ INPPd
mol wt	681.32	739.86
syst	monoclinic	orthorhombic
space group	P2 ₁	P2 ₁ 2 ₁ 2 ₁
a, Å	16.996(4)	18.017(3)
b, Å	9.006(2)	14.204(2)
c, Å	9.655(2)	11.978(2)
α, deg	90.00	90.00
β, deg	91.61(3)	90.00
γ, deg	90.00	90.00
V, Å ³	1477(1)	3065(1)
d _{calc} , g cm ⁻³	1.531	1.603
Z	2	4
F(000)	688.0	1456.0
cryst size, mm ³	0.1 × 0.1 × 0.2	0.1 × 0.1 × 0.2
μ(Mo Kα), cm ⁻¹	9.65	17.02
λ(Mo Kα), Å	0.710 69	0.710 69
T, °C	25	25
no. of rflns coll	3834	3348
no. of rflns with I ≥ 2.5σ(I)	2595	3162
R	0.064	0.050
R _w	0.067	0.049
no. of params refined	367	380
max shift/esd	0.3	0.1
max peak, e Å ⁻³	0.3	0.3
min peak, e Å ⁻³	-0.3	-0.3

in any case. The number of collected reflections and the range are listed in Table 5. Lorentz-polarization corrections, but not absorption corrections, were made. The structures were solved by direct methods, using the SHELXS computer program,²⁷ and refined by the full-matrix least-squares method, with the SHELX76 computer program.²⁸ The function minimized was $\sum w||F_o| - |F_c||^2$, where $w = (\sigma^2(F_o) + 0.0037|F_o|^2)^{-1}$ for **5a-(E)** and where $w = (\sigma^2(F_o) + 0.005|F_o|^2)^{-1}$ for **7b-(Z)**. f , f' , and f'' were taken from ref 29. All hydrogen atoms were located from a difference synthesis for the crystal structure of **5a-(E)**. For compound **7b-(Z)** 9 hydrogen atoms were located from a difference synthesis and the remaining 18 were computed. All hydrogens were refined with an overall isotropic temperature factor, using a riding model for computed atoms. The final R and R_w factors, the number of parameters refined for each structure, maximum shift/esd, and the maximum and minimum peaks in the final difference synthesis are presented in Table 5. Both enantiomorph configurations were refined, giving the atomic coordinates of the lowest R factor.

Acknowledgment. We thank the DGICYT (Grant No. PB 93-0804) for financial support, the Serveis Científico-Tècnics de la Universitat de Barcelona for many facilities in recording NMR spectra, Johnson Matthey Inc. for a loan of palladium chloride, and Mr. Erwan Le Pape and Ms. Anna Luque for doing part of the experimental work.

Supplementary Material Available: Tables of all distances and angles, final hydrogen coordinates, anisotropic thermal parameters, and least-squares planes and atomic deviations for **5a-(E)** and **7b-(Z)** (10 pages). Ordering information is given on any current masthead page.

OM9407969

(27) Sheldrick, G. M. *Acta Crystallogr., Sect. A* 1990, 46, 467.

(28) Sheldrick, G. M. SHELX, Computer Program for Crystal Structure Determination; University of Cambridge, Cambridge, U.K., 1976.

(29) *International Tables for X-ray Crystallography*; Kynoch Press: Birmingham, U.K., 1974; Vol. IV, pp 99–100, 149.

Oxidative Addition of Br₂ to Ru(η^5 -C₅Me₅)(η^4 -diene)Br Complexes. Effect of Substituents of the Diene on the Course of Reaction. Formation of a Novel Cationic Ruthenium(IV) η^4 -Diene Complex

Christian Gemel,^{1a} Kurt Mereiter,^{1b} Roland Schmid,^{1a} and Karl Kirchner*^{1a}

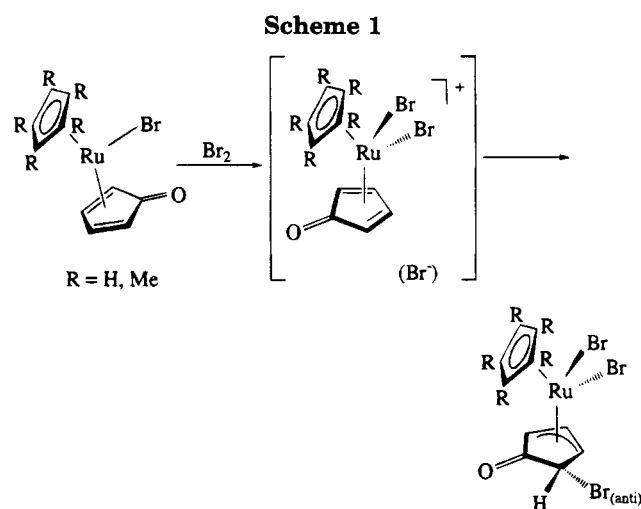
Institute of Inorganic Chemistry and Institute of Mineralogy, Crystallography, and Structural Chemistry, Technical University of Vienna, Getreidemarkt 9, A-1060 Vienna, Austria

Received October 14, 1994[®]

The products of bromine addition to Ru(η^5 -C₅Me₅)(η^4 -diene)Br (**1**) vary with the substituents of the diene moiety. In the case of 1,3-butadiene and 2-methyl-1,3-butadiene the corresponding Ru(η^5 -C₅Me₅)(η^3 -allyl)Br₂ complexes (**2**) are readily formed. For 2,3-dimethyl-1,3-butadiene, in contrast, a η^4 -diene Ru(IV) complex is obtained, which is unstable in solution and tentatively formulated as Ru(η^5 -C₅Me₅)(η^4 -CH₂CMeCMeCH₂)Br₃ (**3**). Among the decomposition products the unusual complex [Ru(η^5 -C₅Me₅)(η^4 -CH₂CMeCMeCH₂)Br₂][Ru(η^5 -C₅Me₅)Br₄] (**5**) is found. With AgCF₃SO₃, complex **3** affords, in a reversible reaction, the novel cationic complex [Ru(η^5 -C₅Me₅)(η^4 -CH₂CMeCMeCH₂)Br₂]⁺CF₃SO₃⁻ (**4**). By X-ray diffraction techniques, the molecular structures of **2b**, **4**, and **5** have been determined. **2b** crystallizes in space group *P2₁/c* (No. 14), with *a* = 12.910(4) Å, *b* = 11.293(4) Å, *c* = 12.615(4) Å, β = 105.05(1)°, *V* = 1776.1(10) Å³, and *Z* = 4. The structure was refined to *R*(*F*) = 0.045 (*F* ≥ 4σ(*F*)). **4** crystallizes in space group *Pnma* (No. 62), with *a* = 17.424(4) Å, *b* = 11.830(3) Å, *c* = 10.550(3) Å, *V* = 2174.6(10) Å³, and *Z* = 4. The structure was refined to *R*(*F*) = 0.039 (*F* ≥ 4σ(*F*)). **5** crystallizes in space group *Pna2₁* (No. 33), with *a* = 28.239(8) Å, *b* = 12.564(3) Å, *c* = 9.006(2) Å, *V* = 3195.3(14) Å³, and *Z* = 4. The structure was refined to *R*(*F*) = 0.049 (*F* ≥ 4σ(*F*)).

Introduction

Cyclopentadienone complexes Ru(η^5 -C₅R₅)(η^4 -C₅H₄O)-Br (R = H, Me) react with Br₂ to give bromo-substituted η^3 -cyclopentenoyl Ru(IV) complexes (Scheme 1).² In this process, the relatively weak nucleophile Br⁻ adds to the cyclopentadienone ligand regioselectively at an α -carbon atom from an antifacial direction. It seems, therefore, likely that the reaction proceeds through a reactive cationic cyclopentadienone Ru(IV) intermediate as depicted in Scheme 1. The enhanced electrophilicity of the cyclopentadienone moiety, dominating at the α -carbon atoms, is a consequence of the strong electron-withdrawing effect of the metal center.^{3,4} With this in mind it was deemed worthwhile to examine whether the course of reaction is maintained when simple acyclic dienes are used as the ligands instead of cyclopentadienone. This process could, thus, provide ready access to new bromo-substituted Ru(IV) η^3 -allyl complexes which, as has been shown recently,^{2c,5} (i) may be further derivatized by replacement of the halide of the allyl moiety by other nucleophiles and (ii) may yield new



functionalized olefins via reductive elimination in the presence of CO. Moreover, from these investigations we will attempt to get some further evidence in favor of the above proposed cationic intermediate.

We report here on the oxidative addition of Br₂ to Ru(η^5 -C₅Me₅)(η^4 -diene)Br complexes, where diene = 1,3-butadiene (**1a**), 2-methyl-1,3-butadiene (**1b**), and 2,3-dimethyl-1,3-butadiene (**1c**). Whereas the reactivity pattern of **1a** and **1b** conforms to Scheme 1, a dramatic change is seen in the reaction of **1c**, that is, upon the introduction of a further methyl group.

Experimental Section

General Information. Manipulations were performed under an inert atmosphere of purified nitrogen by using

[®] Abstract published in *Advance ACS Abstracts*, February 1, 1995.

(1) (a) Institute of Inorganic Chemistry. (b) Institute of Mineralogy, Crystallography, and Structural Chemistry.

(2) (a) Kirchner, K.; Mereiter, K.; Schmid, R. *J. Chem. Soc., Chem. Commun.* **1994**, 161. (b) Kirchner, K.; Mereiter, K.; Umfahrer, A.; Schmid, R. *Organometallics* **1994**, *13*, 1886. (c) Mauthner, K.; Mereiter, K.; Schmid, R.; Kirchner, K. *Organometallics* **1994**, *13*, 5054.

(3) Davies, S. G.; Green, M. L. H.; Mingos, D. M. P. *Tetrahedron* **1978**, *34*, 3047.

(4) Collman, J. P.; Hegedus, L. S.; Norton, J. R.; Finke, R. G. *Principles and Applications of Organotransitionmetal Chemistry*, 2nd ed.; University Science Books: Mill Valley, CA, 1987.

(5) Nagashima, H.; Mukai, K.; Shiota, Y.; Yamaguchi, K.; Ara, K.; Fukahori, T.; Suzuki, H.; Akita, M.; Moro-oka, Y.; Itoh, K. *Organometallics* **1990**, *9*, 799.

standard Schlenk techniques and/or a glovebox. All chemicals were standard reagent grade and were used without further purification. The solvents were purified according to standard procedures.⁶ The deuterated solvents were purchased from Aldrich and dried over 4 Å molecular sieves. ¹H and ¹³C{¹H} NMR spectra were recorded on a Bruker AC 250 spectrometer operating at 250.13 and 62.86 MHz, respectively, and were referenced to SiMe₄. Microanalyses were done by the Microanalytical Laboratories, University of Vienna. Ru(η^5 -C₅-Me₅)(η^4 -diene)Br complexes (diene = 1,3-butadiene (**1a**), 2-methyl-1,3-butadiene (**1b**), and 2,3-dimethyl-1,3-butadiene (**1c**)) have been synthesized according to the literature.⁷

Synthesis. Ru(η^5 -C₅Me₅)(η^3 -CH₂CHCH₂Br)Br₂ (2a**).** To a stirred solution of **1a** (250 mg, 0.675 mmol) in CH₂Cl₂ (20 mL) at -60 °C Br₂ (1 equiv), dissolved in CH₂Cl₂ (5 mL), was added dropwise within a period of 30 min. The solution was then warmed to room temperature, and the volatiles were removed under vacuum. The remaining red solid was washed with anhydrous diethyl ether and dried under vacuum. Yield: 330 mg (92%). Anal. Calcd for C₁₄H₂₁Br₃Ru: C, 31.72; H, 3.99; Br, 45.22. Found: C, 31.79; H, 4.02; Br, 45.32. ¹H NMR (δ , CDCl₃, 20 °C): 5.90–5.60 (m, 1H), 5.48–5.35 (m, 1H), 4.38 (m, 1H), 3.59 (m, 1H), 2.92 (m, 1H), 2.86 (m, 2H), 1.80 (s, 15H).

Ru(η^5 -C₅Me₅)(η^3 -CH₂CMeCHCH₂Br)Br₂ (2b**).** This complex was synthesized analogously to **2a** with **1b** as starting material. Yield: 96%. Anal. Calcd for C₁₅H₂₃Br₃Ru: C, 33.11; H, 4.26; Br, 44.05. Found: C, 32.96; H, 4.17; Br, 44.06. ¹H NMR (δ , CDCl₃, 20 °C): 5.07 (ddd, 1H, *J* = 12.9 Hz, *J* = 3.8 Hz, *J* = 1.9 Hz), 3.79 (d, 1H, *J* = 1.9 Hz), 3.73 (dd, 1H, *J* = 8.5 Hz, *J* = 3.8 Hz), 3.01 (dd, 1H, *J* = 12.9 Hz, *J* = 8.5 Hz), 2.97 (s, 1H), 2.40 (s, 3H), 1.74 (s, 15H). ¹³C{¹H} NMR (δ , CD₂Cl₂, 20 °C): 108.2, 105.5 (C₅Me₅), 71.4, 56.4, 35.3 (CH₂Br), 22.4 (Me), 11.1 (C₅Me₅).

Ru(η^5 -C₅Me₅)(η^4 -CH₂CMeCMeCH₂)Br₃ (3**).** This complex was synthesized analogously to **2a** with **1c** as starting material. Yield: 93%. Anal. Calcd for C₁₆H₂₅Br₃Ru: C, 34.43; H, 4.51; Br, 42.95. Found: C, 34.45; H, 4.48; Br, 42.78. ¹H NMR (δ , acetone-*d*₆, 20 °C): 3.97 (d, 2H, *J* = 4.5 Hz), 3.12 (d, 2H, *J* = 4.5 Hz), 2.07 (s, 6H), 1.82 (s, 15H).

A CH₂Cl₂ solution of **3** was set aside for crystallization by vapor diffusion with diethyl ether. Small dark brown crystals were formed after 1 day. Upon examination of the crystalline solid under a microscope, it was observed that several products were formed. The major product could be separated manually and was crystallographically analyzed.

[Ru(η^5 -C₅Me₅)(η^4 -CH₂CMeCMeCH₂)Br₂]CF₃SO₃ (4**).** **3** (330 mg, 0.591 mmol) was dissolved in 10 mL of CH₂Cl₂. AgCF₃SO₃ (152 mg, 0.592 mmol) was added, and the mixture was stirred for 1 h. The resulting precipitate of AgBr was removed by filtration. On addition of diethyl ether a red precipitate was formed which was collected on a glass frit, washed with diethyl ether, and dried under vacuum. Yield: 275 mg (74%). Anal. Calcd for C₁₇H₂₅Br₂F₃O₃RuS: C, 32.55; H, 4.02; Br, 25.47. Found: C, 32.46; H, 4.07; Br, 26.42. ¹H NMR (δ , acetone-*d*₆, 20 °C): 3.65 (d, 2H, *J* = 1.7 Hz), 2.72 (s, 6H, Me), 2.53 ppm (d, 2H, *J* = 1.7 Hz), 2.16 (s, 15H). ¹³C{¹H} NMR (δ , CD₂Cl₂, 20 °C): 140.7, 116.0 (C₅Me₅), 72.0, 22.2 (Me), 12.4 (C₅Me₅).

Attempted Metathesis of 3 with NBu₄CF₃SO₃. **3** (30 mg, 0.053 mmol) was dissolved in 0.5 mL of CD₂Cl₂ and treated with NBu₄CF₃SO₃ (37 mg, 0.107 mmol). The reaction mixture was loaded into a NMR tube, and a ¹H NMR spectrum was recorded.

Attempted Reaction of 4 with NET₄Cl. **4** (30 mg, 0.047 mmol) was dissolved in 0.5 mL of CD₂Cl₂ and treated with NET₄Cl (7.8 mg, 0.047 mmol). The reaction mixture was loaded into a NMR tube, and a ¹H NMR spectrum was recorded.

Table 1. Crystallographic Data^a

	2b	4	5
formula	C ₁₅ H ₂₃ Br ₃ Ru	C ₁₇ H ₂₅ Br ₂ F ₃ O ₃ RuS	C ₂₆ H ₄₀ Br ₆ Ru ₂
fw	544.13	627.32	1034.18
cryst size, mm	0.08 × 0.22 × 0.68	0.13 × 0.19 × 0.24	0.07 × 0.21 × 0.44
space group	<i>P</i> 2 ₁ / <i>c</i> (No. 14)	<i>P</i> <i>n</i> <i>m</i> a (No. 62)	<i>P</i> <i>n</i> a2 ₁ (No. 33)
<i>a</i> , Å	12.910(4)	17.424(4)	28.239(8)
<i>b</i> , Å	11.293(4)	11.830(3)	12.564(3)
<i>c</i> , Å	12.615(4)	10.550(3)	9.006(2)
β , deg	105.05(1)		
<i>V</i> , Å ³	1776.1(10)	2174.6(10)	3195.3(14)
<i>Z</i>	4	4	4
ρ_{calc} , g cm ⁻³	2.035	1.916	2.150
<i>T</i> , K	297	300	301
μ , cm ⁻¹	76.2	45.3	84.6
θ_{max} , deg	25	23	25
index ranges	-15 ≤ <i>h</i> ≤ 14, 0 ≤ <i>k</i> ≤ 13, 0 ≤ <i>l</i> ≤ 14	0 ≤ <i>h</i> ≤ 19, 0 ≤ <i>k</i> ≤ 12, 0 ≤ <i>l</i> ≤ 11	0 ≤ <i>h</i> ≤ 33, 0 ≤ <i>k</i> ≤ 14, 0 ≤ <i>l</i> ≤ 10
no. of rflns measd	3299	1771	3230
no. of unique rflns	3123	1604	3012
no. of rflns > 4 σ (<i>F</i>)	2348	919	1957
no. of params	184	144	328
<i>R</i> (<i>F</i>) (<i>F</i> > 4 σ (<i>F</i>))	0.045	0.039	0.049
<i>R</i> (<i>F</i>) (all data)	0.070	0.101	0.099
<i>wR</i> (<i>F</i> ²) (all data)	0.108	0.087	0.084

$$^a R(F) = \sum |F_o| - |F_c| / \sum |F_o|. \quad wR(F^2) = [w(F_o^2 - F_c^2)^2 / \sum wF_o^4]^{0.5}. \quad w^{-1} = \sigma^2(F_o^2) + (g_1P)^2 + g_2P. \quad P = (F_o^2 + 2F_c^2)/3.$$

Reactions of 4 with NET₄Br and NET₄I. These reactions were performed on a scale suitable for a NMR experiment. NMR tubes (5 mm) were charged with **4** (30 mg, 0.047 mmol) in CD₂Cl₂ (0.5 mL). NET₄Br (1 equiv) or NET₄I (1 equiv), respectively, was added, and the samples were transferred to a NMR probe. ¹H NMR spectra were immediately recorded.

X-ray Structure Determination for 2b, 4, and 5. Crystal data and experimental details are given in Table 1. X-ray data were collected on a Philips PW1100 four-circle diffractometer using graphite-monochromated Mo K α (λ = 0.710 69 Å) radiation and the θ - 2θ scan technique (**2b**, **4**) or the ω -scan technique (**5**). Three representative reference reflections were measured every 120 min and used to correct for crystal decay and system instability. Corrections for Lorentz and polarization effects and for absorption were applied. The structures were solved by direct methods.⁸ All non-hydrogen atoms were refined anisotropically, and hydrogen atoms were included in idealized positions.⁹ The structures were refined against *F*². Final positional parameters are given in Tables 2–4.

Results and Discussion

Careful addition of 1 equiv of Br₂ to solutions of **1a** and **1b** in CH₂Cl₂ at -60 °C led to the formation of the η^3 -allyl complexes **2a** and **2b**, respectively, as air-stable solids in >90% yield (Scheme 2). Bromine addition on the diene occurred anti to the coordinated Ru and exclusively at the terminal carbon atoms. A structural view of **2b** (Figure 1), as determined by X-ray diffraction, demonstrates the regio- and stereoselectivity of the underlying process. Very recently analogous Ru(IV) η^3 -allyl complexes have been prepared by the action of acyclic dienes on the polymeric Ru(IV) complex [Ru(η^5 -C₅Me₅)Cl₃]_{*n*}.¹⁰ The authors proposed a cationic Ru(IV) η^4 -diene intermediate to explain the stereochemistry of the reaction products obtained.

(8) Sheldrick, G. M. SHELXS86 Program for the Solution of Crystal Structures; University of Göttingen, Göttingen, Germany, 1986.

(9) Sheldrick, G. M. SHELXL93 Program for Crystal Structure Refinement; University of Göttingen, Göttingen, Germany, 1993.

(10) Masuda, K.; Saitoh, M.; Aoki, K.; Itoh, K. *J. Organomet. Chem.* **1994**, *473*, 285.

(6) Perrin, D. D.; Armarego, W. L. F. *Purification of Laboratory Chemicals*, 3rd ed.; Pergamon: New York, 1988.

(7) Fagan, P. J.; Mahoney, W. S.; Calabrese, J. C.; Williams, I. D. *Organometallics* **1990**, *9*, 1843.

Table 2. Atomic Positional and Isotropic Displacement Parameters (\AA^2) for $\text{Ru}(\eta^5\text{-C}_5\text{Me}_5)(\eta^4\text{-CH}_2\text{CMeCHCH}_2\text{Br})\text{Br}_2$ (2b**)**

	x	y	z	U_{eq}^a
Ru	0.26627(4)	0.42432(4)	0.11890(4)	0.0327(2)
Br(1)	0.38820(8)	0.32604(8)	0.01345(8)	0.0681(4)
Br(2)	0.11733(7)	0.36193(8)	-0.04742(7)	0.0614(3)
Br(3)	0.16594(9)	0.84546(7)	0.10247(9)	0.0773(4)
C(1)	0.2968(6)	0.4355(6)	0.3011(5)	0.039(2)
C(2)	0.3638(6)	0.3472(6)	0.2736(6)	0.043(3)
C(3)	0.2948(7)	0.2541(6)	0.2168(6)	0.046(3)
C(4)	0.1882(6)	0.2855(7)	0.2085(6)	0.051(3)
C(5)	0.1876(6)	0.4002(7)	0.2586(6)	0.046(3)
C(6)	0.3372(8)	0.5312(8)	0.3838(7)	0.069(4)
C(7)	0.4850(6)	0.3449(7)	0.3090(7)	0.059(3)
C(8)	0.3318(9)	0.1359(6)	0.1869(8)	0.074(4)
C(9)	0.0915(8)	0.2090(9)	0.1639(8)	0.085(4)
C(10)	0.0903(7)	0.4547(10)	0.2817(8)	0.081(4)
C(11)	0.3812(7)	0.5690(7)	0.1264(7)	0.057(3)
C(12)	0.2878(7)	0.5903(6)	0.0410(7)	0.049(3)
C(13)	0.1901(7)	0.6019(6)	0.0734(7)	0.052(3)
C(14)	0.1792(7)	0.6820(6)	0.1608(7)	0.055(3)
C(15)	0.2884(9)	0.5959(8)	-0.0782(7)	0.073(4)

$$^a U_{\text{eq}} = \frac{1}{3} \sum_i \sum_j U_{ij} a_i^* a_j^* (\mathbf{a}_i \mathbf{a}_j)$$

Table 3. Atomic Positional and Isotropic Displacement Parameters (\AA^2) for $[\text{Ru}(\eta^5\text{-C}_5\text{Me}_5)(\eta^4\text{-CH}_2\text{CMeCMeCH}_2)\text{Br}_2]\text{CF}_3\text{SO}_3$ (4**)**

	x	y	z	U_{eq}^a
Ru	0.38148(4)	0.2500	0.26054(8)	0.038(1)
Br	0.49084(4)	0.10879(7)	0.25602(9)	0.065(1)
C(1)	0.3884(7)	0.2500	0.4704(10)	0.062(3)
C(2)	0.3451(5)	0.1539(7)	0.4355(7)	0.056(2)
C(3)	0.2767(4)	0.1893(6)	0.3768(6)	0.047(2)
C(4)	0.4600(7)	0.2500	0.5502(11)	0.100(5)
C(5)	0.3626(5)	0.0341(7)	0.4732(8)	0.086(3)
C(6)	0.2103(4)	0.1165(7)	0.3488(8)	0.080(3)
C(7)	0.3206(4)	0.1368(7)	0.1308(7)	0.050(2)
C(8)	0.3722(4)	0.1895(6)	0.0487(6)	0.053(2)
C(9)	0.4277(4)	0.1240(7)	-0.0331(7)	0.074(3)
S	0.7298(2)	0.2500	0.7481(4)	0.065(1)
O(1)	0.7235(6)	0.2500	0.6152(8)	0.122(4)
O(2)	0.7584(3)	0.1482(6)	0.8007(7)	0.111(2)
C(10)	0.6322(7)	0.2500	0.7988(12)	0.070(4)
F(1)	0.6250(5)	0.2500	0.9204(7)	0.135(4)
F(2)	0.5932(3)	0.1620(5)	0.7560(6)	0.118(2)

$$^a U_{\text{eq}} = \frac{1}{3} \sum_i \sum_j U_{ij} a_i^* a_j^* (\mathbf{a}_i \mathbf{a}_j)$$

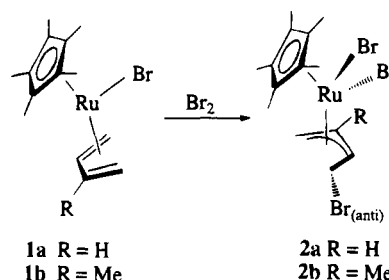
In sharp contrast, the reaction of **1c** does not yield a η^3 -allyl complex but results in the formation of a Ru(IV) η^4 -diene complex in 93% yield, tentatively formulated as $\text{Ru}(\eta^5\text{-C}_5\text{Me}_5)(\eta^4\text{-CH}_2\text{CMeCMeCH}_2)\text{Br}_3$ (**3**; Scheme 3). This formulation is based on elemental analysis and ^1H NMR spectroscopic data. A solution $^{13}\text{C}\{^1\text{H}\}$ NMR spectrum was not available due to the poor solubility as well as stability of **3**. The comparison with the related cationic complex $[\text{Ru}(\eta^5\text{-C}_5\text{Me}_5)(\eta^4\text{-CH}_2\text{-CMeCMeCH}_2)\text{Br}_2]\text{CF}_3\text{SO}_3$ (**4**) described below further supports structure **3**.

The ^1H NMR spectrum of **3** displays the characteristic resonances of the diene ligand. Apart from this, the geminal coupling constants of the CH_2 protons increased from 1.7 Hz in **1c**⁷ to 4.5 Hz. This is indicative of an enhanced sp^3 character of the terminal carbon atoms and points to a metallacyclopentene resonance structure¹¹ rather than that of a classical diene otherwise typical for late-transition-metal η^4 -diene complexes. The values of the geminal coupling constants for terminal CH_2 of $\text{Zr}(\eta^5\text{-C}_5\text{H}_5)_2(\eta^4\text{-CH}_2\text{CMeCMeCH}_2)$ and $\text{Ta}(\eta^5\text{-C}_5\text{Me}_5)_2(\eta^4\text{-CH}_2\text{CMeCMeCH}_2)\text{Cl}_2$ are 10.0 and 7.2 Hz, respectively.^{11b} Several attempts were made to grow

Table 4. Atomic Positional and Isotropic Displacement Parameters (\AA^2) for $[\text{Ru}(\eta^5\text{-C}_5\text{Me}_5)(\eta^4\text{-CH}_2\text{CMeCMeCH}_2)\text{Br}_2][\text{Ru}(\eta^5\text{-C}_5\text{Me}_5)\text{Br}_4]$ (5**)**

	x	y	z	U_{eq}^a
Ru(1)	0.09054(4)	0.25787(8)	0.50000(11)	0.034(1)
Ru(2)	0.37148(4)	0.26543(8)	0.45210(13)	0.042(1)
Br(1)	0.15743(6)	0.12460(12)	0.50579(27)	0.072(1)
Br(2)	0.12142(7)	0.28998(16)	0.23943(19)	0.072(1)
Br(3)	0.41995(6)	0.43635(11)	0.42535(21)	0.061(1)
Br(4)	0.40022(8)	0.24594(19)	0.18430(24)	0.103(1)
Br(5)	0.39404(6)	0.06879(12)	0.44347(27)	0.083(1)
Br(6)	0.41963(5)	0.25404(13)	0.68917(17)	0.053(1)
C(1)	0.1395(5)	0.3796(11)	0.5820(17)	0.046(4)
C(2)	0.1243(6)	0.3198(11)	0.7076(15)	0.045(4)
C(3)	0.0769(5)	0.3385(9)	0.7269(15)	0.037(3)
C(4)	0.0608(5)	0.4092(11)	0.6166(15)	0.037(3)
C(5)	0.1003(5)	0.4331(10)	0.5280(18)	0.052(4)
C(6)	0.1901(5)	0.3908(13)	0.3283(22)	0.082(6)
C(7)	0.1557(7)	0.2654(14)	0.8175(18)	0.091(7)
C(8)	0.0482(5)	0.3071(11)	0.8604(15)	0.059(5)
C(9)	0.0157(5)	0.4685(11)	0.6077(19)	0.069(5)
C(10)	0.1013(6)	0.5177(12)	0.4121(18)	0.086(6)
C(11)	0.0478(6)	0.1414(11)	0.6162(16)	0.049(4)
C(12)	0.0465(5)	0.1014(9)	0.4681(17)	0.044(4)
C(13)	0.0310(5)	0.1721(11)	0.3586(14)	0.036(4)
C(14)	0.0196(4)	0.2753(10)	0.4103(15)	0.041(4)
C(15)	0.0621(5)	-0.0084(10)	0.4285(21)	0.075(5)
C(16)	0.0299(6)	0.1397(11)	0.2036(18)	0.072(5)
C(17)	0.3112(6)	0.3833(13)	0.4613(32)	0.079(7)
C(18)	0.3032(8)	0.3189(22)	0.3502(25)	0.088(7)
C(19)	0.2995(6)	0.2177(14)	0.3967(19)	0.054(5)
C(20)	0.3043(5)	0.2160(14)	0.5608(19)	0.053(5)
C(21)	0.3122(7)	0.3252(19)	0.5979(24)	0.080(7)
C(22)	0.3120(6)	0.5056(12)	0.4733(43)	0.191(17)
C(23)	0.2956(10)	0.3603(23)	0.2010(28)	0.187(15)
C(24)	0.2834(9)	0.1380(21)	0.2939(29)	0.176(16)
C(25)	0.2948(7)	0.1207(18)	0.6563(29)	0.150(12)
C(26)	0.3165(7)	0.3677(28)	0.7527(25)	0.220(21)

$$^a U_{\text{eq}} = \frac{1}{3} \sum_i \sum_j U_{ij} a_i^* a_j^* (\mathbf{a}_i \mathbf{a}_j)$$

Scheme 2

crystals of **3** suitable for X-ray diffraction, but none proved successful.

The different reactivity of **1c** with Br_2 compared to **1a** and **1b** is interesting but difficult to explain with the information at hand. However, we believe that the reactivity difference is electronic rather than steric in origin. Removal of charge from coordinated 1,3-diene ligands by the electron-deficient metal center, typically dominating at the terminal carbon atoms,^{3,4} could be partially compensated for by the electron-releasing effect of the methyl substituents of the diene ligand if this process is charge-controlled. Accordingly, complex **1c** would be less reactive toward nucleophilic attack than complexes **1a** and **1b**.

(11) (a) Krüger, C.; Müller, G.; Erker, G.; Dorf, U.; Engel, K. *Organometallics* **1985**, *4*, 215. (b) Yasuda, H.; Tatsumi, K.; Okamoto, T.; Mashima, K.; Lee, K.; Nakamura, A.; Kai, Y.; Kanehisa, N.; Kasai, N. *J. Am. Chem. Soc.* **1985**, *107*, 2410. (c) Yasuda, H.; Tatsumi, K.; Nakamura, A. *Acc. Chem. Res.* **1985**, *18*, 120. (d) Kingsbury, K. B.; Carter, J. D.; McElwee-White, L.; Ostrander, R. L.; Rheingold, A. L. *Organometallics* **1994**, *13*, 1635.

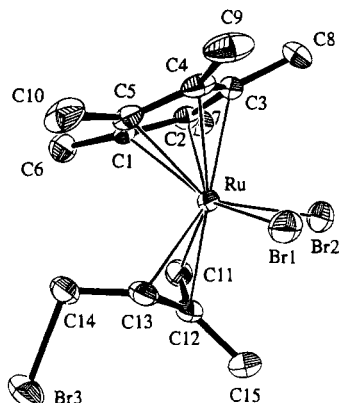


Figure 1. ORTEP drawing of $\text{Ru}(\eta^5\text{-C}_5\text{Me}_5)(\eta^3\text{-CH}_2\text{-CMeCHCH}_2\text{Br})\text{Br}_2$ (**2b**). Selected bond lengths (Å) and angles (deg): Ru–Br(1) = 2.562(1), Ru–Br(2) = 2.550(1), Ru–C(1–5)_{av} = 2.257(7), Ru–C(11) = 2.193(7), Ru–C(12) = 2.168(7), Ru–C(13) = 2.241(7), C(11)–C(12) = 1.413(11), C(12)–C(13) = 1.430(11), C(13)–C(14) = 1.461(11), C(14)–Br(3) = 1.978(7); Br(1)–Ru–Br(2) = 83.5(1), C(11)–C(12)–C(13) = 116.0(7).

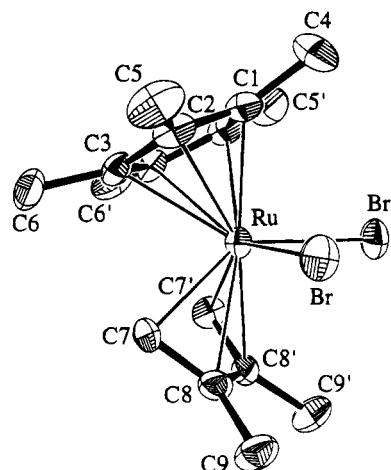
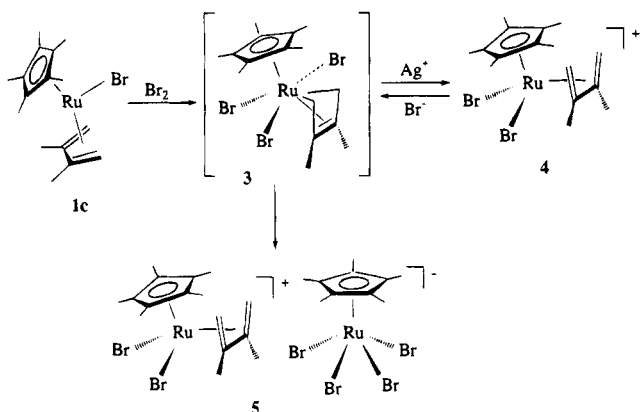


Figure 2. ORTEP drawing of $[\text{Ru}(\eta^5\text{-C}_5\text{Me}_5)(\eta^4\text{-CH}_2\text{-CMeCMeCH}_2)\text{Br}_2]\text{CF}_3\text{SO}_3$ (**4**). Selected bond lengths (Å) and angles (deg): Ru–Br = 2.534(1), Ru–C(1–3)_{av} = 2.263(8), Ru–C(7) = 2.190(7), Ru–C(8) = 2.352(7), C(7)–C(8) = 1.396(9), C(8)–C(8') = 1.431(15), C(8)–C(9) = 1.510(9); Br–Ru–Br' = 82.46(5).

Scheme 3



Addition of AgCF_3SO_3 (1 equiv) converts complex **3** to the novel cationic complex **4** in 74% isolated yield. It is worth mentioning, however, that bromine abstraction was not possible by simple metathesis with $\text{NBu}_4\text{CF}_3\text{SO}_3$. Characterization of **4** was by elemental analysis and ^1H NMR and $^{13}\text{C}\{^1\text{H}\}$ NMR spectroscopy as follows. The ^1H NMR spectrum resembles that of **3**. The major difference is a substantial upfield shift for both syn and anti CH_2 protons of the diene ligand to 3.65 ppm (d, 2H, $J = 1.7$ Hz), and 2.53 ppm (d, 2H, $J = 1.7$ Hz), respectively, while the resonance of the methyl groups of the diene moiety is downfield-shifted to 2.72 ppm (s, 6H, Me). These differences in shifts are significant and cannot be explained merely by a counterion effect. Furthermore, **4** exhibits a smaller geminal coupling constant than **3**, attesting to the much poorer sp^3 character of the terminal carbon atoms. The $^{13}\text{C}\{^1\text{H}\}$ NMR spectrum of **4** shows singlets at 140.7 (internal diene C atoms), 116.0 (C_5Me_5), 72.0 (terminal diene C atoms), 22.2 (Me), and 12.4 ppm (C_5Me_5), respectively (cf. the $^{13}\text{C}\{^1\text{H}\}$ NMR spectrum of **1c**:⁷ 101.5 (internal diene C atoms), 96.0 (C_5Me_5), 55.3 (terminal diene C atoms), 18.7 (Me), 9.4 (C_5Me_5)). The marked downfield chemical shifts are indicative of the high oxidation state of the ruthenium center.

The structure of **4** has been confirmed by X-ray crystallography (see Figure 2). The internal bond of the

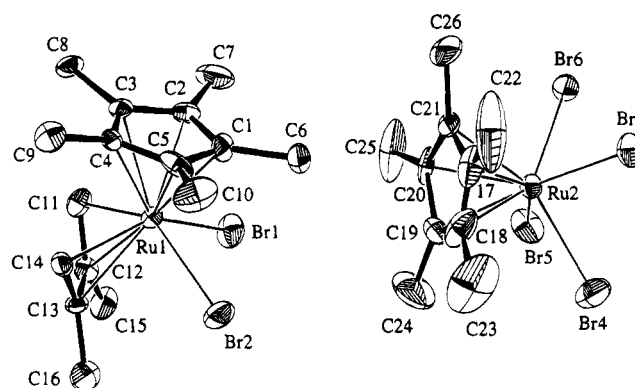


Figure 3. ORTEP drawing of $[\text{Ru}(\eta^5\text{-C}_5\text{Me}_5)(\eta^4\text{-CH}_2\text{-CMeCMeCH}_2)\text{Br}_2][\text{Ru}(\eta^5\text{-C}_5\text{Me}_5)\text{Br}_4]^-$ (**5**). Selected bond lengths (Å) and angles (deg): Ru(2)–Br(3) = 2.558(2), Ru(2)–Br(4) = 2.557(2), Ru(2)–Br(5) = 2.553(2), Ru(2)–Br(6) = 2.535(2), Ru(2)–C(17–21)_{av} = 2.231(18); Br(3)–Ru(2)–Br(5) = 132.1(1), Br(4)–Ru(2)–Br(6) = 128.2(1).

diene ligand of **4** (C(8)–C(8') = 1.431(15) Å) is longer than the terminal bonds (C(7)–C(8) = 1.396(9) Å), in agreement with a diene resonance structure. On the other hand, the significantly shorter Ru–C bonds to the terminal (Ru–C(7) = 2.190(7) Å) than to the internal carbon atoms (Ru–C(8) = 2.352(7) Å) are consistent with metallacyclopentene resonance structures drawn for complexes of electron-deficient early transition metals.¹¹

Noteworthy, **3** is quantitatively recovered when NEt_4Br (1 equiv) is added to **4**, as monitored by ^1H NMR spectroscopy (Scheme 3), while no reaction took place with NEt_4Cl (1 equiv). Surprisingly, on addition of NEt_4I (1 equiv) 2,3-dimethyl-1,3-butadiene was quantitatively liberated. In contrast to **4**, which is stable, **3** decomposes in solution within a matter of hours to several products, most of them as yet not identified. One of the decomposition products could be characterized crystallographically as $[\text{Ru}(\eta^5\text{-C}_5\text{Me}_5)(\eta^4\text{-CH}_2\text{-CMeCMeCH}_2)\text{Br}_2][\text{Ru}(\eta^5\text{-C}_5\text{Me}_5)\text{Br}_4]^-$ (**5**), as depicted in Figure 3, showing a novel $[\text{Ru}(\eta^5\text{-C}_5\text{Me}_5)\text{Br}_4]^-$ anion with a nearly regular RuBr_4^- square pyramid. These results provide

some further evidence for complex **3** containing three bromide ions coordinated at the ruthenium center.

In summary, our preliminary investigations of the reactivity of $\text{Ru}(\eta^5\text{-C}_5\text{Me}_5)(\eta^4\text{-diene})\text{Br}$ complexes revealed a new synthetic approach to bromo-substituted $\text{Ru(IV)} \eta^3$ -allyl complexes. Moreover, a novel cationic $\text{Ru(IV)} \eta^4$ -diene complex has been prepared and crystallographically characterized as the first group 8 transition-metal complex approaching a metallacyclopentene resonance structure. Further reactivity studies of $\text{Ru}(\eta^5\text{-C}_5\text{R}_5)(\eta^4\text{-diene})\text{Br}$ and $\text{Ru}(\eta^5\text{-C}_5\text{R}_5)(\eta^3\text{-allyl})\text{Br}_2$ complexes ($\text{R} = \text{H, Me}$), including density functional

calculations, are in progress and will be the subject of a forthcoming paper.

Acknowledgment. Financial support by the "Fonds zur Förderung der wissenschaftlichen Forschung" is gratefully acknowledged (Project No. 9825).

Supplementary Material Available: Listings of hydrogen atomic coordinates, anisotropic temperature factors, complete bond lengths and angles, and least-squares planes for complexes **2b**, **4**, and **5** (19 pages). Ordering information is given on any current masthead page.

OM940793W

**(C₅H_{5-n}Me_n)₂TiCl₂/Mg/Me₃SnC≡CSnMe₃ (n = 0, 2–5)
Systems. Formation and Crystal Structures of
(C₅Me₅)₂Ti(η²-Me₃SnC≡CSnMe₃) and
[(C₅H_{5-n}Me_n)₂Ti(μ-η²:η¹-C≡CSnMe₃)₂ (n = 0, 2) Complexes**

Vojtech Varga,[†] Karel Mach,^{*†} Jörg Hiller,[‡] Ulf Thewalt,[‡] Petr Sedmera,[§] and
Miroslav Polášek[†]

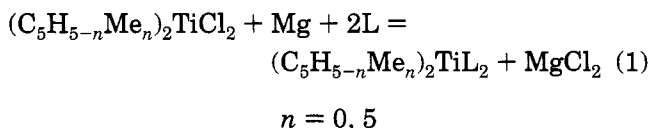
*J. Heyrovský Institute of Physical Chemistry, Academy of Sciences of the Czech Republic,
Dolejškova 3, 182 23 Prague 8, Czech Republic, Sektion für Röntgen- und Elektronenbeugung,
Universität Ulm, D-89069 Ulm, Germany, and Institute of Microbiology, Academy of Sciences
of the Czech Republic, 142 20 Prague 4, Czech Republic*

Received October 24, 1994[®]

The reduction of (C₅H_{5-n}Me_n)₂TiCl₂ (n = 0, 2–5) by Mg in THF and in the presence of bis(trimethylstannyl)acetylene affords mainly single products for n = 0, 2, and 5, which were isolated and characterized. X-ray structure analyses proved the compounds to be the monomeric Ti(II) complex (C₅Me₅)₂Ti[η²-C₂(SnMe₃)₂] (**1**; monoclinic, C2/c, No. 15 (Z = 4), a = 15.879(15) Å, b = 11.851(11) Å, c = 17.555(13) Å, and β = 109.60(5)°), and the diamagnetic dimeric Ti(III) compounds [(C₅H₅)₂Ti(μ-η²:η¹-C≡CSnMe₃)₂] (**2**; orthorhombic, Pbc_a, No. 61 (Z = 4), a = 14.846(2) Å, b = 13.119(2) Å, and c = 15.107(2) Å) and [(C₅H₃Me₂)₂Ti(μ-η²:η¹-C≡CSnMe₃)₂] (**3**; monoclinic, P2₁/n, No. 14 (Z = 2), a = 10.789(3) Å, b = 9.976(2) Å, c = 17.289(2) Å, and β = 98.98(1)°). Compounds **2** and **3** arise from the oxidative addition of C₂(SnMe₃)₂ to a titanocene(II) species followed by thermal elimination of the SnMe₃ radical, yielding Sn₂Me₆. The molecular structures of all the compounds are very similar to those of analogous trimethylsilyl-substituted compounds. The systems for n = 3 and 4 afford mixtures of unidentified products which are different from structural types of **1** and **2** or **3**, as indicated by the infrared data.

Introduction

The reduction of titanocene and permethyltitanocene dichlorides by metallic magnesium in THF generates titanocene species which in the presence of suitable ligands (L) are stabilized by coordination (eq 1). Such



a synthetic pathway has been used for the preparation of titanocene and permethyltitanocene dicarbonyls¹ and phosphines.² In the presence of gaseous nitrogen as a ligand the titanocene systems were found to fix nitrogen in substoichiometric quantities.³ In the presence of 1 equiv of an internal acetylene, titanocene-acetylene complexes (C₅H_{5-n}Me_n)₂Ti[η²-C₂(R)₂] were obtained for n = 0, 5.⁴ Further reaction of these complexes with excess acetylene afforded titanacyclopentadiene complexes for the C₅H₅ complexes and for the acetylenes containing less bulky substituents, e.g., 2-butyne and diphenylacetylene.^{4d,e} The (C₅Me₅)₂Ti(η²-C₂Ph)₂ complex is, however, unreactive toward diphenylacetylene.⁵

Among acetylenes with bulky substituents, bis(trimethylsilyl)acetylene appeared to be the most suitable for the preparation of the whole series of (C₅H_{5-n}Me_n)₂-Ti[η²-C₂(SiMe₃)₂] (n = 0–5) complexes.^{4b,6} The X-ray crystal structures are known for (C₅Me₅)₂Ti[η²-C₂(SiMe₃)₂]^{4a} and (C₅HMe₄)₂Ti[η²-C₂(SiMe₃)₂]⁶ and also for the phenyl(trimethylsilyl)acetylene complexes (C₅H₅)₂-Ti[η²-C₂(SiMe₃)Ph] and (C₅Me₅)₂Ti[η²-C₂(SiMe₃)Ph].^{4c} The parent complex of the series (C₅H₅)₂Ti[η²-C₂(SiMe₃)₂]^{4b} and all other methyl-substituted cyclopentadienyl derivatives⁶ were characterized by spectroscopic methods. Attempts to apply 1,4-bis(trimethylsilyl)buta-1,3-diyne as an acetylene ligand in the (C₅H_{5-n}Me_n)₂TiCl₂/Mg/THF systems afforded products whose structures indicated a cleavage of the diyne. The dimeric acetylide complex [(C₅H₅)₂Ti(C≡SCiMe₃)₂] was obtained from (C₅H₅)₂TiCl₂^{7a} and the tweezer complex [(η⁵-C₅HMe₄)₂Ti(η¹-C≡CSiMe₃)₂]⁻[Mg(THF)Cl]⁺, with the Mg atom embedded between two acetylide arms,

(4) (a) Shur, V. B.; Burlakov, V. V.; Vol'pin, M. E. *J. Organomet. Chem.* **1988**, *347*, 77–83. (b) Burlakov, V. V.; Polyakov, A. B.; Yanovsky, A. I.; Struchkov, Yu. T.; Shur, V. B.; Vol'pin, M. E.; Rosenthal, U.; Görls, H. *J. Organomet. Chem.* **1994**, *476*, 197–206. (c) Rosenthal, U.; Görls, H.; Burlakov, V. V.; Shur, V. B.; Vol'pin, M. E. *J. Organomet. Chem.* **1992**, *426*, C53–C57. (d) Shur, V. B.; Bernadyuk, S. Z.; Burlakov, V. V.; Andrianov, V. G.; Yanovsky, A. I.; Struchkov, Yu. T.; Vol'pin, M. E. *J. Organomet. Chem.* **1983**, *243*, 157–163. (e) Shur, V. B.; Berkovich, E. G.; Vol'pin, M. E.; Lorenz, B.; Wahren, M. *J. Organomet. Chem.* **1982**, *228*, C36–C38.

(5) Cohen, S. A.; Bercaw, J. E. *Organometallics* **1985**, *4*, 1006–1014. (6) Varga, V.; Mach, K.; Polášek, M.; Sedmera, P.; Hiller, J.; Thewalt, U.; Troyanov, S. I. *J. Organomet. Chem.*; submitted for publication. (7) (a) Rosenthal, U.; Görls, H. *J. Organomet. Chem.* **1992**, *439*, C36–C41. (b) Troyanov, S. I.; Varga, V.; Mach, K. *Organometallics* **1993**, *12*, 2820–2824.

[†] J. Heyrovský Institute.

[‡] Universität Ulm.

[§] Institute of Microbiology.

[®] Abstract published in *Advance ACS Abstracts*, February 15, 1995.

(1) Sikora, D. J.; Macomber, J. W.; Rausch, M. D. *Adv. Organomet. Chem.* **1986**, *25*, 317–379.

(2) Fryzuk, M. D.; Haddad, T. S.; Berg, D. J. *Coord. Chem. Rev.* **1990**, *99*, 137–212.

(3) (a) Vol'pin, M. E. *J. Organomet. Chem.* **1980**, *200*, 319–334. (b) Bayer, E.; Schurig, V. *Chem. Ber.* **1969**, *102*, 3378–3390.

from $(C_5HMe_4)_2TiCl_2$.^{7b} On the other hand, 1,4-diphenyl-1,3-butadiyne,^{8a} 1,4-di-*tert*-butyl-1,3-butadiyne, and mixed *tert*-butyl-trimethylsilyl and phenyl-trimethylsilyl 1,3-diyne yield binuclear titanocene complexes containing a μ -(1-3- η):(2,4- η)-*trans,trans*-butadiene bridging unit.^{8b} The reason for the different products obtained has to be sought in the electron donation effect of both the Me groups at the cyclopentadienyl ligands and the SiMe₃ groups at the diyne as well as in the steric effects of all substituents in the formation of products. In contrast, bis(trimethylstannyl)acetylene has not yet been used as a ligand in titanocene chemistry, where only a few tin-containing complexes are known. Those containing a titanium-tin bond were obtained for the triphenylstannyl ligand,^{9a-c} and the X-ray structure of $(C_5H_5)_2Ti(SnPh_3)Cl$ was determined.^{9d} Of others, only (trimethylstannyl)methyl derivatives¹⁰ and 1,3-metallacyclobutane complex, $(C_5H_5)_2Ti(\eta\text{-}CH_2)_2\text{-}SnMe_2$, are known.¹¹

In this work the behavior of bis(trimethylstannyl)acetylene as a ligand in the $(C_5H_5-nMe_n)_2TiCl_2/Mg/THF$ ($n = 0, 2-5$) systems is described and the main reaction products are characterized by X-ray crystal structures.

Experimental Section

General Data. Manipulation with all air-sensitive reagents, syntheses, isolation, and spectroscopic measurements were carried out under vacuum using all-sealed devices equipped with breakable seals. The solvents THF, hexane, and toluene were purified by conventional methods, dried by refluxing over LiAlH₄, and stored as solutions of the dimeric titanocene $(C_{10}H_8)[(C_5H_5/TiH)_2]$.¹² Bis(trimethylstannyl)acetylene, $C_2(SnMe_3)_2$, was synthesized from Me_3SnCl and sodium acetylide (Aldrich) in liquid ammonia.¹³ Its purity was checked by MS analysis and NMR and IR spectra. Magnesium turnings (Fluka, purum for Grignard reactions) were used without preactivation. Commercial $(C_5H_5)_2TiCl_2$ (Fluka) was purified by extraction with hot toluene followed by crystallization from the concentrated toluene extract. Bis(1,3-dimethylcyclopentadienyl)titanium dichloride, $(C_5H_3Me_2)_2TiCl_2$,¹⁴ and the C_5Me_5 , C_5HMe_4 , and $C_5H_2Me_3$ (1,2,3-trimethyl) derivatives were prepared according to literature procedures.¹⁵ The $(C_5H_5)_2Ti[\eta^2\text{-}C_2(SiMe_3)_2]$ and $(C_5H_3Me_2)_2Ti[\eta^2\text{-}C_2(SiMe_3)_2]$ complexes were synthesized as recently described.¹⁴ ¹H and ¹³C NMR spectra were measured on a Varian VXR-400 spectrometer (400 and 100 MHz, respectively) in C_6D_6 at 25 °C. Chemical shifts (given in the δ scale) were referenced to the solvent signal (δ_H 7.15 ppm, δ_C 128.0 ppm). EPR spectra were recorded on an ERS-220 spectrometer (German Academy of Sciences, Berlin) in the X-band at room temperature. Values of g factors were determined using a Mn^{2+} ($M_I = -1/2$ line) standard at $g = 1.9860$ and a MJ-110 R proton magnetometer

(Radiopan, Poznan, Poland). Infrared spectra of hexane solutions were recorded on a UR-75 instrument (Zeiss, Jena, Germany) using KBr cuvettes filled under argon. KBr pellets of crystalline samples were prepared under purified nitrogen in a glovebox (Braun) and were measured in an air-protecting cuvette on a Mattson Galaxy 2020 IR spectrometer. UV-vis spectra were recorded on a Varian Cary 17D spectrometer in the range 270–2000 nm using all-sealed quartz cells (Hellma).

Preparation of $(C_5Me_5)_2Ti[\eta^2\text{-}C_2(SnMe_3)_2]$ (1). $(C_5Me_5)_2TiCl_2$ (0.389 g, 1 mmol) and Mg turnings (24 mg, 1 mmol) were weighed in an ampule equipped with breakable seals, and the ampule was evacuated on a vacuum line. THF (20 mL) was distilled in, and a solution of $C_2(SnMe_3)_2$ in toluene (0.5 M, 2 mL) was added from an attached ampule. The mixture was stirred for 48 h until all magnesium was consumed. All solvents were evaporated under vacuum, and a residue was extracted with hexane. The yellow hexane solution was concentrated and cooled by an acetone/solid- CO_2 mixture. Yellow crystals were separated and dissolved in the same solvent distilled back from the mother liquor. This solution was used to grow crystals for the X-ray analysis and for spectral measurements. The MS of the solid obtained by evaporation of the mother liquor and IR of the mother liquor gave, however, virtually the same spectra as the samples prepared from the crystalline material. The yield of yellow crystalline **1** is 0.34 g (50% based on titanium). **1**: ¹H NMR (C_6D_6) δ 0.09 (s, 18 H), 1.63 (s, 30 H); ¹³C NMR (C_6D_6) δ -4.6 (q, 6 C), 12.4 (q, 10 C), 121.3 (s, 10 C), 244.5 (s, 2 C); UV-near-IR (hexane, 23 °C) 920 nm; MS (70 eV, direct inlet, 120–143 °C; m/e (%)) 672 (M^{++} for $C_{28}H_{48}^{48}Ti^{120}Sn_2$; not observed), 507 ($M - SnMe_3$; 1.0), 339 ($M - (Cp^*Ti + Me)$; 2.0), 318 (Cp^*Ti ; 53), 317 (100), 315 (35), 313 (14); IR (hexane) $\nu(C\equiv C)$ 1580 cm^{-1} . Anal. Calcd for $C_{28}H_{48}Sn_2Ti$: C, 50.2; H, 7.2. Found: C, 49.8; H, 6.9.

Preparation of $[(C_5H_5)_2Ti(\mu\text{-}\eta^2\text{-}\eta^1\text{-}C\equiv CSnMe_3)]_2$ (2). $(C_5H_5)_2TiCl_2$ (0.249 g, 1 mmol) and Mg turnings (24 mg, 1 mmol) were charged into an ampule equipped with a magnetic Teflon-coated stirrer and evacuated. THF (20 mL) was distilled in on a vacuum line, and a solution of $C_2(SnMe_3)_2$ in toluene (0.5 M, 2 mL) was added from an attached ampule. The mixture was stirred at room temperature for 24 h. The bright red solution changed through violet to a final brown-red, at which point all magnesium was consumed. All volatiles were evaporated overnight into a trap cooled by liquid nitrogen, and a dark orange residue was extracted with hexane. A crop of brown-red crystals of **2** was obtained by cooling of the concentrated hexane solution; yield 0.30 g (0.4 mmol, 80% based on titanium). **2**: ¹H NMR (C_6D_6) δ 0.32 (s, 18 H, $SnMe_3$, satellites $J(^1H,^{117}Sn) = 52.9$ Hz and $J(^1H,^{119}Sn) = 55.4$ Hz), 5.18 (s, 20 H, Cp); ¹³C NMR (C_6D_6) δ -6.8 (q, 6 C), 104.6 (d, 20 C), 139.7 (s, 2 C), 236.1 (s, 2 C); UV-vis (hexane, 23 °C) 472 nm; MS (70 eV, direct inlet, 160–190 °C; m/e (%)) 734 (M^{++} for $C_{30}H_{38}^{48}Ti_2^{120}Sn_2$; 1.5), 569 ($M - SnMe_3$; 2.5), 541 ($M - (Cp_2Ti + Me)$; 1.5), 391 (2.0), 380 (4.0), 178 (Cp_2Ti ; 100), 165 ($SnMe_3$; 2), 113 ($CpTi$; 5.5); IR (toluene) $\nu(C\equiv C)$ 1766 cm^{-1} ; IR (KBr) 1768 cm^{-1} . Anal. Calcd for $C_{30}H_{38}Sn_2Ti_2$: C, 49.2; H, 5.2. Found: C, 48.8; H, 5.1.

The volatiles collected from the reaction mixture were carefully evaporated at room temperature to leave a colorless liquid. This was identified by GCMS to be Sn_2Me_6 . Commercial Sn_2Me_6 (Aldrich) was measured as a reference, showing the same peak intensity pattern.

Preparation of **2 from $(C_5H_5)_2Ti[\eta^2\text{-}C_2(SiMe_3)_2]$ and $C_2(SnMe_3)_2$.** A solution of $C_2(SnMe_3)_2$ (0.3 mmol) in toluene (10 mL) was added to a solution of $(C_5H_5)_2Ti[\eta^2\text{-}C_2(SiMe_3)_2]$ (0.3 mmol) in hexane (12 mL) in an ampule with an attached quartz cell ($d = 0.2$ mm). The decrease in the concentration of $(C_5H_5)_2Ti[\eta^2\text{-}C_2(SiMe_3)_2]$ was followed by absorption spectroscopy in the near-IR region. The absorption band at 1060 nm disappeared after 2 days at room temperature, and the color changed from yellow to red. All volatiles were evaporated at 60 °C and collected in a trap cooled by liquid nitrogen. The

(8) Sekutowski, D. G.; Stucky, G. D. *J. Am. Chem. Soc.* **1976**, *98*, 1376–1382. (b) Rosenthal, U.; Ohff, A.; Tillack, A.; Baumann, W. *J. Organomet. Chem.* **1994**, *468*, C4–C8.

(9) (a) Coutts, R. S. P.; Wailes, P. C. *Chem. Commun.* **1968**, 260–261. (b) Kingston, B. M.; Lappert, M. F. *J. Chem. Soc., Dalton Trans.* **1972**, 69–73. (c) Creemers, H. M. J. C.; Verbeek, F.; Noltes, J. G. *J. Organomet. Chem.* **1968**, *15*, 125–130. (d) Zheng, W.; Stephan, D. W. *Inorg. Chem.* **1988**, *27*, 2386–2388.

(10) Jeffery, J.; Lappert, M. F.; Luong-Thi, N. T.; Webb, M.; Atwood, J. L.; Hunter, W. E. *J. Chem. Soc., Dalton Trans.* **1981**, 1593–1605. (11) van de Heistee, B. J. J.; Schat, G.; Akkerman, O. S.; Bickelhaupt, F. *J. Organomet. Chem.* **1986**, *308*, 1–10.

(12) Antropiusová, H.; Dosedlová, A.; Hanuš, V.; Mach, K. *Transition Met. Chem.* **1981**, *6*, 90–93.

(13) Beermann, C.; Hartmann, H. *Z. Anorg. Allg. Chem.* **1954**, *276*, 20–32.

(14) Varga, V.; Mach, K.; Schmid, G.; Thewalt, U. *J. Organomet. Chem.* **1994**, *475*, 127–137.

(15) Mach, K.; Varga, V.; Antropiusová, H.; Poláček, J. *J. Organomet. Chem.* **1987**, *333*, 205–215.

residue was washed out with a minimum amount of hexane to remove traces of unreacted $(C_5H_5)_2Ti[\eta^2-C_2(SiMe_3)_2]$. The remainder was then completely dissolved in warm hexane and crystallized by cooling. Crystalline **2** obtained in this way was, according to all spectroscopic methods, identical with that obtained by the above method; yield 0.18 g (0.25 mmol, 83%). GC analysis of the volatiles revealed the presence of $C_2(SiMe_3)_2$ and Sn_2Me_6 in amounts corresponding to a nearly quantitative reaction.

Preparation of $[(C_5H_3Me_2)_2Ti(\mu-\eta^2:\eta^1-C\equiv CSnMe_3)]_2$ (3**).** $(C_5H_3Me_2)_2TiCl_2$ (0.305 g, 1 mmol) and Mg turnings (24 mg, 1 mmol) were charged into an ampule equipped with a magnetic Teflon-coated stirrer and evacuated. THF (20 mL) was distilled in on a vacuum line, and the solution of $C_2(SnMe_3)_2$ in toluene (0.5 M, 2 mL) was added from an attached ampule. The mixture was stirred at room temperature for 24 h. A purple solution was obtained, at which point all magnesium was consumed. Additionally, the solution was heated to 60 °C for 10 h without any change in color. All the solvents were distilled off at 60 °C overnight into a trap cooled by liquid nitrogen. A dark red residue was extracted with hexane. A crop of dark purple crystals of **3** was obtained by cooling of the concentrated hexane solution; yield 0.28 g (0.33 mmol, 66% based on titanium). **3**: 1H NMR (C_6D_6) δ 0.37 (s, 18 H, $SnMe_3$, satellites $J(^1H, ^{117}Sn) = 51.3$ Hz, $J(^1H, ^{119}Sn) = 53.7$ Hz), 1.91 (s, 6 H, Me), 2.18 (s, 6 H, Me), 4.69 (m, 2 H, Cp), 4.72 (t, 2 H, $J = 2.4$ Hz, Cp), 5.08 (m, 2 H, Cp); ^{13}C NMR (C_6D_6) δ -4.0 (q, 6 C, satellites $J(^{13}C, ^{117}Sn) = 340.5$ Hz, $J(^{13}C, ^{119}Sn) = 356.1$ Hz), 16.8 (q, 4 C), 106.8 (d, 4 C), 108.1 (d, 2 C), 114.2 (s, 4 C), 140.8 (s, 2 C), 242.0 (s, 2 C) (the asymmetry of protons of $C_5H_3Me_2$ rings may arise from the absence of free rotation of $C_5H_3Me_2$ ligands; however, this phenomenon was not observed in the ^{13}C NMR spectrum); UV-vis (toluene, 23 °C) 430 sh, 493 nm; MS (70 eV, direct inlet, 90–250 °C; m/e [assignment]) only fragmentation ions 234 [$(C_5H_3Me_2)_2Ti$] $^+$, 165 [$SnMe_3$] $^+$, 140 [$(C_5H_3Me_2)_2Ti - H$] $^+$ were observed at 90 °C and more extensive decomposition occurred at higher temperatures; IR (toluene) $\nu(C\equiv C)$ 1742 cm^{-1} ; IR (KBr) 1740 cm^{-1} . Anal. Calcd for $C_{38}H_{54}Sn_2Ti_2$: C, 54.1; H, 6.4. Found: C, 53.8; H, 6.2.

Preparation of **3 from $(C_5H_3Me_2)_2Ti[\eta^2-C_2(SiMe_3)_2]$ and $C_2(SnMe_3)_2$.** The procedure using equimolar quantities (0.3 mmol) of both reagents was analogous as for the preparation of **2**. The consumption of $(C_5H_3Me_2)_2Ti[\eta^2-C_2(SiMe_3)_2]$ was followed by the disappearance of the absorption band at 985 nm. The yield of crystalline **3** was 0.2 g (0.255 mmol, 85%). GC analysis of the volatiles gave quantities of $C_2(SiMe_3)_2$ and Sn_2Me_6 similar to those found from the preparation of **2**.

Reactions in the $(C_5HMe_4)_2TiCl/Mg/THF/C_2(SnMe_3)_2$ System. The procedure analogous to that used for obtaining **2** and **3** yielded a mixture of products which could not be isolated in a pure state. The infrared spectra of the reaction mixture after 2 days showed that $C_2(SnMe_3)_2$ was decomposed (the absence of $\nu(Sn-C\equiv)$ at 599 cm^{-1}), and GC analysis revealed Sn_2Me_6 in the volatiles. In the region above 1700 cm^{-1} , medium-intensity bands were observed at 1796, 1819, 1860, 1913, and 1950 cm^{-1} which, together with strong bands indicating the presence of $SnMe_3$ groups at 502 and 522 cm^{-1} ($\nu(Sn-CH_3)$) and at 1182 cm^{-1} ($\delta(CH_3)$), can be attributed to different titanocene acetylide species. These species are, however, different from the dimer analogous to **2** or **3**, which should have an absorption band below 1740 cm^{-1} (cf. the band positions of **2** and **3**).

Reactions in the $(C_5H_2Me_3)_2TiCl_2/Mg/THF/C_2(SnMe_3)_2$ System. The experiment conducted in the same way as that for $(C_5HMe_4)_2TiCl_2$ afforded analogous results. All $C_2(SnMe_3)_2$ was consumed, and Sn_2Me_6 was formed. The presence of probably monomeric titanocene acetylides was indicated by medium-intensity bands at 1836, 1868, 1920, and 1955 cm^{-1} . No individual compounds were isolated from the mixture.

EPR Investigation of the Reaction Solutions. The final reaction solutions contained paramagnetic impurities in amounts estimated to be lower than a few percent. A more

Table 1. Crystallographic Data

	1	2	3
mol formula	$C_{28}H_{48}Sn_2Ti$	$C_{30}H_{38}Sn_2Ti_2$	$C_{38}H_{54}Sn_2Ti_2$
mol wt	669.95	731.77	843.98
cryst syst	monoclinic	orthorhombic	monoclinic
space group	$C2/c$, No. 15	$Pbca$, No. 61	$P2_1/n$, No. 14
a , Å	15.879(15)	14.846(2)	10.789(3)
b , Å	11.851(11)	13.119(2)	9.976(2)
c , Å	17.555(13)	15.107(2)	17.289(2)
β , deg	109.60(5)	90	98.98(1)
V , Å ³	3112(7)	2942(1)	1838(1)
Z	4	4	2
D_{calcd} , g cm^{-3}	1.43	1.65	1.52
cryst size, mm	$0.4 \times 0.4 \times 0.3$	$0.5 \times 0.4 \times 0.3$	$0.4 \times 0.3 \times 0.1$
μ (Mo $K\alpha$), cm^{-1}	17.1	20.6	16.5
2θ range, deg	<44	<50	<50
no. of rflns collectd	1863	2811	3456
no. of rflns with $F_o \geq n\sigma(F_o)$	1297 ($n = 1$)	2340 ($n = 2$)	1396 ($n = 2$)
no; of params refnd	142	156	120
R	0.062	0.048	0.049
R_w	0.062	0.066	0.051
max $\Delta\rho$ in final ΔF map, e Å ⁻³	0.66	0.65	0.95

intense component formed a single line at $g = 1.977-1.979$; $\Delta H = 4-7$ G. A less intense component displayed a single line showing a small coupling to the Ti isotopes ^{49}Ti and ^{47}Ti (natural abundance 5.51 and 7.75%, respectively), $a_{Ti} = 3.0$ G, and a coupling to ^{117}Sn and ^{119}Sn isotopes (natural abundance 7.67% and 8.68%, respectively). The latter species showed a marginal decrease in g value from 1.9950 for the C_5H_5 compound to 1.9945 for the C_5Me_5 compound. The C_5H_5 compound showed $a_{Sn(av)} = 57$ G and the superhyperfine splitting $a = 0.6$ G due to coupling to a number of equivalent protons. The splitting due to the tin isotopes was best resolved for the C_5Me_5 species: $a(^{117}Sn) = 78.6$ G and $a(^{119}Sn) = 82.5$ G, the values being in the ratio of nuclear magnetic moments ($\mu = -0.9951$ and -1.0411 $e\hbar/4\pi mc$, respectively). The EPR spectra are, however, insufficient for the identification of the species. Low values of $a(Sn)$ coupling are probably at variance with an assignment to $(C_5H_5-nMe_n)_2TiSnMe_3$ compounds.¹⁶

X-ray Crystal Structure Analyses of 1-3. Crystal fragments were mounted into Lindemann glass capillaries under purified nitrogen in a glovebox (Braun) and were sealed by wax. The X-ray measurements for **2** were carried out on a Philips PW 1100 four-circle diffractometer. Single crystals of **1** and **3** were measured on the same instrument, which was in the meantime equipped with a STOE electronic control system. In all cases, intensity data were collected by the $\theta/2\theta$ mode using graphite-monochromated Mo $K\alpha$ radiation ($\lambda = 0.71069$ Å) at room temperature. Intensities of three check reflections decreased by about one-third of their starting intensities during the data collection for **1**; therefore, a time-dependent intensity correction was applied. Crystals of **2** and **3** did not show any decomposition. Crystallographic data for **1-3** are summarized in Table 1.

The structures of **1** and **2** were solved by iterative symbolic addition (ISA),¹⁷ and the structure of **3** was solved by the Patterson method. Positional and anisotropic thermal parameters of all non-hydrogen atoms in **1** and **2** were refined by the least-squares method. In **3**, anisotropic temperature factors were assigned to all atoms except those of the dimethylcyclopentadienyl ligands, since one of them showed positional

(16) In a mixture of $LiSnMe_3$ and $[(C_5H_5)_2TiCl]_2$ a stable green compound was formed showing the following EPR parameters: $g = 1.9838$, $\Delta H = 2.0$ G, $a(Ti) = 6.8$ G, $a(^{117}Sn) = 144.4$ G, and $a(^{119}Sn) = 151.4$ G.

(17) Brüggemann, R.; Debaerdemaeker, T.; Müller, B.; Schmid, G.; Thewalt, U. ULM-Programmsystem (1. Jahrestagung der Deutschen Gesellschaft für Kristallografie, Mainz, Germany, June 9-12, 1992; Preprint of Suppl. 5, *Z. Kristallogr.*, p 33) which includes the SHELX-76 Program for Crystal Structure Determination; Sheldrick, G. M. University of Cambridge: Cambridge, England, 1976.

Table 2. Atomic Coordinates and Equivalent Isotropic Temperature Factors (\AA^2) for the Non-Hydrogen Atoms in **1**^a

atom	x	y	z	U_{eq}
Sn(1)	0.0044(1)	0.3729(1)	0.1287(1)	0.051(1)
Ti(1)	0.0000	0.0788(2)	0.2500	0.036(1)
C(1)	0.0015(8)	0.2466(9)	0.2128(6)	0.048(1)
C(2)	0.125(1)	0.466(1)	0.1636(9)	0.120(1)
C(3)	-0.101(1)	0.489(1)	0.112(1)	0.071(1)
C(4)	-0.012(2)	0.300(1)	0.0137(9)	0.122(1)
C(5)	0.1491(8)	0.079(1)	0.2460(8)	0.044(1)
C(51)	0.181(1)	0.150(2)	0.189(1)	0.045(1)
C(6)	0.1195(9)	-0.031(1)	0.2322(7)	0.062(1)
C(61)	0.110(1)	-0.091(2)	0.154(1)	0.130(1)
C(7)	0.1095(8)	-0.072(1)	0.3039(9)	0.056(1)
C(71)	0.100(1)	-0.194(1)	0.327(1)	0.083(1)
C(8)	0.130(1)	0.015(1)	0.3584(7)	0.055(1)
C(81)	0.133(1)	0.003(2)	0.4482(8)	0.100(2)
C(9)	0.159(1)	0.106(1)	0.3261(9)	0.067(1)
C(91)	0.202(1)	0.212(1)	0.368(1)	0.146(1)

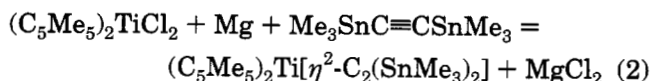
^a Esd's are given in parentheses in this and all subsequent tables.**Table 3.** Atomic Coordinates and Equivalent Isotropic Temperature Factors (\AA^2) for the Non-Hydrogen Atoms in **2**

atom	x	y	z	U_{eq}
Ti(1)	-0.0017(1)	0.1347(1)	0.0175(1)	0.032(1)
C(1)	-0.0723(3)	-0.0267(4)	0.0503(3)	0.031(1)
C(2)	-0.1118(3)	0.0450(4)	0.0873(3)	0.036(1)
Sn(1)	-0.2149(1)	0.0712(1)	0.1818(1)	0.034(1)
C(3)	-0.2374(6)	0.2285(5)	0.2042(6)	0.056(1)
C(4)	-0.1687(5)	0.0006(7)	0.2989(5)	0.057(1)
C(5)	-0.3347(5)	0.0034(6)	0.1301(6)	0.074(1)
C(6)	-0.0484(6)	0.1604(6)	-0.1352(4)	0.060(1)
C(7)	-0.1260(4)	0.1597(7)	-0.0837(5)	0.061(1)
C(8)	-0.1219(6)	0.2446(7)	-0.0271(5)	0.056(1)
C(9)	-0.0463(7)	0.2948(6)	-0.0478(7)	0.081(2)
C(10)	0.0014(6)	0.2445(6)	-0.1110(6)	0.064(1)
C(11)	0.1480(4)	0.1567(7)	0.0777(5)	0.081(1)
C(12)	0.1127(6)	0.2510(6)	0.0731(6)	0.087(2)
C(13)	0.0383(6)	0.2546(8)	0.1323(7)	0.101(1)
C(14)	0.0351(7)	0.1590(9)	0.1719(5)	0.108(2)
C(15)	0.1020(6)	0.1008(7)	0.1368(6)	0.087(1)

disorder preventing anisotropic refinement for its atoms. Hydrogen atoms were included for **1-3** at their optimized positions. An empirical correction for absorption according to Walker and Stuart¹⁸ using the ASC program¹⁷ was applied for **1**; it resulted in a significant improvement of $\langle |\Delta F| \rangle$. The PC ULM package¹⁷ was used for all calculations. Atomic coordinates and isotropic thermal parameters are given for **1-3** in Tables 2-4, respectively. Selected bond distances and bond angles for **1** are listed in Table 5 and for **2** and **3** in Table 6.

Results and Discussion

The reduction of titanocene dichlorides $(C_5H_{5-n}Me_n)_2TiCl_2$ ($n = 0-5$) by Mg in THF in the presence of $C_2(SnMe_3)_2$ bears some features different from the reduction performed in the presence of $C_2(SiMe_3)_2$. The $(C_5H_{5-n}Me_n)_2Ti[\eta^2-C_2(SiMe_3)_2]$ complexes were obtained independently of the number of Me groups at the $C_5H_{5-n}Me_n$ ligand using the molar ratio $Ti:Mg = 1:1$,^{4b,6} whereas the only $C_2(SnMe_3)_2$ complex of this type was obtained for the permethylated titanocene derivative. The $(C_5Me_5)_2Ti[\eta^2-C_2(SnMe_3)_2]$ complex **1** was formed in high yield by the general procedure given in eq 2.

**Table 4.** Atomic Coordinates and Temperature Factors (\AA^2) for the Non-Hydrogen Atoms in **3**

atom	x	y	z	U_{eq}^a
Sn(1)	0.2518(1)	-0.2577(6)	-0.0999(1)	0.039(1)
Ti(1)	-0.0983(2)	-0.1164(2)	-0.0630(1)	0.025(1)
C(1)	0.112(1)	-0.034(1)	-0.0192(6)	0.026(3)
C(2)	0.112(1)	-0.129(1)	-0.0667(7)	0.033(3)
C(3)	0.361(2)	-0.325(2)	0.005(1)	0.068(7)
C(4)	0.186(2)	-0.430(2)	-0.161(1)	0.095(8)
C(5)	0.367(2)	-0.348(2)	-0.170(1)	0.117(7)
C(6)	-0.117(1)	-0.100(1)	-0.2045(7)	0.038(3)
C(61)	-0.041(2)	-0.180(2)	-0.2558(9)	0.057(4)
C(7)	-0.239(1)	-0.130(2)	-0.1876(8)	0.046(3)
C(8)	-0.281(1)	-0.027(1)	-0.1460(8)	0.043(3)
C(81)	-0.404(2)	-0.012(2)	-0.118(1)	0.061(4)
C(9)	-0.184(1)	0.077(1)	-0.1379(7)	0.032(2)
C(10)	-0.086(1)	0.030(1)	-0.1752(7)	0.036(3)
C(11)	-0.199(1)	-0.265(2)	0.0341(6)	0.040(3)
C(111)	-0.274(2)	-0.175(2)	0.0928(9)	0.061(4)
C(12)	-0.249(1)	-0.288(1)	-0.0386(8)	0.046(3)
C(13)	-0.155(2)	-0.357(2)	-0.0689(9)	0.041(4)
C(131)	-0.173(2)	-0.445(2)	-0.143(1)	0.060(4)
C(14)	-0.040(1)	-0.340(1)	-0.0148(7)	0.036(3)
C(15)	-0.0711(9)	-0.261(3)	0.0478(6)	0.039(3)

^a U_{eq} is given for atoms refined with anisotropic temperature factors, and U_{iso} is given for other atoms.**Table 5.** Selected Bond Distances (\AA) and Angles (deg) for **1**

Ti(1)-CE(Cp ring)	2.115(14)	C(1)-C(1')	1.323(16)
Ti(1)-C(Cp ring) (av)	2.42(2)	Sn(1)-C(1)	2.114(11)
C-C(Cp ring) (av)	1.38(2)	Sn(1)-C(2)	2.117(17)
C(Cp ring)-C(Me) (av)	1.53(2)	Sn(1)-C(3)	2.114(19)
Ti(1)-C(1)	2.096(11)	Sn(1)-C(4)	2.131(19)
CE-Ti(1)-CE'	141.2(5)	Ti(1)-C(1)-C(1')	71.6(7)
C(1)-Ti(1)-C(1')	36.8(4)	Sn(1)-C(1)-C(1')	134.9(9)

Table 6. Selected Bond Distances and Bond Angles for **2** and **3**

	2	3
(a) Bond Distances (\AA)		
Ti(1)-Ti(1')	3.573(1)	3.631(1)
Ti(1)-CE(1)(Cp(1) ring)	2.113(8)	2.116(13)
Ti(1)-CE(2)(Cp(2) ring)	2.119(9)	2.161(15)
Ti(1)-C(Cp(1) ring) (av)	2.41(1)	2.43(1)
Ti(1)-C(Cp(2) ring) (av)	2.42(1)	2.46(7)
Ti(1)-C(1)	2.413(5)	2.424(11)
Ti(1)-C(1')	2.065(5)	2.088(11)
Ti(1)-C(2)	2.273(5)	2.287(12)
C(1)-C(2)	1.242(7)	1.252(16)
C(2)-Sn(1)	2.120(5)	2.125(12)
Sn(1)-C(Me) (av)	2.12(1)	2.09(2)
(b) Bond Angles (deg)		
CE-Ti(1)-CE	129.2(3)	129.8(5)
Ti(1)-C(1)-Ti(1')	105.6(2)	107.0(5)
Ti(1)-C(2)-C(1)	81.0(4)	80.7(8)
Ti(1)-C(1')-C(2')	174.1(5)	175.0(10)
Ti(1)-C(2)-Sn(1)	138.4(3)	142.0(6)
C(1)-Ti(1)-C(2)	30.6(2)	30.6(4)
C(1)-Ti(1)-C(1')	74.4(2)	73.0(4)
C(1)-C(2)-Sn(1)	140.1(4)	135.0(10)

Pure crystalline **1** was, however, obtained in only 50% yield because of difficult separation of paramagnetic impurities whose yield was estimated to be less than 5%, based on EPR measurements. The molecular structure of **1** in the solid state has been determined by X-ray crystallography, and it is shown in Figure 1. The ¹H and ¹³C NMR data for complex **1** are consistent with the solid-state structure. A large chemical shift of acetylenic carbon atoms δ 244.5 ppm (cf. δ 116.1 ppm in free acetylene¹⁹) is due to the donation of the four electrons from the alkyne ligand to the metal.²⁰ In the

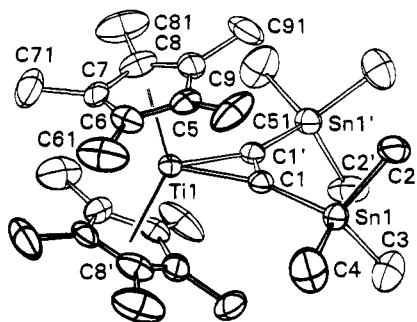


Figure 1. ORTEP drawing of **1**, with ellipsoids drawn at the 50% probability level. Atoms Sn(1'), C(1'), etc. are related to atoms Sn(1), C(1), etc., respectively, by the symmetry operation $-x, y, 1/2 - z$.

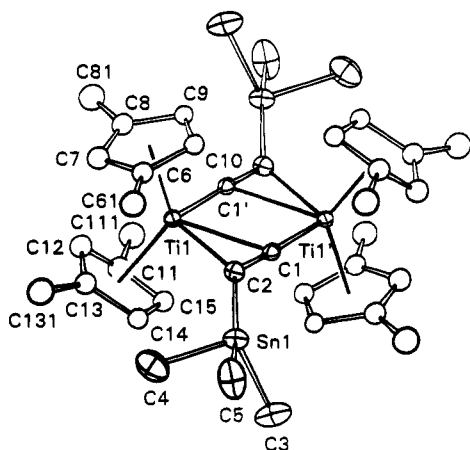


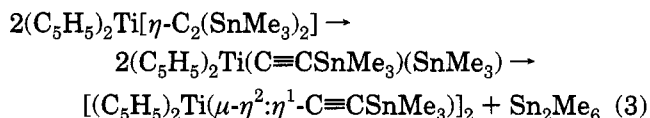
Figure 2. ORTEP drawing of **3**, with ellipsoids drawn at the 50% probability level. Atoms Ti(1'), C(1'), etc. are related to atoms Ti(1), C(1), etc., respectively, by the symmetry operation $-x, -y, -z$.

analogous $(C_5H_5-nMe_n)_2Ti[\eta^2-C_2(SiMe_3)_2]$ complexes the value $\delta(C\equiv C)$ varied from 244.7 to 248.5 ppm on going from the C_5H_5 to C_5Me_5 compound.^{4b,6} Correspondingly, the $\nu(C\equiv C)$ band at 2070 cm^{-1} for free $C_2(SnMe_3)_2$ ¹⁹ was shifted to 1580 cm^{-1} in **1**, which is comparable to the average of corresponding values of 1598 and 1563 cm^{-1} in $(C_5Me_5)_2Ti[\eta^2-C_2(SiMe_3)_2]$.^{4b} A small difference in the effects of $SiMe_3$ and $SnMe_3$ substituents on the electronic structure of $(C_5H_5-nMe_n)_2Ti[\eta^2-C_2R_2]$ complexes also follows from the presence of an electronic absorption band at 920 nm for **1**, which is virtually at the same position as the band at 916 nm for $(C_5Me_5)_2Ti[\eta^2-C_2(SiMe_3)_2]$.⁶

Unexpectedly, analogous reaction systems with $(C_5H_5)_2TiCl_2$ and $(C_5H_3Me_2)_2TiCl_2$ as starting reagents afforded the dimeric titanocene acetylide complexes $[(C_5H_5)_2Ti(\mu-\eta^2:\eta^1-C\equiv CSnMe_3)]_2$ (**2**) and $[(C_5H_3Me_2)_2Ti(\mu-\eta^2:\eta^1-C\equiv CSnMe_3)]_2$ (**3**) in virtually quantitative yields. The molecular structures of **2** and **3** were determined by single-crystal X-ray diffraction, and their skeleton structures were found to be very similar. The ORTEP plot for **3** is shown in Figure 2. Both structures are compatible with spectral data, which closely resemble those of the silicon-containing analogue $[(C_5H_5)_2Ti(\mu-\eta^2:\eta^1-C\equiv CSiMe_3)]_2$.^{7a,21} The chemical shifts of the two acetylenic carbon atoms differ widely in both **2** (139.7 and

236.1 ppm) and **3** (140.8 and 242.0 ppm). Similar chemical shifts (δ 142.85 and 236.79 ppm) were also found in $[(C_5H_5)_2Ti(\mu-\eta^2:\eta^1-C\equiv CSiMe_3)]_2$ ²¹ and recently in its zirconium analogue (151.4 and 245.2 ppm).²² The downfield-shifted signals were assigned to the inner acetylide carbon atom^{7a,21,22} which seems to be, however, at variance with the data for the $(C_5H_5-nMe_n)_2Ti[\eta^2-C_2R_2]$ complexes, where the π -bonded acetylenic carbon atoms resonate above 200 ppm.^{5,6,20} An expected shielding effect of Ti^{III} in the $Ti-C_\alpha$ σ -bond of these binuclear titanocene acetylide complexes and a shorter distance from the π -coordinated titanium atom to the C_β atom than to the C_α atom (vide infra) indicate a reverse assignment. No spectroscopic evidence for either assignment is so far available. The $\nu(C\equiv C)$ vibration is strongly shifted to lower frequencies, 1766 cm^{-1} for **2** and 1742 cm^{-1} for **3**, although to a much lesser extent than in **1** (1580 cm^{-1}).

The electron donation effect of Me groups at the cyclopentadienyl rings in **3** is demonstrated by larger shifts of the above-mentioned δ and $\nu(C\equiv C)$ values for **3** compared to **2**. The intense electronic absorption band of **2** at 472 nm is also shifted to 493 nm in **3**. This shift is consistent with an expected $d-\pi$ nature of the transition where the energy of the LUMO is decreased by the Me substituents whereas the energy of the HOMO occupied by two spin-paired d electrons is virtually unaffected. In both the systems producing **2** and **3** the volatiles contained hexamethylditin in the amount which, according to the GC estimate, was comparable to the yield of **2** or **3**. Moreover, the smooth formation of **2** or **3** in the $(C_5H_5-nMe_n)_2Ti[\eta^2-C_2(SiMe_3)_2]/C_2(SnMe_3)_2$ systems was accompanied by the liberation of Sn_2Me_6 and bis(trimethylsilyl)acetylene in an approximately 1:2 molar ratio. These observations imply that a cleavage of the trimethylstannyl group from the acetylene is a titanium(II)-assisted process. We assume that an unstable [titanocene- $C_2(SnMe_3)_2$] complex is obtained either by coordination of the acetylene to a titanocene species at the onset of its formation in the $(C_5H_5-nMe_n)_2TiCl_2/Mg/THF$ system or by exchange of acetylenes in the $(C_5H_5-nMe_n)_2Ti[\eta^2-C_2(SiMe_3)_2]/C_2(SnMe_3)_2$ systems. The oxidative addition of $C_2(SnMe_3)_2$ to a titanocene moiety probably affords a labile (trimethylstannyl)titanocene(Ti^{IV})(trimethylstannyl)acetylide, which easily releases the Me_3Sn^\cdot radical and dimerizes to give the Ti^{III} dimer **2** or **3** (e.g., eq 3). In



contrast to ionic processes where the $(SnMe_3)^-$ group is known to be a stable substituent (leaving group),²³ the Me_3Sn^\cdot radicals recombine to give Sn_2Me_6 . The titanocene(Ti^{III})-tin-containing impurities observed by EPR spectroscopy need not be the intermediates in the cleavage process but byproducts. Although the analogous cleavage reaction involving $C_2(SiMe_3)_2$ has not been observed in titanocene chemistry, it is known that the

(21) Wood, G. L.; Knobler, C. B.; Hawthorne, M. F. *Inorg. Chem.* **1989**, *28*, 382-384.

(22) Rosenthal, U.; Ohff, A.; Baumann, W.; Kempe, R.; Tillack, A.; Burlakov, V. V. *Organometallics* **1994**, *13*, 2903-2906.

(23) Adcock, W.; Clark, C. I. *J. Org. Chem.* **1993**, *58*, 7341-7349.

(19) Mitchell, T. N.; Walter, G. J. *Organomet. Chem.* **1976**, *121*, 177-184.

(20) Rosenthal, U.; Oehme, G.; Burlakov, V. V.; Petrovskii, P. V.; Shur, V. B.; Vol'pin, M. E. *J. Organomet. Chem.* **1990**, *391*, 119-122.

complex (COD)IrCl₂ (COD = cycloocta-1,5-diene) and the (COD)RhCl₂/MeLi (1:6.4) system react with C₂-(SiMe₃)₂ to yield [(COD)M(μ-η²:η¹-C≡CSiMe₃)₂] (M = Ir, Rh) and Me₃SiCl and Me₃Sn, respectively.²⁴ Instead, a scission of 1,4-bis(trimethylsilyl)-1,3-butadiyne was observed for all the (C₅H_{5-n}Me_n)₂Ti derivatives to give either the dimeric titanocene acetylide complex for $n = 0$,^{7a} structurally analogous to **2** or **3**, or tweezer complexes [(η⁵-C₅H_{5-n}Me_n)₂Ti(η¹-C≡CSiMe₃)₂]⁻[Mg(THF)-Cl]⁺ ($n = 3-5$).^{7b}

In the case of permethyltitanocene a strong electron donation effect of Me substituents is probably responsible for a strong back-bonding interaction enhancing the stabilization of **1**. A small amount of liberated Sn₂Me₆ and a well-resolved EPR spectrum of a titanocene-(Ti^{III})-tin complex (vide supra), however, indicate the minor abundance of the above-mentioned cleavage of the SnMe₃ group.

Reactions of (C₅HMe₄)₂TiCl₂ or (C₅H₂Me₃)₂TiCl₂ with Mg and C₂(SnMe₃)₂ (1:1:1) in THF yielded a mixture of complexes which were not separated and characterized. The GC analysis revealed the complete consumption of the acetylene and the liberation of an approximately stoichiometric amount of Sn₂Me₆. Infrared spectra of the reaction mixtures showed several absorption bands in the region 1796–1955 cm⁻¹ and no bands between 1550 and 1750 cm⁻¹. The absence of absorption bands in the latter region implies the absence of products analogous to **1**, **2**, or **3**. The above-mentioned ν(C≡C) bands together with strong bands at 502, 522, and 1182 cm⁻¹, characteristic of the ≡C–SnMe₃ group, are attributable to various titanocene (trimethylstannyl)-acetylide complexes. Among them, complexes of the tweezer type can be ascribed to components with ν(C≡C) ~1990 cm⁻¹ on the basis of the comparison with the silicon-containing tweezer acetylide complexes.^{7b} Attempts to isolate a pure complex from these mixtures have failed.

An excess of magnesium led in all cases to the formation of a gray sediment of metallic tin and to lower yields of tin-containing complexes. In contrast, for the bis(trimethylsilyl)acetylene systems, the (C₅H_{5-n}Me_n)₂Ti[η²-C₂(SiMe₃)₂] complexes are stable toward excess Mg for $n = 3-5$, whereas for $n = 0-2$ they react further with Mg to give binuclear [(C₅H_{5-n}Me_n)₂Ti][μ-η²:η²-C₂(SiMe₃)₂][(C₅H_{5-n}Me_n)Mg] and trinuclear [(C₅H_{5-n}Me_n)₂Ti][μ-η²:η²-C₂(SiMe₃)₂]₂[Mg(μ-Cl)₂][(C₅H_{5-n}Me_n)Mg(THF)] complexes containing perpendicularly bridging acetylene ligands.¹⁴

Description of the Crystal Structures of 1–3. The X-ray analysis revealed that compound **1** is a permethyltitanocene complex containing one π-bonded bis(trimethylstannyl)acetylene ligand. The molecular structure of **1** is shown in Figure 1. Important bond lengths and bond angles are listed in Table 5. The molecule of **1** has crystallographic C₂ symmetry. It closely resembles the molecular structures of the analogous silicon complexes (C₅Me₅)₂Ti[η²-C₂(SiMe₃)₂]^{4b} and (C₅HMe₄)₂Ti[η²-C₂(SiMe₃)₂].⁶ The bonding parameters for the titanocene–acetylene skeleton are virtually the same in the silicon complexes and **1**, except for the longer Sn–C bonds compared to the Si–C bonds. Within experimental error the C–C bond length in the

C₂(SnMe₃)₂ ligand (1.32(2) Å) is comparable to that of a C=C double bond of 1.34 Å. The angle (Sn–C–C = 134.9(9)° in **1** is consistent with some sp² hybridization at the carbon atoms and agrees well with the angles in the silicon-containing complexes. The intramolecular steric hindrance between two C₅Me₅ ligands in a staggered conformation induces bending of Me substituents out of the best plane of the cyclopentadienyl ring away from the titanium atom. The maximum deviation (0.36 Å) was found for the methyl groups in positions where the C₅Me₅ ligands closely approach each other.

Compounds **2** and **3** are dimeric molecules of the same structural type, and most of their common geometrical parameters are identical within the accuracy of the measurements. The ORTEP plot and atom-numbering scheme for **3** is shown in Figure 2. Compound **2** is described using the same numbering scheme for non-hydrogen atoms. Important bond lengths and bond angles for both compounds are listed in Table 6. Both **2** and **3** exhibit a crystallographic center of inversion, and their titanocene moieties are in a staggered conformation. Two molecules of titanocene (trimethylstannyl)acetylide are linked by a π-bonding interaction between the titanium atom of one molecule and the acetylide group of the other one. The dimeric titanium–acetylide skeleton is essentially planar. The C(2) and C(2′) atoms deviate from the plane defined by Ti(1), Ti(1′), C(1), and C(1′) atoms by 0.011 Å in **2** and 0.053 Å in **3**. The tin atoms deviate from this plane differently for **2** (Sn(1) –0.17 Å) and **3** (Sn(1) –0.53 Å). The Ti(1)–Ti(1′) distances for **2** (3.573(1) Å) and for **3** (3.631(3) Å) are considerably longer than the sum of the Ti van der Waals radii (2.896 Å). The Ti(1′)–C(1)–C(2) fragments are almost linear (174.1(5)° in **2** and 175.0(10)° in **3**), and this is consistent with a largely preserved sp hybridization at the acetylide carbon atoms. On the other hand, a strong bending in the C(1)–C(2)–Sn(1) fragment (140.1(4)° for **2** and 135.0(10)° for **3**) apparently results from a strong π-bonding coordination of the adjacent titanium atom from the opposite direction. This angle and the bond length C(1)–C(2) (1.242(7) Å) are attributable to a partial sp² hybridization of the carbon atoms. Comparison of these parameters with the bond length and C(1)–C(2)–Sn(2) angle in **1** (1.323(16) Å and 134.9(9)°) implies a stronger π-coordination of the acetylene in **1**. The π-bonding in **2** and **3** is, however, asymmetrical, as the Ti(1)–C(2) distance is shorter by more than 0.1 Å than the Ti(1)–C(1) distance (Table 6). The comparison of the structure of **2** with that of the trimethylsilyl analogue^{7a,21} revealed that all the parameters of both complexes except the different lengths of Sn–C and Si–C bonds are virtually the same.

The structure of **3** was determined with a lower accuracy. Within this limitation, most of the molecular parameters of **2** fall in the range of parameters of **3** (Table 6), therefore prohibiting us from evaluating the stereochemical influence of the effects of Me substituents in 1,3-dimethylcyclopentadienyl ligands of **3** on its structure in detail.

Conclusion. The formation of a stable (C₅Me₅)₂Ti[η²-C₂(SnMe₃)₂] complex with a very congested coordination space for the acetylene ligand due to bulky C₅Me₅ ligands and a large CE–Ti–CE′ angle implies that electronic factors are decisive for the alternative reaction

(24) Müller, J.; Tschampel, M.; Pickardt, J. *J. Organomet. Chem.* **1988**, *355*, 513–524.

pathway affording $[(C_5H_5)_2Ti(\mu-\eta^2:\eta^1-C\equiv CSnMe_3)]_2$ (**2**) and $[(C_5H_3Me_2)_2Ti(\mu-\eta^2:\eta^1-C\equiv CSnMe_3)]_2$ (**3**). The liberation of a nearly stoichiometric amount of Sn_2Me_6 and the alternative formation of **2** and **3** from relevant $(C_5H_{5-n}Me_n)_2Ti[\eta^2-C_2(SiMe_3)_2]$ compounds and $C_2(SnMe_3)_2$ are consistent with a titanium(II)-induced homolytic cleavage of the $SnMe_3$ group from the acetylene.

Acknowledgment. This work was supported by the

Grant Agency of the Czech Republic (No. 203/93/0143) and by the Fonds der Chemischen Industrie.

Supplementary Material Available: Tables of crystal data, atomic coordinates, anisotropic thermal parameters, bond distances, valence angles, least-squares planes and atomic deviations therefrom, and important intermolecular contacts and figures giving views of the unit cell for **1–3** (46 pages). Ordering information is given on any current masthead page.

OM9408122

Reduction of Acetonitrile Ligand on W(PhC≡CPh)₃(NCMe) and W(η⁴-C₄Ph₄)(PhC≡CPh)₂(NCMe): Crystal Structure of W(PhC≡CPh)₃(NH=C(Me)₂)

Wen-Yann Yeh* and Che-Sheng Ting

Department of Chemistry, National Sun Yat-Sen University, Kaohsiung, Taiwan 80424

Shie-Ming Peng† and Gene-Hsiang Lee

Department of Chemistry, National Taiwan University, Taipei, Taiwan 10764

Received October 13, 1994[§]

The imine complexes W(PhC≡CPh)₃(NH=C(Me)₂) (1) and W(PhC≡CPh)₃(NH=C(Ph)Me) (2) have been prepared by sequential treatment of W(PhC≡CPh)₃(NCMe) with MeLi and PhLi, respectively, and H₂O. However, treating W(PhC≡CPh)₃(NCMe) with LiHBt₃ and H₂O in sequence produces the amine complex W(PhC≡CPh)₃(NH₂Et) (3). Similar treatment of W(η⁴-C₄Ph₄)(PhC≡CPh)₂(NCMe) with LiHBt₃/H₂O and PhLi/H₂O yields W(η⁴-C₄Ph₄)(PhC≡CPh)₂(NH₂Et) (4) and W(η⁴-C₄Ph₄)(PhC≡CPh)₂(NH=C(Ph)Me) (5), respectively. Compound 1 crystallizes in space group P2₁/c with *a* = 10.075(2) Å, *b* = 10.474(3) Å, *c* = 32.906(7) Å, β = 94.88(2)°, *V* = 3460(1) Å³, *Z* = 4, and *R_F* = 0.026.

Introduction

Reduction of nitriles to amines with either pressurized hydrogen or hydride reagents is a common reaction.¹ Conversion of metal-bound nitriles to metal imine or amine complexes has also been reported.² For instance, Venanzi showed²ⁱ that treatment of [(triar)sRu(NCMe)₃]²⁺ with NaBH₄ in methanol produced [(triar)sHRu(NH₂Et)₂]⁺. Wilkinson reported^{2b} the protonation of Cp₂Mo(NCMe) with HBF₄ in NCMe to give [Cp₂Mo(NCMe)(NH=CHMe)]²⁺. Templeton revealed^{2l-n} the sequential hydride and proton addition reactions with [Tp'(CO)(RC≡CR)W(NCMe)]⁺ yielding [Tp'(CO)(RC≡CR)W(NH₂Et)]⁺ (Tp' = HB(C₅H₈N₂)₃), and characterized each of the intermediates as azavinylidene (-N=CHMe), imine (-NH=CHMe), and ethylamido (-NHEt) species. Recently, we showed³ that hydrolysis

of W(η⁴-C₄Ph₄)(PhC≡CPh)₂(NCMe) in alkaline solution led to alkyne-alkyne coupling to form an acetamido complex W(η⁴-C₄Ph₄)(η⁴-C₄Ph₄H)(η²-NHC(=O)Me). An unstable azavinylidene species W-N=C(OH)Me, presumably formed by OH⁻ attack at the acetonitrile ligand, was postulated as intermediate but not observed. We then moved to investigate the reactivity of W(η⁴-C₄Ph₄)(PhC≡CPh)₂(NCMe) and W(PhC≡CPh)₃(NCMe) toward organic nucleophiles. Presented in this paper are results concerning the reactions with PhLi, MeLi, and LiHBt₃ and subsequent hydrolysis to produce imine and amine complexes (Scheme 1).

Experimental Section

General Procedures. Manipulations involving air-sensitive reagents were performed under a dry nitrogen atmosphere with standard Schlenk techniques. W(PhC≡CPh)₃(NCMe)⁴ and W(η⁴-C₄Ph₄)(PhC≡CPh)₂(NCMe)⁵ were prepared from W(PhC≡CPh)₃(CO)⁶ as described previously. Lithium triethylborohydride (LiHBt₃, 1.0 M in THF, Aldrich), lithium triethylborodeuteride (LiDBt₃, 1.0 M in THF, Aldrich), methyllithium (MeLi, 5% in ether, Merck), phenyllithium (PhLi, 2 M in cyclohexane-ether, Aldrich), and D₂O (99%, Aldrich) were used as received. Tetrahydrofuran (THF) was dried over sodium benzophenone ketyl and distilled before use. Preparative thin-layer chromatographic (TLC) plates were prepared from silica gel (Merck GF254). ¹H, ³¹P, and ¹³C NMR spectra were obtained on a Varian VXR-300 spectrometer at 300, 121.4, and 75.4 MHz, respectively. IR spectra were taken on a Hitachi 2001 spectrometer. Elemental analyses were performed at the NSC Regional Instrumentation Center at National Cheng Kung University, Tainan. Fast atom bombardment (FAB) mass spectra were obtained on a VG-5022 mass spectrometer.

* To whom inquires concerning the X-ray crystallographic work should be addressed.

[§] Abstract published in *Advance ACS Abstracts*, February 1, 1995.

(1) (a) March, J. *Advanced Organic Chemistry*, 3rd ed.; Wiley Interscience: New York, 1985; pp 809 (see also references therein). (b) Rabinovitz, M. In *The Chemistry of the Cyano Group*; Rappoport, Z., Ed.; Interscience: New York, 1970; pp 307-340. (c) Rylander, P. N. *Catalytic Hydrogenation in Organic Synthesis*; Academic: New York, 1979; pp 138.

(2) (a) Adams, R. D.; Horvath, I. T. *Prog. Inorg. Chem.* **1985**, *33*, 128. (b) Storhoff, B. N.; Lewis, H. C. *Coord. Chem. Rev.* **1977**, *23*, 1. (c) Osby, J. O.; Heinzman, S. W.; Ganem, B. *J. Am. Chem. Soc.* **1986**, *108*, 67. (d) Andrews, M. A.; Kaesz, H. D. *J. Am. Chem. Soc.* **1979**, *101*, 7238, 7255. (e) Andrews, M. A.; van Buskirt, G.; Knobler, C. B.; Kaesz, H. D. *J. Am. Chem. Soc.* **1979**, *101*, 7245. (f) Bernhardt, W.; van Schnering, C.; Vahrenkamp, H. *Angew. Chem., Intl. Ed. Engl.* **1986**, *25*, 279. (g) Barron, A. R.; Salt, J. E.; Wilkinson, G. *J. Chem. Soc., Dalton Trans.* **1987**, 2947. (h) McGilligan, B. S.; Wright, T. C.; Wilkinson, G. *J. Chem. Soc., Dalton Trans.* **1988**, 1737. (i) Thorburn, I. S.; Rettig, S. J.; James, B. R. *J. Organomet. Chem.* **1985**, *296*, 103. (j) Rhodes, L. F.; Venanzi, L. M. *Inorg. Chem.* **1987**, *26*, 2692. (k) Maatta, E. A.; Du, Y. *J. Am. Chem. Soc.* **1988**, *110*, 8249. (l) Feng, S. G.; Templeton, J. L. *J. Am. Chem. Soc.* **1989**, *111*, 6477. (m) Caldarelli, J. L.; White, P. S.; Templeton, J. L. *J. Am. Chem. Soc.* **1992**, *114*, 10097. (n) Feng, S. G.; Templeton, J. L. *Organometallics* **1992**, *11*, 1295. (o) Pomeroy, A. J. L.; Hughes, D. L.; Richards, R. L. *J. Chem. Soc., Chem. Commun.* **1988**, 1052. (p) Bakir, M.; Fanwick, P. E.; Walton, R. A. *Inorg. Chem.* **1988**, *27*, 2016.

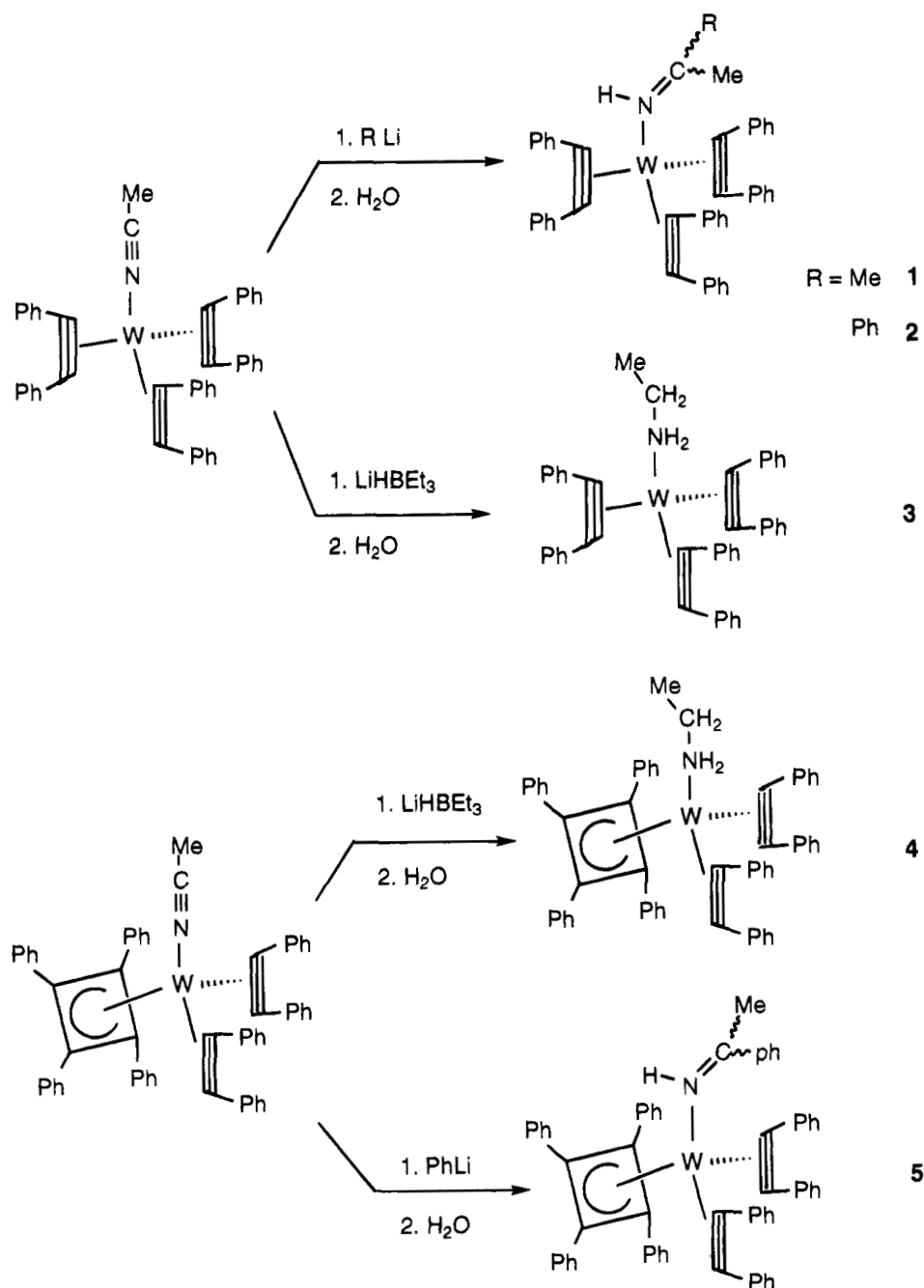
(3) Yeh, W.-Y.; Peng, S.-M.; Liu, L.-K. *Inorg. Chem.* **1993**, *32*, 2965.

(4) Yeh, W.-Y.; Ting, C.-S.; Chih, C.-F. *J. Organomet. Chem.* **1991**, *427*, 257.

(5) Yeh, W.-Y.; Liu, L.-K. *J. Am. Chem. Soc.* **1992**, *114*, 2267.

(6) (a) Tate, D. P.; Augl, J. M. *J. Am. Chem. Soc.* **1963**, *85*, 2174. (b) Tate, D. P.; Augl, J. M.; Ritchey, W. M.; Rose, B. L.; Grasselli, J. G. *J. Am. Chem. Soc.* **1964**, *86*, 3261.

Scheme 1



Preparation of $W(\text{PhC}\equiv\text{CPh})_3(\text{NH}=\text{C}(\text{Me})_2)$. $W(\text{PhC}\equiv\text{CPh})_3(\text{NCMe})_2$ (200 mg, 0.263 mmol) was dissolved in THF (5 mL) in an oven-dried, 20 mL Schlenk flask, equipped with a magnetic stir bar and a rubber serum stopper under nitrogen, and MeLi (116 μL , 0.263 mmol) was added slowly via a microsyringe at ambient temperature. The mixture was stirred for 1 h, and then 20 μL of water was added to the flask. The volatile materials were removed under vacuum, and the residue was subjected to TLC, eluting with *n*-hexane/dichloromethane (3:1, v/v). Crystallization of the material forming the major colorless band from dichloromethane/*n*-hexane yielded air-stable, colorless crystals of $W(\text{PhC}\equiv\text{CPh})_3(\text{NH}=\text{C}(\text{Me})_2)$ (**1**) (110 mg, 0.14 mmol, 53%). Mass spectrum (FAB): m/z 775 (M^+ , ^{184}W), 718 ($M^+ - \text{NH}=\text{CMe}_2$). ^1H NMR (CDCl_3 , 25 $^\circ\text{C}$): δ 11.47 (br, 1H, NH), 7.49–7.11 (m, 30 H, Ph), 2.23 (s, 3H, CH_3), 1.23 (s, 3H, CH_3). $^{13}\text{C}\{^1\text{H}\}$ NMR (CDCl_3 , 25 $^\circ\text{C}$): δ 199.2 (s, $\text{C}\equiv$), 187.4 (s, $\text{C}=\text{N}$), 184.2 (s, $\text{C}\equiv$), 143.5 (s, ipso-Ph), 141.4 (s, ipso-Ph), 129.5, 128.3, 127.6, 127.4, 127.0, 125.9 (s, meta-, ortho-, and para-Ph), 31.3 (s, CH_3), 25.4 (s, CH_3). IR (KBr disk): 3284 ($\nu_{\text{N-H}}$), 3056, 3010 ($\nu_{\text{C-H}}$), 1668 ($\nu_{\text{C}=\text{C}}$) cm^{-1} .

Anal. Calcd for $\text{WC}_{45}\text{H}_{37}\text{N}$: C, 69.68; H, 4.81; N, 1.81. Found: C, 69.33; H, 4.79; N, 1.83.

Preparation of $W(\text{PhC}\equiv\text{CPh})_3(\text{NH}=\text{C}(\text{Ph})\text{Me})$. $W(\text{PhC}\equiv\text{CPh})_3(\text{NCMe})_2$ (200 mg, 0.263 mmol) was reacted with PhLi (0.132 mL, 0.263 mmol) and water by the same method as described above, producing air-stable, pale-yellow crystals $W(\text{PhC}\equiv\text{CPh})_3(\text{NH}=\text{C}(\text{Ph})\text{Me})$ (**2**) (106 mg, 0.126 mmol, 48%). Mass spectrum (FAB): m/z 837 (M^+ , ^{184}W), 718 ($M^+ - \text{NH}=\text{CMePh}$), 659 ($M^+ - \text{C}_2\text{Ph}_2$). ^1H NMR (CDCl_3 , 25 $^\circ\text{C}$): δ 12.22 (br, 1H, NH), 7.54–7.11 (m, 30H, Ph), 1.65 (s, 3H, CH_3). $^{13}\text{C}\{^1\text{H}\}$ NMR (CDCl_3 , 25 $^\circ\text{C}$): δ 199.1 (s, $\text{C}=\text{C}$), 184.1 (s, $\text{C}=\text{N}$), 184.0 (s, $\text{C}=\text{C}$), 143.5, 141.3 (s, ipso- C_2Ph_2), 138.9 (s, ipso- $\text{PhC}\equiv$), 131.5, 129.2, 125.6 ($\text{PhC}\equiv$), 129.6, 128.4, 127.7, 127.5, 127.1, 126.0 (C_2Ph_2), 23.0 (s, CH_3). IR (KBr disk): 3288 ($\nu_{\text{N-H}}$), 3048 ($\nu_{\text{C-H}}$), 1656 ($\nu_{\text{C}=\text{C}}$) cm^{-1} . Anal. Calcd for $\text{WC}_{50}\text{H}_{39}\text{N}$: C, 71.69; H, 4.69; N, 1.67. Found: C, 71.32; H, 4.68; N, 1.58.

Preparation of $W(\eta^4\text{-C}_6\text{H}_6)(\text{PhC}\equiv\text{CPh})_2(\text{NH}=\text{C}(\text{Ph})\text{Me})$. $W(\eta^4\text{-C}_6\text{H}_6)(\text{PhC}\equiv\text{CPh})_2(\text{NCMe})_2$ (200 mg, 0.212 mmol) was treated with PhLi (0.106 mL, 0.212 mmol) and H_2O by the same method as described above. $W(\eta^4\text{-C}_6\text{H}_6)(\text{PhC}\equiv\text{CPh})_2$ -

Table 1. Experimental Data for the X-ray Diffraction Study of Compound 1

chem formula: $\text{C}_{45}\text{H}_{37}\text{NW}$	fw: 770.60
$a = 10.075(2)$ Å	space group: $P2_1/c$
$b = 10.474(3)$ Å	$T = 25$ °C
$c = 32.906(7)$ Å	$\lambda = 0.70930$ Å
$\beta = 94.88(2)$	$Q_{\text{calcd}} = 1.479$ g/cm ³
$V = 3460(1)$ Å ³	$\mu = 3.44$ mm ⁻¹
$Z = 4$	$R_F^a = 0.026$
$2\theta_{\text{max}} = 44.9$	$R_w^a = 0.020$

$$^a R_F = \frac{\sum ||F_o| - |F_c||}{\sum |F_o|}; R_w = \left\{ \frac{\sum [w(|F_o| - |F_c|)^2]}{\sum |F_o|^2} \right\}^{1/2}$$

($\text{NH}=\text{C}(\text{Ph})\text{Me}$) (**5**) (99 mg, 0.098 mmol, 46%) was isolated as air-stable, orange crystals. Mass spectrum (FAB): m/z 1015 (M^+ , ^{184}W), 896 ($\text{M}^+ - \text{NH}=\text{CMePh}$), 837 ($\text{M}^+ - \text{C}_2\text{Ph}_2$). ^1H NMR (CDCl_3 , 25 °C): δ 10.79 (br, 1H, NH), 7.45–6.82 (m, 45H, Ph), 1.24 (s, 3H, CH_3). $^{13}\text{C}\{^1\text{H}\}$ NMR (CDCl_3 , 25 °C): δ 184.0 (s, $\text{C}=\text{N}$), 135.0, 129.6, 127.4, 124.9, 131.0, 128.7, 126.0, 125.6 (Ph), 85.8 (s, C_4Ph_4), 20.4 (s, CH_3). IR (KBr disk): 3260 ($\nu_{\text{N-H}}$), 3056, 2924 ($\nu_{\text{C-H}}$), 1670 ($\nu_{\text{C}=\text{C}}$) cm^{-1} . Anal. Calcd for $\text{WC}_{64}\text{H}_{49}\text{N}$: C, 75.66; H, 4.86; N, 1.38. Found: C, 75.29; H, 4.90; N, 1.37.

Preparation of $W(\text{PhC}\equiv\text{CPh})_3(\text{NH}_2\text{Et})$. $W(\text{PhC}\equiv\text{CPh})_3(\text{NCMe})$ (200 mg, 0.263 mmol) and THF (5 mL) were added into an oven-dried, 20 mL Schlenk flask, equipped with a magnetic stir bar and a rubber serum stopper under nitrogen, and LiHBEt_3 (530 μL , 0.53 mmol) was introduced via a microsyringe. The mixture was stirred at 25 °C for 1 h, and then water (20 μL) was added. The solvents were removed under vacuum, and the residue was subjected to TLC, eluting with *n*-hexane/dichloromethane (3:1, v/v). Crystallization of the material forming the second colorless band from dichloromethane/*n*-hexane yielded air-stable, colorless crystals of $W(\text{PhC}\equiv\text{CPh})_3(\text{NH}_2\text{Et})$ (**3**) (104 mg, 0.14 mmol, 52%). Mass spectrum (FAB): m/z 763 (M^+ , ^{184}W), 718 ($\text{M}^+ - \text{NH}_2\text{Et}$). ^1H NMR (CDCl_3 , 25 °C): δ 7.45–7.02 (m, 30 H, Ph), 4.85 (t, $^3J_{\text{H-H}} = 9$ Hz, NH_2), 2.92 (dt, CH_2), 0.86 (t, $^3J_{\text{H-H}} = 7$ Hz, CH_3). $^{13}\text{C}\{^1\text{H}\}$ NMR (CDCl_3 , 25 °C): δ 200.2 (s, $\text{C}\equiv$), 184.8 (s, $\text{C}\equiv$), 143.3 (s, ipso-Ph), 143.0 (s, ipso-Ph), 129.7, 128.5, 127.6, 127.2, 126.1, 125.7 (s, meta, ortho, and para-Ph), 43.3 (s, CH_2), 19.5 (s, CH_3). IR (KBr disk): 3344, 3284 ($\nu_{\text{N-H}}$), 3052, 3016, 2984 ($\nu_{\text{C-H}}$), 1660 ($\nu_{\text{C}=\text{C}}$) cm^{-1} . Anal. Calcd for $\text{WC}_{44}\text{H}_{37}\text{N}$: C, 69.21; H, 4.88; N, 1.83. Found: C, 69.06; H, 4.89; N, 1.85.

Preparation of $W(\eta^4\text{-C}_4\text{Ph}_4)(\text{PhC}\equiv\text{CPh})_2(\text{NH}_2\text{Et})$. The reaction of $W(\eta^4\text{-C}_4\text{Ph}_4)(\text{PhC}\equiv\text{CPh})_2(\text{NCMe})$ (200 mg, 0.212 mmol) with LiHBEt_3 and H_2O was carried out and worked up in a fashion identical with that above, forming air-stable, orange crystalline product $W(\eta^4\text{-C}_4\text{Ph}_4)(\text{PhC}\equiv\text{CPh})_2(\text{NH}_2\text{Et})$ (**4**) (96 mg, 0.102 mmol, 48%). Mass spectrum (FAB): m/z 941 (M^+ , ^{184}W), 896 ($\text{M}^+ - \text{NH}_2\text{Et}$), 718 ($\text{M}^+ - \text{NH}_2\text{Et} - \text{C}_2\text{Ph}_2$). ^1H NMR (CDCl_3 , 25 °C): δ 7.17–6.77 (m, 40H, Ph), 3.92 (t, 2H, NH_2), 2.69 (dt, CH_2), 0.68 (t, $^3J_{\text{H-H}} = 7$ Hz, CH_3). $^{13}\text{C}\{^1\text{H}\}$ NMR (CDCl_3 , 25 °C): δ 134.9–124.0 (m, Ph), 87.2 (s, C_4Ph_4), 43.7 (s, CH_2), 19.8 (s, CH_3). IR (KBr disk): 3304, 3252 ($\nu_{\text{N-H}}$), 3056, 3012 ($\nu_{\text{C-H}}$), 1690 ($\nu_{\text{C}=\text{C}}$) cm^{-1} . Anal. Calcd for $\text{WC}_{58}\text{H}_{47}\text{N}$: C, 73.96; H, 5.03; N, 1.83. Found: C, 73.75; H, 5.03; N, 1.50.

Structure Determination for $W(\text{PhC}\equiv\text{CPh})_3(\text{NH}=\text{C}(\text{Me})_2)$. A crystal of $W(\text{PhC}\equiv\text{CPh})_3(\text{NH}=\text{C}(\text{Me})_2)$ (**1**) with approximate dimensions 0.05 × 0.10 × 0.17 mm was mounted in a thin-walled glass capillary and aligned on the Nonius CAD-4 diffractometer. Diffraction data were collected with Mo $K\alpha$ radiation ($\lambda = 0.7093$ Å) using the $\theta/2\theta$ scan mode. Lattice parameters were determined from 25 randomly selected reflections with the 2θ angle in the range 16.84–25.60°. All data were corrected for Lorentz and polarization effects and for the effects of absorption. The structure was solved by the heavy-atom method and refined by least-squares cycles; all non-hydrogen atoms were refined with anisotropic thermal parameters. The program used is the NRCSDP-VAX package. The data collection and refinement parameters are given in Table 1. Atomic positional parameters are collected in Table

Table 2. Atomic Parameters for Compound 1

	x	y	z	B_{eq}^a
W	0.39014(2)	0.15150(2)	0.129509(8)	2.71(1)
N	0.3146(4)	0.3475(5)	0.1346(1)	3.2(2)
C1	0.3039(5)	0.1212(5)	0.1834(2)	2.7(3)
C2	0.3626(5)	0.0152(5)	0.1735(2)	2.8(3)
C3	0.2838(5)	0.1449(6)	0.0736(2)	3.2(3)
C4	0.3355(5)	0.0338(6)	0.0805(2)	3.2(3)
C5	0.5718(5)	0.2389(6)	0.1328(2)	3.0(3)
C6	0.5908(5)	0.1179(5)	0.1282(2)	2.6(3)
C7	0.1996(5)	0.4010(5)	0.1336(2)	3.6(3)
C8	0.1824(6)	0.5394(6)	0.1417(2)	5.6(4)
C9	0.0758(5)	0.3234(6)	0.1273(2)	5.1(4)
C11	0.225(5)	0.1789(6)	0.2141(2)	3.3(3)
C12	0.1050(6)	0.1254(6)	0.2232(2)	4.3(3)
C13	0.0288(6)	0.1847(7)	0.2511(2)	5.8(4)
C14	0.0723(7)	0.2947(7)	0.2695(2)	6.9(4)
C15	0.1895(7)	0.3483(8)	0.2610(2)	6.9(5)
C16	0.2645(6)	0.2924(6)	0.2330(2)	4.3(3)
C21	0.3895(5)	-0.1109(5)	0.1903(2)	3.2(3)
C22	0.3272(6)	-0.1566(6)	0.2238(2)	4.5(3)
C23	0.3552(6)	-0.2757(6)	0.2396(2)	5.2(4)
C24	0.4464(6)	-0.3538(6)	0.2237(2)	4.5(3)
C25	0.5092(6)	-0.3104(6)	0.1905(2)	4.5(3)
C26	0.4814(5)	-0.1912(6)	0.1747(2)	3.9(3)
C31	0.1981(5)	0.2081(5)	0.0424(2)	3.3(3)
C32	0.0750(5)	0.1570(6)	0.0284(2)	4.0(3)
C33	-0.0089(6)	0.2193(6)	0.0003(2)	4.6(3)
C34	0.0271(6)	0.3342(7)	-0.0156(2)	4.9(4)
C35	0.1479(6)	0.3867(5)	-0.0028(2)	4.4(4)
C36	0.2319(5)	0.3248(6)	0.0262(2)	3.8(3)
C41	0.3439(5)	-0.0857(5)	0.0577(2)	2.9(3)
C42	0.3385(6)	-0.2058(6)	0.0758(2)	4.1(3)
C43	0.3516(6)	-0.3165(6)	0.0533(2)	4.8(4)
C44	0.3744(6)	-0.3075(6)	0.0130(2)	5.0(4)
C45	0.3802(6)	-0.1926(6)	-0.0055(2)	5.2(4)
C46	0.3636(6)	-0.0828(6)	0.0165(2)	3.9(3)
C51	0.6464(5)	0.3590(6)	0.1334(2)	2.9(3)
C52	0.6214(6)	0.4483(6)	0.1030(2)	4.4(3)
C53	0.6904(7)	0.5624(6)	0.1027(2)	5.8(4)
C54	0.7838(6)	0.5893(6)	0.1339(2)	5.8(4)
C55	0.8088(6)	0.5053(6)	0.1645(2)	4.7(3)
C56	0.7411(5)	0.3916(6)	0.1651(2)	3.9(3)
C61	0.7051(5)	0.0373(5)	0.1193(2)	3.0(3)
C62	0.6923(5)	-0.0546(6)	0.0892(2)	3.3(3)
C63	0.8013(5)	-0.1187(6)	0.0775(2)	3.8(3)
C64	0.9256(5)	-0.0974(6)	0.0966(2)	4.1(3)
C65	0.9414(5)	-0.0095(6)	0.1276(2)	4.2(3)
C66	0.8316(5)	0.0586(5)	0.1386(2)	3.4(3)
HN	0.386	0.412	0.139	3.9

$$^a B_{\text{eq}} = \frac{1}{3} \pi^2 \sum_i \sum_j U_{ij} a_i^* a_j^* a_i a_j$$

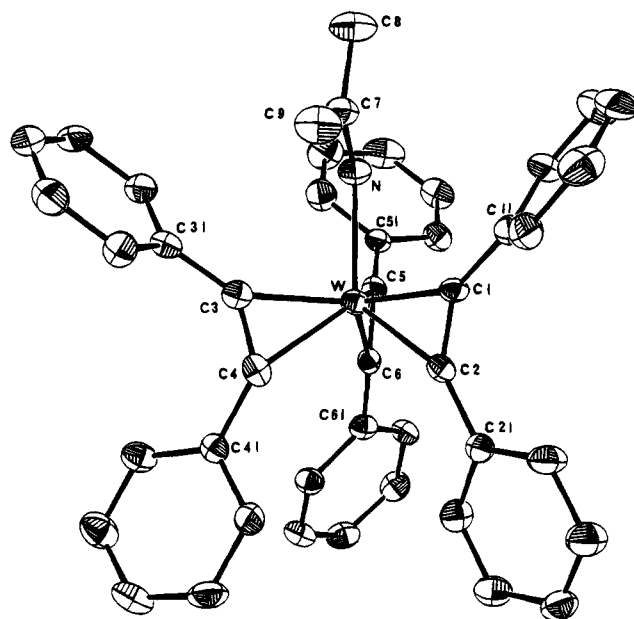
2. Selected bond distances and bond angles are given in Table 3.

Results and Discussion

Synthesis and Characterization of $W(\text{PhC}\equiv\text{CPh})_3(\text{NH}=\text{C}(\text{Me})_2)$. Treating $W(\text{PhC}\equiv\text{CPh})_3(\text{NCMe})$ with an equimolar amount of MeLi in THF solution at ambient temperature, followed by adding a slight excess of water, produces $W(\text{PhC}\equiv\text{CPh})_3(\text{NH}=\text{C}(\text{Me})_2)$ (**1**) in 53% yield. Replacing H_2O by D_2O in the second step affords $W(\text{PhC}\equiv\text{CPh})_3(\text{ND}=\text{C}(\text{Me})_2)$ (**1-d**). Thus, it is likely that initial Me^- attack occurs at the nitrile carbon to form $[W(\text{PhC}\equiv\text{CPh})_3(\text{N}=\text{C}(\text{Me})_2)]^-$, and subsequent protonation at the nitrogen lone pair by water seems more attractive than metal protonation followed by hydrogen migration to give compound **1**. The ^1H NMR spectrum of **1** shows two sharp singlets at δ 1.23 and 2.23 for the two inequivalent methyl protons, a multiplet in the range δ 7.49–7.11 for the phenyl protons, and a broad singlet at δ 11.47 for the imine

Table 3. Selected Bond Distances (Å) and Bond Angles (deg) of Compound 1

Bond Distances			
W-N	2.201(5)	C2-C21	1.449(8)
W-C1	2.064(5)	C3-C4	1.288(8)
W-C2	2.068(5)	C3-C31	1.445(8)
W-C3	2.049(5)	C4-C41	1.465(8)
W-C4	2.067(5)	C5-C6	1.293(8)
W-C5	2.041(5)	C5-C51	1.465(8)
W-C6	2.057(5)	C6-C61	1.477(7)
N-C7	1.284(7)	C7-C8	1.487(9)
C1-C2	1.313(7)	C7-C9	1.489(8)
C1-C11	1.465(7)		
Bond Angles			
N-W-C1	84.5(2)	W-C1-C2	71.7(3)
N-W-C2	121.6(2)	W-C1-C11	145.1(4)
N-W-C3	86.6(2)	C2-C1-C11	143.3(5)
N-W-C4	123.0(2)	W-C2-C1	71.3(3)
N-W-C5	83.8(2)	W-C2-C21	149.9(4)
N-W-C6	120.6(2)	C1-C2-C21	138.6(5)
C1-W-C2	37.0(2)	W-C3-C4	72.5(3)
C1-W-C3	122.6(2)	W-C3-C31	149.1(4)
C1-W-C4	118.3(2)	C4-C3-C31	138.4(5)
C1-W-C5	117.7(2)	W-C4-C3	71.0(3)
C1-W-C6	118.6(2)	W-C4-C41	152.4(4)
C2-W-C3	120.9(2)	C3-C4-C41	136.2(5)
C2-W-C4	95.2(2)	W-C5-C6	72.3(3)
C2-W-C5	116.4(2)	W-C5-C51	147.4(4)
C2-W-C6	95.0(2)	C6-C5-C51	139.7(5)
C3-W-C4	36.5(2)	W-C6-C5	70.9(3)
C3-W-C5	117.5(2)	W-C6-C61	152.4(4)
C3-W-C6	114.5(1)	C5-C6-C61	135.2(5)
C4-W-C5	119.2(2)	N-C7-C8	122.6(5)
C4-W-C6	94.5(2)	N-C7-C9	120.6(5)
C5-W-C6	36.8(2)	C8-C7-C9	116.6(5)
W-N-C7	136.2(4)		

**Figure 1.** Molecular structure of $W(\text{PhC}\equiv\text{CPh})_3(\text{NH}=\text{C}(\text{Me})_2)$ (**1**), showing the atomic labeling used in the text.

missing ^1H NMR signal at δ 11.47 and the IR $\nu_{\text{N-D}}$ band shifted to 2432 cm^{-1} due to the heavier-atom isotope effect.¹³

Crystal Structure of $W(\text{PhC}\equiv\text{CPh})_3(\text{NH}=\text{C}(\text{Me})_2)$.

Crystals of $W(\text{PhC}\equiv\text{CPh})_3(\text{NH}=\text{C}(\text{Me})_2)$ (**1**) contain an ordered array of discrete monomeric molecule units which are mutually separated by normal van der Waals distances. The labeling of atoms within the molecule is shown in Figure 1. Taking the centers of C1C2 (cen1), C3C4 (cen2), and C5C6 (cen3), the coordination about the tungsten atom can be described as a distorted tetrahedron from the angles: cen1-W-N = $104.4(2)^\circ$, cen2-W-N = $104.9(2)^\circ$, cen3-W-N = $102.2(2)^\circ$, cen1-W-cen2 = $114.4(2)^\circ$, cen1-W-cen3 = $115.5(2)^\circ$, and cen2-W-cen3 = $113.5(2)^\circ$. The imine group is η^1 -coordinated to W with W-N = $2.201(5)\text{ \AA}$ and N-C7 = $1.284(7)\text{ \AA}$, characteristic of a W-N single bond^{2m,14} and C-N double bond.¹⁵ The N, C7, C8, and C9 lie in a plane, and the tungsten atom lies only $0.12(1)\text{ \AA}$ out of this plane. The three diphenylacetylene ligands are essentially eclipsed with respect to the W-N vector, as evidenced by the torsional angles N-W-C2-C1 = $2.2(3)^\circ$, N-W-C4-C3 = $4.8(3)^\circ$, and N-W-C6-C5 = $2.5(3)^\circ$. However, the coordinated imine ligand is sterically forcing the alkyne ligands from being parallel, thus C1C2 is tilted from the W-N vector by 13.01° , C3C4 by 14.6° , and C5C6 by 11.72° . This gives rise to a slight difference between the upper and lower C-W distances; such that W-C1 = $2.064(5)\text{ \AA}$, W-C3 = $2.049(5)\text{ \AA}$, and W-C5 = $2.041(5)\text{ \AA}$ are slightly shorter than W-C2 = $2.068(5)\text{ \AA}$, W-C4 = $2.067(5)\text{ \AA}$, and W-C6 = $2.057(5)\text{ \AA}$. The C=C lengths are not equal, ranging from $1.313(7)\text{ \AA}$ (C1C2) to $1.288(8)\text{ \AA}$ (C3C4), and the phenyl groups are bent back from the C=C axis with an averaged angle of 138.6° (range, $135.2\text{--}143.3^\circ$).

proton, probably due to N-14 quadrupole relaxation.⁷ The $^{13}\text{C}\{^1\text{H}\}$ NMR spectrum reveals the alkyne C=C carbon resonances at δ 199.2 and 184.2, the imine carbon resonance at δ 187.4, the phenyl carbon resonances between δ 143.5 and 125.9, and the two methyl carbon resonances at δ 31.3 and 25.4. The alkyne carbon resonances are comparable with those measured for $W(\text{PhC}\equiv\text{CPh})_3(\text{CO})^6$ (δ 192.6 and 174.5), $W(\text{PhC}\equiv\text{CPh})_3(\text{PMe}_2\text{Ph})^8$ (δ 197.8 and 180.4), $W(\text{PhC}\equiv\text{CPh})_3(\text{NCMe})$ (δ 196.4 and 182.4), and $[W(\text{PhC}\equiv\text{CPh})_3(\text{SnPh}_3)]^-$ (δ 193.7 and 183.3).⁹ Since the imine group is normally considered as a two-electron donor, the remaining three alkyne ligands must provide ten electrons, presumably from three $\pi(\parallel)$ and two $\pi(\perp)$ orbitals,¹⁰ to the neutral tungsten atom to satisfy the 18-electron rule. This gives a time-averaged $3\frac{1}{3}$ electron donor for each alkyne ligand. It has been demonstrated^{11,12} that the acetylene carbon resonances of *ca.* δ 220 and 160 are expected for a four-electron and three-electron donor alkyne ligand, respectively. The IR spectrum in a KBr disk shows the $\nu_{\text{N-H}}$ peak at 3284 cm^{-1} and the $\nu_{\text{C=C}}$ peak at 1668 cm^{-1} , consistent with the proposed formulation.

The spectroscopic data for $W(\text{PhC}\equiv\text{CPh})_3(\text{ND}=\text{C}(\text{Me})_2)$ (**1-d**) are identical with those for **1**, except for the

(7) Drago, R. S. *Physical Methods in Chemistry*, 2nd ed.; Saunders College Publishing: New York, 1992; pp 604.

(8) Wink, D.; Cooper, N. J. *Organometallics* **1991**, *10*, 494.

(9) Maher, J. M.; Beatty, R. P.; Cooper, N. J. *J. Am. Chem. Soc.* **1984**, *106*, 2347.

(10) King, R. B. *Inorg. Chem.* **1968**, *7*, 1044.

(11) Templeton, J. L. *Adv. Organomet. Chem.* **1989**, *29*, 1 and references therein.

(12) Wink, D. J.; Greagan, T. *Organometallics* **1990**, *9*, 328.

(13) Shriver, D. F.; Atkins, P. W.; Langford, C. H. *Inorganic Chemistry*; Oxford University Press: Oxford, U.K., 1990; pp 266.

(14) Cotton, F. A.; Wilkinson, G. *Advanced Inorganic Chemistry*, 5th ed.; John Wiley & Sons: New York, 1988.

(15) Michelin, R. A.; Bertani, R.; Mozzon, M.; Bombieri, G.; Benetollo, F.; Angelici, R. J. *Organometallics* **1991**, *10*, 1751.

Synthesis and Characterization of $W(\text{PhC}\equiv\text{CPh})_3(\text{NH}=\text{C}(\text{Ph})\text{Me})$ and $W(\eta^4\text{-C}_4\text{Ph}_4)(\text{PhC}\equiv\text{CPh})_2(\text{NH}=\text{C}(\text{Ph})\text{Me})$. Treating $W(\text{PhC}\equiv\text{CPh})_3(\text{NCMe})$ with 1 equiv of PhLi in THF solution at ambient temperature followed by hydrolysis produces $W(\text{PhC}\equiv\text{CPh})_3(\text{NH}=\text{C}(\text{Ph})\text{Me})$ (**2**) in 48% yield. Again, Ph^- seems to attack the nitrile carbon initially to generate an azavinylidene species $[W(\text{PhC}\equiv\text{CPh})_3(\text{N}=\text{C}(\text{Ph})\text{Me})]^-$, which is then protonated by H_2O to give the observed products. The same treatment with $W(\eta^4\text{-C}_4\text{Ph}_4)(\text{PhC}\equiv\text{CPh})_2(\text{NCMe})$ produces $W(\eta^4\text{-C}_4\text{Ph}_4)(\text{PhC}\equiv\text{CPh})_2(\text{NH}=\text{C}(\text{Ph})\text{Me})$ (**5**) in 46% yield.

$W(\text{PhC}\equiv\text{CPh})_3(\text{NH}=\text{C}(\text{Ph})\text{Me})$ (**2**) forms air-stable, pale yellow crystals. The IR spectrum in a KBr disk includes a weak, sharp band at 3288 cm^{-1} , assigned to $\nu_{\text{N-H}}$, and a medium, broad band at 1656 cm^{-1} , assigned to $\nu_{\text{C}\equiv\text{C}}$. The ^1H NMR shows a sharp signal at δ 1.65 for the methyl protons, the phenyl protons in the range δ 7.54–7.11, and the imine proton at δ 12.22. The room temperature $^{13}\text{C}\{^1\text{H}\}$ NMR spectrum in CDCl_3 exhibits the alkyne carbon resonances at δ 199.1 and 184.0, the imine N=C carbon resonance at δ 184.1, the phenyl carbon resonances ranging from δ 143.5 to 126.0, and the methyl carbon resonance at δ 23.0. If the alkyne orientations in **2** are assumed to be the same as those in **1**, the carbon signals at δ 199.1 and 184.0 can be assigned to the distal and the proximal $\equiv\text{CPh}$ groups,⁸ respectively.

$W(\eta^4\text{-C}_4\text{Ph}_4)(\text{PhC}\equiv\text{CPh})_2(\text{NH}=\text{C}(\text{Ph})\text{Me})$ (**5**) forms air-stable, orange crystals. The IR spectrum in a KBr disk presents the $\nu_{\text{N-H}}$ band at 3260 cm^{-1} and the $\nu_{\text{C}\equiv\text{C}}$ band at 1670 cm^{-1} . The ^1H NMR spectrum shows the methyl protons at δ 1.24, the phenyl protons between δ 7.45 and 6.82, and the imine proton at δ 10.79 which is significantly upfield of that for **2** (δ 12.22). The $^{13}\text{C}\{^1\text{H}\}$ NMR spectrum at room temperature exhibits the imine N=C carbon resonance at δ 184.0 and the cyclobutadiene carbon resonance as a sharp singlet at δ 85.8, suggesting a facile ring rotation for the cyclobutadiene ligand. The alkyne C=C carbon signals coalesce at room temperature and remain undetectable at $-50\text{ }^\circ\text{C}$. In contrast, the slow-exchange alkyne carbon resonances are recorded at room temperature for $W(\eta^4\text{-C}_4\text{Ph}_4)(\text{PhC}\equiv\text{CPh})_2(\text{CO})$ (δ 175.9 and 158.9) and $W(\eta^4\text{-C}_4\text{Ph}_4)(\text{PhC}\equiv\text{CPh})_2(\text{NCMe})$ (δ 186.5 and 174.8).⁵ One possible explanation for a low barrier to alkyne rotation in **5** could be that the steric crowding caused by the imine group destabilizes the ground state and stabilizes the transition state, with the C=C vector parallel and perpendicular to the W–N bond, respectively.⁸

Synthesis and Characterization of $W(\text{PhC}\equiv\text{CPh})_3(\text{NH}_2\text{Et})$ and $W(\eta^4\text{-C}_4\text{Ph}_4)(\text{PhC}\equiv\text{CPh})_2(\text{NH}_2\text{Et})$. Treating $W(\text{PhC}\equiv\text{CPh})_3(\text{NCMe})$ and $W(\eta^4\text{-C}_4\text{Ph}_4)(\text{PhC}\equiv\text{CPh})_2(\text{NCMe})$ with 2 equiv of LiHBEt_3 and then water in THF solution affords the amine complexes $W(\text{PhC}\equiv\text{CPh})_3(\text{NH}_2\text{Et})$ (**3**) and $W(\eta^4\text{-C}_4\text{Ph}_4)(\text{PhC}\equiv\text{CPh})_2(\text{NH}_2\text{Et})$ (**4**) in 52% and 48% yields, respectively. Applying LiDBEt_3 at the first stage produces $W(\text{PhC}\equiv\text{CPh})_3(\text{NH}_2\text{CD}_2\text{CH}_3)$ (**3-d**₂) and $W(\eta^4\text{-C}_4\text{Ph}_4)(\text{PhC}\equiv\text{CPh})_2(\text{NH}_2\text{CD}_2\text{CH}_3)$ (**4-d**₂). However, contrary to the results found for **1**, replacing H_2O by D_2O in the second step does not incorporate the deuterium atoms in the amine position. Moreover, the amine protons of **3** and **4** do not undergo H/D exchange with added D_2O

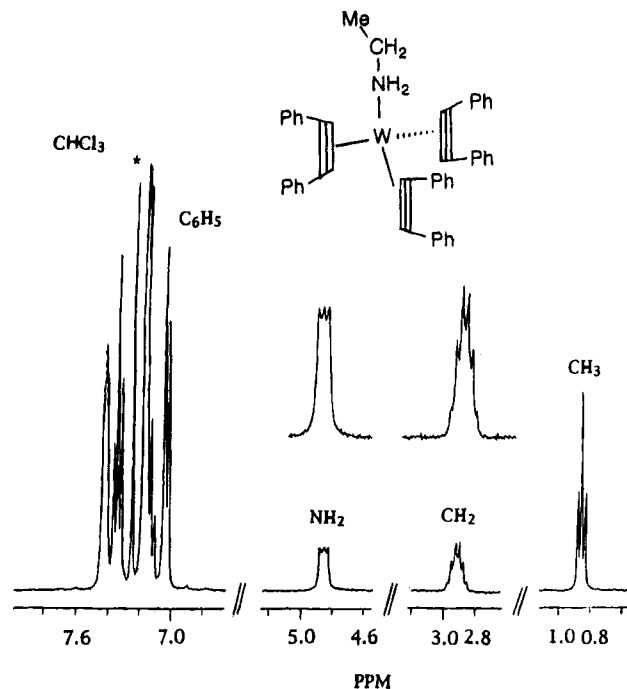


Figure 2. 300 MHz ^1H NMR spectrum of $W(\text{PhC}\equiv\text{CPh})_3(\text{NH}_2\text{Et})$ (**3**) in CDCl_3 .

in CD_2Cl_2 solution, and the ^1H NMR spectrum of $W(\text{PhC}\equiv\text{CPh})_3(\text{NCMe})$ combined with LiHBEt_3 in THF-d_3 shows no formation of compound **3** before introducing water into the reaction mixture. This suggests that the nitrogen lone pairs abstract protons not directly from water, but presumably from solvent or the alkyl groups of the borate reagent after hydrolysis. We have no mechanistic information. It seems that repeated H^- attack at the nitrile carbon occurs to generate a nitrene species $[\text{L}_n\text{W}=\text{N}-\text{CH}_2\text{Me}]^{2-}$ followed by protonation at the nitrogen atom to give the amine products. However, we cannot rule out the possibility of stepwise H^-/H^+ additions to the carbon–nitrogen triple bond, as observed in the reduction of $[\text{Tp}'(\text{CO})(\text{RC}\equiv\text{CR})\text{W}(\text{NCMe})]^+$ by Templeton.^{21–23} Note that protonation of coordinated phenylnitrene ($\text{M}=\text{N}-\text{Ph}$) to release aniline was previously reported in a Cr system.¹⁶

$W(\text{PhC}\equiv\text{CPh})_3(\text{NH}_2\text{Et})$ (**3**) forms air-stable, colorless crystals. The ^1H NMR spectrum, shown in Figure 2, consists of a complex multiplet in the range δ 7.45–7.02 for the phenyl protons, a triplet at δ 4.84 with $^3J_{\text{H-H}} = 9\text{ Hz}$ for the amine protons, a pseudosextet at δ 2.92 for the methylene protons, and a triplet at δ 0.86 with $^3J_{\text{H-H}} = 7\text{ Hz}$ for the methyl protons. The ^1H NMR spectrum of $W(\text{PhC}\equiv\text{CPh})_3(\text{NH}_2\text{CD}_2\text{CH}_3)$ (**3-d**₂) shows no signal at δ 2.92 and the resonances at δ 4.84 and 0.86 appearing as a broad and a sharp singlet, respectively. The $^{13}\text{C}\{^1\text{H}\}$ NMR spectrum reveals the alkyne carbon resonances at δ 200.2 and 184.8, the phenyl carbon resonances in the range δ 143.3–125.7, the methylene carbon resonance at δ 43.3, and the methyl carbon resonance at δ 19.5. The IR spectrum in a KBr disk includes two weak bands at 3344 and 3284 cm^{-1} , assigned to $\nu_{\text{N-H}}$, and a medium, broad band at 1660 cm^{-1} , assigned to $\nu_{\text{C}\equiv\text{C}}$, consistent with the proposed formulation.

$W(\eta^4\text{-C}_4\text{Ph}_4)(\text{PhC}\equiv\text{CPh})_2(\text{NH}_2\text{Et})$ (**4**) forms air-stable, orange crystals. The ^1H NMR spectrum resembles those

recorded for compound **3**, showing the amine protons at δ 3.92 as a broad triplet, the methylene protons at 2.69 as a sextet, and the methyl protons at δ 0.68 as a triplet. The $^{13}\text{C}\{^1\text{H}\}$ NMR spectrum reveals the phenyl carbon resonances ranging from δ 134.9 to 124.0, the cyclobutadiene carbon resonance at δ 87.2, the methylene carbon resonance at δ 43.7, and the methyl carbon resonance at δ 19.8. The alkyne carbon resonances collapse at room temperature and no distinct signals are observed down to -60°C .

Although amines are classical ligands in coordination chemistry, these are not often used with organotransition-metal complexes. Recently, we showed⁴ that $\text{W}(\text{PhC}\equiv\text{CPh})_3(\text{NCMe})$ underwent facile ligand substitution with phosphines to give $\text{W}(\text{PhC}\equiv\text{CPh})_3\text{L}$ ($\text{L} = \text{PMe}_3$, PPh_3 , or $(\text{PPh}_2)_2\text{CH}_2$), whereas treating $\text{W}(\text{PhC}\equiv\text{CPh})_3(\text{NCMe})$ or $\text{W}(\eta^4\text{-C}_4\text{Ph}_4)(\text{PhC}\equiv\text{CPh})_2(\text{NCMe})$ with ethylamine does not lead to the corresponding amine com-

plexes. The reaction of $\text{Cl}_2\text{Pt}(\text{NCMe})_2$ with aziridine to generate the imine complex $\text{Cl}_2\text{Pt}(\text{NH}=\text{C}(\text{NC}_2\text{H}_4)\text{Me})$ was previously reported by Michelin.^{15,17} Thus, it is not surprising if ethylamine attacks the acetonitrile ligand instead of replacing it. The details are still under investigation.

Acknowledgment. This research was supported by the National Science Council of the Republic of China.

Supplementary Material Available: Lists of crystal data, atomic coordinates, anisotropic thermal parameters, bond lengths, and bond angles (7 pages). Ordering information is given on any current masthead page.

OM940790J

(17) (a) Calligaro, L.; Michelin, R. A.; Uguagliati, P. *Inorg. Chim. Acta* **1983**, *76*, L83. (b) Uguagliati, P.; Belluco, U.; Michelin, R. A.; Guerriero, P. *Inorg. Chim. Acta* **1984**, *81*, 61.

Ligand Substitution at 17-Electron Centers. Electroactivation of Functionalized Cyclopentadienylmanganese Tricarbonyl Complexes to Single- and Double-CO Substitution

Y. Huang, G. B. Carpenter, and D. A. Sweigart*

Department of Chemistry, Brown University, Providence, Rhode Island 02912

Y. K. Chung and B. Y. Lee

Department of Chemistry, Seoul National University, Seoul 151-742, Korea

Received October 3, 1994[®]

Electrochemical oxidation of (MeCp)Mn(CO)₃ (**1**) in the presence of P(OEt)₃ leads to rapid single- and double-CO substitution. With analogous complexes (**3**–**5**) having bulky substituents on the cyclopentadienyl ring, the 17-electron species produced by electroactivation also undergo rapid single CO substitution, but at rates significantly reduced from that observed with **1**⁺; substitution of a second CO in **3**⁺–**5**⁺ is even more retarded. Digital simulations of an associative mechanism closely reproduced experimental data and allowed the reactivities of the 17-electron complexes to be quantified. The ability of bulky substituents to hinder the approach of a nucleophile to the metal was examined by determining the X-ray structure of (1,3-dimethyl-2-phenylcyclopentadienyl)Mn(CO)₃ (**3**): monoclinic, space group *P*2₁/*c*, *a* = 11.019(2) Å, *b* = 7.5631(10) Å, *c* = 17.716(2) Å, β = 103.381(12)°, *Z* = 4, 3273 unique reflections with *I* > 2σ(*I*), *R* = 0.0376, wR2 = 0.0912.

Introduction

The enhanced reactivity of 17-electron organometallic complexes to ligand substitution and atom abstraction is well documented.^{1–3} Published kinetic studies of CO substitution³ indicate that these radicals generally follow an associative mechanism and that the rate enhancement in comparison to 18-electron complexes is many orders of magnitude. In the present study, we show that the normally inert⁴ (MeCp)Mn(CO)₃ (**1**), as well as analogues variously functionalized on the cyclopentadienyl ring (**3**–**5**; see Figure 1), undergo extremely rapid substitution of one or two CO ligands

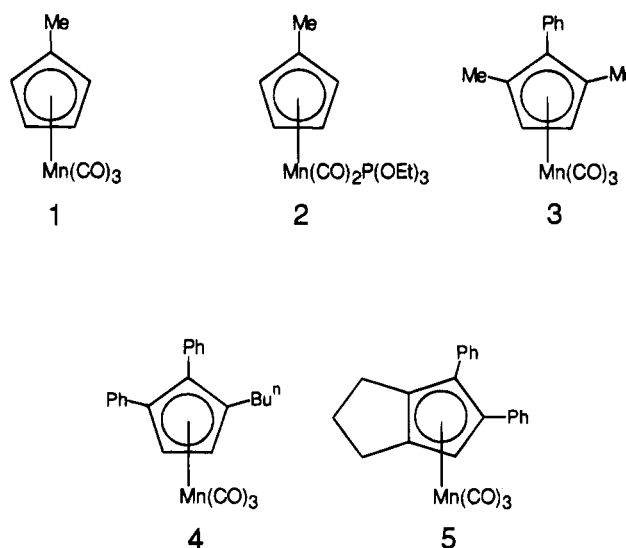


Figure 1. Numbering code for the complexes in this study.

upon oxidation in the presence of P(OEt)₃. The chemistry involved is illustrated in Scheme 1 (the nucleophile L is P(OEt)₃). The extent of single versus double substitution is markedly influenced by steric congestion in the vicinity of the metal due to substituents (R) on the cyclopentadienyl ring. Sufficiently bulky groups hinder access of the nucleophile to the metal center and inhibit the rate; the X-ray structure of **3** was determined in order to examine this effect.

As discussed below, oxidatively promoted CO substitution in (RCp)Mn(CO)₃ is not catalytic; the transformation (RCp)Mn(CO)₃ → (RCp)Mn(CO)₂L requires an initial stoichiometric oxidation, followed by CO substi-

[®] Abstract published in *Advance ACS Abstracts*, January 15, 1995.

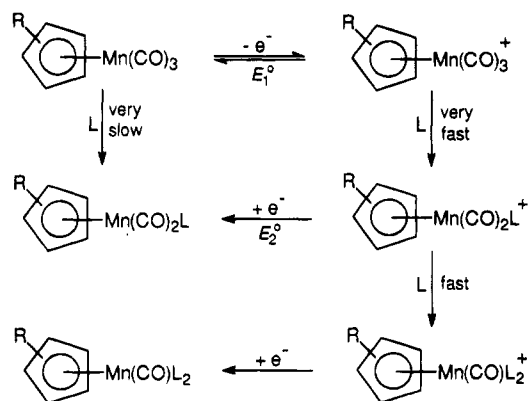
(1) (a) Tyler, D. R. *Prog. Inorg. Chem.* **1988**, *36*, 125. (b) Baird, M. C. *Chem. Rev.* **1988**, *88*, 1217. (c) Kuksis, I.; Baird, M. C. *Organometallics* **1994**, *13*, 1551. (d) Huber, T. A.; Macartney, D. H.; Baird, M. C. *Organometallics* **1993**, *12*, 4715. (e) Scott, S. L.; Espenson, J. H.; Zhu, Z. *J. Am. Chem. Soc.* **1993**, *115*, 1789. (f) Zhu, Z.; Espenson, J. H. *Organometallics* **1994**, *13*, 1893. (g) *Organometallic Radical Processes*; Trogler, W. C., Ed.; Elsevier: Amsterdam, 1990.

(2) (a) Hershberger, J. W.; Klingler, R. J.; Kochi, J. K. *J. Am. Chem. Soc.* **1983**, *105*, 61. (b) Zizelman, P. M.; Amatore, C.; Kochi, J. K. *J. Am. Chem. Soc.* **1984**, *106*, 3771. (c) Kochi, J. K. *J. Organomet. Chem.* **1986**, *300*, 139. (d) Poli, R.; Owens, B. E.; Linck, R. G. *Inorg. Chem.* **1992**, *31*, 662. (e) Legzdins, P.; McNeil, W. S.; Shaw, M. J. *Organometallics* **1994**, *13*, 562.

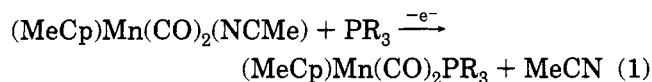
(3) (a) Pöe, A. *Transition Met. Chem.* **1982**, *7*, 65. (b) Fabian, B. D.; Labinger, J. A. *Organometallics* **1983**, *2*, 659. (c) Shi, Q.-Z.; Richmond, T. G.; Trogler, W. C.; Basolo, F. *J. Am. Chem. Soc.* **1984**, *106*, 71. (d) Herrinton, T. R.; Brown, T. L. *J. Am. Chem. Soc.* **1985**, *107*, 5700. (e) Turaki, N. N.; Huggins, J. M. *Organometallics* **1986**, *5*, 1703. (f) Kowaleski, R. M.; Basolo, F.; Trogler, W. C.; Gedridge, R. W.; Newbound, T. D.; Ernst, R. D. *J. Am. Chem. Soc.* **1987**, *109*, 4860. (g) Watkins, W. C.; Hensel, K.; Fortier, S.; Macartney, D. H.; Baird, M. C.; McLain, S. J. *Organometallics* **1992**, *11*, 2418. (h) Meng, Q.; Huang, Y.; Ryan, W. J.; Sweigart, D. A. *Inorg. Chem.* **1992**, *31*, 4051. (i) Shen, J. K.; Freeman, J. W.; Hallinan, N. C.; Rheingold, A. L.; Arif, A. M.; Ernst, R. D.; Basolo, F. *J. Am. Chem. Soc.* **1992**, *11*, 3215.

(4) Angelici, R. J.; Loewen, W. *Inorg. Chem.* **1967**, *6*, 682.

Scheme 1



tution in the 17-electron radical and then stoichiometric reduction. In order for an oxidatively promoted ligand substitution to be catalytic (i.e., electron transfer catalyzed), it is necessary that the 18-electron product be more difficult to oxidize than the reactant, which in turn requires that the reduction potentials in Scheme 1 be in the order $E_2^\circ > E_1^\circ$. In most substitutions, departing ligands are replaced by ones that increase the electron density at the metal so that $E_1^\circ > E_2^\circ$. Therefore, catalytic oxidative activation of organometallic complexes to ligand substitution is expected to be uncommon. (The same reasoning implies that catalytic reductive activation should be common.) Rare examples of catalytic oxidatively promoted ligand substitutions have been reported by Kochi et al.,^{2a-c} who studied a series of reactions typified by eq 1. Detailed electro-



chemical investigations by these workers showed that the 17-electron complex $(\text{MeCp})\text{Mn}(\text{CO})_2(\text{NCMe})^+$ is activated to rapid associative substitution of the MeCN ligand.

Experimental Section

Syntheses. Complex 1 was purchased from Strem Chemical Co. Photochemical substitution of CO in 1 by $\text{P}(\text{OEt})_3$ to give 2 was accomplished by a procedure analogous to that reported by Connelly and Kitchen⁵ for the synthesis of $(\text{MeCp})\text{Mn}(\text{CO})_2[\text{P}(\text{OMe})_3]$. Thus, UV irradiation of 1 (2.2 mmol) and $\text{P}(\text{OEt})_3$ (3.0 mmol) in 60 mL of THF produced a 2:1 mixture of 2 and $(\text{MeCp})\text{Mn}(\text{CO})[\text{P}(\text{OEt})_3]_2$, along with other unidentified species. Separation of 2 from the product mixture was effected by TLC on silica gel with diethyl ether/hexanes (1:25) as eluant. The purity of 2 (obtained in 15% yield) was established with certainty by electrochemical, ¹H NMR, and IR measurements (IR (THF) 1942, 1875 cm^{-1}). Complexes 3–5 were prepared by published procedures.^{6,7}

Crystal Structure of Complex 3. A crystal of 3 was grown by cooling of a hexane/diethyl ether solution. X-ray data collection was carried out using a Siemens P4 single-crystal diffractometer controlled by XSCANS software. ω scans were used for data collection, at variable speeds from 10 to 60°

(5) Connelly, N. G.; Kitchen, M. D. *J. Chem. Soc., Dalton Trans.* 1977, 931.

(6) Lee, B. Y.; Moon, H.; Chung, Y. K.; Jeong, N. *J. Am. Chem. Soc.* 1994, 116, 2163.

(7) Lee, B. Y.; Moon, H.; Chung, Y. K.; Jeong, N.; Carpenter, G. B. *Organometallics* 1993, 12, 3879.

Table 1. Crystal Structure Data for Complex 3

formula	$\text{C}_{16}\text{H}_{13}\text{MnO}_3$
fw	308.2
space group	$P2_1/c$, monoclinic
cryst dimens, mm	$0.35 \times 0.38 \times 0.65$
scan type	ω
a, Å	11.019(2)
b, Å	7.5631(10)
c, Å	17.716(2)
β , deg	103.381(12)
V, Å ³	1436.3(4)
Z	4
ρ_{calcd} , g cm^{-3}	1.425
F(000)	632
radiation	Mo K α , 0.710 73 Å
μ , cm^{-1}	9.22
2 θ limits, deg	1.90–27.50
no. of observns	4338
no. of unique data, $I > 2\sigma(I)$	3273
no. of variables	181
R^a ($I > 2\sigma(I)$)	0.0376
wR2 ^b ($I > 2\sigma(I)$)	0.0912
R (all data)	0.0589
wR2 (all data)	0.0986
GOF	0.905 ^c

^a $R = \sum ||F_o| - |F_c|| / \sum |F_o|$. ^b $wR2 = [\sum w(F_o^2 - F_c^2)^2 / \sum wF_o^4]^{1/2}$. ^c Based on F^2 .

Table 2. Atomic Coordinates ($\times 10^4$) and Isotropic Thermal Parameters ($\text{Å}^2 \times 10^3$) for Complex 3

	x	y	z	U_{eq}
Mn	2978(1)	2300(1)	662(1)	44(1)
O(1)	2386(3)	-115(3)	-666(1)	101(1)
O(2)	347(2)	3238(4)	514(1)	103(1)
O(3)	3509(3)	5174(3)	-330(1)	103(1)
C(1)	4077(2)	253(3)	1340(1)	44(1)
C(2)	3136(2)	830(3)	1720(1)	38(1)
C(3)	3352(2)	2684(3)	1899(1)	42(1)
C(4)	4393(2)	3200(3)	1619(1)	48(1)
C(5)	4840(2)	1723(3)	1276(1)	49(1)
C(6)	2651(2)	3843(3)	2342(1)	55(1)
C(7)	4282(3)	-1618(3)	1114(2)	60(1)
C(8)	2210(2)	-318(3)	1967(1)	40(1)
C(9)	1305(2)	-1268(3)	1451(1)	54(1)
C(10)	513(3)	-2400(3)	1717(2)	63(1)
C(11)	602(2)	-2594(3)	2501(2)	63(1)
C(12)	1472(2)	-1648(3)	3017(2)	58(1)
C(13)	2277(2)	-517(3)	2760(1)	47(1)
C(14)	2607(3)	844(4)	-147(1)	61(1)
C(15)	3282(3)	4060(4)	56(1)	66(1)
C(16)	1370(3)	2895(4)	554(1)	66(1)

min^{-1} . Three standard reflections were measured every 97 reflections with no systematic decrease in intensity observed. Data reduction included profile fitting and an empirical absorption correction based on separate azimuthal scans for eight reflections (maximum and minimum transmission 0.398 and 0.350). The structure was determined by Patterson methods and refined initially by use of programs in the SHELXTL 5.1 package. All of the hydrogen atoms appeared in a difference map. The hydrogen atoms were inserted in ideal positions, riding on the atoms to which they are bonded; they were refined with isotropic temperature factors 20% greater than that of the attached atom. All other atoms were refined with anisotropic thermal parameters. Final refinement on F^2 was carried out using SHELXL 93. Relevant structural data are given in Tables 1–3.

Electrochemical Studies. Voltammetric experiments were done under a blanket of nitrogen that was saturated with solvent. The electrolyte was 0.10 M Bu_4NPF_6 , which was synthesized by metathesis of Bu_4NBr and HPF_6 , recrystallized from $\text{CH}_2\text{Cl}_2/\text{hexanes}$, and dried under vacuum. The solvent in all experiments was CH_2Cl_2 , which was purchased in HPLC grade from Fisher Scientific (catalog numbers D143-1 and D150-1). Additional "purification" by distillation was not

Table 3. Selected Bond Lengths (Å) and Bond Angles (deg) for 3

Bond Lengths			
Mn-C(1)	2.153(2)	Mn-C(2)	2.151(2)
Mn-C(3)	2.154(2)	Mn-C(4)	2.131(2)
Mn-C(5)	2.133(2)	Mn-C(14)	1.779(3)
Mn-C(15)	1.790(3)	Mn-C(16)	1.794(3)
C(14)-O(1)	1.151(3)	C(15)-O(3)	1.149(3)
C(16)-O(2)	1.143(3)	C(1)-C(5)	1.414(3)
C(1)-C(2)	1.430(3)	C(1)-C(7)	1.502(3)
C(2)-C(3)	1.445(3)	C(2)-C(8)	1.481(3)
C(3)-C(4)	1.407(3)	C(3)-C(6)	1.504(3)
C(4)-C(5)	1.412(3)	C(8)-C(9)	1.387(3)
Bond Angles			
Mn-C(14)-O(1)	178.8(3)	Mn-C(15)-O(3)	178.2(3)
Mn-C(16)-O(2)	177.1(2)	Mn-C(1)-C(7)	129.0(2)
Mn-C(2)-C(8)	129.6(1)	Mn-C(3)-C(6)	127.5(2)
C(1)-C(2)-C(3)	107.4(2)	C(5)-C(1)-C(7)	126.2(2)
C(2)-C(1)-C(7)	125.7(2)	C(1)-C(2)-C(8)	125.8(2)
C(3)-C(2)-C(8)	126.4(2)	C(2)-C(3)-C(6)	127.0(2)
C(4)-C(3)-C(6)	125.6(2)	C(2)-C(8)-C(13)	118.7(2)
C(2)-C(8)-C(9)	123.3(2)	C(1)-C(5)-C(4)	108.4(2)

necessary (or desirable), as judged by the solvent potential window and the chemical reversibility of the oxidation of (benzene)Cr(CO)₃, a complex known⁸ to be very sensitive to trace nucleophilic impurities. Once opened, the solvent was kept under argon or nitrogen and contact with the atmosphere was kept to a minimum.

Cyclic voltammetry was done with EG&G 173/175/179 potentiostatic instrumentation. The working electrode was a 1 mm diameter platinum or glassy-carbon disk, and the counter electrode was a platinum wire. The reference was a Metrohm Ag/AgCl electrode filled with CH₂Cl₂/0.10 M Bu₄NClO₄ and saturated with LiCl; this was separated from the test solution by a salt bridge containing 0.10 M Bu₄NPF₆ in CH₂Cl₂. IR spectroelectrochemistry was done with an optically transparent thin-layer electrode (OTTLE), the construction and use of which have been reported.⁹ Bulk electrolyses were done with a platinum-basket working electrode and a platinum-mesh counter electrode, which was separated from the test solution by a salt bridge. Digital simulation of proposed mechanisms utilized the program DigiSim.¹⁰ This program utilizes an efficient fast implicit finite difference algorithm and is able to simulate moderately complex mechanisms within a few minutes on a PC with a 486 chip. Data input includes an *E*⁰ value for each heterogeneous electron-transfer step and an estimate of the rate constants for any homogeneous reactions. In agreement with experimental data, the relevant heterogeneous electron transfers were taken as Nernstian. The simulation results were found to be quite sensitive to the input values of the homogeneous rate constants, which were altered in a systematic manner until the voltammetric shapes and current ratios closely matched the experimental ones. A reasonable estimate of the precision with which the rate constants were determined is ±20%.

Results and Discussion

The results of the voltammetric oxidation of **1** in CH₂Cl₂ are illustrated in Figure 2. In the absence of a nucleophile and at ordinary scan rates the cyclic voltammogram (CV) corresponds to a one-electron chemically

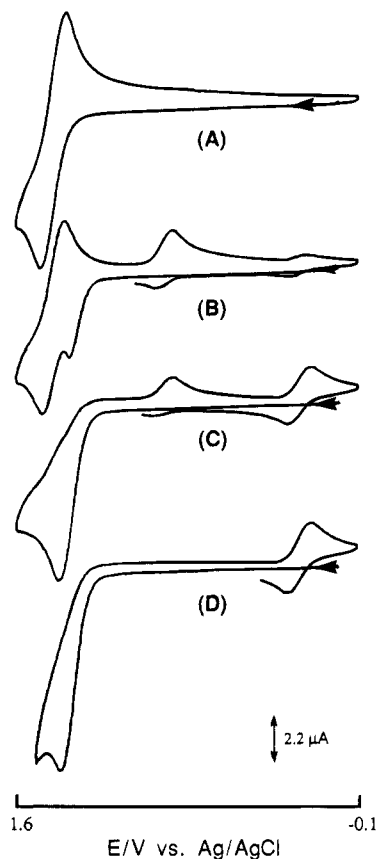


Figure 2. Cyclic voltammograms of 1.11 mM complex **1** in CH₂Cl₂/0.1 M Bu₄NPF₆ at 25 °C with P(OEt)₃ present at the following concentrations (mM): (A) none; (B) 0.41; (C) 1.26; (D) 3.60. The working electrode was a 1.0 mm diameter glassy-carbon disk, and the scan rate was 0.50 V s⁻¹. All potentials are relative to *E*_{1/2}(ferrocene) = 0.55 V.

reversible process (*E*_{1/2} = 1.40 V¹¹), in agreement with results from previous studies.^{5,12} We found, however, that the reversibility is lost in the presence of P(OEt)₃ and that in this case the oxidation of **1** leads to the appearance of two new reversible couples at *E*_{1/2} = 0.85 and 0.18 V¹¹ (Figure 2B–D). IR spectra taken after the electrochemical experiments verified that there was no reaction in the bulk solution. IR OTTLE experiments suggested that the two new complexes resulted from rapid single- and double-CO substitution in **1**⁺ to give the cations [(MeCp)Mn(CO)_{3-n}[P(OEt)₃]_n]⁺ (*n* = 1, 2). In Figure 2B a deficiency of P(OEt)₃ limits the reaction to the single substitution **1**⁺ → **2**⁺, with the reduction wave near 0.85 V being attributed to **2**⁺. As more P(OEt)₃ is added, double substitution to yield (MeCp)-Mn(CO)[P(OEt)₃]₂⁺ becomes competitive (Figure 2C) or dominant (Figure 2D). Verification of these assignments was provided by a comparison of *ν*_{CO} bands found in IR OTTLE oxidation and subsequent reduction of [1, P(OEt)₃]_n mixtures in CH₂Cl₂ with published⁵ *ν*_{CO} data for [(MeCp)Mn(CO)_{3-n}L_n]⁺⁰ complexes (L = PR₃, P(OR)₃) and with IR data for genuine samples of (MeCp)Mn(CO)₂P(OEt)₃ (**2**) and (MeCp)Mn(CO)[P(OEt)₃]₂. Furthermore, voltammetric experiments with **2** gave a reversible couple at exactly the *E*_{1/2} value shown in Figure 2B.

(8) Stone, N. J.; Sweigart, D. A.; Bond, A. M. *Organometallics* **1986**, *5*, 2553.

(9) (a) Bullock, J. P.; Boyd, D. C.; Mann, K. R. *Inorg. Chem.* **1987**, *26*, 3086. (b) Pike, R. D.; Alavosus, T. J.; Camaioni-Neto, C. A.; Williams, J. C.; Sweigart, D. A. *Organometallics* **1989**, *8*, 2631.

(10) (a) DigiSim 1.0 program; Bioanalytical Systems, Inc., West Lafayette, IN. (b) Rudolph, M.; Reddy, D. P.; Feldberg, S. W. *Anal. Chem.*, submitted for publication.

(11) All potentials reported are relative to ferrocene, *E*_{1/2} = +0.55 V.

(12) Denisovich, L. I.; Zakurin, N. V.; Gubin, S. P.; Ginzburg, A. G. *J. Organomet. Chem.* **1975**, *101*, C43.

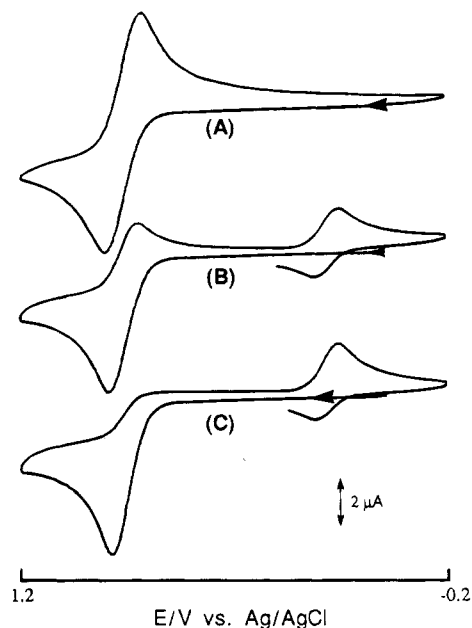


Figure 3. Cyclic voltammograms of 1.00 mM complex **2** in $\text{CH}_2\text{Cl}_2/0.1 \text{ M Bu}_4\text{NPF}_6$ at 25°C with $\text{P}(\text{OEt})_3$ present at the following concentrations (mM): (A) none; (B) 1.20; (C) 5.90. The working electrode was a 1.0 mm diameter platinum disk, and the scan rate was 0.50 V s^{-1} . All potentials are relative to $E_{1/2}(\text{ferrocene}) = 0.55 \text{ V}$.

The replacement of CO in 2^+ by $\text{P}(\text{OEt})_3$ to give $(\text{MeCp})\text{Mn}(\text{CO})[\text{P}(\text{OEt})_3]_2^+$ was probed directly by the voltammetric oxidation of **2** in the presence of $\text{P}(\text{OEt})_3$. Figure 3 gives some results. The electrochemical behavior indicates that 2^+ undergoes clean CO substitution. Digital simulation of the observed CV's in 14 experiments covering a scan rate range of $0.50\text{--}50 \text{ V s}^{-1}$ and a $[\text{P}(\text{OEt})_3]$ range of 1.0 to 20 mM (with **2** at 1.0 mM) established that the rate law for CO substitution in 2^+ is first order in both the metal complex and $\text{P}(\text{OEt})_3$, with a second-order rate constant of $(3.1 \pm 0.5) \times 10^3 \text{ M}^{-1} \text{ s}^{-1}$ at 25°C .

We next examined what effect substituents on the cyclopentadienyl ring have on single- and double-CO substitution in the 17-electron cationic radicals. Figure 4 illustrates the behavior of complex **3**. It can be seen that one CO in 3^+ is readily replaced by $\text{P}(\text{OEt})_3$. However, by comparison to the results shown in Figure 2, it is apparent that double-CO substitution is much more difficult in 3^+ than in 1^+ . In particular, the CV's in Figure 2D and 4D, which refer to experiments with similar $\text{P}(\text{OEt})_3$ concentrations, illustrate the difference rather strikingly. Electrochemical experiments performed with complexes **1** and **3–5** showed that all undergo chemically reversible one-electron oxidation at 0.50 V s^{-1} in $\text{CH}_2\text{Cl}_2/\text{Bu}_4\text{NPF}_6$ with $E_{1/2}$'s in the range 1.37–1.43 V.¹¹ The propensity for double-CO substitution by $\text{P}(\text{OEt})_3$ was found to follow the reactivity order $1^+ > 3^+ \approx 4^+ > 5^+$ (vide infra).

The obvious interpretation of the above order is that it is steric in origin; i.e., it seems likely that bulky substituents inhibit the approach of the nucleophile $\text{P}(\text{OEt})_3$ to the metal. This would be particularly true for the second CO substitution, since the presence of the first $\text{P}(\text{OEt})_3$ would only serve to enhance the steric congestion in the transition state for an associative process. In order to examine the proposed steric effects more closely, the X-ray structure of **3** was obtained.

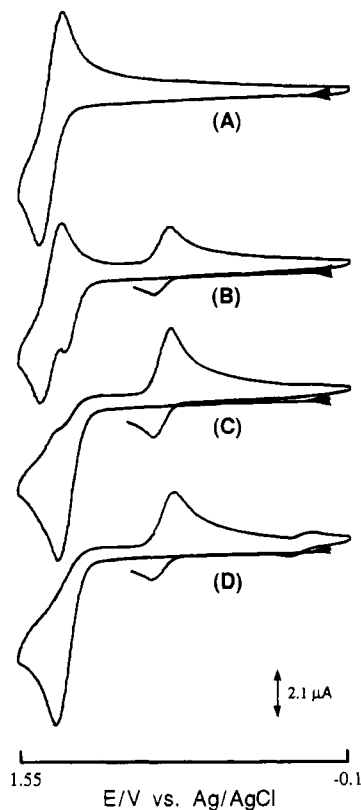


Figure 4. Cyclic voltammograms of 1.00 mM complex **3** in $\text{CH}_2\text{Cl}_2/0.1 \text{ M Bu}_4\text{NPF}_6$ at 25°C with $\text{P}(\text{OEt})_3$ present at the following concentrations (mM): (A) none, (B) 0.36; (C) 0.79; (D) 3.40. The working electrode was a 1.0 mm diameter glassy-carbon disk, and the scan rate was 0.50 V s^{-1} . All potentials are relative to $E_{1/2}(\text{ferrocene}) = 0.55 \text{ V}$.

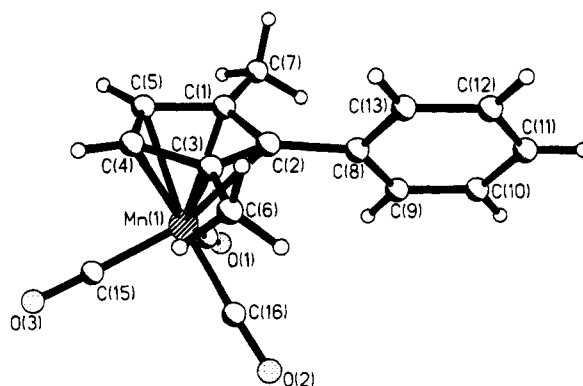


Figure 5. Structural drawing and atomic numbering scheme for complex **3**.

Figures 5 and 6 illustrate the molecular geometry, and Tables 1–3 provide pertinent structural data. Bond lengths and most bond angles in **3** are ordinary and require no comment. However, there is an interesting structural feature shown in Figure 6 that is relevant to the present discussion. The cyclopentadienyl ring C(1)–C(5) is highly planar (mean deviation 0.003 Å), with attached carbons C(6), C(7), and C(8) being about 0.11 Å above this plane and away from the metal. Because of the methyl groups, the phenyl ring is prevented from being coplanar and in conjugation with the Cp ring. The angle between these two planes is 61.6° in the solid. As a result, the phenyl group partially blocks the access of a nucleophile to the metal, and the rate of CO substitution decreases.

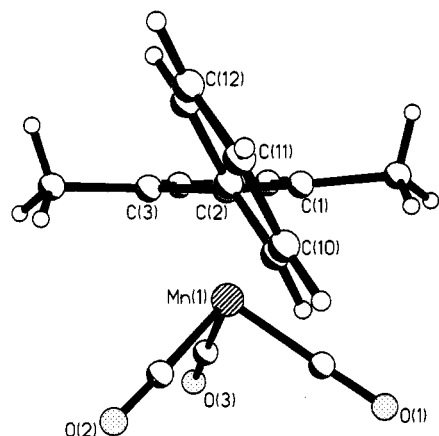


Figure 6. Structural drawing of complex **3** showing the rotation of the phenyl ring from the cyclopentadienyl plane.

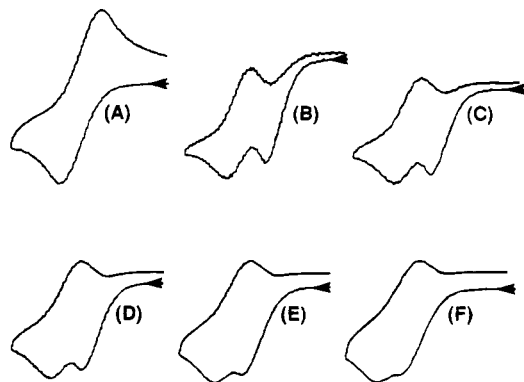
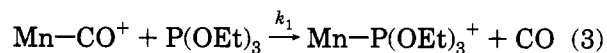
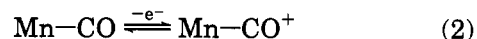


Figure 7. Cyclic voltammograms showing splitting of the oxidation wave of 1.00 mM complex **3** in $\text{CH}_2\text{Cl}_2/0.1 \text{ M Bu}_4\text{NPF}_6$ at 25 °C with $\text{P}(\text{OEt})_3$ absent in A but present at 0.55 mM in B–F. The scan rate (V s^{-1}) was (A) 0.050, (B) 0.10, (C) 0.20, (D) 0.50, (E) 1.0, and (F) 2.0. The working electrode was a 1.0 mm diameter glassy-carbon disk. The current scale was normalized for clarity.

In order to quantify the reactivity of the 17-electron radicals 1^+ and $3^+–5^+$ with $\text{P}(\text{OEt})_3$, the pre-wave method of Parker et al.¹³ was employed. In Figures 2B and 4B it can be seen that the principal oxidation wave is split into two. This occurs because the following requirements are fulfilled: (1) the second-order reaction with nucleophile is very rapid and (2) there is a deficiency of nucleophile. Figure 7 illustrates the wave splitting for the oxidation of **3** with the nucleophile to metal complex concentration ratio, $[\text{P}]/[\text{M}]$, equal to 0.55. At the onset of oxidation of **3** to 3^+ , rapid reaction with $\text{P}(\text{OEt})_3$ causes a cathodic kinetic shift of the wave. Because of the deficiency of $\text{P}(\text{OEt})_3$ at the electrode surface, the supply of nucleophile is quickly exhausted and the remainder of the oxidation wave then occurs at the normal unshifted potential. The result is a splitting of the oxidation into a kinetic pre-wave and the normal Nernstian wave. (If the nucleophile is present in excess, only a single kinetically shifted wave occurs.) The separation of the two waves is a sensitive function of the $[\text{P}]/[\text{M}]$ ratio, the rate of the homogeneous second-order reaction, and the scan rate (Figure 7). The pre-wave method is applicable only to very rapid reactions; under ordinary experimental conditions, the

second-order homogeneous rate constant must be at least $10^6 \text{ M}^{-1} \text{ s}^{-1}$, or a pre-wave will not be seen.

Digital simulation of the mechanism represented by eqs 2–4 accurately reproduced experimental results for complexes **3**–**5**. Useful kinetic information was ob-



tained (via the pre-wave method) for $0.25 \leq [\text{P}]/[\text{M}] \leq 0.75$ and for scan rates between 0.10 and 10.0 V s^{-1} . The behavior of complex **1** was rather more difficult to simulate because concurrent single- and double-CO substitution had to be considered. However, this was easily accomplished because the second CO substitution was studied independently (via complex **2**), as described above. Thus, the only unknown for simulation of the mechanism representing the behavior of **1** was k_1 , the rate constant for the first CO substitution (eq 3). The simulations produced the following second-order rate constants for CO substitution at 25 °C in $\text{CH}_2\text{Cl}_2/0.1 \text{ M Bu}_4\text{NPF}_6$:

	1^+	3^+	4^+	5^+
$10^{-6}k_1/\text{M}^{-1} \text{ s}^{-1}$	100	40	14	7.0

It seems reasonable to conclude that the reactivity order $1^+ > 3^+ > 4^+ > 5^+$ reflects increasing steric congestion near the metal, which causes a decrease in the rate of associative CO substitution in the 17-electron radicals. The steric effects are probably larger than indicated by the k_1 values because of concomitant electronic effects, which would be expected to influence the rates in approximately the opposite direction. Whatever the quantitative interplay of steric and electronic effects, it is pertinent to note that the rate with even the most sterically congested complex (5^+) is very large ($7.0 \times 10^6 \text{ M}^{-1} \text{ s}^{-1}$). Thus, $1^+–5^+$ conform to the generalization^{1–3} that 17-electron organometallic complexes are vastly more reactive than their 18-electron analogues. As a striking example of this, consider that **1** does not undergo thermal CO substitution by PPh_3 at 140 °C over 3 days,⁴ yet it reacts with $\text{P}(\text{OEt})_3$ within milliseconds when oxidized to a 17-electron species.

Substitution of the second CO in 1^+ by $\text{P}(\text{OEt})_3$ is slower than the first substitution by a factor of $k_2/k_1 = (3.1 \times 10^3)/(1 \times 10^8) \approx 3 \times 10^{-5}$. Such rate lowering is normal behavior^{3c} for associative reactions and is dependent on the nature of the nucleophile. If the steric congestion argument made above for k_1 is valid, one would expect that the decrease in reactivity for the second CO substitution (k_2) would not be constant in the series $1^+, 3^+–5^+$. Rather, the ratio k_2/k_1 should be smaller (or k_1/k_2 larger) in the sterically demanding complexes $3^+–5^+$. By matching of digital simulations to experimental data at relatively high concentrations of $\text{P}(\text{OEt})_3$, at which a discernable amount of double-CO substitution occurred, it was possible to estimate ($\pm 30\%$) the rate constant (k_2) for this step:

(13) Jensen, B. S.; Parker, V. D. *Electrochim. Acta* **1973**, *18*, 665. Parker, V. D.; Tilset, M. *J. Am. Chem. Soc.* **1987**, *109*, 2521.

	1 ⁺	3 ⁺	4 ⁺	5 ⁺
$k_2/M^{-1} s^{-1}$	3100	40	40	6
$10^4 k_1/k_2$	3	100	40	100

In agreement with expectations, the k_1/k_2 ratio indeed increases significantly in 3⁺–5⁺ as compared to 1⁺.

In conclusion, we have demonstrated the electroactivation of (cyclopentadienyl)Mn(CO)₃ complexes to facile CO substitution by P(OEt)₃. Similar electroactivation of (arene)M(CO)₃ complexes (M = Cr, Mo, W) has recently been reported;^{3h} in both systems oxidation to 17-electron species initiates the substitution process. It is important to note that the redox-promoted reactions reported herein are stoichiometric (as expected) and not electron transfer catalyzed, as often obtains^{14,15} in reductively initiated substitutions.

Acknowledgment. This work was supported by grants from the National Science Foundation (Grant Nos. CHE-8821588 and CHE-9400800). The X-ray equipment was purchased with assistance from an

instrument grant from the National Science Foundation (Grant No. CHE-8206423) and a grant from the National Institutes of Health (Grant No. RR-06462).

Supplementary Material Available: Tables of crystallographic data, bond lengths, bond angles, H atom positional parameters, and thermal parameters and a packing diagram for 3 (5 pages). Ordering information is given on any current masthead page.

OM940764L

(14) (a) Bezems, G. J.; Rieger, P. H.; Visco, S. *J. Chem. Soc., Chem. Commun.* **1981**, 265. (b) Darchen, A.; Mahe, C.; Patin, H. *J. Chem. Soc., Chem. Commun.* **1982**, 243. (c) Miholova, D.; Vlcek, A. A. *J. Organomet. Chem.* **1985**, 279, 317. (d) Hinkelmann, K.; Mahlendorf, F.; Heinze, J.; Schacht, H.-T.; Field, J. S.; Vahrenkamp, H. *Angew. Chem., Int. Ed. Engl.* **1987**, 26, 352. (e) Neto, C. C.; Baer, C. D.; Chung, Y. K.; Sweigart, D. A. *J. Chem. Soc., Chem. Commun.* **1993**, 816. (f) Neto, C. C.; Kim, S.; Meng, Q.; Sweigart, D. A. *J. Am. Chem. Soc.* **1993**, 115, 2077. (g) Huang, Y.; Neto, C. C.; Pevear, K. A.; Banaszak-Holl, M. M.; Sweigart, D. A.; Chung, Y. K. *Inorg. Chim. Acta* **1994**, 226, 53. (h) Pevear, K. A.; Banaszak-Holl, M. M.; Carpenter, G. B.; Rieger, A. L.; Rieger, P. H.; Sweigart, D. A. *Organometallics* **1995**, 14, 512.

(15) See ref 2a–c for rare examples of oxidatively promoted ligand substitutions that are catalytic.

Vinylaminocarbenes of Group 6 Metals by Metathesis Reaction of 2-Amino-1,3-butadienes. Reactivity toward Electron-Deficient Alkenes

José Barluenga,* Fernando Aznar, and Alfredo Martín

*Instituto Universitario de Química Organometálica "Enrique Moles",
Campus del Cristo, Universidad de Oviedo, 33071-Oviedo, Spain*

Received October 18, 1994*

A new method for the synthesis of chromium, molybdenum, and tungsten Fischer-type vinylaminocarbenes **3** by the metathesis reaction of 2-amino-1,3-butadienes and phenyloxy-carbenes is reported. In addition, the reaction of **3** with electron-deficient alkenes to afford, after hydrolysis, the vinyl ketones **6** has been studied. In order to explain this behavior, a cyclopropanation process has been proposed, which is supported by the formation of the seven-membered ring **8** from diene **7**.

Introduction

Heteroatom-stabilized group 6 metal carbene complexes have been widely used in organic synthesis in the last few years.¹ The first, widely developed process discovered involving these types of compounds has been the cyclopropanation of alkenes.² Many examples of this reaction have been described using alkyl, aryl, and vinyl oxycarbenes of chromium, molybdenum, and tungsten. It is known that either the metal and/or the carbon substituent plays an important role in the reactivity of these complexes; thus, the mildest reaction conditions have been reported for carbenes containing either an alkenyl substituent³ or molybdenum.⁴ Although their potential has been outlined,⁵ aminocarbenes have been much less explored than the oxygen analogues.⁶ This might be due to the lack of general methods for preparation of aminocarbenes, especially

vinylaminocarbenes,⁷ and to their lower reactivity as compared with the oxygen-stabilized derivatives. In this regard, some benzannulation⁸ and [4 + 2]^{6,9} processes have been described for vinylaminocarbenes, while only two intermolecular cyclopropanation reactions involving chromium aminocarbenes have been reported, to the best of our knowledge.¹⁰

We wish to report in this paper a direct general entry into group 6 metal vinylaminocarbene complexes, which is the first one described for molybdenum derivatives, based on the metathesis reaction between 2-amino-1,3-butadiene derivatives and Fischer oxycarbenes, as well as some examples showing the remarkable reactivity of those systems toward electron-deficient olefins; the behavior of molybdenum and tungsten derivatives is reported here for the first time.

Results and Discussion

2-Morpholino 1,3-dienes **1** react with methoxyphenyl complexes **2a–c**, giving rise to the vinylaminocarbenes **3**, in quite good yields, and α -methoxystyrene **4** (Scheme 1, Table 1). It is accepted that the metathesis reaction takes place through a formal [2 + 2] cycloaddition followed by ring opening of the metallacyclobutane intermediate **I**.¹¹ Although the process is probably reversible at the microscopic level, the equilibrium is displaced toward the formation of amino derivatives due to the higher stability of aminocarbenes compared with alkoxy-carbenes. In all cases variable amounts of 1,2-

(6) (a) Schwindt, M. A.; Miller, J. R.; Hegedus, L. S. *J. Organomet. Chem.* **1991**, *413*, 143. (b) Grotjahn, D. B.; Dötz, K. H. *Synlett* **1991**, 381.

(7) (a) Macomber, D. W.; Maudhukar, P.; Roger, R. D. *Organometallics* **1989**, *8*, 1275. (b) Baldoli, C.; Buttero, P. D.; Licandro, E.; Maiorana, S.; Papagni, A.; Zanotti-Gerosa, A. *Synlett* **1993**, 935.

(8) (a) Yamashita, A. *Tetrahedron Lett.* **1986**, *27*, 5915. (b) Dötz, K. H.; Erben, H.; Harms, K. *J. Chem. Soc., Chem. Commun.* **1989**, 629. (c) Dötz, K. H.; Grotjahn, D.; Harms, K. *Angew. Chem., Int. Ed. Engl.* **1989**, *28*, 1384. (d) Dötz, K. H.; Schäfer, T.; Harms, K. *Angew. Chem., Int. Ed. Engl.* **1990**, *29*, 176.

(9) (a) Dötz, K. H.; Noack, R.; Harms, K. *Tetrahedron* **1990**, *46*, 1235. (b) Anderson, B. A.; Wulff, W. D.; Powers, T. S.; Tribbitt, S.; Rheingold, A. L. *J. Am. Chem. Soc.* **1992**, *114*, 10784. (c) Rahm, A.; Wulff, W. D. *Organometallics* **1993**, *12*, 597.

(10) Wienand, A.; Reissig, H. *Organometallics* **1990**, *9*, 3133. (b) Sierra, M. A.; Soderberg, B.; Lander, P. A.; Hegedus, L. S. *Organometallics* **1993**, *12*, 3769.

(11) Casey, C. P.; Tuinstra, H. E.; Saeman, M. C. *J. Am. Chem. Soc.* **1976**, *98*, 608.

* Abstract published in *Advance ACS Abstracts*, February 1, 1995.

(1) For reviews on the synthetic applications of Fischer carbene complexes, see: (a) Dötz, K. H.; Fischer, H.; Hofmann, P.; Kreissel, F. R.; Schubert, U.; Weiss, K. *Transition Metal Carbene Complexes*; Verlag Chemie: Deerfield Beach, FL, 1984. (b) Dötz, K. H. *Angew. Chem., Int. Ed. Engl.* **1984**, *23*, 587. (c) Casey, C. P. *React. Intermed.* **1985**, *3*. (d) Dötz, K. H. In *Organometallics in Organic Synthesis: Aspects of a Modern Interdisciplinary Field*; tom Dieck, H., de Meijere, A., Eds.; Springer-Verlag: Berlin, 1988. (e) Schore, N. E. *Chem. Rev.* **1988**, *88*, 1081. (f) *Advances in Metal Carbene Chemistry*; Schubert, U., Ed.; Kluwer: Boston, MA, 1989. (g) Wulff, W. D. In *Advances in Metal-Organic Chemistry*; Liebeskind, L. S., Ed.; JAI Press: Greenwich, CT, 1989, Vol. 1. (h) Harrington, P. *J. Transition Metals in Total Synthesis*; Wiley: New York, 1990; pp 346–399. (i) Wulff, W. D. In *Comprehensive Organic Synthesis*; Trost, B. M., Fleming, I., Eds.; Pergamon Press: New York, 1991; Vol. 5.

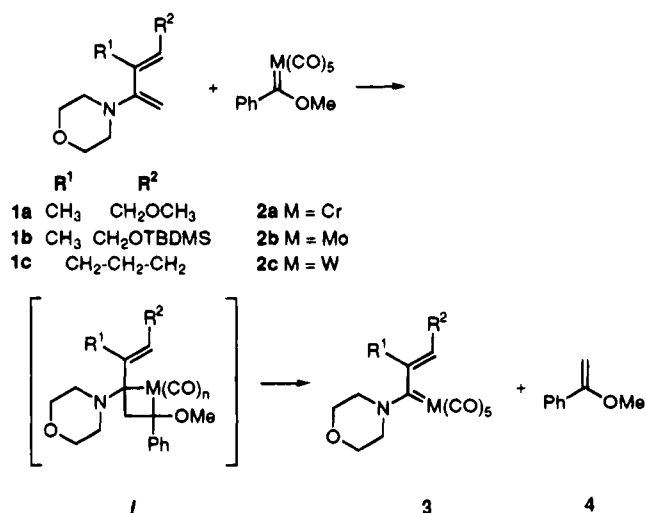
(2) For recent examples, see: (a) Brookhart, M.; Studabaker, W. B. *Chem. Rev.* **1987**, *87*, 411. (b) Wienand, A.; Reissig, H.-V. *Tetrahedron Lett.* **1988**, *29*, 2315. (c) Herndon, J. W.; Tumer, S. U. *Tetrahedron Lett.* **1989**, *30*, 4771. (d) Wienand, A.; Reissig, H.-U. *Angew. Chem., Int. Ed. Engl.* **1990**, *29*, 1129. (e) Murray, C. K.; Yang, D. C.; Wulff, W. D. *J. Am. Chem. Soc.* **1990**, *112*, 5660. (f) Söderberg, B. C.; Hegedus, L. S.; Sierra, M. A. *J. Am. Chem. Soc.* **1990**, *112*, 4364. (g) Herndon, J. W.; Tumer, S. U. *J. Org. Chem.* **1991**, *56*, 286. (h) Hegedus, L. S.; Bates, R. W.; Söderberg, B. C. *J. Am. Chem. Soc.* **1991**, *113*, 923. (i) Barluenga, J.; Tomás, M.; Ballesteros, A.; Santamaría, J.; Lopez-Ortiz, F. *J. Chem. Soc., Chem. Commun.* **1994**, 321.

(3) (a) Wulff, W. D.; Yang, D. C.; Murray, C. K. *J. Am. Chem. Soc.* **1988**, *110*, 2653. (b) Barluenga, J.; Aznar, F.; Martín, A.; García-Granda, S.; Salvadó, M. A.; Pertierra, P. *J. Chem. Soc., Chem. Commun.* **1993**, 319. (c) Barluenga, J.; Aznar, F.; Valdés, C.; Martín, A.; García-Granda, S.; Martín, E. *J. Am. Chem. Soc.* **1993**, *115*, 4403.

(4) (a) Harvey, D. F.; Brown, M. F. *Tetrahedron Lett.* **1990**, *31*, 2529. (b) Harvey, D. F.; Lund, K. P. *J. Am. Chem. Soc.* **1991**, *113*, 8916.

(5) Anderson, B. A.; Wulff, W. D.; Powers, T. S.; Tribbitt, S.; Rheingold, A. L. *J. Am. Chem. Soc.* **1992**, *114*, 10784.

Scheme 1

Table 1^a

entry	R ¹	R ²	M	t (h)	3 (%)
a ^b	CH ₃	CH ₂ OCH ₃	Cr	6	75
b ^c	CH ₃	CH ₂ OCH ₃	Mo	4	57
c ^d	CH ₃	CH ₂ OCH ₃	W	38	64
d ^b	CH ₃	CH ₂ OTBDMS	Cr	5.5	65
e ^b	CH ₃	CH ₂ OTBDMS	Mo	1	35
f ^d	CH ₃	CH ₂ OTBDMS	W	40	18
g ^c		CH ₂ CH ₂ CH ₂	Cr	3	69
h ^c		CH ₂ CH ₂ CH ₂	Mo	2.5	55
i ^d		CH ₂ CH ₂ CH ₂	W	12	46

^a Yields are based on amino diene **1**. Reactions were performed in sealed tubes. ^b In toluene at 110 °C. ^c In tetrahydrofuran at 66 °C. ^d In tetrahydrofuran at 100 °C.

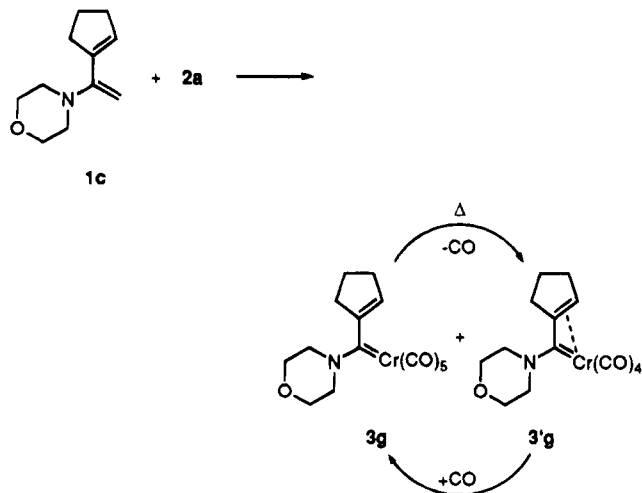
diphenyl-1,2-dimethoxyethane, resulting from the dimerization of carbene,¹² could be detected in the reaction mixture as a byproduct; because of that, an excess (20–70 mol %) of **2** was used in order to improve the yield by total consumption of the amino diene.

As can be deduced from Table 1, tungsten methoxyphenyl carbene is less reactive in the metathesis process than the corresponding chromium and molybdenum derivatives (entries c, f, and i), and an increase in the temperature and/or the reaction time is required in order to take the reaction to completion. On the other hand, due to the greater tendency of molybdenum carbenes toward cyclopropanation, small amounts of cyclopropane derivatives (5–10%) can be isolated as a mixture of diastereoisomers in the case of reactions involving the molybdenum complex **2b**.

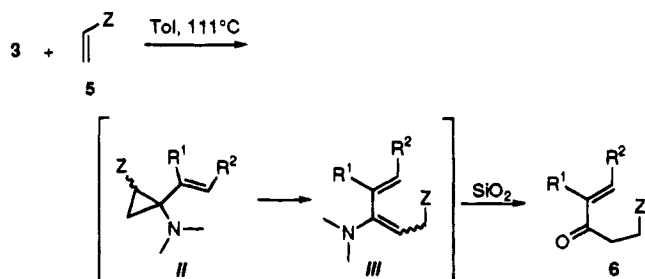
In the reaction of **1c** with complex **2a** (see Scheme 2), the new carbene **3'g**,¹³ formed from **3g** by loss of one CO ligand under the reaction conditions, could be isolated along with **3g**. Compounds **3g** and **3'g** can be easily interconverted; thus, bubbling CO into a THF solution of **3'g** leads quantitatively to **3g**, while **3'g** can be in turn formed in good yield by heating **3g** to 66 °C (see Experimental Section).

The availability of these new chromium, molybdenum, and tungsten aminocarbene complexes encouraged us to investigate their ability to cyclopropanate electrophilic olefins and the influence of the metal as well. Thus, the reaction of complexes **3** with electron-poor

Scheme 2



Scheme 3

Table 2^a

entry	carbene	Z	t (h)	6 (%)
a	3a	CO ₂ CH ₃	1.5	66
b	3b	CO ₂ CH ₃	1	70
c	3c	CO ₂ CH ₃	10	30
d	3b	CN	1	78
e	3b	COCH ₃	1	45
f	3h	CO ₂ CH ₃	1	75

olefins **5** in toluene at 110 °C yielded the new 1-substituted 2-amino dienes **III**. Compounds **III** could not be isolated due to their instability toward aqueous media or chromatographic conditions (silica gel, hexane–ethyl acetate) required for purification, but they were identified on the basis of the NMR analysis of the crude reaction mixtures (for instance, in the reaction of the complex **3g** and methyl acrylate, the most remarkable ¹³C NMR signals for **III** are those at 174.0, 95.9, 67.5, and 50.0 ppm, assigned to the ester, the β-enamine, and the morpholine carbon atoms, respectively). In addition, the hydrolysis in SiO₂ of the reaction mixture affords the expected derivatives **6** (Scheme 3, Table 2).

A plausible mechanism accounting for the formation of the amino diene **III** involves the formation of the donor–acceptor disubstituted cyclopropane **II**, which is not stable under the reaction conditions¹⁴ but undergoes cyclopropane ring opening to give **III**.

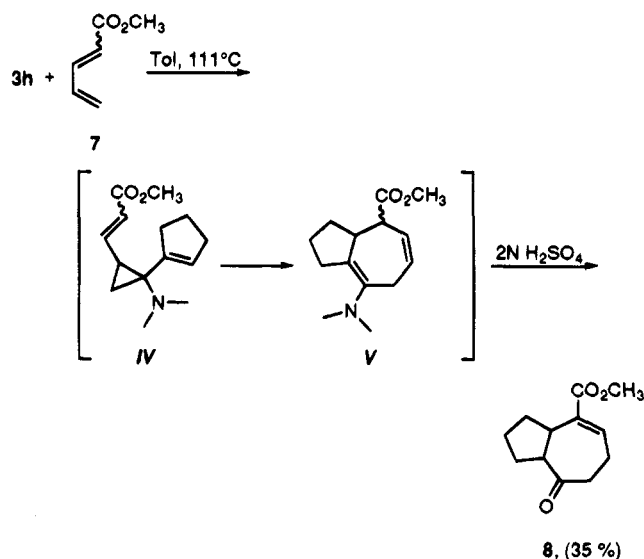
As recorded in Table 2, the reaction yields are higher in the case of the chromium and molybdenum carbenes (entries a and b) than for the tungsten derivative (entry c), probably because of the higher M–CO energy of the latter that impedes the CO ligand dissociation necessary for the olefin–metal coordination.

(12) Casey, C. P.; Cesa, M. C. *Organometallics* **1982**, *1*, 87.

(13) Barluenga, J.; Aznar, F.; Martín, A.; García-Granda, S.; Pérez-Carreño, E. *J. Am. Chem. Soc.* **1994**, *116*, 11191.

(14) (a) Reissig, H. *Top. Curr. Chem.* **1988**, *114*, 73. (b) Wong, H. N.; Hon, M.; Tse, C.; Yip, Y.; Tanko, J.; Hudlicky, T. *Chem. Rev.* **1989**, *89*, 165.

Scheme 4



From Table 2, it seems that the olefin electron-withdrawing group plays an important role in the cyclopropanation reaction; thus, the best results for molybdenum complexes were obtained with methyl acrylate and acrylonitrile (entries b and d), but yields fall when methyl vinyl ketone is used (entry e).

The generality of this reaction toward the electron-deficient diene **7** was further explored (Scheme 4). In this case, the divinylcyclopropane **IV**, resulting from the cyclopropanation of the less sterically hindered double bond of the diene, undergoes Cope rearrangement under the reaction conditions, affording **V**. As far as we know, this is the first example of a seven-membered-ring formation by the tandem intermolecular cyclopropanation/Cope rearrangement reaction involving an amino-vinyl Fischer type carbene and an electron-deficient diene.¹⁵ The attempted purification of that azulene derivative resulted in partial hydrolysis of the enamine group, but treatment of **V** with aqueous acid allowed us to isolate **8** in 35% overall yield from **3h**. The results of this process complement earlier reports on the preparation of seven-membered rings by the reaction of electron-rich dienes and Fischer type oxyvinylcarbenes.³

In conclusion, we have reported a simple and direct synthesis of Fischer type aminovinylcarbenes, which are unknown in the case of molybdenum, from 2-amino-1,3-butadienes. The chromium and molybdenum complexes thus obtained react with electron-deficient alkenes to furnish insertion products resulting from a cyclopropanation process; moreover, the first example of a tandem intermolecular cyclopropanation/Cope rearrangement between a Fischer-type vinylcarbene and an electron-deficient diene has been shown.

Experimental Section

General Considerations. Tetrahydrofuran (THF) and toluene were distilled from benzophenone ketyl under nitrogen. Chromatographic purifications of carbenes **3** were performed

(15) During the evaluation process of this paper, one example of a tandem intramolecular cyclopropanation/Cope rearrangement has been observed for a vinylcarbene complex and an electron-deficient diene: Harvey, D. F.; Grenzer, M. E.; Gantzel, P. K. *J. Am. Chem. Soc.* **1994**, *116*, 6719.

under nitrogen on previously degassed silica gel 60, 230–400 mesh (Merck or Scharlau). TLC was performed on glass-backed plates coated with silica gel 60 F₂₅₄ (Merck or Scharlau). Components were located by treating the plates with an acidic solution of Mo(VI) and Ce(IV) and heating. Chromatographic solvents were distilled and degassed for carbenes **3** by bubbling nitrogen for 15 min prior to their use. NMR measurements were recorded on Bruker AC-200 or AC-300 spectrometers. IR analyses were obtained on Mattson 3000 FTIR spectrometer. MS spectra were recorded on a Hewlett-Packard 5987-A spectrometer. Elemental analyses were obtained on a Perkin-Elmer 240-B analyzer.

2-Amino-1,3-butadienes (**1a–c**)¹⁶ and carbene complexes (**2a–c**)¹⁷ were prepared according to the literature procedures.

General Procedure for the Reactions of Amino Dienes 1 with Carbenes 2. Method A (for Chromium and Molybdenum Metal Complexes). To a 0.2 M solution of diene **1** in the solvent indicated are added 1.2–1.5 equiv of carbene **5**, and the solution is refluxed until TLC (silica gel, hexane–ethyl acetate 3:1 for **1a,c** and hexane–ether–dichloromethane 4:1:1 for **1b**) shows the absence of **1** in the reaction mixture. Partial decomposition of **2** and cyclopropanation in the case of molybdenum complexes afford the metal hexacarbonyl. When the solvent is toluene and the metal used is chromium, hexacarbonylchromium sublimes and can be recovered on a cold finger; in other cases the hexacarbonylmetal species can be recovered by crystallization from the reaction mixture at –20 °C. After that, the solvent is removed at reduced pressure and the crude reaction mixture chromatographed on silica gel with the solvent indicated. Typically, the red, first-eluted fraction contains the starting carbene **2** and α -methoxystyrene (**4**) and the yellow, second one contains the aminocarbene **3**.

Method B (for Tungsten Complexes). 2-Amino diene **1** and 1.7 equiv of metal carbene **2** are dissolved in 70 mL of THF and heated in a sealed tube to 100 °C during the time indicated; then, the reaction mixture is cooled to –20 °C in order to crystallize tungsten hexacarbonyl, filtered, and worked up as in method A.

Pentacarbonyl[(E)-1-morpholino-4-methoxy-2-methyl-2-buten-1-ylidene]chromium(0) (3a; Method A). A 2 mmol (0.394 g) amount of *N*-[(E)-4-methoxy-2-methyl-1-methylenbut-2-enyl]morpholine (**1a**) and 2.4 mmol (0.749 g) of pentacarbonyl(methoxyphenylmethylene)chromium(0) (**2a**) are refluxed in toluene over 6 h. Column chromatography: **4** was first eluted with hexane–ethyl acetate (3:1) and **3a** with hexane–ethyl acetate (1:1); *R_f* 0.08 (hexane–ethyl acetate (3:1)). Yield: 0.562 g (75%). Mp: 71–73 °C (yellow prisms, recrystallized from hexane–dichloromethane). ¹H NMR (CDCl₃): δ 1.71 (s, 3H), 3.28 (s, 3H), 3.62–3.80 (m, 4H), 3.89–3.98 (m, 4H), 4.26 (t d, 1H, *J* = 5.2, 13.3 Hz), 4.36 (t d, 1H, *J* = 4.7, 13.3 Hz), 4.95 (t, 1H, *J* = 6.8 Hz). ¹³C NMR (CDCl₃): δ 14.7 (CH₃), 54.2 (CH₂), 58.0 (CH₃), 59.7 (CH₂), 67.7 (CH₂), 67.8 (CH₂), 115.3 (CH), 147.9 (C), 217.1 (C), 222.9 (C), 273.4 (C). IR (CH₂Cl₂, cm⁻¹): 2054 m, 1927 s. Anal. Calcd for C₁₅H₁₇NO₇Cr: C, 48.01; H, 4.57; N, 3.73. Found: C, 47.94; H, 4.53; N, 3.69.

Pentacarbonyl[(E)-1-morpholino-4-methoxy-2-methyl-2-buten-1-ylidene]molybdenum(0) (3b; Method A). A 2 mmol (0.394 g) amount of *N*-[(E)-4-methoxy-2-methyl-1-methylenbut-2-enyl]morpholine (**1a**) and 2.4 mmol (0.854 g) of pentacarbonyl(methoxyphenylmethylene)molybdenum(0) (**2b**) are refluxed in tetrahydrofuran over 4 h. Column chromatography: **4** was first eluted with hexane–ethyl acetate (3:1) and **3b** with hexane–ethyl acetate (1:1); *R_f* 0.09 (hexane–ethyl acetate (3:1)). Yield: 0.478 g (57%). Yellow oil. ¹H NMR (CDCl₃): δ 1.76 (s, 3H), 3.32 (s, 3H), 3.68 (s, 2H), 3.77–4.01 (m, 6H), 4.21–4.39 (m, 2H), 4.99 (t, 1H, *J* = 6.3 Hz). ¹³C NMR

(16) Barluenga, J.; Aznar, F.; Valdés, C.; Cabal, M. P. *J. Org. Chem.* **1991**, *56*, 6166.

(17) Tumer, S. U.; Herndon, J. W.; McMullen, L. A. *J. Am. Chem. Soc.* **1992**, *114*, 8394.

(CDCl₃): δ 14.1 (CH₃), 53.0 (CH₂), 57.8 (CH₃), 61.2 (CH₂), 67.5 (CH₂), 67.6 (CH₂), 115.3 (CH), 147.8 (C), 206.0 (C), 213.2 (C), 265.9 (C). IR (CH₂Cl₂, cm⁻¹): 2054 m, 1927 s. Anal. Calcd for C₁₅H₁₇NO₇Mo: C, 42.97; H, 4.09; N, 3.34. Found: C, 42.89; H, 4.14; N, 3.30.

Pentacarbonyl[(E)-1-morpholino-4-methoxy-2-methyl-2-buten-1-ylidene]tungsten(0) (3c; Method B). A 2 mmol (0.394 g) amount of *N*-[(E)-4-methoxy-2-methyl-1-methylenebut-2-enyl]morpholine (**1a**) and 3.4 mmol (1.510 g) of pentacarbonyl(methoxyphenylmethylene)tungsten(0) (**2c**) were reacted for 38 h. Column chromatography: **4** was first eluted with hexane-ethyl acetate (3:1) and **3c** with hexane-ethyl acetate (1:1); *R_f* 0.08 (hexane-ethyl acetate (3:1)). Yield: 0.649 g (64%). Yellow oil. ¹H NMR (CDCl₃): δ 1.72 (s, 3H), 3.28 (s, 3H), 3.61–3.80 (m, 4H), 3.88 (t, 2H, *J* = 4.8 Hz), 3.96–4.02 (m, 2H), 4.16–4.35 (m, 2H), 4.98 (t, 1H, *J* = 6.7 Hz). ¹³C NMR (CDCl₃): δ 14.6 (CH₃), 53.1 (CH₂), 58.1 (CH₃), 62.1 (CH₂), 67.7 (CH₂), 116.1 (CH), 148.5 (C), 198.1 (C), 202.8 (C), 256.0 (C). IR (CH₂Cl₂, cm⁻¹): 2054 m, 1923 s. Anal. Calcd for C₁₅H₁₇NO₇W: C, 35.53; H, 3.38; N, 2.76. Found: C, 35.40; H, 3.41; N, 2.78.

Pentacarbonyl[(E)-1-morpholino-4-(tert-butylidimethylsiloxy)-2-methyl-2-butenylidene]chromium(0) (3d; Method A). A 2 mmol (0.594 g) amount of *N*-[(E)-4-(tert-butylidimethylsiloxy)-2-methyl-1-methylenebut-2-enyl]morpholine (**1b**) and 3 mmol (0.936 g) of pentacarbonyl(methoxyphenylmethylene)chromium(0) (**2a**) are refluxed in toluene over 5.5 h. Column chromatography: hexane-ether-dichloromethane (4:1:1); *R_f* 0.26. Yield: 0.617 g (65%). Red oil. ¹H NMR (CDCl₃): δ 0.02 (s, 6H), 0.83 (s, 9H), 1.68 (s, 3H), 3.64 (s, 2H), 3.68–3.86 (m, 2H), 3.93 (t, 2H, *J* = 5.1 Hz), 4.19 (d, 2H, *J* = 6.3 Hz), 4.25–4.44 (m, 2H), 4.90 (t, 1H, *J* = 6.3 Hz). ¹³C NMR (CDCl₃): δ -5.5 (CH₃), -5.4 (CH₃), 14.6 (CH₃), 18.1 (C), 25.7 (CH₃), 54.1 (CH₂), 58.2 (CH₂), 59.7 (CH₂), 67.7 (CH₂), 118.4 (CH), 145.6 (C), 217.2 (C), 223.0 (C), 274.0 (C). IR (CH₂Cl₂, cm⁻¹): 2054 m, 1927 s. Anal. Calcd for C₂₀H₂₉NO₇SiCr: C, 50.52; H, 6.15; N, 2.95. Found: C, 50.63; H, 6.18; N, 2.97.

Pentacarbonyl[(E)-1-morpholino-4-(tert-butylidimethylsiloxy)-2-methyl-2-butenylidene]molybdenum(0) (3e; Method A). A 2 mmol (0.594 g) amount of *N*-[(E)-4-(tert-butylidimethylsiloxy)-2-methyl-1-methylenebut-2-enyl]morpholine (**1b**) and 3.0 mmol (1.068 g) of pentacarbonyl(methoxyphenylmethylene)molybdenum(0) (**2b**) are refluxed in toluene over 1 h. Column chromatography: hexane-ether-dichloromethane (5:1:1); *R_f* 0.33. Yield: 0.363 g (35%). Red oil. ¹H NMR (CDCl₃): δ 0.00 (s, 6H), 0.82 (s, 9H), 1.67 (s, 3H), 3.63 (s, 2H), 3.85–3.99 (m, 4H), 4.12–4.41 (m, 4H), 4.90 (t, 1H, *J* = 6.3 Hz). ¹³C NMR (CDCl₃): δ -0.7 (CH₃), -0.6 (CH₃), 14.2 (CH₃), 18.2 (C), 25.7 (CH₃), 53.0 (CH₂), 58.9 (CH₂), 61.3 (CH₂), 67.8 (CH₂), 118.5 (CH), 145.5 (C), 206.1 (C), 213.3 (C), 267.2 (C). IR (CH₂Cl₂, cm⁻¹): 2054 m, 1933 s. Anal. Calcd for C₂₀H₂₉NO₇SiMo: C, 46.24; H, 5.63; N, 2.70. Found: C, 46.37; H, 5.69; N, 2.73.

Pentacarbonyl[(E)-1-morpholino-4-(tert-butylidimethylsiloxy)-2-methyl-2-butenylidene]tungsten(0) (3f; Method B). A 2 mmol (0.594 g) amount of *N*-[(E)-4-(tert-butylidimethylsiloxy)-2-methyl-1-methylenebut-2-enyl]morpholine (**1b**) and 3.4 mmol (1.510 g) of pentacarbonyl(methoxyphenylmethylene)tungsten(0) (**2c**) were reacted for 40 h. Column chromatography: hexane-ether-dichloromethane (5:1:1); *R_f* 0.35. Yield: 0.218 g (18%). Red oil. ¹H NMR (CDCl₃): δ 0.00 (s, 6H), 0.82 (s, 9H), 1.67 (s, 3H), 3.61 (s, 2H), 3.81–3.88 (m, 4H), 4.12–4.32 (m, 4H), 4.93 (t, 1H, *J* = 6.3 Hz). ¹³C NMR (CDCl₃): δ -5.4 (CH₃), -5.3 (CH₃), 14.4 (CH₃), 18.2 (C), 25.7 (CH₃), 52.9 (CH₂), 58.7 (CH₂), 62.1 (CH₂), 67.7 (CH₂), 67.8 (CH₂), 119.2 (CH), 146.1 (C), 198.2 (C), 202.9 (C), 256.4 (C). IR (CH₂Cl₂, cm⁻¹): 2052 m, 1923 s. Anal. Calcd for C₂₀H₂₉NO₇SiW: C, 39.55; H, 4.81; N, 2.31. Found: C, 39.44; H, 4.79; N, 2.29.

Pentacarbonyl[morpholino(1-cyclopentenyl)methylene]chromium(0) (3g; Method A). A 2 mmol (0.358 g) amount of *N*-(1-cyclopent-1-enylethenyl)morpholine (**1c**) and 2.4 mmol (0.749 g) of pentacarbonyl(methoxyphenylmethylene)

chromium(0) (**2a**) are refluxed in THF over 3 h and cooled to room temperature. In order to improve the yield of **3g**, CO is bubbled over 15 min. Then, the reaction mixture is cooled to -20 °C overnight. Column chromatography: hexane-ethyl acetate (3:1); *R_f* 0.33. Yield: 0.493 g (69%). Mp: 117–119 °C (yellow needles, recrystallized from hexane-dichloromethane). ¹H NMR (CDCl₃): δ 1.85 (br, 1H), 1.99 (br, 2H), 2.36 (br, 1H), 2.50 (br, 1H), 2.75 (br, 1H), 3.64 (s, 2H), 3.67–3.80 (m, 2H), 3.91 (t, 2H, *J* = 4.7 Hz), 4.28–4.36 (br, 2H), 5.13 (s, 1H). ¹³C NMR (CDCl₃): δ 23.2 (CH₂), 33.0 (CH₂), 35.7 (CH₂), 54.4 (CH₂), 59.7 (CH₂), 67.8 (CH₂), 119.4 (CH), 152.6 (C), 217.3 (C), 223.3 (C), 272.1 (C). IR (CH₂Cl₂, cm⁻¹): 2054 m, 1929 s. Anal. Calcd for C₁₅H₁₅NO₆Cr: C, 50.43; H, 4.23; N, 3.92. Found: C, 50.24; H, 4.18; N, 3.88.

Tetracarbonyl[(η^2 -1-cyclopentenyl)morpholinomethylene]chromium(0) (3'g). The complex **3'g** was isolated from the reaction of **1c** and **2a** in 34% yield, but this yield can be increased by the following procedure: 1.52 mmol (0.543 g) of **3g** is dissolved in THF and heated under reflux until TLC (*R_f* 0.33, hexane-ethyl acetate (3:1)) shows the total consumption of **3g**. The reaction mixture is then concentrated under reduced pressure (10⁻² Torr). The red solid formed is redissolved in CH₂Cl₂ (10 mL) and filtered through a pad of Celite, and the solution is diluted with 25 mL of hexane. Crystallization of compound **3'g** from the solution at -20 °C yielded 0.451 g (90%) (*R_f* 0.19, hexane-ethyl acetate (3:1)). Mp: 137–139 °C (red prisms). ¹H NMR (CDCl₃): δ 1.35–1.64 (m, 1H), 1.71–1.88 (m, 1H), 1.96 (d, *J* = 7.8, 14.0 Hz, 1H), 2.20–2.35 (m, 2H), 2.51–2.67 (m, 1H), 3.63–4.01 (m, 8H), 4.67 (s, 1H). ¹³C NMR (CD₂Cl₂, 233 K): δ 21.0 (CH₂), 31.1 (CH₂), 35.4 (CH₂), 57.0 (CH₂), 58.5 (CH₂), 67.1 (CH₂), 67.5 (CH₂), 85.0 (CH), 86.6 (C), 222.0 (C), 224.2 (C), 234.9 (C), 235.8 (C), 257.6 (C). IR (CH₂Cl₂, cm⁻¹): 1879, 1908, 2011, 2045. Anal. Calcd for C₁₄H₁₅NO₅Cr: C, 52.79; H, 4.43; N, 4.10. Found: C, 52.58; H, 4.44; N, 4.05.

Pentacarbonyl[morpholino(1-cyclopentenyl)methylene]molybdenum(0) (3h; Method A). A 2 mmol (0.358 g) amount of *N*-(1-cyclopent-1-enylethenyl)morpholine (**1c**) and 2.4 mmol (0.854 g) of pentacarbonyl(methoxyphenylmethylene)molybdenum(0) (**2b**) are refluxed in THF over 2.5 h. Column chromatography: hexane-ethyl acetate (3:1); *R_f* 0.33. Yield: 0.441 g (55%). Mp: 122–125 °C (yellow needles, recrystallized from hexane-dichloromethane). ¹H NMR (CDCl₃): δ 1.87–1.97 (m, 2H), 2.44 (br, 4H), 3.66 (s, 4H), 3.88 (t, 2H, *J* = 4.8 Hz), 4.21–4.32 (m, 2H), 5.10 (s, 1H). ¹³C NMR (CDCl₃): δ 23.4 (CH₂), 33.2 (CH₂), 35.4 (CH₂), 53.4 (CH₂), 61.3 (CH₂), 67.8 (CH₂), 119.6 (CH), 152.4 (C), 206.2 (C), 213.6 (C), 265.3 (C). IR (CH₂Cl₂, cm⁻¹): 2053 m, 1931 s. Anal. Calcd for C₁₅H₁₅NO₆Mo: C, 44.90; H, 3.77; N, 3.49. Found: C, 44.94; H, 3.81; N, 3.51.

Pentacarbonyl[morpholino(1-cyclopentenyl)methylene]tungsten(0) (3i; Method B). A 2 mmol (0.358 g) amount of *N*-(1-cyclopent-1-enylethenyl)morpholine (**1c**) and 3.4 mmol (1.510 g) of pentacarbonyl(methoxyphenylmethylene)tungsten(0) (**2c**) were reacted for 12 h. Column chromatography: hexane-ethyl acetate (3:1); *R_f* 0.31. Yield: 0.450 g (46%). Mp: 154–156 °C (yellow needles, recrystallized from hexane-dichloromethane). ¹H NMR (CDCl₃): δ 1.95 (br, 3H), 2.51 (br, 3H), 3.68 (s, 4H), 3.89 (t, 2H, *J* = 4.7 Hz), 4.27 (br, 2H), 5.17 (s, 1H). ¹³C NMR (CDCl₃): δ 23.4 (CH₂), 33.0 (CH₂), 35.5 (CH₂), 53.3 (CH₂), 62.0 (CH₂), 67.8 (CH₂), 120.4 (CH), 153.2 (C), 198.3 (C), 203.2 (C), 254.0 (C). IR (CH₂Cl₂, cm⁻¹): 2052 m, 1924 s. MS (*m/e*, relative intensity): (489, 6) M⁺, (461, 47), (431, 89), (401, 84), (372, 45), (345, 68), (317, 64), (290, 100). Anal. Calcd for C₁₅H₁₅NO₆W: C, 36.83; H, 3.09; N, 2.86. Found: C, 36.93; H, 3.06; N, 2.86.

General Procedure for Ketones 6. A 1 mmol amount of carbene complex **3** and 1.1 mmol of alkene **5** are dissolved in 3 mL of toluene and refluxed until TLC shows the total consumption of starting carbene **3** (see Table 2). The M(CO)₆ formed is crystallized at -20 °C and the solution concentrated

and chromatographed on silica gel in the solvent indicated below to give the products as colorless oils.

(E)-Methyl 7-methoxy-5-methyl-4-oxo-5-heptenoate (6a): 0.375 g of **3a**, 0.419 g of **3b**, or 0.507 g of **3c** and 99 μL of methyl acrylate. Column chromatography: hexane-ethyl acetate (3:1); R_f 0.19. Yield: 0.132 g, 66% (**3a**); 0.140 g, 70% (**3b**); 0.060 g, 30% (**3c**). ^1H NMR (CDCl_3): δ 1.69 (s, 3H), 2.55 (t, $J = 6.7$ Hz, 2H), 2.96 (t, $J = 6.7$ Hz, 2H), 3.33 (s, 3H), 3.61 (s, 3H), 4.11 (d, $J = 5.7$ Hz, 2H), 6.64 (t, $J = 5.7$ Hz, 1H). ^{13}C NMR (CDCl_3): δ 11.5 (CH_3), 27.9 (CH_2), 31.8 (CH_2), 51.6 (CH_3), 58.5 (CH_3), 69.4 (CH_2), 136.9 (C), 138.5 (CH), 173.2 (C), 198.8 (C). IR (neat, cm^{-1}): 1675, 1740. MS (m/e , relative intensity): 200, 1 (M^+); 168, 56; 114, 100; 109, 35; 87, 47; 85, 45. Anal. Calcd for $\text{C}_{10}\text{H}_{16}\text{O}_4$: C, 59.98; H, 8.05. Found: C, 59.91; H, 8.04.

(E)-7-Methoxy-5-methyl-4-oxo-5-heptenenitrile (6d): 0.419 g of **3b** and 72 μL of acrylonitrile. Column chromatography: hexane-diethyl ether-dichloromethane (2:1:1); R_f 0.19. Yield: 0.130 g (78%). ^1H NMR (CDCl_3): δ 1.72 (s, 3H), 2.57 (t, $J = 7.3$ Hz, 2H), 3.03 (t, $J = 7.3$ Hz, 2H), 3.34 (s, 3H), 4.12 (d, $J = 5.6$ Hz, 2H), 6.61 (t, $J = 5.6$ Hz, 1H). ^{13}C NMR (CDCl_3): δ 11.4 (CH_3), 11.7 (CH_2), 32.6 (CH_2), 58.6 (CH_3), 69.3 (CH_2), 119.1 (C), 136.4 (C), 139.8 (CH), 196.1 (C). IR (neat, cm^{-1}): 1672, 2249. MS (m/e , relative intensity): 167, 5 (M^+); 127, 42; 95, 100; 85, 67. Anal. Calcd for $\text{C}_9\text{H}_{13}\text{NO}_2$: C, 64.65; H, 7.84; N, 8.38. Found: C, 64.71; H, 7.90; N, 8.35.

(E)-8-Methoxy-6-methyl-6-octene-2,5-dione (6e): 0.419 g of **3b** and 91 μL of methyl vinyl ketone. Column chromatography: hexane-diethyl ether-dichloromethane (2:1:1); R_f 0.24. Yield: 0.083 g (45%). ^1H NMR (CDCl_3): δ 1.69 (s, 3H), 2.15 (s, 3H), 2.67 (t, $J = 7.3$ Hz, 2H), 2.91 (t, $J = 7.3$ Hz, 2H), 3.33 (s, 3H), 4.11 (d, $J = 5.1$ Hz, 2H), 6.67 (t, $J = 5.1$ Hz, 1H). ^{13}C NMR (CDCl_3): δ 11.6 (CH_3), 30.0 (CH_3), 30.1 (CH_2), 37.0 (CH_2), 58.6 (CH_3), 69.5 (CH_2), 137.0 (C), 138.5 (CH), 199.3 (C), 207.4 (C). Anal. Calcd for $\text{C}_{10}\text{H}_{16}\text{O}_3$: C, 65.19; H, 8.75. Found: C, 65.11; H, 8.72.

Methyl 4-(1-cyclopentenyl)-4-oxobutanoate (6f): 0.401 g of **3h** and 99 μL of methyl acrylate. Column chromatography: hexane-ethyl acetate (3:1); R_f 0.37. Yield: 0.137 g (75%). ^1H NMR (CDCl_3): δ 1.85 (quintet, $J = 7.7$ Hz, 2H), 2.46–2.51 (m, 4H), 2.56 (t, $J = 6.9$ Hz, 2H), 2.94 (t, $J = 6.9$ Hz, 2H), 3.62 (s, 3H), 6.74 (s, 1H). ^{13}C NMR (CDCl_3): δ 22.6 (CH_2), 27.8 (CH_2), 30.5 (CH_2), 33.4 (CH_2), 33.8 (CH_2), 51.7 (CH_3), 143.8 (CH), 145.0 (C), 173.5 (C), 196.4 (C). IR (neat, cm^{-1}): 1668, 1739. MS (m/e , relative intensity): 182, 1 (M^+); 150, 44; 95, 100. Anal. Calcd for $\text{C}_{10}\text{H}_{14}\text{O}_3$: C, 65.92; H, 7.74. Found: C, 66.04; H, 7.72.

6-(Methoxycarbonyl)-5-bicyclo[5.3.0]decen-2-one (8). A solution of 0.401 g (1 mmol) of **3h** and 129 μL (1.1 mmol) of methyl 2,4-pentadienoate in toluene is refluxed for 7.5 h. The reaction mixture is cooled to -20 $^\circ\text{C}$ for 10 h, filtered, and concentrated. The residue is treated with a mixture of tetrahydrofuran (5 mL) and 2 N aqueous H_2SO_4 (5 mL) for 1 h, extracted with diethyl ether, dried with anhydrous Na_2SO_4 , and concentrated. The resulting oil is chromatographed (silica gel, hexane-ethyl acetate (3:1)); R_f 0.36. Yield: 0.073 g (35%). ^1H NMR (CDCl_3): δ 1.02–1.55 (m, 3H), 1.55–1.88 (m, 4H), 1.96, 2.47 (m, 3H), 2.47–2.72 (m, 1H), 3.25 (d t, $J = 16.2$, 11.4 Hz, 1H), 3.68 (s, 3H), 7.24 (d d, $J = 8.1$, 5.2 Hz, 1H). ^{13}C NMR (CDCl_3): δ 25.4 (CH_2), 26.5 (CH_2), 29.8 (CH_2), 30.6 (CH_2), 33.7 (CH_2), 42.9 (CH), 52.0 (CH_3), 57.4 (CH), 135.2 (C), 147.7 (CH), 165.1 (C), 202.4 (C). IR (neat, cm^{-1}): 1725, 1696. MS (m/e , relative intensity): 205, 4 (M^+); 176, 84; 148, 80; 139, 45; 126, 60; 121, 57; 120, 74; 108, 75; 98, 100; 91, 53; 79, 61; 68, 57; 67, 42. Anal. Calcd for $\text{C}_{12}\text{H}_{16}\text{O}_3$: C, 69.21; H, 7.74. Found: C, 69.12; H, 7.79.

Acknowledgment. This research was supported by the Dirección General de Investigación Científica y Técnica (DGICYT; Grant No. PB92-1005). An MEC Fellowship to A.M. is gratefully acknowledged.

OM9408021

Reactions of Coordinated Phosphines and Arsines. Iron(II)-Facilitated and Direct Syntheses of Three- to Seven-Membered Heterocycles Containing Phosphorus and Arsenic. Crystal Structures of Iron(II) Complexes of 1-Phenylphosphetane and 1-Phenylarsetane

Armin Bader, Yew Beng Kang, Michael Pabel, Devendra D. Pathak, Anthony C. Willis, and S. Bruce Wild*

Research School of Chemistry, Institute of Advanced Studies, Australian National University, Canberra, ACT 0200, Australia

Received November 21, 1994[⊗]

The complexes $(R^*, R^*)-(\pm)-[(\eta^5-C_5H_5)\{1,2-C_6H_4(PMePh)_2\}FeL]PF_6$, where L = 1-phenylphosphetane, -phospholane, -phosphorinane, and -phosphhepane, have been prepared in high yields from the corresponding phenylphosphine complex by treatment with the appropriate α, ω -dibromoalkanes and potassium *tert*-butoxide. The 1-phenylarsetane complex was obtained by deprotonation of the corresponding complex of (\pm) -(3-chloropropyl)phenylarsine. The 1-phenylphosphirane, the 1-phenylphosphetane, and the 1-phenylarsetane complexes were also prepared by direct reactions of the free ligands with $(R^*, R^*)-(\pm)-[(\eta^5-C_5H_5)\{1,2-C_6H_4(PMePh)_2\}FeMeCN]PF_6$. The molecular structures of $(R^*, R^*)-(\pm)-[(\eta^5-C_5H_5)\{1,2-C_6H_4(PMePh)_2\}Fe(PhPCH_2CH_2CH_2)]PF_6$ and $(R^*, R^*)-(\pm)-[(\eta^5-C_5H_5)\{1,2-C_6H_6(PMePh)_2\}Fe(PhAsCH_2CH_2CH_2)]PF_6$ have been determined by X-ray crystallography. The phosphetane complex crystallized in a solvated form with two independent cations of slightly different geometries in each unit cell; the four-membered phosphetane rings are puckered with the angles between the C-P-C and C-C-C planes being 18(2) and 24(2)[∘] for the respective cations. The four-membered ring of the arsetane complex is also puckered with the corresponding angle being 25(1)[∘].

Introduction

Compared with the long history of five- and six-membered heterocycles containing phosphorus or arsenic,¹ the chemistry of similar three- and four-membered rings has developed only recently.² Routes to four-membered saturated phosphetanes have involved treatment of appropriately substituted alkenes with $RPdCl_2-AlCl_3$ adducts,^{1,5} insertion of phosphonium ions (R_2P^+) into the carbon-carbon bonds of cyclopropanes,⁶ and [2

+ 2] cycloadditions between phosphalkene complexes and activated olefins.⁷ These syntheses often lead to rings containing phosphorus in the +5 oxidation state or, more importantly, to rings that are highly substituted. The first structurally characterized arsirane was reported in 1985,³ and unsaturated four-membered dihydroarsete rings were described some years later.⁴ Unsubstituted oxiranes⁸ and oxetanes⁹ are subject to ring opening and subsequent cyclooligomerization into crown ethers in the presence of metal salts, and similar reactions have also been reported for thiiranes¹⁰ and thietanes.¹¹ This strategy presents the enticing prospect of the synthesis of macrocyclic poly(tertiary phosphines and arsines) from three- and four-membered phosphorus and arsenic heterocycles; such compounds are difficult to obtain in configurationally homogeneous form by conventional methods.¹² The formation of linear oligomers or polymers by the thermally induced

[⊗] Abstract published in *Advance ACS Abstracts*, February 1, 1995.

(1) Quin, L. D.; Hughes, A. N. In *The Chemistry of Organophosphorus Compounds*; Vol. 1 *The Chemistry of Functional Groups*; Hartley, F. R.; Patai, S., Eds.; J. Wiley & Sons Ltd.: Chichester, UK, 1990.

(2) Recent reviews: (a) Mathey, F. *Chem. Rev.* **1990**, *90*, 997. (b) Mathey, F.; Charrier, C.; Maignot, N.; Marinetti, A.; Ricard, L.; Huy, N. H. T. *Comments Inorg. Chem.* **1992**, *13*, 61.

(3) Appel, R.; Gaitzsch, T.; Knoch, F. *Angew. Chem., Int. Ed. Engl.* **1985**, *24*, 419.

(4) (a) Tumas, W.; Suriano, J. A.; Harlow, R. L. *Angew. Chem., Int. Ed. Engl.* **1990**, *29*, 75. (b) Li, X.; Lukehart, C. M.; McPhail, A. T.; McPhail, D. R. *Organometallics* **1991**, *10*, 372.

(5) (a) Jungermann, E.; McBride, J. J., Jr.; Clutter, R.; Mais, A. J. *Org. Chem.* **1962**, *27*, 606. (b) McBride, J. J., Jr.; Jungermann, E.; Killheffer, J. V.; Clutter, R. J. *J. Org. Chem.* **1962**, *27*, 1833. (c) Cremer, S. E.; Chorvat, R. J. *J. Org. Chem.* **1967**, *32*, 4066. (d) Bergesen, K. *Acta Chem. Scand.* **1967**, *21*, 1587. (e) Gray, G. A.; Cremer, S. E. *J. Org. Chem.* **1972**, *37*, 3458. (f) Cremer, S. E.; Weitl, F. L.; Farr, F. R.; Kremer, P. W.; Gray, G. A.; Hwang, H.-O. *J. Org. Chem.* **1973**, *38*, 3199. (g) Emsley, J.; Middleton, T. B.; Williams, J. K. *J. Chem. Soc., Dalton Trans.* **1976**, 979. (h) Gray, G. A.; Cremer, S. E.; Marsi, K. L. *J. Am. Chem. Soc.* **1976**, *98*, 2109. (i) De'Ath, N. J.; Denney, D. B.; Denney, D. Z.; Hsu, Y. F. *J. Am. Chem. Soc.* **1976**, *98*, 768. (j) Vilkas, E.; Vilkas, M.; Sainion, J.; Meunier, B.; Pascard, C. *J. Chem. Soc., Perkin Trans. 1* **1980**, 2136. (k) Yao, E.; Szewczyk, J.; Quin, L. D. *Synthesis* **1987**, 265.

(6) Weissman, S. A.; Baxter, S. G. *Tetrahedron Lett.* **1988**, *29*, 1219.

(7) Marinetti, A.; Mathey, F. *J. Chem. Soc., Chem. Commun.* **1990**, 153.

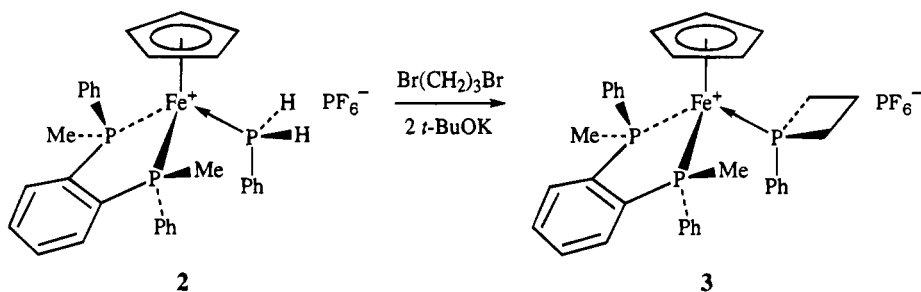
(8) (a) Kern, R. J. *J. Org. Chem.* **1968**, *33*, 388. (b) Dale, J.; Daasvatn, K. *J. Chem. Soc., Chem. Commun.* **1976**, 295. (c) Jones P. G.; Gries, T.; Grützmacher, H.; Roesky, H. W.; Schimkowiak, J.; Sheldrick, G. M. *Angew. Chem., Int. Ed. Engl.* **1984**, *23*, 376. (d) Kostenko, T. I.; Lebedev, V. S.; Vakhtina, I. A.; Samoilova, N. P.; Botnikov, M. Y. *J. Org. Chem. USSR (Engl. Transl.)* **1988**, *24*, 500. (e) Meier, K.; Rihs, G. *Angew. Chem., Int. Ed. Engl.* **1985**, *24*, 858.

(9) (a) Rose, J. B. *J. Chem. Soc.* **1956**, 542. (b) Dale, J.; Fredriksen, S. B. *Acta Chem. Scand.* **1991**, *45*, 82.

(10) Adams, R. D.; Chen, G.; Sun, S.; Wolfe, T. A. *J. Am. Chem. Soc.* **1990**, *112*, 868.

(11) Adams, R. D.; Pompeo, M. P. *J. Am. Chem. Soc.* **1991**, *113*, 1619.

Scheme 1



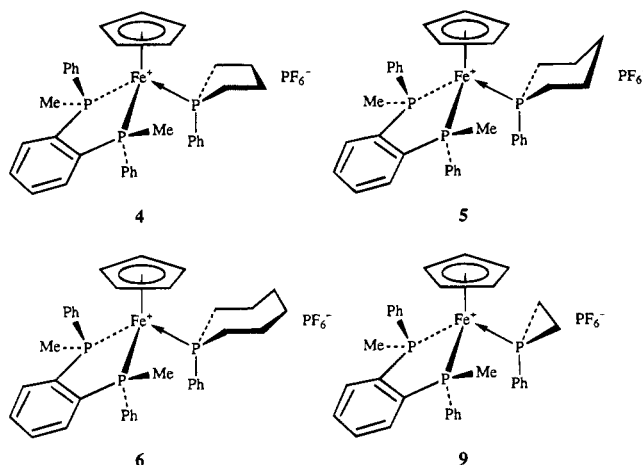
ring opening of 1-phenylphosphetane has been reported.¹³

In previous work, we showed that coordinated primary and secondary phosphines¹⁴ and arsines¹⁵ are readily deprotonated to give reactive phosphido and arsenido species which undergo facile and often highly stereoselective alkylation upon treatment with haloalkanes. As an extension to this work, we have found that α,ω -dihaloalkanes effect ring closures in reactions of appropriate phosphido and arsenido complexes leading to phosphorus and arsenic heterocycles having a range of ring sizes. This strategy was also used recently for the synthesis of 1-diethylaminophosphirane in the coordination sphere of a tungsten complex.¹⁶ Thus, iron(II) complexes of 1-phenylphosphetane, -phospholane, -phosphorinane, and -phosphhepane were prepared from the phenylphosphine complex and the appropriate α,ω -dihaloalkanes in the presence of potassium *tert*-butoxide; the corresponding 1-phenylarsetane complex was obtained from (\pm)-(3-chloropropyl)phenylarsine by a similar strategy. The corresponding 1-phenylphosphirane, -phosphetane, and -arsetane complexes were also prepared by direct syntheses from the free heterocycles by displacement of acetonitrile from the appropriate iron(II) precursor. The crystal structures of the phosphetane and arsetane complexes are reported. A preliminary account of certain aspects of this work has been published.¹⁷

Results and Discussion

Iron(II)-Facilitated Syntheses. Acetonitrile in (R^*,R^*)-(\pm)-[(η^5 -C₅H₅){1,2-C₆H₄(PMePh)₂}Fe(NCMe)]-PF₆ (**1**) is readily displaced by phosphines and arsines.^{14,15,18} Thus, the phenylphosphine complex **2** was obtained in excellent yield from **1** and PH₂Ph in boiling methanol.^{14a} Treatment of **2** with 1,3-dibromopropane and 2 equiv of potassium *tert*-butoxide in tetrahydrofuran (THF) gave the 1-phenylphosphetane complex **3** in high yield (Scheme 1). The reaction is believed to

proceed by a stepwise mechanism involving the (3-bromopropyl)(phenyl)phosphine complex, which, after deprotonation at phosphorus, undergoes cyclization to give the phosphetane complex **3**. The complex was isolated as the dichloromethane solvate (yellow needles) or as a mixed solvate with benzene and chloroform (dark brown prisms); crystals of the latter were suitable for X-ray crystallography (see below). The reaction of **1** with the α,ω -dibromobutane, -pentane, or -hexane in the presence 2 equiv of potassium *tert*-butoxide affords the complexes of 1-phenylphospholane **4**, 1-phenylphosphorinane **5**, and 1-phenylphosphhepane **6**, respectively.



(12) (a) Kauffmann, T.; Ennen, J. *Chem. Ber.* **1985**, *118*, 2692. (b) Ciampolini, M. *Pure Appl. Chem.* **1986**, *58*, 1429. (c) Martin, J. W. L.; Stephens, F. S.; Weerasuria, K. D. V.; Wild, S. B. *J. Am. Chem. Soc.* **1988**, *110*, 4346, and references cited therein.

(13) Tumas, W.; Huang, J. C.; Fanwick, P. E.; Kubiak, C. P. *Organometallics* **1992**, *11*, 2944.

(14) (a) Crisp, G. T.; Salem, G.; Wild, S. B.; Stephens, F. S. *Organometallics* **1989**, *8*, 2360, and references cited therein. (b) Hey, E.; Willis, A. C.; Wild, S. B. *Z. Naturforsch.* **1989**, *44B*, 1041.

(15) Salem, G.; Wild, S. B. *J. Organomet. Chem.* **1989**, *370*, 33.

(16) Mercier, F.; Deschamps, B.; Mathey, F. *J. Am. Chem. Soc.* **1989**, *111*, 9098.

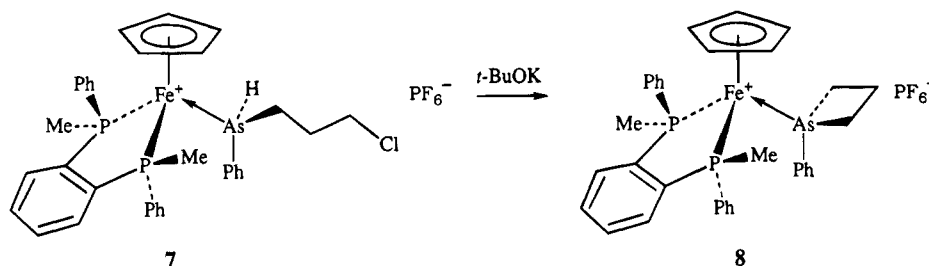
(17) Bader, A.; Pathak, D. D.; Wild, S. B.; Willis, A. C. *J. Chem. Soc., Dalton Trans.* **1992**, 1751.

(18) (a) Schumann, H.; Speis, M.; Bosman, W. P.; Smits, J. M. M.; Beurskens, P. T. *J. Organomet. Chem.* **1991**, *403*, 165. (b) Schumann, H.; Eguren, L. *J. Organomet. Chem.* **1991**, *403*, 183.

The phenylarsine complex (R^*,R^*)-(\pm)-[(η^5 -C₅H₅){1,2-C₆H₄(PMePh)₂}Fe(AsH₂Ph)]PF₆ could not be prepared from **1** and phenylarsine in boiling ethanol, but the secondary arsine (\pm)-(3-chloropropyl)(phenyl)arsine gave [(R^*/S^*),(R^*,R^*)-(\pm)-[(η^5 -C₅H₅){1,2-C₆H₄(PMePh)₂}Fe{PhAs(CH₂)₃Cl}]]PF₆ (**7**) in almost quantitative yield. The yellow complex was isolated as an unequal mixture of the two diastereomers, epimeric at arsenic, each of which gave rise to a characteristic four-line AB ³¹P{¹H} NMR spectrum. Deprotonation of the coordinated secondary arsine in **7** with potassium *tert*-butoxide in THF afforded the deep red arsenido complex, which was not isolated. After 2–3 h at room temperature, the arsenido complex underwent intramolecular nucleophilic substitution at the 3-chloropropyl carbon atom to give the 1-phenylarsetaneiron(II) complex (R^*,R^*)-(\pm)-[(η^5 -C₅H₅){1,2-C₆H₄(PMePh)₂}Fe(PhAsCH₂CH₂CH₂)]-PF₆ (**8**) in high yield.

Direct Syntheses of 3, 8, and 9. The 1-phenylphosphirane complex **9**, which was not accessible by the metal-assisted route from phenylphosphine, was prepared by direct synthesis. Thus, an equimolar mixture

Scheme 2



of **1** and 1-phenylphosphirane¹⁹ in boiling dichloromethane afforded crystalline orange **9** in high yield after 48 h. In a similar reaction, 1-phenylphosphetane, which was used as a 70/30 mixture with its decomposition product poly(phenylphosphino)propane,¹⁹ gave **3**, which was identified by ¹H, ¹³C{¹H}, and ³¹P{¹H} NMR spectroscopy. No attempts were made to isolate **3** from the reaction mixture. The same strategy was employed for the direct synthesis of the 1-phenylarsetane complex **8**. Thus, treatment of a suspension of dilithium phenylarsenide in THF with 1,3-dichloropropane at -78 °C followed by stirring of the reaction mixture at 20 °C for 10 h, evaporation of the solvent, extraction of the residue with petroleum spirit, and removal of the solvent afforded a highly viscous residue. Vacuum distillation gave a few drops of a colorless mobile oil, which solidified in the receiver flask (probably due to polymerization). Heating of a C₆D₆ extract of the distillate with a small quantity of **1** in THF gave **8**, which was identified by ³¹P{¹H} NMR spectroscopy, thus demonstrating the existence of free monomeric 1-phenylarsetane in the original distillate. Free 1-phenylarsetane has also been prepared in low yield by the reductive cyclization of (3-chloropropyl)iodophenylarsine.²⁰

Crystal and Molecular Structures of 3·0.75C₆H₆·0.25CHCl₃ and 8. The crystal obtained from a mixed benzene-chloroform solution of **3** was found to have an asymmetric unit comprising 2 independent cations, A and B, 2 anions, 1.5 molecules of benzene, and a 0.5 molecule of chloroform which was disordered. Crystallographic data, atomic coordinates, and selected molecular parameters are compiled in Tables 1–3, respectively. Figure 1 shows the ORTEP diagrams of cations A and B. The crystal structures of a number of substituted phosphetane derivatives have been determined,^{5j,21} and the parent phosphetane has

Table 1. Crystallographic Data for 3·0.75C₆H₆·0.25CHCl₃ and 8

	3·0.75C ₆ H ₆ ·0.25CHCl ₃	8
formula	C _{38.75} H _{40.75} Cl _{0.75} F ₆ FeP ₄	C ₃₄ H ₃₆ AsF ₆ FeP ₃
mol wt	826.82	782.34
crystal system	monoclinic	orthorhombic
space group	P2 ₁ /n	P2 ₁ 2 ₁ 2 ₁
a, Å	22.491(14)	14.021(2)
b, Å	14.477(14)	14.846(2)
c, Å	25.516(17)	16.504(2)
β, deg	112.55(5)	
V, Å ³	7673(10)	3435.4(7)
Z	8	4
cryst dimens, mm	0.4 × 0.2 × 0.16	0.26 × 0.16 × 0.16
d _{calcd} , g cm ⁻³	1.431	1.512
μ, cm ⁻¹	6.6	64.6
X-ray radiation ^a	Mo Kα (λ = 0.710 73 Å)	Cu Kα (λ = 1.5418 Å)
diffractometer	Nicolet XRD P3	Philips PW 1100/20
T, °C	-125	20(1)
no. of unique data	13243	3211
no. of data used ^b	3484	2221
no. of variables	525	406
R ^c	0.087	0.058
R _w ^c	0.091	0.062
GOF ^c	1.75	2.01
F(000)	3660	1592

^a Graphite monochromator. ^b I > 3σ(I). ^c R = ∑||F_o| - |F_c||/∑|F_o|; R_w = {∑w(|F_o| - |F_c|)²/∑(wF_o)²}^{1/2}; GOF = {∑w(|F_o| - |F_c|)²/(no. ref - no. var)}^{1/2}.

been the subject of theoretical investigations.²² **3** is the first phosphetane complex unsubstituted at carbon to be characterized by X-ray crystallography. Since the original report,¹⁷ however, the complex *fac*-[Mo(CO)₃-(PhPCH₂CH₂CH₂)₃] has been synthesized and structurally characterized.¹⁹ The geometries of the two cations A and B in **3** are similar with small differences occurring only in the conformation of the phosphetane ring. The presence of two unrelated molecules in the unit cell was also found in 2,2,3,4,4-pentamethyl-1-phenylphosphetane 1-oxide.^{21d} The bonding parameters within the [(η⁵-C₅H₅){1,2-C₆H₄(PMePh)₂}Fe] group, as well as the Fe-P(1) bond lengths in the two cations, are in good agreement with those of related compounds.^{14a,21m} The P-C distances in the four-membered rings of the two independent molecules of **3** range from 1.85(2) to 1.90(2) Å with an average value of 1.87(2) Å; P-C bonds for other phosphetanes have been observed as short as 1.788(5) Å^{21e,k} or as long as 1.94(4) Å.^{21b} The C-C distances within the four-membered rings of the two conformers of **3** range from 1.49(3) to 1.60(3) Å. A significant elongation of the C-C bonds in four-membered rings is common for substituted phosphetanes.^{21b-d} The geometry around P(1) is significantly distorted from regular tetrahedral geometry with contracted internal angles at P(1) (77.6(1) and

(19) Kang, Y. B.; Pabel, M.; Willis, A. C.; Wild, S. B. *J. Chem. Soc., Chem. Commun.* **1994**, 475.

(20) Mickiewicz, M.; Wild, S. B. *J. Chem. Soc., Dalton Trans.* **1977**, 704.

(21) (a) Swank, D. D.; Caughlan, C. N. *Chem. Commun.* **1968**, 1051. (b) Moret, C.; Trefonas, L. M. *J. Am. Chem. Soc.* **1969**, *91*, 2255. (c) Mazhar-ul-Haque, *J. Chem. Soc. B* **1970**, 934. (d) Mazhar-ul-Haque, *J. Chem. Soc. B* **1970**, 938. (e) Fitzgerald, A.; Campbell, J. A.; Smith, G. D.; Caughlan, C. N.; Cremer, S. E. *J. Org. Chem.* **1978**, *43*, 3513. (f) Mazhar-ul-Haque, *Acta Crystallogr.* **1979**, *B35*, 2601. (g) Mazhar-ul-Haque; Horne, W.; Cremer, S. E.; Kremer, P. W.; Kafarski, P. K. *J. Chem. Soc., Perkin Trans. 2* **1981**, 1138. (h) Mazhar-ul-Haque; Horne, W. *Acta Crystallogr.* **1982**, *B38*, 2944. (i) Campbell, J. A.; Caughlan, C. N.; Fitzgerald, A.; Campana, C.; Cremer, S. E. *Acta Crystallogr.* **1984**, *C40*, 1918. (j) Mazhar-ul-Haque; Jamil Ahmed; Horne, W. *Acta Crystallogr.* **1985**, *C41*, 975. (k) Campbell, J. A.; Larsen, R.; Campana, C.; Cremer, S. E. *Acta Crystallogr.* **1987**, *C43*, 340. (l) Mazhar-ul-Haque; Horne, W.; Cremer, S. E.; Kremer, P. W.; Kafarski, P. K. *J. Crystallogr. Spectrosc. Res.* **1989**, *19*, 267. (m) Bennett, D. W.; Grubisha, D. S.; Cremer, S. E.; Peterson, A. C. *J. Crystallogr. Spectrosc. Res.* **1992**, *22*, 83.

(22) Bachrach, S. M. *J. Phys. Chem.* **1989**, *93*, 7780.

Table 2. Atomic Coordinates and Equivalent Isotropic Displacement Parameters^a for the Non-Hydrogen Atoms of Species A and B in 3·0.75C₆H₆·0.25CHCl₃

	<i>x/a</i>	<i>y/b</i>	<i>z/c</i>	<i>U/U_{eq}</i>		<i>x/a</i>	<i>y/b</i>	<i>z/c</i>	<i>U/U_{eq}</i>
Cation A									
Fe	0.6963(1)	0.4023(2)	0.6572(1)	0.023(1)	C(16)	0.6266(9)	0.198(1)	0.6430(7)	0.016(5)
P(1)	0.7043(2)	0.3853(3)	0.5747(2)	0.026(3)	C(17)	0.6177(9)	0.100(1)	0.6430(8)	0.030(5)
P(2)	0.7038(3)	0.2565(3)	0.6818(2)	0.027(3)	C(18)	0.556(1)	0.066(1)	0.6128(9)	0.039(6)
P(3)	0.5919(3)	0.3799(3)	0.6220(2)	0.023(3)	C(19)	0.507(1)	0.123(1)	0.5821(8)	0.034(6)
C(1)	0.6641(9)	0.299(1)	0.5189(8)	0.028(5)	C(20)	0.515(1)	0.218(1)	0.5815(8)	0.029(5)
C(2)	0.648(1)	0.370(1)	0.4729(9)	0.053(7)	C(21)	0.5748(9)	0.256(1)	0.6143(7)	0.026(5)
C(3)	0.662(1)	0.459(1)	0.5112(9)	0.047(7)	C(22)	0.715(1)	0.232(1)	0.7554(8)	0.038(6)
C(4)	0.7885(9)	0.389(1)	0.5764(8)	0.031(5)	C(23)	0.539(1)	0.425(1)	0.5360(8)	0.038(6)
C(5)	0.816(1)	0.472(1)	0.5698(9)	0.047(7)	C(24)	0.5498(9)	0.415(1)	0.6682(8)	0.025(5)
C(6)	0.879(1)	0.471(2)	0.573(1)	0.060(8)	C(25)	0.550(1)	0.362(1)	0.7118(9)	0.038(6)
C(7)	0.915(1)	0.395(2)	0.585(1)	0.071(8)	C(26)	0.521(1)	0.388(1)	0.7486(9)	0.044(6)
C(8)	0.889(1)	0.309(2)	0.591(1)	0.061(8)	C(27)	0.488(1)	0.472(1)	0.7374(9)	0.040(6)
C(9)	0.825(1)	0.308(2)	0.5865(9)	0.051(7)	C(28)	0.487(1)	0.524(2)	0.695(1)	0.053(7)
C(10)	0.7667(9)	0.183(1)	0.6734(8)	0.024(5)	C(29)	0.516(1)	0.502(1)	0.6583(8)	0.041(6)
C(11)	0.830(1)	0.196(1)	0.7098(9)	0.036(6)	C(30)	0.768(1)	0.438(1)	0.7367(9)	0.035(6)
C(12)	0.879(1)	0.145(1)	0.7030(9)	0.045(7)	C(31)	0.708(1)	0.473(1)	0.7325(8)	0.034(6)
C(13)	0.864(1)	0.083(2)	0.658(1)	0.055(7)	C(32)	0.687(1)	0.534(1)	0.6871(9)	0.040(6)
C(14)	0.801(1)	0.069(1)	0.6212(9)	0.042(6)	C(33)	0.729(1)	0.536(1)	0.6609(8)	0.030(6)
C(15)	0.7508(9)	0.121(1)	0.6278(8)	0.028(5)	C(34)	0.782(1)	0.476(1)	0.6919(8)	0.037(6)
Anion A									
P(4)	0.4242(3)	0.2420(4)	0.4045(3)	0.046(4)	F(4)	0.411(1)	0.334(1)	0.4254(8)	0.16(2)
F(1)	0.4468(9)	0.156(1)	0.384(1)	0.19(2)	F(5)	0.409(1)	0.205(2)	0.4536(8)	0.19(2)
F(2)	0.437(1)	0.289(1)	0.3566(7)	0.15(2)	F(6)	0.4953(8)	0.260(1)	0.4454(8)	0.15(2)
F(3)	0.3556(7)	0.226(2)	0.3648(7)	0.21(2)					
Cation B									
Fe	0.6658(1)	0.9957(2)	0.2929(1)	0.032(2)	C(16)	0.6706(9)	0.969(1)	0.4234(8)	0.027(5)
P(1)	0.5762(3)	0.9175(4)	0.2566(2)	0.036(3)	C(17)	0.6778(9)	0.936(1)	0.4760(8)	0.028(5)
P(2)	0.7045(3)	0.9241(4)	0.3749(2)	0.030(3)	C(18)	0.6493(9)	0.978(1)	0.5077(8)	0.030(5)
P(3)	0.6301(3)	1.0985(4)	0.3370(2)	0.033(3)	C(19)	0.611(1)	1.056(1)	0.4889(8)	0.029(5)
C(1)	0.522(1)	0.876(1)	0.2918(8)	0.037(6)	C(20)	0.6045(9)	1.092(1)	0.4400(7)	0.025(5)
C(2)	0.461(1)	0.903(2)	0.237(1)	0.069(8)	C(21)	0.6334(9)	1.051(1)	0.4044(8)	0.028(6)
C(3)	0.495(1)	0.969(2)	0.211(1)	0.059(7)	C(22)	0.789(1)	0.937(1)	0.4170(9)	0.042(6)
C(4)	0.579(1)	0.814(1)	0.213(1)	0.045(7)	C(23)	0.552(1)	1.154(1)	0.3071(9)	0.049(7)
C(5)	0.557(1)	0.825(2)	0.154(1)	0.09(1)	C(24)	0.684(1)	1.201(1)	0.3619(9)	0.033(6)
C(6)	0.564(1)	0.741(2)	0.122(1)	0.09(1)	C(25)	0.734(1)	1.197(1)	0.4126(8)	0.036(6)
C(7)	0.588(1)	0.663(2)	0.151(1)	0.071(8)	C(26)	0.778(1)	1.273(2)	0.430(1)	0.065(8)
C(8)	0.609(1)	0.656(2)	0.208(1)	0.054(7)	C(27)	0.764(1)	1.350(2)	0.395(1)	0.061(8)
C(9)	0.605(1)	0.735(2)	0.2393(9)	0.048(7)	C(28)	0.713(1)	1.355(1)	0.346(1)	0.050(7)
C(10)	0.695(1)	0.796(1)	0.3799(8)	0.033(6)	C(29)	0.670(1)	1.280(1)	0.3279(9)	0.046(6)
C(11)	0.736(1)	0.738(2)	0.3655(9)	0.054(7)	C(30)	0.754(1)	0.978(1)	0.2824(9)	0.047(6)
C(12)	0.729(1)	0.641(1)	0.3646(9)	0.047(7)	C(31)	0.743(1)	1.073(2)	0.2870(9)	0.053(7)
C(13)	0.679(1)	0.606(2)	0.3777(9)	0.055(7)	C(32)	0.685(1)	1.099(2)	0.2432(9)	0.048(6)
C(14)	0.640(1)	0.664(1)	0.3907(9)	0.038(6)	C(33)	0.658(1)	1.020(2)	0.2105(9)	0.048(7)
C(15)	0.646(1)	0.760(1)	0.3935(8)	0.033(6)	C(34)	0.702(1)	0.946(2)	0.234(1)	0.051(7)
Anion B									
P(4)	-0.0703(4)	0.8290(5)	0.3462(4)	0.069(5)	F(4)	-0.0004(8)	0.865(2)	0.369(1)	0.20(2)
F(1)	-0.1434(7)	0.800(1)	0.3167(8)	0.12(1)	F(5)	-0.0547(8)	0.735(1)	0.3259(9)	0.17(2)
F(2)	-0.0878(7)	0.9230(9)	0.3675(9)	0.12(1)	F(6)	-0.081(1)	0.871(2)	0.285(1)	0.25(3)
F(3)	-0.064(2)	0.789(1)	0.4007(8)	0.24(3)					
Solvent Molecules									
C(35)	0.202(1)	0.291(2)	0.476(1)	0.083(9)	C(41)	0.508(2)	0.105(3)	0.005(2)	0.14(1)
C(36)	0.242(1)	0.275(2)	0.450(1)	0.069(8)	C(42)	0.557(2)	0.041(3)	0.039(2)	0.14(1)
C(37)	0.226(1)	0.225(2)	0.401(1)	0.059(7)	C(43)	0.547(2)	-0.051(3)	0.031(2)	0.12(1)
C(38)	0.163(1)	0.186(2)	0.380(1)	0.075(8)	Cl(1) ^{b,c}	0.0832(9)	0.881(1)	0.5117(6)	0.11(1)
C(39)	0.121(1)	0.198(2)	0.407(1)	0.09(1)	Cl(2) ^{b,c}	0.0371(7)	1.050(1)	0.4805(6)	0.11(1)
C(40)	0.141(2)	0.254(2)	0.456(1)	0.11(1)					

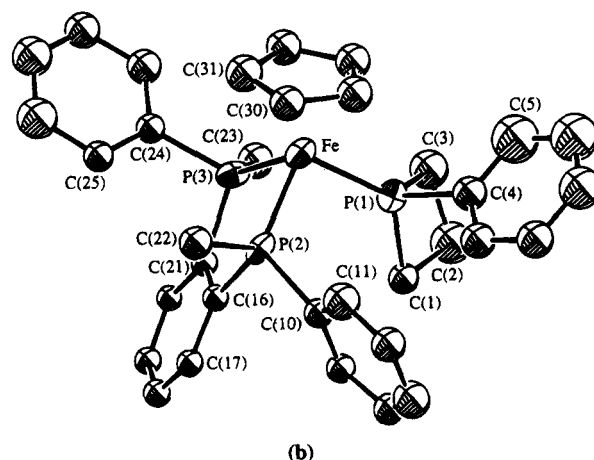
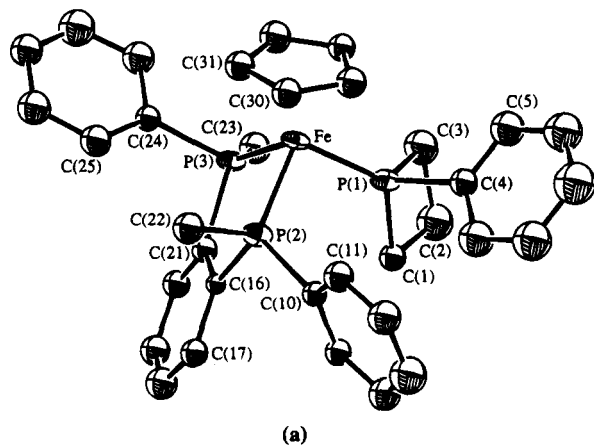
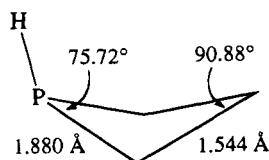
^a $U_{eq} = 1/3 \sum_i \sum_j U_{ij} a_i^* a_j^* a_i a_j$. ^b Two atom sites (and their symmetry-related positions) near 0, 1, 1/2 have been interpreted as arising from disordered CHCl₃ molecule. ^c Occupancy 0.5.

77(1)°). As expected, the phosphetane ring in **3** is decidedly nonplanar. The extent of puckering, as expressed by the angle between the two planes defined by the atoms C(1), P(1), C(3) and C(1), C(2), C(3), is 18(2) (cation A) and 24(2)° (cation B). These values are within the range determined for various substituted systems. Early work^{21e,i} suggested that the magnitude of the puckering angle was related to the number of interactions between substituents that were located on adjacent ring atoms and cis to each other. It is now evident from the crystallographic data for an increasing

number of phosphetane derivatives with a range of substitution patterns that no simple correlation exists between the extent of ring substitution and ring puckering^{21e} and that crystal packing forces also appear to play an important role in the determination of the structures.^{21m} Theoretical studies on the parent phosphetane²² suggest that the lowest energy conformer has the P-H atom axial (endo). The salient bond lengths and angles resulting from the theoretical work are given in Figure 2. Despite the different substituent on the phosphorus atom compared to complex **3**, the agreement

Table 3. Selected Bond Lengths, Bond Angles, and Dihedral Angles for the Cations A and B of $3 \cdot 0.75\text{C}_6\text{H}_6 \cdot 0.25\text{CHCl}_3$

	cation A	cation B		cation A	cation B
Bond Lengths (Å)					
Fe–P(1)	2.193(7)	2.184(6)	P(1)–C(3)	1.87(2)	1.90(2)
Fe–P(2)	2.190(6)	2.194(6)	P(1)–C(4)	1.88(2)	1.87(2)
Fe–P(3)	2.194(6)	2.194(7)	C(1)–C(2)	1.49(3)	1.60(3)
P(1)–C(1)	1.85(2)	1.86(3)	C(2)–C(3)	1.58(3)	1.51(4)
Bond Angles (deg)					
Fe–P(1)–C(1)	128.3(8)	128.9(6)	P(1)–C(1)–C(2)	92(1)	90(1)
Fe–P(1)–C(3)	124.6(8)	124.8(8)	P(1)–C(3)–C(2)	89(1)	91(1)
Fe–P(1)–C(4)	115.3(6)	115.6(8)	C(1)–C(2)–C(3)	98(2)	98(2)
C(1)–P(1)–C(4)	103(1)	101(1)	P(1)–Fe–P(2)	98.1(2)	97.1(3)
C(3)–P(1)–C(4)	100(1)	101.1(9)	P(2)–Fe–P(3)	85.8(2)	85.5(3)
Dihedral Angles (deg)					
C(1)–P(1)–C(3)–C(2)	–11(1)	–16(1)	P(1)–C(1)–C(2)–C(3)	–14(2)	–19(2)
C(1)–C(2)–C(3)–P(1)	12(2)	15(1)	C(1)–C(2)–C(3)–P(1)	14(2)	18(2)

**Figure 1.** ORTEP view of cations A (a) and B (b) of $3 \cdot 0.75\text{C}_6\text{H}_6 \cdot 0.25\text{CHCl}_3$ showing atom labeling of selected atoms. Thermal ellipsoids enclose 50% probability levels.**Figure 2.** Salient distances and angles for the lowest energy conformer of phosphetane.²²

between the calculated values for the parent phosphetane and the crystallographic data for **3** is remarkably good.

Slow crystallization of the 1-phenylarsetane complex **8** from dichloromethane–diethyl ether afforded solvent-free crystals suitable for X-ray crystallography. Crys-

Table 4. Atomic Coordinates and Equivalent Isotropic Displacement Parameters^a for the Non-Hydrogen Atoms in **8**

	<i>x/a</i>	<i>y/b</i>	<i>z/c</i>	<i>U</i> _{eq}
Fe	0.24696(14)	0.46648(11)	0.32933(9)	0.0463(5)
As	0.36285(9)	0.39410(8)	0.25231(8)	0.0510(4)
P(1)	0.1211(2)	0.4221(2)	0.2609(2)	0.048(1)
P(2)	0.2414(2)	0.5899(2)	0.2545(2)	0.0511(9)
C(1)	0.3711(9)	0.2671(8)	0.2174(9)	0.068(5)
C(2)	0.4180(11)	0.2954(13)	0.1362(10)	0.097(7)
C(3)	0.3878(10)	0.3938(11)	0.1327(7)	0.076(6)
C(4)	0.4922(8)	0.4110(8)	0.2936(7)	0.055(4)
C(5)	0.5446(10)	0.4848(9)	0.2701(9)	0.079(6)
C(6)	0.6337(12)	0.5020(11)	0.3048(11)	0.112(8)
C(7)	0.6695(11)	0.4431(12)	0.3593(11)	0.095(7)
C(8)	0.6197(12)	0.3674(9)	0.3818(7)	0.069(5)
C(9)	0.5304(11)	0.3520(9)	0.3502(8)	0.067(5)
C(10)	0.1271(8)	0.3197(7)	0.1987(8)	0.052(4)
C(11)	0.1197(9)	0.2350(8)	0.2369(9)	0.074(5)
C(12)	0.1254(11)	0.1571(8)	0.1920(11)	0.085(7)
C(13)	0.1419(12)	0.1620(12)	0.1118(13)	0.101(8)
C(14)	0.1473(12)	0.2445(11)	0.0733(9)	0.088(7)
C(15)	0.1407(9)	0.3228(9)	0.1160(8)	0.062(5)
C(16)	0.0837(8)	0.5086(7)	0.1905(6)	0.046(4)
C(17)	0.0009(9)	0.5039(8)	0.1419(7)	0.060(5)
C(18)	–0.0247(11)	0.5738(10)	0.0937(8)	0.073(6)
C(19)	0.0317(11)	0.6498(10)	0.0891(7)	0.068(5)
C(20)	0.1132(10)	0.6567(8)	0.1374(7)	0.058(5)
C(21)	0.1400(9)	0.5865(7)	0.1874(6)	0.046(4)
C(22)	0.0098(9)	0.4030(8)	0.3152(8)	0.068(5)
C(23)	0.3369(10)	0.6186(9)	0.1829(9)	0.082(6)
C(24)	0.2202(9)	0.6953(8)	0.3081(7)	0.052(4)
C(25)	0.1388(10)	0.7060(9)	0.3514(8)	0.064(5)
C(26)	0.1246(11)	0.7821(12)	0.4000(9)	0.085(6)
C(27)	0.1965(16)	0.8465(12)	0.4041(11)	0.095(8)
C(28)	0.2787(14)	0.8354(10)	0.3615(11)	0.091(7)
C(29)	0.2895(9)	0.7620(9)	0.3164(9)	0.071(5)
C(30)	0.2041(13)	0.3994(12)	0.4336(8)	0.077(6)
C(31)	0.1771(12)	0.4895(13)	0.4397(8)	0.081(7)
C(32)	0.2617(14)	0.5397(9)	0.4362(7)	0.073(6)
C(33)	0.3392(10)	0.4821(10)	0.4275(8)	0.066(5)
C(34)	0.3008(13)	0.3935(12)	0.4281(8)	0.078(6)
P(3)	0.3713(3)	0.1052(2)	0.4571(2)	0.070(1)
F(1)	0.2795(8)	0.0511(8)	0.4540(8)	0.172(6)
F(2)	0.3734(12)	0.0821(18)	0.5425(8)	0.28(1)
F(3)	0.4266(13)	0.0290(9)	0.4367(17)	0.31(1)
F(4)	0.4669(10)	0.1558(10)	0.4655(11)	0.221(8)
F(5)	0.3742(16)	0.1396(19)	0.3784(8)	0.32(1)
F(6)	0.3172(15)	0.1805(8)	0.4882(16)	0.30(1)

$$^a U_{eq} = 1/3 \sum_i \sum_j U_{ij} a_i^* a_j^* a_i a_j$$

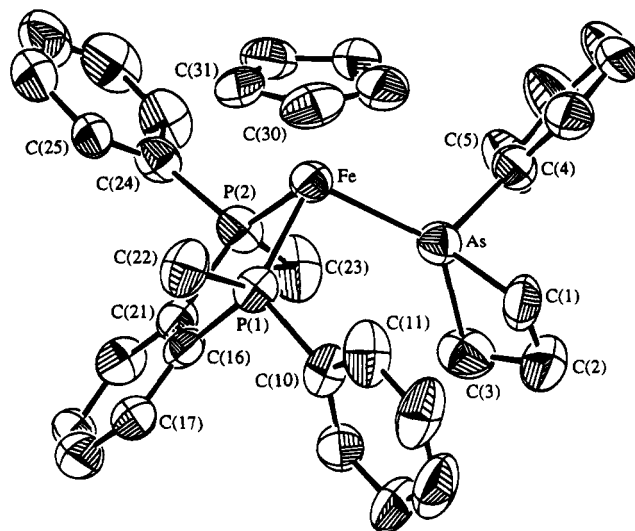
tallographic data and atomic coordinates are presented in Table 1 and Table 4, respectively. Pertinent bonding parameters are compiled in Table 5. The molecular structure of the cation of **8** is depicted in Figure 3. The complex has a piano-stool geometry with pseudooctahedral coordination around the iron. To our knowledge, **8** is the first arsetane derivative to be structurally characterized. Substituted arscyclobutenes, however,

Table 5. Selected Bond Lengths, Bond Angles, and Dihedral Angles in **8**

Bond Lengths (Å)			
Fe-As	2.326(2)	As-C(3)	2.004(12)
As-C(4)	1.953(12)	As-C(1)	1.974(13)
Fe-P(2)	2.210(3)	Fe-P(1)	2.196(3)
C(2)-C(3)	1.52(2)		
Bond Angles (deg)			
Fe-As-C(1)	129.9(4)	Fe-As-C(3)	131.4(4)
Fe-As-C(4)	113.5(4)	C(1)-As-C(3)	72.5(6)
C(1)-As-C(4)	99.8(5)	C(3)-As-C(4)	100.5(5)
As-C(1)-C(2)	91.0(9)	As-C(3)-C(2)	90.8(9)
C(1)-C(2)-C(3)	100(1)	P(1)-Fe-P(2)	86.17(12)
As-Fe-P(1)	98.16(10)	As-Fe-P(2)	95.87(10)
Dihedral Angles (deg)			
C(1)-As-C(3)-C(2)	-15.6(8)	C(3)-As-C(1)-C(2)	15.6(8)
As-C(1)-C(2)-C(3)	-20(1)	C(1)-C(2)-C(3)-As	20(1)

have been isolated and their structures have been determined.⁴ The geometry within the $[(\eta^5\text{-C}_5\text{H}_5)\{1,2\text{-C}_6\text{H}_4(\text{PMePh})_2\}\text{Fe}]$ fragment of **8** is similar to that found in **3**. The Fe-As bond is similar to that in $[(\eta^5\text{-C}_5\text{H}_5)(\text{CO})_2\text{Fe}(\text{AsPh}_3)]\text{BF}_4$.²³ The arsetane ring in **8** is nonplanar with a puckering angle between the planes C(1), C(2), C(3) and C(1), As, C(3) of 25(1)°. The As-C and C-C distances within the heterocycle are typical of single bonds. As expected, the internal angle at arsenic (72.5(6)°) is smaller than the corresponding angle at phosphorus in the phosphetane complex **3**, viz. 77.6(8) and 77(1)° for the two independent cations, respectively.

NMR Spectra. Phosphorus heterocycles are of considerable interest because of their NMR properties. In particular, the chemical shifts of the various nuclei in such rings have been thoroughly analyzed.²⁴ Experimental data suggest that in bis(tertiary phosphine)-metal chelate complexes the ³¹P NMR resonances for the phosphorus atoms are shifted to higher field for four- and six-membered rings and to lower field for five-membered rings.^{5e,24} The situation is less clear in phosphacycloalkanes, where the trends are often in opposite directions.^{24a} The ³¹P{¹H} NMR data for the series of complexes **3-6** and **9** are given in Table 6. The three phosphorus nuclei in each complex give rise to an ABX resonance pattern. The AB portion of the spectrum originates from the phosphorus nuclei of the bis(tertiary phosphine) ligand. The extraordinarily large downfield shift of this subspectrum is due to the incorporation of the phosphorus nuclei into a five-membered metal chelate ring. The X part of the ABX spectrum arises from the phosphorus atom of the unidentate phosphorus heterocycle. The ³¹P{¹H} NMR signals for the phosphorus in the heterocyclic phosphine rings in **3-6** and **9** show pronounced downfield shifts with regard to the free heterocycles.²⁵ The minimum and maximum chemical shift values are found for the phosphirane complex **9** and the phosphetane complex **3**, respectively, thus paralleling the findings for the free heterocycles.²⁵ The ³¹P{¹H} NMR spectrum of **8** consists of an AB pattern; the ¹³C{¹H} NMR spectrum of the

**Figure 3.** ORTEP view of **8** showing atom labeling of selected non-hydrogen atoms. Thermal ellipsoids enclose 50% probability levels.**Table 6.** ³¹P{¹H} NMR Data for the Complexes **3-6** and **9**^a

complex	$\delta(\text{P}_A)$	$\delta(\text{P}_B)$	$\delta(\text{P}_X)$	$ ^2J(\text{P}_A\text{P}_B) $	$ ^2J(\text{P}_A\text{P}_X) $	$ ^2J(\text{P}_B\text{P}_X) $
3	79.7	80.7	99.5	44.2	50.7	49.2
4	79.6	79.7	65.3	44.9	56.2	47.0
5	78.8	77.7	37.8	43.5	55.0	52.1
6	78.8	78.1	51.0	42.9	54.8	49.9
9	81.8	80.6	-114.9	43.9	62.2	58.4

^a P_A and P_B represent the phosphorus atoms of the bis(tertiary phosphine) ligand; P_X belongs to the coordinated heterocycles.

complex contains three sets of resonances for the nonequivalent methylene groups of the arsetane ring.

Conclusion

Saturated 1-phenyl four- to seven-membered phosphorus heterocycles are readily synthesized from phenylphosphine in certain iron(II) complexes by reaction with the appropriate α,ω -dibromoalkane and 2 equiv of potassium *tert*-butoxide. The three-membered 1-phenylphosphirane complex had to be prepared by direct synthesis from the free ligand and the iron(II) precursor, however. The first complex of 1-phenylarsetane was also prepared in high yield by the metal-assisted route from the (\pm)-(3-chloropropyl)phenylarsine-substituted precursor complex. The four-membered 1-phenylphosphetane and arsetane complexes can also be prepared directly from the free ligand and the iron(II) precursor complex, but in each case the metal-facilitated route is the most efficient and expedient synthesis. The interatomic distances and angles for coordinated 1-phenylphosphetane are in remarkable good agreement with those calculated elsewhere for the parent phosphetane.

Experimental Section

All reactions were performed in an atmosphere of dry argon using the Schlenk technique. Solvents were purified by conventional literature methods. ¹H, ¹³C{¹H}, and ³¹P{¹H} NMR spectra were recorded at 25 °C on a Varian VXR 300 S spectrometer at 299.95, 75.43, and 121.42 MHz, respectively. The NMR spectra are referenced to Me₄Si (¹H, ¹³C) or external 85% aqueous H₃PO₄ (³¹P) with downfield chemical shifts as positive. Fast atom bombardment (FAB) mass spectra were recorded on a VG analytical ZAB-2SEQ mass spectrometer

(23) Schumann, H.; Smits, J. M. M.; Beurskens, P. T. J. *Crystallogr. Spectrosc. Res.* **1989**, *19*, 1033.

(24) (a) Review: Garrou, P. E. *Chem. Rev.* **1981**, *81*, 229. (b) Lindner, E.; Fawzi, R.; Mayer, H. A.; Eichele, K.; Hiller, W. *Organometallics* **1992**, *11*, 1033, and references cited therein. (c) Gray, G. A.; Cremer, S. E.; Marsi, K. L. *J. Am. Chem. Soc.* **1976**, *98*, 2109.

(25) Quin, L. D. *The Heterocyclic Chemistry of Phosphorus*; Wiley: New York, 1981; p 212.

(ionization, 30 keV Cs⁺ ions) in a matrix of 3-nitrobenzyl alcohol and methanol as solvent. Elemental analyses were performed by staff within the Research School of Chemistry. (*R**,*R**)-(±)-[(η⁵-C₅H₅){1,2-C₆H₄(PMePh)₂}Fe(NCMe)]PF₆ (**1**),^{14a} (*R**,*R**)-(±)-[(η⁵-C₅H₅){1,2-C₆H₄(PMePh)₂}Fe(PH₂Ph)]PF₆ (**2**),^{14a} and AsH₂Ph²⁶ were prepared according to published procedures.

(*R**,*R**)-(±)-(η⁵-Cyclopentadienyl)[1,2-phenylenebis(methylphenylphosphine)](1-phenylphosphetane)-iron(II) Hexafluorophosphate-0.5-Dichloromethane (3·0.5CH₂Cl₂). A solution of (*R**,*R**)-(±)-[(η⁵-C₅H₅){1,2-C₆H₄(PMePh)₂}Fe(PH₂Ph)]PF₆ (**2**; 0.42 g, 0.6 mmol) in THF (250 mL) was treated with 1,3-dibromopropane (0.13 g, 0.6 mmol) and *t*-BuOK (0.15 g, 1.34 mmol) at 20 °C to give a red solution of the phosphido complex. After stirring for 16 h, the solvent was removed *in vacuo*. The residue was dissolved in dichloromethane, and the solution was passed through a short column of alumina. The eluate, after drying over MgSO₄ and evaporation, gave the crude product. Recrystallization from dichloromethane by slow addition of petroleum ether (bp 40–60 °C) yielded pure 3·0.5CH₂Cl₂ as yellow needles: mp 198–201 °C (dec); yield 0.4 g (85%). Anal. Calcd for C₃₄H₃₆Fe-FeP₄·0.5CH₂Cl₂: C, 53.1; H, 4.8; Cl, 4.5; P, 15.8. Found: C, 52.7; H, 4.9; Cl, 4.1; P, 15.5. ¹H NMR (CDCl₃): δ 0.85–2.40 (m, 6 H, CH₂), 2.09 (d, 3 H, ²J(HP) 8.19 Hz, PCH₃), 2.43 (d, 3 H, ²J(HP) 8.79 Hz, PCH₃), 4.06 (m, 5 H, C₅H₅), 5.32 (s, 1 H, CH₂Cl₂), 6.70–8.00 (m, 19 H, aromatics). ¹³C{¹H} NMR (CDCl₃): δ 17.94 (dd, ¹J(CP) 24.48 Hz, ³J(CP) 2.11 Hz, PCH₃), 24.43 (dd, ¹J(CP) 28.66 Hz, ³J(CP) 2.11 Hz, PCH₃), 80.87 (s, C₅H₅), 128.00–145.58 (m, aromatics); (phosphetane ring) 25.79 (d, ¹J(PC) 31.91 Hz), 28.56 (d, ¹J(PC) 34.02 Hz), 23.36 (d, ²J(CP) 18.48 Hz). FAB-MS: *m/e* 593 (M – PF₆)⁺.

Direct Synthesis of 3. A solution of 1-phenylphosphetane²⁰ (47 mg, 70% purity, 0.22 mmol) in dichloromethane (5 mL) was added to a solution of **1** (140 mg, 0.22 mmol) in the same solvent (15 mL). After 15 min reflux, the solvent was removed *in vacuo*. ¹H, ¹³C{¹H}, and ³¹P{¹H} NMR spectroscopic data for the reaction product in CDCl₃ clearly showed the presence of **3**. No attempts were made to isolate **3** from the mixture.

(*R**,*R**)-(±)-(η⁵-Cyclopentadienyl)[1,2-phenylenebis(methylphenylphosphine)](1-phenylphospholane)-iron(II) Hexafluorophosphate (**4**). A solution of **2** (0.33 g, 0.47 mmol) in THF (200 mL) was treated with 1,4-dibromobutane (0.10 g, 0.47 mmol) and *t*-BuOK (0.11 g, 0.94 mmol). After ca. 12 h at room temperature, the initially deep red solution had become clear yellow. After evaporation of the solvent *in vacuo*, the residue was dissolved in dichloromethane (100 mL). The solution was thoroughly washed with 5% aqueous NH₄PF₆ (50 mL) and purified by chromatography on alumina with dichloromethane as eluent. The eluate was dried over MgSO₄, reduced to ca. 5 mL, and diluted with petroleum ether (bp 40–60 °C). The product crystallized as orange needles: mp 218–220 °C (dec); yield 0.29 g (83%). Anal. Calcd for C₃₅H₃₈FeP₄: C, 55.8; H, 5.1; P, 16.4. Found: C, 55.5; H, 5.1; P, 16.2. ¹H NMR (CD₂Cl₂): δ 0.40–2.55 (m, 8 H, CH₂), 2.00–2.14 (m, 3 H, PCH₃), 2.26–2.35 (m, 3 H, PCH₃), 4.09 (m, 5 H, C₅H₅), 6.50–8.15 (m, 19 H, aromatics). ¹³C{¹H} NMR (CD₂Cl₂): δ 18.11 (dd, ¹J(CP) 18.86 Hz, ³J(CP) 8.80 Hz, PCH₃), 25.24 (dd, ¹J(CP) 21.42 Hz, ³J(CP) 7.69 Hz, PCH₃), 80.89 (s, C₅H₅), 128.00–147.50 (m, aromatics); (phospholane ring) 26.39 (d, ²J(CP) 19.84 Hz), 29.30 (d, ¹J(CP) 24.14 Hz), 32.51 (d, ¹J(CP) 26.40 Hz). FAB-MS: *m/e* 607 (M – PF₆)⁺.

(*R**,*R**)-(±)-(η⁵-Cyclopentadienyl)[1,2-phenylenebis(methylphenylphosphine)](1-phenylphosphinane)iron(II) Hexafluorophosphate-1.5-Chloroform (5·1.5CHCl₃). 1,5-Dibromopentane (0.14 g, 0.60 mmol) and *t*-BuOK (0.15 g, 1.33 mmol) were added to a solution of **2** (0.36 g, 0.56 mmol) in THF (175 mL) at 20 °C. The color of the solution changed immediately from yellow to brown-red. After

heating the reaction mixture for 12 h, the yellow solution was evaporated and the residue was extracted with dichloromethane (2 × 100 mL). The combined extracts were washed with aqueous 5% NH₄PF₆ (40 mL). The organic layer was separated off, concentrated to ca. 5 mL, and purified by chromatography on alumina with dichloromethane as eluent. The eluate was dried (MgSO₄), reduced to 4 mL, and diluted with diethyl ether (12 mL). Dark red crystals of the crude product separated: mp 223–225 °C (dec); yield 0.36 g (84%). Recrystallization of the crude product from chloroform afforded red crystals of the solvate 5·1.5CHCl₃. Anal. Calcd for C₃₆H₄₀FeP₄·1.5CHCl₃: C, 47.6; H, 4.4; Cl, 16.9; P 13.1. Found: C, 48.3; H, 4.4; Cl, 17.5; P, 12.6. ¹H NMR (CD₂Cl₂): δ 0.44–2.45 (m, 10 H, CH₂), 2.04 (d, 3 H, ²J(HP) 8.10 Hz, PCH₃), 2.51 (d, 3 H, ²J(HP) 8.40 Hz, PCH₃), 4.08 (m, 5 H, C₅H₅), 7.30 (s, CHCl₃), 6.60–8.25 (m, 19 H, aromatics). ¹³C{¹H} NMR (CD₂Cl₂): δ 18.21 (dd, ¹J(CP) 23.08 Hz, ³J(CP) 4.37 Hz, PCH₃), 25.50 (dd, ¹J(CP) 27.34 Hz, ³J(CP) 3.31 Hz, PCH₃), 80.89 (s, C₅H₅), 128.00–147.50 (m, aromatics); (phosphorinane ring) 22.15 (d, ²J(CP) 7.69 Hz), 22.64 (d, ²J(CP) 7.69 Hz), 25.69 (d, ³J(CP) 3.24 Hz), 26.10 (d, ¹J(CP) 24.21 Hz), 28.36 (d, ¹J(CP) 24.21 Hz). FAB-MS: *m/e* 621 (M – PF₆)⁺.

(*R**,*R**)-(±)-(η⁵-Cyclopentadienyl)[1,2-phenylenebis(methylphenylphosphine)](1-phenylphosphepane)-iron(II) Hexafluorophosphate-1-Dichloromethane (6·CH₂Cl₂). The compound was prepared from **2** (0.43 g, 0.61 mmol) in THF (225 mL) by the addition of 1,6-dibromohexane (0.15 g, 0.61 mmol) and *t*-BuOK (0.16 g, 1.45 mmol) as described for **5**, but with a heating time of 48 h. Crystallization of the crude product from dichloromethane-petroleum ether (bp 40–60 °C) yielded orange needles of the solvate 6·CH₂Cl₂: mp 204–206 °C (dec); yield 0.30 g (63%). Anal. Calcd for C₃₇H₄₂FeP₄·CH₂Cl₂: C, 52.7; H, 5.1; Cl, 8.2; P, 14.3. Found: C, 53.1; H, 5.1; Cl, 7.6; P, 14.7. ¹H NMR (CDCl₃): δ 0.52–2.45 (m, 12 H, (CH₂)₆), 2.02 (d, 3 H, ²J(HP) 7.20 Hz, PCH₃), 2.49 (d, 3 H, ²J(HP) 8.40 Hz, PCH₃), 4.03 (m, 5 H, C₅H₅), 5.30 (s, 2 H, CH₂Cl₂), 6.48–8.15 (m, 19 H, aromatics). ¹³C{¹H} NMR (CD₂Cl₂): δ 18.38 (dd, ¹J(CP) 22.28 Hz, ³J(CP) 4.93 Hz, PCH₃), 25.82 (dd, ¹J(CP) 29.15 Hz, ³J(CP) 2.76 Hz, PCH₃), 80.75 (s, C₅H₅), 128.15–144.50 (m, aromatics); (phosphepane ring) 22.89 (d, ²J(CP) 8.83 Hz), 23.25 (d, ²J(CP) 8.83 Hz), 26.58 (s), 26.93 (s), 29.53 (d, ¹J(CP) 20.89 Hz), 32.32 (d, ¹J(CP) 23.08 Hz). FAB-MS: *m/e* 635 (M – PF₆)⁺.

(±)-(3-Chloropropyl)(phenyl)arsine. Phenylarsine (20.0 g, 129.8 mmol) in THF (300 mL) was treated with sodium (3.2 g, 139.2 mg atom), and the mixture was stirred at room temperature until the evolution of hydrogen had ceased. After removing excess sodium, the orange-red solution of Na[AsHPH] was slowly added with vigorous stirring to a cooled (–78 °C) solution of 1,3-dichloropropane (45.0 g, 398.3 mmol) in THF (300 mL). The reaction mixture was allowed to warm to room temperature. After evaporation of the solvent *in vacuo*, the residue was extracted with diethyl ether and water. The organic layer was dried over MgSO₄ and evaporated, and the desired product was isolated by fractional distillation of the residue as a colorless oil: bp 116 °C (0.05 mmHg); yield 24.0 g (80%). Anal. Calcd for C₉H₁₂AsCl: C, 46.9; H, 5.3; Cl, 15.4. Found: C, 46.1; H, 5.4; Cl, 14.4. ¹H NMR (CDCl₃): δ 1.85–2.00 (m, 4 H, AsCH₂CH₂), 3.46–3.52 (m, 2 H, CH₂Cl), 3.72–3.75 (m, 1 H, AsH), 7.20–7.55 (m, 5 H, aromatics). ¹³C{¹H} NMR (CDCl₃): δ 18.75, 31.96, 45.96, 127.97, 128.59, 134.40, 135.92.

[(*R**),(*R**,*R**)/(*R**),(*S**,*S**)]-[(3-Chloropropyl)(phenyl)arsine](η⁵-cyclopentadienyl)[1,2-phenylenebis(methylphenylphosphine)]iron(II) Hexafluorophosphate (**7**). (±)-PhAsH[(CH₂)₃Cl] (2.31 g, 10.0 mmol) was added to a suspension of **1** (5.0 g, 7.95 mmol) in ethanol (100 mL), and the mixture was heated under reflux for 3 h. The yellow suspension was reduced in volume to ca. 50 mL and cooled to –10 °C. The crystals were collected, washed with cold ethanol-diethyl ether (1/2, v/v) and diethyl ether, and dried *in vacuo*: Yield 5.5 g (91%). Anal. Calcd for C₃₄H₃₇AsClF₆FeP₃: C, 49.9;

H, 4.6; Cl, 4.3; F, 13.9. Found: C, 49.2; H, 4.1; Cl, 4.6; F, 14.2. $^{31}\text{P}\{^1\text{H}\}$ NMR (CD_2Cl_2): δ 83.0, 81.8 (2d, AB system, $^2J(\text{P}_\text{A}\text{P}_\text{B})$ 43.5 Hz, major diastereomer); 83.3, 80.7 (2d, AB system, $^2J(\text{P}_\text{A}\text{P}_\text{B})$ 44.0 Hz, minor diastereomer). FAB-MS: m/e 673 ($[\text{M} - \text{PF}_6]^+$).

(*R*,R)-(±)-(η⁵-Cyclopentadienyl)(1-phenylarsetane)-[1,2-phenylenebis(methylphenylphosphine)]iron(II) Hexafluorophosphate (8).** A solution of **7** (5.5 g, 6.72 mmol) in THF (50 mL) was treated with *t*-BuOK (0.9 g, 8.0 mmol). The rapid formation of the intermediate arsenido complex was indicated by the deep red color. Stirring of the mixture was continued for 12 h at 20 °C to give a yellow suspension. The solvent was evaporated *in vacuo*, and the residue was extracted with water (50 mL) and dichloromethane (50 mL). The organic layer was separated, washed once with water, and dried over MgSO_4 . The product was isolated as orange microcrystals having a decomposition point at >205 °C; yield 4.6 g (85%). Solvent-free single crystals of the pure product were obtained by repeated recrystallization of the crude material from dichloromethane-diethyl ether. Anal. Calcd for $\text{C}_{34}\text{H}_{36}\text{AsF}_6\text{FeP}_3$: C, 52.2; H, 4.6; F, 14.6. Found: C, 52.4; H, 4.5; F, 14.8. ^1H NMR (CD_2Cl_2): δ 2.14 (d, 3 H, $^2J(\text{HP})$ 8.1 Hz, PCH_3), 2.39 (d, $^2J(\text{HP})$ 8.7 Hz, PCH_3), 4.12 (m, 5 H, C_5H_5), 6.80–8.00 (m, aromatics); (arsetane ring) 1.22–1.34 (m, 1 H), 1.64–1.76 (m, 1 H), 2.02–2.12 (m, 2 H), 2.46–2.62 (m, 2 H). $^{13}\text{C}\{^1\text{H}\}$ NMR (CD_2Cl_2): δ 19.1 (dd $^1J(\text{CP})$ 24.7 Hz, $^3J(\text{CP})$ 4.37 Hz, PCH_3), 23.6 (d, $^1J(\text{CP})$ 28.6 Hz, PCH_3), 79.1 (s, C_5H_5): (arsetane ring) 24.41, 26.14, 26.23. $^{31}\text{P}\{^1\text{H}\}$ NMR (CD_2Cl_2): δ 82.1, 80.9 (2d, AB system, $^2J(\text{P}_\text{A}\text{P}_\text{B})$ 44.6 Hz). FAB-MS: m/e 637 ($[\text{M} - \text{PF}_6]^+$).

Direct Synthesis of 8. Dilithium phenylarsenide (11.37 g, 68.53 mmol), which was prepared from phenylarsine and 2.2 equiv of *n*-butyllithium, was suspended in THF (1 L), and 1,3-dichloropropane (6.27 g, 55.49 mmol) was added at –78 °C; the solution was allowed to warm to room temperature. After 10 h the solvent was removed *in vacuo*. The residue was extracted with petroleum spirit (bp 40–60 °C, 120 mL), and the solution was filtered; removal of solvent and distillation of the residue under reduced pressure (0.05 mmHg) afforded

five drops of a clear colorless liquid that solidified in the receiver flask. The distillate was extracted with C_6D_6 (1 mL). Addition of a small amount of **1** and THF (0.5 mL) to the obtained solution followed by heating to 55 °C for 14 h afforded **8**, which was identified in the mixture on the basis of its $^{31}\text{P}\{^1\text{H}\}$ NMR data (see above).

(*R*,R)-(±)-(η⁵-Cyclopentadienyl)[1,2-phenylenebis(methylphenylphosphine)](1-phenylphosphirane)-iron(II) Hexafluorophosphate (9).** A solution of 1-phenylphosphirane (0.39 g, 2.86 mmol) in dichloromethane (5 mL) was added to a solution of **1** (1.80 g, 2.86 mmol) in the same solvent (50 mL), and the stirred mixture was heated under reflux for 48 h. After removal of the solvent *in vacuo*, the residue was dissolved in acetone (20 mL) and the solution was filtered through Celite. Evaporation of the solvent from the filtrate followed by dissolution of the residue in acetone (5 mL) and slow addition of diethyl ether (14 mL) afforded orange crystals of **9**. Recrystallization in the same way afforded the pure product: mp 210 °C (dec); yield 1.76 g (85%). Anal. Calcd for $\text{C}_{33}\text{H}_{34}\text{F}_6\text{FeP}_4$: C, 54.7; H, 4.7. Found: C, 54.8; H, 4.5. ^1H NMR (acetone-*d*₆): δ 0.15–0.38 (m, 2 H, $(\text{CH}_2)_2$), 1.06–1.25 (m, 2 H, $(\text{CH}_2)_2$), 2.23 (d, 3 H, $^2J(\text{HP})$ 8.70 Hz, PCH_3), 2.34 (d, 3 H, $^2J(\text{HP})$ 9.60 Hz, PCH_3), 4.45 (quart., 5 H, $^3J(\text{HP})$ 1.80 Hz, C_5H_5), 6.90–8.15 (m, 19 H, aromatics). $^{13}\text{C}\{^1\text{H}\}$ NMR (acetone-*d*₆): δ 16.67 (d of m, $^1J(\text{CP})$ 26.32 Hz, PCH_3), 22.77 (dd, $^1J(\text{CP})$ 30.02 Hz, $^3J(\text{CP})$ 3.24 Hz, PCH_3), 81.25 (s, C_5H_5), 128.50–146.00 (m, aromatics); (phosphirane ring) 8.98 (d, $^1J(\text{CP})$ 12.07 Hz), 9.75 (d, $^1J(\text{CP})$ 12.07 Hz). FAB-MS: m/e 579 ($[\text{M} - \text{PF}_6]^+$).

Supplementary Material Available: Experimental details, ORTEPs, and tables of positional and isotropic displacement parameters, interatomic distances and angles, torsion angles, and selected least-squares planes for **3**·0.75 C_6H_6 ·0.25 CHCl_3 and **8** (47 pages). Ordering information is given on any current masthead page.

OM940881G

Stepwise Mechanism for Oxidative Addition of Iodine to Organotellurium(II) Compounds As Observed by Stopped-Flow Spectroscopy

Michael R. Detty,^{*,†} Alan E. Friedman,[‡] and Martin McMillan[§]

Office Imaging Research and Technical Development, Clinical Diagnostics Research Laboratories, and Analytical Technology Division, Eastman Kodak Company, Rochester, New York 14650

Received November 7, 1994[⊗]

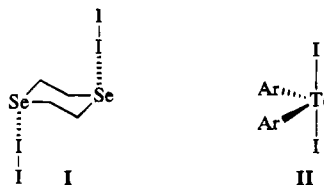
The reaction of iodine with a series of diorgano tellurides was monitored by stopped-flow spectroscopy. For dihexyl telluride (**1**), diphenyl telluride (**2**), di-*p*-anisyl telluride (**3**), and phenyl 2-((dimethylamino)methyl)phenyl telluride (**4**), an initial "fast" reaction was first order in substrate and second order in iodine. For 2,6-di-*tert*-butyltelluropyran-4-one (**5**), the "fast" reaction was second order overall and first order in iodine. The "fast" reaction is actually two reactions: the addition of iodine to the tellurium atom to form an η^1 -R₂Te-I₂ complex followed by the addition of a second iodine to form presumably an η^1 -R₂Te-I₄ complex. The first reaction is faster than the second leading to a rapid preequilibrium and apparent inverted Arrhenius behavior in the temperature dependence of the rate constants. The "fast" reaction(s) is followed by a "slow" reaction, which is first order overall and independent of iodine concentration. The rate constant for the "slow" reaction increases with increasing solvent polarity, which is consistent with a dissociative process leading to ionic intermediates.

Introduction and Background

Among the oldest reactions of diorganotellurium(II) and diorganoselenium(II) compounds are the addition reactions of halogens to these materials.¹⁻³ While the additions of bromine and chlorine to both diorganotellurium(II) and diorganoselenium(II) compounds give products of oxidative addition with nearly linear halogen-chalcogen-halogen bonds,⁴⁻⁶ the additions of iodine to these materials give different products, depending upon the chalcogen atom.

In the 1-chalcogena-4-selenane and 1,4-diselenane systems, McCullough and Chao⁷⁻⁹ observed that the addition of iodine did not give products of oxidative addition. Instead, association complexes with nearly linear chalcogen-I-I arrays were characterized by X-ray crystallographic analysis (structure I for the iodine association complex with 1,4-diselenane). Dissociation constants show that the selenide-iodine complexes ($K_c \approx 5 \times 10^{-4}$ M) are stronger than corresponding sulfide-iodine complexes ($K_c \approx 5 \times 10^{-3}$ M).¹⁰

The addition of iodine to diorganotellurium(II) compounds gives different products. Iodine oxidative-ad-



dition products from diaryl tellurides have been characterized by X-ray crystallography¹¹ and have been shown to have the general structure II. The tellurium-(IV) adduct II is a trigonal bipyramid with the C-Te bonds and a Te atom lone pair of electrons occupying the equatorial sites and with a nearly linear, *trans*-diaxial array of the iodide ligands to the Te atom. Tellurium analogues of association complexes I have not been characterized, although one might postulate their formation along the path to II.

Iodine association complexes with diorganochalcogen species can involve more than one molecule of iodine. Sulfur-iodine complexes with two iodine molecules are known. Both Ph₃P=S-I₄ (III) and ethylenethiourea-I₄ (IV) complexes have been isolated and characterized by



X-ray crystallographic analysis.^{12,13} Materials that are

[†] Office Imaging Research and Technical Development. Current address: Department of Medicinal Chemistry, School of Pharmacy, University at Buffalo, Buffalo, NY 14620.

[‡] Clinical Diagnostics Research Laboratories.

[§] Analytical Technology Division.

[⊗] Abstract published in *Advance ACS Abstracts*, February 1, 1995.

(1) Lederer, K. *Ber. Bunsen-Ges. Phys. Chem.* **1916**, *49*, 2002.

(2) Lederer, K. *Ber. Bunsen-Ges. Phys. Chem.* **1916**, *49*, 1076.

(3) Lederer, K. *Justus Liebigs Ann. Chem.* **1916**, *391*, 326.

(4) McCullough, J. D.; Hamburger, G. *J. Am. Chem. Soc.* **1941**, *63*, 803.

(5) Christofferson, G. D.; McCullough, J. D. *Acta Crystallogr.* **1958**, *11*, 249.

(6) McCullough, J. D.; Marsh, R. E. *Acta Crystallogr.* **1950**, *3*, 41.

(7) McCullough, J. D.; Chao, G. Y.; Zuccaro, D. E. *Acta Crystallogr.*

1959, *12*, 815.

(8) Maddox, H.; McCullough, J. D. *Inorg. Chem.* **1966**, *5*, 522.

(9) McCullough, J. D. *Inorg. Chem.* **1964**, *3*, 1425.

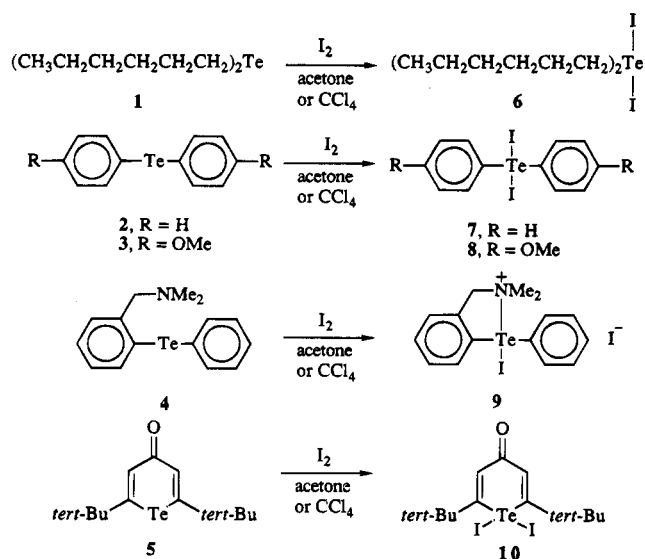
(10) McCullough, J. D.; Brunner, A. *Inorg. Chem.* **1967**, *6*, 1251.

(11) Chao, G. Y.; McCullough, J. D. *Acta Crystallogr.* **1962**, *15*, 887.

(12) (a) Schweikert, W. W.; Meyers, E. A. *J. Phys. Chem.* **1968**, *72*, 1561. (b) Bransford, J. W.; Meyers, E. A. *Cryst. Struct. Commun.* **1978**, *7*, 697.

(13) Herbstein, F. H.; Schwotzer, W. *J. Am. Chem. Soc.* **1984**, *106*, 2367.

Scheme 1



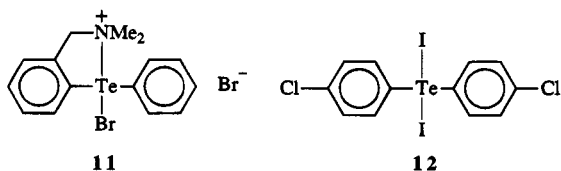
analyzed as covalent R_2Te-I_4 complexes with intact $I-I$ bonds from spectroscopic analysis have been prepared by the addition of excess iodine to telluracyclopentane¹⁴ and telluracyclohexane (tellurane).¹⁵ However, these materials have not been characterized by X-ray crystallographic analysis. Similar complexes with selenium-containing molecules have not been described although it is not clear that they have been sought.⁷⁻¹⁰

One might expect the oxidative addition of iodine across organochalcogen species to follow a reaction course similar to that observed for oxidative addition of bromine in which an initial fast reaction, which is first order in both bromine and substrate, is followed by one or more slower first-order reactions leading to the final product(s).¹⁶ In this paper, we describe a multistep process for the oxidative addition of iodine, which is characterized by a second-order dependence in iodine for the initial fast reaction. Furthermore, the initial reaction(s) in some substrates shows pronounced inverted Arrhenius behavior.

Results and Discussion

Product Studies for the Oxidative Addition of Iodine to Diorganochalcogen(II) Compounds. The diorganotellurium(II) compounds 1–5 react with iodine in either acetone or carbon tetrachloride to give oxidative-addition products 6–10, respectively, as shown in Scheme 1. The products 6–10 were spectroscopically identical with the final products produced by oxidative addition of iodine in the stopped-flow spectrophotometer in experiments described below.

Absorption and infrared spectra for compound 9 are nearly identical with those of compound 11, whose structure has been established by X-ray crystallography.¹⁶ Crystals of 9 were highly twinned and were not



suitable for X-ray crystallographic analysis. For both

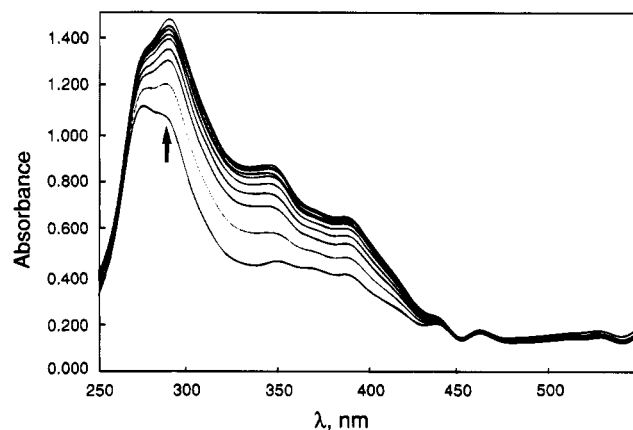


Figure 1. Transient spectra for the fast reaction for oxidative addition of iodine (5×10^{-5} M) to di-*p*-anisyl telluride 3 (5×10^{-5} M) at 295.1 K in carbon tetrachloride. Transient spectra were determined at 0.012, 0.0375, 0.0875, 0.1375, 0.2125, 0.325, 0.4125, 0.587, 0.800, and 2.687 s (traces are sequential from the arrow).

9 and 11, 1H NMR spectra were highly broadened due to exchange processes. From the spectral similarities, we have assumed compound 9 to have a structure similar to that of 11.

The structures of compounds 6–8 and 10 should be similar to that reported for 12, which is trigonal bipyramidal.³

Stopped-Flow Spectroscopic Study of the Oxidative Addition of Iodine. The oxidation of organochalcogen compounds 1–5 with iodine in several solvents was monitored via stopped-flow spectroscopy. As was observed with bromination reactions of similar substrates,¹⁶ several kinetically distinct steps were observed in the oxidation of 1–5 with iodine. A fast reaction was followed by sequentially slower reactions to give the final products.

Unlike the “fast” reactions of bromine with diaryl tellurides, which were too fast for accurate kinetic measurements with our system, the “fast” reactions with iodine were observable. Typical spectral changes for the “fast” reaction are illustrated in Figure 1 for iodine (5×10^{-5} M) and 3 (5×10^{-5} M) in carbon tetrachloride between 0.012 and 2.687 s. Kinetic traces of this process for equimolar concentrations of iodine and diorgano telluride follow second-order behavior, as illustrated in the second-order curve fitting of the kinetic trace at 310 nm of Figure 2 for the fast reaction between iodine (5×10^{-5} M) and diphenyl telluride 2 (5×10^{-5} M) at 281.8 K.^{17,18}

The “fast” reaction is followed by one or more “slow” reactions. Typical spectral changes for the “slow” reaction are illustrated in Figure 3 for iodine (5×10^{-5} M) and 3 (5×10^{-5} M) in carbon tetrachloride between 25.0 and 1000 s. Kinetic traces for the “slow” process follow first-order behavior, as illustrated in Figure 4 for the slow reaction between iodine (5×10^{-4} M) and telluropyranone 5 (5×10^{-5} M) at 288.8 K as monitored at 310 nm.

(14) Srivastava, T. N.; Srivastava, R. C.; Singh, M. *Indian J. Chem.* **1979**, *17A*, 615.

(15) Morgan, G. T.; Burstall, F. H. *J. Chem. Soc.* **1931**, 180.

(16) Detty, M. R.; Friedman, A. E.; McMillan, M. *Organometallics* **1994**, *13*, 3338.

(17) The dead time of our stopped-flow instrument has been measured to be 1.2 ms: Tonomura, B.; Nakatani, H.; Ohnishi, M.; Yamaguchi-Ito, J.; Hiromi, K. *Anal. Biochem.* **1978**, *84*, 370–383.

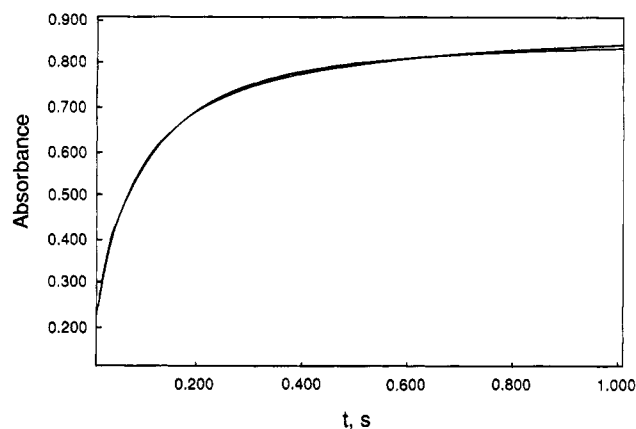


Figure 2. Kinetic trace obtained at 310 nm for the fast reaction between iodine (5×10^{-5} M) and diphenyl telluride **2** at 281.8 K with second-order curve fitting.

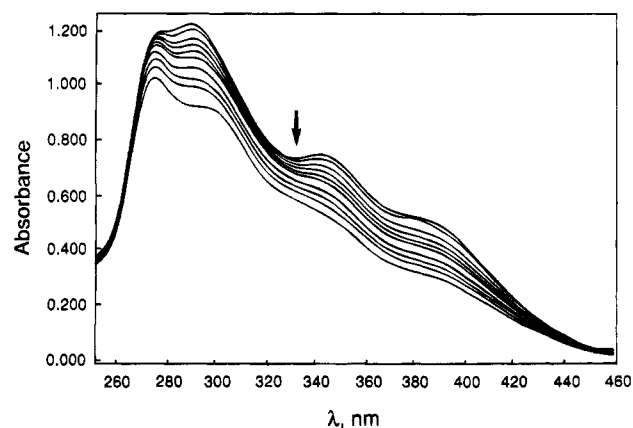


Figure 3. Transient spectra for the final slow reaction for oxidative addition of iodine (5×10^{-5} M) to di-*p*-anisyl telluride **3** (5×10^{-5} M) at 298.0 K in carbon tetrachloride. Transient spectra were determined at 25.0, 50.0, 100, 150, 200, 250, 375, 625, 875, and 1000 s (traces are sequential from the arrow). The spectral window is smaller than in Figure 1 to shorten the acquisition time of the spectral region of interest (20 min/10 nm).

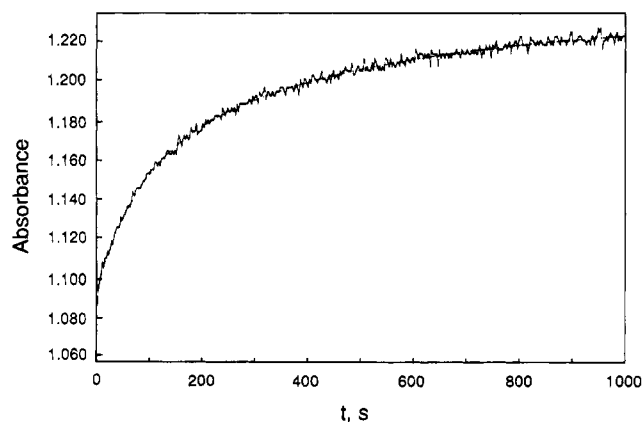


Figure 4. Kinetic trace obtained at 310 nm for the slow reaction between iodine (5×10^{-4} M) and telluropyranone **5** (5×10^{-5} M) at 288.8 K with first-order curve fitting.

The "Fast" Reaction. A. Concentration Studies. The effects of concentration on the initial "fast" reaction are compiled in Table 1. Although the kinetic traces for these systems follow second-order behavior at 5×10^{-5} M concentrations in both substrate and iodine, the

Table 1. Effects of Concentration on the Observed Rate Constants in the "Fast" Reactions of Iodine Oxidations of Diorgano Tellurides and Calculated Third-Order Rate Constants in Carbon Tetrachloride^a

R_2Te	$[R_2Te], M$	$[I_2], M$	T, K	λ_{obs}, nm	$k_{obs}(fast), s^{-1}$	$k_{fast}, L^2 mol^{-2} s^{-1}$
2	5×10^{-5}	5×10^{-5}	292.8	310	$(1.05 \pm 0.06) \times 10^1$	4.2×10^9
	5×10^{-5}	5×10^{-4}	293.2	310	$(1.0 \pm 0.1) \times 10^3$	4.0×10^9
	5×10^{-5}	3×10^{-4}	293.2	310	$(3.58 \pm 0.06) \times 10^2$	3.98×10^9
	2.5×10^{-5}	5×10^{-4}	292.6	310	$(7.9 \pm 0.3) \times 10^2$	3.2×10^9
3	5×10^{-5}	5×10^{-5}	297.3	310	$(2.6 \pm 0.1) \times 10^1$	1.0×10^{10}
	5×10^{-5}	1.5×10^{-4}	297.3	310	$(2.4 \pm 0.1) \times 10^2$	1.1×10^{10}
	5×10^{-5}	5×10^{-4}	297.3	310	$(2.6 \pm 0.3) \times 10^3$	1.0×10^{10}
5	5×10^{-5}	5×10^{-5}	293.2	280	$(2.5 \pm 0.3) \times 10^{-1}$	5.0×10^3 ^d
	5×10^{-5}	5×10^{-4}	292.8	280	3.1 ± 0.7	6.2×10^3 ^d
13	5×10^{-5}	5×10^{-5}	283.7	300	$(6.8 \pm 0.3) \times 10^1$	1.4×10^6 ^d
	5×10^{-5}	5×10^{-4}	283.7	300	$(5.0 \pm 0.1) \times 10^2$	1.0×10^6 ^d
	5×10^{-4}	5×10^{-4}	293.0	300	$(1.8 \pm 0.6) \times 10^3$ ^c	3.6×10^6 ^d
	5×10^{-4}	5×10^{-5}	293.0	300	$(2.5 \pm 0.5) \times 10^3$ ^b	5.0×10^6 ^d
	5×10^{-4}	5×10^{-5}	293.0	300	$(2.5 \pm 0.5) \times 10^3$ ^b	5.0×10^6 ^d

^a Second-order curve fitting at 5×10^{-5} M iodine, pseudo-first-order curve fitting at higher iodine concentrations. ^b First-order curve fitting in s^{-1} . ^c Second-order curve fitting. ^d Second-order rate constant in $L mol^{-1} s^{-1}$.

observed rate constants at 5×10^{-4} M iodine for **2** and **3**, which followed pseudo-first-order behavior, suggested that the reaction was second order in iodine. For both **2** and **3**, a 10-fold increase in iodine concentration gave a 100-fold increase in observed rate (Table 1). The reactions of di-*n*-hexyl telluride (**1**) or diaryl telluride **4** with iodine at concentrations $\geq 1 \times 10^{-4}$ M in carbon tetrachloride were too fast for meaningful measurement.

Under pseudo-first-order conditions in iodine (5×10^{-4} M) a decrease in substrate concentration from 5×10^{-5} M in **2** to 2.5×10^{-5} M in **2** had little effect on the observed rate constant (k_{obs} , Table 1). This is consistent with a first-order dependence on substrate in the kinetics of the reaction.

The "fast" reaction of **5** with iodine followed second-order kinetics with a first-order dependence in iodine concentration. Second-order rate constants of 5.0×10^3 and $6.2 \times 10^3 L mol^{-1} s^{-1}$ at 5×10^{-5} and 5×10^{-4} M iodine, respectively, were calculated at 293 K (Table 1).

The higher order kinetic behavior with respect to iodine concentration has not been previously described for reactions of diorgano chalcogenides with iodine. For comparison purposes, the reactions of diphenyl selenide, diphenyl sulfide, and dihexyl sulfide (**13**) with iodine were followed by stopped-flow spectroscopy. Surprisingly, no spectral changes were observed in the reactions

(18) Concerns have been raised with respect to the measurements of rate constants of $\geq 3.5 \times 10^2 s^{-1}$ under pseudo-first-order conditions ($\tau \leq 2$ ms). With a "dead time" of 1.2 ms¹⁷ and the assumption that mixing is instantaneous, a value of τ of ≥ 0.4 ms ($k \leq 1.7 \times 10^3 s^{-1}$) and an absorbance change of 1.0 during the course of reaction would leave an absorbance change of at least 0.12 (after 3 half-lives) for the collection of kinetic data. Of the 17 pseudo-first-order observed rates listed in Tables 1 and 2, 15 are less than $1.7 \times 10^3 s^{-1}$, one is comparable in magnitude, and one is 50% larger ($k = 2.6 \times 10^3 s^{-1}$). Some of the "dead time" of the instrument is undoubtedly consumed by a finite mixing time and, for the reactions studied here, by the time involved in establishing a preequilibrium. Consequently, a pseudo-first-order observed rate of $2.6 \times 10^3 s^{-1}$ is not without significance. Similar concerns were expressed with respect to second-order observed rates of 1.4×10^4 and $1.7 \times 10^4 s^{-1}$ contained in Table 2. Although the initial value of the half-life, τ , is described by $1/k_{obs}[A]$, where $[A]$ is arbitrarily 1 M in the curve fitting, τ is continually increasing as reagent is consumed. After 3 half-lives, τ is a factor of 8 larger. Thus, initial half-lives of 70 and 60 μs , respectively, have increased to 0.57 and 0.47 ms after 3 half-lives. Again, an absorbance change of 1.0 during the course of reaction would leave an absorbance change of at least 0.12 for the collection of kinetic data after 3 half-lives.

Table 2. Observed Second-Order or Pseudo-First-Order Rate Constants and Calculated Third-Order Rate Constants for the "Fast" Reactions in the Oxidative Addition of Iodine to Diorgano Tellurides 1–6 in CCl₄, EtOAc, or CH₃CN^a

R ₂ Te	solvent	[I ₂], MM	T, K	λ _{obs} , nm	k _{obs} (fast), s ⁻¹	k _{fast} , L ² mol ⁻² s ⁻¹		
1	CCl ₄	5 × 10 ⁻⁵	292.8	290	≥ 2 × 10 ⁴			
		5 × 10 ⁻⁵	297.9	290	(1.4 ± 0.2) × 10 ⁴	5.5 × 10 ¹²		
2	CCl ₄	5 × 10 ⁻⁵	281.8	310	(1.79 ± 0.06) × 10 ¹	7.18 × 10 ⁹		
		5 × 10 ⁻⁵	288.0	310	(1.43 ± 0.02) × 10 ¹	5.72 × 10 ⁹		
		5 × 10 ⁻⁵	292.8	310	(1.06 ± 0.07) × 10 ¹	4.24 × 10 ⁹		
		5 × 10 ⁻⁵	307.3	310	7.1 ± 0.4	2.8 × 10 ⁹		
		5 × 10 ⁻⁵	311.1	310	6.2 ± 0.3	2.5 × 10 ⁹		
		EtOAc	5 × 10 ⁻⁵	293.0	360	(1.7 ± 0.3) × 10 ⁴	6.8 × 10 ¹³	
		CH ₃ CN	5 × 10 ⁻⁵	293.1	310	≥ 10 ⁴		
3	CCl ₄	5 × 10 ⁻⁵	282.7	300	(4.5 ± 0.2) × 10 ¹	1.8 × 10 ¹⁰		
		5 × 10 ⁻⁵	287.3	300	(3.8 ± 0.1) × 10 ¹	1.5 × 10 ¹⁰		
		5 × 10 ⁻⁵	293.0	300	(3.1 ± 0.2) × 10 ¹	1.2 × 10 ¹⁰		
		5 × 10 ⁻⁵	297.3	300	(2.6 ± 0.1) × 10 ¹	1.0 × 10 ¹⁰		
		5 × 10 ⁻⁵	302.2	300	(2.16 ± 0.07) × 10 ¹	8.64 × 10 ⁹		
		5 × 10 ⁻⁵	307.8	300	(1.72 ± 0.04) × 10 ¹	6.88 × 10 ⁹		
		EtOAc	5 × 10 ⁻⁵	312.9	300	≥ 10 ⁴		
		CH ₃ CN	5 × 10 ⁻⁵	293.1	310	≥ 10 ⁴		
		4	CCl ₄	5 × 10 ⁻⁵	282.6	290	(10 ± 1) × 10 ³	4.0 × 10 ¹²
				5 × 10 ⁻⁵	287.6	290	(8 ± 2) × 10 ³	3.2 × 10 ¹²
5 × 10 ⁻⁵	292.4			290	(6 ± 1) × 10 ³	2.4 × 10 ¹²		
5 × 10 ⁻⁵	297.5			290	(4.2 ± 0.2) × 10 ³	1.7 × 10 ¹²		
5 × 10 ⁻⁵	301.8			290	(3.0 ± 0.5) × 10 ³	1.2 × 10 ¹²		
EtOAc	5 × 10 ⁻⁵			286.9	300	(6.2 ± 0.1) × 10 ²	2.5 × 10 ¹¹	
EtOAc	5 × 10 ⁻⁵			295.6	300	(4.1 ± 0.2) × 10 ²	1.6 × 10 ¹¹	
EtOAc	5 × 10 ⁻⁵			302.9	300	(3.9 ± 0.7) × 10 ²	1.6 × 10 ¹¹	
EtOAc	5 × 10 ⁻⁵			312.8	300	(3.12 ± 0.03) × 10 ²	1.25 × 10 ¹¹	
CH ₃ CN	5 × 10 ⁻⁵			293.1	310	≥ 10 ⁴		
5	CCl ₄	5 × 10 ⁻⁴	288.8	280	2.3 ± 0.6	4.6 × 10 ^{3 a}		
		5 × 10 ⁻⁴	292.8	280	3.1 ± 0.7	6.2 × 10 ^{3 a}		
		5 × 10 ⁻⁴	298.0	280	5.2 ± 0.2	1.0 × 10 ^{4 a}		
		5 × 10 ⁻⁴	308.5	280	6.2 ± 0.75	1.2 × 10 ^{4 a}		
13	CCl ₄	5 × 10 ⁻⁵	283.7	300	(6.8 ± 0.3) × 10 ¹	1.4 × 10 ^{6 a}		
		5 × 10 ⁻⁵	295.3	300	(7.9 ± 0.2) × 10 ¹	1.6 × 10 ^{6 a}		

^a Second-order rate constant in L mol⁻¹ s⁻¹.

of either diphenyl selenide or diphenyl sulfide (5 × 10⁻⁵ M) with iodine (5 × 10⁻⁴ M) at 293.0 K. However, a "fast" reaction was observed for the reaction of iodine with **13** and could be followed at 5 × 10⁻⁵ and 5 × 10⁻⁴ M combinations of both reagents (Table 1). The rate behavior for the reaction of **13** with iodine was second order overall and first order in each of the reagents. No spectral changes were observed over a time frame of several hours following the initial second-order reaction with iodine.

B. Inverted Arrhenius Behavior for the "Fast" Reaction of Diorgano Tellurides with Iodine. Observed rate constants at different temperatures under second-order conditions for 1–5 (5 × 10⁻⁵ M in both substrate and iodine) are compiled in Table 2. Solvents examined in this study were carbon tetrachloride, ethyl acetate, and acetonitrile. For comparison purposes, the temperature dependence of the reaction of iodine with dihexyl sulfide **13** was also followed.

The rate of reaction increased with increasing solvent polarity in 1–3. Rate increases of several orders of magnitude were observed at a common temperature from carbon tetrachloride to ethyl acetate to acetonitrile in these systems. For telluride **4**, the observed rate in ethyl acetate was actually somewhat slower than in carbon tetrachloride. However, the rate of reaction in acetonitrile was faster than in either carbon tetrachloride or ethyl acetate.

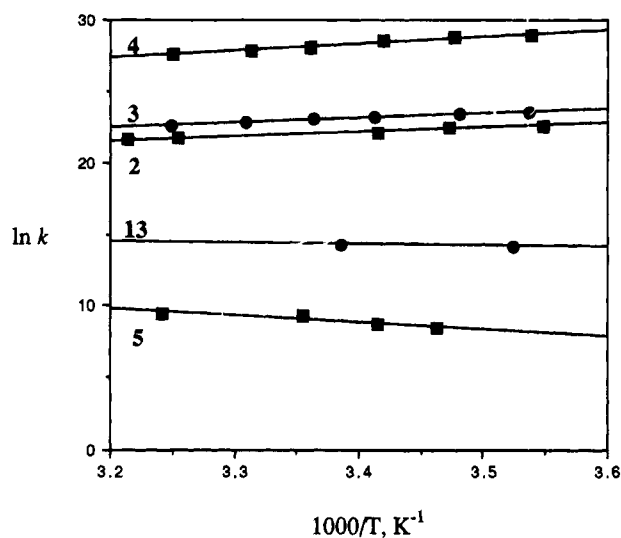


Figure 5. Inverted Arrhenius behavior for $\ln k$ as a function of $1000/T$ for 2–4 (5 × 10⁻⁵ M in both substrate and iodine): **2**, $E_a = -6.2 \pm 0.2$ kcal mol⁻¹; **3**, $E_a = -6.6 \pm 0.4$ kcal mol⁻¹; **4**, $E_a = -9.6 \pm 0.2$ kcal mol⁻¹. These data can be contrasted with the normal Arrhenius behavior observed for **13** (for two points) and for **5** (5 × 10⁻⁵ M in substrate and 5 × 10⁻⁴ M in iodine): **5**, $E_a = 9 \pm 2$ kcal mol⁻¹.

Inverted Arrhenius behavior was observed in carbon tetrachloride for 2–4 with 5 × 10⁻⁵ M iodine as shown in Figure 5. For dihexyl telluride (**1**), the rate of reaction was too fast to measure at temperatures between 282.5 and 292.8 K. However, at 297.9 K the observed rate of reaction had slowed such that a rate constant could be measured, which suggested that the apparent rate of this reaction was slowing with increasing temperature as well. The initial reactions of iodine with 1–4 in acetonitrile were too fast for meaningful measurements of rate constants.

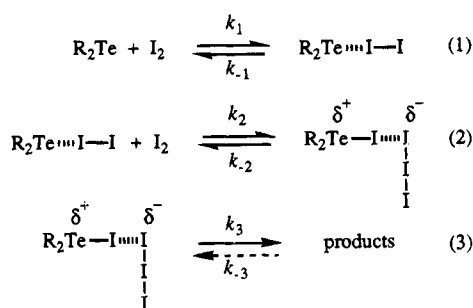
In contrast to these results, the reactions of iodine with **5** at 5 × 10⁻⁴ M iodine and di-*n*-hexyl sulfide (**13**, over a small temperature range) show normal Arrhenius behavior (Figure 5, Table 2).

In carbon tetrachloride, the rate of reaction in the "fast" reactions is a function of the electronic environment of the tellurium atom. The fastest rates are observed in the two most electron-rich systems: dihexyl telluride (**1**) and the (dimethylamino)methyl-substituted derivative **4**, which can form a chelate between the amine and the tellurium atom. The slowest rate is observed for telluropyranone **5**, which has the most electron-withdrawing organic ligands of the compounds of this study. Di-*p*-anisyl telluride (**3**), which is more electron rich than **2**, is faster than diphenyl telluride (**2**).

Mechanistic Implications of the "Fast" Reaction. On the basis of oxidative-addition reactions of bromine with diorgano chalcogenides,¹⁶ the initial "fast" reaction between iodine and diorgano telluride is most likely the formation of an η^1 -association complex. The second-order dependency in iodine suggests that the association complex may involve more than one molecule of iodine. The structure of such complexes might resemble that of complexes **III** and **IV**.

The initial association of iodine with diorgano telluride might be viewed as the formation of an η^1 -R₂Te–I₂ complex (reaction 1), which then reacts with a

Scheme 2



second iodine molecule to give an $\text{R}_2\text{Te}-\text{I}_4$ complex (reaction 2). In analogy to structures **III** and **IV**, the $\text{R}_2\text{Te}-\text{I}_4$ complex may be an η^1 -complex of I_4 , although an association complex of two $\eta^1-\text{I}_2$ ligands cannot be excluded in the absence of structural proof. The $\text{R}_2\text{Te}-\text{I}_4$ complex presumably goes on to products via the "slow" reaction as shown in reaction 3 (*vide infra*). If one assumes that reactions 1 and 2 describe the "fast" reaction and that k_3 in reaction 3 is much smaller than the products $k_1[\text{I}_2]$ and $k_2[\text{I}_2]$, then one can describe the formation of $\text{R}_2\text{Te}-\text{I}_4$ species as an equilibrium process. The $\text{R}_2\text{Te}-\text{I}_4$ complex reacts to give products as shown in reaction 3 of Scheme 2 on a much longer time scale such that k_{-3} can be ignored in establishing the initial equilibrium concentrations of $\text{R}_2\text{Te}-\text{I}_2$ and $\text{R}_2\text{Te}-\text{I}_4$ from reactions 1 and 2, respectively.

The rate expressions for the "fast" reactions as described by reactions 1 and 2 of Scheme 2 can be combined to generate an overall rate expression for formation of an iodine-diorgano telluride association complex ($\text{R}_2\text{Te}-\text{I}_4$) as described by eq 4. In this analysis,

$$\frac{d[\text{products}]}{dt} = k_3 \frac{k_1}{k_{-1}} \frac{k_2}{k_{-2}} [\text{R}_2\text{Te}][\text{I}_2]^2 \quad (4)$$

the final rate expression in eq 4 shows an apparent second-order dependence in iodine for the process, which is consistent with the 100-fold increase in observed rates of reaction for **2** and **4** when the iodine concentration is increased by a factor of 10. The ratios of k_1/k_{-1} and k_2/k_{-2} , the equilibrium constants for the two steps, cannot be measured directly in our studies. However, from dissociation studies of iodine-sulfide and iodine-selenide complexes,¹⁰ one can approximate the k_1/k_{-1} ratio as 10^4 if one assumes that dissociations of $\text{R}_2\text{Te}-\text{I}_2$ complexes are similar to dissociations of $\text{R}_2\text{Se}-\text{I}_2$ complexes.¹⁰

Inverted Arrhenius behavior typically is associated with intermediate complex formation (a preequilibrium) prior to the rate-determining transition state.¹⁹ For the condition $k_1 > k_2$ in reactions 1 and 2 of Scheme 2, a preequilibrium for $\text{R}_2\text{Te}-\text{I}_2$ could be established for reaction 1. If the proportional decrease in K_1 is greater than the increase in k_2 with increasing temperature,

then inverted Arrhenius behavior would be observed in the apparent rate of formation of $\text{R}_2\text{Te}-\text{I}_4$.

The "fast" reaction for the addition of iodine to telluropyranone **5** follows second-order kinetics overall and is first order in iodine. The tellurium atom of telluropyranone **5** is electron deficient relative to the other diorgano tellurides of this study and may follow a different mechanism. An $\text{R}_2\text{Te}-\text{I}_4$ species need not be invoked in the chemistry of this substrate, or its rate constant for formation (and equilibrium concentration) is sufficiently small that it is unimportant in the kinetics scheme.

One precedent for $\text{R}_2\text{Te}-\text{I}_4$ complexes is the isolation of sulfur- η^1 -iodine complexes $\text{Ph}_3\text{P}=\text{S}-\text{I}_4$ (**III**) and ethylenethiourea- I_4 (**IV**).^{12,13} In the tetraiodo-sulfur complexes **III** and **IV**, the $\text{S}-\text{I}_4$ array is L-shaped with the linear $\text{S}-\text{I}1-\text{I}2$ array and linear $\text{I}2-\text{I}3-\text{I}4$ array at nearly right angles. The $\text{S}-\text{I}1$ distance in the $\text{S}-\text{I}_4$ complexes is shorter (roughly 2.50 Å in **IV**) than the $\text{S}-\text{I}1$ distances found in $\text{R}_2\text{S}-\text{I}_2$ complexes (roughly 2.7–2.8 Å).^{13,20} Furthermore, the $\text{I}1-\text{I}2$ distances in the $\text{S}-\text{I}_4$ complexes are longer than the $\text{I}1-\text{I}2$ distances found in the $\text{R}_2\text{S}-\text{I}_2$ complexes. The $\text{I}2-\text{I}3-\text{I}4$ array, which is not symmetrical, is the same length as symmetrical I_3^- found in ionic complexes, and the short $\text{S}-\text{I}1$ bonds suggest that partial separation of charge to sulfonium and triiodide species has occurred in these covalent complexes.¹³

Although $\text{R}_2\text{Te}-\text{I}_4$ complexes are not plentiful in the literature,^{14,15} the larger, more polarizable tellurium atom might be more prone to formation of tetraiodo complexes such as shown in reaction 2 of Scheme 2 than the sulfur atom of similar organosulfur compounds. The formation of this complex from $\text{R}_2\text{Te}-\text{I}_2$ complexes plus I_2 or from R_2Te plus I_4 might involve changes in the bonding of Te to $\text{I}1$ from the former or bond formation in the latter to give telluronium character as well as formation of the "triiodide" interactions of $\text{I}2$, $\text{I}3$, and $\text{I}4$. The development of partial positive character at tellurium would be consistent with the observations that $k(\text{fast})$ is accelerated with increased electron donation from the organic groups attached to tellurium and with increased solvent polarity. (On the basis of data described below for the presence of "slow" reactions and for the addition of excess iodide as well as the dissociation constant of triiodide,²¹ we do not believe that the "fast" reactions are forming a telluronium species and triiodide as the second "fast" reaction.)

In ethyl acetate, which is more polar than carbon tetrachloride, the observed rates of reaction are typically accelerated relative to the observed rates in carbon tetrachloride (Table 2). For **4**, which could be studied over a fairly wide temperature range, inverted Arrhenius behavior was found in ethyl acetate (Table 2). Unfortunately, the spectral changes associated with the reaction of **5** with iodine in ethyl acetate were not well suited for kinetic analysis.

Effects of Added Iodide in Sequential Stopped-Flow Experiments. The reaction of iodide with iodine to give triiodide has been studied in several solvents.

(19) For illustrative examples: (a) Turro, N. J.; Hrovat, D. A.; Gould, I. A.; Padwa, A.; Dent, W.; Rosenthal, R. *J. Angew. Chem., Int. Ed. Engl.* **1983**, *22*, 625. (b) Maharaj, U.; Winnik, M. A. *J. Am. Chem. Soc.* **1981**, *103*, 2328. (c) Turro, N. J.; Lehr, G. F.; Butcher, J. A.; Moss, R. A.; Guo, W. *J. Am. Chem. Soc.* **1982**, *104*, 1754. (d) Gorman, A. A.; Gould, I. R.; Hamblett, I. *J. Am. Chem. Soc.* **1982**, *104*, 7098. (e) Gould, I. R.; Turro, N. J.; Butcher, J.; Doubleday, C.; Hacker, N. P.; Lehr, G. F.; Moss, R. A.; Cox, D. P.; Guo, W.; Munjal, R. C.; Perez, L. A.; Feydorynski, M. *Tetrahedron* **1985**, *41*, 1587. (f) Nicovich, J. M.; van Dijk, C. A.; Kreutter, K. D.; Wine, P. H. *J. Phys. Chem.* **1991**, *95*, 9890. (g) Chen, Y.; Tschuikow-Roux, E. *J. Phys. Chem.* **1993**, *97*, 3742.

(20) (a) Chao, G. Y.; McCullough, J. D. *Acta Crystallogr.* **1960**, *13*, 727. (b) Ahlsen, E. L.; Strømme, K. O. *Acta Chem. Scand., Ser. A* **1974**, *28*, 175. (c) Rømming, Chr. *Acta Chem. Scand.* **1960**, *14*, 2145. (d) Hartl, H.; Steidl, S. *Z. Naturforsch., B* **1977**, *32B*, 6.

(21) Turner, D. H.; Flynn, G. W.; Sutin, N.; Beitz, J. V. *J. Am. Chem. Soc.* **1972**, *94*, 1575.

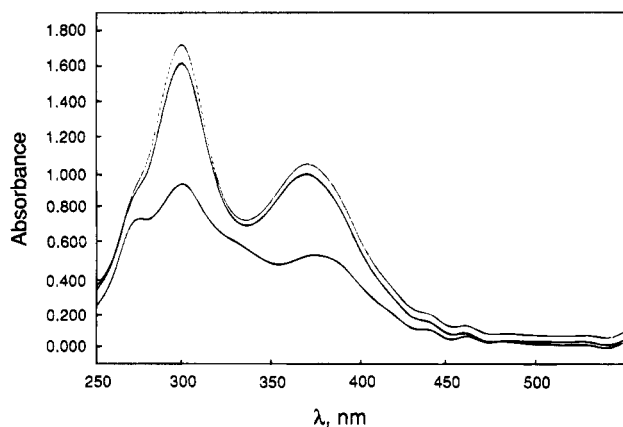
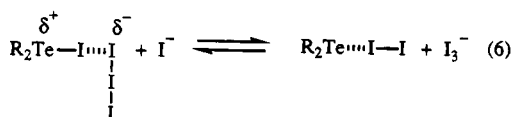


Figure 6. Spectra generated by sequential stopped-flow spectroscopy. The bottom trace is starting di-*p*-anisyl telluride (**3**, 5×10^{-5} M in CCl_4). The top trace was generated by premixing 250- μL aliquots of 2×10^{-4} M iodine and 2×10^{-4} M di-*p*-anisyl telluride (**3**) at 298 K followed by injection of 500 μL of 1×10^{-4} M tetra-*n*-butylammonium iodide 0.500 s later. Sampling was at 0.5 s. The middle trace was taken 1000 s after the time of the top trace at 298 K.

Scheme 3



The second-order rate constant for the reaction of iodide and iodine has been measured as $6.2 \times 10^9 \text{ L mol}^{-1} \text{ s}^{-1}$ in water at 298 K, while the first-order rate constant associated with dissociation of triiodide has been measured as $8.5 \times 10^6 \text{ s}^{-1}$ at 298 K.²¹ The resulting dissociation constant, K_c , is $1.4 \times 10^{-3} \text{ M}$ at 298 K.²¹ In carbon tetrachloride, K_c for KI_3 is only slightly smaller at $1.1 \times 10^{-3} \text{ M}$ at 288 K and $1.5 \times 10^{-3} \text{ M}$ at 303 K.²² The dissociation constants associated with triiodide are similar in magnitude to dissociation constants measured for association complexes of diorgano chalcogenides and iodine.¹⁰ Added iodide should compete with diorgano tellurides for iodine as shown in Scheme 3. Ideally, added iodide would compete more effectively for iodine from the $\text{R}_2\text{Te}-\text{I}_4$ complex than from the $\text{R}_2\text{Te}-\text{I}_2$ complex, which would shift the equilibrium from the "fast" sequence of reactions and allow observation of the $\text{R}_2\text{Te}-\text{I}_2$ complex.

We were able to add iodide to the reaction sequence following the "fast" reaction of iodine with **3** through the use of sequential stopped-flow techniques. In this process, 250- μL aliquots of 2.0×10^{-4} M iodine and 2.0×10^{-4} M **3** in carbon tetrachloride were premixed and a 500- μL aliquot of 1.0×10^{-4} M tetra-*n*-butylammonium iodide in carbon tetrachloride was added 0.500 s later in the stopped-flow spectrophotometer (5×10^{-5} M each in total R_2Te , iodine, and iodide). The spectral results of the sequential stopped-flow experiment are shown in Figure 6 along with the spectrum of starting diaryl telluride **3**. Similar behavior was observed with **2** under identical conditions.

Table 3. Effects of Concentration on the Observed Rate Constants in the "Slow" Reactions of Iodine Oxidations of Diorgano Tellurides **1–3** and **5** in CCl_4

R_2Te	$[\text{R}_2\text{Te}]$, M	$[\text{I}_2]$, M	T , K	λ_{obs} , nm	$k_{\text{obs}}(\text{slow})$, s^{-1}
1	5×10^{-5}	5×10^{-5}	292.8	290	$(3.4 \pm 0.6) \times 10^{-2}$
	5×10^{-5}	5×10^{-4}	293.0	330	$(3.8 \pm 0.5) \times 10^{-2}$
	1×10^{-4}	5×10^{-5}	293.0	290	$(3.6 \pm 0.3) \times 10^{-2}$
2	5×10^{-5}	5×10^{-5}	291.5	310	$(3.83 \pm 0.06) \times 10^{-3}$
	5×10^{-5}	5×10^{-4}	292.6	310	$(3.7 \pm 0.1) \times 10^{-3}$
3	5×10^{-5}	5×10^{-4}	281.6	380	$(9.5 \pm 0.3) \times 10^{-4}$
	1×10^{-4}	5×10^{-4}	281.6	380	$(1.09 \pm 0.06) \times 10^{-3}$
	5×10^{-5}	5×10^{-5}	295.1	380	$(7.2 \pm 0.3) \times 10^{-3}$
	5×10^{-5}	5×10^{-4}	297.3	380	$(1.25 \pm 0.09) \times 10^{-2}$
5	5×10^{-5}	5×10^{-5}	307.5	280	$(5.1 \pm 0.2) \times 10^{-3}$
	5×10^{-5}	5×10^{-4}	307.5	280	$(4.5 \pm 0.7) \times 10^{-3}$

In the presence of added iodide, the spectrum of the product mixture is quite different from that observed in Figure 1 after 0.5 s for the reaction of 5×10^{-5} M **3** and 5×10^{-5} M iodine. In particular, the absorbances are much larger and the band structure of the complex in the presence of iodide is quite similar to that of the starting telluride **3**. The spectral features of the product mixture in the presence of iodide are little changed after 1000 s (Figure 6). It is intriguing to consider the spectrum of the complex of Figure 6 as being primarily due to the $\text{Ar}_2\text{Te}-\text{I}_2$ complex.

Interestingly, the spectral features of Figure 6 can be generated by the addition of iodide to **8**, the final product from iodine oxidation of **3**, which suggests that the entire oxidative-addition sequence is reversible in the presence of added iodide. Furthermore, the "slow" reaction of Figure 3 at 310 nm and the "slow" reaction to 1000 s in the presence of iodide in Figure 6 at 310 nm have identical first-order rate constants ($7.2 \times 10^{-5} \text{ s}^{-1}$ at 295.1 K in the absence of iodide, $7.4 \times 10^{-5} \text{ s}^{-1}$ at 295.8 K in the presence of iodide). While the presence of added iodide has shifted the equilibrium concentrations of the various diorgano tellurium species, the "slow" rate constant, which is the final process observed in these studies, is the same in both systems.

"Slow" Reactions. A. Concentration Studies. A "slow" reaction (or reactions) was observed for **1–5** in carbon tetrachloride. As shown in Table 3, increasing concentrations of iodine have little effect on the observed first-order rate constants for the "slow" step, which suggests that the rate expression for the "slow" step is not dependent on iodine concentration at the concentrations of this study. A discrete "slow" step was not always observed in ethyl acetate or acetonitrile.

The "slow" reactions are the rate-limiting processes for the generation of the oxidative-addition products **6–10** in the compounds of this study. Furthermore, in the reactions of Scheme 2, k_3 in reaction 3 leading to products can be defined as k_{slow} .

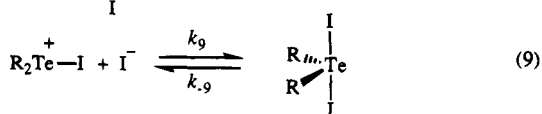
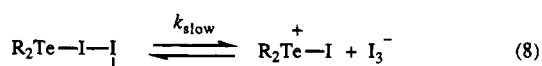
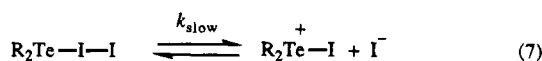
B. Temperature and Substrate Dependence for the "Slow" Reactions. The "slow" reactions followed normal Arrhenius behavior as shown in the rate data of Table 4 for reactions in carbon tetrachloride, ethyl acetate, and acetonitrile. For **2–5**, the observed rates of reaction at 293 K are surprisingly constant, varying by less than a factor of 4. For the "fast" reaction, relative rates for these same substrates varied by 10^5 – 10^6 . If a common "slow" process is described in all three solvents, then one may assume several characteristics of this process: (1) the reaction is little influenced by

(22) Watts, H. *Aust. J. Chem.* **1961**, *14*, 15.

(23) Detty, M. R.; Hassett, J. W.; Murray, B. J.; Reynolds, G. A. *Tetrahedron* **1985**, *41*, 4853.

Table 4. Observed First-Order Rate Constants for the "Slow" Reactions in the Oxidative Addition of Iodine to Diorgano Tellurides 1–5 in CCl₄, EtOAc, and CH₃CN

R ₂ Te	solvent	[I ₂], M	T, K	λ _{obs.} , nm	k _{obs} (slow), s ⁻¹	E _a , kcal mol ⁻¹	
1	CCl ₄	5 × 10 ⁻⁵	292.8	290	(3.4 ± 0.6) × 10 ⁻²		
2	CCl ₄	5 × 10 ⁻⁵	283.6	310	(1.6 ± 0.1) × 10 ⁻³	17.1 ± 0.6	
	CCl ₄	5 × 10 ⁻⁵	291.5	310	(3.8 ± 0.4) × 10 ⁻³		
	CCl ₄	5 × 10 ⁻⁵	300.5	310	(8.8 ± 0.5) × 10 ⁻³		
	EtOAc	5 × 10 ⁻⁵	287.9	360	(4.9 ± 0.2) × 10 ⁻²	11.6 ± 0.6	
	EtOAc	5 × 10 ⁻⁵	293.0	360	(7.8 ± 0.3) × 10 ⁻²		
	EtOAc	5 × 10 ⁻⁵	301.9	360	(1.30 ± 0.02) × 10 ⁻¹		
EtOAc	5 × 10 ⁻⁵	310.6	360	(2.21 ± 0.04) × 10 ⁻¹			
3	CCl ₄	5 × 10 ⁻⁵	282.7	380	(3.9 ± 0.3) × 10 ⁻³	7.7 ± 0.2	
	CCl ₄	5 × 10 ⁻⁵	287.3	380	(5.3 ± 0.1) × 10 ⁻³		
	CCl ₄	5 × 10 ⁻⁵	295.1	380	(7.2 ± 0.3) × 10 ⁻³		
	CCl ₄	5 × 10 ⁻⁵	305.0	380	(1.1 ± 0.2) × 10 ⁻²		
	EtOAc	5 × 10 ⁻⁵	287.9	300	(2.23 ± 0.03) × 10 ⁻¹	12.6 ± 0.4	
	EtOAc	5 × 10 ⁻⁵	293.0	300	(3.3 ± 0.6) × 10 ⁻¹		
	EtOAc	5 × 10 ⁻⁵	301.7	300	(5.8 ± 0.1) × 10 ⁻¹		
	EtOAc	5 × 10 ⁻⁵	310.6	300	1.11 ± 0.03		
	CH ₃ CN	5 × 10 ⁻⁵	284.5	360	1.245 ± 0.02		3.1 ± 0.3
	CH ₃ CN	5 × 10 ⁻⁵	293.2	360	1.54 ± 0.03		
	CH ₃ CN	5 × 10 ⁻⁵	304.6	360	1.8 ± 0.1		
	CH ₃ CN	5 × 10 ⁻⁵	309.8	360	2.0 ± 0.3		
4	CCl ₄	5 × 10 ⁻⁵	282.6	380	(1.113 ± 0.003) × 10 ⁻³	7.7 ± 0.4	
	CCl ₄	5 × 10 ⁻⁵	293.0	380	(1.635 ± 0.003) × 10 ⁻³		
	EtOAc	5 × 10 ⁻⁵	286.9	370	(1.3 ± 0.3) × 10 ⁻¹		
	EtOAc	5 × 10 ⁻⁵	295.6	370	(2.1 ± 0.1) × 10 ⁻¹		
	EtOAc	5 × 10 ⁻⁵	302.9	370	(2.7 ± 0.4) × 10 ⁻¹		
	EtOAc	5 × 10 ⁻⁵	312.8	370	(4.1 ± 0.2) × 10 ⁻¹		
5	CCl ₄	5 × 10 ⁻⁵	292.8	280	(2.6 ± 0.9) × 10 ⁻³	6.6 ± 0.1	
	CCl ₄	5 × 10 ⁻⁵	298.0	280	(3.6 ± 0.3) × 10 ⁻³		
	CCl ₄	5 × 10 ⁻⁵	307.5	280	(4.5 ± 0.7) × 10 ⁻³		

Scheme 4

the concentration of iodine, (2) increasing solvent polarity facilitates reaction, and (3) the reaction is little influenced by the electronic character of the organo groups attached to tellurium in the substrate.

Mechanistic Implications of the "Slow" Reaction. The characteristics of the "slow" reaction are consistent with a first-order, dissociative process to generate ionic intermediates as shown in Scheme 4. Telluronium salt **9** is an example of such intermediates. Dissociation to generate telluronium intermediates could occur from either the R₂Te–I₂ or R₂Te–I₄ complexes. If dissociation were to occur from the latter species, triiodide would be largely dissociated at the concentrations of this study. The final oxidative-addition products **6–8** and **10** are formed by iodide addition to the tellurium atom of the telluronium intermediate. In telluronium salt **9**, the attack of iodide is blocked by the (dimethylamino)methyl substituent.

Summary and Conclusions

The oxidative addition of iodine to diorgano tellurides is a complex process. An initial "fast" series of reactions

can form either 1:1 or 2:1 iodine–diorgano telluride complexes. In the case of substrate **5**, the "fast" reaction with iodine is second order overall and first order in both substrate and iodine. The other diorgano tellurides of this study (**1–4**) show a second-order dependence on iodine and presumably form 2:1 iodine–diorgano telluride complexes. The formation of the 1:1 complex follows normal Arrhenius behavior. Formation of the 2:1 complexes displays inverted Arrhenius behavior, which can be rationalized in terms of a rapid preequilibrium to form the 1:1 complex from diorgano telluride and iodine followed by reaction with a second iodine molecule.

The initial association complexes with iodine can dissociate to telluronium intermediates, which generate the final tellurium(IV) species by addition of iodide to the tellurium atom of the telluronium salt. The dissociative process follows first-order rate behavior and is much slower than the initial reactions. The rates of reaction for both the "fast" and "slow" processes increase with increasing solvent polarity, which is consistent with partial charge separation in both processes.

Experimental Section

Melting points were determined on a Thomas-Hoover melting point apparatus and are uncorrected. ¹H NMR and ¹³C NMR spectra were recorded on a General Electric QE-300 spectrometer or on a Varian Gemini-200 spectrometer. UV–visible–near-infrared spectra were recorded on a Perkin-Elmer Lambda 9 spectrophotometer. Infrared spectra were recorded on a Beckman IR 4250 instrument. Microanalyses were performed on a Perkin-Elmer 240 C, H, and N analyzer. Dichloromethane, ethyl acetate, acetonitrile, tetrahydrofuran (THF), and carbon tetrachloride were obtained as anhydrous solvents from Aldrich Chemical Co. and were used as received. Diphenyl selenide and diphenyl telluride (**2**) were obtained from various commercial sources and were distilled prior to use. Diaryl telluride **3** was prepared according to refs 1 and 2. Telluropyranone **5** was prepared according to ref 21.

Preparation of Di-*n*-hexyl Telluride (1). Sodium borohydride (1.9 g, 0.050 mol) was added in several portions every 15 min to a refluxing slurry of tellurium powder (2.55 g, 0.0200 mol) in 50 mL of 0.3 M sodium ethoxide in ethanol. After the tellurium was consumed and a chalky white mixture was obtained, hexyl bromide (6.6 g, 0.040 mol) in 20 mL of ethanol was added. The reaction mixture was stirred for 3 h at ambient temperature and was then poured into water. The products were extracted with hexanes (3 × 50 mL). The combined organic extracts were washed with brine, filtered through Celite, dried over magnesium sulfate, and concentrated. The residue was purified via short-path distillation over the range 75–100 °C (0.1 Torr) to give 5.85 g (98%) of a colorless oil: ¹H NMR (CDCl₃) δ 2.58 (t, 4 H, *J* = 7.6 Hz), 1.70 (m, 4 H), 1.26 (m, 12 H), 0.85 (t, 6 H, *J* = 6.7 Hz); ¹³C NMR (CDCl₃) δ 30.89, 30.37, 29.82, 21.17, 12.63, 1.27; IR (film, NaCl) 2955, 2919, 2850, 1455, 1211, 1150 cm⁻¹; UV–vis (CH₂Cl₂) λ_{max}, nm (ε) 352 (900); FDMS, *m/z* 300 (C₁₂H₂₆¹³⁰Te).

Preparation of Phenyl 2-((Dimethylamino)methyl)-phenyl Telluride (4). *n*-Butyllithium (10 mL of 2.5 M solution in hexanes) was added dropwise via syringe to dimethylbenzylamine (2.70 g, 0.020 mol) in 50 mL of ether at ambient temperature under an argon atmosphere. After 5 h, a 0.5 M solution of phenyltellurenyl bromide in THF was added dropwise via syringe. After the addition of 38.5 mL, the color of the reaction mixture darkened with the characteristic orange-red color of the phenyltellurenyl bromide. The reaction mixture was poured into 100 mL of ether. The combined organics were washed with brine (3 × 50 mL), dried over magnesium sulfate, and concentrated. The residual oil was

mostly the desired product by ^1H NMR. The residue was purified by chromatography on silica gel eluted with 1:9:90 methanol-ethyl acetate-dichloromethane to give 3.14 g (46.5%) of the amine as an off-white solid, mp 51–54 °C; ^1H NMR (CDCl_3) δ 7.88 (d \times d, 2 H, $J = 1, 8$ Hz) 7.4–6.8 (multiplets, 7 H), 3.51 (s, 2 H), 2.26 (s, 6 H); IR (KBr) 3057, 2976, 2944, 2874, 2850, 2780, 1458, 1449, 1440, 1430, 1026, 1017, 845, 747, 731, 693 cm^{-1} ; UV-vis (CH_2Cl_2) λ_{max} , nm (ϵ) 283 (10 300), 231 (12 400), 226 (12 000); FDMS, m/z 341 ($\text{C}_{15}\text{H}_{17}\text{N}^{130}\text{Te}$). Anal. Calcd for $\text{C}_{15}\text{H}_{17}\text{NTe}$: C, 53.16; H, 5.06; N, 4.13. Found: C, 52.83; H, 4.94; N, 4.03.

The phenyltellurenyl bromide solution was prepared by the addition of 4.80 g (30.0 mmol) of bromine to 12.30 g (30.0 mmol) of diphenyl ditelluride in 120 mL of anhydrous THF. The resulting solution was stirred at ambient temperature for 0.5 h prior to use and was stored under an inert atmosphere in the dark at ambient temperature.

General Procedure for the Oxidative Addition of Iodine on a Preparative Scale. Tellurium-containing substrate (2.0 mmol) was dissolved in 10 mL of acetone. Iodine (0.51 g, 2.0 mmol) was added, and the resulting solution was stirred at ambient temperature for 0.5 h and was then chilled. The crystalline product was collected by filtration. The crystals were washed with small portions of cold acetone and dried.

For **6**: 98%, red oil; ^1H NMR (CDCl_3) δ 3.60 (t, 4 H, $J = 7.9$ Hz), 2.14 (m, 4 H), 1.45 (m, 4 H), 1.37 (m, 8 H), 0.91 (t, 6 H, $J = 6.9$ Hz); IR (film, NaCl) 2950, 2918, 2848, 1450, 1400, 1215, 1160, 705 cm^{-1} ; UV-vis (CH_2Cl_2) λ_{max} , nm (ϵ) 355 (2100). Anal. Calcd for $\text{C}_{12}\text{H}_{26}\text{I}_2\text{Te}$: C, 26.12; H, 4.75. Found: C, 26.53; H, 5.05.

For **7**: 95%, mp 232–235 °C (lit.³ mp 237–238 °C); ^1H NMR (CDCl_3) δ 8.14 (m, 4 H), 7.58 (m, 2 H), 7.45 (m, 4 H); IR (KBr) 3053, 3047, 1572, 1472, 1431, 1326, 1155, 1050, 993, 910, 833, 729, 680, 457, 444 cm^{-1} ; UV-vis (CH_2Cl_2) λ_{max} , nm (ϵ) 372 (13 100), 286 (26 400). Anal. Calcd for $\text{C}_{12}\text{H}_{10}\text{I}_2\text{Te}$: C, 26.91; H, 1.88. Found: C, 27.00; H, 1.95.

For **8**: 73%, mp 167.5–169 °C (lit.² mp 166–167 °C); ^1H NMR (CDCl_3) δ 8.03 (AA'BB', 4 H, J ("doublet") = 9 Hz), 6.95

(AA'BB', 4 H), 3.87 (s, 6 H); IR (KBr) 1581, 1569, 1489, 1296, 1256, 1177, 1053, 1021, 818, 511 cm^{-1} ; UV-vis (CH_2Cl_2) λ_{max} , nm (ϵ) 380 (sh, 13 000), 340 (20 100), 288 (26 800). Anal. Calcd for $\text{C}_{14}\text{H}_{14}\text{I}_2\text{O}_2\text{Te}$: C, 28.23; H, 2.37. Found: C, 28.15; H, 2.35.

For **9**: 73%, mp 178–179 °C; IR (KBr) 2859, 2830, 2785, 1715 (acetone of crystallization), 1479, 1461, 1452, 1438, 1431, 1425, 1159, 1053, 1023, 996, 972, 843, 823, 756, 730, 688, 453, 432, 423 cm^{-1} ; UV-vis (CH_2Cl_2) λ_{max} , nm (ϵ) 381 (12 300), 340 (10 000), 279 (31 500). Anal. Calcd for $\text{C}_{15}\text{H}_{17}\text{I}_2\text{NTe}-\frac{1}{2}$ -acetone: C, 31.87; H, 3.22; N, 2.25. Found: C, 31.99; H, 3.27; N, 2.18.

For **10**: 46%, mp 114–130 °C dec; ^1H NMR (CDCl_3) δ 6.95 (s, 2 H), 1.35 (s, 18 H); IR (KBr) 1970, 1625, 1585, 1280, 1190, 1155 cm^{-1} . Anal. Calcd for $\text{C}_{13}\text{H}_{20}\text{I}_2\text{OTe}$: C, 27.2; H, 3.5; Te, 22.2. Found: C, 27.0; H, 3.5; Te, 22.5.

Stopped-Flow Experiments. All stopped-flow experiments were performed on a Sequential DX17 MV stopped-flow spectrometer (Applied Photophysics, Leatherhead, U.K.). All experiments incorporated the instrument in stopped-flow mode only. The sample handling unit was fitted with two drive syringes that are mounted inside a thermostated-bath compartment, which allowed for variable-temperature experimentation. The optical-detection cell was set up in the 10-mm path length. First- and second-order curve fitting and rate constants used a Marquardt algorithm²⁴ based on the routine Curfit.²⁵ Absorption spectra at indicated time points were calculated through software provided by Applied Photophysics. This consisted of slicing the appropriate time points across a series of kinetic traces (at different wavelengths) and then splining the points of a specific time group. Stock solutions of substrates and iodine at appropriate concentrations described in the text were utilized in the stopped-flow experiments.

OM940846+

(24) Marquardt, D. W. *J. Soc. Ind. Appl. Math.* **1963**, *11*, 431.

(25) Curfit is found in: Bevington, P. R. *Data Reduction and Error Analysis for the Physical Sciences*; McGraw-Hill: New York, 1969.

Organotin Chemistry. 17.¹ Reactions of Stannane with Olefins

Gerald H. Reifenberg and William J. Considine*²

Elf Atochem North America, Inc., King of Prussia, Pennsylvania 19406

Received November 3, 1994[®]

The reactions of stannane with olefins in the presence of catalysts has been investigated. In the presence of a cobalt naphthenate/*tert*-butyl hydroperoxide catalyst mixture, stannane adds to olefins such as ethylene, propylene, but-1-ene, isobutylene, oct-1-ene, cyclohexene, and acrylonitrile. The only organotin compound isolated in each case was the corresponding tetraalkyltin. In the absence of the catalyst, stannane reacted only with acrylonitrile. No reaction occurred with stannane and the catalyst with the following olefins: 2,3-dimethylbut-2-ene, 1,3-butadiene, 1,5-hexadiene, styrene, methyl acrylate, and methyl crotonate. Palladium on carbon (10%) and hexachloroplatinic acid also catalyze the addition of stannane to but-1-ene.

Introduction

In a preliminary communication,³ we reported some results of our investigation of the catalytic addition of stannane to olefins. This paper discusses these results in detail and expands on the scope of this reaction.

The addition of alkyltin hydrides to simple olefins is catalyzed by free-radical initiators.⁴ The conditions are mild, and temperatures of ~40 °C will generally give good yields of the expected adducts. Because of the thermal instability of stannane, reactions carried out above room temperature are not practical. Of necessity, the reactions of stannane are conducted at or below room temperature.

Stannane, a gas with bp = -52.5 °C, was prepared by the LiAlH₄ reduction of SnCl₄.⁵ While relatively stable, stannane decomposes slowly at room temperature. To minimize decomposition, we worked under an atmosphere of nitrogen containing 0.1% O₂. We have already reported that no reaction occurs when stannane is mixed with but-1-ene or oct-1-ene at low temperatures in the absence of a catalyst.³

Results and Discussion

Azobis(isobutyronitrile) and di-*tert*-butyl peroxide, known to be catalysts for the addition of alkyltin hydrides to olefin,⁴ do not decompose to give radicals in the presence of stannane/olefin mixtures at temperatures ranging from -78 °C to room temperature and are recovered unchanged. Benzoyl peroxide and *tert*-butyl hydroperoxide also were not effective catalysts for stannane addition under the same conditions.

We found a cobalt(II) naphthenate⁶/di-*tert*-butyl peroxide (or *tert*-butyl hydroperoxide) mixture to be an effective catalyst system that allowed stannane to be added to several α -olefins and one internal olefin. The one-electron oxidation of the Co(II) proceeds at a sufficiently rapid rate at these low temperatures to generate radicals from the peroxides and catalyze the addition.

The yields ranged from poor to moderate, as might be expected at the low temperatures of our study. In each case, the product isolated was the tetraalkyltin. No organotin hydrides were found. No attempt was made to optimize experimental conditions to increase yields.

Further work was directed to expanding the scope of the stannane additions. The fact that stannane adds to olefins at all is surprising in view of its thermal instability and the necessity of running reactions at low temperatures.

As noted above, no organotin hydrides were detected in any of the runs. However, with alkyl- and aryltin di- or trihydrides as starting materials, hydride products can be isolated.⁴ We were surprised at this result and speculated that the organotin hydrides were more reactive than stannane toward olefins.

To test this idea we reacted tri-*n*-propyltin hydride with propylene in the presence of the cobalt(II) naphthenate/*tert*-butyl hydroperoxide catalyst mixture and obtained a 45% yield of tetrapropyltin. This yield is better than that obtained when stannane reacts with propylene (45% vs 20%) and would tend to lend credibility to our hypothesis.

To expand the range of usable catalyst systems, we investigated the reaction of but-1-ene and stannane in the presence of soaps of metals other than cobalt in *tert*-butyl peroxide mixtures. No reaction occurred with naphthenates of Mn, Pb, Zn and Zr or with iron(II) octoate.

(6) Naphthenic acids are complex carboxylic acids found in petroleum. The salts of several metals are technically important. Cobalt naphthenate is a common paint dryer (oxidation catalyst) and is sold in commerce as a solution in saturated aliphatic hydrocarbons. See, for example: Fieser, L. F.; Fieser, M., D. C. *Organic Chemistry*; Heath: Boston, 1944; p 88.

[®] Abstract published in *Advance ACS Abstracts*, February 15, 1995.

(1) Part 16: Reifenberg, G. H.; Considine, Wm. J., *Organometallics* 1993, 12, 3015. Much of the subject matter in this paper is covered in U.S. Patents 3,607,892 September 21, 1971.

(2) Present address: P.O. Box 96, Pearl River, NY 10965. Work was done at M&T Chemicals Inc., Rahway, NJ.

(3) Reifenberg, G. H.; Considine, Wm. J. *J. Am. Chem. Soc.* 1969, 91, 2401.

(4) Neumann, W. P.; Nierman, H.; Sommer, R. *Angew. Chem.* 1961, 73, 768; *Justus Liebigs Ann. Chem.* 1963, 659, 27. Also: Neumann, W. P. *The Organic Chemistry of Tin*; J. Wiley: New York, 1970; *Synthesis* 1987, 584.

(5) The preparation and characterization of stannane is covered in detail in ref 1 and will not be repeated here.

Noble metal catalysts are known to be promoters of the addition of organosilicon hydrides to olefins.⁷ But-1-ene was chosen as the olefin in the investigation of these systems. It was found that palladium on charcoal and hexachloroplatinic acid catalyze the addition of stannane to but-1-ene. In both cases, tetra-*n*-butyltin was isolated, in yields of 32% and 23%, respectively, based on the stannane charged. No organotin hydrides were detected in the product. Again, no attempt was made to increase yields.

When palladium on charcoal was used, the reaction "puffed" and the head of the reaction vessel popped off. We were able to recover and complete the run.

We also investigated palladium on charcoal as a catalyst for the addition of tri-*n*-propyltin hydride to propylene. In this case, there was a more violent explosion and a fire resulted. Systems containing tin hydrides and palladium on charcoal *must be handled with caution*. In spite of the upset, we were able to work up the reaction mass and isolated hexa-*n*-propylditin, as the only product, in 89% yield.

Since our first communication,³ we have attempted reaction of stannane with some other olefins. None of these olefins (2,3-dimethylbut-2-ene, 1,3-butadiene, 1,5-hexadiene, styrene) gave any organotin adducts under the experimental conditions. Again, no attempt was made to optimize these conditions. With styrene, non-tin-containing compounds were obtained which probably were polymers. Undoubtedly, with certain monomers free-radical-catalyzed polymerization is more rapid than the addition of SnH to a double bond.

As part of this study, we attempted to react stannane with three activated olefins, acrylonitrile, methyl crotonate, and methyl acrylate, since Van der Kerk and co-workers⁸ had reported the addition of organotin hydrides to these olefins. In the presence or absence¹ of the cobalt catalyst system, stannane did not react with methyl acrylate. Methyl crotonate also did not react in the presence of a catalyst. However, stannane did react with acrylonitrile in the presence or absence of the catalyst.¹ The only product in either case was tetrakis(2-cyanoethyl)tin; no (cyanoethyl)tin hydrides were detected.

Experimental Section

Vapor phase chromatography was performed on a Model 720 F&M gas chromatograph. Infrared spectra were obtained with a Beckman IR-8 infrared spectrophotometer.

SnH₄ was prepared by the reduction of SnCl₄ by LiAlH₄.⁵ The preparation and the techniques to collect SnH₄ and subsequently transfer it to the reaction vessel were described previously.¹ Cobalt naphthenate was used as a 10% solution in a hydrocarbon solvent as obtained from Nuodex Products Co., Elizabeth, NJ.

The traps used to collect and store SnH₄ consisted of Schlenk tubes fitted with two side arms, each with a stopcock. This facilitated the transfer of SnH₄ to a suitable reaction vessel.

The solubility of SnH₄ has been determined in several different solvents at -78 °C, including diethyl ether (1.4 g/100 mL), hexane, (1.8 g/100 mL), and tetrahydrofuran (2.4 g/100 mL).¹

(7) Armitage, D. A. In *Comprehensive Organometallic Chemistry*; Wilkinson, G., Stone, F. G. A., Abel, E. W., Eds.; Pergamon: Oxford, U.K., 1982; Vol. 2, p 117, and references therein.

(8) Van der Kerk, G. J. M.; Noltes, J. G.; Luijten, J. G. A. *Chem. Ind.* 1956, 352.

Table 1. Attempted Reactions of Stannane with Catalyst Candidates

material	recovered stannane (%)
Me ₂ C(CN)N=N(CN)CMe ₂	98.5
PhC(O)OOC(O)Ph	98.2
Me ₃ COOCMe ₃	98.5
Me ₃ COOH	98.2

Survey of Catalyst Candidates. The reaction vessel was a special trap as described above but with a removable head to facilitate workup. The candidates, azobis(isobutyronitrile), benzoyl peroxide, di-*tert*-butyl peroxide, or *tert*-butyl hydroperoxide, were dissolved in diethyl ether or tetrahydrofuran. To one of the arms of this trap were attached two other traps in series. These were immersed in liquid nitrogen (-195 °C) and were used to collect any unreacted SnH₄. After establishing a 99.9% N₂/0.1% O₂ atmosphere, a known weight of SnH₄ was slowly bubbled through the solution while it was held in the temperature range of -78 to -60 °C. When all of the SnH₄ was added, the reaction mixture was allowed to warm to room temperature. The recovered SnH₄ was weighed.

Preparation of Tetra-*n*-butyltin. (a) **Co/Peroxide Catalyst.** For this and other reactions of SnH₄ with olefins, the following general procedure was used. The reaction vessel was a special trap as described above with a removable head to facilitate workup. A CaCl₂ drying tube was attached to one of the arms of this trap. After establishing the 99.9% N₂/0.1% O₂ atmosphere, the vessel was immersed in a liquid nitrogen bath. SnH₄ (2.6 g, 0.021 mol) was condensed into the vessel followed by but-1-ene (6.0 g, 0.11 mol). Di-*tert*-butyl peroxide (60 mg) and cobalt naphthenate (6.0 mg on a dry basis) were then added.

After the reactants had been added, the reaction mixture was allowed to warm to room temperature by changing the immersion baths every 15 min and keeping the reaction vessel in each bath for 10 min. The baths were used in the following sequence: liquid nitrogen (-195 °C); dry ice/acetone (-78 °C); ice/methanol (-23 °C), and ice/water (0 °C).

At the end of the reaction, the vessel contained a slightly cloudy, pale green liquid which weighed 2.4 g. Gas chromatographic analysis showed that it was composed of 99 wt % tetra-*n*-butyltin and 1 wt % solvent (from the catalyst). An infrared spectrum of the product was identical to that of authentic material and showed no evidence of Sn-H bands. The conversion to tetra-*n*-butyltin, based on SnH₄ charged, was 33%.

(b) **Pd/C Catalyst.** The reaction was carried out as above with SnH₄ (2.4 g, 0.020 mol), 0.2 g of 10% Pd on charcoal (Pd/C), and but-1-ene (4.6 g, 0.08 mol). When the reaction vessel was first placed in the dry ice/acetone bath, a pressure surge popped off the head of the reaction vessel. The head was replaced, and the reaction was continued. At the end of the reaction period, the mass was filtered and 2.2 g of tetra-*n*-butyltin was obtained as a pale yellow liquid. Its identity was established by GLC and its IR spectrum. The yield, based on SnH₄ charged, was 32% (0.008 mol).

(c) **H₂PtCl₆.** This reaction was carried out as above except that the catalyst was 0.25 g of H₂PtCl₆·6H₂O (10% by weight of SnH₄ charged). At the end of the reaction period, 1.6 g of a slightly yellow liquid was obtained. The liquid was identified as tetra-*n*-butyltin by GLC and its IR spectrum. The yield was 23% (0.005 mol).

Reaction of Tri-*n*-propyltin Hydride with Propylene. (a) This reaction was carried out as above with tri-*n*-propyltin hydride (10.0 g, 0.04 mol), propylene (2.8 g, 0.067 mol), 90 mg of *tert*-butyl hydroperoxide, and 150 mg of a 6% cobalt naphthenate solution. At the end of the reaction period, the liquid reaction mixture containing suspended purple solids was filtered to give 10.9 g of a clear yellow liquid. The composition of this liquid was determined by GLC to be tri-*n*-propyltin hydride (39%), tetra-*n*-propyltin (48%), hexa-*n*-propylditin,

Table 2. Further Reactions of Stannane with Olefins

identity	olefin		SnH ₄ charged		product	yield (%)
	amt charged		g			
	g	mol	g	mol		
propylene	4.0	0.09	2.6	0.021	Pr ₄ Sn	20
isobutylene	5.0	0.090	2.4	0.020	<i>i</i> -Bu ₄ Sn	14
oct-1-ene	10.0	0.084	2.7	0.021	Oct ₄ Sn ^a	7
acrylonitrile	12.0	0.22	1.9	0.015	(NCCH ₂ CH ₂) ₄ Sn ^a	16 ^b

^a The crude reaction mixture was concentrated to remove excess olefin before GLC analysis and IR spectral measurements were made. ^b This yield was obtained when freshly distilled acrylonitrile (to remove inhibitor) was used. When undistilled material was used the yield fell to 9%.

(4%) and solvents and unknown components (8.7%). Based on this analysis, the yield of tetra-*n*-propyltin was 46% (0.018 mol).

(b) This reaction was carried out as above except that 150 mg of 10% Pd/C was used as catalyst. As the reaction vessel was warming, at ~0 °C a violent explosion occurred which was followed by a fire. **CAUTION!** The reaction vessel was not shattered, and after extinguishing the fire, the remaining liquid was filtered to give 9.7 g of a clear yellow liquid. GLC analysis showed that it contained 92% (0.0184 mol) hexa-*n*-propyltin with no tri-*n*-propyltin hydride.

Preparation of Tetraethyltin. SnH₄ (2.6 g, 0.021 mol) and ethylene (3.0 g, 0.11 mol) were condensed in a reactor containing 90 mg of *tert*-butyl hydroperoxide and 150 mg of 6% cobalt naphthenate solution as in the general procedure under tetra-*n*-butyltin.

At the end of the reaction period, 1.7 g of a hazy purple liquid was isolated. GLC analysis showed that it was composed of 96% tetraethyltin and 4% solvents. The IR spectrum of the material was identical to that of tetraethyltin, with no Sn-H bands. The yield was 35% (0.007 mol).

Reaction of SnH₄ With Other Olefins. The olefins listed in Table 2 were reacted in the same procedure as ethylene to give the results in the table. GLC analyses and IR spectra confirmed the identity of the products. In no case was an Sn-H band visible in the IR spectrum of the respective products.

Preparation of Tetracyclohexyltin. SnH₄ (2.0 g, 0.016 mol), cyclohexene (8.0 g, 0.095 mol), 90 mg of *tert*-butyl hydroperoxide, and 150 mg of a 6% cobalt naphthenate solution were mixed. At the end of the reaction period, a clear pale green liquid containing a suspended white solid was obtained. The solids, isolated by filtration, when air-dried weighed 1.2 g and had mp = 262–264 °C undepressed when mixed with authentic tetracyclohexyltin. Another 0.3 g of white solid was recovered from the filtrate after it had been evaporated in a rotary evaporator. This second crop had mp = 261–263 °C undepressed when mixed with authentic material. An IR spectrum of the first crop was identical to that of authentic material. The yield was 20% (0.003 mol).

Attempted Reactions of SnH₄ and Styrene. Freshly distilled (to remove the inhibitor) styrene (8.1 g, 0.078 mol)

Table 3. Other Attempted Reactions of Stannane with Olefins

identity	olefin		SnH ₄ charged		SnH ₄ recovered		
	amt charged		g		g		
	g	mol	g	mol	g	mol	%
hexa-1,5-diene	3.6	0.044	2.7	0.022	1.9	0.015	70
dodec-1-ene	14.1	0.084	2.6	0.022	2.1	0.017	81
methyl acrylate	8.0	0.093	2.6	0.022	2.1	0.017	80
methyl crotonate	7.6	0.076	2.3	0.019	2.0	0.016	87

and SnH₄ (2.6 g, 0.022 mol) were charged into the usual apparatus along with the catalyst mix from the general (Bu₄Sn) procedure. At the end of the reaction, 88% of the SnH₄ (21 g, 0.018 mol) was recovered from the liquid nitrogen traps. The reaction vessel contained a small amount of a dark brown liquid. (low molecular weight polystyrene is soluble in styrene). Complete combustion of this liquid gave no ash residue. No organotin product was formed.

When the reaction was repeated with freshly distilled styrene, but with 0.2 g of 10% Pd/C as the catalyst in place of the Co/peroxide mixture, the result was the same. In this case, no pressure buildup was observed. When this reaction was repeated with undistilled styrene and the Co/peroxide catalyst, the result was the same.

When the reaction was repeated with freshly distilled styrene dissolved in diethyl ether (8.1 g in 25 mL), a suspended white solid (polystyrene?) was observed. Filtration and air-drying gave 5.3 g (65%) of white solid. Evaporation of the filtrate gave no additional solids. Complete combustion of the solid left no ash.

Attempted Reaction of SnH₄ and 1,3-Butadiene. The general procedure (Bu₄Sn) was used with SnH₄ (2.5 g, 0.020 mol) and 1,3-butadiene (4.9 g, 0.090 mol). At the end of the reaction period, nothing remained in the reaction vessel. However, 7.4 g, 93% of the material charged, was recovered from two traps immersed in liquid nitrogen connected in series to the reaction vessel.

Other Attempted Reactions of SnH₄ and Olefins. The four olefins listed in Table 3 were subjected to the general procedure (Bu₄Sn) with the results shown. In each case, combustion of the liquid remaining in the reaction vessel at the end of the reaction period left no residue.

Acknowledgment. The authors are grateful to Mr. John Saraka for his technical assistance. Analyses were performed by Messrs. I. L. Simmons and P. D. Branigan. We benefitted from the opportunity to discuss this work while ongoing with Professor Dietmar Seyferth. We are especially grateful for his encouragement and help in preparing the manuscript for publication. We thank the management of Elf Atochem North America, Inc., King of Prussia, PA 19406, the successor to M&T Chemicals Inc., for permission to publish this article.

OM940835G

The Use of Tetradentate (N₂O₂) Ligands To Form Monomeric, Trimetallic Aluminum Complexes

David A. Atwood,* Jolin A. Jegier, Kyli J. Martin, and Drew Rutherford

Department of Chemistry, North Dakota State University, Fargo, North Dakota 58105

Received November 9, 1994[⊗]

Members of the SalanH₄ class of tetradentate (–N₂O₂) ligand, *N,N'*-bis(*o*-hydroxybenzyl)-1,2-diaminoethane (SaleanH₄), *N,N'*-bis(*o*-hydroxybenzyl)-1,3-diaminopropane (SalpanH₄), *N,N'*-bis(*o*-hydroxybenzyl)-1,2-diaminobenzene (SalophanH₄), and *N,N'*-bis(*o*-hydroxybenzyl)-1,2-diamino-4,5-dimethylbenzene (SalomphanH₄), demonstrate a wide range of chemistry with AlMe₃. For instance, SalpanH₄ will react with 1 and 2 equiv of AlMe₃ to produce the complexes SalpanH₂(AlMe) (**1**) and [SalpanAl(AlMe₂)₂]₂ (**2**), respectively. When 3 equiv of AlMe₃ is added to the appropriate ligand, the novel trimetallic derivatives Salean(AlMe)(AlMe₂)₂ (**3**), Salpan(AlMe)(AlMe₂)₂ (**4**), Salophan(AlMe)(AlMe₂)₂ (**5**), and Salomphan(AlMe)(AlMe₂)₂ (**6**) result. A general feature of **3**–**6** is the presence of a rigid solution-state geometry as evidenced by the ¹H NMR. A crystallographic study of **3** has shown that the molecules are comprised of a central AlMe group coordinated in a planar array to the nitrogens and oxygens of the ligand. The two AlMe₂ groups each bridge an oxygen and nitrogen atom. The overall morphology of **4** and **5** is similar to that shown for **3**. However, structural characterization of **4** and **5** indicates that the AlMe₂ groups are inequivalent, with one bridging the two oxygens and the other bridging the two nitrogens. Crystal data for **3**: C₂₁H₃₁Al₃N₂O₂, space group *P* $\bar{1}$ (No. 2) with *a* = 7.946(3) Å, *b* = 9.662(3) Å, *c* = 15.804(6) Å, α = 89.192(5)°, β = 84.434(6)°, γ = 79.926(4)°, *V* = 1189.0(7) Å³ and *Z* = 2. With 253 parameters refined on 2954 reflections having *F* > 4.0σ(*F*), the final *R* values were *R* = 0.0667 and *R*_w = 0.0651. Crystal data for **4**: C₄₄H₆₆Al₆N₄O₄, space group *P* $\bar{1}$ (No. 2) with *a* = 7.821(7) Å, *b* = 17.890(15) Å, *c* = 18.668(16) Å, α = 89.10(4)°, β = 89.86(4)°, γ = 89.78(5)°, *V* = 2612(4) Å³, and *Z* = 2. With 523 parameters refined on 2068 reflections having *F* > 4.0σ(*F*), the final *R* values were *R* = 0.0690 and *R*_w = 0.0691. Crystal data for **5**: C₃₉H₄₇Al₃N₂O₂, space group monoclinic *P*2₁ (No. 4) with *a* = 10.881(7) Å, *b* = 17.170(10) Å, *c* = 11.288(7) Å, β = 113.275(12)°, *V* = 1937(2) Å³ and *Z* = 2. With 401 parameters refined on 4313 reflections having *F* > 4.0σ(*F*), the final *R* values were *R* = 0.0619 and *R*_w = 0.0642.

Introduction

Schiff base molecules, derived from the condensation of a diamine with 2 equiv of salicylaldehyde,¹ have been used extensively as ligands in transition-metal chemistry.² With regards to the main-group elements, the majority of research has involved the reaction of such Schiff base complexes as *N,N'*-bis(*o*-hydroxybenzyl)ethyleneimine (SalenH₂; Figure 1a) with aluminum³ and gallium⁴ alkyls and various aluminum alkoxides.⁵ Novel complexes of the group 13 elements may also be expected to result when using the reduced version of this ligand (Figure 1b).⁶ By comparison, however, this potentially tetracoordinate ligand, known generally as SalanH₄, may be anticipated to show an even more

diverse chemistry, with the capacity to form σ bonds through the amine groups.

In this paper are described a series of products resulting from the reaction of AlMe₃ with the SalanH₄ ligands *N,N'*-bis(*o*-hydroxybenzyl)-1,2-diaminoethane (SaleanH₄), *N,N'*-bis(*o*-hydroxybenzyl)-1,3-diaminopropane (SalpanH₄), *N,N'*-bis(*o*-hydroxybenzyl)-1,2-diaminobenzene (SalophanH₄), and *N,N'*-bis(*o*-hydroxybenzyl)-1,2-diamino-4,5-dimethylbenzene (SalomphanH₄) (Figure 1b–e). Specifically, complexes with ligand/Al stoichiometries of 1:1 (SalpanH₂AlMe (**1**)), 1:2 ([SalpanAl(AlMe₂)₂]₂ (**2**)), and 1:3 (Salean(AlMe)(AlMe₂)₂ (**3**), Salpan(AlMe)(AlMe₂)₂ (**4**), Salophan(AlMe)(AlMe₂)₂ (**5**), Salomphan(AlMe)(AlMe₂)₂ (**6**)) are reported. The structures of compounds **3**–**5** have been determined by single-crystal X-ray analysis.

Results and Discussion

Synthesis and Characterization. Compounds **1** and **2** were prepared by the exothermic reaction of AlMe₃ with SalpanH₄ in a 1:1 and 2:1 stoichiometry (paths a and b in Scheme 1, respectively). For **1**, the proton NMR data indicated four broad resonances that could be attributed to the propylamine methylene groups. The PhCH₂ groups were manifested as a broad

[⊗] Abstract published in *Advance ACS Abstracts*, February 1, 1995.

(1) Dubsky, J. V.; Sokól, A. *Collect. Czech. Chem Commun.* **1931**, *3*, 548.

(2) Holm, R. H.; Everett, G. W., Jr.; Chakravorty, A. *Prog. Inorg. Chem.* **1966**, *7*, 83.

(3) Dzuga, S. J.; Goedken, V. L. *Inorg. Chem.* **1986**, *25*, 2858.

(4) Chong, K. S.; Rettig, S. J.; Storr, A.; Trotter, J. *Can. J. Chem.* **1977**, *55*, 2540.

(5) Gurian, P. L.; Cheatham, L. K.; Ziller, J. W.; Barron, A. R. *J. Chem. Soc., Dalton Trans.* **1991**, 1449.

(6) The synthesis and characterization of a series of these ligands, including SaleanH₄, SalpanH₄, SalophanH₄, and SalomphanH₄, is reported in: Atwood, D. A.; Benson, J.; Jegier, J. A.; Lindholm, N. F.; Martin, K. J.; Rutherford, D. *Main Group Chem.*, in press.

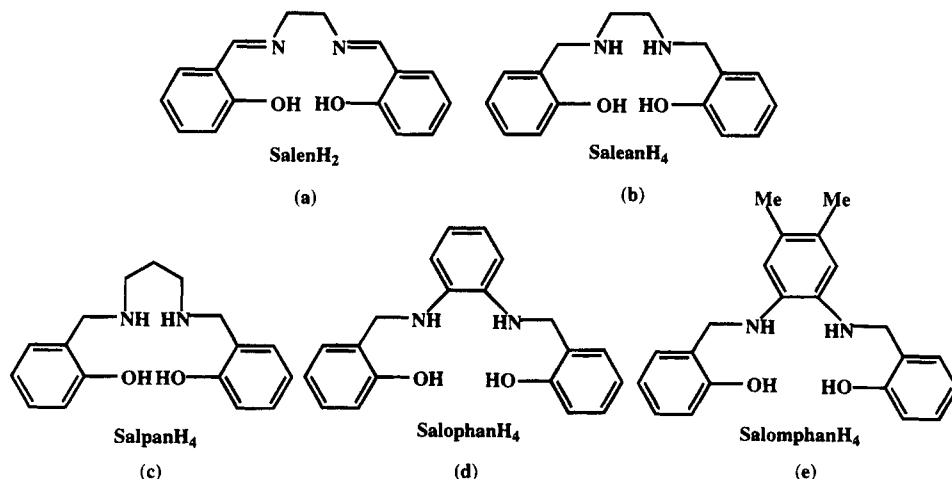
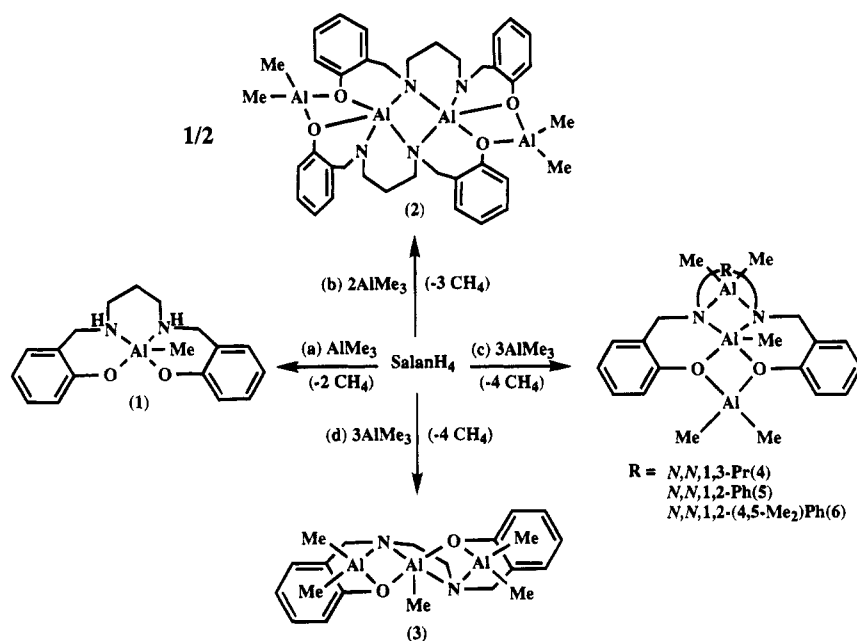


Figure 1. Example of a Schiff base ligand (a) and a display of ligands used in this study (b–e).

Scheme 1. Syntheses of Compounds 1–6



resonance centered at δ 3.95 ppm. This may be indicative of a nonplanar arrangement of the PrN_2Al six-membered ring or an indication that the complex is fluxional in solution. A similar situation was observed for the Schiff base analog SalenAlEt . Crystal structure data for SalenAlEt have demonstrated a square-pyramidal geometry for the central aluminum atom.³ A similar structure is proposed for 1. Additionally, a broad ($w_{1/2} = 6249$ Hz)²⁷Al resonance for 1 at δ 15 ppm is also indicative of a five-coordinate geometry for the aluminum atom.

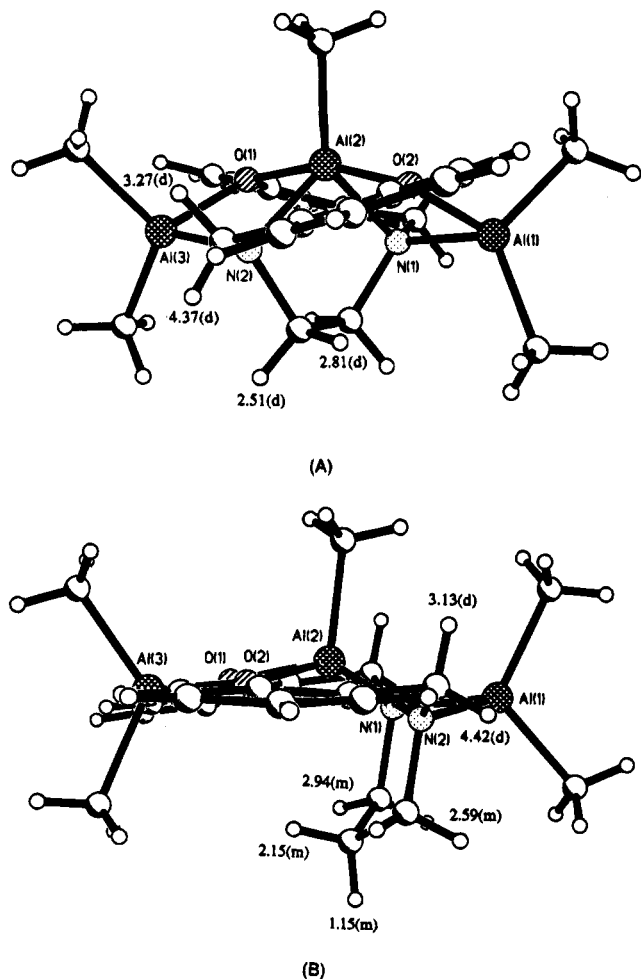
The reaction of 2 equiv of AlMe_3 with SalpanH_4 proceeds through elimination of 4 mol of CH_4 to form $[\text{SalpanAl}(\text{AlMe}_2)]_2$ (2; path b in (Scheme 1)). This formulation is supported by the mass spectral data and by the presence of ^1H NMR resonances for two AlMe_2 groups and two Al resonances in the ^{27}Al NMR at δ 75 ($w_{1/2} = 3645$ Hz) and 155 ($w_{1/2} = 3125$ Hz) ppm. In keeping with the literature precedent,⁷ the broader of the two peaks is assigned to the central aluminum atom,

which may be in a five-coordinate geometry as a result of the dimerization. In comparison to 1, the ^1H NMR data for the Salpan ligand in 2 are indicative of a more symmetrical solution-state structure. There are two resonances for the propylamine backbone at 2.14 and 2.80 ppm, which are integrated in a 2:4 ratio. Additionally, there is one PhCH_2 resonance at 3.85 ppm. Considering the ^1H NMR spectra of complexes 3–6 (vide infra), this may be interpreted as a tendency for the ligands in these complexes to adopt a more rigid geometry as each additional alkylaluminum moiety is added. We propose that the structure of 2 is a dimeric molecule containing bridging nitrogens (for the central Al atoms) and that the AlMe_2 groups bridge one oxygen from each ligand (Scheme 1b). With regards to the group 13 elements, it is important to note that this complex marks the first deviation of the chemistry of the SalanH_4 ligands from that of the SalenH_2 derivatives. For example, the composition of 2 contrasts with that found in the gallium derivative $\text{Salen}(\text{GaMe}_2)_2$, wherein the ligand acts as a bidentate chelate for the two GaMe_2 groups.⁴

(7) Delpuech, J. J. In *NMR of Newly Accessible Nuclei*; Laszlo, P., Ed.; Academic Press: New York, 1983; Vol. 2, p 153.

Table 1. Selected NMR Data (ppm) for Compounds 1–6

compd	¹ H, ppm				²⁷ Al, ppm (w _{1/2} , Hz)	
	PhCH ₂	NCH ₂	NCH ₂ CH ₂	AlCH ₃	Al (central)	AlMe ₂
SalpanH ₂ AlMe (1)	3.95	2.10, 2.95	0.90, 1.13	-0.79	15 (6249)	
[SalpanAl(AlMe ₂) ₂] ₂ (2)	3.85	2.80	2.14	-0.82	75 (3645)	155 (3125)
Salean(AlMe)(AlMe ₂) ₂ (3)	3.27, 4.37	2.51, 2.81		-0.66 to -0.28	55 (6770)	185 (9374)
Salpan(AlMe)(AlMe ₂) ₂ (4)	3.13, 4.42	2.59, 2.94	1.15, 2.15	-0.41 to -0.10	85 (3126)	185 (9374)
Salophan(AlMe)(AlMe ₂) ₂ (5)	3.89, 4.70			-1.22 to -0.11	66 (3645)	182 (16143)
Salomphan(AlMe)(AlMe ₂) ₂ (6)	4.00, 4.53			-1.25 to -0.10	60 (5208)	147 (2083)

Figure 2. Side views and selected ¹H NMR assignments for compounds 3 (A) and 4 (B).

When 3 equiv of AlMe₃ is added to each of the SalanH₄ ligands, followed by reflux in toluene, compounds 3–6 result (paths c and d in Scheme 1). Interestingly, in each case the ¹H NMR data revealed a complex pattern of coupling indicative of a rigid solution-state geometry for the complexes. A hallmark of this behavior is the presence of a doublet of doublets which can be assigned to the PhCH₂ groups (see Table 1). In this interpretation, each of the methylene groups are equivalent, while the protons within the methylene group are inequivalent as an AB spin system, giving rise to two doublets. The alkyl backbones of 3 and 4 also demonstrate a complex pattern of coupling (parts A and B of Figure 2, respectively). In 3 the N–CH₂ resonances result in two doublets of doublets centered at δ 2.51 and 2.81 ppm. In 4 the propyl resonances were manifested as multiplets at δ 1.15 and 2.15 ppm for the NCH₂CH₂ group and as multiplets at δ 2.59 and 2.94 ppm for the NCH₂CH₂ groups. Although such rigid solution-state geometries as observed for 3–6 are

Table 2. Crystal Data for Salean(AlMe)(AlMe₂)₂ (3), Salpan(AlMe)(AlMe₂)₂ (4), and Salophan(AlMe)(AlMe₂)₂ (5)

compd	3	4	5
formula	C ₂₁ H ₃₁ Al ₃ N ₂ O ₂	C ₄₄ H ₆₆ Al ₆ N ₄ O ₄	C ₃₉ H ₄₇ Al ₃ N ₂ O ₂
fw	424.4	876.9	656.7
cryst syst	triclinic	triclinic	monoclinic
space group	P1̄	P1̄	P2 ₁
a (Å)	7.946(3)	7.821(7)	10.881(7)
b (Å)	9.662(2)	17.890(15)	17.170(10)
c (Å)	15.804(4)	18.668(16)	11.288(7)
α (deg)	89.192(5)	89.10(4)	
β (deg)	84.434(6)	89.86(4)	113.275(12)
γ (deg)	79.926(4)	89.78(5)	
V (Å ³)	1189.0(7)	2612(4)	1937(2)
Z	2	2	2
D _{calc} (g/cm ³)	1.185	1.115	1.126
cryst size (mm)	0.6 × 0.6 × 0.6	0.4 × 0.2 × 0.2	0.4 × 0.4 × 0.8
radiation, K _α	Mo; 0.710 73	Mo; 0.710 73	Mo; 0.710 73
λ (Å)			
temp (K)	298	298	298
2θ range (deg)	2.0–45	2.0–45	2.0–45
scan type	2θ–θ	2θ–θ	2θ–θ
scan speed (deg/min)	1–60	1–60	1–60
scan range (deg)	0.55	0.55	0.55
no. of rflns collected	4464	4034	7272
no. of indep rflns	3265	3864	4913
no. of obsd rflns	2068	4313	2954
	(F > 4.0σ(F))	(F > 4.0σ(F))	(F > 4.0σ(F))
no. of params	253	523	401
R	0.0667	0.0690	0.0619
R _w	0.0651	0.0691	0.0642
GOF	0.89	2.28	3.11
largest diff peak (e/Å ³)	0.34	0.21	0.41

uncommon for the heavier main-group elements, a similar solution-state geometry was found for [Ph(CH₂O)₂]₂AlMe(AlMe₂)₂.⁸

The chief difference between compound 3 and compounds 4–6 lies in the disposition of the AlMe₂ groups. In 3, these groups give rise to two ¹H NMR resonances, indicating the symmetrical bridging of a nitrogen and oxygen atom by each aluminum. In 4–6, however, these groups are manifested as four distinct resonances. There are two for the AlMe₂ bridging the oxygens and two for the bridging group on the nitrogens. There are also two resonances in the ²⁷Al NMR spectrum of these compounds. One corresponds to the central five-coordinate Al which is assigned to the resonances in the range δ 60–85 ppm, and the other to the peripheral four-coordinate Al atoms, assigned to the resonances in the range δ 147–185 ppm. The formulations for compounds 3–5 were confirmed by X-ray crystallography.

An X-ray crystallographic study of 3–5 was undertaken in order to correlate the proposed solution-state structures with the solid state. A summary of crystallographic data for these molecules is given in Table 2. Selected bond distances and angles are given in Table

(8) Pasykiewicz, S.; Ziemkowska, W. *J. Organomet. Chem.* **1992**, *423*, 1.

Table 3. Bond Lengths (Å) and Angles (deg) for Compounds 3–5

atoms	3	4A	4B (not shown)	5
Bond Lengths				
Al(1)–Al(2)	2.870(2)	2.854(6)	2.839(6)	2.869(3)
Al(2)–Al(3)	2.868(2)	2.969(7)	2.963(7)	2.897(3)
Al(1)–N(1)	1.960(4)	2.001(14)	2.031(10)	1.970(5)
Al(1)–N(2)		2.022(12)	2.060(13)	1.994(4)
Al(2)–O(1)	1.982(3)	1.942(10)	1.911(9)	1.886(4)
Al(2)–O(2)	1.959(3)	1.931(8)	1.946(11)	1.891(3)
Al(2)–N(1)	1.931(3)	2.005(10)	1.956(12)	2.002(5)
Al(2)–N(2)	1.931(4)	2.002(15)	2.014(16)	1.983(5)
Al(3)–O(1)	1.849(4)	1.903(8)	1.886(11)	1.847(3)
Al(3)–O(2)		1.873(10)	1.902(8)	1.848(5)
Al(1)–O(2)	1.847(3)			
Al(3)–N(2)	1.947(4)			
Bond Angles				
N(1)–Al(1)–N(2)		80.1(5)	78.3(5)	73.7(2)
O(1)–Al(2)–O(2)	163.0(1)	76.7(4)	77.3(4)	77.3(2)
O(1)–Al(2)–N(1)	87.9(1)	90.8(5)	90.3(4)	89.2(2)
O(1)–Al(2)–N(2)	80.1(1)	142.4(6)	141.5(5)	135.4(2)
O(2)–Al(2)–N(1)	80.5(1)	146.0(5)	144.8(5)	137.9(1)
O(2)–Al(2)–N(2)	88.7(1)	90.4(5)	88.4(4)	88.9(2)
N(1)–Al(2)–N(2)	95.7(2)	80.5(5)	81.1(4)	73.3(2)
O(1)–Al(3)–O(2)		79.0(4)	78.9(4)	79.3(2)
Al(2)–O(1)–Al(3)	96.9(2)	101.1(4)	102.6(5)	101.8(2)
Al(2)–O(2)–Al(3)		102.6(4)	100.7(4)	101.6(2)
Al(1)–N(1)–Al(2)	95.0(2)	90.9(5)	90.8(5)	92.5(2)
Al(1)–N(2)–Al(2)	95.4(3)	90.3(6)	88.3(5)	92.3(2)
N(1)–Al(1)–O(2)	82.6(1)			
Al(1)–O(2)–Al(2)	97.8(2)			
N(2)–Al(3)–O(1)	83.0(2)			

Table 4. Atomic Coordinates ($\times 10^5$) and Equivalent Isotropic Displacement Coefficients ($\text{Å}^2 \times 10^4$) for 3

atom	<i>x</i>	<i>y</i>	<i>z</i>	<i>U</i> (eq)
Al(1)	72 855(19)	19 965(15)	60 833(9)	682(5)
Al(2)	45 064(16)	32 671(13)	72 738(8)	567(5)
Al(3)	38 821(19)	33 202(14)	90 919(9)	669(5)
N(1)	58 451(44)	14 165(35)	70 554(22)	591(13)
N(2)	56 793(43)	6 751(34)	82 303(20)	547(12)
O(1)	31 576(37)	24 276(31)	82 019(20)	675(12)
O(2)	64 052(37)	37 696(30)	65 155(17)	620(11)
C(1)	26 389(62)	11 262(53)	81 910(33)	711(20)
C(2)	13 374(66)	8 790(61)	87 836(37)	873(24)
C(3)	7 871(87)	–4 052(81)	87 954(49)	1 116(34)
C(4)	15 523(102)	–14 280(77)	82 124(54)	1 198(39)
C(5)	28 477(82)	–11 724(57)	76 458(41)	948(27)
C(6)	34 516(65)	1 068(50)	76 010(35)	726(20)
C(7)	48 260(65)	2 936(49)	69 125(32)	753(20)
C(8)	67 610(56)	11 511(44)	78 393(28)	624(17)
C(9)	72 064(53)	25 170(44)	81 743(27)	594(16)
C(10)	62 240(62)	50 686(46)	82 255(28)	675(18)
C(11)	71 118(52)	55 357(43)	74 108(28)	577(16)
C(12)	79 291(58)	66 997(47)	74 516(32)	695(18)
C(13)	87 073(63)	72 534(53)	67 539(37)	796(22)
C(14)	87 270(65)	66 466(55)	59 721(37)	816(22)
C(15)	79 391(61)	54 855(51)	59 023(30)	706(19)
C(16)	71 603(52)	49 363(44)	66 094(27)	563(16)
C(17)	97 443(61)	14 206(57)	61 608(33)	846(22)
C(18)	63 814(80)	17 776(62)	50 032(32)	1 014(27)
C(19)	26 446(63)	44 041(55)	67 577(36)	894(23)
C(20)	45 699(75)	20 323(52)	100 034(31)	869(23)
C(21)	22 740(72)	50 549(56)	93 649(40)	1 048(26)

3, and positional parameters are given in Tables 4–6. Molecular structures and atom-numbering schemes are shown in Figures 3–5. In the structure of **3**, the Salean ligand is coordinated in a tetradentate fashion to a central AlMe unit which is in a distorted-trigonal-bipyramidal geometry. In this geometry, the oxygen atoms are located at the axial positions and the nitrogens and methyl carbon in equatorial positions. All of the bond angles are distorted from ideal. However, the most significant deviations occur for the N–Al–C

Table 5. Atomic Coordinates ($\times 10^5$) and Equivalent Isotropic Displacement Coefficients ($\text{Å}^2 \times 10^4$) for 4

atom	<i>x</i>	<i>y</i>	<i>z</i>	<i>U</i> (eq)
Al(1)	33 623(58)	126 662(29)	36 594(18)	585(20)
Al(2)	15 758(59)	134 496(29)	25 460(17)	574(20)
Al(3)	7 435(62)	146 660(30)	15 027(18)	669(21)
O(1)	3 284(111)	143 887(51)	24 758(34)	634(40)
O(2)	21 420(107)	138 182(51)	15 973(34)	600(39)
N(1)	18 911(155)	135 828(73)	36 018(49)	468(51)
N(2)	39 359(184)	130 261(84)	26 556(60)	650(62)
C(1)	53 155(186)	127 346(96)	43 605(66)	1 078(87)
C(2)	21 662(187)	116 801(90)	36 978(65)	834(78)
C(3)	–1 399(195)	126 515(97)	23 696(70)	792(78)
C(4)	21 459(227)	155 929(90)	14 016(72)	1 048(94)
C(5)	–13 295(202)	144 969(107)	9 073(68)	1 197(94)
C(6)	2 555(168)	137 436(85)	39 835(55)	614(64)
C(7)	–6 697(168)	144 590(88)	37 453(55)	515(60)
C(8)	–15 314(168)	148 924(84)	42 375(60)	547(60)
C(9)	–23 734(186)	155 641(94)	40 563(69)	762(75)
C(10)	–22 506(189)	158 649(92)	33 547(65)	824(74)
C(11)	–13 778(174)	154 496(87)	28 484(62)	663(67)
C(12)	–5 391(165)	147 868(83)	30 180(59)	412(57)
C(13)	32 997(187)	134 986(92)	10 935(57)	735(70)
C(14)	33 414(191)	137 943(87)	3 897(60)	721(69)
C(15)	44 421(190)	134 818(97)	–1 304(66)	789(77)
C(16)	55 516(219)	129 103(106)	673(70)	1 075(95)
C(17)	55 430(192)	126 101(98)	7 793(64)	884(77)
C(18)	44 488(179)	129 189(83)	13 150(57)	639(65)
C(19)	44 595(189)	125 257(90)	20 761(57)	757(71)
C(20)	51 976(244)	136 438(119)	27 519(78)	1 139(113)
C(21)	44 289(199)	143 997(103)	30 629(61)	923(86)
C(22)	32 104(233)	142 340(109)	37 185(62)	690(77)
Al(4)	16 463(60)	76 770(30)	36 601(18)	683(23)
Al(5)	34 052(57)	84 512(29)	25 443(17)	532(21)
Al(6)	42 660(66)	96 561(31)	14 993(18)	676(22)
O(3)	28 633(124)	88 053(55)	16 004(41)	530(42)
O(4)	46 645(113)	93 854(55)	24 744(39)	472(40)
N(3)	10 827(141)	80 646(71)	26 597(47)	596(54)
N(4)	30 937(137)	86 357(68)	35 981(45)	476(49)
C(23)	–3 163(201)	77 147(90)	43 714(62)	925(80)
C(24)	27 902(210)	66 775(81)	37 029(69)	876(78)
C(25)	51 259(179)	76 397(90)	23 463(64)	784(78)
C(26)	28 638(216)	10 564(91)	13 999(69)	1 137(93)
C(27)	63 477(220)	95 077(109)	9 099(70)	1 301(106)
C(28)	5 458(197)	75 131(85)	20 674(57)	665(69)
C(29)	6 210(207)	79 170(109)	13 003(71)	525(70)
C(30)	–5 126(197)	76 186(82)	7 713(71)	667(72)
C(31)	–5 532(263)	79 049(121)	652(90)	903(109)
C(32)	5 324(229)	84 665(118)	–1 170(82)	740(92)
C(33)	16 885(202)	88 056(91)	3 852(63)	785(74)
C(34)	17 124(254)	85 038(110)	11 053(72)	651(83)
C(35)	55 403(247)	97 602(138)	30 014(68)	735(91)
C(36)	63 496(262)	10 461(115)	28 295(81)	685(84)
C(37)	72 735(190)	10 8703(87)	33 375(81)	639(72)
C(38)	73 820(281)	10 5965(125)	40 731(92)	847(100)
C(39)	65 866(292)	99 248(128)	42 381(78)	827(96)
C(40)	56 120(209)	94 942(109)	37 388(77)	597(78)
C(41)	47 438(219)	87 652(104)	39 784(60)	595(72)
C(42)	17 576(189)	92 512(97)	37 227(58)	822(81)
C(43)	5 718(173)	93 694(84)	30 530(66)	472(64)
C(44)	–2 394(197)	87 032(88)	27 458(64)	652(74)

angles. This may be explained by the fact that the ligand is distorting toward a square-pyramidal geometry wherein the oxygen and nitrogens form the basal plane. Through one oxygen and one nitrogen atom the ligand also acts as a bidentate chelate for the two peripheral AlMe₂ groups, which adopt distorted-tetrahedral geometries. The ethylene group of the ligand and the central Al–Me are oriented trans to one another to reduce steric interactions. In keeping with the electronegativity difference between oxygen and nitrogen, the Al–O bond distances for these atoms are somewhat shorter than the Al–N distances. However, for Al(2) the opposite trend is observed. The oxygen atoms are occupying the

Table 6. Atomic Coordinates ($\times 10^5$) and Equivalent Isotropic Displacement Coefficients ($\text{\AA}^2 \times 10^4$) for 5

atom	x	y	z	U(eq)
Al(1)	9 979(18)	73 080(3635)	29 743(16)	932(8)
Al(2)	16 345(14)	65 197(3635)	10 480(13)	673(6)
Al(3)	15 566(15)	64 146(3635)	-15 424(14)	766(7)
O(1)	25 911(30)	68 289(3635)	515(30)	711(14)
O(2)	5 701(31)	61 248(3635)	-6 057(30)	734(15)
N(1)	20 437(39)	75 531(3635)	19 411(36)	674(18)
N(2)	-236(37)	68 687(3635)	12 228(37)	727(19)
C(1)	36 470(47)	73 546(3635)	3 301(49)	733(24)
C(2)	42 870(55)	73 801(3635)	-5 043(56)	924(28)
C(3)	53 330(72)	78 834(3635)	-2 797(90)	1 209(42)
C(4)	57 673(65)	83 178(3635)	7 761(90)	1 233(42)
C(5)	51 083(61)	83 236(3635)	15 864(68)	1 050(33)
C(6)	40 422(50)	78 395(3635)	14 095(49)	736(23)
C(7)	34 079(48)	78 538(3635)	23 891(50)	836(26)
C(8)	340(50)	79 871(3635)	9 161(46)	655(23)
C(9)	11 336(54)	86 911(3635)	3 897(52)	791(26)
C(10)	-235(68)	89 830(3635)	-5 779(58)	914(30)
C(11)	-12 202(62)	85 713(3635)	-10 280(60)	919(30)
C(12)	-12 941(56)	78 758(3635)	-4 764(59)	842(29)
C(13)	-1 832(53)	75 806(3635)	4 983(50)	677(23)
C(14)	-12 011(51)	63 443(3635)	8 090(52)	856(27)
C(15)	-16 021(57)	59 910(3635)	-5 114(52)	797(26)
C(16)	-29 305(58)	57 620(3635)	-11 575(65)	929(31)
C(17)	-33 688(72)	54 137(3635)	-23 108(82)	1 184(41)
C(18)	-25 332(83)	52 807(3635)	-29 308(71)	1 171(37)
C(19)	-12 093(62)	55 243(3635)	-23 184(56)	932(29)
C(20)	-7 653(55)	58 842(3635)	-11 402(47)	733(25)
C(21)	18 158(66)	65 456(3635)	43 393(53)	1 301(36)
C(22)	1 458(74)	82 128(3635)	33 428(65)	1 394(44)
C(23)	25 792(51)	56 401(3635)	20 603(52)	918(27)
C(24)	24 502(66)	55 292(3635)	-19 513(63)	1 231(38)
C(25)	6 617(55)	72 162(3635)	-27 710(51)	990(29)

axial positions of the trigonal bipyramid and experience a stronger steric repulsion than the equatorially located nitrogens.

In the structure of **4**, there are two identical molecules in the independent unit and no solvent of crystallization. The metrical parameters for these two molecules are the same to within experimental error, and only one representative molecule is depicted in Figure 4. As demonstrated for Salean, the Salpan ligand acts in both a chelating (Al(2)) and bridging (Al(1) and Al(3)) capacity, giving rise to square-pyramidal and tetrahedral geometries, respectively. Additionally, the alkyl or aryl group of the ligand "backbone" is oriented trans to the central Al-Me group. A similar bonding arrangement is observed for the isostructural Salophan compound (**5**). Interestingly, the arrangement of the AlMe₂ groups in **4** and **5** contrasts with that seen for **3** in which each AlMe₂ unit bridges both an oxygen and a nitrogen atom. The reason for this difference can be understood when the structure of SaleanH₂Sn is considered (Figure 6).⁹ In this structure the Sn atom adopts a square-pyramidal geometry in which the ligand is approximately planar with both oxygen and nitrogen atoms located on the same side of the N₂O₂ plane. The distance between the nitrogens in this structure is 2.886 Å. The same value for **3** is 2.863 Å. By comparison, these distances in **4** and **5** are 2.588 and 2.378 Å, respectively. Thus, if this type of cis structure is considered for the Salean ligand in **3**, then the AlMe₂ bridging group would have to adopt a significantly widened N-Al-N bond angle due to the wide N-N spread. To avoid this, the molecule adopts a trans orientation for the nitrogen and oxygen atoms leading to bond angles around the bridging aluminum

atoms that are comparable to those seen in **4** and **5**. Thus, the structure observed for **3** is dictated by the steric requirements of the ethylamine backbone.

Some structures similar to those seen for **3-5** have been observed for the bidentate alkylamine complexes HAl[(EtN(CH₂)₂NEt)AlH₂]₂¹⁰ and MeAl[(HN(CH₂)₂NH)-AlMe₂]₂.¹¹ It is interesting to note that in the tridentate open-chain amine complexes [(MeAl)₂C₈H₂₀N₆](AlMe₂)₂¹² and [(MeAl)₂C₁₂H₂₈N₆](AlMe₂)₂¹³ the central five-coordinate Al atoms also adopt trigonal-bipyramidal geometries.

Conclusion. We have demonstrated that there is an interesting range of complexes that are accessible in reactions involving AlMe₃ and the SalanH₄ class of ligands. For instance, the trimetallic derivatives of general formula SalanAlMe(AlMe₂)₂ offer evidence for solution-state rigidity. Additionally, the solution-state geometry of these molecules was shown by X-ray crystallography to be the same as that of the solid state. Future research will focus on the use of other SalanH₄ ligands in the synthesis of novel group 13 compounds.

Experimental Section

General Considerations. All manipulations were conducted using Schlenk techniques in conjunction with an inert-atmosphere glovebox. All solvents were rigorously dried prior to use. The Schiff bases SalenH₂, SalphenH₂, SalophenH₂, and SalomphenH₂ were synthesized according to literature techniques.² NMR data were obtained on JEOL-GSX-400 and -270 instruments at 270.17 (¹H), 67.94 (¹³C), and 104.17 (²⁷Al) MHz. Chemical shifts are reported relative to Si(CH₃)₄ (for C and H) and Al(H₂O)₆ (for Al) and are in ppm. All data were taken at 295 K unless otherwise noted. Elemental analyses were obtained on a Perkin-Elmer 2400 analyzer. Mass spectral data were obtained on a Hewlett-Packard 5988 spectrometer using electron impact ionization (70 eV) with a direct ionization probe (DIP). Infrared data were recorded as KBr pellets on a Matheson Instruments 2020 Galaxy Series spectrometer and are reported in cm⁻¹.

Synthesis of SalpanH₂AlMe (1). Trimethylaluminum (0.122 g, 1.70 mmol) in 20 mL of toluene was added to a rapidly stirred solution of SalpanH₄ (0.488 g, 1.70 mmol) in toluene (20 mL) at 25 °C. The vigorous exothermic reaction subsided after a few seconds to give a colorless solution which was stirred for 2 h. The volatiles were removed under reduced pressure to give 0.483 g (87%) of a white solid, mp 238 °C dec. ¹H NMR (C₆D₆): δ -0.79 (3H, s, AlCH₃), 0.90 (1H, m, CH₂CH₂), 1.13 (1H, m, CH₂CH₂), 2.10 (2H, br s, NCH₂), 2.95 (2H, br s, NCH₂), 3.95 (4H, br s, PhCH₂), 6.60-7.35 (8H, m, Ph H). ¹³C NMR (C₆D₆): δ = -11.3 (AlCH₃), 25.8 (CH₂CH₂), 46.0 (NCH₂), 50.5 (PhCH₂), 117.4, 119.9, 120.0, 123.5, 130.1, 160.1 (Ph). ²⁷-Al NMR (C₆D₆): δ 15 (w_{1/2} = 6249 Hz). IR: 3253 m, 2920 m, 1602 s, 1573 m, 1487 s, 1298 s, 1037 m, 893 s, 757 s, 668 s, 686 s. MS: m/e 326 (M⁺), 311 (M⁺ - Me), 267 (M⁺ - Me - Pr). Anal. Calcd: C, 66.26; H, 7.06. Found: C, 66.53; H, 6.67.

Synthesis of [SalpanAl(AlMe₂)₂] (2). The procedure was similar to that described for **1**, except 2 equiv of trimethylaluminum (0.252 g, 3.50 mmol) was used (SalpanH₄; 0.500 g, 1.75 mmol). After removal of volatiles, 0.563 g of an off-white solid remained: yield 88%; mp 265 °C dec. ¹H NMR (THF-d₈): δ -0.82 (6H, s, AlCH₃), 2.14 (2H, m, NCH₂CH₂), 2.80 (4H,

(10) Perego, G.; Del Piero, G.; Corbellini, M.; Bruzzone, M. *J. Organomet. Chem.* **1977**, *136*, 301.

(11) Zhiping, J.; Interrante, L. V.; Kwon, D.; Tham, F. S.; Kullnig, R. *Inorg. Chem.* **1991**, *30*, 995.

(12) Robinson, G. H.; Sangokoya, S. A. *J. Am. Chem. Soc.* **1987**, *109*, 6852.

(13) Robinson, G. H.; Moise, F.; Pennington, W. T.; Sangokoya, S. A. *Polyhedron* **1989**, *8*, 1279.

(9) Atwood, D. A.; Jegier, J. A.; Martin, K. J.; Rutherford, D. J. *J. Organomet. Chem.*, submitted for publication.

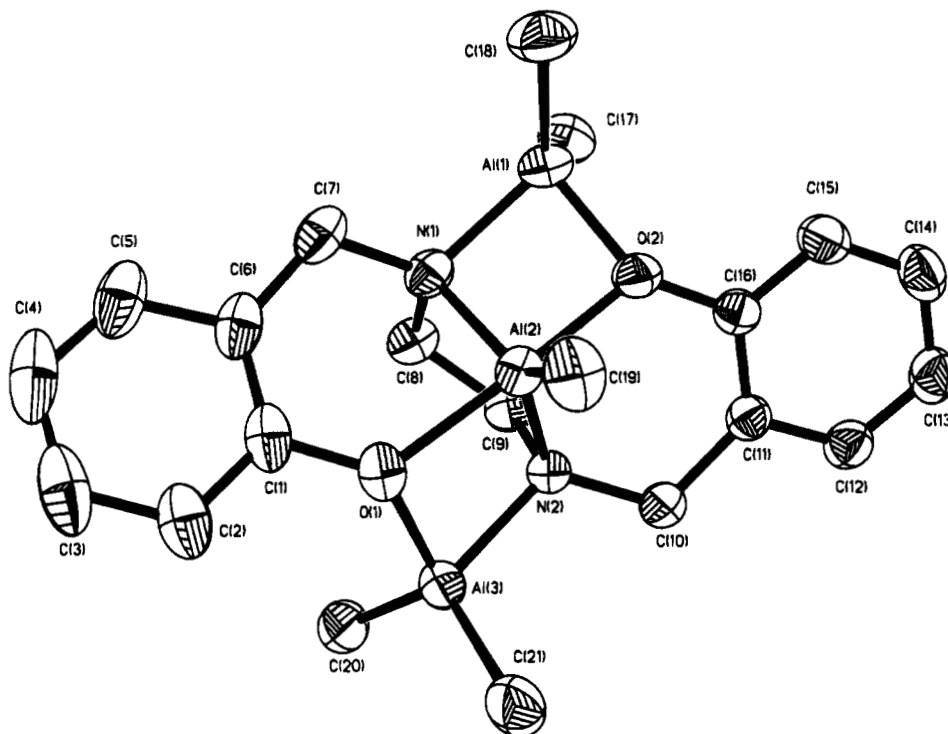


Figure 3. Molecular structure and atom-numbering scheme for **3**.

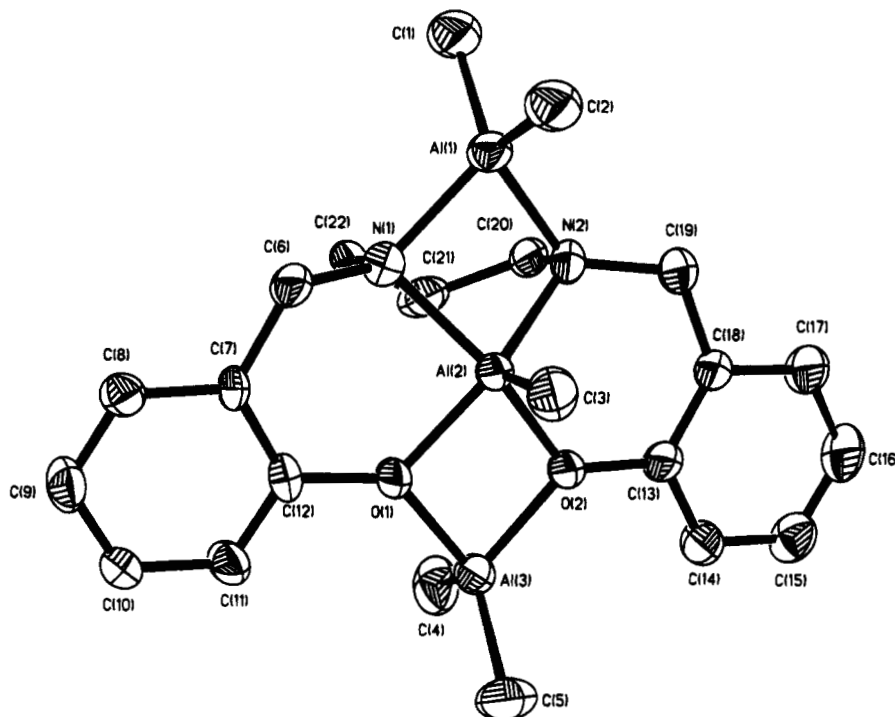


Figure 4. Molecular structure and atom-numbering scheme for **4**.

m, NCH_2), 3.85 (4H, *m*, PhCH_2), 6.45–7.25 (8H, *m*, PhH). ^{13}C NMR ($\text{THF-}d_6$): δ -11.0 (AlCH_3), 24.7 (CH_2CH_2), 47.0 (NCH_2), 50.6 (PhCH_2), 116.8 (Ph), 120.0 (Ph), 126.0 (Ph), 128.9 (Ph), 129.7 (Ph), 162.0 (Ph). ^{27}Al NMR (C_6D_6): δ 75 ($w_{1/2} = 3645$ Hz), 155 ($w_{1/2} = 3125$ Hz). IR: 2928 *m*, 1602 *s*, 1574 *w*, 1488 *s*, 1298 *s* (br), 759 *s*, 688 *m* (br). MS: *m/e* 732 (M^+), 367 (monomer), 351 (monomer - Me), 309 (SalpanAl^+), 307 ($\text{SalpanAl} - 2\text{H}^+$), 190 ($[\text{PhO}(\text{AlMe})\text{CH}_2\text{N}(\text{CH}_2)_2]^+$), 176 ($[\text{PhO}(\text{AlMe})\text{CH}_2\text{NCH}_2]^+$), 162 ($[\text{PhO}(\text{AlMe})\text{CH}_2\text{N}^+]$). Anal. Calcd: C, 62.29; H, 6.60. Found: C, 62.36; H, 6.67.

Synthesis of Salean(AlMe)(AlMe)₂ (3). Trimethylaluminum (0.394 g, 5.47 mmol) was added to a rapidly stirred

solution of SaleanH₄ (0.495 g, 1.82 mmol) in 50 mL of toluene at 25 °C. The exothermic reaction mixture was stirred until the evolution of gas ceased (15 min); then it was refluxed for 5 h. After filtration and concentration, colorless crystals were grown at -30 °C (0.679 g, 88%): mp 165 °C dec. ^1H NMR (C_6D_6): δ -0.66 (*s*, 6H, AlCH_3), -0.35 (*s*, 3H, AlCH_3), -0.28 (*s*, 6H, AlCH_3), 2.51 (*d*, $J = 8$ Hz, 2H, NCH_2), 2.81 (*d*, $J = 8$ Hz, 2H, NCH_2), 3.27 (*d*, $J = 17$ Hz, 2H, PhCH_2), 4.37 (*d*, $J = 17$ Hz, 2H, PhCH_2), 6.63 (*d*, $J = 9$ Hz, 2H, PhH), 6.66 (*d*, $J = 9$ Hz, 2H, PhH), 6.76 (*m*, 2H, PhH), 6.92 (*m*, 2H, PhH). ^{13}C NMR (C_6D_6): δ -13.9, (AlCH_3), -9.6 (AlCH_3), 47.6 (NCH_2), 50.8 (PhCH_2), 121.1, 122.3, 123.4, 128.5, 129.7, 151.2 (Ph).²⁷

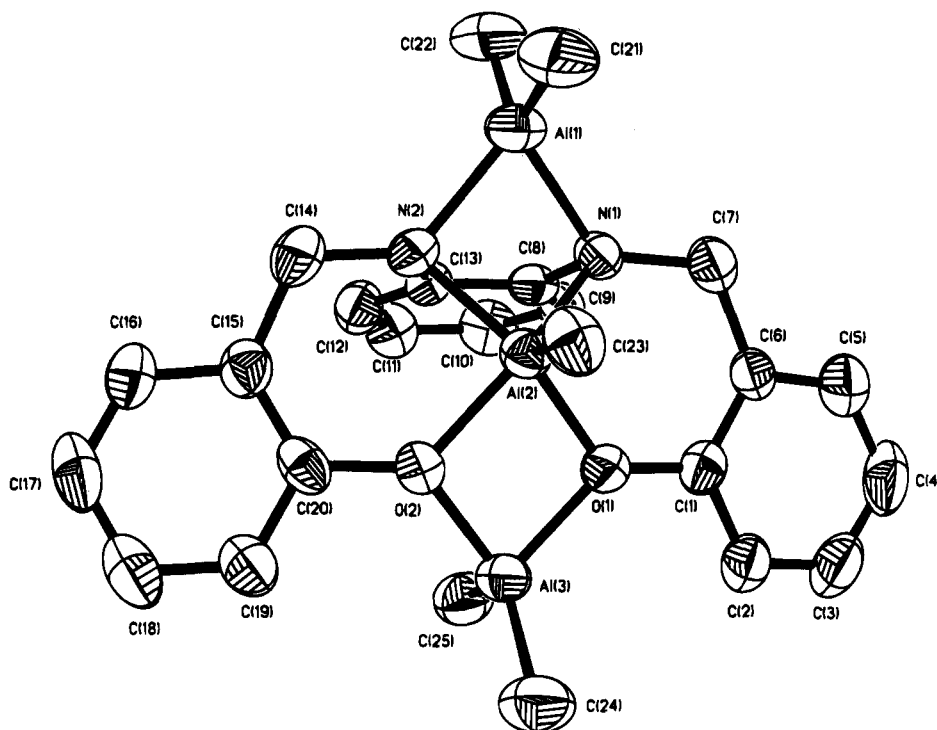


Figure 5. Molecular structure and atom-numbering scheme for **5**.

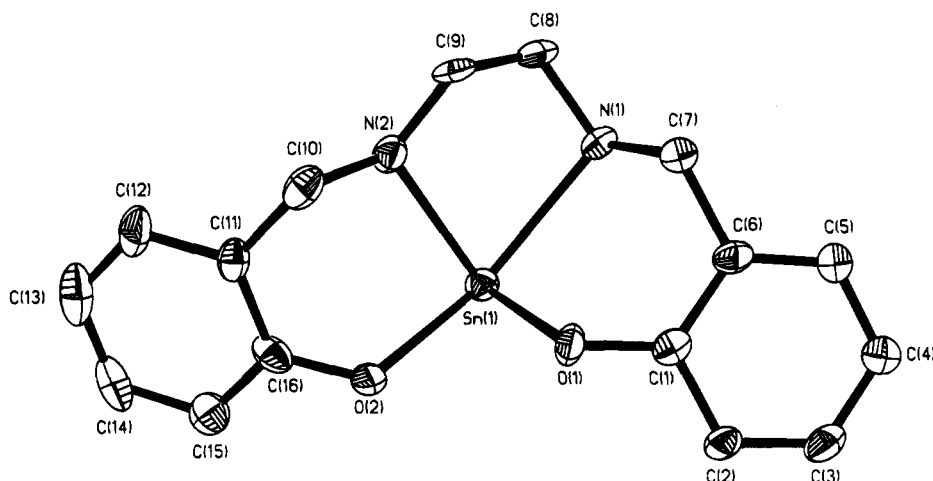


Figure 6. Molecular structure and atom-numbering scheme for SalpanH₂Sn.

Al NMR (C₆D₆): δ 55 ($w_{1/2}$ = 6770 Hz), 185 ($w_{1/2}$ = 9374 Hz). IR: 2932 s, 2888 m, 1604 m, 1581 s, 1491 vs, 1452 vs, 1268 vs, 1239 vs, 1200 vs, 1079 vs, 885 vs, 759 vs, 703 vs, 639 vs, 591 s. MS: m/e 424 (M⁺), 409 (M⁺ - Me), 351 (M⁺ - Me - AlMe₂ - H), 293 (M⁺ - Me - 2AlMe₂ - 2H), 176 ((PhO)CH₂N-(AlMe)CH₂⁺), 162 ((PhO)CH₂N(AlMe)⁺), 57 (AlMe₂⁺). Anal. Calcd: C, 59.43; H, 7.36. Found: C, 59.26; H, 7.29.

Salpan(AlMe)(AlMe₂)₂ (4). Trimethylaluminum (0.440 g, 6.11 mmol) was added to a rapidly stirred solution of SalpanH₄ (0.500 g, 1.75 mmol) in 50 mL of toluene at 25 °C. The exothermic reaction mixture was stirred until the evolution of gas ceased (15 min); then it was refluxed for 5 h. After filtration and concentration, colorless crystals were grown at -30 °C (0.637 g, 83%): mp 211–213 °C. ¹H NMR (C₆D₆): δ -0.41 (s, 3H, AlCH₃), -0.39 (s, 3H, AlCH₃), -0.31 (s, 3H, AlCH₃), -0.25 (s, 3H, AlCH₃), -0.10 (s, 3H, AlCH₃), 1.15 (m, 1H, CH₂CH₂), 2.15 (m, 1H, CH₂CH₂), 2.59 (m, 2H, NCH₂), 2.94 (m, 2H, NCH₂), 3.13 (d, J = 16 Hz, 2H, PhCH₂), 4.42 (d, J = 16 Hz, 2H, PhCH₂), 6.66–6.93 (m, 8H, Ph H). ¹³C NMR (C₆D₆): δ -9.99 (AlCH₃), -6.25 (AlCH₃), 24.5 (CH₂CH₂), 47.5 (NCH₂), 52.6 (PhCH₂), 118.7, 122.0, 124.7, 128.2, 131.2, 152.7 (Ph). ²⁷Al NMR (C₆D₆): δ 85 ($w_{1/2}$ = 3126), 185 ($w_{1/2}$ = 9374).

IR: 2942 s, 1603 m, 1580 m, 1491 s, 1200 s, 1036 s, 80 s, 754 vs, 696 vs, 644 vs. MS: m/e 423 (M⁺ - Me), 365 ([M⁺ - Me - AlMe₂ - H]), 307 ([M⁺ - Me - 2AlMe₂ - 2H]), 190 ([PhO-(AlMe)CH₂N(CH₂)₂⁺]), 176 ([PhO(AlMe)CH₂NCH₂⁺]), 162 ([PhO-(AlMe)CH₂N⁺]), 57 (AlMe₂⁺). Anal. Calcd for C₂₂H₃₃N₂O₂Al₃: C, 60.25; H, 7.60. Found: C, 60.11; H, 7.37.

Salophan(AlMe)(AlMe₂)₂ (5). Trimethylaluminum (0.350 g, 4.86 mmol) was added neat to a rapidly stirred solution of SalophanH₄ (0.500 g, 1.56 mmol) in 50 mL of toluene at 25 °C. The exothermic reaction mixture was stirred until the evolution of gas ceased (15 min); then it was refluxed for 5 h. After filtration and concentration, colorless crystals were grown at -30 °C (0.633 g, 86%): mp 185 °C dec. ¹H NMR (C₆D₆): δ -1.22 (s, 3H, AlCH₃), -0.96 (s, 3H, AlCH₃), -0.22 (s, 3H, AlCH₃), -0.19 (s, 3H, AlCH₃), -0.11 (s, 3H, AlCH₃), 3.89 (d, J = 17 Hz, 2H, PhCH₂), 4.70 (d, J = 17 Hz, 2H, PhCH₂), 6.35–7.12 (m, 12H, Ph H). ¹³C NMR (C₆D₆): δ -7.8, -8.9, -10.2, -13.5, -14.3 (AlCH₃), 45.9 (PhCH₂), 114.0, 119.0, 122.7, 122.8, 123.2, 128.1, 128.2, 128.5, 129.2, 129.7, 138.7, 151.3 (Ph). ²⁷Al NMR (C₆D₆): δ 66 ($w_{1/2}$ = 3645 Hz), 182 ($w_{1/2}$ = 16 143 Hz). IR: 2935 m, 1605 m, 1585 s, 1495 vs, 1450 vs, 1223 vs, 1113 s, 1030 s, 879 vs, 765 vs, 698 vs, 663 vs, 445 m.

MS: m/e 472 (M^+), 457 ($M^+ - \text{Me}$), 400 ($M^+ - \text{Me} - \text{AlMe}_2$), 341 ($M^+ - \text{Me} - 2\text{AlMe}_2 - 2\text{H}$), 237 ($[(\text{PhO})\text{CH}_2\text{NPhNAl}^+]$), 57 ($[\text{AlMe}_2^+]$). Anal. Calcd: C, 63.55; H, 6.61. Found: C, 63.68; H, 6.32.

Salomphan(AlMe)(AlMe₂)₂ (6). Trimethylaluminum (0.331 g, 4.60 mmol) was added neat to a rapidly stirred solution of SalomphanH₄ (0.500 g, 1.44 mmol) in 50 mL of toluene at 25 °C. The exothermic reaction mixture was stirred until the evolution of gas ceased (15 min); then it was refluxed for 5 h. After filtration and concentration, pale green crystals were isolated after cooling to -30 °C (0.649 g, 90%): mp 148 °C dec. ¹H NMR (C₆D₆): δ -1.25 (s, 3H, AlCH₃), -0.88 (s, 3H, AlCH₃), -0.22 (s, 3H, AlCH₃), -0.17 (s, 3H, AlCH₃), -0.10 (s, 3H, AlCH₃), 1.71 (s, 6H, PhCH₃), 4.00 (d, $J = 18$ Hz, 2H, PhCH₂), 4.53 (d, $J = 18$ Hz, 2H, PhCH₂), 6.31 (s, 2H, Ph H), 6.80-7.12 (m, 8H, Ph H). ¹³C NMR (C₆D₆): δ -14.4, -13.8, -8.7, -7.5, -7.1 (AlCH₃), 19.5 (PhCH₃), 45.9 (PhCH₂), 115.5, 119.0, 122.8, 128.5, 129.2, 129.6, 130.1, 136.2, 151.3 (Ph). ²⁷Al NMR (C₆D₆): δ 60 ($w_{1/2} = 5208$ Hz), 147 ($w_{1/2} = 2083$ Hz). IR: 2935 m, 1605 m, 1585 s, 1495 vs, 1450 vs, 1223 vs, 1113 s, 1030 s, 879 vs, 765 vs, 698 vs, 663 vs, 445 m. MS: m/e 500 (M^+), 485 ($M^+ - \text{Me}$), 428 ($M^+ - \text{Me} - \text{AlMe}_2$), 369 ($M^+ - \text{Me} - 2\text{AlMe}_2 - 2\text{H}$), 57 (AlMe₂⁺). Anal. Calcd: C, 64.53; H, 7.42. Found: C, 64.65; H, 7.11.

X-ray Experiment. Details of the crystal data and a summary of data collection parameters for **3-5** are given in

Table 2. Data were collected on a Siemens P4 diffractometer using graphite-monochromated Mo K α radiation. The check reflections, measured every 100 reflections, indicated a less than 5% decrease in intensity over the course of data collection; hence, no correction was applied. All calculations were performed on a personal computer using the Siemens software package SHELXTL-Plus. The structures were solved by direct methods and successive interpretation of difference Fourier maps, followed by least-squares refinement. All non-hydrogen atoms were refined anisotropically. The hydrogen atoms were included in the refinement in calculated positions using fixed isotropic parameters.

Acknowledgment. Gratitude is expressed to the National Science Foundation NSF-EPSCoR program (Grant RII-861075) and the NDSU Grant-in-Aid program for generous financial support.

Supplementary Material Available: Tables giving structure determination summaries, bond lengths and angles, positional parameters, and anisotropic thermal parameters and figures giving unit cell views for **3-5** and a figure showing the shortest intermolecular contacts for **4** (41 pages). Ordering information is given on any current masthead page.

OM9408526

Organic Syntheses via Transition Metal Complexes. 77.¹ 2-Butene-1,4-diones by Photoinduced Acyl Migration of {[2-(Acyloxy)ethenyl]carbene}chromium Complexes

Rudolf Aumann* and Beate Jasper

Organisch-Chemisches Institut der Universität Münster, Orleans-Ring 23,
D-48149 Münster, Germany

Received November 2, 1994²

Photolysis of [(Z)-2-(acyloxy)ethenyl]carbene complexes (CO)₅Cr=C(OEt)CH=C(OCOR¹)R [(Z)-3] (R = C₆H₅, *t*-Bu, *c*-Pr; R¹ = C₆H₅, *c*-Pr, *c*-C₇H₇CH₂, *t*-Bu, Me₂C=CH) with UV light of >300 nm affords 2-butene-1,4-diones R¹COC(OEt)=CHCOR [(E)-6] (60–68%), by a novel metal-mediated acyl migration. Compounds (Z)-6 and furans 7 are formed as minor products.

Methodologies based on reactions of Fischer carbene complexes have become major tools in organic synthesis. Both thermal and photochemical reactivity of such compounds has been utilized. The thermal reactions are exemplified by the cyclization of carbene complexes with alkynes² or isocyanides,³ by cyclopropanation,⁴ by electrophilic substitution and aldol-type condensation of alkylcarbene ligands,⁵ by nucleophilic additions to α,β unsaturated carbene ligands,^{2f} and by metathesis reactions.⁶ Light-induced reactions involve the generation of chromium (alkoxy or amino) ketene complexes,⁷ by

which route β -lactams,⁸ cyclobutanones,⁹ α -amino acids,^{7,10} and aromatic compounds¹¹ have been obtained.

We report on a novel photoreaction of Fischer carbene complexes, by which [(Z)-2-(acyloxy)ethenyl]carbene complexes (Z)-3 of chromium are transformed into 2-butene-1,4-diones (E)-6 and chromium hexacarbonyl. This transformation appears to be attractive in view of the applicability of 1,4-dicarbonyl compounds as precursors to the synthesis of five-membered heterocycles¹² and also in view of the ready availability of [(Z)-2-(acyloxy)ethenyl]carbene complexes, (Z)-3, as starting materials.¹³

The migration of acyl groups as such is a well-known process. Rearrangements of phenyl esters to mixtures of acylphenols were described as early as 1908 by Fries.¹⁴ A considerable number of reports have appeared since this time in connection with mechanistic and synthetic aspects.¹⁵ The Fries reaction is catalyzed by acid, but 1,3 oxygen-to-carbon (and also nitrogen-to-carbon) acyl migration characteristics of the Fries rearrangement can also be achieved without acid catalysis through metalation (anionic Fries rearrange-

* Abstract published in *Advance ACS Abstracts*, February 1, 1995.

(1) Part 76: Aumann, R.; Kössmeier, M.; Roths, K.; Fröhlich, R. *Synlett* **1994**, 1041–1044.

(2) For reviews see: (a) Dötz, K. H. *New J. Chem.* **1990**, *14*, 433. (b) Wulff, W. D. *Adv. Met. Org. Chem.* **1989**, *1*, 209–393. (c) Dötz, K. H. *Angew. Chem.* **1984**, *96*, 573–594; *Angew. Chem., Int. Ed. Engl.* **1984**, *23*, 587–608. (d) Dötz, K. H. In *Organometallics in Organic Synthesis: Aspects of a Modern Interdisciplinary Field*; tom Dieck, H., de Meijere, A., Eds.; Springer: Berlin, 1988; p 85 ff. (e) Wulff, W. D.; Bauda, W. E.; Kaesler, R. W.; Lankford, P. J.; Miller, R. A.; Murray, C. K.; Yang, D. C. *J. Am. Chem. Soc.* **1990**, *112*, 3642–3659. (f) Wulff, W. D. In *Comprehensive Organic Synthesis*; Trost, B. M., Fleming, I., Eds.; Pergamon Press: New York, 1990; Vol. 5.

(3) Review: Aumann, R. *Angew. Chem.* **1988**, *100*, 1512–1524; *Angew. Chem., Int. Ed. Engl.* **1988**, *27*, 1456–1467.

(4) (a) Fischer, E. O.; Dötz, K. H. *Chem. Ber.* **1970**, *103*, 1273. (b) Dötz, K. H.; Fischer, E. O. *Chem. Ber.* **1972**, *105*, 1356. Review: (c) Reissig, H. U. *Top. Curr. Chem.* **1988**, *144*, 73. (d) Brookhart, M.; Liu, Y. In *Advances in Metal Carbene Chemistry*; Schubert, U., Ed.; Kluwer Academic Publisher: Dordrecht, The Netherlands, 1989; pp 251–270. (e) Brookhart, M.; Studabaker, W. B. *Chem. Rev.* **1987**, *87*, 411.

(5) (a) Kreiter, C. G. *Angew. Chem.* **1968**, *80*, 402; *Angew. Chem., Int. Ed. Engl.* **1968**, *7*, 390. (b) Casey, C. P.; Anderson, R. L. *J. Am. Chem. Soc.* **1974**, *96*, 1230. (c) Casey, C. P.; Boggs, R. A.; Anderson, R. L. *J. Am. Chem. Soc.* **1972**, *94*, 8947. (d) Xu, Y.-Ch.; Wulff, W. D. *J. Org. Chem.* **1987**, *52*, 3263. (e) Wulff, W. D.; Gilbertson, S. R. *J. Am. Chem. Soc.* **1985**, *107*, 503. (f) Alvarez-Toledano, C.; Parlier, A.; Rose-Munch, F.; Rudler, H.; Daran, J. C.; Knobler, C.; Jeannin, Y. *J. Organomet. Chem.* **1987**, *323*, 371. (g) Macomber, D. W.; Madhukar, P.; Rogers, R. D. *Organometallics* **1989**, *8*, 1275. (h) Macomber, D. W.; Hung, M.; Puttannachetty, M.; Liang, M.; Rogers, R. D. *Organometallics* **1991**, *10*, 737. (i) Aumann, R.; Heinen, H. *Chem. Ber.* **1987**, *120*, 537–540. (j) Aumann, R.; Hinterding, P. *Chem. Ber.* **1990**, *123*, 611–620. (k) Aumann, R.; Hinterding, P. *Chem. Ber.* **1990**, *123*, 2047–2051. (l) Breimair, J.; Weidmann, T.; Wagner, B.; Beck, W. *Chem. Ber.* **1991**, *124*, 2431–2434. (m) Niemer, B.; Breimair, J.; Völkl, T.; Wagner, B.; Pohlborn, K.; Beck, W. *Chem. Ber.* **1991**, *124*, 2237. (n) Beck, W.; Breimair, J.; Fritz, P.; Knauer, W.; Weidmann, T. *Transition Metal Carbene Complexes*; Kreissl, F. R., Ed.; Kluwer Academic Publishers: Dordrecht, The Netherlands, 1993; 189–199. (o) Kelley, C.; Terry, M. R.; Kaplan, A. W.; Geoffroy, G.; Lugan, N.; Mathieu, R.; Haggerty, B. S.; Rheingold, A. L. *Inorg. Chim. Acta* **1992**, *198*, 200, 601–611. (p) Aumann, R.; Runge, M. *Chem. Ber.* **1992**, *125*, 259–264.

(6) (a) Ivin, K. J.; Kress, J.; Osborn, J. A.; Rooney, J. J. In *Advances in Metal Carbene Chemistry*; Schubert, U., Ed.; Kluwer Academic Publisher: Dordrecht, The Netherlands, 1989; 313–322. (b) Weiss, K.; Hoffmann, K. *Ibid.* pp 351–270.

(7) (a) Hegedus, L. S., In *Advances in Metal Carbene Chemistry*; Schubert, U., Ed.; Kluwer Academic Publisher: Dordrecht, The Netherlands, 1989; pp 233–246. (b) Hegedus, L. S.; de Weck, G.; D'Andrea, S. *J. Amer. Chem. Soc.* **1988**, *110*, 2122.

(8) (a) Hegedus, L. S.; Mc Giure, M. A.; Schultze, L. M.; Yijun, C.; Anderson, O. P. *J. Am. Chem. Soc.* **1984**, *106*, 2680. (b) Narukawa, Y.; Juneau, K. N.; Snustad, D.; Miller, D. B.; Hegedus, L. S. *J. Org. Chem.* **1992**, *57*, 5453. (c) Thompson, D. K.; Suzuki, N.; Hegedus, L. S.; Satoh, Y. *J. Org. Chem.* **1992**, *57*, 1461. (d) Betschart, C.; Hegedus, L. S. *J. Am. Chem. Soc.* **1992**, *114*, 5010.

(9) (a) Hegedus, L. S.; Bates, R. W.; Söderberg, B. C. *J. Am. Chem. Soc.* **1991**, *113*, 923. (b) Söderberg, B. C.; Hegedus, L. S. *J. Org. Chem.* **1991**, *56*, 2209. (c) Sierra, M. A.; Hegedus, L. S. *J. Am. Chem. Soc.* **1989**, *111*, 2335.

(10) Hegedus, L. S.; Lastra, W.; Narukawa, Y.; Snustad, D. *J. Am. Chem. Soc.* **1992**, *114*, 2991.

(11) (a) Merlic, C. A.; Xu, D. *J. Am. Chem. Soc.* **1991**, *113*, 7418. (b) Merlic, C. A.; Xu, D.; Khan, S. I. *Organometallics* **1992**, *114*, 412.

(12) (a) Trost, B. M. *Chem. Soc. Rev.* **1982**, *11*, 141–170. (b) Lu, X.; Ji, J.; Ma, D.; Shen, W. *J. Org. Chem.* **1991**, *56*, 5774–5778. (c) Kaupp, G.; Pogodda, U.; Atfah, A.; Meier, H.; Vierengel, A. *Angew. Chem.* **1992**, *104*, 783–785; *Angew. Chem., Int. Ed. Engl.* **1992**, *31*, 768–770.

(13) (a) Aumann, R.; Jasper, B.; Läge, M.; Krebs, B. *Organometallics* **1994**, *13*, 3502–3509. (b) Aumann, R.; Jasper, B.; Läge, M.; Krebs, B. *Organometallics* **1994**, *13*, 3510–3516.

(14) Bestian, H. *Chem. Ber.* **1984**, *117*, XIII.

(15) (a) Miranda, M.; Garcia, H. In *The Chemistry of Functional Groups: The Chemistry of Acid Derivatives*; Patai, S., Ed.; Wiley: New York, 1992; Suppl. B2, pp 1271–1394. (b) Garcia, H.; Martinez-Utrilla, R.; Miranda, M. A. *Tetrahedron Lett.* **1980**, *21*, 3925–3926. (c) Algarra, F.; Baldovi, M. V.; Garcia, H.; Miranda, M. A.; Primo, J. *Monatsh. Chem.* **1993**, *124*, 209–215.

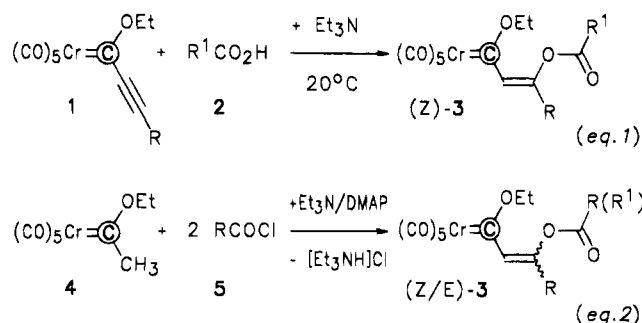
Table 1. Isolated Yields of **3** and (Z/E) Product Ratio

1-5	R	R ¹	% 3	(Z/E)	a	ref
a	C ₆ H ₅	C ₆ H ₅	76	100	eq 1	13a,b
b	C ₆ H ₅	c-Pr	60	100	eq 1	b
c	C ₆ H ₅	c-C ₇ H ₇ CH ₂	48	100	eq 1	b
d	C ₆ H ₅	Me ₂ C=CH	61	100	eq 1	b
e	t-Bu	t-Bu	57	4/1	eq 2	13b
f	c-Pr	c-Pr	69	3/1	eq 2	13b

^a Method of preparation. ^b This paper.

Scheme 1. Routes to

[(Z)-2-(Acyloxy)ethenyl]carbene Complexes



ment¹⁶) or photochemical activation (photo-Fries rearrangement). The mechanisms of these processes are completely different from that of the classical Fries reaction; however the synthetic result is equivalent. Concerning the photochemical-induced Fries rearrangement, a considerable number of reports have appeared during the last years in connection with its mechanistic as well as synthetic aspects.^{15b,c} The advantage of the photo-Fries rearrangement over the classical acid-catalyzed process is mainly due to the mildness of the reaction conditions.

[2-(Acyloxy)ethenyl]carbene Complexes **3**

{[2-(Acyloxy)ethenyl]carbene}chromium complexes **3** are required as precursors to 2-butene-1,4-diones. They are obtained by two different routes: either by the addition of carboxylic acids to an (alkynylcarbene)-chromium complex **1** (eq 1, Scheme 1)^{13a} or by the acylation of a methylcarbene chromium complex **4** (eq 2, Scheme 1).^{13b,17}

The former method (eq 1) is superior with respect to its high stereoselectivity, which leads to the formation of (Z) isomers of **3** as the only products. As a further advantage, two different groups R and R¹ may be introduced into **3** by this route. The application of the second method, shown in eq 2, is restricted to the introduction of two identical groups R = R¹, and it usually affords (Z/E) mixtures of stereoisomers.

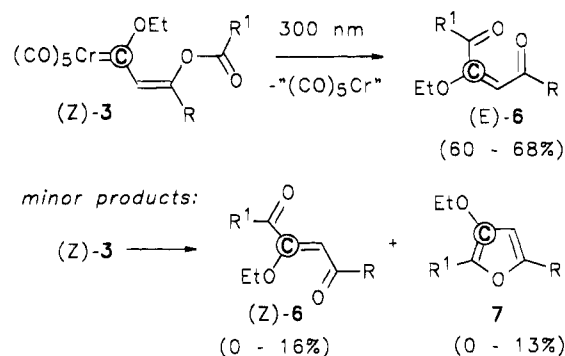
2-Butene 1,4-diones **6** and Furans **7**

Dark brown solutions of [(Z)-2-(acyloxy)ethenyl]carbene complexes, (Z)-**3**, in ether, when irradiated with UV light of >300 nm (in a Rayonet RPR-100 chamber reactor) become yellow within 2–4 h at 20 °C. Chromatography on silica gel affords 2-butene-1,4-diones and

Table 2. Product Ratio from Photolysis of (Z)-**3**

6, 7	R	R ¹	% (E)- 6 /(Z)- 6 / 7
a	C ₆ H ₅	C ₆ H ₅	68/0/12
b	C ₆ H ₅	c-Pr	62/16/0
c	C ₆ H ₅	c-C ₇ H ₇ CH ₂	67/0/0
d	C ₆ H ₅	Me ₂ C=CH	67/0/0
e	t-Bu	t-Bu	60/0/13
f	c-Pr	c-Pr	65/16/8

Scheme 2. Photolysis of

[(Z)-2-(Acyloxy)ethenyl]carbene Complexes **3**

small amounts of furans **7** (Scheme 2, Table 2). Chromium hexacarbonyl is recovered to a great extent.

The configurational assignment of compounds (Z)-**6** is based on the downfield shift of the OCH₂ signal by 0.7 ppm relative to (E)-**6** [e.g. (E)-**6b** 3.30; (Z)-**6b** 4.00] and of 2-H by 1.1–1.2 ppm [e.g. (E)-**6b** 5.85; (Z)-**6b** 6.95] in the ¹H NMR spectra, due to the anisotropic deshielding by the corresponding neighboring C=O groups. A γ effect, resulting from the steric interaction between the acyl functions in (E)-**6** leads to a significant downfield shift of the carbon signals C–OEt by 9–11 ppm [e.g. (E)-**6b** 168.9, (Z)-**6b** 158.5]. NOE effects were observed between the proton signals of OCH₂ and =CH in (E)-**6b** but not in (Z)-**6b**.

Mechanistic Considerations

Photoinduced acyl migrations of organic molecules involve the formation of a radical pair enclosed in a solvent cage, from which radical recombination leads to the rearranged products.¹⁵ The photoinduced acyl migration of [(Z)-2-(acyloxy)ethenyl]carbene complexes, (Z)-**3**, which leads to the formation of 2-butene 1,4-diones (E)-**6** by the elimination of Cr(CO)₆, seems to follow a quite different route. It is metal-mediated and could be initiated by generation of an intermediate **A** by extrusion of carbon monoxide.¹⁸ A subsequent migration of the O-acyl group in **A** may yield **B**, and a reductive elimination from **B** with retention of configuration finally gives (E)-**6**. Small amounts of stereoisomers (Z)-**6b,f** are obtained, which may possibly result from a (photo)isomerization of (E)-**6b,f**, and the captodative C=C bond in **B**, respectively. Furans **7** are formed as minor products. They seem to arise from a Hegedus-type insertion of carbon monoxide into the Cr=C bond.⁷ A consecutive cyclization of **C** to **D** and the elimination of CO₂ from **D** finally could give **7**.¹⁹

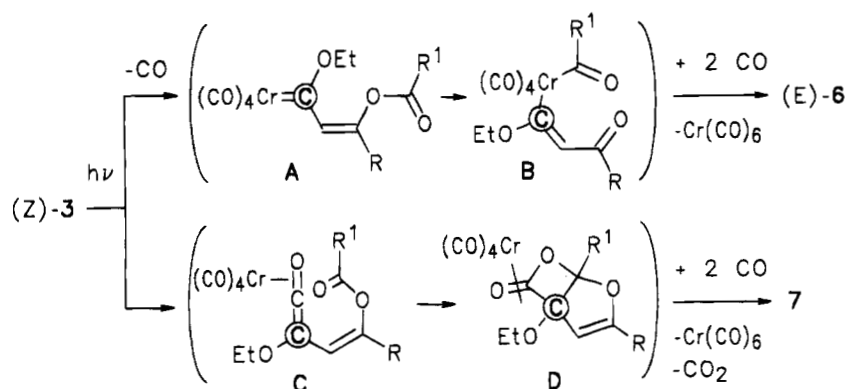
(16) (a) Sibi, M. P.; Snieckus, V. *J. Org. Chem.* **1983**, *48*, 1937. (b) Hellwinkel, D.; Lämmerzahl, F.; Hofmann, G. *Chem. Ber.* **1983**, *116*, 3375.

(17) Casey, C. P.; Boggs, R. A.; Anderson, R. L. *J. Am. Chem. Soc.* **1972**, *94*, 8947–8949.

(18) See, e.g.: Foley, H. C.; Strubinger, L. M.; Targos, T. S.; Geoffroy, G. L. *J. Am. Chem. Soc.* **1983**, *105*, 3064.

(19) For a related type of reaction see: Aumann, R.; Jasper, B.; Goddard, R.; Krüger, C. *Chem. Ber.* **1994**, *127*, 717–724.

Scheme 3. Metal-Mediated Acyl Migration in (Z)-3



Experimental Section

All operations were performed under argon. Solvents were dried by distillation from sodium/benzophenone. ^1H NMR and ^{13}C NMR: Bruker WM 300. Multiplicities were determined by DEPT. Chemical shifts refer to $\delta_{\text{TMS}} = 0.00$ ppm. IR: Digilab FTS 45. MS: Finnigan MAT 312. Elemental analysis: Perkin-Elmer 240 elemental analyzer. Melting points are uncorrected. Column chromatography: Merck-Kieselgel 100. TLC: Merck DC-Alufolien Kieselgel 60 F 254. R_f values refer to TLC tests.

Pentacarbonyl[(2Z)-3-(cyclopropylcarboxy)-1-ethoxy-3-phenyl-2-propenylidene]chromium [(Z)-3b]. To pentacarbonyl(1-ethoxy-3-phenyl-2-propynylidene)chromium (1) (350 mg, 1.00 mmol) in 3 mL of dichloromethane/diethyl ether (1:1) is added cyclopropanecarboxylic acid (2b) (86 mg, 1.00 mmol) and triethylamine (80 mg, 0.80 mmol) at 20 °C in a 5 mL screwtop vessel. After a few minutes the formation of (Z)-3b can be detected by TLC [$R_f = 0.3$ in pentane/dichloromethane (3:1)]. Chromatography on silica after 2–4 h yields (Z)-3b [262 mg (60%), dark-brown crystals from diethyl ether/pentane (1:6), mp 78 °C]. ^1H NMR (C_6D_6): δ 7.63 (1 H, s, 2-H), 7.55, 6.95, 6.90 (2:1:2 H, *o*-,*p*-,*m*-H, 3-Ph), 4.60 (2 H, q, OCH_2), 1.30 (1 H, m, 1'-H *c*-Pr), 1.10 (3 H, t, OCH_2CH_3), 0.90 and 0.45 (2 H each, m each, 2 CH_2 *c*-Pr). ^{13}C NMR (C_6D_6): δ 335.9 (Cr=C), 225.0 and 217.2 [1:4, *trans*- and *cis*-CO, $\text{Cr}(\text{CO})_5$], 171.6 (O—CO), 139.8 (C3), 134.6 (*i*-C, 3-Ph), 130.9 (CH, 2-C), 129.5, 128.0, 127.1 (2:1:2, *o*-,*p*-,*m*-CH, 3-Ph), 77.5 (OCH_2), 15.2 (CH_3 , Et), 13.2 (CH, C1' *c*-Pr), 9.7 (2 CH_2 , *c*-Pr). IR (hexane), cm^{-1} (%): $\nu = 2059.5$ (30), 1986.5 (5), 1948.5 (100) [$\nu(\text{CO})$]. IR (diffuse reflection): 1757.3 (30) [$\nu(\text{OC}=\text{O})$], 1589.9 (20) [$\nu(\text{C}=\text{C})$]. MS (70 eV), m/e (%): 436 (10) [M^+], 408 (10), 380 (20), 352 (20), 324 (40) [$\text{M}^+ - 5\text{CO}$], 296 (20), 252 (80), 239 (20), 199 (20), 149 (100), 139 (60), 105 (50) [PhCO], 81 (80) [*c*-PrCO]. Anal. Calcd for $\text{C}_{20}\text{H}_{16}\text{CrO}_8$ (436.3): C, 55.05; H, 3.70. Found: C, 55.10; H, 3.71.

Pentacarbonyl[(2Z)-3-(α -cycloheptatrienyl)acetoxy]-1-ethoxy-3-phenyl-2-propenylidene]chromium [(Z)-3c]. Pentacarbonyl(1-ethoxy-3-phenyl-2-propynylidene)chromium (1) (350 mg, 1.00 mmol) and α -cycloheptatrienylacetic acid (2c) (149 mg, 1.00 mmol) in 3 mL of dichloromethane/diethyl ether (1:1) are treated as described above with triethylamine (80 mg, 0.80 mmol) at 20 °C. Chromatography after 8–10 h yields (Z)-3c [$R_f = 0.5$ in pentane/dichloromethane (2:1), 240 mg (48%), red-brown crystals from diethyl ether/pentane (1:4), mp 68 °C]. ^1H NMR (C_6D_6): δ 7.70 (1 H, s, 2-H), 7.65, 7.10, 7.06 (2:1:2 H, *o*-,*p*-,*m*-H, 3-Ph), 6.50, 6.05, 5.10 (2:2:2 H, each m, 2'-H to 7'-H, cycloheptatrienyl), 4.60 (2 H, q, OCH_2), 2.65 (2 H, d, $\text{OC}-\text{CH}_2$), 2.50 (1 H, m, 1'-H, cycloheptatrienyl), 1.10 (3 H, t, OCH_2CH_3). ^{13}C NMR (C_6D_6): δ 336.8 (Cr=C), 224.9 and 217.2 [1:4, *trans*- and *cis*-CO, $\text{Cr}(\text{CO})_5$], 168.9 (O—CO), 139.5 (C3), 134.6 (*i*-C, 3-Ph), 131.6 (CH, 2-C), 130.8, 129.4, 126.1 (1:2:2, *p*-,*o*-,*m*-CH, 3-Ph), 129.3, 127.2, 124.7 (CH each, 2:2:2, cycloheptatrienyl), 77.4 (OCH_2), 37.4 ($\text{OC}-\text{CH}_2$), 35.8 (C1', cycloheptatrienyl), 15.3 (CH_3 , Et). IR (hexane), cm^{-1} (%): $\nu = 2059.9$ (30), 1986.9 (5), 1949.2 (100) [$\nu(\text{CO})$]. IR (diffuse reflection): 1761.1 (20) [$\nu(\text{OC}=\text{O})$], 1589.2 (20) [$\nu(\text{C}=\text{C})$]. MS (70 eV), m/e (%): 500 (5) [M^+], 472 (10), 444 (20), 416 (40), 389 (30), 360 (60) [$\text{M}^+ - 5\text{CO}$], 303 (60), 220 (70), 131 (80), 105 (100) [$\text{CH}_2\text{C}_7\text{H}_7^+$], 91 (100) [C_7H_7^+]. Anal. Calcd for $\text{C}_{25}\text{H}_{20}\text{CrO}_8$ (500.4): C, 60.00; H, 4.03. Found: C, 60.14; H, 3.93.

Pentacarbonyl[(2Z)-3-[(2-methyl-1-propen-1-yl)carboxyl-1-ethoxy-3-phenyl-2-propenylidene]chromium [(Z)-3d]. Pentacarbonyl(1-ethoxy-3-phenyl-2-propynylidene)chromium (1) (350 mg, 1.00 mmol) and 3,3-dimethylacrylic acid (2d) (100 mg, 1.00 mmol) in 3 mL of dichloromethane/diethyl ether (1:1) are treated as described above with triethylamine (80 mg, 0.80 mmol) at 20 °C. Chromatography after 3 h yields (Z)-3d [$R_f = 0.5$ in pentane/dichloromethane (2:1), 275 mg (61%), brown crystals from diethyl ether/pentane (1:6), mp 73 °C]. ^1H NMR (C_6D_6): δ 7.80 (1 H, s, 2-H), 7.60, 6.95, 6.90 (2:1:2 H, *o*-,*p*-,*m*-H, 3-Ph), 5.70 (1 H, sept, $^4J = 1.1$ Hz, 1'-H), 4.65 (2 H, q, OCH_2), 1.98 and 1.40 (3 H each, d each, $^4J = 1.1$ Hz each, $=\text{CMe}_2$), 1.15 (3 H, t, OCH_2CH_3). ^{13}C NMR (C_6D_6): δ 335.0 (Cr=C), 225.1 and 217.3 [1:4, *trans*- and *cis*-CO, $\text{Cr}(\text{CO})_5$], 162.8 and 162.0 [C(q) each, O—CO and $=\text{CMe}_2$], 139.8 (C3), 134.9 (*i*-C, 3-Ph), 130.9 (CH, C2), 129.4, 127.3, 127.2 (1:2:2, *o*-,*p*-,*m*-CH, 3-Ph), 115.1 ($\text{OC}-\text{CH}=\text{C}$), 77.5 (OCH_2), 27.4 and 20.6 [$=\text{C}(\text{CH}_3)_2$], 15.0 (CH_3). IR (hexane) cm^{-1} (%): $\nu = 2058.9$ (30), 1984.8 (5), 1947.9 (100) [$\nu(\text{CO})$]. IR (diffuse reflection): 1743.2 (20) [$\nu(\text{OC}=\text{O})$], 1644.8 and 1588.7 [$\nu(\text{C}=\text{C})$]. MS (70 eV), m/e (%): 450 (5) [M^+], 422 (5), 394 (4), 366 (10), 338 (15), 310 (30) [$\text{M}^+ - 5\text{CO}$], 266 (40), 149 (80), 105 (90), 83 (100) [$\text{OC}-\text{CH}=\text{CMe}_2$]. Anal. Calcd for $\text{C}_{21}\text{H}_{18}\text{CrO}_8$ (450.4): C, 56.01; H, 4.03. Found: C, 56.06; H, 3.96.

(2E)-2-Ethoxy-1,4-diphenyl-2-butene-1,4-dione [(E)-6a] and 3-Ethoxy-2,5-diphenylfuran (7a). [(Z)-3-(Benzoyloxy)-1-ethoxy-4-phenyl-2-propenylidene]pentacarbonylchromium¹⁸ [(Z)-3a] (238 mg, 0.50 mmol) in 20 mL of dry ether is photolyzed with >300 nm light in a Rayonet RPR-100 chamber reactor for 3–4 h. The initially brown solution turns gradually yellow. The reaction is followed by TLC. According to the ^1H NMR spectra in C_6D_6 a mixture of (E)-6a:7a = 5:1 is obtained. Chromatography on silica gel with pentane affords colorless $\text{Cr}(\text{CO})_6$ [98 mg (89%), $R_f = 0.9$ in pentane, colorless crystals]. Elution with dichloromethane gives 7a [$R_f = 0.8$ in dichloromethane, 18 mg (12%), colorless oil], and (E)-6a [$R_f = 0.5$ in dichloromethane, 95 mg (68%), colorless crystals from dichloromethane/pentane 1:4 at -15 °C, mp 98 °C].

(E)-6a. ^1H NMR (C_6D_6): δ 8.10, 7.10, 6.95 (2:1:2 H, *o*-,*p*-,*m*-H, 4-Ph), 7.80, 7.05, 6.90 (2:1:2 H, *o*-,*p*-,*m*-H, 1-Ph), 6.30 (1 H, s, 3-H), 3.50 (2 H, q, OCH_2), 0.95 (3 H, t, OCH_2CH_3). ^{13}C NMR (C_6D_6): δ 190.8 (C=O, C1), 188.0 (C=O, C4), 169.2 [C(q), C2], 138.6 and 135.7 (*i*-C, Ph each), 133.2, 132.5, 129.1, 128.8, 128.0, 127.7 (2:2:1:2:1:2, CH each, 2 Ph), 98.5 (CH, C3), 66.2 (OCH_2), 13.9 (CH_3). IR (diffuse reflection), cm^{-1} (%): $\nu = 1686.0$ (60) and 1654.7 (55) [$\nu(\text{C}=\text{O})$], 1584.0 [$\nu(\text{C}=\text{C})$]. MS (70 eV), m/e (%): 280 (45) [M^+], 252 (40), 251 (50) [$\text{M}^+ - \text{Et}$],

236 (30), 235 (35), 149 (60), 175 (40), 105 (80), 69 (100). Anal. Calcd for $C_{18}H_{16}O_3$ (280.3): C, 77.12; H, 5.75. Found: C, 77.23; H, 5.80.

7a. 1H NMR (C_6D_6): δ 8.15, 7.30, 7.05 (2:2:1 H, *o*-,*m*-,*p*-H, 5-Ph), 7.65, 7.20, 7.03 (2:2:1 H, *o*-,*m*-,*p*-H, 2-Ph), 6.35 (1 H, s, 3-H), 3.60 (2 H, q, OCH_2), 1.05 (3 H, t, OCH_2CH_3). GC-IR, cm^{-1} (%): $\nu = 1620.5$ (80), 1598.6 (85) and 1494.9 (90) [$\nu(C=C)$] and [$\gamma(C-H)$]. MS (70 eV), m/e (%): 264 (75) [M^+], 236 (30), 235 (20) [$M^+ - Et$], 207 (10), 179 (5), 131 (5), 105 (100), 77 (50), 51 (20).

1-Cyclopropyl-2-ethoxy-4-phenyl-2-butene-1,4-dione [(E)-6b and (Z)-6b]. Pentacarbonyl[(2Z)-3-(cyclopropylcarboxy)-1-ethoxy-3-phenyl-2-propenylidene]chromium [(Z)-3b] (218 mg, 0.50 mmol) in 20 mL of dry ether is photolyzed with >300 nm light in a Rayonet RPR-100 chamber reactor for 2 h. The initially brown solution turns yellow gradually. The reaction is followed by TLC. According to 1H NMR spectra (C_6D_6) a mixture of (E)-6b:(Z)-6b = 4:1 is formed. Chromatography on silica gel affords colorless $Cr(CO)_6$, (Z)-6b [$R_f = 0.7$ in dichloromethane/diethyl ether (10:1), 20 mg (16%)] and (E)-6b [$R_f = 0.6$ in dichloromethane/diethyl ether (10:1), 77 mg (62%), yellowish crystals from dichloromethane/pentane 1:4 at $-15^\circ C$, mp $65^\circ C$].

(E)-6b. 1H NMR (C_6D_6): δ 8.12, 7.10, 7.00 (2:1:2 H, *o*-,*p*-,*m*-H, Ph), 5.85 (1 H, s, 3-H), 3.30 (2 H, q, OCH_2), 2.20 (1 H, m, 1'-H, *c*-Pr), 1.30 and 0.70 (2H each, CH_2 , *c*-Pr), 1.05 (3H, t, OCH_2CH_3). ^{13}C NMR (C_6D_6): δ 199.9 (C=O, C1), 189.3 (C=O, C4), 168.9 [C(q), C2], 139.2 (*i*-C, Ph), 132.8, 128.9, 128.0 (2:2:1, CH each, Ph), 98.7 (CH, C3), 65.9 (OCH_2), 20.9 (CH, *c*-Pr), 14.3 (CH_3), 12.2 (2 CH_2 , *c*-Pr). IR (diffuse reflection), cm^{-1} (%): $\nu = 1695.6$ (60) and 1655.0 (55) [$\nu(C=O)$], 1564.7 [$\nu(C=C)$]. MS (70 eV), m/e (%): 244 (30) [M^+], 216 (40), 215 (50) [$M^+ - Et$], 175 (40), 105 (70), 69 (100). $C_{15}H_{16}O_3$ (244.3): Anal. Calcd for C, 73.75; H, 6.60. Found: C, 73.60; H, 6.50.

(Z)-6b. 1H NMR (C_6D_6): δ 8.10, 7.15, 7.05 (2:1:2 H, *o*-,*p*-,*m*-H, Ph), 6.95 (1 H, s, 3-H), 4.00 (2 H, q, OCH_2), 2.50 (1 H, m, 1'-H, *c*-Pr), 1.20 and 0.59 (2 H each, CH_2 , *c*-Pr), 0.95 (3 H, t, OCH_2CH_3). ^{13}C NMR (C_6D_6): δ 198.3 (C=O, C1), 190.5 (C=O, C4), 158.5 [C(q), C2], 138.8 (*i*-C, Ph), 132.8, 128.8, 127.5 (2:2:1, CH each, Ph), 105.5 (CH, C3), 70.2 (OCH_2), 30.2 (CH, *c*-Pr), 14.2 (CH_3), 12.6 (2 CH_2 , *c*-Pr). IR (diffuse reflection), cm^{-1} (%): $\nu = 1705.5$ (60) and 1678.3 (55) [$\nu(C=O)$], 1588.4 [$\nu(C=C)$]. MS (70 eV), m/e (%): 244 (40) [M^+], 216 (40), 215 (60) [$M^+ - Et$], 175 (50), 105 (70), 69 (100).

(2E)-5-Cycloheptatrienyl-3-ethoxy-1-phenyl-2-pentene-1,4-dione [(E)-6c]. Pentacarbonyl[(2Z)-3-[(α -cycloheptatrienyl)acetoxyl]-1-ethoxy-3-phenyl-2-propenylidene]chromium^{13b} [(Z)-3c] (250 mg, 0.50 mmol) in 20 mL of dry ether is photolyzed with >300 nm light in a Rayonet RPR-100 chamber reactor for 2 h. The reaction is followed by TLC. The initially brown solution turns yellow gradually. 1H NMR spectra of the mixture indicate a smooth conversion. Chromatography on silica gel results in partial decomposition of (E)-6c [$R_f = 0.5$ in dichloromethane, 103 mg (67%), colorless crystals from dichloromethane/pentane 1:4 at $-15^\circ C$]. 1H NMR (C_6D_6): δ 8.10, 7.15, 7.10 (2:1:2 H, *o*-,*p*-,*m*-H, 4-Ph), 6.60, 6.10, 5.50 (2:2:2 H, 1-H through 6-H, *c*-C₇H₇), 5.90 (1 H, s, 3-H), 3.30 (2 H, q, OCH_2), 3.15 (2 H, d, 5-H₂), 2.80 (1 H, 7'-H, *c*-C₇H₇), 1.05 (3 H, t, OCH_2CH_3). ^{13}C NMR (C_6D_6): δ 197.9 (C=O, C4), 188.9 (C=O, C1), 169.9 [C(q), C3], 139.2 (*i*-C, Ph), 132.8, 131.6, 128.6 (1:2:2, CH each, Ph), 129.0, 128.8, 126.3 (2 CH each, *c*-C₇H₇), 97.2 (CH, C2), 66.1 (OCH_2), 44.1 (CH_2 , C5), 34.8 (CH, C7', *c*-C₇H₇), 14.3 (CH_3). IR (diffuse reflection), cm^{-1} (%): $\nu = 1719.3$ (60) and 1651.0 (55) [$\nu(C=O)$], 1563.1 [$\nu(C=C)$]. MS (70 eV), m/e (%): 308 (30) [M^+], 279 (40), 262 (20), 204 (40), 105 (100), 91 (80). Anal. Calcd for $C_{20}H_{20}O_3$ (308.4): C, 77.90; H, 6.54. Found: C, 78.00; H, 6.70.

(2E)-3-Ethoxy-6-methyl-1-phenyl-2,5-heptadiene-1,4-dione [(E)-6d]. Pentacarbonyl[(2Z)-3-[(2-methyl-1-propenyl)carboxyl]-1-ethoxy-3-phenyl-2-propenylidene]chromium [(Z)-3d] (250 mg, 0.50 mmol) in 20 mL of dry ether is photolyzed with >300 nm light in a Rayonet RPR-100 chamber reactor

for 2–3 h. The reaction is followed by TLC. According to 1H NMR spectra (C_6D_6) a smooth conversion has occurred. Chromatography on silica gel affords colorless $Cr(CO)_6$ and (E)-6d [$R_f = 0.4$ in dichloromethane, 89 mg (69%), colorless crystals from dichloromethane/pentane 1:4 at $-15^\circ C$, mp $102^\circ C$]. 1H NMR (C_6D_6): δ 8.00, 7.15, 7.10 (2:1:2 H, *o*-,*p*-,*m*-H, Ph), 7.28 (1 H, q, $^4J = 1$ Hz, 5-H), 5.89 (1 H, s, 2-H), 3.35 (2 H, q, OCH_2), 2.20 (3 H, s, 6- CH_3), 1.50 (3 H, q, $^4J = 1$ Hz, 7-H₃), 1.03 (3 H, t, OCH_2CH_3). ^{13}C NMR (C_6D_6): δ 189.3 (C=O, C4), 189.2 (C=O, C1), 170.5 [C(q), C3], 156.9 [C(q), C6], 139.5 (*i*-C, Ph), 132.8, 132.7, 129.1 (1:2:2, CH each, Ph), 123.2 (CH, C5), 97.9 (CH, C2), 65.8 (OCH_2), 27.7 and 21.4 (CH_3 each, 6- CH_3 and C7), 14.3 (CH_3). IR (diffuse reflection), cm^{-1} (%): $\nu = 1682.9$ (60) and 1652.0 (55) [$\nu(C=O)$], 1618.4 and 1563.1 [$\nu(C=C)$]. MS (70 eV), m/e (%): 258 (60) [M^+], 243 (40), 229 (40), 215 (40), 187 (40), 153 (70), 125 (60), 105 (80), 84 (90), 83 (100) [$Me_2C=CHCO^+$]. Anal. Calcd for $C_{16}H_{18}O_3$ (258.3): C, 74.40; H, 7.02. Found: C, 74.23; H, 7.14.

(4E)-4-Ethoxy-2,2,7,7-tetramethyl-4-octene-3,6-dione [(E)-6e] and 2,5-Di-tert-butyl-3-ethoxyfuran (7e). Pentacarbonyl[(Z)-3-[1-ethoxy[(1,1-dimethylethyl)carboxyl]-4,4-dimethyl-2-pentenylidene]chromium^{13b} [(Z)-3e] (216 mg, 0.50 mmol) in 20 mL of dry ether is photolyzed with >300 nm light in a Rayonet RPR-100 chamber reactor for 2–3 h. The reaction is followed by TLC. According to 1H NMR spectra (C_6D_6) a >90% conversion into a mixture of (E)-6e:7 = 5:1 has occurred. Chromatography on silica gel affords colorless $Cr(CO)_6$ and 7 [$R_f = 0.8$ in dichloromethane, 15 mg (13%), colorless oil] and (E)-6e [$R_f = 0.4$ in dichloromethane, 67 mg (60%), yellowish oil].

(E)-6e. 1H NMR (C_6D_6): δ 5.35 (1 H, s, 3-H), 3.25 (2 H, q, OCH_2), 1.35 and 1.03 (9 H each, s each, *t*-Bu), 0.85 (3 H, t, OCH_2CH_3). ^{13}C NMR (C_6D_6): δ 206.7 (C=O, C3), 203.4 (C=O, C6), 170.7 [C(q), C4], 96.2 (CH, C5), 65.7 (OCH_2), 43.4 and 43.1 [C(q) each, CMe_3], 27.4 and 27.2 (3 CH_3 each, *t*-Bu), 14.3 (CH_3 , Et). IR (diffuse reflection), cm^{-1} (%): $\nu = 1708.7$ (60) and 1672.5 (55) [$\nu(C=O)$], 1570.2 [$\nu(C=C)$]. MS (70 eV), m/e (%): 240 (50) [M^+], 225 (30), 209 (30), 184 (70) [$M^+ - Me_2C=CH_2$], 169 (100), 155 (20), 141 (20), 95 (50) [t -Bu CO^+], 57 (50) [t -Bu $^+$]. Anal. Calcd for $C_{14}H_{24}O_3$ (240.3): C, 69.96; H, 10.07. Found: C, 70.43; H, 10.45.

7e. 1H NMR (C_6D_6): δ 5.85 (1 H, s, 4-H), 3.65 (2 H, q, OCH_2), 1.45 and 1.23 (9 H each, s each, *t*-Bu), 1.15 (3 H, t, OCH_2CH_3). ^{13}C NMR (C_6D_6): δ 158.7 [C(q), C3], 143.9 [C(q), C5], 141.5 [C(q), C2], 97.1 (CH, C4), 67.4 (OCH_2), 33.1 and 33.0 [C(q) each, CMe_3], 29.3 and 29.0 (CH_3 each, 2 *t*-Bu), 15.4 (CH_3 , Et). GC-IR, cm^{-1} (%): $\nu = 1622.2$ and 1479.5 (55) [$\nu(C=C)$] and [$\gamma(C-H)$]. MS (70 eV), m/e (%): 224 (30) [M^+], 209 (100) [$M^+ - CH_3$], 181 (50) [209 - C_2H_4], 166 (30) [181 - CH_3].

1,4-Dicyclopropyl-2-ethoxy-2-butene-1,4-dione [(E)-6f] and (Z)-6f] and 2,5-Dicyclopropyl-3-ethoxyfuran (7f). Pentacarbonyl[3-cyclopropyl-3-(cyclopropylcarboxy)-1-ethoxy-2-propenylidene]chromium^{13b} [(Z)-3f] (200 mg, 0.50 mmol) in 20 mL of dry ether is photolyzed with >300 nm light in a Rayonet RPR-100 chamber reactor for 2 h. The reaction is followed by TLC. According to 1H NMR spectra (C_6D_6) a >90% conversion into a mixture of (E)-6f:(Z)-6f:7f = 4:1:0.3 has occurred. Chromatography over silica gel affords colorless $Cr(CO)_6$, small amounts of unpolar 7f [$R_f = 0.9$ in dichloromethane, 8 mg (8%), colorless oil], followed by (Z)-6f [$R_f = 0.35$ in dichloromethane, 16 mg (16%)] and (E)-6f [$R_f = 0.3$ in dichloromethane, 68 mg (65%), colorless crystals from dichloromethane/pentane 1:4 at $-15^\circ C$].

(E)-6f. 1H NMR (C_6D_6): δ 5.35 (1 H, s, 3-H), 3.30 (2 H, q, OCH_2), 2.10 (1 H, m, 1'-H, 1-*c*-Pr), 1.75 (1 H, m, 1'-H, 4-*c*-Pr), 1.30 and 0.80 (2 H each, CH_2 , 1-*c*-Pr), 1.15 and 0.65 (2 H each, CH_2 , 4-*c*-Pr), 1.10 (3 H, t, OCH_2CH_3). ^{13}C NMR (C_6D_6): δ 198.9 (C=O, C1), 196.2 (C=O, C4), 166.4 [C(q), C2], 99.9 (CH, C3), 64.5 (OCH_2), 21.2 and 20.8 (CH each, *c*-Pr), 13.8 (CH_3), 11.6 and 10.5 (2 CH_2 each, *c*-Pr). IR (diffuse reflection), cm^{-1} (%): $\nu = 1696.4$ (60) and 1689.2 (55) [$\nu(C=O)$], 1577.3 [$\nu(C=C)$].

MS (70 eV), m/e (%): 208 (30) [M^+], 180 (40), 179 (30) [$M^+ - Et$], 140 (40), 114 (40), 69 (100) [$C_3H_5CO^+$]. Anal. Calcd for $C_{12}H_{16}O_3$ (208.3): C, 69.21; H, 7.74. Found: C, 69.54; H, 7.62.

(*Z*)-**6f**. 1H NMR (C_6D_6): δ 6.60 (1 H, s, 3-H), 4.05 (2 H, q, OCH_2), 2.15 (1 H, m, 1'-H, 1-*c*-Pr), 2.00 (1 H, m, 1'-H, 4-*c*-Pr), 1.20 and 0.70 (2 H each, CH_2 , 1-*c*-Pr), 1.15 and 0.60 (2 H each, CH_2 , 4-*c*-Pr), 1.05 (3 H, t, OCH_2CH_3). ^{13}C NMR (C_6D_6): δ 199.0 and 198.9 (C=O each, C1 and C4), 157.3 [C(q), C2], 111.2 (CH, C3), 69.6 (OCH_2), 22.2 and 21.3 (CH each, *c*-Pr), 15.2 (CH_3), 12.4 and 11.2 (2 CH_2 each, *c*-Pr). IR (diffuse reflection), cm^{-1} (%): $\nu = 1684.4$ (60) [$\nu(C=O)$], 1604.2 (55) [$\nu(C=C)$]. MS (70 eV), m/e (%): 208 (30) [M^+], 216 (40), 215 (50) [$M^+ - Et$], 175 (40), 105 (70), 69 (100).

7f. 1H NMR (C_6D_6): δ 5.80 (1 H, s, 4-H), 3.75 (2 H, q, OCH_2), 1.90 and 1.65 (1 H each, m each, 1'-H, *c*-Pr), 1.25 (3 H, t, OCH_2CH_3), 0.95, 0.65, 0.60 (4:2:2 H, m each, CH_2 , *c*-Pr). GC-IR, cm^{-1} (%): $\nu = 1637.1$ and 1422.0 [$\nu(C=C)$] and [$\nu(C-H)$]. MS (70 eV), m/e (%): 192 (80) [M^+], 164 (30), 163 (40) [$M^+ - Et$], 149 (20), 137 (10), 95 (10), 69 (100).

Acknowledgment. This work was supported by the Volkswagen-Stiftung and the Fonds der Chemischen Industrie.

OM940834O

Naphthyl: Osmium and Ruthenium Cluster Derivatives

William R. Cullen,* Steven J. Rettig, and Tu Cai Zheng

Chemistry Department, University of British Columbia, Vancouver,
British Columbia, Canada V6T 1Z1

Received November 7, 1994[®]

Reaction of the 1-naphthyl derivatives $E(1-C_{10}H_7)_3$ ($E = P, As$) with $M_3(CO)_{12}$ ($M = Ru, Os$) affords the series of naphthyl complexes $M_3(CO)_8(\mu-H)_2[\mu_3-\eta^4-(C_{10}H_7)_2E(C_{10}H_5)]$ (**5-8**) in moderate to good yield, via double metalation of the unsubstituted aromatic ring. Metalation of the substituted aromatic ring results in one complex, $Os_3(CO)_9(\mu-H)[(C_{10}H_7)_2P-(C_{10}H_6)]$. Cleavage of an As-naphthyl bond affords a low yield of the naphthyl complex $Ru_4(CO)_{10}(\mu-CO)[\mu_4-As(C_{10}H_7)][\mu_4-C_{10}H_6]$ (**11**), in which the aryl ring is at an angle of 75° to the Ru_4 plane and acts as a four-electron donor, making **11** formally electron deficient. Crystals of **5** are monoclinic, with $a = 25.746(1) \text{ \AA}$, $b = 9.688(2) \text{ \AA}$, $c = 33.521(1) \text{ \AA}$, $\beta = 108.647(3)^\circ$, $Z = 8$, and space group $C2/c$. Those of **11** are triclinic, with $a = 11.433(3) \text{ \AA}$, $b = 14.746(2) \text{ \AA}$, $c = 9.958(1) \text{ \AA}$, $\alpha = 96.81(1)^\circ$, $\beta = 102.34(2)^\circ$, $\gamma = 78.69(2)^\circ$, $Z = 2$, space group $P\bar{1}$. The structures were solved by the Patterson method and were refined by full-matrix least-squares procedures to $R = 0.033$ and 0.030 ($R_w = 0.031$ and 0.028) for 5308 and 4933 reflections with $I \geq 3\sigma(I)$, respectively.

Introduction

The thermolysis of phosphine or arsine derivatives of $M_3(CO)_{12}$ ($M = Ru, Os$) is a well-established method of preparing aryl derivatives of metal clusters such as the benzyne, ferrocene, and (benzyne)chromium tricarbonyl derivatives **1-4**.¹⁻⁴ In some cases the derivatives

There are no reports of naphthyl complexes of metal clusters; therefore, it was of interest to establish if these could be prepared by pyrolysis reactions. The present paper describes the successful synthesis of such derivatives via the reaction of tris(1-naphthyl)arsine and -phosphine with $M_3(CO)_{12}$ ($M = Ru, Os$).

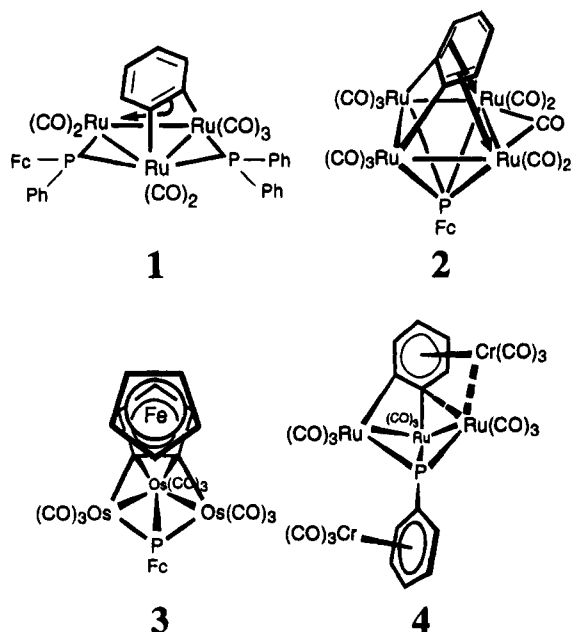
Experimental Section

The methodology used for the experiments described below was essentially the same as that described in earlier papers from these laboratories.^{3,4} Tris(1-naphthyl)phosphine was obtained from Strem Chemicals; the corresponding arsine was prepared from arsenic trichloride and 1-bromonaphthalene.⁵

Pyrolysis of $Os_3(CO)_{12}$ with $As(1-C_{10}H_7)_3$. A solution of $Os_3(CO)_{12}$ (200 mg, 0.22 mmol) and $As(1-C_{10}H_7)_3$ (90 mg, 0.20 mmol) in octane (40 mL) was refluxed for 25 h. TLC revealed the presence of at least 10 products, while 1H NMR spectroscopy showed only two major hydride resonances at -17.69 and -21.65 ppm. The reaction solvent was removed in vacuo, and the residue was chromatographed on silica with 4/1 petroleum ether/ CH_2Cl_2 as eluent. The major second band (65%) contained complex **5**. Crystals of **5** suitable for X-ray structure analysis were obtained from a 2/1 hexane/ CH_2Cl_2 solution.

5: yellow solid; 1H NMR (400 MHz) δ 8.51 (m, 1H), 8.45 (m, 1H), 8.20 (m, 1H), 8.03 (m, 2H), 7.93-7.82 (m, 3H), 7.79 (m, 1H), 7.70 (m, 1H), 7.50-7.38 (m, 5H), 7.38-7.31 (m, 3H), 7.27 (m, 1H), -17.69 (s, 1H, Os satellite, $J_{H-Os1} = 27.6$, $J_{H-Os2} = 43.8$ Hz), -21.65 (s, 1H, Os satellite, $J_{H-Os1} = 28.0$, $J_{H-Os2} = 45.6$); mass spectrum (FAB) m/e 1252 (P^+ , base peak), 1224, 1196, 1167, 1138, 1110, 1094, 1080, 1066, 1052, 1037, 1024, 982, 969, 954, 940, 928, 912, 898, 884, 870, 856, 843, 829, 703. Anal. Calcd for $C_{38}H_{21}AsO_8Os_3$: C, 36.48; H, 1.69. Found: C, 36.55; H, 1.74.

Pyrolysis of $Ru_3(CO)_{12}$ with $As(1-C_{10}H_7)_3$. A solution of triruthenium dodecacarbonyl (128 mg, 0.20 mmol) and $As(1-C_{10}H_7)_3$ (95 mg, 0.21 mmol) in cyclohexane (30 mL) was refluxed for 10 h. 1H NMR spectroscopy revealed the presence



are more easily obtained by pyrolyzing $M_3(CO)_{12}$ with the appropriate arsine or phosphine.

[®] Abstract published in *Advance ACS Abstracts*, January 15, 1995.
(1) Bennett, M. A.; Schwemlein, H. P. *Angew. Chem., Int. Ed. Engl.* **1989**, *28*, 1296. For a recent example see: Cullen, W. R.; Rettig, S. J.; Zhang, H. *Organometallics* **1991**, *10*, 2965.
(2) (a) Zheng, T. C.; Cullen, W. R.; Rettig, S. J. *Organometallics* **1994**, *13*, 3594. (b) Knox, S. A. R.; Lloyd, B. R.; Morton, D. A. V.; Nicholls, S. M.; Orpen, A. G.; Vinas, J. M.; Weber, M.; Williams, G. K. *J. Organomet. Chem.* **1990**, *394*, 385. (c) Bruce, M. I.; Cullen, W. R.; Humphrey, P. A.; bin Shawkataly, O.; Snow, M. R.; Tiekink, E. R. T. *Organometallics* **1990**, *9*, 2910.

(3) Cullen, W. R.; Rettig, S. J.; Zheng, T. C. *Organometallics* **1992**, *11*, 928.

(4) (a) Cullen, W. R.; Rettig, S. J.; Zhang, H. *Organometallics* **1991**, *10*, 2965. (b) Cullen, W. R.; Rettig, S. J.; Zhang, H. *Organometallics* **1992**, *11*, 1000.

(5) Michaelis, A. *Justus Liebig's Ann. Chem.* **1902**, *321*, 242.

of two hydrides of equal intensity. The solvent was removed in vacuo, and the residue was chromatographed on silica with 4/1 petroleum ether/CH₂Cl₂ as eluent. The first band gave Ru₃(CO)₁₂ (5%). The third and major band contained complex **7** (70%); the fourth band contained trace amounts of **11**, which on evaporation afforded crystals and which was identified only by X-ray crystallography.

7: yellow solid; ¹H NMR (200 MHz) δ 8.46 (m, 2H), 8.08 (d, 1H), 8.02 (d, 1H), 7.91 (m, 2H), 7.86–7.72 (m, 4H), 7.58 (m, 1H), 7.44–7.14 (m, 8H), –15.93 (s, 1H), –20.35 (s, 1H); mass spectrum (FAB) *m/e* 984 (P⁺, base peak), 956, 928, 900, 871, 843, 815, 787, 759, 630. Anal. Calcd for C₃₈H₂₁AsO₈Ru₃: C, 46.40; H, 2.15. Found: C, 46.57; H, 2.09.

Pyrolysis of Os₃(CO)₁₂ with P(1-C₁₀H₇)₃. A solution of Os₃(CO)₁₂ (180 mg, 0.19 mmol) and P(1-C₁₀H₇)₃ (80 mg, 0.19 mmol) in octane (30 mL) was refluxed for 24 h. TLC revealed the presence of more than eight products. ³¹P NMR spectroscopy revealed three major resonances at 51.1, 42.4, and 30.9 ppm, and a number of minor ones. The reaction solvent was removed in vacuo, and the residue was chromatographed on Florisil with 3/1 petroleum ether/CH₂Cl₂ as eluent. The first band contained unreacted Os₃(CO)₁₂ (3%), identified by TLC and microanalysis. The fourth, fifth, and sixth bands contained complexes **6** (35%), **9** (30%), and **10** (10%), respectively.

6: yellow solid; ³¹P NMR (121.4 MHz) δ 30.9; ¹H NMR (200 MHz) δ 8.86 (m, 2H), 8.1–6.8 (m, 17H), –17.59 (d, 1H, *J* = 5.6 Hz), –21.47 (d, 1H, *J* = 30.8); mass spectrum (FAB) *m/e* 1208 (P⁺, base peak), 1180, 1152, 1124, 1096, 1068, 1039, 1011, 983, 856, 730. Anal. Calcd for C₃₈H₂₁O₈Os₃P: C, 37.81, H, 1.75. Found: C, 37.89; H, 1.79.

9: brown solid; ³¹P NMR (121.4 MHz) δ 51.1; ¹H NMR (200 MHz) δ 8.3–6.8 (m), –18.53 (d, *J* = 37.7, satellite, *J*_{H–Os1} = 44.0, *J*_{H–Os2} = 31.2 Hz); mass spectrum (FAB) *m/e* 1236 (P⁺, base peak), 1208, 1181, 1151, 1124, 1095, 1067, 1039, 1011, 984, 855, 731. Anal. Calcd for C₃₈H₂₁O₉Os₃P: C, 37.92; H, 1.71. Found: C, 37.99; H, 1.84.

10: orange solid; ³¹P NMR (121.4 MHz) δ 42.3; ¹H NMR (200 MHz) δ 8.6 (m), 8.2–7.7 (m), 7.6–6.8 (m); mass spectrum (FAB) *m/e* 1292 (P⁺), 1264, 1236, 1208 (base peak), 1181, 1153, 1125, 1096, 1067, 1039, 1011, 984, 856. Anal. Calcd for C₄₁H₂₁O₁₁Os₃P: C, 38.14; H, 1.64. Found: C, 38.00; H, 1.87.

Pyrolysis of Ru₃(CO)₁₂ with P(1-C₁₀H₇)₃. A solution of Ru₃(CO)₁₂ (130 mg, 0.20 mmol) and P(1-C₁₀H₇)₃ (80 mg, 0.20 mmol) in cyclohexane (30 mL) was refluxed for 24 h. TLC and ³¹P NMR spectroscopy revealed the presence of two major products and three minor ones. The solvent was removed in vacuo, and the residue was chromatographed on silica with 4/1 petroleum ether/CH₂Cl₂ as eluent. The first band contained unreacted Ru₃(CO)₁₂ (5%). The second band contained complex **8** (50%). The third band contained complex **12** (15%), which was not further identified.

8: yellow solid; ³¹P NMR (81.0 MHz) δ 68.7; ¹H NMR (400 MHz) δ 9.05 (m, 1H), 8.27–8.15 (m, 2H), 8.10 (d, 2H), 8.04 (m, 1H), 7.92–7.78 (m, 4H), 7.73 (m, 1H), 7.46–7.34 (m, 4H), 7.30 (m, 1H), 7.22 (m, 1H), 7.16 (m, 1H), 7.07 (m, 1H), –15.78 (d, 1H, *J* = 5.2 Hz), –19.88 (d, 1H, *J* = 37.4); mass spectrum (FAB) *m/e* 941 (P⁺), 913, 885, 857, 829, 800, 771, 743, 728, 714 (base peak), 585. Anal. Calcd for C₃₈H₂₁O₈PRu₃: C, 48.57; H, 2.25. Found: C, 48.66; H, 2.32.

12: pink-brown solid; ³¹P NMR (81.0 MHz) δ 71.9; ¹H NMR (200 MHz) δ 8.30–8.65 (complex m); mass spectrum (FAB) *m/e* 1067 (P⁺, base peak), 1038, 1012, 984, 956, 928, 914, 900, 883, 872, 855, 844, 827, 814, 800, 771, 744, 714, 645, 615, 596, 568, 540, 527, 512.

X-ray Crystallographic Analyses of 5 and 11. Crystallographic data for **5** and **11** appear in Table 1. The final unit-cell parameters were obtained by least-squares refinement on the setting angles for 25 reflections with 2θ = 33.5–37.1 and 33.8–38.5°, respectively, for **5** and **11**. The intensities of 3 standard reflections, measured every 200 reflections throughout the data collections, showed only small random fluctua-

Table 1. Crystallographic Data^a

compd	5	11
formula	C ₃₈ H ₂₁ AsO ₈ Os ₃	C ₃₁ H ₁₃ AsO ₁₁ Ru ₄
fw	1251.10	1040.64
cryst syst	monoclinic	triclinic
space group	C2/c	P1
<i>a</i> , Å	25.746(1)	11.433(3)
<i>b</i> , Å	9.688(2)	14.746(2)
<i>c</i> , Å	33.521(1)	9.958(1)
α, deg	90	96.91(1)
β, deg	108.647(3)	102.34(2)
γ, deg	90	78.69(2)
<i>V</i> , Å ³	7922(2)	1602.9(6)
<i>Z</i>	8	2
<i>ρ</i> _{calc} , g/cm ³	2.098	2.156
<i>F</i> (000)	4592	992
μ, cm ⁻¹	104.81	29.33
cryst size, mm	0.25 × 0.30 × 0.35	0.10 × 0.15 × 0.30
transmissn factors	0.62–1.00	0.79–1.00
scan type	ω	ω–2θ
scan range in ω, deg	1.04 + 0.35 tan θ	1.31 + 0.35 tan θ
scan speed, deg/min	16 (up to 8 rescans)	32 (up to 8 rescans)
data collected	+ <i>h</i> , + <i>k</i> , ± <i>l</i>	+ <i>h</i> , + <i>k</i> , ± <i>l</i>
2θ _{max} , deg	60	60
cryst decay, %	negligible	negligible
total no. of reflns	12 461	9766
total no. of unique reflns	12 919	9330
<i>R</i> _{merge}	0.044	0.036
no. of reflns with <i>I</i> ≥ 3σ(<i>I</i>)	5308	4933
no. of variables	452	424
<i>R</i>	0.033	0.030
<i>R</i> _w	0.031	0.028
GOF	1.84	1.42
max Δσ (final cycle)	0.02	0.001
residual density, e/Å ³	–0.72 to +1.17 (near Os)	–0.52 to +0.64

^a Conditions: temperature 294 K, Rigaku AFC6S diffractometer, Mo Kα radiation (λ = 0.710 69 Å), graphite monochromator, takeoff angle 6.0°, aperture 6.0 × 6.0 mm at a distance of 285 mm from the crystal, stationary background counts at each end of the scan (scan/background time ratio 2/1, up to 8 rescans), σ²(*F*²) = [*S*²(*C* + 4*B*)]/Lp² (*S* = scan rate, *C* = scan count, *B* = normalized background count), function minimized Σw(|*F*_o| – |*F*_c|)², where *w* = 4*F*_o²/σ²(*F*_o²), *R* = Σ||*F*_o| – |*F*_c||/Σ|*F*_o|, *R*_w = (Σw(|*F*_o| – |*F*_c||)²/Σw|*F*_o|²)^{1/2}, and GOF = [Σw(|*F*_o| – |*F*_c||)²/(*m* – *n*)]^{1/2}. Values given for *R*, *R*_w, and GOF are based on those reflections with *I* ≥ 3σ(*I*).

tions in each case. The data were processed⁶ and corrected for Lorentz and polarization effects and absorption (empirical, based on azimuthal scans for 3 reflections).

Both structures were solved by heavy-atom methods, the coordinates of the heavy atoms being determined from the Patterson functions and those of the remaining non-hydrogen atoms from subsequent difference Fourier syntheses. In both cases there were space group ambiguities. The structure analyses were initiated (and successfully completed) in centrosymmetric space groups (C2/c and P1) on the basis of the number of molecules in the unit cell and the Patterson functions. All non-hydrogen atoms were refined with anisotropic thermal parameters. One of the metal hydrides of **5** was included in a difference map position, and the other could not be located. The carbon-bound hydrogen atoms were fixed in idealized positions (C–H = 0.98 Å, *B*_H = 1.2*B*_{bonded atom}). A secondary extinction correction (Zachariasen isotropic type I) was applied for **5**, the final value of the extinction coefficient being [3.51(7)] × 10⁻⁸. Neutral atom scattering factors for all atoms and anomalous dispersion corrections for the non-hydrogen atoms were taken from ref 7. Final atomic coordinates and equivalent isotropic thermal parameters are given in Tables 2 and 3, and selected bond lengths and angles appear

(6) (a) TEXSAN/TEXRAY Structure Analysis Package; Molecular Structure Corp., The Woodlands, TX, 1985. (b) *teXsan*, Crystal Structure Analysis Package; Molecular Structure Corp., The Woodlands, TX, 1985 and 1992.

(7) (a) *International Tables for X-Ray Crystallography*; Kynoch Press: Birmingham, England, 1974; Vol. IV, pp 99–102. (b) *International Tables for X-Ray Crystallography*; Kluwer Academic: Boston, 1992; Vol. C, pp 200–206.

Table 2. Final Atomic Coordinates (Fractional) and B_{eq} Values (\AA^2) for 5^a

atom	x	y	z	B_{eq}
Os(1)	0.235704(14)	0.53486(4)	0.074674(11)	3.01(1)
Os(2)	0.33844(2)	0.37428(5)	0.079042(12)	4.01(2)
Os(3)	0.34416(2)	0.59720(4)	0.131375(12)	3.82(2)
As(1)	0.17907(3)	0.63425(9)	0.11367(3)	2.92(4)
O(1)	0.1581(3)	0.2962(8)	0.0464(2)	5.9(4)
O(2)	0.1899(3)	0.7004(8)	-0.0070(2)	7.3(4)
O(3)	0.4552(4)	0.2719(12)	0.1208(3)	10.1(6)
O(4)	0.2949(5)	0.0940(10)	0.0436(3)	9.4(6)
O(5)	0.3633(4)	0.4995(9)	0.0023(3)	8.4(5)
O(6)	0.4503(3)	0.5124(10)	0.1977(3)	8.3(5)
O(7)	0.3232(4)	0.8095(11)	0.1913(3)	9.5(6)
O(8)	0.4086(4)	0.7661(13)	0.0878(3)	12.5(7)
C(1)	0.2763(3)	0.4505(9)	0.1347(2)	2.8(3)
C(2)	0.3196(4)	0.3637(10)	0.1363(3)	3.7(4)
C(3)	0.3448(4)	0.2885(10)	0.1746(3)	4.3(5)
C(4)	0.3271(4)	0.2977(11)	0.2080(3)	4.3(4)
C(5)	0.2830(4)	0.3871(9)	0.2071(3)	3.3(4)
C(6)	0.2622(5)	0.4010(11)	0.2414(3)	4.9(5)
C(7)	0.2189(4)	0.4879(11)	0.2390(3)	4.2(5)
C(8)	0.1930(4)	0.5567(9)	0.2034(3)	3.4(4)
C(9)	0.2111(3)	0.5454(9)	0.1687(2)	2.7(3)
C(10)	0.2565(3)	0.4613(9)	0.1703(2)	2.9(4)
C(11)	0.1032(3)	0.5719(9)	0.0958(3)	3.2(4)
C(12)	0.0905(4)	0.4564(11)	0.1132(3)	4.3(4)
C(13)	0.0370(5)	0.4046(11)	0.1005(3)	5.4(5)
C(14)	-0.0035(4)	0.4714(14)	0.0714(4)	6.1(6)
C(15)	0.0080(4)	0.5903(12)	0.0521(3)	4.7(5)
C(16)	-0.0338(4)	0.6606(14)	0.0197(4)	6.3(6)
C(17)	-0.0230(5)	0.7713(14)	-0.0006(4)	6.4(6)
C(18)	0.0301(4)	0.8201(11)	0.0095(3)	5.0(5)
C(19)	0.0724(4)	0.7571(11)	0.0401(3)	4.4(4)
C(20)	0.0627(3)	0.6421(10)	0.0626(3)	3.3(4)
C(21)	0.1785(3)	0.8311(9)	0.1243(3)	3.3(4)
C(22)	0.2162(4)	0.9071(10)	0.1120(3)	4.2(4)
C(23)	0.2247(5)	1.0491(11)	0.1207(4)	5.5(6)
C(24)	0.1975(5)	1.1112(11)	0.1440(4)	5.8(6)
C(25)	0.1583(4)	1.0422(11)	0.1583(3)	4.7(5)
C(26)	0.1297(5)	1.1106(12)	0.1822(4)	6.3(6)
C(27)	0.0917(6)	1.0419(15)	0.1947(4)	6.9(7)
C(28)	0.0786(5)	0.9000(14)	0.1821(4)	6.2(6)
C(29)	0.1059(4)	0.8305(10)	0.1595(3)	4.3(5)
C(30)	0.1472(4)	0.8966(10)	0.1471(3)	3.8(4)
C(31)	0.1852(4)	0.3898(11)	0.0567(3)	3.8(4)
C(32)	0.2068(4)	0.6368(11)	0.0229(3)	4.6(5)
C(33)	0.4111(5)	0.3060(14)	0.1051(4)	6.8(7)
C(34)	0.3114(5)	0.1976(14)	0.0551(3)	6.1(6)
C(35)	0.3553(4)	0.4523(11)	0.0308(4)	5.0(5)
C(36)	0.4101(4)	0.5414(12)	0.1729(3)	5.2(5)
C(37)	0.3302(4)	0.7297(13)	0.1688(4)	5.7(6)
C(38)	0.3842(5)	0.7018(15)	0.1045(4)	7.5(7)

$$^a B_{\text{eq}} = \frac{8}{3}\pi^2 \sum U_{ij} a_i a_j (\mathbf{a}_i \cdot \mathbf{a}_j)$$

in Tables 4 and 5, respectively. Hydrogen atom parameters, anisotropic thermal parameters, complete tables of bond lengths and bond angles, torsion angles, intermolecular contacts, and least-squares planes are included as supplementary material. Structure factors are available from the authors on request.

Results and Discussion

Pyrolysis of $\text{Os}_3(\text{CO})_{12}$ with $\text{As}(\text{1-C}_{10}\text{H}_7)_3$ in octane for 25 h affords one major product (**5**) and some minor ones as judged by TLC.

Complex **5** gives a parent ion at m/e 1252 in the mass spectrum, corresponding to the formula $\text{Os}_3(\text{CO})_8[\text{As}(\text{1-C}_{10}\text{H}_7)_3]$. The ^1H NMR spectrum shows the presence of only 19 naphthyl protons and two hydrides; consequently, a formulation such as $\text{Os}_3(\text{CO})_8(\text{H})_2[(\text{1-C}_{10}\text{H}_7)_2\text{As}(\text{1-C}_{10}\text{H}_5)]$ seems likely. A single crystal structure determination confirms this formulation, and an ORTEP diagram of the molecule is shown in Figure 1.

The molecular structure of **5** consists of a closed Os_3 triangle capped on one face by a naphthyl moiety

Table 3. Atomic Coordinates and B_{eq} Values for 11^a

atom	x	y	z	B_{eq}
Ru(1)	0.71132(4)	0.26098(3)	0.05264(4)	2.829(9)
Ru(2)	0.77466(4)	0.12764(3)	0.24448(4)	3.023(9)
Ru(3)	0.86849(4)	0.26004(3)	0.45879(4)	2.877(9)
Ru(4)	0.79901(4)	0.39849(3)	0.25808(4)	3.040(9)
As(1)	0.90783(4)	0.24035(3)	0.22430(5)	2.62(1)
O(1)	0.5779(3)	0.1000(2)	-0.0027(4)	5.0(1)
O(2)	0.4993(4)	0.3501(3)	-0.1573(4)	6.4(1)
O(3)	0.8266(4)	0.1682(3)	-0.1824(4)	5.8(1)
O(4)	0.6683(6)	-0.0182(3)	0.3435(6)	10.8(2)
O(5)	0.9307(4)	-0.0304(3)	0.1099(4)	5.5(1)
O(6)	0.7629(4)	0.3744(3)	0.6960(4)	6.3(1)
O(7)	0.9473(4)	0.0758(3)	0.5878(4)	6.4(1)
O(8)	1.1162(4)	0.3172(4)	0.5616(4)	7.0(1)
O(9)	0.6731(5)	0.5379(3)	0.4555(5)	8.5(2)
O(10)	0.7028(4)	0.5023(3)	-0.0005(4)	6.5(1)
O(11)	1.0369(4)	0.4735(3)	0.3255(5)	7.1(1)
C(1)	0.6795(4)	0.2618(3)	0.3538(5)	3.0(1)
C(2)	0.6472(4)	0.3266(3)	0.2540(5)	3.0(1)
C(3)	0.5233(5)	0.3676(3)	0.2095(5)	3.5(1)
C(4)	0.4340(5)	0.3427(3)	0.2597(5)	3.7(1)
C(5)	0.4605(5)	0.2785(3)	0.3624(5)	3.3(1)
C(6)	0.3675(5)	0.2570(4)	0.4203(6)	4.3(1)
C(7)	0.3942(6)	0.2020(4)	0.5255(7)	4.9(2)
C(8)	0.5156(6)	0.1649(4)	0.5788(6)	4.8(2)
C(9)	0.6070(5)	0.1837(4)	0.5242(6)	4.0(1)
C(10)	0.5838(5)	0.2399(3)	0.4126(5)	3.1(1)
C(11)	1.0665(4)	0.1895(3)	0.1815(5)	3.2(1)
C(12)	1.1332(5)	0.1154(3)	0.2531(5)	3.7(1)
C(13)	1.2473(5)	0.0725(4)	0.2267(7)	5.2(2)
C(14)	1.2962(5)	0.1042(4)	0.1312(7)	5.1(2)
C(15)	1.2313(5)	0.1807(4)	0.0590(6)	4.0(1)
C(16)	1.2796(5)	0.2140(5)	-0.0435(7)	5.4(2)
C(17)	1.2180(7)	0.2864(6)	-0.1135(7)	6.5(2)
C(18)	1.1031(6)	0.3299(5)	-0.0902(6)	5.8(2)
C(19)	1.0526(5)	0.2998(4)	0.0061(5)	4.3(1)
C(20)	1.1140(4)	0.2252(3)	0.0820(5)	3.4(1)
C(21)	0.6514(5)	0.1405(3)	0.0638(5)	3.5(1)
C(22)	0.5779(5)	0.3182(4)	-0.0767(5)	4.1(1)
C(23)	0.7827(5)	0.2047(4)	-0.0947(5)	3.8(1)
C(24)	0.7066(7)	0.0391(4)	0.3117(7)	5.9(2)
C(25)	0.8703(5)	0.0291(3)	0.1616(5)	3.6(1)
C(26)	0.8018(5)	0.3315(3)	0.6076(5)	3.7(1)
C(27)	0.9122(5)	0.1418(4)	0.5322(5)	4.2(1)
C(28)	1.0259(5)	0.2937(4)	0.5260(5)	4.4(1)
C(29)	0.7208(6)	0.4877(4)	0.3820(6)	5.2(2)
C(30)	0.7356(5)	0.4588(3)	0.0924(6)	4.1(1)
C(31)	0.9466(6)	0.4479(4)	0.2990(6)	4.5(1)

$$^a B_{\text{eq}} = \frac{8}{3}\pi^2 (U_{11}(aa^*)^2 + U_{22}(bb^*)^2 + U_{33}(cc^*)^2 + 2U_{12}aa^*bb^*(\cos \gamma) + 2U_{13}aa^*cc^*(\cos \beta) + 2U_{23}bb^*cc^*(\cos \alpha))$$

which is attached to an arsenic atom coordinated to Os(1). There are eight terminal carbonyls, three each bonded to Os(2) and Os(3), two to Os(1), and two bridging hydrides, with only one being located in the structure refinement. The Os(1)–Os(2) bond at 3.0316(6) Å is the longest, and Os(2)–Os(3) at 2.7564(7) Å is the shortest. Os(1)–Os(3) has an intermediate length of 2.8950(5) Å. H(1), which was located, bridges the Os(1)–Os(3) bond, and the other hydride is believed to bridge the shortest Os(2)–Os(3) bond rather than the longest Os(1)–Os(2) bond. This argument is based on the fact that in the analogous phosphine complex **6** described below the two hydrides show very different couplings to the phosphorus atom, indicating that most likely one hydride is two bonds and the other three bonds away from the phosphorus atom. The whole cluster is electron-precise. The naphthyl moiety is bonded to Os(1) and Os(2) via two σ bonds (Os(1)–C(1) = 2.112(8), Os(2)–C(2) = 2.128(9) Å), and to Os(3) via a η^2 bond (Os(3)–C(1) = 2.281(8), Os(3)–C(2) = 2.369(9) Å). This bonding mode is very similar to that found in **1**¹ and in $\text{Os}_3(\text{CO})_9(\text{H})_2(\text{C}_6\text{H}_4)$:⁸ the C(1)–C(10) plane of **5** makes an angle of 63.64° with the Os_3 plane; in Os_3 –

Table 4. Selected Bond Lengths (Å) with Estimated Standard Deviations for **5** and **11**

Compound 5			
Os(1)–Os(2)	3.0316(6)	Os(3)–H(1)	1.87
Os(1)–Os(3)	2.8950(5)	C(3)–C(4)	1.34(1)
Os(1)–As(1)	2.446(1)	C(4)–C(5)	1.42(1)
Os(1)–C(1)	2.112(8)	C(5)–C(6)	1.42(1)
Os(1)–H(1)	1.61	C(5)–C(10)	1.40(1)
Os(2)–Os(3)	2.7564(7)	C(6)–C(7)	1.38(1)
Os(2)–C(2)	2.128(9)	C(7)–C(8)	1.34(1)
Os(3)–C(1)	2.281(8)	C(8)–C(9)	1.39(1)
Os(3)–C(2)	2.369(9)	C(9)–C(10)	1.41(1)
Compound 11			
Ru(1)–Ru(2)	2.7892(7)	Ru(1)–C(2)	2.320(4)
Ru(1)–As(1)	2.5051(8)	Ru(2)–Ru(3)	2.8934(7)
Ru(2)–As(1)	2.5146(7)	Ru(2)–C(1)	2.330(4)
Ru(3)–As(1)	2.4445(6)	Ru(3)–Ru(4)	2.9062(7)
Ru(4)–C(2)	2.195(5)	Ru(3)–C(1)	2.187(5)
C(1)–C(2)	1.403(6)	Ru(4)–As(1)	2.4399(6)
C(2)–C(3)	1.424(6)	C(1)–C(10)	1.450(6)
C(4)–C(5)	1.421(7)	C(3)–C(4)	1.355(7)
C(5)–C(10)	1.418(7)	C(5)–C(6)	1.414(7)
C(7)–C(8)	1.401(8)	C(6)–C(7)	1.348(8)
C(9)–C(10)	1.414(7)	C(8)–C(9)	1.363(7)
Ru(1)–Ru(4)	2.8704(7)		

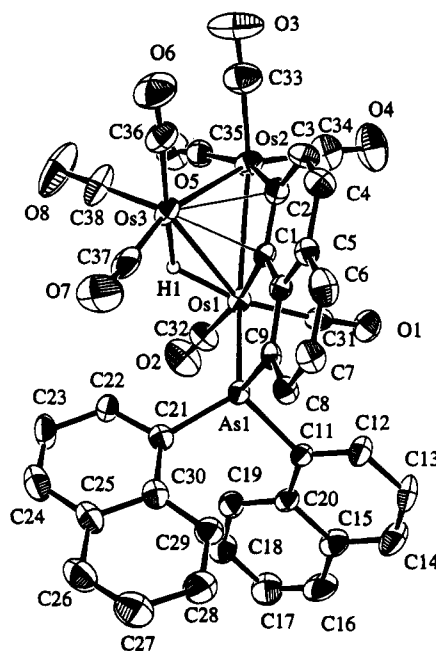
Table 5. Selected Bond Angles (deg) with Estimated Standard Deviations for **5** and **11**

Compound 5			
Os(2)–Os(1)–Os(3)	55.37(1)	Os(1)–Os(2)–Os(3)	59.80(1)
Os(2)–Os(1)–As(1)	146.76(3)	Os(1)–Os(2)–C(2)	67.7(3)
Os(2)–Os(1)–C(1)	66.2(2)	C(2)–C(1)–C(10)	120.2(8)
Os(2)–Os(1)–C(31)	97.8(3)	C(1)–C(2)–C(3)	118.2(8)
Os(3)–Os(1)–C(1)	51.4(2)	Os(1)–Os(3)–Os(2)	64.83(1)
Compound 11			
Ru(2)–Ru(1)–Ru(4)	91.14(2)	Ru(2)–C(1)–C(2)	104.7(3)
Ru(2)–Ru(3)–Ru(4)	88.37(2)	Ru(2)–C(1)–C(10)	109.5(3)
Ru(1)–Ru(2)–Ru(3)	91.18(2)	Ru(3)–C(1)–C(10)	125.9(3)
Ru(1)–As(1)–Ru(4)	70.95(2)	Ru(1)–C(2)–Ru(4)	78.9(1)
Ru(2)–As(1)–Ru(3)	71.37(2)	Ru(1)–C(2)–C(3)	104.4(3)
Ru(2)–C(1)–Ru(3)	79.6(1)	Ru(4)–C(2)–C(3)	122.8(3)
Ru(1)–Ru(4)–Ru(3)	89.31(2)	Ru(1)–C(21)–Ru(2)	86.1(2)

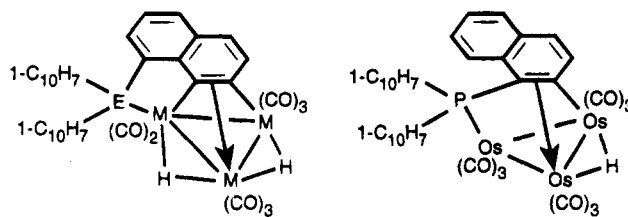
(CO)₉(H)₂(C₆H₄) the corresponding angle is 63.9 (and 69.0°).⁸ The torsion angle Os(2)C(2)C(1)Os(1) is 64.7°, with Os(1) and Os(2) on opposite sides of the naphthyne plane at distances of 0.230 and 0.048 Å, respectively.

In naphthalene the C–C bond lengths are of three types, as follows (using the numbering shown in Figure 1): "C(1)–C(2)", "C(3)–C(4)", "C(6)–C(7)", and "C(8)–C(9)", 1.377(2) Å; "C(2)–C(3)", "C(7)–C(8)", 1.411(2) Å; the remainder, 1.424(2) Å.⁹ This pattern is seen in the bond lengths of the naphthyne moiety of **5** with no apparent difference being observed for the η²-bound C(1)–C(2) bond (1.38(1) Å), although the data are not good enough for much comment. The shortening of C(7)–C(8) to 1.34(1) Å may be unusual.

Pyrolysis of Os₃(CO)₁₂ with P(1-C₁₀H₇)₃ in octane for 24 h affords more than eight products with three (**6**, **9**, **10**) in major quantities, as judged by TLC and ³¹P and ¹H NMR spectroscopy. Complex **6** shows a ³¹P NMR resonance at 30.9 ppm, suggesting the presence of a phosphine. The ¹H NMR spectrum shows complex resonances in the aromatic proton region and the presence of two hydrides. The hydride chemical shifts are very similar to those of **5**. The mass spectrum (parent ion at *m/e* 1207) and the microanalysis are consistent with the formulation Os₃(CO)₈(H)₂[(1-C₁₀H₇)₂P-

**Figure 1.** ORTEP diagram for **5** (33% probability thermal ellipsoids).

(1-C₁₀H₅). Complex **6** undoubtedly has the same basic structure as **5**.



M	E
5	Os As
6	Os P
7	Ru As
8	Ru P

Pyrolysis of Ru₃(CO)₁₂ with As(1-C₁₀H₇)₃ in cyclohexane for 10 h affords one major product, complex **7**. This derivative shows a complex ¹H NMR spectrum, but a 2D proton–proton correlation NMR study supports the presence of 19 naphthyl protons with one unique naphthyl group containing only five hydrogen atoms. The two hydride resonances are similar to those of the osmium naphthyne complexes **5** and **6**, and the mass spectrum gives the parent ion at *m/e* 984, consistent with the formula Ru₃(CO)₈(H)₂[(1-C₁₀H₇)₂As(1-C₁₀H₅)]. The structure of **7** is undoubtedly analogous to that of **5**. Likewise, complex **8**, obtained from the reaction of Ru₃(CO)₁₂ with P(1-C₁₀H₇)₃, shows spectroscopic properties that are consistent with formulation as the naphthyne complex Ru₃(CO)₈(H)₂[(1-C₁₀H₇)₂P(1-C₁₀H₅)].

Compounds **7** and **8** are not only the first naphthyne complexes of a ruthenium cluster to be isolated, they are also the first aryne complexes of a ruthenium cluster known to have a structure analogous to the osmium benzyne derivative Os₃(CO)₉(H)₂(C₆H₄) discussed above. It is interesting to note that naphthyne complexes of this structure are formed in all the reactions of M₃(CO)₁₂ (M = Ru, Os) with E(1-C₁₀H₇)₃ (E = P, As). This is a rare example of a series of complexes in both Ru₃ and Os₃ systems with both phosphorus- and arsenic-based ligands. The best known series of benzyne complexes

(8) Goudsmit, B. T.; Johnson, B. F. G.; Lewis, J.; Raithby, P. R.; Rosales, M. J. *J. Chem. Soc., Dalton Trans.* **1983**, 2257.

(9) Ponomarev, V. I.; Filipenko, O. S.; Atovmjan, L. O. *Kristallografiya* **1976**, *21*, 392.

for both Ru₃ and Os₃ systems is M₃(CO)₇(C₆H₄)(ER₂)₂ of structure **1**; however, the combination M = Ru, E = As is unknown at this present time.¹

The naphthyne complexes from As(1-C₁₀H₇)₃ are formed in higher yield than from P(1-C₁₀H₇)₃ for both the Os₃ series (65% compared to 35%) and the Ru₃ series (70% compared to 50%). This may correlate with the increased length of the As–C₁₀H₇ bond.

Complex **9**, obtained from the reaction of Os₃(CO)₁₂ with P(1-C₁₀H₇)₃, shows a ³¹P NMR resonance at 51.1 ppm, suggesting the presence of a phosphine. The ¹H NMR spectrum is very complex between 6.8 and 8.3 ppm, but a hydride resonance at –18.53 ppm is present. The mass spectrum gives a parent ion at *m/e* 1236 corresponding to the formulation Os₃(CO)₉(H)[(1-C₁₀H₇)₂-P(1-C₁₀H₆)]. The hydride chemical shift is similar to that of related aryl complexes such as Os₃(CO)₉(H)[(C₅H₄-PPhC₆H₄)Fe(C₅H₅)]¹⁰ and Os₃(CO)₉H(PMePh(C₆H₄)),¹¹ and a corresponding structure is proposed. This complex would be formed via an initial ortho-metalation reaction. Complex **10**, isolated from the same reaction mixture, shows a ³¹P NMR resonance at 42.4 ppm, suggesting the presence of a phosphine. The ¹H NMR spectrum again is very complex. The mass spectrum gives the parent ion at *m/e* 1292, consistent with the monosubstituted complex Os₃(CO)₁₁[P(1-C₁₀H₇)₃]. The microanalytical data are in accord.

Ortho-metalation reactions such as that leading to **9** are believed to be the first step in the formation of cluster-bound arynes such as **1–4**: cluster-assisted P(As)–C bond cleavage completes the reaction. However, P(As)–naphthyl cleavage does not seem to be a major reaction pathway largely because of the ready formation of **5–8**, and only a few crystals of a complex (**11**) in which As–C cleavage did occur were isolated. The structure of **11** is shown in Figure 2.

The aryne moiety in **11** is bound to one side of a Ru₄ plane and an arsinidene to the other. The resemblance to the benzyne derivative **2** is immediately apparent; however, there are important structural differences.

First, the naphthyne sits at an angle of 75.3° to the metal plane. This is much closer to 90° than is found in any other aryne of structure **1** or **2**. For example in **2** the dihedral angle between the benzyne and the Ru₄ plane is 51.1°.² Second, in **2** two of the ruthenium atoms lie close to the benzyne plane (0.056 and 0.027 Å); i.e., they are almost coplanar with the aryne. In **11** Ru(3) and Ru(4) lie respectively 0.767 and 0.976 Å from the naphthyne plane. Third, Ru(4)–C(2) (2.195(5) Å) and Ru(3)–C(1) (2.187(5) Å) are longer than the corresponding bonds in **2** (2.116(6) and 2.119(6) Å), and the pair Ru(2)–C(1) (2.330(4) Å) and Ru(1)–C(2) (2.320(4) Å) seem to be slightly longer than the corresponding bonds in **2** (2.306(6) and 2.317(6) Å).

The net result of this increase in tilt angle and bond lengths of **11** is that the distances Ru(2)–C(10) and Ru(1)–C(3) at 3.199(5) and 3.256(5) Å are too great to permit any significant bonding interaction. In **2**, where there is η² interaction, the equivalent distances are 2.625(7) and 2.612(7) Å. Thus, it seems that the bonding of the naphthyne moiety in **11**, unlike the benzyne in **2**, is not satisfactorily explained in terms of

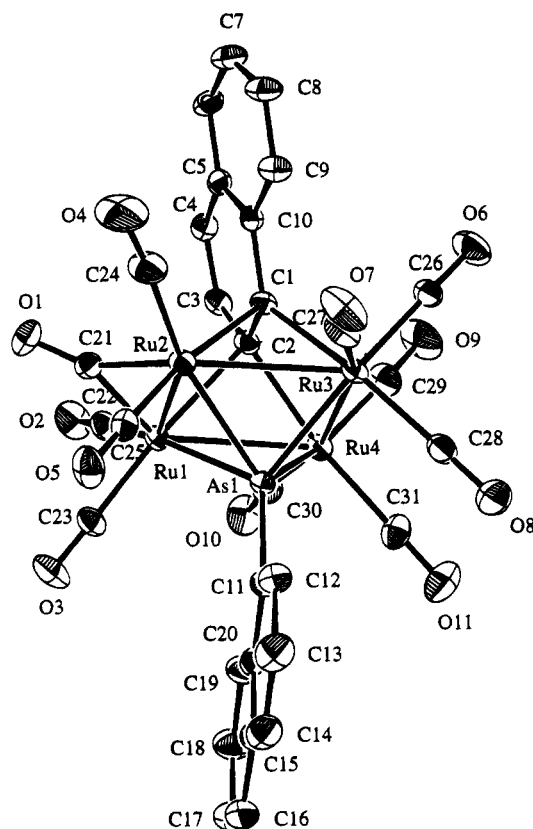


Figure 2. ORTEP diagram for **11** (33% probability thermal ellipsoids).

a six-electron donor comprising two σ plus two η² interactions.

The naphthyne in **11** seems to be a four-electron donor to the cluster, as is the aryne in **1**, **3**, and **5**; however, in **11** the four electrons are supplied via four σ bonds, whereas in the others the source is two σ and one η² bond. This model formally makes **11** electron deficient, as there is nothing in the other metrical data to indicate an alternative source of these electrons, in contrast to the situation found in **4**, where Cr–Ru bonds are unexpectedly present.

When the C–C bond lengths of the naphthyne moiety of **11** are compared with those of naphthalene, listed above, the shortest bonds in **11** are as expected C(3)–C(4) (1.355(7) Å), C(6)–C(7) (1.348(7) Å), and C(8)–C(9) (1.363(7) Å), with the exception of C(1)–C(2) (1.403(6) Å), whose length has increased as a consequence of the μ₄ bonding. Other changes are less significant; for example, the lengths of the pairs C(2)–C(3) (1.424(6) Å) and C(7)–C(8) (1.401(8) Å) are much the same as in naphthalene (1.411(2) Å).

Acknowledgment. We thank the Natural Sciences and Engineering Research Council of Canada for financial support.

Supplementary Material Available: Tables of hydrogen atom parameters, anisotropic thermal parameters, all bond lengths and bond angles, torsion angles, intermolecular contacts, and least-squares planes for **5** and **11** (42 pages). Ordering information is given on any current masthead page.

OM9408425

(10) Cullen, W. R.; Rettig, S. J.; Zheng, T. C. *Can. J. Chem.* **1992**, *70*, 2215.

(11) Deeming, A. J.; Kabir, S. E.; Powell, N. J.; Bates, P. A.; Hursthouse, M. B. *J. Chem. Soc., Dalton Trans.* **1987**, 1529.

Photolysis of Vinyltris(trimethylsilyl)silane. Formation and Observation of a Silene and a Silylene in Primary Steps

S. Zhang, M. B. Ezhova, and R. T. Conlin*

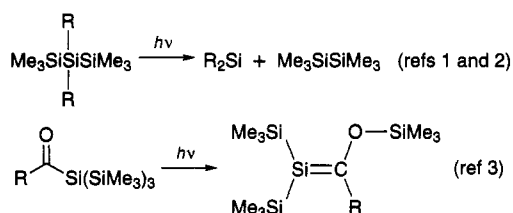
Center for Organometallic Research and Education, Department of Chemistry,
University of North Texas, Denton, Texas 76203

Received November 15, 1994[®]

Photolysis of cyclohexane solutions containing vinyltris(trimethylsilyl)silane produces both the isomeric silene and silylene fragmentation products (trimethylsilyl)vinylysilylene and hexamethyldisilane as primary pathways. Both types of transients produced the expected five- and six-membered rings from reactions with dienes as shown by chemical trapping studies. In reactions with 2-trimethylsiloxybutadiene, the position of the trimethylsiloxy substituent on the π bond in both silacycloalkenes, initially allylic to silicon, isomerized at room temperature to the presumably more stable vinylic isomer. Low-temperature UV spectra as well as chemical trapping studies with triethylsilane, methanol, and a variety of dienes support this mechanistic interpretation.

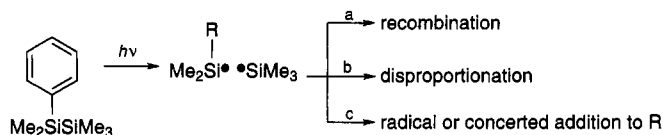
Introduction

Polysilanes containing three consecutive silicon atoms and an additional chromophore on the central metalloid atom have been especially useful photochemical sources of divalent silicon.^{1,2} On the other hand, when the silicon atoms of the polysilane are arranged in a tris(trimethylsilyl)silyl group with an acyl chromophore on the central silicon, photochemical isomerization cleanly leads to 2-trimethylsiloxy-substituted silenes³ that are significantly less reactive^{4,5} than a typical silylene.⁶



Of interest to us has been the possibility of photolyzing a single precursor that yields both types of reactive

silicon-containing transients, silenes and silylenes, from elementary steps.⁷ It may seem that numerous precursors are capable of such processes from absorption of a photon,⁸ but radical pathways can complicate the interpretation.⁹ For example, it has been pointed out that, from photolysis of arylsilylanes, radical pathways can intervene and provide products that appear to require primary silene intermediates.¹⁰ When such silyl radicals, produced from Si-Si bond homolysis by absorption of a 254-nm photon,¹¹ are formed in close proximity (solvent cage), they may initiate a variety of secondary reactions. Among these are (a) recombination of the geminate radicals, (b) disproportionation to hydridosilanes and the corresponding silene intermediates,¹² and (c) addition of one silyl radical to an unsaturated substituent of the other radical. This latter pathway might also proceed with a concerted component, geometry permitting.^{9,13}



A possible distinction between reaction paths suggested from product studies and those paths supported

[®] Abstract published in *Advance ACS Abstracts*, January 15, 1995.

(1) Ishikawa, M.; Kumada, M. *Adv. Organomet. Chem.* **1981**, *19*, 51.

(2) Michalczyk, M. J.; Fink, M. J.; De Young, D. J.; Carlson, C. W.; Welsh, K. W.; West, R.; Michl, J. *Silicon, Germanium, Tin Lead Compd.* **1986**, *9*, 75. West, R.; Fink, M. J.; Michl, J. *Science (Washington, D.C.)* **1981**, *214*, 1343.

(3) For reviews of silene chemistry, see: (a) Brook, A. G.; Baines, K. *Adv. Organomet. Chem.* **1986**, *25*, 1. (b) Raabe, G.; Michl, J. In *The Chemistry of Organic Silicon Compounds*; Patai, S., Rappoport, Z., Eds.; Wiley: New York, 1989; Vol. 2, p 1015. (c) Wiberg, N. *J. Organomet. Chem.* **1984**, *273*, 1984. (d) Guse'nikov, L. E.; Nametkin, N. S. *Chem. Rev.* **1979**, *79*, 529.

(4) For a discussion of stabilization of silenes by the 2-siloxy substituent, see: Apeloig, Y.; Karni, M. *J. Am. Chem. Soc.* **1984**, *106*, 6676.

(5) Zhang, S.; Conlin, R. T.; McGarry, P. F.; Scaiano, J. C. *Organometallics* **1992**, *11*, 2317.

(6) For recent examples of solution kinetics of silylene reactions, see: (a) Conlin, R. T.; Netto-Ferreira, J. C.; Zhang, S.; Scaiano, J. C. *Organometallics* **1990**, *9*, 1332. (b) Konieczny, S.; Jacobs, S. J.; Braddock Wilking, J. K.; Gaspar, P. P. *J. Organomet. Chem.* **1988**, *341*, C17. (c) Levin, G.; Das, P. K.; Bilgrien, C.; Lee, C. L. *Organometallics* **1989**, *8*, 1206. Levin, G.; Das, P. K.; Lee, C. L. *Organometallics* **1988**, *7*, 1231. (d) Shizuka, H.; Tanaka, H.; Tonokura, K.; Murata, K.; Hiratsuka, H.; Ohshita, J.; Ishikawa, M. *Chem. Phys. Lett.* **1988**, *143*, 225. (e) Gaspar, P. P.; Holten, D.; Konieczny, S.; Corey, J. *Acc. Chem. Res.* **1987**, *20*, 329.

(7) Some stable silenes have been reported to rearrange on photolysis: Baines, K. M.; Brook, A. G.; Ford, R. R.; Lickiss, P. D.; Saxena, A. K.; Chatterton, W. J.; Sawyer, J. F.; Behnam, B. A. *Organometallics* **1989**, *8*, 693.

(8) Miller, R. D.; Michl, J. *Chem. Rev.* **1989**, *89*, 1359.

(9) Slugget, G. W.; Leigh, W. L. *J. Am. Chem. Soc.* **1992**, *114*, 1195. More recent results from Professor Leigh's group suggest that both concerted and stepwise eliminations can occur in competition: Slugget, G. W.; Leigh, W. *Organometallics* **1992**, *11*, 3731. A possible silatriene intermediate has been identified by nanosecond flash photolysis experiments on phenylpentamethyldisilane: Shizuka, H.; Okasaki, K.; Tanaka, M.; Ishikawa, M.; Sumitani, M.; Yoshihara, K. *Chem. Phys. Lett.* **1985**, *113*, 89.

(10) Sakurai, H.; Nakadaira, Y.; Kira, M.; Sugiyama, H.; Yoshida, K.; Takiguchi, T. *J. Organomet. Chem.* **1980**, *184*, C36.

(11) The amount of energy available to 1 from a 254-nm photon corresponds 112 kcal/mol and clearly is sufficient to achieve silicon-silicon bond homolysis.

(12) Hawari, J. A.; Griller, D.; Weber, W. P.; Gaspar, P. P. *J. Organomet. Chem.* **1987**, *326*, 335.

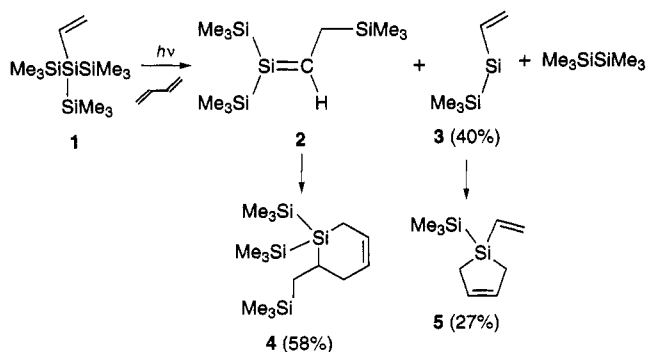
by spectral observation must be recognized. The difficulty is the sometimes tenuous connection between the spectral signal and the reaction pathway attributed to the reactive intermediate. The anticipated correspondence between the macro- and microscopic experiments can be misleading when the method of spectral detection (electronic transitions as UV, ESR, LIF, etc.) is typically many orders of magnitude more sensitive than the techniques used for product analysis (NMR, IR, etc.). Within these constraints, however, direct observation of the transient species in combination with chemical trapping studies can offer valuable support for a reaction mechanism.

Vinyltris(trimethylsilyl)silane (**1**), a structure containing both the polysilanyl and vinyl chromophores, was a likely photochemical precursor to such reactive intermediates. Previous photolyses of 1,2-divinyltetramethyldisilanes^{14–16} indicated an uncomplicated isomerization to a transient silene that was captured by a variety of trapping agents. At the outset of this study, several questions pertinent to mechanisms of the photolysis of functionalized polysilane were addressed. For example, what primary intermediates can be observed by UV/visible spectroscopy using a low-temperature organic glass for matrix isolation of the reactive species? Of additional importance was the possibility of supporting the spectral assignments with unambiguous chemical trapping studies.

Results and Discussion

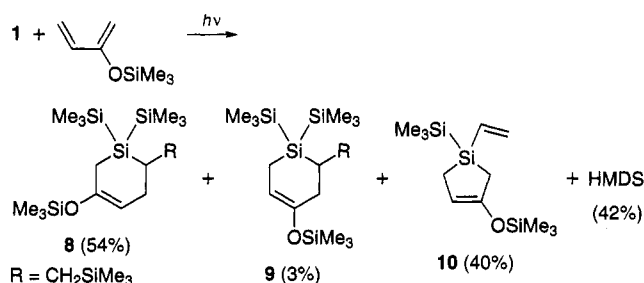
Reactions. Vinyltris(trimethylsilyl)silane (**1**) was synthesized in good yield by addition of vinylmagnesium bromide to tris(trimethylsilyl)chlorosilane and isolated by distillation at reduced pressure. Cophotolysis of hexane solutions of **1** was done with different trapping agents, such as 1,3-dienes, and those containing a heteroatom, such as alcohols and also silyl hydrides. It has been shown previously that the first two groups of reagents yield characteristically different products from silylenes and silenes while silyl hydrides are unreactive with silenes.

Photolysis of **1** (0.28 M) in a 20-fold excess of butadiene in hexane yielded adducts of 1,1-bis(trimethylsilyl)-2-(trimethylsilyl)methylsilene (**2**) and of vinyl-(trimethylsilyl)silylene (**3**) to butadiene. Three new products, silacyclohex-3-ene **4** (58% yield), silacyclopent-3-ene **5** (27%), and hexamethyldisilane (HMDS, 40%) were detected by analytical gas chromatography after 16 h photolysis based on ~80% decomposition. Products were isolated and characterized by NMR and mass spectroscopy.

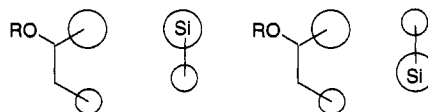


The five-membered ring **5**, from silylene addition to butadiene, is also photosensitive and undoubtedly subject to the secondary photochemical reactions of vinyl-disilanes described above.¹⁷ This suggestion is supported by detection of a product, <1%, whose mass, 236, indicated a product containing a 1:1 ratio of **5** and butadiene and also by the slightly smaller yield of **5** than HMDS. Similar results have been obtained from photolysis of **1** and 2,3-dimethylbutadiene: silacyclohex-4-ene **6** (58%), silacyclopent-3-ene **7** (27%), and HMDS (40%) were isolated and identified. Again, some secondary photodecomposition of the vinyl-disilane **7** can account for formation of small amounts of a product, *m/z* 292, containing one silylene unit and two parts 2,3-dimethylbutadiene.¹⁸

When the diene π system is polarized by an electron donor as in 2-(trimethylsiloxy)-1,3-butadiene, addition of silene **2** yielded both six-membered ring regioisomers, **8** (54%) and **9** (3%); as well as the silylene product **10** (40%) and HMDS (42%).



The orientation of the major Diels–Alder cycloadduct is consistent with predictions from frontier orbital theory, *i.e.*, interaction of the silene LUMO and the 2-(trimethylsiloxy)butadiene HOMO. We consider a picture in which the cycloaddition commences with formation of the stronger silicon–carbon bond (I) preceding formation of the slightly weaker carbon–carbon bond (II). Orbital interactions between the larger lobes of the β -substituted carbon atom of the siloxy-substituted diene HOMO and of the silicon atom of the silene LUMO can account for the greater than 10-fold preference of **8** over **9**.⁴ It is also noteworthy that silene **2**, unlike many other silenes generated photochemically or thermally, did not yield products from insertion into the silicon–oxygen bond of the siloxydiene but instead added exclusively to the organic π electron system.



The position of the double bond in the major cycloadducts **8** and **10** is relatively unstable as both structures

(13) For permutations of the arylsilylene photorearrangement, see: Ishikawa, M.; Sakamoto, H.; Kanetani, F. *Organometallics*, **1989**, *8*, 2767. A mechanistic distinction between path *c* and a direct 1,3 silyl shift (concerted) depends on the depth of the potential well describing the putative radical pair.

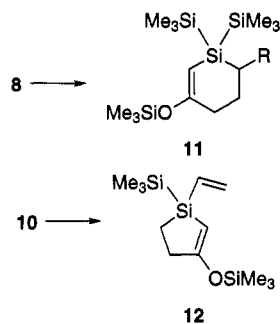
(14) Ishikawa, M.; Fuchikami, T.; Kumada, M. *J. Organomet. Chem.* **1978**, *149*, 37.

(15) Conlin, R. T.; Bobbitt, K. L. *Organometallics* **1987**, *46*, 1406.

(16) Ishikawa, M.; Nishimura, Y.; Sakamoto, H. *Organometallics* **1991**, *10*, 2701.

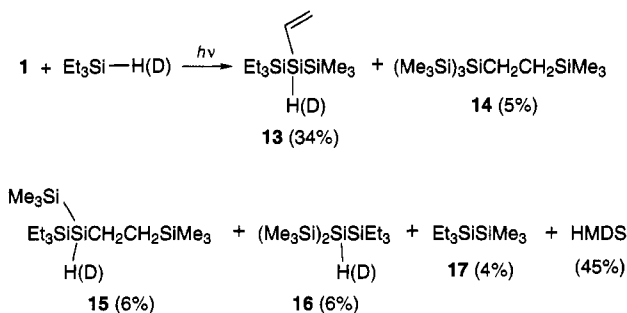
(17) Kira, M.; Maruyama, M.; Sakurai, H. *J. Am. Chem. Soc.* **1991**, *113*, 3986.

rearrange at room temperature in CDCl_3 to vinylsilanes **11** and **12** over days.



The rate of isomerization of **8** is dependent on the solvent, proceeding about twice as fast in chloroform as in benzene. A possible explanation for the faster rate of isomerization in chloroform is that a small amount of ethanol, typically present in tenths of a percent as a stabilizing agent in chloroform, is sufficient to catalyze migration of the π bond.¹⁹ This result, apparently at equilibrium, suggests that the position of the π bond is thermodynamically more stable when it is vinylic to silicon instead of allylic.

In contrast to the apparently uncomplicated trapping studies of 1,3-dienes that offer convincing evidence for both silene **2** and silylene **3** reaction pathways, probing the photolysis with triethylsilane leads to a complex mixture of products. The major product **13** (34% yield), from insertion of vinyl(trimethylsilyl)silylene (**3**) into the silicon hydrogen bond of the silane, is a trisilane and also photosensitive. Indicative of secondary photolysis is the formation of triethyltrimethyldisilane **17** (4%), the mixed disilane, possibly a secondary product from irradiation of the **13**. Secondary photolysis of the products is suggested by increased formation of HMDS (60%). This result suggests that trimethylsilyl radicals are formed in some part of the reaction sequence. The mechanistic origin of products **14** (5%), **15** (6%), and **16** (6%) is less clear but at some step in the formation of products **14** and **15**,

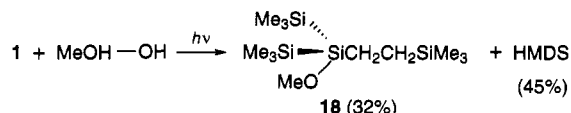


however, it appears that a trimethylsilyl radical has added to the terminal position of the vinyl group on silyl-substituted silicon. A third type of trapping experiment, one that takes advantage of the polarity of the $\text{Si}=\text{C}$ π bond, is the formal insertion into a protic O-H

(18) An alternative mechanistic description of products containing two butadienes and one silylene unit has been reported: Bobbitt, K. L.; Gaspar, P. P. *Organometallics* **1991**, *10*, 2772. In those experiments, it is believed that the primary product, a transient 2-vinylsilylirane, reacted with another molecule of butadiene.

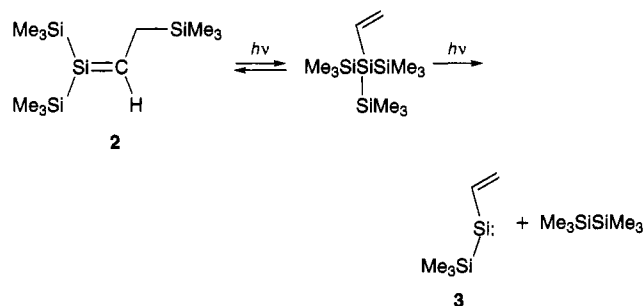
(19) Another possibility is that chloroform solutions, when exposed to air, can become slightly acidic: Gordon, A. G.; Ford, R. A. In *The Chemist's Companion*; Wiley, Inc.: New York, 1972.

bond.^{20,21} Cophotolysis of a methanol solution of **1** yields **18** (32%), the methanol adduct to the silene **2**, and HMDS (43%).



Curiously the silylene insertion product was not formed in sufficient yield to isolate but was detected by GC/MS in trace amounts (<2%). It is quite likely that the product from the silylene insertion, a vinyldisilane, is also photolabile.²²

Although the product yields reported in this work indicate that both a silene and silylene are produced from irradiation of **1**, we have reservation about commenting on the ratio of the two pathways. There are at least two reasons for deferring a mechanistic discussion of factors influencing the ratio. One is that the extent of secondary photolysis of the products, a function of quantum yields of photolysis for the five- and six-membered rings, the respective silylene and silene products, is unknown. Another possible complication is that the relatively long-lived silene **2**, in the absence of effective trapping agents, may also undergo secondary photoreactions as well as scavenge the vinyl(trimethylsilyl)silylene.²³ When triethylsilane is the silylene trap, anomalies in the product distribution (relatively higher yields of HMDS than those observed with diene reactants) suggest that **2** can photoisomerize back to starting material **1**. On continued irradiation, photolysis of regenerated **1** in turn can produce increased amounts of silylene and HMDS.



Spectroscopy. The silene and silylene intermediates can be observed by photolysis of **1** (10^{-3} M) in a 3-methylpentane (3-MP) glass at 77 K. Two new absorptions were observed at 316 and 376 nm (Figure 1) and, on the basis of the lifetime of the two signals upon warming the matrix, were assigned to silene **2** and silylene **3**, respectively. In a 3-MP glass doped with 10^{-2} M triethylsilane, the disappearance of the signal at 376 nm was essentially instantaneous while the 316-nm

(20) Brook, A. G.; Safa, K. D.; Lickiss, P. D.; Baines, K. M. *J. Am. Chem. Soc.* **1985**, *107*, 4339.

(21) Jones, P. R.; Bates, T. F. *J. Am. Chem. Soc.* **1987**, *109*, 4339.

(22) A preliminary report of the photolysis of $\text{MeOSi}(\text{SiMe}_3)_3$ has been described for the synthesis of 1,1-bis(trimethylsilyl)silyliranes: Gaspar, P. P.; Berger, D. L. XXVII Organosilicon Symposium, Rensselaer Polytechnic Institute, Troy, NY, March 18-19, 1994. For additional examples, see: Lei, D.; Chen, Y. S.; Boo, B. H.; Frueh, J.; Svoboda, D. L.; Gaspar, P. P. *Organometallics* **1992**, *11*, 559.

(23) We thank a reviewer for offering the interesting suggestion that the photoisomerization of **1** to the corresponding silene, **2**, may be reversible. Such reactions have been reported for variously substituted silenes in refs 3 and 7.

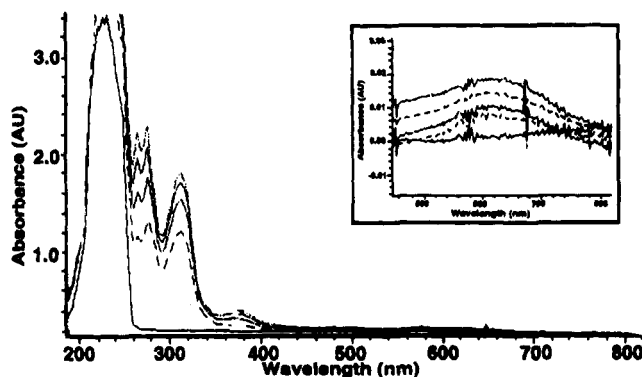


Figure 1. Low-temperature UV spectrum of the photolysate of **1** (1.4×10^{-3} M) at 77 K in 3-methylpentane. Spectra were recorded at 5-min intervals. The inset is an expansion ($\times 10$) of the region between 500 and 800 nm.

signal persisted with a half-life of ~ 2.5 min during warming of the matrix. Both the position and lifetimes of the absorptions seemed in accord with similar spectral assignments.^{4,24} Analysis of the matrix melt by GC/MS allowed identification of the silylene insertion product **13** and a product whose mass spectrum, m/e 548, indicated a dimer of silene **2**. Presumably at lower temperatures and in a medium that efficiently removes the silylene, the concentration of the silene was sufficiently high for dimerization. The position of the absorption for the silylene at 376 nm appeared to be consistent with the only literature report² of a silyl-substituted silylene 368 nm. Nonetheless, recent theoretical calculations of the position for the $n \rightarrow p$ electronic transition in a variety of substituted silylenes predict that the long-wavelength absorption of a silyl-silylene should exhibit a pronounced "red" shift.²⁴

In view of this prediction and observations of broad and relatively weak absorptions at > 600 nm for the low-temperature spectra of several trimethylsilyl-substituted silylenes,^{25,26} we have looked closely for weak absorptions in the photolysis of **1** (see inset of Figure 1). Upon expansion of the region from 500 to 800 nm in the low-temperature UV spectrum, a very weak absorption at ~ 619 nm may be the $n \rightarrow p$ transition of the vinyl(trimethylsilyl)silylene. Also noted is a gradual change in the position of an absorption from 284 to 278 nm when the 3-MP glass is warmed (Figure 2). The position of this relatively high-energy transition is typical of alkyl-substituted silyl radicals²⁷⁻²⁹ as well as other reactive organosilicon transients.^{30,31} Given the possible complexities of reactions between silene and silylene intermediates and new, uncharacterized transients,^{32,33} an assignment of this signal is open.

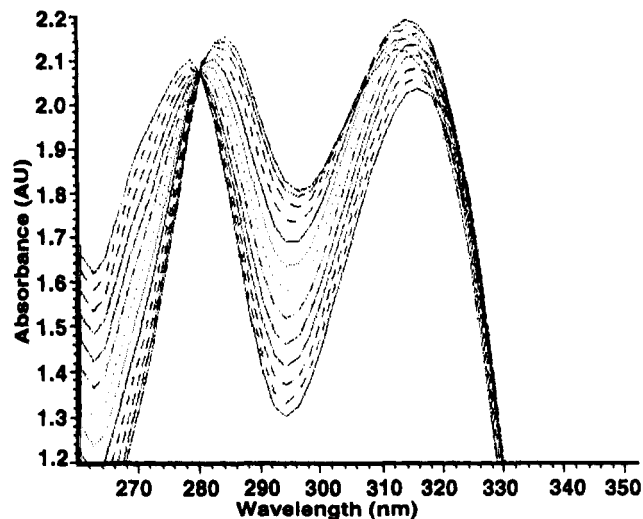


Figure 2. Expansion of the low-temperature UV spectrum for the photolysate of **1** upon annealing the 3-MP glass. Spectra were recorded at 2-min intervals starting from the uppermost trace.

The use of three different types of chemical traps provides different methods of indirectly detecting the reactive species obtained from photolysis of the polysilane **1**. The bimolecular trapping studies that provided the fewest number of reaction products were those with dienes. From the product studies with 2-(trimethylsilyloxy)butadiene, it appears that isomerization of **1** to the silene is the major pathway, accounting for $\sim 60\%$ of the products. Formation of both HMDS and the five-membered rings in slightly smaller amounts suggests that silylene production from **1** is the minor path, $\sim 40\%$.

Some possible reaction pathways were supported and others eliminated by chemical trapping with deuterio-triethylsilane. The product from insertion of trimethylsilyl(vinyl)silylene into the Si-D bond, **13**, bears the new Si-D bond on the formerly divalent silicon atom. From the well-established assumption that products containing a deuterium atom geminal to a triethylsilyl group originate from insertion into the silicon-deuterium bond of triethyldeuteriosilane, it appears that **15** is a secondary product from addition of a trimethylsilyl radical to **13**. Similarly, addition of the same silyl radical to the starting material, **1**, can account for formation of **14**. The immediate precursor to the silyl radicals is not known nor is the reaction sequence leading to **16**. It is interesting, however, that no evidence for radical intermediates is observed when dienes are the trapping agents.

Unlike the silene produced from photolysis of 1,2-divinyltetramethyldisilane that yielded *cis*- and *trans*-3-vinylsiletanes as the major products from **2** + **2** cycloadditions,¹⁴ only **2** + **4** adducts were observed from

(31) The position of λ_{\max} for the UV spectra of silenes can range from relatively short wavelengths, 244 nm for matrix-isolated dimethylsilene,^{30a} to longer wavelength absorptions for 1,1-disilylated silenes (~ 340 nm).^{3a} A comparison between the λ_{\max} of silene **2** and 1,1-dimethyl-2-trimethylsilylmethylsilene from photolysis of vinylpentamethyldisilane, both in a 3-MP glass, shows that replacement of the two methyl groups with trimethylsilyl groups displaces the silene absorption from 272 to 318 nm: Zhang, S.; Conlin, R. T., unpublished results.

(32) Slugget, G. W.; Leigh, W. J. *Organometallics* **1993**, *11*, 3731.

(33) Spectral shifts of the transients from low-temperature UV spectra of oxy-substituted polysilane photolyses have been attributed to conformational changes of the reactive intermediate: Gillette, G. R.; Noren, G.; West, R. *Organometallics* **1991**, *9*, 2925.

(24) Apeloig, Y.; Karni, M. *J. Chem. Soc., Chem. Commun.* **1985**, 1048.

(25) Conlin, R. T.; Banks, K. E.; Wang, Y., XXVth annual Silicon Symposium, U. of Southern California, Los Angeles, CA, April 3-4, 1992.

(26) Kira, M.; Maruyama, T.; Sakurai, H. *Chem. Lett.* **1993**, 1345. Marshall, P.; Tan, C.; Wang, Y.; Conlin, R. T., to be submitted for publication.

(27) Chatgililoglu, C.; Scaiano, J. C.; Ingold, K. U. *Organometallics* **1982**, *1*, 466.

(28) Chatgililoglu, C.; Guerra, M. *J. Am. Chem. Soc.* **1990**, *112*, 2854.

(29) Brix, T.; Paul, U.; Potzinger, P.; Reimann, B. *J. Photochem. Photobiol. A* **1990**, *54*, 19.

(30) (a) Gusel'nikov, L. E.; Volkova, V. V.; Avakyan, V. G.; Nametkin, N. S.; Voronekov, M. G.; Kirpichenko, S. V.; Suslova, E. N. *J. Organomet. Chem.* **1983**, *254*, 173. (b) Maier, G.; Mihm, G.; Reisenhauer, H. P. *Chem. Ber.* **1984**, *117*,

silene **2**. When 2,3-dimethylbutadiene was the trapping agent, both silene **2** and silylene **3** adducts were formed in addition to HMDS. "Ene" products, however, commonly formed in gas and liquid phase reactions between allylic C-H bonds of methyl-substituted dienes and olefins,³ were not detected.

Experimental Section

General Information. Photolyses were done on deoxygenated solutions at room temperature in a Rayonet reactor equipped with 16 medium-pressure Hg lamps. All syntheses were carried out in an atmosphere of Ar or dry nitrogen. ¹H, ¹³C, and ²⁹Si NMR spectra were recorded on a Varian Gemini 200 or Varian VXR 300 spectrometer using C₆D₆ or CDCl₃ as lock solvents. Mass spectra were determined on a HP 5970 mass-selective analyzer coupled to a HP 5790A gas chromatograph. Ultraviolet spectra were recorded on a HP 8451A diode array spectrometer. High-resolution mass spectra were obtained at Rice U. Reaction products were isolated by gas chromatography (20% OV-17 column, 15 ft × 0.24 in. on Chromosorb W). Elemental analyses were performed by E + R Microanalytical Laboratories. Yields were based on the percent photodecomposition of **1** using octane as an inert internal standard and are approximate as discussed below.

The ratio of silene to silylene pathways is suggested from the relative amounts of six- and five-membered ring products when dienes were the trapping agent. A complication is that the ratio of **6** to **5** (a trisilane and a disilane, respectively), changed from 1.8 after 5 h irradiation to 2.2 after 16 h when butadiene was the trapping agent. Since one or both of the products might undergo some secondary photolysis, product yields were subject to some error, ±10%. Photolysis yields, measured with triethylsilane, were more difficult to measure accurately because the major reactive intermediate, a relatively long-lived silene produced in ~60% yield, does not react with silyl hydrides but most certainly scavenges the trimethylsilyl(vinyl)silylene. The reported yields are based on percent decomposition of **1** measured with *n*-octane and the percent formation of hexamethyldisilane. The difference between these numbers was taken to be the yield of silene from **1** that was available for reaction. For example, after 16 h of irradiation, decomposition of **1** was ~60–80% and the relative amount of the silylene available for reaction was ~30%. When triethylsilane served as the trapping agent, the yields were based on the percent decomposition and formation of the insertion product, **13**, but have an ambiguous meaning as discussed in the text. The purpose of trapping with triethylsilane was to provide a wider overview of the reactivity of (trimethylsilyl)vinylsilylene.

Synthesis of Vinyltris(trimethylsilyl)silane (1). Vinylmagnesium bromide, 38 mL (1 M THF; 38 mmol), was added dropwise to an ice-cooled solution of 5.4 g (19 mmol) of tris(trimethylsilyl)chlorosilane^{34,35} in 100 mL of THF. After 4 h stirring at room temperature the solution was poured onto 100 g of crushed ice; this was followed by three extractions with diethyl ether (50-mL portions). The combined organic layers were dried over anhydrous sodium sulfate and distilled under reduced pressure to yield 3.9 g (75%) of **1** as a clear semisolid. Pure samples of **1** used for photolysis were obtained by preparative GLC on a OV-17 column at 150 °C; mp = 118 °C.

Vinyltris(trimethylsilyl)silane ((Me₃Si)₃SiCH=CH₂, **1):** ¹H NMR (CDCl₃) δ 0.18 (27 H, s, SiMe₃), 5.66 (1H, d of d, *J*_{HaHb} = 3.9 Hz, *J*_{HcHa} = 19.5 Hz, =CH_a), 5.93 (1H, d of d, *J*_{HaHb} = 3.9 Hz, *J*_{HcHb} = 13.9 Hz, =CH_b), 6.08 (1H, d of d, *J*_{HaHc} = 19.5 Hz, *J*_{HbHc} = 13.9 Hz, CH_c=); ¹³C NMR (CDCl₃) δ 0.7 (q), 132.62 (d), 132.77 (t); ²⁹Si NMR (CDCl₃) δ -12.95, -83.95; MS

m/z 274 (6, M⁺), 259 (6), 201 (11), 185 (20), 174 (44), 159 (22), 129 (23), 73 (100); high-resolution MS calcd for C₁₁H₃₀Si₄ 274.1425, found 274.1430. Anal. Calcd for C₁₁H₃₀Si₄: C, 48.18; H, 11.01. Found: C, 48.33; H, 10.90.

Photolysis of **1 in 1,3-Butadiene.** A solution containing 150 mg (0.55 mmol) of **1**, 1.0 mL (-5 °C) of 1,3-butadiene (11.5 mmol), and 2 mL of cyclohexane was placed in a 25-mm-o.d. quartz tube. After degassing by three freeze/thaw cycles on a vacuum line, the solution was irradiated for 20 h. Two new adducts, 1,1-bis(trimethylsilyl)-2-((trimethylsilyl)methyl)-1-silacyclohex-4-ene (**4**, 58%) and 1-trimethylsilyl-1-vinylsilacyclohex-3-ene (**5**, 27%) as well as hexamethyldisilane (40%) were isolated by preparative gas chromatography (percentage yields are based on percent of **1** photolyzed, 73%).

1,1-Bis(trimethylsilyl)-2-[(trimethylsilyl)methyl]-1-silacyclohex-4-ene ((Me₃Si)₂SiCH₂(CH₂H_cSiMe₃)CH₂-CH=CHCH₂, **4):** ¹H NMR (CDCl₃) δ 0.01 (9H, s, SiMe₃), 0.10 (9H, s, SiMe₃), 0.14 (9H, s, SiMe₃), 0.54 (1H, d of d, *J*_{bc} = 12.6 Hz, *J*_{ab} = 15.0 Hz, H of CH₂SiMe₃), 0.72 (1H, d of d, *J*_{bc} = 12.6 Hz, *J*_{ac} = 2.1 Hz, H of CH₂SiMe₃), 1.40 (3H, m, CH_a, CH₂Si), 1.85 (1H, m, CHC=), 2.46 (1H, d of triplet, *J* = 17.1 Hz, *J* = 6.0 Hz, CHC=), 5.57 (1H, m, CH=), 5.80 (1H, m, CH=); ¹³C NMR (CDCl₃) δ -0.64 (q), -0.51 (q), 0.55 (q), 7.31 (t), 14.59 (d), 21.52 (t), 34.13 (t), 126.23 (d), 129.93 (d); ²⁹Si NMR (CDCl₃) δ -45.14, -16.60, -16.22, 1.61; GC/MS *m/e* (relative intensity) 73 (100), 131 (15), 155 (15), 167 (6), 181 (6), 199 (3), 255 (2), 328 (1); high-resolution MS calcd for C₁₅H₃₆Si₄ 328.1894, found 328.1898.

1-(Trimethylsilyl)-1-vinyl-1-silacyclohex-3-ene (Me₃-Si(CH₂=CH_aH_b)Si(CH₂CH=CHCH₂, **5):** ¹H NMR (CDCl₃) δ 0.11 (9H, s, SiMe₃), 1.48 (4H, d, *J* = 0.9 Hz (coupling between geminal protons of nonequivalent methylene protons, CH₂-SiCH₂), 5.88 (2H, t, *J* = 0.9 Hz, CH=CH), 5.72 (1H, d of d, *J*_{HaHb} = 3.9 Hz, *J*_{HcHa} = 20.1 Hz, =CH_a), 5.97 (1H, d of d, *J*_{HaHb} = 3.9 Hz, *J*_{HcHb} = 14.4 Hz, =CH_b), 6.21 (1H, d of d, *J*_{HaHc} = 20.1 Hz, *J*_{HbHc} = 14.4 Hz, H_cC=); ¹³C NMR (neat) δ -2.21 (q), 14.96 (t), 130.51 (d), 131.75 (t), 136.04 (d); GC/MS *m/e* (relative intensity) 73 (86), 85 (30), 113 (100), 139 (26), 154 (32), 167 (43), 182 (11); high-resolution MS calcd for C₉H₁₈Si₂ 182.0947, found 182.0846. A small amount of a secondary photolysis product from **5** with butadiene was observed by GC/MS, *m/e* (relative intensity) 236 (M⁺, 12), 221 (7), 208 (10), 163 (25), 162 (17), 154 (20), 141 (25), 139 (19), 135 (59), 121 (13), 109 (33), 73 (100).

Photolysis of **1 in 2,3-Dimethylbutadiene.** A solution containing **1** (150 mg, 0.55 mmol), 2,3-dimethylbutadiene 1 mL (8.8 mmol), and 1 mL of cyclohexane was placed in a 25-mm quartz tube. After purging with argon, the solution was irradiated for 16 h. Two new products, 1,1-bis(trimethylsilyl)-2-(trimethylsilyl)methyl-4,5-dimethyl-1-silacyclohex-4-ene (**6**, 55%) and 1-(trimethylsilyl)-1-vinyl-3,4-dimethyl-1-silacyclohex-3-ene (**7**, 32%), and hexamethyldisilane (43%) were isolated by preparative GC. Decomposition of **1** was 65%.

1,1-Bis(trimethylsilyl)-2-[(trimethylsilyl)methyl]-4,5-dimethyl-1-silacyclohex-4-ene ((Me₃Si)₂SiCH₂(CH₂H_cSiMe₃)CH₂H_cC(Me)=C(Me)CH₂, **6):** ¹H NMR (CDCl₃) δ 0.01 (9H, s, SiMe₃), 0.04 (9H, s, SiMe₃), 0.05 (9H, s, SiMe₃), 0.47 (1H, d of d, *J*_{bc} = 14.9 Hz, *J*_{ab} = 12.2 Hz, H of CH₂SiMe₃), 0.66 (1H, d of d, *J*_{bc} = 14.9 Hz, *J*_{ac} = 2.3 Hz, H of CH₂SiMe₃), 1.22 (1H, m, CH in ring), 1.28 (2H, br s, CH₂Si in ring), 1.61 (3H, s, CH₃), 1.66 (3H, s, CH₃), 1.82 (1H, d of d, *J*_{dc} = 13.2 Hz, *J*_{ad} = 10.0 Hz, one of H in CH₂ in ring), 2.22 (1H, d of d, *J*_{dc} = 13.2 Hz, *J*_{ac} = 6.0 Hz, H in CH₂ in ring); ¹³C NMR (neat) δ -0.59 (q), 0.45 (q), 14.76 (t), 15.80 (d), 21.00 (q), 22.63 (t), 41.29 (t), 125.31 (s), 128.04 (s); GC/MS *m/e* (relative intensity) 356 (2), 823 (9), 209 (8), 183 (30), 131 (13), 123 (13), 73 (100); high-resolution MS calcd for C₁₇H₄₀Si₄ 356.2207, found 356.2200.

1-(Trimethylsilyl)-1-vinyl-3,4-dimethyl-1-silacyclohex-3-ene ((Me₃Si)Si(CH₂=CH_aH_b)CH₂C(Me)=C(Me)CH₂, **7):** Spectral data given in ref 36.

(34) Gilman, H.; Smith, C. L. *J. Organomet. Chem.* **1967**, *8*, 245.

(35) We currently use a variation of the procedure for the synthesis of tris(trimethylsilyl)silane: Dickhaut, J.; Giese, B. *Org. Synth.* **1991**, *70*, 164. We thank Professor Giese for a preprint of this method.

(36) Barton, T. J.; Burns, G. T. *Tetrahedron Lett.* **1983**, *24*, 159.

Photolysis of 1 in 2-(Trimethylsilyloxy)-1,3-butadiene. A solution containing 150 mg (0.55 mmol) of **1**, 0.3 mL (1.7 mmol) of 2-(trimethylsilyloxy)butadiene (purified by preparative GLC), and 2 mL of cyclohexane was placed in a 25-mm-o.d. quartz tube. After purging with argon, the solution was irradiated for 40 h. Three products, 1,1-bis(trimethylsilyl)-3-(trimethylsilyloxy)-6-[(trimethylsilyl)methyl]-1-silacyclohex-3-ene (**8**, 57%), 1-trimethyl-1-vinyl-3-(trimethylsilyloxy)-1-silacyclopent-3-ene (**10**, 40%), and hexamethyldisilane (42%), were isolated. A small amount of 1,1-bis(trimethylsilyl)-4-(trimethylsilyloxy)-6-[(trimethylsilyl)methyl]-1-silacyclohex-3-ene (**9**), an isomer of **8**, was found both by ^1H NMR and GC/MS. Due to the low yield, product **9** was not isolated but the ratio of **8** to **9** was established by ^1H NMR as 9.5:1. Both **8** and **10** isomerized at room temperature over days to 1,1-bis(trimethylsilyl)-3-(trimethylsilyloxy)-6-[(trimethylsilyl)methyl]-1-silacyclohex-2-ene (**11**) and 1-trimethyl-1-vinyl-3-(trimethylsilyloxy)-1-silacyclopent-2-ene (**12**), respectively. Decomposition of **1** was 80% after 20 h.

1,1-Bis(trimethylsilyl)-3-(trimethylsilyloxy)-6-[(trimethylsilyl)methyl]-1-silacyclohex-3-ene ($(\text{Me}_3\text{Si})_2\text{SiCH}_2(\text{CH}_2\text{H}_c\text{SiMe}_3)\text{CH}_2\text{CH}=\text{C}(\text{OSiMe}_3)\text{CH}_2$, **8**): ^1H NMR (CDCl_3) δ 0.00 (9H, s, SiMe_3), 0.10 (9H, s, SiMe_3), 0.14 (9H, s, SiMe_3), 0.18 (9H, s, SiMe_3), 0.60 (1H, d of d, $J_{bc} = 11.2$ Hz, $J_{ab} = 9.0$ Hz, one of CH_2SiMe_3), 1.22 (1H, d of d, $J_{bc} = 11.2$ Hz, $J_{ac} = 7.6$ Hz, one of CH_2SiMe_3), 1.55 (1H, m), 1.86 (2H, m), 2.40 (1H, m), 4.85 (1H, m, =CH); ^{13}C NMR (CDCl_3) δ -1.08 (q), -1.00 (q), 0.19 (q), 0.16 (q), 12.27 (t), 13.73 (d), 20.06 (t), 32.31 (t), 107.55 (d), 149.09 (s); GC/MS *m/e* (relative intensity) 416 (1), 343 (3), 243 (3), 205 (4), 147 (30), 133 (16), 117 (13), 73 (100); high-resolution MS calcd for $\text{C}_{15}\text{H}_{35}\text{Si}_4$ ($P - \text{Me}_3\text{Si}$) 343.1765, found 343.1771.

1,1-Bis(trimethylsilyl)-4-(trimethylsilyloxy)-6-[(trimethylsilyl)methyl]-1-silacyclohex-3-ene (**9**). Spectroscopic evidence for **9** is limited due to the difficulty in isolating in this minor product. ^{13}C NMR spectra displayed two peaks at δ 104.00 (d) and 156.80 (s) for the sp^2 carbons while the ^1H NMR spectrum showed a multiplet centered at δ 5.07 for the olefinic H.

1-(Trimethylsilyl)-1-vinyl-3-(trimethylsilyloxy)-1-silacyclopent-3-ene ($(\text{Me}_3\text{Si})\text{Si}(\text{CH}_2=\text{CH}_a\text{H}_b)\text{CH}_2\text{C}(\text{OSiMe}_3)=\text{CHCH}_2$, **10**): ^1H NMR (CDCl_3) δ 0.12 (9H, s, SiMe_3), 0.18 (9H, s, SiMe_3), 1.42 (2H, appd s, CH_2), 1.56 (2H, appd s, CH_2), 4.93 (1H, br s, CH in ring), 5.75 (1H, d of d, $J_{\text{HaHc}} = 19.5$ Hz, $J_{\text{HaHb}} = 3.6$ Hz, = CH_a), 6.00 (1H, d of d, $J_{\text{HbHc}} = 14.3$ Hz, $J_{\text{HaHb}} = 3.6$ Hz, = CH_b), 6.23 (1H, d of d, $J_{\text{HbHc}} = 14.3$ Hz, $J_{\text{HaHc}} = 19.5$ Hz, = CH_c); ^{13}C NMR (CDCl_3) δ -2.01 (q), 0.41 (q), 11.31 (t), 18.49 (t), 106.24 (d), 132.44 (t), 136.68 (d), 154.46 (s); GC/MS *m/e* (relative intensity) 73 (100), 117 (15), 133 (29), 143 (59), 169 (6), 197 (3), 227 (14), 255 (9), 270 (4); high-resolution MS calcd for $\text{C}_{12}\text{H}_{26}\text{OSi}_3$ 270.1291, found 270.1284.

1,1-Bis(trimethylsilyl)-3-(trimethylsilyloxy)-6-[(trimethylsilyl)methyl]-1-silacyclohex-2-ene ($(\text{Me}_3\text{Si})_2\text{SiCH}_2(\text{CH}_2\text{H}_c\text{SiMe}_3)\text{CH}_2\text{CH}_2\text{C}(\text{OSiMe}_3)=\text{CH}$, **11**): ^1H NMR (CDCl_3) δ 0.00 (9H, s, SiMe_3), 0.09 (9H, s, SiMe_3), 0.12 (9H, s, SiMe_3), 0.20 (9H, s, SiMe_3), 0.49 (1H, d of d, $J_{ab} = 12.3$ Hz, $J_{bc} = 13.5$ Hz, one of CH_2SiMe_3), 0.76 (1H, appd d, $J_{bc} = 713.5$ Hz, one of CH_2SiMe_3), 1.04 (1H, appd t, CH in the ring), 1.46 (1H, m, ring H), 1.82 (1H, m, ring H), 2.3 (2H, m, ring H), 4.32 (1H, s, =CH); ^{13}C NMR (CDCl_3) δ -0.69 (q), 0.32 (q), 14.99 (d), 19.99 (t), 32.11 (t), 34.76 (t), 92.34 (d), 162.36 (s); GC/MS *m/e* (relative intensity) 73 (100), 131 (13), 133 (13), 147 (40), 181 (12), 195 (8), 205 (7), 243 (12), 255 (6), 343 (7), 401 (1, M - 15); high-resolution MS calcd for $\text{C}_{15}\text{H}_{35}\text{Si}_4$ ($M - 73$) 343.1765, found 343.1771; high-resolution mass spectra on a mixture of **8**, **9**, and **10**, calcd for $\text{C}_{12}\text{H}_{26}\text{OSi}_3$ 270.1291, found 270.1284.

1-(Trimethyl)-1-vinyl-3-(trimethylsilyloxy)-1-silacyclopent-2-ene ($(\text{Me}_3\text{Si})\text{Si}(\text{CH}_2=\text{CH}_a\text{H}_b)\text{CH}=\text{C}(\text{OSiMe}_3)\text{CH}_2\text{CH}_2$, **12**): ^1H NMR (CDCl_3) δ 0.07 (9H, s, SiMe_3), 0.21 (9H, s, SiMe_3), 0.92 (2H, m, CH_2), 2.34 (2H, m, CH_2), 4.42 (1H, t, $J = 1.5$ Hz, CH in ring), 5.68 (1H, d of d, $J_{\text{HaHc}} = 19.5$ Hz, $J_{\text{HaHb}} = 3.5$ Hz, = CH_a), 5.93 (1H, d of d, $J_{\text{HbHc}} = 14.5$ Hz, $J_{\text{HaHb}} = 3.5$

Hz, = CH_b), 6.20 (1H, d of d, $J_{\text{HbHc}} = 14.5$ Hz, $J_{\text{HaHc}} = 19.5$ Hz, = CH_c); ^{13}C NMR (neat) δ -2.08 (q), -0.26 (q), 5.14 (t), 33.94 (t), 93.06 (d), 131.42 (t), 137.73 (d), 169.79 (s); GC/MS *m/e* (relative intensity) 73 (100), 117 (13), 133 (23), 143 (45), 155 (6), 189 (2), 277 (10), 255 (7), 270 (3); high-resolution MS calcd for $\text{C}_{12}\text{H}_{26}\text{OSi}_3$ 270.1291, found 270.1284.

Photolysis of 1 in Triethylsilane. A solution containing 150 mg (0.55 mmol) of **1**, 1 mL (6.3 mmol) of triethylsilane, and 2 mL of cyclohexane was placed in a 25-mm-o.d. quartz tube. After purging with argon, the solution was irradiated for 10 h. The major products, isolated by preparative GC, were 1,1,1-trimethyl-3,3,3-triethyl-2-vinyltrisilane (**13**, 34%), tris(trimethylsilyl)[2-(trimethylsilyl)ethyl]silane (**14**, 5%), 1,1,1-trimethyl-3,3,3-trimethyl-2-[2-(trimethylsilyl)ethyl]trisilane (**15**, 6%), bis(trimethylsilyl)(triethylsilyl)silane (**16**, 6%), and trimethyltriethylsilane (**17**, 4%). Hexamethyldisilane (60%) and a trace amount of trimethylsilane were also determined by GC/MS. Trace amounts (<2%) of several other products were observed by GC/MS but were not formed in sufficient yield for isolation. Trimethyltriethylsilane was characterized by comparison with the mass spectra and ^1H and ^{13}C NMR spectra of the known compound.³⁷ Photolysis time was 12 h, and decomposition was 90%.

1,1,1-Trimethyl-3,3,3-triethyl-2-vinyltrisilane (**13**): ^1H NMR (CDCl_3) δ 0.15 (9H, s, SiMe_3), 0.69 (6H, t, $J = 5.9$ Hz, $\text{Si}(\text{CH}_2\text{C})_3$), 0.95 (9H, q, $J = 5.9$ Hz, $\text{Si}(\text{CCH}_3)_3$), 3.41 (1H, d, $J = 5.1$ Hz, SiH), 5.70 (3H, m, $\text{CH}=\text{CH}_2$); ^{13}C NMR (neat) δ -0.46 (q), 4.49 (t), 8.00 (q), 131.29 (d), 132.92 (t); GC/MS *m/e* (relative intensity) 73 (59), 87 (100), 113 (41), 115 (32), 144 (14), 159 (22), 215 (10), 216 (16), 244 (4); high-resolution MS calcd for $\text{C}_{11}\text{H}_{28}\text{Si}_3$ 144.1499, found 244.1495.

Tris(trimethylsilyl)[2-(trimethylsilyl)ethyl]silane (**14**): ^1H NMR (CDCl_3) δ -0.02 (9H, s, SiMe_3), 0.17 (27H, s, SiMe_3), 0.61 (4H, AA'BB' coupling pattern, CH_2CH_2); ^{13}C NMR (CDCl_3) δ -2.27 (q), -0.25 (t), 1.24 (q), 15.59 (t); ^{29}Si NMR (CDCl_3) δ -76.61, -12.94, 1.92; GC/MS *m/e* (relative intensity) 73 (100), 131 (13), 173 (11), 175 (17), 187 (16), 275 (11), 348 (3); high-resolution MS calcd for $\text{C}_{14}\text{H}_{40}\text{Si}_5$ 348.1976, found 348.1978.

1,1,1-Trimethyl-3,3,3-triethyl-2-[2-(trimethylsilyl)ethyl]trisilane (**15**): ^1H NMR (neat) δ -0.27 (9H, s, SiMe_3), -0.08 (9H, s, SiMe_3), 0.40 (10H, m, $\text{Si}(\text{CH}_2\text{C})_3$, CH_2CH_2), 0.74 (9H, t, $J = 5.7$ Hz, SiCH_2CH_2), 3.50 (1H, t, $J = 3.9$ Hz, SiH); ^{13}C NMR (neat) δ -2.41 (1), -0.13 (t), 0.32 (q), 4.81 (t), 8.13 (q), 15.28 (t); GC/MS *m/e* (relative intensity) 73 (100), 87 (45), 115 (31), 159 (21), 174 (47), 187 (24), 188 (26), 215 (22), 216 (81), 244 (35), 318 (2); high-resolution MS calcd for $\text{C}_{14}\text{H}_{38}\text{Si}_4$ 318.2051, found 318.2054.

Bis(trimethylsilyl)(triethylsilyl)silane (**16**): ^1H NMR (neat) δ -0.07 (18H, s, SiMe_3), 0.50 (9H, q, $J = 5.8$ Hz, $\text{Si}(\text{CH}_2\text{CH}_3)_3$), 0.71 (9H, t, $J = 5.8$ Hz, $\text{Si}(\text{CH}_2\text{CH}_3)_3$), 2.34 (1H, s, Si_3SiH). We note the unusually high field position for the hydrogen bonded to silicon. Such effects have been reported previously for the ^1H NMR spectrum of tris(trimethylsilyl)silane, in which the central atom is bonded to three trimethylsilyl groups.³⁸ ^{13}C NMR (neat) δ 1.69 (q), 5.66 (t), 7.93 (q); GC/MS *m/e* (relative intensity) 73 (100), 87 (66), 113 (21), 115 (48), 129 (23), 145 (20), 159 (32), 160 (95), 173 (13), 188 (20), 216 (22), 290 (5); high-resolution MS calcd for $\text{C}_{12}\text{H}_{34}\text{Si}_4$ 290.1738, found 290.1734.

1,1,1-Trimethyl-3,3,3-triethyl-2-vinyltrisilane (**17**): ^1H NMR (CDCl_3) δ 0.15 (9H, s, SiMe_3), 0.69 (6H, t, $J = 5.9$ Hz, $\text{Si}(\text{CH}_2\text{CH}_3)_3$), 0.95 (9H, q, $J = 5.9$ Hz, $\text{Si}(\text{CH}_2\text{CH}_3)_3$), 3.41 (1H, d, $J = 5.1$ Hz, SiH), 5.70 (3H, m, $\text{CH}=\text{CH}_2$); ^{13}C NMR (neat) δ -0.46 (q), 4.49 (t), 8.00 (q), 131.29 (d), 132.92 (t); GC/MS *m/e* (relative intensity) 73 (59), 87 (100), 113 (41), 115 (32), 114 (14), 159 (22), 215 (10), 216 (16), 244 (4); high-resolution MS calcd for $\text{C}_{11}\text{H}_{28}\text{Si}_3$ 244.1499, found 244.1495.

Photolysis of 1 in Deuteriotriethylsilane. When Et_3SiD was used instead of Et_3SiH in the photolysis, similar

(37) Fritz, G. Z. *Naturforsch.* **1952**, *7B*, 207.(38) Burger, H.; Kilian, W. J. *Organomet. Chem.* **1969**, *16*, 299.

products were isolated by preparative GC. In products **13**, **15**, and **16**, the Si-H bond became Si-D as indicated by the disappearance of an Si-H from the absorptions in ^1H NMR spectrum and an increase of one mass unit for the parent ions in the mass spectra.

Photolysis of 1 in Methanol. In a 25-mm-o.d. quartz tube were placed 150 mg (0.55 mmol) of **1** and 2 mL of methanol. After being purged with argon, the solution was irradiated for 9 h. Bis(trimethylsilyl)[2-(trimethylsilyl)ethyl]methoxysilane (**18**, 32%) and hexamethyldisilane (43%) were isolated by preparative GC. Trace amounts of the silylene insertion product methoxy(trimethylsilyl)vinylsilane were detected by GC/MS: m/e (relative abundance) 160 (1, M^+), 145 (21), 117 (43), 73 (100). Less than 5% of **1** remained after 9 h of irradiation.

Bis(trimethylsilyl)[2-(trimethylsilyl)ethyl]methoxysilane (18): ^1H NMR (neat) δ -0.33 (9H, s, SiMe_3), -0.19 (18H, s, 2SiMe_3), 0.34 (4H, AA'BB' coupling pattern, 2CH_2), 3.05 (3H, s, OCH_3); ^{13}C NMR (neat) δ -2.34 (q), -0.65 (q), 6.44 (t), 9.36 (t), 52.61 (q); GC/MS m/e (relative intensity) 73 (100), 89 (17), 117 (19), 131 (53), 175 (38), 203 (7), 233 (8), 291 (4) ($\text{M}-15$) $^+$; high-resolution MS calcd for $\text{C}_{11}\text{H}_{31}\text{OSi}_4$, ($\text{M}-\text{CH}_3$) 291.1452, found 291.1453.

Photolysis of 1 in 3-Methylpentane Matrix. A solution of vinyltris(trimethylsilyl)silane (**1**; 10^{-3} M) in 3-MP was placed in a 1-cm 3 quartz cell with a Teflon stopcock. After three

degassings by freeze/thaw cycle on a vacuum line, the cell was placed in a Dewar flask with optical quartz windows and cooled by liquid nitrogen. The matrix formed in 77 K was irradiated with a Rayonet reactor equipped with 16 medium-pressure Hg lamps and monitored by UV at every 15 min. Four major UV bands were clearly observed at 268, 280, 316, and 376 nm after 2 h of photolysis (Figure 1). When the matrix was annealed at about -150 $^\circ\text{C}$, the 376-, 268-, and 280-nm bands disappeared rapidly. The 316-nm absorption, however, decayed slowly with a half-life ~ 2.5 m. When the matrix was doped with 3×10^{-2} M triethylsilane, similar spectra were observed during the irradiation. After annealing, silylene insertion product **13** was identified by GC/MS and from co-injection with an authentic sample by analytical GC. Another product, **19** (<1%) with a parent peak 548 in the mass spectrum, the molecular weight of a dimer of silene **2**, was observed by GC/MS in the solution. Mass of **19**: m/e (relative intensity) 73 (100), 131 (12), 227 (9), 255 (8), 313 (31), 327 (42), 401 (21), 548 (9).

Acknowledgment. We gratefully acknowledge the Robert A. Welch Foundation for financial support of this work. We also thank Dr. T. D. Marriott of Rice University for obtaining high-resolution mass spectra.

OM940868W

Thermal and Photochemical Substitution and Disproportionation Reactions of the Heterodinuclear Compound $\text{CpMo}(\text{CO})_3\text{-Co}(\text{CO})_4$

Xiaoqing Song and Theodore L. Brown*

School of Chemical Sciences, University of Illinois, Urbana-Champaign,
Urbana, Illinois 61801

Received December 12, 1994[®]

The thermal and photochemical substitution and disproportionation reactions of the heterodinuclear $\text{CpMo}(\text{CO})_3\text{-Co}(\text{CO})_4$ complex (**1**) with phosphorus-donor ligands in 3-methylpentane (3MP) and CH_2Cl_2 were investigated. A CO dissociative pathway, leading to substitution, and a radical chain pathway initiated by associative attack of the ligand, leading to disproportionation, have been found to be operative in the thermal reactions. Reaction products differ, depending on the electronic and steric requirements of the ligand. Substitution on Co is observed for all the phosphorus ligands. For $\text{P}(n\text{-Bu})_3$, PPh_3 , $\text{P}(\text{OMe})_3$, and $\text{P}(\text{OPh})_3$, small amounts of substitution on Mo have also been observed in addition to the major Co substitution. For ligands such as PPh_3 , $\text{P}(i\text{-Pr})_3$, $\text{P}(c\text{-Hx})_3$, and $\text{P}(\text{OPh})_3$, monosubstitution is the only observable process in 3MP; it occurs exclusively on Co for very bulky ligands $\text{P}(i\text{-Pr})_3$ and $\text{P}(c\text{-Hx})_3$. Reactions with $\text{P}(n\text{-Bu})_3$ and $\text{P}(\text{OMe})_3$ under normal thermal conditions favor a disproportionation pathway, forming the ionic product $[\text{CpMo}(\text{CO})_2\text{L}_2]^+[\text{Co}(\text{CO})_4]^-$ ($\text{L} = \text{P}(n\text{-Bu})_3$ or $\text{P}(\text{OMe})_3$). Trace quantities of oxygen in the solution quench the thermally-induced radical chain processes. Upon photochemical initiation of the disproportionation reaction in CH_2Cl_2 , small amounts of $[\text{Co}(\text{CO})_3\text{L}_2]^+$ and $[\text{CpMo}(\text{CO})_3]^-$ are also formed in addition to $[\text{CpMo}(\text{CO})_2\text{L}_2]^+$ and $[\text{Co}(\text{CO})_4]^-$ ($\text{L} = \text{PPh}_3$, $\text{P}(i\text{-Pr})_3$, or $\text{P}(c\text{-Hx})_3$). The X-ray crystal structure of $[\text{CpMo}(\text{CO})_2(\text{P}(n\text{-Bu})_3)_2][\text{Co}(\text{CO})_4]$ is reported.

Studies of reaction pathways characteristic of metal carbonyl compounds containing one or more metal-metal bonds continue to be a challenge. For the extensively studied homodinuclear complexes, sufficient mechanistic information is available that specific and overall patterns of thermal and photochemical reactivity can be perceived, depending on such factors as the electronic and steric properties of reactants.¹ The homodinuclear complexes $\text{Co}_2(\text{CO})_8$ and $[\text{CpMo}(\text{CO})_3]_2$ have been extensively studied in the past two decades.¹⁻⁸ Both complexes undergo reaction with Lewis bases (i.e., phosphines, phosphites, arsines, etc.) to give various products, depending on the particular base and reaction condition. A dissociative CO loss mechanism⁹ has been proposed for the substitution reaction of $\text{Co}_2(\text{CO})_8$ with a weak Lewis base such as AsPh_3 or ^{13}CO . A radical chain pathway for reaction with trialkylphosphines of modest steric requirement leads to disproportionation products.⁹ Both mechanisms have been found to be

operative in the reaction of $[\text{CpMo}(\text{CO})_3]_2$ with a variety of Lewis bases, except that these reactions usually require more rigorous conditions.¹⁰

Reactivity and mechanistic information regarding heterodinuclear metal-metal-bonded systems is limited, although some attention has been given to the substitution reactions and photochemistry of these complexes.¹¹⁻¹⁵ Pope and Wrighton^{11b} reported a low-temperature photochemical study of $\text{CpFe}(\text{CO})_2\text{Mn}(\text{CO})_5$ showing that substitution of CO by P-donor ligands occurs exclusively on Mn. Poliakoff, Turner, and co-workers showed that photochemical loss of CO from $\text{MnRe}(\text{CO})_{10}$ occurs exclusively from Mn.^{13a} Nevertheless, in thermal substitution reactions of $\text{MnRe}(\text{CO})_{10}$ the substituting ligand is found on Re.^{13b,c} Photochemical substitution of PPh_3 into $(\text{CO})_5\text{ReMn}(\text{CO})_3(\alpha\text{-diimine})$, leads exclusively to $(\text{CO})_5\text{ReMn}(\text{CO})_2(\text{PPh}_3)(\alpha\text{-$

[®] Abstract published in *Advance ACS Abstracts*, February 1, 1995.

(1) Meyer, T. J.; Caspar, J. V. *Chem. Rev.* **1985**, *85*, 187.
 (2) Heck, R. F. *Organotransition Metal Chemistry*; Academic Press: New York, 1974.
 (3) Geoffroy, G. L.; Wrighton, M. S. *Organometallic Photochemistry*; Academic Press: New York, 1979.
 (4) Allen, D. M.; Cox, A.; Kemp, T. J.; Sultana, Q. J. *J. Chem. Soc., Dalton Trans.* **1976**, 1189.
 (5) McCullen, S. B.; Brown, T. L. *Inorg. Chem.* **1981**, *20*, 3528.
 (6) Haines, R. J.; Nyholm, R. S.; Stiddard, M. H. B. *J. Chem. Soc. A* **1968**, 43.
 (7) King, R. B.; Pannell, K. H. *Inorg. Chem.* **1968**, *7*, 2356.
 (8) King, R. B.; Pannell, K. H.; Eggers, C. A.; Houk, L. W. *Inorg. Chem.* **1968**, *7*, 2353.
 (9) (a) Forbus, N. P.; Oteiza, R.; Smith, S. G.; Brown, T. L. *J. Organomet. Chem.* **1980**, *193*, C71. (b) Absi-Halabi, M.; Atwood, J. D.; Forbus, N. P.; Brown, T. L. *J. Am. Chem. Soc.* **1980**, *102*, 6248.

(10) (a) Stiegman, A. E.; Tyler, D. R. *J. Am. Chem. Soc.* **1982**, *104*, 2944. (b) Stiegman, A. E.; Stieglitz, M.; Tyler, D. R. *Ibid.* **1983**, *105*, 6032. (c) Goldman, A. S.; Tyler, D. R. *Ibid.* **1984**, *106*, 4066. (d) Philbin, C.; Goldman, A. S.; Tyler, D. R. *Inorg. Chem.* **1986**, *25*, 4434.
 (11) (a) Abrahamson, H. B.; Wrighton, M. S. *J. Am. Chem. Soc.* **1977**, *99*, 5510. (b) Pope, K. R.; Wrighton, M. S. *Ibid.* **1987**, *109*, 4545.
 (12) Schmidt, S. P.; Basolo, F.; Jensen, C. M.; Trogler, W. C. *J. Am. Chem. Soc.* **1986**, *108*, 1894.
 (13) (a) Firth, S.; Hodges, P. M.; Poliakoff, M.; Turner, J. J. *J. Organomet. Chem.* **1987**, *331*, 347. (b) Sonnenberger, D.; Atwood, J. D. *J. Am. Chem. Soc.* **1980**, *102*, 3484. (c) Darling, E. L.; Robinson, D. J.; Coville, N. J. *J. Organomet. Chem.* **1986**, *310*, 203.
 (14) (a) Johnston, P.; Hutchings, G. J.; Denner, L.; Boeyens, J. C. A.; Coville, N. J. *Organometallics* **1987**, *6*, 1292. (b) Ingham, W. L.; Billing, D. G.; Levendis, D. C.; Coville, N. J. *Inorg. Chim. Acta* **1991**, *187*, 17. (c) Ingham, W. L.; Coville, N. J. *Inorg. Chem.* **1992**, *31*, 4084.
 (15) (a) Rossenaar, B. D.; van der Graaf, T.; van Eldik, R. S.; Langford, C. H.; Stufkens, D. J.; Vleck, A., Jr. *Inorg. Chem.* **1994**, *33*, 2685. (b) van Dijk, H. K.; Haar, J.; Stufkens, D. J.; Oskam, A. *Inorg. Chem.* **1989**, *28*, 75.

diimine), through photodissociation of CO from Mn.^{15a} Irradiation of $(\text{CO})_4\text{CoM}(\text{CO})_3(\text{bpy})$ ($\text{M} = \text{Mn}, \text{Re}$) in the presence of PR_3 leads to ionic photoproducts $[\text{M}(\text{CO})_3(\text{bpy})\text{L}]^+[\text{Co}(\text{CO})_4]^-$.^{15b} For the Mn complex the reactions with PR_3 were reported to be radical chain in character.

The compound $\text{CpMo}(\text{CO})_3\text{-Co}(\text{CO})_4$ (**1**), which exemplifies heterodinuclear metal carbonyls, affords an opportunity to examine the relative reactivity of the distinct metal carbonyl centers and the reactivity of the molecule as a whole. Complex **1** was first synthesized in 1978 by photolysis of a mixture of the homonuclear metal carbonyls $\text{Co}_2(\text{CO})_8$ and $[\text{CpMo}(\text{CO})_3]_2$ in a CO-purged benzene solution.¹⁶ Photoexcitation of **1** in degassed benzene solution results in the formation of a 1:1 ratio of $\text{Co}_2(\text{CO})_8$ and $[\text{CpMo}(\text{CO})_3]_2$. **1** reacts with alkynes and alkenes, forming alkynyl- or alkenyl-bridged complexes which further react with excess ligands to give mono- or disubstituted products.¹⁷ Co-substituted complexes $\text{CpMo}(\text{CO})_2(\mu\text{-RC}\equiv\text{CR})\text{Co}(\text{CO})_2\text{L}$ were obtained by refluxing benzene solutions of alkynyl-bridged complexes $\text{CpMo}(\text{CO})_2(\mu\text{-RC}\equiv\text{CR})\text{Co}(\text{CO})_3$ with phosphorus-donor ligands, L .^{17b} Complex $\text{CpMo}(\text{CO})_2[\mu\text{-C}_2(\text{CO}_2\text{Me})_2]\text{Co}(\text{CO})_3$ reacts preferentially at Co with PPh_2H , P_2Ph_4 , and $\text{PPh}_2(\text{SPh})$ to give initially the monosubstituted products. In the case of PPh_2H further reaction takes place at the Mo center to give the disubstituted product.^{17c}

To our knowledge, no mechanistic studies of reactions of **1** with common Lewis bases such as phosphines and phosphites have been reported. It has been shown that the basicity and steric properties of the attacking ligand are both important in determining the reaction pathway for the homodinuclear compounds from which **1** may be thought to be derived.^{9b,10b,18} The question arises how the two different metal centers affect one another, and whether the unsymmetrical character of the metal-metal interaction gives rise to new chemical effects. We describe here a study of the reactions of **1** with selected Lewis bases ($\text{P}(n\text{-Bu})_3$, $\text{P}(i\text{-Pr})_3$, PPh_3 , $\text{P}(c\text{-Hx})_3$, $\text{P}(\text{OMe})_3$, and $\text{P}(\text{OPh})_3$) in 3-methylpentane and in CH_2Cl_2 at room temperature, undertaken to clarify the relative reactivities of the two different metal centers and to understand the general patterns and mechanisms of the reactions.

Experimental Section

General Procedure. All experiments were carried out under an atmosphere of purified argon by employing Schlenk techniques. Hamilton gastight syringes were used for transferring liquids under positive gas pressure, using carefully purged equipment. Except where irradiation is indicated, exposure to light other than red photographic safelight was rigorously minimized in all experiments.

Spectra. All IR spectra were recorded on a PE 1710 FTIR spectrophotometer (2-cm⁻¹ resolution) using either a 1-mm path length CaF_2 IR cell (Specac S/N 21500) or a 0.05-mm path length NaCl cell. Photochemical studies were conducted using a high-pressure xenon flash lamp; at room temperature usually one or two flashes were employed. The IR spectra of the

sample solution before and after flashing were recorded. The UV-vis spectra were obtained using a HP8452 diode array spectrophotometer. ¹H and ³¹P NMR spectra were recorded on a General Electric QE300 (300 MHz) or GN 300 NB (300 MHz) NMR spectrometer. Elemental analyses were done by the Microanalytical Laboratory; mass spectra were obtained using a VG ZAB-SE spectrometer at the Mass Spectrometry Laboratory at the School of Chemical Science, University of Illinois.

Solvents. Hexane was purified as described previously.¹⁹ 3-Methylpentane (3MP) was distilled over CaH_2 and collected under an Ar atmosphere. The distillate was stored over 4-Å molecular sieves and was further degassed via three freeze-pump-thaw cycles in a Schlenk flask. Toluene was purified by distillation over Na under nitrogen before use.

Materials. $\text{Co}_2(\text{CO})_8$ (Strem Chemicals) was used after sublimation at 35 °C under vacuum. $[\text{CpMo}(\text{CO})_3]_2$ (Pressure Chemicals) was used without further purification. $[\text{Co}(\text{CO})_3\text{P}(n\text{-Bu})_3]_2$ was prepared by R. J. Sullivan¹⁹ in this lab. $\text{CpMo}(\text{CO})_2(\text{P}(n\text{-Bu})_3)\text{Cl}$ was prepared by a literature method.²⁰ $\text{P}(n\text{-Bu})_3$, $\text{P}(i\text{-Pr})_3$, PPh_3 , $\text{P}(c\text{-Hx})_3$, $\text{P}(\text{OMe})_3$, and $\text{P}(\text{OPh})_3$ were obtained from Strem Chemicals ($n\text{-Bu} = n\text{-butyl}$, $i\text{-Pr} = \text{isopropyl}$, $c\text{-Hx} = \text{cyclohexyl}$). $\text{P}(n\text{-Bu})_3$, $\text{P}(\text{OMe})_3$, and $\text{P}(\text{OPh})_3$ were purified by distillation over CaH_2 under vacuum before use. PPh_3 and $\text{P}(c\text{-Hx})_3$ were recrystallized from ethanol. The other phosphines were used as received.

$\text{CpMo}(\text{CO})_3\text{Co}(\text{CO})_4$ (1**)** was prepared by following a literature method¹⁶ with some modifications. $[\text{CpMo}(\text{CO})_3]_2$ (0.5 g, ~1 mmol) and 0.43 g of $\text{Co}_2(\text{CO})_8$ (~1.2 mmol) were added to a 250-mL Schlenk round bottom flask to which was added 125 mL of freshly distilled toluene. The solution was degassed by freeze-pump-thaw cycles and CO added. It was irradiated with a 275-W sunlamp for 18 h. The solution was filtered to remove some dark solids and the filtrate rotary-evaporated to dryness (35 °C), during which most of the unreacted $\text{Co}_2(\text{CO})_8$ was sublimed out with the solvent. The residue was slurried with 50 mL of pentane and filtered to remove the less soluble starting $[\text{CpMo}(\text{CO})_3]_2$ dimer. The product was separated on a grade I neutral alumina column (2 × 25 cm) in the dark. It was eluted with pentane and then with 15% CH_2Cl_2 in pentane (v:v); the mixed dimer comes out first, followed by a small amount of $[\text{CpMo}(\text{CO})_3]_2$. The product was obtained by rotary evaporation of the solvent. IR bands in 3MP are listed in Table 1. Anal. Calcd for $\text{C}_{12}\text{H}_5\text{CoMoO}_7$: C, 34.64; H, 1.21. Found: C, 34.67; H, 1.27.

$\text{CpMo}(\text{CO})_3\text{-Co}(\text{CO})_3\text{P}(n\text{-Bu})_3$ (2**)**. The preparation follows a route similar to that for **1**. In a typical synthesis, 0.24 g of $[\text{CpMo}(\text{CO})_3]_2$ (0.5 mmol) and 0.34 g of $\text{Co}_2(\text{CO})_8(\text{P}(n\text{-Bu})_3)_2$ (0.5 mmol) were dissolved in 80 mL of degassed toluene (three cycles of freeze-pump-thaw), and the flask was filled with 1 atm of CO. The solution was irradiated with a 250-W sunlamp for about 19 h. The orange-red solution was then filtered to remove some black solids and the filtrate rotary-evaporated to remove solvent. The red solids were slurried in 20 mL of pentane, and the solution was filtered again. The filtrate was loaded onto an alumina column (grade I, neutral, 2 × 25 cm) and eluted with pentane first. Increasing percentages of CH_2Cl_2 in pentane from 5% to 15% (v:v) were used for elution, and the mixture was separated into three bands (from orange to red). The first-eluted light orange band was identified by its IR spectrum to be the unreacted cobalt dimer $[\text{Co}(\text{CO})_3\text{P}(n\text{-Bu})_3]_2$. The monosubstituted dimer product was eluted next as a major orange band. The eluent was collected and the solvent was rotary-evaporated, yielding 0.23 g of red-brown crystals (81%). IR (3MP): 2024, 1966, 1937, 1923, 1909 cm⁻¹. Anal. Calcd for $\text{C}_{23}\text{H}_{32}\text{CoMoO}_6\text{P}$: C, 46.79; H, 5.46; P, 5.25; Mo, 16.25; Co, 9.98. Found: C, 46.74; H, 5.45; P, 5.19; Mo,

(16) Abrahamson, H. B.; Wrighton, M. S. *Inorg. Chem.* **1978**, *17*, 1003.

(17) (a) Yanez, R.; Lukan, N.; Mathieu, R. *Organometallics* **1990**, *9*, 2998. (b) Dickson, C.; Coville, N. J. *J. Organomet. Chem.* **1992**, *427*, 335. (c) Martin, A.; Mays, M. J.; Raithby, P. R.; Solan, G. A. *J. Chem. Soc. Dalton Trans.* **1993**, 1431.

(18) Fobus, N. P.; Brown, T. L. *Inorg. Chem.* **1981**, *20*, 4343.

(19) Sullivan, R. J.; Brown, T. L. *J. Am. Chem. Soc.* **1991**, *113*, 9155.

(20) (a) Mawby, R. J.; White, C. J. *Chem. Soc., Chem. Commun.* **1968**, 312. (b) Faller, J. W.; Anderson, A. S. *J. Am. Chem. Soc.* **1970**, *92*, 5852.

Table 1. IR Spectral Data for Selected Compounds in 3MP and CH₂Cl₂ at 298 K

compd	molecular formula	IR bands, cm ⁻¹
1	CpMo(CO) ₃ -Co(CO) ₄	2076 (s), 2022 (s), 1986 (sh), 1978 (s), 1949 (m), 1941 (m) ^a 2073 (s), 2017 (s), 1975 (s), 1940 (m, sh), 1930 (m, sh) ^b
2	CpMo(CO) ₃ -Co(CO) ₃ P(<i>n</i> -Bu) ₃	2024 (m), 1966 (s), 1937 (vs), 1923 (m, sh), 1909 (w, sh) ^a 2019 (m), 1959 (s), 1932 (vs), 1895 (w, sh) ^b
2'	CpMo(CO) ₂ (P(<i>n</i> -Bu) ₃)-Co(CO) ₄	2056 (s), 1971 (m), 1960 (s), 1927 (w), 1865 (s) ^a
2-P(<i>c</i> -Hx) ₃	CpMo(CO) ₃ -Co(CO) ₃ P(<i>c</i> -Hx) ₃	2022 (m), 1964 (s), 1936 (vs), 1924 (m, sh), 1896 (w) ^a 2017 (m), 1958 (s), 1929 (vs), 1894 (w, sh) ^b
2-P(<i>i</i> -Pr) ₃	CpMo(CO) ₃ -Co(CO) ₃ P(<i>i</i> -Pr) ₃	2023 (m), 1965 (s), 1937 (vs), 1926 (m, sh) ^a 2018 (m), 1959 (s), 1930 (vs), 1895 (w, sh) ^b
2-PPh ₃	CpMo(CO) ₃ -Co(CO) ₃ PPh ₃	2028 (m), 1971 (s), 1944 (vs), 1926 (m), 1913 (w) ^a 2023 (m), 1966 (s), 1939 (vs) ^b
2-P(OMe) ₃	CpMo(CO) ₃ -Co(CO) ₃ P(OMe) ₃	2036 (m), 1976 (s), 1948 (vs), 1929 (m) ^a 2032 (m), 1971 (s), 1947 (vs), 1928 (m) ^b
2-P(OPh) ₃	CpMo(CO) ₃ -Co(CO) ₃ P(OPh) ₃	2038 (m), 1981 (s), 1954 (vs), 1933 (m), 1922 (w, sh) ^a 2035 (m), 1977 (s), 1951 (vs), 1927 (m, sh) ^b
3	[CpMo(CO) ₂ (P(<i>n</i> -Bu) ₃) ₂][Co(CO) ₄]	2007 (w), 1954 (m), 1915 (s), 1889 (s,sh), 1880 (vs), 1866 (w,sh) ^a 2006 (vw), 1964 (w), 1886 (vs) ^b
5	CpMo(CO) ₂ (P(<i>n</i> -Bu) ₃)-Co(CO) ₃ P(<i>n</i> -Bu) ₃	1993 (m), 1925 (vs), 1914 (vs), 1900 (m, sh), 1843 (s) ^a

^a In 3MP. ^b In CH₂Cl₂.

16.07; Co, 9.91. ¹H NMR (CDCl₃): δ 0.96 (t, *J* = 69 Hz, 9H), 1.40–1.57 (m, 12H), 1.76–1.85 (m, 6H), 5.37 (s, 5H, Cp).

[CpMo(CO)₂(P(*n*-Bu)₃)₂][Co(CO)₄] (3). CpMoCo(CO)₇ (1) (0.8 g, ~2 mmol) was dissolved in 150 mL of hexane, and 2 mL (~10 mmol) of P(*n*-Bu)₃ was added to the solution. The mixture was quickly cooled with liquid nitrogen and degassed by three freeze-pump-thaw cycles. The frozen sample was then warmed to room temperature with stirring. A yellow precipitate formed and was collected by filtration. The yellow product was recrystallized twice from toluene under an argon atmosphere and dried in vacuum. IR in 3MP: 2007, 1954, 1915, 1888, 1880, 1866 (sh) cm⁻¹. Anal. Calcd for C₃₅H₅₉CoMoO₆P₂: C, 53.03; H, 7.50; P, 7.82; Mo, 12.10; Co, 7.43. Found: C, 53.43; H, 7.77; P, 7.98; Mo, 12.35; Co, 7.56. ¹H NMR (CDCl₃): δ 0.98 (t, *J* = 63 Hz, 18H), 1.48 (s, br, 24H), 1.99 (s, br, 12H), 5.40 (s, 5H, Cp).

X-ray Crystal Structure of [CpMo(CO)₂(P(*n*-Bu)₃)₂][Co(CO)₄] (3). The light yellow, tabular, data crystal was mounted using oil (Paratone-N) to a thin glass fiber. Data were measured at 198 K on an Enraf-Nonius CAD4 diffractometer. Crystal and refinement details are given in Table 2. The structure was solved by direct methods;²¹ correct positions for Mo, Co, and phosphorus atoms were deduced from an *E* map. One cycle of isotropic least-squares refinement followed by an unweighted difference Fourier synthesis revealed positions for the remaining non-H atoms, including disordered positions for C(3E) and C(4E). Disordered C atom positions were restrained to equivalent 1,2- and 1,3-distances with an effective standard deviation of 0.01 Å. Methyl H atom positions, C-CH₃, were optimized by rotation about C-C bonds with idealized C-H, C-H, and H-H distances. Remaining H atoms were included as fixed idealized contributors. H atom *U*'s were assigned as 1.2 times the *U*_{eq} of the adjacent C atoms. Non-H atoms were refined with anisotropic thermal coefficients. Successful convergence of the full-matrix least-squares refinement on *F*² was indicated by the maximum shift/error for the last cycle.²² The highest peak in the final difference Fourier map was in the vicinity of the Mo atom; the final map had no other significant features. A final analysis of variance between observed and calculated structure factors showed no dependence on amplitude or resolution. Parts a and b of Figure 1 show the ORTEP plots of the anion and cation of the molecule, respectively. Table 3 lists the bond distances and bond angles.

CpMo(CO)₂(P(*n*-Bu)₃)-Co(CO)₃P(*n*-Bu)₃ (5). A 140-mg sample of [CpMo(CO)₂L₂][Co(CO)₄] (3) was dissolved in 15 mL

Table 2. Crystal Data and Structure Refinement for [CpMo(CO)₂(P(*n*-Bu)₃)₂][Co(CO)₄] (3)

empirical formula	C ₄₂ H ₆₇ CoMoO ₆ P ₂
fw	884.77
temp, K	198(2)
wavelength, Å	0.71073
cryst syst	monoclinic
space group	A2/n
unit cell dimens	
<i>a</i> , Å	27.150(6)
<i>b</i> , Å	14.031(5)
<i>c</i> , Å	27.439(8)
α, deg	90
β, deg	117.97(2)
γ, deg	90
volume, Å ³	9232(5)
Z	8
density (calcd), Mg/m ³	1.273
abs coeff, mm ⁻¹	0.741
<i>F</i> (000)	3728
cryst size	0.64 × 0.30 × 0.14
θ range for data collcn, deg	1.68–22.97
index ranges	-26 ≤ <i>h</i> ≤ 29, 0 ≤ <i>k</i> ≤ 15, -30 ≤ <i>l</i> ≤ 0
reflns colld	6565
ind reflns	6408 [<i>R</i> (int) = 0.0369]
abs corr	integration
max and min transm	0.914 and 0.610
refinement method	full-matrix least squares on <i>F</i> ²
data/restraints/params	6407/12/496
goodness-of-fit on <i>F</i> ²	1.056
final <i>R</i> indices [<i>I</i> > 2σ(<i>I</i>)]	<i>R</i> 1 = 0.0371, <i>wR</i> 2 = 0.0840
<i>R</i> indices (all data)	<i>R</i> 1 = 0.0659, <i>wR</i> 2 = 0.0990
largest diff peak and hole, e/Å ³	+0.398 and -0.296

of degassed toluene under a stream of argon, and the yellow solution was heated and refluxed. IR spectra were taken at intervals to monitor the progress of the reaction. After about 5 h the reaction was complete, as shown by the disappearance of bands at 2006, 1951, 1910, and 1879 cm⁻¹ due to **3**. New bands appeared at 1988, 1919, 1907, and 1833 cm⁻¹. The resulting red solution was then filtered to remove insoluble dark solids. The filtrate was purified by chromatography on a grade I alumina column. A small, light-orange band was eluted first with pentane; it was identified as the homonuclear cobalt dimer [Co(CO)₃P(*n*-Bu)₃]₂ by its IR spectrum (1952 cm⁻¹). The product was eluted next as a red band with 10% CH₂Cl₂ in pentane. The product was collected as a red oil after evaporating the solvents. IR bands of the product in 3MP appeared at 1993, 1925, 1914, 1990 (sh), and 1843 cm⁻¹. Two very small bands which were eluted last with 20% CH₂Cl₂ in pentane were not further investigated. Anal. Calcd for C₃₄H₅₉CoMoO₅P₂: C, 53.41; H, 7.78. Found: C, 54.75; H, 8.67.

(21) Sheldrick, G. M. SHELXS-86. *Acta Crystallogr.* **1990**, *A46*, 467.(22) Sheldrick, G. M. SHELXS-93. In preparation for *J. Appl. Crystallogr.*

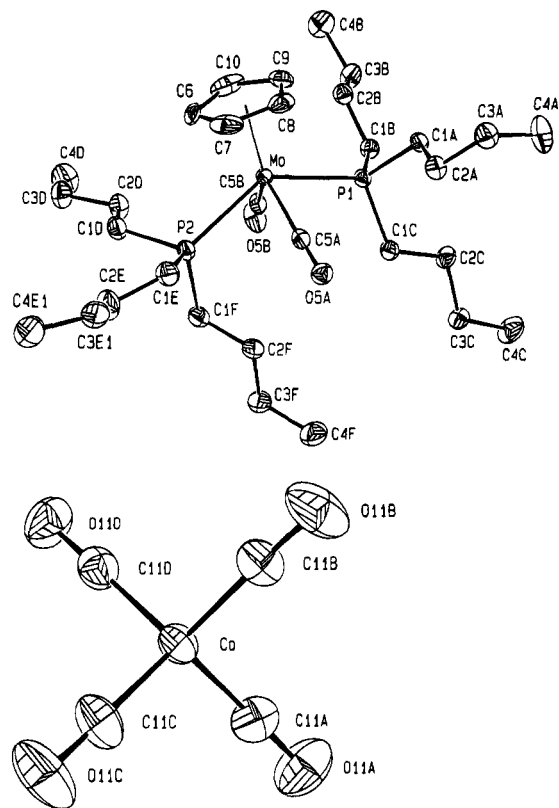


Figure 1. X-ray structure of $[\text{CpMo}(\text{CO})_2(\text{P}(n\text{-Bu})_3)_2][\text{Co}(\text{CO})_4]$.³⁰ (a, top) ORTEP plot of the cation showing 35% probability ellipsoids for non-H atoms; (b, bottom) ORTEP plot of the anion showing 35% probability ellipsoids for non-H atoms.

Table 3. Selected Bond Lengths (Å) and Angles (deg) for **3**

Mo-C(5A)	1.970(5)	P(1)-C(1B)	1.833(4)
Mo-C(5B)	1.974(4)	P(1)-C(1C)	1.836(4)
Mo-C(7)	2.308(4)	P(2)-C(1D)	1.834(4)
Mo-C(6)	2.320(4)	P(2)-C(1E)	1.836(4)
Mo-C(8)	2.322(4)	P(2)-C(1F)	1.838(4)
Mo-C(9)	2.340(4)	Co-C(11B)	1.754(5)
Mo-C(10)	2.350(4)	Co-C(11A)	1.757(5)
Mo-P(2)	2.5069(12)	Co-C(11D)	1.760(5)
Mo-P(1)	2.5070(11)	Co-C(11C)	1.764(5)
P(1)-C(1A)	1.831(4)		
C(5A)-Mo-C(5B)	108.5(2)	C(11B)-Co-C(11C)	107.9(2)
P(2)-Mo-P(1)	134.09(4)	C(11A)-Co-C(11C)	110.5(2)
O(5A)-C(5A)-Mo	174.7(3)	C(11D)-Co-C(11C)	108.8(2)
O(5B)-C(5B)-Mo	177.3(3)	O(11A)-C(11A)-Co	178.7(5)
C(11B)-Co-C(11A)	108.5(2)	O(11B)-C(11B)-Co	179.1(4)
C(11B)-Co-C(11D)	111.3(2)	O(11C)-C(11C)-Co	179.0(4)
C(11A)-Co-C(11D)	109.9(2)	O(11D)-C(11D)-Co	178.8(4)

Results

Substitution and disproportionation products of **1** with various phosphines and phosphites have been either isolated and fully characterized or identified by comparing their IR spectra to independently prepared authentic samples.

a. Reaction with $\text{P}(n\text{-Bu})_3$. Reaction products and product distributions in 3MP were different depending on experimental conditions such as the concentrations of ligand and complex or whether light was involved in the reaction. Figure 2a shows the UV-vis spectra during reaction of **1** (0.1 mM) with $\text{P}(n\text{-Bu})_3$ (2.0 mM) at room temperature. Substitution of CO by $\text{P}(n\text{-Bu})_3$ in **1** ($\lambda_{\text{max}} = 356 \text{ nm}$) resulted in slow formation of **2** ($\lambda_{\text{max}} = 368 \text{ nm}$) over a period of 200 min. The IR spectrum

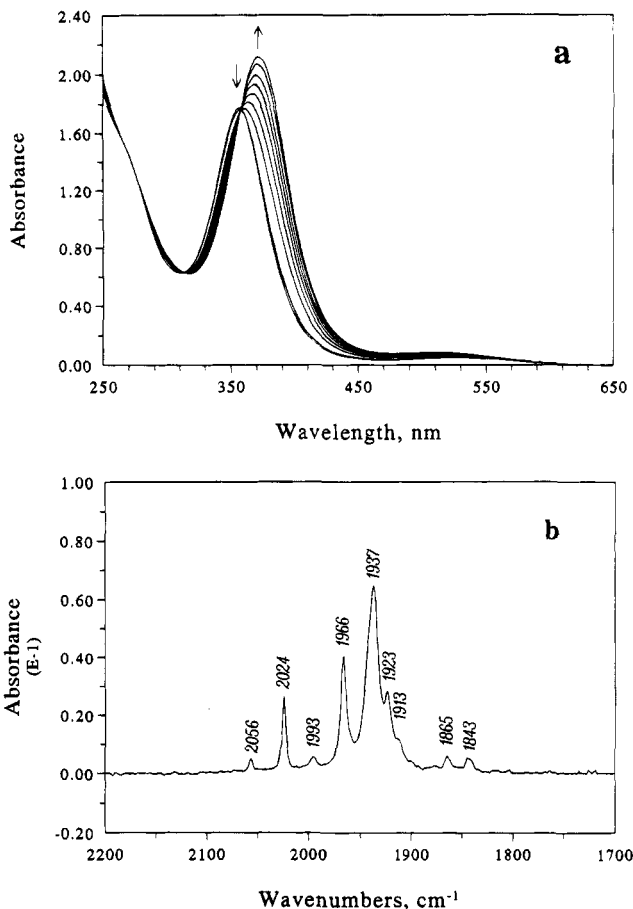
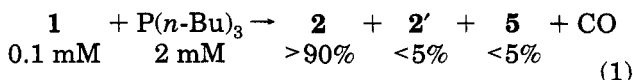


Figure 2. (a) UV-vis spectra of the reaction of **1** (0.1 mM) with $\text{P}(n\text{-Bu})_3$ (2 mM) in 3MP over a period of 200 min. Down and up arrows show the disappearance of **1** (356 nm) and formation of **2** (368 nm). (b) IR spectra of the products formed in the thermal reaction in 3MP. IR bands: for **2** 2024, 1966, 1937, 1923, 1913 cm^{-1} ; for **2'** 2056, 1865 cm^{-1} ; for **5** 1993, 1843 cm^{-1} .

of the product mixture (Figure 2b) showed that three products are formed. The major product ($\sim 90\%$) is the monosubstituted compound **2**, identified by comparing its IR spectrum to the spectrum of an independently prepared sample of **2**. The second product, formed in a small amount ($< 5\%$), has been identified as the disubstituted compound, $\text{CpMo}(\text{CO})_2(\text{P}(n\text{-Bu})_3)\text{-Co}(\text{CO})_3\text{P}(n\text{-Bu})_3$, **5**, also by comparing its IR spectrum with that of an authentic sample. There was yet another set of well-separated low-intensity peaks at 2056 and 1865 cm^{-1} not assignable to either of the above two products. This set of peaks was identified later with a previously unknown Mo-substituted product, $\text{CpMo}(\text{CO})_2(\text{P}(n\text{-Bu})_3)\text{-Co}(\text{CO})_4$ (**2'**), by flash photolysis of a mixture of $\text{Co}_2(\text{CO})_8$ and $\text{CpMo}(\text{CO})_2(\text{P}(n\text{-Bu})_3)\text{-Co}(\text{CO})_3\text{P}(n\text{-Bu})_3$ (**5**) in 3MP solution (vide infra). Thus at a low concentration of $\text{P}(n\text{-Bu})_3$, the reaction proceeds according to eq 1.



Using higher concentrations of **1** ($\sim 1 \text{ mM}$), the reaction with 2 mM $\text{P}(n\text{-Bu})_3$ was monitored by IR spectroscopy. The IR spectra of the products showed that in addition to products **2**, **2'**, and **5** (eq 1), a new product with IR bands at 2007, 1916, 1888, and 1880 (sh) cm^{-1} ,

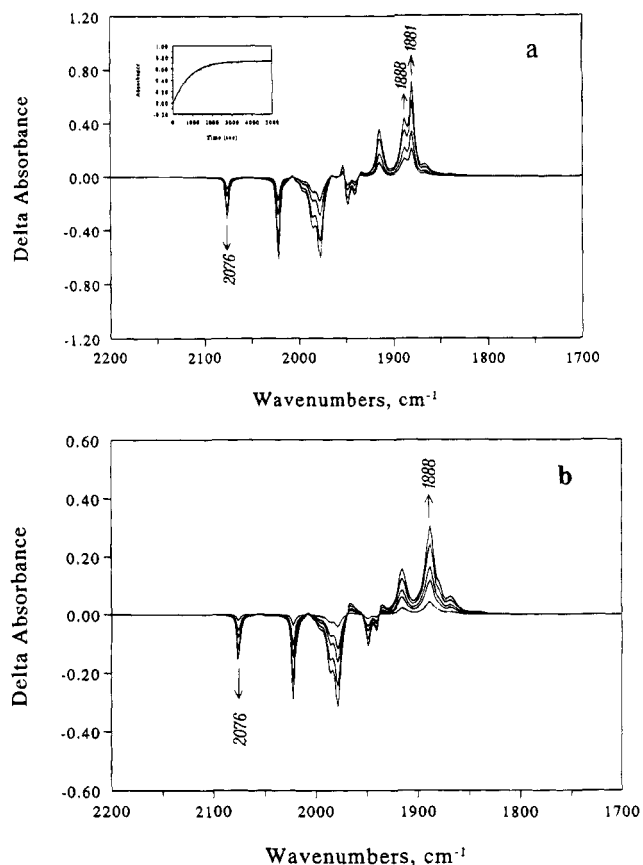
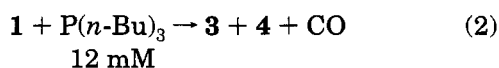


Figure 3. (a) Difference IR spectra of the reaction of **1** with $P(n\text{-Bu})_3$ (20 mM) in a carefully degassed 3MP solution at different times. Positive and negative bands indicate the formation of **3** (1888, 1881 cm^{-1}) and the consumption of **1** (2076 cm^{-1}), respectively. Insert is the time dependence of the band at 1881 cm^{-1} . (b) Difference IR spectra of the reaction of **1** with $P(n\text{-Bu})_3$ (12 mM) in a less rigorously degassed 3MP solution at different times between 1 and 16 min. Positive and negative bands indicate the formation of **4** (1888 cm^{-1}) and the consumption of **1** (2076 cm^{-1}), respectively.

accounting for about 30% of the reaction, was also formed. This new product was identified as $[\text{CpMo}(\text{CO})_2(\text{P}(n\text{-Bu})_3)_2][\text{Co}(\text{CO})_4]$ by comparison with the independently synthesized and characterized ionic compound $[\text{CpMo}(\text{CO})_2(\text{P}(n\text{-Bu})_3)_2][\text{Co}(\text{CO})_4]$ (**3**). Figure 3a shows the IR spectrum of product **3** in 3MP solution (note that the 1880- cm^{-1} peak is more intense than the 1888- cm^{-1} peak). Positive and negative ion mass spectra by FAB show the parent cation $[\text{CpMo}(\text{CO})_2(\text{P}(n\text{-Bu})_3)_2]^+$ ($m/z = 623.3$, the most abundant m/z value within the molybdenum isotopic mass distribution spectrum) and anion $[\text{Co}(\text{CO})_4]^-$ ($m/z = 171$). In the negative FAB mass spectrum, there is also a very small set of peaks due to the fragment ion $[\text{CpMo}(\text{CO})_2\text{P}(n\text{-Bu})_3]^-$ ($m/z = 421.1$) which is produced in the mass spectrometer chamber after loss of a $\text{P}(n\text{-Bu})_3$ from the cation.

When the reaction was carried out at a higher concentration of $\text{P}(n\text{-Bu})_3$ (i.e. 12 mM and above), the disproportionation product **3** (eq 2) constitutes more



than 90% of the product, with only minor amounts of substitution products (eq 1). Unexpectedly, under dif-

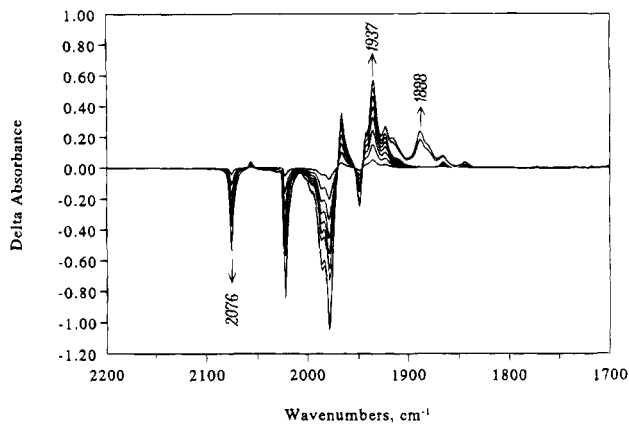


Figure 4. Difference IR spectra of the reaction of **1** with $\text{P}(n\text{-Bu})_3$ in 3MP solution measured in a closed IR cell. The solution is prepared under an air atmosphere. Spectra were taken at each 20 min interval. The feature at 1937 cm^{-1} initially formed is due to **2**. The band at 1888 that formed later is assigned to **4**.

ferent conditions (e.g., depending on how the reaction mixture was degassed or on the concentration of **1**) we obtained yet another set of IR bands formed in the reaction, assigned to product **4**, very similar to yet distinct from those of **3**. Figure 3b shows the IR spectrum of **4**, which has a new band at 1956 cm^{-1} , with the 1888- cm^{-1} absorbance the most intense and with a very weak shoulder at 1880 cm^{-1} . The relative intensities of the IR bands at 1888 and 1880 cm^{-1} varied in different experiments, suggesting that the spectrum in Figure 3b is due to a mixture of **3** and **4**. No interconversion of the two products was observed in 3MP or hexane solution at room temperature for at least one day in the dark. Initially, by using a low concentration of **1** (2.4 mM) and 75 mM $\text{P}(n\text{-Bu})_3$ in hexane, we were able to repeat the experiment on a preparative scale that maximizes the formation of **4**. It was later found that it is not the concentration of **1** per se that determines the product distribution; rather, trace amounts of oxygen present in the solution lead to formation of **4**. Deliberate addition of air to the reaction mixture leads to the formation of **4** as the major product and **3** as the minor product. However, for the disproportionation reaction to occur under these conditions, irradiation is required. The thermal reaction in a solution mixture that contains O_2 results in formation of substituted products only. Figure 4 shows the time development of the different IR spectra in a closed IR cell in which the solution is prepared under an air atmosphere. Initially, only substitution reactions (on both Co and Mo) occur. However, at the point at which the oxygen originally dissolved in the solution is consumed in an initial step, ionic product **4** begins to form immediately. For comparison, the same stock solution used in Figure 4 was kept in the dark in a Schlenk tube with occasional admittance of air. The product IR spectrum shows, as expected, only substitution complexes.

The positive FAB mass spectrum of **3** shows the most abundant peak at m/z 623.1 for cation $[\text{CpMo}(\text{CO})_2(\text{P}(n\text{-Bu})_3)_2]^+$ with a negligible amount of second set of peaks at m/z 639.1, while the mass spectrum of the ionic product mixture (contains **3** and **4**) shows two sets of peaks in comparable intensities that belong to two cations. One cation is $[\text{CpMo}(\text{CO})_2(\text{P}(n\text{-Bu})_3)_2]^+$ ($m/z =$

623.1), and the second has an m/z of 639.1, 16 mass units higher. A high-resolution mass spectrum of the m/z 639.1 set of peaks shows that the 16-unit difference is due to $[\text{CpMo}(\text{CO})_2(\text{P}(n\text{-Bu})_3)_2]^+$ plus an oxygen atom. The anion mass spectra of pure sample **3** and the product mixture show a major peak at 171 units due to $[\text{Co}(\text{CO})_4]^-$. There are also two small sets of peaks centered at 421.1 and 437.1 mass units (also 16 mass units higher) present in the negative ion mass spectrum. The ratio of their intensities is proportional to that of the two sets of cation peaks. As in the case of the negative ion mass spectrum of pure sample **3**, the m/z 421.1 and 437.1 sets of peaks, present in small amounts, are due to loss of a $\text{P}(n\text{-Bu})_3$ ligand from the cations, giving rise to the peaks at m/z 623.1 and 639.1, respectively. We do not know how the oxygen atom is incorporated into the structure of the parent cation from which it is derived. Attempts to separate **3** from **4** by recrystallization and chromatography have been unsuccessful. We plan to further investigate this matter.

The reaction of **1** (~ 2 mM) with $\text{P}(n\text{-Bu})_3$ (~ 20 mM) in 3MP forming **3** is approximately first order in **1** (the reaction is much slower at lower concentrations of both **1** (0.1 mM) and $\text{P}(n\text{-Bu})_3$ (2 mM) when substitution reactions are the only pathway). At 25 °C, the half-life of the disappearance of **1** is about 13 min and it decreases to about 6 min at 40 °C. When the solution containing **1** and $\text{P}(n\text{-Bu})_3$ is irradiated with a sunlamp for 10 s, the strong orange color of the solution changes to light yellow immediately and the reaction is complete, forming the ionic compounds, with only trace amounts of substitution products. The set of low-intensity peaks at 2056 and 1856 cm^{-1} due to **2'** has been detected in all IR spectra of the reaction products.

In CH_2Cl_2 , thermal reaction of **1** with $\text{P}(n\text{-Bu})_3$ results in the formation of disproportionation product **3** with small amounts of monosubstituted product **2**, and trace amounts of **2'** and the cation $[\text{Co}(\text{CO})_3(\text{P}(n\text{-Bu})_3)_2]^+$ (1995 cm^{-1}). When the solution is irradiated, more $[\text{Co}(\text{CO})_3(\text{P}(n\text{-Bu})_3)_2]^+$ is formed than $[\text{CpMo}(\text{CO})_2(\text{P}(n\text{-Bu})_3)_2]^+$ (1961, 1883 cm^{-1}).⁶ The counterion formed in both the thermal and photochemical reactions is $[\text{Co}(\text{CO})_4]^-$ (1887 cm^{-1}). There is no evidence for the formation of $[\text{CpMo}(\text{CO})_3]^-$ (1774 cm^{-1}) in the reactions.

b. Reaction with PPh_3 . Reaction of **1** with PPh_3 in 3MP at room temperature without irradiation results in slow substitution to form the monosubstituted compound $\text{CpMo}(\text{CO})_3\text{-Co}(\text{CO})_3\text{PPh}_3$ (**2-PPh₃**) almost exclusively (characteristic IR bands at 2028, 1971, and 1944 cm^{-1} as compared to 2024, 1966, and 1937 cm^{-1} for the monosubstituted compound **2**). During the reaction, a set of IR bands at 2057 and 1874 cm^{-1} grows in during the early phase of the reaction, then gradually decreases as the reaction proceeds to completion. By comparison with the corresponding peaks of **2'** at 2056 and 1865 cm^{-1} , one can reasonably attribute this set of peaks to the analogous compound, $\text{CpMo}(\text{CO})_2(\text{PPh}_3)\text{-Co}(\text{CO})_4$.

The overall substitution reaction rate is first-order in **1**, with no dependence on the concentration of phosphine, with a first-order rate constant ranging between 1.3×10^{-4} and $1.6 \times 10^{-4} \text{ s}^{-1}$ at room temperature under argon. Adding CO (1 atm) to the reaction mixture slightly slows the reaction compared to that under an argon atmosphere; a first-order rate constant of $1.2 \times$

Table 4. First-Order Rate Constants for Substitution Reaction of **1 with Phosphines in 3MP**

ligand	concn, mM	$10^4 k, \text{ s}^{-1}$
PPh_3	12	1.3 ± 0.2
PPh_3	22	1.3 ± 0.2
PPh_3	50	1.6 ± 0.2
PPh_3	32 ^a	1.2 ± 0.2
$\text{P}(i\text{-Pr})_3$	50	1.7 ± 0.2
$\text{P}(c\text{-Hx})_3$	50	1.3 ± 0.1
$\text{P}(\text{OPh})_3$	50	1.2 ± 0.2

^a Under added CO (1 atm).

10^{-4} s^{-1} was obtained. To test if there was any effect of visible radiation from the IR beam on the substitution reaction, a Kodak IR TRANS filter was used to block the visible radiation in the IR beam while the reaction was monitored. No difference in the rate constant was observed when keeping other conditions identical. Table 4 gives the observed rate constants for various concentrations of PPh_3 . Although there were no ionic compounds formed in the reaction when light was rigorously excluded, irradiation of the solution mixture of **1** and PPh_3 with a sunlamp for 20 s resulted in a small amount of yellow precipitate in 3MP or hexane solution, presumably due to ionic products formed via light-induced disproportionation. However, the disproportionation reaction is clearly slower than the corresponding reaction with $\text{P}(n\text{-Bu})_3$ (eq 2).

In CH_2Cl_2 , the thermal reaction of **1** with PPh_3 results in the formation of a small amount of disproportionation products (<10%) with well-separated IR bands at 2013, 1898, and 1774 cm^{-1} in addition to the monosubstituted neutral product **2-PPh₃** (IR in CH_2Cl_2 : 2023, 1966, 1939 cm^{-1}). The ionic products were identified as $[\text{CpMo}(\text{CO})_2(\text{PPh}_3)_2]^+$ (1898 cm^{-1}),⁶ $[\text{Co}(\text{CO})_3(\text{PPh}_3)_2]^+$ (2013, 2005, 1890 cm^{-1}),^{9b} $[\text{CpMo}(\text{CO})_3]^-$ (1774 cm^{-1}),⁶ and $[\text{Co}(\text{CO})_4]^-$ (1889 cm^{-1}) from the IR spectra.²¹ Irradiation of the reaction mixture by sunlamp or xenon flash lamp results in formation of mainly ionic products, as described above with small amounts of neutral substituted **2-PPh₃**. A small amount of the Mo dimer $[\text{CpMo}(\text{CO})_3]_2$ was also detected in the product mixture, as shown by IR bands at 2014, 1958, and 1912 cm^{-1} .

c. Reaction with $\text{P}(i\text{-Pr})_3$. Reaction of **1** with $\text{P}(i\text{-Pr})_3$ in 3MP at room temperature without irradiation also results in slow substitution, forming exclusively the monosubstituted compound $\text{CpMo}(\text{CO})_3\text{-Co}(\text{CO})_3(\text{P}(i\text{-Pr})_3)$ (**2-P}(i\text{-Pr})_3**). The product was identified by its characteristic IR bands at 2023, 1965, and 1937 cm^{-1} , nearly identical with the band positions for **2**. No peak at around 2056 cm^{-1} was observed in this reaction, which follows a first-order rate law with a first-order rate constant of $1.7 \times 10^{-4} \text{ s}^{-1}$ at room temperature. Irradiation of the reaction by sunlamp for 15 s produced a very small amount of off-white precipitation.

In CH_2Cl_2 , under thermal condition, substitution product $\text{CpMo}(\text{CO})_3\text{-Co}(\text{CO})_3(\text{P}(i\text{-Pr})_3)$ accounts for more than 90% of the reaction (IR bands at 2018, 1959, and 1930 cm^{-1}). A small band at 1992 cm^{-1} (broad) assignable to $[\text{Co}(\text{CO})_3(\text{P}(i\text{-Pr})_3)_2]^+$ (1988–1994 cm^{-1}) was also observed in the IR spectrum. Absorption bands of anionic species are obscured in the strong absorption bands of the substitution product. Irradiation of the reaction mixture with a sunlamp results in the formation of the ionic species $[\text{Co}(\text{CO})_3(\text{P}(i\text{-Pr})_3)_2]^+$ (1992 cm^{-1}),¹⁸ $[\text{CpMo}(\text{CO})_2(\text{P}(i\text{-Pr})_3)_2]^+$ (1896 cm^{-1}), $[\text{CpMo}(\text{CO})_3]^-$, and

[Co(CO)₄]⁻. Substitution products are not clearly seen in the IR spectrum because they are produced in very small quantities.

d. Reaction with P(*c*-Hx)₃. Results similar to those obtained for P(*i*-Pr)₃ were obtained for the reaction of **1** with P(*c*-Hx)₃ in 3MP. The monosubstituted compound CpMo(CO)₃-Co(CO)₃(P(*c*-Hx)₃)₂ (**2**-P(*c*-Hx)₃), identified by its IR spectrum (2022, 1964, and 1936 cm⁻¹), was the sole product under similar conditions, with no evidence for an absorbance at 2056 cm⁻¹. The reaction follows a first-order rate law with a rate constant of 1.3 × 10⁻⁴ s⁻¹ at 25 °C. Irradiation with sunlamp for 20 s resulted in very small amounts of off-white precipitate.

In CH₂Cl₂, photoirradiation with a sunlamp results in formation of both substitution and disproportionation products. The photochemical products are **2**-P(*c*-Hx)₃ (2016, 1958, 1929 cm⁻¹), [Co(CO)₃(P(*c*-Hx)₃)₂]⁺ (1994, 1979 cm⁻¹), [CpMo(CO)₂(P(*c*-Hx)₃)₂]⁺ (1897 cm⁻¹), [CpMo(CO)₃]⁻ (1774 cm⁻¹), and [Co(CO)₄]⁻ (1889 cm⁻¹). Comparisons of IR bands were made with the ionic species produced in the photochemical reactions of [Co(CO)₄]₂ and [CpMo(CO)₃]₂ with P(*c*-Hx)₃ in CH₂Cl₂. Interestingly, when the reaction mixture was irradiated by a xenon flash lamp, the above ionic products were not observed in detectable amounts in the reaction of **1** with P(*c*-Hx)₃; neutral substitution product **2**-P(*c*-Hx)₃ was the only product observed.

e. Reaction with P(OMe)₃. Reaction with P(OMe)₃ in 3MP under an inert argon atmosphere without irradiation produced a mixture of neutral and ionic products (off-white precipitation). As for reaction with P(*n*-Bu)₃, in which both substitution and disproportionation occur, the reaction with P(OMe)₃ proceeds much faster (half-life of 25 min) compared to the reactions with the three bulky phosphines, PPh₃, P(*i*-Pr)₃, and P(*c*-Hx)₃, in which substitution was the only pathway (half-life of 130 min). The neutral product is the monosubstituted compound (**2**-P(OMe)₃) as indicated by the characteristic IR absorption bands at 2036, 1976, and 1948 cm⁻¹. Low-intensity IR bands in the solution at 1998, 1955, 1918, and 1885 cm⁻¹ are due to an ionic product. These bands initially grow in and then decrease as more product forms and precipitation occurs. In this reaction, an absorption at 2059 cm⁻¹ was also observed (other peaks of this product are obscured in the spectrum). The IR spectrum of the solid product dissolved in CH₂Cl₂ shows three symmetrical bands at 2001, 1927, and 1890 cm⁻¹, as expected for an ionic compound [CpMo(CO)₂(P(OMe)₃)₂][Co(CO)₄].²³ Thermal reaction in CH₂Cl₂ leads to formation of [CpMo(CO)₂(P(OMe)₃)₂][Co(CO)₄] as the major product with small amounts of **2**-P(OMe)₃. Irradiation with the sunlamp for 1 min results in formation of trace amounts of [CpMo(CO)₃]⁻ (1774 cm⁻¹) in addition to the two products of the thermal reaction.

f. Reaction with P(OPh)₃. Neutral substitution products were the only observable products formed in the reaction of **1** with P(OPh)₃ in 3MP. Monosubstitution product **2**-P(OPh)₃ on Co was identified by its characteristic IR bands at 2038, 1981, 1954, 1933, and 1922 (sh) cm⁻¹. A small amount of a Mo-substituted complex absorbing at 2063 and 1892 cm⁻¹ was also observed. This reaction rate is first-order in **1**, with a

rate constant of 1.2 × 10⁻⁴ s⁻¹ at 25 °C. No disproportionation products such as those described above for reactions with phosphines have been observed in the photochemical reactions, either in 3MP or in CH₂Cl₂.

g. Thermal Reaction of [CpMo(CO)₂(P(*n*-Bu)₃)₂][Co(CO)₄] (3**).** Refluxing the ionic compound **3** in toluene under argon for 5 h resulted in formation of the disubstituted compound CpMo(CO)₂(P(*n*-Bu)₃)-Co(CO)₃(P(*n*-Bu)₃) (**5**) plus trace amounts of [Co(CO)₃P(*n*-Bu)₃]₂ and other unidentified products. In addition to elemental analysis and NMR spectroscopy, the molecular formula of compound **5** was further supported by the following experiments: flash photolysis of a 3MP solution of **5** under an argon atmosphere results in the formation of the homonuclear dimer [Co(CO)₃P(*n*-Bu)₃]₂ (as indicated by a strong peak at 1952 cm⁻¹ in the IR spectrum of the product). The cobalt dimer was formed as a result of recombination of Co(CO)₃P(*n*-Bu)₃ radicals produced in homolysis of the Mo-Co bond in **5**. No other peaks were observed in the CO stretching region, which indicates that the substituted Mo radical, CpMo(CO)₂P(*n*-Bu)₃, does not recombine to give a symmetrically substituted dimer in solution (in fact, this compound has never been reported). Nevertheless, CpMo(CO)₂P(*n*-Bu)₃ can be trapped via halogen atom transfer. Irradiation of **5** with 0.1 M CCl₄ in 3MP solution under an argon atmosphere produced two major products, the cobalt dimer [Co(CO)₃P(*n*-Bu)₃]₂ and CpMo(CO)₂(P(*n*-Bu)₃)Cl. The latter presumably forms as a result of abstracting a Cl from CCl₄ by the CpMo(CO)₂P(*n*-Bu)₃ radical. This product has two nearly equally intense CO stretch bands²⁴ at 1972 and 1882 cm⁻¹, the same as for an independently prepared sample of CpMo(CO)₂(P(*n*-Bu)₃)Cl. Another minor peak in the product spectrum at 1992 cm⁻¹ is assigned to the product of the reaction of Co(CO)₃P(*n*-Bu)₃ with CCl₄. The same peak at 1992 cm⁻¹ is seen as the only product peak following flash photolysis of [Co(CO)₃P(*n*-Bu)₃]₂ and 0.1 M CCl₄ in 3MP solution. A barely observable peak at 2024 cm⁻¹ is probably due to trace amounts of **2** formed in the reaction as the result of ligand loss from Mo (the photochemistry of this and other related complexes will be reported in another paper²⁵).

h. Flash Photolysis of CpMo(CO)₂(P(*n*-Bu)₃)-Co(CO)₃(P(*n*-Bu)₃) (5**) with Co₂(CO)₈.** Hepp and Wrighton have shown that photolysis of an M-M-bonded carbonyl compound in solution results in reversible M-M bond rupture and, to a less extent, CO loss in the absence of other coordinating ligands.²⁶ In order to confirm the product CpMo(CO)₂(P(*n*-Bu)₃)-Co(CO)₄ (**2'**) formed in the reaction of **1** with P(*n*-Bu)₃, flash photolysis of a mixture of CpMo(CO)₂(P(*n*-Bu)₃)-Co(CO)₃(P(*n*-Bu)₃) (**5**) and Co₂(CO)₈ was carried out at room temperature in 3MP solution. The homolysis of **5** and Co₂(CO)₈ results in the formation of CpMo(CO)₂P(*n*-Bu)₃, Co(CO)₃P(*n*-Bu)₃, and 2 equiv of Co(CO)₄. These radical species can either recombine to form starting materials or react with one another to form cross reaction products. Figure 5 shows the IR spectra of the products formed in the cross photochemical reaction of CpMo(CO)₂(P(*n*-Bu)₃)-Co(CO)₃(P(*n*-Bu)₃) (**5**) with Co₂(CO)₈ in 3MP solution. IR bands at 2078, 2022,

(24) Barnett, K. W.; Slocum, D. W. *J. Organomet. Chem.* **1972**, *44*, 1. Two peaks listed here are 1977 and 1884 cm⁻¹.

(25) Song, X.; Brown, T. L. To be reported.

(26) Hepp, A. F.; Wrighton, M. S. *J. Am. Chem. Soc.* **1983**, *105*, 5934.

(23) Haines, R. J.; Nolte, C. R. *J. Organomet. Chem.* **1970**, *24*, 725.

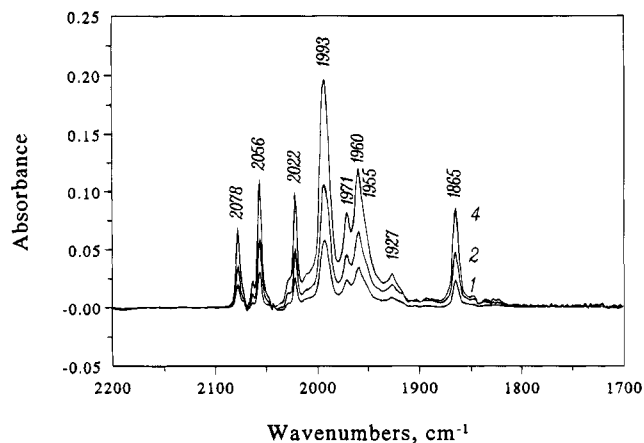


Figure 5. IR spectra of the products formed in the photochemical reaction of $\text{CpMo}(\text{CO})_2(\text{P}(n\text{-Bu})_3)\text{-Co}(\text{CO})_3\text{P}(n\text{-Bu})_3$ (**5**) and $\text{Co}_2(\text{CO})_8$ in 3MP at 25 °C. 1, 2, and 4 denote the number of flashes employed with a xenon flash lamp. IR bands at 2078, 2022, 1993, and 1955 cm^{-1} are due to $\text{Co}_2(\text{CO})_7\text{P}(n\text{-Bu})_3$; IR bands at 2056, 1971, 1960, 1927, and 1865 cm^{-1} are assigned to a new compound $\text{CpMo}(\text{CO})_2(\text{P}(n\text{-Bu})_3)\text{-Co}(\text{CO})_4$. Absorption bands due to the two starting complexes have been subtracted from the spectra of the reaction mixture.

1993, and 1955 cm^{-1} are assigned to $\text{Co}_2(\text{CO})_7\text{P}(n\text{-Bu})_3$,²⁷ the product of recombination of $\text{Co}(\text{CO})_3\text{P}(n\text{-Bu})_3$ and $\text{Co}(\text{CO})_4$ radicals. Recombination of $\text{CpMo}(\text{CO})_2\text{P}(n\text{-Bu})_3$ and $\text{Co}(\text{CO})_4$ results in the formation of $\text{CpMo}(\text{CO})_2(\text{P}(n\text{-Bu})_3)\text{-Co}(\text{CO})_4$ (**2'**), which accounts for the additional IR bands at 2056, 1971, 1960, 1927, and 1865 cm^{-1} .

Discussion

Both basicity and steric requirements of the ligands have been found to affect the course of the reaction of **1** with phosphorus ligands. The homodinuclear compounds $\text{Co}_2(\text{CO})_8$ and $[\text{CpMo}(\text{CO})_3]_2$ exhibit different dependencies on ligand characteristics in their substitution reactions. For example, reaction of $\text{Co}_2(\text{CO})_8$ with $\text{P}(i\text{-Pr})_3$ results in formation of the disproportionation product $[\text{Co}(\text{CO})_3\text{L}_2][\text{Co}(\text{CO})_4]$ as the major product,¹⁸ while the sole product of the reaction between $[\text{CpMo}(\text{CO})_3]_2$ and $\text{P}(i\text{-Pr})_3$ is the monosubstituted compound $\text{Cp}_2\text{Mo}_2(\text{CO})_5\text{L}$.^{10b} No disproportionation products were obtained in the latter reaction, even when the reaction mixture was irradiated with ultraviolet or visible light.

For the heterodinuclear compound **1**, we have observed significantly different reactivities toward certain bases compared to the respective homodinuclear compounds. Table 5 lists the electronic and steric parameters of the phosphorus bases employed in this study; they were chosen so that the electronic and steric effects of the base on the reaction could be probed. $\text{P}(n\text{-Bu})_3$ is small and strongly electron-donating; $\text{P}(i\text{-Pr})_3$ and $\text{P}(c\text{-Hx})_3$ are strongly electron-donating, but are comparatively bulky; PPh_3 is intermediate in terms of both properties. $\text{P}(\text{OMe})_3$ and $\text{P}(\text{OPh})_3$ are both small and comparatively weak bases.

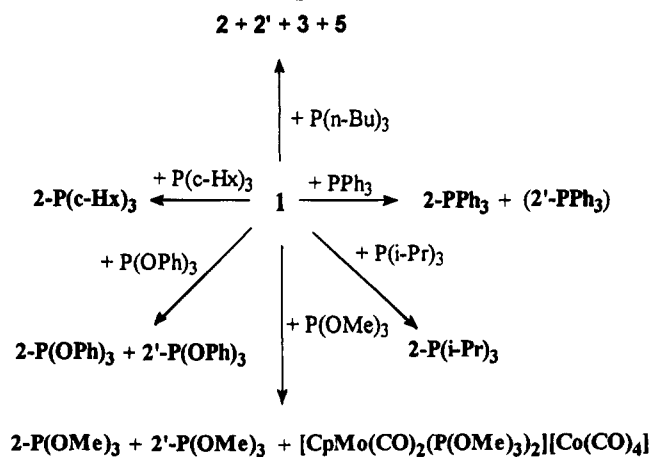
There are three possible pathways for the thermal substitution reaction of **1** with the bases to form the monosubstituted compound $\text{CpMo}(\text{CO})_3\text{-Co}(\text{CO})_3\text{L}$:

Table 5. Electronic and Steric Parameters of Lewis Bases Used in This Paper

ligand	δ^a	Θ^b deg	E_R^c kcal mol ⁻¹
$\text{P}(c\text{-Hx})_3$	6.32	170	116
$\text{P}(i\text{-Pr})_3$	6.20	160	109
$\text{P}(n\text{-Bu})_3$	5.69	132	64
PPh_3	4.30	145	75
$\text{P}(\text{OMe})_3$	3.18	107	52
$\text{P}(\text{OPh})_3$	1.69	128	65

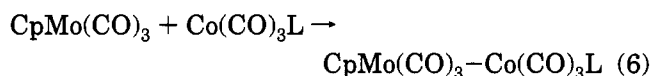
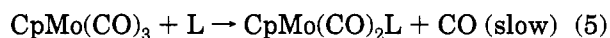
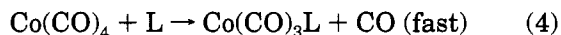
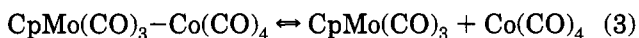
^a ¹³C chemical shift in $\text{LNi}(\text{CO})_3$ complexes, downfield in ppm, from $\text{Ni}(\text{CO})_4$.^{29a} ^b Reference 29b. ^c Reference 29c.

Scheme 1. Thermal Reactions of **1** with Phosphorus Ligands in 3MP at Room Temperature^a

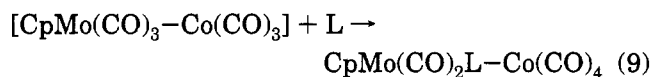
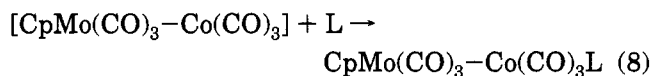
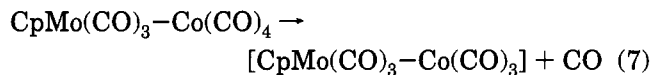


^a Product in parentheses indicates an unstable product at room temperature.

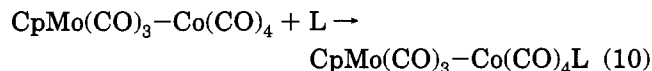
1. Homolytic dissociation via rupture of the Mo–Co bond:



2. Dissociative loss of CO:



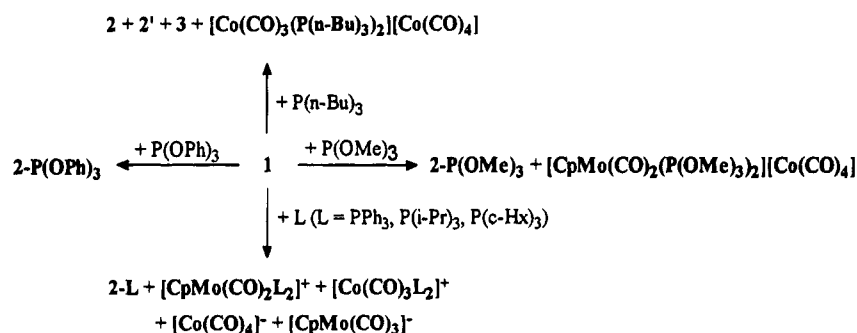
3. Associative interaction of L with **1**:



The product might then lose a CO from Co to form the substituted compound or undergo metal–metal bond rupture to form radicals and then radical recombinations.

(27) Szabo, P.; Fekete, L.; Bor, G.; Nagy-Magos, Z.; Marko, L. *J. Organomet. Chem.* **1968**, *12*, 245.

Scheme 2. Thermal and Photochemical Reactions of 1 with Phosphorus Ligands in CH₂Cl₂ at Room Temperature



Thermal Reaction of 1 with PPh₃, P(*i*-Pr)₃, or P(*c*-Hx)₃ in 3MP. Pathway 1 for the thermal reaction is ruled out by the fact that dimers such as [Co(CO)₃L]₂, [CpMo(CO)₃L]₂, or [CpMo(CO)₂L]₂ are not observed in the course of the reaction. If the reaction involves radical intermediates like Co(CO)₄, Co(CO)₃L, CpMo(CO)₃, or CpMo(CO)₂L, one would expect one or more of these dimers should be formed, at least to some extent.

The bimolecular association pathway, 3, is not consistent with the observed kinetics; i.e., the reaction rate is independent of entering ligand and of ligand concentration for L = PPh₃, P(*i*-Pr)₃, and P(*c*-Hx)₃.

The kinetics of reaction of 1 with L to form the monosubstituted compound 2-L (L = PPh₃, P(*i*-Pr)₃, and P(*c*-Hx)₃) are most clearly consistent with the dissociative CO loss pathway, 2. The first-order rate law implied by this pathway contains no term in the entering ligand, consistent with our observation that closely similar rate constants were obtained for the three different ligands, despite large differences in their electronic and steric properties. The observed behavior is similar to that seen in the reaction of Co₂(CO)₈ with AsPh₃, ¹³CO, or H₂^{9b,28} in which the loss of CO is postulated as an initial step for the substitution reactions.

In pathway 2, the rate-determining step is CO dissociation, forming an unsaturated intermediate. This intermediate may well adopt a CO bridging structure, as revealed by the low-temperature flash experiments.²⁵ If no other ligand is presented, it simply recombines with CO to re-form the starting material. In the presence of a strongly coordinating ligand, it quickly reacts to form the substituted products. In eq 7, if the intermediate indeed adopts a bridging structure, two products would be expected to form if the ligand can attack the intermediate at either metal center. For PPh₃, P(*i*-Pr)₃, and P(*c*-Hx)₃, the final product is invariably the Co-substituted complex (eq 8). In the case of PPh₃, the Mo-substituted species (2'-PPh₃) was observed in the early stage of the reaction (eq 9), but its characteristic absorbance slowly decays as the reaction proceeds and finally disappears when the reaction is complete. Similar bands at 2056, 2059, and 2063 cm⁻¹ were observed in the reaction of 1 with smaller ligands, P(*n*-Bu)₃, P(OMe)₃, and P(OPh)₃; however, in these cases the species were stable under reaction conditions. The spectra showed no evidence of a similar band in the case of the two bulky phosphines.

Because the Mo center is quite crowded, it is conceivable that very bulky ligands, such as P(*i*-Pr)₃ and P(*c*-

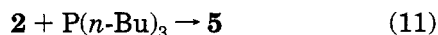
Hx)₃ are unable to bind there, or do so weakly. The smaller P(*n*-Bu)₃, P(OMe)₃, and P(OPh)₃ can approach the Mo center more easily, with formation of stable Mo-substituted species. PPh₃ may be just small enough that the substitution does occur, but the substituted molecule is probably too crowded to be stable in solution. These observations thus suggest that the steric requirement of the ligand is the major factor affecting the rate of formation or the stability of the Mo-substituted product.

The highest frequency CO stretching band of 1 at 2076 cm⁻¹, assigned to a CO stretch mode largely localized at the Co center, is shifted down about 20 cm⁻¹ to 2056 cm⁻¹ following replacement of a CO by L on the Mo in 2'. The direction and magnitude of shift of the CO bands, to 2056, 2057, 2059, and 2063 cm⁻¹ for P(*n*-Bu)₃, PPh₃, P(OMe)₃, and P(OPh)₃, respectively, on Mo are consistent with the expected small effect that replacement of CO by a phosphorus ligand of varying donor strength should have on the frequency of a CO stretching mode associated with the other center. Because the CpMo(CO)₃-Co(CO)₃L products are all stable in a degassed solvent for at least a few hours, we can exclude the possibility that 2' is formed from them. The fact that 2' did not decrease in concentration or disappear after the reaction for L = P(*n*-Bu)₃ indicates that it is not an intermediate in the reaction leading to 2. Since 2' is a minor intermediate product in the reaction of 1 with PPh₃, we cannot be certain as to what product it converts to as it decays; it is likely that PPh₃ dissociates, with formation of starting reactants or conversion to product 2 via a CO shift.

In CH₂Cl₂, thermal reaction of PPh₃ with 1, unlike that in 3MP in which no disproportionation occurs, results in formation of a small amount of [Co(CO)₃(PPh₃)₂]⁺ (2013 cm⁻¹), [CpMo(CO)₂(PPh₃)₂]⁺ (1898 cm⁻¹), and [CpMo(CO)₃]⁻ (1774 cm⁻¹). Since a more polar solvent is expected to stabilize ionic products, it is not surprising that a small amount of ionic products are formed in CH₂Cl₂ but not in 3MP. When the reaction is irradiated, major disproportionation products are formed in addition to small amounts of CpMo(CO)₃-Co(CO)₃(PPh₃) and [CpMo(CO)₃]₂.

Reaction of 1 with P(*n*-Bu)₃. Disproportionation products dominate under some conditions in the reaction with P(*n*-Bu)₃, which suggests that an alternative mechanism is operative. Different reaction products were obtained as reactant concentrations were varied. Reaction of 1 (0.12 mM) with P(*n*-Bu)₃ (2 mM) resulted in the formation of monosubstituted product 2 with minor amounts of 2' and 5, without formation of any

ionic product. The appearance of product **2** follows a first-order law with a rate constant of about $1.8 \times 10^{-4} \text{ s}^{-1}$. The kinetics of the major substitution is consistent with pathway 2 in which the major product is **2** and the minor product is **2'**. **5**, formed in a small quantity, is probably a secondary product between **2** and $\text{P}(n\text{-Bu})_3$ according to eq 11.²⁵



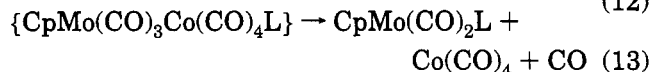
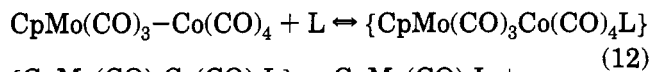
Product **4** is formed when the reaction mixture contains oxygen. The mass spectrum shows that an oxygen atom has been incorporated into the cation, but the mode of incorporation is not clear at present. The ^{31}P NMR spectrum of an impure sample of **4** shows a singlet at 33.42 ppm and a doublet of 32.50 and 32.31 ppm. A singlet ^{31}P NMR peak is obtained at 33.42 ppm for pure sample of **3**.

When higher concentrations of **1** and $\text{P}(n\text{-Bu})_3$ are employed, the reaction gives rise to disproportionation products. Reaction of 2 mM **1** with 2 mM $\text{P}(n\text{-Bu})_3$ results in the formation of about 20% ionic product, while more than 80% of the products are the result of disproportionation when a 12 mM or higher concentration of $\text{P}(n\text{-Bu})_3$ is used. The increasing intensity of any one of the IR bands due to the ionic product can be fitted to a first-order rate law. The observed rate constants vary between 1.3×10^{-3} and $1.7 \times 10^{-3} \text{ s}^{-1}$ at 25 °C for 20 and 50 mM $\text{P}(n\text{-Bu})_3$, respectively. At 40 °C, a rate constant of $2.9 \times 10^{-3} \text{ s}^{-1}$ was obtained using 20 mM $\text{P}(n\text{-Bu})_3$.

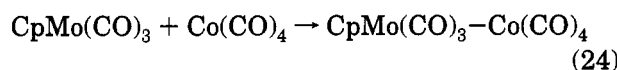
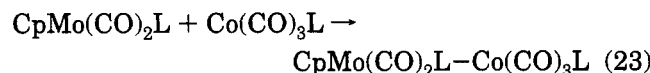
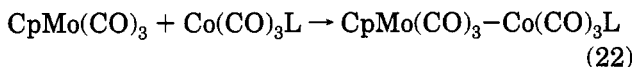
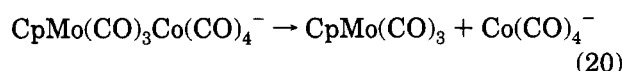
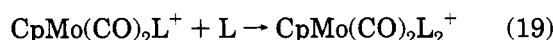
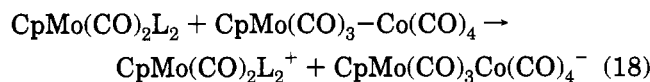
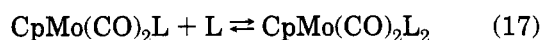
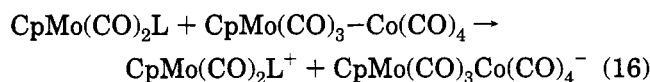
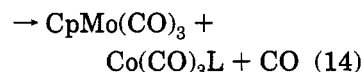
Irradiation of the reactant mixture with a sunlamp for 10 s led to very rapid formation of ionic products, and only very small amounts of neutral substitution products. Under these circumstances the much slower thermal substitution reaction is largely masked by the photoinduced disproportionation reaction. The fact that irradiation (which produces Mo-Co bond homolysis) does not increase the yield of monosubstituted product reinforces our earlier conclusion that the substitution reaction is not rate-determined by metal-metal bond homolysis.

A radical chain mechanism involving electron transfer analogous to the mechanisms proposed for the reactions of homonuclear dimer $\text{Co}_2(\text{CO})_8$ ^{9a,18} and $[\text{CpMo}(\text{CO})_3]_2$,^{10b} eqs 12–24, is suggested for the thermal reaction of **1** with $\text{P}(n\text{-Bu})_3$.

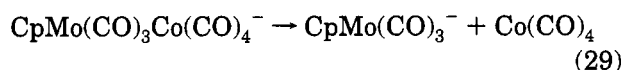
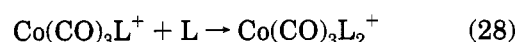
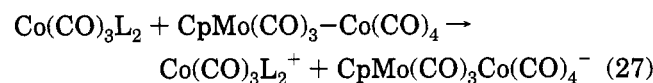
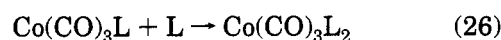
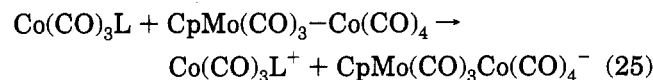
As described by the reaction mechanism, eqs 12–21, the disproportionation reaction with $\text{P}(n\text{-Bu})_3$ in 3MP under thermal conditions gives rise to the formation of only one ionic product, $[\text{CpMo}(\text{CO})_2(\text{P}(n\text{-Bu})_3)_2][\text{Co}(\text{CO})_4]$. Other possible ionic product species such as $[\text{Co}(\text{CO})_3(\text{P}(n\text{-Bu})_3)_2]^+$ (1995 cm^{-1} in hexane^{9a}) or $[\text{CpMo}(\text{CO})_3]^-$ (1894, 1774 cm^{-1} in CH_2Cl_2)²³ were not detected in the reaction. Irradiation of a CH_2Cl_2 solution, however, leads to the formation of small amounts of $[\text{Co}(\text{CO})_3(\text{P}(n\text{-Bu})_3)_2]^+$ in addition to $[\text{CpMo}(\text{CO})_2(\text{P}(n\text{-Bu})_3)_2]^+$; but $[\text{CpMo}(\text{CO})_3]^-$ was not observed. Photo-initiated disproportionation in CH_2Cl_2 with PPh_3 , $\text{P}(i\text{-Pr})_3$, or $\text{P}(c\text{-Hx})_3$, however, results in formation of all four possible ionic species, $[\text{CpMo}(\text{CO})_2\text{L}_2]^+$, $[\text{Co}(\text{CO})_3\text{L}_2]^+$, $[\text{Co}(\text{CO})_4]^-$, and $[\text{CpMo}(\text{CO})_3]^-$; their relative quantum yields are different depending upon the properties of each ligand. For PPh_3 , considerable amounts of $[\text{CpMo}(\text{CO})_3]^-$ are formed in CH_2Cl_2 solution, even under thermal conditions. These results suggest that ad-



or



ditional steps exist in the radical chain mechanism in addition to those described in eqs 12–24. These possible steps are described in the following equations:



The comparative roles of the 17-electron and 19-electron radicals, $\text{CpMo}(\text{CO})_2\text{L}$ or $\text{Co}(\text{CO})_3\text{L}$ and $\text{CpMo}(\text{CO})_2\text{L}_2$ or $\text{Co}(\text{CO})_3\text{L}_2$, respectively, in the radical chain are not readily discernible. When L is a strongly electron-releasing ligand such as a trialkylphosphine, both species should be capable of electron transfer to the parent dimer. While the reducing potential of the 19-electron radical is undeniably higher than that of the 17-electron species, it may be much less abundant in the solution. In any case, the rates of the electron transfer steps eq 16 or 18 and eq 25 or 27 should depend on both the donor and steric properties of L. Bulky ligands such as $\text{P}(i\text{-Pr})_3$ and $\text{P}(c\text{-Hx})_3$ fail to sustain an efficient radical chain process under thermal conditions. Under irradiation, ionic products are formed, but the quantum yields are clearly much smaller than with $\text{P}(n\text{-Bu})_3$. This suggests that while substitution into CpMo -

(CO)₃ and the subsequent electron-transfer do occur, they are not sufficiently fast to compete with one or more chain termination processes, eqs 22–24. For the thermal reaction, in order for the preequilibrium to lead successfully to chain initiation, the interaction between the attacking base and **1** must be sufficiently strong to promote Mo–Co bond rupture. Both the nucleophilicity and steric requirement of the base are important in determining how favorable the preequilibrium will be. If the base is so bulky that a close approach to the metal center is prevented, the interaction will not be strong enough to cause metal–metal bond homolysis. Under these circumstances, irradiation is required to initiate the radical chain processes. The nucleophilicity of the base may be less important than the steric requirements, since a much weaker base P(OMe)₃ also leads to significant formation of ionic products. This is consistent with an earlier study of the reaction of Co₂(CO)₈ with different phosphines. In that case, P(*t*-Bu)₃ ($\delta = 6.37$, cone angle = 182°, $E_R = 154$),²⁹ even though it is strongly nucleophilic, nevertheless failed to initiate a chain process, presumably because it is too bulky. However, if the nucleophilicity of the base is too weak, as for P(OPh)₃, even irradiation does not give rise to the disproportionation reaction.

In summary, we have in this paper demonstrated that the two distinct mechanisms proposed for reactions of homodinuclear complexes with nucleophiles are also operative for reactions of CpMo(CO)₃–Co(CO)₄ (**1**) with a series of Lewis bases in hydrocarbon solvents. We have shown how the reaction course is influenced by the nucleophilicity and steric requirements of the ligand and by solvent effects. For bulky ligands such as PPh₃, P(*i*-Pr)₃, or P(*c*-Hx)₃, neutral monosubstituted complexes are the only products formed in the thermal reaction in 3MP. Substitution occurs exclusively on Co for P(*i*-Pr)₃ and P(*c*-Hx)₃. There is evidence that an unstable Mo-substituted complex is also formed in small amounts during the reaction with PPh₃. The kinetics of the substitution reactions with these three ligands are consistent with a dissociative CO loss pathway. Irradiation of the solution with a sunlamp, however, results in formation of small amounts of disproportionation ionic products. The disproportionation quantum yield is higher in CH₂Cl₂ than in 3MP. Reaction of **1**

with P(*n*-Bu)₃ leads to predominantly ionic products in both thermal and photochemical reactions. However, the product distribution depends on concentrations of both reactants employed, as well as whether light or oxygen is involved. When the concentrations of both reactants are dilute, the concentration-independent CO dissociative pathway dominates, leading to the formation of neutral substitution products. Substitution of a CO by P(*n*-Bu)₃ also occurs preferably on Co, with very small amounts of a stable Mo-substituted product. At higher concentrations, the associative pathway takes over, leading to the formation of mainly ionic products. Because the latter pathway is a radical chain process, irradiation of the reaction for a few seconds results in very fast completion of the reaction, forming ionic products. Trace amounts of oxygen in the solution effectively quench the radical chain process. Reaction with a small but less nucleophilic base, such as P(OMe)₃, results in formation of both substitution (similar to that with P(*n*-Bu)₃, in which substitution occurs preferably on Co) and disproportionation products under thermal conditions. A poorly nucleophilic ligand like P(OPh)₃, even though it may be sterically favorable, fails to initiate the radical chain mechanism to produce ionic products; only neutral substitution products are observed in the thermal reaction. In CH₂Cl₂ solution, photoinitiated disproportionation leads to different ionic species for different ligands.

Acknowledgment. This research was supported by the National Science Foundation under grant NS-FCHE92-13531. The crystal structure determination of [CpMo(CO)₂(P(*n*-Bu)₃)₂][Co(CO)₄] was carried out in the X-ray Diffraction Center of the School of Chemical Sciences by Scott Wilson. The ZAB-SE mass spectrometer was purchased in part with grants from the Division of Research Resources, National Institute of Health (RR 01575), the National Science Foundation (PCM 8121494), and the National Institute of General Medical Sciences (GM 27029).

Supplementary Material Available: Tables of positional parameters, anisotropic displacement parameters, and bond lengths and angles for [CpMo(CO)₂(P(*n*-Bu)₃)₂][Co(CO)₄] (**3**) (14 pages). This material is contained in many libraries on microfiche, immediately follows this article in the microfilm version of the journal, and can be ordered from the American Chemical Society. See any current masthead page for ordering information.

OM940942A

(29) (a) Bodner, G. M.; May, M. P.; McKinney, L. E. *Inorg. Chem.* **1980**, *19*, 1951. (b) Tolman, C. A. *Chem. Rev.* **1977**, *77*, 313. (c) Brown, T. L.; Lee, K. J. *Coord. Chem. Rev.* **1993**, *128*, 89.

(30) Johnson, C. K. ORTEP-II. Fortran thermal ellipsoid plot program, ORNL-3794, Oak Ridge National Laboratory, Oak Ridge, TN, 1971.

Synthesis of the New Chiral Aminodiphosphine Ligands (*R*)- and (*S*)-(α -Methylbenzyl)bis(2-(diphenylphosphino)ethyl)amine and Their Use in the Enantioselective Reduction of α,β -Unsaturated Ketones to Allylic Alcohols by Iridium Catalysis

Claudio Bianchini,^{*,†} Erica Farnetti,[‡] Lionel Glendenning,[†] Mauro Graziani,^{*,‡}
Giorgio Nardin,[‡] Maurizio Peruzzini,[†] Eliana Rocchini,[‡] and Fabrizio Zanobini[†]

*Istituto per lo Studio della Stereochimica ed Energetica dei Composti di Coordinazione del
CNR, Via J. Nardi 39, 50132 Firenze, Italy, and Dipartimento di Scienze Chimiche,
Università di Trieste, Via Giorgieri 1, 34127 Trieste, Italy*

Received December 7, 1994[®]

Synthesis of the potentially tridentate, optically pure ligands $C_6H_5C^*H(Me)N(CH_2CH_2-PPh_2)_2$ (*R*)-(+)- and (*S*)-(-)-PNP*, **5a,b** from their corresponding chiral primary amines was achieved with excellent yields. The catalytic hydrogen-transfer reduction of $PhCH=CHCOME$ and other α,β -unsaturated or unsymmetrical ketones in the presence of $[Ir(COD)(OMe)]_2$ and **5a,b** is reported. These catalytic systems show high activity and chemoselectivity for the reduction of the carbonyl group (up to 94%). Due to the presence of the stereogenic center on the PNP* ligands **5a,b**, asymmetric induction was also achieved with enantioselectivities up to 54%. Discussion concerning the catalytic pathway and the intermediates involved is reported in conjunction with independent reactions of isolated, optically active compounds. Some of these are the iridium(I) cyclooctadiene complexes (*R*)- and (*S*)- $[IrH(COD)\{C_6H_5C^*H(Me)N(CH_2CH_2PPh_2)_2\}]$ (**8a,b**) and the iridium(III) ortho-metalated dihydrides *fac-exo*-(*R*)- *fac-exo*-(*S*)-, *fac-endo*-(*R*)-, and *fac-endo*-(*S*)- $[IrH_2\{C_6H_4C^*H(Me)N(CH_2CH_2PPh_2)_2\}]$ (**10a,b** and **11a,b**). X-ray crystal data are given for *fac-exo*-(*R*)- $[IrH_2\{C_6H_4C^*H(Me)N(CH_2CH_2PPh_2)_2\}]$ (**10a**), a distorted octahedron. The (*R*)-PNP* ligand facially coordinates to the iridium metal center, with the two hydride ligands *cis* to one another. The sixth coordination site is occupied by the ortho carbon atom of the phenyl substituent bound to the stereocenter. Crystal data: monoclinic, $P2_1$, with $a = 12.623(2)$ Å, $b = 18.265(3)$ Å, $c = 14.032(3)$ Å, $\beta = 92.55(1)^\circ$, $V = 3232$ Å³, $Z = 4$, $R = 0.037$, and $R_w = 0.041$.

The development of a universally applicable homogeneous catalyst for use in the stereoselective reduction of a variety of prochiral substrates (olefins, ketones, imines, enamines) is still a diverse and intriguing area of asymmetric synthesis.

As phosphines are highly efficient ligands in many catalytic reactions, there is a continuing effort to develop and design new chiral phosphines and especially chelating diphosphines for use in asymmetric catalysis.¹ In step with these developments in chiral phosphine ligands, transition-metal complexes with chiral amine ligands have also been shown to have a number of significant applications in asymmetric catalysis.^{1,2} It is thus conceivable that a chiral ligand containing two

phosphorus and one nitrogen donor atom would have a diverse and wider use in catalysis. Also, the combination of *soft* (phosphorus) and *hard* (nitrogen) donor atoms in the same ligand framework may offer the advantage of providing free coordination sites along the catalytic pathway by the alternative decoordination of either the phosphorus or nitrogen donor, depending on the nature of the reactant and of the formal oxidation state of the metal.

(2) Togni, A.; Venanzi, L. M. *Angew. Chem., Int. Ed. Engl.* **1994**, *33*, 497–526. For recent applications of chiral diamine ligands in asymmetric catalysis, see: Brookhart, M.; Wagner, M. I.; Balavoine, G. A.; Haddou, H. A. *J. Am. Chem. Soc.* **1994**, *116*, 3641. Nishiyama, H.; Itoh, Y.; Matsumoto, H.; Park, S.-B.; Itoh, K. *J. Am. Chem. Soc.* **1994**, *116*, 2223. For applications of P–N ligands in asymmetric catalysis, see: (a) Brunner, H.; Mokhlesur Rahman, F. M. *Chem. Ber.* **1984**, *117*, 710. (b) Mashima, K.; Akutagawa, T.; Zhang, X.; Takaya, H.; Taketomi, T.; Kumobayashi, H.; Akutagawa, S. *J. Organomet. Chem.* **1992**, *428*, 213–222. (c) Mashima, K.; Akutagawa, T.; Zhang, X.; Takaya, H.; Taketomi, T.; Kumobayashi, H.; Akutagawa, S. *J. Am. Chem. Soc.* **1993**, *115*, 3318. (d) Albinati, A.; Lianza, F.; Berger, H.; Pregosin, P. S.; Ruegger, H.; Kunz, R. W. *Inorg. Chem.* **1993**, *32*, 478–486. (e) Brown, J. M. *Book of Abstracts*, 9th International Symposium on Homogeneous Catalysis, Jerusalem, Israel, Aug 21–26, 1994; Abstract K-4, p 7. (f) Basoli, C.; Botteghi, C.; Cabras, M. A.; Chelucci, G.; Marchetti, M. *Book of Abstracts*, 9th International Symposium on Homogeneous Catalysis, Jerusalem, Israel, Aug 21–26, 1994; Abstract A-11, p 106. (g) Burk, M. J.; Harlow, R. L. *Angew. Chem., Int. Ed. Engl.* **1990**, *29*, 1462. (h) Burk, M. J.; Feaster, J. E.; Harlow, R. L. *Tetrahedron: Asymmetry* **1991**, *2*, 569.

[†] ISSECC, CNR.

[‡] Università di Trieste.

[®] Abstract published in *Advance ACS Abstracts*, February 1, 1995.

(1) (a) Morrison, J. D., Ed. *Asymmetric Synthesis: Chiral Catalysis*; Academic Press: London, 1985; Vol. 5. (b) Jardine, F. H. In *Chemistry of the Platinum Group Metals*; Hartley, F. R., Ed.; Elsevier: Oxford, U.K., 1991; pp 420–424. (c) Ojima, I., Ed. *Catalytic Asymmetric Synthesis*; VCH: New York, 1993. (d) Brunner, H.; Zettlemeier, W. *Handbook of Enantioselective Catalysis with Transition Metal Compounds: Ligands*; VCH: New York, 1993; Vol. 2. For recent applications of chiral diphosphine ligands in asymmetric catalysis see: Rajanbabu, T. V.; Casalnuovo, A. L. *Pure Appl. Chem.* **1994**, *66*, 1535. Hayashi, T.; Ohno, A.; Lu, S.; Matsumoto, Y.; Fukuyo, E.; Yanagi, K. *J. Am. Chem. Soc.* **1994**, *116*, 4221. Gorla, F.; Togni, A.; Venanzi, L. M.; Albinati, A.; Lianza, F. *Organometallics* **1994**, *13*, 1607.

The potentially tridentate aminodiphosphine ligands $\text{RN}(\text{CH}_2\text{CH}_2\text{PPh}_2)_2$ ($\text{R} = \text{H, Me, Pr}^n$; PNP) have received little attention in coordination chemistry.³ Recent studies, however, have shown that the use of these ligands allows the formation of many new types of transition-metal complexes,⁴ exhibiting a number of unusual reactivity patterns,⁵ and also provides novel applications in homogeneous catalysis.⁶ In a previous paper⁶ we reported the hydrogen-transfer reduction of benzylideneacetone, $\text{PhCH}=\text{CHCOMe}$, in the presence of $[\text{Ir}(\text{COD})(\text{OMe})]_2$ (COD cycloocta-1,5-diene) and $\text{Pr}^n\text{N}(\text{CH}_2\text{CH}_2\text{PPh}_2)_2$ (PNPPⁿ). The major product of this reaction was the allylic alcohol formed by reduction of the carbonyl group, whereas reduction of the C=C bond appeared to be disfavored. Introduction of the stereogenic center $\text{NC}^*\text{H}(\text{Me})\text{Ph}$ into the PNP ligand framework was expected to form a catalytic system with reductive activity and chemoselectivity comparable to that exhibited before but also with the added desirable property of asymmetric induction.

This paper details our endeavors to design, synthesize, and characterize a new variety of optically pure ligand containing the PNP donor atom set for use in asymmetric catalysis. We also report our first results of the catalytic activity of new organometallic iridium species stabilized by $\text{C}_6\text{H}_5\text{C}^*\text{H}(\text{Me})\text{N}(\text{CH}_2\text{CH}_2\text{PPh}_2)_2$ (**5a,b**) in the chemo- and enantioselective reduction of α,β -unsaturated or unsymmetrical ketones *via* hydrogen transfer from alcohols.

Experimental Section

All the reactions and manipulations were routinely performed under a nitrogen or argon atmosphere, by using standard Schlenk-tube techniques. Propan-2-ol and cyclopentanol were distilled over CaO. All the substrates were purified by either recrystallization or distillation under an inert atmosphere prior to use. Optically pure (*R*)-(+)- and (*S*)-(-)- α -methylbenzylamine (**1a,b**, respectively) were obtained from Aldrich and used without further purification. Diphenylchlorophosphine was purchased from Fluka AG and distilled prior to use. All the other chemicals were reagent grade and were used as received by commercial suppliers. $[\text{Ir}(\text{COD})(\text{OMe})]_2$ was prepared according to a published procedure.⁷

Infrared spectra were recorded on a Perkin-Elmer spectrophotometer interfaced to a Perkin-Elmer 3600 data station. ¹H, ¹³C, and ³¹P NMR spectra were recorded on a JEOL EX400 spectrometer (operating at 399.77, 100.54, and 161.82 MHz, respectively) or a Bruker AC 200P spectrometer (operating at 200.13, 50.53, and 81.01 MHz, respectively). ¹H and ¹³C chemical shifts were reported relative to tetramethylsilane. ³¹P NMR chemical shifts were reported relative to external 85% H_3PO_4 , with downfield values taken as positive.

Chemical yields and ee's of the catalytic reactions were determined by GC-MS using a Hewlett-Packard 5971A mass

detector coupled with a 5890II gas chromatograph, on a Chrompack CP-CYCLODEX B 236M capillary column (50 m \times 0.25 mm, film depth 0.25 mm). Alternatively, chemical yields were determined by GLC on a Perkin-Elmer Sigma 3B gas chromatograph equipped either with a Supelcowax 10 wide-bore capillary column (30 m \times 0.75 mm) or with a Cp-Sil-5 CB wide-bore capillary column (25 m \times 0.53 mm), and ee's were determined by optical rotation measurements on a Perkin-Elmer 241 polarimeter.

Preparation of (*R*)-(+)- and (*S*)-(-)-(α -Methylbenzyl)-bis(2-(diphenylphosphino)ethyl)amine (PNP*; **5a,b).** (i) **Preparation of (*R*)-(+)- and (*S*)-(-)-(α -Methylbenzyl)bis(2-hydroxyethyl)amine (**2a,b**).** (*R*)-(+)- α -Methylbenzylamine (**1a**) (10.0 g, 82.5 mmol) was dissolved in an ethanol/water mixture (1:2, v/v, 75 mL) under nitrogen and the stirred reaction mixture cooled to -10°C . Ethylene oxide (9.5 g, 215 mmol, 2.6 equiv) was introduced directly into the reaction mixture (~ 2.0 h) at such a rate as to minimize loss of unreacted oxirane. The reaction mixture was warmed to room temperature and stirred for a further 18 h. Ethanol and water were removed by distillation, and the crude diol was purified by fractional distillation under reduced pressure (163–165 $^\circ\text{C}$ /1.0 mmHg) to give (*R*)-(+)-(α -methylbenzyl)bis(2-hydroxyethyl)amine (**2a**) as a clear oil (14.4 g, 84%).

(*S*)-(-)-(α -Methylbenzyl)bis(2-hydroxyethyl)amine (**2b**) was prepared from its corresponding primary amine by following a method similar to that described above. **2b** was obtained as a clear oil (80%) (167–168 $^\circ\text{C}$ /1.0 mmHg). Anal. Calcd for $\text{C}_{12}\text{H}_{19}\text{NO}_2$: C, 69.0; H, 9.09; N, 6.70. Found: C, 69.2; H, 8.58; N, 6.15. MS (*m/e*): 206 (3%), 178 (51), 105 (100), 77 (19), 74 (75). ¹H NMR (CDCl_3 , 20 $^\circ\text{C}$, 200.13 MHz; δ): 1.41, d, ³ $J_{\text{H}_1,\text{H}_2^*}$ 6.8 Hz, 3 \times H1; 2.55, dd, ³ $J_{\text{H}_1,\text{H}_2^*}$ 5.4 Hz, ³ $J_{\text{H}_1',\text{H}_2'}$ 5.4 Hz, 4 \times H2'; 2.57, dt, ² $J_{\text{H}_1',\text{H}_1''}$ 13.7 Hz, ³ $J_{\text{H}_1',\text{H}_2'}$ 5.4 Hz, 2 \times H1' α ; 2.72, dt, ² $J_{\text{H}_1',\text{H}_1''}$ 13.7 Hz, ³ $J_{\text{H}_1',\text{H}_2'}$ 5.4 Hz, 2 \times H1' β ; 3.68, br s, 2 \times OH; 3.97, q, ³ $J_{\text{H}_1,\text{H}_2^*}$ 6.8 Hz, 1 \times H2*; 7.18–7.37, m, 5 \times H Ph. ¹³C{¹H} NMR (CDCl_3 , 20 $^\circ\text{C}$, 50.53 MHz; δ): 16.1, s, C1; 52.8, s, 2 \times C2'; 59.9, s, C2*; 60.9, 2 \times C1'; 127.7, s, C_{para} ; 128.6, s, C_{ortho} ; 128.9, s, C_{meta} ; 143.4, s, C_{ipso} .

(ii) **Preparation of (*R*)-(+)- and (*S*)-(-)-(α -Methylbenzyl)bis(2-chloroethyl)ammonium Chloride (**3a,b**).** To a stirred solution of thionyl chloride (11.3 mL, 18.4 g, 155 mmol) in dry chloroform (15 mL) under nitrogen was added dropwise a solution of (*R*)-(+)-(α -methylbenzyl)bis(2-hydroxyethyl)amine (**2a**; 10.0 g, 47.8 mmol) in dry chloroform (15 mL). The reaction mixture was refluxed for 10 min and then stirred at room temperature for 18 h. The solvent was then removed *in vacuo*, to leave the crude salt (*R*)-(+)-(α -methylbenzyl)bis(2-chloroethyl)ammonium chloride (**3a**) as a viscous oil. Removal of excess thionyl chloride was achieved by repeated addition and evacuation of chloroform (3 \times 20 mL) and ethanol (2 \times 10 mL). The purified **3a** was dried to constant weight at the pump. **3a** (11.0 g, 82%), as a clear oil, was stored under nitrogen prior to use in preparation iii.

Correspondingly, (*S*)-(-)-(α -methylbenzyl)bis(2-chloroethyl)ammonium chloride (**3b**; 75%) was obtained as a clear oil.

(iii) **Preparation of (*R*)-(+)- and (*S*)-(-)-(α -Methylbenzyl)bis(2-(diphenylphosphino)ethyl)amine (**5a,b**).** To an aqueous solution of sodium hydroxide (10 mL, 7 M) was added (*R*)-(+)-(α -methylbenzyl)bis(2-chloroethyl)ammonium chloride (**3a**; 11.0 g, 38.7 mmol) in water (20 mL). The two immiscible layers which form were separated, and the organic layer, (*R*)-(+)-(α -methylbenzyl)bis(2-chloroethyl)amine (**4a**), was dried over sodium hydroxide pellets. Anal. Calcd for $\text{C}_{12}\text{H}_{17}\text{NCl}_2$: C, 58.8; H, 6.94; N, 5.71. Found: C, 57.9; H, 6.60; N, 5.94. MS (*m/e*): 246 (1.1%, $\text{M}^+ + 1$), 245 (1.1, M^+), 231 (3.5), 197 (12.5), 105 (100), 77 (12.7), 63 (10.6). ¹H NMR (CDCl_3 , 20 $^\circ\text{C}$, 200.13 MHz; δ): 1.44, d, ³ $J_{\text{H}_1,\text{H}_2^*}$ 6.8 Hz, 3 \times H1; 2.72–2.85, m, 4 \times H1'; 3.47, t, ³ $J_{\text{H}_1',\text{H}_2'}$ 6.7 Hz, 4 \times H2'; 3.97, q, ³ $J_{\text{H}_1,\text{H}_2^*}$ 6.8 Hz, 1 \times H2*; 7.25–7.47, m, 5 \times H Ph. ¹³C{¹H} NMR (CDCl_3 , 20 $^\circ\text{C}$, 50.53 MHz; δ): 15.0, s, C1; 41.6, s, 2 \times C2'; 52.2, s, C2*; 58.9, s, 2 \times C1'; 125.9, s, C_{para} ; 126.3, s, C_{ortho} ; 127.0, s, C_{meta} ; 141.9, s, C_{ipso} .

(3) (a) Sacconi, L.; Morassi, R. *J. Chem. Soc. A* **1969**, 2904. (b) Sacconi, L.; Morassi, R. *J. Chem. Soc. A* **1971**, 492. (c) Di Vaira, M.; Midollini, S.; Sacconi, L. *Inorg. Chem.* **1978**, *17*, 816. (d) Bianchi, A.; Dapporto, P.; Fallani, G.; Ghilardi, C. A.; Sacconi, L. *J. Chem. Soc., Dalton Trans.* **1973**, 1973. (e) Bertini, I.; Sacconi, L.; Morassi, R. *Coord. Chem. Rev.* **1973**, *11*, 343.

(4) (a) Bianchini, C.; Innocenti, P.; Masi, D.; Peruzzini, M.; Zanolini, F. *Gazz. Chim. Ital.* **1992**, *122*, 461. (b) Marchi, A.; Marvelli, L.; Rossi, R.; Magon, L.; Uccelli, L.; Bertolasi, V.; Ferretti, V.; Zanolini, F. *J. Chem. Soc., Dalton Trans.* **1993**, 1281.

(5) Bianchini, C.; Glendenning, L.; Peruzzini, M.; Romerosa, A.; Zanolini, F. *J. Chem. Soc., Chem. Commun.* **1994**, 2219.

(6) Bianchini, C.; Farnetti, E.; Graziani, M.; Nardin, G.; Vacca, A.; Zanolini, F. *J. Am. Chem. Soc.* **1990**, *112*, 910.

(7) Farnetti, E.; Kaspar, J.; Spogliarich, R.; Graziani, M. *J. Chem. Soc., Dalton Trans.* **1988**, 947.

A solution of potassium diphenylphosphide in tetrahydrofuran (130 mL) under nitrogen was prepared *in situ* from diphenylchlorophosphine (12.1 g, 55.0 mmol) and potassium metal (4.4 g, 112 mmol). To this stirred solution was added dropwise (*R*)-(+)-(α -methylbenzyl)bis(2-chloroethyl)amine (**4a**; 6.8 g, 27.5 mmol) and the temperature maintained at 50 °C during the addition. During the course of the addition the initial red solution gradually changed to a creamy color. The reaction mixture was then refluxed for 5 min and cooled and water (100 mL) added. The two immiscible layers were separated, and the aqueous layer was extracted with ether (2 \times 100 mL). The combined organic layers were dried (Na₂SO₄) and filtered, and the ether was removed by distillation to leave a clear/ivory oil. The crude product was purified by recrystallization from acetone/ethanol (1:1 v/v) to give (*R*)-(+)-(α -methylbenzyl)bis(2-(diphenylphosphino)ethyl)amine (**5a**) as white crystals (78%).

By a method similar to that described above, (*S*)-(–)-(α -methylbenzyl)bis(2-(diphenylphosphino)ethyl)amine (**5b**) was obtained as white crystals (78%). Anal. Calcd for C₃₆H₃₇NP₂: C, 79.3; H, 6.79; N, 2.57. Found: C, 78.8; H, 6.75; N, 2.57. MS (*m/e*): 360 (59%), 346 (44), 185 (68), 105 (100). ¹H NMR (CD₂Cl₂, 20 °C, 200.13 MHz; δ): 1.23, d, ³J_{H₁H₂' 6.8 Hz, 3 \times H1; 2.10, dd, ³J_{H₁' α ,H₂' 8.3 Hz, ³J_{H₁' β ,H₂' 8.3 Hz, 4 \times H2'; 2.59, dt, ²J_{H₁' α ,H₁' β 13.2 Hz, ³J_{H₁' α ,H₂' 8.8 Hz, 2 \times H1' α ; 2.65, dt, ²J_{H₁' α ,H₁' β 12.7 Hz, ³J_{H₁' β ,H₂' 8.8 Hz, 2 \times H1' β ; 3.85, q, ³J_{H₁,H₂' 6.8 Hz, 1 \times H2*; 7.26–7.39, m, 25 \times H Ph. ¹³C{¹H} NMR (CD₂Cl₂, 20 °C, 50.53 MHz; δ): 18.3, s, C1; 26.8, d, ¹J_{P,C₂'} 12.2 Hz, 2 \times C2'; 46.7, d, ²J_{P,C₁'} 23.2 Hz, 2 \times C1'; 59.8, s, C2*; 128.8, s, C_{para}; 129.0, s, C_{meta}; 133.1, d, ²J_{P,C_{ortho}} 3.7 Hz, 2 \times C_{ortho}; 133.5, d, ²J_{P,C_{ortho}} 3.7 Hz, 2 \times C_{ortho}'; 139.2, d, ²J_{P,C_{ipso}} 13.0 Hz, C_{ipso}; 139.4, d, ²J_{P,C_{ipso}} 13.0 Hz, C_{ipso}'. ³¹P{¹H} NMR (CDCl₃, 20 °C, 81.01 MHz; δ): –20.0, s, 2 \times P. **5a**: [α]_D²⁰ = +12.0° (c = 1, CHCl₃). **5b**: [α]_D²⁰ = –11.2° (c = 1, CHCl₃).}}}}}}}}

Preparation of (*R*)-(+)-(α -Methylbenzyl)bis(2-(diphenylphosphino)ethyl)ammonium Chloride (6a**).** Concentrated hydrochloric acid (4.0 mL, 10 M) was slowly added to (*R*)-(+)-(α -methylbenzyl)bis(2-(diphenylphosphino)ethyl)amine (**5a**; 270 mg, 0.50 mmol) to give a viscous oil. Slow addition of water (10 mL) induced the precipitation of the (*R*)-(+)-(α -methylbenzyl)bis(2-(diphenylphosphino)ethyl)ammonium chloride salt. This white precipitate was filtered and washed with water until the filtrate was neutral. (*R*)-(+)-(α -methylbenzyl)bis(2-(diphenylphosphino)ethyl)ammonium chloride (**6a**; 288 mg, 90%) was used without further purification. ¹H NMR (CDCl₃, 20 °C, 200.13 MHz; δ): 1.71, d, ³J_{H₁,H₂' 6.8 Hz, 3 \times H1; 2.00–3.50, m, 4 \times H2' and 4 \times H1'; 4.12, qd, ³J_{H₁,H₂' 6.8 Hz, ³J_{H₁,H₂' 6.6 Hz, 1 \times H2*; 7.14–7.54, m, 25 \times H Ph; 12.52, br s, 1 \times HN. ³¹P{¹H} NMR (CDCl₃, 20 °C, 81.01 MHz; δ): –19.7, s, 1 \times P; –20.0, s, 1 \times P.}}}

Preparation of (*R*)- and (*S*)-[(α -Methylbenzyl)bis(2-(diphenylphosphino)ethyl)amine]iridium Hydride Cyclooctadiene [IrH(COD)(PNP*)]; **8a,b.** [Ir(COD)(OMe)]₂ (663 mg, 1.0 mmol) was dissolved in dichloromethane (20 mL) under nitrogen. PNP* (**5a,b**; 1.09 g, 2.0 mmol) was added, and the reaction mixture was stirred at room temperature for 1 h. The reaction mixture was concentrated and methanol (15 mL) added to induce precipitation of an off-white crystalline solid. This precipitate was filtered under nitrogen and washed with methanol and pentane to give [IrH(COD)(PNP*)] (**8a,b**; 740 mg, 69%). IR spectrum (Nujol mull): ν (Ir–H) 2108 (s) cm^{–1}. Anal. Calcd for C₄₄H₅₀IrNP₂: C, 62.4; H, 5.95; N, 1.65. Found: C, 62.8; H, 5.80; N, 1.57. ¹H NMR (C₆D₆, 20 °C, 200.13 MHz; δ): –13.44, t, ²J_{H₁hydride,P} 22.0 Hz, 1 \times H hydride; 1.12, d, ³J_{H₁,H₂' 6.7 Hz, 3 \times H1; 1.65–3.25, m, 4 \times H2' and 8 \times H COD; 3.46, q, ³J_{H₁,H₂' 6.3 Hz, 1 \times H2*; 4.02, m, 4 \times H1'; 7.20 to 8.10, m, 28 \times H Ph. ¹³C{¹H} NMR (C₆D₆, 20 °C, 100.54 MHz; δ): 19.9, s, C1; 31.7, d, ¹J_{P,C₂'} 5.1 Hz, 2 \times C₂' (COD); 33.8, d, ¹J_{C,P} 23.6 Hz, 1 \times CH₂–P; 34.3, d, ¹J_{C,P} 23.6 Hz, 1 \times CH₂–P; 36.1, dd, ¹J_{C,P} 10.8 Hz, ¹J_{C,P} 3.2 Hz, 2 \times CH₂ (COD); 46.1, d, ¹J_{C,P} 2.5 Hz, 1 \times CH₂–N; 47.7, d, ¹J_{C,P} 3.2 Hz, 1 \times CH₂–N; 47.9, dd, ¹J_{C,P} 27.0 Hz, ¹J_{C,P} 6.4 Hz, 2 \times CH (COD); 61.4, s, C1*; 79.2,}}

dd, ¹J_{C,P} 17.6 Hz, ¹J_{C,P} 3.2 Hz, 2 \times CH (COD); 127.0–134.2, m, 30 \times C Ph. ³¹P{¹H} NMR (C₆D₆, 20 °C, 81.01 MHz; δ): –2.49, d, ²J_{P,P} 23.1 Hz, 1 \times P; 1.24, d, ²J_{P,P} 23.1 Hz, 1 \times P. **8a**: [α]_D²⁰ = +12.9° (c = 1, CHCl₃). **8b**: [α]_D²⁰ = –13.0° (c = 1, CHCl₃).

Preparation of (*R*)- and (*S*)-[(α -Methylbenzyl)bis(2-(diphenylphosphino)ethyl)amine]iridium Dihydride (*fac-exo*-[IrH₂{C₆H₄C*H(Me)N(CH₂CH₂PPh₂)₂}]]; **10a,b.** [IrH(COD)(PNP*)] (**8a,b**; 540 mg, 1.0 mmol) was dissolved in a minimum amount of tetrahydrofuran prior to addition of propan-2-ol (30 mL) under nitrogen. The resulting solution was refluxed for 9 h. The reaction mixture was concentrated to half its volume and *n*-hexane added to induce precipitation of an off-white solid. This product was filtered and washed with propan-2-ol and *n*-hexane to give a mixture of the *fac-exo* iridium dihydride (**10a,b**) and the *fac-endo* iridium dihydride (**11a,b**) in a 10:1 ratio (*vide infra*). Recrystallization of this crude reaction mixture from dichloromethane and propan-2-ol gave pure *fac-exo*-[IrH₂{C₆H₄C*H(Me)N(CH₂CH₂PPh₂)₂}] (**10a,b**; 300 mg, 70%) as a cream-colored solid. IR spectrum (Nujol mull): ν (Ir–H) 1975 (s), 2079 (s) cm^{–1}. Anal. Calcd for C₃₆H₃₈IrNP₂: C, 58.5; H, 5.02; N, 1.90. Found: C, 58.8; H, 5.12; N, 1.85. ¹H NMR (C₆D₆, 20 °C, 399.77 MHz; δ): –18.4, td, ²J_{H₁hydride,P} 11.8 Hz, ²J_{H₁hydride,H₁hydride} 4.9 Hz, 1 \times H_{apical}; –7.7, ddd, ²J_{H₁hydride,P_{trans}} 139.2 Hz, ²J_{H₁hydride,P_{cis}} 22.0 Hz, ²J_{H₁hydride,H₁hydride} 4.9 Hz, 1 \times H_{meridional}. ¹³C{¹H} NMR (C₆D₆, 20 °C, 100.54 MHz; δ): 12.7, s, C1; 34.3, d, ¹J_{P,C₂'} 12.2 Hz, 1 \times C2'; 39.3, d, ²J_{P,C₂'} 23.2 Hz, 1 \times C2'; 53.4, s, 1 \times C1'; 58.8, 1 \times C1'; 76.6, s, C2*; 120.0 to 141, 29 \times C Ph; 154.9, dd, ²J_{P_{trans},C_{ortho}} 82.5 Hz, ²J_{P_{cis},C_{ortho}} 10.3 Hz, 1 \times C_{ortho}. ³¹P{¹H} NMR (C₆D₆, 20 °C, 161.82 MHz; δ): 13.9, ²J_{P,P} 7.7 Hz, 1 \times P; 17.7, ²J_{P,P} 7.7 Hz, 1 \times P. **10a**: [α]_D¹⁵ = +124.0° (c = 1, CHCl₃). **10b**: [α]_D¹⁵ = –123.8° (c = 1, CHCl₃).

Isomerization of *fac-exo*-(*R*)-[IrH₂{C₆H₄C*H(Me)N(CH₂CH₂PPh₂)₂}] (10a**) to *fac-endo*-(*R*)-[IrH₂{C₆H₄C*H(Me)N(CH₂CH₂PPh₂)₂}] (**11a**).** Refluxing *fac-exo*-(*R*)-[IrH₂{C₆H₄C*H(Me)N(CH₂CH₂PPh₂)₂}] (**10a**; ³¹P{¹H} NMR (C₆D₅CD₃, 161.82 MHz) δ 12.7, ²J_{P,P} 8.7 Hz; 16.2, ²J_{P,P} 8.4 Hz) in propan-2-ol under nitrogen gave *fac-endo*-(*R*)-[IrH₂{C₆H₄C*H(Me)N(CH₂CH₂PPh₂)₂}] (**11a**; 15%) after 2 h, with the following spectroscopic properties. ¹H NMR (C₆D₆, 20 °C, 399.77 MHz; δ): –20.4, dt, ²J_{H₁hydride,P} 12.1 Hz, ²J_{H₁hydride,H₁hydride} 5.2 Hz, 1 \times H_{apical}; –9.9, ddd, ²J_{H₁hydride,P_{trans}} 140.9 Hz, ²J_{H₁hydride,P_{cis}} 22.8 Hz, ²J_{H₁hydride,H₁hydride} 4.8 Hz, 1 \times H_{meridional}. ³¹P{¹H} NMR (C₆D₅CD₃, 20 °C, 161.82 MHz; δ): 13.2, ²J_{P,P} 7.3 Hz, 1 \times P; 15.8, ²J_{P,P} 7.3 Hz, 1 \times P. The equilibrium concentration between **10a** and **11a** does not appreciably change after a further 8 h of refluxing in propan-2-ol, which indicates the attainment of the equilibrium system to a stationary state.

Preparation of (*R*)- and (*S*)-[(α -Methylbenzyl)bis(2-(diphenylphosphino)ethyl)amine]iridium Carbonyl Hydride ([IrH(CO){C₆H₄C*H(Me)N(CH₂CH₂PPh₂)₂}]]; **14a,b.** *fac*-[IrH₂{C₆H₄C*H(Me)N(CH₂CH₂PPh₂)₂}] (**10a,b**; 200 mg, 0.27 mmol) was dissolved in toluene (40 mL). The resulting clear solution was placed in an autoclave and charged with carbon monoxide (5.0 atm). The autoclave was then heated to an internal temperature of 80–90 °C for 3 h. The resulting deep yellow solution was removed and the solvent evaporated *in vacuo* to leave a yellow powder. [IrH(CO){C₆H₄C*H(Me)N(CH₂CH₂PPh₂)₂}] (**14a,b**; 200 mg, 97%). IR spectrum (Nujol mull): ν 1906 (s), 1957 (s) cm^{–1}. IR spectrum (CHCl₃): ν 1914 (s), 1971 (s) cm^{–1}. Anal. Calcd for C₃₇H₃₈IrNOP₂: C, 57.9; H, 4.99; N, 1.83. Found: C, 57.0; H, 4.85; N, 1.77. ¹H NMR (THF-*d*₈, 20 °C, 200.13 MHz; δ): –11.03, t, ²J_{H₁hydride,P} 28.4 Hz, 1 \times H hydride; 1.15, d, ³J_{H₁,H₂' 7.0 Hz, 3 \times H1; 2.40–3.10, m, 4 \times H1' and 4 \times H2'; 3.75, q, ³J_{H₁,H₂' 6.9 Hz, 1 \times H2*; 7.12–7.81, m, 25 \times H Ph. ¹³C{¹H} NMR (THF-*d*₈, 20 °C, 50.53 MHz; δ): 21.2, s, C1; 31.9, d, ¹J_{P,C₂'} 26.6 Hz, 2 \times C2'; 48.1, s, 2 \times C1'; 62.6, s, C2*; 128.9–135.1, 30 \times C Ph; 185.7, t, ²J_{P,C} 10.6 Hz, 1 \times CO. ³¹P{¹H} NMR (THF-*d*₈, 20 °C, 81.01 MHz; δ): –7.0, s, 2 \times P.}}

Catalytic Experiments with the System *in Situ*. In a typical experiment, a three-necked thermostated glass reactor

equipped with a condenser, an argon inlet, a rubber septum, and a magnetic bar was charged under an argon flow with propan-2-ol (or cyclopentanol) (50 mL). Addition of [Ir(COD)-(OMe)₂] (6.63 mg, 0.01 mmol) was followed by addition of the PNP* ligand (**5a,b**; 10.91 mg, 0.02 mmol). The resulting pale yellow solution was heated to the desired temperature in the instances where the reaction was performed at 83 or 60 °C, whereas catalytic reactions at temperatures lower than 60 °C were performed by heating the solution at 60 °C for 2 h before lowering the temperature as desired. After the solution was stirred at the final temperature for 10 min, the substrate (2.0 mmol) was added.

Catalytic Experiments with 8a,b or 10a,b as Precursors. A three-necked thermostated glass reactor equipped as described above was charged under an argon flow with propan-2-ol (50 mL). Addition of **8a,b** (16.94 mg, 0.02 mmol) or **10a,b** (14.80 mg, 0.02 mmol) gave after a few minutes a pale yellow solution, which was heated to the desired reaction temperature. After 10 min the substrate (2.00 mmol) was added.

NMR Studies. A three-necked 10-mL flask equipped with a reflux condenser, a rubber septum, an argon inlet, and a magnetic bar was charged under an argon flow with propanol-2-ol (2 mL), the iridium dimer (19.9 mg, 0.03 mmol), and the PNP* ligand (**5a**; 32.7 g, 0.06 mmol). The resulting pale yellow solution was heated to 60 °C for 2 h; after this time, the temperature was raised to 83 °C. Samples of about 0.4 mL of the solution were withdrawn after the initial 2 h at 60 °C, after 2 h at 83 °C, and after 6 h at 83 °C. Each of these samples were transferred to an NMR tube containing about 0.3 mL of previously degassed C₆D₆. ³¹P NMR spectra showed the formation of compounds **8a**, **9a**, **10a**, **11a**, and **12a** (*vide infra*) with yields calculated from the integration of the NMR signals.

An alternative method was to perform the reaction in propan-2-ol-*d*₈, thus allowing monitoring of the ¹H NMR spectra. In such a case, samples of about 0.7 mL of the reaction mixture were withdrawn, and transferred to an empty NMR tube under an inert atmosphere.

The same procedure was employed for the NMR studies of the reactivity of compounds **8a** and **10a** in propan-2-ol: in these cases the above described reactor was initially charged with propan-2-ol (2 mL) (or alternatively in propan-2-ol-*d*₈) and 0.06 mmol of either **8a** or **10a**.

X-ray Data Collection and Processing. Crystals of *fac*-(*R*)-[IrH₂{C₆H₄C*(H)(Me)N(CH₂CH₂PPh₂)₂}] (**10a**) were grown from a dichloromethane/methanol solution at 25 °C under an argon atmosphere. A colorless crystal of dimensions 0.15 × 0.20 × 0.35 mm was mounted on an Enraf-Nonius CAD4 diffractometer, and lattice parameters were obtained by a least-squares refinement of 25 accurately centered reflections.

A summary of the crystal data and the details of the intensity data collection and refinement are provided in Table 1. No significant change in intensities, due to crystal decay, was noticed throughout the data collection.

The structure was solved by conventional Patterson and Fourier methods. The coordinated hydrides were located from the difference Fourier map after anisotropic refinement and then isotropic refinement in the final full-matrix least-squares cycles. The positions of all the other hydrogen atoms were calculated and confirmed by the difference Fourier map. Residual peaks were found only near the heavy atoms. Scattering factors, anomalous dispersion terms, and programs were taken from the Enraf-Nonius MOLEN library.⁸ Final positional and equivalent thermal parameters are given in Table 2. Lists of anisotropic thermal parameters and hydrogen atom coordinates are available as supplementary material.

The crystal structure of **10a** consists of two similar crystallographically independent neutral complexes, as suggested by the comparison of the corresponding bond distances and angles (see Tables 3 and 4, respectively). Figure 2 is an ORTEP

Table 1. Summary of Crystal Data for **10a**

formula	C ₃₆ H ₃₈ IrNP ₂
fw	738.87
cryst syst	monoclinic
space group	P2 ₁
a, Å	12.623(2)
b, Å	18.265(3)
c, Å	14.032(3)
β, deg	92.55(1)
Z	4
V, Å ³	3232(1)
d _{calcd} , g cm ⁻³	1.60
F(000), e	1552
μ(Mo Kα), cm ⁻¹	42.4
cryst dimens, mm	0.15 × 0.20 × 0.35
diffractometer	Enraf-Nonius CAD4
temp, K	294 ± 1
radiation Mo Kα	0.710 69
(graphite monochromated), Å	
scan type	Ω
scan speed, deg min ⁻¹	2–10
scan range, deg	1 + 0.35 tan θ
2θ range, deg	4–56
no. of rflns measd	±h,k,l
no. of total measd data	8342 total, 8032 unique
abs cor	empirical from ψ scan
no. of unique data with I > 3σ(I)	5451
no. of variables	376
R ⁺	0.037
R _w ⁺	0.041
w	1
highest peaks in final diff map, e Å ⁻³	-0.9, +1.2

drawing of one of the two independent molecules. Refinement of the other enantiomer gave R⁻ = 0.043 and R_w⁻ = 0.049. The value R = R_w/R_w⁺ = 1.2 confirms the correct assignment of the absolute R configuration of the C7 atom as shown in Figure 2.⁹

Results

Synthesis of the Ligands (*R*)-(+)- and (*S*)-(-)-(*α*-Methylbenzyl)bis(2-(diphenylphosphino)ethyl)amine (5a,b**).** Synthesis of the PNP* ligands **5a,b** was achieved by following the method illustrated in Scheme 1. Nucleophilic attack with the chiral primary amines **1a,b** and 2.0 equiv of ethylene oxide (and consequent ring opening) in ethanol/water at 0 °C gave the corresponding chiral diols **2a,b**, as clear viscous oils, in excellent yields (80–84%). Subsequent transformation of these diols into their dichloroammonium salts **3a,b** was achieved using thionyl chloride in dry chloroform (yields 75–82%). Addition of concentrated sodium hydroxide to these ammonium salts **3a,b** gave the corresponding dichloro tertiary amines **4a,b**. These dichloro tertiary amines were added immediately to stirred solutions of potassium diphenylphosphide in tetrahydrofuran maintained at a constant temperature of 50 °C. During the course of the reaction, the initial red solution gradually changed to a creamy color. After workup, the crude PNP* ligands were purified by recrystallization from acetone/ethanol to give (*R*)-(+)- and (*S*)-(-)-(*α*-methylbenzyl)bis(2-(diphenylphosphino)ethyl)amine (**5a,b**) as white microcrystals (yields 75–78%). Full details of the conditions used and results are given in the Experimental Section.

The presence of the stereogenic carbon, NC*(H)(Me)-Ph, in the PNP* ligand (**5a,b**) imparts asymmetry to the molecule and hence inequivalence of the two phosphorus atoms of the ligand. It therefore initially proved

(8) MOLEN, An interactive Intelligent System for Crystal Structure Analysis; Enraf-Nonius: Delft, The Netherlands, 1990.

(9) Rogers, D. *Acta Crystallogr.* **1981**, A37, 734.

Table 2. Positional Parameters and Their Estimated Standard Deviations for 10a

atom	x	y	z	$B (\text{\AA}^2)^a$	atom	x	y	z	$B (\text{\AA}^2)^a$
Molecule A									
Ir	0.83286(3)	0.913	0.11033(3)	3.070(7)	C16	1.063(1)	0.7567(9)	0.253(1)	4.9(3)*
P1	0.9813(2)	0.8430(2)	0.0971(2)	3.35(6)	C17	1.027(1)	0.8052(7)	-0.0152(9)	3.9(2)*
P2	0.8546(2)	0.9923(2)	-0.0133(2)	3.55(6)	C18	1.132(1)	0.7971(9)	-0.032(1)	5.4(3)*
N1	0.9375(7)	0.9875(6)	0.1939(6)	3.4(2)	C19	1.161(2)	0.765(1)	-0.116(1)	7.9(5)*
C1	0.807(1)	0.8743(7)	0.2448(9)	3.5(2)*	C20	1.088(1)	0.745(1)	-0.183(1)	6.7(4)*
H	0.760(7)	0.854(5)	0.046(7)	2(2)*	C21	0.984(2)	0.753(1)	-0.172(1)	7.4(5)*
H1	0.74(1)	0.986(9)	0.14(1)	8(4)*	C22	0.951(1)	0.7846(9)	-0.085(1)	4.9(3)*
C2	0.766(1)	0.8087(8)	0.275(1)	4.4(3)*	C23	0.947(1)	1.0596(7)	0.1461(9)	3.8(2)*
C3	0.752(1)	0.7941(9)	0.372(1)	5.3(3)*	C24	0.960(1)	1.0513(8)	0.040(1)	4.5(3)*
C4	0.784(1)	0.841(1)	0.439(1)	5.9(4)*	C25	0.899(1)	0.9707(7)	-0.1324(9)	4.2(3)*
C5	0.826(1)	0.909(1)	0.413(1)	5.1(3)*	C26	0.824(1)	0.9633(9)	-0.206(1)	5.6(3)*
C6	0.8406(9)	0.9251(7)	0.3190(8)	3.9(2)*	C27	0.855(1)	0.943(1)	-0.298(1)	7.2(4)*
C7	0.8815(9)	0.9996(9)	0.2872(9)	4.3(2)*	C28	0.956(1)	0.928(1)	-0.311(1)	7.3(4)*
C8	0.944(1)	1.0428(9)	0.363(1)	5.8(3)*	C29	1.033(1)	0.935(1)	-0.243(1)	6.9(4)*
C9	1.0430(9)	0.9530(7)	0.2193(9)	3.7(2)*	C30	1.005(1)	0.9570(9)	-0.150(1)	5.2(3)*
C10	1.0863(9)	0.9065(7)	0.1396(8)	3.7(2)*	C31	0.7474(9)	1.0577(7)	-0.0412(9)	3.5(2)*
C11	0.9954(9)	0.7609(7)	0.1716(9)	3.6(2)*	C32	0.649(1)	1.0465(8)	-0.0090(9)	4.1(3)*
C12	0.932(1)	0.7022(9)	0.149(1)	5.1(3)*	C33	0.568(1)	1.097(1)	-0.027(1)	6.1(4)*
C13	0.938(1)	0.6387(9)	0.203(1)	5.3(3)*	C34	0.590(1)	1.159(1)	-0.079(1)	6.5(4)*
C14	1.005(1)	0.636(1)	0.280(1)	5.9(4)*	C35	0.687(1)	1.1715(9)	-0.112(1)	5.6(3)*
C15	1.067(1)	0.693(1)	0.306(1)	6.5(4)*	C36	0.767(1)	1.1207(8)	-0.094(1)	4.8(3)*
Molecule B									
Ir	0.33382(4)	0.99434(4)	0.32972(3)	3.672(8)	C16	0.508(2)	1.207(1)	0.226(2)	9.0(6)*
P1	0.4626(3)	1.0827(2)	0.3315(3)	4.24(7)	C17	0.541(1)	1.1067(9)	0.440(1)	4.9(3)*
P2	0.3612(3)	0.9376(2)	0.4725(3)	4.62(8)	C18	0.643(1)	1.078(1)	0.459(1)	6.0(3)*
N1	0.4584(7)	0.9226(7)	0.2782(6)	3.7(2)	C19	0.698(1)	1.094(1)	0.547(1)	6.7(4)*
C1	0.312(1)	1.0144(7)	0.1858(9)	4.1(2)*	C20	0.646(2)	1.136(1)	0.613(1)	7.2(4)*
H	0.251(8)	0.923(7)	0.304(7)	5(3)*	C21	0.550(1)	1.162(1)	0.595(1)	6.4(4)*
H1	0.22(1)	1.046(8)	0.38(1)	8(4)*	C22	0.497(1)	1.1484(8)	0.509(1)	5.2(3)*
C2	0.256(1)	1.0679(9)	0.136(1)	5.5(3)*	C23	0.474(1)	0.8584(8)	0.347(1)	4.7(3)*
C3	0.249(1)	1.066(1)	0.034(1)	6.6(4)*	C24	0.480(1)	0.8843(9)	0.451(1)	6.0(4)*
C4	0.292(1)	1.014(1)	-0.016(1)	6.4(4)*	C25	0.385(1)	0.9832(9)	0.587(1)	5.5(3)*
C5	0.352(1)	0.959(1)	0.030(1)	6.6(4)*	C26	0.469(2)	0.968(1)	0.651(1)	8.1(5)*
C6	0.362(1)	0.9571(8)	0.130(1)	4.4(3)*	C27	0.471(2)	1.009(1)	0.740(1)	8.3(5)*
C7	0.414(1)	0.8958(7)	0.1808(9)	4.2(3)*	C28	0.404(2)	1.060(1)	0.757(2)	8.5(5)*
C8	0.493(1)	0.852(1)	0.126(1)	6.3(4)*	C29	0.319(2)	1.075(1)	0.695(2)	8.7(5)*
C9	0.564(1)	0.9602(7)	0.2712(9)	4.2(3)*	C30	0.310(2)	1.038(1)	0.609(1)	7.6(5)*
C10	0.555(1)	1.0413(8)	0.2513(9)	4.1(2)*	C31	0.265(1)	0.8668(8)	0.506(1)	4.9(3)*
C11	0.437(1)	1.1729(9)	0.282(1)	5.1(3)*	C32	0.297(1)	0.809(1)	0.570(1)	6.7(4)*
C12	0.343(2)	1.207(1)	0.300(1)	8.0(5)*	C33	0.223(2)	0.758(1)	0.590(1)	7.3(4)*
C13	0.318(2)	1.276(1)	0.259(2)	9.5(6)*	C34	0.120(1)	0.761(1)	0.555(1)	6.7(4)*
C14	0.388(2)	1.305(2)	0.205(2)	11.9(8)*	C35	0.090(1)	0.8184(9)	0.496(1)	5.3(3)*
C15	0.484(2)	1.277(2)	0.181(2)	11.3(8)*	C36	0.162(1)	0.8699(9)	0.472(1)	4.9(3)*

^a Starred temperature factors were refined isotropically. Anisotropically refined atoms are given in the form of the isotropic equivalent displacement parameter defined as $\frac{1}{3}(a^2B_{11} + b^2B_{22} + c^2B_{33} + ab(\cos \gamma)B_{12} + ac(\cos \beta)B_{13} + bd(\cos \alpha)B_{23})$.

puzzling to find only one peak in the ³¹P NMR spectrum (and not two) for these compounds. Rapid inversion at nitrogen is a well-known and documented dynamic process of amino compounds with only a small energy barrier separating the two epimers.^{10a} Protonation of the ligand (at nitrogen) effectively "blocks" the epimerization process while not altering the integral makeup of the molecule. Such a protonation experiment was performed on the (*R*)-(+)-C₆H₅C*H(Me)N(CH₂CH₂-PPh₂)₂ ligand (**5a**) to give the ammonium hydrochloride salt **6a**. Protonation of the chiral tertiary amine **5a** was achieved by addition of concentrated hydrochloric acid. Addition of water to the acidic solution induced precipitation of the ammonium salt. Filtration of this precipitate gave **6a** (90%). Blocking of epimerization at nitrogen gave the expected two singlets in the ³¹P NMR spectrum of the ammonium hydrochloride salt, at -19.7 and -20.0 ppm.

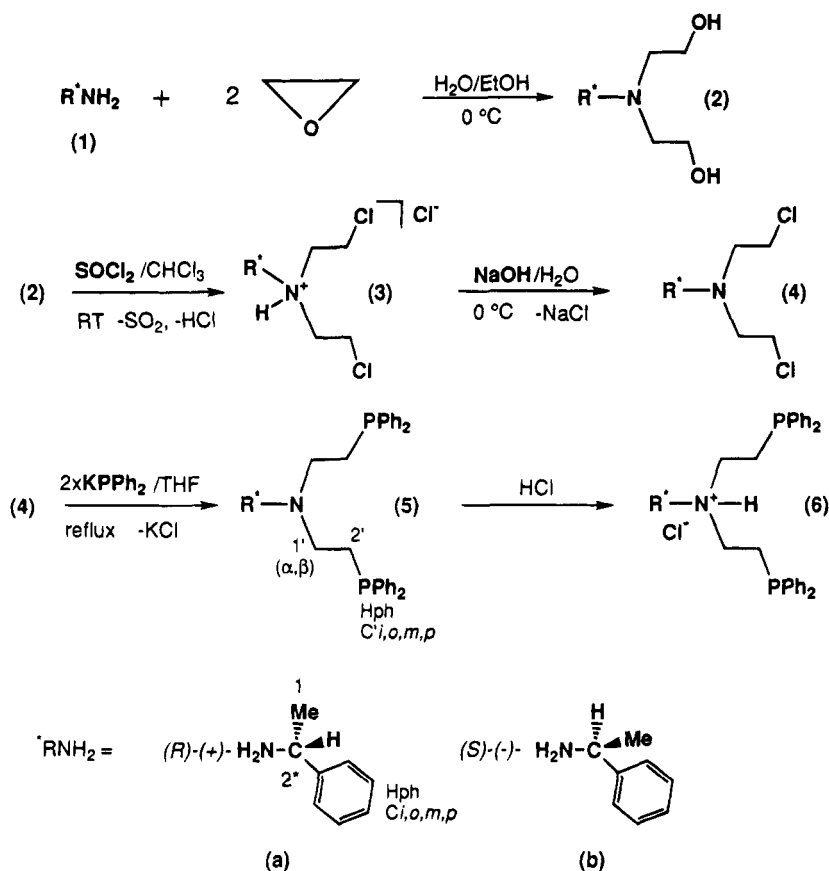
By simply using the three-step process for preparation of chiral PNP* ligands described in this paper and an appropriately chosen starting chiral primary amine, it

is possible to easily and routinely prepare a large range of chiral PNP* ligands. For example, we have, in addition to the preparation of the PNP* ligands (**5a,b**) bearing phenyl and methyl substituents, also prepared mixed-donor chiral ligands with methyl/ethyl and methyl/naphthyl substituents. The investigation of the catalytic activity and organometallic chemistry of these new chiral ligands in association with a variety of platinum-group metals will be the subject of some forthcoming publications.

Synthesis and Characterization of (*R*)- and (*S*)-[IrH(COD){C₆H₅C*H(Me)N(CH₂CH₂PPh₂)₂]} (8a,b**)**
 [IrH(COD){C₆H₅C*H(Me)N(CH₂CH₂PPh₂)₂]} (**8a,b**) was prepared routinely, in good yields (70–80%), *via* addition of 2 equiv of the PNP* ligand (**5a,b**) to the iridium methoxy dimer [Ir(COD)(OMe)]₂ in dichloromethane at room temperature. (*S*)-[IrH(COD){C₆H₅C*H(Me)N(CH₂CH₂PPh₂)₂]} (**8b**) was found to have the following diagnostic spectroscopic properties: a strong Ir–H stretch in the IR spectrum at 2099 cm⁻¹, an upfield triplet (²J_{H,P} 22.0 Hz) in the ¹H NMR (C₆D₆, 20 °C) spectrum corresponding to the terminal hydride proton, and an AM system in the phosphorus spectrum cor-

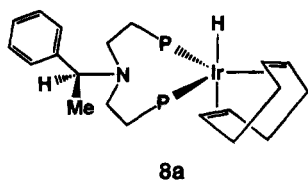
(10) (a) March, J. *Advanced Organic Chemistry*; Wiley: New York, 1985; p 86. (b) *Ibid.*, p 124.

Scheme 1



responding to the two inequivalent phosphorus atoms of the PNP* ligand. In the aliphatic region of the ^1H NMR spectrum signals due to coordinated cyclooctadiene are observed at 3.80 ppm (CH) and between 2.10 and 1.90 ppm (CH_2), while two downfield signals at δ 47.9 and 79.2 ppm in the $^{13}\text{C}\{^1\text{H}\}$ NMR spectrum, which do not disappear in a DEPT90 experiment, are illustrative of the four olefinic carbons of the COD ligand.⁶

Both $[\text{IrH}(\text{COD})\{\text{C}_6\text{H}_5\text{C}^*\text{H}(\text{Me})\text{N}(\text{CH}_2\text{CH}_2\text{PPh}_2)_2\}]$ stereoisomers (**8a,b**) can be described structurally as trigonal-bipyramidal species, with the PNP* ligands (**5a,b**) and the COD moiety being η^2 -bound to the iridium(I) and the hydride adopting an apical position. This structural assignment precludes the bonding of the nitrogen donor and is confirmed by a recent X-ray crystal structure¹¹ of $[\text{IrH}(\text{COD})\{\text{C}_6\text{H}_5\text{C}^*\text{H}(\text{Me})\text{N}(\text{CH}_2\text{CH}_2\text{PPh}_2)_2\}]$ (bearing methyl/ethyl groups on the asymmetric carbon) conducted in conjunction with our studies of the PNP* ligands. A view of the molecular geometry of the complex $[\text{IrH}(\text{COD})\{\text{C}_6\text{H}_5\text{C}^*\text{H}(\text{Me})\text{N}(\text{CH}_2\text{CH}_2\text{PPh}_2)_2\}]$ is shown in Figure 1.



(11) Bianchini, C.; *et al.* X-ray Crystal Structure of (R) - $[\text{IrH}(\text{COD})\{\text{C}_6\text{H}_5\text{C}^*\text{H}(\text{Me})\text{N}(\text{CH}_2\text{CH}_2\text{PPh}_2)_2\}]$. To be submitted for publication. Crystal data: space group $P1$ (No. 2); $a = 9.852(2)$ Å, $b = 12.689(2)$ Å, $c = 15.776(3)$ Å, $\alpha = 68.66(3)^\circ$, $\beta = 75.27(3)^\circ$, $\gamma = 78.95(4)^\circ$, $V = 1765.8$ Å³; $d_{\text{calcd}} = 1.503$ g cm⁻³; $R = 0.036$; $R_w = 0.041$.

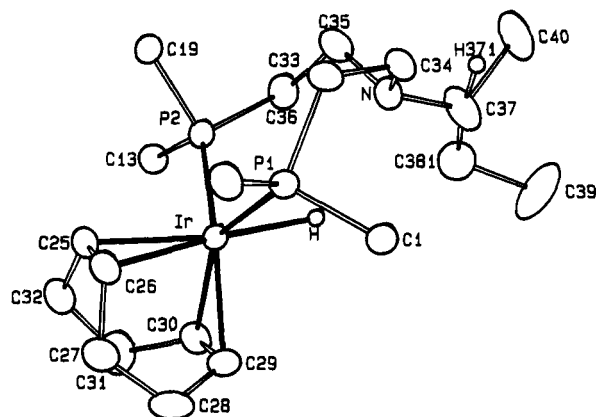
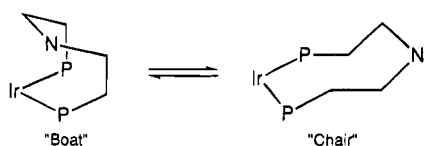


Figure 1. View of the molecular geometry of (R) - $[\text{IrH}(\text{COD})\{\text{C}_6\text{H}_5\text{C}^*\text{H}(\text{Me})\text{N}(\text{CH}_2\text{CH}_2\text{PPh}_2)_2\}]$.

The AM spin system in the ^{31}P NMR room temperature spectrum of $[\text{IrH}(\text{COD})(\text{PNP}^*)]$ (**8a,b**) is due to the inequivalence of the two phosphorus atoms attached to iridium. This inequivalence is believed to be the result of the presence of the asymmetric center $\text{NC}^*\text{H}(\text{Me})\text{Ph}$ in the molecule. A thorough investigation, by means of variable-temperature (VT) NMR experiments, was performed in order to exhaustively study and explain this phenomenon.

The VT NMR experiment involved collection of ^1H and ^{31}P spectra over the temperature range $+75$ to -100 °C. Heating a sample of $[\text{IrH}(\text{COD})(\text{PNP}^*)]$ (**8a,b**) in $\text{C}_6\text{D}_5\text{CD}_3$ to a final temperature of 75 °C showed no physical change of the ^{31}P or ^1H NMR spectra. The ^{31}P NMR maintained its AM structure ($\delta -2.5$ and 1.2) and the ^1H NMR showed the illustrative triplet ($\delta -13.5$) of the *cis* hydride, with all signals in both spectra showing

Scheme 2^a

^a For clarity only the skeleton of the eight-membered ring has been illustrated.

an anticipated increase in resolution. In light of these high-temperature spectra having the same physical makeup of the ¹H and ³¹P NMR spectra acquired at room temperature, it follows that the trigonal-bipyramidal structure described above is maintained at 75 °C. Lowering the temperature of [IrH(COD)(PNP*)] (**8a,b**) in C₆D₅CD₃ to a final temperature of -100 °C produced some very interesting spectra. The ¹H NMR spectrum showed an anticipated loss of resolution with temperature, as the tumbling motion of the complex molecules in solution is slowed and the viscosity of the solution increased. The upfield hydride (δ -13.5 at 25 °C) maintained its chemical shift position but during the course of the NMR experiment lost its fine structure such that at -100 °C only a broad lump was visualized. Similarly, the signals of the COD system showed no physical change during the course of the NMR VT experiment to -100 °C. In light of these results it is apparent that the structural integrity of the hydride and the COD ligand do not undergo any thermodynamically induced change during the course of the VT experiment and the trigonal-bipyramidal system is maintained.

Analysis of the ³¹P NMR VT spectra to -100 °C proved most interesting, with the initial AM spin system coalescing at -45 °C and finally at -100 °C giving four broad signals (δ 13.2, 5.4, 1.9, and -11.2) with a number of smaller peaks (δ 14.6, -5.5, -6.2, -10.8, and -14.5). The four major peaks appear as two AM spin systems corresponding to four unique environments for the phosphorus atoms. Considering the physical rigidity displayed by the complex during the course of the ¹H VT NMR experiment, it proved puzzling that such a dramatic change in the ³¹P NMR would occur. We suggest that this intriguing result may be the consequence of conformational isomerization between two minimum-energy conformations, for example a "boat" and a "chair", depicted in Scheme 2. Such a hypothesis explains the occurrence of four distinct environments (and hence spin systems) for the two phosphorus atoms. Interconversion of cyclic (nonaromatic) systems consisting of six or more atoms between two minimum-energy conformations, for example, chair and boat conformations, is a well-documented process in organic chemistry.^{10b} Conformational changes in large rings (>C₈) proceed through various "twisted" conformers of the ring, which may explain the occurrence of the minor peaks in the ³¹P NMR at -100 °C. Typical values of ΔG[‡] for the interconversion of cyclic C₈ ring systems lie in the range 8.1–10.5 kcal mol⁻¹.¹² At the coalescence temperature of -45 °C a rough evaluation of ΔG[‡] associated with the overall dynamic process exhibited by **8a,b** can be made with the use of eq 1.¹³ Values

$$\Delta G^{\ddagger} = 4.57T[10.32 - \log(k_{\text{coalesc}}/T)] \quad (1)$$

$$k_{\text{coalesc}} \approx 2.22\Delta\nu$$

varying from 9.4 to 9.3 kcal mol⁻¹ can be calculated for Δν between 1800 and 2780 Hz, which are the frequency differences observed for the two major AM systems in the slow-exchange regime.

Synthesis and Characterization of (R)- and (S)-[(α-Methylbenzyl)bis(2-(diphenylphosphino)ethyl)amine]iridium Dihydride (10a,b). Refluxing [IrH(COD){C₆H₅C*H(Me)N(CH₂CH₂PPh₂)₂}] (**8a,b**) under nitrogen in propan-2-ol for 9 h liberates, on workup, an off-white precipitate of *fac*-[IrH₂{C₆H₄C*H(Me)N(CH₂CH₂PPh₂)₂}] (**10a,b**; yield 80–90%) with the following illustrative spectroscopic properties; two strong bands in the IR spectrum at 1975 and 2079 cm⁻¹ indicative of two terminal hydrides,¹⁴ two upfield signals in the proton NMR spectrum corresponding to the two hydride hydrogens, a doublet of doublet of doublets (²J_{H hydride,P_{trans}} 139.2 Hz, ²J_{H hydride,P_{cis}} 22.0 Hz, ²J_{H hydride,H hydride} 4.9 Hz) corresponding to the hydride *trans* to phosphorus, and a triplet of doublets (²J_{H hydride,P_{trans(a)}} ≈ ²J_{H hydride,P_{trans(b)}} 11.8 Hz, ²J_{H hydride,H hydride} 4.9 Hz) further upfield corresponding to the *cis* hydride,¹⁴ and an AM system in the ³¹P NMR spectrum corresponding to the two inequivalent phosphorus atoms of the PNP* ligand. The ¹H-coupled ³¹P NMR spectrum shows that the signal at δ 17.72 corresponds to the phosphorus atom *trans* to the hydride. The ¹³C{¹H} NMR spectrum (C₆D₆, 20 °C) shows in the low-field region a doublet of doublets attributable to the carbon atom of an *ortho*-metalated phenyl group¹⁵ (δ 154.9, J_{C,P_{trans}} 82.5 Hz, J_{C,P_{cis}} 10.3 Hz). For the unambiguous identification of compound **10a**, an X-ray crystal structure of a single crystal grown from dichloromethane/methanol was solved. The crystal structure of **10a** consists of neutral monomeric molecules of the complex without interposed solvent molecules in the lattice. In the monoclinic unit cell there are two crystallographically independent, but practically equivalent, molecules. The structure of one of the independent molecules is depicted in Figure 2 together with the atomic numbering scheme. For the sake of clarity, only the first carbon atom of the phenyl groups on the phosphorus atoms is labeled.

Selected bond distances and angles are given in Tables 3 and 4, respectively. The complex has a distorted-octahedral configuration in which the iridium center is surrounded by the two phosphorus and nitrogen atoms of a **5a** ligand, by an *ortho*-metalated phenyl ring which lies *trans* to one of the phosphorus donors, and by two hydrides in mutually *cis* positions. The hydrides have been located clearly in the Fourier difference map in the expected positions. They exhibit almost identical distances from the metal in the two independent complexes (*d*_{Ir-H} = 1.64(9) and 1.8(2) Å in complex **A**; *d*_{Ir-H} = 1.8(2) and 1.7(1) Å in complex **B**). The Ir-H bond lengths are in excellent agreement with the values determined by X-ray methods for several hydride complexes of iridium.¹⁶ The Ir-N (2.19(1) Å)

(14) Barbaro, P.; Bianchini, C.; Meli, A.; Peruzzini, M.; Vacca, A.; Vizza, F. *Organometallics* **1991**, *10*, 2227.

(15) Bianchini, C.; Masi, D.; Meli, A.; Peruzzini, M.; Zanobini, F. *J. Am. Chem. Soc.* **1988**, *110*, 6411.

(16) See for example: Milstein, D.; Calabrese, J. C.; Williams, I. D. *J. Am. Chem. Soc.* **1986**, *108*, 6387.

(12) Anet, F.; Anet, R. *Dynamic Nuclear Magnetic Resonance Spectroscopy*; Academic Press: New York, 1975; pp 567–572.

(13) Gunther, H. *NMR Spectroscopy: An Introduction*; Wiley: New York, 1980; pp 242–243.

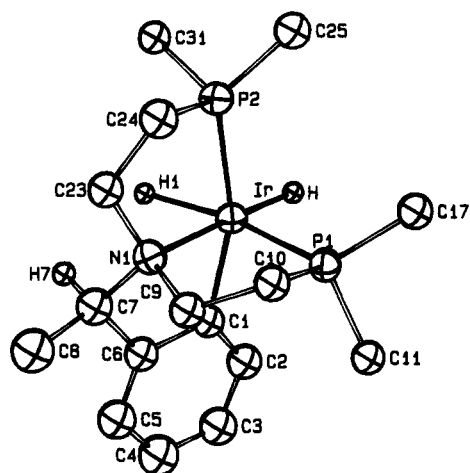


Figure 2. ORTEP plot of one of the two crystallographically independent molecules of *fac-exo-(R)*-[IrH₂{C₆H₄-C*H(Me)N(CH₂CH₂PPh₂)₂}] (**10a**).

Table 3. Selected Bond Distances (Å) for **10a**^a

	molecule A	molecule B
Ir-P1	2.287(3)	2.290(4)
Ir-P2	2.282(3)	2.267(4)
Ir-N1	2.19(1)	2.19(1)
Ir-C1	2.06(1)	2.06(1)
Ir-H	1.64(9)	1.8(2)
Ir-H1	1.8(2)	1.7(1)
P1-C10	1.84(1)	1.82(1)
P1-C11	1.84(1)	1.81(2)
P1-C17	1.84(1)	1.83(1)
P2-C24	1.84(1)	1.82(2)
P2-C25	1.83(1)	1.82(2)
P2-C31	1.84(1)	1.84(2)
N1-C7	1.52(2)	1.53(2)
N1-C9	1.50(2)	1.51(2)
N1-C23	1.48(2)	1.53(2)
C1-C6	1.44(2)	1.47(2)
C23-C24	1.51(2)	1.53(2)
C6-C7	1.53(2)	1.47(2)
C7-C8	1.52(2)	1.52(2)
C7-H7	0.95(1)	0.95(1)
C9-C10	1.52(2)	1.51(2)

^a Numbers in parentheses are estimated standard deviations in the least significant digits.

and Ir-P distances (2.267(4)–2.290(4) Å) fall within the ranges reported for iridium–amine and iridium–phosphine complexes¹⁷ and are quite comparable with those reported for the iridium complex [(PNPPr)Ir(σ,η²-C₈H₁₃)], for which a distorted-trigonal-bipyramidal geometry about iridium has been determined by X-ray methods.⁶ The C,N-coordination from the cyclometalated aryl group gives rise to a five-membered C(sp²)–Ir–N(sp³) ring in which the C(1)–Ir–N angle is acute (80.8(4)° in complex A and 81.3(4)° in complex B). The Ir–C(1) bond distance of 2.06(1) Å in both independent molecules matches well the values reported for several (σ-aryl)iridium complexes ($d_{\text{Ir}-\text{C}(\text{aryl})}(\text{av}) = 2.070 \text{ \AA}$).^{17,18}

Compound **10a** is therefore identified as the dihydride *fac*-[IrH₂{C₆H₄CH(Me)N(CH₂CH₂PPh₂)₂}] (see Scheme 3), formed *via* loss of cyclooctadiene from **8a** and sub-

Table 4. Selected Bond Angles (deg) for **10a**^a

	molecule A	molecule B
P1–Ir–P2	99.6(1)	103.4(1)
P1–Ir–N1	85.1(3)	84.5(3)
P1–Ir–C1	92.5(4)	87.1(4)
P1–Ir–H	92(3)	99(5)
P1–Ir–H1	164(5)	167(4)
P2–Ir–N1	85.8(3)	86.3(3)
P2–Ir–C1	161.2(4)	162.9(4)
P2–Ir–H	95(3)	91(5)
P2–Ir–H1	81(5)	85(4)
N1–Ir–C1	80.8(4)	81.3(4)
N1–Ir–H	177(3)	176(5)
N1–Ir–H1	79(4)	86(4)
C1–Ir–H	99(3)	101(5)
C1–Ir–H1	84(4)	83(4)
H–Ir–H1	104(6)	91(6)
Ir–P1–C10	101.4(4)	100.2(5)
Ir–P1–C11	118.2(4)	121.4(5)
Ir–P1–C17	124.9(4)	122.3(5)
C10–P1–C11	106.2(6)	104.6(7)
C10–P1–C17	105.4(6)	106.0(6)
C11–P1–C17	99.1(6)	100.4(7)
Ir–P2–C24	99.8(5)	101.1(6)
Ir–P2–C25	127.5(5)	125.5(6)
Ir–P2–C31	117.5(4)	117.9(5)
C24–P2–C25	104.6(6)	106.6(7)
C24–P2–C31	102.5(6)	102.6(8)
C25–P2–C31	101.6(6)	100.5(7)
Ir–N1–C7	104.8(7)	104.2(7)
Ir–N1–C9	111.9(8)	113.5(8)
Ir–N1–C23	111.3(7)	108.7(7)
C7–N1–C9	107.0(9)	112.2(9)
C7–N1–C23	108(1)	111(1)
C9–N1–C23	113.0(9)	107.7(9)
Ir–C1–C6	112.7(9)	111.1(9)
C1–C6–C7	117(1)	118(1)
N1–C9–C10	114(1)	114(1)
P1–C10–C9	108.1(8)	109.6(9)
N1–C23–C24	112(1)	111(1)
P2–C24–C23	110.7(9)	108(1)

^a Numbers in parentheses are estimated standard deviations in the least significant digits.

sequent cyclometalation of the phenyl group bound to the chiral carbon atom. The loss of the diene occurs by reduction to cyclooctene effected by propan-2-ol and subsequent decoordination of the olefin, as evidenced by quantitative formation of free cyclooctene detected in the propan-2-ol solution when **8a** is completely transformed into **10a**.

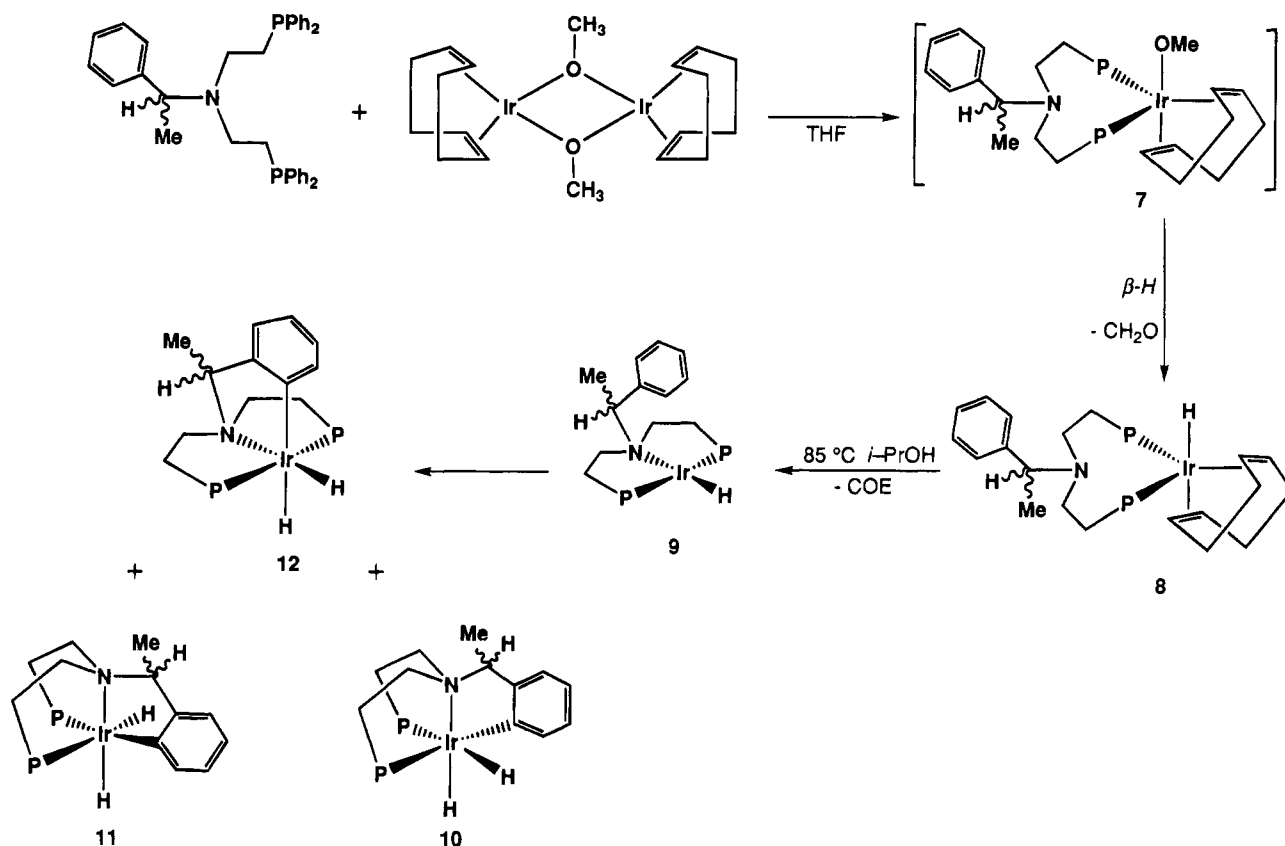
Isomerization of *fac-exo-(R)*-[IrH₂{C₆H₄C*H(Me)N(CH₂CH₂PPh₂)₂}] (10a**) to *fac-endo-(R)*-[IrH₂{C₆H₄C*H(Me)N(CH₂CH₂PPh₂)₂}] (**11a**).** Serendipitously it was noted that prolonged heating of [IrH(COD){C₆H₅C*H(Me)N(CH₂CH₂PPh₂)₂}] (**8a,b**) under nitrogen in propan-2-ol to form the dihydride *fac-exo-(R)*-[IrH₂{C₆H₄C*H(Me)N(CH₂CH₂PPh₂)₂}] (**10a**) also gave small quantities (2–10%) of *fac-endo-(R)*-[IrH₂{C₆H₄C*H(Me)N(CH₂CH₂PPh₂)₂}] (**11a**). A controlled experiment to examine this isomerization process involved the refluxing of **10a** in propan-2-ol. After 2 h of refluxing 15% conversion to the *endo* isomer **11a** was determined by ³¹P NMR spectroscopy. Further refluxing, for up to 9 h, failed to convert more of the *fac-exo-(R)* isomer (**10a**) into the isomer (**11a**), which suggests the occurrence of a steady state.

In a NOEDIFF experiment performed on a sample containing both **10a** and **11a**, the effect of irradiating either the methyl or the hydrogen bound to the asymmetric carbon on the intensity of the hydride multiplet was measured. When the NCHMe group of compound

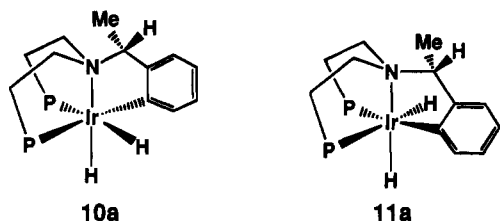
(17) Orpen, A. G.; Brammer, L.; Allen, F. H.; Kennard, O.; Watson, D. G.; Taylor, R. *J. Chem. Soc., Dalton Trans.* **1989**, S1.

(18) (a) van der Zeijden, A. H.; van Koten, G.; Luijk, R.; Nordeman, R. A.; Spek, A. L. *Organometallics* **1988**, *7*, 1549. (b) Albeniz, A. C.; Schulte, G.; Crabtree, R. H. *Organometallics* **1992**, *11*, 242. (c) Manotti Lanfredi, A. M.; Tiripicchio, A.; Ugozzoli, F.; Ghedini, F.; Neve, F. *J. Chem. Soc., Dalton Trans.* **1988**, 651. (d) Neve, F.; Ghedini, M.; Tiripicchio, A.; Ugozzoli, F. *Inorg. Chem.* **1989**, *28*, 3084.

Scheme 3

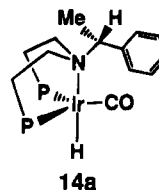


10a was irradiated, the intensity of the hydride signal was increased, whereas irradiation of NCHMe has no effect on the hydride multiplet. The opposite result was observed for compound **11a**, as irradiation of NCHMe caused an increase in the intensity of the hydride signal. We can therefore conclude that complexes **10a** and **11a** are both formulated as *fac*-[IrH₂{C₆H₄CH(Me)N(CH₂CH₂PPh₂)₂}], their difference lying in the reciprocal orientation (*exo* vs *endo*) of the hydride and the NCHMe hydrogen atom.



Synthesis and Characterization of (R)- and (S)-[(α -Methylbenzyl)bis(2-(diphenylphosphino)ethyl)amine]iridium Carbonyl Hydride (14a,b**).** A 10:1 mixture of *fac-exo*- and *fac-endo*-[IrH₂{C₆H₄CH(Me)N(CH₂CH₂PPh₂)₂}] (**10a,b**) in toluene was placed in an autoclave and charged with carbon monoxide to 5.0 atm. The autoclave was then heated to an internal temperature of 80–90 °C for 3 h. Discharging the autoclave and removing the solvent gave the monocarbonyl compound [IrH(CO){C₆H₅CH(Me)N(CH₂CH₂PPh₂)₂}] (**14a,b**), in quantitative yield. The following spectroscopic observations were noteworthy for **14a**. Two bands in the IR spectrum (1971 and 1914 cm⁻¹) were observed in both the solid and liquid phases. The ¹H NMR spectrum contained an upfield triplet diagnostic of a hydride

positioned *cis* to two phosphorus atoms (²J_{H hydride,P_{cis}} 26.9 Hz). The ³¹P NMR spectrum displayed a broad singlet at room temperature with the ¹³C NMR displaying the carbonyl carbon as a downfield triplet at 185.7 ppm (²J_{C carbonyl,P} 10.6 Hz). Experimental evidence for the incorporation of only 1 equiv of carbon monoxide, in **14a**, was obtained by dissolving **14a** in pyridine and adding an excess of iodine, using a closed gas buret.¹⁹ On the basis of these results, it has been concluded that the carbonyl species **14a** is best described as trigonal bipyramidal. In such a species the η^3 (*R*)-PNP* ligand adopts a *fac* orientation (the phosphorus atoms being meridional and the nitrogen donor being diagonally opposed and apical to the hydride). Such a conformation allows the addition of the carbonyl moiety in the phosphorus–phosphorus plane to participate in π – π bonding interactions (back-bonding) with iridium.²⁰



Reduction of Benzylideneacetone and Other Prochiral Ketones Catalyzed by the Ir/PNP* System. The catalytic reactions were initially performed under the same experimental conditions used previously for the achiral ligand (PNPPⁿ).⁶ The catalyst was prepared *in situ* by starting with [Ir(COD)(OMe)]₂ and

(19) Thanks are due to Prof. F. Calderazzo, University of Pisa, Pisa, Italy, for his assistance in performing this experiment.

(20) Rossi, A. R.; Hoffmann, R. *Inorg. Chem.* **1975**, *14*, 365.

Table 5. Reduction of PhCH=CHCOMe Catalyzed by [Ir(COD)(OMe)₂] + PNP*^a

entry no.	PNP*	temp (°C)	t (min)	conversion (%)	selectivity (%) ^d	ee ^b
Hydrogen Donor: Propan-2-ol						
1	(R)-PNP	83	15	93	90	22
2	(S)-PNP	83	15	93	90	17
3	(R)-PNP	60	45	83	92	33
4	(S)-PNP	60	45	90	91	27
5	(R)-PNP	40 ^c	150	85	95	41
6	(S)-PNP	40 ^c	150	86	92	32
7	(R)-PNP	30 ^c	240	84	95	50
8	(R)-PNP	25 ^c	300	65	97	54
9	(S)-PNP	25 ^c	360	64	97	42
Hydrogen Donor: Cyclopentanol						
10	(R)-PNP	60	60	84	80	21
11	(R)-PNP	40 ^c	240	82	92	44
12	(R)-PNP	25 ^c	900	93	89	40

^a Experimental conditions: [Ir] = 4 × 10⁻⁴ M; [Sub]/[Ir] = 100; solvent hydrogen donor. ^b With (R)-PNP the main product is the R allylic alcohol, and with (S)-PNP the main product is the S allylic alcohol. ^c The catalytic system was heated to 60 °C for 2 h prior to lowering the temperature as indicated and adding the substrate. ^d Selectivity % = ((% unsaturated alcohol)/(% yield)) × 100.

2 equiv of the PNP* ligand **5a,b**, with propan-2-ol used as both hydrogen donor and solvent.

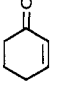
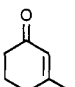
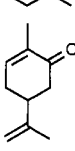
The reactions performed at 83 °C were fast and highly chemoselective (Table 5, entries 1 and 2). The rate of the reaction and yield, in the allylic alcohol, were both higher than those obtained for the system with no chiral auxiliary ligand.⁶ The enantioselectivities of the reactions were similar (approximately 20%), with the (R)-(+)-enantiomer of the ligand PNP*, **5a**, giving a higher yield of (R)-PhCH=CHCH(OH)Me, whereas the S enantiomer of the allylic alcohol is predominantly obtained with the PNP* ligand **5b**. When the reaction temperature was lowered to 60 °C, the ee increased with the expected loss in the reaction rate. In contrast, when the reaction was performed at 40 °C, with an initial induction period of about 3 h, a marked loss in the catalytic activity was observed. However, when the reaction is performed with the catalytic system kept at 60 °C for 2 h before the substrate is added at 40 °C, the induction period is negligible, and the reaction selectivity is improved (chemoselectivity greater than 95%, ee approximately 40%; see Table 5, entries 5 and 6). All the other reactions at temperatures lower than 60 °C were performed by following this procedure; that is, the catalyst was maintained at 60 °C for 2 h before lowering the temperature as desired, and then the substrate was added.

When the reaction temperature was lowered to 25 °C, the enantiomeric excess was more than 50%. Further attempts to raise the ee by lowering the reaction temperature were ineffective, as the catalytic activity was extremely low at 0 °C.

Similar values of chemo- and enantioselectivity have been obtained by Takaya *et al.* using [Ir(BINAP)(COD)]⁺ in the presence of Ph₂P(*o*-C₆H₄NMe₂) as the catalyst in the hydrogenation of benzylideneacetone.^{2b} However, hydrogen donors, as in the present case, have distinct advantages over the use of molecular hydrogen, in that they avoid the risks associated with the reagent, which requires the use of high-pressure apparatus.

When cyclopentanol was employed instead of propan-2-ol as both solvent and hydrogen donor, the catalytic reactions have comparable selectivities but slightly

Table 6. Reduction of Ketones Catalyzed by [Ir(COD)(OMe)₂] + (R)-PNP^a

entry no.	substrate	t (h)	conversion (%)	selectivity (%) ^b	ee
1	PhCH=CHCOPh	5	91	61	9 [S (-)]
2	CH ₃ CH=CHCOC ₂ H ₅	5	0		
3		1	85	51	12 [S (-)]
4		7	52	100	17 [S (-)]
5		8	31	96	6 [R (+)]
6	PhCOCH ₃	3	87		4 [R (+)]
7	CH ₃ (CH ₂) ₅ COCH ₃	5.5	86		25 [S (+)]

^a Experimental conditions: [Ir] = 4 × 10⁻⁴ M; [Sub]/[Ir] = 100; temperature 60 °C; solvent and hydrogen donor propan-2-ol. ^b Selectivity % = ((% unsaturated alcohol)/(% yield)) × 100.

lower reaction rates. This is a consequence of the lower volatility of the ketone formed by dehydrogenation of the hydrogen donor (cyclopentanone vs acetone).²¹

With conjugated enones other than benzylideneacetone the catalytic system appears to be both less active and less selective (see Table 6). The reduction of chalcone, PhCH=CHCOPh (Table 6, entry 1), only gives a 60% yield of the substituted allylic alcohol, which is formed together with the saturated ketone and the saturated alcohol. The ee is less than 10%.

The aliphatic enone 4-hexen-3-one (Table 6, entry 2) is not reduced by this catalytic system, which is most likely due to the irreversible coordination of this substrate to iridium, as suggested by the observation that reduction of benzylideneacetone does not occur in the presence of 4-hexen-3-one. Cyclic unsaturated ketones do not lead to catalyst poisoning. Such substrates are selectively reduced at the carbonyl group only when the C=C bond is sterically hindered (see Table 6, entries 4 and 5), the ee being in all cases below 20%.

Prochiral saturated ketones such as acetophenone or octan-2-one are also reduced by this catalytic system (see Table 6, entries 6 and 7), but both catalytic activity and enantioselectivity are markedly lower than those observed for benzylideneacetone.

The Catalytic System. Further investigations of the catalytic system prepared *in situ* were expected to provide information concerning the nature of the catalytically active species and their possible intermediates. From the catalytic reactions it was apparent that the active species was formed in significant amounts from a propan-2-ol solution of [Ir(COD)(OMe)₂] and an equivalent amount of (R)-PNP* (**5a**), which had been heated to 60 °C for 2 h (*vide supra*). By repeating such reactions at higher concentration in propan-2-ol, it was possible to detect the species formed by ³¹P and ¹H NMR spectroscopy. The ³¹P NMR spectrum (propan-2-ol/C₆D₆) recorded after 30 min at 60 °C shows three main sets of signals: (i) the AM system of **8a** (~85% yield); (ii) an AB spin system (compound **9a**, ~5%) at δ_A 23.29

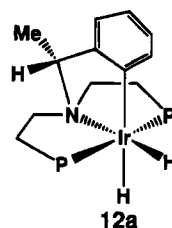
(21) Bianchini, C.; Farnetti, E.; Graziani, M.; Peruzzini, M.; Polo, A. *Organometallics* **1993**, *12*, 3753.

and δ_B 15.37 (J_{PP} 419.7 Hz); (iii) a complex set of signals between -4.00 and -11.00 ppm ($\sim 10\%$). No significant change in the spectrum was observed after further heating of the mixture to 60°C . When the solution was cooled, a yellow solid was obtained. Complete precipitation of the above species cannot be effected by addition of either *n*-pentane or diethyl ether, as the compound appears to be soluble in both solvents. The product is then recovered by cooling in an alcoholic solution (-10°C). NMR spectroscopy unambiguously indicates that the yellow solid is product **8a**. Compound **8a** was the main species formed in our catalytic system and was subsequently tested as a catalytic precursor for the reduction of benzylideneacetone. The reaction performed at 83°C is slower than the corresponding reaction performed with the catalyst prepared *in situ* (90 vs 15 min for 90% conversion), whereas chemo- and enantioselectivities are very similar. When the catalytic reaction was repeated with **8a** at 60°C , a larger difference in the catalytic activity, with the corresponding reaction *in situ*, was observed, as the reaction of **8a** shows an induction period of about 2 h, although chemoselectivity and ee are once again very similar. The reaction of **8a** at 60°C was then repeated, but with the following modification. The propan-2-ol solution of **8a** was refluxed at 83°C for 2 h, before the temperature was lowered to 60°C and the substrate was added. The change in the experimental procedure resulted in a higher catalytic activity (2 vs 9 h for 85% conversion), with disappearance of the induction period.

From these experimental data it was concluded that **8a** is not a catalytically active species, albeit it acts as a catalyst precursor. As a matter of fact, a comparison of the catalytic data obtained starting from **8a** with those for the catalyst prepared *in situ* suggests that the same catalytically active species is involved. Further, one can infer that the induction period observed for the reaction at 60°C is connected with the formation of the catalyst, which is faster at 83°C . Therefore, it seemed interesting to record the ^{31}P NMR spectrum of a solution of **8a** in propan-2-ol which had been refluxed for 2 h. After this period the ^{31}P NMR spectrum showed formation of **10a** (18%) at the expense of **8a**. Complete transformation of **8a** occurred after 9 h of refluxing. After this time, together with the signals of **10a**, two new sets of signals are observed in the ^{31}P NMR spectrum: (i) the AM spin system of the *exo* isomer **11a** (yield 10%); (ii) an AB spin system (compound **12a**, yield 2%) with δ_A 33.02 and δ_B 24.18 (C_6D_6 , J_{PP} 385.7 Hz).

For the unambiguous identification of compounds **11a** and **12a** we recorded the ^1H NMR spectrum of the crude reaction products of **8a** in propan-2-ol, after evaporating the solvent and dissolving the residue in C_6D_6 . As for **10a** and **11a**, **12a** also appears to be a dihydride, with a doublet of doublet of doublets at δ -11.58 (hydride *trans* to carbon, $J_{\text{H hydride, P}_a}$ 26.5 Hz, $J_{\text{H hydride, P}_b}$ 14.1 Hz, and $J_{\text{H hydride, H hydride}}$ 4.9 Hz) and a triplet of doublets at -19.16 ppm (hydride *trans* to nitrogen, $J_{\text{H hydride, P}}$ 14.9 Hz, $J_{\text{H hydride, H hydride}}$ 4.9 Hz). From this set of data^{15,22} **12a** appears to be an isomer of both **10a** and **11a** in which the two inequivalent phosphorus atoms

of PNP* are *trans* to each other. Thus, **12a** is formulated as *mer*-(*R*)- $[\text{IrH}_2\{\text{C}_6\text{H}_4\text{C}^*\text{H}(\text{Me})\text{N}(\text{CH}_2\text{CH}_2\text{PPh}_2)_2\}]$.



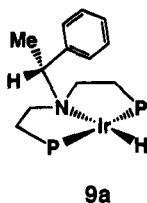
As **10a** was the main species formed from **8a** using the experimental conditions described, the obvious conclusion was that **10a** might be a close precursor of the catalytically active species used in these reactions. However, the presence of **10a** was not detected when the system was generated *in situ* at 60°C and followed by NMR (*vide supra*). This indicates that the catalytic species was not formed *in situ* using the experimental conditions employed. In fact, when the system *in situ* was maintained for 2 h at 83°C rather than 60°C , formation of a small amount of **10a** was detected. From these data the role of **10a** in the catalytic reactions was not definitely established. Such a complex was tested as a catalyst precursor for the reduction of benzylideneacetone in order to get additional information. The catalytic reaction performed at 60°C was rather slow (80% conversion in 6 h vs 45 min of the system *in situ*), both chemo- and enantioselectivity being similar to those observed with the catalytic system prepared *in situ*. No induction time was observed in this case, at variance from what we observed using **8a** as a catalyst precursor. When the catalytic reaction was repeated with **10a** after the precursor was maintained at 83°C for 2 h, no difference in the catalytic activity was observed.

The evolution of **10a** in refluxing propan-2-ol was followed via NMR, and after 2 h the only product formed was **11a** ($\sim 15\%$). At this stage a more detailed investigation of the system formed *in situ* was needed in order to formulate a hypothesis regarding the nature of the catalytically active species. The system formed *in situ* was then monitored by ^{31}P NMR under the following conditions: 2 h at 60°C (see NMR data above) and then further heating to 83°C . After 2 h at 83°C the partial transformation of **8a** into **10a** and **11a** was observed, together with the lowering of intensity of the set of signals corresponding to the so far unidentified compound **9a**. Heating to 83°C for a longer time, together with an expected increase in the yield of **10a** and **11a**, shows the disappearance of the signals of **9a**, and at the same time the set of signals of **12a** appears.

To acquire more information on the nature of species **9a**, the ^1H NMR spectrum of the propan-2-ol- d_3 solution of the system *in situ* after 2 h at 60°C was recorded. In the hydride region of the spectrum, together with the signals of compound **8a**, a new set of signals is observed (δ -9.17 , $J_{\text{H hydride, P}_a}$ 24.3 Hz, $J_{\text{H hydride, P}_b}$ 10.9 Hz), the intensity ratio of the two sets being comparable to that of the ^{31}P NMR signals of **8a** vs **9a**. Compound **9a** therefore appears to have in the coordination sphere of iridium one hydride and one (*R*)-(+)-PNP* ligand, with the two phosphorus atoms in a mutually *trans* configuration. We therefore propose that species **9a** is the square-planar iridium(I) complex $[\text{IrH}(\text{PNP}^*)]$, formed

(22) (a) Pregosin, P. S.; Kunz, R. W. In ^{31}P and ^{13}C NMR of Transition Metal Phosphine Complexes; Diehl, P., Fluck, E., Kosfeld, R., Eds.; Springer-Verlag: New York, 1979. (b) Garrou, P. E. *Chem. Rev.* **1981**, *81*, 229.

via decoordination of cyclooctadiene from **8a**.²³ Such a hypothesis is supported by the fact that when a C₆D₆ solution of **8a** is heated at 80 °C no formation of **9a** is detected: the presence of a hydrogen donor such as propan-2-ol is necessary to perform the reduction of cyclooctadiene to cyclooctene, which is then released from the coordination sphere of iridium.



Identical results have been obtained when **5b** is substituted for **5a**.

Discussion

The Chemistry of Iridium with the PNP* Ligands 5a,b. When a propan-2-ol solution of equivalent amounts of [Ir(COD)(OMe)]₂ and PNP* (**5a,b**) was heated to 60 °C, a catalyst was formed, which showed interesting features of high catalytic activity and chemoselectivity for the reduction of enones. Due to the presence of the stereogenic center on the PNP* ligands (**5a,b**), asymmetric reduction was also achieved. The experiments reported above have thrown light on the organometallic chemistry of the Ir-PNP* system, by allowing the identification of a number of novel iridium complexes.

The initial stages of the reaction sequence consist of coordination of the PNP* ligand (**5a,b**) to the metal, which causes splitting of the methoxy bridge with formation of [Ir(OMe)(COD)(PNP*)]. Such a complex undergoes β-hydrogen elimination to form **8a,b**.^{6,24} Catalytic experiments using **8a,b** as a precursor have shown that such a species is not catalytically active but is capable of evolving into a catalyst. Refluxing **8a,b** in a hot propan-2-ol solution results in its reduction, effected by the secondary alcohol of coordinated cyclooctadiene to give cyclooctene, which leaves the coordination sphere of iridium. Such a reaction results in the formation of a mixture of as many as four complexes, the first one formed being **9a,b**, square-planar iridium(I) species with only one hydride and a PNP* ligand in the coordination sphere. **9a,b** are apparently the common precursors for the subsequent formation of three isomers of [IrH₂{C₆H₄C*H(Me)N(CH₂CH₂PPh₂)₂}], **10a,b**, **11a,b**, and **12a,b**, which are formed *via* ortho metalation of the phenyl ring bound to the asymmetric carbon. The relative amounts of the three products are related to their respective stability. The major product (**10a,b**) was the only one formed from **8a,b** after a short reaction time. Formation of **11a,b** and **12a,b** were detected only

after several hours at 83 °C and can occur either *via* isomerization of **10a,b** (which has been proven to be the case for species **11a,b**) or directly from **8a,b**. The isomerization of **10a,b** to **11a,b** in refluxing propan-2-ol indicates the reversibility of the phenyl C-H oxidative addition even though the former compound appears to be thermodynamically favored.

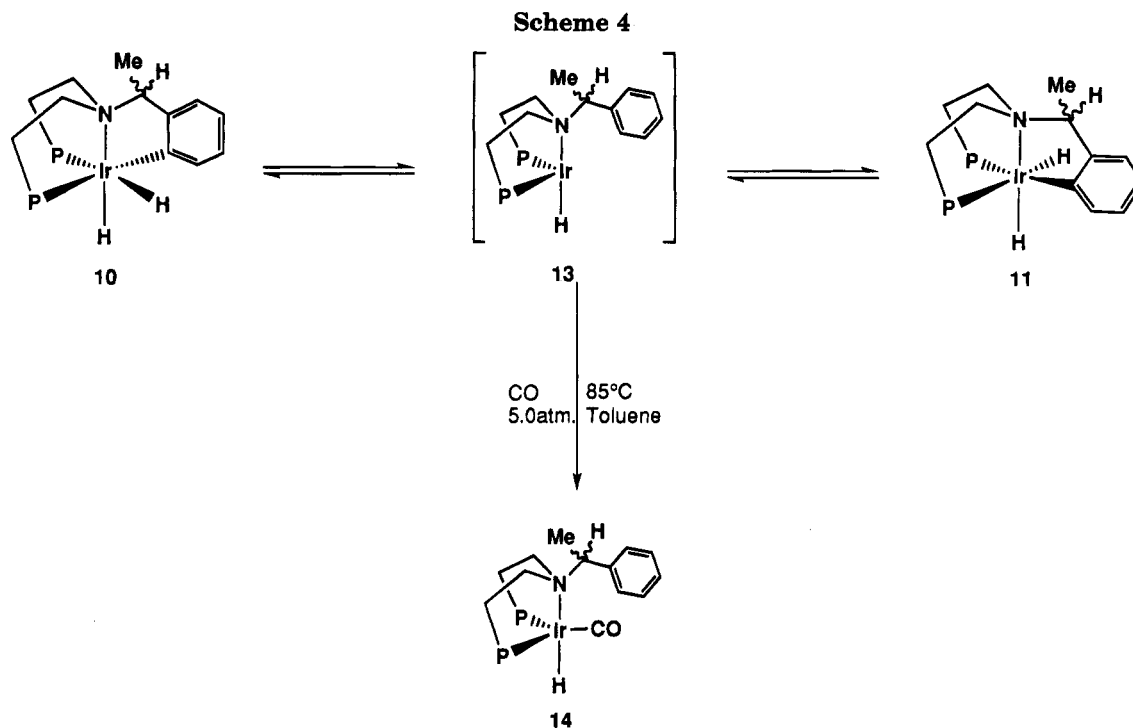
If we assume that the catalysis observed was not due to other iridium species, which were formed in small amounts and were not spectroscopically detectable, we can make the prediction that the catalytically active species was (or was formed from) one of the four complexes formed *via* loss of cyclooctadiene from **8a,b**. In fact, complexes **10a,b**, **11a,b**, and **12a,b** appear to be all related to each other in a reversible fashion through formation of a tetracoordinate iridium(I) intermediate that would be a good candidate for the catalytically active species. In this hypothesis, complexes **10a,b**, **11a,b**, and **12a,b** might all behave as catalyst precursors proceeding through reductive elimination of the phenyl C-H group. However, it is evident that the ease of such reductive elimination will be different for each of these Ir(III) complexes.

Compound **10a,b** slowly isomerizes in refluxing propan-2-ol to give **11a,b** (see Scheme 4). Such a reaction likely proceeds *via* C-H reductive elimination followed by oxidative addition of the aromatic C-H group in the *ortho* position *via* a four-coordinate *fac*-PNP* transient species (**13a,b**). A fluxional movement of one or both hydrides could also accomplish the isomerization. We are inclined to disfavor this interpretation, since both **10** and **11** appear stereochemically rigid on the NMR time scale (see also the carbonylation reactions shown in Scheme 4). Species **13a,b**, once formed, might rearrange to give the square-planar complexes **9a,b**. However, formation of **9a,b** was never observed as an intermediate in the isomerization **10a,b** ↔ **11a,b**, which suggests that **13a,b**, once formed, readily re-form either **10a,b** or **11a,b**. Evidence for the formation of **13a,b** as a transient species in the isomerization **10a,b** ↔ **11a,b** was obtained by trapping the iridium(I) species with CO (*vide infra*) to give **14a,b**. On the other hand, if we consider the results obtained using **10a,b** as a precursor, in the hypothesis that the catalytic activity is bound to the formation of a tetracoordinate iridium(I) species, we must infer that both **10a,b** and **11a,b** can act equally as a catalyst precursor, which is in agreement with the observation that transformation of **10a,b** into **11a,b** does not result in any difference in the catalytic results (see Results; compare the catalytic reactions starting from **10a,b** with and without pretreatment of the catalyst at 83 °C).

In comparison with the results of **10a,b** as a precursor, when **8a,b** was the starting species a higher catalytic activity was observed. From the NMR data we know that, **10a,b**, **11a,b**, and a small amount of **12a,b** are formed in the reaction, and we can reasonably assume that the last species is responsible for the higher catalytic activity. Such a hypothesis appears to be reasonable if we compare the structure of compounds **12a,b** to that of **10a,b** (and **11a,b**). In complex **12** the PNP* ligand is in a *mer* configuration, and one of the hydrides is in a *trans* position with respect to the phenyl carbon atom. Such a configuration results in the Ir-C bond being more labile, and it is consequently easier

(23) A square-planar complex of the formula [IrH(PNP*)] has been isolated in high yield and fully characterized with the use of the ligand (*R*)-(+)-(C₆H₅)C*H(CH₃)N(CH₂CH₂P(C₆H₁₁)₂)₂, which differs from (*R*)-(+)-**5a** only in the phosphorus substituents. ¹H NMR (C₇D₈, 37 °C, 200.13 MHz; δ): -18.6, dd, ²J_{H hydride, P_{cis}} 13.4 Hz, ²J_{H hydride, P_{trans}} 13.4 Hz, 1 × H hydride. ³¹P{¹H} NMR (C₇D₈, 37 °C, 81.01 MHz; δ): AB system, δ_A 30.1, δ_B 25.0, ²J_{PP} 355.0 Hz. Bianchini, C.; *et al.* To be submitted for publication.

(24) Bianchini, C.; Peruzzini, M.; Farnetti, E.; Kaspar, J.; Graziani, M. *J. Organomet. Chem.*, in press.



for C–H reductive elimination to occur.²⁵ In contrast, in complex **10a,b** (and **11a,b**) the phenyl carbon is in a position *trans* to a phosphorus atom, which has a lower *trans* effect in comparison to the hydride.²⁵ Therefore, in the hypothesis that the catalytic activity is related to the ease of C–H reductive elimination, we can expect **12a,b** to be a more efficient catalytic precursor in comparison to **10a,b** (and **11a,b**).

The catalytic cycle proposed in Scheme 5 summarizes all the considerations made so far. The iridium(III) complexes **10a,b**, **11a,b**, and **12a,b** can all act as catalyst precursors to give via C–H reductive elimination the coordinatively unsaturated species **13a,b**, which, before rearranging to the square-planar species **9a,b**, is approached by the ketone which may coordinate in $\eta^1(\text{O})$ fashion. Indeed, this type of coordination for benzylideneacetone was shown to be operative in a similar hydrogen-transfer reduction catalyzed by the complex $[(\text{PP}_3)\text{Os}(\text{H}_2)\text{H}]^+$.²⁰ Migration of the hydride to the carbonyl carbon gives an alkoxy species which in turn is protonated by propan-2-ol and released from the coordination sphere of iridium. Finally the cycle is closed by a hydrogen β -elimination step and loss of acetone to give the iridium hydride **13a,b**.

In order to obtain further support for the hypothesis of formation of the common intermediate **13a,b** starting from **10a,b**, **11a,b**, or **12a,b** the reactivity of these complexes with CO was tested. When a toluene solution of **10a,b** and **11a,b** was treated with CO at 85 °C, the only product formed was the carbonylic complex **14a,b** (see Scheme 4). Similarly, when a catalytic reaction was stopped by quenching with CO (5.0 atm), the only product formed was once again species **14a,b**. Such a complex can be easily formed by addition of CO to the coordinatively unsaturated species **13a,b**, which appears to be the common intermediate.

Scheme 5 rationalizes the enantioselectivity of this reaction; that is, (*R*)-PNP* gives predominantly the (*R*)-PhCH=CHCH(OH)Me enantiomer. Preceding the σ -bond metathesis reaction with propan-2-ol, preliminary chemical events may involve the π - π stacking of the phenyl rings on the substrate, asymmetric carbon, and phosphine groups. The methyl substituents on the ligand and the substrate can then adopt sterically less strained positions in directions opposite to each other. Such an intermediate species would have the PhCH=CHCOMe ketone in the plane of the phosphorus–phosphorus atoms, thus allowing attack of the hydride onto the *Si* face of the ketone.²⁶

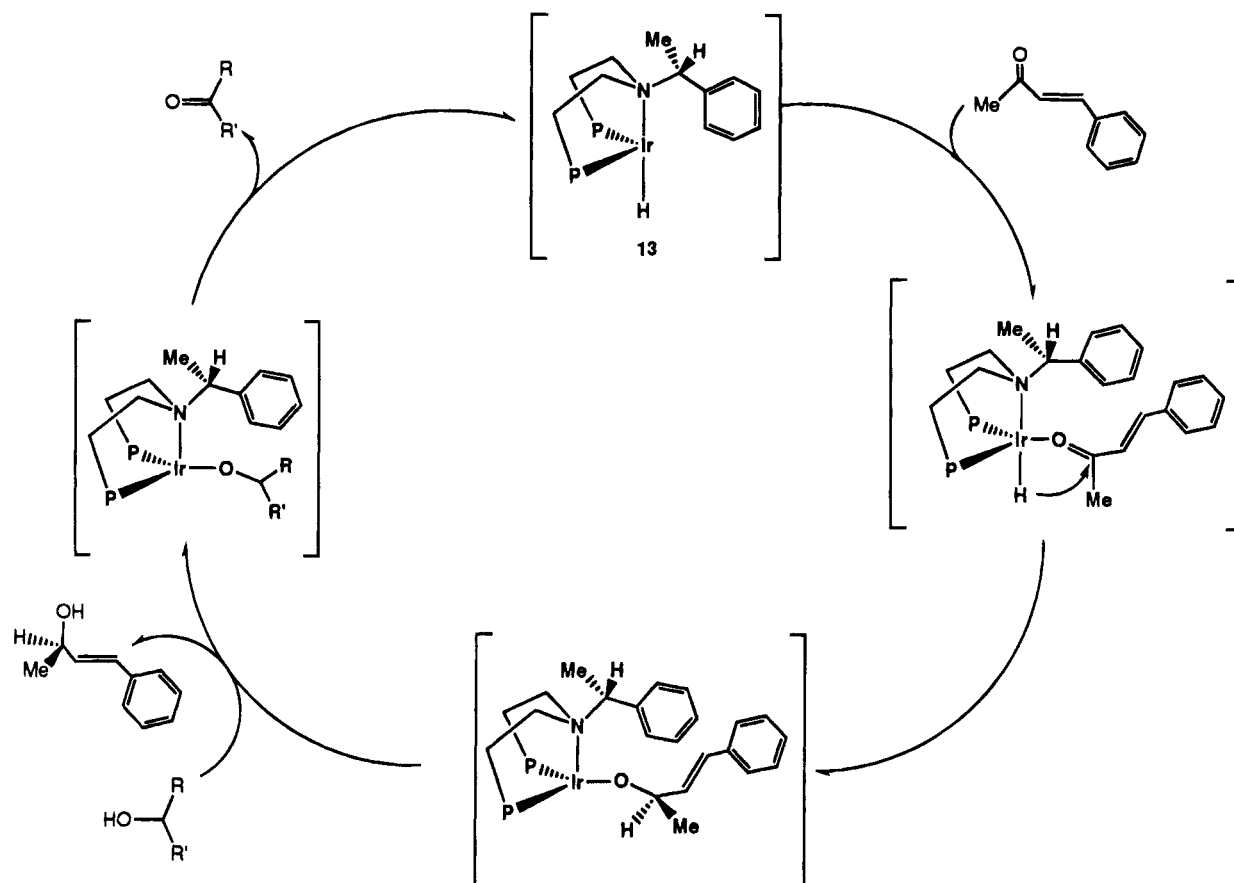
Conclusions

In this paper we have reported a study of the selective reduction of α,β -unsaturated ketones to optically pure allylic alcohols, using a new, chiral iridium complex as catalyst and propan-2-ol as the hydrogen-transfer reagent. Indeed, the utility of delivering optically active allylic alcohols in high enantiomeric excess is highly desirable, as these synthons can then be used in the synthesis of several biologically active compounds.

Chemoselective reduction of α,β -unsaturated ketones to allylic alcohols is shown only by a restricted number of transition-metal complexes.²⁰ Enantioselective reduction is even more rare, being limited to the present PNP*–Ir complexes and to Takaya's $[\text{Ir}(\text{BINAP})(\text{COD})]^+/\text{Ph}_2\text{P}(o\text{-C}_6\text{H}_4\text{NMe}_2)$ system,^{2b} which is fairly efficient only for benzylideneacetone. In both cases, asymmetric induction does not exceed 60%; thus, the production of optically active allylic alcohols in high yield is still a challenging task.

(25) Collman, J. P.; Hegedus, L. S.; Norton, J. R.; Finke, R. G. *Principles and Application of Organotransition Metal Chemistry*; University Science Books: Mill Valley, CA, 1987; Chapter X.

(26) (a) Zassinovich, G.; Bettella, R.; Mestroni, G.; Bresciani-Pahor, N.; Geremia, S.; Randaccio, L. *J. Organomet. Chem.* **1989**, *370*, 187–202. (b) Zassinovich, G.; Mestroni, G.; Gladiali, S. *Chem. Rev.* **1992**, *92*, 1051.

Scheme 5. Reaction Scheme for the Chemo- and Enantioselective Reduction of Benzylideneacetone^a

^a **13** was formed either (i) *in situ* or (ii) from complexes **10**–**12**.

In light of the results presented in this paper, we are, at present, continuing our investigations of the chemistry of the PNP* mixed-donor ligands. Studies include the use of methyl/ethyl- and naphthyl/methyl-substituted PNP* systems in the reduction of a variety of prochiral ketones. Also under investigation is a detailed mechanistic study of the role played by the (a) stereogenic substituent, (b) phosphorus substituents, (c) metal center, (d) nature of the ketone, and (e) solvent system employed in effecting asymmetric reduction. Current investigations center on developing a rationale for the chemical events leading up to the incorporation of the ketone with the catalyst.

Acknowledgment. We thank the Progetto Strategico "Tecnologie Chimiche Innovative", CNR, Rome, Italy, and the EC (Contract No. ERBCHRXT930147) for financial support. L.G. thanks the Italian Ministry of Foreign Affairs for financial support. Thanks are due to Prof. G. Pitacco (University of Trieste) for helpful discussion.

Supplementary Material Available: Tables of anisotropic thermal parameters and hydrogen atom coordinates for the two independent molecules of **10a** (3 pages). Ordering information is given on any current masthead page.

OM9409332

Photochemistry of $[\text{CpMo}(\text{CO})_3]_2$. Direct Detection and Kinetics of the Radical $\text{CpMo}(\text{CO})_3$ in *n*-Heptane Solution at Room Temperature by Fast Time-Resolved Infrared Spectroscopy

Jonas Peters, Michael W. George,* and James J. Turner*

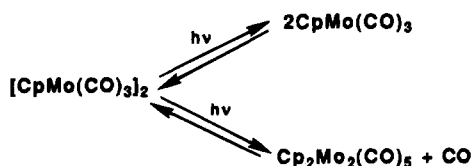
Department of Chemistry, University of Nottingham, University Park, Nottingham NG7 2RD, U.K.

Received November 9, 1994[®]

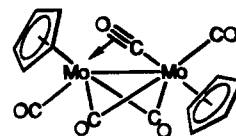
Fast (nanosecond) time-resolved infrared spectroscopy has been used to follow the visible (532 nm) and UV (308 nm) flash photolysis of *trans*- $[\text{CpMo}(\text{CO})_3]_2$ ($\text{Cp} = \eta^5\text{-C}_5\text{H}_5$), in *n*-heptane solution, at room temperature. With visible irradiation, the primary photoproducts observed, on this time scale, are $\text{CpMo}(\text{CO})_3$ (major) and *gauche*- $[\text{CpMo}(\text{CO})_3]_2$. The $\text{CpMo}(\text{CO})_3$ radical dimerizes ($k_2 = 3(\pm 1) \times 10^9 \text{ M}^{-1} \text{ s}^{-1}$) to form both *trans*- and *gauche*- $[\text{CpMo}(\text{CO})_3]_2$. The *gauche*- $[\text{CpMo}(\text{CO})_3]_2$ isomer decays ($k = 2(\pm 0.5) \times 10^2 \text{ s}^{-1}$) to the more stable *trans* isomer. Upon UV flash photolysis the CO-loss intermediate, $\text{Cp}_2\text{Mo}_2(\text{CO})_5$, is observed as a primary photoproduct together with the $\text{CpMo}(\text{CO})_3$ radical and *gauche*- $[\text{CpMo}(\text{CO})_3]_2$.

Introduction

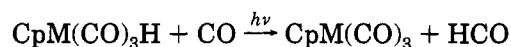
There has been considerable interest in the photochemistry of $[\text{CpM}(\text{CO})_3]_2$ complexes, ($\text{M} = \text{Cr}, \text{Mo}, \text{W}$).^{1–7} Attention has also focused on the intermediates in these photoreactions. Early flash-photolysis experiments⁸ suggested that photolysis of $[\text{CpMo}(\text{CO})_3]_2$ yields *two* species, the radical $\text{CpMo}(\text{CO})_3$ and the CO-loss species $\text{Cp}_2\text{Mo}_2(\text{CO})_5$, which recombine rapidly and slowly, respectively:



More recent flash photolysis studies⁹ proposed rate constants for these rates of recombination. The species $\text{Cp}_2\text{M}_2(\text{CO})_5$ ($\text{M} = \text{Mo}, \text{W}$) was identified in low-temperature matrix isolation experiments by photolysis of $\text{Cp}_2\text{M}_2(\text{CO})_6$, and on the basis of the matrix $\nu(\text{CO})$ infrared spectra, it was proposed¹⁰ that the structure of $\text{Cp}_2\text{M}_2(\text{CO})_5$ ($\text{M} = \text{Mo}, \text{W}$) is

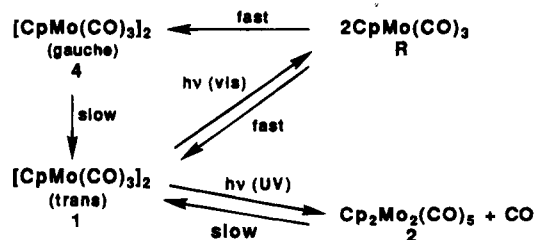


Although it is assumed that matrix photolysis yields both $\text{CpM}_2(\text{CO})_5$ and $\text{CpM}(\text{CO})_3$, only the former is seen because the large size of the radical encourages its in-cage recombination. The matrix $\nu(\text{CO})$ infrared spectrum of the radical has been obtained by a quite different route; photolysis of $\text{CpM}(\text{CO})_3\text{H}$ ($\text{M} = \text{Mo}, \text{W}$) in a solid CO matrix yields $\text{CpM}(\text{CO})_3$, as well as HCO :¹¹



Knorr and Brown¹² (KB) have carried out a thorough study of the photochemistry of $[\text{CpMo}(\text{CO})_3]_2$ including low-temperature photolysis with IR detection, as well as conventional flash-photolysis experiments.

The current situation can be summarized (employing KB's notation):



Some explanatory remarks follow.

(i) In nonpolar solvents, $[\text{CpMo}(\text{CO})_3]_2$ exists almost entirely in the *trans* configuration 1 with the concentration of the *gauche* form 4 too low to detect by IR.¹³

(11) Mahmoud, K. A.; Rest, A. J.; Alt, H. G. *J. Organomet. Chem.* **1983**, *246*, C37.

(12) Knorr, J. R.; Brown, T. L. *J. Am. Chem. Soc.* **1993**, *115*, 4087.

[®] Abstract published in *Advance ACS Abstracts*, February 1, 1995.
(1) Burkett, A. R.; Meyer, T. J.; Whitten, D. G. *J. Organomet. Chem. B* **1974**, *67*.

(2) Wrighton, M. S.; Ginley, D. S. *J. Am. Chem. Soc.* **1975**, *97*, 4246.

(3) Hepp, A. F.; Wrighton, M. S. *J. Am. Chem. Soc.* **1981**, *103*, 1258.

(4) Stiegman, A. E.; Stieglitz, M.; Tyler, D. R. *J. Am. Chem. Soc.* **1983**, *105*, 6032.

(5) Philbin, C. E. W.; Goldman, A. S.; Tyler, D. R. *Inorg. Chem.* **1986**, *25*, 4434.

(6) Covert, K. J.; Askew, E.; Grunkemeier, J.; Koenig, T.; Tyler, D. R. *J. Am. Chem. Soc.* **1992**, *114*, 10446.

(7) Abrahamson, H. B.; Marxen, H. *Organometallics* **1993**, *12*, 2835.

(8) Hughey, J. L.; Bock, C. R.; Meyer, T. J. *J. Am. Chem. Soc.* **1975**, *97*, 4440.

(9) Van Vlierberge, B. A.; Abrahamson, H. B. *J. Photochem. Photobiol.* **1990**, *52*, 69.

(10) (a) Hooker, R. H.; Mahmoud, K. A.; Rest, A. J. *J. Organomet. Chem.* **1983**, *254*, C25. (b) Hooker, R. H.; Rest, A. J. *J. Chem. Soc., Dalton Trans.* **1990**, 1221. (c) Baker, M. L.; Bloyce, P. E.; Campen, A. K.; Rest, A. J.; Bitterwolf, T. E. *J. Chem. Soc., Dalton Trans.* **1990**, 2825.

(ii) KB showed that experiments previously thought to be^{8,9} monitoring the conversion $2 \rightarrow 1$, were in fact measuring the rate of $4 \rightarrow 1$.

(iii) The UV/visible absorption spectrum of **R** (Cr, Mo, W) is very weak. Hence in earlier^{8,9} and more recent^{14,15} experiments for Mo and W and for Cr¹⁶ the rate of $R \rightarrow 1$ has been monitored by the recovery of **1**. The rate constant depends on solvent but in cyclohexane is between 2 and $5 \times 10^9 \text{ M}^{-1} \text{ s}^{-1}$. Although, as described above, **R** has been characterized in low-temperature matrices, its detection by infrared spectroscopy at room temperature has not been published (although $\text{CpMo}(\text{CO})_3$ was described in a thesis¹⁷); the time scale of KB's infrared experiments was too long, even at reduced temperatures, to detect the highly reactive **R**.

(iv) On the basis of the thesis,¹⁷ KB¹² suggested that **4** might be produced via the recombination of **R** rather than directly from **1**. Since they also showed that **4** and **1** have different absorption spectra ($\lambda_{\text{max}} = 362 \text{ nm}$ and $\lambda_{\text{max}} = 390 \text{ nm}$, respectively), this complicates the measurement of the recombination of **R** by the monitoring of parent regrowth.

(v) Depending on the solvent viscosity, the "in-cage" recombination of radicals such as $\text{CpMo}(\text{CO})_3$ is an important feature of the photochemistry.⁶

In this paper we show that the IR spectrum of the radical **R** can be obtained in room temperature solution, and the kinetics of its recombination can be measured directly and compared with other estimates. We also show that some **4** is produced "instantaneously" (presumably by in-cage recombination or direct $1 \rightarrow 4$ conversion) on the fastest time scale of these experiments, and that **4** is also produced from recombination of **R**. The conversion of **4** to **1** is also measured. There has also been recent debate over the spectral characterization of **2** in fluid solution,¹² and we report the infrared spectrum of **2** in *n*-heptane solution at room temperature.

Experimental Section

The Nottingham TRIR apparatus has been described elsewhere.¹⁸ Briefly, it consists of a pulsed UV source, either a XeCl excimer laser (Lumonics HyperEx 440; 308 nm, 20 ns pulse) or a Nd:YAG laser (Quanta-Ray GCR-11; 532 nm, 7 ns pulse), to initiate photochemical reactions and continuous wave IR lasers to monitor the transient IR absorptions. IR spectra are built up on a "point-by-point" basis. The work described here has involved two different monitoring lasers, an Edinburgh Instruments PL3 CO laser, line tunable in steps of ca. 4 cm^{-1} over a limited wavenumber range (2000–1550 cm^{-1}), and a Müttek IR diode laser (Model MDS 1100, fitted with Müttek MDS 1200) which has much lower power but is continuously tunable so that much higher resolution TRIR spectra can be obtained. For low resolution ($\pm 0.5 \text{ cm}^{-1}$), calibration is obtained using the MDS 1200 monochromator.

(13) Adams, R. D.; Cotton, F. A. *Inorg. Chim. Acta* **1973**, *7*, 153. Adams, R. D.; Collins, D. M.; Cotton, F. A. *Inorg. Chem.* **1974**, *13*, 1086.

(14) Scott, S. L.; Espenson, J. H.; Chen, W.-J. *Organometallics* **1993**, *12*, 4077.

(15) Scott, S. L.; Espenson, J. H.; Bakac, A. *Organometallics* **1993**, *12*, 1044.

(16) Yao, Q.; Bakac, A.; Espenson, J. H. *Organometallics* **1993**, *12*, 2010.

(17) Moore, B. D. Ph.D. Thesis, University of Nottingham, October 1985.

(18) (a) Dixon, A. J.; Healy, M. A.; Hodges, P. M.; Moore, B. D.; Poliakov, M.; Simpson, M. B.; Turner, J. J.; West, M. A. *J. Chem. Soc., Faraday Trans. 2* **1986**, *82*, 2083. (b) George, M. W.; Poliakov, M.; Turner, J. J. *Analyst* **1994**, *119*, 551.

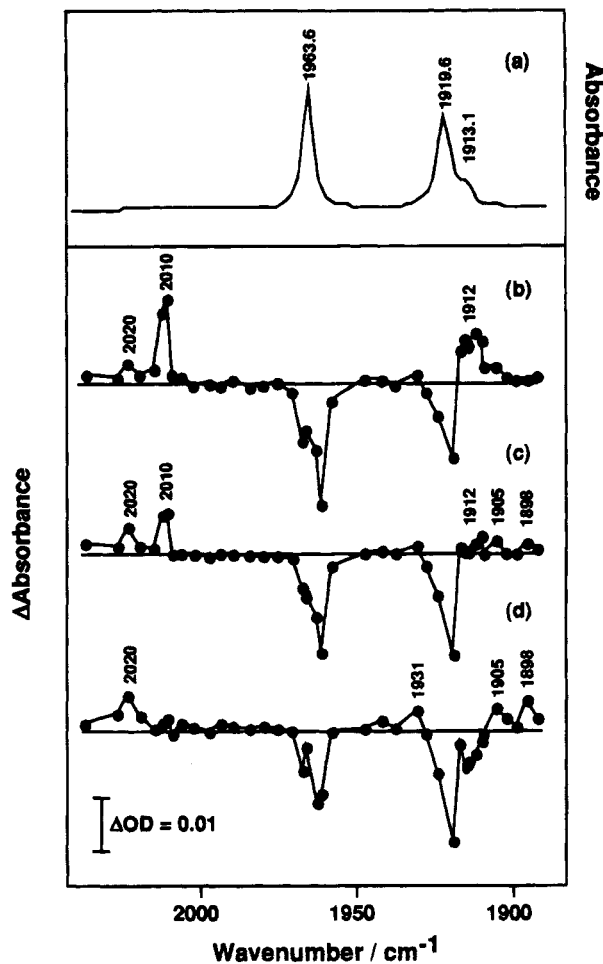


Figure 1. (a) FTIR spectrum, in the $\nu(\text{CO})$ region, of $[\text{CpMo}(\text{CO})_3]_2$ in *n*-heptane. Time-resolved IR difference spectra of $[\text{CpMo}(\text{CO})_3]_2$ in *n*-heptane ($3 \times 10^{-4} \text{ mol dm}^{-3}$): (b) $1 \mu\text{s}$, (c) $30 \mu\text{s}$, and (d) $80 \mu\text{s}$ after the visible (532 nm) laser pulse.

More precise IR frequency measurements can be achieved by external calibration using a high-resolution FTIR spectrometer (Perkin-Elmer System 2000).¹⁹ Standard infrared spectra were obtained with a Nicolet 730 interferometer. *n*-Heptane (Aldrich HPLC grade) was distilled over CaH_2 prior to use. $[\text{CpMo}(\text{CO})_3]_2$ (Aldrich) and argon (Air Products) were used as supplied.

Results and Discussion

Photolysis of $[\text{CpMo}(\text{CO})_3]_2$ with 532 nm Excitation. (a) Identification of $\text{CpMo}(\text{CO})_3$ Radicals and *gauche*- $[\text{CpMo}(\text{CO})_3]_2$. Figure 1a shows the FTIR spectrum of $[\text{CpMo}(\text{CO})_3]_2$ (**1**) in *n*-heptane. Figure 1b shows the TRIR spectrum obtained $1 \mu\text{s}$ after 532 nm excitation of **1** in *n*-heptane ($3 \times 10^{-4} \text{ mol dm}^{-3}$). It is clear from Figure 1b, that visible excitation causes depletion of **1** and the production of two strong IR absorption bands at 2010 and 1912 cm^{-1} . There is a much weaker IR absorption at 2020 cm^{-1} . The bands at 2012 and 1912 cm^{-1} decay at the same rate (see below) and hence can be assumed to be from the same species. By comparison with the $\nu(\text{CO})$ data from the $\text{CpMo}(\text{CO})_3/\text{HCO}$ matrix experiment, these two stronger bands can be assigned to the radical species **R** (see Table

(19) George, M. W.; Haward, M. T.; Hamley, P. A.; Hughes, C.; Johnson, F. P. A. J.; Popov, V. K.; Poliakov, M. *J. Am. Chem. Soc.* **1993**, *115*, 2286.

Table 1. Infrared Spectral Data (cm^{-1}) in the $\nu(\text{CO})$ Region for the Species Involved in the Photochemistry of $[\text{CpMo}(\text{CO})_3]_2$

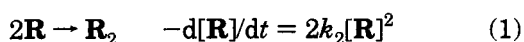
species	<i>n</i> -heptane (298 K) ^a		3-methylpentane ^b		CH_4 (12 K) ^c	CO (12 K) ^d
	93 K	200 K	93 K	200 K		
$[\text{CpMo}(\text{CO})_3]_2$ (<i>trans</i>) (1)	1963.6				1693.0	
	1919.6				1918.5	
	1913.1				1912.5	
$[\text{CpMo}(\text{CO})_3]_2$ (<i>gauche</i>) (4)	2022	2021				
	~1960	1966				
	1931	1930				
	1905	1905				
	1898	1895				
$\text{CpMo}(\text{CO})_3$ (R)	2010				2008.9	
	1912				1915.5/1908.4	
$\text{Cp}_2\text{Mo}_2(\text{CO})_5$ (2)	1982	1982			1981.5	
	1944	1942			1939.5	
	~1910	1913			1885.5	
	1872	1868			1865.5	
		1667			1667.0	

^a This work. ^b Reference 12. ^c Reference 10c. ^d Reference 11; assuming R adopts a C_3 structure, the band at 2008.9 cm^{-1} is assigned to the a_1 mode and the broad "matrix-split" band at $1915.5/1908.4$ to the e mode.

1). The TRIR spectra at $30 \mu\text{s}$ (Figure 1c) and $80 \mu\text{s}$ (Figure 1d) show the decay of the IR bands of R. This decay shows second-order kinetics (see below) which is further proof that the two decaying bands belong to R.

The weak absorption at 2020 cm^{-1} (Figure 1b) increases in intensity over the first $80 \mu\text{s}$. There are other weak bands at 1931, 1905, and 1898 cm^{-1} which all grow in with the same rate as the increase of the 2020 cm^{-1} absorption. (These bands at 1931, 1905, and 1898 cm^{-1} are not seen in Figure 1b either because of overlap with the strong radical bands or because of low intensity at early times). The change in intensity at approximately 1960 cm^{-1} indicates the presence of another, overlapping, band which grows in as the band due to R decays away. By comparison both with Cotton's early work¹³ and with KB's¹² low-temperature work, these weak absorptions at ~ 1960 , 1931, 1905, and 1898 cm^{-1} can be assigned to the *gauche* isomer of $[\text{CpMo}(\text{CO})_3]_2$ (4) (see Table 1). Finally, it should be noted that at the photolysis wavelength of 532 nm, there was no evidence for the formation of any CO-loss species 2.

(b) Determination of Radical Recombination Kinetics. Figure 2a shows a trace in which the change in IR absorbance at 2010.2 cm^{-1} (a frequency at which only R absorbs) is monitored as a function of time. A plot of $1/\Delta A$ versus time, Figure 2b, shows that the decay of the radical follows second-order kinetics and is consistent with a simple bimolecular recombination process, eq 1.



In principle the concentration of R is easily determined. Since the IR extinction coefficient of 1 at a particular frequency is easily measured, the change in concentration of 1 is readily monitored from the change in absorbance of 1 at that frequency; if all of 1 that is photolyzed is converted to R, then the concentration of R is obtained. In practice this is difficult for two reasons: there is overlap between the bands of 1 and the products (see Figure 1); not all of the loss of 1 can be assigned to the formation of R, since there is

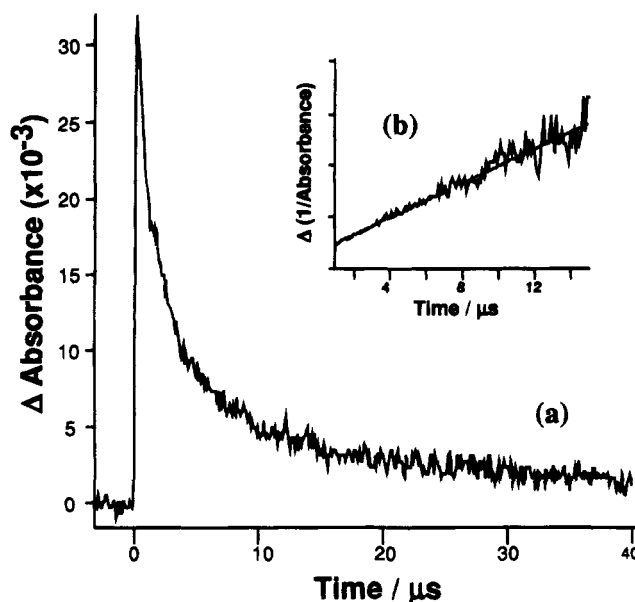


Figure 2. (a) Time-resolved IR decay trace of $\text{CpMo}(\text{CO})_3$, recorded at 2010 cm^{-1} , following 532 nm flash photolysis of $[\text{CpMo}(\text{CO})_3]_2$, in *n*-heptane ($3 \times 10^{-4} \text{ mol dm}^{-3}$). (b) Plot of $1/\Delta A$ versus time for the decay trace shown in (a).

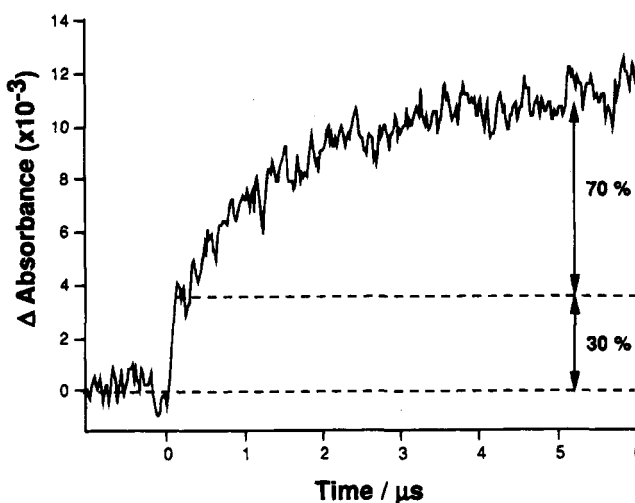


Figure 3. Time-resolved IR trace, recorded at 2020 cm^{-1} , following the 532 nm flash photolysis of $[\text{CpMo}(\text{CO})_3]_2$, in *n*-heptane ($3 \times 10^{-4} \text{ mol dm}^{-3}$) showing the formation of *gauche*- $[\text{CpMo}(\text{CO})_3]_2$.

"instantaneous" formation of some *gauche* isomer 4 (see Figure 1b). We have overcome these problems as follows.

Careful examination of the kinetic traces in the region $1950\text{--}1970 \text{ cm}^{-1}$ shows that at the IR diode laser frequency of $\sim 1960 \text{ cm}^{-1}$, there is no overlap with the developing band of 2. However, it is clear from Figure 1a that this frequency corresponds to the steeply sloping, lower frequency, side of the band of 1; this in turn presents two problems—accurate measurement of the diode laser frequency and accurate determination of the extinction coefficient at this frequency. We have used a high-resolution FTIR spectrometer to measure the diode frequency, 1960.1 cm^{-1} , and the same spectrometer to measure, as accurately as possible, the extinction coefficient ($2500 \text{ M}^{-1} \text{ cm}^{-1}$) of 1 at the same frequency.

Figure 3 shows the grow-in of the *gauche* isomer, monitored at 2020 cm^{-1} . There is the instantaneous

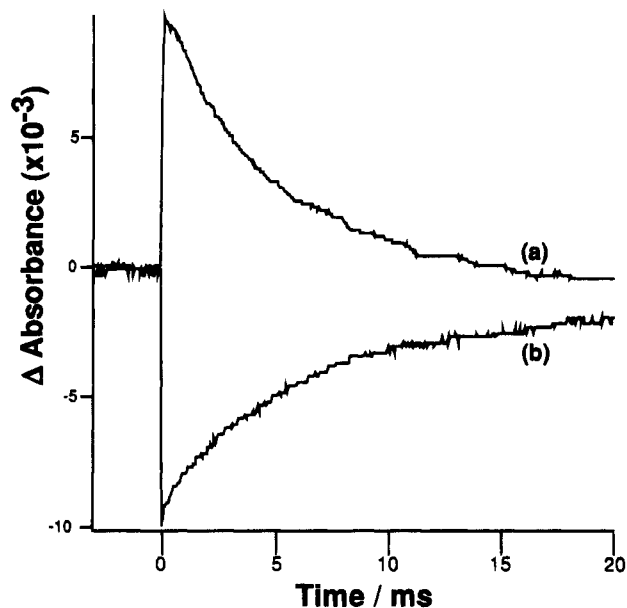


Figure 4. Time-resolved IR decay traces recorded at (a) 1930 cm^{-1} and (b) 1961 cm^{-1} , following 532 nm flash photolysis of $[\text{CpMo}(\text{CO})_3]_2$ in *n*-heptane (3×10^{-4} mol dm^{-3}) showing the decay of *gauche*- $[\text{CpMo}(\text{CO})_3]_2$ and reformation of *trans*- $[\text{CpMo}(\text{CO})_3]_2$.

(detector limited) process, followed by a slower, second-order, process. The first, fast process occurs either because of direct **1** to **4** conversion or because of in-cage recombination of **R** to form **4**; any in-cage recombination to re-form **1** will not affect the observed kinetics. In either case it is clear that approximately 30% of **4** forms immediately and hence an approximately 30% loss of **1** is due to this route. The ratio of in-cage recombination to out of cage recombination is dependent on the solvent viscosity.⁶

With these two considerations, we estimate the IR extinction coefficient of **R** at 2010.2 cm^{-1} to be 4300 $\text{M}^{-1} \text{cm}^{-1}$ and calculate k_2 to be $3(\pm 1) \times 10^9 \text{ M}^{-1} \text{ s}^{-1}$, which compares well with previously determined values.

(c) Rate of Isomerization of *gauche*- to *trans*- $[\text{CpMo}(\text{CO})_3]_2$ (4** \rightarrow **1**).** Following the rapid reaction of **R** to form either **1** or **4**, there is a much slower process involving the isomerization of **4** to **1**. After 80 μs the IR bands due to **R** have disappeared, and hence the bands at ≈ 1960 and $\approx 1930 \text{ cm}^{-1}$ assigned to **1** and **4**, respectively, are free of interference from **R**. Thus the rate of isomerization can be measured directly. Figure 4a shows the first-order decay of **4** at 1930 cm^{-1} ($k_{\text{obs}} = 2(\pm 0.5) \times 10^2 \text{ s}^{-1}$) which is identical to the rate of reformation of **1** at 1961 cm^{-1} ($k_{\text{obs}} = 2(\pm 0.5) \times 10^2 \text{ s}^{-1}$) shown in Figure 4b. This observed rate is consistent with that reported by KB ($3 \times 10^2 \text{ s}^{-1}$), and we agree with them that earlier measurements of radical kinetics were in fact measuring the rate of **4** to **1** isomerization.

Detection of $\text{Cp}_2\text{Mo}_2(\text{CO})_5$ Using 308 nm Excitation. In quoting from the early thesis, whose results were not published in the refereed literature, KB expressed surprise at the incompleteness of the characterization of **2**. We show here that, with the exception of the lowest frequency band at $\approx 1665 \text{ cm}^{-1}$, bands assigned to **2** are readily observed in TRIR experiments. Figure 5a shows the TRIR spectra of $[\text{CpMo}(\text{CO})_3]_2$ in

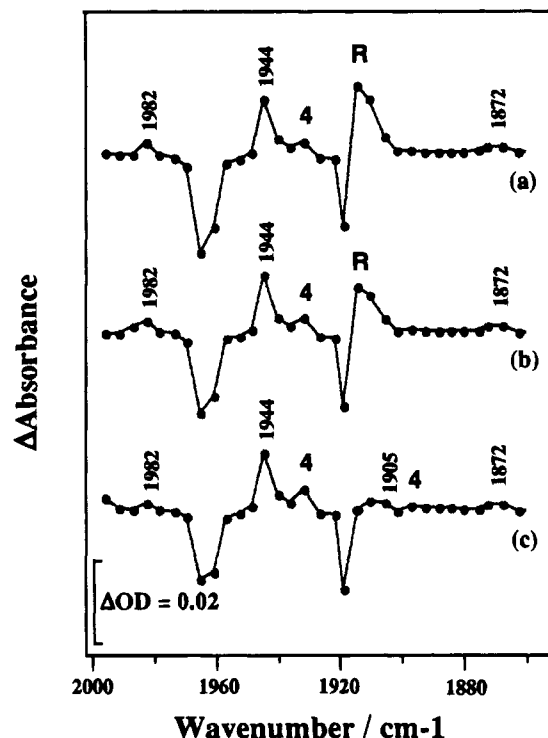


Figure 5. Time-resolved IR difference spectra of $[\text{CpMo}(\text{CO})_3]_2$ in *n*-heptane (3×10^{-4} mol dm^{-3}): (a) 1 μs , (b) 30 μs , and (c) 80 μs after the UV (308 nm) laser pulse. The bands labeled **R** and **4** are due to the previously characterized $\text{CpMo}(\text{CO})_3$ radical and the *gauche* isomer of $[\text{CpMo}(\text{CO})_3]_2$.

n-heptane (3×10^{-4} mol dm^{-3}) obtained 1 μs after the UV pulse (308 nm). The spectrum clearly shows that the UV pulse causes a depletion of **1** and the production of **R** and **4** together with new absorptions at 1982, 1944, and 1872 cm^{-1} . The kinetic behavior of **R** and **4** is identical to that under visible excitation. **R** has partially decayed after 40 μs (Figure 5b) and has fully decayed after 80 μs (Figure 5c). Meanwhile the bands due to **4** grow in. The new $\nu(\text{CO})$ bands at 1982, 1944, and 1872 cm^{-1} do not change in intensity over the first 80 μs , and they remain unchanged for at least 20 ms. In Figure 1d the parent shoulder at 1913 cm^{-1} was clearly seen; in Figure 5c the shoulder is absent, implying that there is a band of **2** coincident with it. The new absorptions produced by UV excitation of $[\text{CpMo}(\text{CO})_3]_2$ can readily be assigned to the long-lived species $\text{Cp}_2\text{Mo}_2(\text{CO})_5$ by comparison with data obtained from matrix isolation and low-temperature solutions (see Table 1).

Conclusions

We have shown that TRIR spectroscopy can be used to determine the kinetics of the recombination of the radical $\text{CpMo}(\text{CO})_3$ and the *gauche* to *trans* isomerization of $[\text{CpMo}(\text{CO})_3]_2$ in *n*-heptane at room temperature.

Acknowledgment. We thank Prof. M. Poliakoff and Dr. B. D. Moore for helpful discussions. We also acknowledge the EC, SERC (GR/H63296), and the Marshall Foundation for a scholarship (J.P.).

OM940850L

Notes

Expansion of Three-Membered Rings by the Insertion of Methyl(methylidene)borane $\text{MeB}=\text{C}(\text{SiMe}_3)_2$

Ulli Englert, Rudi Finger, Peter Paetzold,* and Burkhard Redenz-Stormanns

Institut für Anorganische Chemie, Technische Hochschule Aachen, D-52056 Aachen, Germany

Zbigniew Pawelec and Wiesław Wojnowski*

Instytut Chemii i Technologii Nieorganicznej, Politechnika Gdańska, Ul. G. Narutowicza 11, PL-80-952 Gdansk, Poland

Received October 18, 1994*

Summary: The methyl(methylidene)borane $\text{MeB}=\text{C}(\text{SiMe}_3)_2$ (**1**) and dimethylsilylene react in a 2:1 ratio to give the 1-sila-3,4-diboracyclopentane $[-\text{B}(\text{Me})-\text{B}(\text{Me})-\text{C}(\text{SiMe}_3)_2-\text{Si}(\text{Me})_2-\text{C}(\text{SiMe}_3)_2-]$ (**2**), which crystallizes in the triclinic space group $P\bar{1}$, with lattice constants $a = 16.648(5)$ Å, $b = 17.073(4)$ Å, $c = 11.490(3)$ Å, $\alpha = 102.79(2)^\circ$, $\beta = 104.80(2)^\circ$, $\gamma = 62.76(2)^\circ$, and $V = 2786(2)$ Å³; $Z = 4$. It is assumed that **2** is formed via the cyclic 1:1 adduct of **1** and SiMe_2 , $[-\text{B}(\text{Me})-\text{C}(\text{SiMe}_3)_2-\text{Si}(\text{Me})_2-]$ (**3**), the B–Si bond of which is subsequently added to the B–C double bond of a second molecule of **1**. The azadiboriridine $[-\text{B}(t\text{-Bu})-\text{B}(t\text{-Bu})-\text{N}(t\text{-Bu})-]$ (**4**) undergoes a similar addition to **1** to give the 1-aza-2,3,5-triboracyclopentane $[-\text{B}(\text{Me})-\text{C}(\text{SiMe}_3)_2-\text{B}(t\text{-Bu})-\text{N}(t\text{-Bu})-\text{B}(t\text{-Bu})-]$ (**5**).

Silylenes SiR_2 are readily added to iminoboranes $\text{R}'\text{B}=\text{NR}''$. The primary reaction product, a three-membered ring with a $-\text{B}-\text{N}-\text{Si}-$ skeleton, can be isolated in the case of the reaction of the bulky dimethylsilylene and the iminoborane $t\text{-BuB}=\text{N}t\text{-Bu}$.¹ In order to complete our investigations on the reactions of two-coordinate boron species with silylenes, we added SiMe_2 to the methylideneborane $\text{MeB}=\text{C}(\text{SiMe}_3)_2$ (**1**).²

The silylene SiMe_2 was generated photolytically from its cyclohexamer $\text{Si}_6\text{Me}_{12}$ ^{3,4} in pentane at -60 °C in the presence of **1**. A 77% yield of the crystalline 1:2 adduct **2** from SiMe_2 and **1** was isolated. Three ¹H NMR signals in an intensity ratio of 6:1:1 correspond to three ¹³C NMR signals, two of which are quartets, indicating SiMe groups, and the third of which may be identified as a BMe group by its typical large half-width. Apparently, two molecules of **1** remain equivalent in the product **2** in an equivalent way, and the two methyl groups of the SiMe_2 moiety are incorporated as well. The ¹¹B NMR signal (94.8 ppm) is somewhat high-field-shifted from the range which is typical for tetraalkyldiboranes(4), $\text{R}_2\text{B}-\text{BR}_2$ (103–106 ppm);⁵ such a shift could be caused by $\alpha\text{-SiMe}_3$ groups in the alkyl ligands of $\text{R}_2\text{B}-\text{BR}_2$. The NMR data of **2** are in accord with a siladiboracyclopentane structure, formed according to eq 1.

The proposed structure of **2** is confirmed by an X-ray structural analysis. There are two symmetrically independent molecules **2a** and **2b** in the asymmetric unit of the triclinic cell. The structure of **2a** is shown in

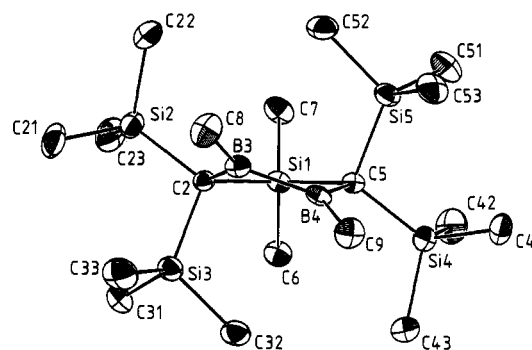


Figure 1. Molecular structure of **2a**, showing 30% probability ellipsoids and the atomic numbering scheme, which is analogously valid for **2b**.

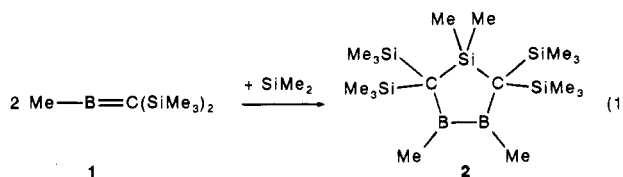


Figure 1. Atomic coordinates and selected bond lengths and angles of **2a** and **2b** appear in Tables 1 and 2. The differences between the molecular parameters of **2a** and **2b** turn out to be small. The central structural unit is a five-membered, nonplanar ring. The eight ring ligands are arranged in a way that allows optimal space for the four bulky SiMe_3 groups. Bond lengths and angles do not deviate remarkably from well-documented standard values. The three bond angles at each of the B atoms sum up to 360° , thus providing planarly coordinated boron atoms. The C_1 point group symmetry of **2a** and **2b** in the crystal is close to C_2 point group symmetry, with the assumed C_2 axis passing through Si1 and the center of the B1–B2 bond. Real C_2 point group symmetry may describe the structure of **2** in solution, leaving neighboring SiMe_3 groups nonequivalent. The observed equivalence of all four SiMe_3 groups, according to NMR data, can then be ascribed to a dynamic process that transforms the two enantiomers of **2** into each other. Actually, the SiMe_3 groups give rise of a ¹³C NMR signal in $\text{THF}-d_8$, the half-width of which is increased from less than 6 Hz at room temperature to

* Abstract published in *Advance ACS Abstracts*, February 1, 1995.

Table 1. Atomic Coordinates ($\times 10^4$) and Equivalent Isotropic Displacement Parameters ($\text{\AA}^2, \times 10^3$) for **2a and **2b**^a**

atom	x	y	z	U_{eq}
Si1	7619.4(8)	8148.4(7)	595(1)	32.0(4)
	1727.8(7)	7619.4(7)	4313(1)	34.2(4)
Si2	6267.3(8)	8364.3(9)	2362(1)	45.3(4)
	1822.5(9)	8903.9(8)	2707(1)	48.8(5)
Si3	8226.7(8)	6835.2(8)	2548(1)	43.7(4)
	3077.3(9)	6885.1(8)	2404(1)	46.8(4)
Si4	8850.9(8)	7169.3(8)	-1517(1)	43.5(4)
	2491.7(9)	6248.4(8)	6295(1)	48.8(4)
Si5	6739.4(9)	7806.7(8)	-2169(1)	42.4(4)
	2322.1(9)	8163.7(8)	7133(1)	44.7(4)
B3	7031(3)	6879(3)	445(5)	37(2)
	3277(3)	7831(3)	4580(5)	37(2)
B4	7711(3)	6573(3)	-636(5)	36(2)
	3463(3)	7114(3)	5551(5)	39(2)
C2	7223(3)	7586(3)	1463(4)	31(1)
	2455(3)	7856(3)	3525(4)	34(1)
C5	7802(3)	7383(3)	-911(4)	32(1)
	2524(3)	7223(3)	5806(4)	34(1)
C6	8674(3)	8304(3)	1439(4)	44(2)
	1293(3)	6801(3)	3368(5)	56(2)
C7	6793(3)	9330(3)	404(4)	49(2)
	596(3)	8590(3)	4539(4)	51(2)
C8	6324(3)	6483(3)	360(5)	65(2)
	3875(3)	8367(3)	4771(5)	57(2)
C9	8203(3)	5570(3)	-1202(5)	55(2)
	4453(3)	6423(3)	6089(5)	59(2)
C21	6100(3)	7839(4)	3493(5)	69(2)
	2469(4)	9010(3)	1681(5)	72(2)
C22	5117(3)	8829(4)	1385(5)	67(2)
	708(4)	8961(4)	1710(6)	79(2)
C23	6486(4)	9331(3)	3267(5)	69(2)
	1533(4)	9964(3)	3763(5)	68(2)
C31	8574(3)	7568(3)	3970(4)	60(2)
	3571(4)	5776(3)	2949(5)	64(2)
C32	9289(3)	6127(3)	1886(5)	53(2)
	2315(4)	6818(4)	918(5)	76(2)
C33	7967(4)	5994(3)	2974(5)	80(2)
	4107(4)	6936(4)	2100(5)	76(2)
C41	8905(3)	6552(4)	-3091(4)	66(2)
	3141(4)	6001(4)	7871(5)	77(2)
C42	8949(3)	8219(3)	-1563(5)	73(2)
	1284(3)	6438(3)	6277(5)	74(2)
C43	9955(3)	6462(3)	-606(5)	50(2)
	3028(4)	5175(3)	5342(5)	74(2)
C51	6716(4)	8670(3)	-2951(5)	64(2)
	2061(4)	9268(3)	6694(5)	71(2)
C52	5605(3)	8286(4)	-1648(5)	62(2)
	1368(4)	8351(3)	7878(5)	63(2)
C53	6674(4)	6891(3)	3365(5)	63(2)
	3374(4)	7930(4)	8346(5)	74(2)

^a Values of crystallographically different molecules **2a** and **2b** one below the other. Atoms refined using anisotropic displacement parameters are given in the form of their equivalent isotropic parameters, defined as one-third of the trace of the orthogonalized U tensor. Numbers in parentheses here and in Table 2 are estimated standard deviations in the least significant digit.

50 Hz at -80°C , thus indicating a slowing down of the fluctuation process with respect to the NMR time scale.

The product **2** will certainly not be formed from three components by a one-step mechanism. The head-tail cyclodimerization of **1**, well known to occur above ambient temperature,² is not likely to be possible at -60°C and would not give the B-B bond found in **2**. We therefore assume the formation of a three-membered ring **3** in a first step, analogous to the cited reaction of

(1) Paetzold, P.; Hahnfeld, D.; Englert, U.; Wojnoski, W.; Dreczewski, B.; Pawelec, Z.; Walz, L. *Chem. Ber.* **1992**, *125*, 1073.

(2) Boese, R.; Paetzold, P.; Tapper, A.; Ziembinski, R. *Chem. Ber.* **1989**, *122*, 1057.

(3) Ishikawa, M.; Kumada, M. *J. Organomet. Chem.* **1972**, *42*, 325.

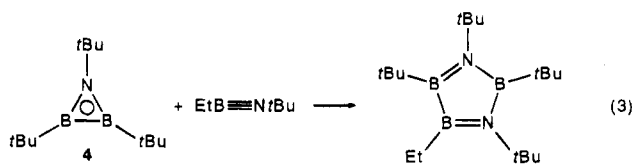
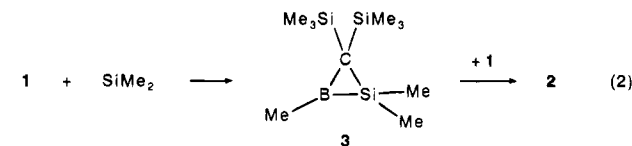
(4) Fink, M. J.; Michalczyk, M. J.; Haller, K. J.; West, R.; Michl, J. *Organometallics* **1984**, *3*, 793.

(5) Nöth, H.; Pommerening, H. *Chem. Ber.* **1981**, *114*, 3044.

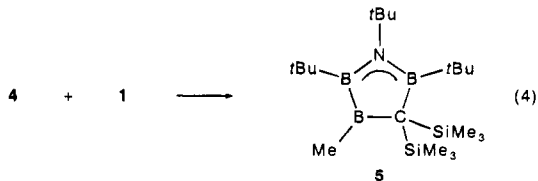
Table 2. Selected Bond Lengths (\AA) and Bond and Torsional Angles (deg) for $[-\text{B}(\text{Me})\text{B}(\text{Me})\text{C}(\text{SiMe}_3)_2\text{SiMe}_2\text{C}(\text{SiMe}_3)_2-]$ (Isomers **2a/2b)**

B3-B4	1.729(8)/1.709(9)	C2-Si2	1.913(4)/1.911(4)
B3-C2	1.570(6)/1.566(6)	C2-Si3	1.916(4)/1.918(4)
B4-C5	1.563(8)/1.582(8)	C5-Si5	1.930(4)/1.924(4)
C2-Si1	1.922(6)/1.913(6)	C5-Si4	1.896(5)/1.879(5)
C5-Si1	1.923(4)/1.921(4)	Si1-C5	1.880(5)/1.874(5)
B3-C3	1.578(9)/1.566(6)	Si1-C6	1.874(4)/1.888(4)
B4-C4	1.588(6)/1.582(8)		
C2-B3-B4	110.3(5)/110.4(5)	C2-B3-C8	127.1(5)/126.9(5)
C5-B4-B3	111.8(3)/111.1(5)	B3-B4-C9	121.8(5)/123.4(5)
B3-C2-Si1	101.7(3)/101.2(3)	C5-B4-C9	126.3(5)/125.5(5)
B4-C5-Si1	101.2(3)/100.3(3)	Si2-C2-Si3	108.0(2)/108.1(2)
C2-Si1-C5	103.4(2)/103.7(2)	Si4-C5-Si5	108.3(2)/108.3(2)
B4-B3-C8	122.6(4)/122.7(4)	C6-Si1-C7	100.1(2)/99.3(2)
C2-B3-B4-C5	-39.11(52)/-42.02(49)		
Si1-C2-B3-B4	27.52(39)/29.57(40)		
Si1-C5-B4-B3	26.75(44)/28.74(38)		
C8-B3-B4-C9	-42.25(68)/-43.43(66)		
B3-C2-Si1-C5	-11.42(33)/-11.83(30)		
B4-C5-Si1-C2	-9.62(34)/-10.49(20)		

t-BuB≡N*t*-Bu and SiMe₂. The product **2** is then formed by the addition of a second molecule of **1** to the B-Si bond of **3**, eq 2. The formation of a B-B bond during a kind of redox process is made possible by the higher electronegativity of boron as compared to that of silicon. This second step is related to the opening of the B-B bond of the three-membered ring **4** by the B-N triple bond of EtB≡N*t*-Bu,⁶ eq 3.



The assumed addition of **1** to **3** and the known addition of an iminoborane to **4** prompted us to try the addition of **1** to **4**. The 1:1 adduct **5** is isolated in a 81% yield as described in eq 4, and its structure is concluded from NMR spectra, which indicate three different B atoms, three nonequivalent *t*-Bu groups, but two equivalent SiMe₃ groups. It should be noted that the 3-methyl



derivative **5** cannot be distinguished by our NMR data from an isomeric 5-methyl derivative **5'**, which would be the product of the addition of **1** to one of the B-N bonds of **4**. The addition of EtC≡Cet,⁶ CO,⁷ BuN₃,⁷

(6) Paetzold, P.; Redenz-Stormanns, B.; Boese, R. *Chem. Ber.* **1991**, *124*, 2435.

(7) Paetzold, P.; Redenz-Stormanns, B.; Boese, R. *Angew. Chem., Int. Ed. Engl.* **1990**, *29*, 900.

(8) Paetzold, P.; Redenz-Stormanns, B.; Boese, R.; Bühl, M.; Schleyer, P. v. R. *Angew. Chem., Int. Ed. Engl.* **1990**, *29*, 1059.

Table 3. Crystallographic Data for 2

formula	C ₁₈ H ₄₈ B ₂ Si ₅
fw	426.6
space group	P1 (No. 2)
a, Å	16.648(5)
b, Å	17.073(4)
c, Å	11.490(3)
α, deg	102.79(2)
β, deg	104.80(2)
γ, deg	62.76(2)
V, Å ³	2786(2)
ρ _{calc} , g/cm ³	1.017
Z	4
F(000)	944
λ, Å	1.5418
μ(Cu Kα), cm ⁻¹	24.20
cryst dimens, mm	0.6 × 0.3 × 0.3
T, K	233
scan mode	omega
scan range, deg	5 < θ < 60
total data	6484
unique obs dat (I > 3σ(I))	5503
no. of variables	548
R, R _w [w ⁻¹ = σ(F _o) ²]	0.052, 0.076
max resid dens, e Å ⁻³	0.3

BH₃,⁸ etc. proceeds, however, across the B–B bond of **4**, which is certainly a weaker bond than one of the B–N bonds. Therefore, the isomer **5** is the more probable product.

Experimental Section

General Procedure. All manipulations of air-sensitive materials were carried out under a nitrogen atmosphere using standard Schlenk or vacuum line techniques.

Synthesis of 1,1,3,4-Tetramethyl-2,2,5,5-tetrakis(trimethylsilyl)-1-sila-3,4-diboracyclopentane (2). A solution of dodecamethylcyclohexasilane (0.70 g, 2.00 mmol) and a mixture of MeB=C(SiMe₃)₂ (1.70 g, 9.23 mmol) and HC(SiMe₃)₃ (0.43 g)² in 20 mL of pentane is photolyzed at –60 °C by means of a high-pressure mercury lamp for 20 h. Another portion of Si₆Me₁₂ (0.70 g) is added, and the photolysis is continued for 20 h. All volatile materials are removed in vacuo, finally at 60 °C/0.004 mbar. The remaining solid is sublimed at 90 °C/0.000 07 mbar. Recrystallization at –30 °C from pentane gives **2** (1.51 g, 77%) as colorless crystals. ¹H NMR (499.84 MHz, CDCl₃): δ 0.16, 0.51, 1.18 (3 s in the ratio 6:1:1). ¹¹B NMR (164.36 MHz, CDCl₃): δ 94.8. ¹³C NMR (125.70 MHz, CDCl₃): δ 5.8 (q, SiMe₃), 7.7 (q, SiMe₂), 15.4 (br, BMe), ca. 39 (br, C_{ring}, sharp signal at δ 39.4 on cooling down to –80 °C in

THF-d₈). MS (MAT 95, Finnigan MAT): calcd for ¹²C₁₈¹H₄₈-¹¹B₂²⁸Si₅ 426.2789, found 426.2773.

X-ray Structure Determination of 2. Geometry and intensity data were collected on an Enraf-Nonius CAD4 diffractometer with Cu Kα radiation (1.5418 Å, graphite monochromator). A summary of crystallographic data, data collection parameters, and refinement parameters is given in Table 3. Metric reduction of the observed triclinic unit cell to a monoclinic C-centered cell could not be achieved within reasonable tolerances. An empirical absorption correction was applied using the program DIFABS.⁹ The structure was solved by Direct methods with SHELXS-86¹⁰ and refined with the SDP system.¹¹ All hydrogen atoms could be located in difference Fourier syntheses. In the final full-matrix refinement, nonhydrogen atoms were refined with anisotropic thermal parameters, and hydrogen atoms were included with refined isotropic displacement parameters and fixed coordinates. In order to maintain an acceptable ratio between observations and variables, no attempt was made to refine the positional parameters of the H atoms.

Synthesis of 1,2,5-Tri-tert-butyl-3-methyl-4,4-bis(trimethylsilyl)-1-aza-2,3,5-triboracyclopentane (5). A solution of tri-tert-butylazadiboriridine (1.51 g, 7.26 mmol) (**4**)¹² is added at –78 °C to a mixture of MeB=C(SiMe₃)₂ (0.74 g, 4.02 mmol) and HC(SiMe₃)₃ (0.185 g)² in 10 mL of pentane. The solution is slowly brought to ambient temperature, and stirring is continued for 48 h. After all volatiles are removed, finally at 50 °C/0.002 mbar, the product **5** (1.28 g, 81%) is obtained by sublimation at 100 °C/0.002 mbar. ¹H NMR (60 MHz, CDCl₃): δ 0.21, 0.87, 1.14, 1.17 (4 s in the ratio 6:1:3:3). ¹¹B NMR (332.08 MHz, CDCl₃): δ 58.6, 67.8, 101.7 (1:1:1). ¹³C NMR (67.28 MHz, CDCl₃): δ 5.3 (q, SiMe₃), 13.4 (br, BMe), 30.1, 31.8, 33.7 (3 q, t-Bu), 55.6 (NC). Anal. Calcd for C₂₀H₄₈-NB₃Si₂: C, 61.40; H, 12.37; N, 3.58. Found: C, 60.41; H, 12.31; N, 3.20.

Supplementary Material Available: Complete tables of H atom parameters, bond distances, bond angles, torsional angles, and anisotropic thermal parameters for **2a** and **2b** (16 pages). Ordering information is given on any current masthead page.

OM940804L

(9) Walker, N.; Stuart, D. *Acta Crystallogr.* **1983**, *A39*, 158.

(10) Sheldrick, G. M. *SHELXS-86, Program for Crystal Structure Solution*; University of Göttingen, Göttingen, Germany, 1986.

(11) Frenz, B. A. *Enraf-Nonius SDP*, Version 5.0; Delft, The Netherlands, 1988.

(12) Boese, R.; Kröckert, B.; Paetzold, P. *Chem. Ber.* **1987**, *120*, 1913.

Selectivity for Hydrogenation or Hydroformylation of Olefins by Hydridopentacarbonylmanganese(I) in Supercritical Carbon Dioxide

Philip G. Jessop, Takao Ikariya, and Ryoji Noyori*,†

ERATO Molecular Catalysis Project, Research Development Corporation of Japan,
1247 Yachigusa, Yakusa-cho, Toyota 470-03, Japan

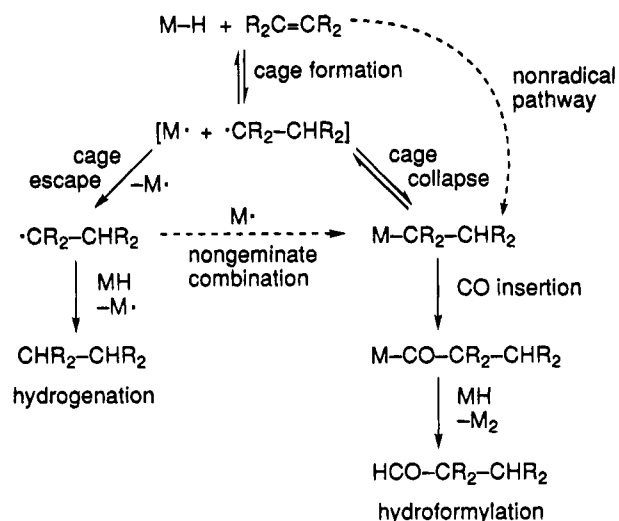
Received July 19, 1994[®]

Summary: The stoichiometric and catalytic hydrogenation and hydroformylation of activated olefins by $MnH(CO)_5$ are generally believed to proceed by a free radical caged pair mechanism, the selectivity of which is affected by solvent. However, the stoichiometric reaction with a test olefin in supercritical CO_2 ($scCO_2$), with its low viscosity, gives a selectivity for hydrogenation almost identical to that found in alkanes or without solvent. Aside from the possibility of coincidentally equal cage strengths, the most likely explanation is that the aldehydes are primarily formed by nonradical pathways which are independent of solvent viscosity.

Introduction

Recent reports of homogeneous catalytic hydrogenation^{1,2} and hydroformylation^{3,4} reactions in supercritical carbon dioxide ($scCO_2$) are examples of what should become a very important new field: homogeneous catalysis in supercritical fluids (SCF). As a medium for chemical reactions, $scCO_2$ has many practical advantages such as ease of separation of products, and it lacks many of the undesirable properties of liquid solvents such as flammability, solvent residues, and disposal costs. Among the chemical advantages^{5,6} are the very high concentrations of dissolved gases possible in SCF.^{1,7-9} Because of the latter advantage, homogeneous hydrogenation and hydroformylation in such fluids are likely to be particularly important in the future. However, altered rates or selectivities compared to those in liquid solvents may be observed because of the unusual physical properties of $scCO_2$. For example, hydrogenation and hydroformylation reactions of some metal carbonyls are believed to have radical pair mechanisms (Scheme 1) and cage effect-controlled selectivities.¹⁰⁻¹⁴ $scCO_2$, with its very low viscosity, may have weaker cage effects than liquid solvents.⁶

Scheme 1. Free Radical Mechanism Proposed for Hydrogenation and Hydroformylation of Olefins by $MnH(CO)_5$ and Related Complexes^{a,11,24}



^a Alternative nongeminate and nonradical routes are indicated by dashed arrows.

Comparisons of the cage effects in $scCO_2$ versus liquid solvents are rare in the literature. DeSimone et al.^{15,16} reported that the initiation efficiency f of AIBN for radical polymerization in $scCO_2$ was 1.5 times higher than in benzene, suggesting a weaker cage effect. The distribution of products from the photolysis of unsymmetrical dibenzyl ketones in liquid solvents¹⁷ and in $scCO_2$ ¹⁸ shows no evidence of cage effects, while the results in inclusion complexes show significant cage effects.¹⁹ Otto et al.^{20,21} found that the quantum yield of the photolysis of I_2 in near-critical liquid CO_2 at 346 atm is comparable to the value in liquid heptane at lower pressures, suggesting comparable cage effects despite the lower viscosity of CO_2 . Reactions which are

† Permanent address: Department of Chemistry, Nagoya University, Chikusa, Nagoya 464-01, Japan.

[®] Abstract published in *Advance ACS Abstracts*, February 1, 1995.

(1) Jessop, P. G.; Ikariya, T.; Noyori, R. *Nature* **1994**, *368*, 231-233.

(2) Jessop, P. G.; Hsiao, Y.; Ikariya, T.; Noyori, R. *J. Am. Chem. Soc.* **1994**, *116*, 8851-8852.

(3) Rathke, J. W.; Klingler, R. J.; Krause, T. R. *Organometallics* **1991**, *10*, 1350-1355.

(4) Rathke, J. W.; Klingler, R. J.; Krause, T. R. *Organometallics* **1992**, *11*, 585-588.

(5) Boock, L.; Wu, B.; LaMarca, C.; Klein, M.; Paspek, S. *CHEMTECH* **1992**, *22*, 719-723.

(6) Subramaniam, B.; McHugh, M. A. *Ind. Eng. Chem. Process Des. Dev.* **1986**, *25*, 1-12.

(7) Howdle, S. M.; Poliakov, M. *J. Chem. Soc., Chem. Commun.* **1989**, 1099-1101.

(8) Howdle, S. M.; Healy, M. A.; Poliakov, M. *J. Am. Chem. Soc.* **1990**, *112*, 4804-4813.

(9) Tsang, C. Y.; Street, W. B. *Chem. Eng. Sci.* **1981**, *36*, 993-1000.

(10) Nalesnik, T. E.; Orchin, M. *Organometallics* **1982**, *1*, 222-223.

(11) Sweany, R. L.; Halpern, J. *J. Am. Chem. Soc.* **1977**, *99*, 8335-8337.

(12) Wassink, B.; Thomas, M. J.; Wright, S. C.; Gillis, D. J.; Baird, M. C. *J. Am. Chem. Soc.* **1987**, *109*, 1995-2002.

(13) Feder, H. M.; Halpern, J. *J. Am. Chem. Soc.* **1975**, *97*, 7186-7188.

(14) Halpern, J. *Pure Appl. Chem.* **1979**, *51*, 2171-2182.

(15) DeSimone, J. M.; Guan, Z.; Elsbernd, C. S. *Science* **1992**, *257*, 945-947.

(16) Guan, Z.; Combes, J. R.; Menciloglu, Y. Z.; DeSimone, J. M. *Macromolecules* **1993**, *26*, 2663-2669.

(17) Robbins, W. K.; Eastman, R. H. *J. Am. Chem. Soc.* **1970**, *92*, 6077-6079.

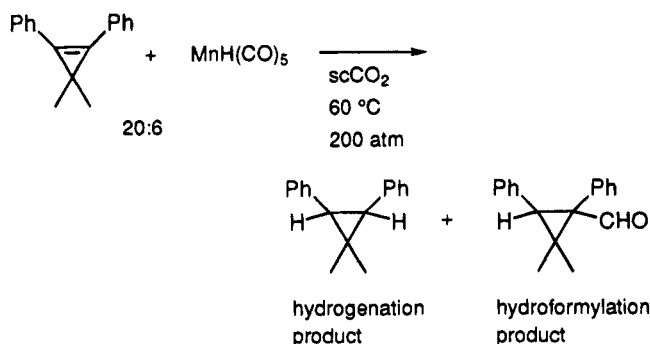
(18) O'Shea, K. E.; Combes, J. R.; Fox, M. A.; Johnston, K. P. *Photochem. Photobiol.* **1991**, *54*, 571-576.

(19) Rao, B. N.; Turro, N. J.; Ramamurthy, V. *J. Org. Chem.* **1986**, *51*, 460-464.

(20) Otto, B.; Schroeder, J.; Troe, J. *J. Chem. Phys.* **1984**, *81*, 202-213.

(21) Luther, K.; Schroeder, J.; Troe, J.; Unterberg, U. *J. Phys. Chem.* **1980**, *84*, 3072-3075.

Scheme 2. Test Reaction of MnH(CO)₅ with 3,3-Dimethyl-1,2-diphenylcyclopropene



much slower than the rate of cage escape are independent of cage effects and solvent viscosity.²² It is therefore not clear whether liquid solvents and SCF have differing cage effects or whether such differences could result in differing selectivities.

The existence of the radical pair mechanism (Scheme 1) has been demonstrated for the stoichiometric hydrogenation of olefins with MnH(CO)₅ by observation of CIDNP emissions for the hydrogenated products.^{11,12,23} CIDNP absorptions for the hydrometalated intermediates^{12,23,24} suggest, though not convincingly, a radical pair mechanism for hydroformylation by the same reagent. Such evidence does not establish the predominance of these mechanisms over nonradical pathways, but this predominance has on occasion been assumed. The stoichiometric reaction of MnH(CO)₅ with 3,3-dimethyl-1,2-diphenylcyclopropene at 60 °C (Scheme 2) was chosen as a test of the selectivity in scCO₂, because the selectivity of the reaction in liquid solvents is almost evenly split between hydrogenation and hydroformylation.^{23,24} Previous studies²³⁻²⁵ of this reaction in solution showed that the selectivity for hydrogenation was lower in micelle-containing solutions than in hexane or pentane, a difference which was attributed to a stronger cage effect in the former solutions. Importantly, these earlier studies also established that the selectivity is unchanged whether the reaction is performed under CO or argon.

Experimental Section

Materials. The preparation of 3,3-dimethyl-1,2-diphenylcyclopropene was performed by the published method,²⁶ after which the crude product was heated to 45 °C for 1.5 h under strong vacuum to remove unreacted 1-phenylpropyne. The desired product was the first fraction obtained by column chromatography (silica gel, hexane eluent) of the remaining liquid. MnH(CO)₅ was obtained by the literature method.²⁷

Safety Warning. Operators of high-pressure equipment such as that required for the following experiments should take proper precautions, including but not limited to the use of blast

shields and pressure relief mechanisms, to minimize the risk of personal injury. The cooling of the reactor may cause weakening of the vessel walls. The use of liquid nitrogen for this purpose should be avoided.

Reactions in scCO₂. The solubility of the olefin (3×10^{-4} mol) in scCO₂ was confirmed by visual inspection using a 50-mL reactor equipped with windows; at room temperature and normal pressure the liquid was clearly visible, while at 60 °C and 200 atm of CO₂ none could be seen. An equivalent test with 2×10^{-3} mol of MnH(CO)₅ had the same result. The qualitative solubility of MnH(CO)₅ in scCO₂ has already been reported.²⁸

Reactions were performed in 50-mL unlined stainless steel reactors manufactured by JASCO. Before each reaction, the reactor was dried at 70 °C and cooled to room temperature under strong vacuum. The 3,3-dimethyl-1,2-diphenylcyclopropene (66 mg, 3×10^{-4} mol) was placed in the reactor, which was then reevacuated and filled with argon to a slight positive pressure. The MnH(CO)₅ complex (0.11 mL, 1×10^{-3} mol) was injected by syringe through a threaded opening in the top of the reactor, which was plugged at all other times. CO₂ was introduced by pumping from a cooled (-5 °C) reservoir by an HPLC pump, after which the reactor was heated to 60 °C for 4 h. The total pressure at the reaction temperature was ca. 200 atm. A magnetic stir bar was used to encourage solubilization and mixing; variation of the stir rate had no effect on the selectivity or yield. An alternative method involved heating the olefin in the reactor to 60 °C under 1 atm of argon before adding the Mn complex and then CO₂ pressure. The results obtained by the two methods were identical.

After the expiration of the desired reaction time, the reactor was cooled with acetone/dry ice to constant pressure. The remaining pressure was vented and the reactor thawed. CDCl₃ solutions of the products were passed through a short column of silica gel (CDCl₃ as eluent) to remove insoluble Mn products, before being analyzed by ¹H NMR spectroscopy. The spectral data of the products have been reported.²³ Complete conversion of the olefin was observed. From the integrals, product ratios were calculated. The experiment in scCO₂ was performed six times in order to measure the scatter, and the highest and lowest values were rejected, the mean percent hydrogenation not being significantly altered by such rejection. The standard deviation of the percent hydrogenation was 3.4. The experiment under 5 atm of CO₂ without solvent was performed once.

In order to determine the dependence of selectivity on the MnH(CO)₅ concentration, a series of experiments were performed at a lower concentration of olefin and several concentrations of the complex. However, problems of NMR signal broadening were encountered at high concentrations of Mn, so a slightly different method of analysis was adopted for this series. The Mn products were removed or solubilized by stirring the CDCl₃ products with dilute aqueous HCl, separating, drying with K₂CO₃, and then analyzing as before by NMR spectroscopy. Tests showed that this method does not alter the observed selectivity. The mass balance was confirmed ($\geq 90\%$ recovery of organic products) by adding 1,2-dichloroethane as an internal standard immediately after the reaction.

Results and Discussion

At 60 °C, the selectivity for hydrogenation in scCO₂ (200 atm) or neat under 5 atm of CO₂ was the same as or slightly higher than that reported for hexane and pentane, and considerably higher than that found in micellar solution (Table 1).

As mentioned in the Introduction, metal carbonyl hydrides such as CoH(CO)₄ and MnH(CO)₅ are generally believed to catalytically and stoichiometrically hydro-

(28) Clarke, M. J.; Howdle, S. M.; Jobling, M.; Poliakov, M. *Inorg. Chem.* **1993**, *32*, 5643-5644.

(22) Brennecke, J. F. In *Supercritical Fluid Engineering Science: Fundamentals and Applications*; Kiran, E., Brennecke, J. F., Eds.; ACS Symposium Series 514; American Chemical Society: Washington, DC, 1993; Chapter 16, pp 201-219.

(23) Nalesnik, T. E.; Orchin, M. *J. Organomet. Chem.* **1981**, *222*, C5-C8.

(24) Nalesnik, T. E.; Freudenberger, J. H.; Orchin, M. *J. Organomet. Chem.* **1982**, *236*, 95-100.

(25) Matsui, Y.; Orchin, M. *J. Organomet. Chem.* **1983**, *244*, 369-373.

(26) Friedrich, L. E.; Fiato, R. A. *Synthesis* **1973**, 611-612.

(27) McNeill, E. A.; Scholer, F. R. *J. Am. Chem. Soc.* **1977**, *99*, 6243-6249.

Table 1. Reactions of $\text{MnH}(\text{CO})_5$ with 3,3-Dimethyl-1,2-diphenylcyclopropene

solvent	gas (pressure, atm)	[Mn]/[olefin], mM	temp, °C	time, h	selectivity, % (cis:trans)	
					alkane	aldehyde
hexane ²³	CO	3200/1100	55	5	66 (7:1)	34 (7:1)
pentane ²⁴	Ar or CO	89/87	60	2–4	63 (7:1)	37 (7:1)
micelle ²⁵	CO	8/2	50	15	8 (only cis)	92 (6:1)
none	CO ₂ (5)	20/6	60	4	66 (5:1)	34 (mostly cis) ^a
scCO ₂	CO ₂ (200)	20/6	60	3.5	66 (6:1)	34 (mostly cis) ^a
scCO ₂	CO ₂ (236)	18/6	35	16	61 (4:1)	39 (15:1)

^a The trans hydroformylation product was observed in very small amounts, so that accurate cis:trans ratios could not be determined.

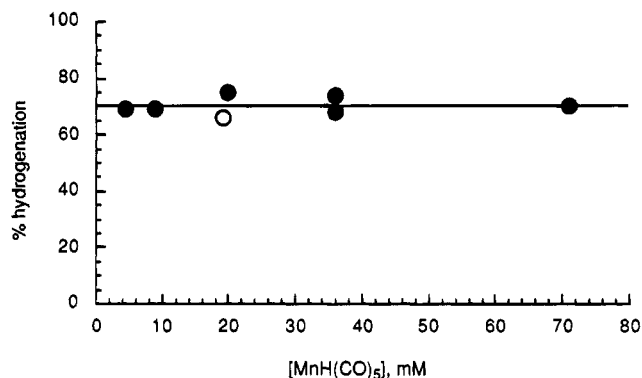
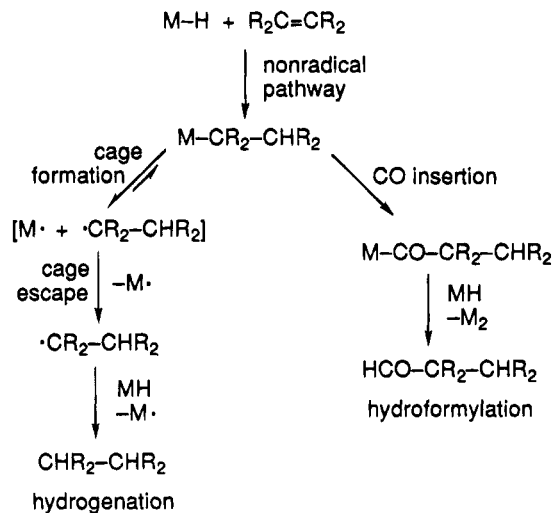


Figure 1. Dependence of the selectivity for hydrogenation on the concentration of $\text{MnH}(\text{CO})_5$ in 200–230 atm of scCO_2 at 60 °C, 1.6 mM olefin. The open circle shows the result at 6 mM olefin.

genate and hydroformylate activated olefins by radical mechanisms.^{10–14} The product-determining steps are escape from the radical cage, leading to hydrogenation, competing with collapse of the radical cage, leading to hydroformylation (Scheme 1). Additional hydroformylation could occur if the escaped alkyl radical encounters a metal complex radical before it reacts with a metal hydride; this process is nongeminate radical combination. If the cage escape and cage collapse processes have comparable rates, then a weaker cage effect in scCO_2 should increase the selectivity for hydrogenation. However, we found that reactions with scCO_2 as a solvent had essentially the same selectivity as that with no solvent under 5 atm of CO_2 and those^{23,24} with hexane or pentane (Table 1). Thus, the selectivity for hydrogenation in scCO_2 is comparable to that in hydrocarbons, despite the greater diffusivity of the supercritical phase. It is possible that the cage effects are coincidentally identical in all of these media. Perhaps it is more likely that the observed selectivity of 66% hydrogenation represents that to be found in the absence of a significant cage effect. The aldehydes must then be formed mostly by nongeminate combination or nonradical²⁹ pathways (Scheme 1). The possibility of nongeminate combination was eliminated by determining the dependence of the selectivity on the concentration of $\text{MnH}(\text{CO})_5$ (Figure 1). If nongeminate combination had been significant, one would have observed a saturation-type curve,³⁰ with concentration-dependent selectivity for hydrogenation at low concentrations and constant selectivity at high concentrations of the complex. The observed independence of the selectivity on concentra-

Scheme 3. Mechanism Consistent with the Observations



tion allows us to reject the nongeminate pathway.³¹ We are thus left with two pathways to aldehyde formation: the cage collapse and the nonradical routes. It is possible that both pathways operate, the cage collapse pathway being favored in viscous media (Scheme 1). The selectivity could also be determined by a competition between homolysis and CO insertion reactions of the metal alkyl complex, which would be formed by a nonradical pathway (Scheme 3).³¹ If the geminate recombination of M^\cdot and $\cdot\text{CR}_2\text{CHR}_2$ occurs to some extent, then this would account for both the CIDNP results and the dependence of selectivity on the medium.

It is only possible to roughly estimate whether a cage effect should have been expected. Although calculations have not been made for scCO_2 , the lifetime of the solvent cage has been estimated to be on the order of picoseconds for other SCF.³² This is too short to be an effective cage for all but the very fastest reactions. The rate of the geminate recombination reaction in the present system is not known, but it should be at least as fast³³ as the rates of the self-dimerizations of $\text{Mn}(\text{CO})_5$ or alkyl radicals (second-order rate constants $\sim 1 \times 10^9 \text{ M}^{-1} \text{ s}^{-1}$).^{33,34} Thus, the rate of reaction of the alkyl radical with the $\text{Mn}(\text{CO})_5$ radical must be close to the diffusion limit in liquid solvents but would have to be a few orders of magnitude faster in order to be affected by the cage of a SCF.

(31) Examination of the dependence of selectivity on $\text{MnH}(\text{CO})_5$ concentration was suggested by a reviewer. We also appreciate the comments suggesting Scheme 3.

(32) Petsche, I. B.; Debenedetti, P. G. *J. Chem. Phys.* **1989**, *91*, 7075–7084.

(33) Ingold, K. U. In *Free Radicals*; Kochi, J. K., Ed.; John Wiley and Sons: New York, 1973; Vol. 1, Chapter 2, pp 37–112.

(34) Baird, M. C. *Chem. Rev.* **1988**, *88*, 1217–1227.

(29) Treichel, P. M. In *Comprehensive Organometallic Chemistry*; Wilkinson, G., Stone, F. G. A., Abel, E. W., Eds.; Pergamon Press: Oxford, 1982; Vol. 4, Chapter 29, pp 1–159.

(30) (a) Jacobsen, E. N.; Bergman, R. G. *J. Am. Chem. Soc.* **1985**, *107*, 2023–2032. (b) Hammond, G. S.; Sen, J. N.; Boozer, C. E. *J. Am. Chem. Soc.* **1955**, *77*, 3244–3248.

The effect of clustering near the critical point of a SCF has been greatly discussed,³⁵⁻³⁷ but the effect is reportedly strongest near the critical point. The conditions of the reactions in Table 1 are too far from the critical point to exhibit significant clustering effects.

The selectivity for cis rather than trans hydrogenation products is similar in scCO₂, neat, and hydrocarbon solutions. However, the trans hydroformylation product was barely detectable in our experiments. In all media, the cis products are preferred for both hydrogenation and hydroformylation. The reason for the preference for cis addition is not known, but steric approach control^{38,39} seems likely. This idea assumes that steric effects acting in an early transition state would direct

the entering reagent to the less hindered trans position.

An experiment at 35 °C in scCO₂ was considerably slower, giving 15% conversion after 16 h. The selectivity for hydrogenation was only slightly lower.

In conclusion, identical selectivities for the stoichiometric reaction of MnH(CO)₅ with the test olefin have been found in three media, hexane, neat olefin, and scCO₂, suggesting that cage effects are either coincidentally identical or that the aldehydes are primarily formed by nonradical pathways (Scheme 3). The cage collapse and nonradical pathways could be in competition, with viscous media favoring the former. Nongeminate radical combination pathways are not significant under the conditions tested. By analogy to the present results, cage effects are not expected to be a factor in catalytic hydrogenations or hydroformylations by carbonyl catalysts in scCO₂.

OM940573I

(35) Ikushima, Y.; Saito, N.; Arai, M. *J. Phys. Chem.* **1992**, *96*, 2293-2297.

(36) Ellington, J. B.; Brennecke, J. F. *J. Chem. Soc., Chem. Commun.* **1993**, 1094-1095.

(37) Combes, J. R.; Johnston, K. P.; O'Shea, K. E.; Fox, M. A. In *Supercritical Fluid Technology*; Bright, F. V., McNally, M. E. P., Eds.; ACS Symposium Series 488; American Chemical Society: Washington, DC, 1992; Chapter 3, pp 31-47.

(38) Dauben, W. G.; Fonken, G. J.; Noyce, D. S. *J. Am. Chem. Soc.* **1956**, *78*, 2579-2582.

(39) Skell, P. S.; Allen, R. G. *J. Am. Chem. Soc.* **1958**, *80*, 5997-6000.

Synthesis and X-ray Structure of $[(\eta^5\text{-C}_5\text{H}_5)\text{Fe}(\text{CO})\text{C}(\text{O})\text{Me}](\mu\text{-}\eta^1\text{:}\eta^1\text{-dppe})[(\eta^4\text{-exo-MeC}_5\text{H}_5)\text{Fe}(\text{CO})_2]$

Lung-Shiang Luh and Ling-Kang Liu*

*Institute of Chemistry, Academia Sinica, Nankang, Taipei, Taiwan 11529, ROC, and
 Department of Chemistry, National Taiwan University, Taipei, Taiwan 10767, ROC*

Received August 22, 1994[⊗]

Summary: The 1:1 mixture of $(\eta^5\text{-C}_5\text{H}_5)\text{Fe}(\text{CO})_2\text{I}$ and $(\eta^5\text{-C}_5\text{H}_5)\text{Fe}(\text{CO})\text{C}(\text{O})\text{Me}(\eta^1\text{-dppe})$ in THF reacts with MeLi at -78°C to produce a novel complex $[(\eta^5\text{-C}_5\text{H}_5)\text{Fe}(\text{CO})\text{C}(\text{O})\text{Me}](\mu\text{-}\eta^1\text{:}\eta^1\text{-dppe})[(\eta^4\text{-MeC}_5\text{H}_5)\text{Fe}(\text{CO})_2]$ in which a dppe links two isomeric, methylated $[(\text{C}_5\text{H}_5)\text{Fe}(\text{CO})_2]$ units, one end being in the form of $(\eta^5\text{-C}_5\text{H}_5)\text{Fe}(\text{CO})\text{C}(\text{O})\text{Me}$ and the other end in the form of $(\eta^4\text{-exo-MeC}_5\text{H}_5)\text{Fe}(\text{CO})_2$. The X-ray structure of the title complex exhibits a dppe-bridged unsymmetrical pseudooctahedral Fe(II) / pseudosquare pyramidal Fe(0) complex without any metal–metal bonding. The embedded structural parameters of Fe(II) and Fe(0) centers give evidence of an Fe(II) smaller than Fe(0), as suggested by the Fe(II)–P length of 2.178(2) Å simultaneously present with that of Fe(0)–P, 2.212(1) Å. The shortening of 0.034 Å is significant as it represents a difference greater than 10 ESDs.

Introduction

The diphosphine $\text{Ph}_2\text{P}(\text{CH}_2)_2\text{PPh}_2$ (dppe) has been regarded as a very good chelating ligand.¹ Nevertheless, it is employed in this study as a bridging ligand to provide one of its PPh₂ groups in assisting the methyl migratory insertion reaction of $(\eta^5\text{-C}_5\text{H}_5)\text{Fe}(\text{CO})_2\text{Me}^2$ and the other PPh₂ in bringing up the ring alkylation reaction with $(\eta^5\text{-C}_5\text{H}_5)\text{Fe}(\text{CO})_2\text{I}$ and MeLi,³ the ring methylation being a reverse in polarity—the $(\eta^5\text{-C}_5\text{H}_5)$ ligand of the iodide becomes the center for Me[−] nucleophilic addition.

Results and Discussion

$(\eta^5\text{-C}_5\text{H}_5)\text{Fe}(\text{CO})_2\text{Me}$ is known to proceed with a PR₃-assisted methyl migratory insertion to yield $(\eta^5\text{-C}_5\text{H}_5)\text{Fe}(\text{CO})\text{C}(\text{O})\text{Me}(\text{PR}_3)$.² Accordingly, the unidentate complex $(\eta^5\text{-C}_5\text{H}_5)\text{Fe}(\text{CO})\text{C}(\text{O})\text{Me}(\eta^1\text{-dppe})$ (**1**) has been prepared by reacting $(\eta^5\text{-C}_5\text{H}_5)\text{Fe}(\text{CO})_2\text{Me}$ with dppe in 1:1 molar ratio to give both the unidentate product **1** (38%) and the bridging product $[(\eta^5\text{-C}_5\text{H}_5)\text{Fe}(\text{CO})\text{C}(\text{O})\text{Me}]_2(\mu\text{-}\eta^1\text{:}\eta^1\text{-dppe})$ (**2**; 49%). Since complex **1** is an intermediate to give complex **2**, the reaction of $(\eta^5\text{-C}_5\text{H}_5)\text{Fe}(\text{CO})_2\text{Me}$ with dppe in 2:1 molar ratio easily proceeds to complex **2**.

The elaboration of the acetyl Me group in $(\eta^5\text{-C}_5\text{H}_5)\text{Fe}(\text{CO})\text{C}(\text{O})\text{Me}(\text{PPh}_3)$ by the nucleophile–electrophile sequence is of much use in organic synthesis,^{4–6} taking

advantage of the chiral Fe center. With similar bonding on the half-sandwich Fe center, the unidentate complex **1** had been expected to proceed with a deprotonation by MeLi, producing the anionic intermediate $(\eta^5\text{-C}_5\text{H}_5)\text{Fe}(\text{CO})(\eta^1\text{-dppe})\text{C}(\text{O})\text{CH}_2^-$ to receive an electrophile, e.g., $(\eta^5\text{-C}_5\text{H}_5)\text{Fe}(\text{CO})_2\text{I}$, in this study. Treating complex **1** with MeLi and then trapping with $(\eta^5\text{-C}_5\text{H}_5)\text{Fe}(\text{CO})_2\text{I}$ in sequence produced very complex Fe-containing species which were not resolved.

The reaction of equal amounts of $(\eta^5\text{-C}_5\text{H}_5)\text{Fe}(\text{CO})_2\text{I}$ and MeLi in the presence of 1 equiv of unidentate complex **1** at -78°C followed the reaction pattern reported earlier³ and gave a novel complex $(\eta^5\text{-C}_5\text{H}_5)\text{Fe}(\text{CO})\text{C}(\text{O})\text{Me}(\mu\text{-}\eta^1\text{:}\eta^1\text{-dppe})(\eta^4\text{-MeC}_5\text{H}_5)\text{Fe}(\text{CO})_2$ (**3**; 76%) that has been characterized with IR, NMR, melting point, MS, elemental analysis, and X-ray crystallography.

The molecular connectivity of **3** was readily derived from the spectroscopic data: the IR ν_{CO} bands of 1910 and 1603 cm^{-1} and ³¹P NMR chemical shift of δ 75.9 are typical of $(\eta^5\text{-C}_5\text{H}_5)\text{Fe}(\text{CO})\text{C}(\text{O})\text{Me}$ linked to dppe as exhibited in **1** and **2**. On the other hand, the IR ν_{CO} bands of 1963 and 1910 (overlapping) cm^{-1} , ³¹P NMR chemical shift of δ 70.3 and ¹H NMR shifts at δ 4.88, 2.62, and 2.11 (integration 2:1:2) are indicative of the presence of a $(\eta^4\text{-RC}_5\text{H}_5)\text{Fe}(\text{CO})_2(\text{PR}'_3)$ fragment in **3** as well, in good comparison with $(\eta^4\text{-MeC}_5\text{H}_5)\text{Fe}(\text{CO})_2(\text{PPh}_3)$ ³, which shows relevant IR ν_{CO} bands of 1964 and 1904 cm^{-1} , chemical shifts at δ 73.2 (³¹P) and 5.03, 2.72, and 2.41 (¹H, integration 2:1:2). Thus, for the first time a dppe linking two isomeric, methylated $[(\text{C}_5\text{H}_5)\text{Fe}(\text{CO})_2]$ units was obtained, one end in the form of $(\eta^5\text{-C}_5\text{H}_5)\text{Fe}(\text{CO})\text{C}(\text{O})\text{Me}$ and the other end in the form of $(\eta^4\text{-MeC}_5\text{H}_5)\text{Fe}(\text{CO})_2$.

In the absence of phosphines, the electrophile $\text{Fe}(\text{CO})_2\text{I}$ is known to react with nucleophilic MeLi to give $(\eta^5\text{-C}_5\text{H}_5)\text{Fe}(\text{CO})_2\text{Me}$,⁷ where the halide exchange is indirect: the electrophile $(\eta^5\text{-C}_5\text{H}_5)\text{Fe}(\text{CO})_2\text{I}$ initially receives RLi at the coordinated CO site rather than the Fe center or the $(\eta^5\text{-C}_5\text{H}_5)$ ligand,⁸ followed by Fe–I bond cleavage and CO deinsertion. A neutral $(\eta^5\text{-C}_5\text{H}_5)\text{Fe}$ skeleton is resistive to modification in the η^5 -bonding.⁹ If a $(\eta^5\text{-C}_5\text{H}_5)$ ligand is the site of reaction, RLi usually deprotonates the $(\eta^5\text{-C}_5\text{H}_5)$ ring, evidenced

(4) (a) Davies, S. G. *Organotransition Metal Chemistry: Applications to Organic Synthesis*; Pergamon: Oxford, U.K., 1982. (b) Davies, S. G. *Aldrichim. Acta* **1990**, 23, 31, and references within.

(5) For practical preparation of optical chiral auxiliaries: Case-Green, S. C.; Costello, J. F.; Davies, S. G.; Heaton, N.; Hedgecock, C. J. R.; Prime, J. C. *J. Chem. Soc., Chem. Commun.* **1993**, 1621.

(6) Libeskind, L. S.; Welker, M. E.; Fengl, R. W. *J. Am. Chem. Soc.* **1986**, 108, 6328.

(7) (a) Piper, T. S.; Wilkinson, G. *J. Inorg. Nucl. Chem.* **1956**, 3, 104. (b) Li, H.-j.; Turnbull, M. M. *J. Organomet. Chem.* **1991**, 419, 245.

(8) Wong, A.; Pawlick, R. V.; Thomas, C. G.; Leon, D. R.; Liu, L.-K. *Organometallics* **1991**, 10, 530.

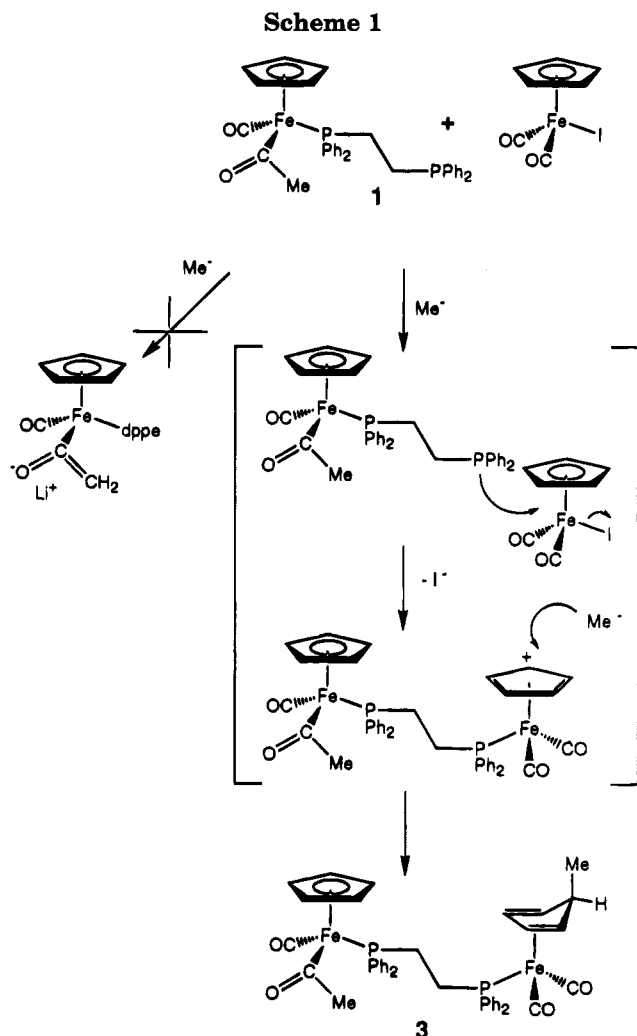
* To whom correspondence should be addressed at Academia Sinica.

⊗ Abstract published in *Advance ACS Abstracts*, January 15, 1995.

(1) Cotton, F. A.; Wilkinson, G., Eds. *Advanced Inorganic Chemistry*, 5th ed.; Wiley: New York, 1988; Section 2.4.

(2) (a) Bibler, J. P.; Wojciki, A. *Inorg. Chem.* **1966**, 5, 889. (b) Butler, I. S.; Basolo, F.; Pearson, R. G. *Inorg. Chem.* **1967**, 6, 2074. (c) Green, M.; Westlake, D. J. *J. Chem. Soc. A* **1971**, 367.

(3) (a) Luh, L.-S.; Liu, L.-K. *Bull. Inst. Chem., Acad. Sin.* **1994**, 41, 39. (b) Liu, L.-K.; Luh, L.-S. *Organometallics* **1994**, 13, 2816. (c) Liu, L.-K.; Luh, L.-S.; Eke, U. B. *Organometallics*, in press.



by the RLi-induced migration reactions of $(\eta^5\text{-C}_5\text{H}_5)\text{Fe}(\text{CO})_2\text{E}$ (E = alkyl, silyl, germyl, stannyl, etc.) being transferred from Fe–E to $(\eta^5\text{-C}_5\text{H}_4\text{-E})$.^{10,11} In the presence of PPh_3 , however, $(\eta^5\text{-C}_5\text{H}_5)\text{Fe}(\text{CO})_2\text{I}$ is reduced by RLi via the cationic intermediate $[(\eta^5\text{-C}_5\text{H}_5)\text{Fe}(\text{CO})_2(\text{PPh}_3)]^+$, which is more electrophilic toward RLi, to produce $(\eta^4\text{-exo-RC}_5\text{H}_5)\text{Fe}(\text{CO})_2(\text{PPh}_3)$.³ Within reasonable extension, Scheme 1 is a plausible mechanism toward the preparation of **3**—the dangling PPh_2 group of **1** coordinates to $(\eta^5\text{-C}_5\text{H}_5)\text{Fe}(\text{CO})_2\text{I}$ to first form a cationic intermediate that is attacked by MeLi , the methylation of $(\eta^5\text{-C}_5\text{H}_5)$ occurring *via* an *exo* direction, which is consistent with the results of an X-ray structure analysis. Figure 1 shows the ORTEP plot of the molecule in which an *exo*-Me group is seen on the cyclopentadiene ring, indicating retrochemically no Fe mediation.

Shown in Figure 1, dppe is a bridging ligand. To the best of our knowledge, the compound is the first to

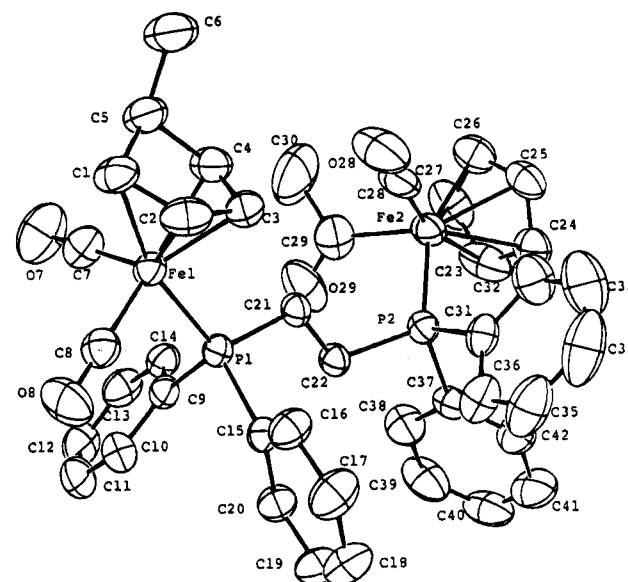


Figure 1. Molecular plot of $[(\eta^5\text{-C}_5\text{H}_5)\text{Fe}(\text{CO})\text{C}(\text{O})\text{Me}](\mu\text{-}\eta^1:\eta^1\text{-dppe})[(\eta^4\text{-MeC}_5\text{H}_5)\text{Fe}(\text{CO})_2]$ (**3**). Selected bond lengths, bond angles, and torsion angles: Fe(1)–P(1) 2.212(1), Fe(1)–C(1) 2.102(3), Fe(1)–C(2) 2.043(3), Fe(1)–C(3) 2.054(3), Fe(1)–C(4) 2.124(3), Fe(1)–C(7), 1.768(4), Fe(1)–C(8) 1.746(4), Fe(2)–P(2) 2.178(1), Fe(2)–C(23) 2.103(4), Fe(2)–C(24) 2.123(4), Fe(2)–C(25) 2.120(3), Fe(2)–C(26) 2.098(4), Fe(2)–C(27) 2.115(4), Fe(2)–C(28) 1.735(4), Fe(2)–C(29) 1.928(4), O(7)–C(7) 1.144(5), O(8)–C(8) 1.150(4), O(28)–C(28) 1.140(5), O(29)–C(29) 1.193(6), C(1)–C(2) 1.414(5), C(1)–C(5) 1.504(5), C(2)–C(3) 1.403(5), C(3)–C(4) 1.408(5), C(4)–C(5) 1.508(5), C(23)–C(24) 1.398(7), C(23)–C(27) 1.396(8), C(24)–C(25) 1.385(6), C(25)–C(26) 1.389(6), C(26)–C(27) 1.403(7) Å; P(1)–Fe(1)–C(7) 97.8(1), P(1)–Fe(1)–C(8) 89.8(1), C(7)–Fe(1)–C(8) 100.1(2), P(2)–Fe(2)–C(28) 91.6(1), P(2)–Fe(2)–C(29) 92.7(1), C(28)–Fe(2)–C(29) 89.6(2)°; Fe(1)–P(1)–C(21)–C(22) –175.7(2), Fe(2)–P(2)–C(22)–C(21) –59.7(1), P(1)–C(21)–C(22)–P(2) –162.9(2), C(28)–Fe(2)–C(29)–O(29) –125.4(3)°.

exhibit the dppe bridge between a pseudooctahedral, formally Fe(II) center of $(\eta^5\text{-C}_5\text{H}_5)\text{Fe}(\text{CO})\text{C}(\text{O})\text{Me}(\text{PR}_3)$ skeleton and a distorted square-pyramidal, formally Fe(0) center of $(\eta^4\text{-MeC}_5\text{H}_5)\text{Fe}(\text{CO})_2(\text{PR}_3)$ skeleton. There is no Fe–Fe bond between the Fe(II) and Fe(0) centers. The coordination geometry of Fe(II) can be described as a piano stool with the $(\eta^5\text{-C}_5\text{H}_5)$ ring occupying the *fac* sites and the three legs being orthogonal.¹² That of Fe(0) can be described as a square-pyramid with the diene group occupying the *cis* sites of the basal plane as joined by CO and PR_3 , the remaining CO being at the apical position. In the literature, the Fe(II)–P lengths and the Fe(0)–P lengths are very scattered in their numerical values. For PMe_3 , the hexacoordinated Fe(II)–P length is seemingly shorter than the penta-coordinated Fe(0)–P length, 2.230(37) *vs* 2.265(42) Å.¹³ For other phosphines, the Fe–P lengths have been tabulated only collectively. Figure 2 reveals a histogram summarizing the Fe(II)–P and the Fe(0)–P lengths, with values retrieved from the Cambridge Structural Database¹⁴ for structures containing a fragment of $\text{Fe}(\text{CO})_2(\text{PR}_3)$ (R = alkyl, aryl) with no differentiation toward the identity of the PR_3 . The structures with

(9) Wilkinson, G.; Stone, F. G. A.; Abel, E. W., Eds. *Comprehensive Organometallic Chemistry: The Synthesis, Reactions, and Structures of Organometallic Compounds*; Pergamon: Oxford, U.K., 1982; Vol. 4, pp 491–2.

(10) Abbott, S.; Baird, G. J.; Davies, S. G.; Dordor-Hedgecock, I. M.; Maberly, T. R.; Walker, J. C.; Warner, P. J. *Organomet. Chem.* **1985**, *289*, C13.

(11) (a) Berryhill, S. R.; Clevenger, G. L.; Burdurlu, F. Y. *Organometallics* **1985**, *4*, 1509. (b) Pannell, K. H.; Cervantes, J.; Hernandez, C.; Cassias, J.; Vincenti, S. *Organometallics* **1986**, *5*, 1056. (c) Cervantes, J.; Vincenti, S. P.; Kapoor, R. N.; Pannell, K. H. *Organometallics* **1989**, *8*, 744.

(12) Seeman, J. I.; Davies, S. G. *J. Am. Chem. Soc.* **1985**, *107*, 6522.

(13) Orpen, A. G.; Brammer, L.; Allen, F. H.; Kennard, O.; Watson, D. G.; Taylor, R. *J. Chem. Soc., Dalton Trans.* **1989**, S1.

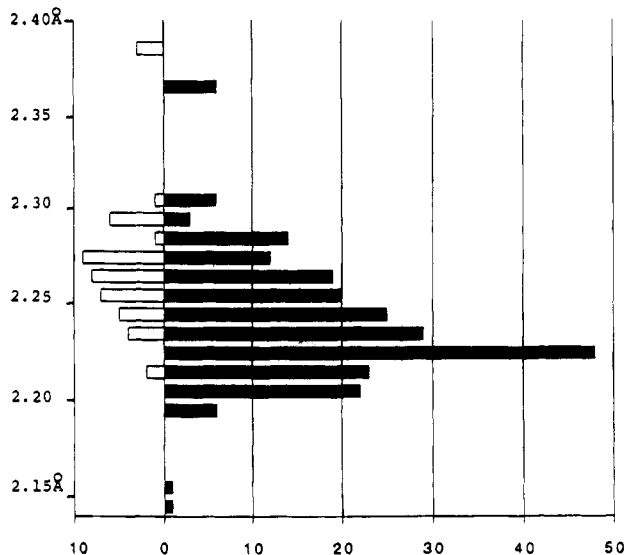


Figure 2. Histogram of Fe(0)–P lengths (filled bar) and Fe(II)–P lengths (open bar) with a step size of 0.01 Å for crystal structures containing a molecular fragment of Fe(CO)₂(PR₃).

disordering problems, and those with an *R* factor greater than 0.10 were discarded. The structures were then sorted into Fe(0), Fe(I), and Fe(II) complexes by hand. The results indicate that the average Fe(0)–P length is 2.242(34) Å for 68 structures totaling 235 fragments whereas the average Fe(II)–P length is 2.270(35) Å for 21 structures and 55 fragments. Statistically, the Fe(II)–P length and the Fe(0)–P length are not different. The structure analysis of the novel complex **3** gives one rare chance for direct comparison. The Fe(II)–P length of 2.178(2) Å is 0.034 Å shorter than that of Fe(0)–P, 2.212(1) Å. Being greater than 10 ESDs, this difference is small yet significant, giving experimental support for Fe(II) smaller in size than Fe(0).

Experimental Section

General Procedures. All manipulations were performed under an atmosphere of prepurified nitrogen with standard Schlenk techniques. All solvents were distilled from an appropriate drying agent.¹⁵ Infrared spectra were recorded in CH₂Cl₂ using CaF₂ optics on a Perkin-Elmer 882 spectrophotometer. The ¹H NMR and ¹³C NMR spectra were obtained on Bruker AC200/AC300 spectrometers, with chemical shifts reported in δ values relative to the residual solvent resonance of CDCl₃ (¹H 7.24 ppm, ¹³C 77.0 ppm). The ³¹P{¹H} NMR spectra were obtained on Bruker AC200/AC300 spectrometers using 85% H₃PO₄ as an external standard (0.00 ppm). The melting points (uncorrected) were determined on a Yanaco MPL melting point apparatus. (η⁵-C₅H₅)Fe(CO)₂I was prepared according to the literature procedure.¹⁶ Other reagents were obtained from commercial sources, e.g., Aldrich and Merck, and used without further purification.

Reaction of 1:1 (η⁵-C₅H₅)Fe(CO)₂Me and PPh₂(CH)₂PPh₂ (dppe). (η⁵-C₅H₅)Fe(CO)₂Me (0.384 g, 2 mmol) and dppe

(0.796 g, 2 mmol) were dissolved in CH₃CN (50 mL) and refluxed for 12 h. The solution was then cooled to room temperature. Filtration followed by removal of the solvent and then column chromatography (SiO₂, eluting with 1:2 EtOAc/*n*-hexane) yielded three bands. The first band was the starting materials. The second band was the orange-yellow compound (η⁵-C₅H₅)Fe(CO)C(O)Me(η¹-dppe) (**1**; 0.438 g, 38%). The third band was the orange compound [(η⁵-C₅H₅)Fe(CO)C(O)Me]₂(μ-η¹:η¹-dppe) (**2**; 0.386 g, 49%).

1: gummy solids, no well defined mp; IR (CH₂Cl₂) ν_{CO} 1916 (s), 1600 (m) cm⁻¹; ³¹P{¹H} NMR (CDCl₃) δ 75.3 (d), -12.1 (d), ³J_{PP} = 40.6 Hz; MS (*m/z*) 591 (M⁺ + 1). Anal. Calcd for C₃₄H₃₂FeO₂P₂: C, 69.17; H, 5.46. Found: C, 69.18; H, 5.68.

2: mp 106–110 °C; IR (CH₃CN) 1912 (s), 1591 (m) cm⁻¹; ³¹P{¹H} NMR (CDCl₃) δ 76.33 (s), 76.27 (s), presumably due to the *meso* and *D,L* forms; MS (*m/z*) 782 (M⁺). Anal. Calcd for C₄₂H₄₀Fe₂O₄P₂: C, 64.47; H, 5.15. Found: C, 64.09; H, 5.02.

Reaction of 1:1 (η⁵-C₅H₅)Fe(CO)₂I and MeLi in the Presence of 1. (η⁵-C₅H₅)Fe(CO)₂I (0.225 g, 0.74 mmol) and **1** (0.437 g, 0.74 mmol) were dissolved in THF (100 mL) and maintained at -78 °C. MeLi (1.6 M, 0.5 mL, 0.8 mmol) in 15 mL of ether at -78 °C was added dropwise to the solution. The mixture was stirred for an additional 1 h before being warmed to room temperature and stirred overnight. The solution was then quenched with water. The organic layer was combined with the benzene extracts of the H₂O layer, dried over MgSO₄, and then evaporated to dryness under vacuum. The resulting oillike concentrates were mixed with 10 mL of CH₂Cl₂ and 5 g of silica gel and pumped dry before being loaded on top of the column. Purification by chromatography (SiO₂, eluting with ethyl acetate/*n*-hexane) gave the yellow [(η⁵-C₅H₅)Fe(CO)C(O)Me](μ-η¹:η¹-dppe)[(η⁴-*exo*-MeC₅H₅)Fe(CO)₂(PPh₃)] (**3**; 0.439 g, 76%), the orange **2** (0.017 g, 3%), and a trace of yellowish (η⁵-C₅H₅)Fe(CO)₂Me. **3** could also be obtained as a byproduct (6.7%) in the reaction of 1:1 (η⁵-C₅H₅)Fe(CO)₂I and MeLi in the presence of dppe.^{3c}

3: mp 159–160 °C; IR (CH₂Cl₂) ν_{CO} 1963 (s), 1910 (s), 1603 (m) cm⁻¹; ¹H NMR (CDCl₃) δ 0.28 (d, ³J_{HH} = 15 Hz, 3H, Me), 1.83, 2.39 (b, 4H, CpFePCH₂CH₂P), 2.04, 2.16 (b, 2H, CH=CHCHMe), 2.51 (s, 3H, C(O)Me), 2.63 (b, 1H, CH=C-HCHMe), 4.31 (s, 5H, Cp), 4.83, 4.95 (b, 2H, CH=CHCHMe), 7.18–7.37 (m, 20H, Ph); ¹³C NMR (CDCl₃) δ 25.28 (d, ¹J_{PC} = 24.7 Hz, CpFePCH₂CH₂P), 27.23 (d, ¹J_{PC} = 22.0 Hz, CpFePCH₂CH₂P), 28.21 (d, ⁴J_{PC} = 5.5 Hz, Me), 51.0 (s, C(O)Me), 51.58 (d, ³J_{PC} = 4.8 Hz, CH=CHCHMe), 57.8 (s, 1C, CH=C-HCHMe), 82.05 (d, ³J_{PC} = 4.9 Hz, CH=CHCHMe), 84.7 (s, C₅H₅), 128.0–138.4 (m, phenyl region), 219.49 (d, ²J_{PC} = 14.0 Hz, CO), 219.5 (d, ²J_{PC} = 10.1 Hz, CO), 220.7 (s, CO), 275.32 (d, ²J_{PC} = 21.9 Hz, CO), ³¹P{¹H} NMR (CDCl₃) δ 75.9 (d, ³J_{PP} = 41.6 Hz), 70.3 (d, ³J_{PP} = 41.6 Hz); MS (*m/z*) 782 (M⁺). Anal. Calcd for C₄₂H₄₀Fe₂O₄P₂: C, 64.47; H, 5.15. Found: C, 64.09; H, 5.02.

X-ray Structure Analysis. The single-crystal X-ray diffraction measurements were performed on a Nonius CAD-4 automated diffractometer using graphite monochromated Mo Kα radiation. Twenty-five high-angle reflections were used in a least-squares fit to obtain accurate cell constants. Diffraction intensities were collected up to 2θ < 45° using the θ/2θ scan technique, with background counts made for half the total scan time on each side of the peak. Three standard reflections, remeasured every hour, showed no significant decrease in intensity during data collection. The reflections with I_o > 2.5σ(I_o) were judged as observations and were used for solution and structure refinement. Data were corrected for Lorentz and polarization factors. An empirical absorption correction based on a series of ψ scans was applied to the data. The structure was solved by direct methods¹⁷ and refined by a full-matrix least-squares routine¹⁸ with anisotropic thermal parameters for all non-hydrogen atoms (weight = 1/[σ(F_o)² +

(14) (a) Cambridge Structural Database; the associated software, Cambridge Structural Database System; Cambridge Crystallographic Data Centre: Cambridge, U.K., Release April 1994. (b) Buerger, H. B., Dunitz, J. D., Eds. *Structural Correlation*; VCH: Weinheim, Germany, 1994; pp 71–110.

(15) Perrin, D. D.; Armarego, W. L. F.; Perrin, D. R. *Purification of Laboratory Chemicals*; Pergamon Press: Oxford, U.K., 1981.

(16) (a) Dombek, B. D.; Angelici, R. J. *Inorg. Chim. Acta* **1973**, *7*, 345. (b) Meyer, T. J.; Johnson, E. C.; Winterton, N. *Inorg. Chem.* **1971**, *10*, 1673. (c) *Inorg. Synth.* **1971**, *12*, 36. (d) *Inorg. Synth.* **1963**, *7*, 110.

(17) Main, P. In *Crystallographic Computing 3: Data Collection, Structure Determination, Proteins and Databases*; Sheldrick, G. M., Krueger, C., Goddard, R., Eds.; Clarendon Press: Oxford, U.K., 1985; pp 206–215.

0.0001(F_o^2), $\sigma(F_o)$ from counting statistics). All of the hydrogen atoms were placed isotropically at their calculated positions (C-H = 1.00 Å) and fixed in the calculations. Atomic scattering factor curves f_o , $\Delta f'$, and $\Delta f''$ of Fe, P, O, and C, and f_o of H were taken from ref 19. Selected bond distances and angles were given in the caption of Figure 1.

Crystal data of **3**: $C_{42}H_{40}Fe_2O_4P_2$, triclinic, space group $P\bar{1}$; $a = 11.967(2)$, $b = 12.066(1)$, $c = 14.855(4)$ Å; $\alpha = 106.51(1)$, $\beta = 97.84(2)$, $\gamma = 108.20(1)^\circ$; $V = 1893.1(6)$ Å³; $fw = 782.42$, $Z = 2$, $F(000) = 811.88$; $\rho_{calc} = 1.373$ g/cm³, $\mu = 0.89$

(18) (a) Gabe, E. J.; Le Page, Y.; White, P. S.; Lee, F. L. *Acta Crystallogr.* **1987**, *43A*, S294. (b) Gabe, E. J.; Le Page, Y.; Lee, F. L. In *Crystallographic Computing 3: Data Collection, Structure Determination, Proteins and Databases*; Sheldrick, G. M., Krueger, C., Goddard, R. E., Eds.; Clarendon Press: Oxford, U.K., 1985; pp 167-174.

(19) Ibers, J. A., Hamilton, W. C., Eds. *International Tables for X-ray Crystallography*; Kynoch: Birmingham (Current distributor D. Reidel, Dordrecht, The Netherlands), 1974; Vol. 4, Tables 2.2A, 2.3.1D.

mm⁻¹, Mo K α $\lambda = 0.7093$ Å, Nonius CAD-4, $2\theta \leq 50^\circ$, $-12 \leq h \leq 11$, $0 \leq k \leq 12$, $-15 \leq l \leq 15$; transmission factors 0.935-0.999, 90 atoms, 451 parameters, 4052 observations [$I_o > 2.5\sigma(I_o)$], $R = 0.031$, $R_w = 0.037$, GOF = 1.81, $\Delta/\sigma = 0.020$.

Acknowledgments. The authors take this chance to thank Academia Sinica and the National Science Council, ROC, for their kind financial support. Thanks are due to Mr. Y.-S. Wen for assistance with the single-crystal X-ray diffraction data collection.

Supplementary Material Available: For Figure 2, listings of the retrieved crystal structures with bibliographic data and, for the structure of **3**, listings of crystallographic data, positional and anisotropic thermal parameters, and bond distances, angles, and structural parameters (23 pages). Ordering information is given on any current masthead page.

OM940672W

Synthesis and Characterization of New Silyl Niobocene Complexes. X-ray Molecular Structure of $d^0 \text{Nb}(\eta^5\text{-C}_5\text{H}_4\text{SiMe}_3)_2(\text{H})_2(\text{SiPh}_2\text{H})$

Antonio Antiñolo,[†] Fernando Carrillo,[†] Mariano Fajardo,[‡] Antonio Otero,^{*,†} Mauricio Lanfranchi,[§] and Maria Angela Pellinghelli[§]

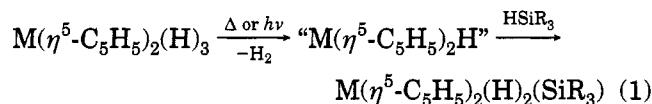
Departamento de Química Inorgánica, Orgánica y Bioquímica, Facultad de Químicas, Campus Universitario, Universidad de Castilla-La Mancha, 13071 Ciudad Real, Spain, Departamento de Química Inorgánica, Campus Universitario, Universidad de Alcalá, 28871 Alcalá de Henares, Spain, and Dipartimento di Chimica Generale ed Inorganica, Chimica Analitica, Chimica Fisica, Università degli Studi di Parma, Centro di Studio per la Strutturistica Diffraattometrica del CNR, Viale delle Scienze 78, I-43100 Parma, Italy

Received August 3, 1994[®]

Summary: Thermal treatment of $\text{Nb}(\eta^5\text{-C}_5\text{H}_4\text{SiMe}_3)_2(\text{H})_3$ (**1**) with organosilicon hydrides (HSiR_3) affords bis((trimethylsilyl)cyclopentadienyl)niobium dihydride silyl complexes, $\text{Nb}(\eta^5\text{-C}_5\text{H}_4\text{SiMe}_3)_2(\text{H})_2(\text{SiR}_3)$, $\text{SiR}_3 = \text{SiMe}_2\text{Ph}$ (**2**), SiMePh_2 (**3**), SiPh_2H (**4**), SiPh_2H (**5**), or SiPh_3 (**6**), in excellent yields. Spectroscopic data indicate the presence of only one of two possible structural isomers in which the silyl substituent is central in the equatorial plane with a symmetrical structure. Compound **5** has been characterized by X-ray diffraction: monoclinic space group $P2_1/n$ with $a = 13.233(4)$ Å, $b = 20.843(6)$ Å, $c = 11.043(7)$ Å, $\beta = 99.17(2)^\circ$, $V = 3007(2)$ Å³, $Z = 4$, $D_{\text{calcd}} = 1.221$ g/mL, $R = 0.0543$, and $R_w = 0.0570$. The coordination polyhedron may be described as a distorted tetrahedron with a centered edge. The complex adopts a "bent sandwich" coordination with the two hydrides flanking either side of the Nb-Si bond ($2.616(3)$ Å).

Introduction

In the last few years, the oxidative addition of organosilicon hydrides to coordinatively unsaturated hydride group 5 metal complexes has been successfully applied to the preparation of silyl derivatives.¹ Using this method, several silyl complexes, $\text{M}(\eta^5\text{-C}_5\text{H}_5)_2(\text{H})_2(\text{SiR}_3)$, have been prepared^{1a,b,e} from trihydride metallocene derivatives of niobium and tantalum, $\text{M}(\eta^5\text{-C}_5\text{H}_5)_2(\text{H})_3$ ($\text{M} = \text{Nb, Ta}$), eq 1. The process presumably

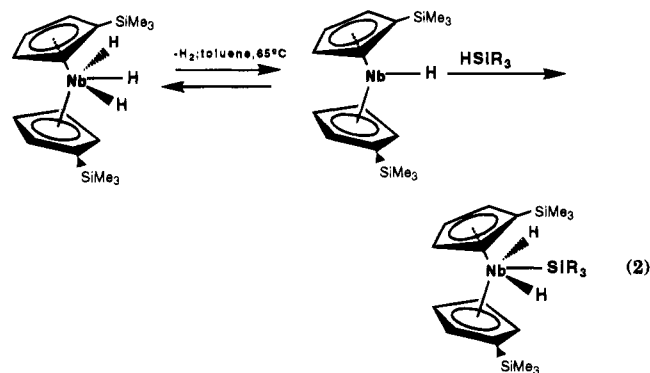


proceeds by reductive elimination of H_2 from the trihydride to give $\text{M}(\eta^5\text{-C}_5\text{H}_5)_2\text{H}$, which then adds the silane. We have previously described² the anomalous spectroscopic properties of various niobocene trihydride complexes bearing electron-withdrawing substituents, SiMe_3 , in the cyclopentadienyl rings, which show large H-H

coupling constants, in agreement with the importance of a near dihydrogen state. This has led us to study the behavior of $\text{Nb}(\eta^5\text{-C}_5\text{H}_4\text{SiMe}_3)_2(\text{H})_3$ (**1**) toward organosilicon hydrides, HSiR_3 .

Results and Discussion

We have found **1** reacts readily with several organosilicon hydrides to give niobocene silyl dihydride species (eq 2), with **2**, $\text{SiR}_3 = \text{SiMe}_2\text{Ph}$; **3**, $\text{SiR}_3 = \text{SiMePh}_2$; **4**,



$\text{SiR}_3 = \text{SiPh}_2\text{H}$; **5**, $\text{SiR}_3 = \text{SiPh}_2\text{H}$; and **6**, $\text{SiR}_3 = \text{SiPh}_3$.

The initial step presumably is formation of the 16e coordinatively unsaturated $\text{Nb}(\eta^5\text{-C}_5\text{H}_4\text{SiMe}_3)_2\text{H}$ by thermolytic loss of H_2 . This then is followed by oxidative addition of the organosilicon hydride so that a closed-shell 18e configuration in the silyl dihydride derivative is achieved. The formation of the intermediate species $\text{Nb}(\eta^5\text{-C}_5\text{H}_5\text{-}n\text{R}_n)_2(\text{H})$ in the preparation of complexes such as $\text{Nb}(\eta^5\text{-C}_5\text{H}_5\text{-}n\text{R}_n)_2(\text{H})(\text{L})$, $\text{L} = \pi\text{-acid ligand}$, from a mixture of $\text{Nb}(\eta^5\text{-C}_5\text{H}_5\text{-}n\text{R}_n)_2(\text{H})_3$ and L via thermal or photochemical treatments³ has been proposed previously.

Although the preparative method has been previously^{1b,d,e} employed in the synthesis of several families of tantalocene silyl hydride derivatives, only two related niobocene complexes, $\text{Nb}(\eta^5\text{-C}_5\text{H}_5)_2(\text{H})_2(\text{SiPhMe}_2)$ and $\text{Nb}(\eta^5\text{-C}_5\text{H}_5)_2(\text{H})_2(\text{SiMe}_2\text{OSiMe}_3)$, prepared by Curtis and co-workers,^{1b} have been described. Complexes **2-6** crystallize as air-sensitive microcrystalline materials

(3) See, for example: (a) Doherty, N. M.; Bercaw, J. E. *J. Am. Chem. Soc.* **1985**, *107*, 2670. (b) Burger, B. J.; Santarsiero, B. D.; Trimmer, M. S.; Bercaw, J. E. *J. Am. Chem. Soc.* **1988**, *110*, 3314. (c) Antiñolo, A.; Fajardo, M.; Jalón, F. A.; López-Mardomingo, C.; Otero, A.; Sanz-Bernabé, C. *J. Organomet. Chem.* **1989**, *369*, 187.

[†] Universidad de Castilla-La Mancha.

[‡] Universidad de Alcalá.

[§] Università degli Studi di Parma.

[®] Abstract published in *Advance ACS Abstracts*, November 15, 1994.

(1) (a) Allison, J. S.; Aylett, B. J.; Colquhoun, H. M. *J. Organomet. Chem.* **1976**, *112*, 67. (b) Curtis, M. D.; Bell, L. G.; Buttler, W. M. *Organometallics* **1985**, *4*, 701. (c) Berry, D. H.; Jiang, Q. *J. Am. Chem. Soc.* **1987**, *109*, 6211. (d) Aitken, C.; Barry, J.-P.; Gauvin, F.; Harrod, J. F.; Malek, A.; Rousseau, D. *Organometallics* **1989**, *8*, 1732. (e) Jiang, Q.; Carroll, P. J.; Berry, D. H. *Organometallics* **1991**, *10*, 3648.

(2) Antiñolo, A.; Chaudret, B.; Commenges, G.; Fajardo, M.; Jalón, F.; Morris, R. H.; Otero, A.; Schweitzer, C. T. *J. Chem. Soc., Chem. Commun.* **1988**, 1210.

from hexane or ethanol. Their stability to air is increased by the presence of phenyl substituents in the silyl group, so that complex **6** survives several hours of exposure to air. Attempts to prepare a complex with Et_3SiH were not successful. A complex mixture of products was obtained which could not be characterized. A similar observation had been made previously^{1b} with $\text{Nb}(\eta^5\text{-C}_5\text{H}_5)_2(\text{H})_3$. Complexes **2–6** have been characterized spectroscopically. Their IR spectra show a weak single, broad band at $\sim 1700\text{ cm}^{-1}$ assigned to $\nu(\text{Nb-H})$. In addition, the IR spectra of **4** and **5**, which contain hydrogen on the silyl groups, exhibit $\nu(\text{Si-H})$ as a medium single band at 2957 and 2040 cm^{-1} , respectively. The ^1H NMR spectra of the complexes clearly show that of the possible symmetrical or unsymmetrical isomers $\text{Nb}(\eta^5\text{-C}_5\text{H}_4\text{SiMe}_3)_2(\text{H})(\text{SiR}_3)(\text{H})$ and $\text{Nb}(\eta^5\text{-C}_5\text{H}_4\text{-SiMe}_3)_2(\text{H})(\text{H})(\text{SiR}_3)$, only the symmetrical one was present in solution. In fact, the spectra show a broad singlet at $\delta \sim -4.50$ for the two equivalent hydride ligands in accordance with a time-averaged C_{2v} symmetry with the silyl group in the central position. The cyclopentadienyl rings are equivalent, showing two broad resonances (see Experimental Section) for an A_2B_2 spin system, which indicates a symmetrical disposition on the niobium center with a rapid rotation of the SiR_3 around the Nb-Si bond. This symmetrical disposition has been confirmed by means of the corresponding ^{13}C NMR spectra in which the three expected resonances for the cyclopentadienyl carbon atoms are present (see Experimental Section). The thermodynamically more favorable symmetrical isomer is obtained under our experimental conditions. Attempts to detect the unsymmetrical isomer were carried out by recording the ^1H NMR spectra for **2–6** at low temperature, but in all cases isomerization was never observed. ^{29}Si NMR data can be used to detect the presence of a H-Si interaction in the silyl hydride derivatives.⁴ Corriu and co-workers⁵ showed that the $^1J(\text{Si},\text{H})$ for the H-Si interaction is ~ 65 Hz, thus appearing between that characteristic of classical silyl hydrides (~ 6 Hz) and that of free silanes (~ 200 Hz). The ^{29}Si NMR spectrum of **5** shows a doublet at $\delta 23.8$ for the silyl group with $^1J(\text{Si},\text{H}) = 177$ Hz. This coupling disappears when the hydrogen of the silyl group is irradiated. In the ^1H NMR spectrum, the coupling also is observed for the resonance of this hydrogen, and in addition, the line width of the signals for the two hydride ligands (~ 6 Hz) is characteristic of classical silyl hydrides. In the ^{29}Si NMR spectrum of **3**, where there is no hydrogen in the silyl group, the resonance for this group appears as a singlet at $\delta 26.7$. These spectroscopic data allow us to establish the classical nature of these silyl hydrides. In order to confirm this, we determined the molecular structure of **5**.

X-ray Structure of $\text{Nb}(\eta^5\text{-C}_5\text{H}_4\text{SiMe}_3)_2(\text{H})_2(\text{SiPh}_2\text{H})$ (5**).** Figure 1 provides a view of complex **5** which adopts a familiar "bent sandwich" coordination. The two centroids of the two Cp' rings and the two hydrides surround the niobium atom at the vertices of an irregular tetrahedron. Moreover, the metal atom interacts with the Si atom of the $\text{Si}(1)\text{HPh}_2$ moiety, the Nb-Si(1) bond roughly bisects the H(1T)-Nb-H(2T) bond angle, and the four atoms Nb, Si(1), H(1T), and H(2T)

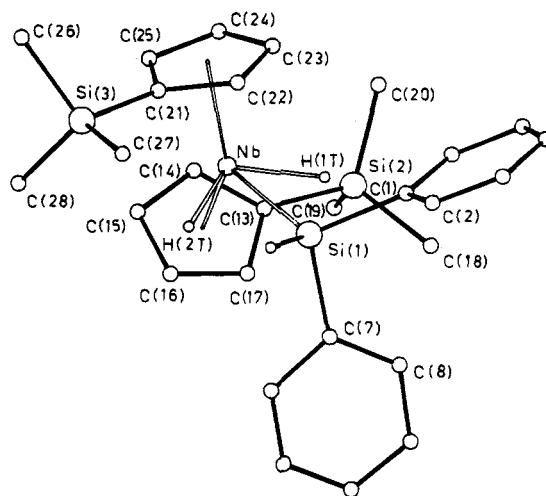


Figure 1. View of the molecular structure of $[\text{Cp}'_2\text{Nb}(\text{H})_2(\text{SiHPh}_2)]$ with the atom-numbering scheme. Selected distances (\AA): Nb-CE(1) 2.064(9); Nb-CE(2) 2.050(10); Nb-H(1T) 1.77(6); Nb-H(2T) 1.76(6); Nb-Si(1) 2.616(3); Si(1)-H(1T) 2.37(6); Si(1)-H(2T) 2.21(6). Selected angles (deg): CE(1)-Nb-CE(2) 141.3(4); CE(2)-Nb-H(1T) 110.7(18); CE(1)-Nb-Si(1) 115.2(3); CE(2)-Nb-H(2T) 101.2(18); CE(1)-Nb-H(1T) 88.9(18); Si(1)-Nb-H(1T) 62.0(19); CE(1)-Nb-H(2T) 99.6(19); Si(1)-Nb-H(2T) 56.6(18); CE(2)-Nb-Si(1) 103.5(3); H(1T)-Nb-H(2T) 115.4(26). CE(1) and CE(2) are the centroids of the C(13)-C(17) and C(21)-C(25) Cp' rings, respectively.

are roughly coplanar (maximum deviation $0.29(6)\text{ \AA}$ for H(2T)). The coordination polyhedron thus can be described as a tetrahedron with a centered edge. Therefore, this complex belongs to the class of bent metallocene complexes containing their ligands in the equatorial wedge with the two hydrides flanking either side of the Nb-Si bond in the symmetrical isomeric form. The Nb-Si(1) distance, $2.616(3)\text{ \AA}$, corresponds to a single, covalent bond and is shorter than that observed in $[\text{Cp}_2\text{Nb}(\text{SiMe}_3)(\eta^2\text{-C}_2\text{H}_4)]^6$ (Nb-Si = $2.669(1)\text{ \AA}$). This shortening can be due to the different oxidation state of the niobium atoms. Silyl complexes of tantalum have received relatively more study, but only two molecular structures of silyl hydride complexes of tantalum have been reported, $[\text{Cp}_2\text{Ta}(\text{H})_2(\text{SiMe}_2\text{Ph})]^{1b}$ and $[\text{Cp}_2\text{Ta}(\text{H})(\text{SiMe}_2\text{H})_2]^{1e}$.

The two hydride ligands were clearly located in **5**. The two H(1T) and H(2T) atoms are at $1.77(6)$ and $1.76(6)\text{ \AA}$ from Nb with a bond angle of $115.4(26)^\circ$. They adopt a symmetrical position with respect to the Si(1) atom, and the two Nb-H(1T)-Si(1) and Nb-H(2T)-Si(1) angles ($76.9(20)$, $81.6(22)^\circ$) are similar. Unfortunately, the hydride ligands were not located^{1b} or not clearly located^{1e} in the two above-cited silyl complexes of tantalum and hence we cannot make any comparison. On the basis of Schubert's work,⁴ it seems reasonable to assume no significant Si-H interaction at distances greater than 2.00 \AA , but can we exclude any interaction between the hydrides and the silicon atom on the basis of van der Waals radii?

The two cyclopentadienyl rings are nearly eclipsed, while the two SiMe_3 groups are trans to each other. The angle subtended by the two Cp' ring centroids ($141.3(4)^\circ$) is greater than that observed in $[\text{Cp}_2\text{Ta}(\text{H})_2(\text{SiMe}_2-$

(4) Schubert, U. *Adv. Organomet. Chem.* **1990**, *30*, 151.

(5) Colomer, K.; Corriu, R. J. P.; Mazin, C.; Vioux, A. *Inorg. Chem.* **1982**, *21*, 368.

(6) Arnold, J.; Tilley, T. D.; Rheingold, A. L.; Geib, S. J. *Organometallics* **1987**, *6*, 473.

Table 1. Crystallographic Data for Compound [Cp'₂Nb(H)₂(SiHPh₂)]

formula	C ₂₈ H ₃₉ Si ₃ Nb
fw	552.781
diffractometer	Siemens AED
radiation	nickel-filtered Cu Kα, λ = 1.541 838 Å
cryst syst	monoclinic
space group	P2 ₁ /n
a, Å	13.233(4)
b, Å	20.843(6)
c, Å	11.043(7)
β, deg	99.17(2)
V, Å ³	3007(2)
Z	4
D _{calcd} , g cm ⁻³	1.221
F(000)	1160
cryst size, mm	0.18 × 0.19 × 0.20
μ(Cu Kα), cm ⁻¹	44.90
temp, K	295
scan speed, deg min ⁻¹	3–9
scan width, deg	1.20 + 0.142 tan θ
scan mode	θ/2θ
2θ range, deg	6–140
reflms measd	h, k, ±l
no. of unique total data	5700
no. of unique obsd data [I ≥ 2σ(I)]	2505
transm factors (max, min)	1.000, 0.759
function minimized	Σw(F _o - F _c) ²
weighting scheme	
w = k/[σ ² (F _o) + gF _o ²]	k = 1.1167, g = 0.0004
no. of variables	328
max shift/error, final cycle	0.63
max/min diff peaks, e/Å ³	0.42/-0.60
goodness of fit	1.5952
R, R _w ^a	0.0543, 0.0570

$$^a R = \sum |F_o| - |F_c| / \sum |F_o|. R_w = [\sum w(|F_o| - |F_c|)^2 / \sum w(F_o)^2]^{1/2}.$$

Ph)] and [Cp₂Ta(H)(SiMe₂H)₂] (138.0(2), 1380.0°). The two centroids, the Nb and Si(1) atoms, are coplanar as in the dihydride silyl tantalum complex and the asymmetrical angles around the metal atoms are due to steric hindrance between the C(13)–C(17) Cp' ring and the C(7)–C(12) phenyl ring (C(7)–H(17) = 2.69(9), and C(7)–C(17) = 3.30(1) Å).

Experimental Section

General Procedures. All operations were performed under an inert atmosphere using standard vacuum line (Schlenk) techniques. Solvents were purified by distillation from appropriate drying agents before use. NMR spectra were obtained on a Varian Unity FT-300 instrument. IR spectra were recorded as Nujol mulls between CsI plates (in the region between 4000 and 200 cm⁻¹) on a Perkin-Elmer PE 883 IR spectrometer. Elemental analyses were performed on a Perkin-Elmer 2400 microanalyzer. Nb(η⁵-C₅H₄SiMe₃)₂(H)₃ was prepared as described earlier.² Organosilicon hydrides (Aldrich and Fluka) were used without purification.

Nb(η⁵-C₅H₄SiMe₃)₂(H)₂(SiR₃), SiR₃ = SiMe₂Ph (2); SiR₃ = SiMePh₂ (3); SiR₃ = SiPh₂H (4); SiR₃ = SiPh₂H (5); and SiR₃ = SiPh₃ (6). To a solution of Nb(η⁵-C₅H₄SiMe₃)₂(H)₃ (300 mg, 0.81 mmol) in 20 mL of toluene was added R₃SiH (0.81 mmol) by syringe. The solution was warmed to 65 °C and stirred for 3 h. The resulting red-brown solution was filtered and evaporated to dryness. The brown, oily residue was extracted with 20 mL of ethanol. After concentration and cooling, white or pale yellow crystals of complexes 2–6 were obtained.

2: pale yellow crystals, 88% yield. IR (Nujol; cm⁻¹): 1685, ν(Nb–H). ¹H NMR (C₆D₆; δ): -4.96 (s, br, 2H, Nb–H), 0.13 (s, 18H, C₅H₄SiMe₃), 0.74 (s, 6H, SiMe₂Ph), 4.20 (s, 4H), 4.90 (s, 4H) (η⁵-C₅H₄, exact assignment not possible), 7.10–7.70 (m, 5H, SiMe₂Ph). ¹³C{¹H} NMR (C₆D₆; δ): 0.40 (SiMe₃), 19.2

Table 2. Atomic Coordinates (×10⁴) and Isotropic Thermal Parameters (Å² × 10⁴) with ESDs in Parentheses for the Non-Hydrogen Atoms of Compound [Cp'₂Nb(H)₂(SiHPh₂)]

	x/a	y/b	z/c	U ^a
Nb	5133.8(6)	2297.8(4)	3710.2(7)	689(3)
Si(1)	6636(2)	2793(1)	2741(2)	768(10)
Si(2)	3442(2)	3769(1)	3799(3)	863(12)
Si(3)	6545(3)	693(2)	3980(4)	1357(19)
C(1)	7467(7)	3441(5)	3637(8)	767(38)
C(2)	8499(8)	3476(6)	3511(10)	1049(51)
C(3)	9142(9)	3941(7)	4105(12)	1085(60)
C(4)	8783(11)	4355(6)	4842(13)	1167(65)
C(5)	7792(10)	4333(5)	5022(11)	1143(58)
C(6)	7142(9)	3868(5)	4414(10)	1018(51)
C(7)	6237(7)	3150(6)	1173(9)	894(44)
C(8)	6208(9)	3797(7)	921(11)	1184(59)
C(9)	5894(11)	4031(9)	-262(15)	1701(87)
C(10)	5617(15)	3607(12)	-1184(15)	1939(124)
C(11)	5624(13)	2986(11)	-955(15)	1659(103)
C(12)	5945(9)	2740(7)	184(11)	1190(57)
C(13)	3647(7)	2964(4)	3190(8)	709(34)
C(14)	3331(7)	2366(6)	3622(10)	875(40)
C(15)	3516(8)	1876(6)	2790(11)	921(47)
C(16)	3924(8)	2146(6)	1865(10)	971(50)
C(17)	4046(7)	2801(6)	2083(9)	849(44)
C(18)	4124(9)	4375(5)	3006(11)	1267(58)
C(19)	2018(7)	3904(5)	3447(11)	1276(58)
C(20)	3889(10)	3804(5)	5467(9)	1380(63)
C(21)	6098(8)	1427(5)	4688(9)	887(44)
C(22)	6663(8)	2006(5)	5011(9)	832(42)
C(23)	6115(9)	2390(5)	5716(8)	862(43)
C(24)	5224(9)	2079(5)	5837(9)	935(47)
C(25)	5200(9)	1496(5)	5211(10)	927(47)
C(26)	6768(12)	43(6)	5121(15)	1997(98)
C(27)	7769(18)	839(7)	3503(22)	4155(213)
C(28)	5554(17)	396(8)	2829(15)	3474(160)

^a Equivalent isotropic U, defined as one-third of the trace of the orthogonalized U_{ij} tensor.

(SiMe₂Ph), 89.2, 91.6, 94.0 (C₅H₄SiMe₃), 128, 133.5 (SiMe₂Ph). Anal. Calcd for C₂₄H₃₉Si₃Nb: C, 58.29; H, 5.87. Found: C, 58.45; H, 5.91.

3: pale yellow crystals, 87% yield. IR (Nujol; cm⁻¹): 1726, ν(Nb–H). ¹H NMR (C₆D₆; δ): -4.66 (s, br, 2H, Nb–H), 0.03 (s, 18H, C₅H₄SiMe₃), 0.77 (s, 3H, SiMePh₂), 4.20 (s, 4H), 4.90 (s, 4H) (η⁵-C₅H₄, exact assignment not possible), 7.10–7.84 (m, 10H, SiMePh₂). ¹³C{¹H} NMR (C₆D₆; δ): 0.33 (SiMe₃), 19.2 (SiMePh₂), 91.7, 94.0, 94.7 (C₅H₄SiMe₃), 129.7, 134.7, 150.0 (SiMePh₂). ²⁹Si NMR (C₆D₆; δ, ref TMS): -3.0 (s, C₅H₄SiMe₃), 26.7 (s, SiMePh₂). Anal. Calcd for C₂₉H₄₁Si₃Nb: C, 62.59; H, 5.57. Found: C, 62.69; H, 5.64.

4: white crystals, 92% yield. IR (Nujol; cm⁻¹): 2057, ν(Si–H); 1729, ν(Nb–H). ¹H NMR (C₆D₆; δ): -4.90 (s, br, 2H, Nb–H), 0.13 (s, 18H, C₅H₄SiMe₃), 4.10 (s, 4H), 4.90 (s, 4H) (η⁵-C₅H₄, exact assignment not possible), 5.24 (2H, SiPh₂H), 7.10–7.97 (m, 5H, SiPh₂H). ¹³C{¹H} NMR (C₆D₆; δ): 0.44 (SiMe₃), 91.5, 93.0, 96.8 (C₅H₄SiMe₃), 135.6, 146.5 (SiPh₂H). Anal. Calcd for C₂₂H₃₅Si₃Nb: C, 56.65; H, 5.36. Found: C, 56.70; H, 5.23.

5: white crystals, 93% yield. IR (Nujol; cm⁻¹): 2040, ν(Si–H); 1728, ν(Nb–H). ¹H NMR (C₆D₆; δ): -4.64 (s, br, 2H, Nb–H), 0.14 (s, 18H, C₅H₄SiMe₃), 4.10 (s, 4H), 4.90 (s, 4H) (η⁵-C₅H₄, exact assignment not possible) 5.86 (1H, SiPh₂H), 7.10–7.90 (m, 10H, SiPh₂H). ¹³C{¹H} NMR (C₆D₆; δ): 0.55 (SiMe₃), 91.9, 94.3, 94.9 (C₅H₄SiMe₃), 135.6, 146.8 (SiPh₂H). ²⁹Si NMR (C₆D₆; δ, referenced TMS): -0.3 (s, C₅H₄SiMe₃), 23.8 (d, ¹J_{SiH} = 177 Hz, SiPh₂H). Anal. Calcd for C₂₈H₃₉Si₃Nb: C, 61.99; H, 5.35. Found: C, 62.06; H, 5.43.

6: white crystals, 98% yield. IR (Nujol, cm⁻¹): 1720, ν(Nb–H). ¹H NMR (C₆D₆; δ): -4.27 (s, br, 2H, Nb–H), 0.06 (s, 18H, C₅H₄SiMe₃), 4.10 (s, 4H), 4.90 (s, 4H) (η⁵-C₅H₄, exact assignment not possible), 7.10–7.97 (m, 15H, SiPh₃). ¹³C{¹H} (C₆D₆; δ): -0.55 (SiMe₃), 90.5, 92.1, 95.6 (C₅H₄SiMe₃), 134.6, 145.5 (SiPh₃). Anal. Calcd for C₃₄H₄₃Si₃Nb: C, 66.02; H, 5.33. Found: C, 66.10; H, 5.29.

X-ray Data Collection, Structure Determination, and Refinement of Nb(η^5 -C₅H₄SiMe₃)₂(H)₂(SiPh₂H) (5). Crystals suitable for X-ray analysis were obtained by recrystallization from ethanol. A single crystal was sealed in a Lindemann capillary under dry nitrogen and used for data collection. Table 1 contains a summary of data collection conditions and results. Lattice parameters were determined from a least-squares refinement of 30 reflection settings ($20 < \theta < 37$ deg) obtained from an automatic centering routine. Three standard reflections were monitored every 50 measurements; no significant decay was noticed over the time of data collection. The individual profiles have been analyzed following the method of Lehmann and Larsen.⁷ Intensities were corrected for Lorentz and polarization effects. A correction for absorption was applied.⁸ Only the observed reflections were used in the structural solution and refinements. The structure was solved by Patterson and Fourier methods and refined by full-matrix least squares, first with isotropic thermal parameters and then with anisotropic thermal parameters for all the non-hydrogen atoms. The methyl carbon atoms bonded to Si(3) show very large thermal parameters with the major axis roughly in the plane of the three carbon atoms. Attempts to resolve a possible disorder of this group were unsuccessful. The two niobium hydrides, the hydrogen atom of Si(1) and the hydrogen atoms of the Cp' rings were clearly located in the ΔF map and refined isotropically. The positional parameters of the two hydride ligands were tested by means of a "potential energy" technique using the HYDEX program.⁹ All the other hydrogen atoms were placed at their geometrically calculated positions (d_{C-H}

= 1.00 Å) and refined "riding" on the corresponding carbon atoms, with isotropic thermal parameters. The analytical scattering factors, corrected for the real and imaginary parts of anomalous dispersion, were taken from ref 10. All calculations were carried out on the GOULD POWERNODE 6040 and ENCORE 91 computers of the Centro di Studio per la Strutturistica Diffraattometrica del CNR, Parma, using the SHELXS-86 and SHELXS-76 systems of crystallographic computer programs.¹¹ Table 2 provides the atomic coordinates.

Acknowledgment. A.A., F.C., M.F., and A.O. gratefully acknowledge financial support from DGICYT (Grant PB92-0715) of Spain. M.L. and M.A.P. gratefully acknowledge financial support from the Ministero dell'Università della Ricerca Scientifica e Tecnologica (MURST) and Consiglio Nazionale delle Ricerche (CNR) (Rome, Italy).

Supplementary Material Available: Tables of hydrogen atom coordinates (Table SI), anisotropic thermal parameters for the non-hydrogen atoms (Table SII), complete bond distances and angles (Table SIII), and least-squares planes and lines (Table SIV) (12 pages). Ordering information is given on any current masthead page. A list of structure factors is available upon request from the authors.

OM940617N

(7) Lehmann, M. S.; Larsen, F. K. *Acta Crystallogr., Sect. A* **1974**, *30*, 580.

(8) (a) Walker, N.; Stuart, D. *Acta Crystallogr., Sect. A* **1983**, *39*, 158. (b) Ugozzoli, F. *Comput. Chem.* **1987**, *11*, 109.

(9) Orpen, A. G. *J. Chem. Soc., Dalton Trans.* **1980**, 2509.

(10) *International Tables for X-Ray Crystallography*; Kynoch Press: Birmingham, England, 1974; Vol. IV.

(11) Sheldrick, G. M. SHELXS-86 Program for the Solution of Crystal Structures; University of Göttingen, Göttingen, Germany, 1986. SHELX-76 Program for Crystal Structure Determination; University of Cambridge, Cambridge, England, 1976.

Photochemical C–Sb Bond Fission in a Palladium–Distibine Complex. Synthesis and Structure of $[\text{Pd}_2(\mu\text{-Ph}_2\text{SbCH}_2\text{SbPh}_2)_2\text{Cl}_2\text{Ph}_2]$

Andrew F. Chiffey, John Evans, William Levason,* and Michael Webster

Department of Chemistry, University of Southampton, Southampton SO17 1BJ, U.K.

Received September 8, 1994[©]

Summary: Photolysis of $[\text{Pd}(\text{Ph}_2\text{SbCH}_2\text{SbPh}_2)_2\text{Cl}_2]$ in CH_2Cl_2 generates the dimeric *o*-phenyl complex $[\text{Pd}_2(\mu\text{-Ph}_2\text{SbCH}_2\text{SbPh}_2)_2\text{Cl}_2\text{Ph}_2]$. The X-ray structure of the title compound was found to be monoclinic with space group $P2_1/a$ ($a = 11.527(8)$, $b = 20.264(5)$, $c = 12.717(4)$ Å, $\beta = 112.12(8)^\circ$, $Z = 2$). The data was refined to $R = 0.033$ on the basis of 3462 reflections ($F > 4\sigma(F)$). The dimeric discrete centrosymmetric molecule contains bridging distibine ligands (Pd–Sb 2.560(1), 2.530(1) Å). The square planar geometry at Pd has *trans* Sb donors and *trans* Cl and phenyl groups.

We have recently examined the use of group 16 donor ligands including RSCH_2SR and RSeCH_2SeR ($\text{R} = \text{Me}$ or Ph) as building blocks to heterobimetallic complexes.¹ In an extension of this work, we examined similar reactions of $[\text{M}(\text{Ph}_2\text{SbCH}_2\text{SbPh}_2)_2\text{Cl}_2]$ ($\text{M} = \text{Pd}$ or Pt). These complexes were reported some years ago and, on the basis of conductance and molecular weight data and IR spectroscopy, assigned *cis* planar structures with η^1 -coordinated ditertiary stibines.² In order to confirm that, we attempted to determine the structure of the palladium complex.

Vapor diffusion of diethyl ether into a solution of $[\text{Pd}(\text{Ph}_2\text{SbCH}_2\text{SbPh}_2)_2\text{Cl}_2]$ in CH_2Cl_2 produced a number of small pale yellow crystals over a period of four days, during which the solution was exposed to laboratory sunlight. The structure determination of these crystals revealed a discrete centrosymmetric dimeric molecule $[\text{Pd}_2(\mu\text{-Ph}_2\text{SbCH}_2\text{SbPh}_2)_2\text{Cl}_2\text{Ph}_2]$. The geometry at the palladium is square planar with *trans* antimony donors and with each ditertiary stibine bridging to two palladium atoms (Figure 1, Table 1). The two square planar units are aligned parallel ("face-to-face") to each other and this is clearly shown in Figure 2. The Sb–Pd distances (2.530(1), 2.560(1) Å) are similar to those found in palladium(II)–triphenylantimony complexes^{3,4} ($[\text{Pd}_2(\text{MeCO}_2)_4(\text{Ph}_3\text{Sb})_2]$ 2.508(4), $[\text{Pd}_3(\text{MeCO}_2)_4(\text{Ph}_3\text{Sb})_2\text{Ph}_2]$ 2.473(4), *trans*- $[\text{Pd}(\text{Ph}_3\text{Sb})_2\text{I}_2]$ 2.578(1) Å). This complex appears to be the first structurally characterized example of this ligand⁵ and only the second reported structure of a distibine complex;⁶ the majority of structural chemistry involves triphenylstibine.⁵ The

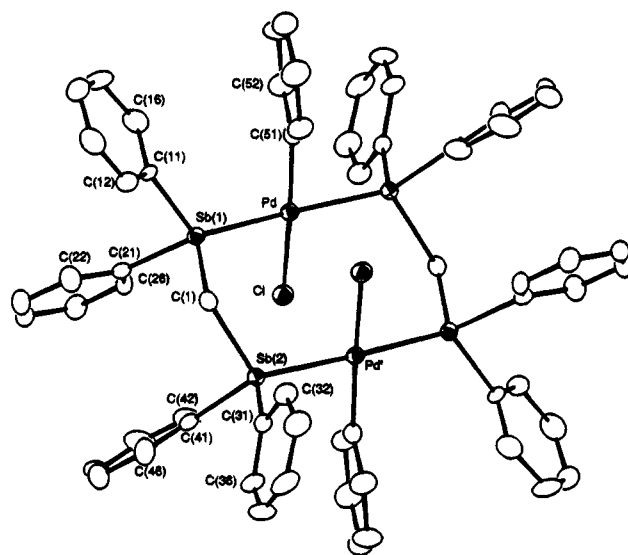


Figure 1. View of the molecule showing the atom numbering scheme. Thermal ellipsoids are drawn at the 50% probability level and hydrogen atoms are omitted for clarity. Primed atoms are symmetry related to unprimed as $-x, -y, 1 - z$.

Table 1. Selected Interatomic Distances (Å) and Angles (deg)^a

Pd–Sb(1)	2.560(1)	Pd–Cl	2.411(1)
Pd–Sb(2')	2.530(1)	Pd–C(51)	2.023(5)
Sb(1)–C(1)	2.115(6)	Sb(2)–C(1)	2.158(5)
Sb(1)–C(11)	2.128(5)	Sb(2)–C(31)	2.128(5)
Sb(1)–C(21)	2.132(5)	Sb(2)–C(41)	2.133(5)
C(51)–C(52)	1.390(8)	C(54)–C(55)	1.390(9)
C(52)–C(53)	1.393(8)	C(55)–C(56)	1.395(8)
C(53)–C(54)	1.370(8)	C(56)–C(51)	1.382(7)
C–C (phenyl on Sb atoms)	min 1.364(8)	max 1.403(7)	
Sb(1)–Pd–Sb(2')	173.0(1)	Sb(2')–Pd–Cl	88.5(1)
Sb(1)–Pd–Cl	94.3(1)	Sb(2')–Pd–C(51)	89.0(2)
Sb(1)–Pd–C(51)	89.2(2)	Cl–Pd–C(51)	170.3(2)
Pd–Sb(1)–C(1)	113.1(1)	Pd'–Sb(2)–C(1)	114.7(2)
Pd–Sb(1)–C(11)	122.3(2)	Pd'–Sb(2)–C(31)	111.8(1)
Pd–Sb(1)–C(21)	121.1(1)	Pd'–Sb(2)–C(41)	123.2(2)
C(1)–Sb(1)–C(11)	101.0(2)	C(1)–Sb(2)–C(31)	100.1(2)
C(1)–Sb(1)–C(21)	99.6(2)	C(1)–Sb(2)–C(41)	100.3(2)
C(11)–Sb(1)–C(21)	95.7(2)	C(31)–Sb(2)–C(41)	103.8(2)
Pd–C(51)–C(52)	117.8(4)	Pd–C(51)–C(56)	124.1(4)
Sb(1)–C(1)–Sb(2)	115.0(2)		
C–C–C (phenyl)	min 118.1(6)	max 121.4(5)	

^a Symmetry transformation: prime (') $-x, -y, 1 - z$.

Pd–C and Pd–Cl distances are unexceptional as is the angle at the methylene atom (Sb(1)–C(1)–Sb(2)) (115.0(2)[°]); there is no evidence for any interaction between Cl and Pd'. Inspection of Figure 2 and the angles around Pd (Table 1) show that the Cl appears to have moved away from the nonbonded Pd atom.

[©] Abstract published in *Advance ACS Abstracts*, February 1, 1995.
(1) Chiffey, A. F.; Evans, J.; Levason, W.; Webster, M. *J. Chem. Soc., Dalton Trans.* **1994**, 2835.

(2) Levason, W.; McAuliffe, C. A. *J. Coord. Chem.* **1974**, *4*, 47.
(3) Matthew, M.; Palenik, G. J.; McAuliffe, C. A. *Acta Crystallogr. Sect. C* **1987**, *43*, 21.

(4) Barton, D. H. R.; Khamsi, J.; Ozbalik, N.; Reibenspies, J. *Tetrahedron* **1990**, *46*, 3111.

(5) Champness, N. R.; Levason, W. *Coord. Chem. Rev.* **1994**, *133*, 115.

(6) The other example is $[\text{Co}\{\text{o-C}_6\text{H}_4(\text{SbMe}_2)_2\text{Cl}_2\}_2[\text{CoCl}_4]]$: Jewiss, H. C.; Levason, W.; Spicer, M. D.; Webster, M. *Inorg. Chem.* **1987**, *26*, 2102.

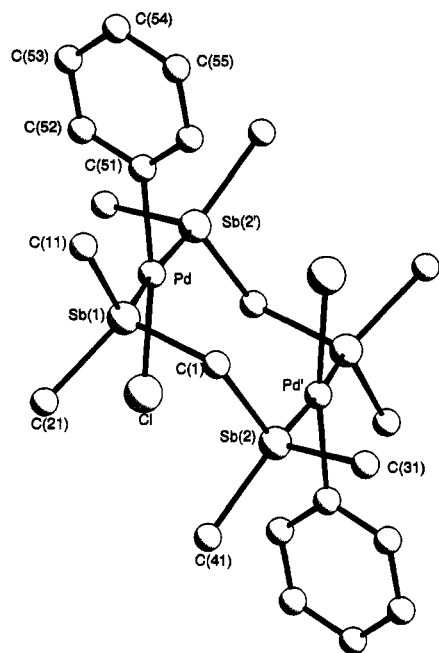


Figure 2. Partial view of the molecule showing the relationship between the two square planar groups. Only the C atoms bonded to Sb are shown. Pd' is related to Pd as $-x, -y, 1 - z$.

Bulk samples of $[\text{Pd}_2(\mu\text{-Ph}_2\text{SbCH}_2\text{SbPh}_2)_2\text{Cl}_2\text{Ph}_2]$ were obtained by photolyzing CH_2Cl_2 solutions of $[\text{Pd}(\text{Ph}_2\text{SbCH}_2\text{SbPh}_2)_2\text{Cl}_2]$ either with a 30 W fluorescent tube (method 2) or simply by exposure to bright sunlight (method 1), as described in the Experimental Section. The ^1H NMR spectra obtained from the crystals and from the products of both the bulk photolysis routes were identical, and showed only a single methylene resonance at 2.60 ppm, which may be compared with a value of 2.44 ppm in the starting material. The ^1H NMR data also show that only a single palladium-containing product was formed in all three preparations. During the course of this work both bulk photolysis routes were carried out several times with identical results. The shift to high frequency in $\delta(\text{CH}_2)$ is consistent with the change from monodentate to bridging bidentate coordination of the ligand. The σ -phenyl group must come from the cleavage of one distibine ligand, but the other products have not been identified. Fragmentation of tertiary stibines, on reaction with metal carbonyls and unsaturated metal centers, is well established and usually indicated by the appearance of black solids.⁵ In very few cases have the products been identified. Barton *et al.*⁴ structurally characterized the $\sigma\text{-Ph-Pd}$ species, $[\text{Pd}_3(\text{MeCO}_2)_4(\text{Ph}_3\text{Sb})_2\text{Ph}_2]$, obtained by heating (47 °C) palladium acetate and Ph_3Sb in tetrahydrofuran/dioxan, while $[\text{Rh}(\text{Ph}_3\text{Sb})_3(\sigma\text{-Ph})\text{Cl}_2]$ was formed from $\text{RhCl}_3 \cdot 3\text{H}_2\text{O}$ and Ph_3Sb in refluxing ethanol.⁷ The formation of $[\text{Pd}_2(\mu\text{-Ph}_2\text{SbCH}_2\text{SbPh}_2)_2\text{Cl}_2\text{Ph}_2]$ is the first example of cleavage of a distibine ligand on a metal center and occurs under unusually facile conditions. A solution of $[\text{Pd}(\text{Ph}_2\text{SbCH}_2\text{SbPh}_2)_2\text{Cl}_2]$ in CH_2Cl_2 in a vessel covered with aluminum foil to exclude light was unchanged after several days, proving that the reaction is photochemically induced.

Table 2. Atomic Coordinates and Isotropic Temperature Factors ($\times 10^3$)

atom	x	y	z	$U(\text{\AA}^2)^a$
Pd	0.13578(4)	0.05571(2)	0.58089(3)	16.8(2)
Sb(1)	0.01266(3)	0.15515(2)	0.47016(3)	16.4(2)
Sb(2)	-0.23431(3)	0.04554(2)	0.30367(3)	16.8(2)
Cl	0.13518(13)	-0.00117(6)	0.41414(11)	23.8(6)
C(1)	-0.1823(5)	0.1376(2)	0.3945(4)	20.6(25)
C(11)	0.0159(5)	0.2484(2)	0.5482(4)	16.0(24)
C(12)	-0.0886(5)	0.2856(3)	0.5303(5)	25.1(28)
C(13)	-0.0794(6)	0.3482(3)	0.5749(5)	33.4(32)
C(14)	0.0361(6)	0.3753(3)	0.6370(5)	33.6(31)
C(15)	0.1431(6)	0.3388(3)	0.6540(5)	37.5(32)
C(16)	0.1340(5)	0.2740(3)	0.6124(5)	29.9(30)
C(21)	0.0444(5)	0.1931(2)	0.3269(4)	18.6(24)
C(22)	-0.0152(5)	0.2493(3)	0.2739(5)	25.8(28)
C(23)	0.0034(6)	0.2748(3)	0.1796(5)	29.1(29)
C(24)	0.0850(5)	0.2423(3)	0.1400(5)	25.2(27)
C(25)	0.1467(5)	0.1864(3)	0.1927(5)	25.6(28)
C(26)	0.1273(5)	0.1618(2)	0.2874(5)	21.6(26)
C(31)	-0.4315(5)	0.0478(2)	0.2601(5)	18.7(25)
C(32)	-0.4762(5)	0.0579(3)	0.3463(5)	27.7(29)
C(33)	-0.6037(5)	0.0527(3)	0.3253(6)	32.6(31)
C(34)	-0.6862(5)	0.0381(3)	0.2169(6)	33.2(31)
C(35)	-0.6435(5)	0.0291(3)	0.1314(5)	32.2(30)
C(36)	-0.5173(5)	0.0318(3)	0.1526(5)	26.5(29)
C(41)	-0.2129(5)	0.0710(2)	0.1492(5)	22.0(26)
C(42)	-0.1047(6)	0.0514(3)	0.1331(5)	33.9(32)
C(43)	-0.0843(6)	0.0732(3)	0.0396(5)	40.8(36)
C(44)	-0.1711(6)	0.1129(3)	-0.0404(5)	40.6(35)
C(45)	-0.2797(7)	0.1312(3)	-0.0276(5)	37.5(33)
C(46)	-0.3001(6)	0.1104(3)	0.0675(5)	32.4(31)
C(51)	0.1676(5)	0.1053(2)	0.7271(4)	21.7(26)
C(52)	0.2894(5)	0.1260(3)	0.7891(5)	29.6(30)
C(53)	0.3167(6)	0.1655(3)	0.8851(5)	33.0(31)
C(54)	0.2241(6)	0.1844(3)	0.9216(5)	32.5(31)
C(55)	0.1022(6)	0.1634(3)	0.8612(5)	35.9(33)
C(56)	0.0749(5)	0.1233(3)	0.7657(5)	28.0(29)

^a Equivalent isotropic temperature factor from anisotropic atom. Phenyl groups are labeled C(IJ) where I (1–5) indicates the group and J (1–6) indicates the atoms within one group.

Experimental Section

Physical measurements were made as described previously.¹ The yellow $[\text{Pd}(\text{Ph}_2\text{SbCH}_2\text{SbPh}_2)_2\text{Cl}_2]$ was prepared as described² from $[\text{PdCl}_4]^{2-}$ and the ligand in a 1:2 mol ratio in aqueous acetone: yield 45%; $E_{\text{max}} 32\,000\text{ cm}^{-1}$ ($\epsilon_{\text{mol}} = 27\,400\text{ mol}^{-1}\text{ dm}^3\text{ cm}^{-1}$); $\nu(\text{Pd-Cl}) = 297$ (sh), 278 cm^{-1} , ^1H NMR (CD_2Cl_2 relative to TMS) $\delta(\text{CH}_2) = 2.44$, $\delta(\text{Ph}) = 7.0\text{--}7.5$. Anal. Calcd for $\text{C}_{50}\text{H}_{44}\text{Cl}_2\text{PdSb}_4$: C, 45.9; H, 3.4. Found: C, 45.6; H, 3.4%.

$[\text{Pd}_2(\mu\text{-Ph}_2\text{SbCH}_2\text{SbPh}_2)_2\text{Cl}_2\text{Ph}_2]$. Solutions of $[\text{Pd}(\text{Ph}_2\text{SbCH}_2\text{SbPh}_2)_2\text{Cl}_2]$ (0.04 g, 0.03 mmol) in CH_2Cl_2 (5 cm^3) were photolyzed in two ways.

Method 1. The sample in a pyrex flask was exposed to direct sunlight for a total of 24 h over a period of 3 days. The solution was evaporated to dryness and the residue washed with diethyl ether (5 cm^3) and dried thoroughly *in vacuo*: yield >90% on Pd; $E_{\text{max}} 32\,100\text{ cm}^{-1}$ ($\epsilon_{\text{mol}} = 20\,700\text{ mol}^{-1}\text{ dm}^3\text{ cm}^{-1}$); $\nu(\text{Pd-Cl}) = 271\text{ cm}^{-1}$; ^1H NMR (CD_2Cl_2 relative to TMS) $\delta(\text{CH}_2) = 2.60$, $\delta(\text{Ph}) = 7.0\text{--}7.6$. Anal. Calcd for $\text{C}_{62}\text{H}_{54}\text{Cl}_2\text{Pd}_2\text{Sb}_4$: C, 47.4; H, 3.4. Found: C, 47.9; H, 3.2%.

Method 2. A sample in a pyrex vessel was photolyzed for 24 h with a 30 W fluorescent tube, and the product was worked up in the same manner: yield essentially quantitative based on Pd; ^1H NMR (CD_2Cl_2 relative to TMS) $\delta(\text{CH}_2) = 2.60$, $\delta(\text{Ph}) = 7.0\text{--}7.6$. An identical solution of $[\text{Pd}(\text{Ph}_2\text{SbCH}_2\text{SbPh}_2)_2\text{Cl}_2]$ in CH_2Cl_2 kept in the dark by covering the vessel completely with aluminum foil was unchanged after 3 days.

Crystal Growth. A solution of $[\text{Pd}(\text{Ph}_2\text{SbCH}_2\text{SbPh}_2)_2\text{Cl}_2]$ (ca. 0.05 g) in CH_2Cl_2 (2 cm^3) in a small sample tube was placed in a 100 cm^3 stoppered flask containing 10 cm^3 of diethyl ether, which was left for 4 days exposed to laboratory sunlight. Crystals grew on the walls of the tube, one of which was used

Table 3. Crystal Data for [Pd₂(μ-Ph₂SbCH₂SbPh₂)₂Cl₂Ph₂]

mol formula	C ₆₂ H ₅₄ Cl ₂ Pd ₂ Sb ₄
mol wt	1569.86
cryst syst	monoclinic
space group	<i>P2₁/a</i>
<i>a</i> , Å	11.527(8)
<i>b</i> , Å	20.264(5)
<i>c</i> , Å	12.717(4)
β, deg	112.12(8)
<i>V</i> , Å ³	2751.8
<i>T</i> , K	120
density (calcd), g cm ⁻³	1.895
<i>Z</i>	2
<i>F</i> (000), e	1512
cryst size, mm	0.24 × 0.20 × 0.14
type of data collection	ω
total no. of observations	12226
total no. of unique observations	4240
abs cor	Difabs
no. of data used in refinement	4240
no. of parameters	317
weighting scheme (w ⁻¹)	σ ² (F _o ²) + (0.0368P) ² where P = [Max(F _o ² , 0) + 2F _c ²]/3
λ, Å (Mo Kα)	0.71069
μ, cm ⁻¹	27.2
max 2θ, deg	50.2
<i>S</i>	0.98
max shift/esd	0.01
<i>R</i> (<i>F</i> > 4σ(<i>F</i>), 3462 refs) ^a	0.033
<i>R</i> (all data)	0.045
w <i>R</i> 2 (all data) ^b	0.078

$$^a R = \sum |F_o| - |F_c| / \sum |F_o|, \quad ^b wR2 = [\sum w(F_o^2 - F_c^2)^2 / \sum wF_o^4]^{1/2}.$$

for the X-ray study below: ¹H NMR (CD₂Cl₂) δ(CH₂) 2.60, δ-Ph) 7.0–7.6.

X-ray Structure Determination of [Pd₂(μ-Ph₂SbCH₂SbPh₂)₂Cl₂Ph₂]. The air-stable platy rhomb-shaped crystal was mounted on a glass fiber using the oil–film method⁸ and mounted on an Enraf-Nonius FAST area detector diffractometer. The temperature was maintained at 120 K using an Oxford Cryostream unit. Cell dimensions were obtained from

250 reflections and intensity data for approximately half of reciprocal space recorded.⁹ Systematic absences established the space group *P2₁/a* (no. 14) and the direct method in SHELXS86¹⁰ yielded the heavy atom positions which were fully consistent with the Patterson function. Repeated structure factor and electron density calculations revealed the C atoms. The H atoms were not convincingly located and were added to the model in calculated positions. Ten reflections which overflowed the data collection system were omitted from the refinement. The Difabs absorption correction¹¹ was applied to the isotropic model (correction: max 1.10, min 0.91) and full-matrix least-squares¹² refinement on *F*² converged satisfactorily. Neutral atom scattering factors were taken from ref 13 (Pd, Sb) and SHELXL93¹² (Cl, C, H). Diagrams were prepared using ORTEPII¹⁴ and PLUTO.¹⁵ Additional experimental details are given in Table 3, and Table 2 lists the atomic coordinates.

Acknowledgment. We thank the SERC and B.P. Chemicals Ltd for support (A.F.C.), and Professor M. B. Hursthouse for the X-ray data collection by the SERC X-ray service.

Supplementary Material Available: Listings of anisotropic thermal parameters, hydrogen calculated atomic coordinates, and bond distances and angles (4 pages). Ordering information is given on any current masthead page.

OM940707S

(9) Hursthouse, M. B.; Karaulov, A. I.; Ciechanowicz-Rutkowska, M.; Kolasa, A.; Zankowska-Jasinska, W. *Acta Crystallogr. Sect. C* **1992**, *48*, 1257.

(10) Sheldrick, G. M. *SHELXS86, Program for the Solution of Crystal Structures*; University of Göttingen: Göttingen, FRG, 1986.

(11) Walker, N.; Stuart, D. *Acta Crystallogr. Sect. A* **1983**, *39*, 158.

(12) Sheldrick, G. M. *SHELXL93, Program for the Refinement of Crystal Structures*; University of Göttingen: Göttingen, FRG, 1993.

(13) *International Tables for X-ray Crystallography*; Kynoch: Birmingham, England, 1974; Vol IV.

(14) Johnson, C. K. *ORTEP-II*; Oak Ridge National Laboratory: Oak Ridge, TN, 1976; Report ORNL-5138.

(15) Motherwell, W. D. S.; Clegg, W. *PLUTO, Program for Plotting Molecular and Crystal Structures*; Universities of Cambridge and Göttingen: Cambridge and Göttingen, 1978.

(8) Hope, H. *Acta Crystallogr. Sect. B* **1988**, *44*, 22.

Synthesis, Characterization, and Carbonylation of the Asymmetric Mono-Ring-Functionalized Zirconocenes, $(\eta^5\text{-C}_5\text{H}_5)(\eta^5\text{-C}_5\text{H}_4)\text{P}(\text{C}_6\text{H}_5)_2\text{Zr}(\text{CH}_3)\text{X}$ ($\text{X} = \text{CH}_3, \text{Cl}$)

Wayne Tikkanen,* Amy L. Kim, Karen B. Lam, and Karlos Ruckert

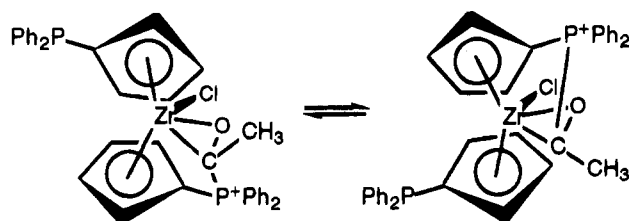
Department of Chemistry and Biochemistry, California State University Los Angeles,
5151 State University Drive, Los Angeles, California 90032

Received September 26, 1994[®]

Summary: The preparation of alkyl, ring-functionalized zirconocenes, $(\eta^5\text{-C}_5\text{H}_5)(\eta^5\text{-C}_5\text{H}_4)\text{P}(\text{C}_6\text{H}_5)_2\text{Zr}(\text{CH}_3)\text{X}$ ($\text{X} = \text{CH}_3$ (**1**), $\text{X} = \text{Cl}$ (**2**)) is described. These compounds insert one molecule of CO to give products which interconvert between an acyl complex and a phosphonium alkoxide at ambient temperatures. The position of equilibrium between the acyl and phosphonium alkoxide complexes depends on the identity of X.

Introduction

We have reported the preparation and carbonylation of two ring-functionalized zirconocenes, bis((diphenylphosphino)cyclopentadienyl)dimethylzirconium(IV) and bis((diphenylphosphino)cyclopentadienyl)chloromethylzirconium(IV).¹ Carbonylation of these molecules gives fluxional products involving phosphine exchange at the carbon derived from CO; the process is illustrated below for $(\eta^5\text{-C}_5\text{H}_4)\text{P}(\text{C}_6\text{H}_5)_2((\eta^5\text{-C}_5\text{H}_4)\text{P}(\text{C}_6\text{H}_5)_2\text{Zr}(\text{OCCCH}_3)\text{Cl}$ (**1**) (the solid state structure of **1** was determined by X-ray methods¹).



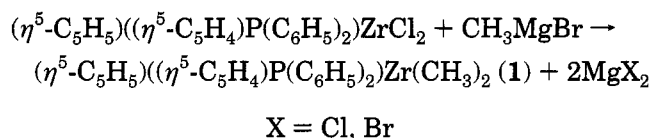
Phosphine Exchange in **1**

We proposed two possible mechanisms for the fluxional process: a dissociative mechanism where phosphine dissociation occurs followed by attack on the coordinated acyl or a displacement or $\text{S}_{\text{N}}2$ type mechanism where attack by the other phosphine displaces the bound phosphorus. To discriminate between these mechanisms, we prepared the ring-functionalized zirconocenes, $(\eta^5\text{-C}_5\text{H}_5)(\eta^5\text{-C}_5\text{H}_4)\text{P}(\text{C}_6\text{H}_5)_2\text{Zr}(\text{CH}_3)\text{X}$ ($\text{X} = \text{CH}_3$ (**1**) and $\text{X} = \text{Cl}$ (**2**)) to examine the behavior of their carbonylation products. The absence of the second phosphine is expected to simplify any fluxional behavior since no second phosphine is present to act as a nucleophile, as required for a displacement mechanism. In addition, **2** is chiral and along with a few other mono-ring-functionalized complexes^{2,3} forms a class of chiral group 4 metallocenes, which, unlike chiral ring bridged

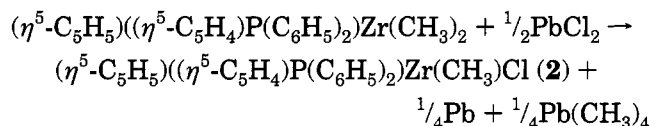
group 4 metallocenes that have been reported,²⁻²¹ have a protecting group blocking access to one of the reactive faces of a coordinated substrate.

Results and Discussion

The preparation of complex **1** is accomplished through interaction of 2 equiv of methylmagnesium bromide (or methyllithium) with the parent dichloro ring-functionalized zirconocene²² in ether:



Complex **2** is prepared by the reaction of **1** with 0.5 equiv of lead chloride:²³



These complexes were characterized by proton and phosphorus NMR spectroscopy and C/H analysis. Sev-

(4) Chen, Z.; Eriks, K.; Halterman, R. L. *Organometallics* **1991**, *10*, 3449-58.

(5) Erker, G.; Berg, K.; Benn, R.; Schroth, G. *Chem. Ber.* **1985**, *118*, 1383-97.

(6) Duthaler, R. O.; Hafner, A.; Alsters, P. L.; Rothe, S. P.; Rihs, G. *Pure Appl. Chem.* **1992**, *64*, 1897-910.

(7) Erker, G.; Aul, R. *Chem. Ber.* **1991**, *124*, 1301-10.

(8) Grossman, R. B.; Davis, W. M.; Buchwald, S. L. *J. Am. Chem. Soc.* **1991**, *113*, 2321-2.

(9) Grossman, R. B.; Doyle, R. A.; Buchwald, S. L. *Organometallics* **1991**, *10*, 1501-5.

(10) Gutmann, S.; Burger, P.; Hund, H. U.; Hofmann, J.; Brintzinger, H. H. *J. Organomet. Chem.* **1989**, *369*, 343-57.

(11) Hoveyda, A. H.; Morken, J. P. *J. Org. Chem.* **1993**, *58*, 4237-44.

(12) Ikegami, S.; Katsuki, T.; Yamaguchi, M. *Chem. Lett.* **1987**, 83-4.

(13) Huang, Q.; Quian, Y.; Tang, Y. *Transition Met. Chem. (London)* **1989**, *14*, 315-8.

(14) Huang, Q.; Qian, Y.; Tang, Y. *J. Organomet. Chem.* **1989**, *368*, 277-86.

(15) Ito, H.; Taguchi, T.; Hanzawa, Y. *Tetrahedron Lett.* **1992**, *33*, 4469-72.

(16) Itsuno, S.; Sakurai, Y.; Shimizu, K.; Ito, K. *J. Chem. Soc., Perkin Trans* **1990**, *1*, 1859-63.

(17) Nugent, W. A. *J. Am. Chem. Soc.* **1992**, *114*, 2768-9.

(18) RajanBabu, T. V.; Nugent, W. A.; Taber, D. F.; Fagan, P. J. *J. Am. Chem. Soc.* **1988**, *110*, 7128-35.

(19) Rheingold, A. L.; Robinson, N. P.; Whelan, J.; Bosnich, B. *Organometallics* **1992**, *11*, 1869-76.

(20) Rieger, B. *J. Organomet. Chem.* **1991**, *420*, C17-C20.

(21) Wild, F. R. W. P.; Wasiucionek, M.; Huttner, G.; Brintzinger, H. H. *J. Organomet. Chem.* **1985**, *288*, 63-7.

(22) Casey, C. P.; Nief, F. *Organometallics* **1985**, *4*, 1218-20.

(23) Wailes, C.; Weigold, H.; Bell, A. P. *J. Organometallic Chem.* **1972**, *34*, 155-64.

[®] Abstract published in *Advance ACS Abstracts*, February 1, 1995.

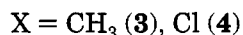
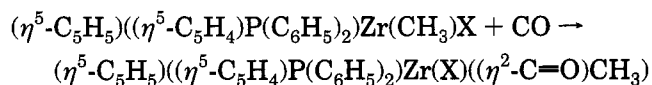
(1) Tikkanen, W.; Ziller, J. W. *Organometallics* **1991**, *10*, 2266-73.

(2) Tainturier, G.; Gautheron, B.; Renaut, P.; Etievant, P. C. R. *Hebd. Seances Acad. Sci., Ser. C* **1975**, *281*, 1035-6.

(3) Renaut, P.; Tainturier, G.; Gautheron, B. *J. Organomet. Chem.* **1978**, *148*, 43-51.

eral samples of **1** and **2** which contained no detectable impurities by ^1H NMR all analyzed somewhat low on carbon. The NMR chemical shifts of the methyl groups and the phosphine-bearing cyclopentadienide are similar to those observed in previously characterized bis-(diphenylphosphinocyclopentadienyl)zirconium complexes.¹

Treatment of pale yellow dichloromethane solutions of **1** and **2** with CO leads to a color change to yellow-orange which accompanies the following reaction:



Although solutions of **3** and **4** are stable at ambient temperatures, attempts to isolate these products as pure solids failed. Removal of solvent from solutions of **3** gave a yellow solid which turned brown after several minutes at room temperature. The NMR spectrum of this brown solid showed no appreciable quantities of **3** present. Analogous workup of **4** gave similar results, although complete decomposition in this case occurs over the course of days.

The ambient temperature proton NMR spectra of **3** showed signs of dynamic behavior, so variable temperature NMR studies of **3** and **4** were undertaken. The spectral changes are completely reversible over this temperature range, and no signs of CO loss are observed. CO loss is not observed even if the samples are freeze-thaw-degassed after carbonylation is complete. This behavior is analogous to that observed for **I**.¹

The region containing the resonances for the methyl and "acyl" groups of **3** is shown in Figure 1. At low temperatures (218 K and lower) a doublet is observed for the "acyl" resonance at δ 1.82 ($J_{\text{P-H}} = 17.3$ Hz) and the methyl signal appears as a singlet at δ -0.47. The region between δ 8.5 and δ 4.5 contains a distinct multiplet for each of the four protons on the functionalized cyclopentadienyl ring, a singlet for the C_5H_5 ring, and two multiplets for the phenyl rings of the phosphine. As the temperature increases, the methyl signal shifts downfield and broadens until about 258 K when the signal sharpens and then until 323 K when a sharp singlet is observed at δ -0.13. The "acyl" doublet similarly broadens and shifts downfield, again, beginning to narrow, finally giving a doublet with $J_{\text{P-H}} = 3.7$ Hz at δ 2.46 at 323 K, the highest temperature investigated. In the downfield region, all the signals broaden and shift with increasing temperature, finally sharpening at 323 K to give a singlet for the cyclopentadienyl ring, four signals for the functionalized cyclopentadienyl ring, and a single complex signal for the phenyl groups.

The proton-decoupled ^{31}P NMR of **3** shows a single singlet at δ 12.6 at 233 K which broadens with increasing temperature. Use of ^{13}CO gives a doublet at low temperatures, $J_{\text{C-P}} = 40.7$ Hz. The proton-decoupled ^{13}C NMR (using enriched ^{13}CO) shows a doublet at δ 39.30 ($J_{\text{P-C}} = 40.7$ Hz). As the temperature is increased, the carbon signal of the labeled CO shifts downfield and broadens without sharpening, even at the warmest temperatures explored. In the ^{31}P NMR, a broad peak can be discerned centered about δ -10 at 318 K.

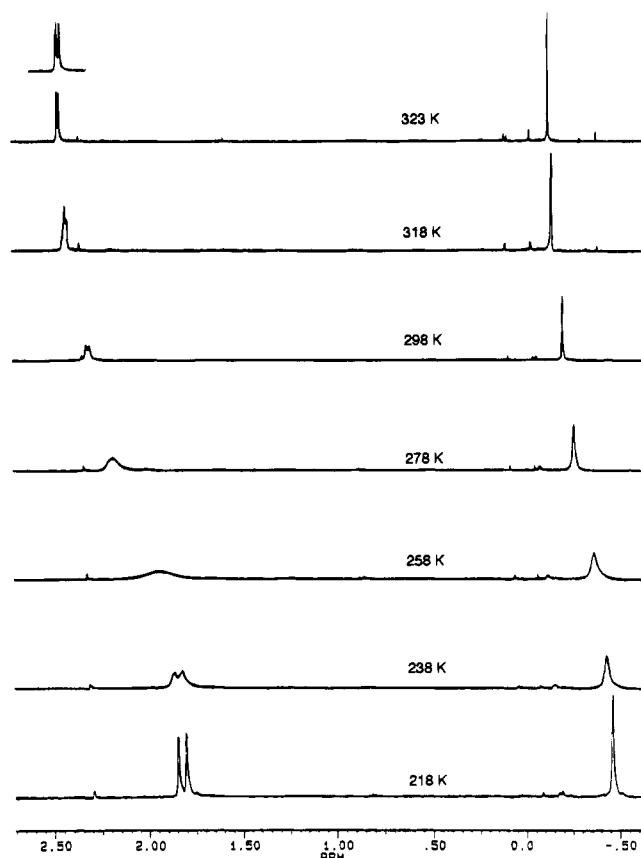


Figure 1. ^1H NMR spectrum of **3** in CD_2Cl_2 between δ -0.5 and δ 2.5 at selected temperatures.

Complex **4**, over the temperature range studied, shows features similar to those of **3** at low temperatures. In the proton NMR, a doublet is observed for the methyl acyl group at about δ 2 at temperatures from 273 (δ 2.02, $J_{\text{P-H}} = 16.8$ Hz) to 314 K (δ 2.07, $J_{\text{P-H}} = 16.2$ Hz). Note the much smaller change in the phosphorus-hydrogen coupling constant. The other spectral features are essentially unchanged over this temperature range, showing only small changes in chemical shifts and some broadening of the lines at higher temperatures. The proton-decoupled phosphorus NMR similarly shows little change; a singlet is observed at about δ 10 ppm over the same temperature range with a slight upfield shift with increasing temperature (δ 8.96 at 314 K; δ 10.73 at 273 K). The ^{31}P resonance at the low-temperature limit of the phosphonium phosphorus in **I** is quite similar, δ 11.68.¹

Scheme 1 shows the processes believed to occur upon carbonylation. Rapid initial lateral insertion of CO and similar unsaturated molecules into the Zr-C bond has been observed by other workers^{1,23-43} and is supported

(24) Erker, G.; Rosenfeldt, F. *J. Organomet. Chem.* **1980**, *188*, C1-C4.

(25) Sonnenberger, D. C.; Mintz, E. A.; Marks, T. J. *J. Am. Chem. Soc.* **1984**, *106*, 3484-91.

(26) Sikora, D. J.; Macomber, D. W.; Rausch, M. D. *Adv. Organomet. Chem.* **1985**, *25*, 318-79.

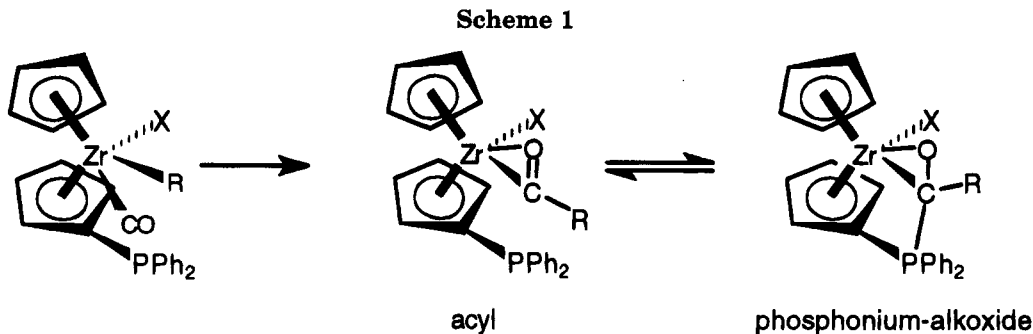
(27) Roddick, D. M.; Bercaw, J. E. *Chem. Ber.* **1989**, *122*, 1579-87.

(28) Marsella, J. A.; Moloy, K. G.; Caulton, K. G. *J. Organomet. Chem.* **1980**, *201*, 389-98.

(29) Martin, B. D.; Matchett, S. A.; Norton, J. R.; Anderson, O. P. *J. Am. Chem. Soc.* **1985**, *107*, 7952-9.

(30) Manriquez, J. M.; McAlister, D. R.; Sanner, R. D.; Bercaw, J. E. *J. Am. Chem. Soc.* **1978**, *100*, 2716-24.

(31) Larson, A. L.; Baker, D. L.; Towne, R. W.; Straus, D. A. *Tetrahedron Lett.* **1991**, *32*, 5893-4.



by theoretical studies;^{44–46} this process forms an acyl complex whose presence is inferred from the NMR data. The chemical shifts of the alkyl groups at the high-temperature limit are similar to that observed by Floriani in the carbonylation of dimethyl- and dibenzylzirconocene.^{36,38} Rapid, reversible attack of the “carbenium-like” carbon leads to an equilibrium between the acyl complex (center) and the phosphonium alkoxide (right) shown in Scheme 1. We describe the structure as a phosphonium alkoxide because of the structural parameters found in the analogous complex **I**¹ and the difference in the phosphorus NMR parameters between **3** and **4** and a complex described as a coordinated η^2 -ylide complex, $\text{Cp}(\text{NO})(\text{I})\text{Mo}(\eta^2\text{-}(\text{CO})(\text{PMe}_3)\text{-}p\text{-tol})$.⁴⁷

The mechanism for the fluxional process is apparently dissociative in nature since the fluxional process is active in the absence of other nucleophiles, demonstrated by the fluxional behavior of **3**. However, the “phosphonium alkoxide” form shown on the right predominates at lower temperatures in complexes **3** and at ambient temperatures in **4**, as shown by the observed P–H couplings. Comparison of the P–H coupling constants at the low- and high-temperature limits for **3** shows that, on average, P is bonded to the acyl carbon about 22% of the time at 323 K. Complex **4** is quite different; the ¹H NMR spectra shows that the phosphonium alkoxide form is predominant at ambient temperatures ($J_{\text{P-H}}$ at 294 K is nearly the same as $J_{\text{P-H}}$ at 273 K, ca. 16 Hz, nearly the same as $J_{\text{P-H}}$ at the low-temperature limit in **3**), a dramatic change in the position of equilibrium. However, the broadening of

signals and lowering of the P–H coupling constant strongly suggests that the same dynamic behavior observed in **3** and **I** also occurs in **4**. The similarity of the coalescence temperatures and NMR spectra for **3** and **I** strongly suggests that the same (dissociative) mechanism occurs in these molecules.

We are currently directing our efforts at investigations of the reactivity and stereochemistry of nucleophilic attack at the acyl carbon in related complexes.

Experimental Section

General Considerations. The compounds described are air sensitive and were prepared using either Schlenk or high-vacuum techniques. Solid compounds were manipulated in a Vacuum Atmospheres Corp. (VAC) HE-43 Dri-Lab with a HE-63P Pedatrol pressure regulator and HE-393 Dri Train. The inert gas used in the glovebox and Schlenk and vacuum lines is either nitrogen or argon which is further purified by passage through activated Chemalog R3–11 catalyst and activated 4A molecular sieves. Solvents were all reagent grade and further purified by standard techniques. $[(\text{C}_5\text{H}_4\text{P}(\text{C}_6\text{H}_5)_2)(\text{C}_5\text{H}_5)\text{ZrCl}_2]$ was prepared as previously described²² or using $\text{C}_5\text{H}_5\text{ZrCl}_3 \cdot \text{DME}$ ⁴⁸ instead of $\text{C}_5\text{H}_5\text{ZrCl}_3$.

Physical Measurements. ¹H and ³¹P NMR spectra were obtained with either Bruker AM-400 or AM-300 spectrometers. Proton NMR spectra were referenced by either the residual proton resonance or internal TMS; ³¹P NMR spectra were referenced against external $\text{P}(\text{OCH}_3)_3$. Elemental analyses were performed by Schwarzkopf Microanalytical Laboratories, Woodside, NY.

$[(\text{C}_5\text{H}_4\text{P}(\text{C}_6\text{H}_5)_2)(\text{C}_5\text{H}_5)\text{Zr}(\text{CH}_3)_2]$ (**1**). $[(\text{C}_5\text{H}_4\text{P}(\text{C}_6\text{H}_5)_2)(\text{C}_5\text{H}_5)\text{ZrCl}_2]$ (5.76 g, 12.1 mmol) was loaded into a Schlenk flask in the glovebox. Then 80 mL of anhydrous ether was added, and the suspension was stirred for about 10 min in an ice bath. Methylmagnesium bromide in ether (8.5 mL, 3 M, 25.4 mmol) was added to the solution and the solution stirred for about 4 h at room temperature. The solvent was removed in vacuo and the residue dried overnight. The brown gray solid was extracted with refluxing pentane overnight in a Soxhlet-type extractor. Removal of the solvent in vacuo gave an off-white solid from the filtrate with a tan solid remaining on the filter. The pentane soluble fraction was extracted a second time in an identical fashion for 16 h (contaminants are present in the solid obtained in the first extraction). The pentane was removed in vacuo and 4.38 g (81% based on $[(\text{C}_5\text{H}_4\text{P}(\text{C}_6\text{H}_5)_2)(\text{C}_5\text{H}_5)\text{ZrCl}_2]$ of **1** were obtained. Proton NMR (CD_2Cl_2): CH_3 , δ –0.41 (s, 6H); C_6H_5 , δ 5.97 (s, 5H); C_5H_4 , δ 6.07 (m, 2H), 6.32 (m, 2H); $\text{P}(\text{C}_6\text{H}_5)_2$, δ 7.34 (m, 10H); $(\text{C}_6\text{D}_6)\text{CH}_3$, δ –0.080 (s, 6H); C_5H_5 , δ 5.75 (s, 5H); C_5H_4 , δ 5.84 (m, 2H), 5.85 (m, 2H); $\text{P}(\text{C}_6\text{H}_5)_2$, δ 7.02 (m, 6 H), 7.40 (m, 4H). ³¹P{¹H} NMR (CD_2Cl_2 ; δ –19.40 (s). Anal. Calcd (found) for $\text{C}_{24}\text{H}_{25}\text{PZr}$: C, 66.17 (64.17); H, 5.78 (5.81); P, 7.11 (6.57).

$[(\text{C}_5\text{H}_4\text{P}(\text{C}_6\text{H}_5)_2)(\text{C}_5\text{H}_5)\text{Zr}(\text{CH}_3)\text{Cl}]$ (**2**). The dimethyl complex, $[(\text{C}_5\text{H}_4\text{P}(\text{C}_6\text{H}_5)_2)(\text{C}_5\text{H}_5)\text{Zr}(\text{CH}_3)_2]$ (2.478 g, 5.69 mmol), was

(32) Lappert, M. F.; Ngoc, T. L. T.; Milne, C. R. C. *J. Organomet. Chem.* **1979**, *174*, C35–C37.

(33) Karsch, H. H.; Müller, G.; Krüger, C. *J. Organomet. Chem.* **1984**, *273*, 195–212.

(34) Guram, A. S.; Guo, Z.; Jordan, R. F. *J. Am. Chem. Soc.* **1993**, *115*, 4902–3.

(35) Gell, K. I.; Schwartz, J. *J. Organomet. Chem.* **1978**, *162*, C11–C15.

(36) Fachinetti, G.; Fochi, G.; Floriani, C. *J. Chem. Soc., Dalton Trans.* **1977**, 1946–50.

(37) Fachinetti, G.; Floriani, C.; Roselli, A.; Pucci, S. *J. Chem. Soc., Chem. Commun.* **1978**, *1978*, 269–70.

(38) Fachinetti, G.; Floriani, C.; Marchetti, F.; Merlino, S. *J. Chem. Soc., Chem. Commun.* **1976**, *1976*, 522–3.

(39) Erker, G. *Acc. Chem. Res.* **1984**, *17*, 103–9.

(40) Erker, G.; Dorf, U.; Krueger, C.; Angermund, K. *J. Organomet. Chem.* **1986**, *301*, 299–312.

(41) Blackburn, T. F.; Labinger, J. A.; Schwartz, J. *Tetrahedron Lett.* **1975**, *35*, 3041–4.

(42) Berry, D. H.; Bercaw, J. E. *Polyhedron* **1988**, *7*, 759–66.

(43) Berg, F. J.; Petersen, J. L. *Organometallics* **1989**, *8*, 2461–70.

(44) Hofmann, P.; Stauffert, P.; Tatsumi, K.; Nakamura, A.; Hoffmann, R. *Organometallics* **1985**, *4*, 404–6.

(45) Lauher, J. W.; Hoffmann, R. *J. Am. Chem. Soc.* **1976**, *98*, 1729–42.

(46) Tatsumi, K.; Nakamura, A.; Hoffmann, P.; Stauffert, P.; Hoffmann, R. *J. Am. Chem. Soc.* **1985**, *107*, 4440.

(47) Bonnesen, P. V.; Yau, P. K. L.; Hersh, W. H. *Organometallics* **1987**, *6*, 1587–90.

(48) Lind, E. C.; Livinghouse, T. *Organometallics* **1990**, *9*, 2426–7.

weighed in the glovebox and dissolved in about 20 mL of toluene, and the solution was filtered into a Schlenk flask. The off white lead chloride (0.805 g, 2.89 mmol) was added to the solution, and the suspension was stirred for 72 h. At that time, the suspension had turned black. The flask was then taken to the vacuum line, and the solvent was removed in vacuo. The dry solid was taken to the glovebox, and the solid was extracted overnight with refluxing toluene. After extraction, most of the solvent was removed in vacuo to give an orange, oily liquid after pumping for several hours. The liquid was layered with an equal amount of pentane and left to mix by diffusion. The solution was left overnight, giving a crystalline product. The supernatant liquor was decanted off, and the crystals were washed twice with 2 mL portions of pentane. The washings and supernatant were discarded. The crystals were then dried under vacuum. The dry crystals were collected, giving 1.92 g of **2** (74% based on **1**). Proton NMR (C_6D_6): CH_3 , δ 0.478 (s, 3H); C_5H_5 , δ 5.80 (s, 5H); C_5H_4 , δ 6.06 (m, 2H), 5.85 (m, 1H), 5.76 (m, 1H); $P(C_6H_5)_2$, δ 7.03 (m, 6H), 7.38 (m, 4 H). Proton NMR (CD_2Cl_2): CH_3 , δ 0.243 (s, 3H); C_5H_5 , δ 6.09 (s, 5H); C_5H_4 , δ 6.54 (m, 1H), 6.30 (m, 1H), 6.24 (m, 1H), 6.17 (m, 1H); $P(C_6H_5)_2$, δ 7.36 (m, 10H). $^{31}P\{^1H\}$ (C_6D_6): δ -18.61 (s). Anal. Calcd (found) for $C_{23}H_{22}PZrCl$: C, 60.57 (59.35); H, 4.86 (5.08); P, 6.79 (6.35).

Carbonylation of 1 and 2. The preparations of **3** and **4** were accomplished by treatment of solutions of the parent complex in dichloromethane- d_2 with excess CO. Typically, a solution about 0.2 M (about 0.015 g in 0.8 mL) was frozen, the inert gas was removed by vacuum, and CO was admitted at pressures from 0.3 to 0.7 atm. The solution was thawed and stirred at room temperature for a period greater than 20

min, at which time carbonylation was invariably complete. NMR data for **3** at 208 K (CD_2Cl_2): 1H C_5H_5 , δ 5.79 (s, 5H); C_5H_4 , δ 5.14 (m, 1H), 5.66 (m, 1H), 5.79 (m, 1H), 6.30 (m, 1H); CH_3 , δ -0.47 (s, 3H); $-CO-CH_3$, δ 1.81 (d, 3H, $J_{P-H} = 17.2$ Hz); $P(C_6H_5)_2$, δ 7.68 (m, 4H), 7.57 (m, 6H); $^{31}P\{^1H\}$ δ 12.6. NMR data for **3** at 310 K (CD_2Cl_2): 1H C_5H_5 , δ 5.62 (s, 5H); C_5H_4 , δ 5.48 (m, 1H), 5.68 (m, 1H), 5.80 (m, 1H), 5.94 (m, 1H); CH_3 , δ -0.18 (s, 3H); $-CO-CH_3$, δ 2.36 (d, 3H, $J_{P-H} = 6.0$ Hz); $P(C_6H_5)_2$, δ 7.43 (m, 10 H); $^{31}P\{^1H\}$ δ 4.4 (br). 1H NMR data for **4** at 294 K (CD_2Cl_2): C_5H_5 , δ 6.04 (s, 5H); C_5H_4 , δ 5.49 (s, 1H), 5.69 (s, 1H), 6.28 (s, 1H), 6.63 (s, 1H); $-CO-CH_3$, δ 2.03 (d, 3H, $J_{P-H} = 16.4$ Hz); $P(C_6H_5)_2$, δ 7.62 (m, 10H).

Acknowledgment. The purchase of the Bruker AM-400 NMR spectrometer was supported in part by PHS grant RR-08101 from the NIH-MBRS program, NSF Grant DMB-8503839, and grants from the W. M. Keck Foundation and the Camille and Henry Dreyfus Foundation. The NSF is acknowledged for partial support of the purchase of the Bruker AM-300 spectrometer. K.L. thanks the Department of Energy for support through the MAERC program, and A.L.K. thanks the Council on Undergraduate Research for summer support through an AIURP fellowship. K.R. was supported by the NIH Bridges to the Future program. Acknowledgment is also made to the donors of the Petroleum Research Fund, administered by the American Chemical Society, for partial support of this research.

OM940745B

Hybrid Phosphorus and Sulfur Donor Ligands. Bridged Thiolato Complexes

Shiuh-Tzung Liu,* Duen-Ren Hou, Tu-Chen Lin, Ming-Chu Cheng, and Shie-Ming Peng

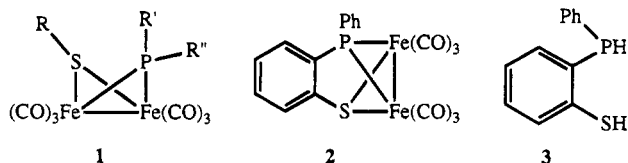
Department of Chemistry, National Taiwan University, Taipei, Taiwan 106, Republic of China

Received October 3, 1994[®]

Summary: Reaction of *o*-C₆H₄(PPhH)(SH) (**3**) with Mn(CO)₅Br and Re(CO)₅Br in chloroform provided sulfido-bridged binuclear complexes {*fac*-[*o*-C₆H₄(PPhCl)(μ₂-S)]Mn(CO)₃]₂ (**4**) and [*o*-C₆H₄(PPhH)(μ₂-Br)Re(CO)₇] (**5**), respectively. Both complexes **4** and **5** were characterized by spectral and crystal structural analyses. The hydrogen atom of the secondary phosphine moiety (P–H) of **3** was replaced by a chlorine atom in dimanganese complex **4** to form P–Cl but was retained in rhenium complex **5**. Methanolysis of **4** gave methoxyl-substituted product {*fac*-[*o*-C₆H₄(PPh(OCH₃))(μ₂-S)]Mn(CO)₃]₂.

Introduction

Bridging phosphido- and sulfidometal complexes have received much attention due to their uncommon coordination modes and properties,^{1–4} and few metal complexes containing both functionalities in the same molecule, such as **1** and **2**, are known.^{5–8} Synthesis of



a mixed thiolato- and phosphidodiiron species **1** was reported by Evertz and Huttner and its reactivity was investigated by Seyferth and co-workers. These works were mainly devoted to iron carbonyl complexes. Here, we present work on selective formation of sulfidometal complexes from the reaction of mixed donor ligand **3** with BrMn(CO)₅ and BrRe(CO)₅.

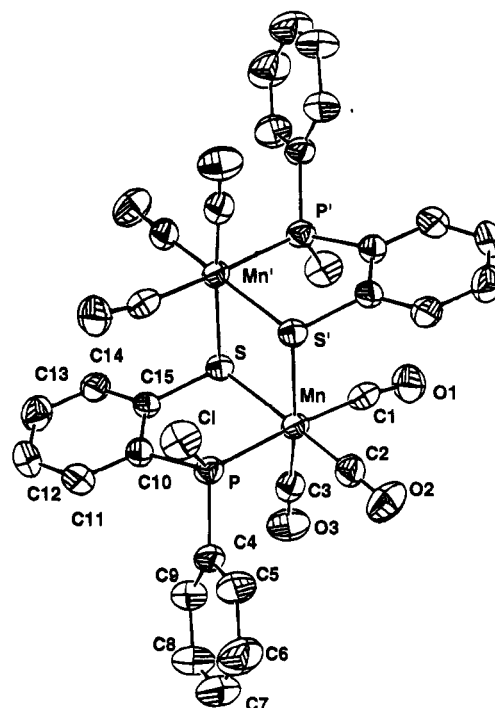


Figure 1. ORTEP plot of manganese(I) complex **4**.

Results and Discussion

Reaction of **3** with two equimolar quantities of Mn(CO)₅Br in refluxing chloroform overnight provided crude product **4** (Scheme 1). Upon recrystallization from a mixture of tetrahydrofuran and ether, binuclear manganese complex **4** was obtained as a yellow-orange crystalline solid in 53% yield. Spectral data of complex **4** include three absorptions (2024, 1963, 1931 cm⁻¹) for carbonyl ligands in the infrared spectrum, a singlet at 173 ppm in the ³¹P NMR spectrum, and a multiplet absorption in the range 7.94–7.71 ppm for aromatic protons in the ¹H NMR spectrum, but these spectral data are insufficient to determine the exact structure of **4**. X-ray crystal structural analysis confirms the formulations of **4** (Figure 1) that clearly indicates the complex to be a sulfido-bridged binuclear species.

Atomic coordinates and selected bond lengths and angles of complex **4** are given in Tables 1 and 2, respectively. Complex **4** possesses a crystallographic center of symmetry. Both manganese atoms are in identical octahedral environments constituted by three facially coordinated carbonyl ligands, one phosphorus, and two sulfur donors. These sulfur donors act as bridges between two metal ions to form a four-membered core; the Mn–Mn distance at 3.598(2) Å indicates

[®] Abstract published in *Advance ACS Abstracts*, February 1, 1995.

(1) Collman, J. P.; Hegedus, L. S.; Norton, J. R.; Finke, R. G. *Principles and Applications of Organotransition Metal Chemistry*; University Science Books: Mill Valley, CA, 1987; p 66.

(2) Reviews of sulfido complexes: (a) Stephan, D. W. *Coord. Chem. Rev.* **1989**, *95*, 41. (b) Seyferth, D.; Anderson, L. L.; Villafane, F.; Cowie, M.; Hiltz, R. W. *Organometallics* **1992**, *11*, 3262. (c) Seyferth, D.; Brewer, K. S.; Wood, T. G.; Cowie, M.; Hiltz, R. W. *Organometallics* **1992**, *11*, 2570 and references therein.

(3) Reviews of phosphido complexes: (a) Adams, M. R.; Gallucci, J.; Wojcicki, A.; Long, G. J. *Inorg. Chem.* **1992**, *31*, 2. (b) Braunstein, P.; de Jesus, E.; Tiripicchio, A.; Ugozzoli, F. *Inorg. Chem.* **1992**, *31*, 411. (c) Baker, R. T.; Calabrese, J. C.; Krusic, R. J.; Therien, M. J.; Trogler, W. C. *J. Am. Chem. Soc.* **1988**, *110*, 8392 and references therein.

(4) Huttner, G.; Knoll, K. *Angew. Chem., Int. Ed. Engl.* **1987**, *26*, 743.

(5) Mckennis, J. S.; Kyba, E. P. *Organometallics* **1983**, *2*, 1249.

(6) Evertz, K.; Huttner, G. *Chem. Ber.* **1988**, *121*, 143.

(7) Seyferth, D.; Brewer, K. S.; Womack, G. B.; Archer, C. M. *J. Organomet. Chem.* **1993**, *446*, 167.

(8) Song, L.-C.; Li, Y.; Hu, Q.-M.; Wang, J.-T.; Zhao, W.-J.; Fang, Y.-Q.; Zhang, S. *Chem. J. Chin. Univ.* **1990**, *11*, 154.

(9) Kyba, E. P.; Clubb, C. N. *Inorg. Chem.* **1984**, *23*, 4766.

Scheme 1

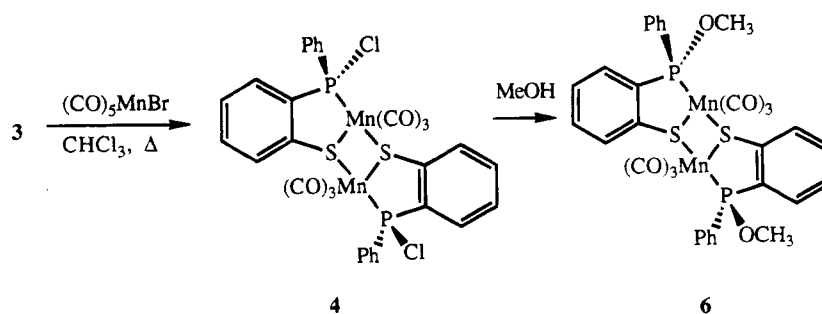


Table 1. Atomic Coordinates and Thermal Parameters of 4

	x	y	z	$B_{\text{iso}}, \text{\AA}^2$
Mn	0.12326(5)	0.52913(3)	0.98610(11)	2.73(3)
S	-0.01342(9)	0.47796(6)	0.77501(18)	2.77(6)
P	0.18839(10)	0.43758(6)	1.06479(20)	2.97(6)
Cl	0.17512(11)	0.39987(7)	1.33580(21)	4.85(8)
O1	0.0563(3)	0.65309(17)	0.8666(6)	4.78(21)
O2	0.2932(3)	0.58421(19)	1.2743(6)	5.58(22)
O3	0.2358(3)	0.53258(19)	0.6580(5)	5.10(22)
C1	0.0754(4)	0.6045(3)	0.9085(7)	3.2(3)
C2	0.2257(4)	0.56270(24)	1.1651(8)	3.5(3)
C3	0.1917(4)	0.53059(23)	0.7871(8)	3.31(24)
C4	0.3242(4)	0.42724(22)	1.0757(8)	3.4(3)
C5	0.3937(4)	0.4381(3)	1.2527(9)	5.0(3)
C6	0.4969(5)	0.4337(3)	1.2526(12)	6.5(4)
C7	0.5276(5)	0.4197(3)	1.0784(14)	6.9(5)
C8	0.4595(5)	0.4098(3)	0.9029(11)	6.2(4)
C9	0.3577(4)	0.4138(3)	0.9009(9)	4.5(3)
C10	0.1238(4)	0.38465(22)	0.8836(7)	2.99(24)
C11	0.1552(4)	0.32531(24)	0.8724(8)	3.8(3)
C12	0.0966(5)	0.28583(24)	0.7390(9)	4.3(3)
C13	0.0076(4)	0.3053(3)	0.6171(8)	4.2(3)
C14	-0.0244(4)	0.36343(24)	0.6272(7)	3.45(25)
C15	0.0322(3)	0.40356(21)	0.7605(7)	2.73(23)
A1	0.5743(24)	0.7557(17)	0.248(20)	47.0(54)
A2	0.572(3)	0.7688(22)	-0.006(18)	55.5(52)
A3	0.706(3)	0.250(3)	0.16(3)	45.8(101)
A4	0.697(3)	0.237(4)	-0.10(3)	63.7(85)

Table 2. Selected Bond Lengths (\AA) and Angles (deg)

Mn-S	2.368(2)	S-Mn-S _a	82.24(6)
Mn-S _a	2.408(2)	S-Mn-P	85.30(6)
Mn-P	2.242(2)	S-Mn-C1	95.1(2)
Mn-C1	1.839(6)	S-Mn-C2	174.4(2)
Mn-C2	1.795(6)	S-Mn-C3	90.7(2)
Mn-C3	1.780(6)	S _a -Mn-P	92.57(5)
S-C15	1.780(5)	P-Mn-C1	176.0(2)
P-C10	1.789(5)	P-Mn-C2	90.8(2)
P-Cl	2.055(2)	P-Mn-C3	87.6(2)
C1-O1	1.135(7)	Mn-S-Mn _a	97.76(6)
C2-O2	1.147(7)	Mn-P-C1	118.81(8)
C3-O3	1.152(7)		

no metal-metal bond. The metal-carbon bond *trans* to the phosphorus donor (Mn-C1) is longer than those *trans* to the sulfur ones due to the *trans* influence. A chlorine atom, instead of the expected hydrogen atom, is identified as a substituent on the phosphorus atom consistent with the absence of P-H coupling in the NMR spectrum.

Reaction of **3** with $\text{Re}(\text{CO})_5\text{Br}$ under similar conditions provided a sulfido complex **5**. The ^{31}P NMR spectrum of **5** in CDCl_3 shows a singlet at δ 26.7 ppm, and the ^1H NMR spectrum shows, besides the signal due to aromatic protons, a doublet at 7.44 ($J_{\text{P-H}} = 373$ Hz) ppm for the shift of P-H. Both spectral data clearly indicate the coordination of a secondary phosphine to the metal ion. Unlike the manganese complex **3**, the P-H moiety in complex **5** was not replaced by a chlorine atom to form P-Cl. The structure of this complex is confirmed by

Table 3. Atomic Coordinates and Thermal Parameters of 5

	x	y	z	$B_{\text{iso}}, \text{\AA}^2$
Re1	0.62462(9)	0.83726(5)	0.11278(7)	2.73(4)
Re2	0.40797(9)	0.66407(6)	0.07815(7)	3.43(5)
Br	0.44577(25)	0.77640(15)	-0.04839(18)	4.21(13)
S	0.6100(6)	0.7150(3)	0.2027(4)	3.1(3)
P	0.7795(6)	0.7694(3)	0.0313(4)	2.8(3)
Cl	0.4914(22)	0.8799(12)	0.1787(15)	3.9(12)
O1	0.4121(15)	0.9082(9)	0.2202(12)	5.2(10)
C2	0.6383(23)	0.9255(13)	0.0285(17)	4.2(13)
O2	0.6459(16)	0.9778(9)	-0.0233(13)	6.0(11)
C3	0.7554(19)	0.8774(1)	0.2280(16)	2.9(11)
O3	0.8316(15)	0.8999(9)	0.3009(11)	5.5(9)
C4	0.9224(20)	0.8119(11)	0.0018(15)	2.9(10)
C5	0.9770(20)	0.8746(13)	0.0549(16)	4.1(14)
C6	1.0840(24)	0.9077(13)	0.0279(20)	5.3(16)
C7	1.1416(22)	0.8794(12)	-0.0538(18)	4.4(13)
C8	1.0857(23)	0.8155(14)	-0.1087(17)	5.0(14)
C9	0.9780(22)	0.7809(12)	-0.0824(17)	3.9(12)
C10	0.8292(21)	0.6850(11)	0.1097(14)	3.4(12)
C11	0.9307(22)	0.6423(12)	0.0947(17)	4.3(12)
C12	0.948(3)	0.5717(13)	0.1492(20)	5.8(15)
C13	0.865(3)	0.5470(14)	0.2149(18)	5.5(16)
C14	0.7679(24)	0.5926(13)	0.2327(16)	4.5(14)
C15	0.7438(19)	0.6611(13)	0.1773(14)	3.3(11)
C16	0.518(3)	0.5991(12)	0.0042(19)	5.0(16)
O16	0.5845(16)	0.5633(9)	-0.0388(12)	5.5(9)
C17	0.3853(20)	0.5898(13)	0.1767(18)	4.2(13)
O17	0.3746(18)	0.5454(9)	0.2430(14)	7.0(11)
C18	0.2546(23)	0.6327(12)	-0.0189(21)	5.2(15)
O18	0.1624(18)	0.6123(10)	-0.0855(15)	7.8(12)
C19	0.2976(22)	0.7290(12)	0.1464(16)	3.8(12)
O19	0.2350(15)	0.7652(9)	0.1903(11)	4.8(9)

Table 4. Selected Bond Distances (\AA) and Bond Angles (deg) of 5

Re1-Br	2.661(3)	Re2-Br	2.633(3)
Re1-S	2.479(6)	Re2-S	2.510(6)
Re1-P	2.414(6)	Re2-C16	2.00(2)
Re1-C1	1.92(2)	Re2-C17	1.85(2)
Re1-C2	1.92(2)	Re2-C18	1.88(3)
Re1-C3	1.90(2)	Re2-C19	1.96(2)
Br-Re1-S	82.6(2)	Br-Re2-S	82.6(1)
Br-Re1-P	84.8(2)	Br-Re2-C16	90.0(6)
Br-Re1-C1	91.2(6)	Br-Re2-C17	175.5(7)
Br-Re1-C2	93.1(7)	Br-Re2-C18	93.8(7)
Br-Re1-C3	178.0(6)	Br-Re2-C19	88.7(5)
S-Re1-P	81.5(2)	S-Re2-C16	89.9(7)
S-Re1-C1	92.4(6)	S-Re2-C17	93.9(7)
S-Re1-C2	173.4(6)	S-Re2-C18	176.0(7)
S-Re1-C3	95.9(6)	S-Re2-C19	91.0(7)
P-Re1-C1	173.1(7)	Re1-Br-Re2	92.32(8)
P-Re1-C2	93.2(6)	Re1-Br-Re2	99.9(2)
P-Re1-C3	93.6(6)		

X-ray structural analysis. Atomic coordinates and selected bond distances and angles are listed in Tables 3 and 4, respectively. As the ORTEP plot of **5** (Figure 2) shows, both rhenium fragments are bridged unsymmetrically by bromide and thiolato ligands. The large distance of Re-Re [3.819(2) \AA] indicates no bonding

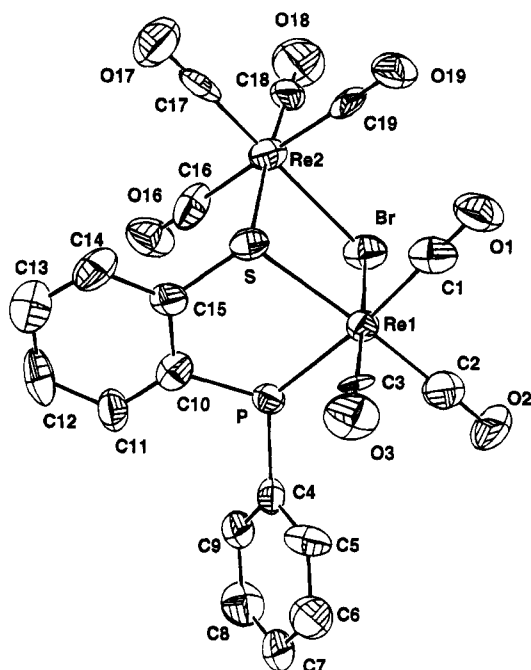
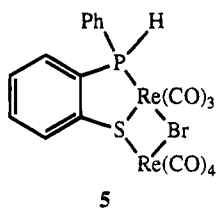


Figure 2. ORTEP plot of rhenium complex 5.

interaction between them. Inspection of the core of the four-membered ring [torsional angles: S–Re1–Br–Re2 11.7(1)°; Re1–Br–Re2–S –11.5(1)°; Br–Re2–S–Re1 12.6(1)°; Re2–S–Re1–Br –12.4(1)°] reveals that one atom in the ring is bent from the plane of the other three by about 12°. The coordination spheres of both Re1 and Re2 are roughly octahedral with three carbonyl ligands occupying a *facial* arrangement around Re1 and substituted donors (thiolato and bromide) in a *cis* relationship around the other rhenium atom (Re2). The bond distances of rhenium to carbonyl ligands (Re–C) decrease according to the order of *trans* ligands of phosphine, thiolate, and bromide (Table 4), which is a consequence of the *trans* influence, as previously seen in the manganese complex 4.



From these results, it appears that the reaction of 3 with Mn(CO)₅Br or Re(CO)₅Br tends to form a sulfido-bridged complex instead of a phosphido complex, but the formation of dinuclear cores differs for the two metal complexes because the bromide ligand is retained by the rhenium complex, whereas the manganese complex loses its bromide ligand, allowing two sulfur donors to form the dinuclear species. As expected, the phosphorus–chloride bond readily underwent methanolysis to give methoxyl-substituted product 6. The P–Cl bond in 4 is similarly reactive to those in (μ -chlorophosphido) species.^{6,7}

Experimental Section

¹H and ³¹P NMR spectra were determined on a Bruker AC-E 200 or a Bruker AM-300WB spectrometer. Chemical shifts

Table 5. Crystal Data for Complexes 4 and 5

compd	4 ^a /5(ether)	5
formula	C ₁₅ H ₉ ClMnPSO ₃ ^c 4/5[(CH ₃ CH ₂)O]	C ₁₉ H ₁₀ BrPSO ₇ Re ₂
fw	450.07	865.67
cryst syst	monoclinic	monoclinic
space group	P2 ₁ /c	P2 ₁ /c
temp, K	298	298
a, Å	13.431(8)	10.478(4)
b, Å	22.319(5)	17.946(14)
c, Å	6.751(1)	12.361(4)
β , deg	102.08(3)	102.31(3)
V, Å ³	1979(1)	2271(2)
F(000)	918.4	1584
Z	4	4
D _{calc} , gcm ⁻³	1.510	2.532
2 θ range, deg	19.18–24.28	18.44–22.56
μ , mm ⁻¹	0.99	5.58
scan type	ω -2 θ	ω -2 θ
radiation	Mo K α	Mo K α
cryst dims, mm ³	0.30 × 0.30 × 0.30	0.35 × 0.35 × 0.40
scan width, deg	0.80 + 0.35 tan θ	0.75 + 0.35 tan θ
transm range	0.87, 1.00	0.23, 1.00
2 θ max, deg	45.0	45.0
reflns, measd	2588	2963
no. of unique refln	2587	2963
no. of refln obsd ^d	2072	2051
computation	NRCS DP-VAX ^b	NRCS DP-VAX
soln method	heavy atom	heavy atom
no of params	236	280
R ^c	0.037	0.054
R _w ^c	0.039	0.057
S ^c	2.81	4.33

^a $I > 2\sigma(I)$. ^b Reference 11. ^c $R = \sum |F_o - F_c| / \sum F_o$; $R_w = [\sum w(F_o - F_c)^2 / \sum w(F_o)^2]^{1/2}$; $S = [\sum w(F_o - F_c)^2 / (\text{no. of reflns} - \text{no. of params})]$.

are given in parts per million relative to 85% H₃PO₄ for ³¹P NMR spectra in CDCl₃, unless otherwise noted. Infrared spectra were recorded on a Bio-Rad FTS-40 instrument. Elemental analyses were made on a Perkin-Elmer 240C instrument. All reactions, manipulations, and purification steps involving phosphines were performed under a dry nitrogen atmosphere. Ligand 3 was prepared according to the previously reported method.⁹ Chloroform was filtered through alumina and distilled over phosphorus pentoxide under nitrogen.

Synthesis of {*fac*-[*o*-C₆H₄(PPhCl)(μ -S)]Mn(CO)₃}₂ (4). A mixture of Mn(CO)₅Br (348.8 mg, 1.27 mmol) and ligand 3 (138.2 mg, 0.63 mmol) in chloroform (14 mL) was heated to reflux for 3 h. Concentration of the reaction mixture yielded the crude product, which was recrystallized from ether and tetrahydrofuran to give 4 as an orange-yellow crystalline solid (202.5 mg, 52%); mp 218–222 °C dec; IR (CH₂Cl₂) ν_{CO} = 2024, 1963, 1931 cm⁻¹; ¹H NMR δ 7.94–7.71 (m); ³¹P NMR (CDCl₃) δ 173. Anal. Calcd for C₃₀H₁₈Cl₂O₆P₂S₂Mn₂: C, 46.12; H, 2.32. Found: C, 46.15; H, 2.31.

Synthesis of [*o*-C₆H₄(PPhH)(μ -S)](μ -Br)Re₂(CO)₇ (5). A mixture of Re(CO)₅Br (370 mg, 0.91 mmol) and 3 (100 mg, 0.458 mmol) in chloroform (7 mL) was heated to reflux for 16 h. The reaction mixture was concentrated, and the residue was chromatographed on silica gel eluted with chloroform and hexane. A yellow band fraction was collected and concentrated to give the desired product as a light yellow solid (187 mg, 47%); mp 156–158 °C dec; IR (KBr) ν_{CO} = 2109, 2038, 2005, 1958, 1944, 1898 cm⁻¹; ¹H NMR δ 7.8–7.2 (m, 9 H), 7.44 (d, $J_{\text{P-H}}$ = 373 Hz, 1 H); ³¹P NMR δ 26.9. Anal. Calcd for C₁₉H₁₀BrO₇PSRe₂: C, 26.36; H, 1.16. Found: C, 26.57; H, 1.29.

Synthesis of {*fac*-[*o*-C₆H₄(PPh(OCH₃))(μ -S)]Mn(CO)₃}₂ (6). A solution of 4 (57.2 mg, 0.073 mmol) in methanol was heated to reflux for 1 h. Upon concentration of the reaction mixture, the residue was filtered through silica gel to give the desired product 6 as a yellow solid (48.0 mg, 85%); IR (KBr) 2015, 1951, 1921 cm⁻¹; ¹H NMR δ 7.8–7.2 (m, 18 H), 3.93 (br, singlet, 6 H); ³¹P NMR δ 179.6. Anal. Calcd for C₃₂H₂₄O₈P₂S₂Mn₂: C, 49.76; H, 3.13. Found: C, 49.50; H, 3.50.

Crystallography. Suitable single crystals of complexes **4** and **5** for X-ray analysis were obtained by recrystallization from ether and tetrahydrofuran at about $-20\text{ }^{\circ}\text{C}$. Data were measured and collected on an Enraf-Nonius CAD-4 diffractometer. The heavy-atom method was used and least-squares refinement was undertaken with all non-hydrogen atoms anisotropic. Atomic scattering factors were taken from ref 10. The computing program was the NRCC SDP VAX package.¹¹ Refinement details follow: F_o and F_c are the observed and calculated structure factor amplitudes, respectively; the function minimized was $\sum w(F_o - F_c)^2$, with $w^{-1} = \sigma^2(F_o)$, $\sigma(F_o)$ from counting statistics; $R_F = \sum |F_o - F_c| / \sum (F_o)$; $R_w = [\sum w(F_o - F_c)^2 / \sum w(F_o)^2]^{1/2}$; $S = [\sum (w(F_o - F_c)^2) / (\text{no. of reflections} - \text{no. of params})]^{1/2}$. Molecules of complex **4** are aligned along the axis

(10) *International Tables for X-ray Crystallography*; Kynoch Press: Birmingham, U.K., 1974; Vol. IV.

(11) Gabe, E. J.; Lee, F. L. *Acta Crystallogr.* **1981**, *A37*, S339.

perpendicular to the plane defined by Mn-S-Mn_a-S_a, and solvent molecules are disorderly distributed between the stack of the complex molecules. The computation of solvent molecules was treated as atoms A1-A4 using the atomic scattering factor of an oxygen atom.

Acknowledgment. We thank the National Science Council (NSC 83-0208-M002-063) of the Republic of China for financial support.

Supplementary Material Available: Lists of thermal parameters and complete bond distances and bond angles of both complexes **4** and **5** (4 pages). Ordering information is given on any current masthead page.

OM940769I

Synthesis and Molecular Structure of $[(\text{Me}_3\text{Si})_2\text{P}\{\text{Me}_2\text{Ga}\}_2\text{PMe}]_2$. A Phosphinogallane Containing a P–P Bond

Jaye A. Burns, William T. Pennington, and Gregory H. Robinson*

Howard L. Hunter Chemistry Laboratory, Department of Chemistry, Clemson University,
 Clemson, South Carolina 29634-1905

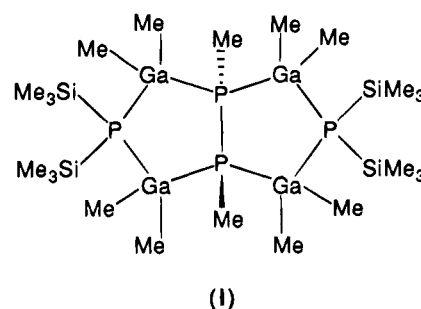
Received October 18, 1994[®]

Summary: The $\text{Me}_3\text{Ga}-\text{PMe}_3$ Lewis acid–base adduct has been prepared by reaction of Me_3Ga with PMe_3 in toluene and characterized by ^1H NMR, ^{31}P NMR, melting point, elemental analyses (C and H), and single crystal X-ray diffraction. The adduct, possessing approximate C_{3v} symmetry, crystallizes in the orthorhombic space group Pnma (No. 62) with unit cell parameters $a = 12.704(1) \text{ \AA}$, $b = 11.1736(9) \text{ \AA}$, $c = 7.8059(6) \text{ \AA}$, $D_{\text{calcd}} = 1.14 \text{ g/cm}^3$, and $V = 1114 \text{ \AA}^3$ for $Z = 4$. Refinement converged at $R = 0.048$, $R_w = 0.062$ for 482 observed reflections. The $\text{Ga}-\text{P}$ distance in $\text{Me}_3\text{Ga}-\text{PMe}_3$ is $2.455(4) \text{ \AA}$. Reaction of $\text{Me}_3\text{Ga}-\text{PMe}_3$ with tris(trimethylsilyl)phosphine ($\text{P}(\text{SiMe}_3)_3$) in toluene affords the novel

phosphinogallane $[(\text{Me}_3\text{Si})_2\text{P}\{\text{Me}_2\text{Ga}\}_2\text{PMe}]_2$, which has been characterized by ^1H NMR, ^{31}P NMR, elemental analyses (C and H), IR, and single crystal X-ray diffraction. This complex resides about a center of symmetry and crystallizes in the triclinic space group $\text{P}\bar{1}$ (No. 2) with unit cell parameters $a = 9.983(2) \text{ \AA}$, $b = 11.628(2) \text{ \AA}$, $c = 9.859(1) \text{ \AA}$, $\alpha = 94.06(1)^\circ$, $\beta = 106.69(1)^\circ$, $\gamma = 91.98(2)^\circ$, $D_{\text{calcd}} = 1.29 \text{ g/cm}^3$, and $V = 1091 \text{ \AA}^3$, for $Z = 1$. Refinement converged at $R = 0.074$, $R_w = 0.092$ for 1133 observed reflections. The mean $\text{Ga}-\text{P}$ distance in the title compound is $2.44(4) \text{ \AA}$. This bicyclic phosphinogallane consists of two fused planar Ga_2P_3 five-membered rings sharing a common base with a $\text{P}-\text{P}$ distance of $2.25(3) \text{ \AA}$.

Introduction

The interaction of phosphorus-containing compounds with organogallium moieties, affording phosphinogallanes, is of current interest.¹ Although the corresponding chemistry of aluminum–nitrogen systems, aminoalanes,² has been developed to a greater extent than that of phosphinogallanes, there are some characteristics of aminoalanes that may be germane to phosphinogallane chemistry—specifically, the molecular assembly of larger Al–N systems from intermolecular condensation reactions. To this end, we sought to explore the feasibility of assembling larger Ga–P oligomers from reactions involving discrete molecular phosphinogallanes. The Lewis acid–base adduct $\text{Me}_3\text{Ga}-\text{PMe}_3$ was prepared, its solid state structure determined, and its reaction with $\text{P}(\text{SiMe}_3)_3$ to give the bicyclic phosphinogallane, $[(\text{Me}_3\text{Si})_2\text{P}\{\text{Me}_2\text{Ga}\}_2\text{PMe}]_2$ (I), was studied.



This novel compound, containing two fused Ga_2P_3 five-membered rings, is the first phosphinogallane containing a $\text{P}-\text{P}$ bond.

Experimental Section

General Comments. Standard Schlenk techniques were employed in conjunction with an inert atmosphere drybox (Vacuum Atmospheres HE-43 Dri-Lab). Solvents were distilled over sodium benzophenone under an atmosphere of argon prior to use. Trimethylgallium was obtained from Ethyl Corp., and trimethylphosphine was purchased from Strem Chemical Co.; both were used as received. Tris(trimethylsilyl)phosphine ($\text{P}(\text{SiMe}_3)_3$) was prepared in this laboratory by published procedures.³ Elemental analyses were performed by E + R Microanalytical Laboratories (Corona, NY). NMR spectra were recorded on a Bruker AC300 FT-NMR spectrometer and referenced to residual CDCl_3 for ^1H (δ 7.26) and to 85% H_3PO_4 for ^{31}P . X-ray diffraction data were collected either on a Syntex P2₁ or Rigaku AFC7R single crystal diffractometer.

Synthesis of $\text{Me}_3\text{Ga}-\text{PMe}_3$. A reaction vessel was charged with 10 mL of toluene and Me_3Ga (5 mmol) inside the drybox. To this solution was added trimethylphosphine (5 mmol), resulting in a colorless, homogeneous solution. After being stirred at room temperature for a few hours, the system was placed in the freezer (-10°C). After several days in the freezer and subsequent concentration of solvent, a multitude of rectangular, colorless, crystals ($\text{mp} = 56^\circ\text{C}$) resulted (0.812 g, 85.0% yield). ^1H NMR (CDCl_3): δ -0.65 (d, 9H, GaCH_3), 1.13 (d, 9H, PCH_3). $^{31}\text{P}\{^1\text{H}\}$ NMR (CDCl_3): δ -144.1 (s). Anal. Calcd (found) for $\text{C}_6\text{H}_{18}\text{PGa}$: C, 37.75 (38.02); H, 9.50 (9.27).

Synthesis of $[(\text{Me}_3\text{Si})_2\text{P}\{\text{Me}_2\text{Ga}\}_2\text{PMe}]_2$ (I). A reaction vessel was charged with freshly prepared $\text{Me}_3\text{Ga}-\text{PMe}_3$ (1.1 mmol) and toluene (10 mL). To this solution, $\text{P}(\text{SiMe}_3)_3$ (1.5 mmol) was added. The resulting solution was clear and homogeneous and was stirred at room temperature overnight before being placed into the freezer. Concentration of solvent after several days resulted in a conglomerate of small, colorless, crystals (0.225 g) ($\text{mp} = 249^\circ\text{C}$). ^1H NMR (CDCl_3): δ 0.147 (d, 36H, SiCH_3), $0.258-0.342$ (m, 24H, GaCH_3), 2.193

(3) Becker, G.; Schmidt, H.; Uhl, G.; Uhl, W. *Inorg. Synth.* **1990**, *27*, 243.

[®] Abstract published in *Advance ACS Abstracts*, January 15, 1995.
 (1) (a) Wells, R. L.; McPhail, A. T.; Jones, L. J.; Self, M. F. *Organometallics* **1992**, *11*, 2694. (b) Wells, R. L.; Aubuchon, S. R.; Self, M. F.; Jasinski, J. P.; Woudenberg, R. C.; Butcher, R. J. *Organometallics* **1992**, *11*, 3370.

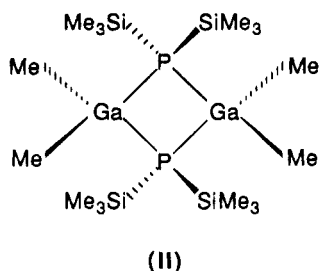
(2) Robinson, G. H. In *Organoaluminanes: Unusual Al–N Systems*. *Coordination Chemistry of Aluminum*; Robinson, G. H., Ed.; VCH: New York, 1993; p 57.

(t, 6H, PCH₃). ³¹P {¹H} NMR (CDCl₃): δ -108.7 (t, PMe), -238.2 (t, PSiMe₃), ²J_{PP} = 30.5 Hz. IR (Nujol mull) 627 (m), 568 (m), 528 (m), 454 (s), 433 (vw), 392 (m), 364 (vw), 344 (w), 304 (vw), 223 (s), 166 (s) cm⁻¹. Anal. Calcd (found) for C₂₂H₆₆-Si₄P₄Ga₄: C, 31.24 (32.25); H, 7.87 (8.07).

Crystal Structure Determinations. X-ray intensity data for single crystalline samples of Me₃Ga-PMe₃ and I, both mounted in thin-walled glass capillaries under an atmosphere of argon, were collected on a Syntex P2₁ and Rigaku AFC-7R single crystal diffractometer, respectively, with Mo Kα radiation (λ = 0.710 73 Å) at 22 °C. Both structures were solved by direct methods. The non-hydrogen atoms for Me₃Ga-PMe₃ were refined anisotropically. Hydrogen atoms were located by standard difference Fourier techniques and were allowed to ride upon the atom to which they were bonded. An isotropic group thermal parameter (*U*_{iso} = 0.20(2) Å²) was refined for all of the hydrogen atoms. A 60/40 disorder about the H₃CP-PCH₃ fragment of the fused ring system was observed for I. The non-hydrogen atoms (other than the disordered methyl groups) were refined anisotropically (the methyl groups were refined isotropically). Hydrogen atoms (except those of the disordered methyl groups) were located by standard difference Fourier techniques and were included in the structure factor calculation at idealized positions (*d*_{C-H} = 0.96 Å) and were allowed to ride on the atom to which they were bonded. An isotropic group thermal parameter (*U*_{iso} = 0.24(3) Å²) was refined for all of the hydrogen atoms. Structure solution, refinement, and calculation of derived results for both compounds were performed using the SHELXTL⁴ and TEXSAN⁵ package of computer programs. Table 1 provides summaries of crystallographic data, data collection, and structural refinement for both compounds while atomic coordinates for both compounds is given in Tables 2 and 3. The molecular structures of both compounds is given in Figures 1 and 2.

Results and Discussion

The interest of this laboratory in the chemistry of phosphinogallanes originated with the reaction of Me₃Ga with P(SiMe₃)₃ affording the corresponding [Me₂Ga-P(SiMe₃)₂]₂ (II) dimer.⁶



The reaction that yields II proved to be remarkably facile, affording the dimer in essentially quantitative yield as large, colorless, crystals. Our inability to isolate higher-order phosphinogallanes led to further interest in this system. In an effort to approach higher-order phosphinogallanes from a fresh route, we explored the reaction of discrete molecular complexes of gallium and phosphorus with an additional reactant phosphine moiety. To this end, we prepared the trimethylgallium-trimethylphosphine adduct (Me₃Ga-PMe₃) and allowed it to react with excess P(SiMe₃)₃—thus affording the title compound I.

(4) Sheldrick, G. M. *SHELXTL, Crystallographic Computing System*; Nicolet Instruments Division: Madison, WI, 1986.

(5) Swepston, P. N. *TEXSAN: Structure Analysis Software*; Molecular Structure Corp.: The Woodlands, TX, 1993.

(6) Dillingham, M. D. B.; Burns, J. A.; Byers Hill, J. J.; Gripper, K. D.; Pennington, W. T.; Robinson, G. H. *Inorg. Chim. Acta* **1994**, *216*, 267.

Table 1. Crystallographic Data for Me₃Ga-PMe₃ and

	Me ₃ Ga-PMe ₃	[(Me ₃ Si) ₂ P{Me ₂ Ga} ₂ PMe] ₂ (I)
Crystal Data		
empirical formula	C ₆ H ₁₈ PGa	C ₂₂ H ₆₆ Si ₄ P ₄ Ga ₄
fw	190.89	845.87
color; habit	colorless;	colorless; parallelepiped
size (mm)	0.17 × 0.23 × 0.35	0.12 × 0.18 × 0.18
space group	orthorhombic, <i>Pnma</i> (No. 62)	triclinic, <i>P1</i> (No. 2)
unit cell dimens		
<i>a</i> (Å)	12.704(1)	9.983(2)
<i>b</i> (Å)	11.1736(9)	11.628(2)
<i>c</i> (Å)	7.8059(6)	9.859(1)
α (deg)		94.06(1)
β (deg)		106.69(1)
γ (deg)		91.98(2)
formula unit/cell	4	1
vol (Å ³)	1114	5289
<i>D</i> _{calc} (g/cm ³)	1.14	1.29
<i>F</i> (000)	400	438
Data Collection		
diffractometer	Syntex P2 ₁	Rigaku AFC7R
unit cell reflns	57	22
2θ range (deg)	3.5–45.0	5.0–50
scan type	ω/2θ	ω/2θ
scan speed (deg/min)	3.0	32.00, four rescans
no. of reflns collected	773	4073
no. of unique reflns (<i>R</i> _{int})	773	3832
indices	(13,12,8)	(12,±14,±12)
cryst decomp	negligible (±2%)	linear (-14.5%)
abs coeff (mm ⁻¹)	2.56	2.71
min/max transm	0.62/1.00	0.73/1.00
Refinement		
final residuals	<i>R</i> = 0.048;	<i>R</i> = 0.074; <i>R</i> _w = 0.092
	<i>R</i> _w = 0.062	
goodness of fit	<i>S</i> = 1.56	<i>S</i> = 2.68
largest Δσ	0.085	0.017
no. of obs reflns (<i>I</i> > 3σ(<i>I</i>))	482	1133
no. of params refined	44	163
max/min diff peaks (e/Å ³)	0.44/-0.31	0.74/-0.56

Table 2. Atomic Coordinates (×10⁴) and Equivalent Isotropic Displacement Coefficients (Å² × 10³) for Me₃Ga-PMe₃

	<i>x</i>	<i>y</i>	<i>z</i>	<i>U</i> _{eq} ^a
Ga(1)	410(1)	2500	1595(2)	81(1)
P(1)	1712(3)	2500	-714(4)	83(1)
C(1)	-923(9)	2500	316(18)	129(7)
C(2)	747(8)	4003(10)	2835(14)	137(5)
C(3)	3052(10)	2500	-163(21)	213(14)
C(4)	1630(12)	3695(13)	-2194(18)	237(9)

^a Equivalent isotropic *U* defined as one-third of the trace of the orthogonalized *U*_{ij} tensor.

Trimethyl-group III metal complexes of trimethylphosphine have been known for decades as investigations may be traced to coordination and NQR studies of Me₃In-PMe₃^{7,8} and to the gas-phase electron diffraction structure of Me₃Al-PMe₃.⁹ It is noteworthy, therefore, that the first solid state examination of Me₃Ga-PMe₃ is described in this report. We have also structurally characterized the Me₃Al- and Me₃In-trimethylphosphine adducts.¹⁰ The Ga-P bond distance

(7) Coates, G. E.; Whitcombe, R. A. *J. Chem. Soc., London* **1956**, 3351.

(8) Patterson, D. B.; Carnevale, A. *J. Chem. Phys.* **1973**, *59*, 6464.

(9) Almenningen, A.; Ferholt, L.; Haaland, A.; Weidlein, J. *J. Organomet. Chem.* **1978**, *145*, 109.

(10) Burns, J. A.; Robinson, G. H., unpublished results.

Table 3. Atomic Coordinates ($\times 10^4$) and Equivalent Isotropic Displacement Coefficients ($\text{\AA}^2 \times 10^3$) for

	[(Me ₃ Si) ₂ P{Me ₂ Ga} ₂ PMe ₃] ₂ (I) ^a			<i>U</i> _{eq} ^b
	<i>x</i>	<i>y</i>	<i>z</i>	
Ga(1)	4936(3)	7512(2)	5473(3)	70(1)
Ga(2)	7643(3)	5203(3)	7304(3)	70(1)
P(1)	7106(7)	7226(6)	7286(7)	59(3)
P(2)	4040(14)	5483(13)	4983(14)	61(6)
P(3)	4649(23)	5565(16)	4229(26)	83(10)
Si(1)	8878(8)	8286(7)	6931(8)	80(4)
Si(2)	6918(10)	7895(9)	9444(9)	102(5)
C(1)	5306(33)	8252(24)	3871(27)	129(19)
C(2)	3448(30)	8145(25)	6281(39)	143(22)
C(3)	9386(31)	4868(26)	6840(34)	135(20)
C(4)	7415(36)	4486(29)	8996(30)	169(22)
C(5)	9149(30)	7748(27)	5207(26)	109(16)
C(6)	8580(34)	9842(20)	6967(36)	132(21)
C(7)	10591(26)	8076(31)	8336(32)	142(19)
C(8)	5486(30)	6919(32)	9784(30)	141(20)
C(9)	6814(42)	9500(26)	9652(43)	203(31)
C(10)	8621(36)	7672(37)	10855(32)	188(26)
C(11)	3399(41)	5033(33)	6354(42)	52(11)
C(12)	6134(50)	5304(38)	3237(50)	22(12)

^a (Atoms P(2) and C(11)/P(3) and C(12) represent a 60:40 disorder model; the carbons atoms of this model are refined with isotropic thermal parameters.) ^b Equivalent isotropic *U* defined as one-third of the trace of the orthogonalized **U**_{ij} tensor.

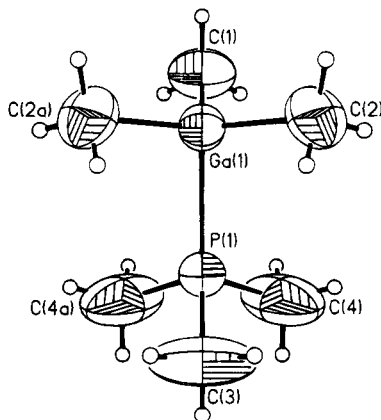


Figure 1. Molecular structure of Me₃Ga-PMe₃ (thermal ellipsoids are shown at 35% probability levels). Selected bond distances (Å): Ga(1)-P(1), 2.455(4); Ga(1)-C(1), 1.97(2); Ga(1)-C(2), 1.99(1); P(1)-C(3), 1.76(1); P(1)-C(4), 1.77(2).

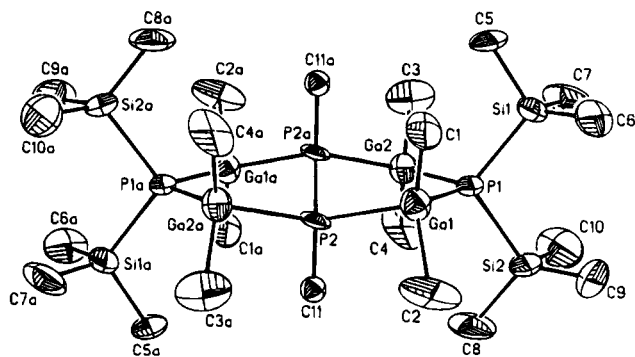


Figure 2. Molecular structure of [(Me₃Si)₂P{Me₂Ga}₂PMe₃]₂ (I) (thermal ellipsoids are shown at 35% probability levels). Selected bond distances (Å): Ga(1)-P(1), 2.431(6); Ga(1)-P(2), 2.46(2); Ga(2)-P(1), 2.430(7); Ga(2)-P(2a), 2.45(1); P(2)-P(2a), 2.25(3).

of 2.455(4) Å in Me₃Ga-PMe₃ is in good agreement with those values reported for Ph₂(Cl)Ga-P(SiMe₃)₃ (2.45(2) Å), Ph₃Ga-P(SiMe₃)₃ (2.539(3) Å),^{1b} and [Me₂Ga-

P(SiMe₃)₂]₂ (2.456(1) Å).⁶ The coordination about the Ga and P atoms in Me₃Ga-PMe₃ may be described as slightly distorted tetrahedral as the molecule approximates C_{3v} symmetry—essentially quite similar to the gas-phase electron diffraction structure (and solid state structure) of Me₃Al-PMe₃ (Me₃In-PMe₃ has a similar structure).¹⁰

There are a number of points relative to structure and bonding concerning I. The title compound, consisting of two fused five-membered Ga₂P₃ rings, resides about a center of symmetry. Furthermore, as symmetry demands, the Ga₄P₄ molecular core is planar. While the quality of the crystal data coupled with the crystallographic disorder present in the molecule prohibits quantitative comparison of bond distances and angles, gross features, nonetheless, emerge. For example, the Ga-P bond distances observed for I (Ga1-P1, 2.431(6) Å; Ga1-P2, 2.46(2) Å; Ga2-P1, 2.430(7) Å; Ga2-P2a, 2.45(2) Å), are in reasonable agreement with the values found for Me₃Ga-PMe₃ and [Me₂Ga-P(SiMe₃)₂]₂.⁶ Similarly, the Ga-C and P-C distances are unremarkable. The coordination about each of the gallium and phosphorus atoms may be described as distorted tetrahedral. It is noteworthy that I demonstrates a measure of stability in air, unlike related phosphinogallanes which decompose immediately upon exposure to air.

Although the literature reveals a number of synthetic methods for the formation of P-P bonds,¹¹ P-P bonds in contemporary III-V chemistry are conspicuously absent. To the best of our knowledge, I represents the first report of a phosphinogallane containing a P-P bond. The P-P bond of distance of 2.25(3) Å observed in I, albeit a bit long, is within the range 2.21–2.35 Å expected for P-P single bonds.¹¹ The ³¹P NMR spectrum of I, as expected, revealed two triplets, indicative of two sets of phosphorus nuclei, centered at -108.7 and -238.2 ppm. The former is attributed to the MeP centers while the latter peak is assigned to the silylphosphine centers, (Me₃Si)₂P. For comparison, the ³¹P chemical shift for Me₃Ga-PMe₃ is centered at δ -144.1 ppm (CDCl₃) while that for P(SiMe₃)₃ is observed at -250.25 ppm (CDCl₃) (both referenced to 85% H₃PO₄).

Although the mechanism which affords I is unclear, this cyclic phosphinogallane may be obtained in reproducible, if modest, yields. Furthermore, the formation of I by reaction of Me₃Ga-PMe₃ with P(SiMe₃)₃ is unexpected and intriguing. Forthcoming studies will address similar Ga-P and In-P systems.

Acknowledgment. We are grateful to the National Science Foundation (CHE-9100518) and to the donors of The Petroleum Research Fund, administered by the American Chemical Society, for support of this work.

Supplementary Material Available: A textual summary of data collection and refinement, and tables of crystal data, bond distances and angles, final fractional coordinates, and thermal parameters (14 pages). Ordering information is given on any current masthead page.

OM9408019

(11) Cowley, A. H., Ed. *Compounds Containing Phosphorus-Phosphorus Bonds*; Dowden, Hutchinson and Ross, Inc., Stroudsburg, PA, 1973. A listing of typical P-P single bond values is found on page 6 and references cited therein.

High-Nuclearity Ruthenium Carbonyl Cluster Chemistry. 2. Reaction of $[\text{Ru}_2(\mu\text{-H})(\mu\text{-NC}_5\text{H}_4)_2(\text{CO})_4(\text{NC}_5\text{H}_5)_2][\text{Ru}_{10}(\mu\text{-H})(\mu\text{-C})(\text{CO})_{24}]$ with Triphenylphosphine: Stepwise Apical Substitution on a "Giant Tetrahedral" Cluster

Marie P. Cifuentes, Mark G. Humphrey, Brian W. Skelton, and Allan H. White

Organometallics, 1995, 14 (3), 1536-1538 • DOI: 10.1021/om00003a069 • Publication Date (Web): 01 May 2002

Downloaded from <http://pubs.acs.org> on March 9, 2009

More About This Article

The permalink <http://dx.doi.org/10.1021/om00003a069> provides access to:

- Links to articles and content related to this article
- Copyright permission to reproduce figures and/or text from this article



ACS Publications
High quality. High impact.

High-Nuclearity Ruthenium Carbonyl Cluster Chemistry. 2.¹ Reaction of [Ru₂(μ-H)(μ-NC₅H₄)₂(CO)₄(NC₅H₅)₂][Ru₁₀(μ-H)(μ₆-C)(CO)₂₄] with Triphenylphosphine: Stepwise Apical Substitution on a “Giant Tetrahedral” Cluster

Marie P. Cifuentes

Department of Chemistry, University of New England, Armidale, NSW 2351, Australia

Mark G. Humphrey*

Department of Chemistry, Australian National University, Canberra, ACT 0200, Australia

Brian W. Skelton and Allan H. White

Department of Chemistry, University of Western Australia, Nedlands, WA 6009, Australia

Received October 28, 1994[®]

Summary: The (hydrido)(carbido)decaruthenium cluster anion [Ru₁₀(μ-H)(μ₆-C)(CO)₂₄]⁻ reacts with triphenylphosphine in a stepwise manner to afford [Ru₁₀(μ-H)(μ₆-C)(CO)_{24-x}(PPh₃)_x]⁻ (x = 1–4), with initial ligand displacement on the apical ruthenium associated with the hydride ligand and subsequent ligand substitution at the other apices; the location of the phosphine substituent of the monosubstituted cluster anion [Ru₁₀(μ-H)(μ₆-C)(CO)₂₃(PPh₃)]⁻ has been confirmed by a single crystal X-ray diffraction study.

of the (hydrido)(carbido)decaruthenium cluster anion [Ru₁₀(μ-H)(μ₆-C)(CO)₂₄]⁻ as its [Ru₂(μ-H)(μ-NC₅H₄)₂(CO)₄(NC₅H₅)₂]⁺ salt¹ and have been investigating its reactivity toward nucleophiles. We report herein its behavior toward triphenylphosphine. In sharp contrast to the osmium system, nucleophilic substitution of [Ru₁₀(μ-H)(μ₆-C)(CO)₂₄]⁻ occurs in a stepwise manner under exceptionally mild conditions to afford a unique series of (hydrido)(carbido)decaruthenium cluster anions containing from one to four phosphine ligands.

Introduction

High nuclearity carbonyl clusters of transition metals are ideal models for metal crystallites with chemisorbed ligands; their chemistry is therefore of fundamental importance. The chemistry of the “giant tetrahedral” cluster [Os₁₀(μ₆-C)(CO)₂₄]²⁻ has been reported in depth;² a range of electrophiles can be added, but the cluster is reported to have a “remarkable resistance to ... nucleophiles”,^{2d} requiring Os–Os cleavage by halogens and harsh reaction conditions. The development of high-nuclearity ruthenium cluster chemistry has lagged behind that of its extensively investigated heavier congener osmium, primarily due to the lack of facile, high-yielding syntheses. However, where comparative studies between ruthenium and osmium systems have been possible (e.g. carbonylation), the ruthenium clusters have shown greatly enhanced reactivity.^{2e,3} We have recently developed a near quantitative synthesis

Results and Discussion

Addition of an approximately equimolar amount of PPh₃ to [Ru₂(μ-H)(μ-NC₅H₄)₂(CO)₄(NC₅H₅)₂][Ru₁₀(μ-H)(μ₆-C)(CO)₂₄] (1) at room temperature results in an immediate change in the IR spectrum. Crystallization from CH₂Cl₂ affords green-black needles of [Ru₂(μ-H)(μ-NC₅H₄)₂(CO)₄(NC₅H₅)₂][Ru₁₀(μ-H)(μ₆-C)(CO)₂₃(PPh₃)] (2) in high yield. In similar reactions, addition of 2–4 equiv of PPh₃ to 1 at room temperature has afforded the bis- and tris(phosphine)-substituted decaruthenium complexes [Ru₂(μ-H)(μ-NC₅H₄)₂(CO)₄(NC₅H₅)₂][Ru₁₀(μ-H)(μ₆-C)(CO)₂₂(PPh₃)₂] (3) and [Ru₂(μ-H)(μ-NC₅H₄)₂(CO)₄(NC₅H₅)₂][Ru₁₀(μ-H)(μ₆-C)(CO)₂₁(PPh₃)₃] (4), respectively. Formation of the tetrakis-substituted cluster anion, [Ru₁₀(μ-H)(μ₆-C)(CO)₂₀(PPh₃)₄]⁻ (5), requires addition of a 12-fold excess of the ligand and reaction in refluxing acetone for 2 h. Spectroscopic data of the resultant product is consistent with a bis(phosphine)-substituted diruthenium cation [Ru₂(μ-H)(μ-NC₅H₄)₂(CO)₄(PPh₃)₂]⁺, where the σ-bound pyridines of the cation precursor have been replaced; σ-pyridine often has a “lightly stabilizing” role in polynuclear chemistry,⁴ but in this system substitution at the “giant tetrahedral” cluster anion apices is so facile that it occurs before replacement of the σ-bound pyridines of the cluster cation. In contrast to the unsubstituted cluster, the mono- (2) and bis(phosphine)-substituted (3) clusters are relatively stable as solids in air, and in solution under an inert atmosphere. The

* To whom correspondence should be addressed.

[®] Abstract published in *Advance ACS Abstracts*, February 1, 1995.

(1) Part 1: Cifuentes, M. P.; Humphrey, M. G.; Skelton, B. W.; White, A. H. *Organometallics* 1993, 12, 4272.

(2) (a) Braga, D.; Henrick, K.; Johnson, B. F. G.; Lewis, J.; McPartlin, M.; Nelson, W. J. H.; Puga, J. *J. Chem. Soc., Chem. Commun.* 1982, 1083. (b) Dearing, V.; Drake, S. R.; Johnson, B. F. G.; Lewis, J.; McPartlin, M.; Powell, H. R. *J. Chem. Soc., Chem. Commun.* 1988, 1331. (c) Drake, S. R.; Henrick, K.; Johnson, B. F. G.; Lewis, J.; McPartlin, M.; Morris, J. *J. Chem. Soc., Chem. Commun.* 1986, 928.

(d) Goudsmit, R. J.; Jackson, P. F.; Johnson, B. F. G.; Lewis, J.; Nelson, W. J. H.; Puga, J.; Vargas, M. D.; Braga, D.; Henrick, K.; McPartlin, M.; Sironi, A. *J. Chem. Soc., Dalton Trans.* 1985, 1795. (e) Cifuentes, M. P.; Humphrey, M. G. In *Comprehensive Organometallic Chemistry II*; Wilkinson, G.; Stone, F. G. A., Abel, E. W., Eds.; Pergamon Press: Oxford, U.K., 1995, Volume 7, Chapter 16.

(3) Coston, T.; Lewis, J.; Wilkinson, D.; Johnson, B. F. G. *J. Organomet. Chem.* 1991, 407, C13.

(4) Cifuentes, M. P.; Humphrey, M. G.; Skelton, B. W.; White, A. H. *J. Organomet. Chem.* 1994, 406, 211.

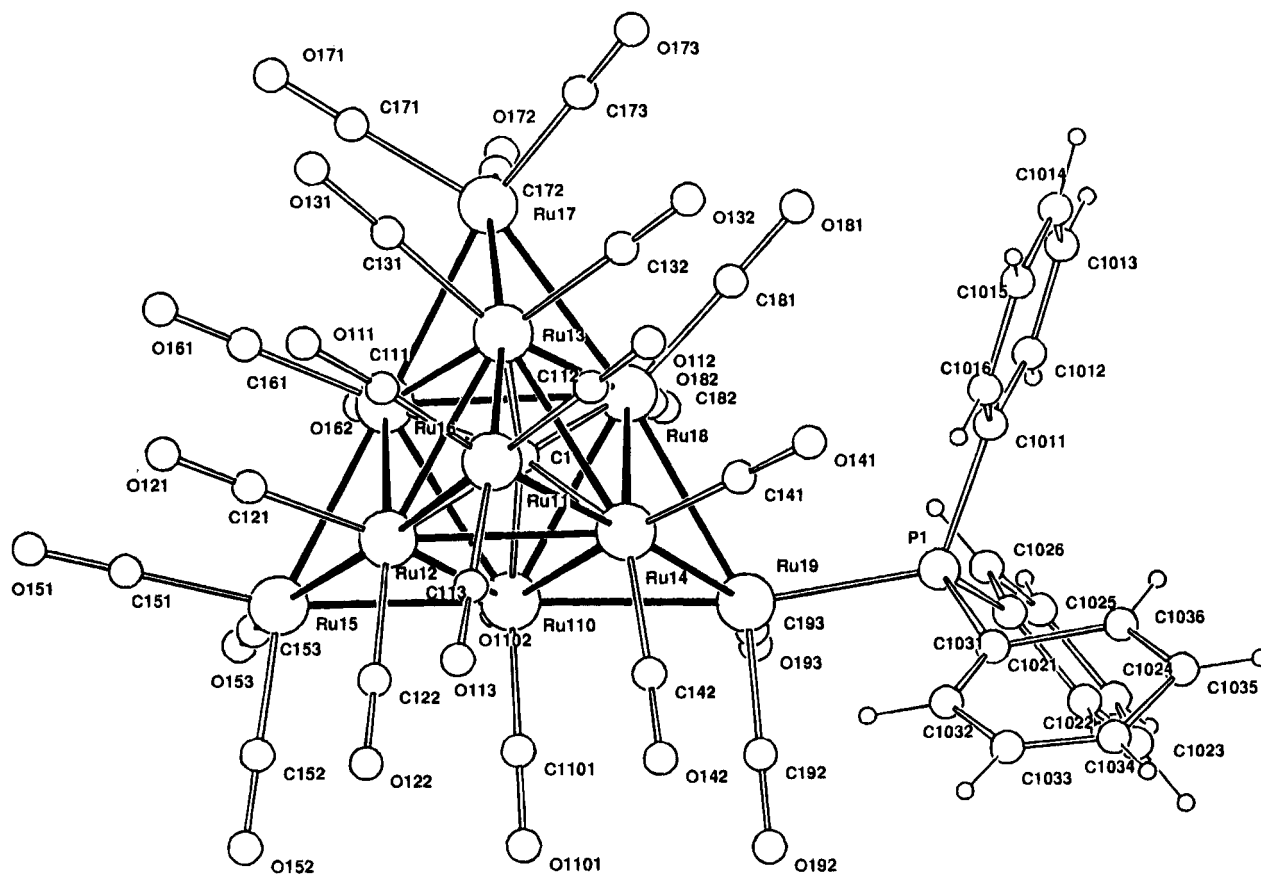


Figure 1. "Molecular" plot of one of the anions of $[\text{Ru}_2(\mu\text{-H})(\mu\text{-NC}_5\text{H}_5)_2(\text{CO})_4(\text{NC}_5\text{H}_5)_2][\text{Ru}_{10}(\mu\text{-H})(\mu_6\text{-C})(\text{CO})_{23}(\text{PPh}_3)]$ (**2**).

tris(phosphine)-substituted cluster **4** forms **3** slowly at room temperature, the PPh_3 conceivably being replaced by CO scavenged from slight decomposition of the cluster anion or cation, chemistry which is mirrored in the FAB MS of **4** where $[\text{M} - \text{PPh}_3 + \text{CO}]^-$ is observed. The initial site of ligand substitution was inferred from spectroscopic data and subsequently confirmed through an X-ray crystallographic study of **2**; complexes **3**–**5** have been spectroscopically characterized.

The ^1H NMR spectrum of **2** shows a doublet signal [$J(\text{HP})$ 7 Hz] due to the metal-bound hydride of the anion, and the $^{13}\text{C}\{^1\text{H}\}$ NMR spectrum shows carbonyl signals in the ratio 3:3:6:2:9 (low field to high field), suggesting substitution on the apical ruthenium atom associated with the bridging hydride ligand (Lewis and co-workers have previously assigned upfield carbonyl resonances to apical sites).⁵ The molecular structure of the anion of **2** is shown in Figure 1. The metal framework has a tetrapped octahedral geometry, with the interstitial carbide sitting in the octahedral cavity, the same core structure as that observed in the unsubstituted parent compound. The structural study confirms substitution of an apical carbonyl by the triphenylphosphine, although bond length and angle data do not allow confirmation of the spectroscopically-assigned hydride ligand site. The $^{31}\text{P}\{^1\text{H}\}$ NMR spectra of complexes **2**–**5** show signal ratios consistent with successive apical substitutions of the decaruthenium anion and the expected upfield shifts of the signals as the electron density at the anion is increased.

These results demonstrate (i) that high-nuclearity group 8 cluster chemistry can embrace nucleophilic as well as electrophilic reagents and (ii) that reactions on high-nuclearity clusters can proceed with control of extent and specificity under very mild conditions. This chemistry is now being extended to a wide variety of nucleophilic reagents.

Experimental Section

$[\text{Ru}_2(\mu\text{-H})(\mu\text{-NC}_5\text{H}_5)_2(\text{CO})_4(\text{NC}_5\text{H}_5)_2][\text{Ru}_{10}(\mu\text{-H})(\mu_6\text{-C})(\text{CO})_{24}]$ (**1**) was synthesized by the literature procedure.¹ Triphenylphosphine (Hopkin and Williams) was used as received. Petroleum ether refers to the fraction with boiling point between 60 and 80 °C. Reactions were carried out using Schlenk techniques⁶ under an atmosphere of dry nitrogen; subsequent workup was carried out without any precautions to exclude air. IR spectra were recorded using a Perkin-Elmer model 1600 Fourier transform spectrophotometer with CaF_2 optics. NMR spectra were recorded on a Varian Gemini 300 spectrometer (^1H spectra at 300 MHz, ^{13}C at 75 MHz and ^{31}P at 121 MHz) in acetone- d_6 unless otherwise stated. References for the ^1H and ^{13}C NMR spectra were set to residual solvent peaks; the latter were proton decoupled. The ^{31}P NMR spectra were recorded using approximately 0.2 M $\text{Cr}(\text{acac})_3$ as a relaxation agent, or a recycle delay of 40 s; they are reported relative to external 85% H_3PO_4 at 0.0 ppm and are proton decoupled. Mass spectra were recorded using a VG ZAB 2SEQ instrument (30 kV Cs^+ ions, current 1 mA, accelerating potential 8 kV, 3-nitrobenzyl alcohol matrix) at the Australian National University; peaks were recorded as m/z . Thin layer chromatography (tlc) was on glass plates (20 × 20 cm) coated with Merck GF_{254} silica gel (0.5 mm) using 1:1 acetone/

(5) Bailey, P. J.; Duer, M. J.; Johnson, B. F. G.; Lewis, J.; Conole, G.; McPartlin, M.; Powell, H. R.; Anson, C. E. *J. Organomet. Chem.* **1990**, 383, 441.

(6) Shriver, D. F.; Drezdson, M. A. *The Manipulation of Air Sensitive Compounds*, 2nd ed.; John Wiley and Sons: New York, 1986.

petroleum ether as eluent. Cluster **1** was not isolated; rather, calculated yields for reactions involving **1** assume complete conversion of its triruthenium precursor $\text{Ru}_3(\mu\text{-H})(\mu\text{-NC}_5\text{H}_4)(\text{CO})_{10}$.

Reactions of 1 with PPh₃. (a) One Equivalent—Synthesis of [Ru₂(μ-H)(μ-NC₅H₄)₂(CO)₄(NC₅H₅)₂][Ru₁₀(μ-H)(μ₆-C)(CO)₂₃(PPh₃)₂] (2). Triphenylphosphine (7 mg, 0.027 mmol) was added to a stirred solution of [Ru₂(μ-H)(μ-NC₅H₄)₂(CO)₄(NC₅H₅)₂][Ru₁₀(μ-H)(μ₆-C)(CO)₂₄] (**1**, 63 mg, 0.027 mmol) in acetone (20 mL). An IR spectrum at this stage showed complete consumption of **1**. The solution was taken to dryness and crystallized from CH₂Cl₂ at -20 °C to give green-black needles identified as **2** (45 mg, 0.018 mmol, 65%). IR (CH₂-Cl₂), $\nu(\text{CO})/\text{cm}^{-1}$: 2077 (w), 2047 (s), 2016 (m), 2000 (m). ¹H NMR (CDCl₃): δ 8.13 (m, 6H), 7.82 (m, 2H), 7.59 (m, 8H), 7.41 (m, 15H), 6.89 (m, 2H), -10.93 (s, Ru₂-H), -11.68 [d, 1H, $J_{\text{H-P}} = 7$ Hz, Ru₁₀-H]. ¹³C NMR (CDCl₃): δ 378.8 (μ₆-C); 197.2, 194.0 (ratio 1:1, Ru₂CO); 210.5, 210.0, 207.9, 199.3 (d, $J_{\text{C-P}} = 9$ Hz), 190.3 (ratio 3:3:6:2:9, Ru₁₀CO); 174.9, 153.9, 153.1, 140.2, 139.0, 135.7, 133.5 (d, $J_{\text{C-P}} = 11$ Hz), 130.5, 128.5 (d, $J_{\text{C-P}} = 10$ Hz), 126.3, 121.6 (aromatic carbons). ³¹P NMR: δ 44.4. Positive ion FAB MS: m/z 630 (630, M⁺). Negative ion FAB MS: m/z 1930 (1930, M⁻). Anal. Calcd for C₆₆H₃₅N₄O₂₇PRu₁₂: C, 30.97; H, 1.38; N, 2.19. Found: C, 31.10; H, 1.32; N, 2.18.

(b) 2–4-fold Excess of PPh₃. Triphenylphosphine (45 mg, 0.172 mmol) was added to a solution of **1** [from Ru₃(μ-H)(μ-NC₅H₄)(CO)₁₀, 200 mg, 0.172 mmol] in acetone (20 mL) and the mixture stirred for 90 min. An IR spectrum indicated the presence of some mono-PPh₃-substituted decaruthenium anion, so a further portion of PPh₃ was added (7 mg, 0.198 mmol) and the solution stirred for 30 min. The solution was taken to dryness *in vacuo*; tlc of the resulting black residue afforded a number of brown-green bands. The first green band was found to contain a minor amount of the bis-PPh₃-substituted anion [Ru₁₀(μ-H)(μ₆-C)(CO)₂₂(PPh₃)₂]⁻ identified by IR, NMR, and negative ion FAB mass spectra, although the cation could not be identified (positive ion FAB MS: m/z 769). The second green band was isolated as a green-black solid by trituration with petroleum ether and identified as [Ru₂(μ-H)(μ-NC₅H₄)₂(CO)₄(NC₅H₅)₂][Ru₁₀(μ-H)(μ₆-C)(CO)₂₂(PPh₃)₂] (**3**, 70 mg, 0.0250 mmol, 33%). IR (CH₂Cl₂), $\nu(\text{CO})/\text{cm}^{-1}$: 2064 (m), 2041 (s), 2011 (s sh), 2006 (s), 1990 (s). ¹H NMR (CDCl₃): δ 8.14 (m, 6H), 7.82 (m, 2H), 7.60 (m, 2H), 7.41 (m, 36H), 6.93 (m, 2H), -10.93 (s, Ru₂-H), -11.69 (d, 1H, $J_{\text{H-P}} = 7$ Hz, Ru₁₀-H). ³¹P NMR: δ 52.1, 43.0 (1:1). Positive ion FAB MS: m/z 630 (630, M⁺). Negative ion FAB MS: m/z 2165 (2165, M⁻). The contents of the third green band were identified as [Ru₂(μ-H)(μ-NC₅H₄)₂(CO)₄(NC₅H₅)₂][Ru₁₀(μ-H)(μ₆-C)(CO)₂₁(PPh₃)₃] (**4**, 25 mg, 0.008 mmol, 11%). IR (CH₂Cl₂), $\nu(\text{CO})/\text{cm}^{-1}$: 2063 (w), 2040 (m), 2013 (s), 2000 (vs), 1985 (m sh). ¹H NMR: δ 8.15 (m, 6H), 7.69–7.48 (m, 57H), -10.75 (s, Ru₂-H), -11.54 (d, 1H, $J_{\text{H-P}} = 7$ Hz, Ru₁₀-H). ³¹P NMR: δ 50.0 (s, 2P), 41.9 (s, 1P). Positive ion FAB MS: m/z 630 (630, M⁺). Negative ion FAB MS: m/z 2399 (2399, M⁻). Attempts to crystallize these samples for analyses proved unsuccessful; repurification by tlc resulted in further conversion of the diruthenium cation

to unknown products. Reactions using up to 4-fold equivalents of PPh₃ (with respect to complete conversion of the triruthenium precursor to a product containing a decaruthenium anion and a diruthenium cation) resulted in the formation of both the bis- and tris-substituted decaruthenium cations in yields of up to 30% each.

(c) 12-fold Excess—Synthesis of [Ru₂(μ-H)(μ-NC₅H₄)₂(CO)₄(PPh₃)₂][Ru₁₀(μ-H)(μ₆-C)(CO)₂₀(PPh₃)₄] (5). Triphenylphosphine (140 mg, 0.534 mmol) was added to a solution of **1** [from Ru₃(μ-H)(μ-NC₅H₄)(CO)₁₀, 118 mg, 0.178 mmol] in acetone (20 mL) and the mixture heated at reflux for 2 h. Purification by tlc afforded one main green band which was crystallized from acetone/*n*-butanol to afford a green-black microcrystalline solid identified as **5** (58 mg, 0.016 mmol, 36%). IR (CH₂Cl₂), $\nu(\text{CO})/\text{cm}^{-1}$: 2050 (w), 2024 (w), 1996 (s), 1972 (m sh). ¹H NMR: δ 7.69–6.82 (m, 90H), -11.54 (m, 1H, $J_{\text{H-P}} = 7$ Hz, Ru₁₀-H), -12.65 (t, $J_{\text{H-P}} = 11$ Hz, Ru₂-H). ³¹P NMR: δ 47.9 (s, 3P, Ru₁₀P), 40.4 (s, 1P, Ru₁₀P), 26.7, 25.0 (1:1, Ru₂P). Positive ion FAB MS: m/z 997 (997, M⁺). Negative ion FAB MS: m/z 2633 (2633, M⁻). Anal. Calcd for C₁₄₃H₁₀₀N₂O₂₅P₆Ru₁₂: C, 47.33; H, 2.78; N, 0.76. Found: C, 48.34; H, 2.69; N, 0.37.

Crystal Data for 2: C₆₆H₃₅N₄O₂₇PRu₁₂, $a = 21.625(5)$ Å, $b = 14.80(1)$ Å, $c = 12.387(4)$ Å, $\alpha = 81.73(4)^\circ$, $\beta = 80.07(2)^\circ$, $\gamma = 88.53(2)^\circ$, $V = 3864$ Å³, D_c ($Z = 2$) = 2.20 g cm⁻³; μ_{Mo} = 23.7 cm⁻¹; specimen 0.20 × 0.12 × 0.08 mm; $A^*_{\text{min,max}}$ (Gaussian correction) = 1.20, 1.34; $2\theta_{\text{max}} = 50^\circ$; $N(\text{indep}) = 13\ 664$, $N(\text{obs})$ ($I > 3\sigma(I)$) = 3226; $R = 0.075$, R_w (statistical weights) = 0.067; $T \sim 295$ K; unique diffractometer data, $2\theta/\theta$ scan mode, monochromatic Mo K α radiation, $\lambda = 0.71073$ Å.

Considerable difficulties imposed by small specimen size, pseudocentrosymmetric symmetry (triclinic, $P1$, quasi- $P\bar{1}$), and crystal decomposition during data collection (~60%; data rescaled) resulted in the adoption of a model with considerable constraints (anisotropic thermal parameter refinement for Ru and P only; (x, y, z, U_{iso})_H estimated; refinement of six-membered rings as rigid bodies). The determination is inferior and is useful only inasmuch as it determines general non-hydrogen atom disposition and connectivity, establishing the location of the PPh₃ substituent on the anionic cluster. Hydrido species were not located.

Acknowledgment. We thank the Australian Research Council for support of this work and Johnson-Matthey Technology Centre for the loan of ruthenium salts. M.P.C. holds a UNE Postgraduate Research Scholarship. M.G.H. is an ARC Australian Research Fellow.

Supplementary Material Available: Tables of crystallographic data, atomic coordinates and isotropic displacement parameters for all atoms, anisotropic displacement parameters for ruthenium and phosphorus atoms and all bond distances and angles (39 pages). Ordering information is given on any current masthead page.

OM9408268

Germylene and Stannylene Anion Radicals: Generation and Electronic Structure

Michael P. Egorov* and Oleg M. Nefedov

N. D. Zelinsky Institute of Organic Chemistry, Leninsky Prospekt 47, Moscow B-334, Russia

Tien-Sung Lin and Peter P. Gaspar*

Department of Chemistry, Washington University, St. Louis, Missouri 63130-4899

Received July 6, 1994[®]

Summary: Germylene and stannylene radical anions $[(\text{Me}_3\text{Si})_2\text{CH}]_2\text{M}^{\cdot-}$ ($\text{M} = \text{Ge}, \text{Sn}$) have been generated and their ESR spectra recorded. The $a(\text{M})$ hyperfine coupling constants of both species clearly indicate a low degree of s -character associated with π -radicals.

Radicals, ions, ion radicals, carbenes, and their analogs are well-known and intensively studied classes of reactive intermediates. The ion radicals of carbenes and their analogs are an extension of this series and have often, since the early 1970s, been suggested as intermediates in redox reactions of diazo compounds and other molecules, both in the liquid and gas phases.^{1,2} The first direct unequivocal ESR detection of a carbene ion radical, the diphenylcarbene cation radical was, however, accomplished only very recently.³ Carbene anion radicals have not yet been detected by ESR.

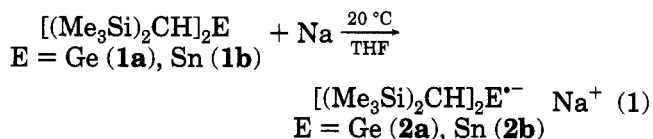
Very little is known about ion radicals of heavier group 14 element carbene analogs.^{4–7} The silylene anion radical $\text{SiH}_2^{\cdot-}$ has been produced in a low-pressure discharge source upon admission of SiH_4 and has been studied by laser photoelectron spectroscopy.⁴ Photoionization mass spectrometry has been used to study silylene $\text{SiH}_2^{+\cdot}$ and germylene $\text{GeH}_2^{+\cdot}$ cation radicals.^{5,6} The $^{28}\text{SiH}_2^{+\cdot}$ and $^{29}\text{SiH}_2^{+\cdot}$ cation radicals have been detected by ESR upon generation by photoionization of SiH_4 in a neon matrix at 4 K.⁷

In the cases mentioned above, the silylene and germylene ion radicals were generated by discharge or photoionization under severe conditions. However, the relatively low ionization potentials and appreciable electron affinities of a number of carbene analogs⁸ allow them to participate in electron-transfer interactions with a variety of electron acceptors and donors. Indeed, the formation of germylene cation and anion radicals as intermediates in the course of germylene reactions has recently been suggested.⁹ A correlation between

reduction potentials of halogen-containing substrates and their reactivity toward dimethylgermylene was found.⁹ For these reactions, an ion radical mechanism was suggested in which a key step is an electron transfer from dimethylgermylene that forms an ion radical pair. Electron transfer from the stable stannylene $[(\text{Me}_3\text{Si})_2\text{N}]_2\text{Sn}$ to organic halides has also been proposed as the first stage of reaction between R_2Sn and RX .^{10,11}

Reactions that can be rationalized by electron transfer from a reducing agent to a germylene have also been reported, including the reaction between the GeCl_2 -dioxane complex and a good reducing agent, hexamethylditin.⁹ This did not result in insertion of dichlorogermylene into the Sn–Sn bond, but in Sn–Sn bond cleavage with concomitant chlorination. The products were Me_3SnCl and $(\text{GeCl})_x$ oligomers.

Here we report the first successful generation of germylene and stannylene anion radicals and their direct detection by ESR. The anion radicals were obtained by reduction of stable $[(\text{Me}_3\text{Si})_2\text{CH}]_2\text{E}$ ($\text{E} = \text{Ge}$ (**1a**), Sn (**1b**)) by sodium:



A 6×10^{-3} M solution of stable germylene $[(\text{Me}_3\text{Si})_2\text{CH}]_2\text{Ge}^{12}$ (**1a**) in THF was allowed to react for 10–15 s at 20 °C with a sodium mirror. The characteristic yellow-orange color of **1a** ($\lambda_{\text{max}} = 410$ nm in THF) immediately turned to green ($\lambda_{\text{max}} = 666$ nm in THF), and a strong ESR signal appeared. The ESR spectrum is displayed in Figure 1a. The 1:2:1 triplet with a hyperfine splitting $a = 2.6$ G arises from two equivalent protons. The spectrum of Figure 1a is shown at higher gain in Figure 1b, in which four weak satellite lines appear on both sides of the central peak. These can only arise from the $I = 9/2$ nucleus of ^{73}Ge (7.8% abundance) with $a(^{73}\text{Ge}) = 12.5$ G. Two other satellite peaks of the total of 10 expected overlap with the strong central peak and are not observed. Under even higher gain, each of the satellite lines splits further into a triplet due to coupling with two equivalent protons. The g -value of this radical species is 2.0125, which is typical for

[®] Abstract published in *Advance ACS Abstracts*, January 15, 1995.

(1) Bethell, D.; Parker, V. D. *Acc. Chem. Res.* **1988**, *21*, 400.
 (2) McDonald, R. N. *Tetrahedron* **1989**, *45*, 3993.
 (3) Bally, T.; Matzinger, S.; Truttman, L.; Platz, M. S.; Admasu, A.; Gerson, F.; Arnold, A.; Schmidlin, R. *J. Am. Chem. Soc.* **1993**, *115*, 7007.
 (4) Kasdan, A.; Herbst, E.; Lineberger, W. C. *J. Chem. Phys.* **1975**, *62*, 541.
 (5) Berkowitz, J.; Greene, J. P.; Cho, H.; Ruscic, B. *J. Chem. Phys.* **1987**, *86*, 1235.
 (6) Ruscic, B.; Schwarz, M.; Berkowitz, J. *J. Chem. Phys.* **1990**, *92*, 1865.
 (7) Knight, L. B.; Winiski, M.; Kudelko, P.; Arrington, C. A. *J. Chem. Phys.* **1989**, *91*, 3368.
 (8) Nefedov, O. M.; Egorov, M. P.; Ioffe, A. I.; Menchikov, L. G.; Zuev, P. S.; Minkin, V. I.; Simkin, B. Ya.; Glukhovtsev, M. N. *Pure Appl. Chem.* **1992**, *64*, 265.
 (9) Egorov, M. P.; Gal'minas, A. M.; Basova, A. A.; Nefedov, O. M. *Dokl. Akad. Nauk.* **1993**, *329*, 594.

(10) Gynane, M. J. S.; Lappert, M. F.; Miles, S. J.; Carty, A. J.; Taylor, N. J. *J. Chem. Soc., Dalton Trans.* **1977**, 2009.

(11) Lappert, M. F.; Misra, M. C.; Onyszczuk, M.; Rowe, R. S.; Power, P. P.; Slode, M. J. *J. Organomet. Chem.* **1987**, *330*, 31.

(12) Fjeldberg, T.; Haaland, A.; Schilling, B. E. R.; Lappert, M. F.; Thorne, A. J. *J. Chem. Soc., Dalton Trans.* **1986**, 1551.

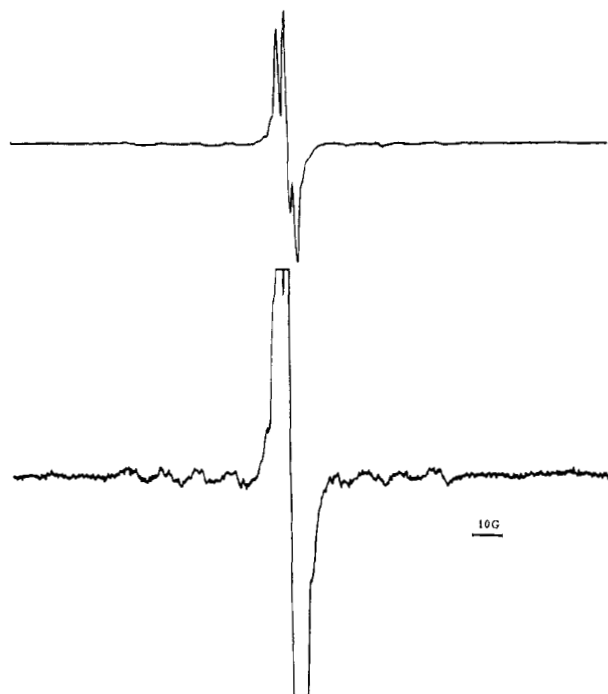
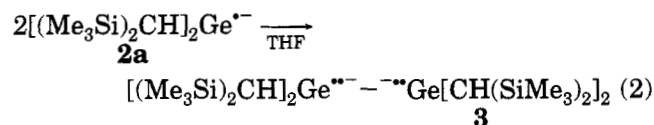


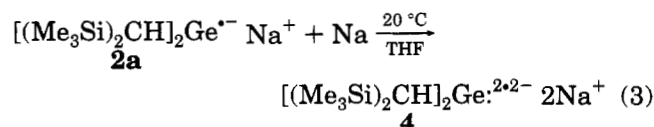
Figure 1. (a) ESR spectrum of $[(\text{Me}_3\text{Si})_2\text{CH}]_2\text{Ge}^{\bullet-}$ (**2a**). (b) Same spectrum at increased gain.

germanium-centered radicals ($g \sim 2.0078\text{--}2.0100$).¹³ On the basis of the hyperfine splitting patterns and the g -value, we can unequivocally assign it to $[(\text{Me}_3\text{Si})_2\text{CH}]_2\text{Ge}^{\bullet-}$ anion radical **2a**.

Anion radical **2a** is quite stable in solution at room temperature. It has a half-life $t_{1/2} = \sim 1.5$ h, which is however considerably shorter than the lifetime of the neutral species $[(\text{Me}_3\text{Si})_2\text{CH}]_3\text{Ge}^{\bullet}$ whose $t_{1/2}$ is greater than 4 months.²² The intensities of the ESR signal and of the electronic absorption maximum at 666 nm decrease at the same rate, consistent with the assignment of the $\lambda_{\text{max}} = 666$ nm absorption to anion radical **2a**. The disappearance of **2a**, simultaneously monitored by visible and ESR spectroscopy, obeys a second-order rate law, suggesting dimerization of **2a**, a reaction typical for sterically nonoverloaded $\text{R}_3\text{Ge}^{\bullet}$ radicals.¹³ Calculations have indicated that dimerization of the methylene anion radical anion $\text{CH}_2^{\bullet-}$ is feasible.¹⁴



Further contact (1–2 min) of solutions of **2a** with sodium results in complete disappearance of the ESR signal. Presumably the anion radical **2a** is reduced by sodium to the diamagnetic dianion **4**.



Both 1,2-dianion **3** and 1,1-dianion **4** have prototypes in products $\text{Ph}_2\text{Ge}(\text{Li})\text{Ge}(\text{Li})\text{Ph}_2$ and Ph_2GeLi_2 that are

(13) Sakurai, H. *Organomet. Chem. Rev.* **1981**, *12*, 267.

(14) Davidson, R. B.; Hudak, M. L. *J. Am. Chem. Soc.* **1977**, *99*, 3918.

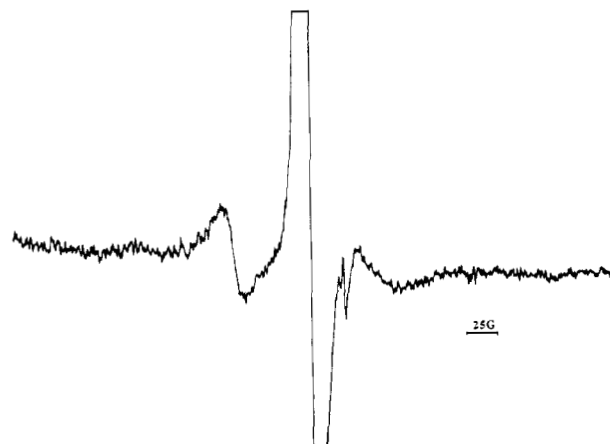


Figure 2. ESR spectrum of $[(\text{Me}_3\text{Si})_2\text{CH}]_2\text{Sn}^{\bullet-}$ (**2b**) at high gain.

believed to be formed from reaction of Ph_2GeH_2 and $n\text{-BuLi}$.¹⁵ Silicon analogs of **3** and **4**, $\text{Mes}_2\text{Si}(\text{K})\text{Si}(\text{K})\text{-Mes}_2$ and Mes_2SiK_2 , respectively, have recently been obtained by potassium reduction of $\text{Mes}_2\text{Si}=\text{SiMes}_2$.¹⁶

Stannylenes anion radical $[(\text{Me}_3\text{Si})_2\text{CH}]_2\text{Sn}^{\bullet-}$ (**2b**) was obtained by brief contact (5–10 s) with a precooled sodium mirror of a 6×10^{-3} M solution of stable stannylenes **1b**¹⁷ in THF cooled to -80°C . The reaction mixture was quickly transferred into a precooled ESR tube, and the ESR spectrum was recorded at -80°C . A broad singlet (line width 7 G) was observed with a g -value of 2.0177, similar to that of the related neutral radical $[(\text{Me}_3\text{Si})_2\text{CH}]_3\text{Sn}^{\bullet}$ ($g = 2.0094$).¹⁸ Under increased gain, two broad unresolved satellites from ^{117}Sn ($I = 1/2$, 7.7% abundance) and ^{119}Sn ($I = 1/2$, 8.7% abundance) were observed with a splitting of $a(^{117,119}\text{Sn}) = 116$ G (Figure 2). As in the case of the neutral radical, $[(\text{Me}_3\text{Si})_2\text{CH}]_3\text{Sn}^{\bullet}$, the high-field satellite line is considerably broader than the one at low field.

The lack, probably caused by spectral broadening, of an observed hyperfine splitting due to the two adjacent CH protons, makes the structural assignment for the tin radical species less certain. The spectral broadening could arise from a slow tumbling motion of the radical at low temperatures, but is more likely due to a slow exchange processes with excess neutral species. Unfortunately the radical decomposes in minutes at 20°C , and it was therefore not possible to obtain spectra at higher temperatures. This is in sharp contrast to the neutral $[(\text{Me}_3\text{Si})_2\text{CH}]_3\text{Sn}^{\bullet}$, species which has a lifetime of 1 year.²²

Nevertheless we can safely interpret the spectrum in Figure 2 as belonging to the stannylenes anion radical $[(\text{Me}_3\text{Si})_2\text{CH}]_2\text{Sn}^{\bullet-}$ on the basis of the small value of the tin hyperfine coupling constant $a(^{117,119}\text{Sn}) = 116$ G, clearly indicative of the π -character of this radical.

In the ion radicals of carbenes and their analogs, an unpaired electron can occupy either a σ - or π -orbital. Experimental data on diphenylcarbene³ and silylene⁷ cation radicals reveal that these species are σ -radicals and have a 2A_1 electronic ground state. Calculations

(15) Cross, R. J.; Glockling, F. *J. Chem. Soc.* **1964**, 4125.

(16) Sohn, H.; West, R. *Abstracts of XXVth Silicon Symposium, Indianapolis, 1993*, P-30.

(17) Davidson, P. J.; Harris, D. H.; Lappert, M. F. *J. Chem. Soc., Dalton Trans.* **1976**, 2268.

(18) Davidson, P. J.; Hudson, A.; Lappert, M. F.; Lednor, P. W. *J. Chem. Soc., Chem. Commun.* **1973**, 829.

predict that the unpaired electrons in methylene¹⁹ and silylene⁷ anion radicals should occupy a π -orbital. It is well-known that the $\alpha(M)$ splitting is proportional to the degree of s character in the orbital on the M atom occupied by the unpaired electron. Therefore σ -radicals have considerably larger $\alpha(M)$ values than do π -radicals. For example, most ¹³C hyperfine coupling constants for carbon-centered σ -radicals are in the range 100–140 G vs 24–26 G for π -radicals.³ For the Ph_2C^+ cation-radical, which is a σ -radical, $\alpha(^{13}\text{C}) = 98.3$ G.³ The experimentally observed $\alpha(^{29}\text{Si})$ for SiH_2^+ is 301 G, which is in the range of hyperfine coupling constants $\alpha(^{29}\text{Si}) = 160$ –500 G found for pyramidal R_3Si^* radicals.²⁰ Recent calculations have indicated that the hybridization of the tricoordinate silicon atom of an $\text{Z}_3\text{-Si}^*$ radical is not directly related to the geometry at the radical center.²¹ The widely accepted designation of $\text{Z}_3\text{-Si}^*$ radicals as σ -radicals may need revision in light of the calculational result that the 3s character of the electron in the SOMO can vary from as low as 3.4% to as high as 41.8% with increasing electronegativity of the substituent Z, without substantial change in the nearly tetrahedral geometry.²¹

Germanium- and tin-centered radicals are also pyramidal, with a high degree of s-character in the orbital containing the odd electron. The range of hyperfine coupling constants $\alpha(^{73}\text{Ge})$ for R_3Ge^* is 70–220 G,¹³ and $\alpha(^{117,119}\text{Sn})$ for R_3Sn^* occurs in the range 1400–1800 G.²² The $\alpha(^{73}\text{Ge})$ value for $[(\text{Me}_3\text{Si})_2\text{CH}]_3\text{Ge}^*$ is 92 G;²³ for $[(\text{Me}_3\text{Si})_2\text{CH}]_3\text{Sn}^*$ $\alpha(^{117}\text{Sn}) = 1698$ G, $\alpha(^{119}\text{Sn}) = 1776$ G.^{18,22} Therefore the very small values of $\alpha(^{73}\text{Ge}) = 12.5$ G for $[(\text{Me}_3\text{Si})_2\text{CH}]_2\text{Ge}^{\cdot-}$ and $\alpha(^{117,119}\text{Sn}) = 116$ G for $[(\text{Me}_3\text{Si})_2\text{CH}]_2\text{Sn}^{\cdot-}$ clearly indicate the small degree of s-character of the unpaired electrons in these germylene and stannylene anion radicals and point to their ²B₁ ground electronic states. Thus both **2a** and **2b** would traditionally be described as π -radicals, but given the reported lack of correlation between the hybridization of silyl radicals and their geometry,²¹ one should have reservations about the use of the σ , π -nomenclature.

Experimental Section

ESR spectra were recorded on a Bruker ER-200D EPR spectrometer (X-band, 9.4 GHz) equipped with an Oxford EPR cryostat (4.2–300 K). UV–visible spectra were recorded on a Varian Cary 219 spectrometer.

All reactions were carried out in an evacuated (10^{-4} – 10^{-5} Torr) sealed glass apparatus equipped with a quartz ESR tube or with both a quartz ESR tube and a quartz UV cell for recording UV–visible spectra. Germylene **1a** and stannylene **1b** were synthesized as described in the literature.^{12,17} THF, distilled from sodium–benzophenone under an argon atmosphere, was degassed and then distilled in vacuum into a tube on the glass apparatus containing a sample of **1a** (**1b**). After an additional cycle of degassing of the resulting THF solution of **1a** (**1b**), the apparatus was sealed. In another tube, isolated from the rest of the apparatus by a breakseal, there was a

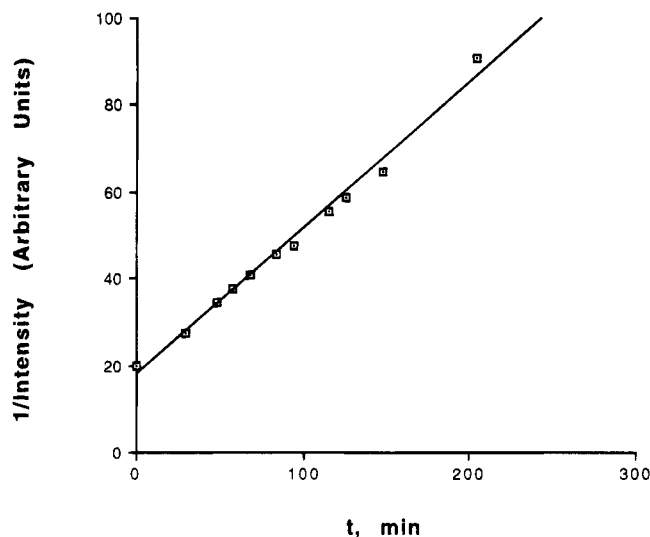


Figure 3. Plot of 1/intensity of the ESR spectrum of $[(\text{Me}_3\text{Si})_2\text{CH}]_2\text{Ge}^{\cdot-}$ (**2a**) vs time.

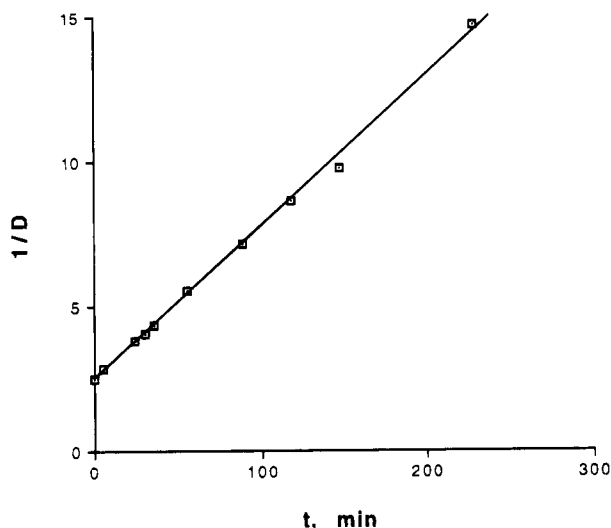


Figure 4. Plot of 1/OD at $\lambda_{\text{max}} = 666$ nm of a THF solution of $[(\text{Me}_3\text{Si})_2\text{CH}]_2\text{Ge}^{\cdot-}$ (**2a**) vs time.

sodium mirror obtained by sublimation of the metal in vacuum. After the breakseal was ruptured, the solution of **1** was allowed to briefly contact the sodium at 20 (**1a**) or -80 °C (**1b**). The solution was then transferred to the ESR tube or the UV cell, and spectra were recorded.

The decomposition of **2a** was monitored by measuring as a function of time the intensity of its absorption at $\lambda_{\text{max}} = 666$ nm in UV–visible spectra and the intensity of the ESR signal for the same sample. Slopes that differed by less than 3% were obtained for the linear plots over more than 2 half-lives ($R = 0.998$ UV–visible, 0.990 ESR) of 1/OD (UV–visible) and 1/ I ($I =$ ESR signal intensity in arbitrary units) vs time.

Acknowledgment. This work received financial support from the National Science Foundation under Grant CHE-9108130. We thank S. I. Weissman for advice and assistance.

OM9405302

(23) Hudson, A.; Lappert, M. F.; Lednor, P. W. *J. Chem. Soc., Dalton Trans.* **1976**, 2369.

(19) Rodriguez, C. F.; Hopkinson, A. C. *J. Phys. Chem.* **1993**, *97*, 849.

(20) Rhodes, C. J. *J. Chem. Soc., Perkin Trans. 2* **1992**, 1475.

(21) Guerra, M. *J. Am. Chem. Soc.* **1993**, *115*, 11926.

(22) Davies, A. G.; Smith, P. J. *Comp. Organomet. Chem.* **1982**, *2*, 521.

First X-ray Structure Analysis of cis/trans Paired Diastereoisomeric Chlorobismuthanes Bearing a Chiral Bismuth Center Induced by the (R)-1-(Dimethylamino)ethyl Group as a Chiral Source. Unexpected Axial Disposition of the Benzylic Methyl Group Causing the Equilibrium Isomer Ratio in Solution To Be Insensitive to Steric Congestion around the Bismuth Atom

Toshihiro Murafuji, Nagao Azuma, and Hitomi Suzuki

Organometallics, 1995, 14 (3), 1542-1544 • DOI: 10.1021/om00003a071 • Publication Date (Web): 01 May 2002

Downloaded from <http://pubs.acs.org> on March 9, 2009

More About This Article

The permalink <http://dx.doi.org/10.1021/om00003a071> provides access to:

- Links to articles and content related to this article
- Copyright permission to reproduce figures and/or text from this article



ACS Publications
High quality. High impact.

First X-ray Structure Analysis of *cis/trans* Paired Diastereoisomeric Chlorobismuthanes Bearing a Chiral Bismuth Center Induced by the (*R*)-1-(Dimethylamino)ethyl Group as a Chiral Source. Unexpected Axial Disposition of the Benzylic Methyl Group Causing the Equilibrium Isomer Ratio in Solution To Be Insensitive to Steric Congestion around the Bismuth Atom

Toshihiro Murafuji*

*Department of Chemistry, Faculty of Science, Yamaguchi University,
Yoshida, Yamaguchi 753, Japan*

Nagao Azuma

*Department of Chemistry, Faculty of General Education, Ehime University,
Bunkyo-cho, Matsuyama 790, Japan*

Hitomi Suzuki*

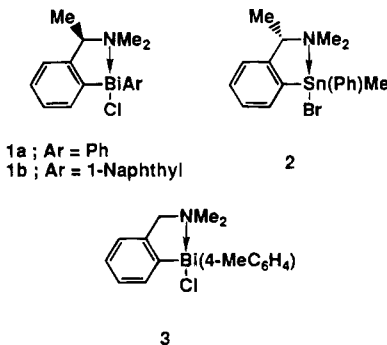
*Department of Chemistry, Faculty of Science, Kyoto University,
Sakyo-ku, Kyoto 606-01, Japan*

Received December 1, 1994[®]

Summary: *cis/trans* paired diastereoisomeric chlorophenyl[2-[(*R*)-1-(dimethylamino)ethyl]phenyl]bismuthanes, 2-[(*R*)-Me₂NCHMe]C₆H₄BiPhCl (**1a**), have been characterized by X-ray structure determination. The crystal structure involves the packing of two pairs of discrete mononuclear molecules in the unit cell, and the asymmetric unit contains a pair of diastereoisomeric molecules, the configurations of which are identical as to the chiral ligand but different as to the chirality of the bismuth atom. The benzylic methyl group of the chiral ligand prefers the axial disposition, which is in contrast to the related organotin bromide 2-(Me₂NCHMe)-C₆H₄SnMePhBr (**2**), where the equatorial location is much preferred.

Introduction

Recently, we have reported the first synthesis of diastereoisomeric chlorobismuthane **1a** with a chiral bismuth center by introducing the 2-[(*R*)-1-(dimethylamino)ethyl]phenyl group as a chiral source onto the bismuth atom.¹ The diastereoselection observed for



compound **1a** was only moderate (77:23). Expecting

that an increase in steric crowdedness around the bismuth atom would enhance the degree of diastereoselection, we prepared compound **1b** similarly. Rather surprisingly, however, the diastereoisomeric ratio was found to be almost the same (78:22). This unexpected result may be accounted for by two possibilities. One is that the methyl group at the chiral benzylic position takes a favorable equatorial site in the chelate ring of compound **1**, and its bulkiness is not enough to induce a high diastereoselection. The other is that the methyl group is forced to occupy an unfavorable axial position due to some steric reason, leading it to be a spectator substituent. The former is the case with the related chiral tin compound 2-(Me₂NCHMe)C₆H₄SnMePhBr (**2**).^{2,3} As an example of the latter case, we now report a full characterization of the *cis/trans* paired diastereoisomeric chlorobismuthanes **1a** by X-ray structure analysis. Comparison of the molecular structure of compound **1a** with that of compound **2** revealed that the disposition of the benzylic methyl group is closely related to the equatorial bond angles of the chiral metal center, *i.e.*, axial for **1a** and equatorial for **2**, the former disposition making the equilibrium ratio of the diastereoisomers in solution insensitive to the bulkiness of the aryl group at the equatorial site.

Results and Discussion

According to our reported procedure,¹ the diastereoisomeric chlorobismuthane **1a** was synthesized from the corresponding lithiated dimethyl[(*R*)-1-phenylethyl]amine and chlorodiphenylbismuthane. A single crystal of compound **1a** obtained by crystallization of the diastereoisomeric mixture from methanol was examined

(2) van Koten, G.; Jastrzebski, J. T. B. H.; Noltes, J. G.; Pontenagel, W. M. G. F.; Spek, A. L. *J. Am. Chem. Soc.* **1978**, *100*, 5021.

(3) High diastereoselectivity (>98%) was realized by substituting the methyl group for the *tert*-butyl group. See: Jastrzebski, J. T. B. H.; Boersma, J.; van Koten, G. *J. Organomet. Chem.* **1991**, *413*, 43.

[®] Abstract published in *Advance ACS Abstracts*, February 15, 1995.
 (1) Suzuki, H.; Murafuji, T.; Matano, Y.; Azuma, N. *J. Chem. Soc., Perkin Trans. 1* **1993**, 2969.

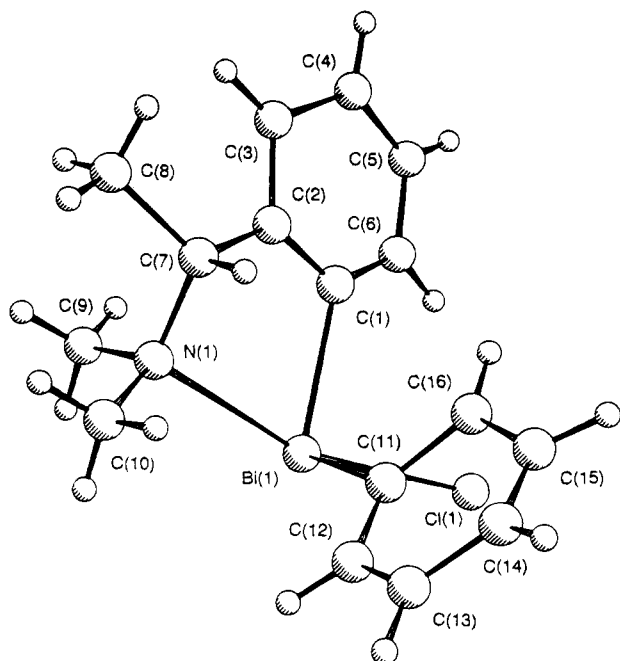


Figure 1. Crystal structure of the *trans* isomer of compound **1a**. For the definition of *cis* and *trans* isomers, see text.

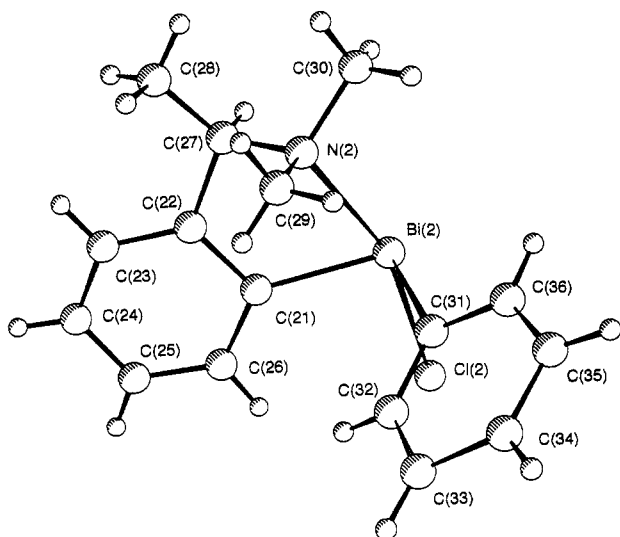


Figure 2. Crystal structure of the *cis* isomer of compound **1a**. For the definition of *cis* and *trans* isomers, see text.

by X-ray analysis, which revealed that the asymmetric unit contains a pair of independent molecules with a configuration different at the chiral bismuth center, where the benzylic methyl and equatorial phenyl groups are disposed in a *cis* or *trans* fashion as shown in Figures 1 and 2, respectively. The bismuth center of both isomers was shown to have a distorted-pseudotrigonal-bipyramidal configuration with two aryl groups in an equatorial plane. The lone pair of electrons is considered to occupy the remaining equatorial position. The apical positions are occupied by the nitrogen and chlorine atoms through the formation of a hypervalent three-center–four-electron bond.⁴ The intramolecular Bi–N distance of the *trans* isomer (2.55(2) Å) is a bit shorter than that of the *cis* isomer (2.57(2) Å), suggesting the operation of a stronger Bi–N interaction in the

Table 1. Selected Bond Lengths (Å) and Angles (deg) for *cis/trans* Paired Diastereoisomeric Chlorobismuthanes **1a**^a

	<i>trans</i> isomer	<i>cis</i> isomer	
Bi(1)–N(1)	2.55(2)	Bi(2)–N(2)	2.57(2)
Bi(1)–C(11)	2.25(2)	Bi(2)–C(31)	2.26(2)
Bi(1)–C(1)	2.30(2)	Bi(2)–C(21)	2.16(2)
Bi(1)–Cl(1)	2.646(6)	Bi(2)–Cl(2)	2.634(6)
N(1)–Bi(1)–Cl(1)	162.7(4)	N(2)–Bi(2)–Cl(2)	161.7(4)
N(1)–Bi(1)–C(1)	72.7(7)	N(2)–Bi(2)–C(21)	72.0(6)
N(1)–Bi(1)–C(11)	88.9(6)	N(2)–Bi(2)–C(31)	86.6(6)
C(1)–Bi(1)–C(11)	95.6(7)	C(21)–Bi(2)–C(31)	98.0(8)
C(7)–N(1)–Bi(1)	106(1)	C(27)–N(2)–Bi(2)	102(1)
N(1)–C(7)–C(2)	105(2)	N(2)–C(27)–C(22)	107(2)

^a Numerals in parentheses are estimated standard deviations.

former compound (Table 1).⁵ In accordance with this, the Bi–Cl bond length of the *trans* isomer (2.646(6) Å) is longer than that of the *cis* isomer (2.634(6) Å). The C(Ar)–Bi–C(Ph) angle of the *cis* isomer (98.0(8)°) is larger than those of the *trans* isomer (95.6(7)°) and of the chlorobismuthane **3** (93.7(2)°).¹ All these observations support the view that the *cis* isomer is forced into a more strained geometry than the *trans* isomer by the presence of the methyl group at the benzylic position. The short intermolecular bismuth–chlorine bond distances of 3.717(7) Å for Bi(1)–Cl(2) and 3.696(8) Å for Bi(2)–Cl(1) indicate the operation of strong interaction between the pairs of *cis/trans* isomers, which are linked together by the sharing of chlorine atoms into the infinite chains in the crystallographic *a*-axis direction.

The most unusual structural feature of compound **1a** concerns the methyl group at the benzylic position. Despite the steric compression by the neighboring dimethylamino group and nearby *ortho* hydrogen atom of the phenylene ring, this methyl group has a tendency to adopt an apparently unfavorable axial position in the five-membered chelate ring. This is in contrast to a similar situation observed for compound **2**, where the benzylic methyl group preferentially occupies the equatorial position. This discrepancy in the preferred configurations may well be attributed to the difference of the equatorial bond angles of the respective chiral metal centers. The large C(Ar)–Sn–C(Ph) angle of 116.1(3)° in compound **2** would lessen the steric repulsion between the methyl and phenyl groups, making the equatorial location of the methyl group more favorable in the organotin compound **2**. In contrast, the smaller C(Ar)–Bi–C(Ph) angle of 98.0(8)° in compound **1a** would give rise to high steric congestion between these two groups, thus enforcing the benzylic methyl group to occupy the axial position in both diastereomers. The reason the methyl group does not prefer the equatorial position in the *trans* isomer may be attributed to the stereoelectronic repulsion between the methyl group and the lone pair of electrons, which should arise when such a position is adopted.

¹H NMR inspection of the diastereoisomeric mixture of **1a** revealed that the structural feature in the solid state is also reflected in solution. When dissolved in CDCl₃, compound **1a** forms an equilibrium mixture of two diastereoisomers (77:23) through the Bi–N dissociation–association process. The methine proton signal of the ethylidene group of the major isomer was observed at appreciably high field (δ 3.57) relative to that of the minor isomer (δ 3.89), showing the former methine proton to be subject to the shielding effect of

(4) Suzuki, H.; Murafuji, T.; Azuma, N. *J. Chem. Soc., Perkin Trans. 1* **1993**, 1169.

(5) The corresponding Bi–N distance and Bi–Cl bond length in chlorobismuthane **3** are 2.525(6) and 2.700(2) Å, respectively.

Table 2. Chemical Shifts (δ) of the 1-(Dimethylamino)ethyl Group^a

isomer	NMe ₂		$\Delta\nu$, Hz	α -Me	α -H	
1a	major (<i>trans</i>)	2.36	2.39	6	1.31	3.57
	minor (<i>cis</i>)	2.03	2.70	134	1.09	3.89
1b	major (<i>trans</i>)	2.12	2.37	50	1.26	3.62
	minor (<i>cis</i>)	1.84	2.67	166	1.01	3.84

^a Determined in CDCl₃ at room temperature.**Table 3. Positional Parameters and Isotropic Thermal Parameters (\AA^2) for 1a^a**

atom	x	y	z	B(eq) ^b
Bi(1)	0.5955(1)	0	0.83191(6)	3.93(3)
Bi(2)	0.1010(1)	-0.23315(5)	0.81021(6)	4.02(3)
Cl(1)	0.3234(8)	-0.0371(5)	0.8853(6)	7.4(4)
Cl(2)	-0.1560(8)	-0.1909(5)	0.8796(6)	7.5(4)
N(1)	0.818(2)	0.079(1)	0.769(1)	5.0(8)
N(2)	0.301(2)	-0.318(1)	0.727(1)	4.0(7)
C(1)	0.541(3)	0.140(1)	0.838(2)	4(1)
C(2)	0.639(3)	0.188(1)	0.803(2)	5(1)
C(3)	0.635(4)	0.276(2)	0.821(2)	9(2)
C(4)	0.509(3)	0.304(2)	0.876(2)	7(1)
C(5)	0.419(3)	0.250(2)	0.920(2)	9(2)
C(6)	0.438(3)	0.167(2)	0.899(2)	7(1)
C(7)	0.748(2)	0.160(1)	0.722(2)	5(1)
C(8)	0.871(4)	0.225(2)	0.696(3)	12(2)
C(9)	0.932(3)	0.090(2)	0.874(2)	8(1)
C(10)	0.884(3)	0.033(2)	0.686(2)	7(1)
C(11)	0.476(2)	-0.017(1)	0.648(1)	3.4(8)
C(12)	0.529(2)	-0.073(1)	0.581(2)	5(1)
C(13)	0.458(3)	-0.085(2)	0.472(2)	6(1)
C(14)	0.336(3)	-0.038(2)	0.427(2)	7(1)
C(15)	0.281(2)	0.013(2)	0.485(2)	7(1)
C(16)	0.355(3)	0.036(2)	0.599(2)	6(1)
C(21)	0.049(2)	-0.364(1)	0.824(1)	3.2(8)
C(22)	0.177(2)	-0.423(1)	0.823(1)	4(1)
C(23)	0.152(3)	-0.508(1)	0.843(2)	5(1)
C(24)	0.015(4)	-0.540(2)	0.864(2)	8(2)
C(25)	-0.109(3)	-0.487(2)	0.863(2)	5(1)
C(26)	-0.094(2)	-0.402(1)	0.844(2)	5(1)
C(27)	0.337(2)	-0.387(1)	0.809(2)	5(1)
C(28)	0.450(3)	-0.448(2)	0.791(2)	10(2)
C(29)	0.246(3)	-0.349(1)	0.611(2)	7(1)
C(30)	0.446(3)	-0.263(2)	0.737(2)	7(1)
C(31)	-0.032(2)	-0.214(2)	0.629(1)	5(1)
C(32)	-0.164(3)	-0.258(1)	0.576(2)	5(1)
C(33)	-0.249(3)	-0.247(2)	0.461(2)	7(1)
C(34)	-0.183(3)	-0.177(2)	0.404(2)	6(1)
C(35)	-0.056(3)	-0.129(2)	0.460(2)	6(1)
C(36)	0.022(3)	-0.150(2)	0.569(2)	6(1)

^a Numerals in parentheses are estimated standard deviations. ^b B(eq) = 1.33 [a²B₁₁ + b²B₂₂ + c²B₃₃ + ab(cos γ)B₁₂ + ac(cos β)B₁₃ + bc(cos α)B₂₃].

the aryl group at the equatorial position (Table 2). This indicates that the major and minor isomers possess the *trans* and *cis* geometry, respectively, for the benzylic methyl and equatorial phenyl groups in the five-membered chelate ring. A high-field shift of the benzylic methyl absorption of the *cis* isomer may be accounted for by flipping of the puckered chelate ring. The *N*-methyl groups are also subject to the anisotropic effect of the aryl ring, but the degree is considerably dependent on the geometry of the respective isomers. As has been shown in Figure 2, one of the *N*-methyl groups in the *cis* isomer is located above the aromatic ring, which is well reflected by a marked difference between the $\Delta\nu$ values for the diastereotopic *N*-methyl protons of both diastereoisomers (Table 2). Such a remarkable anisotropic effect was not observed for the *trans* isomer. These observations confirm that the preferred conformation of compound **1a** in solution is similar to that in the solid state, the benzylic methyl group being preferentially fixed at the axial position in

both diastereoisomers. Thus, we have finally reached a unique answer to the puzzling phenomenon why the diastereoisomeric ratios of compounds **1a** and **1b** are so insensitive to the steric bulkiness of another aryl group attached to the chiral bismuth center.

Experimental Section

Chlorophenyl[2-(*R*)-1-(dimethylamino)ethyl]phenyl]bismuthane (**1a**) was obtained in a crystalline form of a 1:1 diastereoisomeric mixture according to our reported procedure.¹ ¹H NMR spectra were recorded in CDCl₃ on a Varian Gemini-200 (200 MHz) spectrometer with tetramethylsilane as an internal standard.

X-ray Crystallography of Compound 1a. A crystal of dimensions 0.230 × 0.380 × 0.350 mm grown from methanol at ambient temperature was used for X-ray crystallography.

Crystal Data. C₁₆H₁₉NBiCl, *M*_r = 469.77, monoclinic, space group *P*2₁, *a* = 8.672(5) Å, *b* = 16.041(7) Å, *c* = 12.058(4) Å, β = 102.63(3)°, *V* = 1637(1) Å³, *Z* = 4, *D*_c = 1.906 g cm⁻³, colorless prisms, μ (Mo *K* α , λ = 0.710 69 Å) = 108.93 cm⁻¹. Intensity data were collected on a Rigaku AFC5R diffractometer with graphite-monochromated Mo *K* α radiation and a 12 kW rotating-anode generator using the ω -2 θ scan technique to a maximum 2 θ value of 55.0°. Scans of (1.47 + 0.30 tan θ)° were made at a speed of 16.0° min⁻¹ (in ω). Of the 4142 reflections which were collected, 3898 were unique (*R*_{int} = 0.093). Data were corrected for Lorentz, polarization, and absorption effects. Empirical correction for the absorption was made on the basis of azimuthal or ψ scans⁶ (transmission factors 0.57–1.00). The structure was solved by the Patterson method.⁷ The non-hydrogen atoms were refined anisotropically. The final cycle of full-matrix least-squares refinement was based on 2174 observed reflections (*I* > 3.00 σ (*I*)), and 343 variable parameters converged with unweighted and weighted agreement factors of *R* = 0.041 and *R*_w = 0.036. The residual electron densities in the final difference Fourier map ranged from -1.20 to 1.10 e/Å³. The weighting scheme $w = 1/\sigma^2(F_o)$ was employed. Neutral atom scattering factors were taken from Cromer and Waber.⁸ Anomalous dispersion effects were included in *F*_c⁹ the values for $\Delta f'$ and $\Delta f''$ were those of Cromer.¹⁰ All calculations were performed on a VAXstation 3200 computer using the TEXSAN¹¹ crystallographic software package from Molecular Structure Corp. The PLUTO program¹² was used to obtain the drawings in Figures 1 and 2. Selected bond lengths and bond angles are given in Table 1, and atomic coordinates are given in Table 3.

Acknowledgment. The present work was supported by Grants-in-Aid for Scientific Research from the Ministry of Education and Culture of Japan (No. 05236101 and 06740550). T.M. thanks the Japan Society for the Promotion of Science for the Fellowship (No. 1339).

Supplementary Material Available: Full details of crystal data, fractional atomic coordinates, bond lengths, bond angles, hydrogen coordinates, and thermal parameters for **1a** and unit cell and ORTEP diagrams (29 pages). Ordering information is given on any current masthead page.

OM940921G

(6) North, A. C.; Phillips, D. C.; Mathews, F. S. *Acta Crystallogr., Sect. A* **1968**, *24*, 351.

(7) Structure solution method: Calabrese, J. C. PHASE: Patterson Heavy Atom Solution Extractor. Ph.D. Thesis, University of Wisconsin—Madison, 1972.

(8) Cromer, D. T.; Waber, J. T. *International Tables for X-ray Crystallography*; Kynoch Press: Birmingham, England, 1974; Vol. IV, Table 2. 2 A.(9) Ibers, J. A.; Hamilton, W. C. *Acta Crystallogr.* **1964**, *17*, 781.(10) Cromer, D. T. *International Tables for X-ray Crystallography*; Kynoch Press: Birmingham, England, 1974; Vol. IV, Table 2.3.1.

(11) TEXSAN-TEXRAY Structure Analysis Package, Molecular Structure Corp., The Woodlands, TX, 1985.

(12) Motherwell, S.; Clegg, W. PLUTO Program for Plotting Molecular and Crystal Structures; University of Cambridge, Cambridge, England, 1978.